

John K. Warren

EVAPORITES

SEDIMENTS, RESOURCES
AND HYDROCARBONS

 Springer

John K. Warren

Evaporites : Sediments, Resources and Hydrocarbons

John K. Warren

Evaporites : Sediments, Resources and Hydrocarbons

With 654 Figures

 Springer

Professor John K. Warren
Department Petroleum Geoscience
University Brunei Darussalam
Brunei

E-mail: jkwarren@ozemail.com.au

ISBN-10 3-540-26011-0 Springer Berlin Heidelberg New York
ISBN-13 978-3-540-26011-0 Springer Berlin Heidelberg New York

Library of Congress Control Number: 2005932089

This work is subject to copyright. All rights are reserved, whether the whole or part of the material is concerned, specifically the rights of translation, reprinting, reuse of illustrations, recitation, broadcasting, reproduction on microfilm or in any other way, and storage in data banks. Duplication of this publication or parts thereof is permitted only under the provisions of the German Copyright Law of September 9, 1965, in its current version, and permission for use must always be obtained from Springer-Verlag. Violations are liable to prosecution under the German Copyright Law.

Springer is a part of Springer Science+Business Media

springer.com

© Springer-Verlag Berlin Heidelberg 2006

Printed in Germany

The use of general descriptive names, registered names, trademarks, etc. in this publication does not imply, even in the absence of a specific statement, that such names are exempt from the relevant protective laws and regulations and therefore free for general use.

Typesetting: Camera-ready by author
Cover design: E. Kirchner, Heidelberg
Production: Almas Schimmel
Printing and binding: Stürtz AG, Würzburg, Germany
Printed on acid-free paper 32/3141/as 5 4 3 2 1 0

Preface

My aim in writing this book is to offer a comprehensive synthesis of the low temperature (sedimentary) realm of evaporite evolution. It's now more fifteen years since the last comprehensive book on evaporite sedimentology was published; an excellent piece, edited by Judy Melvin (1991). There are also the earlier efforts of yours truly in 1989 and the volume edited by Charlotte Schreiber back in 1988. The present volume follows on from my previous book on evaporites (Warren, 1999). That book attempted to address the diversity of evaporites from deposition into the igneous and metamorphic realms. To achieve this in a single volume without destroying large areas of rainforest meant I had to brush over substantial parts of our wealth of knowledge in evaporite sedimentology, especially in terms of modern depositional studies. In this volume I have attempted to redress this, while also attempting to publish for the first time a comprehensive discussion of the role of evaporites in hydrocarbon generation and trapping. The pulling together of diverse sources of knowledge on exploitable salts, along with a summary of evaporite karst hazards as well as a summary of exploitation methods and pitfalls in dealing with evaporites in conventional and solution mining has not, to my knowledge, been done before.

After an introduction to evaporite textures and depositional brine chemistries (Chapters 1 and 2) this book goes on to present detailed discussions of; Quaternary environments (Chapters 3, 4), ancient salts (Chapter 5), salt tectonics (Chapter 6), evaporite karst and its indicators (Chapter 7), burial hydrology (Chapter 8), life in evaporitic settings and their potential for sourcing hydrocarbons (Chapter 9), the role of evaporites and seals as instigators of hydrocarbon reservoirs and traps in many sedimentary settings (Chapter 10). The last two chapters deal with the characteristics of exploitable salts (Chapter 11) and the methods for their exploitation and utilisation as waste storage receptacles via solution mining (Chapter 12). Chapter 12 also discusses some of the environmental problems that overzealous exploitation or ignorance has created. Parts of this book are updated and expanded versions of some of the chapters in my 1999 book (Chapters 1, 2, 5, 6, 7 and 11), the other chapters are completely new.

I would like to thank the following individuals and companies who allow me to work at the things I enjoy most; geological research and training. First and foremost my thanks to his Majesty, Sultan Haji Hassanal Bolkiah Mu'izzadin Waddaulah Sultan Yang Di-Pertuan of Brunei Darussalam for allowing me to live and work in Brunei. Thanks to the Universiti Brunei Darussalam, which has generously allowed me the time to write this book and also through the UBD research facility funded some of the trips to various libraries to facilitate the gathering of the reference material so necessary in compiling a comprehensive text. Thanks to Brunei Shell (BSP) and to Total Brunei for their foresight in funding the Department of Petroleum Geoscience at UBD and so allow a centre of excellence to grow in this part of the world. My thanks to my fellow faculty and staff in Petroleum Geosciences at Universiti Brunei - Chris, Joe, Angus, Martin, Iqbal, Farrah and Lim. Thanks also to Schlumberger, Earth Sciences at Flinders University, King Fahd University of Petroleum and Minerals, to Ian Cartwright's Group at Monash University in Melbourne and to the former National Centre of Petroleum Geology at Adelaide University for allowing the use of their library facilities in compiling this book. Thanks to Chess at the DMR in Thailand and to Mahbub at King Fahd University, Saudi Arabia, and to all the other groups and individuals who over the years have challenged and changed my ideas on evaporites.

Most importantly and most completely, my thanks to my wife Jennifer, who even after more than 30 years of marriage still manages to live with her at times abstracted other half.

Lastly, I would like to acknowledge NASA. The numerous Landsat images used throughout this book to illustrate modern depositional patterns were cut from larger scenes downloaded from the GeoCover Orthorectified Landsat Thematic Mapper Mosaics site (<https://zulu.ssc.nasa.gov/mrsid/>). The data set was produced by the Earth Satellite Corporation for NASA and came from satellite imagery acquired by Landsat 5 & 7, circa 1990 & 2000. It is an excellent scientific resource published on the internet for free use by the world community but now perhaps superseded by Google Earth.

John K. Warren, November, 2005
Department of Petroleum Geoscience
Universiti Brunei Darussalam
<jkwarren@ozemail.com.au>

TO MY WIFE, JENNIFER
AND MY SONS,
MATTHEW AND TRISTAN

Eppur si muove

(And yet, it does move)

Galileo Galilei after recanting Copernican beliefs

Contents

Chapter 1: Interpreting evaporite texture.....	1
Evaporites defined?.....	2
Primary evaporites	5
Evaporitic carbonates.....	5
Carbonate laminites (subaqueous sediment?).....	5
Strandzone associations: Microbialites, pisolites and tepees	6
Stromatolites and microbialites	6
Vadose pisolites, ooids and other coated grains.....	16
Tepees	18
Carbonates - present and past	20
Primary evaporite salts.....	22
Gypsum beds	23
Halite beds (chevrons and crusts)	26
Halite cumulates, rafts and coated grains	27
Pedogenic and wind reworked salts.....	28
Laminites from settling of pelagic salts.....	33
Can growth-aligned evaporite crystals, interlayered with laminites, be deep?	35
Salt reefs, are they real?.....	36
Secondary (diagenetic) evaporites	38
Intrasediment salts ...	38
Sabkha nodules and crystals	40
Syn depositional karst in crusts	40
Nearsurface crystal and crust dissolution	41
Coming and going of salt crusts	41
Lenticular mudcracks.....	42
Haloturbated and chaotic halite	43
Shallow mineralogic re-equilibration	43
Porosity loss.....	44
Deeper burial - mosaic halite?	45
Limpid dolomite in mosaic halite	46
Burial of sulphate evaporites	47
Nodular anhydrite and water loss	47
Burial Salts: Nodules and stylolites	50
Evaporites as uplift indicators.....	51
Fibrous gypsum and halite (satinspar)	52
Saline clay authigenesis	54
Textural Synthesis	56
Chapter 2: Depositional chemistry and hydrology	59
Quaternary climatic hydrology	59
Chemical evolution of surface and nearsurface brines	67
Marine brines	67
Chemical composition and phase chemistry.....	67
Brine mixing drives precipitation or dissolution	74
Nonmarine brines.....	76
Trona- nahcolite chemistry (Path I brine).....	78
Are most continental salt lakes hydrologically closed?.....	79
Separating marine from nonmarine	83
Back reactions.....	83
Marine aerosols supply continental lakes	86

Acid groundwater in continental saline systems.....	88
Contributions from evaporite bedrock	91
Indicators of brine parenthood.....	92
Bromine profiles - brine genesis or stability?	92
Sulphur and oxygen isotopes	94
Boron Isotopes	96
Chlorine isotopes	98
Fluid Inclusions and brine temperatures	100
Seawater evolution.....	101
A Phanerozoic dilemma: marine versus nonmarine potash?	101
Precambrian oceanic chemistry	105
Hydrology is depositional style	112
Active phreatic/vadose regime.....	113
Hydrologies in saline basins	113
Mudflat aggradation mirrors water table changes	117
Indicators of fluctuating water tables.....	118
Stokes surfaces.....	119
Stokes surfaces and palaeohydrology	121
Degrading hydrology and playa capture.....	124
Salinity stratification and textures.....	126
Brine stability and evaporite textures	129
Brine reflux drives substrate alteration	130
Can reflux really work?.....	136

Chapter 3: Sabkhas, saline mudflats and pans 139

Introduction.....	139
What is a Sabkha?	139
Marine coastal sabkhas	141
Carbonate-hosted coastal sabkhas in the southern Arabian Gulf.....	143
Abu Dhabi facies associations	145
Island shoal and bank facies	145
Subtidal Facies.....	145
Intertidal facies (strandline sands)	148
Intertidal Facies (Lagoon-edge muds)	149
Supratidal Facies	151
Sabkha hydrology and hydrogeochemistry.....	152
Siliciclastic-hosted coastal sabkhas, western and northern Arabian Gulf	159
Coastal sabkhas of eastern Saudi Arabia	160
Sabkhas of coastal Kuwait.....	161
Sabkhas of Kadmah Bay.....	161
Al-Khiran Sabkha	164
Other coastal sabkhas.....	166
Gulf of Suez.....	167
Beach-dune and fluvial sabkhat on deltas.....	168
Western Nile delta coast, Mediterranean Egypt.....	168
Eastern Mediterranean Coast of the Nile Delta and Northern Sinai.....	170
Shatt el Arab estuarine sabkha, Iraq	172
Interpretive limitations of models based on Holocene sabkhas	173
Lacustrine sabkhas and pans.....	176
Depositional characteristics	176
The saline mudflat.....	178
Groundwater transport and fractionation in saline mudflats.....	178
Saline pan.....	179
Styles of continental sabkhas.....	181

Alluvial fan–ephemeral saline lake.....	181
Sabkha Yotvata, Israel.....	181
Basin and Range playas, USA.....	182
Salars of South America.....	187
Ephemeral stream floodplain - dune field–ephemeral saline lake.....	201
Lake Eyre, Australia.....	202
Lake Frome, Australia.....	208
Lake Callabonna, Australia.....	210
Perennial stream floodplain–perennial saline lake.....	210
Eolian sabkhas.....	211
Sea-margins with elongate eolian sabkhat.....	212
Sheets of eolian sabkhat.....	215
Salt pans (marshes) and diapirs.....	219

Chapter 4: Subaqueous salts: salinas and perennial lakes 221

Introduction.....	221
Sea-margin subaqueous salts.....	222
Coastal salinas of Australia.....	222
Carbonate salinas.....	223
Gypsum salinas.....	227
Halite salinas.....	230
Coastal salinas of the Middle East.....	231
Solar Lake, Gulf of Elat.....	231
Ras Muhammad Pool, Southern Sinai.....	232
Late Pleistocene salinas on the Egyptian Red Sea Coast.....	234
South American coastal salinas.....	236
Continental subaqueous basins.....	238
Perennial saline lakes.....	238
Great Salt Lake, Utah.....	239
Mono Lake, California.....	243
Lake levels and conditions.....	244
Tufa mound and pinnacles.....	244
Hydrological and hydrogeochemical evolution.....	246
Saline lakes of Turkey.....	247
Lake Van, Turkey.....	247
Salda Lake, Turkey.....	250
Lake Tuz, Turkey (Tuz Gölü).....	252
Lake Aci, Turkey.....	253
Lake Urmia, NW Iran.....	254
Lake Natron and Lake Magadi, East Africa.....	255
Brine chemistry.....	257
Holocene sediments.....	258
Late Pleistocene sediments.....	260
Diagenesis - magadiite and evaporitic chert.....	262
Dead Sea, Middle East.....	264
Geological Setting.....	265
Water level changes.....	266
Density stratification: Holomixis versus meromixis.....	268
Deep water Halite.....	270
Deep water laminites.....	273
Basin margin sediments.....	275
Lake Lisan, Jordan Valley.....	277
Lake Asal, Republic of Djibouti.....	280
Are all modern saline lakes shallow?.....	282

Chapter 5: Ancient basins and stratigraphic evolution..... 287

Linking present to past aridity	288
Varying extent of ancient evaporites.....	293
Building blocks of ancient salt beds	296
Evaporites: broad scale models.....	300
Lacustrine evaporites	301
Eocene Lake Gosuite, USA	304
Oligo-Miocene lake, Calatayud Basin, Spain	306
Permian lacustrine redbeds , Kansas	308
Other Lacustrine Red Bed Associations	310
Platform evaporites on epeiric shelves	310
Evaporitic epeiric ramps	312
Evaporites atop rimmed epeiric shelves	318
Marine versus nonmarine stages in epeiric seaways	323
Basinwide evaporites	324
Depositional styles.....	327
Tectonic styles.....	329
Importance of hydrographic isolation.....	332
Problems in correlation <i>sans</i> hydrology	335
Dolomite aprons in a drawdown basin	337
Sequence stratigraphy in evaporite basins?	340
Does sealevel control salt sequences?	342
Icehouse and greenhouse eustacy	343
Marine-margin platform evaporites	345
Platform evaporites in a greenhouse earth?	346
Basinwide evaporites	347
Basinwide sequence stratigraphy?.....	348
Basinwide examples	351
Messinian evaporites of the Mediterranean	351
Sequence stratigraphy in the Zechstein	362
Sequence stratigraphy in the Silurian Salina Group of the Michigan Basin	368
Summary	372

Chapter 6: Salt tectonics 375

Introduction	375
Physics of salt systems—	376
Density, viscosity, strength & buoyancy.....	376
Pressure effects	382
Thermal effects	384
Flow textures and rates	384
Triggers, drivers and outcomes of salt flow	389
Diapirs and extension.....	389
Diapirism and differential loading	391
Sedimentation rate controls diapir shape	394
Extension, falling diapirs and turtles	396
Falling diapirs and raft tectonics.....	396
Salt allochthons (salt breakout).....	398
Sheets, welds and basal (subsalt) shear zones	401
Near-diapir suprasalt shear (drag zones).....	404
Welds, loading detachments and growth faults	406
Minibasins floors become welds.....	408
Fault families in allochthons.....	410
Linking allochthons at the basin scale	413

Compressional salt tectonics.....	414
Shortening with gravity gliding	414
Thin-skinned fold and thrust belts	419
Inverted basins	422
Mild shortening in tectonically confined basins	423
Can extrusion indicate extreme shortening?.....	425
Distinguishing downbuilt and reactivated (mildly squeezed) diapirs.....	428
Sediments and flowing salt	430
Sediments and evolving salt structures	432
Siliciclastic patterns	435
Carbonate patterns	436
Sediments tied to salt basin evolution.....	440
Suprasalt clastic sedimentation.....	440
Suprasalt carbonate sedimentation.....	441
Subsalt sections.....	446
Caprock Formation (diagenesis).....	447
Complications of shale diapirism	450
Summary	452

Chapter 7: Karst, breccia, nodules and cement: Pointers to vanished evaporites 455

Introduction.....	455
Evaporite landforms....	458
Local scale karst.....	458
Dolines or sinkholes	458
Suffosion dolines	459
Collapse dolines.....	459
Solution Dolines	459
Breccia Chimneys and Pipes.....	460
Landscape residuals; karst domes and castiles	460
Expansion morphotypes at outcrop.....	462
Regional scale karst	463
Subsidence basins or troughs.....	463
Hutchison Salt, Kansas	464
Delaware Basin, west Texas	466
Holbrook Anticline, Arizona.....	468
Black Hills, South Dakota	469
Subsidence and landscape in diapiric regions.....	469
Five Islands, Gulf of Mexico	470
Zagros/Hormuz region, Arabian (Persian) Gulf	471
Salt Dissolution: Solution breccias and residues	472
Defining evaporite dissolution breccia	472
Bedded solution collapse breccias	474
Breccia extent	478
Stratiform breccias	478
Hydrology and texture	479
Diapiric solution breccias	481
Diapiric breccia versus salt ablation (retreat) breccia.....	485
Salt-cored thrust breccias, rauhwacke and orogeny.....	486
Partial salt dissolution: residues of less-soluble salts	493
Focused rapid dissolution - Evaporite clasts.....	493
Diffuse dissolution- Markers and residue beds.....	495
Gentle dissolution at the top	495

Maha Sarakham salt, Thailand.....	495
Palo Duro Basin, west Texas	497
Dissolution at the bottom	498
Basal anhydrite, Thailand	498
Caves in salt karst	500
Gypsum caves.....	501
Phreatic gypsum caves.....	502
Vadose gypsum caves	504
Miocene karst in the Madrid Basin, Spain.....	504
Modern karst in Cretaceous gypsum, Texas	506
Modern gypsum karst in Saudi Arabia	508
Halite Caves.....	509
Modern halite karst in the Dead Sea depression.....	510
Modern halite karst in crests of diapiric Hormuz salt (Precambrian) in the Arabian Gulf.....	512
Evaporite speleothems in carbonate karst.....	514
Karst hazards in evaporites	515
Problems in the Ripon area, UK	517
Problems with Miocene gypsum, Spain	519
Gypsum karst beneath Mosul, Iraq.....	520
Solving the problem?.....	521
Sulphuric acid speleogenesis	521
Mineralised breccias	528
Filled vugs and nodules	531
Silicified evaporites	532
Calcitisation and dedolomitisation.....	539
Calcitisation of evaporites	539
Dedolomitisation of matrix	545
Celestite as an indicator?	548
Fluorite as an indicator?.....	553
Baryte as an indicator?.....	555
Authigenic anhydrite as a burial salt.....	559
Enigmatic outlines in pseudomorphs.....	564
Summary	565

Chapter 8: Burial hydrology and chemistry..... 567

Burial hydrology	567
Fluids in subsiding sedimentary basins	569
Compactional fluids	570
Therobaric fluids.....	571
Deep flow in pull-apart basins	573
Flow in and adjacent to Collision Belts.....	574
Flow in post-orogenic hydrologically-mature basins	575
Alteration, pressure cells and salinity-driven convection.....	581
Haloes, convection and saltout	581
Evaporites as pressure seals	583
Salt-maintained overpressure.....	585
Pressure changes and drilling	591
Salt-generated Underpressure.....	592
Temperature anomalies and brine flow	593
Fluid flow in halokinetic basins	596
Suprasalt fluid flow and alteration	596
Burial dewatering of hydrated salts	601
Brine-rock burial evolution.....	604
Brine chemistry at depth.....	604

Effects and indications of water-salt interactions	610
Crustal cycling of brines?	612

Chapter 9: Halotolerant life in feast or famine (a source of hydrocarbons and a fixer of metals)..... 617

Introduction.....	617
Evaporitic Source rocks	619
Halobiota: adaptations and bio-markers	628
Metabolic pathways in producers and consumers	629
Salinity tolerance in the halobiota	635
Primary producers	636
The ingesters, grazers and pelletizers	639
The vertebrates..	643
Bacterial decomposers and chemosynthesisers	643
Bacterial sulphate reducers	643
Bacterial chemosynthesisers (sulphur oxidizers).....	644
Extremophiles (mostly Archaea)	644
Cellular adaptations to hypersalinity.....	646
Life in a layered microbial mat?	650
Biomarkers and microbial responses to changing salinities	652
Do biomarkers indicate hypersalinity?	655
Organic enrichment.....	658
Biological responses to variably layered brines: Cycles of “feast or famine”.....	660
Salinity change influences organic productivity: The flamingo connection in East Africa lakes.....	661
”Feast or Famine” in the Dead Sea.....	666
Feast or Famine in the Messinian	668
The where and when of productivity	670
Predicting preservation of benthic organics.....	672
Life, brine seeps and dissolving salt allochthons.....	676
Subsurface organic-sulphate reactions.....	685
Bacterial sulphate reduction (BSR)	686
Thermochemical sulphate reduction (TSR).....	689
H ₂ S, natural gas and metallogeny	692
Importance of mesohaline organics and sulphate reduction in stratiform base metal ores	694
Hydrothermal cracking in saline rift lakes.....	699
Summary.....	701

Chapter 10: Oil and gas associations 705

Introduction.....	705
Seal capacity of evaporites	708
So why do evaporites seal?.....	708
Environments favouring seal continuity	711
Reservoirs and traps....	713
Bedded salt seals....	713
“Peritidal” muddy carbonate with evaporitic mudflat seals	716
Ordovician Red River Fm., Williston Basin, USA and Canada	716
Platform carbonates with saltern seals	720
Jurassic Arab Formation, Arabian Gulf	721
Slaughter-Levelland Trend, west Texas and New Mexico	733
Dolomitised limestones Central Basin Platform, west Texas	737
Reservoirs in the Jurassic Smackover Fm., Gulf of Mexico	737
Middle East reservoirs sealed by bedded basinwide evaporites	742

Eocene and Miocene associations, Middle East	742
Silurian pinnacle reef fields, Michigan Basin	746
Evaporite-sealed platform and reefs, Devonian, Canada.....	748
Reservoir quality tied to bedded seals	752
Yates Field, west Texas.....	752
North Ward-Estes Field, Texas	754
Rotliegende sands of Northern Netherlands and North Sea	758
Personalised ramblings on the bedded-evaporite hydrocarbon association.....	759
The importance of recognising depositional differences	759
The importance of recognising dissolution.....	761
Changing directions of brine flux in an evaporite-sealed system	762
Halokinetic salt traps ..	763
Supradiapiric traps	765
Allochthon plays in the deepwater realm	769
Regional plays in the Gulf of Mexico.....	771
How suprasalt becomes subsalt	775
Intrasalt halokinetic plays	776
Subsalt reservoirs in compressional provinces	780
Zagros Fold belt, Iran.....	780
Alpine fold belt in Albania and Romania	784
Rocky Mountain fold belt, USA.....	784
Evaporite Solution	786

Chapter 11: Evaporites as exploited mineral resources..... 791

A history of salt usage.....	791
Potash salts.....	793
Quaternary potash..	796
Playas of the Qaidam Basin.....	796
Danakil Depression, Ethiopia	799
Inland chotts and coastal sabkhas in North Africa.....	801
Sylvite in the Amadeus Basin, Australia.....	804
Potash from brine pumping	805
Ancient (Pre-Quaternary) potash.....	808
Rhine Graben ...	809
Khorat Plateau, Thailand	810
Permian potash, Europe and North America	815
German potash	815
Boulby potash, UK	815
New Mexico potash, USA	817
West Canadian potash (Devonian)	818
Potash geology.....	819
The fluids	821
Other significant potash deposits	822
Canadian Maritimes (Mississippian of Nova Scotia and New Brunswick)	822
Cretaceous trans-Atlantic potash: west Africa and Sergipe Basin, Brazil.....	824
Moroccan Meseta (Late Triassic)	826
How does potash form?	826
Controls on potash quality: Anomalies, leaching and problematic mine waters	827
Other economic salts...	831
Borate salts (tincals).....	831

Turkish borates	834
South American Borates	838
North American borates	841
Other Borate deposits	844
Rock gypsum and rock salt	845
Gypsum.....	845
Rock salt (halite).....	846
Iodine, bromine and lithium salts	847
Nitrate salts (nitratite and salt petre).....	852
Magnesite and magnesia salts.....	854
Sodium carbonate salts (trona)	859
Trona in North America.....	861
Trona in the African rift	865
Sodium sulphate salts (Glauber's salts).....	865
Canadian deposits	868
Spanish deposits	870
Turkish Deposits	871
Other sodium sulphate deposits	872
Sulphur salts (brimstone)	877
Usage history and industry trends.....	878
Types of sulphur deposits	879
Biology of native sulphur	880
Occurrences and textures	880
Zeolites - molecular sieves	882
Geological controls on saline zeolitization	883
Summary	888

Chapter 12: Solution mining and cavern use..... 893

Introduction.....	893
The solution mining process	894
History of salt solution wells	894
Well and cavern design	896
Solution well styles	898
Techniques in potash operations	900
Lithology effects shape	901
Well pad design.....	903
Blinding and phase chemistry.....	904
Phase chemistry - trona solution mining.....	905
Use of Salt Caverns.....	907
Hydrocarbon Storage	907
Waste Disposal	910
Nonradioactive waste disposal.....	911
Radioactive waste	911
Problems in salt mines, well-bores and storage facilities	912
Case histories: caving brinefields	914
Ocnele Mari Brinefield, Romania.....	914
Subsidence in Old Belvedere Spinello, Italy	915
Brinefield and mine collapse near Krakow, Poland.....	916
Induced collapse in the Gellenoncourt saltworks, France	919
Retsof Mine, New York State, USA	920
Sinkhole problems Cargill saltworks, Kansas	921
Brinefield subsidence, Windsor, Ontario	922
Sinkholes in the Detroit River	922
Case histories: caving and leaking wells	924

Wink Sink, west Texas.....	925
Panning Sink, Barton County, Kansas.....	926
Gorham oil field, Russell County, Kansas,	926
Sinkhole at Bayou Choctaw Dome, Louisiana	927
Grand Saline sinkhole, Texas.....	927
Haoud Berkaoui oilfield, Algeria	927
Lake Peigneur, Louisiana.....	928
Case Histories: storage caverns	930
Weeks Island, Louisiana	930
Explosions and fires from cavern leakage	932
The West Hackberry explosion.....	932
The Brenham explosion.....	933
Barber’s Hill explosion and collapse.....	934
Mineola propane fire.....	935
Hutchinson explosion	935
Recognising and preventing potential cavern problems	936
Salt Creep.....	936
Salt falls versus roof collapses.....	938
Ground subsidence.....	938
Surface indicators of breached caverns	939
Monitoring and minimizing collapse	940
So how stable is a storage cavern?.....	941
Cavern Plugging	941
Summary	943
References.....	945
Index.....	1019

Chapter 1: Interpreting evaporite texture

Salts such as halite, gypsum and trona, have long been significant in the affairs of man, both as a preservative and as an industrial feedstock. Gypsum and halite are listed, along with several other salts, in the Sumero-Assyrian dictionaries written during the rule of the Assyrian king Assurbanipal (668-626 BC). By then the ancient Egyptians had been using *natrum*, an impure mixture of trona and other sodium salts, for several thousand years, both as an important part of the mummification process and for salting food. Today halite is a major feedstock to the chemical manufacturing industries, as are several other varieties of salt. Salts are also important in the trapping, sealing and perhaps generation of hydrocarbons and various metal deposits. Manufactured salt cavities are used as long term waste repositories, as receptacles for the safe storage and cycling of liquids and gases and even for the manufacture of peak load electricity. This book is all about where, how and why this is so in the sedimentary realm.

What are the basic requirements to form and preserve a bed of salt? We need; 1) a surface and nearsurface brine body that is saline enough to precipitate and preserve salt, this typically means an arid to semi-arid climatic setting with a drawdown hydrology capable of maintaining substantial volumes of brine at or near the landsurface, 2) accommodation space in a sedimentary depression that is not filled by other sediment, and 3) a burial environment that does not allow sufficient undersaturated throughflow to completely dissolve the buried salts (Figure 1.1).

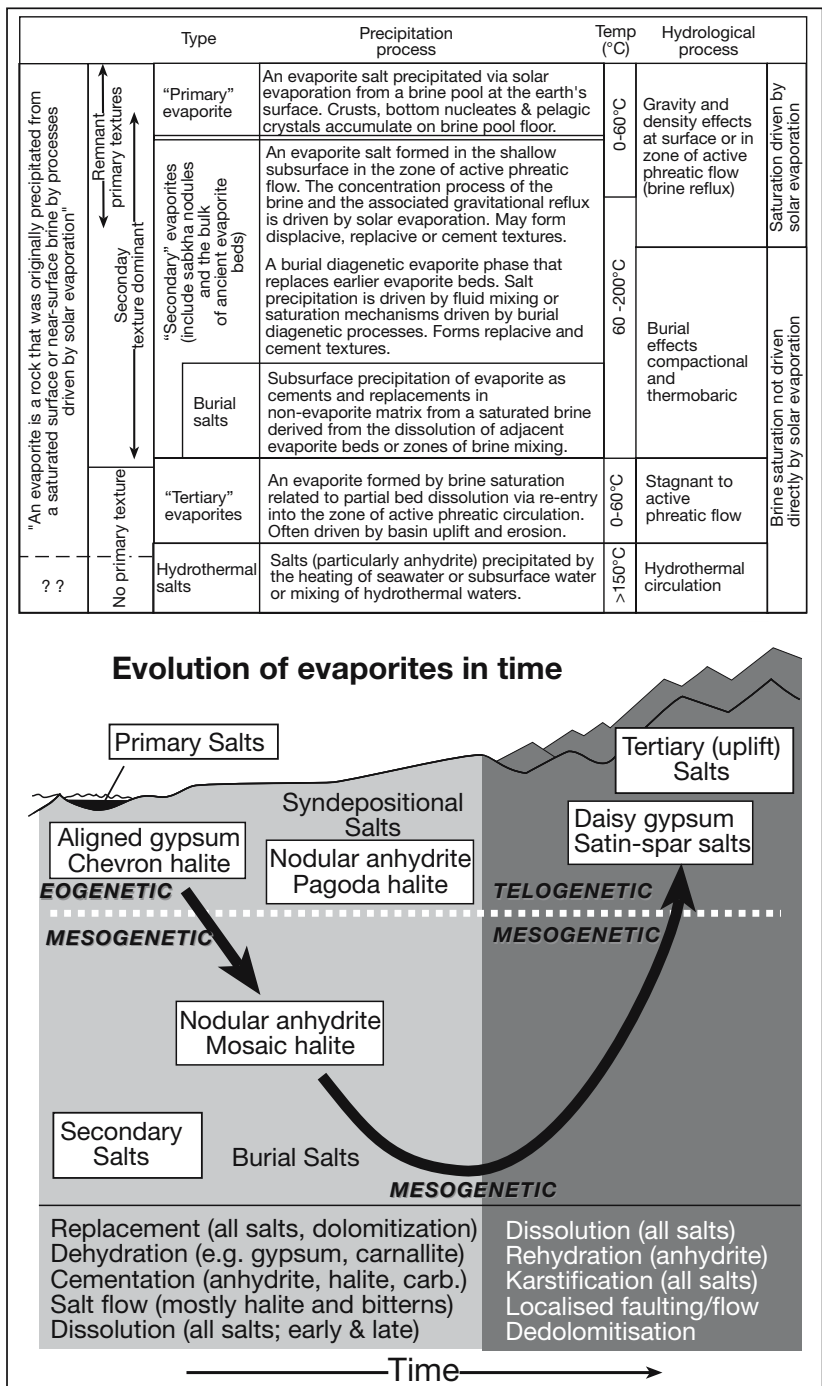


Figure 1.1. Classification of evaporite formation in the depositional-diagenetic realms emphasizing ongoing postdepositional evolution of mineralogy and texture.

Evaporites defined?

I define an evaporite as a salt rock that was originally precipitated from a saturated surface or nearsurface brine by hydrologies driven by solar evaporation (Figure 1.1). This simple definition encompasses a wide range of chemically precipitated salts and includes alkali earth carbonates (Table 1.1). Some workers restrict the term evaporite to those salts formed directly via solar evaporation of hypersaline waters at the earth's surface. In order to emphasise the highly reactive nature of evaporites in the sedimentary realm I think of such evaporites as primary, that is, precipitated from a standing body of surface brine and retaining crystallographic evidence of the depositional process (e.g. bottom-nucleated or current-derived textures). Outside of a few Neogene examples, there are few ancient evaporite beds with textures that are wholly and completely “primary” (Figure 1.1).

Almost every subsurface evaporite texture is secondary; it is diagenetically altered, frequently with fabrics indicating pervasive early recrystallisation and perhaps some later crossflow of basinal waters. Under this definition of a primary versus secondary salt, even the nodules in Holocene mudflats, including those in the type area for sabkhas the Arabian (Persian) Gulf, are secondary textures. They are a porewater overprint superimposed on a primary matrix of mud and sand. Ancient bedded evaporites are typically dominated by secondary textures, although beds may still retain “ghosts” or partial relicts of primary textures such as laminae, aligned anhydrite nodules after growth-aligned gypsum, or patches of aligned halite chevrons floating in a matrix of mosaic halite spar. Even when evaporite beds are extensively recrystallised, most retain laminae made up of impurities that define primary depositional laminae.

In the subsurface it is the ability of evaporites to flow easily, even as they backreact or dissolve, that distinguishes them from other types of sediment. Earliest secondary evaporites are syndepositional precipitates, forming cements and replacements even as the primary matrix accumulates around them. Early replacement sometimes preserves remnants of the original depositional texture, such as gypsum ghosts in nodular anhydrite or aligned halite chevrons. Nodular anhydrite ghosting lenticular gypsum was recognised in Permian mudflats in the early 1960s by Kerr and Thomson (1963), they interpreted it as a subaqueous saline pan indicator. Unfortunately, for the next two decades their results were overlooked by workers in the Permian Basin who incorrectly applied supratidal capillary models based on the Arabian Gulf sabkha anhydrite (Warren and Kendall, 1985).

Early diagenetic overprints and effects of later compaction-driven flow and pressure solution destroy much of the depositional evidence in any ancient evaporite bed. This means retention of primary crystal textures is at best patchy in both halite and anhydrite beds. Many ancient bedded halites are dominated by coarsely crystalline halite spar. Much of it was deposited in multiple episodes of early diagenetic (syndepositional) cementation, leaving less than 10-15% of the bed as primary growth-aligned chevrons. This syndepositional coarse sparry halite formed in multiple dissolution-precipitation events in microkarst pits and was precipitated between successive depositional episodes of chevron halite crust formation (Chapter 3). Other coarsely crystalline halite spar, especially in halokinetic beds, shows pervasive and multiple flow-aligned textures created by pressure-solution. Textures are driven by numerous salt creep and recrystallisation episodes, which occur millennia to millions of years postdeposition, and after hundred to thousands of metres of burial (Chapter 6).

Secondary evaporites form in subsurface settings equivalent to the eogenetic and mesogenetic porosity realms as defined for carbonates by Choquette and Pray (1970). Tertiary evaporite textures tend to form in the telogenetic realm (Figure 1.1) And, as in carbonate diagenesis, the most pervasive alteration of evaporites is either early in the burial history (eodiagenesis) or it occurs much later during uplift (telodiagenesis). Both the eogenetic and telogenetic settings are characterised by relatively permeable evaporites and hydrologies capable of high volumes of pore fluid crossflow. Alteration of a salt mass in the mesogenetic realm consists largely of recrystallisation overprints within a flowing salt mass, but with substantial alteration and dissolution possible about the edge of a bed or a flowing salt mass. In carbonates the mesogenetic overprint tends to be pervasive throughout the bed (Choquette and Pray, 1970). In evaporites the pervasive early loss of porosity and permeability in the shallow diagenetic/eogenetic realm means that deep burial (mesogenetic) alteration tends to be concentrated about the edges of a buried salt body (see discussion of dissolving salt “block of ice” model in Chapters 7 and 8). Unlike carbonates and siliciclastics, the core of the subsurface salt unit is largely unaffected by processes of burial alteration, although they are ongoing in the encasing nonevaporitic sediments and will only cease when the adjacent nonevaporite beds lose their effective porosity. Preservation of the unaltered core of the salt unit is why viable Permian halobacteria can be cultured from brine inclusions in remnant chevrons in Permian salt from west Texas (Vreeland et al., 2000).

Mineral	Formula	Mineral	Formula
Anhydrite	CaSO ₄	Leonhardtite	MgSO ₄ ·4H ₂ O
Antarcticite	CaCl ₂ ·6H ₂ O	Leonite	MgSO ₄ ·K ₂ SO ₄ ·4H ₂ O
Aphthitalite (glaserite)	K ₂ SO ₄ ·(Na,K)SO ₄	Loewite	2MgSO ₄ ·2Na ₂ SO ₄ ·5H ₂ O
Aragonite **	CaCO ₃	Mg-calcite **	(Mg _x Ca _{1-x})CO ₃
Bassanite	CaSO ₄ ·1/2H ₂ O	Magnesite**	MgCO ₃
Bischofite	MgCl ₂ ·6H ₂ O	Meyerhoffite	Ca ₂ B ₅ O ₁₁ ·7H ₂ O
Bloedite (astrakanite)	Na ₂ SO ₄ ·MgSO ₄ ·4H ₂ O	Mirabilite	Na ₂ SO ₄ ·10H ₂ O
Borax (tincal)	Na ₂ B ₄ O ₇ ·10H ₂ O	Nahcolite	NaHCO ₃
Boracite	Mg ₃ B ₇ O ₁₃ ·Cl	Natron	Na ₂ CO ₃ ·10H ₂ O
Burkeite	Na ₂ CO ₃ ·2Na ₂ SO ₄	Nitratite (soda nitre)	NaNO ₃
Calcite**	CaCO ₃	Nitre (salt petre)	KNO ₃
Carmallite	MgCl ₂ ·KCl·6H ₂ O	Pentahydrate	MgSO ₄ ·5H ₂ O
Colemanite	Ca ₂ B ₅ O ₁₁ ·5H ₂ O	Pirssonite	CaCO ₃ ·Na ₂ CO ₃ ·2H ₂ O
Darapskite	NaSO ₄ ·NaNO ₃ ·H ₂ O	Polyhalite	2CaSO ₄ ·MgSO ₄ ·K ₂ SO ₄ ·H ₂ O
Dolomite**	Ca _(1+x) Mg _(1-x) (CO ₃) ₂	Proberite	NaCaB ₅ O ₉ ·5H ₂ O
Epsomite	MgSO ₄ ·7H ₂ O	Priceite (pandermite)	CaB ₄ O ₁₀ ·7H ₂ O
Ferronatronite	3NaSO ₄ ·Fe ₂ (SO ₄) ₃ ·6H ₂ O	Rinneite	FeCl ₂ ·NaCl·3KCl
Gaylussite	CaCO ₃ ·Na ₂ CO ₃ ·5H ₂ O	Sanderite	MgSO ₄ ·2H ₂ O
Glauberite	CaSO ₄ ·Na ₂ SO ₄	Schoenite (picromerite)	MgSO ₄ ·K ₂ SO ₄ ·6H ₂ O
Gypsum	CaSO ₄ ·2H ₂ O	Shortite	2CaCO ₃ ·Na ₂ CO ₃
Halite	NaCl	Sylvite	KCl
Hanksite	9Na ₂ SO ₄ ·2Na ₂ CO ₃ ·KCl	Syngenite	CaSO ₄ ·K ₂ SO ₄ ·H ₂ O
Hexahydrate	MgSO ₄ ·6H ₂ O	Tachyhydrite	CaCl ₂ ·2MgCl ₂ ·12H ₂ O
Howlite	H ₅ Ca ₂ SiB ₅ O ₁₄	Thernadite	Na ₂ SO ₄
Ikaite**	CaCO ₃ ·6H ₂ O	Thermonatrite	NaCO ₃ ·H ₂ O
Inyoite	Ca ₂ B ₆ O ₁₁ ·13H ₂ O	Tincalconite	Na ₂ B ₄ O ₇ ·5H ₂ O
Kainite	4MgSO ₄ ·4KCl·11H ₂ O	Trona	NaHCO ₃ ·Na ₂ CO ₃
Kernite	Na ₂ B ₄ O ₇ ·4H ₂ O	Tychite	2MgCO ₃ ·2NaCO ₃ ·Na ₂ SO ₄
Kieserite	MgSO ₄ ·H ₂ O	Ulexite	NaCaB ₅ O ₉ ·5H ₂ O
Langbeinite	2MgSO ₄ ·K ₂ SO ₄	Van'thoffite	MgSO ₄ ·3Na ₂ SO ₄

Table 1.1. Major evaporite minerals: less saline alkaline earth carbonates or evaporitic carbonates are indicated by **, the remainder are the more saline evaporite salts. Documented dolomite composition ranges from Ca_{1.16}Mg_{0.84}(CO₃)₂ to Ca_{0.96}Mg_{1.04}(CO₃)₂. Less common evaporite minerals, such as borates, iodates, nitrates and zeolites are not listed here, but are discussed in detail in Chapter 11.

Unlike quartzose and aluminosilicate sediments, buried evaporite beds can flow as ductile masses from the surface down to 8-10 km of burial and even into the metamorphic realm. At the same time their dissolving edges supply ions to adjacent nonevaporitic sediments. Salt flow can be: a) early diagenetic, coinciding with syndepositional fractionation, reflux or dissolution; b) later diagenetic, associated with complex

burial-stage bed dissolution or reprecipitation and driven by subsurface fluid flow in the zone of free convection below the zone of overpressure; c) widespread and pervasive, as occurs during halokinesis (salt tectonics); and d) postdiagenetic and extending well into the metamorphic realm where daughter minerals, such as scapolite and tourmaline, can act as a source of volatiles and lubricants long after the precursor salts have gone (Warren 1999; Chapter 6).

	Siliciclastic: (continental, fluvio-deltaic, shelf, submarine)	Carbonate: Humid-Oceanic/marine Tropical/subtropical	Carbonate-evaporite: Arid, land-locked Subtropical/Temperate
Early marine cementation	Rare	Local occurrence	Pervasive (especially in mesohaline platform)
Dolomitisation	Rare	Locally in mixing zones (?)	Pervasive (brine reflux and burial)
Leaching	Uncommon, mostly related to freshwater leaching, rare in burial diagenesis	Common, related to subaerial exposure and karstification	Intensive, related to hypersaline brines
Calcite cementation	Uncommon, locally common (mostly related to burial)	Common	Rare to local occurrence (mostly burial)
Anhydrite-halite	Uncommon	Rare to absent	Common to pervasive
Porosity types	Intergranular	1) Mouldic, vuggy and chalky microporosity (common) 2) Fracture and intercrystalline porosity (local occurrence)	1) Intergranular, mouldic, vuggy, and intercrystalline (dolomitic) porosity (very common) 2) Fracture and chalky microporosity (locally common)
Controls on reservoir quality	1) Stratigraphic position 2) Depositional facies	1) Stratigraphic position 2) Depositional facies 3) Karst in zones on meteoric influx	1) Depositional facies 2) Accessibility of sulphate- and chloride-bearing and later corrosive fluids (karstic or deep)
Geometry	Layered	Layered	1) Carbonate-basinwide evaporite: Massive irregular 2) Carbonate-salttern-mudflat evaporite: layered

Table 1.2. Characteristics of siliciclastic and carbonate depositional systems (in part after Sun and Esteban, 1994).

Exhumed or uplifted evaporite beds also undergo pervasive alteration, dissolution and replacement as they re-enter the zone of active phreatic flow (telogenesis) and regain permeability. Once again, alteration tends to occur from the edges inward. Soluble components from the altering and dissolving bed can be reprecipitated in adjacent shales as alabastrine and satinspar gypsum or fibrous halite. Exhumed evaporite textures are termed tertiary (Figure 1.1) and are varying combinations of competitive crystal alignment and geopetal void fills. The resulting fabrics can duplicate “primary” crystal alignments, especially when parts of a cavern fill can only be studied at a limited scale, as in core or a mine face. Not recognising a telogenetic overprint typically misidentifies tertiary evaporite textures as primary and so creates interpretive confusion (Chapter 7).

Adjacent nonevaporitic sandstones, shales and limestones also undergo diagenetic reactions when flushed by evolving pore fluids, but the diagenetic rock/fluid framework is slower to respond and requires years to millennia to overprint an original depositional texture. But, given enough time the textures of many other sediments, like evaporites, evolve during burial (Table 1.2).

Evaporite mineralogy and texture will change with time, but all ancient secondary and tertiary evaporites occur within the volume of rock that was originally precipitated as the primary or syndepositional salts. Outside of these evaporite sediments

there are two other classes of salts that are not “true evaporites” in that they did not form via hydrologies first driven by solar evaporation and are precipitates that do not necessarily occupy the same position in earth space as the precursor evaporites. I term the two classes, burial salts and hydrothermal salts (Figure 1.1). Burial salts are made up of minerals, such as anhydrite or halite, which do not necessarily occupy the same rock volume as the original sediment. Their occurrence is related to subsurface fluid flow, hydrofracturing, brine mixing and brine cooling. Burial salts typify the commonplace authigenic cements and replacement salts that precipitate in a nonevaporite matrix from subsurface brines derived by dissolution of an adjacent evaporitic salt bed. Because of the proximity to a “true” evaporite bed, most authors would consider burial salts a form of “true” secondary evaporite.

In contrast, hydrothermal salts do not require a nearby dissolving evaporite to form. Hydrothermal anhydrite forms by heating of seawater or by the subsurface mixing of CaSO_4 -saturated hydrothermal waters, either during ejection of hot hydrothermal water into a standing body of seawater, or during convective magmatic circulation. Hydrothermal salts are poorly studied, but often intimately intermixed with sulphides in areas of base-metal accumulations, such as the Kuroko ores in Japan or the exhalative brine deeps in the Red Sea. Hydrothermal anhydrite is a commonplace salt in many such active volcanogenic-hosted massive sulphide deposits (see Warren, 1999; Chapter 9).

Primary evaporites

The simplest subdivision of evaporite minerals is into evaporitic alkaline earth carbonates – aragonite, dolomite, low-Mg calcite and high-Mg calcite – and evaporite salts – gypsum, anhydrite, halite, trona, carnallite, etc. (Table 1.1). Primary evaporitic carbonates tend to form in the initial stages of brine concentration, whereas the other primary evaporite salts are precipitated in the more saline stages of concentration (Chapter 2). Evaporitic carbonates can contain and preserve elevated levels of organic matter that subsequently generate hydrocarbons or act as reductants for base metal sulphides (Chapter 9).

Evaporitic carbonates

Evaporitic alkaline earth carbonates are the first evaporite minerals to precipitate from a concentrating hypersaline surface water and are usually composed of aragonite, high- and low-Mg-calcite, magnesite or even primary dolomite. The essential hydrology of any evaporite depositional setting is that evaporative outflow exceeds inflow. This results in two characteristics of the carbonate depositional system, which hold also for the more saline evaporite salts. First, rapid changes in water level are possible, especially in the more marginward facies, leading to interlayering of strandzone and subaqueous units. Under such a regime any subaqueously precipitated carbonate is liable to subaerial exposure and syndepositional subaerial diagenesis. Second, the solute content, especially the Mg/Ca ratio, of shallow hypersaline water fluctuates as the salinity fluctuates. For example, the Ca content of any brine is depleted by the early precipitation of calcite or low-Mg calcite. Subsequent carbonate precipitates drop out of an increasingly saline water and so will have a higher Mg/Ca ratio and tend to be dominated by high-Mg calcite, aragonite, magnesite, or even dolomite.

Carbonate laminites (subaqueous sediment?) Mm-scale lamination is volumetrically the dominant

sedimentary structure in modern and ancient evaporitic carbonates as well as in higher salinity salts, but its origins are varied and complex (Figure 1.2). Sometimes it is an inorganic cumulate, other times it is biologically structured (biolaminite - see next section). Beds dominated by finely laminated, regular alterations of two or more sediment types are called laminites or rhythmites. Many evaporitic carbonate laminites form couplets or even triplets by the regular superposition of micrite with siliciclastic clay, organic matter or evaporite salts. Such couplets and triplets are frequently referred to as varves, yet are not necessarily “true” varves in that the layers do not define annual couplets.

As an example of a contemporary carbonate laminite, consider deep bottom sediments deposited prior to 1979 in the Northern Basin in the Dead Sea, Israel (Figure 4.48). They are made up of alternating light and dark mm laminae that accumulated beneath a density-stratified brine column more than 350 m deep. The whitish laminae are composed of stellate clusters of aragonite needles (5-10 μm diameter), which precipitated each summer at the air-brine interface and then sank. The darker laminae consist of clay minerals, quartz grains, detrital calcite and dolomite that washed in as suspended sediment from the surrounding highlands during occasional storm floods (Garber

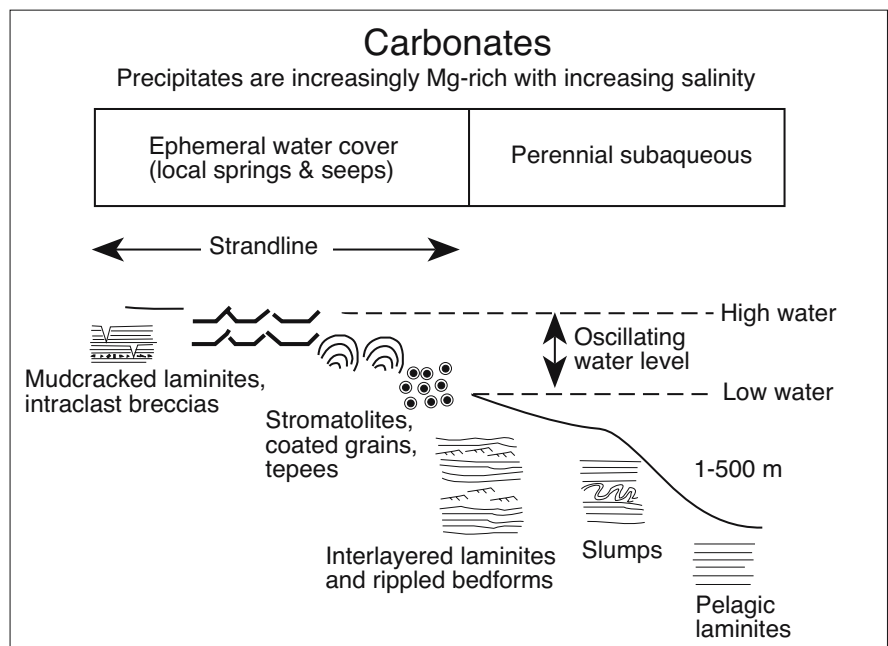


Figure 1.2. Depositional significance of evaporitic carbonate textures. Note the distinction between subaqueous and strandline (ephemeral water) indicators.

et al., 1987). Thus laminites in the Dead Sea are not annual layers, but indicate flood events that occur every 3-5 years.

Permanent water column stratification, with periodic algal blooms at the surface, characterises the waters of Lake Tanganyika. Deep bottom laminites (seasonal varves) containing between 7% and 11% total organic carbon (TOC) accumulate as modern lake bottom sediments where waters are anoxic and more than 250m deep (Cohen, 1989). Or consider the shallow lacustrine laminites of the more saline Holocene Coorong Lakes, Australia (Warren, 1988, 1990). Coorong laminites make up more than 80% of the Holocene sediment volume in the Coorong Lakes and are composed of alternating dark-grey organic-rich and light-grey organic-poor laminae. Matrix mineralogies range from hydromagnesite to aragonite to Mg-calcite to dolomite and organic levels can be as high as 16% TOC. As in the Dead Sea, the Coorong laminites formed subaqueously on the floor of a chemically stratified lake. Unlike the 250+ metres depths of the Dead Sea and Lake Tanganyika, Coorong laminites accumulated as microbially entrained pelletal wackestone/mudstones beneath seasonally stratified perennial lake waters, less than 1-5 metres deep (Figure 4.4b). Once on the bottom these pellets are easily eroded and redeposited as wave-driven bedload, the resulting laminite layering is not a varve.

Laminites can also be preserved under conditions of ephemeral subaerial exposure. Algal-bound laminites (algal mats or biolaminites) crosscut by mudcracks characterise the algal channel and strandzone facies in many modern and ancient evaporitic carbonates such as the sabkhas of the Arabian Gulf (Figure 3.4e). Modern and ancient laterally extensive carbonate laminites, without evidence of subaerial exposure, indicate subaqueous deposition under fluctuating surface water chemistries. They indicate water depths that may have ranged from a few decimetres to hundreds of metres and are not necessarily associated with deepwater conditions (Warren, 1985; Kendall, 1992). They do indicate a lack of burrowing metazoans in saline carbonate sediments deposited across this wide range of water depths.

Strandzone associations: Microbialites, pisolites and tepees

The strandzone in many evaporitic carbonate systems is characterised by an association of stromatolites, mud-cracked cryptalgalaminites (biolaminites), pisolites, ooids, intraclasts, cemented crusts and tepees (Figure 1.2). Strandzones typify deposition associated with fluctuating shorelines about the

edge of a more permanent brine lake or seaway and form in areas of groundwater springs, mudflats and ponds. Rapid fluctuations of strandlines (wet and dry cycles) and associated high rates of capillary crossflow mean this facies association is syndepositionally cemented as it aggrades into stacked layers of intraclast breccia, biolaminites, pisolites and tepees, typically separated by salt beds or their dissolution breccias. Biofilms and mats, in otherwise muddy and granular matrices of any uncemented strandzone sediment, gives a leathery depositional strength to this sediment that encourages the preservation of rip-ups, tears and overfolds due to storm-induced erosion. Biostabilization also tends to encourage the preservation of fenestrae and gas-filled cyanobacterial domes in the surface crusts of many modern strandzones of saltflats and playas.

Stromatolites and microbialites

Microbialites are biogenic structures, the mineralised result of the metabolic activities of microphytic algae, cyanobacteria or archaeobacteria (Figure 1.3; Riding, 2000). Microbialitic structures are commonplace sediments in evaporitic strandzones, textures range from biolaminites (\approx cryptalgalaminites) and stromatolites (matrix-supported agglutinated microbial reefs) through tufa/travertine (cement-supported) reefs to thrombolites (agglutinated reef). Stromatolites and cyptalgalaminates are the most easily recognised microbialites in ancient evaporitic settings (Figure 1.3). Quaternary tufas and travertines tend to characterise the humid hydrological stages of saline lakes when water levels tend to be high and surface water less saline. Internally, microbial textures can be stromatolitic (fine planar-undulating to wavy-crenulated lamination), oncologic (concentrically laminated), thrombolitic (with mesoscale clotted textures, not to be confused with clotted or grumous microfabrics, which occur in both thrombolites or stromatolites) or cryptic (no obvious internal structure).

Biology of stromatolites and microbial layers

Stromatolites to some researchers are a specific layered type of microbialite, often defined as laminated organosedimentary structures with positive relief away from a point or limited surface of attachment (e.g. Burne and Moore, 1987). In this sense stromatolites are equivalent to agglutinated microbial reefs in the terminology of Riding, 2002. To others, stromatolites are not necessarily a biological construct. Microbes and biofilms may be present at the time chemical sediments accumulate, but they play a passive role in textural style during the deposition of this type of stromatolite. Researchers with this view of stromatolites like to add the phrase "it may or may not be of

biological origin” to any definition of an ancient stromatolite. This distinction becomes important as we shall see in a later discussion of pre-Mesozoic evaporitic stromatolites, but reliably defining the contribution of a biofilm to rock texture in ancient evaporitic carbonates is at times near impossible.

Stromatolite shapes range from columnar to domal to subspherical. Internal layers of most modern stromatolites define the successive positions of an agglutinating bioplexi (algal/bacterial community), with each accreting layer produced by trapping and binding of sand to mud-sized sediment. In some settings agglutination occurs in conjunction with direct carbonate precipitation onto or within cyanobacterial trichomes, a process driven by changes in ambient $p\text{CO}_2$ (Figure 1.4a). Modern lacustrine stromatolites tend to be precipitative biochemical structures, while modern marine-margin stromatolites tend to be largely agglutinated structures; both possess surface microbial communities that evolve as the stromatolites prograde (Duane and Al-Zamel, 1999). Many coarser-grained stromatolites in the modern marine and marine margin realms, as in Lee stocking Island and Shark Bay, are poorly layered agglutinated forms and are transitional into thrombolitic structures. Fine-grained mm-laminated stromatolites tend to form best in or near seepage zones in modern hypersaline lakes, such as Marion Lake in South Australia, Gotomeer in the Netherlands Antilles and the Dead Sea in the Middle East, rather than in the open marine realm (Warren, 1982a; Kobluk and Crawford, 1990; Druckman, 1981).

Dominant members of modern microbial plexi range from archaea to eubacteria to cyanobacteria to algae with the proportions and species changing with depth in the sediment and salinity of the water column (Figures 9.16, 9.17). The most common biotal constituents of well-preserved stromatolitic bioherms in Phanerozoic evaporitic settings are filamentous and coccoid cyanobacteria, with lesser halobacteria (Figure 1.4b, c). Species components not only change with water depth and brine salinity but have changed over the course of geological evolution (Figure 1.4b). Modern cyanobacteria typically extrude a mucilaginous sheath that protects the contributing biota from UV radiation. The gooey mucilage also captures sediment particles creating further UV screening, but too thick a sediment layer can cut the necessary exposure to light and so slow photosynthesis. Large amounts of water are held in the mucous sheath and so it also serves as a buffer against osmotic stress.

Modern mesohaline stromatolites exhibit regular occurrences of the halotolerant cyanobacterial species

Microcoleus chthonoplastes, *Lyngbya* sp., *Entophysalis* sp. and *Synechococcus* sp. (Gerdes et al., 2000a). *Microcoleus* is one of a number of cosmopolitan cyanobacteria that form ensheathed filamentous cellular bundles in most growing biolaminites. It grows best in the salinity range 80-160‰ but is present as living filaments in salinities as high as 300‰.

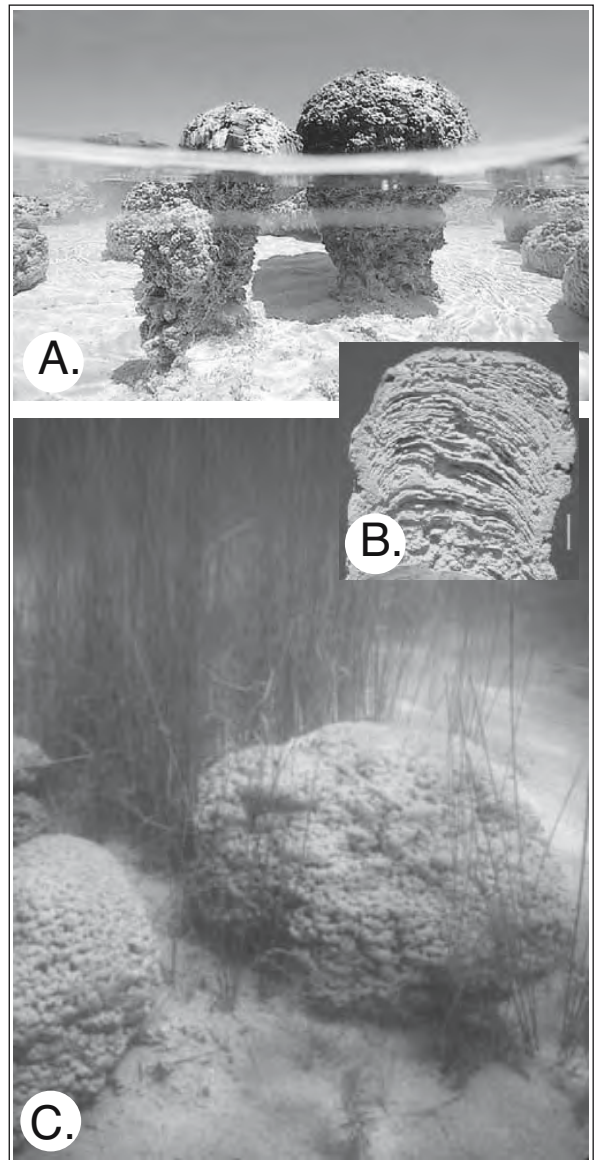


Figure 1.3. Modern agglutinated stromatolite reefs. A) Intertidal stromatolites in Hamelin Pool, Shark Bay Australia (image courtesy of DiscoverWest). B) Cross section of a Shark Bay intertidal stromatolite showing internal mm lamination with truncated edges. C) Lacustrine stromatolites from Cuatro Ciénegas Posas, Mexico. Most particles are captured by the mucilage are diatom frustules (Image courtesy of Alan Riggs).

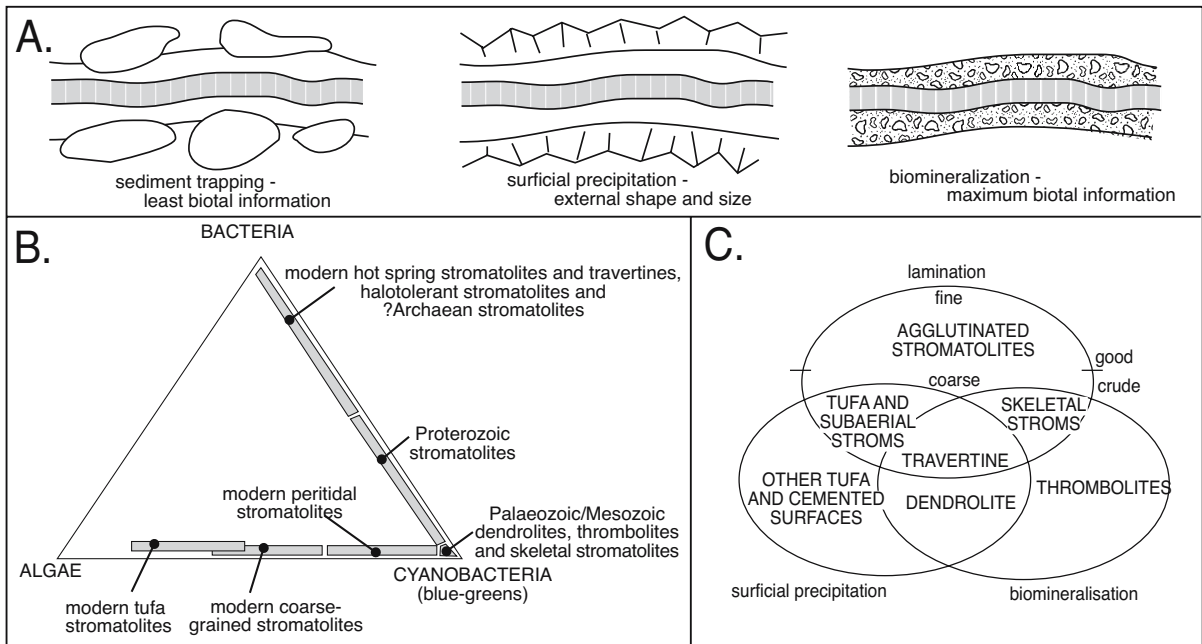


Figure 1.4. Microbialites. A) Styles of mineral accretion about a trichome. B) Biological components that construct various microbialites and the changes over geological setting and time. C) Classification of microbialites according to dominant constituents (after Riding, 1991; 2000).

Fibrillar cyanobacteria are able to glide up and down through nearsurface sediment in order to position themselves in optimal light conditions. This is done by hormogonia, a part of a filament of a photosynthetic cyanobacterium that detaches and grows by cell division into a new filament. Hormogonia are motile and respond phototactically so that, if too much sediment accretes to the mat or if a deepening brine cover reduces the light reaching the filaments, they move upwards to where they accumulate on or just below the sediment surface. It is this periodic repositioning that creates the internal laminated structure and phototropic thickening seen in modern stromatolites and algal mats. Left behind in the sediment matrix are the abandoned sheaths, immotile filaments, cells and mucilage that after passing through the decomposer community becomes buried organic matter (Chapter 9).

Coccolids in modern biolaminites tend to create slime-sheathed pustules and individual cells grow by binary fission (Gerdes et al., 2000a). *Gloeotheca* and *Synechococcus* are two of a number of such coccoid cyanobacteria that make up the other major component of a cyanobacterial plexi. These organisms increase their slime content in order to deal with phototoxicity and tend to dominate exposed surfaces of algal mats and stromatolites, as in the algal mats of the Abu Dhabi and Saudi sabkhas. Coccolids tend to occur in zones about edges of water-covered biolaminites flourishing on the floors of tidal channels (Chapter 3).

Pleurocapsalian cyanobacteria are a cosmopolitan type of coccoid bacterial that dominate modern pustular and pinnacle mats. The typical internal structure in a pustule is colonial, with individual nodules showing discontinuous but more or less concentric layers. Slime production is stimulated by an increase in light intensity, salinity or temperature. This creates sediment with a yoghurt-like consistency made up of polysaccharides interwoven with sediment matrix. The slime coat not only protects the coccolids, but also insulates the other species of the mat community from the lethal effects of increasing light, salinity and temperature. Microbial metabolism facilitates or even drives the precipitation of primary dolomite in many evaporitic carbonates (van Lith et al., 2002).

It is the alternation between mm-scale layers dominated by the filamentous forms and layers enriched in the coccolids that creates the biolamination of modern marine and marine margin stromatolites (Reid et al., 2001). Aggradation in a modern marine-edge stromatolite represents a dynamic balance between sedimentation and intermittent lithification within the cyanobacterial mat. Periods of rapid sediment accretion, during which stromatolite surfaces are dominated by pioneer communities of gliding filamentous cyanobacteria, alternate with hiatus intervals. Microscale discontinuities in sedimentation are characterized by development of surface films of exopolymer and subsequent heterotrophic bacterial decomposition, which

forms thin crusts of microcrystalline carbonate. During prolonged hiatus, climax communities develop, which include endolithic coccoid cyanobacteria. These coccoids modify the sediment micro-environment to create thicker lithified laminae. Subsequence preservation of lithified layers at depth creates the millimetre-scale biolamination that characterises modern and ancient stromatolites.

At the broader scale, successive layers in modern biolaminites can indicate seasonal changes. *Microcoleus*-dominated layers (often associated with diatoms) accumulate in the winter, while coccoid-dominated layers typify the more saline summer growth layers. Alternations of coccoid and filamentous layers in a mat can create lamination even in the absence of agglutinated sediment, although the preservation potential of such organic-only layers is low unless deposited on the anoxic floor of a perennial stratified brine lake (Chapter 9).

Non-stromatolitic lacustrine microbialites

Stromatolites are one part of a much wider group of layered microbialites growing in a wide range of saline marine and nonmarine settings (Figure 1.4c; Riding, 1991, 2000). According to Riding, sediment trapping by filamentous plexi in a modern biolaminite results in an agglutinated stromatolite reef, which is characterised by a particulate microstructure that preserves few, if any, details of the original size, shape or orientation of the biotal plexi responsible for capturing sediment (Figure 1.4a).

On the other hand, biomineralized deposits, such as tufa/travertine cement reefs described by Riding 2002, retain considerable palaeontological detail about the constituent organisms preserved as skeletal microfossils. Mineralisation is especially important in nonmarine microbialites, as in lacustrine tufa cement reefs that define the water-covered margins of the less saline high-water stages of many Quaternary salt lakes. These tufa cement reefs are porous, unbedded or only poorly bedded, and created by cyanobacteria, algae, grasses, and reeds thriving in brackish to fresh lake and river waters and groundwater seeps along the landward side of the saline pan or lake edge. Rapid CaCO_3 precipitation veneers living plants, which would otherwise be masses of soft vegetation, with cement crusts (Riding, 2000; Pedley et al., 2003). Relief on a tufa buildup can be high, with commonplace steep to overhanging, locally cavernous, cemented masses. Tufas tend to occur where inorganic CaCO_3 precipitation is enhanced by CO_2 degassing of venting spring waters.

Likewise travertines, which tend to form layered deposits of CaCO_3 near the outflow points of groundwater and thermal springs, can preserve details of the contributing microbes. Travertine cement reefs are layered microbialites with “shrub” and crystalline fabrics associated with non-skeletal organisms (Figure 4.3; Riding 2002). Deposits tend to form steep-sided mounds, with elevated rimmed pools, normally developed atop and about the mounds. Smoothly banded crystalline crusts construct horizontal, sloping, vertical or overhanging sheets with pisoids typically developing at the bottom of water-filled pools and polygonal saucers. Chafetz and Folk (1984) and Folk (1993, 1999), along with many others working in travertines, document microtextures such as spheroidal dolomite, dumbbell-shaped crystals, fine diurnal-layered dendrites and bushes, all of which indicate a strong bacterial contribution to travertine precipitation. Reeds and grasses can be preserved as moulds within bacterial travertines, but most macro-organisms are excluded by the elevated temperatures and high levels of dissolved minerals (salinity) that typify travertine carbonates. Most travertines are only a few kilometers in lateral extent and, as in tufa cement reefs, subaerial surfaces are common, as are gradations into adjacent marsh and fluvial environments.

CO_2 degassing, in combination with evaporation and rapid microbial growth, can drive extreme carbon isotope enrichment in the organic matter and co-precipitates in many CO_2 -limited organic-enriched sediments, including evaporitic marls, tufas and travertines (Schouten et al., 2001). Enriched $\delta^{13}\text{C}$ values of up to +13‰ in calcite and -10‰ in organic matter were measured in calcite tufas accumulating in well-oxygenated carbonate saturated waters in El Peinado and San Francisco lakes, both high altitude saline lakes in the southern Andean Altiplano, northwestern Argentina (Figure 1.5). Valero-Garces et al. (1999) argue that the large enrichments of the heavier carbon isotopes in the algally bound sediments indicate non-equilibrium gas-transfer fractionation of the carbon isotopes during CO_2 degassing. Parent waters were derived from thermal springs and subject to subsequent evaporative concentration. In general most ions in lacustrine tufas in volcanic settings ultimately come from geothermal and volcanic CO_2 sources. Physical fractionation, rather than biological enrichment in these settings, may have a greater significance than credited in the commonly accepted biological metabolism arguments typically used to explain carbon isotope records in evaporitic carbonates (see Schouten et al., 2001 for opposing argument). Likewise, the dilution of the isotopic signature by C-14-free CO_2 from volcanogenic sources may hinder accurate C-14 chronologies of lake sedimentation when based on samples of lacustrine organic matter and other aquatic plants.

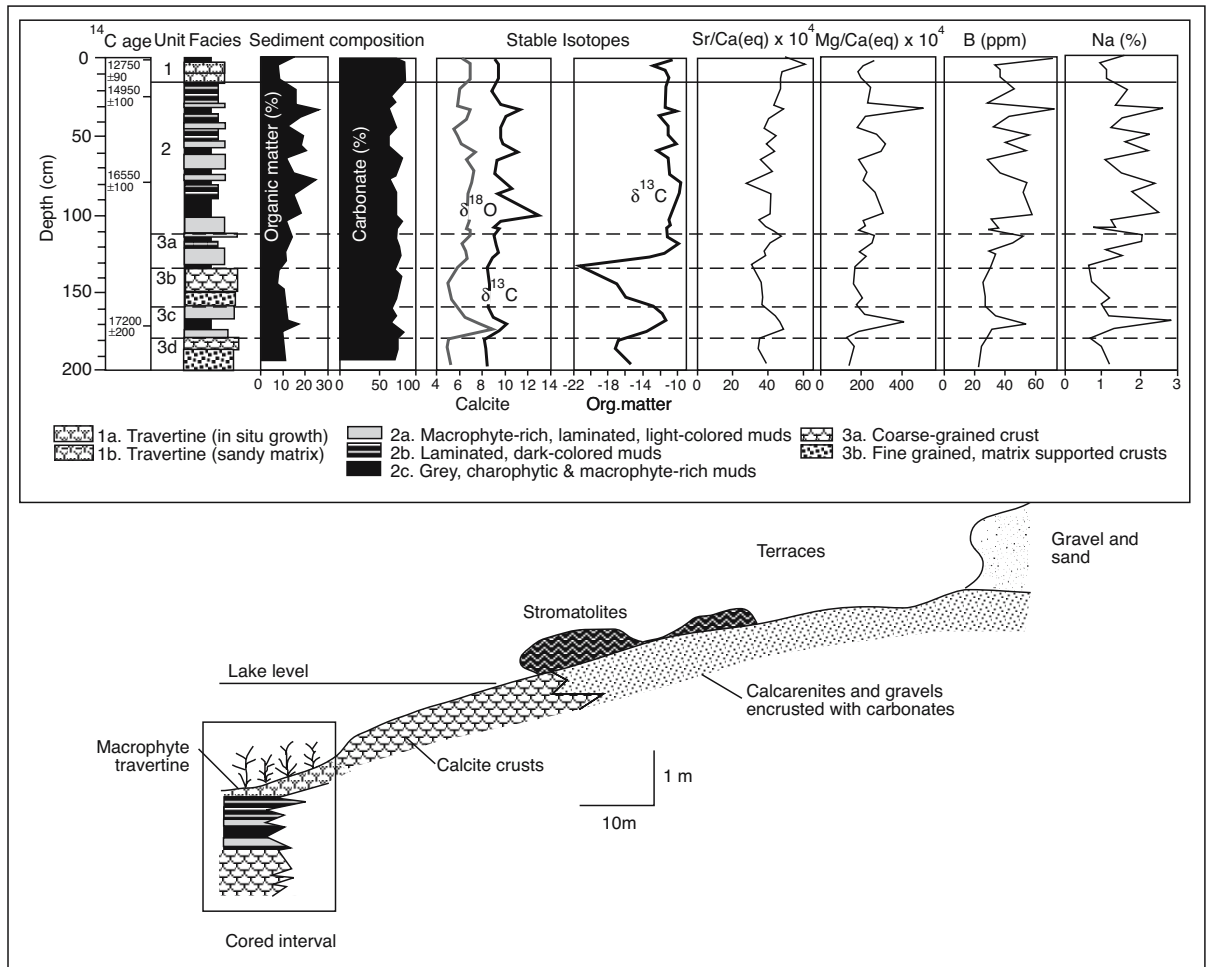


Figure 1.5. Sedimentary facies, sediment composition, stable isotopes and geochemistry of the Lake El Peinado core, Andean Altiplano. Core was collected in the perennially subaqueous carbonate margin of the lake (after Valero-Garcés et al, 1999, 2001). Macrophytes are the current active carbonate binders. Stromatolites today are not active, but grew at an earlier time of more saline water when conditions did not favour macrophytes. Dates are uncorrected AMS ¹⁴C ages (years BP). All isotopic measurements are reported as δ values vs. the PDB standard.

Microbialite sedimentology in saline lakes

Mineralisation associated with biofilm metabolism is much more important than simple agglutination in many Holocene lacustrine stromatolites. Niches occupied by stromatolites and tufa/travertine cement reefs in saline lacustrine settings circumscribe a much wider range of salinities and water conditions than evidenced by modern marine thrombolites and stromatolites. Isopachous biomineralized subaqueous stromatolite reefs, texturally identical to their ancient mm-laminated counterparts, still grow in the mesohaline carbonate-saturated seepage waters of some modern marine-fed gypsum lakes (von der Borch et al., 1977; Warren 1982a). The coarse-layered sandy agglutinated forms of Shark Bay and the mud-cracked supratidal algal mudstones of the Abu Dhabi sabkha have fewer ancient evaporitic counterparts.

Similarly, healthy carbonate-precipitating microbialites communities in the upper parts of less-saline carbonate-rich littoral and slope breaks about many prograding lacustrine margins in modern temperate and tropical carbonate lakes, can be used as analogues for microbial growth in the high water stages of some ancient saline basins (Dean and Fouch, 1983). For example, modern thrombolites, tufas and stromatolites occur in littoral waters (10-60m deep) about the edges of Lake Tanganyika (Cohen and Thouin, 1987) and Salda Gölü in Turkey (Braithwaite and Zeder, 1996). Near identical fresh to brackish water stromatolites, along with oncoids, travertines and tufas, occur in Plio-Pleistocene sediments of the East African Rift Valley lakes (Casanova, 1986). Similar marginward microbial tufa cement reefs (bioherms) reached thicknesses of 7 metres, with diameters of 15 metres, in the Oligocene Ries Basin (Rid-

ing, 1979; Arp, 1995). Freshwater to mesohaline stromatolites characterise Oligocene lake margins in France (Casanova and Nury, 1989) and the 1-10m deep freshwater-filled evaporite karst pond fills (posas) in a modern gypsiferous playa, Cuatro Ciénegas in Coahuila, Mexico (Figure 1.3c; Minckley, 1969; Winsborough et al., 1994). Other examples of ancient lacustrine counterparts include the Tertiary of southern France (Truc, 1978) and the Eocene Green River Formation of the USA (Surdam and Wolfbauer, 1975).

Widespread mm-laminated evaporitic stromatolites also accumulate in more saline lacustrine settings, settings where surface brines are waters supersaturated with respect to a carbonate phase, typically aragonite. In these settings the role of biology is less obvious in the laminates. Biofilms of archaea, eubacteria and algae may be passive rather than active participants during the formation of domal to massive laminar stromatolites. It is in this group of structures that the phrase “may or may not be of biological origin” comes into play. Modern examples of such enigmas include manganiferous aragonitic stromatolites that define the northwestern strandplain margin of the Northern Basin of the Dead Sea (see Druckman, 1981 vs. Garber and Friedman, 1983). Texturally identical evaporite-associated biomineralized stromatolites and biolaminites have characterised the mudflat and strandzone margins of saline and alkaline playa lakes and marine evaporite basins throughout much of the Phanerozoic, especially at times or in regions of transition into or out of episodes of basinwide evaporite precipitation (Figure 1.8a).

Mineralogy of most modern lacustrine stromatolites is dependent on what carbonate phase is precipitating in the ambient lake water. This is true even when biotal metabolism plays a significant role in driving carbonate precipitation. Stromatolites and microbial bioherms are aragonitic in many modern saline lakes (e.g. Great Salt Lake, Eardley, 1938; Marion lake, South Australia, von der Borch et al., 1977) and the precipitation process is often facilitated by the metabolic activities of bacteria (Pedone and Folk, 1996). Hydromagnesite-aragonite mm-laminated stromatolite domes and mats dominate in the schizohaline ephemeral waters of North and South Stromatolite Lakes in the Coorong region of South Australia (Figure 4.5a), while poorly preserved hydromagnesite-magnesite stromatolites characterise much of the present-day playa surfaces of the Caribou Plateau in Canada (Renaut, 1993a). Similar stromatolite domes characterise the highly alkaline

(pH>9) fresh to brackish waters of Salda Golu (Lake) in Turkey where lake margin subaqueous stromatolites are composed mostly of hydromagnesite, along with entrapped diatom tests (Figures 1.6, 4.29; Braithwaite and Zedef, 1994, 1996).

At the basin scale, Quaternary calcitic and aragonitic algal tufa and travertine reefs form atop spring vents in groundwater outflow zone where they can construct substantial spring mounds (Habermehl, 1988). Tufa growth rates can be impressive; Rosen et al. (2004) documented aggradation rates of 30 cm/year in the modern subaqueous tufas of Big Soda Lake in Nevada. Some impressive thinolitic tufa reef mounds in temperate and high-altitude saline lakes were originally constructed of an unusual but interesting variety of low temperature calcite called ikaite (Chapter 4). This hexahydrate form of calcite is found today forming ephemeral precipitates in near freezing brines around spring vents of CO₂-rich waters in Mono Lake and in Quaternary sediments of the Lohanton Basin (Pyramid Lake), Nevada. Similar spectacular tufa mounds occur in groundwater outflow zones on the subaqueous floor of Lake Van, Turkey. Once the water temperature about a spring mound rises above 3-4°C the ikaite dehydrates to calcite, but the calcite can preserve the characteristic lenticular and twinned outline of its precursor. But a lenticular to lozenge shape in a calcite pseudomorph is easily confused with other evaporite minerals, such as gypsum and gaylussite, which also are readily pseudomorphed by calcite (Chapter 7). Ikaite pseudomorphs can have little to do with an evaporite precursor, and occur in modern marine shelf sediments of the Antarctic and in modern and ancient glacial outwash fans from around the world (Shearman and Smith, 1985; Larsen, 1994; Riccioni et al., 1996).

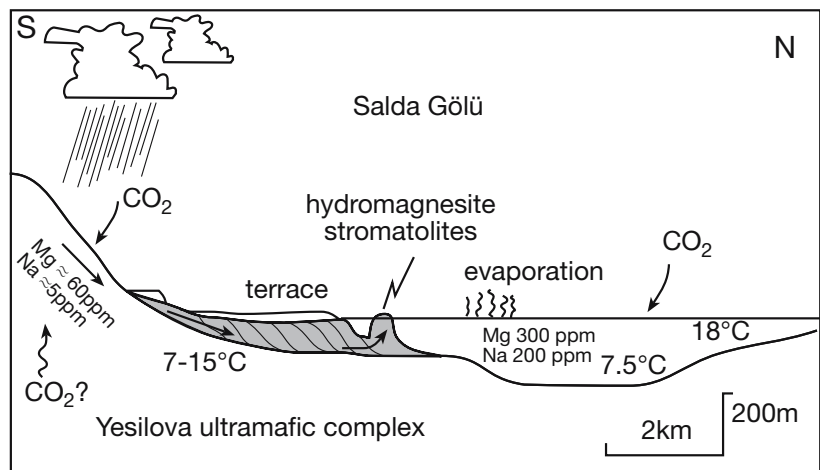


Figure 1.6. Schematic cross section of Salda Gölü showing hydromagnesite stromatolite growing subaqueously in front of the carbonate tufa terrace (after Russell et al., 1999).

Microbialite sedimentology in marine settings

Unlike modern stromatolites and microbialites, which tend to construct significant rock masses in salinity or temperature stressed environments, Precambrian stromatolites were environmentally diverse and abundant across hypersaline, normal marine and nonmarine settings. They first appeared around 3.45 Ga and dominated biogenic sedimentation from 2800 to 1000 Ma (Riding, 2000). The beginning of their Proterozoic decline and environmental restriction, variously identified at 2000, 1000 and 675 Ma, has been attributed to reduced marine cementation or to eukaryote competition. The former was perhaps tied to higher calcium concentrations in Precambrian oceans compared to oceans of today (Laval et al., 2000), while the latter related to the evolution of the gastropod radula (Garrett, 1970). The previously enigmatic lack of calcified cyanobacteria filaments in stromatolite-bearing Precambrian sequences is now explained as a likely result of high concentrations of dissolved inorganic carbon in the Precambrian ocean (Arp et al., 2001) or by the postulate that many Archaean stromatolites were inorganic precipitates (Pope et al., 2000).

Precambrian stromatolites were not confined to the more arid peritidal marine or marginward lacustrine seep situations that characterise most Phanerozoic stromatolites. Such high stress environments (hypersalinity/exposure) tend to exclude many metazoan marine grazers that otherwise browse and destroy algal mats. Modern areas of thick extensive marine-margin stromatolites/cryptalgal laminites are located at the edge of the cropping range of marine grazers, examples of gastropod restriction include the seaward side of the algal facies of the Arabian Gulf (Figure 3.4d; Kendall and Skipwith, 1969) and the hypersaline intertidal flats of Shark Bay, Western Australia (Figure 1.3a; Logan, 1987).

Various thrombolites and dendrolites, mainly formed by calcified cyanobacteria, became important marine microbialites early in the Palaeozoic and reappeared in the Late Devonian, as marine stromatolite populations declined. Microbial marine carbonates retained their importance through much of the Mesozoic, they became scarcer in marine environments in the Cenozoic, but locally re-emerged as large agglutinated domes, possibly reflecting increased algal involvement in sediment binding and cementation.

There are still a few modern normal-marine settings where metre-scale stromatolites flourish. Holocene columnar stromatolites grow as part of a thrombolite-stromatolite association on the floor of modern tidal channels off Lee Stocking Island, Exuma Cays. These bio-columns show three

associations of internal sedimentary structures: (1) prokaryotic stromatolites comprised of alternating layers of coarse-grained ooids and peloids, and fine micrite that are formed exclusively by microbial activity; (2) eukaryotic stromatolites comprised of microbially-induced micritic layers alternating with detrital layers bound and cemented by eukaryotic algae; and (3) thrombolites displaying irregular, clotted fabrics and formed by communities of microbes, algae, and metazoans (Figure 1.7a; Feldmann and McKenzie, 1998).

Onshore in San Salvador in shallow turbid water, beneath the modern mesohaline waters of Storr's Lake, marine-influenced thrombolite layers alternate with stromatolite layers to create mushroom shaped mounds. This alternating layering perhaps reflects changes in salinity and light penetration (Figure 1.7b; Mann and Nelson, 1989). Formation of many modern marine thrombolites has been attributed to carbonate precipitation driven in large part by sciaphile (dark-loving) bacteria, which flourish under low sedimentation rates, low water energies and higher turbidity, hence the preservation of a clotted fabric and lack of lamination (Dupraz and Strasser, 1999; Riding, 1991). Phanerozoic marine thrombolites, in contrast, are mostly interpreted as non-laminated microbialites (not a stromatolites) constructed by cyanobacteria and are not usually interpreted as sciaphiles.

According to Feldmann and Mckenzie (op cit.) the contemporaneous formation of prokaryotic stromatolites, eukaryotic stromatolites, and thrombolites under identical conditions within the present marine environment is unlikely. They suggest that the prokaryotic stromatolites in the Lee Stocking bioherms represent microbial forms that began to develop in an environmentally-stressed intertidal setting during the early Holocene flooding of the Great Bahama Bank. In contrast, thrombolites began to form under the present, normal-marine subtidal conditions (Figure 1.7a). The eukaryotic stromatolites represent intermediate forms between prokaryotic stromatolites and thrombolites, with a gradual change from stromatolite to thrombolite reefs tied to rising sealevel. With the deepening, there would have been a decrease in salinity, an increase in energy, and possibly an increase in nutrient supply; all factors that favour thrombolite growth.

Unfortunately, most environmental and depositional models for Phanerozoic stromatolites tend to draw heavily on Holocene peritidal marine-margin analogues, such as Shark Bay, a hypersaline setting where sand grain trapping (agglutination), rather than micrite precipitation, is the dominant mode of sediment accretion. Accordingly, using modern analogues, many

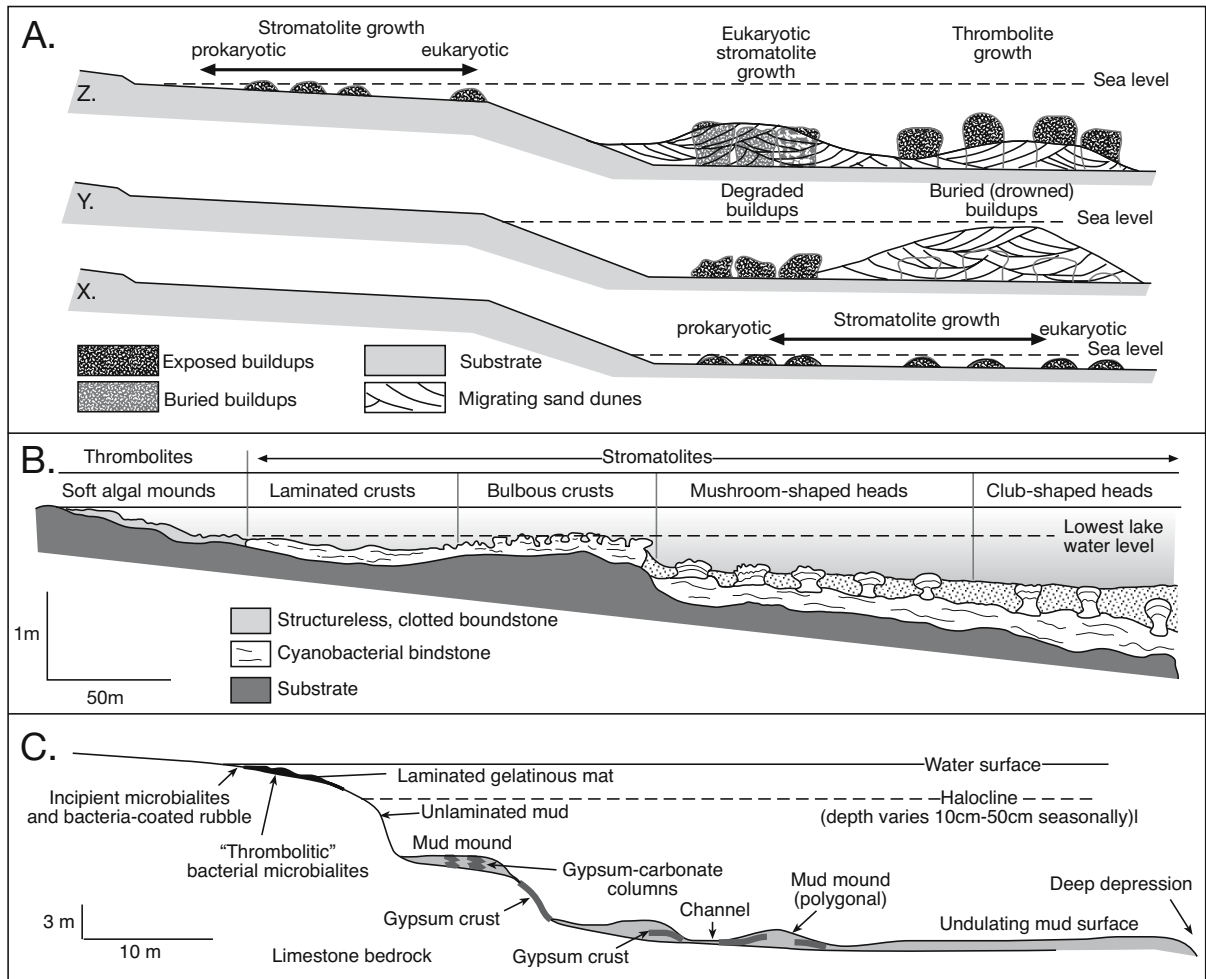


Figure 1.7. Thymbolites in mesohaline to marine settings. A) Evolution of microbialites during a rise in sea level from time X to time Z in the formation of marine subtidal stromatolites in Lee Stocking Island in the Bahamas (after Feldmann and Mckenzie, 1998). B) Distribution of algal/thymbolitic structures in mesohaline aragonite muds of Storr's Lake, San Salvador (after Neumann et al., 1988; Mann and Nelson, 1989). C) Thymbolites (aragonitic) passing into gypsiferous mud mounds below the halocline at the southern end of the channel in Gotomeer, Bonaire (after Kobluk and Crawford, 1990).

sedimentologists assume that well-preserved Phanerozoic stromatolites must have formed in intertidal to supratidal marine settings. As we shall see in Chapter 5, a marine-connected basin is not the best way to model evaporitic carbonates associated with thick evaporites. Microbes living in ancient saline systems constructed a far more diverse and wide ranging biotal association in evaporitic settings than simplistic Shark Bay analogs imply (Chapter 9).

Microbialites typify marine to evaporite and evaporite to marine transitions

Throughout the rock record, Pope et al. (2000) noted that a transition between a carbonate platform or an isolated carbonate

buildup and the overlying evaporites is commonly defined by assemblages of stromatolites or interlaminated carbonates and evaporites. The stromatolites display lamination textures that vary from peloidal and discontinuous on a scale of a millimetre to a few centimetres, to isopachous and continuously laminated on a scale of a centimetre to a few metres. The isopachous lamination may be composed of either: (1) micrite or radial-fibrous calcite, or (2) dolomite. The isopachous laminae are remarkably uniform, varying little in thickness over a given lateral distance, whereas stromatolites formed of peloidal laminae, also show marked variations in thickness over an equivalent lateral distance (phototactic thickening). They observed that isopachous textures are uncommon on most open-marine carbonate platforms and apparently developed in transitional

Location	Units	Carbonate Fabrics	Composition
Great Slave Lake, Canada, Palaeoproterozoic (1.8-1.9 Ga)	Perthei Grp. (c) Stark Fm. *e)	Tufa, isopachously laminated stromatolite at contact in shallow water; Fibrous marine cements throughout platform	Basinwide evaporite Halite >> gypsum (no anhydrite)
Oman, Vendian (570-543 Ma)	Buah Fm. (c) Ara Fm. (e)	Fibrous marine cements throughout platform and isolated thrombolitic bioherms; Isopachously laminated stromatolites at contact; tufa-like crusts in carbonates within evaporites	Basinwide evaporite Halite >> gypsum
Michigan Basin, Silurian (≈ 400 Ma)	Guelph Fm. (c) Salina Fm. (e)	Fibrous marine cements within pinnacle reefs; Isopachously laminated stromatolites (travertine-like coatings) cap marine reefs; Calcite laminites in interpinnacle reef areas	Basinwide evaporite Halite >> anhydrite, potash salts
Western North America; Middle Devonian (≈385 Ma)	Winnepegosis (c)	Stromatolites cap marine reefs, fibrous marine cements in reefs and carbonate-evaporite laminites between reefs in deeper-water settings	Basinwide evaporite Halite >> anhydrite
Sverdrup Basin, Carboniferous, Arctic Canada	Nansen (c) Otto Fiord (e)	Carbonate-evaporite laminites in basinal setting, fibrous marine cements throughout shelf-margin reefs and buildups	Halite ≈ anhydrite
Zechstein Basin, England, Late Permian (≈ 260 Ma)	Middle Magnesian Limestone (c) Hartlepool Anhydrite (e)	Fibrous marine cements throughout reef complex; Isopachously laminated stromatolites (Crinkly Beds) in bioherm capping marine reef complex; Laminar coatings within bioherm, neptunian dikes and cavities; Laminites in basinal setting between buildups	Basinwide evaporite Halite >> anhydrite Locally on platform: Anhydrite >> halite
Mediterranean Messinian (Middle Miocene)	Terminal Carbonate Complex (c)	Thinly laminated stromatolites at transition from marine carbonate to evaporite; fibrous marine cements within reefs underlying stromatolites	Basinwide evaporite Halite >> gypsum
Abu Shaar Complex, Egypt; Messinian (Middle Miocene)	Ruidais Fm. (c) Kareem Fm. (e)	Fibrous marine cements throughout marine reef complex; Thinly laminated stromatolites with fibrous cements on toe of slope; Unique pisoids with distinctive fibrous fabric	Basinwide evaporite Anhydrite > gypsum > halite

Table 1.3. Selected examples of unique evaporitic carbonate fabrics in basinwide transition facies passing from carbonate through mesohaline to hypersaline deposition. Carbonate = (c), Evaporite = (e). (after Pope et al., 2000 and contained references).

carbonate-to-evaporite settings because of basin isolation and drawdown leading to increasing temperature, salinity, and anoxia related to water stratification (Table 1.3; Figure 1.8a). The resulting ecologic restriction created an opportunity for isopachous stromatolite growth.

Stromatolites with isopachous lamination are interpreted to form via in situ precipitation of sea-floor-encrusting calcite and possibly dolomite, whereas the stromatolites composed of peloidal, discontinuous lamination are inferred to have formed by trapping and binding of loose carbonate sediment in microbial mats and can be unrelated to the onset of basinwide evaporite restriction and drawdown. According to Pope et al. (2000), isopachous stromatolites may have accumulated by chemogenic precipitation in the absence of microbial mats, while peloidal stromatolites grew by agglutination in the presence of microbial mats and since the onset of the Phanerozoic have been largely restricted to environmentally stressed biogenic sediment. I would not exclude biofilms from isopachous stromatolites, it is just that high inorganic precipitation rates can swamp the phototactic effects used to interpret biofilms.

Pope et al. (2000) went on to note that when compared to pre-Mesozoic occurrences, stromatolites with thin, isopachous lamination and radial-fibrous textures, though present, are rare to absent in transition facies in Jurassic and younger evaporite basins, such as the Messinian of the Mediterranean region. Instead, the isopachous precipitative facies have been replaced by stromatolites with peloidal, clastic phototropic textures and by mesohaline mudstones with a low-diversity diatomaceous and coccolith biota. These stromatolites are sometimes interlayered with thrombolites (as in Storrs Lake, Caribbean). They interpret the shift away from chemogenic stromatolites to agglutinated stromatolites as a change in seawater chemistry tied to the evolution of the nannoplankton. Accumulation of the biogenic planktonic mudstones in deeper ocean waters since the Mesozoic has had two important effects: (1) Production of coccolith tests in the world's oceans (chalks) helped extract calcium carbonate from seawater, thus lowering the growth potential for inorganic precipitation of sea-floor-encrusting stromatolites. (2) Settling of both coccoliths and diatoms would have created a sediment flux to the sea floor, which would have served to impede growth of chemically precipitated stromatolites because of ongoing smothering of any growing seafloor crystals.

Post-Mesozoic peloidal stromatolites (bio-agglutinates) and thrombolites tend to characterise transitions into and out of episodes of basinwide evaporite deposition. One of the best-preserved transitions of this style of stromatolite/thrombolite occurrence comes from the Late Miocene of SE Spain in cyclic stromatolitic carbonates deposited during and at the termination of the Messinian salinity crisis (Figure 1.8b; Chapter 5). For example, large microbial carbonate domes (both stromatolites and thrombolites) defined the margins of the Sorbas and Alboran Basin during the uppermost Messinian. They occur in a unit overlying the Messinian evaporite succession and were deposited in a variety of environments, including fan deltas (Martín et al., 1993; Braga et al., 1995), beaches, and oolitic shoals (Riding et al., 1991).

Their abundance and continuity in the transitional marine setting is comparable in many respects to their omnipresence as transitional forms in the Precambrian. There is, however, an important difference in some parts of the Messinian sequences. Although major unconformities separate normal marine reefs

from the carbonates of the “terminal complex complex (TCC),” an impoverished and depauperate, normal-marine biota of Late Miocene corals (*Porites*), coralline algae, serpulids, bivalves, and encrusting foraminifers at times lived alongside the stromatolitic microbes as the TCC was accumulating (Martín et al., 1993; Braga et al., 1995). The intimate association of stromatolites with a stressed, but stenohaline, marine biota rules out the possibility of continually elevated salinities at the onset of TCC deposition, as suggested by several earlier authors to account for the occurrence and proliferation of widespread microbial structures in the Messinian strata (Esteban, 1980; Rouchy and Saint-Martin, 1992). The most plausible explanation for this transition into and out of hypersaline into normal marine waters is that microbes acted as opportunistic biota and, for a time, outcompeted other organisms, settling and growing successfully in most of the available and rapidly expanding marine niches (Pope et al., 2000; Feldmann and McKenzie, 1997). This happened during the initial stages of marine recolonization of the Mediterranean Sea, after drawdown and deposition of either the lower or upper evaporite sequences.

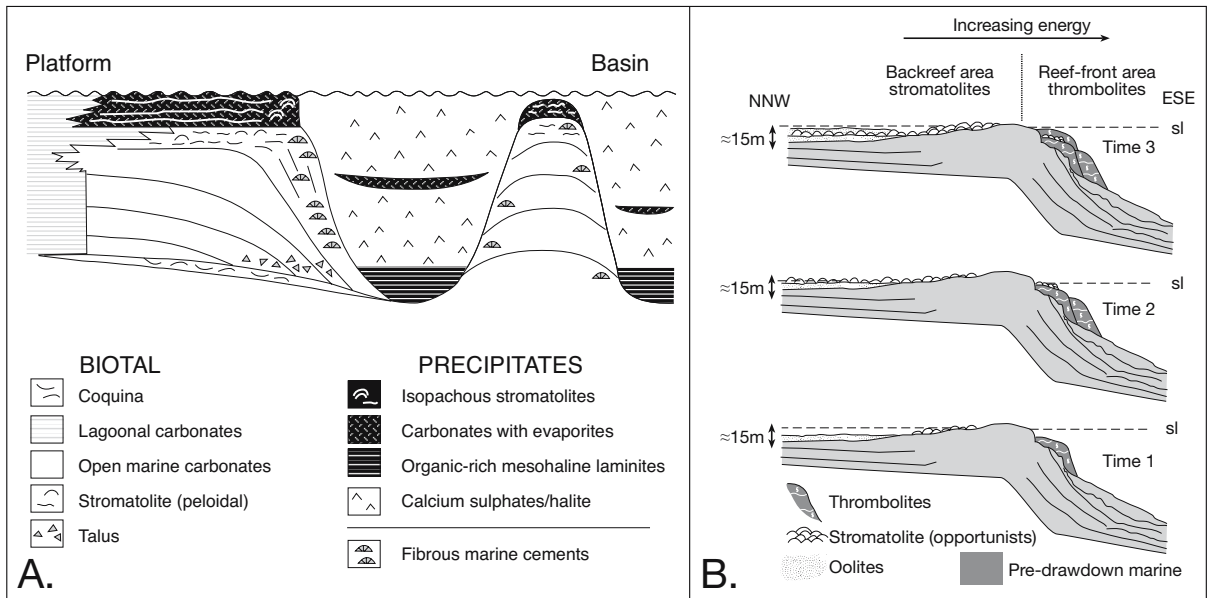


Figure 1.8. Schematics of marine carbonate to evaporite transitions. A) Typical transitions, showing relative positions in the basin stratigraphy of precipitated isopachous stromatolites and the precipitated carbonate fabrics that typify sediments accumulating mesohaline carbonates immediately prior to complete basin isolation and drawdown that defines the onset of basinwide calcium sulphate and/or halite evaporite deposition (after Pope et al., 2000). B) Platform edge distribution of stromatolites and thrombolites relative to cyclic sea-level changes during the Intra-Messinian flooding event in a marginal Mediterranean sub-basin. Time 1) Relative high sea-level stand with thrombolite growth in the subtidal zone at the front reef, oolite deposition in the deeper parts of the back-reef area, and stromatolite growth in the intertidal zone of the back-reef area. Time 2) Relative low sea-level stand promoting thrombolite growth in the basinward migrated subtidal zone at the front reef and opportunist stromatolite growth in the intertidal zone on both the previously deposited ooid sands and thrombolites. Time 3) Relative high sea-level stand with thrombolites growing over the preceding stromatolites in the subtidal zone at the front reef, opportunist stromatolite growth in the intertidal zone of the back-reef area, and sand deposition in the deeper water of the back-reef area (after Feldmann and Mackenzie, 1997).

Thus, the development of microbial structures during the Messinian seems to be related, although indirectly, to the end of each “salinity crisis” and the creation of unoccupied marine ecologic niches as seawater encroached on drawdown unconformities. Earlier but ecologically comparable vacant niche scenarios are found atop Phanerozoic platform carbonates at the onset of basinwide evaporite stages (Table 1.3); examples include the Silurian of Michigan Basin (Sears and Lucia, 1979) and the Permian of the Zechstein Basin (Paul, 1980). The abundance of stromatolites and thrombolites in normal marine environments in the aftermath of a mass extinction of the pre-existing marine benthic biota via drawdown can be explained by the stromatolite and thrombolite communities acting as opportunistic disaster forms taking advantage of vacant ecologic niches (Schubert and Bottjer, 1992).

Vadose pisolites, ooids and other coated grains

Fenestral carbonates, sometimes intercalated with grainstones, are frequently interpreted as peritidal sediments (Shinn, 1983).

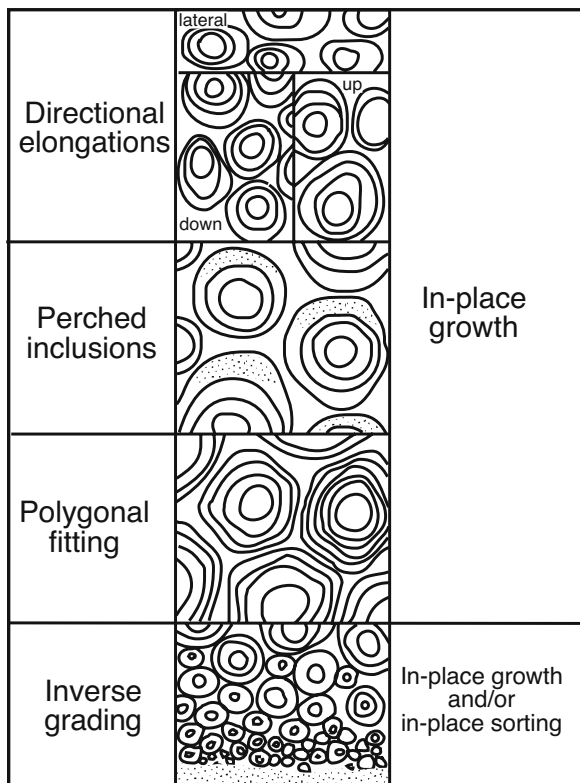


Figure 1.9. Fabrics of pisolites created by in-place processes. Although all these features have been interpreted as requiring vadose pore conditions, only downward directional elongation (micro-stalactite) require such an interstitial condition (after Esteban and Pray, 1983).

Often the grainstones facies are dominated by coated grains, including oolites, and their wave-agitated mechanical genesis is indicated by well preserved crossbed sets. A marine conception is indicated by nuclei of marine shell fragments and intercalation with packstones and wackestones containing marine fossils. More typically in evaporitic settings these metre-thick beds of coated grains lack obvious crossbeds or marine fossils and are intercalated with biolaminites and sharp crosscutting truncation surfaces. Units tend to be inverse graded and coarsen upward into pisolitic rudstones, they are commonly interlayered with evaporite solution breccias (Figures 1.9, 1.10a). Pisolitic beds show many textural features, such as bridged coats and polygonal fitting of pisoids, that imply they formed “in situ” under conditions of little or no wave-induced agitation. Individual pisolites, now composed of calcite or dolomite, can show nonconcentric internal truncation surfaces and brick-like crystal terminations indicative of exposure and an aragonite parent (Figure 1.10b, c; Assereto and Folk, 1976).

Pisolite rudstones tend to be caught up in tepee structures and other strandzone layers and beds that also contain internal structures and cements indicative of alternating vadose and phreatic conditions. Such features include perched inclusions, inverse graded pisolite beds, and pendulous circumgranular cements (Figures 1.9; Dunham, 1972; Esteban and Pray, 1983; Handford et al., 1984). They indicate a depositional setting that was part of a strandzone, typified by the “to and fro” of the strandline edge of a brine lake or seaway in a zone of groundwater seepage. The associated water table rose and fell as, pore water conditions alternated between vadose and phreatic.

Pisolite crust cements formed in a strandzone retain infiltrated micrite and pendulous grain underhangs that indicate the sediment spent at least a part of its time above the water table. The term vadose pisolite is sometimes used to distinguish these evaporitic pisolites from permanently subaqueous isopachous “marine” pisolites or the pedogenically formed calcrete pisolites. The prefix marine is a little misleading when describing isopachous pisolite crusts. Modern examples of isopachous pisolites, along with fitted, pisolith crusts define CaCO_3 -saturated peripheral marine seepage areas on the strandplain of evaporite-filled coastal lakes in western and southern Australia (Warren 1982a, 1983a; Handford et al., 1984) and the thermal spring-fed margins of large halite-filled continental salars in the Andean Altiplano (Risacher and Eugster, 1979; Jones and Renaut, 1994). Both settings lack a surface connection to marine waters. The term seepage should perhaps replace the term marine when describing strandzone pisolites.

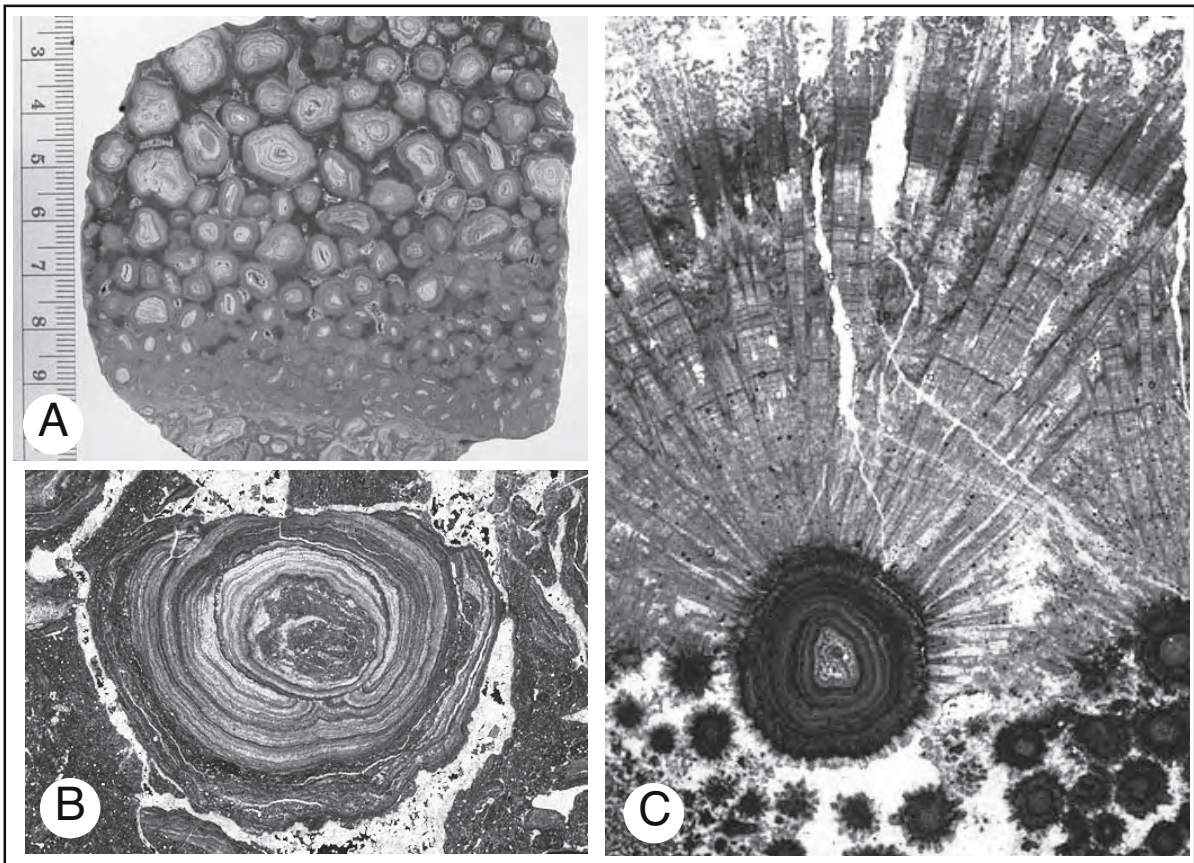


Figure 1.10. Pisolites from Permian of west Texas. A) Polished slab of pisolitic dolomite from the uppermost Yates Formation. Note reverse grading of grains, and "fitted fabric" in which grains have interlocked boundaries produced by compromise growth of outer coatings. Sample from roadside outcrop at "hairpin turn" on New Mexico Highway 7 in Carlsbad Caverns National Park, Eddy Co., NM. B) Thin-section photomicrograph (cross-polarized light) of a pisoid from the Yates Formation. Note irregular, lumpy, partially concentric coatings; fracturing ("autobrecciation") of micritic-peloidal matrix; and evaporite plugging of remnant intergranular porosity. Sample is from 1708.1 ft depth in Gulf/Chevron PDB-04 well on Northwestern Shelf of Delaware basin, 30 km ENE of Carlsbad, Eddy Co., NM. Long axis of photo = 14.5 mm. C) Thin-section photomicrograph (plane-polarized light) of a marine-cemented pisolitic dolomite showing transition from pisoid to botryoidal cement crust. Note that the extremely elongate rays of cement which extend from upper surface of the pisoid show squared crystal terminations. This is used as evidence for an originally aragonitic composition for the cement. Sample from 1739.3 ft depth in Gulf/Chevron PDB-04 well on Northwestern Shelf of Delaware basin, 30 km ENE of Carlsbad, Eddy Co., NM. Long axis of photo = 16 mm. (Images and descriptions courtesy of P. Scholle, <http://geoinfo.nmt.edu/staff/scholle/guadalupe.html>; accessed 11 Dec, 2004).

Ancient pisolites may be marine-fed or continental; all accumulated in CaCO_3 saturated waters. Seepage pisolites are part of a sedimentological association where pisolite crusts are forming mainly as accretionary chemogenic particles in areas of cooling, degassing and concentrating resurgent groundwater. Many are coated with microbial communities, which through their photosynthetic activity help drive the process of carbonate supersaturation. Seepage pisolites occur within confined saline groundwater seepage areas that are located on, or adjacent to, extensive carbonate mudflats about saline waterways. Such systems are not restricted to marine seepage settings but also

form about the strandzone margins of continental saline lakes and salars.

Esteban and Pray (1983) argue vadose (seepage) pisolites characterise the Permian island shoal and sandflat facies of west Texas (Figure 1.10). There pisolitic crusts were thicker and most obvious within the central depressions of decametre-diameter saucers in what was an extensive tepee-overprinted megapolygonal terrain. Warren (1983a) argued the same pisolites were part of a marine seepage facies about the edge of a widespread saltern/mudflat depression that covered the platform interior behind a sandy island shoal.

Nominal “marine” pisolites are characterised by isopachous rim cements, little or no grain fitting and few vadose textures. They are commonplace in normal marine Proterozoic carbonates compared with the Phanerozoic marine (Swett and Knoll, 1989). Their greater abundance reflects a more carbonate-saturated marine chemistry in Precambrian seas (see below). But, throughout geological time, an isopachous pisolite texture has also been a boiler-plate feature of the hypersaline lacustrine realm.

Work by Gerdes et al. (1994) has shown that in addition to “seepage” pisolites other carbonate grains, such as ooids and peloids, typically thought of as indicators of marine conditions and mechanical agitation, can precipitate *in situ* in CaCO_3 -saturated evaporitic settings. They grow within modern microbial mats in hypersaline settings and require no wave-agitated or pelagic phase to precipitate concentric laminar grain coats. Laboratory experiments with unconsolidated muds, and comparisons with fenestral and grainstone textures in evaporitic Guadalupian backreef strata in west Texas by Mazzullo and Birdwell (1989), demonstrated that intense *in situ* alteration of fenestral mudstones can create peloidal grainstones. They go on to argue that such diagenetic grainstones may be the precursors of some forms of pisolitic rudstone.

Wave-agitated shore-parallel crossbedded ooid sand belts, very similar to their modern marine look-alikes, can accumulate in a lacustrine strandzone. For example, cross-stratified oolitic lacustrine grainstones and packstones typify wave-agitated strandzone or lake margin sediments of contemporary Great Salt

Lake, Utah (Eardley, 1938), the Upper Cretaceous to Eocene lacustrine strandzone of Green River Formation of the Uinta Basin, Utah, USA (Williamson and Picard, 1974) and the high energy, lake-shoreline carbonates of the Upper Triassic Mercia Mudstone Group of southern Britain (Milroy and Wright, 2000). Texturally these hypersaline ooids show a radial texture that contrasts with the more typical tangential structure of modern marine ooids. Eardley (1938) noted that ooid sand bodies in Great Salt Lake are concentrated along relatively narrow, wind-swept coasts, adjacent to steep basement promontories and in waters that are less than 2 metres deep (Figure 4.19b). In contrast, strandzone algal bioherms are typically, although not exclusively, associated with wider, less exposed and more gradually inclined shorelines distal to basement uplands. Work by Halley (1977) on ooids from the Great Salt Lake showed that in an agitated setting radial ooids are structurally weaker than comparable tangential marine ooids. He argued that a statistically significantly proportion (>1%) of syndepositionally broken ooids is a reliable indication of radial aragonite ooids associated with hypersaline shorelines (Chapter 4).

Tepees

Tepees are the buckled and broken margins of saucer-like megapolygons in limestone or dolomite crusts that appear as an inverted “V” in vertical two-dimensional exposures (Figures 1.11, 1.12a, b; Adams and Frenzel, 1950). Tepees are commonplace strandzone features in both modern and ancient settings (Assereto and Kendall, 1977; Warren, 1982a, b, 1983a; Esteban and Pray, 1983; Kendall and Warren, 1987;

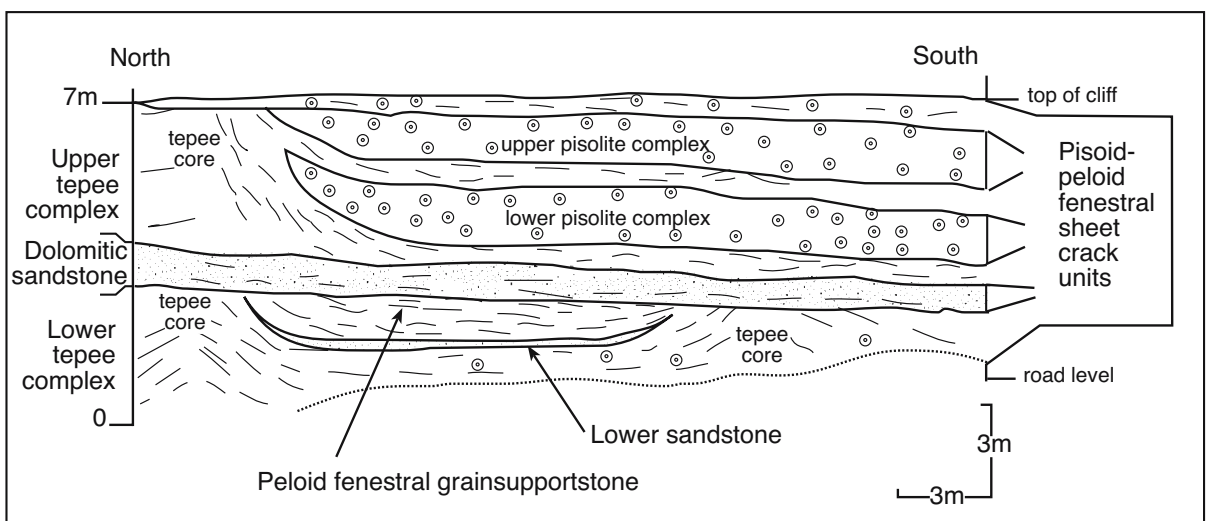


Figure 1.11. Cross section of a field locality of the Permian Tansill Formation at Hairpin Curve in Guadalupe National Park, west Texas. Note the prominent development of pisolites in intertepee depressions within the upper tepee complex and the erosional surfaces that truncate the tepee complexes (after Esteban and Pray, 1983).

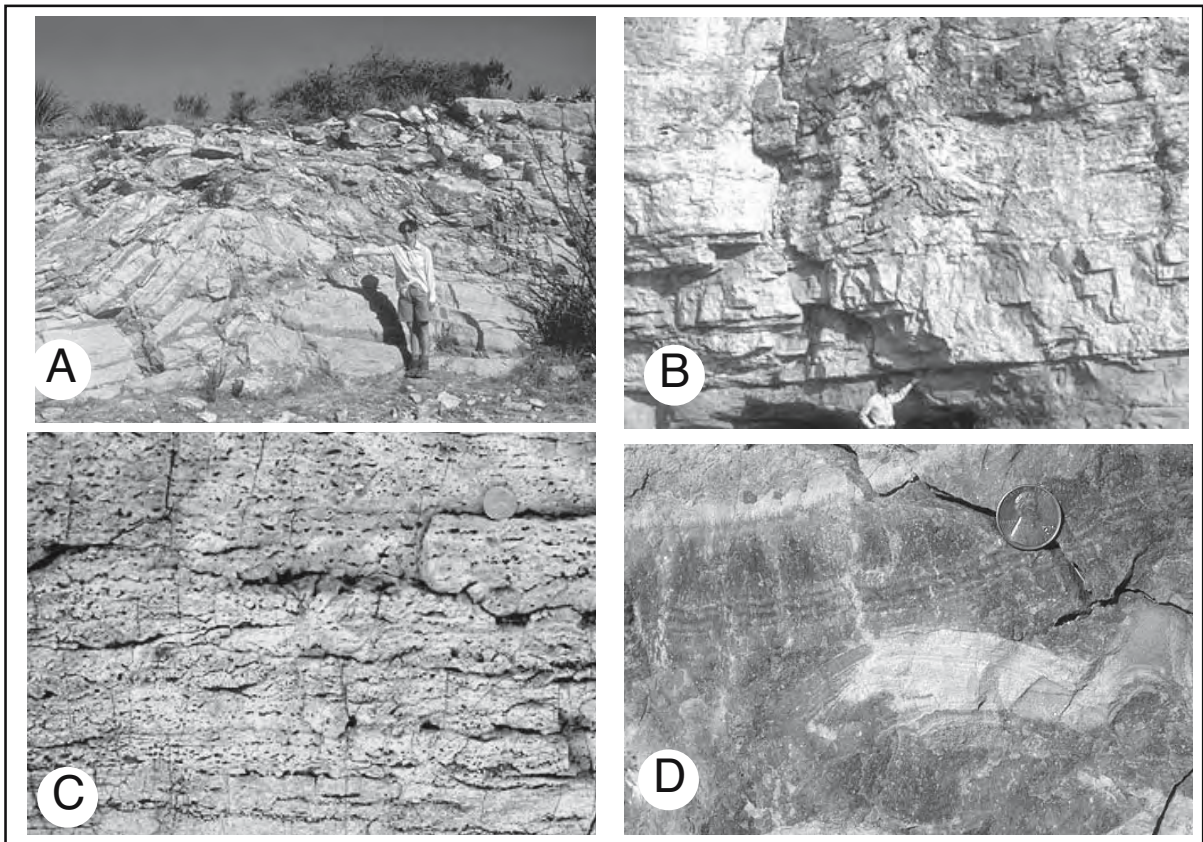


Figure 1.12. Tepee Structures, Permian Basin, west Texas. A) Tepee structure in Tansill Formation. Note that if the upturned margins of the structure were returned to a horizontal position, they could not be accommodated on a flat bedding plane; this shows that these are expansion polygons. Light yellow layers are dolomitized pisolitic and fenestral sediment; darker, gray layers are zones of sheet spar (aragonitic cement crusts). Interstitial growth of aragonite (in marine or coastal spring settings) was the most likely cause of sediment expansion and buckling. Outcrop at southwest end of parking lot at Carlsbad Caverns visitor's centre, Carlsbad Caverns National Park, Eddy Co., NM. B) Stacked sequence of tepees, associated with fenestral and pisolitic dolomites, in the basal part of the Tansill Formation. A 1.8 m thick sandstone at the base of the exposure (at level of man) has truncated tepee stacks in the underlying Yates Formation and possibly acted as an aquifer for the resurging brines that precipitated these tepees. The sandstone sheets, which thin to a feather edge toward the shelf margin, have been interpreted as sabkha sandflats formed by eolian processes during sealevel lowstands. Roadside outcrop on Dark Canyon road approximately 2 km west of the canyon mouth, Eddy Co., New Mexico. C) Peloidal and skeletal grainstones with fenestral fabric in the near-back-reef Tansill Formation. These strata were probably deposited on a relatively high-energy mudflat. Outcrop on south side of Dark Canyon, less than 1 km west of the canyon mouth, Eddy Co., NM. Coin is 2.4 cm in diameter. D) Close-up of sheet spar (aragonite cement) crust from within a tepee structure. Note growth of banded cements from top as well as bottom of cavity and incorporation of fragments of matrix sediment. Roadside outcrop at hairpin turn on New Mexico Highway 7 in Carlsbad Caverns National Park, Eddy Co, NM. (Images and descriptions courtesy of P. Scholle, see <http://geoinfo.nmt.edu/staff/scholle/guadalupe.html>; accessed 11 Dec, 2004 for more details on this region of New Mexico).

Logan, 1987; Kendall, 1989; Smoot and Lowenstein, 1991; Last, 1992; Jones and Renault, 1994; Mutti, 1994; Armstrong, 1995). Some authors have extended the use of the term tepee to pressure ridges in crusts of gypsum or halite. I prefer to restrict usage of the term tepee to overthrust ridges in carbonate crusts and to use the term pressure ridge for overthrust ridges in halite or gypsum crusts. That is, although I use the term tepee nongenetically, I restrict its usage to carbonate crusts and add a

prefix to describe its genesis, e.g. groundwater/seepage tepee, seafloortepee, sabkha tepee, caliche tepee (Kendall and Warren, 1987); some may even be seismic (Pratt, 2002) or microbial (Chow and George, 2004). Others workers restrict the use of the term tepee to inorganic overthrust structures (carbonate and salt hosts) and use the term petee to describe overfolded to overthrust ridges in what were originally biogenically-bound surface layers. Petees can occur in layers and crusts composed

of both evaporitic carbonates and more saline salts, the ridge crest need not be fractured, but can be a series of polygonally linked folds. See Gavish et al., 1985 for the original definition of petee and Noffke et al., 2003 for a comprehensive discussion of petees and other microbially induced sedimentary structures that are commonplace in evaporitic settings. Microbial petees typically have synoptic relief measured in centimetres, but range up to a metre high in the lagoonal strata of the Devonian Lennard Shelf in the Canning Basin of northwest Australia (Chow and George, 2004).

Tepees, along with vadose pisolites are characteristic features of cemented carbonate crusts in areas of a strandplain that experience wetting and drying cycles, CaCO_3 -saturated groundwater seepage, fluctuating salinity conditions, and marked diurnal changes in surface and nearsurface temperatures (Figure 1.12c). Successive episodes of tepee development often stack one bed atop another, with the tepee-overprinted units separated by erosion surfaces, breccias or carbonate-cemented quartz sands (Figures 1.11, 1.12d). Pisoids in the Permian strata of west Texas appear to accumulate best within intertepee depressions or saucers (Figure 1.11; Esteban and Pray, 1983). Subsequent expansion episodes, along with local buckling, may rework beds formed in these pisoid-rich depressions into new tepees. When the pace of resurgence was strengthened during times of increased groundwater outflow, tepee crests were capped by domal stromatolites (Figure 4.5c; Warren, 1982a; Kendall and Warren, 1987).

Many ancient tepee-influenced horizons are interbedded with evaporite solution collapse breccias. This characteristic intercalation reflects the to and fro of a brine sheet edge over the strandzone carbonate facies, typically at times when the platform was isolated from a surface connection to the ocean and brine levels were fluctuating in response to the vagaries of evaporitic drawdown (Chapter 5). Some evaporite solution collapse may postdate the depositional hydrology of the cycle that formed the tepee, but, based on modern analogues such as Marion Lake and Lake McLeod, the schizohaline brine hydrology that forms the marginward saline seeps where tepees flourish is dominated by pore waters that are undersaturated with respect to halite and gypsum. Resurging groundwaters dissolve nearby evaporite beds as they form the tepee/pisolite beds (Warren 1982a). The end result of this ongoing dissolution is the collapse of the overlying tepee-affected strata. Any subsequent prograding of the seepage margin into the evaporite basin means the tepee zone is cannibalised from below and along its landward margin by its own groundwaters. All that may be preserved as widespread evidence of a prograding tepee hydrology within an ancient platform cycle is a terra rosa

profile mixed with remnant breccias composed of fragments of tepee crusts, stromatolite breccias and other residues of the strandplain (Burri et al., 1973; Assereto and Kendall, 1977; Bogoch et al., 1994; Mutti, 1994).

At a broader scale, the occurrence of a substantial tepee-rich unit in a platform interior carbonate succession indicates an episode of exposure and water table drawdown. For example, in the Italian Alps the principal tepee-dominant unit is interpreted as a sequence boundary and forms a regional marker in the highly cyclic Latemar (Triassic) platform interior (Hardie et al., 1986). This 300m thick tepee facies separates the lower cyclic facies and the upper cyclic facies of the Schlern Formation in the Latemar platform (Egenhoff et al., 1999; Mutti, 1994). It is characterized by 79 tepee zones (0.2 to 13m thick) alternating with intervals of thinning-upward, caliche-capped mudstone to packstone cycles.

Some authors have suggested a Milankovitch cyclicity may be preserved in thickness variations within the platform interior sediments of the Latemar (Hinnov and Goldhammer, 1991). If so, the highly altered, overprinted and collapsed origin of at least some of the tepee intervals, probably means individual eustatic parasequences are no longer recognisable within the tepee facies. The predominance of tepees in the Latemar platform also suggests periodic evaporative drawdown in the platform interior. Seepage hydrology needed to form pisolites and tepees implies an exposed but somewhat elevated platform rim at the time the tepees of the interior were active. In contrast, the thicknesses of the transgressive systems tracts (subtidal successions) also preserved in the platform interior indicate flooding and are more likely to retain finer-scale eustatically/climatically distinctive thicknesses.

Carbonates - present and past

Phanerozoic evaporitic carbonates accumulate in CaCO_3 -saturated waters and the consequent aragonite/dolomite muds and cements are distinctive and quite easily separated from open marine shelly carbonate shelf textures. The separation between marine and hypersaline settings is much less distinctive in Proterozoic strata or older. In fact, the best modern textural analogues for many Precambrian marine carbonates are to be found in Holocene evaporitic carbonates and not in modern normal marine carbonates. The dichotomy reflects two major events in earth history: 1) the evolution of an increasingly bicarbonate-depleted and sulphate-enriched ocean by the Proterozoic, and 2) the rise of a shelly marine macrofauna at the Cambrian-Precambrian boundary.

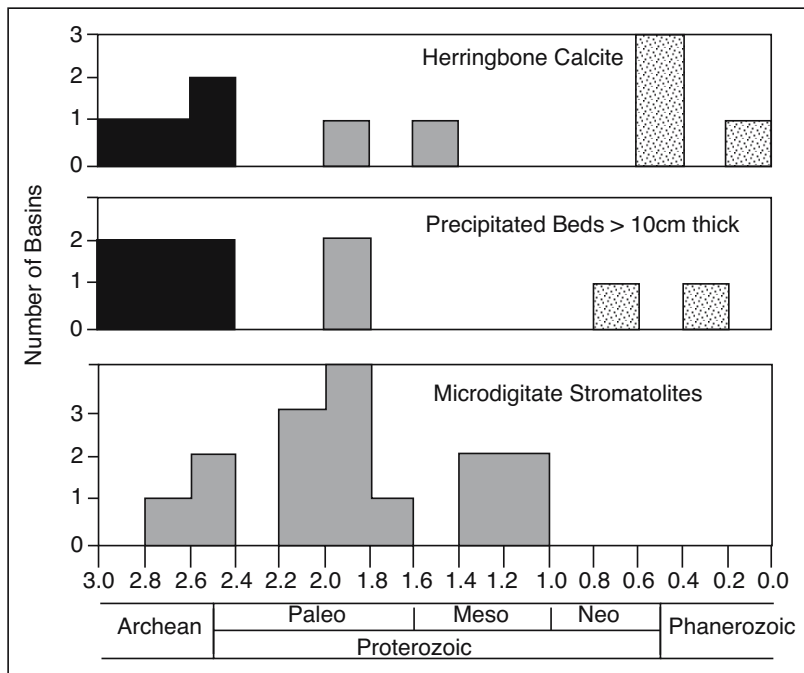


Figure 1.13. Carbonate precipitation from seawater through time. Black fill represents basins where the textures are abundant across a range depositional settings. Grey fill represents basins where the textures are present in a limited number of depositional settings. Stippled pattern indicates textures and minor components with limited extents (after Sumner and Grotzinger, 1996).

During much of the Precambrian, CaCO_3 was extracted from seawater by a combination of inorganic and microbial processes, the same two sets of processes that dominate in modern evaporitic carbonate settings. Archean carbonate sediments entrain numerous and prolific giant botryoids of aragonite that can be up to 1 metre in radius, as well as widespread Mg-calcite precipitates (Grotzinger and Read, 1983; Grotzinger and Kasting, 1993; Grotzinger and Knoll, 1995; Sumner and Grotzinger, 2004). These beds sometimes formed cementstone sheets several metres thick with strike lengths of more than 100 km, with no modern counterparts in normal marine carbonates (Figure 1.13).

By the Palaeoproterozoic, marine carbonates entrained less spectacular masses of aragonite and calcite, although cementstone crusts and microdigitate stromatolites in tidal flats remained a characteristic style of carbonate platform aggradation. In contrast, Meso- through Neoproterozoic carbonate sedimentation saw a progressive decline in the precipitation of massive widespread carbonate cements and an increase in widespread precipitation of micritic whittings. Throughout the Precambrian, periodic high-energy events ripped up and transported fragments of these cementstone crusts and whiting beds to redeposit them

as intercalated intraclast conglomerates and breccias. The secular decrease in the volume of seafloor precipitates reflects a change in the chemical state of the ocean. The much lower sulphate concentrations and much higher bicarbonate to calcium ratios reflect the elevated levels of CO_2 in the Archean atmosphere (Chapter 2; Grotzinger and Kasting, 1993).

The change in the earth's atmosphere and ocean chemistry is also reflected in the evolving nature of microbialites (Grotzinger and Knoll, 1999). During the Archean and early Proterozoic, when CO_2 levels were much higher than today, stromatolites formed by "in situ" precipitation of laminae and coniform stromatolites were commonplace. But younger Proterozoic marine stromatolites grew largely through the accretion of carbonate sediments, mostly through the physical process of microbial trapping and binding (agglutination) and coniform stromatolites had by then largely disappeared from

the world's oceans (Sumner and Grotzinger, 1996) and today are found only as tufas in hypersaline lakes (Warren, 1982a). The carbonate supersaturation of Archean seawater has led some to question the biogenicity of the 3.43 Ga stromatolites at North Pole, Australia - historically interpreted as the world's oldest biological fossils (Grotzinger and Rothman, 1996 vs Hoffman et al., 1998).

The dramatic rise of a skeleton-secreting and sediment ingesting macrofauna at the beginning of the Phanerozoic further changed the nature of marine shelf sedimentation. The proportion of chemically precipitated open-marine mud and cement decreased and new sedimentary particles, such as abundant shell fragments, faecal pellets and biologically derived muds, came to dominate the marine carbonate realm. The formation of widespread cementstone sheets on the seafloor had ceased several hundred million years before the rise of the shelly macrofauna. It was only in hypersaline environments that carbonate supersaturation persisted throughout the Phanerozoic. There isopachous stromatolites and other halotolerant microbialites continue to flourish in the absence of bioturbation and gastropod grazing.

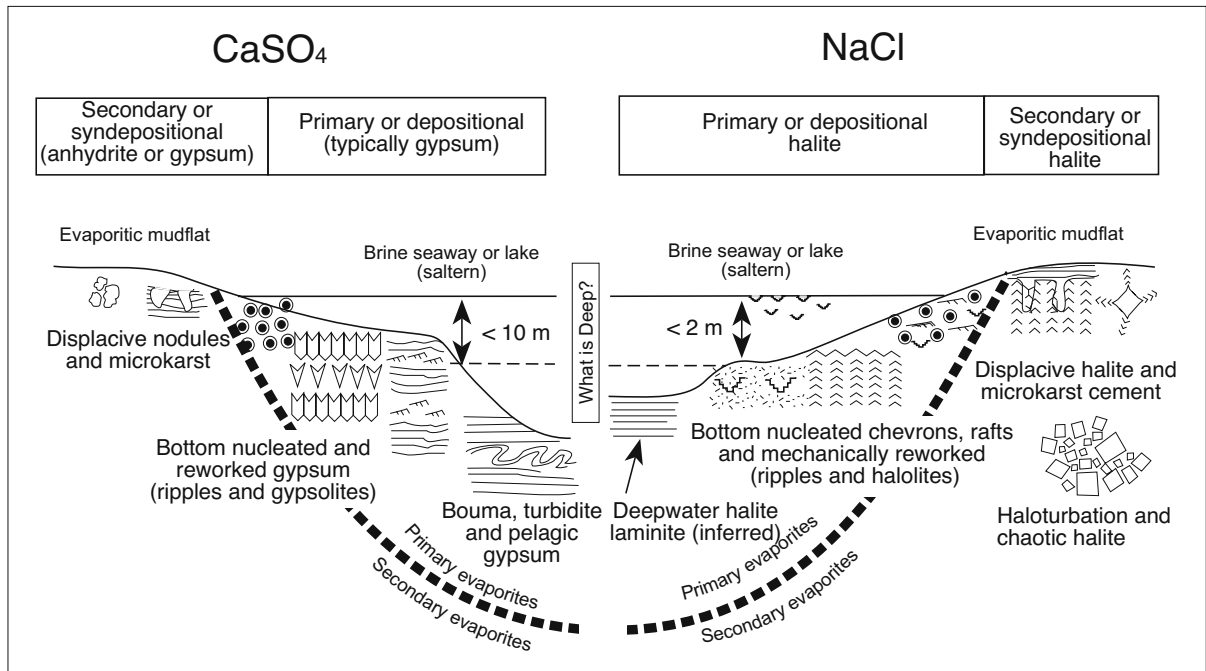


Figure 1.14. Depositional signature of primary evaporite textures and syndepositional secondary evaporites for CaSO_4 and NaCl salts. Secondary textures related to burial are discussed later in this chapter.

Primary evaporite salts

Evaporite salts are deposited in a brine pan or seaway after the brine has precipitated the alkaline earth carbonates. The salts, dominantly CaSO_4 or halite, show a range of crystal textures that indicate relative stability, depth and permanence of the precipitating brine (Figure 1.14).

Simple monomineralic carbonate, sulphate or halite layers and laminae, as well as beds composed of complex interlayered mixtures, dominate subaqueous deposits of many saline lakes and seaways. Laminae created by chemical settling are a typical subaqueous stratification style at the onset of primary salt accumulation. Some laminae outline underlying crystal morphologies, others are flat-planar and can be correlated for long distances across the basin. Biolaminae, including microbial bedding and accretionary tufa and travertine deposits described previously, are common intercalations and indicate less saline intervals in the same brine body. Mechanically reworked laminae (ripples, dunes and slumps) are less common in subaqueous evaporites than in their carbonate or siliciclastic counterparts. This is due to the predominance of chemical sedimentary processes operating in the brine bodies at the salt precipitating stage whereby early crystal precipitates interlock and cement as they evolve into growth-aligned crystals.

Widespread layers or crusts composed of cm-dm sized aligned bottom-nucleated crystals are one of the most widely recognised shoalwater textures. Depending on the salinity of the precipitating brine this bottom-nucleated unit is typically composed of halite chevrons or aligned gypsum crystals. Beneath deeper waters, crystals may accumulate on the bottom as a silt-sized “rain from heaven” pelagic deposit or as a mass of coarsely crystalline monomineralogic bottom meshworks. A range of slope deposits, dominated by reworked shoal water crystals, typifies the subaqueous region separating the shallow from the basinal (Chapter 5).

Over time, decimetre-to-metre thick salt beds can stack one atop the other to form evaporite units that can be hundreds of metres thick. When conditions are suitable, huge thicknesses of shoalwater evaporite can accumulate in very short time frames. For example, a more than one-km-thick sequence of interbedded halite and clay has accumulated in less than 10,000 years in the Danakil Depression of the Ethiopian rift (Figure 11.4). No other type of sediment, carbonate or siliciclastic, can aggrade as rapidly as a subaqueous evaporite bed (Warren, 1991).

Gypsum beds

A few thousand years ago subaqueous crystals of gypsum, up to 1 metre tall, grew in stable bottom waters of shallow (<10m deep) Holocene brine pans of southern Yorke Peninsula, South Australia (Chapter 4; Warren, 1982b). The crystals coalesced into crusts and beds dominated by swallowtail and palmate gypsum crystals. Similar giant growth-aligned subaqueous gypsum with single crystals up to 10 metres tall have been documented in the Lower Miocene evaporites of Poland (Babel, 1990) and the various Late Miocene Messinian sub-basins of the Mediterranean (Rouchy and Saint-Martin, 1992). Growth cycles in these subaqueous gypsum deposits range from mm couplets to decametre beds to brining cycles that are tens of metres thick (Figure 1.15a,b).

Large aligned gypsum crystals that make up the bottom-grown beds typically entrain curved growth faces interspersed among parallel-sided prisms. Very few natural gypsum beds are made up of growth-aligned crystals that first formed as aggregates of upward-oriented simple twins. That is, natural crusts and bed of growth oriented gypsums are not conjoins of the simple prisms shown in Figure 1.16a. In fact, the crystal forms illustrated in Figure 1.16a, and given in many mineralogy texts as typical gypsum morphologies, are the least common forms of gypsum in natural subaqueous systems.

Where a curved face encapsulates a crystal, a single lensoidal crystal forms (Figure 1.16b). The term “bird-beak” gypsum is sometimes used to describe its distinctive lenticular shape. The characteristic hooked termination can be used

with pseudomorphs to help separate gypsum from the truncated lenticular “axe-head and keg barrel” forms of diagenetic anhydrite. Individual lenticular gypsum crystals range from sand-size to boulder-size. Lenticular sand-sized forms make up the uppermost lake sediments and the gypsum lunettes about the saltflat edges of many coastal and continental salt lakes in Australia (Chapter 4; Warren, 1982b). Holocene lenticular gypsum crystals are intimately associated with algal sediments in marine-seepage-fed Ras el Shetan mudflats in the Gulf of Aqaba, Egypt (Aref, 1998a).

Bedded gypsum growing on the shallow bottom of a perennially subaqueous lake or seaway typically precipitates as masses of large parallel-sided megacrystals that show varying levels of expression of the curved faced (Figure 1.16c). Individual growth-aligned crystals are decimetres to metres long in gypsum beds in marine seepage fed Holocene salina such as Marion Lake and Lake Asal, while ancient counterparts in the Middle Miocene of Poland are more than 10 metres long (Babel, 1990). Varying degrees of curvature lead to the growth of distinctive gypsum twins with acute (narrow) to obtuse (wide) angles along the twin plane. Doug Shearman described this form of overlapping curvature along the twin plane as “arms of Siva” gypsum. Strong vertical development of the upper half of some twins creates beds of upward aligned gypsum crystals showing strong curvature of the intercrystalline faces. Such forms are sometimes called palmate gypsum. Some purists would argue that most of these natural forms of growth aligned gypsum are not true twins (Babel, 1990). The varying degrees of curvature entrained in the crystal generate changes

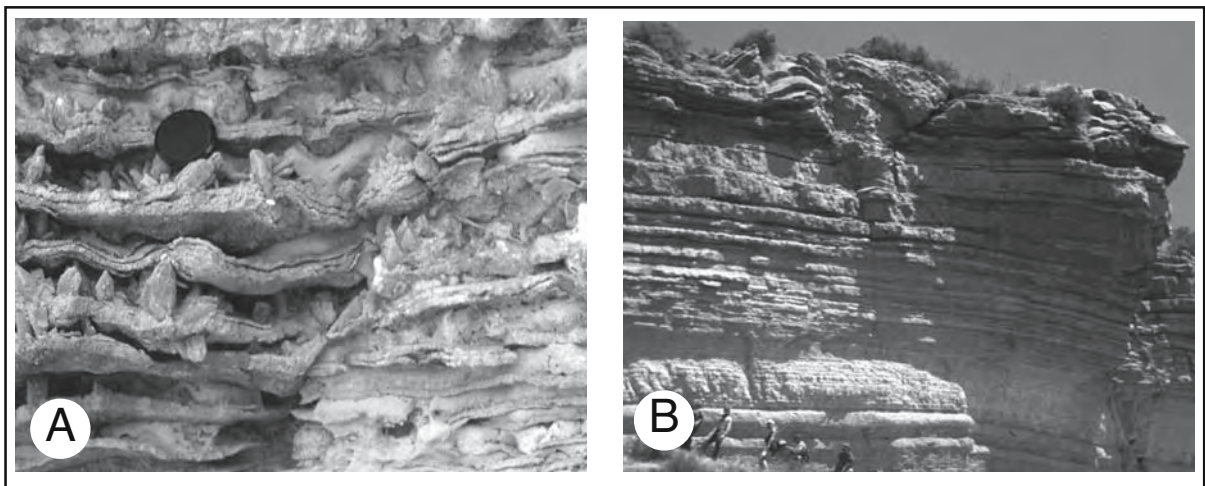


Figure 1.15. Subaqueous gypsum from the late Miocene of Sicily. A) Stacks of layers of aligned cm-scale gypsum crystals, each layer indicates growth competition from a marly gypsarenite base (lens cap for scale). B) Metre-scale layers showing a larger subaqueous growth cycle from a finely laminated marly base through coarsely-bedded aligned gypsum to a series of domal mounds capping the cycle (people for scale).

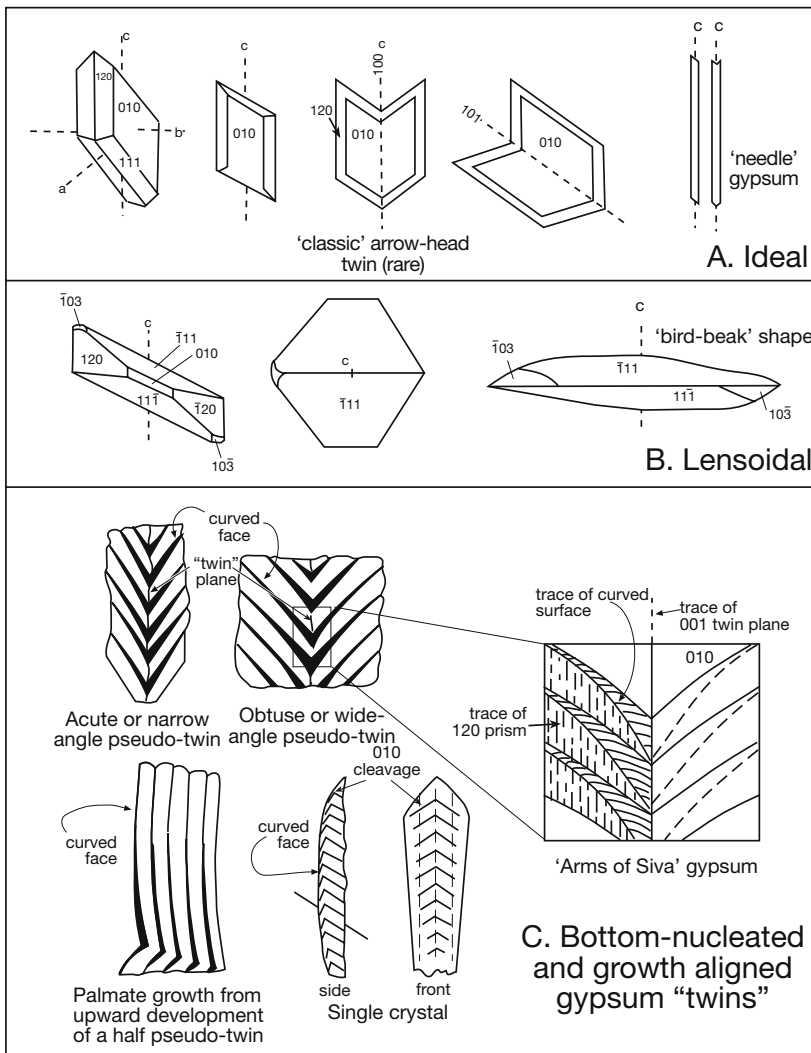


Figure 1.16. Gypsum. A) Prismatic forms of gypsum parallel to (010) with arrow head twins along (100) or (101) and extreme acicular forms of prism and twin on the right. B) Lenticular form of gypsum. Note how the lenticular form (on right) is dominated by the curved faces that are much less important on a typical prism as seen in the side and top views of a crystal (on left). C) Various forms of typical subaqueous "zig-zag" gypsum growth as described in text (after Shearman, 1978; Orti-Cabo and Shearman, 1977; Rouchy et al., 1994).

in the apparent twin angle, even in a single crystal. This breaks the rule of constancy of twin angle, leading some to refer to them as pseudo-twins (e.g. Schreiber, 1988a). Whatever the crystallographic semantics, these large aligned crystals only grow on the gypsum-saturated bottoms of shallow subaqueous brine lakes and seaways.

The reason why the curved face comes to dominate some gypsum crystals (e.g. lenticular crystals and displacive rosettes) is not well

understood. On the basis of a number of laboratory-based growth experiments using brine columns separated by gel growth media, Cody and Cody (1988) argued the lenticular shape of displacive gypsum (intrasediment sediment growth) reflects influence of temperature and the presence of humic compounds in the parent brine (Figure 1.17). Two temperature dependant trends were obvious in the precipitates. At low temperatures the hemipyramidal habit, dominated by the $1\{111\}$ faces dominate. At higher temperatures the lenticular $3\{103\}$ is obvious in all crystals. They concluded that elongate prisms grow best at low temperatures and in the absence of habit-modifying organics.

They found that the modifying influence of temperature on morphology was swamped by the presence of low levels of organics in all the growth experiments. With increasing polytannate concentrations (analog for terrestrial humics), crystals become less elongate and penetration twinning along the $a\{100\}$ develops. This is followed by secondary complex nucleation near twin faces as rosette and rosette-like aggregates form (aka desert roses). The changes in morphology are interpreted as the result of a high degree of adsorption of organic compounds on the $\bar{1}03$ and $\bar{1}11$ faces that inhibits their growth and consequently minimizing growth parallel to the crystallographic c-axis (Cody, 1976). This adsorption is thought to reflect the peculiar surface structure of the face, which unlike the other faces of gypsum is almost entirely composed of Ca^{++} ions and these Ca^{++} ions bond readily with organics (Aref et al., 1998a).

Warren (1982b) found that masses of sand-sized lenticular gypsum crystals make up near surface beds deposited in seasonally vadose settings in the numerous coastal salinas of southern Australia. He argued the lenticular shape tends to form

best in the upper seasonally vadose parts of the brine pan fill subject to periodic short-term dissolution and regeneration. The pristine parallel-sided gypsarenite prisms that constitute the underlying thick bed of gypsarenite or growth-aligned laminar selenite were not present at this level in the lake stratigraphy. However, the vadose gypsum in these salinas grows in surface and near-surface pore waters that are more influenced by surface runoff from nearby vegetation-covered calcareous dunes and so entrain higher tannic acid levels.

Growth-aligned coarse-grained gypsum beds form in Holocene coastal lakes of Southern Australia beneath the waters of perennial subaqueous brine pans that are density stratified for more than 6-8 months of the annual depositional cycle. In the early stages of infill of the salina, the perennial bottom brine was always saturated with respect to gypsum. Salinity conditions were stable and allowed the upper euhedral surface of the aggrading crystal bed to preserve the upper outlines of crystals in each growth stage. If the gypsum precipitating today in Lake Inneston, South Australia, is indicative of the subaqueous growth style, then throughout much of their growth, any large upward facing gypsum crystals are covered by a microbial mat or film that captures aragonite pellets and can be considered a type of gypsum stromatolite (Figure 4.5d). Similar subaqueous gypsum mounds, coated with cyanobacteria, line the southern end of the brine channel leading into Gotomeer in the Netherlands and pass into laminated aragonitic microbialites in the shallower waters along the channel edge (Figure 1.7c; Kobluk and Crawford, 1990)

Rapid bottom growth of gypsum probably only takes place when stratification of the brine column is lost via seasonal concentration of the fresher surface water body to the same salinity as the dense gypsum-saturated bottom waters. Once this happens the whole water column is supersaturated with respect to gypsum and gypsum growth

begins anew on a metres-deep brine pool floor. As the aggrading euhedral gypsum bed surface encloses CaCO_3 impurities, it encapsulates and preserves zig-zag laminae within the bed.

Aragonite pellets that mantle the re-entrant laminae in the salina gypsum are a combination of a pelagic “rain from heaven” and faecal pellets excreted by a grazing biota grazing the biofilm that covers the gypsum. Metazoan life flourishes during the freshened salina stage when a less saline surface water body ($\approx 50\text{cm}$ thick) floats atop the lower brine mass from spring to early summer). Pellets in Lake Inneston and Deep Lake salinas signify the feeding activities of ubiquitous ostracodes and the Southern Hemisphere brine shrimp (*Parartemia zietziana*). When salinities in the surface waters are suitable, this

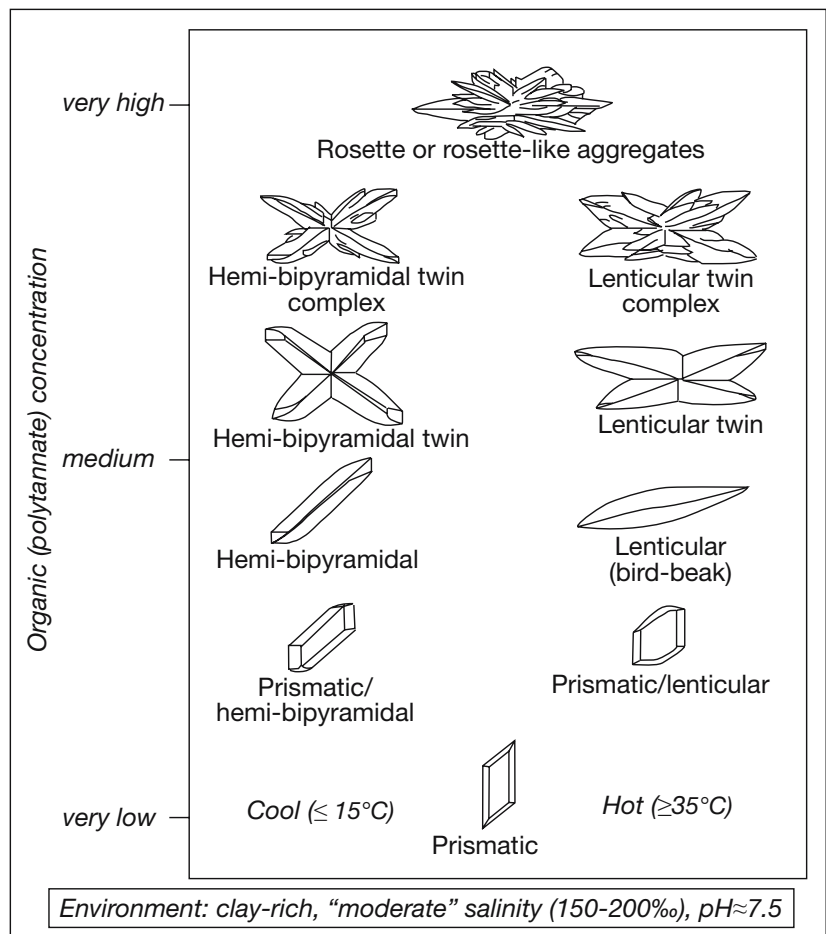


Figure 1.17. Laboratory based changes in gypsum growing in a muddy (bentonite) sediment matrix at moderate salinity and neutral pH in environments characterized by increasing temperatures and dissolved polytannate concentrations. Polytannate is considered to be an analog for terrestrial humic material. c-axis vertical in all examples (after Cody and Cody, 1988).

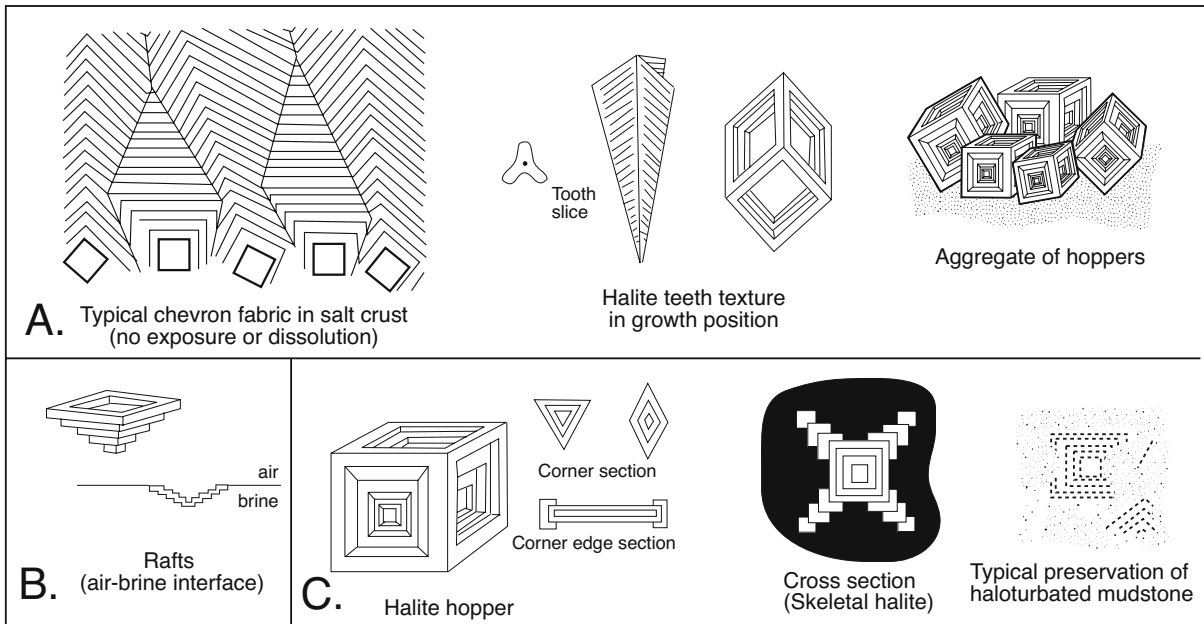


Figure 1.18. Halite. A) Growth aligned forms of subaqueous halite and typical chevron growth fabric outlined by inclusions in the crystals. Those crystallite cubes with upward-aligned edges, rather than faces, come to dominate the growth fabric as a series of merged chevron crystals. Other bottom growth forms include upward-growing halite teeth and aggregates of hoppers on the bottom that were created by overgrowths on sunken rafts. B) Halite raft growth, where crystals hang from the air-brine interface. C) Various forms of skeletal or intrasediment halite hoppers. Notice how the outline of the halite shape or its pseudomorph can vary from rectangular to triangular depending on the plane of intersection of the viewing horizon with the crystal hopper (in part after Shearman 1970; Rouchy et al., 1994).

halotolerant biota spreads through surface waters over the whole brine lake (Chapter 9). When surface salinities later increase to levels that can no longer support a metazoan population, mass mortality occurs. Soon after, the upper and lower brine masses equilibrate/mix and lakewide gypsum precipitation begins again. Even so, small populations of brine shrimp and ostracodes flourish about seawater-fed seeps in the tepee and mound-spring dominated salina strandzone.

Over millennia, the depositional surface of the salina aggraded as successive gypsum layers infilled the centre of the brine lake depression (Warren, 1982b). As the top of the salina gypsum bed aggraded, it reached a level where even the dense bottom water mass was seasonally freshened. Then the perennial bottom waters, as well as surface waters, were undersaturated with respect to gypsum for a number of months each year. At that time the upper gypsum surface dissolved each winter to form a flat planation surface. Now the seasonal growth of the aggrading bed surface enclosed CaCO_3 pellets laying atop this dissolution surface to form a flat mm-laminated gypsum bed (Figures 2.49, 4.5f).

Halite beds (chevrons and crusts)

Crystals in halite crusts first precipitated on the floors of shallow hypersaline brine pools as upward-growing chevrons, cubes and cornet-shaped crystals (Figure 1.18a, 1.19a,b). Chevron structures preserve the outlines of successive crystal growth edges and are defined by enclosed brine inclusions. Remnants of aligned chevrons are the most commonplace primary texture preserved in ancient halites. Abundant inclusions impart a cloudy or milky appearance to the chevron crystals, a feature that is often used in ancient counterparts to distinguish primary halite from clear or spar-like crystals of secondary or diagenetic halite. Crystals can accumulate as successive layers of growth-aligned prisms or can form as syntaxial overgrowths on floundered rafts and other cumulate crystals that have settled to the pan floor. As for all isotropic crystals growing in crowded conditions, the crystal edges of halite cubes that point upward into the brine grow more rapidly than crystals with upward-pointing crystal faces. The upward pointing “V’s” of the edges quickly dominate and so creates an aligned chevron texture that characterises many subaqueous halite crusts (Figure 1.18a). Less common are thin crusts and beds composed of upward-facing cornets and plates. There the

crystals grew by the upward aggradation of the horizontally aligned faces, and perhaps indicate less crowded conditions of bottom growth (Handford, 1990, 1991).

Such crystals accumulations form halite beds up to 5 metres thick in Lake McLeod, Western Australia where the beds are composed of stacked decametre-thick crusts dominated by bottom-nucleated aligned chevrons. Brine sheets that precipitated the halite were always less than two metres deep and usually less than 0.5 m deep (Logan, 1987). Similar units of stacked crusts, but with obvious truncation surfaces and capillary overprints, characterise saline pans in Salar Uyuni and other pans worldwide (Figure 3.30). Patchy remnants of chevron halite crusts, deposited in shallow to ephemeral brines, are also preserved in ancient thick halite beds such as the Ordovician-Silurian Mallowa Salt of the Canning Basin (Cathro et al., 1992) and the Permian San Andres Formation of west Texas (Hovorka, 1987).

Elevated cell densities of halobacteria in extremely hypersaline brines can change the precipitation behaviour of halite (Gerdes et al., 2000a, b). Proteinaceous compounds coating the surface of the growing halites encourage the growth of dendritic crystals rather than chevrons. Crystals forming in organic-enriched brines contain more and larger brine inclusions than crystals growing at the same salinities from sterile brines. Cells are smaller and much more numerous in the organic-enriched brines and the cells are thought to create templates for halite nucleites.

Halite cumulates, rafts and coated grains

Crystallites grow in the uppermost part of a standing body of water where water is rapidly lost by evaporation and salinities are at their highest. Silt and sand-sized crystals settling to the bottom of the brine pool then form layers and beds of cumulate crystals (e.g. “salt and pepper” halite and massive gypsinites). Periodic influxes of freshened surface waters, followed by evaporative concentration, can produce laminites composed of bottom cumulates, which contain increasing fractions of the more saline minerals. Such “rain-from-heaven” laminites are composed of alternate carbonate-sulphate and sulphate-halite couplets and triplets.

When surface water salinities are suitable and surface waters are undisturbed by wind and waves, crystals can continue to grow as rafts held by surface tension at the air-brine interface (Figure 1.19b). Rafts float and grow until the crystal mass becomes so heavy that it exceeds the holding ability of the interfacial surface tension and sinks to the bottom. Halite rafts in quiescent waters can be centimetres to decimetres across before they sink to the bottom. Eventually, increasing wind and wave action breaks up the rafts while they are out in the brine lake and still well away from the strandzone. These remnants then sink to mix with the smaller crystals and so make up part of the texture of the cumulate beds of the brine lake floor. Later, when the lake shallows and further desiccates, these cumulate beds are covered by crusts and beds of bottom-nucleated chevron halite or swallowtail gypsum. This upward transition from cumulates to crusts is commonplace in modern crusts.

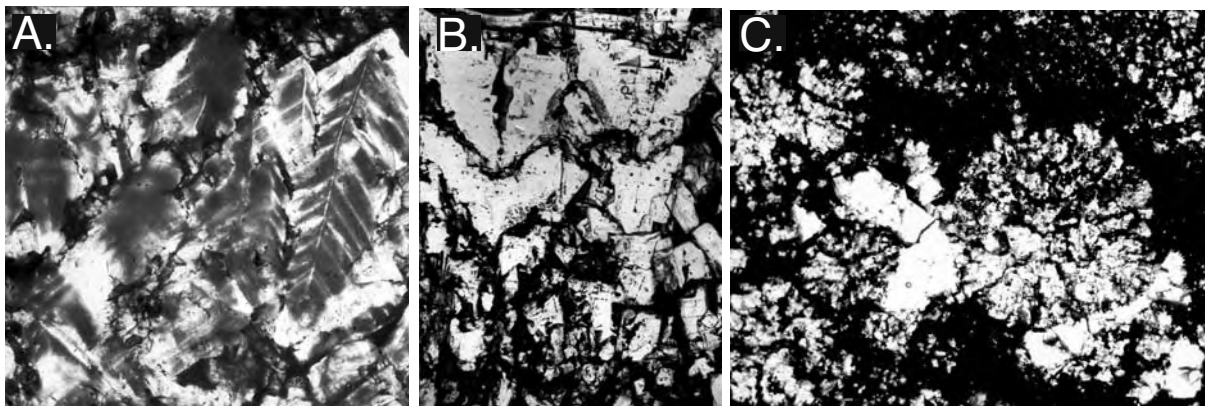


Figure 1.19. Subaqueous halite A) Thin section photomicrograph of halite from perennial saline lake interval, Death Valley core, depth of 8.1 m. Halite chevrons with dense fluid inclusion banding (dark) and vertical, competitive growth fabrics. Horizontal field of view is 4 mm. B) Thin section photomicrograph of halite from perennial saline lake interval, Death Valley core, depth of 15.8 m. Bottom-grown halite crystals with vertical growth fabric. Note that halite crystals widen upward and contain faint fluid inclusion banding. Some mud (dark patches) is trapped within or between crystals. Horizontal field of view is 4 mm. C) Thin section photomicrograph of halite from perennial saline lake interval, Death Valley core, depth of 8.6 m. Halite pisoids, 2-5 mm in diameter and with faint radial fabric, from the upper shallow saline lake interval. Note mud drape (black) and fine-grained halite cumulates above the largest pisoid. Horizontal field of view is 10 mm. (images and descriptions courtesy of Tim Lowenstein; see <http://www.geol.binghamton.edu/faculty/lowenstein/dv/deathvalley.html> - accessed Dec 7, 2004).

Rafts and other cumulate crystals in very shallow to ephemeral brine pans may be blown or carried by bottom currents to the strandzone to accumulate as subaerially exposed masses of strandzone crystals. Such deposits characterise surface carnallite/halite shores about the brine pan edge of Lake Qaidam in China and trona cumulates about the edges of Lake Natron and Lake Magadi. Whenever the adjacent lake water body freshens and expands, the dissolution of the strandzone salts generates dense brine plumes that cement underlying sediment (Casas et al., 1992; Hovorka, 1992; Schubel and Lowenstein, 1997).

Ancient cumulate crystal beds, not covered by bottom-nucleated crusts, were sometimes mechanically reworked by storm and wave-induced bottom currents into crossbeds and ripples. This tended to happen on the bottoms of ancient perennial brine seaways and lakes that were above wavebase and covered by brines that were less than 5-10 m deep. In even shallower nearshore positions that were subject to higher wave-energies, fine-grained cumulate crystals formed the nuclei to concentric ooids composed of gypsum and halite (gypsolite and halolite respectively). Today, such coated grain textures are precipitating immediately basinward of the strandzone of Lake Asal in the African Rift Valley and along the southern end in the Dead Sea (Castanier et al., 1992, 1999), they are also preserved in perennial brine halites in Death Valley California (Figure 1.18c). In a recent paper, Perthuisot and Castanier (2000) have argued that the process of halolite formation is bacterially mediated. The significance of bacterial activity in precipitating evaporitic oolites is widely debated. It is much like the unresolved debate on the importance of bacteria in marine ooid formation that has gone on for decades amongst carbonate sedimentologists.

Pedogenic and wind reworked salts

Many arid to semi-arid desert soils are gypsiferous in areas surrounding the perennial saline lakes, the brine pan depressions and their dune margins. Where gypsum dominates the pedogenic profiles, the soils are typically described as gypcretes, gypsites, gypsicretes, *croûte de nappe* or *croûte gypseuse zonée*. Currently, something like 2×10^6 km² of gypsum-entraining soils cover the world landscape (Nettleton, 1991). Gypsum crusts have been reported from all the continents, including Antarctica (El-Sayed, 1993). They typify soils in arid areas where mean monthly evaporation exceeds mean monthly precipitation, Watson (1985) notes a close association of gypsum soils with areas receiving less than 250 mm annual rainfall.

Use of the term gypcrete often has a connotation of gypsum being the dominant hardpan cement, while the term gypsite im-

plies a fine-grained (silt-sized) powdery soil. According to Aref (2003) gypsum crusts and soils are surficial and penesurficial accumulations that have the following specifications: 1) a minimum thickness of 0.1 metre; 2) a minimum gypsum content of about 15% by weight; and (3) a gypsum content at least 5% greater than the underlying rocks. If the soil contains less than 15% gypsum it is classified as a gypsiferous soil. Watson (1985) also grouped the consolidated gypsum, together with weakly cemented and powdery gypsum accumulations under the term gypsum crust.

Four mechanisms or processes precipitate most gypsum soils and crusts worldwide: 1) in-situ pedogenic weathering of existing gypsiferous or volcanogenic (ash) parent material; 2) eolian or fluvial input of gypsum or SO₄-rich sediment; (3) an oceanic aerosol source, creating in sulphate-enriched rainfall that evaporatively concentrates within the regolith (4) in-situ oxidation of sulphide minerals. The first two sources are direct evaporite associations, while the third is typically associated with salt lakes, sabkhas and playas in semi-arid or desert settings within 500-1000 km of the coast. Many gypsic soil horizons are combinations of both pedogenically precipitated and detrital wind- reworked gypsum.

Soils with gypsic horizons form in various parent materials such as alluvium, eolian sediments and weathered geologic formations, many in regions of pre-existing gypsiferous sediments (Taimeh, 1992). For example, differentiated gypsum soils 0.5 to 1.5 metres thick, largely formed by capillary evaporation, cover much of the area east of the Fayum depression (chott) in the north central part of Egypt (Figure 1.20; Aref, 2003). These pedogenic gypsum crusts only cap Middle Eocene carbonate rocks that are interbedded with thick gypsiferous shale beds and the soils are mostly a result of the hydrological reworking of this Eocene source. The soils show a three-part layering from top to bottom of: (1) massive powdery gypcrete, (2) massive indurated gypcrete, and (3) massive mottled gypcrete. All layers are composed of variable amounts of microcrystalline gypsite, fine to coarse lenticular gypsum, as well as porphyroblastic, prismatic and fibrous gypsum. Precipitation of the various types of gypsum is driven by capillary evaporation of CaSO₄-enriched meteoric waters, so most of the gypsum occurs as vadose surficial crust dominated by displacive gypsum growth. In the lower vadose zone, gypsum accumulates by illuviation, interspersed with hydromorphic (sparry) accretion when water table levels are higher (Aref, 2003). The resulting gypsum carapace, although susceptible to dissolution, tends to preserve the residual landforms from severe erosion or weathering and so form gypsum-capped mesas.

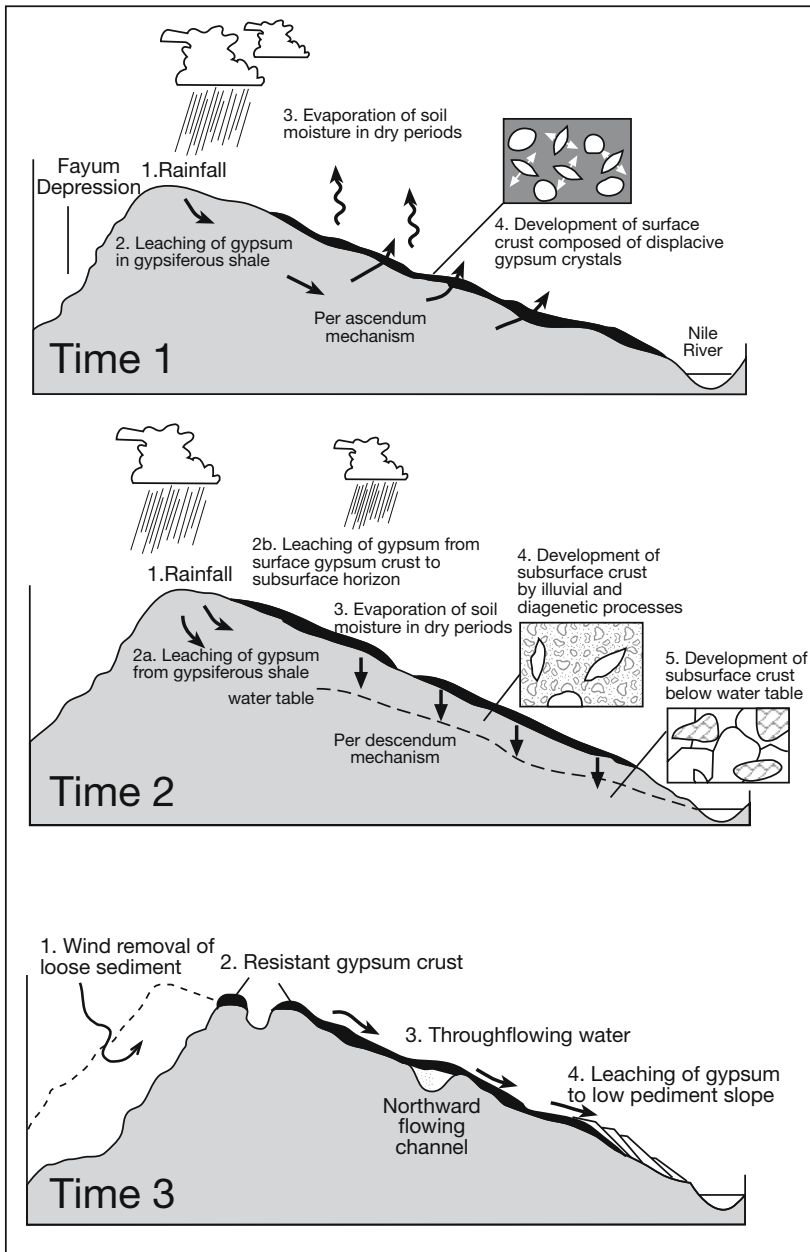


Figure 1.20. Formation of pedogenic gypsum crusts at the eastern side of the Fayum depression Egypt (after Aref, 2003). During dry periods, the gypsum-rich meteoric waters are drawn to the surface by capillarity (per ascensum), which leads to gypsum crystallization and crust accretion on the lower slope. During a subsequent wetter period, the surface gypsum crust is partially dissolved by meteoric water that moves downward and is mixed with laterally moving gypsum-rich meteoric water from the gypsiferous beds, which leads to deposition of subsurface gypsic crust. During subsequent weathering of the landscape the gypsum crusts can preserve residual landforms from subsequent erosion and weathering.

Elsewhere, marine aerosols are focused into playa sinks and then reworked by eolian processes, as in much of the Namibian Desert and in soils about the arid salt lakes areas of southwestern and southeastern Australia. Other evaporite salts, with their inherently higher solubilities, tend to dissolve too rapidly in most vadose situations to form soil crusts and so do not form thick preservable accumulations in most of the world's deserts. Impressive exceptions to this generalisation can be found in the hyperarid Atacama Desert of South America. There pedogenic accumulations of nitrates and iodates, along with halite and gypsum, are accumulating in the desert regolith; and have been doing so since the mid Miocene, when uplift of the Andes first created desert conditions (Figure 11.42). For the same reason, namely hyperaridity, small parabolic dunes of halite (0.7-1.3 m in width and length) are today blowing across the saline pan floor of Salar de Uyuni (Svendsen, 2003).

Pedogenic gypsum horizons can sometimes stack to substantial thicknesses. This is especially so in arid subsiding groundwater basins where ancient evaporite beds exposed by diapirism or uplift about the basin edge are being recycled by karstification. For example, there is a 25 metre thick gypcrete hosted in Miocene alluvial fan sediments in the Calama Basin of northern Chile. The gypcrete is a single horizon in the alluvial bajada and it surrounds an ancient endorheic basin. It formed via stacking of gypsum-cemented soil horizons (Hartley and May, 1998). It was probably preserved, despite its high susceptibility to meteoric recycling, by its 9.5 Ma carapace of ignimbrite. This relatively impervious volcanoclastic ashfall isolated it from downward-percolating meteoric waters.

Locality	Style	Reference
Bonneville Salt Flats, Utah	Gypsum dunes along the edges of an active continental sabkha formed atop a now deflated perennial saline lake	Jones, 1953
White Sands, New Mexico	Gypsum dunes created by active deflation of gypsiferous sediments of Pleistocene Lake Otero	Langford, 2003
Salt Flat Playa, New Mexico	Gypsum dunes along the edges of an active continental sabkha forming atop a former perennial saline lake	Hussain and Warren, 1988
Laguna Ojo de Liebre area of Baja California	Gypsum dunes along the mudflat edges of coastal lagoons	Kinsman, 1969
Continental playas or salt lakes of inland Australia	Gypsum lunettes in most salt lakes in zones of continental seepage outflow in the interior of Australia including; Lake Eyre, Lake Frome, Lake Fowler, Lake Malata-Greenly, Lake Amadeus, Prungle Lakes, Lake Lefroy and Lake Cowan. Other less saline pans are lined by lunettes of pelleted clay or sand	Bowler, 1983 Chen et al., 1990 Dutkiewicz et al., 2002 Magee, 1991 Zheng et al., 2003
Salinas of coastal western and Southern Australia	Gypsum dunes formed by late Holocene deflation of lacustrine gypsarenites in a marine seepage lake that is currently filled to within a few cm of sea level (e.g. Lake Macdonnell, Marion Lake, Streaky Bay Lakes, Hutt Lagoon)	Arakel, 1980 Warren, 1982b
Dunes in chotts in South-central Tunisia	Gypsum dunes derived by the subaerial break-up and deflation of gypsum crusts that cover much of the seepage areas in the chott	White and Drake, 1993

Table 1.4. Some regions where gypsum dunes (lunettes) are associated with the deflation of saline lake (playa) sediment.

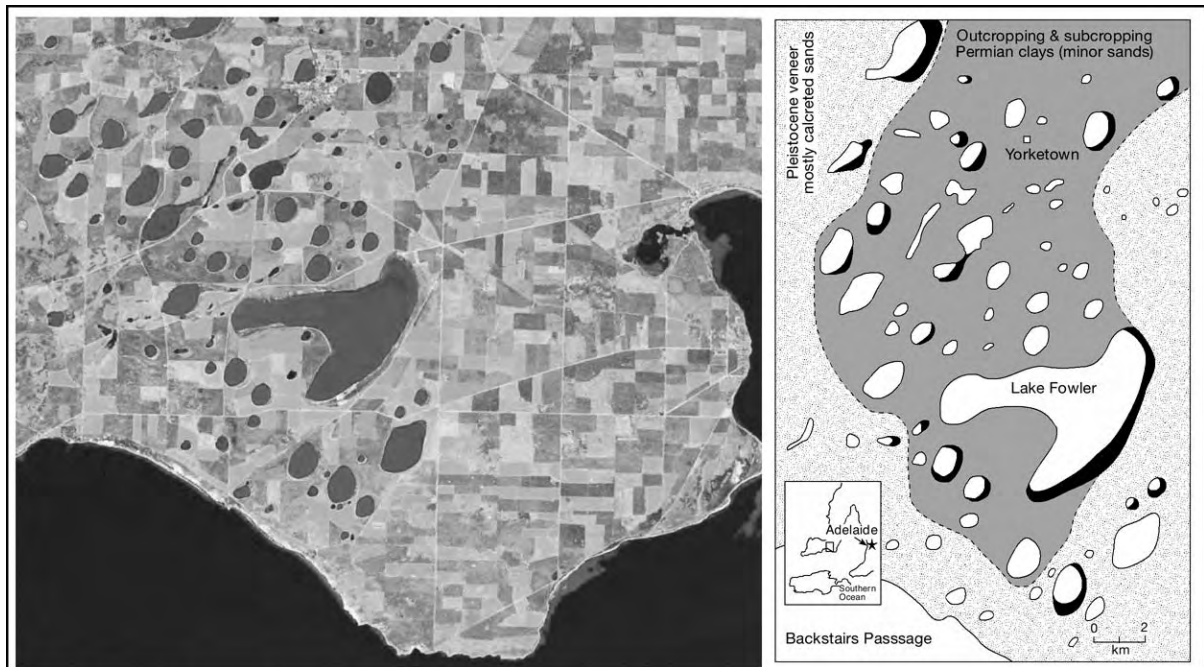


Figure 1.21. Late Pleistocene lunettes in saline pans (salt lakes) in semi-arid southern Australia near the town of Yorketown showing gypsum lunettes at the edges of some of the wind-oriented lakes at the southeastern end of Yorke Peninsula. The largest is a gypsum lunette some 2 km long 100 metres wide and 30 metres thick at the southeastern strandline of Lake Fowler, the large T-shaped lake with a long axis ≈ 6 km (see Warren 1982b for description of gypsum in the lunette). It was extensively quarried in the early part of last century. Larger gypsum dunes (lunettes) are shaded black in the geological map (Landsat image courtesy of NASA).

Gypsum dunes, stabilised by gypsite-soil caps, form wind-reworked vadose deposits around the margins of many Holocene and Quaternary brine lakes throughout the world (Table 1.4). For example, gypsum dunes line the salt pan edges of undisturbed continental salt lakes and coastal salinas in southern and western Australia. Today all lakes are in the penultimate stages of their Holocene brine pan fill; hydrologies are characterised by ephemeral surface waters interspersed with long periods of deflation. In the coastal zone these are the same pans that precipitated large bottom-aligned gypsum crystals in the earlier perennial brine stages of their Holocene infill. But now, with the aggradation of the gypsum fill to near sealevel elevations, the lake surface is at hydrological equilibrium with current sealevel and can aggrade no further (Warren, 1982b). Surface brine sheets come to saturation quickly and dry up by late spring. Rapid multiple nucleation of gypsum crystallites takes place across the floor of the brine pool. Beds of sand-sized gypsum (gypsarenite) now accumulate on the floor of ephemeral brine lakes, only to be subject to later desiccation and deflation.

Each summer, as undisturbed salinas exsiccate, the water table falls and the upper part of any newly formed gypsarenite layer leaves the capillary zone and is blown into dunes that line the margins of the lake (lunettes). Capillary zone deflation forms the characteristic truncation or Stokes surfaces in regions sourcing eolian sediments worldwide (Table 2.11). When dune growth ceases, a stabilised and vegetated gypsum dune is subject to the set of pedogenic processes that form gypsite and gypcrete. Gypsum rhizoliths and bioturbation structures, as well as bioturbated gypsum soils (gypsites) form atop eolian crossbeds (Figure 4.5g).

Gypsum and pelleted clay dunes (lunettes) line the edges of many salt lakes and playas in southeastern, southern and southwestern Australia; Prungle Lakes and Lake Fowler (gypsum lunettes) Lake Tyrell (clay lunette) and Lake Mungo (quartz sand lunette; Figure 1.21; Table 1.4). These lunettes are relicts of a Late Pleistocene deflationary period, when the lacustrine hydrology changed from perennial water-filled lakes to desiccated mudflats. Likewise, there are gypsum dunes in deflationary depressions in Salt Flat Playa and the Bonneville/Great Salt Lake region of Utah (Table 1.4). Internal sedimentary structures in many of these lake gypsum dunes or lunettes show tabular cross beds with consistent bedform orientation. Many lack abundant trough or festoon cross beds, suggesting consistent wind directions (Figure 1.22a; Jones 1953; Bowler, 1973, 1983). Grain constituents clearly indicate deflation of former lake sediments, which were vadose prior to deflation and passage into the dunes (Figure 1.22b).

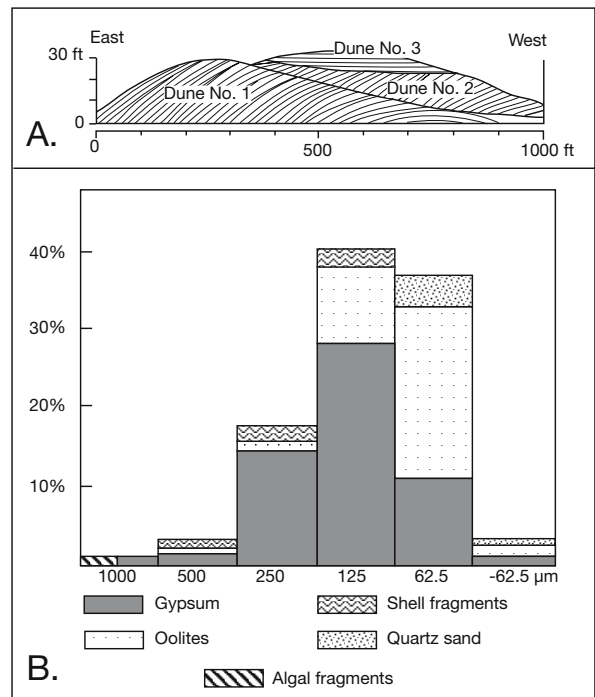


Figure 1.22. Eolian gypsum in the Bonneville saltflats, Utah. A) Cross section through the dune complex near Knolls, Utah. B) Grain size distribution and mineralogy of the sands showing it is the result of deflation of sediments laid down in highstand conditions in the Bonneville/Great Salt Lake Basin (after Jones, 1953). See Chapter 4 for a discussion of Great Salt Lake.

Gypsum dunes are part of a much broader lake-edge eolian sandflat association with the lakes often supplying large volumes of eolian sediment into adjacent sand seas or ergs (Chapter 2). Dunes described as ‘lunettes’ have a characteristic crescentic shape, other lake edge dunes may show more linear or longitudinal outlines (Figure 1.21; Bowler 1973, 1986). Lunette sediments range in composition from quartz-rich, sandy clay, through gypseous clay to nearly pure gypsum. Pure quartz dunes formed under lake-full conditions and are distinct from that of the clay and gypsum-rich varieties, which formed by flocculation and deflation from adjacent subaerially exposed lake floors. In arid to semi-arid zones throughout the Quaternary the interplay between salinity of lake waters and groundwater levels is critical in lunette growth and the mineralogy of the lunette (Bowler, *op cit*).

Although body fossils are rare in most evaporite beds, many subaerial and subaqueous gypsum soils preserve abundant trace fossils that, in addition to track and trails, also include rhizoliths and other pedotubules. Rhizoliths in a gypsiferous lacustrine system form at times of freshening of lake waters, they indicate periodic subaerial exposure and colonisation by terrestrial plants.

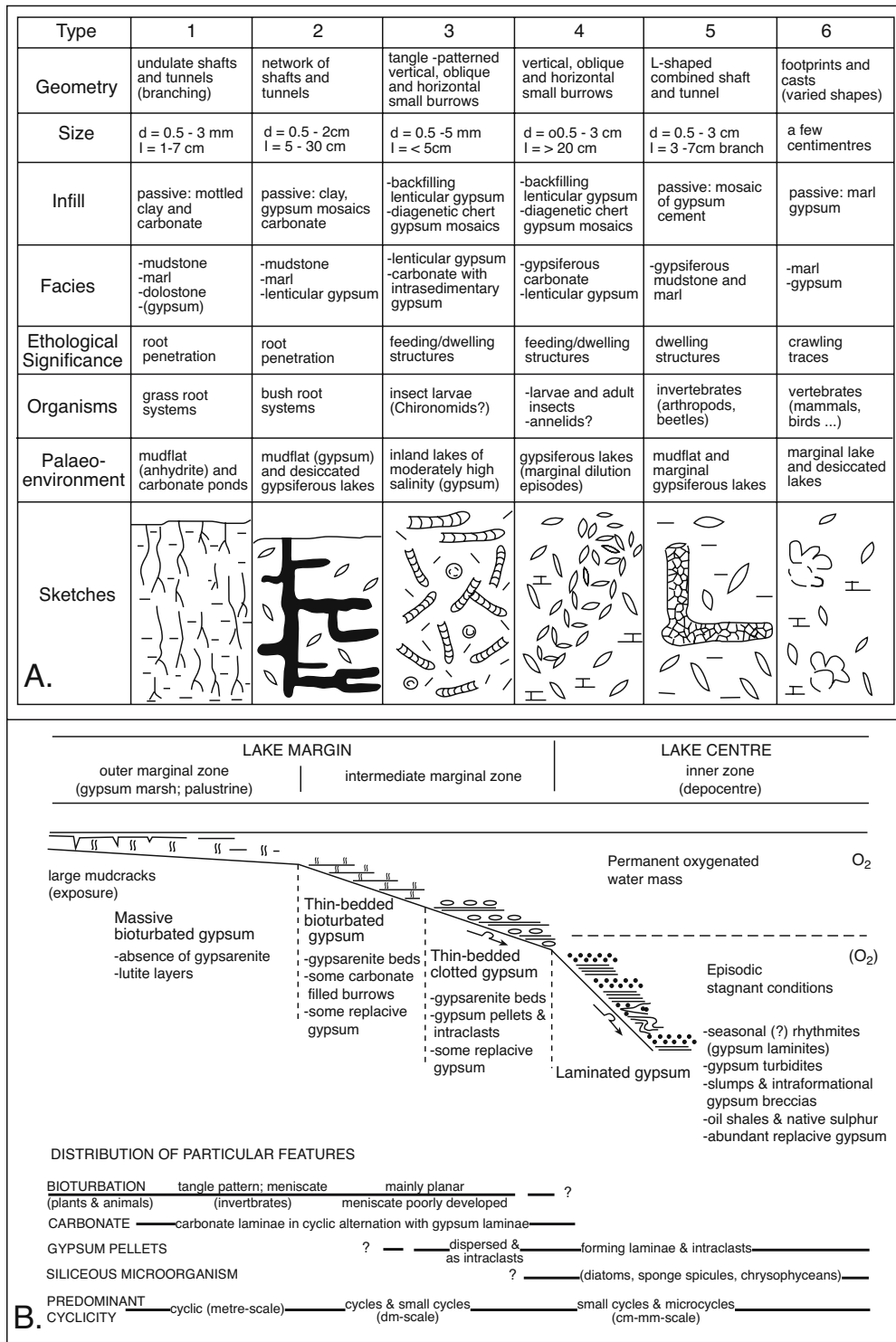


Figure 1.23. Summary of trace fossil and rhizolith types in continental evaporite beds in Spanish Miocene Lacustrine Basins. A) Spectrum of bioturbation structures, mostly from plants and animals in the lake margin facies (after Rodriguezaranda and Calvo, 1998). B) Distribution of bitoturbation structures in relation to lacustrine gypsum textures and water depths (after Orti et al. 2003).

Rodriguezaranda and Calvo (1998) identified six associations of trace fossils in subaerially exposed evaporitic sediments of the continental Tertiary basins of Spain: (1) networks of small rhizoliths; (2) large rhizoliths; (3) tangle-patterned small burrows; (4) isolated large burrows; (5) L-shaped traces; and (6) vertebrate tracks (Figure 1.23a). The rhizoliths occur both in the marginal areas of hypersaline lakes and across lakes characterised by ephemeral but moderately high salinity waters (Figure 1.23 b). In either setting, pedoturbation indicates colonization by grasses and bushes and so indicates vadose conditions at the sediment surface that were tied to a drying of the lake and a lowering of the water table.

According to Rodriguezaranda and Calvo (1998) burrowing invertebrates were especially active in

those Spanish evaporite lakes where gypsum was the main mineral phase, not the more saline salts. They define a separate, sometimes pedogenic, facies in these lakes they called a “bioturbated gypsum deposit.” It is typified by tangle-patterned small burrows and minor isolated large burrows; they are interpreted as burrows of insect larvae, probably chironomids, coleopterans and annelids. Similar organisms typify modern lake environments with water concentrations averaging 100–150 g/l, they flourish in lake areas subject to frequent drying and terrestrial encroachment (Chapter 9).

What is interesting about the bioturbation of these Miocene gypsum lakes in Spain is that the mm-scale layers rich in faecal pellets and associated with this bioturbation can be composed of gypsum and not the aragonite typically seen in Holocene coastal salinas (Figure 1.23b). For example, the gypsum-pellet-rich Libros Gypsum was deposited in the southern Teruel Basin (NE Spain) during the Miocene (Orti et al., 2003). It accumulated in a deep saline lake in which the water stratification became unstable with progressive shoaling. In the basin depocentre, a continuum of lacustrine evaporite lithofacies was influenced by the activity of organisms. Rhythmites, composed of laminae of pelletal gypsum and laminae of very fine lenticular gypsum crystals mixed with siliceous microorganisms, formed in addition to gypsum turbidites, intraformational gypsum breccias and slump structures.

The pelletal laminae originated from the faecal activity of animals (crustaceans?) ingesting gypsum crystallites in the lake water during episodes of maximum evaporation, whereas the laminae of very fine lenticular gypsum mixed with microorganisms accumulated during episodes of relative dilution. In the wide marginal zones of the basin, the Libros Gypsum unit consists of massive to thin-bedded bioturbated gypsum and thin-bedded clotted gypsum, which formed in intermediate to very shallow (palustrine) water depths. The bioturbated gypsum lithofacies were produced by the action of diverse organisms, presumably worms and coleopterans, and chironomid larvae to a lesser extent; the massive lithofacies precipitated in very shallow water; and the thin-bedded lithofacies formed in shallow to deeper settings. The thin-bedded clotted gypsum is a relatively deep facies that may have diverse origins (e.g. bioturbation, compaction, disruption of soft sediments and early diagenesis). There is a well-developed metre-scale cyclicity in the marginal lake sequences, which is not observed in the inner lake deposits. This suggests a depth change in the various lacustrine subenvironments is needed to record cyclic evaporitic processes. The isotopic composition of the pelletal gypsum indicates early sulphate-reducing bacterial activity in the bottom of the lake (Orti et al., 2003).

Biological metabolism drives substantial fluctuations in pedogenic pore pressures and salinity in gypsiferous and magnesitic soils in many lake margins and vegetated areas of coastal sabkhas. This is especially so in the immediate vicinity of plant roots, and it can precipitate CaSO_4 nodules around the plant roots. Anhydrite and gypsum nodules are growing about halophyte roots in the modern gypsiferous supratidal sabkha succession of the Al-Khiran sabkha of Kuwait (Gunatilaka et al., 1980). Anhydrite nodules in pedogenic horizons in the bedded Miocene magnesites of the lacustrine Calatayud Basin in Spain evolved into vertically aligned textures that today resemble gypsum ghosts (Sanz-Rubio et al., 1999). Early stages of this nodule growth were associated with typical pedogenic features such as rhizoliths and clotted to peloidal textures. The consequent anhydrite nodules, which replaced dissolving gypsum during very shallow burial, developed a strong vertical orientation as nodules precipitated along what were mostly vertical soil fissures. It is this nodular texture, mimicking a ped structure, that still dominates most clayey soils in the region. Much of the soil fissuring reflects expansion and contraction driven by root metabolism and a changing soil moisture profile.

Laminites from settling of pelagic salts

At the other end of the mechanically-reworked evaporite spectrum from lunettes and soils are the continuously subaqueous basin-centre “rain-from-heaven” accumulations composed of laminar couplets of sand- and silt-sized evaporite crystals. Crystals originally precipitated at the air-brine interface or within the upper metre or two of the perennial brine body. This uppermost part of a deep brine body is most subject to freshening or concentration (Figure 2.37b). The resulting finely layered and laminated bottom cumulates are thought to typify many ancient “deepwater” evaporite-laminites. Such deposits are often found in basinal positions located well away from the evaporite platform margin.

In some ancient basinal settings, such as in the Castile Formation – a widespread Permian laminite in west Texas, water depths on the drawdown seaway bottom were mostly sub-wavebase and the sediment-brine interface lay beneath anoxic gypsum-saturated bottom waters. Repetitive layering in laminites is resolvable at two scales, 1) at the scale of individual 1.5–2.0 mm laminar couplets of calcite and anhydrite with calcite making up about 6% of a typical couplet, and 2) at the coarser scale of millennial brining upward parasequences ≈ 4 m thick (Figure 1.24a). The mm-couplets are remarkably regular in thickness, and are commonly repeated thousands of times without interruption (Kirkland et al., 2000). The evaporitic sediments that formed the anhydrite-calcite couplets were cumulates.

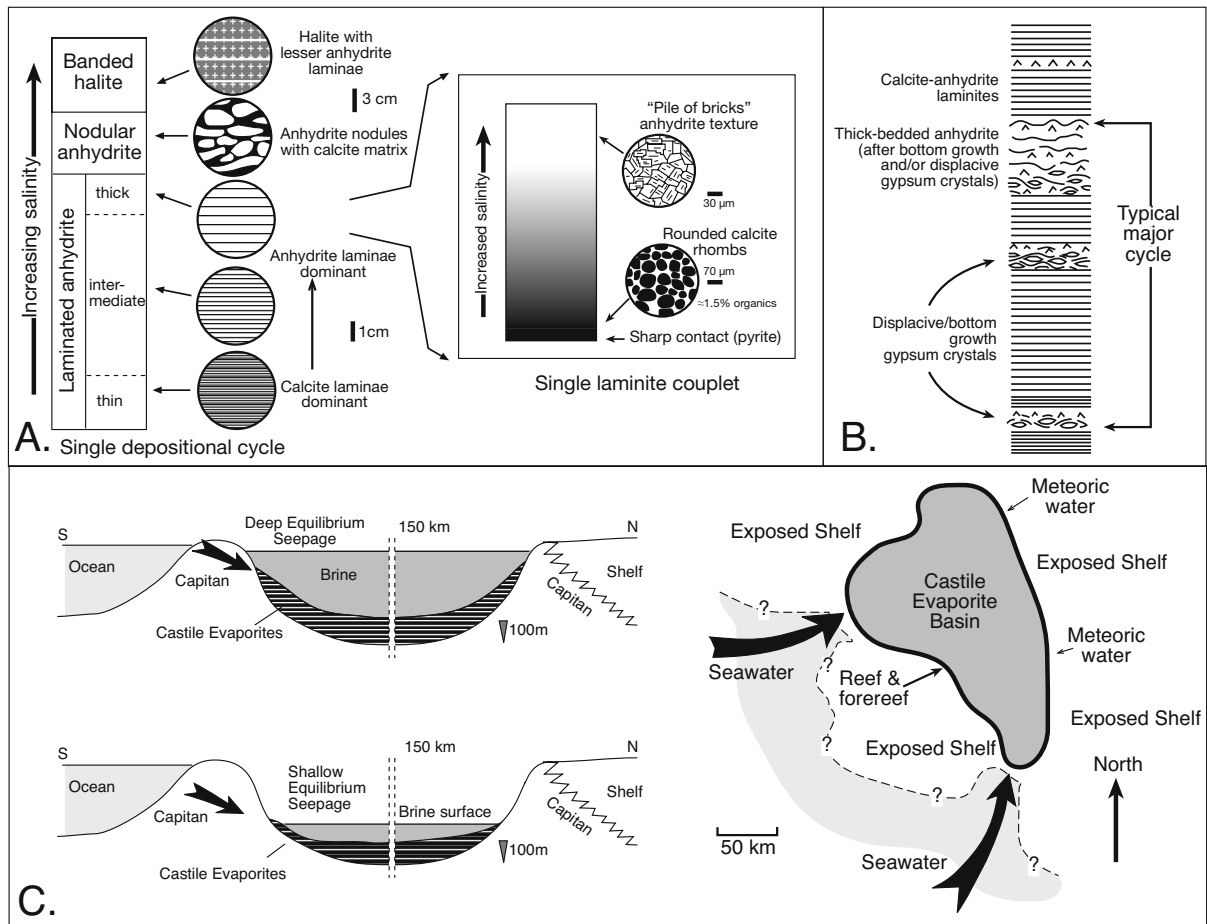


Figure 1.24. Castile Formation, Delaware Basin, west Texas. A) Representative section of a millennial cycle in the Permian Castile Formation of west Texas with a typical thickness of 1.4 metres. Inset shows a typical calcite-anhydrite couplet with typical thickness of 1.5 - 2.0 mm. (after Kirkland et al., 2000). B) Typical sedimentary cycle within the Anhydrite 1 Member, it is capped by thick-bedded anhydrite after displacive and bottom-growth gypsum. Laminae at the base of most cycles are thinner with less anhydrite and more calcite. This cycle is overlain by a layer of laminated anhydrite with less calcite. The top of the Anhydrite 1 Member (which is made up of 5 cycles) is overlain by the Halite 1 Member (after Leslie et al., 1997). C) Alternate models for Castile deposition, both based on a closed-basin, deep-marine-brine model. Brine drawdown either came to drawdown-seepage equilibrium when the brine depth was hundreds of metres or when the brine depth was tens of metres. Seawater seeped into the isolated basin along one or more segments of the reef front. These seepage areas were possibly most active near location of the what were former open marine surface channels through which seawater had entered the Delaware Basin during Guadalupian time (in part after Kirkland et al., 2000).

Crystallites formed at the brine surface or in the upper part of the brine column and "rained" onto the basin floor. Thickness variations of anhydrite laminae in parts of cores dominated by alternating laminae of calcite and anhydrite have been correlated from well to well over distances of up to 113 km (Anderson et al., 1972; Dean and Anderson 1982). Many laminar groupings can be correlated throughout the entire basin to within a fraction of a millimetre (Kirkland et al., 2000).

Spacing variations indicate cyclicity due to Milankovitch fluctuations in solar intensity and so are often interpreted as true

varves (Dean and Anderson, 1982). If so, it means the broader scale brining upward cycles were deposited in something like 1800 - 3000 years per cycle, with an average of 2700 years and something like 175,000 years to deposit the Castile Formation (Kirkland et al., 2000). A cycle generally begins with couplets of calcite-anhydrite in which the anhydrite lamina are thin, and calcite may form as much as 80-99 wt % of the couplet. Above the basal carbonate-rich portion, anhydrite laminae increase in thickness, forming the calcite-banded anhydrite typical of the bulk of the Castile where calcite constitutes 10-15 wt % (Figure 1.24a). Upward within a cycle, anhydrite laminae

become thicker, with calcite laminae constituting about 5 wt %. Farther upward within these thick anhydrite laminae are nodules of anhydrite.

Some beds, typically about 1 m thick, are made up of nodular anhydrite mosaics and, like the laminae, can be correlated across the basin (Leslie et al., 1997). Sporadically associated with these beds of nodular mosaic anhydrite are centimetre-size, anhydrite pseudomorphs after upward-growing gypsum crystals (Figure 1.24b; Hovorka, 1989). These textures suggest that at times the basin was not as “deep” as many have postulated from the laterally extensive laminites. Rather, they represent time intervals when the basin brines became sufficiently shallow (<50 m) to allow supersaturated surface brines to come into contact with the basin floor (Kendall and Harwood, 1989). These supersaturated brines caused precipitation of bottom-growth gypsum on the basin floor and precipitation of displacive gypsum in the upper few decimetres of the sediment column. In about one in ten cycles, nodular mosaic anhydrite is overlain by anhydrite-banded halite where the halite is coarsely crystalline and recrystallised. Although the contact with the halite is abrupt, deposition was regular and uninterrupted and perhaps tied to basinwide evaporitic drawdown (Chapter 5).

Rather than indicating shoalwater drawdown, Leslie et al. (1996) interpreted abundant, structureless interbeds of coarse nodular mosaic anhydrite up to 10 m thick in Castile Formation cores from the Union 4 University 37 borehole to be re-sedimented beds and not aligned nodules after bottom-growth gypsum (Figure 1.24b). Whatever their origin, these intervals do not exhibit the mm-scale laminae that typify most of the Castile anhydrite. Leslie et al. (op. cit.) interpreted these beds as the product of turbidity currents that originated in sulphate shoals along the eastern margin of the Delaware Basin. Thick turbiditic units are less common nearer the centre of the basin, as seen in cores from the PDB-03 research well, where laminites dominate. Differences in the interpretation of brine depth during deposition of the Castile remain unresolved (Figure 1.24c).

Slumped and current-reworked deepwater anhydrite laminites and turbidites have been recognised in slope and rise areas near platform margins in many other ancient evaporites, e.g. Zechstein basinal evaporites in NW Europe (Schlager and Bolz, 1977), the Triassic lacustrine slope deposits of Northern Chile (Bell, 1997) and the Middle Miocene (Belayim Formation) evaporites of the Red Sea Rift (Rouchy et al., 1995). These deepwater reworked sequences are defined by entrained turbidite textures and Bouma cycles sandwiched in anhydritic mm-laminites. The source for this reworked anhydrite was

either clastic CaSO_4 crystals eroded from the adjacent, but much shallower, platform or gravitationally unstable “pelagic” salts. These deepwater sequences are discussed in “depth” in Chapter 5.

Deepwater ancient halites are rarely documented, perhaps because cumulate halite is more liable to recrystallisation and flowage. By analogy to ancient anhydrite laminites “deep” water halite has been thought to be thin bedded and intercalated with anhydritic laminites, but documented examples are not forthcoming. Primary textures patchily preserved in most ancient bedded halite are aligned chevrons. The formation of possible analogs to “deep water” halite on the bottom of the modern Dead Sea suggests the deepwater halite texture is a massive meshwork of poorly aligned clear coarsely crystalline halite prisms, far different from the commonly accepted notion of a “deep water laminite” (Chapter 4).

One of the few documented examples of an ancient “deep water” halite mass flow comes from the lower Miocene Vorotyshcha Suite in the Ukrainian part of the Carpathian foreland basin (Peryt and Kovalevich, 1997). These halite breccias have traditionally been interpreted as tectonically deformed units related to the overthrust nappes of the Carpathians. Most clasts in the breccia consist of intrabasinal sandstone, marlstone, halite, and anhydrite, but exotic clasts consisting of rocks that are characteristic of the Carpathian flysch rocks are also present. Breccia beds are intercalated with salt layers containing chevron crystals and cubic hopper crystals, and some layers are composed of detrital salt. These salt layers rarely display graded bedding or cross-lamination, and continue over great distances. There are also slump structures associated with the bedded salts., where “deep water” halite breccias are interlayered with beds of potash. Deposition versus deformation is an ongoing debate in the interpretation of these sediments.

Can growth-aligned evaporite crystals, interlayered with laminites, be deep?

Textural interlayering of beds of aligned cm-scale nodules with beds of laminites, like those of the Permian Delaware Basin fill, underline a broader interpretation problem in our current notions of what constitutes a deepwater evaporite signature. Can layers of growth-aligned coarse bottom crystals, intercalated with laminites, ever have accumulated on the bottom of a deepwater brine lake or seaway? The high degree of supersaturation required for primary growth-aligned crystal growth means that brine depths are generally shallow during crust growth in all modern examples. Maximum brine depths

are measured in metres atop gypsum laminites in modern coastal salinas and decimetres to centimetres for halite crusts in saline pans. Halite chevrons and aligned laminated gypsum prisms retain intracrystal evidence of successive growth pulses as either thin layers of less saline salts or varying densities of entrained brine inclusions. This style of microlaminated intracrystal layering reflects changes in crystal precipitation rates induced by short-term changes (daily to monthly) in salinity on the subaqueous floor of the shallow to ephemeral brine pan (Warren 1982b; Handford, 1991).

One inference made from modern evaporite textures is that laminated beds separating “in situ” bottom-growth aligned crystals do not necessarily form in deep (>2 m) water in the salinas of Australia, the Red Sea and Sicily (Figure 2.49 and Chapter 4). This has had significant implications in water depth interpretations of the Castile and other “deep water” laminite formations. Bottom brines in deep stratified brine columns are probably too dense and too stable to change with the rapidity required to form the mm-scale intracrystal discontinuities or layers seen in modern coarsely crystalline beds. Hence, laminated bottom-nucleated coarsely-crystalline growth-aligned textures do not form widespread bottom precipitates in modern deeper water settings (Chapter 4).

Rather, the bottom waters of a deep stratified brine system reach saturation and accumulate coarse salts only if the total brine column is at saturation all the way up to the air brine interface. This deposits monomineralic deep bottom beds made up of meshworks of poorly oriented fine to coarse crystals like those forming halite beds on the deep bottom of the Dead Sea and the mirabilite beds on the bottoms of decametre deep saline lakes in western Canada (Figure 5.6).

Thus, a modern analogy doesn't exclude a notion of deepwater halite or gypsum laminates interlayered with coarsely crystalline beds. But it does exclude the notion of this coarsely crystalline beds (be they halite or gypsum) entraining regular discontinuities or finely intrabed layers. Otherwise one must ask, what mechanism could act over the floor of an ancient brine seaway, which was up to hundreds of metres deep and hundreds of kilometres across, to rapidly displace or cool dense halite- or gypsum-saturated bottom waters with short-lived pulses of less-dense freshened or cooler water, which would then pulse the rate of bottom crystal growth? Freshened water will always float atop a dense brine. The volume of less dense water required to displace and dilute a brine column hundreds of metres deep, or the time required for complete mixing to the bottom, excludes a deepwater “in situ” origin for fine layering

in coarsely crystalline bottom-nucleated fabrics. But it does not prevent “rain from heaven” carbonate laminates accumulating in deep brines, as happened in the Dead Sea when it was a stratified water mass prior to 1979 (Figure 4.43).

As more studies are completed on modern deepwater evaporites it is increasingly obvious that laminated beds alternating with growth aligned beds are not the typical signature of a deep subwave-base evaporite in a meromictic brine column. It suggests that if the elongate nodules in the Castile and other deepwater evaporites are after coarse gypsum then they were deep bottom crystal meshworks that indicate times of holomictic brines in a hydrographically isolated seaway. Then when the brine column returned to more typical meromictic conditions it became a seaway where laminites accumulated on the deep sea floor. This explains the correlatable lamina spacings over distances of more than 100 km in laminite beds. As in many evaporite interpretation quandaries, part of the problem lies in the pervasive diagenetic overprinting of primary gypsum texture by a mosaic of overprints that were driven by ongoing compaction and flow. The other part of the interpretation quandary lies in the observation that the present icehouse climate mode limits the range of modern marine-fed evaporite basins available for study (Chapter 5).

If a crystal crust is growing near a deepwater hydrothermal spring, there is also the possibility of pulsing crystal growth in the bottom waters due to temperature fluctuations or changes in the rate and saturation of the spring outflow. This last scenario is not volumetrically important in terms of widespread beds of ancient growth-aligned evaporite textures.

Salt reefs, are they real?

Halite in modern pans and salinas typically constructs beds made up of stacked subaqueous crusts, which may locally entrain recrystallised cumulates and have been periodically subaerial. Beds tend to be dominated by flat layers with synoptic relief of no more than decimetres related to the formation of pressure ridges. However, mushroom-shaped halite buildups or reefs, with steep near vertical sides and a relief measured in metres, are currently forming in artificial solar ponds on the southern margin of the Dead Sea (Chapter 11). Halite reefs began to form in the 1970s and 1980s, after dykes were built to enclose most of the southern basin of the Dead Sea (>200 km²) and so create two sets of solar evaporation ponds on either side of the Truce Line Channel (Figure 11.9; Talbot et al., 1996). At that time the reefs were attributed to salting-out via common-ion mixing between natural Dead Sea brines and end-brines from

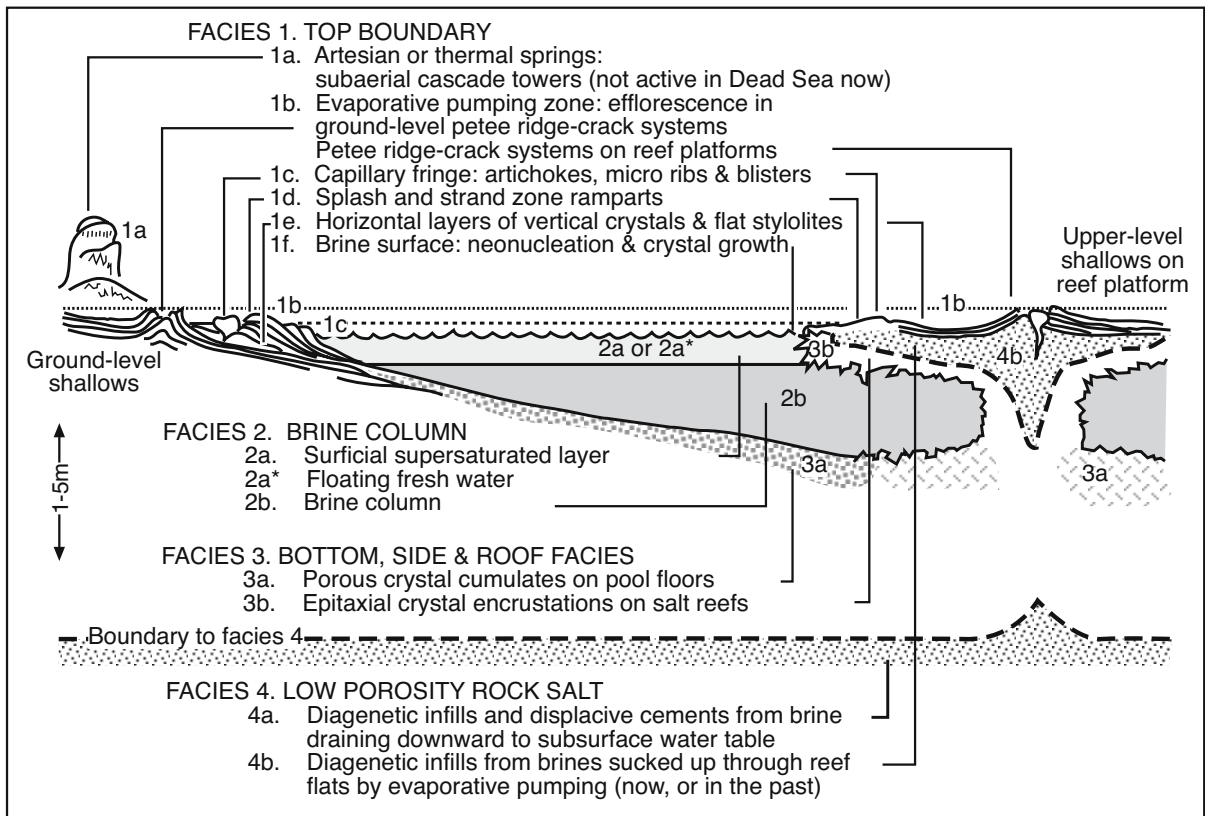


Figure 1.25. Subdivision of the mushroom-shaped salt reefs of the southern Dead Sea is related to the permanency and salinity of stratification in the perennial pond brines in the inter-reef areas (after Talbot et al., 1996).

the first potash plant (Chapter 2). However, tens of thousands of new salt reefs continued to grow in the enclosed salt ponds long after the pans were re-engineered and end-brines from both plants were channelled directly back to the depths of the northern Dead Sea basin (Charrach, 1986; Ram et al., 1988).

The reefs grow in metres-deep perennial halite saturated brine pans as large isolated vegetable-like shapes that merge to form networks of polygonal salt walls (Figure 1.25; Talbot et al., 1996). The walls subdivide large salt concentrator ponds into thousands of small compartments that resist brine throughflow. This is contrary to the engineer’s plan of large subaqueous pans filled with brines that were easily homogenized by wind. Instead of following a designed flow path of homogenisation and downstream fractionation, brines in the compartments between the halite reef walls stratify, ultimately allowing unrecoverable carnallite precipitation in depressions between the walls.

In the inter-reef polygons is an evaporatively-maintained supersaturated 10-cm-thick surficial layer floating atop brines that are halite saturated all the way down to a cumulate covered

floor (Figure 1.25). Epitaxial halite overgrowths expand along the supersaturated uppermost brine layer and the salt reefs develop botryoidal overhangs. Salt projections can merge into a hollow platform roofing over a cell of encased brine. Reefs and their overhangs prolong the crystallization season in the halite-saturated pans by breaking up the continuity of brine throughflow to the carnallite pans. Depositionally, they replace the planned cumulates with brine compartments walled by expanding overhangs. Salt-crustured shallows on bridged-over reef platforms and around the pan strandlines are typically made up of thin flat salt beds with vertical palisade and chevron textures that characterise ephemeral brine pans everywhere (Figure 1.25).

In the 1980s, in order to destabilise the problematic salt reefs, brine levels in the compartments were allowed to draw down by lowering the rate of supply of pumped brine. But, rather than diminishing the evaporation area available for reef growth, the damp emergent salt reefs seemed to act as giant transpirative pumps. This further accelerated salt crystallization rates in the remaining brine compartments, which continued to reconfigure

the evaporation ponds into smaller and smaller areas. Even today the problem is not solved and once an inter-reef area is isolated from brine throughflow, waters caught up in reef-walled depressions concentrate to bitter saturation. Bottom-nucleated carnallite drops out before reaching the target crystallizer pans. Thus, pervasive salt reefs lessen the volume of suitable brine product reaching the final fractionation pans. The solution to this problem is not subtle, reefs in both the Israeli and Jordanian saltworks are periodically removed by a combination of dredging and blasting.

The densest halite reef complex occurs in a broad band that crosses both the Israeli and the Jordanian salt ponds (and their pre-enclosure depth contours), despite each suite of ponds being different distances from the northern basin (Figure 11.9). The most vigorous salt reefs within this band nucleated on an old road incorporated into the Jordanian ponds. The natural end of salt reef formation is probably when shallow brines on hollow reef platforms become ephemeral on solid salt flats. But if pans in the saltworks are allowed to evolve and fill to this stage, they are no longer suitable brine concentrators for the continuous feed bitter crystallisers further down the fractionation string.

Reefs seem to evolve from cracks along pressure-ridged salt crusts, and once supersaturated surface brine layers form, grow rapidly outward and upward via epitaxis. Compared to natural saline pans, brine depths in the pans of the Dead Sea saltworks are maintained at artificially deep levels by pumping Dead Sea brine into the pans. Zones of new salt reefs grow alongside recently flooded pan shores and quickly become unrecognizable as former pressure ridges once the brines deepen. Salt reefs are not seen in modern natural brine pans and salars as the water depths where stacked salt crusts accumulate are always too shallow or ephemeral for pervasive reef growth. Talbot et al. (1996) argued epitaxis in supersaturated surface brine layers helps account for the rapid deposition of modern thick beds in the Dead Sea prior to the building of the salt works. He argues that similar structures probably formed in marine-fed regions of pure salt accumulation on the floors of ancient rifts that periodically opened to the ocean.

Domal gypsum reefs occur in modern salinas and in the Messinian of the Sorbas Basin, Spain (Figures 4.5d, 1.15b), but as yet no ancient halite reefs have been documented. They should be distinguishable as botryoidal layers of nonvertically-aligned chevron crystals, which would follow a megapolygonal pattern between saucers of recrystallised cumulates. Part of the problem of recognition lies in the scale of outcrop exposure needed to

recognise such a salt reef. Bedded gypsum outcrops entraining reefs and domes are commonplace, but nonhalokinetic ancient halite never makes it to the surface. Halite reef textures would be next to impossible to document in cores, but should be visible in mine walls in the same way that ancient halite megapolygon and pressure ridges are, but would easily be misinterpreted as mesoscale syndeositional karst features. Another part of the problem is a lack of expectation of halite reef structures, which are not a commonly listed texture in sedimentology textbooks. And yet another problem is that rapid infill means metres-deep perennial halite-saturated brine bodies are not found in modern salt lakes, only in anthropogenic ponds as in Israel and in quarried coastal pans in Saudi Arabia (Figure 3.15). But, as will be seen in Chapter 5, there are many ancient saline seaways where salt reefs were possible in halite-saturated brine bodies with depths measured in metres to tens of metres.

Secondary (diagenetic) evaporites

Most ancient evaporites show strong evidence of secondary or diagenetic textural overprints. Providing brine is saturated with respect to a particular evaporite mineral it has the potential to precipitate that mineral. This potential exists both at the surface and in the subsurface. So far, we have discussed the primary processes of evaporite precipitation in the context of single-phase primary evaporite crystals deposited on the floor, or about the margins, of brine pans, lakes, salterns or saline seaways. However, evaporites also precipitate as intrasediment crystal growths and replacements, or as cements in preexisting evaporite and nonevaporite hosts.

Processes of secondary evaporite formation are reflected in crystals and textures that indicate displacive growth, recrystallisation, back reactions and replacement. Such events indicate a superimposed brine chemistry that differs in terms of chemical composition, or salinity, or temperature from the brine chemistry that formed the primary or preexisting evaporitic sediments (see Chapter 2).

Intrasediment salts

The well-studied nodular anhydrites and gypsums of the Abu Dhabi sabkha in the Arabian Gulf are probably the most widely recognised examples of syndeositional intrasediment evaporites (Figure 3.4g). The nodules form displacively and replacively from concentrated pore fluids in the capillary and upper phreatic zones beneath the sabkha surface (Figure 1.26a). In the type area these intrasediment crystal growths precipitate

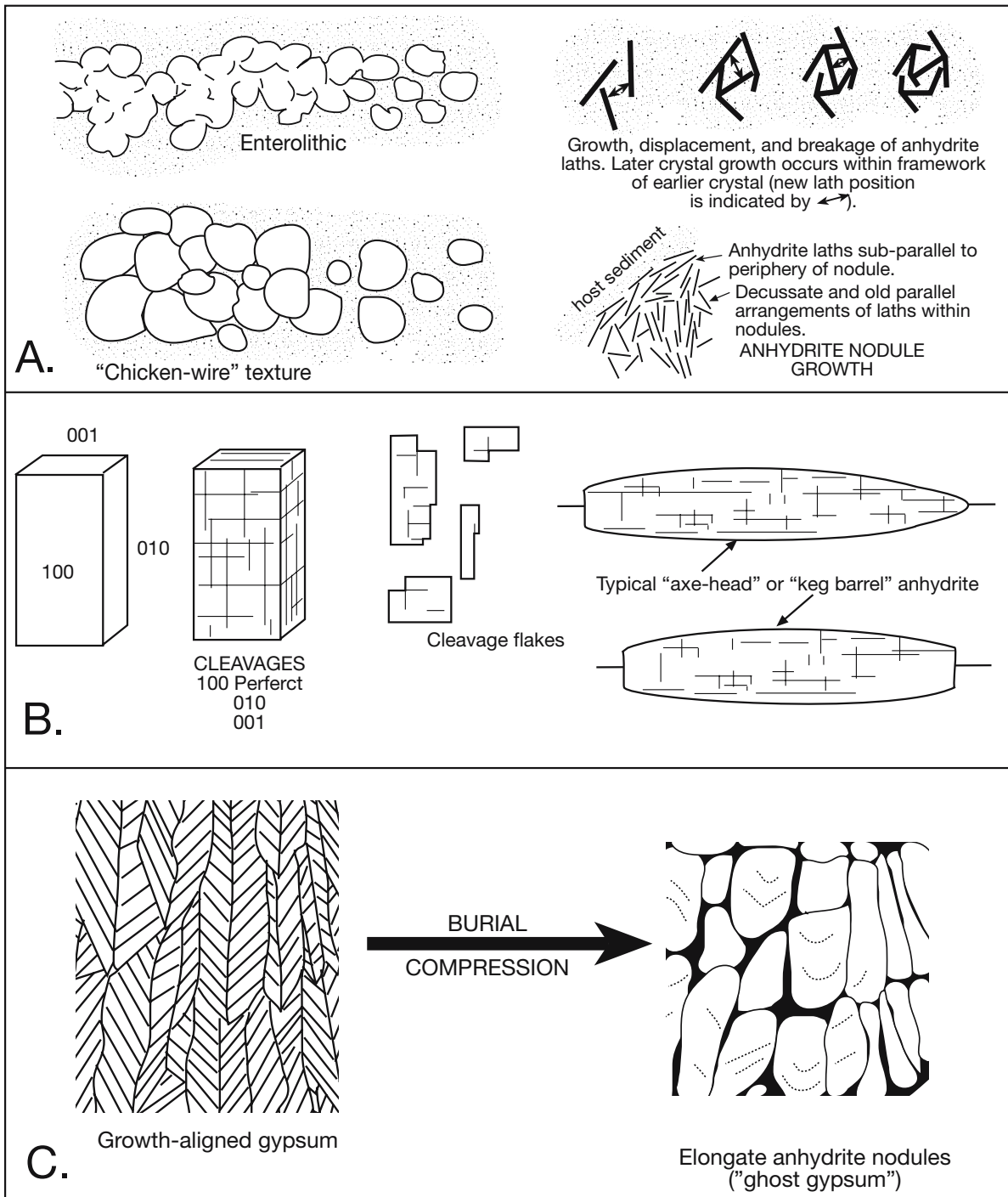


Figure 1.26. Anhydrite characteristics. A) Anhydrite nodule growth into chicken wire and enterolithic anhydrite. Also shows how successive new anhydrite laths break and rotate earlier formed laths. The end result is a nodule with a margin composed of laths aligned subparallel to the its edge. Many nodule interiors preserve clusters of subparallel laths showing large nodules grow by accretion of smaller nodules. B) Crystallographic characteristics of anhydrite laths showing well developed orthorhombic cleavage. Large isolated anhydrite spar crystals in mudstones sometimes have a lenticular form. It or its pseudomorphs can be distinguished from lenticular gypsum by a typical "axe-head" and "beer-keg morphology" with well developed cleavages at one or both ends of the lens. C) Preservation of gypsum ghosts as elongate anhydrite nodules created during burial. (after Shearman and Fuller, 1969; Warren and Kendall, 1985).

in a matrix of upper intertidal and supratidal sediments. But in addition to anhydrite capillary salts, gypsum and halite also precipitate displacively in numerous continental and pedogenic settings. Salts and their crusts may come and go, driven by the vagaries of groundwater resurgence, surface flooding and reconcentration, so that all that may be left as indicators of their former presence are highly disturbed sediments with a few halite or gypsum pseudomorphs.

The amount and variety of intrasediment salt is highly variable. Some mudstones contain scattered crystals and nodules that make up less than 1% of the rock volume. Others are made up of approximately equal volumes of host matrix and evaporite salts, while yet others are characterised by layers composed almost entirely of intrasediment salts. The thickness of the layer over which intrasediment salts can precipitate is controlled by the style of brine supply. If the salts are precipitating by capillary evaporation beneath a subaerially exposed mudflat then the thickness is controlled by the pore throat size of the host sediment. Capillary zones can be metres thick in fine clays, while they are only centimetres thick in sands. If the intrasediment salts are precipitating by the downward percolation of dense cooling brines from a subaqueous water body then the thickness is dependent on the rate of diffusion or reflux into the underlying clay. Handford (1991) estimates intrasediment halite can precipitate in brine-saturated soft muds down to depths of 1-2 metres below the sediment-brine interface.

Sabkha nodules and crystals

As gypsum and anhydrite nodules grow and coalesce in highly saturated pore waters of the capillary zone, they form enterolithic, contorted fold (ptygmatic) and chickenwire textures, which typify the supratidal portion of a coastal sabkha sequence. New laths of anhydrite form between older laths as such anhydrite nodules grow “from the inside out” (Shearman and Fuller, 1969). Successive laths crystallise, displace, rotate and perhaps break the older laths, while the expanding nodule pushes aside the adjacent host matrix. Figure 1.26a illustrates this process and the position of each successive new lath is indicated by a double-ended arrow in the figure. The end result of this “inside-out” growth is a near pure anhydrite nodule, with laths about the edge of the nodule rotated into a subparallel alignment to the nodule margin. Many nodules are constructed of a number of subsets of this subparallel arrangement, implying large nodules grow by accretion of smaller nodules.

Capillary halite crystals typically show an incomplete development of the cube face, and in soft muds with supersaturated

pore brines there is intense development of the cube edges at the expense of the cube faces to create dendritic or pagoda-like morphologies. Rapid crystal growth often entrains some of the mud matrix within the halite, usually parallel to the cube faces. Such rapid growth is thought to indicate a rapidly attained and high degree of supersaturation with respect to halite (Arthurton, 1973; Southgate, 1982) or perhaps growth in organic-rich brines (Gerdes et al., 2000a, b).

Displacive halite grows by capillary evaporation of supersaturated pore waters in soft brine-soaked mudflat or sabkha sediments (Figures 1.18c). Such hoppers are found growing in carbonate muds along the western shore of the Dead Sea (Gornitz and Schreiber, 1981). Similar halite crystals are found actively growing as much as metres below the surface of present day mudflats in Bristol Dry Lake in California (Handford, 1991). Growing about the edges of the same lake are unusual capillary pavements of growth-aligned seepage gypsum (Rosen and Warren, 1990). Dendritic or pagoda forms of halite cannot easily grow in deeper burial environments where rates of salinity fluctuation and kinetics of reactions are much slower. The surrounding matrix is more likely to be indurated, so secondary crystals formed at depth tend to be fracture or mould fills.

Syn depositional karst in crusts

Crusts and beds dominated by primary subaqueous textures (chevrons and palmate/zig-zag structures) can be partially dissolved by more dilute surface brines or by subaerial exposure. Freshening can be via a rise in the brine-pool level associated with rainfall and sheetflooding, by seawater flooding, or by morning dew dissolution associated with the complete drying of the brine pan. The resultant dilution creates a truncating dissolution surface that crosscuts crystal faces in both subaerial and freshened subaqueous settings (Figure 1.27). In a subaerially exposed halite crust numerous cm-dm-scale vertical to subhorizontal karst cavities typically form beneath an upper crystal-truncating exposure surface. Cavities subsequently fill with clear evaporite cement sometimes atop a cavity-lining rind of detrital mud and clay (Figure 3.30). In chevron halite beds these cavities are often filled with a clear inclusion-poor halite spar cement. Void infill is often related to the depositional event that precipitated an immediately overlying chevron halite or swallowtail gypsum layer (Handford, 1991; Warren, 1982a). Using bromine signatures, Cathro et al. (1992) found the Silurian brines that precipitated the cloudy primary halite in the Mallowa Salt of the Canning Basin were indistinguishable from the signatures in the secondary spar-like halite that

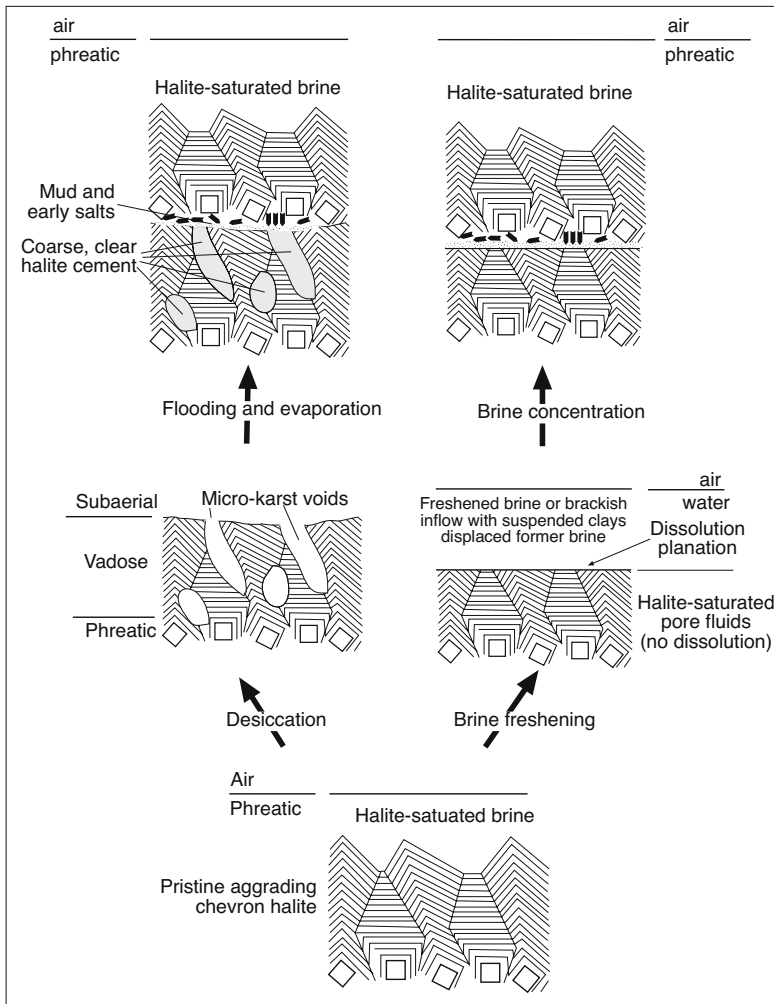


Figure 1.27. Syndepositional overprints on chevron halite. The textural evolution illustrated on the left shows the formation of vadose microkarst, while that on the right illustrates the effect of bottom freshening on the floor of a perennial brine pool and the formation of a planation surface with no vadose karst development.

filled voids in the primary halite, implying an early origin from the same depositional/syndepositional brine. This is a depositional signature still preserved in these beds more than 400 million years later.

Intensity and frequency of dissolution overprints in salt crusts are largely determined by brine depth, frequency of dilute water floods and the permanency of the brine body. Most modern and ancient halite salt pan crusts preserve evidence of syndepositional dissolution in the form of dissolution surfaces and halite-spar-filled cavities. Lowenstein and Hardie (1985) emphasised that the presence of such features in a halite bed is the unequivocal signature of ephemeral surface waters.

The texture reflects dissolution events that accompany subaerial exposure of any salt crust and the periodic flooding of the halite pan by fresh to brackish meteoric water (Figure 3.30). Dissolution cavities are less likely to occur in bottom-nucleated beds deposited in evaporite basins covered by deeper perennial brine bodies. Freshened inflow waters tend to float atop the denser halite-saturated brine body at least until its density equalises that of the underlying brine. If brine freshening does occur in a perennial brine situation then a planation surface without vadose cavities is the likely result (Figure 1.27, 2.49).

Nearsurface crystal and crust dissolution

The following section focuses on small-scale syndepositional features indicative of the groundwater cycling of salt crystals and crusts, Chapter 7 looks broader and deeper in a discussion of dissolution mechanisms creating “the salt that was.”

Coming and going of salt crusts

Salt crusts and isolated crystals on many modern saline mudflats are ephemeral; they are not preserved in the final sediment matrix, yet their growth and subsequent dissolution on or within nearsurface sediments can alter sedimentary structures and textures to such an extent that it is difficult to identify the original texture. Areas

dominated by this set of processes occupy large schizohaline areas of modern salt flats in SE Arabia such as Sabkhat Rumadan in Saudi Arabia, Sabkhat Matti and the At Taf coastal region, both in the Emirate of Abu Dhabi, and the Umm as Samim region in Oman (Figure 3.15; Goodall et al., 2000).

These salt flats are affected by varying combinations of tidal-marine, alluvial and eolian depositional processes and the resulting sediments include both clastic- and carbonate-dominated successions. The efflorescent and precipitated salt crusts in these areas can be grouped into two main types: 1) thick crusts, with high relief (> 10 cm) and 2) a polygonal or blocky morphology; or thin crusts, with low relief (< 10 cm)

and a polygonal or blister-like appearance. The thin crusts may assume the surface morphology of underlying features, such as ripples or biogenic mats (petees).

A variety of small-scale textures resulting from the interaction of detrital sediments with the salt crusts were observed by Goodall et al. (2000), they include: pustular growths, hair-like spikes and irregular wrinkles. Evolution of crusts over time creates a variety of distinctive sedimentary fabrics by salt-growth sediment deformation, salt-solution sediment collapse, sediment aggradation and compound mixtures of these processes. Preservation ranges from completely preserved crust to highly disturbed siliciclastics where only suggestions of former salt crusts remain (haloturbation).

When a subaerial sabkha surface is marked by a salt crust with pressure ridges, the lee side of a ridge acts as a trap to cross-drifting sands that become enmeshed and cemented by further salt growth. Eolian-dominated sabkhas accrete via a set of processes that begin with a sandstorm, followed by a

new salt ridge episode, followed by another sandstorm (Figure 1.28a). The resulting sediment is an irregularly layered sandy mud, disturbed by ongoing intrasediment salt and carbonate growth and solution (Fryberger et al., 1984; Goodall et al., 2000). In other words haloturbation, rather than obvious crust preservation, is the dominant texture in many eolian sabkhas (Figure 3.60).

Salt-crust processes can produce features that may be confused with eolian adhesion structures. For example, distinctive wavy-laminated facies in the Lower Triassic Ormskirk Sandstone Formation in the Morecambe Field of the Irish Sea Basin had previously been interpreted as the product of fluvial sheetfloods modified by soft-sediment deformation and bioturbation. Close inspection of laminations in core revealed many of the same sedimentary fabrics seen in Sabkha Matti (Goodall et al., 2000). This facies is the product of salt growth on eolian sediment and is not of fluvial origin.

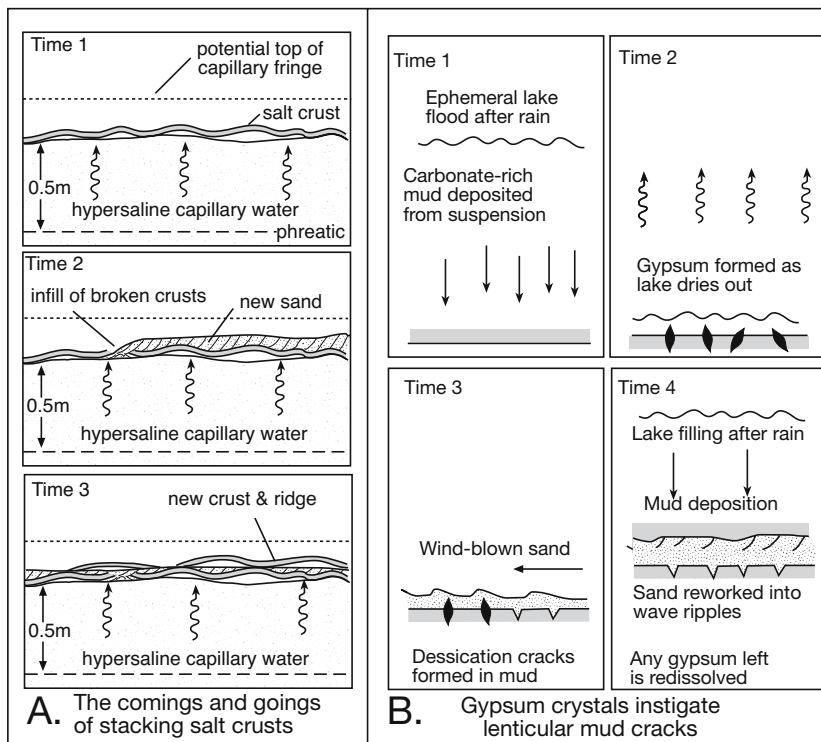


Figure 1.28. Residual evaporite textures indicating syndepositional precipitation and dissolution. A) Salt crust accretion mechanism. Time 1) Development of salt crust at top of capillary zone. Time 2) Covering of crust by windblown sand. Time 3) Incorporation of crust and salt cover by capillary wicking, portions of the old crust may dissolve and collapse (after Fryberger et al., 1984). B) Instigation of lenticular mud cracks (syneresis mimics) by early gypsum growth and dissolution in an ephemeral mudflat/saline pan (after Astin and Rogers, 1991).

Lenticular mudcracks

Evaporites growing in association with drying muddy sediments and eolian sands can also produce mudcracks that may be confused with syneresis cracks. There are numerous mud cracks in irregular arrays and often showing lenticular outlines in the Orcadian (Devonian) laminites of Scotland. They are considered one of the type examples of syneresis cracking and were used as evidence that these sediments were deposited in a shallow (<30 m) lacustrine environment. Yet, lenticular shaped features seem to initiate many of the mudcracks. Rather than a subaqueous origin, these mudcracks are equally characteristic of the incipient stages of subaerial shrinkage with what appear to be gypsum pseudomorphs in some of the straight cracks (Astin and Rogers, 1991).

Cracks are abundant and irregularly clustered because early gypsum crystals acted as nuclei for cracking and controlled crack morphology (Figure 1.28b). The majority of the lenticular

cracked surfaces formed as the ephemeral lakes waters dried up and deposited lenticular or bird-beak gypsum. The crystals were modified to varying degrees before being covered by wind blown sand laminae and buried. Subsequently the gypsum, along with minor halite, dissolved to leave the characteristic cracks in the lake sediments. In a review of other documented examples of subaqueous syneresis cracks, Astin and Rogers (op. cit.) argue that many can be reinterpreted as the result of gypsum instigation, followed by desiccating cracks centred on the crystals and then burial. They go on to conclude that syneresis cracks, although well documented in the laboratory, are rare and insignificant in nature and that evaporites growing in mudcracks are commonplace. King had noted carnallite-filled mudcracks in the salt clays of the Permian Salado Fm., west Texas, as early as 1946.

Haloturbated and chaotic halite

Percolation of capillary waters periodically saturated and undersaturated with a particular evaporite salt can also create textural havoc in a nonsalt matrix. For example, displacement halite grows via capillary evaporation during the supersaturated phase of pore flushing of the saline mudflat facies surrounding many brine pans. The growth of this halite disturbs and rotates primary mechanical structures in the original sediment matrix (laminae, ripples, mudcracks, etc.). But with each flooding of the brine pan there is a freshening of surface waters and nearsurface pore fluids, driven by sheet flood runoff followed by seepage down to a depressed water table. Near surface pore waters become undersaturated with respect to halite and the displacement halite dissolves. Sediment matrix then collapses into the voids so formed, further disrupting any primary structures in the sediment matrix. As the pore fluids are again concentrated by capillary evaporation, intrasediment halite and gypsum begin to grow once more, further displacing and disrupting existing textures. This process of alternate wetting and drying with the associated destruction of primary stratification in the matrix is known as haloturbation (Smith, 1971). If the sediment is preserved with halite still present, it is termed chaotic halite. If the halite is completely dissolved, all that may be left is a haloturbated massive mudstone.

Because it is largely a syndepositional process that occurs prior to induration of the clayey matrix, one of the effects of

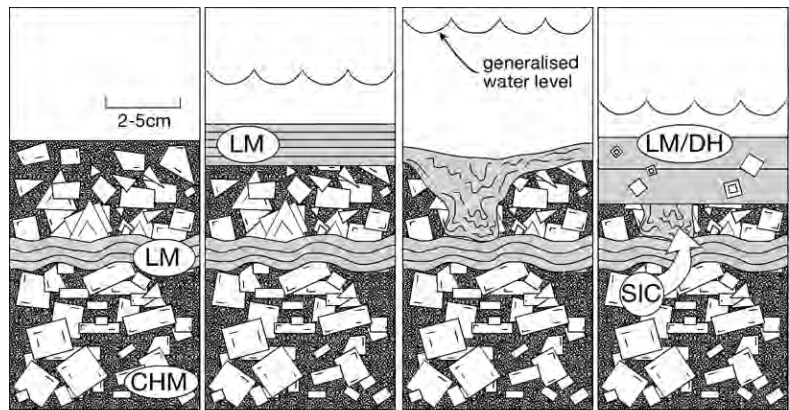


Figure 1.29. Evolution of smeared intraclasts by collapse of lacustrine mudstone into void space created by dissolution of halite crystals during the freshened stage of a wet-dry cycle in an evaporitic mudflat. LM = lacustrine mudstone; CHM = chaotic halite mudstone; SIC = smeared intraclast; DH = displacive halite (after Powers and Holt, 2000).

haloturbation is to create highly deformed intraclasts within the haloturbated or chaotic-halite bed. Powers and Holt (2000) use the term “smeared intraclasts” to describe this form of salt-related mudflat texture. It can be used to recognise a hypersaline capillary mudflat unit, even if the original displacive salt is leached. Smeared intraclasts are typically 2-5 cm across, are made up of the same lithology as the surround matrix and show distorted or smeared internal thin beds or laminae (Figure 1.29). The facies transition layered and undisturbed mudflat to haloturbated mudflat to chaotic halite indicates increasing proximity to a perennial saltpan (Chapter 3).

Shallow mineralogic re-equilibration

Dense saturated bottom brines percolating down through a shallowly buried primary evaporite unit can create diagenetic havoc within the original texture. For example, saturated bottom brines percolating through a buried cumulate halite deposit can convert it into a tightly cemented coarsely crystalline halite mosaic retaining little evidence of the primary texture (Smoot and Lowenstein, 1991; Cathro et al., 1992). Dense halite-saturated brines flushing down through shallowly buried subaqueous gypsum beds that are dominated by bottom-nucleated gypsum crystals can set up diagenetic conditions where the gypsum is replaced by halite/anhydrite pseudomorphs of the original aligned gypsum. In Permian evaporites of west Texas the replacement mimics the crystal shapes in beds composed of bottom-nucleated gypsum precursor, as well replacing internal layering within crystals. This tends to happen early and be driven by reflux of halite-saturated brines into gypsum beds. Ambient high temperatures and salinities mean much of the finer grained gypsum matrix has already converted to nodular

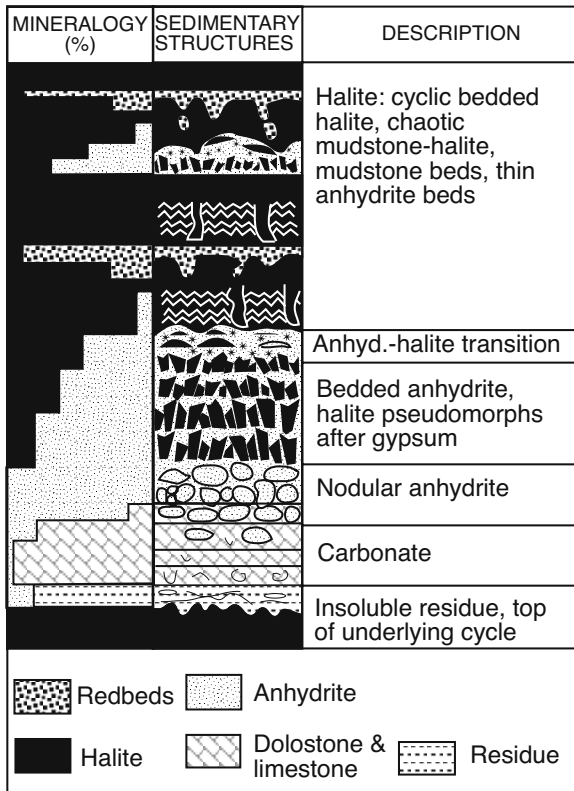


Figure 1.30. Typical depositional cycle in the Permian evaporites of the Texas Panhandle where gypsum (rather than anhydrite) was the dominant sulphate precipitated, even at salinities near halite saturation. Large gypsum crystals grew vertically on floors of brine pools, surrounded by a matrix of autochthonous transported gypsum sand and silt. Most or all of the primary gypsum was altered to anhydrite or leached and replaced by halite in the very shallow (<2m) burial environment under the influence of halite-saturated diagenetic brines (after Hovorka, 1992).

anhydrite. Reflux in ancient brine platforms drove a process of gypsum dissolution and halite replacement a few metres beneath the brine-covered sediment surface in ancient brine seaways (Figures 1.30, 2.54; Hovorka, 1992).

In a similar fashion, changes in the near surface hydrology within the modern saline mudflats of Salt Flat playa in west Texas, have “sabkha-ized” a subaqueous laminated lacustrine gypsum bed (Hussain and Warren, 1989). The process was driven by the superposition of a Holocene capillary hydrology onto subaqueous gypsiferous laminites originally laid down in a Pleistocene salt lake. This capillary zone overprint precipitated nodular displacive gypsum within a matrix of laminated gypsum/dolomite. The change in hydrology indicates a change in climate from more humid Late Pleistocene to more arid Holocene

conditions. It also set up shallow subsurface pore chemistries, whereby lenticular gypsum crystals were pseudomorphed and replaced by halite spar.

Owing to the mixing of waters of two salinities, reflux dolomitization beneath a platform evaporite can take place concomitantly with CaCO_3 dissolution (Sun, 1992). Relative rate of limestone solution compared to dolomite growth is a likely control on porosity levels during the later stages of the reflux dolomitization process (Sun, 1995). If the rate of dolomite growth keeps pace with the rate of CaCO_3 dissolution, then the mimetic replacement of micrite matrix and micritised grains occurs with little change in porosity levels, as in many ancient evaporitic peritidal dolomites. If the rate of reflux dissolution exceeds the rate of dolomite replacement, as in open marine platform carbonates beneath the seaward edge of a platform evaporite, then there is large scale skeletal aragonite dissolution, along with an increase in effective porosity in the dolomitized interval compared to precursor limestone. During shallow subsurface brine reflux in the Permian in the Palo Duro Basin, Texas, the flow of such refluxing waters dissolved marine carbonate to form anhydrite-filled moulds (Bein and Land, 1983), while in the Levelland-Slaughter interval it enhanced reservoir porosity (Figure 10.24; Elliott and Warren, 1989).

Porosity loss

Syndeositional alteration, cementation and porosity loss, in a halite bed continues into the shallow subsurface until the bed can no longer support fluid flushing. This occurs once all effective porosity is occluded by compaction and secondary evaporite cementation. In halite-dominated continental sequences this loss of effective porosity is typically early and shallow (Figure 1.31). Casas and Lowenstein (1989) showed that Quaternary halite layers only 10 m below the land surface have typical porosities of <10% and that layers at depths below 45m are tightly cemented without visible porosity. By 100m of burial, almost all the halite units were tight and impervious. Diagenetic porosity occlusion by surface-driven hydrology in these halite beds was essentially over. No further porosity change can occur until beds start to dissolve deep in the mesogenetic realm or even in the metamorphic realm as the dihedral intercrystalline angle of halite begins to change as the beds approach greenschist conditions (Lewis and Holness, 1996).

From a few hundred metres burial until it reaches the zone of metamorphism, a halite unit maintains permeabilities that are measured in no more than microdarcies or nanodarcies. Thus halite beds and allochthonous sheets provide a highly effec-

tive seal to sediments beneath. To move closer to the surface, trapped basal fluids must either flow laterally around such a salt barrier or dissolve it. If the trapped pore fluids are hydrocarbons then no dissolution can occur as halite is virtually insoluble in gas and oil. Retention of pore fluids below a salt barrier means porosity in the host sediment is maintained to a much greater depth and that sediments below a salt barrier in an actively subsiding basin are typically overpressured.

The pervasive early loss of porosity from more than 50% near the surface to zero by 100m burial also has important implications for textural and geochemical studies of ancient bedded halite. Casas and Lowenstein (1989) showed that this porosity loss was entirely due to early post depositional diagenetic cementation by clear halite. Other mechanisms of porosity loss by chemical or mechanical compaction were dismissed for lack of evidence. There were no strained or broken crystals, pressure solution boundaries nor stylolites, and patches of chevrons preserved in among the mosaic halite spar were all undeformed.

Many Phanerozoic halite beds that have not undergone halokinetic deformation also contain patches of relict depositional and early diagenetic textures, which have remained unchanged for hundreds of millions of years. For example, the Ordovician-Silurian Mallowa Salt (formerly Carribuddy Forma-

tion) in the Canning Basin, West Australia, retains aligned halite chevrons crosscut by syndepositional karst and an overprint of coarse mosaic recrystallised halite (Figure 1.32a; Cathro et al., 1992). Such textures are thought to be syndepositional, yet are not dominated by large volumes of pristine chevron halite. Rather, they preserve evidence of early porosity loss brought on by numerous syndepositional cycles of dissolution and recementation. Lowenstein and Hardie (1985) showed that patchy remnants of chevrons and cornets in a dominantly coarse-grained mosaic of halite spar are not necessarily a burial fabric. All “mature” saltpan halites have this fabric within tens of metres of the depositional surface.

The mechanisms that allow a shallow brine to become supersaturated with respect to halite and to precipitate intercrystalline cements/replacements are still not well understood. One possible mechanism is brine mixing. When compositionally distinct brines mix in the subsurface a new halite-saturated brine may result. This is the case when MgCl₂ brines are mixed with CaCl₂-rich brines (Raup, 1970). Casas and Lowenstein (1989) have questioned whether this is the dominant mechanism that forms pervasive halite cements in most shallowly buried playa sediments. Rather, they suggest a simple temperature drop is the dominant control. Surface brines in halite-forming surface waters can be heated to temperatures in excess of 60 - 70°C, while groundwater brines typically have temperatures of 15 - 30°C. They suggest that the cooling associated with the downward reflux of a surface water is all that is required to saturate a brine and so precipitate widespread halite cements.

Deeper burial - mosaic halite?

Formation of pervasive mosaic halite spar early in the burial history of a salt bed creates a problem in recognising those parts of a halite unit that have been subjected to later burial recrystallisation as a deeper burial environment is also thought to form mosaic halite spar. Diagenetic textures in most ancient bedded halite units are dominated by sutured mosaic textures, where grain boundaries suture in the same fashion as neomorphic pseudosparite in calcite (Spencer and Lowenstein, 1990). Individual crystals display curved boundaries that tend to meet at triple junctions with angles approaching 120°, and interstitial impurities concentrate along the crystal boundaries (Figure 1.32b).

Mosaic texture is comparable to the polygonal equigranular mosaic texture that forms in annealing metals, where cooling grains tend to optimise their size, shape and orientation in order

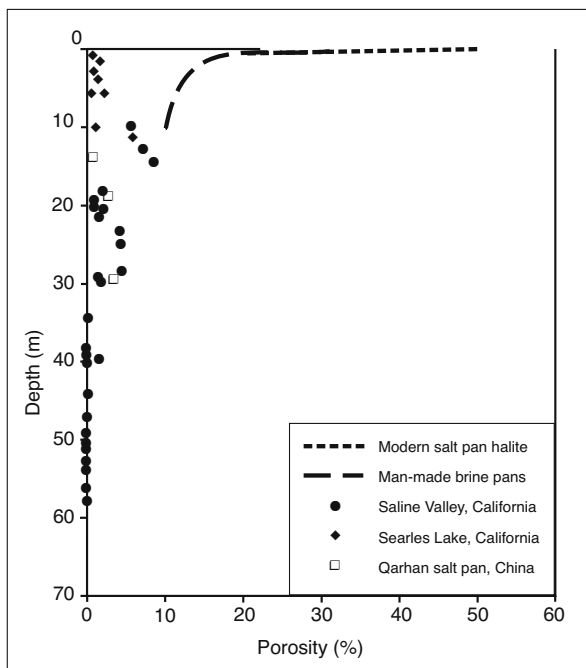


Figure 1.31. Porosity in Quaternary halite beds versus depth (after Casas and Lowenstein, 1989). All effective porosity is lost by 70 m burial.

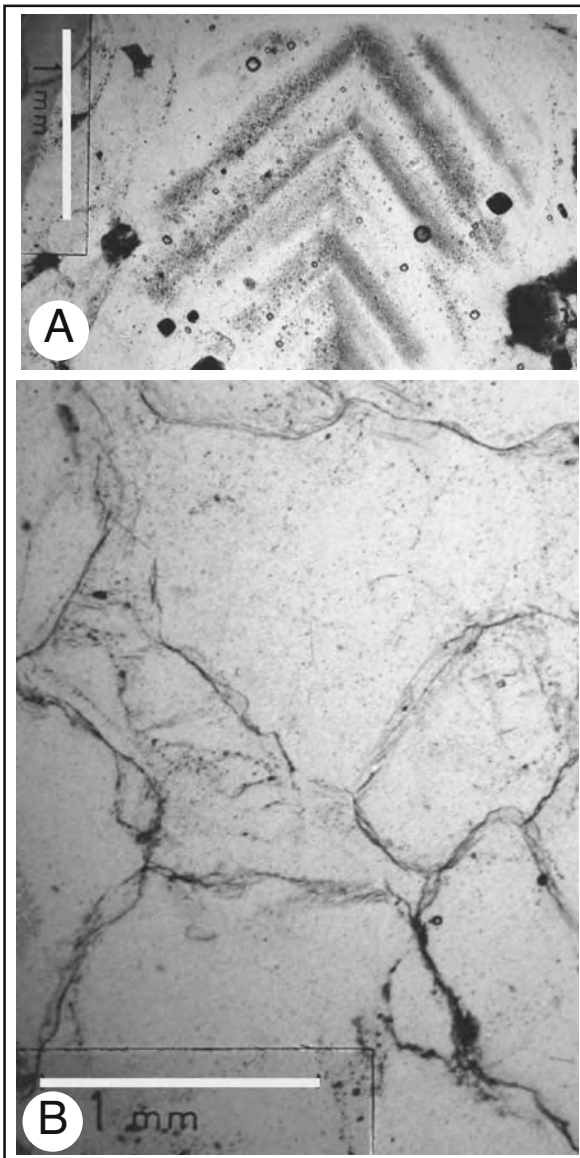


Figure 1.32. Halite textures in the Silurian Mallowa Salt, Canning Basin. A) preserved halite chevron in growth position with erosionally truncated crest implying periodic bottom freshening and hence fairly shallow brine. B) Recrystallised mosaic halite, an enigmatic texture that dominated most of the crust textures in the unit (after Cathro et al., 1992).

to minimise energy. The same mosaic texture can also be found in a soap foam as bubble boundaries with 120° triple junctions. The exact mechanism that controls the formation of mosaic textures in halite is still not well understood. It forms either early during brine reflux cementation or later during burial driven compaction and pressure-solution recrystallisation. During burial it can form a pervasive overprint in flowing

halite. Flowing salt sometimes tends to flatten in the direction of maximum stress and this flattening can be used to distinguish it from other forms of mosaic halite (Figure 6.10a).

Limpid dolomite in mosaic halite

Late, ordered, stoichiometric, euhedral to subhedral limpid dolomite along the contact between bedded halites and interbedded mudstones in the platform evaporites of the San Andres Formation of the Palo Duro Basin, Texas is the outcome of focused burial diagenesis in halite-mudstone successions (Gao et al, 1990). In the Permian example documented by these authors, the limpid dolomite is characterised by a low Sr content and depleted $\delta^{13}\text{C}$ and $\delta^{18}\text{O}$ signatures (Figure 1.33). This they interpret as indicating meteoric or structural waters held in adjacent deeply buried mudstones are a source of ions for the dolomite. This limpid dolomite is not the product of reflux brines, which created the pervasive dolomite in the interlayered San Andres platform carbonates. Limpid dolomite crystallises locally under favourable sulphate-reduction conditions during burial compaction and salt dissolution. Compaction mixed the waters, released from the dewatering mudstones, with brines derived by the dissolution and recrystallisation of adjacent impervious halite beds. Limpid dolomite sparry precipitates along halite-shale contacts where escaping shale waters caused the halite to dissolve and recrystallise as mosaic spar. This mode of dolomite formation is part of a larger set of fluid flow processes that precipitate sparry burial dolomite at the contact between a dissolving salt bed and crossflowing basinal waters

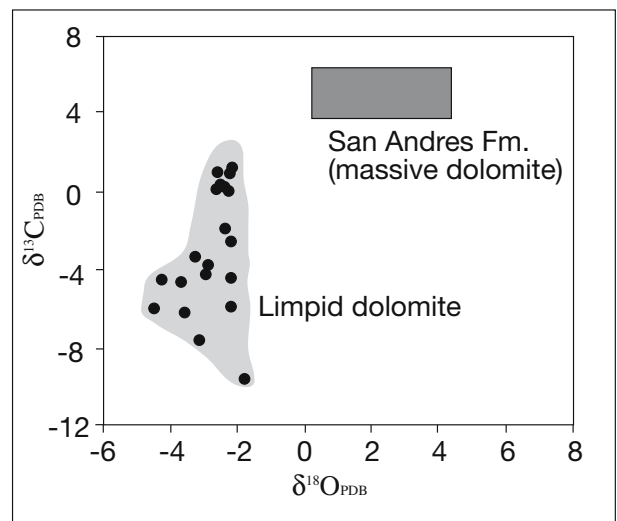


Figure 1.33. Limpid dolomite in halite of San Andres Fm. Palo Duro Basin. Limpid dolomites are depleted in carbon-13 and oxygen-18, compared to typical isotopic signatures in the massive (reflux) dolomite of the San Andres Fm (after Gao et al., 1990).

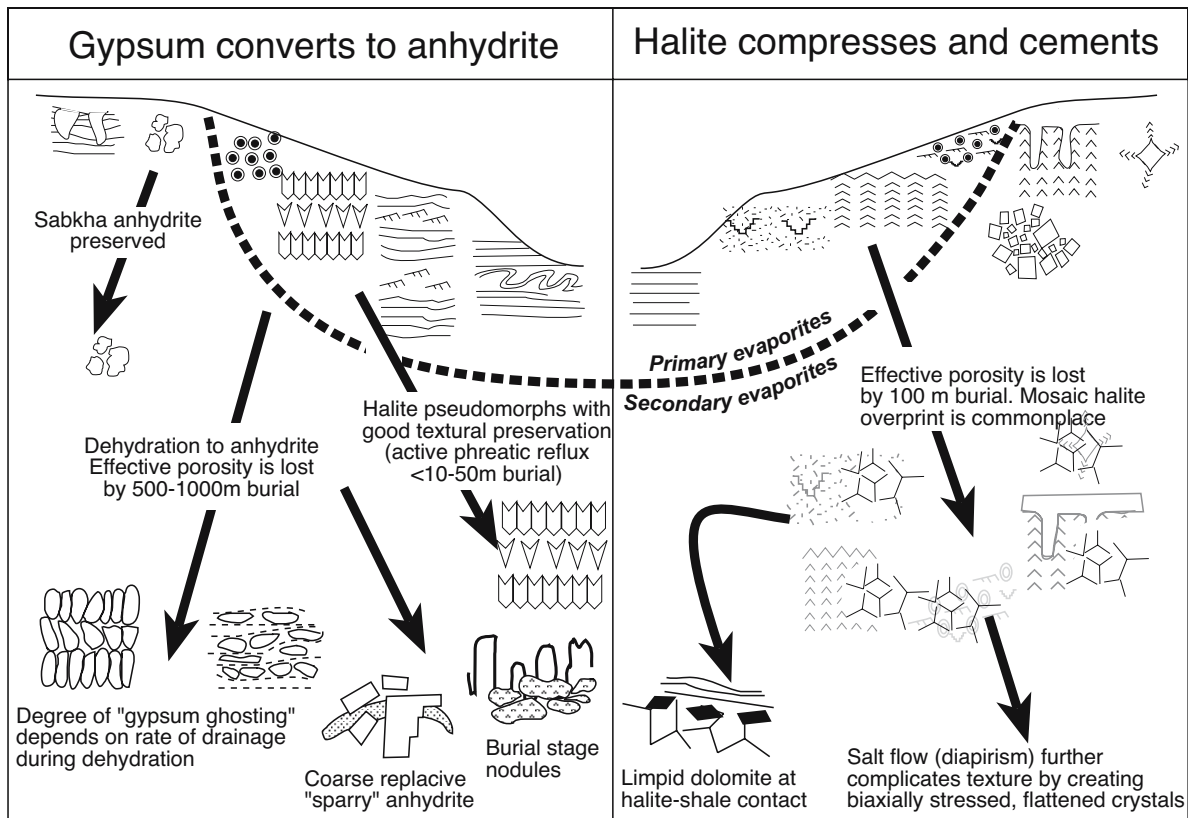


Figure 1.34. Evaporite diagenesis showing evolution of burial-related secondary evaporite textures (includes burial salts).

(e.g. dolomite formation in the basal anhydrite NE Thailand, Figure 7.34a).

Burial of sulphate evaporites

Due to water release, gypsum and other bedded evaporite units made up of hydrated salts with entrained structural water show an inherently more complicated textural response to burial than the simple mosaic overprint of halite beds (Figure 1.34; Warren, 1991). Gypsum releases structural water as it converts with burial to nodular mosaic anhydrite (Figure 1.35). Carnallite ($KCl \cdot MgCl_2 \cdot 6H_2O$) releases Mg and water as it converts to sylvite (KCl) by incongruent dissolution associated with burial diagenesis or phreatic flushing by meteoric waters. Loss of structural water during burial dehydration means syndepositional textures in the converting bed are modified by this flush of escaping water.

Nodular anhydrite and water loss

Gypsum rather than anhydrite is the most common form of sedimentary $CaSO_4$ at earth surface temperatures. Intense

solar heating in very arid regions can dehydrate gypsum to form bassanite/anhydrite at the surface. Gypsum also converts to anhydrite in the capillary zones of sabkhas and evaporitic mudflats where the gypsum is bathed in highly saline NaCl brines. But thick anhydrite beds deposited in ancient saline giants were laid down on the subaqueous floors of perennial brine lakes and seaways not mudflats. Prior to anhydritisation, beds of primary saltern gypsum extended across tens of thousands of square kilometres. Such beds compacted and converted by burial dehydration to nodular anhydrite during early burial, so releasing large volumes of water (Warren, 1991).

As gypsum is buried and ambient temperature rises above 50-60°C, it converts to nodular anhydrite. The depth of transformation is between a few metres to more than a kilometre. The exact depth in any region will depend on lithostatic pressure, local geothermal gradient and pore brine salinity (Figure 8.25). For example, in Miocene Lower Fars evaporites of the United Arab Emirates, with its relatively saline pore brines, the conversion depth ranges from 60 to 245 m across a zone some 10 metres thick (Billo, 1986). In the Salton Sea region with

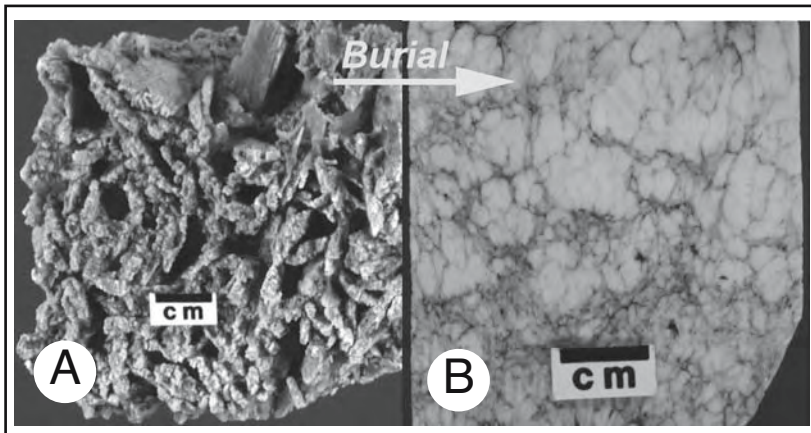


Figure 1.35. Gypsum converted to anhydrite by burial in Bristol Dry Lake, California. A) Lenticular gypsum meshwork from a lake floor sediment sample a metre below the lake surface. B) nodular anhydrite still retaining the outline of the gypsum precursor. Sample from a lake core some 140 metres below the lake surface.

its high geothermal gradients, the conversion from gypsum to anhydrite occurs at 80-105°C and at depths of less than 200-250m (Osborn, 1989). Similar anhydrite conversion was noted at 150-200m depth in cores from the Pleistocene evaporites in nearby Bristol Dry Lake, California; but here the isotopic evidence suggests sulphate-reducing bacteria also play a role in the conversion (Figure 1.35; Rosen and Warren, 1990).

If the nearsurface pore-fluid salinity approaches halite saturation, the conversion from gypsum to anhydrite can occur at shallower depths and much lower temperatures $\approx 35 - 45^\circ\text{C}$. Such temperatures occur as shallow as 1-2 metres below the depositional surface of a halite-saturated brine pool where sediments reside in the zone of active phreatic flow or brine reflux (Figure 2.54). At such depths the buried gypsum bed retains well-developed intercrystalline porosity and inherently high permeabilities. This facilitates the leaching of the gypsum crystals and their infill by clear halite spar, which pseudomorphs the various forms of the precursor gypsum (e.g. Figure 1.30).

With less saline brines in the pores of a buried CaSO_4 bed, the conversion of gypsum to anhydrite may not occur until burial depths of hundreds of metres. By such depths, natural compaction has greatly depleted intercrystalline porosity in the gypsum bed. Release of water from already compressed and cemented gypsum will create 40% water-filled porosity in an otherwise impervious anhydrite unit. Over the long term this water is not retained but escapes into the subjacent sediments. A likely effect within the converting CaSO_4 bed is a decrease in its inherent strength; and in compressive situations, an increased ability to act as a lubricating horizon or décollement, even if no halite is present (Figure 8.26). If the water cannot drain freely

from the dewatering gypsum, the bed may convert to a quicksand-like consistency. This explains some of the intense deformation and enterolithic textures with flow orientations that are commonplace even in flat-lying and otherwise undeformed ancient bedded anhydrites.

As it converts, the more deeply buried and compressed CaSO_4 unit loses almost all of its original texture. Rare indistinct elongate, and partially flow-aligned, nodular “ghosts” may be all that remain of the primary bottom-nucleated textures in many ancient anhydrite beds (Figure 1.26c). Loss of water of crystallisation also affects units subjacent to the dehydrating

gypsum/anhydrite. The escaping water is saturated with respect to CaSO_4 , but undersaturated with respect to other evaporite minerals, including any nearby carbonates, as well as halite and the bittern salts. The onset of anhydritisation will be effected by the salinity and temperature of pore waters and the volume of pore water throughflow (Table 7.12).

Such a complex anhydritisation history is well documented in the varying onset of anhydritisation in calcium sulphate sediments of the Middle Miocene Badenian evaporite basin in the Polish Carpathians. Three distinct, now anhydritised, facies associations record a range of depositional environments from nearshore to deeper basinal settings (Figure 1.36; Kasprzyk, 2003). Coarsely crystalline platform sulphates were deposited in subaerial and shallow-marine environments (shoreline and inner platform-lagoon system) mainly as autochthonous selenitic gypsum. These were reworked and redistributed into deeper waters (outer platform-lagoon, slope and the proximal basin floor system) to form resedimented facies composed mostly of allochthonous clastic gypsum and minor anhydrite. In contrast small gypsum prisms tend to accumulate in water characterised by rapidly fluctuating bottom brine conditions. The prisms were often mechanically reworked into rippled and ooid-like accumulations or captured in algal mats. These laminites were deposited in brine depths ranging down to hundreds of metres, but most accumulate in shallow brines less than a metre or two deep or as pelagites in the deeper part of the basin. It is the rapid salinity fluctuations associated with very shallow waters that favour rapid crystallite formation and multiple nucleation.

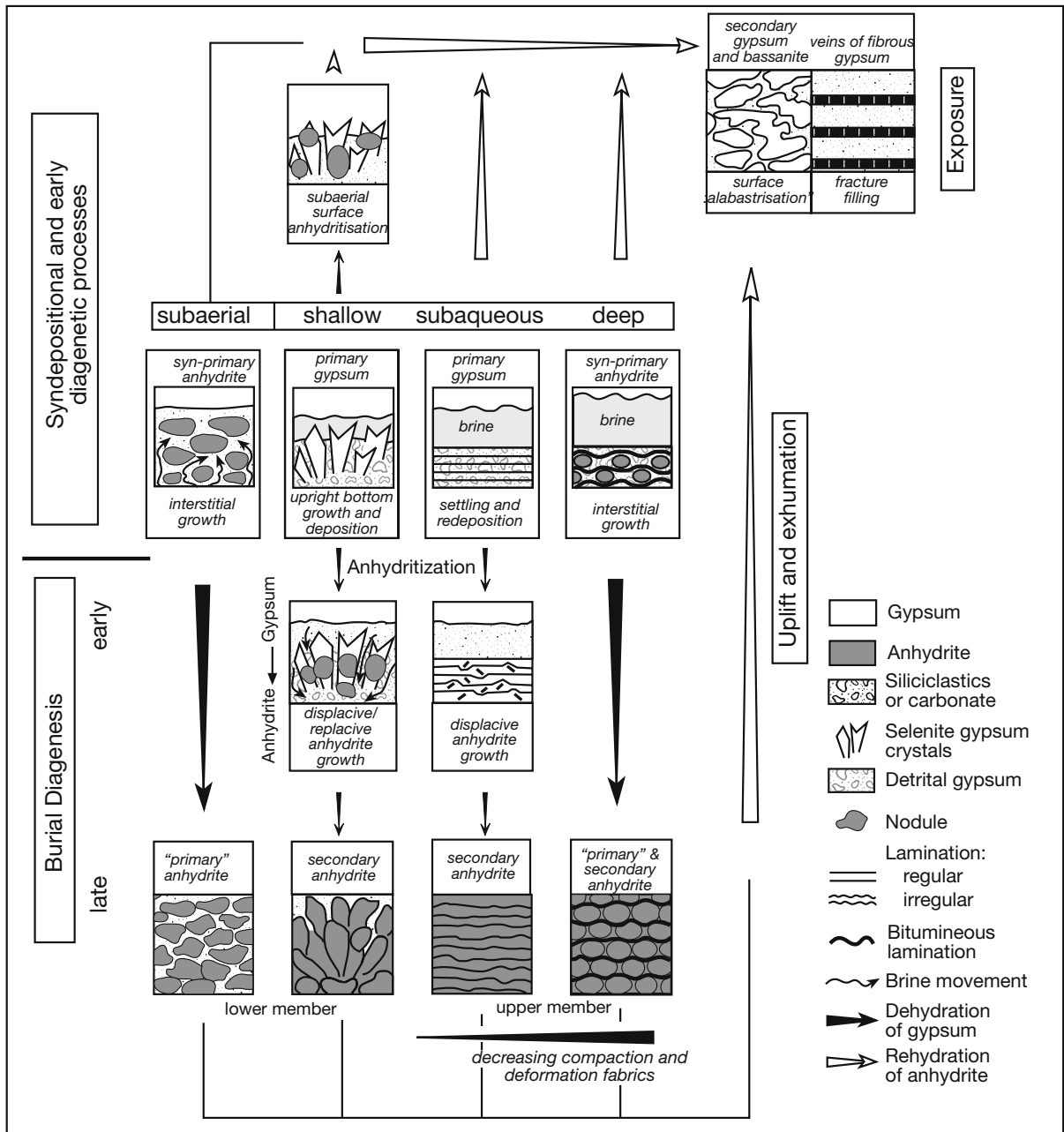


Figure 1.36. Sulphate textural evolution is clearly seen in Middle Miocene sulphates in the Carpathians (after Kasprzyk, 2003). Platform sulphates were deposited in subaerial (sabkha) and shallow-marine environments (shoreline and inner platform-lagoon), mainly as autochthonous coarse-grained aligned (selenitic) gypsum. This platform sediment was reworked and redistributed into deeper waters (outer platform-lagoon, slope and the proximal basin floor system) to form resedimented facies composed mostly of allochthonous clastic gypsum and minor anhydrite. Burial and the conversion to anhydrite subjected these sulphates (mostly gypsum) to two different hydrological styles: (1) syndepositional anhydritisation of gypsum deposits by highly concentrated brines or elevated temperatures in surficial to shallow-burial environments (mostly in the lower member of these Badenian sulphates), and (2) successive phases of anhydrite formation (syndepositional de novo growth, early diagenetic to late diagenetic replacement of former gypsum), which occurred during progressive burial (mostly in the upper member). Finally, the succession was uplifted and re-entered the active meteoric realm where various fibrous and alabastrine textures formed.

Subsequent anhydritization was superimposed on depositional gypsum facies. It was the result of interactions between concentrated seawater, meteoric runoff and highly saline, residual pore fluids. And so two different anhydrite styles overprinted the original Badenian sulphates (Kasprzyk, 2003): (1) syndepositional anhydritisation of gypsum deposits driven by highly concentrated brines and elevated temperatures (mostly in the lower member), (2) successive phases of anhydrite formation (syndepositional *de novo* growth, early diagenetic to late diagenetic replacement of former gypsum) during progressive burial (mostly took place in the upper member). In the basin the anhydrite started to grow in a fine-grained bottom host under very early, probably syndepositional conditions and formed a displacive micromodular laminated lithofacies. Likewise the onset of anhydritisation was very early in clastic gypsum of the strandline. It formed abundant displacive anhydrite with intense syndepositional deformation structures related to nodule growth. This environment was subject to early exposure, high temperatures and high salinities. Later, a deeper burial anhydrite phase spread through the coarsely crystalline gypsum of the shelf. This created replacive nodular anhydrite in sediment hosts so that primary crystal textures are well preserved.

Porosity loss in these units is essentially complete by burial depths of 500m. After this, these anhydrous units, like halite at even shallower depths, are essentially impervious and act as aquitards and pressure seals to any crossflow of pore water, hydrocarbons or metals. Evaporite salt beds below 500-1000 metres typically respond to further burial by flowage and edge-focused dissolution.

Burial Salts: Nodules and stylolites

Subsurface sulphate-rich waters derived from deeply buried dissolving evaporites can precipitate anhydrite nodules in adjacent nonevaporitic strata. Such nodules are a form of burial salt fed by saline compactional and thermobaric waters. Superficially these nodules can resemble those of a sabkha anhydrite, but there are a number of distinguishing features (Machel, 1993; Machel and Burton, 1991; Warren, 1991). Most obvious is that the burial nodules precipitate in porosity zones that are not depositionally defined. They can occur within or adjacent to faults, or within open marine shelf carbonates, which are not intertidal/supratidal units. They often occur within, or juxtaposed to, dark, bituminous argillaceous seams and pockets, or within zones of anastomose bituminous veinlets and carbonaceous

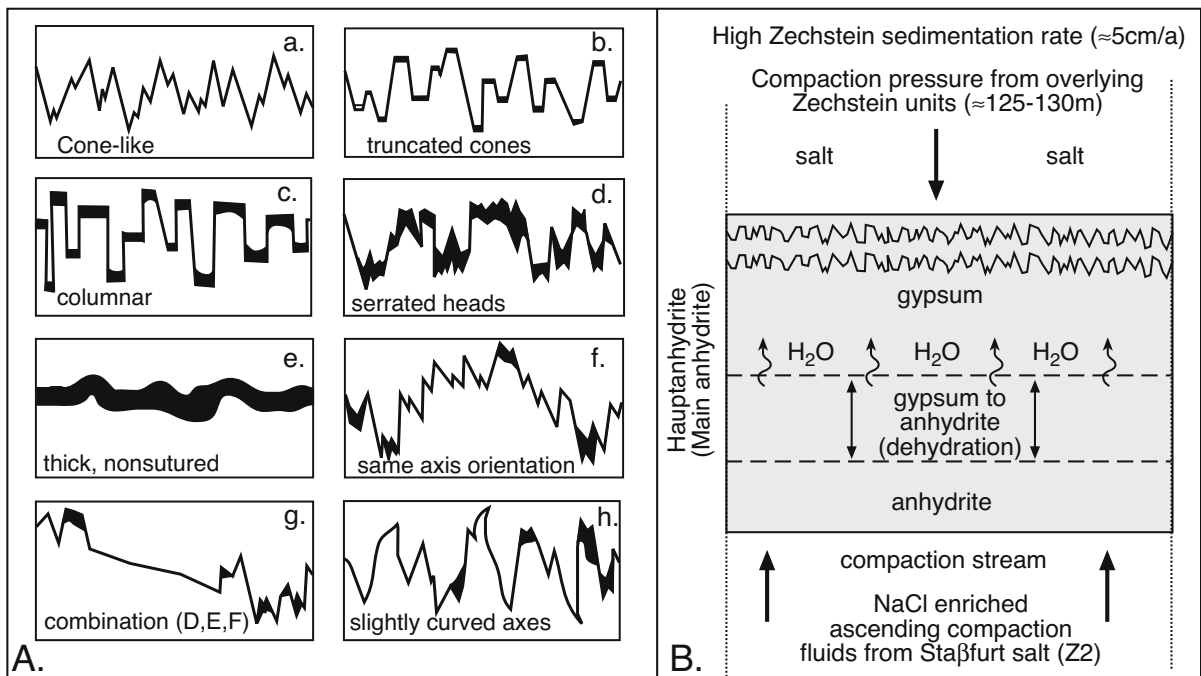


Figure 1.37. Stylolites in anhydrite beds. A) Types of stylolite seams or sutures hosted in the Hauptanhydrit (Zechstein) of the Gorleben salt dome, Germany. B) model for the development of stylolites in the upper part of the Hauptanhydrit during deposition of the younger Zechstein beds. Stylolitisation is restricted to a gypsum matrix (pre-anhydritisation) and occurred less than 150 m below the sedimentation surface (after Bäurele et al., 2000).

haloes, all of which are the result of pressure solution and stylolitisation. They typically replace the host rock and crosscut stylolite boundaries in the carbonate matrix. Thus, they enclose material generated during burial diagenesis, such as authigenic pyrite and saddle dolomite, and show little evidence of mechanical compaction. They are often associated with coarsely crystalline, late-stage poikilotopic and pore-filling anhydrite spar cements.

Stylolites hosted in a limestone or dolomite matrix are widely recognised pressure solution features though to indicate burial depths in excess of 0.5-1.0 km (Bathurst, 1980). Stylolites in evaporite beds are not common and may not necessarily form by such deep burial. Some have argued that anhydrite and halite can not exist at the pressure necessary to form stylolites without pervasive recrystallisation. But stylolite horizons do occur in the Gorleben Zechstein salt dome in the Bänderanhydrit located near the top of the Zechstein Hauptanhydrit (Bäurele et al, 2000). Stylolites were also noted by Peryt et al. (1993) in the Werra Anhydrit (Zechstein 1) of western Poland and by El Tabakh et al. (1998a) in the Basal Anhydrite of the Cretaceous Maha Sarakham of Thailand. The latter can be related to differential salt solution during burial flushing (Figure 7.33).

Bäurele et al. (2000) tied the pressure-solution seams in the Hauptanhydrit to the presence of thin magnesite-clay interlayers and distinguished five principal stylolite morphologies (Figure 1.37a). The orientation of the sutured seams is generally bedding-parallel with the stylolite axes vertical to the bedding surface. Some seams have been deformed by salt flow and the anhydrite beds with bedding parallel stylolites are now steeply inclined to the horizontal. There is no relation between stylolite formation and pressures created by the modern salt dome crest. Solution rates of up to 26% were calculated by measuring maximum stylolite amplitudes in core.

The bedding-parallel occurrence of the Hauptanhydrit stylolites, in combination with the observation that the stylolite seams are crosscut by anhydrite pseudomorphs after gypsum, argues that the stylolites formed before the dehydration of gypsum to

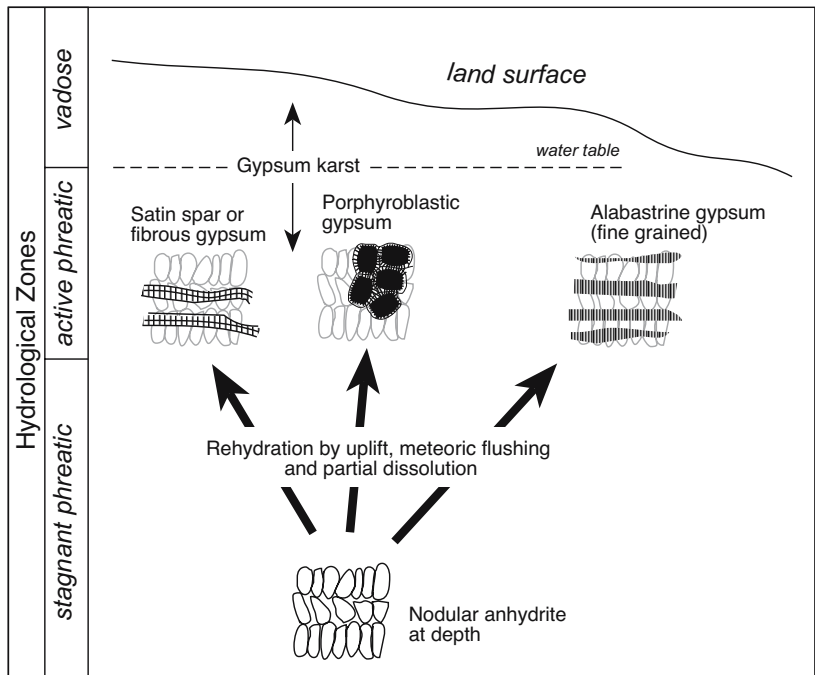


Figure 1.38. Rehydration fabrics in calcium sulphate from uplift, meteoric flushing and dissolution. These are the tertiary evaporites of Figure 1.1.

anhydrite was complete. The lower parts of the Hauptanhydrit were excluded from the stylolitisation process as they had already been converted to anhydrite by ascending compaction fluids of the underlying Zechstein 2 Salt (Figure 1.37b; Bäurele et al., 2000). Porosity and permeability loss that is an integral part of the conversion process prevents the formation of stylolites once any interval had converted to anhydrite. The transition depth in the Zechstein was around 125 m. Pervasive dehydration of gypsum to anhydrite in the Hauptanhydrit was probably complete before the end of Zechstein sedimentation. The arguments of Bäurele et al. (2000) imply that the formation of stylolites occurs in gypsum, not anhydrite, and is a relatively shallow burial process ($\approx 100-150\text{m}$).

Evaporites as uplift indicators

At the other extreme of the burial cycle is the conversion of exhumed and uplifted evaporite beds entering the telogenetic realm. Most common is the conversion of anhydrite into diagenetically regenerated gypsum (Figure 1.38). Uplifted halite beds first undergo differential dissolution to leave behind layers of residual nodular anhydrite, which are then dissolved by ongoing meteoric flushing (Figure 7.29). Two commonplace gypsum fabrics are the result of exhumation: coarse

porphyroblastic gypsum and fine-grained alabastrine gypsum (Holliday, 1970; Warren et al., 1990). Porphyroblastic gypsum often retains dispersed relics of the precursor anhydrite. Crystal forms are coarse, up to two cm across, and can be euhedral or anhedral, thin and acicular or thick and stubby. Porphyroblasts often aggregate into cm-scale rosettes or blebs with acicular gypsum rinds. This creates a texture that is sometimes described as “daisywheel gypsum.”

Daisy wheel gypsum is a response to rehydration under the relatively homogenous conditions of uplift hydrology in a massive nodular anhydrite unit entering the lowermost parts of the telogenetic zone. Rates of fluid crossflow are low, so chemical dissolution is slow and dissolution fronts tend to be focused about the bed contacts between aquifers and the anhydrite (gypsum is not stable at such depths). As an anhydrite bed is uplifted into the telogenetic zone it once again comes into contact with low salinity, low temperature waters. In many uplift situations there is also an artesian flow system established so that both karstification and rehydration to gypsum tends to at first be focused on the edge of the bed where satinspar gypsum tends to dominate. As rehydration to gypsum becomes more pervasive within a bed, it tends to penetrate first along the impurity-rich more permeable edges of anhydrite nodules. Sparry aligned gypsum crystals grow toward the centre of the nodules to form daisywheel gypsum (Warren et al., 1990). As the rehydration proceeds through the bed, some of the gypsum then dissolves to give greater access to undersaturated waters to the gypsum bed to create caverns. Because of the destructive nature of porphyroblastic overprinting, interpreting original

depositional environment is next to impossible in nearsurface and outcropping CaSO_4 units, they are composed almost entirely of diagenetically regenerated gypsum.

Alabaster is the other form of telogenetic gypsum and is created where anhydrite pervasively rewaters to gypsum in the zone of active phreatic flow. Individual gypsum grains are typically less than $50\ \mu\text{m}$, with grain boundaries that range from poorly defined to equidimensional granuloblastic. The change from porphyroblastic to alabastrine may be depth-related (Warren et al., 1990). Porphyroblastic gypsum defines the re-emergence of nodular anhydrite from the stagnant phreatic into the deep portion of the zone of active phreatic flow. Alabastrine gypsum forms in the zone of more diffuse active phreatic flow. This re-emergence is also associated with the formation of gypsum karst and the formation of evaporite-dissolution breccias (Chapter 7).

Excess amounts of trace elements, especially strontium and boron, are released from some bedded anhydrites as they reconvert to gypsum. The released elements may precipitate in the regenerating alabastrine gypsum as celestite or boron-bearing minerals, such as proberite, ulexite, tyreskite and priceite.

Fibrous gypsum and halite (satinspar)

Veins and fractures filled with fibrous satinspar CaSO_4 (typically gypsum) or halite are widespread in the mudstones and shales adjacent to bedded evaporite units undergoing dissolution. Fractures may be subhorizontal and lie roughly parallel to the contact with the bedded evaporite unit or may form as conjugates. The fractures form and fill with fibrous cements in response to stresses set up in the bed by the formation of nearby stratiform cavities (Figure 1.39). The fracture filling is usually zoned and made up of two or more parallel layers of either fibrous CaSO_4 or fibrous halite. Fracture-fill crystals are oriented with their long axes perpendicular to the fracture walls. Coarse calcite crystals can occasionally fill the centre of the fracture. Most fracture fills are monomineralic and gypsum is the dominant mineral in most nearsurface fracture systems. Internal fracture zonation is pronounced and reflects episodic and ongoing opening and



Figure 1.39. Meshwork of satinspar gypsum veins created by dissolution of an adjacent anhydrite bed in the Permian of eastern Saudi Arabia (car key for scale).

filling of the fractures. Some fibrous fills are sigmoidally deformed showing fracture fill was ongoing as adjacent blocks slid and rotated in response to changes in nearby dissolution cavities (El Tabakh et al., 1998b).

Fibrous halite and satinspar formation are linked to fracture and cavity formation in active hydrological systems. Fractures filled with satinspar are linked to uplift and either the generation of open fractures induced by subsidence associated with salt dissolution and uplift (Figure 1.40; Gustavson et al., 1994) or to hydraulic fracturing associated with the conversion of anhydrite to gypsum (Cosgrove, 2001). Thus fracture-filling satin-spar may be a passive process in open fractures or a more active process with fractures forced open by overpressured CaSO_4 -saturated artesian waters.

Superimposed on these processes may be the force of crystallisation of gypsum. Shearman et al. (1972) suggested that displacive satinspar veining is a feature of anhydrite hydration, which may have been due to hydrofracturing by overpressured confined groundwater as exhumed anhydrite reconverted to gypsum. Shearman et al. (1972) pointed out that if all the calcium sulphate is retained within the system, the hydration of anhydrite to gypsum should result in an increase in volume of 63%. They noted that in many secondary gypsum rocks, former anhydrite is replaced on a volume-for-volume basis, and the additional volume of gypsum appears as fibrous or satinspar veins that cut the associated rock. Gypsum grew in the water-filled fractures, whenever the overburden was supported by pressurised water.

Progressive sediment fracturing (hydrofracturing?) is thought to be a response to unroofing. Unloading and release of overburden weight drives the formation of near surface fractures parallel to the earth's surface. Fibrous halite and satinspar

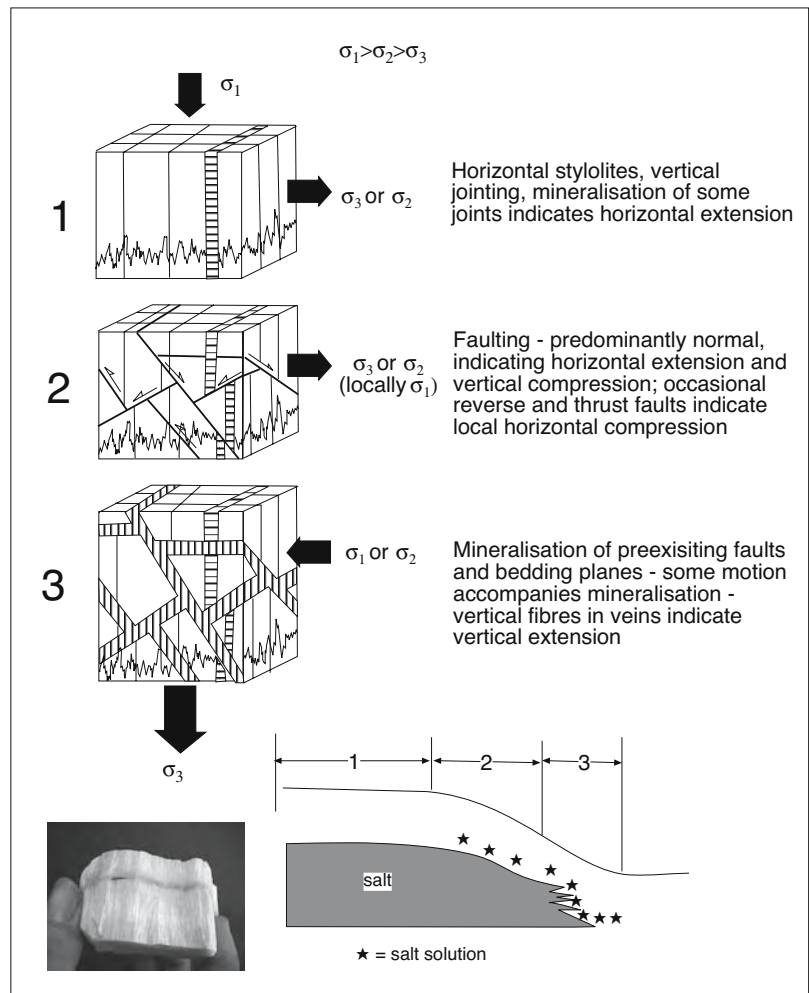


Figure 1.40. Conceptual model of deformation above salt dissolution zone showing structural sequence and proposed location relative to dissolution front. Stage 1 occurs prior to salt dissolution and is characterised by jointing resulting from normal burial. Late stage 1 and stage 2 occur as salt dissolution begins. Early stage 2 is characterised by a few vertical gypsum veins with horizontal fibres. Later stage 2 is characterised by normal faults and uncommon reverse faults. In stage 2 layer parallel extension results from the onset of dissolution and subsidence. Stage 3 is characterised by gypsum veining of bedding planes and faults. In stage 3 vertical extension results from widespread dissolution and collapse of underlying evaporites (after Gustavson et al., 1994).

CaSO_4 are commonly associated with, but not exclusive to, zones of exhuming evaporites (Figure 1.38). It is not known if satinspar filled fractures can also form at greater depths (1000s of metres) in mesogenetic realms associated with overpressuring and compactional or thermobaric waters.

Cosgrove (2001) describes networks of satinspar filled hydraulic fractures preserved only in the exhumed evaporite horizons of the Mercia Mudstones of the Bristol Channel Basin of south-

west England. Like Shearman et al. (op. cit.), he concludes its preservation relates to the volume changes associated with the hydration of anhydrite to gypsum, which occurred as the rock mass was exhumed and the relatively low temperature and pressure conditions necessary for the formation of gypsum were encountered (e.g., Jowett et al., 1993). Hydration in the Mercia Mudstones occurred during the tectonic inversion of the basin as basin sediments experienced tectonic compression during exhumation. This caused an increase in fluid pressure and facilitated the formation of hydraulic fractures that then fill with satinspar. Cosgrove goes on to argue that hydraulic fractures also formed in the muddy evaporite-free horizons. But the fractures reclosed and healed as soon as the fluids had passed through them and pressure had dropped as the appropriate brine required for their preservation as satinspar veins was not present within the nonevaporite sections.

The mechanism of creating satinspar filled fractures as documented by Gustavson et al. (1994) is a much more passive process. They note that most satinspar veins occur in highly fractured or brecciated strata that overlie or are associated with exhumed bedded halite, anhydrite and gypsum. There are often saline springs in the vicinity of a satinspar occurrence indicating active halite dissolution. In this scenario satinspar is a response to several hydrologically driven processes (Figure 1.40). Cavernous porosity is created as halite is dissolved by crossflows of low salinity active-phreatic waters down to depths of 200-750 metres. Extensional fractures form in the strata above these dissolution zones and anhydrite is rehydrated to gypsum either via a dissolution-precipitation interface or through a bassanite intermediary (Holliday, 1970). The deeply circulated groundwater is now saturated with respect to gypsum and any further anhydrite hydration results in supersaturation. Excess CaSO_4 now carried in solution by groundwaters flowing out of the dissolution zones precipitates gypsum in open high permeability fractures created during overburden collapse.

It may well be that the satinspar and the associated fracturing are a response to both active and passive modes of formation. Perhaps active hydrofracturing, as envisaged by Shearman et al. (1972), is more significant in driving satinspar fracture fill at greater depths where the dissolving evaporites and adjacent beds are still relatively tight and are first entering the telogenetic realm (via the zone of stagnant phreatic circulation. As exhumation and dissolution continues the fracture and fill process evolves into a more passive set of collapse induced features. This occurs once beds are shallower and have become more permeable. They have moved into the zone of active phreatic circulation and are closer to the landsurface (see Chapter 7 for more hydrological detail on the effects of telogenetic alteration).

Saline clay authigenesis

So far we have focused on the formation and alteration of the various evaporite salts, but the same evolving saline hydrologies can also drive the formation and alteration of clays (Table 1.5). Many authigenic clay minerals formed in hypersaline settings are enriched in magnesium (Fisher, 1988), but authigenic clays do not make up the greater volumes of clay in modern or ancient salt lakes. Most of the clays in salt lakes and playas are detrital and reflect compositions of older argillaceous formations in the palaeodrainage areas. Illite, kaolinite, chlorite, dioctahedral smectite and a number of mixed-layers clays are commonplace detrital clay minerals in saline formations (Calvo et al., 1999). Widespread flocculation of clays is an effective sedimenter of suspended clay wherever freshwater runoff and streams flood an area of standing saline water. Thus the composition of initial clay sediments in a playa largely reflects that of the minerals carried as suspended load into the lacustrine depression.

The magnitude of detrital clastic input is thought to be a significant factor in the relative volume of authigenic clay. Regions with rapid deposition of clays, tied to high detrital inputs, tend to be areas where the authigenic clay component is swamped by the high detrital input. Clay authigenesis in evaporitic basins is favoured in marginal playa areas where rates of detrital clay input are low (Figure 1.41). This encompasses interdunal depressions, peripheral sandflats

	Structural Formula	Mg/Si	Al/Si
Saponite	$(\text{Ca}, \text{Na})_{0.3}(\text{Mg}, \text{Fe})_3(\text{Si}, \text{Al})_4\text{O}_{10}(\text{OH})_2(\text{OH})_2 \cdot 4\text{H}_2\text{O}$	0.76-0.87	0.07-0.18
Kerolite	$\text{Mg}_3\text{Si}_4\text{O}_{10}(\text{OH})_2 \cdot \text{H}_2\text{O}$	0.75	0.0
Stevensite	$\text{Na}_{0.15}\text{Mg}_3\text{Si}_4\text{O}_{10}(\text{OH})_4$	0.75	0.0
Hectorite	$\text{Na}_{0.3}(\text{Mg}, \text{Li})_3\text{Si}_4\text{O}_{10}(\text{F}, \text{OH})_2$	0.67	0.0
Sepiolite	$\text{Mg}_4\text{Si}_6\text{O}_{15}(\text{OH})_2 \cdot 6\text{H}_2\text{O}$	0.67	0.0
Palygorskite	$(\text{Mg}, \text{Al})_2\text{Si}_4\text{O}_{10}(\text{OH}) \cdot 4\text{H}_2\text{O}$	0.17-0.49	0.02-0.31

Table 1.5. Main authigenic clay minerals occurring in continental evaporitic environments (after Calvo et al, 1999).

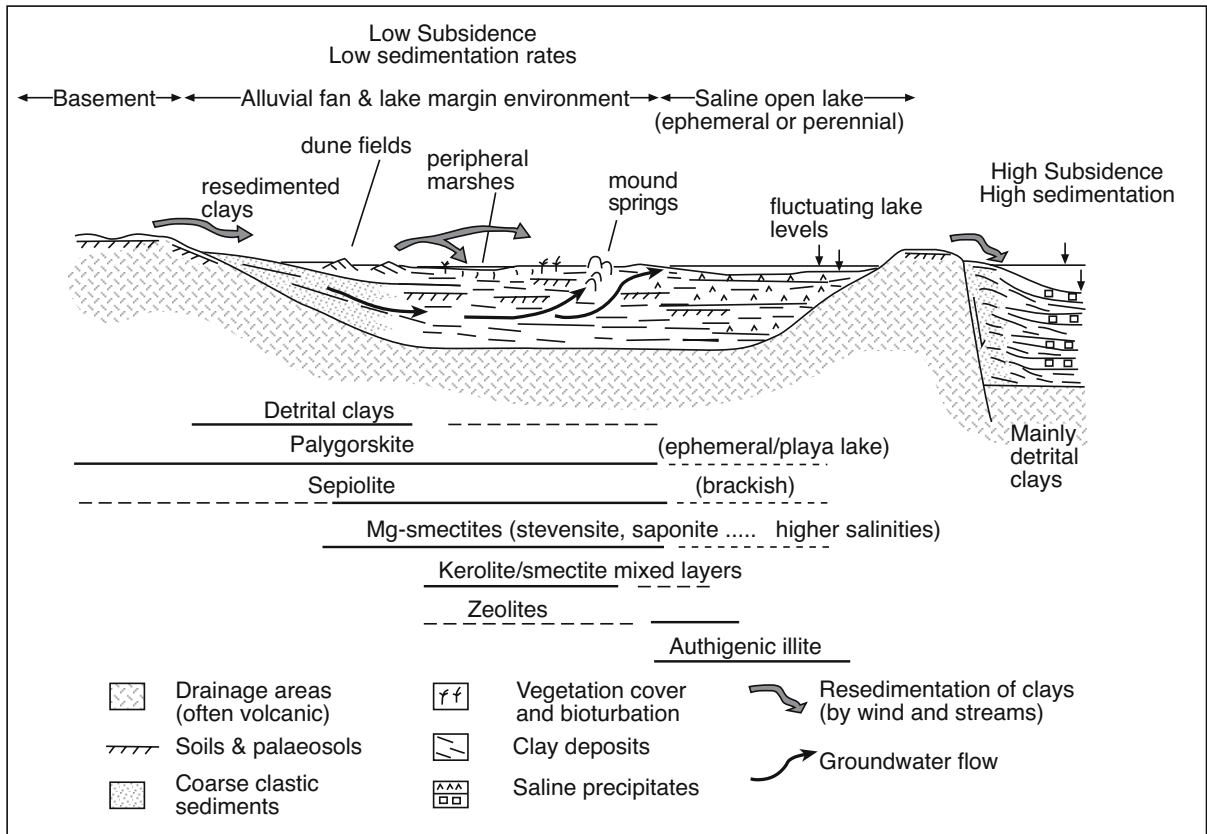


Figure 1.41. Commonly observed distribution of authigenic clays in saline continental environments emphasising the differences between basins undergoing slow and rapid subsidence. Authigenic clays form mostly in saline lake-margin environments. Formation of authigenic clays in open-lake environments is dependent on the degree of schizohalinity. (after Calvo et al., 1999).

and muddy carbonate flats. In these low sedimentation areas the transformation of precursor clays is more effective, driven by episode surface inflow and groundwater discharge (Calvo et al., 1999). Highly reactive nearsurface and surface conditions are favoured by inherently large variations in pore water salinity, pH and pCO₂ levels.

Clay authigenesis in many saline depressions is driven by pedogenesis, especially in the marginal areas where sedimentation rates are low and subaerial exposure dominates at the sedimentation surface. Below the surface episodic wet-dry cycles means neoformed clays are the byproduct of complex reactions between Na and Mg-rich interstitial brines and detrital silicates. Pedogenic processes account for the formation of widespread lake margin palygorskite and sepiolite, typically in association with the creation of calcretes, dolocretes and silcretes. In cases where palygorskite dominates the soil profile, they are sometimes described as palycretes. Zeolites can also form from saline groundwaters in saline lake-margin pedogenic settings (Figure 11.61). Artesian and phreatic groundwater

discharge through springs into the lake margin areas also plays a significant role in the formation of other authigenic clays, as in saline lakes at the foot of Mt Kilimanjaro, in Tanzania and Kenya (Hay et al., 1995).

Once precipitated, authigenic clays can be retransported further out into the playa depression and in more humid climatic stages may even end up on the floor of freshwater lakes. This situation is seen in lacustrine sequences from the Miocene formations of the Madrid Basin (Bellanca et al., 1992) where significant amounts of palygorskite and sepiolite occur as either mud chips or clay aggregates in the basal part of a fresher water lacustrine unit. Eolian transport of saltating clay pellets or dust suspensions may also contribute to the transport of authigenic clays from marginal to more central areas. This sometimes leads to problems of interpretation of detrital versus authigenic in ancient lacustrine successions subject to oscillations in climate, especially when detrital clays are partially or fully inherited from arid soils.

Sepiolite, interstratified Mg-Smectite and palygorskite form authigenic phases in the Quaternary sediments of the Double Lakes Formation, Texas (Webster and Jones, 1994). The dominance of each of these minerals in separate horizons represents evaporative shifts in salinity at the time they precipitated. Sepiolite is thought to indicate a brackish lake, while Mg-smectite indicates more saline conditions. Palygorskite is interpreted as a saline pore water precipitate in the arid soils of the playa stage. Likewise Jones (1986) interpreted authigenic Mg-smectites (e.g. stevensite) as requiring higher salinity than sepiolite. Mg-silicates also define saline lake clays in Great Salt Lake (Spencer, 1983) and some Bolivian salars (Badaut and Risacher, 1983). In Bolivia, the authigenic Mg-smectite replaces the biogenic silica in diatom frustules and requires a pH in excess of 8.2. Authigenic stevensite occurs in unconsolidated muds underlying saline crusts in the interdunal depressions of northern Lake Chad and as small aragonite-associated oolites on the lake floor (Gac 1980, Darragi and Tardy, 1987). Similar stevensite oolites have been found in the Eocene Green River lacustrine basin. Authigenic sepiolite associated with calcite, gypsum and dolomite occurs about the margin of Saline Valley Playa, California and the edges of saline pans in the Kalahari of southern Africa (Hardie, 1968; Kautz and Porada, 1976). Palygorskite, sepiolite and authigenic smectite are common-place precipitates in calcretes of groundwater discharge playas in inland Australia (Arakel et al., 1990).

Clearly, palygorskite and sepiolite (both two-chain structure fibrous clays) occur worldwide as authigenic phases in the soils and palaeosols of arid and semi-arid regions, but the mode of precipitation is still not well understood (Singer, 1979). Jones (1983) concluded sepiolite in the calcic soils of southwest Nevada required percolation of high salinity groundwaters. Magnesium and silica solutes were supplied by the weathering of nearby pyroclastics and carbonates. Sepiolite has replaced magnesite pebbles, from the edges in, during freshened highstand intervals in Miocene Lake Eskisehir in Turkey (Ece, 1998). Palygorskite in calcic soils is thought to be the result of incongruent dissolution of preexisting clays (Jones and Galán, 1988). Fibrous clays degrade when climate becomes more humid and alter to smectite. Paquet and Millot (1972) conclude that the transformation takes place when mean rainfall exceeds 300 mm and Calvo et al. (1999) suggested the transformation can be used as a palaeoclimatic indicator.

Alunite ($KAl_3(SO_4)_2(OH)_6$) is a common clay product in acid saline lacustrine settings (Figure 2.20), but can also form diagenetically in regions where sulphate reduction is occurring. It is thought to be derived by the reaction of clay minerals

with sulphuric acid created by oxidation of sulphides or H_2S at a redox boundary. It is a common product where clays are present in zones of sulphate reduction and examples have been documented in the Middle Miocene gypsums of the Gulf of Suez (Rouchy et al., 1995) and the Upper Miocene gypsums of the Lorca Basin in Spain (Rouchy et al., 1998).

Even the smectite to illite transformation, which is used as an indicator of diagenetic intensity and clay transformations occurring at higher temperatures may be influenced by salinity. This makes illite crystallinity a less reliable indicator of diagenetic stage in environments with saline pore fluids (Honty et al., 2004). Turner and Fishman (1991) found illite-smectite mixed layer clays having a range of expandabilities in altered tuff beds in a Jurassic lake in the Morrison Formation (Eastern Colorado Plateau, USA). The observed clays did not experience deep burial, and did not undergo hydrothermal alteration. The illite content generally increases from the lake margin (100–70% smectite) to the lake centre (30–0% smectite) and follows a lateral hydrogeochemical gradient, which was characterized by increasing salinity and alkalinity (Figure 11.62). It seems that in a saline depositional setting, solution chemistry is a principal factor controlling the smectite to illite proportion. Illite-smectite can form from smectite at low temperatures in several ways (see Honty et al., 2004), but forms best in saline environments subject to wetting and drying cycles, which is a hydrology exemplified in salt lakes and playas. In the presence of K^+ ions, alternating wetting and drying leads to irreversible fixation of K and the formation of illite layers. Illite-smectite clays forming at elevated pH may not even require wetting and drying cycles.

Textural Synthesis

Evaporitic settings can accumulate evaporitic carbonates as well as more saline salts dominated by gypsum and halite beds. Evaporitic carbonates accumulate across the whole range of brine depths from ephemeral to shallow perennial to deep. Carbonate laminites tend to dominate in the deeper brine areas, while a whole range of textures and features, including laminites, form in the shallow and strandzone settings. Strandzone regions are often characterised by pisolites and algal structures of various types, ranging from cryptalgalaminites to stromatolites and tufas. The ephemeral water and groundwater seepage systems that characterise strandzones facilitate the cementation and ongoing growth of carbonate crusts. Over time, these marginward carbonate crusts can grow and deform into overthrust V-shaped carbonate ridges called tepees.

The typical evaporite accumulating on the floor of a stable brine pool or a shallow shelf is composed of upward or growth-aligned crystals. Depending on the stability, salinity, and permanence of the overlying bottom brine, various mineralogical and dissolution surfaces can be superimposed on the upward growing prisms. When the overlying brine column is not subject to marked salinity fluctuations, then pristine crystal outlines are made up of stacked halite chevrons or zig-zag gypsums, with varying degrees of face curvature. When the overlying perennial brine body mixes and freshens, subaqueous crystal truncation surfaces can form. Similar surfaces can form where the brine body dries up. Desiccation-related dissolution surfaces are distinguished from subaqueous truncation surfaces by an inherent abundance of vadose, karst and geopetal features. These three are all features that form during complete drying and falling of the water table into the evaporite bed.

But evaporites do not just form on the bottom of a brine lake or seaway. They can also form where porewaters attain supersaturation in a preexisting nonevaporite matrix (secondary evaporites). Probably the best-documented textures of this type are sabkha nodules composed of anhydrite and gypsum in the supratidal sediments of the Arabian Gulf. Large crystals of displacive halite form in a similar fashion beneath the mudflats of the Arabian Gulf, where the capillary pore fluids are at halite supersaturation. Dense brines, created during the formation of primary and early secondary salts, can sink into the underlying sediments where they can facilitate backreaction and alteration processes in the now buried evaporite beds.

At greater depths of burial, evaporite salts can reprecipitate as pore-filling cements and burial salts. Many primary and early secondary textures are overprinted at this stage by dewatering and recrystallisation processes associated with compactional dewatering and thermobaric alteration. Brines created by the subsurface dissolution of evaporites may also reprecipitate as burial salts in nearby nonevaporite beds.

If evaporites beds survive the rigours of deeper burial, they can be uplifted and re-enter the active phreatic zone where they are once again subject to dissolution and recrystallisation. Satinspar fractures and alabastrine textures are common indicators of this style of alteration. Such evaporites can be classified as tertiary evaporites.

All of the textural and re-equilibration processes outlined in this chapter reflect the ongoing evolution of the brines that bathe the beds throughout their formation, burial and dissolution. Brine hydrology and its evolution is the fundamental control

on evaporites. In the next chapter we look at how brine evolution controls evaporites from the time they precipitate until the time they are completely dissolved.

Chapter 2: Depositional chemistry and hydrology

An evaporite is defined in Chapter 1 as a rock originally precipitated from a saturated surface or nearsurface brine by hydrologies driven by solar evaporation. There is no assumption as to the origin of the parent brine; it may be marine (thalassic), nonmarine (athalassic) or a hybrid. By definition, there is a need for aridity and for water loss to exceed inflow. This means deposition and diagenesis in evaporites is more climate dependant than in either siliciclastic or carbonate sediments. Reaction rates and reversibility are an order of magnitude faster. Suites of precipitated salts follow the geochemical make-up of the parent brine, while primary textures indicate hydrological stability and energy levels of the time of precipitation.

All evaporite salts are ionic salts, containing the major ions Na, Ca, Mg, K, Cl, SO_4 , CO_3 in varying proportions along with other less common ionic constituents, such as B, Ba, Sr, Br and I and varying amounts of structural water (Table 1.1). The mineralogy and order of precipitates in any brine pool is controlled by the ionic make up of the parent brine. This, in turn, reflects the chemical composition of lithologies contributing dissolved ions to the parent water on its way to the site of precipitation. Because of consistent ionic proportions in seawater worldwide, the modern marine evaporite series is predictable and tied to increasing salinity. With nonmarine brines, proportions vary according to source terrain and levels of hydrothermal input. Hence, the proportions of minerals and sequence of precipitation is more variable. But, we now know that the ionic proportions in seawater were not constant through time and that the modern evaporite series is not always a one-for-one analog for past marine-fed precipitates.

Quaternary climatic hydrology

Modern continental evaporites typically accumulate within ground-water discharge regions in semi-arid to hyperarid^{2.1} deserts (Figure 2.1a; Table 2.1). Coastal evaporites occur at the oceanic edge of the same deserts, typically in coastal depressions fed by marine seeps or by rising groundwaters along coast-parallel mudflats. Evaporites also form lake precipitates and efflorescences in cold polar deserts in Antarctica, but the volumes of salt in these cryogenic regions pale to insignificance compared to arid settings closer to the equator. Brine freezing

and mixing, rather than direct solar concentration, plays a much more important role in the crystallisation of most cold climate salts (Carlson et al., 1990; Marion et al., 1999).

Salt-accumulating continental depressions typically define the discharge areas of endorheic (internal drainage) basins; these are areas where more water is leaving the via evaporation than entering as rainfall, snowmelt, surface, or subsurface inflow (Table 2.1). They are found in: 1) tectonic basins, which include fault-defined intermontane basins and intracratonic structural sags, 2) interdune or inter-draa depressions about the edges of sand seas or ergs, 3) wind-deflation hollows, 4) abandoned fluvial valleys 5) bolide-impact or volcanic craters, or 6) interior drainage depressions created by a combination of the preceding. The greatest volumes of desert salts today accumulate within arid to hyperarid depressions in continental rifts, compressional sags and transforms.

Climate drives evaporite deposition at scales ranging from broad latitudinal belts (100s km) down to microclimates (cms; Table 2.2). At the broadest scale, evaporites in deserts are the result of large-scale atmospheric circulation. Modern deserts cover more than 30% of the world's landsurface, mostly within two belts lying 15° to 45° north and south of the equator (Figure 2.1b). Belts of aridity sit beneath cold dry descending air masses of the Hadley Cells, which define high-pressure belts known as the subtropical Trade-Wind Belts or Horse Latitudes. Global-scale atmospheric circulation is driven by varying intensities of solar irradiation, which is most intense directly above the equator and lessens toward the poles (Figure 2.1c). Hence, the equatorial belt experiences greater insolation than the adjacent temperate latitudes. Equatorial air warms as it rises, creating a tropical belt of low pressure. As it rises it cools, losing most of the water vapour as rainfall to the tropical jungles and rainforests below. This now moisture-depleted air moves up and away from the equator and further cools and compresses. Finally, it sinks back to the earth's surface at around 30° latitude north and south of the equator. The cool descending dry air is reheated as it returns to the lower atmosphere, garnering an enhanced potential to absorb moisture, and so the major desert belts of the world are created (Figure 2.1c).

Earth-scale distribution of Holocene climatic belts reflects current atmospheric dynamics. When the icecaps expand the circulation belts are pushed and compressed toward the equator and they have done so numerous times in glacial maxima of the current icehouse climate mode. This increases the intensity

^{2.1} Semi-arid deserts have a mean annual precipitation of between 250 and 500 mm. Arid deserts have less than 250 mm of annual rainfall. Extremely arid or hyperarid deserts have at least 12 consecutive months without rainfall.

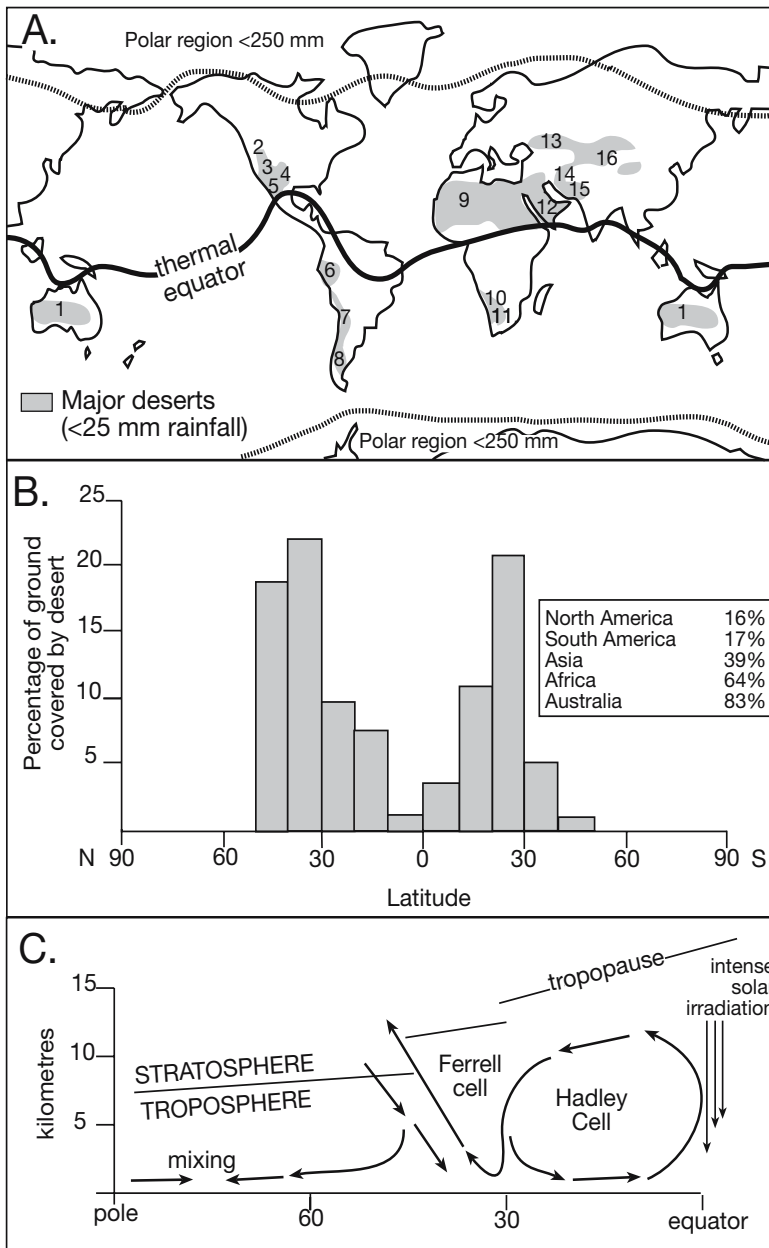


Figure 2.1. A) World distribution of modern deserts as determined by plotting areas with less than 250 mm annual precipitation. 1. Australian, 2. Great Basin, 3. Mojave (Sonoran), 4. Chihuahuan, 5. Baja California, 6. Peruvian, 7. Atacama (Chilean), 8. Patagonian, 9. Sahara, 10. Namibian, 11. Kalahari, 12. Arabian, 13. Turkestan, 14. Iranian, 15. Thar, 16. Gobi. Also shows polar regions with less than 25 cm precipitation. B) Latitudinal distribution of the world's modern deserts. Inset gives proportion of each continent that is arid or semiarid. C) Longitudinal cross section through the earth's atmosphere showing major circulation cells. Belts of cool dry descending air at 30° N and S of the equator create the main arid zones of the world (after Warren, 1989).

of circulation and alters the latitudinal distribution of climate belts. It has a marked effect on climate in Quaternary deserts, so that almost all modern continental playas in the Horse Latitudes have experienced numerous water-full versus dry stages in the last few hundred thousand years.

For example, the strontium-isotopic composition of preserved gypsum in Lake Frome, a large discharge playa in South Australia, records periods of high rainfall at 3-6, 12-15, and >17 Ka, and drier periods at ≈ 10 and ≈ 17 Ka (Ullman and Collerson, 1994). In the last interglacial (early in oxygen isotope stage 5) a nearby and much enlarged Lake Eyre maintained a perennial freshened water body upto 25 m deep (Magee et al., 1995). Subsequently, as climate deteriorated into glacial mode, there were a number of dry periods separating successively less effective wet phases, culminating in the deposition of a substantial halite salt crust around the time of the last glacial maximum. Lake Eyre only attained its present saline mudflat/ephemeral playa status some 3-4 Ka. The drying trend over the last hundred thousand years in Lake Eyre corresponds to a longterm lessening of monsoon intensity in the northern part of Australia, which is the main source area for waters flowing into the lake depression.

In Death Valley, USA, there were dry mudflats, characterised by abundant glauberite, gypsum and minor calcite from 0-10 Ka and 60-100 Ka (Li et al., 1997). In contrast, the wet period from 10-60 Ka was typified by halite and mud layers, with relatively abundant calcite. It encompasses sediments deposited 10-35 Ka, when Death Valley contained a perennial halite lake. This change matches a predominately Na-Ca spring-fed inflow during dry climatic periods and increased volumes of bicarbonate-rich river waters in the wetter periods.

Local topography induces variation in climate that can drive desert and playa formation. For example, the playas and midlatitude deserts of central Asia and central Australia are in part a product of their isolation from the nearest ocean. Continentality is the term that describes the geographic isolation of a desert by its large distance from the ocean. It explains why the highly continental Takla Makan Desert of central China is a hyperarid desert at 50°N latitude, well north of the world's subtropical high pressure belts. The other factor helping form this type of desert is the rain shadow effect.

Rain shadow deserts, also known as adiabatic deserts, form where air masses move up and over mountain ranges (Figure

2.2a). As air rises over a mountain range it cools, moisture develops into clouds and falls as rain on the side of the mountain range facing into the prevailing wind. Subsiding air on the other side of the range is dry and its moisture-bearing capacity increases further as it sinks and warms. For example, the deserts of Patagonia lie on the lee side of the Andes, while the deserts of Nevada and Utah are in the rain shadow of the Sierra Nevada. Adiabatic deserts can also be found behind the Himalayas, the Ethiopian uplands and Eastern Highlands of Australia. Extreme examples include the Dead Sea rift and the Afar depression, both areas are subsealevel depressions surrounded by high mountain ranges of the rift rim. Rain shadow effects increase where the region inland of the mountains lacks relief.

	Region	Location and setting	Notable evaporite features
Africa	East	Continental Danakil Depression, Lake Magadi, Lake Natron, Lake Kivu, Lake Tanganyika, Lake Turkana, Lake Urmia	Continental evaporites. In addition to large volumes of halite and CaSO_4 , potash salts and trona are important salts in particular lakes with mineral evolution dependent on inflow chemistry.
	North	Continental Saharan ergs, Lake Chad, chotts of northern Africa	Sodium carbonate is the dominant primary mineral in Lake Chad, while sodium sulphate and sodium chloride occur in subordinate amounts. Potassium and magnesium salts occur in near negligible amounts.
		Coastal Coastal sabkhas and salinas of Algeria, Tunisia, Libya, Morocco, the Nile delta and the Red Sea	Coastal sabkhas and salinas dominated by gypsum and anhydrite with small volumes of potash in modern chotts and sabkhas of Tunisia.
	Southern	Continental Pretoria, Otjiwalundo and other salt pans, interdunal sabkhas of Namibia	Thousands of small wind-aligned salt pans, often with downwind lunettes, dot the arid landsurface. They form preferentially on a clayey substrate that is made up of the Ecca and Dwyka Shales in South Africa, the Karoo in Namibia and the Kalahari Beds in Botswana.
	Middle East	Continental Rub al Khali ergs, Dead Sea evaporites	Dead Sea is accumulating pan halite in the shallow southern basin, along with carbonate laminites and massive halite in the deepwater northern basin.
Coastal Coastal sabkhas and salinas of the Arabian Gulf		Nodular calcium sulphate with minor halite in classic coastal sabkha successions of Abu Dhabi, Saudi Arabia and Kuwait.	
Antarctica	Continental Lake Bonney, Taylor Valley; Lake Vanda, Wright Valley, Organic Lake, Deep Lake and Ekho Lake in the Vestfold Hills.	Aragonite in the Taylor Valley and the Vestfold Hills. Sulphate minerals predominate in the Wright Valley. Halite and mirabilite are widespread (brine freezing). Trona and thermonatrite in the East Taylor Valley, and soda nitre, bloedite, and darapskite in the Wright Valley. Antarctite ($\text{CaCl}_2 \cdot 6\text{H}_2\text{O}$) in Don Juan Pond.	
Asia	Central	Continental Qaidam Basin, Gulf of Kara Bogaz, Lake Inder	Potash salts (especially carnallite) are accumulating as karstic fills in bedded halite in perennial lakes and playas of the Qaidam Basin. Borates occur in Lake Inder.
	Southern	Continental Iranian playas; Van Golü, Salda Golü and Tuz Golü, Turkey; Didwana Lake and other playas of Thar desert	Iranian playas show complex facies interactions with rising salt diapirs. Turkish lakes are accumulating large volumes of magnesium carbonate and dolomite.
		Coastal Coastal sabkhas of Ranns of Kutch, India	Gypsum and halite sabkhas, widespread fluidization textures from earthquakes.

Table 2.1. Quaternary examples of evaporite accumulations in various deserts.

	Region	Location and setting	Notable evaporite features
Australia	Eastern	Continental Lake Tyrell, Lake George, Maar Lakes, Lake Victoria	Continental salt lakes (playas), some with gypsum/clay lunettes that rim brine pans; others, especially in volcanic maars, are characterised by Mg-rich carbonate sediments and crusts.
	Central	Continental Lake Amadeus (Karinga Creek lakes), Lake Eyre, Lake Frome, Lake Torrens Simpson and Victoria deserts	Continental salt lakes (playas), typically with gypsum lunettes that rim the deposit's brine pan. Many lunettes were more active in the Late Pleistocene. Salt crusts are now largely recycling through the lakes, with no massive accumulations. There is a fresher artesian aquifer beneath many continental lakes. Mostly halite and gypsum accumulate in the lakes, minor thermadite/mirabilite accumulating in the Karinga Creek area.
		Coastal Marion Lake complex, Lake Macdonnell, Streaky Bay Lakes, Fisherman Point sabkhas	Coastal lakes or salinas are classic Holocene areas for coarse-grained gypsum beds up to 10-15m thick, pisolite seepage pavements, modern tepees, mm-laminated domal stromatolites.
	Western	Continental Lake Lefroy, Lake Cowan, Lake Dundas, Lake Ballard, Lake Carey, Lake Raeside	Continental playa lakes within elongate and sinuous Tertiary palaeodrainages on the Yilgarn Craton. Evaporitic fill in the lakes is upto 10 m thick and mostly gypsum with lesser halite. Wind and wave-driven currents rework sediments that are then deflated by the wind to be redeposited in marginal gypsum dunes (lunettes).
Coastal Lake McLeod, Hutt Lagoon, Leeman Lagoon		Coastal lakes or salinas with gypsum and halite in beds up to 10-15m thick in Lake McLeod.	
Europe	Spain	Continental Playas of Los Monegros and Bajo Aragon, Laguna de Tirez in La Mancha	Glauberite and other sodium sulphates accumulating in modern playas.
Americas	Central Canada	Continental Ceylon Lake, Freefight Lake, Deadmoose Lake, Little Manitou Lake and many other saline lakes and playas on the Great Plain of central Canada	Salt pan and perennial subaqueous evaporites containing mirabilite, thenardite, and bloedite. Some lakes, such as Freefight and Deadmoose, are accumulating salts in perennial "deep" waters (10-30m).
	Northern USA	Continental Saline lakes and interdunal sabkhas, Nebraska and North Dakota. Draas of the southwest USA	Salt pans containing sodium sulphate salts, as in Central Canada.
	Southern USA	Continental Salt Flat playa, west Texas; playas in Rio Grande Rift	Pleistocene continental lacustrine accumulations of mostly gypsum±halite, now deflated and overprinted by Holocene sabkha signatures.
		Coastal Laguna Madre	Coastal mudflats with displacive gypsum.
	Western USA	Continental (Basin and Range) Death Valley, Saline Valley, Deep Springs lake, Searles Lake, Bristol Dry Lake, Great Salt Lake, Owens Lake, Salton Sea	Quaternary continental lakes with diverse range of salts including thick halites, lesser anhydrite, trona, glauberite and other salts depending on chemistry of inflow waters. Holocene is a time of saline mudflats, at other times in the Pleistocene the depressions were beneath the waters of a saline/brackish lake.
South Americas	Continental Salar de Atacama, Salar Uyuni, Salar Coipasa, Pastos Grandes, Laguna Salinas, Salar de Pintados	Large volumes of continental evaporites accumulated within the central Andes during Neogene uplift of the Altiplano-Puna plateau with associated development of the Andean volcanic arc. Halite and gypsum are dominant minerals, along with local and economically important borates, nitrates and potash salts.	
	Coastal Bocana de Virilá, Peru	Large volumes of marine-fed estuarine evaporites in a drowned river valley.	

Table 2.1 continued. Quaternary examples of evaporite accumulations in various deserts.

Rainshadow deserts and bedded evaporites are often part of a longer term tectonic association between sedimentation and

climate in both extensional and compressional settings and are a climatic response independent of whether the earth is in

greenhouse or icehouse climate mode (Hay, 1996). Over millions of years, the rifting of continental blocks involves broad upwarping, followed by subsidence of a central valley and uplift of marginal shoulders. The result is an evolving regional climate-sediment association that is repeated many times in the Phanerozoic: first a vapour-trapping arch with centripetal fluvial drainage forms. This is followed by a rift valley, first with fresh-water lakes, culminating in an arid subsealevel evaporitic rift bordered by mountains intercepting incoming precipitation (adiabatic desert). Convergence tectonics also affects climate on a large scale. A rising mountain range is a barrier to atmospheric circulation, especially if perpendicular to the incoming circulation. The uplift of the Tibetan Plateau in the Late Tertiary created an easterly jet stream, which now flows from Tibet across the Arabian Peninsula toward Somalia. This stream of dry air accentuated the existing aridity and created an adiabatic desert that lies almost on the Equator. In the past both extensional sag and compressional tectonism have helped induce hyperaridity atop large subsealevel seepage depressions, which were capable of accumulating thick halite and gypsum successions (Figure 5.27).

Upwelling ocean waters off continental landmasses in the trade wind belts favour coastal deserts. Cold upwelling ocean water creates a belt of coast-parallel cool water. And, as evaporation is a function of heating, cold offshore oceans provide less moisture and less cloud to the adjacent land. The cool air above creates relatively dry onshore winds. As this colder air moves across the land it is heated, so developing an increased capacity to absorb rather than shed moisture (Figure 2.2b).

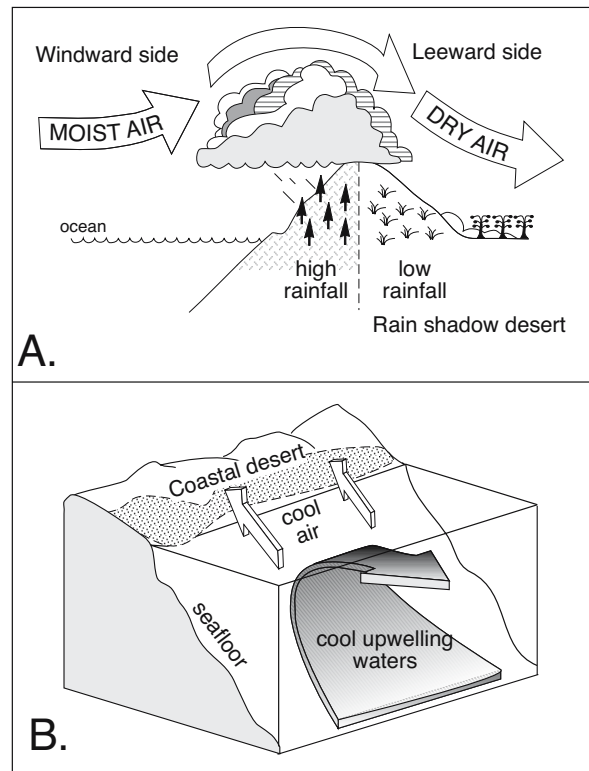


Figure 2.2 Local controls on deserts. A) Adiabatic or rain shadow desert where rain tends to fall on the seaward side of the mountains. B) Coastal deserts form in response to cool upwelling ocean waters and the cool dry onshore winds warming as they pass overland.

Cause	Locations	Examples
Descending or stagnant air mass	Subtropical regions. Regions beneath the descending limbs of Hadley cells (centred around 20-30° north and south of the Equator.	Sahara, Namibia, Kalahari (Africa) Chihuahuan and Sonoran (North America) Great Sandy and Simpson deserts (Australia) Arabian, Iranian, Thar deserts (Middle East and India)
Continentality	Regions within the continental interior. Locations isolated by distance from moisture sources, principally the oceans.	Saharan (Africa) Turkestan, Talimaklan, Gobi (Asia) Great Basin (North America)
Adiabatic or Rainshadow	Regions located in the lee of topographic barriers, such as mountains and plateaus. Cooling of rising airmass creates rainfall on the windward/ seaward side of a mountain range or barrier. As airmass subsides on the leeward side it warms and dries.	Turkestan, Talimaklan (Asia) Great Basin, Colorado Plateau (North America) Monte, Patagonian (South America)
Cool sea surface temperatures	Continental regions adjacent to cool (upwelling) seawater zones. The amount of moisture evaporated from the ocean surface is less under cooler conditions, so yielding drier air. Cooler sea surface temperatures also stabilize air masses, reducing convective rainfall.	Western Sahara, Namibia (Africa) Peruvian, Atacama, (South America) Rub'Al Khali (Saudi Arabia)

Table 2.2 Causes of modern deserts. (see Figure 2.1a for locations), typically more than one factor drives desertification.

Offshore, these cool strips of water are frequently engulfed in winter sea fogs, created by a blanket of warmer air atop cold seawater. Such cold upwelling ocean currents account for the deserts of Baja California and the Namib of southwest Africa (Benguela Current). The Peru Current, as it upwells along the west coast of South America, helps maintain hyperaridity in the Atacama Desert of Chile, which receives around 1 mm of rain every 5-20 years making it the driest desert in the world.

Fog, rather than rain, is the main supplier of moisture to coastal deserts in such areas and it also moderates the coastal air temperature. A range of unusual desert plants and animals have evolved behaviours and physical adaptations to make maximum use of this foggy water. For example, in the early morning some Namibian desert insects with water-capturing fluted carapaces stand on the coastal dunes with sails-high to collect condensation from foggy onshore morning breezes.

The present western edges of most tropical or Trade Wind deserts are washed by cool ocean currents driven by large scale ocean gyres, which rotate anticlockwise in the Southern Hemisphere and clockwise in the Northern Hemisphere. Throughout much of the Phanerozoic, coastal deserts in ancient trade wind belts, indicated by eolian dunes and evaporites, have characterised the western sides of continents (Hay, 1996).

At finer climatic scales, variations in effective evaporation rates influence salinity of any brine body or pore waters in nearby mudflats/sandflats. This in turn influences mineralogy and the preservation potential of precipitated salts. Water vapour pressure over a free-standing brine decreases with increasing salinity. Saturated water vapour pressure over any salt solution is always lower than the vapour pressure of pure water at a given temperature. This is due to the binding of water molecules into hydration sheaths about the various charged ions dissolved in the brine. As the concentration of a surface brine increases, the water vapour pressure decreases in the overlying air mass, reaching its lowest value when the brine is saturated (Kinsman, 1976). At very high salinities the pressure difference between the brine and the air immediately above the brine can become so small that evaporation effectively shuts down and the higher salinities necessary to precipitate the bitter salts may not be reached (Figure 2.3a).

Aerodynamically, the evaporation rate of a surface brine is the product of wind velocity and the difference in water vapour pressure between the main air mass and the air above the surface of the evaporating brine. Complete humidity-induced shutdowns are rare as the air above an evaporating brine body is usually

in continual motion, driven by adiabatic, catabaric and onshore breezes. Salinity of a freestanding brine is a function of wind speed, surface roughness and atmospheric stability in the air above the brine (Figure 2.3; Myers and Bonython, 1958).

Elevated above-brine humidity and limited lateral extent (tens of kilometres) creates a natural buffer to evaporation above modern coastal lakes or sabkhas. Lower salinity evaporites, gypsum and halite, are the dominant precipitates in modern coastal lakes beneath humid marine air, such as the coastal pans of the Saudi Gulf coast and the coastal salinas of southern and western Australia. Gypsum with minor anhydrite is the dominant salt in both the capillary zone and the phreatic zone of most modern arid coastal hydrologies such as the sabkhas of Abu Dhabi (Kinsman, 1976). Any efflorescences or crusts of bitter salts cannot last long, and are recycled or washed away by occasional rainstorms and sheet floods.

Evaporitic shutdown will have an interesting effect on the currently falling water level of the Dead Sea basin. Asmar and Ergenzinger (1999) conclude that the actual evaporation rate of the surface brines in the Dead Sea will become zero at a salinity of 483 - 486 g/l. As water loss can then no longer be driven by evaporation, the currently falling Dead Sea level should stabilise when currently increasing salinities reach this level (Figure 2.3b). The evaporation rate data were calculated using a modified Penman method and were fitted as a function of salinity, where salinity (S) is in g/l and evaporation rate (E) is in mm/year. The relationship is

$$E = 1826.1 - 1.6405S + 0.0116S^2 - 3 \times 10^{-5}S^3$$

Asmar and Ergenzinger emphasize that this equation is an estimate and should be used with caution.

Intrabasin variations in temperature and effective evaporation influence the volume and mineralogy of precipitated sediments and there is often a feedback between these various factors. For example, there is a decrease in the efficiency of capillary evaporation wherever a white salt crust covers the surface of a saline mudflat. The decrease is not just related to a humidity increase in the air above the mudflat, but also to the increased albedo (reflectance) created by the white surface of the salt crust. The amount of short-wave radiation absorbed by any soil surface is largely a function of its albedo (a measure of the amount of light reflected). It varies from 0.2 (20%) for a water saturated soil surface to 0.75 (75%) for a salt-encrusted surface (Malek et al., 1990). A salt-encrusted mudflat on a clear calm sunny day makes use of only a quarter of the incoming energy

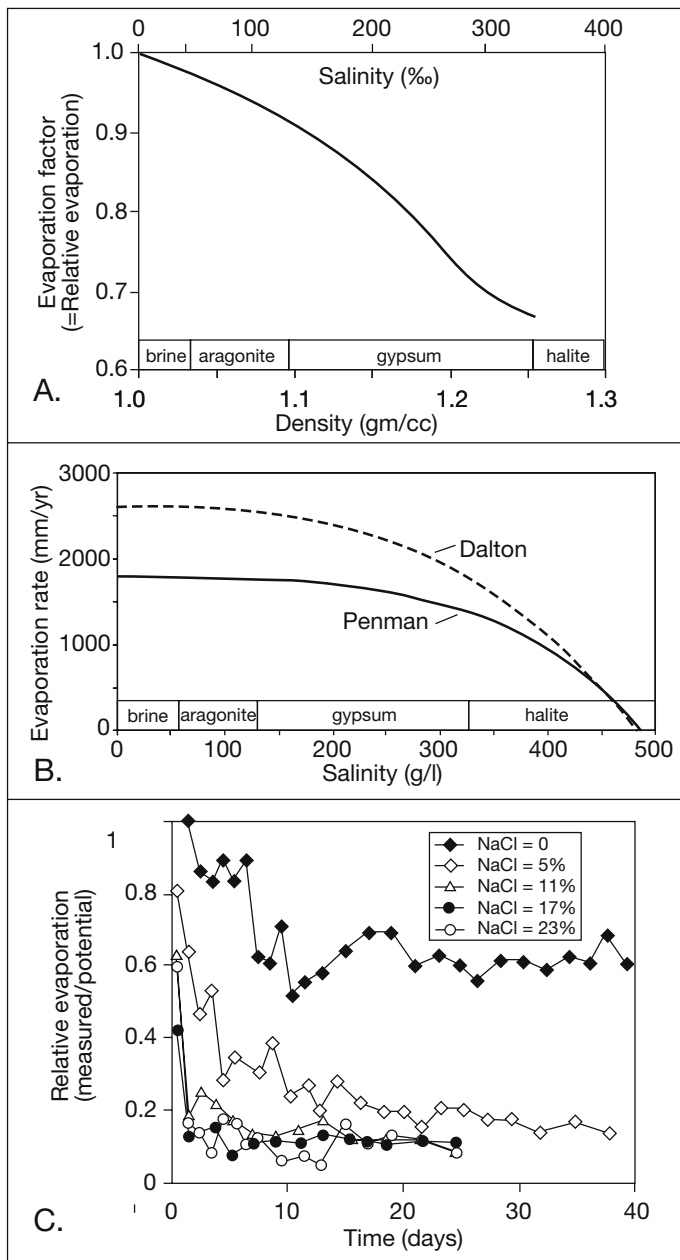


Figure 2.3. Evaporation and salinity. A) Evaporation efficiency decreases as salinity/density of the surface brine increases. Evaporation factor is applied to measured pan evaporation to attain a more realistic estimate. For example, a brine with a salinity around 200‰ has an actual evaporation rate that is only 85% of the measured evaporation rate (after Myers and Bonython, 1958). B) Effect of salinity on evaporation rates in the Dead Sea using the predictive formulae of Penman or Dalton (after Asmar and Ergenzinger, 1999). C) Effect of salt crust formation on the relative evaporation (measured evaporation rate/potential pan evaporation) with waters of variable concentration lying beneath the subaerial crust (after Newson and Fahey, 2003).

(drives evaporation) compared to a damp crust-free seepage mudflat. For the same reason, sediment below a white salt crust will stay moister for longer in the absence of ongoing inflow/seepage.

To quantify the effects of salt crust formation on evaporation rate, Newson and Fahey (2003) conducted a series of laboratory evaporation experiments using artificial soils saturated by water with various NaCl contents ranging from freshwater to concentrations of 23% (mass salt/mass solution). Their aim was to develop an understanding of salt crust formation in order to increase the efficiency of desiccation in mine tailing dams and so improve remediation efficiency. But their results are pertinent to the hydrology of any salt-crust mudflat. Relative evaporation (ratio of actual to pan evaporation) for the freshwater system fell to about 0.6 after about 10 days, and then remained near constant (this indicates capillary equilibrium with fresh water in pores = no salt crust). However, for all other experimental runs using saline water of varying initial concentrations, the relative evaporation ratio was much lower, and once the salt crusts had formed consistently reached values around 0.1–0.2 of potential freshwater evaporation rates (Figure 2.3c). For the high concentration pore waters the reduction occurred almost immediately, and somewhat more slowly for the starting solution with the lowest NaCl concentration ($C = 5\%$). Their results indicate that even a moderate amount of salinity in any feed brine in a semi-arid to arid setting will quickly form a salt crust that severely reduces the relative evaporation rate above the crust.

Their experimental data compares well with observations made for salt-encrusted surfaces on playas and salt lakes around the world. Natural salt encrusted mudflats typically display relative evaporations of the order of 0.03–0.2, for potential evaporation rates of 1.5–3.5 m/year (Malek et al., 1990). For example, the measured effective evaporation rates above salt-free mudflats in Lake Frome, Australia range from 90 to 230 mm/year and average 170 mm/year (Allison and Barnes, 1985). In areas in the same lake covered by white salt crusts the effective evaporation rate falls to 5–30 mm/year (equivalent to relative evaporation of 0.03–0.18; Ullman, 1995).

Newly formed salt crusts are porous, variably buckled layers (pressure ridges and petees) that lack direct contact with the underlying sediment over at least 50% of the crust base (Newson and Fahey, 2003). Air-filled cavities reduce areas beneath the crust where capillary moisture can be transferred in a liquid phase through the salt crust to the air during evaporation. Coupled with this, the high porosity and broader pore throats in newly-formed salt crust, drastically reduces the rate of capillary rise of water compared to a clay or mud and so further reduces the liquid phase continuity to the crust/air interface. Once a crust forms, the only widespread effective mechanism for moisture transfer from the underlying mud to the overlying air mass is by diffusion in the vapour phase. This means mechanisms involved in reduction of the effective evaporation rate from any salt-encrusted mudflat are varying combinations of; 1) an increase in albedo, 2) resistance to moisture transfer and, 3) a decrease in the saturation vapour pressure of the pore fluid.

In a brine pool-entraining modern playa there is substantial cross-playa variation in effective evaporation rate depending on sediment type, proximity of the water table to the landsurface, the presence or absence of salt crusts and the permanence of surface brine sheets. An excellent set of data illustrating this complexity was collected during 1993-1996 in Owens Lake, California using monitored lysimeters and evaporation pans (Figure 2.4; Tyler et al., 1997). Measurements were not made during the period autumn (fall) 1994 to winter 1995 due to playa-wide flooding that marked the end of a long drought period. Rain preceded each summer and autumn measurement period in 1993 and 1994 by at least 15 days and was not significant (1 mm or less). Spring measurements may have been

influenced by prior rainfall, with 3 mm falling 1 day before the 1994 measurements and 19 mm falling 21 days before the 1995 measurements.

Figure 2.4 plots the averaged daily evaporation rate as a function of season of measurement from the three study areas in Owens Lake (sandflat, mudflat and free surface brine; Tyler et al., 1997). Evaporation from the sandflat appears to steadily decline from initial measurements in summer 1993 to autumn (fall) 94 and may reflect the prolonged drought and subsequent decline of the water table in this area. In contrast, evaporation from the salt-crust mudflat shows similar summer rates in 1993 and 1994. The insensitivity to drought in these saline clayey soils may be related to the continued high water contents maintained by capillary rise to elevations well above the water table. The mudflat site also shows highest evaporation rates during spring periods (0.5 mm day^{-1}), when near-surface soil moisture is at its highest level. During these periods, the overlying salt crust is less desiccated and so may also maintain better hydraulic contact with the underlying sediments.

Malek et al. (1990) postulated that loss of hydraulic contact between lake sediment and an overlying salt crust impedes capillary evaporation loss by effectively forming the equivalent to a mulch layer over the clayey substrate. During both spring measurement periods in Owens Lake, no decline in evaporation rate was observed throughout the period of measurement, suggesting that rain before the measurement dates had little influence on the evaporation rates. Winter evaporation rates were slightly higher than those recorded during the autumn months, although they are similar. The winter measurement period was

characterized by warmer than average daytime temperatures, which may have slightly increased the evaporation rates. However, wind conditions were uncharacteristically calm, with maximum daily wind speeds rarely exceeding 1 m s^{-1} , which may have reduced the evaporative flux.

Rates measured in the brine pool in spring 1994 were below those in the previous summer, owing to lower temperatures and decreased net radiation (Tyler et al., 1997). However, evaporation in the brine pool area in the following summer and autumn of 94 were much lower than expected for a free-standing saline water body. The

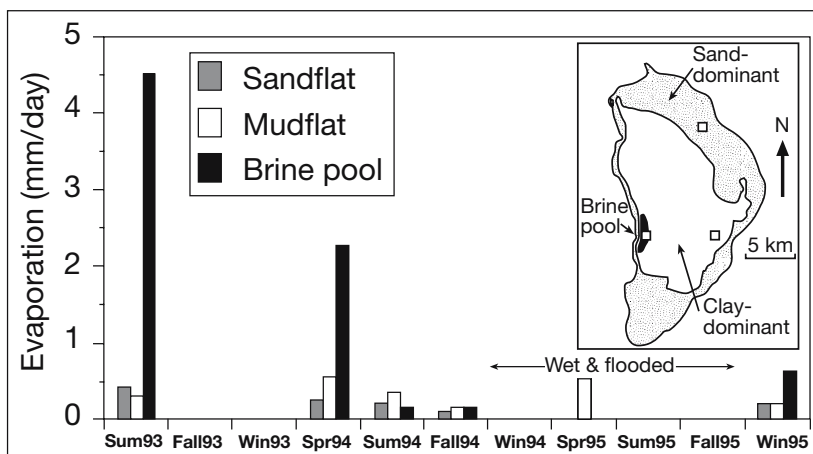


Figure 2.4. Seasonally measured evaporation from the three dominant types of surface sediment in Owens Lake, California. Squares in the inset map show monitored sites (after Tyler et al., 1997).

dramatic reduction in evaporation in 94 was due to a thin (less than 2 mm) floating crust of halite rafts that covered the entire extent of the brine pool. Both periods of measurements in the brine pool were characterized by calm conditions, which allowed the crust to remain intact and effectively cut off evaporation. Winter evaporation rates over the raft-covered brine pool averaged 0.6 mm day^{-1} , almost an order of magnitude below that measured during the raft-free summer of 1993. Rafted crusts are a part of the evaporation setting of most halite-saturated brine pools/sheets and are another reason why brine sheets remain for extended periods in some salt lakes. Surface water sheets in nearby less saline raft-free lakes tend to dry much more quickly. Rafts generally break up and sink or are washed to the lake shore during windy periods.

Yearly estimates of groundwater evaporation from the three dominant surface areas in Owens Lake (sandflat, mudflat, brine pool) were calculated by Tyler et al. (1997) using the data shown in Figure 2.4. Yearly average evaporation was taken as the arithmetic average of the four seasonal rates for each area. For both the sandflat and mudflat areas, autumn rates were well below those measured in the spring, implying that evaporation is more strongly controlled by groundwater conditions rather than potential evaporation rates above the sedimentation surface. Groundwater levels tend to decline in late summer and autumn, owing to evaporative demand, and therefore it is conceivable that winter rates, when the water table is nearer the lake floor, may actually exceed autumn rates. The coincidence of a prolonged drought (1993 to fall 1994) with the main measurement period appears to have affected evaporative flux in both the sandflat area and the brine pool. Consecutive summer measurement of evaporation at both these sites showed a considerable decrease owing to drought conditions. For this reason, summer evaporation rates from 1993 were considered more representative and used to estimate the yearly evaporation from the sandflat to produce a more representative average annual evaporation. At the brine pool site, autumn rates were assumed to be equal to those measured in spring 1994, when open raft-free water was extensive. Using this approach, the seasonally adjusted annual evaporation rate from the sand-dominated areas was $\approx 88 \pm 22 \text{ mm year}^{-1}$. Clay-salt crust-dominated (sabkha) regions in Owens Lake have an evaporation rate $\approx 104 \pm 26 \text{ mm year}^{-1}$. Yearly evaporation from the brine pool surface was $\approx 872 \pm 218 \text{ mm year}^{-1}$ although this is substantially less whenever a cover of salt rafts floats at the air-brine interface.

All these local climatic effects combine to make the high salinities needed to precipitate bittern salts unlikely in most modern marine-fed hypersaline settings. To produce and accu-

mulate primary bittern salts, like carnallite, sylvite and kieserite, to where they constitute a bed, rather than an efflorescent crust, requires a degree of aridity so extreme that it is difficult to envision it as a large-scale process in any modern marine-fed setting and even contemporary continental examples are rare. For example, carnallite is a precipitate in saltwork pans of the Dead Sea where it is the end result of anthropogenic management of fractionated brines (Figure 11.10). The only substantial natural Holocene potash accumulation is a syndepositional karst fill in bedded halites of the Qaidam Basin of western China, located some 1500 km from the nearest ocean. Even there, the potash ultimately comes from reworked subcropping Plio-Miocene potash evaporites. One must go to pre-Quaternary sediments to understand how a widespread potash bed can accumulate with a lateral extent measured in tens to hundreds of kilometres and thicknesses measured in metres (Chapters 5 and 11).

Chemical evolution of surface and nearsurface brines

Until recently, most geologists assumed ancient marine evaporites were precipitated from seawater brines with chemical make-ups very similar to that of today. Now, there is a growing body of evidence that the ionic make-up of Phanerozoic seawater has varied to where magnesium sulphate was not always a dominant bittern precipitate. In modern seawater bitters, it is. As well, varying intensities of evaporite dissolution, dolomite precipitation and hydrothermal flushing contributed varying ionic proportions to the brine feed of ancient salt systems (Hardie, 1984, 1991). This leads to a dilemma in deciding what is marine, what is nonmarine and what is a hybrid brine, based on mineralogical suites found in ancient bedded evaporites.

Marine brines

Chemical composition and phase chemistry

Today the chemical make-up and the proportions of the major ions in seawater are near constant in all the world's oceans. Seawater is dominated by Na and Cl, with lesser amounts of SO_4 , Mg, Ca, K, CO_3 and HCO_3 . Using the brine classification of Eugster and Hardie (1978), modern seawater is a Na-(Mg)-Cl-(SO_4) water, with a density of 1.03 gm/cc and a salinity of $35 \pm 2\%$. When seawater evaporates, a predictable suite of primary evaporite salts crystallise from increasingly concentrated hypersaline waters (Figure 2.5; Table 2.3). The sequence of marine precipitates was first documented by Usiglio

	Brine Stage	Mineral Precipitate	Salinity (‰)	Degree Evap.	Water Loss (%)	Density (gm/cc)
	Normal marine or euhaline	Skeletal carbonate	35-37	1x	0	1.040
Hypersaline	Mesohaline or vitahaline	Alkaline earth carbonates	37 to 140	1-4x	0-75	1.040-1.100
	Penesaline	CaSO ₄ (gypsum/anhydrite)	140 to 250	4-7	75-85	1.10-1.126
		CaSO ₄ ± Halite	250 to 350	7-11x	85-90	1.126-1.214
	Supersaline	Halite (NaCl)	>350	>11x	>90	>1.214
Bittern salts (K-Mg salts)		Extreme and variable	>60x	≈99	>1.290	

Table 2.3. Salinity based classification of mineral paragenesis and brine properties based on concentrated seawater. Hypersaline is defined as >35‰. Biologists working in saline waters use a somewhat different classification of; fresh water (less than 1‰), subsaline (1-3‰), hyposaline (3-20‰), mesosaline (20-50‰), and hypersaline (greater than 50‰). Geohydrologists tend to refer to fresh water as less than 1‰, brackish water as 1-10‰, saline water as 10-100‰, and brine as greater than 100‰.

(1849), while later work by Carpenter (1978) and McCaffrey et al. (1987) focused on the details of the evolving chemistry of the residual bitterns as the various supersaline salts precipitate (Figure 2.5).

As seawater concentrates, the first mineral to precipitate is CaCO₃, usually as aragonite. This begins in mesohaline waters where the brine reaches twice the concentration of seawater (40 to 60‰) and achieves a density ≈1.10 gm/cc. As the brine continues to concentrate and approaches four to five times the concentration of seawater, that is 130 to 160‰, gypsum precipitates from penesaline waters with densities around 1.13 gm/cc (Figure 2.6a). At 10 to 12 times the original seawater concentration (340 to 360‰) and densities around 1.22 gm/cc, halite drops out of supersaline marine waters. After halite, the bittern salts (potassium or magnesium sulphates/chlorides)

precipitate from supersaline waters at concentrations that are more than 70-90 times that of the original seawater. Carnallite and epsomite are the dominant bittern precipitates from modern marine brines. Brine density by this stage of concentration is in excess of 1.30 gm/cc and brine viscosity and feel approach that of olive oil (Figure 2.6b).

Modern coastal lagoonal systems do not naturally attain high salinities until the surface (hydrographic) connection to the ocean is lost and they evolve into marine-seepage groundwater sinks (Figure 5.28). Brines then evolve into mesohaline to penesaline waters with seawater-like (thalassic) ionic proportions (Table 2.4).

Ongoing evaporation of seawater produces two types of high density, high viscosity brine: Na-Cl brines and Mg-Cl-SO₄

Locality	Salinity (‰)	Na	Mg	Ca	K	Cl	SO ₄	HCO ₃	Br
Solar Lake, Sinai	70	890	99	21	19	1040	53	3	2
	146	1815	205	47	30	2189	37	4	-
Ras Mohammad, Sinai	244	3394	391	12	72	3903	147	3	5
	Bardawil Coastal, Sinai	140	1857	197	8	43	2146	31	0.8
		4219	712	28	143	4625	232	5.8	11
Bardawil Inland, Sinai	140	1666	193	31	3	1775	3	0.3	2
		4035	1088	693	92	5124	129	3.5	11
Christmas Island ponds	21	279	27	7	5	331	19	-	-
	247	1893	213	17	34	3490	48	-	-
Lake Hayward, Australia	214	3053	90	23	52	3569	106	-	-
Mangrove Lake, Caribbean	32	-	-	9	-	480	24	3	-
Seawater (average)	35	468	53	10	10	546	28	2	1
River water (average)	0.11	0.31	0.15	0.37	0.04	0.23	0.12	0.89	-

Table 2.4. Examples of the hydrogeochemical make-up of some marine-fed brine systems, salinity is expressed in ‰ and ions in mmol/kg (see Chapters 3 and 4 for discussion of the geology of marine-fed systems).

brines. Na-Cl brines dominate in the salinity range 35-330‰. Brines become progressively dominated by Mg-Cl-SO₄ at higher salinities, indicating preferential removal of Na by halite precipitation. At first, Mg is the dominant cation in the bittern brines, but as the various MgSO₄ bitterns crystallise its place is taken by K. Chlorine remains the dominant anion throughout the evaporation sequence (Figure 2.5).

Much of the field and laboratory work done on evaporating water has been done in closed conditions. Usiglio (1849) simply took a container of seawater and monitored its progress as he evaporated it to complete dryness. McCaffrey et al. (1987) studied the evolution of seawater in a series of man-made salt ponds in the Bahamas and supplemented this with laboratory work at higher salinities and densities not found in the ponds. Ideally, after depositing gypsum and halite, supersaline seawater evaporated to complete dryness deposits a predictable suite of Mg and K sulphate minerals (Usiglio, 1849). However when one tries to compare the suite of bittern salts seen in ancient marine evaporites to modern bitterns there are some obvious discrepancies. These problems can be addressed at varying levels of chemical, hydrological and chronological complexity. In the end many of the discrepancies can be related to the simple statement, "In nature, there is no such thing as a totally closed static system."

One of the first to attempt to deal with the chemical discrepancies between a modern seawater precipitation suite and the bittern suites seen in the Permian Zechstein salts of the Stassfurt β

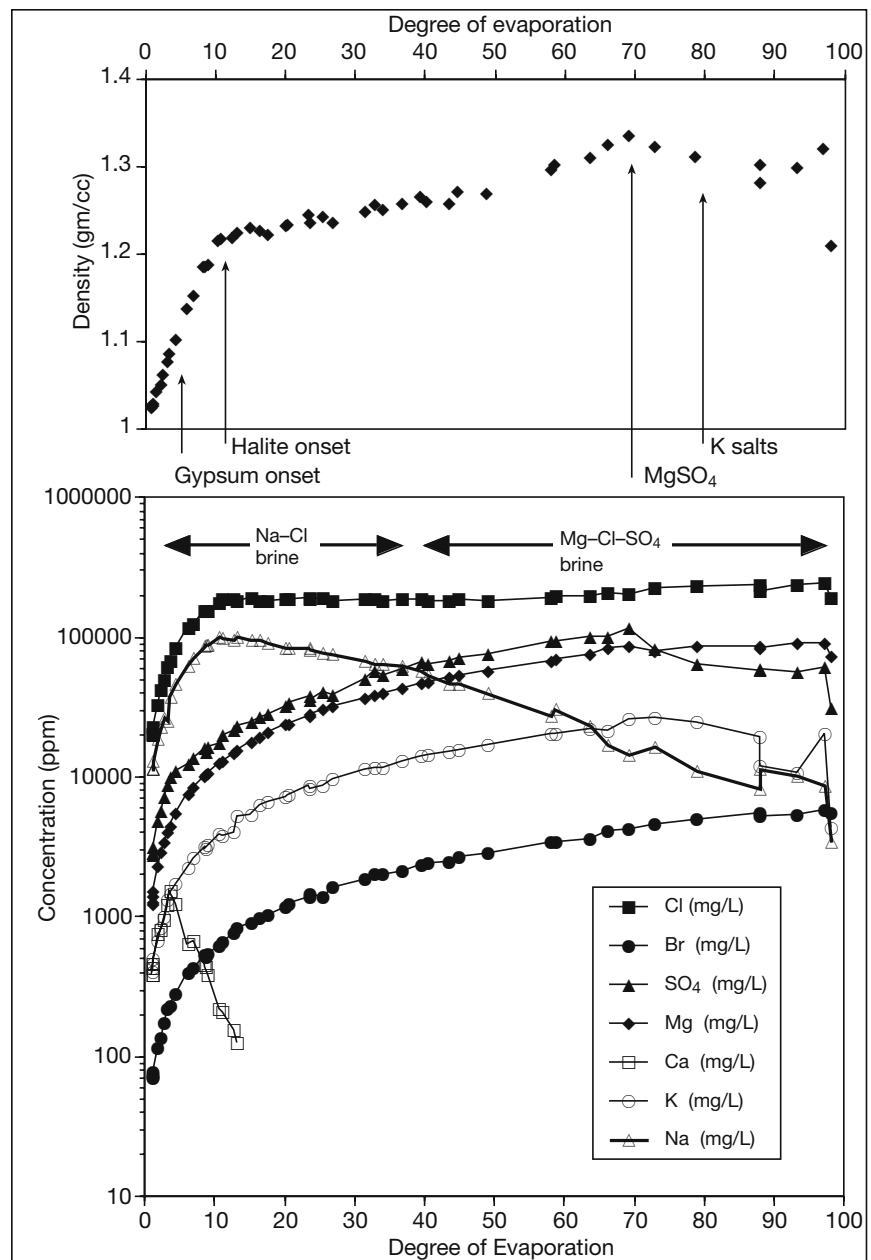


Figure 2.5 Evaporation pathway of modern seawater showing how density increases and the proportions of various ions in solution change as the brine concentration increases. Recompiled from data in appendices in McCaffrey et al., 1987.

was Van't Hoff, a 19th Century German chemist. He reasoned that the best way to study evaporites was to start with a simple solution of two salts and add components one by one, studying the behaviour of the various mixtures at each stage of the experiment. From this work he formulated a series of rules of behaviour for salts in concentrated brines.

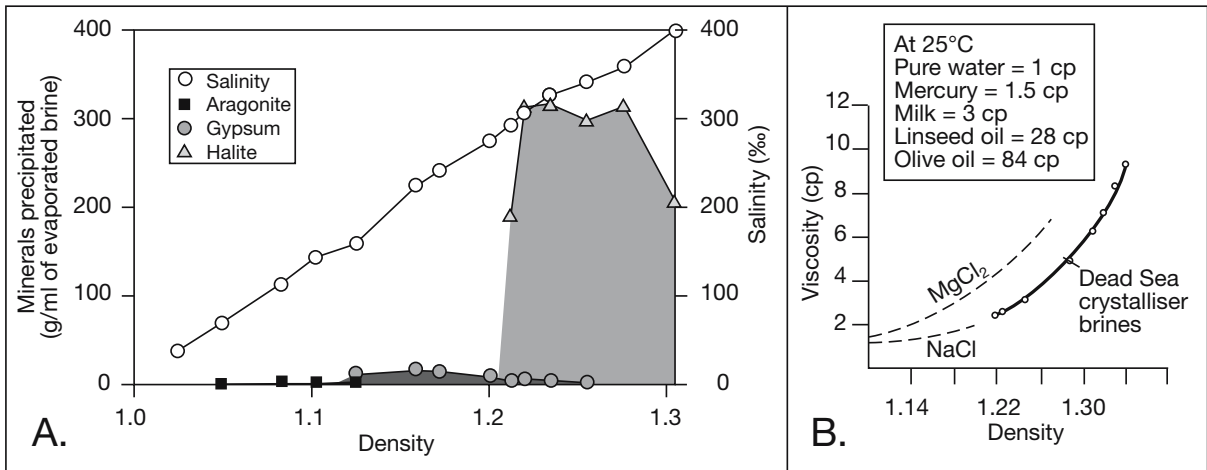


Figure 2.6. Brine evolution. A) Pre-bittern mineral precipitation sequence in a concentrating marine brine (replotted from Table 1 in Briggs, 1958). B) Viscosity increases with brine concentration (replotted from Karcz and Zak, 1987).

- If two salts are in solution, precipitation depends on the relative solubilities of the salts and their concentrations.
- If two salts have a common ion, the solubility of each in a solution of the other is less than in pure water.
- If two salts do not have a common ion, the solubility of each in the other is greater than in pure water.
- Solubility is markedly influenced by increases in temperature, much less so by pressure.

When studying bittern evolution the phase diagrams Van't Hoff developed experimentally are still useful today. Consider a KCl-NaCl system at 25°C and 100°C, this is an example of a salt pairs with a common ion (Figure 2.7a; Borchert and Muir, 1964). Points A and B represent solubilities in pure water at 25°C. Points G and H represent the solubilities in 1:10 NaCl-

KCl solution and 10:1 NaCl-KCl solutions, respectively. Point C represents the point at which the mixture is saturated with respect to both NaCl and KCl salts. Any point below line ACB is undersaturated at 25°C, above it is saturated with the solid salt. Let's now consider the effects of crystallisation and dissolution in this simple system. With concentration, a solution of composition X moves away from the origin until reaching the line ACB at Y, where KCl precipitates (Figure 2.7a). The ratio of NaCl/KCl increases as the solution composition moves along line Y-C (less water, less KCl in brine as NaCl increases). At C, both salts precipitate until dryness. With dissolution, a mixed salt of composition F remains solid until sufficient water has been added to begin its dissolution. At that point

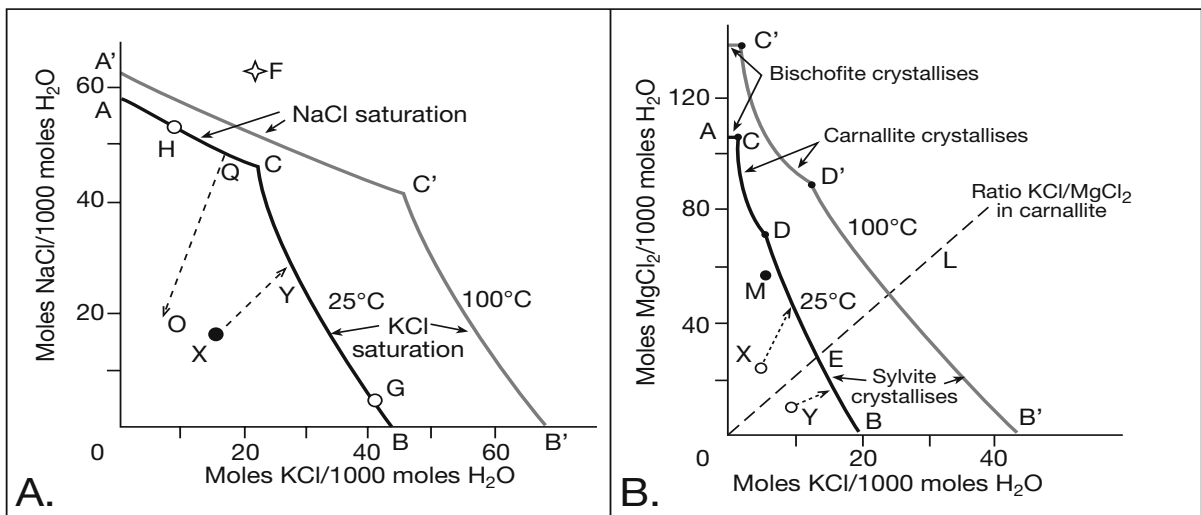


Figure 2.7 Van't Hoff plots. A) Crystallisation of solutions containing NaCl and KCl at 25° and 100°C. B) Crystallisation of solutions containing MgCl₂ and KCl at 25° and 100°C.

both KCl and NaCl begin to dissolve (point C). When all KCl has dissolved some NaCl remains and the composition shifts along C-Q as NaCl continues to dissolve. At Q the final NaCl dissolves and continued dilution moves the composition of the solution toward the origin along line Q-O.

Figure 2.7b is the Van't Hoff plot of the KCl-MgCl₂ system, an example of a salt pair with a common ion forming a double salt. In addition to the two end members (bischofite and sylvite) it has an intermediate double salt KCl.MgCl₂.6H₂O (carnallite). Points A and B represent saturation with MgCl₂.6H₂O (bischofite) and KCl (sylvite) respectively. The dashed line O-L shows the ratio of KCl to MgCl in carnallite. When a dilute solution of composition X is evaporated its composition shifts directly away from the origin until encountering line ACB. At the intersection point sylvite begins to crystallize and continues to crystallize as the composition of the solution shifts along line B-D, well below the composition of the double salt. Only when the solution has reached composition D does carnallite appear. At this point the composition of the solution remains fixed as carnallite crystallizes, both directly out of solution and by partial reaction of dissolved ions with some of the previously precipitated KCl. The resulting solid is a mixture of carnallite and sylvite.

Or with a more KCl-rich initial solution of composition Y, as it concentrates it moves away from the origin until it intersects line ACB where sylvite once again begins to crystallize. It continues to crystallize as the composition of the solution moves up along B-D. At D, carnallite begins to crystallize as the sylvite is used up. If evaporation continues, the composition of the solution now moves along line D-C until it reaches point C, where bischofite crystallizes, along with carnallite. The composition of the solution now remains constant until evaporation is complete.

We can also use this Van' Hoff plot to visualise how carnallite dissolves in this simple system. We begin with carnallite which has an initial composition D. Since this solution is much richer in MgCl₂ it is preferentially dissolved (it lies to the left of the dashed line EL). Once all the carnallite has dissolved, the net result is a solid residue of KCl (sylvite) (incongruent dissolution). Further solution of the residual will move composition of the solution down along line D-B. When it reaches E, the last of the sylvite is dissolved, and further dilution shifts the composition along line E-O (origin).

So, we can describe the section of the saturation line B-D as the 'sylvite region', since here KCl alone is in equilibrium with saturated solutions; CD is the 'carnallite region', and CA

the 'bischofite region'. Point C represents the composition of a saturated solution in equilibrium with both bischofite and carnallite, point D the composition in equilibrium with both carnallite and sylvite. Note that point D differs from point C in that during evaporation it can be approached from only one side, the KCl side, whereas C can be approached from either the carnallite or bischofite side. In other words the bitter precipitation sequence sylvite followed by carnallite, carnallite followed by a bischofite-carnallite mixture, or bischofite followed by a bischofite-carnallite mixture are possible, but never carnallite followed by sylvite.

If two salt pairs do not have a common ion they form a reciprocal salt pair such as a KCl-MgSO₄ system. In an evolved seawater brine it is possible to have four end members plus any number of intermediate double salts. Rather than depicting such a system as this on a simple Van't Hoff binary plot, it becomes necessary to use a ternary diagram. A ternary plot of reciprocal salts is handy, as fixing the relative concentration of three of the four ions also fixes the fourth, providing the system is at equilibrium. This is the basis for seawater ionic reconstructions in many micro-inclusion studies in halite. The most commonly used type of ternary plot in evaporite bitter studies is a Janecke Diagram (Figure 2.8). In many respects it is analogous to the ternary diagrams used in igneous and metamorphic petrology where plotting of two components fixes the relative proportion of the third component and it is very useful in the interpretation of brine inclusion chemistry (Zimmermann, 2001).

Evaporation on a Janecke plot is represented by the reciprocal salt pair MgCl₂-K₂SO₄. The solution remains saturated with NaCl at all times and thus this ubiquitous component can be ignored.

The corners of the diagram are represented by:

- Mg²⁺ = 100% bischofite (MgCl₂.6H₂O)
- K₂²⁺ = 100% sylvite (KCl)
- SO₄²⁻ = 100% thenardite (Na₂SO₄)

Points along the triangle edges are pure salts with only two end members:

- c = carnallite KCl.MgCl₂.6H₂O
- ks = kieserite MgSO₄.H₂O
- hx = hexahydrite MgSO₄.6H₂O
- bl = bloedite Na₂Mg(SO₄)₂.4H₂O
- gl = glaserite K₃Na(SO₄)₂
- e = epsomite MgSO₄.7H₂O

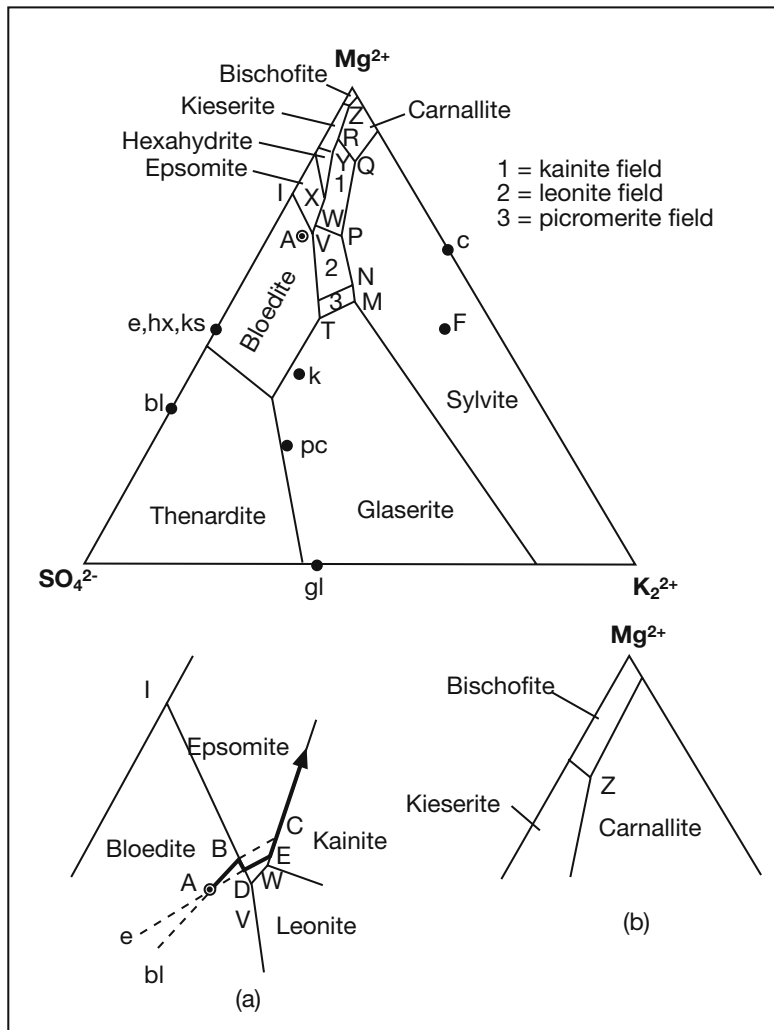


Figure 2.8. Janecke diagram for system $\text{NaCl} \cdot \text{MgCl}_2 \cdot \text{Na}_2\text{SO}_4 \cdot \text{H}_2\text{O}$ at 25°C . Salt points: c = carnallite, bl = bloedite, gl = glaserite, e = epsomite, hx = hexahydrite, ks = kieserite, k = kainite, pc = picromerite. Point A defines the composition of seawater. (a) enlargement near I to show part of the crystallisation path of seawater; (b) shows detail of the Mg corner.

Points within the triangle contain end members such as:

- k = kainite $\text{KMgClSO}_4 \cdot 11/4\text{H}_2\text{O}$
- pc = picromerite $\text{K}_2\text{Mg}(\text{SO}_4)_2 \cdot 6\text{H}_2\text{O}$

If the bulk composition lies within the field, the fields represent the composition of the first salt to precipitate. However, the point representing the actual salt composition often lies outside the field where the ideal salt would precipitate. This is analogous to the previous binary Van't Hoff plots in which point F (carnallite composition) lay far outside the "carnallite region."

In the evaporation of seawater, the average seawater composition is represented by point A on Figure 2.8. This point lies in the bloedite field. Thus, bloedite is the first bittern mineral to crystallize. As bloedite crystallizes the composition moves away from point A along a line which is a projection of the bloedite compositional point projected through point A. At B (seen in the expanded part of the plot) there are two possible pathways:

a) If bloedite has settled out and does not react further, epsomite begins to crystallize and the composition of the salt solution migrates across the epsomite field to point C, the path of migration from point B to C is a projection through B to the epsomite point on the triangle edge.

b) If, however, bloedite is free to backreact with the solution, crystallisation takes a different path. The composition of the solution shifts along line B-D with bloedite being consumed as epsomite forms. At D, the last of the bloedite disappears. At this point the composition of the solution is free to migrate through the epsomite field to point E, which is a projection from the epsomite compositional point at the edge of the triangle through D.

At either point C or E kainite begins to crystallize with epsomite (2 phase boundary) and the composition of the solution moves along the kainite - epsomite boundary. At X, epsomite becomes unstable with respect to hexahydrite. It reacts in the same way, consuming earlier precipitates or not, depending on how isolated precipitates are from the evolving brine. With further evaporation the composition of the solution moves along the kainite-hexahydrite boundary and both crystallize simultaneously. At Y, hexahydrite becomes unstable with respect to kieserite. At R, kainite becomes unstable with respect to carnallite. Thus, we have kainite and kieserite remaining when we leave point R. If concentration continues (we are now well into the bittern field) we move to Z, where we reach a three-phase boundary. Bischofite begins to crystallize with carnallite and kieserite. The solution remains at this point until dryness.

If equilibrium is maintained so that earlier salts are re-absorbed (backreacted) during ongoing crystallisation, the final product should be only three salts (bischofite, carnallite and kieserite), plus halite, plus small amounts of some calcium salts. If equilibrium had not been maintained other salts could be present, but they should be layered in a vertical sequence predicted by the crystallisation path.

The problem with all this 19th-Century laboratory-based bittern phase chemistry is that the prediction rarely matched the reality. For example, polyhalite is an abundant component in the Stassfurt Salt of the Permian Zechstein. This was the salt bed that formed the test case for much of Van Hoff's and Janecke's work, yet polyhalite did not appear in Janecke's plot. One reason for its absence is our inability to precipitate polyhalite from seawater in the laboratory at earth surface temperatures. Little was known about the stability of polyhalite. Where we do find it in the Holocene is as a replacement of gypsum in zones of mixing between marine brines and continental groundwaters. According to the marine brine evolution predicted by the Janecke plot of seawater, kainite should be absent, or present only in the lower portion of the Stassfurt Salt. Yet, in reality it occurs near the top of the Stassfurt bed. Unusual salts, such as loeweite, picromerite, vanthoffite and langbeinite, should not be present at all, yet they are not uncommon in the Stassfurt. A sylvite-kieserite assemblage is forbidden by the phase diagram, but is present in the Stassfurt.

In order to explain some of these problems Van't Hoff suggested that the temperature at the time of salt formation in the Zechstein Basin was as high as 83°C. This explained some of the unusual mineralogies and the sylvite-kieserite association. If the temperature drops to 55°C near the end of the deposition, it allows kainite to be present near the top of the Stassfurt. Geologists found his suggestion of temperatures close to boiling in surface evaporite environments, cooling to 55°C at the end of a cycle, a little unlikely. Janecke proposed that the high temperatures suggested by Van't Hoff were diagenetic and had developed during burial (Borchert and Muir, 1964). He proposed that the problematic polyhalite had formed by secondary alteration as calcium-bearing brines reacted with kainite (addition of calcium, subtraction of chlorine) and that most sylvite formed by incongruent solution of carnallite (loss of magnesium). The more unusual salts, he argued, represented high temperature burial metamorphism. Harvie et al. (1980) recalculated the order of onset for the marine bittern salts in the Zechstein as: glauberite, polyhalite, epsomite, hexahydrate, kieserite, carnallite, bischofite. They concluded that the type of bittern salt and the salinity at which it precipitates varied according to temperature and levels of impurities in the residual brines.

In reality, hydrology of the system is more significant than idealised chemistry in controlling bittern evolution. Brine leakage, mixing with freshened recharge about the basin's margin and the influence of humid air layers lingering above the brine body

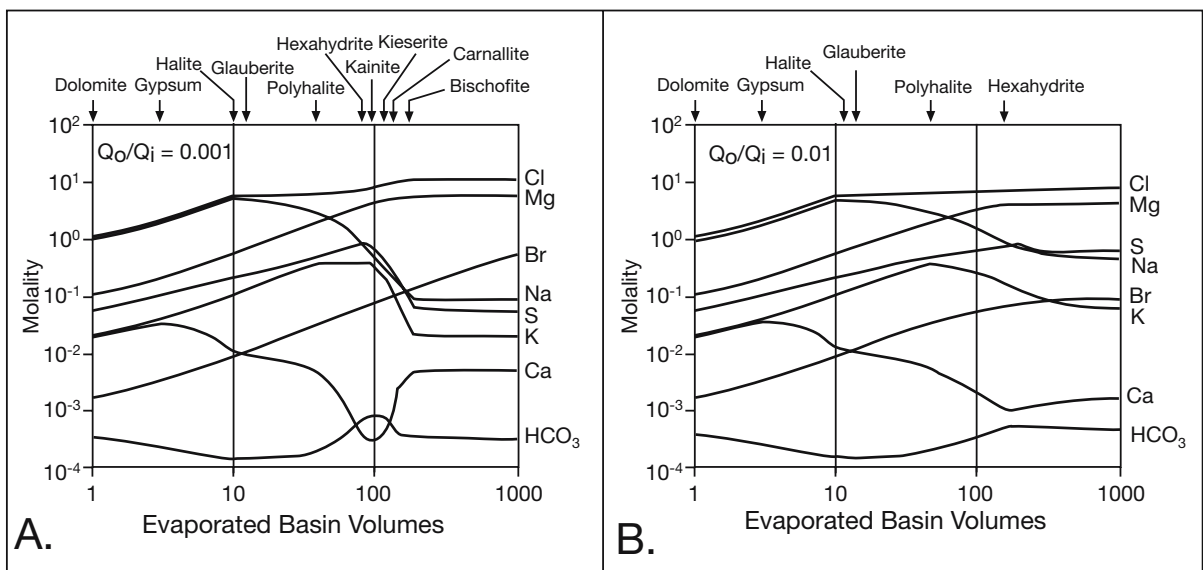


Figure 2.9. Effects of varying levels of basin leakage on ionic proportions and the precipitated mineral suite with a seawater parent brine and measured as a function of the number of evaporated basin volumes (after Sanford and Wood, 1991). A) Leakage ratio of 0.001 (\approx closed basin) shows bittern precipitation. B) Leakage ratio of 0.01, the system never reaches the upper end of the bittern field.

mean a standing body of modern seawater-derived brine liquor rarely moves to the bitter stage in a single primary desiccation cycle. Sanford and Wood (1991) modeled the changes in fluid composition and the sequence of primary salts that would precipitate under a leaky brine hydrology where bottom brine slowly discharges through underlying sediments (leakage via brine reflux). They found that the leakage ratio (ratio of water outflow to inflow) has a profound effect on both the evaporite mineral suites precipitated and the thickness (or volume) of a deposit (Figure 2.9). A system with a leakage ratio of 0.001 (that is, a 1x volume of water escapes from the basin for every 1000x volumes of inflow), the resulting salt evolution sequence is near identical to that of a completely closed system, as first documented by Usiglio (1849). However, with leakier systems there are significant reductions in the maximum salinities that the surface brines can attain and it is increasingly difficult to reach salinities sufficient to precipitate upper-end bitter salts. With a leakage ratio of 0.01 the final brine composition, reached after about 600 basin volumes have evaporated, has higher Na, K and SO_4 compositions and the four most soluble salts, kainite, kieserite, carnallite and bischofite, are not present (Figure 2.9b). This is reflected in the geological reality that textures in most natural bitter salts, such as carnallite and sylvite, indicate nearsurface brine cooling and backreactions drive their crystallisation (Figure 11.3).

There is another problem with much chemical/mineralogic modelling of ancient salts. It is predicated on an assumption that the major ion proportions of seawater do not change with

time. But were the ionic proportions of Phanerozoic seawater constant? Ionic proportions and the precipitation order of ancient seawater bitterns may have changed according to variations in the flux rates of river inflow relative to flux rates through mid-ocean ridges or the volumes of magnesium carbonate accumulating in the world's oceans (i.e., the "zip and split" of supercontinents) may have changed through time. Variations in either mechanism would have changed the proportions of major ions in seawater (Figure 2.30).

Brine mixing drives precipitation or dissolution

Van't Hoff's work also showed that salts can precipitate at a brine interface. All that is needed is mixing of waters of two saturation states with respect to the mineral of interest (Figure 2.10a). When two waters that are saturated with a particular phase are mixed, the resulting solution may be undersaturated or supersaturated with respect to that particular phase (two salt problem discussed earlier). The saturation state during mixing depends on the solubility curve of the mineral phase of interest and the parameter of interest (ion concentration, temperature, salinity, etc.; Runnels, 1969). The only requirement is that the solubility curve for that particular component is nonlinear. Raup (1970, 1982) in a number of experiments showed how halite and gypsum can be precipitated by the mixing of two seawater brines of differing salinity and densities. Figure 2.10b plots experimental results for the mixing of various low and high-density seawater brines and the resulting amount of gypsum precipitated (Raup, 1982). A similar plot can be drawn for the

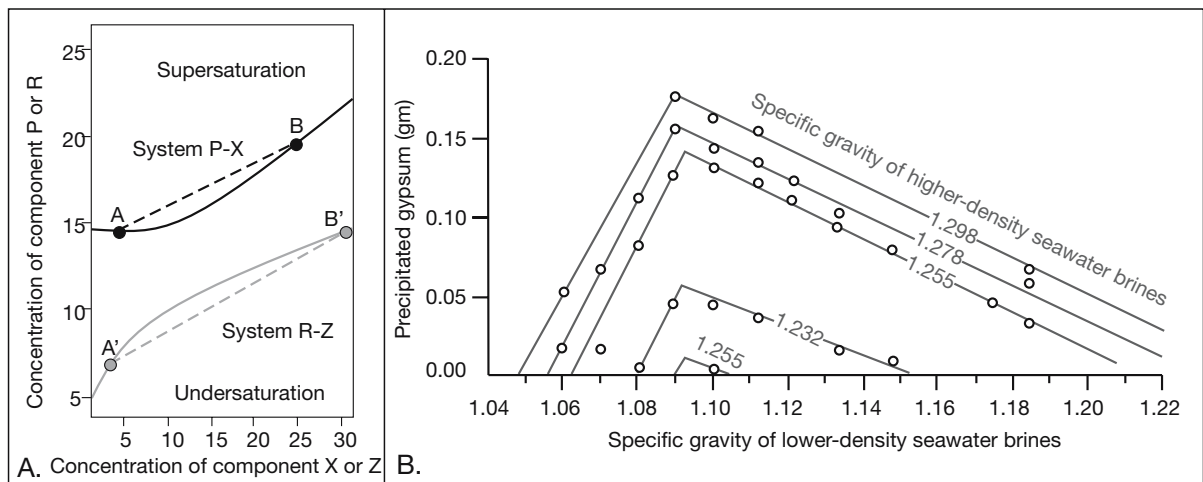


Figure 2.10. Brine mixing. A) Schematic showing effects of brine mixing on supersaturation in two styles of saturation curves - component system P-X and component system R-Z. Solid lines shows equilibrium saturation curve for their respective systems, while the dashed lines are the mixing lines. When solutions A and B mix in system P-X, the resulting solution is supersaturated and liable to precipitate. When solutions A' and B' mix, the resulting solution is undersaturated and liable to drive dissolution of the component of interest. B) Amount of gypsum (in grams) precipitated by mixing of 50 ml each of two seawater brines in various concentrations at 25 °C (after Raup, 1982).

mixing of more saline seawater brines, where halite is the precipitate (Raup, 1970). For similar reasons, gypsum can precipitate in mixing zones in coastal aquifers when seawater first intrudes and displaces freshwater (Gomis-Yagües et al., 2000).

Mixing brines with different temperatures or salinities can be an important salting mechanism in the calcium sulphate (gypsum/anhydrite) salt system as it follows a nonlinear solubility trend, as does the halite-MgCl₂ bittern system (Raup, 1970, 1982). Figure 2.11a shows the solubility curves of gypsum and anhydrite with respect to increasing temperature in pure water. For gypsum, it clearly shows that when two gypsum-saturated waters of different temperature mix then the resulting solution is undersaturated and gypsum tends to dissolve. It also shows that gypsum follows a prograde solubility curve, whereby in the temperature range where gypsum is the stable CaSO₄ phase (<40°C) it is increasingly soluble with increasing temperature. In contrast, at higher temperatures (>40–50°C) anhydrite and gypsum follow a retrograde solubility curve whereby they are less soluble with increasing temperature. Thus, when two anhydrite-saturated waters of different temperatures mix the result is supersaturated brine with a propensity to precipitate anhydrite. This helps to explain why anhydrite is a commonplace hydrothermal precipitate in many mid-oceanic ridges and smoker chimneys (see discussion in Warren, 1999; p.362 ff.). On land, beneath the surface of the Abu Dhabi sabkha, the heating of desert waters rising through the capillary zone to temperatures above 30°C drives the precipitation of CaSO₄ (Figure 3.13; “thermalites”).

Anhydritic systems drive complex diagenetic effects when CaSO₄-saturated brines are diluted via dispersion into adjacent less saline waters (Figure 2.11b). This happens in brine reflux systems where dense CaSO₄-saturated brine plumes, derived

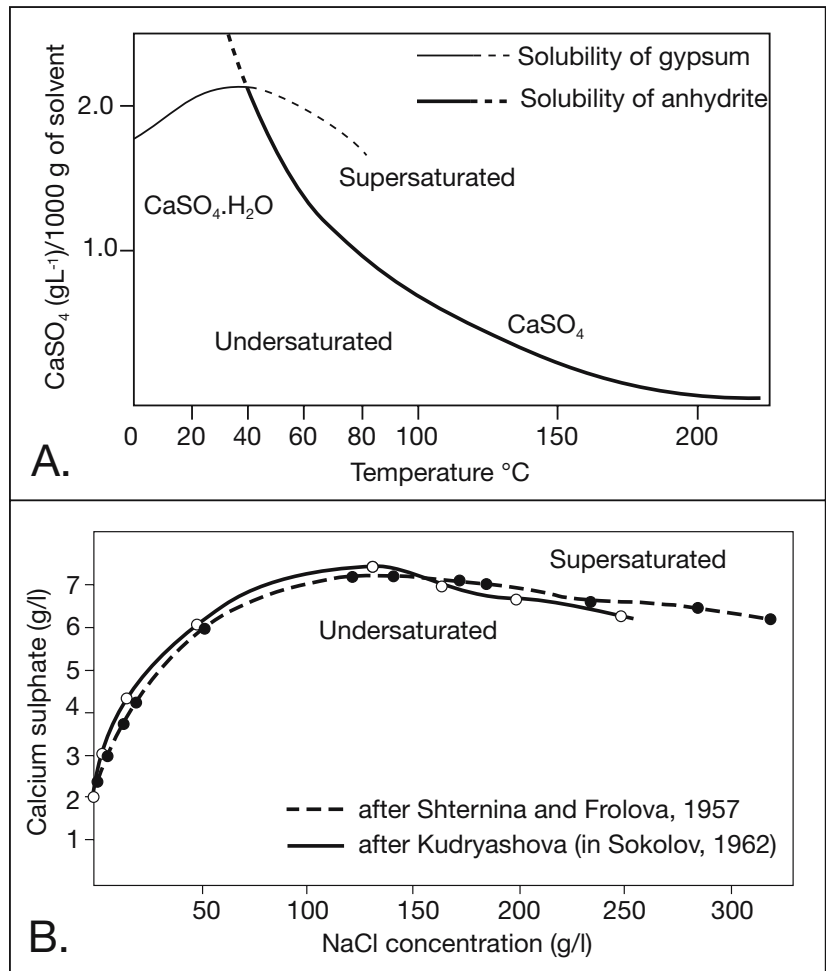
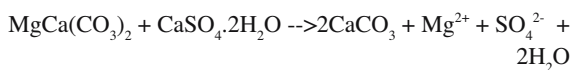


Figure 2.11. Calcium sulphate solubility. A) Idealised gypsum and anhydrite solubility with respect to temperature (after Zverev, 1967). B) Anhydrite solubility first increases then decreases slightly with respect to increasing NaCl content at temperatures of >100°C (Blount and Dickson, 1969).

at the surface at halite saturation, sink into, and interact with less saline brines held in underlying or adjacent anhydritic carbonates. If temperature remains near constant the tendency in this zone of dispersion or mixing is to dissolve anhydrite cements, creating vugular porosity in the interval below or adjacent to a thick salt sequence. If temperature decreases and the brine plume cools, with little change in ionic proportions due to mixing, then the tendency is to precipitate anhydrite. It is not a simple system, with temperature and mixing processes pulling the brine chemistry in opposite directions. It is of economic interest as brine reflux in ancient evaporitic carbonate platforms created diagenetic conditions suitable for the formation of potential hydrocarbon reservoirs via extensive dolomitization (Figure 10.24).

Later in the history of a calcium sulphate bed, during its uplift and dissolution (telogenesis), the mixing of sulphate-enriched waters with waters in adjacent aquifers drives dedolomitization. This is a process that can also create extensive karst in the absence of soil-derived carbonic acid and is doing so today in the Lake Banyoles region of northeast Spain (Bischoff et al., 1994). Lake Banyoles is a karst lake fed by sublacustrine springs, where dedolomitisation-driven karstic collapse drives ongoing subsidence in the immediate vicinity of the lake. The lake lies within the outcrop area of the middle Eocene Banyoles Fm.; a marine marl and mudstone that is organic-rich and pyritiferous. The marls are underlain by the 200–300m thick massive gypsum of the Eocene Beuda Formation, which is in turn underlain by the 100–200m thick dolostones of the Perafita Fm.

Gypsum dissolution drives the local precipitation of calcite, both in the lake and in the aquifer (dedolomitization), thus consuming ions released by dissolving dolomite and facilitating further dissolution in the aquifer (see Chapter 7 for details).



Lake waters reflect this process, they are dominated by Mg–Ca and $\text{SO}_4\text{--HCO}_3$ and are supersaturated with calcite, which is actively accumulating in lake sediments at a rate of $38 \text{ mg} \cdot \text{cm}^{-2} \cdot \text{yr}^{-1}$. Modelling of the regional hydrology based on the chemistry of lake and aquifer waters, along with measures of the annual water flow through the lake, shows that artesian waters create $\approx 9,500 \text{ m}^3$ of subsurface void space per year, enough to create the present karst depression of Lake Banyoles in 1,800 years (Bischoff et al., 1994). One could argue that gypsum dissolution alone can account for 55% of the lake volume. However, when coupled with the ionic removal from the dedolomitization process, gypsum solubility is enhanced by a factor of 1.56, as presumably is the rate of dissolution. Bischoff et al. (1994) go on to argue that gypsum-driven dedolomitization may be

responsible for extensive limestone karst in other exhumed CaSO_4 terrains in semiarid to arid settings, heretofore attributed solely to soil-generated carbonic acid.

Nonmarine brines

Unlike marine-derived brines, evaporating continental waters do not draw on the near isochemical reservoir of an ocean. A more diverse, less predictable, suite of evaporite minerals precipitates during evaporation of continental waters. In nonmarine settings, rivers and groundwaters are the source of most of the ions that are ultimately deposited as evaporite salts. In a closed hydrological system the composition of nonmarine brines depends on the lithologies that are leached in the drainage basin surrounding a salt lake (Eugster and Hardie, 1978; Eugster 1980a). Flow through limestone aquifers in hydrologically-closed basins produces inflow waters rich in Ca and HCO_3 , dolomite dissolution generates Mg, igneous and metamorphic matrices yield silica-rich Ca–Na– HCO_3 waters. Pyritic shales and other sulphide-rich sediments will contribute sulphate ions, whereas basic and ultrabasic rocks tend to produce alkaline Mg– HCO_3 waters.

In all, Eugster and Hardie (1978) distinguished five major water types in what they termed “hydrologically closed” continental evaporite basins (Figure 2.12):

1. Ca–Mg–Na–(K)–Cl
2. Na–(Ca)– SO_4 –Cl
3. Mg–Na–(Ca)– SO_4 –Cl
4. Na– CO_3 –Cl
5. Na– CO_3 – SO_4 –Cl waters

Brine Composition and Source	Major Saline Minerals	Key Minerals
Na–K– CO_3 –Cl– SO_4 Non-marine waters (mainly meteoric)	Alkaline earth carbonates, mirabilite, thenardite, trona, nahcolite, natron, thermonatrite, shortite, halite.	Na_2CO_3 minerals
Na–K–Mg– SO_4 –Cl Seawater, non-marine water or hybrids	Alkaline earth carbonates, gypsum, anhydrite, mirabilite, thenardite, glauberite, polyhalite, epsomite, bloedite, kainite, halite, carnallite, sylvite, bischoffite.	MgSO_4 and Na_2SO_4 minerals
Na–K–Mg–Ca–Cl Non-marine waters (hydrothermal and basinal brines or seawater with different ionic proportions from today)	Alkaline earth carbonates, gypsum, anhydrite, sylvite, carnallite, bischoffite, tachyhydrite, antarcticite.	$\text{KCl} \pm \text{CaCl}_2$ minerals in the absence of Na_2SO_4 and MgSO_4 minerals

Table 2.5. Mineral occurrences and parent brines (after Hardie, 1991).

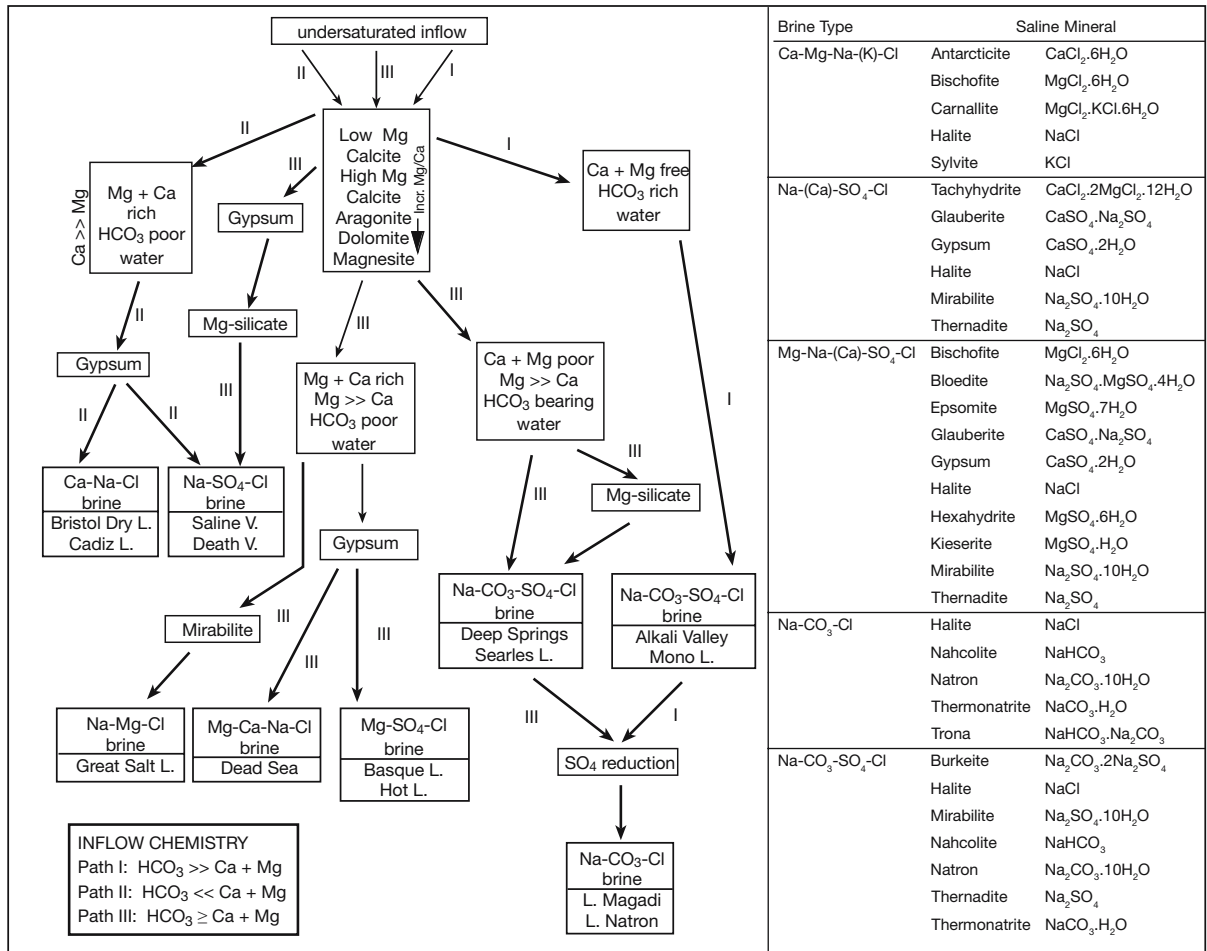


Figure 2.12. Hydrologic classification and brine evolution pathways of concentrating nonmarine waters and a listing of major evaporite minerals associated with the different brine types (after Eugster and Hardie, 1978). L = Lake, V = Valley.

As any one of these waters concentrates within a particular evaporite basin, it deposits a characteristic suite of evaporite minerals (Figure 2.12; Table 2.5). First precipitates are the alkaline earth carbonates: low-magnesian calcite, high-magnesian calcite, aragonite, and dolomite. The mineralogy of this initial precipitate depends on the Mg/Ca ratio of the parent brine. The subsequent evaporation pathway of a basin brine is determined by the proportions of calcium, magnesium, and bicarbonate ions in the brackish inflow waters. It sets up geochemical divides early in the evolution of a lake brine, these divides define the subsequent geochemical and mineralogical evolution of a lake basin.

If the lake waters are enriched in HCO₃ compared to Mg and Ca (i.e. HCO₃ >> Ca+Mg), then the brine follows path I (Figure 2.12). Ca and Mg are depleted during the initial precipitation of alkaline earth carbonates, leaving excess HCO₃ in the brine. As HCO₃ is the next most abundant ion in these waters it

combines with Na in the next stage of concentration. Sodium carbonate minerals, such as trona, natron and nahcolite, precipitate. Little or no gypsum can form from pathway-I brines as Ca is completely used up during the preceding alkaline earth carbonate stage. In contrast, during the evaporation of modern seawater, all the HCO₃ is depleted in the initial alkaline earth precipitates (mostly as aragonite and Mg-calcite). The excess Ca then combines with SO₄ to form gypsum. It is chemically impossible for sodium carbonate to form by evaporation of modern seawater. The assumption that the proportions of calcium to bicarbonate in seawater have not changed much in the last 600-800 m.y. implies that trona salts or their pseudomorphs indicate nonmarine settings throughout the Phanerozoic and much of the Neoproterozoic.

If initial inflow waters have (Ca + Mg) >> HCO₃ then, after the initial evaporitic carbonate precipitates, the brines become enriched in the alkaline earths but depleted in HCO₃ and CO₃,

If the relative volume of HCO_3^- is low, little carbonate can precipitate with further concentration. Brine evolution follows path II, whereby excess alkaline earths (Ca, Mg) left after depletion of carbonate combine with sulphate ions to precipitate large volumes of sulphates (gypsum and/or epsomite). Path II precipitates a suite of continental salts and bitterns similar to that derived from modern seawater. If the ratio of $(\text{Ca}+\text{Mg})/\text{HCO}_3^-$ is near unity (path III) carbonate precipitation can be extensive and voluminous. As Ca is progressively removed there is a progressive increase in the Mg/Ca ratio of the residual brine until large volumes of high-Mg calcites, dolomites and even magnesites precipitate.

Trona- nahcolite chemistry (Path I brine)

Clearly, path I brines cannot be derived by solar evaporation of waters with the ionic proportions of modern seawater. An occurrence of primary trona or its pseudomorphs in Phanerozoic evaporites is evidence of a nonmarine brine with an excess of bicarbonate (Figure 2.12). The three best-known trona deposits in the world are the Pleistocene and Holocene sediments of Lake Magadi, Searles Lake and the Eocene Green River Formation (Table 11.13). All regions show the appropriate bicarbonate excess in their inflow waters that differentiates them from seawater brine. But, as we shall see later in this chapter, there is increasing evidence that early Archean marine evaporites are most likely represented in the rock record by silica replacements of widespread nahcolite or trona, as well as halite. So, it's worth considering in more detail what is the phase chemistry of a sodium bicarbonate system.

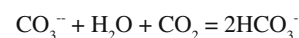
By definition, there must always be an excess concentration of bicarbonate ions in an inflow water to force it into a path I composition (Figure 2.12). This means trona-forming brine is always an alkaline solution, typically with a pH above 9, as seen in all modern soda lake waters (Eugster, 1971; Eugster et al., 1978). Alkalinity is the result of the required solution's inherent chemistry. Trona cannot form in acidic waters, it is a matter of basic chemistry. Any carbonate ion in any aqueous solution tends to bump into and react with whatever ionic species are around. When there is not much free hydrogen around, carbonate in effect steals a hydrogen ion from a water molecule, leaving a hydroxyl ion behind and so, *ipso facto*, produces an alkaline solution.

A number of conditions must be present to create natural Path I brines and so produce trona beds: (1) an underfilled tectonic basin in which downwarping exceeds the rate of sedimentation, (2) a closed hydrographic basin in which evaporation exceeds outflow, (3) evolution of solutes in the lake waters that lead to

high $\text{Na}/(\text{Ca}+\text{Mg})$ and $(\text{HCO}_3^-+\text{CO}_3^{2-})/(\text{SO}_4+\text{Cl})$ ratios, that is alkaline brines, (4) a more-or-less permanent body of nutrient-rich water, (5) a warm climate favouring high primary productivity by microbes and algae, and (6) a high rate of bacterial sulphate reduction. Given the presence of these requisite conditions, varying intensity of photosynthesis, temperature and changes in the amount or volume of degassing spring waters then control the CO_2 content of the sodium bicarbonate precipitating brines and hence the mineralogy of the sodium bicarbonate precipitates (Figure 2.13a).

Trona evaporites in Lake Magadi accumulate as the surface brine is losing (degassing) a substantial portion of its CO_2 to the atmosphere. As that happens the increasingly concentrated brine follows a path similar to the dashed line moving away from point A (Figure 2.13b; Eugster, 1970, 1980a,b). Trona precipitation then occurs at ambient equilibrium (point B). Natron rather than trona is likely to form when ambient temperature is below 25°C (left hand dashed line). Once native trona deposition in Lake Magadi has begun, the CO_2 resupply from the atmosphere is too slow to allow ongoing equilibrium between atmospheric CO_2 levels and levels of CO_2 in the brine. The deposition of the later salts, along with the observed HCO_3^- depletion in increasingly saline brines (levels not buffered by CO_2), suggested to Hardie (op. cit.) that fractional crystallisation likely controls trona deposition in Lake Magadi. Thermonatrite/halite can sometimes precipitate in the later stages of evaporative concentration in Lake Magadi. At higher temperatures, earlier formed natron and trona can be replaced by thermonatrite.

Kinetic effects, especially those governing equilibration between dissolved and atmospheric CO_2 , are extremely important in determining the final mineralogy of sodium carbonate precipitates (Eugster, 1970; Whittig et al., 1982). Evaporative concentrations under conditions of equilibrium with atmospheric CO_2 at 25°C follow path AB in Figure 2.13b and at B, trona begins to crystallize. Crystallisation of trona, together with further evaporation, results in the solution composition moving towards C, i.e., it causes a decrease in the $\text{HCO}_3^-/\text{CO}_3^{2-}$ ratio because this ratio in trona is greater than that in the solution. However, if equilibrium with atmospheric CO_2 is maintained, this ratio should be buffered, and only trona is produced because addition of atmospheric CO_2 stabilizes (buffers) the $\text{HCO}_3^-/\text{CO}_3^{2-}$ ratio via the following reaction:



Under conditions where atmospheric disequilibrium is promoted, i.e., where the $\text{HCO}_3^-/\text{CO}_3^{2-}$ ratio is not buffered, path

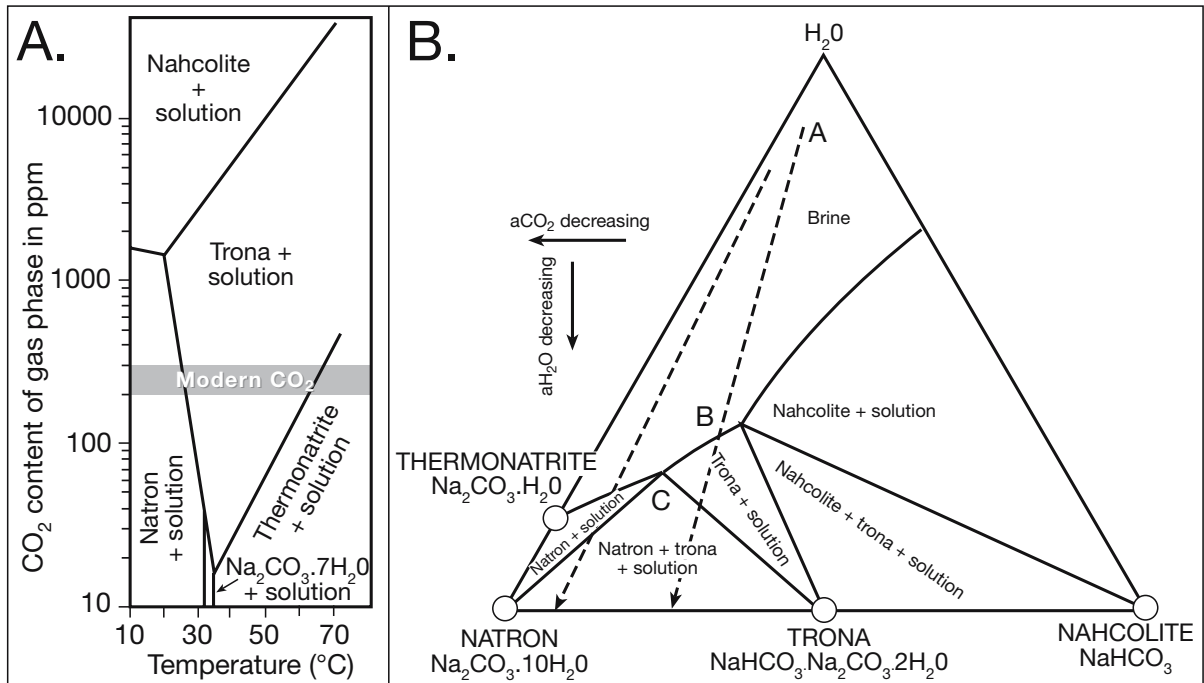
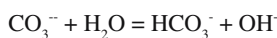


Figure 2.13. Phase chemistry of sodium carbonate salts. A) Sodium carbonate phases in equilibrium with a saturated solution as a function of CO₂ content of the gas phase and temperature. CO₂ content of today's atmosphere is plotted as a grey band (in part after Eugster, 1971). B) Phase diagram for the sodium carbonate, sodium bicarbonate, water system at 25°C. Trona saturation occurs at B where the brine trajectory arrow passes into boundary of trona stability field (after Eugster, 1971).

BC is followed, producing thermonatrite and trona at C. The removal of HCO₃⁻ along path BC under these conditions also causes a marked rise in the pH (alkalinity), as the solution compensates for HCO₃⁻ removal by the reaction,



In spite of this compensation, the HCO₃⁻/CO₃²⁻ ratio in lake Magadi brines falls well below that of atmospheric equilibrium, especially in nutrient-rich waters with a flourishing photosynthesising microbial community (Figure 2.13a).

The shaded interval in Figure 2.13a shows the range of CO₂ values typically present in brines in equilibrium with present-day atmospheric CO₂. Trona is the stable phase in the 25–60°C temperature range typical of most modern surface brines in modern soda lakes where sodium bicarbonate minerals are precipitating. CO₂ values were higher (10 to 200 times; Kaufman and Xiao, 2003) in the Archean atmosphere (as were CH₄ levels), favouring the widespread co-occurrence of nahcolite with trona along with halite, not gypsum, in marine evaporites of the time (Figure 2.32).

Are most continental salt lakes hydrologically closed?

Hydrogeochemical studies do not always draw the distinction between hydrographic closure (endorheic basin) and hydrological closure (no leakage). The former situation is commonplace in evaporite basins, the latter is rare. Studies of the nonmarine hydrogeochemistry of low-relief desert terranes detailed in this section show that varying degrees of brine leakage, rather than hydrological closure, characterise large-scale endorheic lakes and playas located well into the continental interior. Even in modern near-coastal settings the hydrology tends to be open and leaky rather than a closed cumulative systems. For example, evolved path III continental brines, in combination with varying degrees of brine leakage, explain the diversity of evaporitic carbonate mineralogies in the lakes of the Coorong, South Australia (Warren, 2000a). Individual lakes, less than 1 km apart and with sediment surfaces above sealevel, are filled with up to 6 m of Holocene carbonate and show mineralogies that range from low Mg-calcite to high Mg-calcite to calcian dolomite to magnesian dolomite±magnesite to aragonite±hydro-magnesite to aragonite+gypsum (Figure 4.4a). Calcites and calcian dolomites tend to dominate in lakes with lower average annual salinities, while the magnesian

carbonate phases, along with aragonite/gypsum, tend to dominate lakes with higher average salinities (Warren, 1990). During the desiccated stage of the late summer, halite-MgSO₄ efflorescences form atop carbonate mudflats in many Coorong lakes, but are flushed from the system by winter rains. Mineral variation in the Coorong lakes illustrates the importance of relative rates of brine loss (residence time and leakage) in controlling mineralogy in this hydrologically-open continental system. Average brine residence times in the different lakes ultimately control mineralogic assemblage. Those lakes with leakier basements allow a more rapid throughflush of waters and so show lower longterm salinities and so accumulate less saline precipitates.

Yet in the literature, many of our ideas on the nature and evolution of continental evaporite brines and the resulting salts are based on hydrochemical analysis of high topography, "closed-basin" (effectively non-leaking), rain shadow lacustrine systems such as the Basin and Range province of the southwest USA and the continental lakes of the African Rift system. Uplifted bedrock lithologies surrounding these lakes tend to contain abundant labiles in their tectonically-active high-relief catchments. Bedrock alteration with rapid weathering is a major contributing factor to variations in ionic proportions of the final lake brine (Figure 2.14). In contrast, saline groundwaters in playas and salt lakes of low-relief tectonically-stable deeply leached regions such as the interiors of Australia and southern Africa

tend to have salt lakes with seawater-like Na-Cl dominated brines (Type II or thalassic brines). Many Australian playas are hydrologically open; the outcropping parts of mixed local and deeply circulating regional discharge systems (Chapter 3). Aridity and deeply weathered soil profiles have characterised these areas since the early to mid Tertiary. Ionic proportions and chemical constituents of surface waters and brines vary little, even across regions of variable bedrock lithologies (Table 2.6). Gypsum, with lesser volumes of halite, are common precipitates in some, and all lake floors show varying degrees of brine leakage.

Jankowski and Jacobson (1989, 1990) and Jacobson and Jankowski (1989) showed that in such deeply weathered and leached systems the amount of rainfall in a given part of a catchment area is a more important determinant of the chemical composition of the final playa brine, rather than bedrock lithology. In the Lake Amadeus region of central Australia, higher rainfall regions of the catchment generate playa inflow waters that are bicarbonate-dominated, while lighter rainfall regions generate chloride-dominated inflow waters. Differences in brine chemistry can be related to the rate of cycling of pedogenic carbonate within the catchment profile, not to differences in basement lithology. More carbonate is dissolved in the nearsurface when rainfall is relatively high, and so contributes a greater proportion to the brine composition. Higher rainfall regions also flush greater volumes of water

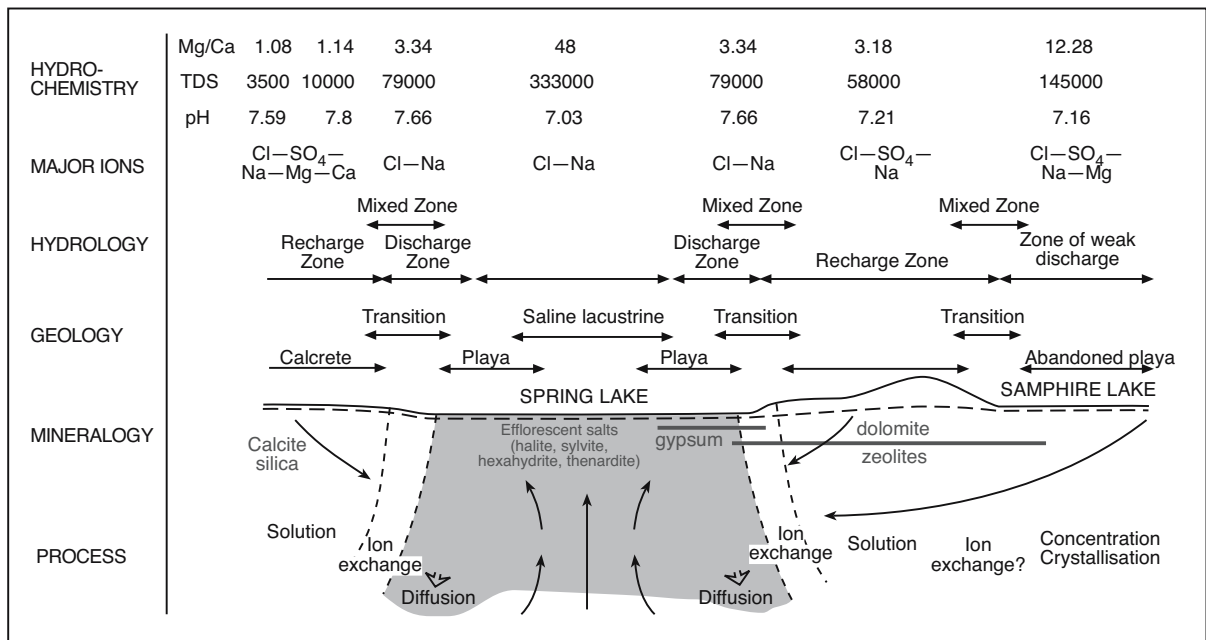


Figure 2.14. Schematic of hydrochemical processes in a groundwater discharge playa complex, Spring Lake, Curtin Springs, Central Australia (after Jacobson et al., 1989).

	TDS	pH	HCO ₃	Cl	SO ₄	Na	K	Ca	Mg	Br
Lake Eyre North, SA	36,800	-	87	21,400	1,100	13,800	35	300	42	-
Lake Eyre South, SA	25,500	-	100	14,300	1,300	9,100	-	600	100	-
Lake Frome, SA	305,900	-	104	173,400	14,100	116,219	366	570	1,030	151
Lake Torrens, SA	301,000	-	-	185,000	7,000	103,000	700	600	4,300	-
Lake Greenly, SA	207,400	7.47	124	109,700	3,500	84,810	1,299	1,170	6,600	314
Lake Malata, SA	224,300	7.49	196	137,200	3,600	71,620	1,609	970	8,690	407
Lake Tyrell, NSW	232,300	-	105	131,000	15,500	77,159	660	510	7,100	347
Lake Amadeus, NT	217,200	7.62	9	118,000	1,440	77,060	2,530	612	2,680	-
Spring Lake, NT	358,000	6.65	72	143,000	55,000	90,000	5,500	250	14,700	-
Glauberite Lake, NT	361,200	6.80	1,102	185,550	31,700	107,000	3,800	39	11,700	369
Palaeochannel, WA	238,800	7.20	50	110,000	18,000	98,000	2,400	430	9,800	-
Seawater	35,700	8.20	140	19,350	2,710	10,760	390	410	1,290	67

Table 2.6. Major ion composition of waters (ppm) in various Australian playas, all showing Na-Cl dominance and seawater-like ionic proportions (after Dutkiewicz et al., 2000; Jacobson et al., 1989 and references therein).

through the same profile in a given time and so are characterised by shorter residence periods per given water volume for rock/fluid interaction. In low rainfall regions chloride tends to remain mobile in the catchment profile, while bicarbonate is more likely to remain fixed as carbonate minerals in the soil profile (Figure 2.14).

The buildup of more soluble salts as pedogenic residuals in low rainfall regions can be impressive. Salt-rich soil profiles near Lake Eyre, South Australia sit atop a widespread flat-lying and deeply weathered pyritic Cretaceous Bulldog Shale. Deep leaching has created a pedogenic unit of epsomite, with a thickness measured in metres and an area measured in thousands of square kilometres (Lock, 1986). Pedogenic nitrates in the hyperarid Atacama Desert have a similar pedogenesis (Figure 11.42).

Hydrological leakage through a brine-covered lake floor varies over time in response to climate change driving rising and falling watertables. Variation occurs across time frames of hundreds to thousands of years, and periodic deflation is typically part of the sedimentary history of these playas. Variations create regional disconformities in the upper few metres of lacustrine sediment. This hydrological regime begs the question, how useful are the major ions proportions in the present surface waters in understanding the mineralogical evolution of the preserved lake precipitates? In other words, how valid is the assumption, typically made in "closed lake" settings, that the chemistry of the concentrating surface waters gives an understanding of the hydrogeochemical parentage of the preserved sediments?

Studies by Dutkiewicz et al. (2000) underline the significance of varying rates of phreatic leakage (both upwelling and downwelling/reflux) in controlling the mineralogy of lacustrine sediments in more hydrologically open playas. Using a steady-state isotopic model of lacustrine carbonates they concluded that present-day leakage in the Malata-Greenly playa complex in South Australia is 75% to 90% of regional inflow. Mineralogy of nearsurface sediment beneath all the lakes in the Greenly-Malata system is relatively simple, dominated by alternating layers of chemically-precipitated gyparenite and carbonate muds, which are either dolomites or calcites, all with relatively minor amounts of transported calcareous sand (Figure 2.15a; Dutkiewicz and von der Borch, 1995). Under present conditions of high leakage, only low magnesian calcite precipitates are preserved along with gypsum. The lake water experiences somewhat reduced effects of evaporation, gas and vapour exchange and, consequently, reduced isotopic and chemical enrichment compared to more arid times in the past when dolomite accumulated.

Using regional groundwater values, Dutkiewicz et al. (2000) calculate that any precipitated carbonate in a salt lake in the region will be calcite that becomes increasingly Mg-rich as brine concentration continues, until the brine reaches a chemistry favourable for dolomitisation. Thus dolomite intervals preserved in the cores but not forming in the present climate, probably reflect more arid climate or times of slower leakage of brine from the lake. Their modelling predictions are confirmed by isotopic measurements over the length of a 2.5 m core taken in the dolomitized carbonates of the lake complex, where the $\delta^{18}\text{O}$ and $\delta^{13}\text{C}$ of the lacustrine carbonates show excursions on

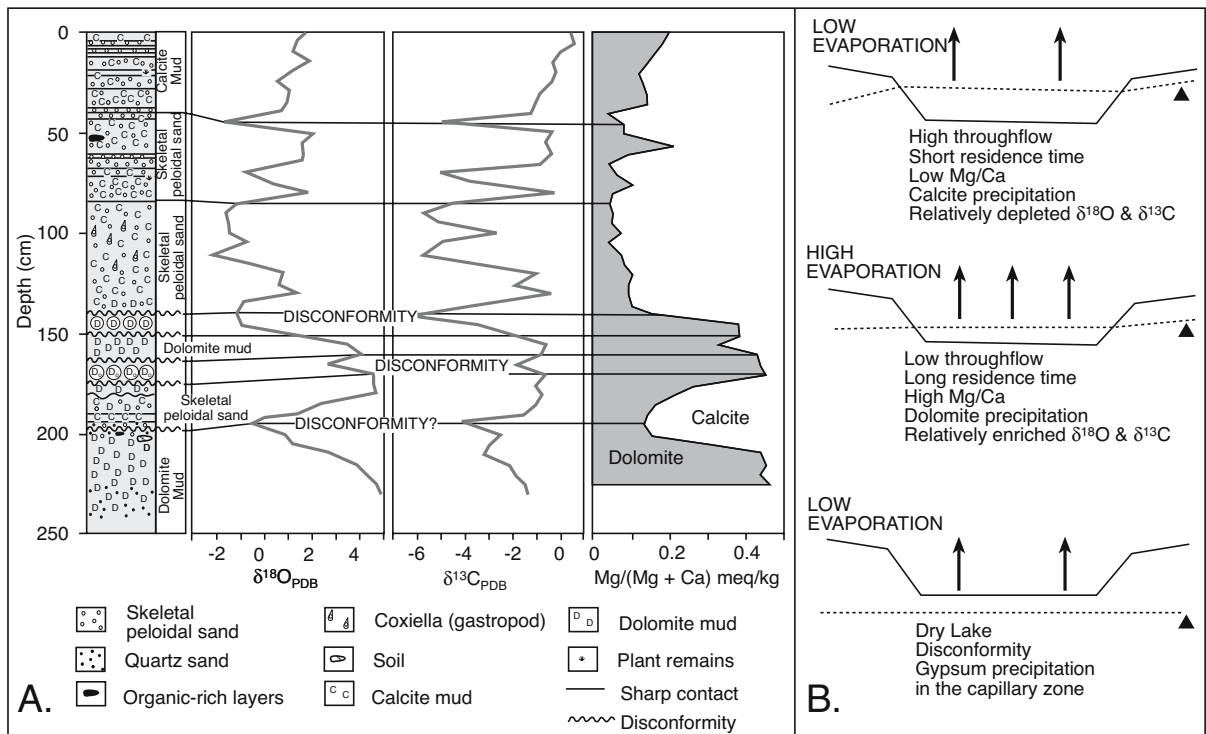


Figure 2.15. Lake Malata-Greenly complex, South Australia. A) Stable isotopes and Mg/(Mg+Ca) ratios plotted against depth and sedimentology of core C17 in Lake Greenly. B) Schematic of the three playa hydrological stages with varying water tables indicated by dashed lines (after Dutkiewicz et al., 2000).

the order of 5‰ (Figure 2.15a). At one end of the hydrological spectrum are past times of throughflow-dominated leaky conditions, when low-Mg calcite accumulated (with characteristic depleted $\delta^{18}\text{O}$ and $\delta^{13}\text{C}$ levels). These were times defined by a high water table, perennial waters and a humid climate (Figure 2.15b) with relatively short residence times in the pore brines. Then there were times of decreased leakage and higher rates of evaporation. These more arid climatic episodes were characterised by the accumulation of high Mg-calcite/dolomite (relatively enriched in $\delta^{18}\text{O}$ and $\delta^{13}\text{C}$ (Figure 2.15a). Dolomite precipitation dominated in Lake Greenly when leakage was reduced to some 55% to 70% of present inflow.

Then there is the climatic situation where deflation or a lowering of the regional water table causes the water level to sink into the lake sediment column to become a water table. The system is then driven by capillary evaporation, the formation of widespread erosional surfaces (disconformities) and net loss of sediment (via deflation) from the lake. This creates breaks or disconformities in the sedimentation history and it can effect both dolomite and calcite successions. It tends to occur more frequently during dolomite depositing episodes, as these were times of greater aridity. Using the modern isotopic signatures

of the regional groundwaters as a baseline, signatures in the preserved lake sediments indicate variable, but high, rates of throughflow or leakage throughout the Late Quaternary (55–90% of today's).

Yet, when mass balance calculations are done using the surface water chemistry in the lake and an assumption that Cl and Br are conservative, there is apparent hydrochemical closure in surface waters of the lake system (ionic proportions indicate < 1% leakage of waters from the lake). Clearly, the surface brine chemistry does not match the leakage history shown by isotopic signatures of the preserved sediments beneath the lake floor (Dutkiewicz et al., 2000). Surface waters reflect the ongoing cycling of a seasonal halite crust, which redissolves each winter. The crust formed during the previous summer under conditions dominated by evaporative discharge into the lake. Circulation of surface waters and the periodic creation of secondary surface brines by halite leaching takes place above a separate widespread mixing zone where older lake brines interact with regional groundwater inflow. Thus the annual solute cycle of surface waters and the halite crusts is decoupled from the subsurface water cycle preserved in the carbonates of the playa sediments. This decoupling is true of

many inland playas across Australia, where reflux and mixing of the lake brines into the regional outflow hydrology prevents the accumulation of thick sequences of bedded gypsum or halite (Figure 3.55).

Decoupling also explains a general observation that in many Quaternary salt lakes around the world, the relative abundance of preserved authigenic minerals in the sediment column is different from that predicted by conventional solute mass balance calculations using surface brine compositions. Conventional hydrogeochemical mass balance models assume that chloride (and bromine) behave conservatively over long periods of time. Such models of ionic evolution fail to take into account the role of diffusion, deflation and fractional crystallisation/dissolution of salts. That is, not all water exchange in a saline system is closed and so can be tied to a simple relationship between runoff and evaporation; in reality all salt lakes will reflux, seep and leak brine to varying degrees.

This decoupled hydrogeochemistry illustrates a general observation on evaporite deposition, underlined by Sanford and Wood (1991) and Rosen (1994), namely, there are very few truly “closed” hydrological systems in evaporite basins in either marine or nonmarine settings. All natural groundwater systems in salt-accumulating areas leak to varying degrees. Geological evidence for leakage through the floor of an evaporite basin includes the formation of reflux dolomite, the longterm stability of brine plumes beneath lakes that are accumulating thick salt sequences, the loss of halite porosity by 30 metres burial, the near surface dissolution of marginward portions of salt beds, the diverse suite of early burial alterations and backreactions, and the formation of burial salts in brine curtains beneath saline depositional systems.

As for seawater biterms (Figure 2.9), the geochemical divides defining the evolution of Type I through III nonmarine brines are perhaps more dependant on the ratio of leakage to inflow rather than the lithology of the surrounding basin. Only in high-relief reactive catchments with very low basin floor leakage (near-closed) hydrologies will surface brine chemistry and crust mineralogy correlate with the suite of minerals and salts accumulating as the lacustrine fill. There the rapid rates of subsidence in the lacustrine sink mean the accumulated salts largely reflect catchment lithologies.

In more hydrologically open systems, with slower rates of lacustrine subsidence and sediment accumulation, the rate of solute input from precipitation and meteoric outflow via pedogenic leakage in the surrounding low-relief deeply

weathered and flushed catchment is often more significant in controlling inflow chemistry than the rate of labile bedrock weathering. Hydrogeochemical proportions of ions in waters throughout the continental groundwater profile are then controlled by a combination of rates of leakage and the ionic composition of the precipitation entering the system. Solutes from the shallowest portions of the groundwater profile are recycled through the seasonal formation and dissolution of salt crusts on the lowest parts of the playa floor and so are typically decoupled from the mineralogy in the immediately underlying lacustrine sediments. The proportion of leakage of solutes into the sediment below the cycling crust is controlled by longer term climate change and the interactions between tectonism, subsidence and deflation.

Separating marine from nonmarine

Hydrological requirements needed to accumulate large-scale thick salt deposits complicates our ability to separate marine from nonmarine water sources in ancient evaporites. A high degree of isolation or “continentality” is required for stable longterm evaporative drawdown, which is always needed to accumulate a thick sequence of bedded salts (see Chapter 5 for detail). That is, a marine evaporite basin may have been supplied seawater by marine seepage or occasional surface seawater breakthrough via narrow ephemeral surface inlets, but, if the basin is to accumulate thick salt beds, it must be a longterm topographically-isolated regional low. The inherent hydrological requirement of isolation from any continuous surface connection to the ocean means it is by definition a subsealevel basin surrounded by land with a marine-phreatic groundwater feed. The salt accumulating area is either surrounded by continental sediments and hydrologies or is a depression within or behind a subaerially exposed carbonate platform. Invariably in some parts of the basin, marine chemistries are overprinted by deeply circulated meteoric waters, thalassic surface waters can be diluted by occasional rainstorms and by the effects of pulses of highly labile volcanic ash. This next section is an attempt to present some of the possible complexities that characterise ancient hybrid (mixed marine/continental) brine systems.

Back reactions

Backreactions complicate the interpretation of brine parentage in ancient evaporite salt sequences. At the start of the last century they were recognised as significant controls on mineralogy by van Hoff and others (Figures 2.7, 2.8). Backreactions can occur both at the sediment-brine interface and within shallow subsurface brine plumes that displace and mix with less dense

underlying pore brines. Pseudomorphs and reaction rims are common indicators of this process, as are relict mineral cores encased in the mineral that replaced it. Documented examples include pseudomorphs of halite after subaqueous gypsum, reaction rims of polyhalite and glauberite around earlier gypsum or anhydrite, bloedite after epsomite, relicts of carnallite in secondary sylvite, and pseudomorphs of sylvite plus kieserite after earlier langbeinite (Table 2.7).

Backreaction means relevant bittern chemistry and associated brine evolution is poorly modeled by studying brine evolution in man-made seawater ponds. In such salt works the evolved brines are separated from earlier precipitated mineral species by sluice gates and pumps. The aim of the saltwork engineer is to create harvestable monomineralic or bimineralic salts and brines in the various fractionating pans. Backreaction either does not occur or is kept to a minimum.

Many secondary (replacive and displacive) salts in natural systems, such as sylvite, glauberite and polyhalite, form syndepositionally via interaction between highly evolved nearsurface brines and earlier formed minerals (Figure 2.16; Table 2.7). For example, during the equilibrium evaporation of seawater at 25°C, glauberite and polyhalite form by backreaction of the brine with earlier formed anhydrite and gypsum. Harvie et al. (1980) modeled much of the variability present in the bittern salts of the Permian Zechstein deposits in Germany via a combination of equilibrium batch evaporation interspersed with times of fractionation and backreaction. As seawater concentrates to slightly below halite saturation, anhydrite replaces gypsum. As evaporation continues, anhydrite is partially replaced by glauberite. Glauberite in turn is replaced by polyhalite and levels of anhydrite are further reduced. These replacements change the residual brine composition so that kainite does not supersaturate, a problem that plagued earlier geochemical models of marine-derived potash precipitation in the Zechstein Series. The Harvie et al.

(1980) model not only explained the absence of primary kainite in the Zechstein deposits, but also explained the pseudomorphic replacement of gypsum and anhydrite by glauberite or polyhalite and the replacement of glauberite by polyhalite. Previous authors had attributed these replacements in the Stassfurt Salt to burial-stage thermal and solution metamorphism (Borchert and Muir, 1964).

Likewise, textures in beds of polyhalite in the Lower Werra Anhydrite (Zechstein - Upper Permian) of northern Poland show they are a very early replacement of anhydrite formed within platform sulphates by diagenetic backreaction with a highly evolved marine brine (Peryt et al., 1998). Formation of polyhalite was preceded by the anhydritisation of the original gypsum. Anhydritisation of primary platform and slope gypsum was an early subsurface alteration driven by syndepositional brine plumes, with ghosts of the primary gypsum texture still visible. Later brines, which were potassium and magnesium rich and nearly saturated with respect to halite, were created by ongoing reflux during more hypersaline conditions on the platform. These more highly evolved brines reacted with anhydrite to precipitate polyhalite along the slopes of the Zdrada Platform. The oxygen and sulphur isotopic compositions of

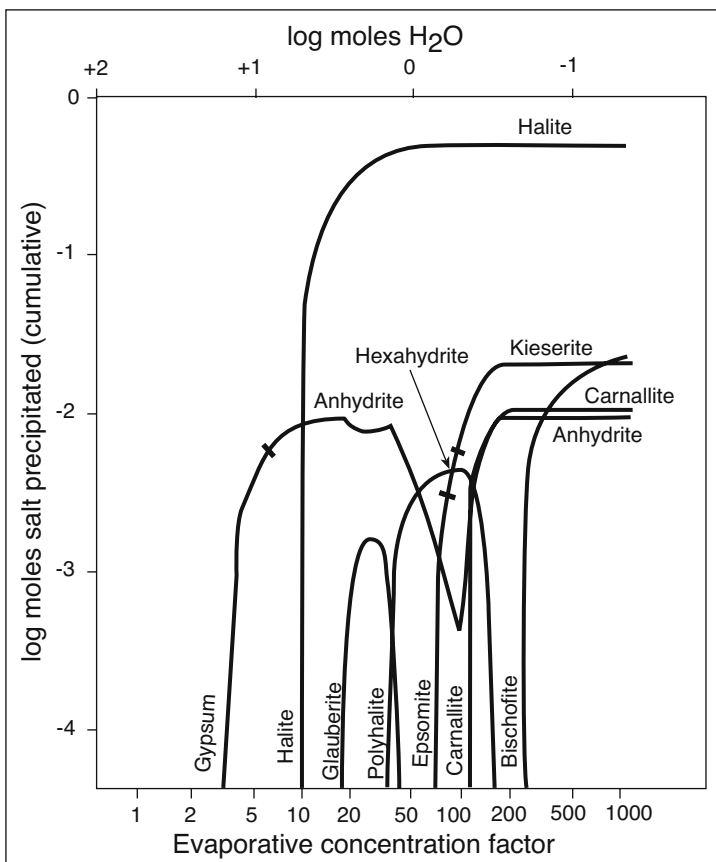


Figure 2.16. Evaporative concentration of modern seawater simulated using the computer program of Harvie et al. (1980) showing cumulative masses of minerals precipitated and resorbed by backreaction as evaporation proceeds. Initial seawater has a concentration factor of 1, with an initial mass of 1 kg of H₂O (after Hardie, 1991).

Secondary mineral phase	Syn depositional origin (<30°C)
Anhydrite CaSO ₄	Dehydration of early formed gypsum as a _{H₂O} of evaporating brine decreases.
Bloedite Na ₂ SO ₄ ·MgSO ₄ ·4H ₂ O	Back-reaction between previously precipitated epsomite and concentrating brine.
Gaylussite CaCO ₃ ·Na ₂ CO ₃ ·5H ₂ O	Back-reaction of evaporating alkaline brine with early formed aragonite or calcite.
Glauberite CaSO ₄ ·Na ₂ SO ₄	Back-reaction of evaporating Na ₂ SO ₄ -brine with early formed gypsum or halite.
Kieserite MgSO ₄ ·H ₂ O	Dehydration of early formed hexahydrate as a _{H₂O} of evaporating brine decreases.
Polyhalite 2CaSO ₄ ·MgSO ₄ ·K ₂ SO ₄ ·2H ₂ O	Back-reaction of evaporating K-Mg-SO ₄ brine with early formed gypsum, anhydrite or glauberite.
Sylvite KCl	Incongruent dissolution of carnallite in undersaturated waters.

Table 2.7. Examples of diagenetic (secondary) evaporites that form easily below 30°C (after Hardie, 1990; Sanchez-Moral et al., 1998).

sulphate evaporites indicate that marine solutions were the only source of sulphate ions supplied to the drawdown Zechstein Basin.

Hypersaline groundwaters can also react with adjacent nonevaporite minerals to form indicator clays and authigenic phases. For example, in reactive volcanogenic margins associated with many rift-valley evaporites there are suites of authigenic zeolites and clays (Figure 11.61). Many formed by the diagenetic reaction of nearsurface saline pore waters with metastable clays derived by weathering and alteration of labile volcanics. The best studied authigenic phases are the sodium silicates, such as magadiite; the borosilicates, such as searlesite; and the zeolites of the alkaline saline lakes, such as clinoptilolite, erionite and analcime. Sepiolite (meerschaum) clays form beds and nodules in saline lake deposits in the Miocene Eskisehir Lake of Turkey. These Mg-rich clays were deposited by direct precipitation out of silica-saturated saline and alkaline lake waters (Ece and Coban, 1994). The rather unusual inflow water was derived by the weathering of a Cretaceous ophiolite complex that contained abundant serpentinite and magnesite. Many of the saline lakes in this region of Turkey also contain widespread evaporitic micrites dominated by primary magnesite.

Volcanogenic ash and debris can be a substantial component in the drainage basins of salt lakes and playas in active rift and collision belts. For example, in the Central Andes various volcanic formations

overlie Cenozoic evaporites and the longterm meteoric recycling of salts from these labile carapaces into the present endorheic basins is a well documented process. But, pulsed short term recycling of fractionated ions into the salar hydrology following a volcanic eruption is another widespread, yet less well documented phenomena (Risacher and Alonso, 2001).

During a recent eruption of the Lascar Volcano in northern Chile around 10⁹ metric tonnes of air-fall tephra was deposited over the surrounding endorheic basins. Leachate experiments on this ash near the volcano summit and the nearby Talabre Valley produced fluids that were almost pure CaSO₄ and near neutral on the summit ashes, while leachates of valley floor ashes were alkaline (pH as high as 10.5) and more enriched in minor components compared to the CaSO₄ leachate of summit ashes (Figure 2.17; Risacher and Alonso, 2001).

Sulphur isotope compositions of leached sulphate are consistent with volcanogenic recycling from Tertiary gypsum that underlies the volcanic cordillera. Risacher and Alonso (op. cit.) estimate that 700,000 tons of easily soluble CaSO₄ were added to nearby endorheic basins by three days of eruption. The high pH of the valley floor leachates indicates hydration of alkali and alkali-earth metal-oxides via pyrolysis of vegetation during ash fall. Efflorescent salts encrusted on plants and dissolution of volcanic glass also provided some of the minor leachate components.

The almost pure CaSO₄ composition of summit leach waters is compositionally distinct from any present inflow waters in the central Andes. Addition of volcanogenically cycled CaSO₄

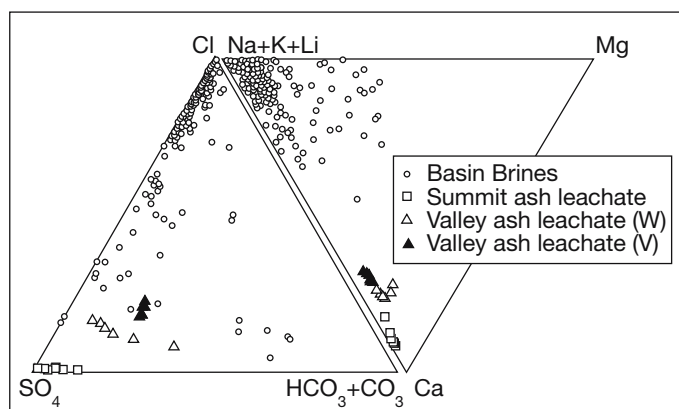


Figure 2.17. Ionic composition of ash leachate from Lascar volcano summit and Talabre Valley floor (V=valley floor, W =valley on west side of volcano) compared with basin brines of northern Chile (after Risacher and Alonso, 2001).

may explain some of the differences between the observed brine compositions and those predicted by computed simulations of the evaporation series based on the chemistry of longer-term inflows. Rapid recycling of sedimentary gypsum and short-term pulses of salts from labile ashfall is probably not restricted to Lascar volcano. The recycling of ancient salts, and possibly the pyrolysis of vegetation, may have been crucial processes in controlling the ionic proportions of closed basins during episodes of intense volcanic activity in the Tertiary. Some of the anomalies in salt mineralogies in ancient salts may reflect pulses of volcanism rather than variations in short term climate or the degree of leakage. Lascar brine chemistry is an example of a decoupled hydrogeochemical brine system where short term brine chemistries are decoupled from longterm chemistries in the drainage basin.

Marine aerosols supply continental lakes

Brine sources in ancient settings are usually inferred by a study of the regional palaeogeography and a definition of drawdown, seepage and hydrothermal brine supply using outcrop or seismic interpretation. Seepage drawdown or periodic storm floods are thought to be the predominant mechanisms for supplying substantial volumes of marine ions to larger ancient basins. But aerosols are a viable ionic supply mechanism in the hydrochemistry of modern continental arid-zone systems up to a thousand kilometres from the coast (Figure 2.18a). There is even a modern aerosol-defined marine versus nonmarine salt-line in the saline depressions of the Vestfold Hills of Antarctica (Gore et al., 1996).

Modern aerosol supply routes are best seen in isotopic signatures of the resulting salt, but this leads a circular argument if marine aerosols are invoked as brine sources for ancient evaporites in continental settings (i.e. I assume a portion of the input is marine therefore a proportion is marine), underpinning once more the numerous difficulties involved in separating marine and nonmarine brine sources for ancient salts.

Aerosols from salt spray can supply substantial quantities of ions to precipitative hydrologies in modern continental salt lake depressions located hundreds of kilometres from the continental margin (Figure 2.18a). For example, the Murray Basin, in southeast Australia, contains a 500m thick sequence of Palaeocene to Recent sediments deposited in fluvial to marine settings (Jones et al., 1994). The upper 100m in the central part of the basin now entrains large volumes of subsurface brines with salinities in excess of 100,000 mg/l. These brines feed many of the discharge playas in the region. They are

type II brines with major solute compositions and proportions very much like that of evaporated marine waters (thalassic groundwater). Their isotopic composition, however, is that of evaporated meteoric water. This led Jones et al. (1994) to the conclusion that the brines have been derived by the longterm accumulation of salt from marine aerosols, mixed with continental waters. The marine salts are blown into the basin either as dry salt suspensions or arrived as rainfall. Evapotranspiration in this semi-arid basin greatly exceeds rainfall and so solutes accumulate as brackish nearsurface waters. These shallow waters are further concentrated via capillary evaporation before escaping into saline discharge lakes. Regionally, the shallow groundwater flow regime is sluggish and not capable of dispelling these brines, so they infiltrate and accumulate above a regional aquitard.

Likewise, the $\delta^{34}\text{S}$ values of gypsum accumulating in modern playa lakes in the ancient landscape of southwestern Australia show little relationship with underlying bedrock types or the $\delta^{34}\text{S}$ values of any nearby bedrock sulphur (Chivas et al., 1991). Analysis of $\delta^{34}\text{S}$ from surficial lacustrine and pedogenic gypsum on a regional scale, in both Western Australia (Yilgarn Block) and South Australia, shows distance-related dispersal patterns over distances of 500 to 1000 km from the coast. The highest values ($\approx 21\text{‰}$) occur near coastlines decreasing to $\delta^{34}\text{S}$ values of $\approx 14\text{‰}$ further inland (Figure 2.18b). Marine sulphate is the dominant source of sulphur to the lakes investigated, with the proportion decreasing from approximately 100% near coastlines to around 55% further inland. For tens of kilometres inland of the modern coast, one can argue for a seepage origin of gypsum in many subsealevel lows (salinas) with active seawater seeps and appropriate drawdown surfaces. Further inland the gypsum in the various salt lakes reside in depressions that intersect a regional continental water table. This water table is metres or more above sealevel and it slopes seaward, so phreatic seawater seepage is not viable, yet the gypsum still has a marine isotope signature.

In some of the more interior Australian salt lakes, there can be a significant weathered bedrock component to the ionic components in the salt lake waters, especially where the bedrock contains abundant soluble sulphur and high levels of iron. Lake Cadibarrawirracanna (inland South Australia), for example, receives approximately 10% of its sulphur from weathering of the pyritic Bulldog Shale (Cretaceous); brine in nearby Lake Amadeus receives up to one-third of its sulphate from leaching of evaporites from the Neoproterozoic Bitter Springs Formation.

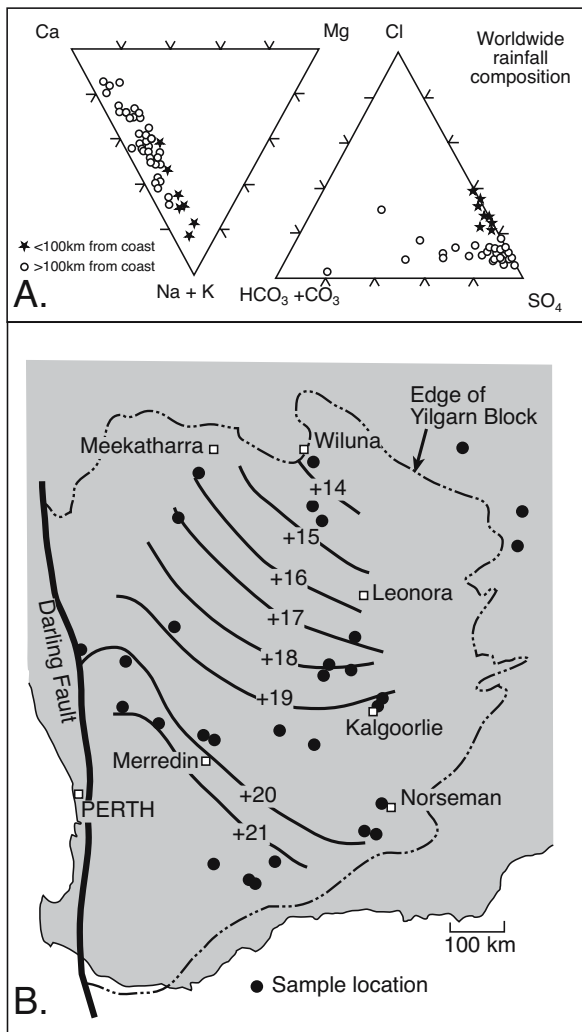


Figure 2.18. Marine aerosols can supply ions in solution to inland playas and lakes in low relief landscapes. A) Major ion content of worldwide rainfall in relation to distance from coastline, compiled from various sources listed in text. B) Changes in sulphur isotope values (mostly gypsum, occasionally from alunite; after Chivas et al., 1991).

Like much of arid inland Australia situated up to a thousand kilometres from the coast, the Namib Desert, which hosts one of Africa's most extensive accumulations of modern pedogenic and playa gypsum, is largely supplied by a variable combination of regolith runoff and marine aerosols (Figure 2.19a; Eckardt and Spiro, 1999; Eckardt et al., 2001). An extensive pedogenic gypsum accumulation forms a 50-70 km wide band parallel to the shore in the Central Namib Desert between the Kuiseb and Omaruru rivers. $\delta^{34}\text{S}$ analysis of calcium sulphate in this belt and the associated brines, along with an analysis of the brine chemistry shows marine aerosols are a major ion contributor

to the gypsum budget (Figure 2.19b). Marine aerosol sulphates are stored within widespread terrestrial gypsum deposits on the hyperarid gravel plain and are traceable as groundwater precipitates, including gypsum, in near coastal sabkhas and inland playas.

$\delta^{34}\text{S}$ values for the gypsum crusts are between +13.0 and +18.8‰, with lower values ($\delta^{34}\text{S} = +3.1$ to 3.4‰) in crusts near local bedrock sulphur sources, which are typically metal sulphide bodies. These Damaran bedrock sulphides show a wide $\delta^{34}\text{S}$ range from -4.1 to +13.8‰ but are significant sulphur sources only on a local scale. Dissolved sulphate in playa, sabkha, spring, borehole and ephemeral river waters have an overall $\delta^{34}\text{S}$ range between +9.8 and +20.8‰ but, unlike Australia, do not show a systematic geographical trend tied to distance from the coast. Even so, marine aerosols are the only viable supply mechanism for pedogenic sulphate over such a large arid near coastal area.

Atmospheric sulphates in the Namib are carried landward as marine aerosols, with a large proportion ultimately derived from decomposition of the dimethyl sulphide of phytoplankton. The plankton are an integral part of high levels of primary production driven by the upwelling of the cool Benguela current, the same oceanic system that creates the onshore aridity. The Central Namib Desert lies onshore from the thickest organic-rich sediment accumulations on the Namibian Shelf (Figure 9.11a). This suggests that some of the sulphate component in Namib gypsum is derived from marine H₂S during the anaerobic decomposition of this organic-rich sediment. The gas is probably carried into the desert by frequent advective fogs. Sea salt, decompositional marine biogenic and local bedrock sulphide sources, once invoked as the main sulphate source in these widespread gypsum accumulations in the Namib Desert, cannot account for the volumes of calcium sulphate unless the substantial dimethyl sulphide from plankton is also included in the sulphur supply cycle (Eckardt and Spiro, 1999). That is, most of the marine aerosol that drives extensive onshore gypsum accumulations is a mixture of marine sources of sea spray and atmospheric non-sea-salt (NSS) sulphate, largely supplied by oxidation of biogenic sulphur compounds - dimethyl sulphide, CH₃SCH₃ (DMS). Many organisms, including plankton and seaweeds, rid their bodies of sulphur (a biochemical waste product) by attaching it to various methyl compounds. They do the same with mercury, antimony and arsenic and other toxins. Such compounds are much more volatile than the original and so readily escape from cellular cytoplasm. Hence, a substantial portion of the sulphur isotope signature of pedogenic gypsum in the Namibian Desert reflects a biogenic marine source for

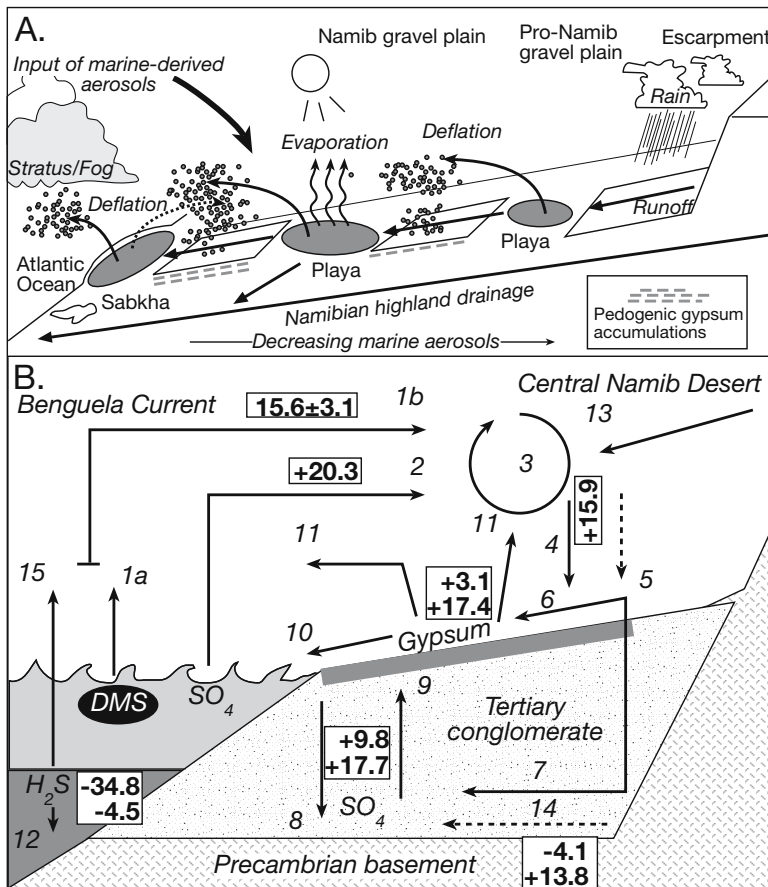


Figure 2.19. Pedogenic gypsum and the origin of sulphate in waters and sediments of the Namib Desert. A) Model of pedogenic gypsum formation for the Namib Desert where marine-derived dry aerosols are dissolved and mobilized through moisture provided by fog and rain water. Primary gypsum formation takes place in playas and is subjected to eolian and fluvial dispersal. Pedogenic gypsum accumulations increase towards the coast as the volume of marine supplied aerosol increases. B) Schematic representation of hydrogeochemical sulphur cycle along the Atlantic - Namib Desert interface (after Eckardt and Spiro, 1999). Solid arrows show sulphur pathways, potential sulphur pathways are indicated by dashed arrows. Range of $\delta^{34}\text{S}$ composition is indicated in boxed numbers. 1a = Dimethyl sulphide (DMS) released from phytoplankton; 1b = Non-sea-salt (NSS) sulphur; 2 = SO_4 release in sea spray; 3 = mixing of aerosols in the atmosphere; 4 = dry aerosol deposition; 5 = wet aerosol deposition; 6 = runoff and gypsum formation; 7 = infiltration and groundwater flow; 8 = capillary rise and gypsum precipitation; 9 = gypsum dissolution and infiltration; 10 = gypsum dissolution and runoff; 11 = eolian gypsum dust dispersal; 12 = in-situ sulphide and sulphate formation in Benguela sediments; 13 = subcontinental dust input; 14 = sulphide oxidation by groundwater; 15 = H_2S release to atmosphere. (after Eckardt et al, 2001).

the sulphur. The Benguela Current has been a major upwelling system dating back to the Late Miocene (10 Ma) and is likely to have generated DMS for a significant amount of that time.

Likewise, much of the gypsum in Atacama Desert soils below 1300m and within 90 km of the coast receive a portion of their

sulphate from coastal fogs. Soils within 50 km of the coast and below 800m elevation, receive 50% of their calcium and sulphur from marine aerosols (Rech et al., 2003).

In summary, the occurrence of modern continental evaporites, especially sulphates, exhibiting largely marine-like (thalassic) brine ionic chemistries and isotopic signatures, is in part due to marine aerosol input and in part due to regionally open or leaky meteoric hydrologies. Mineralogies of preserved evaporitic sediments in low relief depressions on stable cratons can be largely uncoupled from the surface lake chemistries and salt crusts. This leaky hydrology, in a landscape dominated by deep weathering, deep regionally circulating groundwaters, with variable reflux intensity (leakage) drives the evolution of seawater like ionic proportions in the subsurface. It is common to many modern, low-latitude, tectonically stable desert areas and differs from the less aerially extensive but better documented hydrologies of the Basin and Range and East African rift valleys. Perhaps the hydrologically open setting is the more relevant hydrochemical analog for the continental hydrologies of ancient interior redbed deserts of ancient continents. If so, models based on assumptions of evaporite mineralogies in desert redbeds as being indicators of various "closed basin" hydrologies are largely irrelevant. If so, it makes the hydrochemical distinction between marine and nonmarine evaporites in the geological record even more difficult.

Acid groundwater in continental saline systems

Many playas atop the deeply weathered ancient regolith in central and southern Australia have elevated iron and sulphur contents. Salt lakes with more elongate shapes outline Tertiary palaeovalley fills in palimpsest landforms that were created under a different climate than that of today (Figure 11.8; Clarke, 1994). From the mid-Eocene, the climate in

Australia became progressively drier until by Miocene times much of central Australia was dominated by perennial alkaline lakes (Alley, 1998). The subtropical style of weathering that prevailed in the Early Eocene slowly changed with the passage into the Neogene, resulting in the development of a more arid siliceous and ferruginous regolith. The present elevated iron and sulphur levels in the modern Australian landscape ("the Red Centre") were derived, to a large extent, from earlier deep weathering profiles and even today these relicts of a more tropical time are still cycling through the now-arid Australian regolith. Passage into drier conditions allowed the buildup of minerals such as alunite and gypsum in the weathered profiles. The resulting low relief, gently undulating landsurfaces formed partial etchplains with topography controlled largely by the elevation of the palaeoweathering front and associated erosional topography of an incised Tertiary-age palaeodrainage and duricrusts. Hilltops may today be composed of fresher rock, while valley slopes, pediments and pediplains are typically composed of fresh to saprolitic rock, along with residual ferricretes that form low mesas.

Palaeodrainage fills can locally be more than 100-200 m thick, with many palaeodrainage networks currently occupied by elongate playa lakes, often with lunette margins and separated by wide areas of desert soils and dune sands. Formation of the weathered regolith largely predated the incision of the palaeodrainage which, in its deepest parts, has cut through to fresh rock (Clarke, 1994). The older relict saprolite in the current landscape dates back to the Late Permian-Middle Jurassic. Stripping of this regolith occurred in the Middle Jurassic-Early Eocene during the formation of the seaward-sloping palaeodrainage system. For example, about 400 m of material was denuded from the Yilgarn Craton, to infill the Perth, Eucla and Great Australian Bight Basins. Ongoing deep weathering occurred concurrently with erosion as increasing aridity led to disorganization of the drainage to form numerous chains of lakes, which by the Pliocene had evolved into saline lakes. Some of these palaeovalleys today contain economic capillary uranium (calcrete) deposits.

The great age of the Australian landscape and the buildup of remobilised iron in the modern regolith has led to natural acid brine systems feeding into many inland playas such as Lake Tyrell in Victoria and Lake Yaninee in South Australia. The salt lakes are recharge depressions which supply free-convecting dense saline brine (Na-Cl-SO₄ reflux brines) to their underlying aquifers.

For example, Lake Tyrell, with an area of 185 km², is the largest of three salt lakes in the Tyrell Basin, a structural downwarp located some 10 km east of the N-S trending Tyrell Fault in

the riverine plain of the Murray river in semi-arid northwestern Victoria (Figure 2.20; Macumber, 1992). It is a well-studied example of a lunette-fringed lake where deflation plays a major role in controlling morphology and sediment thickness. It evolved into a dry lake some 32 ka, but is today water-covered for up to 3 months in the winter and early spring (Teller et al., 1982). Despite ongoing deflation, up to 5 metres of lacustrine sediment is found in the lake centre and consists of varying proportions of clay, silt and sand, covered by an ephemeral halite crust up to 30 cm thick. The lakebeds are underlain by the Parilla Sand, a regional sulphate-rich aquifer.

Lake Tyrell is part of the outcropping expression of a regional oxidised acidic groundwater mass with characteristically low pH of 2-4 and salinities between 35 and 115‰. In contrast to the regional acidic system, the reflux brine plume beneath the lake is neutral (pH ≈ 7) but with salinities around 240‰. Direct rainfall in the winter months provides the bulk of the surface water currently entering the lake, whereas regional discharge and evaporation of westward-flowing Parilla groundwaters contributes most of the salt load. Faulting to the west of the lake uplifts the Parilla Sand aquifer and effectively closes the basin to ongoing throughflow or outward seepage and augments groundwater discharge by halving the saturated thickness of the aquifer. An additional groundwater divide separates the shallower parts of the hydrology of Lake Tyrell from that of Lake Wahpool (Figure 2.20).

As the regional Fe and S-rich acidic groundwaters resurge into the spring zone about the saline lake edge they precipitate varying proportions of characteristic lacustrine mineral suites made up of varying proportions of alunite, jarosite, halite, gypsum, opaline silica and iron oxyhydroxides. All these mineral phases are rich in Al, Fe and SO₄ giving the oxidised portions of the spring-zone sediments a classic "red bed" appearance (McArthur et al., 1989, 1991; Long et al., 1992a,b; Alpers et al., 1992; Macumber, 1992; Benison and Goldstein, 2002).

Hemley et al. (1969) showed by experiment that a high H₂SO₄ concentration is needed for alunite (KAl₃(SO₄)₂(OH)₆) and jarosite (KFe₃(SO₄)₂(OH)₆) to form in any low pH lacustrine environment. Associated acid minerals in the alunite-jarosite family include; natroalunite, alunogen, jurbanite, basaluminite, and rostitite (all in the system Al₂O₃-SO₄-H₂O), along with natrojarosite, schwertmannite, halotrichite, melanterite, and copiapite (all in the system Fe₂O₃-SO₄-H₂O; Nordstrom, 1982a, b; Van Breemen, 1982; Bigham and Nordstrom, 2000). Once formed in acid settings, these acid minerals may undergo further reactions, breaking down into more stable forms of iron

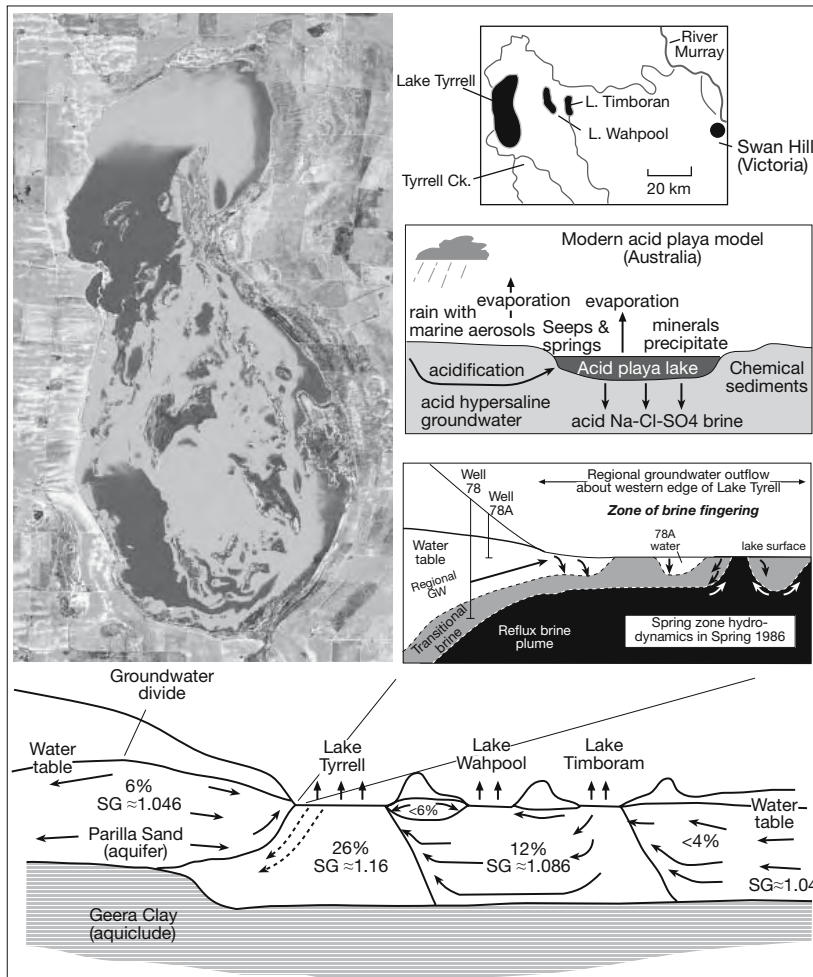


Figure 2.20 Acid lake formation based on modern natural acid lake and groundwater systems centred on Lake Tyrrell in southern Australia (after Macumber 1992; Lyons et al., 1995). These redbed siliciclastic sediments of the Parilla sand aquifer host sulphuric acid-rich saline lakes and groundwaters (pHs of 2–4) which precipitate alunite, jarosite, halite, gypsum, opaline silica, and possibly iron oxyhydroxides. Acidification may occur in the groundwater by processes such as oxidation of pyrite, ferrollysis, and microbial reduction of iron oxyhydroxides. Brine fingering typifies the mixing zone between regional groundwater outflow and the brine reflux prism beneath Lake Tyrrell (Landsat image courtesy of NASA).

oxides (i.e., goethite or haematite; Bigham and Nordstrom, 2000), sulphates (i.e., gypsum or anhydrite; Van Breemen, 1982), and aluminosilicates (i.e., microcline or albite; Long et al., 1992a).

What make them interesting is that these lacustrine redbeds indicate the influence of groundwaters carrying elevated levels of sulphuric acid (pH in the modern systems of Australia typically in the range 2–4) interacting with the neutral hypersaline waters of the lake itself. The regional waters of the regolith are very

different brines to the alkaline waters of well documented continental soda lakes and the marine-fed groundwaters of coastal salinas. Acid groundwaters in arid to semi-arid Australia indicate a landscape that has undergone a transition from tropical to arid conditions, perhaps related in part to Australia's northward drift, but more controlled by climate deterioration created by the transition from greenhouse to icehouse climate mode (Chapter 5).

Similar acid regolith/playa systems probably characterised much of the continental redbed interior of the USA in the Permian. Benison and Goldstein, (2002) argue such acidic saline deposits are commonplace in the rock record but largely unrecognised. They propose the following as criteria for the recognition of ancient acid saline lakes and groundwater deposits: (1) high HSO_4 in fluid inclusions in depositional and early diagenetic halite (or other evaporite minerals); (2) elevated concentrations of Al, as well as Fe and Si, in the same fluid inclusions; (3) identified remains of acidophilic bacteria or other acidophilic microbes; (4) acid minerals such as alunite or jarosite (or, more likely, the diagenetic products of acid minerals, such as gypsum or anhydrite); (5) presence of continental red beds; and (6) lack of widespread carbonate minerals. They go on to argue that many ancient red bed-hosted evaporite saline-pan and saline-lake deposits, which lack widespread bedded carbonates, are likely arid-zone outputs from ancient acidic hydrologies (Figure 5.13).

The spring seep region in the Lake Tyrrell outflow zone was one of the first wet playas documented with sinking brine plume fingers in the axial saucers of polygons of convective upwelling groundwater across the zone of phreatic mixing about the lake edge (Figure 2.20; Lyons et al., 1995). As upwelling regional groundwater reaches the Lake Tyrrell depression, it evaporates

and concentrates and so becomes denser. It then sinks to mix into the regional groundwater crossflow atop the Geera Clay aquiclude. Rather than sinking as a homogenous front these descending waters sink as denser brine fingers surrounded by upward flowing polygonal cells of fresher resurging groundwater that continually resupply the evaporating water surface (Figure 2.20). This convective counterflow creates large variations in fluid composition in short horizontal distances. Migration of the fingers over time creates numerous laterally migrating redox and salinity interfaces where diagenetic minerals can backreact and precipitate. This patchy diagenesis further complicates simple models for the distribution of the original “red-bed” precipitates and explains the complex counterplays of salinity indicators seen in ancient spring-seep strandzones (Chapter 1).

Based upon theoretical and experimental evidence, Wooding (1960) and Tyler and Wooding (1991) postulated that near the evaporating water surface, the downward movement of dense brine is confined to fingers or plumes of dense fluids, surrounded by an upward flow of fresher water supplying the evaporating surface. Similar convective polygons can also occur in freestanding zones of mixing near the strandzone edges of coastal salinas and saltworks. Tyler and Wooding (1991) showed that the conditions necessary for the onset of fingered polygonal convection beneath an evaporative wet playa surface are characterized by a modified Rayleigh number, R_c of the form:

$$R_c = (kg\Delta\rho)/(\mu\varepsilon)$$

where k is the intrinsic permeability (in cm^2), $\Delta\rho$ is the difference in density between the evaporated brine and the regional groundwater (in gm/cc), μ is the dynamic viscosity, ε is the evaporation rate and g is the acceleration due to gravity.

For a playa groundwater system to exhibit brine fingering, Tyler and Wooding (1991) and Ferguson et al. (1992) suggested that the Rayleigh criteria (R_c) must be around 10 or higher. Controlling factors leading to brine instability and convective fingering are sediment permeability, density contrast between the brine and regional groundwater outflow, and the evaporation rate. Using typical playa parameters of $\Delta\rho = 0.3 \text{ g.cm}^{-3}$ and $\varepsilon = 30 \text{ cm.year}^{-1}$, then the sediment permeability must be 10^{-9} cm^2 (100 md) or higher for the playa groundwater system to begin to polygonally convect. This permeability lies between that of unconsolidated clay and sand (Figure 10.4), suggesting that spring zones in sandy or permeable carbonate sediments, such as those typically found near playa and marine strandzone margins, are likely to exhibit brine fingering and

laterally migrating redox and salinity interfaces. Perhaps some of the megapolygonal patterns seen in domal stromatolites and tepees about the strandzone of Marion lake and other modern coastal salinas are the result of stable convective polygons in a resurgent brine hydrology (Figure 4.5b, c).

Contributions from evaporite bedrock

Difficulties in distinguishing marine versus nonmarine sources are further complicated by ongoing dissolution of older exhumed evaporites, which can act as chemical feeds into purely continental hydrographically-closed basins. In areas too continental for significant contributions from marine aerosols, this can still create marine-like signatures in the ionic proportions (Na-K-Mg-SO₄-Cl brines). For example, carnallite-sylvite-halite is a modern lake precipitate in Qaidam Basin, northern Qinghai-Xizang on the Tibet Plateau, China (Figure 11.2). This basin lies within a large, tectonically active region that is totally isolated from the effects of the ocean and is filled with Neogene clastics and evaporites. Its modern at-surface discharge playas are subject to intense evaporation and are characterised by ephemeral hypersaline brines as well as halite, potash and borate crusts and layers.

The chemical composition and Na/Cl ratios of the dissolved solutes in the modern brines and waters in the salt lakes of Qaidam Basin reveals three main sources (Vengosh et al., 1995): (1) Inflow of hot springs enriched in sodium, sulphate and boron. Evaporation of these waters leads to a high Na/Cl ratio (>1), a Na-Cl-SO₄ brine and an evaporite mineral assemblage of halite-mirabilite-borate (e.g. Lakes Daqaidam and Xiaoqaidam). (2) Inflow surface river waters, which are modified by preferential dissolution of older halite and potassium and magnesium salts. Evaporation of such waters creates Na-(Mg)-Cl brines with low Na/Cl (<1) and low Br/Cl, Li/Cl and B/Cl ratios. (3) Ca-Cl subsurface brines with chemistries controlled by both salt dissolution and dolomitization processes. Evaporation and salt crystallisation from mixtures of brines (2) and (3) leads to a “marine-like” Na-Mg-Cl brine with Na/Cl ratios <<1. Although more than 1,000 km from the nearest ocean the precipitated sequence of salts in these lakes is similar to that predicted for progressive evaporation of seawater. Lake Dabuxum and Qarhan playa today contain halite-sylvite-carnallite-bischofite successions.

The lower $\delta^{11}\text{B}$ values of the Qaidam basin brines and halites compared to seawater ($\delta^{11}\text{B} \approx 40\text{‰}$) indicate that the boron within these salt lakes is nonmarine (Figure 2.21; Vengosh et al., 1995). The $\delta^{11}\text{B}$ values of the dilute inflow waters to the

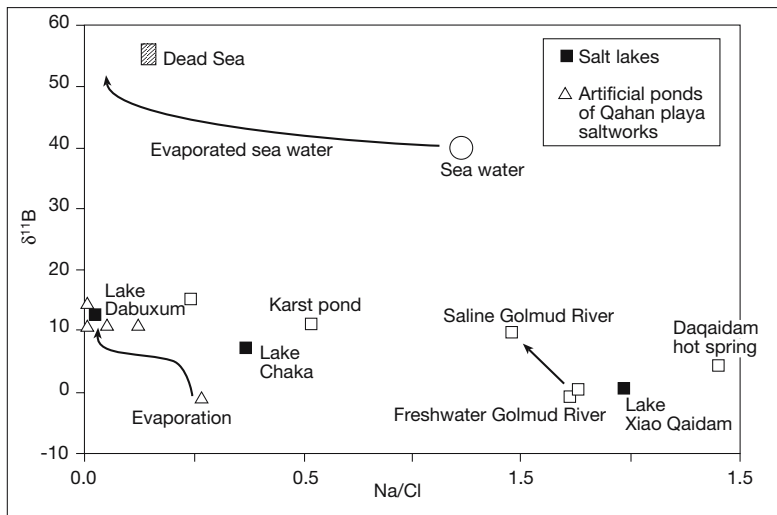


Figure 2.21. Boron isotopic and Na/Cl ratios of waters and brines in the Qaidam Basin, China (after Vengosh et al., 1995). See Figure 11.2 for locations.

Qaidam Basin range from -0.7 to $+10.9‰$, while brines in the various salt lakes range from $+0.5$ to $+15.0‰$ (Vengosh et al., 1995). Both groups overlap and are similar to those of associated granitic rocks ($\delta^{11}\text{B} = -2.12$ to $+3.7‰$) and hence indicate the nonmarine origin of these fluids.

In contrast to the Qaidam playas, the boron isotopic composition of brines, groundwaters and sediments of modern inland salt lakes located nearer the coast across southern Australia have a marine component, probably from aerosols (Vengosh et al., 1991). $\delta^{11}\text{B}$ values of brines in these salt lakes are 25 – $48‰$, with values up to 54 – $59‰$ in volcanic maar lakes in the higher rainfall areas near coastal region of southeastern Australia. Modern seawater has a $\delta^{11}\text{B}$ of $39‰$ (Figure 2.21).

Indicators of brine parenthood

Chemical and isotopic studies of various evaporite salts have been used for more than four decades in an attempt to define brine parentage. Bromine concentration and chlorine isotopes values have been used in this way to separate marine from nonmarine evaporite source brines, but are perhaps better indicators of salinities and stabilities of the parent brine. Sulphur isotopes can be used to indicate parentage, while the boron isotopic signature from brine inclusions in chevron halite is perhaps the best currently used tool for separating a marine from a nonmarine brine source. The lack of fractionation even with alteration and the creation of new indicator minerals well into the metamorphic realm means a boron isotopic signature in meta-evaporitic tourmalinites is still a reliable separator (Peng et al., 1998). Brine inclusions in unaltered sedimentary

halites are also useful indicators of both temperature and salinity, especially when microanalytic techniques are used to interpret the original brine chemistry. In the last two decades the microanalysis of brine inclusions in marine halites has led to a paradigm shift in our notions of the ionic stability of Phanerozoic seawater (Figure 2.30).

Bromine profiles - brine genesis or stability?

Trace elements in halite and other salts can sometimes help support an interpretation of a marine origin of the mother brine, especially if microanalytic techniques are used to determine fluid inclusion contents within the salts of interest and the sampled crystals retain primary sedimentary textures, such as bottom-aligned chevrons in halite. Bromine is fourth in anion abundance in seawater anions after Cl, SO_4 and HCO_3^- ($0.0671\text{ gm}/1000\text{ gm}$ seawater). With an ionic radius of 1.96 \AA it easily substitutes for chlorine (1.81 \AA) in the halite crystal lattice as well as in the other chloride salts. Numerous experiments have found halite's Br-concentration increases in tandem with the bromide concentration of the parent brine, its level in a halite crystal also increases with increases in parent brine temperature and in the speed of crystallisation.

Fixation of Br in the halite lattice is also dependant on the level of other ionic species present in the solution. Cl is strongly preferentially partitioned over Br into Na, K and Mg halogen salts during their precipitation and Br preferentially remains behind in solution (Figure 2.5). Br content decreases with increasing MgCl_2 content in the mother brine and with any increase in the degree of secondary recrystallisation (Dean, 1978). Its conservative behaviour in marine brines means that it has commonly been used as a salinity indicator in ancient halites and other chloride minerals.

The distribution of bromine between a halite crystal and the co-existing solution is described by its partition coefficient (D):

$$D = (\text{Br}_{\text{mineral}}/\text{Cl}_{\text{mineral}})/(\text{Br}_{\text{solution}}/\text{Cl}_{\text{solution}})$$

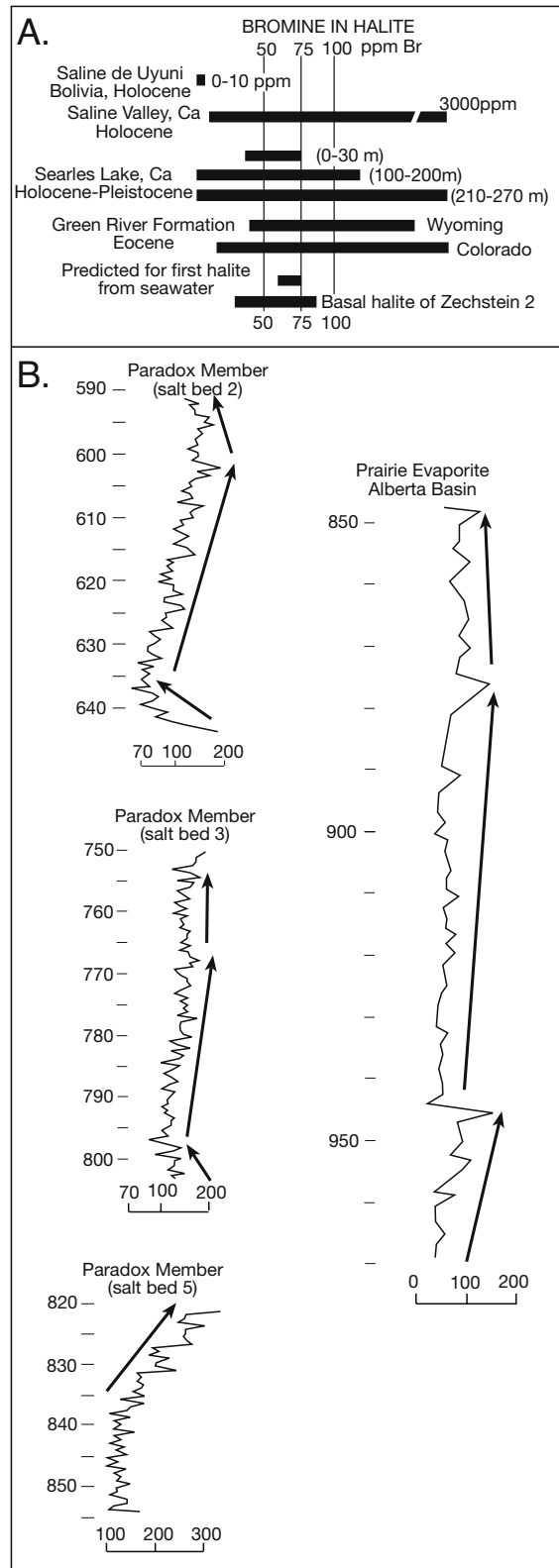
During initial evaporation of seawater, both Br and Cl increase in concentration in the residual brine, and the Br/Cl content of these waters does not vary (Figure 2.5). When halite saturation

is reached, Cl is preferentially removed over Br from the brine. A small fraction of the Br is also partitioned out into the halite, but most remains behind in the brine. As saturation with the bitterns (K-Mg-Cl) salts is reached, the slope of the Br-Cl curve flattens out as these minerals discriminate somewhat less in terms of Br incorporation (higher partition coefficients).

In earlier studies the Br content of ancient rock salt was used to separate marine from nonmarine precipitates (Dean, 1978; Holser, 1979; Wilgus and Holser, 1984). Fresh seawater contains around 65 ppm bromine and reaches 500 ppm by the onset of halite precipitation (Figure 2.5). Halite from a normal marine feed purportedly contains 50 to 100 ppm bromide and it should increase up to a maximum of around 270 ppm at the onset of bittern precipitation (Valyashko, 1956, p. 578). Halite that has been recrystallised in a second cycle of solution and reprecipitation in a brine of lower Br content than the original brine should have a bromide content of 20 ppm or less, especially if the recycling waters were nonmarine. But variations in salinity and the dilution by shallow to ephemeral residual brines, along with recrystallisation and backreaction, all influence the final Br content of any halite crystal in both marine and nonmarine settings (Figure 2.22a). Hardie (1984) discussed the limitations of using whole rock Br content as a depositional indicator and clearly showed the possible confusion that results if Br levels in wholerock halite samples are used in an attempt to separate marine from nonmarine halite.

Even if Br content of halite is not always a reliable indicator of the source of the mother brine, perhaps it can tell us something about brine stability at the time a salt was precipitated. Figure 2.22b plots bromine profiles from halites in two saline giants, the Paradox and the Prairie evaporites where values change in a predictable fashion upsection. Increasing upward trends indicate an increase in average annual brine salinity, while decreases indicate freshening (shown by arrows in Figure 2.22b). The trend to very high values (Br > 250 ppm) near the upper part of salt member 5 of the Hermosa Formation in the Paradox occurs beneath a potash bed and indicates higher salinities needed for the precipitation and preservation of bittern salts. The upward trends for the Prairie evaporite, although sampled at a some-

Figure 2.22. Bromine in halite. A) Bromine levels in halite in marine and nonmarine settings clearly showing that bromine levels have a degree of spread that does not support the assumption that nonmarine or recycled halite will always show values less than first cycle precipitates (in part after Hardie, 1984). B) Br profiles from the Paradox Member, Hermosa Formation in the Paradox Basin and the Prairie Evaporite in the Alberta Basin. All wells drawn to the same depth scale (after Holser, 1966, 1979).



what coarser spacing than the Hermosa, show similar brining upward profiles beneath potash beds. In a similar fashion Bein et al. (1991) used Br variations in brine inclusions in halite to define a southerly brine source for Permian San Andres halite in the Palo Duro Basin, Texas.

Contents of most other trace elements in marine evaporite salts are typically very low and not diagnostic of brine source. Iodine has very low partition coefficients in halite, sylvite, carnallite and the other bitterns, so they contain very little iodine. Its relatively large ionic radius impedes its replacement of chlorine ions in the respective lattices, so any residual liquor (marine or nonmarine) is strongly enriched. Iodate salts form pedogenic phases in the hyperarid Atacama desert (Chapter 11). Fluorine minerals occurs principally in sulphate deposits and salt clays that possibly have been influenced by hydrothermal inflows, although some Russian authors have argued for a marine evaporite association (Figure 7.68). There is no published data on fluorine behaviour during seawater concentration. However, if fluorine concentrates at the same rate as Cl during evaporation, then seawater should have a fluorine concentration around 10 mg/l at the onset of halite saturation. Rubidium and ammonium substitute for potassium in crystal lattices of the bittern chlorides (e.g. sylvite, carnallite). Cesium does not occur in halite, and lithium in water-soluble form is only found in concentrations up to 0.2 ppm. The colouring of halite often feigns higher amounts of heavy metals. Only 2 ppb of trivalent iron can give halite a yellow colour, while a few more parts per billion can turn salt red (Sonnenfeld, 1995).

Sulphur and oxygen isotopes

Modern seawater sulphate has a homogeneous and well-defined isotopic composition for both sulphur and oxygen:

$$^{34}\text{S}_{\text{SO}_4} = +20 \pm 0.5\text{‰ CDT}$$

$$^{18}\text{O}_{\text{SO}_4} = +9.5 \pm 0.5\text{‰ SMOW}$$

Likewise, the fractionation of sulphur and oxygen, which occurs during the transition from aqueous to solid state of sulphate is also near constant at earth surface temperatures. For gypsum, the mean values of the isotope enrichment factor are (Pierre, 1988):

$$\epsilon^{34}\text{S}_{\text{gypsum}-\text{SO}_4} = 1.65\text{‰}$$

$$\text{and, } \epsilon^{18}\text{O}_{\text{gypsum}-\text{SO}_4} = 3.5\text{‰}$$

Thus the $\delta^{34}\text{S}$ and $\delta^{18}\text{O}$ values of sulphate evaporites are directly related to the state of the aqueous sulphate reservoir where precipitation occurred. A plot of ancient marine CaSO_4 evaporites shows the sulphur curve for seawater has varied across time from +30‰ in the Cambrian, to around +10‰ in the Permian and it increased irregularly in to Mesozoic to its present value of +20‰. Oxygen values show much less variability (Figure 2.23a). Variations are reflected in all major marine evaporites and were most likely controlled by major input or removal of sulphides from the oceanic reservoirs during changes in tectonic activity and weathering rates. Simple removal of oceanic sulphate (increase in evaporite formation) would probably not be accompanied by such dramatic isotopic effects.

Rather, variations within the global sulphur cycle are controlled by a redox balance, which is also linked to the carbon cycle and the atmospheric oxygen budget. The oxidative part of the global sulphur cycle is governed by continental weathering (especially of marine black shale), riverine transport and evaporite deposition, while the reduced part is controlled by levels of fixation of reduced sulphur-bearing compounds in the sediment column, mostly as pyrite via bacterial sulphate reduction. The latter process will preferentially remove isotopically light sulphur from seawater and so increase its $\delta^{34}\text{S}$ value in the ocean and any subsequent marine evaporite salt. Another cause of variation in the evaporite-derived sulphur isotope curve of seawater is variation in the rate of high-temperature flushing of seawater through the ocean ridge system and varying input of mantle sulphur to the labile volcanics of the mid-ocean ridges. Thus, the sulphur isotopic composition of seawater sulphate in marine evaporites documents variation in longterm earth-scale processes (i.e. uplift and erosion, mantle input) and aspects of biological evolution (e.g. bacterial sulphate reduction).

The ^{18}O content in seawater sulphate is more stable than sulphur values over geologic time. The isotopic composition of sulphate minerals varied only slightly from the Neoproterozoic to the Palaeozoic decreasing from +17 to +14‰ (Figure 2.23a). Values then rose during the Devonian to reach +17‰ during the Early Carboniferous (Mississippian). Values then fell to +10‰ during the Permian, mimicked by a similar decline in sulphur values in the Late Permian to Early Triassic. Since a rise to +15‰ in Early Triassic values of marine sulphate minerals have remained close to +14‰ (add 3.5‰ to mineral determined value to give ambient seawater value). Overall, oxygen values show little correlation with marine sulphate variation and are perhaps controlled by sulphide weathering reactions that contribute sulphate to seawater and the dissolution of sulphate evaporites. Further discussion on global controls

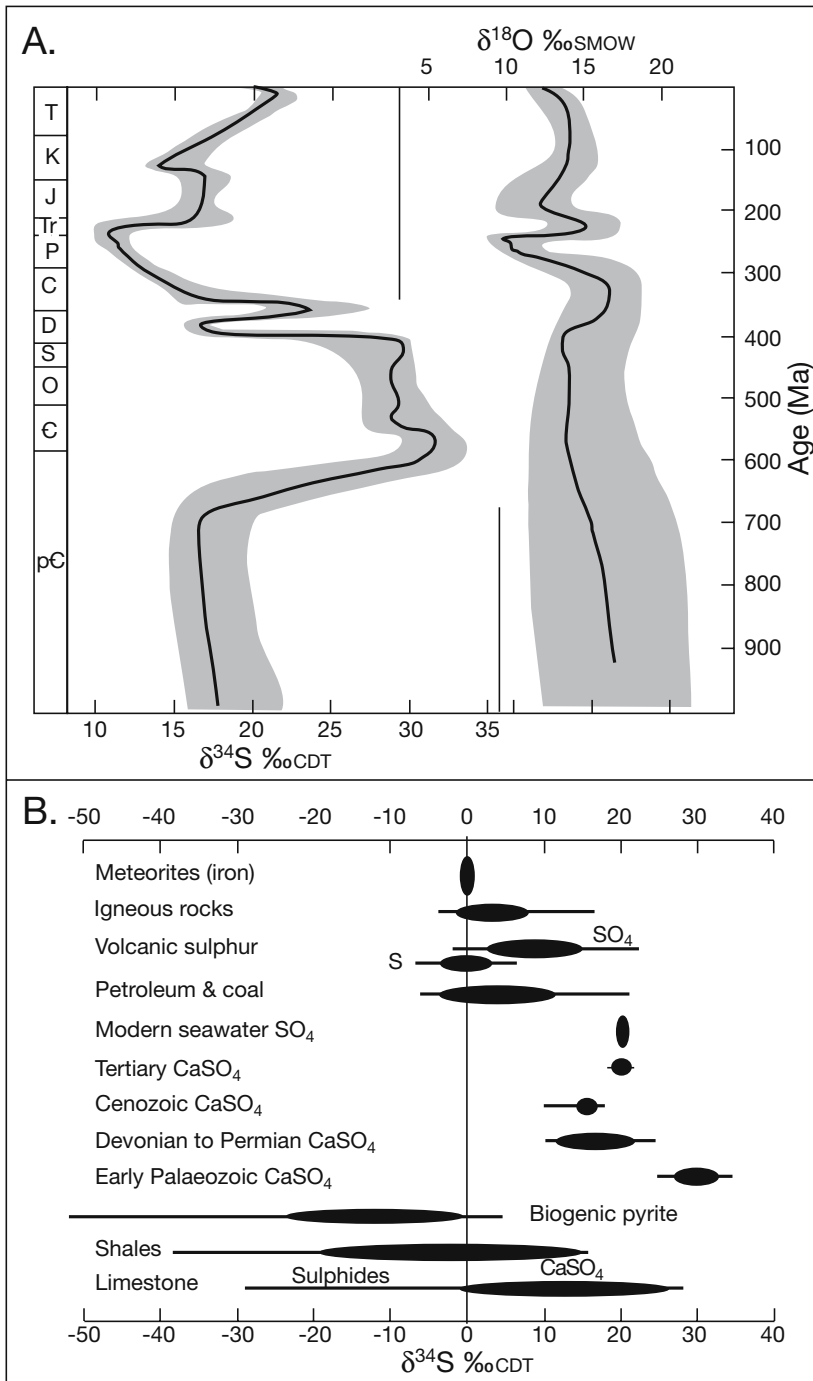


Figure 2.23. Sulphur and oxygen isotopes. A) Sulphur and oxygen isotope age curves for marine sulphate evaporites. The heavy lines are the best estimates of $\delta^{34}\text{S}$ and $\delta^{18}\text{O}$ values of calcium sulphate minerals in equilibrium with world ocean sulphate at that time. Shaded areas are estimated uncertainty envelopes of these curves. B) Isotope range of various systems and selected seawater sulphate (after Pierre, 1988; Veizer et al., 2000).

of isotope chemistry lies outside the evaporite focus of this book. What is significant is that, given the now well established sulphur isotope age curve, a comparison of a measured $\delta^{34}\text{S}$ value from an anhydrite or gypsum of known geological age to the curve allows an interpretation of a possible marine origin to the salt. A value which differs from the marine signature does not necessarily mean a nonmarine origin, but at the least it does mean diagenetic reworking or, more likely, a groundwater-induced recycling of sulphate ions into a nonmarine saline lake (Pierre, 1988). Such oxygen and sulphur isotopic crossplots have been used to establish the continental (nonmarine) origin of the Eocene gypsum of the Paris Basin and the upper Miocene gypsum of the Granada basin, with sulphate derived from weathering of uplifted Mesozoic marine evaporites (Fontes and Letouolle, 1976; Rouchy and Pierre, 1979; Pierre, 1982). Sulphur in evaporitic sulphate can come from a number of sources other than reworked marine evaporites, likely isotopic ranges of possible sources are given in Figure 2.23b.

Crossplots of oxygen with carbon or deuterium isotopes are useful in defining the origin of evaporitic carbonates. If these carbonates are interlayered with gypsum or anhydrite at the mm scale, then their signatures are very useful in determining the origin of the waters precipitating both the carbonates and the sulphates. This was the rationale used by Bellanca and Neri (1986) in a study of the origin of gypsum and associated carbonates in the Messinian of Sicily. The oxygen and hydrogen isotope compositions of crystal water from the laminar gypsum indicate primary precipitation of the sulphate from marine waters concentrated by evaporation (Figure 2.24a). The iso-

topic data also show compositional changes due to periodic influx of continental waters into the depositional basin seen by the clustering of the laminar gypsum values along the SMOW concentration-dilution line with a regression coefficient of 0.98. The massive gypsum signature indicates rehydration by meteoric waters (probably modern). Open-marine-water incursions probably led to the deposition of carbonate layers overlying the laminar gypsum. These contain abundant aragonite with textural features and isotopic compositions suggesting precipitation in shallow and quiet marine waters slightly enriched in ^{18}O by evaporation (Figure 2.24b).

Sulphur is largely resistant to isotopic fractionation during burial alteration and transformation (Worden et al., 1997). Primary marine stratigraphic sulphur isotope variation is preserved in anhydrites of the Permian Khuff Formation, despite subsequent dehydration to anhydrite during burial ($\approx 1,000\text{m}$) and initial precipitation as gypsum from Permian and Triassic seawater. Gypsum dehydration to anhydrite did not involve significant isotopic fractionation or diagenetic redistribution of material in the subsurface. At depths greater than 4300 m, the same sulphur isotope variation across the Permian-Triassic boundary is still present in elemental sulphur and H_2S , both products of the reaction of anhydrite with hydrocarbons via thermochemical sulphate reduction (Figure 9.44). Clearly, thermochemical sulphate reduction did not lead to isotope fractionation. Worden et al. also argues that significant mass transfer has not occurred in the system, at least in the vicinity of the Permian-Triassic boundary, even though elemental sulphur and H_2S are both fluid phases at depths greater than 4300 m. Primary differences in sulphur isotopes have been preserved in the rocks and fluids, despite two major diagenetic overprints

that converted the sulphur in the original gypsum into elemental sulphur and H_2S by 4300 m burial and the potentially mobile nature of some of the reaction products. That is, all reactions occurred must have occurred *in situ*; there was no significant sulphur isotope fractionation, and only negligible sulphur was added, subtracted, or moved internally within the system.

Boron Isotopes

Boron isotope determinations on halite, borate salts, and brines are all capable of distinguishing between marine and nonmarine sources (Figures 2.25; Vengosh et al., 1992; Swihart et al., 1986). Marine evaporites are characterised by distinctly higher $\delta^{11}\text{B}$ values (+18.2 to +31.7‰) than non-marine evaporites (-30.1 to +7.0‰; Swihart et al., 1986). The latter span the range typical of the boron isotope signatures of most other rock types (Palmer and Helvacı, 1997). Likewise, there is a clear isotopic separation between marine and nonmarine brines (Figure 2.25a, c).

The separation reflects the enrichment of the ^{11}B isotope in seawater compared with both oceanic crust and continental crust. Differences are due to the original isotopic fractionation that occurred when boron was extracted from seawater into detrital clays, weathered basalts and carbonate minerals. Continental evaporite brines are derived from the weathering of these various lithologies, while the boron in seawater comes straight from the concentration of seawater. Much of the boron signature that is measured when whole rock halites and other salts are analysed comes from the fluid inclusions and not from boron in the lattice structure. The low level of fractionation between the brine and its precipitate at the time of halite deposition

means boron isotope analysis can reliably distinguish nonmarine and marine brine parents in modern salts, even in complex multisource systems such as Lake Qaidam (Liu et al., 2000).

Beyond the halite precipitation field $\delta^{11}\text{B}$ values tend to increase with increasing concentration in both brine and the associated bittern precipitates. In all fields the $\delta^{11}\text{B}$ values and boron contents are higher in brine than in its precipitated halite suite (Figure 2.25b; Vengosh et al., 1992). However the boron is not

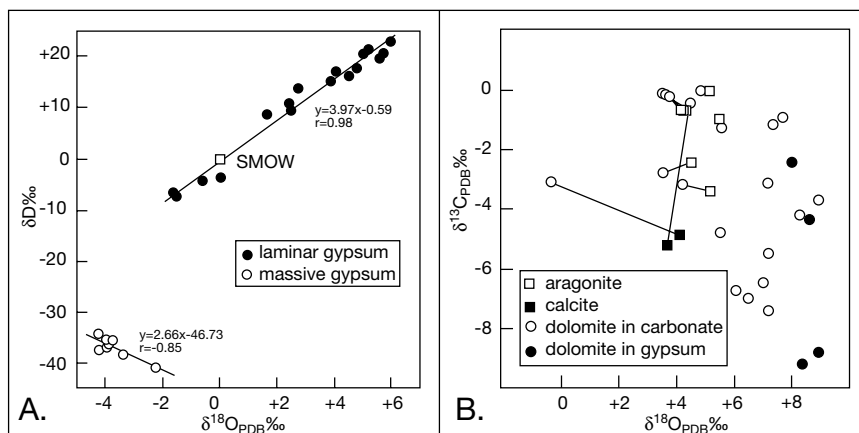


Figure 2.24. Isotope crossplots in Messinian evaporites, Sicily. A) Isotopic associations (carbon and oxygen) in water of crystallisation. B) Deuterium-carbon relationships in carbonate layers in the same units (after Bellanca and Neri, 1986).

Lake Name	Constituents in brine				Constituents in halite				
	pH	B(μg/ml)	Na/Ca	δ ¹¹ B(‰)	B(μg/g)	δ ¹¹ B(‰) Run1	δ ¹¹ B(‰) Run 2	δ ¹¹ B(‰) Run 3	δ ¹¹ B(‰) Average
Gasikule	7.11	101.6	193.8	17.9	8.0	12.1±0.3	12.5±0.1	-	12.3
Mahai	7.98	162.9	208.3	-4.0	11.6	-4.7±0.2	-5.1±0.1	5.3±0.1	-5.0
Balun	6.50	10.1	12.1	31.4	0.4	25.7±0.3	25.9±0.1	-	25.5
Xiaochaidam	8.14	285.6	167.0	-0.5	13.0	0.4±0.1	0.4±0.1	-	0.4
Dachaidam	7.78	404.3	255.7	5.3	16.0	3.7±0.1	3.7±0.1	-	3.8
Chaikai	7.68	15.4	130.6	9.9	7.4	5.6±0.1	5.6±0.1	6.1±0.1	5.9
Niulang	5.34	53.6	0.7	24.5	3.8	-	-	-	20.0

Table 2.8. Boron isotopes in the brines and halite crusts of various salt lakes in the Qaidam Basin, China (after Liu et al., 2000).

behaving in an absolutely conservative fashion and there is a deficiency of boron in the increasingly saline brines and a concurrent increase in the boron content of the associated salts (Table 2.8; Liu et al., 2000). The highest δ¹¹B values in the Qaidam Basin are associated with fluids with low B/Li ratios, indicating selective removal of elemental boron and ¹⁰B by

adsorption onto clay minerals along the flow path into the basin (Table 2.8; Liu et al., 2000). The magnitude of ¹¹B enrichment due to adsorption differs by 15-20‰ from the supply, and thus nonmarine brines are still distinguished from marine-derived evaporitic brines, which have much higher δ¹¹B signatures in the range +39 to +59‰ (Figures 2.25a, d).

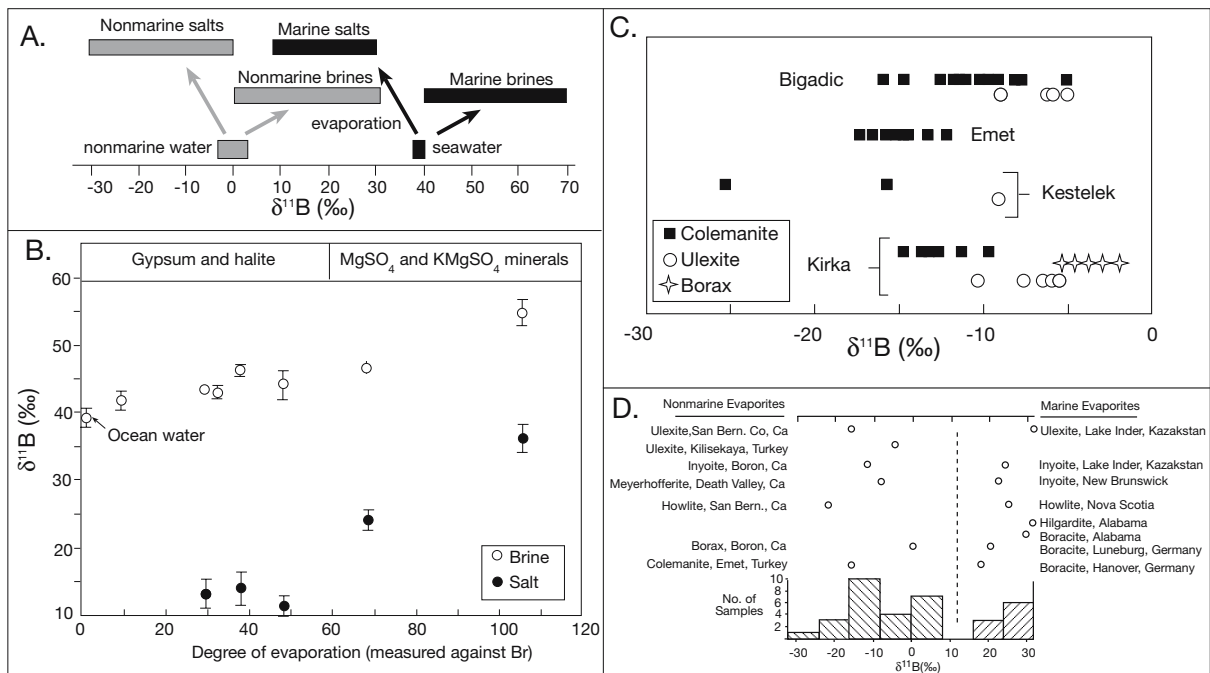


Figure 2.25. A) Isotopic distribution of boron in evaporatively formed marine and nonmarine brines and salts related to signature of original water source. B) δ¹¹B values of evaporated seawater (open circles) and co-existing precipitated halite (closed circles) versus degree of evaporation as calculated from Br values. Note the relative enrichment of ¹¹B in brines relative to salt and the difference in magnitude of enrichment during different stages of evaporation (after Vengosh et al., 1992). C) Ranges of boron isotope values in various minerals in the main Turkish borate deposits- see also Figure 11.30 (after Palmer and Helvacı, 1997). D) Isotopic analysis of evaporitic borates worldwide showing clearly separate fields for marine and nonmarine samples (dashed line). The upper part of figure shows analytical determinations from various deposits, the lower part shows a histogram where these values are grouped (after Swihart et al., 1986).

Palmer and Helvacı (1997) found that the isotopic values of the main borate minerals in the major Turkish borate deposits are largely controlled by their mineralogy and the pH of the brines from which they precipitated. For example, the differences in the $\delta^{11}\text{B}$ values of the three main borate minerals at Kirka (colemanite, ulexite and borax) are greater than would be expected if they had precipitated in equilibrium with one another from a solution with the same $\delta^{11}\text{B}$ value and pH (Figure 2.25c). The data are consistent with all three minerals being primary precipitates from a concentrated brine, with colemanite precipitating from a brine of lower pH than ulexite, and borax precipitating from a brine of higher pH than ulexite. The only other Turkish deposit in which there are significant amounts of coexisting primary borate minerals is at Bigadic, which contains coexisting ulexite and colemanite (Figure 11.31). There the average $\delta^{11}\text{B}$ value of ulexite is -6.8‰ , this is 3.6‰ higher than that of colemanite -10.4‰ (Figure 2.25c). This difference suggests that colemanite precipitated at a lower pH than ulexite (Palmer and Helvacı, 1995).

Chlorine isotopes

Unlike the stable isotopes of boron and sulphur, which can be used as indicators of parent brine type, ^{37}Cl interpretation is more problematic due to its inherently low levels of fractionation during evaporation. Prior to the early 1980s, this meant analytical methods lacked the precision needed to detect small variations in chlorine isotopes levels that occur

in nature. Measurements have now improved to where even small fractions in natural halites can be reliably and accurately determined (Long et al., 1993). Earlier work also suffered from a poor understanding of evaporitic fractionation mechanism and it was only in the mid 1990s that our understanding of ^{37}Cl determinations evolved into a useful environmental tool in an evaporite basins (Eggenkamp et al., 1995). Ongoing impermeability and a lack of reactivity away from the edge of a halite mass means that depositional isotope values will persist, even in tectonised evaporites or in evaporites that have undergone recrystallisation (Eastoe and Peryt, 1999).

Eggenkamp et al. (1995) determined a fractionation of $0.26 \pm 0.07\text{‰}$ between halite and a NaCl solution at 25°C . Halite crystallising from a 0.00‰ NaCl solution will therefore have an initial value of $0.2\text{--}0.3\text{‰}$. Halites precipitated from seawater brines show decreasing values from 0.2‰ at the onset of halite precipitation to -0.5‰ by the hexahydrite precipitation stage (Eastoe et al., 1999). Using seawater, Eggenkamp et al. (1995) showed that the $\delta^{37}\text{Cl}$ value decreases in the halite stage from 0.0 to -0.45‰ . During the subsequent kainite and carnallite stages the fractionation factor is close to unity and the $\delta^{37}\text{Cl}$ of the brine is only 0.04‰ . In the subsequent bischofite stage the fractionation factor is < 1 and $\delta^{37}\text{Cl}$ increases during the final stages of evaporation. The $\delta^{37}\text{Cl}$ values of precipitates in the halite stage decreases from 0.26 to -0.19‰ (Figure 2.26). In the kainite stage, the precipitate (a mixture of salts) has a $\delta^{37}\text{Cl}$ that decreases to -0.34‰ and then to -0.47‰ in the carnallite stage. However in the last stage, typified by the precipitation of bischofite in the mix, the $\delta^{37}\text{Cl}$ value increases from -0.55‰ back into positive values in the very latest stages of evaporation before complete dryness. Error ranges in determinations increases after the end of the halite stage. Because $\delta^{37}\text{Cl}$ values decrease monotonically with concentration in the halite stage, it is possible to use $\delta^{37}\text{Cl}$ values in unaltered halites (chevron halite) to estimate the concentration stage at the time of precipitation of an ancient halite (palaeosalinity determination). At later bittern stages this methodology is less effective and more subject to ambiguities (Eggenkamp et al., 1995).

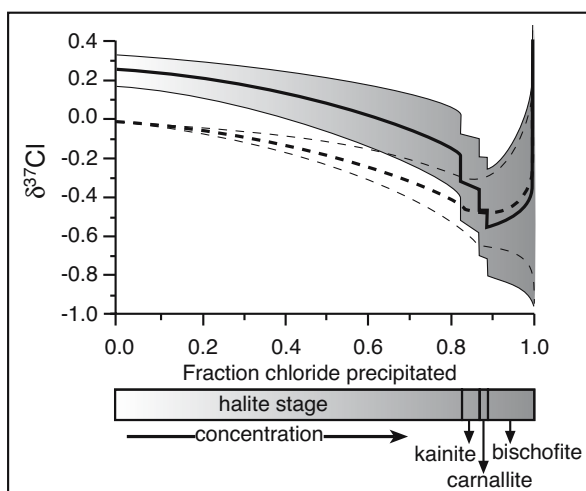


Figure 2.26. Calculated $\delta^{37}\text{Cl}$ values of the precipitate and residual brine during seawater concentration. The shaded area indicates the error range for the precipitates (solid line), while the area between the dashed lines is the error range for the residual brine. Note the discontinuities in the curve for the precipitates (after Eggenkamp et al., 1995).

That this methodology works is clearly seen in a study of the $\delta^{37}\text{Cl}$ signatures of the ZIII interval of the Permian Zechstein salts in the TR-2 well in the Netherlands (Figure 2.27a). The interval is a combination of halite and bittern stage salts. The halite-dominated interval (Z.III.2a) has a simple salt chemistry with minor amounts of carnallite, bischofite and kieserite. $\delta^{37}\text{Cl}$ values tend to decrease upward into the overlying carnallite-kieserite interval at 1660 m, implying increasing salinities as the unit passes up into the bittern-dominated succession. Sam-

ples in the bittern-dominated intervals (Z.III.1b and Z.III.2b) show high levels of carnallite, kieserite and bischofite and values that tend to be toward the lower end of the $\delta^{37}\text{Cl}$ value scale, consistent with higher supersaline salinities needed to precipitate these salts, sylvite ore brines show a similar highly negative signature.

Other ancient bedded halites also lie in the marine supersaline range. For example, bedded Permian halites in the Palo Duro basin, situated immediately above and below a halite bed preserving chevrons, show primary $\delta^{37}\text{Cl}$ values of 0.4 to around 0.0 ‰ (Figure 2.27b). Waters driving the recrystallisation cannot have been generated by later meteoric dissolution and recrystallisation. Rather, these recrystallised halites preserve their Permian depositional signatures (Eastoe et al., 1999). This conclusion supports the notion that subsurface salt beds intercalated with remnant chevrons are largely impervious closed systems that dissolve from the edges inward (Figure 8.7). It means any temperature and salinity values measured in brines in microinclusions in the chevron halite will indicate ambient conditions at the time of halite precipitation (e.g. Figure 2.28). It is also why viable Permian haloarchaea can be cultured from such inclusions (Vreeland et al., 2000).

In contrast, nonmarine chloride contributions to a basinal brine precipitate halite with a more positive $\delta^{37}\text{Cl}$ value. Carpathian (Middle Miocene) halokinetic halite has $\delta^{37}\text{Cl}$ values greater than 0.4 ‰, as do some halites in the Gulf of Mexico, the North Sea and the Paris Basin (Figure 2.27b). Such positive values cannot arise solely from seawater evaporation and require a considerable input of nonmarine chloride, either from a continental meteoric or igneous/hydrothermal source (Eastoe and Peryt, 1999).

The contrast between halite with a hydrothermal signature and that preserving original syndepositional values is clear in

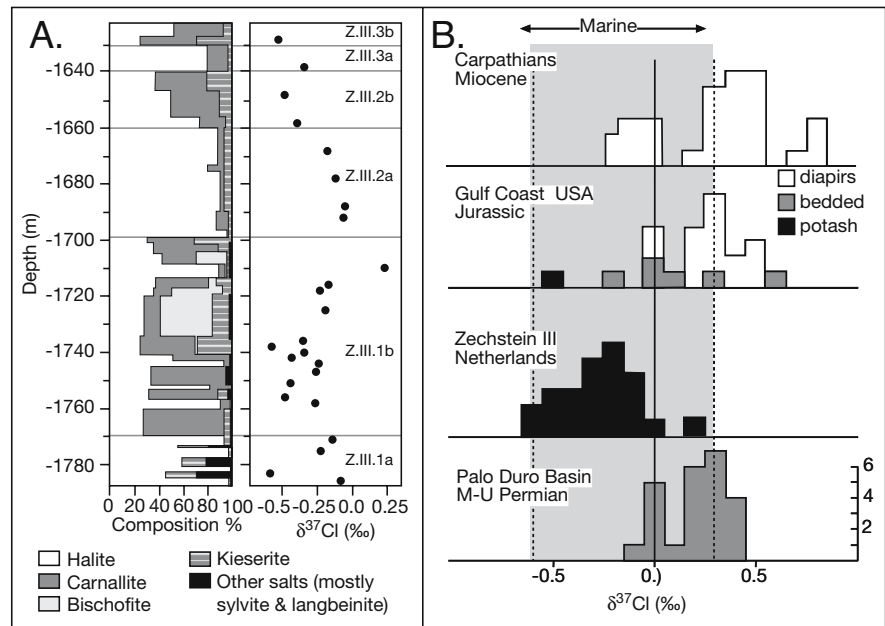


Figure 2.27. $\delta^{37}\text{Cl}$ isotope as an environmental indicator. A) Isotopic and mineralogic composition of Zechstein III showing that in these marine salts the $\delta^{37}\text{Cl}$ isotopic values are typically higher in the halite layers than in carnallite and bischofite layers (after Eggenkamp et al., 1995). B) Isotopic values of selected halites showing marine values are typically less than 0.4 ‰ and centred on 0.0 ‰ (after Eastoe et al., 2001).

Jurassic halite in the Gulf Coast Basin (Eastoe et al., 2001). Halite has a $\delta^{37}\text{Cl}$ range of -0.5 to 0.3 ‰ in most bedded salt and 0.0 to 0.5 ‰ in diapiric salt. The values for bedded salt are consistent with a $\delta^{37}\text{Cl}$ value of 0.0 ‰ for Jurassic seawater chloride, as in modern oceans. The slightly higher values for diapiric salt are possibly caused by incongruent solution of halite (Figure 8.30).

Chloride isotopes in subsurface waters can indicate their provenance and show a $\delta^{37}\text{Cl}$ range of -1.9 to 0.7 ‰ (Eastoe et al., 2001). Formation waters in the Gulf of Mexico with $\delta^{37}\text{Cl} < -0.6$ ‰ are confined to geopressed Eocene to Miocene strata at depths of 2500m or greater. Strongly negative values do not occur in Plio-Pleistocene strata, which retain the values of seawater (connate brines), nor do they occur in Mesozoic strata, which are marine carbonates. It seems that the strongly divergent values come from chloride in waters released from shales undergoing the smectite-illite transformation in the zone of geopressure.

Low $\delta^{37}\text{Cl}$ values in such waters are related to low $m_{\text{Cl}}/m_{\text{Na}}$ (a parameter indicating dewatering) but show no general relationship to Cl/Br ratios (Eastoe et al., 2001). They are consistent with diffusion of chloride from an allochthonous brine. Dif-

fusion can generate domains of water with negative $\delta^{37}\text{Cl}$ on a scale of hundreds of metres in 10^4 – 10^6 years, and may also generate positive $\delta^{37}\text{Cl}$ chloride in residual source brine. The expulsion of such brines into an evaporite basin may account for most non-0 ‰ chloride sources in evaporite basins.

The experiments of Eggenkamp et al. (1995; Figure 2.26) were limited to a single seawater evaporation cycle, but evaporites accumulating in shallow pans in marine and continental settings are subjected to multiple cycles of dissolution and partial reprecipitation before their burial. This can bring about measurable changes in $\delta^{37}\text{Cl}$, but also leaves little residual halite within the total halite mass.

Fluid Inclusions and brine temperatures

When halite and other salts are precipitated, they can capture and enclose inclusions of ambient brine. Such inclusions form the cloudy lamina that outline milky halite chevron and cornet textures and are used to indicate primary growth orientations of crystals in ancient salt beds (Figure 1.32a). Inclusion-rich bands indicate episodes of rapid growth, while clearer bands indicate slower growth rates. Chevron banding may indicate diurnal temperature changes in a shallow brine pan, with rapid growth spurts encouraged by the cooling of brine each evening.

Halite's high solubility and potential for deformation sometimes raises doubts about longterm preservation of the integrity of fluid inclusions. Even ancient halite that still retains abundant growth-aligned textures, if exposed to even moderate heating it may contain fluid inclusions that have leaked. Halite's propensity to flow also means its fluid inclusions are more vulnerable to stretching, leaking, and necking-down compared to most other minerals. But Petrichenko (1979) and Roedder (1984a,b) have shown that even when deformation has occurred, only the outer portions of halite crystals are affected, the centres of crystals typically remain unaltered. Alteration textures in ancient bedded halites with crystals suitable for micro-inclusion analysis are thus defined by altered, clear, outer rims and unaltered, cloudy, primary inclusion-rich cores that retain meaningful inclusion data (Petrichenko, 1979; Roedder, 1984a,b). The problems of defining inclusion leakage, coupled with the possibility of bedded and halokinetic salt being used as repository sites for radioactive waste, has generated valuable research on the validity of fluid inclusion data in halite (Chapter 12).

Lowenstein and Spencer (1990) obtained some of the first reliable and consistent estimates of ancient syndepositional brine temperature estimates using solid-liquid homogeniza-

tion temperatures of sylvite daughter crystals in halite from the Devonian Prairie Formation. They show Devonian brine temperatures were similar to those in Quaternary continental equivalents and that many ancient potash deposits still retained evidence of very early diagenetic features, created by the cooling of syndepositional reflux brines.

Many geologists have maintained a healthy scepticism toward fluid inclusion data derived from evaporites, especially from non-chevron halite (Roedder and Skinner, 1968; Kovalevich, 1975, 1976; Petrichenko, 1979; Roedder and Bassett, 1981). Work by Roberts and Spencer (1995) and by Benison and Goldstein (1999) has shown how petrographically controlled microthermometric testing can define and avoid zones of inclusion alteration in ancient halite. If the tests suggested by these authors show that primary fluid inclusions have not been altered since entrapment, then fluid inclusions from the unaltered portions of a salt bed may be considered representative of evaporative parent waters and can even be used to define palaeotemperatures of the mother brine (Figure 2.28). This is now a widely used approach for determining surface water palaeotemperatures from ancient halites whose fluid inclusions lack daughter crystals (Benison and Goldstein, 1999).

An all-liquid primary inclusion in halite at room temperature indicates mineral growth below approximately 50°C (Kovalevich, 1975; Petrichenko, 1979). Vapour bubbles can be nucleated artificially in some all-liquid inclusions by placing samples in a freezing chamber so that homogenization temperatures below 50°C can be measured. Roberts and Spencer (1995) found that when primary fluid inclusions in newly precipitated halite in ephemeral-lake salt-pans in Death Valley, California, were cooled (in order to nucleate vapour bubbles) and homogenization temperature were measured, the resulting temperature ranges were equivalent to the measured temperatures of the shallow brine sheets from which the halite had precipitated (Figure 2.28a).

Likewise detailed inclusion analysis, centred on chevrons and cornets in unaltered portions of halite beds in the mid-Permian Nippewalla Group of Kansas gave cooling-induced homogenization temperatures representative of the temperature range of the original mother liquor (Figure 2.28b, c). What was even more interesting was the intimate and consistent relationship between temperature and position in the inclusion rich layer in the chevron bands in this mid Permian halite (Figure 2.28b, c). It probably preserves daily temperature changes and shows the propensity of inclusion-rich bands to precipitate when the overlying halite saturated brine cools each evening or with the passage of a cold front.

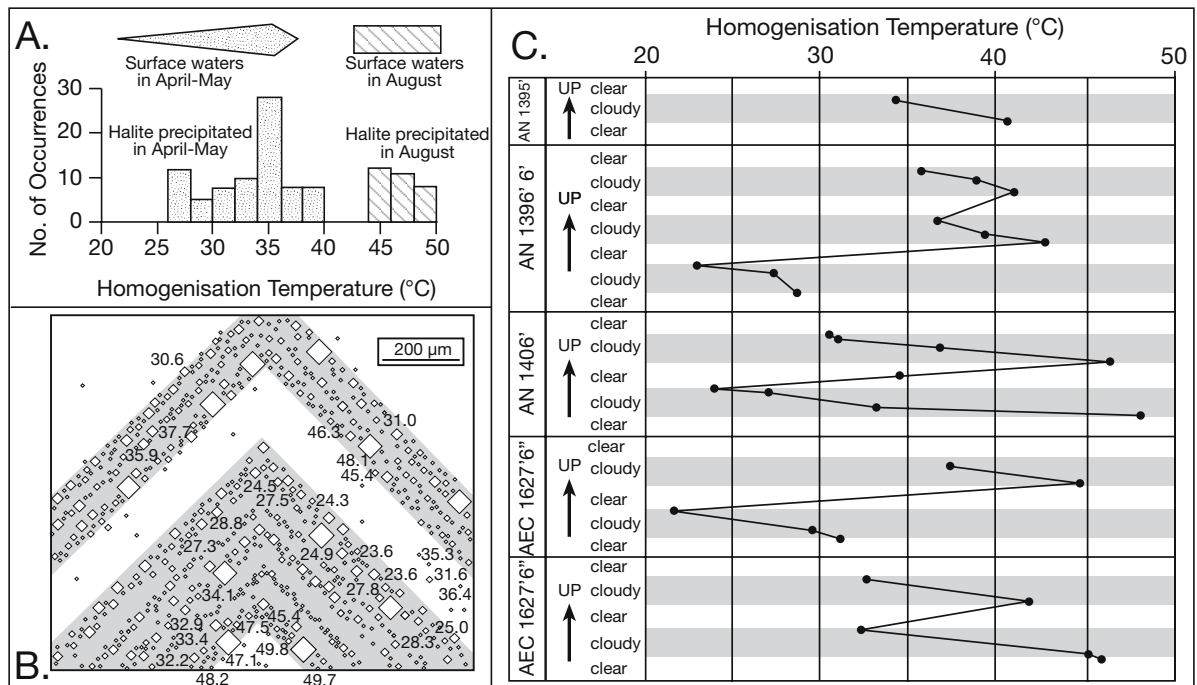


Figure 2.28. Inclusions in chevron halite. A) Histogram of homogenization temperatures measured by the 'cooling nucleation' method in initially all-liquid primary fluid inclusions from modern Death Valley halite. Plotted above the histogram are the temperature ranges of the brines from which these halite crystals grew (after Roberts and Spencer 1995). B) Representation of chevron bands in a halite crystal from the Anadarko Davis No. 1 core (1406 ft depth). Note homogenization temperatures in relation to bands; although homogenization temperatures are consistent within individual fluid inclusion assemblages thin, high frequency growth bands, they decrease from base to top of chevrons (after Benison and Goldstein, 1999). C) Graphic representation of homogenization temperature trends within and among cloudy, inclusion-rich and clear, inclusion-poor growth bands in five chevron halite crystals from the Nippewalla Group. Black circles mark average homogenization temperatures within thicker chevron growth bands. Lines connecting black circles are extrapolated temperature trends. Upward decrease in homogenization temperatures from base to top of individual cloudy chevron bands probably reflect daily fluctuations in surface water temperatures perhaps related to evening cooling (after Benison and Goldstein, 1999).

The fact that halite can retain such intimate precipitational detail supports the notion that growth-aligned chevrons are subsurface survivors. This means microanalysis of the chemical make-up of a brine inclusion in an unaltered halite chevron or cornet is indicative of the chemical composition of the water that precipitated the crystals (Timofeef et al., 2001). This gives an ability to map temporal changes in the ionic proportions of seawater and once again also suggests why Permian halobacteria can be cultured from brine inclusions in Permian salt (Vreeland et al., 2000).

Seawater evolution

So far in this chapter three things are clear: 1) it is difficult to separate marine and nonmarine parent brines based on mineralogy; 2) isotopes and microinclusions can sometimes separate brine parentage; 3) it is increasingly obvious that the proportions of major ions in seawater are probably not constant

across geological time. The significance of various indicators of chemical evolution of seawater over time is now considered in two parts. First, in the Phanerozoic where actual salts are available for sampling and analysis. Second, in the Precambrian, where much of the evidence of brine composition comes from pseudomorphs of evaporite salts.

A Phanerozoic dilemma: marine versus nonmarine potash?

Phanerozoic potash evaporites fall into two categories: 1) potash deposits with $MgSO_4$ salts, such as polyhalite, kieserite and kainite; and 2) potash deposits with halite, sylvite and carnallite, and entirely free or very poor in the magnesium-sulphate salts. This latter group makes up more than 60% of ancient potash deposits (Hardie, 1990). The former group may well be marine-derived as they contain the bittern suite predicted by the evaporation and backreaction of modern marine brines,

but the latter group must have precipitated from Na-Ca-Mg-K-Cl brines with ionic proportions quite different from that of concentrated modern seawater.

MgSO₄-depleted potash evaporites have been explained by some as modified marine evaporites thought to result from backreactions during burial diagenesis of normal marine evaporites (Borchert, 1977; Dean, 1978; Wilson and Long, 1993). If so, then they were derived from an ancient seawater source with modern ionic proportions that were altered via; a) dolomitization, b) sulphate reducing bacterial action, c) mixing of brines with calcium bicarbonate-rich river water, or d) rock-fluid interaction during deep burial diagenesis.

Alternatively, Hardie (1990) suggested that MgSO₄ depleted potash evaporites formed from sulphate-depleted inflow waters seeping into an evaporite basin via springs and faults. Springs were fed either by CaCl₂-rich hot hydrothermal brines or by cooling resurging deep basinal brines. Such fault-fed deeply-circulating evaporite brines occur today in springs in the Dead Sea, Qaidam Basin, Salton Sea and the Danakil Depression. The upwelling of the brines in these regions is driven either by thermally induced density instabilities related to magma emplacement, or by the creation of topographic gradients that force deeply-circulated basinal brines to the surface. Ayora et al. (1994) demonstrated that such a continental Ca-Cl system operated during deposition of sylvite and carnallite in the upper Eocene basin of Navarra, southern Pyrenees, Spain (Figure 8.10).

Thirdly, there is the distinct likelihood that seawater chemistry has evolved throughout the Phanerozoic and that changing ionic proportions define whether or not MgSO₄ salts were typical marine evaporites. Work by Kovalevich et al. (1998)

on inclusions in primary-bedded halite from many evaporite formations of northern Pangaea, and subsequent work using micro-analyses of fluid inclusions in numerous chevron halites (Lowenstein et al., 2001, 2003a), shows that during the Phanerozoic the chemical composition of marine brines has oscillated between Na-K-Mg-Ca-Cl and Na-K-Mg-Cl-SO₄ types. The former does not precipitate MgSO₄ salts when concentrated, the latter does.

A detailed analysis of the ionic make-up of Silurian seawater using micro-inclusion analysis of more than 100 samples of chevron halite from various Silurian deposits around the world was recently published by Brennan and Lowenstein (2002), and clearly supports the notion that ionic proportions in the world's Silurian oceans were different from those of today (Figure 2.29). Samples were from three formations in the Late Silurian Michigan Basin, the A-1, A-2, and B Evaporites of the Salina Group, and the Early Silurian in the Canning Basin (Australia) in the Mallowa Salt of the Carribuddy Group. The Silurian ocean had lower concentrations of Mg²⁺, Na⁺, and SO₄²⁻, and much higher concentrations of Ca²⁺ relative to the ocean's present-day composition. Furthermore, Silurian seawater had Ca²⁺ in excess of SO₄²⁻. Bittern stage evaporation of Silurian seawater produced KCl-type potash minerals that lack the MgSO₄-type late stage salts formed during the evaporation of present-day seawater and allowed sylvite as a primary precipitate.

There is now convincing evidence that the chemistry of seawater has varied across the Phanerozoic, what is not so well understood are the processes driving this change (Figure 2.30a). Spencer and Hardie (1990) and Hardie (1996) have argued that the level of Mg in the Phanerozoic oceans has been relatively constant, but changes in the rate of seafloor spreading have changed the levels of Ca in seawater. Their postulate was also supported

Flux Ratio	Na	K	Ca	Mg	Cl	SO ₄	HCO ₃	Order of appearance of saline minerals during evaporative concentration of seawater
0.96	490	3.7	4.8	111	548	59.0	2.7	CaCO ₃ - gypsum - anhydrite - glauberite - halite - polyhalite - epsomite - hexahydrate - kieserite - kainite - carnallite - bischofite
1.00	470	10.2	20.3	106	548	53.9	0.6	CaCO ₃ - gypsum - anhydrite - glauberite - halite - polyhalite - epsomite - hexahydrate - kieserite - carnallite - bischofite
1.05	448	17.6	36.2	101	548	53.8	0.6	CaCO ₃ - gypsum - anhydrite - halite - polyhalite - sylvite - carnallite - kieserite - bischofite
1.10	427	24.3	51.8	97	548	51.4	0.4	CaCO ₃ - gypsum - anhydrite - halite - sylvite - carnallite - bischofite - tachyhydrite
1.25	376	41.2	91.4	85	548	45.3	0.3	CaCO ₃ - gypsum - anhydrite - halite - sylvite - carnallite - antarcticite - tachyhydrite

Table 2.9. Predicted composition of seawater (meq l⁻¹) as a function of variations in the ratio of mid-ocean ridge hydrothermal brine flux compared to river water flux into the ocean, and the saline mineral paragenesis of the resulting seawater (after Spencer and Hardie, 1990). Only the first appearance of each mineral is listed (see Figure 2.12 for backreaction effects).

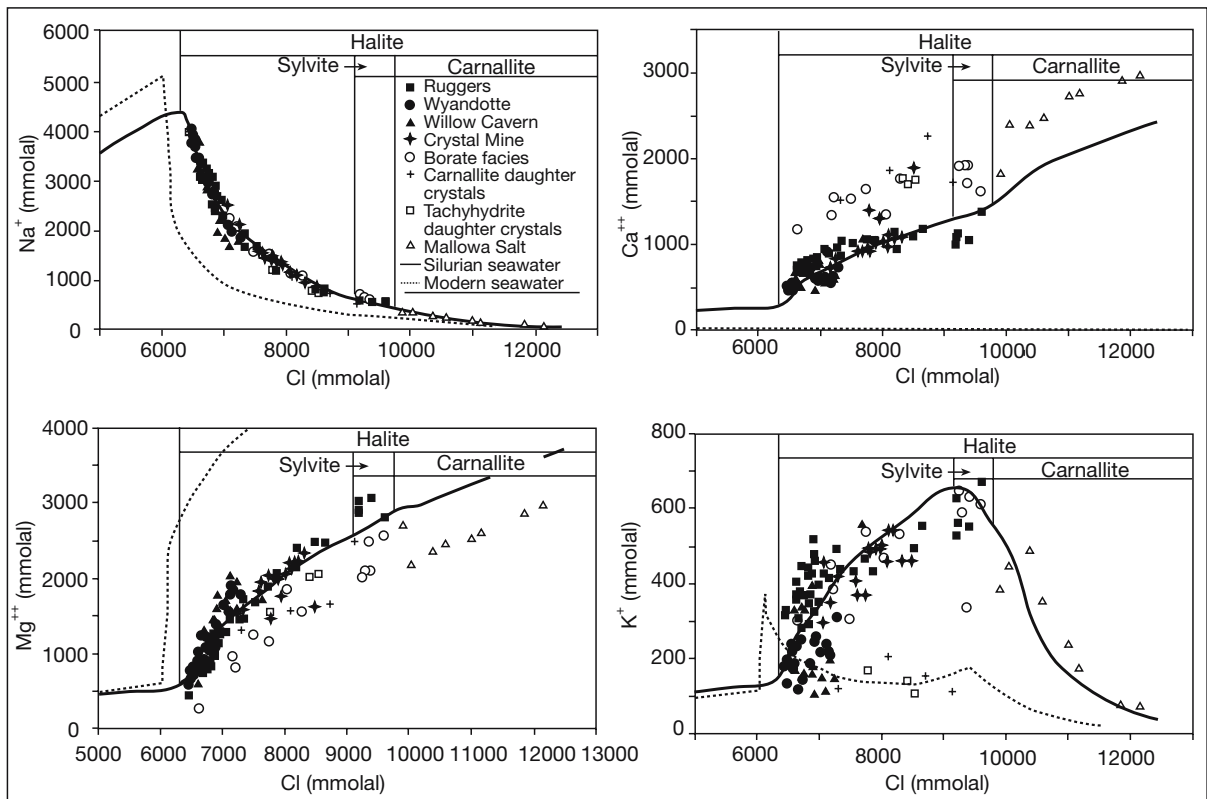


Figure 2.29. Plots of the major-ion concentrations of the fluid inclusions versus chloride concentrations in Silurian salt with preserved primary structures (after Brennan and Lowenstein, 2002). Closed symbols represent fluid inclusions from pristine marine halites, open symbols represent suspect fluid inclusions from halites associated with potash mineralization or high degrees of evaporation. Only the closed symbols were considered for determining Silurian seawater. The evaporation pathway of modern seawater is shown with a dashed line, and the best-fit evaporation pathway for the Silurian data is shown with a solid line. All the plots show that the evaporation pathways defined by Silurian fluid inclusions are different from the modern seawater pathways. The Silurian fluid inclusions all have an excess of calcium, and no measurable sulphate. Modern seawater evaporated to halite saturation has abundant sulphate, and negligible amounts of calcium. Salts expected to precipitate at given Cl concentrations in evaporated "best-fit" Silurian seawater are indicated along the top of each plot. Sylvite is a primary precipitate from concentrated seawater with these ionic proportions.

by Lowenstein et al. (2001, 2003). Timing of the increase in the amount of Ca in the world's oceans was synchronous with a decrease in the SO_4 ion concentration, which at times was as much as three times lower than the present concentration of that ion in seawater.

Simple mixing models show that changes in the flux rate of mid-oceanic hydrothermal brines can generate significant changes in the Mg/Ca, Na/K and SO_4/Cl ratios in seawater (Table 2.9). Such changes of molal ratios in seawater would have generated significant changes in the type and order of potash minerals at the bittern stage. For example, Spencer and Hardie's model predicts that an increase of only 10% in the flux of mid-ocean ridge hydrothermal brine over today's value would create a marine bittern that would precipitate sylvite and calcium-chloride salts instead of the Mg-sulphate miner-

als expected during bittern evaporation of modern sea water. This Ca-Cl ocean corresponds to times of "calcite oceans" and contrast with the lower calcium, higher magnesium "aragonite oceans" of the Permo-Triassic and the Neogene (Figure 2.30a; Hardie, 1996).

Yet many sources have argued, including earlier work by Hardie, that bittern salts lacking MgSO_4 components indicate a nonmarine CaCl source. The strong possibility of temporal changes in Phanerozoic seawater chemistry from a MgSO_4 to a KCl ocean confuses a mineralogical distinction between marine and nonmarine brine sources. It can be used to argue that many extensive ancient evaporites, such as the Devonian Prairie Evaporite Fm. of Canada and the Cretaceous Maha Sarakham salts of Thailand are in fact marine and formed by the evaporation of a KCl ocean.

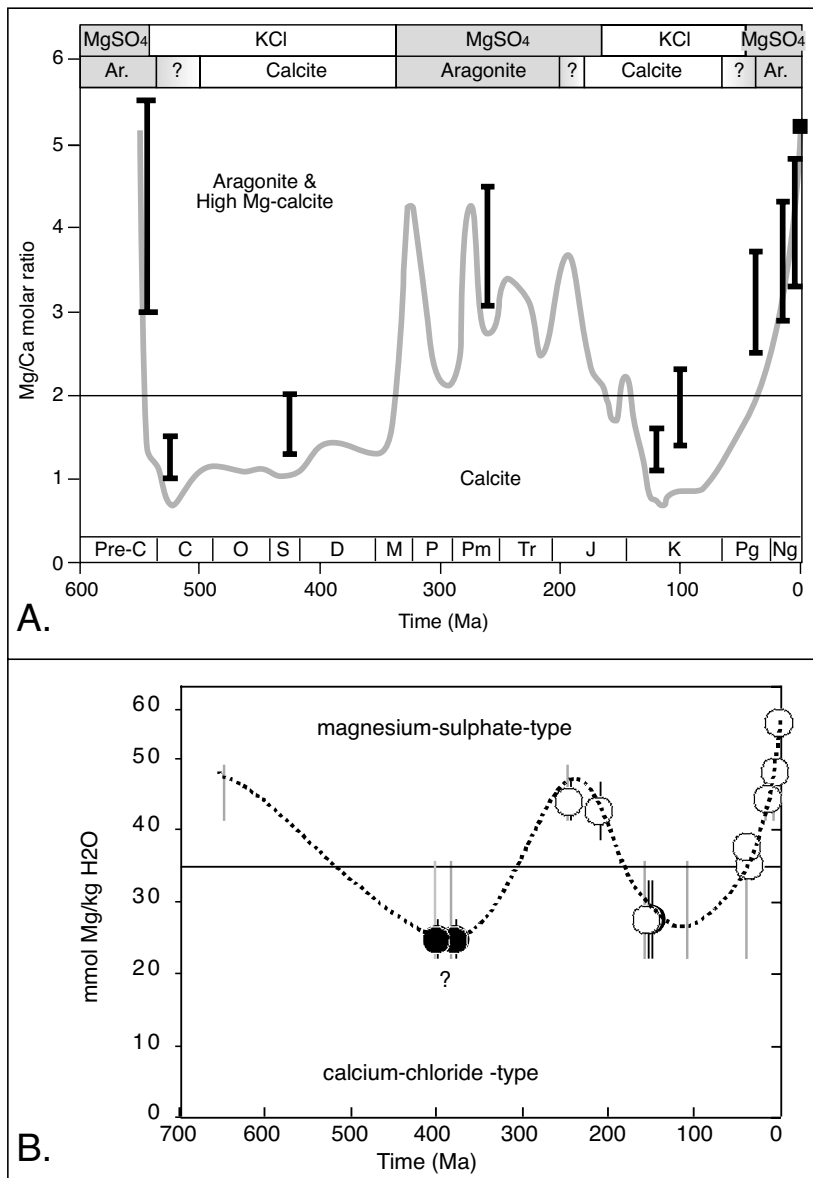


Figure 2.30. Potash and the secular evolution of Phanerozoic seawater. A) Secular variation in the Mg/Ca ratio of seawater estimated from fluid inclusions in marine halites (vertical bars), compared to predicted seawater secular variations. The horizontal line at Mg/Ca = 2 is the approximate divide between calcite seas and aragonite seas. Also plotted are the temporal distributions in the primary mineralogies of Phanerozoic nonskeletal carbonates (calcite and aragonite) and periods of KCl and MgSO₄ evaporites (after Lowenstein et al., 2001). B) Secular changes in seawater chemistry based on microanalysis of fluid inclusions in marine halites (after Zimmermann, 2000a).

Holland et al. (1996), while agreeing that there are changes in ionic proportion of Phanerozoic seawater and that halite microinclusions preserve evidence of these changes, recalculated the effects of changing seafloor spreading rates on global

seawater chemistry used by Hardie and others. They concluded changes in ionic proportions from such changes in seafloor spreading rate were modest. Instead, they pointed out that the composition of seawater can be seriously affected by secular changes in the proportion of platform carbonate dolomitized during evaporative concentration, without the need to invoke major changes in global seawater composition. In a later paper, Holland and Zimmermann (2000) suggest changes in the level of Mg in seawater were such that the molar Mg/Ca ratio of Palaeozoic global seawater (based on dolomite volume) was twice the present value of 5.

Using micro-inclusion studies of halites of varying ages, Zimmermann (2000a, b) has proposed that the evolving chemistry of the Phanerozoic ocean is more indicative of changing volumes of dolomite than it is of changes in the rates of seafloor spreading (Figure 2.30b). Using halite inclusions she showed that the level of Mg in seawater has increased from ≈ 38 mmol/kg H₂O to 55 mmol/kg H₂O in the past 40 million years. This increase is accompanied by an equimolar increase in the level of oceanic sulphate. Over the longer time frame of the Palaeozoic to the present the decrease in Mg/Ca ratio corresponds to a shift in the locus of major marine calcium carbonate deposition from Palaeozoic shelves to the deep oceans, a change tied to the evolution of the nannoplankton. Prior to the evolution of foraminifera and coccoliths, some 150 Ma, the amount of calcium carbonate accumulating in the open ocean was minimal. Since then, a progressively larger portion of calcium carbonate has been deposited on the floor of the deep ocean. Dolomitization of these deep water carbonates has been minor. Reasons for the increase in Mg in the past 40 million years are still not clear.

Ayora et al. (2001) called for caution in applying general models of secular changes in seawater chemistry based on assumptions of worldwide sulphate depletion at various times in the past. They reconstructed the chemical evolution of several European Mesozoic and Tertiary marine evaporite basins using mineral associations, primary fluid-inclusion analyses, and numerical simulations of evaporation scenarios. The solute proportion recorded in the fluid inclusions in all basins could be explained using the evaporation of present-day seawater as a major re-charge. Sulphate depletion in the brines was responsible for the type of potash deposit formed, namely potassium-magnesium sulphates or sylvite. But this sulphate depletion was due either to dolomitization or to the addition of a CaCl_2 -rich solution to the basin. Sulphate depletion occurred in varying intensity in basins of the same age, as well as throughout the evolution of the same basin negating the notion of changes in seafloor spreading. They concluded changes in potash mineralogy and sulphate depletion based on fluid inclusions are not conclusive arguments in favour of secular variations in the composition of the ocean.

But, most evaporite workers would now agree that based on a growing database of worldwide synchronous changes in brine chemistry in fluid inclusions in chevron halite (e.g. Figure 2.29) there were secular changes in seawater chemistry, which drove the two potash endmembers. What is not clear is the magnitude of this change or the dominant driving mechanism (seafloor spreading versus dolomitization) nor why the proportion of K in seawater appears to change very little throughout the Phanerozoic. What is also not considered by some involved in the argument are the pitfalls and analytical needs for exact fluid inclusion interpretation in sediments that may have been subject to subtle diagenetic alteration (see Goldstein 2001 for an excellent review and discussion of inclusion studies).

Precambrian oceanic chemistry

Given that ionic proportions of major ions in seawater have probably changed through the Phanerozoic, how constant was the chemistry of the world's oceans since the early Archaean? For example, does the evaporite evidence support the possibility of a primordial reducing atmosphere or higher levels of bicarbonate in an ancient ocean?

Some authors postulate that there have been no significant changes in the major ion proportions in seawater for the past 4 Ga (Morse and Mackenzie, 1998). Others assert that the Archaean was dominantly a time of little or no atmospheric oxygen and that ocean waters were reducing fluids (Krupp et

al., 1994). Yet others propose that the bicarbonate to calcium ratio was so high in Archaean and Palaeoproterozoic seawater compared to today that all the calcium was used up in widespread abiotic marine aragonite and Mg-calcite precipitates (Sumner and Grotzinger, 2000). In this case trona or nahcolite are likely marine evaporites in the early Archaean. Still others have theorised cyclic changes in oceanic chemistry occurred throughout the Phanerozoic and much of the Precambrian. Such changes were related to changes in styles and rates of sea floor spreading-hydrothermal circulation in midoceanic ridges (Channer et al., 1997) and the development of tonalitic continents (Knauth, 1998). Can Precambrian evaporites and their pseudomorphs give some indirect clues as to which scenario is the more likely?

Given the paucity of preserved evaporite salts prior to the Mesoproterozoic, the discussion must centre on mineralogical evidence left as evaporite pseudomorphs. The resulting detail is far less than when modelling Phanerozoic chemistries, which can use micro-inclusions and isotope signatures of marine salts.

Pseudomorphs, especially of halite hoppers, occur in marine rocks as old as Archaean, but are far more common, as are the actual salts, in Proterozoic and Phanerozoic strata (Figure 2.31). Halite or its pseudomorphs characterise areas of widespread marine chemical sedimentation from the Archaean to the present. CaSO_4 distribution is more enigmatic. Possibly the oldest documented CaSO_4 pseudomorphs are cm-sized growth-aligned barytes that are interpreted to replace bottom-nucleated gypsum in 3.45 Ga metasediments in the Pilbara/North Pole region of Western Australia (Figure 7.71; Barley et al., 1979; Lowe, 1983; Buick and Dunlop, 1990). They were precipitated in volcanoclastics in association with what are possibly the world's oldest stromatolites (Hofmann et al., 1999). Similar growth aligned baryte crystals, which are also possible gypsum pseudomorphs, formed in the Nondweni greenstones in South Africa some 3.4 Ga (Wilson and Versfeld, 1994).

Sequences in both regions are now completely silicified or barytised. At the time they were first documented, the recognition of what were considered shallow-water Early Archaean gypsum pseudomorphs at North Pole, Pilbara Craton, caused a re-evaluation of models of a totally reducing Archaean atmosphere (Dimroth and Kimberley, 1975; Clemmey and Badham, 1982). The presence of free sulphate in surface brines of the Archaean world was thought to imply at least locally oxygenated hydrosphere. Gypsum precipitating in Archaean ocean waters also meant calcium levels in the ocean waters were in excess of bicarbonate, as is in the modern oceans (Figure 2.5). The presence of free-standing gypsum on the seafloor is

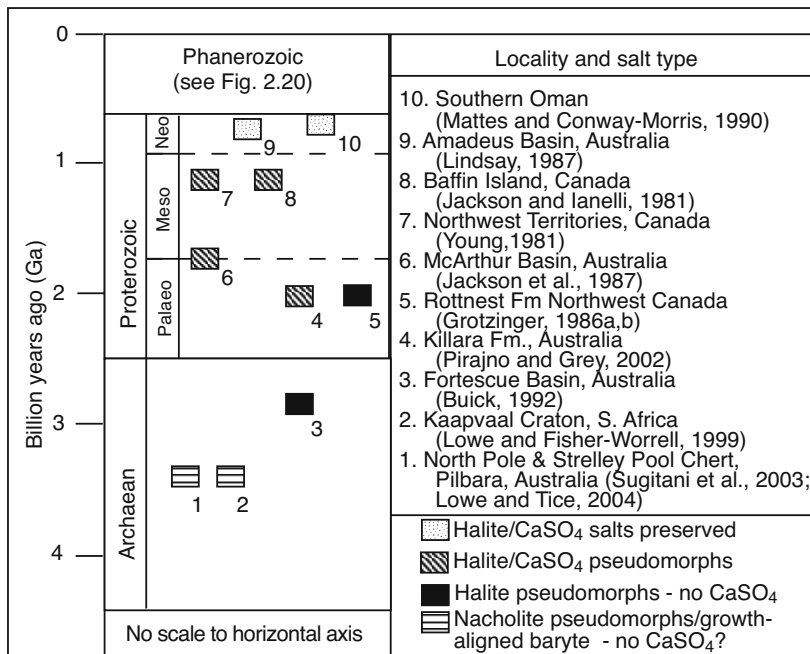


Figure 2.31. Precambrian evaporite occurrences and mineralogies (compiled from listed sources).

incompatible with any model of the Early Archaean ocean as a “soda lake.”

However, in both the Pilbara and the South African sequences there are no actual calcium sulphate evaporites preserved, only growth-aligned crystal textures now preserved as baryte. Textures in baryte ore from Frasnian sediments in Chaudfontaine, Belgium, are near identical to those observed at North Pole, Australia. The Belgian barytes are primary sea-bottom precipitates with no precursor mineral phase (Dejonghe, 1990). Some workers in the Pilbara feel that the growth-aligned baryte in this region is also a primary precipitate, formed in the vicinity of hydrothermal vents (Vearncombe et al., 1995; Nijman et al., 1999; Runnegar et al., 2001). As such, it is not secondary after gypsum. A similar hydrothermal discharge model has been developed for aligned barytes in the Barberton Greenstone belt (de Ronde et al., 1994, 1996).

Levels of Archaean sulphate in the world ocean were probably less than a few percent of the current levels and probably remained so until the evolution of an oxygen-producing biota well into the Proterozoic (Habicht and Canfield, 1996; Kah et al., 2004). Barium sulphate is highly insoluble in modern oxygenated seawater. To carry large volumes of barium or sulphur (as sulphide) in solution to the precipitation site re-

quires anoxic conditions. If the aligned baryte crystals are primary, their formation still requires sulphate to be locally present on the seafloor, at least in the vicinity of the depositional site. A possible source for local sulphate production in the shallow waters that characterised the North Pole site was shortwave ultraviolet photooxidation of volcanic SO₂ (Runnegar et al., 2001). According to Nijman et al. (1999) the occurrence of the North Pole baryte in sedimentary mounds atop growth faults meant sulphate was locally derived via boiling of escaping hydrothermal vent waters enriched in Ba, Si and sulphide. As these hydrothermal waters vented in waters perhaps 50 metres deep, they boiled or violently degassed. Consequent mixing with normally stratified seawater, caused instantaneous oxidation of sulphide into sulphate that then, on cooling, combined with the Ba to precipitate as growth aligned baryte crystals on the seafloor.

Conflicting notions (replaced gypsum versus primary baryte) mean that at this stage of our understanding, the bedded baryte evidence cannot be reliably used to support an evaporite paragenesis of gypsum and so infer an Archaean ocean with ionic proportions similar to those of today.

Archaean and Proterozoic distributions of gypsum have been further complicated by the misidentification of primary aragonite splays and pinolitic siderite marbles as gypsum replacements (Warren 1999; Chapter 8). When these misidentifications are removed from the record it is obvious that calcium sulphate precipitating directly from Archaean seawater to form widespread beds did not occur, and that precipitation of aragonite as thick crusts on the sea floor was significantly more abundant than during any subsequent time in earth history. In contrast to gypsum, halite pseudomorphs are found throughout the Precambrian (e.g. Boulter and Glover, 1986; Figure 2.31; Table 7.1).

Grotzinger and Kasting (1993) argue that high levels of atmospheric CO₂ meant HCO₃/Ca ratios were much higher in the Archaean and the Palaeoproterozoic oceans than today. All the calcium in seawater was deposited as marine cementstones

and other alkaline earth precipitates well before bicarbonate was depleted and there was no Ca left over to precipitate as gypsum. The early Archaean ocean was perhaps a Na–Cl–HCO₃ sea, and not the Na–Cl ocean of today (Kempe and Degens, 1985; Maisonneuve, 1982). This early Archaean hydrosphere had a chemistry similar to that found in modern soda lakes like Lake Magadi and Lake Natron (pathway I brines in Figures 2.12, 2.13). This rather different marine brine chemistry would have precipitated halite and trona/nahcolite, not halite/gypsum. It probably meant that if gypsum did ever precipitate from Archaean seawater it did so only in minor amounts well after the onset of halite precipitation. Excessive sodium in the ocean may help explain the ubiquity of stratiform albitites in much of the Archaean. They would have formed throughout the marine realm as early diagenetic replacements of labile volcanoclastics/zeolites in volcanogenic/greenstone terranes (See Chapter 11, zeolite).

A case for nahcolite (NaHCO₃) as a primary evaporite, along with halite in the 3.42 Ga rocks of the Barberton greenstone belt was documented by Lowe and Fisher-Worrell (1999). Sugitani et al. (2003) reported silicified nahcolite (the high CO₂ form of sodium carbonate salts; see Figure 2.13a) in ≈3.2 Ga rocks in the northern part of the Eastern Pilbara block, Western Australia. Coarse, upward-radiating, silicified evaporite crystals in the ca. 3.47–3.46 Ga Strelley Pool Chert (Lowe, 1983) show the same habit, geometry, and environmental setting as nahcolite in the Barberton belt and also probably represent silicified NaHCO₃ precipitates (Lowe and Tice, 2004).

Marine nahcolite in the 3.5–3.2 Ga sedimentary record is thought to be evidence of surface temperatures around 70±15°C (Figures 2.13a, 2.32; Lowe and Tice, 2004). Con-

temporary early Archaean nahcolite (NaHCO₃) as a primary evaporitic mineral in a very aggressive weathering regime, in the absence of land vegetation, is best explained by a mixed CH₄ and CO₂ atmospheric greenhouse. CH₄/CO₂ ratios were <<1 and pCO₂ was at least 100–1000 times the present value, perhaps as high as several bars (Kaufman and Xiao, 2003). The formation of large areas of continental crust at 3.2–3.0

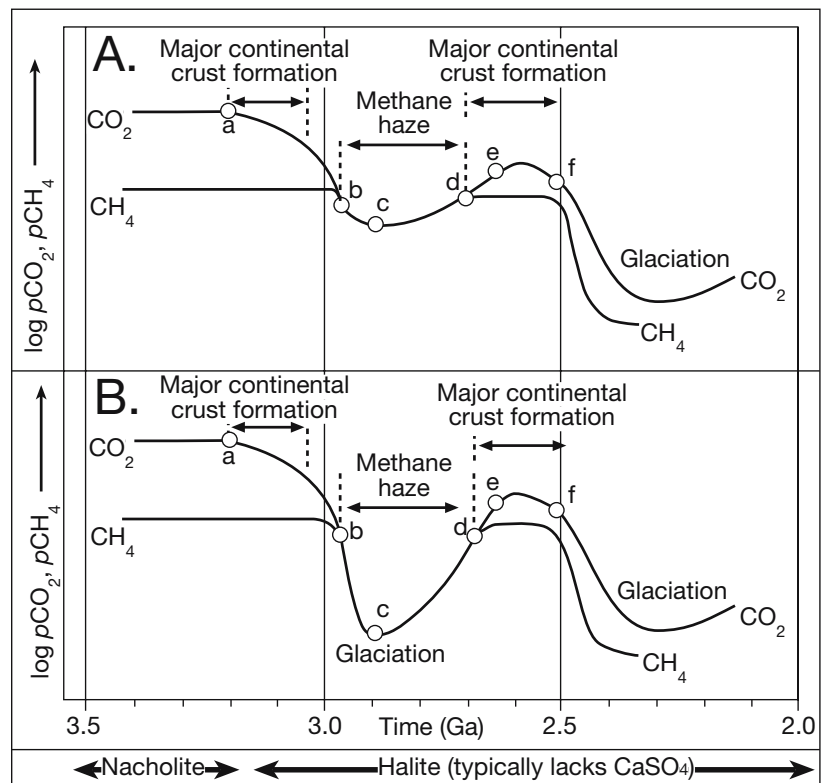


Figure 2.32. Schematic diagrams showing proposed atmospheric $p\text{CH}_4$ and $p\text{CO}_2$ evolution during Archean and earliest Proterozoic, 3.5–2.2 Ga (after Lowe and Tice, 2004). Diagrams show atmospheric evolution A) without and B) with glaciation at 2.9 Ga. High surface temperatures, $70\pm 15^\circ\text{C}$, were maintained from before 3.5 to at least 3.2 Ga by mixed CO_2 and CH_4 atmospheric greenhouse with $\text{CH}_4/\text{CO}_2 \ll 1$. Starting ca. 3.2 Ga (point a), enhanced weathering associated with continent formation began to deplete atmospheric CO_2 , leading eventually to $\text{CH}_4/\text{CO}_2 \approx 1$ some 2.9 Ga (point b) and formation of organic haze, which began to reduce $p\text{CH}_4$ along a path defined by $\text{CH}_4/\text{CO}_2 \approx 1$. Declining $p\text{CO}_2$ and $p\text{CH}_4$ at 2.9–2.7 Ga resulted in global cooling and possibly glaciation (point c in lower diagram). Reduced weathering and continued tectonic recycling 2.7–2.6 Ga led to increasing $p\text{CO}_2$ (line c–d–e), allowing a coupled increase in $p\text{CH}_4$ while maintaining $\text{CH}_4/\text{CO}_2 \approx 1$. When upper limit of CH_4 production was reached (point d), CH_4/CO_2 became < 1 and methane haze formation ceased. Enhanced weathering ca. 2.6 Ga (point e) associated with continent building at 2.7–2.5 Ga once again initiated rapid depletion of atmospheric CO_2 and decline in surface temperatures. Increased O_2 production—associated with latest Archean spread of oxygenic photosynthetic microbes onto large, shallow-water, continental shelves developed on older (pre-3.0 Ga) blocks of continental crust (point f)—concurrently lowered $p\text{CH}_4$, maintaining $\text{CH}_4/\text{CO}_2 < 1$ and preventing the formation of organic haze. Widespread glaciation at 2.4–2.2 Ga resulted from decreasing $p\text{CO}_2$ due to weathering and declining $p\text{CH}_4$ due to oxidation.

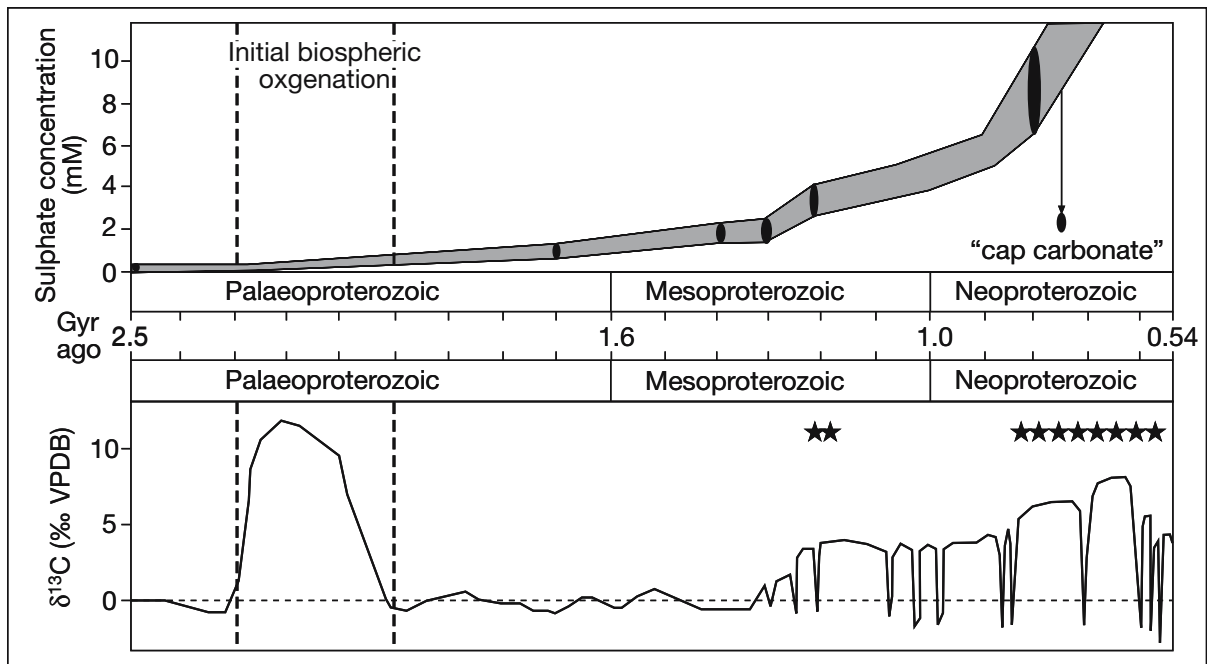


Figure 2.33. Proterozoic marine sulphate concentrations. Filled ovals mark data determinations (after Kah et al., 2004). Marine sulphate concentrations probably remained below 2mM until about 1.3 Gyr ago, rose to, 4.5mM by 1.2 Gyr ago, and possibly as high as 7–10mM by the mid-Neoproterozoic, although near-complete reduction of oceanic sulphate may have occurred during Neoproterozoic glacial intervals (arrow). Increased sulphate concentrations coincide with changes in marine $\delta^{13}\text{C}$ associated with biospheric oxygenation and are marked by the appearance of bedded gypsum (stars) in the late Mesoproterozoic and more frequent gypsum deposition in the last two-thirds of the Neoproterozoic.

Ga, including the Kaapvaal and Pilbara cratons, resulted in the gradual depletion of atmospheric CO_2 through weathering and a lack of marine nacholite since the early Archaean. By 2.9–2.7 Ga, declining $p\text{CO}_2$ was associated with climatic cooling and siderite-free soils.

Transitory CH_4/CO_2 ratios of ~ 1 may have resulted in the sporadic formation of organic haze from atmospheric CH_4 , and are reflected in one or more isotopic excursions involving global deposition of abnormally ^{13}C -depleted organic carbon in sediments of this age. Surface temperatures of $<60^\circ\text{C}$ after 2.9 Ga may have allowed an increase in the distribution and productivity of oxygenic photosynthetic microbes (and a decrease in sulphur dependant thermophiles). Eventual lowering of new formed continental blocks by erosion, reduced loss of atmospheric CO_2 due to weathering, and continued long-term tectonic recycling of CO_2 resulted in rising $p\text{CO}_2$ and decreasing CH_4/CO_2 ratios in the later Archaean and eventual re-establishment of a mainly CO_2 greenhouse. Similar events may have been repeated in the latest Archaean and earliest Proterozoic, but gradually rising production of O_2 effectively kept CH_4/CO_2 ratios to $\ll 1$.

By 2.2–2.0 Ga, reliable examples of pseudomorphs after primary calcium sulphate first appear in the rock record (Figure 2.31; Table 7.9). Undeniable pseudomorphs are widespread in the Late Palaeoproterozoic to Mesoproterozoic sediments of the McArthur Basin, Northern Territory, Australia, and in rocks of Great Slave Lake in northern Canada. For example, in the Malapunyah Formation of the Northern Territory, Australia, the outer portions of numerous decimetre to metre-diameter silicified anhydrite nodules still retain outlines of felted anhydrite laths (pers. obs). The oldest reliable sulphate pseudomorphs after anhydrite and gypsum come from Palaeoproterozoic cherts in the 2.0–2.2 Ga Bartle Member of the Killara Formation, western Australia (Pirajno and Grey, 2002). These cherts locally retain small amounts of anhydrite (verified by XRD, as well as appearing as highly birefringent flecks in thin sections). Other widespread but younger sulphate pseudomorphs occur in the 1.2 Ga Borden Basin, Baffin Island, and the 1.2 Ga Amundsen Basin in the Canadian Arctic Archipelago. Currently the world's oldest documented CaSO_4 beds outcrop in the 1.2 Ga Society Cliff Formation in Baffin and Bylot Islands of the Canadian Archipelago (Kah et al., 2001, 2004). Sulphate evaporites in all these basins formed beds up to tens of metres thick and with lateral extents measured in hundreds

of square kilometres. All were laid down in shallow marine, coastal, and alluvial environments under an oxygenated Mesoproterozoic atmosphere (Jackson et al., 1987; Walker et al., 1977). By then the hydrosphere contained free sulphate and Ca/HCO₃ ratios were lower.

The work of Kah et al. (2004) shows that prior to 2.2 Ga, when oxygen began to accumulate in the Earth's atmosphere, sulphate concentrations in the world's oceans were <1 mM and possibly <200 μM (Figure 2.33). By 0.8 Ga, oxygen and thus sulphate levels had risen significantly. Sulphate levels were between 1.5 and 4.5 mM, or 5–15% of modern values, for more than a billion years after initial oxygenation of the Earth's biosphere some 2.2–2.4 Ga and mid-ocean depth waters were anoxic for most of that time (Brocks et al., 2005). Marine sulphate concentrations probably remained low, no more than 35% of modern values, for nearly the entire Proterozoic. A significant rise in biospheric oxygen, and thus oceanic sulphate, may not have occurred until the latest Neoproterozoic (0.54 Ga), just before the Cambrian explosion, when sulphate levels may have reached 20.5 mM, or 75% of present day levels. This is a time when thick sulphate platforms first characterised the salt basins of Oman.

In yet another proposal of hydrosphere-atmosphere evolution, Huston and Logan (2004) argue that the presence of relatively abundant bedded sulphate deposits before 3.2 Ga (as baryte) and after 1.8 Ga (as CaSO₄ salts), and the peak in banded iron formation abundance between 3.2 and 1.8 Ga, and the aqueous geochemistry of sulphur and iron, when taken together suggest that the redox state and the abundances of sulphur and iron in the hydrosphere varied widely during the Archean and Proterozoic. They propose a layered hydrosphere prior to 3.2 Ga in which sulphate was enriched in an upper oceanic layer, whereas the underlying layer was reduced and sulphur-poor. The sulphate was produced by atmospheric photolytic reactions with volcanic gases in a reducing atmosphere. Mixing of the upper and lower water masses allowed the banded barytes to form prior to 3.2 Ga and created an ocean chemistry where nahcolite was a marine evaporite. Between 3.2 and 2.4 Ga, decreasing volcanogenesis and sulphate reduction removed sulphate from the upper layer, producing broadly uniform, reduced, sulphur-poor and iron-rich oceans.

As a result of increasing atmospheric oxygenation around 2.4 Ga, the flux of sulphate into the hydrosphere by oxidative weathering was greatly enhanced, producing layered oceans, with sulphate-enriched, iron-poor surface waters and reduced, sulphur-poor and iron-rich bottom waters. Gypsum evaporites

were increasingly likely as marine precipitates. The rate at which this process proceeded varied between basins depending on the size and local environment of the basin. By 1.8 Ga, the hydrosphere was relatively sulphate-rich and iron-poor throughout. Gypsum was now a widespread marine evaporite. Variations in sulphur and iron abundances suggest that the redox state of the oceans was buffered by iron before 2.4 Ga and by sulphur after 1.6 to 1.8 Ga.

Gypsum in combination with halite was the marine evaporite association from then until now. Seawater was a Na-Cl-SO₄ ocean. Neoproterozoic sulphates along with widespread bedded halite, occur in the Bitter Springs Formation of the Amadeus basin, central Australia, its equivalents in the Officer Basin, the Callana beds of the Flinders Ranges and the Infracambrian salt basins of the Arabian (Persian) Gulf (Wells, 1980; Cooper, 1991; Mattes and Conway-Morris, 1990; Edgell, 1991).

The transition to calcium sulphate textures in evaporite pseudomorphs mirrors a marked change in the style of marine carbonates around 2.2 to 2.3 Ga when herringbone calcite and precipitated carbonate beds become much less common and the precipitation mode shifted from the seafloor to the water column (Figure 1.13; Sumner and Grotzinger, 1996, 2000). The boundary also corresponds to the “rusting” of the oceans when oxygen levels became high enough to precipitate widespread banded iron deposits on the seafloor. Microdigitate stromatolites cross this boundary with little effect, suggesting the marked decrease in dissolved iron exerted little influence on them.

The relative scarcity of actual Pre-Phanerozoic salts, not pseudomorphs, especially in the Archaean has been used by some to argue that conditions were less favourable for widespread evaporite deposition in the early Precambrian (Cloud, 1972). Others, myself included, feel that the relative scarcity of preserved evaporites in older sequences reflects the greater likelihood of fluid flushing, evaporite dissolution and metasomatism in progressively older rocks. It may well be that sulphate evaporites were less common in the Archaean, and that sodium carbonates mixed with halite were dominant evaporite salts in seawater-fed saline giants of the Early Archaean. But widespread evaporite deposition from sodium-dominated brines did occur throughout the Archaean in large drawdown basins isolated from a surface connection with the ocean. A paucity of preserved bedded evaporite salts in the Precambrian reflects an increased probability of partial or complete evaporite dissolution, remobilisation and metasomatism with increasing geological age.

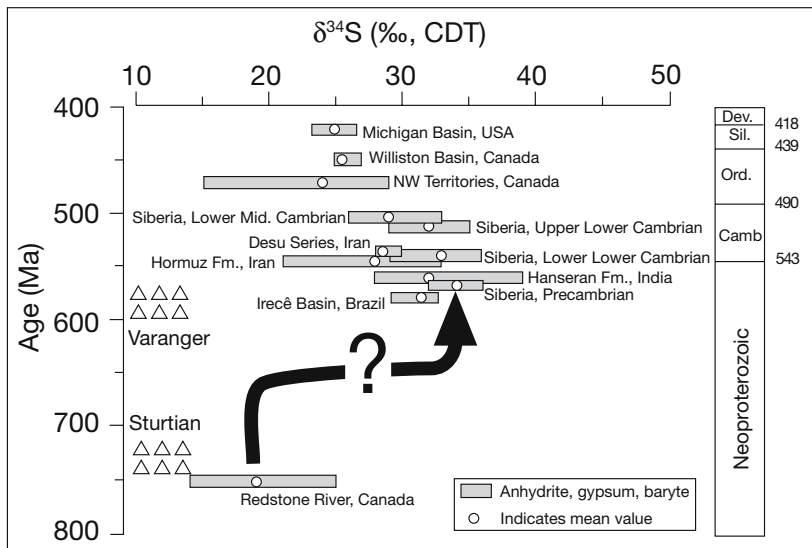


Figure 2.34. Temporal evolution of $\delta^{34}\text{S}$ from marine chemical sediments (anhydrite, gypsum, baryte) during the terminal Neoproterozoic and early Palaeozoic (after Strauss et al., 2001 and references therein).

So, by the Late Neoproterozoic marine sulphates are preserved as actual chemical sediments (anhydrite, gypsum, baryte). Their impermeable nature means their isotopic signatures are useful supplements to the much better preserved marine carbon and sulphide records in defining the transition from the Terminal Neoproterozoic into the early Palaeozoic. Holser 1977, 1984 was the first to address the specific conditions required to produce the rapid rise in $\delta^{34}\text{S}$ of seawater sulphate during the terminal Neoproterozoic which he termed the “Yudomski event” after the regional stratigraphy preserved in SE Siberian evaporites. His model of stratification-stagnation and subsequent ventilation of the deep ocean and mixing of different sulphur isotope signatures for dissolved marine sulphate between surface and deep water was reinforced by subsequent workers (Goodfellow and Jonasson, 1984; Logan et al., 1995). Recently it has been placed in the contextural framework of a possible “Snowball Earth” (Figure 2.34; Strauss et al., 2001). The enrichment in $\delta^{34}\text{S}$ signature of chemical sediments across the boundary is real, but its ultimate cause is still a matter of debate.

Holser (1977) favoured brine generation and density/salinity stratification of the Neoproterozoic ocean. Alternatively, Hoffman et al. (1998) proposed extreme climatic conditions and coverage of the global ocean with sea ice (Snowball Earth) followed by a rapid termination of glacial conditions as a consequence of the build-up of large quantities of volcanogenic CO_2 in the deeper ocean. Subsequent mixing of water masses triggered the precipitation of large quantities of cap carbonates

following the glacial horizons. This scenario (sometimes called “freeze then fry”) results in a major reorganisation of the biogeochemistry for the entire water column and is interpreted by some to be documented in the extreme fluctuations of the carbon isotopic composition, which must reflect major changes in the make-up of the world's carbon cycle as we move across the boundary (Chapter 5).

The Precambrian-Cambrian sulphur cycle preserved in marine evaporites is intimately linked to the carbon cycle (Holser et al., 1988). This is expressed through a negative correlation of their isotopic compositions i.e. carbonate carbon and sulphate sulphur, reflecting the biological aspects of the exogenic cycle (Figures 2.23, 2.34; Strauss et al., 2001). The temporal record of

the carbon isotopic composition displays intervals of strongly ^{13}C -enriched values preceding the Neoproterozoic glacials, a decline in $\delta^{13}\text{C}$ immediately prior to the glacial horizons, and low $\delta^{13}\text{C}$ values in the cap carbonates followed by an evolution back to more ^{13}C -enriched values (Figures 2.33, 5.2c).

In part, this may reflect severe changes in primary productivity associated with varying sea ice coverage. Hand in hand with evolving anoxic conditions in the water column under sea ice, heterotrophic recycling of organic matter by sulphate reduction became an important process in the water column, leading to ^{34}S -enriched seawater sulphate. This is clearly documented in the isotopic composition of resulting sedimentary sulphides (e.g. Strauss, 1997). Deglaciation and rapid ocean turnover then transferred ^{34}S -enriched water on to the shelf, where marine-fed sulphate evaporites record this isotopic signature.

Next in the geological history of Precambrian seawater as preserved in evaporite chemistry comes what is, at least from an anthropocentric viewpoint, the most significant time in the evolution of life. It is when metazoans evolved mineralised hardparts and there was the concurrent evolution of the phylum Chordata (animals with backbones and our distant ancestors). Comparisons of chemical compositions of primary fluid inclusions in marine halite chevrons from terminal Proterozoic Ara Salt (≈ 544 Ma) and Early Cambrian (Toyonian) Angarskaya Formation of eastern Siberia (≈ 515 Ma) indicate that Ca

concentrations in seawater increased approximately threefold across the Precambrian–Cambrian boundary and into the Early Cambrian (Figure 2.35; Brennan et al., 2004).

The timing of this marked increase in Ca in seawater broadly coincides with the Cambrian explosion in life, as well as a brief drop in marine $^{87}\text{Sr}/^{86}\text{Sr}$ values, and an increase in tectonic activity at mid ocean ridges (see earlier in this chapter for discussion of how midoceanic spreading rates may link to oceanic chemistry). Their coincidence suggests a link between the advent of biocalcification, increased hydrothermal mid-ocean-ridge brine production, and the changed composition of seawater (Figure 2.35).

Brennan et al. (2004) suggest that the evolution of widespread biomineralization might be a metabolic detoxification process induced by large increases in intracellular Ca^{2+} as identified by increases in Ca levels in halite inclusions. During the Early Cambrian, the ambient oceanic calcium level may have risen to such a degree that cells could no longer effectively exclude or expel Ca^{2+} ions, causing intracellular Ca^{2+} in certain marine organisms to reach toxic levels (Simkiss, 1977, 1989; Kempe and Kazmierczak, 1994). Furthermore, high phosphate levels in Early Cambrian seawater may have amplified the uptake of Ca^{2+} by organisms (Kempe and Kazmierczak, 1994). Opportunistic organisms may have modified their existing cellular waste-removal systems by binding Ca^{2+} as relatively insoluble minerals (calcium carbonate or calcium phosphate). This

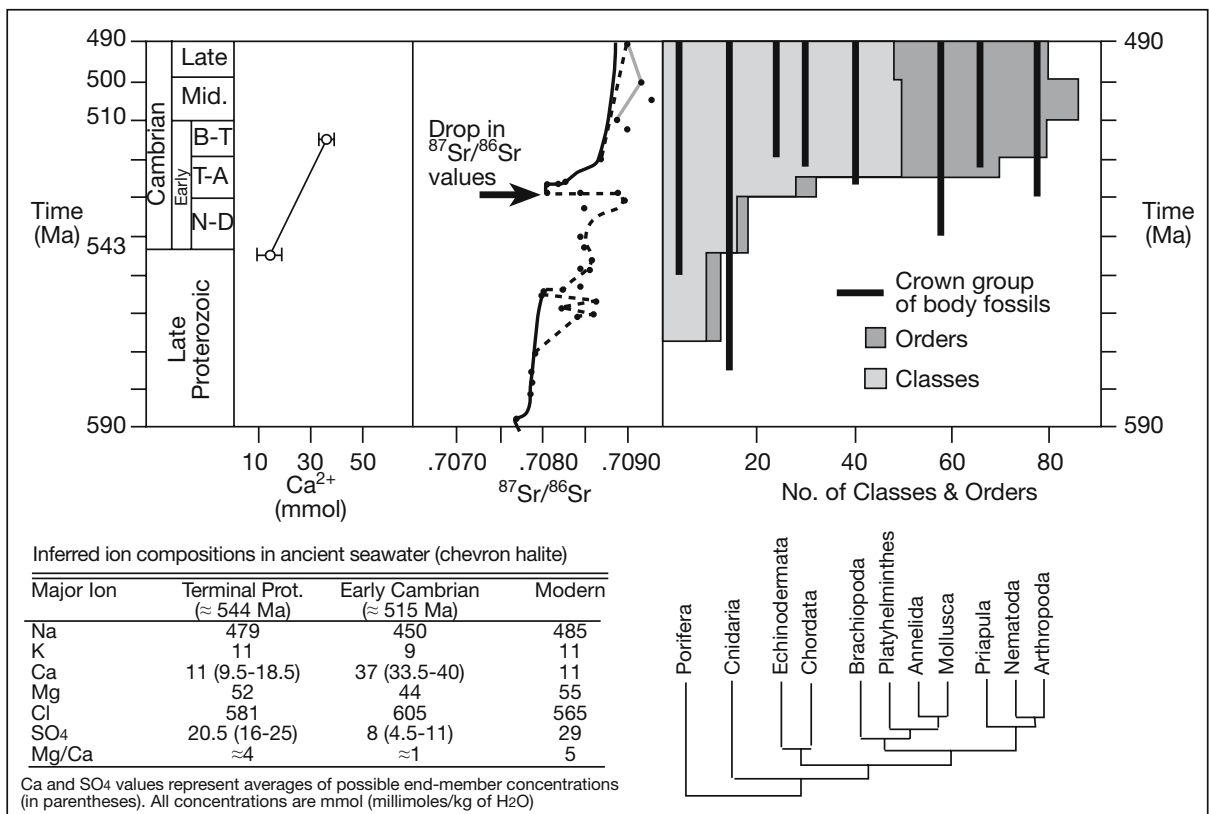


Figure 2.35. Geological and biological changes in oceanic realm during terminal Proterozoic and Cambrian (after Banner et al., 2004 and references therein). Stages in Early Cambrian are Nemakit-Daldynian (N-D), Tommotian–Atdabanian (T-A), and Botomian–Toyonian (B-T); Middle (M) and Late (L) Cambrian are also shown. There was dramatic increase in diversity of animal classes and orders starting in Tommotian time. Phylogeny and corresponding crown group first appearances (time line) show diversification of animal clades from the earliest Cambrian. Crown groups are the last common ancestor of all living members of a clade plus all its descendants. Decrease in marine $^{87}\text{Sr}/^{86}\text{Sr}$ ratios ≈ 530Ma during an otherwise increasing trend in $^{87}\text{Sr}/^{86}\text{Sr}$ ratios likely indicates increase in mid-ocean-ridge spreading rates. Bars indicate possible ranges of oceanic Ca^{2+} determined from inclusions in chevron halite; open circles represent average values with measured ranges shown in parentheses in inset table of computed values of seawater composition for the terminal Proterozoic and Early Cambrian with the composition of modern seawater listed for comparison.

transition in oceanic chemistry, preserved in halite inclusions, could have been the starting point of the complex process that led to exo- and endo-skeletons (and us!).

Hydrology is depositional style

Grains in siliciclastic sediments indicate sediment source or provenance, grains in a carbonate setting indicate biological parentage, mineralogy and textures in an evaporite indicate the nature of the hydrology that created them. During deposition, the hydrologic framework of an evaporite basin consists of surface and near subsurface waters flowing into and out of the areas accumulating salts. It is the upper part of a larger geohydrology made up of several regimes: 1) the active phreatic/vadose, 2) the compactional, 3) the thermobaric, and 4) the active-phreatic-

exhumation/uplift regime (Figures 1.1b, 2.36a). Boundaries are typically indistinct and transitional. The remainder of this chapter concentrates on syndepositional hydrologies of the active phreatic regime, where fluid circulation is driven by solar evaporation and gravity (eogenesis and mesogenesis). Chapter 8 takes this discussion deeper into the subsurface of evaporite basins in thermobaric, compactional and uplift regimes (mesogenesis and telogenesis). In the deep subsurface, where ancient salt masses have spent most of their time, rates of brine flow are slower, alteration events are longer term and driven by a combination of temperature, pressure and density differentials.

Brines and meteoric waters in the zone of active phreatic flow move under the influence of density/salinity or temperature gradients at rates controlled by the permeability of the aquifer.

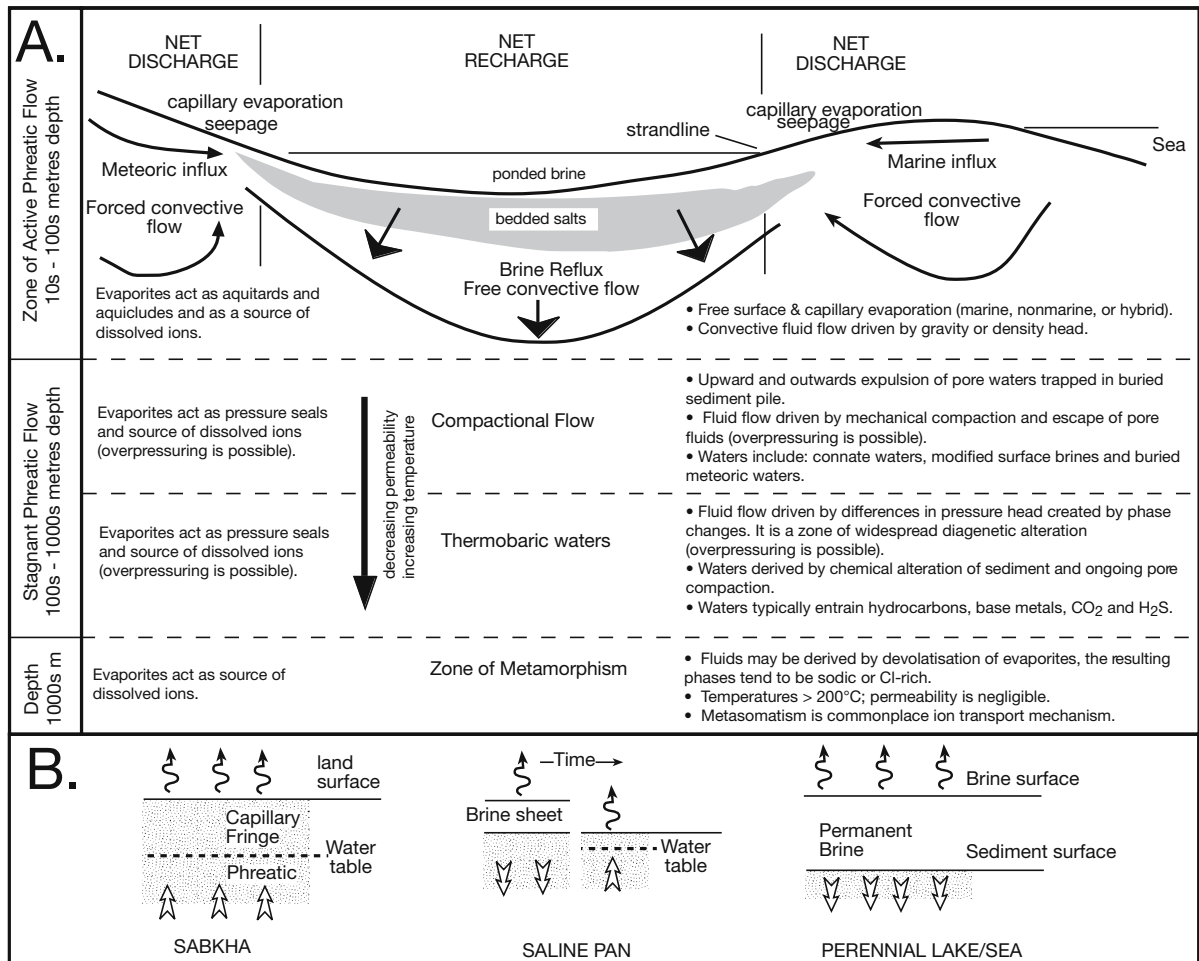


Figure 2.36. Hydrological regimes and processes in evaporitic systems. A) Depth related mechanisms and processes influencing evaporites. B) Simplified hydrology of the three depositional settings that accumulate evaporites.

Where areas of strong topographic relief define the basin margin, as in a continental rift valley or in a transtensional basin-and-range setting, unconfined and confined meteoric water typically discharge into the edges of a brine-saturated depression. Further out, beneath the more central and topographically lowest parts of the depression, density-induced brine reflux, and not meteoric throughput, is the dominant process driving shallow subsurface flow (Figure 2.36a). In a large evaporite drawdown basin, such as in the Mediterranean in the Late Miocene, the level of the discharge zone and the water surface of the perennial brine discharge lake was at times thousands of metres below sea level. Gravity seepage then moved huge volumes of marine/meteoric waters into the depression.

Active phreatic/vadose regime

All primary and syndepositional evaporites first precipitate from brines outcropping at the top of the active phreatic zone or its capillary fringe. This setting is capable of maintaining the density or gravity heads necessary to drive, pond and concentrate large volumes of brines needed to deposit and preserve thick salt beds. An active phreatic flow regime encompasses the zones of seepage outflow, brine ponding, brine reflux and meteoric flow (Figure 2.36a). The surface of a perennial brine lake or seaway is the outcropping expression of the regional water table. In the surrounds, where the regional water table comes near the landsurface, the top of a capillary fringe may be the outcrop expression of the same regional water table and evaporitic mudflats dominate. Solar evaporation drives water loss at the surface of both settings to form bottom nucleated and pelagic salts in a standing water body and capillary salts in a mudflat. Depressions with surface and nearsurface brines in arid settings indicate groundwater discharge zones and their ongoing desiccation creates discharge playas and ancient evaporite seaways. Water lost is replaced by water seeping in from the surrounds creating a replenishment hydrology sometimes described as evaporative drawdown. The replacement water can be continental or marine, and can be supplied via unconfined nearsurface aquifers or via deeply circulating artesian systems.

Hydrologies in saline basins

Hydrologies that precipitate salts can be divided into two end members (Figure 2.36b), 1) a perennial brine lake or seaway (saltern) that at times is density stratified and 2) an evaporitic mudflat (sabkha) with a landsurface defined by deflation at the top of the capillary fringe. A common intermediary stage is an evaporitic mudflat occasionally covered by thin sluggish

brine sheets (salt pan). Before discussing the significance of hydrology to evaporitic sedimentation, we first must define some general hydrological principles (Figure 2.37).

The hydrology of an evaporitic saline mudflat and its landward surrounds (dry mudflat or sandflat) is controlled by the position of the water table in the sediments (Figure 2.37a). Pores below the water table are filled by water of variable salinity and constitute the phreatic or saturated zone where the water volume saturation is total (equals 1 or 100%). The phreatic zone is the region where gravity-driven groundwaters seep down the potentiometric slope toward discharge zones (forced-convection) and dense free-convecting brines, which are created by the evaporation of free surface waters, sink into underlying strata (brine reflux).

Above the water table is the vadose zone, where pores are filled by a combination of soil air and varying levels of water and brine, water volume saturation is less than one. The vadose zone in dry mudflats or sandflats contains an uppermost interval known as the soil moisture zone where the water content can vary considerably over short time frames. Light rains typically penetrate the soil moisture zone but are not sufficient to saturate the whole vadose zone. Pore water returns to the atmosphere, via evapotranspiration, without ever replenishing the water table. Fluctuating evapotranspiration levels in this zone vary widely between storms, reflected in variable metabolic activities of the soil biota, variable mean moisture contents, and varying O₂ and CO₂ levels. Pedogenic carbonates and more soluble salts are typically precipitated as surface crusts and near surface cements as a result of these fluctuations. With the next heavy rain the less soluble carbonate precipitates remain, while any more soluble salts tend to be flushed back into the subsurface, through a now saturated vadose profile, to re-enter the phreatic water mass.

Sediments	Capillary Rise (cm)
Fine silt	750
Coarse silt	300
Very fine sand	100
Fine sand	50
Medium sand	25
Coarse sand	15
Very coarse sand	4
Fine gravel	1.5

Table 2.10 Representative thickness of the capillary zone in various host sediments.

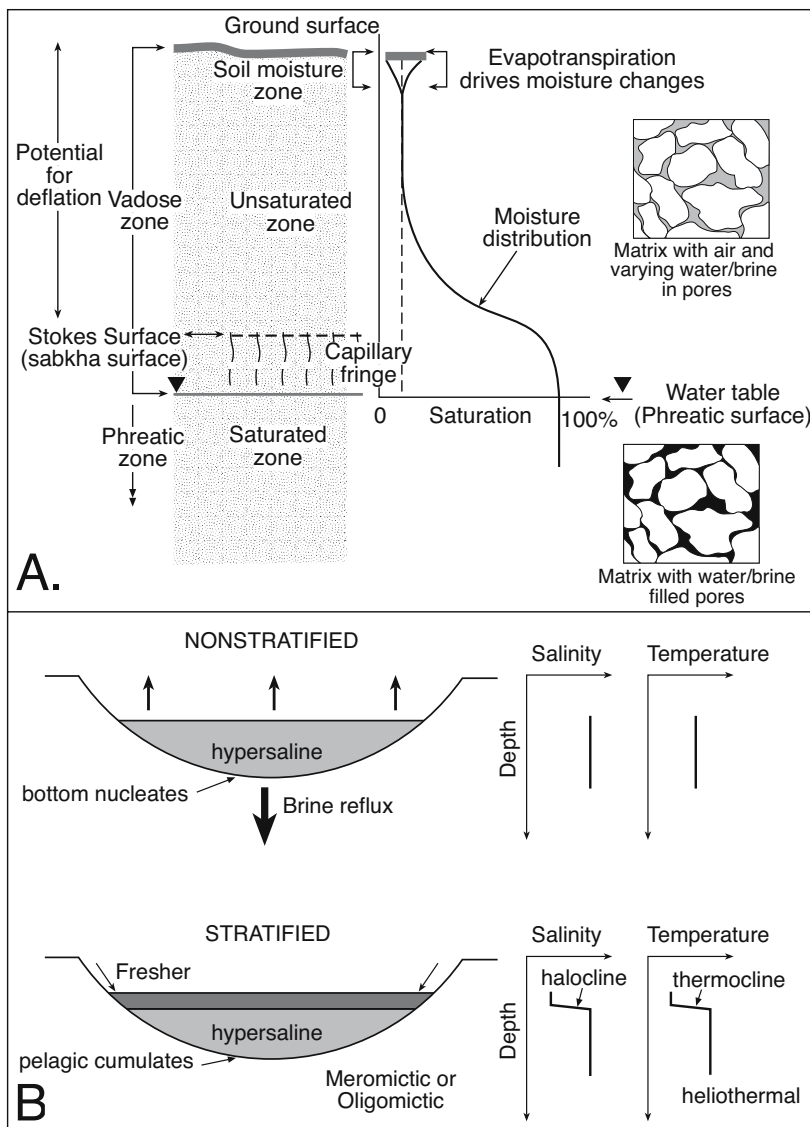


Figure 2.37. Hydrological classification in saline settings. A) Hydrological zonation in the mudflat and its landward surrounds. B) Water mass zonation in a perennial brine lake or seaway.

The process of flushing surface waters to the phreatic zone is known as infiltration. In a homogeneous medium it requires the whole vadose profile to be water saturated. In an inhomogeneous medium, such as a karstic or a fractured and fissured evaporitic landscape, replenishment to the water table can be more focused. Once the more soluble ions are back in the phreatic mass they continue to flow as dissolved load down the potentiometric gradient and ultimately into the discharge depression where, driven by solar concentration, emerging waters once again can precipitate salts in sabkhas, pans, brine lakes and seaways.

The lower part of the vadose zone beneath a dry mudflat is made up of the capillary fringe (aka tension-saturated or wetting zone). In a saline mudflat the capillary fringe extends all the way to the landsurface. The diameter of pore throats in the capillary zone controls the thickness of the capillary zone; the smaller the throat, the thicker the capillary zone. It is a few mm thick in sands and metres thick in fine clays (Table 2.10). Pores in the capillary fringe are not completely filled with water until its lowermost regions, there 100% water/brine saturation defines the top of the phreatic zone and the position of the water table (Figure 2.37a). Water film and gas phases coexist in the interstitial pore space of much of the capillary zone. The relative humidity of the gas phase (saturated vapour pressure) is, however, equal to the thermodynamic activity of water, and so no evaporative concentration can occur in the capillary zone unless it is very close to the landsurface. Loss of pore water from the capillary fringe in a mudflat typically only occurs in its uppermost few centimetres.

There are some simple principles of soil physics associated with capillary fringes in groundwater discharge zones (sabkhas) that at times have been ignored in sedimentological models of sabkha deposition. First, if the capillary fringe is relatively thick, say 0.5 - 1.0 m, then host sediments must (by definition) have small pore throats and so must have low permeabilities. A sabkha, by definition, is a zone characterised by the growth of displacive and replacive capillary salts. Salinity of pore water in this capillary fringe is elevated (indicated by the preservation of gypsum, anhydrite, halite etc.). This low permeability means that high rates of transient short-term rapid lateral or vertical flow through a sabkha capillary fringe is impossible. When a sheet flood covers the 0.5-1.0 m thick saline capillary fringe of a sabkha with a sheet of fresher surface water (rainwater or

seawater) this water does not begin to infiltrate until its density exceeds that of water in the underlying capillary pores. Then, even when densities do exceed that of the underlying waters, the low permeability of the narrow pore throats means the rate of recharge is slow.

To accumulate salts in the capillary fringe the overall solute-carrying water flow vector over time must be upward, not downward. It also means that almost all of the water in occasional fresher water sheets covering a sabkha are lost to the atmosphere. Low permeabilities mean a sabkha is not capable of maintaining longterm downward reflux flow of water or solute to the phreatic mass. This is true in all evaporitic mudflats. This notion of *per ascendum* rather than *per descendum* hydrologies is correctly accommodated in water flow models for most continental sabkhas and mudflats. This was less so in some sedimentological models of modern marine margin sabkhas, or at least this was so until the last decade when detailed hydrological data sets were collected, and coastal sabkha hydrologies quantified, rather than assumed.

As Wood et al. (2002) has clearly shown in the Abu Dhabi sabkha (Figure 3.12b) and Dutkiewicz et al. (2000) demonstrated in Lake Greenly mudflats and pans (Figure 2.15), solute flux in the capillary fringe of saline mudflats is largely decoupled from the effects of water cycling in ephemeral sheets of surface water and their salt crusts. Most of the solute load precipitated as salts in a sabkha comes from rising, sometimes deeply circulating groundwater. It does not come from recharge by occasional surface floods atop the sabkha. Floods (marine or meteoric) in a sabkha tend to do little more than redissolve and reprecipitate surface salt crusts and flush the dissolved contents to the sea or the basin pan. Floods of surface waters to a sabkha flat tend to evaporate, not infiltrate. We shall return to this discussion in more detail in Chapter 3, for now we will just note that any secondary salts actively accumulating in a sabkha or evaporitic mudflat at depths of more than a few centimetres below the landsurface are precipitated by physical and chemical changes in ascending, not descending, pore waters.

Quantified hydrological observations in the capillary zone of Owens Lake mudflats by Tyler et al. (1997) underline some other significant general characteristics of the hydrology of evaporitic mudflats (Figure 2.4):

- 1) Effective evaporation rates are higher over brine pools than evaporitic mudflats, especially those mudflats covered by a salt crust.
- 2) Depth to the water table in a mudflat is a significant control

on the volume of capillary salt precipitated in an evaporitic mudflat or saline pan. That is, much higher volumes of salt accumulate in regions where the saline water table resides closer to the sediment surface for longer periods of time.

3) Because winter and spring water tables are higher (typically cooler with more precipitation) than summer water tables, the rate of capillary salt accumulation in some mudflats can be greater than in the hottest and driest part of a year, when water tables are lower.

The top of the capillary fringe is the landsurface in those parts of an evaporitic mudflat (sabkha) that are actively accumulating surface salt crusts. Heating of pore waters moves liquid water into vapour that leaks into the atmosphere only in the uppermost few centimetres of the capillary zone, immediately beneath the landsurface. The salinity of the residual brines in this uppermost zone increases to where various salts precipitate (Figure 2.38). Lost waters are replaced by the rise of capillary waters from below in the process known as capillary rise.

There is another general principal of soil physics in operation here that many sedimentologists working in sabkhas have ignored. To concentrate a brine to where water is lost in large amounts happens largely in the uppermost parts of the capillary fringe, not throughout its whole extent. This is why in every capillary fringe in every discharging sabkha in every modern example, the most saline pore waters (and the most saline salts, sometimes including bitterns) occur in the uppermost portion of the capillary fringe or in the efflorescent crusts at its surface (Figure 2.38). The underlying capillary waters show upward increasing salinities but never attain the salinities of this uppermost few centimetres where salts can evaporatively precipitate (Figure 2.38).

And yet, from the displacive evaporite textures seen in the capillary fringe of most sabkhas and evaporitic mudflats it is obvious that sabkha salts do not only precipitate as surface and uppermost nearsurface efflorescences and crusts (Figure 3.6c). This leads to the conclusion that preserved calcium sulphate salts in the classic Abu Dhabi sabkha and probably many other sabkhas are a type of retrograde evaporite precipitate known as thermalite salts (Wood et al., 2005). Such salts form passively and displacively in the bulk of the capillary fringe, below the uppermost interval of ephemeral evaporative halite and bitterns. The precipitation mechanism is heating of a rising capillary pore water solution that is dominated by a retrograde phase (anhydrite, gypsum) to temperatures above 25–30°C (see Chapter 3 for details). Sabkha salts in a capillary zone are “true” evaporites in that the overall precipitation hydrology is driven by solar evaporation, but the local precipitation mechanism in

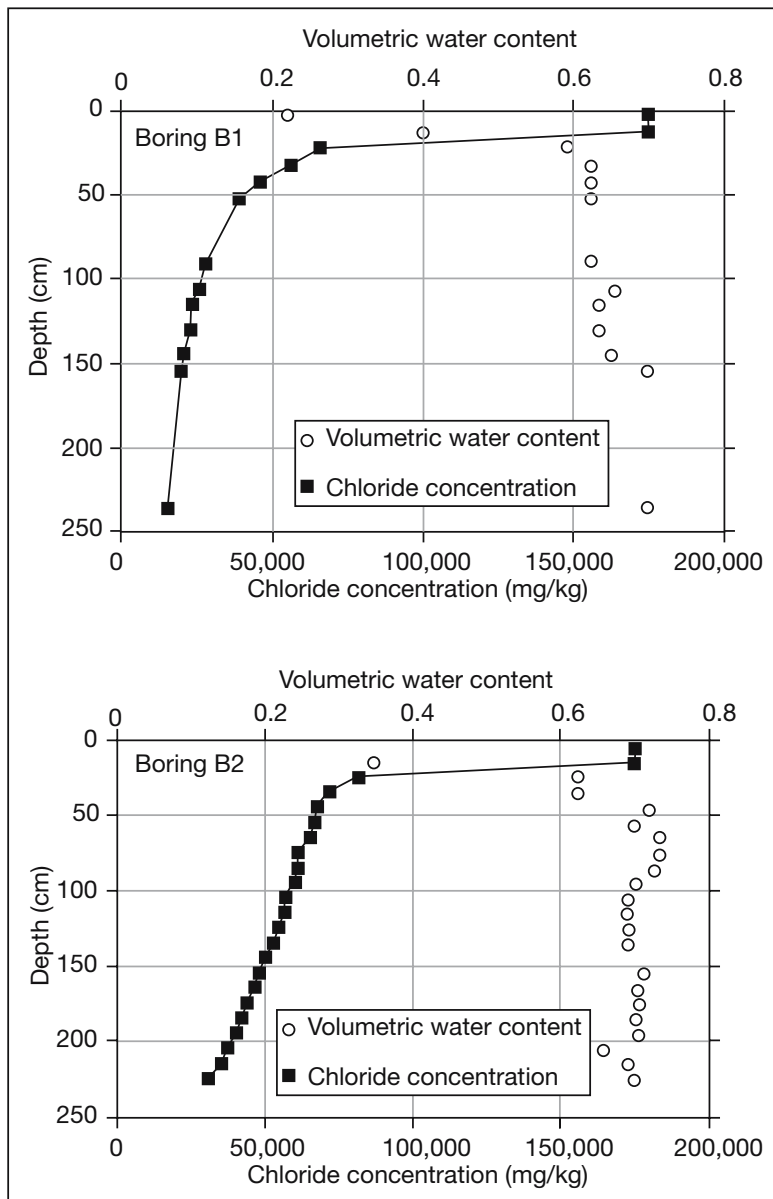


Figure 2.38. Measured moisture and chloride profiles in the vadose zone of two monitored boreholes in the salt-crusted clay-dominated saline mudflats in Owens Lake, California. Measurements were made in summer of 1994 and 67 days after last recorded rain in the region (after Tyler et al., 1997). A water saturated profile would have a volumetric water content or saturation of 1 or 100%. See figure 2.4 for location, both boreholes are from the saline mudflat site.

the bulk of the capillary zone is more a response to temperature change than to evaporative concentration.

In contrast, the hydrology that preserves modern bitterns (carnallite) in the bedded halites of Qaidam Basin is not that of a capillary fringe in a sabkha about the lake edge. By defi-

nition, sabkha pore waters are rising and heating. Rather, the precipitation mechanism in Qaidam salt flats is one of sinking and cooling dense brines precipitating prograde salts, following an episode of halite karstification (Figure 11.3c). Modern carnallite precipitation is a passive pore filling process that takes place *per descendum*, beneath a freestanding and concentrating holomictic brine sheet, which is feeding a dense descending brine plume (brine reflux). It is a recharge mechanism and not a capillary rise process.

Surface waters within freestanding perennial brine lakes or seaways routinely fluctuate between stratified and nonstratified conditions. In the stratified system an upper fresher (less dense) water mass sits atop a more saline (denser) lower water mass (Figure 2.38b). The narrow zone of transition between the two masses in the brine column is called the halocline. Often a stratified saline lacustrine system is also thermally stratified, with warmer waters in the lower water mass and a zone of transition is called the thermocline. Its position is typically identical in the column to that of the halocline. Thermal stratification with a cool top and a hot base is opposite to that found seasonally in many temperate freshwater lakes and so is sometimes called reverse stratification and also described as heliothermal layering. The term meromictic is used to describe a permanently stratified water mass where surface layers may mix, but the bottom layer does not disappear. The upper water mass that periodically mixes is the mixolimnion, the lower permanent mass is the monolimnion. Oligomictic is used to describe stratified water masses that mix or homogenise for short irregular periods every few years.

Mixing in a saline water mass is controlled by the evaporation and concentration of the upper water mass until it reaches a density equivalent to the lower water mass. Then mixing or overturn occurs. Substantial density differences between the

upper and lower masses in most density stratified systems means diffusive mixing across the halocline is insignificant. A stratified system is a stable system, so that when a hypersaline water mass is density stratified there is little bottom precipitation of salts. Sedimentation is mainly by a pelagic rain of crystallites, which first formed either in the uppermost part of the upper water mass or by brine mixing at the halocline. Whenever the upper and lower water masses equilibrate and homogenise, bottom nucleation of salts is possible even at the base of deep brine columns, as is occurring in the Dead Sea today (Chapter 4). Whenever a homogenised water mass restratifies, the rate of brine reflux in to sediments below the sediment brine interface slows and ultimately stops, for there is no ongoing mechanism to resupply brines denser than pore waters in the substrate.

Refluxing brine plumes beneath homogenized surface water masses sink and at the same time start to spread laterally toward the basin fringes where they mix with incoming forced-convection waters of the seaway or playa margin. Ultimately plume waters can return to the surface in a diluted form as a component of spring or seep waters or they can be lost to the regional hydrological flow. Reflux-driven convective flow is an effective way of moving salt load through large volumes of basin sediments in modern saline depressions (e.g. Lake Tyrell, Australia: Figure 2.20) and also explains the distribution of salts, pseudomorphs and dolomites in ancient sediments that underlay or were adjacent to areas accumulating bedded salts.

Mudflat aggradation mirrors water table changes

Unconfined meteoric and marine groundwaters seeping and discharging into the edges of an evaporitic depression have a potentiometric head defined by the position of the regional water table. The unconfined meteoric water table surrounding a modern coastal marine-seepage lake is typically a few centimetres higher than sea level. In a continental saline lake or an ancient drawdown saline giant, the water table about the basin margin is higher than the brine level within the evaporite-accumulating depression (Figure 2.39a). Once meteoric/marine groundwater seeps into discharge zones within the salt-accumulating region of the central depression, it comes into contact with more saline and denser surface and pore brines. On average, the throughflowing waters beneath a mudflat or bajada margin are less dense (fresher) than hypersaline waters in the brine-saturated lowermost parts the saline depression. After a heavy rainstorm or a flood, a shallow fresher groundwater layer forms along the strandline edge of the permanent brine lake or seaway as freshwater floats atop a wedge of denser hypersaline pore waters (Figure 2.39a, b).

Shallow meteoric sheets and groundwater lenses are typically transient mudflat features, so without ongoing recharge, these freshened groundwater outflows within the mudflat dissipate via capillary evaporation and are replenished by more saline pore waters. Alkaline earth carbonates and lower salinity salts can precipitate as surface crusts or nearsurface pedogenic nodules and crystals in the vadose portions of the basin edge. During prolonged dry spells, capillary evaporation continues to lower the saline mudflat water table until flow directions may be reversed. Brines in aquifers from the basin centre and more deeply circulating region groundwaters begin to seep into the margin to replace the lost capillary fluids. Increasingly saline pore waters in a saline mudflat, mean salts, which crystallised earlier, can now evolve into more saline precipitates via backreaction and replacement (Figure 2.39c).

With the next influx of freshened recharge the water table rises once more in the marginward vadose zone of the saline depression. At the same time a thin sheet of fresh rainwater or seawater can cover the surface of the saline mudflat. This redissolves highly soluble salts of the uppermost capillary zone, along with any of the more soluble surface efflorescences (Figure 2.39b). A wedge of freshened water now floats above a stable body of dense brine, both atop pore waters of the saline mudflat and atop a dense lower brine mass the central density-stratified perennial brine lake. This blanket of freshened water shuts down evaporation of saturated waters and prevents further accumulation of salts, both in the uppermost parts of the capillary mudflat and in the salt brine covered regions of the perennial lake or seaway. The style of surface sedimentation at this time is sheet flood sands followed by accumulation of suspended load clays.

Then, as the depression begins to dry out, the brine sheet shrinks until it only covers the lowermost parts of the lake depression, the zone of perennial lake waters. Once the saline mudflats are re-exposed, capillary evaporation begins once more. At some point in this desiccation stage, surface water becomes saturated and crystallites formed at brine surface sink through the brine column to the lake/seaway floor (pelagic sedimentation of carbonate and gypsum). Bottom nucleation and intrasediment prograde precipitation of reflux salts beneath a standing brine lake recommence when the rising salinity (density) of the upper water mass comes to equal that of the lower brine mass. The two water bodies then mix and precipitation of bottom salt begins anew (Figure 2.39a).

Near surface sediments in saline mudflat margins experience the effects of schizohaline pore waters. Salinities in sediments beneath perennial (meromictic) brine-covered depressions

tend to be more stable, although a body of freshened surface water comes and goes. Textures in schizohaline salt beds are dominated by ongoing re-equilibration reactions, backreactions, dissolution-reprecipitation and haloturbation, while textures in beds deposited in perennial brine seaways and lakes tend to be more stable and dominated by large growth-oriented crystal beds and brine reflux re-equilibration textures below.

As an evaporite basin aggrades toward its hydrological equilibrium level (Figure 2.39c) the depositional surface aggrades into ephemeral brine sheet (pans) and ultimately mudflats (filled accommodation space). The progression brine lake to

a mudflat induces schizohaline textures in the uppermost parts of each shallowing upward hydrological cycle. If there is no rise in regional watertable, the same textural shoaling occurs across the whole discharge zone.

Indicators of fluctuating water tables

Because evaporites form by the evaporation of discharging and ponding waters, any longterm water table fluctuations in an evaporite basin influence sedimentation style and mineralogy on scales coarser than the stacked gypsum and tepee truncation layers and parasequences described in Chapters 1, 3 and

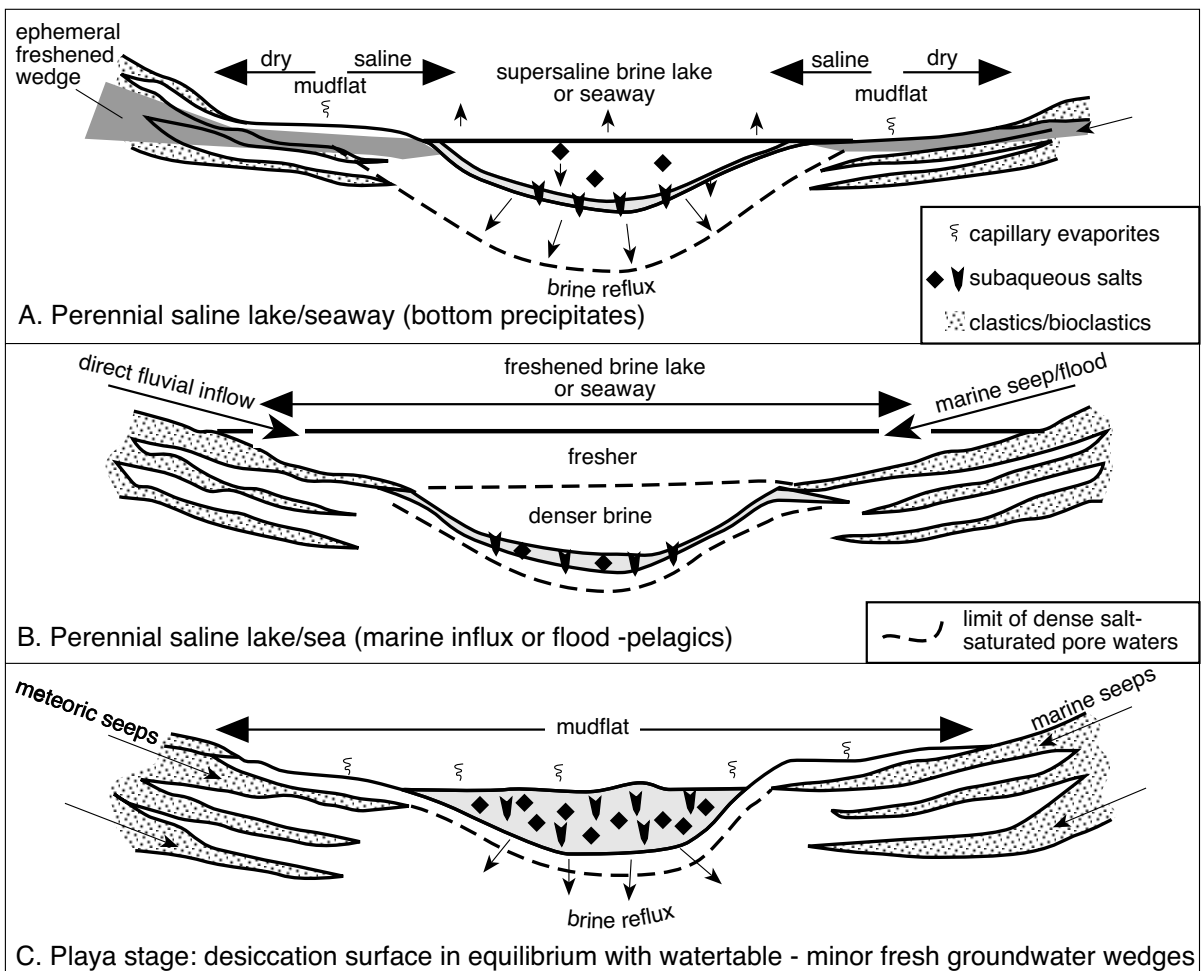


Figure 2.39. Cross sections showing hydrological stages in the active phreatic zone in an evaporitic seaway or a continental lake. A) Perennial saline lake accumulating widespread subaqueous evaporites from a nonstratified brine body. Capillary evaporation of fresher water lenses about the lake margin. B) Perennial saline lake or water full stage with subaqueous brine lens isolated from solar evaporation processes by a layer of surface water. This shuts down widespread crystallisation in lower brine body and slows brine reflux. C) Playa stage where ongoing evaporite fill, or lowering of regional water level, means the sediment surface is mostly subaerial and in capillary equilibrium with saline lake water table. This is a classic evaporitic mudflat or sabkha hydrology. No fresh water lens exists until after the next flood event.

Locality	Geological setting of Stokes Surfaces	References
Arabian Gulf sabkhat, United Arab Emirates	Coastal saltflats prograding into Arabian Gulf	Patterson and Kinsman, 1981 Warren, 1991
Jafurah Sand Sea, Saudi Arabia	Interdunal saltflats in sand sea (erg) migrating into the Arabian Gulf	Fryberger et al., 1983, 1984
Samphire Lake and Spring Lake, Australia	Playa capture and deflation driven by a lowering of the regional water table	Jacobson and Jankowski, 1989
Guerrero Negro dune field, Mexico	Coastal barchan dunes migrating landward over lagoonal sediments	Fryberger et al., 1983, 1984
White Sands dune field, New Mexico, USA	Continental saltflat and gypsum dunes deflated from Lake Lucero	Loope, 1984 Langford, 2003
Great Salt Lake desert, Utah, USA	Continental dunes and lacustrine saltflats	Stokes, 1968

Table 2.11. Some examples of modern capillary deflation surfaces or Stokes surfaces.

4. Longterm aggrading water tables (or regional subsidence) in an evaporite basin enable the capture of formerly vadose sediment by the damp, sticky to wet conditions that characterise the capillary and phreatic zones and so facilitate the preservation of formerly vadose and nonevaporite sediment in the depositional system - sediment that would otherwise be blown away (e.g. Newell, 2001). It is aggrading water tables that ultimately preserve almost all ancient sabkha, brine lake and dune sediments.

Falling water tables enable entry of vadose conditions into former capillary and phreatic sediments. This leads to the dissolution of salt beds, to eolian deflation and to the formation of residual sediment layers that come to lie at or just above the regional water table. Episodes of active deflation in the Late Quaternary have periodically fed the extensive quartzose and gypsum sand dunes that abut numerous playas in Australia, Saudi Arabia and the southwest USA. Deflation to the top of the capillary fringe creates the characteristic flat surfaces of many modern playas, sabkhas and interdunal depressions. The hydrological process has been called watertable bevelling as it is tied to the erosional top of the capillary zone (Bowler, 1986, Warren and Kendall, 1985). The capillary surface erosionally truncating underlying sedimentary structures is termed a Stokes surface.

Stokes surfaces

Stokes surfaces accompany changes in the base level of erosion/deflation and are commonplace in eolian sand seas or ergs abutting ancient evaporite beds. At the local scale a Stokes surface defines the top of the sedimentation surface in a degrading wet interdunal depression (Table 2.11; Stokes, 1968). A succession of such truncation surfaces can be preserved atop a number of depositional cycles as successive packages of sediments aggrade

and stack, driven by longterm water table rise. Changes in water table level may indicate climatic change or episodic basin floor subsidence. At the regional scale an extensive truncation surface in an ancient desert succession, which passes through various arid lithofacies, is called a super-surface or a super bounding surface by sequence stratigraphers, but it is really a glorified Stokes surface.

Stokes surfaces create sharp planation surfaces in eolian crossbeds, sometimes outlined by a thin veneer of lag sediment (Fryberger et al., 1983, 1984). Water table control on their creation is clearly seen in the Umm Said portion of the Qatar coast south of Doha where large transverse and barchan dunes still migrate into the sea (Figure 2.40a). This eolian-fed progradation of the shoreline and the creation of the associated Stokes surface has been taking place since the early Holocene sea first intersected the sand sheet (Figure 2.40b, c). The Stokes surface is the surface of uppermost eolian preservation and it migrates seaward as the dunes build out into the Arabian Gulf. In all modern coastal dune successions the Stokes surface is the top of the capillary zone and it approximates sealevel.

Erosion surfaces, defined by the top of the capillary zone also truncate anhydrite nodules or enterolithic folds in the upper parts of the coastal sabkhas of the United Arab Emirates (Figure 3.4g). In the fine grained matrices of a sabkha the erosional truncation of an evaporite is typically up to a metre above the water table. Stokes surfaces are an integral part of the capillary hydrology of a sabkha and are very useful in distinguishing ancient mudflats from subaqueous evaporites (Warren and Kendall, 1985).

Aggrading water tables in discharge depressions in sand-rich eolian environments can promote the passive precipitation of pore cements in the uppermost part of the capillary zone. In

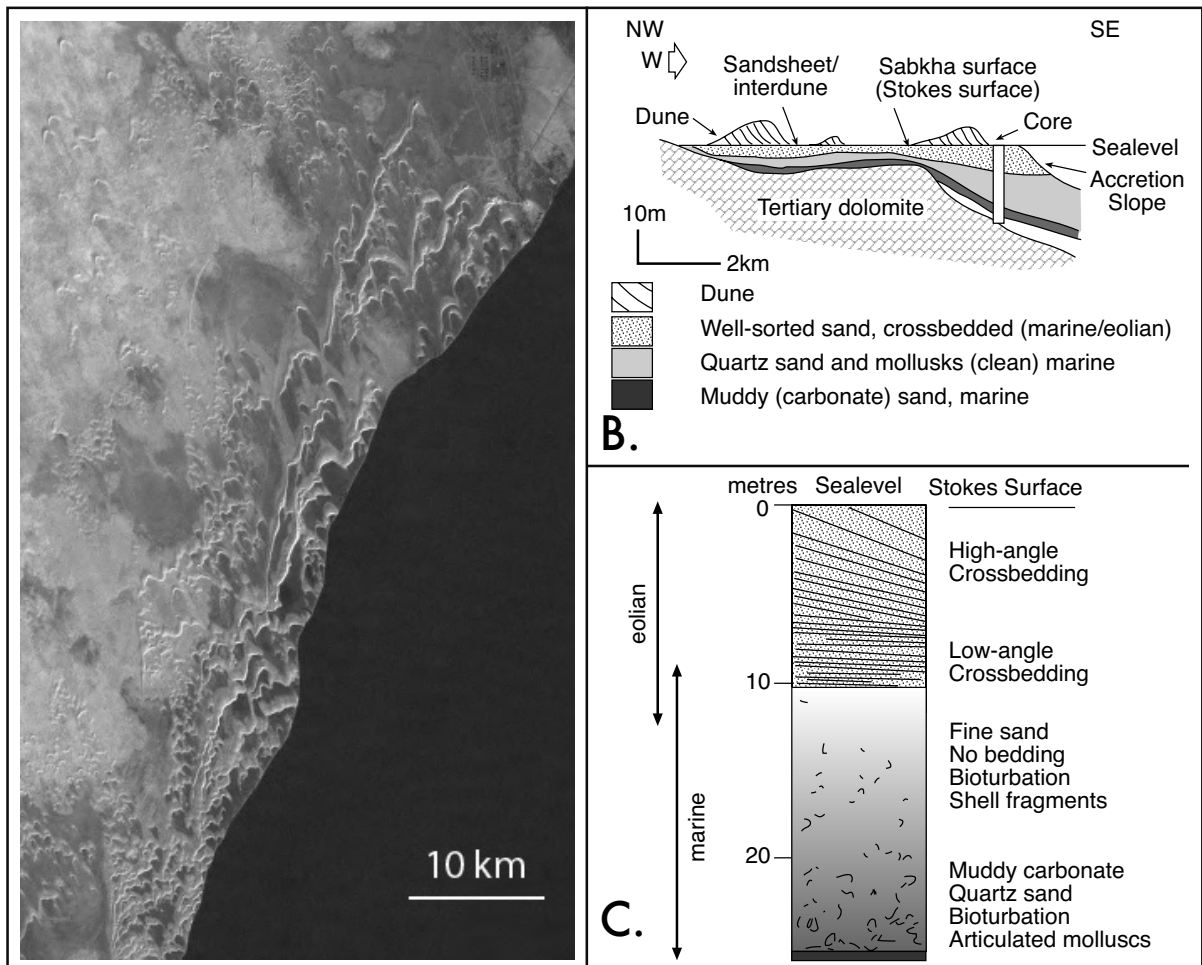


Figure 2.40. Umm Said Sabkhat, Qatar. A) Transverse and barchan dune moving seaward atop sandflat and coastal sabkha (Image courtesy of NASA). B) Cross section and core from an Umm Said sabkha in coastal Qatar showing how the deflation surface that defines sealevel and the top of modern coastal sabkhas is also a Stokes equilibrium surface (indicates the top of the capillary zone). C) Schematic core taken in position shown in B. (B and C after Shinn, 1973).

modern dunes and sandflats these aggrading salt-cemented intervals are sometimes called salcretes, the evaporite equivalent of capillary calcretes. They are made up of passive pore-filling cements (gypsum or halite), not the active displacive nodules and crystals that typify sabkhas. Schenk and Fryberger (1988) noted such massive phreatic-gypsum cemented zones act as a lower limit to any subsequent eolian deflation in the gypsum dunes of the White Sands dune field, New Mexico. They create a cemented near-horizontal base level to erosion, now seen as a widespread Stokes surface in the interdunal corridors. Aggrading salcretes, tied to a rising water table, can help preserve capillary and eolian sedimentary structures. Salcretes were the main reason why dune topography is preserved in some transgressive settings where ancient ergs are overlain by evaporite beds (e.g. Entrada-Todilto and Rotliegende-Zechstein formations).

Megapolygonal desiccation cracks are another expression of the hydrology associated with a Stokes surface and form in deflating mudflat or playa sediments in conjunction with a regionally falling water table (Figure 2.41). Megapolygons can be up to 300 m wide and separated by fissures up to 5 m deep, they characterise the modern surfaces of a number of Basin and Range playas in Oregon, Nevada, California, Arizona and New Mexico (Neal et al., 1968). Fissures are hosted in fine-grained playa sediments rich in clays and carbonate minerals. The fissures, which are up to 1 metre wide, are routinely filled or partly filled with wind blown sands (mixture of quartz and gypsum). Individual fissures tend to be discontinuous across the playa surface and often display en-echelon patterns.

Megapolygons are the result of shrinkage in fine-grained lake sediments and indicate water loss following a fall in the piezometric head. In some cases the water table lies 3-20 m below the megapolygonal surface. As pore waters evaporate from the upper part of the newly created vadose zone, tensile stresses accumulate in the muds until they eventually rupture into the polygonal fissure network. Neal et al. (1968) interpret the fissures as indicating vigorous desiccation over a number of years. Some playa fissures may be related to overexploitation of the local groundwater resources in the last 50-100 years, most indicate the rigorous climatic transformation that occurred during the Pleistocene-Holocene transition. Identical sand-filled fissures, up to 18 cm wide and 5.7 m deep, have been documented in the Pennsylvanian Hermosa Formation of southeastern Utah (Loope and Haverland, 1988).

Stokes surfaces and palaeohydrology

Recognition of Stokes surfaces, associated interdunal sabkhas and wet mudflats/interdunes has broader scale implications in terms of regional hydrological evolution over time frames measured in thousands of years and to permeability models. Most modern Stokes surfaces either are a coastal groundwater response to progradation since the last rise in sea level some 6,000 years ago, or are a hydrological response related to marked climatic changes in deserts from the Late Pleistocene to the present, usually toward increasing aridity (Table 2.11).

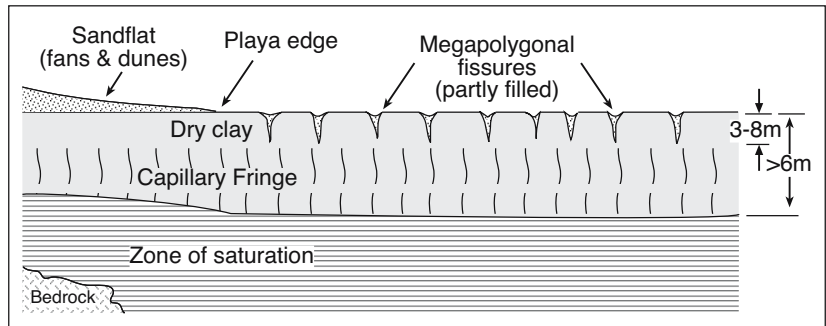


Figure 2.41. Megapolygonal desiccation cracks, partly filled with sand captured as it saltated across the deflationary playa surface. Fissures formed by a lowering of the regional water table and the associated shrinkage during drying of lacustrine clays (after Neal et al., 1968).

Changes in the level of ancient regional water tables and aggradation of base level (creation of accommodation space) is often preserved in ergs (sand seas) abutting the edges of evaporite basins in the USA and elsewhere (Mountney and Thompson, 2002). For example, Havholm and Kocurek (1994) used the presence of regional discontinuities in the erg succession to interpret the depositional history of the Jurassic Page Sandstone of the Colorado Plateau, USA (Figure 2.42). The Page Sandstone was deposited in a coastal erg where there was a constant rise and fall of the strandzone of the adjacent epeiric seaway. These eolian sediments encompass a number of regional erosion surfaces known as super bounding surfaces or supersurfaces. Sometimes the interdunal portions of these supersurfaces preserve giant (5 m high) stromatolites indicating flooding and longterm at-surface brines in the interdunal corridors (Eisenberg, 2003).

Correlation of super-surfaces between outcrops defined inter-relationships between the dune sands and the interlayered

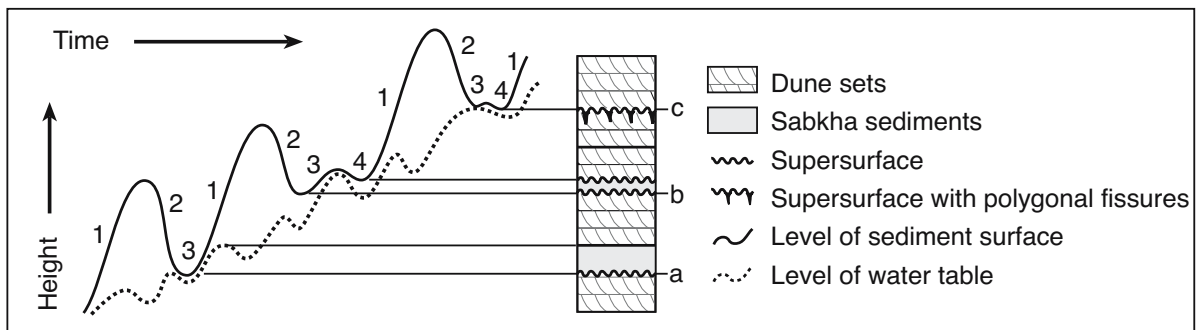


Figure 2.42. Accommodation space for Jurassic Page Sandstone (30-50 m thick) sedimentation was controlled by interaction during subsidence between deflation (solid curve) and changes in the level of the water table (dashed curve). Surface a is overlain by sabkha sediments that were not eroded, surface b is overlain by partly eroded sediments, and surface c is an erosional surface with polygonal fissures. Numbers 1-4 on sedimentation curve indicate type of activity: 1) dune accumulation, 2) deflation, 3) sabkha formation or formation of polygonal fissures, 4) deflation of surface features (from Havholm and Kocurek, 1994).

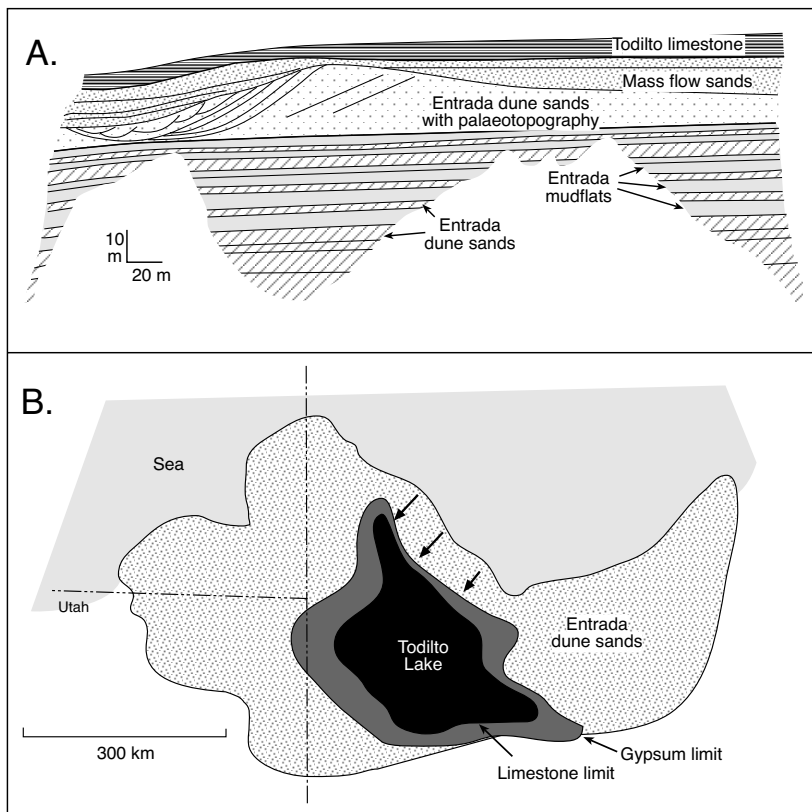


Figure 2.43. A) Outcrop drawing showing preserved dune palaeorelief with onlapping structureless sandstones and overlying limestones of the Todilto Formation. The Entrada Sandstone underlying the preserved relief consists of interbedded dune sets and evaporitic mudflat (sabkha) deposits (after Benan and Kocurek, 2000). B) Approximate Late Callovian-Oxfordian(?) palaeogeography of the Four Corners area after partial marine transgression of the Entrada. Extent of the Todilto Formation shown with concentric limits of limestone and gypsum within the unit, with surrounding eolian units (after Lucas and Anderson, 1994).

sabkha and interdunal successions (Figure 2.42; Havholm and Kocurek, 1994). Sand accumulation in the Page was episodic and punctuated by the formation of supersurfaces tied to substantial lowerings of the regional water table. This created both Stokes surfaces and megapolygonal fissures. Sabkhas and interdunes aggraded as the water table rose until sedimentation surfaces sat above the top of the capillary zone. Then vadose sedimentation, typically eolian crossbedded dunes sands, dominated once more. Thus the Page Sandstone is a collection of desert dune-interdune successions preserved in accommodation space created by an overall rise in the water table (basin subsidence). The smaller scale sequence packaging (dune alternating with wet interdune) reflects periodic rises in the water table, tied to shorter-term variations in climate, tectonics (subsidence) and changes in the strandline positions of nearby seaways or lakes.

The Jurassic Entrada Formation shows a similar water table control with its sea-marginal setting, promoting numerous internal truncation surfaces tied to deflation to the top of the capillary fringe (Crabaugh and Kocurek, 1993). Sediments deposited in the passage of the Entrada Fm. into the overlying evaporitic Todilto Fm. are unusual for an eolian system. The upper part of the Entrada is characterised by mass flow deposits and preserved eolian dune palaeotopographies beneath sandy subaqueous strata, rather than the more typical erosional top with the eolian unit passing up into continental deposits (Figure 2.43a; Benan and Kocurek, 2000). Preserved dune remnants have relief of up to 35 m and are buried by onlapping, subaqueous, largely structureless sandstones. The latter are derived by mass wasting of the upper portions of the dunes as regional water levels rose. Eolian sands were redeposited as sediment-gravity flows, which infilled depressions between the dunes. Preservation of dune palaeotopography beneath mass-flow deposits argues that flooding of the Entrada dune field was geologically rapid and energetically gentle.

Flooding heralded the onset of a restricted density-stratified brine lake/seaway, which deposited the evaporitic Todilto Formation. This seaway was a marine-seepage fed drawdown depression within what was the lowest part of the erg. This type of seepage encroachment converting the erg to a lake meant there was no transgression of a high energy marine coastline across the top of the sand sea (Figure 2.43b). Rather, aggradation of the saline water table was a relatively gentle process, with preservation of dune topography beneath lacustrine laminites perhaps aided by the formation of ephemeral capillary-fed salcrettes. Salcrettes precipitate where the capillary zone intersects the eolian landscape in any arid zone transition from an erg to a brine lake. A similar preserved dune palaeotopography, also with ephemeral salcrettes, formed atop the Permian Rotliegend/Wiessliegend sands of the North Sea and heralded the onset of evaporite deposition in the saline giant that deposited the Zechstein salts (Glennie and Buller, 1983).

The position of the water-table in many ancient sand seas controlled the depositional style and facies continuity of various windblown sand units (Figure 2.44). Less permeable lenses of salcrete-cemented, damp and wet interdune strata and interdunal sabkhas exhibit an intertonguing, transitional relationship to the toe-sets of adjacent and overlying eolian dune units (Mountney and Thompson, 2002). Intercalation signifies vadose dune migration (eolian cross beds) was contemporaneous with water table-controlled accumulation in adjacent interdunes. Eolian crossbedding can only form in the vadose zone. Down-wind changes in the geometry and facies of the interdune units indicate periodic expansion and contraction of the interdunes in response to changes in the elevation of the groundwater table with respect to the landsurface. Changes in geometries and extents of the various vadose, capillary and lacustrine units in an erg are a response to climatic change, subsidence and episodic flooding.

Understanding that hydrology (depth to watertable) creates permeability layering during deposition of ancient dune sand succession adds another level of reality to previous dry erg models for fluid flow in eolian reservoir sands deposited below evaporite seals. Older engineering models guiding hydrocarbon recovery from oil and gas fields from eolian sands below evaporite seals typically assumed that the spectrum of internal flow discontinuities in the eolian sands were largely defined by 1st- through 4th-order bounding surfaces, that is, the primary sedimentary structures control permeability. At the reservoir scale the sands were assumed to respond as largely homogenous flow units during hydrocarbon extraction, with permeability variation tied to grain size variation. This is after all what is seen in the impressive Quaternary ergs of

the Sahara, Arabia and Mongolia. But these analogs are all purely continental settings, located a long way from the ocean and from any other permanent body of surface water with a hydrology capable of depositing a widespread evaporite seal over the top of the erg.

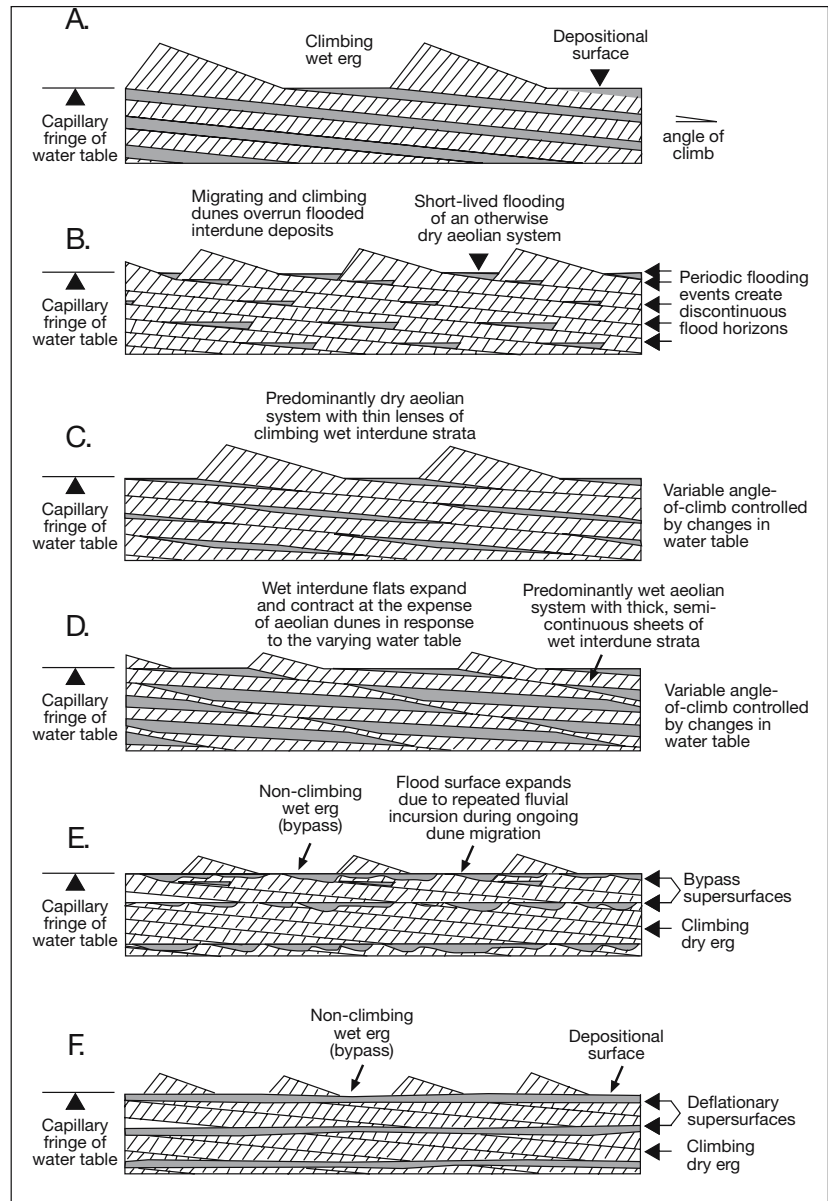


Figure 2.44. Spectrum of interdune geometries generated by variations in the frequency and magnitude of water-table change, the rate of dune migration and the net eolian sediment budget. (a) Entrada Sandstone, (b) Navajo Sandstone, (c) and (d) Helsby Sandstone Formation, (e) Cedar Mesa Sandstone, (f) White Sands (after Mountney and Thompson, 2002 and references therein).

The reality is that homogenous eolian sand reservoirs are not all that commonly associated with bedded evaporite seals that overlie windblown sediments. Typically, thick homogenous dune sand units are not preserved at or immediately beneath the contact with an encroaching evaporite seal. The encroaching hydrology associated with the passage from an eolian system to an evaporite system simply does not allow widespread vadose conditions during the transition. Rising water tables feed capillary salts that patchily cement the reservoir sands during passage into deposition of an evaporite seal. Reservoir quality in these systems is typically a reflection of intergranular cement intensity (anhydrite or halite) and is not a direct reflection of primary depositional geometries or primary sedimentary structures. By the time an evaporite seal covers a unit dominated by windblown sands any loose sands have already blown on and away into the interior, as is the case in the central Arabian Peninsula, or have been dispersed into the shoreface, as in the southeastern Qatari and northeastern Saudi coastal zones (Figure 3.57).

Preserved sandflats about the edges of most aggrading and transgressive evaporite seaways are tied to deflation controlled capillary fringes and aggrading marine water tables. Such a hydrology must deposit evaporite cements wherever the capillary fringe intersects the land surface and reflux cements where brine plumes sink into the underlying sands beneath brine-filled interdunal corridors (Figures 10.40 - 10.42). In this hydrological setting the sabkhas, mudflats and salcrettes that characterise the transition to the seal facies create low permeability cement patches within any underlying eolian sediment sheet. Thick piles of more homogenous vadose crossbedded dune sand that may have once been present in the region prior to the encroachment of the evaporite precipitating hydrology now lie deeper in the succession, and so are of less interest in terms of modelling hydrocarbon production from sediment beneath the evaporite seal.

Reservoir models for flow response in eolian sandflats sealed by evaporites should not assume intraformational continuity in the sands beneath the seal. Instead, a competing model with two end-members is more appropriate. At one end of the depositional spectrum are damp/wet interdune strata in wet eolian sandflats with shallow water tables. At the other end of the depositional spectrum are dry dunes with deep water tables that are flooded by the rapid entry of seawater into the continental depression. Inputs to the model can be quantified by the relative proportion of dry eolian versus wet interdune structures seen in core or core-calibrated FMI imagery. Scaling of reservoir geometries can be done using analogues

for the various styles of watertable encroachment on coastal dunes as seen in modern marine and lacustrine settings (e.g. Figures 3.58 - 3.61).

A climbing dune model (relevant for much of the Entrada Sandstone, in Utah) requires moderate-high sediment supply in balance with a relatively deep water table. It has a relatively low potential for widespread capillary salcrettes and fine-grained interdunal sediments (Figure 2.44a). The non-climbing dune model at the other end of the hydrological spectrum is characterised by widespread episodes of non accumulation or hiatus (relevant for climatically controlled supersurfaces as in the coastal zone of modern NE Saudi Arabia, Sabkha Matti in the UAE, the White Sands of New Mexico, the Late Quaternary sandflats surrounding Lake Eyre and their Pre-Khuff counterparts in the subsurface of Saudi Arabia). It requires periodically low rates of sediment supply, high rates of deflation and longterm low rates of creation of watertable controlled preservation space for the sand sheets. It has a much higher potential for large areas of the system to be deflationary, for large areas of the sedimentation surface to intersect the capillary fringe and for the preservation of widespread capillary salcrettes (Figure 2.44f).

Defining which of the various intervening styles of sediment accumulation in the eolian succession under study is important in modelling porosity and permeability extents and in correlating lateral extents of high permeability zones in ancient sand bodies (Mountjoy and Thompson, 2002; Figure 2.44b-e). Textures indicative of dry or wet eolian systems and interdunal sabkhas are discussed in the next chapter. Wet interdune textures are described in detail by Goodall et al. (2000).

Degrading hydrology and playa capture

Aside from Stokes surfaces, the effects of a degrading (falling) hydrology and associated deflation are seen in sediment and drainage patterns in many Late Quaternary playas, including those in Central Australia located in and around Lake Amadeus and Curtin Springs (Jacobson et al., 1989). Longterm reduction in groundwater levels associated with increasing aridity at the end of the Pleistocene led to a change in the status of some inland playas from discharge playas to recharge playas (with solution fissures and karst holes) via a process known as playa capture. It occurs when a fall in the level of regional groundwater, perhaps driven by the deflationary deepening of one playa floor leads to the removal of one or more adjacent playas from the discharge level of regional groundwater outflow (Figure 2.45; Jacobson and Jankowski, 1989). Groundwater head in the Curtin Springs area has decayed over the last several thousand

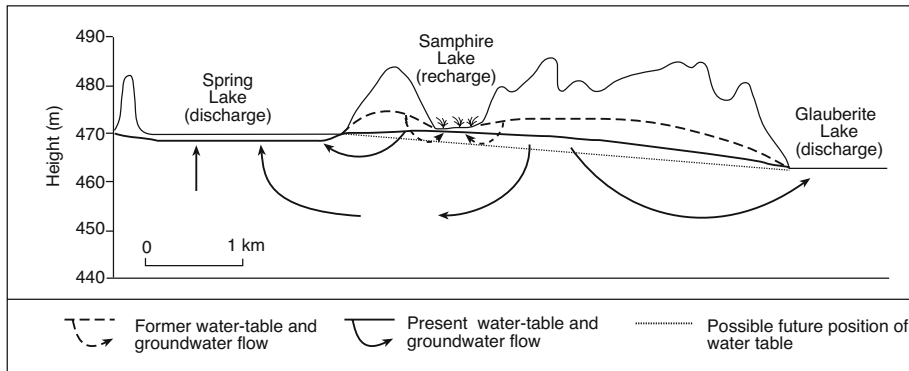


Figure 2.45. Schematic of playa capture or abandonment via decay of groundwater head. Samphire Lake was once a discharge playa (dashed line indicates former water table) that was accumulating gypsum, but it was converted to a recharge playa as Glauberite Lake progressively captured the regional groundwater flow system (after Jacobson and Jankowski, 1989).

years and so changed the nature of playa sedimentation. A few thousand years ago Samphire Lake was a discharge playa and it still retains thick deposits of groundwater-derived lacustrine gypsum from that time (Figure 2.45). Today the discharge system is no longer active in the lake as the regional water table lies metres below the playa floor. Samphire Lake has evolved into a vegetation-covered recharge playa and regional discharge is focused into nearby Spring Lake and Glauberite Lake. This has rendered the Samphire Lake surface sediment susceptible to eolian deflation, karstification and vegetation coverage. Over time Glauberite Lake will become the primary focus of groundwater activity in this region and will ultimately form a regional groundwater sump.

Falls in local hydrological base level can be driven by changes in climate, uplift or tectonic isolation. It drives local processes such a karstification and carnallite precipitation in bedded halites in the Quaternary playas of Qaidam Basin, China and in Lake Asal, Djibouti (Figures 11.2, 4.56). An impressive example of the effects of a local lowering of the saline base level on karst intensity is seen in evaporite-cemented sediments that increasingly exposed about the margins of the Dead Sea in the Middle East. Lake water level has been falling since the 1940s and the rate of fall has accelerated since the 1960s with increasing anthropogenic extraction of fresh water (Figure 4.42a). This fall in water level drags with it the brackish groundwater lens that floats atop dense lake brines about

the lake edge (Figure 2.46; Salameh and El-Naser, 2000). Sediments that were evaporite-cemented and mineralogically stable when bathed by hypersaline lake brines become subject to dissolution and collapse with the encroachment of brackish to fresh pore waters. The process of dissolution is especially obvious at the contact between the less permeable Lisan Formation and the overlying salt-cemented gravels.

Away from the pervasive collapse dolines tied to the retreating shoreline, other areas of reactivated subsidence in the Dead Sea depression are tied to fault intersections and radial uplift fractures atop and about areas of active diapir uplift in the Lisan Straits (Closson, 2005). Groundwater preferentially flows along faults, joints and fractures so that chemical and physical erosion of saline sediments takes place along such weaker zones. Underground voids then appear, creating growing cavities, which come up to the surface after successive roof collapses (Chapter 12). For example, the falling water levels of the Dead Sea lake has created problems for the salt works in the Southern Basin with newly-formed solution collapse structures weakening some of the dykes enclosing the evaporation ponds. Between 2000 and 2002, the Arab

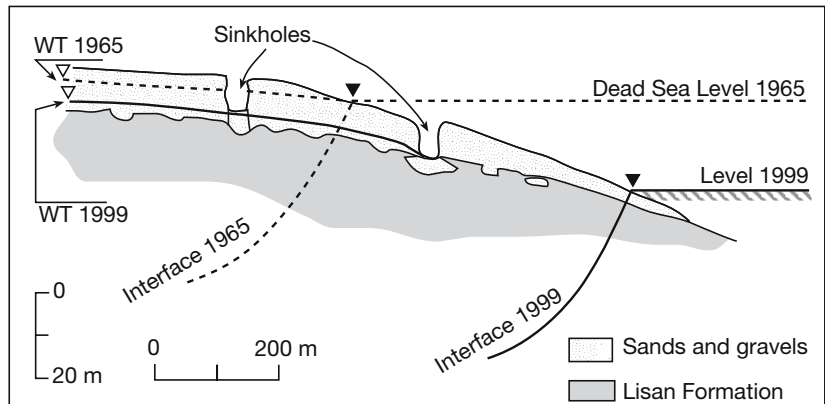


Figure 2.46. Dissolution and removal of salts due to lowering of water level and the associated flow of freshwater along the interface of the sandy gravels and the salty Lisan Formation deposits at the Dead Sea margin and the accompanying cavity, collapse, and sinkhole formation in the gravels (after Salameh and El-Naser, 2000).

Potash Company (APC) lost two salt evaporation ponds due to solution-breaching of dykes resulting in a loss of \$70 million. The breached zones show a strong structural control tied to regional lineaments. The southern Dead Sea is by far the most affected by sinkholes and decametric to kilometric subsidence phenomena.

At a broader scale, longterm watertable falls in any saline basin drive a redistribution of salt sinks within large isolated drawdown sedimentary basins. Drawdown changes the distribution of marginal versus basin-centre evaporite accumulations (Figure 5.40b). It can create regional mega-surfaces or unconformities, which are recognisable on seismic sections and can cross continental and marginal marine sequences (e.g. the Messinian M-horizon of the Mediterranean). These surfaces are sometimes described as mega-bounding surfaces by sequence stratigraphers. If they are incorrectly interpreted as eustatically induced contacts, rather than watertable or climatic responses to subaerial exposure in a continental settings, they can greatly complicate any attempt at age fitting a sealevel curve to the seismic sequence stratigraphic signature (Chapter 5).

Salinity stratification and textures

The occasional surface input of freshened waters into the central discharge depressions of evaporitic seaways (salterns) or perennial saline lakes tends to create stratified surface water bodies with less-dense lower-salinity waters floating atop more-dense saline bottom brines (Figure 2.37b). If there are large salinity contrasts between the two water masses, they tend not to mix until their densities equilibrate. The emplacement of a freshwater body atop a lower dense brine slows and stops the concentration process in the lower brine body that drives brine reflux. It can start up again once the freshwater body has concentrated to where it mixes with the underlying brine. This ongoing stop-start mechanism probably explains the finer scale layering seen in the many anhydrite cements and replacement dolomites created by reflux hydrologies.

Brine stratification occurs today in marine-fed coastal salinas in Australia, in perennial saline lakes in the African Rift Valley and in the Dead Sea, Israel (Chapter 4). Lake Hayward, a coastal salina in Western Australia, typifies such a stratified brine system and has ionic proportions in the bottom brines similar to that of seawater. Carbonate muds are accumulating on the microbially bound floor of its small perennial brine pool (2-3 m deep) under a limnology that is density and thermally stratified for much of the year (Rosen et al., 1995). Meteoric inflow creates a well-defined longterm mixolimnion; this upper,

less dense and cooler water mass has salinities ranging from 50,000 to 210,000 ppm. It exists from late autumn to early summer (May to February) as it floats atop a lower denser and warmer water mass (monolimnion) with salinities in the range 150,000 to 210,000 ppm (Figure 2.47).

Stratification disappears for a few months each year from mid-summer to mid-to-late-autumn (Figure 2.47a). During summer the waters of the upper water mass evaporate and concentrate as their bicarbonate content steadily increases. From the onset of stratification in late autumn, across mid winter and on into to early summer the temperature trends of the two water masses are parallel. They form a heliothermic system where the lower water mass is some 15-20°C hotter than the upper water mass. By mid summer (e.g. January 1992) lower water mass begins to cool, while the temperature of the upper water mass continues to rise. Once the temperatures (and densities) of the two water masses equalise they mix as the lake overturns. Waters of the lower water mass (the monolimnion) now come into contact with the atmosphere once more. While the water masses are stratified, the chemocline and the thermocline are sharply defined across a 10cm interface with a salinity contrast that may be as much as 135,000 -140,000 ppm and a temperature difference of up to 19°C.

The time of mixing is immediately preceded by a sharp fall in the level of bicarbonate in the mixolimnion, suggesting the precipitation of calcium carbonate (mostly aragonite) occurs in the upper water mass from late summer to autumn (Figure 2.47a; Rosen et al., 1995). The lower water mass in Lake Hayward was supersaturated with respect to gypsum and anhydrite from late 1990 to February 1992 (Figure 2.47b; Rosen et al., 1996). When the lake mixed from January 1991 to May 1991 and from March 1992 until early May 1992, the entire water body was at gypsum saturation, but slightly undersaturated with respect to anhydrite. A 'whiting' (a cloudy white appearance to the water body) was observed in the lake in March 92, just at the time of first mixing of the lake. Analysis by scanning electron microscopy (SEM) of the collected filtrate indicated that the 'whiting' was composed of gypsum and diatom tests. At that time, there was also a thin (10-20 mm) crust of gypsum on the lake floor. After the 'whiting', when the water was unstratified, both the monolimnion and mixolimnion were near saturation with respect to gypsum.

After mixing, the stratification begins to reform with the next influx of meteoric waters onto the lake surface. In the early stages of setup leading into the longterm stratification it appears stratification is not stable and the water bodies may

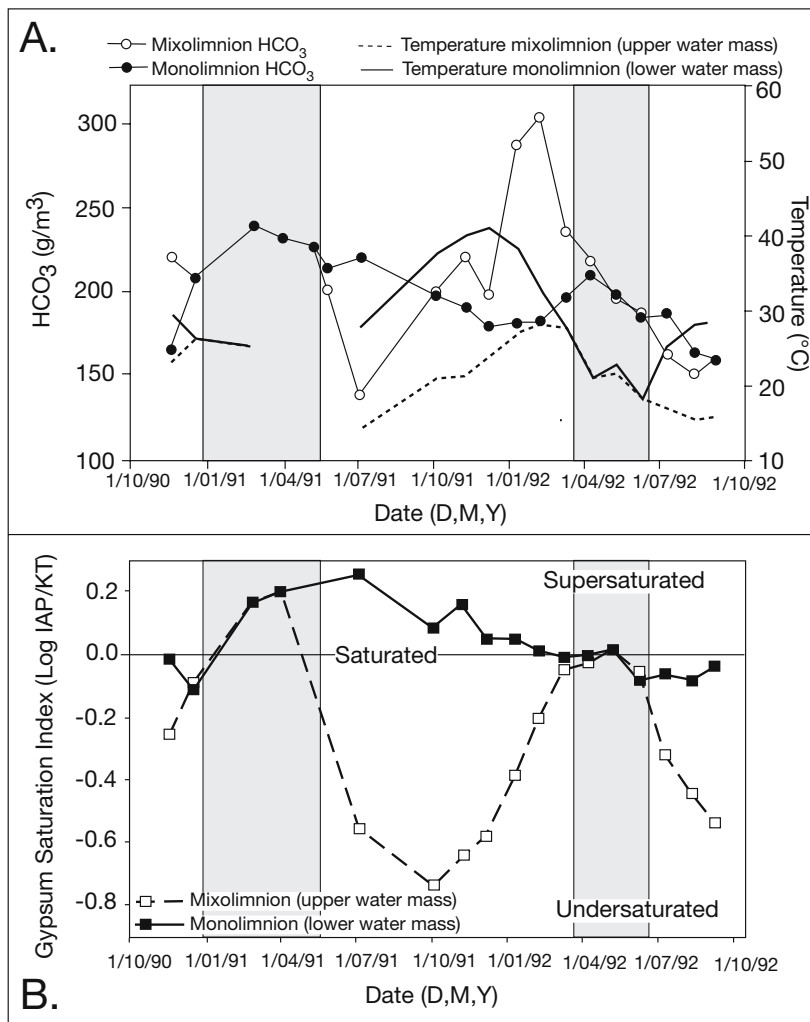


Figure 2.47. Hydrogeochemistry of Lake Hayward waters, Western Australia. A) Plot of temperature regime in upper (mixolimnion) and lower (monolimnion) water masses and bicarbonate content. As the lake mixes, the thermal and density stratification disappears. Immediately prior to mixing the bicarbonate concentration decreases suggesting precipitation of calcium carbonate (aragonite) (after Rosen et al., 1995). B) Saturation state with respect to gypsum. The monolimnion was saturated with respect to gypsum from summer 1991 to autumn 1992 and was again near saturation at the start of summer 1992-1993. The mixolimnion was only saturated when the lake water column was homogeneous (after Rosen et al., 1996).

remix before stable stratification sets in by mid winter (e.g. May-June 1992; Figure 2.47). Lake Hayward illustrates an aspect of pelagic evaporite precipitation that is probably more generalised in many “deep water” density-stratified settings. Namely that evaporite crystals grow on the bottom only when the water column is unstratified. This is so even when the lower water mass is at saturation almost year round (Figure 2.47b versus Figure 9.31).

Another well-documented heliothermal brine lake is Solar Lake, a small monomictic hypersaline lake located on the Sinai coast of the Gulf of Aqaba (Cytryn et al., 2000). The lake is separated from the ocean by a narrow sand bar (Figures 4.10, 4.11). Water is supplied via seawater seepage through the sand bar and occasional winter precipitation. Brine depth fluctuates between 4 and 6 m, driven by seasonal changes in the intensities of evaporation and the related levels of seawater seepage and brine reflux. High evaporation and aridity in the summer months raises the lake salinity to 200‰. At that time the brine column is completely mixed (holomictic) and the entire water column is oxygenated (Figure 2.48a). Temperature/salinity vary little throughout the brine column and sulphide/methane concentrations are very low.

By autumn, the water column is stratified with a newly introduced seawater brine (50‰) layer overlying residual, highly saline bottom water (180 - 200‰). A well-defined density gradient (halocline or pycnocline) now separates an upper oxygenated cooler (16°C) brine mass (epilimnion) from the lower hotter (45-55°C) anoxic sulphide-rich brine mass (hypolimnion; Figure 2.48b). High sulphide concentrations develop in anoxic waters below the halocline from the activities of sulphate-reducing bacteria, both in the water column and in the underlying cyanobacterial mats. Crossing the halocline into the

lower brine there is a rapid downward increase in sulphide concentration, which reaches a maximal value of 1,240 μM proximal to the sediment brine contact (Cytryn et al., 2000). At the same time a peak in methane concentration develops directly below the halocline, where a maximum value of 6.5 μM was measured in the December 1997 profile and was in part a reflection of the decomposer activities of the methanogenic haloarchaea (Chapter 9).

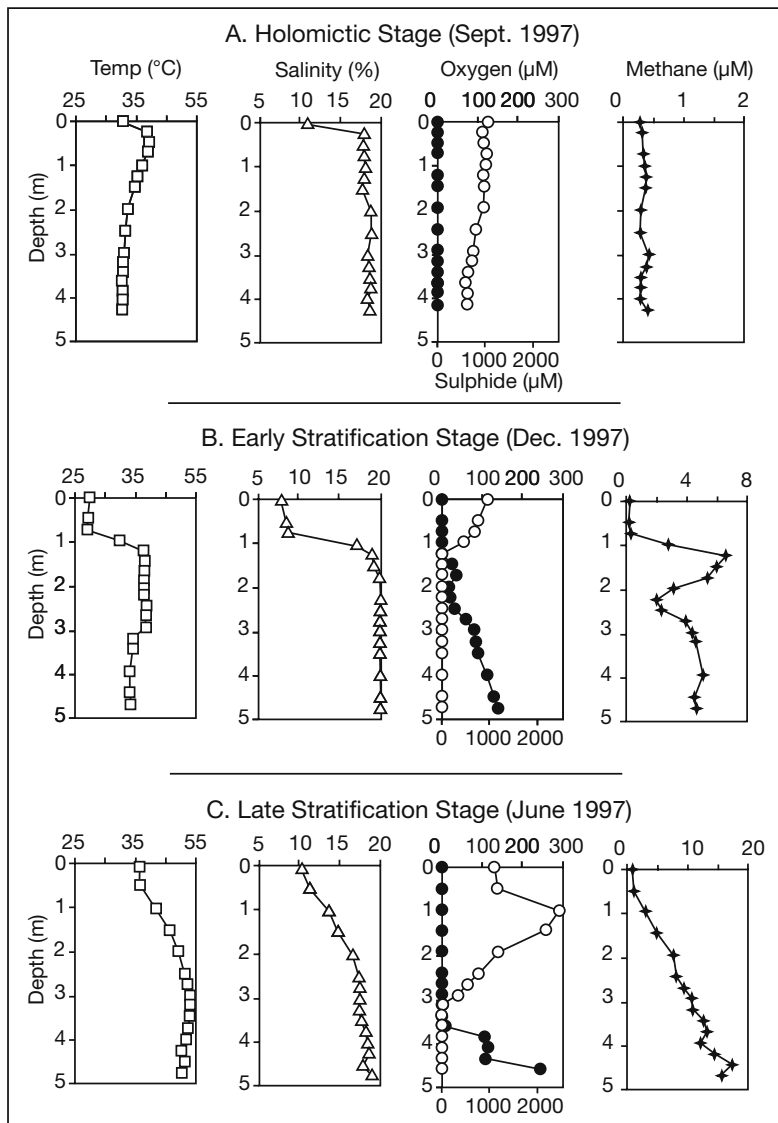


Figure 2.48. Effects of the seasonal development of heliothermic stratification in Solar Lake, Middle East (after Cytryn et al., 2000). Open circles = O_2 , filled circles = sulphide.

As winter passes into spring, a gradual heating and increase in the salinity of the upper water mass degrades the halocline. The data shown in Figure 2.48c was collected in June 1997 and portray a transitional state between late stratification and the beginning of holomixis. Salinity and temperature gradients across the halocline are more gradual and deeper in the water column than those observed in the December 1997 profile. The deepening halocline allows oxygen to penetrate much deeper than in the earlier stages of stratification, and the chemocline is now located 3.25m below the water surface. The oxygen

concentration in the upper water mass reaches a maximum value of $300 \mu\text{M}$ at a depth of 1 m below the water surface. These supersaturated values of oxygen imply intense photosynthetic activity at these depths. Below the chemocline, a sharp rise in sulphide concentration occurs, reaching a maximum value of $2,150 \mu\text{M}$ at the water-sediment interface (Cytryn et al., 2000). Methane concentration increases linearly from the surface and reaches a maximum value of $17 \mu\text{M}$ adjacent to the lake bottom, implying methane, like the bacterially derived H_2S , is escaping from the sediments. Subsequent increasing evaporation rates further disrupt the stratification and ultimately lead to summer holomixis identical to that in the September 1997 profile.

Thick cyanobacterial mats carpet the Solar Lake sediment surface and contain a highly diverse microbial community of cyanobacteria and haloarchaea. Their metabolic activities, along with the lake's planktonic microbes greatly affect the hydrogeochemistry of the lake waters by exporting oxygen, sulphide, and methane into the brine column. Biological interactions with evaporite sediments and brine columns are discussed in detail in Chapters 4 and 9.

Although the daily temperature/stratification records of Lake Hayward and Solar Lake are probably the best documented examples of the hydrology of a naturally stratified brine column, both regions have a number of inherent limitations when attempting to use them as direct analogues for the hydrology of ancient stratified brine seaways. Unfortunately, neither are saline enough nor isolated enough from their seawater feeds to accumulate substantial thicknesses of halite. Neither are hydrological analogues for bottom-nucleated salt beds, such as gypsum or halite units that dominate the central portions of ancient evaporite seaways and lakes. They also suffer from the scale limitations that enfeeble all modern marine-associated evaporite analogues (Figure 5.3). Their small aerial extent ($\leq 0.6 \text{ km}^2$) prohibits a direct hydrological comparison with

bedded salt accumulations in ancient saline giants (areas > 10⁶ km²). Their centripetal unconfined meteoric inflow hydrologies, driven by winter rains and a lowering of evaporation intensity, means they cannot be directly compared to ancient brine seaways where strandlines moved up to hundreds of kilometres in a wet-dry cycle and where unfractionated meteoric waters or seawaters were insignificant in the freshening process in the subaqueous basin centre.

Brine stability and evaporite textures

In ancient evaporitic seaways and lakes the style and permanency of brine stratification is best interpreted from the preserved depositional textures (Lowenstein and Hardie, 1985; Warren and Kendall, 1985). But there are some physical principles common to modern and ancient brine hydrologies. If a stratified brine column forms above a growing crystallisation surface, solar driven crystal growth of gypsum or halite in the bottom waters first slows then stops (Figure 2.37b; Figure 2.49). Once a water body is stratified, no solar mechanism is available to further

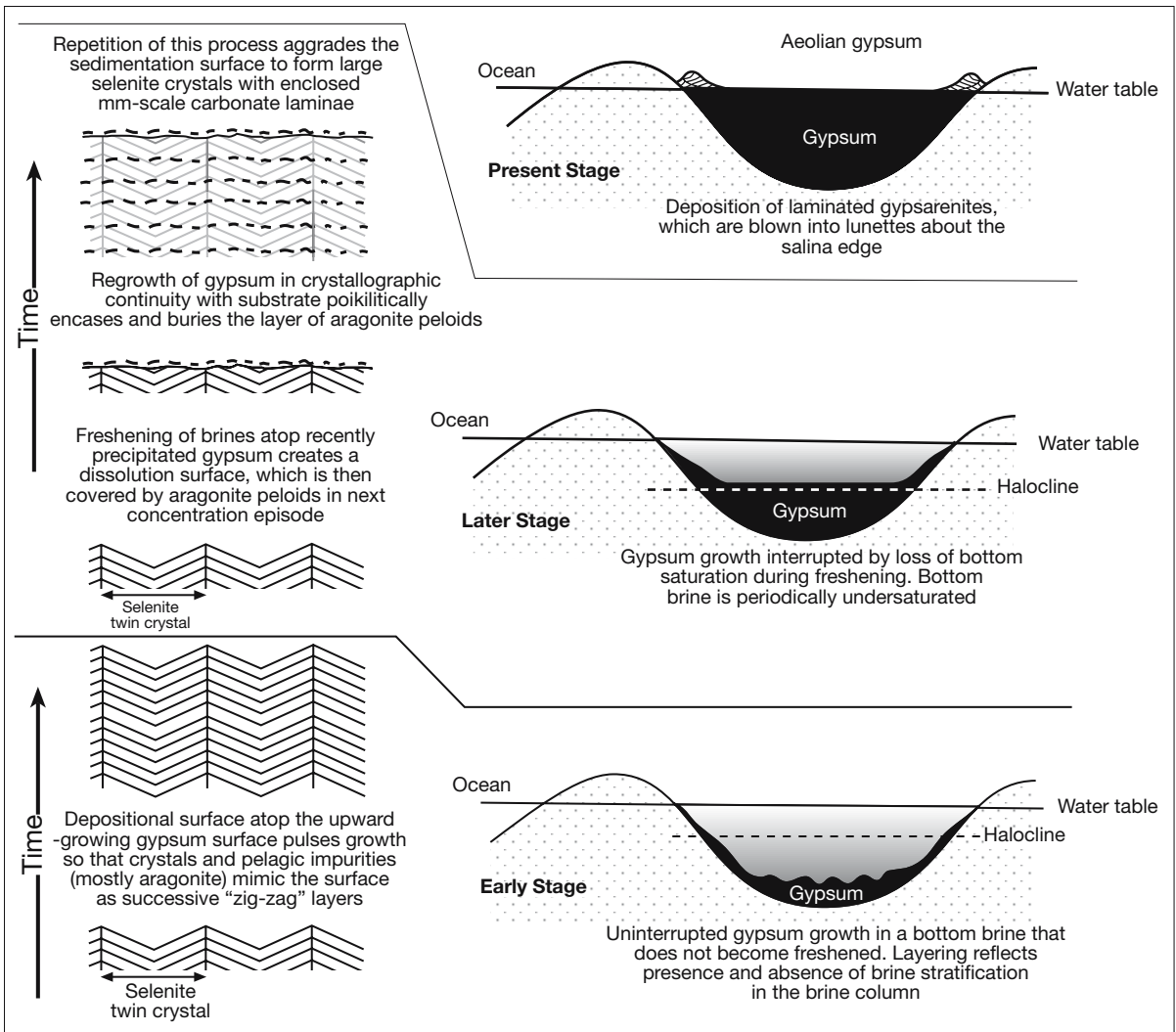


Figure 2.49. Growth-aligned gypsum shows internal textures are controlled by the gypsum growth surface interacting with the stability and salinity of bottom brines. In the early stage of fill, when the brine lake is deeper, the bottom brines are stable and salinities do not ever decrease to where they become undersaturated with respect to gypsum. "Zig-zag" textures result. When the sediment surface aggrades to where bottom brines freshen, then the periodic dissolution of the upper part of the growth surface dissolves and mm-laminated textures form. The present stage of sediment fill is where the brine lake has been filled to equilibrium with the local water table, eolian reworking of seasonal gypsarenite precipitates is the dominant mode of deposition (after Warren, 1982b).

concentrate the bottom waters. Subaqueous crystallisation can only continue in a stratified system in zones of brine mixing or bottom temperature change near subaqueous spring seeps. Once the freshened inflow ceased, ongoing evaporation concentrates the upper brine body until its density matches that of the lower brine body. The two water bodies then mix (holomixis) and crystal growth on the bottom can begin anew (Figure 2.49). This type of holomictic bottom crystal precipitation, where the crystallisation surface is never in contact with undersaturated bottom water, deposits layered euhedral growth-aligned crystal beds on the brine floor (e.g. chevron halite or aligned swallowtail gypsum; Figure 2.49).

If, on the other hand, the freshened upper water body does come into contact with the crystallisation surface of the salt bed then subaqueous horizontal planation surfaces develop. Subhorizontal planation occurs both in saline basins subject to complete desiccation and in those parts of evaporite seaways covered by perennial brine sheets (tens of cm deep) that were subject to periodic freshening. A desiccation stage, followed by a freshened water flood, creates a near horizontal planation surface with intercrystalline karst, which marks a time when the water table was lowered into the salt bed immediately prior to a subsequent freshening event (Figure 1.27). In contrast, freshening of perennial bottom brine creates a horizontal planation surface atop the salt bed with little or no intercrystalline karsting (laminated coarse-grained gypsum in Marion Lake; Figures 2.49, 4.5f).

In both cases the freshened surface water sheet only dissolves the uppermost portion of the salt bed, it does not displace the much denser pore brines that saturated the bulk of the underlying salt bed. A planation surface defines the top of saturated pore brines. Vadose karst in a desiccated salt pan can only extend down to the top of this dense pore brine layer. Below it the pore brines are saturated, above it the waters are undersaturated or nonexistent.

These flat, laterally extensive dissolution surfaces typically truncate the tops of previously growing crystals, be they trona, halite, gypsum or any other bottom nucleating salt (Figure 2.49). As the freshened water body

begins to concentrate it may precipitate a less saline mineral phase, which settles onto the planation surface. It may also be the time when clays, formerly suspended in the floodwaters or blown in by the wind, begin to flocculate and sink through increasingly saline surface waters. As the freshened water body continues to concentrate into salinities that precipitate the dominant salt phase the aggrading crystals that underlie the planation surface can now poikilitically enclose the less saline precipitates (e.g. laminae of aragonite pellets in laminated coarse-grained gypsum; Figure 2.49).

Brine reflux drives substrate alteration

Brine reflux occurs when ponded or concentrating holomictic brines atop the floor of an evaporitic seaway or lake become dense enough to displace underlying pore fluids and so percolate into the underlying succession (Figure 2.50). Descending brines can have chemistries that are supersaturated with different mineral phases to the matrix through which they are flowing and so drive various alteration processes such as dolomitization, backreactions and pseudomorphing. It may also drive the precipitation of widespread authigenic K-feldspars in siliciclastic hosts at burial depths that are much shallower, and in authigenic stages much earlier than those of equivalent precipitates in non- evaporitic siliciclastics (Sandler et al., 2004).

One of the most widely recognized effects of brine reflux is the formation of dolomite in units underlying and adjacent to a thick evaporite sequence. When evaporitic carbonate or gypsum precipitates in hypersaline areas on such platforms, the surface

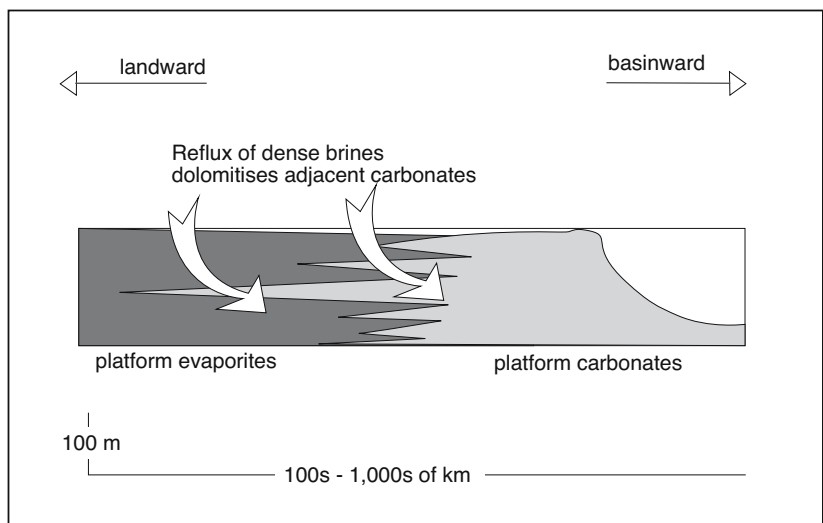


Figure 2.50. Schematic illustrating the process of brine reflux creating secondary dolomite in a carbonate platform (after Warren, 1991).

brine densities are in the range 1.1 to 1.2 gm/cc (Figure 2.5). Concurrent Mg/Ca ratios of the remaining brines rise compared with their seawater seep feed, and so dense Mg-enriched solutions sink through the underlying platform sediments. They displace connate pore fluids with densities around 1.03 gm/cc and slowly seep basinward through underlying platform limestone aquifers. In this way large volumes of Mg-rich brine pass through previously deposited shelf limestones, precipitating dolomite both as a pore fill and as a replacement in the former shelf limestones (Figure 10.24). The first evaporite-generated brine reflux model for ancient dolomites was by Adams and Rhodes (1960). Their model explained the dolomitization of the Permian Capitan reef complex of west Texas; whereby backreef, shelf and lagoonal carbonates are intensely dolomitized, while the shelf edge and slope carbonates are not. They envisioned reflux dolomitization through porous sediments to depths of several hundred metres below the brine source.

By the mid 1960s, seepage reflux dolomitization as proposed by Adams and Rhodes had gained a large number of proponents working in ancient evaporite-associated dolomites (Hsu and Siegenthaler, 1969) but needed, under the dictates of strict geological uniformitarianism prevailing at the time, to be verified in the Holocene (Warren 2000a). In 1965 Deffeyes et al. reported modern Mg-rich brines in a marine spring-fed gypsum salina (Pekelmeer Lagoon) on Bonaire in the Netherlands Antilles in the Southern Caribbean. From the water chemistry, they predicted that concentrated lagoonal brines should be sinking and forming reflux dolomite in underlying sediments. They observed micritic dolomite in Holocene lagoon muds beneath gypsum crusts but, with only a soft-sediment coring device to work with, could not penetrate the cemented Pleistocene base. Outcropping on the opposite end of the island, well away from the present lagoon, they located a dolomite replacing what they interpreted as Pleistocene limestone and inferred that this had formed during an earlier episode of brine reflux.

Lucia (1968) subsequently drilled beneath the Pekelmeer Lagoon and found no widespread dolomites in the underlying Pleistocene carbonates. He also found that porewaters were of normal marine salinity in areas where brine was predicted by a seepage reflux model. A thin clayey ash layer of generally low permeability was found forming a hydroseal that separated sediments below with normal salinity from lagoonal sediments with elevated salinity. Thus, reflux dolomitisation was not occurring beneath the lagoon. Springs supplying seawater to the salina were in areas where the ash bed was broken or missing and formed the terminations of flow pathways in the underlying Pleistocene/Pliocene (Murray, 1969). For most of the year seawater seeps into the Pekelmeer springs driven by

evaporative drawdown. However, during a short period in the late summer, the springs are inactive and the hydrostatic pressure on the landward side is greater than that on the seaward side. Murray concluded that return flow or reflux could occur at such times, but did not appear to do so with sufficient volumes of brine crossflow to form replacement dolomite.

The claim that the Pekelmeer was forming extensive seepage reflux dolomites beneath an evaporite lagoon was further challenged when Sibley (1980) concluded that the solutions responsible for extensive dolomitization in Tertiary sediments on Bonaire (dolomites that were earlier used as evidence for reflux dolomite) were probably fresh to brackish meteoric waters mixed with seawater, and were not derived by reflux of the modern Pekelmeer hydrology. Later work by Fouke et al. (1996) on dolomite in the Seroe Domi (Miocene), a unit more than 20 m thick that extends 115 km across the Netherlands Antilles, has reinforced Sibley's conclusions. However, Lucia and Major (1994) continue to argue for a significant input of marine/hypersaline waters during Neogene dolomitization in the region.

There are, nevertheless, other islands in the tropics where localized brine reflux, associated with hypersaline conditions, is apparently forming local-scale Holocene dolomites. Müller and Teitz (1971) documented brine-reflux dolomite replacing earlier carbonate cement in skeletal grainstones on the shoreline in Fuerteventura in the Canary Islands. Kocurko (1979) found brine-reflux dolomite a few metres above the high tide line, in the spray-zone pools of the shoreline of San Andres, Columbia. Aharon et al. (1977) described small volumes of reflux dolomite forming in Holocene sediments of Solar Lake. Thin, localized brine-reflux dolomites can also be found about the present-day edges of Ras Mohammed on the Sinai Peninsula (Chapter 3). It seems small-scale examples of brine reflux dolomites exist, but pale in comparison to obvious and extensive reflux dolomites of the past (Figure 5.3).

Hydrological modelling of ancient reflux systems by Shields and Brady (1995), using very conservative assumptions of brine head and drawdown, show that reflux can explain platform dolomites within geologically realistic time frames of burial (Figure 2.51). Their flow model used flow lengths varying from 1 to 1000 km and the relative densities of seawater and brines of two end member compositions (Figure 2.51a): brine 1 is anhydrite-saturated (density $\rho = 1120 \text{ kg/m}^3$) and brine 2 is halite-saturated ($\rho = 1200 \text{ kg/m}^3$). Brine 1 is approximately 9.3% denser than seawater ($\rho_{\text{seawater}} = 1024.5 \text{ kg/m}^3$), and brine 2 is 17.1% denser. Using a 100m tall and 1 m wide flow cell

(Figure 2.51b), brine 1 has approximately 9.3 m more hydraulic head than a comparable column of seawater, while brine 2 has a differential hydraulic head of 17.1 m. Shields and Brady (1995) assume a pure calcite precursor and a final product that

is 100% dolomite with 7% porosity; this requires 350 kg/m³ of magnesium. The results (Figure 2.51c) show that reflux flow could circulate the Mg necessary to completely dolomitise carbonate platforms with radii of a few tens of km in a few million years. Shelves with shoreline to basin distances of the same order can be completely replaced in a similar period. Larger platforms require more time or that the evaporite recharge areas migrate with time. Carbonate platforms tens to several hundred kilometres across could be dolomitized by such epeiric hydrologies.

The relative abilities of rocks to transmit brine will control where the bulk of the fluid flux occurs within platform limestones of any age. It is unrealistic to think of reflux dolomitization as a homogenous process uniformly overprinting all platform limestones. The inherent permeabilities of the various precursors clearly play an important role in dolomite intensity. The most permeable lithologies beneath the evaporite lagoon will focus the bulk of flow as the brine seeps seaward. Whatever unit acts as the aquifer at the time of reflux will also be the subject of the most intense dolomitization. High permeability units within flow paths of tens to hundreds of kilometres can channel the volume of necessary brine in time frames \approx 1 Ma. Such high permeability units also have the potential to be dolomitized in regions well removed from the brine source (Figure 10.24).

In a recent paper that models brine circulation and retention in platform evaporites. Jones et al. (2002) has shown that the effects of a single 100,000 year platform evaporite episode can generate a reflux plume that persists for as long as 10 million years in underlying carbonates before it is once again displaced by geothermally driven brines (Figure 2.52). They call this long term effect "latent reflux,"

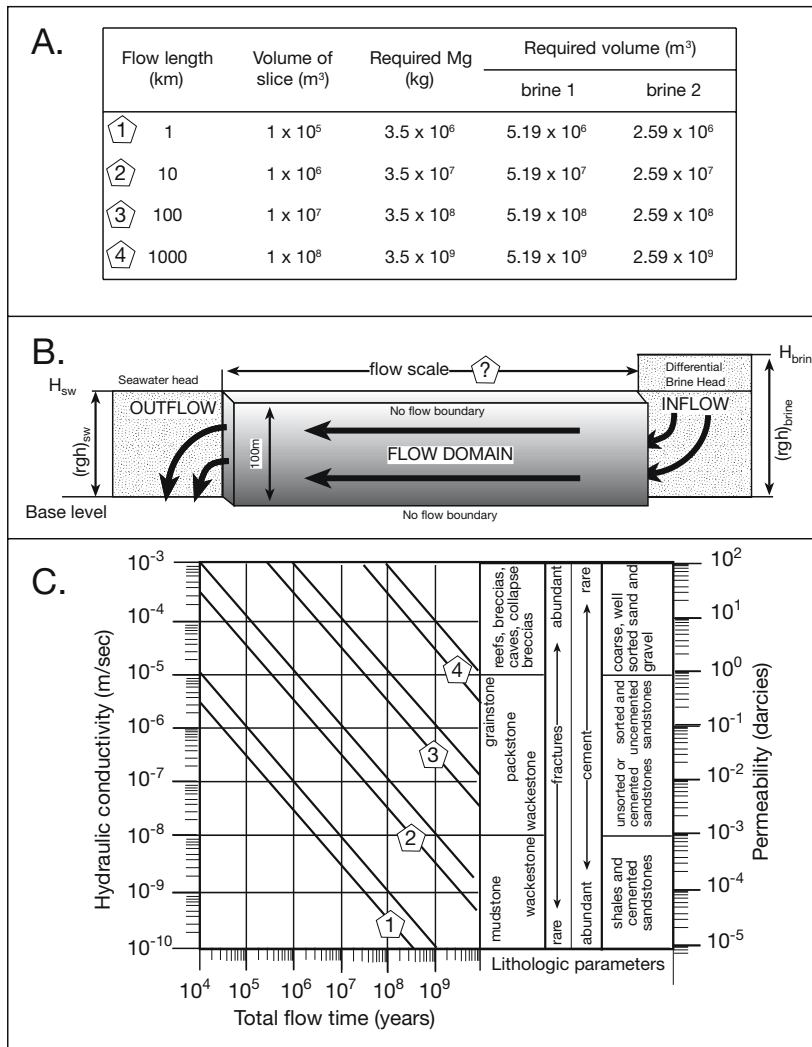


Figure 2.51. Dimensional analysis of seepage reflux (after Shields and Brady, 1995). A) Table of brine properties and amount of Mg required to covert calcite to a dolomite with 7% porosity. B) Dimension of slice model used in their calculations. Slices are similar except that flow length varies from 1 to 1000 km. Base level is 100 m in all cases and head drops are 9.3 m for anhydrite saturated brine 1 and 17.1 m for halite saturated brine 2. C) Dimensional analysis of Darcy's Law for a regional brine reflux system with 100 m base level. Diagram illustrates the time necessary for the minimum volume of dolomitizing brine to flow through a rectangular slice. All slices are 100 m thick and 1 m wide with varying flow lengths (1-4). It is assumed 350 kg/m³ of Mg are required to dolomitise the block. The lower curve for each flow path represents brine at halite saturation with a Mg exchange efficiency of 47%. The upper curve represents brine at anhydrite saturation with a Mg exchange efficiency of 36%. Permeability conversions assume an average brine density of 1160 Kg/m³ and a viscosity of 8.904 x 10⁻³ kg/(m/sec) and a temperature of 40 °C.

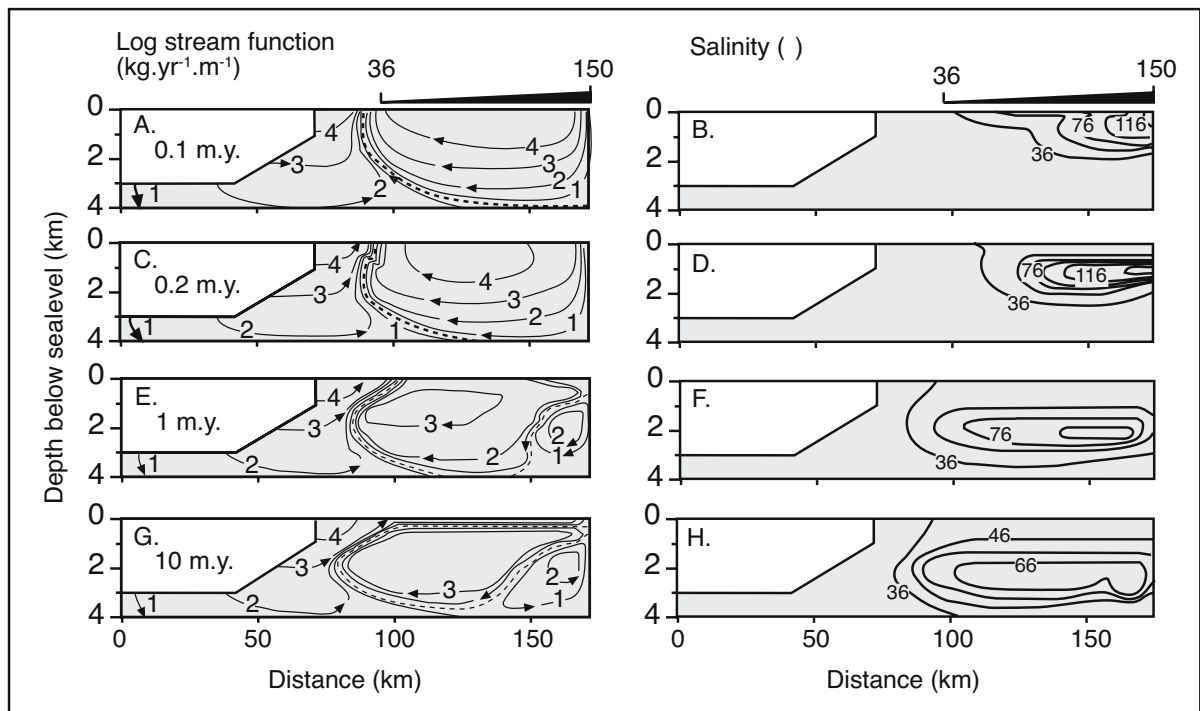


Figure 2.52. Evolution of groundwater circulation and salinity persists for as much as 10 m.y. after a single reflux event at gypsum saturation which lasted 0.1 m.y. Dashed line in the stream-function plots represents interface between geothermal reflux and latent reflux. Only the upper 4 km of platform is plotted; vertical exaggeration = 9 (after Jones et al., 2002).

it documents a hydrological situation where the effects of a sinking reflux brine persist long after the at-surface brine lake or seaway has disappeared. The modelling utilised a single depositional episode and a surface brine at gypsum saturation (150‰). They went on to note that higher salinity waters and longer episodes of evaporite precipitation would generate more widespread and longer acting brine plumes in the underlying sediments (Jones and Xiao, 2005).

Detailed mapping of dolomite distribution across the Permian Capitan shelf, the type area for the brine reflux model, clearly shows reflux works in ancient evaporitic platforms (Melim and Scholle, 2002). Dolomite extent is greatest beneath and adjacent to the drawdown lagoon facies. In contrast, dolomite distribution through the Capitan reef and into the fore reef outlines the distribution of those brine aquifers that were more active at the time of brine reflux, namely fractures and fore reef debris aprons. Aquifers carrying the descending brines out into the adjacent basin were dolomitised, while tighter aragonite-cemented intervals between aquifers were largely isolated from the flushing brines and so remained undolomitised. Garber et al. (1990) used a similar model of reflux but called upon bittern brines, derived from the very saline Salado Formation,

to explain magnesite, not dolomite, distribution in the same basin. They argued that when a brine has a Mg/Ca ratio > 40 it will precipitate a magnesite replacement rather than the more commonly observed dolomite. Similar reflux processes, driven by the deposition of Zechstein evaporites, may have precipitated authigenic magnesite cements in siliciclastic dune sands of Rotliegende reservoirs in the North Sea (Purvis, 1989).

Reflux dolomitisation in a platform setting can often be distinctive, even in core, as the intensity of total dolomitization decreases the further down core or laterally one moves from the evaporite-carbonate contact (Figures 2.53, 10.24). If not completely re-equilibrated during later burial dolomitization, the oxygen isotope signatures in platform dolomites formed by reflux typically follow a lightening trend away from the evaporite unit; that is, the further one moves from the contact, the less was the sediment's isotopic signature influenced by the heavier reflux-derived brines. If the sediments are not extensively recrystallised by later burial dolomitization, trace elements, along with stratigraphic position, can give another clue to a reflux association. In a study of dolomite from Neogene to Permian age, Sass and Bein (1988) found that evaporative dolomites associated with gypsum/anhydrite tend to show

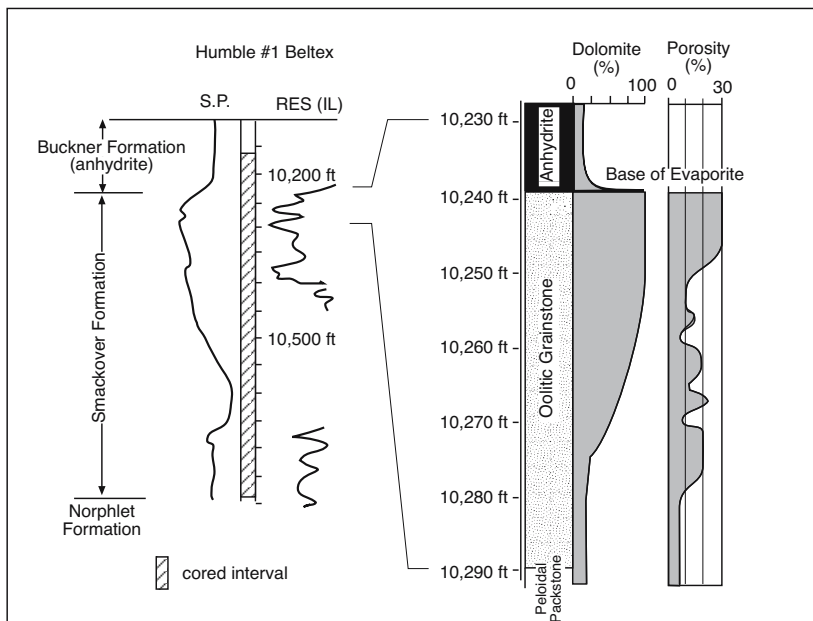


Figure 2.53. Wireline signature and the interpreted core description of the Humble #1 Beltex Well, Bowie County, Texas. Shows a close relationship between Buckner anhydrite and dolomitization in the underlying Smackover Formation. Note changes in proportion of dolomite and porosity in terms of proximity to evaporite contact (after Moore et al., 1988).

50–57% CaCO_3 and the highest levels of sodium (up to 2700 ppm). Marine nonevaporitic subtidal dolomites have a similar range of compositions, but sodium concentrations of only 150–350 ppm.

The present may be the key to the past but it is simply not a good time to document depositional or diagenetic analogues for ancient platform and basinwide evaporites, nor their associated reflux hydrologies. There are no modern depositional counterparts to most types of ancient marine-platform and basinwide evaporites, hence there are no modern counterparts to brine-reflux dolomites (e.g. Figure 5.27). Holocene evaporites are accumulating within an “icehouse” climatic phase. The current “icehouse” mode, typified by waxing and waning polar ice sheets, has dominated the earth’s climate for the last 12 million years. “Icehouse” times, with their high frequency sealevel oscillations, are not conducive to the formation of thick platform evaporites. In contrast, “greenhouse” time, with their inherent lack of polar ice sheets and low amplitude sealevel changes, favour the formation of platform evaporites and hence widespread reflux dolomitization of platform carbonates. Basinwide evaporites and their associated dolomites form via tectonic controls on basin isolation that are independent of “icehouse versus greenhouse” sealevel scenarios.

Most brine reflux models published to date utilise a platform evaporite setting. Examples include: the Cambrian Ouldburra Formation in the Officer Basin, Australia (Kamali et al., 1995); the Devonian Birdbear (Nisku) Formation of Canada (Whittaker and Mountjoy, 1996); Pennsylvanian platform carbonates of west Texas (Dickson et al., 2001) Permian San Andres Formation, USA (Leary and Vogt, 1986; Ruppel and Cander 1988; Elliott and Warren, 1989); the Permian Tansill and Yates Formations of the Central Basin Platform, USA (Andreason, 1992; Garber et al., 1990); the Jurassic Smackover and Haynesville Formations of the Gulf of Mexico (Moore et al., 1988); the Lower Cretaceous Edwards Formation of Texas (Fisher and Rodda, 1969) and the Middle Palaeocene Beda Formation, of the Sirt Basin, Libya (Garea and Braithwaite, 1996). Hydrological geometries of reflux dolomite associated with drawdown basinwide settings are different and are discussed in Chapter 5 after the various styles of saline giant are presented, while a number of oil field examples are discussed in detail in Chapter 10.

As well as long term effects in underlying carbonates, reflux also has significant syndepositional effects on nearsurface salt beds. Sinking supersaturated brines force backreactions and replacement processes in salt beds immediately beneath an evolving brine body. Hovorka (1992) recognised reflux of halite saturated brines through gypsum beds as the dominant control in the formation of halite pseudomorphs of subaqueous gypsum (Figures 1.30, 2.54). The replacement process is driven by the fact that gypsum precipitation is favoured by low temperatures and low salinities, while anhydrite precipitation is favoured by higher temperatures and higher salinities. At the warm temperatures that typify modern low-latitude brine pools (25 to 50°C), the gypsum-to-anhydrite transition is predicted to occur somewhere between the initial precipitation of gypsum and initial precipitation of halite. In contrast, brines at halite saturation are undersaturated with respect to gypsum, while saturated with respect to halite. Textural relationships in such settings, where bottom-aligned gypsum is replaced by halite, are shown to be controlled by nearsurface diagenesis and related to brine pool evolution (Hovorka, 1992).

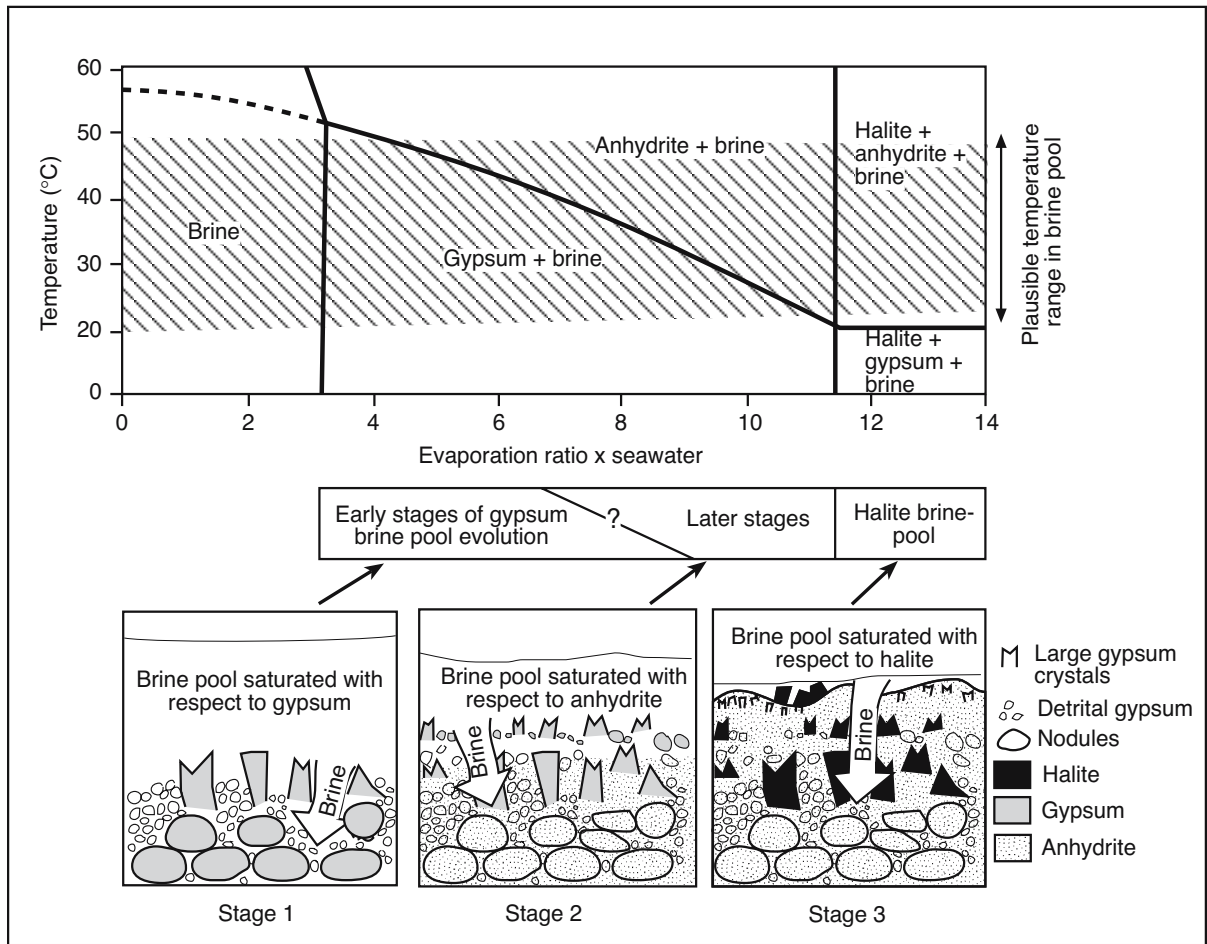


Figure 2.54. Gypsum replacement by halite during brine reflux. Upper part shows phase relationships between the gypsum and anhydrite in NaCl brine. Lower part shows how the alteration and replacement is dependent on the evolution of the overlying brine supplying waters that are refluxing through the gypsum bed. Stage 1: Large gypsum crystals grow vertically from the floor of the brine pool, and gypsarenite accumulates between the crystals. Gypsum is stable in diagenetic fluids concentrated three to approximately six times seawater concentration: alteration to form nodules occurs in shallow subsurface environments. Stage 2: As salinity increases from six to ten times seawater concentration, gypsum continues to precipitate metastably, but is dehydrated to thermodynamically stable anhydrite in the shallow diagenetic environment. Stage 3: When the brine pool evolves to concentrations about 10 times seawater concentration, halite begins to precipitate. Halite-saturated brines introduced into the shallow burial environment dissolve any remaining gypsum and replace it with halite (after Hovorka, 1992).

During Stage 1 the perennial brine body is four to six times the concentration of seawater and is at gypsum saturation (Figure 2.54). In stage 2 brines are at the upper end of the calcium sulphate field (6-10x seawater) and are in the anhydrite stability field. Metastable gypsum continues to precipitate on the brine pool floor, but reflux of this brine converts gypsum to nodular anhydrite. By stage 3 the surface brines lie in the halite saturation field (>10-11x seawater) so that halite is precipitating on the floor of the brine pool. The refluxing brine is now undersaturated with respect to gypsum so that it is dissolved in the shallow subsurface and the resulting voids are filled by

halite cements. This replacement process is thought to take place in the first few metres of burial, but like reflux dolomite has yet to be documented as more than a localised process in a Holocene gypsum deposit. As thick halite beds are tightly cemented by 100m of burial, surface-driven brine reflux and associated backreactions in ancient salt beds are most intense in the first few tens of metres of burial.

In a related paper Schreiber and Walker (1992) argue that pseudomorphous replacement of gypsum by halite at the transition between bedded sulphate and chloride documented

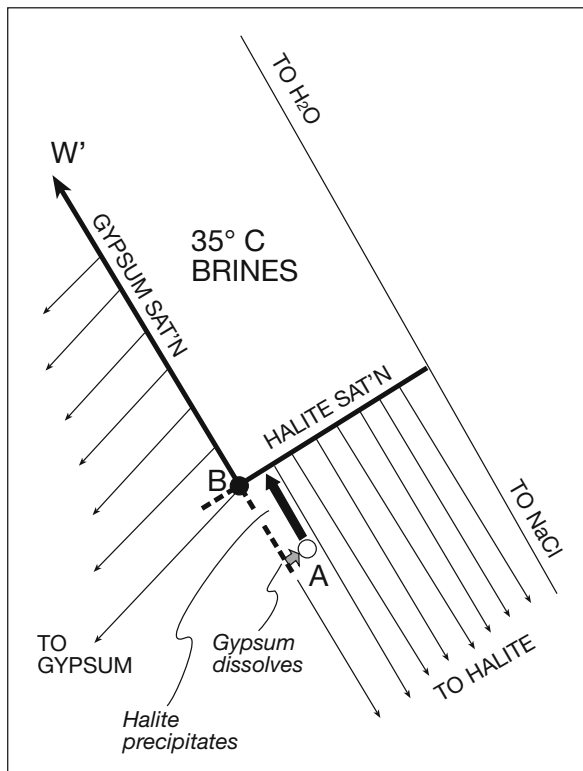


Figure 2.55. Salient features of the metastable gypsum-halite phase curves at 35°C (after Schreiber and Walter, 1992). A co-saturated brine, as plotted at A from 50°C when entering the 35°C environment will be out of equilibrium. Gypsum must dissolve and halite must precipitate in order to move brine A composition to equilibrium at B.

by Hovorka (op. cit.) in cyclic evaporite sequences of Permian age is an early diagenetic reflux process. But they argue it is a thermal disequilibrium process and can not be directly tied to simultaneous conversion of gypsum to anhydrite (Figure 2.55). They argue that in solar salt ponds, hot brines at halite saturation are undersaturated in gypsum and oversaturated in halite with respect to the cooler, previously accumulated gypsum substrate. This is what causes the halite to replace gypsum when suitably hot brine is in contact with the substrate. If this is the mechanism driving replacement it too would take place at or very close to the sediment brine interface.

Solar heating of the brines and production of porosity within the gypsum crystals, both of which are key features of the replacement mechanism suggested by Schreiber and Walker (1992), are materially aided by red pigments from halophilic activity (see Chapter 9). If this is the mechanism driving replacement then it cannot be related to the large-scale transition of gypsum to anhydrite (as argued by Hovorka, 1992). Diluted brines

created by the replacement of gypsum by anhydrite would corrode halite rather than precipitate it. Modern examples of a thermally driven replacement process are rare, perhaps because the appropriate brines are decanted for commercial collection of halite and are not allowed to backreact.

Can reflux really work?

Some have argued that brine reflux cannot be a geologically significant process because we do not see modern marine brines capable of displacing substantial volumes of pore waters at sufficiently rapid rates to drive brine reflux. Rather the deposition of bedded salt creates a “hydroseal” (discussed in Chapter 5). I have just stated and will argue in detail in Chapters 5 and 10, that marine-fed reflux dolomite is not a widespread process in today's marine platforms but is a significant process in ancient evaporitic settings.

Today's carbonate platforms are characterised by laterally discontinuous buildup geometries. They are a response to high-amplitude high-frequency eustatic signals of the current icehouse climate mode whereby continuous reef rims and shoals do not form. Subsealevel marine seepage inflows into an isolated platform lagoon, and consequent reflux of dense brine is impossible in the hydrologies of icehouse mode carbonate shelves. Likewise, there is no where on the world's surface today where subsealevel marine basin floors are totally isolated from the ocean, so no basinwide evaporites and reflux dolomites are accumulating in modern examples of this setting. But the viability of reflux hydrology and its ability to quickly descend into underlying strata can be seen in modern continental systems where man has interfered with natural hydrologies and created saline hydrologies in regions where there were none before. This is perhaps our best set of hydrological analogs to characterise modern counterparts of the hydrologies of ancient platform and basinwide evaporite systems.

One of the best examples comes from Owens Lake, California, where the water needs of the City of Los Angeles converted a moderately saline perennial lake (salinity $\approx 90\%$) into a hypersaline pan accumulating bedded halite and trona. Starting in 1913, the streams that fed the Owens River, which in turn fed Owens Lake, were diverted by Los Angeles Department of Water and Power to feed the Los Angeles Aqueduct. The lake level started to drop quickly and by 1924 the lake had completely dried out. Prior to this the lake was saline, but perennial.

In order to study the Quaternary history of the lake, the US Geological Survey collected a 323 m long core from the lake

(Bischoff et al., 1993). The core encompasses the last 800,000 years of basin fill and was analysed for water content, pore water salinity, sulphate and chloride values (Figure 2.56). Water content, a measure of compaction, varies erratically down the core, generally decreasing from about 60 wt % at the top to about 20 wt % at 240 m (Bischoff et al., 1993). Below 240 metres and to the bottom of the core the water content sharply increases to between 40 and 60 percent by weight. This zone is characterized by an abundance of sandy units. Salinity varies with depth in a smooth pattern, with a minimum at 30 m, gradually increasing to a single broad maximum at about 150 metres depth, and sharply declining thereafter to steady low values at 210 metres and below.

The salinity of the modern lake prior to diversion of the Owens River, was about 9‰ (Bischoff et al., 1993). Assuming that similarly elevated salinity characterizes previous interglacial times when Owens Lake was the terminus to the Owens river, and that fresh waters must have characterized the glacial periods of intense overflow, Bischoff et al. expect about 8 salinity oscillations during the past 800 kyr time span of the core. Such cycles are seen in the solid components of the sediments, particularly for carbonate and organic carbon content (Bischoff et al., 1993)

indicating the lake did indeed experience such climate changes. Yet the salinity-depth profile has been drastically smoothed by post-depositional diffusion of dissolved salts. This is not a hydrologically closed system.

Remnant water, a leftover from the last glacial is the likely explanation only for the first salinity minimum seen at 30-40 m depth (Bischoff et al., 1993). The smooth and gradual increase of salinity in the older sediments below this depth to a maximum at about 150 m is likely the result of diffusional smoothing of waters of older cycles. Diffusion should have had more than sufficient time, therefore, to smooth salinity gradients even lower in the core. The abrupt and erratic decrease of salinity from 150 to 210 m depth, and the erratic and generally low salinities from 210 to the bottom of the hole points to an open throughflow system for the basal pore fluids. The most likely explanation for this pattern is that deeply circulating fresher waters are actively moving through the sandy units below 200 m, diffusively harvesting solute from the overlying fine-grained sediments in the process. Thus ground water is moving at different velocities in the varying permeable sandy units. A diffusional steady state and smoothing of the salinity gradients has not been achieved. This particular depression in the Basin

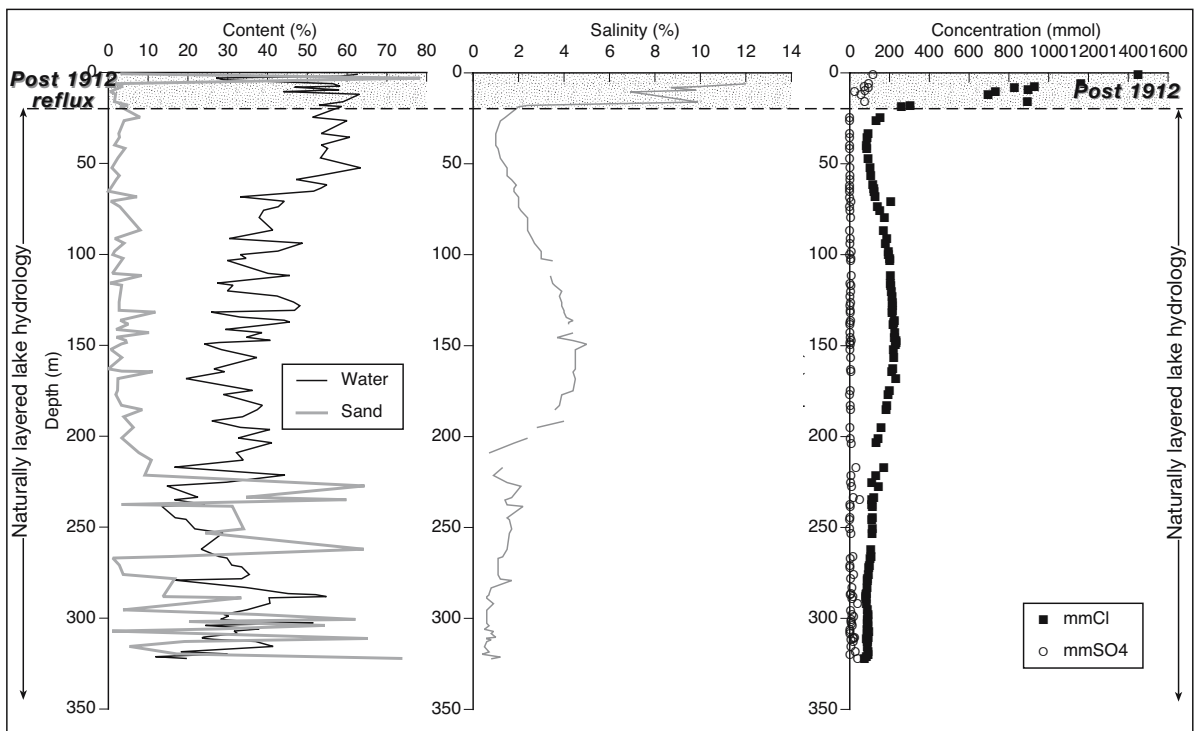


Figure 2.56. Core OL-92 a 327 m core collected in Owens Lake, California. Shows depth plots of sand and water content (%), salinity (%), chloride and sulphate content (mmol) of pore waters squeezed from the core (replotted from data in Table 1 in Bischoff et al., 1993).

and Range province of the USA, is in the type region for what has been argued are “hydrologically closed” lake systems, clearly is not. It is leaking waters vertically and laterally at a rate sufficient to smooth any former climatic layering.

But what is most impressive in the lake's hydrology is what has happened in the upper 20 metres in the last 80-90 years. The pre-1900 waters of Owens Lake had a salinity less than 9%, the lake was alkaline and probably had a pH \approx 9-10. The extremely high salinity of the top 20 metres is not a reflection of the pre-1912 natural lake. Rather, it is a consequence of river diversion and almost complete desiccation of the lake basin since 1924, and the associated downward migration of dense residual-brines (Bischoff et al., 1993). As the post-1924 lake dried out, Na-carbonate minerals precipitated to form a 1 to 2 m thick salt bed now covering the lower parts of the lake depression. Residual brines from the salt bed were denser than the underlying 9% pore water and were also relatively enriched in Cl. Modern brine percolated downward by gravity displacement and ionic diffusion, so that high salinity pore waters now dominate down to about 15-20 m.

Reflux brines derived by the accumulation of 2 metres of bedded salt have penetrated some 20 m of relatively fine-grained water-saturated sediment in 80 years. The original now-displaced pore waters had a salinity up to three times that of seawater and so would have been more difficult to displace than seawater brines in an ancient carbonate platform undergoing reflux, which would have had salinities around 3-4%. Clearly once a holomictic bedded salt system has formed, associated reflux is rapid and ongoing. What is more, the total system leaks water and brine at all levels in the cored hydrology. It possesses an open hydrological base to the lake depression even though the underlying nonevaporite sediments are more than 90% clay. Reflux rules the upper portions of the hydrology, deeper artesian circulation rules the lower part of the hydrology. It is a small, but temporally impressive, example of the hydrological processes that would be active in ancient drawdown platform or basinwide evaporite settings (e.g. Figures 5.7, 5.32).

Chapter 3: Sabkhas, saline mudflats and pans

Introduction

This chapter looks at Quaternary depositional styles in ephemeral saline waters, focusing on evaporitic mudflats (sabkhas) and saline pans (Table 3.1). Until the 1960s there were no well documented modern counterparts to ancient arid zone sediments that entrained evaporite nodules or isolated euhedral crystals floating in a nonevaporite matrix. Then nodular anhydrite was discovered in the mudflats of the saline coastal plain of the southern Arabian Gulf, centred on Abu Dhabi. Models of this saline mudflat setting, now widely known as the Abu Dhabi sabkha, began to be published. For the next 10-15 years the supratidal sabkha model came to dominate depositional interpretations of most ancient nodular sulphates. By the early 1980s subaqueous alternatives for widespread units of calcium sulphate salts had been documented in a number of small-scale Holocene marine-fed salinas. At the same time the concept of what is a sabkha had been expanded to encompass both continental and marine saline mudflats, with continental examples typically located next to ephemeral saline pans.

Ancient sabkhas are typically dominated by matrix, with capillary salts occupying less than 30-50% of a stack of m-scale erosion-capped beds. Saline pans accumulate as metre-scale

stacked masses of salt crusts overprinted by karst and capillary cements. Subaqueous sequences tend to be purer and thicker with far fewer exposure surfaces. Chapter 4 looks at Quaternary examples of subaqueous beds accumulating beneath perennial saline waters (salinas and saline lakes), while Chapter 5 compares models based on Quaternary systems with much larger and thicker ancient evaporites and attempts to answer the question, "Is the present the key to the past?"

What is a Sabkha?

Sabkha is an Arabic word for a salt flat. In the local terminology of the Arabian Gulf region it describes extensive, barren, salt-encrusted, and periodically flooded, coastal and inland mudflats. Geological usage implies intrasediment evaporite growth beneath a flat geomorphic surface with an elevation dictated by the top of the capillary fringe (Warren and Kendall, 1985). Modern sabkhas in the Arabian Gulf (sabkhat is the correct form of the Arabic plural) are occasionally covered by ephemeral marine and continental floodwaters that until recently were thought to be the major suppliers of ions to salts growing displacively in the sabkha matrix. We know now that this is not the case and that deeply circulated resurging continental

Sea-margin saline mudflat (sabkha) with carbonate matrix	Sea-margin mudflat (sabkha) with siliciclastic matrix	Lacustrine mudflat (sabkha) and saline pan - siliciclastic matrix
Abu Dhabi sabkhas, coastal plain of the United Arab Emirates (eolianite, beach ridges and interdunal)	Kadmah Bay Coast, Kuwait, Arabian Gulf (alluvial fan/sand flat/delta)	Salar di Uyuni, Bolivia (ephemeral lacustrine)
Al-Khiran sabkha, Kuwait (beach ridges)	Shatt al Arab, transitional mudflats, Arabian Gulf (delta/estuarine)	Lakes Eyre, Frome, Torrens and Callabonna, South Australia (ephemeral lacustrine and interdunal)
Tidal mudflats at the head of Gulf St Vincent and Spencers Gulf, South Australia (beach ridge and interdunal)	Sabkhas of the Sulaymaniya lagoon, Red Sea coast, Saudi Arabia (beach-ridge and estuarine)	Bristol Dry Lake, Deep Spring Lake and Saline Valley, Basin and Range, California (ephemeral lacustrine)
Tidal mudflats at the southern end of Shark Bay, Western Australia, as well as in nearby interdunal corridors locally known as "boinkas" (eolianite, beach ridges and interdunal)	El Qaa sabkhas, Gulf of Suez, (coastal plain/beach ridges)	Salt Flat Playa, west Texas, USA (ephemeral lacustrine)
	Bitter Lakes, sabkhas, Nile Delta, Egypt (eolianite interdunal corridors)	Sabkha Yotvata, Israel (ephemeral lacustrine)
	Laguna Madre mudflats, Texas (sandflat-barrier coast)	Sabkhas near Dharhan, Saudi Arabia (interdunal) and coastal sabkhas near Half Moon Bay
	Guerrero Negro area, Baja California, Mexico (interdunal)	Ranns of Kutch (eolian and deflation flats)

Table 3.1. Occurrences of Quaternary evaporitic mudflats (sabkhas) and saline pans, parentheses indicative of the origin of dominant matrix hosting the salts. These examples are discussed in detail in this chapter.

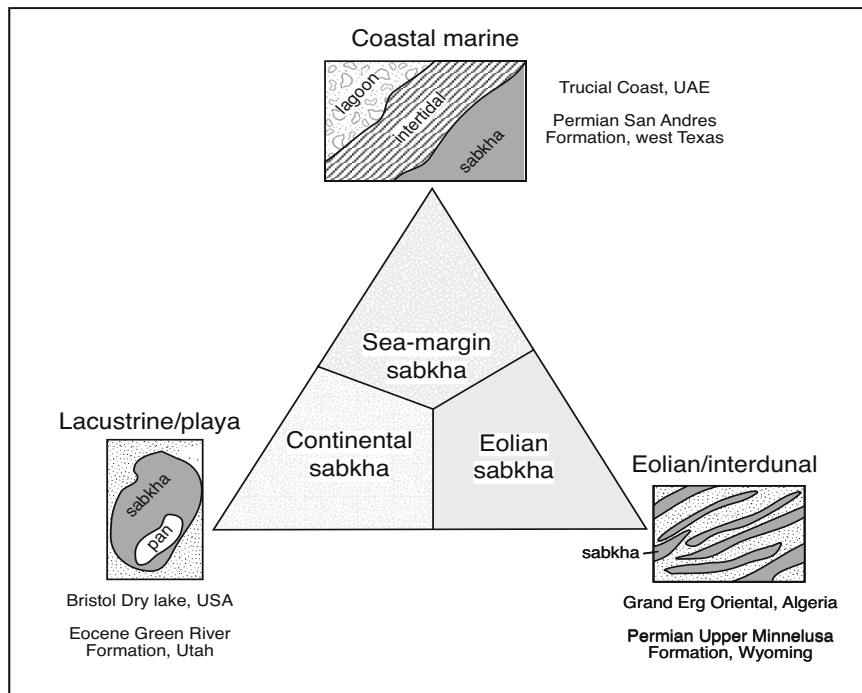


Figure 3.1. Sabkha classification using depositional setting of the matrix material (modified from Handford, 1981).

groundwater is the major supplier of salts to the sabkha. The mudflat surface is dry and subaerial for most of the time. It is held in place by capillary moisture, fed from a shallow saline water table lying a few centimetres to a metre or two below the sediment surface.

The first sedimentological studies of sabkhas were in the Arabian (Persian) Gulf (e.g. Curtis et al., 1963), but similar sediments were soon described along the coast of Baja California, Mexico (Phleger, 1969; Shearman, 1970), the coast of Sinai (Gavish, 1974; Levy, 1977a, b), and in various continental playas worldwide (Moiola, 1965; Surdam and Wolfbauer, 1975).

Occasionally, the term sabkha is used in a narrow sense to describe anhydritic mudflat sediments deposited in a marine coastal or sea-margin sabkha, exemplified by the Arabian Gulf coastal sabkha. But when sabkha is used to imply “salt flat,” it should include both coastal and continental sabkhas and encompass displacive growth of other intrasediment capillary salts like halite or glauberite as well as calcium sulphate. Some coastal sabkhas, such as those along the At Taf coastal strip (formerly known as the Trucial Coast), pass laterally in to continental sabkhas (e.g. Sabkha Matti) without any noticeable change in surface morphology (Kinsman, 1969; Goodall

et al., 2000). The seaward side of a modern coastal sabkha is characterized by a matrix of marine sediments, while the continental portion is characterised by nonmarine sediments and continental groundwaters.

Sometimes, the term playa is used as a geological equivalent to continental sabkha. But, as used in the southwest USA, playa is a much wider ranging descriptor than sabkha. In addition to the salt-crustured evaporitic mudflat (sabkha) a playa encompasses other related settings including, distal alluvial fans, sand flats, saline pans and dune fields. Continental sabkhas may also be encompassed in local usage of other wider ranging terms such as vloer/pan (southern Africa), salt lake (Australia), nor (Mongolia), takir (Russia), kavir (Iran), salar (Chile) and alkali flat/salada/dry lake/playa (southwest USA). Terms in local usage may not necessarily identify geomorphologically and geologically identical features. Even the original usage of the term playa does not mean salt flat, rather its Spanish usage covers the terms beach, shore, strand or coast. Its usage first came across into English to describe abandoned beaches or strandlines that can be seen on the margins of many inland salt lakes and saline pans. Using sabkha and playa interchangeably is very poor usage of what is already a poorly defined set of terms (see Briere, 2000).

In an attempt to clarify the geological usage of the term sabkha so it can be more easily applied to a particular vertical sequence in ancient evaporitic sediments, I define sabkha as a groundwater driven sedimentary system indicated by syndepositional intrasediment capillary evaporites, which precipitate in both marine and continental saline mudflats (Warren and Kendall, 1985; Warren, 1989). The hydrology of precipitation, via capillary evaporation, is the same in both marine and continental settings. Even so, the matrix typically shows evidence of its marine or continental pedigree, as can the hydrogeochemistry of the pore waters. In other words, sabkhas are hydrological settings where resurging groundwaters form displacive and replacive evaporite

minerals (gypsum, anhydrite, halite, polyhalite, glauberite, etc.) in the capillary fringe above a saline water table or in the brine-saturated muds immediately below. The whole capillary sequence is typically made up of more than 50% non-evaporite matrix and is capped by an erosion surface or Stokes surface (Warren and Kendall, 1985). The advantage of this definition is its utility in subsurface studies of ancient sediments where it can be applied using sedimentary textures in a single core; the surrounding depositional sequence does not need to be interpreted. The common thread is the growth of intrasediment salts in the capillary zone and in brine-saturated phreatic muds immediately below the water table, with the whole succession capped by a syndepositional erosion surface (Stokes surface). Sabkha hydrology controls the thickness of an evaporite unit, the style of intrasediment crystal (euhedral outlines to nodules) and most importantly generates the characteristic erosional or hydraulic “jack-up” surface that caps a sabkha cycle.

The host matrix in which sabkha salts grow by capillary evaporation is the sedimentological basis of most sabkha classification, (Figure 3.1: Handford, 1981; Warren 1991). Matrix in modern and ancient sabkhas is deposited as:

- Marine coastal
- Fluvio-lacustrine
- Eolian

Sabkha salts are mostly gypsum or halite and less often anhydrite, or even more unusual salts such as trona, borax or glauberite. Dominance of one of the matrix associations gives rise to sea-margin, continental, or eolian sabkhas. An eolian sabkha can be a subset of both sea-margin and continental sabkhas.

Marine coastal sabkhas

Modern sea-margin sabkhas form as narrow belts along many coastal arid to semi-arid deserts including; the western and southern coasts of the Arabian Gulf, the coast of western and southern Australia, Northern Africa, and the Sinai (Table 3.1). The most complete documentation of modern carbonate sabkhat centres on the southern coast of the Arabian Gulf (Persian Gulf) in the emirate of Abu Dhabi, while siliciclastic sabkhas typify the Saudi Arabian coast between Qatar and Kuwait, and fluvio-deltaic coastal sabkhas are forming atop the Shatt al Arab delta at the northwestern end of the Gulf. Elevated pore water salinities along the coasts of the Arabian Gulf (aka Persian Gulf), reflect a combination of frequent winds (mostly blowing from between 315° and 15°), high temperatures (up

to 45 to 50°C), low precipitation (typically less than 5 cm a year), low fluvial input (except for the Tigris, Euphrates and Karun rivers in the extreme north of the Gulf) and the restricted silled connection via the Strait of Hormuz between the saline waters of the Arabian Gulf and the normal salinity waters of the Gulf of Oman and the Indian Ocean.

Physiographically, the Arabian Gulf is an almost enclosed subrectangular basin that trends in a northwest-southeast direction, it is approximately 850 km in length with a maximum width of 330 km (Figure 3.2a; Wyn-Hughes, 1997; Evans, 1995). The basin floor is markedly asymmetrical, forming a ramp that dips gently (35 cm per km) away from the tectonically stable Arabian side (typical depths of 20 to 40 m), and more steeply (175 cm per km) away from the tectonically active Iranian side (depths of 40 to nearly 100 m). The greatest water depth (100 m) is reached near the entrance to the Gulf at the Straits of Hormuz (Purser and Seibold, 1973).

In terms of its regional tectonic setting, the Arabian Gulf is an epicontinental sea within a foreland basin, located between the geologically stable, low-lying, Precambrian Arabian Shield and the high, geologically unstable Tertiary fold belt of the Zagros Mountains of Iran. The fold belt is a compressional suture, active since the Early Miocene along the Zagros Thrust Zone and driven by the subduction of the Arabian Plate beneath the Eurasian Plate (Wyn Hughes, 1997). The Gulf's bathymetric asymmetry comes from Pliocene to Quaternary tectonic loading on the Iranian side, and tilting of the Arabian Peninsula in the Neogene, during the opening of the Red Sea. The southeastern part of the Arabian Gulf is a very gently sloping ramp. The Qatar Peninsula forms a distinct feature on the near-linear Arabian coastline, and causes anomalous trends in current direction, and possibly of sedimentation, along the southeastern Gulf.

Ramp carbonates, including sabkhas, define the coast along much of the cratonic southern side of the Gulf, while the northern coast is dominated by more steeply dipping siliciclastic alluvial aprons passing landward and northward into the Zagros Mountains. Moving south from the deepest Gulf floor, the bottom changes from deepwater micrites through grainstones and reefs of the Great Pearl Bank into reworked dune and eolianite barrier shorelines into the coastal carbonate sabkhat (the shorelines of the Emirates, Qatar and Saudi Arabia). Entry of siliciclastic sediment to the present Arabian Gulf is mostly longitudinal via the Shatt Al Arab delta at the northwestern end of the Gulf. The Shatt Al Arab is the confluence of the Tigris, the Euphrates and the Karun rivers. It has constructed a huge wedge of fluvio-deltaic sediments, with thin patchy sabkha capstones landward of

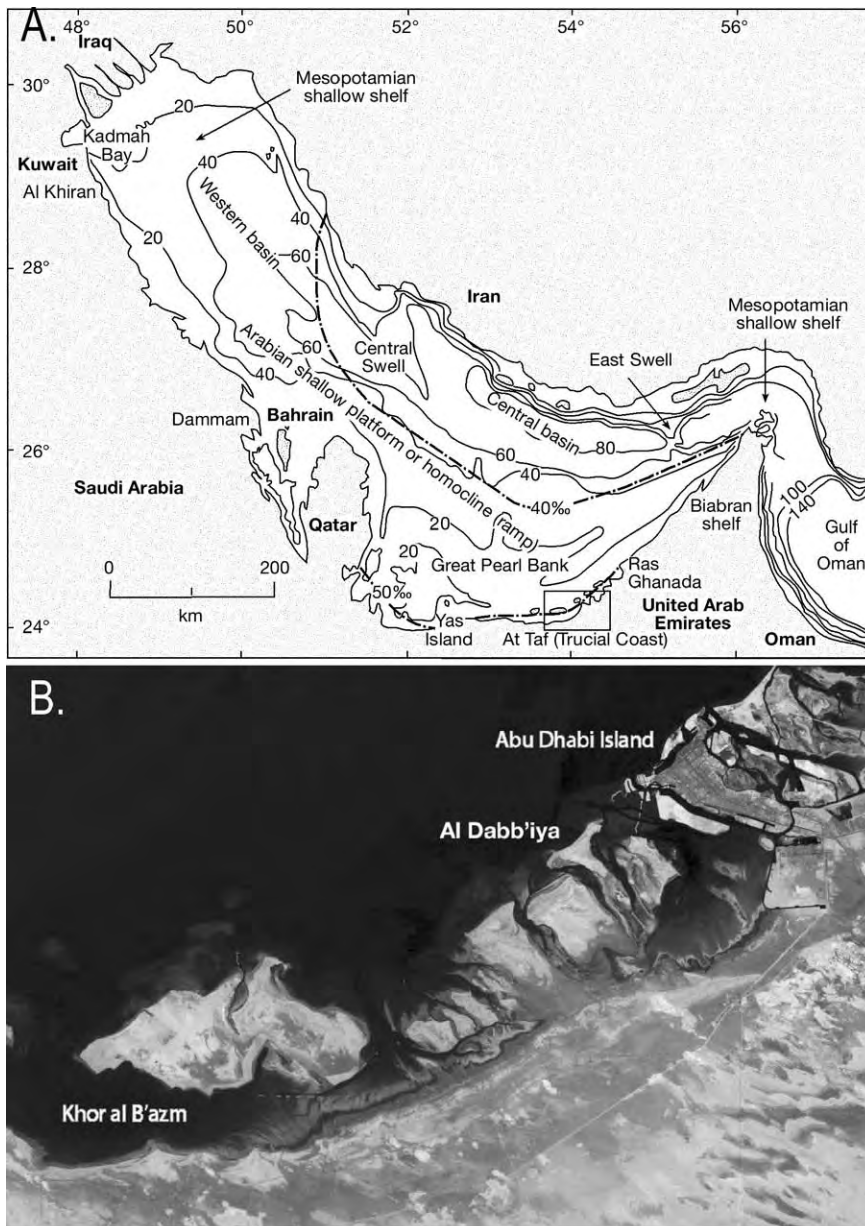


Figure 3.2. Sabkhas of the Arabian (Persian) Gulf. A) Physiography (m) and salinity (‰) in the Arabian Gulf (after Purser, 1973a; Evans, 1995, Wyn Hughes, 1997). B) General sediment distribution of the Trucial Coast of the United Arab Emirates from the entrance to the Khor al B'azm Lagoon to Abu Dhabi Island, showing the shallow water areas of the lagoon and the oolitic ebb-tidal deltas on the seaward side of the tidal channels between the islands (see Figure 3.4). The intertidal zone, defined by intertidal algal mats, is clearly visible as zones of dark-coloured sediment. Landward of the intertidal zone is the supratidal zone of the sabkha, which in turn passes into dune sands across the mesa that defines the erosional edge of the Miocene plateau (Landsat image courtesy of NASA).

the shoreline (coasts of Iraq and Kuwait). Siliciclastics enter also from wadis along the northeastern side of the Gulf and from encroaching dunes along parts of the Saudi coast. Eolian

transport is driven by the north-westerly Shamal winds (*shamal* is Arabic for north) and carries both siliciclastic and carbonate fines well out into gulf waters. In the Late Pleistocene much of the Arabian Gulf floor was covered by active seif dunes. Interestingly, detrital dolomite rhombs make up around 15% of the non-clay component of modern bottom sediments in the northern Arabian Gulf and up to 60% of the 30-125 μm fraction (Al Bakri et al., 1984). Morphologically they are near identical to much of the authigenic sabkha dolomite rhombs that first caused so much interest in sabkhas in the Emirates in the 1960s.

Geologically the Arabian Gulf is unique as it is the only modern example of a modern shallow inland sea in which widespread ramp carbonates are accumulating. This is attributed to its low latitudinal position and relatively clear waters, the result of low terrigenous input, making much of the seafloor suitable to a tropical carbonate-secreting biota (Wyn-Hughes, 1997). The depth of the euphotic zone is around 20 m in turbid waters above the muddy sediments along the Abu Dhabi coastline, but increases to 30 m in the clearer deeper waters in the axial parts of the seaway.

Although it is a marine carbonate system today, 20 ka when sealevel was 120 m below its present level, the whole Gulf was a desiccated basin with active eolian dunes covering much of what is the present seafloor. The Pleistocene-Holocene (Flandrian) transgression covered and reworked much of this dune sand as the gulf waters returned

to the present coastline some 7-10 ka. Much of the Holocene marine carbonate section in the southern Gulf is now underlain by these eolian siliciclastics.

Carbonate-hosted coastal sabkhas in the southern Arabian Gulf

The Arabian Gulf sabkha, centred on Abu Dhabi city, is the eastern part of a sabkha belt known as Sabkhat al Salamiyah that extends along the coast of the United Arab Emirates between Yas Island and Ras Ghanada (Figures 3.2b, 3.3). Further west, adjoining the eastern base of the Qatar peninsula is Sabkha Matti, one of the largest tectonically-induced sabkha depressions in the region (see eolian sabkhas). The sabkha-dominated At Taf coastal strip is approximately 320 km (200 miles) long and the coastal sabkha belt is up to 24 km (15 miles) wide; on average it has prograded 1.5 km (1 mile) every 1000 years. Seaward slopes on the sabkha are low and range from 1:3,000 to 1:4,000, this means whenever water a few centimetres deep arrives on the sabkha, the strandline on the brine sheet will have migrated kilometres.

It was the occurrence of modern nodular anhydrite and dolomite in the sabkhas of Abu Dhabi and Qatar that first attracted the attention of the geological community during the 1960s. The work of Curtis et al. (1963), Illing et al. (1965), Evans et al. (1969), Kinsman (1969), Shearman (1963), Butler (1966, 1969, 1970), and Kendall and Skipwith (1969a, b) provided observational data on which most of our current sabkha models are based. Fieldwork since the 1960s tended to consider specific sedimentological problems within the sabkha setting, such as hydrological zonation (Patterson, 1972; Hsu and Schneider, 1973; McKenzie et al. 1980; Patterson and Kinsman, 1981), the origin of dolomite (McKenzie, 1981; Patterson and Kinsman, 1982), or it has reinforced the facies model of earlier workers (Bush, 1973; Butler et al. 1982; Kendall and Warren, 1988). Excellent recent reviews of this literature and some new insights are given in review papers by Alsharhan and Kendall (2003), Kirkham (1997) and Evans (1995). The most recent addition to this substantial knowledge base is a drastic revision of our understanding of the dynamics of sabkha hydrology by Wood et al. 2002. It changes our understanding of evaporite capillary salts from one of marine-derived floodwaters to one of solutes precipitated in a Holocene marine matrix, but sourced from resurging basinal waters.

To understand sabkha deposition requires an understanding of the climatic and hydrological factors that create conditions suit-

able for sabkha progradation into the southern Gulf. The Arabian Gulf is the warmest sea in the world; in the open Gulf the surface temperatures range from 20°C in February to 34°C in August, with an annual average around 29°C in waters located offshore from Abu Dhabi. Water temperatures on the open platform in the vicinity of Abu Dhabi Island range from 23° to 34°C and from 15° to 40°C in the inner lagoon. Shallow waters in the lagoon can experience daily changes of 10°C. Air temperatures on the adjacent mudflat can be as low as 5°C in the winter and as high as 50°C in summer, with average temperatures ranging from 23° to 33°C. Sediment surface temperatures on the sabkha are even more variable, with reported values up to 60° to 80°C atop dark-coloured microbial mats (Kinsman, 1965). Temperatures a few centimetres below the sabkha surface range from 22° to 40°C. In summer, the sabkha is extremely humid, especially at night, when the humidity reaches 100%. Salinities in the open Gulf are 3 to 4‰ above normal open marine salinities. Where coastal islands restrict exchange with the open Gulf, as in the vicinity of Abu Dhabi Island, lagoon salinities range between 54 and 67‰, near double that of the open ocean.

Evaporation levels on mudflats along the southern coast of the Arabian Gulf are influenced by prevailing onshore winds. In winter the intensity of the onshore winds increases as the Shamal blows seawater and sediment from the lagoon onto the mudflat. At other times offshore winds blow continental dune sand into the back side of the sabkha. Thus the sabkha is furnished with matrix sediment from two sources, carbonates from the lagoon and siliciclastics from the hinterland. Many earlier sabkha models tended to ignore the eolian input, yet some areas of the mainland side of the Abu Dhabi sabkha (e.g. Al Du'yybaya sabkha) have quartz silt and sand as the major matrix material and it is the dominant aquifer supplying water to the coastal plain. Rainfall along the sabkha coast averages 70 mm/year and is very irregular, in some years no rainfall is recorded. In the 6-year period from 1958 to 1964 the highest annual reading on the sabkha was 6.73 cm, the lowest 0.33 cm. When rain does fall it can be torrential. Bottomley (1996) notes that in the last 30 years there was at least one 24 hours period when more than 200 mm of rain fell on the sabkha. Although infrequent, such desert rains can be torrential, especially in coastal sabkhas near the foot of the Oman Mountains, such as at Rams, where flooded wadis typically carry continental sediments as sheet floods many kilometres into the sabkha (Warren, 1991). Rain floodwaters can sometimes cover portions of the sabkha for one to three months and so dissolve and recycle surface and nearsurface halite/bittern crusts, as occurred in late 2003.

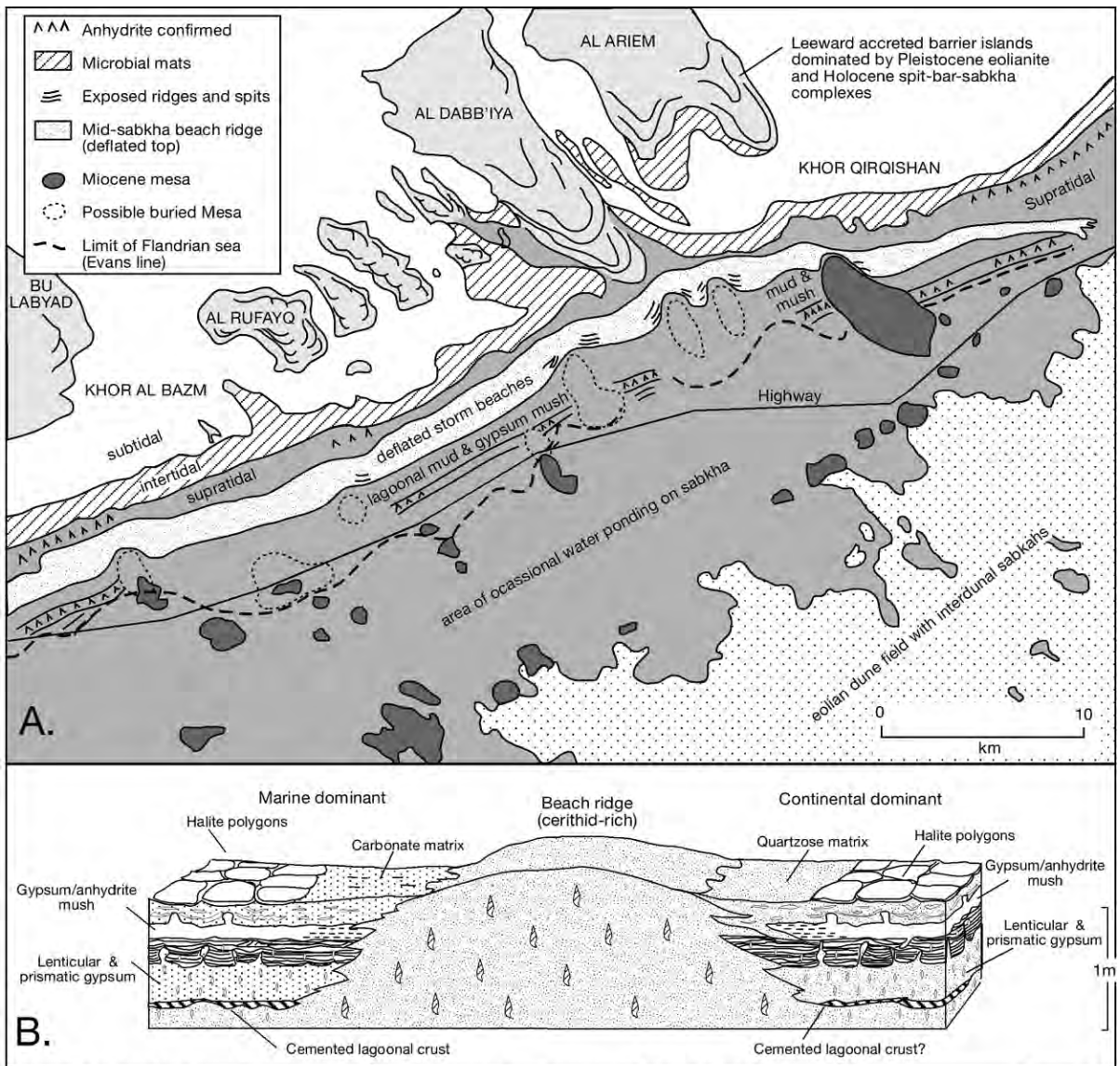


Figure 3.3. Abu Dhabi sabkha. A) Sabkha facies located to the west of Abu Dhabi showing beach ridges encased in sabkha sediment in the vicinity of Bu Labyad - Al Du'yybaya (after Kirkham, 1997). B) Sabkha cross section based on facies present in the vicinity of the beach ridges south of Al Du'yybaya Peninsula and the Mussafah Channel wall (after Warren and Kendall, 1985).

Physiographically, the Abu Dhabi sabkha is characterized by billiard table flatness, a direct reflection of its control by capillary wicking fed from the underlying water table. The sabkha surface is a Stokes surface (Figure 3.4a). In general, the water table control to any sabkha gives them one of the flattest forms of any arid landscape feature. Below this flat surface the Abu Dhabi sabkha preserves an evaporitic mixed-carbonate-siliciclastic stratigraphy (Evans et al., 1969; Kinsman, 1969; Kirkham, 1997). Deposition began some 7,000 years ago when

a rapid transgression flooded interdunal (eolianite) depressions with a veneer of marine-reworked, predominantly quartzose sediments. About 4,000 years ago the Arabian Gulf shoreline reached its maximum Holocene strandline and the edge of this flooding event is defined by a line of well preserved beach-ridge sediment sometimes called the “Evans line.” This was followed by pulsed progradation of the sabkha sequence to its present configuration.

Abu Dhabi facies associations

The peritidal belt that defines the Abu Dhabi sabkha is divided into three: subtidal, intertidal, and supratidal (Figure 3.3a). Tidal range is 2–2.5 m along the seaward side of the islands of the southern Gulf, but it can be as little as 1 m in the more restricted lagoonal areas, which are locally known as khors. As the strandzone progrades, the peritidal belts of the lagoon, cyanobacterial mat and sabkha, all located landward of the present barrier island belt, are stacked one atop the other to create an archetypal shallowing-upward sabkha cycle. We will discuss each peritidal belt in detail, but first let's look at a largely ignored part of the southern Arabian Gulf peritidal trilogy, the island shoal and bank facies. This is the unit that protects the muddy coastal lagoons in the vicinity of Abu Dhabi and allows the various carbonate sabkhas to form. Facies belts basinward of the island shoal are classic carbonate ramp sediments, while peritidal sediments landward of the island shoal make up the sabkha association.

Island shoal and bank facies

Cemented coastal-beach-dune barriers form the core of a belt of northeast trending carbonate islands that are the easternmost extent of the "Great Pearl Bank" (Wyn Hughes, 1997). These barriers enclose lagoons or tidal estuarine sequences and in places may directly abut the mainland (Warren, 1991). Most of the islands are eolianite-cored shoals, composed of varying proportions of Holocene and Pleistocene ooids, along with skeletal and quartz sands. Island cores are stationary, fixed in place by carbonate cements, and are separated by active tidal channels up to several kilometres wide and 7 to 10 metres deep (Figure 3.2b, 3.3a; Purser and Evans, 1973; Loreau and Purser, 1973). Further up the coast on the Qatar Peninsula and along parts of the Saudi coast their place is taken by marine-reworked quartzose eolian dune sand shoals, which still have counterparts building directly into the Gulf (see eolian sabkhas for details). The coastal barriers and spits along the At Taf coastal strip, which form the depositional frame for the Holocene sabkha, formed in the late Pleistocene via carbonate accretion atop reworked eolian quartzarenites as the desert dunes were inundated during the final phase of Flandrian rise (Purser and Evans, 1973; Kirkham, 1998). Up to 9 m of Pleistocene eolian material and 2.7 m of Holocene carbonates overlie Miocene marine carbonates in the vicinity of Abu Dhabi city (Butler et al., 1982). Miocene strata also form mesas and outliers on the landward side of the sabkha (Figure 3.3a).

Holocene vadose and phreatic cements stabilised the transgressive island shoals at the position of the Pleistocene-Holocene stillstand. Previously, the coastal dune/shoreface had migrated

landward in front of the rising late Pleistocene sea. The early Holocene stillstand, in combination with cementation meant the islands evolved into wave-resistive structures fronted by coralgal reefs. This in turn preserved a barrier lagoon, even in the early Holocene when wave-resistive reefs had yet to grow on the seaward side of the now stationary barrier islands. Cemented sands formed a stable substrate for subsequent coralgal reefs and today maintain a relatively fixed focusing grid for wave, longshore and tidal currents.

Island stability in turn maintains the position of numerous active tidal channels as fixed breaches in the cemented eolianite topography. Tidal channels between the islands allow exchange of seawater with the more saline waters of the inner lagoon. The longterm stability of the island shoal facies explains the formation of thick ooid ebb-tidal delta sands on the seaward ends of many channels along the Abu Dhabi coast. Where these ooid sands accumulate above sealevel they are blown into Holocene coastal eolianites, adding volume to the island shoal sediment pile (Figure 3.2). If the islands were not cemented stationary structures, then tidal channels and islands would migrate laterally, ebb sands would spread out as much thinner accumulations and form barrier geometries more akin to classic "drumstick" tidal deltas in mesotidal barrier coasts.

Subtidal Facies

Subtidal sedimentation along the Abu Dhabi coastline can be divided into sediments accumulating seaward of the island shoal facies and sediments in the lagoon (Evans 1995):

1. *Open marine sedimentation* occurs along the seaward side of the northeast trending barrier island coast and has largely buried the underlying Pleistocene eolianites and seif dunes (Figure 3.2). Seaward terminations of shallow channels draining the lagoon are flanked by tidal ebb deltas composed of oolitic sand. These Holocene lobes form lens-shaped bodies 2 to 10 km wide and 1 to 5 m thick. They occur in wave- and tide-agitated areas where ooids are piled into shoals by opposing onshore waves and offshore ebb-tidal currents. The ooid sands (ooid grainstones) are fashioned into various bedforms including break point bars, along with large and small-scale ripples. Skeletal fragments in the shoals indicate a limited macrofauna of molluscs, echinoids and burrowing crustaceans. Broken fragments of this fauna typically form the core or nuclei to ooids.

Within the sand pile the ooid grain size and cortex thickness decreases away from the channel levees. Cemented crusts (aragonite and Mg-calcite) and crust fragments can also be found in the sand pile, much in the same way they occur in

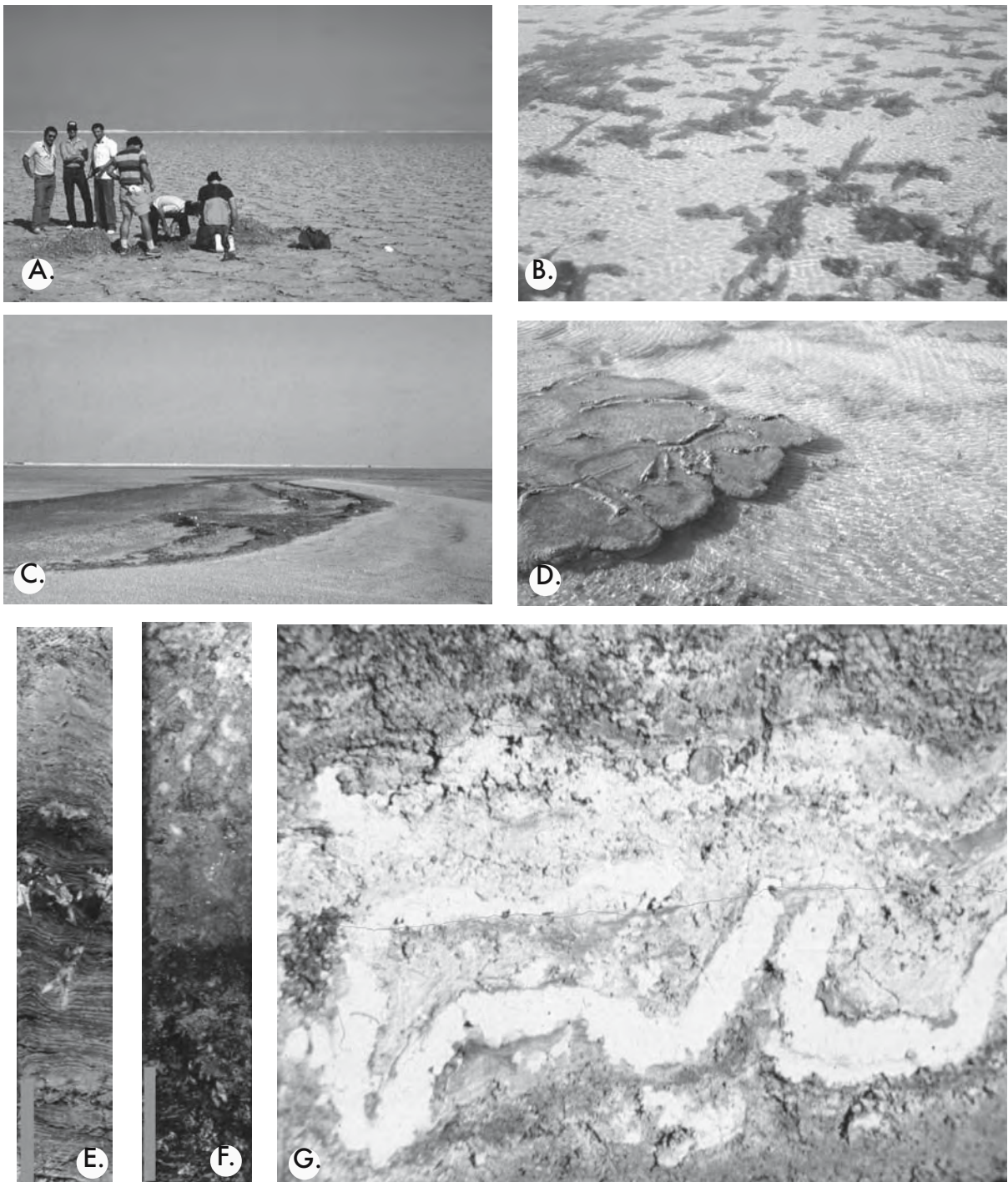


Figure 3.4. Arabian Gulf sabkha, Abu Dhabi. (A) Sabkha surface covered in an ephemeral halite crust; (B) Lagoonal sediments of Khor Al B'azm showing peloidal grainstones and packstones with growing clumps of brown algae covered with calcareous epibionts (photo courtesy of Xris Kendall); (C) Cusped, laterally accreting beach ridge on seaward side of Al Du'yybaya sabkha, Abu Dhabi; (D) Truncated and grazed edge of laminated polygonal mat at the edge of a tidal pool, southern Khor Al B'azm; (E) Core of laminated mat with displacive euhedral gypsum and an overlying unit of supratidal gypsum and anhydrite, sabkha south east of Abu Dhabi City (scale bar = 5 cm); (F) Core of cyanobacterial peat (?pustular mat) with lenticular gypsum and an overlying unit of supratidal gypsum and anhydrite, sabkha south east of Abu Dhabi City (scale bar = 5 cm); (G) Nodular and enterolithic anhydrite with obvious truncation surface preserved in middle of unit, Al Du'yybaya sabkha.

the less active portions of Bahamian ooid shoals. At a water depth of about 2 m on the spillover front of the Abu Dhabi ooid shoals there is an abrupt change into mixed ooid-bioclastic grainstones/packstones. Storms and the wind drive ooid sands onto the island shoal belt and so continue to supply sediment to the barrier islands. High eolian dunes form where active ebb tidal deltas are building out onto the cemented island core. Bedding in these parabolic dunes is inclined landward and retains continental indicators such as occasional rhizoconcretions and insect burrows.

Patchreefs are growing immediately seaward of the Pleistocene-cored islands (island shoal facies) in areas between the ooid shoals. Reefs also extend landward along the sides of some of the more stable open-marine tidal channels, but do not extend far into the more restricted sections of the lagoon. There the waters quickly become too saline for the reef to remain healthy (Kinsman, 1969) and are subject to intense temperature and salinity variations during Shamal storms (Figure 3.5; Riegl, 2003). Shinn (1976) attributed massive coral die-back in the southern Gulf (Qatar) to a severe Shamal, which caused cooling to 4°C at sea surface and to 14.1°C at 18 m depth. Shamals may generate storm seas of up to 6 m wave height (65 kph winds), driving erosion, turbidity and complete vertical mixing of lagoon waters and partial mixing offshore. Clearly, rapid cooling by Shamals, sometimes coupled with extremely low tides, amplified by negative storm surge, are a significant stress factor causing repeated coral mortality and bleaching throughout the southern Arabian Gulf (Riegl, 2003).

When compared to the reefs of the open Indian Ocean, the coral fauna, even on the open marine side of the islands of the Emirates, is somewhat sparse and restricted. It is dominated by genera of *Porites* and *Acropora* with *Platygyra*, *Cyphastrea*, and *Stylophora* calcareous and binders dominated by coralline algae (*Lithothamnion*, *Lithophyllum*, and *Goniolithon*). The reduced reef biota is a response to temperature and salinity stresses inherent to the restricted waters of the Arabian Gulf. Salinity and turbidity oscillations mean many of the corals growing along the sides of tidal channels feeding the lagoons appear unhealthy and at times are covered by flourishing coats of green algae. Like corals, echinoids die out in the lagoons

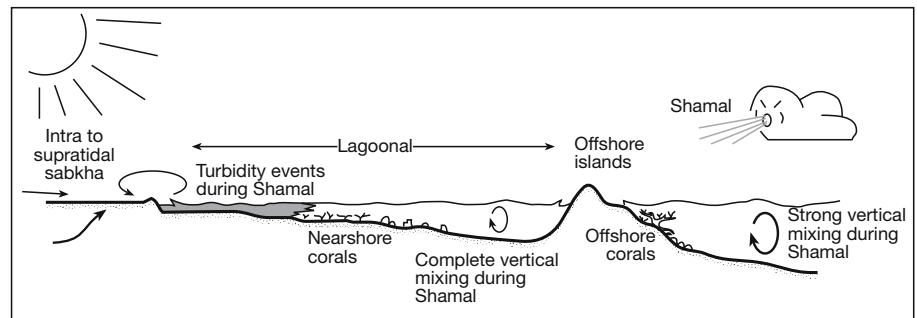


Figure 3.5. Schematic of hydrodynamics in the near offshore and lagoon/sabkha of the southern Arabian Gulf (after Riegl, 2003).

although asteroids, and more particularly ophiroids, extend much further into the lagoons or khors.

Seaward of the islands is a broad gently sloping Holocene platform covered by skeletal sands, which pass offshore into progressively deeper and finer-grained carbonate silts and muds of the Gulf centre. This sloping profile is one of our better modern analogues for ancient carbonate ramps (Evans 1995), while the Great Pearl Bank makes an excellent Holocene analog for Cretaceous rudistid buildups (Wyn Hughes, 1997).

2. *Restricted marine (khor) sedimentation* takes place along the landward side of the barrier islands in areas dominated by lagoon and sabkha sediments (Figure 3.4b). The tidal inlets and khors (*khawrs*) are unique subtidal settings formed behind the grainstones of the island shoals and constitute the protected seaward edge of many sabkhas. They vary in shape and size from large elongate lagoons such as Khor al B'azm and Khor al Baghi (behind Abu Dhabi Island) to the estuarine inlets of Umm Al Qwayn (Warren 1991). Many are dendritic in outline, but lack any permanent surface freshwater inflow (Warren, 1991), except for those khors located close to the mountains near the Straits of Hormuz, which can be periodically flushed by meteoric runoff. Today many khors in the Emirates are dredged to form accessible waterways and sheltered harbours. Some deepened channels can now accommodate large dhows and other seagoing vessels, whereas undredged natural tidal channels into the khors are typically less than a metre or two in depth, even at high water.

Tidally scoured lagoonal channels join the open-marine settings to the restricted-marine lagoons or khors. Channels are floored with skeletal and peloidal sands, which are reworked by tidal and wave action into crossbedded skeletal/peloidal grainstones. Toward their inner parts, in the lagoon proper, the channel floor sediments become sandy muds (peloidal/skeletal packstones and wackestones). Wherever they poke through a thin lag of

coarse shell and intraclasts, cemented calcareous eolian sands (eolianite) sometimes crop out on the channels floors.

Extensive shallow-water lagoons, filling with bioturbated packstones and wackestones, occupy the shallower parts of the khors away from the channels. Because of their higher elevation relative to the lagoonal channel floors, subaqueous areas of khor away from the channel are sometimes described as lagoonal terraces. Terrace sediments entrain a diverse biota made up of many benthic species but relatively few phyla (Kendall and Skipwith, 1968b). Molluscan sands and peneroplid foraminifera dominate the more open terrace areas, whereas pelleted carbonate mudstones with a sparse fauna accumulate in the more protected reaches. Cyanobacterial grain coats and biofilms are abundant on the lower-energy terrace sediments and encourage healthy populations of cerithid gastropods, which through their grazing contribute a large proportion of the pellets in the lagoon. Terrace sediments are also heavily burrowed by crustaceans and worms. The somewhat elevated temperatures and salinities on the lagoon floor drive seafloor cementation of these ubiquitous pellets. In the more marine parts of the terraces various sea grasses and seaweeds (brown algae) form dense carpets on the channel floors, along with healthy epiphyton coats of bryozoans and calcareous algae (Figure 3.4b). There are four species of seagrass in more open marine parts of the khors and further offshore: *Halodule uninervis*, *Halophila stipulacea*, *H. ovalis* and *Syringodium isoetifolium*. *Halodule uninervis* is undoubtedly the dominant species of seagrass in the southern Gulf and is the major food-plant taken by herds of grazing dugongs in the UAE.

Isopachous crystalline rinds and micrite crusts, composed of aragonite and Mg-calcite, bind large areas of the lagoon terraces into cemented layers. Ongoing expansion of the layers creates dm-scale tepee structures, which can also be traced upslope into the base of the intertidal zone (Kendall and Warren, 1987). Tepee-overprinted ridges on the lagoon floor create a stable substrate or holdfast for much of the larger epiflora as well as a healthy population of borers. Seaweeds tend to attach themselves to tepee ridges in preference to the less stable muddy bottom veneer that forms the lagoon bottom away from the tepee crest.

Intertidal facies (strandline sands)

Waves can drive loose terrace sediments shoreward to build narrow sandy beaches and berms of peloidal and skeletal grainstone, typically with landward-directed cross stratification (Figure 3.2a, b, 3.4c, 3.6a; Evans, 1995; Warren and

Kendall, 1985). Cerithid gastropods, which populate the more landward parts of most khors, are a major skeletal component of the ridge sands, as are bivalve fragments and benthic forams. In areas more exposed to wave action the beach ridge sediments are coarser, ranging from coarse sands to skeletal gravels (rudstones). Locally, low-relief tidal levees and ridges enclose mangrove swamps where sediments tend to be highly bioturbated muds crosscut by rhizophores. More typically, the narrow beach ridges in a sabkha coast are transitional into the cyanobacterial-dominated intertidal sediments that typify much of the intertidal zone of the inner lagoon (Figure 3.3a).

I have trenched and cored buried equivalents of these beach ridges within various parts the Abu Dhabi supratidal sabkha succession, they are most obvious in the sabkha to the south and west of the Al Du'yybaya peninsular (Figure 3.3b). They have not been well documented as a facies within the Abu Dhabi sabkha as the tops of older ridges landward of the modern strandline are typically deflated and buried beneath a halite crust (Figure 3.6a). Southeast of Khor al B'azm a line of deflated beach ridges lies behind the currently active area of sabkha sedimentation. It is some 3-4 km inland of the present edge of the lagoon and forms the seaward edge of a 10 km wide belt of older Holocene sabkha sediments (Figure 3.3). Remnants of an older sequence of beach ridges define the maximum extent of the Flandrian (Holocene) transgression (aka the "Evans Line"), the initiation of the seaward progradation of the Holocene sabkha coastline and the occurrence of supratidal CaSO_4 facies. Portions of this system are now buried beneath lagoonal muds. The contact between more oxidised beach-ridge pore waters and the reducing waters of the lagoon muds is defined by an iron-stained band of lenticular and prismatic gypsum (Figure 3.6a).

The presence of Holocene beach ridges along the coast on the seaward side of the present day sabkha supratidal, the presence of older largely buried and deflated Holocene beach ridges in the mid sabkha, and the relicts of early Holocene ridges defining the most landward extent of the Flandrian transgression clearly show Holocene sabkha progradation is not a simple seaward progression of peritidal facies. It is a punctuated and possibly forced regression (Warren and Kendall, 1985; Warren, 1991; Kirkham, 1997). Similar beach ridges within Holocene sabkhas are described from the northern Emirates by Al-Farraj (2005), from Kuwait by Picha (1978) and from northeast Qatar by Shinn (1973).

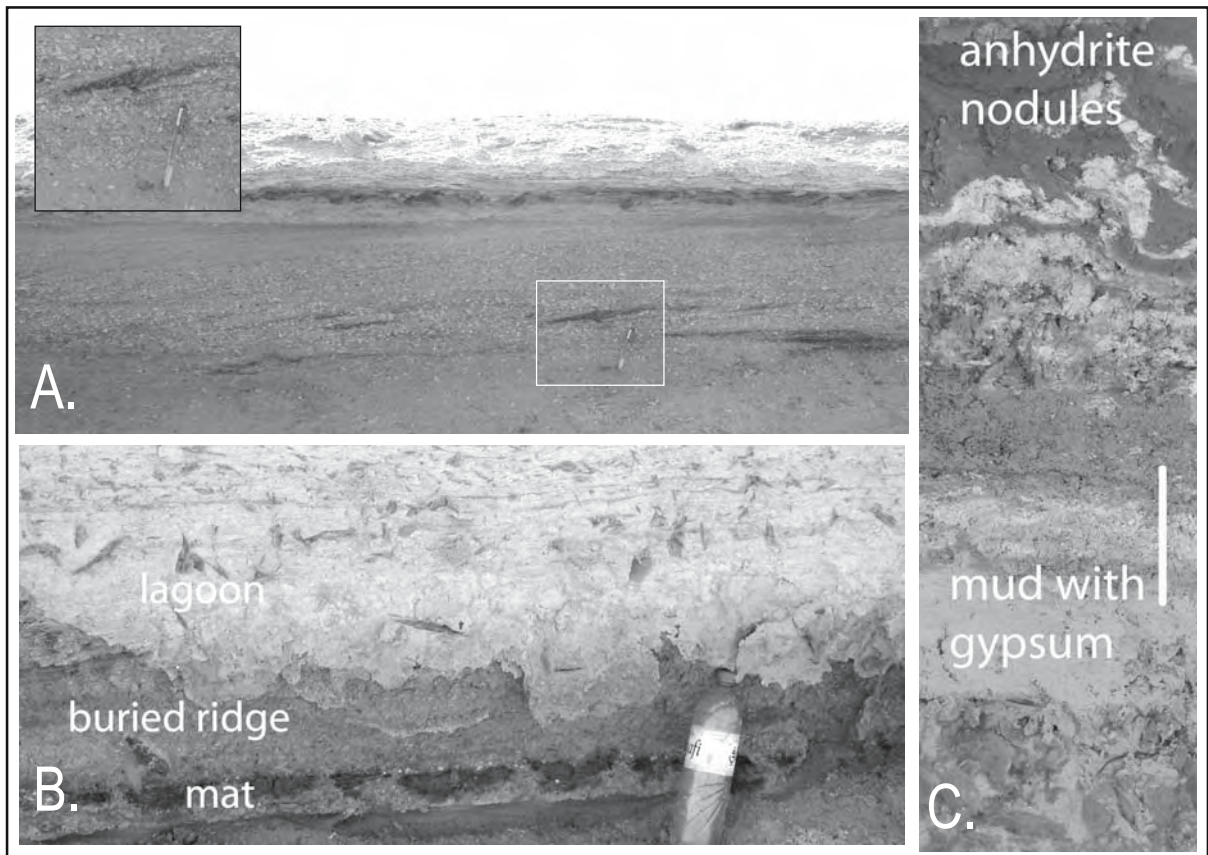


Figure 3.6. Styles of CaSO₄ occurrence exposed in the Mussafah Channel, Abu Dhabi: The trench is actually the wall of a man-made shipping canal cut into the sabkha near the Mussafah Industrial Area. The locality is over 7 kilometers landward of the present-day restricted lagoon and 25 kilometers from the open Arabian Gulf waters. A) Buried beach ridge gastropod rudstone showing landward-directed storm cross bedding and gypsum at the contact with overlying mud (inset shows detail of cross bedding). B) Buried algal mat (dark blebs) overlain by ridge and lagoon sediment, with lenticular gypsum growing in the overlying lagoonal muds. Site is located about 50 m seaward of ridge in 3.6a. C) Enterolithic anhydrite in the supratidal sabkha which is a lateral equivalent of gypsum in 3.6b, the site is located around 200 m northwest of the gypsum in 3.6b. Scale bar is 10 cm long.

Intertidal Facies (Lagoon-edge muds)

Away from the active beach ridges, the intertidal zone is divided into upper and lower intertidal facies, although the lower intertidal facies of some workers is equivalent to the lagoonal terrace facies of others. The confusion stems from the presence of a wide cemented flat along the mainland shore of the various khors; a flat that is covered by rippled peloidal sands or muddy sands (peloidal grainstones and packstones) and hosts a dense population of cerithid gastropods. Some authors place this flat in the shallow subtidal as an extension of the lagoonal terrace, while others place it in the lowermost intertidal. The lack of firm definition of its distribution is due to the flat, shallow nature of the southern Gulf. This means minor variations in wind direction, speed and the barometric

pressure can cause the predicted tides in the khors to remain either “out” or to advance several kilometres further “in” than predicted. Longer term seasonal variations follow a more defined if unusual pattern, with inundation of many otherwise “supratidal” areas, that is large areas of sabkha flat, not occurring until late autumn (post-equinox). Hence, the lateral extent (strandzone) of the intertidal area of sedimentation in the UAE is large, but poorly defined. Even the terms tidal to describe sheets of lagoon water that at times cover the uppermost parts of the sabkha “intertidal” is a little misleading as the process driving the sheets landward is typically the shamal.

Geologically, what defines the muddy intertidal facies is evidence of cyanobacterial (aka algal) mats. Mats first occur as degraded cyanobacterial peats in a transitional 100-200m-wide

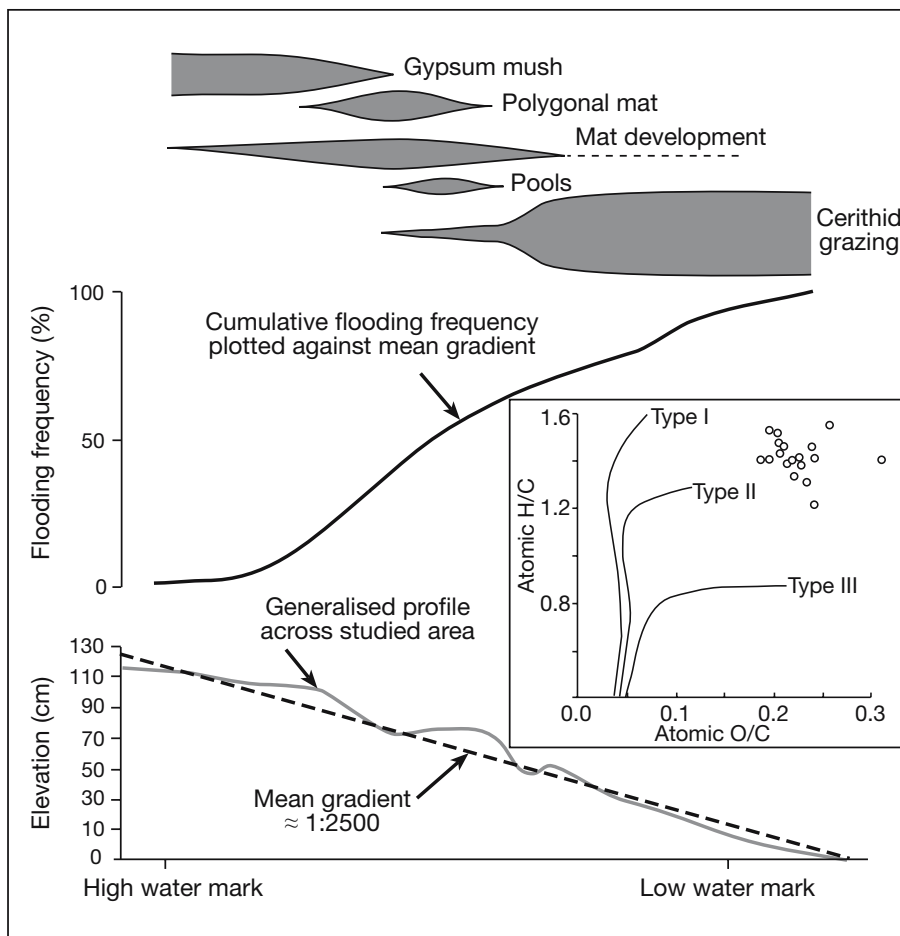


Figure 3.7. Distribution of cyanobacterial mats in relation to tidal range, flooding frequency and cerithid grazing on the Abu Dhabi coast. Inset shows van Krevelen plot of protokerogen type in mat organics (after Park, 1977; Alsharhan and Kendall, 2003).

zone where the bare lagoonal flats pass landward into a belt of well-preserved laminated mats (Figure 3.4e, f, 3.6b; Kendall and Skipwith, 1968a, Park, 1977). Hence, the lower intertidal is defined by degraded oxidised peats composed of the bioturbated remnants of cyanobacterial mat. The upper intertidal facies is variably defined by laminated microbial mats across an extensive belt up to 1 to 2 km wide. These biolaminites accumulate in moist intertidal areas where salinities and temperatures are too hostile for cerithid gastropods and the other grazing animals of the lagoon flat (Figure 3.7). Many mats have sharp edges on their seaward side due to the grazing activities of the cerithids and other salinity-tolerant gastropods (Figure 3.4d). Sediments in the microbial flat are dominated by mm-laminated mudstones up to 50 cm thick composed of cyanobacterial remnants interlayered with aragonite muds. Periodic exposure means many mats are crosscut by desiccation cracks and are termed polygonal mat. Measured TOC contents of the mats vary

between 0.5 to 2.7%, with hydrogen indices between 510 and 675 in a range of type I-II protokerogens, with a $\delta^{13}\text{C}_{\text{PDB}}$ range from -8.41 to -10.78‰ (see inset in Figure 3.7 and Kenig et al., 1990)

Most of the literature on the sabkha gives the impression that laminated cyanobacterial mat is the only type of mat accumulating in the upper intertidal zone. Yet, in almost every area of mat I have visited along the mainland shores of the various khors of the Arabian Gulf, the laminated mat tends to occur beneath the floors of shallow channels and pools (waters a few centimetres deep), separated by interchannel areas of rugose or pustular mat. The sedimentary signature of the pustular mat is a poorly layered organic-rich mush, often with patches of lenticular gypsumarenite. Thus, the intertidal zone in an ancient equivalent need not

be laminated to be microbial in origin.

Many intertidal mats are crosscut by desiccation cracks that contain euhedral or lenticular (diagenetic?) gypsum crystals up to 2 mm long (Figures 3.4e, f, 3.6b). Gypsum is especially common in areas of pustular mat and along the landward side of the cyanobacterial belt, where it passes into the gypsum mush zone. Aragonite, magnesite, and dolomite locally cement surface sediments of the cyanobacterial flat (Butler et al., 1982). When microbially-bound intertidal muds are buried beneath prograding supratidal sediments, they can be extensively dolomitized (McKenzie, 1981). Such dolomites were first documented by Wells (1962). Arabian Gulf sabkhas and are one of two or three areas on the world's surface where Holocene dolomites are forming over aerially extensive regions, even if the extents are somewhat thin and patchy (Warren, 2000a).

Supratidal Facies

That part of the sabkha landward of the microbial mats and active beach ridges is further subdivided into three subfacies: lower, middle and upper supratidal (Figures 3.3, 3.8).

Lower Supratidal Lower supratidal sediment accumulates in a belt just above the high water mark (hwm) in a zone up to 2.5 km wide and flooded perhaps once or twice a month during high spring tides. It is characterized by a mushy gypsum bed, up to 30 cm thick, which passes seaward into cyanobacterial mat. Its lower part is an aragonite mud, crisscrossed by cyanobacterial filaments and isolated gypsum prisms (Figure 3.3b). The upper part is a thixotropic mush of small, mostly sand-sized lenticular gypsum, with an occasional 1-1.5 cm long crystal. Much of the mush is thought to grow as displacive crystals within the capillary zone, from pore waters not saline or hot enough to precipitate anhydrite. The surface of the mush can alter to white bassanite ($\text{CaSO}_4 \cdot 1/2\text{H}_2\text{O}$), or to anhydrite during even longer hot, dry periods.

Middle Supratidal The middle supratidal is a belt of sediment up to 1.6 km wide covered by lagoonal water at less than monthly intervals. It is characterized by growth of nodular anhydrite or gypsum within the sediment matrix. In the subsurface, well away from the lagoon, there is a lateral transition from gypsum to anhydrite (Figure 3.8). Subsurface and surface anhydrite nodules can increase in size and number

in a landward direction until in some areas they eventually form interlocking polygons. Along the Al Du'ybyaya sabkha, pockets of gypsum crystals are mixed with anhydrite nodules and layers, especially on the landward side of this zone, where they are dispersed in a matrix of reworked eolian quartz sand and silt. The middle sabkha surface is sometimes covered by an ephemeral halite crust and thin patches of loose blowing siliciclastic and carbonate sands.

At the same time anhydrite occurs above the water table, displacive and pore-filling gypsum is found in sediments immediately beneath the sabkha water table (Figure 3.6c). Crystal growth breaks up and destroys laminar textures in some buried biolaminites (Figure 3.4e, f). The seaward part of the middle supratidal is also the zone where dolomite is most common. It grows best as a pore cement in aragonite muds and can replace portions of the lower supratidal and intertidal mud facies (McKenzie et al., 1980; Butler et al., 1982).

Upper Supratidal In the vicinity of Abu Dhabi city the upper supratidal zone is up to 4.8 km wide and is rarely flooded by seawater (less than once every 4 to 5 years). In this, the most landward zone of the sabkha, the gypsum mush can be completely replaced by coalesced nodules of "chicken-wire" anhydrite to form near pure intervals that are up to 30 cm thick and lie mostly above the water table, not immediately below the landsurface (Figure 3.4g, 3.6c). Ongoing growth of irregular

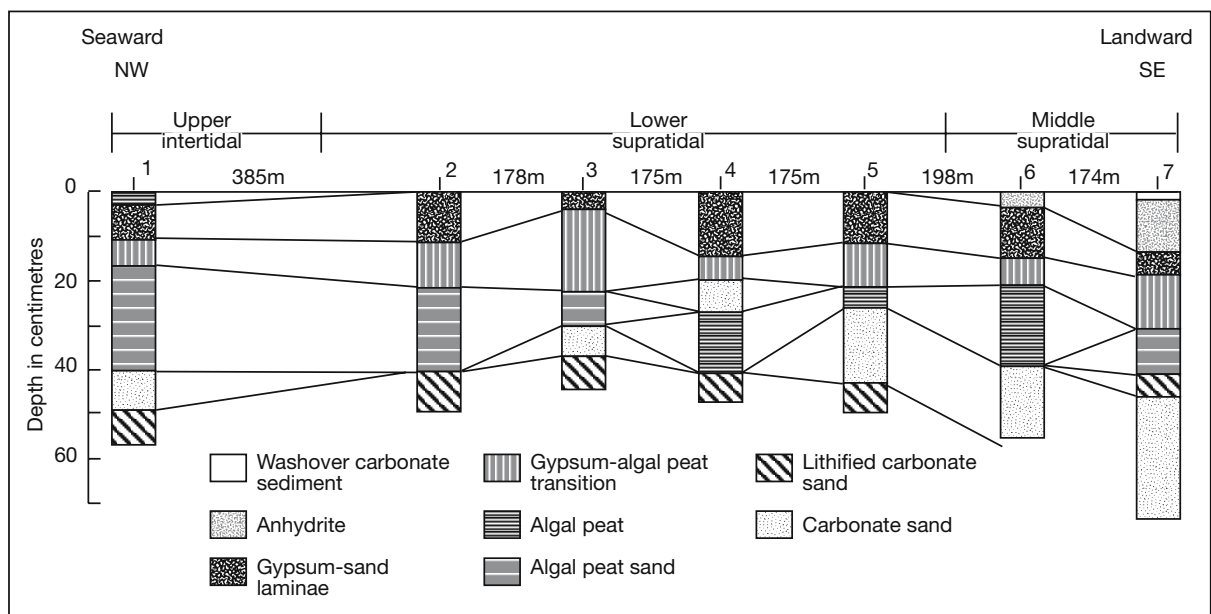


Figure 3.8. Lithofacies distribution in subsurface across the upper intertidal to middle supratidal along the southern shore of the SW Khor al B'zam south of Al Qanatar Island, western Abu Dhabi (after Alsharhan and Kendall, 2003).

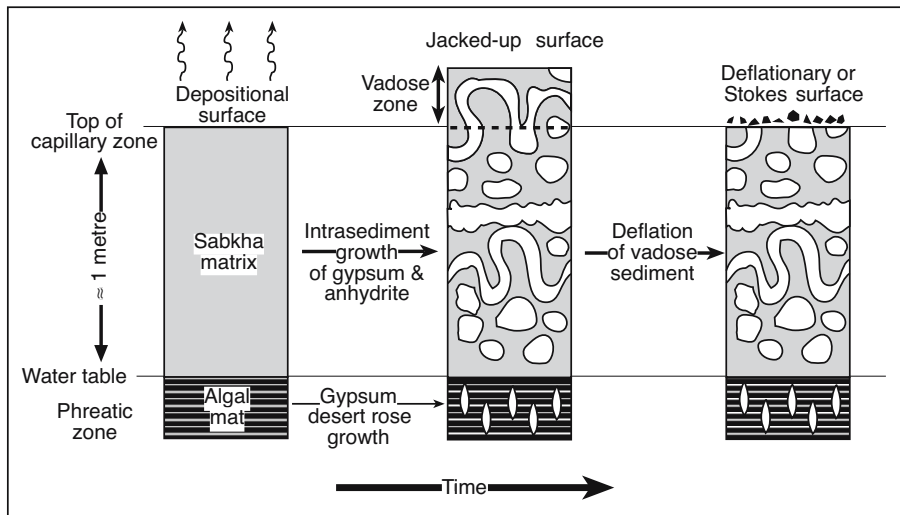


Figure 3.9. Capillary evaporation in the sabkha precipitates nodules and crystals of gypsum and anhydrite in the capillary zone. This increasing volume lifts the upper part of the sediment column out of the zone of capillary water into the vadose zone where it deflates to leave behind the characteristic erosional surface that caps modern and ancient sabkhas. It is a type of Stokes surface (after Warren, 1991).

anhydrite layers creates thrust folds, ptygmatic and enterolithic folds, and diapir-like protuberances. Beneath this zone much of the original cyanobacterial lamination is partially or completely obliterated by the growth of clusters of large prismatic to lenticular gypsum crystals (6 to 25 cm in diameter, locally known as desert roses). Anhydrite and gypsum also fills the interior of hollow aragonitic shells, especially the former living chambers of cerithid gastropods. Sediment accumulating in the upper supratidal zone contains little or no new dolomite. Along its most landward extent, the upper supratidal anhydrite layer can contain gypsum after anhydrite, with some nodules constructed of mixtures of both gypsum and anhydrite.

Widespread displacive calcium sulphate growth in the capillary zone sediments raises the sabkha surface out of the capillary zone to form a widespread erosional surface. As the rising sediments enter the vadose zone they dry and are blown away to leave behind the characteristic erosion surface of a sabkha sequence, covered in places by a deflation veneer (Figure 3.9). This erosion surface, especially where it truncates enterolithic or ridge anhydrite is one of the most useful indicators of the sabkha hydrology. Like other Stokes surfaces it defines the top of the capillary fringe (Figure 3.4g). Its presence in an ancient sabkha clearly distinguishes this style of truncated nodular anhydrite layering as penecontemporaneous and cannot be the result of burial conversion of gypsum to nodular anhydrite.

In drought times much of the middle and upper sabkha is covered by a pock-marked crust of halite, crosscut by pressure ridges and petees. This crust contains a range of efflorescent bittern and nitrate salts, but is dissolved and the soluble products flushed seaward with the next intense rainstorm or sheet flood. It is an ephemeral crust with a decoupled hydrology much like salt crusts in Australian salt lakes, as described in the previous chapter. Cm-sized displacive halite crystals can grow below these ephemeral salt crusts in the uppermost few centimetres of the upper supratidal sediments,

attesting to the infrequency of surface water in this region. The coming and going of the halite crust at the depositional surface of aggrading sections of the Abu Dhabi sabkha strongly influences textures in the remaining “supratidal” sediments (Figure 1.28; Goodall et al., 2000).

Sabkha hydrology and hydrogeochemistry

Hydrologically, much historic argument in the Abu Dhabi sabkha has dealt with the ultimate origin of the pore waters precipitating supratidal sulphate, i.e. marine flooding versus continental storm runoff (Figure 3.10a). Hydrogeochemical work in the 1960s and 1970s argued for a largely marine origin of the sabkha brines, which were supplied and replenished by occasional Shamal-driven tidal/storm seawater floods (Kinsman, 1969; Butler et al., 1973). The seawater flooding model was the first to provide a mechanism for cycling ions through capillary sediments and so account for the observed dolomite and calcium sulphate (Figure 3.10a). An alternate “evaporative-pumping” model was proposed by Hsu and his coworkers (Hsu and Siegenthaler, 1969; Hsu and Schneider, 1973) and included in the layered seawater flood/upwelling models of McKenzie et al. (1980), which suggested a compartmentalised hydrology made up of aquifers and aquitards and that capillary evaporation from the sabkha induced lateral flow of both seawater and continental groundwater (Figure 3.10a). All these early models suggested that seawater, either by flood

recharge or seepage reflux, was the dominant supplier of ions to the salts precipitating in the coastal plain. Much of the base hydrochemical data for a marine source was ambiguous. And some measurements such as strontium isotopes suggested the possibility of at least a partial continental source to the ions in the sabkha groundwaters (Figure 3.10b; Müller et al., 1990). Warren and Kendall (1985) and Warren (1991) noted that much of the matrix hosting the coastal sabkha salts of the Emirates was not marine but was a continental eolian sediment. Warren (op. cit.) also noted that as the sabkha prograded pore waters were replaced by continental fluids and that in ancient counterparts marine hydrologies probably only dominated the most lagoonward portions of the coastal sabkha flat.

Much of this earlier work was based on extrapolation of hydrological processes based on short term observations of the effects of Shamal and storms covering the sabkha with sheets of water and a limited number of trenches and transects. The assumption was that the solutes accumulating in the sabkha were derived and replenished in these occasional floods. Recent detailed groundwater study of the sabkha has concluded much of this earlier hydrological discussion assuming a marine solute source to the sabkha is largely erroneous or irrelevant

(Sanford and Wood, 2001; Wood and Sanford, 2002; Wood et al., 2002; Wood, 2005).

This more recent work uses longterm (1-2 year) monitoring of changing water levels and chemistries in a continually logged database across the sabkha. It is made up of data from 490 wells drilled to 1-2m below the sabkha water table, including a number of piezometer nests (listed as RP wells in Table 3.2) and six deep cased wells to monitor deeper hydrological circulation (listed as GWP wells in Table 3.2). The deep wells were drilled to depths of more than 100m into the Tertiary aquifers that underlie the sabkha (Figure 3.11a, b). These real time measurements, and the resultant realistic hydrologically and geochemically balanced models, show that some 95% of the solutes precipitated in the capillary zone of a sabkha are derived from ascending deeply-circulating continental brines; only minor amounts of the solutes are derived from rainfall or from lateral groundwater flow entering from nearby areas, including the ocean. Solute load in the capillary salts are largely decoupled from the rainwater cycling in the sabkha as are the salt crusts, which dissolve and reprecipitate with each flood-desiccation cycle (Chapter 2). Flood recharge of marine water does not supply ions to the capillary salts of the sabkha, upwelling or ascending continental groundwaters do (Wood and Sanford, 2002).

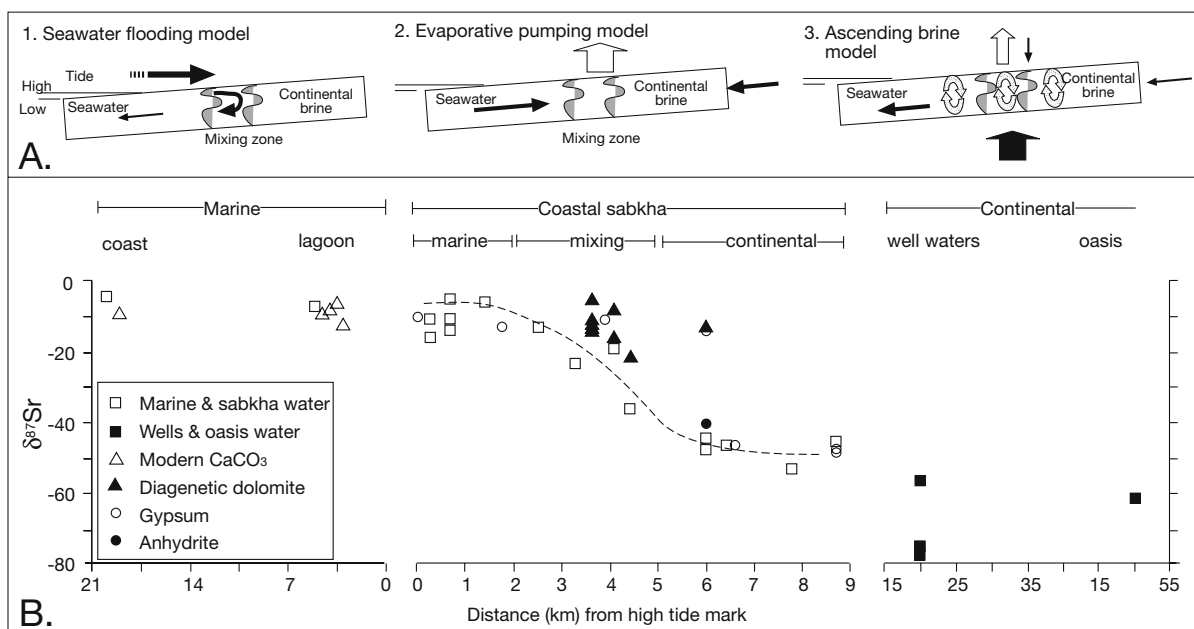


Figure 3.10. Hydrology of the Abu Dhabi Sabkha. A) Schematic of various models for sources of solutes in the (1) seawater-flooding model, (2) evaporative-pumping model, and (3) ascending-brine model. Open arrows indicate vapour loss, solid arrows represent solutes, and width of arrows indicates relative solute mass (after Wood et al., 2002). B) Analysed δ⁸⁷Sr values for water, carbonate and sulphate samples versus distance from the high tide mark. On the basis of these values the sabkha hydrology is divided into marine, mixing and continental zones with the dashed line representing the generalised trend (after Müller et al., 1990).

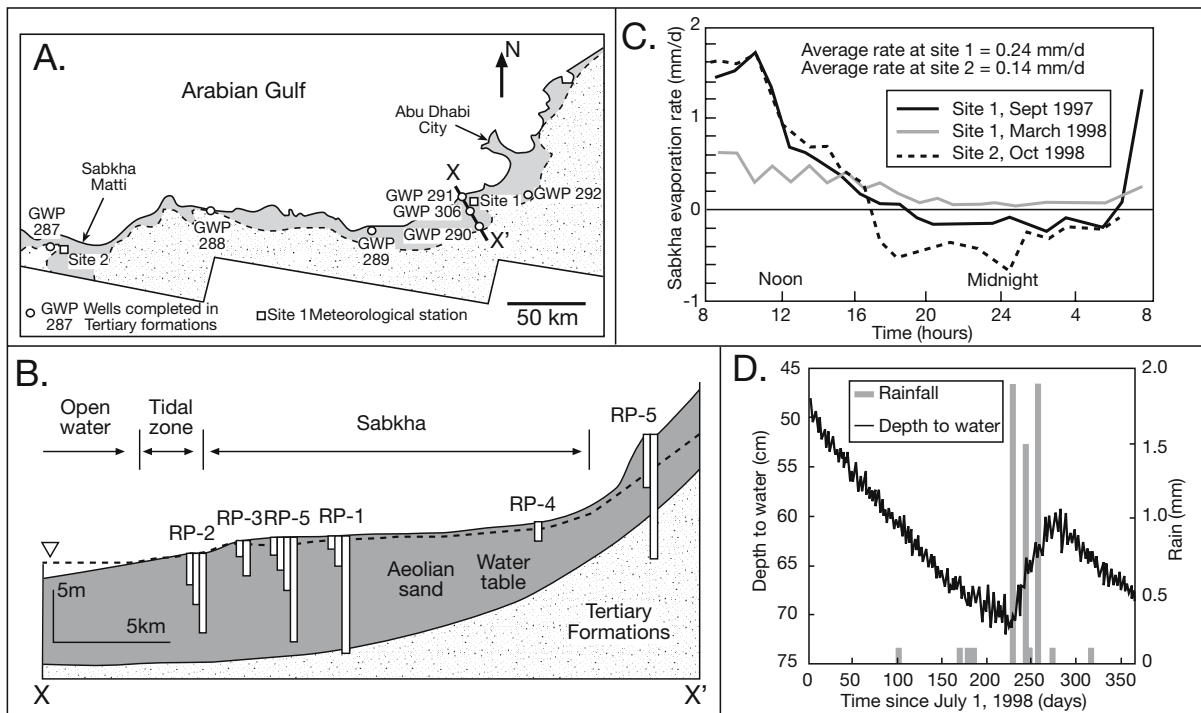


Figure 3.11. Hydrology of the Abu Dhabi sabkha (from Sanford and Wood, 2001; Wood and Sanford, 2002; Wood et al., 2002; Wood et al., 2005). A) Localities of selected monitoring wells, transects and sites. B) Measured evaporation rate at sabkha surface using a humidity chamber. C) Geological section showing thickness and piezometer nests along transect X-X'. D) Groundwater level and rainfall over a year (beginning July 1998) at site 2 in Sabkha Matti.

Potential (pan-measured) evaporation rates of fresh surface water on the sabkha are $\approx 3,500$ mm/year. But free surface water rates are not the same as actual rates of evaporation of pore waters held in the sabkha capillary zone by pore surface tension (Figure 2.3). Measured evaporation rates, using a humidity chamber, were around 0.24 mm/day at site 1 and 0.14 mm/day at site 2, with rates of evaporation changing with time of day (Figure 3.11c, d). These values are 3% of the pan evaporation rates at both measurement sites and correspond roughly to the mean annual rainfall throughput at both sites (90 mm/year for Abu Dhabi City and 50 mm/year at Sabkha Matti). The estimated rainfall recharge to the sabkha occurs at a rate of $640 \text{ m}^3/\text{year}$ in the representative volume illustrated in Figure 3.12. A mean value of 69 mm/year (from humidity chamber values) for evaporation gives a value of $690 \text{ m}^3/\text{year}$ for the volume of water lost in the sabkha, as shown in Figure 3.12. This volume of evaporative loss is about 15 times that of upward leakage from the underlying Tertiary aquifer ($45 \text{ m}^3/\text{year}$), and there is a meteoric-evaporation deficit of $\approx 50 \text{ m}^3/\text{year}$. Put simply, the sabkha is taking up Tertiary groundwaters like a sponge.

The humidity chamber measurements also showed that water flux during the night can be reversed at times when the humidity in the air above the sabkha exceeds the activity of

water on the surface of the salt crusts, causing night dew and some redissolution of the crusts. Periods of reversal are the times when the sabkha evaporation values are less than zero in Figure 3.11c.

Ongoing capillary evaporation means water level in the sabkha is typically around 1 metre below the sabkha surface (Table 3.2). Pore waters above this level are held in the pore throats by capillary pressure. Measurement of squeezed pore waters shows most salinities in the unsaturated zone are in the gypsum/anhydrite saturation range, as are waters at and just below the water table (130–290 mg/l), with brine densities ranging from 1.070 to 1.187. Measured conductivity (permeability) of the sabkha sediment is between 0.3 and 2.0 m/day (≈ 3 –10 md), and is relatively uniform across the sabkha. Using a hydraulic conductivity of 1 m/d, and a density-corrected piezometric gradient of 0.0002, results in a lateral flux of between 7 and 8 cm/yr (Wood et al., 2002). Dividing the flux by porosity from an average of the measured porosities (0.38) gives a seepage velocity of 18–21 cm/yr. This range in itself negates any notion of lateral marine seepage from the lagoon ever being capable of supplying the volumes of solute needed to precipitate the Holocene evaporites of the sabkha coast. These transmissivity calculations show that solute-carrying water simply cannot seep into the sabkha from its sides in sufficient volume to explain the

Well Name	Depth (m)	Unit well screened	Depth to water (m)	Conductivity (m/d)	Dissolved solids (g/l)	Density (g/cc)
GWP-287A	121	Tertiary	-20.6	-	118	1.080
GWP-288A	89	Tertiary	-9.5	-	37	1.026
GWP-289	120	Tertiary	-4.6	--	22	1.025
GWP-290	88	Tertiary	-7.7	-	50	1.037
GWP-291A	142	Tertiary	-22	-	96	1.069
GWP-292	120	Tertiary	-13.0	-	146	1.097
GWP-306A	137	Tertiary	-8.3	-	107	1.082
RP-1-2.5	0.8	-	-	-	275	1.175
RP-1-10	3.0	0.95	0.6	0.6	286	1.187
RP-1-36	11.0	0.96	0.6	0.6	283	1.184
RP-2-4.5	1.4	0.17	-	-	104	1.071
RP-2-12	3.7	0.28	-	-	194	1.132
RP-2-21	6.4	0.19	0.3	0.3	214	1.152
RP-3-3	0.9	0.59	-	-	238	1.197
RP-3-10	3.0	0.59	-	-	232	1.174
RP-4-3	0.9	0.79	-	-	237	1.199
RP-5-16	4.9	1.56	1.0	1.0	131	1.070
RP-5-35	10.7	0.71	-	-	140	1.072
RP-6-2.5	0.8	-	-	-	238	1.178
RP-6-10	3.0	-	1.3	1.3	241	1.180
RP-6-16	4.9	-	2.0	2.0	240	1.180
RP-6-35	10.7	-	0.4	0.4	242	1.183

Table 3.2. Well Information from Abu Dhabi sabkha (after Woods and Sanford, 2001). Minus signs in "depth to water" column indicate water level above landsurface.

volumes of capillary salts now in the sabkha. Solute-carrying waters must be coming from below.

Between 47,600 and 55,500 years are required for a molecule of a conservative (i.e., nonreactive) solute to traverse the 10 km width of the sabkha in the considered rectilinear volume (Figure 3.12). If it is assumed that the average residence time is one-half of the total time required for a conservative solute to traverse the full length (10 km) of the rectilinear volume by horizontal flow, the average steady-state residence time of a conservative solute in this sediment volume is $\approx 26,000$ yr. Because the calculated residence time is greater than the age of the sabkha-aquifer system, it is clear that steady state for the solute flux has not been achieved. Capillary salts are still accumulating across the sabkha and it is this mechanism that is driving the jack-up and formation of Stokes surfaces.

In terms of the water cycle (not the solute cycle), direct rainfall onto the sabkha and subsequent groundwater recharge to the underlying aquifer accounts for 90% of the annual water input to the system; the remaining 10% comes from both lateral and ascending saline groundwater flow (Wood et al., 2002). Less than 1 m³/yr of pore water enters and exits by lateral groundwater flow into a representative rectilinear volume of sabkha aquifer measuring 1 m wide, 10 m deep, and 10 km long (Figure 3.12a). Some 45 m³/yr enters by upward vertical leakage, 640 m³/yr enters by recharge of rainfall, while 690 m³/yr is lost to evaporation. But, and this is what earlier work had not expected, the water and solutes in the sabkha are largely from different sources; they are decoupled as they are in the playas and salt lakes of Australia (Chapter 2). The bulk of the solute load precipitated in the Abu Dhabi coastal sabkha comes from the resurgence of deeply circulated groundwater returning to the surface in the coastal plain via Tertiary limestone aquifers. Solute in the capillary salts are not from seawater or from direct rainfall onto the sabkha. Approximately 100 kg/yr

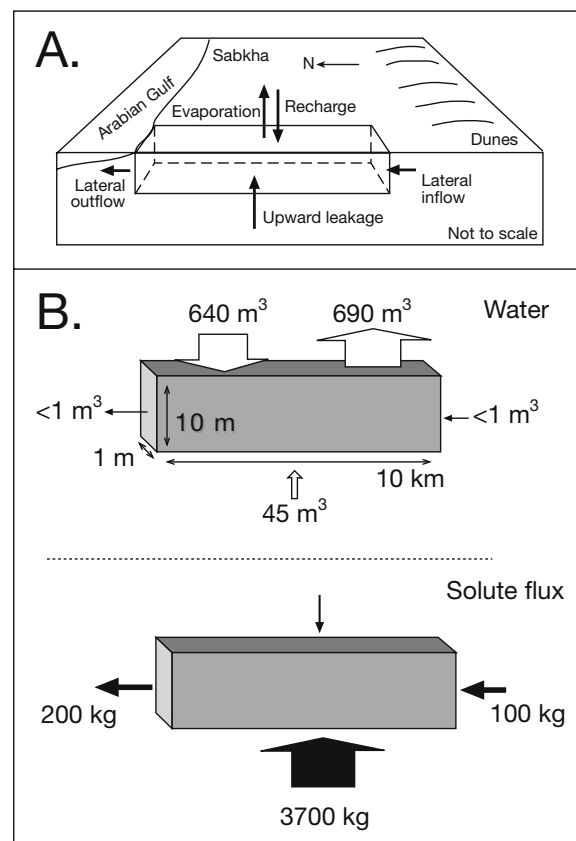


Figure 3.12. Hydrologic fluxes in the coastal sabkha aquifer of the Abu Dhabi sabkha. A) Schematic of hydrologic processes in the Abu Dhabi sabkha. B) Magnitudes of the various annual water fluxes in a 1 m x 10 m x 10 km control volume (after Wood et al., 2002).

Source	Locality	Depth (m)	Date	Ca	Mg	Na	K	Sr	SiO ₂	Alk-HCO ₃	Cl	SO ₄	Br	NO ₃	TDS	Density	pH	δ ³⁴ S	δ ² H (TU)	δ ¹⁸ O
Marine	Arabian Gulf	surface	Apr. 96	625	1750	13000	625	13	4.2	152	24000	3450	72	2	43560	1.0290	7.6	-	17.7	2.63
Marine	Arabian Gulf	surface	Apr. 96	625	1700	13200	625	13	4.3	140	24000	3400	72	1	43658	1.0291	7.6	-	17.7	2.63
Marine	Khor Bazam	surface	Apr. 96	700	2150	16100	750	18	5.0	170	28500	3800	89	1	52150	1.0356	7.9	-	24.6	3.54
RP-53	groundwater	10	May 96	2200	2000	34000	600	50	32	41	61500	5050	-	40	139697	1.0719	7.2	15.91	15.3	5.63
Tertiary	GWP-288A	89	Jan. 98	1450	950	10500	300	25	36	55	15700	4050	11	33	37076	1.0258	8.0	19.80	-0.2	2.37
Tertiary	GWP-289	119	Jan. 98	1150	675	5600	120	23	15	49	10300	4000	5	8	21922	1.0146	7.8	19.84	0.7	2.92
Tertiary	GWP-290A	80	Feb. 98	1500	850	15500	450	27	20	50	25000	5750	15	22	50251	1.0389	7.4	17.72	5.9	4.09
Tertiary	GWP-291A	142	Feb. 98	2200	1350	31500	950	40	18	39	55100	4650	20	36	95667	1.0608	7.8	18.42	5.0	4.64
Tertiary	GWP-292	119	Feb. 98	3600	2400	48000	1500	52	23	34	67300	3300	6	33	145239	1.0971	7.4	17.82	7.5	5.19
Tertiary	GWP-306A	129	Mar. 98	2750	1250	34500	1100	50	16	64	62500	4600	12	50	107056	1.0820	7.7	-	-	-
Sabkha	Av. (n=161)	3	97-98	9280	9929	84039	4156	211	53	49	172649	4417	78	2283	286415	1.1658	6.7	15.77	27.6	6.5
Rain	Av. (n=4)	-	95-97	3.73	0.20	0.82	0.52	-	-	47	1.48	2.85	-	-	39	-	7.7	-	-	-
Bu Hesa	Oilfield brine	16,400	Nov. 95	16400	4900	60500	2100	725	50	180	131500	500	310	650	217400	1.415	6.4	-	-2.8	3.19
Ramaittha	Oilfield brine	14,200	Apr. 96	14200	1600	57900	1350	1000	22	210	110000	350	620	1	186600	1.0289	6.2	-	-5.3	6.47
Jam Yaphour	Oilfield brine	9,700	Apr. 96	9700	1200	40000	600	200	29	142	62000	200	345	0	114000	1.0291	6.6	-	7.1	7.12

Table 3.3. Hydrogeochemistry of source of solutes in Abu Dhabi sabkha; hydrogen and oxygen isotopes in SMOW. Sulphur in PDB (after Wood and Sanford, 2002; Wood, 2005).

of solute enters from lateral flow; ≈ 15 kg/yr enters by rainfall; and ≈ 3700 kg/yr enters by ascending vertical leakage (Figure 3.12b). Some 200 kg/yr is discharged to the Gulf by lateral flow. Upwelling groundwater originally entered the system in feeder zones in the Oman Mountains some tens to hundreds of kilometres to the east and picked up much of its solute load by water-rock interaction on its way to the coast.

Vertical gradients and hydraulic conductivity suggest that approximately seven pore volumes of water from the underlying Tertiary formations have discharged to the original coastal sabkha-aquifer system in the 7,000 years since deposition of those Holocene formations (Wood et al., 2002). Wood et al. (op. cit.) go on to argue that, if there are no other sources or sinks of solutes, then the concentration of a conservative solute should be approximately seven times the concentration of the input Tertiary brine. Bromine, a conservative element in brines, should have a concentration ratio close to the seven fold predicted by the hydrologic analysis if fed by Tertiary aquifers, and this expectation is realized (Figure 3.13a).

Loss of halite from the pore water is clearly shown by the low concentration ratios of both sodium and chloride. Sulphate and calcium concentrations are less than seven because of the precipitation of calcite, anhydrite, and gypsum in the unsaturated zone in the sabkha. Magnesium should be generally conservative in this system because there is no significant mass of clay that could act as an ion exchanger or structural sink for the mineral. Magnesium, like bromine, is not being removed by mineral precipitation of chloride bitterns within the aquifer. The current chemical conditions in the majority of the sabkha aquifer do not favour dolomitization (low concentrations of bicarbonate, low pH, and magnesium/calcium ratio of $\approx 1:1$; Table 3.3; Wood et al., 2002). It means that dolomite observed by previous workers in the sabkha is related to the original volume of trapped seawater. Significant masses of magnesium are not lost or gained from sources other than the brine, and the concentration ratio is approximately seven (Figure 3.13a). Like bromine, it is behaving conservatively.

In solutions without significant concentrations of carbonate species, magnesium hydroxide complexes [MgOH^+ and $\text{Mg}(\text{OH})_2$] can control the pH (Wood

et al., 2002). Observed pH in sabkha brines, which declines with increasing magnesium concentrations is consistent with this hypothesis (Figure 3.13b). The relative concentrations of calcium and sulphate can also be used to define the source of the solutes. Hydrochemical divides, as conceptualised by Hardie and Eugster, 1970, mean that mineral precipitation in a relatively closed system, such as the sabkha, will cause the concentration of one element of a precipitating mineral to approach zero, while the other element or elements will increase in concentration (Figure 2.12). The initial input concentration of the elements determines which element will be limiting. In the case of seawater, there is a greater equivalent

of sulphate compared to calcium; thus, with precipitation of calcite, anhydrite, and gypsum, the thermodynamic activity of calcium will approach zero. In the case of the Tertiary brines and oilfield waters, the average equivalents of calcium are greater than the average equivalents of carbonate and sulphate (Table 3.3). Thus, precipitation of anhydrite and calcite from the concentration of Tertiary brines will result in sulphate and carbonate levels in the brines approaching zero, while calcium increases in concentration. In the Abu Dhabi sabkha system the observed calcium is increasing, and sulphate approaches zero in most cases (Figure 3.13c), consistent with a Tertiary brine source for the sabkha anhydrite and gypsum. The few analyses in which sulphate is greater than calcium are from the supratidal zone nearest the lagoon. The concentration of sulphate does not go to zero because of hydrated complexes formed with magnesium and calcium; however, the thermodynamic activity does approach zero (Wood et al., 2002).

This interpretation of ionic proportions assumes that no other process, such as bacteriogenic sulphate reduction, is removing sulphate from solution. The regional groundwater system is oxidizing, with dissolved oxygen values between 4 and 5

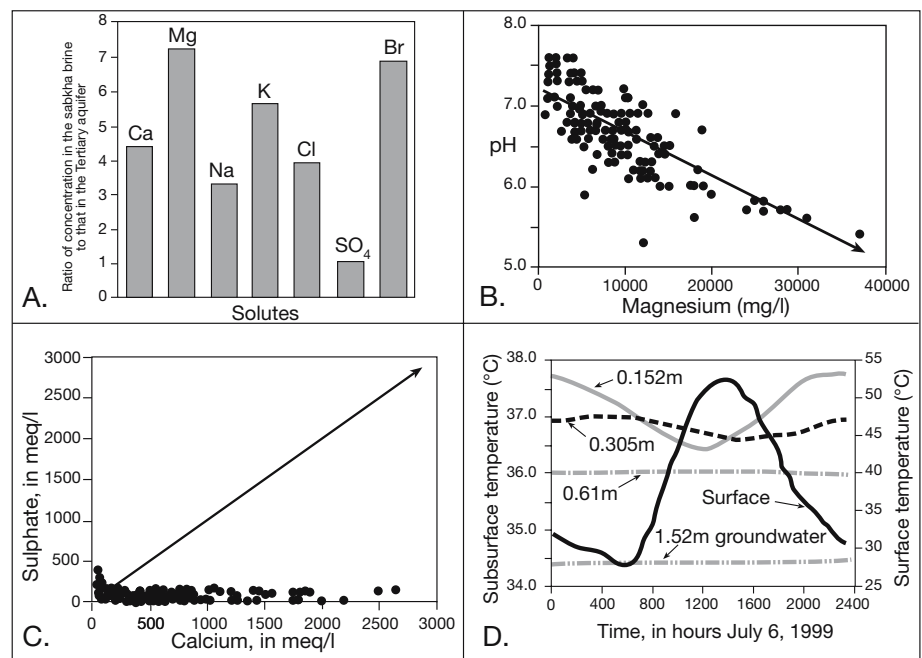


Figure 3.13. Hydrogeochemistry of pore waters in the Abu Dhabi sabkha (after Wood et al., 2002). A) Concentration factor (ratio of existing concentration in the sabkha-aquifer to input concentration of Tertiary brines) in the sabkha aquifer. B) Decline in pH with increasing magnesium in sabkha aquifer. C) Sulphate as a function of calcium in sabkha aquifer. D) One day temperature record of the surface, at various depths in the capillary zone, and of groundwater at site 1 in the coastal sabkha of the Emirates of Abu Dhabi.

mg/l, except at the distal edge of the sabkha. Therefore, it is not likely that bacterial sulphate reduction is removing a substantial mass of sulphate to significantly alter the Ca/SO_4 ratio as this bacterial process requires anoxic pore waters.

Periodic intense recharge by rainwater in the coastal plain dissolves halite and other soluble minerals on the sabkha surface, causing the surface and near surface waters to become more dense and sink (reflux) to the bottom of the aquifer where it vertically mixes with less dense ascending basal brines (Wood et al., 2002). With the next drying cycle solutes are once again returned to the surface by capillary forces (a cycle that is largely decoupled from external solute supply). Thus, the system becomes vertically mixed, but there is essentially no horizontal mixing of seawater with groundwater. In the same way bittern salts are flushed from the uppermost parts of the unsaturated sediment column.

Any observed seawater solutes in the undersaturated zone come from interstitial seawater trapped by the rapid progradation of the sediments into the Arabian Gulf or from marine aerosols, they are not refluxed or laterally mixed marine pore brines as was inferred in the previous hydrological models. For example,

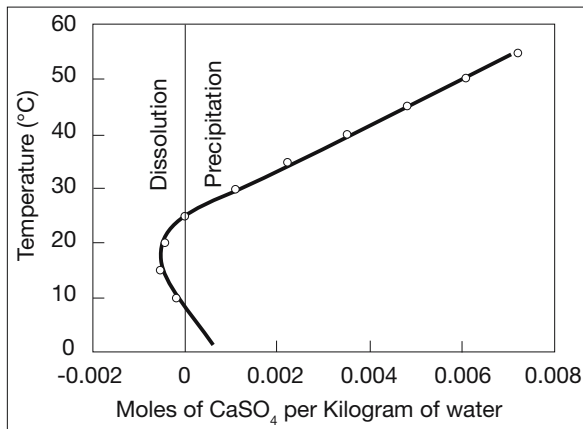


Figure 3.14. Moles of CaSO_4 precipitated per kilogram of water as a function of temperatures for a representative solute sample from the sabkha of the Emirates of Abu Dhabi (after Wood et al., 2005).

Müller et al. (1990) observed a seaward gradient in strontium isotope values perpendicular to the coast, which they attributed to lateral mixing of continental brines and seawater within the sabkha (Figure 3.10b). Wood et al. (2002) reinterpret the significance of this distribution, noting that the inferred lateral mixing is as readily explained as the function of the number of pore volumes of resurging continental brine contributed to a specific area on the sabkha. That is, the distance from the shoreline and the number of pore volumes of Tertiary brine recharged to the sabkha-aquifer system are directly proportional and it is this that controls the Sr isotope values in the Abu Dhabi sabkha, not lateral recharge of seawater. In other words it is not necessary to invoke lateral mixing or transport to obtain the observed strontium isotope distribution.

Wood et al. (op. cit.) go on to note that the area of dolomitization (as identified by Patterson and Kinsman, 1982) is the region closest to the Abu Dhabi shore. This is the zone that retains the largest amount of seawater solutes because it is the area most recently prograded. The mass of dolomite formed on the sabkha is limited to that derived from the magnesium and carbonate concentrations in the initial pore volume of seawater trapped by the prograding sediments. The actual evaporative geochemical mechanism for dolomite formation, as proposed by Patterson and Kinsman (1982) appears to be correct; it is just that there is no ongoing seawater reflux occurring in this dolomitizing system. Arguing that all that is needed is more time to explain extensive dolomite cycles by prograding a set of sabkhas across ancient platforms is not hydrologically viable, syndepositional ancient platform dolomites require a different set of hydrological drives than icehouse sealevel (Chapter 5).

The hydrological mechanism driving the accumulation of calcium sulphate salts in the sabkha is the rise of deeper circulating groundwater to replace waters lost by evaporation. The process moving capillary waters and their solute load through the unsaturated zone of the sabkha is solar driven and so the calcium sulphate in the sabkha is a true evaporite mineral (Chapter 2). Within this evaporative framework, Wood et al. (2005) argues that brine warming drives calcium sulphate precipitation in the Abu Dhabi sabkha. That is, gypsum and anhydrite precipitate in the capillary zone because of their retrograde solubility. As well as belonging to the broader family of “true” evaporites, they are also “thermalites.” A thermalite is defined by Wood (op. cit.) as a mineral formed by changes in temperature, independent of other processes that alter the thermodynamic properties of the solution. He argues that the capillary zone is critical to the development of the authigenic thermalite salts in any sabkha.

Any capillary fringe is the result of two sets of forces: mutual attraction between water molecules (hydrogen bonding), and molecular attraction between water and the different minerals that form the aquifer (Figure 2.37). Thus, for any given mineral, the smaller the interstitial pore size, the greater the vertical rise of water (Table 2.10). The zone of capillary rise (also known as the “zone of tension saturation” or the “wetting front”) is the saturated zone above the water table in which the interstitial pore space is completely filled with water, but this water is under less than atmospheric pressure. There can be no evaporation within this zone of tension saturation (no pore water passing into its gas phase) because water completely fills the narrower pore spaces and the atmospheric pressure is negative. If it does not, capillary rise cannot occur. Above the zone of tension saturation in the unsaturated zone is a zone in which the water film and a gas phase coexist in the interstitial pore space. The relative humidity of this gas phase is, however, equal to the thermodynamic activity of water, and no evaporative concentration can occur in this interval as well.

The physics of the capillary zone means evaporation in the Abu Dhabi sabkha (or any other sabkha) can only occur at the surface, or in the pore spaces a few cm below, in the interval where the relative humidity of the gas phase is less than the thermodynamic activity of the water. Thus, any minerals precipitated lower in the capillary zone must be thermalites with precipitation driven by the retrograde solubility of calcium sulphate and not by an evaporation driven increase in the salinity of the pore fluids (Figure 3.14). The notion of thermalites explains the typical occurrence of the bulk of the CaSO_4 in the sabkha. Nodules and prisms are most common in the interval about the water

table and toward the base of the capillary fringe, not in the few centimetres immediately below the landsurface. This would be the position of maximum anhydrite growth if evaporation of capillary waters, not their heating was the dominant process driving CaSO_4 precipitation.

Wood (op. cit.) argues this conceptual model of thermalite precipitation applies to mineral deposition in the capillary zones of most coastal sabkhat. Water and solutes are transported upward by capillary forces from the shallow water table in response to water evaporating at the surface. As water passes into the gas phase and is removed from the uppermost few centimetres it leaves behind evaporatively precipitated salt residues, including bitterns in the uppermost part of the capillary fringe. It is a diverse suite, dominated by halite (NaCl), but encompasses other more saline salts such as carnallite ($\text{KMgCl}_3 \cdot 6\text{H}_2\text{O}$) and antarcticite [$\text{CaCl}_2 \cdot 6\text{H}_2\text{O}$] as well. Below this uppermost zone, minerals exhibiting retrograde solubility, such as anhydrite (CaSO_4), calcite (CaCO_3), dolomite ($\text{CaMg}(\text{CO}_3)_2$), and gypsum ($\text{CaSO}_4 \cdot 2\text{H}_2\text{O}$), are precipitated as thermalites. They are the result of increasing temperature experienced by solute-rich deeply circulated groundwaters as it moves through the capillary zone toward the surface during the summer months.

A representative summer day temperature profile (July 6, 1999) illustrates a positive gradient of approximately 25°C m^{-1} in the Abu Dhabi sabkha at site 1 (Figure 3.13d). A reverse thermal gradient (upward cooling) in the winter permits dissolution of some of the previously precipitated retrograde minerals. Because the negative thermal gradient is less in the winter than in the summer with nearly the same water flux, the water does not have the capacity to dissolve all of the mineral mass that was precipitated in the preceding summer. Thus, there is a net accumulation of these retrograde (thermalite) minerals in the capillary zone (Wood et al., 2005). Figure 3.14 illustrates the difference in mass of salts precipitated and dissolved as a function of temperature for anhydrite based on measurements made in the sabkha. It clearly shows the relatively small temperature window in the sabkha ($5\text{--}25^\circ\text{C}$) during which winter dissolution can occur.

Detailed hydrological studies of the coastal sabkhas of the Abu Dhabi region show they are no more than the outcropping expression of outflow zones of regional artesian aquifers. Clearly the ascending brine model of Wood et al. (2002), and his subsequent conclusions of sabkha salts accumulating beneath the halite crust as thermalites, contrast significantly with both the seawater-flooding and evaporative pumping models previously proposed and widely accepted as explaining the source of solutes to the coastal sabkha of the Emirate of Abu

Dhabi (Figure 3.10a). Wood's conclusions show solute cycling in the coastal sabkha setting is decoupled and similar to that in continental sabkhas and chotts in many inland deserts with seawater like ionic proportions, as in the Sahara or central Australia (Chapter 2). Outflow of deep seepage throughput in the Abu Dhabi coastal sabkha is focused by a phreatic seawater wedge associated with the modern shoreline. Sediment matrix in some parts of the sabkha may be marine, but the hydrology and the authigenic overprint (mostly CaSO_4) comes largely from ions supplied by a deeply circulating continental aquifer. This new understanding of the large scale sabkha hydrology has significant implications for the preservation potential of ancient marine-margin sabkhas.

Siliciclastic-hosted coastal sabkhas, western and northern Arabian Gulf

An excellent literature base dealing with the sedimentology of the seaward side of the Abu Dhabi sabkhat creates an impression that coastal sabkhas in the Arabian Gulf are characterised by capillary salts hosted in marine carbonate matrices. But this is not the case and many marine-margin capillary salts in the Arabian (Persian) Gulf are hosted in siliciclastics or even in desert loess blown into coastal depressions. Even in the type area, the Abu Dhabi sabkhat, at least 50% of the coastal plain sediments that host capillary evaporites do so in a matrix of mixed carbonate-siliciclastic or pure siliciclastic. Many ancient counterparts to strandzone sabkhas have siliciclastic matrices. Well-documented examples include the Permian sandflats of Europe and much of the Guadalupian lagoonal sediments of the Central Basin Platform in west Texas and New Mexico (e.g. Figure 10.40-10.42). The following section describes some modern coastal sabkhas of the Arabian Gulf with capillary salts growing in mixed siliciclastic/carbonate and pure siliciclastic matrices.

A predominance of siliciclastics in the sabkhas of Kuwait and Saudi Arabia in the northwest of the Gulf versus carbonate in sabkhas along the At Taf coastal strip in the southeast of the Gulf simply reflects sediment transport and coastal dynamics in the seaway (Figure 3.2a). The northwestern shore of the Arabian Gulf passes from the siliciclastics of the shallow Mesopotamian Shelf to the carbonate shoals of Bahrain, Qatar and the At Taf coastal strip. The northern Gulf is an arid, micro to mesotidal region with tides ranging from 1 to 4 metres (Gunatilaka and Mwango, 1988). Anticlockwise tidal currents of the northern Gulf and the prevailing northwesterly Shamal winds produce a shore-parallel largely southeasterly-directed wind-wave energy system, which supplies a combination of desert sand

and loess to this part of the Gulf coastline, with an increasing fluvial contribution toward the northernmost gulf.

Arabia, south of Damman, is characterised by a north-south elongated belt of eolian dune sand, which approaches the coast

From the coast to inland areas along the northwestern Gulf there are three broad depositional environments (Lomando, 1999). Along the coast is a near continuous belt of modern mixed carbonate-siliciclastic deposits with a wide range of depositional styles from interdunal to estuarine to barrier coast. To the immediate landward is a discontinuous belt of active and abandoned marine sabkhas, which pass into a broad desert system of continental sabkhas, desert flats, and dune fields. The inland desert system is the flattest area of Kuwait and northern coastal Saudi Arabia and is part of a zone of regional deflation, providing wind-blown sand to the Jafurah Sand Sea and ultimately accumulating in the northern areas of the Rub Al Khali in Saudi Arabia (Figure 3.57).

Coastal sabkhas of eastern Saudi Arabia

Sabkhas of eastern Saudi Arabia are divisible into coastal and inland sabkhat, both are surrounded and underlain by Pleistocene and Holocene dune sands (Figure 3.15a). Eolian sandflat sediments of the coastal region were documented by Fryberger et al. (1983,1984) in a study of the Jafurah Sand Sea margin and are discussed in detail toward the end of this chapter. The Eastern Province of Saudi

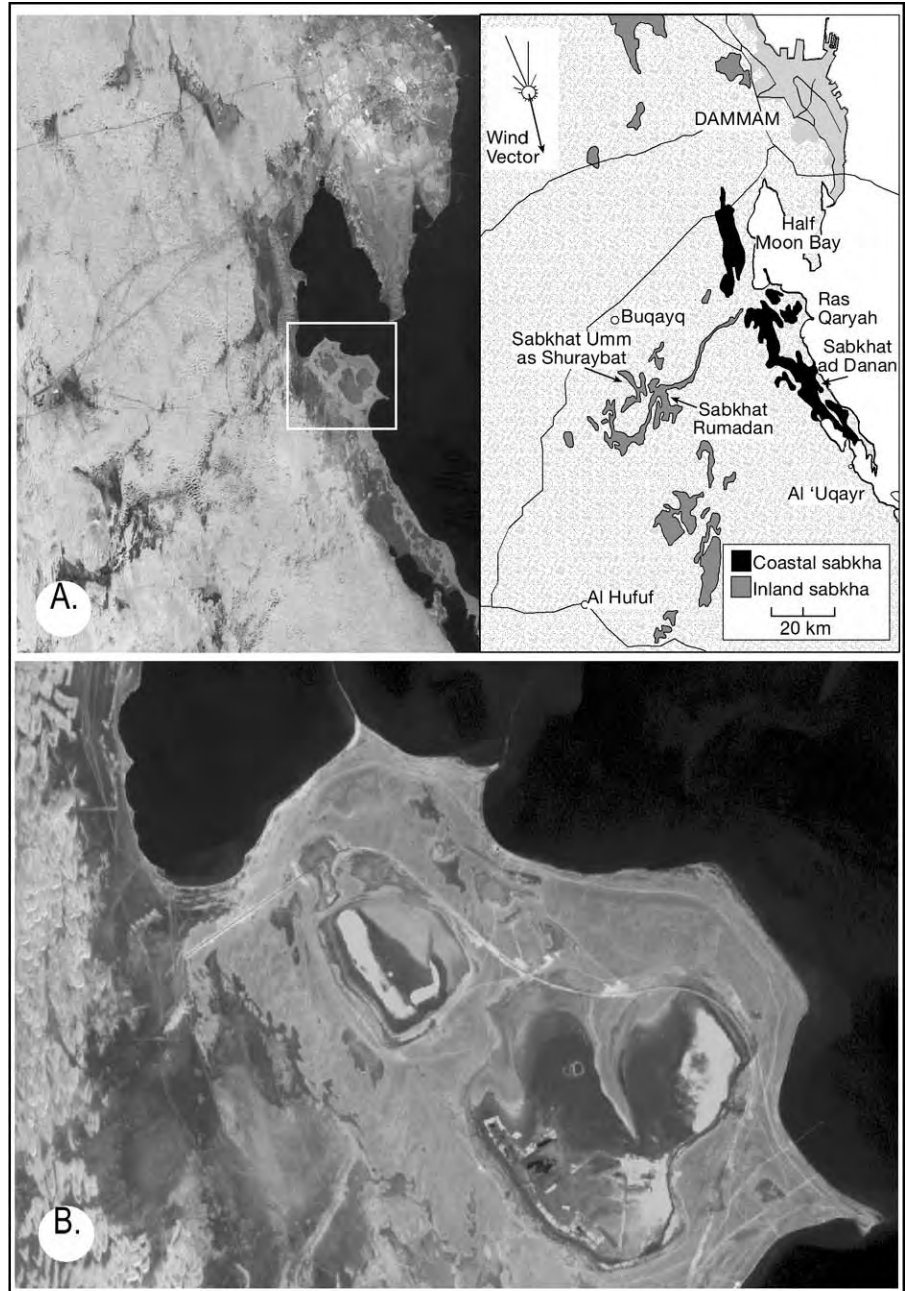


Figure 3.15. Sabkhas of Saudi Arabia southeast of Damman. A) Distribution of coastal and interdunal sabkhas in areas of shallow groundwater resurgence along the Damman coastline. The coastal region defines the modern marine edge of the Jafura sand sea where isolated subsealevel coastal depressions are today filling with capillary salts in a mostly siliciclastic matrix. In the last glacial this sand sea extended well out into the Arabian Gulf (Landsat image courtesy of NASA, wind vector after Fryberger et al., 1984). B) Semi-circular marine seepage sabkhat behind Ras Qaryah and adjacent to the eastern edge of Sabkhat ad Danan.

between Doha Dhalum (Half Moon Bay) and Al-'Uqayr (Figure 3.15a). To its immediate north are the Tertiary limestones and dolomites highlands that define the outcrop expression of the Dammam dome (cored by a salt diapir). This coastal zone is surrounded by siliciclastic sand sheets passing upwind into active barchan sand dunes that are still moving sand into and across the coastal sabkha to a prograding siliciclastic shoreline. Sand movement is principally towards the south-southeast and sand is driven seaward by the Shamal (Figure 3.15a). In areas where the water table approaches the landsurface, sabkha evaporites are growing in sand sheets in both sea-margin coastal sabkhas and in interdunal sabkhas located further inland (Figure 3.15a, b).

The dominant capillary salt is gypsum (Figure 3.16a-c) in both inland and coastal sabkhas in the Eastern Province on Saudi Arabia, with small local areas of halite and anhydrite in the most saline parts of both the inland and coastal sabkhas. Some of the large coastal sabkhas, such as Sabkhat ad Danan, have gypsum lunettes along the sabkha edge (Figure 3.16c). Gypsum is also a widespread pedogenic precipitate in much of the arid landscape of eastern Saudi Arabia. The level of carbonate matrix in the Saudi sabkha increases with proximity to the present coastline with a few wet dune seeps adjacent to the coast even supporting a healthy mollusc population. Coastal margins to the sabkhas show a range of cemented carbonate crusts with some modern lagoonal shorelines showing megapolygons in marine-cemented layers identical to those of the Abu Dhabi lagoonal margin (Figure 3.16d). The important difference in the sabkha between the two areas is the amount of eolian siliciclastics in the upper intertidal and lower supratidal sediments.

Brine seeps through the sand aquifers and replenishes areas depleted by drawdown from capillary evaporation within the lower parts of the sabkha depressions. Gypsum crystals grow in the pore spaces near the water table, poikilolithically enclosing sand grains, to form spectacular crystal clusters or desert roses (Figure 3.16b). Individual crystals can be up to a metre across, but most are measured in centimetres. The proportion of gypsum in the crystals is more than the porosity of the adjacent loose sand, showing that gypsum is not only growing in the pore spaces, it is also displacing the sand as it grows (Warren, 1991).

Gypsum typically grows in a matrix of dark-coloured quartz sand and silt in a capillary zone that can actively precipitate gypsum up to 50 cm above the water table. Some sabkhas, such as Sabkhat ad Danan are currently deflating so that parts of the surface of the sabkha are paved by thousands of isolated

prismatic gypsum blades standing up along fracture polygons and the edge of the adjacent sabkha is lined by a dissected terrain of gypsum lunettes (Figure 3.16c). Most of the crystals at the surface are weathered white and have split along cleavage planes. Immediately below the sabkha surface the gypsum crystals are still entire. The Stokes surface overprint indicates a fall in the regional water table, which has moved the crystals into the vadose zone and may in part reflect regional uplift driven by the nearby salt diapir-cored Dammam dome, which is currently rising at a rate of 5.5 metres per million years (Weijemars, 1999). More likely, it indicates the local vagaries of erosion associated with ongoing autocyclic gypsum crystal growth jacking overlying sediment up and out of the capillary zone, where it is subject to intense wind deflation. In the lowermost parts of the regional sabkha plain there are local depressions a few kilometres across where brines pond and the sediment surface periodically lies below the water table. There salt pans are forming and are filling with successive crusts of chevron halite, rather than the more typical displacive gypsum of the regional sabkha (Figures 3.15b, 3.16e). Around the high salinity edges of these halite pans are zones of nodular anhydrite rather than the ubiquitous sabkha gypsum (Figure 3.16f).

Sabkhas of coastal Kuwait

Modern sea-margin sabkhas in coastal Kuwait are not developed at the same broad scale as those of Abu Dhabi or the Dammam region, but are nonetheless interesting as they illustrate a transition from an alluvial fan-fluvial supplied sabkha in Kadmah Bay (aka Kuwait Bay) to a mixed eolian siliciclastic-carbonate matrix sabkha in the Al Khiran region to the south (Figure 3.2a). Inland Kuwaiti sabkhas are also widespread in depressions more than 10 km from the coast. Both inland and coastal sabkhas of Kuwait are largely hosted in sheets of reworked medium-grained quartz dune sand (Al-Hurban and Gharib, 2004). Compared to inland sabkhas, the detrital matrices in coastal sabkhas are slightly muddier, contain less gravel and show higher levels of gypsum due to their proximity to marine aerosols and marine seeps (Figure 3.17).

Sabkhas of Kadmah Bay

To the north of Al Khiran sabkha, the Holocene sediments of Kadmah Bay (Kuwait Bay) represent the western-most limit of the siliciclastic Shatt Al-Arab delta and the southern limit of the alluvial fans of Jal Az-Zor escarpment (Saleh et al., 1999; Al-Sarawi, 1988). Most of the sediment matrix in the western part of the Kadmah Bay hypersaline system is deposited at the distal end of large alluvial fans, downdip of the Jal Az-

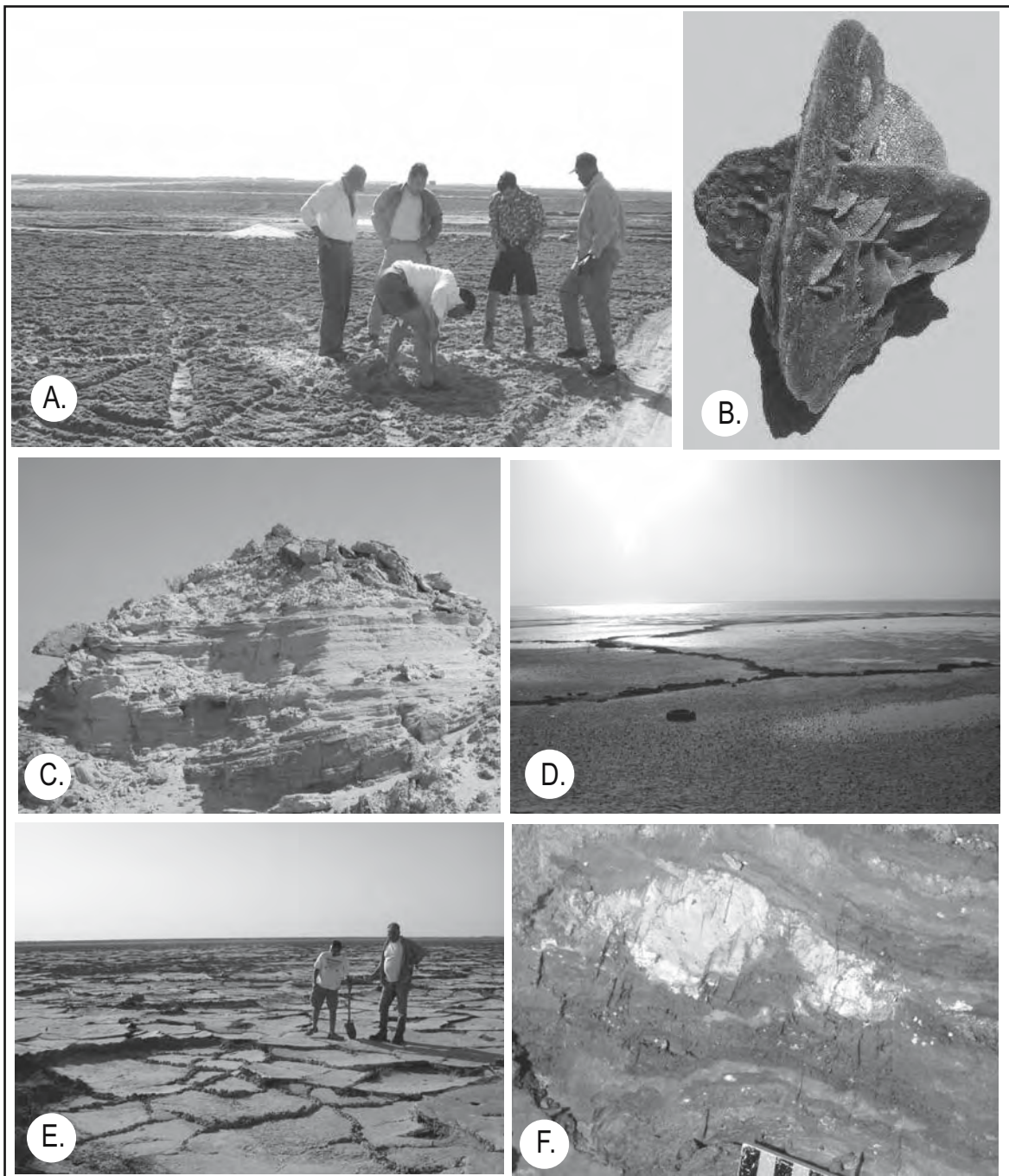


Figure 3.16. Coastal sabkhas of the Eastern Province, Saudi Arabia. A) Flat puffy algally-bound (petee) surface of the Sabkhat ad Danan. B) Typical displacement gypsum (desert rose) growing within a half a metre of the sabkha water table in Sabkhat ad Danan. Crystal is 10 cm across. C) Gypsum lunette showing characteristic eolian cross bedding (outcrop face \approx 1.5m high) D) Megapolygonal tepee ridges in marine cemented intertidal lagoon crusts in southern Half Moon Bay (area locally known as "wrong way spit"). E) Pressure ridges in the halite pan facies (lowest point) of the Ras Qaryah sabkha shown in 3.9b in March 2004. The water table at this time of year is no more than a tens of cm below the sabkha surface. F) Displacive nodular anhydrite growing in the capillary zone in fine detrital clay about the edge of this saline pan facies in the Ras Qaryah sabkha (scale division is in cm).

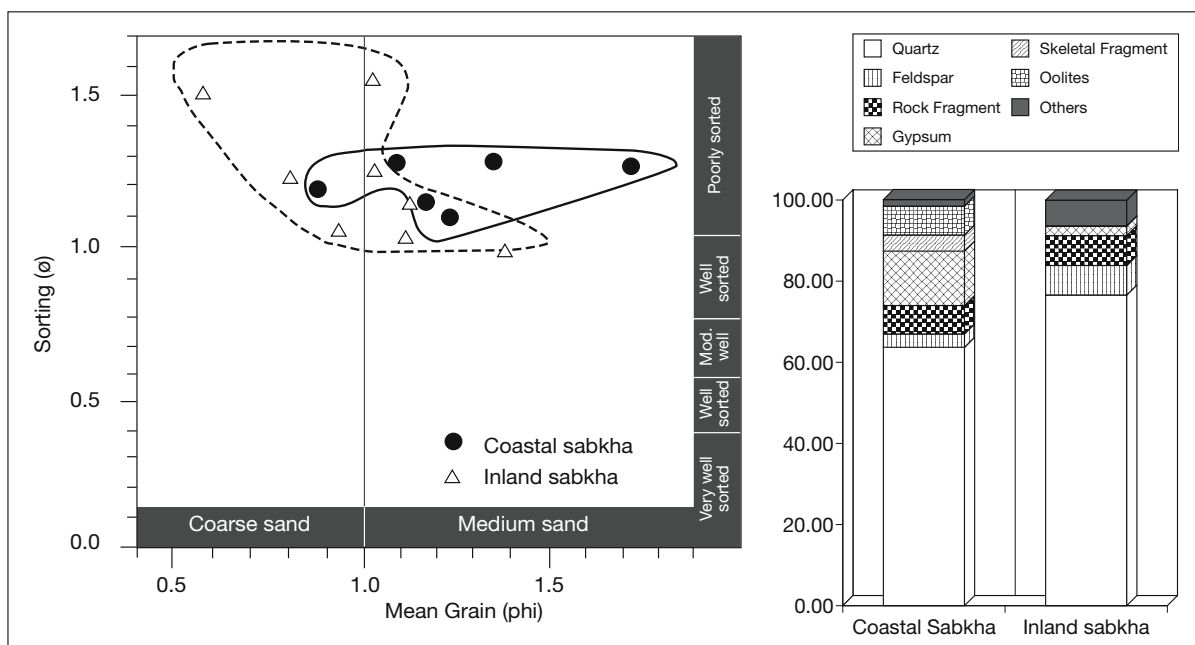


Figure 3.17. Grain-size and mineralogical comparison between sediments of inland and coastal sabkhas of Kuwait (replotted from Al-Hurban and Gharib, 2004).

Zor Escarpment (Figure 3.18 a, b). In contrast, sabkha matrix in the northeastern part of the bay is fed substantial volumes of finer-grained sediment by longshore drift of sediment sourced in distributaries of the Shatt el Arab delta sediments. This higher volume of sediment supply means sabkha at the northeastern end of the bay has prograded further into the bay waters (Figure 3.18a). Today, the bay is about 20 km wide, has a tidal amplitude of almost 2 m and is around two-thirds exposed during very low tide. Although very shallow, the lack of wave energy and the proximity of the muddy Shatt al Arab, means the central bay fill is very muddy and is near impossible to cross on foot at low tide.

Four sedimentary settings define the northwestern Kadmah Bay margin; namely alluvial fans, playas, sabkhas and beaches (Figure 3.18b; Al-Zamel and Al-Sarawi, 1998). Coastal sabkha deposits extend landward to where they interfinger with the distal ends of modern alluvial fans, much like the sabkhas of Ras Al Khaimah at the other end of the Arabian Gulf (Warren, 1991). Distal fan sediments are typically plane-laminated sands interlayered with playa lacustrine muds and are often encrusted by a gypcrete carapace. Mid fan sediments are dominated by crossbedded and parallel laminated sands, while proximal fan sediments are poorly sorted imbricated gravels and poorly stratified pebbly sandstones.

Evaporitic Kadmah Bay sabkha sediments can be divided into two subfacies: (1) dark brown silt mixed with very fine sand,

rich in prismatic gypsum, gypsum roses and gypsum nodules at the level of the water table, along with some halite and aragonite and very minor amounts of anhydrite; and (2) light brown silts mixed with local anhydrite nodules in fine sands in the upper parts of the sabkha plain. Gypsiferous sabkhas dominate.

An erosional or deflationary regime now characterizes the sabkha of the coastal plain of Kadmah Bay (Saleh et al., 1999). Maximum marine flooding of the supratidal area is dependent on the coincidence of high water spring and/or storm tides with southeasterly winds and is an uncommon event. This results in a very limited portion of the tidal zone (0.6-0.7 km wide) being subjected to flood recharge during the normal tidal cycles. Away from the immediate bay waters, much of the active Kadmah Bay sabkha is best described as an evaporitic ‘wind flat’ or sandflat rather than a diurnally flooded carbonate mudflat. The closest comparable modern setting documented in the sedimentological literature is probably the evaporitic mudflat of the Colorado River delta (Shelton et al., 1978). Once again, this is a continental system that just happens to be at the edge of a modern sea and its hydrology is largely continental.

The dominantly-southeast Shamal wind means coastal sabkhas in Kadmah Bay are distinct from carbonate-dominated coastal sabkhas further south in the Gulf. The Shamal blows continental sediment into the bay so that the sabkhas are the seaward edges of deflation flats with matrices characterized by abundant

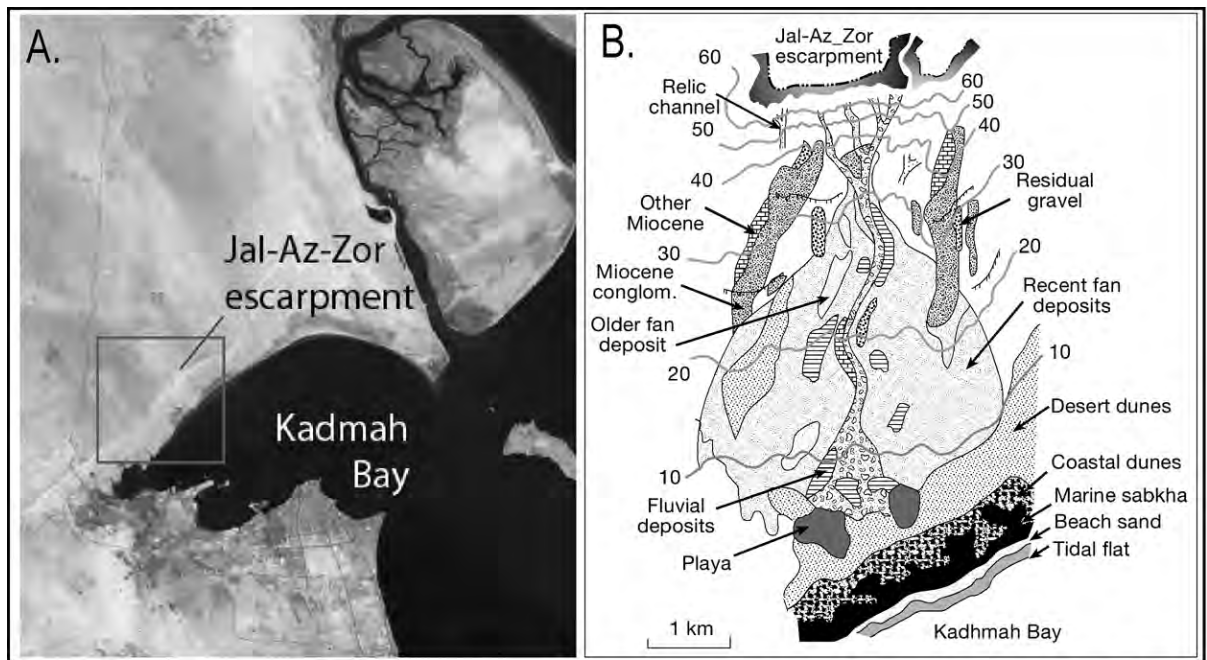


Figure 3.18. Kadmah or Kuwait Bay A) Shows the development of an extensive but narrow coastal sabkha with a siliciclastic matrix on the northern margin of the bay (Landsat image courtesy of NASA). B) Surface geology of the region where Al-Khuwaisat alluvial fan passes south into Kadmah Bay sabkhat, Kuwait (after Al-Sarawi, 1988).

siliciclastics, not carbonates. The dry windy setting means there is an absence of healthy laminated cyanobacterial mat along much of the intertidal sabkha strandline. It is simply too dry, so laminated cyanobacterial mat is mostly confined to small moister areas on the floor and the immediate vicinity of tidal channels. The mud-size fraction in the Kadmah sabkha ($\approx 5\%$ of sediment volume) is dominated by carbonate minerals, but this carbonate is detritus from the north, not diagenetic or marine supplied material from the bay (Saleh et al., 1999; Al-Bakri et al., 1984). Much of it is low-Mg calcite washed in from the surrounding plain where capillary calcretes (*gatch*) are commonplace. Similarly, almost all of the dolomite in the northern Arabian Gulf, including that on the floor of Kadmah Bay is detrital and derived either from longshore transport from the Shatt el Arab delta or is blown in by the Shamal as it scours the desert plains of Iraq (Al-Bakri et al., 1984). Numerous primary sheet flood and eolian structures are preserved beneath the prograding supratidal flat, with only minor disruption to these structures caused by local growth of intra-sedimentary gypsum. Gypsum and other capillary salts never dominate mineral proportions in the supratidal zone of Kadmah Bay (Figure 3.18).

The windblown and deltaic siliciclastic coastline of Kadmah Bay has been prograding into the bay for 3,000 years at a rate of 1.5 to 2 km per 1000 years. More landward, the preceding "Early Holocene" transgressive coastal sediments are made up of patchily distributed, autochthonous carbonates (aragonitic oolites, pellets and micrite), similar to the early Holocene beach ridge carbonates of the At Taf coastal strip. The Mid-Holocene transition to a siliciclastic matrix along the north coast of Kadmah Bay indicates the time when longshore currents flooded the northern bay with reworked muddy fluviodeltaics from the prograding Budyah channel (see Shatt al Arab sabkha).

Al-Khiran Sabkha

To the south, near the Kuwaiti border with Saudi Arabia, Late Pleistocene and Holocene sediments are exposed in and about the sea-margin sabkhas in the Al-Khiran area (Figures 3.2a, 3.19; Gunatilaka et al., 1987; Al-Sarawi et al., 1993). The Al-Khiran sabkha is a carbonate-hosted lagoonal system some 60 km² in area. It lies behind a chenier belt of four oolitic beach-dune ridges where large parts of the inter-ridge sabkha depressions are no longer subject to marine flooding. The oldest and most landward exposed beach ridge is older than the Flandrian transgression. The four younger, accreted ridges, mapped by Al-Sarawi et al. (1993), were dated at 6,800, 5,800, 3,000 and 2,000 years BP.

Sabkha plains in the inter-ridge depressions were formed by sedimentary offlap driven by the relative fall in sea level since the last Holocene transgressive maximum approximately 4.5–4.7 ka. Sabkha evaporites (gypsum and anhydrite) in the inter-ridge depressions are hosted by aragonite-rich pellet muds, which also entrain significant amounts of comminuted marine shell material. Thin layers of blowing sand now cover portions of the sabkha to varying thicknesses depending on depth to the top of the capillary fringe. Some of the anhydrite in the Al Khiran sabkha is unusual compared to the Abu Dhabi sabkha in that it first nucleates in zones of moisture stress around plant roots and so is an evaporitic form of dikaka or rhizoconcretion (Gunatilaka et al., 1980).

In an annual cycle, modern marine waters are confined to two tidal creeks cutting the Al-Khiran sabkha (Gunatilaka et al., 1987). Occasionally, perhaps a few times in a year, a narrow strip up to a 100 m wide adjacent to the creeks is by covered by tidal waters, brought there by exceptionally high spring tides. An absence of significant marine flooding over the rest of the sabkha means much of the current hydrology and pore chemistry is almost entirely controlled by influxes of conti-

ental groundwater. This topographic-continental hydrologic framework is also reflected in the formation of diagenetic continental dolomite in some depressions on the salt flat, as well as the isotopic make-up of the dolomite, which indicates a continental or nonmarine source.

Major ions show a steady evaporative concentration across the sabkha from inland to the coast, with a “high” chloride plateau in the central parts of the marine sabkha similar to the plateau that occurs in the Abu Dhabi sabkha (Robinson and Gunatilaka, 1991). Monitoring of groundwater over a three-year period indicated that: (a) when the water table depths are < 1.2 m, the sabkhas are in a state of depositional equilibrium; (b) water table fluctuations (due to drawdown or recharge) exceed 0.5 m/yr; and (c) calculations based on measured fall in water table levels, porosities of the sediments, and the volume of anhydrite formed in the sabkha all suggest that over the last 4,700 years, since progradation commenced, only 2–4 cm/yr (net) of groundwater is lost from the sabkha surfaces. This is a surprisingly low rate for this arid region and indicates significant replacement by resurging continental groundwaters. This groundwater replenishment maintains longterm stability

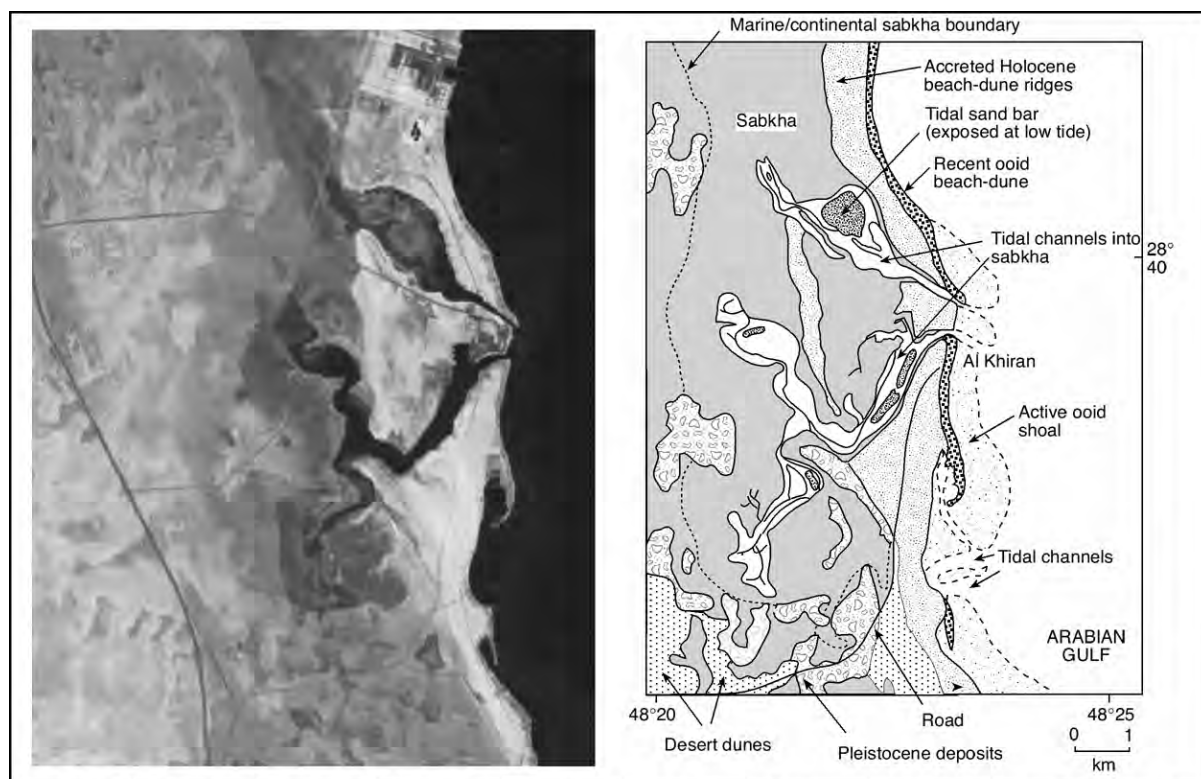


Figure 3.19. Surface geology of part of the Al-Khiran sabkha, Kuwait, showing the importance of accreted ooid beach ridges in forming the structural framework of the coastal sabkha estuary and the passage into dune sands in the sabkha hinterland (Landsat image courtesy of NASA, surface geology after Gunatilaka et al., 1987).

of the sabkha sequence. Without it, deflation would dominate and most of the older sediment would be planed off to the level of the intertidal/subtidal crust, much like what has occurred on the backside of Kadmeah Bay.

Supratidal anhydrite in the Al Khiran sabkha has three distinct morphologies (Gunatilaka, 1990): (a) hair-cream anhydrite which occurs exclusively in association with the halophytic saltbush *Halocnemum strobilaceum*; (b) nodular/laminated cottage cheese anhydrite, which is associated with a bacterial-cyanobacterial mat. This nodular anhydrite forms massive layers up to 4 cm thick with the anhydrite initially pseudomorphing gypsum crystals in the mats. In laminated anhydrites it can form aphanitic layers up to 7 cm thick, made up almost entirely of microcrystalline anhydrite; (c) anhydrite formed by the alteration of prismatic gypsum crystals now exposed in the lowermost parts of some now abandoned and desiccated drainage channels.

With “hair cream” anhydrite, climate and biological influences play a significant role in what is often an annual mineralogical change between gypsum and anhydrite, depending in part on rainfall intensity. On the death of the halophyte, hair-cream anhydrite reverts to microcrystalline alabastrine secondary gypsum and then to a gypcrete. The gypsum-anhydrite transformation is a reversible dissolution-precipitation process and

there appears to be an intimate relationship between the plant, its “soil water” requirements and the hydrodynamic behaviour of capillary groundwater brines in the vadose zone, which interact to control the mineralogy. Compared to “hair cream” anhydrite, type (b) anhydrite is more likely to be preserved as anhydrite, not gypsum, at least into the shallow subsurface above the watertable. Type (c) anhydrite is rare and possibly only forms with complete drying of the channel bottom, it is always susceptible to deflation or rehydration and so has low preservation potential compared to types (a) and (b).

All anhydrite in the Al-Khiran sabkha forms from a gypsum precursor at temperatures $>30^{\circ}\text{C}$ and brine chlorinities >4 mol Cl/kg. Al-Khiran is the northernmost occurrence of widespread patches of anhydrite in the coastal belt of the Arabian Gulf (gypsum dominates further north). It also defines a change in lagoonal matrix in the coastal plain to the fluviodeltaic sabkha coast of northern Kuwait and Iraq.

Other coastal sabkhas

Outside of the southern coast of the Arabian Gulf there are many other coastal deserts where evaporation of a combination of marine and continental waters precipitates capillary salts in a matrix of marine-reworked sediment.

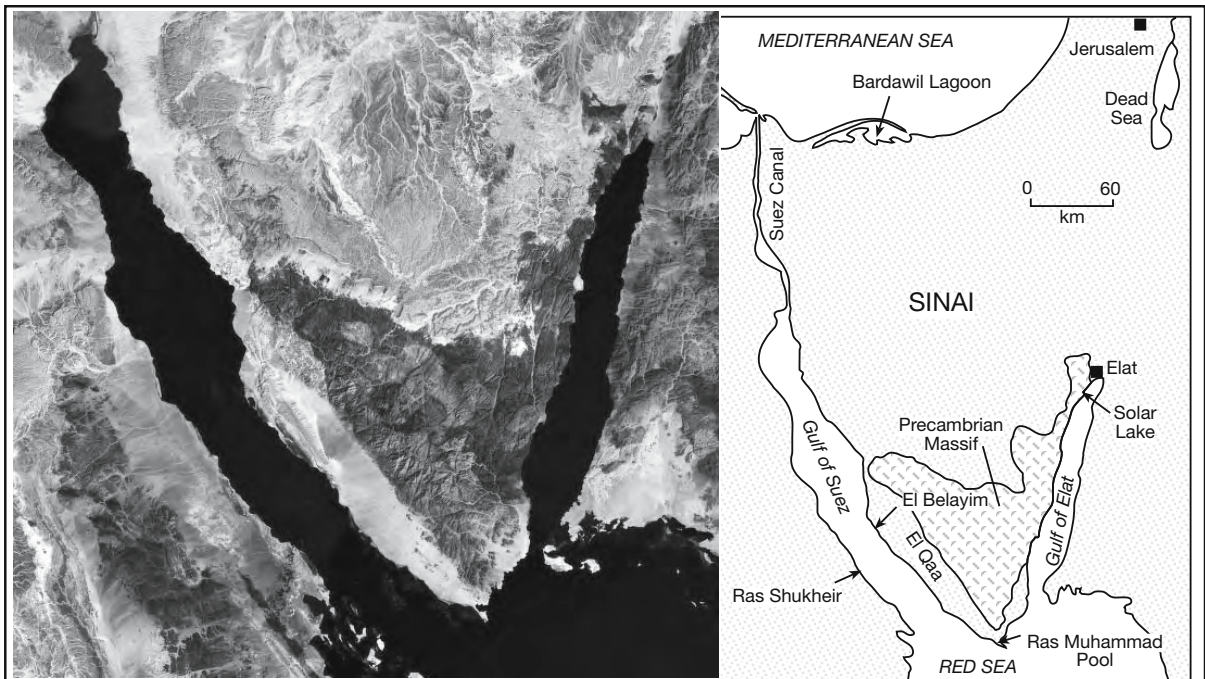


Figure 3.20. Sinai Peninsula showing distribution of some of the studied Holocene sabkhas and salinas in the Quaternary coastal fringe (Landsat image courtesy of NASA).

Gulf of Suez

Sea-margin sabkhas form along both sides of the Gulf of Suez. Small sabkhas are patchily developed along the seaward edge of the El-Qaa, in a coastal strip that runs from Abu Rudeiz to Ras Muhammad (Figure 3.20; Gavish, 1974, 1980). The El Qaa is a near-flat alluvial plain, mostly composed of alluvial silicate minerals weathered from Precambrian metasediments and granitic massifs to the east. The El Qaa area experiences some of the hottest and driest conditions in the Sinai, yet it lacks substantial accumulations of anhydrite. Capillary evaporites where they do occur are mostly scattered patches of interstitial gypsiferous cements within a few hundred metres of the coast (Figure 3.21). Nowhere in the Sinai coast are sabkha salts as extensive as in the Arabian Gulf sabkha (Gavish, 1974). Gypsiferous capillary cements in marine-reworked siliciclastic matrices, are also patchily developed in a narrow coastal strip on the opposite (African) side of the Gulf of Suez (Keheila et al., 1989). At Ras Shukheir the sabkha is unique in that it is developed atop and around one of the world's few examples of a Late Pleistocene coastal salina, which was once filled with laminated subaqueous gypsum, although now the succession is heavily eroded (Figure 4.15).

The sabkha fringe to the Gulf of Suez coastal plain typically extends from the marine shoreline to the seaward base of an alluvial fan apron or bajada, which lines a faulted escarpment located up to a kilometre or more in the hinterland. The sabkha itself usually occupies the first few hundred metres immediately landward of the shoreline where the bajada watertable approaches the landsurface (Figure 3.21a). Matrix sediments are mixtures of clastic fine-sands, derived from alluvials, and marine carbonate washover sands composed of skeletal fragments, pellets, ooids, and some intraclasts (Sellwood and Netherwood, 1984). Finer-grained marine carbonates typically occupy the seaward side and coarser-grained alluvial clastics occur on the landward side, so that the proportion of carbonate decreases upward in a prograding sabkha cycle. In many places there is an elevated sandy berm or a strip of pebbly beachrock defining the upper limit of the intertidal zone and a sabkha flat is developed behind the berm (Figure 3.20a). The supratidal zone generally extends a few hundred metres inland, its width being dependant on the regional slope. Further landward the top of the capillary fringe passes below the landsurface. Storm surge waters occasionally cover large portions of the supratidal flat and a thin ephemeral crust of pressure-ridged chevron halite may form a cm-thick cap to the sabkha as the surface waters disappear. The crust too disappears in the next flood or rainstorm. Once again, it is highly likely the hydrology of the crust is decoupled from that of the underlying sabkha.

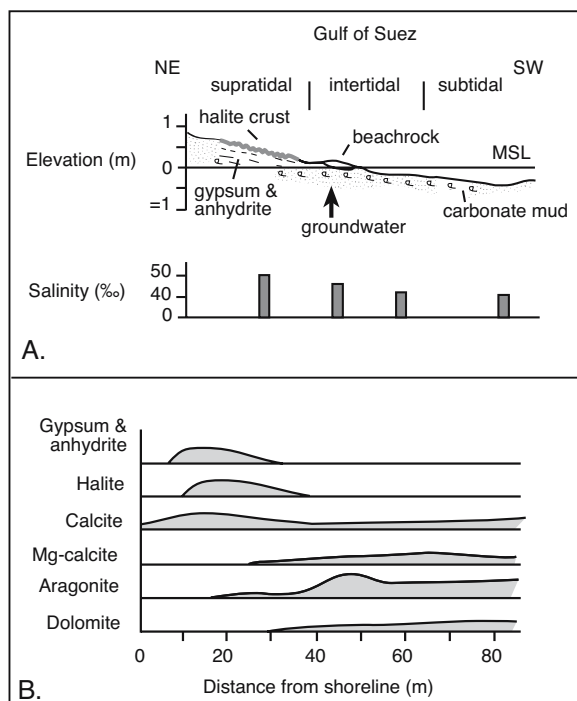


Figure 3.21. Gulf of Suez sabkhas. A) Generalised cross section through sabkhas of the coastal zone of the Gulf of Suez and typical pore water salinities (after Gavish, 1980). B) Distribution of various mineral phases in terms of distance landward from the marine shoreline. Gypsum, anhydrite and halite are the main evaporite minerals (after Gavish, 1980).

Evaporite mineral distribution in a typical Gulf of Suez sabkha is very similar to the mineral suite in an Arabian Gulf sabkha but the volumes of capillary salts are less and depositional belts are much narrower. Like the Arabian Gulf, the Gulf of Suez sabkhas precipitate evaporites mostly as displacive crystals within the supratidal zone (Figure 3.21b). Capillary driven concentration precipitates salt in a matrix-rich supratidal evaporite unit, which is no more than 60 - 80 cm thick - the thickness of the capillary fringe. Most of the gypsum is precipitated as passive pore cements immediately above the water table. Gavish (1974, 1980) attributes most of the ion supply to landward seepage of seawater, driven by capillary evaporation, as per the model of Hsu and Schneider (1973). The hydrology of the Gulf of Suez sabkhat has not been re-assessed since the work by Wood et al. (2002) on sabkhas of the At Taf coastal strip.

One of the most obvious differences between the Gulf of Suez sabkhas and the Arabian Gulf sabkhas is the distribution of the two calcium sulphate phases (Gavish, 1974). In the Gulf of Suez, gypsum is the dominant sabkha mineral in all active parts of the sabkha. Only very minor traces of anhydrite are found and

only in the older more elevated portions of the sabkha where it has locally recrystallised or replaced a gypsum precursor.

Beach-dune and fluvial sabkhat on deltas

Modern sea-margin settings where large river systems are building deltas into the marine realm in arid settings are areas that set up shallow water tables and so can host local near-coastal sabkha systems. They form where the capillary fringe intersects the land surface and so tend to be preserved either in more protected subsealevel depressions behind coastal beach ridges (Nile Delta) or as fringes to coastal lagoons fed by occasional storm surges and marine floods (Bardawil Lagoon).

Western Nile delta coast, Mediterranean Egypt

Interdunal sabkhas of the Nile delta are forming today along the Mediterranean coast near El Hammam, a region halfway between Alexandria and El Alamein (Figure 3.22; Bellah and Hassouba, 1995). There the coastal zone consists of nine or more Quaternary shore-parallel carbonate beach-dune ridges.

All the ridges are cemented with a hard caliche cap, except the most recent dune known as the “coastal ridge.” Lagoonal and desert loess sediments fill large swaths of the elongate depressions between the ridges and act as host matrices to the sabkha precipitates.

The first sabkha depression is situated immediately behind the “coastal ridge” of oolitic sand and is more than 8 km long and a few hundred metres wide (Figure 3.22; Ali and West, 1983; West et al., 1979). Displacive nodular gypsum (with minor palygorskite/attapulgite) is growing in the capillary zone of the carbonate-rich desert loess that has filled this most seaward interdunal depression. Landward and to the south, beyond the Abu Sir limestone ridge (Pleistocene), there are other interdunal sabkhas forming about and within various halite-encrusted, cyanobacterial-mat-fringed lakes.

Sediment behind the third ridge back from the coast is very interesting in that it contains a laminated gypsum fill, which is possibly the preserved remnant of a Pleistocene subaqueous deposit (pers.obs). The beds there are extensively quarried

and well exposed, but as yet its geology is poorly documented and it is not known if it formed as a marine-fed salina or as a lacustrine chott fill. The fact that this laminar gypsum alternates with thin limestone layers preserving articulated shells of *Cardium sp.* argues perhaps for a marine seepage origin.

All the sabkhas in the inter-ridge depressions are characterised by gypsiferous capillary zone units up to 60 cm thick made up of a combination of lenticular to prismatic gypsum crystals, and small spherical to elliptical nodules 1 to 4 cm wide composed of silt-sized gypsum. There is no anhydrite growing in the capillary fringe. Matrix sediment is a mostly brown, laminated, very fine quartzose silt and carbonate sand. It was depos-

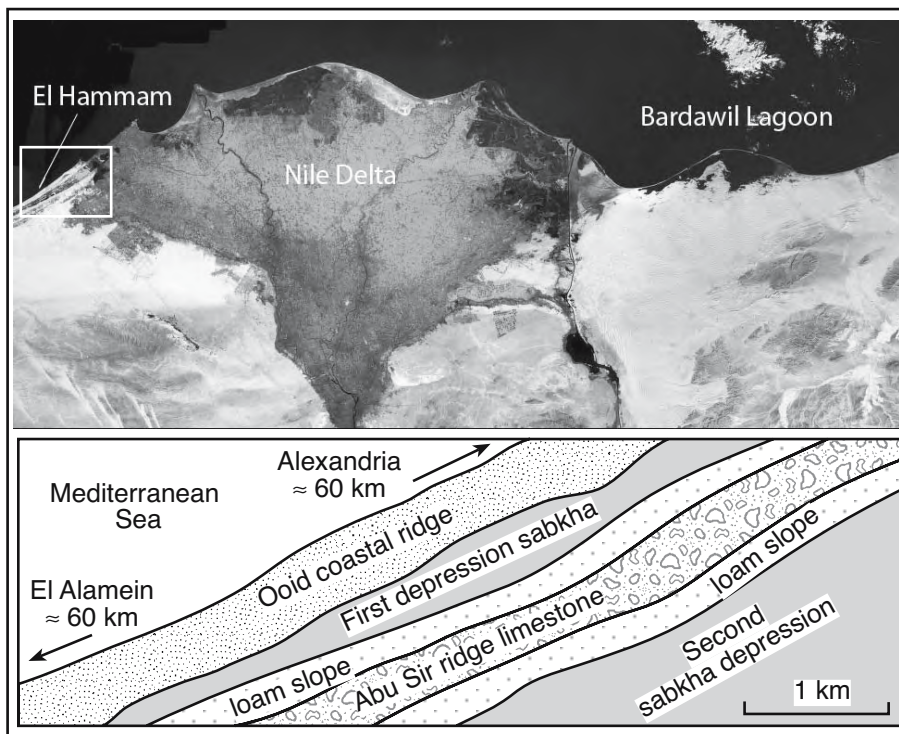


Figure 3.22. Egyptian coast centred on the Nile Delta. Interdunal coastal sabkhas occur on the eastern end of the vegetated Nile cone (rectangular inset, while Sabkhat Yathal Yam occur on the southern side of Bardawil Lagoon beyond the eastern end of the Nile delta (Landsat image courtesy of NASA, surface geology after West et al., 1979).

	No. of samples	Na	K	Mg	Ca	Cl	SO ₄	HCO ₃	Sr	Salinity
Zone V	6	77,500	5,200	21,800	100	173,000	49,200	trace	21	327‰
Zone IV	4	46,000	3,000	11,100	1,100	66,000	19,700	trace	45	148‰
Zone III	6	24,700	1,200	2,500	1,500	54,000	19,300	trace	42	103‰
Zone II	9	16,300	600	2,000	1,000	31,000	7,800	trace	40	59‰
Seawater	-	10,600	380	1,270	400	18,980	2,650	140	8	34‰

Table 3.4. Average compositions of 25 interstitial waters squeezed from evaporitic sediments in the first interdunal corridor, Abu Sir sabkha, Nile coast. Bicarbonate was below the detectable limit in all samples (after Ali and West, 1983).

ited as desert loess and is occasionally reworked by sheet floods shed from the adjacent ridges. Nodules grow most efficiently in Zone III and IV of the inter-ridge sabkha, with more saline pore waters above and less saline waters below (Figure 3.23). Nodules in zone IV and the uppermost part of Zone II are soft, very friable, uncemented and still maintain high intranodule porosity and permeability. Zones of coalesced nodules can create local upward-bulging enterolithic structures. Nodules made of small gypsum crystals typically overlie nodules composed of larger crystals. The relationship between crystal size and distance from the sabkha surface shows that nodules are precipitating in the active capillary zone and do not form by replacement of an anhydrite precursor. As capillary gypsum crystals continue to grow, the nodule expands by pushing aside and deforming adjacent sediment laminae. The fine-grained nature of the hosting loess encourages displacive growth rather than passive interparticle poikilotopic growth. Minor amounts of authigenic calcite and dolomite are also precipitated.

A marine-seepage origin for the gypsum nodules was inferred by Ali and West (1983) based on the seawater-like proportions of the interstitial brines and periodic gypsum saturation in waters of zones III and IV in the waters of the first inter-ridge depression (Figure 3.23; Table 3.4). But as we saw in Chapter 2 seawater-like proportions in a groundwater do not necessarily mean a seawater origin in continental

areas with caliche. Salinities of phreatic groundwaters in Zone II vary from 40-80‰, with a mean of 59‰, which is almost twice as concentrated as seawater. Na, Mg and Cl are present in thalassic proportions, Sr is somewhat in excess, as are Ca and SO₄, an association that probably indicates ongoing dissolution of gypsum. Above Zone II, salinities increase upward in zones III and IV. Zone IV, with a predominance of growing gypsum nodules has an average pore water salinity of 148‰ (Figure 3.23). The uppermost part of the sabkha interval has the highest salinity pore waters, averaging 327‰, a salinity value that is five times that of zone II. Na and Cl maintain their relative

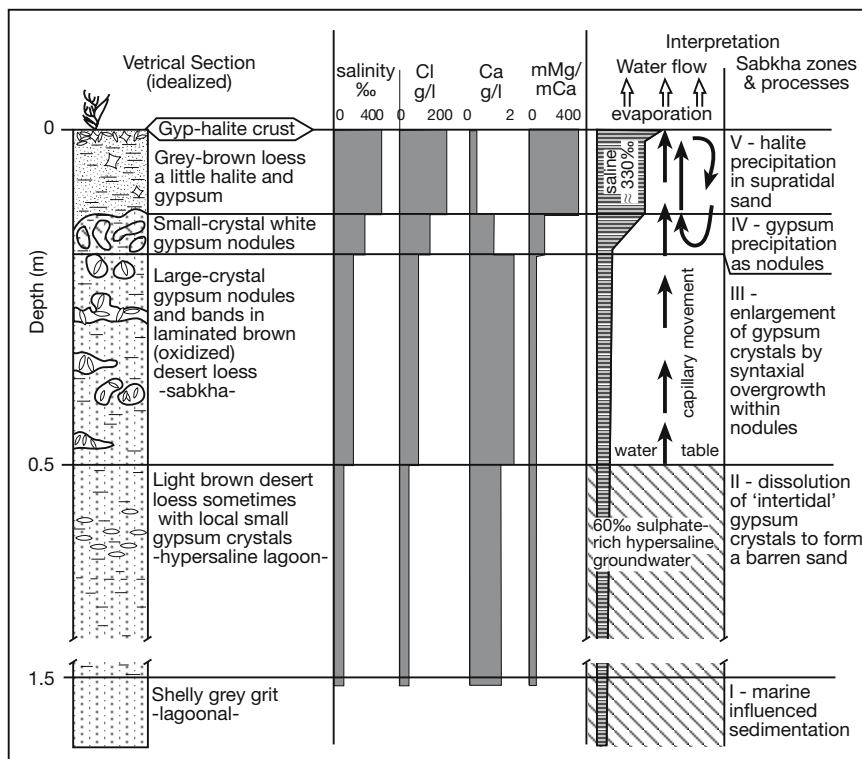


Figure 3.23. Inter-ridge gypsum sabkhas on the Nile delta, Egypt showing idealised vertical section through the first sabkha depression and the interpreted capillary-driven subsurface evaporation hydrology forming the gypsum nodules that define the sabkha sequence (after West et al., 1979; Ali and West, 1983).



Figure 3.24. Southern coast of Bardawil lagoon, northern Sinai, Egypt, shows beach-lagoon and interdunal sabkhas within the coastal portion of a sand sea dominated by longitudinal (seif) dunes. Sabkha deposition was a response to a rise in the regional water table driven by the end-Pleistocene rise in sea level to its present position some 6 ka (Image courtesy of NASA).

proportions tied to brine concentration in Zones II through V (five-fold increase from Zone II to V). K rises nine-fold over the same interval and Mg about eleven-fold. In contrast the Ca content is almost constant in zones II through IV and drops sharply in zone V, showing that gypsum is actively precipitating in zones III and IV. Sr shows a similar trend to Ca, although it does not decrease as sharply in Zone V. SO_4 increases upward to a concentration in Zone V than is a six-fold increase over its levels in the groundwaters of Zone II.

Ali and West (1981) utilised the measured hydrogeochemistry of the interstitial waters to argue for gypsum precipitation by capillary evaporation of thalassic seepage waters via “per ascendum” rather than a “per descendum” model, although at the time they published their work the latter was the prevailing interpretation for a sabkha hydrology.

This series of Egyptian coastal sabkhas is of interest as it is an active sabkha plain in the low-fluvial-supply (desert loess) coastal portion of the prograding Nile delta. It also shows that extremely arid conditions are not a requirement for evaporite nodule growth; it only needs the appropriate seepage hydrology where the capillary fringe intersects the land surface. These sabkhas are actively accumulating gypsum in a region where annual rainfall is ≈ 18 cm. Once again, like the At Taf sabkha, it demonstrates the lack of preservation potential of any salts precipitated in the seepage hydrology of all modern coastal sabkhas. Once the gypsum nodules are buried into Zone II they are seen to dissolve in rising phreatic brines, which are undersaturated with respect to gypsum (Figure 3.23). Gypsum is being recycled through the upper parts of a subsiding profile and its preservation potential is low (implications of this are discussed further later in this chapter).

Eastern Mediterranean Coast of the Nile Delta and Northern Sinai

On the other side of the Nile delta, the northern Sinai coast is bordered for about two-thirds of its length by the Bardawil Lagoon (Figures 3.22, 3.24; Levy, 1977a, b, 1980). It is a broad marine lagoon with smaller evaporitic sabkha/lagoons in interdunal depressions along its southern coastal interface. The southern part of the Bardawil also defines the coastal desert edge of an extensive sand sea or erg dominated by longitudinal or seif dunes. Regional climate is arid, evaporation rates are high (≈ 2 m/yr) and precipitation is low (≈ 100 mm/yr). Marine-influenced sabkhas on the southern side of the lagoon occur wherever the capillary fringe intersects the landsurface and are of two types: 1) coastal sabkhas (also called lagoon-beach sabkhas-see Warren, 1991), which are at present connected to the lagoon and flooded occasionally by seawater - examples include the inner lagoons and Nahal Yam, and 2) near coastal interdunal sabkha depressions, which are now cut off from the lagoon by sand dunes - examples include Sabkhat Mahzin and Sabkhat Hafirdim (Figure 3.25a). Both types of sabkha formed as a rising marine water table, created by the Late Pleistocene-Holocene transgression, encroached upon the erg. There is also a third type of sabkha in the region; it is typified by large inland eolian sabkhas such as Sabkhat el Mustabag and Sabkhat Bir Kasiba. This group of sabkhas is carbonate rich and formed under a Late Pleistocene paludal hydrology, which was active at the edges of this desert sand sea in more humid climatic periods. Eolian-lacustrine sabkhas are discussed in more detail toward the end of this chapter.

The largest documented coastal-beach sabkha, Sabkhat Nathal Yam, is about 7 km long and extends about 1 km inland. To the south of the lagoon beach sabkhas, coastal interdunal sabkhas

extend inland to a distance of about 1-4 kilometres and are accumulating capillary salts from hypersaline capillary water lenses surrounded and underlain by slightly less saline continental phreatic wedges. These “inland” eolian sabkhas tend to be a few kilometres long and less than a kilometre wide (Figure 3.25a). They define a coast-parallel hydrological transition from marine seepage into continental groundwaters carried in the unconfined aquifers of the regional sand sea or erg.

Both types of sabkha are typified by siliciclastic matrices with displacive gypsum within supratidal evaporitic units up to 60 cm thick (Figures 3.25b, c). The intertidal zone in the beach-lagoon sabkha of Nathal Yam is 200-300m wide and is regularly flooded by tidal waters of the lagoon. The intertidal is characterised by cyanobacterial mats, interlayered with low Mg-calcite muds and containing marine gastropod and

lamellibranch shells derived from the lagoon. Lenticular and prismatic gypsum crystals are growing in the cyanobacterial mat layer in the more landward parts of this zone; it is very similar to the gypsum mush zone of the At Taf coastal strip. Landward of the intertidal zone is a 100m-wide outer flood recharge zone, it experiences no more than an occasional marine flood (a few times a year) during a fortuitous combination of storms and high tide. There the cyanobacterial mat is covered by a thin layer of detrital quartz sand and otherwise lies atop the same basic sequence of sediments found in the intertidal zone. Landward still at the southern end is a 500m-wide supratidal zone. This area is not currently flooded by lagoon waters, even during storms and defines the interval where the capillary zone intersects the land surface. Under an ephemeral halite crust it hosts displacive gypsum lenses and prisms in a matrix that is otherwise identical to its more seaward counterparts.

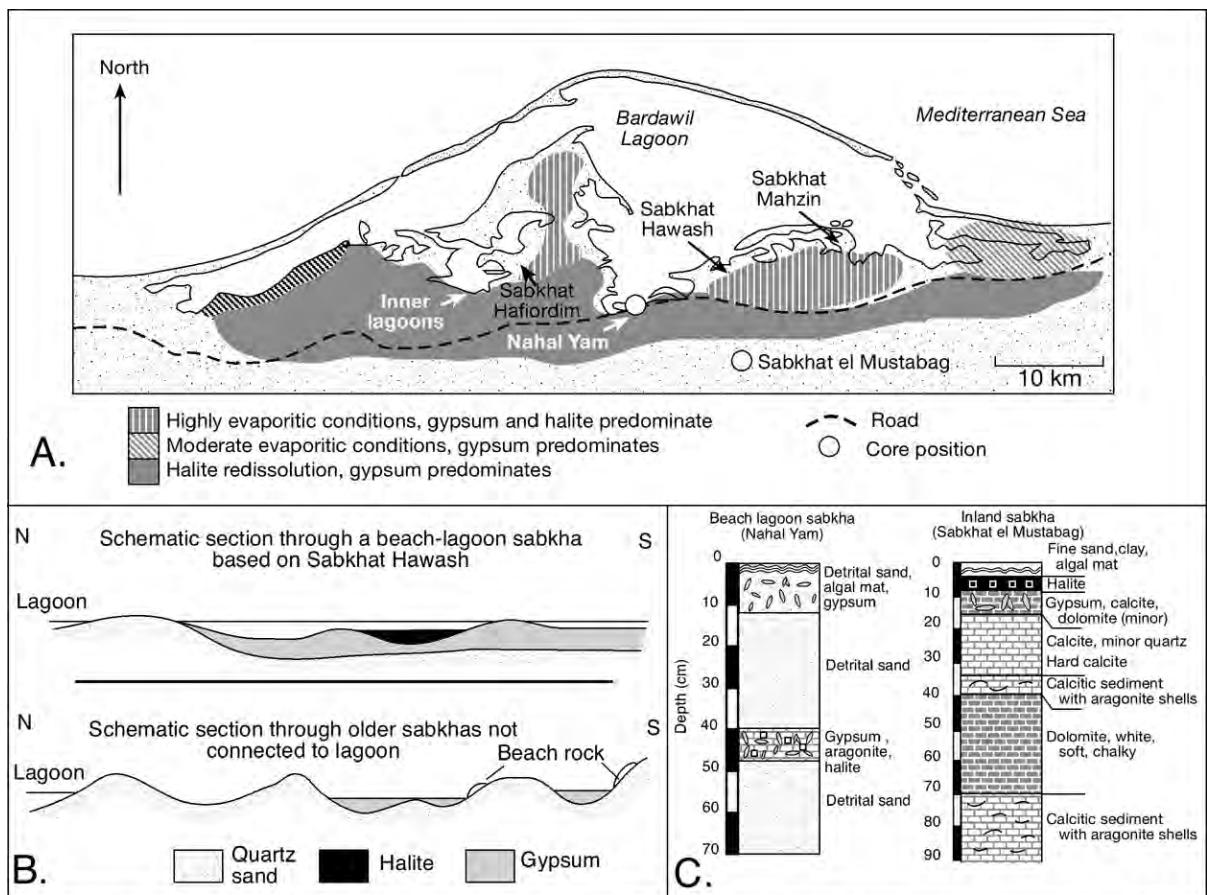


Figure 3.25. Sabkhas of the Bardawil lagoon, Mediterranean Coast, northern Sinai (after Levy, 1977; see Figure 3.22 for locality). A) Distribution and mineralogy of sabkha salts south of the Bardawil Lagoon. B) Schematic cross section through a beach-lagoon sabkha based on Sabkhat Hawash, showing differences in lateral scale with older inter-ridge sabkhas. C) Composite vertical section in a beach-lagoon sabkha based at Nathal Yam, it is based on cores taken at 20m, 500m and 700m from the beach line.

Unconfined continental groundwater, moving north toward the shoreline, periodically seeps into the supratidal zones of all the beach lagoonal and near coast “inland” sabkhas along the southern side of Bardawil Lagoon. Rising water levels occur after heavy winter rains and create ponds of surface water that rapidly evaporate to precipitate thin halite crusts and efflorescences. In fact, most of the present freshened inflow into the supratidal zones both beach-lagoon and coastal interdunal sabkhas comes from a winter groundwater flood from the nearby dunes and not from any influx of storm-derived seawater. This rising water table dissolves most surface halite crusts, as well as some of the gypsum precipitated in the more isolated parts of all sabkhas in the previous summer. The inherent fractionation explains why ephemeral halite crusts are typically found in depressions located seaward of the gypsum-dominated inland sabkhas.

The calcium sulphate mineral in both styles of near-coastal sabkha is a gypsum pore cement, it is not anhydrite. The setting is not saline enough, nor arid enough, to favour the preservation of anhydrite. Groundwater floods in the winter means most crystals of capillary gypsum are periodically flushed by meteoric waters and so show internal layering and lenticular shapes indicative of alternating stages of precipitation and dissolution. Mg-calcite, dolomite and halite are minor authigenic components in some near-coastal sabkhas.

Large inland sabkhas, such as Sabkhat el Mustabag, were possibly once connected to the Bardawil Lagoon, although dunes now cut off all the inland sabkha depressions from the sea (Figures 3.24, 3.25b). More likely, they formed in the Late Pleistocene in an earlier paludal phase at the seepage edge of the Sinai sand sea, when the seacoast was tens of kilometres further out on the exposed shelf. Soft chalky-white calcian dolomite (layer up to 20 - 30 cm thick) caps the upper portions of the sediment fill in some of the larger inland sabkhas (Figure 3.25b). The age of the carbonate precipitates in these older sabkhas is not well constrained. Beneath the dolomitic carapace are well preserved aragonitic gastropod shells, typically embedded in a muddy calcitic groundmass. Radiocarbon dating shows that the dolomite and the underlying unit is older than 35,000 years (Figure 3.25c). It is a lacustral continental sabkha, possibly deposited in a Pleistocene pluvial, with little tie to the present largely vadose hydrology of the inland sabkhas along the landward edge of the Bardawil coastal prism.

Shatt el Arab estuarine sabkha, Iraq

The Shatt el Arab delta lies at the northwestern end of the Arabian Gulf, immediately northeast of Kuwait (Kadmah) Bay. It is an area where three rivers (Tigris, Euphrates, Karun) merge to form the Shatt el Arab delta (Figure 3.26). It is an unusual region in that it is one of a few modern examples of a large modern river delta feeding into an enclosed saline sea and where the amount of eolian sediment in the delta (via the northwesterly Shamal wind) may equal the volume of waterborne fluvial sediment (Evans, 1995).

The Shatt el Arab is fed by a broad funnel-shaped estuarine channel with wide levees on either side. Spreading out from the levees are dense surrounding marshes of reed beds (locally known as *ahwar*). The region was drained under the genocidal policies of Saddam Hussain, but is now being re-engineered to return the reedbed system to its natural state. These areas are flooded each spring and early summer by waters fed from snowmelt in the river headwaters. Large crevasse splays spread into interchannel areas, which in the lower deltaic plain are dominated by brackish to freshwater lakes and dense surrounding reed-bed marshes (Aqrawi and Evans, 1994). Lakes are floored by bioturbated sandy silts and clayey silts, which preserve abundant meshworks of plant roots and a brackish shelly fauna. Crevasse sediments feeding the lakes are well-stratified sandy silts and muds. At its most seaward extent and across Budiyah island an extensive plain of estuarine sabkha takes the place of the reedbed.

Matrix in both the sabkha and the *ahwar* regions is similar. It is rich in detrital carbonates as well as quartz, reflecting the large volumes of outcropping carbonate in the hinterland. What separates the two settings is the lack of higher plants on the estuarine sabkha (instead of root meshworks there are widespread cyanobacterial mats and some local mangroves) and the widespread authigenic precipitation of high-Mg-calcite, calcite, calcian-dolomite, gypsum and perhaps pyrite as capillary salts in the sabkha matrix. Palygorskite is present in the sabkha as both authigenic and allochthonous phases (Aqrawi and Evans, 1994).

The extremely low wave energy attacking the front of the Shatt el Arab delta separates it from other arid-zone deltas, such as the Indus, which show similar 2-3 metre tidal ranges. Due to this low wave energy (limited fetch), only narrow beaches and small coastal dune systems form along the leading edge of this arid zone delta. Rapid progradation of fines forms widespread saline mudflats and sandbars across much of the seaward parts of the delta plain, dissected by tidal channels along the delta

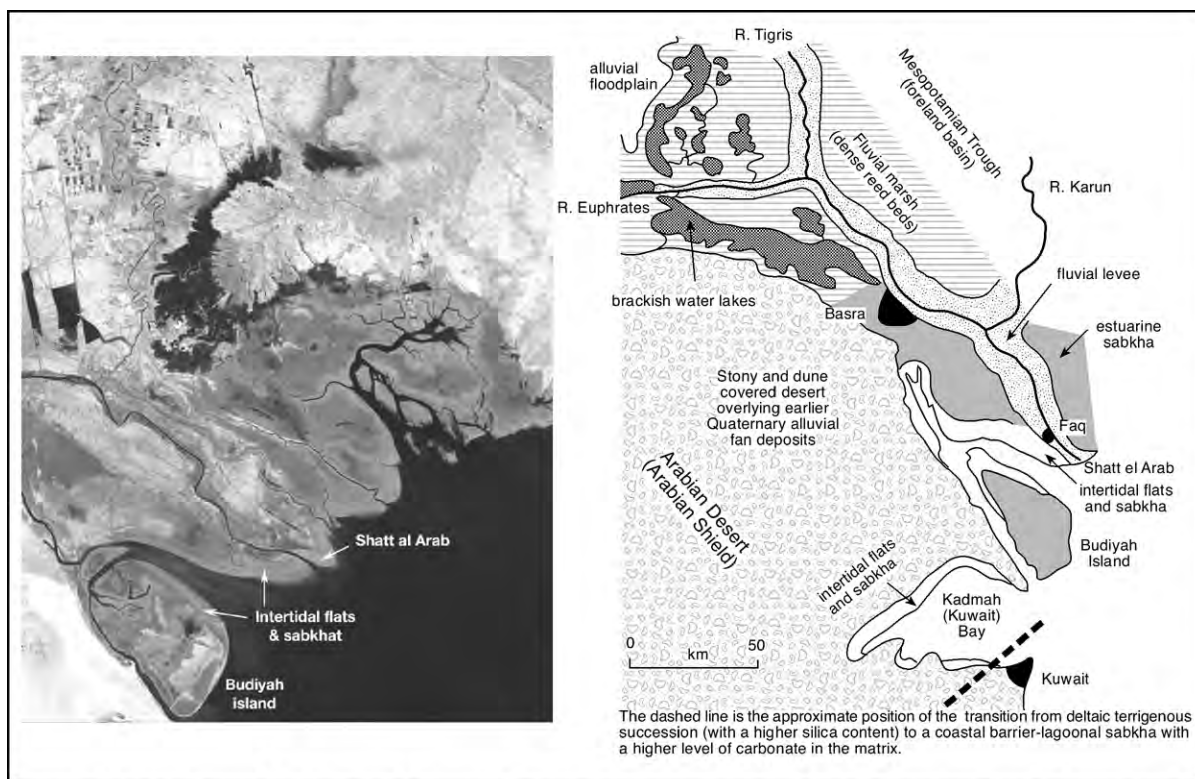


Figure 3.26. Distribution of fluvial related facies including estuarine sabkha with a siliciclastic matrix along the lower length of the Shatt el Arab River. Note Kuwait Bay in lower centre of geology map (Landsat image courtesy of NASA, surface geology after Evans, 1995).

front. Saltpans and gypsiferous sabkhas form behind low relief beach ridges and chenier ridges where surface seawater is trapped after very high tides and storm floods. The resulting evaporitic zones are characterised by crusts of halite and capillary precipitates of gypsum. Anhydrite after gypsum occurs in the most exposed and saline portions of this system.

The seaward extent of this evaporite capped large volume of deltaic sediment is not well established, but the delta lobe probably extends some 100 km from the modern shore (Figure 3.2a; Evans, 1995). Away from the active fluvial-fed portions of the delta lobe, quartzose sands are reworked into a shoalwater complex of elongate tidal bars that passes seaward in prodeltaic marls, which in turn enclose the reef capped Kharg Island off the Iranian coast.

Sabkha sediments, passing updip into dense reed beds, show affinities to similar facies on the Nile Delta. In both, the increasing distance from the active part of the delta explains the change from a quartzose matrix in the delta sabkhas to a more carbonate-rich barrier-lagoon style of sabkha (e.g. Figure 3.26 - dashed line).

Interpretive limitations of models based on Holocene sabkhas

Capillary salts and surface crusts precipitated in Holocene marine-margin sabkhas and many continental sabkhas have low preservation potential. They precipitate in a hydrological fringe underlain by undersaturated waters and below a land surface subject to periodic freshening and flooding. Whether capillary salts form by cooling (thermalites) or pore brine evaporation is irrelevant in terms of their ultimate preservation potential. To pass into the rock record any sequence must, by definition, subside. As it does so, the sabkha nodules, crystals and crusts at the edge of a body of brine of normal seawater salinity must pass back into waters undersaturated with respect to the minerals precipitated in the capillary fringe. At best, what will be preserved of the original salts in the prevailing hydrology at the edge of a normal marine water body will be partially dissolved remnants of the salts and nodules. More likely, the capillary fringe precipitates will become a thin interval of haloturbation textures and dissolution collapse. If, on the other hand, a sabkha succession sits on the edge of a hypersaline saline pan (as in some modern continental sabkhas) or on the

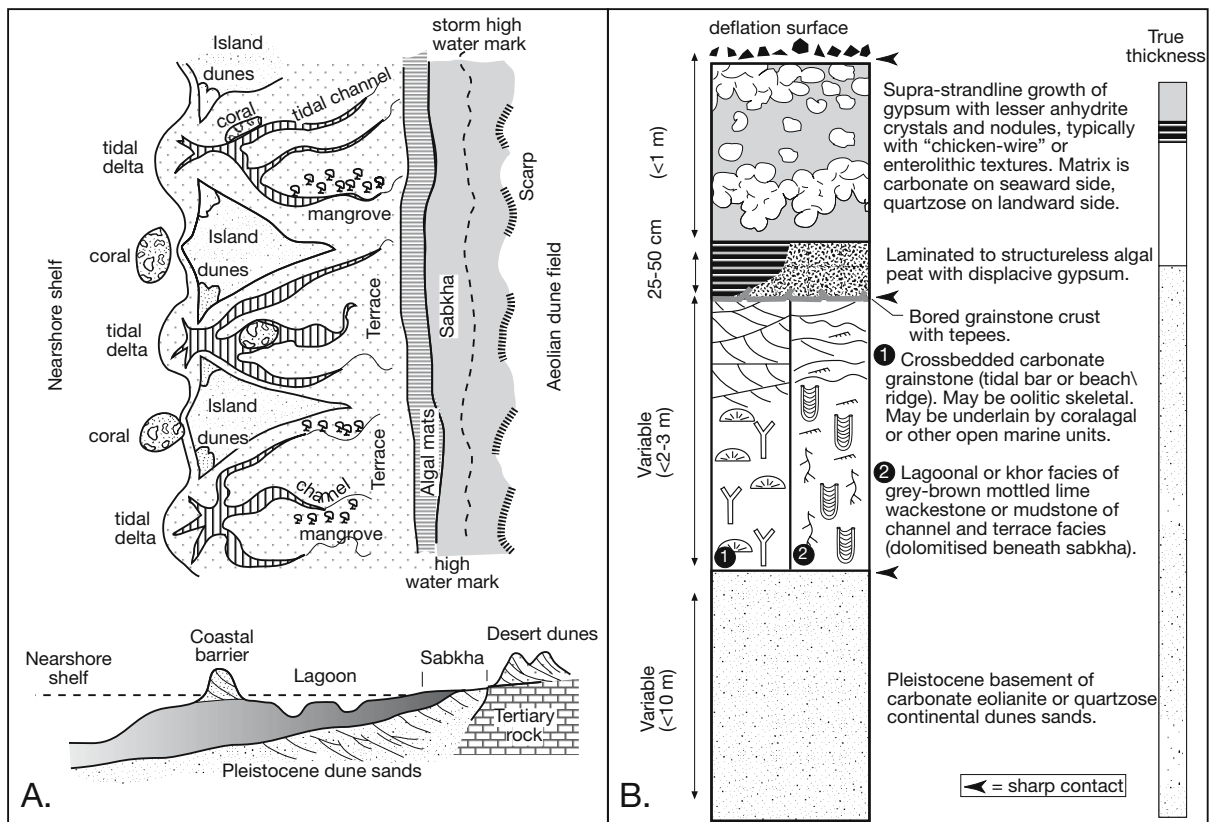


Figure 3.27. Generalised geological model. A) Based on the distribution of the main carbonate facies belts in Abu Dhabi - Khor al B'azm region (in part after Evans, 1995). B) Characteristic vertical succession of sea-margin carbonate sabkha showing typical thickness for each unit, right column shows true relative thickness (in part after Warren, 1991).

edge of an ancient saltern or seaway, then the capillary salts pass into a saturated brine curtain or into the edge of a reflux plume, and so preservation of the original capillary textures is more likely (Figure 5.29).

There are other implications of the sabkha signature always forming in a capillary fringe. A typical sediment distribution model for an ancient sabkha, based on the Abu Dhabi Holocene, looks something like that presented in Figure 3.27. Such models typically do not consider hydrology, bed thickness, lateral extent or structural controls when compiling the sabkha units; they merely use Walthers Law to stack the various peritidal sequences into a vertical succession. Because of this, the Abu Dhabi sabkha analogy is sometimes used to interpret ancient evaporitic platform successions composed of marine carbonate beds interlayered with nodular anhydrites (platform evaporites), without a full understanding of the implications of the requisite sabkha hydrology.

An Arabian Gulf carbonate-hosted sabkha is part of a prograding Holocene ramp where the total succession is composed of subtidal, intertidal, and supratidal sediments. It is capped by a Stokes surface and typically backed by a siliciclastic sand sheet/dune association. The complete Holocene section is no more than 3 metres thick and in the type area centred on the Abu Dhabi region the Holocene sequence is composed predominantly of subtidal lagoonal carbonates. The evaporitic intertidal and supratidal cap is up to a metre thick and always reflects the thickness of the capillary fringe.

Underlying Pleistocene sediments are up to 12 m thick in the vicinity of Abu Dhabi; they are permeable Pleistocene dune sands that directly overlie the Miocene carbonate aquifer supplying solutes to the sabkha (Figure 3.27a). In terms of sediment volume, scaling and perhaps even geometries of accommodated sediment, much of the Abu Dhabi sabkha is best considered to be an eolian sabkha with a water table closer to the landsurface because of proximity to the ocean (eolian sabkhas are discussed in more detail at the end of this chapter).

In its strictest sense, based on relative unit thicknesses, an Abu Dhabi sabkha should only be used as an analogue for ancient successions made up a transgressive subtidal lagoonal carbonate (1-3m thick) with a 0.5 m thick matrix-rich cap containing capillary salts, which is in turn capped by an erosional surface (Figure 3.27b). The whole succession should have been deposited atop a much thicker marine-flooded eolian dune aquifer system (Achauer, 1985). In most Holocene-based analogues for ancient evaporite systems, we modify notions of Holocene thickness and stacking to accommodate great changes in scale and thickness needed to typify ancient epeiric settings. Sometimes this is done without considering inherent hydrological limitations and the laws of fluid physics are unknowingly ignored (see Chapter 2 for hydrological details of various saline hydrologies).

For example, many thick, ancient sequences of pure nodular anhydrite have been interpreted as sabkhat deposited under conditions of slowly rising sea level (transgressive systems tract). There are hydrological and preservation restrictions associated with this hypothesis that are not considered in many sabkha reconstructions. The thickness of nodular anhydrite in any supratidal unit is limited by the thickness of the capillary fringe. Any evaporite sediment lying above the top of the capillary zone is blown away or dissolved (Figure 3.27b). Aside from the preservation issues mentioned earlier, this means that the supratidal evaporite phase in a single sabkha cycle (stillstand) can be no more than 0.5-1 metres thick and by definition it is matrix dominated (Warren and Kendall, 1985). Matrix must exist before capillary salts can grow. Hence the difficulty in explaining metres-thick pure nodular anhydrite as a thick sabkha without any encapsulated erosion surfaces. If in an ancient succession a nodular anhydrite is relatively pure and lacks internal erosion surfaces it cannot be a sabkha, it is some sort of subaqueous succession or subsurface replacement front.

The only exception to ancient sabkha sequences being dominated by non-evaporite matrix is when the matrix is composed of mechanically deposited sulphate or halite, perhaps derived by storm or eolian transport from a nearby saltern or saline pan. If such a succession was buried, the result would be a nearly pure sulphate or halite unit composed of sabkha cycles, each 1 to 2 metres thick, interlayered with saltern or saline pan units many metres thick. No modern examples of this style of evaporite deposition exist outside of the stacked saline pan halites in the South American salars discussed in the next part of this chapter. Modern sulphate equivalents are unknown, although they can be commonplace in stacked saltern-dominated marine-fed platform successions such as the Cretaceous Ferry

Lake Anhydrite of the Gulf of Mexico and the Permian Werra Anhydrite of the Zechstein (Chapter 5).

The need to stack sabkhas into hypersaline, not marine, groundwaters also means that wherever matrix-rich beds of nodular anhydrite are metres to tens of metres thick with no intrabed erosional surfaces (Stokes surfaces) then the sequence is not a sabkha. It may be a reflux-cemented marine platform carbonate, or an interval overprinted by burial cements. In my experience many ancient normal marine platforms overprinted by later patchy diagenetic anhydrite nodules and axe-head cements are often misinterpreted as sabkha indicators. In many sequence stratigraphic reconstructions this leads to such intervals being misinterpreted as being formed in times of lowered sealevel. This is especially so in studies by stratigraphers looking for evidence of times of sealevel lowering in platform successions. They tend to ignore the possibility of diagenetic evaporites or the marked differences in eustatic amplitude and frequency that characterise icehouse and greenhouse climate modes (Chapter 5). The presence of a few anhydrite nodules in a core or an FMI image, floating in a matrix of carbonate or siliciclastics, is not sufficient evidence to interpret the sequence as an ancient sabkha.

In the modern sabkha, the evaporites of the sabkha supratidal zone overlie restricted lagoonal sediments; they never overlie open-shelf carbonates. Yet in ancient platform evaporites, many beds of nodular anhydrites have been interpreted as sabkha. Such units typically seal dolomitized open-marine shelf carbonates. Perhaps insufficient time has elapsed in the Holocene for sabkha progradation to form a geologically realistic sabkha cap atop marine platform carbonates. Or perhaps ancient nodular anhydrite beds were deposited in a subaqueous saltern at a time when the platform was an isolated drawdown lagoon (Figure 5.16).

In a few millennia, and only if the At Taf coastal strip undergoes suitable subsidence, the succession of sabkha evaporites, and its formative hydrology, may prograde over the Holocene carbonates of the oolite shoals and the open shelf. And yet, the modern sabkha progrades across the inshore lagoon in response to the protecting action of the offshore oolite-reef shoal. The barrier islands screen the soft sabkha muds and evaporites from the erosive forces of the open gulf waves and the Shamal storms. Once the sabkha has infilled the lagoon behind this buffer, it is unlikely the sabkha will prograde much further seaward without the deposition of another sand shoal or reef a little further offshore.

Yet the sabkha “Trilogy” used by many to interpret ancient nodular anhydrite is supposedly composed of three laterally continuous facies belts with subtidal overlain by intertidal overlain by supratidal sediments, all merrily marching out into a subsiding basin without a change in facies. In reality, sabkha progradation, using an Arabian Gulf analog, must be a punctuated process over geologically significant time scales with the evaporite salts unlikely to be preserved (Warren and Kendall, 1985). A sabkha succession cannot be a simple continuous seaward movement of the “Trilogy”, never broken up by coquinas, barrier islands, ooid shoals, beach ridges or reefs.

Lastly, models used to interpret ancient sabkhas typically regard the Arabian Gulf as a carbonate province with the siliciclastic components ignored, or mentioned only in passing. This should not be the case. In almost all coastal areas along the southern Arabian Gulf the most landward portion of the sabkha is a sediment belt 2 to 6 kilometres wide with gypsiferous evaporites accumulating in an eolian derived siliciclastic matrix. This zone passes seaward into a predominantly carbonate matrix. There are, in fact, numerous modern siliciclastic continental sabkhas both in the Arabian Gulf and elsewhere, all of which show lateral extents more akin to larger scale ancient counterparts than do any modern carbonate-hosted coastal sabkhas (see eolian sabkha section at the end of this chapter).

Lacustrine sabkhas and pans

So far this chapter has focused on sabkhas and evaporitic mudflats in modern sea-margin settings. But at the 10 ka scale these are aerially-limited and ephemeral hydrologic systems, tied to the Holocene coastal highstand, with inherently poor preservation potentials. To study sabkhas that can stack to greater thicknesses and have sizes and volumes comparable to some of the smaller ancient evaporite systems we must move to Quaternary continental lacustrine settings and include hydrology of the saline pan in our modelling of preservation potential.

Modern continental sabkhas contribute to salt deposits with thicknesses of more than a hun-

dred metres and areas measured in thousands of square kilometres. Evaporites in continental sabkhas grow by displacive crystal growth in the capillary zone or in immediately underlying brine-saturated muds. Ongoing growth of capillary salts above the water table pushes the sabkha surface up out of the capillary zone into the vadose zone. This raised and dried continental sediment deflates to create the characteristic erosion/truncation surface. As in models based on modern marine-margin sabkhas, the presence of a Stokes surface is a key feature in recognising an ancient continental sabkha succession. Brine concentration in the saline mudflat is driven by the intensity of capillary evaporation and occurs adjacent to areas of saline pan and even adjacent to perennial subaqueous salt beds. Pans and holomictic brine lakes are needed to generate stable brine plumes or brine reflux curtains that preserves a stacked sequence of salt beds. The presence of a pan or perennial lake next to a sabkha defines the hydrology needed to preserve subsiding sabkha sequences. Their longterm absence is why Quaternary marine-margin sabkhas have little or no preservation potential.

Depositional characteristics

A continental sabkha is the part of a playa mudflat complex where the capillary fringe intersects the landscape. It sits within a sedimentary transition from the basin margin to the lowest parts of the brine-saturated basin floor (Figure 3.28; Eugster and Hardie, 1978):

alluvial fan/ephemeral stream/floodplain → sand flat → dry mudflat → saline mudflat → salt pan

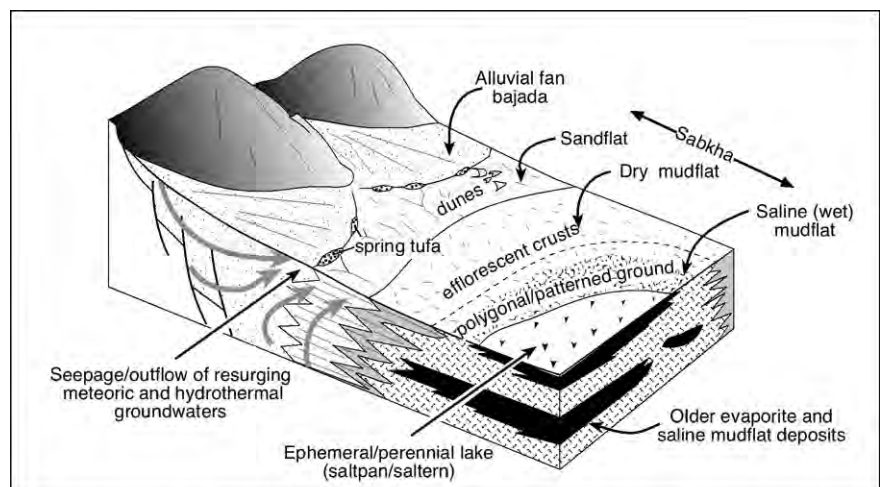


Figure 3.28. Continental sabkha/playa showing various facies belts and processes of solute supply that include surface runoff, meteoric and hydrothermal groundwaters (in part after Kendall, 1992; Eugster and Hardie, 1978).

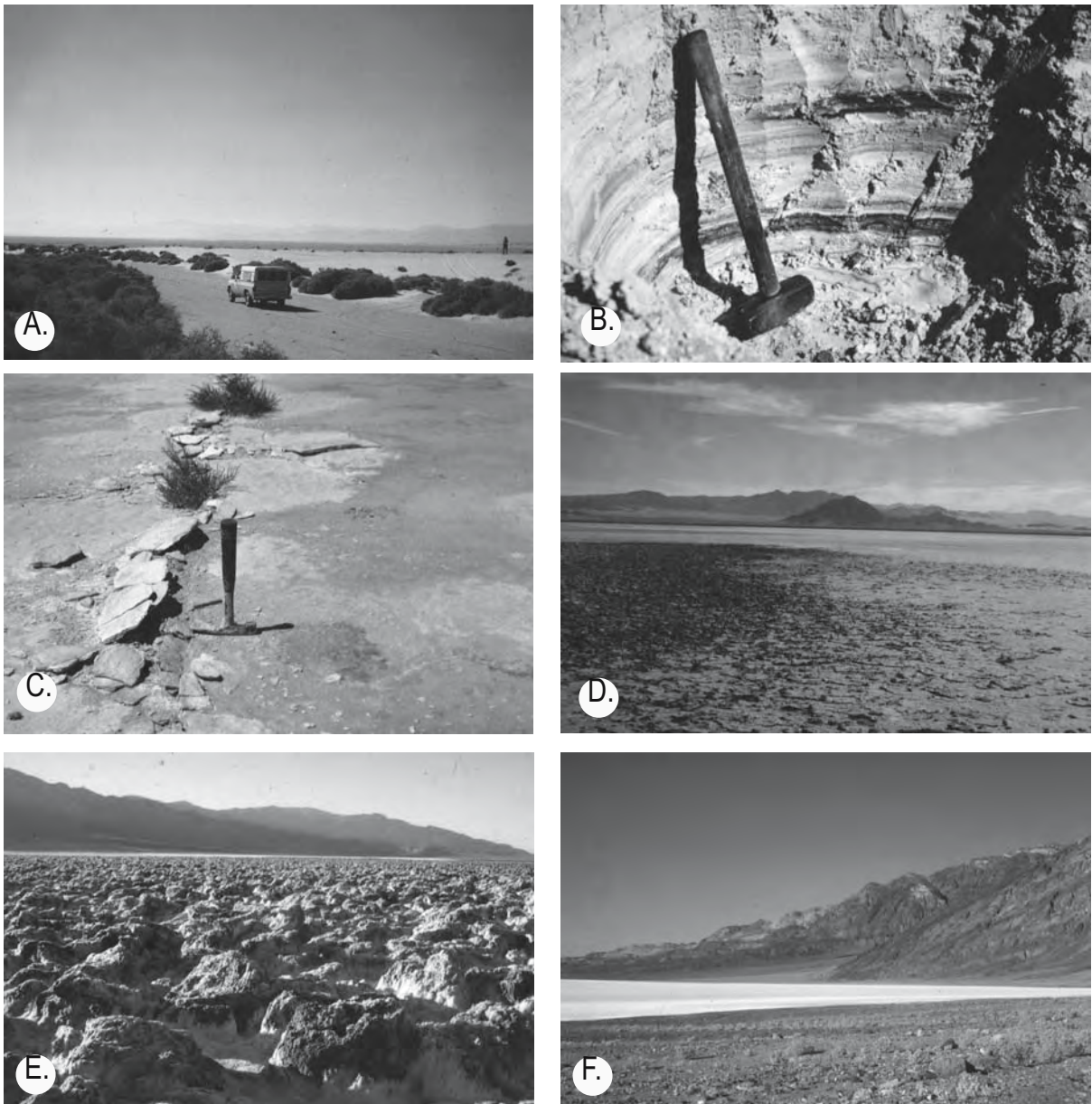


Figure 3.29. Continental sabkhas. A) Dry mudflat with local eolian dunes on the edge of Owens Lake, California. B) Laminated dolomite-gypsum sediment where capillary gypsum is growing above the water table, the hosting matrix is made up of former perennial lake sediments with dark organic rich layers, Salt Basin Playa, west Texas. C) Transition between dry mudflat and wet flat on with a tepee-overprinted dolomite crust, Salt Basin Playa, west Texas. D) Transition between saline mudflat and saline pan facies, Bristol Dry lake, California. E) Highly etched and disturbed salt crust of completely desiccated saline pan (Devil's golf course; Death Valley). F) Panorama of Death Valley showing juxtaposition of alluvial fan with sabkha/saline pan facies due to steepness of valley walls.

The more landward parts of this depositional association are composed of terrigenous alluvial sediments and their reworked eolian residues in the dry sand flat (Figure 3.29a). The water table is usually deep within these alluvials and so sediments do

not retain the more saline capillary salts, which are the focus of this discussion. They can contain caliche horizons formed by soil moisture fluctuations and perched capillary evaporation. We will come back to these less saline margins settings

in our discussion of various specific examples of modern continental sabkhas. For now, we will focus on those parts of the playa system that do preserve substantial volumes of the evaporite salts, namely, the saline mudflat and the outer edge of the saline pan.

The saline mudflat

The saline mudflat, along with the haloturbated parts of the dry mudflat, define the sabkha belt of a continental sabkha and together make up what is also often called the ephemeral saline lake belt (Figure 3.28, 3.29a; Eugster and Hardie, 1978). The sabkha passes basinward into beds of the saline pan, which are made up of stacks of predominantly subaqueous salt crusts, and landward into dry mudflats, sandflats and alluvial fans. Additional sedimentary facies may be found within the sabkha tract at any of several positions depending on short and long-term changes in the basin hydrology. They include dunefields and lunettes, which are composed of terrigenous sands, mud pellets, or evaporite grains; travertine springs or tufa mounds; and shoreline/strandline features such as sheet deltas, beach ridges, or spits.

Continental saline mudflats (sabkhas) are extensive vegetation-free flats composed of fine-grained sediments with displacive intrasediment precipitates of halite, gypsum and anhydrite or, less often, of more exotic salts such as glauberite, mirabilite and trona. Displacive salts may grow randomly in the capillary fringe as crystals and nodules or be concentrated in dm-thick layers (Figure 3.29b). Backreactions, periodic freshening and progradation may drive alteration, leaching and replacement of salts in this zone and mineral precipitation is sometimes aided by bacterial processes (Rosen and Warren, 1990).

Dry mudflats, with their requirement of a somewhat deeper water table, typically lie closer to the landward edge of a playa and form the rim to saline mudflats and saline pans. Sediments are mostly fine-grained, characterised by primary structures formed under alternating upper and lower flow regime conditions, such as sand-rich layers deposited by sheetflood, along with palaeosol horizons indicating periods of landscape stability. Dry mudflats do not retain evaporite salts, but may show disrupted to massive textures created by earlier intrasediment evaporite growth and dissolution (haloturbation), related to earlier times of higher water tables. Occurrences of actual salts on modern dry mudflats are limited to puffy surface efflorescences related to humidity fluctuations in the soil moisture zone and are destroyed/dissolved with the next light rain or fog.

A feature common to many dry mudflats is a pervasively cracked surface with crack diameters ranging from centimetres to giant polygons tens of metres across. Giant polygons or megapolygons indicate a long-term drawdown of the regional water table associated with longer-term climatic change (Figure 2.41; Neal et al., 1968). Cracks may not be a simple V, but may step across layers, show evidence of multiple stages of growth and be filled by a variety of sediments ranging from sands to muds.

Groundwater transport and fractionation in saline mudflats

Sheet floods in ephemeral lakes are relatively rare, most salts move about the lake flats as soluble load in shallow groundwaters, not as mechanically reworked sediment. Surface water and groundwater always flows to the lowermost point on the playa surface. Groundwater on this journey can come near or to the playa surface a number of times in zones defined by capillary salts and ephemeral efflorescent crusts. Crusts and salt assemblages in early stages of their formation can contain metastable high salinity salts such as epsomite and thenardite, which can even occur at the surface of the most landward parts of a mudflat. But when subjected to fluctuating humidities or light rains the less stable (more soluble) salts are quickly leached back into the dissolved load of the groundwaters and continue their journey basinward down the potentiometric gradient. Brines derived from the partial dissolution of efflorescent crusts are usually simple chemical solutions dominated by one or two major solute species (e.g., NaCl, Na₂SO₄, Na₂CO₃). The less-soluble mineral fraction is then left behind, in the more landward parts of the saline mudflat where it forms a carbonate crust, such as the dolomitic crusts of Salt Flat Playa, west Texas. There, the ongoing accumulation of capillary carbonate has forced the surface crust to buckle and crack into lacustrine mudflat tepees (Figure 3.29c; Hussain and Warren, 1988).

Farther out into a salt basin, ongoing capillary evaporation precipitates new salts as efflorescences on the lake surface or as intrasediment nodules and the process of fractionation can begin all over again. Ongoing repetition of this process means shallow sabkha groundwaters become increasingly saline as they seep toward the lowest part of the lake floor – so saline that even the more soluble salts become stable and can accumulate as intrasediment precipitates (e.g. displacive halite, glauberite, thenardite). Only the most soluble salts are carried into the lowermost portions of the lake basin, so that crusts deposited in salt pans define mineralogically simple bull's-eye patterns with the most soluble salts accumulating only in the lowermost portions of the ephemeral lake floor. Such concentric

or “bull’s-eye” fractionation patterns are often assumed for salts making up ancient sabkhas and pans, with the most soluble salts indicating the deepest part of the basin. But this simple pattern can be complicated by periodic near-unidirectional flooding fed from a single inflow channel, as seen today in some of the sabkhas in the salt lakes of central Australia (e.g. the Warburton Channel into Lake Eyre; Figure 3.51).

Saline pan

Saline pans in modern continental salt lakes are closely tied to the formation of saline mudflats and dry mudflats (Figure 3.30; Lowenstein and Hardie, 1985). They define zones on the salt lake floor where surface brines pond and concentrate long enough to stack into layers and beds composed of aggrading salt crusts (Figure 3.30; Stage II). Pans typically form in drainage sinks

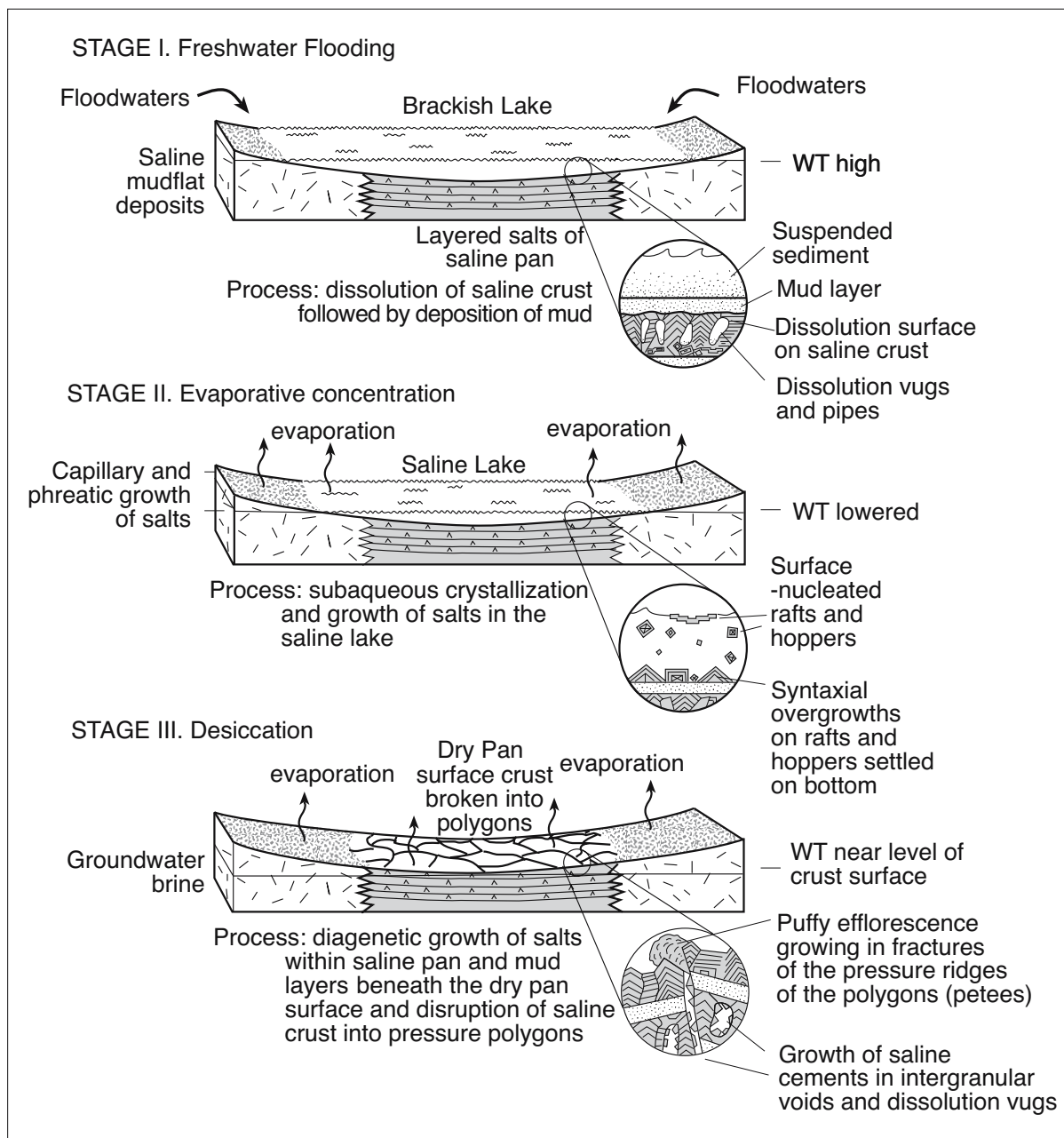


Figure 3.30. Evolution of a depositional cycle in a saline pan setting (after Lowenstein and Hardie, 1985).

situated in the lowest parts of the playa surface. A pan is typically surrounded by a saline mudflat and is frequently underlain by older bedded or layered salt units (Figures 3.28, 3.29d). In Lake Magadi, for example, the pan is defined by a trona bed 40 m thick, while in Bristol Dry lake the saline pan facies can be found intercalated with saline mudflat facies throughout the 400 metres of core recovered from the basin centre.

Pans range in size from small features a few km across to gigantic continental salt sinks as in Salar di Uyuni where the pan area is more than 9,000 km² (Rettig et al., 1980). Textures in the stacked salt layers are a combination of subaqueous aligned features (e.g. chevrons and swallowtails) and exposure overprints (e.g. microkarst pits, subhorizontal erosional bevels and salt-filled polygons) that formed each time pan dried and its surface was exposed (Figure 3.29e). Stacked crusts are usually dominated by halite, but other minerals such as gypsum, mirabilite and trona can be important.

When the pan dries eolian dust is trapped by capillary adhesion on its moist, rough surface or filters down cracks and fissures in the salt crust. Storm waters cover the pan after the next lake flood and the upper part of the salt crust dissolves, while flocculating muds settle onto the solution surface and sink into intercrystalline karst cavities (Figure 3.30, Stage I; Shearman 1970). Ongoing evaporation then creates a new subaqueous salt crust atop the dissolution surface. The knobby surface seen on some playa salt crusts is the result of continual precipitation and fretting of a subaerial salt layer, fed brine by “capillary wicking.”

The halite in the initial crust is often composed of upward-pointing subaqueous halite chevrons (Figure 3.30; Stage II). The freshening episodes plane off the upper part of the chevrons as undersaturated waters eat into the crust along the inter-chevron boundaries and form brine filled pores (Chapter 1). Capillary evaporation and brine reflux then fills the porosity with clear halite cement. Continued dissolution and reprecipitation of halite and other soluble salts in the vadose and capillary portions of the crust can destroy much of the initial aligned chevron texture. The end result of alternating freshening and drying episodes is a bedded stack of salt crusts with pores filled by halite spar, occasional relict zones of aligned chevrons and numerous internal truncation surfaces (Figure 3.30; Stage III).

At the broader scale, the continual addition of new salt crystals from evaporating pore waters causes an increase in the volume of the surface crust, which, once the pan desiccates, lies at the top of the capillary zone. Thickness of the capillary fringe

limits any continued vertical growth of the crust and focuses precipitation into the uppermost parts of the crust, so the crust attempts to expand horizontally. The force of crystallisation creates a biaxial stress in the crust that ultimately forms cracks that grow into overthrust salt polygons or pressure ridges. Freshly exposed thin halite and gypsum crusts in modern pans and sabkhas around the world show this style of polygonal ridging and crestal cracking. But the mechanism creating mature m-thick pressure ridged beds is not crust expansion driven solely via the force of crystal growth. There is also the addition of detrital sediment to the crust via infill of newly formed fissures. Wind-blown detrital sediment fills fissures with successive linings.

Ongoing capillary precipitation means pressure ridges rarely retain the simple inverted V cross section of the infill formed in the initial break in the salt crust. Ongoing salt growth, fissuring and dissolution, along with infiltration of eolian silt and sand into cracks and fissures, deforms and anneals the crust into a variety of knobs, ridges, and pinnacles with a relief of up to a metre above the adjacent mudflat floor (Figure 3.29e). Underlying clays often heave up and out through the axis of the megapolygon suture. Ancient counterparts to salt hosted pressure ridges and megapolygons have been recognised in the Messinian salts of Sicily (Lugli et al., 1999) and the Triassic salts of Cheshire, UK (Tucker, 1981) where they are used as indicators of times of exposure in thick halite sequences. Fissure fills in these ancient counterparts can cut up to 6 metres vertically across stacked halite beds.

Each salt layer in a thick salt pan unit, is in large part derived from the recycling of older salt layers. Layers are separated and crosscut by mud partings composed of detrital material carried in by floodwaters or eolian detritus blowing across the emergent salt surface. The final buried sediment is a thick bedded-salt composed of randomly aligned recrystallised evaporites. Saline pans form relatively pure salt units, which are metres thick, layered, and crosscut by fissures filled with eolian or detrital impurities. This type of bedded salt, which has been subjected to ongoing exposure and capillary evaporation, contains randomly aligned and overprinted crystals precipitated from a brine hydrology characterised by crystallisation, dissolution and recrystallisation. It contrasts with bedded salt deposited in the relatively stable perennial brine hydrologies of a more-or-less continually subaqueous saline lake where, even after burial, the crystals in the stacked crusts still retain a growth aligned fabric of upward pointing large gypsum crystals, chevron halites, or trona prisms (see perennial lake discussion in the next chapter).

Styles of continental sabkhas

Mudflats, sabkhas and saline pans occur as parts of three saline lacustrine settings (Hardie et al., 1978);

- Alluvial fan–ephemeral saline lake
- Ephemeral stream floodplain - dune field–ephemeral saline lake
- Perennial stream floodplain–perennial saline lake

Settings are not static and changes in tectonics or climate can cause one setting to evolve into another. Texture of the capillary precipitates are similar in all three, but differences in lacustrine hydrology means continental sabkhas are more widespread in ephemeral lake systems than in perennial lake systems, which seem to require steeper sided basins (Table 4.7).

Alluvial fan–ephemeral saline lake

The alluvial fan–ephemeral saline lake depositional complex typifies fault-bounded, orogenic basins in tectonically-active arid areas. Tectonism generates topography and increased contrast in thermal gradients, so that water volumes seeping into the evaporitic mudflat (continental sabkha) and adjacent pan can be quite high, fed predominantly from groundwater and occasional storm runoff. Such arid intermontane lows can be covered by extensive continental sabkhas, with areas of saline pans in the lowermost positions on the playa floor (Figure 3.31). Modern examples range across various tectonic settings and include intermontane playas in the Basin and Range of North America, salars of the Central Andes, some East African rift valleys, saline valleys at the southern end of the Dead Sea transform, and playas on the Tibetan Plateau and Mongolia. Of the two ephemeral lake settings, it is the one where thick sequences of evaporitic salts are more likely to be preserved due to rapid subsidence. Ancient counterparts of this style of deposit include the saline mudflat and pan facies in the Wilkins Peak Member of the Eocene Green River

Formation, Utah, the Tertiary borate deposits of Turkey and Cambrian Lake Parakeelya of the Officer Basin, South Australia (Fischer and Roberts, 1991; Helvaci, 1995; Southgate et al., 1989). Let us now look in more detail at the geology of few Quaternary examples.

Sabkha Yotvata, Israel

Sabkha Yotvata is a continental sabkha with an aerial extent of 45 km²; it infills the entire 10 km width of the southern Arava Valley (Figure 3.31a; Amiel and Friedman, 1971). It is located some 45 km north of the Red Sea and 110 km south of the Dead Sea in the Great Rift Valley, the transform depression separating

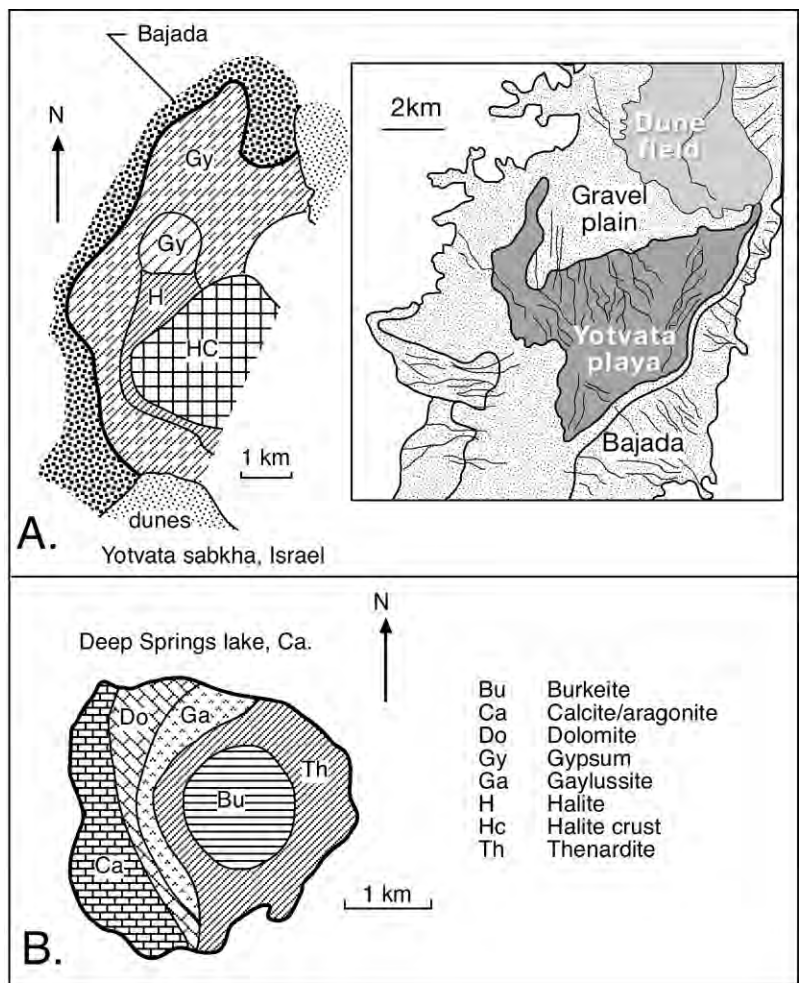


Figure 3.31. Surficial geology of continental sabkhas. A) Sabkha Yotvata, Israel, (Amiel and Friedman, 1971; Amit et al., 1999) and, B) Deep Spring Playa, California (Eugster and Hardie, 1978). Note the off-centre bull's-eye pattern in the distribution saline salts indicating nearsurface seepage fractionation and the accumulation of the most saline salts in the lowermost part of the playa floor.

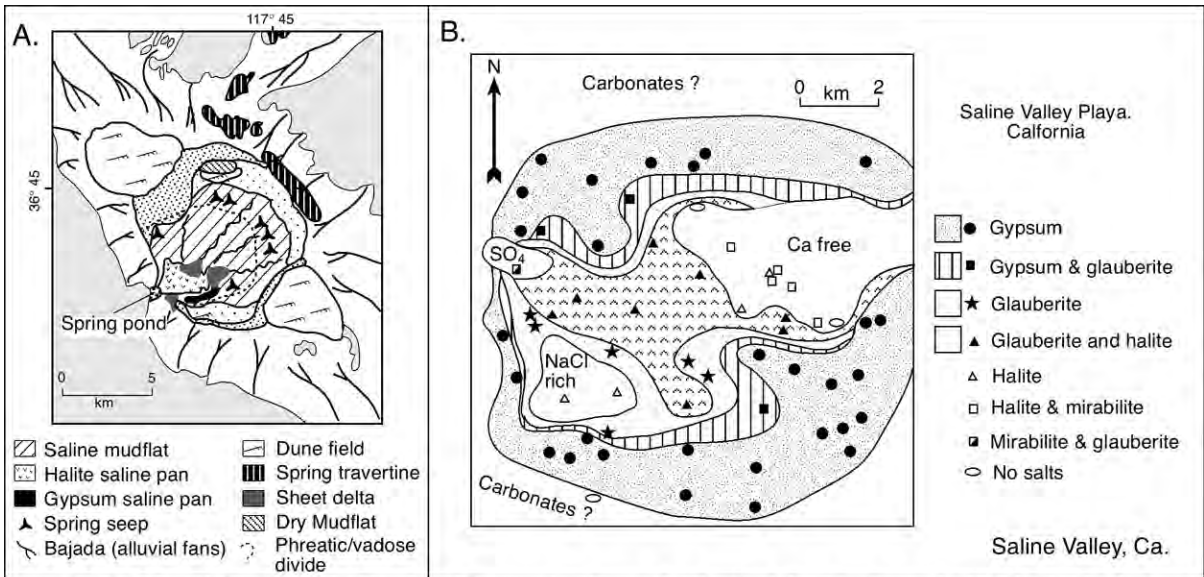


Figure 3.32. Saline Valley Playa, California. A) Regional sediment distribution (after Hardie et al., 1978). B) Distribution of intrasediment evaporite salts in the saline mudflat (sabkha) part of the playa. The concentric of “bull’s-eye” pattern with the more soluble salts in the lowest parts of the area indicates fractionation and progressive concentration of groundwater seepage (after Hardie, 1968 and Smoot and Lowenstein, 1991).

the Jordanian and Palestinian plates. The Yotvata valley floor is only 75 m above sea level. To the east and west the sabkha is bordered by steep-sided valley margins; to the east the valley wall rises up to 1300 m above the valley floor while to the west it rises up to 600 m. Differences in relief are a response to current movement on the Avrona Fault zone. Some 1km wide and 35 km long, the Avrona Fault extends in a NNE direction from the western margin of the northern coast of the Gulf of Elat across the Avrona Playa and up along the steep eastern side of the Yotvata Playa (Amit et al., 1999). North of the Yotvata Playa it dies and merges with the prominent strike-slip fault that trends north to become the Dead Sea Fault.

Steep valley walls have led to the development of an extensive bajada, which interfingers with the evaporitic sediments of the sabkha. In the valley to the north of the sabkha is an extensive dune field extending some 40 km up the valley. To the south is another smaller dune field, which partially covers the southernmost sediments of the sabkha.

Matrix sediments are furnished to the sabkha by sheetfloods and a series of short ephemeral streams (wadis) on the bajada, fine silts and sands are blown into the sabkha by northerly winds from the dunes. Matrix grain size in the sabkha shows a bull’s-eye pattern of distribution with fine to coarse sands and pebbles about the margin and silty to sandy clays in the centre. North and south the grain-size bull’s-eye is complicated by the

presence of dune sands. The displacive evaporite salts of the sabkha grow in the capillary and phreatic zones and also follow a bull’s-eye pattern related to efflorescent/capillary fractionation of the groundwater; gypsum dominates the periphery and halite the lowermost central portion of the sabkha. The water table is as deep as 4 m about the bajada periphery and shallower than 1 m beneath the sabkha. Puffy ground and dissected halite crusts form the ephemeral saline pan facies in the lowest part of the valley, whereas displacive nearsurface gypsum grows in the capillary zone of the adjacent saline mudflat.

Basin and Range playas, USA

Saline lakes with extensive mudflats and smaller areas of saline pans, both surrounded by extensive alluvial aprons (bajada) characterise many of the depressions in the arid zone of the south western USA. These saline systems are locally known as playas. Tectonically, the depressions hosting the sabkhas are a response to extension and transform faulting.

Deep Springs Lake, California

Deep Springs Lake is a small 5-km wide playa in Deep Springs Valley in eastern California, just east of Owens Valley (Figure 3.31b; Jones 1965). Holocene faulting has dropped the valley floor some 1500 m in the southeastern corner to form a 5-km² playa with a 1-km² saltpan near its centre. The playa is fed by

a series of tufa springs with waters that have been in contact with igneous and metasedimentary rocks. The pan in the lowest part of the playa floor is occupied by soluble, mainly Na-rich salts—thenardite, burkeite, trona and halite—deposited as a bedded crust deformed into overthrust pressure ridges. Dolomite precipitates in the more peripheral, less saline areas (Peterson et al., 1963). The playa is surrounded by the distal sediments of a series of alluvial fans with carbonate-cemented tufa springs at their feet. Volumetrically the capillary and pan salts are a minor portion of the valley-fill which is dominated by alluvial fan and sand flat (distal fan) facies.

Saline Valley playa, California

Saline Valley playa is a small continental sabkha-salt pan playa in a fault-bound graben located east of Owens Lake across the Inyo Mountains. Amalgamated alluvial fans (bajada), fed from adjacent mountains, are dominated by debris flow deposits; their slopes are short and steep with little sandflat development around their bases (Hardie, 1968; Hardie et al., 1978). In contrast, fans at the NW and SE ends of the depression are more longitudinal to the basin axis and so show lower gradients allowing eolian sand sheets and dunes to accumulate adjacent to wind-reworked fan toes (Figure 3.32a). Zones of groundwater seepage are marked by Pleistocene travertines and active spring mounds.

Sabkhas (saline mudflats) cover a large portion of the basin floor and are dissected by sinuous seepage channels, while a halite-floored saline pan defines the lowest part of the playa. Pan facies are made up of dm-thick halite beds separated by mud layers with abundant intrasediment crystals of halite, glauberite and thenardite (Figure 3.32b). Glauberite crystals and moulds of mirabilite, now filled with glauberite, are common in the sabkha or saline mudflat. Along the southern zone of the saline mudflat is a belt of layered aligned gypsum that probably formed by intense capillary fringe evaporation like the texturally identical capillary gypsum crusts defining the sabkha edge of Bristol Dry lake (Rosen and Warren, 1991). The sulphate-rich northwest corner of the mudflat is tied to ponding and evaporation of seepage waters from a nearby spring.

Bristol Dry Lake, California

At the surface, the Bristol Dry Lake basin in the Basin and Range province of California exhibits what appears to be a slightly off centre bull's-eye distribution of surface and near surface salts (Figure 3.33; Handford 1982; Rosen 1991). Low-gradient alluvial fans ring the 10-km wide playa, while extensive calcretes and pedogenic calcites, associated with halophyte plants, cement mid-to-distal fan gravels and sands. Basinward of the distal fans, in the playa margin facies, is a gypsiferous sabkha some 300 m wide where celestite precipitation forms

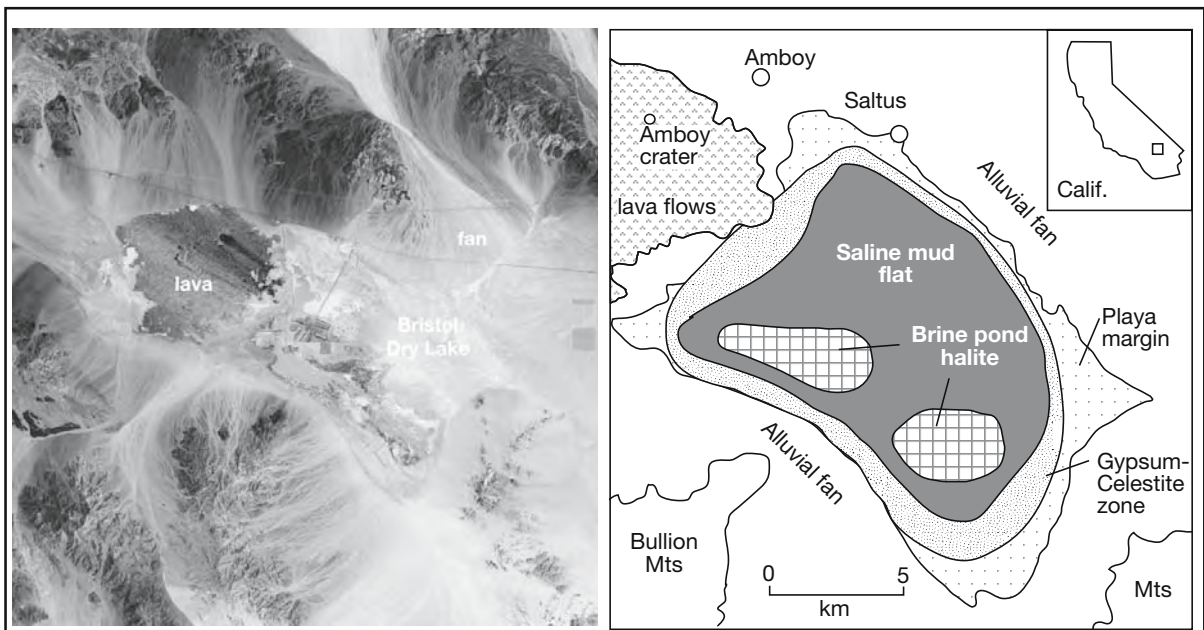


Figure 3.33. Bristol Dry Lake, California. The continental sabkha facies shows concentric pattern of intrasediment salt growth with an outer gypsum capillary pavement and an inner halite saline mudflat, the halite pan facies is slightly offset from the centre and occurs in the lowest parts of the lake in the southern part of the depression (Landsat image courtesy NASA, surface geology after Rosen and Warren, 1990).

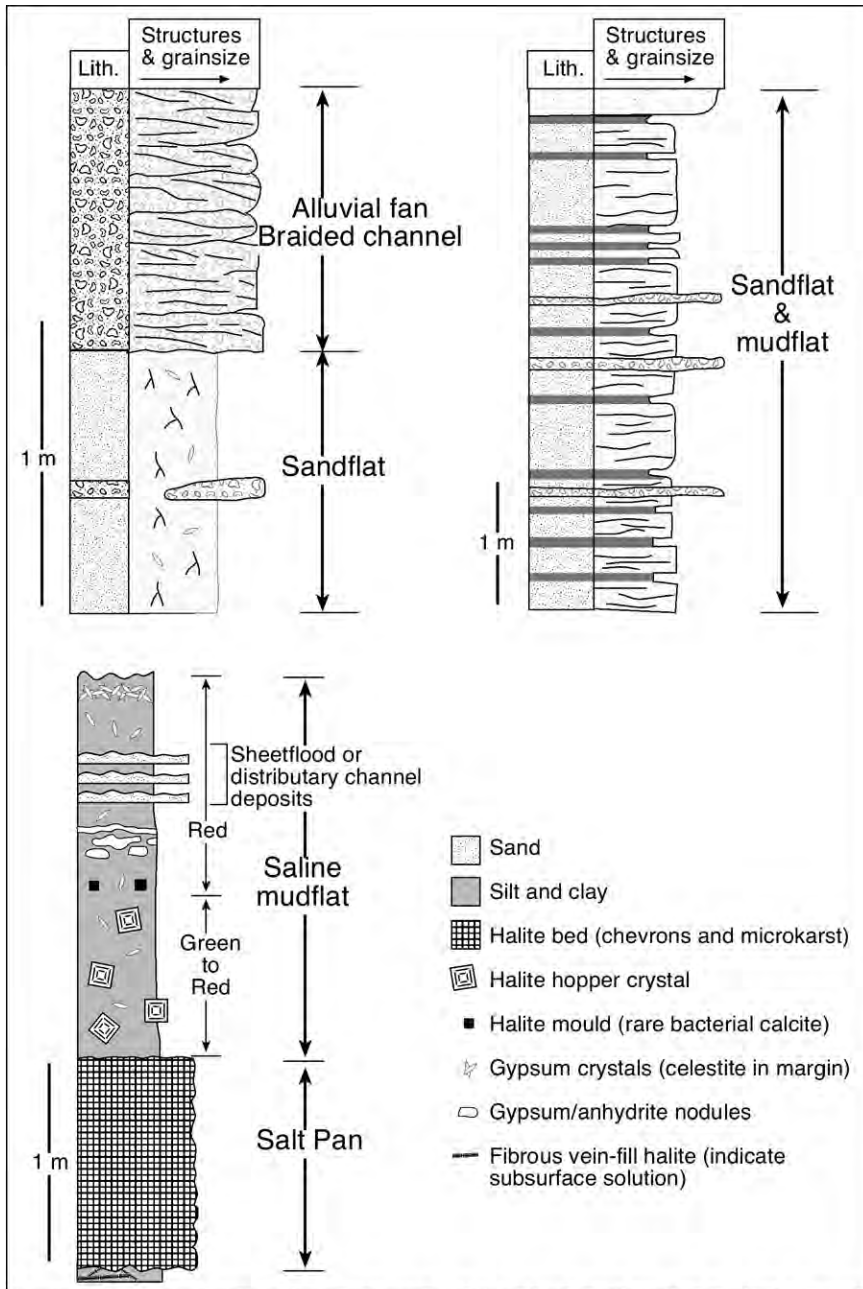


Figure 3.34. Generalized stratigraphy based on Bristol Dry Lake from the alluvial fan margin into the saltflat saline pan centre. (after Handford, 1991; Rosen and Warren, 1990).

large decimetre-size nodules that can coalesce into metre-size patches. The gypsum unit is characterised by a growth-aligned fabric created by competitive alignment of gypsum prisms in a zone of capillary wicking (Figure 3.34; Rosen and Warren, 1990). Once these gypsum crystals are buried and converted to aligned anhydrite nodules it would be next to impossible to

distinguish them from the much more commonplace subaqueous textures. Basinward of the playa margin facies, halite hoppers (up to 0.5 m in diameter) form displacive intrasediment precipitates in brine-saturated muds of the saline mudflat facies. Finally, in the basin-centre depression a 0.2-m thick chevron-halite crust (salt pan) is forming by evaporation of ponded ephemeral waters.

The lateral facies distribution seen at the surface also stacks throughout the entire length of deep cores collected in the playa (Rosen 1991). Saline pan halite beds alternate with halite-saturated siliciclastic muds in a 500-m core from the basin centre. Playa margin cores exhibit alternating beds of playa margin sediments and saline mudflat (sabkha) units for most of their length. Towards the base of the deepest playa-margin core, distal alluvial fan sediments are also present. Rosen (op. cit.) notes that a delicate balance between subsidence and mechanical/chemical deposition of minerals was necessary to maintain a vertically-consistent ephemeral brine environment during the deposition of over 500-m of basin fill.

I would say this is not really an example of some rather unusual delicate balance preserved in the sedimentary signature, so much as it is evidence of a hydrological/deflation forcing mechanism.

It is the same Stokes surface hydrology that drives sedimentation in the sabkha and pan regions of most Quaternary continental playas and sea margin sabkhas. Accommodation space in the Bristol Dry Lake depression is created by subsidence in a tectonically active region, in what has been a variable but

mostly arid climate throughout the basin's Quaternary history. The basin's hydrology dictated the contrast in accumulation styles between the salt rich succession in the basin centre and the coarser siliciclastic dominated basin edge. The volume of sediment accumulating in the basin centre in Bristol Dry Lake can never surpass the ability of the wind to blow any dried sediment out of this depression centre into surrounding areas. That is, the surface of the sedimentation in the basin lowermost parts is maintained by deflation at a position that is always near the water table. The only types of sediment that can remain in the arid basin centre are in equilibrium with the water table and the top of the overlying capillary zone. When the water table was a metre or so below the sedimentation surface, aggrading sediments were held in place by meniscus forces inherent to the capillary fringe and accumulated in saline mudflats as sabkha sediments. When the water table rose to become a water surface, it created a semipermanent saline brine pan that then deposited and stacked salt pan crusts.

Basin edge sedimentation was not hydrologically forced but built up as volumes of centripetally-supplied sediment accumulated. This in turn facilitated the creation of an aggrading potentiometric head feeding ground and surface waters to the basin centre lows. About the edges of Bristol Dry Lake, where the accumulating clastic sediment is closer to its source, it is coarser grained and less liable to deflation. Clastics are accumulating in sufficient volumes to build facies belts situated well above the regional water table, hence the accumulations of alluvial fan, dune and sandflat sediments. At times when the subsidence rate exceeds the rate of sediment supply in this area, its hydrology becomes more like that of the basin centre and saline mudflat facies come to dominate over much of the playa floor. Such a hydrologically forced system means that when regions of maximum subsidence in a basin change position, it moves the position of the hydrologically forced sediments into the new lowermost areas on the playa floor. Ultimately, once the rate of subsidence decreases to where the rate of clastic sediment supply exceeds the ability of the wind to deflate, the margin sediments will cover the whole basin and evaporite sedimentation will cease.

Death Valley playa, California

Death Valley is probably the best known playa of the Basin and Range setting in the USA, yet Death Valley is a very steep sided and unusual lacustrine depression. Its floor is some 24 m below sea level, making it the lowest continental locality in the Western Hemisphere. Its steep sides mean it is likely to become a perennial saline lake with minor changes in climate

(Chapter 4). In many areas of Death Valley the coarse-grained debris flows of the alluvial fan directly abut the salt crusts of the sabkha and the saline pan. Sandflats and dry mudflats, so obvious in most Basin and Range playas, are poorly developed or absent in Death Valley. This too reflects the steep valley walls (Figure 3.29f) and its relatively high water table in relation to the lake surface. It is a rapidly subsiding saline lacustrine system in which more than 50% of the Quaternary sediment fill beneath the lowest parts of the lake floor are dominated by saline lake and pan halite rather than matrix-rich evaporitic mudflat (sabkha).

This is clearly seen in a 90 metre length of core (DV93-1), which returned an interbedded salt and mud sequence extending back some 200,000 years (Figure 3.35; Li et al., 1996, 1997; Lowenstein et al., 1999). Minerals intersected in the core include sodium chloride (halite), sulphate minerals (glauberite, gypsum, and thenardite), and carbonate minerals (calcite and dolomite). Glauberite, gypsum, and thenardite occur in mud layers or partings as randomly oriented, mud-incorporative crystals. They are thought to be early diagenetic and to have precipitated from nearsurface ground waters within saline mudflat or sabkha settings. Carbonate minerals calcite and dolomite occur as rhombs to irregularly shaped crystals that are less than 5 μm in diameter. Vertically, there are significant mineral assemblage variations in the core. Abundant glauberite and gypsum, and relatively small amounts of calcite (13%-35% of > 1 μm size insoluble fraction) are associated with both sabkha and subordinate saline pan settings. They formed in relatively dry periods from 0 to 10 ka and 60 to 100 ka (0-8 m and 60-90 m depths in the core, respectively). Sabkha sediments (0.25-7 m, 60-78 m, 87-90 m) consist of muddy silts with sand patches and mud cracks and accumulated during long periods of desiccation. They indicate sedimentary accretion via formation and incorporation of efflorescent salt crusts in the accreting sediment matrix. These episodes of sabkha and subordinate saline pan deposition indicate periods when Death Valley was relatively arid and the sedimentation surface was the top of the capillary zone over much of the valley floor, similar to the modern setting.

In contrast, most of the remaining intervals in the core are characterised by sparse CaSO_4 -bearing minerals and relatively high amounts of calcite (20%-50% of the >1 μm -size insoluble fraction). These are intervals where much of the sediment is halite rather than mud-dominated. It defines a time 10 to 60 ka (8-60 m) when the basin-floor water table was above the sedimentation surface for long periods of time, including the 25,000 year wet period when Death Valley contained a perennial

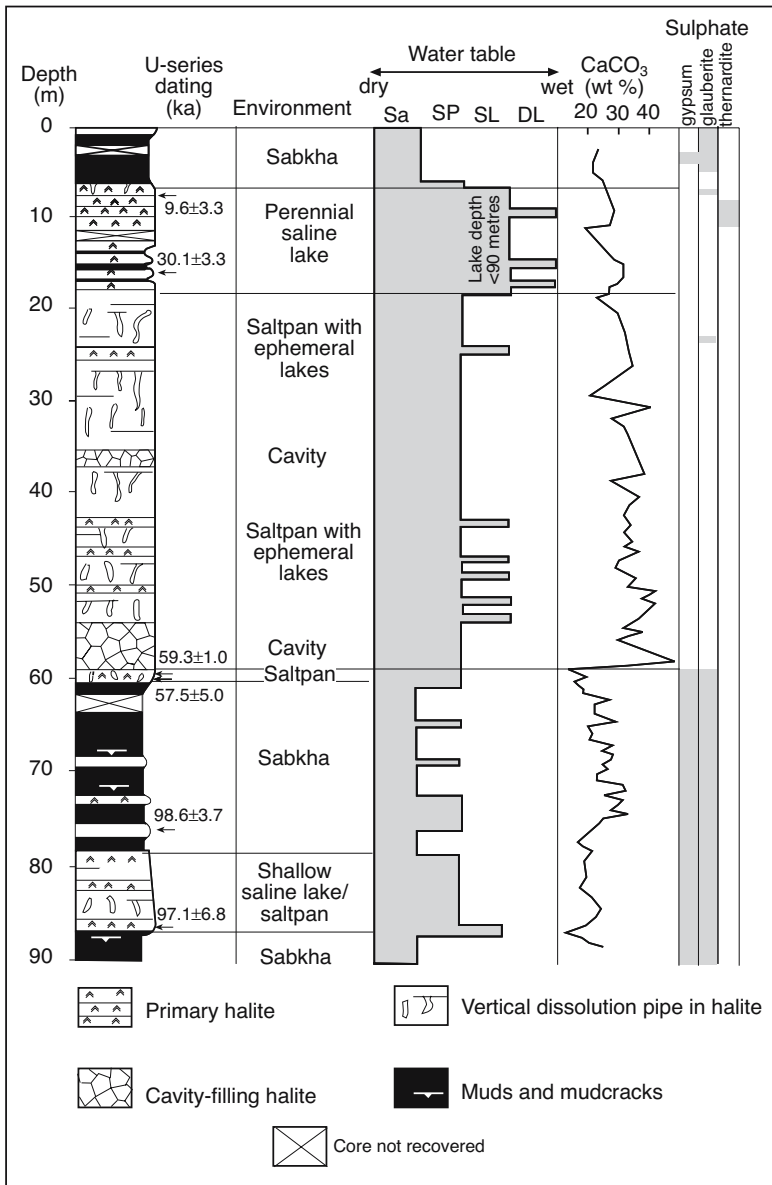


Figure 3.35. Stratigraphic column of upper 90 metres of core DV-93-1 from Death Valley, California (after Li et al., 1997). Lake levels and water table fluctuations are shown ranging from driest (sabkha) through saline pan (SP) to the wettest lacustrine phases of saline lake (SL) and deepest lake (DL). The dominant evaporite mineral is halite and the position of the sulphate evaporites in the core, as well as the weight percent CaCO₃ in the > 1 μm fraction, are also shown.

halite lake (10 to 35 ka; 8-18 m) and the 25,000 year period when the floor of Death Valley consisted of saline pan-ephemeral saline lake environments (35 to 60 ka; 18-60 m; Figure 3.35). Core intervals through saline pan sediments are composed of interbedded halite, chaotic muddy halite, and mud. The halite contains abundant vertical dissolution pipes, cemented with clear halite, indicating the water table periodically dropped below

the surface of the stacking halite crusts. These sediments record repeated flooding by dilute waters, dissolution of subaerially exposed surface salt crusts, deposition of mud from suspension, precipitation of halite during the saline lake phase, and cementation by diagenetic halite (Li et al., 1996). Such deposits document a relatively wet climate with a high ratio of water inflow to evaporation compared to today. Ostrocodes in mud layers represent the least saline, deepest lake phases when, based on the position of beach deposits in the valley walls, water depths in the deepest part of the lake were as much as 90 metres. Halite layers are made of fine-grained cumulates and clear, vertically oriented crystals precipitated during shallower, perennial lake stages. The near complete absence of syndepositional dissolution textures in saline minerals precipitated in the perennial saline lake interval, imply that the accumulating salts were permanently protected from dissolution by an overlying perennially-saline at times holomictic water column (see detailed discussion in Li et al., 1996).

According to Li et al., 1997, the interval with little glauberite and gypsum, and relatively abundant calcite, dated from 10 to 60 ka (8-60 m), corresponds to the last glaciation, i.e., stages 2 and 3 of the marine oxygen isotope record. This was a relatively wet period in Death Valley. The intervals with abundant glauberite and gypsum and relatively low calcite correspond to the Holocene and to stages 4 and 5 of the Quaternary marine record, which were two relatively dry periods in Death Valley. Therefore, mineral assemblages correlate with wet and dry climate cycles in Death Valley (lake versus mudflat), which shows once more that mineral assemblages, depositional style and brine chemistry are all linked to climate changes (Chapter 2).

Salars of South America

The greatest thicknesses and volumes of evaporites currently accumulating anywhere in the world are doing so in the various collision related intermontane depressions and deserts of South America. More than a hundred salt-crusts pans or playas, locally known as salars, characterise depressions in the high-relief arid region of the central Andes and constitute salt deposits with areas ranging from more than 9000 km² to less than 1 km² (Figures 3.36, 3.37). Some have been harvested on a small scale since the mid 19th century for their chloride, nitrate, borate and iodide salts. Huge state-of-the-art brine extraction/processing plants have come to operate in some of these salars in the last two decades and have taken much of the world market from similar older smaller facilities in North America (Chapter 11).

Salars occur within a tectonically active region of largely interior (endorheic) drainage over an area of more than 400,000 km². It extends from the arid to semi-arid deserts of the Andean highland plateau (Altiplano Puna) down to the hyperarid Atacama desert, an area that is so arid that nitrate salts form widespread (and mineable) pedogenic precipitates (Figure 11.42). Altiplano Puna was uplifted in the Miocene and is characterised by an average elevation greater than 3000m and widespread endorheic drainage. Salars of the Puna are either “wet” or “dry” and similar styles of arid deposition have dominated their fills throughout their Neogene histories (Alonso et al., 1990).

Dry salars are characterized by high rates of evaporation and are starved of detrital sediment. Fluvial input is restricted to rare flash floods and groundwater seepage is the dominant source of solutes. Stacked crusts of salar halite are typically in direct contact with basin margin gravels. Desert indicators are abundant in the clastic edge and include, eolian sands, polished clasts, varnished cobble, desert pavements and gypcrete soils. Volcanism, either by ash fall or hydrothermal circulation is the parent to almost all solutes accumulating in the basin. Examples include; Salar de Uyuni, Salar de Atacama, Salar Grande and Salar Arizaro.

Wet salars are fed by permanent streams, in addition to groundwater seepage. These salars have perennial brine lakes and evidence of fluvial deposits, especially alluvial fan deposits, is more significant in the fill than in dry salars. Salar fill is typically alternating beds of clastics and evaporites. The slightly wetter (but still arid) environment of deposition is indicated by mud cracks, raindrop prints, bird tracks, ripple marks, desiccation breccias and preserved plant fragments. Modern examples include the Pastos Grande and Hombre Muerto salars.

The hyperaridity of much of this region of South America reflects a confluence of a number of desert-forming conditions (Table 2.2). First, it lies in the Horse Latitudes, a region of permanent subtropical highs locally blocking influence of the semi-permanent South Pacific Anticyclone and so limiting the influence of winter storm tracks from the south. Second, offshore upwelling of the cold northward Humbolt current creates an atmospheric temperature inversion ($\approx 1000\text{m}$ elevation) that prevents inland penetration of Pacific moisture. And third, the Atacama Desert lies on the western flank of the high Andes and so sits in a rain shadow not subject to tropical/subtropical moisture from the east. The driest part of the Atacama, which is 50 times more arid than Death Valley, California, in effect lies in a “double” rain shadow with the Andes to the east and the Coastal Range to the west (Figures 3.36, 3.37).

The region has experienced arid to semi arid climate as far back as the Middle Miocene, when the modern Andes were first uplifted to form a barrier to easterly trade winds. Uplift anchored the South Pacific Anticyclone to the western bend in the South American continent. Uplift of the Andes to its present elevation may have occurred as early as 15-19 Ma, although palaeobotanical evidence suggests the Central Andes were at half their present elevation some 10 Ma (Vandervoort, et al., 1995; Gregory-Wodzicki, 2000). The Humbolt current has been active since the Early Tertiary, but reached its present intensity either during a major expansion of the Antarctic ice sheet 15 Ma or after the Isthmus of Panama formed some 3.5 Ma (Chapter 5). Onset of Miocene aridity also shut down the meteoric flushing that drove supergene enrichment needed to create the giant porphyry copper deposits of the Southern Atacama (Sillitoe and McKee, 1996).

There are four Neogene evaporite domains in the Andean highplain (Figure 3.38a; Alonso et al., 1990). Deposits change from only travertine in the north, to a mix of travertine, gypsum and minor borate, to completely evolved halite dominated successions in the south, with borate-rich sequences along the eastern Puna. Older halite-rich successions are often caught up in subsequent tectonism and become halokinetic sources to modern salars such as Salar de Uyuni and Salar Atacama. The southward change from travertine to halite is consistent in deposits ranging in age from the Miocene until the present and probably indicates a consistent trend of increasing aridity from north to south since the Andes first arose in the Miocene (Alonso et al., 1990).

Present day rainfall in the Andean Highlands ranges from <50 mm in the vicinity of Salar di Maricunga and nearby areas in

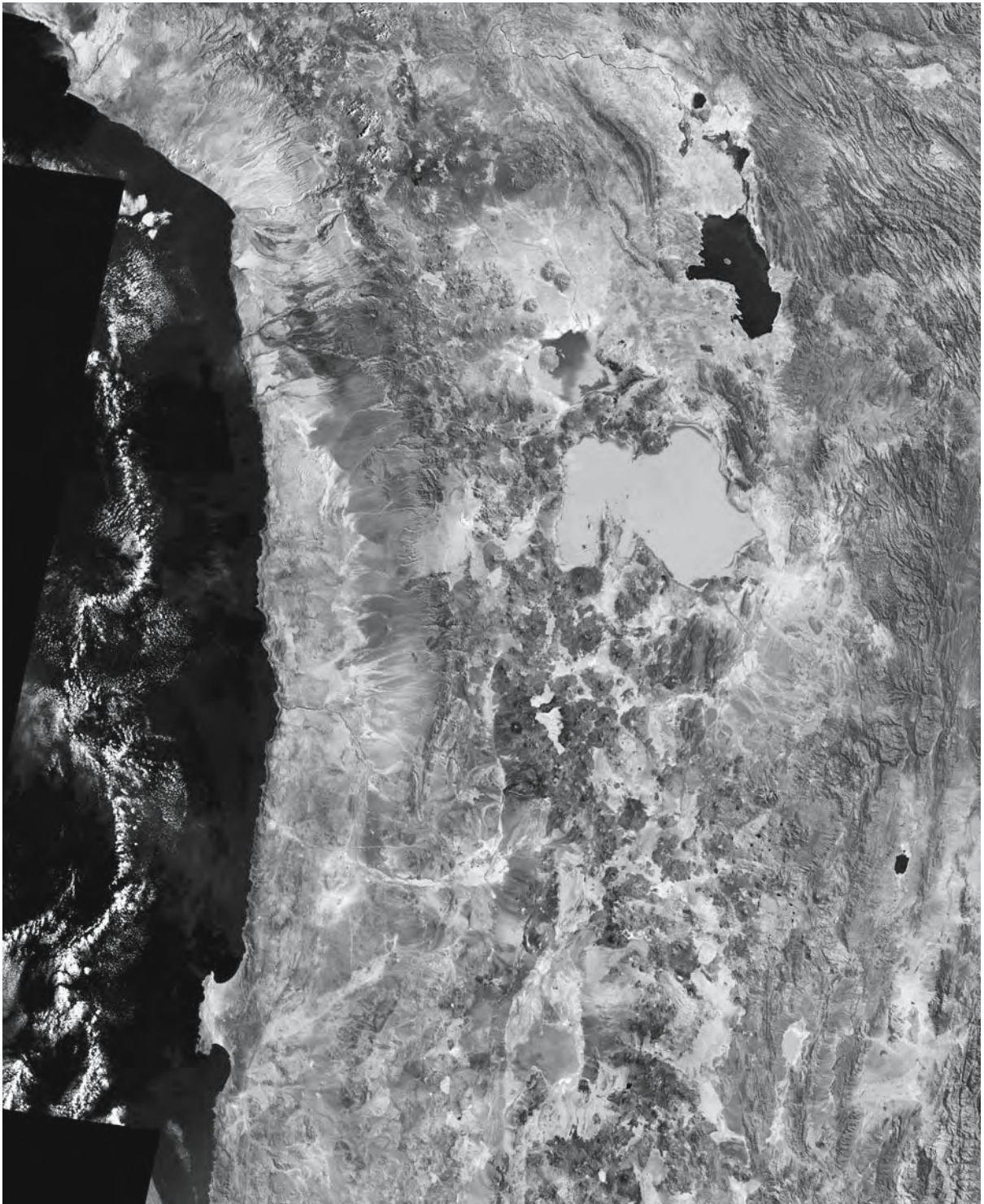


Figure 3.36. Saline lakes (salars) of the desert belt of South America, shows the proximity of many salars to active rhyolitic/andesitic volcanoes in the Altiplano (refer to Figure 3.37 for location of individual lakes and salars (Landsat image courtesy of NASA).

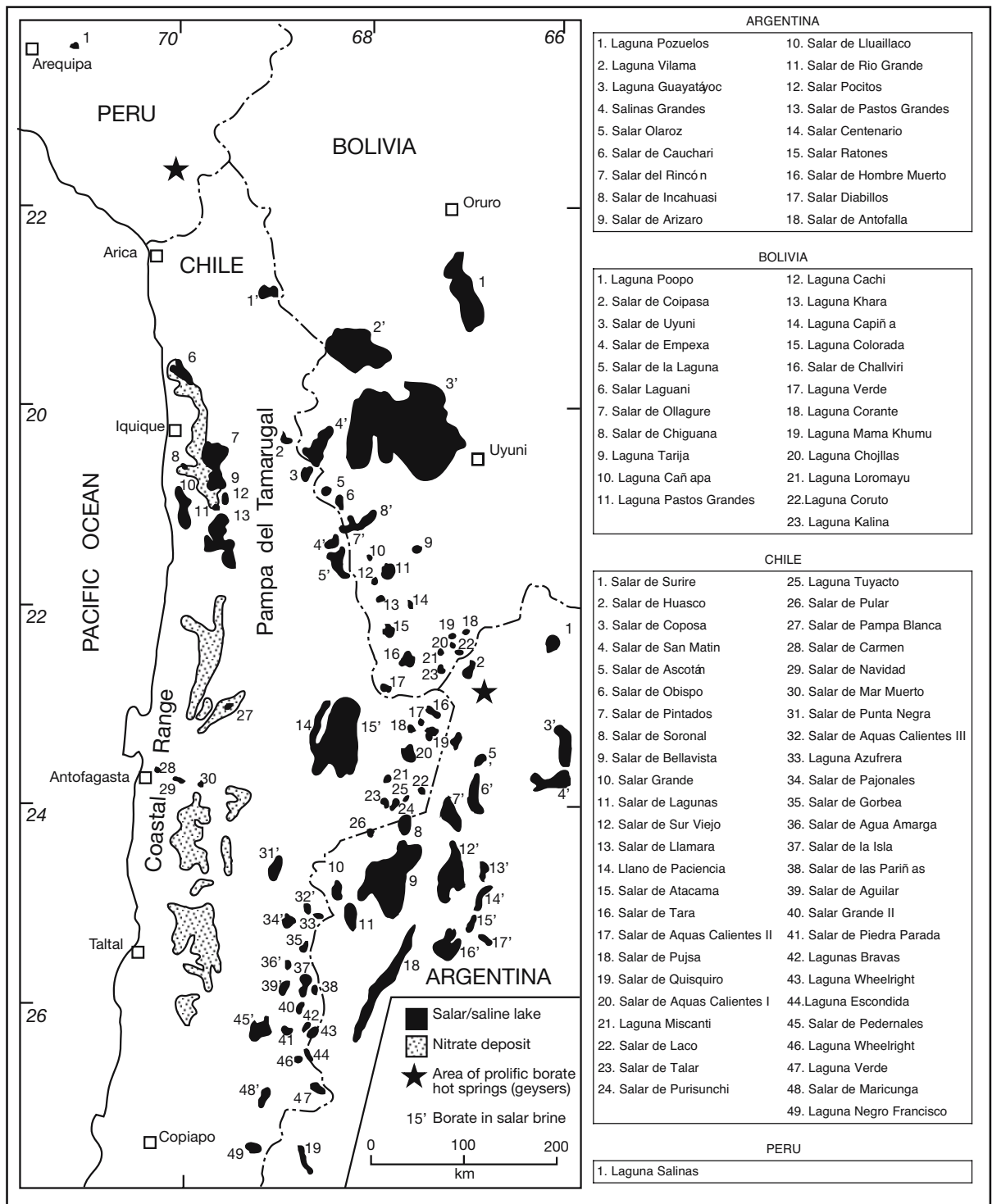


Figure 3.37. Index of the main salars and salinas and nitrate deposits in the central Andes, South America (after Ericksen, 1993).

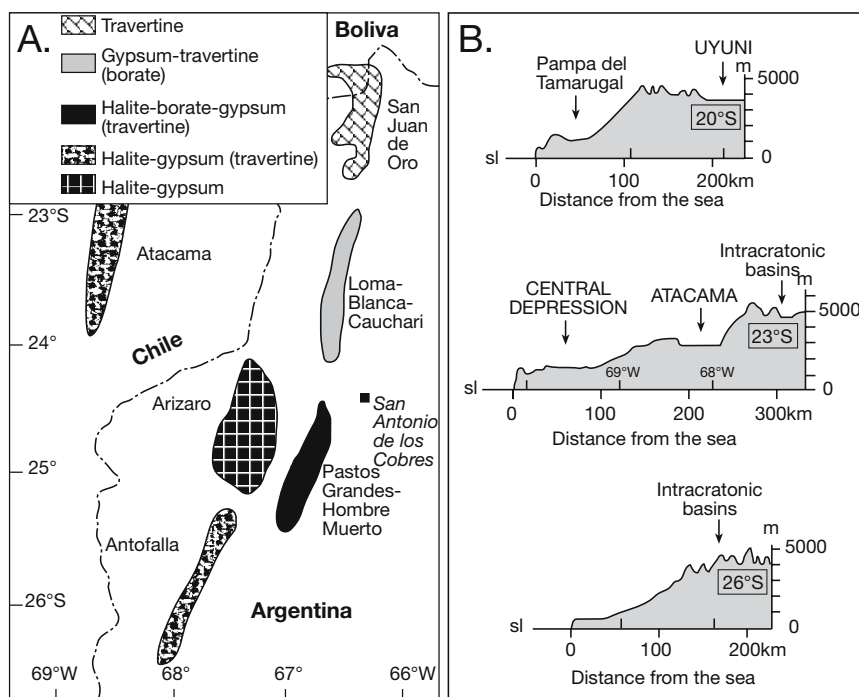


Figure 3.38. A) Evaporite belt and physiography, Andes, South America. A) Generalized latitudinal distribution of Pliocene-Miocene evaporite belts (after Alonso et al., 1990). B) Physiographic profiles at various southern latitudes across the Andes (after Risacher et al., 2003).

Bolivia and Argentina to nearly 300 mm in the area around Lake Titicaca and southern Peru (Figure 3.37; Erickson, 1993). In contrast, the Atacama Desert lacks an annual rainfall and it may rain as infrequently as once every 10 - 20 years. Much of the groundwater in the desert is sourced from runoff in the Andean Highlands. Unlike the playas in the southwest of the USA, dry salars are dominated by pan facies rather than mudflats, perhaps reflecting higher relief and lower permeability substrates in this region creating more opportunities for flooding, followed by extended times of brine ponding.

Active continental volcanism is ongoing, with several west-northwest trending volcanic ridges cutting the Puna. This divides the Puna into several stagnant endorheic basins, further subdivided by north-south trending structural blocks creating local sources for alluvial fans and groundwaters. Thus, many of the salars show elevated lithium and boron contents in their surface and interstitial brines, with solutes sourced in abundant highly reactive volcanics, mostly rhyolitic ash-flow tuffs. Ions are redistributed to the salar by runoff and

ongoing hydrothermal circulation (Figure 2.17; Table 3.5; Erickson, 1993). Evaporative concentration of salar brines leads to the depletion of Ca, HCO_3 , B_2O_3 and SiO_2 , and the enrichment of Li, K and Mg. Ca and SO_4 are removed from the concentrating waters as gypsum, while Ca and HCO_3 are removed early in brine evolution as cyanobacterial limestones, ostracode carapaces and inorganic precipitates, mostly travertines (Risacher et al., 2003). Boron precipitates as ulexite (see Chapter 11), while SiO_2 is removed by incorporation into widespread diatom tests in the fresher water lakes and spring pools. The proportions of Li, K and Mg tend to remain constant in a single lake basin, but vary from basin to basin owing to varying proportions of contributing lithologies from one drainage basin to another.

According to Risacher et al. (2003), sea salts and desert dust are blown eastward over the Cordillera, where they can constitute an appreciable fraction of the solute load of very dilute waters feeding the salars (salt content < 0.1 g/l). But

	Atacama	Uyuni	Hombre Muerto	Del Rincon	Empexa	Ascotan
Cl	189,500	191,800	194,800	191,000	120,000	70,000
SO_4	15,900	13,200	11,100	13,500	34,100	25,000
HCO_3	230	592	n.d.	n.d.	430	2,900
B_2O_3	1,416	1,136	1,455	1,570	702	2,520
Li	1,570	700	914	310	213	186
Na	103,000	94,900	121,900	121,800	67,200	45,000
K	23,600	13,500	9,340	6,260	3,400	3,500
Mg	6,130	11,800	268	2,090	8,480	5,125
Ca	520	461	1,000	480	259	920
TDS	370,000	351,000	340,920	330,000	239,000	153,600

Table 3.5. Chemical analyses of selected brines from salars in the central Andes, South America (in part after Erickson, 1993).

weathering of volcanic rocks contributes most components to inflow waters with salt content ranging from 0.1 to 0.6 g/l. However, the average salt content of all inflows is much higher, about 3.2 g/l. Chemical composition, Cl/Br ratio, and ^{18}O - ^2H isotope contents point to the mixing of very dilute meteoric waters with present lake brines for the genesis of most of the saline inflows. Saline lakes and subsurface brines are a steady-state hydrologic regime. The average residence times of conservative brine components ranges from a few years to some thousands of years and indicate permanent leakage of the brines through bottom sediments. The infiltrating brines are recycled in the hydrologic system where they mix with dilute meteoric waters. High heat flow is the likely driving force that moves the deep waters in this magmatic arc region. According to Risacher et al. (2003), active Chilean salars cannot be considered as terminal lakes nor, strictly speaking, as truly "closed" basin lakes. They leak (see Chapter 2). Almost all incoming salts ultimately leave the basin and are transported elsewhere. Moreover, the dissolution of fossil salt crusts in some of the active salars also carries away important fluxes of components in percolating brines. In effect, the regionally leaky salar hydrology constitutes a broad scale fractionating system that can accumulate relatively pure salts in each of the large salt basins.

Although there is a longterm north to south trend of increasing salinity, evaporite basins and aridity have migrated eastwards with time, driven by the Miocene evolution of the Andean Range. Consequently, many of the westernmost salars, such as Salar Grande, are presently not regions of internal drainage (Pueyo et al., 2001). Worldwide, this migration of precipitative activity in "piggy-back" salt basins characterises the evolution of many evaporite deposits that accumulate in collision belts (e.g. Figure 5.43). The Central Depression is bounded on the west by the Coastal Range and the Pacific Ocean and to the east by the Andean Pre-Range (Figure 3.38b). Throughout the Neogene, it acted as a significant drainage basin for pluvial input from the east that flowed into the area without reaching the sea. Its alluvial fan systems reach dimensions of tens of kilometres wide and hundred of metres in thickness. In the more distal parts of the fans, both perennial and ephemeral lakes developed (e.g. Calama-Chiu Chiu, Batea, Quillagua-Soledad, Bellavista-Pintados, Pisagua basins). The topography responsible for this drainage arrangement was generated during the Upper Paleogene, as a result of the Incaic orogenic pulse. From this time to the Pliocene the Central Depression was an endorheic area, and the Coastal Range acted as a barrier to drainage to the sea.

In plan view, sediment patterns in most of the South American salars with salt fills show a central zone, consisting of a relatively thick stack of halite crusts, surrounded by a thin marginal sulphate zone consisting of a variety of sulphate minerals, as well as minor halite and ulexite (Ericksen, 1993). The zoning may be symmetrical (bull's-eye pattern) with sulphate surrounding a central halite core, or asymmetrical with the halite zone crowded against one side of the salar. This is the situation in Salar de Atacama where tectonic tilting has displaced the lowest part of the brine sink to the southern end of the playa. Alternating arid and pluvial climatic episodes, since the mid-Miocene, means most salars/playas are filled by alternating beds of salt and siliciclastics.

Salar di Uyuni, Bolivian Altiplano

The Salar of Uyuni, at an elevation of more than 3600m in the central Bolivian Altiplano, is an active ephemeral saline lake (salt-crust saline pan) where substantial salt thicknesses have accumulated across an area of a little less than 10,000 km², making it the world's largest salt-filled saline pan (Figures 3.39, 3.40a; Risacher and Fritz, 2000). A 121 m deep well, drilled in the central salar, intersected a complex evaporitic sequence made up of 12 saline pan intervals separated by 11 mud layers deposited mostly as saline mudflats or sabkhas (Figure 3.40b). The thick saline pan beds are composed of stacked salt crusts and alternate with thinner mud units in the lower half of the well. The mud beds show obvious lacustrine features and thicken upwards as salt beds thin. The well indicates a longterm hydrology where tectonics, as well as climate, controlled the level of the regional water table.

Bromine contents of the recovered pan halites range from 1.3 to 10.4 mg/kg (Figure 3.40b). Such low values mean the various halite beds were not precipitated by simple evaporation of meteoric and surface waters. This would be indicated by Br contents of tens of mg/kg in the pan halites (Risacher and Fritz, 2000). Rather the brines were created by dissolution of older evaporites, which subcrop in the drainage basin. Halite from one such nearby gypsum-capped diapir has a very low Br content of 2 mg/kg, strongly suggesting that most of the halite deposited at Salar di Uyuni originated from the leaching of similar diapiric salt. The ubiquity of this salt source is indicated by the numerous gypsum-capped diapirs, which still outcrop in the Altiplano (Figure 3.40a).

The very low and fairly constant Br content (1.6-2.3 mg/kg) of the lower salt beds, along with an abundance of detrital minerals, suggest the deeper and thicker halite beds were

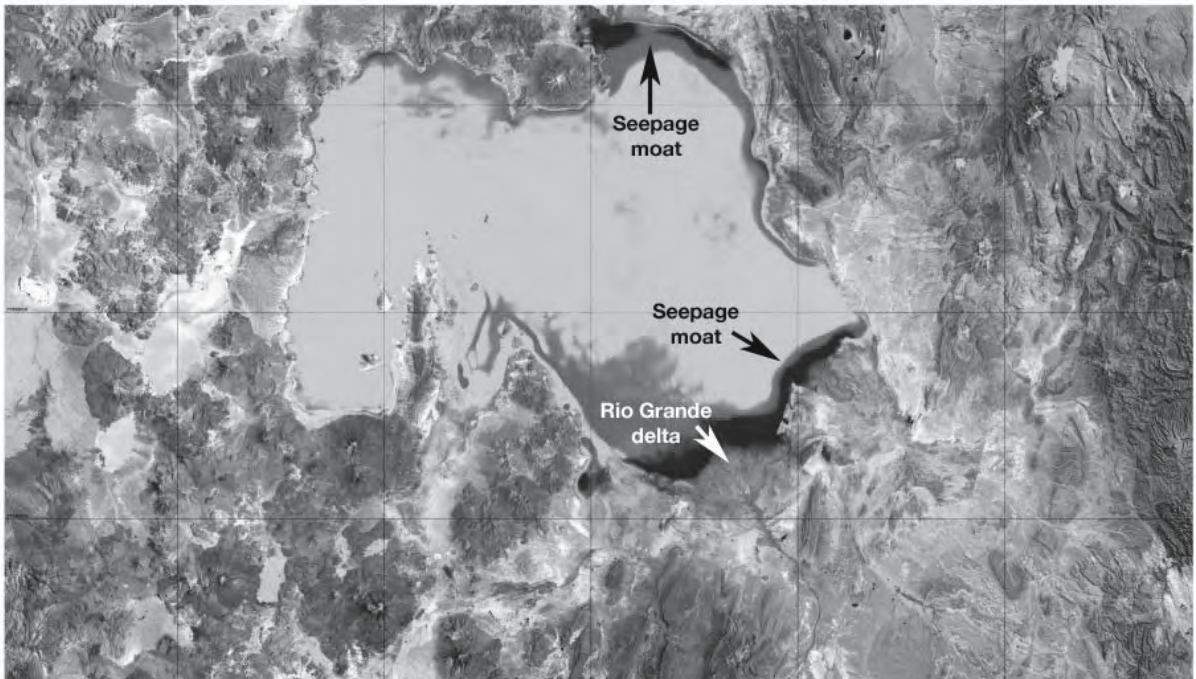


Figure 3.39. Salar di Uyuni, Central Altiplano, Bolivia. Halite crust appears light blue, the moat fringe dark blue, and the Rio Grande delta can be clearly seen in the southwest part of the salar (Image courtesy of Fachrichtung Geoinformatik, FU Berlin).

deposited as saline pan intervals in ephemeral lakes (Figure 3.40b). Thereafter, perennial water episodes of increasing

duration, flooded the central Altiplano. This change is tied to an increase in the volume of dilute meteoric waters entering the

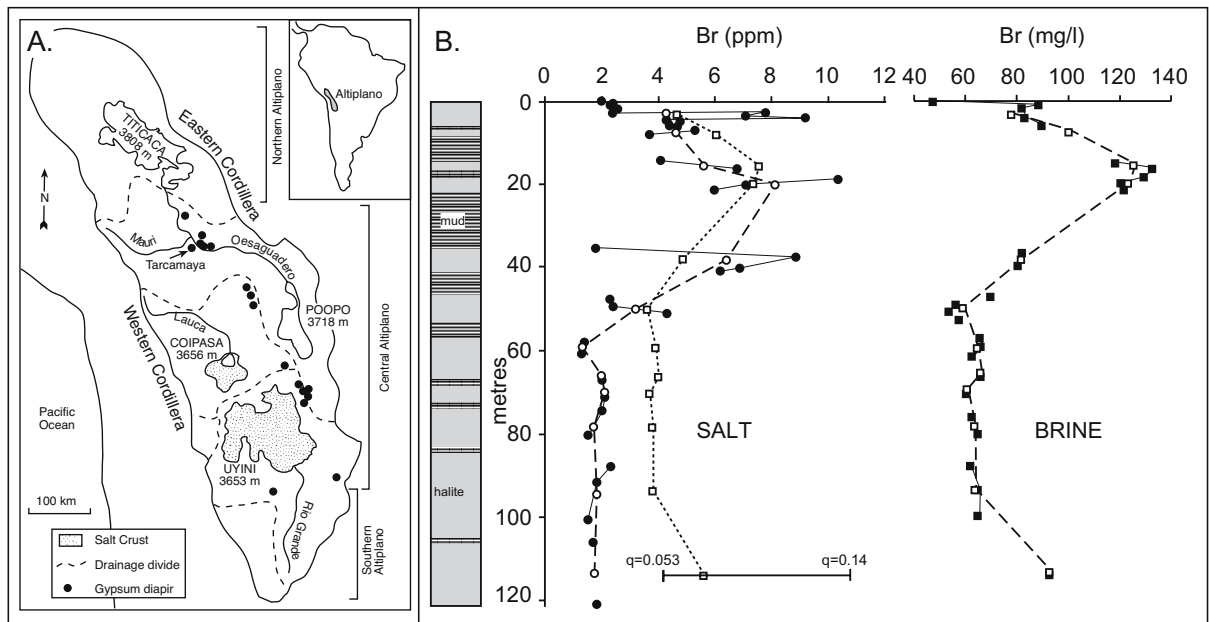


Figure 3.40. Salar di Uyuni, Andean Altiplano. A) Locality map showing hydrological relations with drainages of other salars and lakes of the Altiplano as well as its proximity to diapires. The dissolution of diapor salts has sourced much of the salt accumulating in the Salar di Uyuni. B) Lithology and Br profiles from a 121 metre well in Salar di Uyuni (after Risacher and Fritz, 2000).

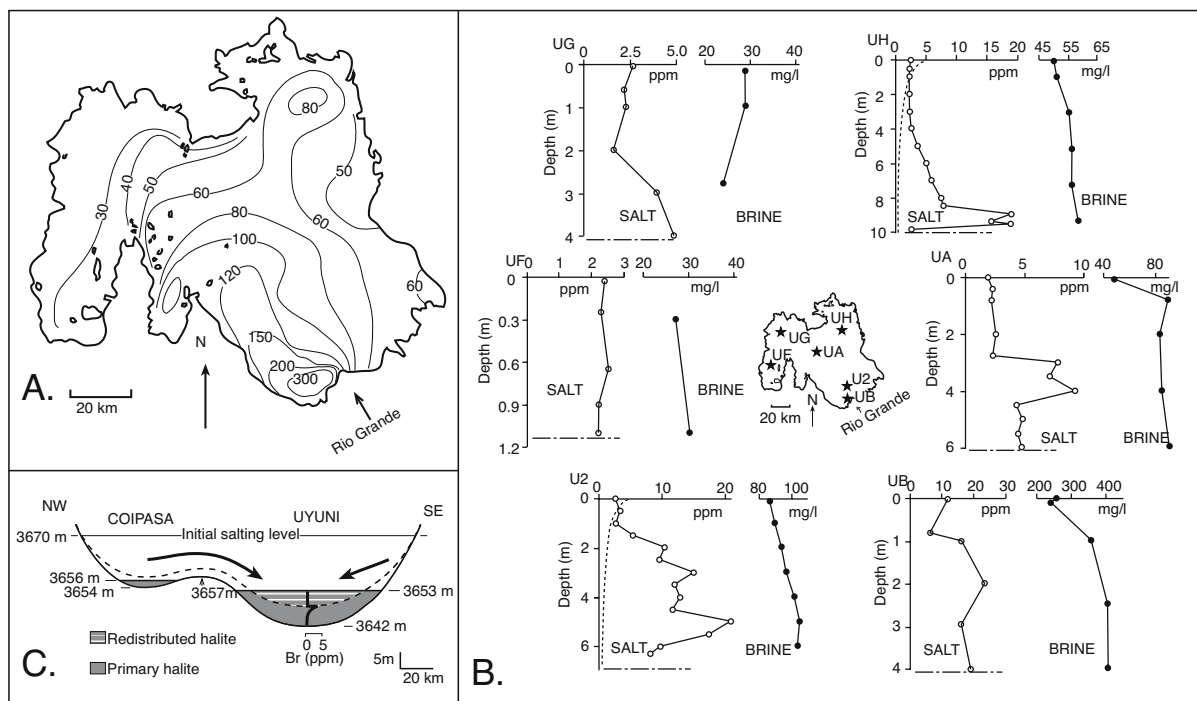


Figure 3.41. Distribution of Br in shallow saline pan sediments of Salar de Uyuni. A) Distribution of Br in near-surface brine. B) Br profiles of pan halite and interstitial brines from selected shallow cores. C) Schematic showing how low bromine salt is reworked and redistributed from initial marginward crusts by a lowering of the perennial water table (after Risacher and Fritz, 2000).

Uyuni drainage basin and in the proportion of mud beds in the salar core. These waters had lower Cl/Br ratios, indicated by an increase in Br to 6–10 mg/l in the pan halite beds between 10 and 40 m depth (Figure 3.40b). The change may have also coincided with the exhaustion of diapiric halite as a source of ions, perhaps related to a decrease in the intensity of tectonism that was driving diapiric salt to the surface. Paleolake levels in the central Altiplano rose at this time, while those in the northern Altiplano (the Titicaca basin) were simultaneously falling. This reflects progressive fluvial erosion of the threshold between the northern and the central Altiplano, which lowered the levels of the northern lakes and allowed more dilute waters with lower Cl/Br ratio to flood the central Altiplano and so move into Salar de Uyuni. The three uppermost salt crusts show a decrease in bromine content, which may reflect a recent modification to the inflow regime.

The salt of the uppermost salt pan layer began to accumulate around 10,000 years ago and continues today. The halite shows a bromine distribution that is low in the shallow parts of the bed (≈ 2 mg/l) but unexpectedly increases with depth to values in excess of 8–10 mg/l (Figure 3.41a, b). This increase is thought to indicate an episode of exposure and recycling of earlier formed marginward salt crust into the current brines

(Figure 3.41c). As the lake dried some 10,000 years ago, the resulting salt crust was initially distributed over a wider area than the crust of the present pan. It covered the topographic surface of the salar depression up to the level of the lake where halite brines first reached saturation (Figure 3.41c). Ongoing lowering of the Holocene water table, and the associated dissolution of the higher parts of the salt crust about the more marginward parts of the pan depression recycled ions (including Br) from crusts about the margins of the lake into the brines feeding the lowered brine levels located further toward the salar centre. Ongoing recycling explains the progressively lowered Br contents in successive pan crusts in the more central parts of the salar. Clearly, the increasing aridity and lowered water table that typifies the current episode of saline pan aggradation has cannibalised earlier versions of itself as ongoing longterm drying of the lake raised marginward crusts above the salar water table.

Many parts of the lake surface about the lake edge still show evidence of salt dissolution and crust recycling. Circular holes appear in the lake crust, especially about the salar edge; surface expression of the holes can be a few tens of centimetres wide but they are typically underlain by brine-filled swallow holes

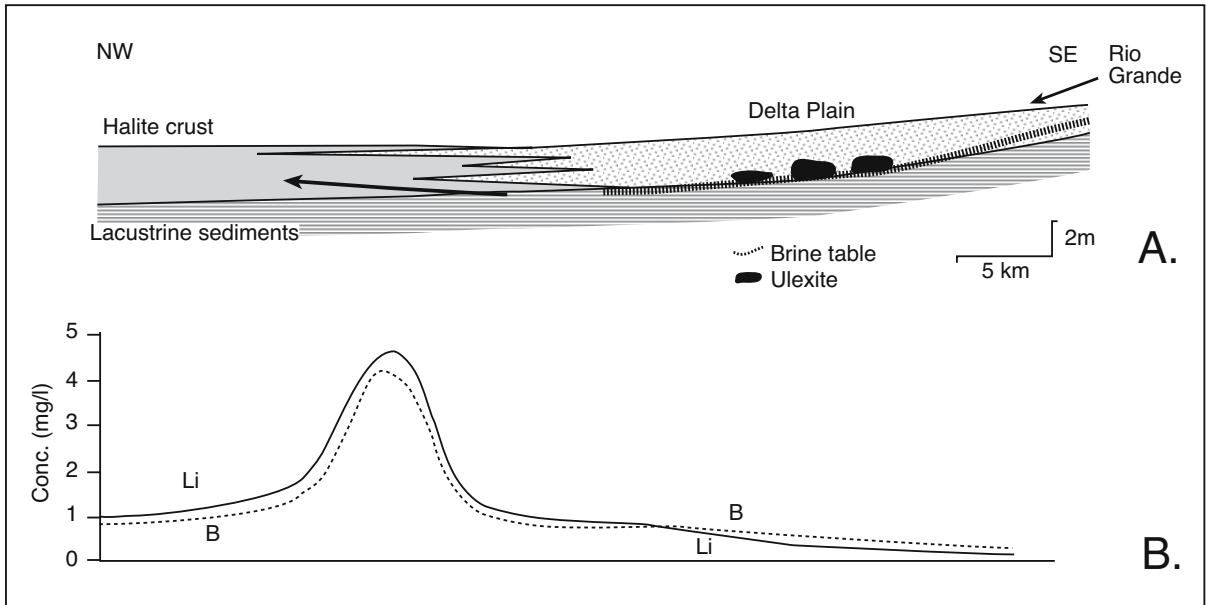


Figure 3.42. Stratigraphy (a) and B-Li content (b) of brine in the southwestern portion of Salar di Uyuni in the Rio Grande delta. Arrows indicate brine flow, Brine chemistry shows a peak in both B and Li at the chemical interface between halite saturated lake brines and the delta prism, but the ulexite precipitates by capillary evaporation at the brine table interface beneath the delta prism (after Risacher and Fritz, 1991). See Figure 3.40 for location of delta.

opening out in to salt cavities that are metres deep and wide. It makes driving on some parts of the salar edge quite hazardous. The local name for these small holes at the surface is “Eye of the Devil” (*ojo del diablo*). Local karst development about the edge of a bedded salt mass is an early diagenetic overprint common to many modern and ancient salt pans. It is driven by changes in the lake water table and the encroachment of

regions of less saturated water into the margins of the bedded salt. The associated preferential leaching and fractionation drives the syndepositional formation of many potash and borate accumulations (e.g. Figure 11.16).

The main fluvial feed to the salar is from the Rio Grande, which enters the salar depression in its southwestern part. There it has

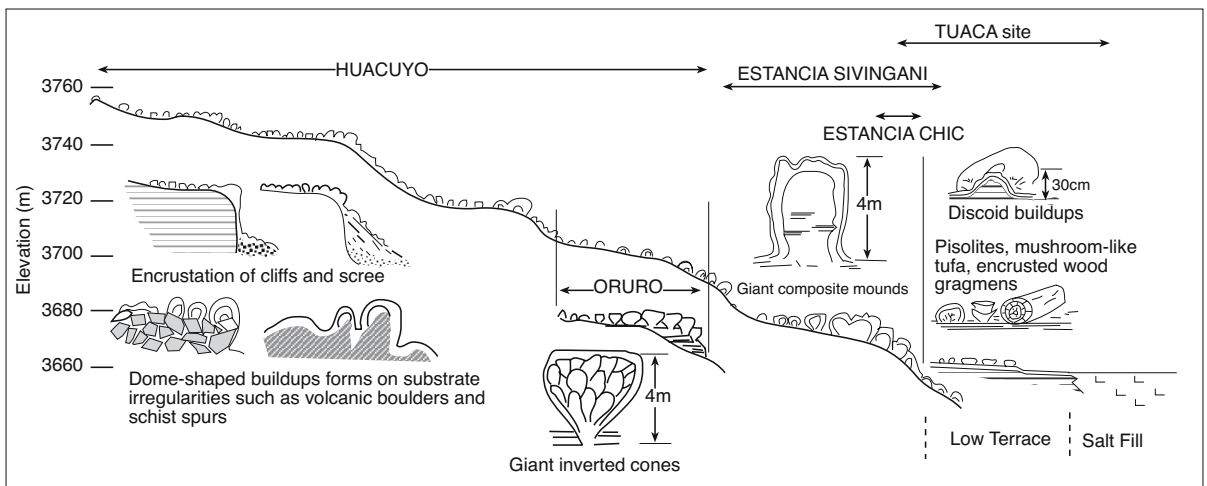


Figure 3.43. Schematic of the distribution of various types of algal bioherms within the outcropping as carbonate veneers in the surrounds of Salar di Uyuni. At the time the bioherms were actively accumulating these areas were shoal water portions of a perennial lake (after Rouchy et al., 1996).

built up a 300-km² delta, characterised by a lens of fresher water and sediment that intertongues with the halite crust unit (Figure 3.39). The delta itself is a complex of silt and clay with local sand lenses indicating fluvial channel fills. Clays are mostly smectite with some illite and minor kaolinite. Overall, the delta prism is characterised by low porosity and permeability (Risacher and Fritz, 1991). Paludal muddy lacustrine sediments underlie both the delta prism and the halite crust facies. The contact between the delta wedge and the halite unit is a brine interface and the watertable of the delta prism today lies close to the surface. It converts much of the delta prism situated some distance from the fluvial channels into an evaporitic mudflat, where capillary evaporation is driving fluid flow. This in turn drives a slow circulation in the underlying mixed waters and so precipitates calcite, gypsum and ulexite ($\text{NaCaB}_5\text{O}_9 \cdot 8\text{H}_2\text{O}$) toward the edge of the delta prism (Figure 3.42). This has created one of the largest borate accumulations in Bolivia where the ulexite interval in the delta prism has an average thickness of 0.1 m over a 120 km² area with a water content of 50% (Risacher and Fritz, 1991). Total boron reserves in this area are estimated to be around 1.6×10^6 tons.

The Salar di Uyuni surrounds also preserve evidence of Upper Pleistocene sedimentation, this was a time when the Central Altiplano of Bolivia was repeatedly flooded by deeper and extensive saline lakes (Rouchy et al., 1996; Baker et al., 2001). These freshening episodes in the Salar di Uyuni area are marked by the development of microbial bioherms defining at least three major periods of lacustrine highstand (Figure 3.43). These calcitic tufas discontinuously cover the 300-km-long and up to 100-km-wide lacustrine slopes and terraces of the surrounds of Uyuni up to an elevation of 100 m above the surface of the modern halite crust. Clearly, Salar di Uyuni was a perennial mega-lake when the bioherms were growing and deepwater diatomaceous siliceous muds were accumulated across the same area where subaerial crust are accumulating today.

The distribution, size and shape of the bioherms are diverse, reflecting various factors such as the nature and morphology of the substrate and the hydrodynamic conditions that prevailed during bioherm growth (Figure 3.43; Rouchy et al., 1996). Build-ups on the larger palaeoterraces

coalesced to form platform-like carbonate reef mound accumulations. Although the morphologies closely resemble those created by cyanobacterial binding, they were predominantly constructed by other plant communities largely dominated by green algae. Cyanobacterial communities flourished in association with the plants, but they did not contribute significantly to the architecture of the bioherms; rather they encrusted the plant stems and microbial bushes, or formed thin laminated layers that covered the last stages of build-up growth. Buildups located between 3660 and 3680 m elevation show one or more of three growth stages or envelopes: (1) a massive inner core formed before 40 ka during an early Minchin highstand; (2) a large peripheral envelope deposited at about 40 ka (late Minchin) and (3) a thinner outermost crust formed during a late glacial event. Many bioherms show composite growth layering indicating episodes of microbial growth during lake highs separated by times of subaerial exposure and moderate erosion.

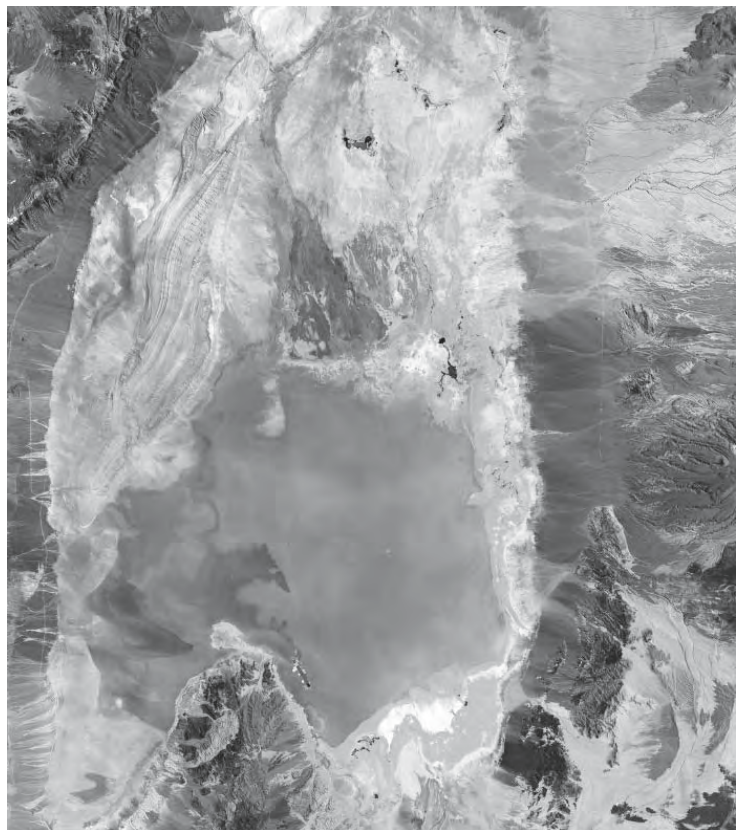


Figure 3.44. Salar de Atacama, Chile showing saline pan facies associated with the influx of the San Pedro River along the northeast side of the salar, the sulphate-rich marginal zone along the east and northeast of the salar and the salt-crusted halite facies dominating the southern portions of the salar (image courtesy of NASA). See also Figure 3.45.

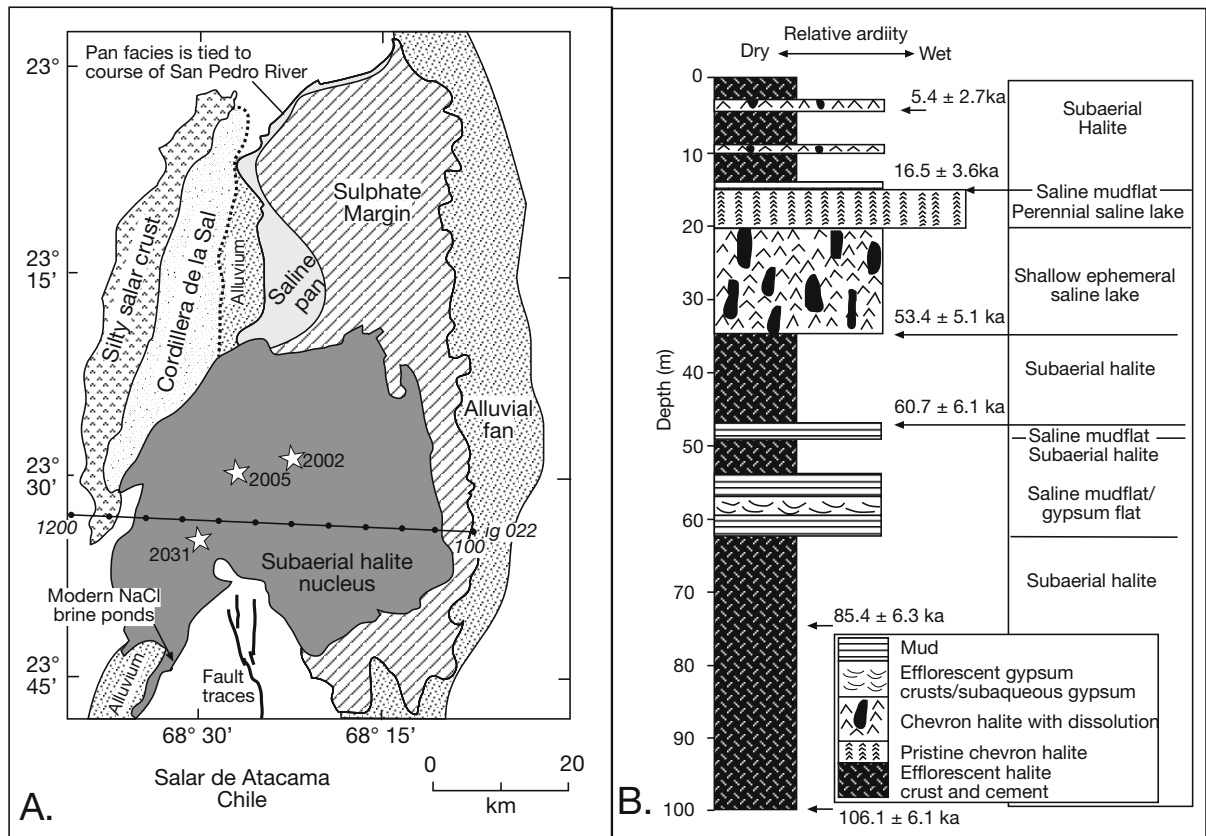


Figure 3.45. Salar de Atacama, Chile (see Figures 3.37, 3.44). A) Surface geology and extent of main salar lithofacies. Also shows onshore position of main salar fault and location of seismic trace ig 022 (with shot point positions). The stars show the position of cores 2002, 2005 and 2031. B) Sedimentology of core 2005 (after Bobst et al., 2001; Jordan et al., 2002).

Salar de Atacama, Chile

Salar de Atacama is the lowest drainage sink in another endorheic basin in the pre-Andean depression of the Atacama desert and contains more than a kilometre of interlayered halite and siliciclastics (Jordan et al., 2002; Rech et al., 2002). At an elevation of 2,300 m above sea level with an area of 3,000 km², it is the third largest saline pan in the world and an excellent barometer of Pleistocene climate change in the southern hemisphere (Figures 3.36, 3.37).

Today the San Pedro River forms an ephemeral stream feed along the western margin of the northern sector of the salar and defines the edge of a saline mudflat dominated by sulphate, carbonate and siliciclastic sediments (Bobst et al., 2001). The mudflat surface is dominated by brown halite-rich crusts and is underlain by silty clays with sand, displacive halite and locally organic-rich mud. A “sulphate marginal zone” dominated by ephemeral streams, eolian dune fields, sand sheets, dry mudflats and spring-fed ponds and marshes, forms

the eastern edge of the salar and lies to the east of the saline mudflat (Figures 3.44, 3.45a). This northern region captures the majority of the siliciclastics entering Salar de Atacama. In general its water table is between tens of centimetres and several metres below the deflationary land surface. Uppermost sulphate zone sediments are typically covered by and cemented with efflorescent sugary gypsum and minor halite. When trenched these gypsum crusts form discontinuous bowl-shaped concave-upward layers tens of centimetres in diameter.

A thick layer or crust of halite today covers the halite nucleus of modern Salar de Atacama (Bobst et al., 2001). The top 40 cm of this crust is made up of millimetre-scale “sugary” inclusion-poor halite crystals along with interstitial mud. The crystals show a well-developed interlocking polygonal texture. At the broader scale the crust appears “wormy” with numerous subvertical to randomly oriented tubular microkarst voids. The crust surface is broken by metre-scale polygons with typical upturned edges showing up to a metre of relief. Mud typically ponds in the centres of saucers between the megapolygonal salt ridges. This

uppermost crust is interpreted as an efflorescent crust formed largely by the capillary evaporation of groundwater brines and contains only a few growth-aligned chevrons.

Below the surficial crust the halites of the saline pan nucleus are massive and mainly composed of cm-sized interlocking crystals separated by mud-filled voids. Most of this halite is clear and inclusion poor indicating slow subsurface growth. Occasional freshwater influx drives dissolution of surface efflorescent halite crusts and creates large voids that then fill with clear cm-scale euhedral halites growing in toward the

centre of the void. This dissolution-precipitation of halite is an ongoing process with evidence of numerous overprinting episodes destroying most primary chevron structures. Layering is poor to nonexistent.

A deep core (No. 2005) through the halite nucleus facies recovered some 100 metres of evaporitic sediment and sampled some 100,000 years of salar sedimentation (Figure 3.45b; Bobst et al., 2001). Deposition was dominated by arid conditions similar to today, with two significant wetter intervals. From 100 m to 62.8 m the core is composed of clear interlocking halite with

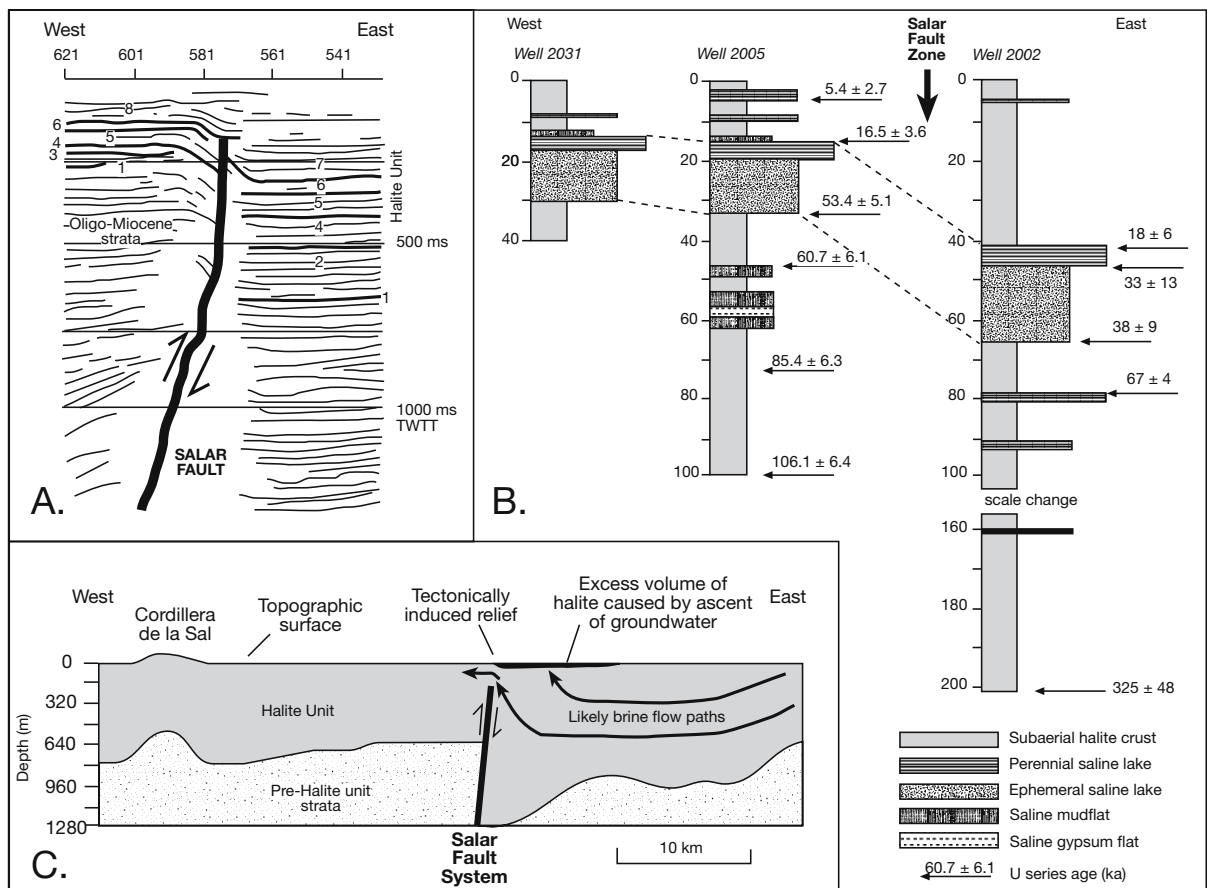


Figure 3.46. Interactions between the Salar de Atacama fault zone and halite sedimentation (See Figure 3.45a for location of seismic line and wells; after Jordan et al., 2002). A) Interpreted seismic line ig 022 across the Salar reverse fault showing monoclin flexure and thickening of beds across the fault. Fault trace dies out before reaching current halite surface. B) Summary of halite facies in sequence 8, documented in SQM cores. Boreholes 2031 and 2005 are located west of the Salar fault system, whereas borehole 2002 is located east of the Salar fault system. U-series dates from boreholes 2005 and 2002 and comparisons of halite depositional environments at the three sites allow temporal correlation among the cores. The top of the perennial saline lake facies, dated as ca. 16.5 ka, is readily identifiable in all three locations. That horizon occurs at similar depths in cores 2005 and 2031, but is vertically displaced ≈ 28 m across the Salar fault system. C) Conceptual model of enhanced halite accumulation east of the Salar fault system, which leads to a horizontal depositional surface across the fault trace. Under the conditions of a desiccated surface environment, halite accumulates because of evaporation of groundwater-fed brines. A drop in permeability at the fault (either due to juxtaposition of lower permeability rocks in the western fault block or due to properties of the fault zone itself) blocks the westward flow of topographically driven groundwater, forcing a high rate of upwelling in the downthrown eastern fault block.

patches of millimetre-scale sugary halite. These textures are near identical to those forming at the surface today and indicate dry mostly subaerial accumulations. From 62.8–47.0m (75.7–60.7 ka) there is a vertical succession passing from mudflat gypsum to mudflat/shallow pond to subaerial halite and mudflat deposits that represent a progressive increase, then a decrease and finally an increase in water supply to Salar de Atacama. This occurred within what were moderately wetter conditions (saline lakes and saline mudflats) than the subaerial conditions of today (Bobst et al., 2001). A similar somewhat wetter interval occurred from 53.4 to 15.3 ka, with the wettest perennial lake interval from 26.7 to 16.5 ka. Short relatively wet periods (chevron halite) also occurred in the Holocene from 11.4 to 10.2 ka and from 6.2 to 3.5 ka. The remaining sections are dominated by halite textures similar to the subaerial dominated capillary fringe conditions of today.

Seismic collected across Salar de Atacama shows a north-northwest–striking fault system that extends for at least 30 km across the salar and can be seen intersecting the lower part of the halite nucleus (Figure 3.46; Jordan et al., 2002). In the southern sector of the salar there is at least 700 m of Pliocene–Quaternary down-to-the-east reverse motion across the fault, but locally the salar fault system deforms the lower halite unit into a monocline with 400 m of structural relief (Figure 3.46a). Rates of displacement throughout the Quaternary have been on the order of 0.1–2.0 mm/yr. And yet, despite these large displacements and large displacement rates so obvious in the seismic, no modern topographic scarp exists in the halite nucleus. Seismically-defined stratal geometries and thicknesses reveal variation between former times when there was a topographic scarp at the deformation zone and times, like today, with no topographic expression. The available borehole data suggest that both the times with and without a topographic scarp were likely dominated by halite accumulation adjacent to the salar fault system (Figure 3.46b).

Jordan et al. (2002) propose that unique sedimentation processes in a groundwater-fed evaporite environment are responsible for the lack of topographic expression of a major fault system that intersects the salt. During desiccated times, groundwater derived from topographically driven flow on the east side of the salar would have been forced upward by a barrier created at the fault zone, enhancing the supply of solutes to the zone immediately east of the fault (Figure 3.46c). This mechanism generates a higher rate of accumulation of halite east of the Salar fault system than to its west. The enhanced deposition on the eastern fault block is sufficient to prevent scarp formation during times of moderate displacement by the Salar fault system, though during times of especially high rates of offset,

this depositional mechanism was not sufficient to prevent temporary formation of scarps. It is not yet known how common “truly blind” faults are beneath the dry salt pans of other salars, but they are not unique to the Atacama basin. Similar occurrences of blind faults beneath the depositional surface of the ephemeral saline pan facies characterise; Salar de Antofalla and Salar de Hombre Muerto in the Altiplano, along with the Badwater salt flat in Death Valley, California and Great Salt Lake in Utah (Figure 4.19; Jordan et al., 2002). Like Salar de Atacama, they indicate the rapid deposition/accumulation rates that typify brine-saturated salt accumulating depressions.

Salar Grande, Central Andes of Chile

The Salar Grande is a 45-km-long (N-S axis), 4–5-km-wide, fault-bounded (pull-apart) Neogene forearc evaporitic basin, located in the Cordillera de la Costa of northern Chile (Figure 3.47). The altitude of the Salar Grande salt surface is currently 640–750 m above sealevel and halite deposition is inactive compared with salars to the east (Pueyo et al., 2001). The salar fill is composed almost exclusively of dry massive halite around 100 m thick, with dry salt in the deepest parts more than 160 m thick (Pueyo et al., 2001; Diaz et al., 1999; Ericksen, 1993). The salt is very pure, locally 99% NaCl, with a lakewide average of 95% over an area of 280 km². It has been mined at least since the mid 19th century and today it supplies all of Chile’s needs, as well as being exported, mostly to Japan.

Halite is in direct contact with igneous lithologies about the salar edge, while something like 10 m of alluvium separates the bottom of the salt body from its andesitic Mesozoic basement. There is no evidence of a concentric pattern of mineral fractionation in the salar, nor of any significant volume of salts other than halite (Diaz et al., 1999). Only a patchy anhydrite belt, several metres thick, caps portions of the salar edge (Ericksen and Salas, 1989). It is made up of saccharoidal CaSO₄, which sometimes retains selenite pseudomorphs (dm-diam), as in the SE margin of the salar (Figure 3.47). This sulphate bed can be traced into the adjacent western Llamara area.

The Neogene depositional history of Salar Grande is closely tied to an adjacent Tertiary lacustrine basin, the Llamara-Quillagua basin to its east (Figure 3.48a). Phreatic waters flowing into the Salar Grande depression from the east (now the Precordillera and Altiplano) were progressively enriched in solutes by interaction with volcanic rocks. These fluids had first drained into the Llamara-Quillagua lacustrine system of the Central Depression to deposit thick sequences of diatomites, carbonates, evaporites and clastic sediments. This lacustrine area eventually filled

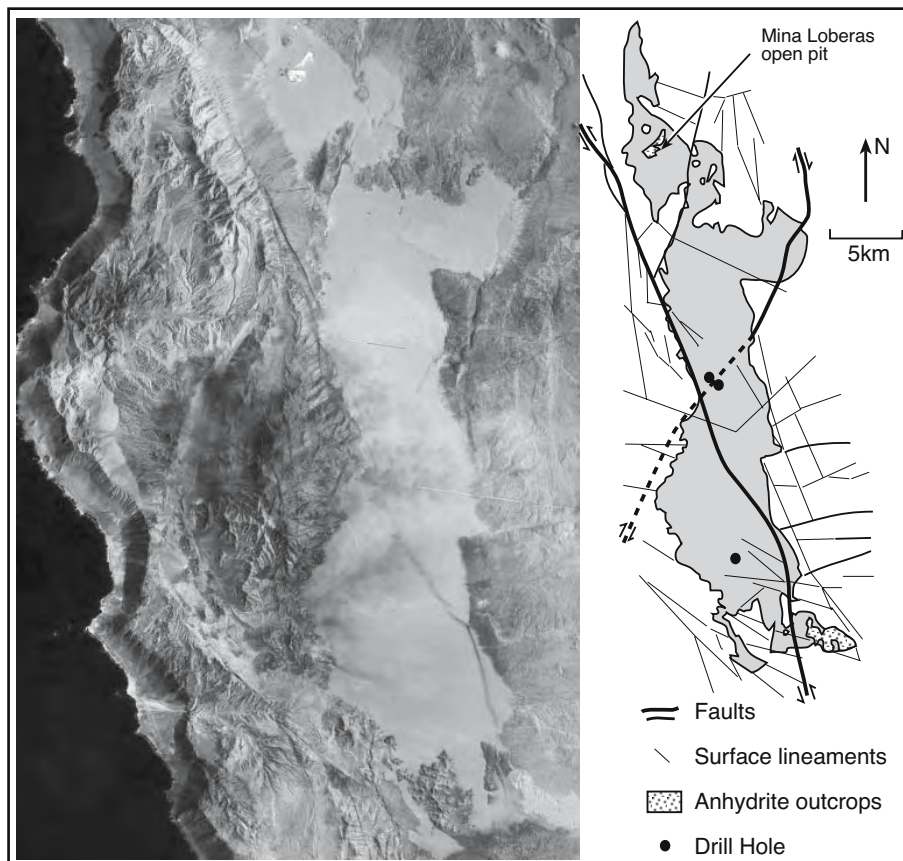


Figure 3.47. Salar Grande, Northern Chile Geological map shows position of 3 drill holes drilled in the 1920s for potash, which established salt in the central portion of the salt was more than 162 thick and underlain by dry alluvium. Also shows main fault of Atacama fault system trending SE-NW as well as other faults and lineaments in and around the salar (Landsat image courtesy NASA).

and dried to where it became a salar filling with anhydrite and halite. During this stage (Late Miocene-Pliocene), the evolved brines of the Llamara-Quillagua area seeped eastwards along structural paths (fractured bedrock?), to reach the Salar Grande basin, which acted as their final sink. Proof of this connection is the anhydrite/selenite bed that overlies the halite in both lakes and links the western Llamara to the southeastern Salar Grande areas via the Montón de Gloria pass (Diaz et al., 1999).

Phreatic brines were subsequently lost from the basin in Pliocene times when the Loa River canyon reached the sea. This was the beginning of the current exorheic hydrology and the opposite of its previous endorheic hydrology. Drainage into the ocean was reflected in a fall of the regional water table, the drying of the salt body and the underlying alluvium, and the creation of a hydrologic situation in Salar Grande that still exists today (Ericksen, 1993).

Large halite sinkholes, up to 10 - 20 m deep are best developed on the eastern side of the salar, while others developed along fault lines where they transect and weaken the now dry salt body (Diaz et al., 1999). Some sinkholes are funnel-shaped, while others are cylindrical, all may be connected laterally by a network of caves. Etched profiles in the sinkholes walls indicate they were brine-filled pools prior to the drainage of brine from the salar much like the "eyes of the devil" in Salar di Uyuni.

The regionally extensive Atacama Fault zone, a major tectonic feature in the region, transects the Salar Grande with its position marked on the salt crusted surface by irregular elongate depressions and mounds, low scarps and fractures (Figure 3.47). Other active faults, defined by open fracture networks, outline tectonic zones in the surrounding and underlying

bedrock. The appearance of the fault trace at the surface of Salar Grande is in marked contrast to Salar de Atacama, which lacks any expression of its active faulting at the surface. That the regional fault intersects the surface of Salar Grande and not the surface of Salar de Atacama shows that the halite accretionary process is today much less active in Salar Grande. Accretion of halite requires a saline water table within a few decimetres of the lake surface; the water table of Salar Grande is much deeper.

Dripping fogs (*camanchacos*), in combination with deflation, capillary evaporation and rain, have sculpted a knobby and pressure-ridged surface to the modern salt crust with relief up to 50 - 60 cm. At the larger scale some pressure ridges outline megapolygons in the salt with saucer diameters measured in tens to hundreds of metres, as well as smaller polygons measuring several metres between ridges (Ericksen, 1993).

Ongoing reworking of the upper boundary of the massive salt crust by fog moisture and the incorporation of eolian, detrital and insoluble clays through time has created a dirty brown salar-capping halite crust, up to 1 metre thick, atop thicker, drier, purer halite.

Mining and coring in the northern part of Salar Grande shows the lower 10m of the salt fill was deposited on the floor of a mostly brine covered saline pan. It is made up of thinly-layered halite composed of cm-mm-sized bands of chevron halite, separated by syndepositional dissolution surfaces. It is depositonally similar to the shallow saline pan facies of Salar di Uyuni and the saline lake facies of Salar de Atacama (Figure 3.48b). Minor amounts of sulphate salts (mostly mm-sized glauberite, thenardite and polyhalite) and clay minerals cap each dissolution surface, indicating settle-out and freshening related to periodic flooding of the basin. The overlying Massive Halite was deposited as displacive or intrasediment halite, still in a saline pan but now

accumulating in the capillary fringe of a pan that was subject to ongoing desiccation and evaporation, much like the majority of the halite filling Salar de Atacama.

The transition between the Lower Banded Halite and the Upper Massive Halite takes place over an interval several metres thick, which shows alternations of both units. Lower banded halite passes by an increase in crystal size into the Upper Massive Halite, which is made up of two halite crystal classes (< 4 cm diam and > 4 cm diameter). The random nature of crystal alignment in the massive halite shows its precipitation as multiple overprints of displacive crystal growth from saturated phreatic and capillary waters at a time when the salar surface was mostly subaerial.

Minor thenardite (Na_2SO_4) crystals occur in the Upper Massive Halite at levels 2 and 3 in the Mina Loberas pit where it appears to be an early, perhaps syndepositional, cement between

displacive halite crystals (Diaz et al., 1999). Thenardite locally replaces the halite, but typically shows poikilotopic textures with solid inclusions of glauberite, clay and micrite. Polyhalite ($2\text{CaSO}_4 \cdot \text{MgSO}_4 \cdot \text{K}_2\text{SO}_4 \cdot \text{H}_2\text{O}$) is the most abundant sulphate mineral in Salar Grande; it outlines grain boundaries and dissolution surfaces in the Massive Halite.

Pockets of very coarsely crystalline halite (>50 cm diameter) occur in the Massive Halite and in parts of the underlying Banded Halite. They show centripetal or geode-like patterns of halite growth and infill. This very coarse halite is thought to be an earlier dissolution tube fill precipitated when the water table was higher. It is a common texture in many other South American salars where it precipitates as halite karst-fill cement in the Ojo de Diablo.

Work on the sedimentology of the halite pans in the South American salars over the last two decades has substantially improved our

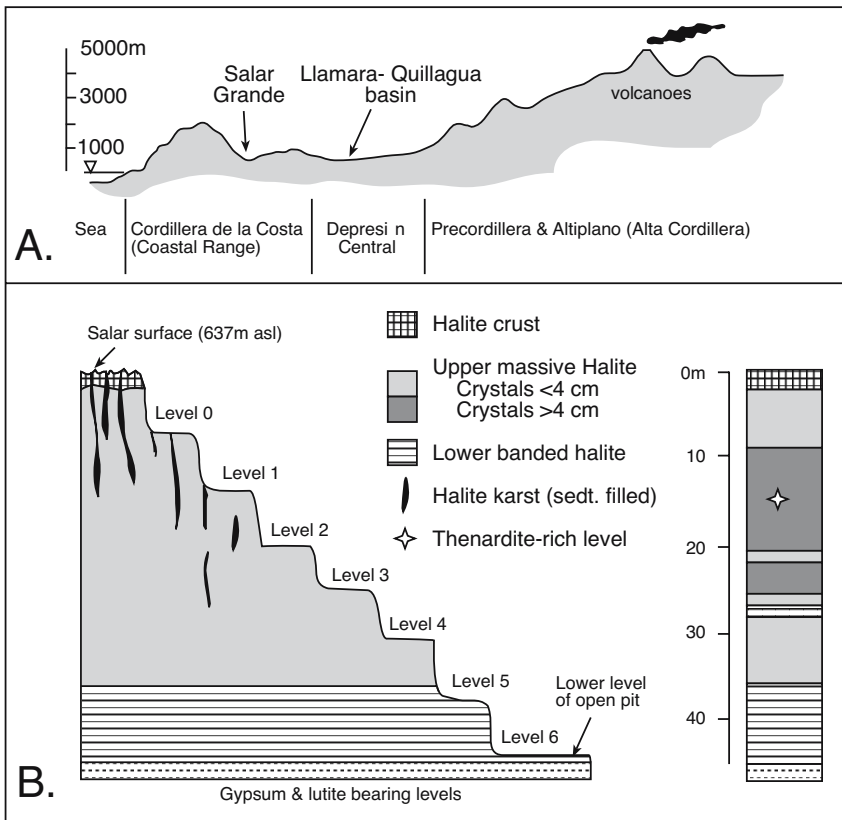


Figure 3.48. Salar Grande. A) Schematic of main physiographic subdivisions and the relative position of the Llamara-Quillagua Basin. Total section length is about 100 km. B) Section through open pit at Mina Loberas in the northern part of the salar showing stratigraphic arrangement of different lithofacies discussed in text. (after Diaz et al., 1999; Ericksen, 1993).

understanding of the hydrological significance of halite textures. It has added a third group of textures to prior notions of: 1) matrix-dominated displacement halite forming in the capillary fringe of a sabkha sitting in a zone of ascending waters above a less saline phreatic water mass and 2) subaqueous chevrons, overprinted by subaerial microkarst forming in areas of ephemeral waters in saline pans. This third textural style is exemplified by the halite units currently forming in Salar de Atacama and dominating the Massive Halite fill of Salar Grande. It is a form of chaotic displacement halite with little or no non-evaporite matrix and little or no preserved chevron textures. It is porous and forms mostly in the capillary fringe above a groundwater fed halite-saturated brine mass or brine curtain. As it forms it cannibalises itself to such a degree that little or no primary texture is preserved.

Ephemeral stream floodplain - dune field-ephemeral saline lake

The ephemeral stream floodplain-dune field-ephemeral saline lake complex typifies tectonically-stable low-relief areas usually located within arid-zone subtropical high-pressure belts. Continental saline mudflats (sabkhas) are commonplace in regions of shallow water tables in this lacustrine complex, but low rates of subsidence and high rates of deflation mean evaporites are less likely to be preserved compared to rapidly subsiding alluvial fan-ephemeral saline lake settings. Rather, sediments are composed of varying combinations of saline mud flats or sandflats, with the more saline intervals showing widespread haloturbation, but little or no preserved salts. The latter were recycled as ≈1m thick at-surface crusts, dissolved and reprecipitated after each flood event.

Most of the large ephemeral lakes in this setting occur in regional outflow zones of large artesian hydrologies or regional artesian seeps in low relief terranes. The rise of less saline resurging water inhibits development of a thick brine curtain or reflux plume beneath the pan and the mudflat, a requirement for longterm preservation of salt beds (Chapter 5). Surface inflow is a combination of local storm runoff and long distance ephemeral floods, with intense flood events often spaced years apart. Lake sediments are subject to the vagaries of climatic changes outside the immediate vicinity of the saline lake. These lakes generally lie at the edges of sand seas or ergs. They tend to preserve relatively thin lacustrine sediment piles with numerous truncations that indicate ongoing deflation. Wind reworking of vadose lacustrine and fluvial sediment supplies substantial volumes of sediments to these adjacent sand seas.

Ephemeral braided stream floodplains, sheet deltas, dunes and sandflats are the dominant facies in the depositional basin, not bedded evaporites. Lake Eyre (9,500 km²), Lake Amadeus (1,032 km²), Lake Frome (2,700 km²), Lake Gairdner (4,351 km²), and Lake Torrens (5,745 km²) in inland Australia are modern well-documented examples of this depositional style (Figure 3.49; Pell et al., 2000). Major flood events are mostly fed by long distance southward transport from intense monsoonal outbursts in northern Australia (Figure 3.49).

Likewise, Lake Chad in North Central Africa, another well documented example of this style, is fed via the Chari/Logone river system from monsoon rains that typically fall in June, July and August. The subtropical position of all these examples means vertical sequences retain evidence of Pleistocene fluctuations in monsoonal intensity. Many lake complexes in southern central Australia (Lake Callabonna, Lake Eyre, Lake Frome, Lake Gairdner, and Lake Torrens) were freshwater to brackish water lakes some 35,000 years ago, yet today are saline

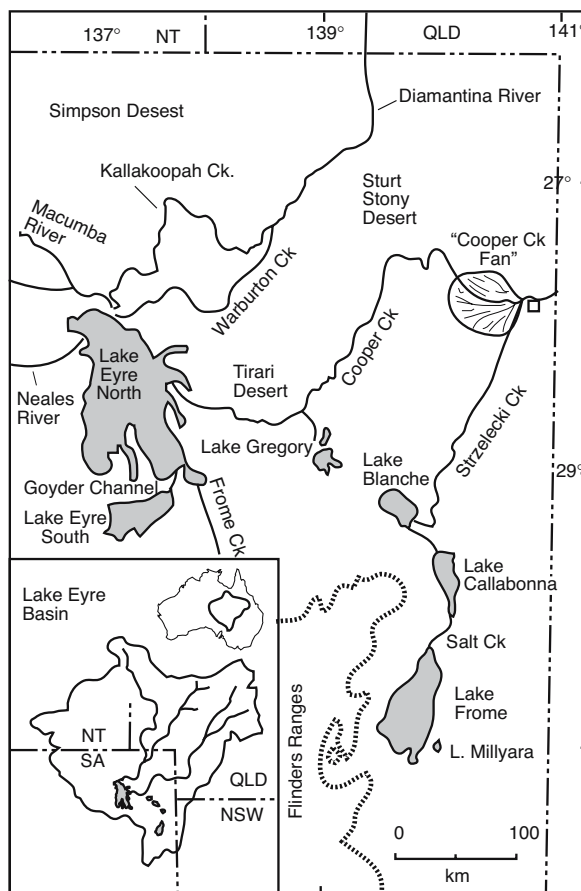


Figure 3.49 Drainage into and between lakes in the Lake Eyre Basin of South Australia.

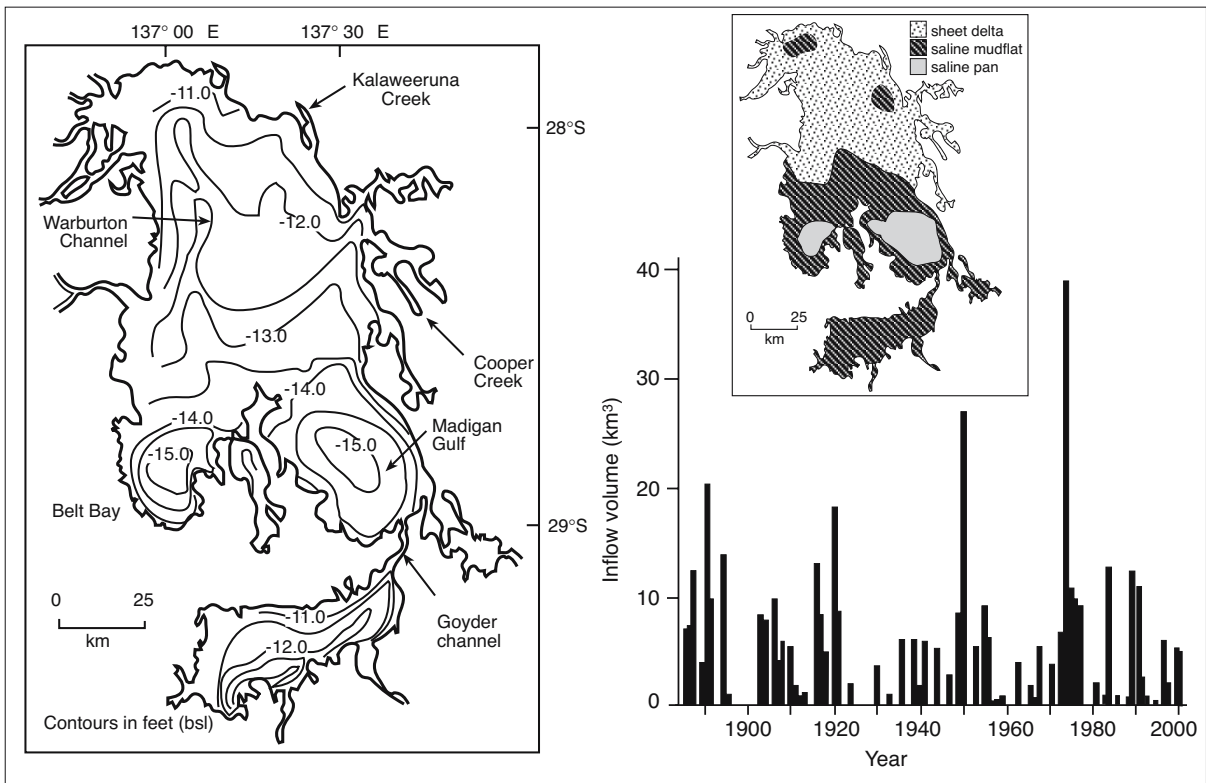


Figure 3.50. Lake Eyre bathymetry, facies and flooding history compiled from Kotwicki (1986), Kotwicki and Allan (1998) and various references cited in text. Lake floor contours are in metres below sea level.

mudflats with only short-term episodes of filling. Likewise, Lake Chad has undergone massive fluctuations in size and salinity; at one point during the Pleistocene it extended to the Tibesti Mountains in northwest Chad, at another point it was sufficiently saline to precipitate natron (Eugster and Maglione, 1979). Droughts since the 1970s have decreased Lake Chad levels so that it is now extremely shallow and divided into northern and southern pools. This drying is not unusual, the lake has dried up completely a number of times in the last 200 years. What is unusual in the lake's long history is the environmental stress created by too many people attempting to eke out a living in and around the lake.

Ancient counterparts to the ephemeral stream floodplain-dune field-ephemeral saline lake association include portions of the Lower Permian Rotliegende of northern Europe, Permian red beds of the US interior centred on Kansas; the Late Triassic of northwest Europe and the Palaeoproterozoic Whitworth Formation of the Mt Isa Block, Australia (Glennie, 1989a, b; Benison and Goldstein, 2000; Talbot et al., 1994; Simpson and Eriksson, 1993).

Lake Eyre, Australia

Lake Eyre North has an area of some 8,430 km² and is 144 km long and 77 km wide. It is joined by the narrow Goyder Channel to Lake Eyre South, which is 64 km long and 24 km wide with an area of 1,260 km². The lowest part of Lake Eyre North is the eastern part of Belt Bay with some areas slightly deeper than -15.2 m and, making it the lowest point on the Australian continent (Figure 3.50). The floor of the Lake is very flat with bottom slopes $\approx 2 \times 10^{-5}$, so the definition of the exact location of the deepest point is rather arbitrary. For the same reason, boundaries of its sedimentary facies tend to migrate large distances with little change in the lake water level. In dry times the lower parts of Lake Eyre North in Belt Bay and Madigan Gulf are covered by a bedded halite crust around 0.5 metre thick. The 4×10^8 tonnes of salt held in this crust completely dissolves during major floods, so the lake floor actually deepens topographically during a flood (Dulhunty, 1977). When the lake is dry, the saline pan crust is surrounded by a saline mudflat facies where gypsum grows displacively in the capillary fringe (Figures 3.50, 3.51).

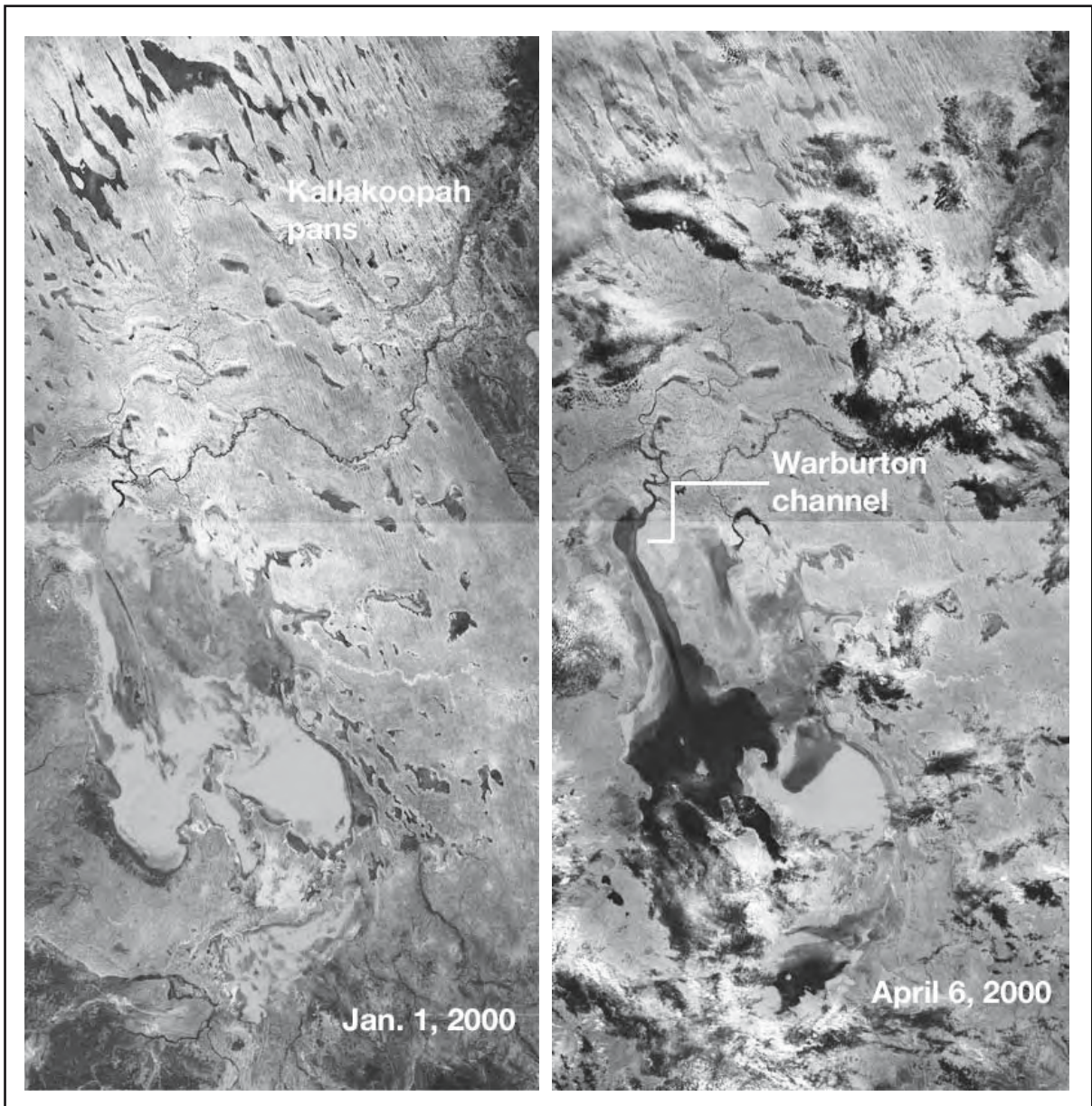


Figure 3.51. Lake Eyre, South Australia. Image on left taken on January 1, 2000 at a time prior to a major flooding event. Partly cloud-obscured image on right taken on April 6, 2000 after a major monsoon-fed flood influx into lake from northern part of lake. The elongate interdunal sabkhas and pans in the northern part of the image constitute the Kallakoopah Pans. Note the water-filled Warburton Channel transecting the northern lake floor (Landsat 7 satellite images acquired and processed by ACRES).

The northern portion of Lake Eyre is where most of its ephemeral streams enter the lake depression. Entry points are defined by a number of low flat amalgamated sheet deltas, which are dominated by fine sands and silts. The lower part of the sheet delta facies are cut by low channels, the largest of

which is a north-south depression that transects the northern two thirds of the lake and is known locally as the Warburton Channel. When the lake floods these channels quickly drain the floodwaters into the lowest part of the lake and dissolve the salt crust (Figure 3.51).

Date	Salinity	Na	K	Ca	Mg	Cl	SO ₄	HCO ₃	CO ₃
14 Feb, 1984	25,331	9,114	<1	545	53	14,290	1,274	55	0
28 Mar, 1984	40,989	14,620	70	876	150	23,000	2,140	35	7
30 Mar, 1984	42,355	15,150	93	887	143	23,350	2,700	32	0
30 Apr, 1984	49,023	17,520	70	1,050	171	27,220	2,950	42	0
7 May, 1984	51,301	18,400	46	1,040	187	28,300	3,280	48	0
28 May, 1984	57,728	20,640	48	1,240	193	31,880	3,670	57	0
25 Jun, 1984	61,278	21,970	49	1,350	173	34,360	3,310	66	0
21 Jul, 1984	64,969	23,320	92	1,350	236	35,910	4,070	81	0
27 Aug, 1984	71,248	25,500	136	1,450	264	39,640	4,170	88	0
24 Sep, 1984	86,710	31,200	68	1,680	310	48,100	5,290	62	0
28 Oct, 1984	117,797	42,600	111	2,050	451	65,700	6,820	65	0
30 Oct, 1984	120,067	43,800	111	1,820	473	67,500	6,300	68	0
26 Nov, 1984	162,697	60,300	129	1,650	725	93,100	6,720	78	0
17 Dec, 1984	217,350	82,000	208	1,220	874	126,200	6,800	48	0
16 Jan, 1985	272,819	101,300	555	459	2,500	155,600	12,300	105	0

Table 3.6. Evolution of the Lake Eyre brine chemistry following the 1984 flood event (after Kotwicki, 1986). Note the marine-like proportions. Values in ppm.

Lake Eyre is an ephemeral playa-salt lake that lies asymmetrically in the southern portion of one of the largest internal drainage basins in the world (1.14 million km²) and covers one-sixth of the Australian continent (Figure 3.49). Drainage topography is flat, with extensive areas of sandy and stony deserts. There are regions with some relief near the boundaries of the drainage basin, but only 30% of the area is elevated more than 250 m above sea level. All streams flowing into Lake Eyre are characterised by extreme variations in discharge and flow duration (Figure 3.50). Mean annual runoff across the basin is 4 km³, equivalent to a water layer 3.5 mm in depth, the lowest runoff level of any major drainage system in the world. The Lake Eyre Basin is large but dry, its drainage spans a number of climatic zones, including the tropical monsoon system to the north and the mid-latitude westerly circulation belt to the south. Some 5 x 10⁵ km² of the drainage basin receives less than 150 mm of rainfall per year (on average). The highest rainfalls, with annual averages around 400 mm, occur in the northern and eastern margins, where rainfall comes from the edge of the monsoon belt.

^{3.1}The El Nino - Southern Oscillation (ENSO) is a global climatic phenomenon marked by see-saw shifts in air pressure between the Indo-Australian and eastern regions of the Tropical Pacific. El Nino and La Nina refer to extreme phases in the 2-7 year cycle. During the warm 'El Nino' phase, the Australian seaboard cools, SE trade winds slacken and extended periods of drought are experienced in the Australian interior. In the cool 'La Nina' phase, the seas around Australia warm, the SE trade winds intensify, and widespread rain and flooding occurs.

The northern end of the Lake Eyre catchment lies barely on the periphery of the planetary monsoon system. The Northern Australian monsoon is erratic both in space and time. Recent lake floods are related to La Nina phases of the El Nino-Southern Oscillation (ENSO^{3.1}) and are out of phase with the Pacific Dry Zone rainfall and El Nino events (Kotwicki and Allan, 1998). Changes in the intensity of the monsoon have controlled the frequency and permanency of Lake Eyre waters throughout much of the Quaternary (Magee et al., 1995; 2004).

Monsoonal outbursts supply water to the Lake Eyre via its eastern tributaries; Cooper Creek, Diamantina and Georgina rivers systems. This water takes weeks to reach the lake and floods much of its flow path on the way, as it deposits sediment in a unique set of anastomose arid-zone fluvial deposits, known locally as "the Channel Country" (Gibling et al., 1998). Trustworthy data on the filling of Lake Eyre reports flooding in 1938, 1955, 1963, 1968, 1973, 1974, 1975, 1976, 1984 and 1989 with exceptional floods occurring every 25 to 30 years (Figure 3.50; Kotwicki, 1986; Kotwicki and Allan, 1998). In 1974, in the largest flood on record, water flowed from Lake Eyre North to Lake Eyre South between March and October when an equilibrium level was obtained. More than 39.3 km³ of surface runoff flowed into the lake at this time, completely dissolving the salt crust. The crust reformed in the following two years as more than 39.5 km³ of water was evaporated (Dulhunty, 1977; Kotwicki, 1986). Large quantities of salt, estimated at 30 million tons (7.5% of Lake Eyre North content), were

transferred into Lake Eyre South during this event, creating, in its lowest portion, a salt crust up to 29 cm thick for the first time on record (Dulhunty, 1977).

As well as the monsoon feed from the north, significant runoff can originate in the desert west of the basin, where it is drained by the Neales and the Macumba Creeks. The 1984 filling, with a total volume of 10 km³, was a relatively minor one but it proved that the western tributaries can fill Lake Eyre in a matter of days. During the 1984 flood, maximum water depths were 5.7 m in Lake Eyre North and 3.7 m in Lake Eyre South. Lake Eyre South this time filled first - an event never previously recorded and considered to be extremely unlikely - and overflowed to Lake Eyre North, reversing the usual flood pattern in the lake (Allan et al., 1986).

Monitoring of the chemistry of the lake brines in the 1984 flood shows the conservative behaviour of all the major ions in Lake Eyre with the exception of Ca, which, relative to the other ions, started to deplete after October 1984 and to sulphate, which flattened its still rising concentration rate. This coincides with the onset of gypsum precipitation around October 1984. Its seawater like brine evolution is typical of most inland waters in Australia (Table 3.6 and Chapter 2).

In 1989 another western-fed flooding event occurred, coinciding with the filling of Lake Torrens on the other side of the Flinders Ranges. Lake Torrens is the second largest Australian playa after Lake Eyre and in 1989 it filled for the first time since 1878. Short term inflow rates into Lake Eyre during both the 1984 and 1989 flooding events were enormous: for example

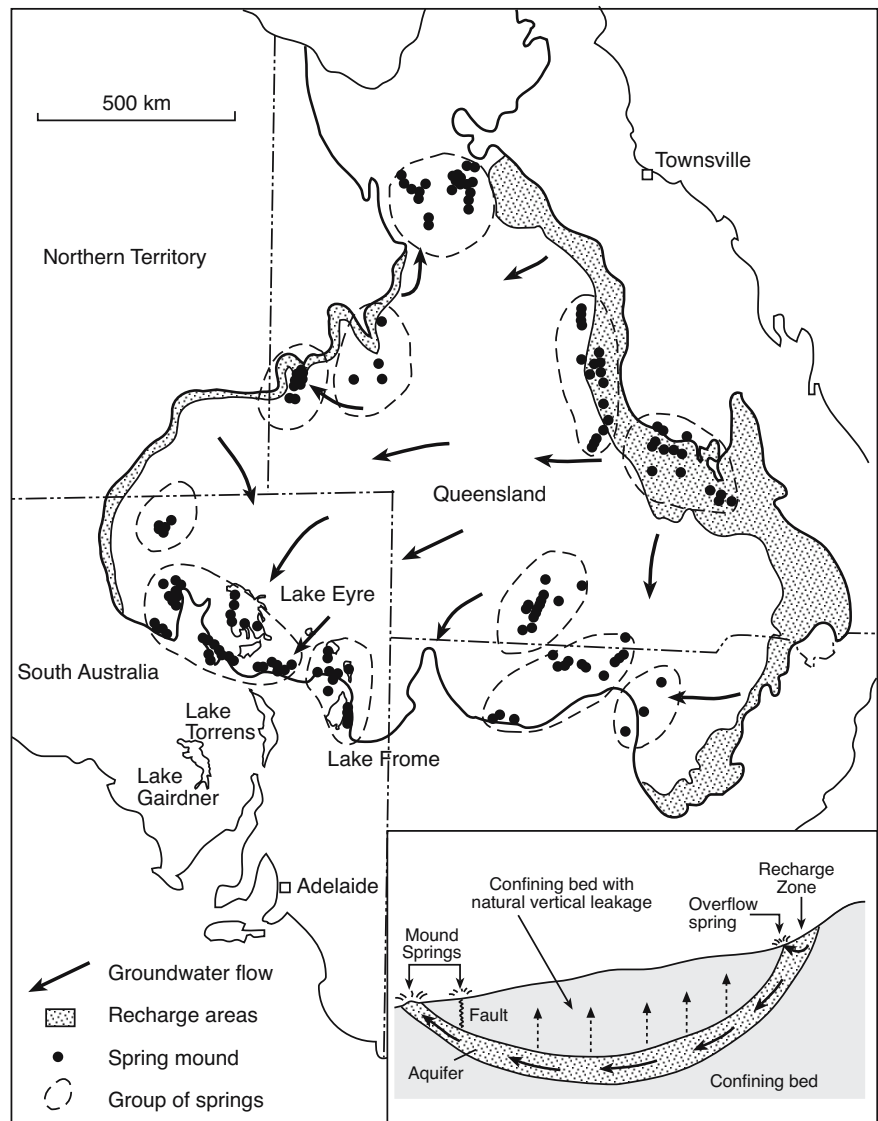


Figure 3.52. Location of spring mound, spring groups and artesian groundwater flow paths in the Great Artesian Basin, Australia. Shows a high density of mounds in the vicinity of Lake Eyre and Lake Frome (after Habermehl, 1982)

in 1984 and in 1989 Lake Eyre received some 8 km³ from western tributaries in three days, which implies discharges of the order of 30 000 m³/s, or one-sixth that of the Amazon. The 1989 “wet” continued into 1990 when, after some of the most devastating floods of the Channel Country in Australian history, water from the Cooper Creek reached Lake Eyre for the first time since 1974.

As well as the being the regional sink for its surface runoff, Lake Eyre’s position also defines the southern outflow or seepage area of the Great Artesian Basin (GAB), which covers an

area of 1.7 million km² (Figure 3.52). The GAB consists of several contiguous sedimentary basins with confined aquifers of Triassic, Jurassic and Cretaceous continental quartzose sandstones, underlain by an impervious pre-Jurassic base (Habermehl, 1980, 1982, 1996). It forms a large synclinal structure, uplifted and exposed along its eastern margin, leaving the overall basin tilted southwest. Recharge to the GAB occurs primarily along the uplifted eastern margins and also on the western margins where the aquifers are exposed or overlain by sandy sediments. Confined groundwater then percolates very slowly towards the terminal base level of Lake Eyre and saline lake sumps, reaching the Lake Eyre area after a calculated travel time of up to three million years (Figure 3.52).

Natural discharge from the GAB comes from two principal processes: 1) diffuse vertical leakage towards the regional water table and, 2) from focused outflow via 600 springs located in 11 groups along the western and southern boundaries of the Lake Eyre basin (Figure 3.52). Many spring mounds define linear fault-controlled surface trends. Flow from the mounds totals 0.03 km³/year and is a minor discharge component of the overall diffuse artesian discharge to the water table. But it creates distinct carbonate spring mounds with the potential to be preserved (Ponder 1986; Mudd, 1998, 2000). Measured flows from various springs range from 0.0001 to 0.23 m³/s totalling around 1 m³/s. Salinities range from 700 to 80,000 ppm, pH from 7.1 to 8.0 and water temperatures from 30 to 40°C.

A typical mound consists of a central pool of water, an outer rim of reeds and vegetation, an outflow channel, and successive layers of carbonate (Figure 3.53). They are composed of micritic marls, invertebrate remains, microbial tufa, pisolites and micrite-cemented eolian sands and are surrounded by gypsiferous sabkha mudflats. Spring mounds are especially obvious in the southern part of Lake Eyre (Habermehl, op cit).

Active mounds are up to 8 m in height and up to 30 m across. The now extinct Hamilton Hill Spring Mound rises more than 40 m above the surrounding hypersaline playa floor, suggesting that late Pleistocene artesian pressures have been higher (Habermehl, op cit.). Flow rates from Lake Eyre springs are directly proportional to the area of wetland vegetation that the spring supports (Williams and Holmes, 1978).

The shores of modern Lake Eyre erode the edges of some now inactive spring mounds and a number of lunette-cored islands within the lake. The southeastern lake coastline, which today consists of eroded dune sand cliffs, is being rapidly cut back, with an erosion rate in the order of 5 m per major flood. The presence of several older strandlines some 0.7, 1.6 and 2.8 m above the 1974 water level, indicate previous unrecorded major flood events. According to Kotwicki (1986), the above levels represent approximate storages of 35, 48 and 67 km³ respectively. The highest potential available storage in the Lake Eyre depression is more than 200 km³, i.e. almost seven times greater than the 1974 storage. The terms “full” or “flooded to capacity” should therefore be used cautiously in Lake Eyre in relation to historical flooding events.

The Lake Eyre basin has been an area of lacustral sedimentation since the Mesozoic. The first documented lacustrine sediments are of freshwater Lake Walloon, which occupied central eastern part of the Australian continent some 150 Ma (Middle Jurassic). By the late Cretaceous (85-75 Ma) it had shrunk to become the much smaller 5 x 10⁵ km² Lake Winton. By the early Miocene (21 Ma) the freshwater lake had assumed a position closely resembling that of Lake Eyre, it even had an indigenous species of freshwater dolphin. This freshwater system in turn evolved into Lake Dieri, a Pleistocene “greater Lake Eyre” which underwent large scale variations in size and salinity from a perennial freshwater lake up to 25 metres deep,

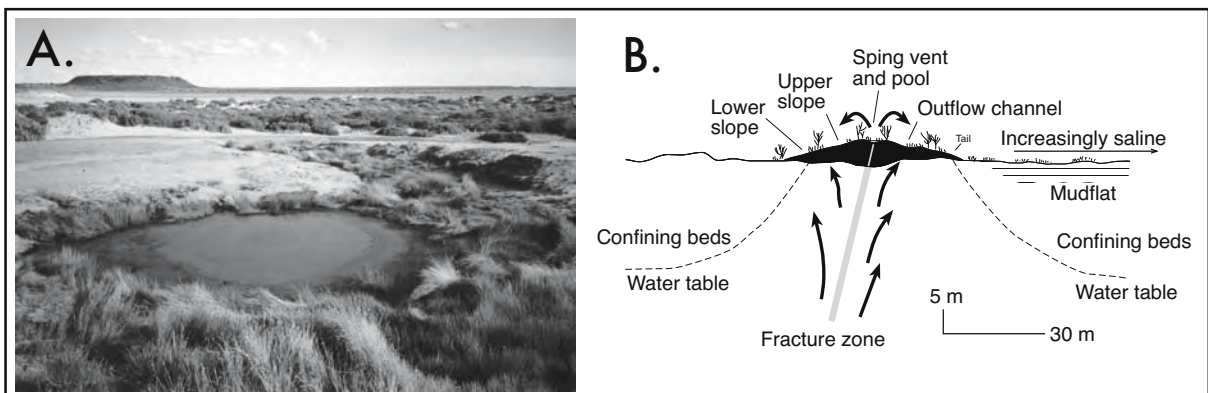


Figure 3.53. A) Active mound spring in the southern margin of the Great Artesian Basin artesian where water up to 3 million years old returns to the surface. B) Schematic cross section of typical Lake Eyre Basin mound spring.

to a groundwater-controlled playa marked by substantial sediment deflation to enter the Holocene as a dry salt pan subject to occasional flooding (Magee et al., 1995; Magee and Miller, 1998). Four Late Pleistocene shorelines have been recognised in those parts of the present Lake Eyre surrounds not located downwind of the depression. They are: a 40 ka shoreline at -10m AHD (Australian Height Datum), a 65 ka shoreline at -3.5m AHD, a 80 ka shoreline at +5m AHD shoreline and a 125 ka shoreline at +10 m AHD, which corresponds to Stage 5e on the Quaternary eustatic curve (Figure 3.54; Magee et al., 2004; DeVogel et al., 2004).

Greatest effective aridity in Lake Eyre in the past 150 k.y. occurred in marine oxygen isotope stage (MIS) 6, when basin deflation was 4.3 m lower than today (Figure 3.54). This arid event was followed abruptly by formation of the deepest perennial lake (phase V at +10m relative to the Australian height datum [AHD—mean sea level]), a level 10 metres above sealevel and some 25 metres above the modern playa floor. At least 6 m of finely laminated gypsiferous and calcareous clay were deposited at this time in conditions characterised by salinity stratification and strongly reducing bottom conditions (Magee et al., 2004). At the same meandering inflowing streams deposited thick, lateral-accretion sediments and fluviodeltaic sediment at the stream mouths.

After this acme level, the lake then shallowed and briefly dried at least once, but no evidence is seen of deflation or pedogenesis (Magee et al., 2004); then the lake refilled to +5 m relative to AHD between 100 and 75 ka (Phase IV), when lacustrine deep-water clays, calcareous nearshore and beach sands, and clastic gypsum evaporites were deposited coevally with renewed fluvial aggradation. Fluctuations in lake level and salinity noted by Magee et al. (op cit.) suggest decreasing regularity of inflow and gradual diminution of the monsoon toward the end of Phase IV.

Sediments of Phase IV were pedogenically modified and eventually truncated by deflation when the lake dried at 75–70 ka and disrupted gypsiferous playa sediments were transported downwind. Incision of tributary rivers into previous fluvial and lacustrine sediments, extending down almost to the modern level, documents a transition to significant aridity.

Lacustrine conditions returned at 65–60 ka (phase III), depositing lake sediment and a prominent beach sand, rich in the brackish water gastropod *Coxiellada gilesii* at -3m relative to AHD; coeval fluvial aggradation and vertical accretion of

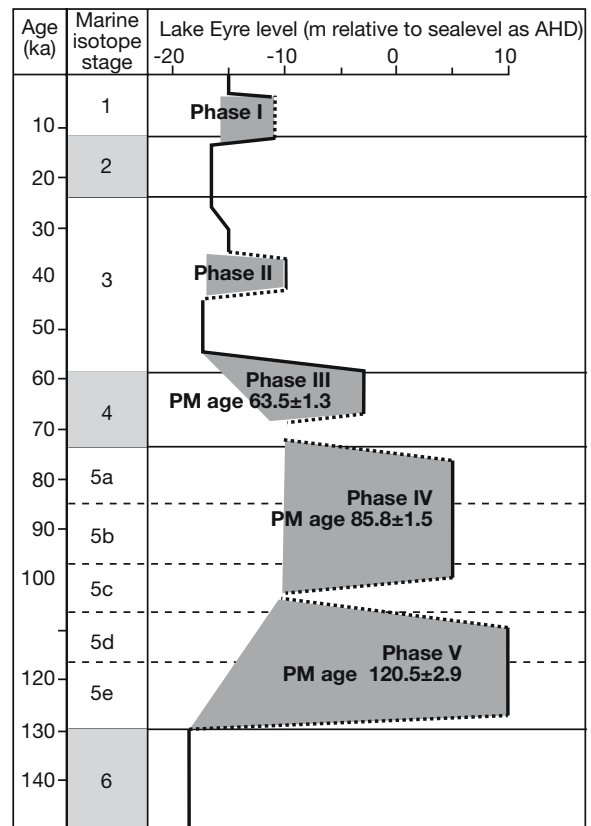


Figure 3.54. Late Quaternary changes in lake level in Lake Eyre (after Magee et al., 2004).

overbank muds occurred. Though having shallower water and shorter duration than Phases V and IV, Phase III had significantly deeper water and longer duration than the modern ephemeral events and represents the last deep-water perennial lake in the basin and the last influence of moderately effective monsoon precipitation.

A major deflation episode between 60 and 50 ka excavated the present Lake Eyre basin to deposit gypsum- and clay-rich lunettes at a number of sites around the lake edge as well as covering former shorelines on the windward side of the lake. After deflation ceased, a thick secondary gypsum soil profile (gypsite) developed on the dunes early in oxygen-isotope stage 3. Between about 30,000 and 12,000 yr. B.P. Lake Eyre was at least as dry as it is today. At many sites a lunette-like, playa-marginal, eolian unit formed from saline mudflat sediments deflated from the playa floor. After 10,000 yr B.P. a minor lacustral phase occurred (Phase I) until the modern ephemeral playa regime became established at 3000–4000 yr B.P.

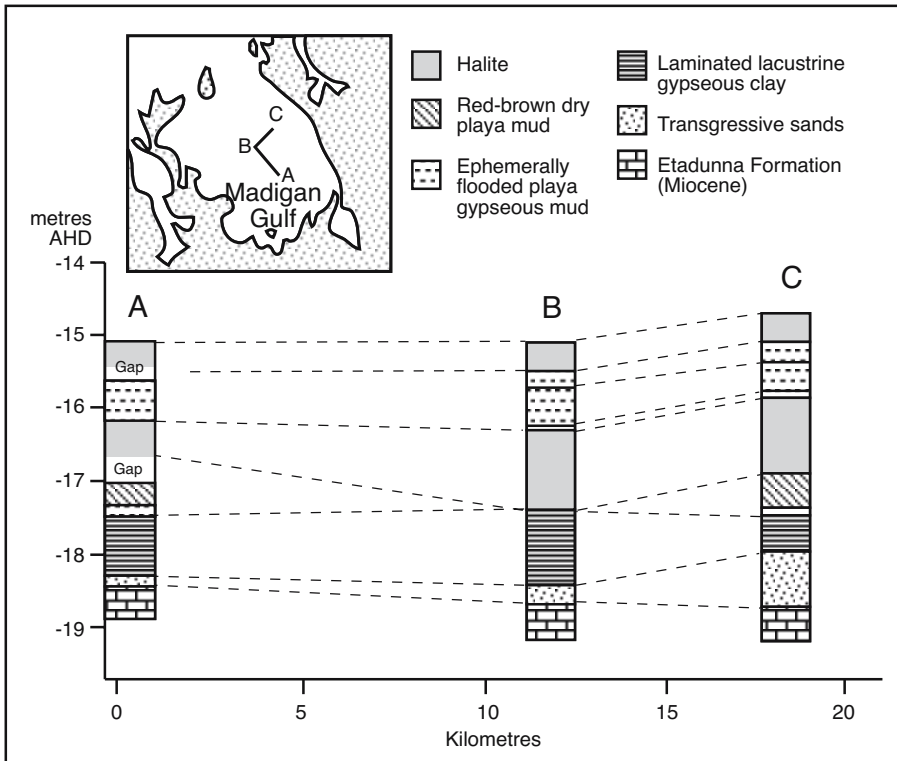


Figure 3.55. Distribution of buried saline pan halite beds and associated sediments in Madigan Gulf, Lake Eyre North (after Magee et al., 1995).

Given the large volumes of water periodically entering the lake depression, and its long history extending back to the Mesozoic, one would perhaps expect large volumes of salt to have at times accumulated in the lake sediments. Certainly, Lake Eyre (Madigan Gulf) is the only Australian playa to retain buried Pleistocene halite beds (Figure 3.55; Magee et al., 1995), but both beds are less than a metre thick. The total Pleistocene thickness is only 3 metres in this the saltiest part of Lake Eyre North. A lack of preservation/accommodation space, tied to ongoing lake floor deflation, reflects the meteoric/artesian recycling hydrology that characterises most large low relief playas of inland Australia (Chapter 2).

Gillespie et al. (1991) interpreted the buried halite in Madigan Gulf is a former salt pan unit, which was partially dissolved during the onset of a minor halite phase in the early Holocene and then preserved by the deposition of the overlying gypsiferous clays. But with thicknesses of less than a metre for each of the two preserved saline pan beds it is not a geologically significant body of halite. Inherent low relief and artesian hydrologies means the ephemeral stream floodplain – dune field – ephemeral saline lake playas of Australia and elsewhere are

unable to accumulate thick sequences of bedded salt in the lowest parts of the drainage basin. It simply blows away. Haloturbation of siliciclastics in continental sabkhas in association with widespread redbed fluvial and eolian deposition is the dominant signature of this style of deposition.

Lake Frome, Australia

Lake Frome, South Australia, is another example of an ephemeral stream floodplain – dune field – ephemeral saline lake complex in the major outflow zone of the Great Artesian Basin (Figures 3.52). Lake Frome is approximately 100 km long and 45 km wide with an area of 2700 km² and lies to the south of Lake Eyre (Figure 3.49). Sediments come

mainly from the west via a series of short, relatively steep gradient streams, originating in the Flinders Ranges some 40 to 50 km away. Overflow waters from Lake Eyre sometimes spill into the north of the lake via Warrawoocara Channel, which also connects lakes Gregory, Blanche and Callabonna. This spillover prevents Lake Eyre water from today rising to a height of more than 12 metres above the Australian height datum (AHD).

The lake contains many islands mainly in the south, where the lake floor is at its lowest, some 2 m below mean sea level (Figure 3.56). These islands are the erosional remnants of earlier now largely deflated Pleistocene sediments and are composed of gypsiferous quartz sands atop a clay surface. Around the edges of the lake there are quartzose spits and bars, beach deposits, and delta fans, as well as Pleistocene transverse and longitudinal desert dunes (Draper and Jensen, 1976). As in Lake Eyre, sheet delta fans define the entry points of the larger ephemeral streams and are built by the coalesce of flat lenses of ephemeral stream sediment and dominated by low angle layering. Stream channels are shallow, straight to gently curved features with few point bars. Oxidised organic-rich muds define lowest parts of the channels. Fine-to-coarse sands

with minor gravels form the bulk of the sheet delta sediment. Interchannel areas are composed mostly of reworked eolian sands. Marginward evaporitic flats with widespread capillary gypsum form large areas peripheral to, but sometimes, atop the sheet delta sand prisms.

Further out into the lake the channels die out and pass into the sands and muds of the saline mudflat, which dominates the lake basin. The bulk of the mudflat matrix is a quartzose sandy

mud or mud with displacive gypsum forming in the capillary fringe and displacive halite in the uppermost 10 cm. Mudflat sediments tend to be massive but can locally show indistinct wispy organic lamination. In the lowest part of the lake floor is the saline pan made up of an ephemeral halite crust up to 20 cm thick and composed of halite rafts and chevrons. The crust completely dissolves during times of flood and is continually underlain by water-saturated muds with large crystals of lenticular and prismatic gypsum.

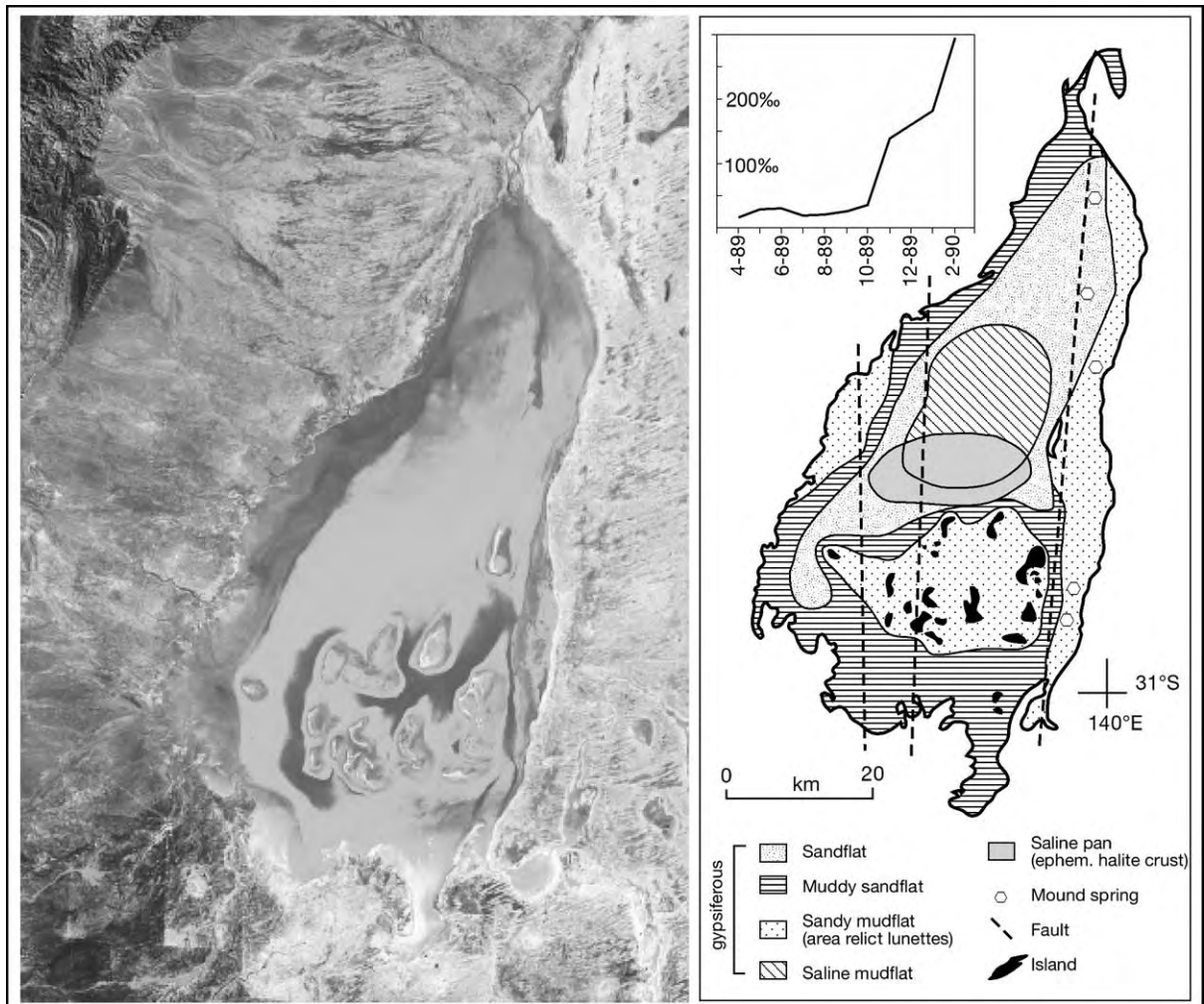


Figure 3.56. Surface sediments in Lake Frome, South Australia. The Flinders Ranges are visible in the upper northeast corner of Landsat image. Sediments in the lake depression show an off-centre bull's-eye pattern related to the presence of a deflationary high in the southern centre with islands dominated by lunette gypsum. The clastic distribution is also inverted with high proportions of sand in the more central positions of the saline mudflat rather than along the current lake strandline. This unusual matrix position indicates detrital flooding from the north fed by overflow from the Warrawoocara Channel, which feeds overflow from Lake Eyre into the northern end of the lake. Note also the association of aragonitic spring mounds along the eastern side of the lake with their positions controlled by upwelling along a north-south trending fault. Inset shows salinity evolution of surface waters after the April 1989 flood (Landsat Image courtesy of NASA, surface geology in part after Draper and Jensen, 1976).

Like Lake Eyre, the lake also displays large active spring mounds along its eastern side. Mound sediments are made up of varying proportions of detrital sediment and authigenic aragonite, calcite, and dolomite cements forming an microbial tufa bindstone. An apron of gypsum fringes the active mounds. As in Lake Eyre, the mounds indicate fault-focused outflow fed from aquifers of the Great Artesian Basin and line up parallel to the major north-south normal fault system that characterises the area.

The inset in Figure 3.56 shows the salinity evolution of a brine sheet from April 1989 until complete desiccation 11 months later in March 1990. The rate of salinity change in the brine sheet was climatically controlled. In April 1989 it was a sheet of mesohaline water (<50‰) covering the previously dry lake floor. Much of the salinity in the water sheet soon after flooding came from dissolution of the salt crust that had previously occupied the central depression. The brine sheet remained for 6 months through the cool months of winter and spring, with little change in its mesohaline salinity. Then, with passage into the hot summer of the Australian interior, brine sheet salinity rose rapidly. In less than a month it moved from its previous salinity plateau into gypsum saturation and then into the halite saturation field before desiccation three months later. By end March-early April, 1990 (almost a year after the flood) the lake floor had dried out and its 30 cm-thick salt crust had reformed. This style of salinity increase, with a long plateau of mesohaline waters, is important to life in the lake as it allows sufficient time for a halotolerant macro and microfauna to breed and survive into adulthood. Plateaus in salinity evolution can control the intensity of the “feast or famine” response in many saline water bodies worldwide (Chapter 9).

Lake Callabonna, Australia

Lake Callabonna, located between Lake Eyre and Lake Frome (Figure 3.49) is another example of climate deterioration in the ephemeral stream floodplain setting in large saline lakes in the Australian interior. Some 0.2-0.7 Ma the lake was a predominantly freshwater lake surrounded by grassy plains and subject to periodic shrinkage and desiccation (Wells and Tedford, 1995). Compared to today this was a time of greater monsoonal supply to the Lake Eyre Basin. Today Lake Callabonna is a dry playa, surrounded by desert. Then the Pleistocene lake was of variable salinity but was several times the size of the present Callabonna saline mudflat and never as dry as it is today. Plant remains associated with this time suggest a more arborescent flora than that near the present-day edge of the evaporitic mudflat but

one containing taxa that still exist in the surrounding region. These facts indicate a seasonal climate with fluctuating water table but a regionally more effective rainfall than at present (the Australian version of Lake Chad?).

This savannah-style vegetation supported large numbers of Diprotodon, a hippopotamus-sized marsupial and the largest marsupial known to ever exist in Australia, as well as other large marsupials including giant kangaroos. These large-bodied vertebrates were mired in the clays during times of low-water or desiccation, while attempting to cross the floor of the lake. Today, fossil carcasses can be found beneath thousands of mud-covered evaporite-cemented mounds littering the exposed lake floor. Geosystems modelling of the Pleistocene hydrology by De Vogel et al. (2004) shows that lakes Callabonna and nearby Blanche were the last two remaining water holes in the catchment whenever the system dried at the end of each wet interval.

Perennial stream floodplain–perennial saline lake

Perennial stream floodplain–perennial saline lake depositional complexes, the third saline lacustrine depositional style of Hardie et al. (1978), occur in several high relief tectonic settings and usually lack extensive sabkhas. Any sabkhas that are present tend to be localised muddy embayments about the lake shoreline. Most perennial saline lakes such as the Dead Sea and the Great Salt Lake are characterised by steep slopes surrounding the lake. The steep slope allows saline water to pond in an arid climate and the lack of sabkhas is often the result of the steep basin sides, with the associated lack of an aerially extensive outcropping of the capillary fringe. These perennial lakes are discussed in detail in the next chapter.

All the ephemeral saline water systems discussed in this chapter have one very obvious feature in common, that is, all are subject to an unpredictable and variable rate of water inflow. Researchers who have not experienced a heavy desert rainstorm often do not appreciate how much and how quickly moisture can enter the system and move large volumes of sediment. It creates debris-charged raging torrents in normally dry streambeds of the hinterland, crossbedded and rippled sheet sands, vast areas of muddy floodplain and in a day or two can convert a saline pan sump into a lake filled with brackish water and teeming with a halotolerant biota (Chapter 9). Table 3.7 lists extreme rates of rainfall in some of the areas that occasionally can feed huge volumes of surface flow into the saline lake depressions. Once this huge volume of water has moved large volumes of

Location of event	Date of event	Annual av.	Storm rainfall (mm/time)
Aozou, Sahara	May, 1934	15 mm	370 mm in 3 days
Tamanrasset, Sahara	Sept., 1950	27 mm	44 mm in 3 hours
El Djem, Tunisia	Sept. 1969	275 mm	319 mm in 3 days
Bisra, Algeria	Sept., 1969	148 mm	210 mm in 2 days
Sharja, UAE	1957	107 mm	74 mm in 50 minutes
Swakopmund, Namibia	1934	15 mm	50 mm
Dead Sea, Middle East	Nov., 1995	90 mm	150 mm in an hour (2.5 mm per minute)
Mt Dare, Australia	March, 1967	126 mm	149 mm in 1 day
Alice Springs, Australia	March, 1988	275 mm	205 mm in 1 day
Innamincka, Australia	Jan., 1974	172 mm	356 mm in 3 days
Balcanoona, Australia	March 1989	200 mm	341 mm in 2 days
Chicama, Peru	1925	4 mm	394 mm in single storm
Lima, Peru	1925	46 mm	1524 mm (more than 30 times annual)

Table 3.7. Rates of extreme rainfall events that create sheetfloods in the arroyos, ephemeral fans and "channel country" fluvial systems feeding surface waters into saline lakes and pans.

siliciclastic sediment into the lake depression, it dries out within weeks to months and the system then can stay dry for years. With desiccation the newly deposited sediment is subject to the vagaries of deflation and with longer term climatic change and lowering of the regional water table can evolve into what can be extensive eolian sand and dust sheets.

Eolian sabkhas

So far, this chapter has described and defined sabkha deposition in either marine-margin or continental settings. In both situations the interpretation of ancient counterparts comes from the matrix, not the salts. Put simply, nodular anhydrite accumulating in a marine sabkha is hosted in and intercalated with marine (fossiliferous) fine-grained sediment, while continental sabkhas are intercalated with, and hosted in fine-grained nonmarine fluvio-lacustrine matrices. But there is a third sabkha association, that of eolian sabkhas where nodular anhydrites, gypsums and displacive halites are hosted in muddy eolian matrices (Figure 3.1). Eolian sabkhas can form in either marine margin or continental lacustrine settings. In either setting their depositional proximity to eolian sands means eolian sabkhas tend to be intercalated with potential eolian reservoirs and can form lateral discontinuities in the eolian sands (Figure 2.44). For this reason I have broken out modern occurrences of eolian sabkhas as a separate topic.

I define an eolian sabkha as being characterised by capillary salts accumulating in any eolian-derived matrix and sitting below a Stokes surface. It may form in interdunal depressions, in sand sheets on the marine or lacustrine edges of ergs, or even in areas of desert loess. By definition, eolian sabkhas, like all sabkhas, require the upper part of the capillary fringe to intersect the landsurface. Fluctuating water levels and water tables will move a sabkha strandline back

and forth over the lower parts of an arid drainage so that eolian sabkha sediments are often intercalated with units deposited in either the ephemeral saline pan or in sand sheets. The ratio of siliciclastic matrix to capillary evaporite in an eolian sabkha unit means it can be further classified into: 1) detritally-dominated (wet eolian sabkha) with a capillary succession showing haloturbation but little or no preserved capillary salts (possible hydrocarbon reservoir), and 2) chemically-dominated (saline eolian sabkha) with abundant capillary salts preserved (possible seal).

Matrix in wet eolian sabkhas has a characteristic association of sedimentary structures associated with ephemeral water and eolian overprints ranging from; subaqueous current and wave ripples, wavy laminae and contorted bedding (wet-surface conditions), through adhesion structures, bioturbation structures, desiccation cracks (damp-surface conditions), megapolygons and Stokes surfaces (falling water tables) to wind-ripple lamination (dry-surface conditions; see Chapter 2; Mounney and Thompson, 2000; Goodall et al., 2000). Similar sedimentary structures occur in chemically-dominated eolian sabkhas but they tend to be overprinted and disturbed by pervasive chaotic salts and associated haloturbation.

Probably the best modern area to study the interrelationships between eolian sabkhas and dune systems is the Arabian Peninsula (Figure 3.57). At least six generations of dunes can be identified on satellite images of the United Arab Emirates and Saudi Arabia (Glennie, 1998). Geomorphic relations indicate

that older periods of Pleistocene dune formation have been modified by later periods of eolian activity, including modern wind flow patterns. In addition, at least two periods of older eolian sedimentation lie beneath the modern dunes. Some dunes sands have a high content of comminuted marine shells and along with wind-reworked oolites have been cemented into calcareous eolianite, locally known as miliolite. They were sourced in sands blown out of the exposed marine shelf during glacial induced sealevel lows (Figure 3.57). Thus, the modern eolian sabkhas on the Arabian Peninsula indicate a complex combination of groundwater overprints interlayered into active dunes and palaeodune bedforms. Those dunes cemented into calcareous eolianites (miliolites) tend to be associated with sea margin sabkhas, as in the vicinity of Al Liwa oasis in the UAE, others form in siliciclastic matrices at the edges of ergs in continental interiors, as at Umm as Samim in Oman.

Older literature discussing eolian sabkhas typically assumes an elongate geometry, inherited from groundwater-driven infill between the partially preserved topography of the underlying

dune ridges (Figure 3.1; Handford, 1981). But dunes are merely loose sediment blowing around above the water table, if the dunes blow on, the remaining sediment is held in place by the capillary fringe and so this type of eolian sabkha can have a sheet-like geometry. It also means the edges of many active ergs are flat laterally extensive erosional sandflats with deflation limited by the top of the capillary fringe. Thus, sheet-like sandflat-hosted styles of eolian sabkha about the edge of a sand sea are much more commonplace in continental interiors than the more typically cited elongate interdunal sabkha geometries (Figure 2.44). Elongate interdunal geometries tend to be most obvious where changing climate or subsidence pushes a rising water table and fluvial floods further into a sand sea. They are typical of low energy desert coastlines preserving the Flandrian transgression, and they are often associated with carbonate-rich (miliolite) hosts. Interdunal geometries are also typical of rising water levels at lacustrine-dune contacts, for example the edge of Lake Chad where rising lake levels pushed the water table to outcrop in nearby dunes in the last 10,000 years and drove the formation of silicates and sodium bicarbonate salts in the

interdunal capillary fringe. Muddy interdunal sabkhas also dominate areas where ephemeral streams flood into a sand sea.

Sea-margins with elongate eolian sabkhat

For an elongate interdunal geometry to be preserved during a marine transgression requires relatively low energy in the zone of marine encroachment. Otherwise, the encroaching high-energy coastal shoreface will erode and transform the depositional signature and destroy any sabkha salts. The landward side of the barrier-lagoon northeast of Abu Dhabi is such a low energy setting located at the sandflat edge of a large sand sea (erg) in the triangle between Abu Dhabi, Dubai

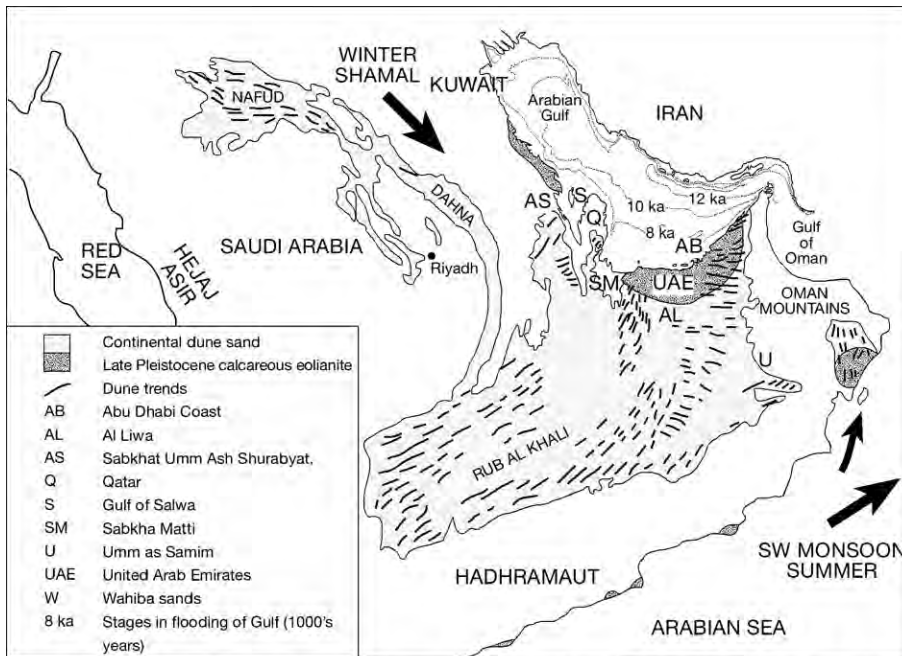


Figure 3.57. Extent of dunes and orientation of their crests on the Arabian Peninsula and approximate extent of the postglacial marine transgression into the Arabian Gulf basin at 12, 10, and 8 ka (after Glennie, 1998; Teller et al., 2000). Dominant modern wind directions are shown by arrows. Occurrence of late Pleistocene eolianite (Miliolite) is indicated by a darker pattern along coast, especially along southern coast of the Arabian Gulf around the Salwa Gulf and in the United Arab Emirates (UAE) where these palaeo-dunes extend as far south as about Liwa Oasis (AL), which is just north of the Saudi Arabian border. AB, SM, U and AS show the position of Abu Dhabi coast, Sabkha Matti, Umm as Samim and Sabkhat Umm Ash Shurabyat, all examples that are discussed in this section on eolian sabkhas.

and Al 'Ayn (Figures 3.57, 3.58a; Abu-Zeid et al., 2001; Teller et al., 2000; Glennie, 1998). Close to the coastal plain these dunes contain a high proportion of marine derived calcareous sand grains (miliolite). The dunes were at their most active in the late Pleistocene glacial maximum when strong winds blew from the west across the Eastern Emirates. Dune surfaces have been subsequently modified by the modern NNW Shamal winds. At the time they were at their most active the ocean had receded from the Arabian Gulf and the Tigris-Euphrates River reached the sea east of the Strait of Hormuz. Along the At Taf this facilitated transport of exposed shelf sediments into a series of E-W trending seif dunes and draas. Then, between 12 and 6 ka, the sea transgressed more than 1000 km from north-west to fill the formerly subaerial Arabian Gulf and in so doing cut off the supply of eolian sand to the dunes of the At Taf (Trucial Coast). At the same time the rising water table and the encroachment of the Flandrian seashore converted the present day coastal area from an eolian-dominated system to the Holocene coastal sabkhat documented earlier in this chapter.

Today the lagoon sabkha system between Abu Dhabi and Ras Ghanada shows broad-scale E-W curvilinear trends that are partially truncated by marine encroachment, so that sabkha-lined dune-cored spits now protrude into the lagoon (Figure 3.58a). To the south, similar now sabkha-covered dune ridges constitute the core to the elongate

trend of the Abu Dhabi and Al Du'yybaya spits. In fact much of the classic sabkha coast of the southern Arabian Gulf shows broad scale thickening patterns in the Holocene section that indicate an initial relatively passive marine encroachment into interdraa depressions (Warren, 1991; Kirkham, 1998).

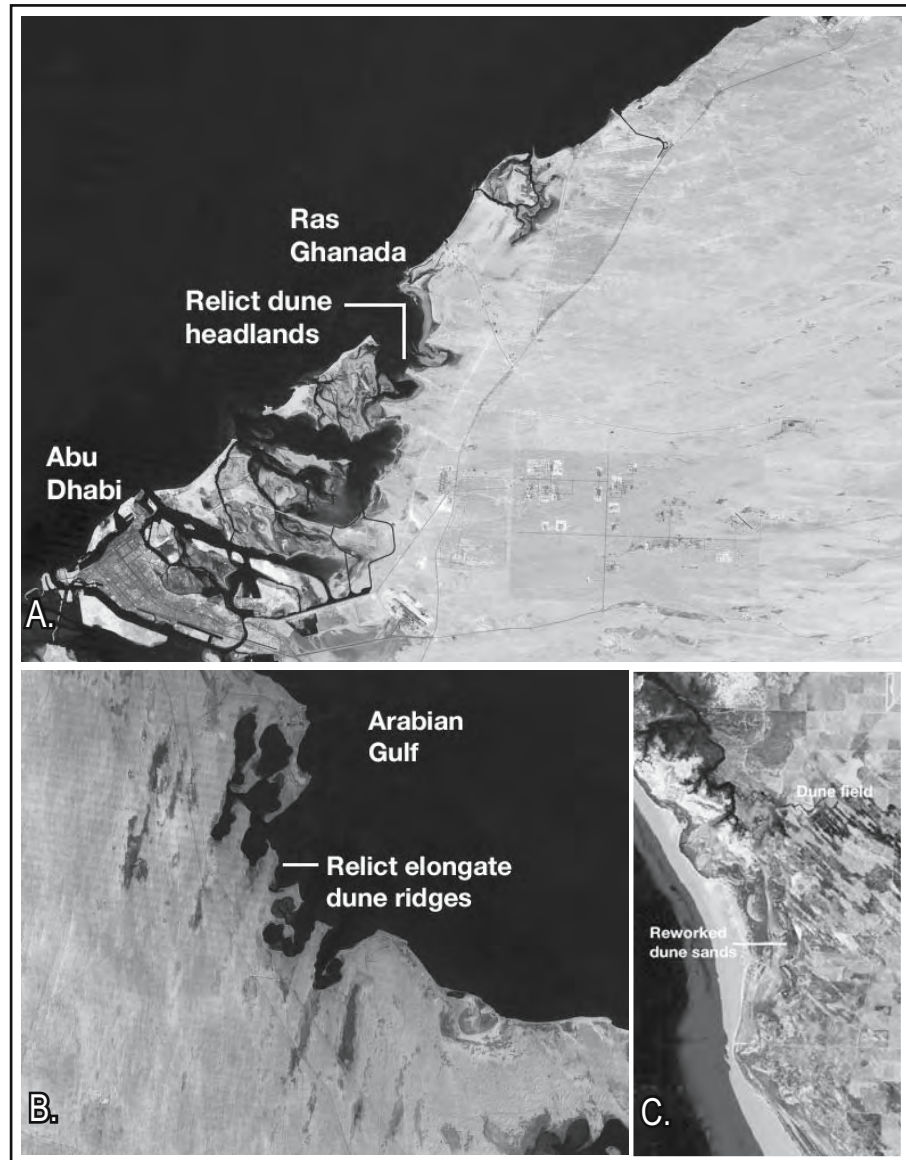


Figure 3.58. Examples of modern eolian sabkhas created by the Flandrian sea level rise and the encroachment of a seawater wedge into what were formerly continental interdunal corridors. A) Embayed sabkha-lagoonal coastline in the coastal zone between Abu Dhabi and Ras Ghanada, UAE. B) Embayed interdunal sabkhas in the coast south of Munfah, Saudi Arabian coast of the Arabian Gulf. C) Interdunal seepage sabkhas near Tickera, Spencer Gulf, South Australia. (All Landsat images are courtesy of NASA).

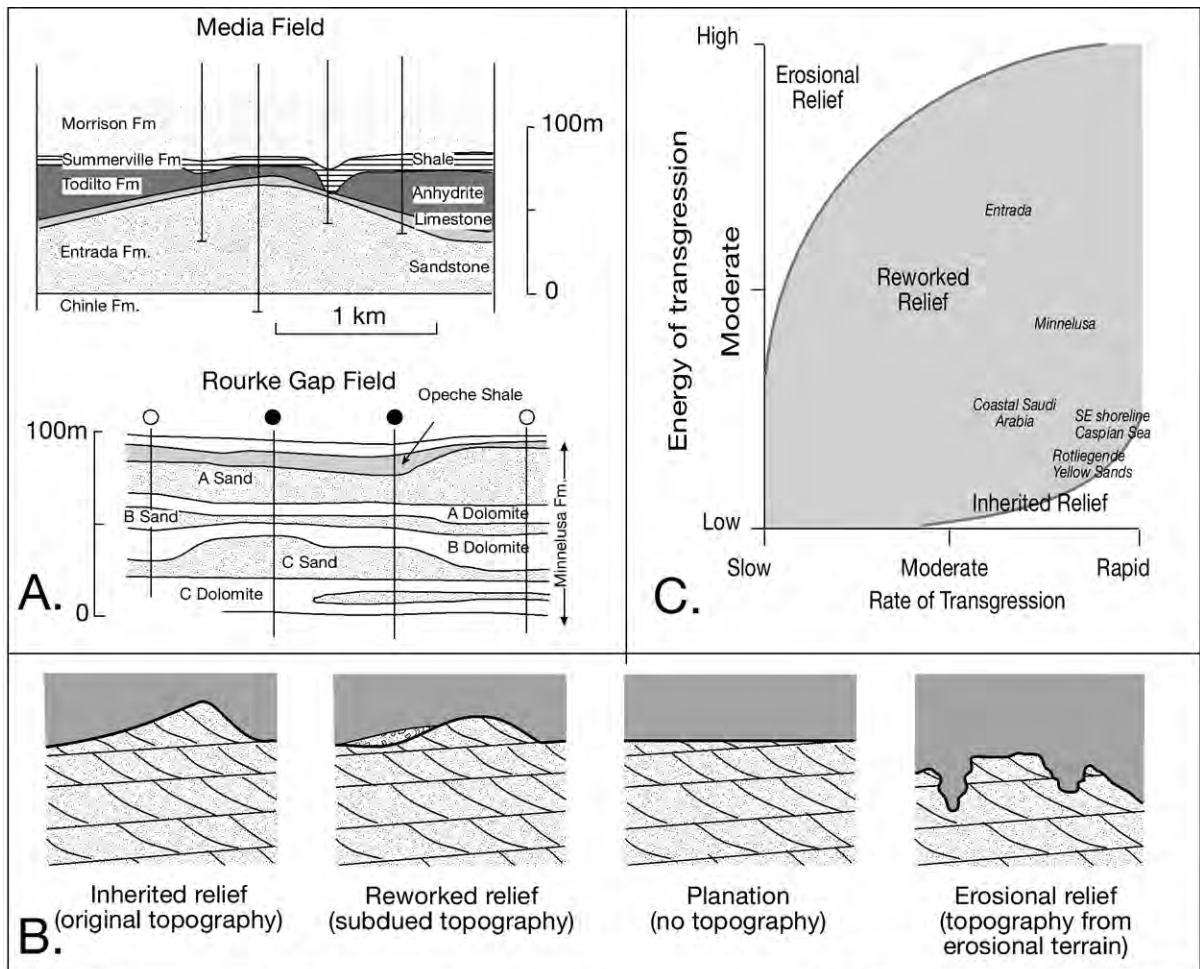


Figure 3.59. Preservation of marine-margin eolian sabkha. A) Ancient dune-hosted oil fields encased by an eolian sabkha seal (after Vincelette and Chittum, 1981; Achauer, 1982). B) Schematic of varying dune-sabkha contacts in transgressive marine-margin situations. C) Controls on the preservation of relict dune topography during a marine transgression (B and C after Eschner and Kocurek, 1988).

Interdraa coastal eolian sabkha geometries are even more obvious further along the coast in the region south of Munfah, Saudi Arabia (Figure 3.58b). There interdunal depressions are dominated by muddy sands with fringes of mm-scale biolaminites and displacive and lenticular gypsum growing at or above the water table (pers obs). Yet another coastal association of low-energy marine encroachment onto interdunal ridges is clearly seen on the northeastern Tickera coast of Spencer Gulf, South Australia (Figure 3.58c). In this case the encroachment was more energetic than on the Saudi coast. Many of the coastal sabkhas near Tickera lie parallel to the coastline in an area immediately behind coastal dune ridges. The most seaward quartzose dune sand ridges were reworked into these coast-parallel beach ridges, so the most seaward portions of the sabkha flat shows a coast parallel orientation.

It changes to a more obvious interdunal orientation a little further from the coast. All three systems are found in coastal zones on the edges of marine gulfs with limited fetch. Solute feeds to the three systems are all from groundwaters, although the proportions of marine versus continental inflow in the feed are still debated.

According to Eschner and Kocurek (1988) and Fryberger (1986), the geometry of preservation of an eolian dune system when undergoing transgression and possible encasement by an evaporite seal, is classifiable into inherited, reworked, and/or erosional dune morphologies at the contact with the sabkha evaporite (Figure 3.59a, b). Their modelling was done prior to our current understanding of the hydrological requirements needed to create platform and basinwide evaporite seals. We

now know that most laterally extensive marine evaporites are seepage fed systems that form when a basin is hydrographically isolated. There are no modern same scale marine analogs for this hydrology (Chapter 5); the dune-embayed coast of the southeast Caspian Sea is perhaps our closest modern analogy. Transgressing brines in an evaporite basin are an inherently low energy system and this is why ancient dune morphologies are best preserved below evaporite seals (Weissliegende and Entrada sands beneath Zechstein and Todilto seals, respectively).

Reworked dune relief, a preservation style which shows significant destruction of original dune topography, but with remnants preserved, is the most typical situation when an erg experiences marine encroachment or transgression in both the modern and the ancient. Modern examples include relict dunes of coastal Australia and the Arabian Gulf (Figure 3.58), Ancient examples include marine transgressed parts of the Jurassic Entrada Sandstone of the San Juan basin, and the Pennsylvanian-Permian Minnelusa Formation of Wyoming (Vincelette and Chittum, 1981; Achauer, 1982).

Whether inherited or reworked, how much dune relief is preserved in a marine transgression depends on the sand budget of the dunes and the erg, the degree of capillary cementation prior to transgression, and to the level of coastal energy in the transgressive environment (Figure 3.59c; Eschner and Kocurek, 1988; Fryberger 1986). Sand budget refers to the maintenance, gain, or loss of dune sand prior to and during initial transgression. Sand can be conserved and the dune form stabilized by vegetation, early capillary salt cementation, or a wind regime conducive to "sand trapping" by the dune as it is encroached by the sea (Eschner and Kocurek, 1988).

With thicker evaporite seals to the preserved dune morphology, the base of the seal tends to be a sabkha cement, hosted in the dune sands or its reworked equivalent, which in turn passes up into subaqueous evaporitic carbonates and salts of the evaporite proper. Cementation is typically due to capillary salts and so is tied to a shallow water table. Hence, the most intense capillary cementation can be associated with interdunal rather than high dune positions in the landscape. This creates a carbonate/evaporite cemented carapace that is more resistant to erosion than mobile loose sands of the draa crests. Upon transgression, this can create an inverted remnant topography with the cemented carapaces forming higher parts of the beleaguered landscape and corridors of marine embayment preferentially entering and reworking the more easily eroded loose draa sands (Fryberger, 1986). Remnants of this style of cementation beneath a platform or basinwide evaporite seal

can give strong directionality to permeability and create fluid flow corridors in the upper parts of an eolian reservoir sand beneath the seal.

Dune building and interdunal cementation can continue during initial transgression by maintenance of sand-drift paths, best accomplished by offshore winds, as seen today along the marine edge of southeastern Qatar (Figure 2.40). In contrast, dune forms can be degraded by deflation, a cutoff of the sand supply, and a variety of marine processes as is seen today along the At Taf coastal strip and the northern end of Sabkha Matti. Factors related to the nature of the transgressive environment and ultimate permeability in the reservoir sand include; (1) orientation of the dunes to destructive marine processes, (2) types of processes, (3) energy level, (4) type and rate of sedimentation, and (5) rate of marine encroachment (Eschner and Kocurek, 1988).

Preservation of inherited to reworked relief requires that the dunes ridges become stabilized or remain active into the early phases of the transgression. Effects of destructive marine processes are minimized by; 1) resistant, early capillary cement in the encroached dunes, 2) an orientation of the dunes such that marine energy is dissipated along a minimum area of the dunes, 3) low-energy, non-wave-dominated transgressive marine environment and 4) rapid transgression that reduces the length of time for reworking, or by high rates of marine sedimentation burying dune forms (Figure 3.59c).

Sheets of eolian sabkhat

This style of eolian sabkha is not as widely documented as elongate interdunal sabkhas. Yet modern examples characterize numerous continental interior situations where a rising water table in a deflationary sand sheet creates conditions suitable for the preservation of eolian sabkhas. They tend to be geomorphologically stable areas in that within a yearly sedimentation cycle they experience less erosion or deposition than nearby dunes sheets. In fact, because they lie in a moist hydrological zone below the top of the influence of the shallow water table, sheets of continental eolian sabkha tend to have much higher preservation potential than most of the crossbedded sands of the dunes. The latter sit above the water table and so have a tendency to blow on through (Figure 2.44f). Eolian sabkha sheets lie beneath exposed surfaces with high rates of sand cross-drift, a direct result of their saline watertable-induced flat topography and lack of vegetation. That is, in regions of shallow desert groundwater the flat bedded eolian sabkha sheets with characteristic capillary salts and Stokes surfaces

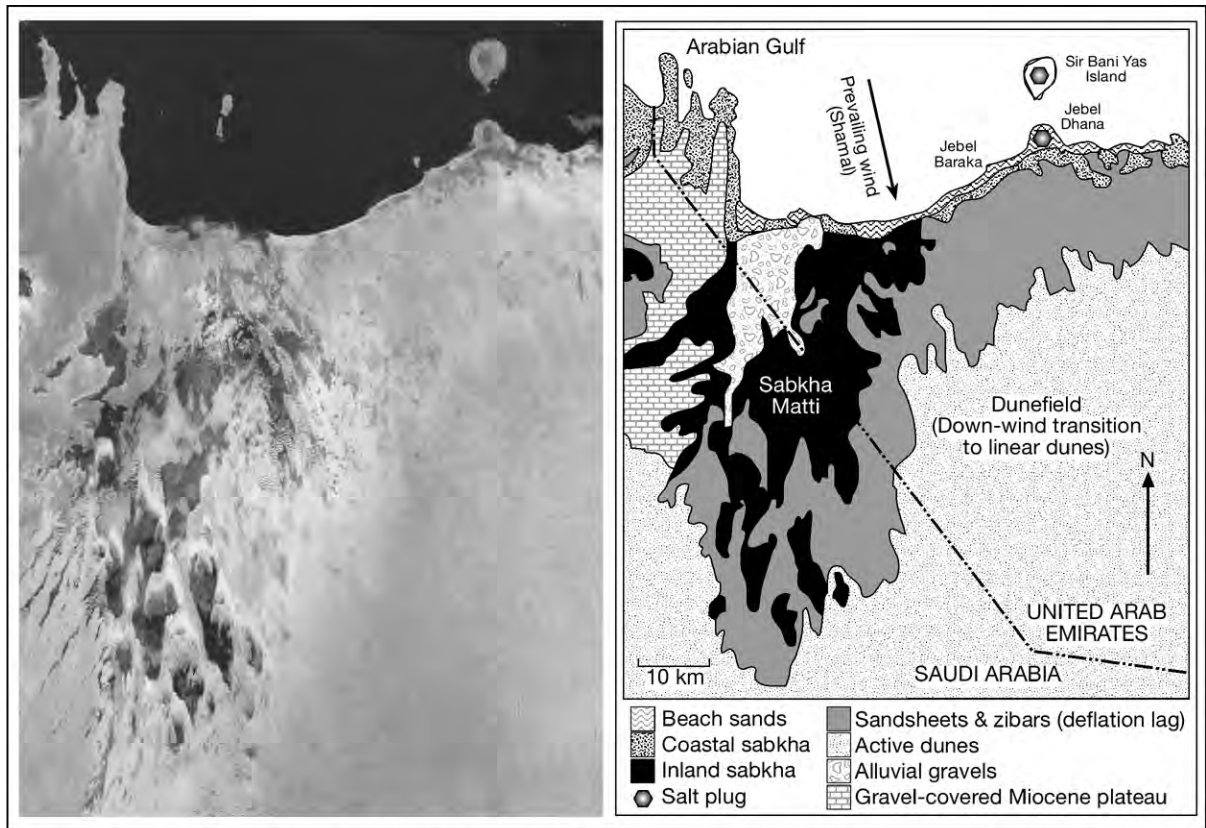


Figure 3.60. Sedimentary facies in Sabkha Matti, and inland sabkha in the southern central Arabian Gulf (in part after Alsharhan and Kendall, 2003; Landsat image courtesy of NASA).

are preserved more often than cross-bedded eolian sand, which by definition is deposited in a vadose environment and subject to ongoing deflation.

Depending on grain size of sediment in the capillary zone and the time of the year, the surface of a modern eolian sabkha sheet can lie up to a metre above the regional water table in the driest times of the year. Fluctuations in the regional water table in ergs can lead to the deflation of gypsiferous inter-draa sabkha and the creation of an eolian gypsum component to the dunes. This is the case in the near coastal region of Saudi Arabia where deflation has formed gypsum lunettes along the deflated pan margin of the gypsum encrusted Sabkhat ad Danan (Figure 3.16c.). Similar long term deflation of saline mudflats led to the downwind formation of extensive quartz dune fields as in the Late Pleistocene Chott Rharsa Basin of Tunisia (Blum et al, 1998) and to the growth of Holocene gypsum dunes along the edge of Lake Lucero in White Sands, New Mexico (Langford, 2003).

Continental eolian sabkha surfaces can be accretional or deflationary, depending on the availability of sand, subsidence rate and whether the water table is rising or falling. Deflationary eolian sabkhas typically leave behind little more than an evaporite-cemented Stokes surface and so have little preservation potential. Modern deflationary sabkhas are commonplace occurrences at the arid endorheic ends of large areas of monsoonal drainages, as in the Kallakooopah interdunal sabkhas and pans north of Lake Eyre and in the extensive dune fields of the Lake Chad Basin. Both are examples of the ephemeral stream-dune field-ephemeral saline lake association, discussed earlier in this chapter.

Accretionary eolian sabkha sheets have higher preservation potential and tend to characterise areas where eolian and alluvial sediment is piling up within rising artesian saline groundwater and surface water outflow zones. Such conditions are typically found at the foot of mountain ranges or in arid continental regions characterised by subsidence (alluvial fan-ephemeral saline lake association). This is the case at Umm as Samim (“Mother of Worries”) sabkha in Oman, which is fed matrix

sediment from the Oman Mountains and groundwater from the limestone aquifers of the Tertiary Umm Er Radhuma Formation. Accretionary sabkhas also occur in the Sabkhat Umm Ash Shuraybat in Saudi Arabia, where a combination of artesian resurgence and encroaching eolian sands facilitate an aggrading and prograding saline water table (pers. obs.).

In the region of subsidence that defines Sabkha Matti, for example, capillary salts are growing in zones of shallow watertables across large expanses within and adjacent to the flat surface of its deflationary sand sheet (Figure 3.60; Goodall et al., 2000). In the Sabkhat Matti region, the supratidal salt flats of the marine margin sabkha grade southwards into inland flats of the continental eolian sabkha with no distinct break in surface topography. The inland sabkha extends southwards for about 130 km and, in this distance, the land surface rarely rises more than 80 m above sea level (Figure 3.60; Goodall et al., 2000). This region constitutes a modern accretionary eolian sabkha sheet and is adjacent to dry mudflats and sand sheets. This in turn passes downwind into an active sand sea that is piling up at the foot of the Oman mountains. Sabkha Matti sand sheets form a sandy plain around the deflationary edge of the sabkha (Figure 3.60; Goodall et al., 2000). There is little information available on rainfall for the inland areas of Sabkhat Matti, but measurements taken on the coast show that average annual rainfall is less than 40 mm and it will be less further inland.

Evaporation of occasional ephemeral brine sheets reforms the salt crusts, which today cover large areas of Sabkha Matti for most of the year. The thickest salt crusts (1 ± 5 cm), with large megapolygonal pressure ridges characterise the Sabkha Matti surface situated within 5–10 km of the modern coast, further inland the Sabkha Matti surface is characterised by thinner salt crusts (≈ 1 cm) and smaller, lower-relief, pressure ridges, along with more numerous blisters and petees interacting with wind-blown sediments to form characteristic haloturbated structures (Fryberger, et al., 1979; Goodall et al., 2000).

The surface of the sabkha-hosting sand sheets of Sabkha Matti are planed by wind action (Stokes surface). Internally the eolian sabkha sheet consists mostly of low-angle eolian stratification (cm-scale laminae) created by migrating ripples and grainfall that can be altered by ongoing haloturbation. Quartz sand fills the saucers between eroded salt ridges and locally gives the Sabkha Matti surface a “leopard-skin” appearance (Goodall et al., 2000). The end result of ongoing wetting and drying in this sandsheet host is a highly disturbed sheet-like body of sediment entraining a variety of distinctive sedimentary fabrics.

They indicate salt-growth sediment deformation, salt-solution sediment collapse, sediment aggradation and compound mixtures of these processes. Salt-crust processes also produce features that may be confused with eolian adhesion structures (Goodall et al., 2000).

Some modern accretionary sabkha sheets are situated adjacent to zones where eolian dune sediment is also accumulating. They tend to be nearer to zones of sediment supply (reworked fluvio-lacustrine sediment) or be in regions where playas abut actively encroaching sand seas, often in association with ephemeral river breakout through the dunes. Sabkhat Umm Ash Shuraybat, an hour's drive southwest of Dammam in Saudi Arabia is one of the more accessible areas to see capillary processes in action in an accretionary eolian sabkha at the edge of a sand sea. It forms a zone of aggrading sabkha sedimentation in association with occasional floodwater ponding behind a sand sea (Figures 3.16a, 3.61a). The dunes are still active and form a cover to the aggrading outflow zone of a regional artesian aquifer. The dunes also store waters from rare periods of heavy rainfall. Because of this, the water table intersects the edges of some dunes and oases can form. They define areas where local fresher water seeps support a halophyte fringe and with evaporation also create the salts of the adjacent sabkha sheet. Spring mounds, cyanobacterial blisters and petees dominate in the seepage zones immediately downstream from the outcropping water tables that define the edge of the dunes (Figure 3.61b). In places the seepage waters are fresh enough to support a flourishing biota of ostracodes and brine shrimp (pers. obs.). Away from the seepage zone the accretionary eolian mudflats (a combination of desert loess and fluvially-supplied sediment) host displacive capillary gypsum, identical in morphology to that described for the coastal sabkhas of Saudi Arabia. Further down the fractionation trend in Sabkhat Umm Ash Shuraybat, the saline waters ponded in the lower parts of the depression and precipitated stacks of saline pan halite crust (Figure 3.61c). The resulting halite beds are up to 4 metres thick and layered at the decametre scale by thin laminae and partings of clay and anhydrite (Collenette and Grainger, 1994).

In addition to its currently active eolian sabkhat the Umm Ash Shuraybat area preserves evidence of a late Pleistocene river, which flowed into the Gulf but is now largely covered by dunes. Ephemeral streams which follow remnants of this old channel still flow into the dunes as periodically water-filled channels before being dammed by the dunes. Ponded water is then lost to the dunes via seepage. Historically, there is no record of the main stream channel breaking through the dunes to the coast in this region, although the satellite imagery suggests

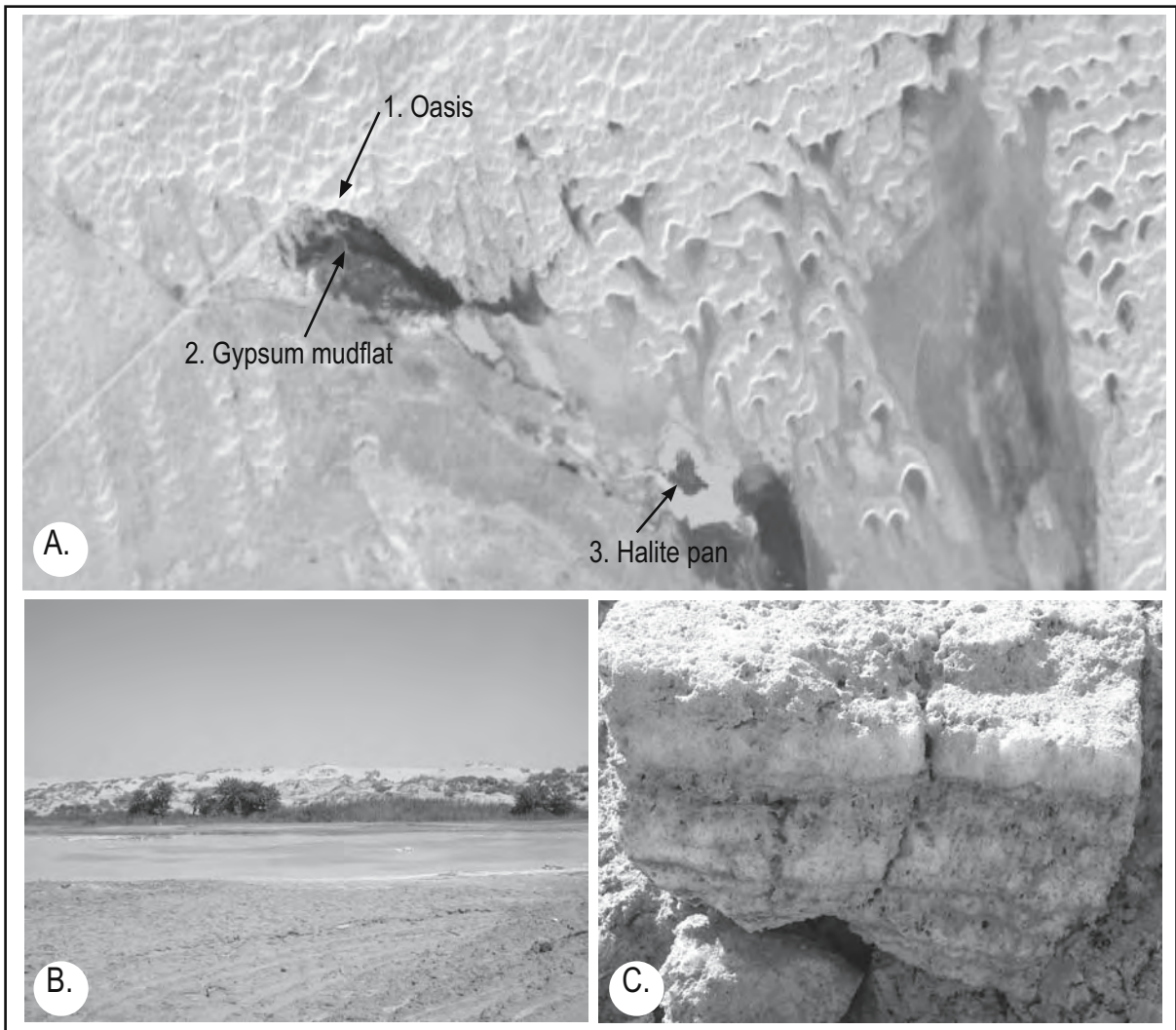


Figure 3.61. Sabkhat Umm Ash Shurabyat, Saudi Arabia (Figure 3.15a for location). A) General location of the sabkha at the edge of the dune field clearly shows the position of the intersection between landscape and dune water table at position 1 where fresh to brackish phreatic water held in the erg seeps into the sand flat margin to create an oasis (position 1 as seen in 3.54b). B) View from puffy ground atop gypsum mudflat (eolian sabkha) and looking north toward oasis at the edge of the sand sea. C) Stacked saline pan halite facies with eolian silt laminae. Sample was extracted from position 3, each pan halite layer is between 5 and 10cm thick.

this may have happened in the last few thousand years. Better examples of catastrophic breakout of flooded rivers through an erg to the sea can be seen in Namibian ergs of the Skeleton Coast of southwest Africa (Svendsen et al., 2003). The result of periodic flooding, ponding and occasional breakout of a stream channel into any dune field is a number of clayey fluvial lenses in the interdunal corridors, which then act as a host for capillary sabkha salts. Such elongate or interdunal geometries fed by streams and deposited in corridors dominated by interdunal fluvial and carbonate marls (pedogenic), have been documented in the Permian sandstones of Utah and Colorado

(Driese, 1985) and in Tertiary “oases” in the Namibian desert (Smith and Mason, 1998).

It seems that some ancient counterparts of continental eolian sabkha sheets are preserved in regions where little or no crossbedded dune sand is preserved; these sheets do not show the elongate interdunal geometries that much of the literature seems to require for an eolian sabkha interpretation. Rather, they possess a sheet geometry associated with capillary evaporite-cemented and haloturbated muddy sands accumulating in large erosional capped flatlands (Figures 2.44f, 3.59b). Their sheet-

like distribution is the sedimentary response to their water table-capillary zone origins. Such sheet-like eolian sabkha systems typify the flat topped depositional setting of the Permian Yates Formation reservoir sands of west Texas and portions of the reservoir sands of the Rotliegende Formation in the northern Netherlands (Chapter 10). It is also the case for muddy sand sheets in parts of the Lower Triassic Sherwood Sandstone Group of offshore NW England (Cowan, 1993; Herries and Cowan, 1997) and parts of the Lower Permian Rotliegende Group in the North Sea (Goodall, 1995). In the North Sea examples, which are offshore reservoirs for gas, the change in understanding of the origin of these facies from fluvial shoestrings to haloturbated sand sheets has had profound implications in planning for the exploitation of the entrapped gas.

This is not to say all evaporite-cemented intervals in reservoir sands beneath an evaporite seal are preserved eolian sabkha caps. But sabkhas will be a commonplace signature of the transition from a completely isolated continental basin into the outcropping hydrology required for widespread evaporite deposition. The limited fetch of hydrographically isolated evaporite seaways, the widespread capillary cementation in the strandzone and across the basin at the onset of evaporite accumulation, along with the consequent low energy of the transgressing hypersaline water edge, will tend to better preserve dune topography. There will be less high energy coastal reworking of sediment compared to a marine transgression into a sand sea (Figure 3.58c). Excellent examples are preserved in the transition from the Rotliegende-Weissliegende into Zechstein evaporites in the Permian Basin of NW Europe and in the transition from the Jurassic Entrada into the Todilto evaporites in the San Juan basin of the USA.

In summary, eolian sabkhas are a response to areas of shallow subcropping water tables within or about the edges of continental sand seas (ergs). The matrix for the displacive evaporite growth comes from the sediments of the dunes blown onto the areas of shallow subcropping water table, or is supplied by fluvial processes periodically cutting through a sand sea. In many cases the geometry of the eolian sabkha is not an elongate shoestring or interdunal trend. Rather the capillary salts accumulate in areas of shallow water table in aggrading sand/mud sheets. Thus, in the rock record, narrow (1-2 km) elongate interdunal eolian sabkha trends have much lower preservation potential than areas of capillary cementation in eolian sand sheets (>5-10 km wide) accumulating in regions of rising water tables (Chapter 2). A rising water table can be driven by subsidence, changing climate, or by a rise in the regional hydrological base level driven by sea level rise. In these situations the eolian sabkha is more

likely to be deposited as the evaporite-cemented portions of a sand sheet with textures dominated by adhesion ripples and haloturbation rather than by preserved salts. High water tables and high salinities in “wet” or chemically-dominant sabkhas can induce widespread early cementation, which through its retention or dissolution may control lateral variations reservoir quality in ancient counterparts. Episodes of deflation during the aggradation of the eolian sabkha are indicated by “Stokes surfaces,” which are easily recognised in ancient eolian counterparts (Newell, 2001).

Salt pans (marshes) and diapirs

So far, we have discussed the various pans and sabkhas in a hydrologic framework of endorheic depressions, with the topography doing little more than supply the gradient to an arid groundwater and hydrographic sump. But there are also a few modern deserts where the drainage topography is not passive, rather it is salt-cored and replenished by halokinesis even as the diapiric salt is simultaneously recycled into salt encrusted depressions. Earlier in this chapter in the various South American salars, such as Salar de Uyuni and Salar de Atacama we saw a more passive mode of diapiric supply whereby ions derived from the dissolution of at-surface diapirs supplied significant volumes of ions (along with weathered acid volcanics), to the groundwater as it seeped into saline sumps floored by hardrock basement. But in parts of the Iranian interior, centred on the holy city of Qum located north of the Zagros Mountains and south of the Alborz Mountains, the role of the diapirs in controlling the drainage and groundwater network is much more active. There the diapirs and their namakiers create the landscape, the drainage patterns and supply ions to various suprasalt groundwater sumps so that recycled diapiric salt (Miocene) accumulates in salt-rich Quaternary playas atop suprasalt rim synclines (Figure 3.62).

The region is known as the Dasht-e Kavir or great salt desert; it is some 800 km long and 320 km wide, located southeast of the Alborz Mountains in north central Iran. It is a huge saline desert basin with endorheic drainage and named after the large kavirs (salt marshes) that characterise salt-floored depressions in the landscape. The Kavir Buzurg (Great Kavir), some 320 km long and 60 km wide, constitutes the lowest part of the desert depression. It lies in a rainshadow desert that is almost rainless. Strong surface evaporation in the salt marshes and wet saline mudflats in the lower regions of the kavir sump precipitates stacked crusts of pan and capillary salt with a high proportion of the ions in the crusts coming from the dissolution of nearby diapir crest. The ease of breaking through the

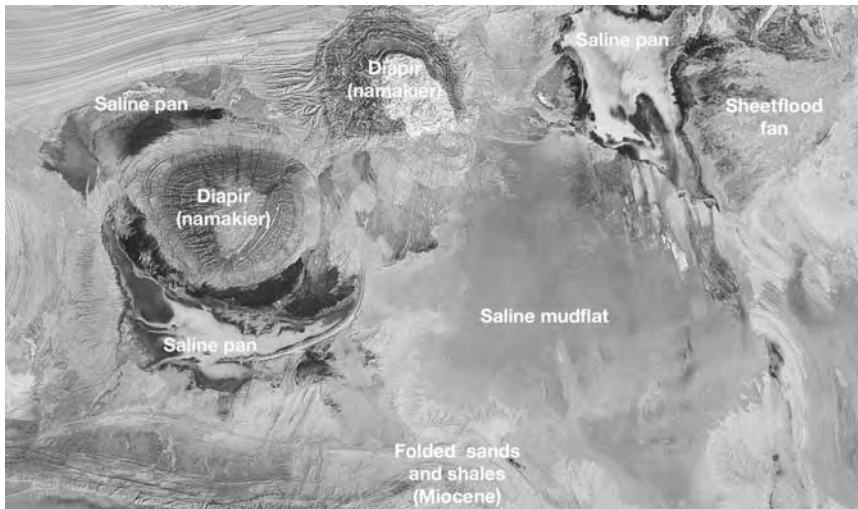


Figure 3.62. Diapirs composed of Miocene salt pierce the surface of the Great Kavir, Central Plateau of Iran (see also Figure 6.8b). Salt is dissolved from the diapir crest and redeposited in a saline pan facies in the rim synclines created by salt withdrawal adjacent to the diapir crest. (Diapir on the left is diapir No 10 in Jackson et al., 1990; Image courtesy of NASA).

surface salt crusts into hot dark saline mush beneath makes travel across the kavirs quite dangerous. The kavir's aridity and hostility means it is almost uninhabited and only partly explored; human settlement is largely restricted to the hills and mountains surrounding the kavir. Extending south from the Dasht-e Kavir is the Dasht-e Lut, which is a more typical sand and stone desert, some 480 km long and 320 km wide. It is dominated by dry mudflats and sandflats with extensive sand dunes and deflationary lag plains. Together the two deserts occupy most of the central Iranian plateau.

Salt in the various active diapirs that have surfaced in the Kavir plateau of Iran is much younger (Lower Oligocene-Miocene) than the Hormuz namakiers of SE Iran (Figure 6.45). This part of North Central Iran is undergoing north-south shortening between the Alborz mountains in the north and the Zagros mountains in the south (Talbot and Aftabi, 2004). Diapirs tend to emerge along releasing bends that have been pulled apart along major dextral transpressive faults in the central plateau of Iran. These structures include the small but mature salt fountain of Kuh-e-namak (mountain of salt in Farsi) near the holy city of Qum. This is probably the salt mountain best known to most Iranians because it dominates the western skyline of Qum, the religious capital of Iran some 140 km SSW of Tehran. It is probably the best described namakier and brief descriptions of Qum Kuh are given in Gansser (1957), Richter-Bernberg (1980), Aghashahi and Zomorodian (1981) and Jackson et al. (1990), with a more detailed analysis by Talbot and Aftabi (2004). Qum Kuh is of economic interest as centimetre to

decimetre thick beds of sylvinite ($KCl \pm NaCl$) are interbedded with the halite and repeated by folds in the extrusion.

The shapes of these extrusions of Tertiary salt indicate that they have followed a history similar to that of extrusions of the older Hormuz salt in the Zagros (Figure 6.45). Gansser (1957) and Jackson et al. (1990) noted that salt deformation in the central Iranian Plateau involves two Tertiary-age salt sequences: a clean white salt at the base of the ductile marls and shales of the Lower Oligocene Lower Red Fm, and a rhythmic sequence of multicoloured salt at the base of the salty marls of the Lower Miocene Upper Red Fm. These

two salt sequences are generally separated by limestones of the Qum Formation that do not surface in emergent salt structures (Talbot and Aftabi, 2004).

Influence of the diapir-induced topography is clearly seen in the position of the various modern saline pan facies, which tend to stack in the lows atop secondary rim synclines adjacent to outcropping salt ridges of the diapir high (Figure 3.62). The dissolution of this Miocene salt supplies most to the salt accumulating in the depressions. Further away from the diapir crest is the saline mudflat interval, which tend to dominate atop turtle-structure anticlines. Based on the Landsat imagery this mudflat succession is topographically higher than the sump of the saline pan floor, arguing that the zone of maximum salt withdrawal (indicated by maximum subsidence at the landsurface) has migrated progressively closer to the stem from the position of the original primary rim syncline (see Chapter 6 for a discussion of topography associated with diapirs and turtles).

Although as yet poorly documented, the sedimentology of this diapir-cored landscapes offers an excellent modern analogue for syndepositional responses to halokinetic highs such as those that once characterise the salt beds of the Triassic Kueper Fm. in Germany and the Cretaceous Maha Sarakham Fm. of Thailand. (Mohr et al., 2004; Warren, 2000c).

Chapter 4: Subaqueous salts: salinas and perennial lakes

Introduction

Ancient shoalwater platform (saltern) and deepwater (slope and basin) evaporites are subaqueous precipitates and, together with saline pan and mudflat evaporites, encompass all the ancient depositional settings where solar-driven evaporites can precipitate (Chapter 5). But, as for mudflats and pans, when we seek analogues for ancient subaqueous salts in the Quaternary marine record we find our choices are limited. As we shall see in Chapter 5, there are two main reasons for this dichotomy between examples of Quaternary and ancient marine-fed evaporites. First, we live in an icehouse earth characterised by climate-driven high-amplitude high-frequency changes in sea level. In marine settings this can only form small-scale coastal ponds and mudflats with limited preservation potential. Widespread marine seepage-fed platform evaporites simply cannot be preserved in this hydrology, they require the hydrological stability associated with much gentler sea level fluctuations that characterised greenhouse earth climate. Second, there are no sizeable areas on the world's surface today where the appropriate combination of tectonics and climate have hydrographically isolated and desiccated whole ocean basins and so turned them into subsealevel seepage-fed marine basins. What we are left with today as depositional analogues for ancient marine

subaqueous systems are transient, limited-scale sea-margin settings or somewhat larger high-relief saline lakes in closed intermontane basins (Table 4.1). Neither setting approaches the scale or setting of most ancient marine-fed systems. To form a permanent body of saline water in the Quaternary, with a lateral extent of more than a few tens of kilometres, and with salt beds accumulating to thicknesses of more than a 50 metres, requires a high relief tectonically-active continental closed basin. It needs a landscape characterised by subsidence of the lake floor and the maintenance of a longterm brine or reflux plume (brine curtain) within and beneath the accumulating salt beds.

Until the 1970s most subaqueous evaporite textures had been documented in ancient halite-rich basins (e.g. Dellwig, 1955) and very few examples of modern subaqueous gypsum or halite deposition had been published. Then Holocene subaqueous gypsum was documented in sea margin settings in Baja California, the Mediterranean, Southern and Western Australia and the Middle East (von der Haar and Gorsline, 1977; Aharon et al., 1977; Schreiber and Kinsman, 1975; von der Borch et al., 1977; Arakel, 1980). This work led to a new understanding of the significance of laminar and bedded textures (both sulphate and

Coastal salinas, subsealevel marine seepage depressions typically with carbonate rim (strandzone)	Continental perennial saline lakes in endorheic basins typically with siliciclastic or mixed rim (strandzone)
<p>Coorong interdunal corridors, South Australia: lacustrine depressions a few km across with a groundwater-fed carbonate fill of dolomite, magnesite, aragonite, Mg-calcite and calcite.</p> <p>Gypsum salinas up to 20 km across in southern and western Australia (Marion Lake complex; New Lake; Lake Macdonnell; Hutt and Leeman Lagoons), some depressions are filled with large palmate and swallow-tail gypsum beds, all show an aragonitic seepage rim with strandzone indicators.</p> <p>Lake MacLeod, Western Australia, 120 km long salina with a halite and gypsarenite fill, aragonitic seepage defines the rim or moat facies. Probably the largest active marine-fed subsealevel coastal salina in the world.</p> <p>Ras Muhammad Pool, southern Sinai, a small desiccated marine seepage pond, a few hundred metres across, filling with laminated microbialites and gypsum.</p> <p>Solar Lake, Gulf of Elat, a small heliothermal seepage pond, a few hundred metres across, filling with laminated microbialites about the rim and a foetid organic-rich gypsiferous mush in the meromictic lake centre.</p> <p>Lagoa Vermelha, Brazil, a small, km-scale, carbonate coastal salina with widespread bacterial dolomite.</p>	<p>Great Salt Lake, Utah: Perennial saline lake currently accumulating rippled and laminated lacustrine carbonates, along with stand line ooids and stromatolites. Earlier, in the Late Pleistocene, it was a saline pan with mirabilite and glauberite.</p> <p>Mono Lake, California: Perennial saline lake, lake level has fallen since 1947 to expose algal tufa mounds and pinnacles as well as organic-rich laminated carbonates on the lake floor. It is a well documented example of cold water carbonate ikaite forming in moderately saline lake.</p> <p>Saline lakes of Turkey: Intermontane perennial to ephemeral saline lakes with fault-defined margins. Sediment accumulations range from hydro-magnesite-aragonite tufa pinnacles, to borates to gypsum-halite laminites.</p> <p>Lake Urmia, northwest Iran, shallow perennial lake currently accumulating laminated aragonite muds, along with organic-rich muds and minor oolites.</p> <p>Rift valley lakes, Magadi and Natron, East Africa: Small fault-defined lakes in subsiding volcanic terranes, dominant sediments are trona crusts, laminated carbonates and diatomaceous siliceous oozes and cherts.</p> <p>Dead Sea, Middle East. Deep, fault-defined steep-sided transtensional basin. Sediments range from shoalwater halite crusts to deep water calcite-aragonite-gypsum laminites.</p>

Table 4.1. Some examples of perennial saline evaporite settings in Quaternary coastal and continental settings.

halite), so that in the last 10-15 years many ancient evaporites, previously interpreted as sabkhas, have been re-evaluated and found to be combinations of a number of mostly subaqueous settings. In the last twenty years we have also documented the beginnings of a partial Holocene analog for ancient deep water evaporites via the ongoing hydrological transformation of the Dead Sea into a halite-accumulating perennial lake.

Let us now look at some modern examples of subaqueous evaporites, first in small coastal subsealevel (sea-margin) settings then in larger Quaternary lacustrine depressions.

Sea-margin subaqueous salts

Modern subaqueous evaporites are forming today in shallow marine-fed coastal lakes or salinas around the edges of the

Mediterranean, the Black Sea, the Red Sea and along the southern and western coast of Australia. All these marine-fed systems are subsealevel depressions, all lack a permanent surface connection to the sea (hydrographically isolated) and are supplied solutes via seawater seeps (marine-fed).

Coastal salinas of Australia

Holocene salinas occupy isolated depressions within Quaternary calcareous coastal dunes along the southern and western coasts of Australia (Figure 4.1). Most are filled, or are filling, with bedded subaqueous evaporites; some are filled with evaporitic carbonates (e.g. Coorong dolomite lakes and Sleaford Mere in Southern Australia, Lakes Clifton and Haywood in southwestern Australia), while others are filled by combinations of carbonate, gypsum and halite (Marion Lake, Lake Macdonnell and Lake MacLeod complexes). Solutes in all the salinas are supplied by

resurging groundwaters, no salina has a surface connection to the sea if subaqueous evaporites are accumulating (hydrographically isolated). Seawater seepage, plus varying amounts of meteoric water, supply coastal salinas filling with gypsum or halite, while carbonate-filled salinas are largely supplied by resurging continental groundwaters. Winter temperatures typically reach 10° to 20°C and rarely fall below freezing, summer temperatures are often in the 30's but can occasionally climb into the 40's. The CaSO₄ phase in coastal Australia is always gypsum, not anhydrite, temperatures are not high enough, nor the basins arid enough, to deposit anhydrite. Its lack tempts one to propose that primary sedimentary anhydrite only forms as a capillary salt in hot arid mudflats (?thermalites) and never forms as a subaqueous precipitate at the sediment-brine interface in nonhydrothermal waters.

The three salina styles -carbonate versus gypsum versus halite- can be separated using annual

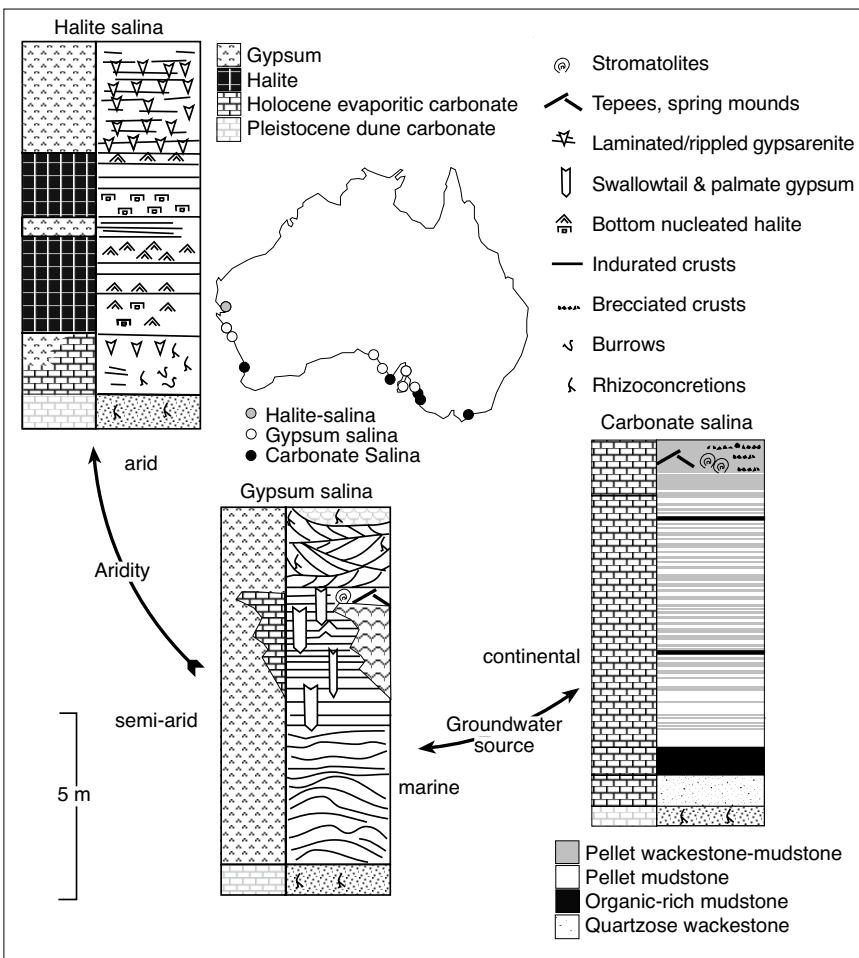


Figure 4.1. Climatic and groundwater spectrum, textures and mineralogies in the Holocene coastal salinas of southern and western Australia (after Warren 1982a,b; 1990).

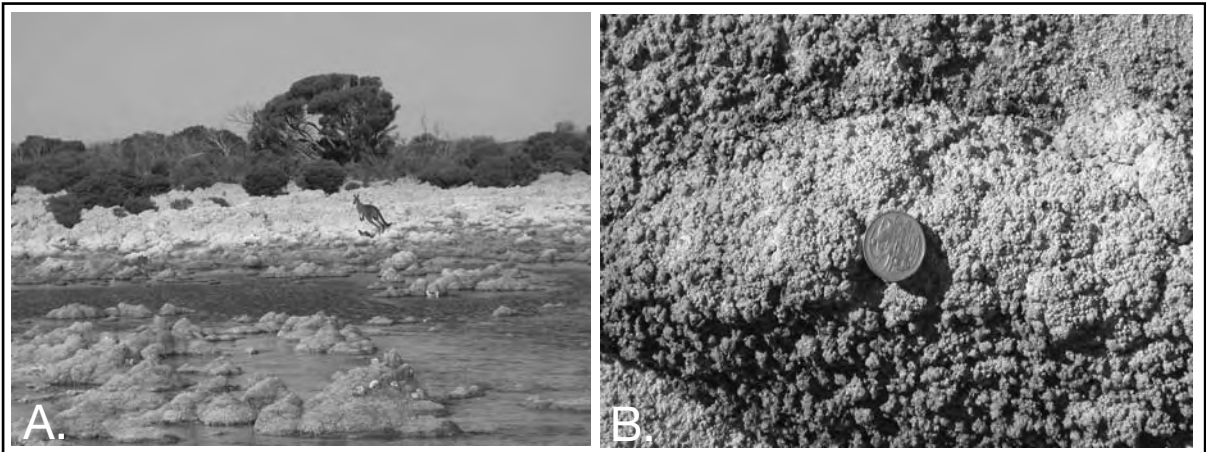


Figure 4.2. Algal tufas of Sleaford Mere, Southern Eyre Peninsula, Australia. A) Tufa reef mounds define the lake strandline (kangaroo for scale). B) Looking down on the cracked, knobby and crenulated surface of indurated calcite tufa mounds (coin for scale).

rainfall, an indirect measure of the degree of coastal aridity. Carbonate salinas dominate in the higher rainfall parts of the southeastern coast of South Australia and the southwestern coast of Western Australia, where annual rainfall is 450-800 mm. Gypsum salinas typically form best along the semi-arid southern Australian coast where annual rainfall is between 300 and 450 mm/year, while the halite-filled salinas such as Lake MacLeod form in arid areas of the central western coast of Australia where annual rainfall is less than 300 mm.

Carbonate salinas

The best documented and most voluminous carbonate fills of Holocene salinas, including some salinas filled with Holocene dolomite, are found in Pleistocene interdunal corridors behind the main Coorong lagoon in South Australia (Figure 4.2). There are numerous less well documented examples of Holocene lacustrine carbonates accumulating in coastal salinas in other parts of southern and western Australia, such as Sleaford Mere on Eyre Peninsula, and Lakes Clifton and Haywood in southwest Australia (Figure 4.1). Actively growing tufas dominate the strandlines in these other settings, they are indurated reef mounds (thrombolites and tufas) unlike many of the leathery Holocene cyanobacterial mats and mounds of the Coorong Lakes. Further out into these tufa-fringed salinas, where water depths can be up to 4-5 metres, bottom sediments are laminated ostracodal pellet wackestones and mudstones. Bioherm shapes around the salina edge range from elongate reef terraces to isolated domal and conical mounds, some with Conophyton-like shapes. Individual mounds can be 2 metres high and extend as reefal terraces for up to 6 km along the salina strandline (Figure 4.2; Warren 1982a; Coshell et al., 1998; Konishi et al., 2001).

The Coorong Region was first documented as an area of modern dolomite precipitation by Mawson (1929), but was not studied in any detail until the work of Alderman and Skinner (1957), von der Borch (1965, 1976), von der Borch and Lock (1979), Rosen et al. (1988, 1990), Rosen et al. (1989) and Warren (1988,



Figure 4.3. Coorong region in the area centred on the township of Salt Creek, South Australia. Part of the 120 km long barrier island, composed of carbonate sand (Youngusband Peninsula), is visible, backed by the waters of the Coorong Lagoon, which is floored by mm-laminated aragonite muds. Laminated lacustrine carbonates, including dolomites, are accumulating in lakes in isolated interdunal corridors behind the Coorong Lagoon -see Figure 4.4 (Landsat image courtesy of NASA).

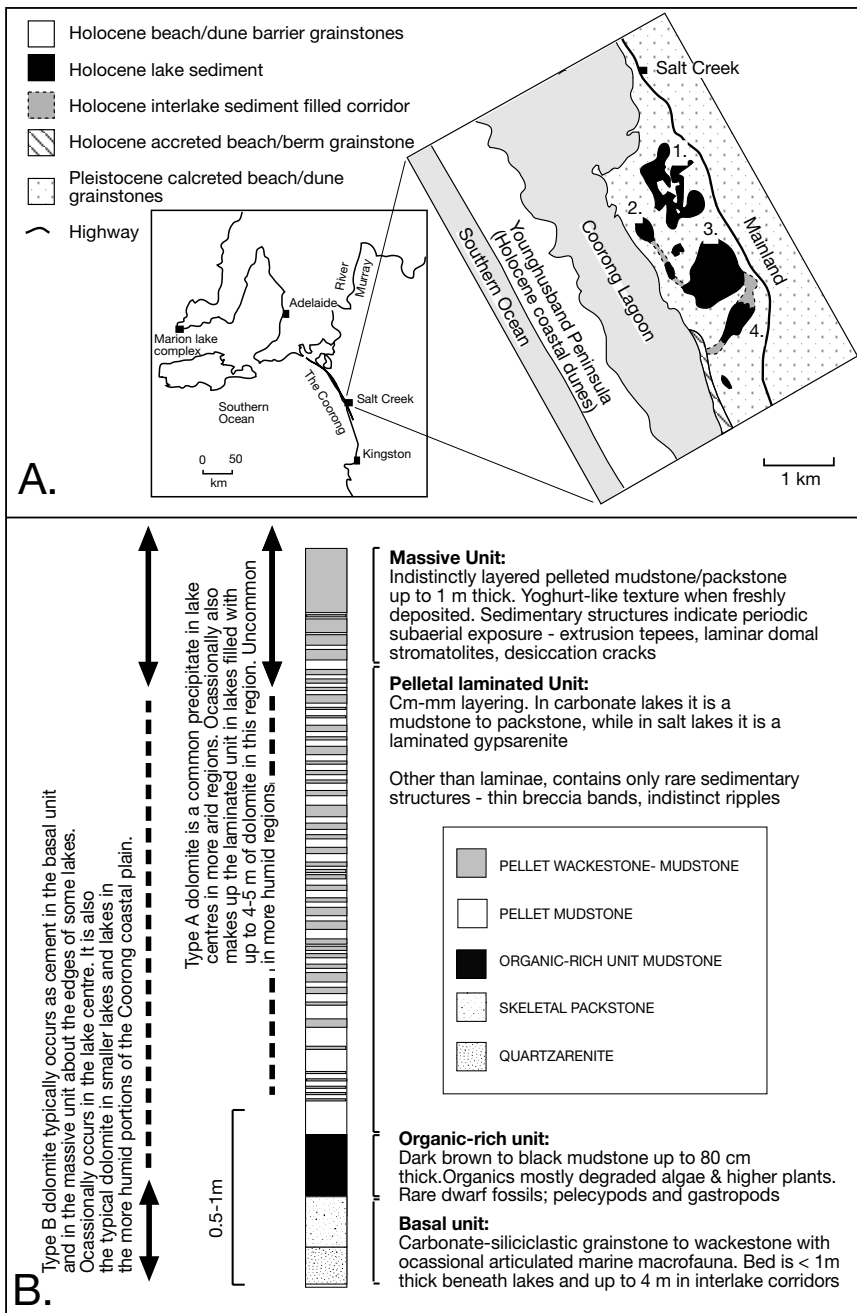


Figure 4.4. Coorong Lakes, South Australia. A) Locality and map of the Coorong region. Geological plan of the Salt Creek region shows how three of the four major lakes are joined by an interdunal corridor and were connected to the Coorong lagoon earlier in the Holocene. Milne Lake, the best dolomite accumulator in the Coorong coastal plain, never had a surface connection with the Coorong Lagoon. Mineralogies: Lake 1 = Milne Lake (dolomite + magnesite), Lake 2 = Halite Lake (gypsum + aragonite overlain by hydromagnesite + aragonite in massive unit and currently covered by ephemeral halite crust), Lake 3 = Pellet Lake (dolomite + hydromagnesite + aragonite), Lake 4 = North Stromatolite Lake (hydromagnesite + aragonite; minor dolomite in basal unit and about lake edge) (after Warren, 1990). B) Typical vertical sequence in Holocene evaporitic lakes of the Coorong coastal plain. (after Warren, 1990; 2000a).

1990). Most work in the region concentrated on salinas that contained dolomite, but there are many salinas, probably the majority, where the fill is dominated by carbonate mineral phases other than dolomite (Warren, 1990). Fills include low and high Mg-calcite, magnesite, hydromagnesite, aragonite, and less commonly gypsum (Figure 4.3). Von der Borch (1976) observed that Holocene dolomite occurs in areas of the coastal plain where rainfall is less than 700 mm, encompassing the area between Kingston and Salt Creek (Figure 4.4a). He suggested that south of the 700 mm isohyet, reduced evaporation rates and higher rainfall prevented the concentration of lake waters to salinities where dolomite could precipitate. Regional sampling of lakes across the area tied to climate confirms his postulate and shows that the more magnesian-rich dolomites tend to occur in the more arid northwestern portion of the Coorong coastal plain, centred on lakes in the vicinity of Salt Creek, while Mg-calcite and calcite filled salinas are increasingly common in the cooler moister parts to the southeast (Warren, 1988, 1990).

Textures in carbonate salinas are largely independent of mineralogy and can be related to salinity, brine depth and permanence (Figure 4.4b; Warren, 1990; 1991). If the salina possessed an early Holocene connection to the marine waters of the Coorong Lagoon, then the lowermost Holocene unit is a marine/estuarine skeletal grainstone/

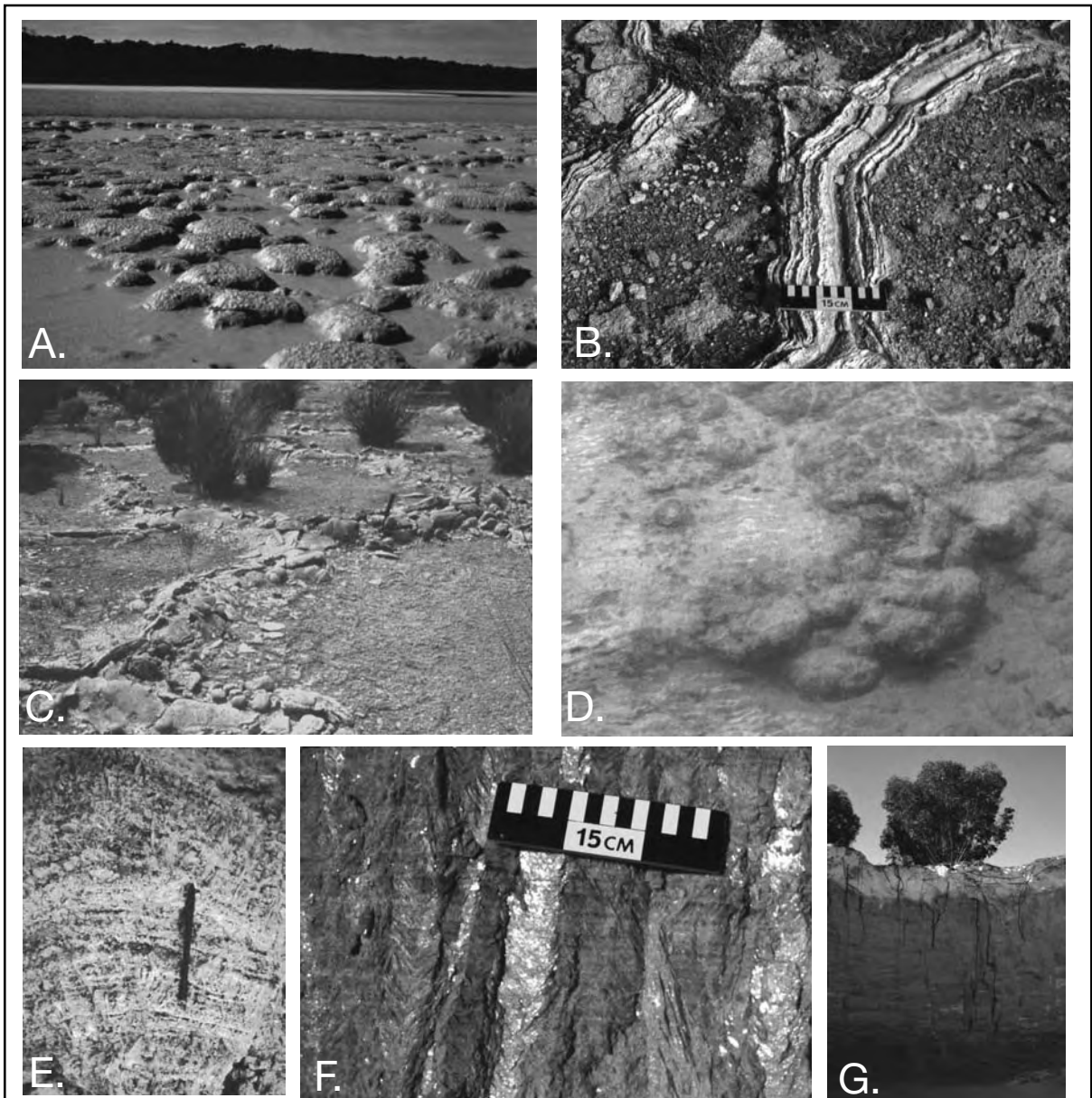


Figure 4.5. Salina geology. A) Domal stromatolite; North Stromatolite Lake. B) Extrusion tepee; North Stromatolite Lake. C) Domal stromatolites capping tepee polygons Marion Lake. D) Actively growing gypsum dome, subaqueous floor Inneson Lake; E) Layered gypsum Dome, New Lake. F) Laminated gypsum, Marion Lake. G) Gypsite soil atop gypsum dune, Cooke Plains.

packstone, similar to Holocene units flooring the more saline salinas of the Marion lake Complex and Lake MacLeod. If there was no marine connection to the Coorong lagoon then the basal unit is a quartzose packstone to wackestone. These lowermost sediments can contain small percentages of diagenetic calcian dolomite (Rosen et al., 1989). Above the lowermost unit is a variably-developed massive to faintly laminated organic-rich

unit. In lakes with an early marine connection the levels of total organic carbon (TOC) in this unit can be as high as 12%, usually as an oil-prone proto-kerogen. Its formation indicates a seasonally stratified water column where fresh water seasonally overlay stagnant marine water during the transition from a surface connected marine estuary to a totally isolated groundwater-fed salina.

Above this is a mm-laminated unit of pelletal packstone to mudstone, deposited on the floors of perennial, but schizohaline, density-stratified brine lakes, which formed in the Salt Creek region once the estuarine connection to the open Coorong Lagoon was cut off by beach-ridge accretion at the entrance to the chain of salinas (Figure 4.4a). The proportion of faecal pellets in the laminated unit is a direct reflection of energy level and organic binding on the subaqueous salina floor. In areas of higher wave energy/bottom currents and little or no algal binding, the sediment is a packstone. Such sediments are more common about the salina edge and in the shallower parts of the more central sediment fill. In areas of lower wave energy in relatively deeper water, or in areas of algal binding, the sediment is a wackestone or at times a mudstone. Muddier sediments are more common in the central parts of a salina. In a few coastal salinas with no early Holocene marine connection, such as Milne Lake, the laminated unit is composed of magnesian dolomite up to 5 metres thick (Figure 4.4a). More typically it is composed of varying proportions of aragonite, hydromagnesite, magnesian calcite and low magnesian calcite. In one marine-seepage lake (Halite Lake) it is made up of laminated gypsum/aragonite couplets.

Capping the lake sediments is a “massive” unit of poorly layered packstone/mudstone. It is usually less than 60-80 cm thick and shows varying degrees of induration from brecciated crusts about the salina edges to domal leathery stromatolites in some of the more central water covered areas. Domal stromatolites seem to flourish in Coorong salinas filling with a mixture of hydromagnesite and aragonite (Figure 4.5a). This, the uppermost part of the sediment fill, usually holds the bulk of the evaporative dolomite in the majority of carbonate salinas containing dolomite, especially in the vicinity of Salt Creek. But the Massive Unit can also be composed of aragonite, hydromagnesite, magnesian calcite and magnesite. It contains numerous terrestrial burrows and root traces, as well as mud cracks, extrusion tepees and breccia fragments - all features indicative of at least occasional desiccation and thorough bioturbation (Figures 4.4b).

Whatever the mineral assemblage, the dominant textural feature in the sediment column of a carbonate salina is lamination passing up section into a more massive unit with evidence of seasonal subaerial exposure of the sedimentation surfaces. Tepee-overprinted carbonate crusts are especially common in the desiccated strandzones of the lake margins (Figure 4.5b), while domal stromatolites and cyanobacterial are common in the area of more permanent brine, especially in salinas precipitating hydromagnesite and aragonite. Brackish lakes, such

as Lake Fellmongery, in the southeastern part of the Coorong coastal plain have well-developed algal tufa fringes, with some tufas first precipitated as monohydrocalcite and quickly altering to calcite. Surfaces of all the carbonate-filled salinas in the Coorong coastal zone are half a metre or more above sea level indicating the current nonmarine supply of waters (as groundwater cannot flow up hill). Some lakes had a marine seepage connection in their earlier stages of infill (e.g. Halite Lake; Figure 4.4a).

Volumetrically, most salina carbonates form by the evaporation of unconfined magnesium-rich continental groundwaters, driven to the surface along the coastal zone as they float up over a more dense seawater wedge. That most dolomite forms where large volumes of resurging continental waters can evaporate explains why the thickest Coorong dolomites form adjacent to the present coast. However, mineralogically similar dolomites are also precipitating 20-40 km further inland as thin capping

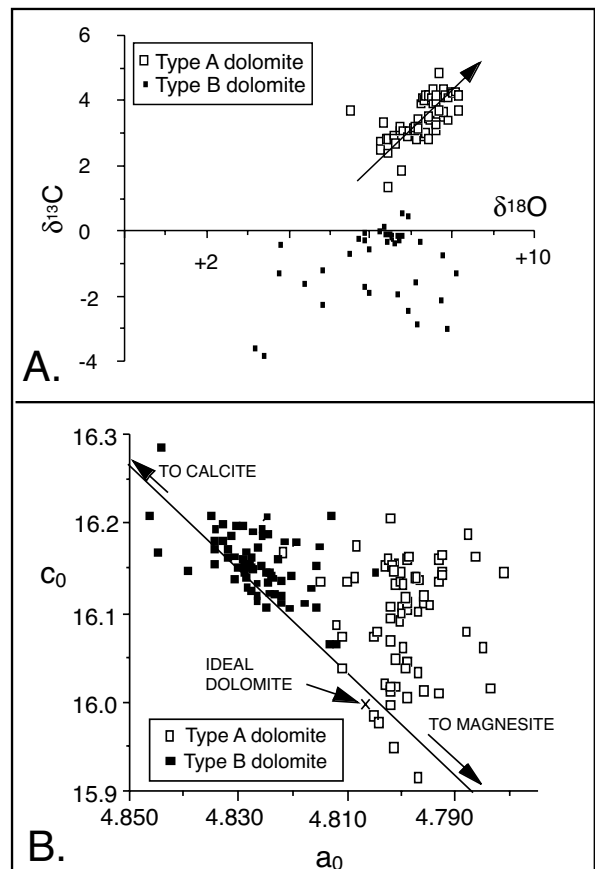


Figure 4.6. Geochemistry of Coorong dolomites. A) Isotopic signatures of Type A and Type B dolomite. B) Unit cell parameters of type A and Type B dolomite (after Rosen et al., 1989; Warren, 1990).

units in fully continental ephemeral lakes. These areas are well away from the seawater wedge, but still in areas where the regional water table intersects the land surface and continental groundwaters can pond and evaporate.

Dolomites in salinas in the Salt Creek region precipitate as two geochemically and isotopically distinct types (Type A and B), typically in association with other carbonate minerals. Type A dolomite has a slightly heavier oxygen isotope signature than type B, and is 3 - 6‰ heavier in ¹³C (Figure 4.6a). Type A dolomite also has distinct unit cell dimensions (Figure 4.6b). It tends to be magnesium-rich with up to 3 mole percent excess MgCO₃, while type B is near stoichiometric or calcian-rich. Type A dolomite commonly occurs in association with magnesite and hydromagnesite, Type B with Mg-calcite. Transmission electron microscopy (TEM) shows that Type A dolomites have a heterogeneous microstructure due to closely spaced random defects, while type B dolomites exhibit a more homogeneous microstructure implying that excess calcium ions are evenly distributed throughout the lattice. TEM studies show that the two types of dolomite are distinct and are not intermixed with other mineral phases; they are primary precipitates, and not replacements (Miser et al., 1987).

Dolomites in carbonate salinas are evaporitic carbonates, once thought to only form in areas free of preserved evaporites (von der Borch and Lock, 1979). Yet, Milne Lake, a salina filled with 4 metres of laminated dolomite-magnesite, lies less than a kilometre from Halite Lake, a depression filled with 2-3 metres

of laminated gypsum-aragonite (Figure 4.4a; Warren, 1990). Milne Lake was fed seaward-flowing continental groundwaters throughout its infill history. Halite Lake during the gypsum stage of its fill was fed by landward-flowing marine groundwaters (evaporative drawdown stage). Today Halite Lake is filled to its hydrological equilibrium level; its present depositional surface lies above the level supplied by marine seepage and it no longer accumulates laminated gypsum-aragonite. Above its laminated gypsum-aragonite unit is a 10-50 cm thick capstone bed of pelleted aragonite-hydromagnesite, a mineral association that indicates the current surface hydrology is dominated by a nonmarine groundwater feed (Warren 1990). Other Coorong Lakes in the same climatic zone, but located further inland, and more isolated from resurging marine groundwaters, are completely filled with this aragonite-hydromagnesite association (Figure 4.4a; North Stromatolite Lake and South Stromatolite Lake).

Gypsum salinas

Gypsum-filled coastal lakes are located mostly to the west of the Coorong coast (Figure 4.1) and are best documented in the region of Marion Lake on the southwestern tip of York Peninsula (Figure 4.7a). Groundwater feeds to these salinas are dominated by seawater, so the current hydrological equilibrium surfaces (Stokes surface) in all the gypsum salinas are still up to 50 cm below sea level. In plan view the surface sediments of a gypsum salina define bull's-eyes, consisting of a carbonate seepage rim and a more central gypsum zone (Figure 4.7b).

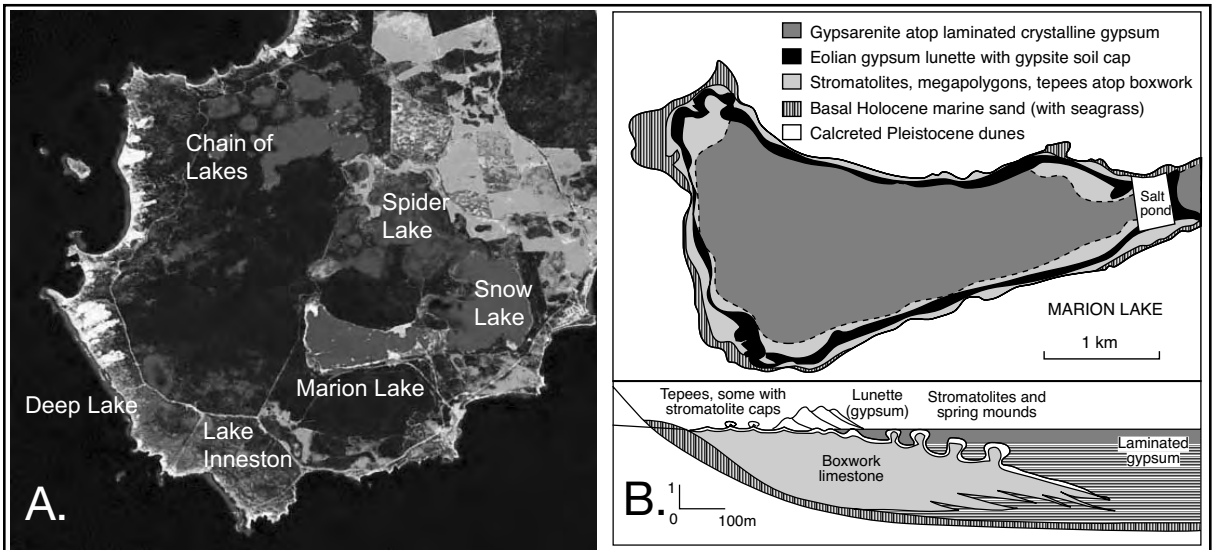


Figure 4.7. Gypsum salinas. A) Seepage fed coastal salinas of the Marion Lake complex at the southwest tip of Yorke Peninsula, South Australia. B) Surface geology and cross section of Marion Lake are after Warren, 1982a,b. (Landsat image courtesy of NASA).

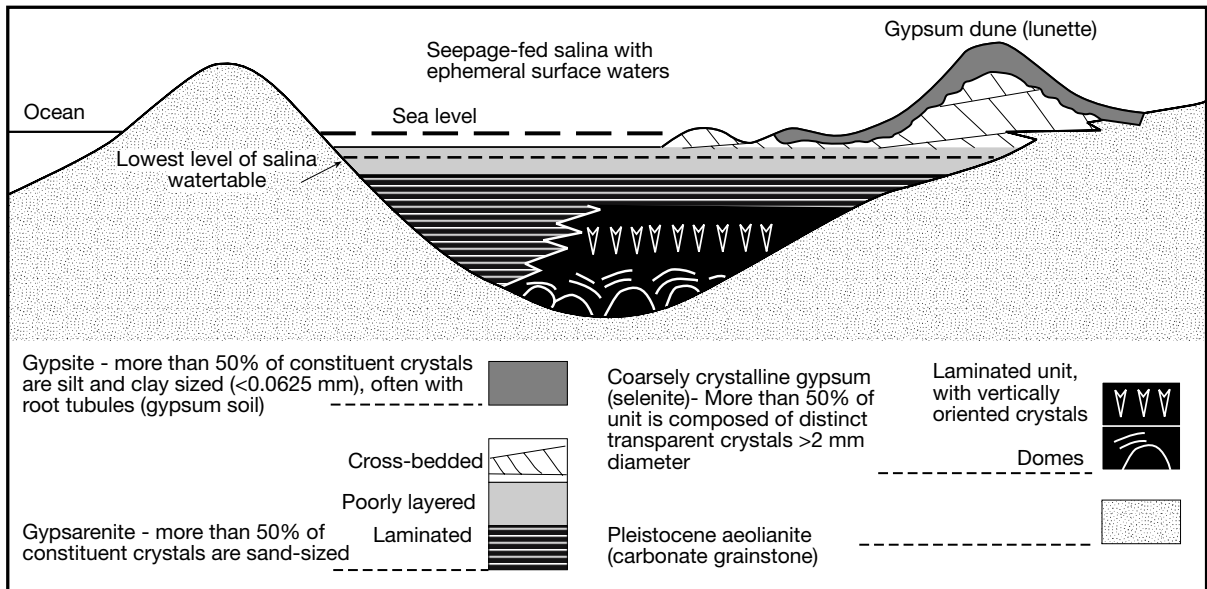


Figure 4.8. Gypsum facies in South Australian salinas, after Warren 1982b, showing domes overlain by laminites and the eolian reworking of upper portions of the lake sediments into gypsosite-capped lunettes. For simplicity, the carbonate rim is not shown (see Figure 4.7b).

Individual gypsum-filled salinas measure up to 20 x 12 km (Lake Macdonnell on the coast of the Great Australian Bight) with centres filled by laminated gypsum units up to 10m thick.

A carbonate unit forms a seepage rim about the salina edge and is composed of a boxwork limestone unit (up to 4 to 5 m thick) overlain by a fenestral limestone sheet or crust, which is less than 1 m thick (Figure 4.7b; Warren 1982a). Boxwork limestone is a diagenetic unit created by the cannibalization of earlier marine-lacustrine carbonates and sulphates by inflowing “fresher,” but still saline, marine-derived groundwaters. The “boxwork” contains relict algal structures, evaporite pseudomorphs and other highly altered bedded fabrics in proportions depending on pre-existing sediment types. Some areas of the limestone sheet above the boxwork limestone consist of tepee-overprinted crusts, others of mm-laminated subaqueous stromatolites and algal mats.

Taller stromatolites in Marion Lake grew as current-aligned mm-laminated elongate domes (up to 40 cm tall) in a brine-filled feeder channel, that focused the flow of marine seepage waters into the perennial gypsum lake of the salina centre (Figure 4.7b). Other smaller domal and encrusting stromatolites define the water-saturated cyanobacterial terrace of the lake strandzone where indurated biolaminites define areas of very shallow and sometimes ephemeral surface waters (von der Borch et al., 1977; Warren, 1982b). Stromatolite domes cap tepee structures in some marine-fed seepage areas (Figure 4.5c). Like stromatolites,

the tepee structures are confined to the capping carbonate unit and form an extensive fenestral limestone sheet up to 60 cm thick. Tepees form readily in areas of resurging groundwater, where seasonal changes in the groundwater head encourage tepee growth (Warren, 1982b). Most of the limestone sheets caught up in the tepee structures are capillary crusts composed of fenestral lime mudstones containing stromatolite-like voids, pisolites, laminar cements, and geopetal internal sediment partially filling pores and vugs. A similar lake-margin recharge hydrology controls the formation of stromatolite-capped tepees in Holocene Lake Walyungup in coastal Western Australia (Coshell et al., 1998).

Salina gypsum in the central portions of Marion Lake is coarse-grained, porous, bottom nucleated and growth aligned; it retains intercrystalline porosity of 15-25%; pore infilling gypsum cement is rare (Figure 4.8). South Australian salinas are one of a few Holocene occurrences where subaqueous gypsum is deposited as widespread units of coarsely crystalline bottom-aligned swallowtail and palmate crystals (Table 4.1; Warren, 1982a). Worldwide, gypsum in most modern salinas is a layered gypsarenite. The cm-scale gypsum crystals are usually more than 90% pure and laid down as characteristic shallowing-upward growth-aligned crystal aggregates (Figure 4.1). At the base of an idealized succession are massive, poorly layered domes of coarsely crystalline palmate and swallow tail crystals (aka selenite; Figure 4.8). Modern growing examples of this style can be found regrowing on the floors of flooded mined-out

salinas such as Lake Inneston (Figure 4.5d). The elongate gypsum prisms in the early stages of dome growth show little or no preferred orientation, with carbonate pellets and flakes distributed randomly through the gypsum porosity. Active domes on the floor of Lake Inneston are coated by microbial slime and can be considered to be a type of coarsely-layered gypsum stromatolite.

Higher in the section the degree of lamination increases and dome amplitude decreases until domes pass into sub-horizontally layered and laminated units of aligned crystals (Figure 4.5e). Higher still, individual laminae of pelletal and micritic aragonite appear to crosscut large upwardly-aligned gypsum crystals (Figure 4.5f, 4.8). Such large crystals at first sight appear secondary and their Miocene equivalents in the Sicilian Basin were once interpreted as secondary gypsum after anhydrite (Ogniben, 1957). Studies of identical Holocene gypsum in the South Australian salinas have shown that the crystals (30 to 50 cm long) are primary, not secondary. They grow with their long axes perpendicular to bedding, an effect of crystal impingement and growth alignment (Figure 2.49; Warren, 1982b).

Gypsum is not only deposited as coarse-grained gypsum (selenite) in South Australian coastal lakes. Some salinas are filled with laminated gypsarenites and are probably as common, if not more common, than those filled with the geologically more interesting coarsely-crystalline gypsum. Laminated gypsarenite fills large interdunal corridors near Streaky Bay and Point Fowler in South Australia and Hutt and Leeman Lagoons in Western Australia (Figure 4.1).

In salinas with coarse-grained fills, the coarsely-crystalline laminated gypsum (selenite) unit, punctuated by carbonate laminae, is in turn overlain by a mm-laminated, sand-sized gypsarenite accumulation (Figure 4.8). Parts of the horizontally laminated gypsarenite unit, especially near the salina strandzone, can be reworked into wave-oscillation ripples. Laminated and rippled gypsarenite is in turn overlain by a thin, massive, poorly-bedded gypsarenite unit deposited under seasonally vadose or subaerial conditions and represents accumulation in the salina capillary fringe.

Topping the whole succession is a unit of cross-stratified eolian gypsum and, in areas stabilized by vegetation, a pedogenic cap of gypsite (silt-sized). This gypsum soil is a degradational profile that is slowly cannibalising depositionally inactive regions of both lacustrine and eolian gypsum throughout coastal and inland Australia (Figure 4.5g).

Carbonate laminae in the various gypsum units form by the precipitation and accumulation of aragonite pellets during the spring and early summer (Chapter 9). The pellets come from the faeces of ostracodes and brine shrimp, mixed with the micritised remnants of algal tubules. At first the pellets mantle any underlying gypsum and often are captured by a cyanobacterial mat that covers the gypsum. During the ensuing summer and autumn, as the lake maintains its gypsum saturation, the pellets are encased by the upward poikilitic growth of large gypsum crystals (Figures 2.49, 4.5e, f).

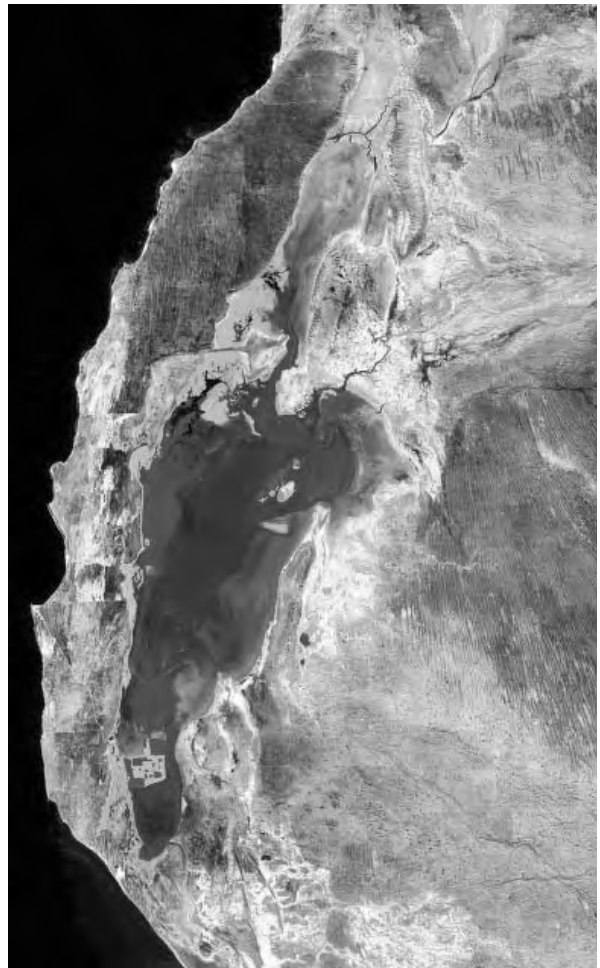


Figure 4.9. Lake MacLeod, Western Australia. It is the largest evaporite-filled coastal salina in the world. Marine-fed brine springs and sheets are visible in the central western and northwestern strandzone, while solar ponds are visible in the south. The interdunal depression only started to accumulate Holocene salts after its surface connection to the ocean at its southern end was cut off by longshore sand drift (Landsat image courtesy of NASA).

Halite salinas

Lake MacLeod is a halite-filled salina some 120 km long and 40 km wide, lying just to the north of Shark Bay (Figure 4.9; Logan 1987; Handford et al., 1984). Climate is arid, with average rainfall around 230-260 mm and annual potential pan evaporation in excess of 2,600 mm. The surface of much of Lake MacLeod still lies well below sea level indicating evaporative drawdown and a groundwater feed from the nearby Indian Ocean. Some parts of the lake depression, especially near the marine seeps, are still covered with semipermanent water sheets. In its northern part, and across the current lake surface, the lake fill is a Holocene gypsarenite unit; it is as much as 5 metres thick along the northern and western (seaward) sides of the lake (Figure 4.10). To the south and beneath the laminated gypsum unit is a widespread halite bed up to 7 m thick. It is made up of stacked halite crusts, dominated by growth-aligned chevrons and cornets. Brines from this halite unit in the south are pumped into saltwork ponds to produce halite for the chemical industries of southeast Asia. Gypsum is also dredged in the northern part of the lake and is mostly used for wallboard manufacture (Chapter 11) Both the gypsum and the halite overlie a thin unit of Holocene lagoonal carbonate deposited prior to the depression's transition from marine embayment to coastal seepage lake.

Lake MacLeod never possessed a surface (hydrographic) connection to the ocean at any time in its salt-accumulating Holocene history. Seawater seeps onto the subsealevel lake floor via a series of marginward carbonate-precipitating spring pavements and beds, fed from fractures and caves in the underlying and surrounding calcareous coastal dune aquifer. As the escaping water exits the dune aquifer it degasses and concentrates to salinities where it precipitates seepage or strandzone carbonates. Aragonite pisolites and tepees are still forming today, especially about seeps along the eastern and northern edges of the MacLeod salina (Handford et al., 1984).

The northern part of the lake is a perennial seepage pond, called Ibis Pond, where perennial waters are over a metre deep (Figure 4.9). When the water first escapes into the pond it has normal to near normal marine salinities and supports a restricted population of halotolerant marine gastropods and small fish. A similar marine biota can be found in marine seepage ponds on the seaward side of gypsum-filled Lake Macdonnell of coastal South Australia. Spring-fed normal marine waters are thought to have supplied the Lake MacLeod brine lake for the last 5,000 years, ever since the Australasian Sea rose to a level that was within a metre or two of its present level. At that time a series of laterally accreting beach ridges cut off the lake's southern

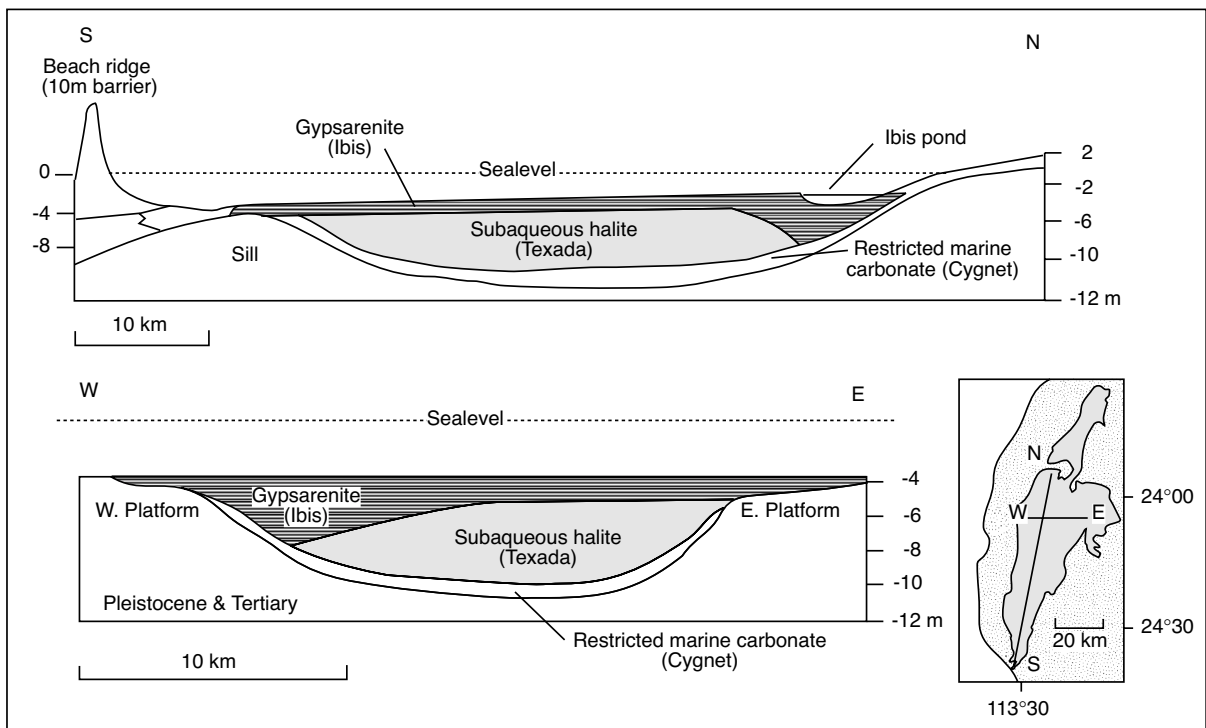


Figure 4.10. Lake MacLeod, Western Australia. Stratigraphic cross sections showing distribution of halite and gypsum as well as the effect of seepage decreasing the salinity so that the gypsum thickness increases toward areas of carbonate seepage defined by Ibis Pond and the western platform (after Logan and Brown, 1986).

surface connection to the Indian Ocean (5,100 years ago). Since then, evaporative drawdown has pulled seawater into the lake depression and bedded salts have accumulated.

From 5,300 to 3,800 years ago, seawater seepage concentrated to halite saturation and deposited some 6 billion tons that is the Texada Halite, with a remaining brine-filled porosity of around 30%. As the salina filled with beds of stacked chevron halite, the depositional surface rose. This meant that the groundwater head drawing water into the lake was reduced. At the same time the once perennial brine lake, depositing the halite and the gypsum, began to dry out each year and evolved into a saline pan. Meteoric input became more important in this later stage in the depositional fill, much in the same way it did in the South Australian salinas (Warren, 1982a). This meant the salinity of the surface brine sheet was reduced to where gypsum was the stable mineral phase throughout the brine lake and the Ibis Gypsite^{4.1} unit was deposited across the lake. Local springs fed the lake throughout its Holocene history, so that aragonitic carbonate was deposited adjacent to the springs, while gypsum and halite filled the salina in an asymmetrical fashion away from these water sources (Handford et al., 1984).

Coastal salinas of the Middle East

In the coastal deserts of the Middle East there are a number of small-scale coastal depressions filling with subaqueous evaporites, mostly aragonite and gypsum. They are flooded by perennial brines and replenished by phreatic seawater drawn into the lakes by evaporative drawdown. Like the Australian salinas, these Holocene fills have low preservation potential and will be largely flushed and dissolved during the next glacial and its sealevel low.

Solar Lake, Gulf of Elat

The Sinai coast of the Gulf of Elat is characterized by steep rifted-margin topography and a clearly defined fringing-reef (Aharon et al., 1977; Gavish, 1980). In most areas

along the northern part of the Gulf the mountainous granitic and metamorphic massif meets with gulf waters to produce a narrow steep shorezone composed of slump blocks, coarse beachrock plates and narrow reef flats. Locally wadis extend as fan deltas into the gulf to produce wider, flatter coastal plains. Small brine ponds or salinas can develop in sub-sealevel depressions in this narrow coastal plain. Probably the best known of these is Solar Lake, a salina located immediately north of a large fan delta (Wadi Murah) some 18 km south of Elat (Figures 3.20, 4.11a).

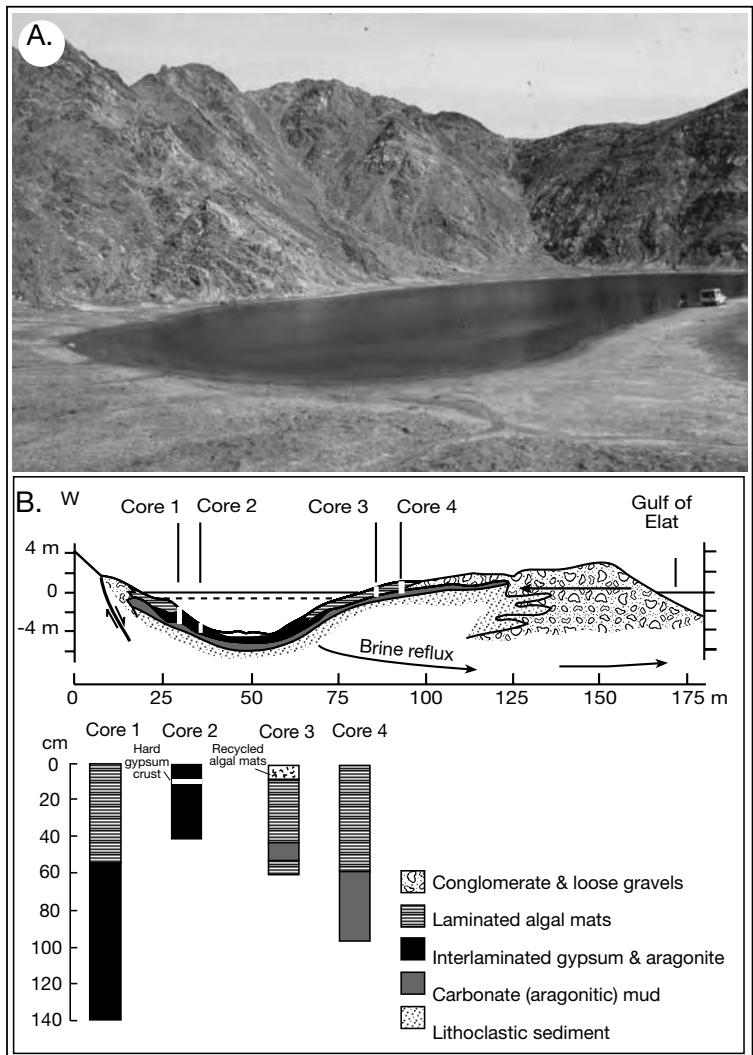


Figure 4.11. Solar Lake, Gulf of Elat. A) View shows cyanobacterial mats rimming the more central gypsum area. Note the steep-sided surrounds of the Precambrian Massif (photo courtesy B. Lyons). Vehicle for scale. B) E-W topographic and lithologic cross section based on cored sediments showing peripheral algal facies and a more central gypsum zone (after Aharon et al., 1977).

Solar Lake is a meromictic brine pond, about 140 m long and 65 m wide, with a maximum depth of 5 m. It is separated from the open sea by a porous beach-barrier, some 60 m wide and up to 3 m high, composed of coarse sand and pebbles of igneous and metamorphic rocks, along with abundant molluscan shell debris (Figure 4.11b). Water is drawn to the pond by evaporative drawdown especially during high tide when the piezometric head is at its maximum. Minor amounts of seawater may also enter the pond by splashing over the barrier during occasional winter storms. Evaporation exceeds inflow each summer, raising the total dissolved solids of the pond brine to 160-180‰ in an unstratified or mixed brine column (May-September). In winter, the combination of lessened evaporation, ongoing inflow of seawater and minor amounts of rainwater combine to create an upper water layer of lower salinity (70-100‰) atop an anaerobic hypersaline hypolimnion (\approx 180‰) and a corresponding seasonal thermocline separating the two brine masses and making the lake a meromictic system (Figure 2.48).

The heliothermal brines of Solar Lake are typical of many density-stratified coastal brine lakes. Its bottom water temperatures reach 57°C in the winter and spring, while year-round surface water temperatures range from 20 to 28°C (Figure 2.48). During stratification, as the lower brine layer absorbs heat, convection between the two layers is inhibited, and the bottom layer becomes hot and anoxic with relatively high levels of H₂S. By summer, the evaporation of the upper water body causes a weakening of the density stratification and finally the overturn of the water body. At that time the water level in the pond is as much as 0.5 m below sea level. With overturn, the water body becomes homogeneous and aerobic, it also cools by convective heat loss to a consistent 28°C.

Sediments accumulating in the pond reflect the style of water supply and the meromictic stratification of pond waters. Down to a bottom depth of 2 metres the margins of the pond are covered by thick halotolerant cyanobacterial mats atop carbonate mud. Slopes of the pond are composed of a white crust of interlayered bottom-nucleated gypsum crystals and aragonite mud, while the deep pond bottom is covered by black mud and a loose gypsum mush (Figure 4.11b; Lyons et al., 1984). There the halobiotial biomass changes to halophilic cyanobacteria with soft flocculent fabrics and an associated increase in the numbers of sulphur-dependant anoxy-photobacteria (Krumbein et al., 1977).

^{4.1}Use of the term gypsite by Logan and coworkers to describe a unit that is laminated and dominated by sand-sized gypsum prisms is unfortunate. Outside of the University of Western Australia, the use of the term gypsite follows general sedimentological usage to define a very fine grained silt or mud-sized sediment (e. g. pelite, micrite, etc.).

A total of about 70 cm of biolaminated sediment has been deposited in 2400 years about the lake margin. Seasonally exposed portions of the biolaminates are crosscut by well-developed polygonal cracks giving the cyanobacterial mat a “lily-pad” appearance identical to the “lily pad” mats of the Abu Dhabi sabkha and the Ras Muhammad pool. Cracks open to their maximum extent during the late summer and autumn when the water level is at its lowest and the mat surface is subaerially exposed. Carbonates in the mat laminae and in the gypsum are composed of aragonite, with lesser Mg-calcite, dolomite and calcite with dolomite forming as a replacement of the aragonite (Friedman et al., 1973; Aharon et al., 1977). The bulk of the dolomite occurs in gypsiferous sediment and not in the algal mats. The dolomite indicates a throughflow of hot hypersaline brines, with a Mg/Ca ratio increased by the precipitation of gypsum, it is a local-scale brine reflux dolomite, possibly facilitated by bacterial sulphate reduction (Aharon et al., 1977). Beneath the cyanobacterial and gypsum layers of the pond is an earlier muddy aragonite unit with numerous *Cerithium* gastropod shells, indicating less saline deposition during the initial isolation of the pond.

Submersed sediments of Solar Lake are rich in organic carbon, a one metre deep core showed TOC values consistently in the range of 5-20% (Schidrowski et al., 1985). Lyons et al. (1982) found significant levels of dissolved organic carbon, in the range 119-818 mg/l, in the pores of the same sediments. They concluded this material is not a “photosynthetic exudate,” rather it is a build up from the early stages of the organic maturation, a response to early-onset catagenesis driven by high temperatures and high salinities attained in the sediment mass (see thermal maturation and early cracking in Chapter 9).

Ras Muhammad Pool, Southern Sinai

At the southernmost tip of the Sinai there is a small peninsula, called Ras Muhammad, constructed by tectonically uplifted Pleistocene reefs (Figures 3.20, 4.12; Gavish, 1980; Kushnir, 1981). At the termination of this spit is a 1 km long tidal inlet with a small perennial brine pool at its end called Ras Muhammad Pool; the pool is an oval feature about 100 to 170 m in diameter and not more than 50 cm deep. It is separated from the inlet by a porous barrier, some 250 m wide, composed of reef material and carbonate sand (oolitic) that can be blown or washed into the pan. Most of the water in this subsealevel pool seeps in via a series of seawater springs around the pool’s edge (Figure 4.13a). It means the pool never dries up, although the extent and depth of water in the pool varies with the seasons. During summer and fall, the water volume in the pond is reduced by



Figure 4.12. Ras Muhammad pool, Southern Sinai Peninsula, clearly shows seepage feed to the perennial pool, tectonic alignment and proximity to seawater source in the tidal inlet (photo courtesy of G. M. Friedman).

high evaporation levels and salinities in the pond can be more than 300‰. In winter and spring the pond expands and surface water salinities fall to 100‰ (Figure 4.13b).

Sediments below the perennial pool are composed of alternating layers of gypsum mush and algal mats; there is no primary or diagenetic anhydrite (Figure 4.14; Kushnir, 1981). Thickness of gypsum layers ranges between 0.3 and 6 cm and averages 1.8 cm. Porosity in the gypsum layers ranges between 64

and 69 percent. The gypsum in the layers is mainly prismatic (crystals up to 6 mm long) and associated with minor amounts of aragonite, calcite, quartz and feldspar. The gypsum in the upper younger layers (e.g. layer 2) consist mainly of small crystals whereas the deeper older layers (e.g. layer 29) have a broader, coarser size distribution (Figure 4.13c). Mid-positions of cores taken through the cyanobacterial sediments can contain lenticular and prismatic gypsum crystals that have grown displacively within these biolaminites. The continued growth of gypsum eventually destroys the original lamination, as in the sabkha of Abu Dhabi. Likewise, much of the evidence of the original nearsurface organic binding (cyanobacterial filaments) is destroyed by the activities of heterotrophic decomposers that live below the surface of the mat. The final fabric as revealed in the lowermost layers of the cores taken by Kushnir (about 80 cm deep) is a laminated and disturbed gypsum mush with thin interlaminae of carbonate crusts and ooids with very little identifiable cyanobacterial material (Figure 4.14, insert).

Strandzone sediments around the pool edge are cemented by an ephemeral halite crust, while beneath the crust and above the water table are rare concentrations of anhydrite after gypsum, but salts in these strandzone sediment are dominated by gypsum. Pore fluids become increasing saline below the sediment surface

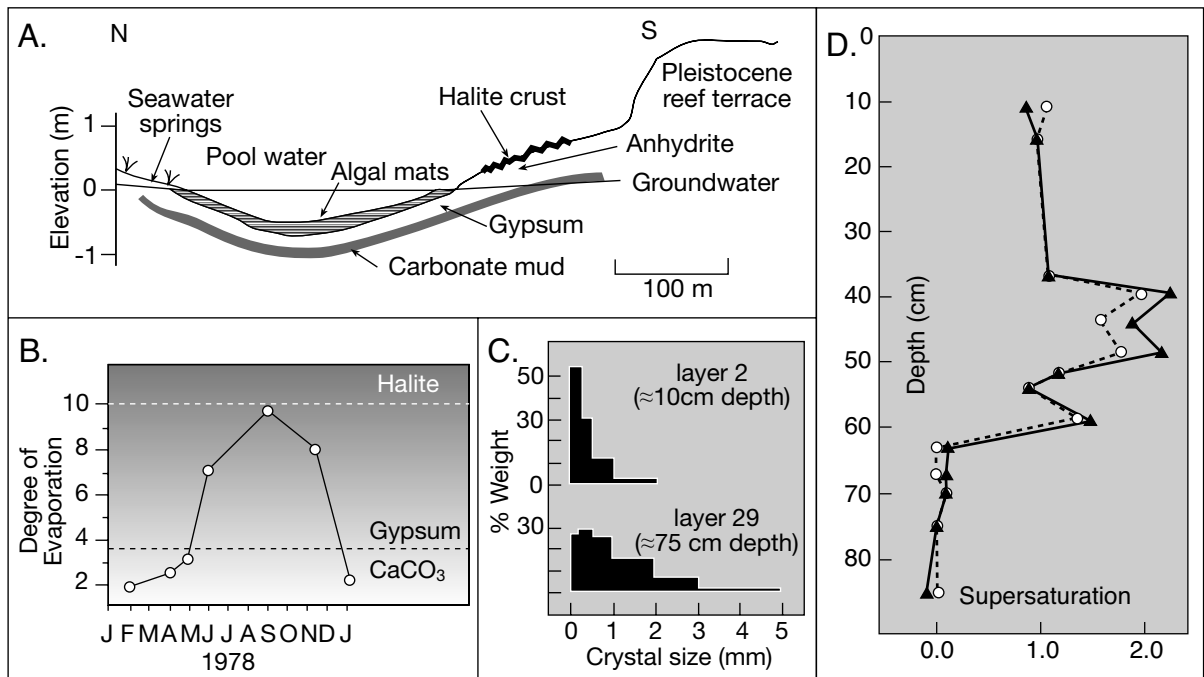


Figure 4.13 Ras Muhammad pool, southern Sinai Peninsula. A) Generalised cross section through the pool showing asymmetrical sediment distribution controlled by zones of seepage outflow. B) Annual brine concentration cycle of surface waters for 1978 - Seawater is unity on the degree of concentration scale. C) Gypsum crystal size distribution in a shallow and a deep sediment layer. D) Gypsum saturation versus depth, using interstitial waters squeezed from gypsum layers (after Kushnir, 1981).

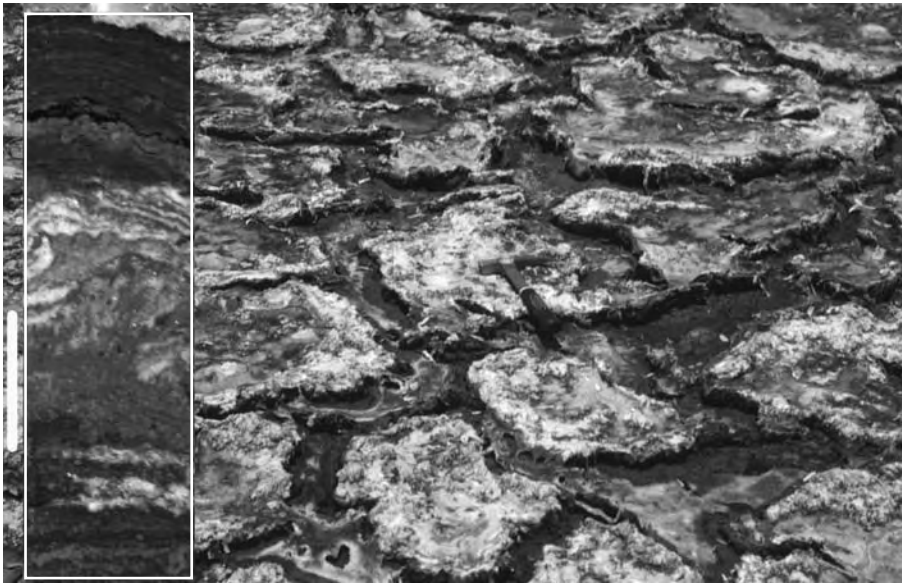


Figure 4.14. Polygonal microbial mats ("lily pads") from the strandzone of Ras Muhammad pool. Mats are seasonally desiccated and underlain by biolaminites and gypsum. Scale bar of core inset is 5 cm and there is a geological hammer atop the mat in the centre of the image. (Originals courtesy of G. M. Friedman).

and down to depths of 50-60 cm can be supersaturated with respect to gypsum by upward of a factor of 2 (Figure 4.13d). High levels of gypsum supersaturation are relieved by the precipitation of gypsum and the growth of coarser prismatic crystals, as is seen in the coarser crystal sizes of layer 29 some 75 cm below the sediment surface (Figure 4.13c). According to Kushnir (1981) precipitation of larger gypsum crystals in the uppermost capillary intervals is perhaps inhibited by high levels of organics in the supersaturated pore fluids (Kushnir 1981). Alternatively, the coarser gypsum just above the water table may indicate thermalitic precipitation. It is very likely that the precipitative mechanism for gypsum in the capillary fringe in Ras Muhammad is the same as in the Abu Dhabi upper intertidal section.

Late Pleistocene salinas on the Egyptian Red Sea Coast

Ongoing aridity along the tectonically stable area of the Egyptian coast of the Red Sea, has locally preserved Pleistocene remnants of embayment salinas (khors) that filled with laminated subaqueous gypsum during the Last Interglacial (Eemian, 5e = 5.5 Marine Isotopic Substage; Plaziat et al., 1995; Orszag-Sperber, et al., 2001). Heavily eroded remnants of the sediments in these small gypsum-filled khors, each up to a kilometre across, are scattered along a 400 km-long narrow coastal strip, backing on to Precambrian basement, between Ras Shukheir on the Gulf

of Elat and Ras Banas on the Red Sea coast (Figure 3.20). Evaporitic sediment was initially deposited as shelly and subaqueous laminated gypsum in erosive depressions elongated parallel to the present shore and behind a subcontinuous Late Pleistocene fringing coral reef (Figure 4.15a, b). The entrenched geometry and the marine to brackish evolution of the pre-evaporite faunas indicate deposition in a hydrographically isolated depression behind a reef rim. Gypsum precipitation occurred during a brief relative sealevel drop that cut off the surface connection with the Red Sea. Both the reefal and gypsum units are

Late Pleistocene with a consistent set of U/Th dates around 123 ka bp. Ages from reef and gypsum are at times so close that there is no statistical difference between their respective ages in spite of the large number of dates collected by Orszag-Sperber et al. (2001).

This is not a matter of poor precision in dates, but indicates the very rapid rate of gypsum infill once the khor lost its surface connection to the waters of the Red Sea. Narrow-mouthed embayments along the present coast quickly develop into kharms or khors that with further isolation and closure of the surface connection to the adjacent ocean of the Red Sea could become evaporitic drawdown basins filling with subaqueous gypsum units composed of coarse growth aligned gypsum crystals up to 5-10 cm long (Plaziat et al., 1995). There is a possible Holocene counterpart to these systems on the Red Sea coast at Ras Shukeir (Aref et al., 1997) but laminar aragonite, rather than gypsum, dominates the fill in all modern kharms (Plaziat et al, 1995).

Textures indicating permanent Late Pleistocene salina waters atop the aggrading gypsum and the mm-laminae of carbonate that interrupted gypsum crystal growth suggests it was very similar in both its marine seepage hydrology and its depositional setting to the salinas of southern Australia and to Lake Asal (Figure 4.15c). That is, it was an anchialine salina

system (littoral saline lake) fed by permanent seawater seeps through the reef.

Tops of the laminated subaqueous gypsum outcrops locally grade up into polygonal gypsum pressure ridges near the top of the gypsum unit implying that the level of freestanding salina waters was about 3 m below the locally derived mean sea level as deduced from the shoreline of the former Late Pleistocene reefal unit (Orszag-Sperber, et al., 2001). This reflects the evaporitic drawdown of the salina water level necessary to drive seawater seepage and gypsum precipitation.

Laminated salina gypsum in the Late Pleistocene Red Sea backreef is transitionally overlain by a massive pedogenic gypsum subunit (with root traces, burrows) interpreted by some as an emergent sabkha facies (Aref et al., 1997). It can grade laterally into older alluvial-fan substratum to become sloping gypsum-crusts (gypcretes) cementing the gravels.

These gypcretes and the sabkha facies clearly differ in process of formation and perhaps solute source from the laminated subaqueous gypsum. Likewise for the gypsum cements in coarse gravelly sand and sandy gravel about the khor edge, which were fed by a combination of marine aerosols and saline continental phreatic waters, seeping slowly seaward (Figure 4.15b). Capillary rise of phreatic seawater is prevented by the elevation and coarseness of the host-material. Holocene gypcrete crusts throughout the Red Sea coast indicate a combination of marine aerosols and sulphate-rich continental water leaching halokinetic Miocene gypsum, which outcrops near these Late Pleistocene salina remnants.

Slightly inland from the coast there are similarly textured laminated gypsarenite lenses in small depressions with heights ranging between 17.5 and 110 m above sea level. These are continental not marine fed salinas and are similar to continental salt lakes inland of El Alamein west of the Nile Delta (Figure

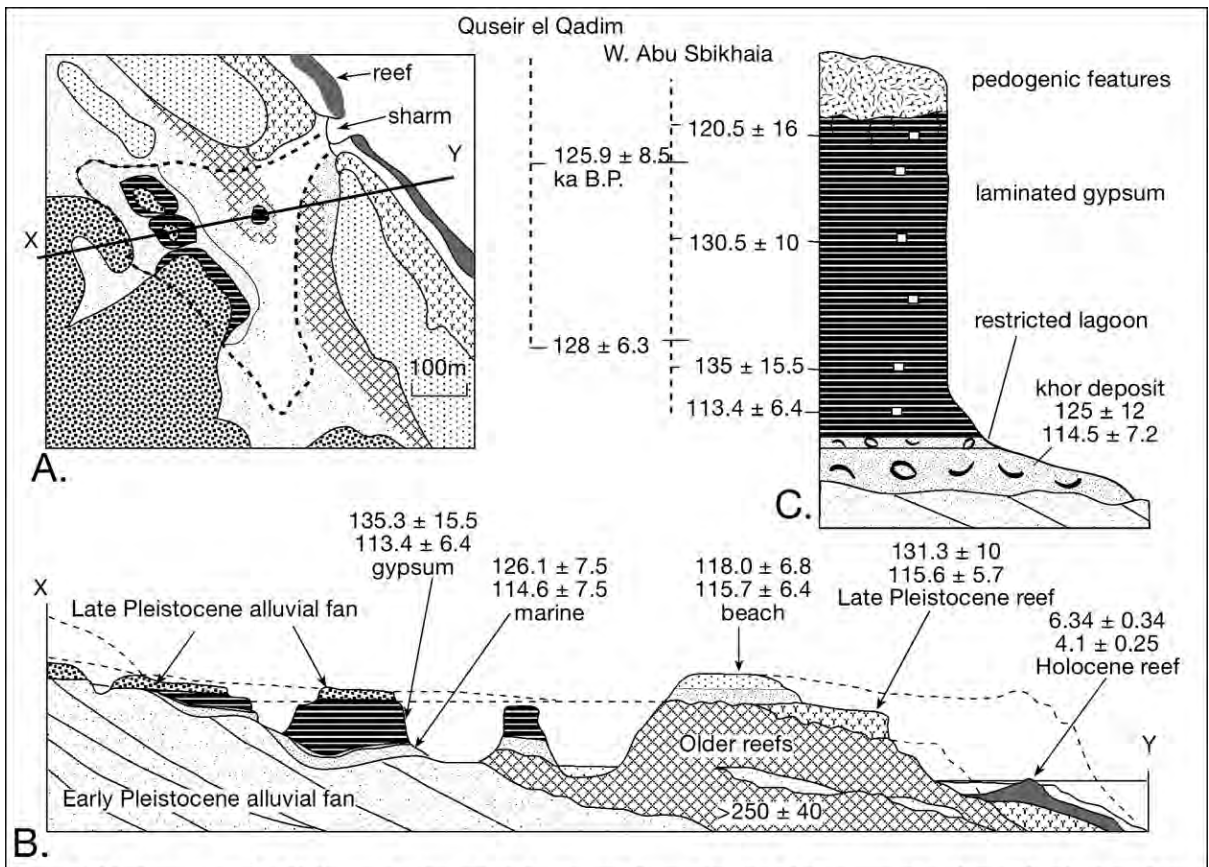


Figure 4.15. Remnants of a Pleistocene salina, Red Sea coast, Egypt showing the geometry and age distribution of Late Pleistocene units and their Early Pleistocene alluvial fan substrate at Quseir el Qadim (A. map; B. cross section), C) vertical section at wadi Abu Sbikhaia. The Late Pleistocene marine khor carbonates give U-Th dates similar to those of the overlying salina gypsum (after Orszag-Sperber et al., 2001).

3.22). The sediment fill lacks the basal marine fossiliferous sands that define the basal succession of many Late Pleistocene coastal salinas. Their watertable heights are so far above sea level that seawater seepage is impossible. Marine aerosol sources are a distinct but as yet untested possibility.

The highly dissected nature of all these 1-km scale examples of Late Pleistocene marine-fed evaporite khors of the Red Sea Coast attests to the low preservation potential of Quaternary coastal salina evaporites worldwide. The high frequency (100,000-year), high amplitude (100 m+) sealevel changes, that are diagnostic of icehouse climate, drive substantial dissolution of marine salts even in the very arid climate of the Red Sea (Chapter 5).

South American coastal salinas

One of the more interesting accumulations of modern evaporitic carbonate to be documented in the last decade occur in a series of coastal depressions centred on Lagoa Vermelha, which is a small shallow isolated hypersaline coastal salina east of Rio de Janeiro, Brazil. Its Holocene fill provides the best evidence to date of the likely involvement of particular species of sulphate-reducing bacteria in producing primary dolomite (Vasconcelos and Mackenzie, 1997; van Lith et al., 2003). Ca-dolomite is crystallizing in Lagoa Vermelha muds at the sediment-brine interface under anoxic hypersaline conditions within a black aragonitic sludge layer (Figure 4.16a).

Unlike the Coorong salinas, the source brines for these evaporitic carbonates are thought to be marine or connate groundwaters drawn into the salina by evaporative drawdown. Marine-fed salinas in the Coorong occupy similar hydrographically-isolated subsealevel depressions (e.g. Halite Lake), but in a more arid setting and precipitate laminated gypsum-aragonite, not dolomite. Both the initial precipitation and early diagenetic evolution of Lagoa Vermelha dolomites is strongly mediated by microbial activity. In fact, sulphate-reducing bacteria from Lagoa Vermelha samples, cultured in brines at low temperatures from artificial seawater, produced highly ordered dolomite in the laboratory at earth-surface temperatures (Vasconcelos and Mackenzie, 1997; Warthmann et al., 2000).

Evaporation lowers the lagoon water level in the dry season and drawdown then allows seawater to enter via seepage through the dune barrier. Elevated organic productivity in the lagoon leads to anoxia at the sediment-water interface and the formation of a black organic-rich carbonate sludge on the meromictic salina floor. The highly saline waters have elevated sulphate levels,

which in the shallow subsurface provide a sulphur source for bacterial sulphate reduction, as well as elevated magnesium that is precipitated as Mg-calcite and calcian dolomite. Microbial activity in the sludge mediates the precipitation of these primary carbonates. Eventually microbial activity ceases, but the diagenetic precipitation of dolomite continues atop the microbially precipitated crystal substrate.

Vasconcelos et al. (1995) first suggested that sulphate-reducing bacteria in hypersaline waters promote the essential conditions needed for dolomite precipitation. Van Lith et al. (2002), after a detailed study of the hydrochemistry in the lagoons, concluded that elevated salinity and sulphate reduction are the main factors inducing dolomite precipitation in these lagoons (Figure 4.16b, c). Their detailed measures of water and sediment conditions during an annual cycle (1996–1997) demonstrated that dolomite formed in May–June which was a time of high salinity. High $\delta^{34}\text{S}$ of pore water sulphate and high sulphide concentrations correlated with dolomitic horizons, demonstrating the association of bacterial sulphate reduction with dolomite formation.

Dolomite forms year round in another small nearby salina, Brejo do Espinho; perennial precipitation is a direct response to its higher year-long salinity compared to Lagoa Vermelha. High salinity apparently provides the ions and saturation state necessary for dolomite precipitation, while the observation that dolomite formed at times or in zones of decreased sulphate concentrations underlies the likely importance of bacterially-driven sulphate reduction in Brejo do Espinho. Bacterially-driven sulphide oxidation may also drive dolomite precipitation in other as yet untested high salinity lakes in the same region (Moreira et al., 2004). The precipitation of dolomite in the lab at earth surface conditions using various strains of halotolerant sulphate-reducing bacteria (Van Lith et al., 2003) underlines the fundamental role of microbial metabolism in many saline environments (Chapter 9; Warren 2000a).

Sulphate ions form strong ion pairs with Mg^{2+} ions and are held together in space like a single particle. When sulphate-reducing halotolerant bacteria metabolize SO_4 ions, they also use the accompanying Mg^{2+} ions inside their cells. Magnesium is essential for many vital physiological functions in the bacterial cell, and makes up 0.5% of the cell's dry weight in halotolerant strains. During bacterial metabolism, excess Mg is released together with other byproducts of sulphate reduction, such as bicarbonate ions and hydrogen sulphide (Chapter 9). Saturation with magnesium in microenvironments around the bacterial cell probably creates conditions favourable for preferential precipitation of dolomite, as is observed in lab-based bacterial culture experiments (Van Lith et al., 2003).

Using the Lagoa Vermelha system as their starting point, Vasconcelos and Mackenzie (1997) proposed a new actualistic model for dolomite formation that they call the microbial dolomite model (Figure 4.16a). An anoxic turbid layer at the sediment surface creates a special environment where photosynthetically produced organic matter can be microbially recycled by sulphate-reducing bacteria on a submicron scale, with concomitant precipitation of high-Mg calcite and Ca-dolomite. In contrast to the sulphate-reduction model of Kastner (1984), which required a lack of sulphate, this model requires a

continuing supply of sulphate in order for halotolerant bacteria to metabolise and so precipitate dolomite (Figure 4.16a). Living sulphate-reducing bacteria are required to overcome the kinetic problems of dolomite formation.

Once dolomite bionucleation has occurred, the Ca-dolomite ages; as is indicated by depth-related trends of larger crystal size, more negative $\delta^{13}\text{C}$ values and increased stoichiometric ordering of the dolomite lattice. Bacteria apparently remain important in shallow burial, as seen by the continued presence

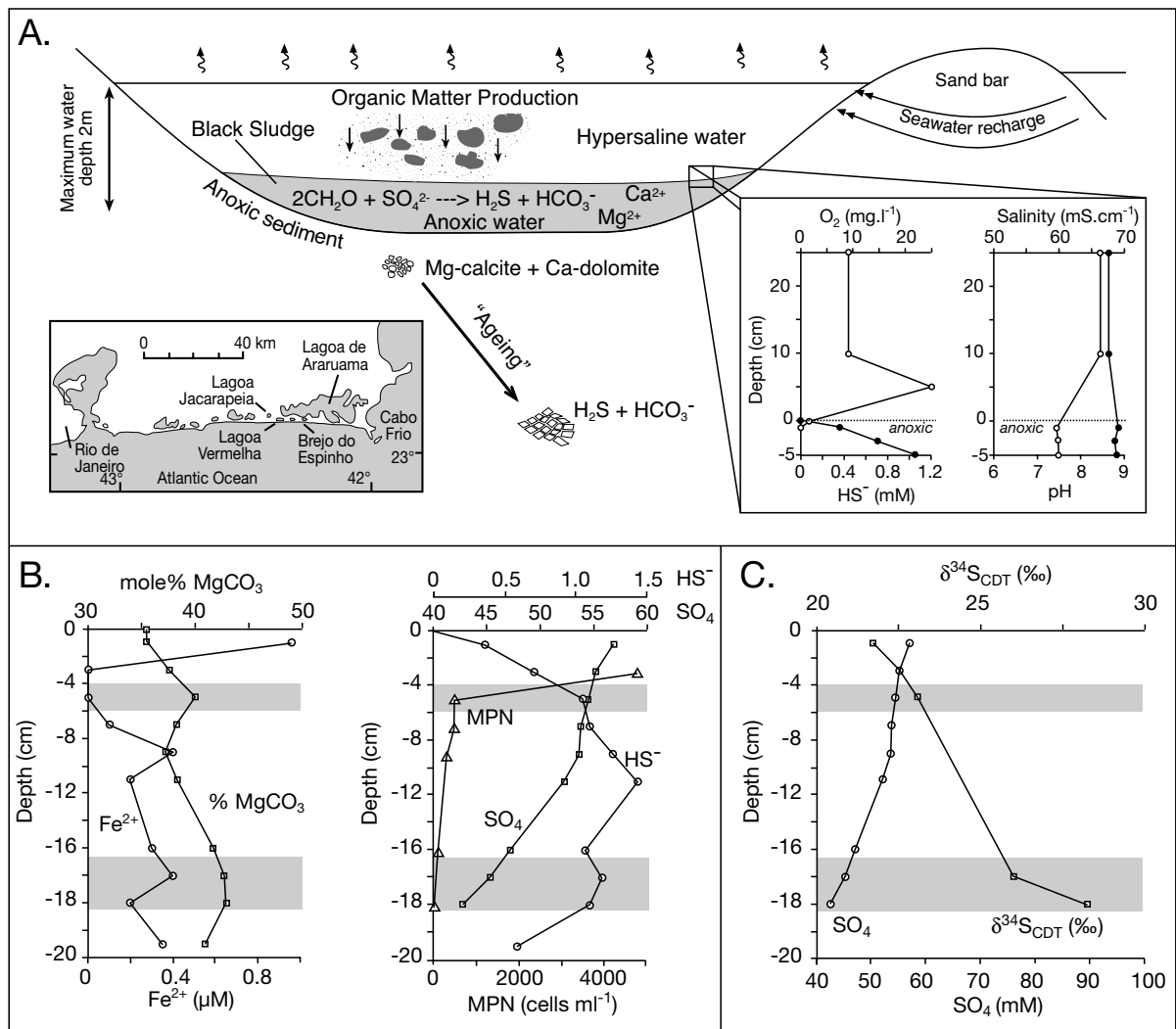


Figure 4.16. Lagoa Vermelha, Brazil. A) Schematic of microbial dolomite formation in Lagoa Vermelha and Brejo do Espinho, Brazil. Insets show the location of the salina on the Atlantic Coast and the pore water conditions immediately above and below the sediment brine interface. B) Mol% MgCO_3 in carbonate, Fe^{2+} , HS^- , and SO_4^{2-} concentrations, and most probable numbers (MPN) of sulphate-reducing bacteria in Lagoa Vermelha sediment from 0–24 cm depth. C) Dissolved sulphate concentration in pore waters of Lagoa Vermelha and its sulphur isotopic composition ($\delta^{34}\text{S}_{\text{CDT}}$). In April 1999 the core illustrated in B and C was taken and pore water extracted. The gray bars indicate Ca-dolomite horizons. (after Vasconcelos and Mackenzie, 1997; van Lith et al., 2002).

of nanobacteria on the surfaces of the “aging” crystals. With time, and deeper in the sedimentary section (70–90 cm), the crystals grow by a layer-by-layer mechanism that creates smoother and euhedral crystals. Apparently, once the dolomite is nucleated, crystals can continue to grow by inorganic processes, but each new layer still appears to be composed of coalesced submicron-size bacterial balls (spheroids). The microbial dolomite model requires an ongoing supply of sulphate to maintain the microbial activity promoting dolomite precipitation. In contrast, it may be that the presence of sulphate in a sterile (bacteria-free) environment may act to inhibit dolomite precipitation as shown in the laboratory experiments of Baker and Kastner (1981) and Morrow and Ricketts (1988).

Wright (1999) and Wright and Wacey (2005) present a similar set of microbial arguments and laboratory experiments to explain the ease of dolomite precipitation in some of the carbonate salinas of the Coorong. In the realm of bacterially mediated dolomites some authors have attempted to draw a dichotomy between bacterial mediation and evaporitic conditions, but this is an extreme view. Both the Brazilian and Coorong salinas pore waters where the bacteria flourish are hypersaline, their waters evaporitic. How else do they thrive at the expense of a less halotolerant biota at salinities up to 4–5 times that of seawater? It is the elevated salinities in surface and near surface waters that allow appropriate halotolerant sulphate-reducing bacteria to flourish in waters that can be marine, nonmarine or hybrid (Chapter 9). High salinity and bacterial mediation of natural primary dolomite are associated, not separated, features in many natural hypersaline waters.

Continental subaqueous basins

Examples of subaqueous evaporite deposits discussed so far occur in hydrographically-isolated subsealevel coastal depressions fed solutes by an inflow of marine groundwaters. The resulting sediments accumulate at limited scales (1–20 km across) with limited thicknesses (<10m). Such deposits have

	Great Salt Lake, USA North Arm (mg/l)	Lake Van, Turkey (mg/l)	Tuz Golu, Turkey Deep Zone June (mg/l)	Tuz Golu, Turkey Main Zone June (mg/l)	Dead Sea, Middle East, Upper water (mg/l)	Dead Sea, Middle East, Lower water (mg/l)	Lake Asal, Djibouti (ppm)
Na	105,120	7,747	31,500	114,717	38,510	39,700	101,200
K	8,480	508	453	1,458	6,500	7,590	5,161
Mg	10,420	95	1,327	3,963	36,150	42,300	12,500
Ca	420	5–10	478	772	16,380	17,180	2,677
Cl	181,730	5,450	50,875	185,454	196,940	219,250	199,155
SO ₄	21,730	2,344	3,485	8,838	580	420	4,320
HCO ₃	-	2,191	-	-	-	-	184
CO ₃	-	3,331	-	-	-	-	-
TDS	328,110	22,000	-	-	300,000	332,000	-
pH	7.3	9.5	8.5	7.3	-	-	7.1
Br	120	-	-	-	4,000	5,270	-
Sr	-	0.70	-	-	-	-	-
Li	50	1.50	-	-	-	-	-
B	40	-	-	-	-	-	-
PO ₄	-	0.52	-	-	-	-	-

Table 4.2. Varying ionic proportions in selected perennial lake waters, compiled from various references listed in text.

little or no longterm preservation potential within the rapidly migrating shorezone hydrologies that typify icehouse eustasy (Warren, 1991). To find examples of thicker more widespread subaqueous evaporites in Quaternary successions, we must move to continental lacustrine settings in lake depressions characterised by perennial saline water bodies. This setting corresponds to the third category of Hardie et al.’s (1978) classification of saline lacustrine settings described in Chapter 3; namely the perennial stream floodplain - perennial saline lake. In such a setting Quaternary evaporites have filled lake basins measuring up to a 100 km across with stacked salt bed units that are more than tens of metres thick.

Perennial saline lakes

Subaqueous lacustrine beds typically alternate with brine pan and sabkha salt beds in most continental saline lakes. Changes from one depositional style to another relate to changes in inflow volume and chemistry and often indicate a change in climate, fluvial inflow or tectonics. Perennial lakes and pans typify the topographically lowest part of an endorheic lake basin. Most subaqueous lake sediments are dominated by carbonates

and siliciclastics, higher salinity salts are less common. This reflects the hydrology needed to form a permanent lake. That is, to maintain a perennial above-surface brine body requires continuous water inflow to the lake depression, either from river inflow or from spring seeps. This means most perennial lakes occur in the bottom-most parts of steep-sided endorheic depressions (Figure 4.57).

The definition of what surface salinity constitutes a modern saline lake varies between the Northern and Southern Hemispheres; Hardie et al. (1978) chose a minimum concentration of 5,000 ppm to define saline lake waters based on Beadle's (1974) definition of the upper salinity tolerance of freshwater organisms. In contrast, most Australian limnologists use 3,000 ppm to separate freshwater and saline biotas (Geddes et al., 1981).

Regardless of its minimum salinity, a perennial brine lake and its biota is at the mercy of variations in the local climate and inflow intensity. Lake water levels and salinities are subject not only to seasonal changes but to long-term fluctuations in climate and tectonism. In the short term the volume of inflow water increases after a storm or winter snow melt; in the long term a change to a more humid climate increases the volume of water in the lake depression, while a change to more arid conditions decreases the volume of water and may convert a perennial saline lake into a saline pan or evaporitic mudflat. Tectonic uplift also affects deposition, it can convert what was formerly a hydrologically open basin into an endorheic basin, or vice versa, volcanism and lava flows can do the same. Tectonism can also change the position of the topographically lowest point in the lake, and through uplift can change the volumes of surface runoff, groundwater seepage and inflow chemistry.

The chemical make-up of continental lake brines is much more variable compared to the near isochemical seawater reservoir that supplies mostly gypsum and

halite to modern coastal salinas (Table 4.2). Proportions of the various ions in perennial saline lake waters are controlled by chemistries of the dilute inflows, which are a combination of rainfall intensity and the lithologies in the drainage area surrounding the lake (Chapter 2).

Great Salt Lake, Utah

Great Salt Lake is a perennial water body and has been so for the last 30,000 years. It is one of the largest perennial saline lakes in the world, measuring some 120 km (75 miles) long and 55 km (35 miles) wide, with a water surface elevation that oscillates around 1,280 m (4,200 ft) above sea level (Figures 4.17, 4.18). At this elevation the lake brines cover an area of 4,180 km² and have a maximum depth of 10 m. In a typical year the water surface fluctuates around 30-60 cm, reaching its highest level in May-July (after snow melt) and dropping to its lowest level in October-November. Since 1847 the water level of Great Salt Lake has varied from a low of 1,277.5 m in 1963 to a high of 1,283.75 m in 1986-87 (Figure 4.18). Because the lake is so shallow and its floor so flat, small changes in water level correspond to large migrations of the strandline.

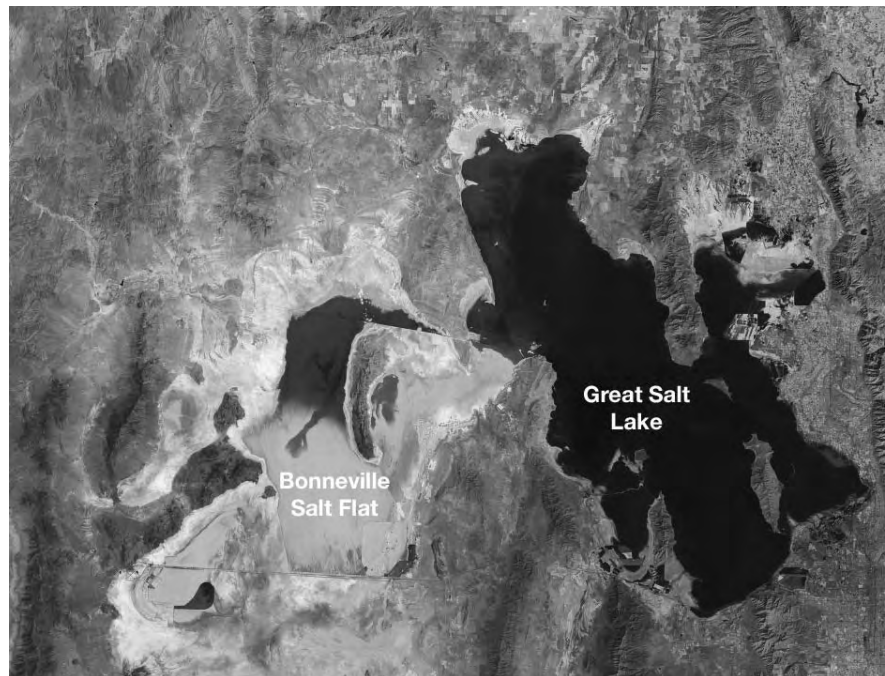


Figure 4.17. Great Salt Lake and the Bonneville Salt Flat, Utah and the adjacent peaks of the Wasatch Mountains east of the lake depression. A railway causeway that transects the northern arm of the lake is visible, as are solar evaporation ponds. The Lake Bonneville salt flats (lighter coloured) lie to the west of the Great Salt Lake. (Landsat image courtesy NASA).

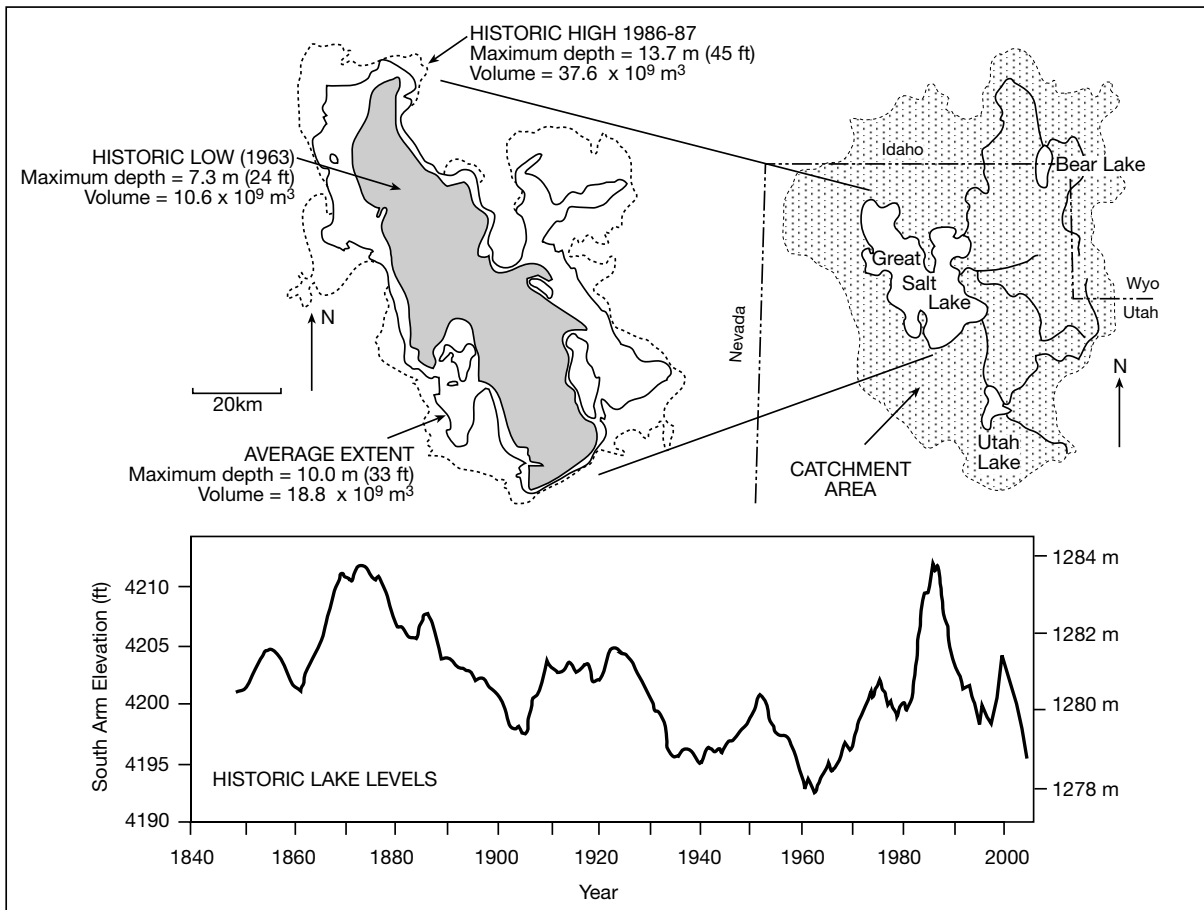


Figure 4.18. Great Salt Lake, Utah. The lake is subject to large changes in the extent of its perennial water body. The upper figure shows the different extent of its highest and lowest levels in historical time. The chart plots yearly changes of lake water level since 1847.

Great Salt Lake lies in an endorheic basin with no surface outlet. The main rivers entering the lake are the Bear River from the north, the Weber and Ogden Rivers from the east, and the Jordan River from the south. Together with small volumes of bajada runoff, they supply around two thirds of the water currently entering the lake. Direct precipitation into the lake supplies some 31 percent, while ground water supplies the remaining 3 percent. The drainage basin of the lake covers an area of about 57,000 km² (21,500 mile²). Water is lost from the lake mostly through evaporation, with something like 3,500 km³ of water evaporating annually (Figure 4.18). When inflow equals evaporation, the level of the lake remains constant. If inflow is greater or less than evaporation, the level of the lake will rise or fall, respectively.

Being situated along the Wasatch Front at the eastern edge of the tectonically active Basin and Range Province, means the size, shape, and location of the Great Salt Lake depression

has been a response to variable intensities of subsidence and faulting, overprinted by the intense climatic vagaries of the Late Pleistocene. Present-day Great Salt Lake is a remnant of a much larger and fresher water body that was once linked into the Pleistocene Lake Bonneville system, as were Utah Lake, Sevier Lake, and the Bonneville Salt Flats (Figure 4.19a). Areas of perennial fluvial inflow into Pleistocene Great Salt Lake are defined by classic “bird’s-foot” or “Gilbert-style” hanging deltas (Figure 4.19a). The downcutting of the current hydrology and the presence of Pleistocene shoreline terraces on higher levels of the delta prism suggest deltas were most active during Pleistocene lake full stages (Lake Bonneville time) when the lake was not accumulating evaporite salts.

Modern strandzone deposits are mostly shorezone spits and bars, which are dominated by aragonitic ooid and peloidal sands (mostly brine shrimp pellets). Carbonates also precipitate about the lake strandline in spring mounds, algal mounds, and

in stromatolites (Figure 4.19b; Eardley, 1938; Halley, 1977). Older algal reef mounds are located further out in the lake and are now buried by lake muds; they grew earlier in the Holocene when lake water levels were lower than today (Colman et al., 2002). Oolite shoals today form sand waves that define the lake strandzone (Figure 4.19b). Individual ooids are aragonite with a radial crystal structure. When and how the individual ooids grew is not well understood, but halobacteria and organic matrices are thought to play a role (Sandberg, 1975; Pedone and Folk, 1996; Reitner et al., 1997).

Laminated mudstones, in large part composed of the faecal pellets of brine shrimp, are currently accumulating further out in the lake (Eardley, 1938). The pellets are a mixture of aragonite and detrital matter, mostly quartz, clays and organics. The brine shrimp *Artemia gracilis* thrives in the lake, it is a filter feeder that flourishes in spring and summer. It supplies a seasonal rain of faecal pellets to the lake bottom and its droppings represent a sampling of the mineral matter suspended in the water column. This implies aragonite is a seasonal precipitate within the upper part of the meromictic water column (see Chapter 9 for biology and feeding styles of brine shrimp and other halozoa).

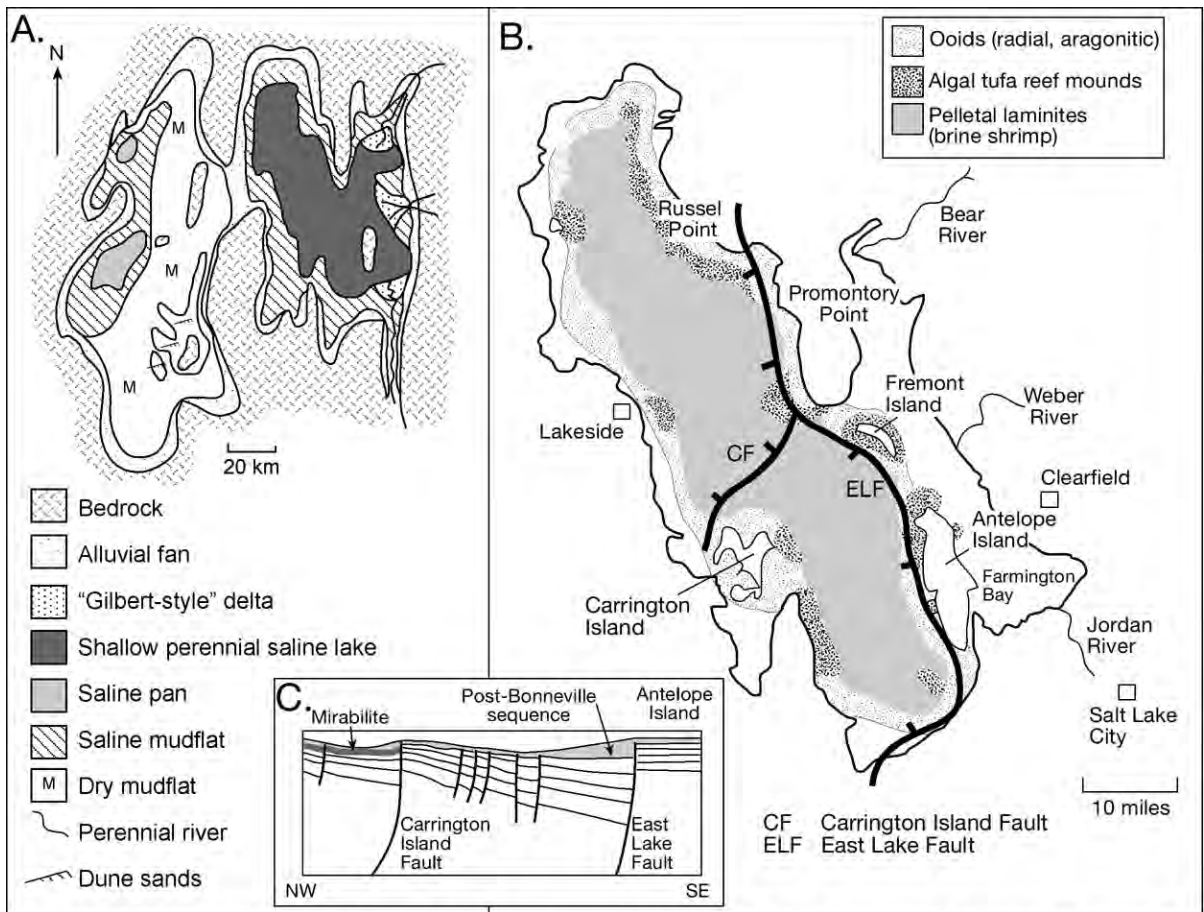


Figure 4.19. Sediment distribution in Great Salt Lake and surrounds. A) Distribution of depositional settings in the Bonneville/Great Salt Lake basin, Utah. The lake itself is a perennial water body fed by rivers with "bird's-foot" deltas at the older entry points into the lakes. The saline pan facies are halite-rich with lesser glauberite, while the dry and saline mudflats are subaerially exposed parts of the old subaqueous floor of Lake Bonneville. Carbonate mudstones, mostly aragonite pellets, dominate sediments currently accumulating on the subaqueous lake floor (after Smoot and Lowenstein, 1991). B) Distribution of algal tufa reefs and ooid sand shoals about the strandzone at the edge of the perennial water body in Great Salt Lake. Positions of the East Lake Fault (ELF) and the Carrington Island Fault (CF) are shown (after Eardley, 1938; Colman et al., 2002). C) Schematic cross section based on seismic lines between Antelope Island and Carrington Island showing the importance of syndepositional faulting in controlling thickness of post Bonneville (<13.5 ka) sedimentary packages (grey) and the distribution of the mirabilite bed in the lake (after Colman et al., 2002).

Rippled sand lamina alternate with mud in the deeper water deposits, with many deeper beds disrupted by the growth of now-dissolved evaporites (Unit I; Spencer, 1983). Remnants of bedded Holocene halite still remain on the deepest parts of the lake floor, preserved by longterm density stratification in the overlying waters. Spencer (1983) recovered euhedral gypsum in the upper 1-2 metres of the now water-covered aragonitic sediments of the lake centre. This sediment also shows evidence of haloturbation and pinch-and-swell bedding. Below this is a 1 m-thick bed of finely laminated aragonitic clay and algal mat partings, which passes laterally into bedded mirabilite (Unit II; Spencer 1983). A later shallow seismic survey showed this mirabilite unit is restricted to a fault-controlled depression north of the Carrington Island Fault (Figure 4.19c). Laminated aragonite is underlain by a laminated calcitic clay with lamination-poor ostracod-rich horizons. Spencer (1983) interpreted this bed (his Unit III) as the deepest water unit recovered in his coring program. Only one core penetrated below this deeper water unit to recover clays and muds of what may be a subaerial mudflat (Unit IV).

Prior to 32 ka, the basin was an ephemeral pan - saline mudflat system (Unit IV). Since then, Great Salt Lake has mostly been a perennial water body, initially a shallow saline brine lake, then a brackish lake between 25 and 19.5 ka. Between 19.5 and 17.5 ka a fresher but somewhat restricted lake occupied the basin, with a water surface near the Provo level (water was 195 m deep). Fresh water conditions and a standline near the Bonneville level existed from about 17 to 15 ka (waters around 310 m deep). A sharp drop in lake elevation occurred about 15 ka. Between 15 and 8 ka the lake was at extremely low levels and at times was divided into two separate saline basins. For the past 8 ka the lake has fluctuated near its present level. Much of the salt now contained in the Great Salt Lake was originally dissolved solute in the waters of Lake Bonneville. An additional two million tons of dissolved salts now enter the lake each year via river and spring inflow, which carries leachate from the surrounding soils and rocks.

Recent study of a single long core that records the last four glacial/interglacial sequences in the Great Salt Lake Basin has shown that salt/freshwater marshes as documented by Spencer (op cit) were common during the interglacials (Balch et al., 2005). Deep freshwater conditions correspond with the maximum global ice volume in Oxygen Isotope Stage 2, and before a maximum in global ice during Oxygen Isotope Stage 6. Immediately following each deep lake period the lake level crashes via rapid desiccation and it resulted in the deposition of thick evaporite units.

Fault-accommodated subsidence in the Great Basin has now filled the depression with more than 3700 m of continental sediment, with most of the sediment carried in by the major rivers. Two currently-active faults underlie Great Salt Lake (Figure 4.19b, c; Colman et al., 2002). The East Lake Fault passes along the west edge of Antelope and Fremont Islands and on northwards by the west side of Promontory Point. The Carrington Fault extends northeastward from Carrington Island to merge with the East Lake Fault of the southwest tip of Promontory Point.

Most of the current strandzone facies along the eastern side of the lake are tied to the topographic escarpment created by the East Lake fault, many now buried Holocene tufa-reef mounds also sit atop subsidiary faults in the lake. Similar broader-scale fault-controls to Late Pleistocene lacustrine geometries are seen in seismic facies throughout the lake basin. Colman et al. (2002) concluded that the Great Salt Lake basin has been, and continues to be, an area of active extensional tectonics and that tectonics has exerted a major effect on the distribution and type of sediments in the lake. Currently, the East Lake Fault is at least as active as any of those along the Wasatch Front, showing at least three episodes of significant faulting since lake water level fell around 13.5 ka from its Pleistocene high. The upthrown side of the Carrington Fault today forms a sill, with a seismically resolvable tip that is only about 5 m below present lake floor. Fluid flow into the lake along this and other fault planes may explain some of the indurated bioherm mounds and pavement sheets present on the lake floor.

A fall of the lake waters marked the end of the high Bonneville phase and led to the formation of a basin-wide seismic horizon associated with lowered lake levels (Colman et al., 2002). Mapping of this reflector shows that the southern basin comprises a distinct sediment wedge thickening toward the East Lake Fault, a geometry that contrasts, to some degree, with the smooth symmetry of the current lake floor (Figure 4.19c). Seismic facies maps also show the lake level during the early Holocene was considerably lower than today; it was a time when the lake was an intermittently flooded playa and when up to 13 metres of post-Provo halite accumulated near the East Lake Fault. At that time small remnant water bodies probably ponded in local lake-floor grabens along the downthrown sides of active fault scarps. Thus fault-controlled tectonics controlled the distribution of the various early Holocene pan evaporites, including the mirabilite/halite beds (Figure 4.19c).

Within this tectonic framework, Late Quaternary climate change across the Great Basin altered solute proportions in the lake

inflows and so influenced mineralogies in the evaporite suites accumulating in low water stages in Great Salt Lake. Spencer (1983) defined three major styles of inflow to the lake system; 1) concentrated Na-Cl dominant spring waters, 2) dilute Ca-HCO₃ river waters, and 3) dilute Ca-HCO₃ precipitation (rainfall and snow melt). During the fresh-water period of the Lake Bonneville and other pluvial times, the inherently higher levels of meteoric discharge to the lake meant inflow chemistries were dominated by calcium bicarbonate waters. Saline stages, as in most of the Holocene, were characterised by lowered meteoric inflow volumes and so fault-fed hydrothermal springs became an increasingly significant solute source. Between 15 and 8 ka the lake waters were cold and relatively depleted in Cl. Mirabilite accumulated on the lowermost parts of the cold, largely subaqueous parts of a meromictic lake floor, in a setting much like the subaqueous salts of the modern meromictic saline lakes of the Canadian interior (Figure 11.51). Since that time, conditions became drier and warmer, with higher proportions of Cl-rich waters entering the perennial lake. Halite was precipitated prior to mirabilite during hypersaline or droughty episodes in the lake and this mirabilite is still an ephemeral mineral in the pans of the North Arm. Before the lakewide drawdown that ended Lake Bonneville, the dominant lake carbonate was calcite. Since that time a more arid climate has dominated and aragonite is the dominant carbonate precipitate.

Mono Lake, California

Mono Lake, an endorheic meromictic saline lake in a volcanically active area at the edge of the Sierra Nevadas (Figure 4.20), has been accumulating laminated lacustral sediments since 760 ka. Current free surface brine volume is ≈3.2 km³, surface area is 184 km², annual total inflow is around 283.7 x 10⁶ km³ and current salinity is around 90,000 ppm. Major anion

content of lake brines is divided almost evenly between chloride, sulphate, and bicarbonate. The high pH (≈9.8) and alkalinity of lake waters leads to high concentrations of volcanic elements that ordinarily have short residence times in lakes (i.e. lanthanides and actinides, including naturally high levels of arsenic in bottom brines; Tomascak et al., 2002). Calcium carbonate (calcite and aragonite) precipitates spontaneously from the lake waters and makes up 3-10 % of the laminite sediment on deeper tufa-free bottoms, the remainder is detrital. Some of

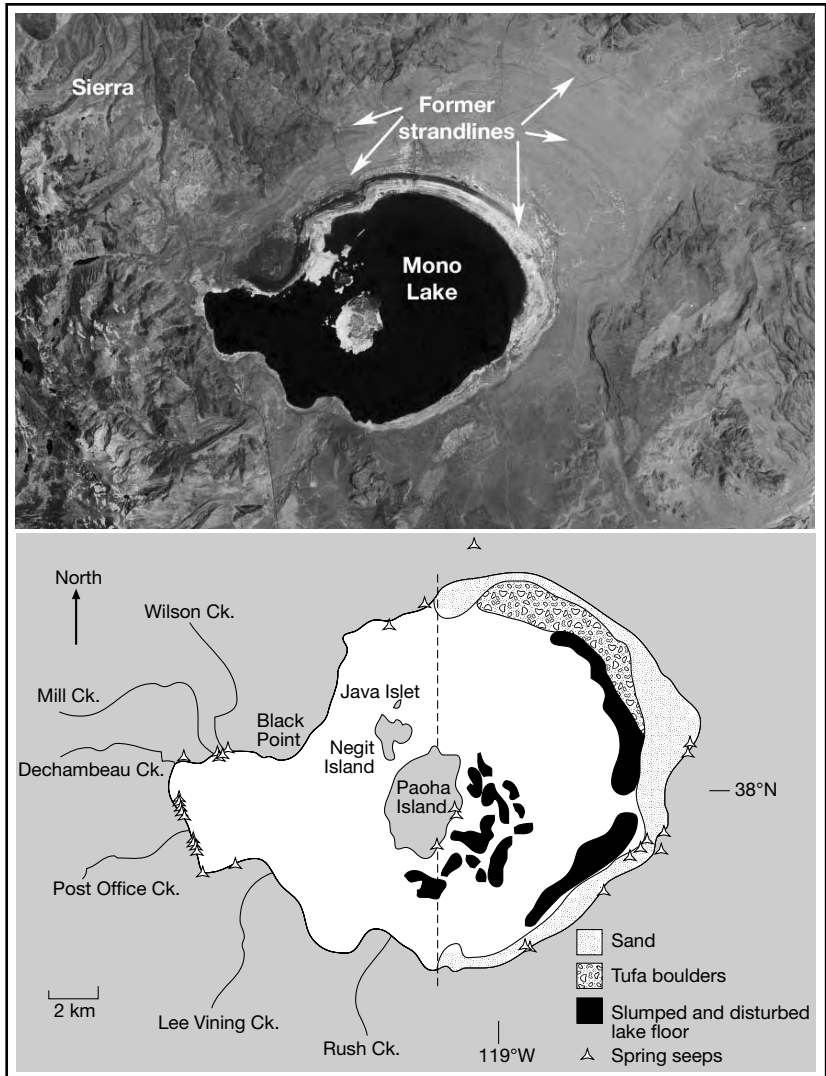


Figure 4.20. Mono Lake, California. Successive strandlines associated with lake shrinkage are visible in the Landsat image, as are the volcanic centres of Paoha Island and the adjacent lake plain to the northwest. High relief drainage source to the west in the Sierra Nevada is clearly seen in the high proportion of creeks entering the western side of the lake (Landsat image courtesy of NASA). Geological interpretation of the type of sediment is only published for the eastern half of the lake - extent indicated by dashed line (in part after Benson et al., 2003).

the lake bottom laminites are slumped, possibly initiated by ongoing volcanic disturbance (Figure 4.20; Benson et al., 2003). Calcite accumulates, sometimes with an ikaite precursor, where resurging groundwaters degas on the lake floor and can form spectacular biogenically-bound towers of tufa.

Lake levels and conditions

From 1850 until the middle of last century the lake water level rose some 5 metres, then the water needs of the City of Los Angeles caused a drastic water fall. In 1941 the distributaries that fed Mono Lake were diverted into the Los Angeles aqueduct. In the 50 years since this diversion, the lake water level dropped more than 10 metres, the lake water volume was cut in half, while the alkalinity and salinity of the lake waters doubled (Figure 4.21). Before the diversions of Mono's tributary streams the water level was as high as 1958 metres above sealevel. Subsequent lower lake levels exposed numerous calcitic tufa mounds and pinnacles on the lake floor and enlarged the portion of the lake floor covered by saline mudflats.

To prevent the complete destruction of the lake, some water from the former distributaries has been rediverted back into Mono Lake, which is now slowly refilling after reaching an all time low of 1942.2 m asl in 1982 (Figure 4.21). The current lake level is 1945 m asl (December, 2004). The projected stabilized lake elevation is 1948.3 m, which should be attained within the next 10-15 years. Interestingly, the anthropogenic lowering of lake water level in the last half-century and the associated increase in lake salinity is still well within the range of natural fluctuations experienced by Mono Lake in the last 4,000 years (Figure 4.22a, b).

In 1982 and 1983 exceptionally large volumes of freshwater runoff led to a rapid 2.6 m rise in surface elevation of the lake and the onset of meromictic stratification (Jellison and Melack, 1993). In 1984 this chemical stratification accounted for a density difference of $1.2\text{--}1.5 \times 10^{-2}$ gm/cc between the 2 and 28 m water depths. At the same time the midsummer density difference between 2 and 28 m depths that was due to temperature was approximately 0.5×10^{-2} gm/cc. Salinities ranged from 77 to 98 gm/l across the interface and sodium, chloride, sulphate, and carbonate were the major ions in both the upper and lower water mass.

Another transition from monomixis to meromixis occurred from 1994 to 1995 (Melack and Jellison, 1998). During the preceding monomictic conditions in 1993 and 1994, the lake had thermally stratified in March and had mixed to the bottom by December. During meromictic conditions in 1995, 1996 and 1997, the absence of holomixis during winter resulted in persistent anoxic conditions beneath the chemocline, the accumulation of ammonium in the monolimnion, its depletion in the mixolimnion, and low mixolimnetic chlorophyll concentrations in the spring and autumn. A comparison of density differences between the 2 and 28 m water depths indicate thermal stratification predominated in 1993 and 1994, while chemical stratification dominated the density differences in 1995, 1996 and 1997.

Tufa mound and pinnacles

The most visually striking geological features of Mono Lake are its metres-tall tufa columns, which protrude from lake waters and line parts of the lake edge. These mounds and needle-like

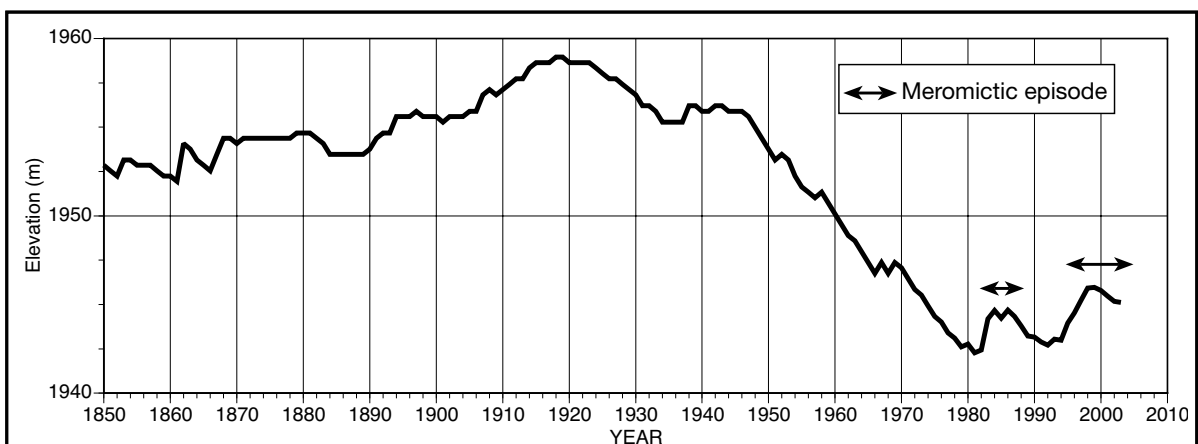


Figure 4.21. Mono Lake levels from 1850 - present (replotted from online data of Mono Lake Preservation Society accessed on March 27, 2004 at <http://www.monolake.org/live/lakelevel/yearly.htm>).

pinnacles of calcium carbonate frequently define linear trends that are the seepage expression of underlying faults and joints (Figure 4.23). Columns are surrounded by soft bottom sediments and many columns are rooted in massive domal buildups of calcite. Dominant growth orientation is vertical and defines the rapid upward rise of less saline CO_2 -rich waters. Branching of lithoid columns is rare and “pseudo-branches” easily explained by the collapse of one or two adjacent columns imply much of the precipitation mechanism is via inorganic degassing of groundwater on reaching the lake floor. Microbial biofilms coat active tufa surfaces beneath the lake waters and create characteristic knobby grumous microtextures in the reef mounds and pinnacles as they capture the precipitated carbonate (Figure 4.23b).

In today's lake waters calcite and aragonite are the carbonate minerals with long-term stability and they dominate the non-siliciclastic fraction accumulating in the lake (Benson et al., 2003). But during the colder Tioga glacial period of the Late Wisconsinan (12 to 9 ka), and during the present day winter season, ikaite ($\text{CaCO}_3 \cdot 6\text{H}_2\text{O}$), was the dominant carbonate precipitate (Whiticar and Suess, 1998). Ikaite is a metastable cryogenic carbonate and the low temperatures needed for ikaite stability are obvious in winter in Mono Lake. In the winter of 1985 ikaite crystals were visible as coatings on the subaqueous surfaces of active spring seep tufas about the shallow lake edge (*pers obs.*). If these small ikaite crystals were removed from the icy cold winter waters of the lake and held in an ungloved hand, the increase in ambient temperature caused the ikaite to deliquesce, so that in a few minutes it disappeared leaving behind a pool of milky water. Council and Bennett (1993) and Bischoff et al. (1993) argued that during winter, calcite precipitation in Mono Lake is inhibited by low temperatures and high concentrations of phosphates and organic carbon. The same factors allow metastable ikaite to form. Ikaite decomposes into calcite during the spring warming, occasionally leaving pseudomorphs of the primary precipitate in the calcitic tufa.

At a broader scale Council and Bennett (1993) demonstrated a strong hydrological control on the position of many of the larger lithoid tufa mounds. The unconfined aquifer that domi-

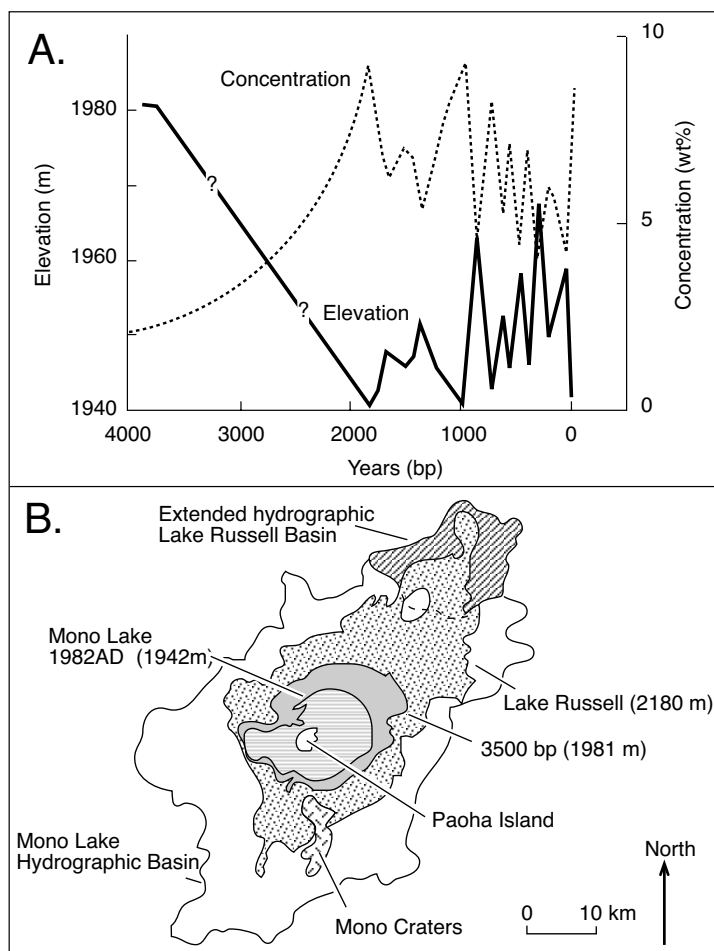


Figure 4.22. Mono Lake, California. A) Hydrological conditions for the last 4,000 years (after Stine, 1990). B) Map outlining different lake areas related to changing water elevations through time (after Rogers and Driese, 1995a, b).

nates the western side of the basin is composed of fluviodeltaic sediment and it controls the modern discharge at many points about the current lake shoreline (Figure 4.23a, c). Currently active diffuse low flow rate seeps are dispersed across the strandzone, and extend from $\approx 200\text{m}$ above the present lake shore to around 1 metre below the present lake water surface (Figure 4.20). Diffuse outflows are geologically defined by flat beachrock-like zones of encrusting tufa and tufa flowers, and most active about the present lake strandline.

Further offshore, where the aquifer is largely confined by lake muds, CO_2 -saturated groundwaters discharge through fault and fracture focused conduits. The associated tufa mounds precipitate along linear trends tied to positions where faults transect the confining clays to intersect the lake floor. Other

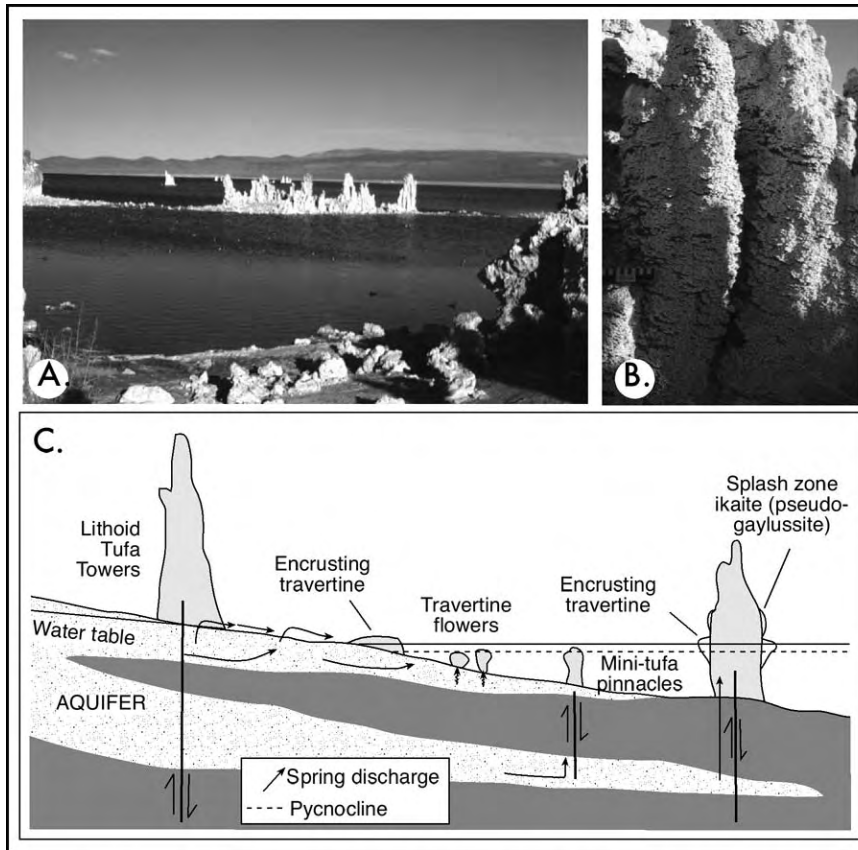


Figure 4.23. Mono Lake, California. A) Tufa pinnacles forming linear growths on the saline linear ridges in the lake floor in Nov. 1985. B) Close up of algal-bound crenulated pinnacle surface and subhorizontal layering (scale bar is 15 cm long). C) Schematic cross section showing aquifer control on the development of modern tufa mounds on the margin of Mono Lake California (after Council and Bennett, 1993).

older, now exposed and mostly inactive linear tufa mounds and encrustations define prior times of higher lake water levels and water tables. Modern springs along the western side of Mono Lake originate along the Sierra front and discharge Ca-HCO_3 waters that are neutral to slightly acidic, whereby their degassing drives present day tufa precipitation. In contrast, springs along the eastern shore typically discharge Na-HCO_3 waters, have lower hydraulic heads and are not generally associated with the formation of modern tufa sheets.

The identification of modern ikaite (pseudo-gaylussite) suggests that portions of many Pleistocene and Holocene tufas in the Mono Basin and other cold saline lakes in the Great Basin first precipitated as ikaite (Whiticar and Suess, 1998; Shearman et al., 1989). These palaeo-ikaite have long since recrystallised to form their calcitic pseudomorphs ('thinolites'). Ikaite pseudomorphs are also found in recent and ancient sediments of polar re-

gions where they are known as 'glendonites', or colloquially as "devil's horns". The environmental occurrence of ikaite and their pseudomorphs deem them as potential palaeoclimatic indicators of cold environments including saline lakes. Larger crystals are typically restricted to colder, deeper organic-rich marine sediments or groundwater outflow zones in cold moderately saline evaporitic basins (Buchardt et al., 2001).

Aside from Mono Lake and its spectacular tufa mounds, the other obvious geological feature in the immediate area of the lake is the Mono Craters (Figure 4.22b). These are the remnants of 24 domes of explosive rhyolite, which erupted over the last 40,000 years, with the last eruption occurring less than 700 years ago to form Panum Crater (actually a plug-dome volcano) located just above the south shore of Mono Lake. Black Point, Negit Island, and Paoha Island are all recent volcanic features of the lake geomorphology, Paoha Island emerged from the lake waters within the last 350 years. This recent volcanism drives hydrothermal circulation and is still active in the surface and subsurface hydrochemistry of the Mono Lake waters. It supplies elevated levels of sodium and bicarbonate ions compared to chlorine, along with higher concentrations of arsenates and rare earths (Tomascak et al., 2002).

Hydrological and hydrogeochemical evolution

Up to 2 km of lacustral and volcanogenic sediments underlie Mono Lake, and saline groundwaters (>18,000 ppm) extend to the bottom of the basin's sediment fill (Rogers and Driese, 1995a, b). The position of the saline-fresh groundwater interface within the lake basin reflects a balance between a dense saline brine plume or curtain beneath the lake and the force of inflowing fresh groundwaters fed from the Sierras and discharge

near the lake's western shore. The rain shadow of the Sierra Nevada to the immediate west of the lake has had a dramatic effect on the asymmetry of surface and groundwater inflow to the lake depression. More than 114 cm of precipitation falls at the Sierra crest, which then supplies waters to the western side of the lake's drainage basin, mostly by surface drainage. Lee Vining Ck., Mill Ck., Rush Ck. and Wilson Ck. together supply $\approx 1.75 \times 10^{11}$ l/a to the lake (Figure 4.20; Tomascak et al., 2003). Less than 13 cm of precipitation falls on the eastern shore of Mono Lake. Altogether surface inflow supplies around 75% of the lake's water and springs supply the remainder.

The much higher recharge rates for fresh surface and groundwater seepage along the western or Sierra Nevada side of the lake have pushed the saline-fresh water interface basinward of the shorezone beneath that side of the lake. This creates the artesian head that facilitates the formation of the more spectacular linear-trending tufa mounds. In contrast, the brine plume-freshwater interface lies near or directly below the shoreline around much of the rest of the lake. There the saline groundwater discharge zone is just below the playa surface and it contributes to development of saline mudflats and flat sandy beachrock/rubble atop recently exposed former lake beds in an area that lacks significant tufa pinnacles.

Simulations by Rogers and Driese (*op cit*) confirm that extensive faulting controls local permeability in the basin fill beneath the lake waters. Faulting increases vertical permeability and leads to focused or channelled regions of outflow and seepage in the lake floor. High permeability zones in the lake substrate on the western side means resurging less-saline groundwater can overcome the opposing force of the saline groundwater density plume and so can issue onto the lake floor where its degassing outflow is marked by linear belts of spectacular tufa precipitation, (Council and Bennett, 1993).

In the longer time frame of the Mono Lake's Quaternary hydrology, the redistribution of the basin's solutes between the lake and underlying saline groundwater body is today still driven by late Quaternary lake level changes (Figure 4.22b; Rogers and Driese, 1995b). At times of low lake levels in the Late Pleistocene, the higher concentration and density of lake waters caused solute loss via free convection (brine reflux). This probably occurred more rapidly and penetrated deeper into the sediment column along open faults or fractures. At higher lake levels, the shoreline discharge zone moved closer to the basin edge (e.g. the Lake Russell strandline; Figure 4.22b). The now-unrestrained saline groundwater mass subsided, drawing solutes from the lake waters into the basin sediments. Subsequent

falling lake levels again constricted the saline groundwater zone beneath the lake, driving saline water and their solutes back into the lake waters and once again increasing solute content of surface waters.

Sediment permeability below the lake is the major control on the solute transfer rate between the lake and its groundwater reservoir. Only the larger, longer-term lake level changes drive saline groundwater movement in the lake margin. Depending on permeability of the basin fill aquifer, the equilibration of the saline groundwater and lake solute content to lake water level requires hundreds to thousands of years. Rogers and Driese (1993a, b) suggest that current conditions, where a more saline Mono Lake brine pool (50,000-90,000 ppm) overlies less concentrated groundwater ($\approx 18,000$ ppm), reflects the still active impact of late Pleistocene lake high stands. In support of this they note that Mono Lake's historical salinity data have a large scatter, but suggest there was a 5% decrease in the lake's solute content over the last 50 years of drawdown; they suggest this indicates a diffusive solute flux into lacustrine sediments for this period. Their conclusions are the opposite of the commonly accepted view of Mono Lake drawdown automatically increasing the salinity of the lake waters.

Saline lakes of Turkey

Turkey, with its active compressional tectonics and semi-arid climate, is ideally situated to form permanent ponded bodies of somewhat saline water in mountainous endorheic depressions. It has some of the largest modern saline lacustrine systems in the Northern Hemisphere in subaqueous settings ranging from perennial water pools about the edges of ephemeral saline mudflat and pan systems like Tuz Golu and Aci Golu (Golu = lake), to large deep bodies of alkaline water, such as Lake Van which have extents comparable to Great Salt Lake and Lake Urmia (Figure 4.24). As in the Andes, ongoing plate to plate compression and associated volcanism throughout the Neogene of Turkey has created rich deposits of exploitable saline minerals, especially borates and zeolites, in the many Tertiary lacustrine depressions of Turkey, (Chapter 11).

Lake Van, Turkey

Van Gölü in eastern Turkey has an area of 3,574 km², a maximum water depth of 451 m, a volume of 576 km³ and a catchment of more than 15,000 km². It is the world's largest soda lake and the 4th largest closed-basin perennial lake in the world. It is the largest lake in Turkey and at its widest point it is some 119 km across (Figures 4.24, 4.25). The main water mass of the

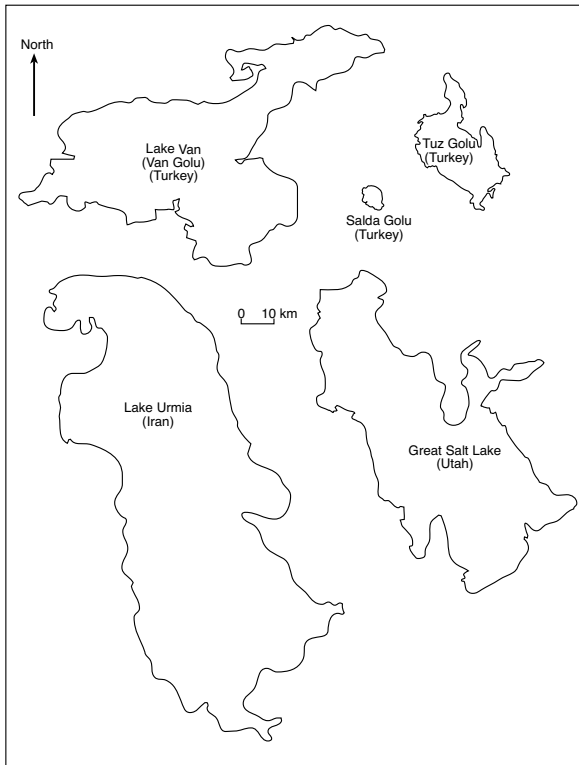


Figure 4.24. Same scale outlines of the various Turkish Salt lakes compared to Lake Urmia (Iran) and Great Salt Lake (Utah).

lake lies in its west, where waters are deeper than 400m. The lake sits in the lower part of a steep-walled, fault-controlled basin, once drained by the Murat River (Figure 4.25). During the mid Pleistocene, some 200 ka, a lava flow from the Nemrut

volcano extended some 60 km across the southwestern end of the basin, blocking westward drainage from the lake via the Murat River and thereby transforming the depression into a endorheic basin.

Climate in the drainage basin is highly continental with hot dry summers and long cold winters. Annual precipitation across the drainage basin is variable and ranges between 400 and 700 mm. Most detrital influx into the lake is in April to June, carried by snowmelt and spring rains. In summer the present day lake waters are thermally stratified and temperatures within the uppermost water column reach as high as 19-20°C (Figure 4.26). Below 50 m depth, water temperatures are less than 3°C and do not change much year round. In winter the shallower northern sections of the lake can freeze over, and the onset of lower surface water temperatures in the autumn drives an annual overturn of the lake waters.

Salinity is 22‰, pH hovers around 9.5 and can be as high as 9.8 making the lake waters highly alkaline (≈ 153 meq/l; Figure 4.26). Free oxygen is present throughout the water column, but drops to values <1 mg/l near the lake bottom. Calcium concentrations in the lake waters are low (≈ 4 mg/l; Thiel et al., 1997) The main cation in the lake waters, sodium, is not only balanced by chloride, but also to a near equivalent extent by high levels of carbonate and bicarbonate ions. As in Mono Lake, the high alkalinity reflects the preponderance of young volcanics in the drainage basin and ongoing hydrothermal circulation. This high alkalinity in the lake's hydrogeochemistry explains the onset of trona deposition when the lake dried out some 15 ka. Relatively high salinity and very high alkalinity means modern

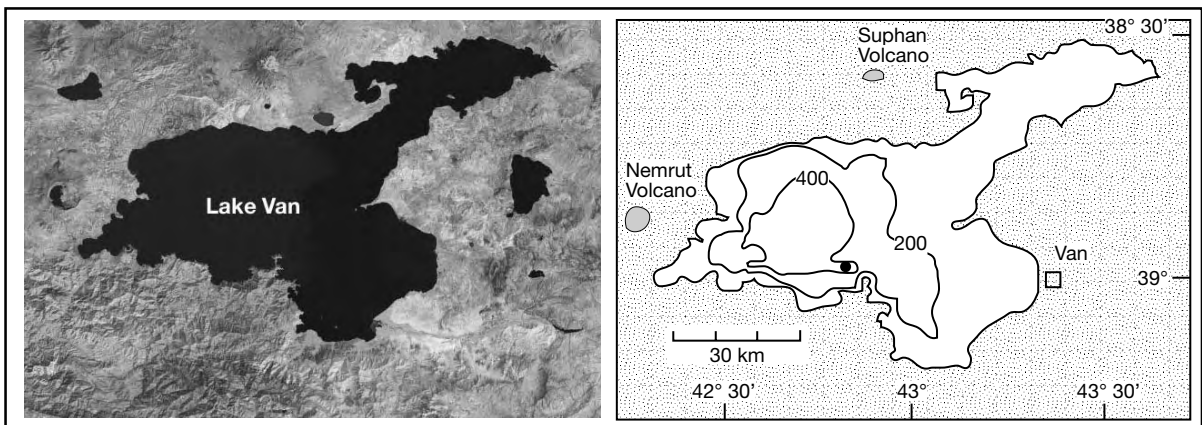


Figure 4.25. Lake Van, eastern Turkey, is the largest perennial saline lake in Turkey. Toward the top of the image are the Satak Mountains, Nemrut Lake, the crater lake of an active volcano, that last erupted in the year 1440 lies to the west. Ercek Lake can be seen to the east of Lake Van. To the north of Lake Van is the extinct Suphan Volcano, a circular volcanic maar with an elevation of 4061 metres. (Landsat image courtesy of NASA). Bathymetry is in metres and the black circle indicates the position of piston core K10, with its geology and chronology illustrated in Figure 4.28.

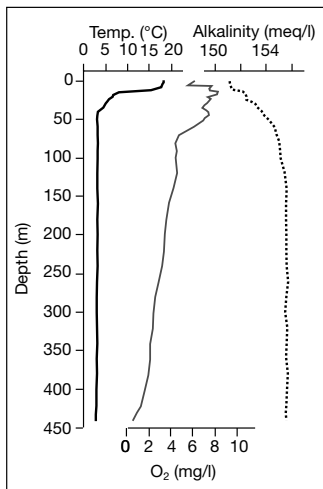


Figure 4.26. Temperature, oxygen and alkalinity profiles in the Lake Van water column (after Thiel et al., 1997).

lake waters host a low diversity, largely endemic phytoplankton population dominated by diatoms and cyanobacteria (primary producers). Copepods and ciliates are the main contributors to the zooplankton.

Today, the lake water level is around 1648m asl and fluctuates around 50 cm annually, being lowest during the winter months and rising after the spring thaw to reach its highest level each July (Figure 4.27a). Longer term lake levels over the

last few decades have been rising at rates as high as 2.6 m per decade, leading to major problems for agriculturalists working lands about the strandzone or lake floodplain. Millennial lake level changes are even more significant. Some 15 ka the lake had dried into a series of saline pans and the water level was more than 450 metres below that of today (Figure 4.27b; Landmann et al., 1996). A few thousand years earlier, at the height of the last glacial, some 18 ka, the water level in Lake Van was 72 m above its present position (Degens et al., 1984). The rapidity of natural water level changes are of the same magnitude as those currently occurring in the Dead Sea Basin (Figure 4.42).

Lake Van deep bottom sediments were collected by a series of piston cores in 1990 and the results published in Landmann et al. (1996) and Thiel et al. (1997). Their work, along with the results of an earlier piston core study by Kempe and Degens (1978), are summarised in the next few paragraphs and a key core (K10) is illustrated in Figure 4.28. Sediments accumulating on the deeper parts of the Lake Van floor are mainly dark-coloured carbonaceous siliceous carbonate laminites/mudstones, with layering that indicates annual deposition cycles and so are true varves. Varve counts imply core K10 recovered some 15,000 years of lake history (Figure 4.28). Lighter coloured laminae in each varve couplet are dominated by micritic carbonate and opaline silica. Darker laminae are characterised by higher amounts of organic material and high proportions of nonchemical detrital sediment matrix, which was carried into the lake by spring melt waters. Dolomite occurs in various

lamina, but is detrital, not authigenic, and comes from eroded Cretaceous dolomites.

Colours in the recovered core are mostly dark and range from dark brown to dark greyish green; they reflect largely anoxic deepwater conditions (Eh of 150 to -280 mV), which have prevailed on the subaqueous lake floor for the last 15 ka. Accordingly, organic contents in the bottom sediments are high, the organics are oil prone, and TOC ranges up to 5-6% (Thiel et al., 1997). The base of the laminite unit is at around 8.5 m in core K10 and is defined by a sandy layer, thought to indicate the drawdown stage in the deeper parts of the lake, some 15 ka (Figure 4.27b).

Material caught in sediment traps in the central parts of the lake show that most of the micritic carbonate in the cored laminite was annual, probably precipitated in the evaporative surface layer each summer to fall (Landmann et al., 1996). Aragonite/calcite ratios, determined by X-ray diffraction analysis on core K10, scatter between 2 and 9 in sediments younger than 3700 yr B.P., and from 1 to 4 in older sediments (Figure 4.28). The other main chemical component in the sediment traps is opaline silica, largely derived from phytoplanktonic diatom tests.

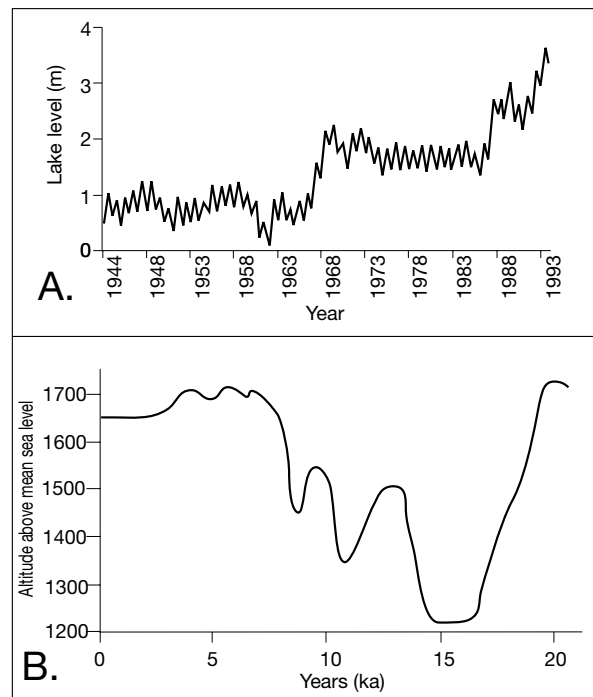


Figure 4.27. Water levels in Lake Van (Vangolu), Turkey. A) Water levels changes in the period 1944-1993 (after Kadioglu et al., 1997). B) Water level changes in the last 20,000 years (after Landmann et al., 1996).

Because present lake waters are supersaturated with respect to alkaline earth carbonates, carbonate precipitation is most obvious in the lake at positions of calcium input where fresher waters mix with more saline lake waters. This can be at the mouths of rivers, where whittings have been documented, or it can occur on the shallow lake floor down to depths of 120 metres, where the degassing of resurging calcium-rich groundwaters escaping into the lake waters creates tufa towers or pinnacles, up to 40m high. These structures constitute some of the largest active microbialite buildups in the world today (Kempe et al., 1991). Lake Van does suffer from severe winters, but these aragonite/calcite tufa samples described by Kempe et al. (1991) were collected in the summer. The possibility of primary ikaite was not considered. So, it not known if some of the initial tufa in Lake Van was once ikaite, which then converted to CaCO_3 . A textural comparison with similar structures in Mono Lake suggests this may be so, especially in older colder stages in the lake history.

The current condition of Vangolu is a useful analog for the Pleistocene freshwater stages in many of the world's soda lakes that are currently in a hypersaline (trona) stage and for many pre-Quaternary alkaline lakes. It serves as a useful analog for the laminites of High Magadi Beds of the Lake Magadi and Lake Natron and for the oil shales of the Eocene Green River Fm, USA.

Salda Lake, Turkey

Saldagolu is another highly alkaline ($\text{pH} > 9$) saline lake in southern Turkey, located in a collision belt at an elevation of 1139 m asl. It is bowl-shaped and occupies the lowest part of a fluvial and seepage-fed endorheic depression at the foot of the Esler Mountains. Lake waters are up to 184 metres deep and cover an area of 43.7 km^2 (Figure 4.29). Lake levels rise about 50-70 cm each spring, but longterm levels are falling and have been doing so for decades exposing widespread beach-rock like terraces and stromatolites of hydromagnesite and aragonite. Inflow waters to Salda Golu are enriched in magnesium and carbonate and when compared to Lake Van are much fresher, they are even capable of supporting the local livestock.

The lake drainage is rimmed on three sides by serpentinites (ophiolites) and on the fourth by a downfaulted block of Upper Cretaceous limestone. Hazburgite is the dominant country rock, though in places it has been metamorphosed to lizardite ($\text{Mg}_3\text{Si}_2\text{O}_5(\text{OH})_4$) and subsidiary dunite, all Mg-rich phases. All the rivers draining into the lake follow faults, flow across peridotites, and under the lowered water levels of today are losing streams. Waters typically seeping into fan deltas or into the lake surrounds before ever reaching the strandzone of Salda Golu (Russell et al., 1999).

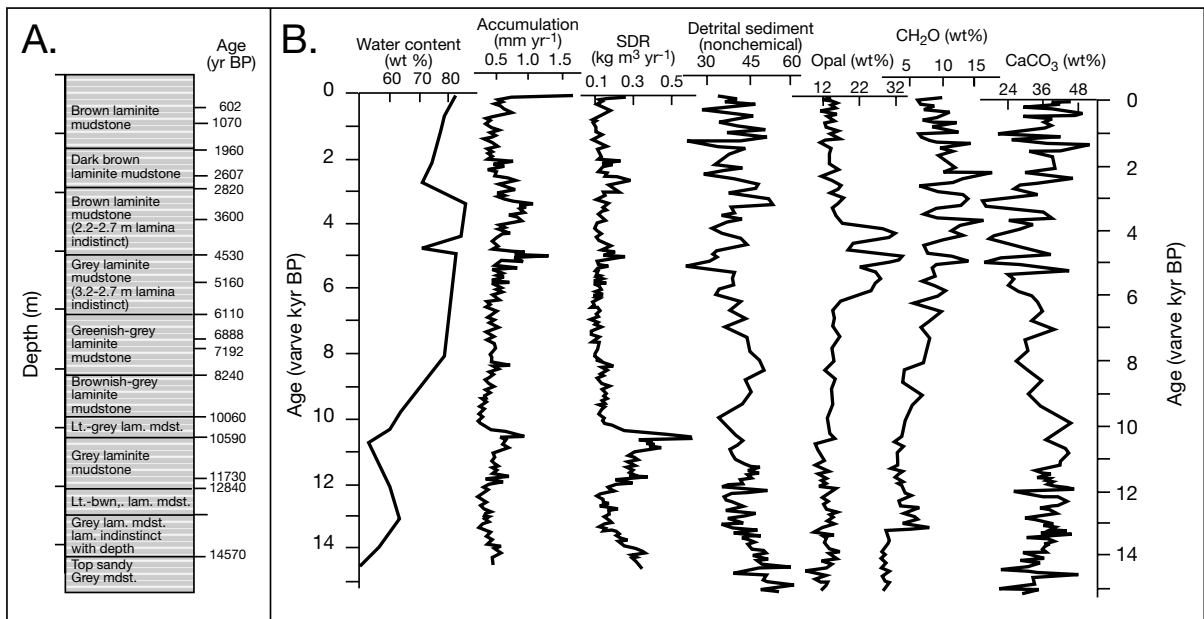


Figure 4.28. Lake Van Core K10 (see figure 4.25 for location). A) Laminate lithology plotted against depth and varve-determined ages. B) Core properties plotted against varve determined time. SDR = rate of sediment deposition. Opal is dominantly from diatom tests and CaCO_3 is mostly from aragonite with lesser calcite (after Landmann et al., 1996).

Magnesium concentration averages 60 ppm in wells and cold springs in the lake surrounds, temperatures range up to 12-15°C and pH lies in the range 8-10 (Braithwaite and Zedef, 1996). Sodium levels in the groundwaters of the lake surrounds are low (\approx 5 ppm) as are most other ions, with the exception of HCO_3^- . In contrast, lake waters contain 300 ppm of Mg and 200 ppm of Na down to a depth of 80 metres, with a pH around 9.1. Mg in the lake has increased by a factor of 6 compared to waters in the surrounding aquifers, while Na in lake water is more than 40 times that in the lake surrounds. Obviously, the bulk of the groundwater seeping into the lake edge gathers Mg as it seeps lakeward through older river mouth fan deltas, which contain abundant cobble of metastable Mg-rich ultramafics such as lizardite (Russell et al., 1999). Lakeward seeping groundwater outside the deltas also picks magnesium, relative to Ca, as it cannibalizes the older hydromagnesite-cemented gravelly strandlines/terraces that circumscribe the present lake. Subsequent hydromagnesite precipitation in the lake is probably related to an increase in pH in the lake waters, tied to HCO_3^- depletion (CO_2 depletion) as it enters the lake, perhaps indirectly brought about by the metabolic activities of microbialites.

Composite stromatolites, several metres high and composed largely of hydromagnesite, line significant portions of the current lake margin; they are best developed atop the now largely inactive fan deltas of the Salda River (Karakova Dere) in the SSW of the lake and the Yesilova delta in the ESE of the lake (Figures 1.6, 4.29). Outside of the fan deltas, smaller stromatolitic mounds of hydromagnesite occur along the lake's western strandzone. Most of the detrital sediment currently accumulating along the strandzone between reef mounds is created by the mechanical (wave-driven) breakdown of former carbonate terraces and hydromagnesite microbialites; it is not derived from longshore transport of fluvial sediment (Braithwaite and Zedef, 1994, 1996; Russell et al., 1999). Hydromagnesite precipitates, now exposed by falling water levels, give the present strandplain its bright white colour. Fine-grained hydromagnesite, reworked

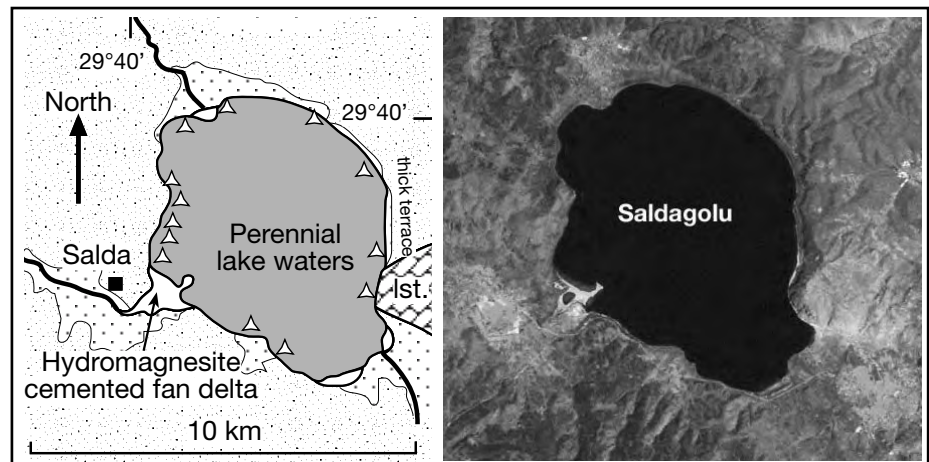


Figure 4.29. Saldagolu, Turkey. A perennial carbonate precipitating lake, currently accumulating hydromagnesite and aragonite. The lake is best known for the subaqueous stromatolites accumulating basinward of hydromagnesite strandline terraces, with most prolific occurrences indicated by triangles (for detail on the stromatolites see Chapter 1).

from tufa shorelines and from the terraces, is suspended in the water column during storms and is probably redeposited as micritic turbidites alternating with laminites in the deeper part of the lake.

Further landward from the present strandline, the earlier hydromagnesite terraces preserve no obvious stromatolites, but include boulders and blocks of reworked hydromagnesite up to 0.5 m across. Many of these circum-lake terraces appear to be inorganic precipitates that started to form when lake levels were higher. It seems that stromatolitic morphologies do not survive long-term exposure and lithification as they quickly degenerate into a porous, coarse-grained poorly lithified floatstone, with the positions of former microbialites sometimes still recognisable as mounded outlines in intervening muds (Russell et al, 1999). Like the hydromagnesite stromatolites of the Coorong region, stromatolites in Saldagolu have poor preservation potential.

Hydromagnesite precipitation and biofilm coating throughout the current lake is facilitated by the metabolic activities of a flourishing flora of diatoms and cyanobacteria. Biofilms cover the surface of the stromatolites and much of the littoral zone of the current lake. But precipitated crystals do not occur in direct contact with cell surface, implying CO_2 fluctuations may be driving precipitation rather than direct biomineralization. Interestingly, diatoms rather than cyanobacteria dominate the phytoplankton assemblage in the current surface waters of the lake and each year take up all the available silica (Russell et al., 1999). Silica averages 16 ppm in the wells and springs about the lake yet is below detection limit (1 ppm) in the lake

surface waters. Opaline diatom tests rapidly dissolve out of the consolidating stromatolites and are rarely found as body fossils in any of the exposed hydromagnesite cliffs about the lake edge, once again a similar situation to that found in the hydromagnesite-aragonite lakes of the Coorong.

Lake Tuz, Turkey (Tuz Gölü)

Lake Tuz (*tuz* = salt; aka Lake Sereflikochisar) has an elevation of 905 m asl and a water full area of 2,600 km². After Lake Van, it is the second largest lake in Turkey (Figure 4.24) and occupies the lowest part of a fault-defined (transtensional) endorheic depression in the arid Central Plateau. Unlike Vangolu, much of the current lake floor is a salt-crusted saline pan for at least six months a year, with a small area of perennial brine along its eastern higher-relief edge.

To the east of the lake lies a mountainous highland of metamorphics dominated by granites and gneisses. Highlands to the north are composed of sandstones and shales, andesitic and basaltic volcanics lie to the northwest, ophiolite hills lie to the west, and rhyolitic tuffs and andesites constitute the lower relief hills to the south and southeast. Flatter areas of the Konya drainage basin between these highlands are covered by gypsiferous lacustrine marls of various Neogene ages (Figure 4.30).

At some 350 mm/year the area receives the lowest annual precipitation in Turkey, while potential monthly evaporation ranges between 1175 and 1390 mm in a yearly cycle. Natural river inflow to the lake depression totals 88×10^6 m³/yr and comes from three main rivers (Peceneközü, Uluiрмаk and Insuyu). Each year a discharge from the artificial Konya drain releases around 75×10^6 m³ of wastewater into the lake.

Maximum brine depth in the lake is 1.5 m, attained in the spring when meltwaters reach the lake from the adjacent highlands. Evaporative evolution of the natural inflow brines shows a continuous trend from Ca-HCO₃ rich spring waters to Na-SO₄-Cl rich brines with considerable variations in ionic proportions in inflow brines related to lithologic variations in the drainage area. There were times in the Late Pleistocene (20-17 ka and 13 ka) when lake levels were 15 metres higher than today and the Tuzgolu depression was filled with permanent water up to 16 metres deep (Kashima, 2002). Older, but undated, Quaternary shoreline terraces occur some 100 metres above the present lake level (Erol, 1978).

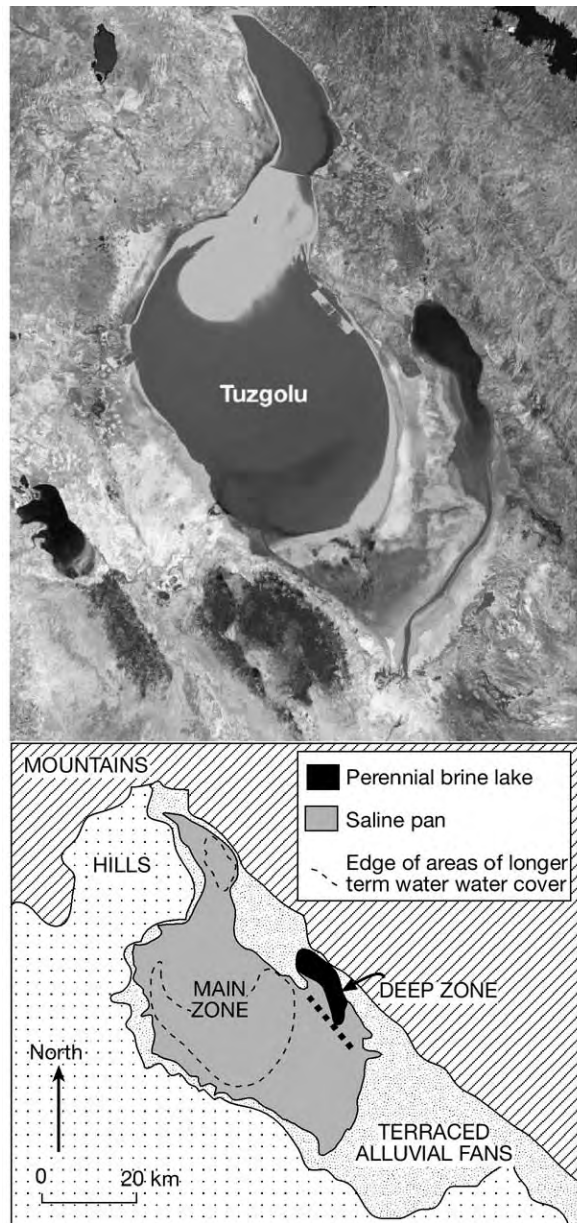


Figure 4.30. Tuz Golu, Turkey. Shows a partially desiccated stage in the lake when much of the saline pan is still water covered. The sill separating the main zone from the deep zone is clearly exposed. The manmade drainage channel and its waste plume cutting into the southwestern part of main zone is also visible. The obvious linear separation between the mountains to the northeast and the terraced alluvial plain reflects the transtensional fault-controlled origin of the Acigolu depression (image courtesy of NASA).

Each year, by mid summer most of the lake floor has dried up and only a few small areas retain permanent surface water in spring-fed seep ponds or brackish marshes (aka moat facies). The largest area of pooled perennial brine lies south of the town of Sereflikochisar, in the eastern part of the lake. It has a permanent brine-covered area of 35 km² called the “deep zone” and it expands with each snowmelt in the nearby mountains. It is separated from the “main” salt pan, which constitutes much of the rest of the lake surface, by a low salt crusted ridge (Figure 4.30).

Waters covering the “main” zone are \approx 70 cm deep in spring, but dry out in summer to early autumn and leave behind a 1-30cm thick halite crust over an area of 1200 ha, which is mined by a large saltworks on the lake shore (\approx 750,000 tonne/year) to provide 55% of Turkish salt needs. In contrast, waters in the deep zone are permanent, are not halite saturated and can be as deep as 1.5 metres in the spring.

Evaporite mineralogy in the seasonal salt crust in the “main zone”, especially in the northern arm studied by Camur and Mutlu (1996), consists of mixtures of halite, gypsum, aragonite and calcite. The unconsolidated sediment for 1-30 cm below the salt crust starts with a gypsum-, huntite- and magnesite bearing levels up to 25 cm thick, with polyhalite in the more central parts of the main zone. This is underlain by a layer up to 35 cm thick composed of gypsum, huntite, magnesite, illite and smectite-bearing sediments. Holocene dolomite was documented in shallow sediment cores from the central parts of the main zone (Irion, 1968) and minor anhydrite was noted along the northern edge of Tuzgolu by Camur and Mutlu, (1996). Each summer halite cumulates cover the chevrons of the salt pan crust and coarsely -crystalline lenticular and prismatic gypsum crystals (0.3 - 4 cm diameter) are commonplace in the sediment immediately beneath the salt crust (up to 50% by volume). They constitute a “desert rose” unit in a micritic matrix made up of varying proportions of magnesite, huntite and dolomite mixed with siliciclastic detritus.

The interaction of microbialites with the recycling salts in the “main” zone has produced disc-like structures in dried halite known as salt biscuits (Mueller and Irion, 1969). Biscuits are 2-7 mm thick crusts, with diameters between 3 and 8 cm. The upper surface tends to be smooth and covered with cumulates of small halite cubes (<2 mm diameter), the lower surface is made up of larger downward-aligned halite crystals up to a centimetre long. Irion and Mueller (1968) concluded that the biscuits are founded halite rafts with ongoing underside growth fed by ongoing capillary rise after surface waters had receded.

A constant freshened, but unnatural, inflow today reaches Tuzgolu via the 150 km long Konya drain (completed in 1974). It feeds a saline sump that drains agricultural wastewater from the Konya irrigation area to the south. In addition, all untreated sewage from Konya city and several hundred industries are periodically released into this drainage channel. This means that each year agricultural waste exuded from the channel into the lake includes the leached residues of more than 1105 tons of pesticides and 446 tons of fertilisers applied to the Konya basin. Industrial waste includes outflows from dairy farms, aluminium and copper plants, leather processing units and a LPG bottling plant. Large amounts of nitrogen, oil, phosphorous, sulphur and organic wastes, as well as heavy metals, including borax, zinc, iron, lead, arsenic, cadmium and mercury today reach the lake depression through the Konya channel. Yet the lake brine is recovered annually for salt manufacture in pans about the lake edge, which supply more than half of the domestic and industrial salt consumed in Turkey. Pumping of industrial and agricultural wastes into salt sumps is an environmental quandary, typical of many developed agricultural and industrial areas in semi arid areas across the world. Only in the last decade have the some of the required hydrological and groundwater studies begun to assess wastewater and salinization effects in such basins in Australia, Egypt, Israel, Mexico, Turkey and the USA.

Lake Aci, Turkey

Acigolu lies in the next major intermontane valley to the northeast of Salda Lake (Figure 4.31). It is a perennial brine lake surrounded by extensive saline pan and mudflat sediments. Like Tuzgolu, the lake is fed by two distinct water sources, less saline Mg-HCO₃ groundwater and local Na-SO₄ springs, while the final lake waters are Na-Cl-SO₄ brines (Mutlu et al., 1999). Differences in composition of the two inflow waters are attributed to different water cycles and different intensities of rock-water interactions.

Dry mudflats in Acigolu are composed of gypsum, calcite, dolomite and huntite, together with clastics. In contrast, wet or brine-soaked mudflats exist locally around saline Na-SO₄ springs and are characterised by efflorescences of halite, bloedite; thenardite and/or mirabilite. Laminated to structureless gel-like sediments composed of aragonite and organic matter typify the bottom sediments of areas of perennial lake brines along the fault controlled southwestern margin and are also zones where halobacteria flourish year-round (Mutlu et al., 1999).

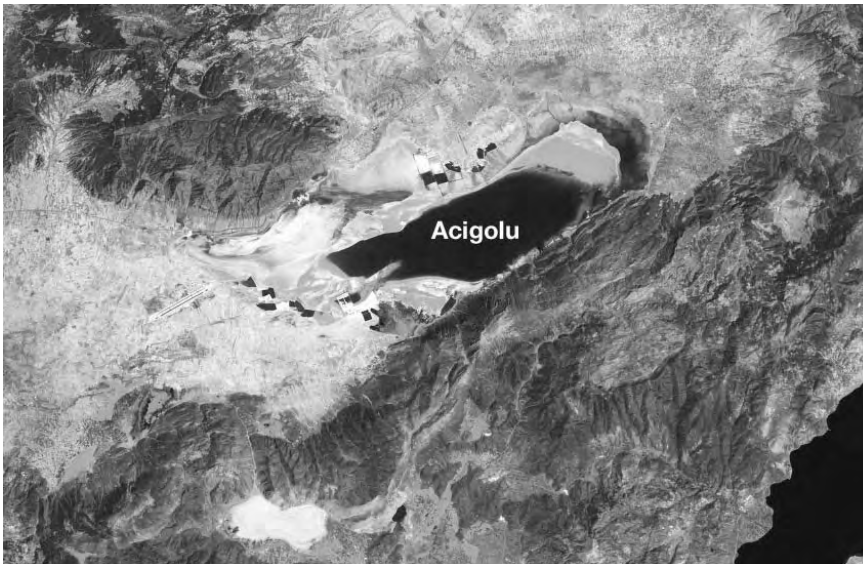


Figure 4.31. Acigolu, SW Turkey. Older strandlines are visible in the north of the lake, while an area of shallow perennial brine (aragonite+organics) occupies the more southerly portion of the lake depression. Part of the fresher water Lake Burdur is discernible toward the bottom right of the image. Near the lower bottom centre of the image is the white salt crust of the now dry Yarash Lake. Numerous faults and lineaments are visible in the surrounding highlands and control the linear orientation of the southwest lake edge (Landsat image courtesy of NASA).

Lake Urmia, NW Iran

Lake Urmia, formerly Lake Rezaieyeh, is a shallow perennial saline lake in the lowest part of an endorheic depression in Azerbaijan Province of northwest Iran. Surface waters have a current elevation of slightly more than 1,280 m asl and surface salinities range annually from 80 to 280‰. The lake is some 140 km long and 80 km wide, with an area of 4,700 - 6,000 km². It is the largest lake in Iran and, with a brine volume around 28 km³, it is also one of the world's largest perennial hypersaline lakes (Figures 4.24, 4.32a). Average water depth is around 5 metres, which deepens to 8 metres in the south, where the maximum water depth is 15 metres.

Lake Urmia lies at the bottom of an endorheic basin located further

along the same alpine collision suture as the Turkish lakes. It was created as the Turkish and Eurasian plates were squeezed sideways along very active strike-slip fault systems. Palaeozoic metamorphics crop out in the Zagros Mountains to the west of Lake Urmia. Infracambrian sediments lie to the south, while the northern and northeastern lake margins are characterised by outcrops and subcrops of the evaporitic Middle Miocene Fars Formation and underlying marine limestones of the Lower Miocene. Several Miocene salt domes pierce the surface of the lake's drainage basin.

Climatically, the lake lies in a semi-arid, almost desert environment, with precipitation averaging 30 cm per year. The climate is harsh with winter temperatures

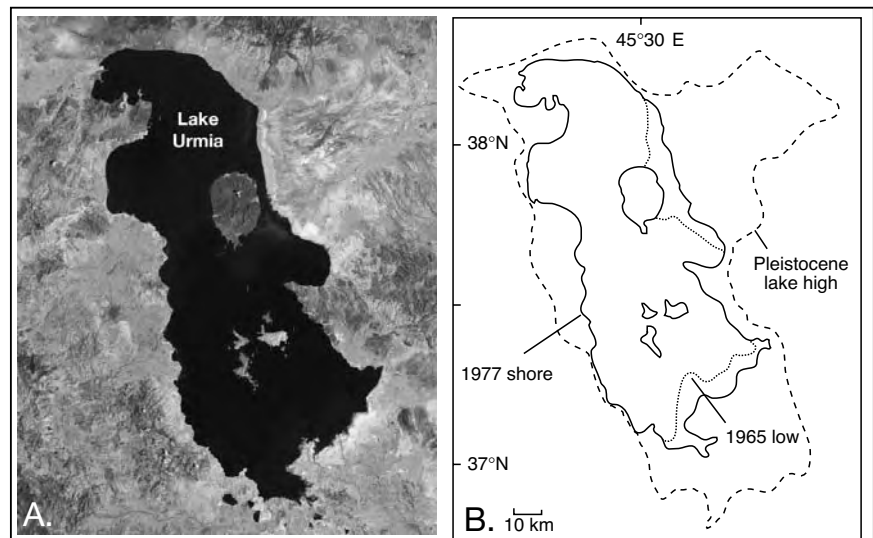


Figure 4.32. Lake Urmia, Iran. A) General distribution of lake sediments clearly showing the Talkerud alluvial braid plain and fan delta to the northwest of the lake and exposed strandline sediments along parts of the northwest and southeastern shores (Landsat image courtesy of NASA). B) Varying extent of Lake Urmia, northwest Iran, shows outline of the lake as defined by its 1977 AD water level, as well as the 1965 AD shoreline and the much more extensive freshened lake that formed during the Pleistocene (in part after Kelts and Sharabi, 1986).

down to -20°C and summers up to 40°C . Surface inflow from the $52,000\text{ km}^2$ drainage basin is strongly seasonal, driving an annual lake water level fluctuation of up to 1-2 metres, especially during the spring melt when the Talkkeh and Simineh Rivers discharge around $57\text{ m}^3/\text{s}$ into the lake (Figure 4.33). By summer the inflow drops to $1.7\text{--}3.7\text{ m}^3/\text{sec}$ and lake levels fall once more.

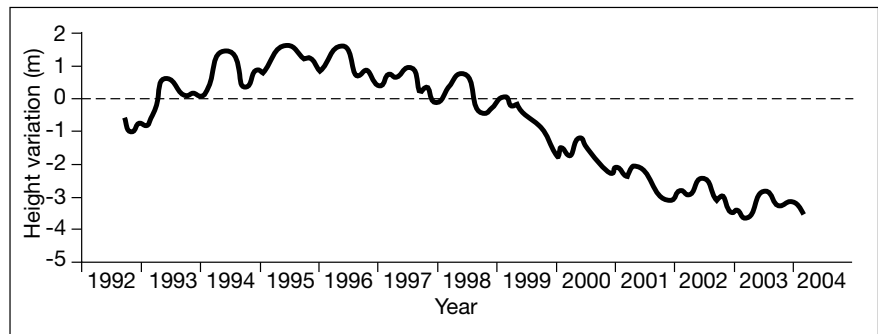


Figure 4.33. Water levels changes in Lake Urmia, Iran, for the period 1992-2004. (replotted from altimetry derived from TOPEX/POSEIDON and Jason-1 satellite passes by the USDA and last accessed on April 2, 2004 at <http://www.pecad.fas.usda.gov/cropexplorer/>).

Topographically, the surrounding region is either plateau or mountain. Mountains west of the lake have peaks that exceed 3350 metres making that side of the lakeshore somewhat steeper. Salt flats and the fan deltas characterise lake sediments along the southern and western shores. Slight changes in water level can drive drastic migrations of the strandline across the evaporitic mudflats of the lake. In 1977 the lake had a water level of 1284 m asl, while in 1965 the water level had hovered around 1278 m; the lake level had risen by 6 metres in a decade and the shoreline had migrated 5-10 km (Figure 4.32b). Similarly, there was a 5 metre fall in lake level from 1996 to 2003 (Figure 4.33).

Modern lake floor sediments are mostly aragonitic pelletal laminites/mudstones, near identical in appearance, depths of deposition and origin to those of Great Salt Lake, Utah. Laminites in both lakes result from the seasonal biologically-mediated precipitation of aragonite (Kelts and Shahrabi, 1986). When salinity and nutrient levels are suitable, Urmia's surface waters support an abundant summer flora of the green alga *Enteromorpha intestinalis* along with species of *Dunaliella* and *Tetraselmis*. Blooms can be so intense in some years that the water changes colour to a deep green and light penetration is measured in tens of centimetres. The algal bloom is followed quickly by a bloom of the brine shrimp *Artemia salina* (upto 4,000 individuals per litre), which graze the alga. While feeding, the shrimp also ingest particulate aragonite that is precipitating in the lake waters. Thus aragonite in the Urmia laminites occurs both as $10\ \mu\text{m}$ long euhedral prisms in pelagic mud and as the major constituent in sand-sized faecal pellets from the brine shrimp. Both of types of aragonite are interlaminated with organic-rich laminae in a matrix dominated by terrigenous sediment brought to the lake by spring melt. The aragonite is sometimes sufficiently cemented to form cm-thick crusts on and beneath the lake floor. The precipitation of aragonite, rather than calcite, reflects the high Mg/Ca ratio of lake waters (molar ratio 28:1).

At some time earlier in the Quaternary the lake level was lower than today and portions of the lake floor became so saline that gypsum precipitated. At the northern end of the lake this gypsum bed is now some 1.5 metres below laminites of the current subaqueous lake floor. It was interpreted as a sabkha unit by Kelts and Shahrabi, (1986). In other parts of the lake dolomitic mudflats were time equivalents to this now buried gypsum. Oolites shoals formed at the northeast end of the lake but they too are now buried beneath 30 cm of putrid, black organic-rich mud.

The biota and the general spectrum of carbonate sediments found in Lake Urmia is near identical to that of Great Salt Lake, Utah. Like Great Salt Lake, sediments formed on the deeper floor of the perennial saline lake are pelletal aragonite laminates, while shallower sediments accumulated in ooid strandzones or as cemented crusts/beachrocks.

Lake Natron and Lake Magadi, East Africa

These two lakes are probably the most often cited saline alkaline lakes in the geological literature. Both are groundwater sumps, are small and lie just south of the equator in the eastern branch of the East African Rift, which extends for more than 3000 km from the Afar Triangle in the north to Mozambique in the south. Lake Natron, the larger of the two, is in northern Tanzania, at latitude $2^{\circ} 20' \text{ S}$, and longitude $36^{\circ} 10' \text{ E}$; it extends some 55 km N-S and 24 km E-W, with a total surface area of about 950 sq. km. Its northern shore touches the territorial boundary with Kenya. Lake Magadi lies within Kenya slightly to the north of Lake Natron at the bottom of a steep-sided valley, which is the lowest point in the eastern or Gregory Rift Valley (Figure 4.34a). It extends roughly 20 km N-S and is up to 6 km wide. Both lakes lie at an altitude of some 600 m above sea level and are surrounded by plateaus and active volcanoes reaching to more than 3,000 m asl (Figure 4.34b). With an area of only

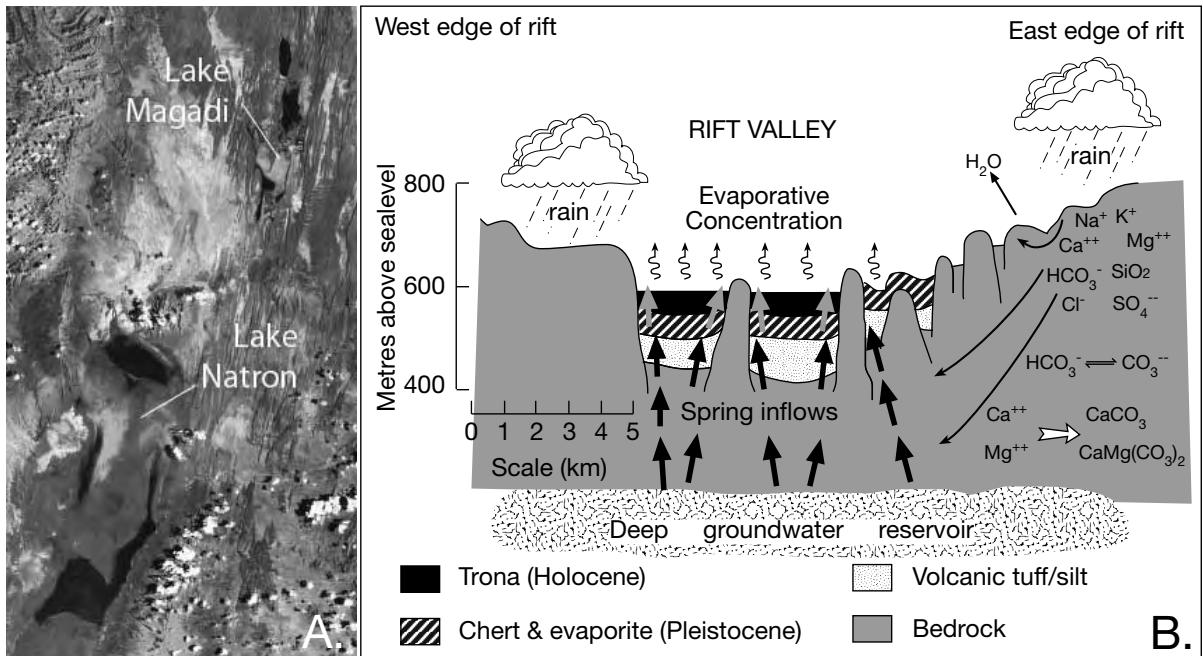


Figure 4.34. Lake Natron and Lake Magadi, East African Rift. A) Position in the East African (Gregory) rift showing adjacent and underlying volcanogenic basement (Landsat image courtesy of NASA). B) Scaled schematic of the distribution of evaporitic lacustrine sediment in the rift valley based on an east-west transect of Lake Magadi (after Jones et al., 1977).

90 km², Lake Magadi is one of the most saline, but also one of the smallest, alkaline lakes in the Rift Valley.

The eastern Rift Valley stretches from Ethiopia to Tanzania and contains numerous endorheic soda lakes of varying salinity. Some lakes are fresh, like Lake Naivasha, others are quite saline Na-CO₃-HCO₃ solute systems like Natron and Magadi. Salinities range from 5% in the more northerly lakes (Bogoria, Nakuru, Elementeria, Sonachi) to around 30% and halite/trona saturation (Magadi, Little Magadi and Natron) in the south of the valley. The pH of surface waters in all is typically above 9, with values ranging up to 11.5 in the more saline alkaline depressions. Hydrographic closure is provided either by location in a volcanic crater or by formation of lake depressions in block-faulted lavas and volcanoclastics. The Rift Valley is volcanically active, with ongoing outpourings of sodic lavas and numerous hot springs (some boiling) about the edges of many of the modern lakes, indicating active hydrothermal circulation. Spring outflows are typically less saline than the lakes they feed and form biological refugia during times of widespread drought.

Climate in the lowermost parts of the rift valley in the vicinity of lakes Natron and Magadi is arid, with high temperatures and an adiabatically reduced mean annual rainfall that is typically less

than 500 mm in non El Nino years. Most precipitation falls in a single rainy season from March to May. Potential evaporation on the rift valley floor exceeds rainfall for most of the year so that the hydrological balance in the drainage region about both lakes is clearly negative. This facilitates the precipitation of aragonite in perennial brine pools about the lake edges and trona in the more central saline pan areas. Air temperatures around the lake can reach 40°C in the dry season, while temperatures can be as high as 66-68°C in dark-coloured mudflat sediment that make up the edge of the moat facies and in the thin brine sheets in megapolygonal saucers in the trona areas.

Both lakes are surrounded by metamorphosed Precambrian basement rocks. Volcanism began in earnest with the Neogene opening of the rift and continues today, with active volcanoes in the vicinity of both lakes. A general rule for volcanoes of the rift valley near Magadi and Natron is: the younger the volcanism the higher the alkalinity. Ol Doinyo Lengai, which is the youngest volcano in the vicinity of Lake Natron (≈20 km south of the lake), spews forth carbonatite lavas that are molten mixtures of sodium carbonate and calcium carbonate salts. Hydrothermal circulation, associated with the numerous active volcanoes and their feeder faults, supplies hot alkaline brines to the many hot springs situated about the edges of both lakes (Table 4.3). More than 20 warm, saline springs, with

temperatures between 32° and 52°C, and release rates between 30 and 300 litres/sec, discharge into Lake Natron from scree slopes adjacent to the salt pan. There is no perennial stream flow into Lake Magadi, but it too has numerous warm surface springs feeding saline brines to the perennial lagoon portions of the Magadi depression (Figure 4.36). Eugster (1970) argued that subterranean seepage from nearby Lake Naivasha contributes a solute load equivalent to that carried by all other saline groundwater springs in the Magadi depression.

Other than spring brines, the only other perennial water source to Lake Natron is the Ewaso Ngiro River, which drains into the north end of the lake. Yet today, no bedload sediment carried by the Ewaso Ngiro reaches Lake Natron. It is almost all deposited in an adjacent swamp created when the river was ponded and dammed behind a recently uplifted horst adjacent to the Shambole volcano. River blockage forced the river to dump its traction/suspended load into the waters of the burgeoning Ewaso Ngiro swamp. River water, minus any sediment load, now continually seeps out of the edge of the swamp into a perennial brine lake at the northern end of Lake Natron (Figure 4.35). The effect of uplift on bedload in Lake Natron implies that mineralogical changes in ancient lacustrine units are not always a response to climatic changes; mineralogy in a lake depression can change due to tectonics.

Brine chemistry

Interstitial groundwaters and hot spring waters come from parent waters with low levels of alkaline earths Mg and Ca, and high levels of Na, Cl and HCO₃ (Table 4.3). This chemistry is ideal for ongoing trona precipitation at higher salinities (Figure 2.12). Rain falling in the drainage basin contains normal levels of Ca²⁺ and Mg²⁺ but on the way to the lake depression the same waters flow over and through highly alkaline and reactive volcanics. By the time these same waters flow out onto the lake as

springs and seeps they have gathered a four-fold dominance in bicarbonate over the alkaline earths (Ca + Mg). They have already passed the calcium carbonate chemical divide and left behind their calcium and magnesium in various pedogenic and phreatic carbonates to become path I brines (Figures 2.12, 4.34).

Chloride in brines in both lakes behaves conservatively, and so its concentration can be used as a brine evolution marker (Eugster, 1970). Chlorine levels show an 18,000 fold increase in concentration in the lake brine compared to river and spring inflow. Yet this is not sufficient to precipitate large volumes of halite within the Natron-Magadi depression, nor does the current warm climate favour the accumulation of natron over trona. Trona is the first Na-carbonate mineral to precipitate in equilibrium with concentrating lake brines. Natron could form as a coprecipitate if the surface brine temperature falls below 25°C (Figure 2.13). But, such low temperatures do not occur in either Lake Magadi or Lake Natron at the times trona precipitates.

As trona forms, there is a marked decrease in the bicarbonate proportion (relative to chloride) in the increasingly saline lake brine. As the brine continues to concentrate, lesser amounts of

	Ewaso Ngiro River	Hot Spring (Natron)	Interstitial brine (Natron)	Surface water (Natron)	Hot Spring (Magadi)	Salt pan brine (Magadi)	Moat brine (Magadi)	Surface water (Nakuru)
Na	7.0	12,166	119,500	104,000	7,000	160,930	64,970	7,500
K	2.3	212	1,470	1,700	75	2,230	1,040	220
Ca	6.5	0.5	n.d.	1.5	0.6	<1	<1	225
Mg	3.7	0.0	n.d.	<1	<0.4	<0.5	<0.5	<0.5
SiO ₂	20	91.0	976	186	36	895	425	200
HCO ₃	48	14,600	3,230	52,000	13,000	237,900	110,820	12,100
CO ₃	0	3,490	94,050	162,700				
SO ₄	2.4	159	2,100	165	52	1680	1,230	50
F	0.2	154	1,440	n.d.	70	n.d.	n.d.	n.d.
Cl	4.0	4,740	71,750	51,970	3,550	112,000	39,900	2,040
Br	n.d.	114	265	n.d.	n.d.	n.d.	n.d.	n.d.
PO ₄	0.08	10	70	400	n.d.	175	22	14
B	n.d.	8.6	88	n.d.	n.d.	n.d.	n.d.	n.d.
TDS	77	29,200	294,000	352,000	24,100	340,000	210,000	22,100
pH	7.0	9.2	10.5	>11.5	9.9	>11.5	>11.5	10.5

Table 4.3. Typical chemistry of waters and brines in saline East African rift valley lakes (ion contents in ppm, cited from various sources listed in text).

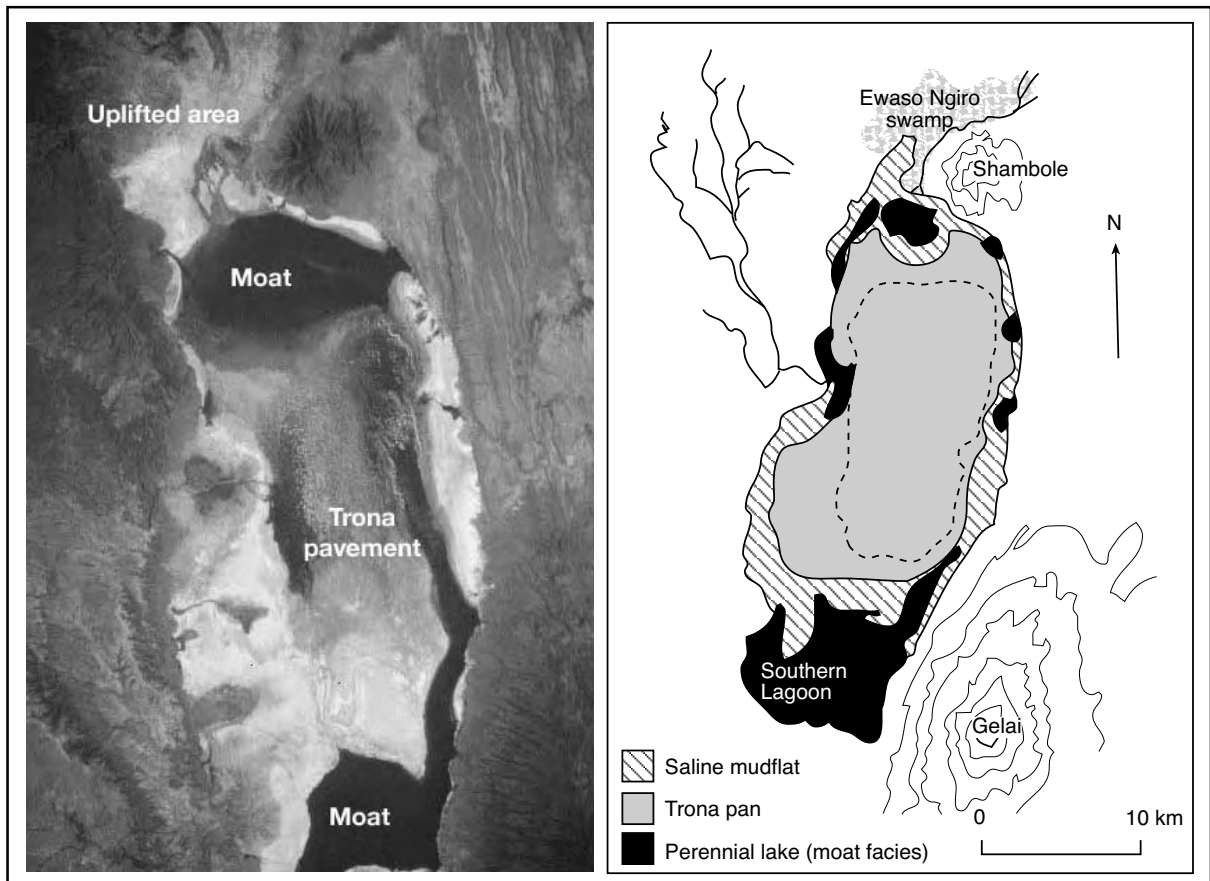


Figure 4.35. Lake Natron. A) Northerly looking view of Lake Natron showing moat facies about the lake edge and the more central trona platform, the water covered area appears pink due to a flourishing haloarchaeal population (Photo courtesy of NASA). B) Geological setting of Lake Natron.

trona precipitate and ultimately halite should crystallise. But, the high humidities maintained over the lake brines in the deep valley bottoms of Lake Magadi and Lake Natron mean surface waters can only rarely attain concentrations where halite can precipitate in large volumes (no more than 5-10% halite is preserved in the trona crusts in either lake). Higher temperatures at the time the various Na-carbonates precipitate from the lake brines means thermonatrite (not natron) is the other sodium carbonate accumulating in both lakes (Figure 2.13); only at rare to minor levels in Magadi, but it can locally constitute up to 30% of the trona pavement in Lake Natron.

Interestingly, the concurrent fluoride increase between inflow and the trona stage of the lake brine is only 7,200 times (compared to 18,000 in chloride in the same waters), indicating its removal as a sodium salt. A lack of Ca in lake brines prevents direct fluorite precipitation in this fluorine-rich hydrothermal province. Accordingly, fluoride concentrations in the interstitial

brines of the trona^{4.2} platform can be more than 1400 ppm. This, and the elevated Na levels in the concentrated lake brines, leads to the precipitation of sodium fluoride salts in the trona crust that include kogarkoite ($\text{Na}_3\text{SO}_4\text{F}$) and villiumite (NaF) (Darragi et al., 1983; Eugster, 1986). Prior to its documentation in a Lake Natron trona crust, kogarkoite had only been observed in hydrothermal deposits.

Holocene sediments

Spring and ephemeral stream-fed carbonate lagoons form permanent water-filled depressions that line the edges of the trona pan in both lakes. Unlike the more central trona depositing saline pan, the lagoons never dry up and are sometimes described as a “moat” to the lakes (Figures 4.35, 4.36). In Lake Natron, which

^{4.2} Use of fluoride-rich trona from Lake Natron as a food tenderiser has led to widespread dental fluorosis in the local population (Mabelya et al., 1997).

year-round contains more freestanding water than Magadi, the lagoon water depths during the wet season can be upwards of 10 m. These perennial brine lakes are floored by black micritic laminites, which are mostly composed of aragonite and dolomite peloids and can contain up to 16% TOC. The lagoon floor laminites and nearby pisolites and cemented crusts of the spring seeps, constitute a carbonate “moat” facies. Although located about the lake edge, this laminated carbonate unit is deposited in waters deeper than the ephemeral brine sheets forming the trona pavement lake centres. Less saline areas near spring seeps in the moat lagoons in both lakes can contain thriving populations of *Tilapia alcalica*, a small fish that survives at temperatures of 39°C and pH up to 10.5. Away from the spring-freshened areas, the lagoon bottom waters and pore waters in pavements become too saline and too anoxic to support vertebrates and a well-adapted halophilic microbial biota flourishes, including endemic alkaphilic archaea, (Chapter 9).

Trona accumulates in the central portions of both lakes as flat pavements composed of stacked saline pan crusts. Some 2,100 km² of the northeastern part of Lake Natron is covered by an impure trona bed averaging 1.5 metres thick (Figure 4.35). The Lake Magadi trona pan is some 74 km² in area and is 7 - 50 m thick, known locally as the “Evaporite Series” (Figure 4.36). It is made up of cm-scale stacked trona-detrital couplets (Baker, 1958). Light-coloured trona layers are composed of rosettes and splays of upward pointing, growth-aligned trona crystals. Thin bands of finer trona coloured by dark, mainly windblown dust separate the crust layers from each other. Even as it stacks and dissolves, each layer retains some porosity between interlocking growth aligned crystal splays.

During the wet season the trona pans in both lakes are covered by shallow brine sheets (<1 m

deep) and are subaerially exposed for the remainder of the year. When not covered by lake brines, the modern surface of both the Magadi and Natron trona pans are rock hard and occupy topographically higher positions compared to the water surface of the adjacent perennial lagoons. This “moat” geomorphology is used as a natural protection from predators by flamingoes that, once waters recede from the trona pan, nest in large numbers on the platform, especially in Lake Natron (see flamingo connection in Chapter 9).

Trona saturation is achieved when the shrinking brine sheets are 2-10 centimetres deep. At that stage the trona prisms grow upward from the pan surface as cm-scale aligned elongate blades and splays. Interlocking of the crystal splays give the accreting trona sheet an inherent strength that allows it to support expansion polygons or pressure ridges, with saucers up

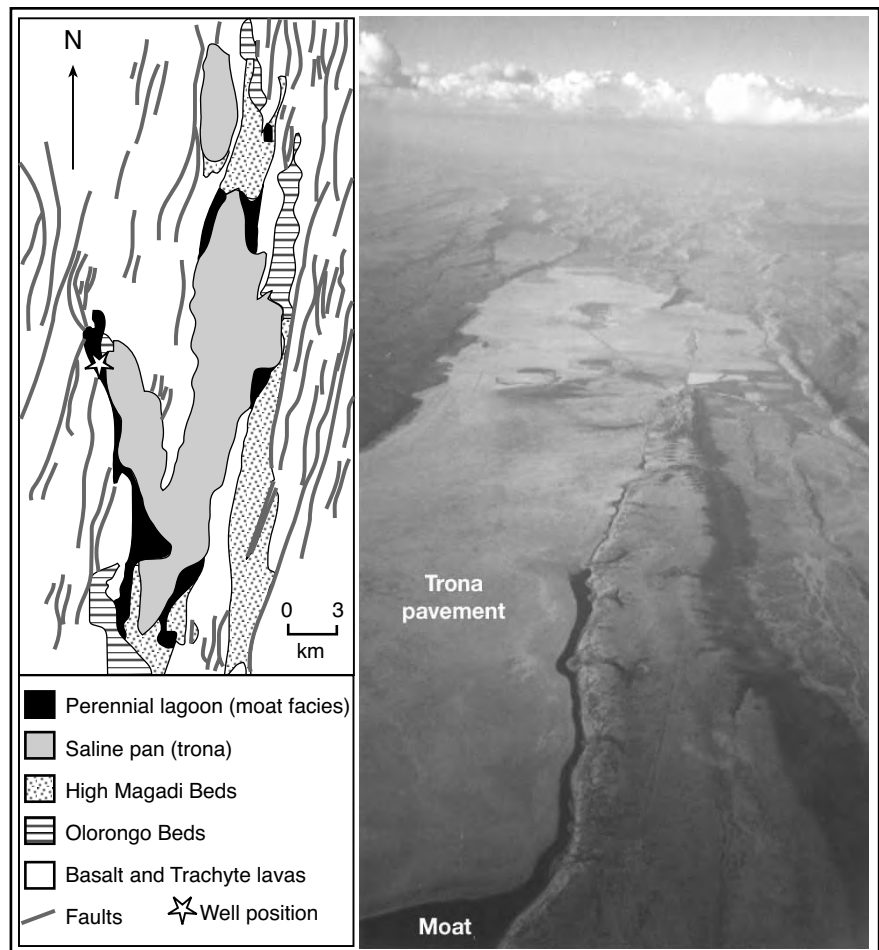


Figure 4.36. Depositional setting of Lake Magadi. Aerial view looks north and shows dark coloured moat facies of perennial lagoon defining lake edge. The well position locates the core in the High Magadi beds documented in Figure 4.37.

to several tens of metres wide and ridges up to a metre high. Ridging is the result of pavement overthrusting, driven by the sideways expansion of trona layers jostling for space in the various growing crystal pavement. The resultant cracking and thrusting of the layers cuts the trona pavement up into a series of overthrust-edged saucers, with small bright pink brine pools in the centre of each polygon; the colour is the result of a haloarchaeal bloom (see Chapter 9).

At the same time the ridges are forming, thin films or rafts float on the surface of the brine sheet. Trona rafts contribute only a minor amount to the total trona volume in the pavement unit, but are important in controlling mineralogy as they slow evaporation and raise the temperature of the underlying brine through a greenhouse effect. Temperatures of 60°-65°C can occur annually within thin brine sheets immediately below the trona rafts and so drive precipitation of thermonatrite (Figure 2.13). As brine level continues to fall, the upward-growing bottom-nucleated trona splays break through the floating rafts. Prior to complete drying, high winds can break up and flounder the rafts or blow them into heaps about the local strandzones of small brine pools.

Finally, the brine level falls below the surface of the newly formed trona crystal crust and the annual primary depositional cycle is complete. Small amounts of trona continues to crystallise as minor amounts of interstitial cement below the surface of the exposed pan. When the pan surface dries out, the brine level stays very close to the surface of the trona pavement. Even during exceptionally dry years it drops no more than 5 cm into the trona layer. Whenever the surface of the layer is exposed during the dry season it can be covered by a thin layer of windblown material.

With the next rainy season the water table rises as the pan is once again covered by water. Initially, these inflow waters are fresh and undersaturated with respect to the pore waters of the trona pavement. So they float above the top of the dense interstitial brines and any trona crystals poking up into these freshened waters start to dissolve. Last season's crystals are truncated by the influx of freshened waters. During this freshened stage, windblown clays and other detritus on the pavement surface can be retransported by waves. Then the wet-season rains cease and the trona precipitation cycle begins anew. Each season a trona layer 2 to 5 cm thick forms on the saline pan in both lakes but subsequent seasonal dissolution means the average Holocene accumulation rate for Lake Magadi trona is at most 0.4 cm/yr. The much thinner layer of Holocene trona preserved in Lake Natron, implies dissolution levels are even higher compared to Lake Magadi. The annual trona crop in Lake Magadi is around

1.5 million tonnes/year, but the bulk of this crop ($\approx 75\%$) is recycled by pan dissolution each wet season. Lake Magadi has been described as an "ephemeral saline lake at the peak of its trona productivity" (Eugster, 1980b). Trona in Lake Magadi has been extracted at various times from 1914 until today using dredging barges. Replenishment of trona in the lake is so rapid that at the rates the Magadi trona is mined (230,000 tonnes/year) it is a renewable resource (Chapter 11).

Late Pleistocene sediments

Aside from the Ewaso Ngiro River, two other rivers flow toward the shores of Lake Natron, the Peninj and Malambo Rivers. Today, these rivers are ephemeral and any surface water sinks into the riverine sediment fans well before it ever reaches the current lake strandline. Some 9,000 to 10,000 years ago during the last high water stage, these rivers, and the Ewaso Ngiro, deposited fan deltas along the edge of a much fresher and higher Lake Natron. Today, these sediments form "hung" delta lobes on the surrounding landscape located well back from the lake shoreline, some 10 to 60m above the present lake level. In earlier lake-full times the flood sands from these highstand deltas probably extended further out into the lake centre and so may now directly underlie the trona-hosting sediments of the lake centre and act as potential aquifers for fresher groundwaters that prevent the accumulation of thick trona units in Lake Natron.

At the time the fan deltas were active Lakes Magadi and Natron were both deeper, larger and fresher water bodies. At such times in the late Pleistocene the two lakes sometimes merged into a single pluvial lake (Hilaire-Marcel et al., 1987). Studies of stromatolites and tufa terraces from various high lake levels in the vicinity of both lakes show that the most recent high lake levels were part of a two-stepped climatic optimum that occurred some 12 to 11 ka (Williamson et al., 1993; Icole et al., 1990). The first humid period (between 12 and 11 ka) created a lacustrine highstand that topped the 635m-elevation barrier (msl) separating the Magadi and Natron depressions. Between 11 and 10.7 ka the lake level dropped below the barrier, once again separating the two lakes. A second maximal high stand occurred around 10 ka, possibly once again joining the lakes. Since that time, and throughout the Holocene, the lake levels have been consistently near their present levels and some 60 m below their former highstands.

The High Magadi Beds were deposited as diatomaceous mudstones when lake waters were more than 13 to 14 metres above the present level and relict shorelines from that time are

still mappable (Figure 4.36). Lake sediments of that time are mostly bedded volcanic muds and cherts, typically deposited as lakefloor laminates with abundant fish scales visible on partings. A 8.7m core taken from this highstand facies in the region of the Flamingo Nursery on the northern edge of Lake Magadi recovered High Magadi beds that were deposited from 40 to 9 ka (Figure 4.37; Damnati et al., 1995; Williamson et al., 1993). The lower (870–740 cm) and upper (295–6 cm) units in the core consist of laminated silts made up of alternating layers of magadiite (zeolite-rich) and organic-rich muds (TOC > 5% dry weight). The middle unit (295–740 cm) contains homogenous inorganic clay silts that are unlaminated, suggesting the lake was not stratified at that time. The upper laminated unit was deposited 12 to 9 ka, the middle unit \approx 23 ka, while the lower laminated unit contains sediments as old as 40 ka. Each unit is separated from the other by a thin sand that is thought to mark a hiatus in chemical sedimentation and to be a flood sand from the feeder deltas.

The laminae episodes in the core indicate times when a relatively deep lake was chemically and thermally stratified. Light laminae in the couplets are in turn comprised of couplets. Each light layer is made up of a microlayer rich in detrital elements (quartz and feldspar) and broken diatom frustules that is overlain by a microlayer of magadiite (Damnati et al., 1995). The dark lamina in each couplet is composed of a microlayer made up mostly of well preserved diatom frustules, covered by a layer of microspherules (probably microbial) associated with autochthonous organics generated in the lake waters. White lamina indicate a more humid season climate and dark laminae indicate drier climatic conditions in the lake depression. Variations in lamina thickness can be tied to year to year variations

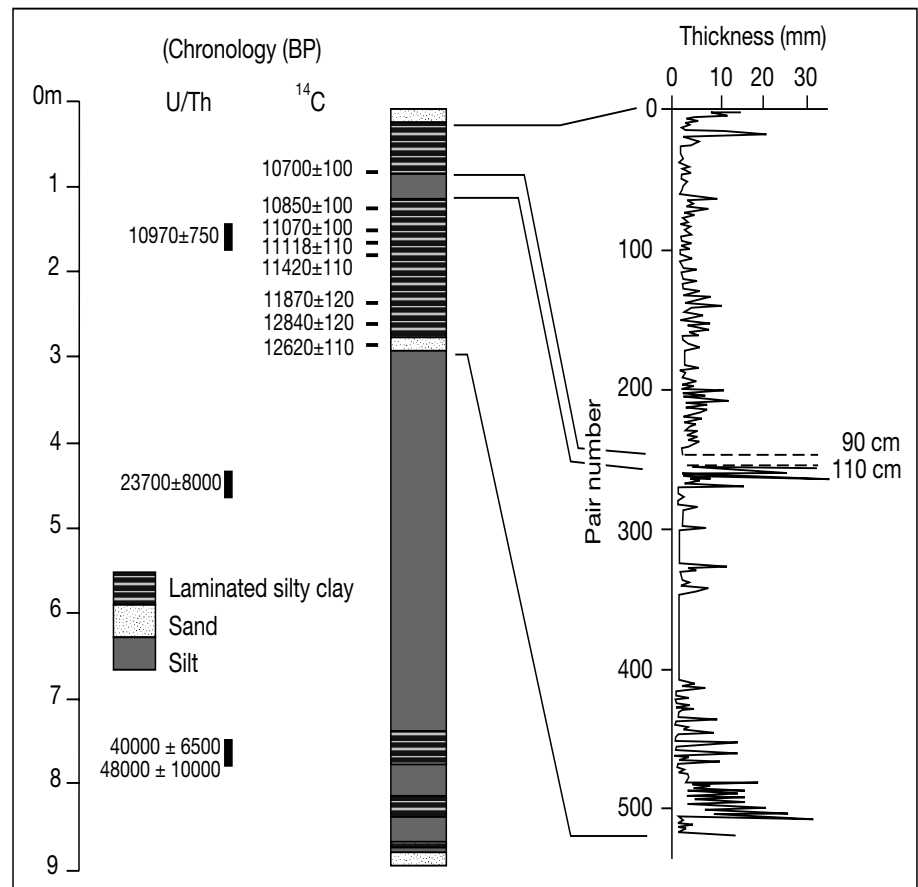


Figure 4.37. Core in the High Magadi beds, Lake Magadi (see Figure 4.36 for location; after Damnati et al., 1995).

in monsoonal intensity and to ENSO years. These Pleistocene laminae are very similar to those accumulating in Lake Van today and the general lake hydrology and humid climates are probably comparable, although one forms in a transtensional tectonic regime and the other is part of a rift valley fill.

Two hundred kilometres north of Magadi is Lake Bogoria, a permanent freshwater lake, which today receives more fluvial inflow than either Magadi or Natron. Lake Bogoria is located in the lower part of what is locally an asymmetric rift valley with active fan deltas forming along the steeper gradient eastern side of the lake, Gilbert-style deltas typify Holocene deposits on the less steep western side and diatomaceous laminae are accumulating in the deep lake centre. It is probably a Holocene counterpart of the Late Pleistocene situation when the High Magadi beds were deposited.

An important general observation for saline systems, based on the African Rift valley lakes, is that perennial continental lakes

do not usually deposit bedded evaporites at the same time that they deposit thick fluviodeltaic successions. Nor do all lakes in a rift valley accumulate evaporites at the same time. Episodes of fluviodeltaic deposition and thick evaporite deposition are separate in time and space – a restriction inherent in the isolated lake hydrology needed to precipitate evaporites. That is, ancient lacustrine evaporite beds occurring in separate but adjacent basins are not necessarily time equivalent. And, it is almost impossible to form evaporites when the lake waters are diluted by fresh water carrying siliciclastics into deltas. However, the time intervals resolvable in the siliciclastic-to-evaporite transition in the African Rift Lakes are less than a few thousand years. In pre-Quaternary lacustrine deposits, such as the Eocene Green River Formation, the two sedimentation styles may appear syndepositional and are easily mis-correlated.

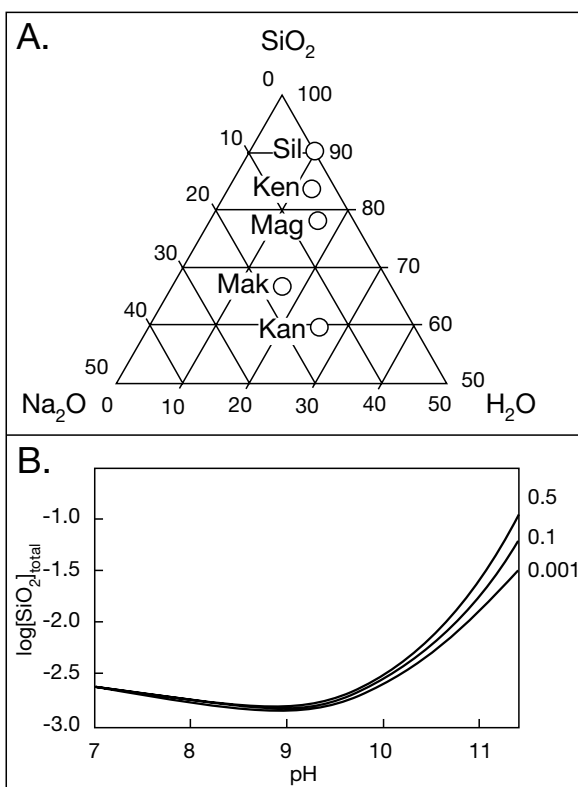


Figure 4.38. Magadiite chemistry. A) Sodium silicates minerals plotted in the upper part of the ternary diagram $\text{Na}_2\text{O}\pm\text{SiO}_2\pm\text{H}_2\text{O}$ showing the position of various hydrous sodium silicates related to varying proportion of the constituent water silica and sodic contents (Ken, kenyaite; Kan, kanemite; Mag, magadiite; Mak, makatite; Sil, silhyrite). B) Concentration of $[\text{SiO}_2]_{\text{total}}$ at equilibrium with magadiite as a function of pH at ionic strengths of 0.5, 0.1 and 0.001 mol Na^+ L^{-1} , 25 °C (after Dietzel and Leftofsky-Papst, 2002).

Diagenesis - magadiite and evaporitic chert

Neoformed sodium silicates (especially magadiite) accumulate in alkaline carbonate-rich hydrogeochemical environments, especially in organic-rich diatomaceous laminites of the freshened stages of soda lakes. Such sodium silicates were first documented in the High Magadi beds (Eugster, 1969, 1980b; Baker, 1958) and also occur in the High Natron beds. There are three sodium silicates in the High Magadi beds: magadiite - $\text{NaSi}_7\text{O}_{13}(\text{OH})_3\cdot\text{H}_2\text{O}$, kenyaite - $\text{NaSi}_{11}\text{O}_20.5(\text{OH})_3\cdot\text{H}_2\text{O}$, and makatite - $\text{NaSi}_2\text{O}_3(\text{OH})_3\cdot\text{H}_2\text{O}$ (Figure 4.38a). Of these, only magadiite occurs in substantial quantities, typically as beds, mounds and nodules. Kenyaite, never occurs as beds, but is not uncommon as nodules in the bedded magadiite laminites of Lake Magadi. Some magadiite nodules have kenyaite at their centres, perhaps implying kenyaite can be created by the weathering of magadiite.

To date, magadiite has been found only in Quaternary alkaline lacustrine settings. In addition to Lake Magadi, Quaternary magadiite has been found in Lake Bogoria, in Lake Chad in western central Africa, Alkali Valley playa in Wyoming, and Trinity County in California (Sebag et al., 2001). On a longer time scale, ancient Magadi-type (crocodile skin) chert has been found in many ancient lacustrine basins, in the Jurassic of Wyoming, the Proterozoic Callana Beds of the Adelaide geosyncline in South Australia, and in Precambrian banded iron formations in Western Australia (see also Table 7.11).

Conditions associated with the precipitation of magadiite from lake brines in Lake Chad, and probably most other soda lake occurrences including Lake Magadi are (Sebag et al., 2001); 1) elevated alkalinity (pH >9), 2) high concentrations of dissolved silica (up to 2700 ppm), 3) incorporation of sodium ions into the silica lattice that precipitates at the time of supersaturation. Depending on the concentrations of Na and Si in the brine, the various sodium silicates will precipitate (Figure 4.38).

Bedded magadiite is widespread in High Magadi laminites, it precipitated in the Pleistocene when Lake Magadi was deeper, fresher and density stratified. Most of this magadiite is an authigenic phase precipitated during shallow diagenesis via the interaction of alkaline brines with reactive siliceous materials such as volcanic glass and zeolites (Jones et al., 1967). Even today, hydro-sodium-aluminosilicate gels precipitate about the edge of Lake Magadi where saline spring waters first emerge. With shallow burial the gels convert to analcime, erionite, and magadiite.

Two mechanisms are thought to drive the precipitation of the sodium silicates. One is intense evaporation, so the resulting

sodium silicates are intimately associated with evaporite indicators, such as evaporite splays and dissolution breccias with evaporite pseudomorphs and moulds in the magadiite host. The other is the pH decrease that occurs when a brine comes into contact with more diluted or more acidic water as when two stratified water masses with differing chemistries mix (Figure 4.38b). Likewise, although the pH change may be as little as 0.5, a decrease in pH from 10.3 to 9.8 lowers amorphous silica saturation more than 500 ppm (Figure 7.58). In contrast to the modern occurrences, the pH and dilution changes needed to form the Pleistocene magadiite of the High Magadi laminites were probably related to the annual overturn of the stratified water mass.

Freshly precipitated, magadiite is a soft plastic white paste (Maglione, 1980), and remains so while bathed in alkaline pore brines. However, when exposed to drying and dehydration it quickly loses its plasticity, cracks and shrinks as it irreversibly hardens into chert. Shrinkage (25% volume change) of the hardening surface creates neoformed chert with a superficial crack network made up of small prisms separated by fissures, comparable to desiccation cracks (Figure 4.39; Icole and Perinet, 1984). It gives the surface of any resulting chert a characteristic “crocodile-skin” or cracked appearance. This is a texture used to support an alkaline lacustrine interpretation in ancient counterparts, such as the crocodile cherts in the Eocene Green River Formation (Figure 4.39). In Phanerozoic hosts, such nodules are readily distinguished from the much more commonplace and nondiagnostic smooth-walled chert nodule, which are widespread in both marine and nonmarine matrices.

Whenever a plastic magadiite horizon in the High Magadi beds is traced from depth (≈ 1 m) to the surface or from subcrop to outcrop, a conversion from magadiite to surface chert is always seen. In the perimeter sediments of Lake Magadi, Eugster (1969) described what he considered to be an impressive syndepositional result of this transformation, namely shrinkage megapolygons up to 50 m across in a bedded chert host with bounding upturned chert ridges up to 2 m high.

More recent work on the same structures by Behr and Röhrich (2000) has concluded the megapolygons do not indicate a response to mineralogical transformation, rather they are part of a suite of prelithification structures in soft siliceous lake sediment. The chert megapolygons are a soft sediment response to strong deformation and local-scale diapirism, as are the associated pillow-chert mounds, chert extrusives along dykes and fault ramps, horizontal liquefaction slides with breccias, slumps, petees, flows and shear-structures in the magadiite

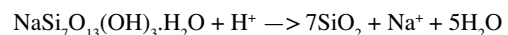


Figure 4.39. Magadiite chert from Lake Magadi showing cauliflower surface texture, also known as crocodile skin.

beds (now all chert at outcrop). Collapse, liquefaction and extrusion of the pre-lithified siliceous matrix were caused by seismotectonic rift activity in the lake basin and it activated fault scarplets and large-scale dyke systems. Seismic activity led to liquefaction and other earthquake-induced intrasediment deformation, especially along fault ramps and on tilted blocks. The textures all indicate the chert megapolygons are a form of seismite and do not indicate volume changes in the transition from magadiite to chert. After liquefaction and extrusion, the exposed magadiite material solidified via spontaneous crystallisation in an environment that was characterised by highly variable pH and salinity.

Since the work of Eugster in the 1960s, three sets of diagenetic processes are now thought to be responsible for driving the conversion of magadiite to chert in Lake Magadi and other soda lakes:

(1) Leaching of sodium by dilute surface runoff during weathering of the High Magadi beds, as evidenced by tracing unweathered beds into outcrop and summarized in the chemical transformation (Eugster, 1969);



(2) Spontaneous release of sodium driving the conversion of magadiite to chert, whatever the nature of throughflushing solutions and environments. In this process sodium is expelled even in the presence of brines; it does not require the fresh water needed for process 1, and perhaps better explains the occurrence of calcite-filled trona casts in cherts and the presence of chert nodules in unweathered magadiite horizons in Lake Magadi (Hay, 1968, 1970).

(3) To this inorganic perspective on the transformation to form chert, Behr and Röhrlich (2000) added a biological one. Based on their field observations and microbiological studies of the cherts in Lake Magadi region, they argue that inorganic cherts are rare at the type locality of Magadi-style cherts. They go on to note that most of the cherts in the Magadi depression are older than the High Magadi Beds and developed from flat-topped calcareous bioherms of *Pleurocapsa*, *Gloecocapsa*, and other coccoid cyanobacteria, along with thinly bedded filamentous microbial mats, stromatolites, bacterial slimes, diatoms, *Dascladiacea* colonies and other organic matter accumulations. Silicification occurred from a silicasol via opal-A to opal-C with final recrystallisation to a chert of quartzine composition. They conclude that metabolic processes of cyanobacteria controlled the pH of the brine and strongly influenced the dissolution-precipitation mechanism that created the chert (Figure 7.58).

Dead Sea, Middle East

The Dead Sea water surface defines what is the deepest continental position (-415 m asl) on the earth's current terrestrial surface. It is our only modern example of bedded salts accumulating on the floor of a brine body where water depths are measured in hundreds of metres. This salt-encrusted depression is 80 km long and 20 km wide, has an area of 810 km², is covered by a brine volume of 147 km³ and occupies the lowest part of a drainage basin with a catchment area of 40,650 km² (Figure 4.40). However, falling water levels in the past few decades mean the permanent water mass now only occupies the northern part of the lake, while saline pans occupy the southern basin so that the current perennial "Sea" is now only some 50 km long. Rainfall in the region is 45 to 90 mm, evaporation around 1500 mm, and air temperatures between 11 and 21°C

in winter and 18 to 40°C in summer, with a recorded maximum of 51°C. The subsiding basin is surrounded by mountain ranges to the east and west, producing an orographic rain shadow that further emphasises the aridity of the adjacent desert (Figure 4.40).

So, until recently, the basin floor was physiographically divisible into two contiguous and permanent brine-covered water bodies, the Northern and Southern basins, largely separated by a diapir-cored shallow sill, the Lisan ridge and joined at the Lisan Straits. But continuing falling water levels means that today the North Basin is the only permanent natural water mass with waters some 320 m deep (Figure 4.42a). The Southern Basin is today a saline pan/mudflat, which would be a subaerially exposed plain, except that brine-filled saltworks now cover much of the former Southern Basin lake. Perennial brine sheets are artificially maintained in these pans by continually pumping of brines from the Northern Basin (Figure 11.10).

The basin floor beneath the waters of the Northern Basin is asymmetric, with the western slopes around 7° and the eastern slopes about 8°. The northern part of the Northern Basin is flatter and smoother than either its eastern and western slopes and is covered by deltaic clays of the Jordan River outfall (Figure 4.40a). Away from the northern slope the outflow zones of the various streams and

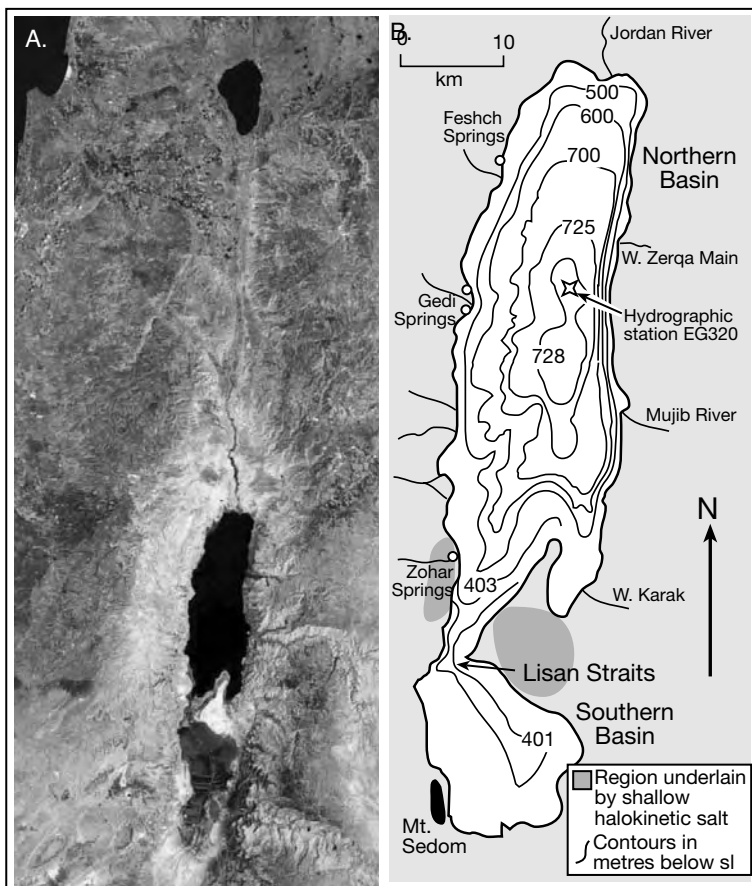


Figure 4.40. Dead Sea depression, Middle East. A) Dead Sea Valley. Image of the depression in the early 1990s, showing the Dead Sea separated into a deep Northern Basin separated by the Lisan Straits from the Southern Basin with its solar ponds. The Jordan River enters the Dead Sea at its northern end. Sea of Galilee is visible in the northern end of image (Image courtesy of NASA). B) Bathymetry of lake floor in metres below sea level, the basin shows E-W basin asymmetry with a somewhat steeper eastern margin.

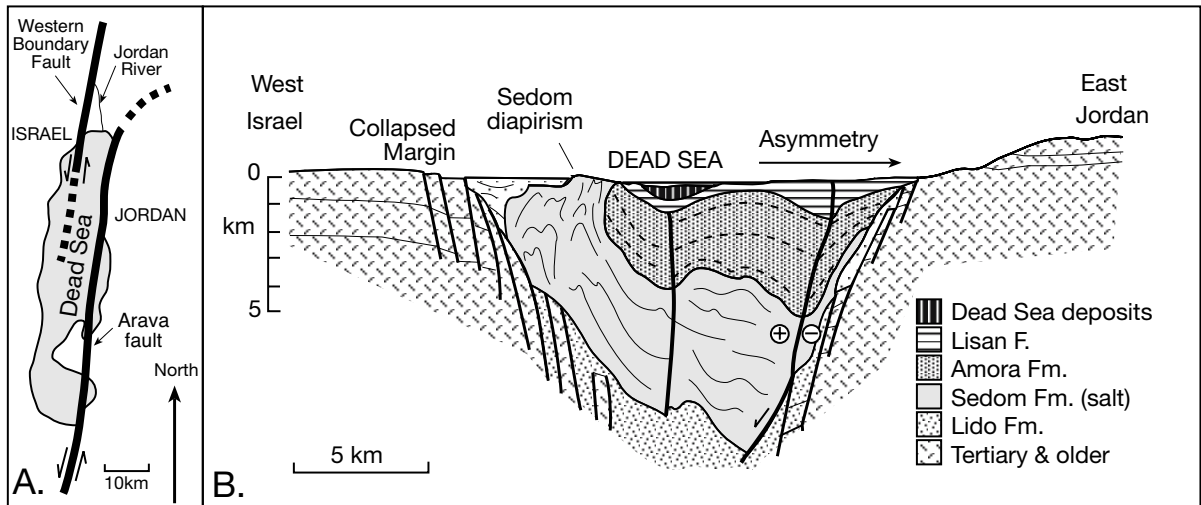


Figure 4.41. Dead Sea, Middle East. A) Plan view show the location of the Dead Sea depression in relation major transensional faulting. B) Schematic cross section of lake geology showing the importance of subsidence, in relation to salt tectonics and strike-slip faults as controls on sediment distribution in the depression (in part after Zak, 1980).

wadis are defined by local clastic aprons or fan deltas, most of which are now “hung” in response to the lowered lake levels (Figure 4.49a).

Geological Setting

The Dead Sea depression is a large strike–slip basin located within the Dead Sea transform; a plate boundary separating the Arabian plate from the African plate and connecting the divergent plate boundary of the Red Sea to the convergent plate boundary of the Taurus Mountains in southern Turkey. Since it formed, 105 km of left-lateral horizontal movement has occurred along the transform. In places where crust is stretched or attenuated, plate stress is accommodated in several rapidly subsiding en-echelon rhomb-shaped grabens separated across west-stepping fault segments. The Dead Sea basin and the Gulf of Elat to its south are the largest of these graben depressions and are separated by the Yotvata Playa basin (Figure 3.31a). The Dead Sea basin fill is 110 km long, 16 km wide and 6–12 km deep and located in the offset between two longitudinal faults, the Arava Fault and the Western Boundary (Jericho) Fault (Figure 4.41a; Garfunkel et al., 1981; Garfunkel and Ben-Avraham, 1996).

Movement began 15 Ma in the Miocene with the opening of the Red Sea and is continuing today at a rate of 5 to 10 mm/yr. The Dead Sea basin floor is more strongly coupled to the western margin (Levantine plate) and is being left behind by the northward moving Arabian plate. Since the Miocene, depocentres in the Dead Sea region have moved 50 km northward along

the shear zone (Zak and Freund, 1981) to create the offlapping style of sedimentation in the Dead Sea–Arava Valley, with a basin geometry reminiscent of the Ridge Basin in California. Continued extensional movement has triggered halokinesis in the underlying Miocene evaporites so that diapirs subcrop along the Western Boundary Fault and its offshoots (Figure 4.41b; Neev and Hall, 1979). Salt in these structures is equivalent to the salt in the outcropping Mount Sedom diapir.

The Holocene to Miocene fill is 8 to 10 km thick beneath the Dead Sea, with at least 90 metres of Holocene fill beneath the Southern Basin. There have been three stages of deposition since the Miocene inception of the Dead Sea valley (Figure 4.41b; Garfunkel and Ben-Avraham, 1996). The bottom 2 to 3 km of fill is made up of continental conglomerates of the Hazeva (Lido) Formation. This represents the first stage of basin fill, during which deposition kept pace with subsidence of the rift. It ended in the late Miocene (8–10 Ma) when differential uplift along the transform edges and rapid subsidence of the basin led to a deep topographic trough. During this second stage (4–6 Ma) the trough was invaded by Mediterranean seawater through the Yizre’el Valley to create a highly restricted arm that was periodically cut off from the ocean and deposited the 2–3 km thick halite-rich evaporites of the Sedom Formation (also known as the Usdum Fm.). This 2 to 3 km-thick section is now halokinetic in the Dead Sea region. In its third stage, the basin was cut off from the Mediterranean seepage to become a closed continental basin. A series of large lakes formed during this time and 3–4 km of fluvial and lacustrine sediments of the Plio-Pleistocene Amora and Samra-Lisan formations were

		Flow	Na	K	Mg	Ca	Cl	SO ₄	HCO ₃	Br
Inflows	Jordan River	400	765	51	276	330	1630	452	436	2
	Mujib River	42	316	40	108	106	573	279	140	0.3
	Zerqa Ma'in River	25	428	56	29	139	709	198	301	7
	Zohar Spring	?	20,500	2,575	22,500	11,400	119,900	1551	130	2,950
	Yesha Spring	3	27,800	3,500	18,700	10,300	11,753	1,060	142	2,206
	Rainfall (µg/l)	-	6.5	0.4	2.5	4.6	14	11.4	-	-
Dead Sea waters	Modern surface	-	39,330	6,500	40,450	17,750	212,600	760	290	6,120
	1960, lower water mass	-	38,510	6,500	36,150	16,380	196,940	580	230	4,600
	1960, upper water mass	-	39,700	7,590	42,430	17,180	219,250	420	220	5,270
	1977, northern basin	-	40,100	7,650	44,000	17,200	224,900	450	270	5,300
	Post-halite crystallizer	-	11,800	21,000	81,700	16,300	302,000	>100	>100	5,000

Table 4.4. Major inputs to the Dead Sea and their solute compositions. Flow is in 10^6 m³/yr and concentrations in mg/l (compiled from data in Azmar and Ergenzinger, 2002; Abu-Jabar, 1998; Karcz, 1987).

deposited (Figure 4.41). The Pleistocene Amora Fm. in the region of the Dead Sea is a fluvio-lacustrine chalky marl with entrained gypsum, anhydrite, sands, conglomerates and thin halite layers. The overlying Lisan-Samra Fm. was deposited in the last large lake that filled the majority of the Dead Sea-Jordan Rift Valley during the later Pleistocene. It consists mostly of finely layered marls, laminites and chinks with gypsum in its more evaporitic portions.

Unlike the marine isotopic signatures of the salts in the Sedom Formation, isotopes in the evaporites of the various Pleistocene sequences indicate their precipitation from lacustral CaCl-rich connate brines. Groundwater inflow chemistries were created by rock-water interactions with an original connate seawater brines first trapped in sediments of the rift walls in "Sedom time" (Raab et al., 2000). After the final Pliocene disconnection from the sea and a lowering of the lake levels, these residual brines gradually seeped and leached back in to the Sedom basin. There was never a hydrographic connection of the Dead Sea to the Gulf of Aqaba in the south and all of the Pleistocene salts in the depression come from the evaporation of continental groundwaters, not from ongoing marine-fed seepage. Neogene parts of the intervening rift valley were always above sea level and even today the Arava Valley is characterised by ridges up to 200 metres above sea level in the Gulf of Aqaba.

The rapid accumulation of Amora and Samra sediments within a subsiding and extending valley, atop thick bedded evaporites of the Sedom Fm. initiated several salt diapirs along the valley floor, the best known being Mt. Sedom (Figure 4.41b; Larsen et al., 2002). The Mount Sedom diapir has pierced the surface atop a 200 m-high salt wall. Throughout the Holocene, salt has

been rising in Mt. Sedom at a rate of 6-7 mm a⁻¹ (Frumkin, 1996a).

Water level changes

The highest recorded level of the Dead Sea (-392 m asl) was reached in the 1920s (Figure 4.42a), since then the lake level has been decreasing and today is around -416 m asl and still falling. At the beginning of 1978 the falling waters reached a level of -399.6 m asl, which dried out the Lisan Straits and divided the water covered area of the Dead Sea into separate Northern and Southern basins (Figure 4.43a). Since 1977, the surface level of the Dead Sea has been falling at a rate ≈60 cm/year. The lake water surface reached -410 m (msl) in 1997 and from 1998 to 2002 the lowering rate reached 100 cm/year. Since the 1930s, the trend of water levels in the Dead Sea lake has been falling or "droughty" (Figure 4.42a). In a "droughty" year the total level rise in winter is smaller than the yearly drop, and in a "rainy" year-larger. For example, in the droughty period 1981-1988, the net level drop in water level in every single year is in the range 70-90 cm yr⁻¹ (Figure 4.42b; Anati, 1998; Yechieli et al., 1998; Gertman and Hecht, 2002). An exactly balanced year, which is the common situation in most of the world's perennial lakes in temperate climates, has never been recorded in the Dead Sea. Dead Sea water level changes underline the general observation that differences in the hydrological balance in a lacustrine setting are the dominant control on the various styles of lake fill and that evaporites only accumulate in underbalanced lacustrine settings (Figure 5.8).

It seems the rate of fall has been accelerating since the 1960s. This more rapid rate of fall is largely a response to the diversion

of river water from the Jordan and Yarmuch Rivers into irrigation projects in Syria, Israel and Jordan. As a result, the inflow of fresh water into the Dead Sea has diminished significantly in the past half century. In the 1950s, the yearly Jordan River input to the Dead Sea was estimated to have been 1,370 million m³, while present annual inflow is between 250 and 300 million m³. Moreover, Israel and Jordan are pumping Dead Sea waters from the northern basin into saltworks in the southern Basin, further contributing to the falling water levels. Streams other than the Jordan River supply surface runoff to the Dead Sea and include; Wadi Mujib, which discharges around 83 x 10⁶ m³, Wadi Karak, which discharges around 18 x 10⁶ m³; Wadi Hasra, which discharges about 34 x 10⁶ m³; and the Zerqa Ma'in Springs which discharge about 23 x 10⁶ m³. Small intervalley catchments provide an additional 30 x 10⁶ m³ (Table 4.4, Figure 4.40b; Abu-Jaber, 1998; Salameh and Bannayan, 1993).

Until the 1960s, the Jordan River, flowing south from the Sea of Galilee, provided 80% of the water received by the Dead Sea (Eugster and Hardie, 1978). Storm runoff provided around 8% and spring inflow the remainder. Historically, the bulk of the water and detrital sediment entering the Dead Sea Basin was carried by the Jordan River into the northern end of the lake. However, even before the current drastic lowering of the Jordan's flow to a quarter of previous levels, the bulk of the solutes forming chemical precipitates in the Dead Sea came from saline springs fed by dissolving Miocene salt and not from the Jordan inflow. Annual spring inflow is thought to be around 80 million cubic metres and up to 300 times more saline than the waters of the Jordan River. As in many other evaporite basins, hydrography and solute cycling in the Dead Sea are largely decoupled.

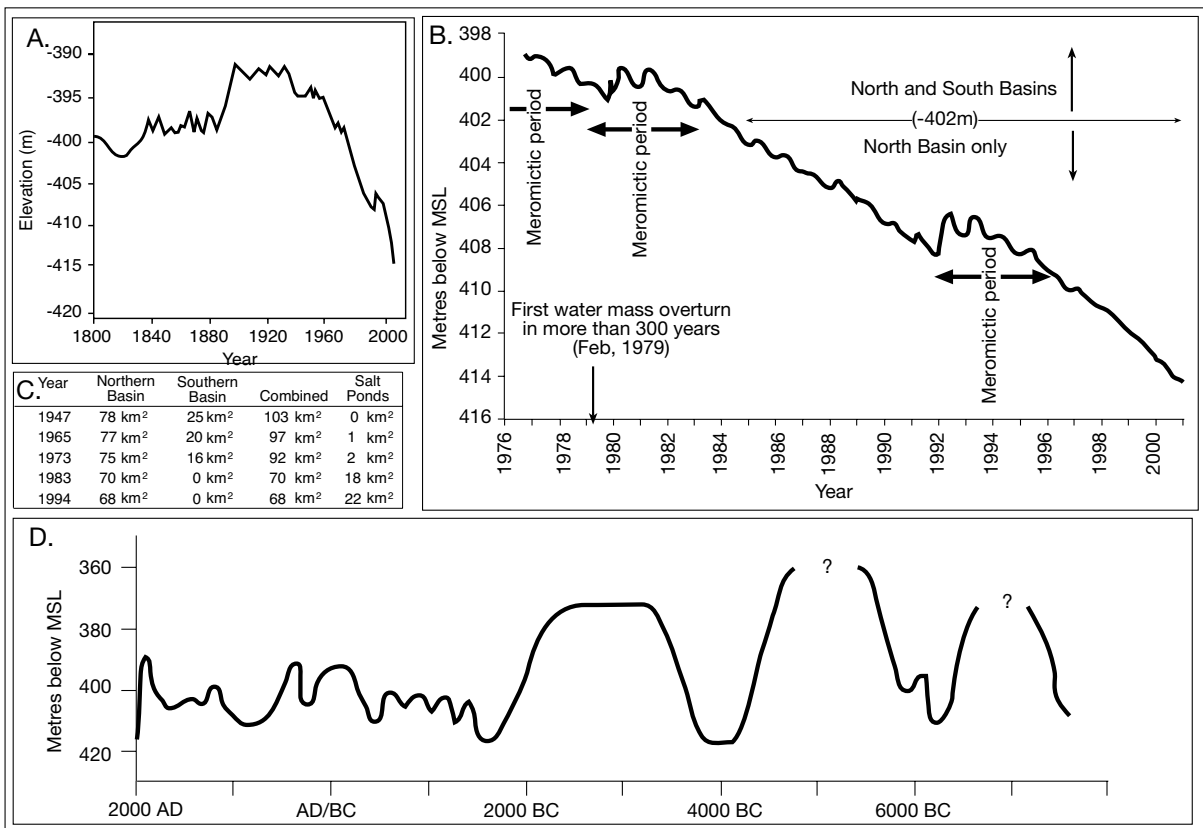


Figure 4.42. Changes in the Dead Sea water level at various time scales. A) Historical changes in the water level of the Dead Sea brine level since 1800, showing obvious acceleration in rate of fall since the 1960s and the “droughty” or falling trend since 1918. B) Detailed curve for the last three decades showing how rapid rises are tied to “wet” years and the consequent meromictic lake hydrology. C) Variations in the areas of the Northern and Southern Basins and the growing area of anthropogenic salt pans as it relates to changing brine levels. C) Changes in the Dead Sea level for the past 8,000 years (A and C replotted from Enzel et al., 2003; B replotted from Gertman and Hecht, 2002).

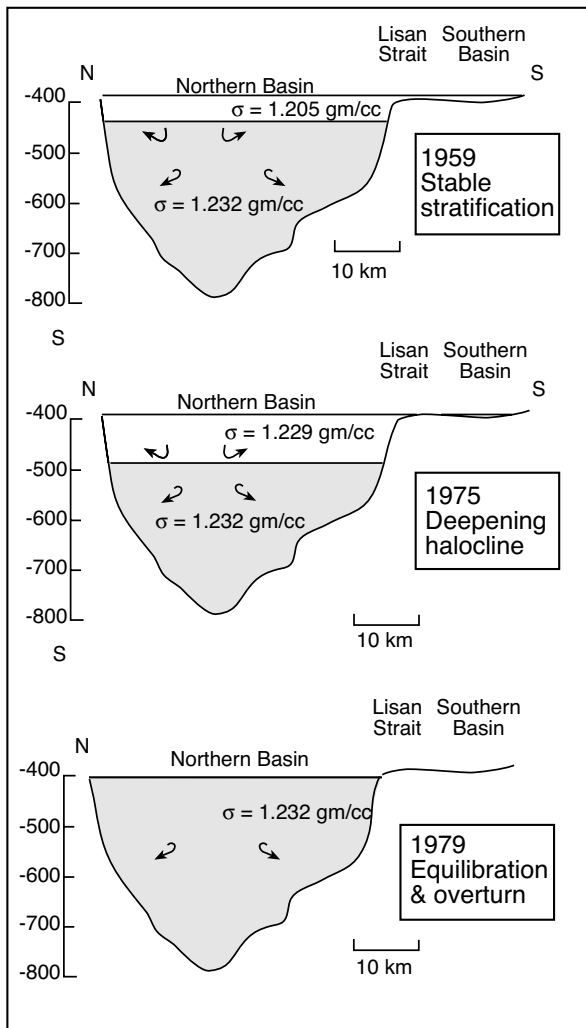


Figure 4.43. Evolution of Dead Sea stratification in the period 1959-1979 showing the loss of brine stratification via lessening of freshened inflow from Jordan River and entry of brine waste from south. This resulted in increased salinity of surface waters, a deepening of the halocline and final equalisation of densities of the two masses and their overturn in 1979.

Given the marked fall in brine level over the last 50 years, Yechieli et al. (1998) addressed the interesting quandary, “Will the Dead Sea ever dry up?” They argue it will not dry up completely as the rate of evaporation will continue to decrease as the salinity of the brine increases. The evaporation rate of fresh water under Dead Sea conditions is about 3.5 m/yr, while the evaporation rate of Dead Sea surface waters is about three times lower (Figure 2.3b). In 1944, when the surface salinity of the Dead Sea was about 280 g/l, the rate of evaporation was 1.7 m/yr. By 1960, it decreased to 1.5–1.6 m/yr at a salinity of

300 g/l, and in 1979–1980, the evaporation rate was 1.3–1.4 m/yr at a salinity of 330 g/l. An extremely low evaporation rate (1.05 m/yr) characterised the period 1983–1987. The present rate of evaporation is believed to be ~1.25 m/yr (range 1.1–1.4 m/yr).

Assuming water inflow remains at present levels, a new equilibrium between evaporation and water input will be reached in about 400 years (Yechieli et al. 1998). The brine surface will then be at –500m, more than 80 m below the present value. The surface area of the lake will be 526 km², and the water volume will have decreased by about one third from its present level. The remaining brine, in equilibrium with the air of 50% humidity, will contain about 380 g/l dissolved salts, and have a density of 1.27 kg/l (Krumgalz et al. 2000). Over longer time frames encompassing the Holocene, the current levels of the lake are not unusual, although the rate at which levels are changing may well be (Figure 4.42c). Similar lake level lows ~–500m asl characterised the Dead Sea some 2.5 and 4 ka (Enzel et al., 2003).

Density stratification: Holomixis versus meromixis

Until 1979 lake waters were meromictic or “permanently stratified” and had been so for 300 years (Stiller and Chung, 1984). In the 1950s there was a well-developed permanent pycnocline and thermocline at a depth of 50 m (Figure 4.43; Neev and Emery, 1967). The average temperature of the upper 50 m of the water body was between 16 and 36°C and density around 1.205 gm/cc, while at brine depths greater than 50 m, the temperature was a constant 21.5°C and the water density was 1.232 gm/cc. But in the 1960s and 70s the lessening inflow from the Jordan meant the surface water mass became increasingly saline and the permanent pycnocline deepened. In 1975 the pycnocline was some 100 metres below the lake surface and the upper water mass had a density of 1.229 gm/cc. In February 1979 the densities of the upper and lower water masses equalised and the lake overturned, whereby the lower water mass mixed with the upper water mass and the lake had become holomictic (Steinhorn, 1983). It was marked by a strong and persistent H₂S smell as bottom waters came into contact with the atmosphere for the first time in centuries. Prior to the 1979 overturn, the lake had been continually stratified (meromictic) since its last holomictic period some 300 years earlier. Overturn has occurred naturally a number of times in the lake’s Holocene history and these episodes are marked by beds of massive coarsely-crystalline deepwater halite.

After 1979 the lake entered a new phase in which its hydrological regime seesawed between holomictic and meromictic regimes, depending on the size of the storm runoff into the lake (Gertman and Hecht, 2002; Anati, 1998). The Dead Sea level rises, typically in winter, in an relatively unpredictable fashion driven by short events of varying intensity (runoff and sudden floods), and drops at a fairly constant rate for the rest of the year. The first holomictic period, 1979–1980, lasted for 2 months only. It was succeeded by a 4-year meromictic period (1980–1983). The second holomictic period lasted for 9 years (1983–1991; Figure 4.42b). Then, during an unusually wet winter in 1991–1992, some $1.5 \times 10^9 \text{ m}^3$ of meteoric water entered the lake. This caused the lake level to rise by 2 metres and formed a freshened stable upper water mass, which persisted until November, 1995 when stratification collapsed and the lake overturned once more (Anati et al., 1995). The upper layer with a relatively low salinity was restored and a new meromictic period began.

During each meromictic period, the hydrological regime of the Dead Sea is characterized by following long-term trends (Gertman and Hecht, 2002): the mixolimnion thickens as the depth of the summer thermocline increases from 12–15 to 25–30 m; the quasi-salinity^{4,3} of the upper layer, initially around 164 kg/m³, increases rapidly at a rate of about 16–18 kg/m³/year; the quasi-salinity of the deep water, initially of about 235 kg/m³, decreases slowly at a rate of about 0.08–0.10 kg/m³/year; and the winter minimal temperature of the upper layer, initially of about 16°C, increases rapidly at a rate of about 2°C/year. In November 1995, the latest meromictic period of the Dead Sea came to an end. In other words, even though the meromictic upper water mass persists for years, its physical properties not

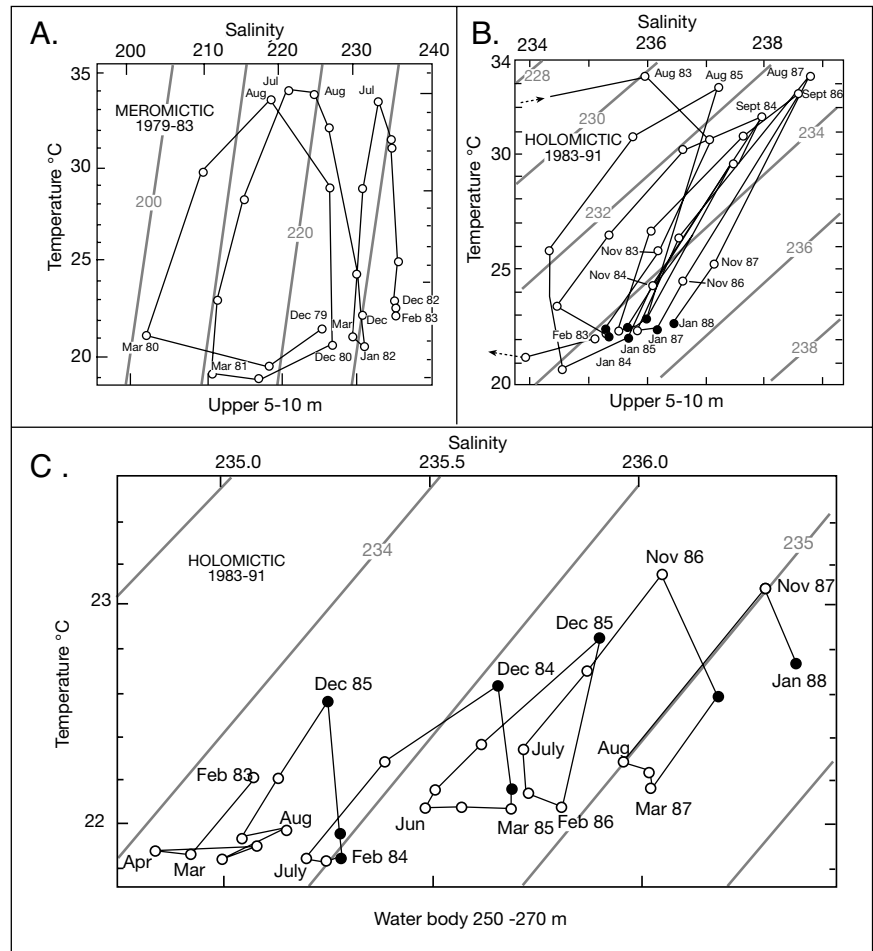


Figure 4.44. Dead Sea hydrological evolution in temperature-salinity space (T-S diagrams after Anati, 1998) A) Upper 5-10 m water trends in the meromictic period 1979-1983. B) Upper 5-10 m water trends in the holomictic period 1983-1991. C) Water trends in lower water mass at 250-270 m depth for much of the holomictic period 1983-1991.

only change annually, driven by seasonal changes in temperature and evaporation intensity, it also evolves from year to year as it becomes increasingly warmer, more saline and denser until its physical properties equal those of the underlying deep water

^{4,3}Solute proportions of the waters of the Dead Sea are relatively rich in calcium, magnesium, potassium and bromine, and relatively poor in sodium, sulphate and carbonate, thus are significantly different from those of modern seawater (Table 4.4). Strictly speaking, in view of the peculiar chemical composition of its waters, the accepted definition of “salinity” based on seawater proportions does not apply to the waters of the Dead Sea and it has been replaced by an “equivalent salinity” based on pycnometry (Anati, 1999; Gertman and Hecht, 2002) and referred to as “quasi-salinity.” Thus, quasi-salinity is defined as the Dead Sea water density anomaly from 1000 kg/m³ at an arbitrary reference temperature of 25°C. For the sake of comparison, a quasi-salinity of 235 kg/m³ is the equivalent of 280‰.

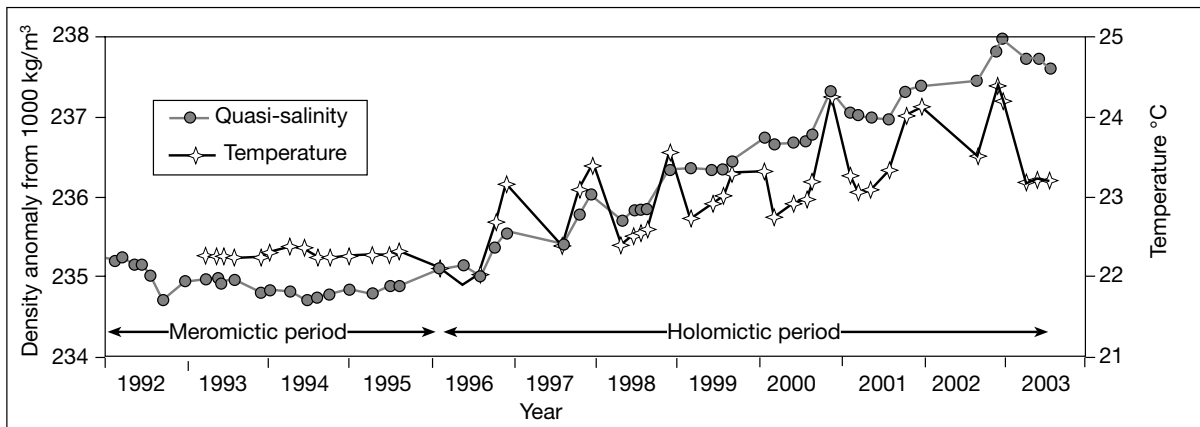


Figure 4.45. Long term changes in quasi-salinity and temperature in the deep water body (below 100m) of the Dead Sea in a meromictic to holomictic period (after Gertman and Hecht, 2002 and replotted data from <http://isramar.ocean.org.il/DeadSea> (last accessed Sept 29, 2004).

mass and the lake waters overturn. This evolution can be clearly seen in maps of the time-based evolution of temperature-salinity space (Figure 4.44a; Anati, 1998).

During holomictic periods, as exemplified by the period 1996–2000, the hydrological regime of the Dead Sea *in toto* is also characterized by long-term trends (Figures 4.44b, c, 4.45; Gertman and Hecht, 2002; Anati, 1998): the quasi-salinity of the entire Dead Sea increased at a rate of about 0.5 kg/m³/year, with practically no decrease during the winters; the temperature of the deep water mass increased with a rate of about 0.25°C/year; and the period of vertical convection of the entire water column, initially about 3 months, increased at a rate of about 1 week/year. Moreover, the temperature and salinity of the bottom layer in the deepest part of the Dead Sea rose by about 0.5–0.6°C and 0.15–0.25 kg/m³ during each holomictic summer.

During holomictic years, a stratification builds during the summer months with a thermocline generally located between 15 and 30 m depth (Figure 4.46a). The density contrast at the base of the upper water mass is large enough to balance an ephemeral destabilizing halocline formed daily in the uppermost few metres as a result of intense evaporation. At night the same uppermost waters cool and mix with underlying waters above the major thermocline. This stable thermocline persists throughout the summer and into autumn when the overlying air mass cools, so driving a cooling of the whole upper water mass until temperature and densities equalise and overturn occurs, usually in November. A temporary dilution of the upper water layers may occur due to winter rain floods, but in a holomictic year it is destroyed by summer evaporation, so

preventing the year round stratification that characterises the lake in its meromictic stage.

Detailed work on the lower Dead Sea water mass by Gertman and Hecht (2002) shows an additional interesting stratification in the lowermost parts of the lower water mass (Figure 4.46b, c). Temperature profiles of the bottom layer exhibit a step-like feature indicating advection of saltier, warmer and denser water into the lowermost parts of the Dead Sea. The differences in the size of the steps indicate the changes in the intensity of the advection in this part of the column. There are three possible sources for such waters; 1) Endbrines pumped back into the Northern Basin from the Dead Sea Works at the southern end of the Dead Sea, 2) Subsurface hot springs similar to those documented by Niemi et al. (1997), 3) Slope convection of warm saline dense brines from the shallow edges of the Dead Sea. At this time there has been insufficient monitoring to determine which of the possibilities is the most likely, or if all can contribute to the bottom anomaly.

Deep water Halite

The transformation of the brine column in the last two decades has allowed substantial halite to accumulate on the deep water floor of the basin for the first time in 300 years. Halite first crystallised in the near surface lake brines in 1979, while massive halite began to crystallise from the entire brine column toward the end of 1982, when ropes suspended in the water would quickly accumulate cm-thick rinds of centripetal halite (Steinhorn and Gat, 1983; Stiller and Sigg, 1990; Stiller et al., 1998). The mass of halite that precipitated between 1976 and 1992 is estimated to be about $2,550 \times 10^6$ tonnes (Gavrieli

1997). The result of this holomictic saturation of the Dead Sea is a layer of coarse crystalline halite accumulating rapidly on the deep lake bottom that today (20 years after it began) is already several tens of centimetres thick. For the period 1983 to 1989 the estimated annual accumulation rate for halite on the Dead Sea floor was 3 - 6 cm/year (Levy, 1991, 1992). This new bed of halite defines the end of several hundred years of longterm brine stratification (meromixis) when halite did not precipitate in the hydrologically isolated lower brine mass. Instead a pelagic/detrital carbonate laminite had accumulated (see next section). Previous episodes of nonstratification in the deep brine column (holomixis) are indicated by similar but now buried beds of widespread metre-thick massive halite beneath the lake floor (Levy, 1984).

Several crystal morphologies define the halites currently accumulating above and on the deep bottom of the Dead Sea (Gavrieli, 1997; Herut et al., 1998); a) Clear aggregates of sedimentary halite crystals forming interlocked aggregates and massive dm-thick bed on the lake floor that are made up of white to clear crystals up to 1 cm in diameter and typically interbedded with layers composed of fine grained (<1 mm diameter) halite crystals and brown mud, b) Individual clear idiomorphic cubes up to a cm long floating within brown mud layers and, c) Large interlocked clear centripetal halite crystals (0.5 - 2.0 cm long) growing on ropes suspended in the brine column. Much of the halite on the Dead Sea floor consists of intercalations of types a and b, with each constituting around 50% of the newly formed halite layer. Clay mud layers are

though to indicate wet years in the lake hydrology such as the period 1992-1993 (Gavrieli, 1997).

Finer-grained halite and gypsum layers are common in shallow waters (< 50 m) about the lake edge, particularly in the western and southern parts of the Northern Basin where they cover much of the lake floor and may well indicate the effects of brine outfall from saltworks in the Southern Basin. Coarser clear cm-scale halite crystals and layers are today common in the deeper waters of the Dead Sea. This is not entirely consistent with many of our current models arguing that pelagic

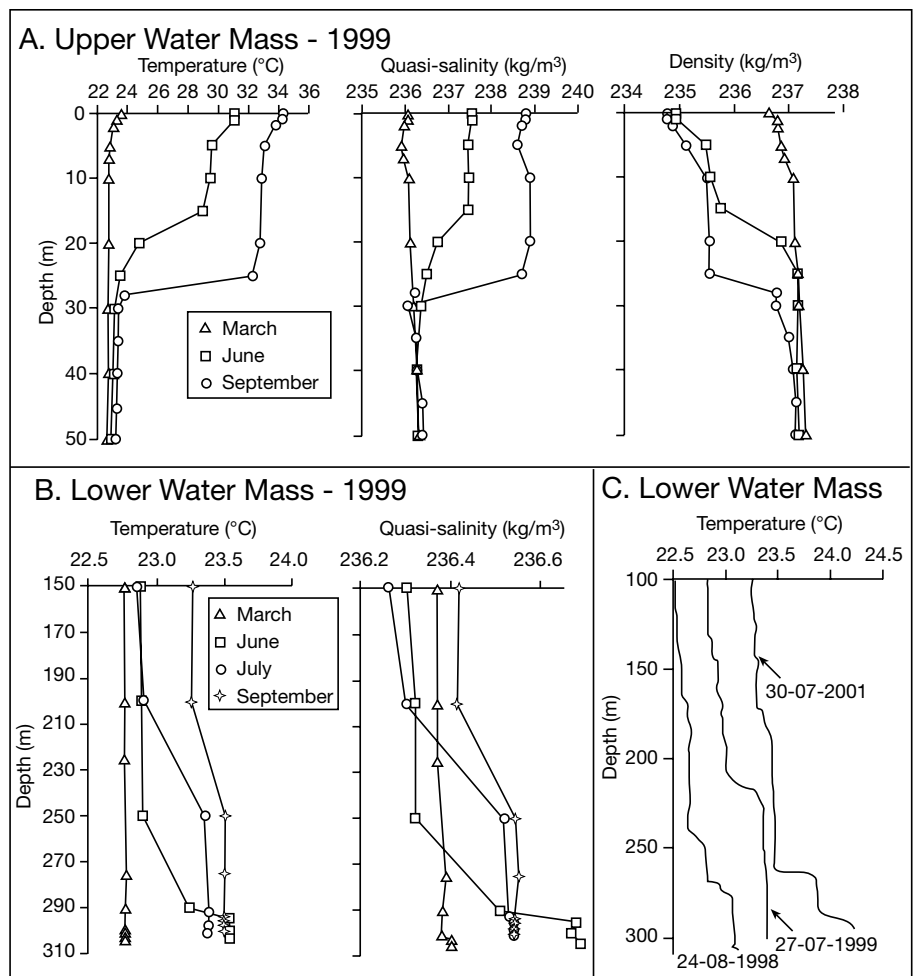


Figure 4.46. Stratification of the Dead Sea during holomictic years as illustrated by temperature, quasi-salinity and density profiles (after Gertman and Hecht, 2002). A) Stratification builds in the upper water mass at a depth of 20-30 m in the summer (June-September) and is destroyed by overturn in the autumn (March). Note the smaller daily increase in temperature and salinity/density in the uppermost 5 metres of the water mass due to intense daily evaporation. B) Temperature and salinity anomalies in the lower water column in September 1999. C) Temperature anomalies in the lowermost part of the lower water column. All profiles were measured at site EG320, its location is shown in Figure 4.40b.

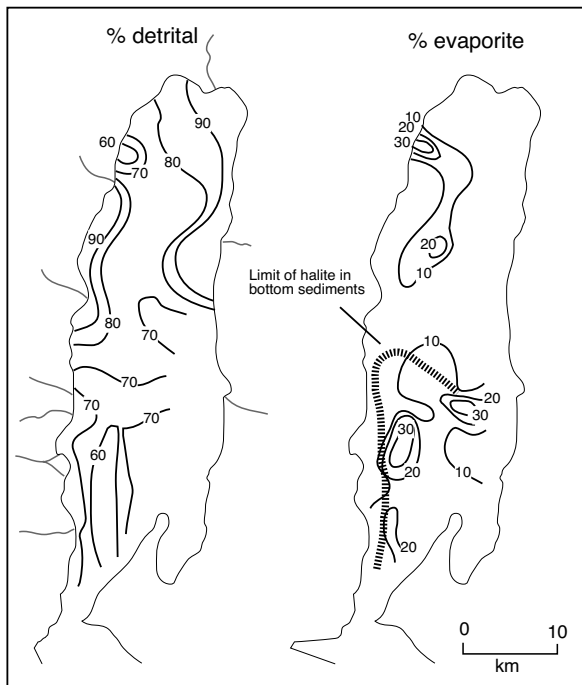


Figure 4.47. Bottom sediment distribution map of sediment mostly created prior to monomictic halite precipitation in 1979. The eastern or Jordanian parts of the Lake floor was not sampled (after Garber, Levy and Friedman, 1987).

deep water “salt and pepper” textured, finely-crystalline halite laminites indicate the deeper water parts of an evaporite basin fill (e.g. Schreiber and El Tabakh, 2000).

Some of the finer-grained salt layers in the Dead Sea are thought to precipitate via outsalting. Prior to 1979 this occurred where dense brine plumes, created in the areas of more intense evaporation about the lake edge sank into the deeper part of the basin. A similar hydrology is perhaps indicated by Figure 4.46c. Outsalting, via mixing between Dead Sea waters and the industrially concentrated end brines pumped into the Northern Basin from the solar operations of the Southern Basin is most obvious in the southern part of the Northern Basin (Figure 4.47; Epstein et al., 1975; Gavrieli, 1997). At 480 g/l these bottom hugging waste brines from potash manufacture are more concentrated than waters of the Northern Basin and have different relative proportions of the major ions. They are depleted in potassium and sodium and are enriched in magnesium and chloride relative to the Dead Sea waters, creating a situation ideal for saltout at the mixing zone between the two waters (Gavrieli, 1997, Yechieli et al., 1998). Saltout has probably occurred in the southern part of the Northern Basin for decades and is defined by bottom sediment areas where finer-grained halite occurs in 1-20 cm thick layers interbedded

with gypsiferous brown mud. Descending brine plumes probably allowed halite and coarse-grained gypsum to accumulate beneath zones of mixing, even prior to the 1979 turnover, as can be clearly seen in preholomictic maps of bottom sediments (Figure 4.47).

But mixing-induced saltout does not explain all of the halite currently accumulating across the floor of the Northern Basin. Another possible mechanism is the annual cooling of the uppermost brine layer in holomictic years (Gavrieli, 1997). Temperatures in summer in the upper water 30 metres in holomictic years are $\approx 34\text{--}36^\circ\text{C}$, while in winter they are $\approx 22\text{--}24^\circ\text{C}$ (Figure 4.46a). Although annual precipitation due to cooling of surface waters creates supersaturated chemistries, no unequivocal halite crystallisation driven by seasonal cooling has been observed in the Dead Sea. Yet, when saturated brines are collected and allowed to cool in the lab, halite precipitation as mm-scale crystals does occur spontaneously (Gavrieli, 1997).

Brine mixing and seasonal cooling explain the formation of finer-grained cumulate halites, but do not explain the formation of cm-scale crystal aggregates and layers. Yet such crystals can and do form in the current waters of the Dead Sea, as evidenced by coarse clusters in the current seafloor bed and large crystals hanging off anchor ropes. Gavrieli (1997) argues that these larger crystals in the bottom layers are authigenic and indicate slower ongoing authigenic growth in halite-saturated pore waters and brine columns situated at or just beneath the present day lake floor. Such saturated growth can only be maintained when the lake waters are holomictic. It seems that authigenic growth and recrystallisation is an ongoing process, as is seen in the pervasive recrystallisation and coarse crystalline overprint preserved in the 500 year old Dead Sea halite layer cored by Levy (1984).

Interestingly, cores taken twenty years earlier in the 1960s, below water depths of 40 m at the southern end of the Northern Basin, bottomed on a hard halite bed after passing through 10 to 80 cm of soft carbonate laminite (Neev and Emery, 1967). This halite was deposited some 300-500 or so years ago during a previous holomictic event. Likewise, four reflectors, so obvious in sediments of the deeper part of the Northern Basin, probably mark contacts between carbonate marls and beds of massive rock salt (Ben-Avraham et al., 1993). If the massive cm-scale inclusion-poor randomly-oriented crystals of the halite bed intercalated with finer-grained halite layers that are currently accumulating on the floor of the Dead are similar to textures in this buried deep water halite, then the notion that deepwater halite is solely a silt-sized “rain from heaven”

laminite is problematic. But, then again, the uniqueness, the small scale, and the continental transform setting of the Dead Sea means its utility as an analog for ancient marine-fed basinwide evaporites is also somewhat problematic.

Deep water laminites

Prior to overturn in 1979, away from the Jordan river delta, away from wadi aprons and away from the influence of end brine mixing, the deep bottom sediments were mostly carbonate laminites accumulating in water depths ranging from more than a few metres down to the deepest parts of the basin. These laminites are today being covered by halite, but prior to the onset of holomixis in 1979 carbonate laminites were the main sediment accumulating on the deep lake floor. Lamina in the mm-scale light-dark couplets are dominated by two time-separate pelagic components, namely terrigenous detritals and chemical precipitates (Garber, 1980; Garber et al., 1987). Light coloured lamina are dominated by chemical precipitates, mostly made up of stellate aragonite clusters precipitated in the upper water mass (Figure 4.48). Dark-coloured detrital layers in laminites contain limestone (calcite) grains, quartz, and silicate clays, along with minor feldspar and dolomite, all allochthonous components carried into the basin as bottom load, suspended load and air-borne detritus. The proportion of terrigenous material in the laminites increases toward the lake shoreline, especially toward river and stream mouths (Figure 4.47). Illite averages about 40% of the carbonate-free clay fraction of the laminites, smectite about 32%, and kaolinite about 28%. Locally, there are lesser and varying proportions of pelagic gypsum and coarser “in situ” gypsum roses within the carbonate/detrital laminites (Figure 4.49b).

Whitening events precipitating the aragonite occurred in the surface waters of the Dead Sea every few years prior to the onset of holomixis. For example, Neev and Emery (1967) sampled two summer “whitenings” of surface waters that occurred in 1959 and determined a gypsum to aragonite weight ratio of 3.14. Yet the aragonite in light lamina in the laminites on the bottom, hundreds of metres below, were almost 100% CaCO_3 . They had identified a chemical discrepancy that needed an explanation and attributed the alternation of aragonite in the lighter lamina and calcite in the darker lamina to the activities of sulphate-reducing bacteria acting on pelagic gypsum settling through the anoxic density stratified water column and converting it to bacterial calcite. Elsewhere, sulphate-reducing bacteria are known to destroy organic matter and gypsum, converting them to sulphides, energy, and H_2S with calcite as a byproduct (Figure 9.41a).

Subsequent isotopic work on the calcite lamina by Garber (1980) showed the calcite was detrital, not bacteriogenic. He also found that the laminites were not annual or “true” varves, only 15 to 20 lamina couplets had been deposited on the Dead Sea floor in the first 75 years of the last century. More recent work on CO_2 flux in the Dead Sea water during the meromictic period from February 1993 to December 1994 showed that summer whitenings are probably not the major source of aragonite in the laminites (Barkan et al., 2001). Rather aragonite precipitation occurs via mixing (salting out) in the upper water mass after a massive bicarbonate input from winter floods. This notion of precipitation resulting from winter flooding and brine mixing is contrary to the accepted notion of summer precipitation of aragonite in the uppermost surface waters of the historic Lake Lisan, the predecessor of the Dead Sea (see next section). But it better explains the lack of annual varving noted by Garber and means that either the origin of the aragonite laminites in the Lisan Fm should be re-evaluated, or the present Dead Sea should not be considered a direct hydrologic analog for the somewhat fresher and deeper waters of Lake Lisan.

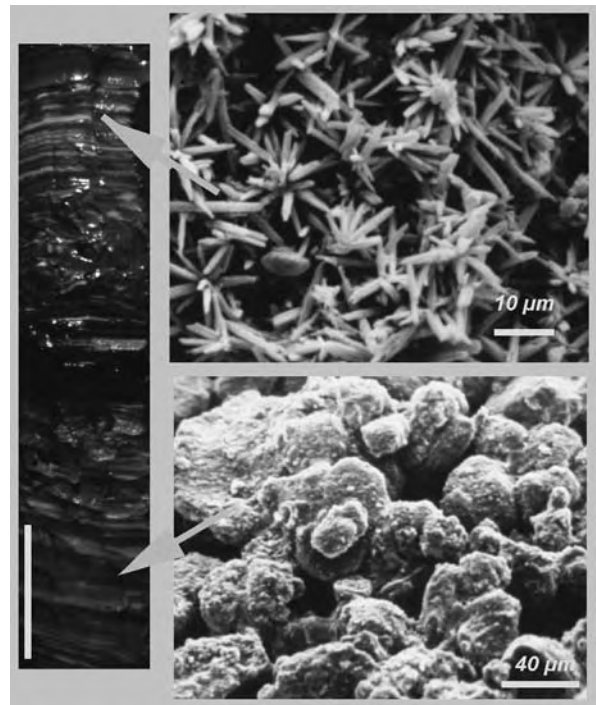


Figure 4.48. Dead Sea deep water laminites in bottom core collected in Northern Basin in water depths of more than 200 m. It was collected in late 1970s when water mass was still stratified. Light coloured laminae are composed of stellate aragonite prisms precipitated as “whitenings”, while dark coloured laminae are dominated by detrital calcite. Scale bar on core is 5 cm (Images courtesy of Ray Garber).

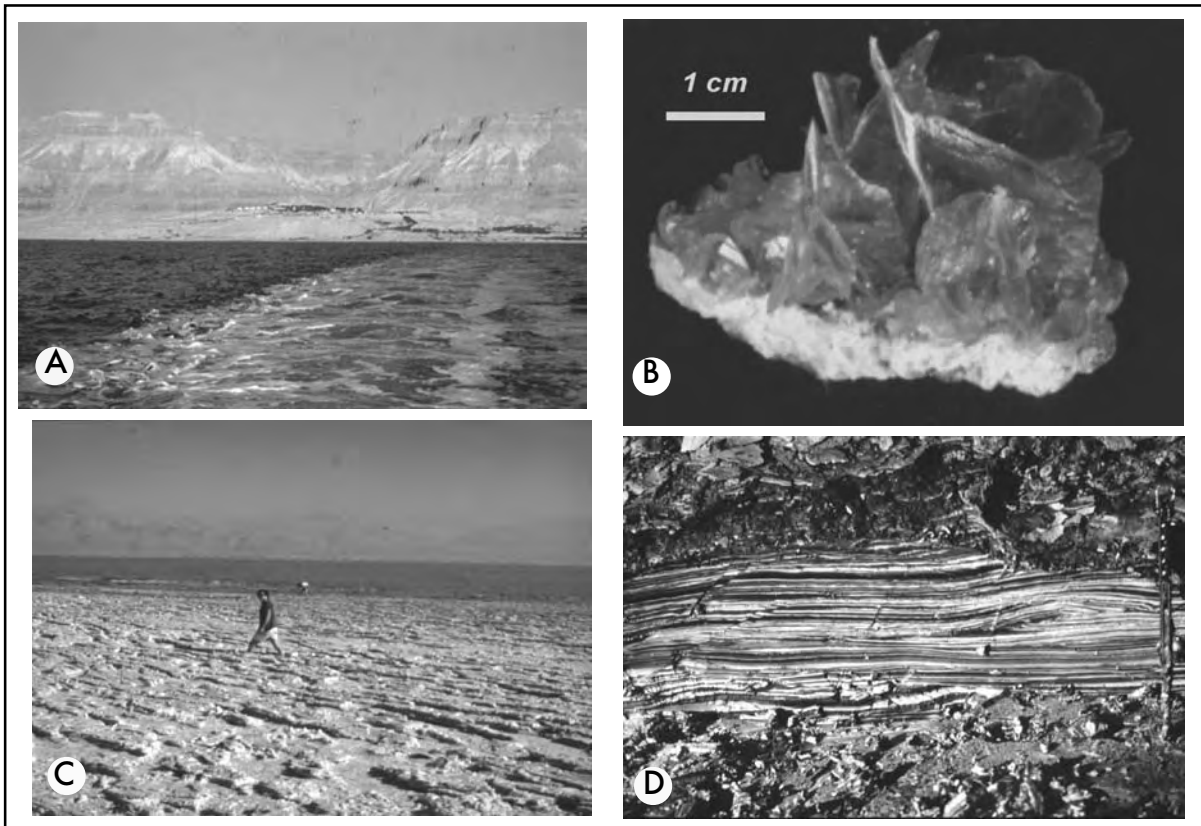


Figure 4.49. Dead Sea. A) Ein Gedi, village located on a “hanging” fan delta of Late Pleistocene age and is evidence of higher lake levels at that time. B) Intrasediment gypsum rose growing in bottom sediment in brine depths of more than 200 metres. Brines may be supplied from brine plumes from dissolving salt diapir crests. C) Exposed unconsolidated laminite muds on the eastern margin of the Dead Sea. D) Trench in muds shown in C); Note the soft sediment deformation in some layers. (All photos courtesy of Ray Garber).

The dark coloured detrital-dominated mm-scale layers of the Dead Sea laminites lack a pervasive microfossil/diatom component, unlike laminites forming in less saline perennial lakes such as Lake Van. Diatom frustules do accumulate on the lake floor where diatoms flourish in areas of longterm freshened water. Their remains are common only in the detrital-rich prodelta laminites of the northern region of the Dead Sea. There, the Jordan River delta is building out into the lake and carries the remains of diatoms, along with abundant clays and silts. Surface waters over the rest of the Dead Sea are too saline to allow diatoms to live.

Prior to the onset of holomixis, intrasediment gypsum made up of individual crystal disks, constituted around 6% of the sediment volume in deep basinal laminites. In fact, contrary to the earlier findings of Neev and Emery (1967), Garber (1980) found gypsum in all cores recovered in the mid 1970s

from laminites in lake bottom settings ranging from shallow sea-marginal, through slope to deep basinal settings. Gypsum rarely formed in discrete laminae, small lenticular crystals were mostly disseminated through the terrigenous (dark) layers but larger crystals cut through both light and dark lamina. Garber (op cit.) concluded that gypsum in the deepwater laminites was probably present even during the studies of Neev and Emery. He argued that finely crystalline sand-sized gypsum was probably the settled-out remnants of gypsum precipitated in the surface waters, either as documented in the whittings by Neev and Emery (1967) or by brine mixing near the contact of the upper and lower water masses. Further gypsum crystal growth into desert-rose like displacive aggregates in the sediment (Figure 4.49b) was interpreted to indicate upward brine diffusion through the bottom sediments. Such upwelling brines were perhaps derived by the dissolution of nearby subcropping salt structures.

The absolute paucity of bedded salts during meromixis was the most surprising thing about the deepwater sediments accumulating in the Dead Sea in the three hundred years prior to 1979. Why were they absent on the bottom when the upper water mass was at gypsum saturation a number of times each summer and the lower water mass was at or near halite supersaturation year round? The answer lay in the permanence of the upper water mass, it prevented chemical change in the lower mass and hence, although the lower waters were supersaturated there was no concentration mechanism to allow it to accumulate salts. Only pelagics made it to the bottom until the brine column mixed and the Dead Sea became a holomictic system in direct contact with the atmosphere. Then large volumes of evaporitic halite could accumulate on the deep basin floor in areas covered by waters hundreds of metres deep. The Dead Sea clearly shows that halite and other salts can accumulate at the base of a brine column several hundred metres deep. But, they do so mostly as coarsely crystalline aggregates, not fine-grained laminites, and can only do so when the whole brine column is a well mixed (holomictic) water mass. When a brine column is

permanently stratified, no “in situ” bottom growth occurs. The dominant depositional style is a “rain-from-heaven” made up of less saline precipitates and siliciclastic fines, with chemical precipitates forming either at the mixing zone between the two water masses, or at the air-brine interface.

Basin margin sediments

Layers of siliciclastic and calcitic detritus in the deep water bottom sediments are generally tied to floods and wind borne dust sourced in the highlands about the basin margins. Fan delta lobes about the basin margin indicate positions where streams and wadis drain into a water-filled depression. In the Dead Sea they show two main styles; 1) Currently active deltas that reach down to the present lake shoreline (Figure 4.50) and, 2) Late Pleistocene fan deltas that are typically smaller in extent than their Holocene counterparts and form “hanging” deltas (Figure 4.49a; Sneh, 1979; Bookman et al., 2004). The more obvious hanging deltas were actively accumulating sediment

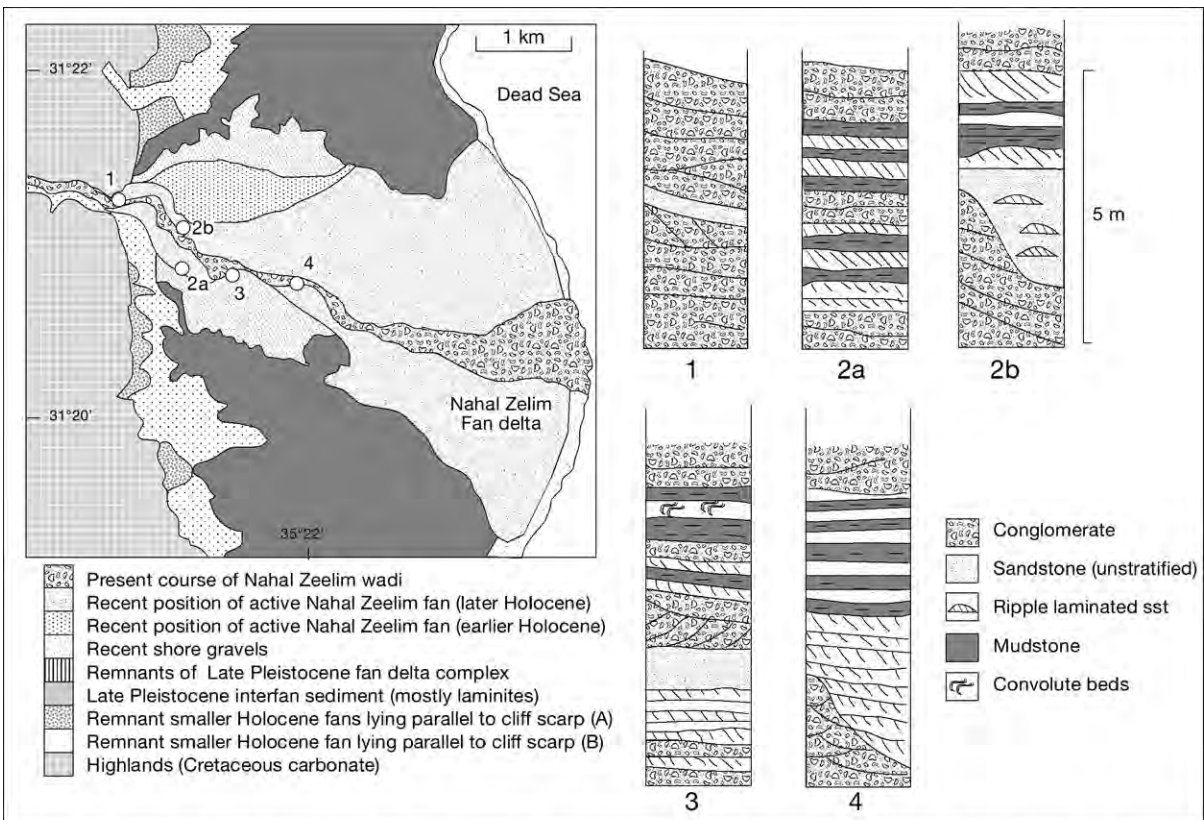


Figure 4.50. Nahal Zeelim fan delta, Dead Sea margin. Map shows multiple overprinted fan delta lobes from avulsion. Lobes of the Holocene delta lie below “hanging” late Pleistocene fan delta sediments deposited when the lake water level was 180 m above its present level. Vertical successions of five measured fan delta sections (1-4; localities shown on map) show a fining into the basin trend in average grain size (after Sneh, 1979).

in Lake Lisan time when lake waters were fresher and lake levels were up to 200 m higher. Size of the fan deltas vary, with the Nahal Zeelim delta being the largest of the active deltas located along the western margin of the depression (Sneh, 1979). In terms of the morphometry of fan deltas worldwide, Nahal Zeelim is relatively small ($\approx 6 \text{ km}^2$), its slope is steep (2.5°), and its catchment (235 km^2) is quite large for the size of the sediment lobe. Its morphometry reflects its arid setting, water supply is low and pulsed with resupply during times of short intense storm floods.

Each delta lobe is made up of several successive fan sequences, with facies changing from dominantly conglomerates at the head of the fan to sands and muds at the foot (Figure 4.50). In the proximal parts of a Dead Sea fan delta lobe, units of crudely stratified conglomerate alternate with coarse to medium sands that show cut and fill textures, along with abundant trough and planar cross beds. In the sand-dominated medial parts, structures range from unstratified or poorly layered sandy beds, through granule and mud-ball layers, into trough and planar crossbedded sands. Many of the finer sands in this zone preserve ripple

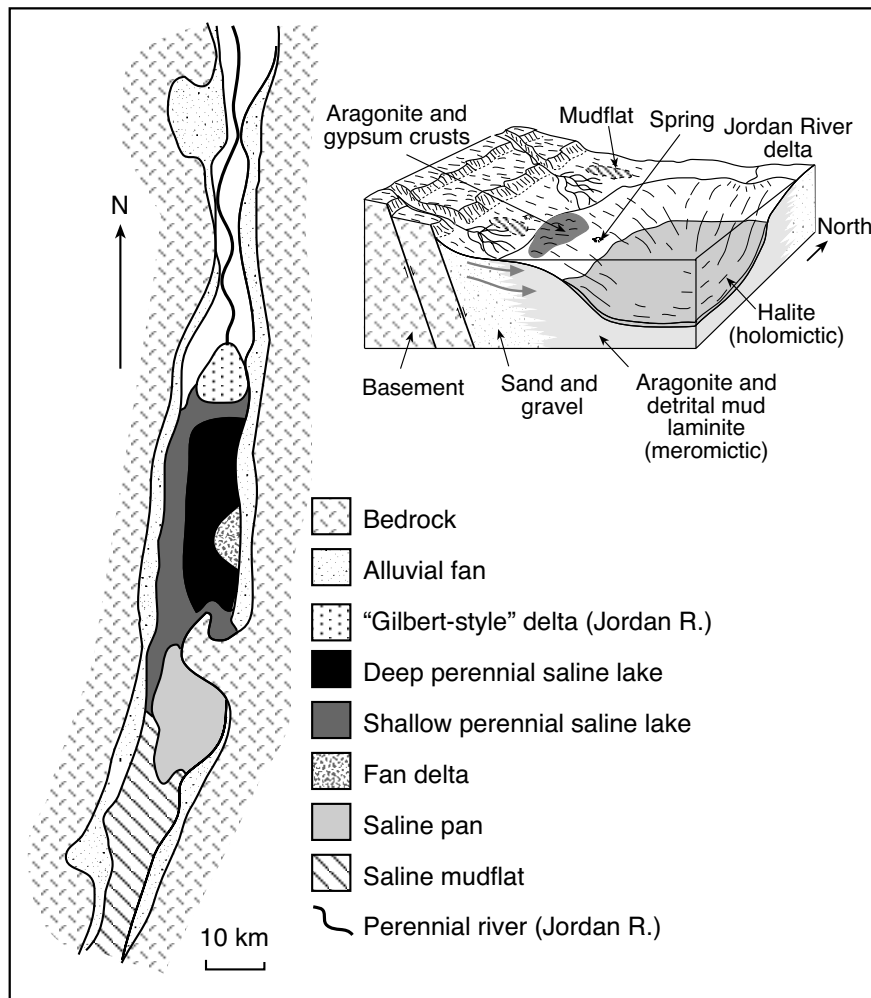


Figure 4.51. Geology of the Dead Sea basin showing the distribution of the various depositional settings in plan view and as a block diagram of the Northern Dead Sea basin. The River Jordan forms a fluviodeltaic wedge in the northern part of the basin. Active transension faulting and block rotation has exposed older lake deposits of the Lisan Formation at higher elevations as well as an apron of alluvial fan sediments with a number of "hung" fan deltas tied to older higher water levels in the lake. The saline pan in the southern basin is dominated by halite, artificial pans fed with deep brines have been constructed in this area to produce sylite and other potash products (see Chapter 11).

cross laminae. Further into the basin, the more distal parts of the fan lobes are composed of interlayered sand/mud facies intercalated with carbonate laminites. Alternations of coarse to medium sand with layers of very fine sand characterise distal fan sediments, as do thin 2-3 cm thick layers of mm-layered aragonitic laminite. Rapid deposition of fan sediments atop water-saturated laminites creates numerous examples of convolute bedding that formed as rapidly deposited sands loaded brine-soaked muds.

In strandzones away from the direct influence of active fan deltas, the grain size of sediments tend to indicate distance of the strandline from the base of the cliffed escarpment that defines the edge of the present Dead Sea basin. Where the present shoreline of the Dead Sea is a long distance from the fan-lined border escarpment, sediments tend to be muddy laminites, deposited during times of relatively higher water (meromictic) during the last few centuries and including blocks derived by reworking of Lisan marls (Figure 4.49c, d). In strandlines closer to the escarpment the shores are moderately steep with beaches and bars of sand and gravel

reworked from the base of the escarpment, especially where waves are eroding older bajada sediments. Where the shoreline is a cliff at the base of a border escarpment, the sediments tend to be reworked blocks and muddy slumps of Pleistocene Lisan Formation (Neev and Emery, 1967). Fluctuations in water levels throughout the Quaternary have created numerous terraces; more than 30 near-horizontal sandy shore terraces and gravel bars have been recognised behind the current lake strandline (Bookman et al., 2004).

The asymmetry of the tectonic setting of the Dead Sea depression is reflected in the granulometry of the fans. The eastern side of the Dead Sea is the more active transform escarpment, so slopes are somewhat steeper and fans are dominated by poorly-sorted debris flows, which often reach all the way to the modern strandline. On the western side of the depression the slopes are not as steep (Figure 4.40b). Based on comparisons with the rift lakes of Africa, there should be sand aprons created by widespread longshore reworking of fan delta sediments along this western side. But this is not happening in the Dead Sea, any clean sands created by wave action on the western side of the depression are swamped with sheets of muds derived by erosive reworking of Lisan Fm. laminites which blanket the depression. In terms of the Dead Sea's ability to act as a Holocene lacustrine analog for modelling reservoir sand distributions in ancient evaporite-sealed lacustrine counterparts, it suffers from the same problems as that other deep hole in the ground with evaporites - Death Valley, California. Both depressions are too deep, with sides simply too steep, to allow well-sorted sand bodies to accumulate in substantial volumes about the lake edge.

Much of the exposed margin of the Dead Sea between active fan delta lobes is made up of soft laminites and intercalated indurated beach-rock-like aragonitic crusts. These exposed recent laminites were deposited from meromictic lake waters and were deposited prior to 1979 (Figure 4.49c, d). Intercalated with the sea margin laminites are gravels and sands reworked from fan sediments and perhaps acting as aquifers or at least zones of high crossflows of waters into the lake margins. Exposed gravels and sands are sometimes cemented into beach rock sheets and have been coated with mm-scale laminated aragonite encrustations and stained with manganese (Garber et al., 1981; Garber and Friedman, 1983). Some of these aragonite precipitates are botryoidal, others are encrusting, yet others are oolitic/pisolitic, all are interpreted by Garber as largely inorganic precipitates. They are reminiscent of the microbial, stromatolitic and pisolitic crusts of the South Australian salinas and like them indicate strandzones and seeps in ancient counterparts.

In summary, surface sediment distribution in the Dead Sea region is a combination of Holocene accumulations and palimpsest Lisan Fm. derivatives (Figure 4.51). Today the lake is holomictic and a bed of coarsely-crystalline, inclusion-free halite is accumulating on the deep water floor of the lake. At the same time detrital accumulations fed from stream inputs, especially the Jordan River, dominate the northern parts of the lake. In the recent past (pre 1979) the lake was permanently stratified and deposition of carbonate laminite was the dominant depositional style on the deep lake floor.

Fluvial input to the fresher surface waters of the lake supplied both the detritals (calcite, aluminosilicate clays and siliciclastics) and drove the mixed water chemistry that created the aragonite rich portions of the laminite couplets. Dust storms also supply detritus to the deep lake bottom.

Lake Lisan, Jordan Valley

Beneath and surrounding the Holocene sediments of the Dead Sea are the sediments of the Quaternary Lisan (70 to 17 ka) and Damya (17 to 12 ka) formations (Bartov et al., 2002). The Lisan Formation forms a blanketing cover throughout the Jordan Valley (Figure 4.54a). *Lisan* is Arabic for tongue and describes the shape of the Lisan Peninsula where the type section was measured. Pleistocene Lake Lisan waters left behind dissected terraces of lacustrine sediment, consisting of laminated marls up to 40m thick, that extend from Lake Tiberias (Sea of Galilee) in the north to a boundary ridge some 35 km south of the Dead Sea (Figure 4.52). The highest outcrops of Lisan

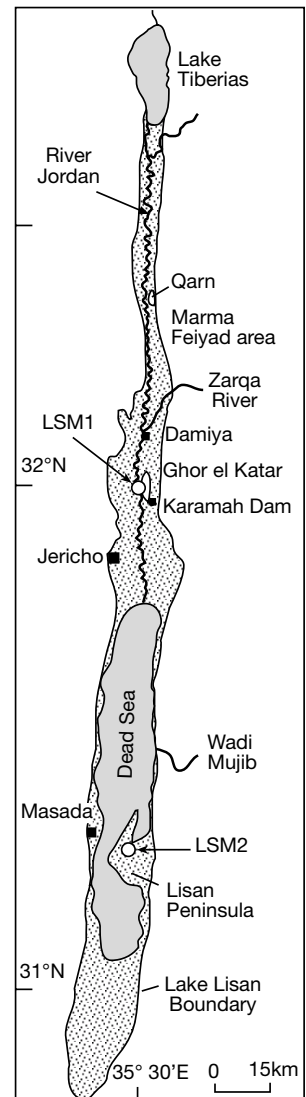


Figure 4.52. Extent of Pleistocene Lake Lisan in the Dead Sea transform. Positions of sites LSM1 and LSM2 are indicated (see figure 4.55 for detail).

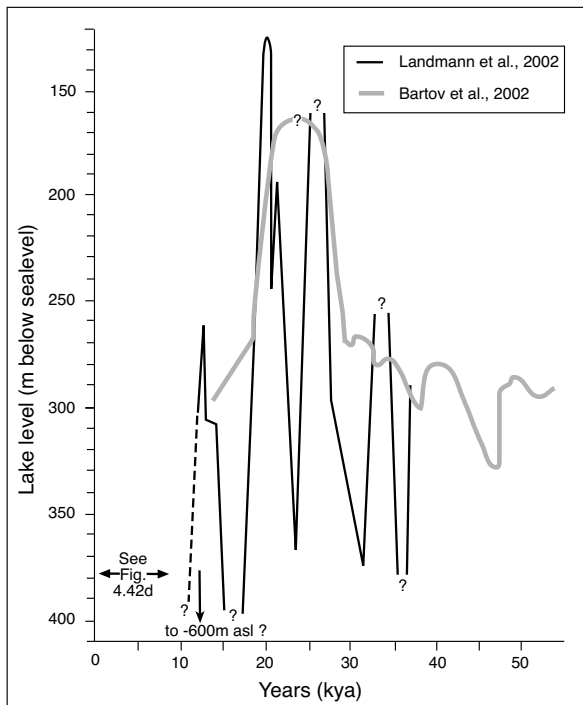


Figure 4.53. Lake Lisan levels between 15,000 and 50,000 years ago.

laminites are found at -180 m asl, but there is morphological evidence for lake waters as high as -150m or even -130 m asl during Lisan time (Figure 4.53). During its highstand, Lake Lisan covered several subbasins in the Jordan Valley, it had a maximum area of some 2,000 km² and a drainage basin of 40,000 km². Pre-Holocene, but post-Lisan, sediments occur in fan delta regions near the current Dead Sea shore and in the vicinity of the city of Damya in Jordan, which is the type area for the Damya Formation.

Mineralogical variations in the Lisan Formation along the Jordan Valley show lake waters varied both in aerial extent and salinity. The lake was permanently stratified for much of its history. In its southern part, the sedimentary sequence consists mainly of laminated evaporites, and salinity is thought to have ranged between 100 and 300 g/l and lake water levels were probably lower. At the higher elevations that characterise Lisan outcrops in the north in the Kinarot basin, sediments of the Lisan Formation are very different, and the sequence is mainly diatomite. The change from south to north probably indicates inflow from the north and a freshening of surface waters during the highest stands of the lake. Salinities throughout Lisan time were hypersaline but probably less than those of the present Dead Sea (Abed and Yaghan, 2000).

Landmann et al. (2002) document two styles of couplet in the Lisan laminites; 1) detritus–aragonite (most common), and 2) detritus–aragonite–gypsum. Begin et al. (1974) documented the lithology and biota of the Lisan Formation along the Jordan Valley west of the Jordan River. They subdivided it into a lower Laminated Member and an upper gypsiferous White Cliff Member. Along the Jordan Valley they described three laminite facies; a gypsum facies in the Dead Sea region, and an aragonite facies north of the Dead Sea up to Marma Feiyad and a diatomite facies further north. Later work by Abed and Yaghan (2000) in the vicinity of Ghor el Katar and the nearby Karameh Dam reclassified the Lisan into three members; Lower Laminite, Middle Clay and Upper Laminite with the White Cliffs making up the upper part of the Upper Laminite. The contrast in gypsum content in laminites of the Lisan formation from the Ghor el Katar region (LSM1) compared with those of the Dead Sea region (LSM2) is clearly documented in the detailed mineralogy of two outcrop sections published by Landmann et al., (2002; Figures 4.52, 4.55).

The Lower Laminite is made up of thinly interlaminated calcareous silt and aragonite with subordinate sand layers. In the Ghor el Katar area (LSM1) the Lower Laminite is 15 m thick and the aragonite proportion is less than 30%. The Middle Clay is composed of massive black clays, and is around 9 metres thick. The clay matrix is mostly mixed layer illite/smectite with minor kaolinite. No gypsum or other evaporites occur in the Middle Clay and its organic content can be as high as 6%. The Upper Laminite is once again mostly interlayered aragonite and detrital silt (Figure 4.55). Thin sand and clay layers are not uncommon in this unit. Its uppermost 5-7 metres outcrops as a conspicuous white cliff that entrains layers with abundant gypsum. This upper portion in section LSM1 is equivalent to the White Cliff Member of Begin et al. (1974) as documented in section LSM2 (Figure 4.55). To the south of Ghor el Katar area, the White Cliff unit thickens until it is more than 25 m thick on the Lisan Peninsula (LSM2; Figure 4.55).

The Lower and Upper Laminated members are composed of very fine, varve-like white and dark laminae. White laminae are usually monomineralic and composed mainly of aragonite needles with diatom frustules. In the White Cliff unit the light-coloured laminae are composed almost entirely of gypsum or mixtures of aragonite and gypsum. Gypsum laminae are dominated by fine lenticular gypsum crystals (0.25 to 0.50 mm) with their long axes arranged parallel to the bedding. Dark laminae are predominantly detrital mud-sized calcite, the reworked remnants of microfossils, nannofossils and rock fragments. Quartz, dolomite, clay minerals (kaolinite, smectite,

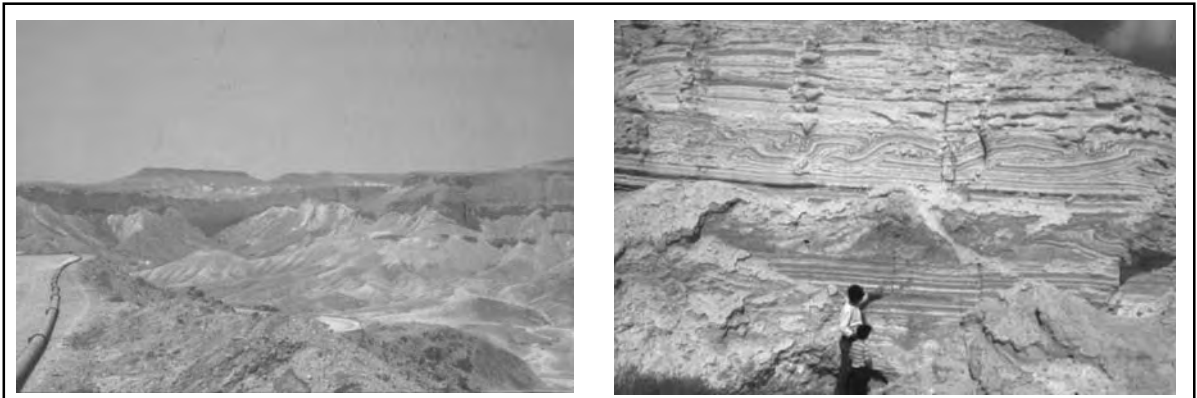


Figure 4.54. Lisan Formation. A) View of Lisan Formation outcropping along the escarpment of the Dead Sea, B) Syndepositional slump in the Lisan Formation.

illite, and palygorskite), halite, and gypsum also occur in these detrital calcitic layers, much like in the laminites of the present Dead Sea floor.

In the vicinity of the modern Dead Sea the laminae in the Lisan Formation are sometimes crenulated and may contain sulphur concretions. Some layers display sediment slumps and overfolds, water escape structures, growth faults, and other evidence of soft sediment deformation (Figure 4.54b). The Lisan Formation was laid down as a water-saturated muddy succession; earthquakes kicked off multiple episodes of sediment movement both syndepositionally and in the shallow subsurface (Weidlich and Bernecker, 2004).

Some of the non-gypsiferous aragonitic couplets are interpreted as accumulating in lake-waters some 400-600 metres deep. But gypsum in some of the Lisan laminites in the White Cliff Member show evidence of much shallower deposition in the form of large vertically

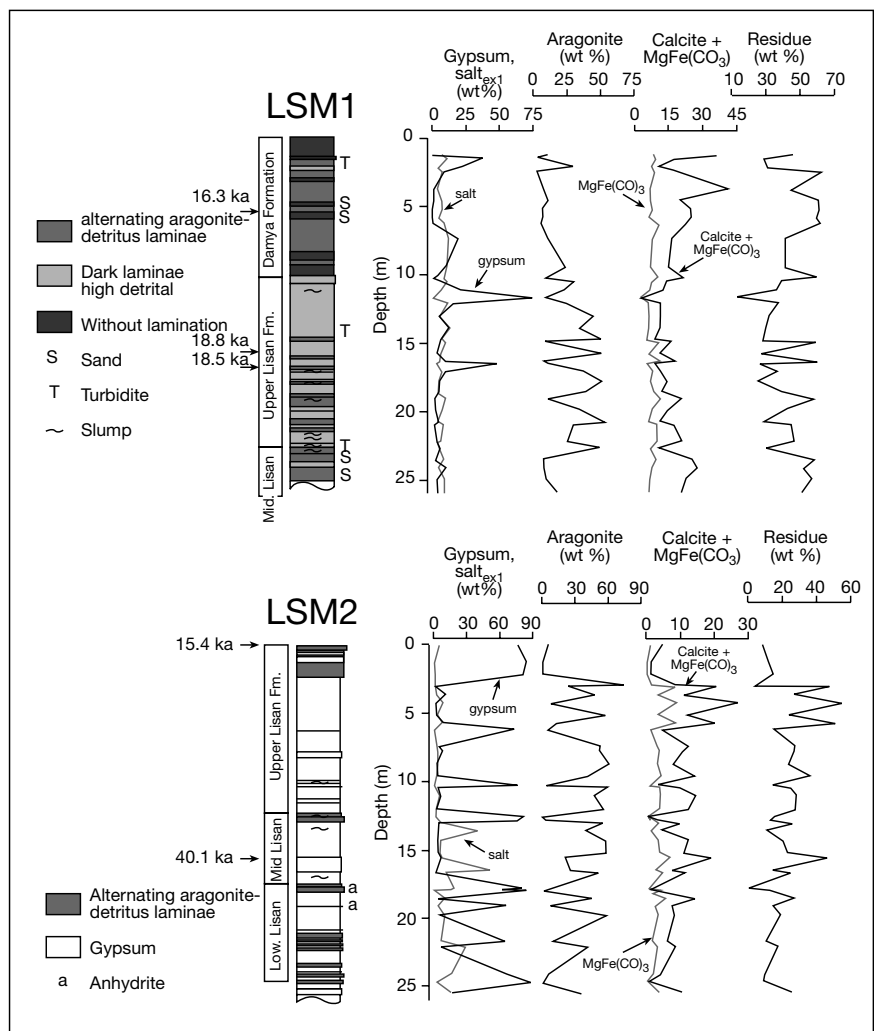


Figure 4.55. Stratigraphy and mineralogy of the Lisan and Damya formations in the Jordan Valley. Positions of the sections are shown in Figure 4.52 (after Landmann et al., 2002).

aligned gypsum crystals. These giant crystals fit better an earlier model of Lisan Formation deposition by Picard (1943) who described the coarsely crystalline gypsiferous parts of the Lisan Formation as being deposited in a combination of settings, a shallow lake, a large playa, and/or a giant sabkha. The presence or absence of gypsum perhaps indicates changing water levels in the Lisan Lake so that when bedded and growth-aligned gypsum is commonplace the Lisan water levels were lower..

Overlying the Lisan Formation is up to 14 m of clastics of the Damya Formation (equivalent to the "unnamed unit" of Begin et al., 1974). Damya sediments are mostly clays, silts and sands, some gravels and no evaporites (Abed and Yaghan, 2000). It was deposited in a freshwater to brackish lake stage with a water level of -160m at the onset of Lake Damya some 15-16 ka. According to Begin et al. (1985), the Lake Damya ended some 10-11 ka with a drop to -700 m asl, a fall in lake level of more than 800 metres in a few thousand years (Figure 4.53). If real, it means the driest period in Lake Lisan's history was immediately preceded by the wettest time in Damya climate. Clearly, waters levels in perennial saline lakes are subject to high frequency, high amplitude changes in water level with rates of change that can be 4 to 8 times greater than marine eustatic changes in an icehouse climatic mode (Chapter 5).

Lake Asal, Republic of Djibouti

Lake Asal, with a water surface some 155 m below sea level, is the lowest place in Africa (Figure 4.56). The lake is small (area 52 km²) and shallow, with a maximum depth of 30 metres and an average depth of 7.4 metres. The lake depression lies in the NW-SE oriented Asal - Ghoubbat al Kharab rift extending northeast into the Gulf of Aden. It is part of a tectonic system considered to be one of two examples where an oceanic ridge outcrops; the other being on the island of Iceland. This part of the rift extends southwest into the East African rift and is at the marine-fed end of what is our type example (Afar triangle) of a spreading centre (triple junction) in an arid part of world's rift systems. Locally, the ridge shows a spreading rate of 30-60 mm/year. Although small, Lake Asal is one of the few modern examples of a marine-fed rift basin that is actively accumulating bedded evaporites. As such, it is the only Quaternary analog for ancient marine-fed rifts including the numerous Mesozoic evaporitic lacustrine basins that underlie passive margins on either side of the Atlantic (Table 5.6).

The lake today is completely continental with no surface connection to the ocean. Yet the fact its -155m asl level has changed

little in the last few centuries argues it is fed a steady flow of seawater through the highly fractured 10 km wide volcanic ridge that separates oceanic water at Ghoubbat al Kharab from the hypersaline waters of Lake Asal. It constitutes an excellent example of a drawdown marine seepage basin fed through a volcanic ridge.

Many actively flowing springs, locally called manda, are dotted along the eastern strandzone of the lake. Their geochemical makeup is very close to seawater proportions (Sanjuan et al., 1990). Total marine inflow to the lake is estimated to be of the order of 60-80 m³ per second, with transit times for waters seeping from the ocean to the lake floor measured in less than tens of years, or at most two centuries (Demange et al., 1971; Fontes et al., 1980). Outflow is focused along shallow narrow fracture networks that cut the volcanic ridge (Mlynarski and Zlotnicki, 2001). There are also several hydrothermal springs and many fumaroles still active in the area and it is clear that the subsurface temperatures are still very high below the fracture meshworks carrying cooler seawater inflows to the lake depression.

Two deep wells were drilled in the Asal area in 1975, Asal-1 had a final depth of 1154 m and Asal-2, a final depth of 1554 m. These thermal test holes were drilled at the southwest edge of the geothermal area in a region where there is no direct inflow from the sea. Asal-1 produced 22 kg/sec of high salinity water with a measured temperature at 1040 m of 255°C prior to flow testing, and 260°C during a flow test in 1981. Water produced by Asal-1 had a very high solids concentration (128 g/l) and during the 1981 flow test, rapid incrustation in the casing had plugged the well in less than 3 months. The other well, Asal-2, was plugged inside the casing, possibly by drilling mud, and is no longer producing steam.

Lake brines reach salinities of 350 ‰ and, like their marine spring feeds have seawater like proportions, dominated by Cl, Na, K, SO₄ and Mg. Salts in the perennial standing body of lake brine are mostly gypsum, which is accumulating with mounded and bottom-nucleated aligned-layer textures identical to those that characterise the South Australian salinas. Gypsum precipitation dominates in this the southeastern part of the lake depression, located next to the seeps that bring seawater to the surface. Fractures also intersect the subaqueous lake floor and seawater can be seen to rise up along fractures cutting the lake bottom. Older layered and mounded gypsum beds crop out around the lake edge to as high as 55 metres above the present lake level (Stieltjes, 1973).

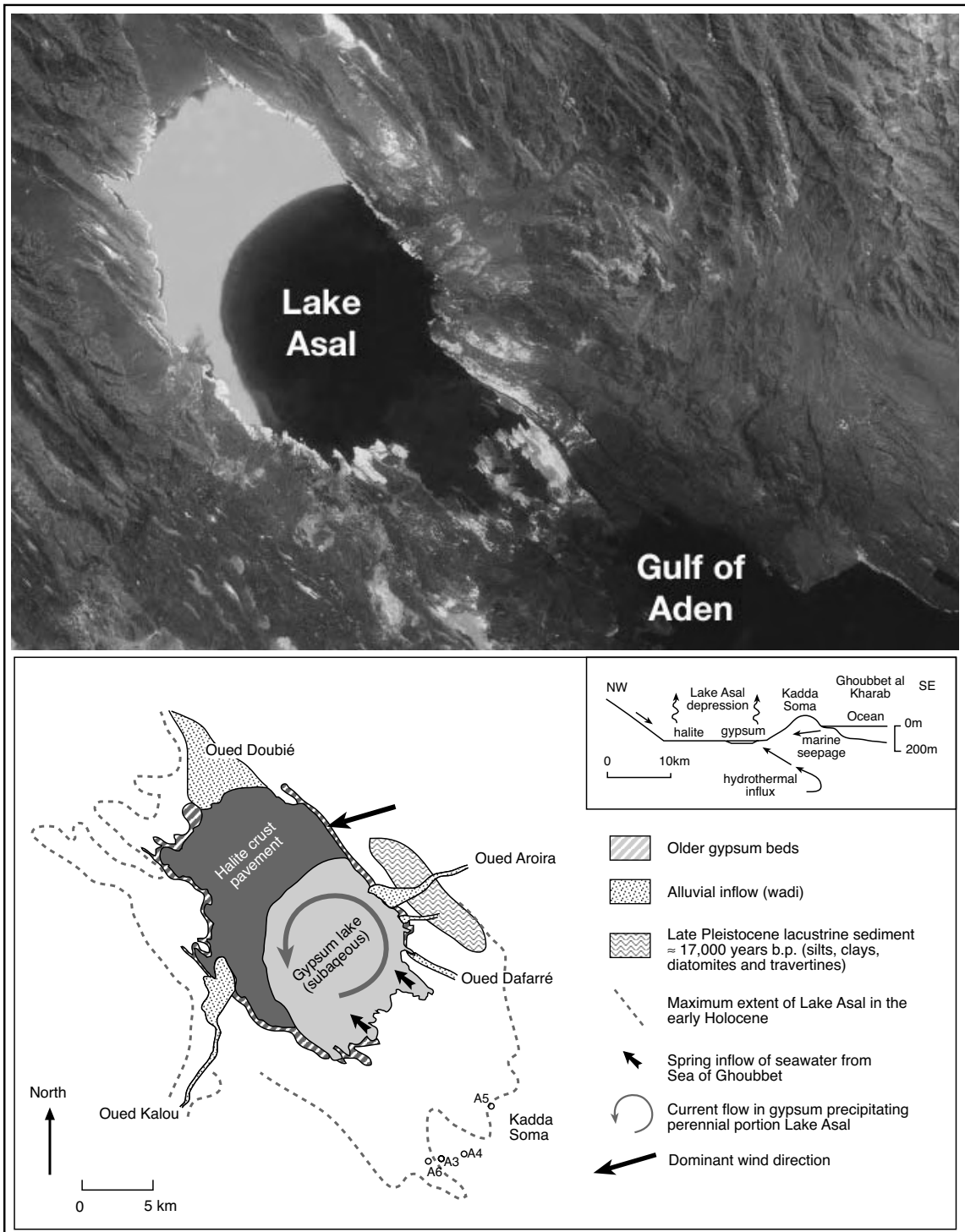


Figure 4.56. Holocene sediment distribution in Lake Asal, Republic of Djibouti (surface geology after Stieljes, 1973). Marine inflow is via fractured basalts of the Kadda Soma. A_{3,4,6} indicate positions of geothermal test wells - A₁ and A₂ lie further to the southwest. The inset is an idealised cross section from the ocean to the lake depression (Landsat image courtesy of NASA).

Hydrological compartment	Volume (1000 km ³)	Percent
Oceans	1,370,000	97.61
Glaciers, ice, snow	29,000	2.08
Subsurface	4,067	0.295
Freshwater lakes, rivers	126	0.009
Saline lakes	104	0.008
Atmosphere	14	0.001

Table 4.5. Water volumes in the global water compartments (after Wetzel, 1988).

Stacked halite crusts characterise the saline pan facies that covers much of the northeastern part of the lake where it forms a wide (≈ 60 km) and thick (20–80 metre) accumulation of pan halite. Prior to 1978 the top of this halite plain lay some 30 to 80 cm above the water surface of the perennial gypsum lake. Then in 1978 renewed volcano-tectonic activity in the region

reopened fractures and faults leading to an increased influx of waters from the Ghoubbat al Kharab and a rise of lake waters which partially submerged the top of the salt pan (Ruegg et al., 1979). Once again, as in most other basins accumulating bedded evaporites, the changes in hydrological base level in this depressed pan are in large part driven by tectonics, not marine eustacy (see Chapter 5). The separation between areas of subaqueous gypsum and pan halite clearly shows how two mineral phases cannot accumulate simultaneously in a single holomictic brine lake, but can be adjacent facies.

Are all modern saline lakes shallow?

Table 4.5 shows the relative importance of saline lakes in the total volume of the world's surface water. There is as much water caught up in the world's saline lakes as there is in freshwater lake systems. Tables 4.6 and 4.7 summarize the physiographic

	Area km ²	Brine surface	Hydrological setting (Brine source)	Tectonic Setting	Characteristics
Lake MacLeod, Australia (Logan, 1987)	2,500	≈ 1 m below sealevel	Evolved from stratified perennial to ephemeral during sediment infill (marine)	Passive margin	Holocene marine-fed coastal salina with 10m thick bottom-nucleated salt beds. Stable brine curtain maintains salt beds and marine-fed seepage margin. Salts have filled an interdunal depression to within a metre of ambient sealevel via seepage of mostly marine-fed groundwater.
Abu Dhabi mudflats (Evans et al., 1969)	≈ 300	≈ 1 m above sealevel (asl)	Ephemeral with water cover during marine flood stage (marine)	Ramp in foreland basin	Holocene marine-fed coastal mudflat with 1-2m thick displacive salts growing in detrital matrix of supratidal and intertidal units. Stable brine curtain is maintained by capillary evaporation and marine seepage.
Dead Sea, Middle East (Ben-Avraham et al., 1999)	1,000	-415 m asl	310 metre deep lake hypersaline lake with alternating longterm meromictic and holomictic brine columns (nonmarine)	Continental transform basin	Quaternary fluvial/seepage-fed deep perennial lake. Thick stable brine curtain bathes multiple stacked subaqueous beds. Beds in Northern Basin deposited in deep water, Southern Basin in saline pan/ salina settings. Much of the solute is fed to the lake from springs carrying dissolved Miocene (4-6 Ma) evaporites (diapirs also outcrop on lake floor).
Kara-Bogaz-Gol, Turkmenistan	13,000	28 m below sealevel	Endorheic basin joined by a narrow inlet to Caspian Sea (nonmarine)	Intramontane basin in a continent-continent collision belt	In the last 0.5 million years three separate Mg-Na-SO ₄ -rich salt layers have formed across the gulf, perhaps forming best in glacial episodes when the connection to the Caspian was reduced compared to today, and year round temperatures were much lower. Such glacial conditions favoured a perennial lake to pan mode of cryogenic mirabilite precipitation (Figure 11.56)
Lake Eyre, Australia (Magee et al., 1995)	9,300	-15 m asl	Ephemeral lake mudflats with up to 6 metres of freshwater cover emplaced during occasional storm flood (nonmarine)	Intracratonic sag atop Precambrian rift	Quaternary fluvial-seepage fed, has changed from fresh (100 ka) to the ephemeral salt lake of today, showing the decreasing effect of the monsoonal feed. Upwelling and throughflushing of freshened artesian waters beneath the lake destroys the brine curtain and so prevents more than 2-3m of halite accumulating beneath the lowermost parts of the lake floor.
Salar Uyuni, Bolivia (Risacher and Fritz, 2000)	10,600	+ 3653 m asl	Saline pan with peripheral mudflat (continental/hydrothermal)	Intramontane basin in a forearc collision belt	Largest salt pan in the world today. A 121m deep well intersected 12 saline-pan beds separated by 11 lacustrine mud beds, all bathed in a stable brine curtain. Mud layers thicken upwards, while the thickness of the salt beds decreases markedly from the base upward.

Table 4.6. Representative listing of variations in Quaternary evaporite deposits.

variety of some Quaternary perennial brine lakes. Admittedly, around 70% of the saline lake water volume listed in Table 4.5 comes from the Caspian Sea. This saline lake and the other saline lakes of western Asia (Kara-Bogaz-Gol, Lake Urmia, Lake Issyk-Kul and Lake Van) are all located in foreland basins created by Neogene collision tectonics and together contribute what appears to be an anomalously high proportion to the world's total volume of saline lake waters. Then again, over 40% of the listed freshwater volume comes from the combined volumes of Lake Baikal and the Great Lakes of the North Americas. Also, most saline water bodies are shallow, so the area of the world's surface covered by saline lakes is probably greater than that covered by freshwater lakes.

In terms of saline lake sediments associated with saline water bodies, the largest contiguous area of Quaternary bedded salt accumulating today is in Salar Uyuni, a continental lake (saline pan/mudflat) with a water level some thousands of metres above sea level. The Dead Sea, with a water surface more than 415 m below sealevel is our onHolocene example of a substantial deepwater evaporite basin currently accumulating halite. Its inflow is a combination of river and saline spring inflow. Our best example of an active marine-fed perennial saline lake, which is still accumulating bedded shoalwater gypsum and pan halite, is Lake Asal, a rift depression lake with a water surface some 155 metres below sea level. In area, it is exceeded by many of the marine seepage-fed Holocene coastal salinas of southern and western Australia. Unlike Lake Asal, the Australian coastal salinas have equilibrated within a metre of the height of their sea level source and are no longer actively accumulating subaqueous bedded salts. Active subsidence in a rift seems to allow a continental lake to maintain permanently subaqueous brines, as is the case in the Dead Sea. After Lake Asal, Death Valley at -86 m asl, is the next deepest hole on the world's surface that is occupied by a saline lacustrine system. In its current form it is a saline pan rather than a perennial halite accumulating lake, but in the Late Pleistocene it was a deep perennial system (Chapter 3). Although well studied, the volume of salts accumulating in Death Valley is relatively minor in terms of the total volume of salt in saline lacustrine settings of the world.

A plot of salinity versus brine depth in the world's perennial saline lakes shows that lakes accumulating salts more saline than calcite/aragonite/dolomite couplets (salinities > 70 ‰) tend to be shallow, with brines less than 10-20 metres deep (Figure 4.57a). In terms of total salts held in the lake waters the less saline lakes (Caspian, Aral Sea, Lake Urmia) dominate (Figure 4.57b). An obvious exception to the more saline

lakes being characterised by shallow to ephemeral surface waters is the current condition of the Dead Sea. The Dead Sea's physiography as a narrow rapidly subsiding basin in the deepest continental position on the world's surface makes it unique amongst the world's modern saline lakes. But the Dead Sea can accumulate halite in its deepest waters only when its longterm density stratification is destroyed (holomixis). The destruction of the halocline is not an annual event, as it is in some of the less saline lakes (e.g. Lake Van), but seems to occur every few hundred years.

All of the largest active perennial saline water bodies, which are depositing substantial volumes and areas of subaqueous salts over time frames measures longer than 10,000 years, are continental not marine depressions. All the largest perennial saline lakes occur in semi-arid rather than arid to hyperarid climates and all are located in tectonically active and subsiding (underfilled) basins such as in the Andes, the tectonic collision zones of Turkey and Iran, and the Basin and Range of USA.

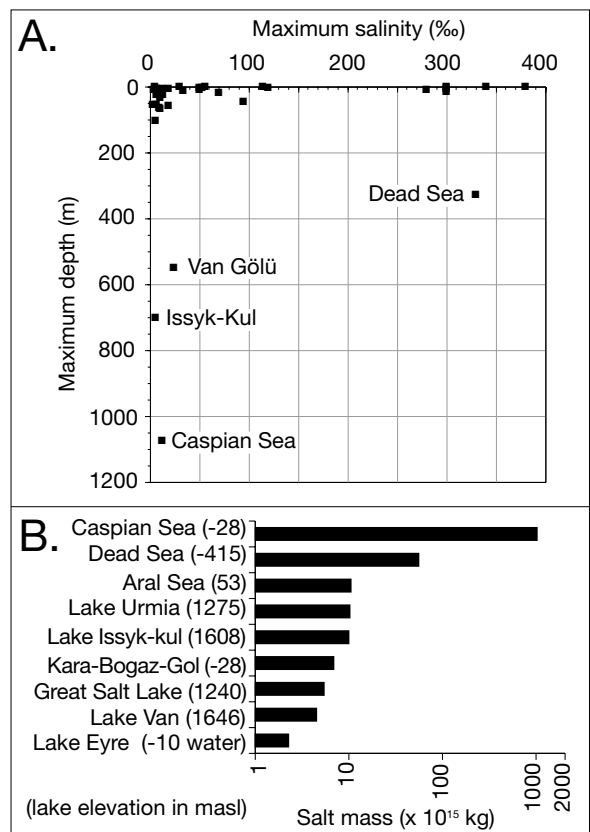


Figure 4.57. Physiography of saline lakes of the world. A) Maximum salinity of saline lake waters versus maximum water depth in the lake (data plotted from Table 4.7). B) Mass of salt held in selected lake waters. Note logarithmic scale.

Lake	Style	Salinity ‰	Area km ²	Vol. km ³	Depth Av. (m)	Depth Max.(m)
Great Salt Lake (USA)	perennial	150-280	4,400	19	4	10
Salton Sea (USA)	perennial	33	891	6.8	7.6	12
Pyramid (USA)	perennial	5.3	446	26.4	59	103
Big Quill (USA)	perennial	43-53	307	0.5	1.5	2.6
Mono (USA)	perennial	95	158	2.8	15.2	45.7
Walker (USA)	perennial	10.6	150	3.5	20	33
Natron (Africa)	perennial	340	900	0.35	0.4	0.5
Magadi (Africa)	perennial	114	95	0.05	0.5	0.6
Nakuru (Africa)	perennial	10-120	40	0.06	1.5	3
Bogoria (Africa)	perennial	50	33	0.18	5.4	9
Elmenteita (Africa)	perennial	29.5	20	0.02	0.9	1.1
Simbi (Africa)	perennial	13	0.3	0.004	13	23
Sonachi (Africa)	perennial	6.8	0.2	0.0007	4	7
Caspian (Asia)	perennial	10-12	422,000	79,000	n/a	1072
Kara-Bogaz-Gol (Asia)	perennial	300-360	13,000	20	3	9
Aral (Asia)	perennial	8-10	66,000	1,064	n/a	69
Balkhash (Asia)	perennial	0.5-7.0	22,000	122	n/a	27
Issyk-Kul (Asia)	perennial	5-6	6,300	1,730	n/a	702
Chany (Asia)	perennial	1.5-4	3,245	7.1	n/a	10
Tengiz (Asia)	perennial	3-19	1,590	n/a	n/a	8
Qinghai (Qinghai)	perennial	12.5	4,600	85	17.5	27
Lop Nor (Sinkiang)	ephemeral	5	3,010	5	n/a	1
Selin (Tibet)	perennial	19	1,628	49.2	30	60
Zarainmu (Tibet)	perennial	12	996	6	6	6
Dabuxun (Qinghai)	ephemeral	380	184-334	>1	n/a	1
Dalai (China)	perennial	5.5	238	1.6	n/a	7
Urmia (Iran)	perennial	>200	5,000	25	5	16
Van Golu (Turkey)	perennial	24	3,600	19	53	550
Niriz (Iran)	perennial	7-56	1,810	1.8	1	1.7
Tuz Golu (Turkey)	ephemeral	>300	1,600	1	0.5	2
Dead Sea (Israel/Jordan)	perennial	>300	940	136	145	330
Eyre North (full -Australia)	ephemeral	>50 - >300	8,430	27.7	3.3	5.7
Corangamite (Australia)	perennial	30-50	233	0.5	2.9	4.9
Bullen Merri (Australia)	perennial	9	4.9	0.2	39.3	66
Gnotuk (Australia)	perennial	70	2	0.03	15.3	18.5

Table 4.7. Physical characteristics of some perennial saline lakes worldwide.

Tectonism facilitates steep topographic gradients, endorheic closure and subsidence within large intermontane depressions, all three factors seem to be needed in order to form a permanent brine body in Quaternary systems. Milder levels

of aridity allow waters to persist above the land surface and do not drive the conversion of the hydrology to sabkhas and evaporitic mudflats that characterise the more arid settings.

The other significant factor common to the formation of large perennial saline lakes is longterm climate change. Ephemeral flood-pan lacustrine systems, such as Lake Eyre and Lake Frome in Australia, which today are combinations of saline pans and evaporitic mudflats, were large perennial lakes in milder climatic episodes in the Late Pleistocene. These southern hemisphere “mega-lake” phases are tied to a more southerly influence of the monsoonal belt during these times. Even historical flooding events in the central Australian playas are frequently tied to La Nina phases in the El Nino-Southern Oscillations (ENS. Laminated Pleistocene (10-12 ka) lacustrine sediments from Lake Magadi also preserve evidence of ENSO changes in the variations of laminae thickness (Damnati and Taieb, 1995). Changes in Pleistocene climate also explain why many modern playas and pans in the Basin and Range were once perennial lakes; during pluvial episodes of the Late Pleistocene some were even freshwater lakes with waters more than 100 metres deep (Smoot and Lowenstein, 1991). Death Valley for example, changed from its modern saline pan/mudflat setting into a perennial saline lake in this time (Chapter 3). Perhaps one of the most impressive Late Pleistocene megalakes was Lake Chad some 8,000 to 10,000 years ago when its water-covered area was equivalent to that of the present Caspian Sea. Other lakes currently in their fresher saline stages (Lake Van and Lake Urmia) experienced times of shrinkage and desiccation in the Late Pleistocene.

To state everything we have discussed so far in its simplest terms: to accumulate bedded salts, you need a large, deep centrally-draining somewhat leaky hole in the ground (a groundwater sump). And, like Goldilocks, it

performs best in a climate that is not “too hot” and not “too cold” and not “too wet” and not “too dry.” If we use Quaternary examples of evaporites as strict uniformitarian analogues for ancient evaporite deposits then we must conclude that thick, laterally extensive salt beds are always continental lacustrine deposits, accumulating in tectonically-induced, rapidly-subsiding intermontane basins.

Marine seepage fed platform and basinwide evaporite settings do not exist today. But, the next chapter will show that most of the largest examples of ancient evaporites are actually marine-fed precipitates, deposited under eustatic and tectonic conditions for which there are no Quaternary counterparts.

Chapter 5: Ancient basins and stratigraphic evolution

Is the present the key to the past in evaporite studies? It's a question that has plagued geologists working with salts since the 17th century, when Werner's neptunist postulates explained world geology (including igneous strata) as layered precipitates from cooling oceanic waters. And like Werner's Scottish protagonists, we are still discussing the merits of strict uniformitarianism. In this chapter I am not questioning the fundamental principle of using present process to interpret the past. Nor am I questioning the utility of detailed studies of modern process to reliably interpret the past. Let me put it plainly for the creationist community and proponents of "intelligent design," all the geological evidence clearly shows the earth is not 8,000, but more than 4 billion years old, that biological evolution is fact, it interacts with and responds to the physical environment and has been in operation for at least the past 3.5 billion years. There is no need to invoke the supernatural to explain biological evolution and other earth processes, and there is no geological evidence for a worldwide biblical flood of epic proportions drowning mankind and covering all the land.

What I am questioning is strict actualistic approaches to sedimentological interpretation of evaporites, whether the depositional diversity we see in our current icehouse climate

mode and eustasy is sufficiently broad to explain the diversity of ancient evaporites (Table 5.1). If our present is the key in terms of all scales of deposition and climate, then why are there no marine platform evaporites forming today and why are there no evaporitic seaways? Chapters 3 and 4 show that the largest and thickest Quaternary evaporites are continental lacustrine deposits, not marine-fed systems. We shall shortly see that such lacustrine systems are directly and completely comparable with their ancient lacustrine counterparts in terms of facies, salt thicknesses and lateral extents. But the scale of lacustrine evaporite development, past and present, pales in comparison to some ancient marine-fed saline systems. There are no modern counterparts to such ancient marine-associated systems. Our inability to compare all aspects of evaporite deposition, past and present, reflects a present-day lack of both longterm shallow epeiric seas and of large drawdown basins fed by seawater seeps.

The Hith Anhydrite of the Middle East, the Zechstein salts of Europe and the Messinian evaporites of the Mediterranean have no modern same-scale counterparts. An understanding of the shortcomings inherent in applying strict uniformitarian models is tied to current styles of continent-scale tectonics and

	ICEHOUSE	GREENHOUSE
Age	Late Cenozoic, Late Carboniferous to Early Permian, Late Neoproterozoic	Cambrian to Middle Carboniferous, Middle Permian to Early Cenozoic
Tectonic style	Collision, telescoping	Stretching, rifting
Seafloor spreading	Slow	Rapid
Subduction/volcanism	Low	High
Marine margin basins	Narrow shelves, limited short-lived interior seaways with small aerial extent	Wide shallow shelves and large long-lived interior seaways (epeiric seas)
Marine eustasy	High amplitude ($\approx 100\text{m}$) change on 100,000 year times scale (4th order). World sealevel is low (caught up in longterm polar ice sheets)	Low amplitude ($>5\text{-}10\text{m}$) change on 100,000 year times scale (4th order). World sealevel is high (no polar ice sheets)
Ocean Basins	Cold, oxygenated	Warm, often anoxic
High latitude climates	Glaciers, taiga and tundra	Deciduous forest
Mid latitude climate	Deciduous forest, glacial advances and steppe	Tropical wet and stressed forest
Low latitude climate	Rainforest, savanna and desert	Desert
Erosion/weathering	Fast/mechanical	Slow, chemical
Depositional styles of large evaporite basins	Tectonically induced endorheic continental depressions (terrestrial lacustrine; no marine-seep platform and basinwide evaporites accumulating at present time; but basinwides can form in suitably isolated icehouse conditions, and did so most recently in the Middle and Late Miocene)	Tectonically and eustatically induced endorheic continental and marine margin depressions (terrestrial lacustrine, marine platform and marine-fed basinwide styles can be widespread whenever suitable combinations of tectonics and eustasy occur)

Table 5.1. Climatic and depositional contrasts between icehouse and greenhouse earth.

icehouse eustasy. Put simply, the rates and amplitudes of seafloor spreading, orogeny and eustasy are not constant across deep time. Widespread marine evaporites require particular tectonic and/or eustatic conditions to accumulate, conditions that are not present on the world's modern surface (Table 5.1). They will be in the future, and they have been many times in the past.

This chapter demonstrates the importance of differences between icehouse and greenhouse climate/eustasy as controls on evaporite style in marine platforms. It shows how particular tectonic and climatic settings are needed to form saline giants in isolated subsealevel drawdown depressions. It also shows how interpretations using sequence stratigraphic marine eustatic frameworks do not work as well in ancient basinwide saline giants as they do in interpreting evaporites laid down on ancient marine platforms. Even on an ancient continental shelf, we need to separate icehouse from greenhouse platforms in order to understand evaporite distribution.

By the end of this chapter, I hope it will be obvious that when trying to predict and model ancient evaporites it is much more

useful to consider tectonics and hydrologies of large evaporite basins as the fundamental controls of basin-scale evaporite geometries, mineralogies and bounding surfaces. One should not force marine-seepage-fed drawdown systems into a marine-eustatic icehouse model. Nor should our interpretations be driven by the hydrologically dubious notions of ongoing surface (hydrographic) connections between ocean waters and restricted basins at the time thick salts accumulate; and yet these assumptions still dominate many interpretations of ancient evaporite basins.

Linking present to past aridity

In order to understand possible linkages between present and past evaporites, we must first understand geological indications of past and present climate. After all, the preceding chapters clearly show it is climate that drives the accumulation of salts in the deserts, lakes and sea margin systems of today and that the same was true in saline giants of the past. Only with a sturdy palaeoclimate understanding can we reliably compare

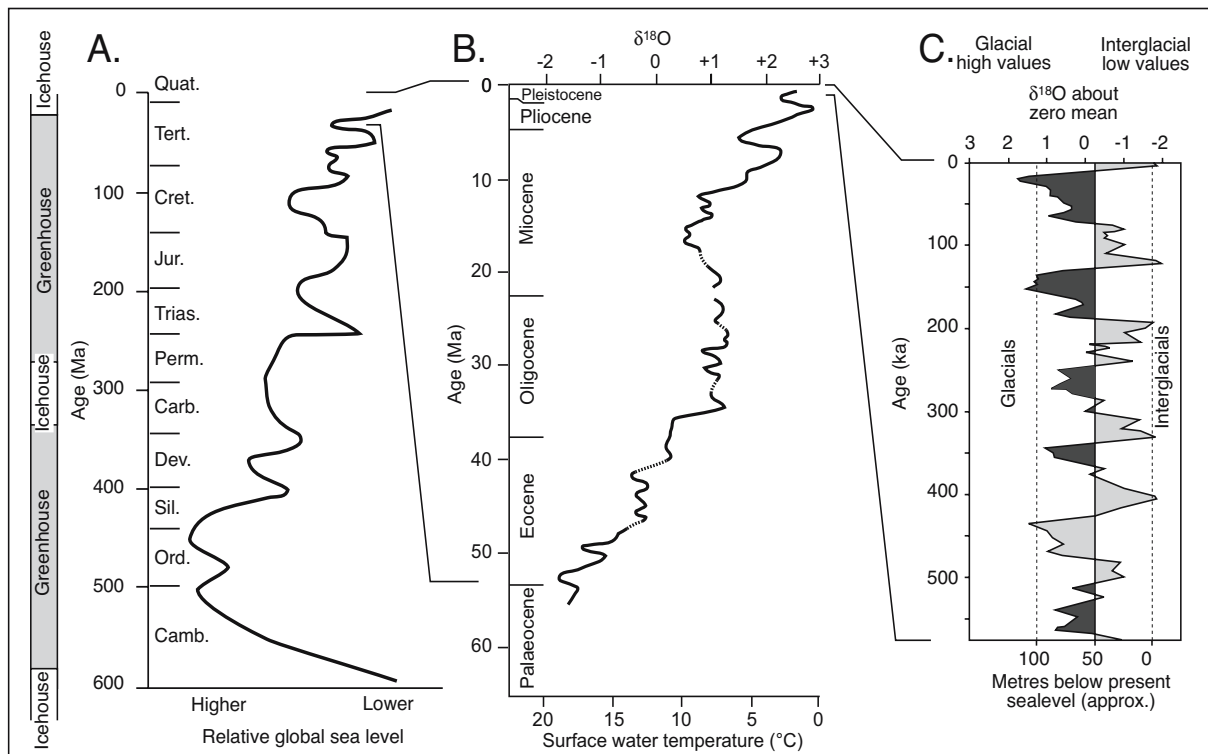


Figure 5.1. Sea level change through the Phanerozoic. A) Relative sea level curve, based on sequence stratigraphy of Vail et al., 1978. Icehouse and greenhouse intervals are not well constrained. B) and C) show Tertiary and Quaternary oxygen isotope/palaeotemperature curve of high latitude seawater and are based on deep marine sediment cores in the Southern Ocean. Isotope scale on the Tertiary curve is relative to SMOW, the Quaternary curve is corrected to a zero mean (both curves are after Williams et al., 1993).

Quaternary to older depositional settings. Quaternary and late Neogene climatic systems, characterised by waxing and waning polar ice sheets, define the current “icehouse” climate mode. Today, some 10% of the world's surface is covered by ice, representing about 80% of surface freshwater, and a further 20% is affected by permafrost. Of these ice-covered lands, Antarctica has 86% by area and Greenland 11%. In the last glacial maximum (18-20 ka) a staggering 30% of the earth's surface was covered by ice.

The current icehouse mode evolved during the latter part of the Tertiary period and is characterised by glacially -driven oscillations in sealevel with amplitudes of more than a hundred metres, with repeat frequencies around 100,000 years (Figure 5.1). Marine-fed evaporite distribution associated with icehouse and its older counterparts at the end of the Palaeozoic and the Neoproterozoic are not the same as that of the “greenhouse” climate mode, which has dominated much of the earth's Phanerozoic history (Table 5.1).

Quaternary climate (icehouse), especially in semi-arid to temperate latitudes, is characterised by repeated rapid temperature swings from levels much like those of today (interglacial) to levels many degrees colder. Colder (glacial) times are associated with growth of huge km-thick circumpolar and high latitude/high elevation ice sheets and lowered sealevels. Ocean surface temperatures were up to a few degrees cooler at such times, while sealevels fell more than a hundred metres compared with its interglacial current level. On the land, mountain tree lines shifted to lower positions, grasslands replaced forests, continental ice- and periglacial-driven processes were more widespread and large volumes of dust and sand were blown about by cold, intense winds. During passage into the cooler climatic phases (glacials) of icehouse mode climate there were rapid pulses of sealevel fall, while in the passage to warmer (interglacial) periods the rates of sealevel rise were even more intense. There have been more than 15 glacial periods in the last 1.7 million years. It was in the latter part of this icehouse regime of rapid change and climatic stress that *Homo sapiens* first came to be some 100 ka.

This remarkable 1.8 Ma climatic period known as the Quaternary is the culmination of a slow and uneven climatic progression toward cooler conditions that typified much of the latter part of the Tertiary and a transition from greenhouse to icehouse earth. At the start of the Tertiary, Antarctica was ice-free. Oxygen isotope palaeotemperatures suggest that the nearby southern oceans were quite warm, perhaps 18°C at the surface and forests were flourishing even at very high latitudes (Figure 5.1; Williams et al., 1993, p 21).

The cooling of the world's oceans, as interpreted from $\delta^{18}\text{O}$ data by Zachos et al. (2001), started during the early Eocene climatic optimum (≈ 50 -52 Ma) when the measured $\delta^{18}\text{O}$ reached a minimum for the Cenozoic with equivalent deep ocean temperatures of +12°C. From ≈ 50 Ma until the early Oligocene the world's ocean seems to have steadily cooled. The reasons for this cooling and the onset of the current icehouse mode are a topic of ongoing debate. All agree the underlying cause was plate tectonics. Interpretations as to mechanism are split between proponents supporting changing oceanic circulation, driven by a widening Southern Ocean and a closing Tethys as the main driving mechanism, versus those arguing that falling CO_2 levels was the major driver, driven by the rising Himalayas and burial of significant quantities of terrestrial biomass. The post-Cretaceous lessening of oceanic ridge activity may be another contributing factor to gradual Cenozoic cooling.

Around 50 Ma Australia began to drift north, opening the Southern Ocean Seaway and so establishing the beginnings of the Antarctic Circumpolar Current (ACC). From that time the ACC completely encircled the Antarctic continent. It acted as a barrier that prevented warm currents of the lower latitudes ever reaching the Antarctic coast and reduced the transport of “sensible” heat to the higher latitudes, so contributing to the growing polar cold. The tropics were little effected and so the equator-pole temperature gradient began to increase, invigorating the intensity of worldscale atmospheric circulation.

Throughout the Paleocene and the Eocene it was still possible for the major equatorial ocean currents to encircle the globe, passages were still open between the Americas, between India and Europe, and between Australia and Indo-China. Worldwide climate was still generally warm. A powerful western equatorial drift passed through the open remnants of the Tethyan Ocean and allowed ongoing transfer of tropical heat to the polar regions. Closure of the Tethys, as India approached the Eurasian continent, ended circum-equatorial circulation and forced circulation south of Africa into the temperate zone. This early Eocene event is the first of four major steps that punctuate the longterm history of Cenozoic cooling (McGowran et al., 1992).

But even when the Tethyan connection closed, the initial effect on Antarctica's cool, but not frigid, climate was relatively minor. As the Eocene progressed, the Southern Ocean continued to widen but the ACC circulation did not develop to its present intensity because of shallow barriers or seafloor baffles between Australia and Antarctica (East Tasman Rise) and in the region of the Drake Passage between South America and Antarctica. Even so, high latitude cooling continued to increase, driven forward by the ongoing widening of the Southern Ocean.

At the end of the Eocene, around 34 Ma, there was a major cooling episode (Lawver and Gahagan, 2003). High latitude deep water temperatures in the Southern Ocean dropped 4–5°C, probably indicating the development of freezing conditions at sealevel around Antarctica and the first formation of sea ice. Land temperatures over high latitudes in both hemispheres probably dropped by 10°C. With the opening of the Drake Passage around 32 Ma to water depths greater than 2000 m, South America completely parted from Antarctica. This enhanced the intensity of the ACC, so producing further cooling and formation of greater volumes of ice on the Antarctic land mass (Lawver and Gahagan, 2003). The very rapid cooling of ocean temperatures at the end of the Eocene probably reflects a positive feedback between growing Antarctic ice and an increase in the world's albedo (increased reflection of sunlight).

The continuing widening of the Southern Ocean and the complete floundering of Drake Passage around 25 Ma allowed the ACC to begin to develop to its full intensity, including the set up of cold bottom water circulation, which effectively cut off Antarctica from any warming equatorial influences. By the Miocene, the ACC had attained levels of flow volume comparable to those of the Quaternary (Rack, 1993).

Widespread thick ice sheets covered Antarctica by the Middle Miocene and ice sheets moved out onto the continental shelf by the Late Miocene, as indicated by ice-rafted continental debris in deep oceanic sediments around much of Antarctica at that time (Lawver and Gahagan, 2003). It heralded the arrival of permanent thick glacial ice at sealevel, a circum-Antarctic condition that persists today. Significant cooling is seen in the oceanic paleotemperature curve at this time. It is still not well understood why it took until the Mid-Miocene for the Antarctic ice to reach extents similar to those of today, long after the development of the ACC in the early Miocene. But the associated effects on equatorial-pole temperature gradients are clear. The resulting strengthened winds intensified Mid-Miocene ocean water circulation, which in turn was associated with increased upwelling and biological activity in many of the world's oceans.

A further global cooling took place in the Late Miocene when world sealevel dropped a further 40–50 m (Kennet, 1982). This regression, in association with local tectonic activity, contributed to the isolation of the Mediterranean from the rest of the world's oceans. It perhaps helped deposit huge thicknesses of salt in giant shallow lakes across the lower parts of the former Mediterranean seafloor in an episode known as the Messinian salinity crisis. But this widely accepted correlation of an icesheet-induced major sealevel fall and widespread

evaporite deposition in the Mediterranean has been questioned by Hodell et al. (2001) who defined a Miocene glacial period that lasted from \approx 6.26 to 5.50 Ma. It consisted of 18 glacial-to-interglacial oscillations that were controlled by the 41-kyr cycle of obliquity. Although the intensification of polar glaciation at 6.26 Ma may have contributed to the restriction of the Mediterranean, it preceded the depositional onset of the lower Messinian evaporite unit at 5.96 Ma by some 300 kyr. It seems that the initiation of evaporite accumulation in the Mediterranean evaporite basin, the world's last "saline giant," was tectonic and not glacio-eustatic.

Whatever the ultimate cause of the Messinian isolation, the volume of oceanic salt deposited in the Mediterranean during the salinity crisis is 40 times that which would be deposited if the present Mediterranean evaporated to complete dryness, illustrating that there was a phreatic inflow of subsurface seawater brines into the drawdown Mediterranean depression. Removal of this volume of salt from the world's oceans lowered the salinity of the open ocean water by 6%. As less saline seawater freezes at a higher temperature, this in turn fed back into global climate by allowing yet more sea ice to develop in higher latitudes, so further reinforcing high latitude cooling.

After a slight warming in the early Pliocene, conditions cooled still further. As North and South America united across the Panama Isthmus, late Pliocene (around 3 Ma) climatic conditions in the Northern Hemisphere had cooled to where ice-rafted debris was being deposited in deep water sediments of the Northern Atlantic. By 2.4 Ma, near the beginning of the Quaternary, permanent moderate-sized ice sheets characterised the high latitude lands of the Northern Hemisphere. This marked the beginning of a climatic phase characterised by the repeated waxing and waning of polar ice sheets in the high latitudes of both the Southern and Northern Hemispheres, further enhancing high amplitude and high frequency changes in sealevel and further intensifying the alternation of warmer (interglacial) and cooler (glacial) climatic episodes.

During the early Quaternary (Matuyama magnetic chron 0.78–1.77Ma) the warm to cool climatic alternations follow a periodicity of 41 ka (Williams et al., 1993). This is equivalent to the repeating cyclicality in the obliquity of the earth's axis in terms of the plane of its ecliptic (21.8°–24.4°). From 0.8 Ma the amplitude of climatic fluctuations recorded in marine sediments seems to increase, reflected in the increased sizes of the cold phase ice sheets. The periodicity of climatic fluctuations in this time also appears to increase to a cycling time of 100 ka. This correlates to the eccentricity of the earth's orbit around the sun as it varies from nearly circular to somewhat elliptical. This 100

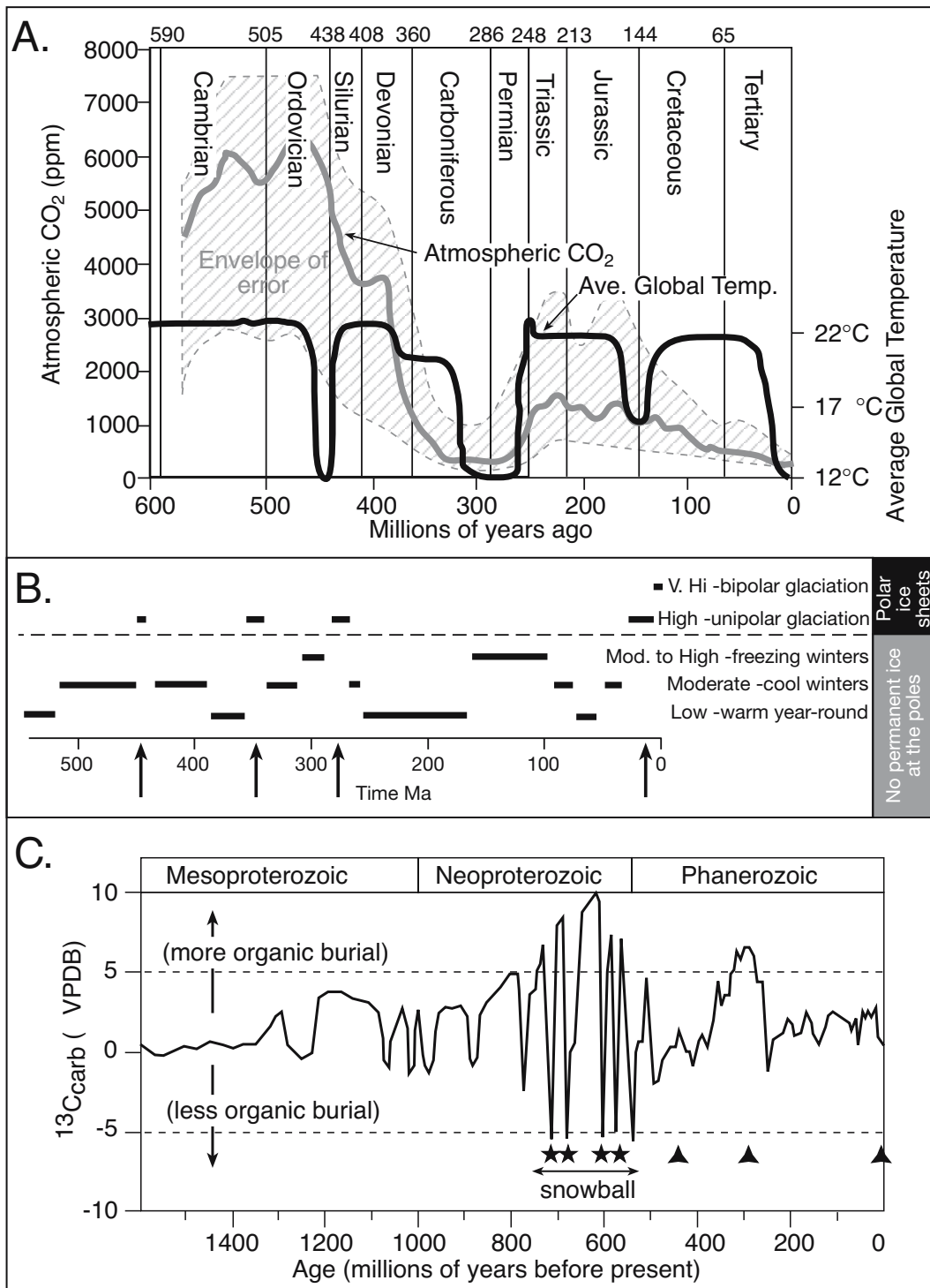


Figure 5.2. Climate change across geological time. A) Global temperature and atmospheric CO₂ change over time (after Berner, 1998). B) Pole to Equator climatic gradient through time, arrows indicate episodes of polar ice (replotted from data in Boucot and Gray, 2001) C) Secular variation in Carbon-13 content of shallow marine carbonates over the last 1600 million years - see also Figure 2.33 (after Kah et al., 2001).

ka periodicity, with sealevel amplitudes of more than 100 m, is especially dominant in the last 400 ka of world history, but superimposed on this are the 41 ka cycles and 23 ka precession cycles of the earth's equinoxes (Figure 5.1).

Rapid climatic change and high amplitude high frequency changes in sealevel are the hallmarks of the Quaternary, and probably most of late Neogene. Relative to the previous 200 million years of climatic history, the climatic fluctuations of the Quaternary were unprecedented in terms of their speed and amplitude. The mean annual temperature difference between the last glacial maximum (18 ± 3 ka) and the early Holocene climatic optimum (9 ± 3 ka) is around 10°C in many temperate land areas of the world (Williams et al., 1993; p. 223). This is roughly equivalent to the inferred longterm drop in temperatures between the early Eocene and early Pliocene in these same regions (Figure 5.1). The surface of the Southern Ocean cooled by $10\text{-}15^\circ\text{C}$ over this 40 million year period. Temperature drops of a similar magnitude occurred in eastern Australia over the 100,000 year time span that separates the last interglacial from the last glacial maximum in this region. Similar high frequency changes typify the Quaternary in many other parts of the world.

Prior to our present "icehouse" climate mode of the last 15-25 million years, the last time when there were widespread polar ice sheets, high amplitude-high frequency sealevel fluctuations, and a similar "ice house" climate was the Permo-Carboniferous some 270-315 Ma (Figure 5.2a, b). Prior to this we must go as far back as the Late Ordovician and then to the Neoproterozoic to see evidence of other worldwide "icehouse" conditions (Figure 5.2c). The late Ordovician glaciation (≈ 440 Ma) was unusual compared to the icehouse episodes that preceded and postdated it. Major glaciation was apparently confined to South America and Northwest Africa and nowhere else. Timewise, it is also the most contentious of the Phanerozoic icehouses. Brenchley et al. (1994) argue it was restricted to the Hirnantian and was some 0.5-1 m.y. long, rather than the 35 m.y. of earlier estimates. In terms of paleogeography, it probably defines the southern polar position of a uniting Gondwana. It was an Ordovician Antarctica equivalent, not associated with the breakdown of worldwide ocean circulation and it probably had no more than local climatic influence in a overall warming greenhouse world (Drury, 1999).

In fact, in the last 600 million years the late Carboniferous to the early Permian (315 -270 Ma) was the only time when atmospheric CO_2 and average global temperature were both as low as they are today. Even so, today's bipolar glaciation

appears to be a unique icehouse scenario compared to the rest of the Phanerozoic (Figure 5.2b). The obvious conclusion is that the last 20 ma, and certainly the last 2 Ma of the Quaternary experienced climate and eustatic styles that are simply not representative of non-icehouse conditions covering the majority of Phanerozoic time.

Prior to the Phanerozoic, preceding Proterozoic icehouse regimes consist of at least three and maybe up to five glacial pulses between 900 and 550 Ma (Figure 5.2c), the latter part of this episode encompasses the notion of a completely ice-covered "snowball earth" (Figure 2.33; Hoffman et al., 1998). If real, this was a cryogenic system far more intense than the bipolar system of today, with its own unique climatic and sedimentologic implications. Prior to this Neoproterozoic icehouse, there is evidence of earlier worldwide glacial (icehouse) conditions at 2200 Ma and possibly at 2500 Ma. If snowball conditions did encompass the Neoproterozoic earth with an ice envelope, and ultimately lead to the Phanerozoic explosion of life, then the only possible "evaporite" salts that could have accumulated in snowball episodes would have been hydrothermal anhydrite in the vicinity of volcanic vents and spreading ridges, or cryogenic hydrohalite precipitates and volumetrically minor slushes of mirabilite and hydrohalite created during the formation of widespread sea ice. Hydrohalite ($\text{NaCl}\cdot 2\text{H}_2\text{O}$) is the stable form of halite below temperatures of 0.1°C , it is anhydrous at higher temperatures, hydrohalite has four times the volume of mirabilite in modern sea ice (Richardson, 1976). The possibility of preservation of either mineral, other than as isolated pseudomorphs, along with ikaite in glacial meltwater deposits is zero.

The rapid melting of the global icesheets of snowball earth and the transition to widespread temperatures as hot as 50°C during the formation of successive cap dolomites, along with the likely encroachment of shallow epeiric seaways via the return of continental glacial waters to the sea, would have encouraged the formation of widespread platform evaporites in association with the cap carbonates. Widespread megapolygonal tepees and/or salt karst does outcrop in the appropriate stratigraphic position in the Neoproterozoic dolomite capstones in Oman (pers. obs.) and atop the Elatina Shale in the Flinders Ranges of Australia. Defining the worldwide timing of such Neoproterozoic evaporites and their dissolution residues may be an interesting test of the validity the "freeze and fry" climate conjectured for snowball earth. Some megapolygons beneath cementstone layers have been interpreted in a very nonuniformitarian fashion by snowball earth proponents. They are tepee-like with unbroken crests and not thought to be true tepees. Rather they are me-

chanically-formed chevron-like wave structures indicative of wave periods of 21-30 seconds and formed by consistent flow velocities of 20 m/sec in megawinds blowing across oceans with unlimited fetch (Allen and Hoffman, 2005).

Clearly, our present icehouse climatic regime does not represent climatic and sealevel regimes throughout much of geological time. As Charles Dickens once wrote on contemporary time, "It was the best of times, it was the worst of times." In terms of marine evaporite deposition, a lack of "strict uniformitarianism" leads to a paucity of Quaternary analogues for most large marine-fed evaporite deposits.

Varying extent of ancient evaporites

Nowhere in Quaternary depositional systems is there Holocene proof of a desiccated ocean basin, yet in the Late Miocene (Messinian) salinity crisis a series of subsealevel saline depressions on the Mediterranean floor filled the lowest parts of the Mediterranean with 2-km-thick sequences of halite and gypsum

in less than 300,000 years (e.g. Balearic Basin; Figure 5.3). These Messinian evaporites were laid down on the floors of a chain of shallow saline seas that were more than a thousand kilometres long, more than two hundred kilometres across, with brine surfaces more than 2,000 metres below ambient sealevel. They formed in the lowermost parts of a hyperarid to semiarid seafloor desert that extended from Spain to Israel and from northern Italy to Libya (Cita, 1983; Hsu et al., 1973).

Similarly, there is no Holocene proof of evaporitic brine-reflux dolomitisation and the associated salt seals, simply because there is no Holocene example of a whole carbonate platform being covered by an evaporite deposit. Yet in ancient evaporite basins, reflux dolomitization was a widespread and pervasive mechanism that yielded substantial intercrystalline porosity in platform carbonates beneath laterally continuous beds of platform evaporite salts (Chapter 10).

Many thick ancient salt accumulations are underlain or overlain, and sometimes intercalated, with thick widespread marine carbonate beds. A major dilemma facing geologists interpreting

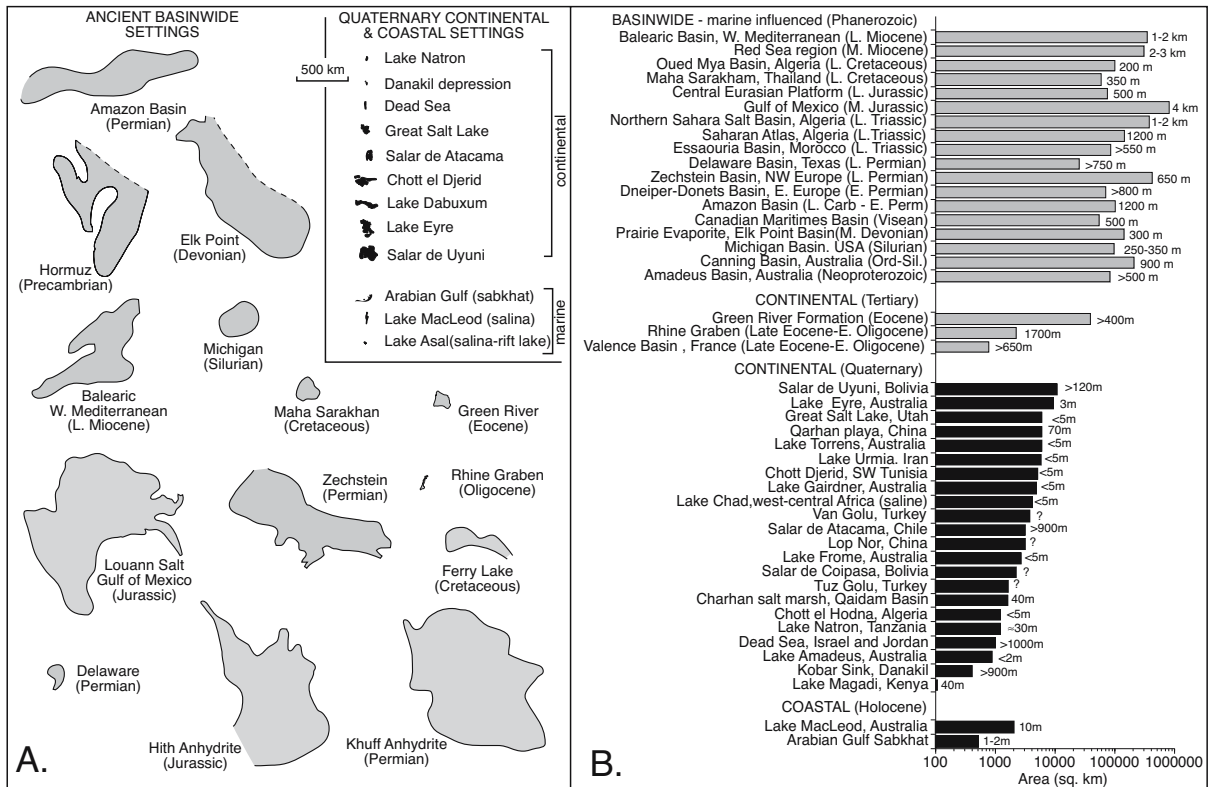


Figure 5.3. Evaporite distribution - modern and ancient. A) Aerial extent of Quaternary and ancient evaporite settings (in part after James and Kendall, 1992; Warren 1999). B) Area and thickness of Quaternary and ancient evaporites (after Herdendorf, 1984; Hardie, 1990; Warren, 1999) Note that the scale is exponential, not linear.

	Area (km ²)	Locality	Age	Evaporite style	References
Continental					
Salar de Uyuni	10,600	Bolivia	Quaternary	saline-pan to mudflat	Risacher and Fritz, 1991, 2000
Lake Eyre	9,300	Australia	Quaternary	saline-pan to mudflat	Alley, 1998; Magee et al., 1995
Great Salt Lake	6,000	USA	Quaternary	saline-pan to mudflat	Eardley, 1938; Spencer et al., 1985
Qaidam Basin	6,000	China	Quaternary	saline-pan to mudflat	Schubel and Lowenstein, 1997
Lake Torrens	5,900	Australia	Quaternary	saline-pan to mudflat	Schmid, 1988a,b; Williams et al., 1998
Lake Urmia	5,800	Iran	Quaternary	brine lake	Kelts and Shahrabi, 1986
Chott Djerid	5,000	Tunisia	Quaternary	saline-pan to mudflat	Bryant et al., 1994a, b; Gueddari, 1984
Lake Gairdner	4,800	Australia	Quaternary	saline-pan to mudflat	Herdendorf, 1984; Johns, 1968
Lake Chad (saline)	4,000	Chad	Quaternary	saline-pan to mudflat	Eugster and Maglione, 1979; Maglione, 1980
Van Golu, Turkey	3,700	Turkey	Quaternary	brine lake	Herdendorf, 1984; Kipfer et al., 1994
Salar de Atacama	3,100	Chile	Quaternary	saline-pan to mudflat	Alonso and Risacher, 1996
Lop Nor	3,100	China	Quaternary	saline-pan to mudflat	Herdendorf, 1984
Lake Frome	2,700	Australia	Quaternary	saline-pan to mudflat	Nanson et al., 1998
Salar de Coipasa	2,200	Bolivia	Quaternary	saline-pan to mudflat	Risacher and Fritz, 1991
Tuz Golu	1,600	Turkey	Quaternary	saline-pan to mudflat	Braithwaite and Zedef, 1994, 1996
Charhan marsh	1,600	China	Quaternary	saline-pan to mudflat	Chen and Bowler, 1986; Yang et al., 1995
Chott el Hodna	1,200	Algeria	Quaternary	saline-pan to mudflat	Guiraud, 1965
Lake Natron	1,200	Tanzania	Quaternary	saline-pan to mudflat	Gueddari, 1984; Manega and Bieda, 1987
Dead Sea	1,000	Israel	Quaternary	brine lake	Ben-Avraham et al., 1999; Talbot et al., 1996
Lake Amadeus	880	Australia	Quaternary	saline-pan to mudflat	Herdendorf, 1984; Jacobson, 1988
Kobar Sink, Danakil	400	Ethiopia	Quaternary	saline-pan to mudflat	Holwerda and Hutchison, 1968
Lake Magadi	105	Kenya	Quaternary	saline-pan to mudflat	Eugster, 1986
Marine-fed					
Lake MacLeod	2,000	Australia	Holocene	coastal salina	Logan, 1987
Arabian sabkhat	500	Emirates	Holocene	coastal sabkha	Evans et al., 1969; Warren, 1991
Lake Asal	52	Djibouti	Holocene	marine-edge rift lake	Fontes et al., 1980

Table 5.2. Some representative examples of Quaternary lacustrine deposits, list is sorted by size of the basins and should be compared to Figure 5.3b.

such strata is the lack of Quaternary marine counterparts with comparable depositional scale and unit thickness (Figure 5.3a, b). All thick Quaternary salt deposits are medium-scale accumulations of continental lacustrine evaporites in tectonically active settings (Table 5.2; Chapters 3 and 4). The ancient evaporite record entrains much larger volumes of salts precipitated in platform or basinwide settings tied to a seawater feed (marine-fed evaporites), as well as ancient continental lacustrine deposits (continental evaporites) with similar thicknesses and extents to the Quaternary examples discussed in Chapters 3 and 4 (Figure 5.3).

The largest marine-fed Holocene subaqueous deposits fill coastal salinas with halite or gypsum beds up to 10 m thick along the semi-arid western and southern coasts of Australia (areas up to 2,500 km²). Preserved Pleistocene salt beds do not underlie these marine-fed Holocene coastal salinas. The term “marine-fed” refers to the dominant source of the inflowing groundwaters at the time the evaporites are deposited, not to the presence of a hydrographic connection to the ocean, which these deposits typically lack. Although they are excellent natural environments to study the textures of precipitation in relation to brine stability and permanence, and to document early alteration mechanisms, even the largest Holocene coastal deposits pale in size and volume when compared to ancient

marine-fed accumulations (Figure 5.3a). There is a similar lack of stacking and extent in the type area for modern marine-fed evaporitic mudflats, or sabkhas, in the Arabian Gulf (Warren and Kendall, 1985; Warren, 1991).

The largest accumulations of ancient marine-fed salts are basinwide deposits, which were laid down in hydrographically-isolated subsealevel depressions, created by divergent, convergent and intracratonic (intraplate) tectonics. Their sediment volumes are not evenly distributed across the Phanerozoic, with the period from the Permian through Jurassic generating the greatest Phanerozoic accumulations of both halite and total evaporites (Figure 5.4). This corresponds to the time of the assembly and disassembly of the Pangaeon supercontinent. A supercontinent is the culmination of a mega-longterm (300 – 600 million year duration) tectonic pattern of continental accretion and fragmentation, whereby a supercontinent gradually assembles then rifts and drifts apart prior to reassembling (e.g. Veevers, 2004). Basinwide evaporites are most likely to accumulate on the floors of isolated subsealevel depressions at times of close proximity of drifting landmasses. This occurs both during the building of the supercontinent and then during times of its early disassembling. Ongoing marine drawdown incursions into marine-fed arid-zone subsealevel basins takes place both as a supercontinent assembles (collision and fore-

land basins) and then as it unzips (rifts and intracratonic sag basins).

Marine platform evaporites are the other major type of ancient marine-fed salt accumulation. They formed on continental margins throughout much more of Phanerozoic time than basinwides. They are characterised by bedded units of calcium sulphates (with lesser halite), typically 10-50 m thick and interbedded with marine carbonates. Stacked platform sections with this style of accumulation encompass depositional time frames of $\approx 1-10$ my. Basinwide evaporite fills tend to be thicker (>100m), more halite prone and purer than platform evaporites and to accumulate rapidly across time frames of less than a million years. Platform evaporite occurrences are largely tied to times in earth history when climate was in greenhouse mode.

The wider extents, greater depositional and diagenetic diversity and greater thicknesses of Phanerozoic marine-fed evaporites reflects two sets conditions not actively influencing modern marine-fed evaporites:

- *Warmer climates of greenhouse earth* creating wider latitudinal distributions of reefs, shoal-rimmed platforms and epeiric seaways under styles of eustatic fluctuation that were more suited to extensive evaporite deposition in the isolated backreef and lagoon.

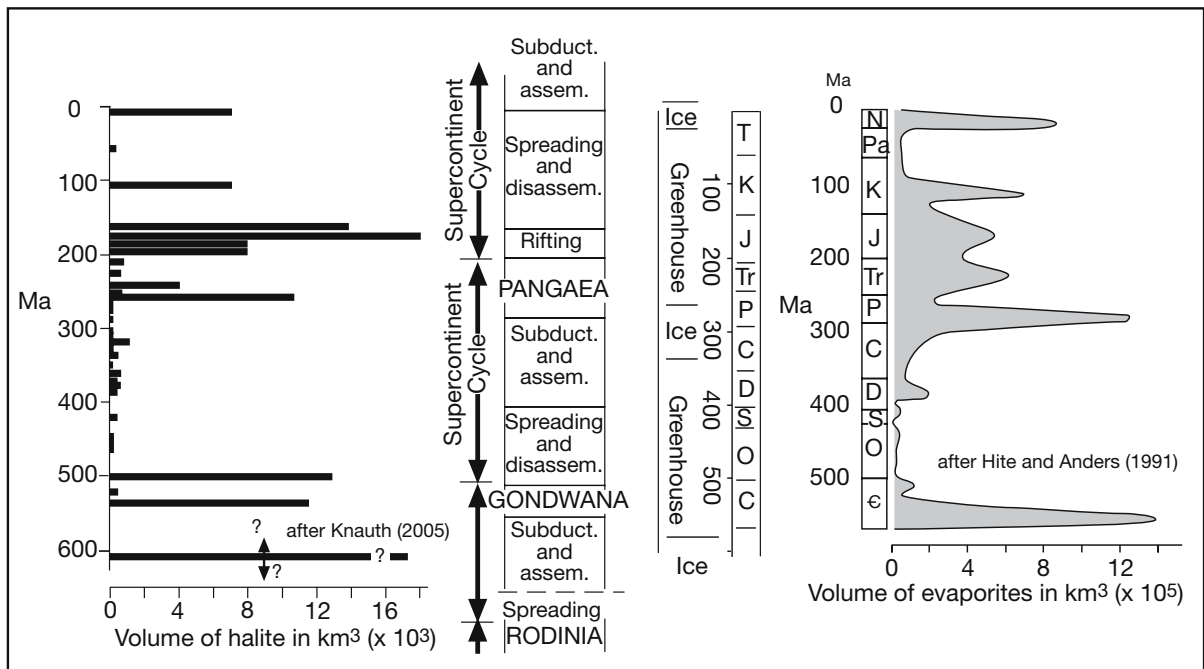


Figure 5.4. Changes in worldwide volumes of evaporites and of halite with time compared to earth climate mode and supercontinent cycles (base data for the sediment volumes from Land et al. (1988) and Zharkov (1981).

- *Set up of the correct tectonic and climatic conditions* for the hydrographic isolation of large subsealevel tracts in a tectonic depression where marine groundwater feed was the dominant source of solutes onto the arid basin floor.

Study of ancient marine evaporite deposits underscores limitations inherent in the strict actualistic application of the Law of Uniformitarianism. Processes and textures of deposition and early diagenesis can be studied in modern settings (as detailed in Chapters 1 through 4), but current climatic eustatic and tectonic interactions do not encompass all the levels of variation that have occurred in deep time.

Building blocks of ancient salt beds

Whatever an ancient evaporite basin's regional or tectonic setting, the depositional signature can be broken down into three main building blocks: mudflats (with sabkhas, salinas and saline pans), salterns and deeper water slope/basin deposits ((Figure 5.5; Table 5.3).

Evaporitic mudflats form laterally extensive units composed of stacked, shoaling-upward, matrix-dominated cycles (1 - 5 m thick). The whole unit is typically widespread and readily correlatable across scales of up to hundreds of kilometres, but individual beds or layers are not easily traced across the same

lateral extent. Salts accumulated as a mosaic of dry and saline mudflats (sabkhas) separated by local brine-filled depressions (salinas/salt pans) in both marine-fed and continental settings. Much of the matrix was deposited by storm-induced sheet floods feeding sediments and surface waters onto the mudflat, both from the land and from the lake or seaway. On its "seaward" side the matrix tended to be carbonate mud, but typically lacked stenohaline marine fossils. On its "landward side" beds are often interlayered with eolian or fluvial braidplain/sheetwash sediments (Figure 5.5a).

As the stormwaters began to dry up, windblown cm-thick evaporating brine sheets oozed and trickled back and forth atop the very flat mudflat surface. The vast extent of the mudflat, and resulting high humidity in the overlying air, greatly slowed the rate of evaporation so that halite and gypsum were the dominant precipitates. Large parts of these ancient mudflats were sabkhat accumulating displacive and replacive capillary salts. Hence, much of an ancient evaporitic mudflat mosaic is characterised by nodular and enterolithic CaSO_4 pseudomorphs after discoidal gypsum, and skeletal and chaotic halite.

Thin sheets of brine covered extensive areas for weeks or months after a storm or flood, depositing thin layers and stringers of pan gypsum or halite a few centimetres thick atop the freshly deposited silts and sands. Later, once the brine sheet had dried

	Evaporitic mudflat	Saltern	Slope and basin
Brine depth and stability	Ephemeral shallow brine sheet to subaerial	Longterm brine sheet to permanent shallow seaway	Permanent brine lake or sea deeper than 2-10 m
Dominant evaporative/ precipitation mechanism	Capillary evaporation, wind-blown thin brine sheets	Solar concentration of permanent brine, typically density stratified for part of its annual depositional cycle	Solar concentration with laminites in density stratified bodies, massive coarsely crystalline in unstratified brines
Textures	Displacive and replacive capillary salts, chicken wire and nodular textures, skeletal and pagoda halite, chaotic halite, haloturbation, Stokes surfaces, syndepositional micro-karst cements, eolian silt and sand ripples in evaporitic beds	Bottom nucleation, growth aligned laminar to chevron textures crosscut by dissolution. Mechanically reworked beds with ripples, cross beds, gypsolites/halolites. Syndepositional exposure with water table drawdown is not common, but does occur	Pelagic settling of cumulates and rafts, dense brine underflows, turbidity currents in density stratified brines. Massive beds of inclusion-free coarsely crystalline bottom growths at the base of unstratified saturated brine bodies
Holocene depositional analogs	Sabkhat, salt pan, salina	Salt pan, salina	Some aspects of deepwater brine lakes (esp. Dead Sea)
Lateral extent and wireline correlation	Whole unit is laterally continuous, but it exhibits strong lateral variability in proportions and distributions of internal salt masses. Tendency to be matrix-rich and show a "spiky" signature in conventional wireline logs. Conventional wireline not calibrated to core can be confused with reflux-generated evaporite cements	Good lateral continuity of whole bed. In a marine shelf this can extend over the whole extent of underlying platform. Good lateral continuity of various internal salt horizons within a saltern unit. Tendency to be evaporite-rich with little matrix and show "blocky" signatures in conventional wireline logs, which can be similar to slope and basin	Good lateral continuity of bed. Internal salt units tend to be laterally continuous in deeper parts of basin and individual layers in laminites can extend for 50-100 km. Slope units tend to show less lateral continuity. Tendency to be matrix-poor. Conventional wireline signature similar to saltern. FMI can be distinctive

Table 5.3. Characteristics of depositional systems that define ancient evaporites. deposits

up or was blown to another locality on the mudflat, it left behind a freshly deposited salt crust exposed to the vagaries of air, sun, wind, haloturbation and diagenesis. Ongoing exposure and deflation of the mudflat surface created Stokes surfaces, drove additional precipitation of intrasediment salts, exposed earlier carbonate crusts, altered gypsum to anhydrite, and meant the partial or complete dissolution of early brine sheet crusts. Throughout, the aggrading mudflat periodically captured influxes of eolian silt blown in from adjacent dry mudflats.

Somewhat longer-term ponding of brine sheets (months to years) occurred within local depressions to form small shallow brine lakes (salinas and pans) atop the mudflat. Water bodies were a few to tens of kilometres across and a few dm to metres deep (Figure 5.5a). Resulting salt crusts and subaqueous beds were purer and somewhat thicker (>1-2 metres) than time-equivalent intervals of capillary salts accumulating in the subaerial surrounds. Such purer units are resolvable in the vertical perspective of a conventional wireline log, especially in an image log, but are not readily correlated using logs from well to well. Overall the matrix-rich evaporite mudflat log is a distinguishable wireline signature. But, if it is not calibrated to core or to an image log, it is readily confused with units of open marine carbonate plugged by evaporite cements precipitated during brine reflux (see Chapter 10).

The term tidal-flat or peritidal evaporite is inappropriate in describing these gigantic epeiric/continental mudflats. Yet, marine-edge terminology is widely used by some sedimentologists in describing ancient evaporitic mudflats. They base its application on textural comparisons with the coastal sabkhas of Abu Dhabi. But as we saw in Chapter 3, nodular and displacive sabkha salts form in capillary settings ranging from continental lacustrine to coastal. Capillary salts, even in the classic sabkha, come mostly from resurging deeply-circulated groundwaters, a transport and emplacement mechanism that is independent of any possible tidal association in some of the matrix. Plus, the huge lateral extent of ancient mudflats, typically constituting the edges of huge interior seaways or shallow brine lakes, meant there was little or no tidal exchange with open ocean waters (Hallam, 1981; Warren, 1991). Strandplain or strandzone evaporite is apropos in describing the vast expanses of ephemeral water in ancient evaporitic mudflats.

Examples of evaporitic mudflat-dominated deposits include; Sequence 4 in the Upper Triassic Argilo-Gréseux Inferieur of the Berkine Basin, Algeria (Turner et al., 2001); the Minnelusa Formation in Wyoming (Achauer, 1982); the seal facies in the Permian Basal Seven Rivers Formation in Yates field, west Texas

(Warren, 1991); the northern regions of the Palo Duro Basin during deposition of the Upper San Andres Formation, Texas Panhandle (Hovorka, 1987); the more landward parts of the Lower Clear Fork Formation of Texas (Handford, 1981); the Cambrian Red Heart Dolomite of the Georgina Basin, Australia (Nicolaidis, 1995); the Archaean Wittenoorn Dolomite of the Hamersley Group, Western Australia (Kargel et al., 1996).

Saltern describes extensive shallow-subaqueous evaporite beds (5-50 m thick) deposited across hundreds of kilometres in the hypersaline portions of an ancient evaporite lake or seaway (Warren, 1991). Deposition took place in both marine-fed and continental settings (Figure 5.5b; Table 5.3). Unlike evaporite mudflats, units tend to lack matrix within the stacks of salt layers that constitute the unit. Internal textures range from aligned crystals layers, or their ghosts, which preserve little evidence of syndepositional exposure through to stacks of salt pan crusts separated by abundant dissolution surfaces.

Unlike the sabkha, pan and salina components of an evaporitic mudflat, there are no modern counterparts for salterns in terms of scale or location. Salterns formed in extensive salt-depositing seaways that covered former open marine platform carbonates or accumulated on 100 km+ wide evaporite shelves about the edges of giant deep brine seas (Figure 5.6). Even so, most saltern texture can be interpreted using analogous textures in subaqueous salt beds in Quaternary lakes (Chapters 1 and 4).

Individual beds were precipitated from meromictic perennial brine sheets that were a few tens of centimetres or more deep and were originally accumulations of growth aligned crystals, rafts, clusters and crusts. Horizontal laminae in calcium sulphate beds were often crosscut or interrupted by coarse-grained to giant, vertically aligned crystals of calcium sulphate or halite. Primary sulphate textures were altered and recrystallised syndepositionally or during burial into nodular and coarsely crystalline textures. Primary halite chevron textures tend to be retained as remnants in a variably recrystallised matrix of halite spar. The end result of saltern deposition is a number of superimposed shoaling-upward beds (parasequences) composed of one or two dominant minerals, usually halite or gypsum (now nodular anhydrite).

Smaller crystals can be reworked by storms into subaqueous traction deposits characterized by graded and reverse-graded beds, rippled and crossbedded layers, and algal rip-up structures. The graded beds and the rippled layers probably recorded waning storm-flood conditions (Hardie and Eugster, 1971). Reverse-graded mechanical beds recorded either episodes of

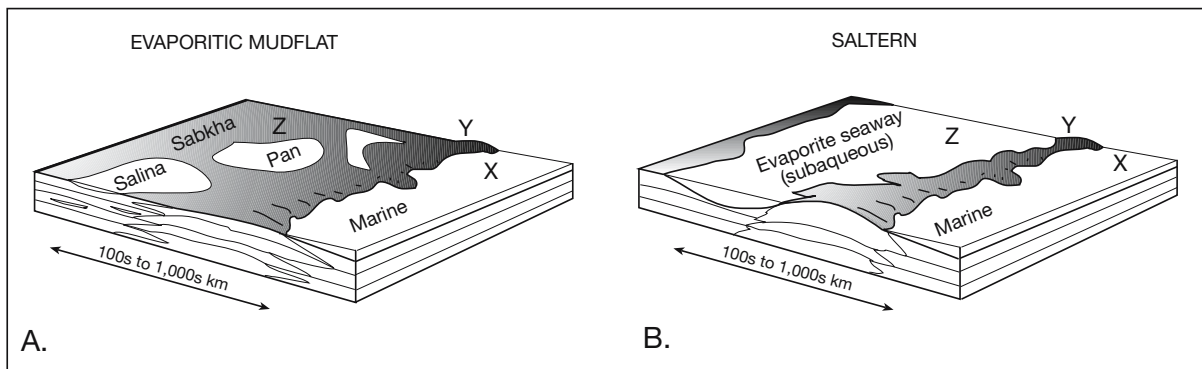


Figure 5.5. Depositional geometries of: A) evaporitic mudflat and B) saltern (after Warren, 1989, 1991). Both can occur in ramp or platform settings, the notation XYZ refers to the ramp subdivisions of Irwin (1965).

storm surging (increasing energy levels) across the saltern, or episodes of brine dilution that had slowed precipitation, so that coarser crystal overgrowths came to dominate the upper part of the lamina or layer.

Freshening of saltern waters to where salinities were undersaturated with respect to halite or gypsum created thin cm-dm mudstone to wackestone layers (calcite or dolomite) entraining intraclast breccias, tepees, pisolites, cross beds, crystalgalaminites, micritic domal stromatolites, often with numerous pellets coming from brine shrimp and ostracodes or other opportunistic halotolerant species. Mud interbeds can also preserve rare vertebrate tracks.

Using shallow-looking conventional wireline logs (e.g. PEF or MSFL), a saltern is typically resolvable into internal beds of relatively pure cyclic sets (parasequences). Core and image logs show cycles are typically shoaling cycles (e.g., domes passing up into laminites) with decimetre to metre scale layering that can be traced over large well to well distances. The relative purity (>95% salts), greater thickness of bed cycles and improved lateral continuity gives saltern beds a blocky wireline signature that frequently allows their distinction from evaporitic mudflats when using wirelines for subsurface correlation (Table 5.3). Mapping this distinction can be an important reservoir quality indicator (Figure 10.37).

Ancient examples of saltern deposits include the Cretaceous Ferry Lake Anhydrite in the northern Gulf of Mexico (Pittman, 1985), the ramp interior evaporite cycles of the Early Cretaceous of the Caohuila platform (Lehmann et al., 1998), the P₁ and P₂ evaporites of the San Andres Formation on the northwest shelf of the Permian Basin, the Lower San Andres Formation of the Texas Panhandle (Elliott and Warren, 1989), the upper Visean anhydrites of southern Belgium (De Putter et al.,

1994), and the Hith Anhydrite of the Middle East (Azer and Peebles, 1998).

Deepwater evaporites accumulated beneath deeper brines of lacustrine and basinwide evaporite successions and encompass the slope, rise and basin deposits (Figure 5.6). Fine-grained halite or gypsum laminites accumulated in the central deeper parts of a density-stratified basin, they were intercalated with less saline salts, as well as with carbonate or organic laminites. The fine layering reflects change in the saturation states of the surface brines or variations in the rate of sediment supply and grain size from the more marginward slope deposit feeds (Figure 5.6a). These “deepwater” laminites accumulated in two main ways; 1) as “rain from heaven” with crystallites first forming in the upper supersaturated metre or two of the brine column and then settling to the deep brine seafloor, 2) as the distal ends of evaporite turbidites and debris flows that characterise the slope and rise in basinwide deepwater settings. Slope deposits accumulate up-dip from the laminites of the basin floor and are mechanically reworked from saltern or mudflat parent. They are characterised by textural associations typical of deeper water in all sedimentary basins and include; turbidite fans, Bouma cycles, slumps and debris flows, sole marks, tool marks, scour and fill, ball and pillow structures. All are relatively high energy features intercalated with laminites deposited during times of quiet bottom settle-out.

Studies of basin-centre and slope evaporites in the Permian of the Delaware and Zechstein basins, the Visean evaporites of the Canadian Atlantic, and the Miocene of Red Sea rift in the Yemen Republic, the Messinian of Spain and the Apennines indicate these ancient deepwater sequences can be interpreted in much the same way that deepwater deposits are interpreted in carbonate and siliciclastic depositional systems (Anderson et al., 1972; Clark, 1980a, b; Richter-Bernburg, 1986; Schlager and Bolz,

1977; Schenk et al., 1994; El Anbaawy et al., 1992; Rouchy et al., 1995; Peryt, 2000; Orti et al., 2003; Roveri et al., 2001). The main difference when compared to other deepwater clastics relates to water depth and the relative importance of “rain from heaven” versus resedimented shelf deposits in depositing the fine laminites of the basin centre.

Interpreting an ancient evaporite as deep water is more difficult than separating subaqueous and subaerial depositional styles (Warren and Kendall, 1985; Warren 1985). A lack of a benthonic microfauna, similar conventional wireline signatures and varying degrees of drawdown during deposition of thick interlayered coarsely crystalline and laminated evaporite sequences, means water depth determinations are difficult in ancient slope and basin evaporites. Varying intensities of drawdown as evaporites accumulate in a basin centre plays havoc with the assumptions of rates of water level change that are inherent in estimating water depths in open marine deposits. Unlike marine basins where sealevel tends to fluctuate tens of metres above and below the shelf break, brine surfaces in basins accumulating evaporites in drawdown basin centres can be 2 km or more below sealevel and the position of the shelf break prior to basin isolation, and it can happen in the space of a few tens of thousands of years.

Using a deep “water full” basin model, Richter-Bernburg (1957) estimates water depths of more than 1000 metres for anhydrite laminites in the centre of the Permian Zechstein basin. Subsequent work by Schreiber (1988a) postulates a minimum relief of 100-200m for the shelf to base-of-slope transition during anhydrite deposition. Warren (1989, 1991) argues that determinations of deep versus shallow in a drawdown basin are difficult, but favours water depths of no more than 100-200m. Kendall (1992) argues deepwater evaporites typically form in water depths greater than 20-40 metres; but, like Warren (1985), notes that “deepwater” sulphate laminates can form in brines less than a few metres deep. The mechanism driving resedimentation

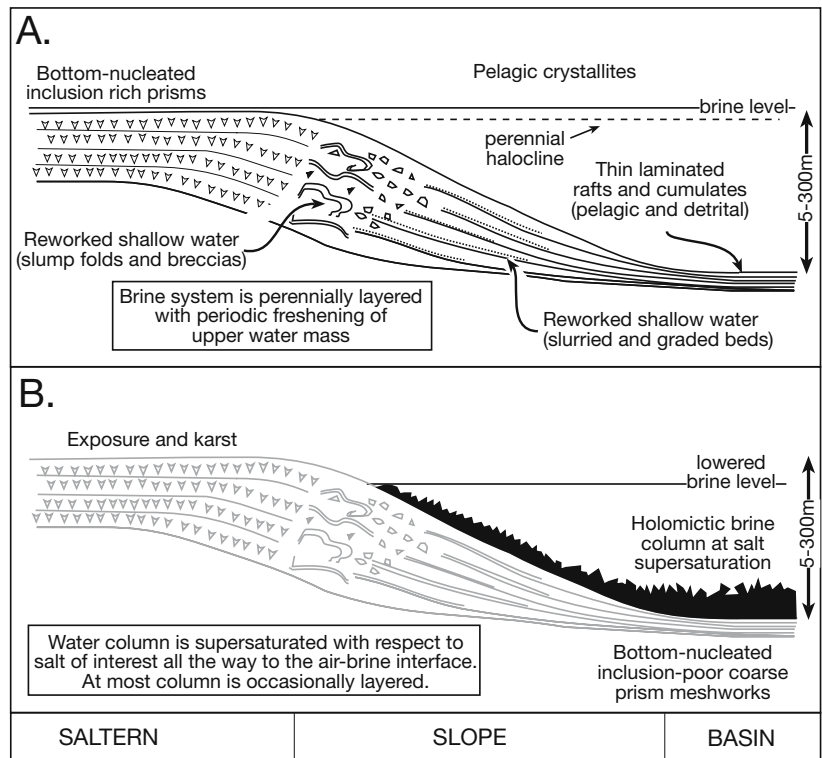


Figure 5.6. Depositional setting and characteristics of deep water evaporites. A) Depositional spectrum accumulating beneath deep and layered brines. B) Depositional spectrum accumulating beneath a deep holomictic and saturated brine column (see Chapter 4).

in “deepwater” salts is also contentious; Schlager and Bolz (1977) favour turbidity currents, while Clark (1980a) favours a control by storm surge instability (Figure 5.6a).

Unlike deepwater anhydritic laminites, resedimented ancient halites are not widely recognised and their interpretation in ancient salt beds typically stems from their entrained nonevaporite clasts, rather than from textures in any finely layered halites (Czapowski 1987). One of the better-documented examples of platform halite being redeposited into deeper water is the halite breccias and olistoliths in Middle Miocene evaporite in the Wieliczka and Stebnyk salt mines of Poland (Peryt and Kovalevich, 1997). There, the salt breccia is interpreted as a series of subaqueous fans, with redeposition of the originally shallow water halite into deep water, driven by vertical tectonic movements and the northward advance of the Carpathian Nappes. Water depths at the time of halite deposition are interpreted to have been between ten and tens of metres deep. Others have interpreted the same mine sequence to be halokinetic.

In understanding ancient deepwater evaporites and reliably tying down water depths, a significant problem is that there are only two Holocene settings, both continental lakes, where “deep water salts” are accumulating in waters deeper than 30 metres (Dead Sea halite and Canadian mirabilite). The deepwater sediments in almost all modern saline lakes are carbonate laminites. Modern deepwater analogues accumulate in small steep sided continental depressions, while deepwater ancient evaporites accumulated across the flat floors of broad drawdown marine basins with no modern counterpart. If we take the two Holocene examples as direct analogues they show the following: Massive beds made up of coarsely crystalline meshworks of sodium sulphate salts are accumulating beneath 30 m deep brine columns in small salt lakes in the interior of Canada (Chapter 11; Last, 1994). Finely-laminated bottom carbonates alternating with massive crystalline halite beds are accumulating on the floor of the Northern basin of the Dead Sea (\approx 300 m deep brine).

Using the current textures in the Dead Sea and Canada as a process analog we should add another style of deepwater evaporite; namely, beds made up of rapidly deposited, coarsely crystalline, meshworks of prisms. The prisms accumulate on stable bottoms and so show little upward crystal orientation with a characteristic lack of inclusion-rich layering in individual prisms. These beds indicate times when the deep brine column was holomictic and saturated with respect to the salt of interest (Figure 5.6b). From strandzone to deep basin floor, this coarsely crystalline halite is a lakewide time-synchronous holomictic unit.

Laminites probably indicate periods when deep bottom brines in the centres of many ancient evaporite basins were density-stratified, sediment starved and anoxic, or at best dysaerobic for long periods (Kirkland and Evans, 1981; Hite and Anders, 1991). The resulting cumulates often entrained significant volumes of pelagic organic matter and, with suitable burial, yielded hydrocarbons or ultimately were converted to graphitic schists. The bottom sediments in the deepwater gypsum of the Gibellina Basin contain up to 7% TOC, similar elevated levels occur in the mesohaline laminite of the Paradox basin. At present the organics entrained in the evaporitic carbonates of the Sicilian basins are still thermally immature, while those in the Paradox are mostly locked in place by pervasive diagenetic salt cements. The evaporite association of many of these deepwater meromictic pelagics means their potential to act as source rocks is limited to a few particular settings (Figure 9.3).

Evaporites: broad scale models

Saltern and mudflat beds, along with varying development of slope and basin deposits, occur in three interrelated regional depositional settings:

Platform evaporites: Stratiform beds typically <50 m thick and composed of stacked <1 to 5 m thick parasequences or cycles with a variably present restricted marine carbonate base. Salts were deposited as mixed evaporitic mudflat and saltern evaporites, sometimes with local accumulations of bitterns. Typically they were deposited across large marine platform areas that pass basinward into deeper water sediments (Figure 5.7a). In marine-margin epeiric settings, such as the Jurassic Arab/Hith and Permian Khuff cycles of the Middle East, these platform evaporites are intercalated with shoalwater marine-influenced carbonate shelf/ramp sediments, which in turn pass basinward across a subaerial sill into open marine carbonates. Landward they pass into arid zone continental siliciclastics or carbonate mudflats. Platform salts intercalated with open marine to restricted marine platform carbonates are termed marine-fed platform evaporites. The intimate association between potential reservoir (frequently reflux-dolomitised limestone) and seal (platform evaporites) in many marine platform evaporite settings has created many of the giant and supergiant Jurassic and Permian oil and gas fields in the Middle East and the Permian Basin of west Texas (Chapter 10). Platform evaporites, often without intercalated carbonate beds, also form shallower circum-basin belts around a deeper water basin-centre in basinwide/(saline giant) systems (Figure 5.7b; e.g. Werra Anhydrite in the Zechstein Basin).

Basinwide evaporites Thick, basinwide units > 50-100 m thick of deepwater/shallow water evaporites retain textural evidence of different but synchronous depositional settings, including mudflat, saltern, slope and basin (Figures 5.6, 5.7b). When evaporite deposition took place, the whole basin was evaporitic typically saturated with the same mineral phase across large areas of the basin (as when halite today forms halite chevrons on the pans and coarse inclusion-poor crystal meshworks on the deep basin floor of the Dead Sea). Bittern salts sometimes accumulate during the most isolated times in the basin's drawdown history, typically in depressions with minimal surface water influx, either in the lowest parts of the basin centre, or in platform depressions behind the shelf break (Chapter 11).

Continental play/lacustrine deposits These are constructed of stratiform salt units, typically with the greater volume of gypsum and halite deposited in evaporitic mudflats and salt pans, rather

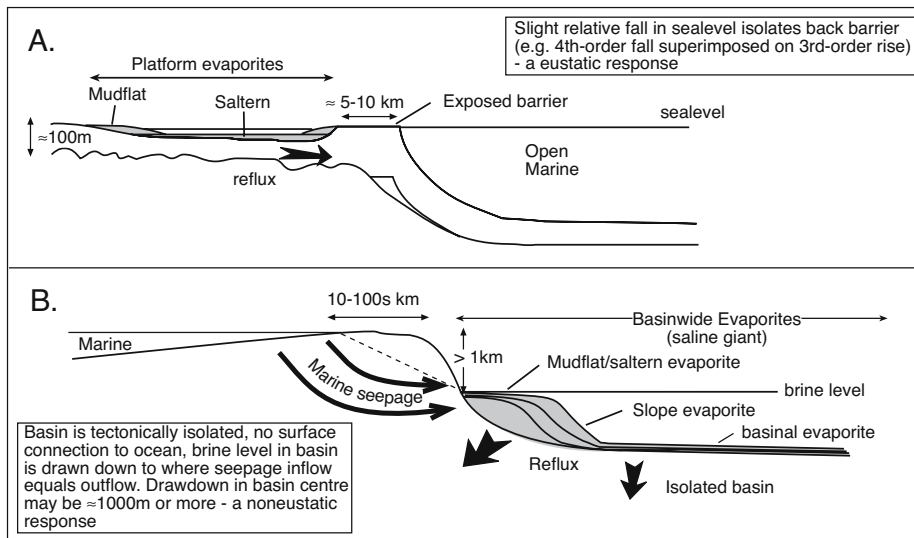


Figure 5.7. Ancient evaporite settings that have no modern analogues. A) Platform evaporites. B) Basinwide evaporites (see text for explanation).

than in perennial lakes (Figure 5.8). Total thicknesses range from metres to hundreds of metres, with lateral extents measured in tens to hundreds of kilometres (Figure 5.3). Such salt beds are separated and often surrounded by deposits of lacustrine muds, alluvial fans, ephemeral streams, sheet floods, eolian sands and rebeds. Typically the salts accumulated in endorheic or highly restricted discharge basins. Basins typically have a shallow water table in the saline mudflat area and a lowermost depression with ephemeral ponded brine pans. Perennial saline lakes formed during more humid periods in the same depression or in parts of the lake floor located below the regional water table (moat facies). Evaporite mineralogy was dependent on composition of inflowing waters; suitable settings accumulated thick sequences of trona, glauberite and thenardite as well as more typical sequences of halite and anhydrite. High water stage perennial sediments tend to be carbonate-rich or silica-rich (diatomaceous) laminites. Ancient examples include the Eocene Green River Formation of Wyoming and the Permian Pingdiqian Formation of the Junggar Basin, China.

Let us now look in a little more detail at sedimentological characteristics that allow a determination of depositional setting of these three ancient evaporite groupings.

Lacustrine evaporites

According to the degree of accommodation space, all ancient lacustrine deposits can be subdivided into 3 types: underfilled, balanced and overfilled (Figure 5.8; Bohacs et al., 2000). Accommodation is the space available for sediment accumulation

below the basins outlet or spill-point. The type of lake is defined by how much of that space is filled by some combination of sediment + plus water over a particular time span. Hence climate (≈ sediment supply + water depth and permanence) and tectonics/inherited topography (≈ potential accommodation) exert coequal controls on the nature and distribution of the various lacustrine deposits. Changes in climate or tectonic subsidence means ancient lacustrine basin fill can evolve from one lake type to another a number of times in the infill history of the basin (Lambiase, 1990).

The fluvial-lacustrine facies association that occurs in overfilled (humid) lakes is composed of marlstone, argillaceous coquina and bioclastic grainstone, along with widespread sandstones, carbonaceous mudstones and coals with a freshwater fauna. Beds retain mixtures of aquatic and terrigenous organic matter and most sedimentary textures are physical, not biogenic (Figure 5.8; Bohacs et al., 2000). The fluctuating-profundal lacustrine facies association is common in balanced lakes and is made up of a complex of interbeds of heterogenous lithologies including carbonates, siliciclastics, argillaceous and organic rich mudstones, with a fresh to saline water biota. Dominantly aquatic organic matter is found in beds and bedsets, while sedimentary structures are typified by a combination of physical and biogenic features.

Evaporitic lacustrine facies typically accumulate in underfilled basins, with lithologies ranging across clastic sandstone and carbonate grainstones, kerogenites (oil shales) and evaporites. Widespread shoalwater evaporites typically fill the lowermost parts of the basin during the most arid or underfilled times in the lake history. Halophilic organic matter can accumulate in moat facies at that time, or halotolerant organic remains can accumulate across larger parts of the lake floor when water levels are somewhat higher and fresher (Chapters 4 and 9). Sedimentary structures include both physical and biogenic structures, as well as textures indicating periodic desiccation (mudcracks) and crystallization (cumulate, growth-aligned and displacive textures).







Lake type & lacustrine facies association	Stratigraphy	Lithologies	Sedimentology	Organic matter	Kerogen-hydrocarbon characteristics
OVERFILLED  Fluvial-lacustrine facies association	Maximum progradation:  • parasequences related to lateral progradation (relatively stable) • maximum fluvial input	Terrigenous sediment dominant • mudstone, marls • sandstone • coal, coaly shale • coquina (isolated highs in basin)	Physical sedimentation dominant: • ripples, dunes, flat bed • root casts • burrows (infaunal and epifaunal)	• freshwater biota charophytic and aquatic alga OM • low to moderate TOC • terrigenous and algal biomarkers	• mixed type I-III kerogen • both oil and gas generative • very waxy, low sulphur oils
BALANCED FILL  Fluctuating-profundal facies association	Mixed progradation & aggradation  • distinct shoaling cycles common • fluvial input variable	Mixed chemical and terrigenous sediment: • marl, mudstone • siltstone, sandstone • carbonate, grainstone, wackestone, micrite • kerogenite	Physical & biogenic sedimentation: • flat beds, • current, wave and wind ripples • stromatolites, pisolites and oncolites • mudcracks • burrows (epifaunal)	• saline tolerant biota aquatic algal OM minimal land plant • moderate to high TOC • algal biomarkers	• predominantly type I kerogen, type I-III mixtures near flooding surfaces • mostly oil generative • paraffinic but relatively nonwaxy oils, low sulphur
UNDERFILLED  Evaporitic facies association	Maximum aggradation minimum progradation  • high-frequency wet-dry cycles • minimum fluvial input • maximum evaporite input	Chemical sediments dominant: • mudstone, kerogenite • evaporite • siltstone, sandstone • grainstone, boundstone wackestone, micrite • flat-pebble conglomerate	Chemical, biogenic & physical sedimentation: • cumulative textures • disjunctive fabrics • stromatolites, pisolites and oncolites • climbing ripples • flat beds • eolian cross beds	• low diversity halotolerant to halophilic biota • algal-bacterial OM • low TOC in oxidised margins • high to very high TOC oil shale in basin centre • "hypersaline" biomarkers	• type I kerogen • mostly oil generative • paraffinic oils, moderate to high sulphur

Figure 5.8. Attributes of the three major styles of lacustrine basins (after Bohacs et al., 2000).

Studies of sizes of modern lakes of all three types, their water depths and the character and thickness of ancient counterparts typically do not correlate with measured or inferred climatic humidity (Bohacs et al., 2000). Interestingly, the drainage basins of the world's largest rivers contain no large lakes, only a few relatively small ones (e.g., Amazon, Congo, Orinoco and Mississippi River basins). Ancient lake systems show a similar lack of correlation between lake size, climate and fluvial volumes (Carroll and Bohacs, 1999). Of the three types of ancient lakes, the focus for the remainder of this section is on the underfilled or evaporitic lakes. For further discussion of the sedimentology of other two lacustrine associations, the interested reader is referred to the excellent review paper by Bohacs et al. (2000) and the references therein.

Ancient saline lacustrine deposits range in age from Neogene to Precambrian (Table 5.4). Facies patterns and distributions in saline lakes are different from marine carbonate or siliciclastic-filled basins as; 1) the depositional base level changes much more rapidly in lakes and with much higher amplitudes, 2) salinity is not constant. As was documented in the various saline lake/playas discussed in chapters 3 and 4, water/brine depth and lake salinity can change hundred of metres in less than a few thousand years, from a highstand deep perennial fresher lake accumulating deepwater chemical laminites, along with lake-plain and highstand deltas, to a shallow or ephemeral lake made up of small saline pans on broad salt flats and mudflats. In Lake Van, Turkey, there was a change of 600 m

in 2-3 thousand years, Lake Malawi in the East African rift dropped as much as 140 m in just 340 years (Owen et al., 1990) and the lake level in the Dead Sea is currently falling at similar rates. Changes are related to local climate and uplift and, unlike the base level changes in marine eustacy, do not show time synchronous change tied to worldwide climate mode (icehouse versus greenhouse). Facies analyses tied to dated

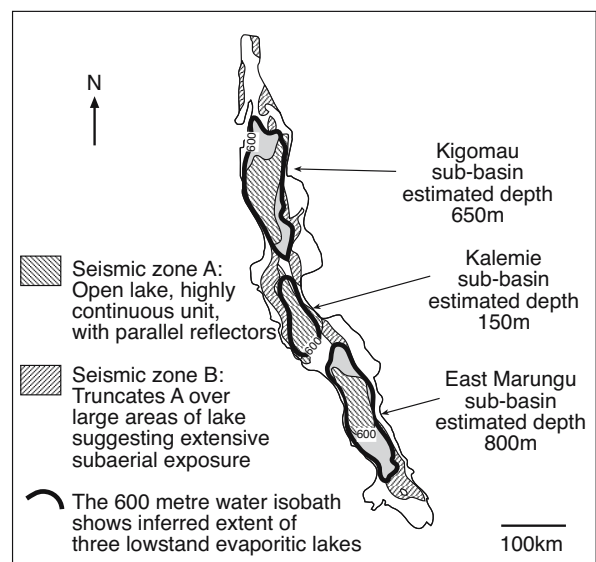


Figure 5.9. Subdivision of Lake Tanganyika into three separate sub-basins during a mid- to late-Pleistocene lowstand (after Tiercelin and Mondeguer, 1991).

cores in Lake Tanganyika, Africa, show the current lake was made up of three separate saline lakes when water levels were lower in the mid to late Pleistocene (Figure 5.9). Compared to Lake Tanganyika, Lake Magadi and Salar Uyuni show the

opposite effects in terms of timing of late Quaternary high water in that their current salt pan surfaces are some tens of metres below what were the much higher lake water surfaces in the late Pleistocene.

Sequence of interest	Basin/setting	Locality	Age	References
Beds of displacive borates	Bigadic, Emet and Kirka basins	Turkey	Neogene	Gundogdu et al., 1996; Gurer and Gurer, 1999
Massive halite of Salar Grande	Cordillera de la Costa forearc	Central Andes, Chile	Neogene	Diaz et al., 1999
Bed I and Bed II	Olduvai Gorge, East African Rift	Tanzania	Pliocene	Hay and Kyser, 2001
Furnace Creek Fm. (borate beds)	Extensional half-graben	Death Valley, USA	Pliocene-Miocene	Tanner et al., 2002
Gypsum as beds and fracture-fills	Sivrihisar/Sultancayir/Cankiri basins	Anatolia, Turkey	Miocene	Orti et al., 1998; Varol et al., 2002
Lacustrine carbonates	Ries-impact-crater	Southern Germany	Miocene	Arp, 1995
2.5 km thick lacustrine halite	Hualapai basin	NW Arizona	Miocene	Faulds et al., 1997
Kirmir Fm.	Bey pazari Basin	NW Turkey	Miocene, Middle - Upper	Yagmurlu and Helvacı, 1994
Juncalito Fm.	Puna Plateau - intra-arc basin	NW Argentina	Miocene, Middle -Upper	Kraemer et al., 1999
Bedded and nodular gypsum (glauberite)	Calatayud Basin	Spain	Miocene, Lower	Orti and Rosell, 2000
Bedded and nodular gypsum (glauberite)	Ebro Basin - foreland basin	Spain	Miocene, Lower	Arenas and Pardo, 1999; Arenas et al., 1999
Creede Fm.	Ancient Lake Creede	Colorado, USA	Oligocene, Upper	Finkelstein et al., 1999
Potash beds of Couche Inferieure	Mulhouse Basin	Rhine Graben, Europe	Oligocene, Lower	Gely et al., 1993; Orti-Cabo et al., 1985
Green River Fm.	Uinta and Piceance basins	Utah and Colorado	Eocene	Dyni, 1981; Surdam and Wolfbauer, 1975
Bembridge Limestone Fm.	Isle of Wight	Southern England	Eocene, Upper	Armenteros et al., 1997
Taleh Fm.	Somalia	El Bur Plateau	Eocene, Lower -Middle	Singer et al., 1998
La Tinaja del Oso (colmenite)	Magdalena extension basin	Mexico	Mid-Tertiary	Mirandagasca et al., 1998
Uhangri Fm.	Yucheon Group	SW Korea	Cretaceous	Chough et al., 1996; Paik and Kim, 1998
Mmashoro Fm.	Basal Kalahari Group	Botswana	Cretaceous, Upper	Du Plessis and Leroux, 1995
El Molino Fm.	Potosi Basin	Bolivia	Cretaceous, Upper - Tertiary, Lower	Camoin et al., 1997; Rouchy et al., 1993
Lagoa Feia Fm.	Campos Basin	Brazil	Cretaceous, Lower	Trindade et al., 1995
Codocedo Limestone Member	Atacama region	Northern Chile	Jurassic, Upper - Cretaceous, Lower	Bell, 1989; Bell and Suarez, 1993
Drakensberg Group	Intercalated in Karoo basalts	Southern Namibia	Jurassic, Lower	Stollhoffen et al., 1998
Kalkrand Fm.	Karoo flood basalt province	Namibia	Jurassic, Lower	Stollhoffen et al., 1998
Mercia Mudstone Group	North Atlantic rift basins	Southern Britain	Triassic, Upper	Milroy and Wright, 2000; Talbot et al., 1994

Table 5.4. Some representative examples of Pre-Quaternary saline lake deposits (underbalanced systems).

Sequence of interest	Basin/setting	Locality	Age	References
Passaic Fm.	Newark Basin	Eastern North America	Triassic, Upper	El Tabakh et al., 1997, 1998b; Smoot, 1991
Blomiden redbeds	Fundy Basin	Nova Scotia	Triassic, Upper	Hubert and Hyde, 1982
Buntsandstein	Helgoland Basin	East Greenland	Triassic, Middle	Clemmensen, 1978; Clemmensen et al., 1984
Pingdiqian Fm.	Junggar Basin	NW China	Permian, Upper	Carroll et al., 1992; Tang et al., 1997
Groden Fm.	Intermontane basins, Alps	Tyrol, Austria	Permian, Upper	Spötl and Burns, 1994
Opeche Shale	Williston Basin	North Dakota, USA	Permian, Middle	Benison and Goldstein, 2000
Nippewalla Group	Continental interior sag basins	Kansas, USA	Permian, Middle	Benison and Goldstein, 2001
Rotliegende sediments	Muhlhausen and Iffeld basins	Germany	Late Carboniferous-Permian	Paul, 1999
Old Red Sandstone (middle)	Orcadian Basin	Scotland	Devonian, Lower	Clarke and Parnell, 1999; Donovan, 1993
Paraakeelya Alkali Member	Officer Basin	Australia	Cambrian	Southgate et al., 1989

Table 5.4 continued. Some representative examples of Pre-Quaternary saline lake deposits (underbalanced systems).

Vertical changes in facies and lithologies are abrupt in many ancient saline lake systems, a reflection of these rapid high amplitude changes in water levels. Large falls in lake water level lead to “hanging” deltas and terraces along with deep incisions through highstand Pleistocene deposits. In arid lowstand lakes, newly exposed lake floor sediments can be overprinted by subaerial weathering and the processes of soil formation. Exposed lake floor laminites can be sabkharized, as is happening today in Salt Flat Playa, west Texas (Hussain and Warren, 1989).

Intuitively, many sedimentologists assume that climate is the major control on water depth and salinity in a saline lake basin. That is, larger deeper lakes with thicker lake sediment packages should accumulate in wet or humid climatic periods, while drier saline periods should be characterised by saline deposits with lesser aerial extents. But the hydrology of all lake basins, including endorheic basins, is never truly closed and varying degrees of reflux and leakage play significant roles in the final salt distribution (Chapter 2). Concurrent saline lakes in Turkey or the African Rift Valley can range from hypersaline to brackish in intermontane valleys located only a few tens of kilometres apart. Assuming all ancient lakes in an area are arid or humid at the same time is not a valid approach to correlation of salt beds in adjacent saline lake basins.

Eocene Lake Gosuite, USA

Lacustrine sediments deposited in Eocene Lake Gosuite are preserved in the Green River Formation, which has several

members corresponding to major lake high- and low-stands, each of which probably lasted several hundred thousand years or more. Saline lacustrine phases of the Green River Formation, such as the Wilkins Peak Member, have two main modes. Lake high-stands are marked by oil shales (laminated dolomitic kerogenites). Lowstands, when water covered areas of the lake contracted and salinity increased, are indicated by salt beds of saltern/pan trona or halite deposited atop the oil shale layers. Dolomitic mudstones were deposited during lowstands as subaerial evaporitic mudflats across over the dried and exposed lake floor. These strandzone to shoalwater carbonates are made up of structureless to laminated muds, algal dolomudstones algal boundstones, oolitic pisolitic grainstones and ostracode grainstones, which a comparison to the massive unit in the Holocene Coorong lakes show are mostly ephemeral to strandzone indicators. Sandstone and siltstone line the basin edge and may be present as thin interbeds in the kerogenites. Roehler (1993) identified 77 depositional cycles of mudflat/kerogenite in cores from the Wilkins Peak Member. Based on an estimated duration of 1.6 My for the member, he calculated an average period of 21 kyr for the cycles and suggested they were probably caused by the earth’s precession, which has periodicities of 19 and 23 kyr.

The oil shales (kerogenites) are composed of mm-scale alternations of amorphous algal organic matter (kerogen) and slightly thicker laminae of carbonate (mostly dolomite) and clay. TOC content can exceed 25%. Comparisons to laminites accumulating in the various Quaternary saline lakes detailed in Chapter 4 means most authors now agree the Eocene kerogenites of the

Green River Basin indicate highstand conditions (Figure 5.10). But the definition of “deep” for the water depths accumulating kerogenite varies from author to author. The thickest beds of oil shale tend to occur toward the basin centre and some oil shale intervals are laterally extensive, perhaps indicating deposition at the bottom of a substantial body of perennial lake waters. Toward the basin margin the oil shales change to marlstones, kerogen-rich marlstones and lean oil shales (Hite and Anders, 1991). Basin centre oil shale accumulations can also contain diagenetic dawsonite, halite and nacholite (Dyner, 1981). They may also entrain mud-cracked horizons and solution breccia beds. To interpret the shales, some authors focus on the large lateral extent of the finely-laminated kerogenites and infer deposition at the bottom of a deep stratified water mass with density-stratified permanent waters more than tens of metres deep (Bradley and Eugster, 1969; Desborough, 1978; Dyner, 1981). Others focus on the intercalation of the oil shales with evaporites and subaerial indicators, along with the dolomitic nature of the matrix and propose a shallow lake/saline pan

depositional model for the widespread kerogenites (Eugster and Surdam, 1973; Smoot, 1983).

Changes in Lake Gosuite water levels may mean the highstand sediments of kerogenite have a somewhat greater areal extent than the salts (Figure 5.10a), but their deposition on the floor of a perennial body of water does not mean they also show greater thicknesses. The freshest “lake-full” organic-enriched sediments of the Green River Formation in Wyoming are actually the thinnest and least aerially extensive of the various members of the Green River Formation (e.g. Luman Tongue). In contrast, the Tipton and Laney members, which accumulated as varved oil shales beneath more saline meromictic lake waters have greater extents and thicknesses (Figure 5.10b; Hite and Anders, 1991).

Within the saline lake phase, those sediments deposited when the lake was at its driest (the Wilkins Peak Member), were deposited much more rapidly than the perennial saline lake

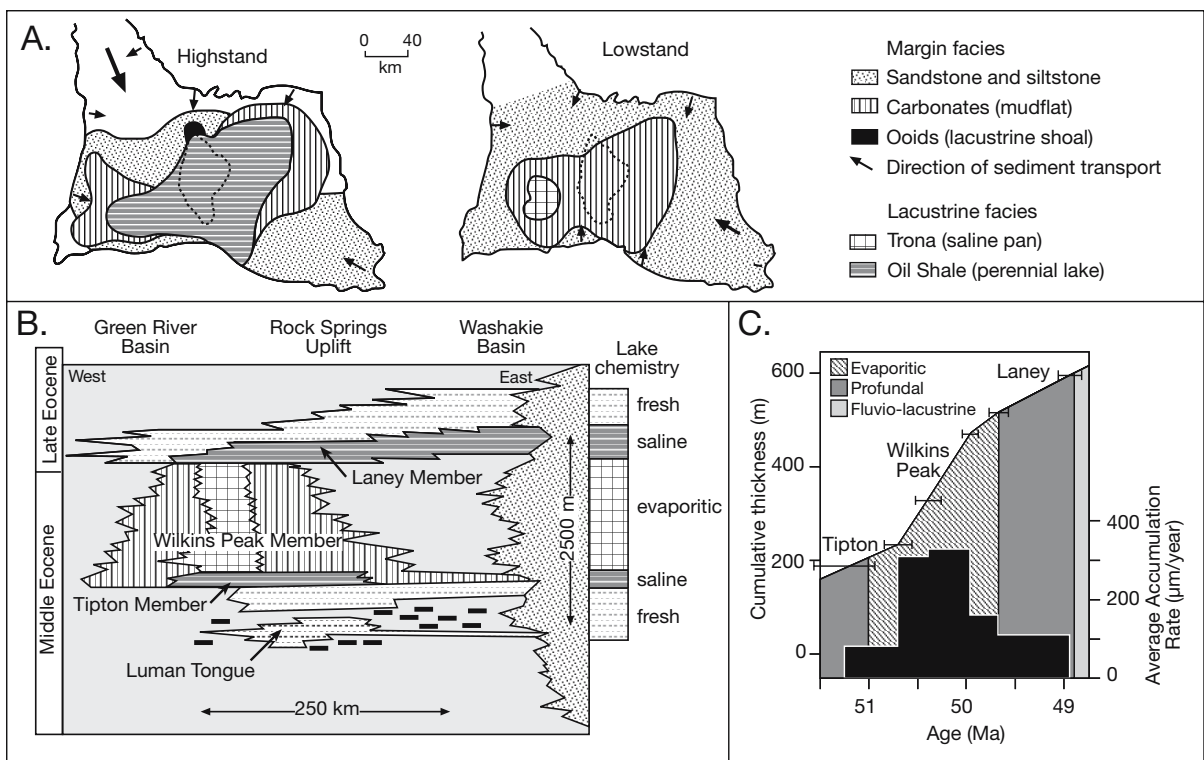


Figure 5.10. Lithofacies distribution of Eocene Lake Gosuite as preserved in the Green River Formation, Wyoming. A) Wilkins Peak time showing highstand conditions with extensive accumulations of oil shale beneath the salinity-stratified waters of a perennial lake versus lowstand conditions when carbonate mudflats dominated and trona was precipitated beneath very shallow to ephemeral waters of a hypersaline brine lake (after Surdam and Wolfbauer, 1975). Dashed line outlines the approximate position of the Rock Springs Uplift. B) Schematic E-W cross section showing lateral extents and thicknesses of various lacustrine units (after Bohacs et al., 2000). C) Average sediment-accumulation rates for the Green River Formation based on a reference section in the southern Greater Green River Basin (after Smith et al., 2003).

laminites either of the Tipton or Laney members. $^{40}\text{Ar}/^{39}\text{Ar}$ based accumulation rates of Smith et al. (2003) are direct measurements of accumulation rates and do not rely on lamina counts being annual varves (Figure 5.10c). For a reference section near the southern Green River Basin depocentre they calculated accumulation rates of 88 ± 34 and $104 \pm 18 \mu\text{m}/\text{yr}$ for the Tipton and Laney members; both values are consistent with an annual origin for the laminae. A much faster accumulation rate emerges from the Wilkins Peak Member. In the same reference section they calculated a net average rate of $327 \pm 85 \mu\text{m}/\text{yr}$, which is three times as fast as for the Tipton or Laney Members.

Their observation of faster accumulation rates is in accord with U-series disequilibrium-based results from Quaternary playa-lake evaporites. Ku et al. (1998) found that accumulation rates in a core from Death Valley were much higher for the salt-pan evaporite facies than for perennial lake muds, and Bobst et al. (2001) noted that accumulation rates during dry phases of the Salar de Atacama were up to three times as high as during wet periods (see Chapter 3). Net accumulation rates in these cases range between 0.5 and 1.8 mm/yr, which are up to five to six times faster than deposition of the Wilkins Peak Member. However, higher rates of Wilkins Peak Member evaporite accumulation may have occurred in the basin's subsurface depocentre, which lies to the west of the reference section (Smith et al., 2003).

Evaporitic sediments of Wilkins Peak Member, which accumulated at a time when the lake's waters were at their shallowest (perennial saline lake) and saltiest (pan/mudflat), are stratigraphically the thickest member of the Green River Formation (Smoot, 1983). This more saline lacustrine phase separating the kerogenites is enriched in sodium bicarbonate minerals such as trona and nacholite in layers and is discussed in more detail in Chapter 11.

The alternation of playa and perennial lake modes explains accumulations of hydrogen-prone organics as oil shales in many saline lacustrine systems (Table 9.1). Boyer (1982) argues that hydrogen-rich oil shales in the Green River Basin accumulated beneath an anoxic lower brine layer in a density-stratified meromictic and relatively shallow saline lake. It was created and maintained by ongoing dissolution of underlying pan evaporites, especially trona/halite. He named this evaporite-induced stratification, ectogenic meromixis. If true, then accumulations of very thick oil shales in the Laney Member of the Bridger-Washakie basins and the Mahogany Bed of the Uinta-Piceance Creek basins are also a likely response

to shallow subsurface dissolution lake evaporites. The lack of similar underlying soluble beds in fresher water lacustrine oil shale basins (as in Honyanchi Fm. of China and the Rundle oil shale of Australia) may help explain why the trona-associated oil shales of the Green River Fm. are unique in their very high oil content. It also explains why virtually the entire Green River fish fauna, so famous for its high quality of preservation, is made up of pelagic freshwater taxa, which flourished in the freshened upper water mass (Grande, 1980). The permanent saline anoxic bottom layer was too nasty to support anything but well adapted microbes (see Chapter 9).

Oligo-Miocene lake, Calatayud Basin, Spain

The Oligocene-Miocene Calatayud basin of Spain is a foreland basin formed by the uplift of the Pyrenean chain to the north and is bounded to the southeast by the Catalanian Coastal Range and the Iberian range to the southwest (Figure 5.11a). Thick beds of lacustrine salts accumulated in the endorheic lower parts of the basin. These deposits entrain a combination of carbonate and sulphate lacustrine environments, fed a combination of Pyrenean waters via resurging groundwaters and alluvial systems. Deposits show strong similarities in distribution patterns and textures with the lacustrine evaporites and clastic aprons of the adjacent Ebro Basin (Figure 8.10; Salvany and Orti, 1994; Arenas and Pardo, 1999).

Miocene climate fluctuated from arid to more humid, but more importantly the mountains to the North of the lake depression were composed of Triassic evaporites and Mesozoic marine carbonates. As they weathered they supplied ions for the salts accumulating in residual brines within the topographically lowest parts of the lake floor. The nearby Ebro Basin is well known for its economic accumulations of lacustrine glauberite that, as in the Calatayud Basin, largely occur in the central part of the basin (Figure 11.53b). Two distinct lake styles alternated through time: a) High lake levels associated with a single body of dilute carbonate water, where massive biogenic carbonate facies proliferated. These lakes had wide palustrine vegetated margins, where bioturbated facies dominated the depositional signature. b) Low lake levels of a playa-lake with extensive development of saline pans and mudflats surrounding a more permanent gypsum-saturated brine body.

In the drawdown or playa stage a subaerial basin floor sloped gently down from a northern marginal mudflat zone to a central saline complex. Gypsum accumulated across the lake depression as both primary beds of mechanically reworked and 'in situ' gypsarenite, as well as early diagenetic precipitates of

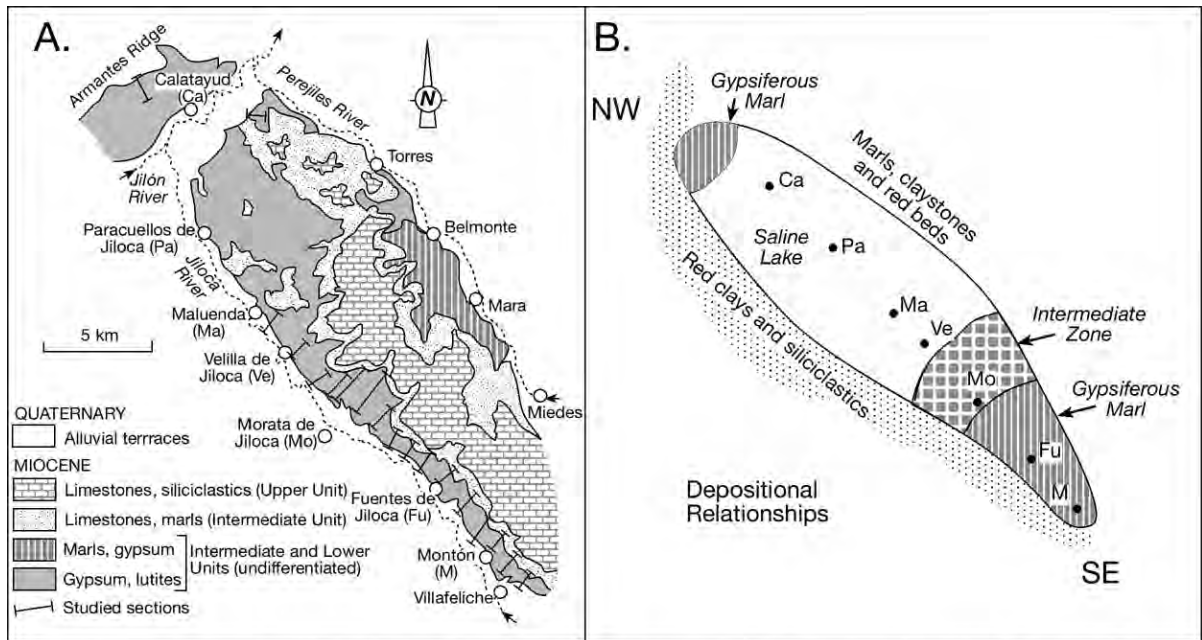


Figure 5.11. Lacustrine sediment distribution in Cataluyud Basin, Spain. A) Lithologic map showing distribution of Miocene lacustrine sediments in the area between the Armantes Ridge in the northwest, the village of Villafeliche in the SE and the area between the Jiloca and Perejiles rivers. B) Schematic of the same area, showing areal distribution of the main lacustrine subenvironments in the lower evaporite unit. (after Orti and Rosell, 2000).

lenticular anhydrite (Figure 5.11a). Surface runoff from nearby highlands constructed a bajada along the southern margin of the lake depression. But the transport of the greater volume of solute into the basin was from the north and largely subsurface, via groundwater flow through an extensive karst systems in the evaporitic Mesozoic limestones. Shallow groundwaters seeping south down the hydrologic gradient supplied increasingly fractionated and saline brines to lakes and pans all the way from the basin margin to the basin centre (Figure 5.11b; Salvany and Orti, 1994; Salvany et al., 1994; Orti and Rosell, 2000).

Calcium carbonate and gypsum precipitated in the fan edges and in marginal palustrine marshes and ponds, while substantial beds of dolomite and charophyte residues accumulated over large parts of the lake floor during more humid climatic episodes (Figure 5.11a). Many of the laminated gypsarenite beds are bioturbated, indicating periodic episodes of freshening and exposure, even as the gypsum was accumulating (Figure 5.12a; Rodriguez-Aranda and Calvo, 1998; Figure 1.23). Margin mudflats, marshes and ponds acted as preconcentrators for the shallow groundwaters seeping slowly toward the central sump of the lake centre. By the time these fractionating brines reached the central

sump, they were highly concentrated and capable of precipitating thick beds of gypsum, halite and glauberite. Much of the glauberite and polyhalite, along with some of the gypsum, was an early diagenetic interstitial precipitate, created by capillary evaporation of cross-seeping brines. The halite beds were predominantly primary saline pan units, composed of hoppers and chevrons interbedded with laminated primary gypsum (Figures 5.12a, 11.53b).

The whole Oligocene Miocene lacustrine succession in the Cataluyud Basin is made up of six 100-200 m thick cycles. The lower part of each cycle commences with beds of saline lake salts (including glauberite) that show typical playa mudflat/pan textures and have the greatest lateral extent (Figure 5.12b; Orti and Rosell, 2000; Salvany and Orti, 1994; Arenas and Pardo, 1999). Saline facies then shrink toward the basin centre as the lakes evolve into a freshened palustrine stage, until the top of each cycle is dominated fine-grained siliciclastics and alluvial fan sediments, which reflect progressive progradation of alluvial fans into the lake centre. The tops of some cycles are composed entirely of clays and fine-grained clastics. Depocentres of successive cycles shift toward the north over time, suggesting the ultimate control on the cyclicity was tectonic, not climatic.

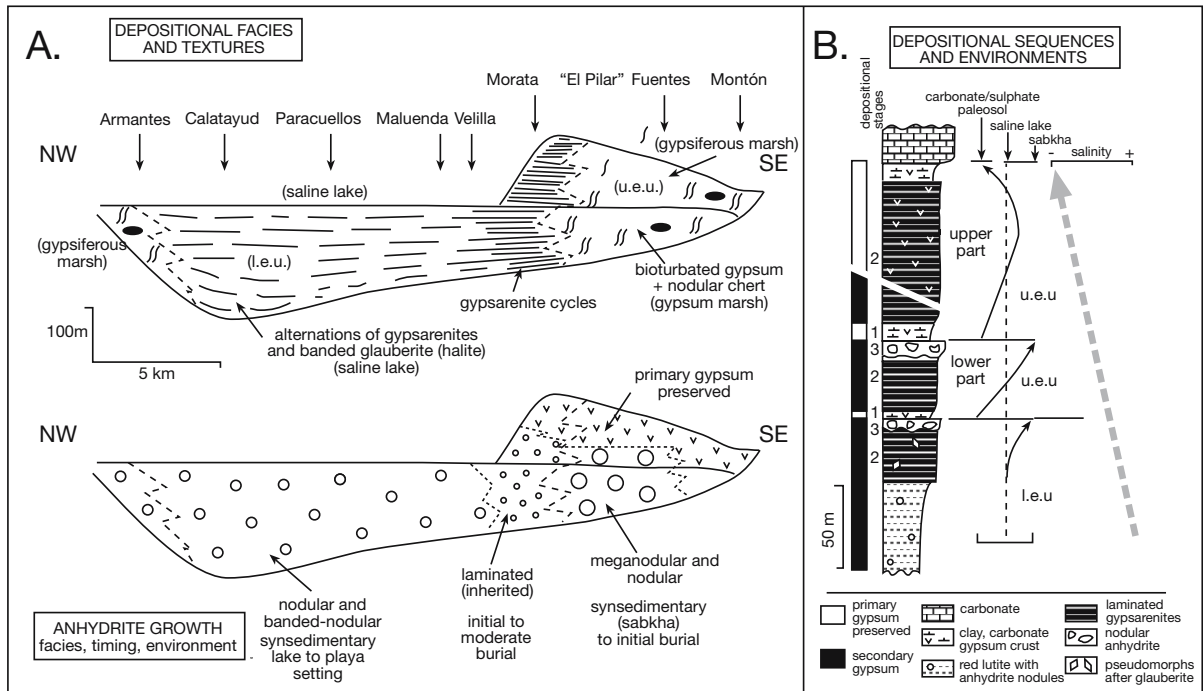


Figure 5.12. Lacustrine evaporites in the Calatayud Basin, Spain. **A)** Depositional facies distribution and their differential conversion to anhydrite: l.e.u., lower evaporite unit; u.e.u., upper evaporite unit (See Figure 5.11 for location of sections and Figure 11.53b for depositional style). **B)** Depositional sequences and evaporite units in the area of the village of Morata. Salinity arrow indicates a decrease in the ionic concentration of the parent brines with time. The lower part of the upper evaporite unit shows a complete depositional cycle with associated salinity increase. Depositional stages: (1) dilution stage: gypsiferous-calcareous horizon (carbonate-sulphate palaeosol); (2) concentration stage: laminated gypsarenite (saline lake); (3) subaerial, hypersaline stage: nodular anhydrite (sabkha) (after Orti and Rosell, 2000).

Much of the Miocene evaporitic sediment in the Calatayud Basin outcrops or subcrops along the southwestern part of the basin where it is liable to rapid karstification and collapse. The proximity to groundwater crossflow throughout the late Tertiary period means many primary evaporite textures in the basin have been diagenetically overprinted at various times in its burial and uplift history (Orti and Rosell, 2000). In the gypsiferous marsh facies, the dominant, massive, bioturbated gypsum was partly replaced very early in the sediment history by syndepositionary chert nodules and siliceous crusts (Figure 5.12a). In the saline lake facies, a replacement of portions of the laminated glauberite by anhydrite also occurred early. Episodes of subaerial exposure and pedogenic/capillary alteration are represented by: 1) pedogenic carbonates (with nodular magnesite) and gypsiferous crusts composed of poikilitic crystals; and 2) nodular anhydrite, which probably formed in the capillary zone of a lacustrine sabkha or mudflat. Additionally, a somewhat later pervasive meganodular secondary anhydrite texture overprints much of the laminated lake gypsum, presumably driven by heating of ascending, highly saline groundwaters. The timing of anhydritization was mainly controlled by the salinity of the

pore solutions, and ongoing from the onset of deposition to moderate burial (Orti and Rosell, 2000). The basin's diagenetic history indicates the complexity of evaporite textural evolution, even in strata that are undeformed and have undergone no more than shallow burial (Figures 7.36, 7.44).

Permian lacustrine redbeds, Kansas

The mid-Permian (Leonardian) Nippewalla Group of Kansas and the Opeche Shale of North Dakota are part of an extensive redbed succession deposited in an arid continental interior sag basin on the Pangaeon megacontinent (Figure 5.13a; Benison and Goldstein, 2000, 2001). Characteristic lithologies comprise bedded pan evaporites, red-bed siliciclastics and grey siliciclastics, all laid down in a series of continental playas (Figure 5.13b, c). Most evaporite deposition took place in a series of halite-dominated ephemeral saline lakes surrounded by saline and dry mudflats, sandflats and sand dunes. It was an environment characterised by acid groundwaters with hydrologies not unlike those of southeastern interior Australia and exemplified by the redbed lacustrine associations forming

today in and around Lake Tyrell, Victoria and the salt lake landscape of southwest Western Australia (Benison and Goldstein 2002; Figure 2.20). Permian climate alternated between arid, when red siltstones and bedded evaporites dominated the various saline lake centres, and more humid when grey siltstones and palustral carbonates were widespread.

Bedded evaporites were deposited as saltpan and chaotic halites, or as less widespread bedded units containing calcium sulphate salts. Like the acid drainage basins of Australia, the system lacked widespread carbonates. These evaporite-depositing depressions were surrounded by extensive redbed mudflats and sandflats. Lithologies and sedimentary features indicate lacustrine and eolian deposition, subaerial exposure and palaeosol formation. Grey siliciclastic mudstones represent a freshwater-brackish perennial lake facies and are characterized by planar and convolute laminations, ostracods, peloids and plant material. Water levels were higher and the climate more humid when the grey siltstones were deposited. Bedded anhydrites containing gypsum-crystal pseudomorphs, clastic anhydrite grains, along with grey mud drapes and partings, all suggest deposition in saline lake depressions. Bedded halites consist of chevron and cumulate crystals, dissolution surfaces and pipes, and mudcracked microcrystalline salt crusts. They were deposited in saline pans subject to flooding, evaporative concentration and desiccation. Chaotic halite, composed of red-bed mudstone and siltstone with displacive halite crystals, formed in saline mudflats surrounding the salt pans. Red-bed mudstone and siltstone with little or no displacive halite, but with abundant cracking, root and plant features were deposited in dry mudflats in areas where water throughputs were less saline and waters were sufficiently fresh to allow halophytes to grow. Red-bed sandstone, composed of well-sorted, well-rounded quartz

grains cemented with halite, indicate eolian and rare shallow-water deposition.

Evaporation, desiccation, flooding and wind reworking played significant roles in this environment (Benison and Goldstein, op. cit.). The Nippewalla Group/Opeche Shale siliciclastics and evaporites represent an evolution from a perennial lacustrine system to a nonmarine, acidic saline pan system in the mid-continent of North America. Inclusion data from primary chevrons in the pan halite preserve temperature fluctuations at the seasonal scale and act as first-rate proxies for Permian climate in an

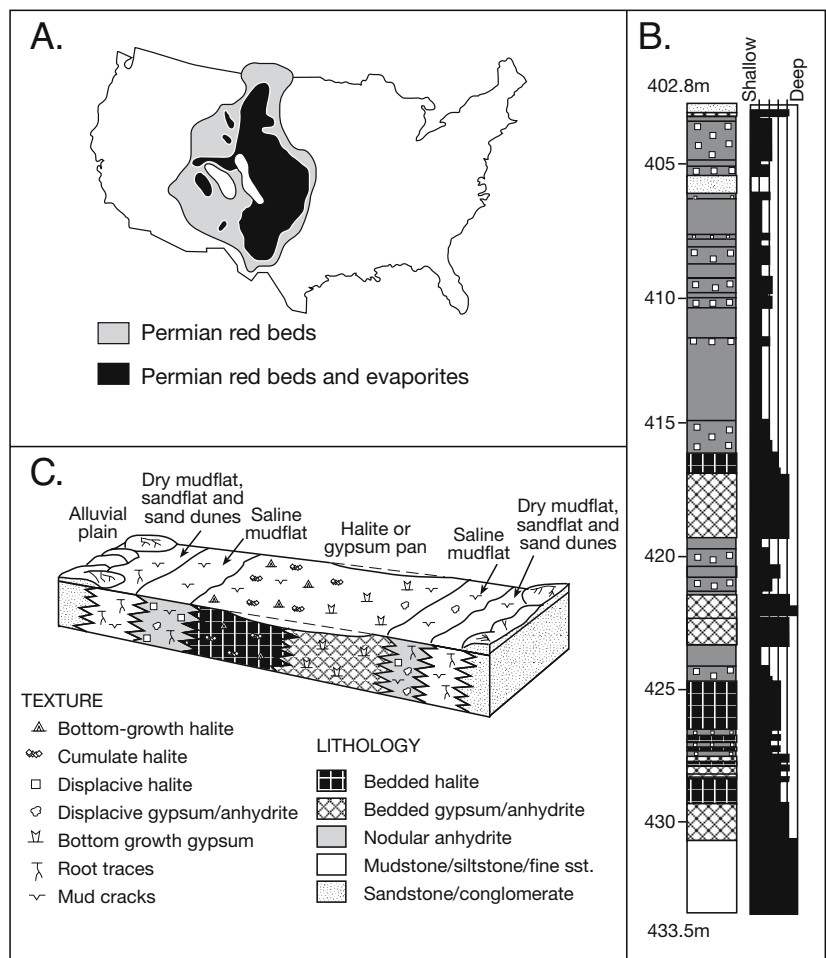


Figure 5.13. Permian redbeds of interior USA. A) Distribution of Permian red beds and evaporites in the USA. B) Lithological description and relative depths of depositional environments of the Nippewalla Group from the subsurface of western Kansas; Anadarko-Davis No. 1 core, Seward County, Kansas. Deeper probably indicates a wetter climate and so this core seems to represent a transition from a wetter to a drier climate. C) Inland playa associations that controlled sediment patterns in red beds of both the Opeche Shale and Nippewalla Group. (after Benison and Goldstein, 2000, 2001).

arid megadesert created by the formation of Pangaea (Figure 2.28). To the south, time equivalent evaporitic sediment in the San Andres and Clear Fork formations of the Palo Duro Basin, show an increasing marine influence in the form of intercalated carbonates. There widespread pan halites and bedded gypsums are intercalated with oolitic, restricted-marine platform carbonates, cryptogalaminites become significant contributors to the sediment volume, and bioturbation from marine burrowers are locally important in some of the carbonate units (Handford, 1981; Hovorka, 1987). Halite pseudomorphs after bedded coarse-grained gypsum is an important early diagenetic fabric in some of these sediments.

This passage to more marine-influenced saline pans and salterns in the south illustrates a correlation problem common to many ancient evaporites deposited atop cratonic landmasses. Namely, what defines an evaporite bed as marine or marine seepage-fed versus continental lacustrine in what where highly restricted settings where even marine-fed depressions had no surface connection to the ocean. This paradox is discussed in more detail later in this chapter.

Other Lacustrine Red Bed Associations

In a number of underfilled lacustrine basins the supply of water may be insufficient to maintain a shallow water table or a perennial lake in the drainage basin sump. In this situation the basin dries to where much of the sediment is reworked by wind action and little evidence of bedded lacustrine evaporites remains. Much of the basin fill is wind-reworked silt and loess. This is the situation in the present day Lake Eyre drainage basin of Central Australia and was also the case in the Triassic across much of northwest Europe (Figure 5.14; Talbot et al., 1994; Reinhardt and Ricken, 2000). This was when the Mercia Mudstone Group was deposited in Great Britain and the Kueper in Germany. Deposition was dominated by a characteristic assemblage of fine-grained facies, the most widespread of which is a variably dolomitic red mudstone. It is typically massive and unfossiliferous except for occasional vague horizontal laminae and irregularly distributed wispy sand

patches (e.g. Brookfield, 2003). Desiccation features are common, as are blocky weathering patterns. Nodular beds of gypsum/anhydrite and celestine are associated with the mudstone, along with gypsum-filled desiccation cracks and pseudomorphs after displacive halite and suggestions of haloturbation. Locally there are also 10-30 cm thick dolomite and limestone beds. These thin beds range from micritic mudstones to ooid grainstones and packstones with freshwater algal remains (charophytes and *Botryococcus*). These local freshwater intervals are interpreted as areas of ponded floodwaters brought to the basin after exceptional rains (Talbot et al., 1994). As for the rest of the lithotypes, they too have their counterparts in times of freshened lacustrine sedimentation tied to flooding of the Quaternary Lake Eyre Basin (Chapter 3).

Details of other saltpan and perennial lacustrine deposits, where the bedded salts are an exploited resource or a intimately associated with an exploited resource, are discussed in Chapter 11 (borates, lithium, magnesites, nitrates, potash, sodium carbonate, sodium sulphate, zeolites).

Platform evaporites on epeiric shelves

Platform evaporites accumulated in epicontinental (epeiric) or pericontinental settings and constitute the salt layers in many stacked shoaling marine platform cycles, where 5-10 m

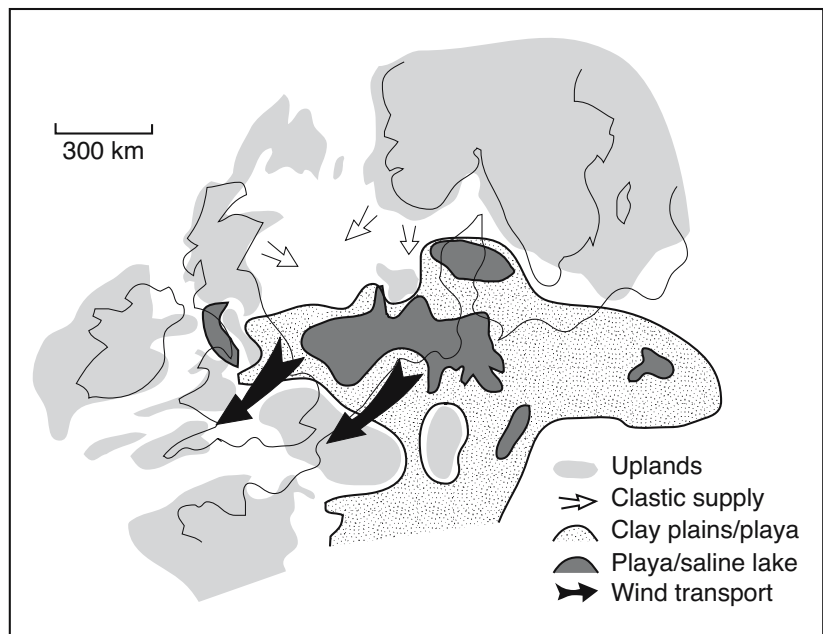


Figure 5.14. Late Triassic palaeogeography of northwest Europe showing how deposition was predominantly in an endorheic basin and wind was blowing dust from mudflats about large discharge playas (after Talbot et al., 1994).

thick evaporite units (typically anhydrite with lesser halite) are repeatedly interbedded with open-marine shoalwater carbonates or continental siliciclastics. Epeiric seaways were huge very shallow shelf and interior seas, up to thousands of kilometres across, that typically held waters no more than tens of metres deep and were usually much shallower during the hydrographically-isolated bedded salt phases (Figure 5.15). Epeiric seaways require large areas of continent to be covered by water and so are commonplace at times when world sealevels are high, as exemplified by greenhouse climate modes. In the world's current icehouse mode, sealevels are low as much of this water is caught up in polar icesheets and so there only are few Quaternary examples of epeiric carbonate seaways; they are all open marine systems (e.g. Gulf of Carpentaria, northern Australia, with its patchy but widespread *Halimeda* mounds and the Yucatan Shelf of Mexico with its well developed strandline of calcareous eolianite).

When an epeiric basin is cut off from a surface connection to the open ocean (hydrographically isolated), deposition occurs in widespread evaporitic mudflats surrounded by desert dunes and wadi plains. Or deposition occurs beneath sluggish, slowly circulating perennial sheets of marine-fed brine that cover the lower parts of the basin, especially near zones of marine seepage. There the surface waters can become holomictic and attain sufficient salinity to precipitate and stack widespread salts beds into units as much as 5-10 metres thick. Subaerial evaporitic carbonate mudflats and sandplains typically separated the brine sheets from the open ocean.

At other times, when the same areas on the epeiric platform had a surface connection to the adjacent ocean (hydrographic connection), they were covered by shallow seawater. It could concentrate into the mesohaline range, especially in more restricted parts away from areas of marine resupply, but could not reach sufficient concentration to produce bedded salts. The greater volume of the platform sediments at times of surface connection were muddy marine carbonates, mostly peloid wackestones and mudstones. Skeletal and peloidal (oolitic)

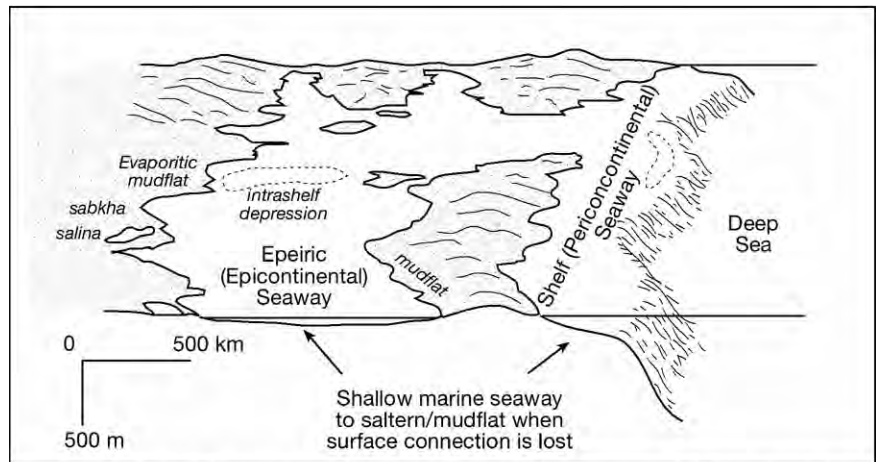


Figure 5.15. Epeiric (epicontinental) seaways covered large areas of the continental interior with shallow marine waters, while pericontinental seaways formed as very wide shelf edges. They have no modern counterparts but were commonplace in greenhouse earth when the continental freeboard was much larger than it is today. Waters were very shallow over areas that were hundreds to thousands of kilometres across. With hydrographic isolation these restricted marine seaways quickly became salterns or evaporitic mudflats (after Heckel, 1974).

grainstone shoals built up in areas where current energies from waves, or possibly tides along the marine edge, were sufficient to winnow lime mud but not grains. This created sand flat islands or shoals with long axes subparallel to the direction of dominant current transport, encased in peloids or muds. These beds constitute the reservoir sands in many mudflat and saltern sealed epeiric sequences, such as the Arab D and Khuff carbonates in the Middle East (Figure 10.9). Repetitive and characteristic shoaling-upward stacks or parasequences accumulated on the platform as the various types of marine sediments aggraded and prograded in this carbonate milieu. The extensive flat arid areas circumscribing the seawater-covered areas of the open seaway were typically huge evaporitic mudflats. Salinities along the low-relief strandzones of these huge shallow seaways were sufficiently elevated that the only fossil evidence of life was the occasional stromatolite in a mass of microbial laminites.

Mudflat edges of these isolated seaways and the marine-fed platform salterns generated dense seaward-flowing seeps of residual reflux liquor. Such brines cycled through and across the underlying platform sediment to create reflux dolomites (Figure 2.49). The fluxes were sometimes sufficiently voluminous to supply longterm chemosynthetic seeps on the open sea floor of the adjacent open marine platform. At times of hydrographic connection, brines escaping from an adjacent mudflat into the seaway would become bottom-hugging waters, which trickled and seeped into local brine sumps on the marine platform floor.

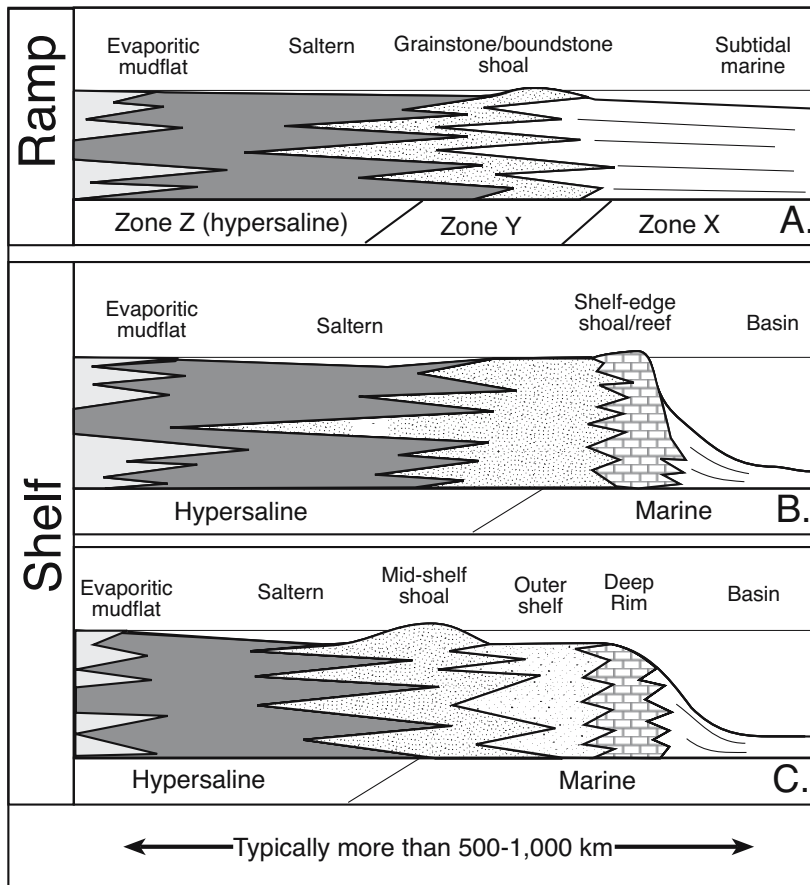


Figure 5.16. Evaporite depositional styles - ramp and shelf. A) Gently deepening ramp with restriction created by exposed zone Y shoal. B) Rimmed shelf with restriction supplied by exposed reef/shoal that defines the platform margin. C) Rimmed shelf with deep rim and restriction supplied by exposed mid-shelf shoal (Warren, 1999).

Ultimately, these denser, bottom waters formed areas characterised by long-term dense anoxic bottom water beneath a column of normal platform seawater. These areas were intraplatform or intrashelf basins that were local, slightly deeper, warmer (heliothermic) depressions on the seaway floor. They could be up to hundreds of kilometres across, but water columns were no more than 10-30 m deep. By the time the mudflat-derived bottom brines finally ponded in the deeper parts of such intraplatform lows, salinities may have been diluted, via mixing, to where they were no more than a few ‰ higher than normal seawater. This was sufficient to maintain a density/thermal stratification, so that the bottom waters were dysaerobic to anoxic. A number of organic-rich oil-prone carbonate laminites and marls (source rocks) accumulated in these lows, such as the Jurassic Hanifa Formation a significant source rock of the Arabian Platform (Figures 9.3, 9.4). At times of hydrographic connection between the epeiric platform and the world's oceans, the platform areas surrounding these intraplatform depressions were shallow and

more oxygenated than the depression floor, with largely normal marine salinities and water depths typically less than 10 metres. This encouraged the local accumulation of reef mounds and sandy shoals.

Hydrographic connection between the open ocean and the epeiric seaway could be lost for a number of reasons; a sand shoal buildup at the platform rim, a slight fall in sealevel, or tectonic tilting. Once portions of epeiric or pericontinental seaways lost their hydrographic connection to the open ocean, bedded marine-fed saltern and mudflat evaporites were laid down. This occurred within one of two carbonate platform settings; either on a *carbonate ramp* or on a *carbonate shelf* (Figures 5.7, 5.16). Carbonate ramps have slopes of less than 1°, the wave agitated zone is typically close to the seashore, and there is no high relief shelf break located some distance seaward from shoreline (Ahr, 1973). Slopes in ancient epeiric ramps in greenhouse times and in intracratonic seas were as low as 1 in 50,000, compared to modern ramp gradients of between 1 in 500 and 1 in 2500 (Burchette and Wright, 1992; Warren 1991). In

contrast, carbonate shelves are shallow water, land-coupled platforms with a pronounced break in slope into deeper water (Figure 5.16b). The break in slope is typically a wave agitated to high-energy feature, it may be composed of a reef rim or a series of mechanically-reworked sand shoals and islands. The slope, seaward of the platform edge, is typically measured in degrees of inclination. In modern reef-rimmed platforms the seaward slope ranges from 30° to vertical.

Evaporitic epeiric ramps

Ahr's original ramp model envisaged a uniform slope from the shoreline into the basin, later termed a homoclinal ramp by Read (1985). However all modern ramps, and some ancient ramps appear to have a subaqueous slope break into deeper water and are termed distally-steepened ramps. The inclination of the slope

is still flat (<1-2°) and never approaches that of a carbonate shelf. Modern ramps characterise the tropical carbonate coasts of the southern Arabian Gulf, the Gulf of Carpentaria and the Yucatan shelf. All these modern ramps face directly into the open ocean and have never shallowed sufficiently to isolate large portions of their lagoons and so lack widespread salt beds. The only well documented example of a modern carbonate ramp with some evaporite deposition is the Trucial Coast of the southern Arabian (Persian) Gulf (Purser and Evans, 1973). But, it is a poor analog for any epeiric or pericontinental counterpart as it is not supplied solute from a seawater source, its evaporite belt is supratidal, less than 10-15 km wide, matrix-rich and less than a metre thick (Chapter 3).

Unlike most modern carbonate ramps, which are tens to a few hundred kilometres wide, ancient epeiric ramps were hundreds to thousands of kilometres across and formed huge evaporitic seaways at the edges of continents (pericontinental seaways;

Figure 5.15) or extended as near-land-locked interior seaways that spread out across large areas of various continental cratons (epicontinental seaways). The Permian red beds discussed in the lacustrine section are the landward end of one such interior evaporitic lake or seaway (a saltern). The world's last development of such a huge interior seaway was in the Eocene in evaporitic platform carbonates of the Middle East (Table 5.5). But these platform evaporites (Radhuma, Rus and Damman formations) are perhaps better considered as basinwide back-bulge or intracratonic sag salts, deposited in a response to flexural sag and basin isolation behind the migrating forebulge of the Zagros Orogeny (Alavi, 2004). If so, this makes the world's most recent episode of marine platform evaporite as old as the Paleocene or the Cretaceous (Table 5.5, Figure 10.29).

The transition into an icehouse climatic mode in the Tertiary, the capture of large volumes of ocean water in oscillating ice caps, and a slowing in the rate of seafloor spreading, meant

Unit	Location	Age	Reference
Siwalik Group	Kohat Plateau, N. Pakistan	Low. Eocene	Pivnik and Wells, 1996
Rus Fm.	Arabian Basin, Qatar	Low. Eocene	Mukhopadhyay et al., 1996
Jirani Dolomite	Jifarah Trough, Libya	Low. Eocene	Mriheel and Anketell, 1995
Beda Fm.	Sirt Basin, Libya	Mid. Palaeocene	Garea and Braithwaite, 1996
Fort Terrett Fm.	Kirschberg Basin, Texas	Low. Cretaceous	Warren et al., 1990
Quintuco-Loma Montosa Fm.	Neuquen Basin, Argentina	Low. Cretaceous	Carozzi et al., 1993
Ferry Lake Anhydrite	Gulf of Mexico, NE Gulf Coast	Low. Cretaceous	Pittman, 1985
Sunniland Limestone	South Florida, USA	Low. Cretaceous	Halley, 1985
Cupido Fm.	Coahuila platform, NE Mexico	Low. Cretaceous	Lehmann et al., 1998, 2000
Smackover/Buckner Fm.	Gulf of Mexico, N Gulf Coast	Up. Jurassic	Lowenstein, 1987a; Mann, 1990
Hith Anhydrite	Arabian Basin, Saudi Arabia	Up. Jurassic	Alsharhan and Kendall, 1994
Arab-C	Arabian Basin, E. Saudi Arabia	Up. Jurassic	Saner and Abdulghani, 1995
Sabatayn Fm.	Wadi Al-Jawf-Marib, Yemen	Up. Jurassic	Youseff, 1998
Lower Bathonian sediment	Causses, Southern France	Mid. Jurassic	Fuersich et al., 1995
San Vincente Limestone	Pucara, Central Peru	U. Tr. - Low. Jur.	Spangenberg et al., 1996, 1999
Interlayered carb/evap.	Kand sub-basin, N. Iraq	U. Triassic	Sadooni, 1995
Mixed sabkha facies	Adriatic offshore, Croatia	Mid. - U. Triassic	Cota and Baric, 1998
Muschelkalk	SW Germany and E. Spain	Mid. Triassic	Schauer and Aigner, 1997
Tripolis Unit	Ionian Zone, NW Greece	Mid. Triassic	Karakitsios and Pomonipapaioannou, 1998
Latemar Massif	Dolomites, Italy	Mid. Triassic	Egenhoff et al., 1999
Sudair Fm.	United Arab Emirates	Low. Triassic	Whittle et al., 1995
Roet salt	Western Poland	Low. Triassic	Czapowski, 1992

Table 5.5. Representative examples of Mesozoic and Tertiary evaporitic platforms. In some, the former evaporite beds are now represented by laterally extensive solution breccia horizons. Some examples are also the margins to tectonically-induced basinwide evaporite fills.

Sequence of interest	Basin/locality	Age	References
Khuff Fm.	Arabian Basin, Middle East	Up. Permian	Al-Jallal, 1991; Alsharan, 1993
Guadalupian backreef	Delaware Basin, west Texas	Up. Permian	Saller and Henderson, 1998
Karstryggen Fm.	East Greenland	Up. Permian	Stemmerik et al., 1988
Bellerophon Fm.	Dolomites and Carnia, Italy	Up. Permian	Massari and Neri, 1997
Haselgebirge Fm.	North Calcareous Alps, Austria	Up. Permian	Spötl, 1989a
Saltern sediments	Dinardides, Croatia and Bosnia	Up. Permian	Tisljar, 1992
Park City Fm.	Wyoming	Up. Permian	Ulmer-Scholle and Scholle, 1994
Saltern sediments	Palo Duro Basin, Texas	Up. Permian	Hovorka et al., 1993; Long et al., 1997
Leadville Fm.	NW Shelf, Paradox Basin, Utah	Low. Carbon.	Miller, 1985
Mission Canyon Fm.	SE Shelf, Paradox Basin, N. Dakota	Low. Carbon.	Lindsay and Kendall, 1985
Dinantian anhydrites	Solway Basin, UK	Low. Carbon.	Crowley et al., 1997
DeBolt Fm.	Western Canada	Low. Carbon.	Al-Aasm and Packard, 2000
Qianheishan Fm.	Northern Qilian fold belt, China	Low. Carbon.	Ma, 1998
Belle Roche Breccia	Vesder Basin, Belgium	Low. Carbon.	Muchez et al., 1994; Swennen et al., 1990
Birdbear Fm.	Western Canada	Up. Devonian	Whittaker and Mountjoy, 1996
Evaporitic carbonate	Barbwire Tce., W. Australia	Up. Devonian	Wallace, 1990
Eday Marls	East Orkney Basin, UK	M.-Up. Devonian	Marshall et al., 1996
Cadjebut Fm.	Lennard Shelf, W. Australia	Mid. Devonian	Warren and Kempton, 1997
Evaporitic carbonate	Cudgegong, NSW Australia	Mid. Silurian	Jones et al., 1987
Interlake Fm.	Cabin Creek field, Montana	Up. Silurian	Roehl, 1985
Red River Fm.	Williston Basin, Montana, USA	Up. Ordovician	Dewing and Copper, 1991
Aleman Fm.	SW New Mexico, USA	Up. Ordovician	Geeslin and Chafetz, 1982
Port Nelson Fm.	Southampton Is., NW Territories	Up. Ordovician	Dewing and Copper, 1991
Queenston Fm.	W. Taconic Wedge, Ontario, Canada	Up. Ordovician	Brogly et al., 1998
Yeongheung Fm.	Yeongheung Platform, Korea	Mid. Ordovician	Yoo and Lee, 1998
Joachim Dolomite	Holstein Basin, Arkansas, USA	Mid. Ordovician	Handford and Moore, 1976
Upper St George Gp.	W. Newfoundland Basin, Canada	Low. Ordovician	Coron, 1982
Ellenberger Dolomite	Tobosa Basin, west Texas, USA	Low. Ordovician	Loucks and Anderson, 1985
Arbuckle Group	Arbuckle platform, Slick Hills, USA	Low. Ordovician	Gao and Land, 1991
Upper Knox Group	Appalachian Basin, USA	Low. Ordovician	Montañez and Read, 1992
Majiagou Fm.	Ordos Basin, N. China platform	Low. Ordovician	Feng et al., 1998; Zhu and Zhang, 1999
Cool Creek Fm.	Arbuckle platform, S. Oklahoma	Low. Ordovician	Ragland and Donovan, 1984
Arrintheta Fm.	Georgina Basin, Central Australia	Up. Cambrian	Kennard, 1981
Ninmaroo Fm.	Georgina Basin, Central Australia	Up. Cambrian	Radke, 1980
Red Heart Dolomite	Georgina Basin, Central Australia	Low.-Mid. Camb.	Nicolaidis, 1995
Ouldburra Fm.	Officer Basin, Australia	Low. Camb.	Kamali et al., 1995

Table 5.5 continued. Representative examples of Paleozoic evaporitic platforms. In some, the former evaporite beds are now represented by laterally extensive solution breccia horizons. Some examples are also the margins to tectonically-induced basinwide evaporite fills.

large evaporite seaways, so conspicuous on the Late Permian and Mesozoic platforms, had disappeared from the face of the earth by the mid Tertiary. A lack of modern analogues means we cannot directly observe the influence that epeiric seaways had on the depositional styles of ramp evaporites. We are forced to scale up sediment patterns in Quaternary coastal evaporites in the knowledge that the high amplitude, high frequency, eustasy of today is not the hydrological or eustatic equivalent of the sea-margin ramps of greenhouse earth.

Epeiric ramps were first modeled by Shaw (1964) and Irwin (1965), they both concluded that the huge areas of restricted stagnant circulation on the backsides of these seaways were capable of periodically accumulating extensive beds of evaporites. Irwin's epicontinental-sea model proposed there were three zones of varying hydraulic energy on ancient platform ramps (Figures 5.16a):

- *Zone X* was a wide low-energy region situated below wavebase on the open-marine side of the platform, so that sediments were mainly bioturbated marine mudstones and wackestones. It was often hundreds of kilometres wide and locally characterized by limited water circulation with occasional stagnation. Now and then, this led to the deposition of organic-rich laminated sediments.
- *Zone Y* was a narrow, intermediate to high-energy belt beginning where waves first bottomed on the seafloor and extending landward to the limit of any tidal action. Sediments in this zone included sand and grainstone shoals, mud banks, reef mounds and patch reefs. These sediments could build elongate shoals that restricted and at times prevented the surface entry of seawater into the adjacent zone Z.
- *Zone Z* was an extremely shallow, restricted low-energy region on the landward side of zone Y. In arid settings, wherever zone Z was hydrographically isolated from zone X, extensive saltern and mudflat evaporites were deposited. At times when zone Z and zone X had a surface connection through zone Y, the seaward portion of zone Z was covered by restricted-marine mostly muddy sediments with local sandier carbonates. The more distal portions on its continental side were evaporitic mudflats.

Marine wave energy was dissipated some distance basinward from zone Z as it spent itself against the seaward side of the shoals, bars, and reefs of zone Y. Shallow wave-agitated facies of zone Y passed down the slope into deeper-water subtidal open-marine facies of zone X without a rapid change in slope angle. Behind the zone Y shoal, bottom slopes in zone Z were even less than on the open marine ramp and had maximum

bottom angles of only a few seconds of arc ($\approx 1:50,000$). Thus, huge areas of zone Z were covered by extremely shallow water sheets, much of it only tens of centimetres deep. This is a setting replicated at a much smaller scale in the modern khors of the United Arab Emirates. During times of widespread evaporite deposition across zone Z there was no hydrographic connection to the ocean and so tidal effects were negligible. Depositional textures were largely akin to those formed in modern saline pans and sabkhas although perennial seaways depositing salterns were a distinct possibility in zones with more relief behind Zone Y.

Zone Z water levels fluctuated most rapidly during intense storms or hurricanes, as sheets of sediment-laden seawater could be washed landward over zone Y into zone Z, or during exceptional episodes of flash-flooding generated by torrential rainstorms in the continental hinterland. Both marine and meteoric influx freshened the surface and nearsurface brines of Zone Z as sheets of water migrated tens of kilometres across the strandplain. At the same time a new pulse of marine or continental clastic sediment matrix was delivered. Evaporite-forming areas in zone Z were up to hundreds of kilometres wide, far wider than any evaporitic area on the modern land surface.

On any evaporitic ramp there was some degree of topographic relief about zone Y, and restriction of water flow across it. When salts were accumulating in Zone Z there were no perennial surface channels connecting it to the waters of Zone X (see later discussion and Figure 5.28). Vertical sequences of evaporites deposited in zone Z were very much dependent on the relative physiography of zone Y. If zone Y was a well developed low-relief shoreline with extensive washover flats behind, then much of zone Z was an evaporitic mudflat; a mosaic of sabkhas and salinas. Or, if zone Y was a higher-relief shoal, it would be backed by a marine seepage-fed evaporite lagoon, and zone Z would consist of saltern evaporites with an increasing proportion of subaerial mudflat indicators (desiccation cracks, karst, erosion features, displacement textures) toward the top of the unit and toward the landward and seaward strandplains (Figure 5.5).

Units P₁ and P₂ of the San Andres Formation in the northwestern platform of the Permian Basin and the Palo Duro Basin illustrate the saltern-ramp end member (Figure 10.22; Elliott and Warren, 1989). Similar saltern signatures dominated the San Andres and Clear Fork formations in the Palo Duro Basin (Figure 5.17). Correlatable units of saltern anhydrite or halite in the Palo Duro Basin have areas of more than 26,000 km². At times of widespread evaporite deposition on the Palo Duro Basin and the northwestern shelf of west Texas, one could

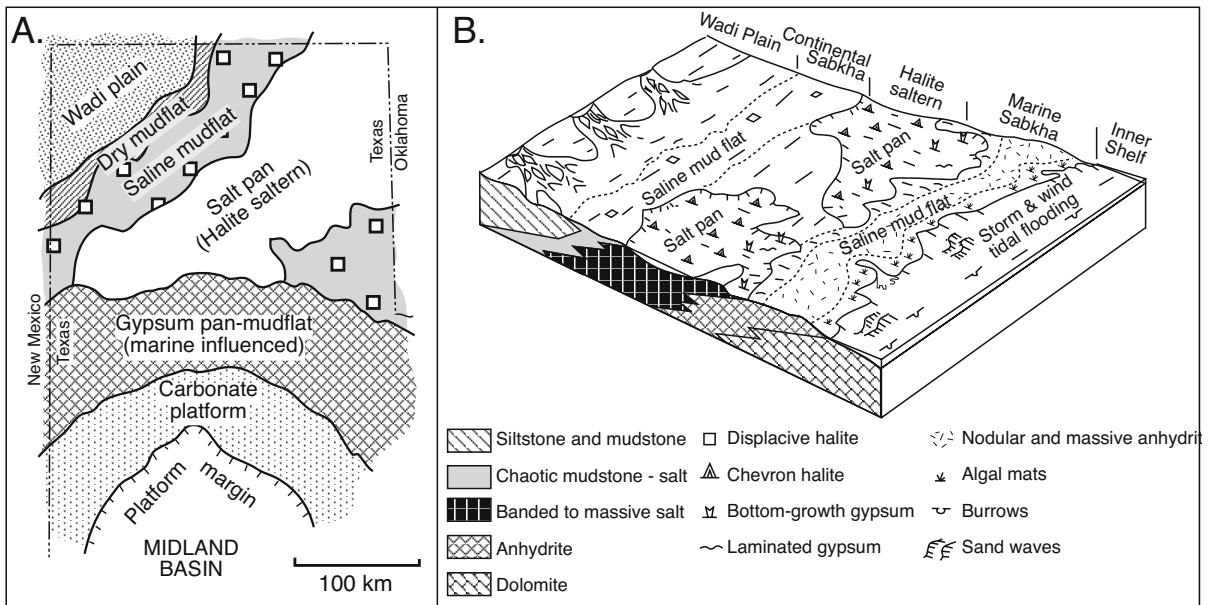


Figure 5.17. Lithofacies and paleogeography of the early Permian Lower Clear Fork Formation, an evaporitic ramp at the northern end of the Midland Basin in the Texas Panhandle. A) Plan View. B) Schematic of depositional relationships between main evaporitic facies (after Handford, 1981).

have travelled 50 to 150 km south and seaward from the strandplain of the brine sheet and never crossed through water that was much more than a few metres deep, nor less saline than gypsum-saturated.

The northern portions of the Lower Clear Fork Formation of the Palo Duro Basin illustrate the evaporitic mudflat-ramp end member where extensive “dirty” halite beds are intercalated with fine-grained siliciclastics (Figure 5.17a; Handford, 1981, 1991). Deposition took place in an evaporitic mudflat and pan complex that passed further northward into the large continental desert made up of salt pans, wadis and dunes documented by Benison and Goldstein, (2001). Southward, the Clear Fork ramp passed from highly continental mudflats into marine-fed saltern deposits and then across the restriction of the Zone Y phylloid buildups into open-marine carbonates of zone X (Figure 5.17b; Ramage, 1987). Deciding where to place a line separating marine from nonmarine brines is near impossible; although it is generally true in this and in most other arid successions passing from the marine into huge interior redbed deserts that the thicker bedded salt accumulations are more likely on the marine side of the system.

Thick evaporitic carbonates and intercalated anhydrites of the Khuff Formation define a huge evaporitic platform (≈ 255 Ma) in the Arabian Gulf, with an upper section that straddles the Permo-Triassic boundary (Figure 5.18; Al-Jallal 1995,

Dasgupta et al., 2002). In eastern Saudi Arabia, the Khuff Formation is divided into five units or members designated as Khuff A through E. However, throughout the Gulf region the Khuff may comprise as many as seven designated mappable subsurface units or members (Al-Jallal, 1995). Most of the Khuff Formation is composed of carbonates and evaporites; major siliciclastic facies increase towards the west and toward the base of the sequence, especially in Saudi Arabia. As many as four of the five units are capable of acting as hydrocarbon reservoirs and correspond to four depositional carbonate-anhydrite cycles where transgressive marine carbonates are capped by regressive anhydrites.

The Khuff Formation thickens from about 260 m in southwestern Saudi Arabia to more than 915 m in the central Rub ‘al Khali Basin, 1,220 m in Oman, and 1,520 m in Iran. Typical thickness for the Khuff ranges between 370 m and 490 m over most of central and eastern Arabia (Al-Jallal, 1995). The basal Khuff section consists mostly of siliciclastics throughout southern Arabia. The “basal Khuff clastics” in Saudi Arabia are made up of shale, carbonaceous shale, limestone streaks, and incised channel-fill sandstones. Individual channel-fill sandstone units of the basal Khuff clastics are as much as 18 m in thickness and can cut deeply into the underlying Unayzah Formation. In the Hazmiyah field of central Saudi Arabia, the reservoir occurs entirely within these channel sandstones in the basal Khuff (Senalp and Al-Duaiji, 1995). The Unayzah and

basal Khuff sandstones form the principal reservoirs in central Saudi Arabia; however, widespread reservoir quality variations occur in these sandstone reservoirs owing to heterogeneous sedimentary facies and variable diagenetic intensity (Aktas and Cocker, 1995; Polkowski, 1997).

Over most of the rest of Saudi Arabia and west into Oman and the UAE the Khuff is more than a 1 km thick and composed of numerous 2-10 m thick shoaling stacked dolomitized carbonate cycles or parasequences. These Late Permian dolomites are major gas reservoirs along the offshore in the Arabian Gulf north and west of Qatar. In contrast, the regionally extensive anhydrite, shale, and tight (low-permeability) carbonates of the Khuff Formation form the major regional seal for Pre-Khuff hydrocarbon accumulations in central and eastern Saudi Arabia (Al-Jallal, 1995; Wender and others, 1998).

Deposition of this thick carbonate succession was initiated as a ramp in the late Khazanian or early Tatarian and had evolved into a reef-rimmed evaporitic platform by the later Permian to early Triassic (Figure 5.18). Most of the cycles in the upper part of the Khuff are capable of producing gas and are variably dolomitised oolite-peloid successions that typically grade upward into fine-grained laminites and nodular mudflat/pan anhydrite. Carbonate cycles atop siliciclastics in the lower part of the Khuff tend to be more dominated by coarsening-upward shoreface/shoal cycles with lesser mudflat laminites.

All the Khuff beds and markers pass westward via a belt of mixed detrital carbonate and siliciclastics onto the palaeohigh of the Arabian Shield. Correlations and definitions of time-equivalence in adjacent wells or outcrops in this belt is problematic due to a lack of appropriate fossils and similarity in wadi/dune depositional styles throughout large passages of Palaeozoic and Mesozoic time in the circum-Arabian Shield area.

The succession is punctuated by numerous intervals of subaqueous and pan anhydrite (after gypsum) with local development of evaporitic mudflat facies atop shoals (pers. obs.). In the middle of the Khuff succession is a

thick saltern sulphate bed called the Middle Anhydrite. It is a regional marker bed originally deposited as a thick sequence of bottom-nucleated subaqueous gypsum. This marker defines a time when the whole of the Khuff platform was converted to a saltern rather than the more typical combinations of evaporitic mudflats and pans (Chapter 10).

The Jurassic section atop the Khuff in Saudi Arabia and the Emirates is another evaporitic platform succession. It constitutes the most significant source-reservoir-seal association for hydrocarbons anywhere in the world (see detailed discussion of Hanifa, Arab D and Hith Anhydrite in Chapters 9 and 10). Both the Arab and the Khuff formations accumulated at different times along the southern shore of the Neo-Tethyan Ocean when sediment accretion atop an original Hercynian horst and block terrain periodically isolated large parts of the platform interior (Figure 10.9). This led to the punctuation of the carbonate platform record with evaporite beds throughout much of the Mesozoic.

Regionally, the Mesozoic in the Middle East was a period of tectonic activity centred around the opening and closing of the Tethys. The Late Permian ocean backed onto the huge land-

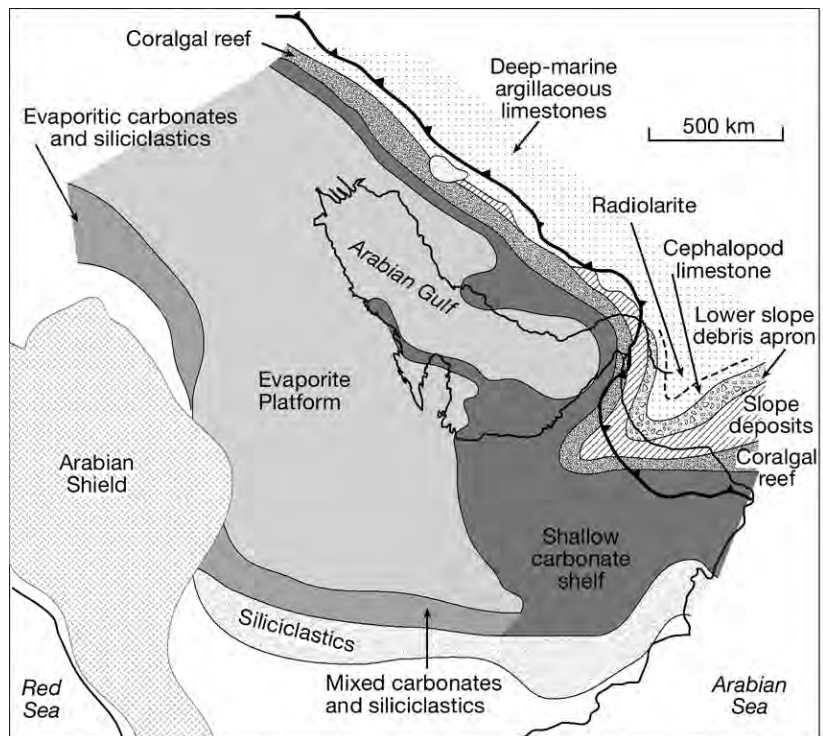


Figure 5.18. Major facies belts and their interrelationships in the Permian Khuff Formation of the Middle East (after Al-Jallal, 1995).

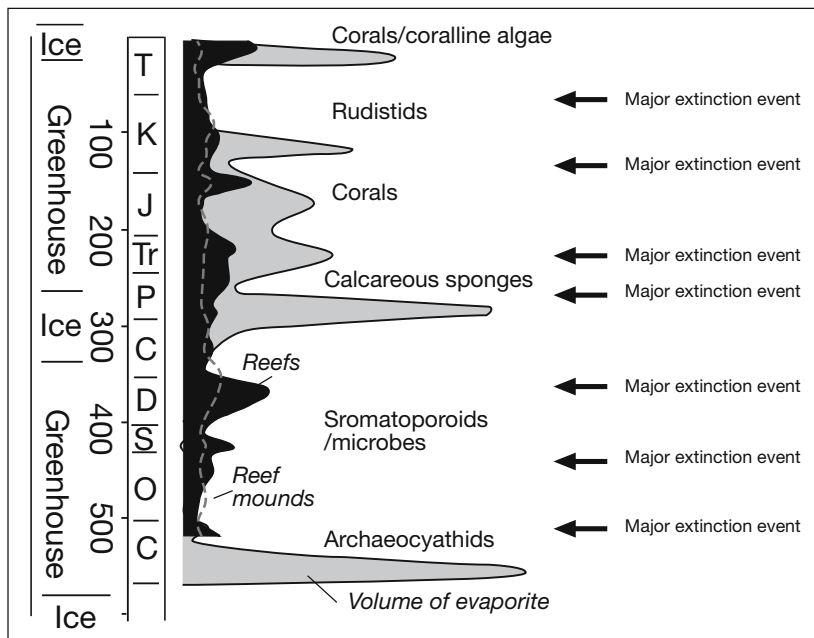


Figure 5.19. Phanerozoic distribution of reefs (black shading), reef mounds (dashed line), major extinctions and the dominant reef formers through time (after Kiessling et al., 1999) versus the worldwide volume of evaporites (after Hite and Anders, 1991).

masses of Pangaea and in both opening and closing stages of the supercontinent the ocean created large subsealevel marine margin areas where epeiric carbonate seas formed that were periodically isolated as intracratonic sags and then filled to hydrologic base level with bedded salts. Similar evaporite entraining epeiric carbonate ramps also characterised the Infracambrian of the Middle East, the lower Palaeozoic of North America and Australia, the late Palaeozoic of America and Russia, and the Triassic and Jurassic of Europe (Table 5.5).

Evaporites atop rimmed epeiric shelves

Ancient rimmed-shelves were shallow-water carbonate platforms with an outer wave-agitated edge marked by biogenically induced buildups or highs and a pronounced increase in slope that was typically a few degrees, less often more than 60° , into deep water (Read, 1985). Platform evaporites can be found behind such rims throughout the Phanerozoic (Table 5.4a, b). Subsurface examples of this style of carbonate deposition, as opposed to ramps, are readily identified seismically using obvious clinofolds and reflection discontinuities that define the shelf edge or shelf break. Many modern reef-rimmed shelves are constructed by combinations of corals and coralline algae, but different organisms have occupied the framebuilder niche in the past; stromatolites in the Proterozoic, stromatoporoids

in the Devonian and rudistids in the Cretaceous. When Phanerozoic reef occurrences are plotted in time against evaporite volumes there is little or no correlation implying reef-rimmed platforms are not the dominant mechanism driving times of widespread evaporites. It implies tectonic isolation during times of continental make-up or break-up, and not eustasy, created the depressions and the drawdown hydrologies that precipitated the greater volumes of world's ancient evaporites (Figure 5.19).

Areas behind platform rims in arid settings are typically made up of seepage-fed evaporitic carbonate flats that pass landward into salterns and then into mudflat evaporites or arid zone siliciclastics (Figures 5.7a and 5.16b, c; Warren, 1991). The platform rim in greenhouse times was continuous to semicontinuous during times of open marine carbonate growth, characterized by high-energy reefs and reef mounds with intervening grainstone shoals and flats. Rimmed shelves require biogenic binding and cementation to maintain an elevated rim, they cannot form on siliciclastic platforms (high turbidity), nor can they flourish if they are connected at the surface to hinterland areas where extensive evaporites are accumulating. Both these scenarios set up inimical seaward-flushing waters; in one the reef-formers are killed off by detrital plugging, in the other by elevated salinity.

The change in the major reef formers through time does create some interesting variations in the degree of proximity of the living reef formers to the evaporite accumulating areas. Precambrian stromatolitic platform-edge reefs could grow in close proximity to an evaporitic mudflat; some stromatolitic horizons are repeatedly intercalated and even penetrate saltern beds in the Neoproterozoic Ara salt of Oman. Cambrian archeocyathids were much more fragile. For example, in the well-exposed reef outcrops of the Flinders Ranges in South Australia the archeocyathids never outcrop in close proximity to evaporitic mudflats. There are always debris aprons and unconformities separating bioherms from overlying evaporite dissolution breccias. Stromatoporoids in lagoonal bioherms in the Alberta Basin appear to have better tolerated exposure to mesohaline waters, at least for short periods. But with no

modern analog it is difficult to define why this is so (e.g. were stromatoporoids related more to calcareous sponges or to cyanobacterial plexi?). Phanerozoic corals (rugose, tabulate and scleractinian) consistently show a poor tolerance to salinity change (stenohaline fauna) and living communities were never able to tolerate salinity changes for more than a few hours. Rudists appear to have been more robust in their salinity tolerance. In core from the subsurface of Texas I have seen small *in situ* buildups forming units adjacent to both oyster bioherms (estuarine) and the least saline portions of ancient evaporitic mudflats. This ability to survive changed salinities is probably related to their molluscan pedigree. When conditions became too saline, too hot or too fresh they could retract their filtering apparatus, pull down their opercular caps and wait out the adverse conditions, at least for a day or two. Even today, chemosynthetic molluscs can survive in close proximity to deep seafloor brine lakes (Figure 9.40).

The degree of restriction in the evaporite-depositing lagoon area behind the platform edge is controlled by the continuity of the rimming shoal. To form a saltern or an evaporitic mudflat in an ancient lagoonal depression requires the rim crest to be at or above sealevel, with any channels cutting across the rim and its sandflat to be choked with sediment (Lucia, 1972). This prevents freshening via the free exchange of marine and back-rim waters. Otherwise, like the carbonate platforms of today, conditions behind the shelf rim or shoal can never become saline enough to deposit widespread evaporites and, at best, restricted marine carbonates are deposited.

The Cretaceous Ferry Lake Anhydrite formed behind a rimmed platform as a 90 m-thick unit extending from east Texas to Alabama (Figure 5.20). It is made up of metres-thick alternating units of carbonate and anhydrite deposited in the lagoonal area of

a broad, shallow reef/shoal-rimmed carbonate platform. Using wireline signatures, individual sulphate beds can be traced over distances of more than 160 km ((Figure 5.20a; Pittman, 1985). Where it subcrops toward its present landward extent the anhydrites have been dissolved by meteoric waters. At the time of deposition they passed further landward into alluvial plain conglomerates and redbeds. Detailed core study in the J. B. Kitchens No. 1 well (Henderson Co, Texas) showed the anhydrite beds are mostly composed of vertical- to near vertical-aligned nodules separated by fine mm-laminated anhydrite (Loucks and Longman, 1982). These structures are diagenetic “ghosts” after original bottom-nucleated gypsum. Throughout much of its subsurface extent the wirelines signature of the correlated anhydrites show a clean blocky appearance with neutron-density crossplots indicating high levels of sulphate purity, making it a saltern deposit (Warren, 1991). Sabkha mudflat signatures in

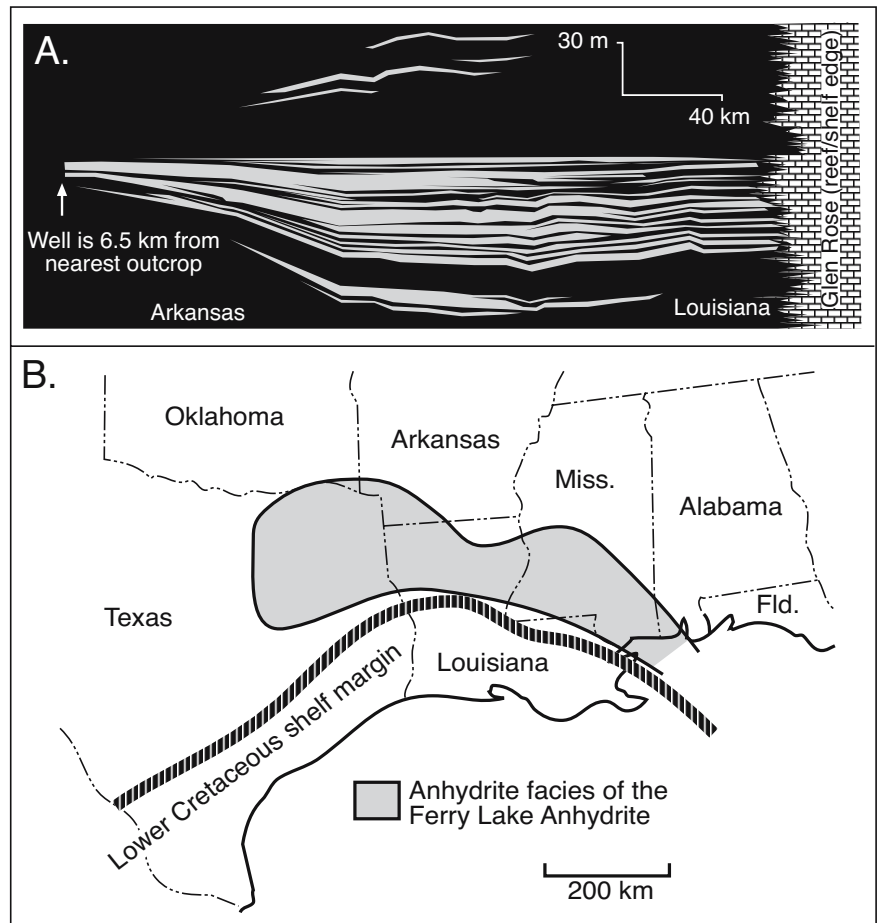


Figure 5.20. Lower Cretaceous Ferry Lake Anhydrite, northern Gulf of Mexico. A) N-S cross section showing distribution of main anhydrite beds from wireline logs (after Pittman, 1985). B) Distribution of anhydrite saltern on the platform behind the rudistid shelf margin shoal (after Loucks and Longman, 1982).

the anhydrites are rare. The saltern/lagoon was up to 260 km (160 miles) wide and was separated from open marine waters by shelf-margin bank or shoals dominated by rudistid debris of the Glen Rose Formation (Figure 5.20b). The position of the shoal was possibly controlled by down-to-the-basin faulting. This in turn was controlled by into-the-basin salt flow and associated growth faulting, driven by halokinetic movement of the underlying Jurassic Louann Salt (Chapter 6).

The anhydrite beds are up to 7 m thick and contain thin mudstone layers with entrained anhydrite rip-up clasts. The thicker carbonate beds, which separate the anhydrites, are near-normal-marine lagoonal bioclastic/oolitic wackestones indicating times of hydrographic connection through the rim facies to the open ocean. The entrained fauna includes ostracodes and molluscs, several units contain *Orbitulina* and echinoid fragments, indicating that normal marine waters were present either during highstands or in times of storm-induced marine floods.

Loucks and Longman's original 1982 interpretation was that the marine carbonate beds were deposited during periodic storm flooding of a restricted carbonate lagoon by marine waters. They also postulated that a single perennial evaporite lagoon was capable of depositing gypsum on its seaward side and halite on its landward side. Given a lack of widespread halite and what we now know about saltern hydrology this surface-connected scenario of marine on one side of a lagoon and halite on the other is somewhat unlikely. To deposit a widespread subaqueous evaporite unit requires total or near total isolation from a surface connection to the ocean in a system where a single perennial brine is at saturation with a single mineral phase (see later hydrological discussion in this chapter). A more likely scenario is that the Ferry Lake Anhydrites were precipitated simultaneously across a gypsum-saturated seaway during times of complete surface isolation from the ocean, and halite was perhaps forming stacked crusts in isolated pan depressions within subaerial mudflats in the most landward parts of the basin (as in Lake Asal today). On the seaward side of the saltern the crests of the rudistid shoals and reefs were subaerially exposed, while the underlying shoal sediment was an unconfined aquifer facilitating the phreatic supply of marine water into the drawdown saltern filled with gypsum-saturated brine sheets up to a few metres deep.

An even more thoroughly documented example of a rimmed evaporitic platform is the Permian margin of the Delaware Basin in west Texas and New Mexico, USA (Figures 5.21a, 7.9). The margin is exposed in the Guadalupe Mountains, while its

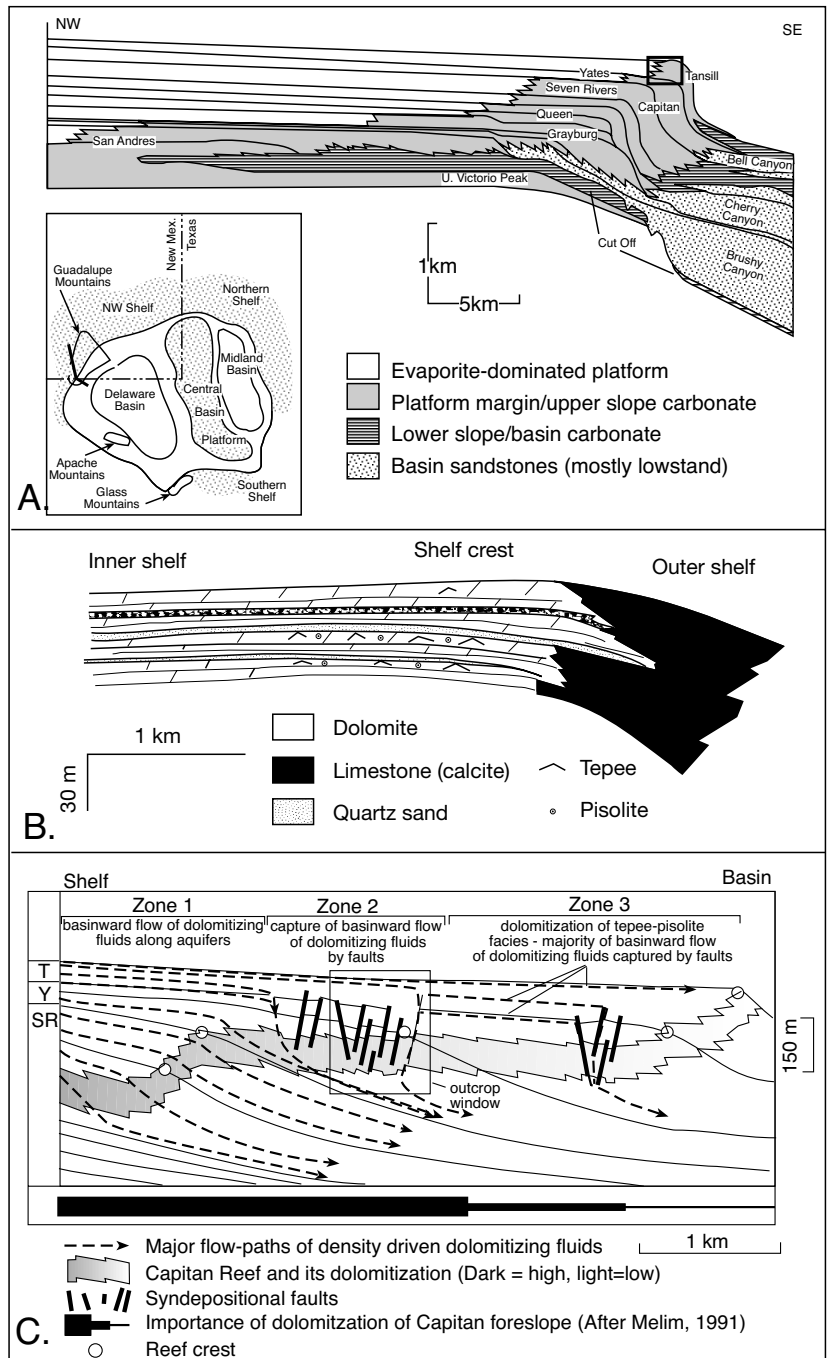
dolomitised, evaporite-sealed, subsurface lagoonal counterparts form the most productive reservoir intervals from the NW shelf into the Central Basin Platform. The Permian Basin of west Texas covers an area of more than 100,000 km² and is almost completely encircled by the reef-rim sediments of the Goat Seep and Capitan formations. Some distance landward of the reef is a 13 km wide belt of highly cyclic platform carbonates made up of widely correlatable stacks of dolomite mudstone and wackestone, capped by anhydritic laminites, which Sarg (1981, 2001) interprets as subaqueous. Even further landward are thick belts of saltern evaporites, which have been largely dissolved from their outcrop expressions in the Guadalupe Mountains.

Seaward of the cyclic platform dolomites, in a position somewhat closer to the reef mass proper, is an 0.8 to 3 km wide belt of carbonate sands and pisolitic rudstones. These were deposited as mostly coarsening-upward, cyclic stacks, which culminate in tepee-overprinted pisolite beds with subaerial exposure or truncation surfaces. These evaporitic carbonates constitute the tepee-overprinted pisolitic strandzone and barrier island shoal facies of the Guadalupe platform (Esteban and Pray, 1983) and were described in some detail in Chapter 1. Evaporite-sealed counterparts to the dolomitized pisolitic cycles also constitute high quality subsurface reservoirs (Chapter 10).

During deposition the pisolite facies constituted a series of shoals that are considered by many to have been the topographically highest part of the platform (Esteban and Pray, 1983; Mutti and Simo, 1993). Located landward of the reef, the island shoal facies distinguishes this style of platform from the more usual reef-rimmed reconstruction, where the reef mass and its sand flat occupy the topographically highest position on the platform profile (Figures 5.16b, 5.21b). The pisolitic high of the Guadalupe region is the type area for what is called a distally-steepened reef rim or deep reef-rimmed shelf. This platform profile occurs in other shelf margins characterised by platform salterns (Figure 5.16c). A little further basinward of the pisolites and tepees are the reef masses of the Goat seep and Capitan formations. Separating the pisolitic shoal zone from the reef rim proper was a narrow belt of carbonate wackestones, typified by a low diversity marine fauna.

The basal part of the reef mass is pervasively cemented by cm-scale aragonite botryoids (now calcite), which can constitute up to 90% of the reef matrix. This zone of intense cementation passes upward into prolific biogenic masses of sponges, bryozoa, brachiopods and *Tubiphytes*, all bound by calcareous algae and marine cements. Some of the calcareous algae are coelobites,

Figure 5.21. Permian reef complex of the Guadalupe Mountains, west Texas. A) Schematic cross section of the Permian carbonate platform based on outcrops in the Guadalupe Mountains of Texas and New Mexico. Note the initial strongly progradational ramp-like profile in the San Andres Formation and its evolution to a reef-rimmed shelf with a well defined slope break, along with steep shelf margin that was several hundred metres high. The platform interior is dominated by saltern evaporites (white) that pass seaward through pisolitic island shoal/strandzone facies into the deep-rim reef of the Capitan Formation (after Kerans et al., 1993; Kerans and Fitchen, 1996). The basinward slope of the evaporite sequence is based on the current configuration of the basin margin and probably does not reflect the original slope. It is created by post depositional regional tilting. Map inset shows major physiographic provinces of the Permian Basin in west Texas and New Mexico. B) Detailed facies and dolomitisation relationships based on measured sections in the Yates/Tansill Formation showing the position of the shelf crest landward of the reefs of the Capitan limestone (after Mutti and Simo, 1993). C) Dolomitisation of the Capitan shelf strata and reef by dense mesohaline fluids that originated in the near back reef evaporitic shelf-lagoon (Hunt et al., 2002). Basinward flow of the dolomitising fluids was along aquifer units within the shelf—the sandstones resting on sequence boundaries. The basinward tilting of the back reef strata between the shelf crest and the Capitan may have helped promote a basinward flow of the dolomitising fluids, but the main hydrological gradient came from natural brine reflux. In areas updip of the faults (zone 1, the basinward flow of the dolomitising fluids would have primarily been along aquifers and downward through the reef and fore reef (both areas here are extensively dolomitised). The flow of fluids through the fore reef followed bedding, and dolomitisation decreases downward through these strata (Melim and Scholle, 2002). Further downdip in the cross-section (zone 2), much of the basinward flow of the dolomitising fluids would have been captured by the syndepositional faults and related fracture systems that reach high into the platform stratigraphy. Here, the sandstone-dominated fill of the faults and fractures provided vertical conduits for the dense dolomitising fluids through the platform. Capture of the flow of the dolomitising fluids by the fault zones in updip locations (zone 2) may have acted to inhibit the extensive dolomitisation of the middle and upper Capitan reef further downdip (zone 3). Here, dolomitisation is mostly limited to tepee–pisolite facies. Hunt et al.’s model is a logical extension of that developed by Melim (1991) and they argue dolomitisation was likely a discontinuous process typical of TST and HST times, while fracture-controlled dissolution prevailed during lowstands.



Further downdip in the cross-section (zone 2), much of the basinward flow of the dolomitising fluids would have been captured by the syndepositional faults and related fracture systems that reach high into the platform stratigraphy. Here, the sandstone-dominated fill of the faults and fractures provided vertical conduits for the dense dolomitising fluids through the platform. Capture of the flow of the dolomitising fluids by the fault zones in updip locations (zone 2) may have acted to inhibit the extensive dolomitisation of the middle and upper Capitan reef further downdip (zone 3). Here, dolomitisation is mostly limited to tepee–pisolite facies. Hunt et al.’s model is a logical extension of that developed by Melim (1991) and they argue dolomitisation was likely a discontinuous process typical of TST and HST times, while fracture-controlled dissolution prevailed during lowstands.

which flourished in dark aragonite-cemented fractures in the growing reef. The reef mass is largely undolomitised and internally shows no evidence of subaerial exposure, implying aragonite cementation was early and that the reef was never capable of growing to sealevel.

It may well be that the stenohaline biota of the reef rim could never grow to sealevel, nor form closer to the pisolitic shoreline, because of the debilitating effect of increased salinities. Dense brines, created by evaporative drawdown on the landward side of the island shoal, refluxed seaward via sandstone aquifers and growth faults beneath the unconfined marine phreatic lens to seep back to the seafloor just seaward of the basin shoreline to create a facies belt characterised by a low diversity, halotolerant biota. Brines mixed freely with seawater in this near coastal seafloor zone and so were dissipated into the huge reservoir of open ocean water that occupied the Delaware Basin (Figure 5.22a). If the deep reef rim grew up toward the sea surface it would create greater restriction immediately behind the reef rim allowing the escaping reflux brines to gather and increase the salinity of the back reef waters. As these more saline waters spilt and washed over the still subaqueous reef rim it would slow the growth of the reef until subsidence allowed freshening of the lagoon once again (Figure 5.22b). Hence the reef could never grow to approach the sea surface in front of a huge area of widespread evaporites and refluxing dolomitising brines. Whenever it did so, it shot itself in the back before it ever reached the sea surface.

Seaward of the reef rim is a 2 km wide belt of carbonate slope and rise sediments, which also defines the shelf break. It is made up of massive to thinly bedded limestones with intercalated slumps of shelf material, breccias and debris flows (Melim and Scholle, 2002). Small downslope buildups are found on the shallower parts of some slopes. Portions of the deepwater carbonate sands and the deeper parts of the shelf margins of the Delaware Basin are dolomitised to lesser degrees than the platform. Even so, the distribution of dolomite in these sediments reflect the influence of widespread evaporite deposition and brine reflux in the hinterland and the more seaward focusing action of syndepositional growth faults (Figure 5.21c; Hunt et al., 2002).

Further out, widespread siliciclastic sand sheets dominate the basin floor. These form a channelised deepwater belt at the foot of the carbonate slope in a zone some 6 km wide and up to 35 m thick. The sand sheets were fed by desert dune sands from the hinterland, which largely bypassed the shelf margin via canyons transecting the reef. Some of these basinal channelised sands are unusual compared to typical deepwater sand channels in that they contain drape muds on the channel floor and a rather homogenous set of sedimentary structures. They are interpreted either as density flows created by bottom-hugging saline brine flows, which originated in the platform salterns (Williamson, 1978) or as settle-out muds and silts carried out over the seaway by intense winds from an adjacent sand sea (erg), much in the same way that silt and mud is carried out into the Atlantic off the Saharan coast of north Africa today (Fischer and Sarnthein, 1988).

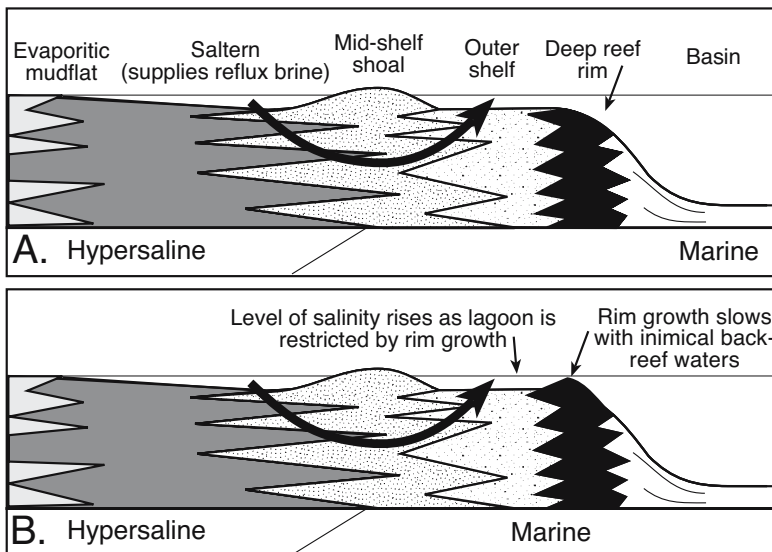


Figure 5.22. Effect of a deep reef-rim growth in a saltern-backed platform.

Saline platform sequences have been recognised as far back as the Archean (Figure 5.23). A number of impure dolomitic limestone beds in the latest Archean (≈ 2.5 Ga) Wittenoom and Carawine dolomites of the Hamersley Group in Western Australia contain features such as mud cracks and evaporite pseudomorphs that indicate shallow water with local evaporitic mudflats (Kargel et al., 1996). The system extended across what was possibly the original extent of the Hamesley Basin as defined by Trendall (1983) in his evaporite-basin model for initial banded iron precipitation. In the barred platform model of initial iron precipitation published by Morris (1993) it also corresponded to what was interpreted to be a broad carbonate platform passing

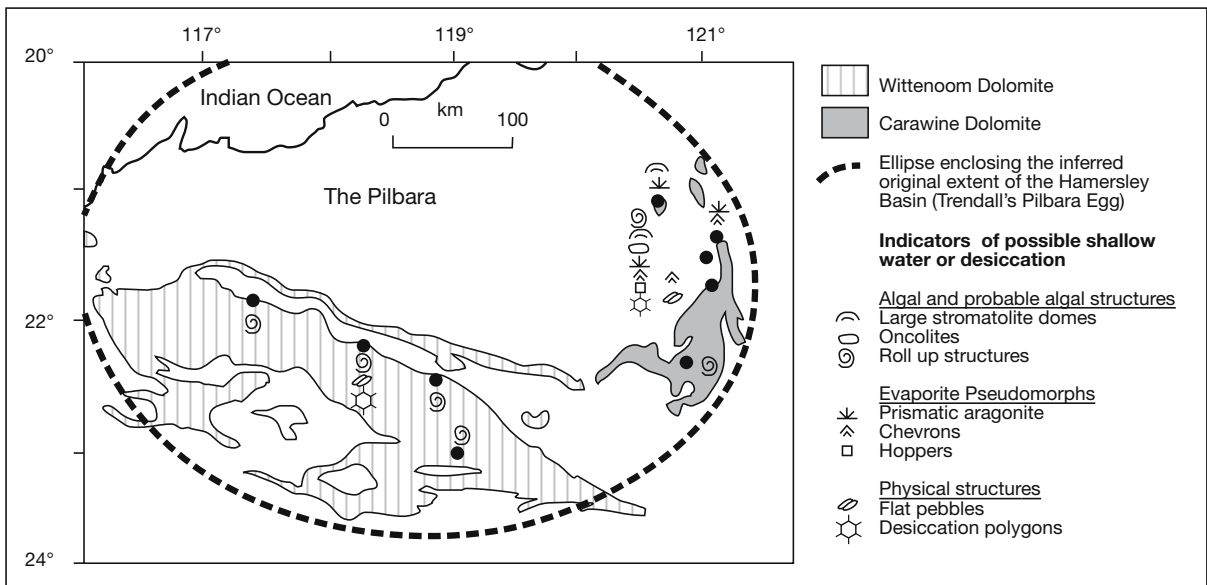


Figure 5.23. Sketch map showing the distribution of sedimentological features that indicate shallow water and evaporitic conditions in the Archean Wittenoom and Carawine dolomites in the Pilbara of Western Australia (after Kargel et al., 1996) and used as evidence to indicate that the widespread banded iron ores in this region first precipitated as saline precipitates in a barred marine platform basin.

into deeper marine waters to the south. In either case, during the accumulation of the Wittenoom and Carawine dolomites the depositional setting was a carbonate platform that at times was evaporitic.

These evaporitic dolomites underlie the world-scale banded iron ores (BIFs) of the Hamersley Basin, deposits that contain 10% of the world's known iron ore reserves. As in all models of ore deposits of this age, explanations for the formation of the banded iron ores are contentious. Trendall (1983) favours an evaporitic basin to explain the precipitation of the ore, Morris (1985) favours supergene enrichment beneath a Paleoproterozoic weathering surface, Li et al. (1993) favour a hypogene origin, while Powell et al. (1999) argue for synorogenic Paleoproterozoic hydrothermal fluids squeezed northward away from the Ophthalmian fold belt.

Marine versus nonmarine stages in epeiric seaways

Correlations across the Clear Fork ramp passing into the siliciclastics of the Opeche Shale or the Khuff Formation anhydrites passing laterally into basin rim continental siliciclastics derived from the Arabian Shield, or Guadalupe salterns passing landward into wadi and dune deposits are all problematic. They underline the everyday problem of reliably tying facies to time horizons in many ancient mixed siliciclastic/evaporite/carbonate platforms. Fossil-lean but

extensive areas of saltern evaporites typically backed onto, and were surrounded by, evaporitic mudflats and fossil-lean sand-sheets with numerous internal unconformities that are Stokes surfaces. The problem is worse in ramps, which lack well developed clinoforms that can be used seismically to define the seaward side of a subsurface carbonate platform. Something as simple as determining whether the platform had a marine or nonmarine brine feed is problematic in many subsurface salterns. Little if any open-marine carbonate matrix was ever transported into the highly isolated parts of the hinterland, even during intense hurricane events. For much of the time the water conditions in the saltern/lagoon were too saline for most marine or carbonate-secreting organisms with the possible exception of cyanobacteria and halophilic mats. When the base of a saltern evaporite cycle is made up of carbonates, they usually retain some evidence of a marine biota so that it is likely that the overlying salt beds were fed by marine seepage. But, if the intrasalt beds are dominantly mud, with no fossils, what was the original depositional setting?

This problem beleaguers depositional interpretations of the Permian (Leonardian) Nippewalla Group of Kansas, a lateral time equivalent succession to the Clear Fork Formation of the Palo Duro Basin. As mentioned earlier, Benison and Goldstein (2001) argue the Nippewalla Group siliciclastics and evaporites represent an evolution from a lacustrine system to a nonmarine, acidic saline pan system in the mid-continent

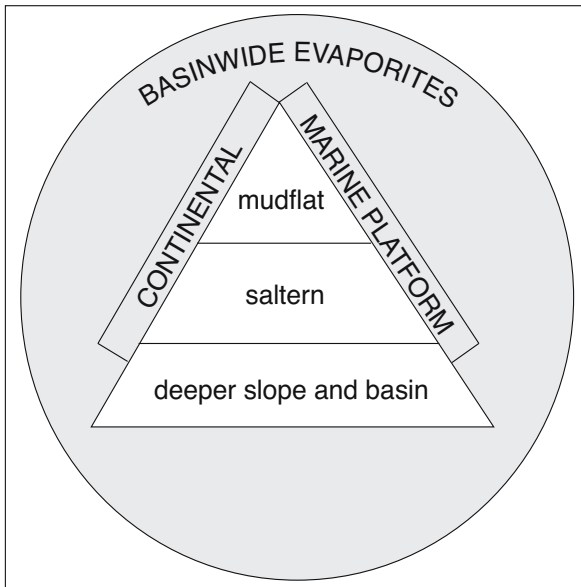


Figure 5.24. Venn plot showing the diversity of environmental settings possible in basinwide evaporites.

of North America. Most evaporite deposition took place in halite-dominated ephemeral saline lakes surrounded by saline and dry mudflats, sandflats and sand dunes. The key to their continental interpretation comes, not from the textures in the nodular anhydrite or the halite and chaotic halite beds, which

are equivocal, but from a volumetrically unimportant grey mudstone facies. This they interpret as a perennial lake deposit akin to the acid redbed lakes in parts of modern Australia. It is a grey siliciclastic mudstone characterized by planar and convolute laminations, ostracodes, peloids and plant material laid down in a freshwater-brackish perennial lake.

More reliable interpretations of a salt bed as marine or nonmarine are usually best done by studying the less saline intrasalt beds. In fact, it is the first feature on the list of four criteria noted by Hardie (1984) as most useful in separating marine and nonmarine evaporites. He listed; 1) sedimentology of the associated non-saline facies, 2) kinds of fossils, 3) kinds and associations of primary evaporite minerals and, 4) geochemical characteristics of evaporite minerals.

Basinwide evaporites

Basinwide evaporites are thick basin-filling evaporite units, often described as “saline giants” or “mega-evaporites.” Salt sequences typically extend across large areas of the central parts of a sedimentary basin and contain textural evidence of a variety of depositional settings ranging from deepwater to saltern to mudflat (Figures 5.7b, 5.24; Table 5.6). Basinwide evaporites are not accumulating anywhere on the surface of the world today as the necessary interactions between tectonics,

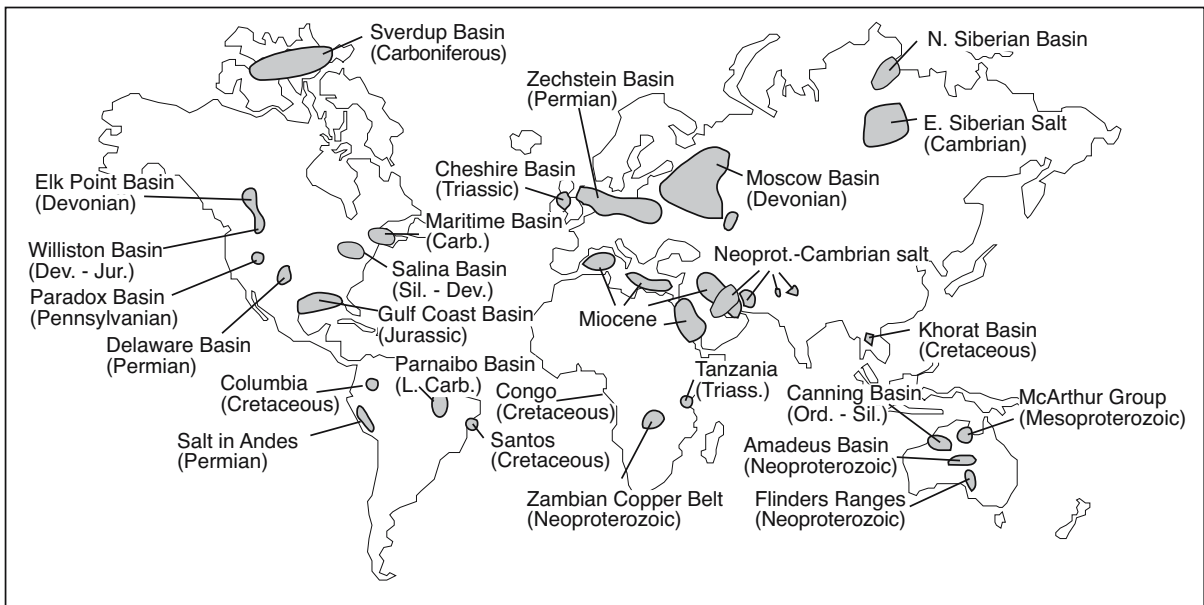


Figure 5.25. Map showing location and age of some of major basinwide evaporite deposits. All of the Proterozoic examples, except the Amadeus Basin of Australia and the Fahud Salt Basin of Oman, are characterised by dissolution breccias and pseudomorphs, not the actual salts. Owing to the small size of the map, basins are drawn for visual clarity not to exact scale.

Sequence of interest	Basin/setting and Location	Age	Basin style	Tectonic event	References
Messinean Evaporites	Lago Mare ("lake sea"), Mediterranean	Miocene, Upper	Flexure	Convergent foreland Alpine	Krijgsman et al., 1999
Belayim and Gharib formations	Gulf of Suez - Red Sea, Middle East	Miocene, Middle - Upper	Extension	Red Sea Breakup and the formation of the Red Sea/Suez Rift	Rouchy et al., 1995; Meshref, 1990
Gachsaran Formation	Mesopotamian Basin, Middle East	Miocene, Middle	Flexure	Convergent foreland Zagros-Taurus	Tucker, 1999
Maha Sarakham Formation	Khorat Basin, Thailand	Cretaceous, Upper	Flexure	Convergent foreland Cretaceous inversion and thrust loading	Ulta-Aroon, 1993; Booth and Sattayarak, 2000
Todilto Formation	Todilto Basin, New Mexico, USA	Jurassic, Middle	Flexure	Convergent foreland Ancestral Rockies	Benan and Kocurek, 2000
Louann Salt	Gulf of Mexico Basin, Gulf Coast	Jurassic, Middle	Extension	Incipient Gulf of Mexico- Atlantic rift	Land et al., 1988, 1995; Salvador, 1987
Argo Formation & Osprey Evaporites	Scotian Basin, and Grand Banks, Canada	Upper Triassic-Lower Jurassic	Extension	Incipient Atlantic rifting	Holser et al., 1988
Northwich Halite	Cheshire Basin, United Kingdom	Triassic	Extension	Incipient Atlantic rifting	Pegrum and Mounterey, 1978
Halite (S1-S4, Las and Dogger Anhydrite units)	Oued Mya Basin, Algeria, Northern Sahara	Upper Triassic-Lower Jurassic (Liassic)	Extension	Intraplate sag basin atop grabens created by incipient Atlantic and Tehyan rifting	Yahi et al., 2001; Turner et al., 2001
Saliferous units	Ghadames (Berkine) Basin, Algeria	Triassic, Upper Jurassic, Lower	Extension	Intraplate sag basin atop grabens created by incipient Atlantic and Tehyan rifting	Yahi et al., 2001; Turner et al., 2001
Argiles d'Argana	Essaouria Basin, Morocco	Triassic, Upper	Flexure	Intraplate sag basin atop grabens created by incipient Atlantic and Tehyan rifting	Hafid, 2000; Evans 1978
Formation Salifere	Saharan Atlas, Algeria	Triassic, Upper	Flexure	Intraplate sag basin; incipient Atlantic and Tehyan rifting	Hardie, 1990; Merabet and Popov, 1971
Salina d'Ourgla	Northern Sahara Salt Basin, Algeria	Triassic, Upper	Flexure	Intraplate sag basin; incipient Atlantic and Tehyan rifting	Hardie, 1990; Merabet and Popov, 1971
Nikitov, Slavyan, and Kramatov Formations	Dnieper-Denets Basin, Ukraine and Russia	Permian, Lower (Kungurian salt)	Flexure	Post-rift sag reactivated by Uralian Orogeny (Hercynian)	Ulmishek, 2001a; Chekunov et al., 1992
Rolliegende	Dniepr-Donets Basin, Eastern Europe	Permian, Lower	Flexure	Foreland Variscan Orogeny	Kabyshv et al., 1998
Zechstein Basin, NW Europe	NW European Basin, NW Europe	Permian, Upper	Flexure	Post Variscan Orogeny collapse	Hardie 1990

Table 5.6. Representative examples of basinwide evaporites (also called saline giants and basin centre evaporites). In some the former evaporite beds are now represented by laterally extensive solution breccia horizons.

Sequence of interest	Basin/setting and Location	Age	Basin style	Tectonic event	References
Castile Formation	Delaware Basin, west Texas	Permian, Upper	Flexure	Marathon-Ouchita	Kirkland et al., 2000
Iren Horizon Kungurian evaporites	North Caspian Basin (aka Pri- or Peri-Caspian), Khazakhstan and Russia	Permian, Lower	Flexure	Foreland, Uralian Orogeny. Collision of Russian Platform with the Siberial/Kazakhstan	Ulmishek, 2001b
Otto Fiord Formation	Sverdrup Basin, Canadian Arctic Islands	Carboniferous	Extension	Synrift stage of post-Caledonian intracontinental rifting	Balkwill, 1978; Stephenson et al., 1992
Paradox Formation	Paradox Basin, Colorado-Utah USA	Carboniferous, Upper	Flexure	Ancestral Rockies	Barbeau, 1999
Caurauri Formation	Amazonas Basin, South America	Carboniferous, Upper	Flexure	Distal effect of Marathon-Ouchita orogeny	Hardie, 1990; Szatmari et al., 1979;
Windsor Group	Magdalen Basin, Eastern Canada	Carboniferous, Lower	Extension	Cabot fault-Belle Isle transensional system	Langdon and Hall, 1994; Lynch and Keller, 1998
Liven Horizon	Dnieper-Denets Basin, Ukraine and Russia	Devonian, Upper Frasnian and Fammenian	Extension	Synrift via crustal stretching (passive margin)	Ulmishek, 2001a; Ulmishek et al., 1994
Prairie Evaporite	Elk Point Basin, Western Canada Plains	Devonian, Middle	Flexure	Intracratonic sag; a distal effect of thrust-loaded compression of the western Laurasian plate	Pysklywec and Mitrovica, 2000
Salina Group	Michigan Basin, USA	Silurian, Middle-Upper	Flexure	Intracratonic sag during Taconian thrust loading, sits atop Mesoproterozoic Midcontinent rift basin	Howell and Van der Pluijm, 1999
Mallowa Salt (Carribuddy Formation)	Canning Basin, Northwest Australia	Ord. -Silurian	Extension	Pre-rift to Synrift stage of intracratonic sag	Cathro et al., 1992
Chandler Formation	Amadeus Basin, Central Australia	Cambrian, Lower	Flexure	Petermann Range Orogeny	Bradshaw, 1991
Lower and upper Usolye Group	Turukhan - Irkutsk - Olekmin salt basin, SE Siberian Craton	Cambrian, Lower	Flexure		Ulmishek, 2001b
Bitter Springs Formation	Amadeus Basin, Central Australia	Neoproterozoic	Extension	Rift - Rodinia breakup	Lindsay, 1987; Southgate, 1991
Callana Formation	Adelaide Geosyncline, South Australia	Neoproterozoic	Extension	Rift - Rodinia breakup	Powell et al., 1994
Hormuz Formation	Arabian Basin, Middle East	Neoproterozoic	Extension	Rift Basin	Edgell, 1991; Husseini, 1989
Ara Salt, Oman	Fahud, Gaba and South Oman Salt Basins, Oman	Neoproterozoic	Extension or transension	Rifts driven by Nejd transfrom fault system	Schröder et al., 2000a; Sharland et al., 2001

Table 5.6 continued. Representative examples of basinwide evaporites (also called saline giants and basin centre evaporites). In some the former evaporite beds are now represented by laterally extensive solution breccia horizons.

hydrology and climate do not exist. Basin-central evaporite is another term to describe this grouping of ancient deposits (Kendall, 1992). I prefer the term basinwide as the evaporite sequence can fill the basin centre and then climb out over the old basin margin (e.g. the transition from Castile to Salado formations in the Delaware Basin).

Basinwide evaporites can constitute large proportions of sediment fill in many ancient evaporitic basins, such as the Delaware Basin of west Texas, the Zechstein Basin of Europe, the Louann Salt Basins in the Gulf of Mexico, the Hormuz Salt Basins in the Arabian Gulf and the Late Miocene Messinian sub-basins in the Mediterranean (Figure 5.25). The total evaporite fill in such basins is often hundreds to thousands of metres thick and composed of numerous stacked “brining upward” evaporite cycles tens to hundreds of metres thick (e.g. the Z1-Z4 of the Permian Zechstein of northwest Europe). Rather than the anhydrite that dominates the mineralogy of many marine platform evaporites, basinwides typically contain thick halite beds that can source halokinetic structures.

Saltern textures (salt pan and salina) dominate basinwide deposits, although basin and slope deposits can also occur, especially in the early stages of each depositional cycle. Sometimes, especially in the gypsum/anhydrite stages of an evaporite fill the saltern constructs a “platform” area in the basin with deeper water sulphate laminites accumulating in the central part of the basin (Figures 5.7a, 5.26a). At other times the basin centre had filled and shallowed to where a saltern extended across the entire depositional area of the basin (Figure 5.26b, c). Stacking of a number of saltern cycles into a thick basinwide sequence indicates the basin did not fill in a single depositional episode, but as a number of brining-upward and/or shoaling-upward depositional cycles typically composed of even finer scale parasequences. Compared with saltern deposits in marine-margin platform evaporites, the salterns in many basinwide evaporite basins tend to accumulate as much thicker units (>100m), and bedded salts are not restricted to the shoalwater/lagoonal portions of any underlying carbonate platform. Rather, they tend to cover and encase underlying carbonate reef rims and pinnacles.

Depositional styles

Basinwide evaporites can be classified into three settings (Figure 5.26; Warren, 1989; Kendall, 1992):

- Deeper water–deep basin
- Shallower water–deep basin
- Shallow water–shallow basin

Deeper water–deep basin evaporites have basin centres dominated by “deepwater” evaporites composed mostly of finely laminated salts (mostly sulphates) or coarsely crystalline inclusion-free halite meshworks. Individual laminar groupings in the basin-centre laminites can be correlated over wide areas (Figure 5.26a). This style of deposition dominates a hydrographically isolated marine-fed basin that reaches hydrologic equilibrium (water inflow = loss) at a time when a relatively deep water mass still covers the basin centre. The contentious part of this model lies in what water depth defines a deepwater brine in the basin centre, is it 30m, 100m or >1000m? Basin slopes at times when the basin water column is meromictic are dominated by reworked saltern evaporites deposited as slumps and turbidites, while pelagic laminites dominate the basin centre (Figure 5.6a). At times when water levels are somewhat lower and the water mass is holomictic then coarsely crystalline evaporites (either gypsum or halite) are deposited across the basin floor (Figure 5.6b).

Seawater flows into the basin as a perennial seepage; if the basin remains hydrographically isolated, evaporites can fill the basin to a water level just below that of the supplying ocean (Figure 5.38). Consequently, the evaporite unit “in toto” is a shallowing upward succession, often composed of smaller shallowing-upward cycles (parasequences). The basin fill starts off dominated by deeper water laminated and resedimented salts that pass up section into shallow-water salterns, pans, mudflats, or continental playas. But it can also preserve coarser crystalline units indicating holomictic but still “deep” episodes in the basin fill.

The Permian Castile Formation and the transition into the overlying Salado Formation in the Delaware Basin in west Texas is a good example of this passage from predominantly deep to predominantly shallow (Figure 1.24). The basin-centre started off relatively deep with the deposition of the varved sediments of the Castile Formation, and with time filled and shallowed into the shoalwater/playa deposits of the Salado Formation. Any sediments that immediately postdate the evaporites of this overall shallowing sequence will also be shoal water or saline mudflat deposits. This is the case with the shoalwater/mudflat deposits of Rustler Dolomite where it overlies the Salado Formation in the Permian Basin, west Texas. Other examples of deeper water deposition occur in the basin-centre deposits of the north and south Zechstein basins of NW Europe and the deeper parts of the marginal basins in the Messinian of the Italian Apennines.

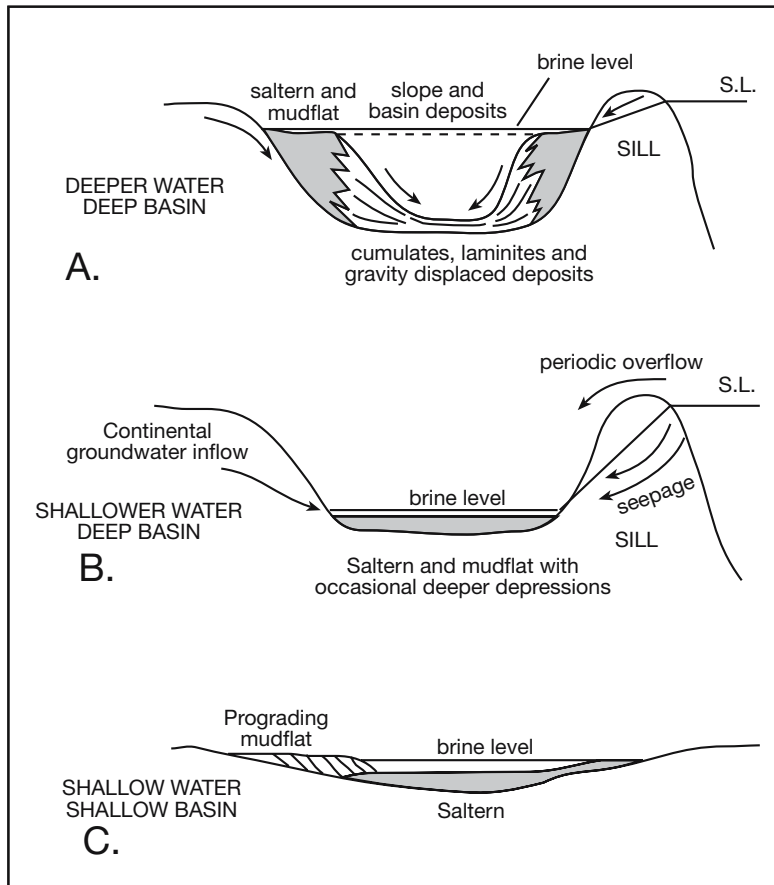


Figure 5.26. Basinwide evaporite settings, see Figure 5.6 for more detail on 5.26a, which only represents the meromictic stage (modified from Warren, 1989; Kendall, 1992).

The *shallower water–deep basin* sequence is dominated by shallow water evaporites deposited as stacked saltern to mudflat cycles in a basin with a hydrological base level hundreds to thousands of metres below sealevel. This type of basin is supplied by evaporative drawdown, pulling seawater into the basin as a series of marginward seeps perhaps interrupted by the occasional waterfall (Figure 5.26b). It characterises the more drawdown stages of evaporite deposition in both soft suture collision belts and some intracontinental rifts. This style of evaporite fill is often intimately related to the deeper water–deep basin style of deposits and indicates a more arid period in the same depositional basin. That is, its hydrological equilibrium is reached when much shallower waters cover the basin centre and there are many topographically deep evaporite basins where deeper fills alternate with shallower fills.

In the collision setting the underlying basin-centre succession is typically a deep marine sediment, often a pelagic carbonate

that passes upward across a disconformity or unconformity into alternating stacked saltern and deeper water evaporites. Normal marine pelagics were deposited before the basin depression was hydrographically isolated from the ocean and can return to dominate the basin fill if a hydrographic connection is re-established. The transition from a deeper marine basin to evaporitic can be marked by organic-rich restricted marine-influenced deposits (Figures 9.3,9.24). Basin margin regions can contain reefal deposits from the preceding marine phase.

Shallower water–deep basin fills dominate the evaporite fill in many marine-fed rift successions, such as the Aptian South Atlantic Salt Basin. Thick salts precipitated atop an endorheic rift valley floor that was hundreds of metres below sealevel (Szatmari, 2000). Unlike the relatively small volumes of marine-fed salts being deposited in today’s best example of a shallow water–deep basin marine-fed rift (Lake Asal depression; Figure 4.56), the volumes of salt deposited in ancient rift sags could be huge. Consider the wedge-shaped body of Upper Aptian salt that was deposited in the South Atlantic Salt Basin as Africa separated from South America about a rotational pole in NE Brazil (Szatmari, 2000). The salt basin was more than 2000 km long, some 400 km wide at its southern end in the Santos Basin and tapered northward to less than 100 km wide in the Sergipe-Alagoas Basin. Prior to halokinesis, the original salt thickness in the various sub-basins was around 2 km. Most of the salt was deposited as halite in a series of saline lakes/salters within a pre-existing continental rift depression, with a floor some 2 km below sealevel. Marine flooding ended the depression’s isolation from the sea in the late Aptian. It required nearly one million cubic kilometres of water to fill the depression to sealevel, an event that would have caused a geologically instantaneous drop of 3 m in global sealevel (Szatmari, 2000).

The *shallower water–shallow basin* association forms under conditions of ongoing subsidence where the rate of evaporite aggradation keeps pace with tectonic subsidence (Figure 5.26c). The basin depositional setting starts off shallow and remains shallow throughout the deposition of the evaporite sequence.

Sedimentary signatures are dominated by interfingering saltern, saline pan and mudflat successions often crosscut by karstic erosional surfaces. There is little or no evidence of deeper water evaporites. Shallow water–shallow basin evaporites are typical of intracratonic sag fills such as in the Williston Basin in the USA and the Silurian–Ordovician Canning Basin in Australia. Salt beds in intracratonic fills are typically intercalated with shallow-water open-marine carbonates and siliciclastics and tend to form stacked cyclic units with thicknesses between 10m and 100 m, unlike the thick rift and collision successions (>100-1000 m thick). Using data from one or two wells it can be very difficult to distinguish intracratonic basinwide evaporites from marine-margin platform evaporites. The distinction requires a thorough knowledge of the basin’s tectonic history and architecture and is often best resolved using regional seismic and well data. This style of deposition also dominates the later stages of basin infill in what were previously deep hydrographically-isolated evaporite basins, as described in the other two members of this classification.

In reality, interpreting basin-filling evaporites is never as simple nor as predictable as a three-end-member classification suggests. Changes in brine level, subsidence rates or climate, play havoc with a simple tripartite breakdown of evaporite basins. Water depths in an evaporite basin are never constant, they rise and fall in response to intensity of tectonism, climate, sealevel change, playa capture and associated changes in the degree of seepage, evaporation intensity and surface runoff in the inflow zones. Basinwide provinces such as the Mediterranean Basin during the Late Miocene, or the Permian Basins of Texas and northern Europe in the Late Permian, are actually composed of a series of large sub-basins. Each sub-basin in an evaporitic province responds in its own fashion, depending on the local topography, tectonics, and climate and the total fill can contain examples of all three end members.

Tectonic styles

Throughout earth history, basinwides tend to accumulate in three tectonic settings: 1) Areas of rifting continental plates; 2) Areas of converging continental plates (collision belts); 3) Areas of intracontinental or intraplate sags, which are often the result of farfield plate stress induced by continental orogeny acting on zones of pre-existing crustal weakness such as an old rift belt or foreland depression (Table 5.6; Figure 5.27). Evaporating brines in

most basinwide lows tend to be maintained by a continuous inflow of marine groundwaters into tectonic depressions (marine-fed hydrological systems). This hydrology is created in an arid setting wherever tectonically-driven subsidence moves the basin floor to sub-sealevel elevations without allowing a surface connection to the open ocean.

Basinwide evaporite style changes as continents accrete and suture. The various salt-filled basins, that together make up the Pangaeen peak in the salt volume curve, were created mostly by plate tectonic mechanisms within what were tectonically-induced arid to hyperarid climatic zones of the latest Palaeozoic to Mesozoic earth (Figure 5.4). Volumes of salts caught up in this association dwarf all Quaternary salt volumes. Zharkov (1981) recognized 95 Permian evaporite basins with a total volume of $1.5 \times 10^6 \text{ km}^3$ (37 were halite-dominated and 48 sulphate-dominated). The basinwides that make up the Pangaeen peak came into being as the continents collided to construct the Pangaeen supercontinent and then as it rifted and sagged during its breakup.

Carboniferous basinwide evaporites were precipitated in the Williston Basin and northern Ellesmere region in North America, in northern Brazil, North Africa, the East-European Platform, and Kazakhstan (Trappe, 2000). Early Permian evaporite basins form a broad belt along western Pangaea, but also in northeastern

<p>Late Palaeozoic formation of Pangean supercontinent</p>	<p>Pennsylvanian collision of Laurussia, Kazakhstania and Siberia to form Laurasia ($\approx 280 \text{ ma}$), followed by Permian collision of Laurasia and Gondwana</p> <p>Associated orogenic events Appalachian/Alleghenian orogeny of eastern North America Mauritanide/Moroccan fold belt of northwest Africa Hercynian orogeny of southern Europe Marathon/Ouachita orogeny of southern North America Uralian orogeny of Europe-Siberia</p>
<p>Mesozoic breakup of Pangean supercontinent</p>	<p>Breakup of Pangea: 220-190 Ma: Newark and other rift basins in northeast North America and northwest Africa 175 Ma: Opening of Neo-Tethys 135 Ma: Separation of South America from Africa (opening of south Atlantic)</p> <p>Breakup of Gondwana (as it unzips around Antarctica): 165 Ma: Rifting of Africa from Antarctica 125 Ma: Separation of India from Antarctica 100 Ma: Separation of Australia from Antarctica 85 Ma: Separation of New Zealand from Antarctica</p> <p>Breakup of Laurasia: 90-50Ma: Opening of the north Atlantic between North America and Eurasia/Greenland</p>

Table 5.7. Timing of the assembly and disassembly of the Pangean supercontinent.

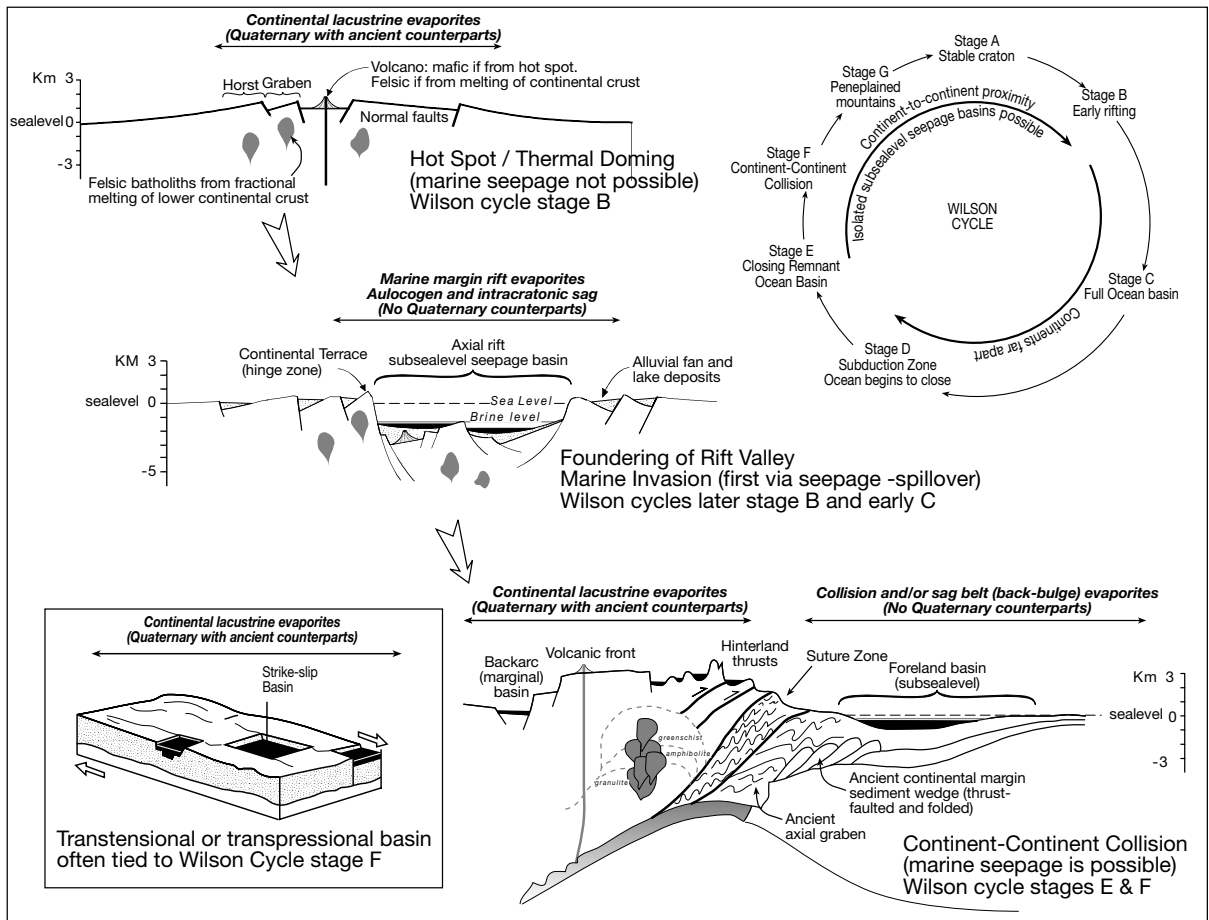


Figure 5.27. Tectonic settings of basinwide evaporite deposition in the past (no current counterparts) and Quaternary setting of large continental evaporite basins in the framework of the Wilson cycle (stages A-G). Strike-slip basins are associated with local readjustments to stresses created by plates moving past each other. Evaporites can only form in hydrographically isolated (typically endorheic) environments and so do not form in open marine stages C or D. Evaporites are shaded black.

North America and eastern Greenland, as well as in northern South America (including western Brazil). Large salt deposits of the same age are found in central Europe including portions of the East-European Platform and the Urals. The largest Early Permian deposit fills the East European Basin from the Caspian to the Black Sea with some $500 \times 10^3 \text{ km}^3$ of halite and $100 \times 10^3 \text{ km}^3$ of anhydrite (Magaritz 1987). Late Permian evaporites include major deposits in the Zechstein Basin of northwestern Europe and the evaporites of west Texas. Together these basins define a broad band of equatorial aridity extending from about 50°N to about 30°S palaeolatitude, with basinwide salt deposition ranging in time and world climate across Carboniferous icehouse to Permian greenhouse.

Permian halite volumes are in their turn dwarfed by those of the Triassic, which account for 22% of all Phanerozoic halite,

while Permian and Triassic halite together make up 35% of the world's halite (Figure 5.4). During the Early Triassic, evaporite formation intensified as huge evaporite pans associated with redbeds developed in southeastern and western USA, western Canada, northwestern Africa, western and southeastern Europe, central South America, south-central Africa and eastern Greenland (Tables 5.6, 5.7) Large evaporite platforms were established in northern Arabia, Iraq, Kazakhstan, and northern China. The increased salt volume reflects intensified rift activity in low latitude regions during the Triassic breakup of Pangaea. Extension, followed by cooling and sagging, established a number of large isolated subsealevel rifts and intracratonic sags, which acted as the preeminent salt accumulators.

Thus, the plethora of Pangaeian basinwide evaporites is associated with three time-plate tectonic associations (Table

5.7; Figure 5.27): 1) Pennsylvanian to Permian accretion of the Pangaea supercontinent, as mostly marine-fed collision basin evaporites were deposited along the soft collision belt of the irregularly embayed margins of Gondwana, Laurussia and Siberia; 2) Intraplate extensional depressions created during the subsequent Mesozoic breakup of Pangaea into Gondwana/Laurasia; salt beds deposited in these widening marine-fed rift basins, including the continental salts of the Newark Basin (Triassic), the marine salts of the Gulf of Mexico (Jurassic), the Campos Basin (Cretaceous) and the various mostly marine-fed salt basins of offshore west Africa (Evans, 1978); and 3) Associated intracratonic sag salt accumulations in basins that typically sit atop the failed arms of earlier more sharply-defined fault-bound rift successions (Youssef, 1998) or in the hinterland or foreland of orogenic belts created by farfield stresses driven by interplate collision (Pysklywec and Mitrovica, 2000). The intracratonic-sag basins in the Pangaea association are especially obvious in the various Triassic and Jurassic salt basins of Northern Africa, which formed isolated subsealevel marine-fed depressions as Pangaea unzipped along its Tethyan and Atlantic axes.

Large intracratonic sags also typify many other subsealevel isolated marine-seep fed saline giants outside of the time of the Pangaea supercontinent (e.g. the Devonian Elk Point Basin, the Palaeozoic Williston Basin, the Silurian Michigan Basin and Ordovician Canning Basin), as do other rift (e.g. Frasnian of Dnieper-Denets of eastern Europe) and collision (Miocene of the alpine Mediterranean and the Zagros foreland) associations (Table 5.7).

Creation and destruction of the Gondwana supercontinent in the Neoproterozoic-Early Cambrian (≈ 550 Ma) defines an earlier, but not as well documented, peak in the evaporite distribution curve shown in Figure 5.4. Thick layers of preserved rock salt (halite) are widespread in the latest Ediacarian to the Early Cambrian. Indeed, these strata contain some of the world's thickest successions of rock salt (Table 5.5). They include the Hormuz Salt of Iran and the Arabian Gulf, the Ara Salt of Oman (both thought to be latest Ediacarian), the Salt Range salt of Pakistan (Atdabanian-Botoman), and the Usolka and equivalent salts of Siberia (Tommotian-Atdabanian). The assembly Gondwana, took place during the Ediacarian to Early Cambrian. It involved the amalgamation of the separate crustal blocks of Avalonia, Europa, Arabia, Africa, Madagascar, South America, and Antarctica (together forming West Gondwana) and resulted in the compressional Pan-African orogeny, which culminated between 560 and 530 Ma. East Gondwana (India,

South China, North China and Australia) collided with West Gondwana along the Mozambique suture between ca. 600 and 550 Ma. The development of thick salts in the Ara Formation, once thought to be rift deposits of Tommotian age, now appear to be foreland basin deposits of late Ediacarian age. Even older (Neoproterozoic) thick halite beds such as the Bitter Springs Fm. in the Amadeus and the halites of the Browne and Madley Fms. in the Officer Basin of Central Australia, as well as the widespread dissolution breccia after Callana Fm. halites in the Flinders Ranges and the Duruchaus Fm. in Namibia and its equivalents in the Katangan copper Belt are perhaps related to the breakup some 850 Ma of the Mesoproterozoic supercontinent known as Rodinia or Kanatia.

Volumes of salt deposited in saline giants can be huge, with individual deposits accumulating over geologically short time frames of no more than a few million years. For example, the deposition of the Jurassic Louann Salt in the Gulf of Mexico some 175 Ma, sequestered approximately 8% of world-ocean NaCl (Land et al., 1988), while the Messinian evaporites of the Mediterranean were deposited in less than 300,000 years, yet lowered oceanic salinities by 6‰. Unlike platform evaporites, which can be tied to climate and eustasy on greenhouse epeiric platforms, the formation of basinwide deposits is not related to icehouse or greenhouse episodes in earth history. Rather, the formation of saline giants can be related to particular plate tectonic stages (A-H) in the Wilson cycle (Figure 5.27). Named in honour of J. Tuzo Wilson, the Wilson cycle encapsulates the notion that as new ocean basins open via the formation of new seafloor, others must close driven by the process of subduction and ultimately by collision (Wilson, 1966).

The requirement that the basin must be hydrographically isolated and that there must be a huge source of brine available to supply the required ions means; 1) all large thick volumes of salts (basinwides) must come from seawater and the only mechanism capable of supplying this volume is seepage into an isolated subsealevel depression, and 2) the isolation of huge tectonic depressions capable of accumulating evaporites must be systems with high continentality. Thus there are only some stages in the plate tectonic cycle where basinwides can form. One is when the incipient ocean basin is first extending and subsiding to become an evaporite-capped seafloor. The salt accumulating basin is floored by continental sediments and basalts and surrounded by continental crust; it is a hydrographically isolated subsealevel incipient ocean depression (Stage B passing into early Stage C in Figure 5.27; north Atlantic margin in Jurassic, South Atlantic Margin in the Cretaceous and possibly

the Hormuz Basin in the Neoproterozoic/Cambrian). Another is as two continental land masses come together along a soft or irregular suture belt to create subsealevel remnant ocean basins and foreland basins (Late Stage E and F in Figure 5.27 as in the Late Miocene in the Mediterranean; Middle Miocene in Poland). Somewhat smaller endorheic accumulations are currently accumulating in Quaternary tectonic depressions with a nonmarine brine feed. Such continental salts characterise the Dead Sea in the Middle East, the various suprasedeal lacustrine deposits of the Andes (salars) and the various saline lakes of the African rift (see Chapters 3 and 4). A third is where farfield tectonic flexure creates intracratonic sags.

Importance of hydrographic isolation

Modern continental lacustrine evaporites all accumulate in underfilled endorheic or hydrographically closed basins (Chapter 2). Likewise, marine-fed evaporite basins require complete hydrographic isolation from the ocean and a subsealevel water surface in order to maintain the required throughput/seepage of brine (Chapters 3 and 4). Both basinwide and platform evaporites are a response to underfilled marine-seepage hydrologies. I use the term hydrographic isolation as distinct from the groundwater connection, which dominates in all evaporite-accumulating depressions. Lucia (1972) studied the interrelationship between

maximum salinity in a modern evaporite basin and the basin's water balance (water loss versus gain). He showed that for marine-fed halite to precipitate any surface inlet from the ocean must be at least one hundred million times smaller in cross-sectional area than the surface area of the basin; for gypsum it must be at least a million times smaller (Figure 5.28). That is, any basin accumulating thick beds of evaporites effectively lacks a continuous surface connection to the ocean or other standing body of brackish water.

Maiklem (1971) in a study of evaporative drawdown in the Elk Point Basin of Canada showed that, once it was hydrographically isolated from the ocean, the Devonian Pesqu'ile barrier it did not have sufficient transmissivity to prevent evaporative drawdown, even with permeability of 73 darcies. Kendall (1989) recalculated Maiklem's figures using more realistic values of 0.9-2.7 darcies for permeability in the barrier and concluded that evaporative losses were as much as 200-800 times greater than the rate of supply. Any saline giant precipitating bedded salts is subject to evaporative drawdown and seepage influx of marine-fed phreatic waters. A corollary is that at the time of thick evaporite precipitation there is a correlative unconformity or hiatus forming in the adjacent nonevaporite lithologies that make up the surrounds of the hydrographically isolated depression.

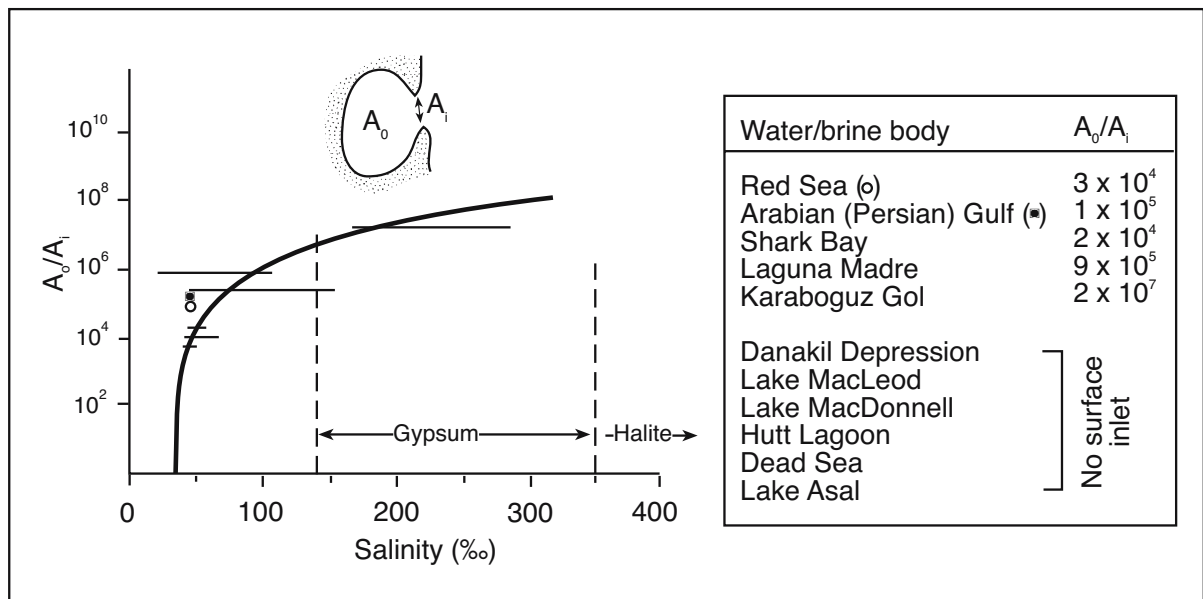


Figure 5.28. Relationship between the ratios of the cross-sectional area of a surface inlet (A_i) and the surface area of the associated hypersaline basin (A_o) plotted against salinity in the basin, with examples from several modern evaporitic depressions. Note that Quaternary examples that are accumulating substantial evaporite beds have no surface connection and are fed either by continental inflow or by marine seepage (modified from Lucia, 1972; Handford, 1991).

An evaporite basin capable of accumulating thick salt beds is always located in a large isolated depression where at the onset of drawdown more water is being lost by evaporation than entering as seepage inflow and runoff. The water level in the basin is drawn down until the volume of water lost equals the volume of inflow (hydrologic equilibrium). A potentiometric gradient (elevation head) then exists between the level of water in the basin and its surrounds, so that by definition an evaporite basin must be an underfilled basin. Such large deep holes in the landsurface attract not just marine seepage, but also ground and formation water seepage from beneath areas adjacent to the hole. In a drawdown saline-giant basin, with a predominantly marine source, the seawater enters mostly as resurging brines through springs in the basin floor. In a saline lake fed by nonmarine water, the water enters by a combination of occasional storm runoff and rainfall, as well as by groundwater and hydrothermal springs (Chapter 4).

Water ponded in an evaporitic depression must remain at the surface or reside just below the land surface in the realm of capillary evaporation. Otherwise, thick sequences of bedded salt could not accumulate, parent waters would seep away before attaining salinities high enough to precipitate salts. In a hydrological setting where the saline water table is rising into a previously vadose environment, the first salts typically precipitate as a capillary cement in previously nonevaporitic sediments of the basin floor. This is the typical situation in marine transgressions and it characterises evaporite accumulation in marine-fed Holocene coastal salinas without a hydrographic connection to the ocean. It is also the hydrology of their larger scale counterparts in subsiding rifts and intracratonic sags where rising relative sealevels force a marine-fed seepage hydrology into a previously continental depression. It also characterises Quaternary continental lacustrine transitions from a dry mudflat or sandflat into a saline pan or perennial saline lake and can be driven by a change to a more humid climate in an arid nonmarine basin.

In a hydrological situation where a previously marine basin becomes a marine-fed depression, the basin waterlevel falls. It is drawdown once the basin-centre or platform lagoon becomes hydrographically isolated from the ocean. Now the water level falls and surface water concentration increases to where dense saline brines begin to sink into the underlying succession. The water level will fall until the volume of water lost from the basin by a combination of evaporation and reflux leakage equals the volume entering by influx seepage of marine and continental waters. Hydrological equilibration in some basins occurs at gypsum saturation, in others at halite saturation. In some basins

it occurs when the water level is a water surface and subaqueous evaporites accumulate. In other basins it does not occur until the water level falls below the surface of the sediments and evaporitic mudflat deposition dominates. Hydrographic isolation drives the formation of marine-fed platform evaporites where a fourth order sealevel fall occurs during a 3rd order rise (Figure 5.37). It also dominates in basinwide evaporite deposits formed in soft-collision continent-continent suture belts (Figure 5.27). It also occurs in continental lakes undergoing a transition from fresher high-waterlevel systems into saline lower-waterlevel lakes. In this purely continental scenario the transition in lake style can be a climatically-driven change from humid to arid, or it can be a tectonically-driven change in the amount of fresh water entering the lake depression (Chapter 4).

In all situations of holomictic subaqueous and salt pan evaporites, the necessary hydrology creates a cone of refluxing brine. This leaky plume of dense brine bathes the accumulating evaporites in saturated and supersaturated water as the plume sinks, spreads and diffuses into the underlying regional hydrology. I call this zone of sinking waters associated with the accumulation of bedded salts the brine curtain (Figure 5.29). The process is brine reflux, the geometry outlined by salt-saturated pore waters defines the brine curtain. Rates of brine escape or brine residence time within the plume of the brine curtain control many of the backreactions discussed in Chapter 2 (e.g. halite pseudomorphs after subaqueous gypsum - Hovorka, 1992; carnallite in Lake Qaidam - Casas et al., 1992; and the mineralogy of the Holocene Coorong Lakes - Warren, 1990).

Once the brine curtain (reflux plume) is established and actively cycling hypersaline groundwaters, it is not easily displaced by short-term inflows of less-dense marine or meteoric groundwaters. The curtain creates an autochthonous hydrology of stable hypersaline pore waters where evaporites can continue to accumulate as secondary cements and alteration haloes (Figure 5.29). It is a plume of dense pore waters with wedgelike margins that force less-saline groundwaters to enter the basin as a series of seeps and springs about the edge of the curtain. Upon burial the evaporite cements associated with the base of the curtain are typically the first part of the evaporite sequence to be dissolved by resurging basinal and compactional waters.

Locally, the brine curtain may be breached atop areas of exceptionally strong upwelling or artesian outflow, which can be situated well out into the salt-saturated parts of the basin. Where resurging artesian waters break through the brine curtain to the

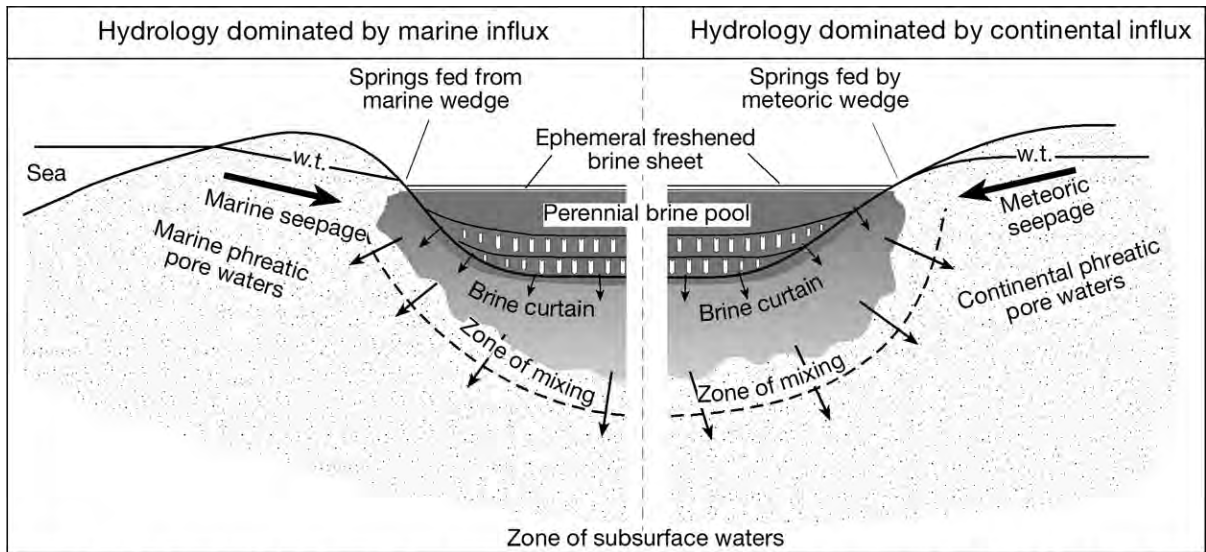


Figure 5.29. Schematic of a brine curtain in a marine-fed and a meteoric-fed evaporitic setting ($V:H \approx 10:1$). Once established the brine curtain is actively maintained by ongoing evaporation and reflux, as well as by the relatively impervious nature of the salt bed (highly effective aquitard). It is difficult to displace the curtain via influx from the margin of less-dense marine or meteoric waters. These tend to float out over the saline water table atop the denser waters of the curtain and move into the salt-filled depression via groundwater wedges that feed spring seeps about its edges. Short-term high-volume runoff or floods of fresher waters tend to form a floating brine sheet across the brine body, which disappears once it is concentrated to where its salinity and density equals that of the underlying brine body. Focused outflow of confined artesian water can locally displace the brine plume. Longer term fluctuations in the volume of all types of freshened inflow can cause changes in the mineral equilibrium that is depositing salts across the perennial brine covered floor. It can lead either to a freshening or a salinity increase in the waters of the brine curtain. Such longterm changes in flow volume favour dissolution, alteration or backreaction of pre-existing mineral phases, as can complete drying of the brine body, which may follow a longterm lowering of the regional water table.

landsurface, as along the fault lines that cut across Lake Frome, they feed prominent lines of spring mounds on the lake floor. In some ancient drawdown basins a localised freshened upflow occurred through zones of exposed pinnacle reefs and were associated with haloes of less saline mineralogies in a sea of halite. Unlike the hydrologies of most ancient basinwide evaporites, the brine curtain in many Quaternary continental lakes in central Australia fades at depths not far below the surface of the lake sediments. In lakes such as Lake Eyre and Lake Amadeus, or the sabkhas of the Abu Dhabi coast, the brine curtain is destroyed at depths of a few metres by dilution from resurging artesian waters. This brackish to mesohaline upwelling of regional groundwater, coupled with periodic surface floods, continually recycles salts into nearsurface sediments. There they are deflated or washed away, so preventing stacking of thick bedded salts within the playa or sabkha depressions. The only bedded salt to accumulate in such settings is a continually recycling pan crust that is never more than a metre thick. Its hydrogeochemistry is largely decoupled from the mineralogies of the underlying sediments (Chapters 2 and 3).

Logan (1987) and Kendall (1992) use the term “hydroseal” to describe the lowermost salt layer in any evaporite sequence. They interpret it, and not the formative reflux hydrology, as the fundamental cause of evaporite accumulation and the varying mineralogies in the basin. The notion of a “hydroseal” is not strictly correct, as secondary or capillary salts precipitated in any zone of refluxing brine must be by definition forming in an aquitard and not an aquiclude. It leaks, to varying degrees, across the whole of the salt-covered basin floor. Even when a salt bed becomes cemented it still dissolves from its underside and becomes a supplier of brines to the base of a more deeply buried brine curtain (Chapter 8). As pore waters making up the brine plume slowly seep and sink, they ultimately mix with underlying compactional and basinal crossflows, as well as any more marginward meteoric or marine inflows. This mixing drives diagenetic reactions that include the precipitation of quartz overgrowths and dolomite cements in units located further away from the brine curtain (Ceriani et al., 2002; Morrow et al., 2002).

Thus, the term “seal” is not appropriate to any reflux situation and the notion of the base of an evaporite bed as a total seal, which is not subject to dissolution or alteration, is one of the reasons why the significance of basal anhydrites and other diagenetic deposits, such as some of the Rote/Faule Kupferschiefer ores, were not attributed to an inherent evaporite dissolution hydrology (Figure 9.46; Warren, 1999, 2000b).

Problems in correlation *sans* hydrology

The need for hydrographic isolation means thick salts are not simultaneous with marine carbonates. Likewise, there are fundamental hydrological problems with the notion that evaporite beds pass laterally below the same sheet of water into contiguous synchronous carbonates and clastic beds. This requires longterm maintenance of subvertical density interfaces in a fluid, which is a physical impossibility. Put simply, if you ignore the unique hydrology needed to deposit a thick evaporite bed, the correlation will fail. Thick evaporites must correlate to unconformities in their surrounds and subaqueous evaporite deposition in a single brine-filled water body (basin) must be a simultaneous holomictic event.

Shaw (1977) in a landmark paper was one of the first geologists to recognise that the classic silled-basin model, with evaporites accumulating in the basin centre and a restricted surface connection to the ocean defined by growing reefs, is hydrostatically unsound. He went on to demonstrate that in such a scenario deepwater evaporites cannot accumulate. Kendall (1988) further develops his arguments by integrating his conclusions with the work of Lucia (1972) to illustrate that when an evaporite basin is depositing widespread salts it must be totally isolated from a surface supply of seawater. Deepwater evaporites are possible in such isolated nonstratified basins (see discussion of the Dead Sea halite in Chapter 4).

Deepwater halite accumulating simultaneously with platform gypsum and basin entry carbonate in a single water mass is not possible, yet it is commonly invoked in models of many ancient evaporite basins. In order to deposit gypsum in a shallow area of a brine body and halite in a deeper area of the same brine body requires an inclined halocline. The required fluid system cannot exist over the longterm in a single brine body. Any body made up of liquids of two different densities cannot support shear. The inclined halocline required by this model will spontaneously collapse in order

to regain its gravitational equilibrium. Once it has restratified to a horizontal interface the precipitation of salts in the deeper brine body ceases until the salinities of the upper and lower brine bodies are equalised by the concentration of the upper less saline water body (Chapters 2 and 4). There never has been and there never will be a brine lake or seaway with a permanently non-horizontal halocline.

In terms of stratigraphy, this means a thick subaqueous bedded halite intersection in one well is an unlikely time correlative of a thick subaqueous anhydrite/gypsum bed in an adjacent well a few kilometres away. The only exception is if they were deposited in nonconnected water bodies in two separate sub-basins or if one or both units were capillary salts not bottom growths. Monomineralogic subaqueous evaporite beds are perhaps one of the few examples of true “layer cake” stratigraphy. Many of the supposed correlations and basin reconstructions in the literature, which propose that a deep subaqueous halite in the basin-centre is time-equivalent to a shallower subaqueous basin marginward anhydrite and to a biologically restricted, but growing, reef carbonate in the seawater inflow area are wrong as they ignore the fundamental principles of physics and hydrology. By implication, the geological interpretations and correlations in the same regions will be marked by the nonrecognition of the significance of erosion surfaces, hiati or dissolution horizons in adjacent wells or in the carbonates or other marine strata that occupy the basin margin. A time of evaporite deposition corresponds to a time of exposure and the creation of a subaerial unconformity in adjacent carbonate sills.

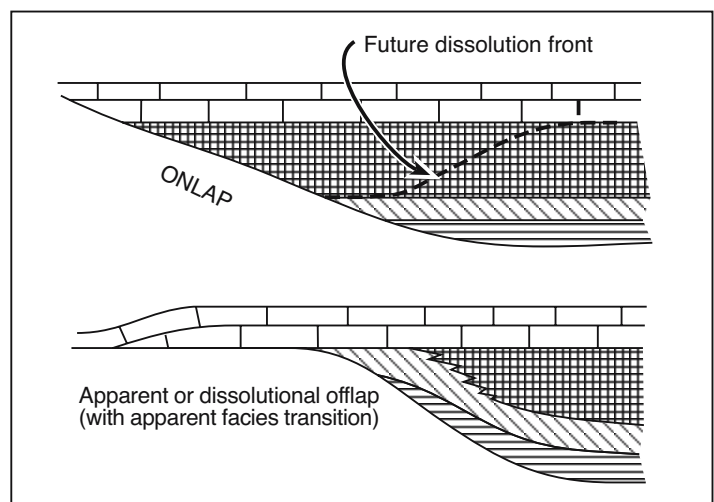


FIGURE 5.30. DISSOLUTION OF EVAPORITES ABOUT THE MARGIN OF A BASIN CAN CREATE AN APPARENT OFFLAPPING STRATIGRAPHY FROM AN ONLAP SITUATION (AFTER KENDALL, 1988).

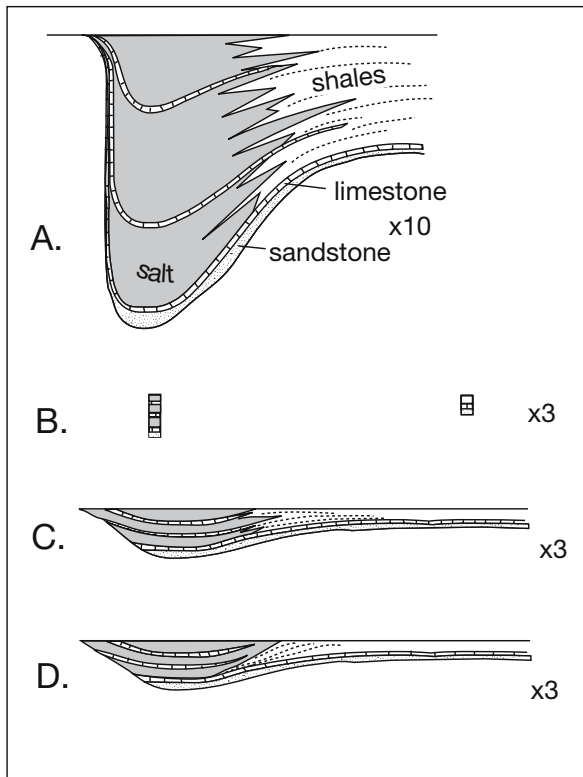


Figure 5.31. Effect of vertical exaggeration on correlation between thick evaporite sequences and marginal clastics or carbonates (after Busson, 1980; Kendall, 1988). A) Conventional correlation with significant vertical exaggeration showing lateral equivalency of evaporites and marginward clastics or carbonates. B) Original data drawn with less vertical exaggeration. C) Conventional correlation with less vertical exaggeration (hydrologically unlikely in an evaporite basin accumulating thick salt beds). D) Alternative correlation, which assumes drawdown is required and so there is no equivalency between salt beds and marginward clastics or carbonates (hydrologically likely in drawdown basin). Alternative D) is reasonable to most geologists when not suffering from a psychological need to draw near-horizontal correlation lines. It implies times of thick salt accumulation were distinct from times of carbonate deposition.

Kendall (1988) lists five factors that should be addressed when correlating evaporite units or applying the principles of sequence stratigraphy to evaporite basins:

1. *A lack of stratigraphic control*; evaporite depositing areas tend to be populated by halotolerant organisms that have low biostratigraphic potential. This means that biostratigraphic faunal analysis can be used to bracket the evaporite group (using fossils in nonevaporite strata above and below the unit of interest); but intra-evaporite biostratigraphic subdivision is near impossible.

2. *The rapidity of evaporite deposition*; evaporites accumulate at some of the most rapid sedimentation rates known. Even if fossils are present in intrasalt units that separate a number of evaporite beds, the very short time required to deposit thick evaporite sequences means the biota are incapable of evolving fast enough to be used for biostratigraphic control of the evaporites.

3. *Complexity of stratigraphic relationships*; stratigraphic relationships between the surrounding nonevaporite lithologies and the evaporites are typically dynamic and problematic. Their hydrology and rapid rate of deposition mean evaporites accumulate so rapidly that lateral correlatives to the evaporite deposit are at best thin, or more typically, are surfaces of erosion or nondeposition.

4. *Early dissolution about basin edge*; A high likelihood of partial to complete subsurface dissolution, especially of the more soluble salts, almost from the time the salts accumulate (Figure 5.30). This means most ancient evaporite deposits show clear evidence of thinning, especially about the edges of a thick evaporite succession where flushing by meteoric and basinal waters is most likely to occur. As we shall see in Chapter 7, a salt bed or halokinetic salt mass shrinks like a block or ice, inwards from its edges. If the evaporite dissolves completely, remnants may be missed (such as layers of insolubles or thin dissolution breccias), and a whole episode of basin history and structural evolution ignored. Even when evaporites remain in the basin, a greater degree of dissolution in zones of freshening about the basin edge means the current distribution of mineralogies may bear no relation to their original distribution in a basin (Figure 5.30). Removal of the marginal portion of a halite layer that had overstepped an earlier anhydrite unit will convert an onlapping situation to an apparent offlapping situation in a seismic section in an area without well control. Likewise many apparent “bull’s-eye” basins may be the result of marginward dissolution of the more soluble evaporite layers.

5. *Inappropriate scaling*; We tend as a profession to use vertically exaggerated cross sections to make relationships more obvious in what are natural systems with thin relative to width ratios (Figure 5.31a). Their training makes most geologists reluctant to draw steeply inclined bed-to-bed correlations when more horizontal possibilities are available (Kendall, 1988; Busson, 1980). A propensity for large vertical exaggeration in basin cross-sections leads to a tendency to draw correlation lines that show transitional facies between the evaporite beds and the surrounding nonevaporites, and to impose age equivalence of evaporites and nonevaporites (Figure 5.31b, c). But the inherent hydrological constraints required to form a platform

or basinwide evaporite fill means salt beds tend to accumulate rapidly in isolated depressions on the land's surface. Times of evaporite deposition correlate to times of isolation and so to times of nondeposition or gaps (unconformities) in adjacent nonevaporite strata. In such situations we should be quite happy to draw inclined correlation lines showing that at the time of evaporite deposition there was little or no deposition taking place in the adjacent nonevaporite strata (Figure 5.31d).

Dolomite aprons in a drawdown basin

Requirements of hydrographic isolation for basinwide evaporites also have consequences for reflux dolomites. In contrast to well documented reflux dolomite geometries and distributions in platform evaporite associations (Figures 2.50, 10.24), outputs from dolomitising hydrologies in saline giants are a little more complicated (Figure 5.32). Brine plume and seawater seepage inflow in a drawdown basinwide evaporite

depression is driven by piezometric head between sealevel and the brine -air interface, which can be of hundreds to thousands of metres below sealevel (Figure 5.7b). With no modern counterpart, one can only infer, not observe, the hydrological and diagenetic character of such basinwide systems by studying the more accessible outcrop examples of platform and basinwide evaporites, as in the Messinian evaporite/dolomite associations of the circum-Mediterranean (Sun and Esteban, 1994; Lu and Meyers, 1998), the Permian Zechsteinkalk dolomites associated with basinwide evaporites of NW Europe (Clark, 1980a; Peryt and Scholle, 1996) and the Devonian basinwide evaporites and associated dolomites of the Keg River- Pine Point Presqu'ile of Canada (Maiklem, 1971; Kendall, 1989).

Maiklem (1971), Cercone (1988) and Kendall (1989) pointed out the potential for widespread dolomitisation via seawater seepage beneath subaerially exposed carbonate slopes about a drawdown basin margin is largely independent of marine

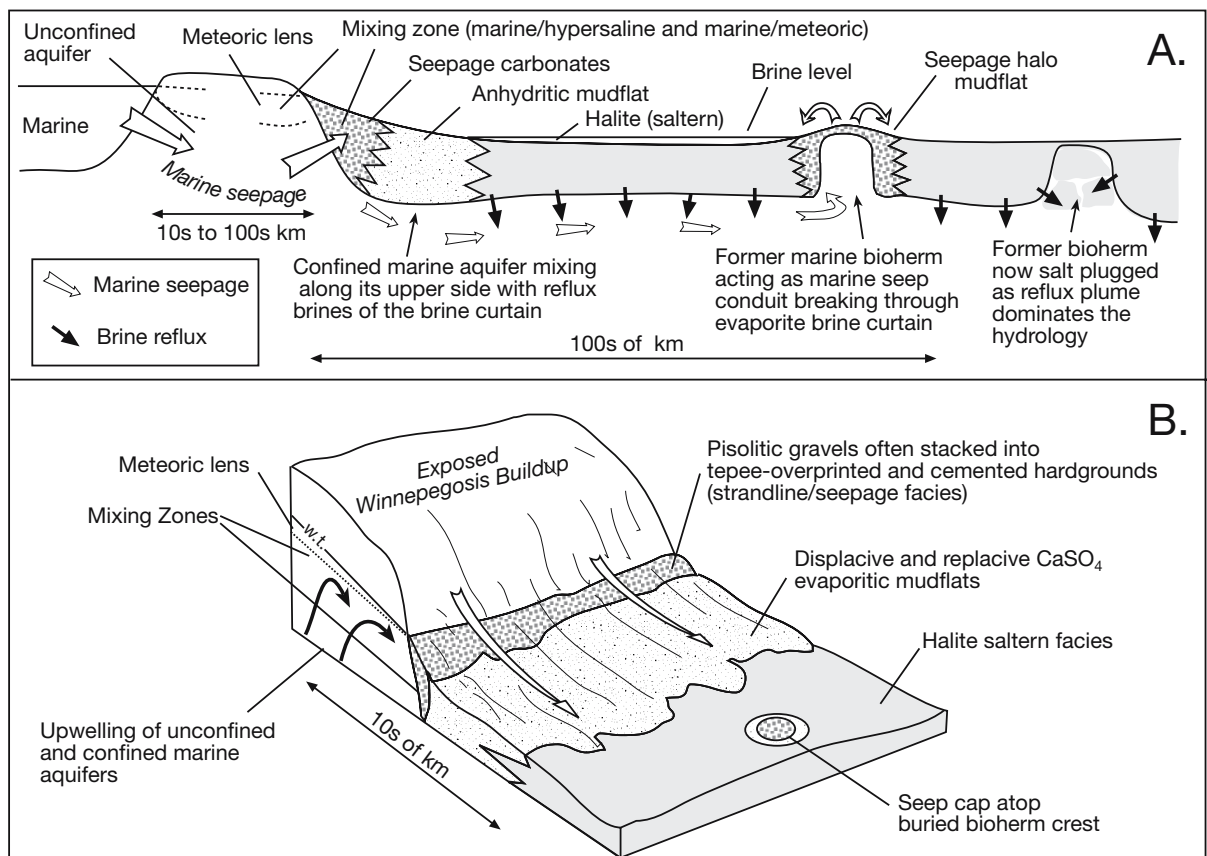


Figure 5.32. Evaporative drawdown dolomitization. A) Hydrology of basin showing seepage facies and halite in basin centre. Note the potential for the mixing of seawater seepage with refluxing brines both about the margin of the drawdown basin and beneath the reflux curtain across much of the basin floor. Diagram is not drawn to any consistent lateral scale. B) Close-up of facies pattern associated with seepage outflow zones and the potential positions of marine/meteoric and marine/hypersaline mixing zones (in part after Warren, 2000a and Kendall, 1989).

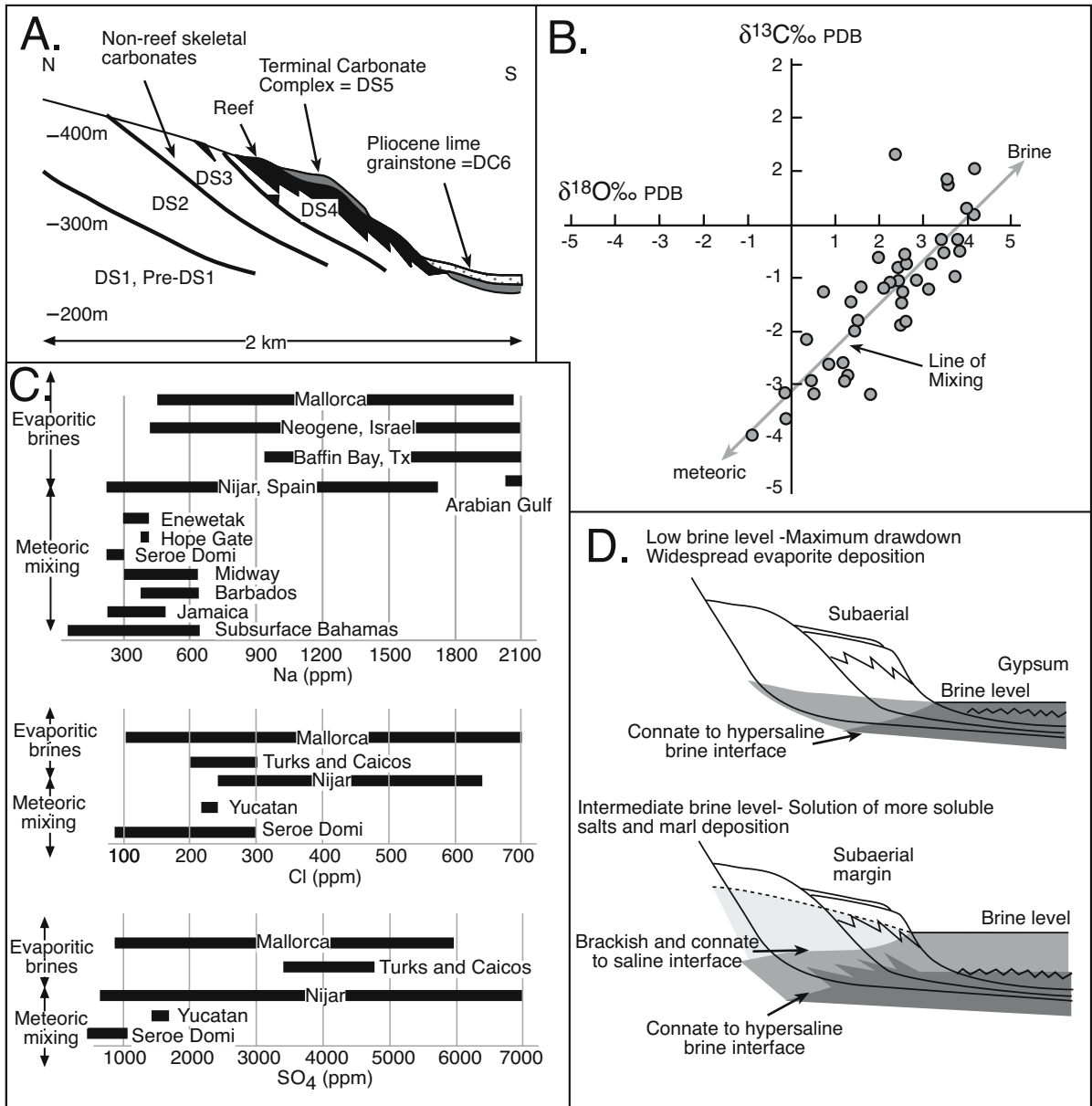


Figure 5.33. Nijar dolomites in the Messinian of Spain. A) Composite stratigraphic cross section of the Tortonian-Messinian carbonate platform at Nijar. DS = depositional sequence. B) Oxygen and carbon isotopes of the Nijar dolomites C) Na, Cl and SO₄ contents of Nijar dolomites compared to other Tertiary and modern dolomites formed in mixing zone, seawater and evaporative brines. D) Model of migration of mixing interfaces between hypersaline brine, connate seawater and meteoric brackish waters. Their position within the carbonate margin is controlled by fluctuation in brine level in the basin (after Meyers et al., 1997; Lu and Myers, 1998; Lu et al., 2002).

eustasy (Figure 5.32). Drawdown basins have the potential to flush huge volumes of phreatic seawater through the basin edge. As the groundwater heads in such systems are measured not in metres but hundreds of metres, and if one accepts that seawater flushing has the potential to dolomitise marine limestone, then the potential for dolomitisation is huge within

carbonate aquifers about the margin of an evaporite drawdown basin. "Mixing" zone dolomites are also likely, but not in a classic seawater-freshwater Ghyben Herzberg interface on the marine side. Rather dolomite will form in rapidly fluctuating and flushed interfaces and outflows in and about the now isolated and exposed carbonate slope and rise shown in Figure 5.32.

The schematic is drawn assuming an unconfined aquifer in the interval separating the marine from the seepage zone. The reality is much more likely to be a combination of confined and unconfined aquifers feeding predominantly seawater into the basin margin. This zone of mixing and seawater spring outflows will move to and fro over the exposed basin edge as the brine level in the basin responds to changes in tectonics and climate.

Outflow points of these predominantly seawater brines develop a characteristic set of pisolitic/tepee cementstone lithologies - the strandline/seepage facies described in Chapter 1. Kendall (1992) showed how such a carbonate seepage facies can be used to define hydrologies in the Devonian Keg River Basin where these spring-aprons were mostly located about exposed former shelf slopes and pinnacle reefs (Figure 5.32b). When part of an inactive pinnacle reef or other aerially exposed bioherm, these permeable carbonates can act as confined aquifer outflow zones capable of breaching the active reflux curtain on the basin floor, much like the modern spring mounds of Lake Eyre and Lake Frome (Figure 5.32a). Slightly down dip of the seepage facies were evaporitic mudflats dominated by anhydrite and in the lowermost sections of the basin floor were widespread areas of perennial surface brine (the halite seaways of the Keg River Basin). Away from seawater and meteoric discharge seeps, the downward reflux associated with the brine curtain moved Mg-rich waters into underlying sediments driving reflux dolomitization and evaporite plugging. This water ultimately mixed with deeply circulating seawater seepage fluids and other subsurface waters (Figure 5.32a).

Such a basinwide hydrology creates both reflux and mixing zone chemistries, which have the potential to dolomitise any limestone host in contact with the outer parts of the brine curtain. Detail of such drawdown mechanisms can be inferred in dolomite distribution within Neogene evaporitic sub-basins of the Mediterranean. For example, Meyers et al. (1997) and Lu and Meyers (1998) have documented pervasive dolomites that cut across intra-Miocene sequence boundaries in the Nijar Platform and also occur in the youngest Messinian reef/oolitic units (Figure 5.33a). The dolomites do not transect the Miocene-Pliocene unconformity, although they do occur as clasts in overlying basal Pliocene lime grainstones. This constrains the dolomitization as being latest Miocene and pre-Pliocene, suggesting this widespread dolomitization occurred within 600,000 years and possibly in less than 200,000 years. It is an excellent indication of the large volumes of phreatic seawater that can be cycled through the rock pores in short times in drawdown hydrologies.

Carbon and oxygen isotopes of Nijar dolomites show marked positive covariation, with most values ranging from +5.4 to -1.2‰ $\delta^{18}\text{O}_{\text{PDB}}$ and +2.5 to -4.3‰ $\delta^{13}\text{C}_{\text{PDB}}$ (Figure 5.33b; Meyers et al., 1997). The highest $\delta^{18}\text{O}$ values are heavier than reasonable estimates of Messinian normal-salinity seawater dolomites, suggesting the involvement of evaporative brines in the dolomitisation process. Calculations of covariations of O and C isotopes during water-rock interaction and fluid-fluid mixing argue against recrystallisation of Nijar dolomites, an interpretation also supported by their Ca richness (49-57 mol %). Mixing calculations show that four-fifths of Nijar data are consistent with dolomitization via mixtures of freshwater and a few tens of per cent of marine-derived evaporative brine, while one-fifth are consistent with mixtures of freshwater and normal-salinity seawater. Modelling of covariations of $^{87}\text{Sr}/^{86}\text{Sr}$ and Sr/Ca ratios that developed during mixing, further supports involvement of evaporative brine, and suggests that any freshwaters involved in the dolomitization had low Sr/Ca ratios and relatively high Sr and Ca concentrations. Na, Cl, and SO_4 concentrations in Nijar dolomites (200-1700 ppm, 300-600 ppm, and 600-6500 ppm, respectively) also argue for involvement of evaporative brines, and for mixtures of brine with freshwater and/or seawater (Figure 5.33c).

Meyers et al. (1997) and Lu and Meyers (1998) proposed that most dolomitization occurred after Messinian reef formation during multiple relative sealevel/brine level changes associated with evaporative drawdown. Marine carbonate deposition of the Nijar shelf occurred during high sealevels, and evaporite deposition during lowered basin water levels associated with evaporative drawdown. During drawdown, basin brines with 5x- to 6x-seawater concentrations (gypsum precipitating) developed on the floor of the Nijar Basin. Brines mixed with freshwater and seawater mainly in a groundwater setting about the basin margin as fluctuating base levels of the brine curtain drove before it a zone of freshened/meteoric water seepages (Figure 5.33d).

Similar drawdown dolomites can be found in the Zechstein of NW Europe where dolomitized algal-bryozoal reefs, oolites and intertidal to shallow subtidal skeletal grainstones to mudstones occur adjacent to the margin of the Zechstein salts. They are interlayered with the platform portion of basinwide evaporite beds composed of anhydrite and halite (see later in this chapter). Evaporite salts were deposited during the complete isolation and drawdown of the Zechstein Basin. It was at this time of drawdown that reflux dolomites replaced the adjacent and underlying Zechstein limestones (Clark, 1980a). At the same time the regression of facies associated with the drawdown of

the brine base level caused the encroachment and displacement of formerly marine to hypersaline porewaters by meteoric waters in the dolomites of the Magnesian Limestone (Kaldi and Gidman, 1982).

Sequence stratigraphy in evaporite basins?

Sequence stratigraphy is the study of ancient rock relationships within a chronostratigraphic framework of repetitive, genetically related strata, bound by surfaces of erosion or nondeposition or their correlative conformities (Posamentier and James, 1993). Stratigraphic sequences are deposited during a single cycle of relative sealevel change and the rise and subsequent fall of sealevel within the shallow marine setting generates a characteristic sedimentary wedge with a specific geometry and vertical stacking pattern. Sequences are conformable successions constructed by genetically related strata, bound at the top and bottom by unconformities and their correlative

conformities (Figure 5.34; Van Wagoner et al., 1988, 1990; Tucker, 1993). Unconformities bounding sedimentary wedges may represent a significant time gap and may die out in more basinward positions where sealevel oscillations do not expose the sedimentation surface.

In classic sequence stratigraphic interpretations of marine sequences the major control on depositional extent and geometry is assumed to be relative sealevel change, determined by rates of eustatic sealevel variation and tectonic subsidence. Depositional sequences are generated by a single cycle of relative sea-level change, and a complete depositional sequence, bounded by unconformities, consists of, from oldest to youngest, lowstand, transgressive, and highstand components (= systems tracts). This evolution creates the characteristic transgressive-regressive pattern of sedimentary facies within a depositional sequence with the outline of a sigmoidal wedge or prism (Figure 5.35); lowstand systems tract (LST), transgressive systems tract (TST) and highstand systems tract (HST)). A seismically resolvable depositional sigmoid typically has a thickness of 10-100 m,

extends laterally for 10-100's km, and represents a depositional episode of 1-5 million years in duration. According to Haq et al. (1987), it is a response to 3rd order sealevel changes (Table 5.8). Internally depositional sequences are constructed of sub-seismic-resolution parasequences (metre- to decametre-scale 4th and 5th order depositional cycles). Parasequences are typically bound by local scale unconformities and disconformities.

Chronostratigraphic correlation is an important application of sequence stratigraphy. It is tied to the notion that sediment wedges form in response to worldwide sealevel cycles of rise and fall. If so, then seismic geometries can be used to extract a global sealevel cycle chart (aka Vail or Exxon sealevel curves). This then leads to the construction of age models for given stratigraphic successions that are based on the correlation of a local stratigraphic sigmoid to this global sealevel curve (Posamentier and James, 1993). Different orders of sealevel change are recognised based on the time interval

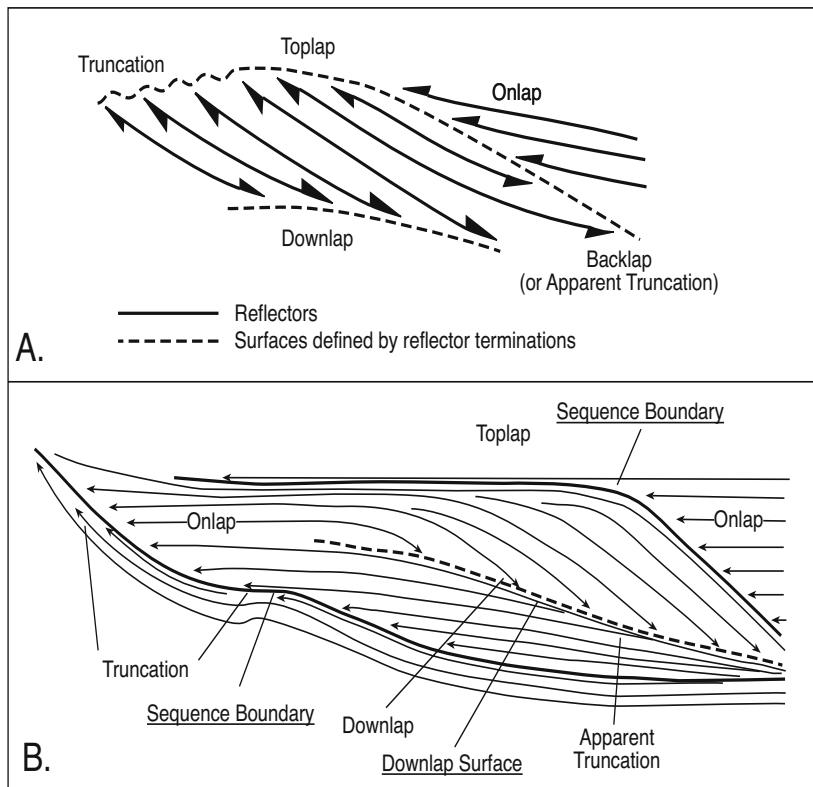


Figure 5.34. Fundamentals of seismic sequence interpretation. A) Terminology used in defining sequence interpretation of seismic reflectors. B) Sequence boundaries define a depositional package.

encapsulated in the sealevel cycle (Table 5.8). The use of sequence stratigraphic principles to construct age-eustatic (chronostratigraphic) models is based on the assumption that stratigraphic successions are a function primarily of eustatic rather than local tectonic fluctuations or that the effect of tectonics can be removed to allow sealevel fitting.

First and second order changes in world sealevel are a response to changes in the volume of the ocean basins caused by continental dispersal and collision. High rates of seafloor spreading during continental dispersal reduce ocean basin volume, leading to high sealevel. Third order changes have durations of 1 to 10 m.y. and are typically about 2.5 m.y. in length. The cause of third order cycles is controversial as they are too short to attribute to most world scale tectonic events affecting the volume of the ocean basins, but too long to attribute to glacio-eustatic responses. Other more local tectonic events, such as changes in plate stress and regional tectonism, are of the correct duration, but do not appear to be capable of generating sufficient change in water depth to account for the magnitude of world scale third order cycles. Fourth order (500 ky - 200 ky) and fifth order (200 ky - 10 ky) cycles are widely documented in marine sediments (outcrop and core based parasequences) in many periods of the Phanerozoic in both shallow marine and pelagic strata. These cycles are possibly the result of changes in global climate driven by cycles in the Earth's orbital parameters and tilt, collectively referred to as Milankovitch Cycles.

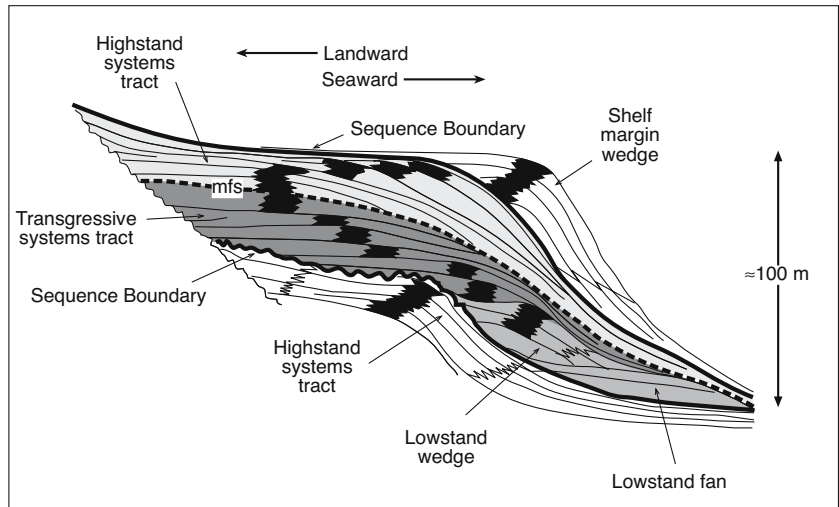


Figure 5.35. The familiar sigmoidal or "slug" model of a marine carbonate depositional sequence used by sequence stratigraphers with the black shaded areas representing carbonate shoal/reef sediments. A single depositional sequence consists of lowstand, transgressive and highstand systems tracts (after Van Wagoner et al., 1988 and other sources). In terms of associated evaporite deposition each sequence boundary (unconformity) may be time equivalent to a thick sequence of basinwide evaporite fill, which accumulated further out in the basin. Saltern evaporites tend to accumulate on the platform landward of the reefs within transgressive system tract sediment packages when higher order sea sealevel falls expose reef crests and isolate lagoons from a surface connection to the ocean.

There is still much debate in the literature as to controls on the magnitude and frequency of the various sealevel changes that could facilitate a correlation of sedimentation packages worldwide; especially at the third order world scale cycles where seismic and rock based interpretations overlap. At that scale, some authors well versed in outcrop and core study go further and question the reality and the scientific basis for the construction of world scale age correlations based on seismic-based third-order eustatic age curves in almost all sedimentary basins (e.g. Miall, 1997).

For evaporites, there is also the problem of different depositional rates inside and outside a hydrographically isolated groundwater

Order	Years	Tectono-eustatic	Rifting and thermal subsidence	Global eustatic	In-plane stress	Glacioeustatic, tectonic, sedimentary	Basinwide Evaporites Time to deposit 1-2 km of fill
1st	10 ⁸	↕	↕	↕	↕	↕	SEISMIC SIGMOIDS ↕ PARASEQUENCES
2nd	10 ⁷						
3rd	10 ⁶	SEISMIC SIGMOIDS		↕	↕		
4th	10 ⁵	↕					
5th	10 ⁴	← -- Typical limit of seismic resolution in siliciclastics and carbonates -- →				↕	
6th	10 ³	PARASEQUENCES					

Table 5.8. Orders of sealevel change and likely driving mechanisms (in part after Tucker, 1993).

sump. Rates of evaporite deposition, especially in basinwide settings, are an order of magnitude higher than that of marine shelf carbonates or siliciclastics (1-2 km in 300,000 to 500,000 years are typical). Seismic geometries resolvable in evaporite fills are typically 4th and 5th order, with parasequence sets resolving time frames of the order of a thousand years (6th order). Comparing seismic stratigraphies inside and outside a basinwide evaporite basin and attempting, based on the evaporites, to relate the eustatic interpretation to the global curve is difficult if not impossible. We are not resolving depositional evolution at the same time scale (Table 5.8).

More generally accepted than worldwide chronostratigraphic correlation is the application of seismic sequence stratigraphy to lithology prediction based on interpretation of depositional geometries and basin architecture using a combination of seismic, wireline, core and outcrop data. For example, the favoured sites for major porosity development in carbonate-dominated depositional sequences include large, isolated buildups within the transgressive phase, massive grainstone aprons located immediately landward of the shelf-margin facies within the regressive phase, and karst-affected platform interior facies immediately beneath the sequence-bounding inter-regional unconformities (Figure 5.35).

There are numerous volumes and papers now published that deal with high resolution sequence stratigraphy of arid zone carbonate shelves and ramps and how they differ from siliciclastic sequences in their response to sealevel changes (Figure 5.35; Read et al., 1995; Budd et al., 1995; Loucks and Sarg, 1993; Tucker, 1993; Posamentier et al., 1993; James and Kendall, 1992). The details will not be repeated here and the interested reader should refer to these volumes. There are only a few published papers that deal specifically with the sequence stratigraphy of evaporite systems; key papers include, Tucker, 1991; Goodall et al., 1992; Strohmenger et al., 1996a, b; Sarg, 2001. The results are contentious and most concentrate on the carbonate (marine-connected?) stage of the evaporite basin. This is understandable as it is in these carbonate units that potential hydrocarbon reservoir facies are to be found, often beneath or adjacent to the evaporite seal.

Does sealevel control salt sequences?

When attempting to interpret eustatic effects (global sealevel) in evaporite basins, a requirement of no effective hydrographic connection to the open ocean during times of extensive evaporite accumulation plays havoc with the fundamental marine eustatic paradigms of sequence stratigraphy. Documented brine level

changes in lacustrine and marine basinwide settings are ≈ 1 km in a few thousand years and there is no simple relationship between sealevel changes going on outside the basin and the geometry of the evaporite body in the isolated evaporite-accumulating basin (Kendall, 1992).

All evaporite basins with a marine-seepage feed have a brine level that is below sealevel. It is, after all, drawdown that drives brine influx in ancient marine-fed basins. The relative difference in water level across the isolating barrier may be no more than a few to tens of metres, as it was in the platform evaporites of Guadalupian backshoal strata in west Texas, or it may be thousands of metres as it was in the late Miocene salinity crisis in the Mediterranean, the Cretaceous evaporites of the southern Atlantic and the early stages of the Permian salinity crisis in the Zechstein Basin of NW Europe. Brine salinities and the rate of salinity change in a brine-filled depression, as well as the absolute brine level in an isolated basin, are controlled by the local climate, the rate of brine leakage through the underlying brine curtain and the rate of seepage replenishment of the inflow waters and brines about the depression's margin. With most ancient saline giants the creation of a depression capable of accumulating and preserving thick lacustrine and basinwide evaporite fill is a response to tectonics, not eustacy (Figure 5.27).

Marine-fed platform evaporites must be distinguished from basinwide evaporites if one wishes to apply the marine eustatic concepts. At our present level of understanding we can probably fit marine-margin platform evaporites and some intracratonic saltern fills (epeiric seaways) into a global eustatic context. In the absence of tectonic tilting in these two settings, the precipitation of large volumes of platform salts is largely dependent on marine phreatic seepage through a carbonate barrier. It requires platform isolation brought about by a slight fall in sealevel, perhaps a 4th order fall on a 3rd order rise in greenhouse mode (Figure 5.7a). The evaporites can fill the depression behind the barrier; but cannot, as they are seepage fed, rise any higher than sealevel. The isolating barriers in turn have geometries and distributions across the platform that are controlled by sealevel changes (Read et al., 1995; Loucks and Sarg, 1993).

In contrast, tectonically-formed subsealevel basinwide evaporite units, with their much lower hydrological base level, are more problematic in terms of using the effects of sealevel fluctuations to understand and predict evaporite geometries and mineralogies. The problem will remain until the hydrologies of large-scale drawdown systems are better understood. Formation

of basinwide evaporite sequences are largely tied to a suitable juxtaposition of tectonics and climate. In such a scenario the decametre sealevel fluctuations on the marine side of the isolating barrier are largely irrelevant to evaporite depositional styles within the lowermost portions of an isolated basin experiencing a drawdown that is up to 1,500 - 2,000 metres below sealevel. Likewise continental lacustrine evaporites are not directly tied to the world sealevel curve. In both basinwide and continental lacustrine scenarios the application of sequence stratigraphic modelling is most useful in a genetic rather than an age (world sealevel) context.

Icehouse and greenhouse eustacy

Sequences in seismic stratigraphy are unconformity-bound packages generated by high amplitude sealevel changes with bounding surfaces typically produced during relative sealevel falls (Tucker, 1993). High amplitude sealevel changes producing regional sequence boundaries can occur on several time scales depending on the presence or absence of polar ice caps. At times of no polar ice cap (greenhouse earth) the high amplitude changes that produce sealevel oscillations of several tens of metres are a response to second and third order processes, while fourth/fifth order processes produce only metre-scale relative sealevel changes and associated parasequences (Figure 5.36). In contrast, when there are polar ice caps (icehouse earth) the high amplitude sealevel changes (typically greater than 100 metres) are brought about by fourth-/fifth order processes. The driving force for these high amplitude/high frequency oscillations is change in polar ice volume driven by Milankovitch rhythms (Figures 5.1, 5.2). During icehouse times the same longer term second-/third-order fluctuations in sealevel that dominate the greenhouse style still occur, but they now have a lower amplitude and longer period than the glacially driven changes. Thus the glacially-driven eustatic cycles swamp these longer term effects, so that in icehouse times fourth-order sequences are produced and are arranged into sequence sets (Tucker, 1993). Greenhouse periods produce third order sequences constructed by fourth-/fifth order parasequences and show a much more prevalent cyclicality in lagoonal parasequences.

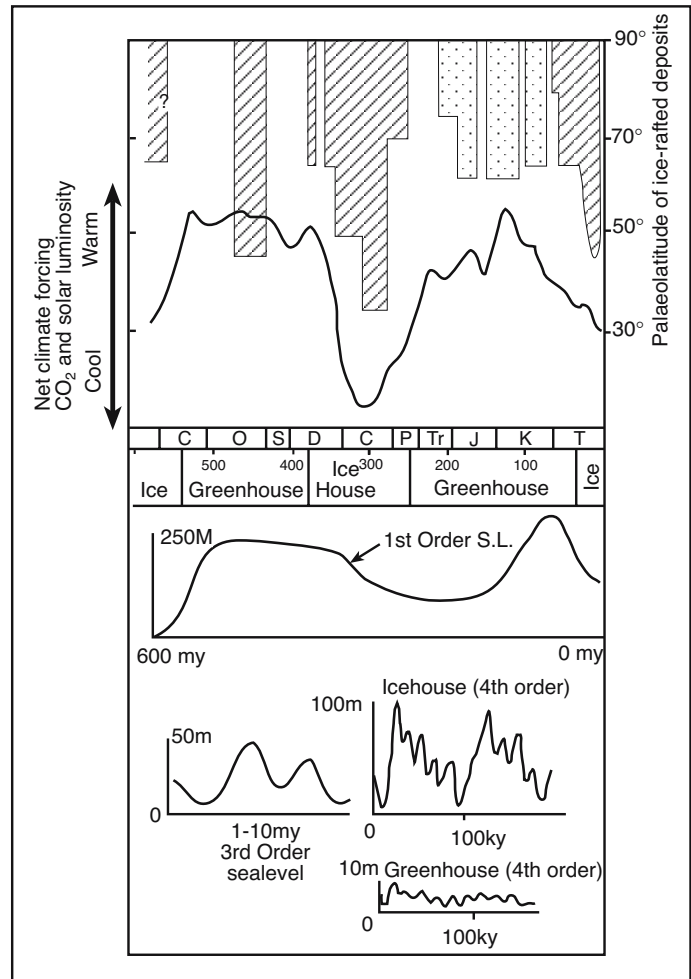


Figure 5.36. Relationship between icehouse and greenhouse conditions, eustacy and global CO₂ (after Read and Horbury, 1993; see Figure 5.2 for more detail and refinement of curves/climate). Upper half of figure shows palaeolatitudinal extent of continental ice-raftered deposits (crosshatched) and marine ice-raftered debris (dots). The curve beneath plots net forcing of climate due to variations in CO₂ and solar luminosity. Inferred times of general icehouse and greenhouse earth are shown on the horizontal axis (icehouse times are narrower if defined on a basis of presence of polar ice, as in Figure 5.2b). Lower half of diagram shows first order Vail sealevel curve in upper part. Bottom diagram shows typical third order sealevel curve with 1-10 my period. Schematic 4th order with superimposed 5th order sealevel curves are drawn for icehouse and greenhouse conditions.

The Neogene sedimentary marine record is an icehouse record, where fourth-order sequences dominate the continental margin as unconformity-bound, relatively thin (5-30 m thick), stratal packages. Other older icehouse intervals include the late Precambrian and the Permo-Carboniferous (Figures 5.2, 5.36). In contrast in greenhouse times (Late Cambrian to Middle Ordovician, Silurian to Early Devonian, Late Permian to

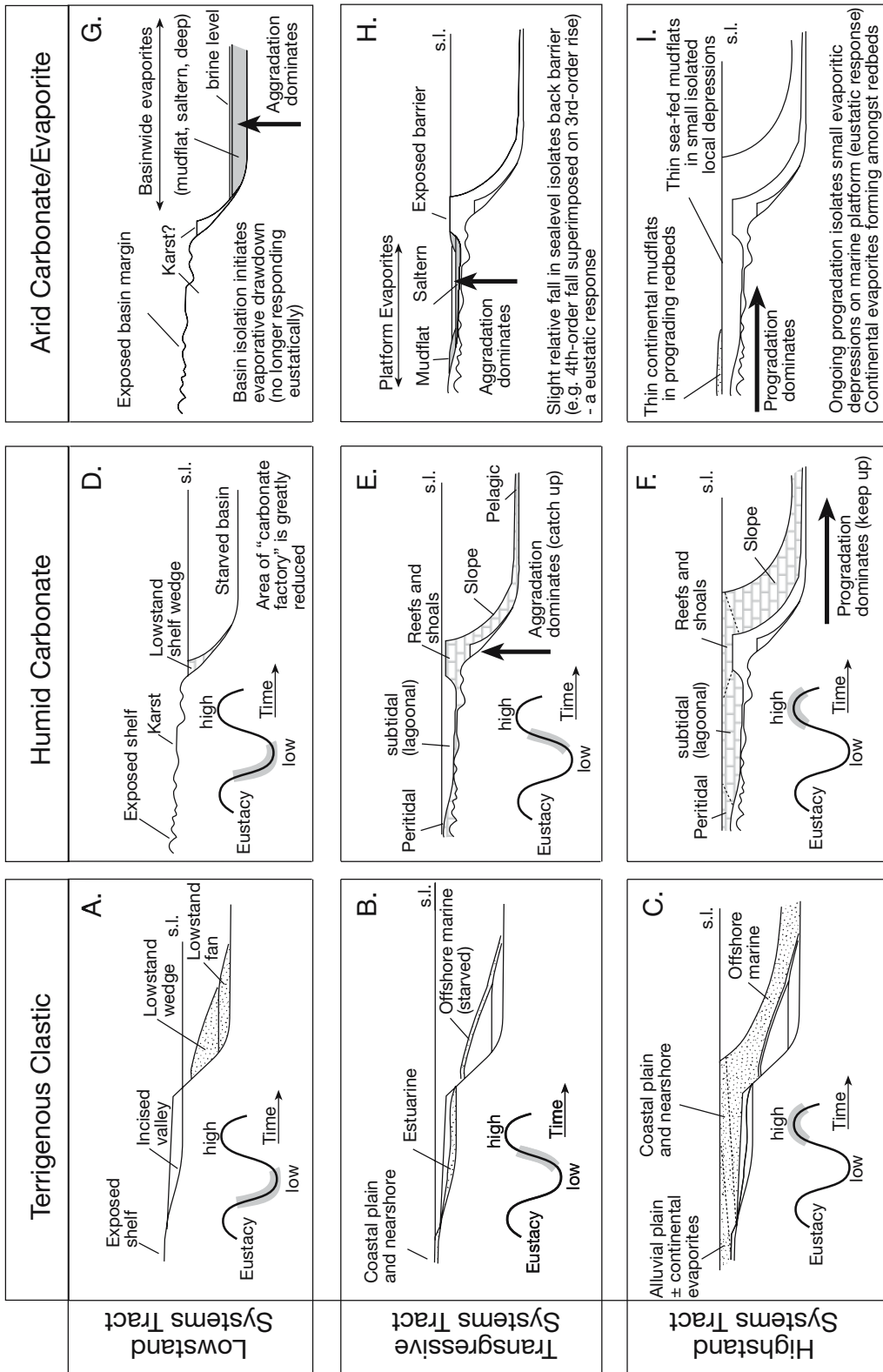


Figure 5.37. Sequence stratigraphic models for terrigenous clastic, humid carbonate and arid carbonate platform systems. Note there are significant differences. In a lowstand systems tract there are substantial volumes of terrigenous sediment deposited at the foot-of-slope, but relatively minor carbonate deposition if sealevel is below the shelf break (lowstand shelf wedge). In an isolated evaporite basin large volumes of basinwide evaporites can accumulate as a lowstand systems tract. In a transgressive systems tract carbonate sedimentation in a humid setting reaches its highest growth potential. If a transgressive systems tract is also subject to a higher order fall that isolates a seepage depression on the shelf, then thick sequences of platform evaporites can form. In a highstand systems tract only thin mudflat evaporite units can form, while thick sequences of platform clastics and carbonates can accumulate. See text for full discussion of this figure.

Oligocene), marine stratal packages consist of much thicker unconformity-bound sequences (50 m to hundreds of metres thick) deposited as third order cycles made up of fourth-fifth order parasequences that are 1 to 10 metres thick.

Marine-margin platform evaporites

Marine carbonate platform systems show a different set of depositional responses to sealevel change compared with siliciclastics (Figure 5.37). This is because almost all marine carbonate is ultimately biogenic. Unlike siliciclastic shelves (Figure 5.37a-c), carbonate shelves most actively aggrade and then prograde both seaward and landward during times when the continental margin and interior is covered by shallow seas. That is, those most rapidly growing parts of any epicontinental platform, usually the reef crest and associated grainstone belts, aggrade most rapidly when part of a transgressive systems tract (Figure 5.37e). In contrast, the marine carbonate platform progrades most rapidly when part of a highstand systems tract (Figure 5.37f). When part of a lowstand systems tract, the much more restricted area of the “carbonate factory” means little or no growth can take place in either deep or shallow water, karstification of exposed platform sediments dominates at the sequence boundary on the platform (Figure 5.37d).

Unlike siliciclastics, carbonate sedimentation rates cannot be assumed to be near-constant across a platform. The variation in unit thickness reflects the strong environmental controls imposed on biogenic sedimentation rates. Thus, changes in geometric stacking patterns in carbonates do not necessarily directly reflect changes in the rates of relative sealevel rise as environmental changes are not always directly linked to changes in sealevel, but may reflect differing rates of deposition due to differing biotal growth rates across the platform (James and Kendall, 1992; Hunt and Tucker, 1992).

In a marine carbonate system the TST is the time when the maximum growth potential of the carbonate platform is realised and the parts of the open marine platform with the greatest growth potential typically aggrade to sealevel and then begin to prograde both seaward and into the lagoon (Figure 5.37e). In contrast, evaporite deposition occurs on a marine platform when a back-reef or lagoonal depression is isolated from a surface connection with the sea (Figure 5.37h). On a ramp, the barrier is usually a buildup of some sort of continuous zone Y shoal, on a rimmed shelf it is typically the reef belt or the associated grainstone/pisolite flat that have built up to sealevel.

Hydrographic isolation across the barrier crest and the onset of thick platform evaporites are usually initiated by a slight fall

in sealevel, following a time of vertical aggradation (catch up) in the more rapidly growing parts of the carbonate platform; e.g. a fourth order fall superimposed on a third order rise in greenhouse mode. Thick platform evaporites are most likely to form as part of a transgressive systems tract (third order) in a greenhouse earth. Any slight fall in sealevel will be marked by an unconformity across the topographic high (rim/shoal), which isolates the marine from the evaporite-depositing areas (Figure 5.37h). Thinner evaporative mudflat (sabkha/salina) units may form as part of a highstand systems tract where ongoing progradation of the shelf (keep up) isolates small depressions further landward (Figure 5.37i).

When platform evaporites were deposited, the subaerial isolation either of the rim/grainstone buildups on a rimmed shelf or of the zone Y shoal facies on a ramp were responsible for the restriction of the lagoon to the point where evaporites could accumulate (Figure 5.28; Lucia, 1972). Otherwise, like the carbonate shoals and reefs on platforms of today, subaqueous conditions behind the shelf rim or shoal would have never become saline enough to deposit subaqueous evaporites and only thin capillary zone sabkha caps (< 1m thick) could prograde across the landward feather edge of marine lagoon sediments. Prior to hydrographic isolation, normal marine to restricted marine sediments had been accumulating in the lagoon, so that in a vertical profile normal marine bioturbated shelf wackestones and mudstones typically underlie bedded platform evaporites. In sequence stratigraphic terms, episodes when platform evaporites accumulate correlate to karstic exposure surfaces or bounding surfaces on the platform crest. But, as it occurs in greenhouse eustasy, 4th-order sealevel did not fall more than a few metres, so it is a type 2 sequence boundary. In contrast all basinwide deposits are defined by type 1 sequence boundaries (in truth, applying marine seashore terminology to a hydrographically isolated and drawdown basin is probably wrong usage, or at least inappropriate).

Once an evaporite lagoon on the platform is hydrographically isolated from the open ocean, two end members can be deposited behind the rim; either saltern sequences or mudflat-dominated successions (Figure 5.7). The dominance of one or the other reflects the response of evaporite drawdown hydrology to changes in relative sealevel on the platform. An evaporitic mudflat mosaic forms when there is intense evaporation and relatively slow rates of marine seepage recharge and longterm surface brine cover is relatively rare. Mudflat fills dominate if there is little difference in elevation between the sealevel on the other side of the exposed barrier crest and the floor of evaporitic depression. Sediments of the rim /shoal (oolite/grainstone/pisolite/boundstone) pass directly upward into thin

intercalated sabkha/salina units or stacked sabkha cycles and back to shoal facies that make up the base of the next cycle, with no intervening saltern sequences.

Saltern fills tend to dominate evaporites of the lagoon fill when evaporation is less intense and/or there is a greater rate of seepage replenishment through the isolating barrier. Salterns are more common if there is a greater potentiometric head across the barrier between ambient sealevel and the water surface in the lagoon. This tends to occur when the platform lagoon was deeper at the time of its isolation. This happens during a transgression in settings where the rim/shoal aggrades relatively rapidly, while the backshoal platform does not keep pace with the same rise in sealevel. Early shoalwater carbonates deposited on the lagoonal side of the rim are not all that different from those on the seaward side of the rim. This is especially true where the rim is incipiently drowned at the onset of the transgression. While the rim was growing and catching up to a new, higher sealevel the waters in the lagoon could freely exchange with the open ocean and so a diverse open-marine biota flourished within the lagoon.

When a rim reef or shoal catches up to the new higher sealevel and coalesces into an isolating barrier, conditions in the carbonate-accumulating epeiric lagoon become more restricted. As the exchange with open ocean waters is reduced; sediments are now deposited as restricted-marine carbonates. With complete restriction across the rim or shoal, the lagoonal waters become sufficiently saline to deposit evaporites and fill the drawdown lagoon with a shoaling-upward saltern cycle, perhaps capped by a mudflat sequence. The saltern evaporite unit is as thick as the lagoon was deep at the inception of evaporite deposition (Figures 5.7a, 5.37h).

Such subaqueous saltern beds tend to be widespread across the evaporite lagoon and so are easily correlated from well to well as metre- to decametre-thick clean evaporites. The ten or so subaqueous cycles of the Cretaceous Ferry Lake Anhydrite in the northern Gulf of Mexico region (Figure 5.20a; Pittman, 1985) and the Permian San Andres cycles on the northern margin of the Delaware Basin (Elliott and Warren, 1989) are examples of stacked saltern beds, while the base of the Late Permian Seven Rivers Formation atop Yates Field on the Central Basin Platform in west Texas is an example of the stacked mudflat mosaic (Figure 10.38). The geology and reservoir/seal properties of these units is detailed in Chapter 10.

Unlike bedded carbonates and siliciclastics, the effects of syndepositional and later evaporite dissolution can greatly complicate any attempt at high-resolution stratigraphic in-

terpretation in an evaporitic platform. Dissolution typically occurs as the subsiding platform evaporite passes from an active phreatic hypersaline hydrology into a compactional or thermobaric regime. This creates thin dissolution breccias and residue layers that extend over large portions of the platform (Chapter 7). Such breccias can be confused with subaerial exposure surfaces and humid/temperate phreatic karst. Unless the significance of evaporite dissolution breccias and the timing of dissolution in relation to burial is recognised, whole episodes of platform isolation may be miscorrelated. Many published outcrop-based studies of high-resolution stratigraphy in carbonate-evaporite platforms are problematic because dissolution breccias, which tend to be thin and recessive, are largely unrecognised or, if recognised, misinterpreted as marine flooding surfaces. And yet, a one-metre thick breccia may mark the position of a former 100m thick salt bed. This is especially true in Precambrian platforms where biostratigraphic checks on correlation are not possible.

Platform evaporites in a greenhouse earth?

The high amplitude rapid to-and-fro of the icehouse sea across Neogene platforms has discouraged the deposition of extensive shallow water platform evaporites. The most recent time of extensive platform evaporites is perhaps the Eocene in the Middle East, centred on Iraq and Iran or the Paleocene of North Africa (Table 5.5). Platform evaporites tend to form under greenhouse earth conditions characterised by lower amplitude sealevel fluctuations and higher world sealevel with marine waters over large parts of the continental masses (epeiric seaways). The high-amplitude high-frequency sealevel changes of icehouse earth encourage local high-relief “catch-up” reefs and banks due to ongoing rapid flooding and exposure of the platform, along with substantial unconformities and pervasive meteoric diagenesis deep in the reefs. Hence icehouse carbonate facies show considerable lateral thickness variations (Read and Horbury, 1993). Throughout the Quaternary there has never been sufficient time for shelf edge reefs and sand belts to grow and accrete into a single continuous shelf margin facies belt similar to those that characterise greenhouse time. Before it can happen, icehouse sealevel falls off the shelf edge every 100,000 years or so.

Thus, platform reefs and shoals typically do not develop into laterally continuous strike-parallel belts under an icehouse scenario. Converting large areas of periplatform lagoons into isolated depressions with marine-seepage hydrologies suitable for precipitating evaporites simply does not happen. The only place where marine-fed isolated seepage depressions can occur

in today's icehouse scenario is in narrow sea-marginal highstand bands, as evidenced by numerous small scale sabkhas and salinas along the marine coasts of many arid areas (Chapters 3 and 4). Sealevel repeatedly falls off the platform in icehouse earth mode (>100m fall; type 1 boundaries) and so any local areas of sea-marginal peritidal or seepage evaporites that may have formed in a highstand are subject to widespread dissolution via vadose flushing, as is seen in the worldwide lack of well preserved Pleistocene marine sabkhat and salinas (Warren, 1991). Even in the hyperarid coastal zone of the Red Sea, only small isolated remnants of marine-fed evaporites from the last 100 ka sealevel high remain and none remain from the previous 200 ka high (Figure 4.15). Thus, modern highstand marine-edge evaporites are small in scale and have little or no longterm preservation potential.

In contrast, the low amplitude low frequency sealevel oscillations that characterise epeiric seaways and shelves in greenhouse earth intervals favour the formation of stable, large, highly restricted, at times evaporitic, depressions on the inner shelf portions of many marine platforms. Sea levels were high and covered more of the craton. Carbonate platform rims had growth potentials that could more than keep pace with the low amplitude fourth order sealevel fluctuations. Wide, flat carbonate platforms with huge back-platform lagoons were commonplace (epeiric seas). A slight fall in sealevel meant seepage waters easily ponded in isolated large shallow shelf depressions behind continuous, now subaerially exposed reef or shoal rims. In areas where epeiric seaways covered large inland portions of the continental interior, the formation of a tectonic or shelf rim barrier followed by a fall in sealevel meant that the entire platform interiors and intracratonic sag basins could become evaporitic.

Thus, stacked platform evaporites tend to form in epeiric and pericontinental seas in greenhouse times as rapidly deposited, but extensive, saltern and mudflat beds precipitated atop marine lagoon sediments. They were part of an overall TST, but only precipitated during short intervals characterised by higher-order low amplitude falls in sealevel. At such times the platform crest was subaerial and much of the platform was brine saturated. Today there are no substantial epeiric seaways and the isolating effects of slight sealevel falls, as well as any possibility of accreting an ongoing laterally continuous carbonate platform rim, are swamped by the overriding influence of rapid, high-amplitude, icesheet-induced 4th order sealevel changes moving across relatively narrow and steeper continental shelves. Conditions suitable for the formation of platform evaporites simply do not exist under today's icehouse eustatic regime.

Basinwide evaporites

Thick basin-filling evaporites (more than 500-1,000 m thick and hundreds of kilometres across) accumulated in both greenhouse and icehouse periods. They did so, not because of fluctuations in sealevel, but as a result of tectonic isolation of large parts of the earth's surface from the direct surface influx of the world's ocean waters. Fills tend to be autocyclic and tectonically induced, although subsequent fluctuations in sealevel may have aided erosional breaching and refilling of the depression by seawater episodes (Table 5.6; Figure 5.27). Once isolated, changes in sealevel outside the basin rim may change potentiometric head with respect to the free brine surface in the basin and so drive changes in the rate of supply of brine. A relatively high sealevel outside of the basin will create a steeper potentiometric gradient and hence encourage more rapid replenishment of brine and a greater volume of brine seeping through the permeable barriers that separate the brine depression from the open ocean (e.g. Kendall, 1992). When relative sealevel is lower, this decreases the potentiometric gradient and slows the rate of brine flow. A fall in sealevel also causes the sea coast to retreat from the isolated depression, which further decreases sea water supply.

But autocyclic mechanisms, including the vagaries of climate, tectonics and adiabatic effects, along with the rate of formation and efficiency of intrabasin brine curtains or hydroseals, all interact to swamp the influence of sealevel changes to the hydrology of the evaporite basin (Chapter 2). For example, the aggradational infill of a tectonic depression by salt beds that create their own underlying aquitard or brine curtain has the same effect as the change in sealevel on potentiometric gradient of the inflow. As the sequence aggrades it decreases the potentiometric gradient and so slows the rate of marine recharge independent of changes in absolute sealevel.

The effect was noted by Warren (1982b) and used to explain the changes in the infill cycle textures in Holocene gypsum-filled salinas in coastal southern Australia. Logan (1987) discusses similar hydrological transitions in controlling vertical sequences and the transition from halite to gypsum with aggradation in Holocene Lake MacLeod, Western Australia. Kendall (1989) used such Holocene analogues to interpret the upward transition from anhydrites to carbonates in the Middle Devonian of northern Alberta (Muskeg and Sulphur Point Formations). Previously the transition was interpreted as reflecting a sealevel rise, but Kendall argued it would more likely reflect a transition related to sealevel fall outside of the basin and a decreasing volume of marine inflow into a marine-

fed basin with no surface connection to the ocean. His model better explains the terminal nonmarine bed that makes up the overlying Watt Mountain unit.

In summary, unless a rise in sealevel breaches the tectonic sill and converts the basin once more to a restricted mesohaline sea-way, decametre-scale sealevel fluctuations outside the isolated basin exert a relatively minor influence on basinwide hydrology and hence on the detailed stratigraphy of a basinwide evaporite unit. While the basin is isolated much of the fill is autocyclic, it reflects changes in the hydrological base level that have more to do with fluctuations in tectonics and climate as they effect inflow/seepage hydrology. In the larger saline giants, such as the Messinian sequences of the Mediterranean and the Zechstein of NW Europe, any changes in relative sealevel that occurred outside the drawdown evaporite basin and probably across a barrier that was hundreds of kilometres from the drawdown strandline were largely irrelevant to the style and geometries of evaporite deposition in the basin.

Basinwide sequence stratigraphy?

Given our rudimentary understanding of hydrology and isolation in basinwide settings, let us now look at some of the implications in terms of high-resolution stratigraphic analysis in basinwide evaporite deposits. Documented examples are few and far between, and tend to concentrate on patterns in the mesohaline to marine carbonate facies. High resolution interpretation of any intercalated thick salt beds is more challenging because:

- Outcrop studies of geometries of evaporite units are near useless as most of the evaporite is dissolved well before it approaches the land surface - differential collapse and flow during dissolution means detailed internal relationships and depositional geometries are lost not just at outcrop but also in the shallow subsurface,
- Seismic analysis tied to well data in bedded saline giants is rarely undertaken because very few oil companies wish to characterise the internal stratigraphy of what is an undeniable seal facies,
- Deeply buried thick basinwide salt sequences are subject to flow into diapiric and other structures - this largely destroys the stratigraphic integrity of internal reflectors in halokinetic parts of the basin and the onset of flow can be very early, even synprecipitational (see Chapter 6).

All authors working on basinwide systems (aka basin-centre and saline giants) agree that they are lowstand deposits (Kendall, 1988; Strohmenger et al, 1996a, b; Tucker 1991;

Warren, 1999; Sarg, 2001). Kendall (1988) and Warren (1999) attempt to address the principles of sequence stratigraphy in terms of the isolated hydrological framework and the need to precipitate widespread and thick salt sequences. Others consider that basinwides require a reduced connection to the world's oceans, yet others allow intrabasinal marine carbonates to be possible syndepositional sediments with basinwide evaporites. The latter expresses a blissful ignorance of the fundamentals of hydrology and hydrography seen in sediment textures and distributions in all modern evaporite basins.

Tucker derives two end member models to interpret the evaporite carbonate relationships in saline giants: Model 1, incomplete drawdown with marginal gypsum wedges and basinal laminated gypsum; and Model 2, complete drawdown with halite basin-fills. However, his hydrological constraints are not clearly stated and his hydrological assumption that marginal gypsum wedges typically form in relation to a lowered sealevel without isolation (his Figure 2) is probably not correct (see Goodall et al., 1992).

Figure 5.38 assimilates some of the concepts of Tucker (1991) as well as the work of Kendall (1988) and my own work. It is a preliminary attempt to place basinwide evaporite geometries and overall basin fills into a sequence stratigraphic context. Unlike Tucker (1991) it is based on the notion that in an isolated basin the drawdown hydrology is largely independent of decametre scale sealevel fluctuations that are going on outside the basin. Most of the internal decametre-scale evaporite geometries in a saline giant are autocyclic, while larger scale geometries reflect ongoing interactions between tectonics and climate. Only if and when the basin is connected at the surface to the world's oceans do the geometries of the carbonate units reflect a marine eustatic control and by then basinwide evaporites are not accumulating.

In the time prior to the onset of hydrographic isolation the basin has a surface connection to the world's ocean (Figure 5.38a). The depositional response at this time is a classic marine carbonate response and the only widespread evaporites that precipitate are typical marine-margin saltern/mudflat evaporites that are intercalated with normal marine platform sediments (see Figures 5.7a and 5.37 for interpretations of this style). Pinnacle reefs and mud mounds may grow on the shelf foreslope during the marine TST (e.g. right-hand part of Figure 5.38a). In the basin centre, thin (condensed) pelagic deepwater carbonates and hemipelagic mudrocks will be deposited, mostly as thin finely-laminated units that pass laterally into slope deposits about the basin edge.

Once sealevel falls below the sill height — either through a eustatic change in sealevel or, more likely, through regional tectonic movement that cuts off the basin from a surface connection with the world’s oceans — evaporative drawdown will

quickly lower the brine level in the evaporite basin to where it is well below the old carbonate shelf break (Figure 5.38b). Under an arid climate, water within the now isolated basin will rapidly become hypersaline. Seawater, along with formation,

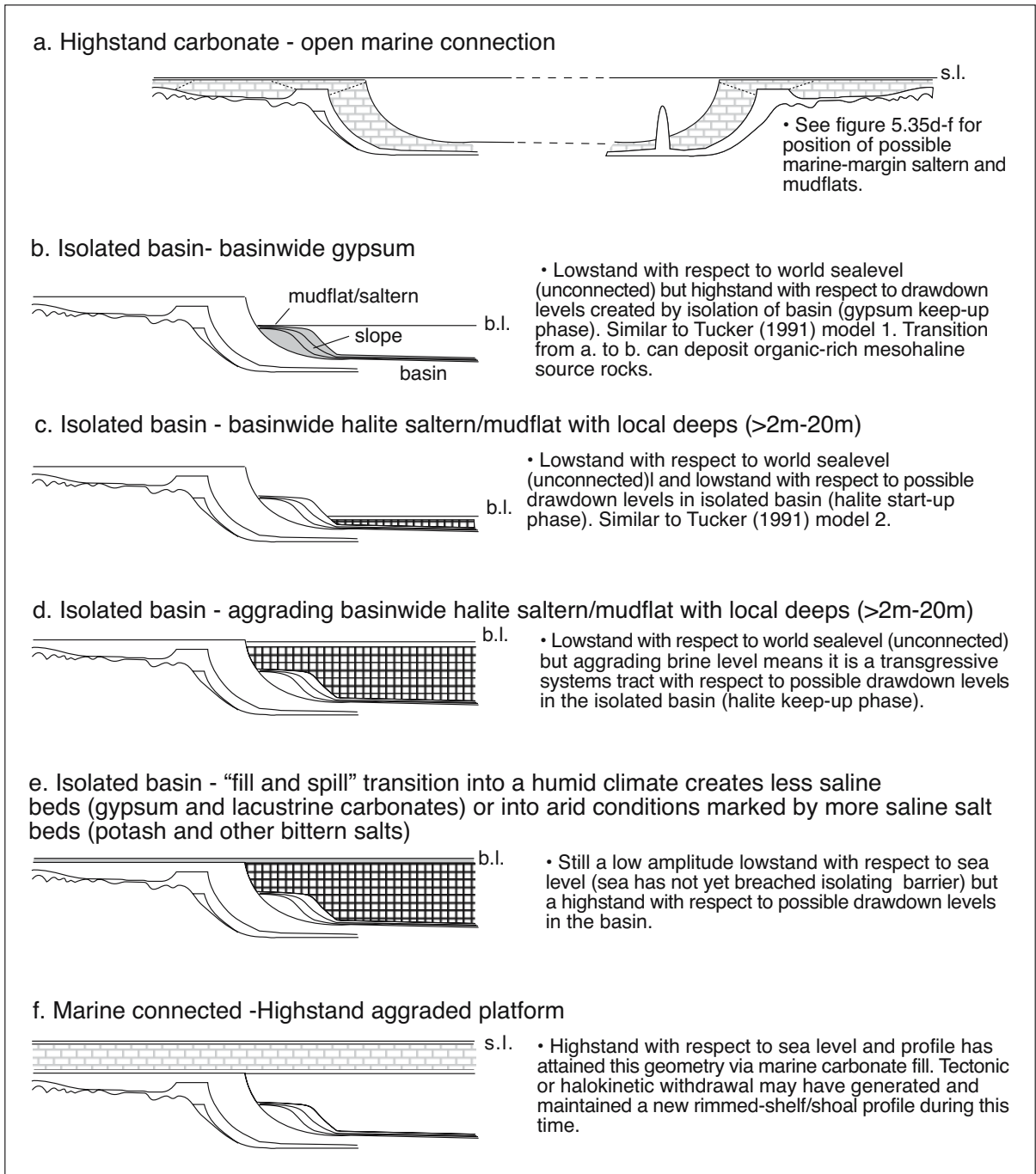


Figure 5.38. Sequence stratigraphic model for basinwide evaporite deposition in a basin undergoing complete isolation from a surface connection to the world’s oceans and subsequent drawdown.

continental, and hydrothermal waters, now seeps into the depression. It enters through permeable, now subaerially exposed, formerly deepwater carbonate slopes and former pinnacle reefs. These outflow zones generate spring and tufa deposits with characteristic textures such as pisolites, tepees, tufas and stromatolites. In the relatively deep subaqueous basin centre, organic-rich mesohaline carbonate laminites typically mark the onset of basin isolation and continue to form until the basin is hydrographically isolated and equilibrium is reached.

If hydrological equilibrium is reached at gypsum saturation then gypsum has the potential to accumulate across the whole basin. When the water column is meromictic coarsely crystalline zig-zag or laminated gypsum forms best in the “chemical factory” of the shallow basin edge while detrital and pelagic laminites accumulate in the basin centre (Figure 5.38b). If the basin does not subside greatly as it becomes isolated, the level of this new gypsum wedge (platform) will first form atop old slope carbonates and below the old carbonate shelf break. With respect to sealevel outside the isolated basin this is a lowstand deposit associated with the creation of a karstic type 1 boundary on the old carbonate shelf prism in areas about the basin edge not covered by brine. But, with respect to the subsequent drawdown hydrology of the basin, it is a highstand system tract.

Resedimentation of the saltern/mudflat sediments of the gypsum wedge into deeper density-stratified waters by storms, slope failures, debris flows and turbidity currents will deposit graded beds, slumps and breccias as gypsum slope deposits and fine-grained “rain-from-heaven” gypsum laminites in the basin centre. At times when the brine column is holomictic, coarse-crystalline gypsum can perhaps accumulate across the deeper basin floor (there are no Holocene analogs for deepwater gypsum, but there are for halite and mirabilite).

If this situation of gypsum saturation is hydrologically stable, that is hydrological inflow balances outflow at gypsum-precipitating salinities, and the situation is maintained for time frames $\approx 10^5$ years or more, the whole basin evaporite fill may be composed of gypsum. Such was the case during precipitation of large portions of the Permian Castile Formation of Texas (Chapter 1). Metre-scale sedimentary cycles (parasequences) will be developed within the prograding gypsum wedge reflecting higher-frequency low-amplitude (5th-6th-order, i.e. $10^4/10^3$ year) autocyclic brine-level changes within the basin (Figure 1.24).

If hydrological equilibrium is still not maintained in the basin, and brine losses continue to exceed inflows, the brine level

will continue to be drawn down and the salinity of the residual brine will increase. Saltern gypsum will begin to precipitate in the basin centre if the brine depth drops below 10-30 m. If a hydrological balance is still not reached and the brine level continues to fall, the brine body next reaches halite saturation (Figure 5.38c). Based on most Holocene analogues (except the current Dead Sea) water depths at the onset of halite deposition are less than a few tens-of-metres to metres and saltern or pan halite will be deposited across the whole basin floor. If the waters are density stratified then locally there may be deeper-water depressions on the basin floor that fill with fine-grained laminated “salt-and-pepper-textured” deepwater halite cumulates lacking any evidence of subaerial exposure (this requires brine depths of 2 metres or more, if Lake MacLeod and the artificial halite pans of the southern Dead Sea Basin are used as textural analogues; Warren, 1991). If the brine column is holomictic then beds of coarsely-crystalline randomly-oriented inclusion-free halite meshworks will accumulate, rather than fine-grained halite or gypsum cumulates. This stage of the sedimentation is still a lowstand with respect to sealevel outside the basin, and is now a lowstand systems tract with respect to the basin hydrology. If the analog of the deep water fill of the Dead Sea is used as an analog then the deeper parts of an ancient basinwide evaporite fill will be composed of beds of coarse-crystalline halite meshworks interlayered with carbonate-gypsum or halite laminites.

Once thick pan halite units begin to accumulate across the basin floor, the degree of permeability loss in salts below the precipitation surface increases drastically, reflecting a near complete loss of porosity in metre-decametre thick halite beds. The brine curtain and its cement aquitard can now support a permanent halite-saturated brine body. This can maintain a near permanent position atop the primary crystallisation surface with only occasional episodes of complete desiccation or flood-induced surface freshening. Thus the halite body begins to aggrade as a series of subaqueous metre-thick autocyclic parasequences, with each metres-thick cycle deposited in time frames of 10^2 - 10^3 years. The maintenance of this aggrading hydrology allows the basin to fill with predominantly saltern halite (Figure 5.38d).

With respect to sealevel outside the isolated basin it is still a lowstand system, but in terms of the intrabasin geometries it is a transgressive systems tract. But it is a transgressive systems tract that has no parallel in the marine realm. It is an autocyclic transgression that aggrades as it maintains and grows its own near impervious base soaked in a saturated brine curtain that is maintained by slowly refluxing brines. There is no suitable eustatic term in the classic sequence stratigraphic literature to

describe this, as there is no concept of autocyclic transgression where the sedimentation surface creates the stabilising hydrology that in turn facilitates the rise of the sedimentation surface. Tucker (1991) terms this unit the lowstand basin-fill-halite; I am more comfortable calling it an intrabasinal transgressive systems tract halite.

As the halite fill continues to aggrade it climbs over the old gypsum wedge and, if the basin is subsiding but still isolated, it can also climb over the old gypsum and then the carbonate shelf margin (Figure 5.38e). As the fill tops an older platform margin it reaches a vast flat karst-etched plain. Before being retained the permanent basin waters must now spread over a much wider area of an older platform top. I call this the “fill and spill” stage of the basin’s sedimentation and hydrology. It is still a lowstand systems tract with respect to external sealevel and the marine groundwater feed, but a transgressive systems tract with respect to intrabasin geometries. It is typically a mudflat system, although salterns may still occur. The fill and spill point horizon is often marked by a change in mineralogy, which indicates a change in depositional hydrology.

In a semi-arid system this spill point is often defined by beds of less saline evaporite minerals such as gypsum or lacustrine carbonates. Rainfall and meteoric influx are an increasingly important part of the ponded surface water volume as they spread outside the former less aerially extensive depression. In contrast, if fill and spill occurs in a very arid setting, the effect of meteoric freshening is minimal and as the piezometric head is less than at the onset of evaporite deposition in the drawdown basin. Surface brines are less diluted and the hydrology may pass into bittern saturation so that syndepositional bittern or potash salts are possible precipitates. A hydrological transition to “fill and spill” under a hyperarid scenario explains why the potash cycles in the Salado Formation of the Delaware Basin are largely confined to regions in the vicinity of the old carbonate platform margin (Figure 11.18a).

Once again the transition is autocyclic and dependent on climate within the basin. The system is still a lowstand with respect to sealevel outside the basin. In terms of the intrabasin geometry it is a transgressive systems tract either atop the older HST gypsum wedge or atop the former HST of the older carbonate margin. Tucker (1991) also recognises this TST (his early TST gypsum or TST retrogradational sabkha evaporite lagoons), but he only allows for a CaSO_4 mineralogy and he relates it to a surface reconnection with the world’s oceans. Unlike Tucker (1991), I feel that this widespread thin unit is deposited subsealevel in a still isolated basin where surface reconnection to the ocean

has yet to occur. I also emphasise that this TST is not always gypsum/anhydrite, it can be composed of a multiplicity of mineralogies depending on the degree of climatic restriction in the basin. Kendall (1992; his Figure 40) also recognises this stage, but he relates the mineralogical transition to less saline minerals to a transgression beyond a hydroseal or basal aquitard, that allows greater volumes of brine to be lost from the system, and so average salinities in the surface brines are lowered. This is a valid concept, but it is not complete as it does not explain why some basins are actually precipitating more hypersaline minerals and bittern salts in the upper parts of the halite basin fill.

Once the basin is reconnected to the open ocean, the formerly exposed carbonate platforms are reflooded and a carbonate TST re-established. In this scenario any subsequent platform evaporite deposits can be considered equivalent to the marine marginal platform evaporites discussed in the preceding section and their internal geometries behind the isolating platform rim or shoal may well once again reflect eustatic controls (Figure 5.38f). Because the aggraded evaporite surface is a flat plain at the time of marine reflooding, the onset of marine carbonate deposition is typically characterised by ramp deposits. If the carbonate biota also contain appropriate binders and reef formers the profile quickly evolves into a rimmed carbonate shelf. The transition to a rimmed shelf in many ancient basins undergoing regional extension is typically focused by halokinetically induced shallowing of the seafloor driven by flow of the thick underlying halite (Chapter 6).

Basinwide examples

Three of the better documented areas where high resolution sequence analysis has been attempted on bedded basinwide evaporites are; 1) gypsum-halite evaporites of Messinian age in the marginal basins of the Mediterranean, 2) the basinwide anhydrite-halite evaporites of Permian Zechstein in NW Europe, and 3) the halite-dominated salt beds of the Silurian Salt of the Michigan Basin.

Messinian evaporites of the Mediterranean

In the icehouse world of Messinian evaporites in the Mediterranean, there are two styles of marine-fed evaporite deposition. One is characterised by high level, marginward circum-Mediterranean deposits, the other by a number of much larger, thicker, basin-centre deposits that now lie below more than 2,000 m of water and Plio-Pleistocene overburden (Hsu et al., 1973). There are excellent onshore exposures of the marginward Messinian

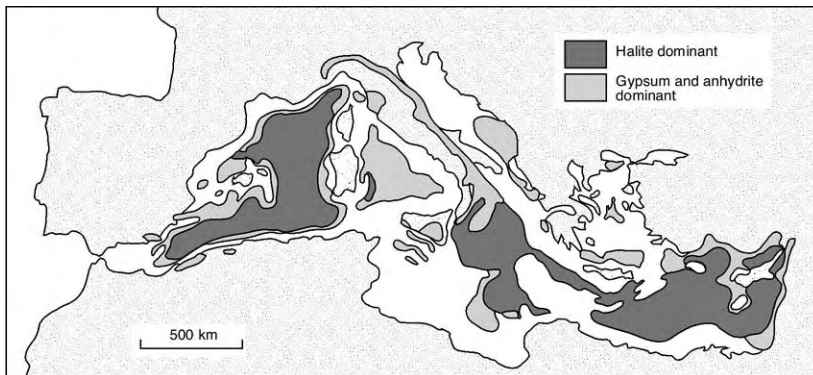


Figure 5.39. Distribution of basinwide Messinian evaporites, both onshore and offshore.

basins in Sicily, Spain and Cyprus (Figure 5.39, 5.40a). In contrast, in the various sub-basins in the deeper parts of the Mediterranean Sea, where seismic lines show thick sequences of salts deposited during times of maximum drawdown, there has been little core sampling and so there is little reliable facies interpretation based on rock samples. DSDP (Deep Sea Drilling Project) wells that did manage to recover salts sampled a combination of salt pan halite and sabkha anhydrite, showing that the salts accumulated on a basin bottom that was covered with brine lakes, which at times dried up to accumulate pan halite (Hsu et al., 1973). While not questioning the hydrographic isolation of the Mediterranean during the Messinian, Hardie and Lowenstein (2004) have questioned the notion of complete desiccation and rather argue for a sub-wave subaqueous origin to much of the evaporite recovered in the DSDP cores.

Aside from this textural evidence for drawdown precipitation in the few deepsea cores recovered from more basin-centre positions in the Mediterranean, there is also evidence for Late Miocene drawdown in the strata and unconformities surrounding the main salt beds. Drawdown to an erosional base level, that at times in the Messinian was 1-2 km below sealevel, created the widespread “M” reflector, a seismic indicator of subaerial exposure about much of the Mediterranean margin. Drawdown also deepened the thalwegs of many major rivers draining into the Late Miocene Mediterranean depression. Wells in the Nile Delta at the eastern end of the Mediterranean, which are more than 300m (1000 feet) deep and enter Messinian strata, do not reach the bottom of Nile canyon (Aal et al., 2001). Said (1993) shows the Messinian incision of the Nile thalweg reached a depth of 170 m at Aswan, 800 m at Assuit and more than 2500 m immediately north of Cairo. Similar deep Late Miocene channels occur at the western end of the Mediterranean in Libya, Algeria, Israel and Syria (Griffin, 2002). Likewise the thalweg

of the northern end of the Rhone River gorge was cut deeply into its granite basement in the Late Miocene and is now filled with marine sediments. For the same reason, some of the deepest karst in the world formed in Yugoslavian (Montenegrin) carbonate hosts during this time of maximum drawdown, with some caves now more than 900 metres deep.

Assuming a surface marine connection to the Atlantic immediately prior to the time of evaporite precipitation, Krijgsman et al. (1999, 2002) argued

that the onset of the Messinian salinity crisis was synchronous over the entire Mediterranean basin, dated at 5.96 +/- 0.02 million years ago (Figure 5.40a). They argue that isolation from the Atlantic Ocean was established between 5.59 and 5.33 million years ago, causing a large fall in Mediterranean water level, followed by circum-Mediterranean erosion and basinwide evaporites (5.59-5.50 million years ago) and in turn followed by deposition (5.50-5.33 million years ago) of nonmarine sediments in a large ‘Lago Mare’ (Lake Sea) basin immediately prior to surface reconnection with the world’s ocean (a likely example of “fill and spill” sedimentation).

Once hydrographically isolated, the cyclic evaporite deposition in the various Messinian basins can be almost entirely related to circum-Mediterranean climate changes driven by changes in the earth’s precession, and not to obliquity-induced glacio-eustatic sealevel changes. Krijgsman et al. argue in favour of a dominantly tectonic origin for the Messinian salinity crisis, although its exact timing of some of its parasequence boundaries may well have been controlled by the \approx 40-kyr component of the Earth’s eccentricity.

Others argue for a somewhat later onset of the salinity crisis (\approx 5.6 Ma) and that rather than a time synchronous deposition of Messinian evaporites throughout the Mediterranean there were two time-separate styles of evaporite deposition (Figure 5.40a): 1) marginward areas around the periphery of the Mediterranean, versus 2) more basinal or central regions (Clauzon et al., 1996; Butler et al., 1995). Yet others argue that within a framework of basin isolation the exact time of onset of evaporite accumulation in the various marginal sub-basins may not be time synchronous around the margin of the Mediterranean and that evaporite sequences in some marginal basins may postdate the main unconformity (Riding et al., 1999).

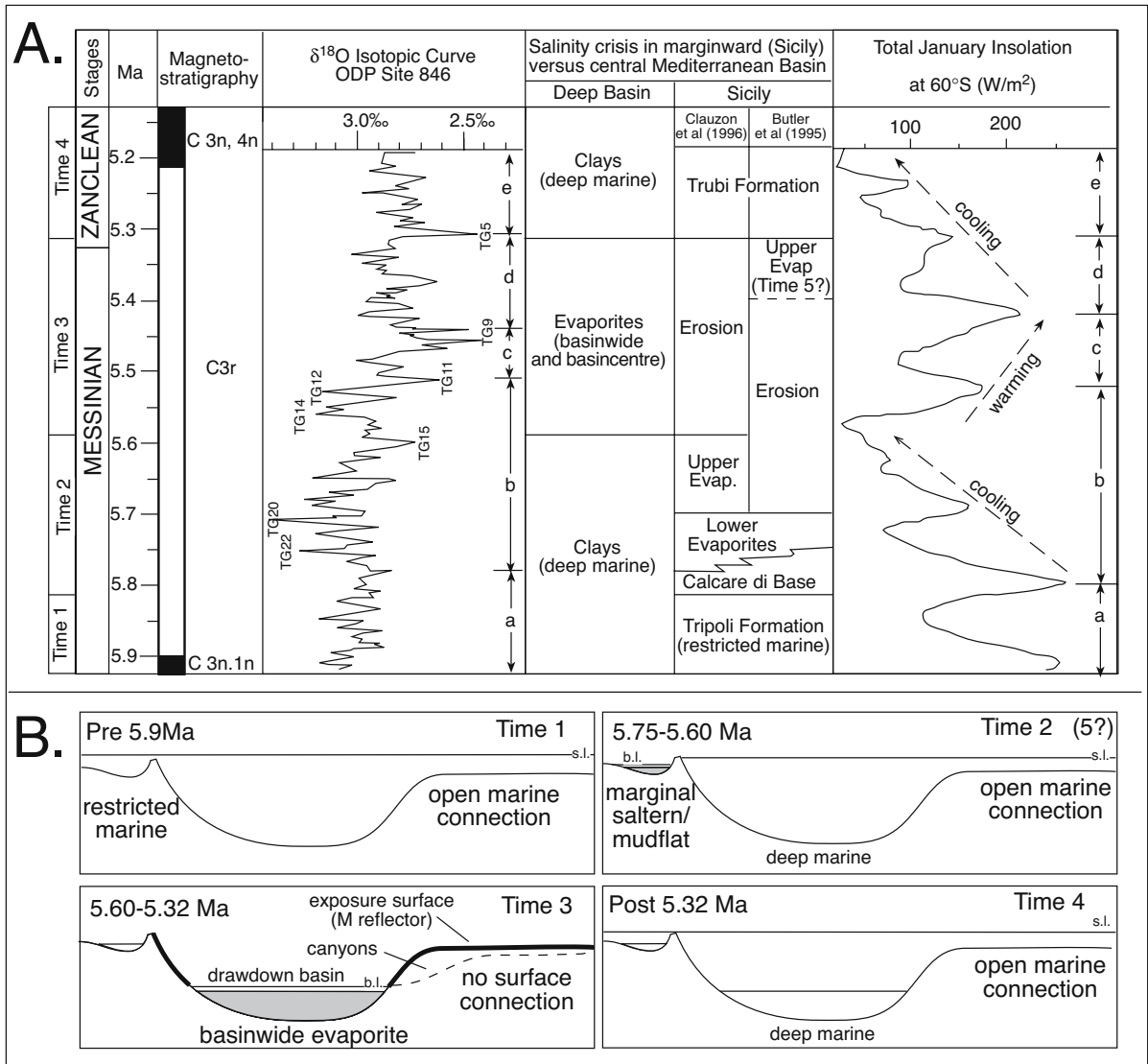


Figure 5.40. Messinian salinity crisis in the Mediterranean. A) Plot of $\delta^{18}\text{O}$ of equatorial Pacific tied to magnetostratigraphy, Messinian stratigraphy and modeled January insolation for that time frame (modified after Clauzon et al. (1996) and Butler et al. (1995)). Note the difference in interpretation of the upper evaporite in Sicily. B) Schematic times sequence showing mode of formation of marginal and basinwide evaporites in the Mediterranean. Note that the interpretation of Butler et al. (1995) requires a time 5.

The diachroneity between the basin margin and basin centre Messinian evaporites can be deduced from the stratigraphic relationships linking the evaporites in the marginal basins to the major Messinian erosional surface (M-reflector) that surrounds the basin centre evaporites. During the first phase of isolation and local drawdown (from 5.75 to 5.60 Ma), the deposition of evaporites took place in Spain and Sicily and other marginward areas in response to a modest sealevel fall in various tectonically isolated (compressional fold belts)

subsealevel basins. In the second interval (from 5.60 to 5.33 Ma), more central parts of the Mediterranean basin became isolated and deposition largely ceased in the marginal basins (Figure 5.40b; Clauzon et al., 1996).

The stratigraphy in marginal basins of the Mediterranean Ridges, Sicily and some of the other Messinian basins, such as Crete and Cyprus, was defined by mineralogies evolving separately in a series of rising “piggy-back” foreland basins,

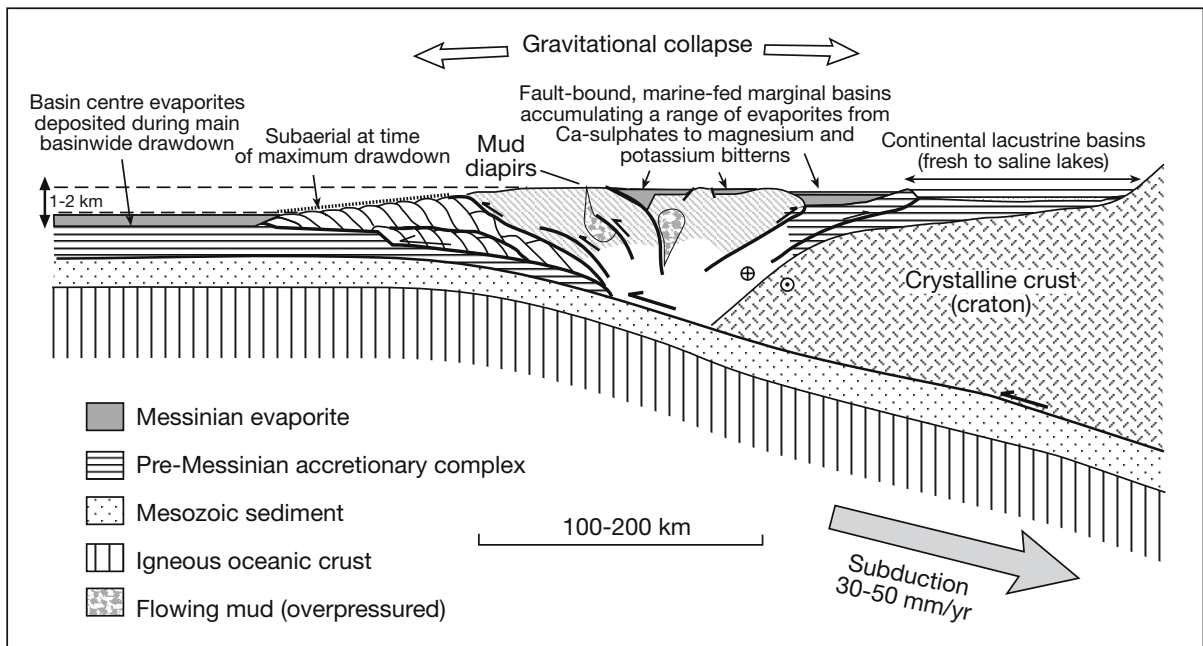


Figure 5.41. Schematic shows tectonism related distribution of continental, marine margin and basin centre lacustrine evaporites around the time of closure of the Mediterranean basin and the Late Miocene salinity crisis. Schematic is constructed based on geology of the Mediterranean Ridges, Sicily and the Italian Peninsula (in part after Westbrook and Reston, 2002).

created during thrusting-related uplift that was active in the Messinian and continues today (Figure 5.41; Westbrook and Reston, 2002). In many marginal basins, such as in Cyprus, the changes in the level of drawdown were related to ongoing transcurrent faulting and rifting. Much of the tectonic drive creating the evaporite fill in the various marginal basins, prior to the main drawdown, was a result of the collision of Africa with Eurasia, which ultimately drove the closure of the surface connection to the Atlantic and ultimately caused the whole Late Miocene Mediterranean deep basin floor to become isolated and evaporitic.

According to Clauzon et al. (1996) the first major evaporite-depositing episode (5.75-5.60 Ma) took place during a cooling period associated with a weak global sealevel fall that isolated numerous tectonically induced circum-Mediterranean marginal basins in Spain, Libya, Morocco, the Apennines, Sicily, and Cyprus. Isolation of these marginal basins occurred while the adjacent Mediterranean Sea still retained a direct surface connection with the Atlantic (Time 2; Figure 5.40b). The next period of evaporite deposition (5.60-5.33 Ma) occurred when the whole Mediterranean was isolated and basinwide evaporites were deposited in a series of giant evaporite sub-basins (hundreds to thousands of kilometres across) and now located beneath the present deep Mediterranean floor (Time 3; Figure 5.40b). Away from halokinetic areas, none of these

areas outcrop and only their uppermost portions have been sampled by a few wells in the DSDP programme. At the time they formed there was a huge drop of some 1500-2000 metres in water level, and widespread basin-centre marine-fed brine lakes of the Mediterranean were completely isolated from any surface connection with adjacent Atlantic or Tethyan remnants. The isolation was driven by the ongoing collision tectonics as Africa collided with Eurasia. At the time of the complete isolation of the Mediterranean Basin there was a worldwide warming trend and a likely global sealevel high, but tectonic isolation completely negated the effects of eustasy within the Mediterranean.

Even so, the onset of evaporite deposition in marginal basins was driven by a combination of eustasy and tectonics. The evaporite phase of the marginal basins was typically preceded by cyclic Late Miocene carbonate ramp or reef cycles; which are readily interpreted using the principles of high-resolution carbonate sequence stratigraphy (e.g. in Spain and Italy- Martin et al., 1996; Esteban, 1996; in Morocco- Benson et al., 1997; Cunningham et al., 1997). Post reef growth, the typical response of the marginward basins to isolation and the onset of basin drawdown was the accumulation of an evaporitic carbonate rim (aragonite/dolomite) about a drawdown bedded-gypsum saltern, with marine-fed bitterns accumulating in the most isolated portions of these subsealevel depressions. Such a

situation outcrops today as the Calcare di Base rim facies circumscribing the bedded salts of the dominantly gypsum saltern fill in the Sicilian Basin (Figure 5.42a). The Calcare di Base indicates the drawdown basin possessed a marine seepage connection to the Mediterranean Sea. The “in situ” occurrences of this dolomitic seepage unit are restricted to the margin of the Sicilian Basin and it has an isotopic signature that becomes increasingly heavy toward the sites of gypsum and halite precipitation (Figure 5.42b: Decima et al., 1988). Once any circum-Mediterranean marginward basin was isolated from a surface connection to the ocean, ongoing tectonics and autocyclic mechanisms controlled the chemistry, cyclicity and textural styles in the various evaporite basins. Stratigraphic relationships between reefs that define the edges of the basin and consequent subaqueous carbonate/gypsum/ halite that then filled these marginal basins are clearly time separate events (Figure 5.42b).

The depocentres of the marginal basins in Sicily are in synclines related to underlying thrust structures of the frontal part of the Maghreian chain (Figure 5.43; Butler et al., 1995). Prior to hydrographic isolation from the Mediterranean seawater, these basins were hydrodynamically linked through the thrust foredeeps to world sealevel. Thus Late Miocene reef and ramp precursors in the various Sicilian basins were linked eustatically. Initial isolation and drawdown of the Mediterranean base level is marked across the thrust belt by first cycle evaporitic carbonates and evaporites on the structural highs and lows, respectively. Vast accumulations of halite and potassium salts (up to 1200 m thick) are restricted to growing thrust synclines. Salts were deposited once the subsealevel depressions were hydrographically isolated. At that time the different evaporite signatures were related to different water conditions, reflecting various continental and marine seepage plumes and circulations across various sub-basins (Butler et al., 1995). Internal cyclicity (parasequence scale) reflect high-frequency autocyclic

variations in brine level, and are not tied to marine eustacy. Thrusting provided accommodation space for evaporites and also controlled the groundwater pathways into the desiccating basins. In similar fashion Messinian sediments of the northern Marcean Apennines form part of a syn-orogenic foreland basin succession. They underwent shortening by thrust-related folding soon after deposition (Mazzoli, 1994).

For the same reasons, that is, varying times of restriction and loss of surface connection, the onset of hypersaline conditions in the various Sicilian basin occurred diachronously. Even the Tripoli Formation began to accumulate locally at various times well before the onset of deposition of the main evaporites (Bellanca et al., 2001). Mesohaline sediments first occur in

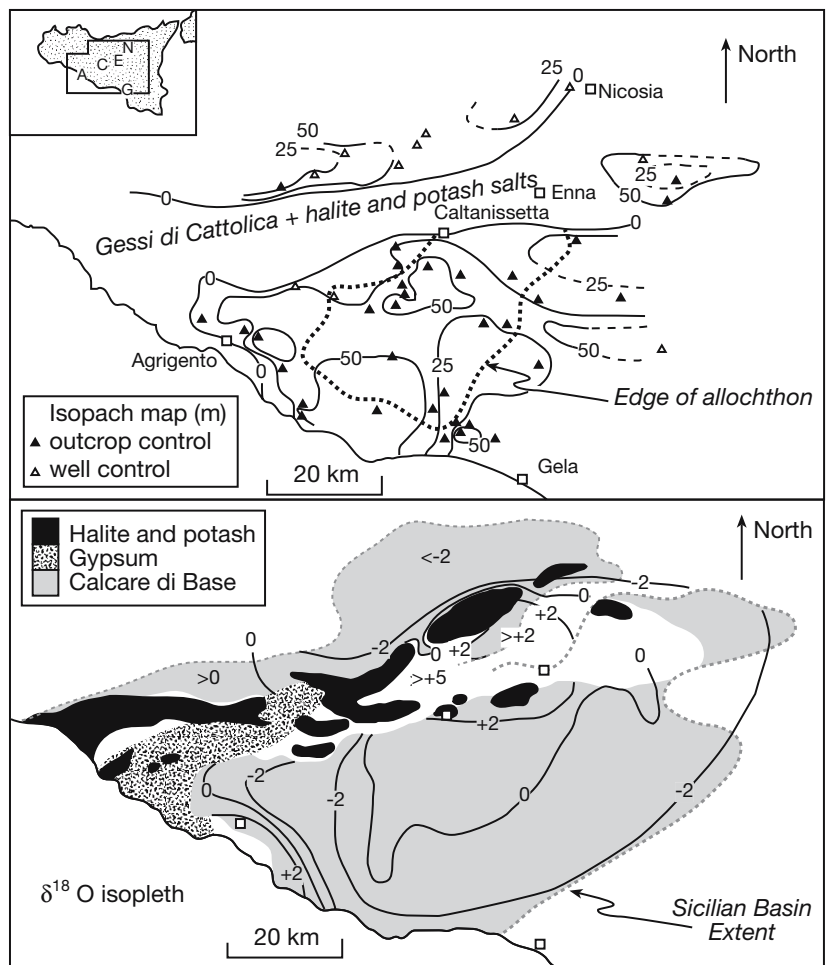


Figure 5.42. Calcare di Base, Sicilian Basin (after Decima et al., 1988) A) Isopach (in metres) and breakdown into an “in situ” unit and an allochthon block that was thrust over the evaporite salts. B) Oxygen isotope distribution in the in situ unit showing depletion in parts of Calcare di Base deposited further from areas of contemporaneous salt deposition (gypsum, halite and potash).

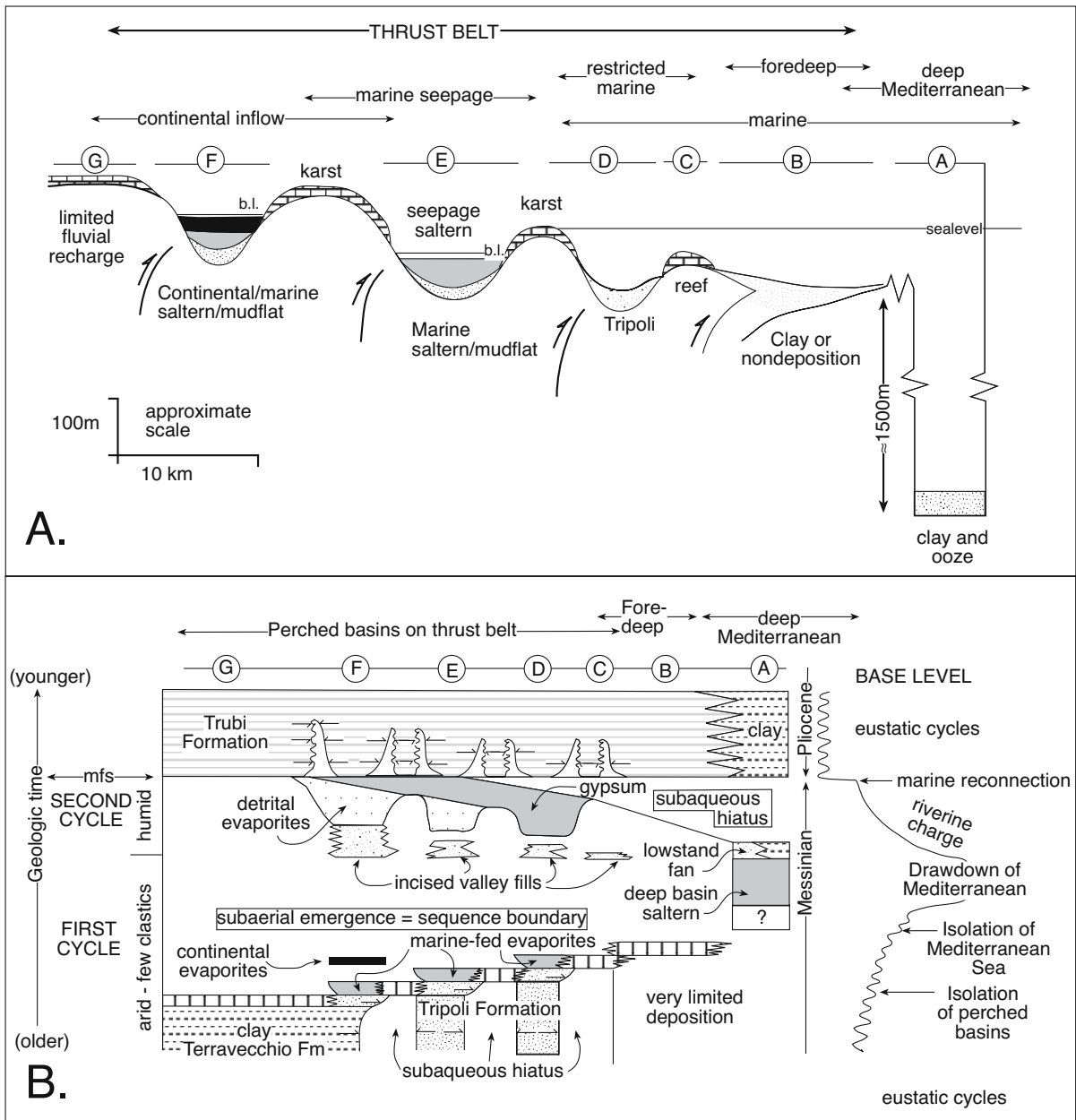


Figure 5.43. Marginal thrust top evaporites in Sicily (modified after Butler et al., 1995). A) Regional model for stratigraphy across different thrust top basins during deposition of the Lower Evaporites (see Figure 5.41). Note the evaporite forming basins are isolated from a surface connection with the Mediterranean, but have a seepage connection. Restricted surface marine circulation facilitates deposition of the Tripoli Formation. Progressive thrusting leads to progressive reduction of import of marine inflow and finally to deposition of potash evaporites under conditions of hyperaridity and predominantly continental recharge. B) A relative chronostratigraphic model for Messinian and Lower Pliocene deposits of Sicily and their correlation with basinwide deposits of the central Mediterranean sub-basins. Note that deposition of basinwide evaporites on the floor of the Mediterranean corresponds to an unconformity (sequence boundary) that separates the Lower and Upper Evaporites. This interpretation contrasts with that of Clauzon et al. (1996).

cycle 34 (6.32 Ma) at Serra Pirciata, cycle 42 (6.15 Ma) at Torrente Vaccarizzo, and cycle 44 (6.12 Ma) at Marianopoli. These changes represent the hydrological and sedimentary response to the thrust induced fragmentation of a larger marine

Tripoli basin into different sub-basins, which ended in the more or less in complete endorheic closure as recorded by the deposition of the overlying evaporite-rich Calcare di Base Formation (true onset of the evaporitic event).

Clauzon et al. (1996) group the deposition of the Upper and Lower Evaporites of Sicily into a single period from 5.75 to 5.60 Ma. The initial eustatically-induced marginward isolation was then followed by complete isolation and drawdown of the whole Mediterranean (Figure 5.43a). In contrast, and although they use only relative time, Butler et al. recognise a major sequence boundary between the Upper and Lower Evaporites of the Sicilian Basin (also called the First and Second cycles). They interpret this sequence boundary as corresponding to the major drawdown of the whole Mediterranean and the formation of a major regional unconformity, which now surrounds all these basinwide deposits (M reflector; see Lofi et al., 2005). They go on to interpret the Upper Evaporite (Second Cycle - mostly saltern gypsum, not halite or bitterns) as being deposited in the isolated marginal seepage basins of Sicily once the Mediterranean was again flooded by seawater entering via a newly re-established surface connection (Figure 5.43b). The contact with the upper evaporites and the overlying deepwater marine Trubi Formation is a maximum flooding surface in both scenarios.

There is also a degree of chronostratigraphic confusion in relating the evaporite fills of many of the marginward basins of Spain to the main Mediterranean drawdown event. The Sorbas basin, Spain, is a good illustration of this. Depending on the author, the main saltern unit (Yesares gypsum) is considered to be time equivalent to the Lower Evaporite unit of the main Mediterranean drawdown event, or it postdates it or predates it (Figure 5.44a). The key

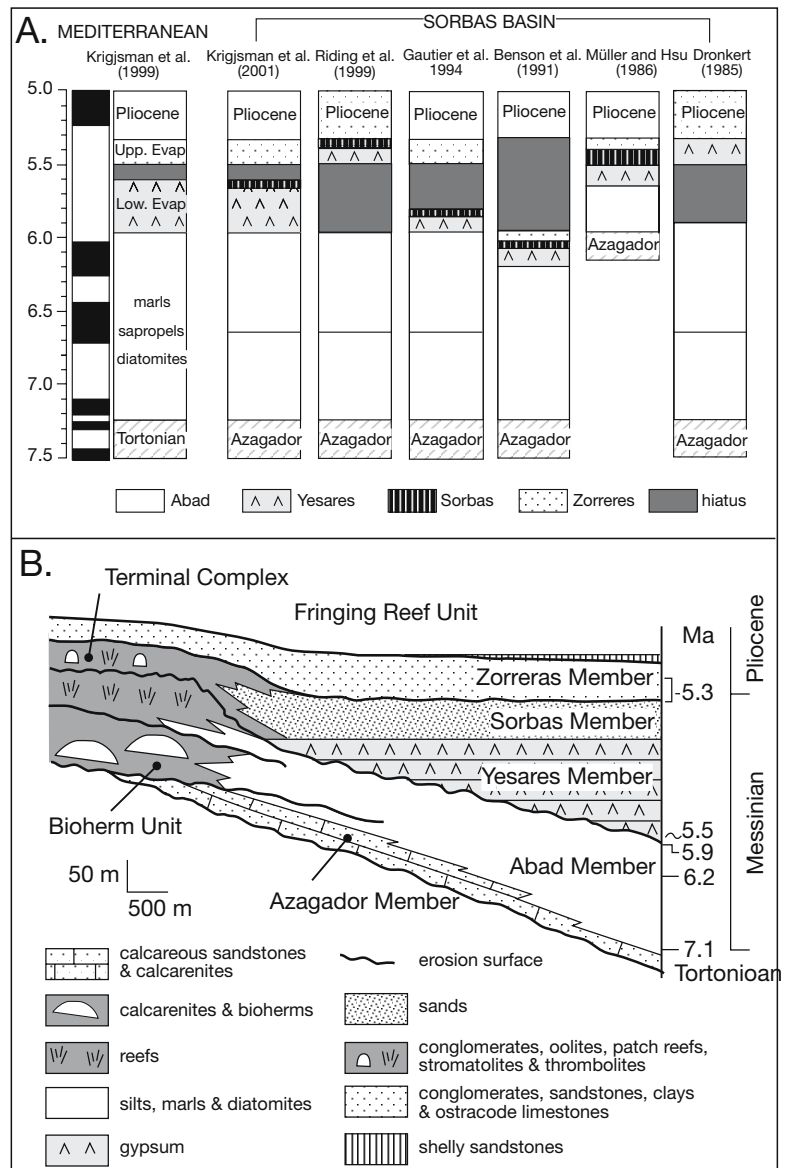


Figure 5.44. Messinian lithofacies, Sorbas Basin, Spain. A) Overview of different chronostratigraphic models for the marginal Sorbas basin showing the large controversies in timing and duration of the various stratigraphic members in relation to the recently established Messinian Mediterranean astrochronology (Krijgsman et al., 2001). The models of Dronkert (1985) and Riding et al. (1998) are based on a correlation of the Yesares Member to the 'Upper Evaporites' of the Mediterranean. The models of Müller and Hsu (1987) and Gautier et al. (1994) are plotted along with the timing by various cited authors of Yesares Member to the 'Lower Evaporites' and the Zorreras to the 'Upper Evaporites'. B) The Messinian-Pliocene succession in the Sorbas Basin. According to Riding et al. (1998) the "Salinity Crisis" sealevel fall occurred within the interval 5.9–5.5 Ma, and the resulting drawdown-driven erosion surface is below the Yesares Gypsum Member, and atop the Fringing Reef Unit. Note the marginal onlap of the Sorbas-Terminal Complex.

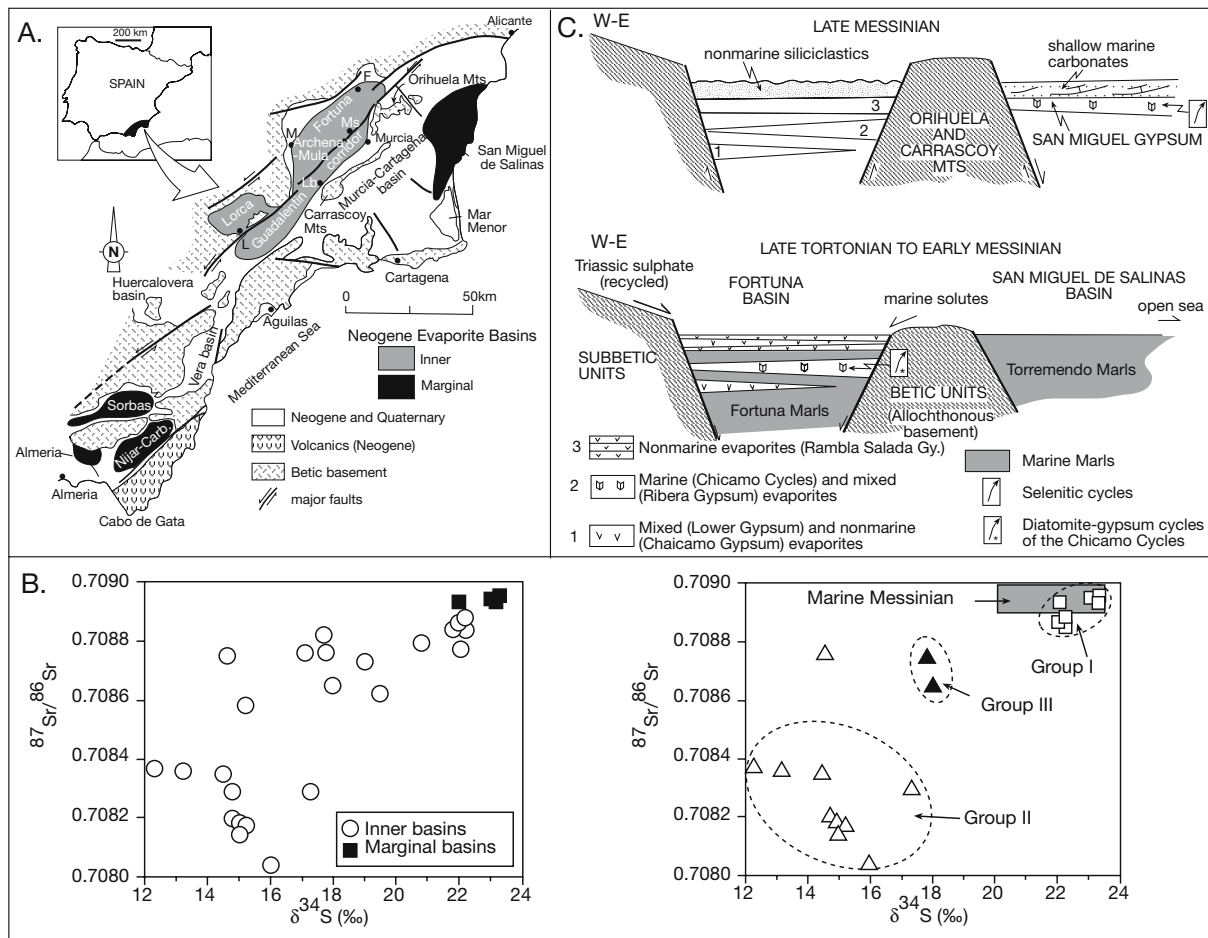


Figure 5.45. Neogene evaporites, Spain (after Playa et al., 2000). A) Location of the Neogene inner and marginal basins in the Eastern Betics. Towns: F: Fortuna; L: Lorca; Lb: Librilla; M: Mula; Ms: Molina de Segura. Ridges: LT: La Tercia Mts. B) Isotopic composition ($^{87}\text{Sr}/^{86}\text{Sr}$ ratio, and $\delta^{34}\text{S}$) of gypsum lithofacies. Plot on left shows primary and secondary gypsum (undifferentiated) samples in the inner and marginal basins. Marine-fed gypsum in the sea-marginal basins shows a much tighter clustering of values reflecting its near isochemical seawater parent. Plot on the right shows primary gypsum samples. Group I: selenites (aligned coarsely crystalline gypsum of the sea-marginal basins). Groups II and III: gypsum lithofacies of the inner more continental basins. The areal distribution of the Messinian marine sulphates from the Mediterranean region is shown shaded in grey. C) Schematic showing the distribution of Neogene evaporite sediments from more continental basins in the west (inner basins such as the Fortuna basin) to the east (sea-marginal basins such as the San Miguel de Salinas basin) in the easternmost part of the Betics (Murcia–Alicante region).

to where it is positioned in the stratigraphy relates to where the equivalent to the main erosion surface (M-equivalent) is placed. Riding et al., (1999) place a regional erosion surface and unconformity (300,000 years exposure) at the base of the Yesares Formation, making the Yesares equivalent to the Upper Evaporite, while Krijgsman et al., (2001) argue any discontinuities at the base of this unit are not regional but reflect no more than local slumping. The debate continues and is yet to be resolved.

The Sorbas Basin is one of a number of marginward basins formed in a complex system of transcurrent faults, with both transpressive and transtensional characteristics. Tectonics controlled depositional geometries in the evaporite fill of the marginal basins of the Betic Cordillera of SE Spain, not sealevel changes outside the hydrographically isolated depression (Figure 5.45a; Playa et al., 2000; Michalzik, 1996). They are seepage basins and there is no evidence for any catacratic-like connection of any of these basins before and during the

formation of Messinian evaporites. Nor is there evidence for a “mega-Niagara Falls,” ending the salinity crisis, as first suggested by Hsu et al. (1973).

The most frequently occurring gypsum lithofacies in all the Spanish basins formed in shallow-water depositional environments and include: crystalline selenitic gypsum (‘grasslike gypsum’), laminated gypsum and crossbedded gypsarenite. Sabkha-type chickenwire alabastrine gypsum are rare in the Spanish sea marginal basins (Michalzik, 1996). Evenly laminated gypsum units interbedded with graded gypsarenites (turbidites), gypsrudites (debrites) and slumps occur in basins or parts of basins with considerable palaeoslopes. Evidence for early diagenetic overprinting includes the formation of giant gypsum twin crystals, ‘super cones’ and alabastrine nodular gypsum. The accumulation of Messinian evaporites in SE Spain was perhaps instigated by a third-order sealevel lowstand that isolated these marginal tectonic basins from the Mediterranean Sea. But all the smaller-scale evaporite units (parasequences) in the various marginal basins, at the scale of shoaling decametre-cycles, are fourth- to sixth-order cyclic and rhythmic responses. They are clearly related to basin dynamics or to autogenetic processes of the local facies (facies dynamics). None are related to high-frequency marine eustacy (Michalzik, 1996).

Inland from the marine fed sea-marginal Messinian basins of Spain are large saline lacustrine basins fed both by seawater seeps and continental waters from the Pyrenees with a substantial solute component coming from the dissolution of Triassic sulphate salts. The saline fills of these largely continental depressions started earlier in the Miocene than the sea-marginal marine-fed depressions (Tortonian versus Messinian) with both their surface and groundwater feeds showing a more continental provenance (Figure 5.45a). For example, in the inner basins of the Murcia-Alicante region, a number of continental-influenced evaporite units were differentiated by Playa et al. (2000). The more continental saltern gypsum lithofacies have the following characteristics (Figure 5.45b): 1) Variable strontium contents, with mean values (primary gypsum) between 1,121 and 2,380 ppm; 2) Isotopic compositions of sulphur ($\delta^{34}\text{S}$) ranging from those characteristic of the Tertiary marine water (+20.3 to +25.5 ‰) to those characteristic of the Triassic sulphates (+8.0 to +16.0 ‰), the latter suggesting recycling of the sulphate anion in meteoric waters; intermediate values (+17.4 to +19.6 ‰) are attributed to mixed mother brines; and, 3) Strontium ratios ($^{87}\text{Sr}/^{86}\text{Sr}$) between 0.70804 and 0.70888; these values range from those of the Tertiary marine water to those exceeding the Triassic sulphates, suggesting additional continental contribu-

tions (from both dissolving country rocks and hydrothermal solutions). The comparison between the sulphur and strontium isotopic compositions of the sulphates, together with the study of the biota present in the marls associated with the gypsum, distinguishes marine, continental, and mixed units (Playa et al., 2000).

In the marine-fed sea marginal basins of the Eastern Betics, where single evaporite units characterized by selenitic gypsum prevail: (1) the strontium contents are more homogeneous, with mean values (primary gypsum) between 493 and 625 ppm; (2) the isotopic compositions of oxygen ($\delta^{18}\text{O}$) and sulphur ($\delta^{34}\text{S}$) between +12.2 and +14.8 ‰, and between +22.0 and +23.5 ‰, respectively; and (3) the strontium ratios ($^{87}\text{Sr}/^{86}\text{Sr}$) varying from 0.70890 to 0.70895. The clear separation between properties of the two gypsum-entraining foreland depressions (Fortuna Basin versus San Miguel de salinas Basin) illustrate that, although gypsum deposition occurred in two side-by-side basins, some units on the continental side started to accumulate bedded gypsum earlier than the Messinian and with signatures that reflect a mixed continental-marine parentage (Figure 5.45c).

At the other end of the Mediterranean in Cyprus, Messinian gypsum units accumulated in a series of semi-isolated tectonically-induced small marginward piggyback basins. They contained landlocked brine sheets (gypsum salterns) located not far below ambient sealevel (Robertson et al., 1995). Evaporites in south Cyprus (Maroni Basin) formed in elongate marginal basins between compressional lineaments instigated by Early Miocene thrusting in a tectonic situation similar to that described for Sicily. In the sub-basins of west, southwest and south Cyprus, large scale slumping of saltern gypsum into deeper water formed megarudite debris flows, which are thought to have been triggered by one or several phases of extensional faulting. The Pissouri and Polemi basins of south Cyprus also preserve sediments of late Messinian-Early Pliocene “Lago Mare” sediments (Figure 5.41).

All the Messinian-Pliocene transitions that define the end of the salinity crisis in Cyprus and in approximately equivalent basinward sediments in the Mediterranean on the edge of the Erathostenes Seamount are marked by a very rapid environmental change, as indicated by sharp variations in lithology, sedimentology, microfaunal assemblages and stable isotope composition (Rouchy et al., 2001). The latest Messinian interval in both regions is known as ‘Lago-Mare’ and is dominated by transitional sediments deposited in mostly oligo-mesohaline conditions. The most striking feature in the Pissouri Basin is the intercalation between the uppermost gypsum bed and the

base of the Zanclean (Early Pliocene) deposits of four main horizons of palaeosols interbedded with carbonates and conglomerates. Palaeosols indicate periods of subaerial exposure in the marginward basins of Cyprus that were long enough to permit pedogenesis during the transition to less evaporitic conditions. Intercalated conglomerates indicate intense erosion of the Troodos Massif and its sedimentary cover. In contrast, shallow oligohaline conditions persisted in the deeper parts of the Mediterranean basin, as indicated at ODP Site 968. Both in the Pissouri Basin of Cyprus and on the flank of the Erathostenes Seamount in the Mediterranean the late Messinian sediments are directly overlain by the lowermost Pliocene sediments deposited in well-oxygenated deep marine conditions. This drastic change of water depth that typifies the basinwide end to the salinity crisis shows that as in the earlier evaporite stages, water levels of the latest Messinian “Lago Mare” were still far below that of the world ocean, by at least more than several hundred metres.

Moreover, the study of the Polemi sections shows that oligohaline conditions had already started during the deposition of the upper gypsum sub-unit. Typical brackish and fresh water assemblages are present in the last two gypsum layers and intergypsum beds (Rouchy et al., 2001). This indicates that freshwater dilution, i.e. the Lago-Mare conditions, resulted from a progressive change of the hydrological budget, which had started during deposition of the upper evaporites and climaxed after the deposition of the uppermost gypsum layer (classic Lago-Mare facies). This basinwide evolution is interpreted as

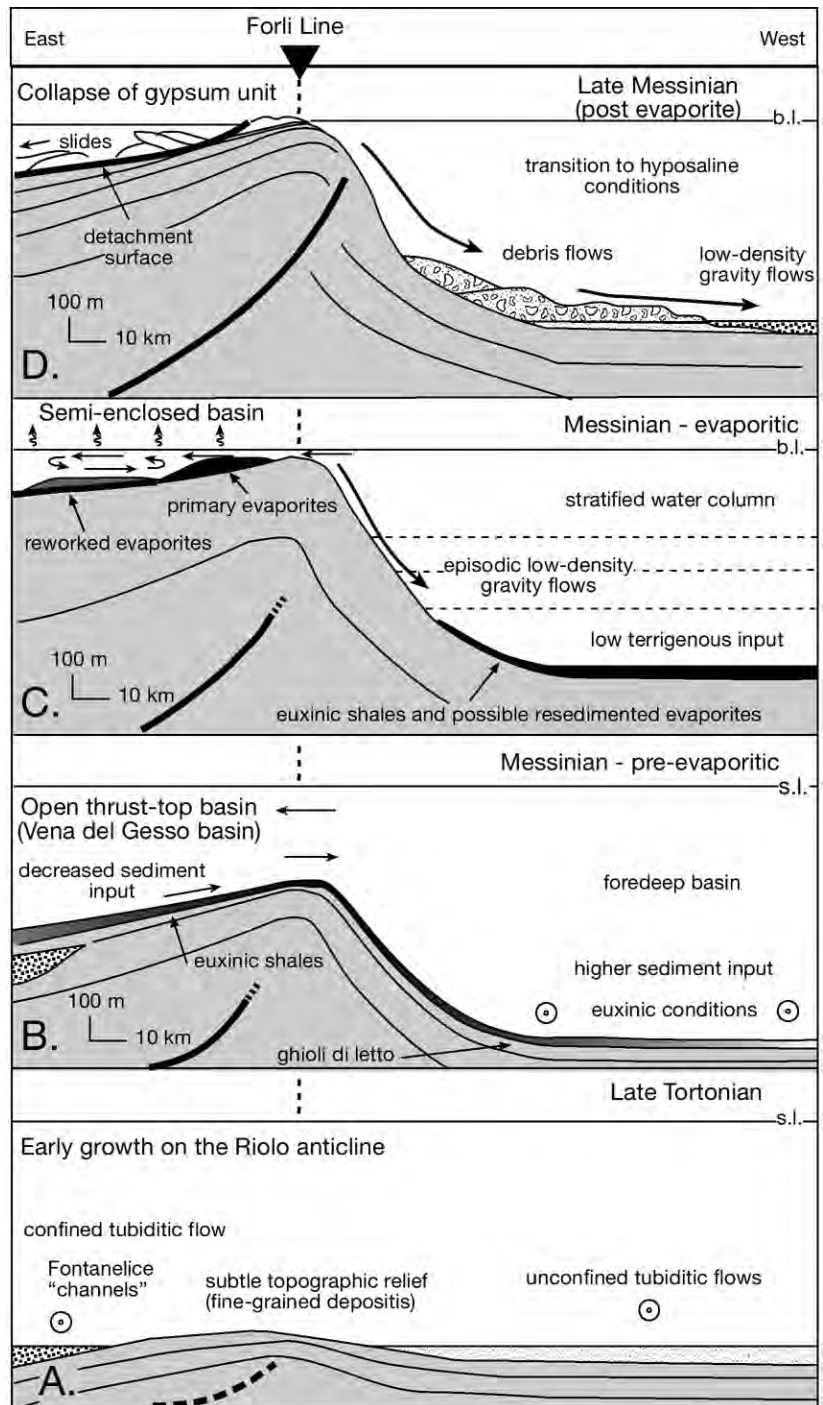


Figure 5.46. Evolution of the Vena del Gesso basin, Italian Apennines, from the Tortonion to the late Miocene with respect to facies and the evolving thrust basin topography indicated by the Forli Line (after Roveri et al., 2003).

being due both to the severance from the marine brine feed and to the increasing contribution of the runoff-precipitation versus marine inputs in the hydrological budget of the Mediterranean toward the end of the salinity crisis, immediately prior to the re-establishment of open marine conditions. In my opinion it reflects a transition into a fill and spill mode of deposition in a relatively humid setting and is not the first time of basin isolation argued by Krijgsman, rather it is the last stage of basin isolation and immediately predates the return to a surface connection to the world ocean.

Further complicating the resolution of a marine eustatic history for cycles in sediments deposited in the Messinian salinity crisis is the ongoing likelihood of gravity tectonics moving large blocks of shallow water evaporites into deeper water settings. Such olistoliths characterise many continent-to-continent collision belts and such a gravity slump system controlled the distribution of Messinian sediments about the Riolo anticline in the Italian Apennines (Roveri et al., 2003; Manzi et al., 2005). Primary, shallow-water evaporites (growth-aligned selenitic saltern gypsum) only occur to the west of the Forli line in Vena del Gesso basin (Figure 5.46a-d). The abrupt vertical facies changes in the region from the euxinic shales to the overlying shallow-water evaporites implies a dramatic relative sealevel fall, on the order of several hundreds of metres, occurring in a very short time span.

But lateral and vertical facies changes within the underlying deepmarine turbidites of the Marnoso-Arenacea Formation show Messinian evaporite precipitation occurred in a thrust-top basin (Vena del Gesso basin), bound to the north and to the east by the thrust-related Riolo anticline, which had been actively growing since the late Tortonian (Figure 5.46a-b). Both gypsum deposition and its subsequent deformation were strongly controlled by evolving palaeobathymetry driven by gravity tectonics.

Primary growth-aligned gypsum accumulated in a shallow, silled marginal basin (Vena del Gesso basin) that lay to the east of the growing Riolo anticline, while organic-rich shales were deposited in the adjacent deeper and larger foredeep basin to the west (Figure 5.46c). These gypsum deposits underwent severe postdepositional deformation related to large-scale gravitational collapse, tied to regional uplift events. Deformation was also coincident with the end of the evaporitic phase in the marginal thrust-top basin. Along the inner, shallower-dipping limb of the anticline bounding the basin, large-scale, weakly deformed gypsum slabs slid downslope along a detachment surface devel-

oped at the contact with the underlying euxinic shales, forming both extensional and compressional features and showing an overall southwestern vergence (Figure 5.46d).

The identification of a south-southwest-dipping palaeoslope by Roveri et al. (2003) suggests that the deformational features affecting the gypsum unit were probably driven by gravity and not by deformation tied to active thrust planes (Figure 5.46d). The steeper frontal limb of the anticline promoted the transformation of gypsum slides into debris flows and turbidite currents that deposited their load in the adjacent deeper basin to the west. This gravitational deformation was sealed by postevaporitic upper Messinian Lago Mare deposits.

The sedimentary history of the Vena del Gesso basin, as documented by Roveri et al. (2003) and Manzi et al. (2005), suggests that the Messinian salinity crisis in the Apennine foredeep, as well as in the Balearic, Tyrrhenian, Sicily, and Eastern Mediterranean Basins, was tightly linked to intrabasinal tectonic processes not worldwide eustasy. The large-scale, postdepositional gravity collapse of primary evaporitic deposits into the deeper parts of adjacent foreland basins is a widespread feature in the Mediterranean basins, and it may have altered the original stratigraphic relationships in some places. It means the amplitude of any waterlevel fall cannot be easily determined in some marginal basins as some beds are allochthonous.

Outside of the Mediterranean there are other complications for notions of world-scale eustasy controlling basinwide evaporite deposition. Work in the Neogene sediments in the Red Sea and the Gulf of Suez has shown that the concept of maximum regional aridity corresponding to times of maximum evaporite accumulation and minimal clastic accumulation is not that simple. Studies of the Miocene/Plio-Pleistocene succession in the Gulf of Suez and the Red Sea have shown that the Messinian (Zeit Formation and equivalent) sediments were deposited at rates greater than other units of the Miocene/Plio-Pleistocene (Griffin, 1999). The Zeit Formation contains a significantly higher clastic content than the underlying evaporitic South Gharib Formation indicating that the Messinian in this region adjacent to the main Mediterranean basin was a time of high rainfall and high sediment yield rates. This period, named the Zeit Wet Phase, stands in marked contrast to the arid conditions of the preceding Tortonian Stage when halite-bearing South Gharib Formation and its equivalents were precipitated in the Gulf of Suez and Red Sea (Griffin, *op cit*). It suggests that the Zeit Wet Phase was marked by high monsoonal activity and that this wet phase peaked in the late Messinian. This was the

time of the lowstand maximum in the Mediterranean driving the Messinian Salinity Crisis.

The preceding discussion of the inherent, and still not fully resolved, largely tectonically controlled climatic and hydrologic complexities in the Messinian of the Mediterranean is based on more than three decades of detailed scientific work, mostly in exposed marginal basin stratigraphies, where the evaporites are still largely preserved as primary gypsum. With the possible exception of an initial third order fall in worldwide sealevel cutting off the basin, all these deposits were isolated via active tectonism. Their finer stratigraphic geometries are not reflective of eustasy but of tectonically induced drawdown and autocyclicity. Much larger volumes of basinwide evaporites are preserved beneath the present deepwater centres of the various Mediterranean basins. These bedded sections currently lie beneath hundreds of metres of Pliocene and Pleistocene sediment; only halokinetic intervals lie within a few tens of metres of the modern deep seafloor. With the exception of a few DSDP holes that intersected the uppermost few metres of bedded salts, the internal stratigraphies of these saline giants are largely unsampled and uninterpreted. And yet we know deposition of 1-2 km-thick basinwide salts took place in less than 300,000-400,000 years. By definition, the total 1+ km package of the Messinian sequence must be a fourth order sequence (Table 5.8). It implies that internal reflectors and cycles seen in seismic sections through thick basinwide evaporites, must reflect fifth and sixth order time frames.

Any eustatic curves, based on seismic that encapsulates the very high accumulation rates of basinwide evaporites in large basin-centre positions in the Mediterranean, will outline very high frequency responses. Even if we ignore the fact that ancient basinwide evaporites are depositional systems with internal responses not related to sealevel changes, comparison of eustatic curves derived from internal geometries of basinwide evaporites with lower order eustatic curves derived from the worldwide study of various marine carbonate or siliciclastic sequences is simply not possible. The internal reflectors and responses that we can resolve seismically within a basinwide evaporite unit are responding to water level changes that are far too short-term to be compared with the eustatic information captured in classic Vail or Exxon-style sealevel curves. We cannot correlate the various eustatic peaks and troughs outlined by the depositional tracts in either system, they are responding to different time-based waterlevel frequencies. The highest seismically resolvable frequencies in a marine sequence are third, and perhaps the occasional fourth, order response. In basinwide evaporite sequence we are looking at

seismically resolvable bounding surfaces that are responses to fifth or sixth order cycles.

Errors arise if intrabasinal correlations attempt to tie thick basinwide evaporite deposits to what are mistakenly considered time-equivalent eustatic curves based on studies of seismic sections through marine carbonates either within or outside the basin. What it most clearly shows is that, using the most recent example we have of a saline giant, the deposition of the one km-plus evaporite units in the various basin centres corresponds to a two dimensional bounding surface or centripetal unconformity (M-marker) immediately outside of the evaporite depositing areas. This should be the starting point for any seismic-based correlation of the evaporites (or subsequent dissolution breccias) with adjacent normal marine sediments.

So, is it also a questionable approach to attempt a sequence stratigraphic age comparison between the marine sediments and deposits sandwiched between the various salt beds of a marine-fed saline giant? Unless we clearly define all sequence boundaries and realise that thick beds of evaporites equate with regional unconformities in surrounding sediments, we may be comparing chalk and cheese. And yet some authors have been courageous enough to attempt internal sequence stratigraphy of ancient saline giants based on various eustatic scales. We shall now look at such a set of studies in the Zechstein evaporites.

Sequence stratigraphy in the Zechstein

During the Late Permian an area of approximately 600,000 km² in northern Europe was covered by the waters of the epicontinental Zechstein Sea (Figure 5.47). The sea was relatively shallow; its maximum basin-centre depth is estimated to have been \approx 300 metres in the early mesohaline stage prior to complete isolation and drawdown (Brongersma-Sanders, 1972). The basin was subdivided into two main east-west oriented basins, called the Northern and Southern Permian Basins, which were separated by a sequence of palaeo-highs, the Mid-North Sea and Ringkøbing-Fyn Highs. Lithostratigraphic similarities between the evaporitic fill of the two basins suggest that the highs did not prevent the free surface exchange of brine between the north and south regions of the Zechstein depression.

During the Late Permian, this part of northern Europe lay at a palaeolatitude of \approx 25°N and within the Pangaeon supercontinent. This, coupled with the restricted and at times marine-fed seepage supply of seawater from the Boreal Ocean to the North and the Tethys Ocean to the Southeast, resulted in deposition of thick sequences of bedded sulphate and halite

evaporites, along with minor volumes of bittern salts. Prior to the onset of marine-fed seepage, the basin accumulated terrigenous sediment known as the Rotliegend/Wiessliedend Formation, in an arid continental playa/eolian/wadi setting in a subsealevel depression created by the final stages of the Variscan Orogeny (Carboniferous-Early Permian). The region at that time was characterised by the development of pull-apart rift basins that evolved into passive margins by the Middle Permian-Triassic period.

This time frame encompasses the main stage of basin subsidence and is characterised by aridity and periodic widespread evaporite deposition including Zechstein evaporites in the Late Permian, followed by Muschelkalk salts in the Middle Triassic and Keuper salts in the Late Triassic (Figure 5.48a). The Mesozoic of NW Europe was also characterised by ongoing metasomatic and hydrothermal activity, as evident from multiphase, cross-cutting, intraformational veinlets. The following Rhaetian through Lower Cretaceous period was marked by intensive faulting, rifting, and the initiation through much of the basin of large-scale halokinesis, sourced in the Zechstein halites.

The Zechstein encompassed the last 5-7 million years of the Permian (Figure 5.48a; Menning, 1995). Most drill intersections and most sequence stratigraphic interpretations have been completed in the southern basin. This is the region associated

with onshore hydrocarbons in the Zechstein of the Netherlands and northern Germany and is also a region where halite and potash salts have been mined for centuries (Chapters 6 and 11). Late Permian fill in the southern Zechstein Basin constitutes a classic basinwide deposit, with circumbasinal transitions from an evaporite platform about the basin edge into a deeper-water centre dominated by laminites (Figures 5.47, 5.48b).

Traditionally, the Zechstein Group is divided by its mineralogy into evaporitic cycles that reflect progressive evaporation from less saline to more saline salts. This method defined four main evaporite cycles (Z1-Z4) and rudimentary fifth and sixth cycles (Z1-Z6; Figure 5.48a). An ideal Zechstein cycle starts with a transgressive nonevaporitic “shale,” followed by carbonates and culminates in thick evaporites (mostly halite/anhydrite). Since most of the classic formation boundaries are picked at what are now considered by sequence stratigraphers to be maximum flooding surfaces (at base Z1: Coppershale or Kupferschiefer Member; base Z3: Grey Salt Clay Member; base Z4: Red Salt Clay Member), the lithostratigraphy of the Zechstein Group closely approaches that of units broken out using the concepts of genetic sequence stratigraphy (Figure 5.48b; Geluk, 2000). It means these basal transgressive units (mfs) provide a base for correlation of the main lithostratigraphic units. The lower three Zechstein evaporite cycles (Z1-Z3) are marine-fed basinwides. They contain evaporitic carbonates in their basal parts that

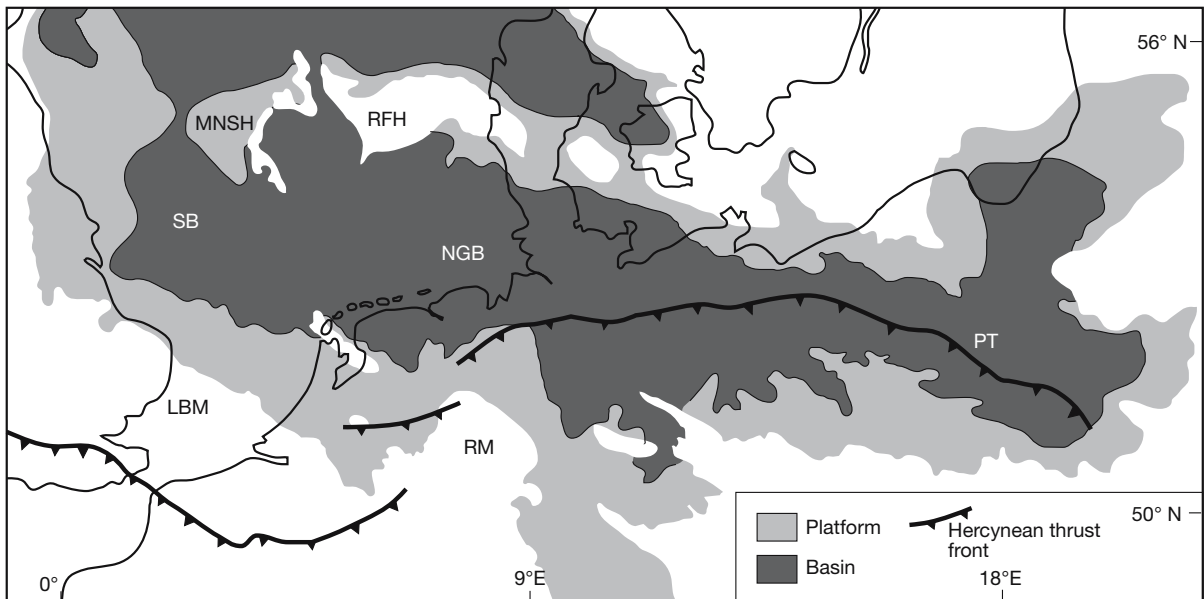


Figure 5.47. Facies distribution in the southern Zechstein Basin (after Geluk, 2000). The basin is bordered to the north by the Mid North Sea High and Ringkøbing-Fyn High and the London-Brabant Massif and Rhenish Massif in the south. The solid black line represents the location of the Variscan Thrust Front. MNSH: Mid North Sea High; RFH: Ringkøbing-Fyn High; SB: Silverpit Basin, LBM: London-Brabant Massif; RM: Rhenish Massif; NGB: North German Basin; PT: Polish Trough.

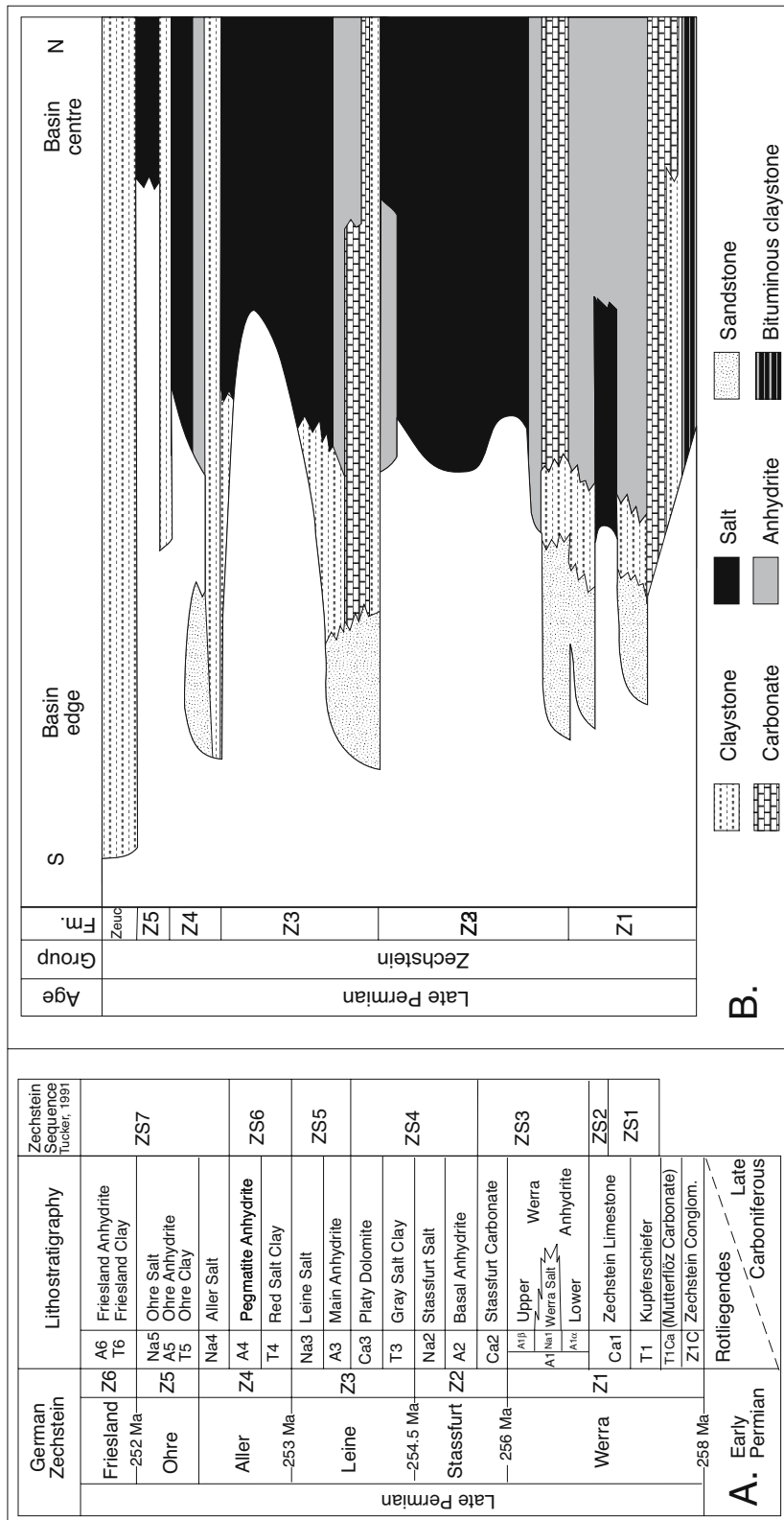


Figure 5.48. Zechstein Stratigraphy. A) Stratigraphy of the Zechstein Series in Germany (after Strohmenger et al. 1996a, b, and sources therein). Shown are the classic Zechstein cycles (Z1-Z6) and the Zechstein sequences (ZS1-ZS7) as proposed by Tucker (1991). B) Classic lithostratigraphic subdivisions from the basin fringe to the basin centre (after Geluk, 2000).

indicate initial precipitation from brines with near normal marine salinities (Taylor, 1990; Leyrer et al., 2001). The overlying anhydrites and salts in these cycles reflect the progressive evaporation of marine-fed salterns and deeper water brine lakes.

Classic transgressive/regressive cycles interpreted in the Z1 and Z2 cycles have been related to glacio-eustatic sealevel fluctuations by Strohmenger et al. (1996a, b) and Leyrer et al. (2001). Earlier, Tucker (1991) published an alternative to the classic Zechstein stratigraphy based on what he interpreted as third order sequences (ZS1-ZS7). In it he correlates evaporites with sealevel lowstands (LSTs) and carbonates with sealevel highstands (TSTs and HSTs). Tucker's approach, in tying evaporites to lowstands, is opposite to that of the classic stratigraphic approach in the basin (pre-sequence stratigraphy) that tied evaporite deposits to highstands, but his approach is more realistic in terms of evaporite hydrology. His classification was criticised firstly by Goodall et al. (1992) on the basis he assumed external sealevel exerted a one-for-one control on evaporite mineralogy and position, and then by Strohmenger et al. (1996a) as his classification did not respect exposure surfaces and stratal geometries.

Strohmenger et al. (1996a, b) and Leyrer et al. (2001) went on to refine a sequence

stratigraphic approach for the basal Zechstein (Z1 and Z2) using facies analysis, geometric relationships, stacking patterns and forward modelling based on core and seismic from the subsurface of northern Germany (Figure 5.49). However, Strohmenger et al. (op. cit.) found that due to the poor quality of internal reflectors in the Zechstein sequence they could not use the usual approach of interpreting the major depositional units from seismic, then establishing a seismic stratigraphic model and then tying well data to seismic. Rather they had to first establish a geological model based on detailed stratigraphic analysis of core and outcrop. Then they developed a sequence stratigraphic framework and then interpreted and forward modeled the intra-Zechstein reflectors. Their analysis (Figure 5.49) shows that reworked sandstones of the Weissliegende and/or the Zechstein conglomerate (Z1C) record the initial transgression of the Zechstein sea and overlie the Zechstein sequence boundary (ZSB1). Transgressive systems tract (TST) deposits of the first Zechstein sequence (ZS1) are also represented by deeper marine carbonates of the Mutterflöz (T1Ca). The overlying Kupferschiefer is interpreted as a condensed section (CS) indicating maximum flooding (mfs) of the first Zechstein sequence. The bulk of the shallow water Zechstein limestone (Ca1) is interpreted as a highstand systems tract (HST). It is separated from the thin uppermost part of the Zechstein Limestone by a karst horizon corresponding to an erosive sequence boundary (ZSB2).

Correlatable shallow water carbonates (oncolites and stromatolites) indicate lowstand systems tracts (LST) of the second Zechstein sequence (ZS2; Figure 4.50). The uppermost part of the Zechstein Limestone represents the transgressive systems tract of the second Zechstein sequence (ZS2). According to Strohmenger et al. (1996a, b) there is no indication of a sequence boundary at the top of the Ca-1 platform carbonates (contrasts with Tucker 1991). They argue Ca1

carbonates, in a basal position, show a deepening upward tendency toward the superimposed deposits of the A1 sulphates. They place the maximum flooding surface (mfs) of the second Zechstein sequence at the top of the Ca1 platform carbonates. The overlying anhydrites of the A-1 sulphate platform (Werra Anhydrite) are interpreted as predominantly highstand systems tract deposits displaying an erosive sequence boundary (ZSB3) at its top. This is in direct contradiction with Tucker (1991) and according to Strohmenger et al. (1996a, b) it is only in the slope and basal environments that the A1 also represents lowstand wedge deposits of the third Zechstein sequence (ZS3).

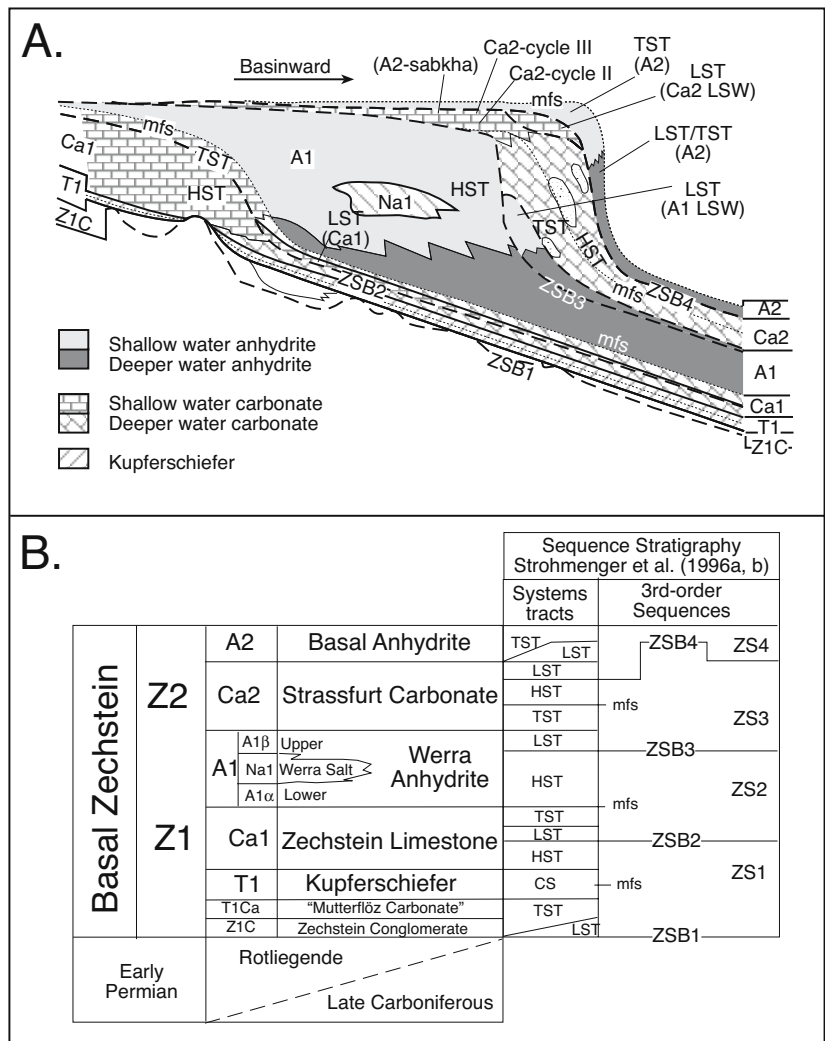


Figure 5.49. Zechstein evaporites of northwestern Germany (after Strohmenger et al., 1996a, b and sources therein). A) Schematic of basal Zechstein relationships on the southern margin of the Zechstein Basin. B) Lithostratigraphy of basal Zechstein showing classic subdivision (Z1-Z2) and Strohmenger et al. (1996a) subdivision (ZS1-ZS4). ZSB = Zechstein sequence boundary.

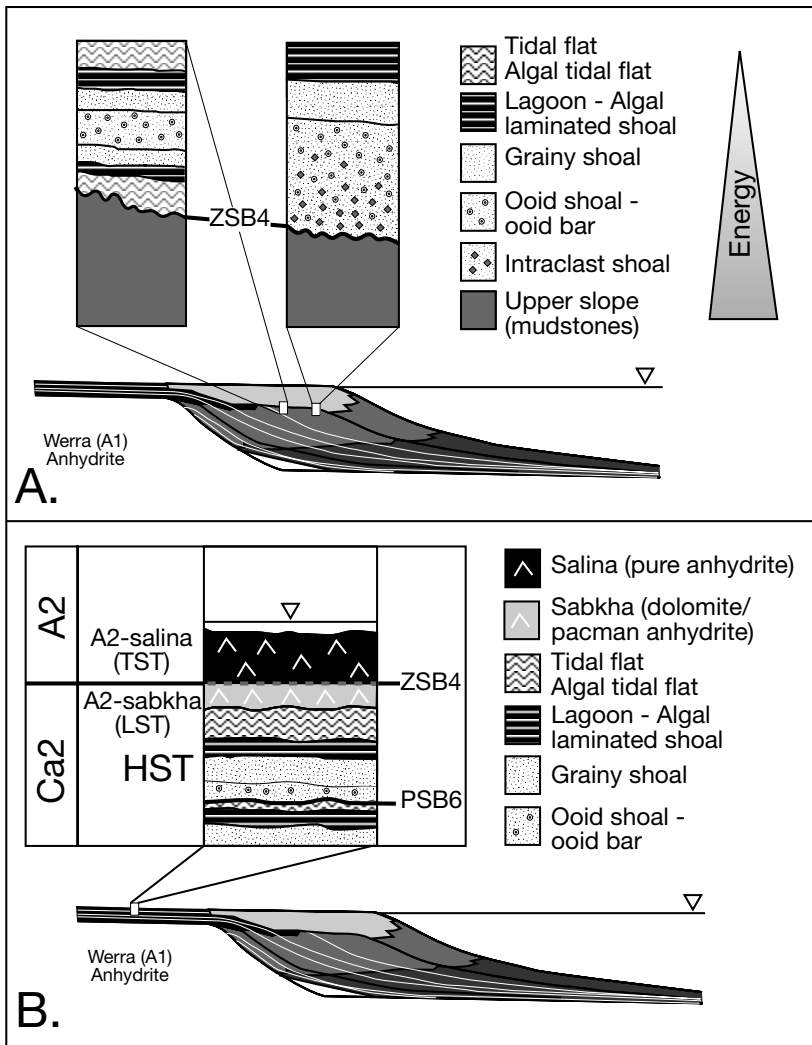


Figure 5.50. Facies associations in Ca₂ carbonate platform, Zechstein Basin, northwest Germany (after Leyrer et al., 2001). A) Slope position (HST of ZS3 to TST of ZS4). B) Platform position (HST of ZS3 to TST of ZS4).

In reality, each of the evaporite cycles is made up of a highly complicated stack of parasequences that sequence stratigraphers argue represent higher order sea-level fluctuations. In my opinion, climate-related intrabasinal autocyclicality is a more likely driving mechanism at the scale of the parasequences. The contradiction underlies the difficulties in sequence stratigraphic analysis of evaporite deposits using models derived from geometries and 3rd order eustatic responses of marine systems. The terms highstand systems tract and lowstand systems tract are largely defined by whether the shelf of the basin that is under consideration is covered by water. There is no concept as yet in the sequence stratigraphic literature that an aggrading

evaporite bed causes its overlying brine level to rise (autocyclic hydrologic feedback).

Most Zechstein interpretations assume a surface connection to the ocean at all times and that there were direct marine eustatic responses in brine base level. We have already discussed the likely errors inherent in this assumption. In the marine realm we are talking about eustatic sealevel amplitudes of no more than a hundred or so metres in icehouse periods and less than decametres in greenhouse periods. There is an inherent assumption in classic sequence stratigraphy that in greenhouse and icehouse times the prime locus of sedimentation is near a shoreline, either on the shelf or just basinward of the shelf break (Type 2 and Type 1 boundaries). In an evaporite basin that is undergoing drawdown we are discussing an initial hydrographic isolation (mesohaline carbonates are considered to indicate the mfs by the sequence stratigraphers) quickly followed by a water level fall of more than 500-1,000 metres and the onset of widespread evaporite precipitation. Any strandline in the system will likely have migrated hundreds of kilometres and be situated well out on the old continental slope at the onset of evaporite accumulation. Once again, marine eustatic models do not apply.

At hydrologic equilibrium (inflow=loss) the whole marine highstand shelf and slope, as well as part of the basin floor, is exposed. Water levels even in the deepest parts of the basin are mostly less than a few tens of metres and no more than one or two hundred metres. In this scenario the locus of maximum deposition is not tied to sediment supply from outside the basin (siliciclastics) or to any need for shallow waters atop a carbonate platform. The maximum locus of evaporite deposition is in the lowest part of the isolated depression in many drawdown basins with no surface connection to the ocean. This area is assumed to be deep water by sequence stratigraphers, but textures from the salts accumulating there are typically saltern or salt pan with local deeper water cumulates.

Defining the stratigraphic significance of sequence boundaries, such as the ZSB2, are more problematic in such hydrographically isolated drawdown scenario (Figure 5.49). Strohmenger argues that the Ca1 carbonates, in basinal position, show a deepening upward tendency toward the superimposed deposits of the A1 sulphates. What he is observing is a gradational transition. The term deepening is probably too categorical in this scenario. If the basin is isolated so that thick gypsum/anhydrite can accumulate, then the brine level in the basin must be lowered with respect to the old shelf. The A1 profile above the ZSB2 sequence boundary is most likely subaqueous throughout, and is a “brining upward” profile. The sequence does not deepen upward, it is continuously subaqueous but brines upward as the regional water level is lowered. That is, the average annual salinity of the brine body is increasing up section and ongoing lowering of the brine level does not stop until an effective brine curtain/inflow equilibrium is established. The brine level is not reflecting marine eustasy but a hydrological/climatic balance.

Stacking patterns laid down in such scenarios are not well understood, but should not be forced to fit the classic paradigms of marine sequence stratigraphy. We are looking at an evaporite system that probably was at any time deeper or shallower depending on the vagaries of climate and tectonics and largely independent of eustasy. All we can say in terms of the A1-sulphates is that at no time during the deposition of the sulphate phase was the water deeper than a few hundred metres and probably was mostly less than tens of metres deep (Warren, 1989; Kendall, 1992). During the preceding carbonate platform phase the water body was obviously less saline and probably deeper on average than during sulphate deposition and tended toward meromictic rather than holomictic conditions.

Even in the carbonate horizons separating the main evaporite phases, thought by many to be marine, the drastic changes in intrabasinal base level create problems in creating a reliable sequence stratigraphic interpretation if interpreters have assumed a hydrographically connected sealevel in the basin. The Zechstein 2 Carbonate (Ca2) overlies the A1-Sulphate (Werra Anhydrite) and according to Strohmenger et al. (1996a, b) and Leyrer et al. (2001) encompasses transgressive systems tract as well as highstand systems tract deposits of Zechstein sequence ZS3. The maximum flooding of the Ca2 is correlated with the flooding of the A1-sulphate platform. Therefore, Ca2-platform carbonates (Main Dolomite) are dominated by shallow-water highstand deposits of the third Zechstein sequence (ZS3). Deposits of the Ca2 transgressive systems tract

are coated-grain and composite-grain packstones/grainstones that contain reworked anhydrite clasts of the underlying A1. Leyrer et al. (2001) clearly demonstrate that the depositional facies, and hence the porosity distribution of the gas-bearing Ca-2 carbonates in the subsurface of northern Germany, are in large part controlled by high energy positions that reflect a shallow “sea” superimposed on the underlying evaporite topography. This topography was created prior to carbonate deposition by saltern to basin transitions in the underlying Werra (A1) Anhydrite.

An upper contact of the Ca2 carbonate is defined by the transition of shallow-water Ca2 carbonates into the overlying anhydrites of the A2 (Strohmenger et al., 1996a, b; Leyrer et al., 2001). The stratigraphic limit between the Ca2 and A2 is highly arbitrary and conventionally drawn in wells by the last up-section occurrence of bedded dolomite, but is gradational. Carbonates near the contact show typical Ca2 facies (e.g. algal-laminated coated-grain and composite-grain wackestones/ packstones and algal bindstones) and are often intercalated with bedded anhydrites of the A2 (Figure 5.50). Furthermore, according to Strohmenger et al. (op. cit.), the platform anhydrites of the A2 at this contact can display ghost structures of Ca2 facies. Leyrer (pers comm.) appropriately describes this as “Pacman” anhydrite, although it is perhaps more widely known as anhydritization. It indicates that the lower part of the A2 can be interpreted as sabkha/pan deposits (A2-sabkha) cannibalising the Ca2 carbonate and indicating the emergence of the Ca2 platform at the end of Ca2 time (Figure 5.50b). Alternately, the widespread evaporites within and replacing A2 carbonates could be a form of reflux-driven cementation/replacement created during deposition of the overlying saltern anhydrite. In my opinion this contact is perhaps tied to the time when the ooid/grainstone shoal along the basin edge became sufficiently well developed to isolate the platform lagoon and so it converted to an evaporitic mudflat or saltern.

According to Strohmenger et al. (1996a, b) the fourth sequence boundary of the Basal Zechstein (ZSB4) occurs not on top of the Ca2 shallow-water carbonates, but somewhere within the A2-platform deposits, once again in contrast to the model of Tucker, 1991. The lower part of the A2 (anhydritised or Pacman-style Ca2 facies) is interpreted as the time equivalent of shallow-water Ca2 carbonates that overlie deeper-marine upper slope carbonates in a basinward position, corresponding to the lowstand systems tract (lowstand wedge) of the fourth Zechstein sequence (ZS4; Figure 5.50a). The uppermost part of the A2 (pure salina-type anhydrites on top of pacman

anhydrites showing ghost structures of Ca₂-platform facies) is thought to represent the transgressive systems tract of the fourth Zechstein sequence (ZS4; Figure 5.50b). The relatively thick anhydrite accumulations of the A2 (approx. 100 m), which occur basinward of the Ca₂ slope, are thought to represent both lowstand systems tract as well as transgressive systems tract deposits of the fourth Zechstein sequence (ZS4).

According to Strohmenger et al. (1996a, b) the basinward progradation of the third-order Basal Zechstein depositional sequences is forced by the tectono-eustatic, first- and second-order sealevel lowstand of the latest Permian. The cyclicities observed within the different systems tracts are thought to be caused by higher order sealevel fluctuations with durations of 0.08-0.5 Ma (fourth-order cycles), 0.03-0.08 Ma (fifth-order cycles) or 0.01-0.03 Ma (sixth-order cycles and related to orbitally controlled Milankovitch cycles (Leyrer et al., 2001). Strohmenger et al. (1996a, b) go on to argue that the 0.1 and/or 0.4 Ma Milankovitch cycles indicate to high-amplitude sealevel fluctuations throughout the Late Permian. They draw analogies to small-scale sequences as described from the Yates Formation (United States, Permian Basin) by Borer and Harris (1991) and from the Wegener Halvø Formation (Jameson Land Basin, East Greenland) by Scholle et al. (1993).

In my opinion, there is a problem in comparing eustatic sealevel models, derived from platform evaporites of the Permian of Greenland and west Texas, to the basinwide drawdown platform evaporites of the Zechstein. Work by Strohmenger et al., (1996a, b) and Steinhoff and Strohmenger (1999) provide excellent core-based facies breakdowns of the evaporite stratigraphy and mapping of water level changes and hence predictors of porosity in units such as the Ca-2 carbonates, which are the major onshore gas reservoir in northern Germany (Leyrer et al., 2001). Where I have a problem is accepting the leap of faith in applying marine-derived Vail-curve age models (timing of cycle orders) to the brine level fluctuations that controlled the shelf to basin geometries of the Basal Zechstein. This approach ignores the need for complete lack of a surface connection with the ocean to deposit thick evaporite sequences. Furthermore, if we look to analogies in the marine-fed saline giants sub-basins of the Messinian, then sedimentation rates used by Strohmenger et al. for sealevel ties to evaporite packages, such as the A1 sulphates, are much too slow. Thick basin-centre evaporites require particular conditions of tectonic isolation to form, when this does occur the evaporites are laid down very rapidly (5th and 6th order cycles), as they were in the Mediterranean.

Sequence stratigraphy in the Silurian Salina Group of the Michigan Basin

The Michigan basin in the Late Silurian was a roughly circular intracratonic sag basin, approximately 400 km in diameter and fringed by reef pinnacles passing updip into an extensive rimmed platform (Figure 5.51a; Brennan and Lowenstein, 2002). The reefs are encased in salts of the Salina Group. When Salina Group evaporite deposition commenced some 423 Ma the palaeolatitude was approximately 26°S, and approximately 20°S at 417 Ma, when Salina Group deposition ended (Brennan and Lowenstein, 2002). Prior to its hydrographic isolation, marine waters entered from the southern Kokomo Sea, via the Clinton Inlet, and from the northern Moose River Basin via the Georgian Inlet (Briggs et al., 1980). A relative sealevel drop in the late Wenlockian produced restriction and isolated the Michigan Basin from the Silurian ocean; throughout, the earth was in greenhouse climate mode (Dellwig, 1955; Dellwig and Evans, 1969). The deep-water A-0 unit (calcite-anhydrite-halite), the first deposit associated with this sealevel drop, is conformably overlain by the A-1 Evaporite and defines the transition into mesohaline conditions as the surface connection to the open ocean was lost (Figure 5.52; Dellwig, 1955; Nurmi and Friedman, 1977; Gill, 1977; Briggs et al., 1980; Cercone, 1988; Leibold and Howell, 1991).

Middle Silurian pinnacle reef reservoirs in the Michigan Basin are isolated stromatoporoid/coral-crinoid buildups, which are encased and sealed by a combination of Upper Silurian halite, anhydrite and fine-grained carbonate (Figures 5.51, 5.52). Reef pinnacles form two hydrocarbon belts some 16 to 24 km (10 to 15 miles) wide that extend basinward from the steep inner face of an extensive, but nonproductive, barrier reef (Figure 10.32). The basinal equivalent of the reefs is a thin carbonate some 18 to 24 m (60 to 80 ft) thick. The reef/bank rimmed platform is dolomitised, as are most of the pinnacles, although a few of the more basinal pinnacles are still limestone (Sears and Lucia, 1979, 1980). Pinnacles are capped by an erosional unconformity and reef growth had ceased well before the basinwide drawdown events that deposited the encasing evaporite cycles (Figure 5.51a; Gill, 1985). Drawdown created the karst horizon that caps the marine reef sediments of the Guelph Formation and immediately underlies the stromatolitic capstones formed during deposition of the A-1 evaporitic carbonates (Mesolella et al., 1974). During drawdown the pinnacles formed topographic highs and were sites of marine groundwater escape (pisolitic/stromatolitic seepage facies) until they were enveloped in aggrading salts of the A-2 cycle.

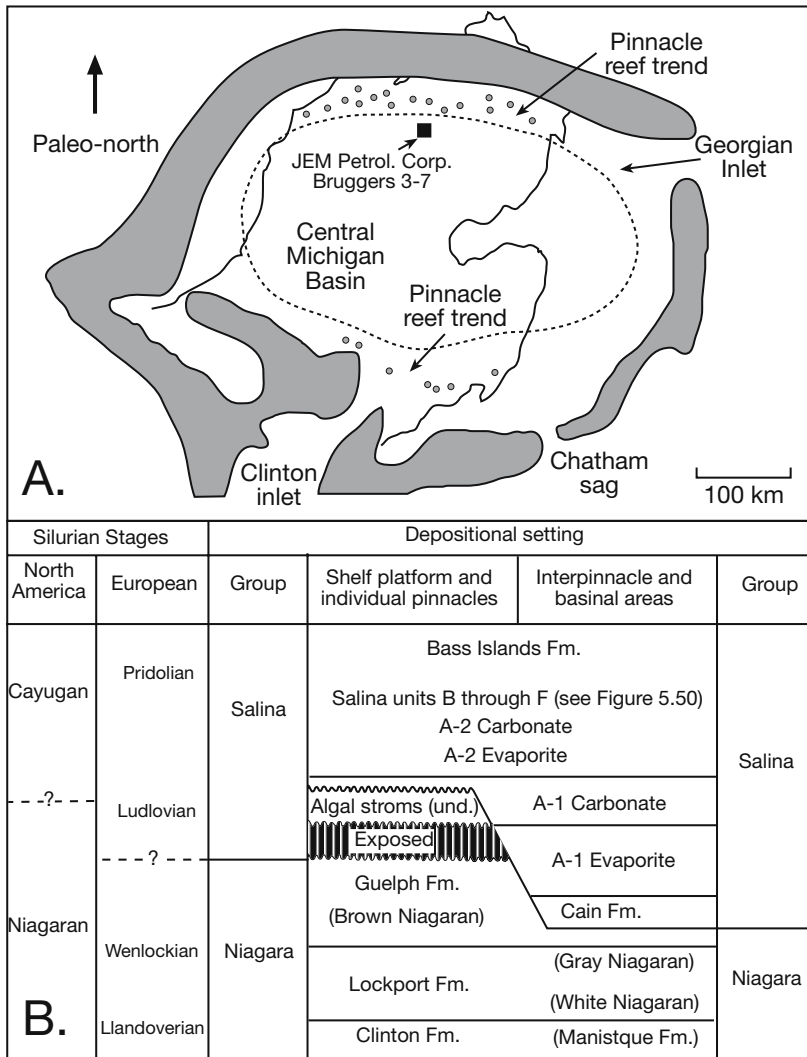


Figure 5.51. Silurian evaporites in the Michigan Basin, USA. A) Location of Salina Group, the evaporite-filled central Michigan Basin is identified by the dotted oval, and the evaporite-sealed northern and southern pinnacle reef trends are shown by the larger dots. Also shown is the position of the JEM Petroleum Corporation Bruggers well, Missaukee County, Michigan. B) Stratigraphic chart of Silurian formations in the Michigan Basin (after Gill, 1979).

The sealing evaporites of the Lower Salina Group were some of the first thick sequences of salt to be interpreted as containing textures of more than one depositional setting. The earliest depositional interpretations of these salts were as deepwater deposits (Dellwig, 1955; Dellwig and Evans, 1969). Nurmi and Friedman (1977) challenged many of Dellwig’s conclusions. They interpreted much of the halite as having formed as stacked halite crusts precipitated beneath shallow brine sheets subject to periodic drying. The arguments of Nurmi and Friedman were rooted strongly in processes observed in Holocene salt crusts.

A shallow to ephemeral water model came to dominate subsequent interpretations and have been reinforced by subsequent detailed geochemical studies (Figure 5.52; Brennan and Lowenstein, 2002).

Thus, the evaporites imply episodes of evaporative drawdown and that there was subaerial exposure of the reef crests prior to their encasement in salt, via a process of “fill and spill.” The complex rapid rise and fall of the brine level over vertical distance of several tens of metres during the accumulation of the Salina Group drove ongoing alteration, dolomitisation and evaporite plugging, not just of the Salina Group but also in the Niagaran, especially in those pinnacles sitting below zones where thick sequences of evaporites were accumulating.

Detailed stratigraphic analysis of the evaporites and evaporitic carbonates in the vicinity of producing pinnacles clearly define the complexity of sequences accumulating under a system of basinwide evaporitic drawdown. Using more than 350 wells and numerous cores, Leibold (1992) and Howell and Leibold (1992), defined four composite sequences: Niagaran, A-1 Unit, A-2 Unit, and the B Unit (Figure 5.52). The Niagara Group carbonates comprise a dominantly intrabasinal highstand composite sequence that was deposited on a preexisting carbonate ramp and was interrupted by at least one major drawdown event. Numerous Type 1 unconformities on the carbonate platform margin were recognised by Leibold (op. cit.) and related to evaporative drawdown events. Thus, the Niagaran is a composite sequence made up of two sequences separated by an unconformity. The lower sequence consists of three parasequence sets: aggradational (“White Niagaran” ramp), transgressive (“Gray Niagaran”), and progradational (“Brown Niagaran”). The Brown Niagaran includes a distinct stromatoporoid shelf-bank margin and a zone of pinnacle

reef growth. Biostratigraphic, lithostratigraphic and isotopic evidence indicates Upper Niagaran water depths in the basin exceeded 250 metres prior to drawdown. The Brown Niagaran parasequence set is interrupted by a drawdown unconformity, represented by the subaerial exposure surface mentioned earlier. It extends below the shelf margin into the inter-pinnacle reef areas and defines a type 1 boundary (Figure 5.52).

A second drawdown event ended Niagaran deposition and initiated the A-1 Unit as a thick (140 m) lowstand evaporite wedge in the basin (Figure 5.52, 5.53). Deposition of the halite-dominated A-1 Evaporite occurred in an initially somewhat deeper brine that progressively shallowed. The JEM Bruggers 3–7 core, Missaukee County, Michigan completely cored the A-1 evaporite (Figure 5.52; Leibold, 1992). The basal 10 m of the A-1 Evaporite is composed of alternating layers of coarse, clear halite (50–150 mm thick) and anhydrite (30–100

mm thick). It was interpreted as a possibly deeper water unit showing widespread halite recrystallisation, but models of meshwork halite (Dead Sea holomictic/meromictic analog) were not available in the early 1990s. This unit is overlain by 25 m of chevron-rich halite, the upper 5 m contains bedding planes dipping up to 40°, which have been interpreted by Leibold (op cit.) as buckled pressure-ridged pan halite crusts, formed during subaerial exposure (Leibold, 1992). This is overlain by the “mid-basin potash facies”, which is up to 60 m thick and composed of halite and sylvite elsewhere in the Michigan Basin (Leibold, 1992). The potash facies in the JEM Bruggers core does not contain bedded sylvite; however, primary fluid inclusions in the halite do contain daughter crystals of sylvite, carnallite, and tachyhydrite (Leibold, 1992). These potash facies also contain borate nodules and buckled salt crust polygons indicating saline-pan deposition with periodic basin desiccation. The mid-basin potash facies is overlain by halite that has been pervasively recrystallized (Leibold, 1992).

pervasively recrystallized (Leibold, 1992).

Leibold (1992) and Raup and Hite (1993) analysed bromide from bulk halite samples in the JEM Bruggers 3–7 core and showed that coarse halite and chevron-rich facies at the bottom of the A-1 Evaporite display a systematic upsection increase in Br concentration, ranging from 25 to 200 ppm. This type of bromine profile, along with the upward increase in the density of chevrons, and buckled crust polygons towards the top of the chevron-rich facies indicate that this lowermost section of the A-1 halite formed by the progressive evaporation of a large shallow body of brine, which dried out at the top of the unit. In contrast, halite from the mid-basin potash facies does not exhibit any systematic increase in the Br concentrations. Instead, the Br is relatively high (210 ppm) throughout, which suggests these halites did not form strictly by the progressive evaporation of a large body of Silurian seawater (Figure 5.52).

The A-1 Evaporite is overlain by the A-1 Carbonate, which signifies

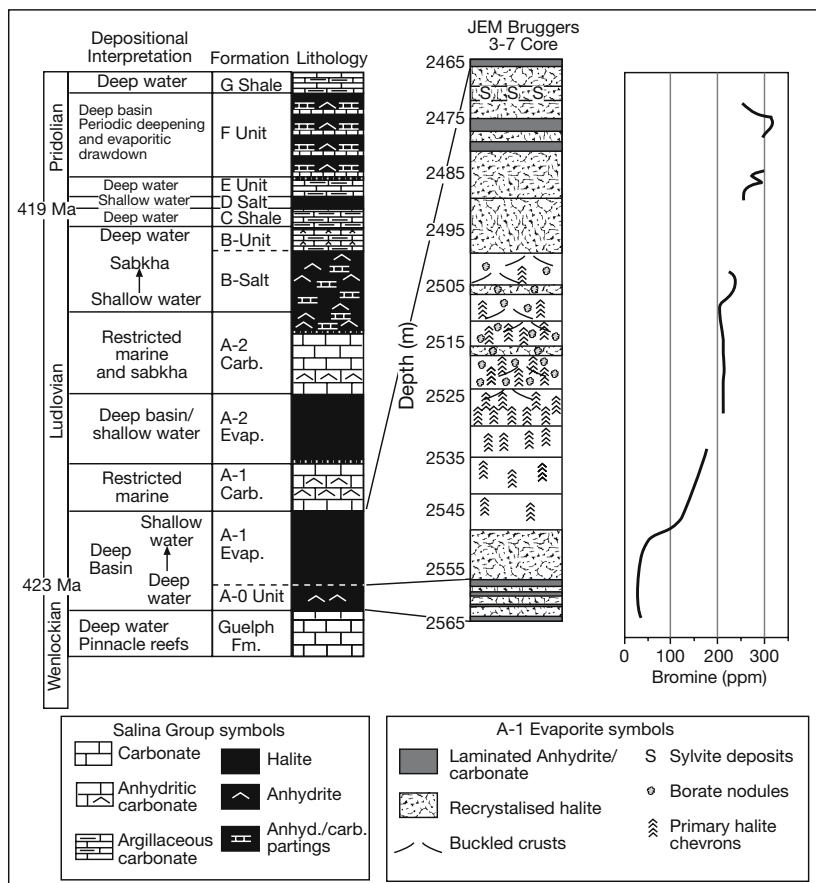


Figure 5.52. Stratigraphy of the Salina Group (left column) and detailed facies of A-0 and A-1 Evaporites in Bruggers 3–7 core (right column), Michigan Basin (Upper Silurian). The thicknesses of the Salina Group Formations are not to scale. The depositional interpretations of the Salina Group are primarily from Leibold (1992). (after Brennan and Lowenstein, 2002).

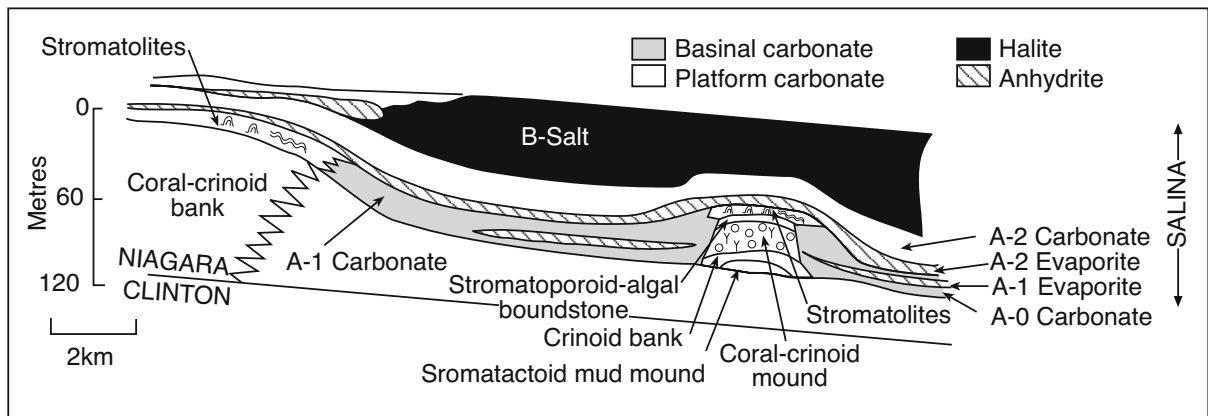


Figure 5.53. Schematic showing facies relationships of a shelf to basin profile in the Silurian of the southern Michigan Basin (in part after Sarg, 2001).

a higher volume of marine brine in the Michigan Basin, this could indicate a more humid climate or a possible renewed surface connection to the Silurian ocean. The A-1 Carbonate is overlain by the A-2 Evaporite, which indicates a second period of increased aridity or the return to isolation of the Michigan Basin from the Silurian ocean. The A-2 carbonate, a gray, nonfossiliferous mudstone, conformably overlies the A-2 Evaporite. The B Evaporite conformably overlies the A-2 Carbonate and is composed of two units, the B-Salt and the overlying B Unit. The B-Salt deposits consist of halite interbedded with anhydrite and dolomite partings (Leibold, 1992), which likely formed within a shallow isolated central basin. The B-Unit is interpreted by Leibold (op. cit.) as a deep-water, anhydrite-rich, argillaceous carbonate, which marks the beginning of a regional transgression. The C Shale, D-Salt, and the E-Unit possibly indicate alternating incursions of seawater and isolation and concentration of the basin waters (Droste and Shaver, 1985) or more likely they are responses to climatically induced transitions from meromictic to holomictic basin waters.

The mid-Pridolian F-Unit is the uppermost evaporite formation of the Salina Group and comprises six separate halite units, F-1 to F-6, that are separated by shales, dolomites, and anhydrites (Sonnenfeld and Al-Asam, 1991). The lowermost F-1-Salt is composed of continuous beds of chevron-rich halite separated by anhydrite partings (Dellwig and Evans, 1969) and resembles similar facies in the A-1 Evaporite. Bromide concentrations increase systematically upsection in the halites of the F-1-Salt (Das et al., 1990), consistent with the profile expected for evaporation of a large body of seawater-fed brine. Sulphur and strontium isotopic analyses of the anhydrite in the F-1 salt are also consistent with Silurian seawater values (Das et al., 1990).

The thickness, orientation and mineralogical zonation of marginal evaporite wedges in the basal A-1 Evaporite overlying the Niagaran sequence required initial minimum brine depths of 20 metres and so imply wind and water currents influenced evaporite deposition (Sarg, 2001). Overlying lower A-1 Evaporite salts were deposited in shallower brines, less than a metre or two deep, as indicated by chevron-rich growth-aligned halite pan textures. Middle and upper A-1 evaporite lithofacies contain evidence of alternating very shallow brine and subaerial depositional conditions (Leibold, 1992). The Middle A-1 lithofacies are sylvite- and borate-rich, with sylvite beds present only in the central Michigan Basin (Figure 5.51a). Upper A-1 evaporite lithofacies, which Sarg (2001) calls transgressive (I prefer fill and spill), are dominated by stacked, saltpan morphologies. The brine level at this time was well below sealevel and the basin had no surface connection to the open ocean.

Periodic seawater flooding or climatically-induced freshening then renewed carbonate deposition as the A-1 carbonate was deposited across the basin and platform region (Leibold, op. cit.). The A-1 composite sequence was terminated by further drawdown, resulting in a second thick lowstand evaporite wedge (A-2 halite). Reflooding and/or climatically induced freshening initiated multiple stacked A-2 carbonate aggradational sequences, separated by several drawdown unconformities. The B Unit is a composite of carbonate/evaporite sequences, each consisting of an aggradational carbonate parasequence and a lowstand evaporite wedge. These sequences mark the final filling of the basinal depression created during Niagaran carbonate deposition. Thus the A-1 and A-2 units of the Salina Group each comprise a lowstand relative to external sealevel, with each evaporite sequence set overlain by a relative highstand carbonate sequence set. Both composite sequences are punc-

tuated by several, widely-correlatable drawdown events. The B-Evaporite is dominantly a “lowstand” composite sequence consisting of stacked, shallowing-upward evaporite cycles.

Sequence stratigraphic interpretation in the Michigan Basin sequence underscores the difficulties in interpreting an isolated intracratonic basin using unconformity/bounding-surface terminology tied to a set of marine sealevel implications. It is very hard to do this reliably in a basin that lacked a marine connection for most of its evaporite history and in a hydrological situation where intrabasinal water level fluctuations were not necessarily related to extrabasinal eustatic changes. Recognising regional unconformities in core and seismic is the key to any reliable sequence stratigraphic interpretations in this situation. Unfortunately unconformities are numerous in drawdown sequences and correlations of supposed regional unconformities from basin edge to basin centre are difficult. Often it is done based on marine eustatic assumptions and this of course leads to circular arguments in interpretations of eustasy based on a sequence stratigraphic interpretation.

Sarg (2001; his Table 1) lists the Michigan Basin as a type example of a third-order basin centre fill (10-100 m thick) with an onlap basin margin and he places it in the same classification category as the Z1-Z4 units in the Zechstein Basin. A fact to remember when attempting unconformity-based correlation and sequence stratigraphic interpretation is that evaporite aggradation rates are so rapid in a basinwide systems that the basin fill quickly aggrades to the intrabasin hydrological equilibrium (time frames of up to 1-2 km of fill in a few hundred thousand years). It means that in the 1-7 million year long history of any evaporite-filled basin there were long periods, post the attainment of hydrological equilibrium, when not much was happening depositionally. That is, based on the hydrologies detailed in Chapters 2 through 4 and the chronology of the Messinian in the Mediterranean, we know that evaporite basins fill rapidly with stacks of 5th and 6th order cycles. Using salt thickness to divide evaporite successions into second order (100-1000 m) versus third order (10-100 m) cycles is an irrelevancy that comes from applying assumptions inherent in a marine eustatic terminology.

Thick-bedded marine-fed evaporites are intrabasinal responses to hydrological evolution and should not be tied to any marine eustatic implication. Marine-fed and the associated concept of hydrological equilibrium (drawdown) are not the same as assuming marine salts fill the basin to sealevel. When 1-2 km thick halite beds were accumulating in the Messinian in Mediterranean basin, the saltpan surface never came within a kilometre of sealevel in the adjacent Atlantic.

Sarg (2001) also argues that the coral-crinoid growth occurred in Michigan Basin pinnacles in a marine reconnection episode, following the A1 evaporite drawdown stage. He equates subsequent coral-crinoid growth to ongoing growth in the Niagaran Platform via a set of regional unconformities. Others have difficulty with this correlation and see stenohaline crinoid-coral deposition ceasing throughout the basin at the end of the Niagaran with subsequent mud mound growth occurring in mesohaline marine-seepage fed conditions. This group of workers choose a different set of unconformity correlations. They see the euryhaline stromatolite/stromatoporoid biomes as the major contributors to mound growth once the Michigan Basin lost its surface connection to the ocean.

This debate of a possible marine surface connection post-A1 carbonate and a definition of the A-0 carbonate, first detailed by Mesolella et al. (1974) in three models of pinnacle-evaporite inter-relationships, continues today. What we have learnt since the early 1970s is that all of the salts in the Michigan basin were deposited in shallow drawdown waters. At the time of evaporite deposition the basin's shelf margin and the crests of the pinnacle reefs were subaerially exposed, the tops of the inactive pinnacles acted as spring mound feeds to the surrounding lows characterised by a halo of anhydritic mudflats passing further out in to halite pans. Anhydrite is present both as a sabkha nodules and as widespread diagenetic cements within marine carbonate hosts. The possibility of widespread early burial anhydrite in Niagaran carbonate is something largely ignored by sequence stratigraphers working in pinnacles in the Michigan Basin, who tend to see anhydrite as a mostly marine mudflat facies not a seepage facies. With the possible exception of the pinnacle crests, no widespread open marine sediments accumulated in the Central Michigan Basin, even at times of freshened (but still evaporitic) carbonate accumulation, such as the A1 and A2 carbonates.

Summary

Modern and ancient evaporite basins can deposit kilometre-thick sequences in less than 300,000 years. Such infills only occur at times of complete basin isolation when there is no surface connection to the world's oceans. Once we realize that thick evaporite accumulations require a stable longterm brine curtain ($\approx 10^5$ - 10^6 years) to accumulate to substantial thicknesses and lateral extents, we reach an understanding of why the present is not a good time to study the scale and diversity of possible evaporite settings. High amplitude, high frequency 4th-order sealevel oscillations of our current “icehouse” climate do not

allow the set up of stable brine curtains in present-day continental platforms. Nor are there suitable rift or collision belts where conditions are suitable for the creation of marine-fed basinwide drawdown deposits. The last such basinwide event occurred in the Mediterranean some 5.5 Ma. Thick stable brine curtains are today only found in continental settings.

Sequence stratigraphic analysis must be tied to a subdivision of ancient evaporites into three depositional styles, continental lacustrine, marine platform and marine basinwide. All three are suitable for high-frequency seismic interpretation and the unique nature of salt mean it is easily recognised and traced in a seismic section. The hydrology needed to form a salt bed also makes it a close approximation to a time line in the basin architecture. But, of the three styles, a marine eustatic interpretation tied to sealevel is only possible in a marine platform evaporite succession.

Chapter 6: Salt tectonics

Introduction

Flowing salt produces some of the most complex and visually impressive low-temperature geological deformation to be seen on the earth's surface. In Iran, flowing glaciers of salt (namakiers) rise up to 1000 metres above the surrounding Zagros landscape. Diapiric salt also outcrops in the Andes, the Canadian Arctic, in Cardona in Spain, and subcrops near Hallestat/Dachstein in Austria and along the banks of the Nam Theun River in Laos. It also is an important mechanism in controlling the formation of many complex traps for hydrocarbons and base metals (Warren, 2000b).

That rising salt can maintain units of highly soluble near-pure halite near the earth's surface is why Neolithic salt exploitation in Europe was inland and centred on mines at Cardona and Hallestat, as opposed to sites of seasonal coastal evaporation on the coastal plain. Some diapiric salt masses even have religious significance; Lot's wife on the edge of the Dead Sea is a 12m-high column of salt lying at the foot of the much larger Mt Sedom (Usdum). It is a dissolutional remnant from a gypsum-capped outcropping diapir composed of Miocene salt, which also makes up Mount Sedom. It was noted by Fulcher of Chartres (Chaplain to King Baldwin) who accompanied the crusader Baldwin I across the Dead Sea valley in December 1100 AD. But Sedom's description as a mountain is somewhat of a

misnomer, it is certainly 8 km across, but only rises a hundred metres or so above the floor of the Dead Sea Valley.

Salt tectonics (syn. halotectonics and halokinesis) is a general term that encompasses notions of lateral and vertical salt flow, trans-stratal salt movement, salt pillowing and diapirism, it refers to tectonic deformation involving halite or other evaporites as a substratum or source layer (Figure 6.1). Concepts of salt tectonics have undergone a major revision in the last fifteen years, due mainly to advances in 3D seismic acquisition and processing, especially 3D prestack depth imaging, and the realisation that salt tectonics is best modeled by considering a salt bed as a pressurized fluid layer overlain by brittle sediment (Hodgkins and O'Brien, 1994; Ratcliff and Weber, 1997).

Salt tectonics can be summarised in two simple geological principles. First, differential loading drives salt tectonics; this makes halokinesis a much more passive process than had been believed. Second, salt is a very weak and incompetent layer in the subsurface; its lateral flow and sliding carries along its overburden in extension and acts as a décollement in compression. Salt sheets, tongues, and allochthonous nappes are major subhorizontal components of the salt tectonic realm (Figure 6.1). Like any less competent layer in extension it undergoes boudinage and drives fracturing in its more brittle overburden.

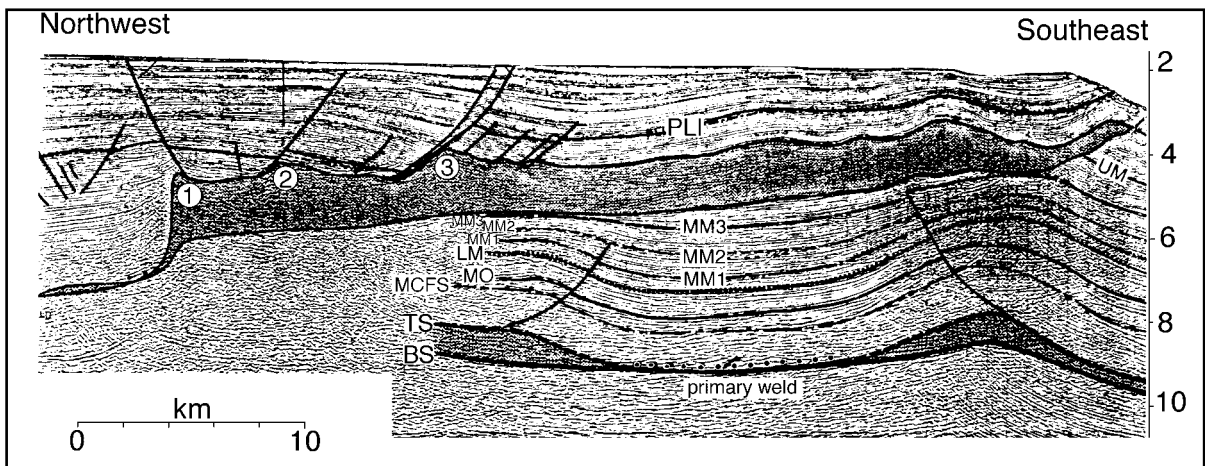


Figure 6.1. Interpreted seismic profile through allochthonous salt sheets that build the Sigsbee Escarpment (to southeast), base of continental slope off Louisiana, Gulf of Mexico (after Wu, 1993; Jackson and Vendeville, 1994). Note how supra-allochthonous faults have initiated diapiric upwelling at 1, 2 and 3. The allochthon is underlain by shortened strata of the Mississippi Fan Foldbelt. BS = base of Jurassic Louann Salt; TS = Top of salt; MCFS = Middle Cretaceous flooding surface equivalent; MO = Middle Oligocene; LM = Lower Miocene; MM1 = Lower Middle Miocene; MM2 = Middle Miocene; MM3 = Upper Middle Miocene; UM = Upper Miocene; PLI = Pliocene. Note how Jurassic salt has climbed the stratigraphy and now overlies and seals Neogene deepwater sediment.

The word diapir originally comes from the Greek *diaperin*, meaning “to thrust-through” and was coined by L. Marzic in 1902 to describe salt features of the Romanian Alps at a time when diapir emplacement was considered to be a forceful intrusive process capable of pushing aside kilometres of overburden. Today, salt diapirs are defined as salt flow features showing discordant contacts with the encasing sedimentary strata. This definition does not uncritically encompass notions of active piercement and the shouldering aside of thick overburden. Where feasible salt constituting a diapir should be further classified as either allochthonous or autochthonous.

Allochthonous salt structurally overlies parts of its (stratigraphically younger) overburden and is often no longer connected to the primary salt bed (mother salt level). For example, spectacular allochthonous salt sheets in the northern Gulf of Mexico form a line of five or so huge asymmetric tongues of Jurassic salt that now overlie and seal Pliocene to Pleistocene sediments. They coalesce behind the Sigsbee Scarp to form a salt tongue canopy and can be considered analogous to gravitational nappes in orogenic belts (Figure 6.1; Worrall and Snelson, 1989). Allochthonous salt bodies climb the stratigraphy via a series of tiers or canopies, leaving evidence of passage as thin salt pods, dissolution residues and alteration aprons along salt welds or overburden touchdowns, much like a garden slug leaves behind a slime trail. Autochthonous salt structures are those still firmly rooted in the stratigraphic level of the primary salt bed. Prior to the application of current seismic imaging and processing techniques most diapiric structures were interpreted as autochthonous thumb-like appendages connected at the level of primary weld.

A whole new realm of salt/sediment configurations and oil exploration plays have opened up in the last two decades with the realization that; a) salt sheets can be allochthonous and subhorizontal over large areas in a sedimentary basin, and b) structures in the salt allochthon overburden are tied either to the trailing edge of the allochthon where salt is evacuating/withdrawing, or the leading edge where salt is flowing at or near the surface. A range of potential subsalt hydrocarbon traps have now been successfully drilled in the Americas, where the move into deeper water revitalised what were considered mature exploration provinces (Montgomery and Moore, 1997; Meisling et al., 2001).

This chapter will concentrate on salt structures; halokinetic breccias that remain after the salt has dissolved will be discussed in Chapter 7, hydrocarbon associations are discussed in Chapter 10 and exploitable diapiric salts in Chapter 11. Diapirs do not just form in salt, they can occur in any geological material

with markedly different pressure and strength compared to its overburden. Some of the principles and concepts developed in describing salt diapirism as newtonian fluid responses can be successfully applied to overpressured shales, serpentinites and even molten granites rising through the mantle (Talbot, 1992a).

Physics of salt systems

Even with our greatly improved ability to seismically outline salt features, the comments made by Richter-Bernburg, more than two decades ago, still hold true today. In a 1980 review he noted that our geological understanding of the world's various salt structures is still very much like that of a sculptor to the human body; the whole figure can be perfectly described, especially using 3D seismic and forward modelling, but the anatomy, the inner organs and the complicated inner structures remain largely disregarded. So before we look at the various geometries sculpted by salt, let us look internally at the properties of salt that drive salt flow and at the internal textures indicative of this flow.

Density, viscosity, strength & buoyancy

After it loses effective porosity by 100-200m burial, halite's density of 2.2 gm/cc remains near constant throughout the diagenetic realm and it is near incompressible to depths of 6-8 km (Figure 6.2a). With entry into greenschist depths, deeply buried halite can experience massive recrystallisation and dissolution, along with a slight decrease in density due to thermal expansion (Figures 6.2a, 8.19; Lewis and Holness, 1996). In contrast, burial compaction in shales and most other sediments is defined by a progressive loss of porosity, with an associated increase in density and strength until it exceeds that of the salt below. This means that salt has positive buoyancy when buried beneath nonevaporitic overburden to depths in excess of a kilometre. With a muddy overburden, the depth of density crossover, sometimes called the level of neutral buoyancy, is typically shallower than 1300 to 1500 metres. It can be much shallower beneath reefs and other cemented carbonates, which can have densities equal to, or greater than, salt almost from the time of deposition. This can lead to rapid foundering and brecciation of reef materials, especially in areas of overburden extension and allochthon spreading.

Few other rocks are as thermally conductive or as close to truly viscous as natural rock salt (Figure 6.2b, c). Viscosity is a measure of a fluid's resistance to flow or its internal fric-

tion and is measured by the ratio of shear stress to the rate of shear strain. Laboratory measurements show wet carnallite can have a viscosity as low as 10^8 Pa.s, while dry halite has a viscosity around 10^{18} Pa.s (for comparison, honey at 14°C has a viscosity ≈ 60 Pa.s; window putty $\approx 10^5$ Pa.s; and road tar $\approx 10^7$ Pa.s; $1 \text{ Pa.s} = 10 \text{ poise}$). The viscosity of salt in the Gulf of Mexico is 10^{13} to 10^{16} Pa.s, depending on moisture content and temperature. The adjacent overburden of clays and sands is less viscous by four to five orders of magnitude. Davison et al. (1996a) estimates the ratio, sedimentary rock: evaporite rock viscosity, ranges from 50 to 10^4 . As different parts of a diapir deform at different rates and by different mechanisms, the effective subsurface viscosity values for diapiric salt vary with position in the diapir, the water content of the salt and time. Due to its much higher moisture content (from meteoric waters), diapiric salt is much less viscous when it reaches the surface as a tongue of extruded salt than at depth.

Over geological time frames, finer-grained wet salt approaches^{6.1} Newtonian viscous behaviour, unless it is atypically coarse grained. And like any fluid it cannot support shear so a mound of wet salt emplaced on the earth's surface will spread under its own weight. Using a viscous fluid model, salt diapirism and its relationship to its overburden can be likened to Rayleigh-Taylor instability with a viscous substratum (salt) and an overlying denser viscous fluid (overburden; e.g. discussions in Koyi, 1991; Talbot, 1992a,b). Under such a fluid-fluid model, diapirism is spontaneously initiated by small irregularities in the fluid-fluid interface that then amplify with time and buoyancy contrast. Diapirs rise continuously and inevitably until the less dense salt overlies its overburden. The only requirement for Rayleigh-Taylor instability in a fluid-fluid system is density inversion; diapirism modeled in such a way does not require any external trigger such as regional extension or differential loading. Under this fluid-fluid scenario, any regional extension thins the fluid overburden and the source layer, so reducing the overall thickness. The resulting diapirs are smaller, more

^{6.1}Newtonian (or viscous) flow occurs when the rate of shear stress is directly proportional to the shear strain.

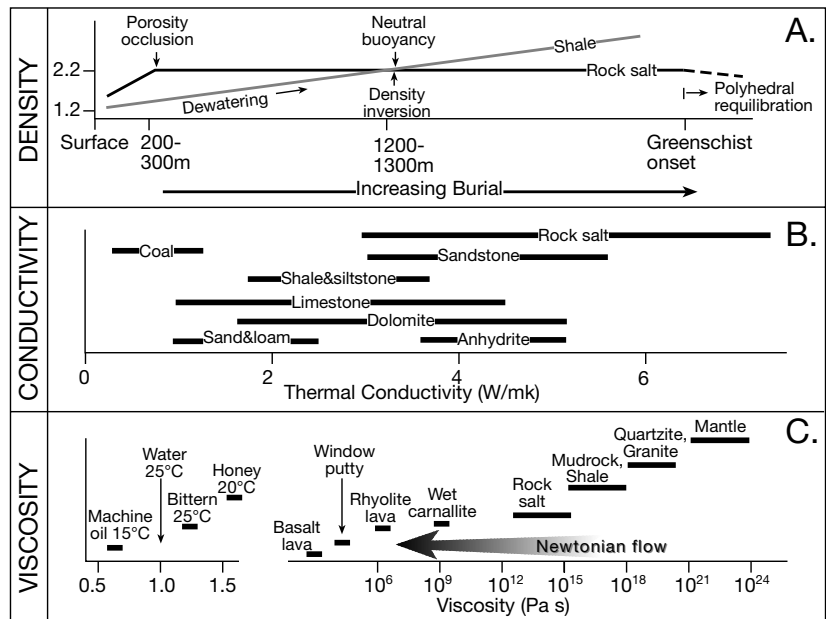


Figure 6.2. Physical properties of rock salt compared to other lithologies. A) Density changes with burial. B) Thermal conductivity (see also Figure 8.19a). C) Viscosity.

closely spaced, and more slowly rising than those in unthinned counterparts (Koyi, 1991).

Rather than model the salt's overburden as a viscous fluid, proponents of the "brittle school" tend to model salt as a pressurized pseudo-fluid at subsurface flow rates, and consider its sedimentary overburden liable to show brittle responses to stress (e.g. Jackson and Vendeville, 1994). In most subsurface situations it means that relative density as a trigger and a subsequent control to halokinesis, is a less important consideration than relative strength of salt and its overburden. This style of modelling is better supported by the geological observations that; diapirs rise episodically rather than continuously, that salt flows when loaded (much like toothpaste is squeezed out of its tube) and that faulting, rather than folding, characterises much of the early deformation in the overburden. In reality, the strength response of a buried salt bed and its overburden will depend on the strain rate and the rate of deformation in the overburden. Salt can fracture and fault at high strain rates (brittle response), but the required strain rate is much higher than experienced in many typical subsurface situations (Jackson and Talbot, 1994).

Subsurface nonevaporitic sediments, including indurated shales, show time-independent, pressure-dependent brittle behaviour under stress and deform most readily by frictional slip along faults. In contrast, bedded salt under stress tends to flow and

deform. Most adherents of the brittle school contend that varying combinations of regional extension, differential loading and gravity sliding, will localise, initiate and promote diapirism of salt and shale. The conclusions of the “brittle” school are supported by studies showing virtually all sediments at shallow crustal depths (<8-10 km) deform as faulted brittle masses, rather than by the creep and folding that typifies deforming evaporite salts. This depth range encompasses much of the realm of salt tectonics in sedimentary basins.

Evaporite salts are unique in their tendency to flow in the diagenetic realm. Representative strain rates and speeds of salt deformation are listed in Table 6.1. A strain value of 10^{-15} s⁻¹ indicates that a rock stretches at a rate of 10^{-15} of its length per second and is representative of the slow strain rates encountered in rock deformation rates in active orogenic belts. A value of 10^{-9} is 1 million times faster and represents strain rates in active (wet) salt glaciers in Iran (1.6×10^{-13} to 1.8×10^{-8} per second; Wenkert, 1979) and equates to an annual rate of rise of ≈ 2 m/year in the salt stem. But the rate of salt supply and surface flow is not constant; salt glaciers (namakiers) in Iran always flow faster after a rain; the Dashti glacier at Kuh-e-Namak flows at upto 0.5 m/day during the few weeks of the annual wet season, but flows little if any during the dry season when the glacier expands and contracts diurnally in response to changes in surface temperature. But what do these observed rates of deformation mean in terms of driving mechanism and how does flow occur at the crystalline scale?

Cataclastic or brittle responses to deformation involve microfracturing and sliding of grains and grain fragments (grain crushing) and are important in non-evaporite indurated sediments at low temperatures and confining pressures (Talbot and Jackson, 1987). The same brittle responses are also seen in salt mines in areas where deformation failure of salt pillars has occurred. In contrast, any fluid responses to deformation result in kinking of crystal lattices by various combinations

of slip, glide or dislocations of grains, known collectively as dislocation creep.

Based on naturally and artificially deformed salt samples, Carter et al. (1983) concluded dislocation creep occurs at temperatures and pressures relevant to subsurface salt deformation. They found that short-term, high stress flow properties of dry salt can be reasonably encapsulated in an empirical power-law equation (Figure 6.3a). This power law explains the rates of creep and differential stress fields interpreted in shallow diapiric salt. It does not explain the much higher strain rates of 10^{-8} to 10^{-11} measured in salt allochthons and salt glaciers (extruded wet salt) at stress differentials estimated to be around 0.5 MPa and at ambient surface temperatures (Talbot and Jackson, 1987a). Nor do their stress/strain triaxial experiments duplicate the elongate recrystallised textures of naturally deformed salt; such textures imply some sort of diffusional flow (Urai et al., 1986).

Classic hard-rock diffusional flow mechanisms allow strain by diffusion of ions along grain boundaries (Coble creep) or through the crystal lattice (Nabarro-Herring creep). In dry salt experiments these mechanisms are largely irrelevant in the low temperature fields that characterise salt deformation in the diagenetic realm. In wet salt, a diffusion mechanism can operate at much lower temperatures and differential stresses (Urai et al., 1986). The high solubility of chloride salts means solution transfer creep (aka solution precipitation creep and pressure solution creep) is the prevalent deformation mechanism in flowing salt in the diagenetic realm (Figure 6.3b). Triaxial deformation experiments by Urai et al., (1986) using carnallite, sylvite and rock salt showed that flow laws based on short-term high-stress experiments conducted on dry salt should not be extrapolated to salt deforming under lower strain rates and nondilatant conditions. They found that both dry salt (≈ 0.05 wt% inherent water) and wet (brine-saturated) salt both deformed by power law creep with $n > 5$ at strain rates faster than 10^{-7} s⁻¹, as found by Carter and Hansen (1983). However, the same rocks

deformed by power law creep with $n \approx 2$ (dry) or $n \approx 1$ (wet) when samples were stained more slowly by suppressing the rate of dilatancy (either by increasing confining pressure to between 5 to 10 MPa, or adding brine under dilatant conditions.

Type of flow	Strain rate (s ⁻¹)	Speed (mm a ⁻¹)	Speed
Lava flow (faster when hotter)	10^{-5} to 10^{-4}	5×10^{11} to 3×10^{13}	1 to 60 km hr ⁻¹
Ice glacier (surges with increased temperature)	10^{-10} to 5×10^{-8}	3×10^5 to 2×10^7	1 to 60 m day ⁻¹
Salt glacier (surges after a rainstorm)	10^{-11} to 2×10^{-9}	2×10^3 to 2×10^6	10 to 100 km Ma ⁻¹
Mantle currents (temperature and pressure controlled)	10^{-15} to 10^{-14}	10 to 10^3	2 m a ⁻¹ to 5 m day ⁻¹
Spreading salt tongue (<30km wide)	8×10^{-15} to 10^{-11}	2 to 20	2 to 20 km Ma ⁻¹
Spreading salt tongue (>30km wide)	3×10^{-16} to 10^{-15}	0.5 to 3	0.5 to 3 km Ma ⁻¹
Rising diapiric salt (increases with water content)	2×10^{-16} to 8×10^{-11}	1×10^2 to 2	10 m to 2 km Ma ⁻¹

Table 6.1. Representative strain and flow rates (after Jackson and Vendeville, 1994).

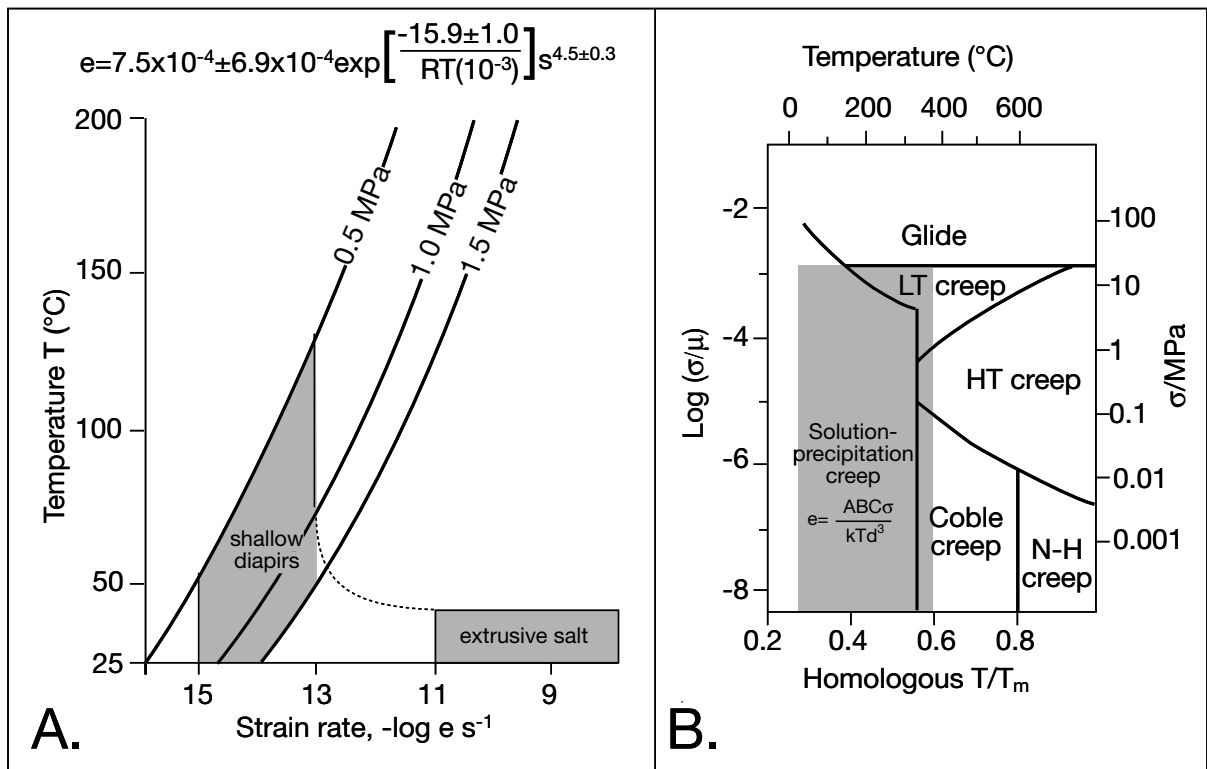


Figure 6.3. Conditions of temperature and strain where salt tends to flow rather than fracture (after Talbot and Jackson, 1987a; Carter and Hansen, 1983). A) Power law behaviour of dry rock salt where the relation between steady-state strain rate (e) and differential stress (σ in MPa) is highly nonlinear (stress exponent, $n = 4.5$). This power law does explain deformation in salt diapirs but not the much higher strain rates of extruded salt/salt glaciers. There much of the flow is periodic and facilitated by the presence of water. R is universal gas constant and T the absolute temperature. B) Deformation mechanism map for damp rock salt showing dominant deformation mechanisms for different temperatures and stresses. Shaded area shows the dominant field for most natural salt flow, which lies mainly in the solution-transfer field (solutant diffusivity term; C = grain boundary structure parameter; k = Boltzmann constant; d = grain size. T_m = melting point of halite; LT and HT is low and high temperature; N-H is Nabarro Herring (after Urai et al., 1986).

They also found that samples deformed under these more geologically realistic conditions had completely recrystallised with flattened fabrics very similar to those of naturally deformed salt. This process of solution transfer creep in the salt produces new gneiss-like crystal textures made up of amoeboid-like strain-free flattened salt grains (a flow parallel fabric). Solution-transfer creep or pressure solution creep occurs in regimes of differential stress as halite grains dissolve in regions of high stress and reprecipitate in regions of low stress. The basic processes involved are the migration of existing grain boundaries and the formation of new high angle grain boundaries (Drury and Urai, 1990). New crystals are less substructured and replace older more substructured grains as migrating crystal grain boundaries consume and sweep through the older milky inclusion-rich portions of the salt. Crystals in an area swept by grain boundary migration tend to be inclusion-free, with fluid inclusions now focused along the grain boundaries and so providing conditions

suitable for pressure-solution induced creep of the salt mass (Urai et al., 1986; Spiers et al., 1990). Much of this new salt is clear and sparry rather than milky.

Grain boundary migration in deforming wet salt typically leads to grain growth during recrystallization, but can also lead to grain size reduction if new grain boundaries are formed at grain boundary bulges or as a result of grain dissection by migrating boundaries (Ter Heege et al., 2005). New grain boundaries may also form from subgrain boundaries, by progressive misorientation of subgrains or by migration of a sub-boundary through an area of cumulative lattice rotation. This is called rotation recrystallization. The relative importance of migration and rotation recrystallization is dependent on the deformation conditions (i.e. temperature, strain rate and stress). The mean grain size D of dynamically recrystallized materials has been found to be related to the steady state flow stress σ by a general

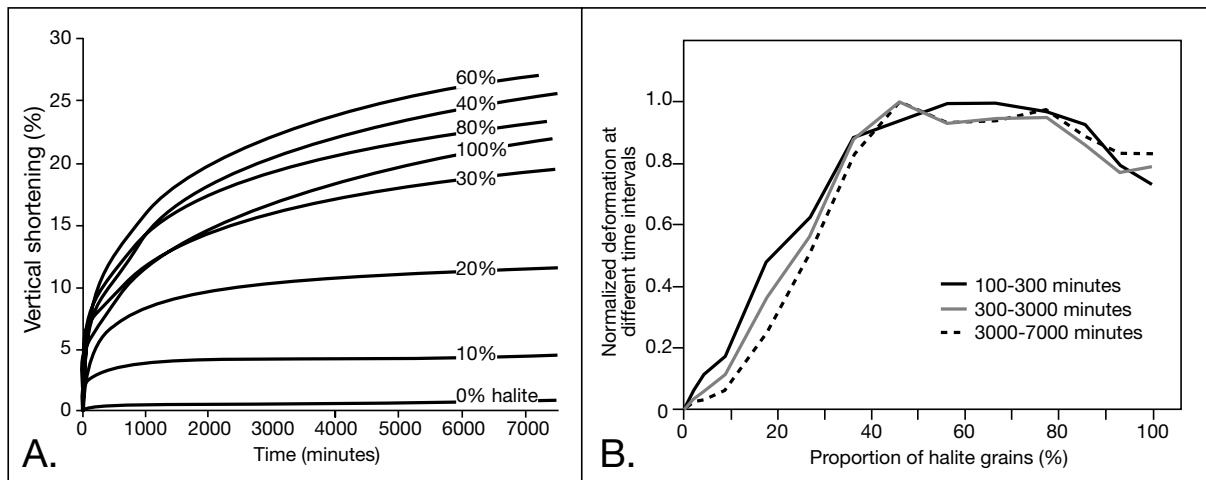


Figure 6.4. Effect of impurities on salt compression, cementation and pressure solution. A) Result of drained compaction experiments. Compaction curves $E(t) = (x_0 - x(t))/x_0$ for different samples show that the total amount of compaction after 7000 min (roughly 5 days) depends on the relative proportion of halite and calcite grains. The highest finite compaction (vertical shortening) does not occur in a sample composed of 100% halite grains. B) Effect of the mineralogical composition on the amount of vertical shortening on a halite-calcite aggregate. The three curves are normalized to the average maximum deformation of the tested samples at the given elapsed time and they show the same trend, within experimental errors. The mixtures with halite contents between 0 to about 40% do not exhibit this behavior. The rate of deformation goes down during progressive deformation for halite proportions ranging between 10% and 40% (after Zubtsov et al., 2004).

theoretical relation of the type $D = K\sigma^p$, a power law, where K and p are material and mechanism specific constants (see also Figure 6.11 and discussion). Ter Heege et al., (2005) have now experimentally modelled the specific deformation of wet salt and concluded that the equation is of the form:

$$(D/\beta) = 10^{-1.55 \pm 0.24} (\sigma/\mu)^{-1.85 \pm 0.23} \exp(14.2 \pm 2.8/RT)$$

with D denoting mean recrystallized grain size, Burgers vector $\beta = 3.99 \times 10^{-4}$ μm and the shear modulus $\mu = 1.5 \times 10^4$ MPa.

The intensity of salt flow and recrystallisation (re-annealing) can in part depend on levels of impurities in deforming and compressing salt. Various lab-created mixtures of crushed halite aggregate and calcite crystals show an interesting set of responses under triaxial compression with free drainage of fluid products (Zubtsov et al., 2004). A 100% halite sample, or an 80:20 halite-calcite mixture, are both less susceptible to compressional shortening than halite-calcite mixtures of between 40% and 60% halite (Figure 6.4a). This is true at all time ranges in the experiment, which ran for periods of up to 5 days (Figure 6.4b). Mixtures with <30% halite show less shortening than all samples with higher proportions of halite in the mix. These responses indicates two mechanisms competing at the grain-to-grain scale: 1) intergranular pressure solution at grain contacts, which facilitates compression, especially across boundaries with different chemical potential

as typically occurs at contacts between grains with different mineralogy, and, 2) grain boundary healing (re-annealing), as occurs between halite-halite grains and studied in pure halites by Urai et al. (1986). It drives the ongoing annealing that then hinders further compaction. As the halite content in the mixture increases, more and more halite-halite grain contacts can heal and so act to resist compression. Volume loss by draining of pressure solution fluids becomes less efficient in such healed or partially healed contacts (Zubtsov et al., 2004). This is another illustration of pure salt's ability to act as an effective seal, it shows that even when faulted salt will quickly anneal itself, unless impurities can enter the fault plane.

When the creep and frictional strengths of wet and dry salt are compared with equivalent strengths of other sedimentary rocks, using a representative strain rate of 10^{-14} s^{-1} , it can be seen that even dry salt is much weaker than any overburden sediment, except perhaps for extremely shallow water-saturated muds less than a few hundred metres deep where water contents can be in excess 50% (Figure 6.5). Damp salt, which deforms by solution-transfer creep is hundreds of times weaker than dry salt, which deforms by dislocation creep, which the movement by slippage along lattice defects (Urai et al., 1986).

The minute quantities of brine caught up as inclusions and intergranular films in confined natural salt have a profound effect on strength. Damp salt does not even require external

water to act as a newtonian fluid (Urai et al., 1986). Water in a deforming salt unit need not come from an external source as its brine-filled inclusions contain sufficient water (up to 4-5% by volume) to allow salt to flow naturally at the earth surface conditions. In other words, salt can flow spontaneously by solution transfer creep, once extruded at the surface it will collapse or spread under its own weight (gravity collapse).

Deforming salt has almost no shear strength at most geological time scales of applied stress; it is a pseudo-fluid (Figure 6.5; Weijermars et al., 1993). The extreme weakness of natural wet salt at the surface is seen in seismic onlap patterns of allochthonous salt sheets deforming by gravity gliding in the Gulf of Mexico. The salt sills are emplaced into low density water-saturated shales at depths of less than 250-300m beneath the sediment-water interface, with a mean depth of 150m (Figure 6.6; Nelson and Fairchild, 1989; Nelson, 1991). Shales deeper than that were too strong to be laterally intruded by a salt sheet. Were density contrast rather than relative strength the controlling factor, then salt sheets would have spread out at depths \approx 1400 metres, which is the level of neutral buoyancy beneath this part of the Gulf of Mexico (Nelson, 1991). Salt weakness, or lack of strength, is thus more significant than buoyancy contrast in controlling the position of flowing allochthonous salt sheets in earth-space.

The weakness of salt at geologic strain rates means the viscous forces in flowing salt cannot easily drag or stretch the overburden. Rather, thick flow-susceptible salt sheets acts as a pressurized layer of lubricant that effectively decouples the overburden from the basement. A thick salt bed tends to act as a ductile "crack stopper" whereby it hinders faults and dykes propagating into higher or lower levels of the stratigraphy. A thick salt layer segments basin sediments into suprasalt and infrasalt layers that can deform independently or even by different processes. The impervious but fluid nature of salt focuses and entraps petroleum and mineralising fluids against a salt seal at the tops of subsalt faults, even if the faulting postdates the subsalt and suprasalt layers (Chapter 10).

Salt layers act as a lubricant in deforming sediment masses. The lubricious effects of salt layers are seen in the widths, taper angles, and internal structures of dynamic wedges at both converging and diverging plate boundaries. By lubricating regional décollements, even thin layers of salt influence how huge areas shorten or extend during gravity gliding. It leads to the complexities of raft tectonics, where rapidly opening ocean basins generate floundering blocks of brittle sediments (tens of kilometres across and kilometres thick) that glide down into the widening basin atop a layer of lubricating salt. For the same reason fold thrust belts in converging plate margins that are deforming over salt layers are much wider, with taper angles

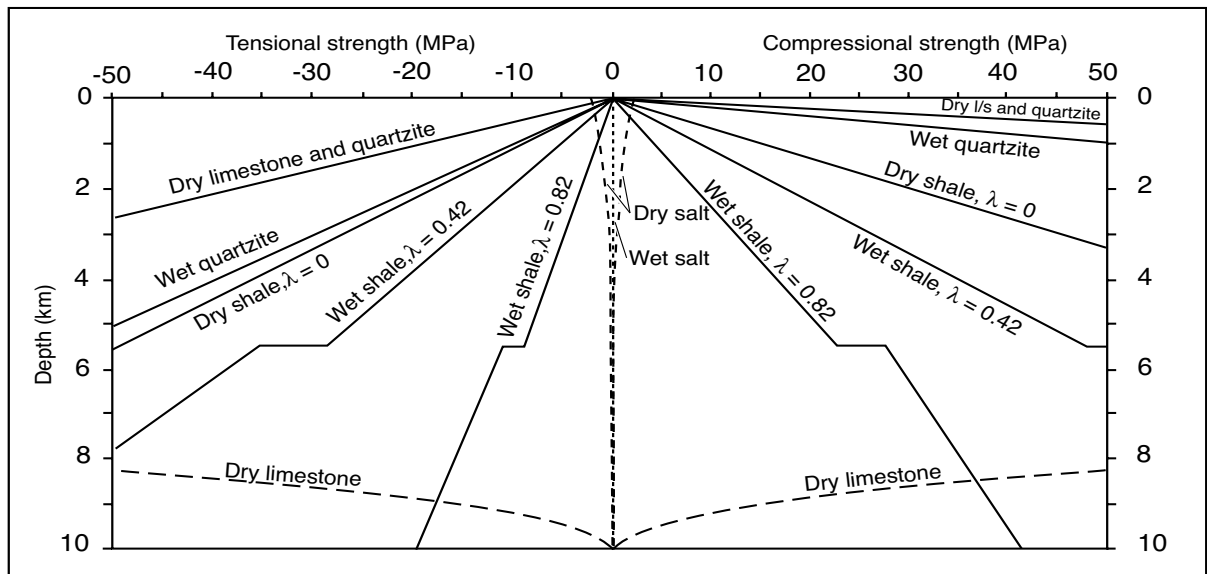


Figure 6.5. Comparison of creep and frictional strength of dry salt with equivalent strengths of dry and wet sedimentary rocks and sediments (after Jackson and Vendeville, 1994). Creep strength is the deviatoric stress required to drive salt flow at a representative strain rate of 10^{-14} s^{-1} . Pore pressure coefficient (λ) is the ratio of pore pressure to lithostatic pressure: $\lambda=0$ for dry rocks, $\lambda=0.46$ for hydrostatically pressured rocks and $\lambda = 0.86$ for overpressured rocks. In contrast wet salt is so weak (strength of 0.01 MPa at this strain rate) that its creep curve plots virtually on the central axis.

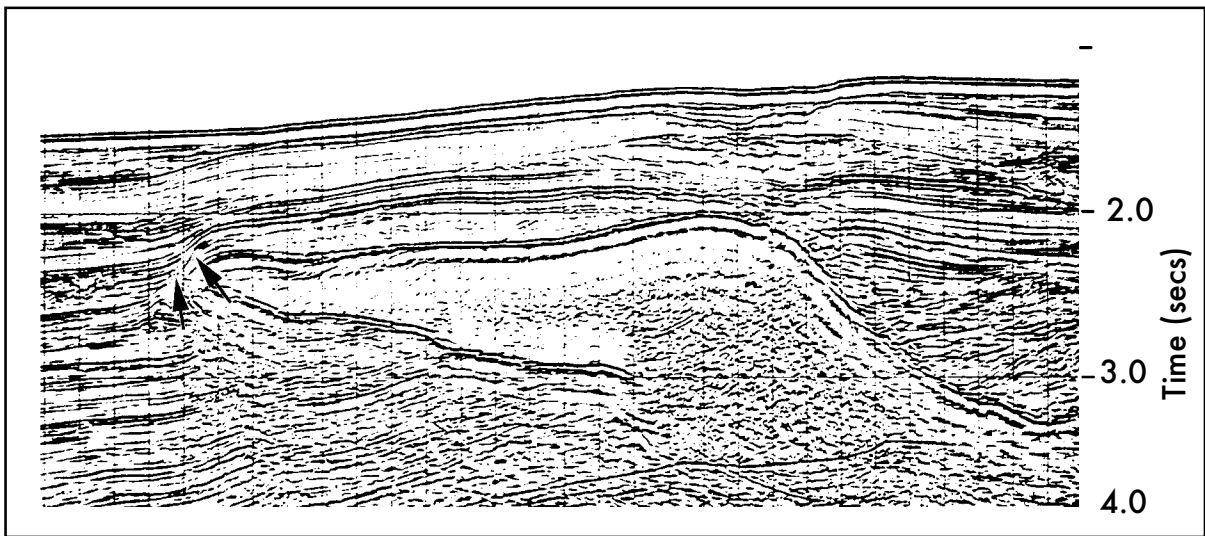


Figure 6.6. Salt allochthon, northern Gulf of Mexico (after Nelson, 1991). Onlap of frontal reflectors above a thin roof, averaging only 100m thick (arrows on left hand edge of salt tongue), indicates shallow emplacement of the allochthonous salt tongue.

$<2^\circ$; while those deforming over more competent décollement layers are narrower, with taper angles nearing 8° (Davis and Engelder, 1987).

In reality, a simple division into brittle versus viscous fluid response models is an oversimplification as salt and the adjacent sediments can, depending on the circumstances, exhibit either brittle or viscous responses (Davison et al., 1996a; Poliakov et al., 1996). Salt at the surface is brittle enough to fault or shear, and such displacements are not uncommon in salt mines or in faults cutting across the surfaces of some dry salars of South America (Figure 3.47). Likewise the overburden can show evidence of viscous behaviour. Sediments atop allochthonous salt sheets in the Mexican fold ridges in the Gulf of Mexico are mostly folded not faulted. Seismic also shows many diapirs have sedimentary margins with smooth drag profiles known as shale sheaths, rather than brittle faulted margins adjacent to fluid salt.

Pressure effects

The realisation that density inversion is not the major force driving the onset of salt diapirism led to an improved understanding of the significance of pressure differences once salt flow has begun. Like all buried sediments, a salt source layer is pressurised by its own weight, along with that of the overburden, to create a pressure head (Ψ). The typical subsurface situation prior to diapirism is where a unit of pressured salt underlies a more competent sedimentary sequence. As hydrostatic fluid

pressures build within the accumulating overburden it fails, typically under extension. Failure is often activated by externally applied stress such as; continental slope/pull-apart, seismic triggering, gravity sliding, or the onset of inversion tectonics. Pressure is released in the overburden via brittle failure and pressurised salt flows in to take up the dilating space. As this occurs the fractured blocks of the more competent overburden simultaneously pull apart and sink into the rising salt.

Flowing salt moves laterally or is dragged into developing gaps, with a speed dependant on the relative rates of overburden sinking and extension, which in turn reflects on the fluidity of the salt. If overburden mostly sinks as blocks into a fluid salt layer, then salt filling the space between the blocks rises relative to the surface of the sinking overburden and so can spill and spread over the surface of the sinking overburden block (see allochthon discussion). However if the salt layer is relatively strong or if separation dominates, then the salt diapir may never rise very high at all and never spill and flow at the surface. If extension continues once the salt has risen to the maximum level dictated by the pressure field, then the salt diapir crest will collapse as the gap between adjacent overburden blocks increases. A graben will develop atop the salt crest, depositing sediments in the top levels of the dilating supra-diapir space (see discussion of falling diapirs).

Active piercing of a brittle sediment overburden can occur wherever the pressure head (Ψ) exerted by the fluid salt creates a buoyancy force that exceeds the strength of the overburden.

Figure 6.7 illustrates pressure head for three situations where the fluid salt layer is rising through its brittle overburden (Jackson and Vendeville, 1994). In all, any net upward force in the salt is resisted by the strength of the overburden roof, which depends on roof thickness. Thin roofs are weak and easily pierced, whereas thick roofs are too strong to be pierced by pressurised salt alone and require regional extension to be diapirically breached. The thickness of sediment that can maintain sufficient strength to hold back a buoyant (pressurised) salt bed defines the piercement threshold layer. If sediment thickness is less than the piercement threshold, then a salt diapir can actively pierce or shoulder aside its overburden (shown by the arrow in Figure 6.7a). Active piercement can occur where the floor of an erosional valley, or sag-focused erosion, thins the overburden layer to such a degree that the trough floor lies below the piercement threshold (Figure 6.7b). This is the mechanism driving salt diapirism in the Canyonlands National Monument, USA, with a diapir formed in a area thinned beyond the piercement threshold by the erosive activity of the Colorado River (Schulz-Ela and Walsh, 2002). Active piercement can also occur in situations where the suprasalt roof is thinned by extension, a commonplace feature in actively spreading rift systems (Figure 6.7c).

Jackson and Vendeville (1994) noted that, the taller or wider the salt ridge or plug, the more easily it pierces its overburden. Likewise, the thinner the roof, the more easily it is pierced. Structures with linear planforms (ridges or troughs) are more easily pierced than those with circular planforms (plugs or cavities). Pressure forces below a surface trough or cavity are set up by the density ratio between overburden and air or water (typical ratios around 2 or higher). Conversely, pressure forces above salt ridges or

plugs reflect the lower density ratio between overburden and salt, typically around 1.1 to 1.2.

Salt's fluidity and ability to reanneal make it a highly effective low permeability barrier to fluids escaping from the underlying

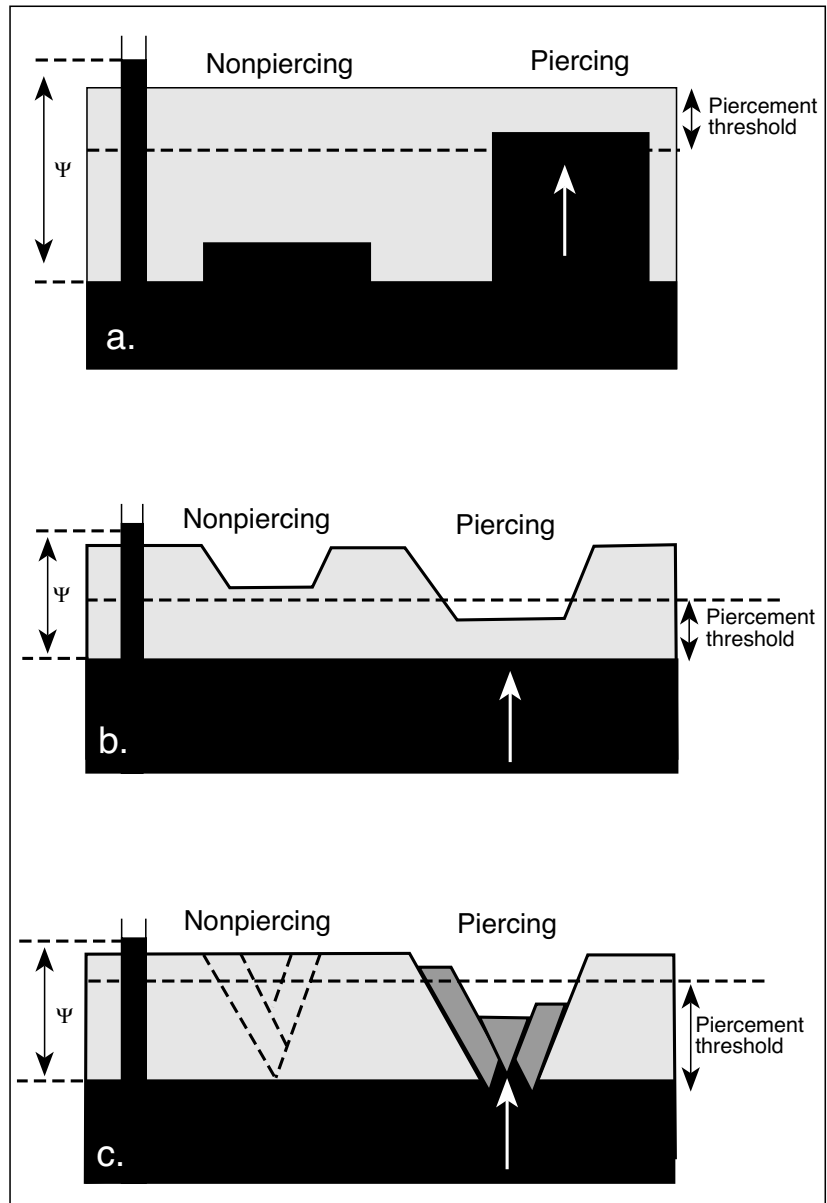


Figure 6.7. Conditions for active piercement of salt (black) overlain by rigid brittle overburden (grey). Where the overburden is thinner than the piercement threshold, the salt can break through (white arrows) under nonextensional conditions above salt ridges (a) or below topographic troughs (b). In (c) the non-stretched salt roof is too thick to permit diapirism but where it is thinned by extension to below the critical thickness a diapir can break through. Ψ is the pressure head of salt (after Jackson and Vendeville, 1994).

sediments. As sediment is deposited atop an impervious but fluid salt layer, pressure beneath it builds as it acts as a pressure blanket. A layer of salt in a subsiding basin exaggerates overpressures in the section beneath the salt and mitigates transfer of overpressure to the section overlying the salt. If there are no breaches in the salt layer this can result in a tremendous increase of overpressure across the lower salt boundary (Figure 8.14). Even thin salt sills can be highly efficient fluid seals. As a result, extremely overpressured sediments can be intersected immediately under a salt sill, creating a drilling hazard. Whenever or wherever a salt sheet is breached by salt dissolution or salt evacuation, a highly pressured pulse of subsalt fluids moves up through the breach. In many situations the sole of a growth fault marks the breach and the extending fault becomes a conduit for the escape of hot basinal fluids, along with their elevated metal contents (Warren, 2000b).

Thermal effects

In addition to pressure/strength interactions, variations in burial temperature gradients can also have an effect on salt flow. In terms of its thermal properties halite is an unusual mineral; as well as being one of the most thermally conductive sediments (at 43°C the thermal conductivity of halite is 5.13 W/m-K, while a typical shale at the same temperature is 1.76 W/m-K), its volumetrics also respond differentially to heating. At a depth of 5 km, under a geothermal gradient of 30°C/km, halite expands 2% due to heat and contracts 0.5% due to pressure (Jackson and Talbot, 1994). Under such a scenario (assuming zero porosity at either depth) the base of a thick salt unit becomes slightly less dense with the increased temperatures associated with burial and so creates a temperature-induced density inversion. Thermally induced convective flow is theoretically possible in a salt layer thicker than 2.9 km under a geothermal gradient of 30°C per km (assuming a viscosity of $<10^{16}$ Pa.s). This mechanism may trigger diapirism in salt-filled rifts characterised by elevated nearsurface temperatures and high geothermal gradients (Talbot, 1978). The volcano-shaped salt mounds associated with hot springs in Ethiopia's Danakil Depression may be located above the tops of thermally convecting plumes of salt, as may the diapiric features on Europa, a moon of Jupiter (Pappalardo and Barr, 2004) and the layered ice diapirs on Triton a moon of Neptune (Schenk and Jackson, 1993).

Gussow (1968) argued that outcropping Iranian salt glaciers were catastrophic extrusives emplaced hot, in a similar way to a lava flow. He thought that heated salt was intrusive and that the salt glaciers have now cooled and are no longer flowing. He was strongly influenced by early experimental work on disloca-

tion creep using coarse-grained dry salt that had indicated salt could only flow at temperatures above 200°C. We now know that most confined salt in the sedimentary realm is wet and capable of flow at earth surface temperatures (see above). Later work on the Iranian glaciers by Kent (1979, 1987) and Talbot (1979) indicated that the salt is still flowing today and that hot intrusion was not a major mechanism of salt emplacement in this or in other sedimentary basins. Temperature triggers, as first noted by Gussow (1968), do become an important consideration that can create intrusive sills and dykes once bedded salt enters greenschist facies conditions, as is perhaps seen in intrusive Neoproterozoic salt remnants in the thrust belt of the Damara Orogen in Namibia and in the Ugandan copper belt (Warren, 1999; Chapter 6 for discussion).

Flow textures and rates

Salt structures are zones where salt has thickened relative to its original stratigraphic thickness and by definition, salt must have flowed into this thickened structure. In salt pillows the sense of flow thickening is mainly horizontal, while in diapirs there is a much greater component of vertical flow. In Zechstein "pillows" the predominantly horizontal flow of halite is indicated by a gross morphology with a gentle nonpiercement style of thickening, but coring shows thickening of the salt structure was driven by stacked large scale flow-folds with near horizontal axial planes, as seen in the Anloo pillow in the Netherlands (Figure 6.8a; Geluk, 1998). In the late "pillow" stage, the flow direction changes from predominantly horizontal to an even less predictable system as the salt starts to pierce its overburden.

By the diapir stage the morphology of a salt structure shows that the sense of salt movement is predominantly vertical and that salt breaks through its cover. Diapiric salt is often mined, so its internal structures have been mapped. By this stage vertical fold axes (curtain folds) have been superimposed on the horizontal fold axes. Frictional interactions between the edges of the diapiric salt and adjacent strata drives even more complex fold patterns as flow vortices are created by irregularities in the thickness of the diapir neck. An analogy for this style flow folding is that created when a handkerchief is poked up and through a napkin ring. Once the salt is at the surface it spreads as a series of salt glaciers (namakers) and allochthons rolling and advancing over the surrounding landscape, much in the same way as a military tank rolls forward on its track.

In many diapiric structures the central part of the salt neck contains salt from the older (lower) part of the salt stratig-

raphy and the margins are made up of younger units. This is true for the diapirs of Dasht-i-Kavir (Figure 6.8b) and many Zechstein diapirs such as Bente, Reidel, Winschoten and Zuidwending diapirs (Figure 6.9a). But, as noted by Geluk (1998), this is a generalisation for there are many Zechstein diapirs where the reverse is true (e.g. Gorleben, Hänigsen and Pieterburen diapirs).

Richter-Bernburg (1980) argues for high levels of structural complexity in all salt deposits and that even our expectations of internally consistent layering in a sequence of stratiform salt beds may not be true. He cites the Silurian Salina Salt in the Wiskey Mine near Cleveland in Michigan where apparent isoclinal folds with horizontal axial planes are exposed on a 3 m-tall mine face in an area of the Canadian Shield where typical formation dips are less than 5°. An underground visit in 1984 by Professor Bernburg and me to another nearby mine in the Salina Salt with similar features lead to a discussion of whether these features were actually isoclinal folds or stacked and backfilled syndepositional erosional channels. However, in other salt basins with structures showing external geometries of pillowing or diapirism, the complexity of the internal structures that form in halokinetic salt is indisputable (Balk, 1953; Talbot and Jackson, 1987a).

Internal complexity is especially obvious in Zechstein diapirs where potash layers have been mapped as part of the extraction and ore control process (Figure 6.9). Characteristic flow folding and shearing is outlined by halite beds swimming or floating in isoclinally-folded carnallite beds, as in diapirs in Miocene potash of Sicily and Poland and Zechstein of Germany. In all these examples, areas of high strain are largely accommodated by the least competent layer, typically potassium salt or purer finer-grained rock salt units (Figure 6.9b). Some halite layers between these high strain intervals can remain relatively undeformed and even retain remnants of primary fabrics, such as megapolygons and microkarst pits. As the structure

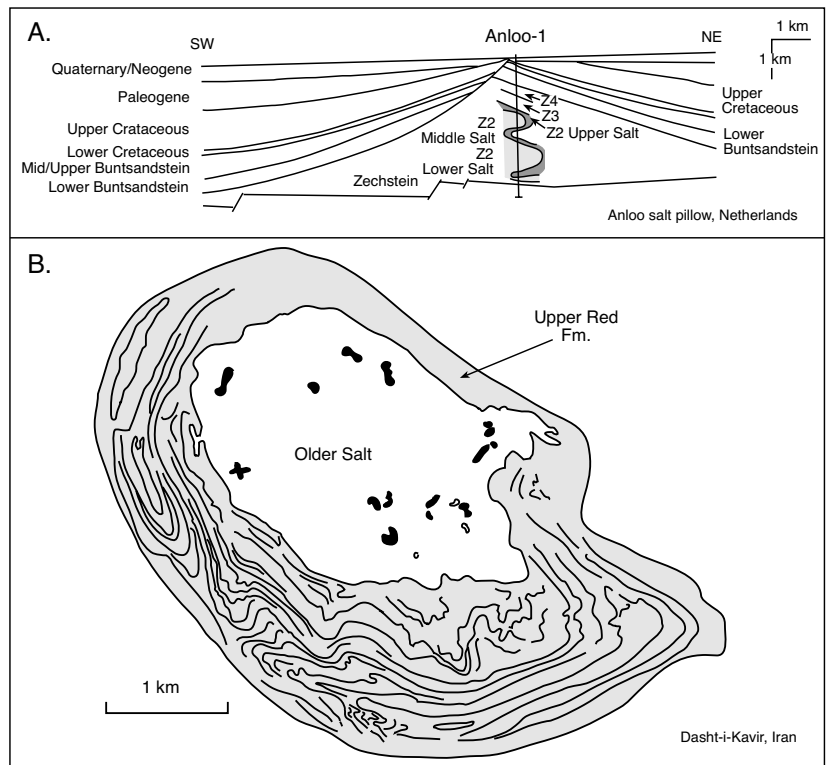


Figure 6.8. Internal fabrics of salt structures. A) Interpreted folded internal structure of the Anloo salt pillow (Permian Zechstein salt) based on regional seismic and fabrics observed in the Anloo-1 Well (after Geluk, 1998). B) Outcropping salt structure (Dome 20 in the Dasht-i-Kavir, Iran). Its central portion is made up of Older Salt (Eocene), which is composed of relatively pure halite. Surrounding this, and making up the outer part of the dome, is the Miocene Upper Red Formation, which entrains alternations of clay, anhydrite and halite. These layers clearly outline the complex folding styles that characterises salt flow (after Jackson et al., 1990 - see also Figure 3.62).

continues to deform these more competent layers also begin to brecciate or stretch into boudins. Finally, these halite layers pervasively recrystallise via pressure solution creep and no primary texture remains.

The internal complexity of salt structures is such that the near-surface portions of salt diapirs may be divided into a number of zones showing differential movement and separated by shear zones. This was first demonstrated by Balk (1953) in a classic paper mapping the internal complexities and shears in mined salt diapirs in the Gulf coast. Subsequent work by Kupfer (1976) on the same structures further refined notions of internal shear in diapirs. A shear forms where adjacent parts of a salt structure rise at different rates. This differential rise at the crest of a structure typically creates an active topographic high and a lack of thick caprock atop a rising spine, as is the case at Jefferson Island salt dome (Balk, 1953, Kupfer, 1976). The

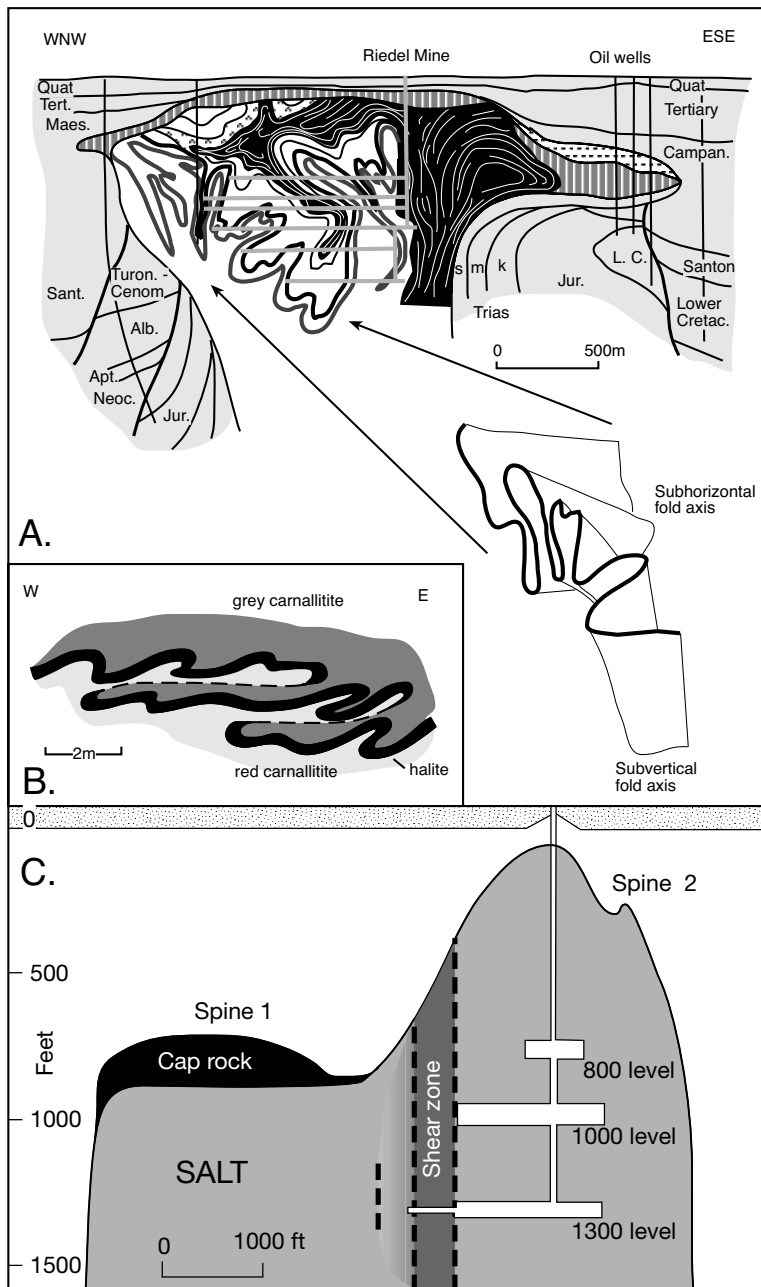


Figure 6.9. Internal structures of salt diapirs, A) Riedel diapir, Germany. The stratigraphically older part of the diapir (grey) of the structure sits atop the younger salt (white). Inset is a three dimensional diagram of the folds outlined by potash beds (ore horizon) in younger salt showing how axes of folds pass from a vertical orientation to a subhorizontal with depth. B) Halite bed (black) defines sheath folds and shear planes floating in deformed carnallitic matrix in a potassic ore zone in the Krügershall Mine near Halle/Saale, Germany (after Richter-Bernburg, 1980). C) Cross section through the Jefferson Island Salt dome, Louisiana, showing a wide boundary shear separating an active salt spine from a less active caprock-capped part of the structural crest. North is to the left and the 800, 1000 and 1300 ft working levels of the mine are shown (after Kupfer, 1976).

younger part of this salt stock is now 250 m (800 ft) higher than the adjacent flat-topped mass, which is also overlain by a cap rock (Figure 6.9c). The boundary separating the spine from the less active portion of the crest is finer-grained and shale rich and it formed a limit to the former salt mining of the pure salt within the spine. Shale-rich shear zones at the edges of active spines are sometimes called “black salt” by the miners and can show a greater propensity to leak water into a mine. The spine and its boundary shear are also seen in the Jefferson landscape, with a solution lake defining the zone of shallower salt created by the active spine. Shear zones within diapirs are potential problem zones if the crestal portions of domes are utilised for any type of fluid storage without an understanding of the significance of “black salt” (Figure 12.26).

In a benchmark paper on the internal complexity of salt structures in Europe Richter-Bernburg (1980) made a number of interesting observations:

- Salt deposits are not, or have not always been, in mechanical equilibrium with their ambient environment and deformations caused by salt flow have to be expected in all subsurface situations
- Isoclinal and overturned folds can occur in simple salt ridges so that stratigraphically older members of a formation can dip into the local area from above a particular horizon.
- By the diapir stage, possibilities are open for building folds of all imaginable - or even unimaginable - features and shapes (including migmatitic and boudinage styles). Axes of curtain folds in a diapir are not simply vertical, they may be inclined in all - mathematically! - possible directions.

He concludes that any prognosis about the interior structure of a halokinetic salt body -even if it is scarcely diapiric- is not possible without seeing it from the inside.

This mesoscale complexity reflects deformation textures that are occurring on the

microscale. As a salt crystal migrates in an actively flowing salt, it recrystallises via pressure solution creep. As it re-anneals, its outline stretches and deforms, leaving behind a strain memory of the stress regime in the various structures and crystal fabrics preserved in the diapir (Raymer and Kendall, 1998; Talbot, 1992a; Zak and Freund, 1980). Like many other crystalline rocks in structurally complex lithologies, such as migmatites and mylonites, the grains in flowing salt have such short strain memories that they rarely strain beyond length to width ratios of 4 or 5 before new crystals are created by the effects of pressure solution creep (Figure 6.10a). Hence, fine-scale grain-shape fabrics in confined flowing salt can record only the later stages of the strain history. Actual strains, resulting from superimposed deformations, are recorded by larger strain markers—primary layering or bedding, nodules, inclusions, and veins—all of which have much longer strain memories than individual halite crystals (Talbot and Jackson, 1987a,b).

Constant readjustments and recrystallisation to the variable stress field experienced during flow does indicate the ambient stress field in a diapir. Most halokinetic salt crystals have long axes that are a few cm long and are steeply inclined to subvertical within a salt stem or wall (Figure 6.10a). Between the elongate crystals are subgrain crystals with diameters that are a response to stress and can be approximated by an experimental power law equation noted by Carter et al., 1993 (see also Figure 6.3):

$$D(\mu\text{m}) = 214\sigma^{-1.15} \text{ (MPa)}$$

where D is the average subgrain size in microns and σ is differential stress in MPa.

A subgrain is a volume of crystalline material surrounded by subgrain walls composed of planar arrays of dislocations (Looft, 2000). The subgrain walls separate crystalline material of the same composition with slightly misoriented crystal lattices (usually less than 1°). Creep proceeds at stresses above a critical shear stress by glide and the multiplication of dislocations (Carter, 1976). Dislocations are linear defects in the crystal lattice that divide slipped regions in the crystal from unslipped regions, allowing localized slip to occur and spread consecutively. With increasing deformation, dislocation density increases and work hardening occurs as the dislocations tangle and interfere with each other, limiting mobility. Recovery occurs by the diffusion of vacancies that allow dislocations to climb normal to their slip planes to avoid obstacles, and form stable subgrain walls. Steady-state creep constitutes the bulk of the creep strain in naturally deformed deeper diapiric salt and occurs when the salt recovers at the same rate that it hardens,

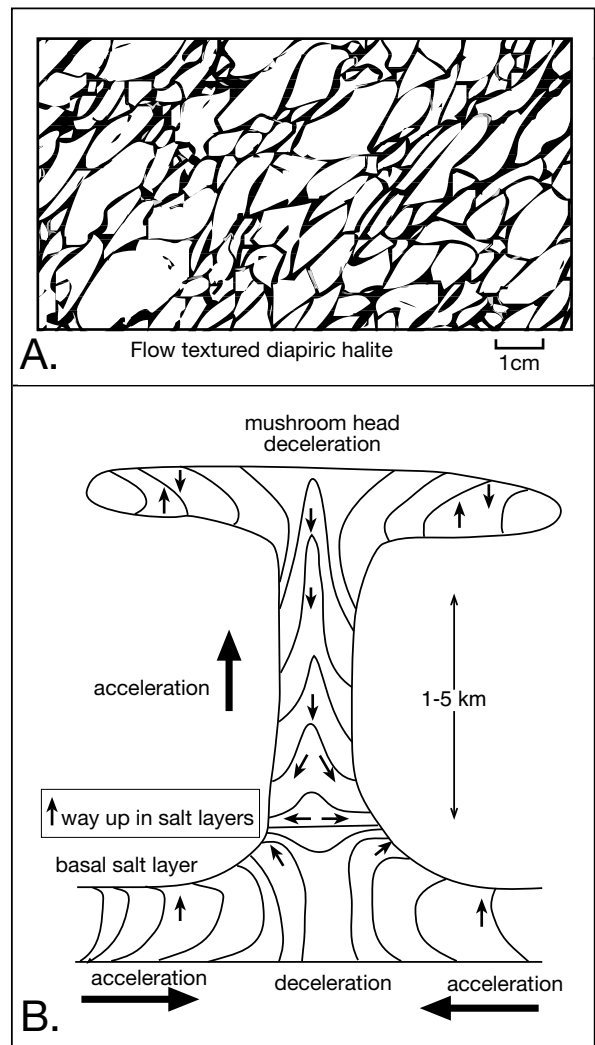


Figure 6.10. Micro and macro scale flow texturing. A) Digitised outline of flow textured halite crystals in a thin section of diapiric salt, no primary texture remains. B) Schematic velocity fields in a flowing diapir derived from physical models. The deformed outlines of originally vertical markers are shown, as well as bed facing directions (after Davison et al., 1996a).

so that large creep strains can be achieved at constant stress and strain-rate (Carter, 1976; Carter et al., 1993).

A detailed analysis of subgrain size immediately below the two-spined crest of the Weeks Island salt dome in Louisiana found differential stresses vary from 0.87 to 2.33 MPa at the 1000 ft level (Figure 6.11; Looft, 2000). More actively moving salt is indicated by higher stress levels and smaller subgrains. Such textures are generally associated with areas of salt spine beneath regions of higher surface topographic relief and lows with zones of coarser-grained, recrystallized salt.

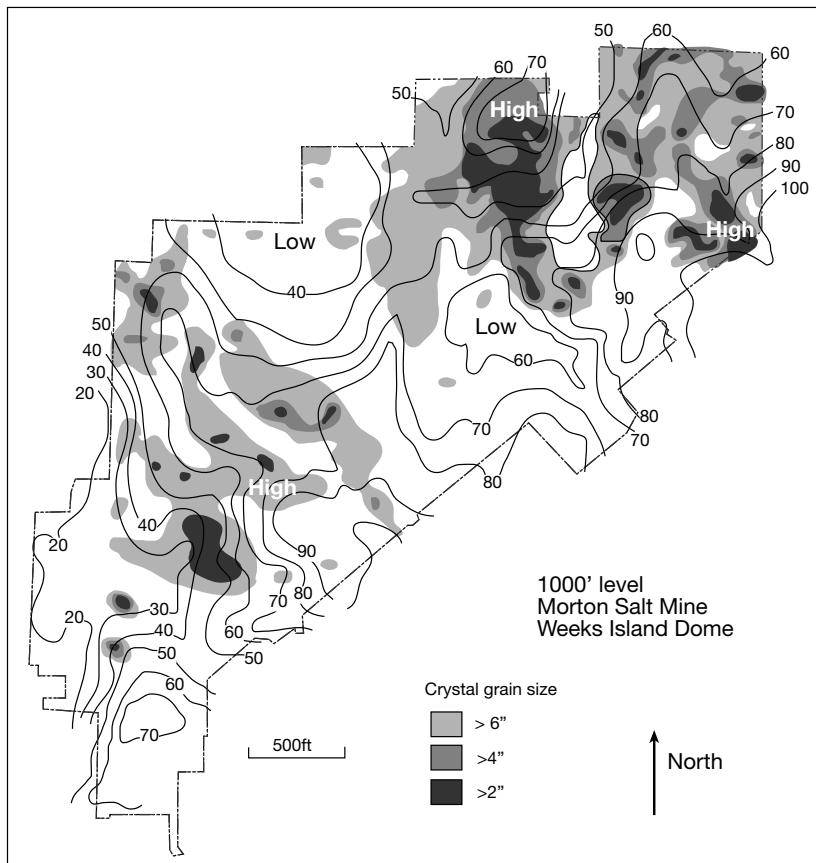


Figure 6.11. Comparison of the salt grain size in the 1000 ft level of the Morton Salt Mine, Weeks Island Louisiana, with surface topography over the mine. The finer-grained salt is generally associated with topographic high areas, while topographic depressions are associated with coarser-grained salt (after Loeff, 2000).

Detailed mapping of internal mesoscale strain markers along with modelling experiments have clearly shown internal flow in deforming salt away from shear zone is also not homogeneous (Kupfer, 1976; Zak and Freund, 1980; Burliga, 1996; Davison et al., 1996a; Sans et al., 1996a, b; Smith, 1996; Talbot and Alavi, 1996; Geluk, 1998). Foliations in deformed salt in a diapir are often axial to folds that develop in the primary layering and to the flow folds that map local gradients in flow rates along internal stream lines and surfaces in the moving salt (Figure 6.10b; Talbot, 1979, 1992b). If these layers approach mechanical passivity then the flowing viscous salt “fluid” picks up internal flow folds wherever the salt slows and thickens to pass obstructions. Beyond the obstruction the flow accelerates and internal folds tighten and almost disappear in the narrowing flow before they refold at the next obstruction. If the internal markers are strain active, the slow (competent) layers fold, while fast (incompetent) layers mullion as they shorten

within the slowing flow. Shears zones forming in a deforming salt body first grow in the least competent (usually potassic) horizons within the flowing salt mass. Between the shear zones, less deformed halite layers are carried laterally and upward into the diapir stem.

Davison et al. (1996a) show that fold wavelengths in Zechstein salt the North Sea (Figure 6.41) are of the order of 20–30 km in layers with an original thickness of more than one kilometre and an overburden that is now more than one kilometre thick. The spacing of the folds controls the amount of salt that drains into any particular structure. With a circular drainage envelope of 10 km radius a 1.5 km-thick salt layer can supply of the order of 470 km³ of salt to a single diapir. This is much greater than the volume of salt held in a typical North Sea diapir, which is around 25–75 km³. It means there has been substantial salt loss by allochthon escape and crestral dissolution. The rate of salt supply is not constant throughout the drainage area as the rate of radial flow increases closer to the diapir. According to Davison et al. (1996a) the constriction associated

with flow into the diapir neck creates strain within the neck up to 80 times greater than in the surrounding source layer. Thus, vertical flow in the centre of a diapiric neck produces extreme prolate strain textures that are in turn nullified at the top of the diapir where vertical flattening takes place via recrystallisation (Figure 6.10b).

Various combinations of pressure solution creep and dislocation creep create the deformed, aligned and recrystallised halite textures seen in cores recovered from salt flows (Figure 6.10a). Average halite grain size in cores from deformed recrystallised salt ranges between 5 and 10 mm in Zechstein salt in the North Sea and in Miocene salt in Mt Sedom in Israel and from 15 to 20 mm in Gulf Coast salt; all with L/S ratios typically greater than 1.5 (Davison et al., 1996a; Zak and Freund, 1980; Talbot and Jackson, 1987a).

Any interbedded sediment within the salt source layer strengthens a salt unit; it initially creates drag zones within the flowing salt, and so induces anisotropic strength and strain effects in the source layer as it moves toward the salt stem. This drag is often sufficient to generate small wavelength sheath folds. Once diapirism is more advanced, intrasalt beds (up to 40m thick) in the mother salt are brecciated or boudinaged. Salt can then flow across former intervening layers, carrying along fragmented and fractured layer remnants, with the whole region then behaving like a pure salt mass. Thus, once the system attains diapiric status, the strength and resistance to flow created by more competent intrasalt beds is drastically reduced by boudinage and breakup. Once the intrasalt beds are broken, diapiric salt can develop internal vortices like a billowing cloud of smoke, which trap, encapsulate and lift the fractured blocks of intrasalt beds. These fragments, usually dolomite anhydrite or dolerite, are referred to as “rafts” although they are not truly floating in the salt mass. Their density is typically higher than that of the salt. Rather, they are being swept upwards on a very slow rising plume. They can be porous and contain gas (including H_2S), oil or water and may create zones of unexpected overpressure when drilling salt. Once salt flow slows or ceases, blocks previously buoyed and caught up in the flowing salt mass of the diapir stem can sink back toward the base of the salt stem (Figure 8.15; Koyi, 2001). The style of intrasalt boudinage depends on the degree of induration of the entrained sedimentary layers. Where the sediments are well indurated the breakup of intrasalt beds tends to create angular clasts, where less consolidated the beds tend to stream, streak and flow plastically, like the adjacent salt. Boudinaged and aligned angular clasts and blocks are a substantial component in any later halokinetic dissolution breccia (Figures 7.22, 7.23).

Triggers, drivers and outcomes of salt flow

We have seen that density inversion does not bring about salt flow; so what is the trigger? From our preceding discussion we can state unequivocally that pure salt is extremely weak compared to its surrounds. Wet salt at the surface collapses under its own weight (gravity spreading) and so behaves like a Newtonian fluid across most geological time scales. In contrast any overlying or adjacent sediment responds brittlely to the same stress field. Salt structures in extensional basins that are accumulating sediment are triggered and driven by two main mechanisms; extension and differential loading. Both are derived from externally applied forces. Later in this chapter we

shall look at salt flow in relation to compressional forces, but we will now focus on extensional systems.

Salt flow can be triggered syndepositionally with the accumulation and gravity-driven extension of overburden or by an episode of regional extension long after bedded salt was first deposited and buried (Vendeville, 2005a,b). Syndepositional movement was the case with the numerous early allochthons and minibasins in the Jurassic of the northern Gulf of Mexico and the Cretaceous of Santos Basin of Brazil. Initial halokinetic-sediment feedback began in the Mesozoic, yet further out in both basins flow continues today as allochthons of Mesozoic salt are emplaced atop Neogene deep-sea floor sediment. Later flow, triggered by regional extension, was the case in the Zechstein salt (Late Permian) over much of the current North Sea; flow was mostly Mesozoic and did not begin until tens of millions of years after salt deposition had ceased. There was yet another episode of salt flow in the Zechstein salt in the North Sea. It took place in the late Mesozoic to Tertiary and was triggered by compression tied to the Alpine orogeny.

Studies of halokinesis conducted in the 1980s tended to place more significance on the triggering and driving effects of differential loading (Trusheim, 1960; Dailly, 1976; Seni and Jackson, 1983a,b; Jackson and Talbot, 1986, 1991; Worrall and Snelson, 1989; Nelson, 1991). Studies in the early 1990s tended to emphasise the role of regional extension (Duval et al., 1992; Vendeville and Jackson, 1992a,b; Demercian et al., 1993; Jackson and Vendeville, 1994). By the late 1990s, differential loading was physically modeled in the same way as extension had been and shown to be an equally valid mechanism for both triggering and driving salt flow in basins accumulating substantial volumes of sediment (Ge et al., 1997).

Now after more than two decades of detailed analysis of salt structuring in active halokinetic regions of the Gulf of Mexico, the Santos Basin and offshore West Africa, we know that both mechanisms can work concurrently from the first onset of salt flow. Waltham (1997) argued that apparent differences in triggers are two end members of a response continuum, depending in large part on the thickness of the salt and the rate of deformation (Figure 6.12).

Diapirs and extension

During regional extension diapirs can “pierce” the overburden in three related ways: reactively, actively and passively (Figure 6.13; Jackson et al., 1994 a, b). A reactive diapir pierces by filling the space created by divergence of faulted overburden

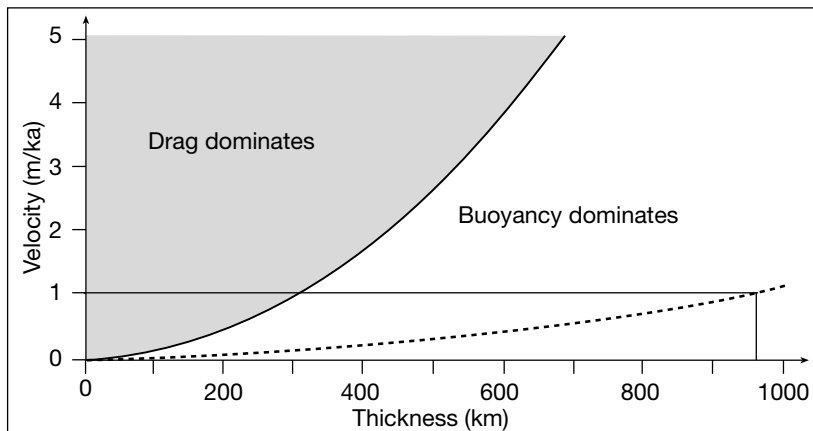


Figure 6.12. Shaded interval shows the overburden velocity field where drag (largely a brittle response in the overburden) dominates over buoyancy contrast as a trigger of salt flow (viscosity is 1×10^{18} Pa.s). The dashed curve shows the overburden velocity field at which drag dominates over buoyancy if the viscosity is 10 times higher (i.e. 1×10^{19} Pa.s). The crossline shows the salt thickness corresponding to an overburden velocity of 1 m/ka (after Waltham, 1997).

blocks. Reactive diapirism occurs during regional extension as salt approaches the surface beneath a subsiding graben in the thinned overburden. This surface graben is matched by development of an “inverse graben” at the underlying salt-sediment interface (isostatic balance). Salt fills the expanding space in the inverse graben and forms a reactive diapir that is triangular in cross section with flanking growth faults that become younger toward the diapir crest. If regional extension ceases before the onset of active diapirism, so does diapirism. Extension typically reflects a more regional set of tectonic processes such as gravity spreading or gliding of shelf and rise sediments in opening rifts. Diapiric salt at the reactive stage is not forcing aside overburden sediment, it merely reacts to regional stretching as it moves into space created by extension.

Extensional faulting is an effective mechanism for initiating diapirism in many situations, regardless of the prior overburden thickness, lithology or density (Figure 6.13; Vendeville and Jackson, 1992a, b). In such settings there is always a low ratio between salt pressure (Ψ) and brittle strength of the overburden. Reactive structures can be found either beneath newly-deposited thin overburden just starting to extend, or atop deeply buried salt beds in regions newly undergoing extension (Figure 6.7).

An active diapir, by definition, lifts and shoves aside its overburden. Unlike reactive diapirism, this style of salt emplacement must deal with a “room” problem. It requires forceful intrusion to remove the roof of sediment atop the salt. It is possible only if the overburden is relatively thin, whereby salt pressure exceeds

the brittle strength of the overburden (Figure 6.13). The roof must be thin enough for the pressure differential to lift it (Figure 6.7). For this to happen the roof is typically less than 20% of the entire thickness of the overburden flanking the diapir (Jackson et al., 1994b). However, once initiated, a diapir can actively pierce each new increment of sediment that buries it. Repetition of active piercement events sheds successive episodes of thin cover sediment into a debris belt around the growing diapir. Over time, an active diapir can pierce large cumulative thicknesses of sediment and create successive stacked unconformities about the diapir stem, which fade away with passage into areas above the withdrawal sink (rim syncline).

Each unconformity defines an episode of active piercement. Fractures formed during shedding of crestal sediment in active diapirism are extensional, often filled with infiltrated sediment and typically show little displacement of sedimentary layering on either side of the fracture (as is the case in fractured Lisan Fm. laminates atop actively flowing Sedom salt in the Dead Sea depression; Marco et al., 2002).

Once a diapir or salt wall emerges and flows onto the earth's surface it becomes a passive diapir, typically rimmed by salt allochthons; its edges spread and collapse under the weight of the extruded salt mass (Newtonian flow). A passive diapir crest maintains its position near the surface, while the adjacent sediment lows, along with the source salt layer they cover, subside. This is called downbuilding and rim syncline maintenance and was first documented by Barton (1933). A passive diapir cannot continue to rise without ongoing sedimentation to load areas adjacent to the at-surface salt, but the area of the salt mound can widen and if extension continues will ultimately subside (falling diapir stage). A thin skin of sediment can form atop the salt high but it is continually breached, pierced and fragmented. Its remnants are erosively shed from the diapir crest, or carried away “conveyor belt style” by divergent lateral flow of the underlying salt allochthon. Thus sediment does not accumulate atop the crest of a passive diapir and most adjustments in the thickness of accumulating sediment in the adjacent subsiding basin is a response to the evacuation or withdrawal of salt at deeper levels below the accumulating sediment pile.

A lack of vertical constraint to the rising salt at the passive stage means there is no “room” problem; flanking strata need not be rotated, faulted or pushed aside as they must be during active diapirism. Faulting and folding are negligible in the sediments adjacent to passive diapirs, apart from a narrow drag zone along the salt-sediment contact (Figure 6.13; Jackson et al., 1994a, b; Schultz-Ela, 2003). Once the source layer is depleted, the diapir ceases to grow and is buried by further sedimentation. Shapes of passive diapirs are primarily a function of the ratio of salt flow rates to sedimentation rates. When balanced, the diapir stem grows vertically; when sedimentation rate is relatively slow, the salt leaks out over its surrounds to give flanges to the diapir and a more mushroom-like allochthonous aspect.

The sequence reactive --> active --> passive can be altered by changes in rates of extension, depletion of the source layer or changes in sedimentation rate, and so various evolutionary paths are possible (Jackson et al., 1994a):

- Although a diapir may appear to be initiated passively it most likely was reactive or active during its earliest stages. If the overburden was thin and unevenly deposited the reactive and active stages are very brief, and the strata faulted during these very early stages can be too thin to be resolved seismically.
- A diapir that appears to have been passive may have passed through numerous cycles. Each cycle could have comprised an episode of passive growth during slow sedimentation, followed by burial during a period of rapid sedimentation and be terminated by a brief active salt breakout. Each active stage removes the overburden roof by doming, local

extension, entrainment, slumping, dissolution collapse and the creation of local unconformities.

- An active diapir can partially break through its roof, but never emerge, as: 1) the salt source layer may become depleted, 2) the salt source may be channelled off (pirated) by an emergent segment of an adjacent salt wall, or 3) without erosion or differential loading an active diapir only partially penetrates all but the thinnest roofs before reaching equilibrium (Schultz-Ela et al., 1993).

If a passive pluglike stock is later stretched during ongoing regional extension, the adjacent country rocks may also stretch, creating normal faults next to the diapir. But more typically the stretching is taken up in the much weaker salt body, so that passive elongated salt walls under extension are widened via ductile flow of salt. The much stronger flanking overburden may remain grossly intact and virtually devoid of normal faults at the scale of seismic resolution. An apparent absence of normal faults in sediments adjacent to a passive diapir wall means that even large amounts of regional extension may remain hidden within the expanding and deforming salt wall. This cryptic extension can be inferred by accurate reconstruction of cross sections backward in time. But this process is far from straightforward and requires additional constraints, such as independent data on the original length of the section or original thickness of salt (Schultz-Ela, 1992).

Diapirism and differential loading

In a series of scaled physical models Ge et al. (1997) demonstrated the importance of progradation as a trigger for salt

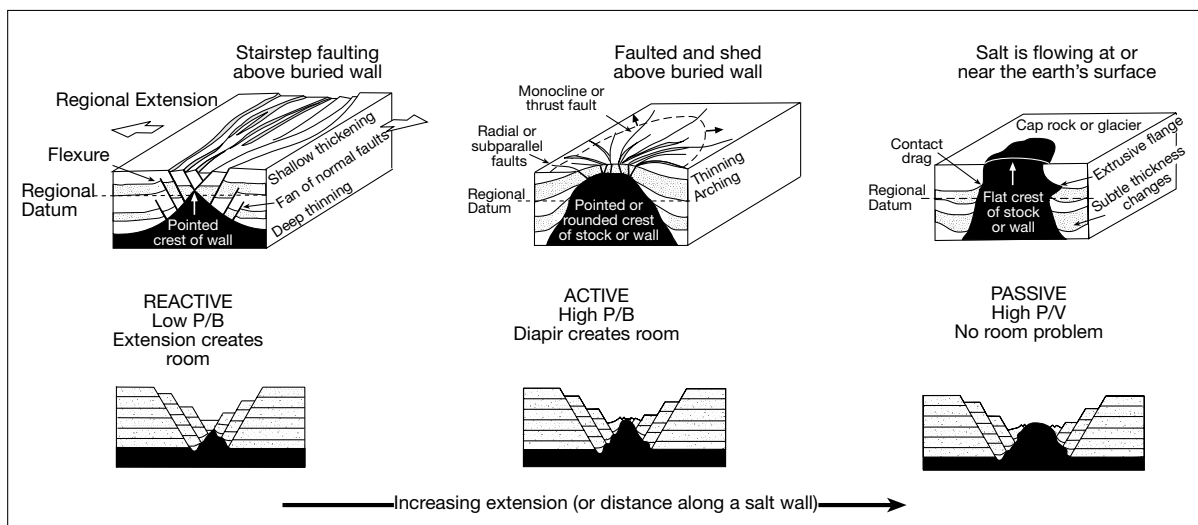


Figure 6.13. Three piercement modes for diapirs (salt is black) and their characteristic structures. Regional datum (dashed line) is the base of the stippled layer. P, V and B refer to stresses due to salt pressure, salt viscosity and overburden brittle strength, respectively. Extension is accommodated by both graben-related faulting and diapir widening (in part after Vendeville and Jackson, 1992a; Jackson et al., 1994a).

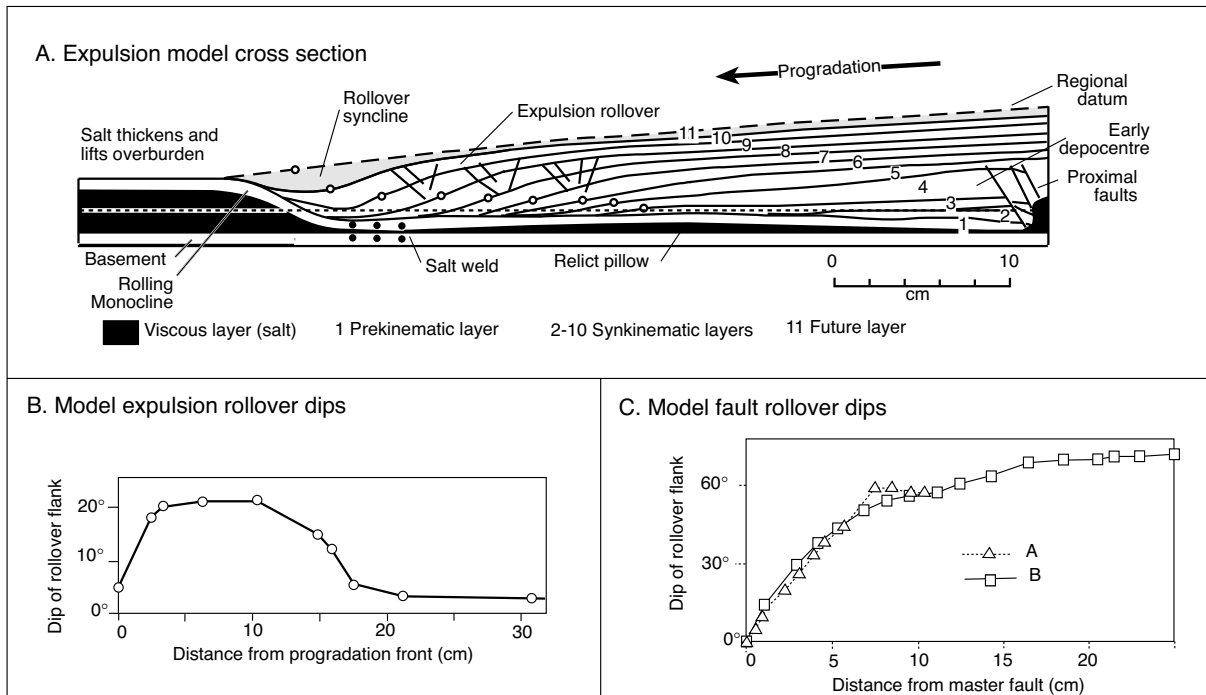


Figure 6.14. Expulsion rolover characteristics. A) Regional cross section with rolling monocline, rolover syncline, and expulsion rolover all migrating basinward with the basinward progression of the progradation front. Dashed horizontal line represents the top on an initially tabular salt body. Open black circles show positions of data points plotted in Figure 6.14b. B) Rollover plots of maximum dip associated with model illustrated in 6.14a. C) Rollover plot of model experiments: result A is from experiment model 188 listed in Ge et al. (1997), result B is from experiment E30 in McClay (1990) (modified from Ge et al., 1997).

tectonics and formation of allochthonous sheets. They considered two end members. One group of experiments modeled salt with an underlying flat top to the basement (Figure 6.14), while another group considered a basement with a stepped top, as would occur in a block faulted basement terrain (Figure 6.15). Regional extension and contraction were excluded in their models.

The prograding wedges above a tabular, buoyant salt layer that was underlain by a flat basement top, expelled the salt basinward in a predictable sequence of structures. From proximal to distal they were: a) sigmoidally distorted initially planar wedges, b) relict salt pillows and salt welds, c) basinward-dipping expulsion rolover and crestal graben, d) rolover syncline, e) landward-facing salt-cored monocline, and f) distal inflated salt layer (Figure 6.14a). This deformation zone amplified and advanced basinward together with the prograding sediment front. Complete evacuation of the salt left a basin-propagating salt weld below the prograding sediment wedge; incomplete evacuation left salt pillows as residual highs, but no diapiric salt structures were formed.

In contrast, progradation over a buoyant salt layer that was underlain by landward-facing basement steps or fault escarpments (Figure 6.15a), initially formed a broad anticline where the salt flow was focused across each basement step (Figure 6.15b). Early on, differential loading by the prograding wedge expelled the salt basinward in an identical fashion to that which occurs in a basin with no basement steps. Then the lateral escape of the salt was altered as it was slowed across the friction point created by the basement step. The salt backed up to form a broad asymmetric salt-cored anticline. Distal aggradation continued to pin the anticline and enhance differential loading. Next the anticline actively pierced its crest, which in the real world may have been thinned by faulting and erosion (Figure 6.15c). Thereafter the diapir grew passively, locally sourcing allochthonous salt sheets. This deformation cycle repeated over each basement step so that the age, amplitude, complexity and maturity of salt-related structures decreased basinward (Figure 6.15d-f).

As each allochthonous salt sheet was buried and evacuated by sediment loading, arcuate peripheral normal faults formed along the sheet's trailing edge, detached wrench faults formed

along its lateral edges, and active piercement at its leading edge allowed the sheet to break out and climb stratigraphic levels. This process formed a multi-tiered complex of salt sheets that migrated basinward with time. Ge et al.'s (1997) modelling clearly shows that immense landward-dipping (counter-regional) pseudofaults can arise entirely by salt expulsion rather than regional extension. Their physical model clearly shows that progradation alone can generate salt anticlines that mature into salt walls, stocks, glaciers or linked, multi-tiered complexes

of evacuated sheets and salt welds. The prograding sediment wedge expels salt basinward regardless of density relationships. In such situations there is a relationship between underlying basement discontinuities and the location of salt diapirs and allochthons. A result that is not obvious in purely extensional regimes where the zones of diapirism tend to begin in zones of overburden thinning that can bear no relationship to subsalt discontinuities.

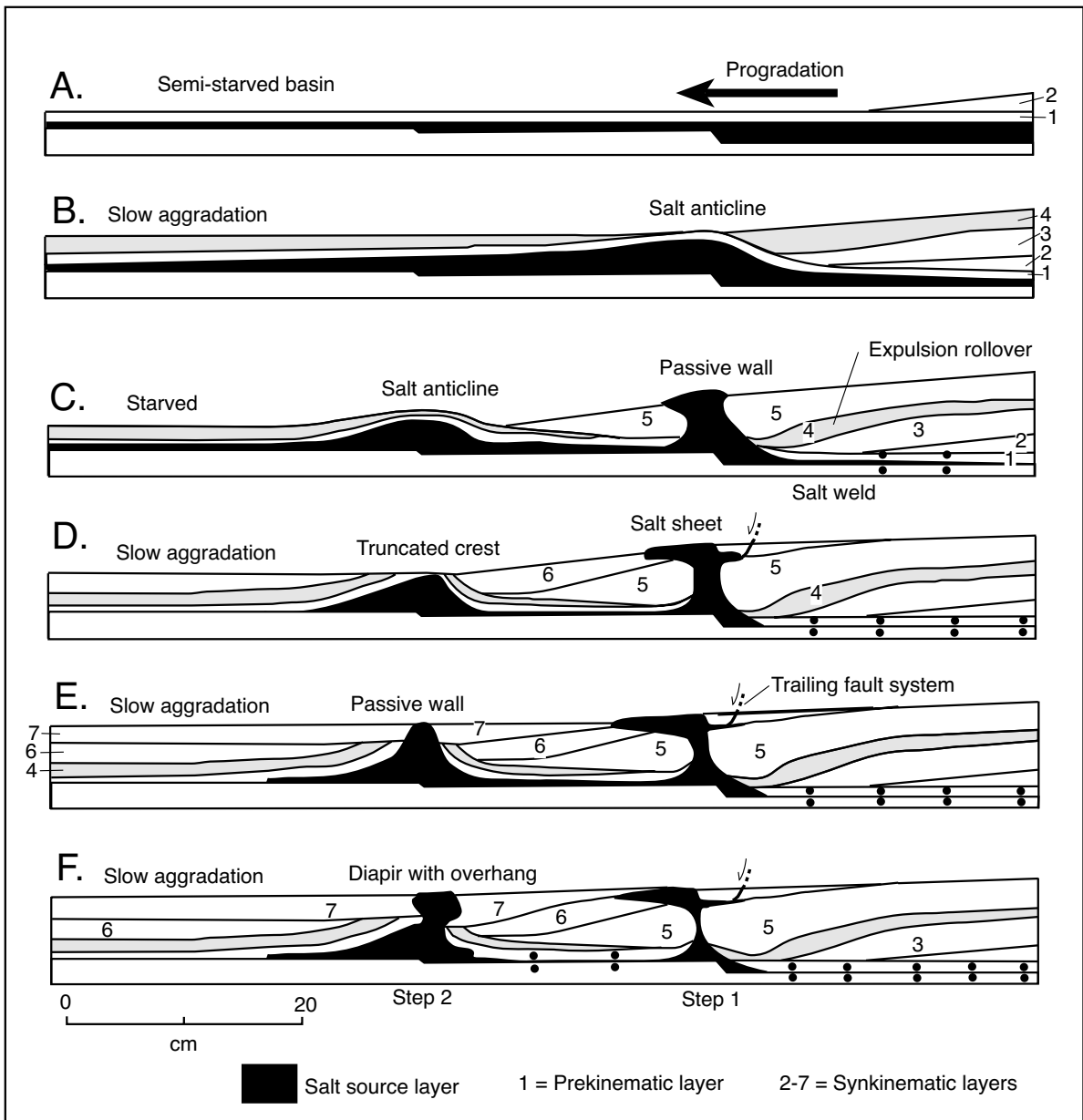


Figure 6.15. Evolution of salt structures during progradation atop a salt basin that is underlain by a stepped basement (modified from Ge et al., 1997).

Salt flows under both regional extension and progradation. Both are typically present and interacting in a sedimentary basin where extension drives the subsidence that in turn creates accommodation space, which is then filled by sediment. Extension is probably the dominant mechanism for triggering diapirism in deeply buried salt bodies, while progradation is a commonplace driving mechanism whenever salt is near the surface. Salt's propensity to flow means that diapirs, initially formed by early progradation of a wedge of continental shelf or platform sediment, can be later reactivated or overprinted during extensional or compressional regimes.

This leads to an obvious problem in distinguishing between expulsion rollover generated by progradation and a fault rollover in the hanging wall of a listric growth fault generated during extension. Ge et al. (1997) clearly show how dip analysis of the rollover plot can be used to help differentiate the two styles (Figure 6.14b, c). They plot the maximum dip of each sediment wedge in the expulsion rollover (open circles in 6.14a, b) versus distance from the present progradation front. Maximum dip was measured on the basinward-dipping flank in the rollover syncline. The rollover plot is shaped like an asymmetric hill with dips increasing rapidly away from the front to a maximum and then decreasing less rapidly. The maximum dip corresponds to where the thickest salt was expelled. The oldest wedges preserved the initial depositional slope (5° in modeled system) and planar shapes, even though they were folded and then unfolded by the passage of the structural monocline that rolled through them as the salt evacuation front passed by. The plot of a fault rollover in the hanging wall of a simple listric fault is quite different and shows no decrease in dip away from the present progradation front (Figure 6.14c). Dips of the hanging wall cut off abruptly and then gradually increase to reach a maximum value away from the surface trace of the listric fault. The constant maximum dip away from the fault corresponds to flattening of the underlying fault. This type of analysis can only be carried out on synkinematic strata, which are distinguished from prekinematic strata as they show local lateral variations in thickness. If a listric fault has multiple flats and ramps, the prekinematic strata generate a tail of data points that are not diagnostic and should not be used. See Ge et al. (1997) for a full explanation of this methodology and its application.

More recent publications subdivide the effects of sediment loading on salt flow into 1) systems with linear progradation fronts moving out over a salt mass (Vendeville, 2005) versus, 2) more lobate styles of sediment loading (Gauillier and Vendeville,

2005). The former are appropriate to linearly-loaded continental margins, as along much of the Atlantic slope-and-rise of South America and the Gulf of Mexico, while the latter models are more appropriate to lobate loaded margins, such as the Gulf of Lions and the Nile Cone.

Sedimentation rate controls diapir shape

The interaction of upwelling salt and accumulating sediment on the diapir's flanks controls the geometry of a passive or downbuilding diapir. If the rate of salt rise is less than the sediment accumulation rate, then a passive diapir narrows upward as onlapping sediments encroach onto the diapir ($R/A < 1$; Figure 6.16a, b). When a large volume of salt is supplied to the growing structure, the diapir rises faster than the surrounding sediment can aggrade. The resulting laterally unsupported salt ridge repeatedly overflows its unsupported margins, thus creating a salt tongue that widens upward over time ($R/A > 1$; Figure 6.16a, b). Eventually, all diapirs are buried by the slowing and eventual cessation of the salt supply. This typically happens once the mother salt (source layer) is thinned or depleted by salt withdrawal and overburden touchdown.

The gross flow rate of salt in passive diapirs reflects the balance between driving forces, retarding forces and salt supply (Jackson et al., 1994a). Any changes in sedimentation rate versus rate of salt supply controls the overall planform (at-surface shape) of a passive diapir. Within a single ovoid or elongate salt structure a diapir's rate of salt flux increases with increasing width. At the diapir's widest part, salt flow rates are high relative to sedimentation rates. Conversely, contact drag at the structure's extremities affects the narrower ends of an elliptical diapir more than at its wider parts. This slows the rate of rise at either end so creating relatively high aggradation rates. Thus salt spreads at the widest part of a diapir and retreats from its elliptical ends. Accordingly, an originally elongate salt wall evolves toward a string of pluglike passive stocks rising from the deeply buried reactive salt ridge. The number of exposed plugs atop a wall declines as they exhaust their salt supply and become buried.

If, during extension, the sedimentation rate is high compared to the rate of regional extension, a reactive diapir evolves into a squat deeply buried salt roller bounded by a listric (upward steepening) fault. Conversely, if the sedimentation rate is low compared to the rate of regional extension, a reactive diapiric ridge evolves into a tall salt wall or a number of adjacent salt

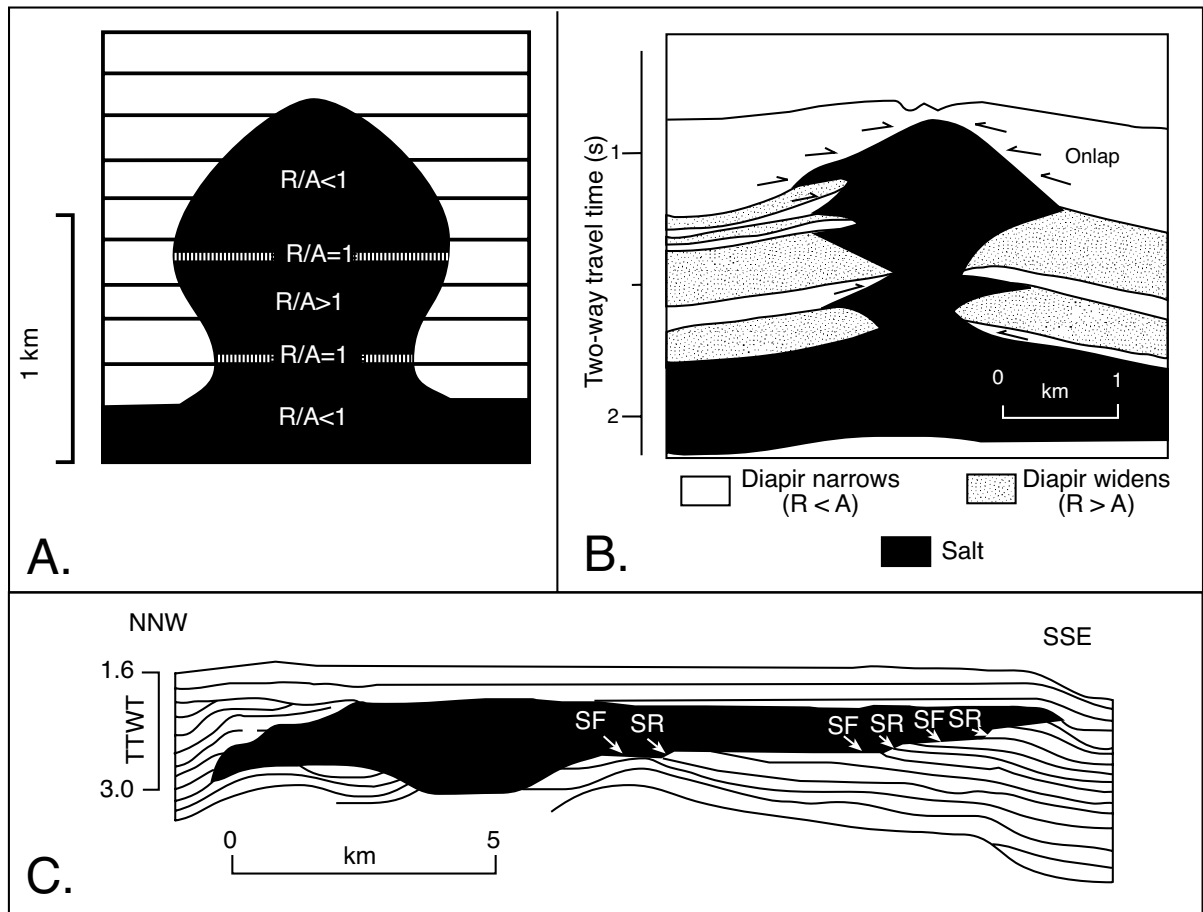


Figure 6.16. Passive diapirs with extrusive flanges overlapped by overburden. A) The shape of a diapir is controlled by the ratio of net diapiric rise R (incorporating the effects of dissolution), to aggradation rate (vertical accumulation of sediment). B) A typical North Sea Diapir with allochthonous salt wings (after Jenyon, 1986). C) The stepped base of Mica (aka Mitchell dome) Garden Banks, offshore Louisiana, shows it was emplaced as an allochthon not a sill; high R/A causes salt flats (SF), low R/A causes salt ramps (SR) (after Vendeville and Jackson, 1993).

plugs that show steep or overhanging discordant contacts and shallowly buried crests (Vendeville and Jackson, 1992a). Likewise sedimentation rate also controls the form of advance of an allochthonous salt sheet (Figure 6.16c). Salt flats indicate times of low sedimentation, while salt ramps indicate higher rates of sedimentation. Salt ramps are the remnants of an allochthon which was an active glacier moving across the seafloor. When the salt is completely evacuated the former ramp becomes a salt weld. Observation in seismic lines collected in the late 1980s across buried salt allochthons of the Gulf of Mexico showed a stepped base of salt (ramps and flats), rather than the older flat or planform interpretations. It changed the notion of salt allochthon emplacement from that of a salt sill injected into marine muds a few hundred metres or more below the seafloor into one of salt glaciers marching out over the seafloor.

As a salt glacier is extruded onto the seafloor it can flow in any direction, depending on the local slope (gravity spreading); it can even flow landward into the depression atop an adjoining rollover syncline (rim syncline). Over time the breakout sites, where the salt climbs the section and breaches to the surface, will ultimately shift basinward as salt is squeezed by the prograding basin fill (Figure 6.15). Regionally, the depocentre of active diapirism in the Gulf of Mexico has been shifting basinward since the Jurassic when the mother salt bed, the Louann Salt, first breached the surface. As each newly emplaced salt sheet is loaded by the prograding sediment pile, it carries its overburden basinward by gravity spreading. Thus, while a sheet evacuates into a new stratigraphic level it also generates halokinetic profiles atop it.

Extension, falling diapirs and turtles

Salt-lubricated extension can initiate and maintain diapirism throughout the reactive, active and passive stages. While connected to an adequate salt supply, passive diapirs can widen between separating blocks of overburden while still maintaining their crest at or near the surface (Vendeville and Jackson, 1992b). That is, once it attains its maximum height, a reactive/passive diapir can continue to widen by viscous flow. Salt inflow fills an ever-widening gap between the faulted extending blocks of overburden that are gliding apart on the salt source layer (Figure 6.17a, b). Eventually the salt supply becomes restricted and ultimately depleted so that the diapir crest sags or falls into a characteristic two-horned profile, even as the diapir body continues to widen (Figure 6.17c).

Turtle-structure anticlines, with crestal keystone grabens, form adjacent to falling diapirs and are another response to source-layer depletion. Historically, these anticlines were attributed to the evolution of a salt pillow as it contracted into a diapir (see Warren 1989 for discussion), but it is now known that they form during the falling diapir stage in an extending basin (Figure 6.17c-e). Once the salt supply to a diapir is restricted, more and more salt from the surrounds is withdrawn into the falling diapir (Figure 6.17c). As this occurs the region of overburden touchdown forms and then widens beneath the rim syncline sediments. Over time, the ongoing widening of this zone of salt withdrawal and touchdown causes the sediments of the rim syncline to invert into a turtle structure anticline, often with a keystone graben in the anticlinal crest (Figure 6.17d). The touchdown and inversion of the rim syncline sediment pile can create a topographic high on the seafloor. Sediments deposited atop the anticlinal crest may be higher energy sands and carbonate buildups, as has occurred in the reefal carbonate reservoirs that characterise buildups in the James Limestone in the Gulf of Mexico (Figure 10.46). Such positionally enhanced potential reservoir intervals can be thought of as self-reservoiring, self-closing and self-draining.

As the diapir crest continues to sag, the crest inverts from a topographic bulge into a subsiding depotrough or graben, which is rapidly filled with sediment. This creates a sediment thick atop the diapir (Figure 6.17c). Slippage along the bounding faults of this deepening graben continues, but no new faults generally form within the graben. Such a crestal graben lacks the stair-step faults that characterise the smaller and shallower crestal graben of a reactive diapir. Adjoining the indentation are hornlike cusps of salt below each bounding fault of the graben.

If extension continues after all salt supply to a passive stage diapir is cutoff, overburden touchdown occurs in the position of the former passive diapir. The falling diapir overburden segments into two flanking triangular relics flanked by glide blocks composed of older overburden (Figure 6.17e). The diapiric relics are now separated by deep, wide depocentres filled with younger sediments. If extension continues, the flanks of these diapiric relics subside until they too touchdown. Thus, ongoing extension and salt depletion causes even the young depocentre to subside until it too eventually inverts into a crestally faulted arch, called a mock-turtle anticline.

But what about the third dimension along the strike of a salt wall or diapir crest? In many diapiric settings, such as the North Sea and the Gulf of Mexico, salt walls can pass along strike from a section of the wall at the passive stage to a falling section of the wall marked by a thickening crestal graben. In other words, stages a-e in Figure 6.17 and a-d in Figure 6.18, can occur along strike within a single salt wall (joined by dashed lines in figures). Where subsidence is accommodating regional extension, salt tends to move into the rising (reactive-passive) sections of the wall and away from subsiding depressions below the crestal grabens. As salt flows into the intervening culminations along the wall they evolve into increasingly pluglike, rounded diapirs. If extension continues, these rising diapirs, which are commonly emergent, continue to widen and accommodate the regional extension without faulting. With sufficient extension, these diapirs ultimately exhaust their salt supply so that they too must subside and also become buried.

Prior to the work of Vendeville and Jackson (1992b) on falling diapirs, many of the crestal structures produced by diapir fall were attributed to salt dissolution or forceful active intrusion at the crest; all three possibilities should be evaluated in any areas of crestal grabens or remnant salt cusps/rollers. A long-standing bias toward salt dissolution causing crestal grabens is partly because criteria for interpreting the origin of crestal grabens are usually neither clearly stated nor consistently applied.

Falling diapirs and raft tectonics

In some areas of falling diapirs the overburden becomes stretched to two or three times its original length by normal faulting, but the sub-salt basement is not involved. This prodigious extension of the overburden over a non-deforming basement is enabled by a weak intervening ductile layer or décollement of salt. This style of overburden deformation is called raft tectonics and defines

an extreme form of thin-skinned^{6.2} extension or gravity sliding where rigid sediment blocks slip downslope atop a décollement layer of evaporite or shale (Spathopoulos, 1996; Cramez and Jackson, 2000; Fort et al., 2004). Raft tectonics characterises areas of large-scale extension where the hanging wall of an extensional salt-soled fault separates completely from the footwall, creating a fault weld via coherent slippage along the salt detachment surface (Figure 6.18a; Duval et al., 1992). In other words these rafts are allochthonous fault-defined overburden blocks that have slipped down-dip to become so far apart they are no longer in mutual contact across the growing fault that once separated them. Rafts characterise extensional geometries beneath the modern shelf and rise of Brazil in South America, Angola in central West Africa and the Gulf of Mexico (Figure 6.18a; Anderson et al., 2000). Similar large rafts characterise blocks of Zechstein sediment in the NW Permian Basin of the North Sea (Clark et al., 1998). In this case, the blocks of sediment are composed of platform anhydrite, which slid into the basin atop a halite lubricated sole.

With less extension the fault blocks are called pre-rafts as they remain in mutual contact across the fault and parts of the hanging wall still rests on its original footwall. Rafting movement produces listric faults and sediment-filled grabens atop a deflating salt mass. These sediment-filled grabens can be substantial structures; the Quenguela Graben in the Kwanza Basin measures 20 km wide and 90 km long, the nearby Gaivota Graben is 15-20 km wide and 225 km long (Figure 6.18b; Cramez and Jackson 2000).

With initial extension between two overburden blocks, a salt wall first rises passively to fill the increasing gap (Figure

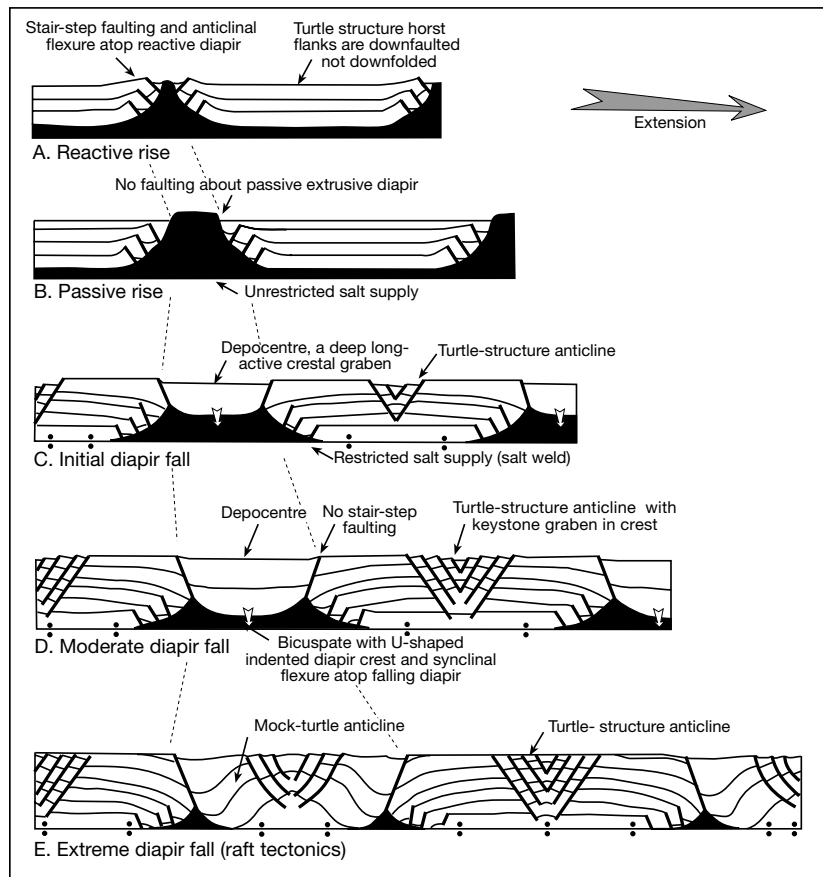


Figure 6.17. Rise and fall of diapirs during synkinematic sedimentation and extension. The dashed line implies the various stages are not necessarily separate in time, but can be found along a single salt wall (after Vendeville and Jackson, 1992b).

6.18b; time 1). Once the supply of salt can no longer keep up with demand, the diapir starts to fall. The crest of the sagging diapir becomes a subsiding trough that fills rapidly with sediment (Figure 6.18b - time 3). While stretching and décollement are active the thickness of the evaporite layer is reduced both by downslope gravity drainage of the salt and ongoing dissolution. Once most of the salt is removed from under the sliding blocks, they ground or weld on the presalt layers and the downslope movement of the blocks stop (Figure 6.18b - time 4). Stretching or extension that drives raft tectonics can usually be attributed to gravity gliding. Gravity gliding is the translation of fault blocks down a gentle slope, driven by the downslope shear stress component of gravity on a tilted mass atop a mobile layer.

Regionally, salt basins characterised by raft tectonics can usually be divided into two different stress regimes (Figure 6.34a; Spathopoulos, 1996; Cramez and Jackson, 2000): an updip

^{6.2}Thin-skin tectonics describes a situation where most of the deformation occurs in sediments above a regional décollement and structures in the basement below the décollement are different to those above. Sometimes called a "no basement" structural interpretation.

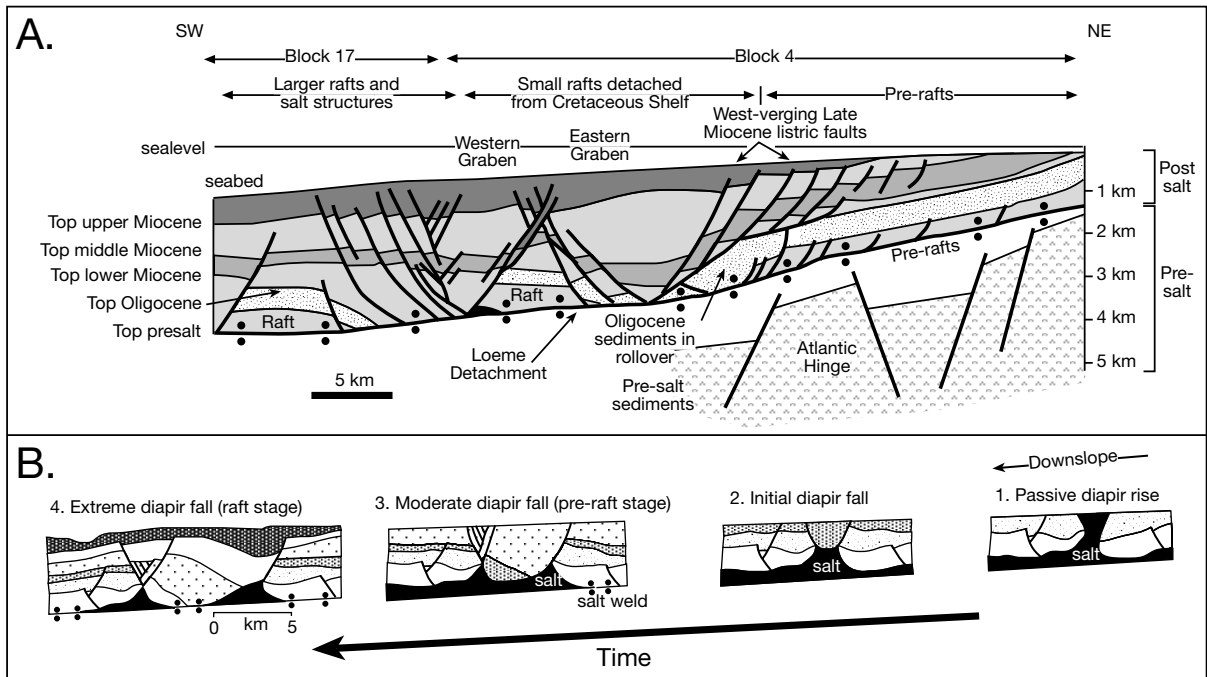


Figure 6.18. Raft Tectonics, Angola. A) NE-SW section through the Block 4 region of the Lower Congo Basin (Anderson et al., 2000). West-dipping listric faults affect the late Cretaceous sediments in the east of the block. Further west, Miocene extensional faults and associated grabens separate an isolated Cretaceous fault block (raft) from the equivalent Cretaceous sediments on the shelf. A similar structural style, characterised by thin-skinned faults, exists to the west but with relatively simple Cretaceous roll-over anticlines. Each of these isolated fault blocks is separated from neighbouring fault blocks by Miocene grabens (Eastern and Western grabens). The Miocene faults flatten downwards onto a salt detachment in the Loeme Formation. B) Restoration model of a falling diapir in the zone of raft tectonics of the Kwanza Basin, Angola (after Schultz-Ela, 1992 and based on a seismic line in Duval et al., 1992).

extensional regime located under the shelf and upper slope where salt décollement has facilitated the breakup of overlying sediments into raft blocks, and a downdip compressional or contractional regime typically under the lower continental slope where the up dip extension is taken up in a fold or thrust province. Raft tectonics requires the creation of substantial lateral space into which the overburden can expand during stretching. Downdip space is generated by: 1) formation of a downdip fold or thrust belt, 2) down dip displacement of autochthonous salt into allochthonous salt sheets that climb the stratigraphy, and 3) generation of new oceanic crust by a spreading ridge with allochthonous salt allowing overlying blocks to slide (Duval et al., 1992). This downdip compressional terrain is discussed in more detail later in the chapter.

Salt allochthons (salt breakout)

Allochthonous salt sheets are flowing salt masses that have been moved by low temperature tectonic processes so that the front edge of the salt flow overlies younger strata and it is typically

no longer connected with the mother salt bed. Allochthons have areas measured in hundreds of square kilometres and thicknesses ranging up to several kilometres. They typically indicate into-the-basin translation of the salt mass and its overburden. When actively inflating with salt they lie at or very near the surface (Figure 6.19). Some authors draw a distinction between an allochthon and a namakier (salt glacier; *namak* is Farsi for salt), using namakier to describe the structure created by the extrusion of allochthonous salt at the surface. Others use the terms salt allochthon and namakier interchangeably.

In contrast to an allochthon, an autochthonous salt structure extends continuously down to the primary source layer and may not have experienced substantial lateral translation (Rowan et al., 1999). Allochthonous salt sheets characterise the present day continental margins of offshore Brazil, the Gulf of Mexico, West Africa, the North Sea and the Red Sea and outcrop as namakiers or their remnants in Iran, Algeria, Yemen, Mexico and Australia (Figure 6.19). Their recognition in the last two decades as potential traps in deepwater petroleum provinces

has opened up possibilities of prodigious subsalt hydrocarbon reservoirs, particularly in continental slope and rise sediments in the various circum-Atlantic salt basins (Chapter 10).

Proposed emplacement mechanisms for salt allochthons include: recumbent folding, deep intrusion, shallow intrusion and surface extrusion (Figure 6.19; Schultz-Ela and Jackson, 1996). In all categories, a massive basinward flow of salt is a major part of the emplacement process in both subaerial and submarine settings. Ewing and Antoine (1966) envisaged the allochthonous Sigsbee Scarp was the basinward flowing edge of an autochthonous diapir (Figure 6.19a). We now know their original interpretation, limited by the state of the seismic art at that time, was not correct in terms of its vertical connectivity to the mother salt bed (Figure 6.1). Amery (1969) discovered that the Sigsbee Scarp was the leading tip of a wedge of allochthonous salt.

Jackson and Cornelius (1987) modeled allochthonous salt sheets as flowing salt bodies ramping up to the nearsurface from a buried sub-salt step. The suprasalt wedge then spread rapidly under gravity as a recumbent fold anticline. They argued the whole system had advanced like a tank track rolling out over itself, with a core of allochthonous salt and a laterally sliding deformed sedimentary overburden (Figure 6.19b). As an allochthon rolls out over the seafloor it carries with it the veneer of accumulating and deforming sediment so that, when later buried and drilled, the sediments atop a salt sheet may be older than those below. This is case in the Vermilion #356 well drilled through a Gulf of Mexico salt sheet by Amoco in 1988. The highly overpressured section beneath the salt sheet is younger than the condensed suprasalt section in the same well (Figure 6.22; Harrison and Patton, 1995).

D'Onfro (1988) modeled allochthonous salt sheets as dykes and sills that were intruded in areas of local compression, such as the toe regions of growth faults (Figure 6.19c). Podladchikov et al. (1993) modeled asymmetric salt sheets as intruding laterally from a diapiric salt mass at depths of approximately 1 km depth. This level, according to the authors, lies just above an abrupt

thousand-fold downward increase in the viscosity in what otherwise are uniformly viscous sediments (Figure 6.19d). Amery (1969, 1978) envisaged shallow allochthonous intrusion of the spreading salt layer as occurring beneath a thin sediment roof that was no more than 200 - 300 m thick. He visualised the salt as coming from an autochthonous diapir source. Nelson (1991) stated that most salt sheets in the Gulf of Mexico had been emplaced shallow at depths of around 100m and never

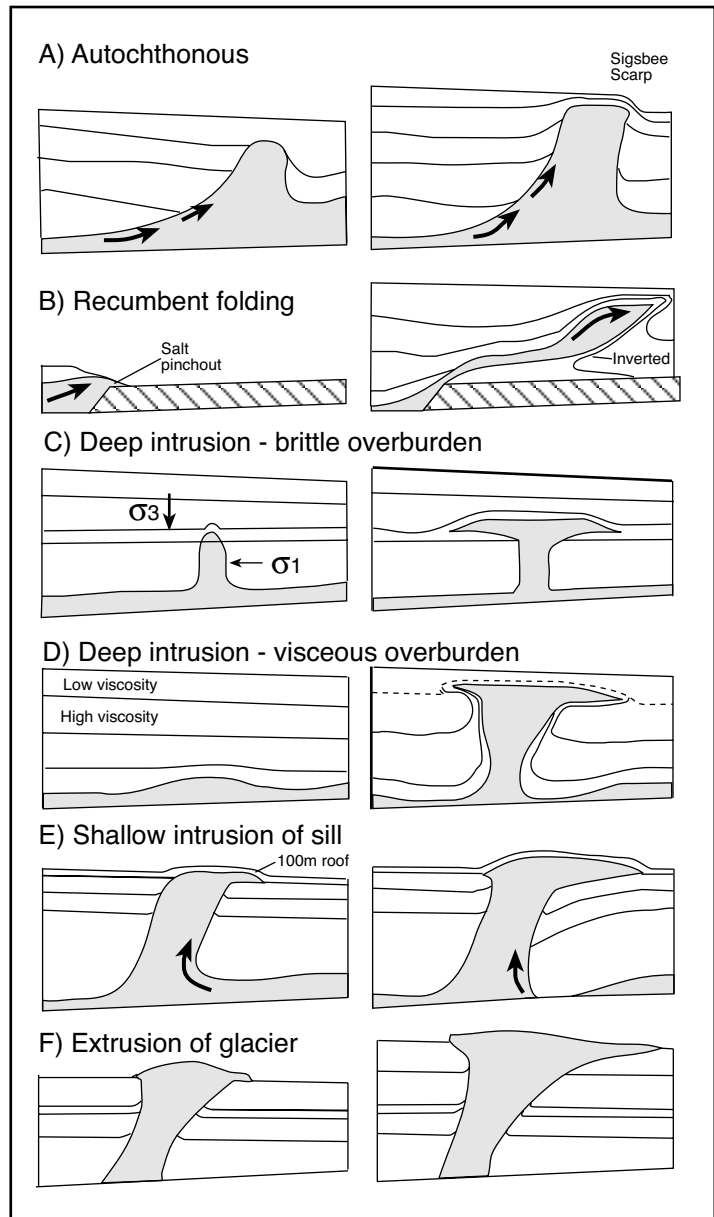


Figure 6.19. Hypotheses for the origin of allochthonous salt sheets. See text for explanation (modified from Schultz-Ela and Jackson, 1996).

more than 300m (Figures 6.6, 6.19e). Talbot (1993) pointed out the resemblance of salt sheet profiles to viscous fountains spreading laterally into unconsolidated surface muds (Figure 6.19f). The stepped base to many salt allochthons attest to their emplacement as surface rather than shallow subsurface features (Figure 6.16c).

Humphris (1978) was the first to postulate extrusion at the front of the vast Gulf of Mexico thrust nappe, which was riding basinward as an allochthonous salt sheet (Figures 6.1, 6.27). Jackson and Cornelius (1987) hypothesised that extrusion was possible if progradation was slow. Vendeville and Jackson (1992a) first modeled allochthonous salt sheets as forming under little or no roof. The concept of extrusive salt sheets on the sea floor under little or no sediment cover is now the most widely accepted mechanism for allochthon emplacement (Figure 6.19b, f; Fletcher et al., 1995; McGuinness and Hossack, 1993; Schultz-Ela and Jackson, 1996; Schuster, 1995). Salt sheets form by the geologically rapid widening of the crest of passive diapirs (Jackson et al., 1994b; Fletcher et al., 1995; Ge et al., 1997). As sediments are deposited around an extruding salt sheet, the salt glacier climbs up across the newly deposited

sediment. Thus a salt allochthon climbs over progressively younger sediment as it moves away from its feeder. The slope at the base of the salt sheet (ramp versus flat) is thus a function of the relative rate of sedimentation (Figure 6.16).

During times of active extrusion a salt sheet forms a bathymetric high with up to several hundred metres of relief above the surrounding seafloor (Fletcher et al., 1995). A feedback occurs between the rate at which salt is pumped to the surface and the rate at which seawater dissolves the salt. The rate of salt pumping is thought to be many times greater than the sedimentation rate during peak growth periods of the allochthon. Expanding salt sheets are protected from dissolution by a combination of: 1) sedimentary veneer, 2) an insoluble residue (or caprock) of anhydrite/gypsum, and 3) an overlying layer of saturated pore brines where circulation of sea water is locally restricted. If continuously deposited, a low-permeability sedimentary roof, alone, can protect underlying salt, even if the roof is continuously breached by deformation and erosion.

Historically, the ancient equivalents of salt glaciers were not widely recognised in the rock record. Now, with our improving

understanding of salt tectonics and the significance of widespread salt evacuation, ancient counterparts are now well documented in Kazakhstan, Algeria, Tunisia, Yemen, the Flinders Ranges and Mexico (Volozh et al., 1994; Vila et al., 1994, 2002; Davison et al., 1996; Dyson, 1998; Giles and Lawton, 1999, respectively). As any salt glacier or allochthon sheet spreads out over the surrounding landscape or seafloor they also laterally transport and deform any roof and can induce drag folds in subsalt sediments to ultimately create transition zones known as basal shears. With the exception of the namakiers of Iran, most areas where allochthons outcrop are no longer characterised by salt actively flowing at the surface. Rather, the former presence of thick flowing sheets of salt are indicated by dissolution breccias and welds and associated deformation in the surrounds of the former sheet (Figures 6.20a, b, 7.23, 7.24, 7.27).

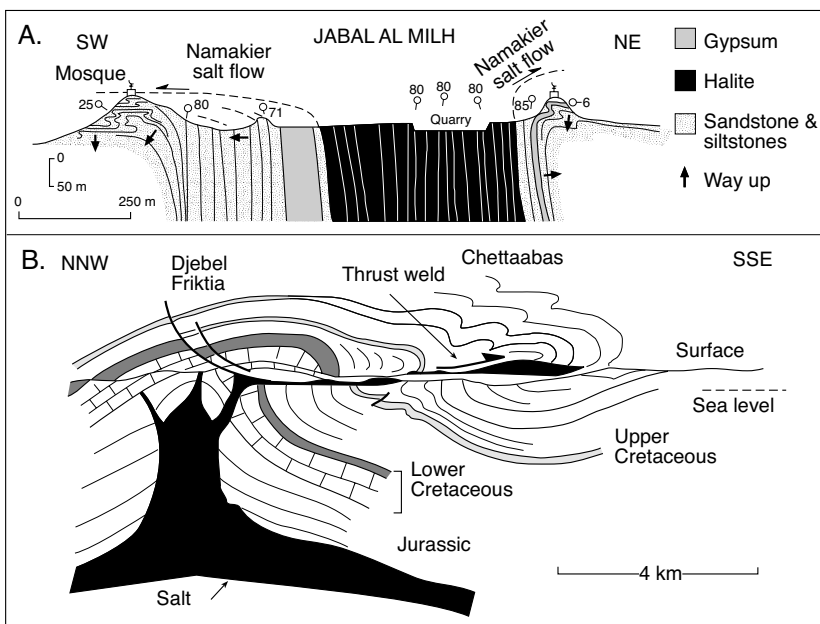


Figure 6.20. Cross sections through outcropping salt allochthon terrains. A) Recumbent folding and thrusting are the main deformation features observed in the siltstones and gypsum layers of the overburden at the Jabal Al Milh diapir, Yemen (after Davison et al., 1996b). B) The Jebel Frikitia allochthon, Algeria, shows how breakout of salt into the next allochthon tier typically evolves into a gravitational collapse 'thrust' off the original salt wall. This thrust is a gravitational adjustment to "down to the basin" extension in the overburden. Breakout occurs in areas where pressurized salt rises faster than extension and sedimentation can accommodate.

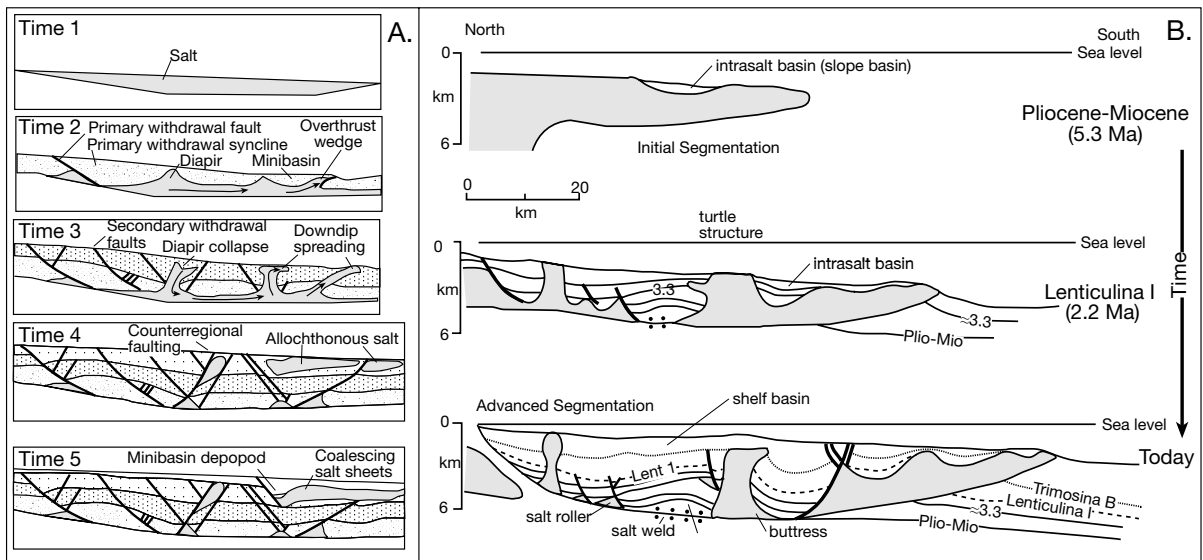


Figure 6.21. Salt allochthon evolution. A) Evolutionary model of the creation of allochthonous salt sheets in the Gulf of Mexico (after Montgomery and Moore, 1997). B) Schematic of evolution of eastern Green Canyon, Gulf of Mexico. At 5.3 Ma the salt sheet was extruded. From 6.3 to 3.3 Ma the ongoing basinward extension of the sheet promoted differential loading within half grabens. From 3.3 to 2.2 Ma the largest intrasalt basin displaced all the salt below it to create a salt weld and a structural inversion that was created by a turtle structure. Subsequently the sheet was further deformed as it continued to flow basinward and climb the stratigraphy (modified from Seni and Jackson, 1992).

Sheets, welds and basal (subsalt) shear zones

There are two major phases of allochthon emplacement (Montgomery and Moore, 1997): 1) initial inflation and loading of a salt mass, which generates zones of salt withdrawal and diapir formation (Figure 6.21a; times 1-3); and 2) subsequent suprasalt loading, which creates complex growth faults classified as regional and counter-regional faults (Figure 6.21a; times 3-5). This second stage occurs in levels of the stratigraphy that lie well above the primary salt level. Emplacement at all stages involves both syndepositional salt dissolution and shearing at the allochthon contacts. It can be associated with the spreading and/or coalescence of a number of salt sheets to form a salt canopy, which is in turn evacuated by later sediment loading (Figure 6.21b). Once emplaced, an allochthonous salt sheet is segmented into smaller second-generation structures. The top and bottom contacts of the initial salt sheet come closer and closer together until touchdown occurs and it becomes a salt weld (e.g. the Fraktia thrust weld in Figure 6.20b).

A salt weld forms when the salt sheet or primary bed is so thinned by withdrawal that salt is no longer resolvable on seismic profiles. The weld can still retain some salt or consist of faulted and brecciated sediment and insoluble residues. Salt welds are also called overburden touchdowns, or simply

touchdowns. A salt weld is usually, but not always, marked by a structural discordance. Another distinctive feature is the common presence of a structural inversion above the salt weld, which often defines some sort of broad anticlinal structure (e.g. turtle and mock-turtle structures; Figure 6.17).

Better-documented examples of weld textures do not come from the subsurface but from salt basin outcrops in regions such as the Flinders Ranges and the Zagros fold belt. One of the best examples is in the La Popa basin, near Monterey, Mexico, where a subvertical salt weld is exposed for 25 km along its strike (Figure 6.59; Rowan et al., 2003). Traverses across the weld indicate significant strike-parallel variability in both weld structure and the geometry of adjacent strata. In some places the weld is a 2 to 4 metre wide fault zone with brecciated and sheared siliciclastics, no remnant evaporites, and evidence of extensive fluid alteration. In other places, the weld contains up to 30 m of remnant gypsum, either massive or sheared, that locally contains inclusions of meta-igneous rocks or Jurassic dolostones that were carried up in the diapir. The La Popa weld ends in the west at an outcrop of gypsum several hundred metres in diameter that represents a remnant salt stock; in contrast, the weld trace is truncated in the south-east by an intra-Maastrichtian unconformity (see later in this chapter for geological detail).

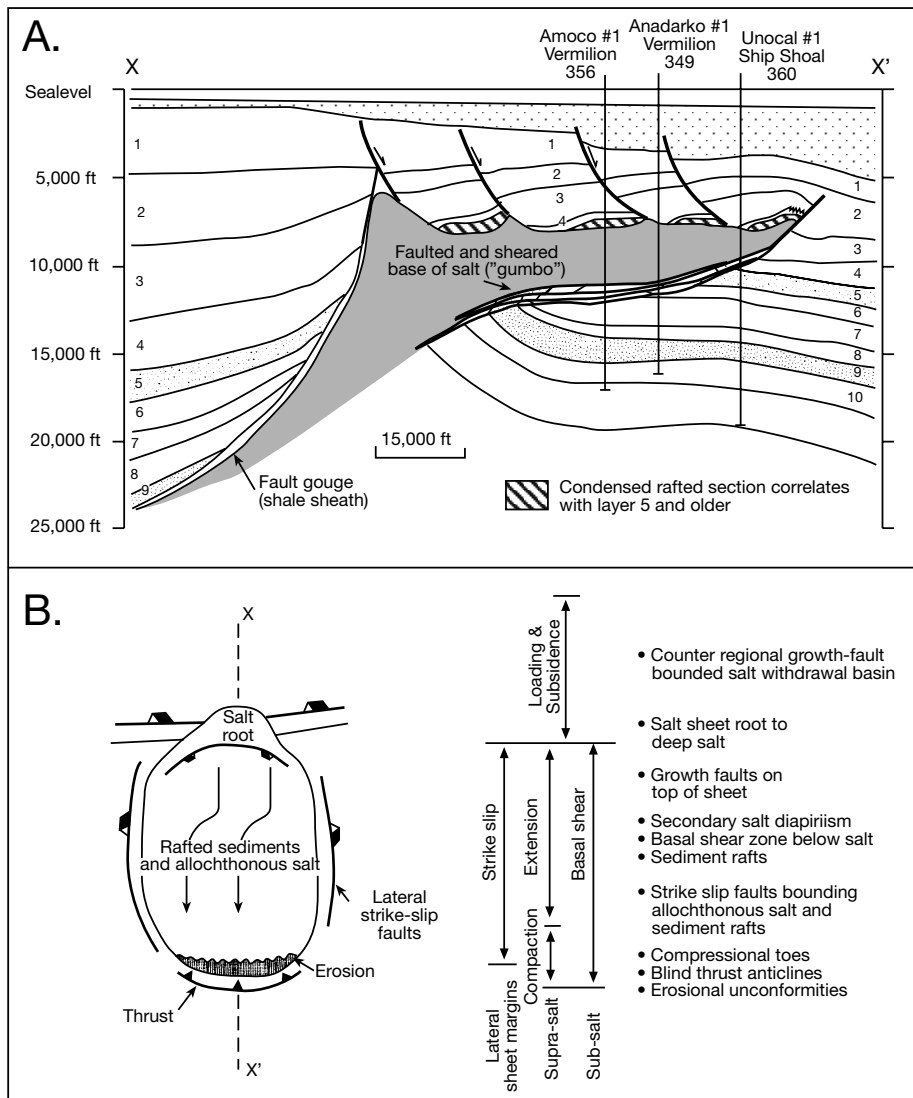


Figure 6.22. Basal shear model (after Harrison and Patton, 1995). A) Cross section view with a thrust fault defining the rising compressional nose of the salt sheet. Relevant Gulf of Mexico wells are placed schematically on this section. B). Map view. Down-to-the-basin translation of the composite salt/sediment glacier forms strike slip shears at the depopod margins. The compressional toe is a complex combination of normal fault and eroded blind-thrust anticlines (see later).

A primary weld joins strata originally separated by gently dipping autochthonous bedded salt. Secondary welds join minibasin or depopod strata originally separated by steep sided salt diapirs (walls or stocks). Tertiary welds join strata originally separated by gently dipping allochthonous salt sheets (Jackson and Cramez, 1989). Each side of the weld can slip relative to the other, as it can in a more steeply inclined fault that is lubricated by salt. The latter structure is termed a fault weld although all welds are tied to some sort of translation or shearing of strata above and below the salt sheet (Figure 6.21a, b). A fault weld

is simply a recognisable fault surface or fault zone joining strata originally separated by autochthonous or allochthonous salt. Thus a fault weld can be a salt weld along which there has been obvious faulting or shearing.

Shearing associated with the margins of salt diapirs has long been recognised as creating shale sheaths and as explaining shear-defined cylinders of differential salt movement within down-building subvertical diapirs (Hanna, 1953). This is especially obvious in subvertical salt structures that have been mined or crop out (Balk, 1953; Kupfer, 1976; Talbot and Jackson, 1987a; Zak and Freund, 1980). What differentiates classic subvertical diapir models and the lateral flow emphasis of allochthon models is the development of minibasins and listric faults in supra-allochthon sediments (Figures 6.21). A minibasin is an suprasalt depositional basin underlain and surrounded by allochthonous salt. The term intrasalt basin is sometimes used to described salt-floored minibasins or depopods. In

my opinion this is confusing as intra means within, these basins are never within, they are initially atop and laterally restrained by salt. Then in more mature extensional and compressional terrains where most of the salt in a former salt wall has been largely squeezed from the system the remaining adjacent depopods can be in lateral contact across a salt weld and flooded by a salt weld (e.g. Figure 6.25). I use the term intrasalt to describe features completely encased in salt.

Once an allochthonous salt sheet is detached from its source layer, pods of condensed sediment are deposited as a roof carapace (e.g. palaeontological equivalent of unit 5 in Figure 6.22a). This suprasalt region loads and splits into a number of growth-fault defined suprasalt depopods (layers 1-4 in Figure 6.22a). Sediment accommodation space is created at the up dip end of this expanding minibasin via growth faulting, while thrusting and erosion is occurring at the same time at the downdip end (Figures 6.21 and 6.22b). The rotation of the suprasalt sediment prism as it accumulates is facilitated by the lateral migration of salt. Internal shear in the advancing salt sheet is greatest in the basal shear zone.

Sediments beneath the base of subhorizontal allochthon sheets or the subsequent welds typically preserve shear features that encompass both external and internal shear zones. They include; evidence of sediment pressurization, entrainment of country rock within the salt body and structurally induced drag folds (Figure 6.22a; Harrison and Patton, 1995; Alsop et al., 1996). Basal shear zones of allochthons are also called transition zones, gumbo zones, unconsolidated rubble zones, and can be considered as a subhorizontal type of shale sheath.

The basal shear zone is a response to thrusting along and within the base of the salt allochthon as it is emplaced at or near the sea floor (Harrison and Patterson, 1995). Consequent sediment loading atop the sheet drives further salt withdrawal and suprasalt sediment deformation (Figure 6.22a). Salt flow within the salt sheet occurs via internal shear and pressure solution creep. A pure salt sheet remains impermeable as it experiences no brittle response to flow deformation as it rolls out over its substrate (Figure 6.5). As the sediment carapace thickens over the salt sheet, overpressures develop in the subsalt transition zone. The resulting anomalously high pore fluid pressures facilitate simple shear beneath the sheet by reducing the effective normal stress, thereby allowing lateral movement of the sheet and its sediment carapace (gravity gliding; Baud and Haglund, 1996). Whether shearing occurs within the salt sheet or in the subsalt sediment is determined by which interval has the lower shear strength. Baud and Haglund (op. cit.) believe post first-emplacment shearing occurs within the salt sheet at least until anomalously high pore pressures develop in sediments below the sheet.

Measured pore pressures in the basal shear zone of Gulf of Mexico allochthons can be much higher than regional pore pressures and approach fracture-inducing pressures in some subsalt shales. Measured gradients as high as 0.88 psi/ft or balanced mud weights of 17 ppg characterise Gulf of Mexico drilling

(Table 8.3; Harrison and Patton, 1995). Field evidence cited in House and Pritchett (1995) indicates that the hyper-pressured interval below a salt sheet is typically 300 to 600 m (1000-2000 ft) thick and its upper part is likely to entrain a lithologically distinct "gumbo" or transition zone. In the Gulf of Mexico, a "gumbo" zone has been encountered beneath salt sheets emplaced into Pliocene, upper Miocene and middle Miocene age sections, but hyper-pressurised cells in the "gumbo" have been documented only below allochthons emplaced into Pliocene and upper Miocene sections (House and Pritchett, 1995). This may indicate that hyper-pressures are a geologically transient allochthon phenomenon and that with sufficient time a pressure equilibrium gradually re-establishes itself.

On passing through the salt allochthon the Amoco #1 well, Vermilion Block 356, immediately intersected such a pressured disturbed transition or "gumbo" zone. Cuttings from the gumbo zone documented a change with increasing depth below base of salt from a grey soft shale with pyrite traces into a firmer, medium to dark shale. Deep resistivities were less than 0.2 ohm.m in the shale in the first 120 m (400 ft) below the salt and increased to 0.4 ohm.m in the next 180 m (600 ft) possibly indicating decreasing pore water salinities or increasing organic content. The lowest resistivity zone corresponds to a wireline density ≈ 2.10 gm/cc that increases to 2.25 gm/cc by 300 m below base of salt. RFT measured pressures in thin sands in the disturbed (gumbo) zone were some 16.7 ppg equivalent, while measured pressures several thousand feet below the gumbo in the same well were 16.1 ppg equivalent.

The South Marsh Island Block 169 Amoco #1 well in a transition zone immediately below its salt sheet intersected pressure gradients of 17.4 ppg equivalent. This pressure level is only 0.3 ppg less than the calculated fracture gradient for the matrix (House and Pritchett, 1995). Below the "gumbo", pressure gradients decrease to more typical regional values of 16.5 ppg equivalent. Pressure data divide this well into a high-pressure zone (hyper-pressure cell) some 335 m (1100 ft) thick immediately below the salt sheet and an underlying pressure transition zone some 245 m (800 ft) thick. Pressures below the transition zone are equivalent to regional overpressures.

Abnormally high pressures in transition zones (gumbo) typically indicate hydrologic isolation of this shale-rich section and a lack of hydraulic continuity (these shales do not readily dewater). Wireline image data show soft sediment deformation features, with higher levels of contortion in proximity to the allochthon contact. A similar style of disturbance outcrops in the transition zone of Jabal Al Milnh diapir, Yemen (Figure 6.20a) and in

subsalt thrust folds that define the Upper Cretaceous section of the Jebel Fraktia allochthon (Figure 6.20b). A basal shear zone in most active allochthon provinces is best considered as a potentially thick, highly pressured, faulted and folded interval. Fluids in this deformed zone may migrate along fault planes but typically not within the blocks of disturbed sediment matrix, which like the overlying salt, acts as vertical barriers to fluid flow. Pressure build-ups within the shales probably lead to periodic matrix fracturing and bleed-off of elevated pressures (seismic pumping).

Hence, the transition zone (gumbo zone) that characterises the lower contact of most active allochthon sheets is outlined by abnormal pressure and temperature gradients. Differential translation is concentrated at and immediately below the base of the salt sheet. Salt-lubricated slivers line up as sub-parallel thrust planes along the pressurised base of the allochthon, as do repeat sections and recumbent subsalt folds (Figure 6.22a; Harrison and Patton, 1995). A lack of fluid movement in a disturbed zone can also lead to anomalously low temperature gradients in this interval with a low thermal gradient halo typically characterising the interval immediately below the thick, thermally conductive salt sheet. Thermal gradients in this halo gradually increase downward until a more normal regional gradient is achieved. The low temperature, high-pressure interval that occurs below most allochthon sheets is a potential problem zone for the drilling engineer (Chapter 8).

Jackson and Hudec (2004) have expanded on Harrison and Patton's notion of basal thrusting (Figure 6.22a) by arguing that as salt allochthons continue to advance over the seafloor they act much in the same way as a glacial ice sheet advances and ploughs over glacial till. As allochthonous salt rides up over its underburden it pushes, deforms and thrusts portions of its water-saturated substrate. This in turn creates thrust ramps and duplexes in subsalt "gumbo" sediments immediately beneath the salt sheet.

When pressurised, the base of salt or gumbo zone tends to act as a permeability barrier to rising basinal fluids, as does the overlying salt (House and Pritchett, 1995). When rising fluids impinge on this zone they are forced to flow laterally, subparallel to the base of salt and through the gumbo until they encounter a breach point or the feather edge of the salt sheet (Chapter 8). But not all "gumbo" transitions are anomalously pressured and pressure character is not easily predicted ahead of drilling. For example, instead of being impervious, extra permeability can be created in a gumbo or transition zone via periodic salt evacuation from salt feeder stocks below an allochthon canopy.

Depending upon its local character, a gumbo zone can be a seal, it can be a path for hydrocarbon migration, or a potential reservoir. When pressurised a gumbo zone provides a potential trapping mechanism, much like a pressure-sealing fault. Hydrocarbons migrating laterally through a highly-pressured transition zone can be injected into low-pressured underlying sands and trapped due to the pressure differential. Or a transition zone can trap hydrocarbons migrating upward through subsalt sands as overpressures in the transition zone prohibit fluid invasion. If not overpressured, a fracture-susceptible gumbo zone can provide a permeability pathway for hydrocarbons migrating upward along base of a salt feeder as buoyant fluids move through the transition zone. Hydrocarbons can also migrate upward through suballochthon sands and then leak into the transition zone wherever the sand and transition zone contact one another. Lastly, subsalt transition zones could prove to be reservoirs themselves, as widespread leakage of hydrocarbons from below, or lateral migration of fluids through the gumbo, can saturate them. But most subsalt transition or "gumbo" zones are probably not of reservoir quality, observed log character shows most are disturbed and shale prone (LeBlanc, 1994). Fluid modelling based on allochthon-focused sub-salt flow has implications for the pulse-like mineralisation episodes and the development of footwall alteration haloes in many Proterozoic base metal deposits (Warren, 2000b).

Near-diapir suprasalt shear (drag zones)

Deformation in the suprasalt sediments immediately adjacent to a growing subvertical diapir or an inflating allochthon edge creates an external shear or drag zone. Drag zones form as beds in the overburden are rotated into steeply dipping attitudes

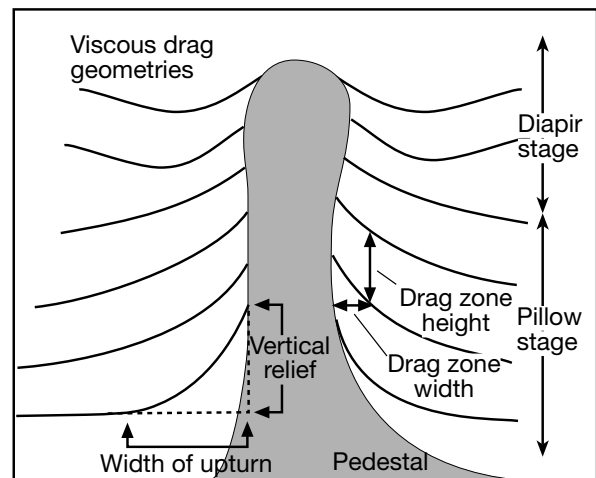


Figure 6.23. Dimensions and parameters of the diapir drag zone (after Davison et al., 2000b).

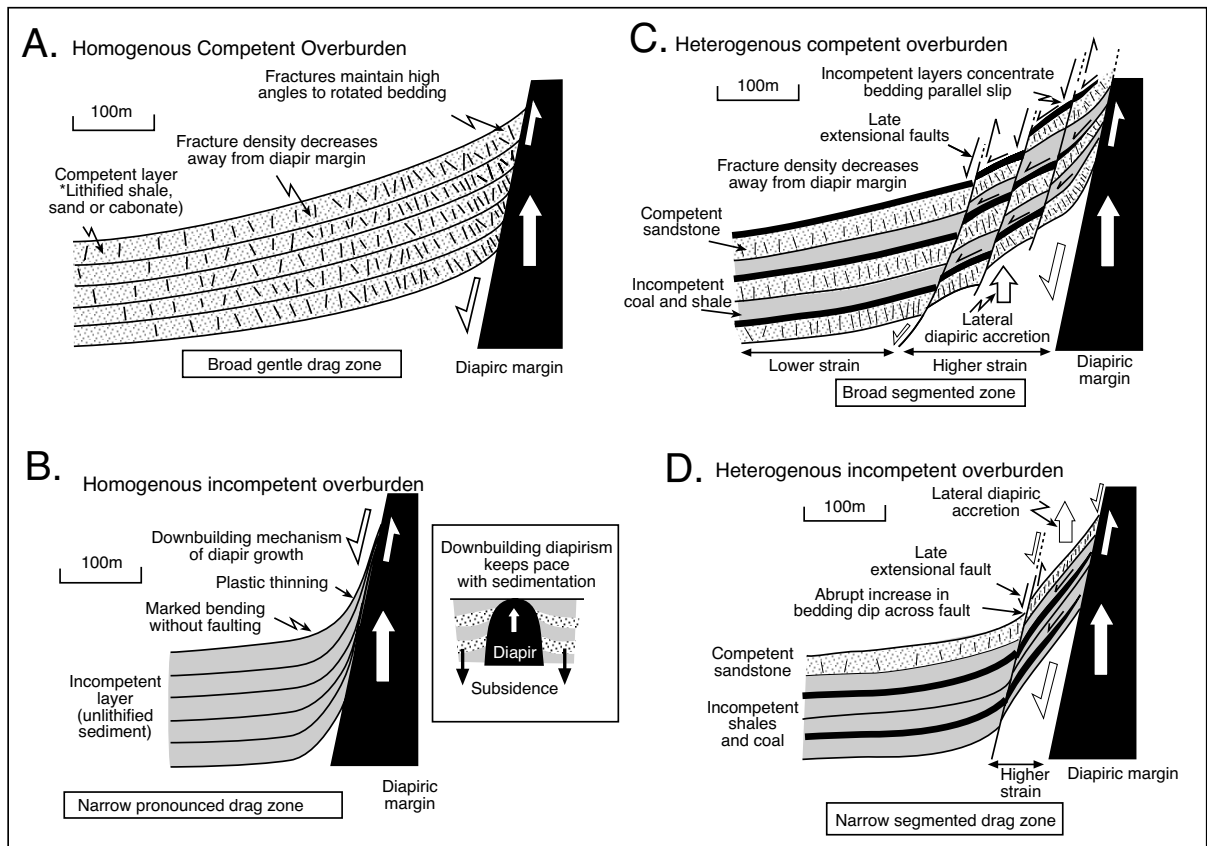


Figure 6.24. Schematic profiles of diapir drag zones (after Alsop et al., 2000). A) Broad drag zone within homogenous competent overburden. B) narrow drag zone with incompetent inhomogeneous overburden. C) Broad segmented drag zone within homogenous incompetent overburden. D) narrow segmented drag zone within heterogeneous incompetent overburden with marked internal competency contrasts. C) and D) also illustrate the process of lateral diapiric accretion where fault-bound material moves upward with the flanks of the diapir relative to sediments further out in the rim syncline.

that lie subparallel to the walls of the salt diapir (Schultz-Ela, 2003; Alsop et al., 2000). Rotations can be as steep as 90° and can even overturn beds. Deformation is driven by a variety of processes including downbuilding, differential compaction, grain boundary sliding, microfracturing, larger-scale faulting and pressure solution. The abutment of an inclined drag zone against a near-diapir fault can form a large number of stacked and compartmentalised oil and gas reservoir sands (Figure 10.45a).

Drag zones develop sequentially; initial salt pillow uplift creates broad gentle overburden flexure that increases in intensity as the structure evolves into a diapir (Figure 6.23). By the diapir stage the width of a drag zone is approximately equivalent to the width of the diapir at the diapiric base and decreases to 25% of the diapir width toward the diapir crest. Vertical relief of the upturn in a bed also decreases upward (Figure 6.23; Davison et al., 2000b). Vertical relief is some 5% of the diapir

height near the crest and increases to 30% near the diapir base, a consequence of the greater relative movement across the pre-movement and early syn-movement layers situated near the base of the diapir stem. The width of the drag zone increases proportionally with increasing diapir size and diapir height, while the total amount of bed upturn increases proportionally with the width of the drag zone.

In one of the few outcrop studies of the characteristics of diapir drag zones Alsop et al. (2000) relate variation across the zone to overburden competence (Figure 6.24). Their work focused on an outcropping diapiric province in Cape Breton Island, Nova Scotia, where five Viséan-age salt diapirs penetrate Upper Carboniferous (Namurian-Stephanian) conglomerates, sandstones, shales and coal seams. The width of diapiric drag zones varies from 70 metres up to 500 metres. Narrow drag zones are a response to the low mean competence of shales and siltstones, which were probably shallowly buried and poorly

lithified at the onset of diapirism (Figure 6.24b). Broader drag zones are dissected by two sets of extensional fractures, together with major faults, suggesting that the overburden was semi-lithified and displayed greater flexural rigidity at the time of salt flow (the beam effect; Figure 6.24a). Overburdens with high internal competency contrasts (e.g. interbedded sand-shale) generated strain localization and partitioning, with pervasive granulation seams and minor faults developed in the more competent sandstones and bedding-parallel shears in the coal and shale horizons. The various drag zones are segmented by steep outward-dipping faults associated with decametric, asymmetric drag profiles (Figure 6.24c, d). These faults facilitate the upward movement of material and effectively enlarge the diapiric process into the adjacent overburden a process they call lateral diapiric accretion.

In the subsurface, seismic of varying quality is usually all that is available to interpret drag zone geometries. Steep dips and irregularities in the distribution and density of adjacent salt means that the shape and extent of the diapiric drag zone is poorly defined in the inner shear zone area, especially when the diapir is bulbous. The width of the upturned zone caused solely by frictional drag is difficult to estimate, as a large section of the upturned interval can be due to the salt pedestal effect (Vendeville and Nilsen 1995). The increased permeability around zones of fracture adjacent to diapirs means that drag zones can act as preferential conduits for fluids escaping from deeper levels. Pervasive fracturing in broader drag zones formed by more competent beds helps explain the pervasive entry of ferroan brines into adjacent carbonates and fracture defining haloes as is seen in the outcropping Proterozoic diapiric province of the McArthur Basin, Australia (Warren, 1999). There the salt has long gone and only siderite/brunnerite haloes remain around fault welds and salt welds.

With prekinematic overburden, substantial drag-induced folds only form in exceedingly weak rock (Schultz-Ela, 2003). Even then, most folding develops by nearsurface upward and outward rotation. Protrusions of overburden into a diapir, where the contact dips shallowly outward, are most susceptible to folding due to frictional drag created by the crossflow of salt. Based on modelling experiments Schultz-Ela (op. cit.) argues synkinematic sedimentation is much more likely to engender large and broad folds in the drag zone because onlapping wedges may be continually produced during downbuilding. These syndepositional folds can even form in strong layers. He argues folding of onlaps over rising salt is really drape folding, so “drag” fold is actually a misnomer. Local gravity fold is perhaps a better descriptor of this style of deformation. Episodically deposited layers further enhance the potential for onlap folding.

For the same average aggradation rate, pulsed deposition of thick layers generates larger folds than do continuously deposited thin layers. Variation in thickness and timing of deposition increases the likelihood of multiple wide onlaps that evolve into substantial folds. Older layers tend to form the broadest and tallest folds because those layers prograded farthest across the diapir crest. As the salt contact steepens, the folded zone narrows as younger layers onlap onto older folds or the salt. Onlap folds can only form for a limited range of relative salt rise and deposition rates. Deposition much faster than the net rate of salt rise buries the diapir. Deposition that is too slow creates steep contacts or salt spilling onto the sediment surface, both of which result in little “drag” folding.

In three dimensions, outcrop and 3D seismic studies have shown that both radial and concentric faults occur in drag/drape zones around diapirs, and that the fault patterns are lithologically dependent (Davison et al., 2000). This pattern can facilitate the creation of a hydrocarbon-bearing column adjacent to a diapir that is more than a km tall. Many fault patterns are approximately sub-radial due to the intersection of multiple fault trends and many faults curve to become roughly tangential to the diapir face to produce cusped salt outlines in plan view (Figure 6.21; Chapter 10).

Welds, loading detachments and growth faults

Many regional growth faults in salt allochthon provinces sole out onto residual fault welds, which can be many tens of kilometres in length (Figure 6.21b). With time and ongoing salt evacuation, the basal shear zones and gumbos depressurize and evolve into normally pressured regions across the salt or fault weld. The link between growth faults and salt welds is an inherited relationship whereby one evolves or passes into the other (Jackson et al., 1994b; Fletcher et al., 1995). A thick salt sheet that was present before welding decouples faulted zones above and below it. This decoupling means most large faults sole out into the level of the former sheet.

Burial of an evacuating salt allochthon beneath loading sediment typically occurs after pinch-off from the feeder diapir (Fletcher et al., 1995). This allows the former sea floor high created by the glacier to relax (deflate), especially at the updip end of the sheet. Sediment can then prograde across the sheet beginning at its updip end (Figure 6.22a, 6.25). Even during burial of its updip end, an evacuating salt sheet typically retains several hundred metres of relief on the downdip end. Thus the downdip sheet continues to advance as a composite salt-sediment glacier. Sediments atop the allochthon are deformed, along with the flowing salt, as the gliding movement creates extensional breakaway zones at the updip end. In turn this

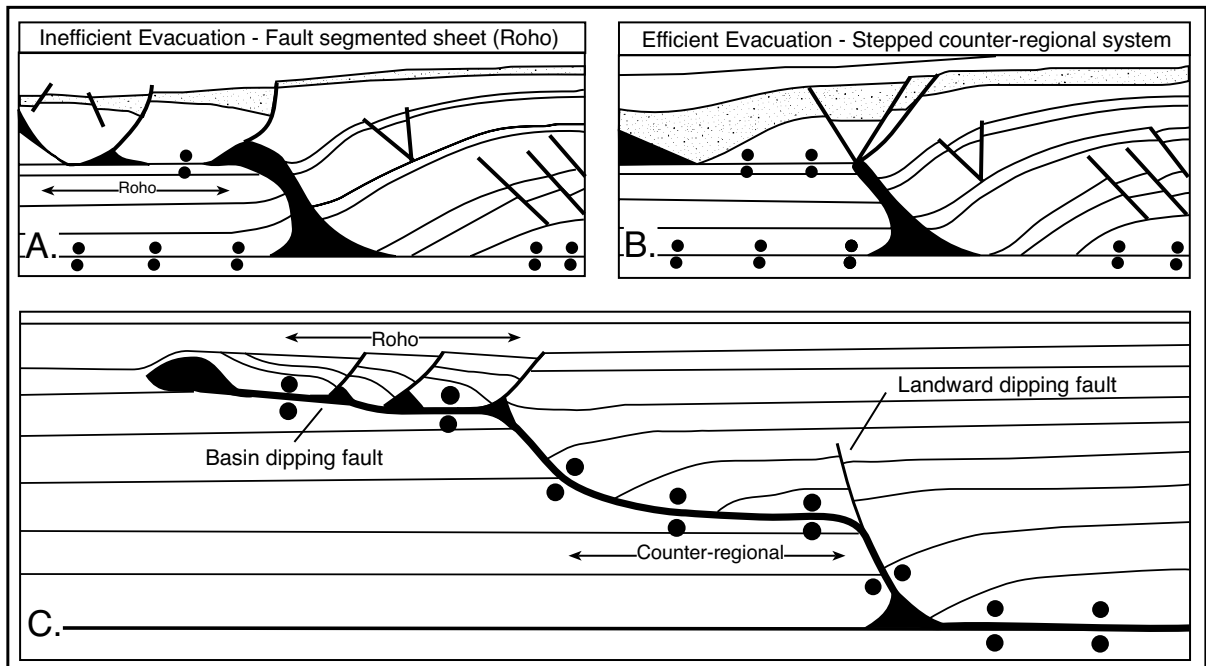


Figure 6.25. Efficiency of evacuation is reflected in the suprasalt structuring. A) With inefficient salt evacuation a fault segmented (Roho^{6,3}) system forms. B) With efficient evacuation a counter-regional system is created. C) Shows how the two systems can be created by the same salt body. Circles show position of salt weld. See text for explanation, black circles define salt welds (in part after Jackson and Vendeville, 1994b; Rowan, 1995).

initiates fault-bound minibasins at the updip end of actively flowing salt sheets (Figure 6.22). Ongoing slippage creates a growth fault rollover anticline as salt continues to extrude at the downdip or compressional end.

The same salt mass can recycle multiple times as tiers ascending into ever higher stratigraphic levels (Figure 6.25). Each time salt activity is transferred to a higher level, a largely welded smear of salt with vestigial salt structures is left behind at the lower levels. Substantial volumes of salt are lost via dissolution each time the salt approaches the seafloor or is bathed in less saline pore fluids. Thus, the ascending salt mass cannot recycle indefinitely and the driving mechanism is lost once a salt weld or overburden touchdown is created beneath the minibasins.

^{6,3}The detachment surface for these into-the-basin “Roho” growth-faults is inefficiently evacuated salt. With 1960s and 1970s vintage seismic data, it was not possible to image below the salt evacuation surface. An early seismic stratigrapher in Shell, Chuck Roripaugh, after being instructed to map to the Moho below areas of salt, jokingly labelled his map of the salt evacuation as “Roripaugh’s Moho” which was later contracted to Roho. This in-house joke has since escaped into the public literature.

A salt sheet that is isolated from its feeder stock can advance further only by cannibalising its trailing edge (Figure 6.21b; Fletcher et al., 1995; Schuster, 1995; Jackson and Vendeville, 1994b). If the salt is inefficiently withdrawn from the trailing edge, the salt becomes progressively sequestered into residual smaller bodies and the overall structure is called a fault-segmented sheet. In the Gulf of Mexico this is also called a “Roho” system or a listric weld (Figure 6.25a). Roho systems are characterised by major, listric, down-to-the-basin growth faults, which in the Gulf of Mexico sole into salt evacuation surfaces known as tertiary salt welds (as opposed to primary and secondary salt welds - see earlier). During shelf progradation over a salt sheet or salt “wing,” the rear (landward) margin of the salt sheet gradually segments and deep withdrawal structures are enhanced. At shallower levels, vestigial salt forms a train of sequestered salt walls formed by the partitioning of a formerly continuous sheet of salt. Each residual salt structure is typically in the footwall of a normal fault or is separated from its neighbour by a syncline. Each residual wall is generally overlain by a splay of extensional faults, which are commonly listric.

If salt is more efficiently withdrawn from the deflating trailing margin shelf progradation then a stepped counter-regional

system results (Figure 6.25b). Strata above the deflating salt sheet subside to form a shallow flat step along the weld of vanished salt. The step resembles a landward dipping growth fault. However, the step can be merely a pseudo-fault, like the contiguous deeper step created by upward evacuation of the original diapir. In three dimensions the shallow step fault is the axis of a partly evacuated sheet that is shaped like a tongue with curled up lateral margins (Figure 6.22b). Along the deepest axis of the tongue lies the deepest, most evacuated part of the salt sheet below the thickest overburden.

These two structures — the fault-segmented sheet (Roho) and the stepped counter-regional system — are end members of a load-induced evacuation series where the counter-regional systems define welds where salt has been completely evacuated and a Roho system defines less efficient evacuation. It is possible that as the salt climbs the stratigraphy the same salt body can create both Roho and counter-regional systems or welds depending on the efficiency of evacuation (Figure 6.25c).

Minibasins floors become welds

Differential loading, created by the emplacement of a depositional lobe atop a salt allochthon, induces a differential fluid pressure in the salt below. Salt squeezes laterally into flanking areas and a bathymetric high, which dams the accumulating sediment, forms a rim adjacent to the sediment accumulating in the growing minibasin (Figure 6.22). A feedback process is created as the sediment-loaded minibasin floor subsides by pushing salt aside, so allowing the basin to receive additional sediment (Figure 6.26a). The process continues until the minibasin floor touches down on the subsalt strata to form a salt weld. At that time, minibasin subsidence ceases. Once the minibasin touches down, subsidence shifts from the centre of the minibasin to the flanks, which are still underlain by salt. Both flanks subside, creating an anticlinal turtle structure. Subsequent depocentres form on both sides of the early depocentre (Figure 6.17).

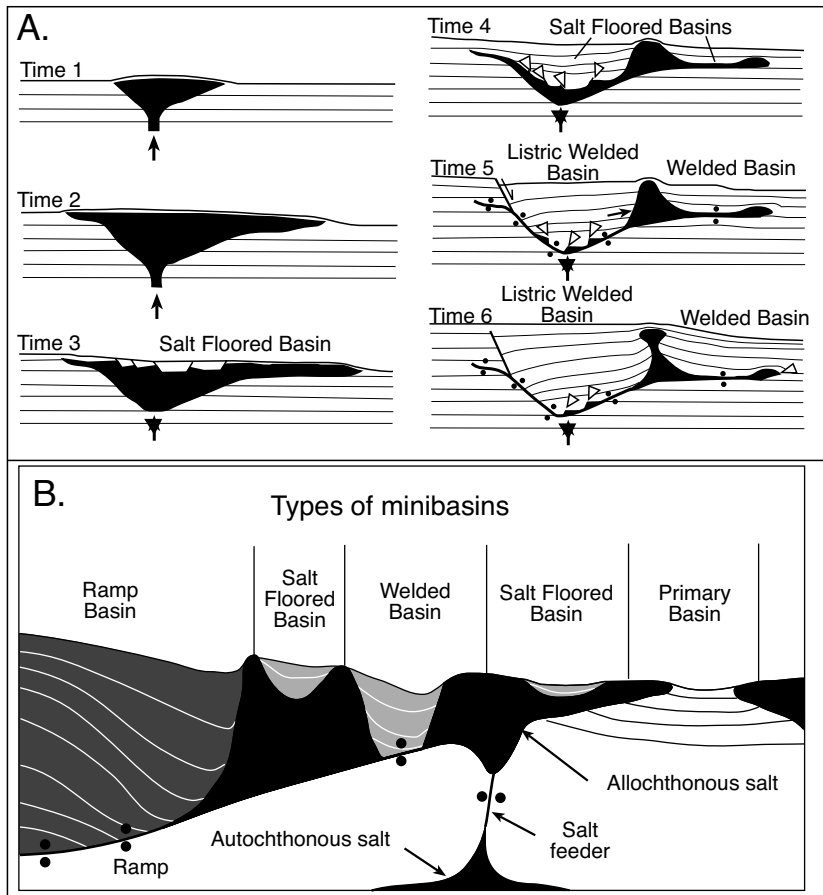


Figure 6.26. Evolution of minibasins atop salt allochthons based on the northern Gulf of Mexico (as in Figure 6.21). **A**) Evolution of a minibasin as sediment loads a salt allochthon (after McBride et al., 1998a). **B**) Types of minibasins (after Koch et al., 1998).

Intrasalt minibasins that form above tabular salt allochthons typically entrain a sediment fill that indicates an evolution from slope basins to shelf basins (Figure 10.52). They are typically bound by arcuate growth faults formed largely by downslope salt withdrawal rather than by extension. Initially, the allochthon acts as a deflating cushion that accommodates sediment deposited in minibasins. After time, loading or extension, the original salt sheet transforms into thin but broad welds, which then act as major subhorizontal detachments for deep growth faults whose slip creates space for further sedimentation. Ultimately, the sheet itself is segmented into discrete salt structures separated by salt welds and fault welds. Second or third cycle tiers of salt structures can rise from these deformed sheets.

Substantial thicknesses of sediment can accumulate in minibasins; in the Green Canyon region of the Gulf of Mexico the intrasalt basins contain more than 5 km of Neogene and

Quaternary sediment fill (Figure 6.21b). Minibasins in the northern Gulf of Mexico are divisible into 5 types based on the relationship of the fill to the presence or absence of a salt weld (Figure 6.26b; Koch et al., 1998):

- Ramp (atop counter-regional)
- Salt-floored minibasin
- Welded minibasin
- Welded Listric minibasin (Roho)
- Primary basin (seaward of the allochthon)

Ramp basins predominate on the slope in Garden Banks and Green Canyon of the Gulf of Mexico. They are characterized by a south-bounding, north-dipping salt ramp (Figure 6.21b). Most ramp basins have young thick depocentres adjacent to the counter regional ramp. Ramp basins tend to be asymmetric and larger in areal extent. Welded basins were previously underlain by allochthonous salt that has been fully or partially evacuated. In the northern Gulf of Mexico they increase in frequency southward into the Walker Ridge and Keathley Canyon protraction areas (Figure 10.51).

Welded listric (Roho) basins in the northern Gulf of Mexico have south-dipping arcuate faults that sole into the evacuating salt. Welded basins have a multitude of internal fault patterns and sediment fills, some are symmetrical with bowl-shaped fills, others have multiple depositional axes and bidirectional stratal fills. Primary basins in the Gulf of Mexico show no evidence of allochthonous salt and display continuous sedimentary fill from Cretaceous to Recent. Salt-floored basins are underlain by continuous allochthonous salt, which typically shields them from the underlying petroleum kitchens. Salt-floored basins occur along the down dip edge of allochthonous salt near the Sigsbee escarpment and above very young salt sheets in Garden Banks and Green Canyon (Figures 6.1, 6.27).

As basin fill changes through geologic time, each of the five types of basin has a differing capability to receive and internally distribute the hydrocarbons it receives via a complex plumbing system from sources at greater depths below the basin (Koch et al., 1998). In

general, hydrocarbon entry points to basin strata in the Gulf of Mexico salt basins are controlled through time by salt movement and geometry. Koch et al (op. cit.) argue ramp basins have attractive plumbing for hydrocarbons as well as an enhanced trapping focus (Chapter 10). Welded and welded-listric basins are dependent on the evacuation of the salt floor for any hydrocarbon charge to occur, therefore the age and areal extent of the weld are factors in assigning prospectivity. Primary basins appear to have access to underlying sources but may lack effective migration pathways and trapping geometries. Salt-floored basins are the lowest ranked basins due to separation from source. Within the four areas studied by Koch et al. (1998), most discoveries have been in ramp and welded minibasins (about 1 BBOE in each basin type). Primary and salt floored minibasins show minor discoveries and none of significant size. The feedback between allochthon style, deposition of potential reservoirs units and hydrocarbon maturation is discussed in detail later in this chapter and in Chapter 10.

At broader scales than minibasin sags, salt sheets can spread laterally as they deform until they eventually coalesce with neighbouring salt sheets. Collectively they create a salt canopy, a feature that dominates much of the foot of slope in the

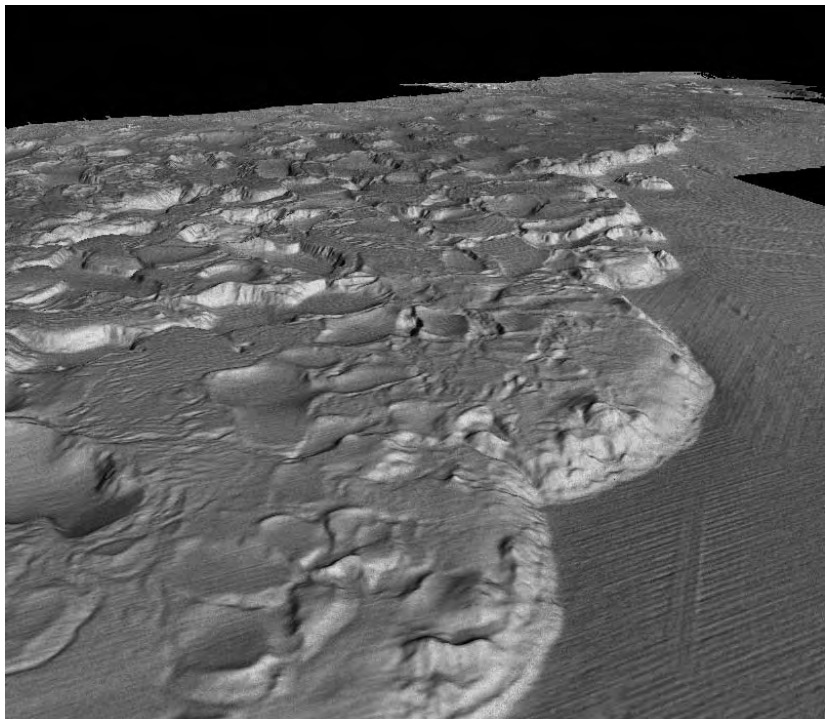


Figure 6.27. Salt canopy along the continental slope of rise of the Northern Gulf of Mexico. Image shows a series of salt-floored minibasin depressions atop a salt canopy (Image courtesy of Martin Jackson).

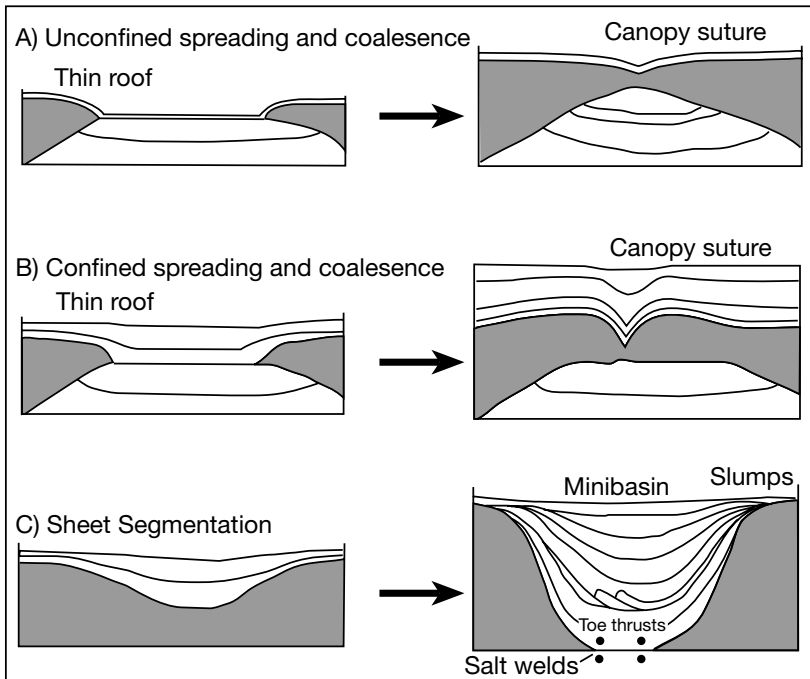


Figure 6.28. Comparison of structures produced by A) coalescence of unconfined salt glaciers, B) coalescence of confined, buried salt sheets, and C) segmentation of salt sheets by loading suprasalt minibasins (Jackson et al., 1994b).

northeastern Gulf of Mexico (Figure 6.27; Talbot, 1993; Wu, 1993). There individual lobate sheets coalesce westward into an extensive salt canopy whose leading edge is the Sigsbee Scarp. Adjoining sheets merge into canopies along salt sutures. The formation of a more or less continuous salt canopy must entail the upward and lateral movement of vast quantities of salt carrying with it an expanding overburden made up of minibasins actively accumulating sediments.

When the canopy roof is thin, the adjoining sheets are salt glaciers. In contrast, when a thicker roof of sediment confines the edges of adjacent sheets, the roof contracts into a cusped sediment-filled syncline associated with small thrust faults and kinks (Figure 6.28; Jackson et al., 1994b). This depositional syncline between suturing salt sheets is different from the depositional synclines created by depositional loading in suprasalt minibasins. Both contain thrusts, but minibasin thrusts are the result of slumping driven by the steepening sides of the subsiding

minibasin. They steepen over time but unlike canopy synclines do not contract laterally. The two types of syncline also differ in plan view, being cusped above salt sutures and bowl-shaped in minibasins atop segmenting salt sheets.

Fault families in allochthons

In the past decade our understanding of gravity gliding and salt flow in the Gulf of Mexico, the Santos Basin of offshore Brazil, the Kwanza Basin of offshore Angola has improved to where linkages between faults and anticlines in allochthon provinces can be predicted. Linkages between anticlines and extensional faults predominate, but links to contractional faults and strike-slip faults can also be predicted within a prograding sediment prism (Figures 6.29, 6.30, 6.31).

The observed diversity of structuration reflects the linked nature of gravity-driven deformation in zones where sedimentary overburden spreads under its own weight and slides basinward atop salt detachments (Rowan et al., 1999). Linked gravitational systems can range in scale from small, isolated, allochthonous salt sheets to the entire continental margin as it detaches and slides above autochthonous salt. Extension characterizes the landward and middle parts of salt-linked continental margin systems, while contraction usually occurs near the basinward

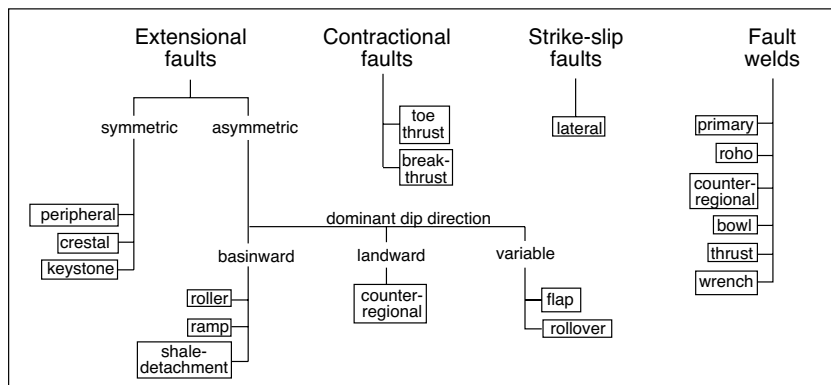


Figure 6.29. Classification system based on fault families and fault welds observed in the northern Gulf of Mexico (after Rowan et al., 1999).

limits of allochthonous salt (Figures 6.30, 6.31). Strike-slip deformation frequently connects these two domains. Where frontal contraction is not observed, downslope translation is usually accommodated by extrusion of allochthonous salt tongues.

Using a synthesis of existing seismic, Rowan et al (1999) reclassified the salt-associated faulting and welding in the Gulf of Mexico into related families (Figure 6.29). The classification is strictly geometric, without reference to kinematics, dynamics, or genesis. But the different families are connected in linked fault systems (inheritance), which, in turn, are associated with different types of salt systems. The transition from one fault family into another is typically related to position of the allochthon within the continental margin sediment prism (Figure 6.29). Each fault family is an array of faults having similar three-dimensional form and geometric relationships with deformed strata and associated salt. A fault family can include not only a dominant style (e.g., a basinward-dipping, listric, growth geometry), but also smaller faults that accommodate the strains and displacements induced by the primary faults. These subsidiary elements include antithetic faults, whose dip is opposite to that of the primary faults, and faults at high angles to the dominant trend. The various fault families and fault welds are tied to five varieties of salt systems: autochthonous salt, salt-tongue systems (both stepped counter-regional and Roho evacuation styles), salt-stock canopies, and salt nappes (Figures 6.30, 6.31).

Autochthonous salt tectonics: Autochthonous salt flow in the Gulf of Mexico is driven by two related mechanisms: gravity gliding and gravity spreading (Rowan et al., 1999). Early salt flow is dominated by gravity gliding (Figure 6.30). Oceanic spreading in the Gulf of Mexico began around the same time the Louann Salt accumulated during the Callovian. Subsequent cooling of the lithosphere probably tilted the continental margin basinward, causing gravity gliding of the thin overburden above autochthonous

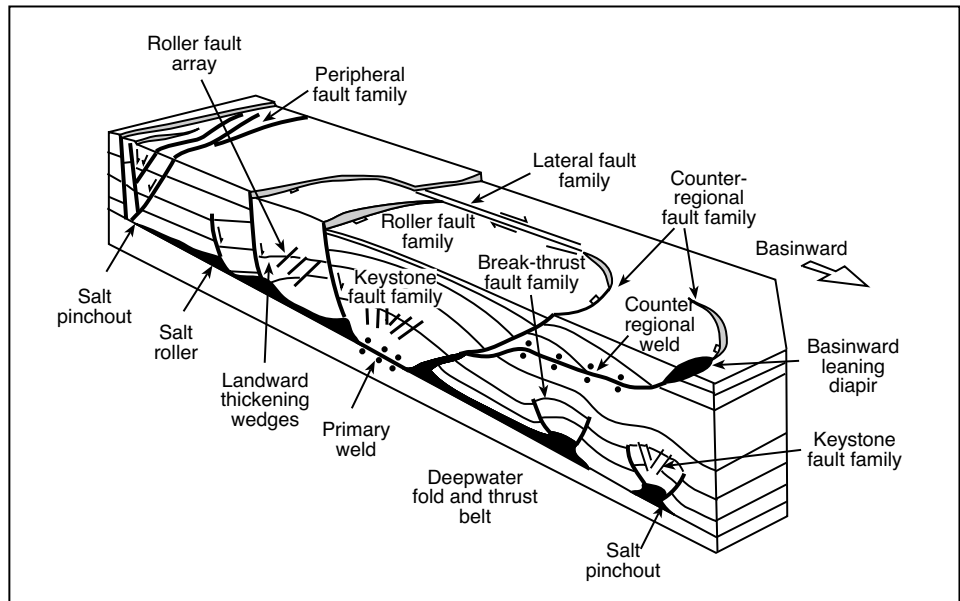


Figure 6.30. Fault families in areas of salt flow centred on the primary salt level (autochthonous salt), which evacuates to leave behind the primary weld (after Rowan et al., 1999).

salt. Increased clastic input along the continental margin created a depocentre that flexed the underlying crust. This flexure probably reversed the basinward tilt of the autochthonous salt below the continental slope, thereby ending gravity gliding at this level in the stratigraphy; however, the continental margin remained gravitationally unstable and spread under its own weight, especially during Cenozoic clastic progradation. Thus, some of the structures established during early gravity gliding probably were reactivated during subsequent gravity spreading related to ongoing sediment loading. As a squeezed salt mass climbs the stratigraphy it separates from the primary salt level to become allochthonous salt. Ongoing allochthon loading and flowage forms the same spectrum of faults seen in autochthonous structures but now at levels well above those of the mother salt bed (Figure 6.30). Peripheral and roller fault families accommodate basinward extension at the landward margin of the basin and throughout the salt basin, respectively. Early reactive diapirism can create crestal fault families in this extensional zone. The extension is balanced by a combination of distributed salt extrusion and contractional deformation at the basinward limit of salt. Salt extrudes mainly from basinward-leaning salt diapirs (overlain by counter-regional fault families), but also from more vertical salt stocks. Contraction at the toe of the system creates detachment folds and break-thrust fault families. Folding, whether due to slip on extensional roller faults, collapse of seaward-leaning feeder diapirs, or contraction, generates a combination of rollover and keystone faults. Lateral fault families segment extensional

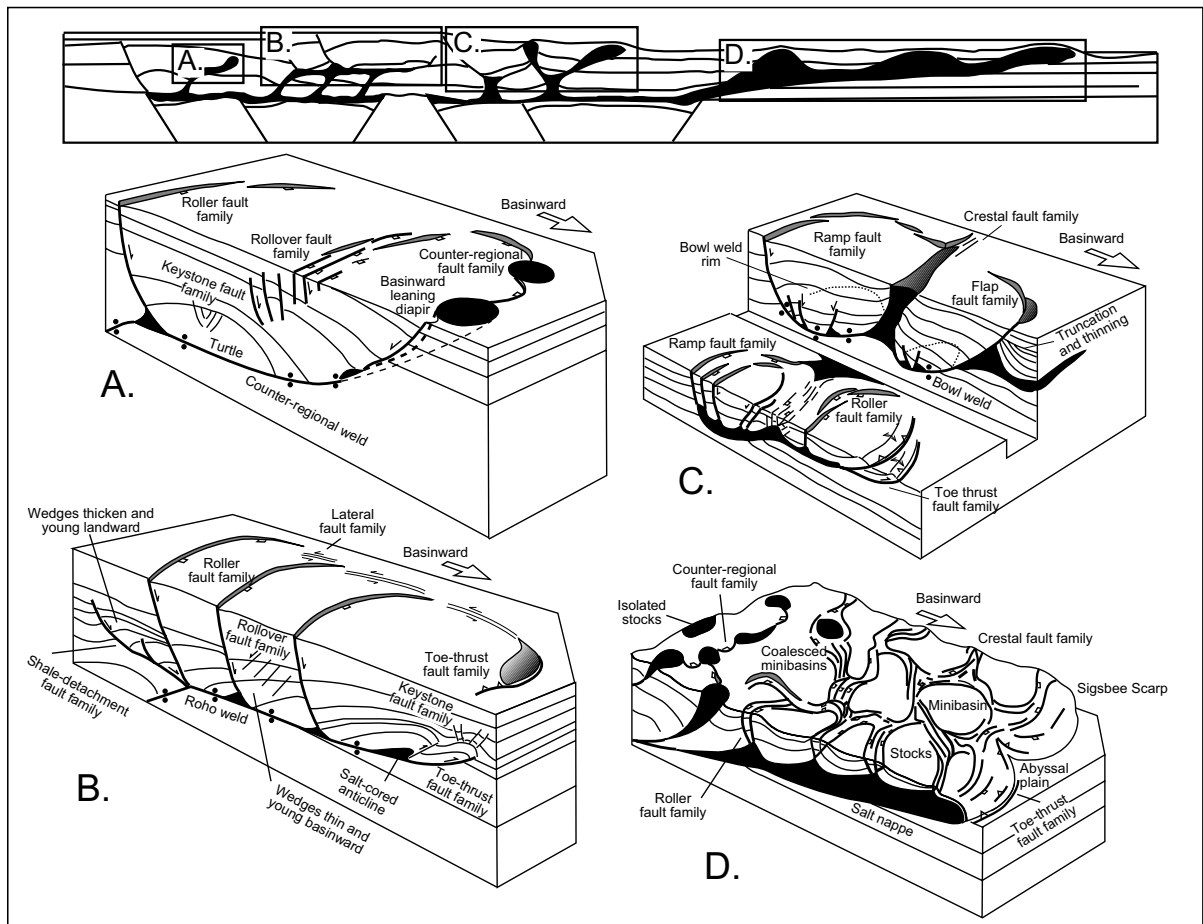


Figure 6.31. Fault families in salt allochthon provinces, based on the Gulf of Mexico (after Rowan et al., 1999). A) Typical assemblage of fault families and salt or fault welds in a stepped counter-regional allochthonous salt system. Roller faults are less common than the other types. B) Typical assemblage of fault families and fault welds in a Roho allochthonous salt system. C) Typical assemblage of fault families and salt or fault welds in an allochthonous salt-stock canopy. The frontal section shows a partially evacuated salt stock; the back cutout shows two coalesced stocks that have been completely evacuated. D) Typical assemblage of fault families in a salt nappe advancing over the abyssal plain. The basinward area shows an immature stage of evolution; the more landward area shows more highly evolved structures.

regimes, possibly controlled by the geometry of faults in the rifted basement (e.g., Watkins et al., 1995; Rowan, 1997). Remnant salt or primary welds provide the common link in autochthonous salt systems.

In a landward to basinward traverse, allochthonous fault associations break down into four interrelated fault families, which are shown in basinward order in Figure 6.31a-d.

Stepped Counter-regional Salt System: Salt-tongue systems comprise subhorizontal salt sheets fed by one or more basinward-leaning feeder diapirs (Rowan et al., 1999). These systems can evolve as stepped counter-regional systems (Schuster, 1995), consisting of a deep feeder weld, an intervening evacu-

ated salt sheet, and higher level basinward-leaning diapirs and landward-dipping salt welds. The linked fault system associated with this counter-regional weld is relatively simple (Figures 6.25b, 6.31a). It is dominated by a counter-regional fault family and associated rollover and keystone fault families. Additionally, a second counter-regional fault family may overlie the deep feeder (not shown), or there may be a roller fault family detaching on the secondary weld if there were any basinward translation during evacuation of the sheet.

Roho Salt System: Salt-tongue systems can also evolve as Roho systems (Schuster, 1995). These are generally longer in the downdip direction than are stepped counter-regional systems. The extra length creates a greater elevation for

the salt and thus more gravity spreading. The result is a linked fault system dominated by a roller fault family (Figures 6.25a, 6.31b). In places, shale-detachment fault families merge into the landward or lateral edges of the salt layer or weld. The extension on the combination of roller and shale-detachment faults is accommodated by salt extrusion or shortening along a to thrust fault family. Extension and contraction are linked by lateral fault families and a Roho weld. Minor structures include rollover fault families in the hanging walls of the roller faults and keystone fault families in the crests of contractional folds.

Salt-Stock Canopy System: Salt-stock canopies can be true or apparent depending on whether amalgamation occurred during stock growth or stock evacuation, respectively (Rowan et al., 1999). In both, a complex linked fault system can develop with the link provided by remnant allochthonous salt and bowl welds (Figure 6.31c). Partly or fully evacuated stocks can have ramp fault families at the landward margins, flap fault families at the basinward margins, and older roller fault families in the central areas. Where the canopy feeds a subhorizontal salt tongue, reactive diapirs and crestal fault families can form at the stretched hinge between the stock and tongue. Translation above the tongue can create roller and to thrust fault families linked by lateral fault families.

Salt-Nappe System: Salt nappes are large allochthonous salt bodies that advance tens to hundreds of kilometres basinward over long periods of time (Worrall and Snelson, 1989; Rowan, 1997). The front of a salt nappe is an arcuate lobe of salt covered by a generally landward-thickening clastic skin. In its most immature, distal regions, the structure is dominated by circular to elliptical minibasins up to 40 km wide. They subside into the salt and are separated by reactive diapirs formed during radial gravity spreading of the salt nappe (Jackson and Vendeville, 1995). Thus, the linked fault system is dominated by a polygonal pattern of crestal fault families (Figures 6.27, 6.31d). Toe thrusts can occur at the front of the nappe. Landward, the regular polygonal pattern degrades as

minibasins coalesce. Interaction between salt deformation and sedimentary loading may result in various fault families (e.g., counter-regional, roller, flap, lateral) and welds; however, the three-dimensional geometry of fault families in mature salt nappes is unknown because mature examples have not yet been identified.

Linking allochthons at the basin scale

Clearly, salt flow in a loading and extending sedimentary basin creates a number of predictable geometries, rollovers and fault patterns that are related by variations in rates of extension and loading as prograding suprasalt sediments evolve into ramps and welded basins (Figure 6.30, 6.31). In the Gulf of Mexico it is important to distinguish between the more landward intervals of salt flow, which are sourced in autochthonous salt and by definition are still linked to the primary salt level, and the more basinward flows sourced in allochthonous salt where the salt slug is no longer connected to the primary weld (Rowan

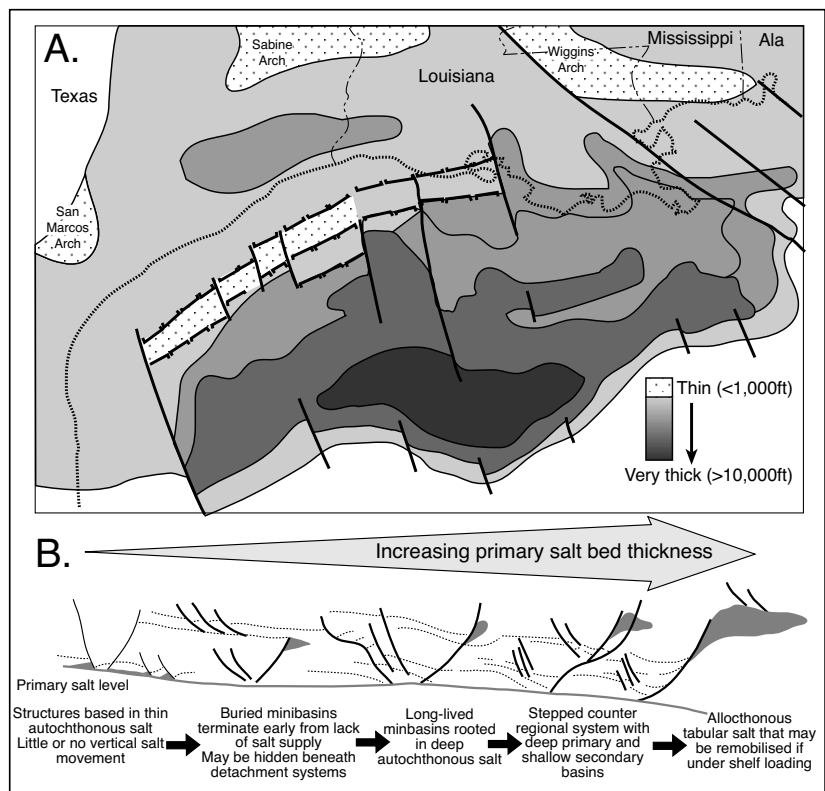


Figure 6.32. Salt tectonic style is controlled by original thickness of the primary salt layer. A) Approximate salt thickness at the time of deposition of the Jurassic Louann Salt. B) Schematic showing that autochthonous salt deformation tends to occur in zones of thinner primary salt, whereas allochthonous salt deformation is favoured by areas of thicker primary salt (after Karlo and Shoup, 2000).

et al., 2001). At the broadest scale of flow, Karlo and Shoup (2000) argue that the thickness of the primary salt bed (Jurassic Louann Salt) is what separates regions of autochthonous and allochthonous salt flow in the Gulf of Mexico. Allochthonous salt tends to be sourced in the thickest portions of the primary salt, while autochthonous flow tends to be sourced in the thinner areas of the primary source bed (Figure 6.32).

The resulting salt features and associated withdrawal basins make up an ordered but gradational sequence of structural styles across the shelf and slope (Figure 6.32; Karlo and Shoup, 2000). The sequence progresses from updip autochthonous basins with static diapirs that aborted and were buried, to the most downdip withdrawal basins that have been active at various levels in the stratigraphy since the Mesozoic and are related to an amalgamated and fully allochthonous salt canopy. They argue that differences in depositional thicknesses of the Louann Salt mean the thicker eastern half of the Gulf of Mexico basin has a full progression of salt-related structural styles, while the western half of the basin has a wide area lacking major salt structures that then abruptly juxtapose against tabular salt. The gravity slide detachments characteristic of the western half of the basin are superimposed over salt related structures where original salt thickness was insufficient to maintain structural growth at higher levels.

The work of Karlo and Shoup (op cit.) is supported by the results of Hall (2002) who found that most of the deep-water region of the northern Gulf of Mexico was underlain by an inflated mother salt layer during the Cretaceous to middle Miocene. The southern edge of this mega-pillow was either the depositional edge of the salt or a basement structure. Partial deflation of this mega-pillow during Late Miocene-Pleistocene sedimentation resulted in the formation of large structures overlying the mother salt. The process of 'deep' structuring was synchronous with progressive emplacement of shallow (allochthonous) salt to form the Sigsbee canopy in the southern part of the present-day deep-water area.

Compressional salt tectonics

Contractional or tectonically shortened salt basins are numerous and can be loosely classified into three conceptually shingled compressional styles (Figure 6.33; Letouzey et al., 1995):

- Zones of shortening at the toe of prograding and gravity-gliding systems (thin-skinned; Figure 6.34a),
- Thin-skinned deformation in fold and thrust belts (Figure 6.34b),

- Intracratonic inverted^{6.4} basins with or without wrench components - thick-skinned^{6.5} with basement involved in the compression (Figure 6.34c).

Contractional salt tectonism is produced either by convergent (including transpressive) plate tectonics, or is restricted to the seaward portions of divergent continental margins, where downslope gravity-sliding stacks and thrusts overburden blocks against each other as they slide basinward atop a salt décollement. Contractional salt tectonics require either the minimum principal stress (s_3) to be vertical (so creating shortening) or the intermediate principal stress (s_2) to be vertical (resulting in transpression; Jackson and Talbot, 1994). Compression in a salt-entraining basin tends to thicken both salt and its overburden units. This increases overburden strength and laterally squeezes the feeding stem of any existing diapir, while the increased overburden strength tends to impede piercement. Shortening or squeezing of diapirs, that earlier formed in extension, is an under-recognized process in gently shortened basins and a later section is allocated to this topic.

Shortening with gravity gliding

Belts of upslope extension are paired or linked to downslope compression on rapidly prograding shelf-slope systems on salt-cored passive continental margins. Overburden sediment slides downslope atop a lubricating salt layer, with the translation largely driven by the increasing weight of sediment accumulating atop the salt (Figure 6.34a). Shortening and compressional structures typify the toes of such systems, while extensional features and welds occur in the upslope position. Areas of extreme extension in the upslope regions evolve into regions of raft tectonics. In the zone between areas of extension and compression some large plates of sediment (up to tens of kilometres across and a kilometre or more thick) can shift or translate downslope with little intraplate evidence of migration until the downslope edge starts to experience compression and pop-up structures, such as squeezed diapirs, form.

The compressional toes of such regions of into-the-basin translation are characterized by rising growth folds and active thrusts. Compressional foot of slope systems lubricated by salt décollement include: the Perdido and Mississippi Fan

^{6.4} Inversion tectonics describes situations where older faults are reactivated and normal faults become compressional.

^{6.5} Thick-skin tectonics describes situations where the basement is involved and so tends to be dominated by higher angle faults compared to thin-skinned deformation.

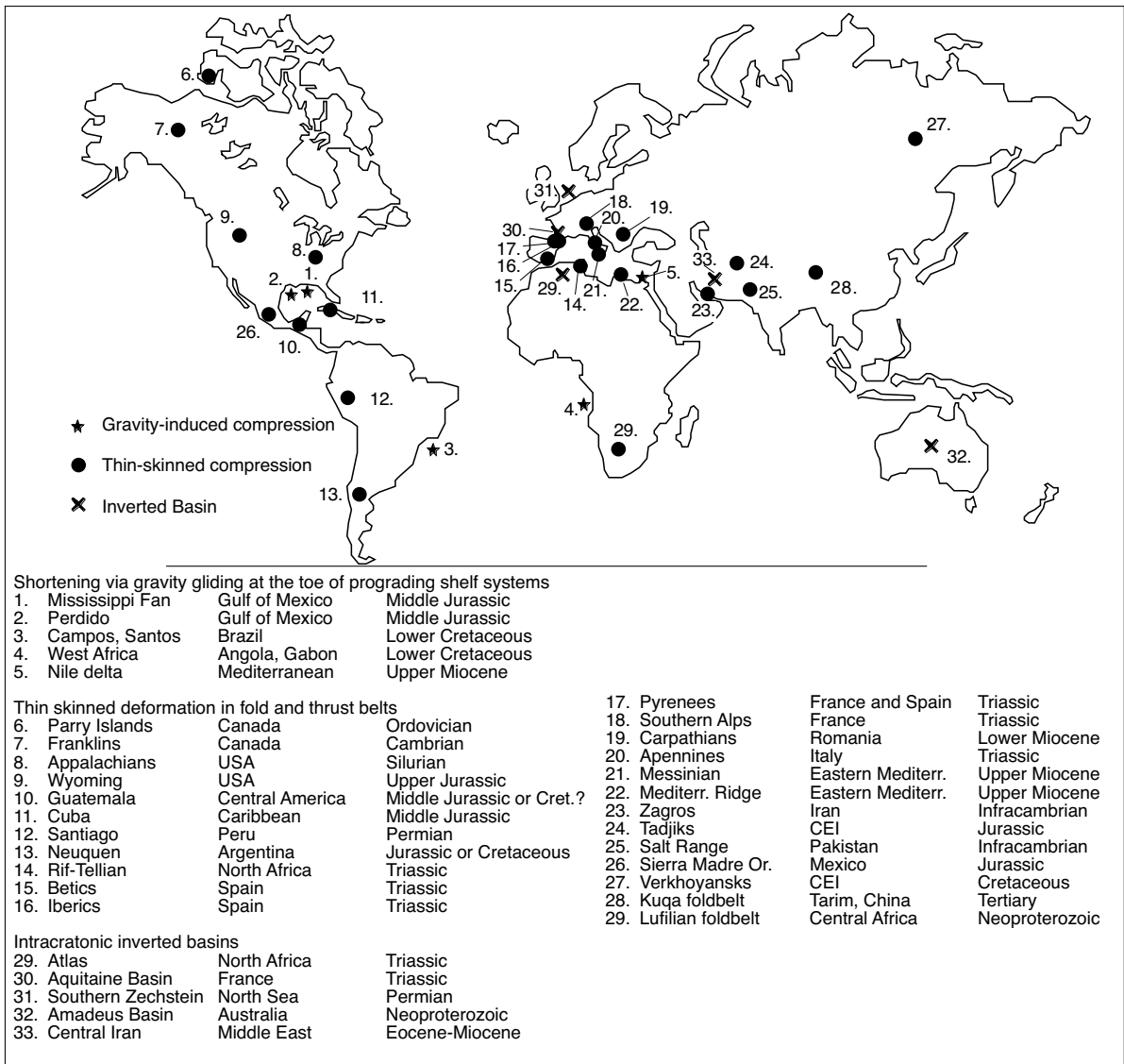


Figure 6.33. Worldwide occurrences of compressive deformation that involves salt sequences (in part after Letouzey et al., 1995; Davis and Engelder, 1985).

foldbelts in the Gulf of Mexico (Schuster, 1995), the deep Campos and Santos Basins of offshore Brazil (Cobbold et al., 1995, 2001), offshore west Africa (Duval et al., 1992; Cramez and Jackson, 2000; Brun and Fort, 2004), the eastern Mediterranean adjacent to the Nile Deep Sea fan (Sage and Letouzey, 1990), and offshore Yemen (Heaton et al., 1995). The salt in all the areas, with the exception of the Mediterranean, was precipitated in early post-rift time with consequent thermal subsidence generating a basinward tilt of the continental margin (typically > 1°-3°). The tilt was an early contributing factor to the décollement and gravity gliding, but was not the triggering

mechanism. That was supplied largely by differential loading tied to the rapid progradation of the up-dip shelf margin sediments. Compressional toe-thrust and diapiric systems are not the sole province of salt-floored systems, but also occur along the deepwater edges of mud-rich evaporite-free continental margins such as the Neogene fluvio-deltaic wedge of Brunei and the Niger Delta of Africa.

Because the extensional domain tends to lie in a more proximal shallower water position within such sedimentary basins they are, to date, better studied than the associated downdip com-

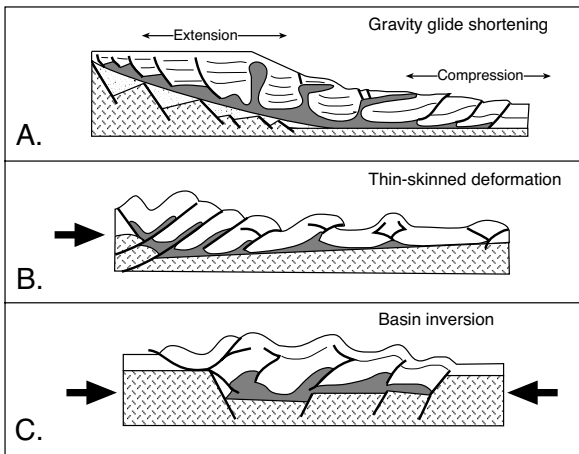


Figure 6.34. Compression tectonics. A) Gravity glide shortening at the toe of the continental slope. The basement is not involved in the deformation. B) Thin skinned deformation in front of the fold and thrust belt where subduction is the driving mechanism in the inner fold belt. C) Intracratonic inverted basin. Driving mechanism is regional contraction, which is orthogonal or oblique to the preexisting graben. Basement, salt and overburden are all shortened together (after Letouzey et al., 1995).

pressional terrain. This is the result of widespread hydrocarbon exploration and development in shelf and upper slope sediments. Structures characteristic of the salt-floored extensional domain include: salt rollers in the footwalls of listric normal growth faults, salt walls with triangular cross sections lying between intersecting conjugate normal faults, turtle anticlines and salt welds (see earlier in this chapter). Contractional or compressional domains tend to lie in deeper water further out into the basin at the foot of a continental slope or a prograding delta front. Many of these offshore compressional areas are covered by waters that are still too deep to be exploited with current drilling technology.

Shortening in gravity-glide salt belts is usually accommodated in salt-cored compressional foldbelts with growth-folds near the toe of the salt layer or at the base of the continental slope (Figure 6.34a). Contractional growth folds are the nearsurface subseafloor expression of a ramping thrust fault at the downdip end of an inflating salt allochthon. If the crest of a salt-cored fold is eroded or weakened enough by crestal faulting, salt may burst through as an active diapir. Once it reaches the surface, it can continue to grow as a passive diapir instigating a new allochthon-floored stratigraphic level of into-the-basin gliding.

The Mississippi Fan Fold Belt lies 200 km SSE of New Orleans and is defined by a such a series of ENE trending thrust-associated anticlines down dip of the current allochthon salt sheet

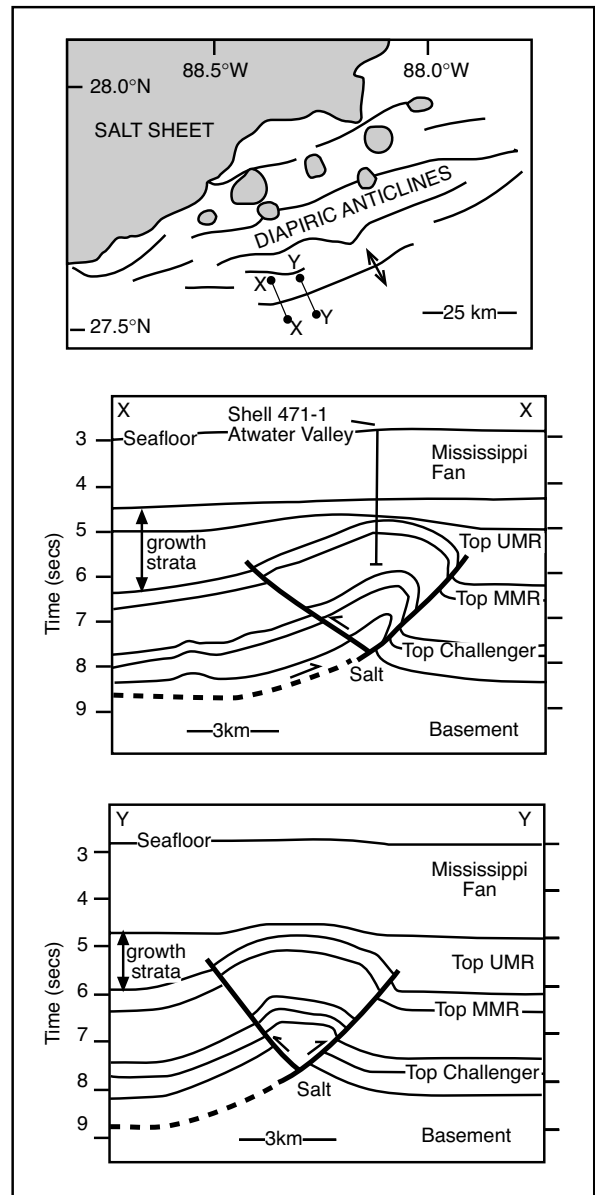


Figure 6.35. Thrust folding in downslope compressional belt, northern Gulf of Mexico (after Rowan, 1997). A) Map showing the location of presumed salt-cored anticlinal structures in the Mississippi Fan fold belt and locations of interpreted sections. B) Interpreted seismic section profile X-X' through a salt-cored anticline showing an asymmetric faulted detachment fold. C) Interpreted seismic section profile Y-Y' further along strike through the same structure, showing a symmetric faulted detachment fold. UMR = Upper Mexican Ridges; MMR = Middle Mexican Ridges.

canopy of the Jurassic Louann Salt (Figure 6.35). The fold belt probably defines the Jurassic limit of the original bedded

Louann Salt (Rowan, 1997). Today it is a zone of compressional response to updip loading and associated gravity spreading/sliding along a salt detachment, linked to updip normal faults (Figure 10.51b). Faults and folds are dominantly south vergent, although symmetric box folds and backthrusts exist. Updip, the shallow allochthonous salt sheets of the Sigsbee Nappe have over-ridden the landward portions of this same fold belt to create a number of hydrocarbon targets. Thickness variations in sediments above the Top MMR and a lack of such variations in more recent sediments of the Mississippi Fan unit suggest structures actively grew near the seafloor prior to the current episode of Tertiary-age shortening (Figure 6.35; Rowan, 1997).

Profile X-X' shows a seismic interpretation of one such asymmetric faulted detachment fold cored by the Louann Salt (Figure 6.35). Data from the Shell 471-1 Atwater well constrain the interpretation in the upper part of the section. The frontlimb of the fold is cut through by a major thrust fault, which is truncated up section by unconformable units of the Upper Mexican Ridges. A back thrust cuts through the backlimb and terminates against the main fault. Both thrusts are characterized by fault to fold transfer, although the displacement of individual units may vary up section. The overall geometry, fold-fault relationship, and the nature of the stratigraphic section, which consists primarily of alternating shales, chalk, marls, and turbidites, are all suggestive of an asymmetric faulted detachment fold (Mitra, 2002). The upper part of the Upper Mexican Ridges consists of growth units, which are strongly thinned and eroded on the crest of the structure, suggesting that the folds formed primarily during the deposition of these units (growth-fold deposition). The growth units thin onto the crest of the structure on both limbs and also are truncated on the backlimb. The salt cored structure shown in profile Y-Y' is located further east along the same ridge (Figure 6.35). It has a more symmetric pop-up geometry with a relatively flatter fold crest. Thrust faults on both limbs terminate upward within the Upper Mexican Ridges and downward within the Louann Salt. The thrust fault on the southern limb has a larger displacement; however, the difference in displacement on the two thrusts is smaller than in profile X-X'. Once again thickness changes in the upper part of the Upper Mexican

Ridges unit show it is also a growth fold, with fold-related seafloor topography controlling depositional patterns on the seafloor. The structural characteristics of this part of the fold ridge are suggestive of the symmetric faulted detachment fold model of Mitra (2002), with thrust faults propagating through rotated segments on both limbs.

Regionally, the style of compression across a salt-lubricated toe of the slope system is largely controlled by the extent of the salt layer (Letouzey et al., 1995). If the mother salt layer extends well out into the basin and beyond the zone of significant compression, the system tends to form a fold belt dominated by salt-cored buckle folds with little or no evidence of thrusting. If, on the other hand, the salt layer pinches out near the toe of the slope, the friction coefficient at the base of the contracting sediment pile is greatly increased and forms a narrower thrust-faulted zone (Figure 6.36).

The degree of shortening in such compressional thrust terrains can be substantial. In the deep water Santos Basin, Brazil, the downdip section is shortened by up to 50% of its original length as the seaward margin of the salt belt flows out over the backstop basalts of oceanic basement (Figure 6.37). Many of these thrust blocks show typical contractional salt thrust assemblages of sediment wedges in their footwall and chronologically older (Aptian) salt in their hanging walls. Interestingly, the giant oilfields of the Campos Basin and the fields of the Santos Basin only occur atop salt breakout windows on the inboard side of the belt of continuous salt or atop the zone of salt welds. This

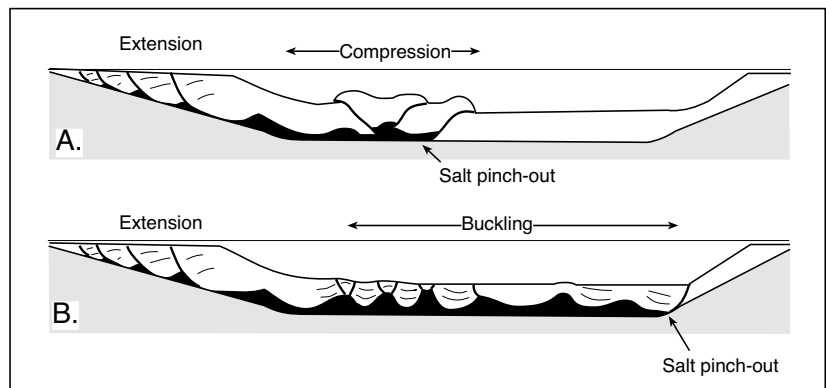


Figure 6.36. Location of basinward pinchout of the salt layer controls the style of contractional/compressional structures. A) Where the salt layer does not extend out far past the foot of the continental slope, the frictional resistance increases at the base of the sedimentary pile and interferes with further basinward movement. This can create an imbricate thrust zone on the updip side of the salt pinchout. B) Where the salt layer extends across the basin and well out from the foot of the continental slope, the contraction is taken up in a series of buckle folds with crests that tend to lack thrust zones (after Letouzey et al., 1995).

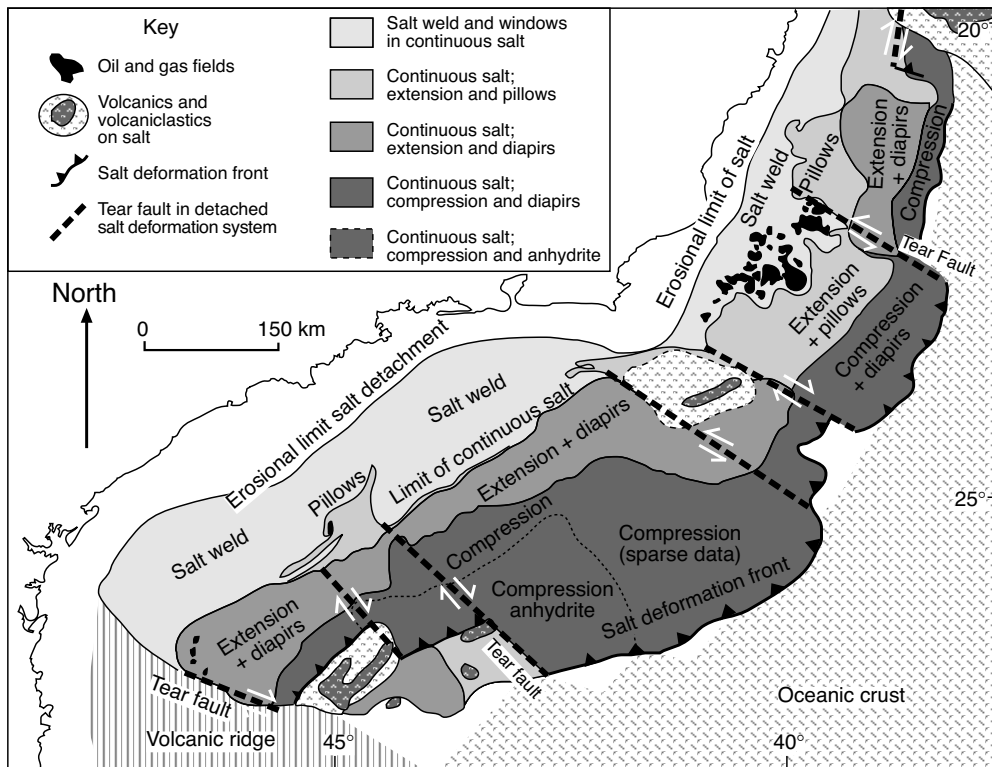


Figure 6.37. Map showing relationships between the various salt-detached basins in the Santos and Campos basins of offshore Brazil. Oil and gas fields only occur updip of the limit of continuous salt in suprasalt turbidite reservoirs that are sourced from sub salt lacustrine sediments (after Meisling et al., 2001).

reflects the high seal integrity of continuous salt sheets, which prevent hydrocarbons generated in the mature subsalt salt source from reaching the suprasalt turbidite reservoirs (Meisling et al., 2001). It is a very positive indicator of the possible presence of large subsalt traps some distance further offshore where halokinetic salt sheets constitute more continuous layers.

At the broad scale of salt flow in passive margin sediments along the edge of a widening ocean basin there is also the process of increasing shelf edge to ridge distance to be considered. Over time this will create an increasingly broad compressional zone in the zone of transitional crust at the foot of the continental slope. This is clearly illustrated in the expanding compressional belt down dip of the zone of raft tectonic in the seaward margin of the Kwanza Basin, Angola (Figure 6.37; Fort et al., 2004). A thick sequence of Cretaceous (Aptian) salt was laid down atop lacustrine sediments in the opening rift, followed by a transition into marine sediments the passive margin. Three groups of sediments make up this marine wedge; The Pinda Group (Albian to Late Cretaceous), consists of a carbonate platform followed by sedimentation increasingly dominated by marls and clays. The Iabe-Landana Group (Late Cretaceous to Eocene)

consists of dominantly siliciclastic sediments, with locally significant carbonates. Most of these deposits are located on the current platform, pinching out seaward into condensed sections, indicating a long-term highstand during the Late Cretaceous. The Malembo Group (Oligocene to the present day) corresponds to a large, prograding clastic wedge. The salt has acted as a décollement allowing updip extension and downdip compression.

The extensional domain is characterised by oceanward-sealed tectonic blocks, rollovers and diapirs, while the downdip compressional terrain is characterised by growth folds, squeezed diapirs and thrusts (Figure 6.38).

The compressional zone is divisible into; 1) an inner more upslope subdomain characterised by formation of contractional diapirs by the compression of former extensional diapirs (squeezed diapirs) and 2) an outer more downdip subdomain characterised by growth folds and thrusts. The upper subdomain indicates the expansion of the compressional domain in a more upslope direction as formerly extensional suprasalt sediments slides and piles at the foot of slope. The ductile diapir salt is trapped and pinched in anticlinal cores, leading to the formation of contractional diapirs that typically do not necessarily extrude at the surface but are stopped and sealed by further sedimentation. This type of updip extension and downdip compression indicates an initial salt geometry that wedged or thinned in both seaward and landward directions at the end of the margin-rifting stage (Aptian; Figure 6.38a). Postrifting cooling of the lithosphere then induced a seaward tilt in the margin and the development of gravitational instability, creating a seaward spreading-gliding system with an extensional upper end and a

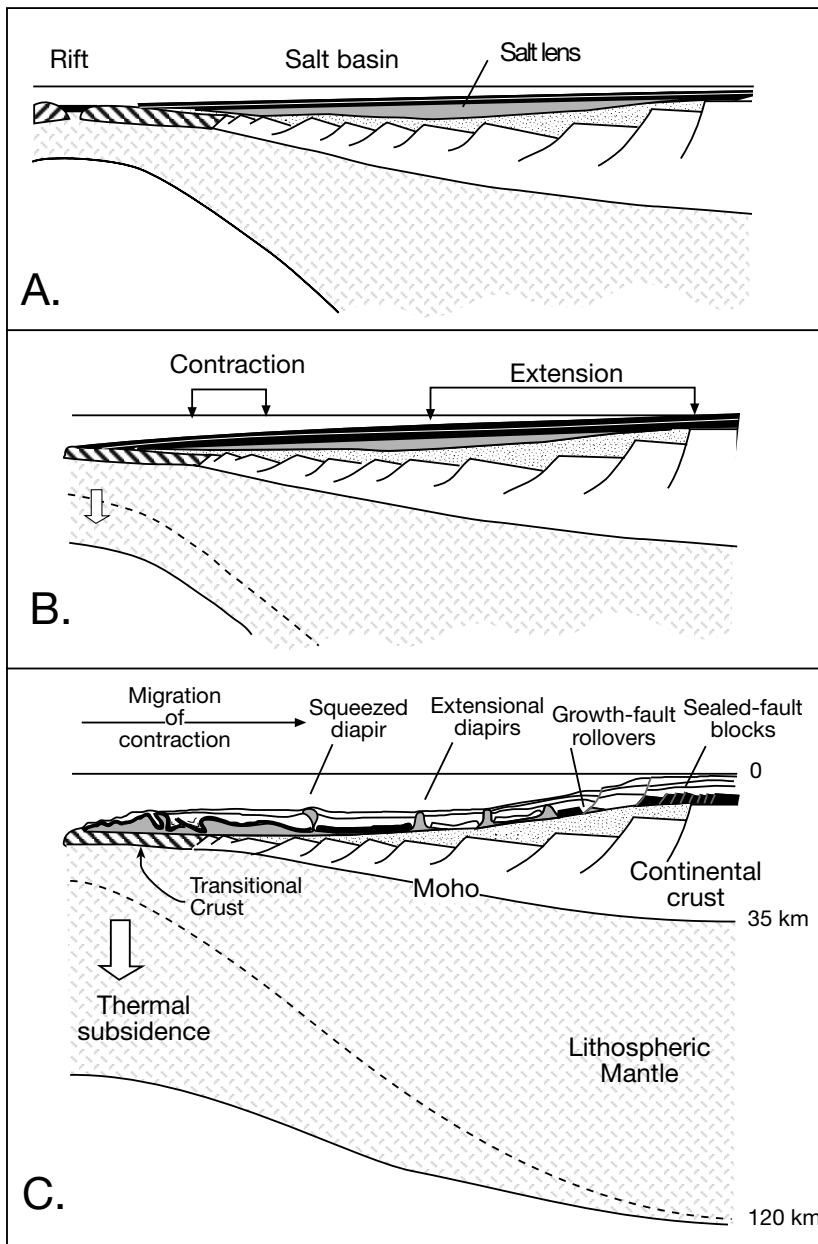


Figure 6.38. Evolutionary model of gravity spreading above salt in a passive-margin tectonic setting, at lithospheric scale based on the offshore region of Angola, central Africa. A) Initial stage following continental breakup. The salt basin is entirely covered by sediments that overlie oceanic crust. B) Synchronous initiation of contraction downslope and extension upslope. The compressional domain initiates at some distance from the salt wedge toe. C) Major displacement of extensional and compression domains during spreading. Compression migrates both downslope and upslope. Downslope migration reaches the salt toe. Upslope migration reaches the downslope part of the extensional domain, thus inducing diapir squeezing. Slope increases during spreading as a consequence of lithospheric cooling and subsequent subsidence. (Fort et al., 2004).

compressional downdip end (Figure 6.38b passing to 6.38c). The increasing into the basin tilt due to thermal subsidence drives an updip migration of the zone of compression or contraction (Figure 6.38c). Over time diapirs that formed by extensional processes become squeezed and take on the structural and trap morphologies of diapiric structures indicative of this compression (Figure 6.47).

Thin-skinned fold and thrust belts

Widening salt-floored rift basins are subject to later closure (Wilson cycle; Figure 5.27), so compressional deformation is often superimposed on originally extensional halokinetic margin (Figure 6.34b) or its aulocogen counterpart in the continental interior (Figure 6.34c). Allochthonous salt acts as a lubricant to any consequent thrust sheet as it pushes landward. Thin-skinned fold and thrust belts form in mountain chains where the basement is not involved in the deformation and evaporite layers are preferred detachment horizons (Letouzey et al., 1995). Resultant structures are predominantly oriented parallel to the intermediate stress direction and perpendicular to the maximum shortening. Examples of thin-skinned fold and thrust belt include: the Parry Islands Foldbelt in Arctic Canada (Harrison, 1995), the European Jura (Philippe, 1994), the Spanish Alps (Flinch et al., 1996), the Lufilian fold belt of Central Africa (Figure 7.27; Jackson et al., 2003), the Adelaidean foldbelt of southern Australia (Marshak and Flottmann, 1996), the Kuqa foldbelt of Tarim Basin of NW China (Liang Je Tang et al. (2004) and the Zagros Foldbelt of Iraq and Iran (Talbot and Alavi, 1996).

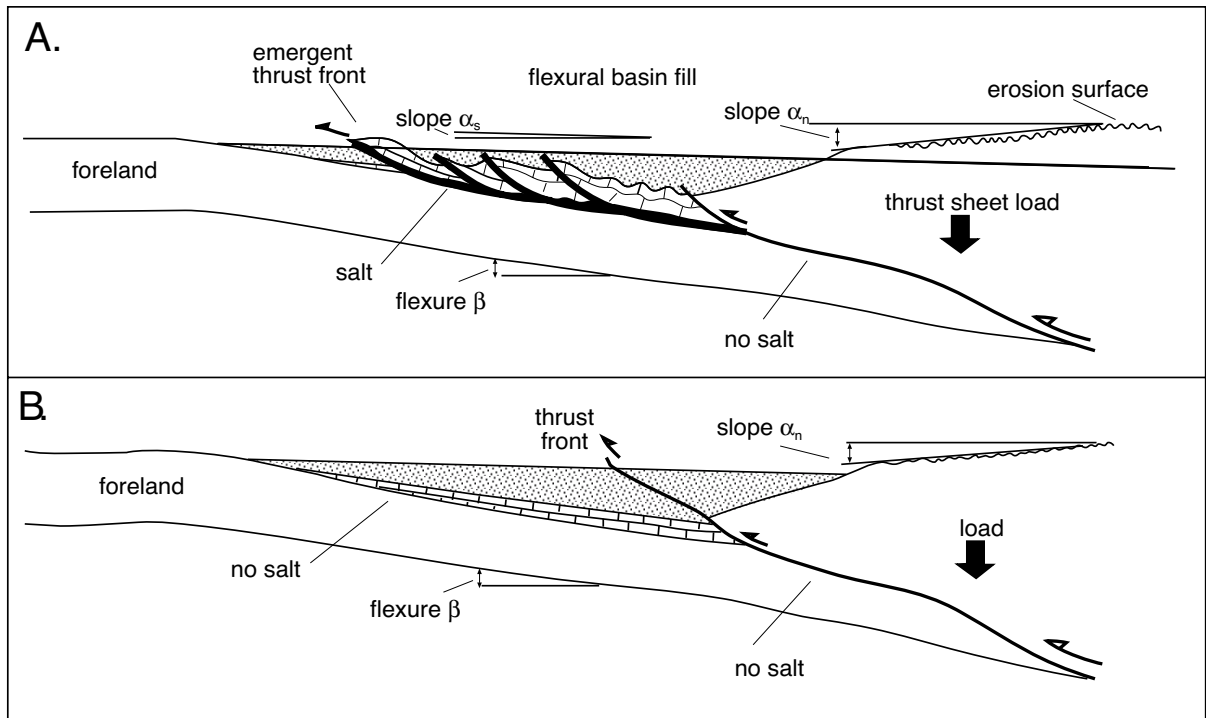


Figure 6.39. Characteristics of thrust propagation and taper angle in a salt cored and nonsalt cored thrust A) Salt lubricates thrust sheets. B) No salt to lubricate thrust sheet. Salt cored thrusts are wider, show more extensive thrust propagation, thinner thrust cross section and taper angles $<2^\circ$; while those deforming over other rock layers are narrower, with taper angles nearing 8° (after Davis and Engelder, 1985, 1987).

The style of deformation is dependent largely on the friction coefficient acting along the detachment level(s). The lower the basal friction level, the further the thrusts propagate out and so the wider the thrust belt, the thinner the cross section of deformation and the lower the taper angle (Figure 6.38: Davis and Engelder, 1985, 1987). A salt décollement in a compressional thrust terrain also enhances the development of major backthrusts and greater outward migration of the deformation front (Luján et al., 2003; Velaj et al., 1999). Preexisting faults and salt welds in a halokinetic prism on a passive margin can be a major zone of weakness in the development of subsequent compressional structures. Hence the very close association between preexisting faults and the current elongated salt structures of the southern North Sea (Figure 6.42).

A fundamental consequence of salt weakness in many salt-detached thrust foldbelts is an absence of a preferred direction of thrust transport (Figure 6.39; Davis and Engelder, 1987; Harrison, 1995; Bahroudi and Koyi, 2003; Luján et al., 2003). The geometry of individual thrusts and anticlines reveals little or nothing about the location of the tectonic hinterland without some independent understanding of the regional geol-

ogy. Angular folds (box folds, chevron folds and mitre folds) predominate in a buckling thin-skinned salt-cored thrust belt, reflecting internal deformation of anisotropic multilayers above the thin, ductile salt substratum. If the deforming salt substratum is thicker, the multilayers tend to buckle as a single unit into large sinusoidal folds, with consequent loss of fold angularity. Mixtures of forethrusts and backthrusts are common even in individual salt-cored anticlines.

An active example of this style of thin-skinned thrust, lubricated by salt, is found in the Salt Range region of Pakistan (Figure 6.40). The Salt Range and Potwar Plateau are the external and most recent expression of Himalayan shortening. This thin-skinned fold-and-thrust belt is detached upon thick Lower Cambrian evaporites of the Salt Range Formation. This basin-wide evaporite unit underlies the Potwar Basin and is roughly equivalent in age to the Hormuz Formation in the Zagros Belt of the Arabian Gulf. The presence of thick salt facilitated rapid thrust propagation of the basal detachment before the main fault plane rose to form the Salt Range thrust above a basement frontal ramp at the southern termination of the basin.

A dextral wrench zone defines the western limit of the Salt Range and corresponds to the edge of the halokinetic Infracambrian evaporite (Cotton and Koyi, 2000). There are three main zones of deformation across the Salt Range and Potwar Plateau: from north to south, these are the Northern Potwar deformation zone, the Soan syncline, and the Salt Range (Figure 6.40). Deformation in the Northern Potwar deformation zone is characterized by the development of an imbricate duplex in the footwall of the Main Boundary thrust of the Himalayas. Deformation of the overlying Main Boundary thrust sequence constrains development of the Northern Potwar deformation zone to younger than 10 Ma. The northern limb of the Soan syncline marks the southernmost limit of uplift in the Northern Potwar deformation zone. The northern limb of the Soan syncline is steeply upturned, forming a monocline. A sequence of salt cored pop-up structures and broad anticlinal swells accommodated shortening formed to the south of the Soan syncline axis. The contrast in deformation styles between the Northern Potwar deformation zone and the Soan syncline, seen in Figure 6.40, is attributed to the lubricating effect of the Infracambrian evaporite sequence (Salt Range Formation).

The Salt Range today forms an approximate east-west hanging wall in a thrust that accommodates ~25–30 km of shortening (Baker et al., 1988). The majority of deformation was accommodated within the hanging wall with some minor imbrication of the footwall. Deformation in the Salt Range area is considered to have occurred in two pulses, commencing ca. 5 Ma with a later pulse at 2 Ma. Lag time between pulses is attributed to breakback thrust development in the northern limb of the Soan syncline. The anomalous thickness of salt that has accumulated beneath the hanging wall of the Salt Range thrust is a result of differential loading by a prograding basin fill and

deformation front moving south from the growing Himalayas. This combination of sedimentary and tectonic loading caused a southward migration of the Salt Range Formation (like squeezing toothpaste). This thickening has been assisted in the central Salt Range by the buttressing effect of a major basement fault in front of the southward-migrating salt (Figure 6.40).

Another well-documented example with more than 200 km of salt-lubricated translation characterises the Triassic section of the external domain of the Betic Cordillera, near Gibraltar in the Mediterranean, where the thrust block is rootless and allochthonous (Flinch et al., 1996; Luján et al., 2003). The frontal accretionary wedge of the Guadalquivir allochthon consists of Triassic evaporites and red beds that form a gypsum-cemented melange mixed with Upper Cretaceous-Palaeogene deepwater sedimentary rocks. Throughout the unit, Jurassic rocks are absent. The widespread Triassic evaporites of the Guadalquivir allochthon were originally emplaced as gravitational allochthonous masses or salt sheets at the foot of the Betic continental slope. This occurred originally in a passive-margin gravity glide setting, much like the present day emplacement of allochthonous sheets of Jurassic salt atop Neogene sediments in the Texas-Louisiana Gulf Coast or the Santos Basin of Brazil. Later, during Neogene formation of the Gibraltar Arc, these evaporites were overthrust as an accretionary wedge to form the Guadalquivir allochthon. This explains the lack of Jurassic sediments within the melange of Guadalquivir allochthon. Triassic halokinetically pierced strata were thrust back up onto the former passive Betic margin, a lateral distance of some 200 km, from an area that lacked Jurassic deposits. Thus the Guadalquivir allochthon ended up atop sediment that was originally located well landward of the Guadalquivir prism.

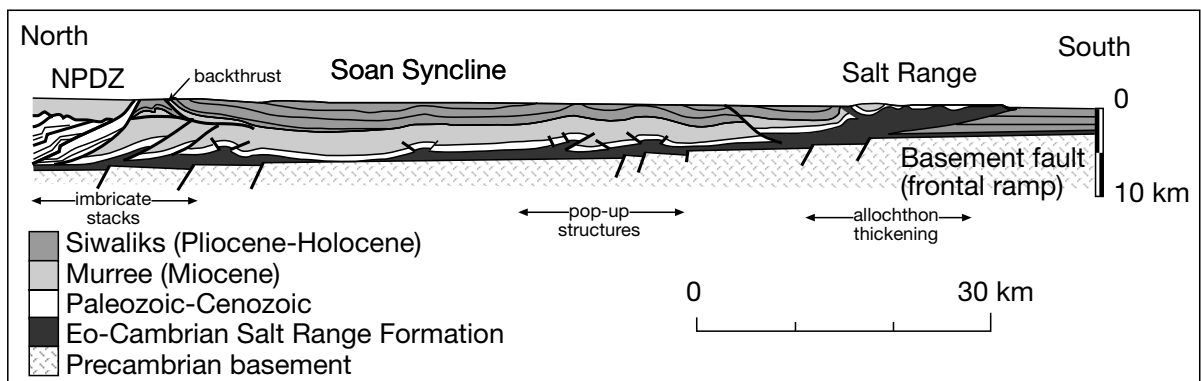


Figure 6.40. North-South cross section in Pakistan across the Northern Potwar deformation zone (NPDZ), Soan syncline, and Salt Range (after Cotton and Koyi, 2000). Three deformation zones can be seen: an imbricate stack (NPDZ) forming a wedge at the rear northern part; a zone of broad anticlines and synclines with pop-up and/or pop-down structures in the middle; and a zone of thickened allochthonous salt (Salt Range) in the south.

Inverted basins

Varying degrees of inversion are common in many intracratonic basins, which tend to evolve into a compressional regime some time after subsidence of the initial extensional rift/sag has ceased (Figures 6.34c, 6.41). Salt-floored inverted basins typically pass laterally into a thin-skinned thrust terrain. By the time inversion occurs much of the sediment atop the primary salt interval is indurated and the basin is laterally confined. Examples of salt-entraining inverted basins include the relatively mild effects of Tertiary shortening of Palaeozoic and Mesozoic sediments in the southern and central North Sea Basins (Hooper et al., 1995; Stewart and Coward, 1995; Eggink et al., 1996) through to more extreme basin overprints as seen in the Cretaceous shortening of Triassic basins in the Atlas fold belt of north Africa (Vially et al., 1994), the Palaeozoic shortening of Neoproterozoic basins in the Flinders Ranges and the Amadeus Basin in central Australia (Stewart et al., 1991), and the Eocene-Miocene shortening of Palaeozoic and Mesozoic basins in the Zagros of central Iran (Jackson et al., 1990). Under a regional shortening event that is orthogonal or oblique to preexisting structures, the inversion typically squeezes hanging wall blocks upward, as the original extensional normal faults become compressional (Figure 6.41). Basement, salt and overlying sediments are all shortened with pre-existing salt structures (pillows, diapirs and walls) frequently taking up much of the initial compression.

Where the horizontal compressive stresses are near orthogonal to preexisting extensional structures and where these are bound by high angle normal faults, much of the inversion above the salt layer is accommodated by forced folding rather than slip along the former faults (Letouzey et al., 1990). New low-angle reverse faults are firmly rooted in the décollement salt and typically

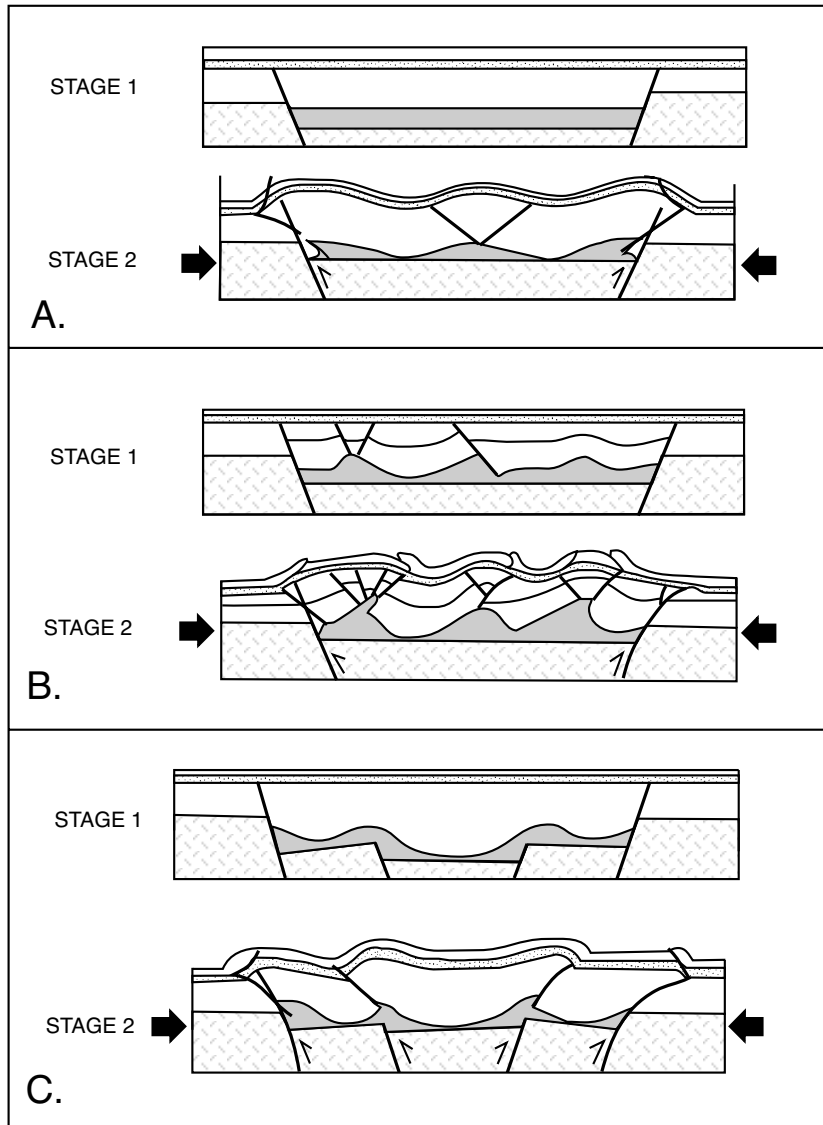


Figure 6.41. Structural evolution of an inverted basement graben varies according to structures present in preexisting graben (salt is grey). A) Folds and short-cut faults develop in homogeneous strata above inverted basement faults. Fold hinges in the graben are perpendicular to the regional compression. B) Thrusts and folds are localised by preexisting salt structures. C) Thrusts and folds are localised by reactivation of basement faults (after Letouzey et al., 1995).

originate at the crest of the upthrown basement block, and so passively transport the former high-angle normal fault planes (Figure 6.41). This initiates short-cut thrust geometries. If the horizontal compression is oblique to the former normal fault, a strike-slip component is induced that can reactivate former high angle normal faults. In addition to conventional inversion features, such as forced folds and short cuts over basement faults, strike slip will also form *en echelon* synthetic faults in

the hanging walls of preexisting basement faults (Letouzey et al., 1995). Such *en echelon* systems define the basin edge of the Sahara flexure in Algeria (Vially et al., 1994).

Lateral pressures on a fluid salt décollement horizon undergoing compression promotes decoupling of the overburden and so create the following associations:

- Folding is more common than thrusting,
- Folds and thrusts lack consistent vergences, being commonly expressed as box folds and backthrusts;
- The cross sectional taper is typically low angle, which results in extremely broad fold and thrust belts;
- Complex three-dimensional edge effects form at the lateral boundary of the salt substratum.

Mild shortening in tectonically confined basins

Salt flow occurs within basins confined on either edge and subject to varying degrees of compression. Pre-existing basement structure is an obvious broad scale control on the development

and location of the various salt features in these basins while formerly extension diapirs experience compressional shortening. Salt walls and ridges of Permian salt in the southern North Sea Basin are type examples of extension followed by basin shortening and inversion. Many ridges tend to follow well-defined trends that parallel reactivated basement faults (Figure 6.41c, 6.42; Remmelts, 1995; Stewart et al., 1997). In other words, present suprasalt patterns in much of the southern North Sea Basin are not decoupled from subsalt structure, unlike the current gravity glide systems of the Gulf of Mexico. North Sea salt structures tend to first develop as extensional features atop the high of the upthrown basement block and are slightly offset but parallel to the controlling basement fault. At the same time salt was rising into these features, into-the-basin flow of salt was also creating downslope compressional buckles. Both these features typically first formed in the early Mesozoic, many millions of years after the Zechstein salt deposition had ceased (Mohr et al., 2004). Many such extensional diapirs were

then further altered during subsequent late Mesozoic compression and inversion.

There are three salt domains (defined by parallel salt ridges) in the southern North Sea (Figure 6.42; Remmelts, 1995). The first, in the north, are elongate salt structures oriented north to northeast in a province that runs from the Central North Sea Graben to northern Germany. The second encompasses the region from English waters to onshore Netherlands where the salt structures are elongated northwest and made up of both pillows and walls. The third encompasses onshore southern Germany where an eastward trend is more obvious and encompasses both pillows and low salt walls. Small structures, with no preferred orientations, separate the three domains. The domains defined by the various salt ridges correspond to the structural grain in the basement.

Triassic extensional faults strike north to north-northeast in the northern part of the basin where they form the boundary of the

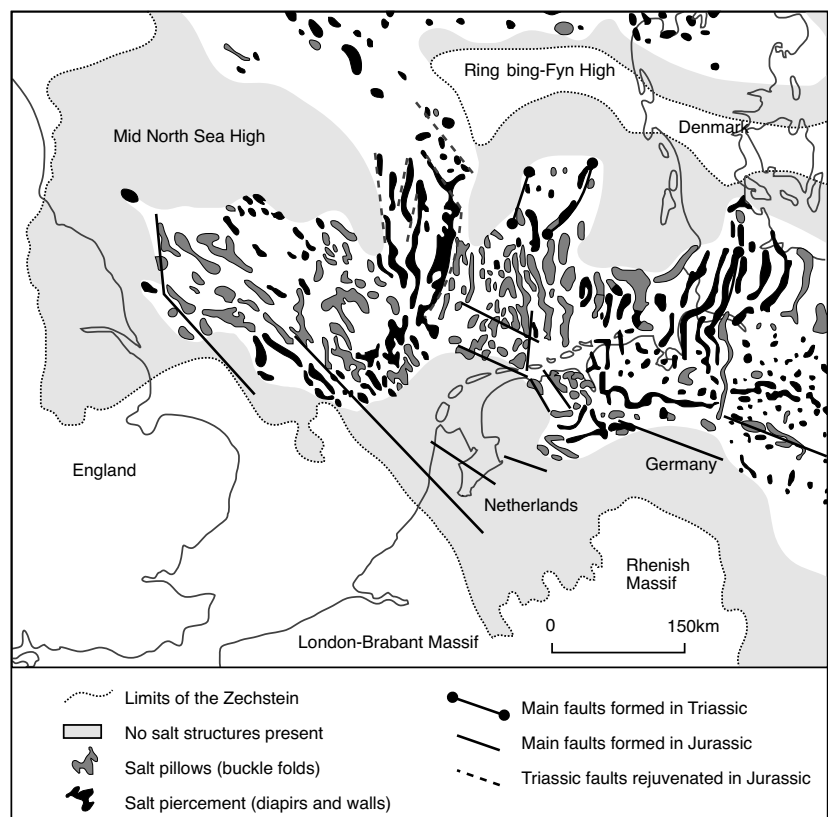


Figure 6.42. Salt structures in the southern North Sea showing that salt flow tends to be restricted to the basin centre. The various structures show a regularity of ridge spacing and there is an association with the major fault directions in the basin (after Remmelts, 1995).

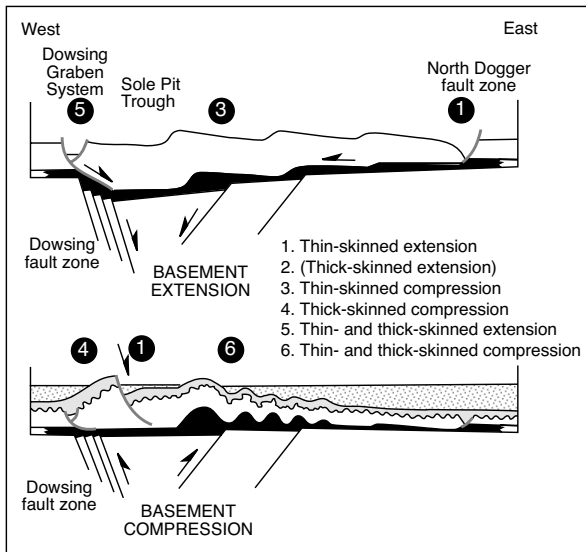


Figure 6.43. Driving mechanisms for the evolution of suprasalt features atop the Zechstein salt in the western part of the southern North Sea Basin. All listed mechanisms, except thick-skinned extension, played a role. Salt structures evolved as the basin tectonics evolved from extension (upper diagram) to compression (lower diagram) and there is always an element of detachment tectonics, such as buckle folding, in the current distribution of the salt layer (after Coward and Stewart, 1995).

Central North Sea Graben, the Horn Graben and the Glückstadt Graben, while in onshore Germany this same orientation defines the Ens Low and the Weser Depression. Further south, extension was accommodated by transtensional slip in a northwest direction. Not only are the orientation of salt ridges and fault trends related across the domains, but so is the timing of salt movement and faulting. Salt piercement and basement fault movement is dominantly Triassic in the northern part of North Germany, while in the south a Jurassic age prevails. Piercement is mostly Late Jurassic in the Central North Sea Graben, as is the main tectonic phase.

Many diapirs in the southern North Sea Basin were initiated along extensional faults that defined half-graben edges in Triassic to Jurassic times (Figures 6.43, 6.44a). The lack of primary rim synclines indicates that many of the structures became diapiric without going through a pillow phase immediately atop the Zechstein salt. In extension the diapirs grew mainly by asymmetric downbuilding with salt rise focused on the upthrown block adjacent to the fault, probably with sporadic periods of bathymetric relief created at diapir crests (Figure 6.43, 6.44a). The associated hanging wall tilt drove gravity gliding of the post-salt section, with resultant low-angle extensional faulting upslope and salt-cored buckling downslope

with structural trends following basement grain (Thomas and Coward, 1996).

Many extensional half-grabens were subsequently tightened or compressed by a phase of thin-skinned inversion, associated with back-steepening of the margin fault system and a resulting reactivation of the extensional detachment system. The effects of this inversion have been noted in many parts of the northern North Sea so that post Early Cretaceous and Tertiary history of the southern North Sea Basin is compressional, not extensional. This is expressed as changes in basin tilt and in reverse slip on individual faults so that parts of the North Sea basin now tilt to the northeast, a reversal of the original Jurassic tilt direction in the UK section of the southern North Sea Basin (Figure 6.43; Stewart and Coward, 1995). This is especially obvious in thrust faults and structures that fringe the Broad Forties basin (Hayward and Graham, 1989 but is seen across the North Sea Graben (Thomas and Coward, 1996) and much of the southern North Sea Basin (Remmelts, 1996; Stewart et al., 1997). Within the South Viking Graben, shortening estimates vary between 14 and 18% and are expressed on seismic data by localized hanging wall folds and the back-steepening of faults along the fault complex of the western margin of the graben, together with out-of-graben thrusting up the hanging wall dip-slope.

In order to fully explain the elongate salt walls and pillows of the southern North Sea Basin the effects of both extension and inversion must be considered in the final analysis of the salt structure geometry. Recognition of significant inversion can change the interpretation of some elongate salt-cored anticlines from salt pillows/swells to compressional buckle folds and squeezing of earlier extensional structures (Figure 6.47). Clearly, any precontractual salt tectonics strongly influences the location of subsequent thrusts and folds (Figure 6.41; Letouzey et al., 1995).

During contraction and inversion, folds and thrusts are initiated where thickness variations in the salt were already present in the overburden (Figure 6.44a; Vendeville and Jackson, 1992a,b; Nalpas and Brun, 1993). Erosional thinning of the overburden over salt ridges or salt walls also localises thrusts and folds, even when they are not related to basement normal faults (Figure 6.44b). Décollement atop the compressed salt also induces normal-fault offsets on the top of salt that then localise thrusting and facilitate subsequent reactive diapirism (Figure 6.44b).

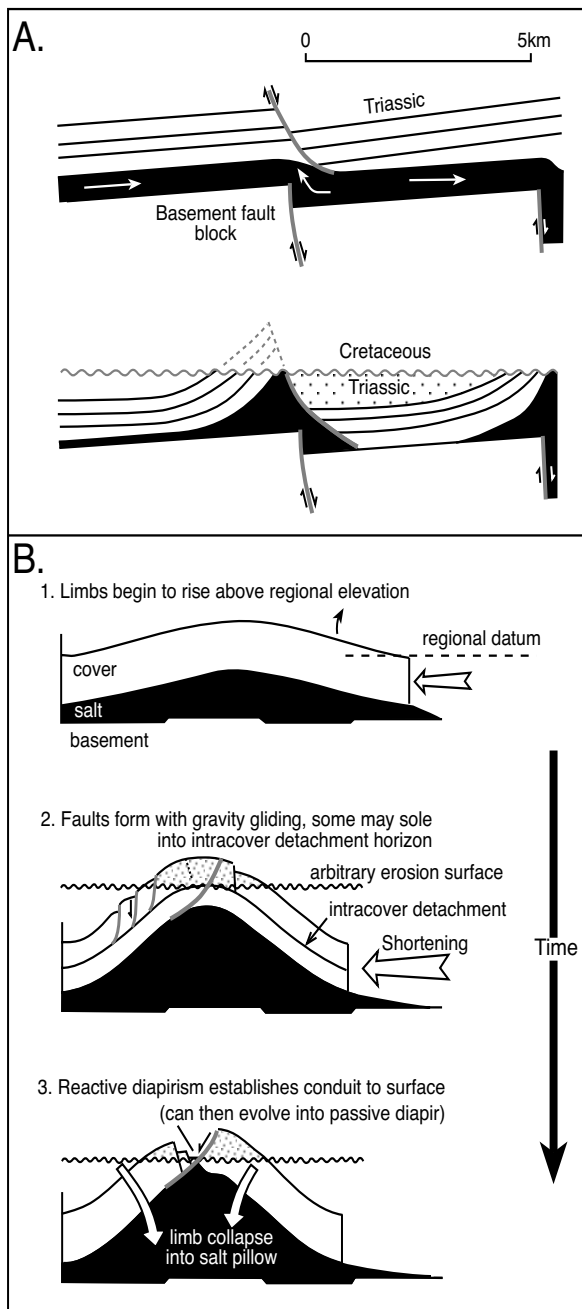


Figure 6.44. Extension and conversion structures, North Sea. A) Evolution of the Step Graben in the North Sea. Triassic extension focused the formation of salt structures atop normal faults in Sub-Zechstein basement. Early block faulting and accompanying rotation causes bedding plane parallel salt flow and pillowing atop the fault plane. This is followed by compression (shortening and inversion), tied to the Cretaceous unconformity and deposition of overlying sealing shales. Shortening drove oversteepening and flow reactivation during the Cretaceous-Tertiary inversion (after Remmelts, 1996). B) Buckle fold evolution with crestal erosion culminating in diapirism (after Coward and Stewart, 1995). See also Figure 6.47.

Can extrusion indicate extreme shortening?

With enough time, a sedimentary basin evolves from extensional to compressional or re-activated diapirs (Wilson Cycle), or a gentle salt anticline can evolve from a pillow created by gravity-driven downslope compressional folding (with an upslope extensional regime) into a compressional buckle fold via inversion (Figure 10.47). Salt can breakout out from anticlinal crests in either scenario and if it escapes onto the landsurface or seafloor it can initiate a new phase of passive diapirism.

Lateral shortening via buckling encourages thickening of salt in the anticlinal core, while the associated folding and crestal erosion can create the structural relief necessary for buoyancy and possible salt emergence, as can pinch-off from the mother salt layer. Such buckled salt-cored anticlines constitute the source to salt in the active namakiers of the Zagros Fold Belt of Iran (Figure 6.45). Once salt is extruded the original salt-cored anticline is subject to collapse and erosion (Figure 7.14).

But physical modelling of salt under compression creates a quandary as to whether the buckling and the thickening of a salt anticline alone can build sufficient pressure to initiate active diapirism, especially if the salt in the buckle-fold core is still connected to the mother salt layer. Physical models of a buckling compressional system using brittle overburden and a viscous salt-analogue silicone gel layer do not show breakout at the thickening anticlinal crests (Vendeville and Jackson, 1992b; Letouzey et al., 1995; Koyi, 1998). The silicone gel initially thickens in the rising anticlinal cores, then is squeezed out back down into the mother salt layer (the squeezed salt/gel takes the path of least resistance compared with breaking through the brittle overburden), or the gel is dragged along thrust planes. In all cases it stays in normal stratigraphic contact with the overlying thrust sheet. Only when there is a pre-existing diapir stem, or there is crestal erosion, or if the salt core is pinched off from the original mother salt level, is salt extruded. Extrusion in physical models with brittle overburden tends to occur whenever the stem is cut off from the mother bed and then the extrusion event is short lived (aka "popping the pimple").

Yet, 300-metre high glaciers of Neoproterozoic salt are flowing today across the landscape in the eastern foldbelt of the Zagros Mountains, Iran. The ubiquity of salt glaciers (namakiers) in this part of the Zagros foldbelt clearly shows salt can breach anticlines within regionally compressed terrains (Figures 6.45a, b, 6.46a). Zagros folds in this area are elongated symmetric whalebacks or box-shaped anticlines trending in a generally NW-SE direction, with the main thrust detachment at the level

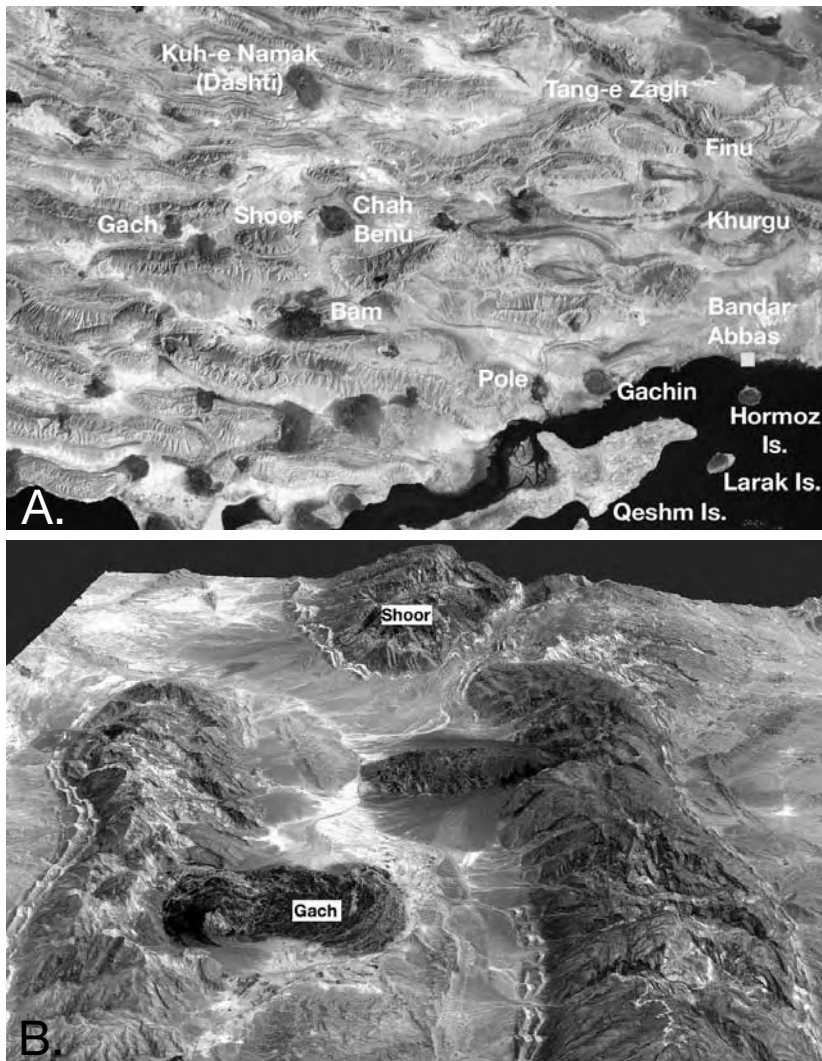


Figure 6.45. Namakiers of Iran. A) Salt glaciers (dark blebs) of Hormuz Salt flowing across the landscape of Iran north and east of the coastal town of Bandar Abbas, offshore islands are also cored by salt diapir and with now inactive glacier residues at surface. B) Later view looking east across the Gach - Shoor region (Images courtesy of NASA, NASA/GSFC/METI/ERSDAC/JAROS, and the U.S./Japan ASTER Science Team; see <http://asterweb.jpl.nasa.gov/gallery>; accessed Dec 7, 2004).

of the Precambrian Hormuz salt (Alavi, 2004). Hundreds of kilometres to the northeast from the Hormozgan district, in the hydrocarbon rich section of foreland fold belt in the Fars district, the Miocene evaporites of the Fars/Gachsaran Formation can act as a secondary detachment level whereby pairs of shallow thrusts are rooted with opposite vergences toward the crest of the anticline (Figure 10.56). Besides gently dipping overthrusts, many salt-cored folds in the Hormozgan region are dissected by subvertical normal and wrench faults (Talbot and Alavi, 1996). The Zagros fold system in this region is

overthrust along, and cut off by, the Zandan Thrust, a branch of the Zagros Main Thrust, approximately 75 km east of Bandar Abbas. Salt breakout in the salt-cored anticline does not occur unless the crest of the anticline is faulted or eroded (Figures 6.44b, 6.46b). Clearly salt undergoing compression in a natural foldbelt does not easily pierce thick brittle overburden, as in the analogue models.

Bosak et al. (1999) and Fürst (1976) note that outcropping salt plugs and associated namakiers are mostly associated with sigmoidal bends in fold axes (the circular plugs of Fürst 1976) or occur near terminations of anticlines (plunge turnovers). Many flows are sourced on anticlinal flanks and not in axial crests (Figure 6.45b). This observation implies that zones of fault-induced extensional shear are more important in controlling the site of salt emergence rather than the zone of extension across the culmination of anticlinal crests (salt leaks out of the sides of sliced structures; we are slicing bladders, not popping pimples!). A few of the salt plugs on the anticlinal flanks lie closer to the synclinal axis than to the anticlinal axis. But in some of the less active namakiers the site of the original emergence can be difficult to define as extruded salt always rolls downslope. If it is cut off from its source, it will end up occupying flanks and synclinal axes. Even so, the following generalizations can be made; most salt plugs outcrop in bends or faulted displaced offsets of the anticlinal axes, salt typically does not breakout in areas of straight (unfaulted) anticlinal axes. This led Talbot and Alavi (1996) to argue that Hormuz salt emerges as namakiers where the salt cored anticlinal crests are cut by faults, such as in the Kazerun and Mangarak fault zones (Figures 6.46b). A similar system of extensional tear faults across salt-cored compressional anticlines also explains emergent salt in Miocene salt diapirs of the Alborz region of Iran and Triassic salt in the Atlas ranges of Algeria (Figure 6.46c; Talbot and Aftabi, 2004; Vially et al., 1994).

Other than faulted and eroded anticlinal buckle folds, most other salt- or salt breccia-defined outcrops in compressional situations are along salt-lubricating thrust planes. Examples include Miocene salts in the Carpathians of Romania (Figures 10.58, 10.59), Triassic salts in alpine thrust belts in southern France and Spain, the Neoproterozoic Roan breccias of the Lufilian fold belt of Central Africa (Figure 7.27) and the Callana Formation breccias of the Flinders Ranges of South Australia (Figure 7.23). Modelling by Vendeville and Jackson (1993) showed that thrusting and strike-slip faulting can initiate asymmetric diapirism and salt allochthons in a compressional setting, but do so much less effectively than in extensional terrains.

Because compression driven emergence is occurring today as spectacular 1,000 m high salt glaciers in the Zagros mountain chain of Iran, allochthons as compressional features tied to later tectonic inversion are perhaps afforded a greater significance in salt tectonic modelling than the much larger but not so visible, compressional allochthons that typify the continental slope and rise positions of salt floored passive margins, as exemplified by the various the Atlantic basins. Interestingly, the Triassic thrust belts of southern Europe examples have now been reconstructed using balanced section techniques and the spectacular salt-cored thrust belts are seen to be centred on reactivated diapirs, first formed in an earlier extensional phase that was then

caught up in the thrust belt (Dardeau and Graciansky, 1990). How widespread the inheritance of salt diapirs and walls from extension into compressional thrust planes is still under debate although the early stages of the expression of the compressive belt are occurring in offshore Angola at a time well before any episode of continent-to-continent collision (Figure 6.38c). There is now widespread agreement that salt plays a fundamental role in controlling the amount of shortening in thin-skinned salt-entraining thrust provinces and outcomes range from mild inversion of an previously extensional system (such as pillow structures of the North Sea; Stewart and Coward, 1995) to fully developed salt-cored detached fold-and-thrust belts in the various alpine chains of Europe, North Africa, southwest Asia and central Australia.

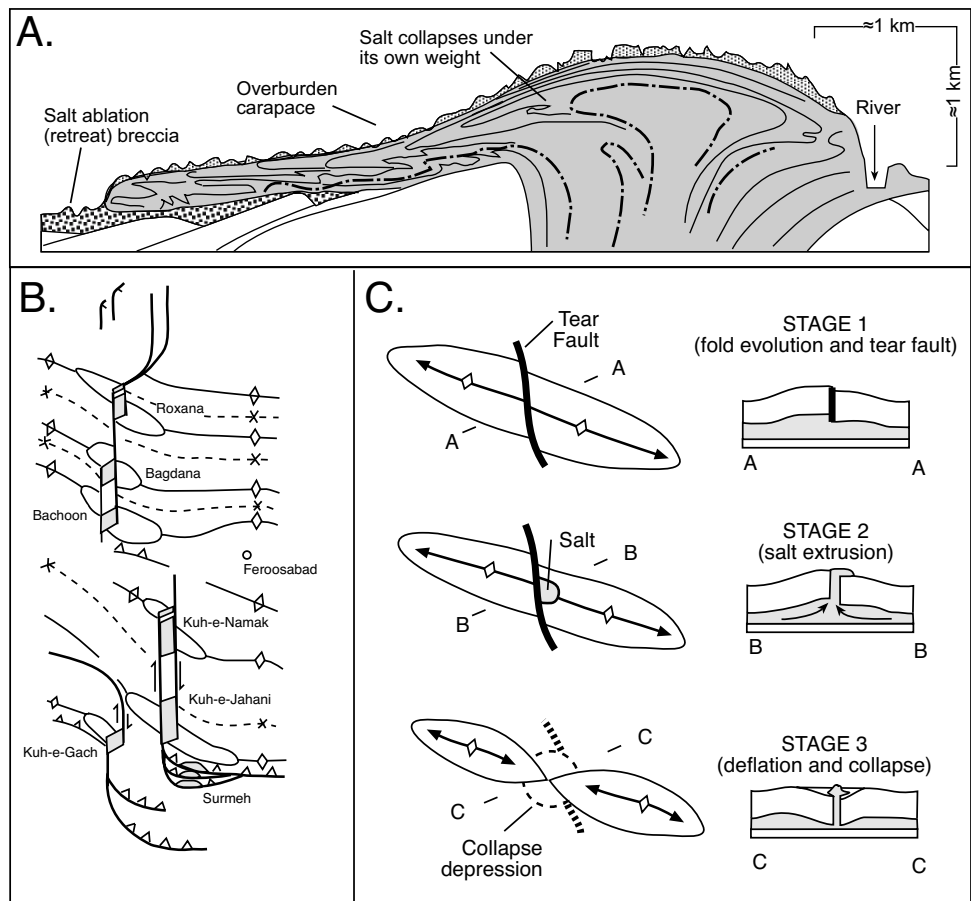


Figure 6.46. The importance of faulting as a control on salt extrusion in compressional buckling regimes. A) Cross section of Kun-e-Namak diapir, Iran. Internal folds show how salt flows over the landscape like the rolling track of a military tank (after Talbot, 1979). B) Current kinematics of Mangarak fault zone, Iran, showing the location of extrusions (grey) in zones where fault zone crosses salt-cored anticlinal culminations, shown as elliptical areas (after Talbot and Alavi, 1996). C) Schematic based on Algerian examples showing how salt extrusions occur where tear faults intersect salt-cored anticlinal culminations (modified from Letouzey et al., 1995). See Figure 6.45 for location of Iranian diapirs.

Criteria	Downbuilding	Rejuvenation driven by compression
Stratal thickness	Thick beds on the flanks thin over the salt, consistent with the syngrowth sedimentation patterns of Trusheim (1960) and Seni and Jackson (1983).	Uniform bed thickness over crest when not tectonically thinned. Large thickness of overburden folded above crest. High angle onlap onto pre-inversion unconformity.
Lithological variation	Thick beds on the flanks thin over the salt, consistent with the syngrowth sedimentation patterns of Trusheim (1960) and Seni and Jackson (1983).	Less concentric lithological variation produced when diapir inactive before inversion period.
Layer parallel shear	Normal sense of movement away from crest, caused by material sliding off crest.	Reverse sense of movement toward the crest.
Faulting	Small displacement normal faults on diapir shoulders, dipping away from the diapir. Crestal graben. Large listric growth faults along part of the salt contact.	Convex upward thrusts in the overburden on the shoulder of the diapir. Crestal horst as well as graben. Normal faults, strike-slip faults and thrust faults directly above the diapir e.g. Withjack and Scheiner (1982).
Drag zone geometry	Narrow and high relief.	Broad and lower relief.
Regional deformation	Regional extension faults.	Regional folds and thrusts and inverted extension structures in the cover.
Fold geometry of concordant overburden	Geometry moulds to the diapir.	Broad at top or, fold shapes unrelated to the underlying diapir shape.
Withdrawal basin	Primary and or secondary rim syncline sometimes present.	Absent when diapir is growing by compression. Diapir continues to grow even when source is severed by welding.

Table 6.2 Criteria for separating downbuilt diapirs from diapirs which have been reactivated by regional compression (after Davison et al., 2000b; Vendeville and Nilsen, 1995).

Distinguishing downbuilt and reactivated (mildly squeezed) diapirs

The preceding discussion of salt in compressional terrains shows that many extensional diapirs suffer later horizontal shortening (squeezed diapirs). Examples are found in all three compressional terrains, namely; a) thin-skinned fold and thrust belts at the toe of gravity-spreading systems on divergent margins, as in the South Atlantic, b) thin-skinned fold and thrust belts driven by plate convergence, as in the foreland fold belt of the Zagros Mountains, and c) inverted, thick-skinned extensional basins, such as the North Sea. Styles range from salt structures that merely acted as foci of mild compression induced folding and faulting to diapirs that underwent considerable rise of salt or reactivation.

Shortening squeezes salt in the diapir stem and so contributes to a short-term increase in salt supply. But this increase is temporary and decreases sharply once shortening closes and empties the feeding stem of the diapir. During shortening diapirs act as stress concentration zones where new folds/thrusts may form and propagate (Koyi, 1998). Thrusts can propagate from the salt pedestal and so cut the feeding stem of the diapir. These diapirs sag with time arguing that some of the inactive diapirs in the Zagros mountain belt may have their feeding stems cut-off during the Zagros orogeny. If breached, these diapirs can form large dissolution craters on the surface outlining the

region where the salt in their dynamic bulge has dissolved (e.g. Figure 6.46c).

In the relatively undeformed autochthonous salt region of the southern North Sea, the importance of Tertiary compression after Mesozoic extension was largely ignored until the early 1990s. Many diapirs cutting through the Tertiary section of the Central Graben, North Sea and the onshore basins of Germany, are now known to be rejuvenated diapirs with later episodes of salt flow driven by compression (Davison et al., 2000a, 2000b; Scheck et al., 2003; Mohr et al., 2004). Similar sets of rejuvenated diapirs can be also found nearby in the southwestern Nordkapp Basin (Henriksen and Vorren, 1996). In all these basins diapirs first formed in Triassic extension and were rejuvenated during Late Cretaceous to Middle Tertiary shortening. It was an event that formed the many Danian chalk reservoirs of the North Sea basin region offshore from Norway and Denmark.

Diapirs reactivated in compressional settings typically show common set of features (Table 6.2 Figure 6.47; Vendeville and Nilsen, 1995; Davison et al., 2000b); 1) Growth was episodic rather than continuous, allowing thick sets of strata to be deposited flat and horizontal as a thick roof atop the diapir crest during periods of diapiric quiescence, 2) Reactivated and compressed diapirs tend to have narrow or pinched-off stems, 3) Strata adjacent to the diapir are little deformed as most of the

deformation is taken up in the diapir salt, 4) Many reactivated and squeezed diapirs show a triangular-shaped basal pedestal. A lack of primary rim synclines around these diapirs during times of tectonic quiescence indicates that the structures went diapiric without necessarily going through a pillow phase.

Most rejuvenated structures grew by localised downbuilding associated with crestal extension and near-crestal gravity sliding with sporadic periods of bathymetric relief at the active diapir crest. For example, salt-cored sea-bed relief controlled the deposition of Palaeocene and Eocene turbidite sandstones in the North Sea, which today thicken away from the compressional re-activated diapir crests to form potential reservoir sands from 0 to 300 m thick (Figure 6.53). The effects of compression on autochthonous salt structures in the North Sea tend to be most obvious around the diapirs and not in the interdiapir areas. Compression in the Central Graben was driven by downslope sliding of overburden above the Zechstein salt on the Eastern Platform area during late Palaeocene, and by regional Alpine shortening across the whole of the Central Graben during middle Miocene times. The various re-activated diapirs of the North Sea are much less deformed than those described in the Triassic-salt cored décollements of Spain and the French Maritime Alps (Roca et al., 1996; Dardeau and Graciansky, 1990) or the Cegonha and similar compressional structures in offshore Angola (Duval et al., 1992; Fort et al., 2004).

Specific features in the overburden atop a North Sea diapir, which may help in determining whether a diapir was rejuvenated by late compression after a phase of downbuilding, are illustrated in Figure 6.47a (see also Letouzey et al., 1995; Vendeville and Nilsen, 1995; Guglielmo et al., 2000). Sediments atop rejuvenated North Sea diapirs exhibit some or all of the following characteristics: (a) localised unconformities with high angles of onlap above the unconformity; (b) thick lid

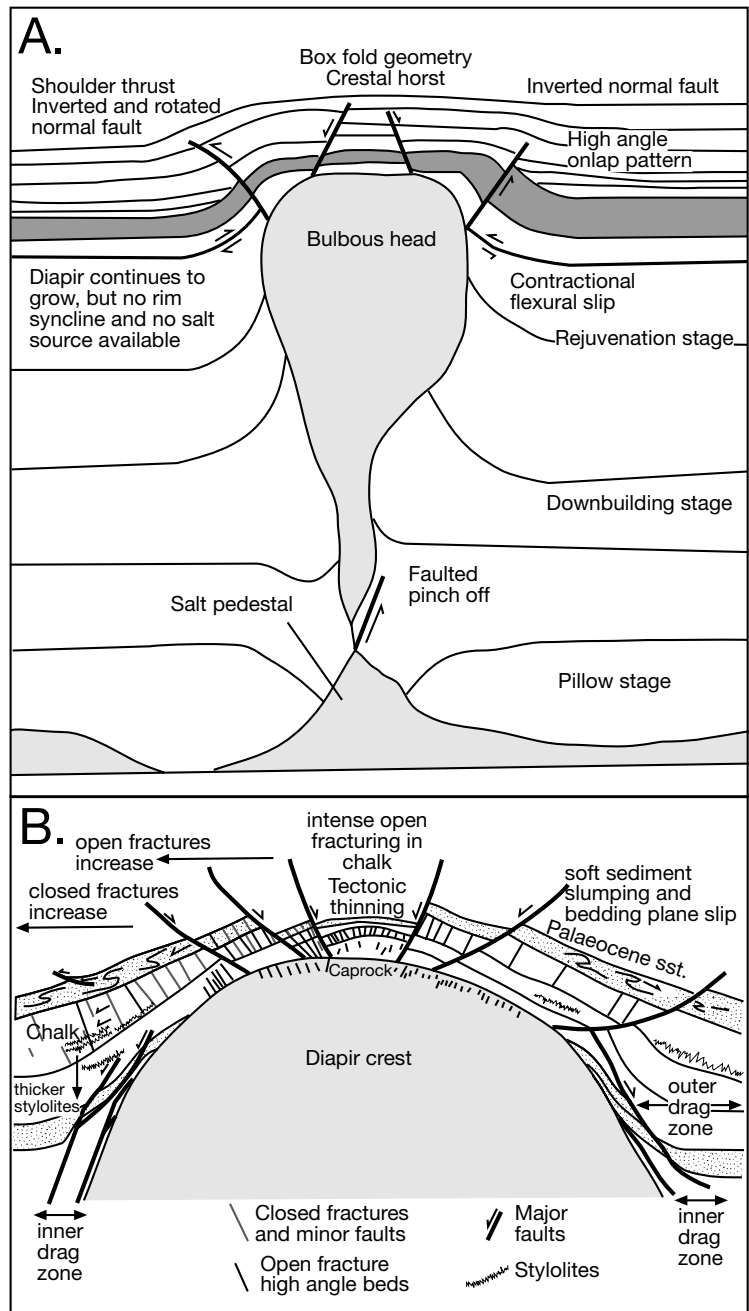


Figure 6.47. Rejuvenated diapirs and suprasalt deformation. A) Typical diapir crest showing deformation style in fractured chalks and Palaeocene sandstones (after Davison et al., 2000a). B) Seismic scale geometry of diapirs affected by late compression with (a) compressional fold in overburden, (b) reverse layer-parallel slip, (c) wide drag zone, (d) thrust faults on shoulders, (e) lack of rim synclines (f) localised unconformities and high angle of onlap above unconformity restricted to immediate diapir vicinity, and (g) thick updomed strata above the diapir (after Davison et al., 2000b).

of overburden strata (>300 m) updomed above the diapir; (c) reverse layer-parallel slip or concentric thrust faults localised at the diapir shoulders; (d) central horst block uplifted above diapir; (e) continued upward movement of the diapir even when pinched off from the source. The presence of layer parallel reverse slip and concentric reverse faults may not occur together. In experiments on active diapirs Schultz-Ela et al. (1993) showed that layer parallel slip occurs in overburden, which is anisotropic, and thrust faults at diapir shoulders occur in isotropic overburden. Crestal collapse graben also occur above some rejuvenated diapirs, but crestal horst structures have only ever been produced in physical models of upbuilt diapirs (Davison et al., 1993). The significance of the various fault patterns associated with the inversion of the diapir is discussed further in terms of hydrocarbons in Chapter 10.

Suprasalt doming influenced the distribution of chalk and sandstone overburden in the North Sea via crestal thinning associated with intense extensional faulting, tensile fracturing, gravity sliding and pressure solution (Figure 6.47b; Davison et al., 2000a). Salt buoyancy created topographic relief about the flanks of the thinned chalk layers, resulting in semi-indurated chalk sliding off the crests of the diapirs as shown by soft-sediment slump folding and bedding-parallel shear zones in the chalk in most producing offshore fields. Debris flows in the Kyle field carry clasts of caprock anhydrite indicating that the salt crest was exposed or was near the seafloor. Lithified angular clasts in the same debris flows indicate that chalk was already indurated and cemented at the time of extrusion, but nevertheless the diapir was able to actively break through and shed this lithified material. Topographic relief of several tens to hundreds of metres above the surrounding seafloor had developed atop reactivated diapir crests during the Late Cretaceous to Palaeocene period.

An associated flow of squeezed pore fluids through the chalk reservoirs in Banff, Machar, Kyle and North Pierce fields in the North Sea resulted in interconnected vuggy fractures filled with calcite. This calcite was probably derived from pressure solution, but much of the dissolved chalk atop the Machar diapir has since been removed from the system, with dissolution waters possibly escaping directly into the sea along major faults. A combination of all the rejuvenation effects produces what is an apparently intrusive single-event geometry. In reality, the overburden was tectonically thinned episodically and removed by gravity sliding, rather than actively pushed aside by rising salt in one event. Typical deformation patterns observed in chalks above a reactivated diapir are summarised in Figure 6.45b.

Palaeocene sands overlie chalks in many diapiric fields in the Central Graben. Bedding-plane slip surfaces, with at least 10 m of displacement, are common in the Palaeocene siliciclastic rocks from South Pierce field in the North Sea (Figure 6.47b; Davison et al., 2000a). Like the chalks, these overlying clastic sediments slid away from the diapir crest to accumulate on the diapir flanks as stacked and slumped deepwater sandstones. Sliding and shedding preferentially took place along mudstones, which preserve commonplace slump folds and polished faulted surfaces. Similar soft-sediment folds are not always present in the sandstones, which rode on the muddy slides and some coherent sandy blocks were translated large distances without any internal deformation. Thicknesses of the Tertiary sandstone packets increase from zero near the crest to 300 m on the flanks and indicate a combination off-crest channel stacking/ponding and crest-induced slumping. Davison et al. (2000a) argue that build-ups of tens of metres of supracrestal sediment were followed by up-doming of the salt diapir crest, which was accompanied by faulting and rotation of the strata until a critical angle was reached and then overburden slid off the diapir. Hence, as for their chalky precursors, these episodically active compressional diapirs were close to or at the seafloor during the Palaeocene to Eocene period, producing bathymetric highs that periodically shed their siliciclastic sediment cover (Figure 6.53).

Sediments and flowing salt

It is not just sediment patterns about reactivated diapirs that respond to salt-induced topography. Wherever flowing salt approaches the land surface in both continental and offshore positions it creates topographic relief in the landscape and so influences the style and pattern of deposition (Table 6.3). Historically, sedimentological studies of this phenomena focused on predicting suprasalt deposition and its utility in predicting associated porosity trends (see summary in Warren, 1989). Conclusions as to the position of sands, reefs and porosity belts in relation to salt structure highs in the landscape are still valid, but our understanding of mechanisms driving salt flow have substantially changed. With increasing recognition of the importance of lateral flow in allochthonous salt, the sedimentology of subsalt systems has become as important to model and predict.

Reactive diapirism typically forms a graben or low atop the diapir crest. Active diapirism, passive diapirism and compressional growth folds are all marked by topographic highs about the crest of the salt body. Salt flow rates are in turn influenced

by loading (sedimentation rates) and tectonics (rates of extension or compression). Interaction creates feedback whereby the geometry of a growing salt body is influenced by, and feeds back into, the depositional rate/water depth of the adjacent sedimentation setting. Once rising salt is sufficiently close to the surface to influence its topography, sedimentary feedback typifies all styles of halokinesis. At the scale of seismic resolution this is recorded in changes in bed thickness (e.g. formation of suprasalt/intersalt basins or minibasins, thickness changes approaching active diapirs ridges and growth folds), as well as varying onlap and offlap relationships, and changes in bed attitude as the salt body is approached. At the lithofacies scale, it is recorded in changing styles of shallowing or deepening of the sequence (sanding or shaling upward parasequences), the development or the drowning of reefs and shoals, syndepositional bed disturbance, slumping and faulting, as well as the formation of local unconformities and karsting.

At the broad scale of seismically resolvable sediment geometries, the style of sedimentation can be broken down into three groupings: prekinematic, synkinematic and postkinematic (Figure 6.48; Jackson and Talbot, 1994). The prekinematic layer records sedimentation before salt movement or any other deformation. A prekinematic sediment layer is an interval of strata where initial stratigraphic thickness is constant above a salt structure or its adjacent rim. That is, the prekinematic sediment layer is isopachous or its depositional thickness varies only as much as would be typical for the same sedimentation style in a region where no salt was present.

In contrast, the synkinematic layers record sediment thickness and facies changes related to salt-cored highs and crestal sloughing. Synkinematic layers thicken above withdrawal basins or locally thin against rapidly rising structures. For example,

in the East Texas Basin in the Gulf Coast, the percentage of stratigraphic or seismic-stratigraphic thinning of synkinematic strata ranges from 10 to 100% in units influenced by the flow of Jurassic Louann Salt (Seni and Jackson, 1983a,b). Changes in bed thickness are frequently recorded by onlap or truncation at all levels of the synkinematic layer (Figures 6.48, 6.49).

The postkinematic layer is the interval of strata deposited by sedimentation after salt flow, or any other deformation, has ceased. Basal postkinematic strata can onlap an underlying, uneven deformed surface but show no thickness changes that can be directly ascribed to deformation induced by local salt-flow. The postkinematic layer typically overlies the synkinematic layer.

Truncations (unconformities) are particularly useful in distinguishing the three packages. Removal and termination of dipping deformed strata by subaerial or subaqueous erosion forms a truncation or sequence boundary. Truncations cutting across anticlines or fault blocks indicate that the structures had surface relief at the time of erosion (Figure 6.48). Undeformed truncations mark the base of the postkinematic layer. Where a truncation is itself folded or faulted, it marks an episode of deformation of the synkinematic layer.

Various terms have also been coined to describe syn-kinematic basins that fill with sediment as they load and subside adjacent to or atop relatively thick allochthonous or autochthonous salt, which ultimately evacuates to leave behind weld and ramp basins (Figure 6.26). An older term for such sediment-filled basin atop a salt allochthon is a depotrough. In its strictest definition depotrough describes a basin filled with deepwater, mass flow or turbiditic deposits that uplap a diapir margin (Spindler, 1977). The term depotrough is used by some as equivalent to

Offshore			
Abu Thama, Arabian Gulf	60 m	Neogene compressional reactivation	Purser, 1973
Cabo St Tome, Brazil	97-144 m	Gravity gliding	Demercian et al., 1993
Allochthons, Gulf of Mexico	130-260 m	Gravity gliding	Liro, 1992; Wu et al., 1990a,b; Rezak, 1985
Offshore Mississippi Delta	100-240 m	Gravity gliding	Jackson et al., 1995
Continental			
Al Salif, Yemen	45 m	Extensional with gravity gliding	Davison et al., 1996b
Jabal al Milh, Red Sea	45 m	Extensional	Davison et al., 1996b
Mt Sedom, Dead Sea	200 m	Transtensional	Frumkin, 1994a, b
Saharan Atlas, Algeria	300 m	Compression with salt source cut-off	Kulke, 1978
Zagros Chain, Iran	300-1500 m	Compression with salt source cut-off	Kent, 1987; Talbot and Alavi, 1996

Table 6.3. Landscape relief around salt structures.

a depopod. But a depopod can also be a basin filled with shallow water deltaic deposits draping over or against a flanking salt diapir. In many prograding shelf situations a depotrough passes upward into a depopod. A better term to describe sedimentary basins created by the coming and going of flowing salt is minibasin. It has no genetic implications. And without drilling there should be no assumption of predominant water depth or lithology accumulating during the fill of a minibasin. In much of the current literature there is a strong bias toward Gulf of Mexico models of sediment fill by deeper water siliciclastics passing up into fluviodeltaics. This bias reflects the excellent, but geographically localised, work that has been widely published on the slope and rise allochthons of offshore Gulf of Mexico. It has led some authors to discuss suprasalt reservoirs solely in terms of siliciclastic models. Outside of the Gulf of Mexico, modern and ancient minibasins are filled by other facies; such as chalks in the North Sea, or by shallow water lagoonal mudstones, grainstone shoals and reefs, as well as Mesozoic sabkhas and salterns in the Middle East (e.g. Davison et al., 1996b).

Sediments and evolving salt structures

The crestal positions of shallow salt structures in extensional regimes are intimately associated with faulting in the first two of the three evolutionary stages of diapirism (reactive and active versus passive). The reactive diapir is triggered by faulting in the extending brittle overburden whereby the hanging wall of an initial fault sinks into the source layer until resisted by increasing pressure forces in the salt source layer and the bending resistance of the overburden (Jackson and Vendeville, 1994a). Continuing expansion is accommodated by subsidence as new faults form repeatedly along the expanding axis of the graben. The central fault block sinks and dwindles, while the diapir rises below it, regardless of overburden density. Progressively smaller fault blocks are supported by fluid pressure of the salt at progressively higher levels flanking the triangular diapir. Syndiapor sedimentation keeps diapirs in the reactive phase longer by continually filling the graben floor with new layers of sediment (Figure 6.50). Reactive diapirism is controlled by the rate of regional extension; whenever regional extension ceases, a reactive diapir stops growing. In contrast both active and passive diapirs are strongly influenced by sedimentation rates and the deposition of sediment wedges (Ge et al., 1997).

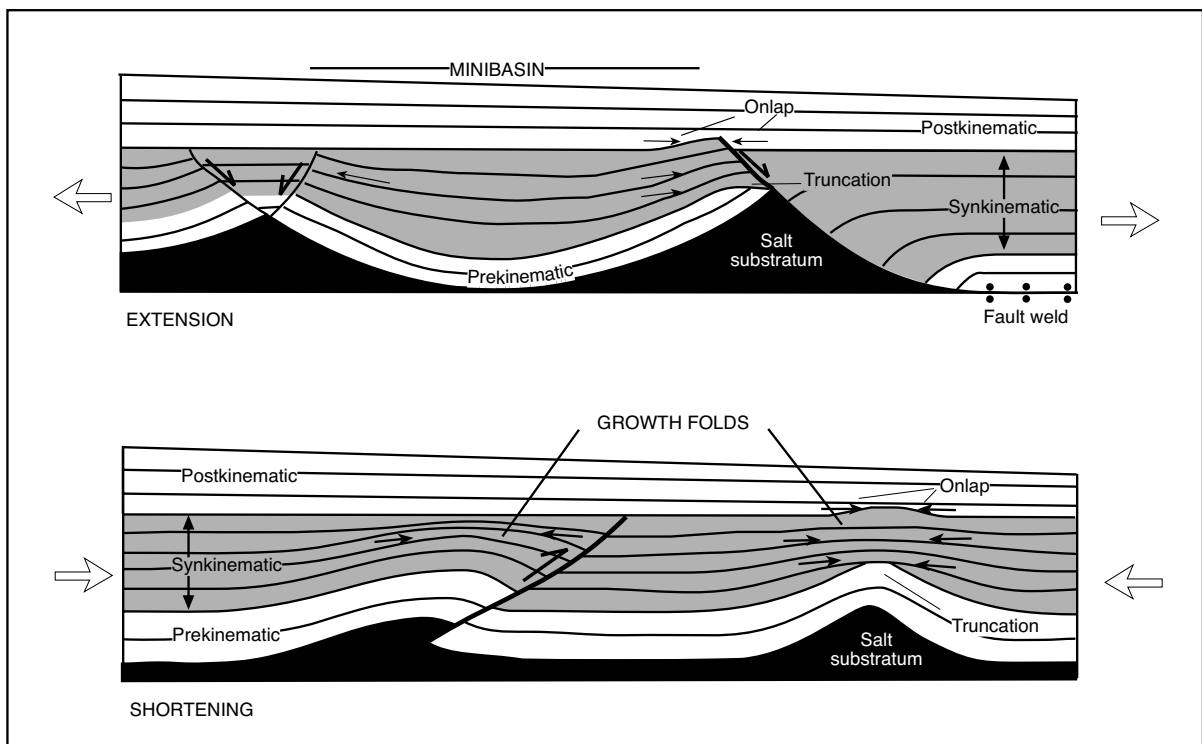


Figure 6.48. Sedimentary record of salt flow during extension (upper panel) or shortening (lower panel). The prekinematic layer was deposited before salt movement began. The synkinematic layer was deposited during salt flow and includes many internal onlap or truncation surfaces. The postkinematic layer was deposited after salt flow ceased. Its base may onlap or truncate originally exposed surfaces in the synkinematic layer (after Jackson and Talbot, 1994).

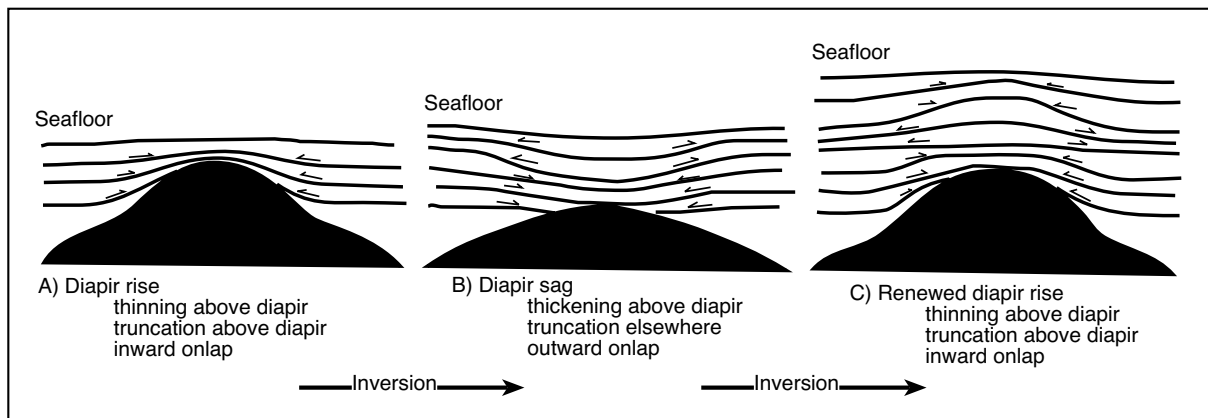


Figure 6.49. Schematic of two episodes of structural inversion caused by subsidence and renewed uplift of a diapir. The inversions are recorded by changes in bed thickness and onlap directions indicated by barbed arrows (after Jackson and Talbot, 1994; Nelson, 1991).

At the time a reactive diapir is forming there is an active depression or graben atop the extending structure (Figure 6.50). There are three depositional settings that can supply sediment to that depression: continental, marine shelf, and deepwater slope to basin. If the extensional graben or depression atop the reactive diapir is in a continental situation, then any surface waters, lakes or rivers will tend to occupy that depression. In hydrologically open settings, the deposits of a series of stacked fluvial channels may infill the lower parts of the depression. In more restricted to hydrographically closed scenarios the graben fills with deposits from a series of elongate saline lakes and mudflats. If the graben depression forms in a marine shelf setting it may fill with deeper water lagoonal muds while shoal water sediments and reefs occupy the very shallow waters atop the edges of the faulted graben margin. If the reactive stage creates a graben depression in deeper waters on the upper part of the continental slope, then a series of growth faults amid thickened deltaic sand traps may occur and help load the system. Conversely the graben may create a deep seafloor depression that stacks successive episodes of submarine channel and fan sands.

Once a reactive diapir becomes sufficiently tall and its roof sufficiently thin, then pressure at the diapir crest impels the system into the active stage. The diapir lifts its roof, as it rotates, breaks through and shoulders aside its overburden. Crestal erosion and near-crest sloughing then disperses the fragmented roof materials as a series of monomict debris aprons composed of sediments that formerly overlay the diapir crest. Throughout this time, and during the following passive stage, the area above and about the diapir or salt wall is a topographic high that does not accumulate sediment. In the continental realm,

fluvial channel sands may stack into the depression created by any adjacent salt withdrawal sink. In the marine realm, the high often lifts the sea floor above wavebase and into shallow euphotic waters suitable for carbonate growth. The higher energy realm about a high on the open marine shelf means the muds are winnowed to leave behind sands and gravels. In the transitional continental marine setting, the high energy shorezone tends to lap up onto the edge of the high and wave action reworks and winnows the debris apron of the active stage into well sorted shorezone sands. Later in the passive stage the shorezone also picks up and redeposits exotic blocks derived by the dissolution of extruded salt to create polymict breccias and conglomerates.

Once salt is emergent at the land surface or on the seafloor the diapir has evolved into its passive stage (Figure 6.50). At this stage the salt is extrusive and any thin sediment roof that may periodically develop atop the salt has little mechanical influence and is destroyed by ongoing active breakout. Dissolution of the salt sheet on the seafloor creates anhydrite/gypsum carapaces and may also supply a cap of exotic blocks that have been dragged up from greater depths. In some Neoproterozoic salt allochthons in Northern Australia the transition from active to passive can be seen in a change of the debris apron constituents from monomict to polymict breccias. The increase in the variety of clasts is driven by dissolution of namakier salt, leaving behind a much broader range of clasts (pers. obs.). If the breccias are not recognised as salt allochthon-generated, such units are easily misidentified as the outcome of long distance transport driven by tectonic uplift. In Proterozoic and Archaean salt allochthons the salt carrier has typically dissolved, even in the feeders to many of these breccias. All that remains are

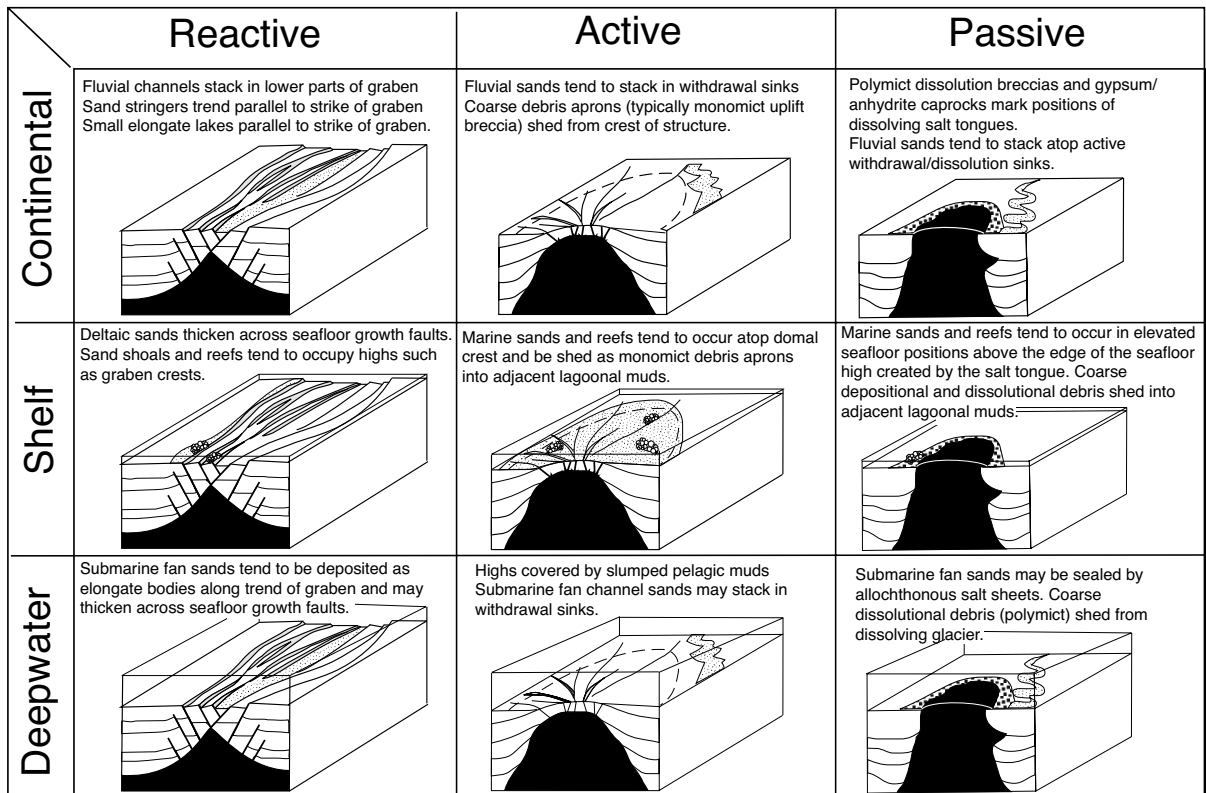


Figure 6.50. Schematic cross sections showing the control exerted by shallow salt (topographic high) on the distribution of sands and reefs in synkinematic sediments. Sand distribution changes with the stage of salt structure and water depth in the depositional setting (modified in part from Warren, 1999). This sequence of schematics is drawn using a diapir outline, but similar depth-related sediment patterns also form about the seafloor highs created by nearsurface salt allochthons or atop turtle structure anticlines in interdiapir areas.

characteristic alteration haloes around salt and fault welds and indicators of the former presence of salt in the matrix of the breccia itself (Chapter 7). This has significance to many base metal deposits and exploration models (Warren, 2000b). For example, in sedex exploration it is the difference between a predictive layered brine pool model as the control on prepared ground for subsequent mineralisation versus no discernable control other than fault proximity.

A salt-induced high on the seafloor can develop substantial relief over the surrounding region. A rich biota of bioherms and associated grainstone flats can form in shoalwater tropical seafloor settings. In the deeper water settings of the allochthons in the Gulf of Mexico the areas atop extrusive salt tongues have a relief measured in hundreds of metres above the surrounding seafloor (Fletcher et al., 1995). Such deep seafloor highs tend to channel turbiditic sands into the relative lows along the allochthon edge. While the salt is replenished (salt fountain), the region about the salt remains a topographic high. The maintenance of the salt at or near the sedimentation surface

by periodic overburden shedding means that both the active and the passive stages are characterised by many unconformities, debris aprons and thinning of strata in the vicinity of the diapir crest.

Three-thousand-year-old coral reefs that now lie some 18 m above sea level along the onshore portion of the active Al Salif diapir, Yemen (Davison et al., 1995, 1996b). This active stage diapir has lifted its roof and continues to do so today. The nearby Jabal al Milh diapir is the much-reduced remnant of a formerly active extrusive structure on a Pleistocene carbonate shelf (Figure 6.20a). In both, the highs atop the structures strongly influence the facies distribution of nearby carbonate and evaporite sediments. Offshore from this region are a number of depositionally similar islands and grainstone shoals that likely indicate sea floor shoaling atop other diapirs and salt walls in the same Miocene salt.

Topographic lows form above peripheral sinks created atop areas of salt withdrawal. These are often areas of preferential

sedimentation, that is, sediment thicks. Loading associated with accumulation of sediment in the sinks drives further salt flow. The lows persist until the salt is completely evacuated and a salt weld forms. Salt-flow induced highs and lows in the sedimentation surface persist until the diapiric ridge or crest is cut off from its supply by the formation of welds or touchdowns. Then the diapir and allochthon crests are buried by sediment that continues to aggrade until its thickness exceeds the piercement potential and the structure is no longer active.

Even though coal is not a sediment typically associated with evaporites the ongoing low created during the formation of suprasalt minibasins lows has preferentially accumulated a thick coal succession in the Pennsylvanian Joggins Formation, in the Cumberland Group of Nova Scotia (Waldron and Rygel., 2005). This 1.5-km-thick coal-bearing unit is famous for upright fossil lycopsid trees, and is preferentially preserved in the Athol syncline in the western Cumberland basin. Seismic profiles show that the Athol syncline sits atop a salt weld and that the Joggins Formation thins on the flanks of adjacent evaporite-cored anticlines. During deposition of the Joggins Formation, at least 1 km of syndepositional subsidence was facilitated by flow of underlying salt into the adjacent anticlines.

Both subaerial and submarine glaciers are topographic highs at the time of salt emplacement so the syndepositional surface adjacent to a glacier is subject to slumping and mass wasting. Like a glacier of ice, a salt allochthon or namakier can spread out over its own moraine, so that the lower contact of a preserved allochthon is disturbed even while the salt rolls out over its own lower surface (Figures 6.22a, 6.46a). It seems that the preservation potential of salt wings and allochthons are higher if emplaced as a submarine glacier compared to a subaerial glacier (Peel et al., 1995). Submarine salt glaciers form in passive margin settings and are protected from pervasive dissolution by a thin membrane of supersaturated salt mud, which maintains its suprasalt position as the salt sheet is loaded and minibasins form in the relative quiescence of the sub-wavebase seafloor. Subaerial glaciers tend to form in compressive continental terrains where the salt source is more limited and their carapaces are exposed to the continuous rigours of subaerial weathering and rainfall dissolution. Caprocks atop glaciers in both settings can form either as biological precipitates or as accumulations of insoluble weathering products.

Siliciclastic patterns

When a diapir crest is near the surface in a continental deltaic or fluvial setting it is a topographic high that focuses sand deposition into a series of stacked channels in the interdiapir area.

Even in a mature salt province, such as the modern siliciclastic Texas Gulf coast, salt structures are capable of maintaining a degree of topographic relief at the land surface and so act as a focus for off-structure fluvial sand accumulations (Figure 6.51) and as a focus for sand distributions further out on the modern siliciclastic dominated shelf (Morton and Suter, 1996).

Through time, the crest's position in earth space is maintained by the withdrawal of salt from an adjacent rim syncline, with the creation of a topographic low in the landscape atop the sediment-accumulating rim syncline. The effect of this topographic differential explains the 10-100% syndepositional thinning of lower Cretaceous Paluxy sands over the Van and Hawkins salt pillows and the Hainesville diapir in east Texas and the associated stacking of fluvial sands in the interdiapir areas (Seni and Jackson, 1983a). A net sandstone map shows that crestal areas contain between 5 and 20% less sand and that Cretaceous Paluxy sands were focused into withdrawal sinks between highs in the landscape created by the growing autochthonous salt structures (Figure 6.52a). Sand pinchout and lateral passage into floodplain muds atop the various salt structures clearly shows that the thinning of the Paluxy sands onto the various salt structure crests is depositional, rather than a response to active piercement. Likewise, sand body distribution in the Paleocene-Eocene Wilcox Group around Bethel and Oakwood domes in the southern East Texas Basin indicate the effects of dome induced topography on coeval fluvio-deltaic sedimentation in this Tertiary landscape (Figure 6.52b; Seni and Jackson, 1983a). For example, there are four stacked channel-fill sands, each more than 15 metres thick, in the rim syncline immediately east of the Bethel Dome. In contrast, there is only one sand body more than 15 metres thick in the strata over the Bethel Dome, yet the percentage of sand in thinned crestal succession is only slightly lower than in the stacked sands. Paluxy sands in the East Texas Basin were deposited around the basin margin as part of the Lower Cretaceous Trinity Group. At the same time, but further out in the basin, shelfal sediments were

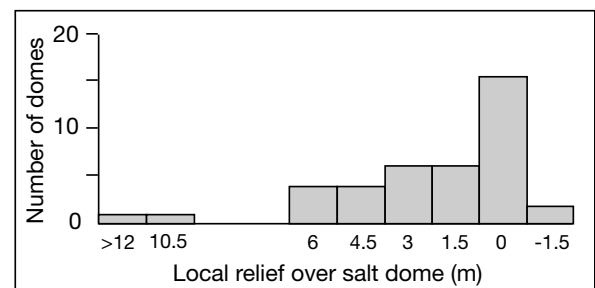


Figure 6.51. Topographic relief developed over buried salt domes in the uppermost Texas coast (Beaumont-Port Arthur area; after Seni and Jackson, 1983a).

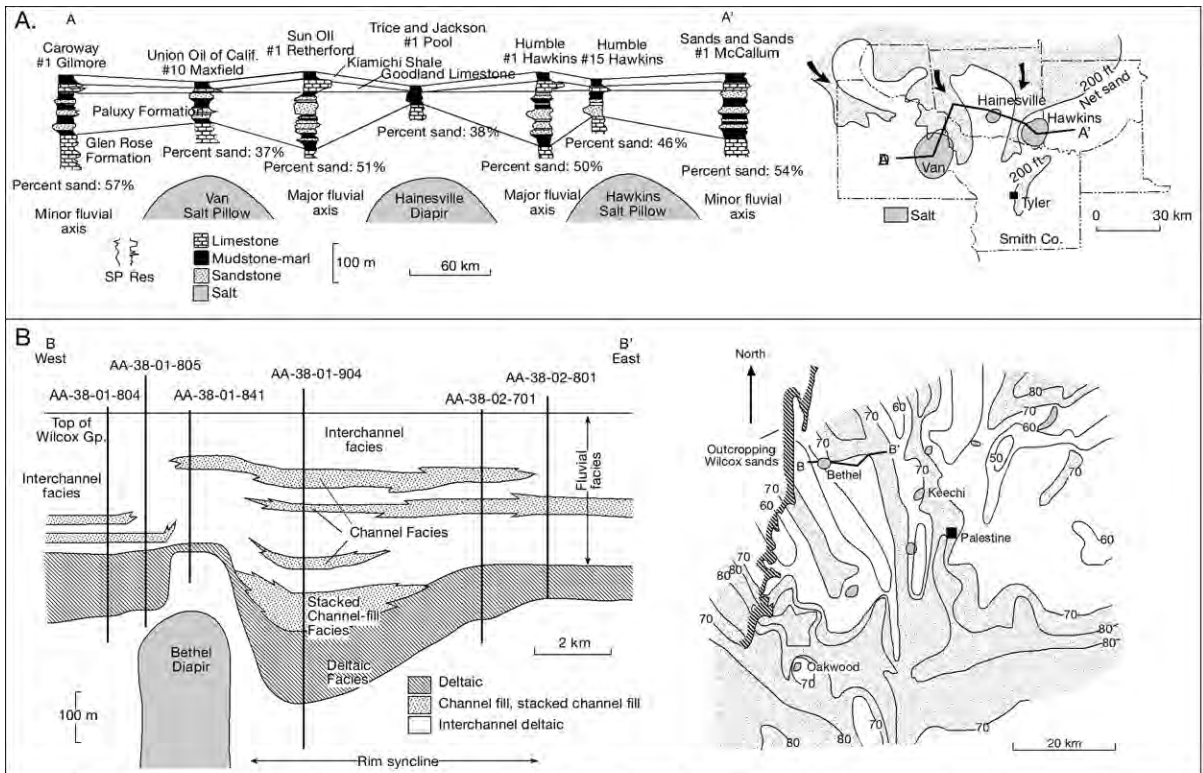


Figure 6.52. Interaction of fluviodeltaic sedimentation and diapirism. **A)** Decreased thickness and sand percentage over Van, Hainesville and Hawkins salt structures in East Texas Basin indicate that fluvial systems bypassed topographic swells over salt structures during Paluxy deposition. **B)** Cross section across top of Bethel diapir and a percentage sandstone map showing how stacked fluviodeltaic sands of the Eocene Wilcox Group in the southern part of the East Texas Basin pinch out over the crest of the structure (after Seni and Jackson, 1983a).

dominantly carbonates of the James Limestone and the Glen Rose Formation. There seafloor highs atop salt structures and turtle structures controlled local patterns of carbonate reef and shoal sedimentation (Figure 10.46).

When a reactivated or squeezed diapir crest is near the deep seafloor of the continental slope it creates a syndepositional high, which then influences deepwater sand patterns (Figures 6.47, 6.53). A squeezed diapir's shape and its freeboard height above its surrounds affect the flow direction, speed, and thickness of turbidite sands accumulating in the various fan lobes atop withdrawal sinks adjacent to the squeezed diapir high. This was the case in the Eocene of the North Sea during the deposition of the deepwater Tay sand, which now forms the reservoir in the various Gannet fields (Figure 6.53a; Armstrong et al., 1987). Reservoir sands are broken down into three units; the lower, middle and upper sands, all deposited in a shoaling submarine fan complex. The area is underlain by various squeezed diapirs and some, like the Gannet North diapir, have exerted a major control on sand thickness and sand distribution. The seafloor

highs, generated by areas of shallow reactivated Zechstein salt structures, created sand pinchouts as salt-cored highs deflected dense turbidity flows away from their edges (Figure 6.53b). This minibasin system shows a classic vertical transition from stacked sheet to channel-levee geometries.

Carbonate patterns

The multiplicity of depositional settings above and around reactivated salt-cored highs in the Arabian Gulf gives an insight into the geometries of carbonate sands and porosity distribution in squeezed salt structures that are no longer extruding salt (Figure 6.54; Warren, 1989). Salt-cored seafloor highs surrounded by deeper gulf waters do not show the effects of widespread current reworking. These structures simply shed shallower water sediments centripetally into deep sub-wave base depths (Figure 6.55). Facies patterns tend to form concentric rings, with the best-sorted sediments at or near the crest of the now buried structure. Sediment patterns tend to become more elongate and stream in the direction of current transport once

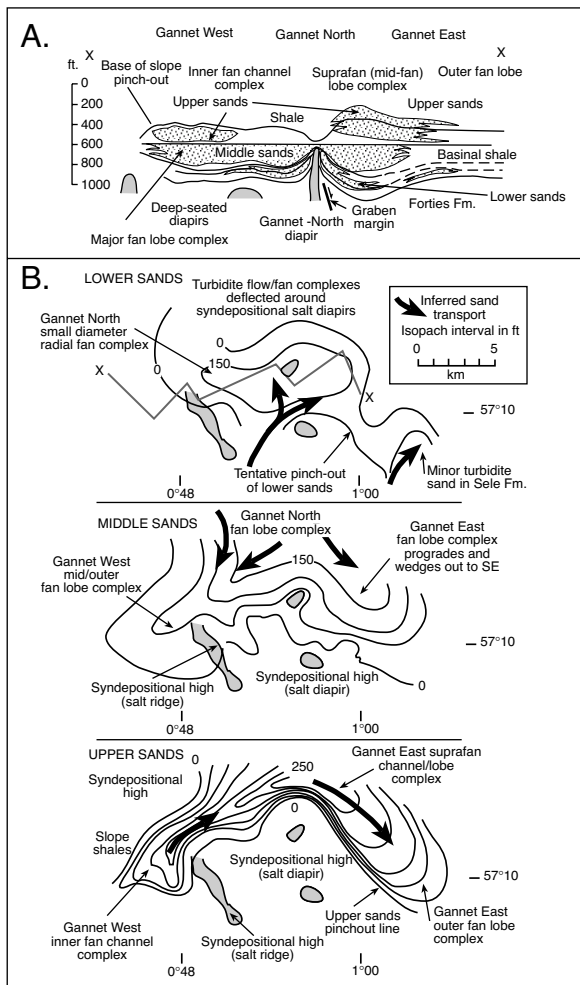


Figure 6.53. Eocene Tay Sands of the Gannet area of the North Sea. A) E-W cross section showing a strike section through the lower and middle sands and a proximal to distal section through the upper sand. Note the influence of re-activated diapirs on sand distribution. B) Palaeogeographic reconstruction for lower, middle and upper sand intervals showing the effects on sand/fan distribution of diapir-induced syndepositional seafloor highs (after Armstrong et al., 1987).

the depositional surface lies above wave base. In the case of the various grainstone and rudstone shoals of the Great Pearl Bank this largely reflects waves driven by the Shamal (Figure 6.54). When exploring for porosity in an ancient counterpart one would drill on or near the crest of the structure, as identified in seismic. Intermediate water depth highs in the Arabian Gulf are surrounded by waters of moderate to shallow depths. Sediment shed from the carbonate high is reworked by tides and other currents, both across the high and into the shoal water areas surrounding the high. Often, this type of structure generates a down current sediment tail, creating a strong asymmetry to

any reef or sand buildup on the structure itself. The sediment tails can be quite thick; off Dalma Island in the Arabian Gulf the modern downwind grainstone tail attains thicknesses of 20 m (Figure 6.54). Exploring for relict primary porosity on the ancient equivalent of this type of marine platform structure involves drilling both on or near the crest of the structure, as well as expecting and drilling sand trends that cut across the structural crest (Lomando et al., 1984; Lomando, 1999).

The observation that sediment tails about Arabian Gulf salt structures tend to trend in the same direction as the prevailing winds of the region is a useful predictive tool. Once the position and trend of any ancient grainstone shoal is established about an individual salt structure, likely grainstone orientation and position of potential reservoirs about other time equivalent diapirs in the region can be predicted as likely to occur in the same quadrant. In the case of the Great Pearl Bank the region about the salt structure highs with the highest probability of sand occurrence lies south to southeast of the salt-cored seafloor high (Figures 6.54, 6.55).

In near coastal settings in the southern Arabian Gulf the wind-wave sediment trend is often modified by coastal parallel (longshore) transport processes. Leeward sediment tails often extend from the high to the shoreline, generating a progressive shallowing between the high and the mainland that ultimately create a tombolo. Studies of the peritidal sand tail that extends from Yas Island onto the mainland at Jebel Dhanna show that shallowing increases the velocity of tidal currents. This causes the sequence to shoal upward from bioclastic grainstones and wackestones into oolite shoals that trend at an oblique angle to the trend of the sediment tail (Figure 6.56; Warren, 1989). The Jebel Dhanna diapir-cored high also controls the seaward extension of Holocene sabkha in the coastal plain behind the headland.

In the modern Gulf of Mexico, a reef system is actively accumulating coarse biogenic sediment atop a salt cored high in the Flower Gardens Bank. Upper-slope siliciclastic deepwater muds completely surround the reef-capped high. Carbonate buildups top the Flower Garden Bank because of the shoaling effects of salt just below the seafloor. A brine lake occupies the central part of East Flower Garden Bank (Rezak and Bright, 1981). Collapse foundering over the crest of the structure generated the graben that houses the lake, while ongoing salt dissolution and the focused escape of basinal brines maintain the dense waters of the lake. Healthy growing corals surround the lake, except where a canyon cuts a brine lip across the bank to the deep open seafloor. Halokinesis beneath the Flower Garden

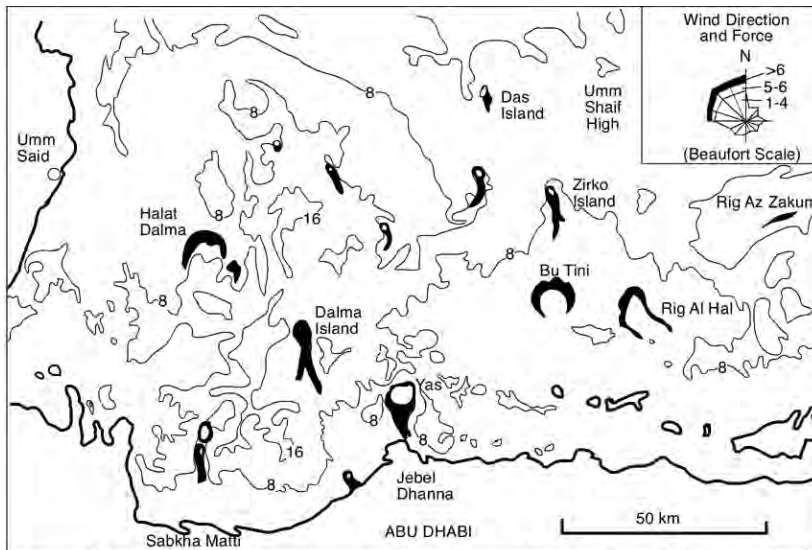


Figure 6.54. Relationship between wind direction and orientation of Holocene sediment tails (black) in shallow waters of the Great Pearl Bank, southern Arabian Gulf. Bathymetry in fathoms (after Purser, 1973; Warren, 1989).

Banks has converted an otherwise muddy siliciclastic platform into a region suitable for carbonate reef growth. Shoaling lifted the seafloor into a clear, well-lit environment and has created a carbonate buildup in what is otherwise a muddy, siliciclastic province. Brine seeps atop salt allochthons, located in much deeper waters at the foot of the continental slope, have allowed chemosynthetic mussel communities (biostromes) to flourish at water depths that are a kilometre or more below the base of

glacigenic units, thereby placing reef growth within the upper Cryogenian. A reef core facies of cumulate stromatolite domes first formed as mounds, which interfingered with the surrounding sediments, then as reefs, which stood well above the sea floor. Many mounds formed preferentially atop large debris blocks carried to the surface by diapiric salt.

the euphotic zone (Figure 9.33).

Ancient counterparts to the salt-cored islands in carbonate seaways, where carbonate sedimentation patterns are controlled by seafloor shoaling, occur in numerous diapir provinces ranging in age from Proterozoic to Neogene. Hydrocarbons and base metals have accumulated in brine lake laminites associated with some of these buildups (Warren, 2000b). For example, a series of Neoproterozoic stromatolite reefs fringe the western edge of the Enorama Diapir in the central Flinders Ranges (Figures 6.57, 7.23; Lemon, 2000). The enclosing stratigraphic unit, the Enorama Shale, is the locally-named interglacial succession, lying between the Sturtian and Marinoan (Varanger equivalent)

The Enorama diapir breccia blocks are typical of many diapir remnants (stems and welds) in the Central Flinders Ranges (Lemon, 2000). The breccias atop former salt stems and their surrounding debris aprons are made up of red and grey shales, sandstone blocks with halite casts, yellow dolomites with chert pseudomorphs of gypsum and anhydrite, and large blocks of amygdaloidal basalt and dolerite. All these blocks were carried up the stratigraphy by allochthonous - autochthonous salt source in the mother salt bed in the Callanna Group. Interaction with the surrounding sediments and inclusion of breccia fragments in the reefs and mounds shows continual movement and exposure of the diapir occurred throughout the deposition of the lower two thirds of the Enorama

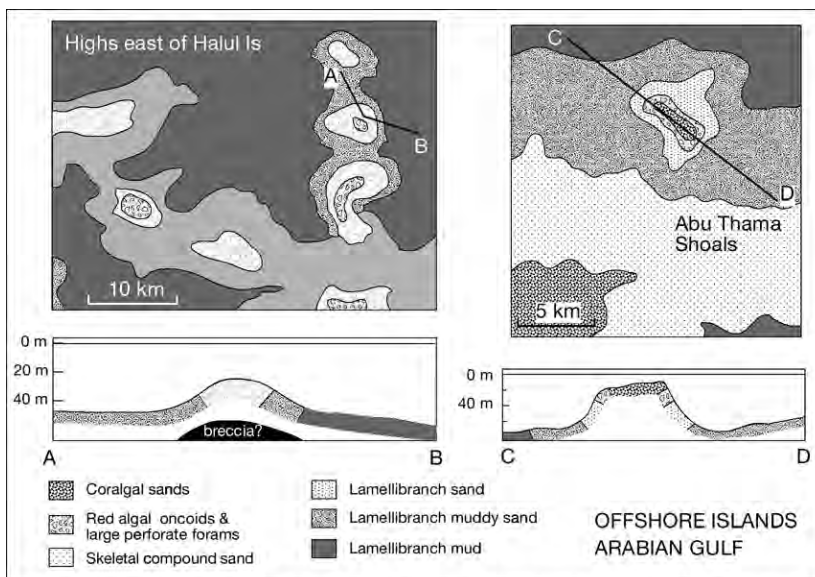


Figure 6.55. Sediment distribution on sea floor shoals atop buried salt structures on the floor of the Arabian Gulf (after Purser, 1973). See also Figure 7.22.

Shale. Lenses of diapir-derived polymict conglomerate are common along the flanks of the Enorama diapir and many of these show extensive evidence of shorezone reworking. Pebbles of conglomerate in cobbles of conglomerate within boulders indicate several phases of deposition followed uplift and erosion. The conglomerates commonly have a dolomicrite matrix which cements very early to allow the reworking to be recorded. Thickening of the Enorama Shale towards the Enorama Diapir is particularly evident in the stacked halokinetic sequences at the northern end of the diapir. Associated stacked conglomerate lenses that thicken toward the diapir stem, show this was an area of ongoing aggradation and syndepositional growth of the diapir stem as it fed salt into various allochthon sheets (aka christmas-tree diapirs; Dyson, 1998).

Not all mounds progressed to reefs, as the edge of the active diapir was unstable at times. The maximum size of a mound plus reef at Enorama is ≈ 50 m high and 200 m across the base. Syndepositional diapir activity is indicated by tilting of the surrounding sediments and by inclusion of insoluble debris shed from the diapiric island. Progressive movement is shown by cannibalisation and reworking of coarse shoreline conglomerates (Figure 6.57). Diapir movement continued after deposition of the reefs ceased so that the entire succession in the drag zone close to the diapir is tilted up to near vertical in what would be called the shale-sheath position in a siliciclastic interval.

Enorama reefs interfinger with both shallow water limestones of the Etina Formation and deep water siltstones of the Enorama Shale. The base to the middle of the Enorama Shale is a transgressive systems tract, deposited during a steady rise in sea level. Onlap onto the diapiric island is marked by backstepping of each reef higher in the section (Figure 6.57). Backstepping occurred as a number of pulses, each marked by channels of conglomerate shed from the diapir and by progressive convergence of local angular unconformity surfaces. Small pulses of salt uplift caused reefs to recolonise on higher ground, sometimes on previous reef growths, sometimes establishing a new mound. The reefs drowned as the sea floor next to the diapir subsided into the peripheral sink that flanked the diapir. On a mesoscale, the reefs are composed of a series of stromatolite mounds up to 6m high and 15m long. Lamination within the mounds is wrinkled and quite unlike nearby isopachous stromatolites characterised by smooth laminated micrite. The latter grew in the shallow water as Etina limestones and are interbedded with the older parts of the widespread reef complex. The microscale wrinkly structure of the reefs show a distinct clotted texture with filamentous linkages, reminiscent of calcareous alga like Epiphyton or Renalcis. The entire reef complex has been completely dolomitised, probably by solutions emanating from the diapir. Early dolomite cement has allowed mimetic preservation of sedimentary textures and some minor porosity.

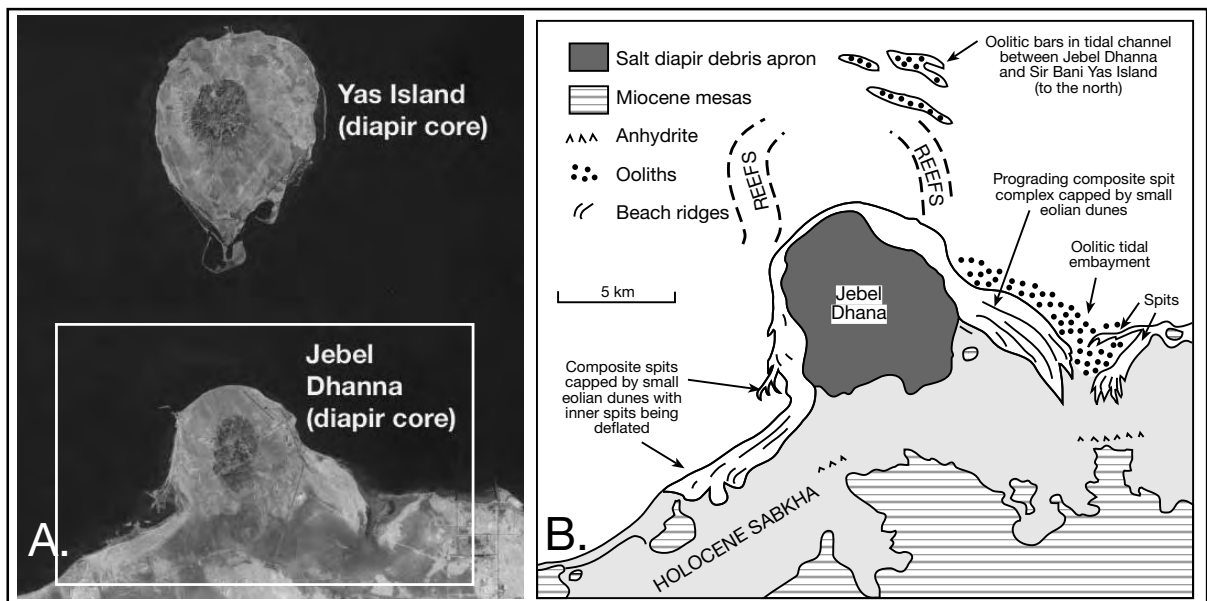


Figure 6.56. Sediment distribution controlled by the near coastal and coastal shoals created by Jebel Dhanna and Yas Island diapirs, coastal Abu Dhabi, see Figure 6.54 for location. A) Landsat image of coastal zone clearly shows diapir breccias forming cores to both diapiric outcrops (Image courtesy of NASA). B) Holocene sediment coastal patterns and tails in the vicinity of Jebel Dhanna (in part after Kirkham, 1997). Note that seaward extension of active reefs and offshore oolite bar thickens both controlled by the position of the diapir.

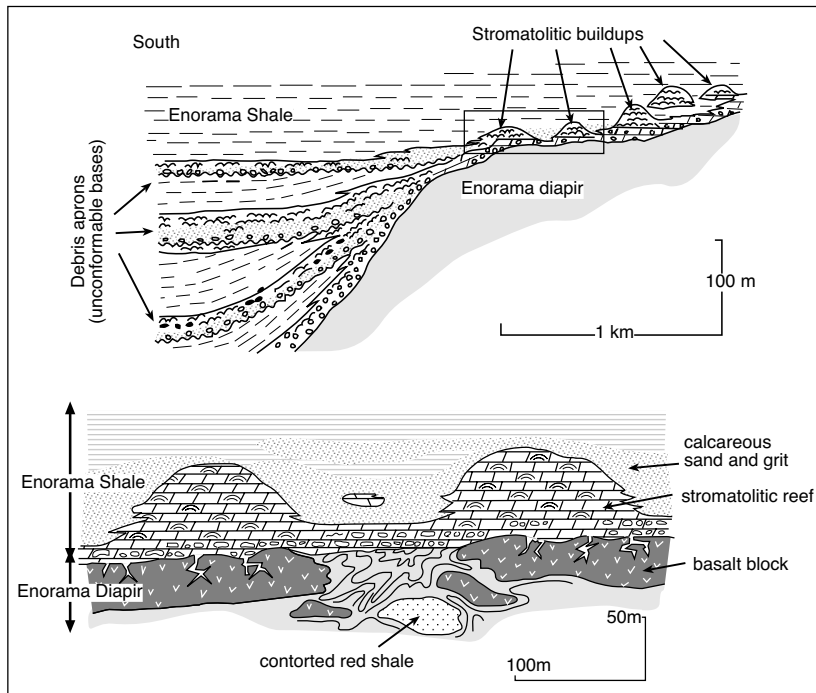


Figure 6.57. Palimpsestic reconstruction of part of the western Neoproterozoic margin of the Enorama diapir, Flinders Ranges, Australia. Lower figure shows detail of contact of reef with diapiric breccia. (after Lemon, 2000).

In summary, the reefs grew during a time of sea level rise and show a close relationship with rises in the Enorama Diapir, with each deepening upward reef succession being a response to a pulse of diapir growth. The diapir provided an area of shallow water around an island at a time when deeper water shale was being deposited in the rest of the basin. The mound to reef transition shows ‘catch up’ and ‘keep up’ growth habit but the sudden demise of each individual reef appears related to a subsequent pulse of salt movement on the diapir, not to broader eustasy.

Sediments tied to salt basin evolution

Suprasalt clastic sedimentation

Alexander and Flemings (1995) documented the spatial and temporal distribution of siliciclastic sand within an evolving Pliocene-Pleistocene salt-withdrawal shelf minibasin in the Gulf of Mexico; the Eugene Island Block 330 field. Part of it is a giant oil and gas field in offshore Louisiana and is located immediately landward of the deeper water Green Canyon area. The minibasin evolved through three phases: prodelta, proximal deltaic, and fluvial (Figures 6.58, 8.16). In the prodelta phase, bathyal and outer neritic shales and turbidites loaded and mobi-

lised the underlying salt sheet (Figure 6.58a). During the proximal deltaic phase, salt continued to withdraw from beneath the minibasin, and lowstand shelf margin deltas remained focused at a regional growth fault zone on the northern margin of the minibasin (Figure 6.58b). Sediment accumulation and fault slip rates were high, as thick sequences of deltaic sands were deposited adjacent to the fault system. During the final fluvial phase, salt withdrawal waned; consequently, the creation of accommodation space within the minibasin ceased (Figure 6.58c). The basin filled and, during lowstands, deltaic systems prograded southward. Unconformities developed in the minibasin during these lowstands. During transgressions, thick packages of shallow-water deltaic and fluvial sands (capped by shales) were deposited on top of the unconformities.

On a salt-floored continental margin that is being loaded by fluvio-deltaic wedges, the transition from deep water, when the floor of the minibasin first begins to subside as it is loaded, into a shelf and deltaic system is a natural evolution. The sedimentation model documented by Alexander and Flemings (1995) has a wider application to other salt-floored passive margins. Some authors in the Gulf of Mexico prefer to divide minibasin sedimentation into shelf-loaded and slope-load subcategories, but recognise it is all part of a feedback between basinward salt flow of the allochthon sheet and sediment loading (Figures 6.31, 10.52). Once the salt is evacuated from beneath a minibasin the basin can no longer subside and the depositional locus shifts basinward into the next minibasin atop the next tier of the allochthon. In the case of the Eugene Island minibasin this did not occur until the basin was filling with shelf sediments. In other basins this can happen while turbidites are still accumulating in the withdrawal sink. In this case the basin no longer accumulates turbidites, which now bypass the basin on their way downslope to the next active depopod.

Turbidite fill in Gulf of Mexico minibasins of the northern Green Canyon and Ewing Bank areas has been modeled by Rowan and Weimer (1998). They found that at the highest

order of scale, external factors dictated the volume and type of systemwide clastic input. Regional factors, such as nearby salt structures and the position of deltas, then controlled the dispersal of the clastics to the continental slope. Local factors, such as the thickness of underlying salt, influenced minibasin-specific evolution. In the deepwater slope setting these factors interact at three scales: (1) a broad transition from sand-rich ponded settings to shale-dominated bypass settings during the Pliocene-Pleistocene, (2) fluctuations over periods encapsulating several sequences creating highly variable stratigraphic stacking patterns, and (3) a progression from ponded to bypass facies within individual sea level cycles. The most sand-rich gravity flows in an ideal sequence are deposited in the minibasin at the beginning of a sea level cycle (i.e. during the lowstand) giving rise to sheet-like geometries. A transition to more mud-rich gravity flows leads to the formation of a channel levee system, where flows tend to be channelised and more organised. The gradual decrease of sediment volume within individual gravity flows during a sea level cycle increases the hemipelagic content (mixed pelagic and gravity flows) and eventually passes into a condensed section typified by pelagic mud-rich sediments or foraminiferal-rich oozes.

The idealised fining upward succession is complicated by varying rates of salt withdrawal from the minibasin, which influences the volume of accommodation space within the minibasin. The distribution of accommodation space can be further complicated if the crest of a diapir undergoes dissolution to create a potential zone for further sediment accumulation. Slides and slumps can occur anywhere within a sequence; they can originate from local slope failures or from oversteepened delta fronts and can be triggered by salt movement, dissolution or can be seismically induced.

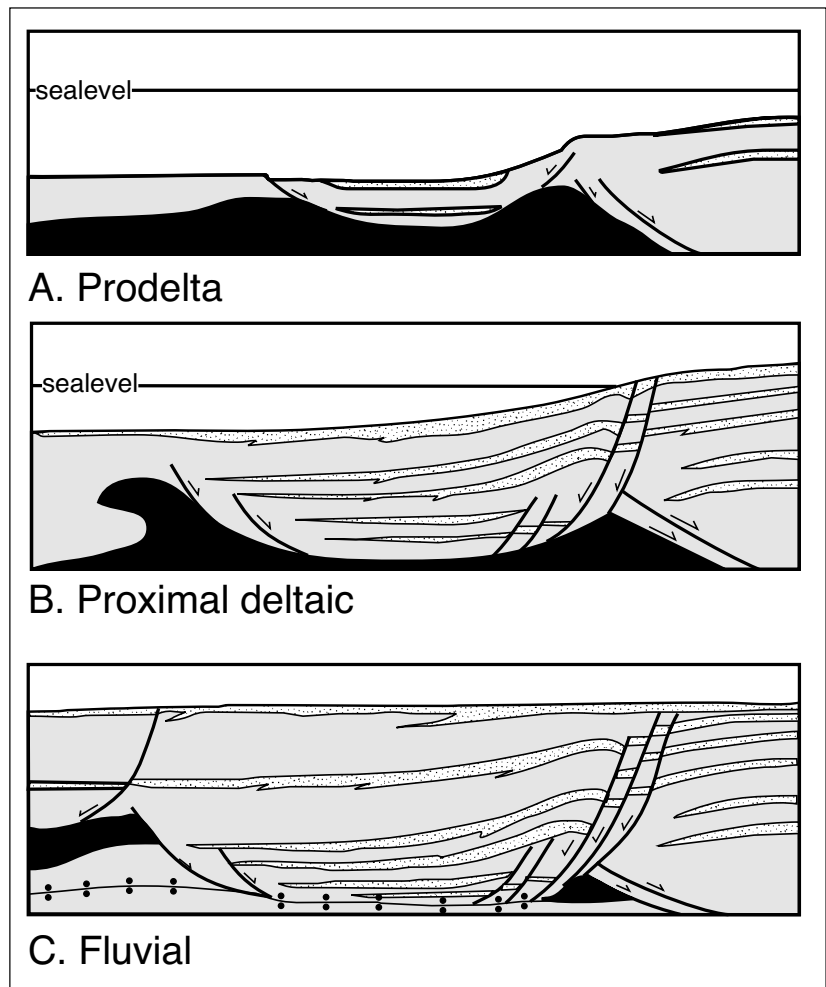


Figure 6.58. Schematic of three-phase depositional evolution of intrasalt basin fill in the 330 Block, Gulf of Mexico (Alexander and Flemings, 1995). Evolution began prior to 2.8 Ma and continues today.

Suprasalt carbonate sedimentation

La Popa Basin, Nuevo Leon, Mexico, is a salt influenced foreland basin near Monterey in Mexico, with excellent exposures of halokinetically influenced sedimentation around three salt stems (La Popa, El Papalote and El Gordo diapirs) and along the 25 km La Popa salt weld/wall (Figure 6.59; Giles and Lawton, 1999; Giles and Goldhammer, 2002). As in the Flinders Ranges, reef growth is a halokinetic response to pulses of diapir growth. A number of thick (<600m) coral, sponge, red algal reefs, exposed as a series of carbonate lentils, are the most obvious sediments associated with halokinetic seafloor shoaling. These carbonate buildups, the La Popa, San Jose, El Toro and El Gordo lentils, developed as shoals atop significant seafloor highs created by the passive rise of salt diapirs during

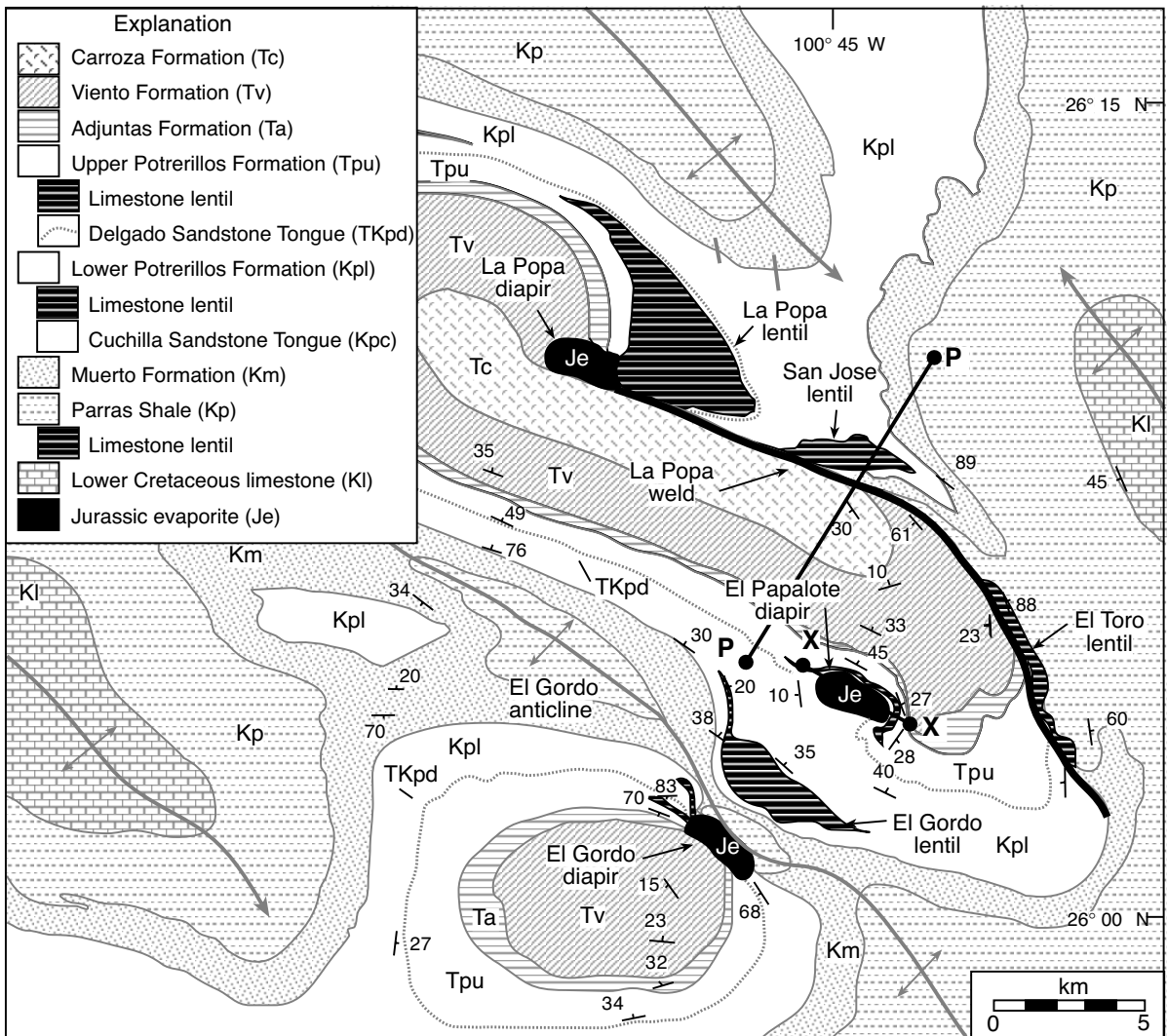


Figure 6.59. Geologic map of the La Popa Basin, Mexico. Anticlinal fold axes indicate structures attributed to the Hildagoan (Laramide) shortening (after Giles and Lawton, 2002). P-P' and X-X' are the locations of cross sections in Figures 6.60 and 6.61.

the Cretaceous and Lower Tertiary in what was a dominantly fine-grained siliciclastic shelfal environment.

The La Popa structure is interpreted as a 25 km long salt weld with parallel flanking synclines, previously it was considered to be a reverse fault (Figure 6.60a, b; Giles and Lawton, 1999). The displacement surface is convex to the southwest and dips south to southwest. Stratigraphic displacement at the surface is zero at either end and increases to ≈ 5 km halfway along the trace of the structure. The structure is the result of hanging-wall subsidence during evacuation of Jurassic salt along a former diapiric salt wall. Sedimentation patterns on either side of the weld indicate the La Popa structure experienced

a two-phase history in Late Cretaceous to Eocene time: 1) A diapiric phase marked by rise of an elongate, arcuate salt wall that was symmetrically flanked by withdrawal synclines; 2) a subsequent evacuation phase recorded by substantially increased subsidence of the hanging wall relative to the footwall and the stratigraphic “welding” of footwall and hanging wall along a steep planar discontinuity (salt weld) created as salt withdrew from the former diapir.

Superb exposures (over 10km along strike) of the largest reef complexes along the northern side of the La Popa Weld show that during the diapir stage these Paleocene lentils initially accreted as coral, sponge, red algal reef and oyster biostrome

complexes atop and immediately adjacent to the La Popa salt wall (Figure 6.60c). Large, steep (200m relief over 0.5km) foreereef clinofolds indicate northward (downwind) progradation of the La Popa lentil away from seafloor high created by the La Popa salt wall. With a probable lowering of the local rate of salt induced uplift near this part of the salt wall, this reefal system was subsequently truncated, onlapped and possibly overlapped by a southward prograding grainstone bar complex. This shoal was derived from a separate source to the north, perhaps from another salt-related bathymetric high tied to the La Popa Diapir. To the north and west of the La Popa diapir the two carbonate complexes coalesced through time to generate a continuous carbonate sheet that now defines the La Popa lentil. It extended more than 5 km within what was at edge of a low created by a salt withdrawal/contractional syncline as salt was evacuated into the rising salt wall (Figure 6.60c).

Carbonate strata thin and become siliciclastic away from the La Popa salt wall and are intercalated with siliciclastics in the footwall syncline. The Delgado Sandstone Tongue of the Potrerillos Formation is a shelfal sandstone/siltstone that was deposited during salt wall growth as a complex, wave-

dominated, eastward-prograding deltaic depositional system. Typical parasequences in the siliciclastic section comprise offshore shales overlain by lower to upper shoreface sandstone. The Delgado Sandstone contains a lower, progradational parasequence set; it is part of a highstand system tract that is in turn part of the underlying Middle Siltstone Member of the Potrerillos Formation. It also contains an upper retrogradational set, which is part of a transgressive system tract that persisted into the Upper Mudstone Member. The two system tracts are separated by an erosional sequence boundary that incises up to 10 m of underlying strata and locally preserves a lowstand system tract within the incised valleys.

During growth of the salt wall in the Early Tertiary, thick prodeltaic and tidally-influenced shoreface siliciclastics periodically accumulated in the adjacent withdrawal syncline. Flute marks on bases of turbidite beds and channel axis orientations indicate a dominant palaeoflow along synclinal axes, with a component of flow away from the salt wall. Siliciclastic units thin and fine toward the salt wall, near which they are upturned and contain numerous synkinematic angular unconformities. During evacuation the volume of the wall declined, causing the

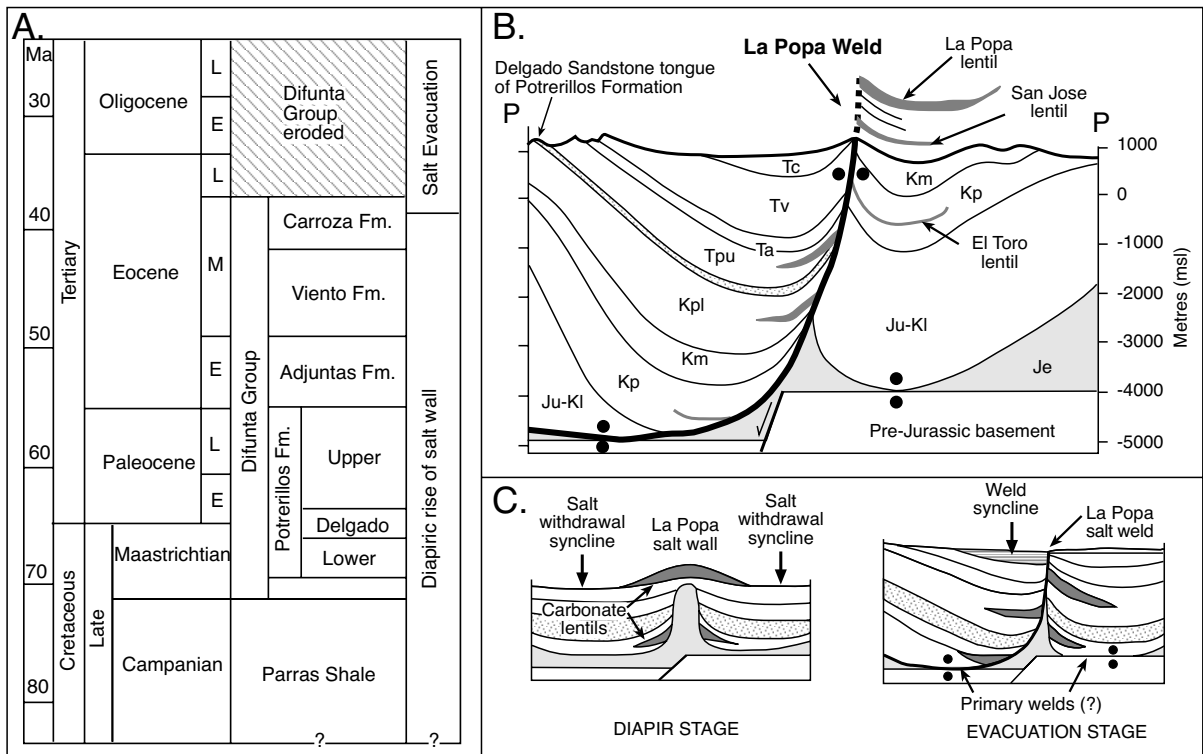


Figure 6.60. The La Popa salt weld. A) Stratigraphy of the La Popa Basin during the time when salt flow occurred (L = Lower; M = Middle; U = Upper). B) Cross section of the La Popa weld (see Figure 6.59 for position). C) Interpreted evolution of the La Popa structure (after Giles and Lawton, 1999).

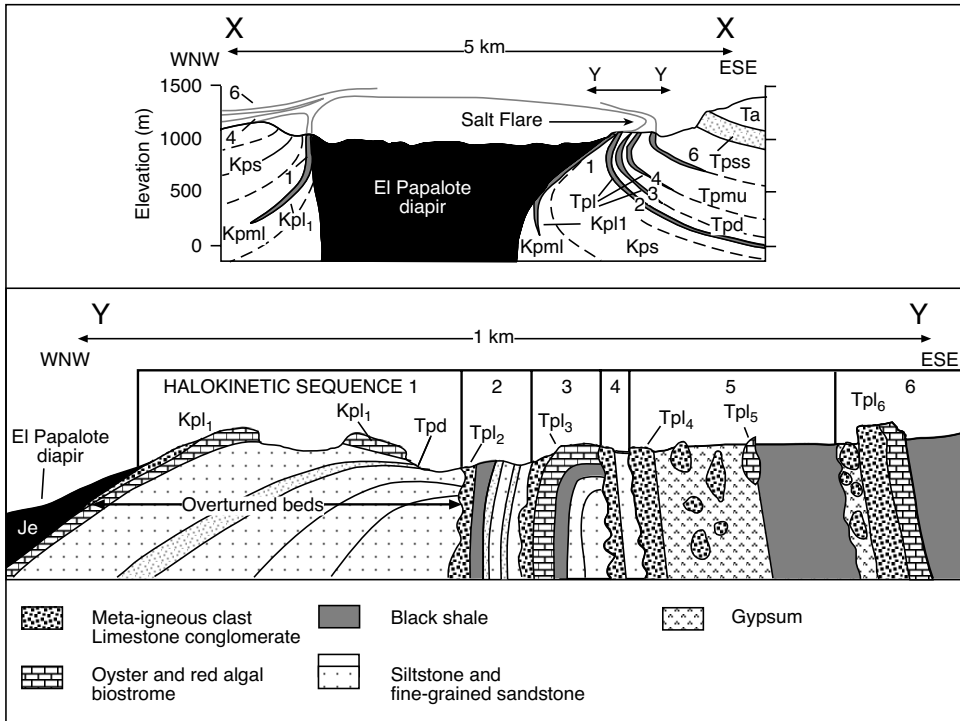


Figure 6.61. Cross sections X-X' and Y-Y' through the El Papalote diapir (after Giles and Lawton, 2002). Locality of cross section X-X' is shown on Figure 6.59.

synclinal hinge of the hanging wall to migrate laterally toward the developing weld. Hangingwall strata deposited during the evacuation phase thicken, rather than thin, toward the weld. They define the weld syncline where sand-rich fluvial channels are concentrated directly adjacent to the weld.

To the south of the La Popa salt weld are the El Papalote and El Gordo diapirs, they have similar dimensions and are located 5 km apart (Figure 6.59). The at-surface diapiric material in both diapirs and portions of the weld is today a complex mixture of gypsum, anhydrite and salt-transported exotic blocks of metamorphosed mafic intermediate igneous rocks and Jurassic carbonates (Garrison and McMillan, 1999). The gypsum is created by rehydration of the anhydrite caprock atop the Jurassic salt of the diapir core. Petrology and geochemistry of the meta-igneous blocks indicate derivation from partial mantle melting during Jurassic rifting with greenschist facies metamorphism dated at 146 Ma ($^{40}\text{Ar}/^{39}\text{Ar}$ dating of biotite and potassium in meta-plutonic blocks). This date is younger than that of the hosting Minas Viejas evaporite beds suggesting high heat flow from the basement continued into the latest Jurassic. The various sedimentary and volcanic blocks were likely intercalated in bedded salt prior to halokinesis, while the plutonics were intruded into the syn-rift fill and all were fragmented by extensional tectonics and salt flow.

El Papalote diapir is located on a major fold limb and has experienced approximately 100 m of net shortening, whereas El Gordo is located along the axis of the same fold and has accommodated over 2 km of shortening (Rowan et al., 2001). The corresponding halo of diapir-related drape folding, which is at most 800 m wide at El Papalote, is up to 2 km wide at El Gordo. Carbonate lentils, which formed over the bathymetric highs associated with both diapirs, are overall shallower, thicker, broader and record fewer halokinetic sequences at El Gordo than at El Papalote.

Sandstone units start thinning within 300-800 m of the edge of El Papalote but within 1000-1500 m at El Gordo. Differences in style and distribution of halokinetic strata about the two diapirs imply that the uplift histories of the two features were different and that the buildup atop the El Gordo structure more closely approached sealevel (Rowan et al., 2003).

Sediments flanking the El Papalote diapir have been studied in more detail than the other two structures with a view to defining typical successions in an ancient withdrawal sink and to test if such successions are amenable to sequence stratigraphic analysis (Figures 6.61, 6.62; Giles and Lawton, 2002). At the time sediments were accumulating, diapir-flanking strata thinned toward the diapir and were characterised by abrupt lateral facies changes and intense local deformation. Strata can be broken out into a series of "halokinetic sequences," which are defined as unconformity-bounded strata, genetically related to halokinetic processes.

Each halokinetic sequence contains a basal debris-flow bed overlying an unconformity, which is angular directly adjacent to the diapir and becomes disconformable to conformable with increasing distance from the diapir. Debris-flow or mass

wasting beds contain polymict clasts derived from the diapir and material that mantled the diapir (Figure 6.62). At the various times these beds were forming the diapir crest was exposed at the sediment-water interface and shedding carapace debris into the surrounding sediments. These mass wasting deposits are dominated by carbonate clasts. They are interlayered with autochthonous reefal and biostromal strata and together constitute the lentils mentioned earlier. Hence, debris and mass wasting beds grade upsection into oyster- and red algal-rich carbonate banks. This carbonate section is then onlapped by black basal shales and capped by upward-shallowing and coarsening, lower shoreface siliciclastic strata, which lack diapir-derived detritus (Figure 6.62). This lack of diapir detritus indicates that the diapir crest was no longer at the surface or had insufficient seafloor relief to act as a sediment source. Lower shoreface deposits are abruptly overlain by outer shelf shales that in turn underlie the angular unconformity of the next halokinetic sequence.

Each halokinetic sequence was generated by the waxing and waning of an episode of salt fountaining and salt glacier flow (Figures 6.60c, 6.62; Giles and Lawton, 2002). Periods of salt rise and salt glacier advance followed by retreat create unconformities near the salt structure. They correspond to times of slow sedimentation and regional black shales in interdiapir withdrawal sinks. These black shales perhaps reflect basin deepening (maximum flooding events). Advances of glaciers over diapir-flanking beds provided a mechanism of deforming and overturning strata that underwent subsequent local truncation

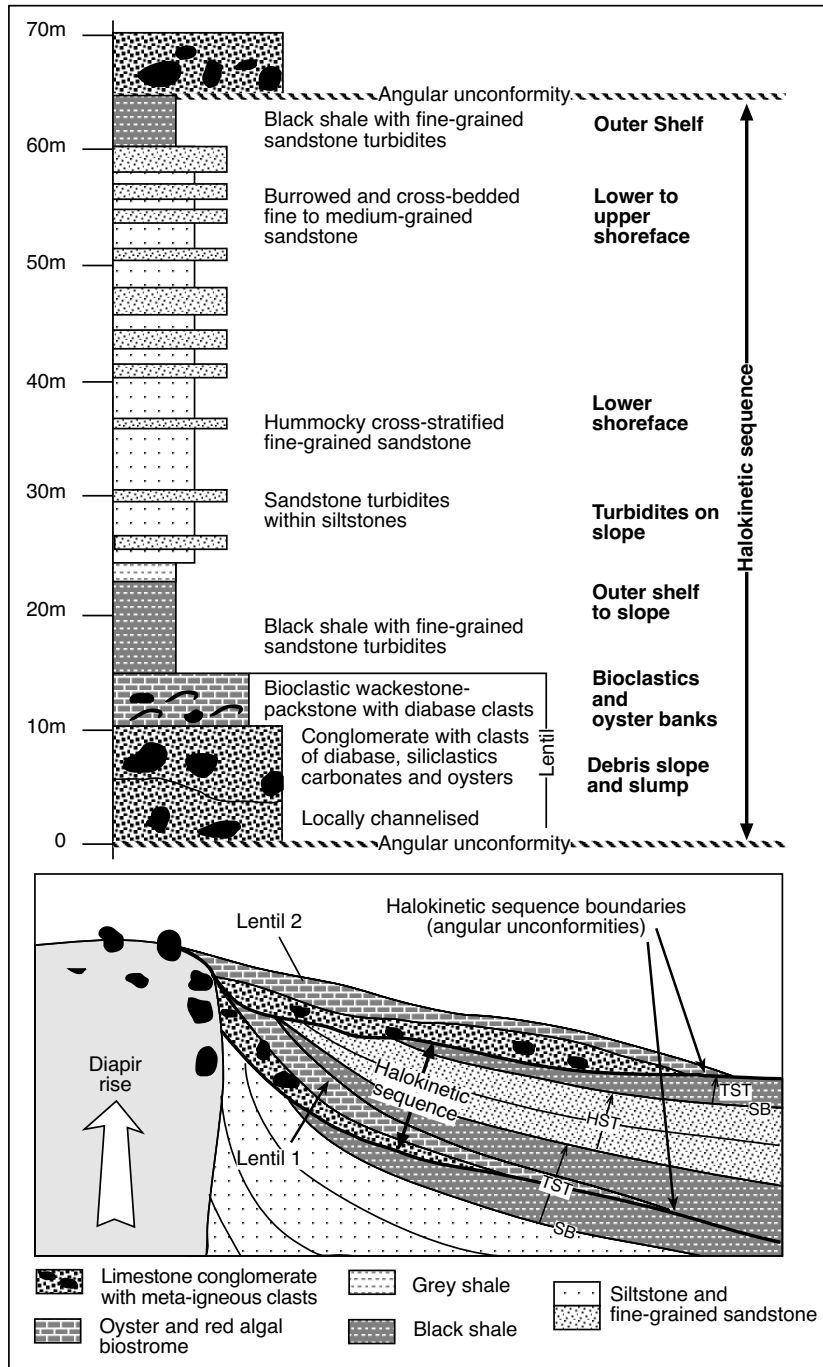


Figure 6.62. Halokinetic sequence in a marine shelf setting, based on the stratigraphy of the lentil and associated sediments in the vicinity of the El Papalote diapir. Lower figure also shows the interpreted relationships between sediments and angular unconformities tied to diapir rise and to the sequence stratigraphic interpretation of the surrounding shelf and slope sediments. SB = sequence boundary; TST - transgressive system tract; HST = highstand system tract (after Giles and Lawton, 1999).

via subaqueous erosion processes during glacial retreat. As in the modern Gulf of Mexico, glacial salt advance was also marked by development of a siliciclastic “shadow zone” on the downcurrent flank of the salt diapir high. Glacier advance at El Papalote is only displayed by strata on the east side of the diapir, indicating a down gradient flow of seafloor salt into the regionally extensive withdrawal syncline created by asymmetric salt supply to the adjacent and inflating La Popa salt wall. Quaternary counterparts to these carbonate debris aprons have been documented in weathering haloes about salt structures in the Arabian Gulf, while older counterparts occur in the Neoproterozoic salt structures in the Flinders Ranges of Australia. For example, Lemon (1985) documented and modeled similar asymmetric salt withdrawal controls on sedimentation about the Neoproterozoic Oratunga diapir in the Flinders Ranges, Australia.

Internally, the various halokinetic sequences show stratal onlap and thinning of beds toward the diapir. Adjacent to the diapir stem each halokinetic sequence is tightly folded and angular unconformities have truncation angle as high as 90 degrees (Figure 6.62b). The intensity of deformation and angle of truncation decrease rapidly away from the diapir and sequences are typically conformable by a distance of 250 m from the diapir. The geometry resembles the hook of the letter ‘J’ (e.g. Sequence 3 in Figure 6.61; Rowan et al., 2003). These ‘J’ hook unconformities terminate directly against the diapir and outline salt cusps created by a combination of drape folding and fault reactivation during halokinesis. The amount of fault reactivation on these unconformities can be significant with the unconformity/fault preserving evidence of brittle shear and sense-of-shear indicators showing older beds were displaced away from the diapir. Away from zones directly influenced by the diapirs and ‘J’ unconformities sediments tend to lack evidence of mass wasting and the interdiapir lows were filled by facies that shallow from middle shelf lower shoreface shale to upper shore-

face foreshore sandstones and tidal-lagoon sequences. These sequences do not terminate at the diapir but are spatially separated by a thick/wide package of older more tightly folded drag-zone strata (Figure 6.61).

Subsalt sections

Subsalt sediments, originally deposited adjacent to a seafloor allochthon and subsequently sealed beneath overflowing salt and its basal shear zone, have been studied most extensively in the Gulf of Mexico, where more than 50 exploration wells have been drilled with subsalt targets (Chapter 10). Sub-allochthon sands in the Gulf of Mexico are mostly Miocene-Pleistocene deepwater-slope submarine fan channel and levee settings. The sandstones were deposited by turbidity currents associated with channel-levee systems carrying sediment from the outer shelf into bathyal water depths in the middle to lower continental slope (Snyder and Nugent, 1995). Drilled facies vary from thick fining upward channelised deposits to thinly bedded levee sands and overbank splays. Sands range from friable to moderately consolidated, very fine to fine-grained, moderately to well sorted and slightly calcareous. Channel orientations can be strongly influenced by the seafloor topography generated by nearby salt allochthons. Once deposited the sands were then overridden and sealed by lateral flow of the allochthon sheets. The encroachment of the salt allochthon is associated with the creation of a salt-sealed gumbo or basal shear zone and defines one of four positions where subsalt sandy reservoirs are likely (Figure 6.63). Economic and stratigraphic aspects of this very

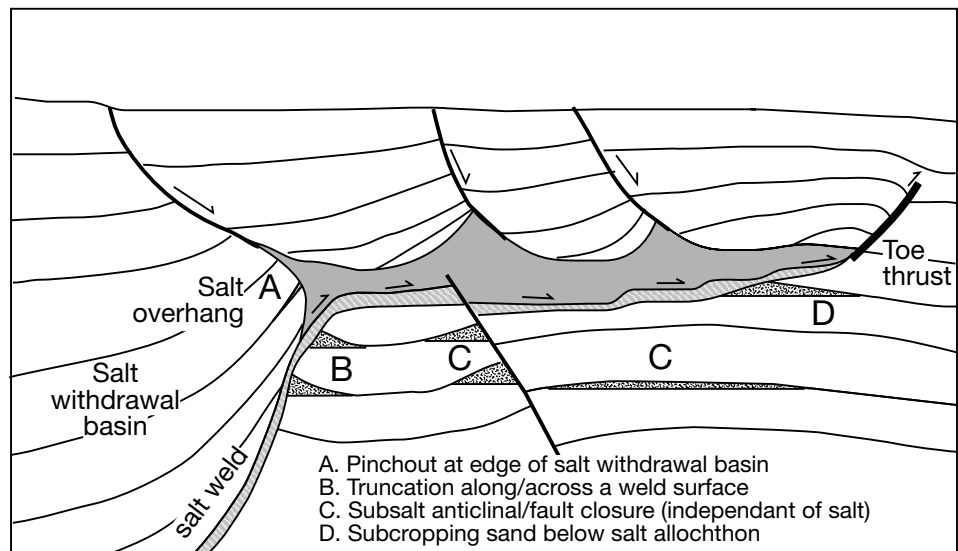


Figure 6.63. Subsalt sediments buried beneath an encroaching allochthon is one (Style D) of four subsalt trap styles discussed in Snyder and Nugent (1995).

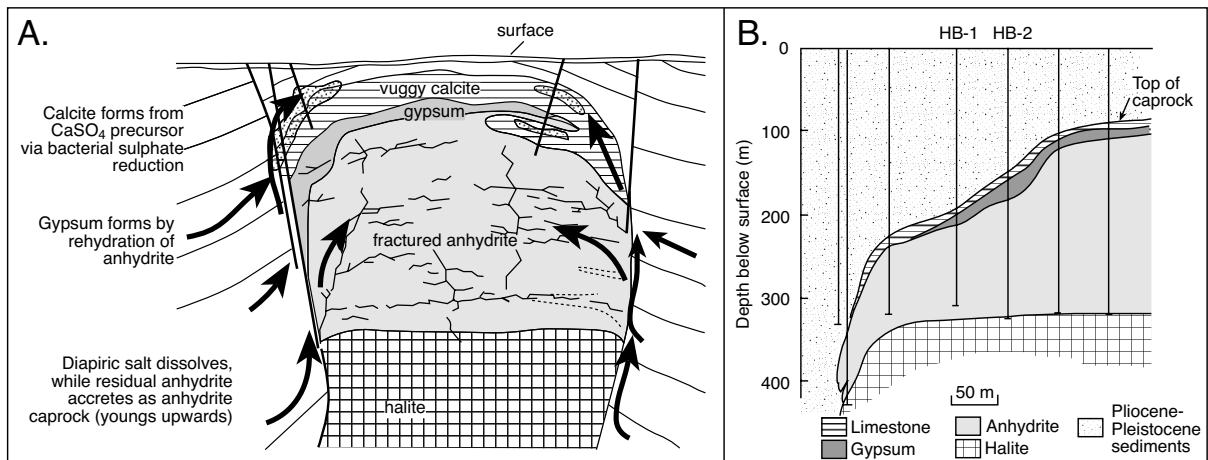


Figure 6.64. Caprock zonation. A) Caprock forms by the dissolution of the upper part of a salt structure once salt supply dwindles the rate of rise slows and it is flushed by undersaturated phreatic waters (black arrows). Dissolution of the halite leaves behind anhydrite that then accretes into an anhydrite caprock. The upper portion of the anhydrite unit rehydrates to gypsum that is then converted to limestone by bacterial sulphate reduction. B) Section of Hockley dome caprock showing relative thickness of the caprock zones and depth below the landsurface based on drilling (after Hallager et al., 1990).

important subsalt-hydrocarbon association are discussed in detail in Chapter 10.

Caprock Formation (diagenesis)

Caprock is a limestone/anhydrite carapace found atop many buried diapirs and allochthons (Figure 6.64a; Halbouty, 1979; Light and Posey 1992; Prikryl et al., 1988; Kyle and Posey, 1991). It forms as a dissolution residue atop diapirs, seafloor allochthons and even buried subaerial namakiers. Suprasalt caprocks thicken once salt supply starts to dwindle and the head of the salt plug or the top of any residual salt sheet is buried to shallow depths where it can no longer actively pierce and shed sediment. The edge of any buried salt mass feels the increased effects of dissolution via the undersaturated crossflow of phreatic waters. Atop a buried but still buoyant diapir, halite preferentially dissolves from the upper part of the salt mass/stem and a CaSO_4 unit accretes via underplating. The caprock underbelly has a continued supply of anhydrite residues as the top of the rising and dissolving salt stem is dissolved (Figure 6.65; Hallager et al., 1990). In zones of longterm fluid crossflow and ongoing slow salt supply, this interface becomes a widespread laminar sulphate carapace, encasing a salt mass with caprocks some tens to hundreds of metres thick.

Caprock is most common and thickest on diapir crests that are currently close to the earth's surface but can be found atop structures buried as deep as 3000 m. Most diapir capstones are 100 to 150 metres thick, but can be thicker than 300 metres. Caprock is thickest over the crest of shallowly

buried diapiric spines and thins toward the flanks. Oil drilling over the Hockley dome, near Houston Texas, clearly defines a mineralogical layering of diagenetic products that is typical of caprocks worldwide (Figure 6.64b). At its crest the Hockley Dome caprock is covered by only 30 m of Plio-Pleistocene sediments. The upper part of the caprock is a calcite unit up to 30 metres thick. Over the crest the calcite is underlain by a gypsum zone up to 30 metres thick. Further toward the flanks and somewhat deeper the gypsum unit is absent or very patchy and the calcite is in direct contact with anhydrite. The calcite zone grades downward across a transition zone into a laminar anhydrite capstone up to 244 metres thick. The Hockley caprock thins toward its edge and disappears, but in some other nearby Gulf of Mexico diapirs the steep vertical walls of the diapir stem are also mantled with caprock.

Caprock extent reflects hydrodynamics about the upper part of the salt stem. The gypsum and limestone intervals in a caprock typically contain accessory minerals such as baryte, celestite, strontianite, metal sulphides, rare tourmaline and fluorite derived from ascending basinal brines (Figure 6.64a, b). Sulphur forms in vugs and fractures in the upper parts of caprocks where H_2S is oxidised by crossflowing waters (Figure 11.58a). Reactivated salt flow and associated carapace destruction means earlier allochthon and namakier residues can be carried to the margins and shed to become part of a polymict debris flow aprons.

The bulk of an actively accreting caprock is laminated and composed of unoriented, interlocking xenoblastic anhydrite crystal mosaics. Laminae are defined by thin intervals of dark

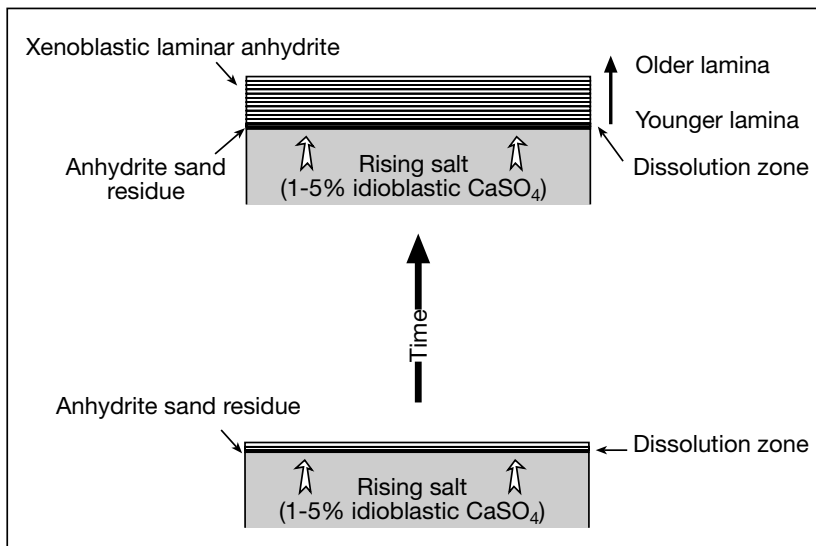


Figure 6.65. Development of laminar anhydrite caprock via underplating across a zone of periodic dissolution at the halite-anhydrite contact.

sulphide/bitumen accumulations or by intervals of more intense pressure-solution-sutured anhydrite. Deformed, banded anhydrite clasts are also contained locally within cm-spaced lamina (Ulrich et al., 1984, 1985). The laminar nature of a caprock reflects its formation via underplating, whereby the less soluble anhydrite and a few carbonate rhombs are left behind as undersaturated groundwaters dissolve halite from the upper part of the buoyant diapir stem (Figure 6.65; Ulrich et al., 1985).

Anhydrite and carbonate typically comprise 1-5% of the original undissolved salt mass in Gulf of Mexico diapirs. The salt/anhydrite contact tends to be subhorizontal to undulose, with local cm-thick metres-wide pockets of unconsolidated idioblastic anhydrite sand (euhedral grains freed from their encasing halite matrix). Above the halite contact and its sand pockets the anhydrite is laminated and consists of tightly interlocked xenoblastic crystals (Ulrich et al., 1985; Hallager et al., 1990). The transition from euhedral idioblastic anhydrite sand to xenoblastic anhydrite mosaics occurs in the first few centimetres above the salt stock. Outside of the sand pockets the porosity and permeability are consistently low to negligible.

Enclosed coarsely crystalline halite pockets, still with disseminated idioblastic anhydrite, can occur along some horizons in the caprock, especially in the lower portions of the anhydrite zone. Pocket shapes vary from tall and thin to broad and squat, maximum dimensions range from less than 0.5 m to about 2.0 m. These moundlike halite structures are mega-inclusion in the

caprock anhydrite and are remnants of former zones of salt spine penetration along the salt-anhydrite contact. As the halite spine dissolves through several cycles of dissolution and accretion, a laminated anhydrite mound is preserved that sometimes contains minor amounts of base metals. Other clasts within the laminar anhydrite caprocks are remnants of anhydrite beds first deposited along with mother salt, and then deformed and boudinaged into anhydrite "pencils" during salt flow (Hoy et al., 1962).

Gypsum forms sporadically along the upper side of the anhydrite portion of a caprock by hydration and is driven by the crossflushing of cooler less saline waters. Depending on permeabilities, this gypsum band is variably developed on and through the anhydrite, but many deeper caprocks in the onshore Gulf of Mexico lack a gypsum zone. Given the relatively high salinities and elevated temperatures that characterise the zone of onset of caprock formation it may well be that gypsum formation postdates the formation of most calcite and sulphide minerals in the caprock and requires the pervasive entry of cooler meteoric water or seawater.

The calcite portion of the caprock occurs in hydrocarbon-bearing zones, mostly in the anhydrite zone where anaerobic SO_4 -reducing bacteria break down the CaSO_4 phase into CaCO_3 and H_2S . Like the anhydrite zone, a calcite cap rock exhibits horizontal banding defined by alternating dark- and light-coloured layers of calcite that formed along the prevailing anhydrite/calcite contact during dissolution of anhydrite, coupled with SO_4 reduction (e.g. Prikryl et al., 1988). Dark calcite bands consist of fine-grained and typically pelletoidal calcite containing minor amounts of Fe, Zn, and Pb sulphides and bitumen. Light-coloured bands consist of coarse-grained euhedral calcite that apparently precipitated in open spaces and can also fill vugs.

Massive amounts of the Sr minerals celestite (SrSO_4) and strontianite (SrCO_3) occur in the lower portions of some calcite cap rocks primarily in the light-coloured bands, along with minor amounts of baryte. Sulphide minerals can also be locally abundant in the lower portions of calcite cap rocks. The calcite cap rock at the Hazlehurst salt dome in Texas is approximately 30

m thick in the 2 drill holes that fully penetrated it (Saunders and Thomas, 1996). The upper half of the cap rock consists of banded calcite similar to other Gulf Coast salt domes. Numerous near-vertical banded calcite-sulphide veins are also present in this part of the cap rock. The lower part of the calcite cap rock consists of horizontal sulphide + calcite bands that alternate with coarse-grained (white) calcite bands. Locally, sulphide-rich zones are more than a metre thick and consist principally of marcasite and pyrite, with minor amounts of sphalerite, galena, pyrrhotite, celestite, baryte and strontianite. Sulphate minerals are commonly intergrown with sulphides.

Fluid inclusion data in the calcite caprock of Hockley Dome, Texas, indicate that baryte and celestite precipitated at temperatures less than $\sim 60^{\circ}\text{C}$, from brines averaging around 200,000 mg/l total dissolved solids (Figure 6.66; $\sim 18\%$ NaCl equiv.; Saunders and Thomas, 1996). Fluid inclusion salinities in caprocks do not vary significantly with depth, suggesting that brine salinity did not change dramatically over time. Sulphur and carbon isotopic evidence also supports a biogenic origin for both carbonate and sulphide minerals in calcite cap rocks (Saunders and Swann, 1994) or a combined basinal and biogenic origin (Hallager et al., 1990).

In the last two decades there have been a growing number of studies dealing with mineralised portions of caprock and the results are used to improve geological understanding of processes that create Mississippi Valley Type (MVT) base metal deposits (Kyle and Price 1986; Bechtel et al., 1999). In Tunisia, some of these mineralised caprocks the associated biolaminated muds and the iron-rich haloes adjacent to the salt stems contain sufficient lead, zinc or siderite to be mineable (Bechtel et al., 1998; Warren, 2000b). Porosity in biogenic calcite caprocks can be as high as 40%, with porosity types ranging from pinpoint to fracture to vuggy to cavernous. Caprock reservoirs^{6.6} are shallow and so were attractive targets in the early heyday of drilling in Texas and many of the famous early discoveries were in caprocks; examples include Spindletop, Sour Lake, and Humble. Caprock reservoirs tend to be relatively small; the most difficult thing about working them in the early 1920s was their lack of predictability.

The earliest-formed anhydrite lies at the top of the anhydrite zone, and the oldest calcite lies at the top of the calcite zone (Figure 6.65). In other words the anhydrite and calcite caprock units grow from the bottom up and can be thought

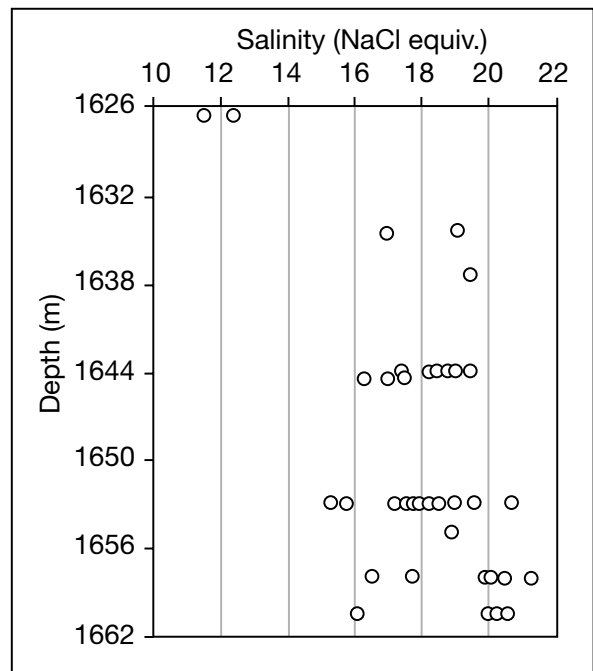


Figure 6.66. Plot of fluid inclusions-based salinities in barite and celestite in calcite cap rock versus depth (ft) in the Hockley Dome, Texas (after Saunders and Thomas, 1996).

of as having a half life, like the basal anhydrites of the Maha Sarakham Fm in Thailand (Figure 7.33). That is, the thickness of any caprock zone is dependant on the rate of fluid flushing at the lower contact where it is forming and at the upper contact where it is being converted to another mineral phase or is dissolving. Ultimately, if crossflow continues, all that will be left of a caprock is a dissolution breccia or a weld. Paleomagnetic age measurement of stratiform laminae of pyrrhotite and other sulphides in anhydrite cap rock, over a sampled section that

^{6.6}The early oil history of Gulf Coast, USA, has an interesting aside. Oldtime drillers found that drilling wells in graveyards led to a significant number of successes. High success rates associated with "graveyard-tology" meant that early last century the church elders and many still-living relatives developed a sudden if somewhat belated attachment to long-since-departed great aunt Maude. Bitter legal battles, fraught with claims along the lines of being the bastard child of aunt Maude, were fought over the percentage of royalties that one would receive for part of, or even a distant ownership of, a small piece of "Boot Hill." A reason exists for these early success rates. Many early east Texas fields were salt-structure associated, with the shallow reservoirs (vuggy and fractured caprock) lying directly over the crest of the structure. The surface expression of an underlying salt structure in the Texas Gulf coast is a small topographic high or hill, and since John Wayne was a whippersnapper, graveyards have been "up on Boot Hill." The first oil discovered in southern Louisiana in 1901 came from a similar salt-formed topographic feature known as Jennings Hill about 100 km west of Baton Rouge.

represents about two thirds of the total anhydrite thickness in the Winnfield salt dome in northern Louisiana, indicate it formed between 157 and 145 Ma (latest Jurassic; Kyle and Gose, 1991). Accumulation rates from these data indicate that the average rate for the oldest cap rock sampled is 5.7 m/m.y. and decreases to 2.8 m/m.y. for the younger lower parts of the caprock, indicating a waning rate of salt supply. The nearby 285 m-thick Hockley Dome cap rock is believed to have developed within the last 45 Ma giving same order of magnitude for the caprock accumulation rate (≈ 6 m/m.y.)

Caprocks are residuum responses to throughflushing waters atop and about largely inactive and buried salt structures. Historically they were interpreted as a diagenetic response to largely continental meteoric hydrologies imposed on dissolving diapir crests. Halbouty (1979), for example, noted that only 5 of 77 offshore wells drilled in diapiric crests intersected a caprock, but this analysis was done before any notions of allochthon shedding had been developed. Without doubt, actively forming caprock is found onshore wherever the active meteoric phreatic comes into contact with the upper part of a buoyant diapir crest (Schelkes et al., 2001). Yet, caprocks also form in offshore halotectonic slope and rise realms atop largely inactive salt structures that have not experienced substantial meteoric crossflow.

For example, a core through the Eureka dome, a structure located in the upper slope of the Gulf of Mexico, encountered 36 m (117 ft) of anhydrite caprock above the salt massif (Lehner, 1969). Assuming an anhydrite content of around 5% in the Louann Salt, this thickness of caprock requires the dissolution of more than 700 metres of salt. Burk et al. (1969) reported caprock in core recovered from the Challenger Knoll in the Sigsbee abyssal plain. The allochthonous Sigsbee salt mass overrode the abyssal plain sediments with its upper surface at or near the seafloor throughout the entire Cenozoic era and was probably never in contact with large volumes of meteoric waters. Apparently, circulating meteoric water is not necessary for salt dissolution and caprock formation. If it is present, its relatively low salinity compared to phreatic seawater does accelerate the process of caprock creation. Substantial caprock can even form subaerially and active salt glaciers in Iran have a brownish laminated gypcrete capstone that can be 3-10 m thick over the actively flowing parts of the salt (Bosak et al., 1999).

The term “cap” may be somewhat of a misnomer as layered CaSO_4 dissolution residues also form offshore in the Gulf of Mexico in zones of active fluid flushing on the undersides of salt beds and allochthon sheets (see fractionated dissolution discussed in Chapter 7). For example, cores taken from the base

salt contact in the Amoco #1 SL 12878 well in Plaquemines Parish, Louisiana, sampled a mineral assemblage of calcite, euhedral dolomite, ferroan dolomite, anhydrite, banded diagenetic calcite and trace mineral, the typical mineral association of a Gulf Coast caprock (House and Pritchett, 1995).

Complications of shale diapirism

Both salt and shale form diapiric structures that, without drilling, can appear quite similar in seismic sections. In a benchmark paper Morley and Guerin (1996) discuss the similarities and differences present in salt and shale diapiric provinces and outline ways to distinguish the two styles of diapirism. Salt's mobility is a fundamental material property; so that structures in a mobile salt belt continue to evolve until the salt is completely dissolved or ongoing salt withdrawal produces sufficient overburden touchdowns to stop further flow. Shale, on the other hand, only “flows” while it is overpressured. Whenever the main shale body depressurizes it freezes. While a shale is mobile it can generate a progression of kinematic geometries similar to those generated by the reactive and active phases of salt diapirism (Figure 6.67a; Morley and Guerin 1996, Van Rensbergen et al., 2003).

Halokinetic flow in a salt province builds diachronous levels and tiers of allochthons all the way up through the basin stratigraphy to the seafloor. Salt flows and evolves at higher levels in the stratigraphy, long after the original salt level has become a primary weld. Movement of a shale diapir tends to be much more episodic and related to particular overpressuring events within the shale-dominated section of a prograding typically deltaic continental margin (e.g. load driven compaction or thermobaric release of water or hydrocarbon generation). Once a mobile and chaotic shale mass approaches the surface and the pressure buildup is released via mud volcanoes, the shale freezes.

Mud diapirs are not the same as salt diapirs, even if they show similar patterns of gravity-driven compressional folding. There is an important distinction to be made between the actual volume of sediment flowing in a mud “diapir” or allochthon versus the distribution of overpressured mud leaking pores fluid. What we resolve seismically as a mud diapir is not sediment that has experienced Newtonian flow. Rather, it is muddy sediment that is disturbed because it contains, or once contained, overpressured fluid. This is not the same as a body of flowing salt in the salt allochthons and diapirs that characterises slope and rise regions in the Gulf of Mexico, the Middle East and the North Sea. This means that there are no equivalents to salt

canopies and tongues in regions of mud diapirism. Rather there are local, often relatively narrow and cylindrical structures (mud diapirs) that define the vent and escape positions of overpressured fluids. Allochthons and diapirs in halokinetic systems act as a focus to fluid flow, in mud diapirs and walls they are the zones of fluid flow.

For this reason shallow allochthons and widespread raft tectonics atop thin shallow décollement layers are much less common in mobile shale belts. Most shale diapirs show affinities to autochthonous rather than allochthonous salt systems. Laterally limited shale allochthons do occur in the Niger Delta, where they form imbricate thrusts that pass down dip into gravity flows and slumped blocks of shale derived from the exposed mobile shale.

Another significant difference between salt and shale diapiric provinces lies in the permanence of the contact between the flowing unit and adjacent strata. While flow in halokinetic terrains only takes place within the salt unit, shale mobility can spread out into adjacent beds as the overpressured interval spreads. While overpressured, a mobile shale interval can cannibalise adjacent shale strata and so cut across time/bed boundaries giving an overpressured shale interval a chaotic indistinctly-layered appearance in seismic (Figure 6.67b).

Morley and Guerin (1996) noted how such differences in mechanical behaviour lead to differences in structural style between shale and salt deformation, although many basic aspects of the gravitational tectonics are the same in both provinces. They note that prekinematic and synkinematic structures occur in both provinces, but much of the prekinematic deformation in mobile shale deltas, such as the Niger Delta of Africa and the Baram/Champion systems of Brunei, are destroyed by aggrading cannibalisation

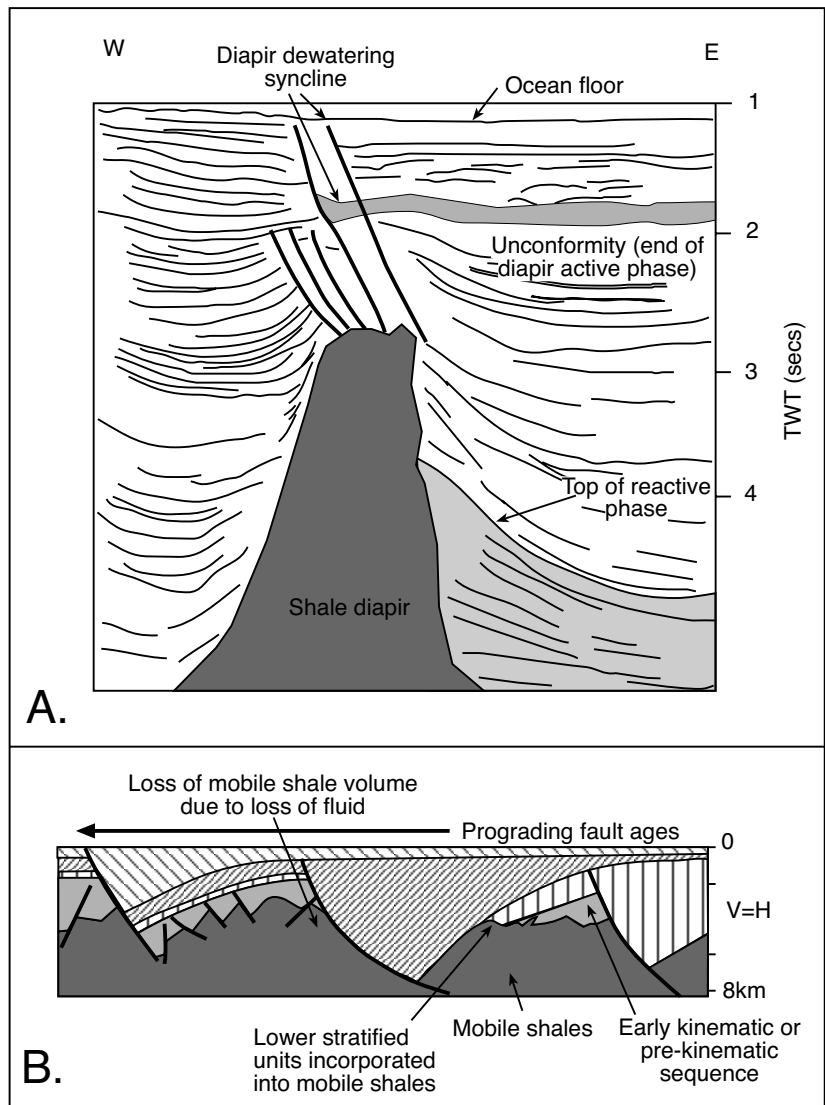


Figure 6.67. Shale diapirs. A) Shale diapir from the offshore diapir province of the Niger Delta, Africa. Adjacent sediments show synkinematic evidence of reactive and active phases of shale diapirism. The reflectors in the shaded region show thickening toward the shale diapir stem, suggesting expansion into an active growth fault during the reactive phase. B) Idealised evolution of growth faults associated with thick mobile shales (after Morley and Guerin, 1996).

of the overpressured shale. Not recognising this cannibalising effect can lead to the inappropriate placement of the lower portions of growth faults during seismic interpretation of shale diapiric belts (Van Rensbergen and Morley, 2000).

Fault-dominated minibasins occur above the flowing unit in both salt and shale mobile belts. For example, in the Niger Delta, the interval of overpressured shales beneath the actively

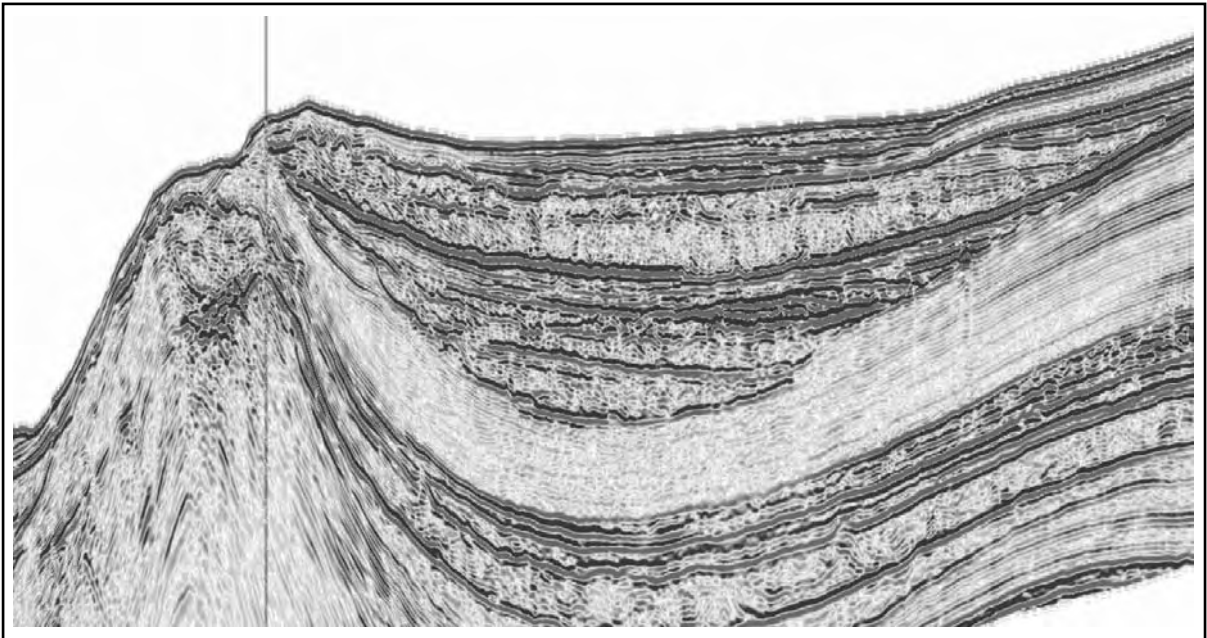


Figure 6.68. Seismic section from the thrust-floored compressional slope and rise of offshore Brunei Darussalam. Vertical line shows the position of a seep atop an erosionally breached anticlinal crest with an overpressured mud diapir core. The growth anticline has ponded deepwater sediment on its updip side.

accumulating delta prism varies from relatively thin intervals to massive chaotic zones some 4-6 km thick. The maximum depopod thickness is the thickness of the mobile shale plus the thickness of the overlying pregrowth fault strata (i.e. some 4-8 km). Such thicknesses are similar to those in salt-induced minibasins in the Gulf of Mexico.

Classic autochthon geometries are common to both salt and shale provinces, as are normal fault haloes that are created during reactive diapirism (Figure 6.67a). Early counter-regional faults and toe thrusts are early controls on the formation and position of depopods. Salt has the potential to completely evacuate as it evolves into salt welds or overburden touchdowns. Mobile shale deformation may also create local touchdown areas, but complete shale collapse is uncommon and large volumes of immobile dewatered shale are usually left after diapirism has ceased. Van Rensbergen et al. (2003) go on to note that due to the requirement of overpressure for shale mobility and the need for hydrocarbon generation to instigate overpressuring, a gas-charged mobile shale can forcibly stope upward through its overburden via a process of shale cannibalisation. This creates narrow near vertical mud pipe typically issuing onto the landscape as mud volcanoes. There are no equivalent narrow pipe-like cannibalistic stoping or diatreme-like features in the realm of salt tectonics.

Compressional growth anticlines cored by salt or overpressured mud can influence the distribution of deepwater sediments in the continental slope and rise in both settings. Such an anticline from the shale diapiric zone of offshore Brunei is illustrated in Figure 6.68. The geometry can be compared with similar anticlines, but with salt cores in the Gulf of Mexico and Angola (Figures 6.35, 6.38).

Summary

With the increasing use of 3D seismic for oil exploration in Phanerozoic basins, it has become obvious that models of predominantly vertical movement of salt from a mother salt bed into thumb-like autochthonous appendages are limiting. We now know that huge salt sheets (allochthons) can climb the stratigraphy as a series of predominantly subhorizontal sheets or tiers that are continually moving and squeezing as they are loaded by ongoing sedimentation. The end result is a feedback system where flowage create lows that fill with sediment, while the filling of the low with sediment triggers further salt flow. The upper side of the deforming salt sheet can flow into more classic thumb-like styles of diapirs.

Prior to the advent of forward-modelling techniques in seismic processing and the gathering of 3D data networks we could not image beneath salt bodies and so tended to interpret the upper salt surface as the primary level of the salt body. We now know this is not the case, many deforming salt beds flow into allochthons, which become rootless once the connection to the primary source or mother salt bed is converted to a salt weld or a fault weld. A salt weld forms as salt migrates or dissolves away to allow the former upper and lower contacts of the salt to come together or touchdown to form a salt weld. A fault weld forms where salt that was once within or lubricating a fault or shear plane is lost and the two sides of the fault come together. When a thrust plane is lubricated by salt that is subsequently lost by migration or dissolution, the plane may convert to a characteristic nearsurface dissolution breccia called *rauhwacke* (Chapter 7).

The end result of salt allochthons climbing through an aggrading and prograding shelf sequence is a layered and faulted stratigraphy with former sheets left as salt welds and fault welds, rather like a slug leaves a slime trail as it moves through a pile of leaf debris. The amount of salt left behind in the basin stratigraphy depends on the efficiency of salt evacuation. When the evacuation of the allochthonous salt sheet is efficient, all that is left behind is a series of stepped counter-regional fault welds and associated landward dipping faults. When the evacuation is less efficient the result is a series of salt rollers along the salt weld and an overlying fault-segmented sedimentary sheet cut by dominantly basin-dipping growth faults (a Roho system).

Wherever a salt allochthon is near the seafloor it can load, deform, coalesce or disaggregate as it continues its climb through the aggrading stratigraphy. Sediment loading atop a deforming allochthon creates fault-defined suprasalt basins or minibasins, often interacting with salt glaciers on the seafloor. Minibasins typically fill with a characteristic upward shoaling pattern of sediments passing from initial deeper-water laminated shales and mud to shallow water sands and carbonates. Processes of ongoing halokinesis and minibasin formation cease once the salt allochthon is sufficiently thinned, dissolved or buried. Thus, throughout the sedimentation history of a passive margin that is underlain by early thick salt beds there are many intervals where thick sheets of flowing allochthonous salt are present just beneath the deep sea floor and sandwiched into what are otherwise normal deeper marine bottom sediments.

Salt tectonics is also active in compressional terrains, which occur at the foot of a gravity glide sheet basinward of the continental slope; but is especially obvious in ancient foreland fold and thrust belts and inverted basins where weak subsurface salt acted a *décollement* layer. The resulting anticlines are narrow and salt cored while the intervening synclines are broad. Most of the thrusts are blind and backthrusts typically occur in association with forward directed thrusts. Much of the salt in the cores of the anticlines is strongly folded and diapiric; although the notion that compressional diapirs can breach their overburden, without being erosively thinned or disrupted by tear faults, has yet to be proven. There is a growing body of evidence that a substantial number of compressional diapirs are actually reactivated extensional structures.

Chapter 7: Karst, breccia, nodules and cement: Pointers to vanished evaporites

Introduction

Given enough time all subsurface evaporites eventually dissolve. Even in the sedimentary realm there are probably more intervals of dissolution residues than there are beds of salts. The rate of evaporite dissolution changes with temperature and rate and volume of crossflowing undersaturated pore waters (Figure 7.1) Solubility of the chloride salts consistently increases with increasing temperature (prograde solubility), with the sulphates and the sodium carbonates it initially increases, but can then decrease at higher temperatures (retrograde solubility). Dissolution typically begins in the shallow subsurface as the edges of salt beds are flushed by meteoric or marine waters and continues deeper in the

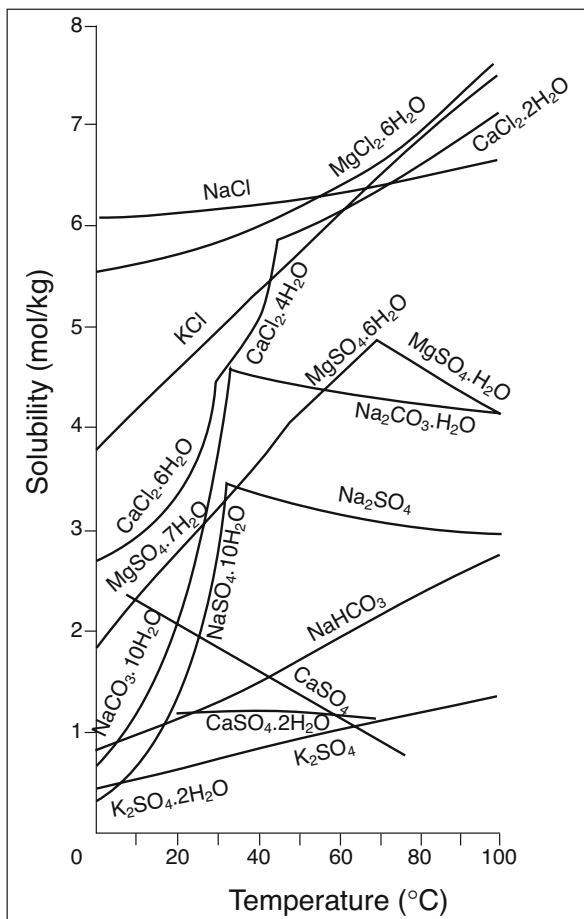


Figure 7.1. Solubility of common salts in pure water as a function of temperature, expressed in mole anhydrous salt per kg H₂O, (after Braitsch, 1964).

Mineral Name	Composition	Solubility in freshwater (moles/litre)	Solubility with respect to limestone
Limestone	CaCO ₃	0.00014	1
Magnesite	MgCO ₃	0.001	7.1
Gypsum	CaSO ₄ ·2H ₂ O	0.014	100
Nahcolite	NaHCO ₃	1.22	8.7 x 10 ³
Mirabilite	Na ₂ SO ₄ ·10H ₂ O	1.96	14.0 x 10 ³
Natron	Na ₂ CO ₃ ·10H ₂ O	2.77	19.8 x 10 ³
Epsomite	MgSO ₄ ·7H ₂ O	3.07	21.9 x 10 ³
Thenardite	NaSO ₄	3.45	24.6 x 10 ³
Hexahydrate	MgSO ₄ ·6H ₂ O	4.15	29.6 x 10 ³
Bischofite	MgCl ₂ ·6H ₂ O	5.84	41.7 x 10 ³
Halite	NaCl	6.15	43.9 x 10 ³
Antarcticite	CaCl ₂ ·6H ₂ O	7.38	52.7 x 10 ³

Table 7.1. Solubilities in freshwater of various evaporite salts in comparison to limestone (relative solubility calculated from molar concentrations).

subsurface, wherever and whenever bed edges are flushed by undersaturated basinal brines. Partial dissolution, whereby crystals of more saline salts (typically halite and bitterns) are flushed, leaves behind residues of the less saline salts (typically gypsum-anhydrite, as in many caprocks).

Solubilities vary from salt to salt (Table 7.1). For example, gypsum is moderately soluble in nearsurface meteoric waters with a saturation concentration of around 2500 ppm at 40°C. Halite is much more soluble, its saturation concentration is ≈350,000 ppm at 25°C and, unlike the calcium sulphate salts, its solubility consistently increases with rising temperature (Figure 7.1). Limestone dissolves more slowly than gypsum or halite, with a saturation concentration that varies according to ambient pH and CO₂ levels, but typically in the range 50-400 ppm. Thus, when exposed to meteoric crossflows, gypsum is one to two orders of magnitude as soluble and halite is more than three orders of magnitude as soluble as limestone. Whatever the mineralogy, an evaporite mass will rapidly dissolve when in contact with a crossflow of meteoric or undersaturated basinal water. Put simply, if a block of gypsum the size of a transit van fell into a river it would completely dissolve in less than two years, a block of halite in days. The same is true in the subsurface; it just takes a little longer because the rate of crossflow is less.

Unlike carbonate karst, the effects of nearsurface evaporite solution on cavern formation and land surface subsidence are obvious in time frames measured in years, not millennia and can be impressive. The cluster of sinkholes atop dissolving evaporites and locally known as Hell's Kettles to the south of Darlington, UK, formed in 1179 AD via catastrophic collapse of the landsurface. A twelfth century annalist describes their formation as follows:

“In the reign of Henry II, the earth rose high at Oxendale, in the District of Darlington, (Oxendale is now Oxney flat) in the likeness of a lofty tower, and so remained from nine in the morning until evening, when it sank down with a terrible noise, to the terror of all that heard it, and being swallowed up it left behind a deep pit.”

This chapter on karst deals with subsurface and near surface regions where hypersaline depositional and burial hydrologies are replaced by pore waters undersaturated with respect to the various evaporite salts. This situation is ubiquitous wherever ancient evaporites are exhumed and have once again entered the active phreatic zone. It is also typical of evaporites in the deeper subsurface wherever undersaturated basinal waters are flushing the edges of impervious evaporite beds (Chapter 8). Dissolution leaves behind solution breccias and other indicators of the former presence of now-leached evaporites (vanished evaporites or “the salt that was”).

Even as an evaporite bed accumulates, or soon after its deposition ceases, the depositional environs can be periodically freshened, either by climatic excursions or by progradation of sheetwash/fluvial/marine flood sediment. In this scenario karstification is part of the ongoing depositional story and explains many microkarst textures described in chapter 1. In one of the first uses of the term “the salt that was,” Schreiber and Schreiber (1977) described Miocene gypsum beds in Sicily where early halite layers were seasonally dissolved, even as the gypsum bed was accreting. This is an example of the syndepositional end of a salt dissolution spectrum that extends into much longer time frames that encapsulate the burial and even the metamorphic realm.

At the millennial scale, the periodic evolution of syndepositional hypersaline hydrology into less saline groundwater system creates karst effects and textures at the contact between the evaporite bed and its overburden. It can drive pervasive karstification into the upper 5-10 metres of an accumulating evaporite bed. This scenario is common in many continental playas where fluvial and bajada sediments periodically build

out over a saline pan or where transgressive coastal zones pass over saltern beds. Its effects are discussed later in this chapter in the section dealing with syndepositional karst. But most of the chapter deals with the various outcomes and indicators of longer time frames where overburden is indurated and the dissolution process effects deeper subsurface (mesogenetic) and uplifted (telogenetic) bedded and diapiric salts.

Because of their high solubility, exhumed ancient evaporites outcrop best in arid or frozen regions of the world. These are areas with lower crossflow volumes of liquid groundwater and so are zones where even halite can make it back to the shallow subsurface before complete disintegration. Exhumed anhydrite typically converts to gypsum some tens to hundreds of metres below the landscape over those areas of the world featuring subcropping and outcropping evaporites. This telogenetic gypsum has a fresh set of textures that make it difficult to interpret its original depositional fabric (Chapter 1). Subcropping halite, with its much higher solubility, tends to dissolve completely before reaching the surface. In all but the most arid environments, gypsum, not halite or anhydrite, is the commonplace outcrop expression of an underlying evaporite mass, be it bedded or halokinetic.

Outcropping gypsum caprock, with well-developed karst, encases salt diapirs in the Middle East, north Africa and central Australia and defines halite subcrop in the Qinghai (Tibetan) plateau, the Pecos Valley of west Texas, the Magdalen Islands in the Gulf of St. Lawrence, Canada, and in the Sierra del Fraile, in northeastern Mexico. Gypsum capstones can occasionally outcrop in humid tropical regions. For example, a gypsum caprock sporadically outcrops along the erosional banks of the Nam Theun river in Laos. This site lies within the axis of an evaporite-floored synclinal trough, it is surrounded by tropical pine forest, and caps an actively dissolving residual mass of stratiform, Cretaceous halite (*pers. obs.*). Halite can reach the surface in arid zones where salt is actively flowing into diapirs and allochthons, as at Mt Sedom in the Dead Sea Valley and in the salt glaciers (namakiers) of Iran.

Individual exposures of outcropping salts are usually no more than a few square kilometres, whereas dissolution breccias, insoluble residues and their characteristic subsidence terrains such as blind-valleys and suffusion karst, subcrop more widely. The mining of rock salt, or the drilling of boreholes into or through rock salt, have accidentally intersected or created caverns leading to a number of large, anthropogenic collapse sinks, subsidence cones and subsrosion features, which are discussed further in Chapter 12. Natural karst hazards are discussed later in this chapter.

Indicator	Examples	Reference
Modern gypsum karst	Miocene gypsum host, Sivas, Turkey	Kacaroglu et al. (1997)
	Late Miocene gypsum host, Sicily	Ferrasse et al. (2003)
	Tertiary gypsum hosts, Ebro and Madrid basins, Spain	Rodriguez-Aranda et al. (2002)
	Permian gypsum host, Ripon, UK	Cooper and Waltham (1999)
	Pennsylvanian - Permian gypsum, Sth Dakota, USA	Epstein, 2001
	Devonian gypsum host, Northern Lithuania	Paukstys et al. (1999)
Modern halite karst	Bedded Quaternary halite, Dead Sea Margin	Frumkin and Raz (2001)
	Miocene halite host (diapiric), Mt Sedom, Dead Sea	Frumkin (1994a, b)
	Neoproterozoic halite host (diapiric), Zagros Chain	Bosak et al. (1999)
Solution collapse breccia	Cretaceous Kirschberg breccia, Texas	Warren et al. (1990)
	Permo-Carboniferous, Central Spitsbergen, Svalbard	Eliassen and Talbot (2005)
	Lower Carboniferous, Vesder, Belgium and Wexford, Ireland	Swennen et al. (1990); Nagy et al. (2005)
	Triassic breccia beds, Ionian Zone, NW Greece	Karakitsios and Pomoni-Papaioannou (1998)
	Pennsylvanian Amsden Formation, Montana	Luebkings et al. (2001)
	Devonian Carbonates, western Canada	Stanton (1966)
	Devonian, Cadjebut area, Lennard Shelf	Warren and Kempton (1997)
Preferential dissolution residues	Miocene gypsum breccias in halite, Poland	Babel (1991)
	Basal Anhydrite, Khorat Plateau, Thailand	El Tabakh et al. (1998a); Warren (1997)
	Anhydrite residues via solution of Maha Sarakham Salts, Khorat Plateau, Thailand	Sessler (1990) Utha-aroon et al. (1995)
	Permian salt beds, Texas Panhandle	Hovorka (2000)
Rauhawacke	Quaternary-weathered brecciated detachment horizons in nappes of European Alps and Spain	Schaad (1995); Warrak (1974); Orozco et al. (1999)
Silicified evaporites and nodules	Miocene lacustrine evaporites, Calatayud Basin, Spain	Orti and Rosell, (2000)
	Miocene gypsum nodules, Mogrha Fm., Western Desert, Egypt	Khoriby (2005)
	Late Palaeozoic carbonates, Bear Island, Svalbard	Folk and Siedlecka (1974)
	Permian Park City Fm., Wyoming	Ulmer-Scholle and Scholle (1994)
	Mississippian strata, Kentucky and Tennessee	Milliken (1979)
Calcitised evaporites	Lower Triassic red mudstones, Central Spain	Bustillo et al. (1999),
	Permian Khuff Formation, Abu Dhabi	Worden et al. (2000)
	Permian Zechstein EZ-1 Carbonates, Europe	Harwood (1980)
	Permian Capitan Fm., Texas and New Mexico	Scholle et al. (1992)
	Mississippian nodular anhydrites, Saskatchewan	Kendall (2001)
Calcitised dolomites (dedolomite)	Permian Blaine Formation, SW Oklahoma, USA	Raines and Dewers (1997)
	Permian Raisby Fm. (Zechstein), NE England	Lee and Harwood (1989); Lee (1994)
	Permian Tansill Fm, New Mexico	Lucia (1961)
	Mesozoic limestones, French Jura	Shearman et al. (1961)
Celestite nodules	Salina Dolostones, Ohio	Carlson (1987)
	Purbeckian of Dorset, UK	Salter and West (1966)
Fluorite cements	Eocene mudstones, Florida	Cook et al. (1985)
	Visean evaporites, France	Rouchy (1986)

Table 7.2. Documented examples of indicators of evaporite dissolution.

Indicator	Examples	Reference
Baryte nodules and cements	Arid soils, central Australia	Sullivan and Koppi (1993)
	Magnet Cove baryte, Nova Scotia	Mossman and Brown (1986)
Authigenic anhydrite/halite cements	Cretaceous Pearsall and Glen Rose Fm., Texas	Woronick and Land (1985)
	Permian Rotliegende Sands, North Sea, Europe	Sullivan et al. (1994); McNeil et al. (1998)
	Jurassic Smackover Fm., USA	Heydari and Moore (1989)

Table 7.2. Continued.

Complete evaporite dissolution means no salt remains, while partial or preferential dissolution means the vertical or lateral extent of the remaining salt sequence is reduced and the more soluble salts have gone. Salt bed dissolution can be syndeositional, as can nodule and crystal replacement, or can occur later during shallow burial with vadose or shallow phreatic flow driving cavern formation and overburden collapse. Bed alteration and solution can occur much later under deeper phreatic basin hydrologies, where circulation is driven by compactional and thermobaric flushing. It can occur later still, when uplifted salts beds are once again flushed by deeply circulating meteoric waters during collision, inversion and overthrusting, (Table 7.2). Dissolution also occurs in the more enigmatic meta-evaporitic and igneous realms, where it is accompanied by deep burial mineral transformations such as scapolitisation, albitisation and tourmalinisation (see Warren, 1999; Chapter 6 for details).

Brines generated at an evaporite dissolution front can seep into adjacent sediments where new authigenic evaporite cements and nodules precipitate. Dissolution brines can be carried up along brine escape conduits, such as faults and fractures, into the higher portions of the sediment pile where they cool or mix with waters of differing chemistries and so precipitate as authigenic cements. Although dissolutional hydrology is transitory, the evidence of former evaporite beds—the evaporite that was—is permanent and ranges from dissolution breccias and residues, to replaced evaporite crystals and nodules, to authigenic evaporite cements near flow conduits such as unconformities, faults and fractures.

Evaporite landforms

As salt dissolves in the shallow subsurface it creates void space into which overlying strata can drape or brecciate to create characteristic landforms at both local (m to km) and regional (km to tens of km) scales (Figure 7.2). We can divide

solution-related landforms into two styles: active karst and palaeokarst. Paleokarst refers to ancient karstic features that are no longer active and were tied to basinal flushing hydrologies or landsurfaces no longer present. Active karst is responding to the ambient hydrology and typifies the landscapes discussed in the following section.

Local scale karst

Regions underlain by evaporite subcrop exhibit dissolution landforms similar to carbonate karst and include many varieties of karren, sinkholes (dolines), blind valleys and poljes (Ford and Williams, 1989). Bedrock exposures of gypsum or salt at a finer scale are sculpted into irregular surfaces called rillenkarrren and other solution flutes (Macaluso and Sauro, 1996; Stenson and Ford, 1993).

Dolines or sinkholes

Dolines (aka sinkholes, esp. in North America) are closed circular to elliptical hollows or depressions, often funnel shaped, with diameters ranging from a few metres to a few kilometres and depths from a metre or so to hundreds of metres (Figure 7.2). They indicate subsidence and/or collapse of underlying salt or carbonates. Because exhumed evaporites make it to the surface or nearsurface in mostly arid to hyperarid climates, sinkholes atop shallow bedded evaporites tend to occur at the terminations of dry arroyos in deserts. Valley sides may be steep and can expose karstified gypsum, or be gentle and covered by desert soils. Larger sinkholes may also enclose one or more smaller sinkholes and can be further subdivided into collapse, suffosion and solution dolines (Figure 7.2). A collapse doline forms by the collapse of a roof span into an underlying solution cavity. Suffosion dolines are smaller features (1-5m diameter) covered and filled with soils and debris washed into its fissures by rainfall or sheetflood. They indicate that the dissolving salt mass is close to the landsurface. Solution (subsidence) dolines tend to be larger downwarped doline craters or bowl-like subsidence depressions. Compared to collapse and suffosion dolines

they have lower slopes into the deeper parts of the doline, the doline walls are usually hosted in nonevaporites and the dissolving salt bed lies some distance below the landsurface. At the larger end of the scale of doline development a subsidence doline merges into a subsidence basin. This is a large solution hollow that creates enough accommodation space to be considered a small sedimentary basin that is filling with varying combinations of fluvial and lacustrine sediments.

Dissolution, collapse and suffosion are more active, more rapid, more frequent and more obvious in evaporite terrains compared to carbonates. In the Perm and Bashkir regions of Russia, Gorbunova (1979) reported doline densities atop weathering evaporites and carbonates of 32 and 10/km² respectively, although densities of up to 1,000/km² can occur in evaporite-cored fold axes or at contacts of evaporites with other lithologies. Densities of 1,100-1,500/km² have been documented in evaporite karst in the Italian Alps. Such high densities occur in regions of high hydraulic gradients and mean the dolines have diameters around 5 m (Belloni et al., 1972). The inherently high solubility of evaporite salts also explains densely-packed schloten depressions and large karren shafts seen in gypsum karst of Antigonish County, Nova Scotia, where extrapolated doline densities range up to 10,000/km² (Martinez and Boeber, 1997). Extrapolated, because such dense networks do not extend over any more than a square kilometre or two and are typically found near retreating escarpment edges underlain by shallow subcropping salts.

It is a form of mantle karst where the dissolving salt bed is never far below the landsurface.

Collapse dolines

Collapse dolines are steep-sided sinkholes, often defined by cave entrances. They form when solution of an underlying evaporite bed creates a roof span in the regolith that can no longer be supported by the overlying lithology. Doline walls are frequently asymmetrical; one wall is steep and the other one is gentle. Doline floors tend to display either concave-up or flat geometries. Apart from blocks of the collapsed roof span, active doline floors can be veneered by thin collapse breccias. The high density of dolines in areas of evaporite subcrop and the ubiquity of the associated breccias indicates the inherently higher solubility of the evaporite salts compared with interbedded and overlying carbonates (Figure 7.2b).

Solution Dolines

Larger sinkholes (subsidence dolines) with characteristic low angle widespread edge flexures and slopes indicate deeper, more widespread salt dissolution compared to collapse dolines and are linked to the creation of a bowl of subsidence (Figure 7.2c). They occur in most regions of deeper evaporite karst including; Italy (Belloni et al. 1972; Burri 1986; Ferrarase et al., 2002), Spain (Gutiérrez, 1996) and the Pecos Valley of

Suffosion dolines

High levels of dispersed impurities in a rapidly dissolving evaporite mass (mostly clays and muds, often dolomitic), means a soil or carapace of insoluble residues quickly covers the subcropping top of a dissolving salt mass (Figures 7.2a, 7.3). This carapace is continually undermined by the rapid solution of the shallow salt mass. Residual debris is washed into the doline crevices to create the characteristic soil-covered dimpled landscape that typifies a high-density doline

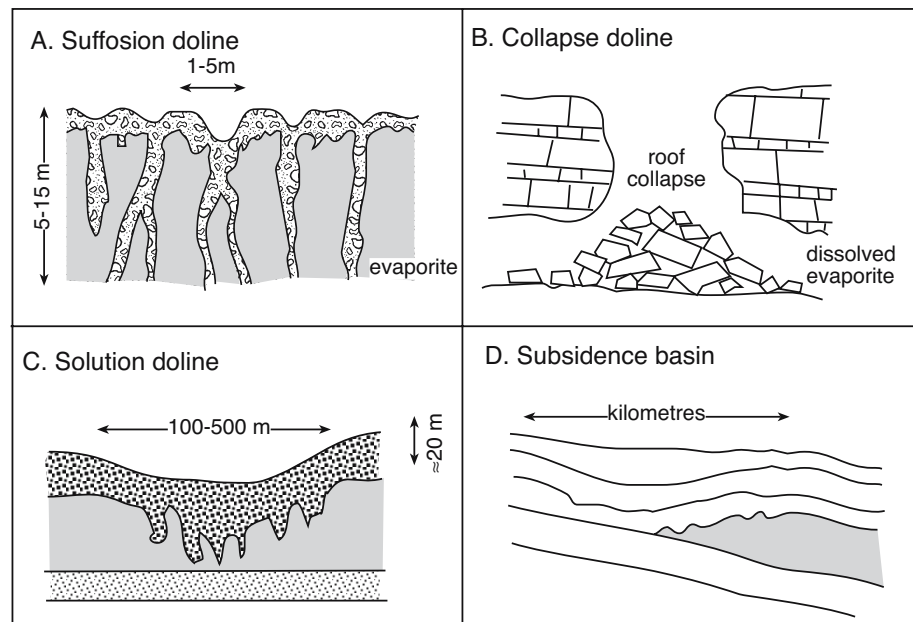


Figure 7.2. Typical scales and origins of evaporite karst features formed at the land surface atop a dissolving evaporite unit (grey).

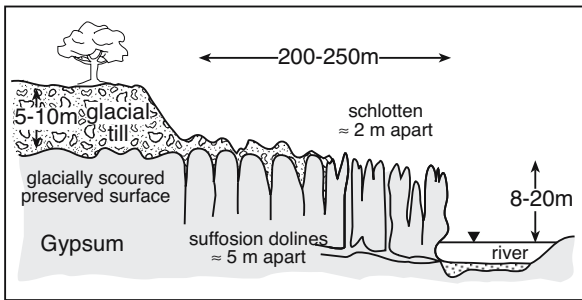


Figure 7.3. Suffosion karst development on subcropping till-covered gypsum in Nova Scotia, Canada.

west Texas and New Mexico (Gustavson et al., 1982; Davies, 1984a, b; Quinlan et al., 1986). In contrast to the numerous small steep-sided suffosion and collapse dolines formed atop shallow subcropping shallow evaporites, these larger, bowl-like dolines can have diameters of 100-500 m and depths of 10-20 m. Most have a soil cover and a thick sediment fill, with dissolving salt units at depths measured in tens to hundreds of metres below the land surface. They are mature dissolution forms and are transitional to subsidence basins where even thicker more widespread sediment fills are to be found (Figure 7.2d).

Breccia Chimneys and Pipes

Breccia pipes develop as landscape features on the same scale as collapse dolines or sinkholes. These steep sided chimney-like features are created by progressive upward stoping from the base of the salt bed, not its upper portions. In regions of thick evaporites the stoping process is driven by the focused upward escape of undersaturated basinal or deeply circulating meteoric waters leaking from levels below the sealing evaporite bed. Waters creating a stoping pipe can be focused into point or line sources via underlying biogenic buildups or fracture networks (Figure 7.4). Quinlan (1978) reviewed the nature and distribution of more than 5,000 breccia pipes within or atop salt or gypsum in the United States. Pipes ranged from 1 to 1,000 m in diameter and up to 500 m in depth. Similar crosscutting pipes in halite of the Devonian Prairie evaporite interrupt workings of potash mines in Saskatchewan, where they may propagate from depths as great as 1,200 m, and may lie beneath 1,000 m or more of cover strata (Figures 7.5). Unexpected intersection with a breccia pipe in an exploited bed can lead to catastrophic flooding and ultimate loss of a mine (Figures 11.27, 11.28).

Breccia pipes in an evaporite mass may exhibit one of four possible states (Figure 7.4): a) Active, and propagating upwards towards the surface, but not yet expressed there - a blind chimney; b) Active or inactive, expressed at the surface as a closed depression or a depression with a surface outflow channel; c) Inactive, and buried by later strata - paleokarst chimney; d) Inactive and standing up as a positive relief feature on the landsurface because the breccia (probably cemented) is more resistant to weathering than the upper cover strata - a residual pipe. Downward flexure in the uppermost strata atop a growing pipe forms a bowl of subsidence and sinkhole.

In some intrasalt pipes the halite or gypsum is entirely removed, leaving only an accumulation of insolubles and collapsed breccia blocks. In others, portions of the less soluble salts remain in the pipe. Mature pipes are typically filled by a jumble of intrasalt and suprasalt breccia blocks. In some, a lower brecciated zone is succeeded by an upper zone in which the overlying strata failed as a coherent block, settling downwards via a cylindrical pattern of steep to vertical faults with downthrows of up to 200 m.

Landscape residuals; karst domes and castles

Karst domes remain as features of positive relief once the surrounding evaporite mass has completely dissolved. Unlike chimneys, the cores of evaporitic karst domes can expose blocks from below, as well as above the original salt level. Some evaporitic karst domes are related to the stratigraphic level of former bedded salt, others are the remains of now dissolved salt thrusts, diapirs and allochthons (see diapiric breccias and rauhwacke). Domes and residuals are dramatic landscape features in the gypsum terrain of northern Alberta, Canada (Wigley et al., 1973; Tsui and Cruden, 1984) and the

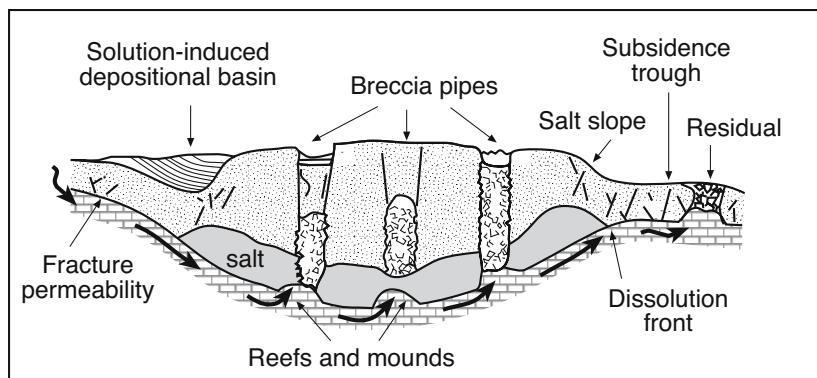


Figure 7.4. Interrelationships between larger scale dissolution features, artesian flow and various types of upward stoping breccia pipes (not to scale; in part after Ford, 1989).

Archangel gypsum karst region inland of the Barents Sea coast of Russia (Korotkov 1974). Canadian karst domes range from 10 to 1000 m or more in length or diameter, and can rise up to 25 m above the surrounding land surface. Many domes are highly fractured, with individual overburden blocks displaced by heaving and sliding, with the residual gypsum showing well-developed flow foliation.

At the extreme end of disturbance and dissolution the domes are megabreccias; positive relief features made up of upthrust jumbles of large blocks the size of houses. The largest reported Canadian example is in a steep-limbed anticline that extends along the shore of Slave Lake for a distance of 30 km, it is up to 175m in height with a crest that is marked by a 'chaotic structure and trench-like lineaments' (Aitken and Cook 1969). These spectacular karst domes occur in regions of widespread permafrost so that accumulation of ground ice in initial fractures in the evaporite layer probably contributes to the heaving and other displacement of breccia fragments in the dome. Tsui and Cruden (1984) attributed the examples that they studied in the salt plains of Wood Buffalo National Park Canada (Lat. 59-60°N) to hydration processes operating on subcropping bedded gypsum during the postglacial period. Ford and Williams (1989) argued such features indicate local injection of gypsum residuals during times of rapidly changing glacial ice loading. Whether they are created by glacial unloading/reworking or are a type of gravitationally-displaced dissolution breccia in a permafrost region is debatable; that they are a type of evaporite residue is not. They characterise the region defined by dissolution of shallow subcropping Devonian salt in Northern Alberta.

Residuals composed of cemented sinkhole or breccia pipe fillings can create hills surrounded by lower relief remnants of the former host bed (Figure 7.5). More than a thousand such hills occur on the gypsum plains of western Oklahoma (Fay

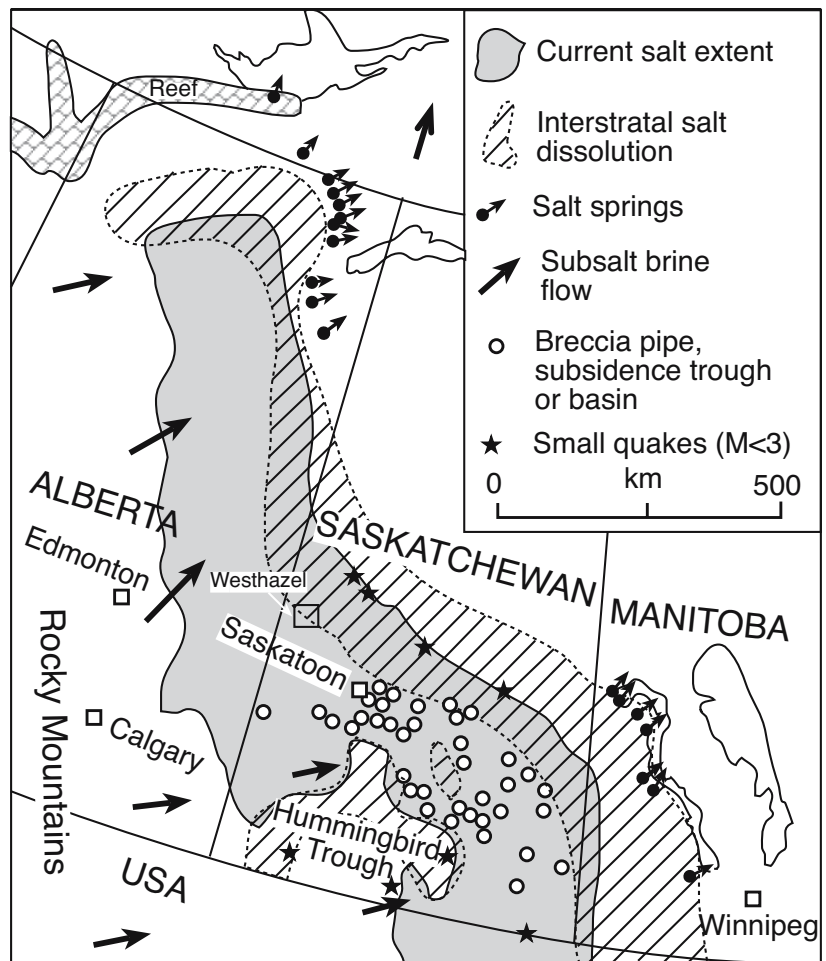


Figure 7.5. Regional distribution of evaporite karst features in the Prairie Provinces of Canada, including a large subsidence basin known as the Hummingbird Trough. These features were created by the dissolution of thick widespread Prairie Evaporite at various times from the Devonian to the present (in part after Ford and Williams, 1989).

and Hart 1978). Those karst mounds or hills with a doughnut form (a central depression) rather than a rounded form are believed to be cemented expressions of former sinkhole fills within bedded evaporites, rather than residual breccia pipes (Myers 1962). Hills of cemented breccia pipe residuals are typically a few tens to hundreds of metres in diameter and can rise 5-40 m above their surrounds.

Castiles are another exhumed feature in a gypsum karst terrain. In their type area of the Delaware Basin, south of Carlsbad Caverns, New Mexico, they make up steep-sided hills and mesas rising 3 to 30 m above the Gypsum Plain (Kirkland and Evans 1976, 1980). They are now exposed by the preferential dissolution of the surrounding bedded gypsum in an area near the solution edge of the sulphate facies of the Castile Forma-

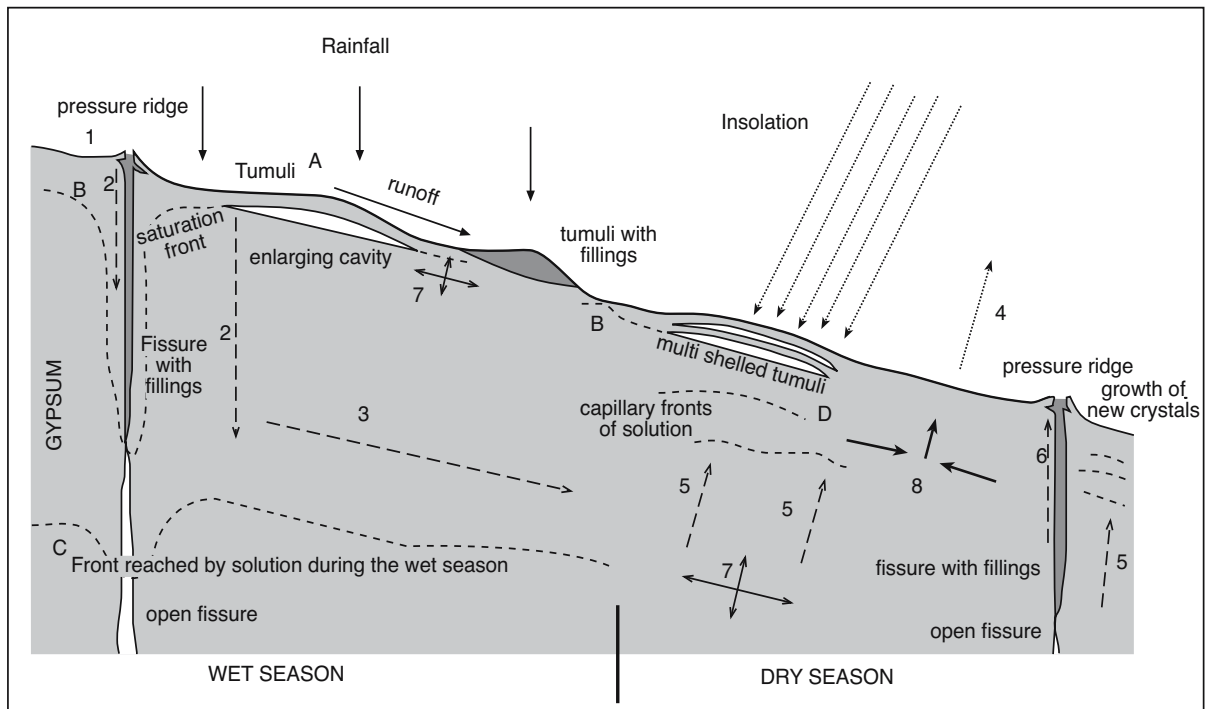


Figure 7.6. Main processes occurring inside an outer gypsum layer directly exposed to the atmosphere in a typical Mediterranean climatic regime. During wet winters, rainfall drives an overland flow and the water dissolves the gypsum at the surface (A) while a portion of the runoff manages to penetrate inside the intercrystalline pores of the rock. The water reaches saturation (with CaSO_4) at the surface and a few decimetres into the rock (the B line (dashed) may be considered a saturation front). The solution continues to penetrate both inside the pores and along fissures and joints (2), creating a downward reaching front of newly arrived meteoric water (C). Near-surface water in this front can also flow laterally (3). During the dry season, the pores lose water by evaporation (4). The inner solution becomes oversaturated and moves by capillary action towards the surface (5). In the D zone, there is precipitation of gypsum both by evaporative loss and by brine heating as it approaches the landsurface (gypsum has retrograde solubility). In the fissures and cavities, the pore fluids now migrate upwards (6) and new gypsum crystals may develop. The mass transfer from the inner towards the outer zone results in pressure relaxation (7) in the C zone, where open fissures may exist, and in pressure increase (8) in the D zone. In the type II environment, the runoff inside the sediment causes solution of the underlying gypsum both at the interface and in the fissures and other discontinuities of the rock. In this way, covered solution pavements and expansion tumuli develop, these features are most obvious after erosion of any soil cover (after Ferrarase et al., 2002).

tion (Figure 7.9). Similar features occur in areas of exhumed Miocene evaporites along the margin of the Red Sea (Aref, 1998b). Castles first form in the subsurface as a byproduct of the metabolic activities of sulphate-reducing bacteria, which locally replace gypsum with biogenic calcite (Figures 7.45a, 9.43).

Expansion morphotypes at outcrop

As well as the classic karst features, which are a response to dissolution and volume loss, some outcropping gypsum beds, especially in regions of anthropogenically induced rapid soil erosion, indicate local volume changes as in parts of Sicily and Spain where weathered late Miocene gypsum is now exposed at the landsurface (Figure 7.6). Such regions are characterised

by extensive alteration and recrystallisation of the gypsum regolith and soil textures that indicate repetitive cycles of expansion and contraction of the near-surface gypsum. The gypsum has evolved into pedogenic mounds and polygons related to exhumation into an active hydrology some millions of years after its deposition (telogenesis). The resulting medium-sized dome-like hills are covered by a mosaic of smaller landforms, related to different types of karren and of “expansion” forms such as tumuli and polygons. According to Ferrarase et al. (2002), the various gypsum morphotypes can be classified into two main categories: those that originated by solution and those that originated through recrystallisation.

Outcrops of gypsum lacking soil cover and influenced by alternating seasonal water conditions of surplus and deficit are

affected by both solution and recrystallisation processes. During the wet season, the water soaks into the rocky subcropping gypsum mass, filling all the fissures and pores of the outer layer from a few centimetres to some metres below the surface. During the dry season, there is a capillary-driven upward motion of the water solution. Near the surface, gypsum precipitates from the oversaturated solution, increasing the crystal size or forming new crystals. In this way, during the dry season, there is a pressure increase in the outer gypsum layers, which is responsible for the development of a “gypsum weathering crust.” It is characterised by many different expansion forms such as gypsum tumuli, pressure ridges and pressure humps. Tumuli are hollow subcircular domes, developed in coarsely crystalline gypsum crusts in the uppermost stratum of the gypsum regolith. They vary from a few centimetres to several metres in diameter and reach maximum heights of a little over a metre. Thicker crusts (≈ 1 m thick) support the development of mega-tumuli and dome-like hills some hm across. Development of dome-like hills does not seem to be controlled by variations in strike, dip, or fissuring of the gypsum beds. Their evolution seems to be linked to the fact that on most of the dome surfaces, the weathering crust is evolving through a nearly isotropic field of stresses, which is a result of capillary-driven volume increase in the outer gypsum layer (Ferrarase et al., 2002).

Regional scale karst

The distribution of landscape features above an actively dissolving salt mass depends on the extent and depth of the underlying salt. That is, at the regional scale is the dissolving salt bedded or diapiric? Elongate depressions, known as subsidence troughs, tend to define the subcropping edges of shallow gently-dipping salt beds. In contrast, smaller zones of circular sinkholes, solution lakes and cenotes tend to form atop the crests of shallow diapiric salt. In regions where the crest of the halokinetic salt is still rising, there is ongoing retention of positive relief atop the structure, even though sinkholes and capstones are continually forming within this zone of positive relief.

Subsidence basins or troughs

Subsidence troughs are large-scale elongate depositional depressions created by interstratal solution along the dissolving edge of shallow salt bodies. They can be filled or partly filled by clastic sediments (Figures 7.7a-c, 7.8; Olive, 1957; Quinlan, 1978). Salt-edge leaching of the shallow dipping salt underscores a set of self-perpetuating processes. Fractures created by the collapse of overburden and intrasalt beds into accommodation space (generated by salt cavities) provide new fissures and

sinks that act as additional conduits for further percolation of meteoric or upwelling of undersaturated basinal waters into the salt. This in turn instigates yet more salt solution in the vicinity of the collapse and typically creates an elongate corridor of subsidence at the surface.

Large solution-induced depositional basins and monoclines outline the edges of the great interstratal salt deposits of the world. Depression corridors some 5-500 km long, 5-250 km wide, with up to 100 to 500 m of subsidence induced relief and sediment fill define saline karst plains along the edges of bedded and dissolving saline giants in the Devonian subcrop of Canada (Tsui and Cruden 1984), the Permian Basin of New Mexico, Oklahoma and Texas (Bachman 1984), the Perm region of Russia (Gorbunova, 1979) and the Jurassic Hith region of Saudi Arabia (Amin and Bankher, 1997a, b). Associated sediment infill typically reduces the regional solution edge landscape to a few tens of metres of relief. For example, the Rosetown Low and the Regina Hummingbird Trough accumulated more than 100 metres of depression trough sediment during interstratal dissolution of the underlying Prairie salt (Devonian) in southern Saskatchewan (Figure 7.5b; DeMille et al., 1964). The concurrence of a supra-unconformity thick, adjacent to the sub-unconformity feather edge of a bedded salt sequence, is at a scale that is easily recognised in seismic and constitutes one of the classic signatures of a salt collapse-induced hydrocarbon trap (Figures 7.7a, 10.63).

A solution depression tends to capture rivers which, via seepage loss, tend to be losing streams in the vicinity of the solution front, so encouraging further salt solution and collapse. Examples of modern fluvial capture by subsidence troughs include the nearsurface edges of the Hutchison Salt Member in Kansas, the Maha Sarakham Formation in NE Thailand and along the Nam Theun valley in Laos (Figure 7.7c; Anderson et al., 1994; Supajanya and Friederich, 1992) and rivers in the Ebro Basin, NE Spain (Benito et al, 2000). The associated accumulation of fluvial and other sediments rapidly fill most modern solution troughs, so that surface relief is usually no more than metres to tens of metres across the subsidence corridor. Pleistocene and Holocene sedimentation rates in active US and Canadian subsidence corridors are ≈ 5 to 10 cm/1000 years. The Uralian troughs of the former Soviet Union are no longer active and so show somewhat lower rates of 0.3 to 3 cm/1000 years.

Interestingly, the foci of many small recent Saskatchewan earthquakes (magnitude $<3-4$ on the Richter scale) are located near the dissolving edge of the Prairie Evaporite salt (Figure 7.5; Gendzwill and Unrau, 1996). As bedded salt dissolves,

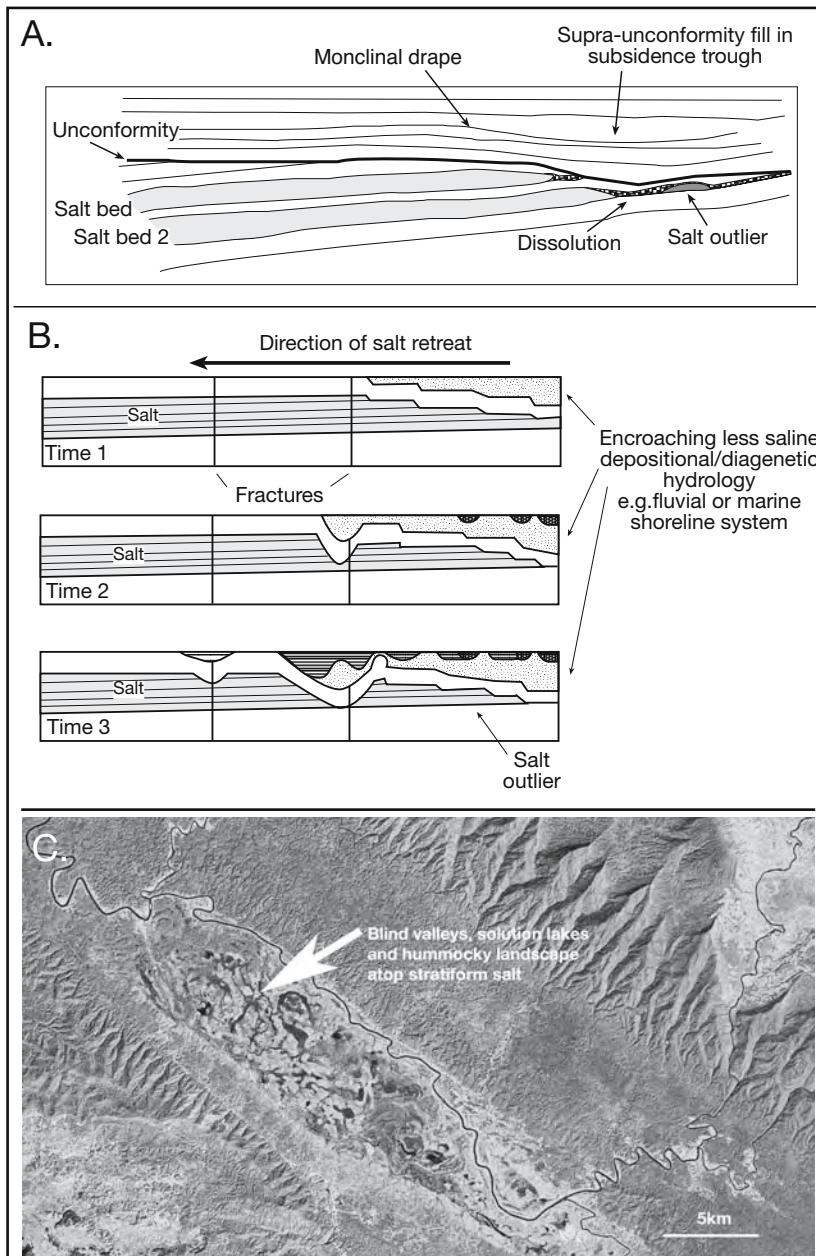


Figure 7.7. A) Subcrop salt dissolution creates characteristic sag geometries visible in seismic reflectors. B) Schematic dip section showing the sequential development of a regional subsidence trough, based on studies of the Hutchison Salt Member, Kansas (modified in part from Anderson et al., 1994). C. Nam Theun syncline, Laos, with Nam Theun River running along the northeastern edge of a dissolving stratiform salt mass that is equivalent to the Cretaceous Maha Sarakham salt of Thailand (Landsat image courtesy of NASA).

support is removed from the overburden, which then slumps. If the overburden is weak or extensively fractured, it settles quietly. However, if the overlying rock is an indurated carbonate, it may resist movement, forming a bridge over the growing

cavern. The roof span can fail violently when the undermined area gets large enough, so causing a small earthquake. Dissolution of the salt is possibly localized by faults and fractures, which provide seepage paths for the entry of undersaturated ground waters. Landscapes above many of the small Saskatchewan earthquakes lack extensive solution lakes, implying they may be sites upward sloping breccia pipes that have not yet breached (blind chimneys). Similar scale earthquakes can also define times of catastrophic failure in some salt mines and brine fields. On March 12, 1994 a 3.5 M quake documented the collapse of a mine panel in the Retsof Mine near Cyberville, New York state. Ensuing flooding caused the loss of the mine, which was until then the largest salt mine in the United States (Figure 12.19).

Hutchison Salt, Kansas

As well as their vertical expression being maintained by dissolution, subsidence troughs also migrate laterally, mirroring the retreat of the dissolving salt front (Figure 7.7b, 7.8a). The westward-dipping Hutchison Salt Member of the Permian Wellington Formation is 50-90 m thick and underlies much of central and south-central Kansas. Ongoing edge dissolution since the late Tertiary has created a subsidence corridor with contemporaneous valley-fill of Quaternary alluvium. In places, the alluvial fill extends more than 25 km to the east of the present-day edge of the main body of contiguous rock salt. The salt margin has receded this distance over the past several million years. Subsidence and collapse atop the active dissolution front creates numerous sinks, blind valleys and other salt karst features in the land surface and a pockmarked irregular thickness in the shallower parts of the salt bed (Figure 7.8b).

Oil well drillers call this region of dissolution cavities and fractures the “Wellington Lost Circulation Zone” and it extends for more than 100 miles N-S parallel to the dissolution edge of the salt bed (Figure 7.8a). Hutchison Salt is leaching vertically from the top down, and horizontally inward along the outer edge of the salt shallow dipping salt bed. Dissolution is driven by sustained contact with a crossflow of unconfined and undersaturated groundwater. As a result, over distances of 5-15 km westward, the eastern margin of the dipping and dissolving salt bed thickens by up to 90 m (from east to west). Locally, the salt member is preferentially leached along NNE-trending palaeoshear/fracture zones to leave behind thick stepped outliers (Figure 7.8b). Walters (1978) calculated an average lateral retreat of 3.2 km per million years since the late Pleistocene. He also pointed out that this rate is not constant. Dissolution was more rapid in the Early Pleistocene as the salt front was shallower. Now, when the front affecting the shallow dipping beds is deeper, groundwater crossflow and associated dissolution is slowing.

Natural subsidence and the rapid appearance of collapse dolines atop the dissolving Hutchison Salt Member has resulted in periodic ponding of surface waters in numerous dolines, abandonment of at least one oil well, and ongoing damage to numerous county roads (Figure 12.24). Because this damage can be in the vicinity of an oilfield much of the surface subsidence has been popularly attributed to poorly controlled drilling and development by unscrupulous oil companies. Any subsidence that occurs significant distances from any known well site is popularly attributed to unrecorded abandoned wells or complex asymmetric patterns of salt dissolution that originates at a drillhole. To test the validity of this widely accepted anthropogenic

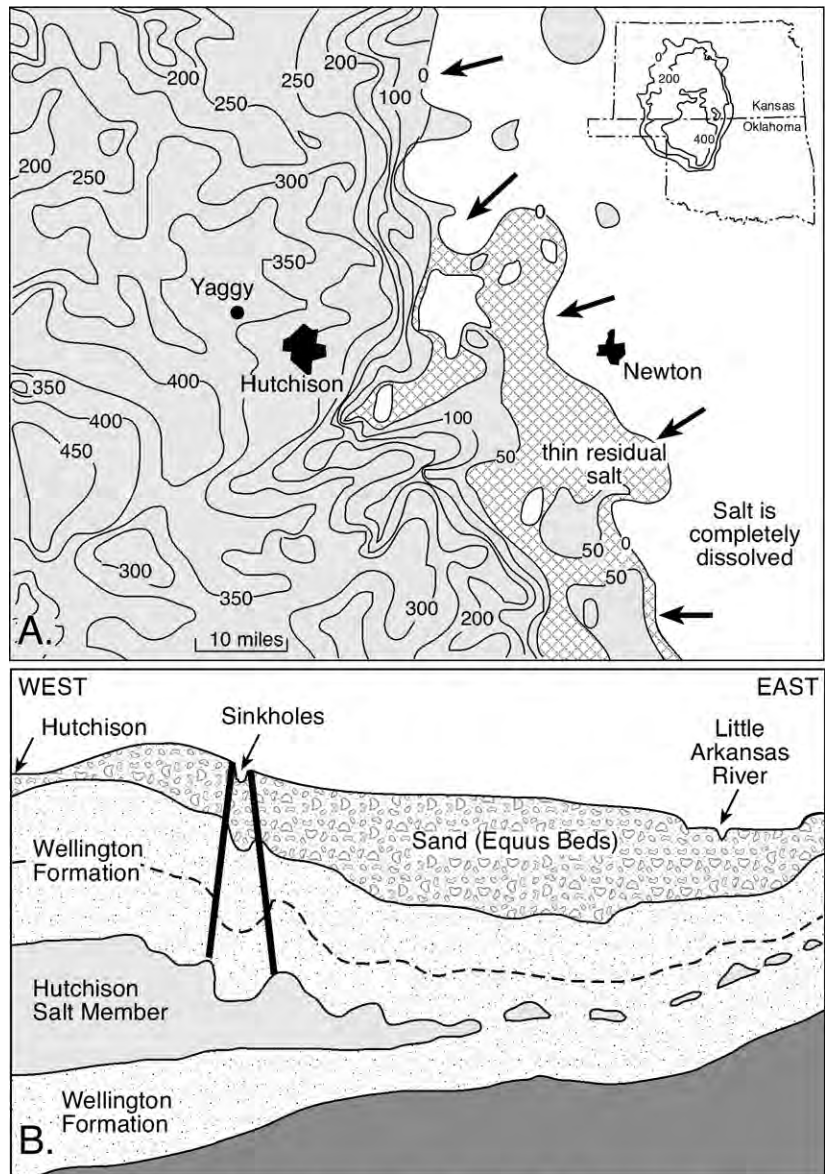


Figure 7.8. Karstified edge of Hutchison Salt Member. A) Thickness of the Permian Hutchison Salt, Kansas. Arrows indicate the direction of retreat of the dissolution feather edge of the salt body, Thickness is in feet and grey shading indicates salt thicker than 50 feet. Note the remnant outliers to the east of the dissolution edge (after Walters, 1978). B) Schematic east-west section in the vicinity of the town of Hutchison (after Watney et al., 2003).

salt-dissolution model, so popular with the environmental movement, a 4 km seismic reflection profile was acquired along an east-west-oriented county road adjacent to an abandoned oil well (Anderson et al., 1998). The expectation was that the residual Hutchinson Salt Member would be anomalously thin near an area of historical subsidence such as near the Burton oilfield. It should be thicker away from intensely drilled areas.

Contrary to expectations, the residual Hutchinson Salt Member is relatively thick (20–30 m) below areas of significant recent surface subsidence.

Nor is there any evidence of recent surface subsidence at locations along the seismic profile where the rock salt edge has been totally leached. Dissolution and subsidence at these sites largely predates European settlement of Kansas. Sinkhole development via catastrophic collapse is apparently a natural phenomenon and should be expected along this irregular salt dissolution front. Anderson et al. concluded that no modern catastrophic sinkhole development in the area has a clear-cut anthropogenic cause. As in the Prairie Evaporite, it seems focused collapse is largely a natural process influenced strongly by preexisting geologic conditions. This means sinkhole formation was only slightly and then rarely enhanced by the poor drilling and well abandonment procedures of 1920 though 1950s. However, the anthropogenic hazards created by a combination of gas storage in

shallow bedded salt and the presence of old poorly-documented solution wells, is another matter (see Hutchison gas explosion; Chapter 12). Natural salt karst collapse occurs quickly, well within a human lifetime. We cannot greatly influence the process of salt karst collapse, so we should plan geographic placement of infrastructure so that as much as possible it avoids it.

Delaware Basin, west Texas

The Delaware Basin of west Texas and southeast New Mexico, in the southwest portion of the Permian Basin, contains bedded evaporites of the Late Permian Castile, Salado and Rustler Formations. Outcrops and subcrops of these three formations constitute an area of widespread subsidence troughs, collapse sinks, dolines and breccia chimneys, all created by ongoing removal of underlying bedded Permian salts. The Delaware is an eastward-dipping basin, largely surrounded by the Capitan Reef and its equivalents (Figure 7.9). The area called the

“Gypsum Plain” of Texas lies to the west of the Pecos River and comprises about 2,600 square kilometres of subcropping gypsum of the Castile Formation. It is where the “Castile” landforms mentioned earlier are to be found. Additional gypsum outcrops are present to the east in the Rustler Hills and to the north in Reeves County, Texas.

In the centre of the Delaware Basin the thick evaporites of the Castile and Salado Formations and the thinner evaporites of the Rustler Formation are underlain by relatively permeable carbonates and siliciclastics, including some prolific hydrocarbon reservoirs in Permian backreef of the Central Basin Platform. Reef mounds, fractures and faults in these underlying sediments have provided focused conduits for upward stoping chimneys through the buried evaporites as well as the subsurface formation of now-exhumed Castiles to the west. An eastward-flowing deeply-circulating regional artesian hydrology, in combination with centripetal escape of buoyant hydrocarbon-rich basal waters, drives the formation of these features, with their surface expressions occurring in areas such as the Wink Sink (chain of breached chimneys) and

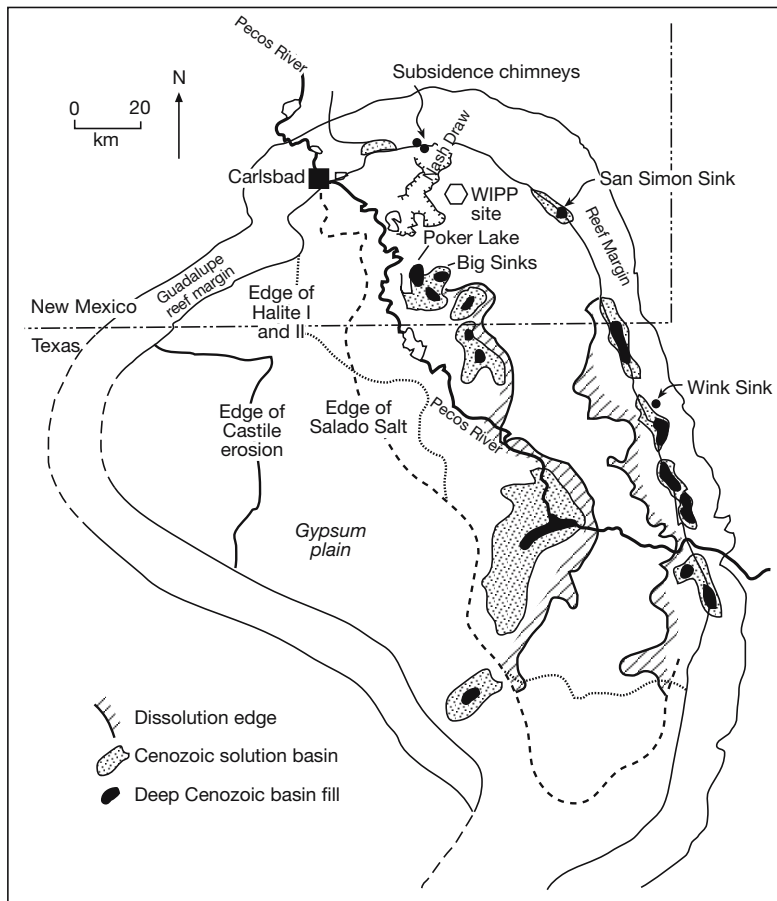


Figure 7.9 Karst features in the Delaware Basin and the positions of dissolution edges of various salt units, USA (after Davies, 1984a, b).

the Gypsum Plain (Castiles).

The upper sides of the shallow dipping salt beds are also affected by the hydrologies of the zone of active phreatic circulation. The Pecos River has migrated back and forth across the top of subcropping evaporites for much of the Tertiary. Its ancestral positions drove substantial salt dissolution, now evidenced by large sediment-filled subsidence

basins and troughs in the centre of the Delaware basin (Figure 7.9). The regional eastward dip of the Delaware basin sediments means first halite and then gypsum has disappeared along the updip eastern edge of the basin. Relatively undisturbed salt remains along the more deeply buried western side of the basin. Bachman and Johnson (1973) estimate the horizontal migration rate of the dissolution front across the basin as high as 10-12 km per million years. Multiple smaller examples of sediment-filled subsidence troughs occur at the edge of the gypsum plain of the Delaware Basin south of Carlsbad Caverns, where depositional troughs, 0.7 to 15 km in length, 100 to 1,500 m wide and no more than 5-10 m deep, are well documented (Quinlan et al. 1986).

The San Simon Swale is a 25 km² depression defining a residual karst feature atop the Capitan Reef on the northeastern margin of the Basin (Figure 7.9). San Simon Sink is the lowest point in the depression and is some 30 m deep and 1 km² in area. It in turn encloses a secondary collapse sink some 100 metres across and 10 metres deep. During a storm in 1918 a sinkhole formed a gaping hole about 25 metres across and 20 metres deep in the sink. In one night, nearly 23,000 cubic metres of soil and bedrock disappeared into the cavern. Annular rings that cut the surface around the San Simon sink today suggest ongoing subsidence and readjustment of the sinkhole is still occurring in response to earlier collapses. The position of

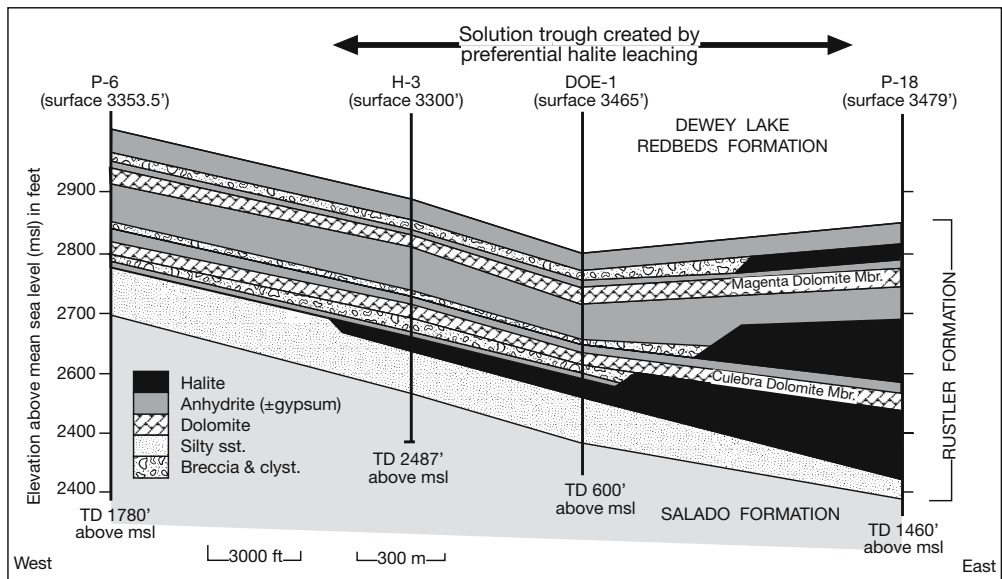


Figure 7.10. Differential dissolution of halite in Rustler Formation in the vicinity of the WIPP site (see Figure 7.9 for location). Note the anhydrite-gypsum and breccia residuals (as distinct from the bedded anhydrite). The solution trough lies some 400 metres above the level of the salt-encased WIPP (waste isolation pilot plant) subsurface waste storage facility in the Salado Formation.

the San Simon sink over the Permian reef crest led Lambert (1983) and many others to suggest that the sinkhole originated as a groundwater cavity breakthrough atop a series of stoping reef-focused breccia pipes.

Nash Draw is a southwesterly trending depression some 25 km long and 5-15 km wide, at the northern end of the Delaware Basin with its sump in a salt lake (Poker Lake) at the southern end of the draw (Figure 7.9). The underlying evaporitic Rustler Formation and parts of the Salado Formation has largely dissolved so that more than 100 caves, sinks, fractures, swallow-holes, and tunnels make up a complex local karst topography, which is apparently still active today (Bachman, 1981). An extensive drilling program conducted for the nearby WIPP site (now a low level radioactive waste repository) showed that dissolution of halite in the Rustler and upper Salado formations is responsible for the subsidence and overall formation of Nash Draw (Lambert, 1983).

To the west of Nash Draw the WIPP/DOE drilling program clearly defines the formation of a solution trough in the Dewey Lake Redbeds, created by preferential leaching of halite beds in the Rustler Formation, with interstratal anhydrite and breccia residuals (Figure 7.10). This dissolution occurred at a level some 400 metres above the salt-encased storage level of the WIPP waste isolation facility. A heated scientific (and at times not so scientific!) debate of just how deep surface karst penetrates

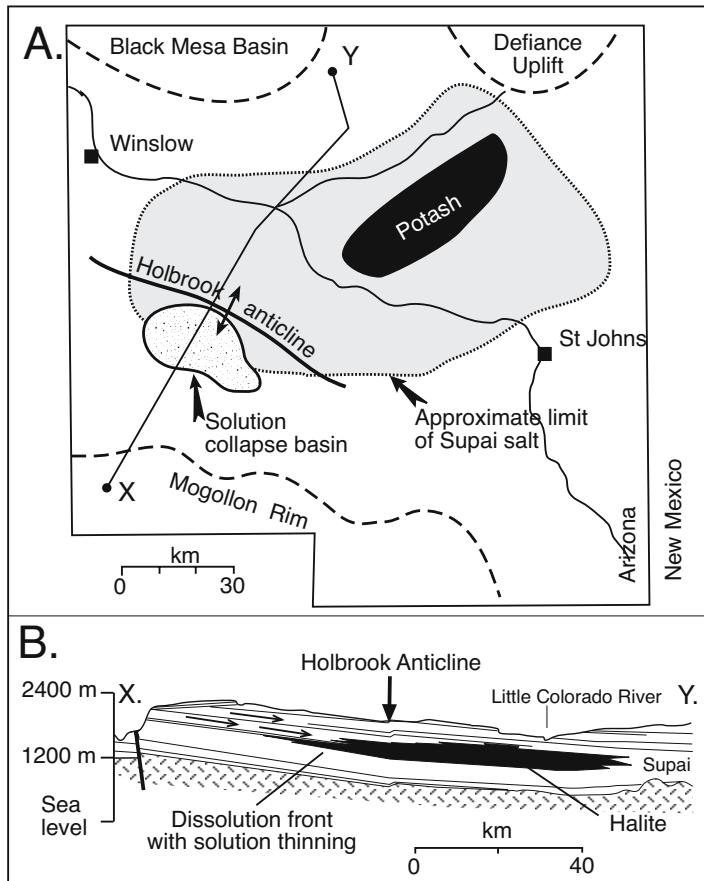


Figure 7.11. Holbrook Anticline, Arizona. A) Distribution of dissolution features seen at the surface and their relationship to the underlying Permian Supai Salt. B) Cross section showing how the Holbrook Anticline is a monocline flexure created by dissolution of the underlying Supai Salt (after Neal, 1995).

into the bedded halite of the Salado Formation in the vicinity of the WIPP site continues today (see Chapter 12 for detail of waste isolation in bedded and diapiric salt).

Further north, near the subcropping western edge of the Northwest Permian Shelf is Bottomless Lakes State Park, located some 20 kilometres east of Roswell. Outcropping about and underlying the lakes are the gypsum, halite, dolomite and red beds of the Artesia Group and San Andres Formation. Away from the lakes the area has numerous other sinkholes and collapse dolines, most of which are circular, steep walled or vertical holes, 50-100 metres across and 30-60 metres deep, with the greatest density of features aligned along the eastern side of the Pecos River floodplain. Water in the various sinks that make up the Bottomless Lakes is crystal clear and generally brackish to saline (6,000-23,000 ppm), attesting to its passage through subsurface layers of gypsum and salt. Although the

lakes are around 30 metres deep, dark-green moss and algae coat the bottoms giving the impression of great depth and hence the name of the park. To the west, many of the playas in depressions near Amarillo in the High Plains of Texas have a similar genesis as solution depressions atop dissolving Permian salt, but most do not intersect the regional water table and so do not hold permanent surface water (Paine, 1994).

Holbrook Anticline, Arizona

Subsidence driven by natural salt solution at depth generates regional-scale drape or monoclinical folding in strata atop the retreating salt edge. This is the corollary of the formation of a subsidence trough (Figures 7.7a, 7.8b). The 70-km long dissolution front in the Permian Supai Formation of Arizona is defined by more than 300 sinkholes, fissures and subsiding depressions (Neal, 1995). Away from the dissolution zone the northeasterly-dipping Supai Formation is composed of up to 150 metres of bedded halite, with local areas of sylvite along its northern extent (Figure 7.11a). Atop the solution front there are a number of topographic depressions with playa lakes that in total cover some 300 km². This expanse of salt removal has produced a regional gravity depression, largely coincident with a surface topographic depression where as much as 100 metres of collapse and topographic displacement has occurred. The solution front is also essentially coincident with the updip end of the Holbrook Anticline, a flexure defined by dip reversal in an otherwise northeasterly dipping succession (Figure 7.11b).

Rather than orogenically driven, the Holbrook Anticline is a subsidence-induced monoclinical flexure created by the northward migrating dissolution front (Figure 7.11b). It may be the largest single solution-collapse fold structure in the world (Neal, 1995). The reverse dip of the flexure directly overlies the salt-dissolution front and marks the location of two major collapse depressions known as The Sinks and Dry Lake Valley, both occur where salt is within 300 m of the surface (Peirce, 1981). Although it has periodically held surface water, reports of several hundred acre-feet of flood water in the Dry Lake Valley playa draining overnight supports the notion of active fissure and cavern formation related to salt removal at depth. Major surface drainage events took place in 1963, 1979, 1984

and 1995, with more than 50 new sinkholes forming in the valley during that period. The continuing rapid appearance of new sinkholes testifies to the ongoing nature of dissolution in the underlying evaporites. According to Neal (1995), dissolution front features began forming in the landscape in the Pliocene and continue to form today.

Other karst features attributed to evaporite dissolution in the Holbrook basin are; pull-apart fissures, graben sinks (downward-dropped blocks), breccia pipes and plugs, and numerous small depressions with and without sinkholes (Neal et al., 1998, 2001). The presence of the more than 500 karst features in the Holbrook basin, some of which formed in days, evokes practical karst hazard and infrastructure concerns, even in such a sparsely populated region (Martinez et al., 1998).

Black Hills, South Dakota

Another area of ongoing evaporite karstification is the Black Hills of South Dakota (Epstein, 2001). There, substratal salt bed dissolution, centred on anhydrites of the Minnelusa Formation (Pennsylvanian - Permian), has produced breccia pipes and pinnacles, regional collapse breccias, sinkholes, and extensive disruption in the overburden of otherwise stratiform beds. Anhydrite removal in the Minnelusa probably dates back to the early Tertiary when the Black Hills were first uplifted and it continues today^{7.1}. Evidence for recent natural collapse includes fresh scarps surrounding shallow depressions, steep-sided sinkholes more than 20 metres deep, and sediment disruption and contamination in water wells and springs. Several sinkholes in the Spearfish Formation west of Spearfish, South Dakota, which today support fish hatcheries and are used for local agricultural water supply, probably originated as the surface expressions of stopping chimneys initiated some 150 metres below in the salts of the Minnelusa Formation (Figure 7.12;).

As the anhydrite dissolution front migrates further down dip and radially away from the centre of the Black Hills uplift, resurgent

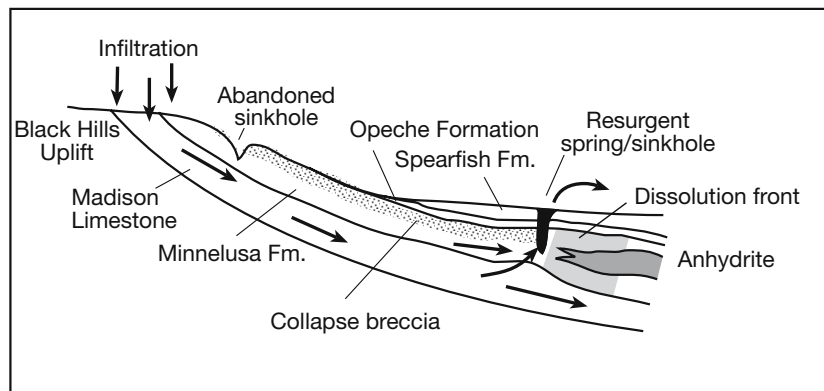


Figure 7.12. Minnelusa dissolution. As the Black Hills are slowly lowered by erosion, the anhydrite dissolution front in the subsurface Minnelusa moves down-dip and radially away from the centre of the uplift. As the front expands the resurgent springs defining the outflow pipes dry up and new ones form down dip (after Epstein 2001).

springs that once defined the active edge of the subsidence trough are overstepped. They dry up and new ones form further down dip. Abandoned sinkholes and breccia pipes, preserved in cross section on downcut canyon walls, attest to the former positions of the outward migrating artesian dissolution front (see also Figure 7.52). The Spearfish Formation, mostly comprising redbed shale and siltstone, is regionally considered to be a confining layer to the aquifer system. However, secondary fracture porosity develops locally within the lower Spearfish Fm. It is the result of cavity creation via salt dissolution in the Minnelusa Fm. (volume contraction fractures) or the hydration of anhydrite to gypsum (volume expansion fractures). Thus, up-dip of the anhydrite solution front, fracturing in overlying lower Spearfish Formation makes a respectable aquifer, especially for a regional shale, and it yields potable water through both pumped wells and springs.

Subsidence and landscape in diapiric regions

When diapiric salt is actively flowing near the surface it typically elevates the landscape (Table 6.3). In continental settings this places highly soluble halite and somewhat less soluble gypsum/anhydrite caprocks in the zone of active phreatic and vadose groundwater flow. This in turn leads to dissolution caverns, cavern collapse, slumping and landscape/gully retreat, typically focused in to the vicinity of subcropping salt dome crests. Sinkholes in such settings tend to form atop landscape highs, rather than in the intervening lows between the diapirs. Such diapir karst landforms dominate the Texas coast of the Gulf of Mexico, the Zagros/Hormuz region and parts of the drainage feeding the Ebro Basin of Spain.

^{7.1} The Plains Indians that inhabited the area 300 years ago trapped and slaughtered thousands of buffalo for their primary food by stampeding the animals over the steep rim of one of the large sinkholes near Beulah, Wyoming (the Vore Buffalo Jump).

Five Islands, Gulf of Mexico

Five salt dome crests, locally known as “the Five Islands,” are located near the western boundary of the Mississippi River delta plain in coastal south Louisiana. The present landscape of the islands reflects a combination of salt induced uplift and salt dissolution (Autin, 2002; Autin and McCulloh, 1995). The islands, aligned in an approximately NW-SE trend, are named Jefferson Island (JI), Avery Island (AI), Weeks Island (WI), Cote Blanche Island (CBI) and Belle Isle (BI) (Figure 7.13a). The five salt domes coring the islands have pierced, uplifted

and shed sediment, while their surrounding flanks subsided and accumulated sediment. Each dome is nearly circular in plan, with maximum elevation ranging from approximately 52 m asl on Weeks Island to 23 m asl on Jefferson Island. Avery, Weeks, and Cote Blanche Islands are large mounds with small sinkhole ponds, whereas the crests of Jefferson Island and Belle Isle are marked by large lacustrine collapse structures (Figure 12.25). Each “island” landform is, surrounded by lowland Pleistocene terraces and/or Holocene delta plain marshes (Figure 7.13a, b). Sediment cover on the mound is made up of the Late Wisconsin Peoria Loess covering alluvial deposits of the Prairie Complex.

The Prairie Complex crops out parallel to the coast and consists of alluvial deposits of the Late Pleistocene Mississippi and Red Rivers.

On Weeks Island the high salt island landform has a base that is marked by a pronounced increase in topographic slope between 15 and 23m MSL. A generally north-south trending ridge is mostly underlain by loess-covered sandy deposits of the Prairie Complex and so forms the “Devil’s Backbone,” which defines the highest part of the island (Figure 7.13b). The middle salt island landform occupies elevations of 8 to 23m, and the low salt island landform occupies lower elevations. Both landforms are underlain by mostly sandy, but locally loam-covered deposits of the Prairie Complex. The lowermost landscapes are tributary gully fills and perimeter colluvial aprons maintained by uplift of the salt core. Geomorphic evidence of ongoing salt-induced uplift on Weeks and the other islands includes; surface lineations, linear gullies, and excessively steep land surface topography coincident with steep topography on spines that define the top of the underlying salt (Autin and McCulloh, 1995).

Thus topographic features on all of the Five Islands were formed by a combination of; (i) rising diapiric salt spines, (ii) sediment reworking and

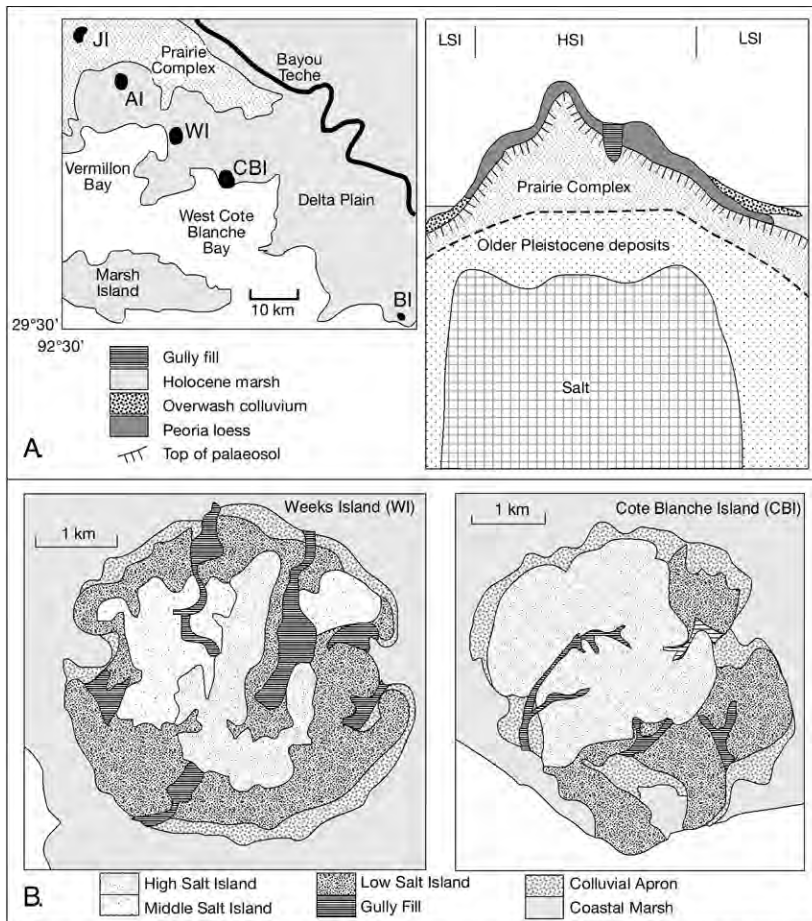


Figure 7.13. Five Islands Domes, after Autin (2002) and Autin and McCulloh (1995). **A)** The Five Islands of south Louisiana are aligned in a NW-SE direction along the western margin of the Mississippi River delta plain. The idealised salt dome cross section illustrates the relationship between salt island landform components and surficial stratigraphy. A palaeosol marks the top of the uplifted Prairie Complex across the islands. Beneath the high salt island landsurface (HSI) the Peoria Loess and local gully fill sediment veneer the Prairie Complex. Holocene marsh and overwash colluvium occur as veneer deposits beneath the low salt island (LSI) landsurface. **B)** Geomorphic features of Weeks Island and Cote Blanche Island, the surface features of Weeks Island largely reflect the dissolution topography of the underlying salt (see Figure 12.26).

development of a drainage network moving sediment away from uplifted areas, and (iii) subsidence creating sediment sinks (Autin, 2002). Uplands are drained by small gullies that dissect the dome landscape and cut into the Peoria Loess. The gullies contain a graded wash fill that passes laterally and down-dip into the aggrading colluvial aprons. Where the low salt island landform approaches sea level, the apron's fill in turn interfingers with finer grained aggrading sediment of the adjacent Holocene coastal marsh. Active dissolution of the salt crest creates sinkholes and water-filled ponds atop the salt and typify degradational dissolution zones on both the high and low salt island landscapes.

The boundary between aggradational and dissolutorial components of the landscape may in part coincide with underlying anomalous zones of differential shear within the underlying salt indicated by shear zones, locally known as black salt (Kupfer, 1976). The problematic development of an active sinkhole on Weeks Island, first noticed in 1992, occurs in a position of sharp change in landform slope (transition from high island to gully fill). It lies atop the projected alignment of what is known as Shear Zone E in the underlying salt (Figure 12.26; Autin and McCulloh, 1995).

Zagros/Hormuz region, Arabian (Persian) Gulf

Active salt glaciers (namakiers) typify the foreland fold region of the Zagros-Hormuz province, in a region made up of a number of E-W trending anticlinal mountain ridges and synclinal valleys (Figure 6.45). Many islands and ridges further to the south also have squeezed salt cores, but salt is now longer at the surface. More than 200 degraded namakiers and salt plugs (diapirs, domes) occur throughout the Arabian Gulf region, many are associated with hydrocarbon and metal shows (Kent, 1979; Talbot and Jarvis 1984).

Salt flow at the surface in the region of Zagros namakiers of southeast Iran began in the Pliocene and continues today with average uplift rates $\approx 2\text{mm/year}$. Actively flowing namakiers retain no deeply penetrating caves beneath their sediment carapace due to ongoing salt replenishment. Karst and karren features are most obvious around the edges of active glaciers,

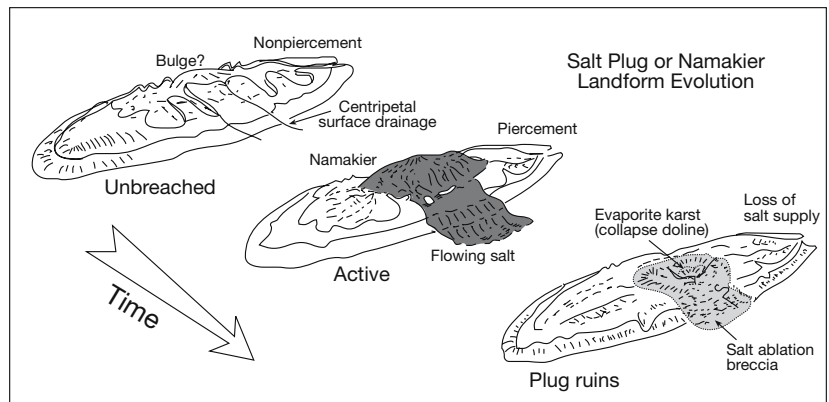


Figure 7.14. Landform evolution in an area where salt is flowing at the surface in a salt glacier (namakier). Based on various salt plugs in the Zagros foreland belt near the Straits of Hormuz (e.g. Figure 6.45).

especially in areas where the salt supply has slowed and the namakier edge is retreating. Iranian namakiers show different diameters (1-15 km) and range in outline from conical to cigar shaped, with varying intensities of surface karst and rilling. Salt plug landscapes can be divided in 4 types based on the intensity of supply versus dissolution (Bosak et al., 1999); active, passive, ruins of plugs and unbreached plug domes (Figure 7.14). Active plugs are positive relief features with centrifugal drainage networks and the plug surface dominated by flowing halite with relatively minor development of karst. Small ephemeral features, including shallow caves, are typical of the salt glacier surface, but in an active namakier the salt is flowing too fast to preserve them.

Once salt flow has ceased, karstification can be so well developed in some former namakiers that only the edges of the relict plug still show any positive relief. Salt plug ruins are even more disturbed and indicate a complete cessation of surface salt flow. Overall, inactive plugs tend to be negative landscape features (depressions) in the local Iranian landscape. Exotic "Hormuz" blocks of various sizes are scattered as dissolution residues about the edges of the "ruined" depressions, but no salt outcrops. Internally draining dendritic stream networks feed into the collapse doline centres of the ruined plug, the reverse drainage to that of an active plug.

To the south of the active namakier province are numerous salt-cored islands such as Hormuz, Das and Yas islands (Figure 6.56). These once diapiric salt masses are now largely inactive with only minor at-surface evaporite present, mostly as gypcretes and caprock remnants. Highest parts of the islands are typically covered by dissolution breccias that form a cap to the salt core below. Salt beneath the breccia carapace is pervasively karstified

and where relatively shallow, as at Hormoz Island, it is covered by suffusion karst and crosscut by tube caves (Figure 7.40). Active flow of the squeezed salt in the various island cores seems to have ceased sometime in the Miocene and much of the surface expression of the former outcropping salt is now defined by terrains of exotic blocks (Figure 7.22).

Salt Dissolution: Solution breccias and residues

Evaporite solution breccias (syn. evaporite collapse breccias) form whenever the removal of evaporite salts allows the intercalated or overlying rock to settle and become fragmented. Breccia horizons and a pile of finer-grained insolubles are the typical end result of complete subsurface dissolution of an evaporite. Frequently, especially in outcrop or about the buried edges of an evaporite bed, they are the only evidence of a former evaporite unit (McWhae, 1953; Middleton, 1961; Stanton, 1966; Elliott and Warren, 1989; Swennen et al., 1990). In evaporite paleokarst such breccias are one of the most reliable indicators of the former evaporites, even in situations where all soluble salts have been flushed.

The impervious internal make-up of a buried salt mass means it dissolves like a melting block of ice. That is, it shrinks via a series of retreating fronts, all moving from the edges inward and all defined by an expanding rind of insoluble residues. Retreat is most rapid along solution fronts in contact with

large volumes of undersaturated pore water crossflow, as occurs along the upper side of shallow salt layers, atop shallow diapir crests, in zones near active faults that intersect bedded or halokinetic salt, or about the feather edge of subcropping inclined beds and allochthons. Pervasive and rapid dissolution creates cavities filling with clasts of the adjacent lithology (solution breccia). Slow dissolution creates higher salinity pores where residual rinds made up of less soluble salts (typically anhydrite or gypsum) can form. As dissolution eats inward it can also create free-flowing residues of sand- to mud-sized insolubles, which in their turn infiltrate, and sometimes fill, the spaces between the breccia clasts. These fines, known as dissolution flour, are varying combinations of quartzofeldspathic muds and microcrystalline dolomite and calcite rhombs, all previously dispersed through the now dissolved salt mass.

Defining evaporite dissolution breccia

Breccia is a nongenetic rock type that ranges across sedimentary, igneous and structural regimes. As a rock descriptor it needs a prefix to define its origin. Depositional breccias can be considered “proto-conglomerates” that is, deposits composed of clasts or eroded fragments which were not transported sufficient distances to become rounded and so become a conglomerate (Figure 7.15). Nonevaporitic sedimentary breccias of this kind are commonplace. They form in glacial or alluvial outwash, can be an outcome of waves impacting reefs or sea cliffs, or can form in response to slope failure. As a group, depositional breccias tends to indicate rapid changes in transport energy, with clast diversity a pointer to lithologic variation in the source area.

In contrast, evaporite dissolution breccias are diagenetic horizons, usually dominated by cm-metre angular collapse clasts in a mud-sand matrix of dissolution flour. Commonly used sandstone and carbonate breccia classifications do not adequately address the variable character of solution breccias as they emphasise depositional energy levels and the style and rate of evaporite dissolution, not overburden and intrasalt collapse. Hence, we need to define a relevant breccia classification (Figure 7.16), then we can discuss how evaporite solution breccias relate to sedimentary breccias.

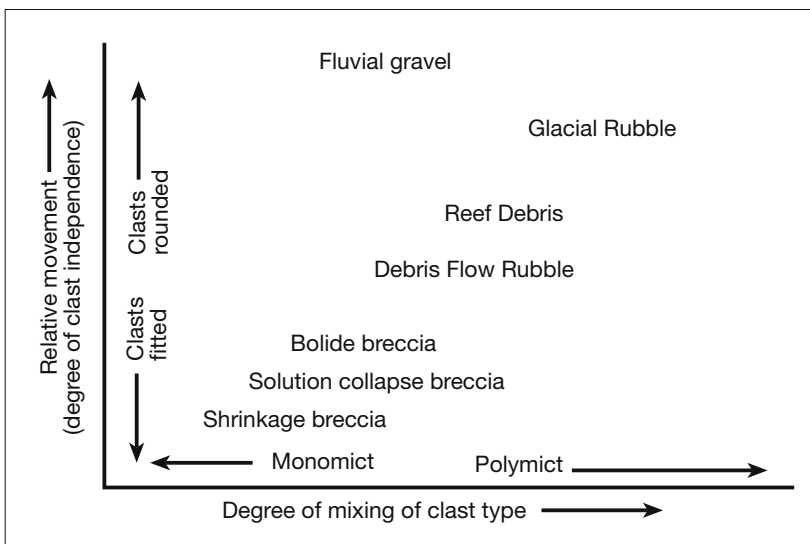


Figure 7.15. Evaporite solution breccias classification (based on the degree of clast movement and mixing after von Engelhardt et al., 1977).

Breccias are by definition composed of angular clasts, typically rock fragments of granule or pebble size and larger. Whenever classifying a breccia one should ask the following (Morrow, 1982):

- Are clasts of a single lithic type (monomict/oligomict) or of widely variable types (polymict); are lithic types in clasts similar or different from the rocks bounding the breccia body; are clasts composed of durable rock fragments or of a mixture of hard and soft clasts?
- Are clasts closely fitted, loosely fitted, or spatially independent, i.e., crackle - mosaic - packbreccia - floatbreccia (Figure 7.16a)?
- Do clast shapes and clast-to-clast contacts indicate either plasticity of clasts or brittle behaviour at the time of sedimentation? What is the nature of the clast edge (Figure 7.16b)?
- Are spaces between clasts filled with cement or with detrital matrix; i.e. clast-support or matrix-support?
- Does a weathering rind or coat extend all around a clast, or is it developed only on one side, or is there no indication of weathering?
- What is the nature and style of clast size and size grading; evidence for bedding; imbrication or other spacial alignment of clasts?
- What is the overall size and shape of the breccia deposit; is there a sharp lower contact and/or sharp upper contact; is the breccia body discordant (trans-stratal) or concordant (interstratal) in relation to bounding rocks?

Packbreccias are clast-supported, while floatbreccia clasts float in a finer matrix of granules, sands or mud. The distinction between crackle, mosaic and rubble breccia depends on whether the clasts are fitted, mildly disoriented or totally independent (Figure 7.16a). Crackle denotes a fabric in which there is little relative displacement of fragments. Mosaic implies fragments are largely but not wholly displaced. Rubble breccias are completely disordered and no fragment boundaries match. Some packbreccias have particulate matrices, others are cemented by spar or silica, indicating clast support. Elements other than fabric, such as the size and shape of the breccia body, its stratigraphic setting, the depositional setting of adjacent sediments and lateral equivalents to the breccia provide evidence of origin.

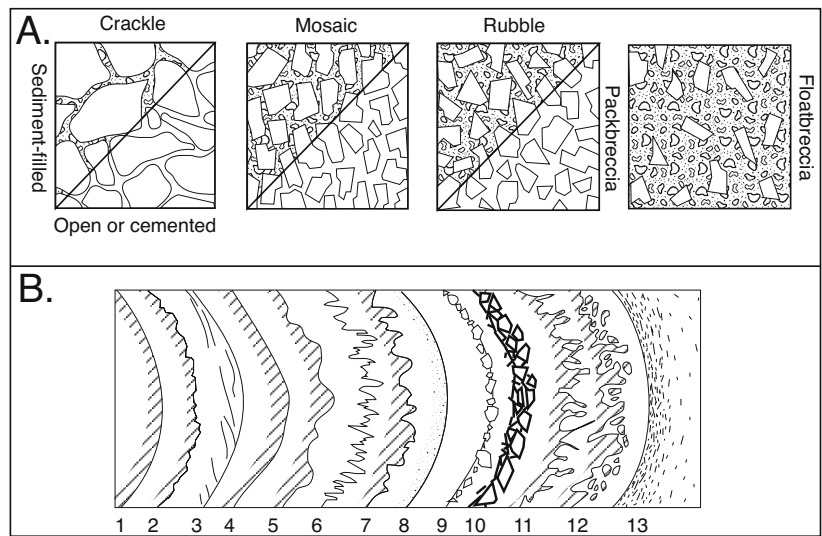


Figure 7.16. Breccia description. A) Nongenetic classification of breccias (after Morrow, 1982). B) Nature of clast contacts; 1. smooth, 2. slightly pitted, 3. striated, polished, 4. faceted, 5. solution rounded and pitted, 6. stylolitic, 7. ragged, 8. weathering rim or alteration rind, 9. microfragment armouring, 10. fragments in process of breaking out, 11. jagged, 12. crumbled, 13. diffuse, gradational (after Laznicka, 1988).

Intrastratal breccias indicate former bedded salts, while trans-stratal breccias characterise breccia chimneys and halokinetic dissolution breccias.

Evaporite solution or collapse breccias tend to form diagenetically as undersaturated pore waters flush a buried evaporite bed. Clasts in the resulting breccia can be derived from a lithology that once overlay the dissolving salt bed or from thin stringers and beds that were entrained in the dissolving salt. In many dissolution breccias the distance travelled by the clasts before being redeposited is negligible, often only centimetres to a few metres. Timing of clast movement may be episodic or a single widespread instantaneous event. Clasts in an evaporite solution breccia may have moved into a cavity in concert, like a school of fish, or they may have gently sloughed and foundered a few at a time, with little breakage or change in orientation. The distance of movement is dependent on the size and lateral extent of the solution cavity into which the clasts move and whether the clasts originally resided in thin interbeds within the dissolving evaporite or if they were part of a thick strong roof-spanning lithology that once overlay the dissolving salt bed. If the cavity is only a few millimetres to centimetres high, the overburden founders gradually and gently and so clast orientation and fitting is little disturbed by the process of dissolution. Crackle and mosaic breccias will be commonplace. If large local cavities develop, the collapse of the roof span is more likely to be catastrophic and the result to be dominated by disturbed rubble or packbreccias (Figure 7.17a).

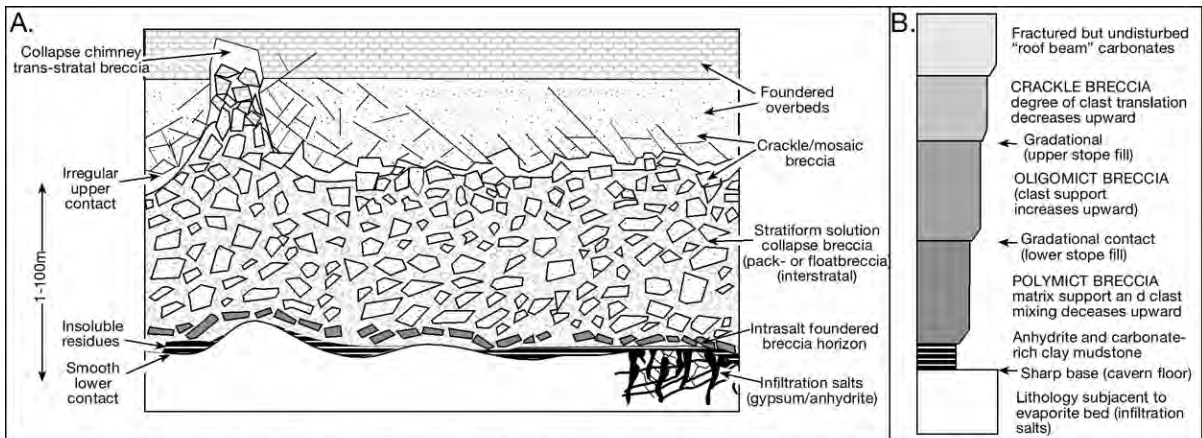


Figure 7.17. Lithological distribution in an evaporite dissolution triggered collapse breccia. A) lateral facies distribution. Left half of figure illustrates relationships in a trans-stratal chimney, right half in a stratiform solution collapse breccia. B) Ideal vertical sequence of breccia cumulates in an evaporite solution breccia.

Bedded solution collapse breccias

Stanton (1966) in a benchmark paper on formation of evaporite dissolution breccias demonstrated solution, subsidence, and evaporite flowage act simultaneously during subsurface brecciation. The resulting evaporite solution breccia in the Upper Devonian Leduc Formation, Alberta Basin, Canada, is made up of cm-dm angular dolomite clasts in a matrix of dolomite mud or anhydrite. He concluded that anhydrite-supported floatbreccias are a transitional stage to a dolomite clast-supported packbreccia in the dissolution of interbedded halite-anhydrite-dolomite. Angular fragments of the dolomite overburden and interburden in an anhydrite-supported breccia (floatbreccia) are loosely supported by solution-thinned, but still abundant, nodular anhydrite with textures indicating viscous flowage during dissolution. As the breccia forms and flows, dolomite fragments are continuously broken and rebroken, while the supporting anhydrite matrix carries a high proportion of loose, whole or broken dolomite rhombs (silt-sand size crystals). Ultimately, a dolomite packbreccia forms by the complete solution of the anhydrite. It consists of tightly packed dolomite fragments and clasts, within a matrix of sand-sized detrital rhombs and dolomite microspar cement.

Evaporite solution breccias typically have planar to slightly irregular, continuous lower contacts, often coated with insoluble residues (Figure 7.17a). The footwall surface to a breccia is usually covered by a few centimetres of mud- to sand-sized insoluble residues. The thickness of a pure evaporite that dissolves to produce a thin layer of insoluble residues may be substantial. For example, the Hartlepool Anhydrite contains only 0.5% - 0.8% insolubles (Smith, 1972). Complete solution of a 100m thick bed produces a layer of insolubles a mere

50-80 cm thick. In many breccia beds the insoluble residues now make up the matrix between clasts that were derived by the breakup of thin beds of carbonates or clastics. These are the fragmented remains of thin intrasalt beds that were once supported and interlayered by the now dissolved salt. This interval tends to be more polymictic than the upper roof-derived parts of the breccia unit.

Insoluble residues typically consist of fragmented chert, detrital quartz, silt, clay and dolomite rhombs, which are later cemented by authigenic phases (typically calcite, dolomite or silica cements). Many evaporite beds originally entrain dispersed syndepositional silt-sized dolomite rhombs. When the encasing salts dissolve, a dissolution residue or matrix is left behind; it is dominated by solution-disaggregated dolomite crystal silts and sands and is sometimes called "chalky dolomite." A high degree of initial intercrystalline porosity in the residue makes it an excellent potential aquifer for later mineralising solutions or hydrocarbons, especially when it forms at burial depths where much of the adjacent nonevaporite sediment is tight, having lost its porosity by mechanical and chemical compaction.

Siliciclastic and carbonate sands bound by early evaporite cements (e.g. halite cements in aeolian, wadi, or oolite sands) can also be leached during burial diagenesis to create permeability in an otherwise tightly cemented sand. In extreme cases the result is disaggregated freeflowing subsurface sand with depositional levels of permeability, which remain until it is recemented by subsurface processes.

Sometimes, rocks in the footwall beneath the breccia bed are locally veined by infiltrations of satin spar and poikilotopic

gypsum or anhydrite. Smith (1972) argues the fractures hosting such footwall stockworks were first created by the pressure of crystallisation of the evaporite itself; others envisage a more passive process of cement fill within preexisting joints or fractures. In my own work I have found the joints are often the result of passive fill in joints and fractures created by the extensional stress in units above or below a dissolving salt unit. Because pure halite has often completely dissolved, its former presence is difficult to determine, especially in core or image logs, but these tell-tale fracture-fills remain in the log signature (especially in image logs) and indicate a much thicker former salt bed.

The basal zone of insoluble residues passes up into the main breccia body, an interval dominated by packbreccia or floatbreccia. Breccia fragments and clasts in the main breccia can be angular or solution-rounded (Figure 7.17a). Almost all rubble texture in a breccia is generated by the collapse of overlying or interbedded lithologies into cavities created by dissolving salt beds. Where the original sequence was made up of interbedded salts and other lithologies, the resulting clast rubble typically collapses in sequential order, so that the rubble pile retains the crude stratigraphic order of the former intrasalt beds.

Clasts are composed of varying amounts of sandstone, dolomite, limestone, mudstone and chert fragments. The main breccia may be polymict or monomict, depending on the nature of the intrasalt beds and the overburden. Breccias can be clast- or matrix-supported (packbreccia versus floatbreccia) depending on the amount of residue entrained in the evaporitic interval prior to dissolution. Pure evaporites, interbedded with indurated dolomites and other nonevaporite strata, tend to produce clast-supported packbreccia fabrics. Evaporite sequences interbedded with, or underlying, nonconsolidated sediments, or evaporites with a high content of dispersed impurities, tend to produce matrix-supported floatbreccia fabrics.

Unlike its lower contact, the upper contact of the main breccia interval is typically gradational, progressing from rubble breccia in the main body into mosaic, crackle then ultimately into unaltered overburden (Figure 7.17b). A breccia begins to accumulate on the bottom of a growing cavern marking the contact of undersaturated pore waters and the salt. As the salt begins to dissolve, the insoluble clay-sized material that was present as impurities in the salt accumulates in thin layers on the floor of the cavern. Later in the dissolution process, and higher in the breccia sequence, angular to etched clasts of mixed intrasalt and roof rock form a polymictic breccia. Polymictic breccia passes upward into a monomict breccia made up of

angular clasts of roof rock. Gradually, the overlying rock is not broken into clasts but is merely fractured and expanded to form crackle breccia. Crackle fractures, if they are not filled with cement, can provide excellent pathways for subsurface mineralising fluids and can act as reservoirs for oil and gas.

The contrast between a sharp lower contact and a gradational upper contact is one of the most reliable characteristics of a solution breccia. It can be used both in outcrop and subsurface studies (core and image logs) to separate an evaporite solution breccia from a depositional breccia, which has evidence of syndepositional infiltration and depositional drape along its upper contact, and a tectonic breccia, which has cataclastic and typically symmetrical contacts related to fault or shear zones.

Where complete removal of less soluble evaporites has not yet occurred, evaporite salts, such as flow-textured laminar to nodular anhydrite, remain as part of the matrix within the main breccia interval. In cores through thick-bedded evaporites the upper bed contact is often defined by a zone of disturbance in the anhydrite textures. The typical fabric is very similar to soft sediment disturbance textures associated with rapid water escape in sands. The anhydrite just below the contact is typically made up of angular but contorted anhydrite blocks in a finer anhydrite matrix. Often, there are also highly distorted and folded blocks or fragments of dolomite and other disturbed intrasalt beds. I have seen these zones at the contacts of many thick anhydrite beds with the adjacent nonevaporite strata including; the San Andres and Seven Rivers formations of west Texas, the Khuff Formation in Abu Dhabi and Saudi Arabia, caprocks to Gulf of Mexico diapirs and Zechstein Formation anhydrites in NW Europe. These disturbed contacts define intervals of subsurface dissolution where the process of dissolution and brecciation is not complete. In many cases dissolution processes may no longer be active, as the adjacent nonevaporite beds no longer have sufficient permeability to transmit undersaturated fluids. They are a form of frozen dissolution breccia that define the early fluidisation stage, where the bed is dissolving from its edges inward like a melting block of ice.

Local reprecipitation of evaporites into the breccia matrix may also generate large poikilotopic crystals, which encase the dissolutional residues. Such cements are typically coarse-grained anhydrites with a somewhat anhedral form and isotopic signatures indicative of elevated temperatures. Pseudomorphs of now dissolved evaporite minerals and nodules, composed of calcite, silica or celestite, may also remain either in the matrix or within clasts. Cement may be a fine-grained crystalline precipitate of equidimensional calcite crystals, as described by

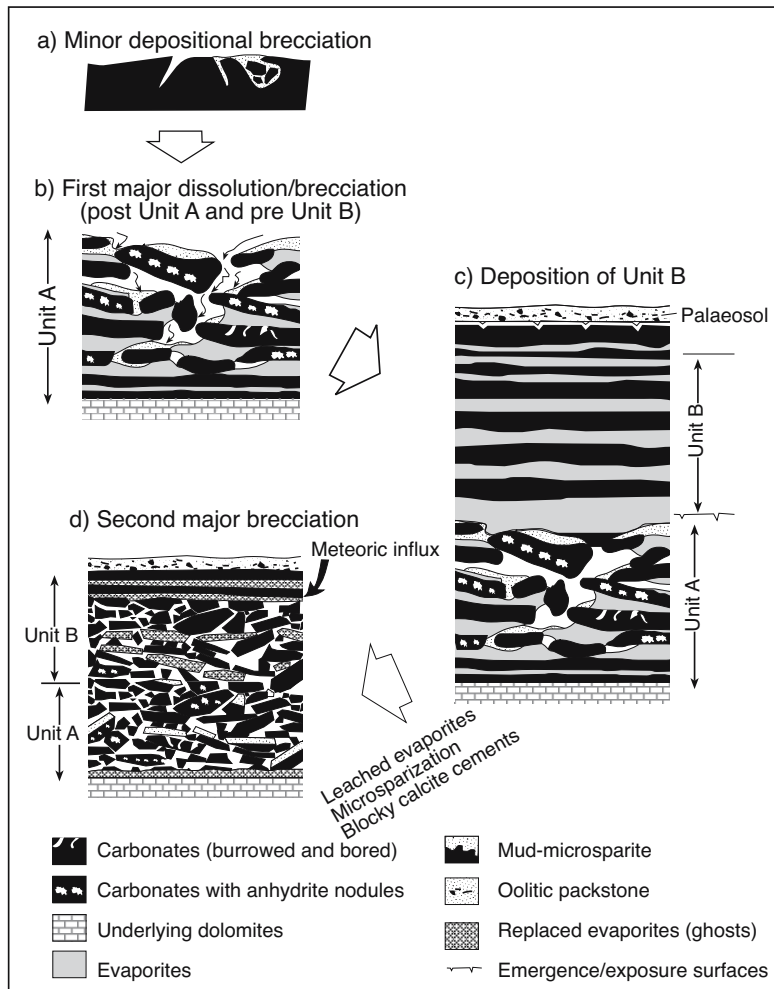


Figure 7.18. Sequential brecciation episodes in the lower Visean Belle Roche breccia (after Swennen et al., 1990). **A)** Minor syndepositional dissolution and fracture brecciation mainly related to shrinkage. **B)** This occurred shortly after deposition of bedded evaporites of unit A and involved incompletely lithified clasts, infiltration of freeflowing mud with ooids. **C)** Resumption of evaporitic sedimentation to deposit unit B with palaeosol cap. **D)** Second major brecciation event driven by meteoric influx. It overprinted both unit B and unit A. The brecciation process was mostly foundering rather than cavern collapse, and so stratigraphic order was retained in the breccia stack. Foundering means the overlying beds parallel the general stratification.

Swennen et al. (1990) in the Belle Roche breccias in Belgium, or a sparry coarsely crystalline dolomite or calcite (burial spar). Coarse sparry or saddle dolomite is often associated with evaporite solution breccias in Mississippi-Valley-type deposits (Olson, 1984; Warren and Kempton, 1997). Isotopic and petrographic character in dolomite burial cements in evaporite solution breccias are often complex and multistage. For example, there are six burial-related stages of dolomite formation and two episodes of breccia formation preserved in the evaporite

solution breccias of the Tripolis Unit, Mainalon Mountain, Greece (Papioanou and Carotsieris, 1993; Karakitsios and Pomonipapaioannou, 1998).

The lower Visean Belle Roche breccia (east Belgium) is a classic multistage evaporite dissolution collapse breccia (Figure 7.18; Swennen et al., 1990). Its origin as a dissolution breccia is indicated by: a) the sharp lower contact of the breccia and a gradual transition into the overlying strata, b) the presence of semicontinuous clast layers within the breccia giving it a crude 'stratification', and c) the existence of several types of evaporite pseudomorphs that are now composed of calcite, dolomite and silica. The majority of the sedimentary carbonates making up the breccia fragments show primary features indicating they were originally deposited under hypersaline subaqueous conditions and were probably interbedded with the now dissolved evaporite beds.

Most Belle Roche breccia has an interlocking packbreccia fabric showing a subparallel clast alignment and crude layering that indicates foundering by gradual subsidence, rather than catastrophic collapse into a large cavity (Figure 7.18b, c; Swennen et al., 1990). Multiple brecciation episodes are obvious in the lower breccia (Unit A), where brecciated and veined fragments occur within a microsparite (neomorphosed mud) matrix. There were at least two major brecciation episodes (Units A and B) driven by the successive dissolution of interlayered evaporite units. The second brecciation event related to infiltration of meteoric water and to the complete dissolution of any remaining evaporites (Figure 7.18d). Meteoric infiltration was probably triggered by uplift related to an orogenic event at the end of the Visean (Sudetic orogenic phase).

Some of the breccias in this region were dolomitized in active-phreatic mixing zones via processes facilitated by bacteria (Nielsen et al., 1997). High degrees of dolomite supersaturation

were produced in the anaerobic to dysaerobic zones of bacterial sulphate reduction. The sulphate came from the dissolving evaporites and the organics from the adjacent interbeds. The resulting dolomite precipitates show characteristic bacterial morphologies, such as spheroidal and dumbbell shaped crystals. The whole breccia was finally cemented by a blocky calcite under deeper burial conditions.

As a thick widespread evaporite bed dissolves, it does so more rapidly and pervasively in zones of greatest fluid access. This can be along a fault-bound edge, along a thinned featheredge, along an upper or lower contact, or along joints and fracture planes that cut the bed. As the salts dissolve, carbonate cements may precipitate as cement rinds within stratiform cavities, or along cross-cutting fracture planes. Alternating episodes of dissolving, fracturing and cementing will form veined fracture infills and fragments with clasts of cement within the disappearing bed. With further collapse, these cements may be brecciated and cemented numerous times into internally complex clasts and fragments. Ongoing repetition of this process can create clasts made up of nothing but multiple episodes of vein and cavity-fill cements (Figure 7.18). Some fracture and block-defining cements can remain, and, with the disappearance of the supporting evaporite, evolve to form an open lacework or cellular grid of cemented materials and residues called a boxwork limestone. Such boxworks are especially obvious in nearsurface dissolution settings, as in rauhwacke terrains or phreatic zones of growing tepee structure crusts. Once a rock is more deeply buried and compressed, the boxwork either collapses or is only preserved as delicate laceworks encased within massive cements. For example, even after burial, local relics of boxwork texture can still be seen beneath the V's of the Permian tepees of west Texas and the Triassic tepees of Italy (Kendall and Warren, 1987).

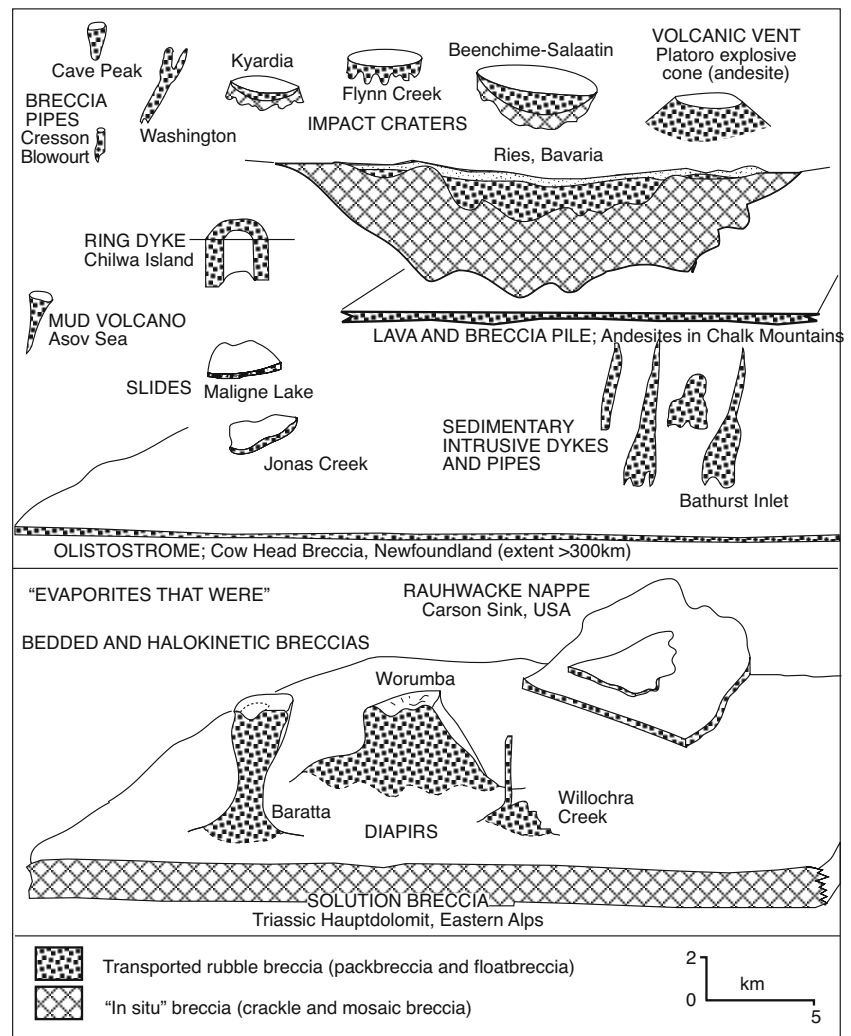


Figure 7.19. Size and shape of various breccia bodies that occur in sedimentary successions (modified in part after Laznicka, 1988). Evaporite-related ("evaporites that were") geometries are illustrated in the lower part of the figure.

Flow of water through cavities during breccia collapse in the active phreatic zone can rework fine-grained matrix material. Localised cm-dm cavities can fill with waterlain laminae that are typically overprinted by water escape features, slumps and, less commonly, with ripples and crossbeds. If the cavity lies in the vadose zone, or if a deeper phreatic cavity contains biogenic or thermochemical gases, such as methane or H₂S, then the cavity may be ornamented with microstalactites, "snottites" and other speleothems. Calcitic vadose speleothems ornament cavities in dissolution breccias in the Kirschberg Evaporite breccia of central Texas (Warren et al., 1990), while pendulous sphalerite stalactites, precipitated in thermochemically-de-

Characteristic features of an interstratal dissolution breccia	Commonplace textures and features of the adjacent crackled matrix. They also occur in some recemented breccia fragments, details on their genesis given later.
<ul style="list-style-type: none"> • Sharp lower contact and irregular upper contact to breccia bed. • Oligomict clasts derived from overlying and intrasalt lithologies. • Breccia body shows a crude stratification, with clasts of differing lithologies often stacked in original stratigraphic order. • Depositional textures in some breccia fragments indicate hypersalinity during deposition. • Zone of insoluble residues (silt, chalky dolomite, etc.) lies atop lower contact, and sometimes has infiltrated into fractures beneath. • Evaporite cements in fractures beneath lower contact. • Several types of evaporite pseudomorphs (nodules, radial textures, length slow chalcedony, etc.) are present in clasts or matrix and interclast cements. 	<ul style="list-style-type: none"> • Pseudomorphs of former crystals retaining shapes after bird-beak gypsum, axe-head anhydrite or halite hoppers, now filled or partially filled (moulds and casts) with calcite, chalcedony or quartz, baryte, celestite, strontianite. • Thumbnail to fist-sized rounded moulds or vugs, in limestone or dolomite host, with irregular edges defining positions of former chicken-wire, nodular or spherical evaporite (cauliflower vugs). Vugs may be filled or partially filled with calcite, chalcedony or quartz, baryte, celestite, strontianite. • Silica fill in vugs (geodes) is a varying combination of length-slow chalcedony (quartzine) and spherulites composed of lutecite. • Euhedral crystals of authigenic limpid dolomite or quartz (some are double-terminated) in dolomites adjacent to breccia horizon. • Minute rectangular relics of anhydrite in quartz or other minerals such as calcite (obvious in quartz because of contrasting moderate birefringence and the rectangular cleavage - but are very small). • Coarsely recrystallized (sparry) limestone and dolomite, often porous, and without skeletal debris. Internally the sparry interval may be massive, laminated or contorted. Form by calcitization of dedolomitization when evaporite dissolved (especially common in association with telogenetic alteration). • Net-textures, a small-scale relic of original bedded gypsum/anhydrite, typically with displaced impurities that outline edges of structures, typically relict patches in secondary, sparry limestone. • Small contortions typically related to flow of insoluble residues and characterised by sedimentary structures that are slumped or fractured during subsurface movement in response to evaporite dissolution.

Table 7.3. Features of an interstratal breccia created by foundering, which is the most common mechanism creating an evaporite solution breccia (in part after West, 1979).

rived H₂S/methane-filled ^{7.2}bathypneatic cavities, typify the evaporite-replacing breccia ores in the Cadjebut Pb-Zn mine, Australia (Warren and Kempton, 1997).

Breccia extent

Evaporite solution breccia beds can be syndepositional, or form much later after millions of years and hundreds to thousands of metres of burial, halokinesis, and uplift. Breccia beds tend to be widespread and stratabound, with geometries that reflect the distribution of the precursor evaporite (Figure 7.19). If the precursor layer was part of a stacked cyclic sequence of platform evaporites interlayered with carbonates or siliciclastics, the breccias tend to stack into interstratal cyclic horizons. This is the most easily recognised style of evaporite solution breccia. If the precursor evaporite was part of a halokinetic or remobilised sequence then the solution breccia is trans-stratal and follows the distribution of former salt stems, salt welds, or thrust planes. Recognising this second type of collapse breccia is more difficult, especially in core.

Intensity of brecciation and the general geometry of the foundered strata in the breccia bed can vary widely from place

to place, even within a single unit (e.g. Smith, 1972). The geometry of collapse is related to variations in:

- a) Inflow geometry of the solution front: water may enter along a fracture, fault, blanket aquifer, reef, diapir margin, etc. The timing of development of the solution front may in turn be related to episodes of seismic or tectonic instability (e.g. seismic pumping driving episodic basin dewatering, or periodic uplift or sea level lowering creating a gravity head to drive meteoric flow).
- b) Rate of evaporite solution: this is dependent on the rate of formation water crossflow and the saturation state of the crossflow. This is in turn controlled by climate, tectonics, regional uplift, development of major unconformities, etc.
- c) Confining pressure: related to thickness of overburden at the time of collapse. This is in turn related to the age of collapse (burial/uplift timing).

Stratiform breccias

The simplest and most general styles of interstratal collapse are typified by blanket aquifers and broad areas of gentle sagging and foundering where diffuse undersaturated water flow over large areas has slowly removed bedded evaporites (Table 7.3; Figure 7.19; Hauptdolomit). The blanket aquifer can lie above, below, or even within the dissolving evaporite bed. Overburden brecciation in such gently foundering regions is minor, so fossils and sedimentary structures are mostly preserved in blocks with

^{7.2}Bathypneatic is used to describe deep, stagnant waters situated at depths well below the zone of active pneumatic circulation.

near upright orientations. Larger interbed and overburden clasts tend to be tabular, and only slightly separated or disorientated, i.e., dominated by mosaic to crackle breccias.

In areas of more focused dissolution where large caverns and solution planes have formed within the dissolving evaporite beds, the whole of an overlying sequence can be reduced by chimney stoping and doline collapse to a rubble breccia — a mass made up of completely disarticulated and rotated (commonly rectangular) blocks and fragments ranging from silts to blocks many metres across. In still other areas the foundered strata can be bound by sharp folds or dislocations that are in effect normal faults. Such areas of intense brecciation are often the end product of localised collapse and can grade laterally and vertically into almost unbrecciated equivalents. These dislocations can be sharp and clean, or associated with areas of intense diagenetic alteration such as calcitisation and precipitation of ferroan carbonates. This latter group of intensely altered and replaced breccia intervals within a carbonate or sandstone host is part of a larger group of fault-focused, often metalliferous, deposits with hydrologies driven by evaporite solution (Warren, 2000b).

Hydrology and texture

Salt beds that dissolve during early burial tend to create characteristic ductile breccia textures and soft sediment slumps in the overburden. These are features that can be used to distinguish syndepositional from later modes of breccia formation related to subsurface or basinal waters or to even later uplift and re-entry into the active phreatic zone. Evaporites dissolving early in their burial cycle, even while subjacent strata are accumulating, tend to evolve into ridge and furrow dissolution geometries that influence thickness and depositional style in the lower parts of the overlying sediments. Overlying clastic beds are typically no more than partially lithified when the underlying evaporite dissolves and so are highly disturbed by ongoing collapse of their substrate. Syndepositional collapse and accommodation creates widespread intrabed slumps, water escape textures and other soft sediment deformation features in the beds immediately above the dissolution horizon. Breccia clasts in such scenarios can be contorted (plastic) and typically show rounded to crumbly edges.

In contrast, bed collapse after induration tends to create angular clasts and breccias dominated by structures indicative of more brittle collapse failure and sharp-edged angular clasts. This group includes trans-stratal joint and chimney stopes that may have tens to hundreds of metres of relief, as well as pervasive interstratal

angular breccias derived from overlying strata where the clasts show little or no evidence of internal deformation (Figure 7.4). Stopes form in the rock above the salt as the roof collapses and accumulates in the cavern formed by dissolution of the salt. Fractures and faults form in the rock layers for some distance above and around stope perimeters. Porosity and permeability created by this fracturing and faulting can provide pathways for late stage cements and can trap or transmit hydrocarbons and metalliferous fluids (Chapters 8 and 10).

Early dissolution of a nearsurface evaporite tends to be a response to facies-controlled permeability corridors in the blanketing unconfined aquifers. Areas of preferential ingress into the evaporite bed are controlled by depositional permeabilities within the overburden (e.g. ingress beneath porous and permeable sand-rich fluvial channels versus less ingress beneath relatively impervious mud-rich floodplain sediments). In contrast, the hydrologies of later dissolutional systems tend to be more directional and focused by secondary permeability features. By then the overlying and underlying beds are indurated and relatively impervious so that major zones of undersaturated infiltration or crossflow are controlled by joints, faults, fractures or reef crests, as well as regional tilting or sag. Water arriving at the site of dissolution can be either from meteoric or basinal sources and enter from above or below the evaporite bed.

The feedback between early shallow salt dissolution and partially consolidated overlying sediment styles can be traced for over 35 km of the outcrop length in the Blomiden Formation (Late Triassic) of the Mesozoic Fundy rift basin of Nova Scotia (Ackermann et al., 1995). This unit exemplifies syn-dissolutional salt loss, which was induced by shallow groundwater freshening tied to fluvial sedimentation. Fluvial sands of variable thickness (unit C) lie atop a highly chaotic and slumped mudstone with evaporite nodules still visible in its lower parts (unit B; Figure 7.20). The primary lamination in clasts in the chaotic mudstone unit preserves much of the evidence of syndepositional collapse of the evaporite substrate. It is characterized by highly disrupted bedding that is commonly cut by small (<0.5 m) domino-style syndepositional normal faults. It also preserves evidence of downward movement of fines, of geopetal structures, of variable thicknesses related to local hollows after evaporite solution, and of irregular, partially faulted contacts with the overlying unit. Unit B is underlain by a normally faulted massive mudstone (unit A).

Although the thickness of the fluvial sandstone (unit C) is highly variable, the overlying flat-bedded mudstone exhibits only gentle

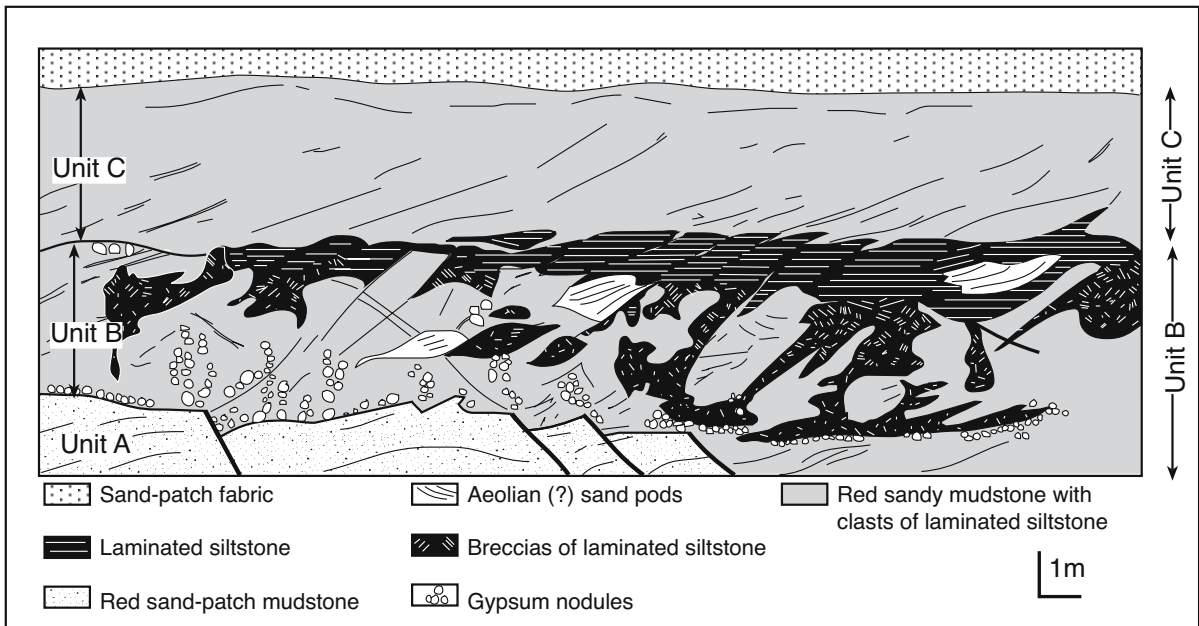


Figure 7.20. Syn depositional collapse features related to dissolution of an underlying evaporite bed in the Lower Blomidon Formation (Late Triassic) near Blomidon, Nova Scotia. See text for discussion of units A-C (after Ackermann et al., 1995).

regional dip, hence the bulk of the evaporite layer must have dissolved prior to the deposition of the flat bedded floodplain mudstones. Like unit B, the sands of unit C exhibit numerous soft sediment deformation features including; dewatering structures, convoluted bedding, kink bands, and convergent small-scale fault fans. The frequency and intensity of these features increases dramatically above low points in its base, showing unit C sands were laid down within local solution depressions or furrows that were still expanding as sediment was deposited. Unit B (the chaotic unit) is characterised by blocks of laminated claystone, which become increasingly disrupted and brecciated downward toward its base where locally abundant gypsum nodules are still preserved. Lenses and fissure fills of mudstone to coarse sandstone within the chaotic unit often entrain clasts of laminated mudstone originally derived from immediately overlying beds.

Both the chaotic unit and the overlying fluvial sands were deposited as an underlying evaporite layer underwent syn depositional subsidence and karst collapse. Groundwaters driving the dissolution were probably tied to the same river system that was depositing units B and C. The former presence of underlying evaporites is now solely indicated by residual gypsum nodules within the lower part of unit B (Figure 7.20).

In contrast, breccias that form after induration of overlying strata tend to be combinations of interstratal and trans-stratal

geometries with breccia clasts that are made up of well-indurated angular blocks. Post-induration interstratal breccias tend to follow the lateral distribution of the evaporite bed from which they formed, while trans-stratal (transformational) breccias tend to cross cut the strata and form by a combination of chimney growth and overburden stopping (Figure 7.17). Soft sediment deformation features are less pervasive in post-induration breccias and are typically restricted to intervals where insoluble residues accumulated in joint and fracture-defined fluid-filled cavities.

Post-induration interstratal breccia beds tend to have sharp flat bases and uneven, wavy to transitional blocky upper surfaces, as described earlier. If the dissolved evaporite was pure, with few intrasalt beds, the resulting rubble breccia unit is thin, but widespread. For example, a clean 100 m thick bed of salt may, when dissolved, leave behind a residue bed and rubble breccia that is no more than 0.5 - 2 m thick, but that residue may form a continuous marker horizon with a lateral extent of hundreds of kilometres. Core recovery from such intervals is often difficult. Even with good core recovery, recognising beds composed of little more than solution residues is difficult, they are easily misinterpreted as unconformities, tectonites, or syn depositional intraclast breccias. Preserved evaporite indicators, such as "cauliflower" chert or calcite concretions, are one way to define the evaporite association of such breccias.

Spectacular breccia-filled trans-statal solution chimneys dominate Silurian outcrops in the Mackinac Straits area of Michigan and western Lake Erie (Carlson 1992, Black 1997). They are paleokarst features created by evaporite dissolution and joint-controlled stoping. There are three styles of breccia in the region: 1) megabreccia beds in which blocks up to several hundred metres in size moved intact except for some minor tilting; 2) relatively thin intraformational or intrastatal breccia developed along the bedding planes both regionally and within layers in the megabreccia blocks; 3) thicker trans-statal breccias extending vertically from a few feet to several hundred metres and abutted by undisturbed bedded strata. The thickest trans-statal breccias slope vertically up to 460 m and at one site the individual blocks have fallen 290 m. Some solution caverns have recently been reactivated on a much smaller scale (Carlson, 1992). But most of the intense evaporite karstification, chimney stoping and celestite replacement took place in the Late Silurian. Not all breccia chimneys reach the surface, and areas of this “blind” salt karst can only be located using geophysical techniques.

Diapiric breccias are always trans-statal and clasts tend to be polymict associations of allochthonous fragments. Clasts of varying diameters are combinations of; a) material that was once an intrasalt bed, b) buoyed material that was plucked or was enclosed by flowing salt, and c) material that was derived from the collapse of overburden as the active diapir deflated and dissolved (Figure 7.21). The complex folding that accompanies salt flow means breccia bodies defining a former diapir are much less likely than bedded solution breccias to

Diapiric solution breccias

Salt diapir (halokinetic) breccias are transtratal features that ultimately contain no salt, but outline a former diapir geometry. Diapiric solution breccias and their reworked debris aprons (salt ablation breccias) are forming today in and around at-surface salt diapirs in the Arabian Gulf and the resulting landscape was discussed earlier in this chapter (Figure 7.14). Once the stem salt or its allochthon has dissolved, the only evidence of former flowing salt may be a few pseudomorphs after halite or calcium sulphate, either in the breccia clasts or in the interclast matrix. The breccia itself is typically an allochthonous assortment of angular clasts in a matrix made up of insoluble residues (sometimes called “rock flour”), which is typically dominated by finely crystalline carbonate, clay, sericite and chlorite. Classic exam-

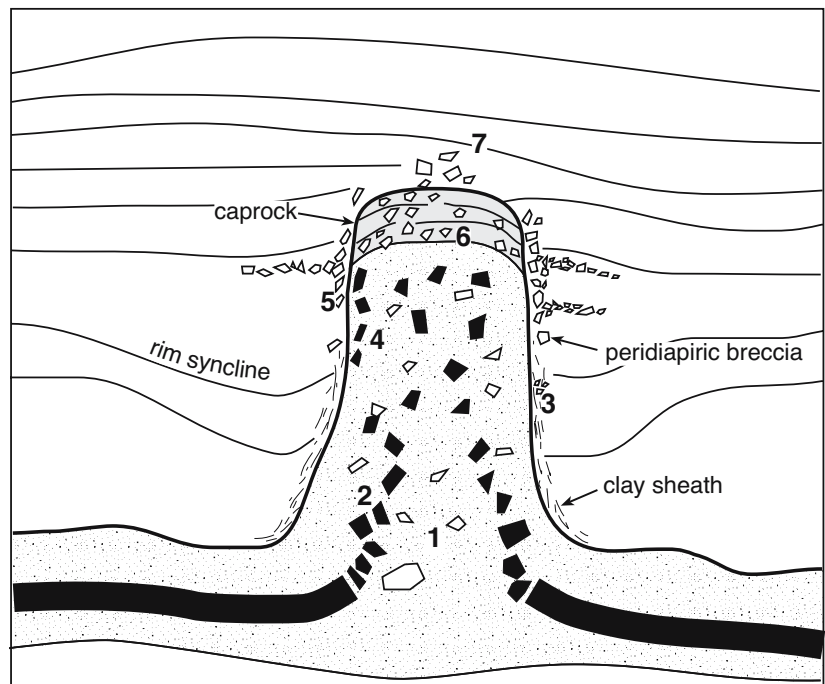


Figure 7.21. Distribution of diapir associated breccias. 1) Slabs of anhydrite in granular halite; 2) internal flowage breccia formed by dismemberment of competent internal beds; 3) breccia pockets in “clay sheath”; 4) transported flowage breccia of wallrock fragments incorporated into outer zones of stock; 5) peridiapiric ablation breccia, extent is greater in zones of former salt glaciers; 6) caprock breccia; 7) false caprock breccia, a dissolution breccia generated by salt collapse (after Laznicka, 1988).

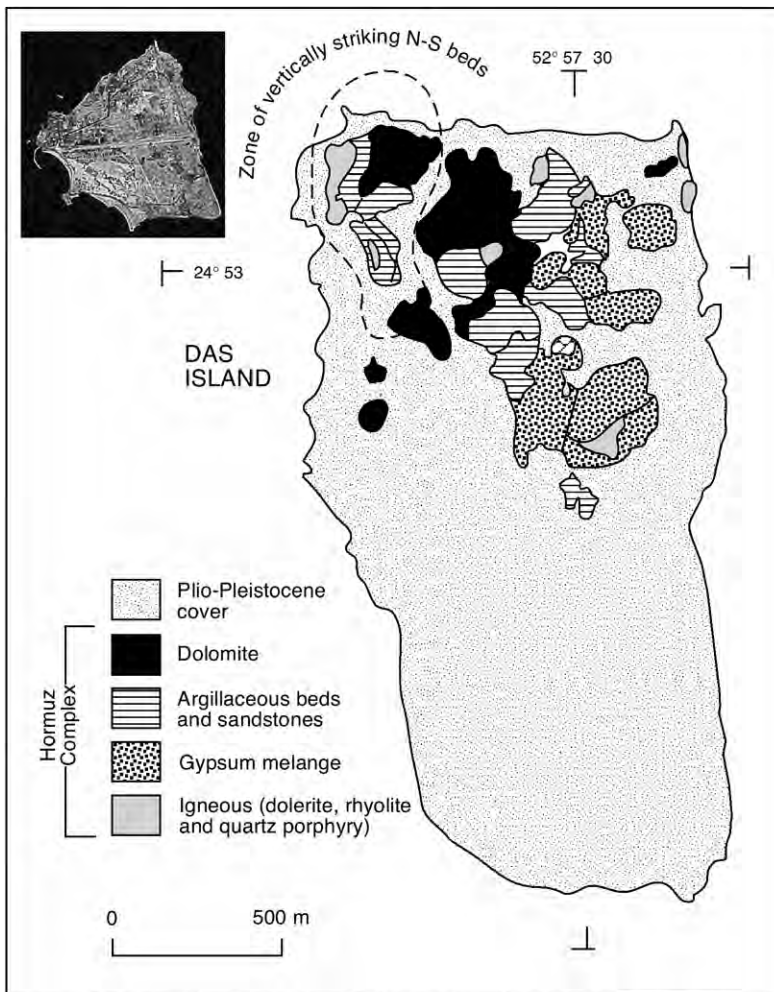


Figure 7.22. Das Island, Arabian Gulf, showing chaotic nature of the Hormuz Complex; it includes blocks of ferruginised and rafted material that are hundreds of metres across (after Kent, 1987). See Figure 6.54 for location. Inset showing a Landsat 2000 view of the island and its adjacent carbonate platform (courtesy of NASA).

preserve original stratigraphic layering of any intrasalt beds (Figures 6.8, 6.9).

Breakage and rotation of intrasalt beds begins once the encasing salt begins to move (Figure 7.21). Flowing salt can also pluck large blocks from strata adjacent to a salt wall or in contact with the flowing bed of the mother salt layer. Once caught up in flowing salt, the clasts are carried toward the surface to accumulate as breccia masses in stratigraphically higher regions of former salt, either in stems and feeders or spread out laterally across areas of former allochthons. Clasts often include metamorphic-grade minerals, such as magnesian-talc, sodian-scapolite and dravite-uvite tourmaline, which indi-

cate the clasts were carried from depths where the metamorphic/diagenetic grade was higher than the current stratigraphic level of the breccia. Solution breccia emplacement in the Damara Orogen also encompasses processes of fluidisation and cataclasis within mobile evaporite units in thrust belts and welds. These breccias were actively forming at greenschist and higher metamorphic grades and so lie outside the sedimentary focus of this book (see Warren 1999 - Chapter 6).

Recognising the occurrence of higher temperature and metamorphic grade indicators is useful when a core has intersected a breccia body and an attempt is made to distinguish interstratal breccias and transtratal chimneys from diapiric breccias and welds, as well as from associated allochthon debris aprons. Halokinetic breccias can also outline former thrust or glide planes after the dissolution of the original halite or calcium sulphate horizons that lubricated the thrust. Such thrust-weld breccias are termed *rauhwacke* and are discussed later in this chapter.

Diapiric dissolution breccias define areas above subcropping salt plugs in numerous islands in the Arabian Gulf, in what is one of the world's largest salt provinces and also one of its largest hydrocarbon provinces. Most of these diapir-cored Gulf Islands are plug ruins that have experienced little salt movement since being squeezed by the mid Miocene collision of the Arabian and Iranian plates (Figures 7.14: 7.22). Today these regions of outcropping Hormuz Complex are heavily eroded and largely covered by Neogene shoal water carbonates and marine cut platforms.

These diapiric breccias are the outcrop expressions of what is locally called the Hormuz Complex, from the type section on Hormoz Island (Figure 6.45a). It is a polygenetic assemblage of lithologies that includes both the nonevaporite blocks carried along by salt flow, as well as the supporting salt and gypsum/anhydrite matrix. The Hormuz Formation was originally deposited as a basinwide evaporite at a time near the

Precambrian/Cambrian boundary and has since been mobilised numerous times into salt structures (Kent, 1987). The range of clasts in the Hormuz Complex is diverse, but uniform over most of the Gulf islands. In none of the outcropping breccias are there any clasts derived from the cubic kilometres of indurated Palaeozoic and later sediment through which the salt passed on its passage to the surface (Kent, 1987). One of the most characteristic raft lithologies is a black foetid finely laminated and bedded dolomite that is often coarsely recrystallised and shows evidence of deep burial diagenesis. It was deposited in the same hypersaline setting that was also responsible for the deposition of the thick salt beds that became the Hormuz Complex. Similar foetid dolomite blocks characterise megabreccias in regions of outcropping diapiric breccias of the Neoproterozoic Ara Formation in Oman (Peters et al., 2003). Siliciclastic blocks composed of sandstones and siltstones are also widespread in the Arabian Gulf breccias, they are mostly reddish, grey or greenish grey and variably indurated. Throughout the region, both dolomites and siliciclastics can outcrop as spectacular rafted blocks up to several hundred metres across (Figure 7.22).

Igneous rocks are another important component of rafted megabreccia blocks in many diapiric breccias worldwide. In Gulf island breccias the igneous rafts tend to be dominated by acid tuffs (trachytes and rhyolites) along with acid intrusives

and dolerites. On the Iranian mainland the igneous rafts in namakier residues are referred to as “greenstone” blocks, as they are dominated more by basalts and dolerites. Throughout the salt-cored Gulf islands and on the Iranian mainland, large volumes of red specular haematite characterise outcrops of the Hormuz Complex. Some rafts of silicified shale are crosscut by malachite stained joints. On Hormoz Island the outermost ring of the salt plug itself is made up of haematitic tuffs, locally so rich in iron oxide that it is mined as a source of pigment (Kent, 1987). The significance of Fe-rich phases in terms of ferroan chloride brine haloes and metal transport in halokinetic provinces is discussed further in Chapter 9 and in Warren (2000b).

Texturally identical Neoproterozoic diapiric megabreccias, breccias and breccia trains crop out in the Flinders Ranges of South Australia (Figures 7.23, 7.69b; Dalgarno and Johnson, 1968). Many breccias in anticlinal cores are still located at or near the level of the mother salt bed (Callanna Beds) and so are remnants of former autochthonous salt pillows or glide planes rather than true diapirs. Others, such as the Oratunga and Wirrealpa diapirs show subcircular patterns of outcrop and breccia wings at stratigraphic positions well above the level of the original mother salt bed. Almost all the transtratal breccias line up along major regional shears and faults (welds)

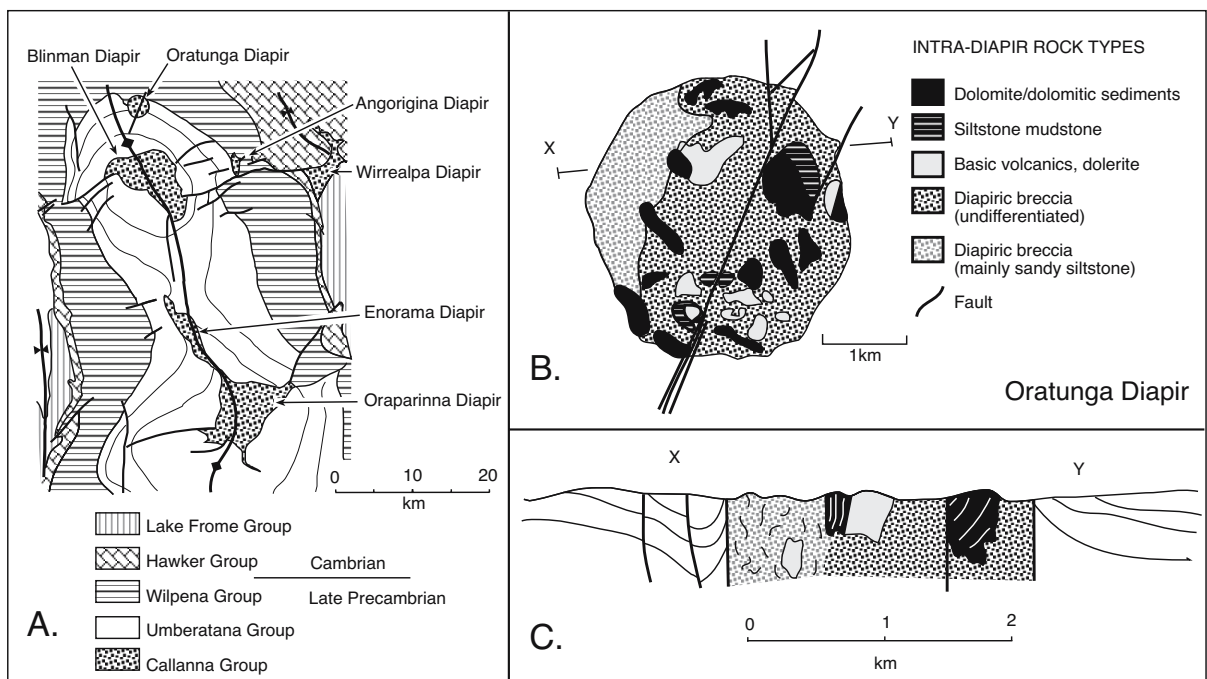


Figure 7.23. Halokinetic breccias, Flinders Ranges, Australia. A) Regional distribution of halokinetic breccia in the Callanna Formation. B) Distribution of large megabreccia lithoclasts or rafts in outcropping breccia matrix that define the Oratunga Diapir. C) East-west cross section of Oratunga Diapir (modified from Lemon, 1985).

surrounded by jostling depopods or minibasins, indicating that the mother salt bed was flowing while the basin was under extension (Figure 7.23a). Lemon (1985, 1988, 2000) clearly illustrates synkinematic controls on sedimentary facies and thicknesses adjacent to many of these breccia masses (Figure 7.23b, c).

Diapiric breccias in Flinders Ranges are heterogenous, with polymict clasts set in a strongly folded and disrupted matrix dominated by weathered pale-grey siltstones and fine sandstones. Clasts are mixtures of dolomites with gypsum and anhydrite pseudomorphs, dolomitic sandstones, siltstones and sandstones with displacive halite casts along bedding planes, and angular igneous fragments of diabase and basic volcanics, including amygdaloidal basalts (Lemon, 1985). The margins of many former diapirs in the Flinders Ranges are also characterised by numerous sub-economic copper shows in a haematitic matrix, much like the copper shows in the Gulf Islands.

Banded and aligned fabrics of clasts in the breccia masses of the Flinders Ranges diapirs indicate that shaping, disruption, mixing, and alignment of clasts occurred during salt-buoyed flow. Rafts showing coherent flow alignment can be blocks of megabreccia up to 500 metres across (Figure 7.23b, c). Long axis alignments of large raft blocks near the edge of a breccia mass are frequently near vertical and aligned subparallel to the diapir margin. Rafts nearer the centre of the breccia mass are more randomly distributed, a feature that indicates frictional alignment of large clasts near the diapir edge at the time salt was flowing or flow was collapsing. There is similarity between the size and lithology of rafts found in Neogene diapir crests in the Arabian Gulf and those in breccia masses in the Flinders Ranges. Steeply dipping bedding in rafts located near the diapir edge is also a feature of both areas and suggests flow alignment (Figure 7.22 and Figure 7.23b).

Matrix minerals in the Flinders Range's breccias include: carbonate, chlorite, feldspars (both detrital and authigenic), haematite, magnesio-riebeckite, quartz, stilpnomelane, and talc. Mount (1975) interpreted them as zeolite facies minerals formed during breccia emplacement via reactions involving hypersaline fluids. Although all the at-surface breccias lack preserved salts he argued conditions during breccia formation were aqueous, low pressure, and hypersaline. Mineral-forming reactions occurred in an oxidative low-grade metamorphic environment replete with CO₂, with open system fluid throughput and low temperatures (150° - 300°C). He concluded this palaeohydrochemical system had strong affinities to natural hydrothermal and geothermal systems. It indicated a later deeper

burial stage comparable to the current salt-filled diagenetic systems of the Iranian namakiers. The matrix minerals formed as solution flour at a time when most of the salt had already dissolved from the system and only the breccia bodies remained to outline the former salt geometry.

The late extension-stage geometries shown by the halokinetic breccias of the Flinders Ranges also means that where the crestal rather than the stem or feeder portions of the diapir breccia crop out they tend to show classic "falling diapir" geometries with suprasalt depopods, along with oversteepening related to subsequent compression and diapir squeezing (Figure 7.69b). Examples include the Wirrealpa and Oraparinna diapirs (Dyson, 1998, 1999). The falling diapir stage is characterised by crestal collapse and the formation of fault-defined graben thicks in the overlying sediments (Figure 6.17). As the diapir was collapsing, the underlying salt was thinning and dissolving. This facilitated the growth-fault focused escape of formerly confined basinal fluids on to the seafloor. This mechanism explains the formation of large fault-fed baryte masses atop many former diapir crests, along with the various small copper shows found in association with the diapir breccia margins (Warren, 2000b).

Mount (1975) noted breccia/host rock contacts were invariably abrupt and coincided with planes of weakness in the host strata. The breccia edge - country rock contacts match across some diapir stems, despite synformational sculpting and quarrying by invading diapir material. Adjacent host strata were rarely brecciated against a diapir, illustrating again the passive nature of the intrusion. His observations help explain why material from overburden strata located adjacent to a rising salt stem is not broken into rafts and transported to the surface. Salt emplacement is predominantly a passive process driven by the flow of pressurised salt into preexisting planes of entry. Where contact deformation has occurred, it usually predates diapirism and was due to glide plane faulting that then controlled subsequent breccia geometry. Mount (op. cit.) termed this style of contact 'permitted intrusion.' He argued it occurred under extension of the cover or overburden, perhaps induced by regional extension. Alteration of the host rock adjacent to contacts was absent but for minor dolomitisation and sideritisation in certain areas.

Instead of using models of forcible injection for diapir emplacement that prevailed in the 1960s and 1970s in the Flinders Ranges, Mount (op. cit.) used the outcrop geometries to stress the passive nature of salt flow into tensional structures. He concluded that "diapir" in terms of the then popular notion of active piercement, was not the most appropriate term to explain

breccia emplacement in the Flinders Ranges. His understanding of the dominantly passive nature of the diapiric process preceded by almost two decades our current models of brittle overburden atop weak flowing salt. In 1975 he stated, "... The overburden was relatively brittle, its weight the prime driving force to the intrusions. Mobility of source material, rather than factors such as density, was paramount to diapirism. The mobility is explained by the former presence of saline evaporites in the interstices of the breccias."

Diapiric breccia versus salt ablation (retreat) breccia

Diapiric collapse breccias are classified as a type of evaporite solution breccias in the preceding discussion (Table 7.4). Diapiric solution or collapse breccias are typically considered to be the result of subsurface dissolution of a diapiric feature that retains the outline of the original subsurface salt stem or allochthon. But this definition does not encompass the notion of breccias created by the leaching of an at-surface salt allochthon or namakier. When a namakier retreats it does so via at-surface dissolution of the salt mass, much in the same way a glacier retreats as it melts (Figure 7.14). Likewise, the outer edge of a salt glacier expands and contracts like the outer edge of an ice glacier. When the salt mass retreats it leaves behind a jumbled mass of material it once buoyed, which can include megabreccia blocks tens of metres across, as well as the insolubles of its carapace and insoluble intrasalt layers. These chaotic breccias are similar to a diapiric collapse breccia, but contain a much more polymict assemblage of clasts than an evaporite collapse breccia (after bedded salt) and often show evidence of mechanical reworking of portions of the breccia material by waves or currents. A separate term is probably needed to distinguish them from the more general term diapiric breccia; I call them salt ablation or salt-retreat breccias (Table 7.4)

Salt ablation breccias are forming today atop and peripheral to the dissolving edges of retreating namakiers in the Zagros of southwestern Iran (Figure 6.46a; Talbot and Jarvis, 1984; Bosak et al., 1999). Wherever an active but shrinking salt tongue subcrops or lies beneath a dissolution-derived gypcrete carapace, the clasts accumulate by breakup of the soft overburden and by stacking of fragments and rafts formerly held within the now dissolved salt matrix. The resulting namakier breccia is composed of a coarse, unsorted, heterolithic (polymict) rubble supported by a fine-grained calcareous matrix dominated by solution flour. This material can be mixed with fluvial and alluvial material or marine carbonate debris from times when the sea encroached on the salt tongue.

Ongoing dissolution of the namakier leaves behind a rubble moraine at the level of the former salt allochthon. Thus, salt ablation breccias associated with salt cores of the various island diapirs of Arabian Gulf are jumbles of exotic material carried to the surface by upwelling salt, which is then combined with the disrupted remnants of the Neogene marine carbonate shoals and buildups that once covered earlier now-dissolved salt tongues (Hormuz Complex). The mixing of contemporary sediment with salt-buoyed megabreccia blocks and insolubles in the salt, and the stratiform circum-stem or circum-weld nature of its occurrence, is what distinguishes a salt ablation breccia from a diapiric breccia (Table 7.4).

Breaking out the age of the former cover sediments within buried salt ablation breccias is useful in attempting to time episodes of at-surface salt in Phanerozoic successions adjacent to former salt stems. Belous et al. (1984) described reworked breccia trains (salt ablation breccias) composed of fragments of Devonian basalt and limestone at several stratigraphic levels in sediments surrounding the Late Palaeozoic Adamovsk salt stock in the southern Ukraine. They attributed breccia trains to lateral redeposition of salt-lifted blocks during periods of stock

Feature of interest	Evaporite collapse breccia (stratiform after bedded salt)	Evaporite collapse breccia (transtratal after diapiric salt)	Salt ablation (retreat) breccia (stratiform after an at-surface allochthon)
Timing of brecciation	Subsurface	Subsurface	Can be at-surface or nearsurface
Overall shape of unit	Stratiform (sometimes with local chimneys) with passive base	Transtratal (includes salt and thrust welds), shale sheath drag zone	Stratiform with disturbed lower contact (former gumbo)
Diversity of breccia clasts	Upward transition from low-polymict to monomict (crackle)	Polymict from intrasalt layers and plucked subsurface material	Polymict intermixed with surface sediments (e.g. fluvial, alluvial, reef)
Metamorphic grade of clasts in breccia	Matches adjacent sediments	Higher than adjacent sediments	Higher than adjacent sediments
Vertical stacking in the breccia mass	Broadly matches the original stratigraphic order, even in any stoped transtratal chimneys	Chaotic (salt flow churns clasts along diapir stem then via dissolution and welding)	Chaotic for salt-carried clasts, but more cover sediment toward its top (e.g. reef carapace on blocks)

Table 7.4. Comparison of salient features for separating three main types of breccias created by dissolving

unroofing, possibly via a salt glacier mechanism. Similarly, drilling in 1991 in the Tapley Hill Formation on the flank of the Blinman Diapir (Flinders Ranges, South Australia) intersected an anhydrite-cemented breccia with most clasts not derived from the enclosing shale (Cooper, 1991). The intra-Tapley breccia is interpreted as a salt ablation breccia, it is a residue of a salt glacier once flowing across the Neoproterozoic seafloor under a relatively deep water mass. Recognition of numerous salt ablation breccia levels in circum-stem positions about the Pinda and Wirrealpa structures in the Flinders Ranges, South Australia, led Dyson (1998, 2004) to describe them as “Christmas-tree” diapirs.

Salt-cored thrust breccias, rauhwacke and orogeny

Rauhwacke horizons are the weathered and leached remnants of what were once ‘weak’ salt-entraining tectonised layers (Jeanbourquin, 1988, 1994; Warren, 1999). Under stress, their evaporitic precursors acted as rheologic inhomogeneities providing surfaces of décollement during orogeny. Halite, or sometimes anhydrite/gypsum, is the main lubricant during the formation of stratiform tectonite or décollement layers. The inherent lack of strength of halite or anhydrite/gypsum under stress, when compared to other lithologies, focuses the greater part of the detachment or thrust plane movement into the salt-entraining interval, which can also move salt into higher levels in the thrust sheet (Chapter 6).

Conceptually a rauhwacke overlaps with both salt and fault welds and in some situations may have once fed salt into what are now salt ablation breccias. It forms a dissolution residue in the nearsurface and at outcrop as the more soluble evaporite components are leached from an unroofed thrust breccia, or deeper in the subsurface as the sheared evaporite and its surrounds are metasomatically converted to less soluble salts, such as calcite spar or dolomite. Halite probably is a major component at depths where translant thrusting occurred, but was subsequently dissolved to leave behind deformed anhydrite at shallower depths. Rauhwacke breccias in outcrop are dominated by carbonate and clastic fragments in a cataclastic matrix. Boxwork and cellular honeycomb textures, so common in rauhwacke horizons, are the outcrop expressions of pervasive weathering of an evaporite precursor.

Rauhwacke are evaporite solution breccias that define outcrops and subcrops of evaporite lubricated thrust-planes and have been described from the Jura Mountains of Switzerland, the Atlas

Mountains of Morocco and the Salt Range of Pakistan. Jordan and Nuesch (1989) and Jordan et al. (1990) describe deformed anhydrite textures in décollement horizons preserved in tunnels intersecting the main Alpine thrust planes. These anhydrites are deeper less-leached equivalents of near-surface zones where meteoric waters create rauhwacke from their evaporitic tectonite precursor. That is, rauhwacke units are the weathered outcrop expressions of evaporite-lubricated thrust planes, glide planes and detachment terranes within orogenic belts. In some older studies, the rauhwacke itself was considered to have facilitated thrusting. In other seemingly conflicting studies rauhwacke was considered to be obviously nontectonic as it could contain channel fill sediments, parallel lamination, cross-lamination, graded bedding, clastic dykes and other sedimentary structures. Now we know that much of this confusion was created by a lack of understanding of its evaporite genesis and poor definition of the term itself. An evaporite-lubricated thrust horizon or décollement is where the rauhwacke protolith forms. Subsequent weathering of the thrust horizon first in subcrop and then outcrop created rauhwacke layers with sedimentary structures. That is, rauhwacke is herein defined as an exhumation-driven post-thrusting evaporite dissolution/alteration overprint on a former salt-lubricated thrust or tectonic melange. Erosional unroofing to the level of the evaporite-facilitated thrust creates rauhwacke, which can then be reworked by fluvial and other surface processes. Rauhwacke is an evaporite dissolution overprint, it is not the cause of the thrust event.

As well as this tectonite specific usage of rauhwacke, the term is sometimes still used interchangeably with the French terms *cornieule* or *cargneule*. It then describes a porous or cavernous carbonate sedimentary rock (especially a cellular dolomite), with angular cavities filled with soft, friable, evaporitic residues that easily dissolves or falls out to leave a rough, corroded and fretted angular surface (e.g. Schreiber 1988). This less specific usage is associated with widespread textures indicating preferred dissolution of dolomite or evaporite clasts leaving behind the surrounding calcite cement. Evaporite boxwork or cellular or honeycomb fabric, all nongenetic terms, and not rauhwacke should be the preferred descriptors when angular salt solution textures cannot be tied to décollement.

Surface-related karsting of different tectonised protoliths forms structurally and geometrically distinct types of rauhwacke in the Swiss Alps. Schaad (1995) identified two end members in rauhwacke outcrop in the region (Figure 7.24a, b): a) dolomite-bearing gypsum, and b) gypsum-bearing dolomite. Dolomite-bearing gypsum rauhwacke develops as karst-fill sediment within the thrust plane, and is typified by unstructured, often

polymictic units, with geometries that reflect the shape of the precursor karst cavity. In contrast, gypsum-bearing dolomite *rauhwacke* makes up stratiform geometries that are dominated by dolomite breccias with crackle to mosaic textures. This form of *rauhwacke* is a solution-collapse breccia developed after the solution of widespread tectonised evaporite beds. Sometimes, karstification of thrust plane evaporites is aided by synformational fluvial or fluvio-glacial processes that are focused into valley depressions created by salt edge retreat, much in the same way as gently-dipping evaporite beds dissolve in the near subsurface (Figure 7.7). Pomoni-Papaioannou and Karakitsios (2002) recognise similar features to Schaad (*op. cit.*) in the *rauhwacke* horizons that define major evaporite (Carnian)

lubricated thrusts in central western Crete and the Ionian zone of the Greek mainland (Figure 7.24c). They go on to note that *rauhwacke* can be observed for more than 700 km along the outcropping base of the external nappes of the Hellenides.

Most of the deformation/lubrication in the precursor horizon to a *rauhwacke* breccia comes from the unique Newtonian flow properties of halite. But there is an under appreciated aspect of gypsum flow in a dissolution zone that may also contribute to the deformation in a *rauhwacke* horizon. Gypsum tends to deform more rapidly when bathed in increasingly saline solutions (de Meer and Spiers, 1999). This means that when an exhumed anhydrite unit has converted to gypsum, those parts of the gypsum subject to crossflow by increasingly saline brines are more susceptible to ongoing deformation.

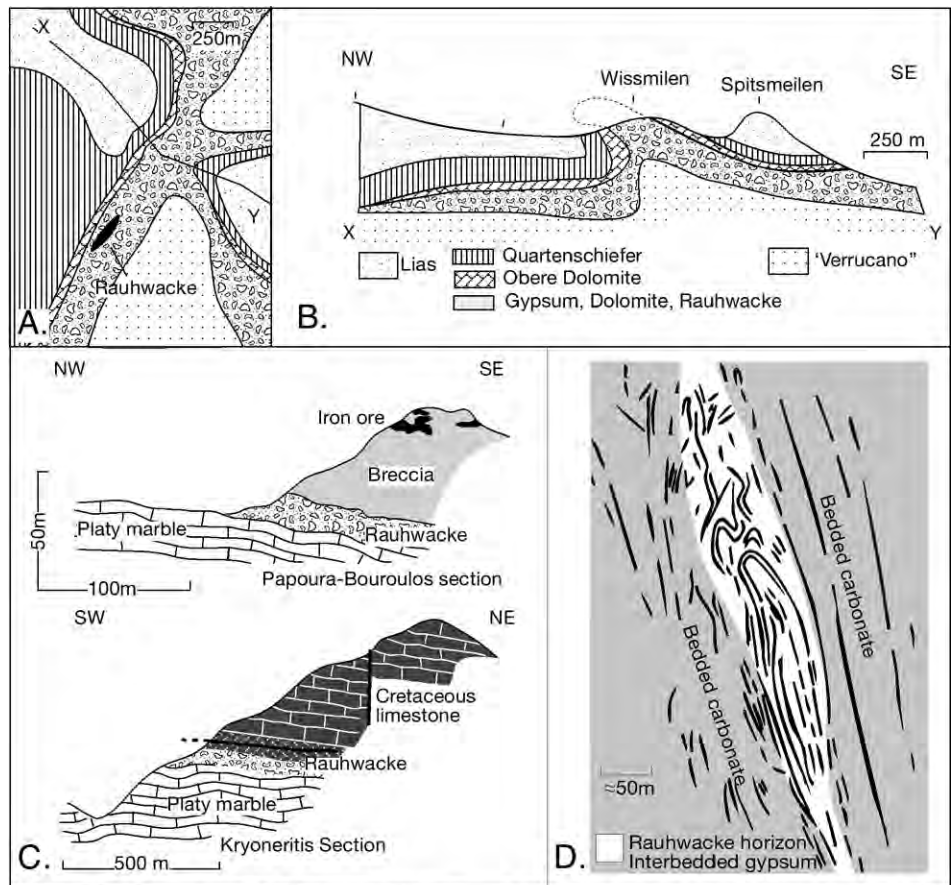


Figure 7.24. *Rauhawacke*. A) Plan view of *rauhawacke* developed atop subcropping gypsum (after anhydrite) in thrust *décollement* of the European Alps (from Schaad, 1995). B) Cross section X-Y, with position shown in 7.22a. C) Geological sections in the Rodakino region, Crete showing development of *rauhawacke* along *décollement*, which was lubricated by Triassic evaporites (after Pomoni-Papaioannou and Karakitsios, 2002). D) Outcrop trace showing increase flow deformation in a *rauhawacke* layer (formerly halite-rich) in the Gillen Member of the Neoproterozoic Bitter Springs Formation, Amadeus Basin, central Australia (after Lindsay, 1987).

As with all evaporite solution breccias, much information relevant to the *rauhawacke* protolith must be inferred rather than directly observed at outcrop. But in some relatively unleached thrust windows in the European Alps there are transitions between salt-cored tectonite protolith and *rauhawacke* that are still preserved as subcrop and even occasional outcrop. In the Austrian Alps, Spötl (1989b) describes tectonised evaporitic breccias that were created, and are still preserved, in the faults and thrusts of the mostly Permian Haselgebirge Formation. All these salty tectonic breccias flowed and fragmented during the Alpine Orogeny (Middle Cretaceous - Late Eocene) and are part of a giant regional tectonic melange. The Haselgebirge Fm. was also involved in tectonism well before the Alpine thrust event.

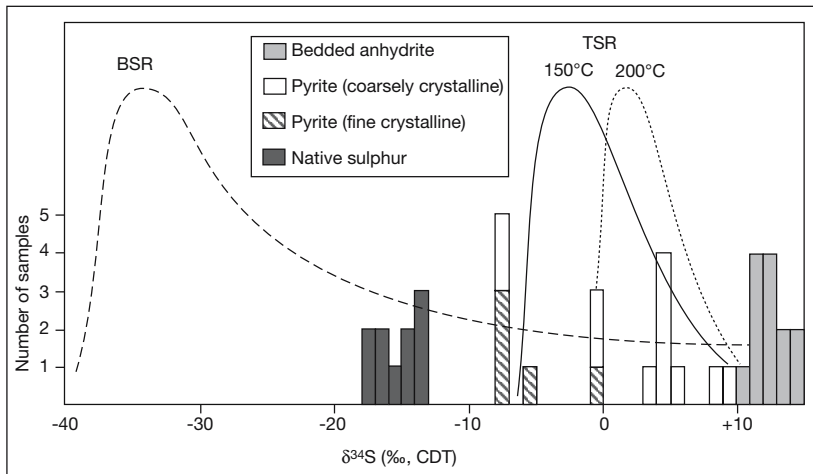


Figure 7.25. Frequency distribution of Sulphur isotope values for sulphates, sulphides and native sulphur from the Haselgebirge Fm. melange, Austria (after Spötl et al., 1998). Theoretical $\delta^{34}\text{S}$ distribution curves for pyrite produced during bacterial (BSR) and abiogenic thermal sulphate reduction (TSR) processes are shown. Note that pyrite $\delta^{34}\text{S}$ values are close to and within compositions expected for TSR.

Haselgebirge Fm. breccias are composed of polymict clasts (from cm to several tens of metres in diameter) that in the subsurface are often embedded in a halite matrix (Spötl et al., 1998). The breccia matrix contains varying amounts of clay and silt impurities (normally in the range of 15–55 %) plus minor quantities of anhydrite. In addition to clasts derived from the tectonic breakup of the initial intrasalt beds (shales, silts, sandstones, anhydrites, scarce pyroclastic rocks), nappe transport drove huge blocks of faulted Mesozoic carbonates, marls and shales into the underlying visco-plastic (halokinetic) Haselgebirge Fm. Like their brecciated surrounds, these partially or completely isolated overburden blocks show evidence of severe strain that includes; internal fragmentation, stretching, translation and rotation. Overburden pressure seems to have controlled the degree of brecciation and slickensides within these detachments.

In the subsurface the tectonised “Haselgebirge” breccias sit within intervals of recrystallised halites and anhydrites, still preserving what at first sight appears to be mm-cm scale depositional lamination. Closer inspection of the layered halites and anhydrites defines preserved isoclinal noses and overfolds, clearly illustrating the tectonite origin of the laminae (Spötl, 1989b). Pervasive salt flow and recrystallisation means any relics of primary structures in the halite beds are almost all destroyed. Preserved remnants of primary sedimentary features in the Haselgebirge Formation only remain within blocks and fragments composed of carbonate and anhydrite.

These fragments and blocks were once more competent intrasalt beds, which were progressively fragmented by tectonism and flowage, and now make up the majority of clasts in the Haselgebirge Fm. breccias. The breccias preserve evidence of their progressive tectonic evolution from limited ductile deformation → brittle fracturing → boudinage → individual rotation of newly developed clasts → development of localised matrix-supported breccias (not laterally persistent) → laterally persistent matrix breccias with increasingly homogenous grain sizes (Spötl, 1989b, 1998). In the early stages of intrasalt bed breakup the clasts were angular. With ongoing clast deformation and rotation, the clasts become rounded and develop slickensided boundaries.

The brecciation of the intrasalt beds reflects the different responses of anhydrite or carbonate to strain, when compared with halite. In response to shear stresses of much less than 1 MPa at geologically significant strain rates, halite typically flows and recrystallises via pressure solution (Figure 6.3a). Due to their higher strength, the shale, carbonate and anhydrite intrabeds respond in a brittle fashion and tend to brecciate, not flow, at the same strain rates.

The higher temperature origin of the diagenetic products in the Haselgebirge is clearly seen in the sulphur isotopic evolution of sulphate reduction products (Spötl et al., 1998). Sulphates in the Haselgebirge matrix largely preserve their Permian-early Triassic marine signatures and range in $\delta^{34}\text{S}$ from +9.8 to +13.8‰ (Figure 7.25). Matrix dolomite alteration was driven by thermochemical sulphate reduction (TSR) and is indicated by the replacement of anhydrite by calcite + pyrite ± native sulphur (See Chapter 9 for detail on TSR and BSR). Pyrite associated with TSR is coarsely crystalline and characterized by a small sulphur isotope fractionation relative to the precursor Permian anhydrite. Interestingly, the carbonates associated with TSR show low Fe/Mn ratios reflecting rapid reaction of ferrous iron during sulphide precipitation. As a result, TSR-related dolomite and calcite typically show bright Mn(II)-activated cathodoluminescence. This is in marked contrast to the dull cathodoluminescence of many (ferroan) carbonate cements in nonevaporitic deep-burial settings. In addition to carbonates and sulphides, authigenic silicate formation was closely related

to TSR, and included quartz, K-feldspar, albite and K-mica. Increasing illite crystallinity in the Haselgebirge also defines the sequence's entry into the anchizone (see Warren, 1999, Chapter 6, for further discussion of meta-evaporites and related clay transformations). The subduction or tectonism driving this salt-cored thrust melange was tied to the closure of the Meliata-Hallstatt ocean to the south of the Northern Calcareous Alps and may have preceded the main Alpine Orogeny by 50 million years (Spötl et al., 1998).

Likewise, the rauhwacke that characterises outcrops of the Triassic Burano Evaporite Formation from the Secchia River Valley of Italy is intensely modified and tectonised as its evaporitic precursor was the main décollement horizon during the formation of the Northern Apennines chain (Lugli, 2001). Inclusion temperatures of the various burial products clearly show a high temperature (greenschist) genesis (Figure 7.26). Regionally, the Burano Formation is up to 2200 m-thick and composed of metre-to decametre-scale interbeds of gypsum-anhydrite and dolostones with minor halite. The deposit has been affected by a complex array of postdepositional modifications, thermal events and large-scale evaporite dissolution, all acting to destroy an evidence of the environment of deposition. Carbonate clasts are composed of; massive and/or laminated dolomitic mudstones, wackestones, oolitic packstones and oolitic, peloidal, bioclastic grainstones. All can appear as mega-boudins within a calcium sulphate groundmass. The dolostones, (with a $\delta^{18}\text{O} = -5.7$ to -3.7‰ ; $\delta^{13}\text{C} = +1.3$ to $+3.0\text{‰}$; PDB) have been overprinted by sparry magnesite during Mg-metasomatic replacement ($\delta^{18}\text{O} = -14.0$ to -2.6‰ ; $\delta^{13}\text{C} = -2.6$ to $+1.4 \text{‰}$; PDB) via orogenically-driven hydrothermal circulation (Lugli 2001; Lugli et al., 2002). Homogenization temperatures of fluid inclusions in hydrothermal magnesite range from 275 to 310°C (Figure 7.26a).

Anhydrites in the Burano are characterized by flow structures such as centimetre-scale pseudolamination composed of aligned prismatic

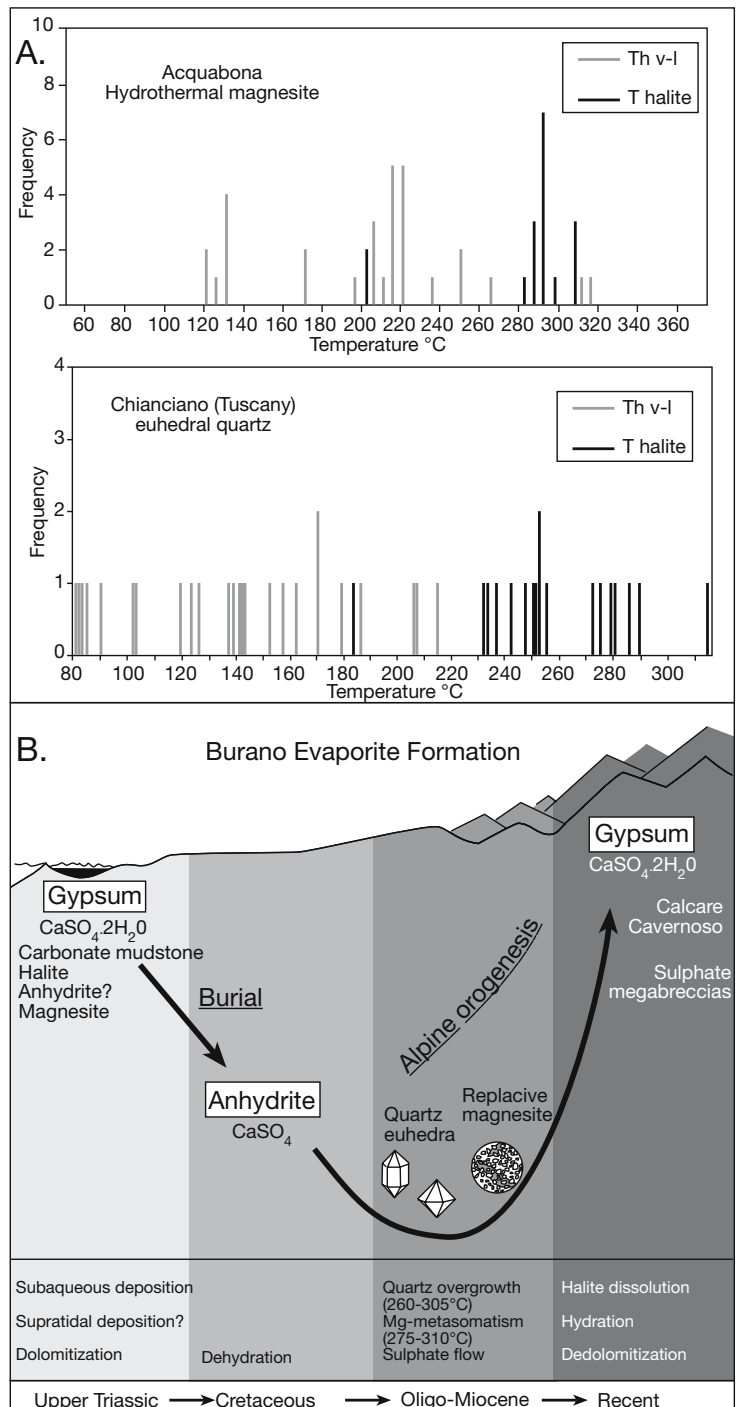


Figure 7.26. Burano Evaporite Formation (after Lugli, 2001), A) Frequency histogram of fluid inclusion results from vapour to liquid homogenization temperatures (v-l) and halite melting temperatures (halite) in fracture-filling sparry magnesite from the Acquabona region and authigenic quartz euhedra from Chianociano region in Tuscany. B) Reconstruction of the geologic history. Not to scale and adapted from the original gypsum-anhydrite-gypsum burial cycle of Murray (1964).

crystals with transposed isoclinal folds outlined by dolostone fragments. No primary textures remain. Homogenization temperatures of fluid inclusions in authigenic quartz incorporated into sulphate rocks range from 260 to 305 °C (in the Emilia area) and from 230 to 315 °C (in the Tuscany area; Figure 7.26a). Outcropping and nearsurface gypsum is composed of xenotopic irregular cloudy crystals and, more rarely, by centimetre-scale idiotopic crystals showing the same structures as the anhydrite rocks. The gypsum is a late alteration product from anhydrite, formed during migration of sharp hydration fronts and meteoric flushing. Hydration is a two step process as indicated by the presence in the gypsum encasing corroded anhydrite micro-relics and by authigenic quartz crystals that still include anhydrite (Figure 7.26b).

Evolution of Burano Evaporites during the Apennines tectogenesis was ongoing and tectonically driven by the processes of burial compression and exhumation (Figure 7.26b; Lugli, 2001). It can be divided into: (a) prevalent deposition of gypsum in the Upper Triassic; (b) gypsum dehydration at burial conditions to form anhydrite (Cretaceous?); (c) syntectonic flow of anhydrite rocks, brecciation of dolostones; syn-growth stage of quartz euhedra at deep burial conditions possibly related to the development of the Oligocene-Miocene greenschist facies of the Apuane metamorphic complex; (d) hydrothermal deposition of sparry magnesite and partial Mg-metasomatic replacement of dolostones by magnesite; (e) sub-surface dissolution of halite to form thick matrix-supported residual caprock-like anhydrite mega-breccias; (f) complete regypsification of anhydrite at sub-surface conditions; and (g) evaporite dissolution at surface exposure producing dolostone breccias with partial calcitisation and removal of most evaporite clasts ("calcare cavernoso" or *rauhwacke*).

Rauhwacke sheets (carbonate thrust breccias) also define outcrop of tectonic slices in nappe piles now dominated by pelitic rocks of Early Mesozoic age in the Carson Sink region of Nevada (Muttlebury and Lovelock Formations; Speed, 1975; Speed and Clayton, 1975). There the most extensive carbonate breccia nappe, the Muttlebury Nappe, extends over an area of 100 km² (Figure 7.19). The outcropping *rauhwacke* sheets are interlayered and interlensed with non-brecciated marble slabs. The coarse grain size and granuloblastic texture of the marbles suggests an origin via metamorphic overprint of at least moderate grade. But the degree of apparent recrystallisation in the marbles contrasts with a lack of recrystallisation and metamorphic alteration in the intercalated limestones and *rauhwacke* breccias. That is, the apparent metamorphic grade of these marbles is seemingly incompatible with that of the

adjacent unmetamorphosed sedimentary carbonates and is best explained by emplacement along an evaporite-lubricated thrust. A nearby 30m -thick gypsum klippe shows internal isoclinal folding due to strong translational movement. Speed and Clayton (op. cit.) correlate it as a lateral equivalent to *rauhwacke* of the Muttlebury Nappe. Remnants of the same folding style are preserved in the matrix of some breccia beds in the *rauhwacke* of the Muttlebury Nappe.

Chert caught up in the granuloblastic calcite marbles, and interlayered with *rauhwacke* sheets of the Muttlebury Nappe, contains ubiquitous length-slow chalcedony, implying a possible evaporite precursor for the marbles. But the genesis of the marble is best resolved using their stable isotopic signatures (Speed and Clayton, 1975). Carbon and oxygen isotope ratios of calcites from various carbonate rocks in the Carson Sink, including the marbles, fall into two distinct trends. One has nearly constant $\delta^{13}\text{C}$ and variable $\delta^{18}\text{O}$; the other has nearly constant $\delta^{18}\text{O}$, and a $\delta^{13}\text{C}$ signature that varies between -7 and -25 ‰ (PDB). The first trend encompasses all the fine-grained carbonate rocks and calcarenites of the region, whereas the second encompasses all analyses of the problematic granuloblastic calcitic marbles. Speed and Clayton's (1975) interpretation of the isotopic trend of the marble is that the marble's precursor was a coarse-grained gypsum or anhydrite-lubricated décollement caught up in active thrust and glide planes. When active it had acted much like the anhydrite-lubricated Alpine thrusts (Figure 8.26).

These calcium sulphate-cored décollement sheets were subsequently calcitised bioepigenetically, with the sulphate-reducing bacteria utilising sulphate from the décollement plane and organic carbon from sources outside of the sulphate beds, perhaps the nearby euxinic limestones, or perhaps hydrocarbons percolating and focused by the now inactive thrust sheet (hence its $\delta^{13}\text{C}$ signature). Thus, Speed and Clayton argue the process of marble formation was similar to that now forming the calcitised sulphurous cap rocks of diapirs in the Gulf of Mexico (Figures 6.64).

Thus the *rauhwacke* breccias in the Muttlebury Formation, interlayered with these enigmatic marbles, are intraformational tectonic breccias. They were created by near-surface meteoric dissolution of calcium sulphate remnants in previously salt-lubricated thrusts. Crossbedded calcarenites and quartz sands are water-reworked matrix components in the *rauhwacke* breccia, much like in the type area of the Alps; they are mechanically reworked accumulations of insoluble residues and stringers that were originally disseminated through the antecedent sulphate beds.

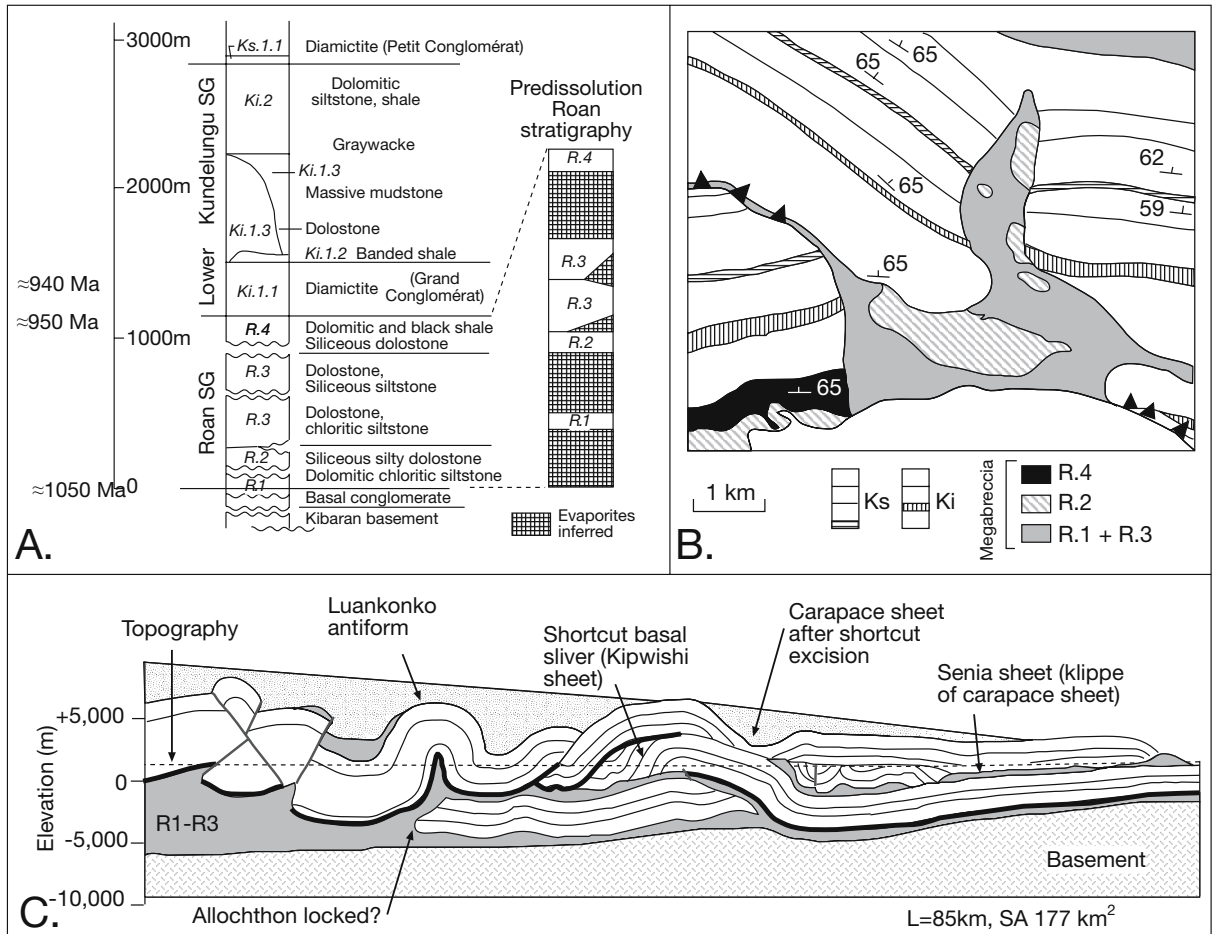


Figure 7.27. Lufilian halokinetic breccia or rauhwacke (after Jackson et al., 2003). A) Katangan stratigraphic column with a side column showing qualitatively restored evaporite thicknesses. Basal units below R.1 are based on the Zambian Copperbelt not the Katanga region. B) Map of Mukondo Diapir, representing a down-plunge oblique section. In the diapir's northern apophysis, the Roan evaporite-gigabreccia passively pierced 2 km upward through accumulating Ki and Ks overburden in the southern limb of Mutaka Synform. This diapir appears to be rooted in autochthonous Roan. The separate Roan diapir in the extreme northeast is allochthonous. C) Regional reconstruction of Katangan thrust section at the end of Lufilian time with no vertical exaggeration. The level of the modern topography indicated by dashed line.

Older but impressive examples of salt-lubricated thrust sheets and evaporite-hosted rauhwacke melange outcrop in Neoproterozoic sediments caught up in orogenic belts in the Katangan copper belt of Central Africa, and in outcrops in the Flinders Ranges of South Australia and the Amadeus Basin of Central Australia (Figures 7.27, 7.23, 7.24d, respectively). The original evaporite matrix to the breccias has long since dissolved in these regions leaving behind a complex highly brecciated melange, sometimes entraining large megabreccia blocks that can be kilometres across. Rauhwacke occurs in close association with diapiric breccias that define an extensional halokinetic stage that preceded compression and thrusting. Both the breccia blocks and the finer-grained matrix still retain a number of indicators of the former presence of widespread

evaporites and include; a) pseudomorphs of gypsum, anhydrite and halite crystals, b) dolomite textures in breccia fragments that mimic anhydrite nodules, enterolithic folds, and chickenwire textures, c) doubly terminated euhedral quartz and length-slow quartz, d) minor volumes of actual calcium sulphate (mostly regypsified at outcrop) as a pore filling cement, e) hypersaline fluid inclusions in authigenic phases and f) meta-evaporitic alteration haloes about the breccias bodies that indicate an evaporite source. These rauhwacke horizons are the structured remnants of much thicker salt masses (Figure 7.27a).

Melanges of dissolution residues in both areas outline both diapiric structures and subsequent thrust welds. The original salt in both areas was precipitated in rifts, which evolved into passive

margins, with both autochthonous diapirs and allochthonous salt tiers, and then into a salt-lubricated thrust belt during subsequent orogenesis. The salt was sourced in the Callanna Group in the Flinders Ranges and the Roan Supergroup in the Katangan Copper belt (Lemon, 1985; Jackson et al., 2003). The details of the diapiric breccias in the Flinders Ranges were discussed in the previous section (Figure 7.23). Many workers in the Flinders Ranges have focused on the diapiric nature of the breccias, although salt-lubricated thrust plane *rauhwacke* breccias are widely visible in outcrop. Work by Jackson et al. (2003) has clearly defined the intimate interrelationship between halokinesis, thrust plane development and salt in the Katangan fold belt. Classic diapiric geometries are outlined by the brecciated residuals of the Roan Supergroup, as in the Mukondo Diapir (Figure 7.27b). Former salt-lubricated thrust planes are now outlined by *rauhwacke* breccia sheets in both the Katangan Copperbelt of Shaba (Democratic Republic of the Congo) and Zambia. These regions also contain the world's largest concentration of stratiform copper-cobalt ores, with their genesis largely focused by the interactions between metalliferous basinal brines and salt sheets (Warren 2000b).

During the Lufilian orogeny, the Katangan basin structure was radically transformed first by extrusion of allochthonous evaporites, then by orogenic shortening (Figure 7.27c; Jackson et al., 2003). Salt tectonics began during deposition and gravity gliding of the Roan Supergroup between 1050 and 950 Ma. In mid-Roan time, salt walls and extrusions of evaporites began to be emplaced (former salt now outlined by breccias and *gigabreccias* - as in Flinders Ranges). In early Kundelungu time (940-850 Ma) the evaporitic diapirs enlarged. Lufilian deformation began by laterally squeezing diapirs to form salt welds between 850 and 650 Ma. Then, a large sheet of commingled Roan evaporite and carbonate-dominated sediments and ores was extruded northward by ≈ 65 km. Extrusion was fast enough to blanket a uniform pre-orogenic footwall unit without overriding any synorogenic deposits, much like the Salt Range in Pakistan today (Figure 6.40). Continued shortening then emplaced large thrust sheets, lubricated by the preexisting salt-sediment extrusive sheet. Restorations by Jackson et al. (2003) suggest that the Lufilian foreland in the Katangan area shortened from 193 km to 85 km and that the depositional northern edge of the evaporite basin controlled the shape of the Outer Lufilian Arc.

Bed geometries in both the Flinders Ranges and the African copper belt show that a post salt-solution distinction between *rauhwacke* and diapiric breccias is difficult in core, and without sufficient outcrop analogues or seismic is near impossible.

Lithologically, at the lower temperature end of the burial spectrum, the components of *rauhwacke* and diapiric breccias are identical. Our increased understanding of tiered allochthon emplacement of salt masses, and the time equivalence of early updip extension and downdip compression, makes such a distinction increasingly irrelevant at the lower temperature end of burial. When formed, updip extensional diapirs pass downdip into compressional toe-of-slope regions and both areas will become compressional later in the Wilson Cycle (Figures 5.27, 6.38).

Rauhwacke and its precursor salt-lubricated thrust planes and alteration haloes tend to be dominantly interstratal stratiform surfaces defined by focused slippage, adjacent fault plane brecciation and subsequent solution collapse. Such thrust planes often separate a brittle-faulted hanging wall from a less altered footwall succession (thin-skinned tectonics discussed in Chapter 6 and illustrated in Figure 7.27c). Occasionally a *rauhwacke* breccia cuts upsection as a thrust ramp or riser. In contrast, diapiric solution breccias tend to be identified by largely trans-stratal geometries that outline the shape of the precursor salt diapir. But salt-lubricated allochthon sheets evolve into thrust planes, while former salt welds and diapirs can be reactivated to become the base of salt-lubricated thrust sheets (see Figure 6.41). When diapirs, allochthons, depopods and detachment surfaces are part of the same salt-lubricated system, the two breccia styles merge and become near impossible to separate. Older 1950s vintage notions that salt diapirs indicated active halite intrusion and so were a separate tectonic style to thrusting, led to heated but possibly unnecessary argument in the 1960s and 70s on ways to separate diapirs from *décollement* in the Flinders Ranges (e.g. Burns, 1977). We now know they are part of the same salt-lubricated association with diapiric intervals and salt tiers often acting as a plane of weakness for subsequent thrusting as the basin passes from extension into compression (Wilson cycle).

Where the concept of salt allochthon breccia versus *rauhwacke* needs to be better defined is in the higher-temperature higher-pressure realm of metamorphism. *Rauhwacke* when used to define a type of breccia has inherent notions of a thrust sheet and an alteration halo about the salt-cored thrust plane. Fluids focused along the salt cored thrust can penetrate, alter and even mineralise adjacent strata. Salts can survive as halite to burial temperatures in excess of 450°C and as anhydrite to temperatures >900°C (Warren, 1999). *Rauhwacke* as a concept explaining near fault alteration has been applied to salt-lubricated thrust residues and alteration/mineralisation haloes within this temperature range (greenschist to amphibolite facies).

But notions of diapirs and salt welds are largely restricted to the sedimentological literature yet they too must pass into the metamorphic realm. Salt allochthon and weld models, based largely on seismic interpretations of sedimentary basins, have no such notion of alteration haloes, yet they have extensive ferroan carbonate haloes as seen in outcrop in Algeria, the Flinders Ranges and the McArthur Basin (Warren, 1999; Chapter 8). Combining the two notions into a single model of structural evolution and mineralised fluid focusing will give increased exploration success in copper and base metal metamorphic/halokinetic terrains such as the Mt Isa-Cloncurry belt of Queensland, Australia and the Yunnan province of China (Warren, 2000b).

Partial salt dissolution: residues of less-soluble salts

Whenever a thick evaporite bed comes into contact with undersaturated waters it dissolves to leave behind a bed of insoluble residues. So far we have concentrated on characteristics of evaporite solution breccias with insoluble residues that no longer retain preserved salts. But there are intermediate stages in many subcropping and subsurface beds and diapirs in sedimentary basins, where less soluble salts remain after the more soluble salts have dissolved. The result is a cumulate laminar layer or breccia dominated by less soluble salts, typically anhydrite, that were originally dispersed through a now largely dissolved halite bed. At the same time as the beds dissolve, pore fluid salinity increases at the dissolution contact. As this water mixes with throughflowing waters in adjacent beds it can precipitate anhydrite or gypsum cements in nonevaporitic strata (burial and telogenetic salts).

If the dissolution is rapid and focused, overburden and intrasalt beds brecciate and fail via incremental crack-seal processes, with residual anhydrite or alabaster matrices surrounding the former intrasalt breccia blocks. If the dissolution is slower and subsidence or “let down” of the overburden gentler, then a residue bed of layered sulphates forms (Figure 7.28). In this case the overburden span or roof tends to subside in parallel, with no more than minor crackle fracturing at the contact with the accreting laminar sulphate bed. If the subsiding overburden is a clay, then satin spar veins fed by high salinity brines coming off the dissolution front can infill any gravitational and hydraulic fractures forming in response to collapse-induced extensional stresses (Figure 1.40).

Less soluble salts tend to accrete at the boundary of the salt bed in contact with the undersaturated crossflow. If dissolution occurs at the top of a salt bed then accretion occurs along the base of the residue bed (younging downward - as in anhydrite caprock atop a diapir). If it occurs along the underside of a thick salt unit, the less soluble salts accrete to the top of the bed (younging upward - an “upside-down” caprock known as a basal anhydrite). In either case, the accretion of less soluble salts generally leads to a distinctive wavy-laminated fabric, either in anhydrite or in mud-sized residual material (that includes carbonates as well as clays). The wavy structure forms as small and disaggregated layers of insolubles are wrapped around larger clasts or nodules of anhydrite.

The mineralogy and thickness of the residue layer depends on the proportion of insolubles in the original evaporite bed and the salinity and chemical composition of the undersaturated waters. Relatively pure halite or potash units tend to produce thin layers of residual impurities. Anhydrite or mudstone insolubles hosted in the original intrasalt beds are typically first incorporated as bedding-parallel elongate clasts in the bed, often with minimal modification to their pre-collapse textures. Ultimately, with enough time, freshening and flushing, all the residual anhydrite dissolves and only nonevaporite clasts and fine-grained insolubles remain (typically muds and loose silt-sized dolomite rhombs).

Focused rapid dissolution - Evaporite clasts

Differing solubilities between bittern, halite and CaSO_4 salts means that breccias can be derived from the collapse of intrasalt beds of less soluble salts into cavities formed by the rapid dissolution of more soluble salts. Brecciated beds of less soluble strata are typically composed of angular blocks of bedded gypsum/anhydrite, which fragment and settle as the supporting halite or bittern beds dissolve. These breccia beds are sometimes encased or underlain by halite showing evidence of flow or slippage into the subsurface space created by differential dissolution. Other times the breccias have characteristic smooth bases and more irregular tops. Sulphate collapse breccias typify parts of the subcropping margin of the Permian Castile Formation of the Delaware Basin in west Texas and New Mexico (Hovorka, 2000), and the Middle Miocene (Badenian) gypsum of southern Poland and the Ukraine (Babel, 1991) and the Permian Khuff Formation of Abu Dhabi and Saudi Arabia (pers. obs.).

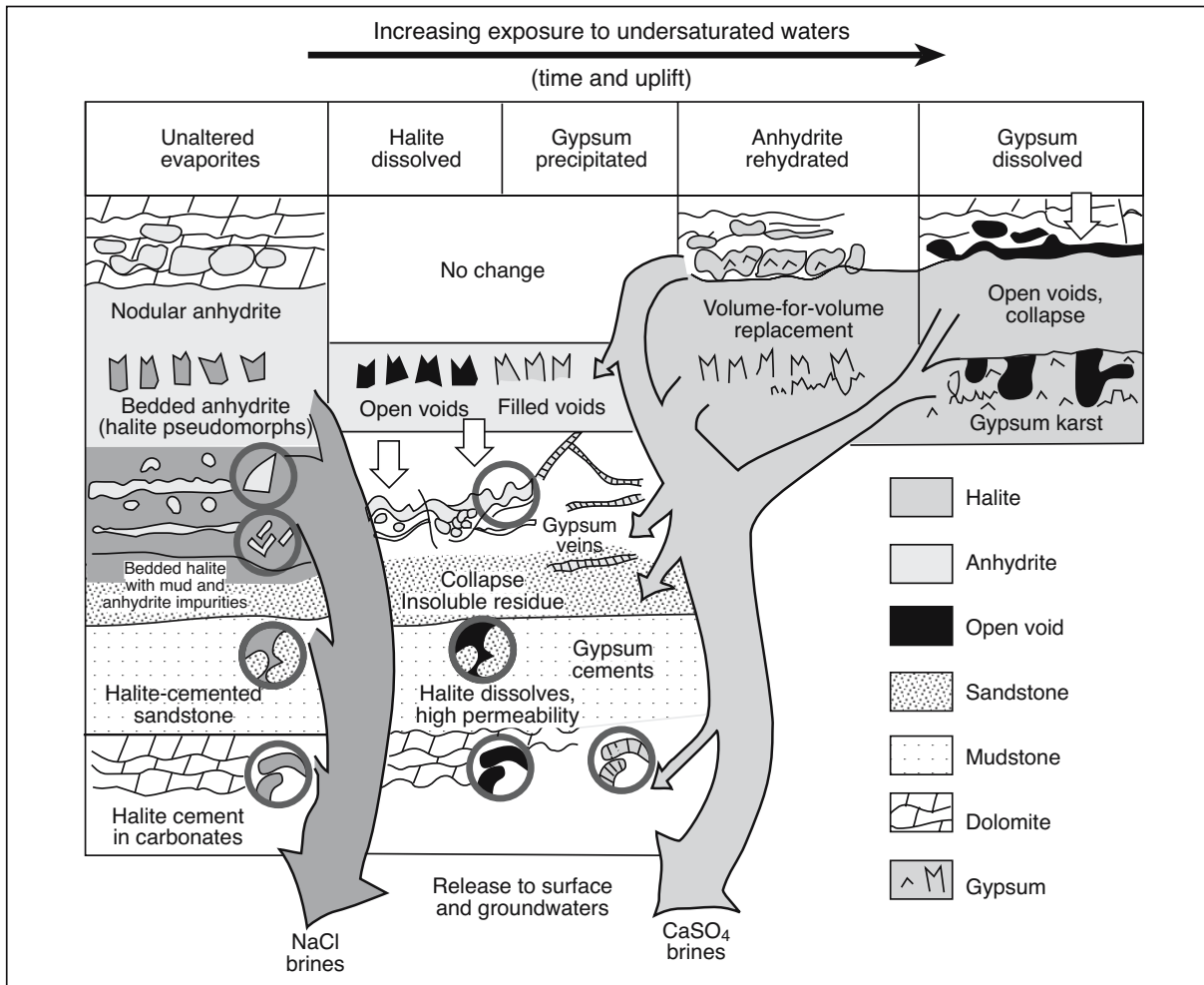


Figure 7.28. Salt-dissolution processes related to ongoing exposure to undersaturated waters. Unaltered evaporite is shown on the left, initial alteration in contact with somewhat undersaturated water in the middle, and intense alteration after prolonged contact with undersaturated water is shown on the right. Degree of exposure to undersaturated water is largely related to uplift and time (after Hovorka, 2000).

Babel (op. cit.) describes preferential intra-evaporite dissolution processes in gypsum of the Middle Miocene (Badenian), southern Poland. Gypsum-clast breccias formed by the early diagenetic dissolution of halite beds within a thick laminated gypsum section. Sometimes the effected interval is a single cm-thick bed and halite dissolution is interpreted to have occurred during a short freshening interval that only affected sediments just below the sediment-brine interface. Other times, the dissolution front was thicker, dissolving substantial thicknesses of halite to form crackle/rubble zones in bedded calcium sulphates that are tens of metres thick. Dissolution in some areas took place while parts of the gypsum beds were still water-saturated and soft, leading to complex soft-sediment deformation textures. Dissolution in other areas occurred after

the gypsum was indurated and created classic collapse breccia intervals, with smooth bases and irregular crackled upper surfaces. Residuals within the gypsum karst are defined by very fine-grained gypsum and clay horizons that typically also define the base of a collapse interval. The brecciated intervals pass up or laterally into faint or unlaminated gypsum alabaster (aka compact gypsum).

Because such partially dissolved evaporite breccias define the edges of many buried evaporite units, and are typically associated with syn-dissolutional flowage of some of the remaining salt layers, they are easily confused with primary debris flows in the evaporite bed. This is especially so when the dissolving salt beds are adjacent to pinnacle reefs, which have acted as

artesian aquifers during evaporite drawdown, as is the case with many of the inter-reef salt beds adjacent to the pinnacle reefs in the Silurian of the Michigan Basin (pers. obs.). Separating primary emplacement from a secondary dissolution origin can be very difficult in such brecciated and clast-rich beds and residues. Genesis is best resolved using oriented core, image logs and ties to detailed seismic mapping of salt collapse haloes above and around pinnacles.

**Diffuse dissolution-
Markers and residue beds**

Gypsum-anhydrite caprocks atop diapirs are widely recognised products of preferential salt dissolution (Figure 6.64). Less widely recognised stratiform equivalents to caprocks occur where undersaturated groundwaters flush the upper and lower contacts of stratiform halite. Such a set of processes affects halite beds in Maha Sarakham evaporites beneath the Khorat Plateau of NE Thailand (Sessler, 1990; Utha-aroon et al., 1995; Warren, 1997) and the San Andres salts of the Palo Duro Basin of west Texas (Hovorka 2000; Gustavson et al., 1994). As a thick salt mass dissolves the mineralogy of the various residues typically depends on how long the evaporites were in contact with invading undersaturated waters and on the chemical make up of the crossflowing waters (Figure 7.28). Invading waters can be meteoric or basinal.

Gentle dissolution at the top
Uplift, or simply the cessation of evaporite deposition allows undersaturated waters to come into contact with a buried salt bed. Undersaturated meteoric pore waters tend to pond atop the relatively impermeous buried salt and so the salt mass dissolves from the top down.

Maha Sarakham salt, Thailand

The Maha Sarakham sediments of NE Thailand are of upper-middle to late Cretaceous age and unconformably overlie continental deposits of the Khorat Group (Utha-aroon, 1992; El Tabakh et al., 1995). Maha Sarakham sediments were deposited as a thick sequence (up to 1000 m) of basinwide evaporite. Beds tend to be stratiform about the basin edge and halokinetic in the thicker, deeply buried beds of the present centre (Figure 7.29a). Three thick evaporite units (informally called the Lower, Middle and Upper Salt), or their residual

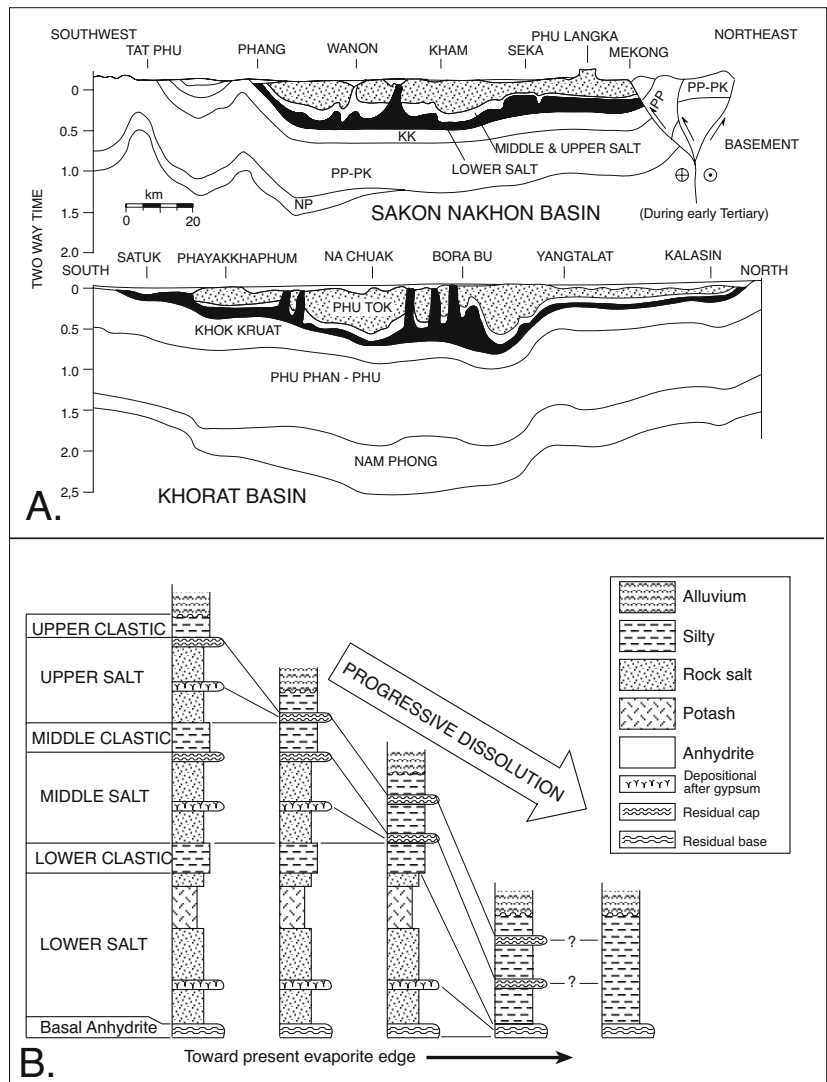


Figure 7.29. A) Regional subsurface structure of Maha Sarakham Formation showing preferential development of diapirs in lower salt toward the basin centre and dissolution toward structural edges of basin. B) Progressive dissolution of halite and accretion of residual anhydrite beds toward the present basin edge (after Utha-aroon et al., 1995). See Figure 11.13 for locality and detailed stratigraphy.

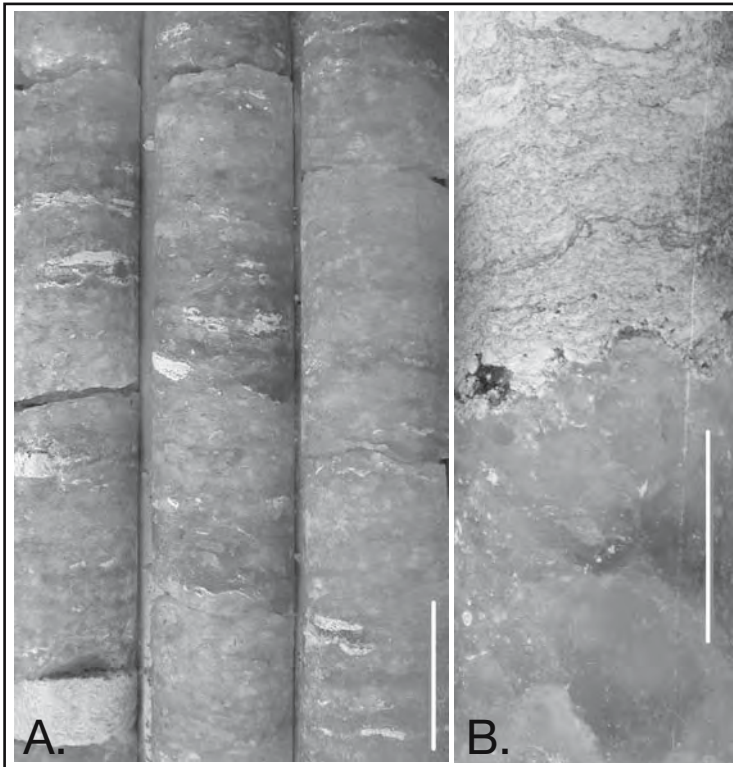


Figure 7.30. Formation of the laminar bed of nodular anhydrite residues at the upper contact of the lower halite member of the Cretaceous Maha Sarakham Formation, NE Thailand. A) General distribution of white-grey anhydrite nodules and layers dispersed in chevron halite in core. B) Contact between dissolving halite and upper white-grey unit of dispersed anhydrite nodules and blebs. This laminar accretionary anhydrite bed defines the upper dissolution contact of the lower halite member. Some 2 metres above this contact are the redbeds of the lower clastic member. The anhydrite unit preserves the shapes and sizes of the anhydrite blebs that were dispersed through the halite prior to its dissolution (as in Figure 7.30a). These nodules and blebs are left behind to form a layered and accreting sulphate unit as halite is dissolved at the halite anhydrite contact (Scale bar is 5 cm long).

equivalents, are present throughout the basin (Figure 7.29b). Evaporite minerals in the various beds include: sulphates, rock salt and potash minerals. Potash is found mostly in the upper part of the Lower Salt unit, but saltern halite is by far the most common salt and many beds preserve pristine chevron textures. The salterns occasionally freshened so that cm-scale gypsum nodules and beds with subaqueous textures (<1m thick) were deposited. All the gypsum converted to anhydrite during shallow burial. The three main halite units that make up the Maha Sarakham Formation are laterally continuous and are traceable basinwide. Nevertheless, ongoing interplays between salt dissolution and flowage has been active from the Cretaceous until today. Lithostratigraphic correlation from one place to another is not a straightforward exercise (Figure 7.29b).

Thick clastic redbeds of mudstone separate each of the three main salt beds and are informally called the Upper, Middle and Lower Clastics (Figure 7.29b). In core the clastic units are largely homogeneous clay beds, with locally laminated and stromatolitic horizons, infrequent nodular caliche horizons, occasional anhydrite nodules, root structures and mudcracks. Near their contact with adjacent salt beds there are beds of anhydrite residues overlain with clays hosting fractures and fissures filled with satinspar anhydrite and halite, indicating dissolution of a portion of the adjacent salt bed (Chapter 1).

Depositionally, the lower halite in the Maha Sarakham is composed of chevron halite with dispersed cm-scale anhydrite nodules and stringers after gypsum (Figure 7.30a). The earliest evidence for salt dissolution is cm-dm karst-pits filled by coarse recrystallised halite cement forming a syndepositional dissolution texture identical to that in the modern Qaidam Basin (Figure 11.3). Salt dissolution next occurred in the shallow subsurface along bed boundaries where clastic units were in contact with bedded salts. Waters undersaturated with respect to halite, moved through adjacent redbed aquifers, initially as the clastics underwent deep weathering then as the buried clastics acted as conduits for compactional and basinal waters. This style of clastic-groundwater-driven dissolution left behind accreting residue textures at each major salt/clastic contact. Where the dissolving salt bed was composed mostly of clean halite all that now remains is a thin laminar residue of accreted insoluble clay residues. Due to the highly saline and anoxic nature of the brine leachate, the iron in these zones is reduced and where the salt bed is still actively dissolving the colour of the adjacent clastic has been altered from red to green.

In other regions of the basin, where the dissolving halite contained numerous anhydrite nodules and stringers, the resulting dissolution residue is composed of stacked anhydrites that can be partially rehydrated to gypsum. These residual beds can occur along both the upper and lower dissolving bed contacts of all three salt units. At the contacts of the Upper and Middle Salt members the CaSO_4 residuals tend to be dm-m thick on

the upper bed contact, but somewhat thinner on the underside (cm-dm). On the underside of the Lower Salt member, the CaSO_4 residual is much thicker ($\approx 1\text{-}2\text{ m}$) and probably reflects a much greater focused throughflushing from the underlying and dewatering Khorat Group sediments (see basal anhydrite discussion).

Each CaSO_4 residual bed is made up of undulose thinly-layered to laminated light grey to off-white anhydrite/gypsum nodules and micronodules. Individual layers may be as thick as 2 cm (Figure 7.30b). Lamina/layer orientation ranges from horizontal to vertical, with clays and organic matter defining the laminae and the nodule edges. Where a halite residual undergoes more localised dissolution the anhydrite beds are broken and brecciated with interclast matrix infiltrating from the adjacent clastic member. Brecciated textures are most common in residues of the Upper Salt member as this unit is more effected by modern nearsurface meteoric leaching. If the Upper Salt member is still present in the stratigraphy it protects the Middle Salt member from surface driven dissolution.

Within the Middle Salt member is a basinwide dm-m-thick anhydrite marker bed. Complete dissolution of the halite encasing the marker bed of the Middle Salt member, and associated gentle foundering of the overlying middle clastic member, stacks the marker bed along with other anhydrite nodules and stringers in their original stratigraphic order (Utha-aroon et al., 1995). This gentle style of oriented solution stacking of the intrasalt sulphate beds even preserves the subaqueous gypsum pseudomorphs of the anhydrite marker bed in their original growth position. Recognition of preferential dissolution occurring in a basin's stratigraphy allows a correlation across areas where halite beds have disappeared and only the anhydrite residuals remain (Figure 7.29b). The final stage of salt dissolution occurs when the anhydrite residuals completely dissolve and brecciate to leave the three clastic members stacked one atop the other.

Where the Upper and Middle Salt members of subcropping Maha Sarakham Fm have completely dissolved, the present-day landsurface is defined by topographic depressions adjacent to a blind valley karst system atop a suprasalt high. Fluvial systems

flow into this depression and feed subsurface waters to the dissolution front, which in turn focuses and stacks Quaternary fluvial channel sands. Outcropping and subcropping examples of this style of sequential halite dissolution define caprock outliers of the Maha Sarakham Formation in the Nam Theun syncline in central Lao (Figure 7.7c). As on the much larger Khorat Plateau, Cretaceous halite along the syncline axis is retreating from the meteoric-flushed edges and top of the salt bed leaving behind distorted and slumped remnants now patchily exposed in erosional banks along the river (pers. obs).

Some geomorphologists working in the salt solution terrains of NE Thailand have not recognised the effects of salt solution on the stacking pattern of fluvial systems. Instead, they have interpreted the thickened sections of Quaternary fluvial sediments as indicating a deepening of the river thalweg and have related it to Quaternary uplift and not dissolution downcutting. Effects of preferential dissolution along the edges of a bedded halite unit further emphasize the pitfalls of using simplistic notions of lateral correlation between thin marginward anhydrite and thick basin-centre halite (Figure 5.30).

Palo Duro Basin, west Texas

Hovorka (2000) has described the textures and effects of salt solution on the widespread Permian salt beds of west Texas (Figure 7.31). She focused on the solution processes occurring beneath the High Plains of the Texas Panhandle, an area typified by landscape stability and the slow, longterm deposition of the overburden. There the upper surface of the salt approximately

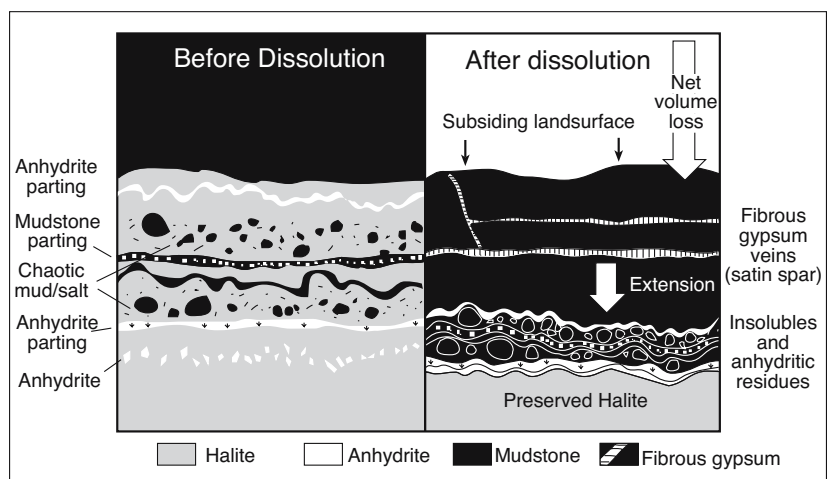


Figure 7.31. Crossflow of undersaturated groundwater at the top of an impure halite bed creates an insoluble residue of anhydrite and mud under conditions of regional, low-angle salt dissolution and passive letdown of overlying strata, which fracture and are cemented by satin spar gypsum (after Hovorka, 2000).

parallels the hydrologic flow lines and so lies at a low angle to the land surface. In the Palo Duro Basin the top-of-salt lies at a depth of 250 - 300m, approximately paralleling the low relief Southern High Plains. This salt dissolution surface regionally crosscuts Permian stratigraphy, so that in the northwest, the Seven Rivers Formation is the uppermost salt-bearing unit and overlying salts have been dissolved; while down hydrologic gradient to the southeast, the younger Salado halite is partly preserved.

Hovorka's examination of the residues left after regional low-angle salt dissolution in the Palo Duro Basin showed that salt dissolved and residues formed by incremental dissolution of the uppermost salt unit over a wide area. It was accompanied by passive stratiform subsidence of overlying strata (Figure 7.31). Horizontal fractures in overlying strata indicate vertical extension, while syntaxial satin spar gypsum fillings show that the fracture opening occurred incrementally as underlying salt was dissolved (Gustavson and others, 1994). Typically, the creation of overburden voids atop most salt beds in west Texas does not lead to catastrophic collapse. Rather, stratiform beds of insoluble residues are the best evidence that impure salt beds have been dissolved.

Diagnostic features of the regional low-angle crosscutting dissolution surface atop salt units in the Palo Duro Basin are: (1) Mixtures of insoluble components from the previously underlying halite with a wavy lamination in anhydritic intervals. This reflects the accretion of newly released insoluble components against existing insoluble residues. (2) Residual beds in positions that are laterally equivalent to preserved salt, (3) Anhydrite residual beds that stack one atop the other with little or no internal deformation, providing there were depositional sulphate beds in the original salt. (4) Syntaxial, horizontal, gypsum-filled fractures in overlying units. These are the same sets of features that define regional dissolution atop Cretaceous halite in the Maha Sarakham of Thailand (Utha-Aroon et al., 1995) and probably characterise all shallow low angle salt beds undergoing exhumation.

Dissolution at the bottom
Undersaturated escaping basinal waters, or deeply circulating meteoric waters, can drive dissolution on the

underside of a thick salt bed. In this situation the salt dissolves from the bottom up, and the residual wavy-layered anhydrite bed has a finite thickness controlled by its inherent crossflushing hydrology. To date this mode of preferential salt solution has only been documented in Maha Sarakham, probably because it is one of the few, if not the only, saline giant where both the upper side and the underside of the thick salt unit has been extensively cored and studied.

Basal anhydrite, Thailand

Preferential dissolution of the underside of the Maha Sarakham Formation of NE Thailand is occurring where it is bathed in a crossflow of compactional and thermobaric waters (Warren 1997; El Tabakh et al., 1998a). The resulting basal anhydrite passes downward, via a thin cm-thick organic-rich residue layer, into underlying nonevaporite sediment made up of calcite-cemented fluvial sands and shales of the Khok Kruat Group. The basal anhydrite bed is characterised by a near constant basinwide thickness and consistent stratigraphic textures across the underside of large portions of the salt (Figure 7.32). In many evaporite basins of the world, similar constant thickness beds are described as basal anhydrites, but are assigned a primary depositional origin.

To explain the subsurface processes that effect the underside of thick evaporite beds, the salts of the Khorat Plateau of Thailand are ideal. The region is unique in that the various salt layers of the Maha Sarakham Formation have been extensively and continuously cored from top to bottom and a simple gamma log suite run in the borehole. This was done in the 1970s and 1980s in a World Bank funded exploration project for potash

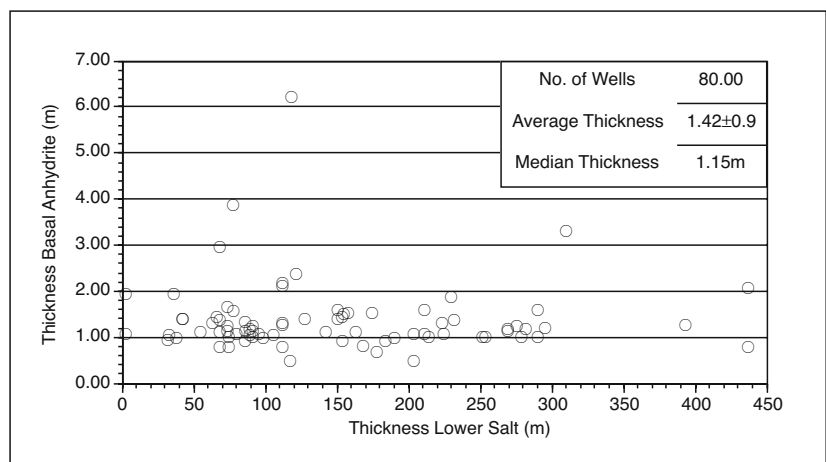


Figure 7.32. Crossplot of thickness of the basal anhydrite unit versus thickness of the overlying "Lower Salt" in the Maha Sarakham Formation, Thailand.

salts. The cores were double-sealed in plastic wrap and archived at a DMR core store in Udon Thani, where they are still available for study. Everywhere it was cored the underside of the thick Lower Salt of the Maha Sarakham Formation is a thin, distinctive basal anhydrite bed composed of nodular anhydrite, with a thickness that is surprisingly consistent (Figure 7.32). Work to date has clearly shown the basal anhydrite is a diagenetic unit created by ongoing salt dissolution. It is a pressure-welded nodular anhydrite unit that accreted in the subsurface as a buildup of insoluble residues on the underside of a basinwide dissolving halite sequence (Figure 7.33a). The process was driven by the escape of undersaturated compactional and thermobaric waters. It is, in effect, an upside-down caprock (Figure 7.33b).

Unlike depositional anhydrites in saline giants, which typically thicken into the lowstand platform wedge, the basal anhydrite of the Maha Sarakham has a near constant thickness across the entire basin that is independent of the thickness of the overlying Lower Salt (Figure 7.34). There are a few wells where the anhydrite is thicker than 1-2 metres, but there the anhydrite shows evidence of flow thickening and the wells are typically located at or near the dissolution edge of the Lower Salt where larger karst cavities can form and suprasalt and subsalt sulphate residues can stack. The near constant thickness of the basal anhydrite across the basin reflects the intrinsic self-limiting permeability of a nodular anhydrite bed accreting beneath a salt overburden. Wherever upwelling basinal waters contact the underside of the Lower Salt unit it dissolves, leaving behind a nodular anhydrite residue. The nodular residue continues to accrete along its top by gathering anhydrite nodules via preferential solution of the salt host. These nodules were originally suspended within the now dissolving bedded halite. At the same time as new nodules are accreting along the upper side of the basal anhydrite, the anhydrite may be dissolving along its underside.

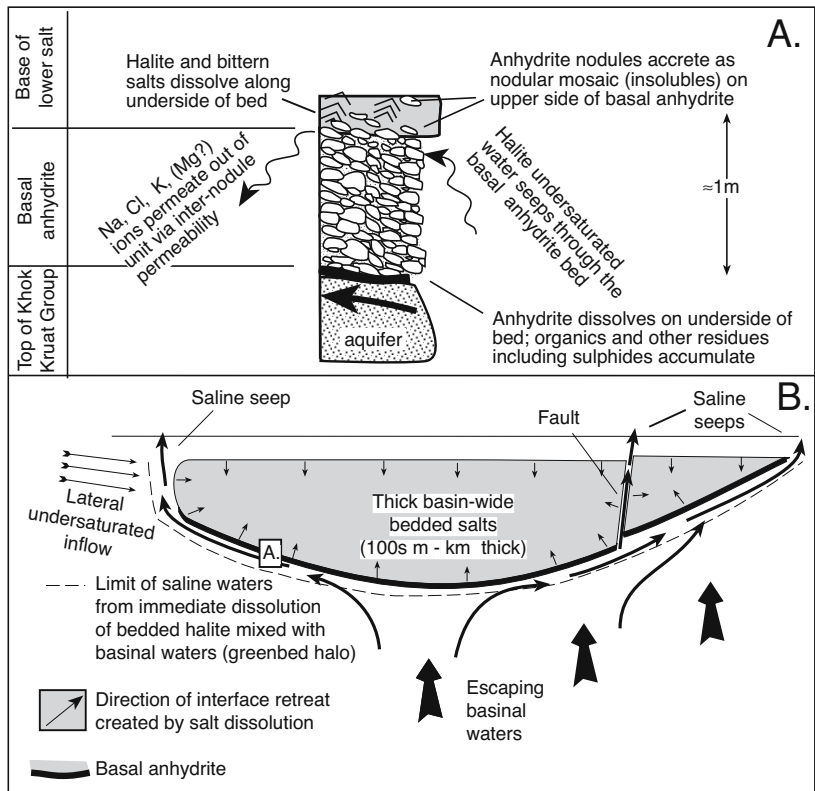


Figure 7.33. Mode of formation of a diagenetic basal anhydrite. A) Vertical profile through a dissolution-generated basal anhydrite. B) Schematic cross section with box showing relative position of vertical profile (modified from Warren, 1997).

The overall dissolution process is driven by escaping compactional waters flushing the underbelly of the salt (Figure 7.33b). If the basal anhydrite accretes to where it is more than a metre or two thick it starts to act as an aquitard for waters seeping through its internodular porosity. This slows water access to the halite contact. Thickness can increase until it reaches a point where undersaturated compactional waters can no longer flow through internodule permeability, to reach the halite-anhydrite dissolution front. Once undersaturated waters no longer access the halite dissolution front, anhydrite accretion slows and even shuts down along the upper side of the anhydrite unit. Even so, compacting undersaturated waters continue to flow along the underside of the basal anhydrite, where anhydrite dissolution occurs. Once sufficient anhydrite dissolves from its underside, undersaturated waters can again reach the halite and dissolve it anew. Basinwide near-constant thickness of the basal anhydrite reflects a buffering interaction between the rate of anhydrite nodule accretion or docking on its upper surface and the rate of anhydrite loss on its lower surface. In effect a basal anhydrite has a “half-life.” The actual thick-

ness is determined by the inherent transmissivity of the material between the nodules.

Coarse and saddle burial-stage calcian dolomite precipitates from brines flushing internodular zones in the basal anhydrite. Crystals continue to grow and re-equilibrate into higher temperature forms in response to ongoing burial. This is shown by the evolving carbon and oxygen isotope signatures, as well as $^{87}\text{Sr}/^{86}\text{Sr}$ ratios, which all define a burial trend from early limpid dolomite through coarsely crystalline dolomite through to saddle dolomite with precipitation signatures indicating increasingly higher temperature basinal fluids (Figure 7.34a, b; El Tabakh et al., 2003; Warren, 2000a).

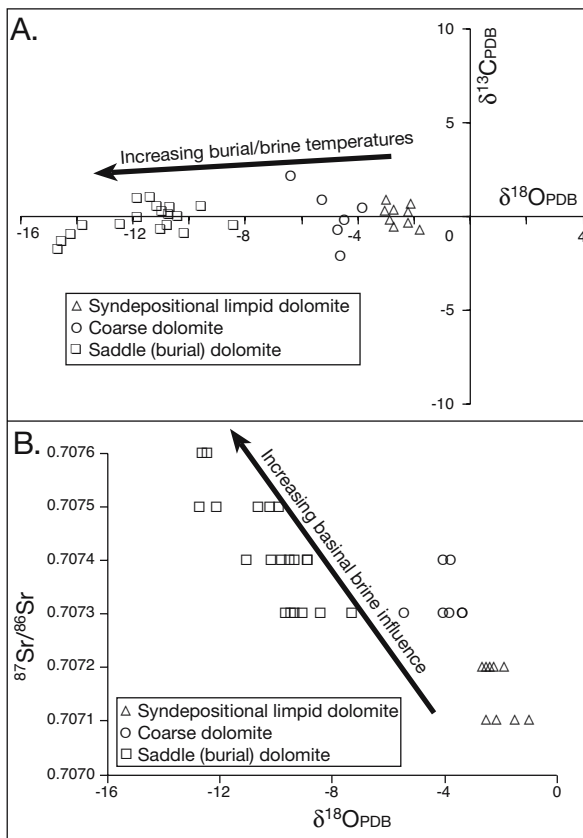


Figure 7.34. Isotopic signatures in the three types of dolomite occurring in the basal anhydrite of the Maha Sarakham Fm. Thailand. A) Cross-plots of dolomite $\delta^{18}\text{O}$ and $\delta^{13}\text{C}$ isotopic values showing influence of increasing temperature related to ongoing burial. B) Crossplot of $\delta^{18}\text{O}$ versus $^{87}\text{Sr}/^{86}\text{Sr}$ showing influence of ongoing basin brine evolution from limpid dolomite through coarse and saddle dolomite precipitates (after El Tabakh et al., 2003).

Basin	Age	Reference
South Pyrenean foredeep	Eocene	Rosell and Orti, 1980
Zechstein	Permian	Peryt, Orti and Rosell, 1993
Delaware Basin	Permian	Presley, 1987
Base of Windsor Group	Carboniferous	Lynch and Giles, 1996
Elk Point Basin	Devonian	Williams, 1984
Canning Basin	Devonian	Cathro et al., 1992
East Siberian Basin	Cambrian	Aitken, 1981
Mackenzie Basin	Early Palaeozoic	Aitken, 1981

Table 7.5. Various basins with possible dissolution-derived basal anhydrites (in part after El Tabakh et al., 2003).

The laminar underside of the basal anhydrite is made up of what remains once the anhydrite is dissolved, namely, an undulose cm-thick microlaminar organic-rich insoluble residue layer. It contains micronodules and fissure fills of metal sulphides (mostly pyrite and bornite) created by metal fixing and driven by thermochemical sulphate reduction (Warren 2000b).

Overall this “upside-down” cap rock is very similar to a pressure solution mega-seam and its mode of formation is not all that dissimilar except that the fluid flow is more one sided. This model, explaining laterally extensive, constant thickness basal anhydrites on the undersides of thick halites as a form of dissolution residue, has implications for other evaporite basins that possess basal anhydrite units with near constant thickness. Table 7.5 lists some other possible regions where dissolution-generated basal anhydrites may characterise the bottoms of thick dissolving halite units.

Caves in salt karst

At first sight, medium to large scale evaporite karst surface landforms, such as dolines, polje-like depressions, subsidence bowls and collapse dolines, appear near-identical to those found in and on carbonate karst. Likewise, all the smaller-scale intracavern features, both dissolutional (pipes and cavities) and constructive (speleothems), can be preserved karst in and above an evaporite host, even when the formative hydrology becomes inactive and the system is buried (palaeokarst). But, as we shall see, the much higher rates of dissolution of halite and gypsum compared to limestone or dolomite means there are differences in rates of formation and cave geometry compared to carbonate caves in nonevaporitic hosts. One cannot simply take models of caves developed by studies of carbonate karst and use them to unreservedly interpret evaporite caves. Differences reflect the inherently higher solubility and flowability

of the host salts at earth surface conditions and means most evaporite-hosted caves have their own peculiarities.

The high solubility of evaporite beds atop deeply circulating pressurised and jointed aquifers means deep phreatic chimneying is a common cave forming mechanism in and atop buried salt beds. When a stoping chimney cave breaches the water table, it can lead to the rapid creation of numerous steep-sided water-filled collapse dolines in suprasalt regions with strong roof spans and high volumes of sediment being swallowed if loose sediment covers the roof span.

Most of the action in uplifting salt beds and masses begins well below the watertable. It takes place hundreds of metres below the surface at bathyphreatic depths where anhydrite is reconvertng to gypsum and where caprocks and other dissolution residues are forming. Early dissolution is greatest at contacts between the salt bed and joints or fractures in adjacent aquifers. Thus patterns of jointing or fracturing control the extent and style of caves in a salt host and typically creates high-density maze caves. With halite, the only type of NaCl mass that makes it to the surface, and so becomes a host to accessible vadose caverns, is in active or recently active diapirs. Prior to its dissolution this cave-hosting diapiric halite was impervious, flowing and reannealing. Hence, most of the karst action accessible for study in halite caves is vadose and tied to perched water tables. If phreatic caves ever do form in diapiric halite, these early cavities are quickly closed by the pressurized salt flow needed to bring salt to surface and make it accessible to speleologists. Some of the metre-scale blebs of finely-layered gravitationally-aligned laminar halite seen in deep salt mines within diapirs and floating in a matrix of flow foliated coarse-crystalline halite is probably the result of mesogenetic salt precipitating in gas-filled open cavities within the diapir mass. They are not relict blocks with primary depositional texture of the mother salt. Nitrogen-filled cavities are a hazard occasionally encountered during potash mining in the diapirs of NE Germany. Their presence and their ability to blow out mine walls clearly show that open gas pockets are not uncommon in flowing salt.

Cave-forming processes are either vadose or phreatic and many caves show textural evidence indicating transit from one realm to the other. At any one time the transition from vadose to phreatic landforms is tied to depth to water table. This is seen in the cap karst to gypsiferous diapirs in Spain (Calaforra and Pulido-Bosch, 1999). The crests of the salt structures are dominated by collapse dolines (vadose), this passes radially out into the belt of solution dolines occupied by seasonal saline

lagoons and further out into rim of saline springs that form wherever the watertable intersects the landsurface (phreatic). Some caves pass from phreatic to vadose a number of times in response to watertable fluctuations tied to varying climate and tectonics.

Vadose processes characterise the uppermost part of a karst aquifer and have air in pores above any water surface or perched water table. Drainage is free-flowing under gravity; cave passages drain downslope and show strong gravitational orientations (numerous sub-vertical features). Because they form above the water table, vadose cave walls are subject to surface seepage, evaporation and drying. Speleothems decorating the cave walls indicate varying combinations of gravity and airflow and include; stalactites, stalagmites, cave popcorn, helictes and flowstones.

Caves can form in a salt bed on its way down (syndepositional to early burial phreatic), on its way up (telogenesis begins at bathyphreatic depths) and at the bottom of the bed's burial history (mesogenetic karst).

Gypsum caves

Active caves beneath gypsum karst landforms first formed as phreatic maze caves and are characterised by dense passage networks with numerous contemporaneously closed loops. Vadose sections of the same system can be quite large due to the high solubility and relative homogeneity of the host, especially if formed in a thick capstone. Heimkehle in the Zechstein anhydrites in the Harz Mountains of Germany has a overall passage length of more than 2 km, with large rooms up to 22 metres high and 65 metres wide. It was large enough to be used in World War II to house a factory manufacturing parts for JU88 aeroplanes. Gypsum caves are well documented in Miocene gypsum hosts in west Ukraine (Table 7.6; Klimchouk, 2000; Klimchouk and Andrejchuk, 2003; Andrejchuk and Klimchouk, 2004) and much of our current understanding of process comes from this region.

Gypsum cave walls in the vadose realm are relatively undecorated compared to carbonate caves. But speleothems can form and are well documented as alabastrine flowstones and selenite rinds on cave walls in northwest Texas (McGregor et al., 1963), in Alabaster Cave in the Blaine Gypsum in western Oklahoma (Bretz, 1952; Myers, 1960a), and in quarries intersecting the gypsum karst system in the Kirschberg Evaporite member near Fredericksburg, Texas (Warren et al., 1990).

Cave location and host lithology	Length, (km)	Area of cave (m ² ×10 ⁶)	Volume of cave (m ³ ×10 ⁶)	Area of cave field (km ²)	Volume of rock (m ³ ×10 ⁶)	Specific volume (m ³ /m)	Passage density (km/km ²)	Cave porosity (%)	Areal coverage (%)
Optimisticheskaja Cave, W. Ukraine, Neogene gypsum	188	0.260	0.52	1.48	26.03	2.8	127.03	2.00	17.57
Ozernaja Cave, W. Ukraine, Neogene gypsum	111	0.330	0.665	0.74	13.20	6.0	150.00	5.04	44.59
Zoloushka Cave, W. Ukraine, Neogene gypsum	89.5	0.305	0.712	0.63	18.93	8.0	142.06	3.76	48.41
Mlynki Cave, W. Ukraine, Neogene gypsum	24	0.047	0.080	0.17	2.38	3.3	141.18	3.36	27.65
Kristalna Cave, W. Ukraine, Neogene gypsum	22	0.038	0.110	0.13	1.82	5.0	169.23	6.04	29.23
Estremera Cave, Madrid, Spain, Neogene gypsum	3.5	0.008	0.064	0.06	0.71	18.3	59.32	9.04	13.56
Mammoth Cave, KY, USA, Carboniferous limestones	550	1.386	8	36.78	3310.2	14.5	14.95	0.24	3.77
Lechuguilla Cave, NM, USA, Permian limestone	180.1	-	-	-	-	-	-	-	-
Carlsbad Cavern, NM, USA, Permian limestone	49.6	-	-	-	-	-	-	-	-

Table 7. 6. Representative morphometry of gypsum maze caves that formed as confined aquifer phreatic systems, compared to Mammoth Cave (unconfined aquifer system) and Carlsbad and Lechuguilla caves (now both unconfined aquifer systems but first formed as sulphuric acid caves with gypsum precipitates; after Klimchouk, 2003; Palmer and Palmer, 2000; and listed references).

Phreatic gypsum caves

Phreatic caves in bedded evaporites atop artesian aquifers typically grow as upward stoping and branching blind flow loops caverns (phreatic cupolas) and chimneys, which begin to grow deep below the water table (bathypheatic karst). For example, deep artesian systems drive cupola karst and blind chimney stopes in the Black Hills of Dakota (Figure 7.13) and the Elk Point Basin of Canada (Figure 7.5). Even deeper in a basin, where bathypheatic caves are bathed by centripetal mesogenetic crossflows, water flow is even slower and phreatic karst is driven by the escape of H₂S and CO₂ rich basinal waters, not meteoric head. Fluid flow at these greater depths is driven by pore water gradients that reflect potentiometric variations in temperature, pressure and salinity of basinal waters.

Passages in mesogenetic and telogenetic caves tend to first develop about fractures and joints in adjacent aquifers and then expand into maze cave networks. Once growing in the main salt mass some phreatic maze passages can show internal upward-directed switchback gradients independent of jointing in adjacent aquifers and tied to internal inhomogeneities in the host bed such as intrasalt beds and changes in mineral proportions.

A phreatic tube is the most common passage shape in smooth-walled blind dissolution pockets and cupolas in bathypheatic gypsum caves. Tube or channelway shapes range in cross section from near-circular (isotopic dissolution of soluble host) to elliptical tubes to canyon-shaped keyholes (Figure 7.35; Klimchouk, 1992, 1996). Ornamentation is minimal where undersaturated crossflow drives the rapid dissolutional breakdown of the cave wall and the resulting passages are smooth, with local scalloped dissolution irregularities. Dense intersecting maze cave networks first form in the early stages of exhumation at the contact between tight but soluble gypsum/anhydrite and a less soluble carbonate or siliciclastic aquifer. This less soluble bed is the supply conduit for groundwaters that dissolve the edges of the initially impervious anhydrite/gypsum bed. The greatest rate of water supply into the dissolving gypsum contact is along joints and fractures in the adjacent aquifer bed (especially with limestone aquifers). Accordingly, the meshwork of caves penetrates the gypsum bed and tends to follow joint and fracture patterns of the adjacent aquifer.

The more stagnant phreatic portions of telogenetic CaSO₄ cave systems can be saturated and so precipitate isopachous crusts and crystal rinds. Gypsum is the commonplace isopachous precipitate in voids in this setting, while anhydrite tends to

dominate in cavities in the deeper mesogenetic realm (Garcia-Guinea et al., 2002). By the time phreatic maze caves are exhumed into a vadose setting, where they are accessible for study, much of the earlier phreatic ornamentation has already been dissolved by the increasing undersaturated throughflow and the cavern interconnection associated with uplift into the more active phreatic realm, which always precedes entry into the vadose realm (Warren et al., 1990).

Some of the longest and most complex phreatic maze cave systems in the world are found in Miocene gypsum in west Ukraine. Optimisticheskaja Cave, with more than 188 km of surveyed passages, is the world's longest gypsum cave and the second or third longest cave of any type (Table 7.6; Klimchouk, 2000, 2003). The world's longest cave, at 550 km, is the carbonate-hosted Mammoth Cave of Kentucky. The West Ukraine region contains the five longest known gypsum caves in the world, accounting for well over half of the total known length of gypsum caves on Earth. By area and volume the world's largest gypsum caves are: Ozernaja (330,000 m² and 665,000 m³; with 122 km of documented passages it is also the world's 10th longest), Zoloushka (305,000 m² and 712,000 m³), followed by Optimisticheskaja Cave (260,000 m² and 520,000 m³). They are all complex joint-controlled maze caves, formed under confined aquifer conditions that existed from the Pliocene to the Early Pleistocene (karstification on the way up - telogenesis or gypsum exhumation). Their growth patterns indicate upward-transverse phreatic groundwater circulation, with ultimate cavern fusion across the gypsum bed. All these west Ukrainian caves were fed by artesian crossflow in sub-gypsum and supra-gypsum aquifers and sourced in the Carpathian Mountains (Figure 7.35a).

High rates of dissolution in phreatic gypsum caves, relative to rates of water crossflow, are

indicated by the bevelled, faceted and “keyhole” cross sections of the Ukrainian caves (Figure 7.35a; Klimchouk, 1996; Pfeiffer and Hahn, 1976). Keyholes indicate density stratification and convectonal circulation in cave-forming waters, with shapes sometimes complicated by lithological discontinuities in the gypsum bed (Figure 7.35b; Kempe, 1972). Convection in caves is most pronounced where sluggish artesian flow and low flow velocities dominate.

This was the case in the Pliocene to early Pleistocene history of the maze caves of the western Ukraine (Figure 7.35c; Klimchouk and Andrejchuk, 2003). At that time the deeply buried gypsum dissolved via upward growing but blind, phreatic cavities, with a reflux of somewhat denser “spent” waters sinking toward the base of the cave. Spent water was replaced by less dense inflow waters supplied from the lower

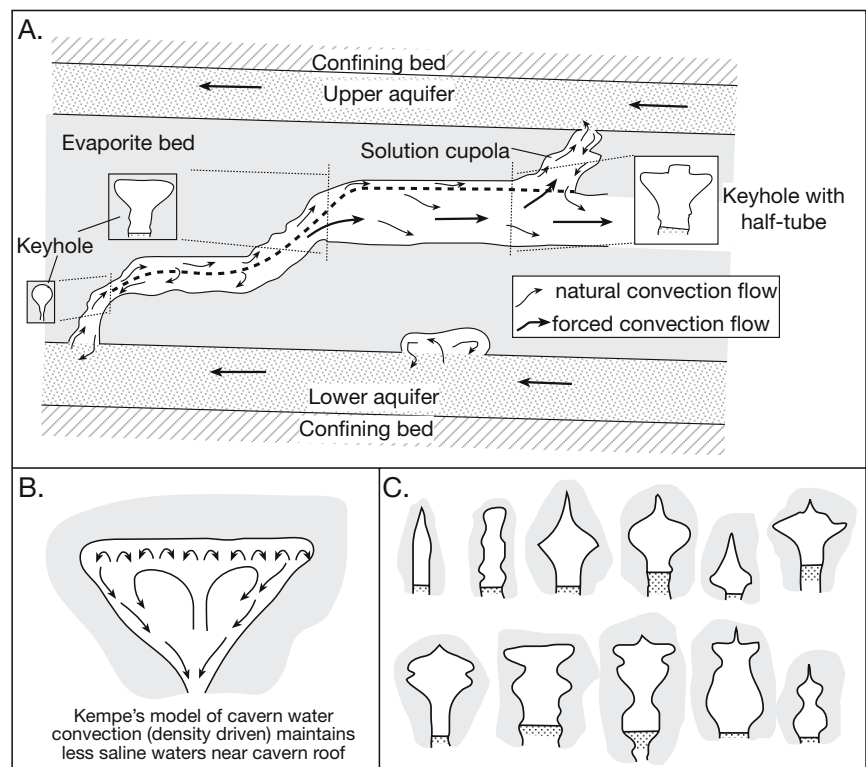


Figure 7.35. Maze caves. A) Formation of upward expanding dissolution cupolas by pressurized buoyant currents, such a system drives the formation of gypsum caves in the western Ukraine. The diagram shows the schematic relationship between lines of natural and forced convection flow on the mature stage of artesian speleogenesis, when conduit connection has already been established through the gypsum, but forced flow is slow due to the major constraint of the upper confining bed. B) Cross section of Kempe's (1972) model for cavern development by dissolution due to natural density convection, C) examples of typical cross-sections from the gypsum caves of the western Ukraine showing varieties of notching or faceting effects from differing rates of lateral expansion (dissolution). (after Klimchouk, 1992, 1996; Kempe, 1972).

aquifer. This sets up a natural density-stratified convection, which maintained fresher (less dense) waters near the phreatic cave roof. Upward growing blind caves tend to expand more at their tops driving the transition from subcircular to keyhole caverns along the cave conduit. After dissolving gypsum and increasing in density, a portion of the “spent” cave water sank all the way back into the underlying aquifer where it once again joined the regional throughflow in the lower aquifer. Once a stoping cave breached the top aquifer water flow direction in the cave was controlled by temperature, pressure and density contrasts between aquifers on either side of the gypsum bed. It seems that post-breach most of the cave water continued to rise through the cave system into the overlying aquifer (Figure 7.35a). Similar keyhole and cupola morphologies are developed in low flow rate bathyphreatic sulphuric acid caves in carbonate hosts (e.g., early stages in the formation of the Carlsbad and Lechuguilla caverns; Figure 7.45).

But the formation of keyhole passages is not an exclusively phreatic phenomenon in density-stratified gypsum caves. Keyholes in the vadose portions of many telogenetic carbonate caves indicate the transition of the cave passage from phreatic, with circular cross sections, to vadose with deepening drainage slots at the base of the passages (e.g. Calaforra and Pulido-Bosch, 2003).

Vadose gypsum caves

A lowering of the water table, either by uplift or climatic change, converts a former phreatic cave into a vadose cave. This is the recent history of the accessible portions of the gypsum maze caves in the western Ukraine and Saudi Arabia where the passage into the middle-upper Pleistocene marks the transition from phreatic to vadose in most of the accessible caves. It is also characteristic of the very recent history of some naturally phreatic caves where watertables were artificially lowered to allow quarrying of gypsum (Klimchouk, 2000). In both cases, the current vadose diagenesis is driven by telogenetic processes. The hydrological regime is passing from phreatic to vadose (the bed is on its way up = exhumation).

Climate change or water table lowering at the other end of the burial cycle can create vadose conditions in gypsum beds in the early stages of burial. That is, the gypsum bed hosting the vadose cave is on its way down, although it may pass through the water table a number of times before its final burial. This is the case today in the captured recharge playas in central Australia (Figure 2.45) and about the edges of some of the halite-filled salars in the Andes (Figure 3.41) and many Ca-

nadian salt lakes (Last, 1993a) Similar change in climate has karstified the gypsiferous sediments of many modern Sinic playas. Yauro and Cooper (1997) documented Pleistocene lake basins in north-west China, such as the Chaidamu Basin, where exposed gypsum beds have karst overprints that include: corroded flutes, fissures, small caves and associated collapse breccias and roof falls. Water table lowering is a hydrological overprint that is preserved as ornamented surfaces in gypsum caves, disconformities and cave fills in many ancient lacustrine gypsum units.

Miocene karst in the Madrid Basin, Spain

The Miocene sedimentary record of the Madrid Basin displays several examples of palaeokarstic surfaces sculpted within the gypsum at the same time that the overlying strata were deposited (Rodriguez-Aranda et al., 2002). The karst indicates a time of freshening in the same lacustrine setting that was depositing the gypsum (early burial karst). One of the better documented of these palaeokarstic surfaces separates the Lower and Intermediate units at the boundary between what are two main lithostratigraphic units in the basin (Figure 7.36). There ^{7.3}epikarst formed in Aragonian lacustrine gypsum as it was covered by terrigenous deposits of the overlying Intermediate unit. Karst features include infiltrations of the overlying Aragonian marls into the gypsum of Lower unit for up to 5.5 m below the epikarst surface. The presence of a shallow water table at the time of karstification, along with low hydraulic gradients in the evaporite basin, were the main factors controlling karst style.

Karstification was extensive and rapid, it took place in a relatively short time frame of several thousands of years (Figure 7.36; Rodriguez-Aranda et al., 2002). Stage 1 of the karstification was the accumulation and bioturbation of a bed of lenticular gypsum in a moderately saline lake (Figure 1.23). During periods when the lake dried out, plants colonised the poorly indurated and exposed gypsum ground (Stage 2). These halophytic plants contributed to the local transformation of primary gypsum to anhydrite through a dissolution–reprecipitation process, similar to that reported from vadose zones in supratidal sabkhas,

^{7.3}*Epikarst*: pertains to the upper/outer layer of karstified rock in the unsaturated zone, immediately below the soil layer.

Exokarst: pertains to features found on a surface karst landscape, ranging in size from karren to dolines and subsidence bowls.

Endokarst: pertains to all features beneath the surface and hosted by a vertically layered karst system. It includes the full spectrum of underground voids and the dissolutional features present on the rock surfaces surrounding them.

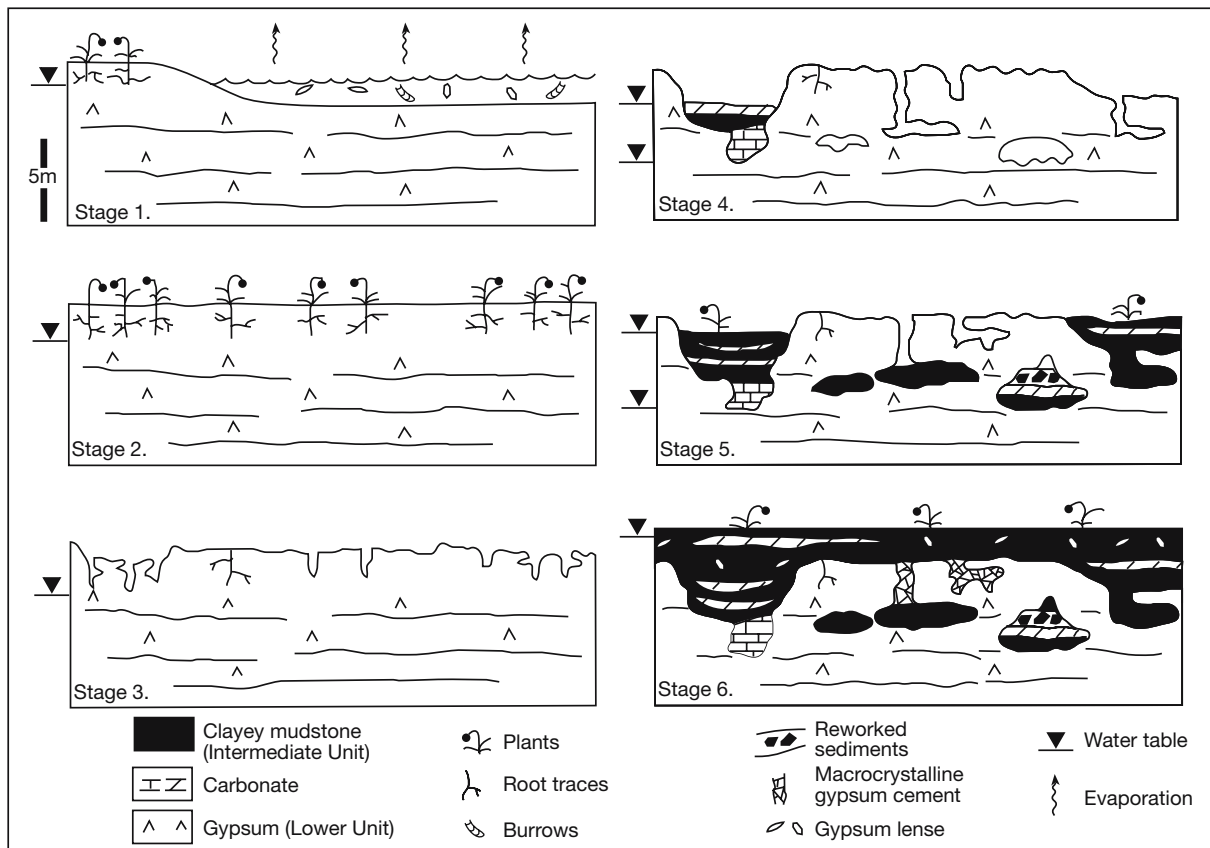


Figure 7.36. Development of epikarstic surfaces and associated endokarst in the Miocene Gypsum of the Madrid Basin. See text for detail of the evolutionary stages (after Rodriguez-Aranda et al., 2002).

salinas and losing playas. Stage 3 corresponds to the death and decay of plants, with the root holes behaving as preferential conduits for entry of meteoric water. Anhydrite, which had formed in the soil via respiring plant roots, was unstable and transformed to secondary gypsum. Continued vadose flushing of the initial conduits resulted in the formation of cylindrical and funnel-shaped pits that mimic, but do not strictly represent, root casts or rhizoconcretions (Stage 4). Both the vertical vadose conduits and gypsum caves only penetrated a few metres below the palaeokarst surface, suggesting the ongoing presence of a shallow, still saline water table. The position of the water table played a critical role throughout (stages 1-6) and limited the depth reached by both exokarst and endokarst features (Figure 7.36). In addition, the formation of roughly planar, horizontal cavities was probably related to the top of the water table, which also represented the maximum depth for root penetration (stage 4).

Formation of horizontal caves was constrained by stratification planes in the gypsum host rock. Conduits and caves were

coeval with larger gypsum dolines, and all were partially to completely filled by varying combinations of clayey mudstone, carbonate and detrital gypsum (stage 5). Clays in the karst fill are mostly coarsely laminated, green mudstone beds, possibly reworked from mudflat and alluvial fan deposits that are laterally associated with the lacustrine gypsum (Rodriguez-Aranda, 1995). Clay infiltration was probably tied to periodic floods of the karstified surface, with the caves and doline floors making depressions where waters ponded with a relatively high concentration of suspended fine-grained siliciclastic material and organic detritus. These mudstone fills in the gypsum caves are similar to the mud-filled cavities observed by Last (1993a) in modern saline lakes of the northern Great Plains of western Canada, and are consistent with the episodic clastic input patterns recognized by Calaforra and Pulido-Bosch (1999) in similar gypsum karst in the Sorbas Basin, SE Spain.

Carbonate is present in the sedimentary fill of both dolines and gypsum caves. Carbonate in the dolines consists of massive to peloidal dolomicrite or nodules developed in laminated

claystone, whereas carbonate in caves typically consists of calcite rafts and patches of reworked calcitised gypsum. The doline carbonates were probably deposited in shallow water that was episodically ponded in the karstic depressions. The carbonate nodules are probably pedogenic, arguing for punctuated deposition with times of subaerial exposure during the sedimentary fill of the dolines. Calcite rafts in clayey cave deposits suggest inputs of clastic sediment alternated with periods of standing water when calcite rafts precipitated at the air–water interface of pools in the caves (Taylor and Chafetz, 2004).

Alluvial fine-grained sediments of the Intermediate unit then accumulated and filled any remaining irregularities in the epikarst surface, which was pocked by numerous doline depressions and unfilled cavities (pits and conduits) (Stage 6). Once dolines were entirely filled by fine-grained sediment and the adjacent epikarst surface was also covered, a sedimentary discontinuity was preserved between the top of the bedded gypsum and the overlying clay. Clay had by then accumulated in the various pits and conduits that were not filled in earlier stages of karstification.

Infill of the remaining cavities includes macrocrystalline gypsum cement meshworks or mosaics that are especially obvious in cavities with little or no earlier detrital fill (Stage 6). They indicate saline phreatic conditions where a rise in the water table accompanied the deposition of the terrigenous sediments that now sealed the palaeokarstic surface. The same saline pore waters, perhaps derived by ongoing subsurface gypsum dissolution, also drove the precipitation of displacive gypsum crystals in some nearsurface clays.

Modern karst in Cretaceous gypsum, Texas

At the other end of the vadose gypsum karst spectrum are caves formed by uplift of buried anhydrite beds and the transition from phreatic maze caves to vadose caves with gypsum and calcite speleothems. Ornamented vadose gypsum caves, a late stage of this conversion, are today exposed within the workings of the Fredericksburg Gypsum Quarry in a 10-metre (30 feet) thick gypsum bed. The gypsum is the nearsurface remnant of the Cretaceous Kirschberg Evaporite Member, which was exposed during the late Tertiary exhumation of the Edwards Plateau. Early stages of the uplift were typified by the rehydration of anhydrite back to gypsum and the formation of fibrous vein fills (Figure 1.38). The complete telogenetic dissolution of the evaporite level is indicated by a widespread evaporite solution breccia.

Relatively impervious nodular gypsum hosts most of the caves, with nodules showing varying overprint by coarser crystalline gypsum daisy textures. Much of the cave fill and ornamentation is made up of a more permeable alabastrine gypsum precipitate (Figure 7.37a). Where a gypsum bed is completely dissolved by cave expansion all that remains of the former gypsum karst is a jumble of speleothem clasts beneath and within a dolomitic crackle breccia. Most of the larger blocks in the breccia were derived from the overlying Edwards Formation and are now encased in a residuum or matrix of silt- to sand-sized dolomite rhombs (“chalky” dolomite). The rhombs were originally floating in a matrix of gypsum/anhydrite and their equivalents can still be found as dispersed rhombs and layers in nearby, as yet undissolved, gypsum beds.

Friable alabastrine gypsum up to 10–20 cm thick coats cave walls in zones of sluggish and perched groundwater crossflow. It is made up of silt-sand sized euhedral prisms with a delicate open “pack-of-cards” texture that could only be preserved in caverns experiencing very low rates of fluid cross flow. Gypsum is also locally reprecipitating as small stalactites and stalagmites in vadose cavities. Walls tend to be smooth and unornamented in other nearby caves with more active throughflow.

The following sequence of exhumation and karsting was listed by Warren et al. (1990) as indicative of the transition from the deep phreatic to the vadose (Figure 7.37b):

- *Formation of nodular “daisy-head” gypsum* As uplift raised this bed of nodular anhydrite into the zone of rehydration, replacement by gypsum was at first slow but pervasive, with near-stagnant phreatic fluids oozing into the calcium sulphate bed. At the microscale, stagnant phreatic waters seeped into the nodular anhydrite bed. Flow was focused along intercrystalline porosity films within the dolomite rims surrounding the calcium sulphate nodules or it was focused along thin-bedded dolomite stringers within the anhydrite bed. Millimetre to cm-sized, aligned gypsum crystals nucleated off these flow paths and grew inward toward the nodule core via dissolution and replacement of the anhydrite to form daisy-textured gypsum. The main mesoscale permeability entries into the gypsum bed were provided by fractures in the adjacent aquifers, which began to render a maze cave network.

With further uplift there was a change to more active hydrologic conditions, which modified the rate of gypsum growth and fine gypsum crystallites that characterise alabaster came to be the dominant precipitate. Replacive gypsum grew more rapidly through the unit as a microcrystalline alabaster texture

overprinted some of the nodules. The adjustment in gypsum texture as the unit was exhumed probably reflects more pronounced fluctuations in temperature and saturation tied to increased groundwater crossflow (Figure 7.37b). This was probably related to greater access of undersaturated phreatic water to the unit as the dense network of joint-controlled maze caves permeated the gypsum and were fed from joints and fractures in the adjacent aquifer.

• *Karst structures and calcite/gypsum speleothems* As the gypsum bed passed into the zone of active phreatic flow and then vadose infiltration, the process of gravity-driven karstification began in earnest. Nodular and alabastrine gypsum now was subject to widespread dissolution. Phreatic groundwater entry was first along joint mazes, while vadose infiltration in the exhumed parts of the unit tended to expand former phreatic caves and to create new vertical pipes with scalloped edges indicating the downcutting process. Gypsum and calcite speleothems formed in caves and pipes with less active vadose crossflow, mainly as popcorn, flowstone and alabastrine laceworks (Figure 7.37a).

• *Brecciation and complete loss of gypsum* Complete dissolution of the gypsum bed produced zones of collapse breccia, with circumclast radial and botryoidal calcite cement (speleothems). Collapse occurred gradually over wide areas of contact between the bedded gypsum and adjacent strata so that the overlying beds tend to be lowered gently into broad folds. Regionally, the overburden stratification was little disrupted by widespread foundering associated with the complete flushing of gypsum. Regionally a residual zone of pulverulent dolomite rhombs (“chalky” dolomite) overlain by packbreccia now defines the cap to the dissolved gypsum bed. Where gypsum remains, some of this unconsolidated dolomite residuum is washed from the upper surface of the dissolving gypsum into karstholes and pipes that cut down into the gypsum to accumulate on the conduit floors with classic “vadose silt” textures.

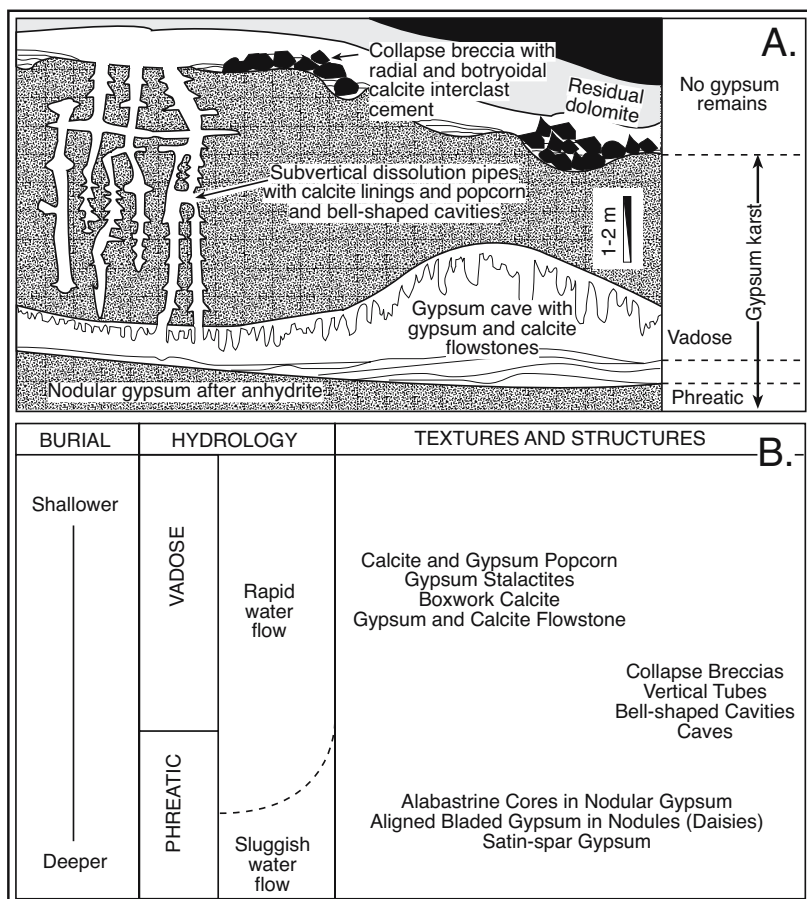


Figure 7.37. Model karst and related calcite textures developed through sequential complete dissolution and retexturing of an uplifted gypsum bed - based on textures in the subcrop of the Fredericksburg Gypsum in central Texas. A) Schematic cross section through the dissolving now vadose gypsum bed. B) Textural evolution related to groundwater regime (modified from Warren et al., 1990).

There is abundant calcite precipitating as void fill in rubble breccia cavities and pipe linings, but there is no discernable conversion of the chalky dolomite to calcite (dedolomitisation) in this system. XRD shows chalky dolomite remains well ordered and near stoichiometric. The lack of dedolomitisation raises the question: Is it commonplace in evaporite beds on the way down in the burial cycle, when newly formed dolomite is more likely to be a less ordered highly metastable form of dolomite? Is it less common in evaporite beds on the way up (see calcitisation of evaporites discussion later in this chapter)?

The end result of unroofing an ancient evaporite bed in this humid region of central Texas, where the karsted gypsum beds never outcrops, is a stratiform chalky calcitic/dolomitic residuum layer that underlies a gently folded and collapsed packbreccia bed. The former position of a regional decametre-

thick CaSO_4 bed is now defined by cm-metre thick interstratal packbreccia characterised by brecciated and rebrecciated fragments of calcite popcorn, boxwork and botryoidal calcite, all intermixed with fragments of the overlying strata and the dolomite residuum. None of the original evaporite salt remains in the final breccia.

Modern gypsum karst in Saudi Arabia

Similar telogenetic gypsum transformations, associated with gypsite/alabaster replacement, brecciation and karstification, are seen at Dahl Hit (*dahl = cave*) at Ain Hit in eastern Saudi Arabia (Figure 7.38a). There the 72 metre-thick type section of the Hith Formation outcrops in the roof and sides of a large collapse-prone doline mouth to a phreatic tube cave. In the subsurface the Hith Anhydrite is a major regional seal to the prolific reservoirs of the Arab Formation of Saudi Arabia and the western Emirates and it is typically more than 120 m thick in these oilfields (Chapter 10). The tubular cave mouth defines the lower part of the breached doline floor and leads down into a phreatic tube cave that has yet to be completely surveyed. The cave entrance is located at the Hith Anhydrite's contact with the limestones of the overlying Sulaiy Formation. The cave is steeply inclined ($\approx 30^\circ$) and floored by a scree slope composed of packbreccia created by gypsum layer breakdown. Blocks in the packbreccia are jumbled combinations of collapsed carbonate overburden and transforming blocks of Hith Formation anhydrite. Larger blocks range up to 3-5 metres across. Like most phreatic tube caves, the cave walls are smooth and unornamented with the floor covered by angular blocks of fallen roof. Much of the fine bottom sediment that covers the packbreccia on floor of the water-filled parts of the tube cave is composed of insolubles from dissolution of the Hith Anhydrite.

For centuries Hit Dahl at Ain Dit was a source of fresh water for the local population (*Ain = water spring*). But overpumping in the last few decades has led to a drastic drawdown of a potable water layer that once floated atop more saline phreatic water in the cave proper. The rapid lowering of the watertable has now destabilised the cave roof. Dahl Hith is now a dangerous cave to visit. On my last visit (November 2003) a large section of the roof had just collapsed in the preceding days. Much of the interior of the cave fissure is now packed with freshly collapsed blocks making cave access much more difficult than in the past.

At outcrop scale (Figure 7.38b) the retreating dissolution edge of the gently dipping Hith Fm. creates an obvious zone of bedding disturbance and folding in the Sulaiy Formation. The

current contact with the dissolved and monoclinally dipping Hith Formation ($\approx 30\text{--}40^\circ$) at Hit Dahl is defined by large collapse features and rotated mega-blocks of overburden in the flexure zone atop the shallow subcrop edge of the anhydritic Hith. A megabrecciated zone defines overburden collapse along the subcropping monoclinally edge of the Hith in Saudi Arabia and it can be traced as an elongate at-surface expression of the Hith for more than 550 km along strike. Similar, also spectacular, collapse dolines and rotated mega-blocks characterise gypsum karst features in the subcrop belt of the Eocene Gachsaran Formation in the foreland fold belt of Iran (Cucchi and Zini, 2003).

Active collapse fractures, visible in the Hit cave wall, show the effects of solution-related extensional collapse on the meteoric conversion of grey anhydrite to white-buff alabastrine gypsum (Figure 7.38c). The layering in the Hith is largely preserved on conversion to the fine alabaster crystals, which create an almost mimetic preservation of precursor texture. Thin extension fractures parallel to the main fracture/collapse allow the formation of thin alabaster streaks, which are clearly visible in the left third of the photo (Figure 7.38c).

The nature of the anhydrite-to-gypsum conversion front at Dahl Hit varies from fracture parallel, as seen in Figure 7.38c to bedding parallel, as seen in Figure 7.38d. In the latter case the upper boundary of the residual anhydrite block shows a nodular replacement contact with the newly precipitated alabaster. In contrast, its lower contact shows a more feathered relationship. White bedding-parallel satin-spar has formed in small fractures in the anhydrite and are parallel to the main entry fracture creating the alabaster zone. Satinspar is the last gypsum phase to form in this and has also grown in bedding-parallel fractures as well steeper veins that crosscut some anhydrite-alabaster contacts. Veins were created by extension in response to the growth of void space. Most of the grey anhydrite is being replaced from the edges inward, but the alabaster, which is less consolidated and somewhat more permeable, can accommodate a much higher density of bedding parallel fractures. It is a largely inhomogeneous response to tension created by dissolution and contrasts with the more isotropic response seen in the satinspar growing in the Permian clays where the Khuff anhydrite subcrops (Figure 1.39).

The replacement sequence at Hit Dahl is laminated anhydrite passing directly into laminated alabaster. It may reflect the much lower rates of fluid rock interaction experienced by the Hith Fm. during uplift as compared to the more humid conversions occurring deeper and earlier in the uplift history at Fredericksburg, Texas. The greater disturbance in the overburden at Hit Dahl

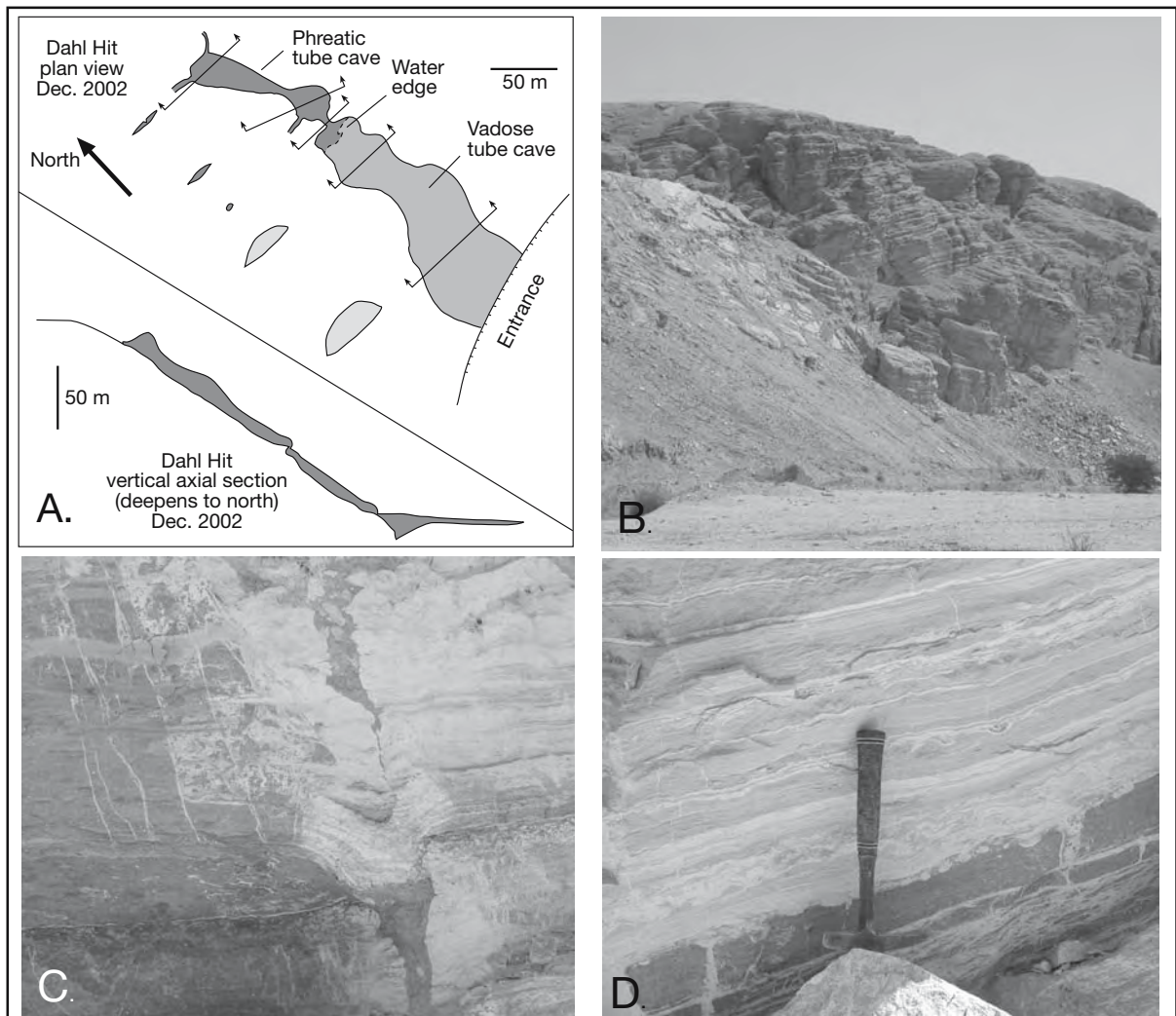


Figure 7.38. Dahl Hit at Ain Hit in Saudi Arabia. A) Surveyed geometry of Dahl Hit (replotted from Gregory et al., 2002). B) Overburden disturbance created by the nearsurface conversion and dissolution of the Hith anhydrite. Cliff \approx 100m . C) Contact between alabastrine gypsum and anhydrite showing a v-shaped breccia- and clay filled cavity some 50 cm across. D) Detail of the conversion front with buff alabastrine gypsum at top, grey remnant anhydrite below, upper conversion contact is nodular, lower transition is feathered, Bedding parallel white veins in the alabastrine gypsum are satin spar gypsum. Images B through D illustrate the effects of anhydrite conversion at the outcrop edge of the Jurassic Hith Fm. anhydrite at Hith Dahl.

compared to Fredericksburg reflects the greater thickness and resulting locally steeper dip of the monoclinical defining the edge of the dissolving CaSO_4 bed and perhaps a greater strength in the roof span in Saudi.

Halite Caves

Because of its high solubility, halite does not make it into outcrop or shallow subcrop as easily as gypsum/anhydrite. Where halite is at the surface it tends to be in regions of Pleistocene halite deposition (salt on its way down) or in zones of active diapirism

(salt coming up very quickly). Chabert and Courbon (1997) noted caves in ancient rock salt in several regions: Algeria (in diapirs, mostly as shafts and short caves up to 280 m long), Chile (diapirs, with caves 250-500 m long), Israel (in a diapir as tube caves several hundred metres in length), Romania (in diapirs, with caves up to several hundred metres long), Spain (in diapirs, with caves up to 650 m long), Tadjikistan (several caves 300 to 2,500 m long and up to 120 m deep), and in the namakers of Iran and the offshore island relicts where cavern lengths range from several hundred metres to kilometres.

Halite in an active namakier rises and spreads rapidly, so any karst in an active salt diapir tends to be a feature associated with the immediate underside of a caprock. Karst processes cannot deeply penetrate while salt is flowing, even when the plug rises more than 300 metres above the surrounds. But halite's susceptibility to rapid dissolution means the length of a cave developed below the caprock can be substantial. There is a report of a single salt halite cave in Iran with a passage length of 5.1 km (Bruthans et al., 2002). Once diapir rise has slowed or ceased the positive topography of the now inactive diapir controls the depth of development of doline collapse on the diapir itself. Deeper collapse dolines can now form in the more central topographically higher portions of a salt structure (e.g. Calaforra and Pulido-Bosch, 1999). The high solubility of halite means a halite cave system can form in a few hundred years rather than the thousands to tens of thousands of years needed to form carbonate karst. This means some of our notions of karst process and cave stability, related to the rate and density of cavern expansion, need to be modified when dealing with halite karst.

Modern halite karst in the Dead Sea depression

Halite caves occur in the Mt. Sedom diapir, where halokinetic Miocene salt is sporadically exposed beneath a weathering and fractured gypsiferous caprock (Figure 7.39a; Frumkin, 1996; Frumkin and Ford, 1995). Water enters the various caves in Sedom diapir through breaches in the caprock. Most of the caves in the higher parts of Mt. Sedom salt are vadose inlet caves; these are meandering steeply inclined tubes and canyon slots located within or immediately below the caprock. They form where salt solution quickly carves out near vertical slots and shafts (typically < 2m wide and much deeper) that lead down from the surface, sometimes along pre-existing fractures and shears in the salt. Inlet caves in the central portions of the mountain can only be accessed through their sinks and appear to have no distinct outlet. All terminate several tens of metres above the regional water table (e.g. Karbolot Cave; Frumkin, 1994a, b, 1996).

The lower parts of inlet caves often contain steep silt and clay banks with surge marks that indicate occurrence of low energy water ponding, with variable residence times. Silt and clay sediments settling at the bottoms of inlet caves impede infiltration, extending the residence time of pond water (Frumkin, 1994a, 1996). Three of the studied caves in northern Mount Sedom had perennial ponds throughout the period 1984-1995. The ponds are perched, without any lithologic control, tens of metres above the nearest potential outlet at the foot of the

mountain. Water level in each pond differs from the others by tens of metres. All pond waters are highly concentrated, up to 324 g/l, with solutes consisting mainly of sodium and chlorine. Fresh inflow waters reach halite saturation within a few hours of reaching the pond. Both dissolution and precipitation features form the pond edges, and their equivalents can be seen on cave walls wherever ponds have dried out. Dissolution is indicated by horizontal notches, which connote density stratification in the ponds when aggressive fresh flood waters temporarily diluting the upper parts of the pond. Subsequent saturation of holomictic pond waters is indicated by the growth of cm-scale halite crystals on the bottom and sides of the ponds.

Towards the periphery of Mt Sedom, the inlet caves lead down to laterally expanding vadose cave levels that drain onto the Dead Sea plain. Sedom Cave, is the longest laterally expanding cave, with an aggregate length between two subparallel conduits of 1.8 km. Malham Cave, another large perched and laterally expanding cave, lies a few hundred metres south of Sedom Cave (Figure 7.39a; Frumkin, 1996). It has an aggregate passage length of more than 5.5 km and reaches to some 194 m below the landsurface. There is an upper tier of largely inactive passages and a lower active channel level. ¹⁴C dates on fossil wood in the upper cave level shows meteoric waters began to sculpt the upper cave more than 5,500 years ago. Ongoing uplift of Mt Sedom salt means the active channel level in Malham Cave is now downcut some 10-12 metres lower than when it began. Malham Cave passages quickly developed an open outlet through which floodwater escaped directly to the Dead Sea floor, proving that during this period some 4000 years ago rock salt had already risen above region hydrological base level at the Malham outlet point within the eastern escarpment (Figure 7.39a). Lashelshet Cave, an inlet cave on the highest point on the diapir cross section, has an even older age of more than 7,000 years since cave initiation. Caves in the northern part of Mt Sedom did not begin to form until some 3,000 years later (Frumkin, 1996).

Based on their study of the caves of Mt Sedom, Frumkin and Ford (1995) concluded cave passages develop in two main stages: (1) an early stage characterized by inlet caves with high downcutting rates into the rock salt bed, and steep passage gradients; (2) a mature laterally expanding stage characterized by lower downcutting rates and the establishment of a wider subhorizontal perched stream bed armoured with alluvial detritus. This style of cave tends to develop toward the periphery of the diapir mound. In the mature expanding stage downcutting rates are controlled by the uplift rate of the diapir and changes of the level of the Dead Sea.

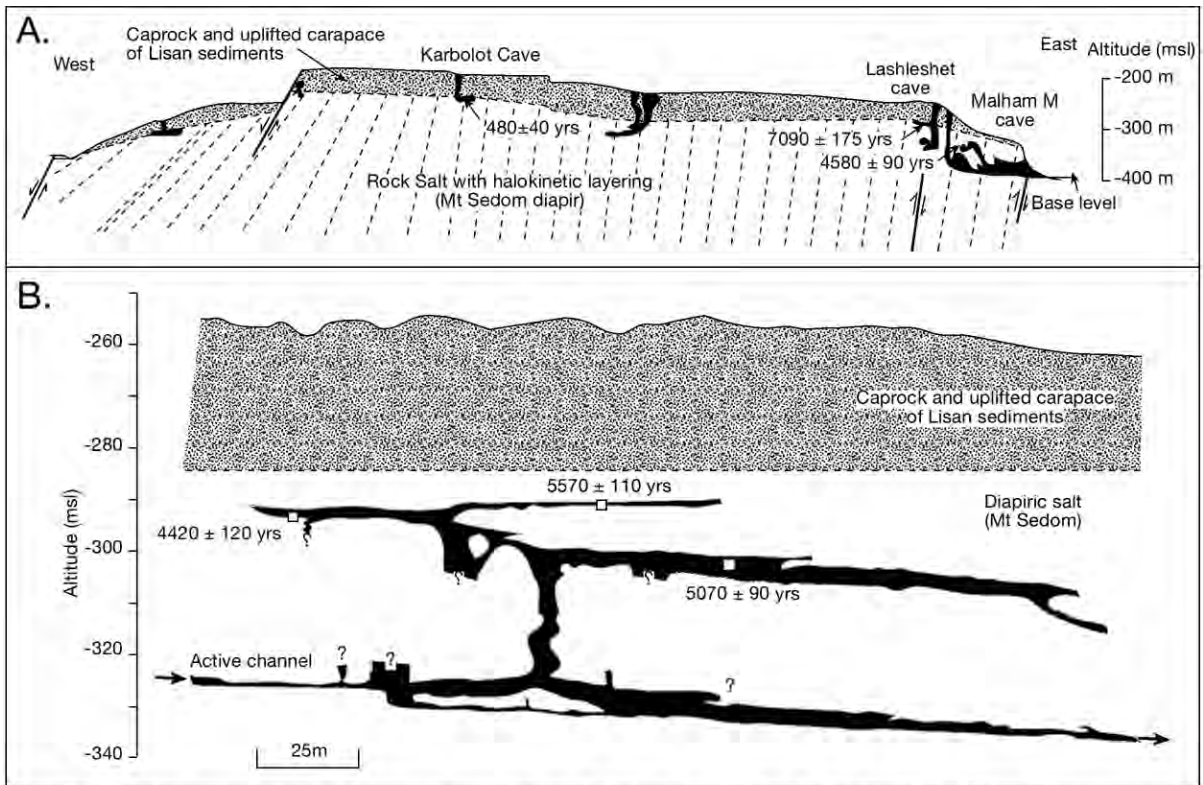


Figure 7.39. Halite caves beneath the caprock carapace of Mt Sedom, Israel (after Frumkin, 1996). A) East-West cross section through the southern part of Mount Sedom, showing ages of upper levels of caves in ¹⁴C yr B.P. Dashed lines indicate dip of salt layers within the diapir. Caves are colored black. The oldest cave date comes from Lashleshet Cave, which lies at the top of the eastern escarpment, implying this was the earliest region on the Sedom uplift to experience vadose flushing. B) Vertical section along part of Malham South Cave, showing several dated levels. The age of the uppermost level (5570 ± 110 yr B.P.) indicate the minimum exposure age of this site created by the halokinetic uplift of the landsurface. See Figure 4.40 for location of Mt Sedom.

Passages may aggrade to create wide flat bevelled passages and slots with thick sediment armoured bases (Frumkin, 1998). A lack of a consistent phreatic level in the blind bottoms of perched water levels and the presence of the horizontal slots in the lower levels of Sedom Cave means dissolution in both types of caves is largely restricted to times of flooding and perched or backed up freshwater in the vadose zone. This explains the tapering passages of inlet caves and the widespread alternation of armouring and bevelling as well as formation of narrow horizontal meandering slots toward parts of the top of the meandering channel that is now Sedom Cave.

Mass balance calculations in the halite caves of Mt Sedom yield downcutting rates of 0.2 mm s⁻¹ during peak flood conditions, this is about eight orders of magnitude higher than reported rates in any limestone cave streams (Frumkin and Ford, 1995). However, floods have a low recurrence interval in the arid climate of Mount Sedom so that longterm mean downcutting

rates are lower: an average rate of 8.8 mm a⁻¹ was measured for the period 1986-1991. This is still at least three orders of magnitude higher than rates established for limestone caves.

The highly impervious nature of halite and its resupply in actively growing diapirs means that, unlike carbonate and gypsum caves, there is no real water table level to define maximum cave development in a rising salt stem. Rather, the inlet caves are simple dissolution tubes where rainwater has accessed halite and sank until it was saturated and then dissolution stopped until the next flood. Toward the edge of the rising stem these inlet caves breached the edge of the salt mound and vented their perched groundwaters to the surrounding plain (Sedom and Malham caves). This creates a downcutting and laterally expanding cave system, which is still some metres to tens of metres above the base level of the regional water table in the surrounding plain. The expanding cave level is dominated by mostly horizontal growth, often with a sediment-armoured

floor. It has numerous benches in the walls that probably reflect changes in the hydrological base level.

Dense anastomosing cave networks that characterise gypsum caves are not found in the halite caves of Mt Sedom. This reflects the ability of diapiric halite to re-anneal and the fact that all exhumed halite that makes it to the surface is diapiric, not bedded. At-surface halite is not sandwiched between jointed aquifers above and below the dissolving layer. Rather it is a growing mound subject to dissolution at its top and sides.

Away from Mt Sedom, there are active collapse sinkholes and caverns forming in the alluvial fans and clastic aprons that overlie the bedded Quaternary lacustrine halite of the Dead Sea (salt on its way down in the burial cycle). In the sediments around the lakeshore the pace of collapse has accelerated in the last 60 years due to a drastic lowering of the circum-lake water table and the associated lakeward migration of the saline-fresh water interface (Figure 2.46; Arkin and Gilat, 2000; Salameh and El-Naser, 2000; Frumkin and Raz, 2001). For example, a series of collapse dolines 2-15 m diameter and up to 7 m deep, appeared in 1990 in the New Zohar area. In January 2001 a large sinkhole, some 20 m deep and 30 m wide, cut through the asphalt surface of the main road along the western shore of the Dead Sea. It was opened by the passage of a busload of tourists on their way from Ein Gedi to the solarium. Existing tourist facilities, such as the Ein Gedi beachside parking, were shut down after the road was damaged and several buildings have since collapsed into sinkholes. Sinkholes have since developed in other areas about the Dead Sea Margin including Qalia, Ein Samar, Ein Gedi and Mineral Beach.

Three main types of sinkhole or doline fill have been recognized atop the dissolving Holocene salt beds; 1) Gravel holes in alluvial fans, 2) mud holes in the intervening bays of laminated clay deposits between fans, and 3) a combination of both types at the front of young alluvial fans where they overlap mud flats. Fossil, relict sinkholes have been observed in the wadi channels cutting into some old alluvial fans, showing this is a natural and ongoing process. While lake levels continue to fall (Figure 4.42), the potential for subsidence hazards related to karst collapse is ongoing.

There is evidence of an older set of widespread ground collapses, sinkholes and caves that are tied to an earlier substantial fall in the Dead Sea water level some 4 ka. It may even be that the events described in Genesis 14 in the Christian Bible took place at the time of a substantially lowered sea level. The described battle, which occurred prior to the fall of Sodom and Gomorrah, perhaps took place on the subaerially exposed flats of the

Southern Basin of the Dead Sea. The “pits of slime” described in the fall perhaps were solution collapse sinkholes activated by the 4000 ka fall in the Dead Sea water level (Frumkin and Elitzur, 2002).

Modern halite karst in crests of diapiric Hormuz salt (Precambrian) in the Arabian Gulf

Namakier outcrops in and about the Arabian Gulf range from structures actively extruding salt to those in ruins where salt has not flowed for tens of thousands of years (Figure 7.14). Likewise the halite caves developed in the namakiers of Iran, or their offshore island counterparts, show a broad range of ages and styles of salt cave development tied to the time since cessation of salt flow.

Surfaces of actively flowing namakiers on the Iranian mainland are characterised by karren flutes and pinnacles, with numerous small-medium dolines, collapse structures, swallow holes and small caves at their base. Caves tend to be sediment-armoured meandering tube caves or subvertical canyon slots that are centred on joints in the salt beneath a thin suffusion mantle. In contrast, the halite caves in the diapiric cores of the many islands in the Arabian Gulf have a more mature bevelled meandering style with thicker sediment armouring on the cavern floor. Many of these caves breach the retreating edges of former namakiers and salt fountains.

Salt movement in the various diapiric cores of these islands is inactive or is greatly reduced compared to the Miocene when these structures were active namakiers. For example, Dragon Breath Cave on Hormuz Island is a linear meander tube cave fed by an ephemeral stream in a shallow valley filling with alluvium (Figure 7.40; Bosak et al., 1999). The surrounding landscape is classic salt karst with numerous depressions, blind valleys, ponors and subsidence sinks. Together they form a highly pockmarked centripetally-ringed topography, which outlines those central parts of the island underlain by shallow subcropping Hormuz salt. The cave itself is one of a number of tube caves exiting about the edge of the zone of diapiric salt. Hosted in steeply dipping diapiric salt, it is around 100 m long with its main passage created by a minor ephemeral stream. Its near flat roof, with an average inclination of 5.4%, is a notable feature and reflects either joint-related dissolutional spalling of the roof or an earlier water table slot related to backup of a freshened water body (Figure 7.40).

The current cave passage has cut down a metre or more into earlier cave floor sediments (sediment armour), which contain clasts up to 50 cm in diameter. The cave formed by initial ingress

along a linear joint, which was then widened by salt dissolution, so allowing meandering of the stream trace within the salt. It is a cave system very similar to the mature stages of laterally expanding caves in Mt Sedom. The base level of the cave correlates with the surface of a widespread marine terrace, which is now uplifted some 20 metres above sealevel and defines much of the periphery of Hormoz Island. The raising of the terrace is related to the ongoing raising of the island via salt flow.

Bruthans et al. (2000) concluded that the style of karst landform developed in dissolving diapiric salt in the Arabian Gulf Islands reflects the thickness of the carapace that caps the dissolving salt core. They distinguished four classes of diapir cap, each with a specific association of superficial and underground karst forms, namely: 1) outcropping salt, 2) thin capping (0.5-2 m), 3) capping with moderate thickness (5-30 m), 4) capping with greater thickness (more than 30 m). Cap thickness controls or reflects: 1) the density of recharge points, with high densities of recharge points in the thinner caps; 2) the amount of concentrated recharge which occurs at each recharge point, with suffusion karst characterising thinner caps; 3) the rate of lowering the ground surface atop the salt, with the faster rates of lowering occurring beneath thinner caps, and 4) the amount of load transported by underground flood-streams into cave systems. The volume of sediment load tends to be locally higher and focused beneath the thicker caps, especially where inflow streams abut the edges of a dissolving salt dome. The thickness of caps atop expanding halite caves does not appear to influence the shape or style of the cave developed within the salt mass; more important seems to be the thickness of cap in the recharge area of the cave and the type of recharge into the salt environment. That is, how much water is passing into the salt and is its flow ongoing or ephemeral?

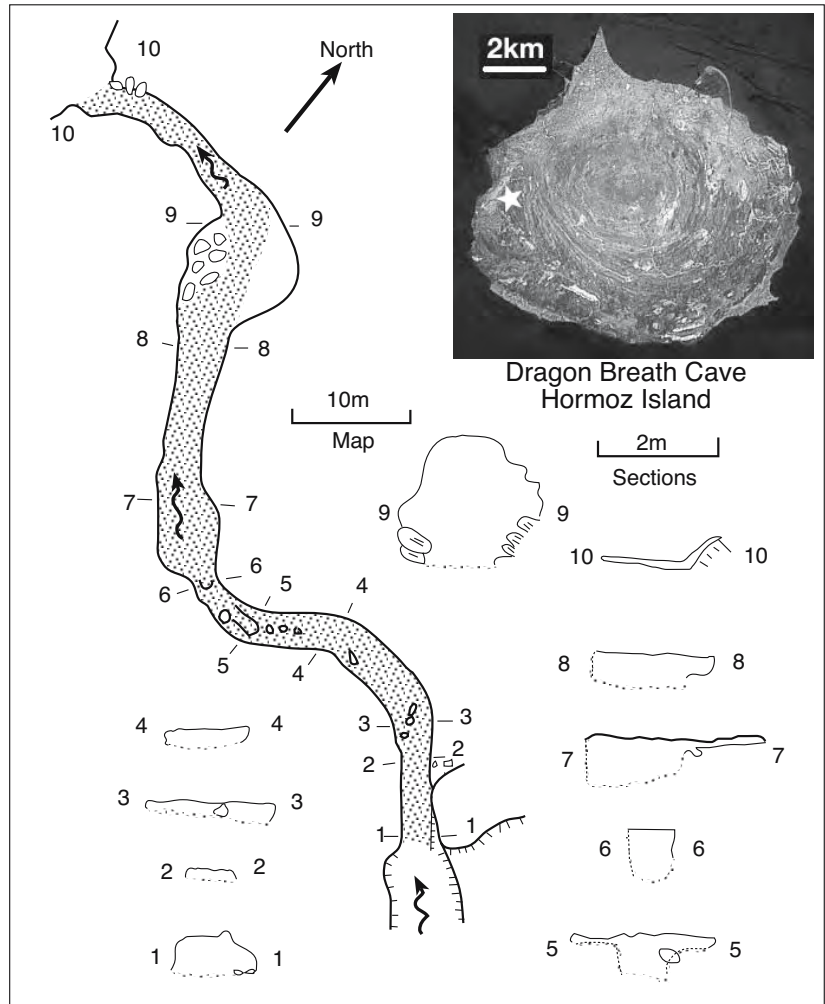


Figure 7.40. Map of Dragon Breath Cave, a meandering karst cavity draining the edge of the inactive diapiric core of Hormoz Island, Arabian Gulf (after Bokacs et al., 1999). Star marks cave position on insert, see Figure 6.45 for location of island. (Landsat image of island courtesy of NASA).

Halite caves in the relatively mature salt stems of the various islands of the Arabian Gulf, unlike carbonate systems, can swallow and store huge volumes of clastic sediment, volumes that would clog the entrance to a carbonate system. The extreme solubility of halite enables the pace of dissolution/corrosion enlargement in a salt cave to keep pace with large amounts of sediment carried into the cave by external inflows. Stream sediments arriving at the cave entrance, including boulders, move inside and are trapped within the salt itself. Sediment is not dumped outside the cave entrance, which is the typical situation in blind valley river mouths at carbonate caves (Bruthans et al., 2003). For example, coarse-grained sediment fractions are carried hundreds of metres into the cave by two large in-

intermittent streams entering the upper part of the Ponor Cave (Hormoz Island). The clasts in the resulting intra-cave alluvial fan conglomerates range from cobble of several centimetres up to 1 m diameter boulders, only sand-sized particles make it to the lower part of the same cave.

Caves capable of storing such coarse alluvium within the cavern itself are halite-specific with no equivalent in a carbonate karst terrain. There the boulder-size fraction in the cave itself is the result of roof fall and almost all stream-borne coarse alluvium is deposited outside the cave.

Cave walls in zones of less intense dissolution and stream crossflow are decorated with halite, gypsum and anhydrite speleothems. Anhydrite forms speleothems in preference to gypsum in those parts of the cave with very high salinity waters. Some of these speleothems can be quite large, up to a few metres long. Compared to the growth rates of calcite speleothems in carbonate caves the growth rates of evaporite speleothems are phenomenal. Halite stalactites, several metres long and curving into the direction of airflow, formed in the mouth of Dragon Breath cave in a few years rather than millennia needed for carbonate counterparts (Bokacs et al., 1999). In August 1997, a network of numerous halite stalagmites and stalactites blocked the entrance to Dragon Breath Cave. In March 1998 there were no remains of the speleothem meshwork, while in February 1999, the stalagmites had reappeared (Bosak et al., 1999). Similar halite structures occur in the caverns of Mt Sedom and on the wet roofs of some salt mines.

Evaporite speleothems in carbonate karst

Evaporites can form speleothems in the drier parts of carbonate caves where airflow dries cave capillary waters to salinities appropriate for precipitation. Gypsum and epsomite speleothems

are especially common in vadose caves in areas receiving less than 250 mm of rainfall per year. Even in the ever-wet climate of New Guinea, powdery gypsum crusts can coat carbonate substrates in caves like Selminum Tem and Atea Kanada in a region where the annual rainfall is more than 4,000 mm. But these are relatively minor portions of the total volume of cave decoration with the sulphate sourced in the weathering of pyritic impurities and are only found in parts of the cavern system subject to vigorous air circulation.

The most common vadose evaporite speleothem is gypsum, which forms as relatively fine-grained granular crusts on the limestone wall of most arid-zone carbonate caves. It grows and accretes via uniform seepage and evaporation of brines escaping from the porous cave wall. This is an ongoing process whereby older crusts become detached, fall off and, if not dissolved by throughflowing waters, accumulate on the cave floor as new crusts continue to form on the walls. It is really a form of salt weathering that just happens to occur inside a cave. Gypsum also accumulates as granular layered rinds in many phreatic and bathyphreatic carbonate caves that were moulded by sulphuric acid speleogenesis in their early stages of formation.

Sulphate speleothems are not restricted to crusts in caves in warmer climates, Harmon et al. (1983) reported at least three sulphates (gypsum, mirabilite and epsomite) in speleothems in Castleguard Cave in the Canadian Rockies, with the most spectacular forming large ice-clear stalactites of epsomite and mirabilite (Table 7.7). Celestite can also form as a crystalline crust or as distinct blue needles atop gypsum crusts, while baryte has been documented as a cement in cave soils. Both minerals, along with fluorite, are also found as phreatic precipitates in hydrothermal bathyphreatic caves.

But the most commonly noticed evaporite speleothems in carbonate karst are not various crusts and prisms but the spectacularly curved gypsum and halite flowers that protrude as lacy intertwined ribbons hanging from ceilings and walls. Epsomite and mirabilite occasionally also form crystal flowers. These cave flowers (oulopholites) typically grow as curved radiating masses of very long (up to 50 cm), narrow crystals. New growth originates at the base of the crystal strings as saturated brines emerge from the cave wall, driven by capillary evaporation. Faster growth in the centre of a bundle of crystals creates the radiating or flower-like pattern. Often they grow from waters issuing

Mineral	Composition	Type of occurrence
Gypsum	$\text{CaSO}_4 \cdot 2\text{H}_2\text{O}$	Dripstone, wall crusts, flowers, bladed crystals, pore cement in cave soils
Halite	NaCl	Dripstone, wall crusts, flowers, pore cement in cave soils
Epsomite	$\text{MgSO}_4 \cdot 7\text{H}_2\text{O}$	Dripstone, flowers, pore cement in cave soils
Hexahydrate	$\text{MgSO}_4 \cdot 6\text{H}_2\text{O}$	Loose crusts on cave floor
Mirabilite	$\text{Na}_2\text{SO}_4 \cdot 10\text{H}_2\text{O}$	Dripstone, flowers, loose tufts of crystals
Bloedite	$\text{Na}_2\text{SO}_4 \cdot \text{MgSO}_4 \cdot 4\text{H}_2\text{O}$	Loose crusts on cave floor
Celestite	SrSO_4	Loose crusts on cave floor

Table 7.7. Evaporite minerals and their mode of occurrence in cave speleothems.

from crevices and fractures in the cave wall and their growth contributes to parts of the cave wall breaking away or spalling (salt weathering). Changes in cave atmosphere and rates of capillary supply drive varying growth rates and hence the curvature of the crystals, much like the controls on helictes (twisted stalactites). Oulopholites are especially sensitive to seasonal changes in cave airflow. The growth of gypsum anemolites (wind-controlled oulopholites) in a cave in the Ukraine was found to vary with changes in cave humidity (Maltsev and Ford, 1991). When air moves into this cave each summer, and cave humidity is 70-90%, accretions of up to 7 mm form. In winter, the airflow reverses, the humidity rises and the same structures tend to dissolve.

Hill and Forti (1986) list ten sulphate salts derived from normal vadose karst processes; many others result from the interaction of karst waters with ore bodies. White (1988) lists four possible sources of cave sulphate, divided into two distinct source groups;

- Carbonate bedrock source:
 - a) Dissolution of sulphate bearing bed
 - b) Oxidation of pyrite in the bedrock
 - c) Weathering of anhydrite nodules
- Deep groundwater source:
 - a) Movement of deep H_2S waters into contact with phreatic karst waters to form sulphuric acid, which may dissolve calcite and deposit gypsum.
- To this list Hill and Forti (1986) add guano and weathering basalt.

As well as flowers in carbonate caves, halite is a rapidly growing vadose speleothem in its own right. Halite speleothems in carbonate caves form best in arid regions, where parent materials are leached from the regolith by circulating brackish groundwaters and redeposited under evaporative conditions in the cave environment. Lowry (1967) discussed halite speleothems from the carbonate caves beneath the Nullarbor, while Goede et al. (1992) notes the region has what may be the world's largest halite speleothems in a carbonate cave. Nullarbor's saline speleothems in Mullamullang Cave include the distinctive "coffee and cream" textures made up of a mixture of fine powdery and more coarsely crystalline magnesian calcite crusts, and varying levels of iron and manganese oxide, intermixed with fragments of halite and gypsum flowers.

Huge single evaporite crystals with geode-like textures can form in zones where saturated brine pools covers the cave floor or can rim a deep phreatic cavern. Where fluid chemistry fluctua-

tions are minimal in these gypsum saturated phreatic waters, clear impurity-free gypsum blades can grow as single crystals up to a metre or more in length and decimetres in width (e.g. phreatic crystals in sulphuric acid caves in Lechuguilla caverns of New Mexico, Almeria caverns in Spain and the Dnestro-vsko-Pricernomorskij karst caves of the western Ukraine. The details of this style of "giant" phreatic cement are discussed later in this chapter.

Karst hazards in evaporites

Unlike the relatively slow formation of limestone karst, gypsum/halite karst develops on a human/engineering time-scale. For instance, at Ripon in Yorkshire, a 3 m cube of undercut gypsum that fell into the River Ure was completely dissolved in 18 months and the nearby gypsum face was undercut another 6 metres in the next 10 years (Cooper, 1998). Although halite is even more susceptible to dissolution, it typically is not an urban engineering problem; large numbers of people simply do not like to live in a climate that allows halite to make it to the surface. However, catastrophic doline collapse atop poorly managed halite/potash mines and solution brinefields can be an anthropogenically-induced problem in developed regions (Chapter 12).

Collapse into nearsurface gypsum caves can create stoping chimneys in the overburden, which break out at the surface as steep sided dolines, often surrounded by broader subsidence hollows. Such swallow holes, up to 20 m deep and 40 m wide, continue to appear suddenly in gypsum areas throughout the world. Natural gypsum karst is a hazard in many parts of Europe

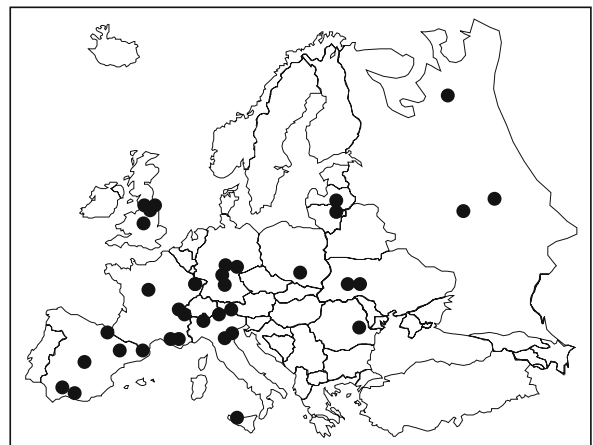


Figure 7.41. Areas in Europe associated with the development of intervals subsidence and collapse associated with gypsum karst.

Action or group of processes	Subsidence mechanisms	Examples
Removal of ground fluid	Loss of buoyant support for soil particles; compaction of sediment; possible failure of material bridging a void, thus, causing catastrophic collapse	Sinkholes overlying gypsum karst in Lithuania (Paukstys et al., 1999)
Shrinkage of organic or clay-rich materials	Consolidation of sediment; net loss of organic material	Shallow depressions from desiccated swelling clays (Biddle, 1983; Driscoll, 1983); subsidence of peat in subsidence hollows (Cooper, 1998)
Hydrocompaction of sediments	Softening and yield of metastable interparticle bonds by the introduction of water	Building subsidence caused by compaction of gypsiferous silt in alluvial fan, e.g., Calatayud Spain (Gutiérrez and Cooper, 2002) This effect is aggravated by broken water pipes in Calatayud and leaking septic tanks in Mosul, Iraq (Jassim et al., 1997)
Fluvial karstification of gypsum bedrock	Loss of mechanical support; syn- and post-sedimentary subsidence of alluvial deposits into depressions forming at the alluvium/gypsum contact	Subsidence depressions on alluvial flood plains, Calatayud Graben, Spain (Gutiérrez, 1996), river valley 'subrosion' (Ford, 1997)
Downwashing of unconsolidated sediments	Downward movement of sediments into existing voids or breccia pipes resulting in gradual growth of shallow depressions	Sinkholes in Lithuania (Paukstys et al., 1999); sinkholes in Ripon (Cooper, 1986)
Gradual collapse of unconsolidated materials overlying gypsum karst	Sagging of materials overlying a void leading to concomitant lowering of the cover/gypsum interface, and growth of a surface depression	Sinkholes in West Ripon (Cooper, 1998)
Catastrophic collapse of unconsolidated sediments into existing voids (may be preceded by a period of gradual subsidence)	Collapse that probably requires a triggering mechanism; ravelling of a void upwards through unconsolidated sediment possibly accompanied by removal of sediment by rapid water flow through the void	Sinkholes in Ripon (Cooper, 1986, 1998); sinkholes in China (Yaoru and Cooper, 1997); sinkholes in glacial drift overlying gypsum karst, Nova Scotia (Martinez and Boehner, 1997)
Catastrophic collapse of competent strata into voids (breccia pipe propagation)	Failure of material bridging void; development of sinkhole generally requires a triggering mechanism	Sinkholes in Ripon (Cooper, 1986), New Mexico (Martinez et al., 1998), NW territories, Canada

Table 7.8. Processes and mechanisms driving the creation of gypsum karst hazards, with examples (after Lamont-Black et al., 2002).

(Figure 7.41) and similar areas of subcropping gypsum in much of the rest of the world (Table 7.8). Areas surrounding the city of Zaragoza in northern Spain are affected as is the town of Calatayud (Gutiérrez and Cooper, 2002). Gypsum dissolution is responsible for subsidence and collapse in urban areas around Paris, France (Toulemont, 1984), in and around Stuttgart and towns peripheral to the Harz Mountains in Germany (Garleff et al., 1997), in Pasvalys and Birzai in Lithuania (Paukstys et al., 1999), in the Perm area of Russia (Reuter and Tolacev, 1990), in the Sivaz region of Turkey (Karacan and Yilmaz, 1997), in the region centred on the city of Mosul in northern Iraq (Jassim et al., 1997) and on a number of areas of rapid urban development in eastern Saudi Arabia (Amin and Bankher, 1997a, b). Large subsidence depressions caused by gypsum dissolution in China have opened up in the Taiyuan and Yangquan regions of Shanxi Coalfield and in the adjacent Hebei Coalfield.

Natural gypsum karst has been responsible for leakage or failure in more than 24 dams worldwide. In the USA they

include: McMillan, Avalon and Rio Hondo dams in New Mexico; San Fernando, Dry Canyon, Buena Vista and Castaic and Olive Hills dams in California; Stanford Dam, Texas; Red Dock Dam, Iowa, Fontanelle Dam, Oklahoma; and the Moses Saunders Tower Dam, New York. Other problem dams include: Kamskaya and Bratsk dams in Russia, El Isiro dam in Venezuela, Allos dam in Spain, Mosul Dam in Iraq, Houspiro dam in China and Hessianheim Dam in Germany.

In the towns of Ripon in the UK and Pasvalys and Birzai in Lithuania about 45,000 people are currently affected by catastrophic subsidence caused by natural gypsum dissolution (Paukstys et al., 1999). Special measures for construction of roads, bridges and railways are needed in these areas and include: incorporating several layers of high tensile heavy duty reinforced plastic mesh geotextile into road embankments and car parks; using sacrificial supports on bridges so that the loss of support of any one upright will not cause the deck to collapse; extending the foundations of bridge piers laterally to an amount that could span the normal size of collapses; and

using ground monitoring systems to predict areas of imminent collapse (Cooper 1995, 1998).

Problems in the Ripon area, UK

The town of Ripon and its surrounds experience the worst gypsum-karst related subsidence in England (Cooper and Waltham, 1999). At least 30 major collapses have occurred in the last 150 years (Figures 7.42 and 7.43). Numerous sags and small collapses also characterise surrounding farmlands. Subsidence features are typically 10-30m in diameter, reach up to 20m in depth and can appear at the surface in a matter of hours to days (Figure 7.43). To the east of the city, one collapse sinkhole in the Sherwood Sandstone is 80 m in diameter and 30 m deep, perhaps reflecting the stronger roof beam capacity of the Sherwood Sandstone.

Shallow subcropping Zechstein gypsum occurs in two subcropping bedded units in this area, one is in the Permian Edlington and the other is in the Roxby Formation. Together they form a subcrop belt about a kilometre wide, bound to the west by the base of the lowest gypsum unit (at the bottom of the Edlington Formation) and to the east by a downdip transition from gypsum to anhydrite in the upper gypsum-bearing unit of the Roxby Formation. The spatial distribution of subsidence features within this belt relates to joint azimuths in the Permian bedrock, with gypsum maze caves and subsidence patterns following the joint trends (Cooper, 1986). Most of the subcropping gypsum is alabastrine in the area around Ripon, while farther to the east, where the unit is thicker and deeper, the calcium sulphate phase is still anhydrite.

Fluctuations in the watertable level tied to heavy rain or long drought are thought to be the most common triggering mechanism for subsidence. Many of the more catastrophic collapses occur after flooding and periods of prolonged rain, which tend to wash away cavern roof span support. Subsidence is also aggravated by groundwater pumping; first, it lowers the water table and second, it induces

considerable crossflow of water in enlarged joints in the gypsum. When recharged by a later flood, the replacement water is undersaturated with respect to gypsum.

Thomson et al. (1996) recognised four hydrogeological flow units driving karst collapse in the Ripon area:

- 1) Quaternary gravels in the buried valley of the proto-River Ure
- 2) Sherwood Sandstone Group
- 3) Magnesian Limestone of the Brotherton Fm. and the overlying/adjacent gypsum of the Roxby Fm.
- 4) Magnesian limestone of the Cadeby Fm. plus the overlying/adjacent gypsum of the Edlington Fm.

Local hydrological base level within this stratigraphy is controlled by the River Ure. Its buried Pleistocene valley (proto-Ure) is filled by permeable sands and gravels (Figure 7.42). In the area around Ripon the palaeovalley cuts down more than 30 m, reaching levels well into the Cadeby Formation, so providing the seepage connections or pathways between waters in all four units wherever they intersect the palaeovalley. There is considerable groundwater outflow along this route with

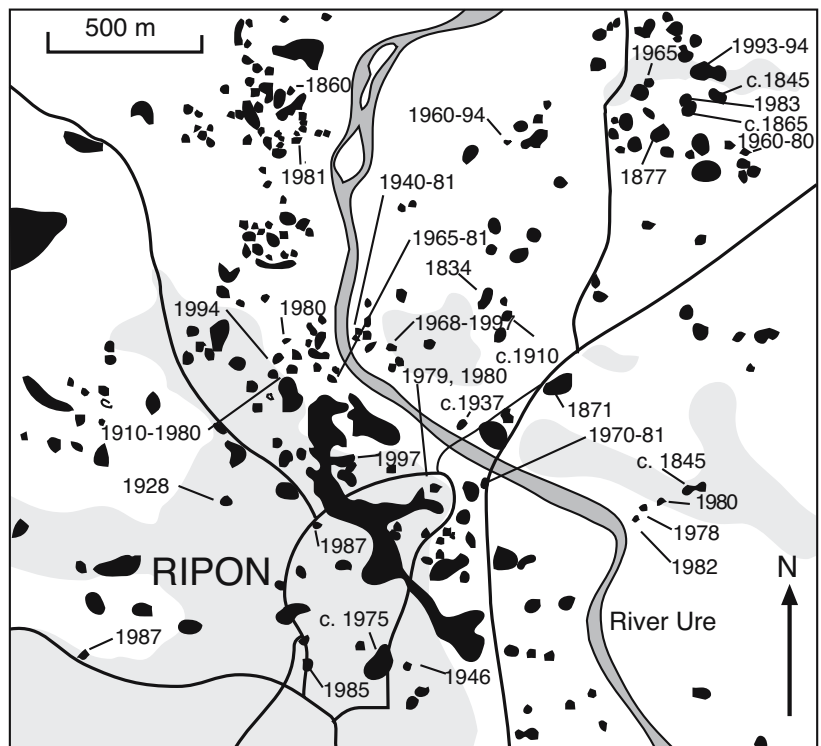


Figure 7.42. Surface distribution (shaded black) and time of formation of subsidence features (where known) in and around the town of Ripon, United Kingdom (after Cooper and Waltham, 1999). Built up areas are shaded grey.

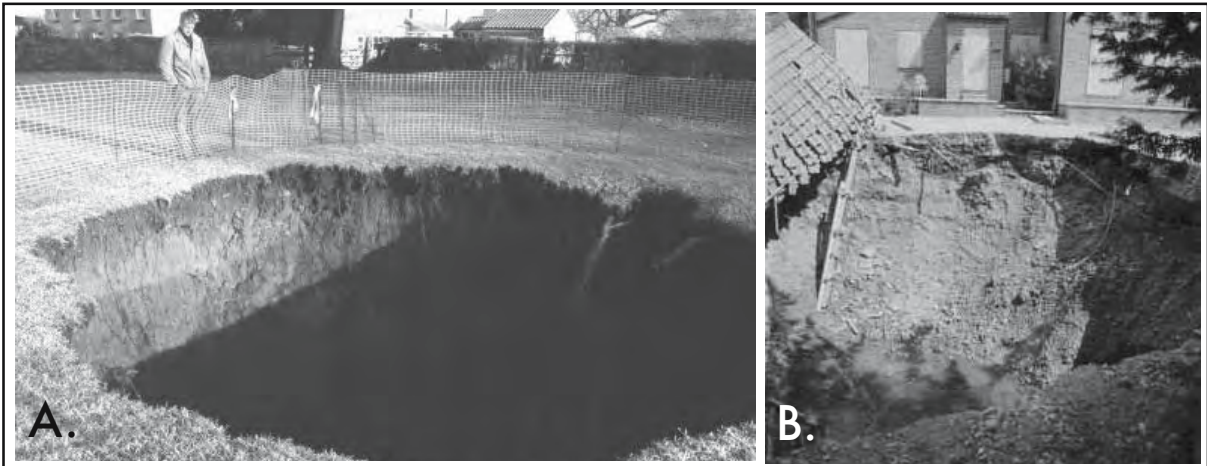


Figure 7.43. Catastrophic collapse areas of gypsum subcrop, UK. A) Subsidence crater caused by the dissolution of Permian gypsum at the village of Sutton Howgrave, North Yorkshire. The hole started to collapse in December 2000, the photograph was taken on 14th February 2001 when the hole was 5-6m in diameter and 11m deep with water at a depth of 8m. B) Collapse at the rear of a house in the village of Ripon, April 1997 (Photographs courtesy of A. H. Cooper and accessible at <http://www.bgs.ac.uk/programmes/envhaz/uggh/karst/home.html>; last accessed Dec 4, 2004).

artesian sulphate-rich springs issuing from Permian strata in contact with Quaternary gravels of the buried valley (Cooper, 1986, 1995, 1998).

The potentiometric head comes from precipitation falling on the high ground of the Cadeby formation to the west and the Sherwood Sandstone to the east. Groundwater becomes largely confined beneath glacial till as it seeps toward the Ure Valley depression, but ultimately finds an exit into the modern river via the deeply incised sand and gravel-filled palaeovalley of the proto-Ure. Waters recharging the Ure depression pass through and enlarge joints and caverns in the gypsum units of the Edlington and Roxby Formations, so the highest density of subsidence features are found atop the sides of the palaeovalley. This region has the greatest volume of artesian discharge from aquifers immediately beneath the dissolving gypsum. Although created as an active karst valley, the apparent density of subsidence hollows is lower on the present Ure River floodplain than the surrounding lands as floodplain depressions are constantly filled by overbank sediments (Figure 7.42).

^{7.4}*Entrenched karst* occurs where the entire thickness of the soluble rock is entrenched along the sides of valleys but the insoluble cap spans most interfluvies.

Subjacent karst occurs where the soluble rock is locally breached by erosion over a minor part of its thickness, karst features may be expressed at the surface as combinations of springs and collapse features.

Mantled karst is wholly or partly covered by a relatively thin veneer of post-karst rock or sediment and is part of the contemporary landscape.

Cooper (1998) defined 16 sinkhole variations in the gypsum subsidence belt at Ripon, all are types of ^{7.4}entrenched, subjacent and mantled karst. Changes in karst style are caused by; the type of gypsum, the nature and thickness of the overlying deposits, presence or absence of consolidated layers overlying the gypsum and the size of voids/caverns within the gypsum.

To the west of Ripon, the gypsum of the Edlington Formation lies directly beneath glacial drift. These unconsolidated drift deposits and the loose residual marl atop the dissolving gypsum gradually subside into a pinnacle or suffusion (mantled) karst. But between Ripon city and the River Ure, the limestone of the Brotherton Formation overlies the Edlington Formation. There the karst develops as large open caverns beneath strong roof spans (entrenched karst). Ultimate collapse of the roof span creates rapid upward-stopping caverns in loosely consolidated sediment. Slopes break through to the surface as steep-sided collapse dolines or chimneys with sometimes catastrophic results. A similar entrenched situation is found east of the Ure River but there karstified gypsum units of both the Edlington and the Roxby formations are involved.

When a chimney breaks through, the associated surface collapse is very ^{7.5}rapid. A recently documented example of one such subsidence crater, which opened up in front of a house on Ure Bank terrace on 23rd and 24th April, 1997, is documented by Cooper (op. cit.) as follows (Figure 7.43a).

“The hole grew in size and migrated towards the house, to measure 10m in diameter and 5.5m deep by the end of Thurs-

day. Four garages have been destroyed by the subsidence. This collapse was the largest of one of a series that have affected this site for more than 30 years. The hole is cylindrical but will ultimately fail to become a larger, but conical, depression. As it does so, it may cause collapse of the house, which is already damaged, and the adjacent road. The house and several nearby properties have been evacuated and the nearby road has been closed. The gas and other services, which run close to the hole, have also been disconnected in case of further collapse.”

Problems with Miocene gypsum, Spain

Karstification has led to numerous problems in areas of subcropping Miocene gypsum in the Ebro and Calatayud basins, northern Spain. Areas affected are defined by subsidence or collapse in Quaternary alluvial overburden and include; urban areas, communication routes, roads, railways, irrigation channels and agricultural fields (Soriano and Simon, 1995; Elorza and Santolalla, 1998). There can be a reciprocal interaction between anthropic activities and sinkhole generation, whereby the ground disturbance engendered by human activity accelerates, enlarges and triggers the creation of new sinkholes. Subsidence is particularly harmful to linear constructions and buildings and numerous roads, motorways and railways have been damaged. Catastrophic collapse in roads and buildings

^{7.5}A. H. Cooper in a lecture to the general public has recently argued that the collapse dolines breaching the landscape between Ripon and Darlington were the inspiration for the rabbit hole in Alice in Wonderland. In Chapter 1, Lewis Carroll wrote.

“The rabbit-hole went straight on like a tunnel for some way, and then dipped suddenly down, so suddenly, that Alice had not a moment to think about stopping herself, before she found herself falling down what seemed a deep well. Either the well was very deep, or she fell very slowly, for she had plenty of time as she went down to look about her, and to wonder what would happen next”

Charles Lutwidge Dodgson, who later adopted the Lewis Carroll pseudonym, was born in Cheshire and spent his early days at Croft, near Darlington. There, a trio of ponds called Hell’s Kettles were believed by locals to be bottomless. The pits are now known to be gypsum collapse features only 22ft deep but they may have inspired this passage from the first chapter. In 1852 Carroll moved with his parents to Yorkshire when his father became Canon Dodgson of Ripon. Here, he first met Mary Badcock. Carroll, a keen mathematician, scientist and photographer, took pictures of Mary that were later adapted by Sir John Tenniel into illustrations in the first edition of Alice in Wonderland.

can have potentially fatal consequences. For example, several buildings have been damaged around the towns of Casetas and Utebo. In the Portazgo industrial estate some factories had to be pulled down due to collapse-induced instability. A nearby gas explosion was attributed to the breakage of a gas pipe caused by subsidence. The local water supply is also disrupted by subsidence and pipe breakage so that 20,000 inhabitants periodically lose their water supply. The most striking example of subsidence affecting development comes from the recently built village of Puilatos, in the Gallego Valley. This was severely damaged by subsidence and abandoned before it could be occupied.

Collapse affects irrigation channels in the countryside with substantial economic losses (Elorza and Santolalla, 1998). In 1996 a doline collapse cut the important Canal Imperial at Gallur village. New dolines often form in close proximity to unlined irrigation canals. The ongoing supply of fresh irrigation waters to field crops can also encourage sinkhole generation in the fields. Though not directly visible, natural sinkholes also form in the submerged beds of river channels cutting regions of subcropping gypsum. On December 19th, 1971, a bus fell from a bridge into the Ebro River at Zaragoza, near where the so-called ‘San Lazaro well’ (a submerged gypsum sinkhole) is located. Ten people lost their lives in this accident, nine of them where never found. Locals suggested that bodies were carried into the sinkhole and sank into the caverns fed by this losing stream.

Variation in the water table level, induced by groundwater pumping, is another anthropogenic trigger for dolines. As the watertable declines it causes a loss of buoyant support to the ground, it also increases the flow gradient and water velocity, which facilitates higher rates of crossflow and deeper aquifer recharge in subsequent floods and so reduces the geomechanical strength of the cover and washes away roof span support. Dolines can also be associated with groundwater quality issues. Collapse dolines or sinkholes are frequently used as areas or sumps for uncontrolled dumping industrial and domestic waste. Because of the direct connection between them and the regional aquifer, uncontrolled dumping can cause rapid dispersion of chemical and bacterial pollutants in the groundwater.

Sometimes even well-intentioned attempts to remediate culturally significant buildings under threat of karst collapse can exacerbate collapse problems. Gutiérrez and Cooper (2002) cite two examples from the city of Calatayud, Spain (Figure 7.44a, b). Subsidence-induced differential loading drives the tilting of the 25 metre high tower of the San Pedro de los Francos church, which leans towards and overhangs the street by about

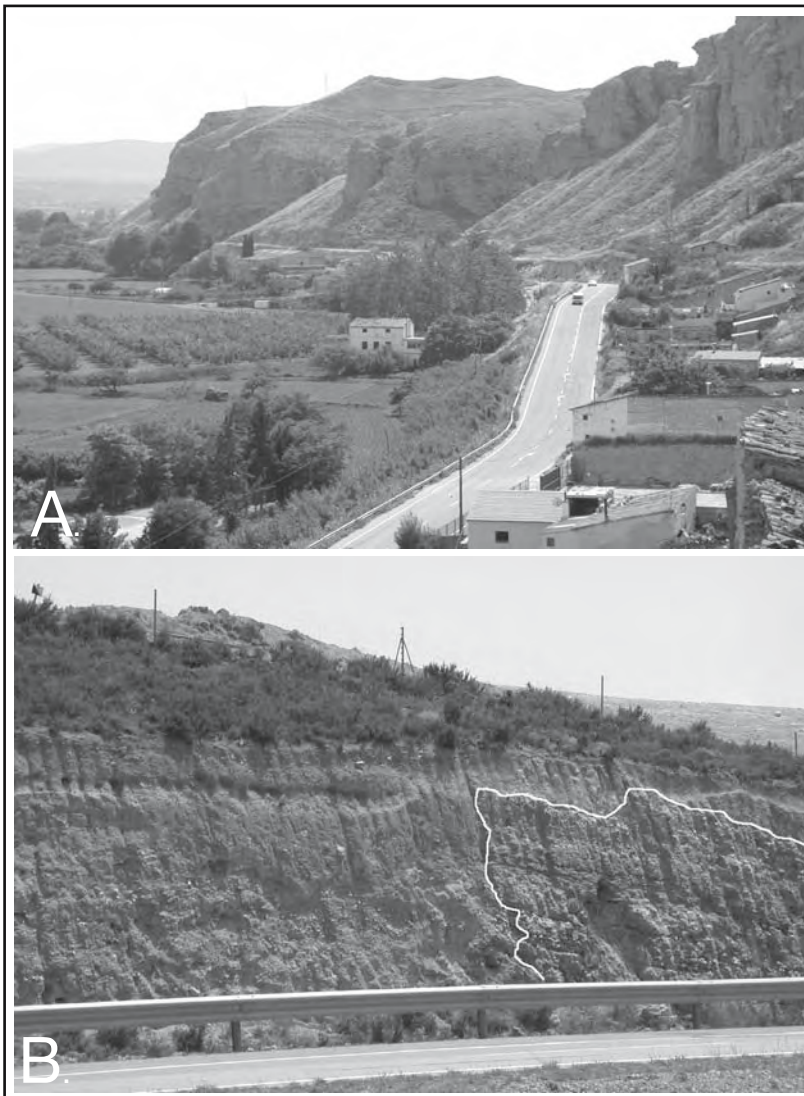


Figure 7.44. Gypsum karst, Calatayud region, Spain. A) View from the town of Calatayud toward the retreating front of Miocene gypsum and the encroaching floodplain of the Río Jalón. B) Mantled steep edge of a collapse doline exposed in a highway cut on the approach to Calatayud. Bedded gypsum makes up the right half of the exposure, alluvium the left.

1.5 metres. In places, the brickwork of the church indents the pre-existing tower fabric, which probably dates from the 11th Century or the beginning of the 12th Century. This indentation and the non-alignment of the church and the tower walls indicates that most of the tower tilting occurred prior to the construction of the church. In 1840, the upper 5m of the tower was removed and the lower part buttressed for the safety of the Royal family, who visited the town and stayed in the palace opposite. On 3rd June 1931, San Pedro de los Francos church was declared a “Monument of Historical and Artistic value.” Due

to its ruinous condition, the church was closed to worship in 1979. Micropiling to improve the foundation was started in 1994, but this corrective measure was interrupted when only half of the building was underpinned. Very rapid differential settlement of the building took place in the following year, causing extensive damage and aggravating the subsidence problem.

Colegiata de Santa María la Mayor was constructed between the 13th and 18th centuries, it has an outstanding Mudéjar (a 72 m high tower) and numerous Renaissance features; it is considered the foremost monument in the city of Calatayud. As with the San Pedro de los Francos Church, recent micropiling work, applied to only one part of the cloister, has been followed by alarming differential movements that have drastically accelerated the deterioration of the building. Large blocks have fallen from the vault of the “Capitular Hall” and cracks up to 150 mm wide have opened in the brickwork of the back (NW) elevation, which has now been shored up for safety. The dated plaster tell-tales placed in these cracks to monitor the displacement demonstrate the high speed of the deformation produced by subsidence in recent years. On the afternoon of 10 September 1996, the fracture of a water supply pipe flooded the cloisters and the church with 100 mm of muddy water. Ten years earlier a similar breakage and flood had occurred. These breaks in the water pipes are most likely related to

karst-induced subsidence. Once they occur, the massive input of water to the subsurface may trigger further destruction via enhanced dissolution, piping and hydrocollapse (Gutiérrez and Cooper, 2002).

Gypsum karst beneath Mosul, Iraq

A similar quandary of multiple areas of structural damage from gypsum-induced subsidence affects large parts of the historic

section of the city of Mosul in northern Iraq (Jassim et al., 1997). The main part of its old quarter is over a century old and some buildings are a few hundred years old. Mosul lies on the northeastern flank of the Albu Saif anticline and near to its northern plunge. It was built on the western bank of the Tigris River on a dip slope of Miocene limestone that is directly underlain by bedded gypsum and green marl (equivalent to Fars Formation). Houses in the old city were built on what seemed to be at the time a very sound rock foundation.

In the early part of last century water distribution in the city was done on mule back and the estimated water consumption did not exceed 10 litres per person per day (Jassim et al., 1997). Discharge from households was partly to surface drainage and partly to shallow and small septic tanks. The modern piped system of water distribution did not start until the 1940s, resulting in a sudden increase in water consumption (presently around 200 litres per person per day) and it was not associated with a complementary sewer system. Increased water consumption meant larger and deeper septic tanks were dug at the perimeter of buildings (which never seemed to fill) resulting in a dramatic increase in water percolating downwards, water which was also more corrosive due to the increased use of detergents and chlorination. This water passes through the permeable and fractured limestone to the underlying gypsum. On its way through the limestone it enlarged and created new dissolution cavities, but eventually found its way into the older gypsum karst maze, which is then further widened as water drains back into the Tigris. Caverns in the gypsum enlarge until the roof span collapses. Since the 1970s more and more buildings in the old city have fractured and many were subject to suddenly collapse. The problem was further intensified due to the expansion of the city in the up-dip direction (west and southwest) including construction of industrial, water-dependant centres. Water draining from the up-dip areas eventually passes under the old city before discharging in the Tigris river. The process was slightly arrested in the 1980s by the completion of a drainage system for the city, but the degradation of the old city continues.

Solving the problem?

Throughout the world, be it in the UK, Spain, eastern Europe, or the Middle East, it is a fact that weathering of shallow gypsum forms rapidly expanding and stoping caverns, especially in areas of high water crossflow, roof beams and unconsolidated overburden. Formative processes and mechanism are commonplace and widespread (Table 7.8). It is fact that natural solution in regions of subcropping evaporites is always rapid,

and even more so in areas where it is encouraged by human activities, especially increased cycling of water via groundwater pumping, burst pipes, septic systems and uncontrolled storm and waste water runoff to the aquifer.

Typically, the best way to deal with a region of an evaporite karst hazard is to map the regional extent of the shallow evaporite solution front and avoid it. In established areas with a karst problem the engineering solutions are largely short term and local. Problems will be ongoing as subsidence and occasional, but rapid, catastrophic collapse are both natural processes. If man-made buildings of significance are to be restored and stabilized, perhaps it is better to wait until funds are sufficient to complete the job rather than attempt partial stabilization of the worst-affected portions of the building. In the words of Nobel prizewinner, Shimon Peres; "If a problem has no solution, it may not be a problem, but a fact - not to be solved, but to be coped with over time."

Sulphuric acid speleogenesis

Historically, most carbonate karst networks have been interpreted as epigenic (surface-driven) responses to vadose/shallow-phreatic leaching of carbonate bedrock, in a hydrology driven by throughflowing fresh to brackish meteoric waters. Leaching and cavern/joint enlargement is seen as a response to waters enriched in carbonic acid. Carbonic acid is derived from CO₂ in the atmospheric and soil zones. Most vadose cave ornamentation is a response to CO₂ degassing at or above the watertable and precipitates are dominantly calcite, with lesser volumes of other carbonate minerals (aragonite, magnesite) and rare sulphates.

We have just seen how gypsum maze caves do not fit neatly into this epigenetic meteoric/watertable dominated template. Telogenetic gypsum karst in an evaporite basin starts much deeper (hypogenic), typically in water crossflows driven by deep artesian circulation or escaping basinal fluids. In the last two decades the importance of similar hypogene leaching of carbonates has been recognised in systems driven by the ascent, mixing and cooling of H₂S and CO₂ rich basinal brines. Examples are now documented in what were once considered classic regions of meteoric leaching (Table 7.9; Davis, 1980; Egemeier, 1981). Caverns can form in carbonate hosts well below the water table where there is frequently a calcium sulphate association in the deeper parts of the hydrology, both in basinal generation of H₂S and in the typical byproducts of cavern creation.

Active sulphidic caves and hypogenic karst	Australia: Odyssey Cave	Jennings, 1985
	Canada: "Sulphur" Cave, Banff National Park	Ford, 1997
	Italy: Frasassi Caves (Grotta Grande del Vento Grotta de Fiume); Submarine caves as in Grotta Azzurra region	Vlasceanu et al., 2000; Galdenzi and Menichetti, 1995; Forti et al., 2002
	Mexico: Cueva de Villa Luz; Miscellaneous coastal cenotes	Hose et al., 2000
	Romania: Movile Cave	Forti et al., 2002
	Turkmenistan: Cupp-Coutum Cave	Maltsev and Malishevsky, 1990
	Ukraine: Zoloushka Cave	Andrejchuk and Klimchouk, 2001
	USA: Cesspool Cave, Virginia; Crystal Beach Cave, Florida; Lower Kane Cave, Wyoming; Parker Cave, Kentucky; Deep portions of the Edwards Aquifer, Texas	Engel et al., 2001, Egemeier, 1981
Inactive sulphidic caves and hypogenic karst	China: Yangcheng gas field	Hao et al., 1998a
	South Africa: Mboho Mkuu Cave	Martini et al., 1997
	Thailand: Nang Nuan oilfield	Heward et al., 2000
	USA: Carlsbad Cavern and Lechuguilla Cave, New Mexico	Hill, 1990

Table 7.9. Active and inactive sulphuric cavern systems, not all are related to evaporite dissolution, but all accumulate gypsum.

Bathypneatic caves are still classified by some carbonate sedimentologists as a form of hydrothermal karst with an implication of hot hydrothermal waters. There certainly are some bathypneatic caves developed as carbonate karst that do have an association with hot circulating waters, especially those caves forming host cavities to some MVT deposits (Warren and Kendall, 1997). But many sulphuric acid groundwaters that form caves and cavern gypsum, such as those of the Carlsbad system, were probably not all that hot. The term hypogene (formed at depth) is more appropriate than hydrothermal (waters with elevated temperature) in classifying caves formed by cooling and mixing of hydrocarbon-rich basinal waters, which have encountered deeply buried beds of sulphate evaporites on their way to the surface.

Hypogene caves in carbonate hosts can contain substantial volumes of gypsum precipitated as cavern fills and limestone replacements at scales ranging from microcrystalline crusts on the cave wall to cavern-filling accumulations of phreatic gypsum crystals deposited either as pelagic laminites or as spectacular crystal-clear prisms that can be metres long and wide (Buck et al., 1994). The accumulation of large volumes of cave-fill gypsum, independent of the climate at the landsurface, does not fit well with older notions of surface-driven meteoric circulation and arid cave atmospheres for gypsum speleothems. Hypogene caverns and their gypsum fills can develop wherever oxygenation of rising H_2S -laden hypogene waters occurs, this typically first occurs at bathypneatic depths, and can be hundreds of metres below the meteoric water table.

Early stages of hypogenic caves display no relationship to meteoric recharge conduits in their overburden. This is typically an epigenic overprint that forms during later uplift. Hypogenic cave passages typically follow ramiform, network, or spongiform patterns (Palmer and Palmer, 2000). Time and ongoing exhumation brings a hypogene cave closer to the land surface and moves it out of its formative bathypneatic hydrology. By the time hypogene caves are accessible to speleologists the evidence of the formative hydrology is largely overprinted by classic meteoric-driven karst textures and precipitates. H_2S needed to drive hypogene cavern formation is carried by escaping basinal waters that have experienced biochemical or thermochemical reduction of sulphate evaporites and petroleum. Less commonly, they are derived by groundwater oxidation of pyrite, or they entrain volcanogenic waters. As anoxic, H_2S -enriched basinal water rise along fractures in the limestone host, it cools and mixes with the underside of a layer of meteoric pore water, which typically is oxygenated. As sulphide-rich waters mix and become oxidized, the most aggressive byproduct of their oxidation is sulphuric acid, which can be biologically-mediated by sulphur-oxidising bacteria. This aggressive water leaches and dissolves the surrounding carbonate aquifer so that hypogene caverns tend to have large chambers with narrow connections and deep shafts along fracture or joint avenues where the sulphide-rich waters rose (inverted tear-drops). As the acid is spent the concentrations of calcium and sulphate in the cave waters build to gypsum saturation and the resulting gypsum ornamentation can be spectacular.

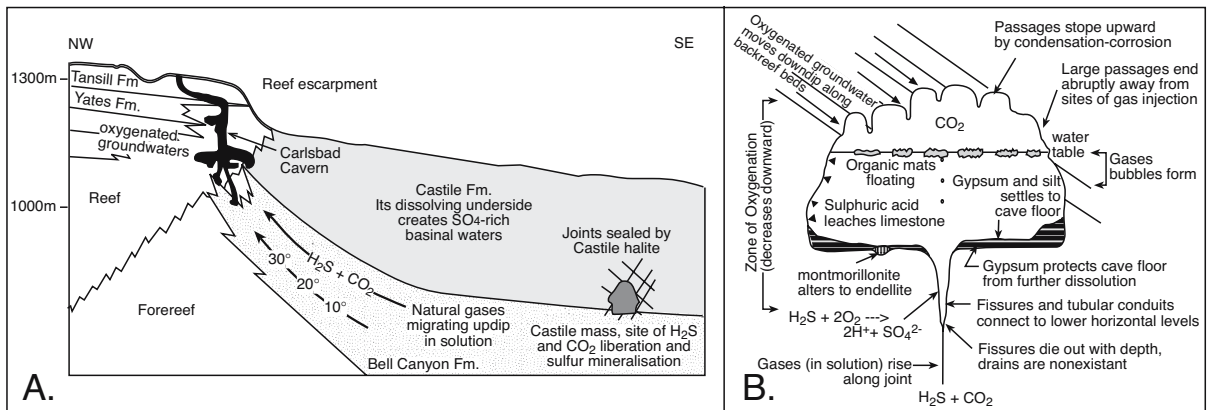


Figure 7.45. Sulphuric acid speleogenesis. A) Schematic section of Delaware Basin. Escape of natural gas from hydrocarbon kitchen in the basin centre is focused along the dissolving underside of the laminated anhydrite of the Castile Formation. It reacts thermochemically with the sulphate ions to produce H₂S, CO₂ and calcite replacement of the anhydrite (this forms the characteristic Castiles when later exhumed). H₂S and CO₂ continue their focused escape through the Bell Canyon Formation toward the basin margin where they enter limestones of the Capitan and Goat Seep Reefs. There the gases mix with oxygenated groundwater, hydrogen sulphide in solution and dissolved oxygen combine to form sulphuric acid, which then leaches the host limestone, especially along the more permeable joints and fissures. B) Hydrogen sulphide reacts with dissolved oxygen to form sulphuric acid which leaches a cavern. The sulphuric acid is neutralised by the limestone so that caverns tend to terminate abruptly away from zones of gas injection. Oxygenation and hence the acidic reaction die out with depth so that large rooms do not extend far below the horizontal extent of the cavern. With successive lowering of base level, driven by uplift and climatic change, new horizontal levels became connected with older horizontal levels by spring shafts and joint chimneys (after Hill, 1990; Forti et al., 2002). The gas-filled cavern top and an associated water table is only present during the more mature stages of exhumation. The process of mixing of H₂S-rich and meteoric waters that creates the hypogene cavern is a totally phreatic system and is largely unrelated to the presence or absence of a water table.

The best documented example of sulphuric acid speleogenesis in the western literature is the Carlsbad-Lechuguilla cavern system in Permian reefal limestones of the Guadalupe Mountains, USA (Figure 7.45a; Hill, 1990; Palmer and Palmer, 2000). Although meteoric processes now form calcitic speleothems in these caves, the early host caverns were etched bathyphreatically by sulphuric acid and walls were free of calcite speleothems. Sulphuric acid caverns created by mixing of H₂S waters with oxygenated phreatic waters began to form in the Carlsbad system some 10-12 Ma and as much as 200 metres below the water table. Remnant blocks of pelagic gypsum, a widespread byproduct of sulphuric acid leaching, still cover the floor of the now largely inactive and exhumed Carlsbad Cavern.

Room” level of Carlsbad Cavern formed 3.9 to 4.0 Ma, while the upper level of Lechuguilla Cave formed 5.7 to 6.0 Ma (Figure 7.46). Other older and now more elevated hypogene caves in the Guadalupe Mountains formed at various times from 6.0 to 11.3 Ma (Polyak et al., 1998). Alunite ages increase with,

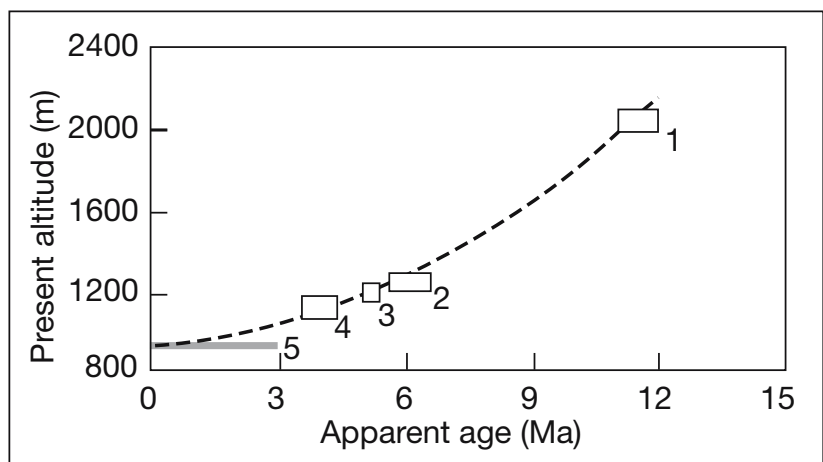


Figure 7.46. Age versus elevation for several cave levels in the Guadalupe Mountains (after Polyak et al. 1998). 1 = Cottonwood Cave and Virgin Cave; 2 = Endless Cave and Glacier Bay (Lechuguilla Cave); 3 = Lake Lebarge (Lechuguilla Cave); 4 = New Mexico Room, Big Room, and Green Clay Room (Carlsbad Cavern); 5 = present water table.

⁴⁰Ar/³⁹Ar dating of fine-grained alunites that were formed during hypogene leaching, and still present in residual clays, show that the “Big

Location	H ₂ S (mg/l)	Reference
Henderson oil field, Delaware Basin, 120 km east of Guadalupe escarpment	600	Wiggins et al., 1993
Sulphur Springs Tabasco, Mexico	394	Palmer and Palmer, 1998
Sharon Springs Sulphur Spa, New York	103	Palmer and Palmer, 1998
Lower Kane Cave, Wyoming	6	Egemeier (1981)
Hellespont Cave, Wyoming	15	Egemeier (1981)
Movile Cave, Romania	10	Sarbu et al., 1996

Table 7.10. Levels in waters from some H₂S enriched settings.

and are strongly correlative to, cave elevation, indicating an 1100-metre decline in the water table tied to ongoing Neogene uplift and tilting (Figure 7.46).

The cavern forming process is driven by chemical changes in oil- and gas-rich basinal waters moving up dip from the evaporite-sealed Delaware Basin (Figure 7.45a). Rising waters derive much of their sulphate content by dissolution of the underside of Castile anhydrite. Some of this sulphate undergoes thermogenic and biogenic sulphate reduction to form H₂S and CO₂, with bacteriogenic “Castile” calcite precipitated as a sulphate reduction byproduct along the contact between the underlying aquifer and the Castile Fm. SO₄. H₂S-enriched basinal waters then enters the Capitan and Goat Seep strata via crosscutting joints, typically along local aquifers created by the steeply dipping fore reef beds, or via lenses of sandy equivalents to Bell Canyon siliciclastics.

Rising basinal waters carry large volumes of H₂S, CO₂ and methane in solution. As it rises it depressurizes and releases the various dissolved phases as gas bubbles (degasses). By

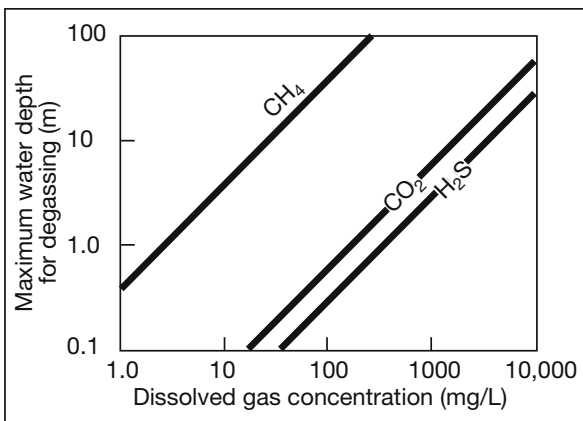
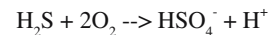


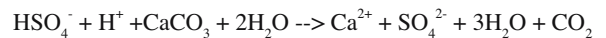
Figure 7.47. Maximum depth at which degassing of H₂S, CO₂, and CH₄ can take place below the unconfined water table. Partial degassing occurs at depths well below the respective lines, but no degassing will occur above the line (after Palmer and Palmer, 2000).

the time the water comes to within a few metres of the water table it has released almost all of its gas as bubbles (Figure 7.47; Table 7.10; Palmer and Palmer, 2000). We shall focus on the H₂S because of its role in precipitating hypogene gypsum fills, but released CO₂ and methane released as gas bubbles from ascending brines also play a role in hypogene caves. Like H₂S, they can create chemosynthetic ecosystems in the deep phreatic, systems which function independent of energy input from the surface (Chapter 9).

On arrival in the shallower phreatic levels of the basin, the H₂S reacts with oxygenated groundwater to form sulphuric acid:



Once formed, the sulphuric acid immediately attacks the limestone host and etched out the Carlsbad caverns via the reaction:



This adds further sulphate to the already sulphate-enriched cave waters. If the dissolving carbonate host is dolomitic, then significant magnesium is also added to the cave water. Expanding horizontal benches in such hypogene caverns reflect intervals of most intense phreatic mixing between H₂S and SO₄ saturated basinal waters. They are located in the lower portion of the oxygenated active phreatic system and may not necessarily be tied the presence of a water table.

Sulphuric acid caves have spongelike edges and no calcitic speleothems ornamenting the growing cavity. Cave walls tend to end abruptly in the horizontal plane as the acidity of the cave waters is quickly quenched away from fissures supplying H₂S. Likewise, since the level of dissolved oxygen in cavern waters decreases with depth, the fissure passages and pits tend to terminate vertically via a rapid narrowing downward channelway. This forms an inverted “tear drop” cavern, a shape less seen in epigenic carbonate karst (Figure 7.45b).

Ongoing leaching means calcium and sulphate levels continue to build in cavern waters, which are already near or at gypsum saturation from earlier leaching of the Castile Formation. Gypsum starts to precipitate in the cave water column and on the cave walls. Fine laminated and layered pelagic gypsum builds up beneath the water-covered parts of the cave floor, typically atop endellitic silts. Huge centripetal splays (metres long and decimetres wide) of ice-clear prismatic gypsum precipitate in

stable phreatic portions of the cavern system. Alabaster crusts can coat vadose areas of the cave walls often in association with the growth of acidophilic archaea and sulphur-oxidising bacteria.

Smectitic clays, released by the leaching of the carbonate bedrock settle through the quiescent cave waters, along with the gypsum crystallites forming in the supersaturated cave waters, to form a pelagic (“rain-from-heaven”) unit of laminated gypsum and silt on the cave floor (Figure 7.45b). Acidic cave waters convert some of the accumulating smectite to endellite ($\text{Al}_2\text{Si}_2\text{O}_5(\text{OH})_4 \cdot 2\text{H}_2\text{O}$), a brightly coloured clay indicative of acidic conditions in hypogene caves. Two other low-pH, sulphuric-acid indicator minerals, alunite and natroalunite, also occur in association with the endellite (Cunningham 1992; Hill 1995). The same sulphuric acid environment facilitates the formation of secondary late-stage, uranium-vanadium minerals tyuyamunite and metatyuyamunite at redox boundaries in the caves and their presence helps explain elevated levels of radon that typify the modern cave air in the various Carlsbad caverns (Hill, 1995).

Even though further uplift has now drained the waters from the caverns, relicts of the gypsum spar and blocks of layered granular pelagic gypsum remain. Such blocks are sporadically scattered over the deeper parts of the floor of the “Big Room” in Carlsbad Cavern as remnants of a former gypsum layer that was up to 10m thick. Internally, the blocks and rinds of the pelagic units show a laminated or microfolded fabric indicative of its subaqueous origin (pers. obs). In Lechuguilla Cave, phreatic spar gypsum ornamentation forms “chandeliers” or “ferro di lancia” accumulations of ice-clear gypsum crystals, which now, with subsequent water table lowering, protrude from the exposed and accessible areas of the cave.

Even more widespread and spectacular examples of gypsum chandeliers line the Cupp-Coutum and other now inactive hypogene sulphuric acid caves of Kugitangtau Ridge, Turkmenistan (Maltsev and Malishevsky, 1990). The phreatic calcium sulphate textures record a phase of hydrothermal activity within a pre-existing karstic groundwater conduit system (Bottrell et al., 2001). Hydrothermal fluids entered the caves through fault zones and deposited sulphate, sulphide and carbonate minerals under phreatic conditions. Locally, intense alteration of limestone wall rocks also occurred at this stage. Elsewhere in the region, similar faults contain economic quantities of galena and elemental sulphur mineralization. Comparisons between the Pb and S isotope compositions of minerals found in cave and ore deposits confirm the link between economic

mineralization and hydrothermal activity at Cupp-Coutum. The predominance of sulphate mineralization in Cupp-Coutum implies that the fluids were more oxidized in the higher permeability zone associated with the karst aquifer.

Following the hydrothermal phase, speleothemic minerals were precipitated under vadose conditions (Bottrell et al., 2001). Speleothemic sulphates show a bimodal sulphur isotope distribution. One group has compositions similar to the hydrothermal sulphates, whilst the second group is characterized by higher $\delta^{34}\text{S}$ values. This latter group may either record the effects of microbial sulphate reduction, or reflect the introduction of sulphate-rich groundwater generated by the dissolution of overlying evaporites. Oxygen isotope compositions show that calcite speleothems were precipitated from nonthermal groundwater of meteoric origin. Carbonate speleothems are relatively enriched in ^{13}C compared to most cave deposits, but can be explained by normal speleothem-forming processes under thin, arid-zone soils dominated by C_4 vegetation. However, the presence of sulphate speleothems, with isotopic compositions indicative of the oxidation of hydrothermal sulphide, implies that CO_2 derived by reaction of limestone with sulphuric acid (‘condensation corrosion’) contributed to the formation of ^{13}C -enriched speleothem deposits.

Blocks composed of white, fine-grained, pelagic (phreatic) gypsum cover large floor areas (over 1000m^3) of the upper cave level of the Grotta Grande del Vento, Italy (Galdenzi, 1990; Galdenzi and Maruoka, 2003). In this case the gypsum does not form the spectacular “ferro di lancia” found in New Mexico and Turkmenistan, although there are some coarsely crystalline aligned prisms that are interpreted to have grown in the cave mud. Today’s gypsum textures in the Frasassi caves are much less diverse and more localised than when sulphate precipitation was at its peak in the hypogene phreatic caverns of the early Pleistocene (Galdenzi and Maruoka, 2003). What makes Grotto Grande so interesting is that the process of gypsum formation is still active in some accessible parts of the cave where H_2S -rich waters mix with oxygenated ground waters. Hollow vaterite spherules have been precipitated in the laboratory from bacterial cultures collected from such caves in Italy and Spain (Sanchez-Moral et al., 2003).

Native sulphur can be found in sulphidic caverns of New Mexico either admixed with gypsum in the remnant pelagic blocks or as canary-yellow sulphur crystal coats on the undersides of dipping beds of the foreereef or the siliciclastic Bell Canyon Formation. $\delta^{34}\text{S}$ values are as low as -25.8‰ (CDT) in this cave sulphur. Similar values in the cave gypsum (-25.6‰) and the

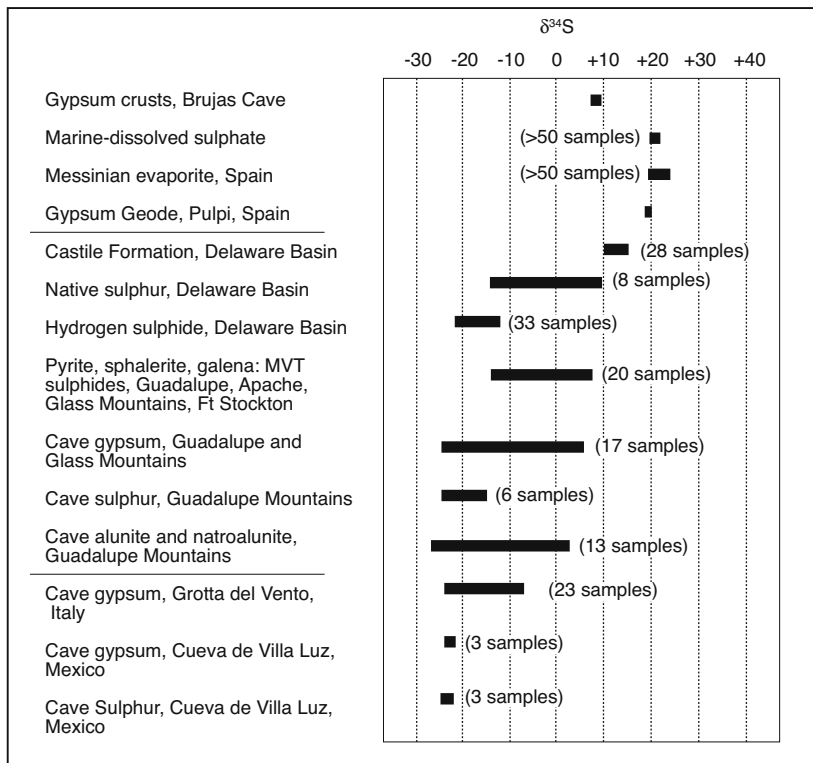


Figure 7.48. Range of sulphur isotope values for various H_2S associated cave deposits in the USA, Italy and Mexico (after Hill, 2000; Hose et al., 2000; Polyak and Güven, 1996; Galdenzi and Maruoka, 2003; Garcia-Guinea et al., 2002; Sancho et al., 2004). Cave gypsum and sulphur in the Delaware Basin are significantly enriched in the light isotopes compared to the Castile Formation. Their isotopically light composition within the basin (H_2S gas, native sulphur) and in the reef (sulphides and sulphur/gypsum cave deposits) reflect bacterial sulphate reduction where sulphate solutions mixed with hydrocarbons to produce isotopically light hydrogen sulphide. Similar products from sulphuric acid caves in Italy and Mexico also plot in the negative sulphur range and are clearly not indicative of a meteoric or marine source.

endellite, indicate that they too are end products of microbial reduction reactions metabolising escaping hydrocarbons. Their isotopic signatures are not products of meteoric diagenesis (Figure 7.48; Hill, 1990).

Throughout the various caves of the Guadalupe Mountains, sulphur isotope results have been crucial in defining its hypogenic speleogenesis (Figure 7.48; Hill, 1990, 2000). Without bacterial mediation (mostly by anoxic sulphate reducers at depth, then sulphate oxidisers near the water table), cave gypsum with such negative values could not have been derived from Castile anhydrite beds. It means inorganic models based on local brine pooling and saturation (Bretz, 1952) or the inorganic cooling of basinal water (Queen et al., 1979) are not directly applicable to Carlsbad precipitates. Such inorganic models are more relevant to the ice-clear 8 metre long, 1 metre wide,

gypsum crystals filling giant geodes in a Triassic limestone host at Pulpí in SE Spain (Garcia-Guinea et al., 2002) and to gypsum crusts in Brujas Cave, Argentina (Sancho et al., 2004). The average isotopic composition of marine-fed Castile gypsum/anhydrite is +10.3‰. If the cave gypsum had precipitated directly from cooling Castile brines, then gypsum in the cave fill should have a similar signature to the Castile Formation, clearly, it does not. Sulphur isotope data also discount sulphate derivation from a pyrite precursor, as proposed by Jagnow (1977). Metal sulphide values in the Guadalupe Mountain samples (mostly pyrites) range from $\delta^{34}S = -9.3$ to +12.6‰ (mean = -2.2‰ for 20 samples; Figure 7.48). As there is no significant isotopic fractionation involved in the subsurface leaching of sulphides (less than 1‰), it must be concluded that the isotopically lighter signatures of cave floor gypsum and sulphur (mean $\delta^{34}S = -16.8$ ‰ for 22 samples) are not derived from a pyrite source. Instead, the consistent isotopically light signature in the cave precipitates support a model of bacterial sulphate reduction acting on Castile Formation sulphate (and hydrocarbons) and ultimately creating sulphuric acid leading to caves with gypsum as a widespread precipitate.

Sulphuric acid speleogenesis is no longer active in the accessible portions of the New Mexico or Turkmenistan caves. But sulphuric acid driven cave expansion is occurring today in the Cueva de Villa Luz in Mexico (Hose et al., 2000), Grotta Grande del Vento in Italy (Galdenzi, 1990) and the Movile Cave in Romania (Sarbu et al., 1994). In all three, the cave water and cave atmosphere is enriched in hydrogen sulphide and the action is centred around the watertable (Table 7.10).

Oxidation of sulphide-rich waters seeping from the cave walls and the associated precipitation of fine-grained gypsum is largely microbially driven (Figure 7.49). It is localised to seepages at or near the water table and the precipitation chemistry is facili-

tated by sulphur-oxidising bacteria. Near identical microbial mat communities float at the air/water interface in the active sulphuric acid lake of Movile Cave, Romania, and coat the cave walls (snottites) in Cueva de Villa Luz, Mexico. In all three, the process today is vadose and tied to the watertable. Textures in the wall gypsum are not the same nor as widespread as the relict phreatic pelagics and gypsum spars we see in palaeohypogene caves in New Mexico and Turkmenistan.

Measured H_2S levels in the cave atmosphere of Cueva de Villa Luz reach 210 ppm, while SO_2 typically exceeds 35 ppm, conditions which require researchers to use masks and breathers. These gases, plus oxygen from the cave air, are absorbed by water films that gather on the cave walls via infiltration and condensation. Sulphur-oxidizing bacterial colonies in water films on cave walls and floating on cave waters facilitate the conversion of the abundant hydrogen sulphide to sulphuric acid. Microbes probably also facilitate the conversion of carbon dioxide to carbonic acid. Low pH waters (0.0-3.0, with a mean of 1.4) drip from microbial veils onto the limestone floor. Growths look like delicate stalactites made of phlegm, locally dubbed “snottites” (Figure 7.49). The acid drips form rillen and incised channels in the wet limestone walls adjacent to the main cave stream. On the cavern slopes above main stream level, the sulphuric acid reacts with the surrounding limestone to produce a pasty plastering composed of microcrystalline (alabastrine) gypsum and microbes, with surface pH values between 0.5-3.0.

Cueva de Villa Luz is fed by at more than 25 groundwater springs, with a combined flow of 200-300 l/s. Inlet water chemistry defines two categories: a) those with high H_2S content (300-500 mg/l), mean $P_{CO_2} = 0.03-0.1$ atm, and no measurable O_2 ; and b) those with less than 0.1 mg/l H_2S , mean $P_{CO_2} = 0.02$ atm, and modest O_2 contents up to 4.3 mg/l. Both water types have a similar source, as shown by their dissolved solid content. However the oxygenated water has been exposed to aerated conditions upstream from the cave inlets so that much of the original H_2S has been largely lost via outgassing and oxidation to sulphate, increasing the sulphate concentration in the waters by about 4%. Modelling of the cave water chemistry shows that it can be produced by dissolution of sulphate, carbonate, and chloride minerals, which are present deeper in the basin (Hose et al., 2000).

Two cave-enlarging mechanisms were identified in the Cueva de Villa Luz (Figure 7.49; Hose et al., 2000): 1) Sulphuric acid from oxidation of hydrogen sulphide prior to exit into the cave, which converts subaerial limestone surfaces to gypsum and

is aided by the activities of sulphur-oxidising bacteria. Most of this gypsum ends up falling into the cave stream where it is redissolved and lost via the stream exiting the system. 2) Strongly acidic droplets, formed on microbial filaments, which dissolves limestone as it drips onto the cave floor. Possible sources of H_2S in the Cueva de Villa Luz system are the evaporites of the Villahermosa petroleum basin, which is less than 50 km downdip and to the northwest, or the hydrothermal system of the El Chichon volcano located some 50 km to the west. Depletion of ^{34}S values for sulphur stabilized from H_2S in the cave atmosphere (-11.7‰), along with the hydrochemistry of the spring waters, favour an evaporite - sulphate reduction origin over a volcanogenic source.

In part, so much more gypsum occurs in the caverns at Carlsbad, compared to the amount of gypsum accumulating on cave walls in other active sulphuric acid caves of today, simply because there was so much more dissolved gypsum entering the cave system along the edge of dissolving evaporite bed. When it was active, the Carlsbad system was located in the outflow zone of a large regionally draining basin with escaping waters focused

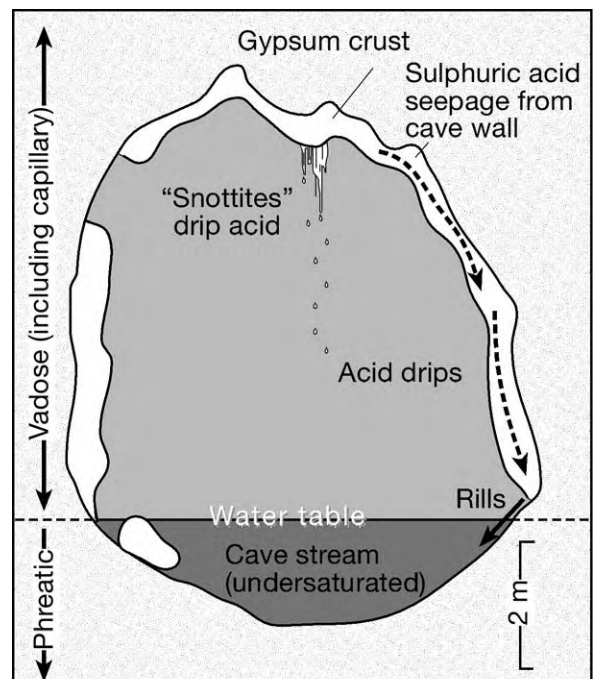


Figure 7.49. Mechanisms for cave enlargement. 1. Conversion of limestone to gypsum crust by sulphuric acid, dissolved by the cave stream and by infiltrating freshwater. 2. Drips of sulphuric acid from the gypsum wall crust and snottites corrode limestone below. Microbial activity enhances the oxidation reactions that produce the acid. 3. Sulphuric acid seeps through the gypsum crust and dissolves the limestone at the base. Solutional rills are common (after Hose et al., 2000).

into the growing cave system by the dissolving underside of a bedded basinwide anhydrite.

But there is another key difference when comparing gypsum precipitation processes at Carlsbad to modern sulphuric acid caves. Gypsum textures in now inactive hypogene karst fills of Carlsbad and similar systems elsewhere (Table 7.9) indicate phreatic gypsum could accumulate within expanding caves situated as much as 100–200 m below the meteoric water table. Today in all the accessible parts of the active sulphuric acid caves of Mexico, Italy and Romania caves the gypsum precipitation process is a microbially-mediated seepage process, where H_2S rich waters condense and seep down cave walls. It leads to unique lithoautotrophic systems centred on the sulphate oxidisers in the vadose zone at or immediately above the water table. But how relevant are these modern biogenic gypsum products to the much more spectacular and voluminous gypsum precipitates forming in inaccessible blind and deep hypogene caverns some tens to hundreds of metres below the water table? We now can study the results of this bathypneumatic hydrology only as relicts that have survived exhumation into the vadose realm.

In terms of models of gypsum precipitation and the relative contribution of sulphur-oxidising microbes to all gypsum formation in hypogene karst systems, we have the same scale and process-comparison problems that plague all studies of ancient evaporite deposition. What we have available to use in modern sulphuric caves, such as Cueva de Villa Luz, is accessible and measurable, but how reliably can we generalise our conclusions on what forms hypogene gypsum using models of vadose cave wall products to interpret what we see in the rock record. Studies of process in active sulphuric acid caves is restricted to parts of a cave system where people can crawl, sweat, swim and sample. These accessible parts are probably not the parts of a hypogene carbonate system where most gypsum precipitates and accumulates. To interpret process for this type of gypsum we must use the textures and extent of the gypsum itself. Even if such places were accessible in some yet to be discovered part of an active cave system, the elevated levels of H_2S would make it extremely toxic to generalist lifeforms like us.

Some carbonate workers would argue that H_2S -related karstification of marine carbonates is not a widespread diagenetic process. They argue that the bulk of published karstification studies in the literature support this contention. To this I would argue that the literature on carbonate karst reflects a sampling bias. That is, most studies of modern karst process are done in caves that are accessible for study. By definition these caves are near or at the surface and so are in

settings where meteoric karst predominates. Most H_2S -related karstification takes place at greater depths. In Chapter 9 we shall see that H_2S (sour gas) is a significant fluid component in most carbonate-evaporite basins and that much of this H_2S is produced by thermochemical sulphate reduction. Evaporite-associated examples from the Gulf of Mexico, the eastern US and Canadian shelf, the Mediterranean and the Middle East will be discussed.

H_2S can even be a significant component in fluids hosted in normal marine shelf sediments. For example fluids collected during the drilling of the southern Australian continental margin (Leg 182 of the Ocean Drilling Program), showed unusually high salinities (to 106‰) in nonevaporitic Miocene to Pleistocene carbonate and siliciclastic sediments (Swart et al., 2000). At three sites (1127, 1129, and 1131), high contents of H_2S (to 15%), CH_4 (to 50%), and CO_2 (to 70%) were encountered and may be associated with H_2S dominated clathrates. These levels of H_2S are the highest yet reported during the history of either the Deep Sea Drilling Project or the Ocean Drilling Program. The high concentrations of H_2S necessary for the formation of hydrates under these conditions were provided by the abundant SO_4 caused by the high salinities of the pore fluids, and the associated high concentrations of organic material. One hypothesis for the origin of these fluids is that they were formed by evaporation of brines on the adjacent continental shelf during previous lowstands of sea level. They then sank into the underlying sediments (brine reflux) where their residuals remain today.

Mineralised breccias

As they form, or after they form, evaporite solution breccias can act as permeable foci for base metal, sulphur hydrocarbon accumulations. Where the dissolving bed contains sulphate evaporites, it can act also as a source of sulphur to base metal sulphide precipitates and so become a locus for ore deposition (Warren 2000b). This is clearly seen in the ores of the now depleted Cadjebut Mine on the Devonian Lennard Shelf, West Australia (Warren and Kempton, 1997). The Cadjebut zinc mine is situated at the southern margin of the Emanuel Range and is hosted by platform carbonates of probable Givetian age near the base of the Pillara Limestone (Figure 7.50a). The orebody lies approximately 500 m to the north of the Cadjebut Fault and trends subparallel to it over a strike length of 3 km. Surface expression of the orebody is the “No Way Gossan,” which crops out 100m to the west of the mine portal. The orebody is roughly linear in shape, trending toward the northwest and dipping with the host dolomite at 5° – 10° to the northeast.

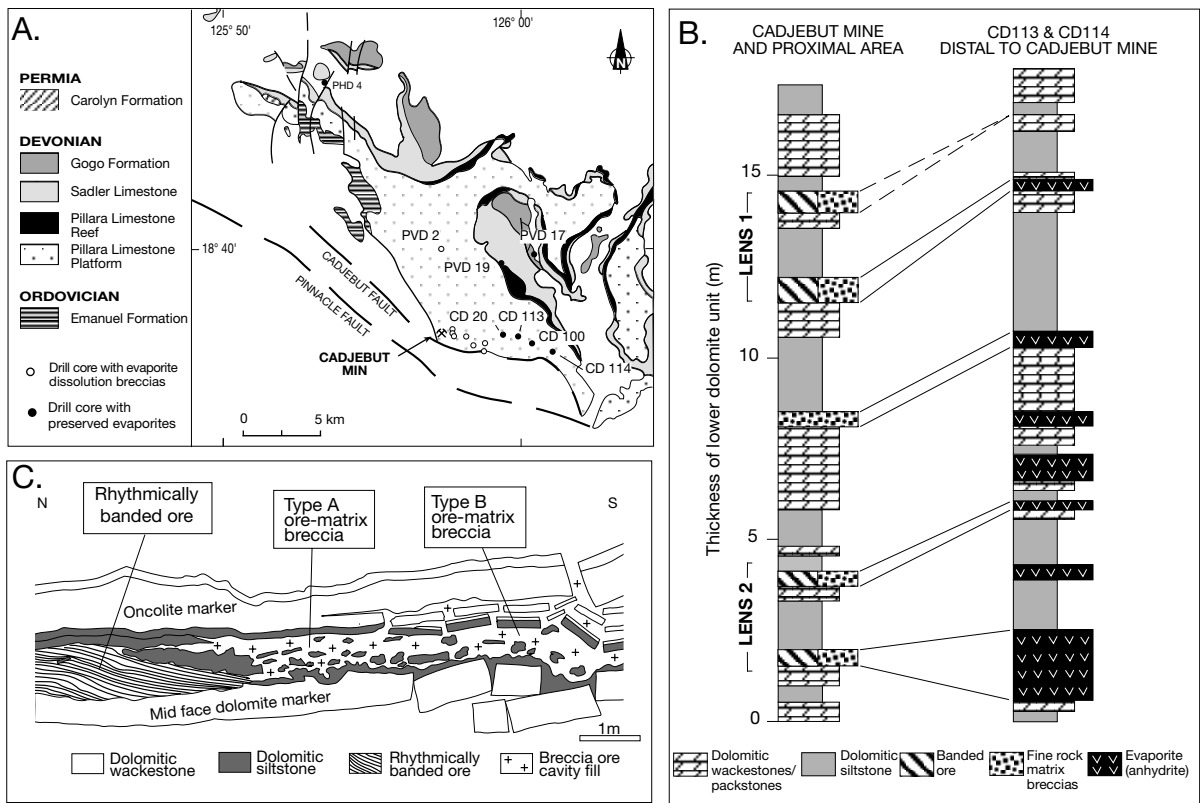


Figure 7.50. Cadjebut evaporites and mineralisation. A) Regional mine geology showing cored wells with and without evaporites. B) Correlation of ore lenses to solution breccias to evaporites in more distal positions from mine. C) Mapped ore face showing the different styles of ore texture in the mine. This ore horizon is laterally equivalent to an evaporite dissolution breccia, which in turn passes into equivalent anhydrite beds (after Warren and Kempton, 1997).

Cadjebut Mine had pre-mining reserves of 3.8 million tonnes of 17% combined zinc and lead. Ore grade mineralization (Zn-Pb) occurs as two stratabound lenses, referred to as “lens 1” and “lens 2” (Figure 7.50b), ranging in thickness from 4 to 6 metres. The width of the orebody varies from 50 to 150 m, as defined by a cut off grade of 7% lead-zinc, and is flanked to the north and south by hypogene alteration haloes of marcasite, calcite and baryte (Tompkins et al., 1994). The contact between ore grade mineralization (>7% Zn+Pb) and the alteration halo is usually abrupt over a distance of a few metres. In section, the ore-bearing lenses are stacked vertically above one another and separated by about 5 to 6m of barren or weakly mineralized dolostone (Figure 7.50b). In plan view, both ore lenses have a broad sinusoidal shape and display the same geometrical congruence.

Two dominant ore types are present (Figure 7.50c): (a) stratiform, rhythmically banded zinc-rich ore; and (b) stratiform to stratabound, lead-rich breccia-hosted cavity-fill ore. The rhythmically banded ore occurs as four stratiform horizons,

two throughout lens 2 and two in the northern part of lens 1. Rhythmically banded baryte and/or rhythmically banded marcasite form a halo around the orebody and are associated with the rhythmically banded zinc-rich ore.

There is a one-to-one correlation of sulphide-mineralised horizons in the Cadjebut Mine with evaporite dissolution breccia horizons in the immediate area around the mine, and with remnant bedded anhydrite units well away from the mine (Figure 7.50b). Evaporite beds were the precursor lithology to the sulphide ore lenses at Cadjebut. The stratabound linear nature of the Cadjebut deposit reflects a time when upwelling metalliferous basinal fluids interacted with bedded stratiform nodular anhydrite beds and trapped hydrocarbons to precipitate lead and zinc sulphides. Current structure in the mine region still preserves a gentle drape anticline, which Warren and Kempton (1997) interpret as a partial artifact of the mineralisation structure, enhanced by the sequential loss of the surrounding evaporites, after ore had locally replaced a bedded anhydrite precursor. The linear nature of the anticlinal structure

indicates some form focusing of ore fluids and hydrocarbons, either atop an active underlying fault, or within a preexisting anticlinal trap, perhaps created as a rollover drape on the edge of an evaporite-dissolving front (e.g. Figure 7.51a). Hydrocarbon residues (bitumens) are still present in the ore zones.

The rate of evaporite dissolution versus the rate of supply of mineralising fluid controlled the large scale textures within the Pb-Zn ores. Lead-zinc mineralisation in the Cadjebut Mine occurs as three distinct ore types (Figure 7.50c):

- stratiform rhythmically banded zinc-rich ore,
- stratiform Type A ore-matrix breccia ore, and
- crosscutting Type B ore matrix breccia ore.

The rhythmically banded ore formed under conditions where the potential for sulphide precipitation exceeded the rate of evaporite dissolution. This occurred in cm-sized laminar dissolution meshworks that ate their way into the anhydrite beds (Figure 7.51b). Millimetre-laminated colloform to pendulous microstalactitic sphalerites were the dominant precipitates.

Type A ore matrix breccia formed in irregular cm-dm stratabound cavities. These formed at times when the rate of sulphide precipitation was slower than the rate of sulphate dissolution. Such cavities were not sufficiently large to instigate catastrophic roof collapse. Type B ore-matrix breccia ores formed in dm-metre sized crosscutting cavities, fractures and veins. Cavern space was sufficiently large to allow the single-event roof span collapse and rotation of metre-sized roof blocks into the caverns. Type B ore-matrix breccias are lead-rich compared to the banded ore and are interpreted by Tompkins et al. (1994) to postdate the formation of banded ore. All the Cadjebut ore textures were created from sulphate supplied by the dissolving evaporites across mm-dm-sized replacement fronts or meshworks under deep bathyphreatic and typically overpressured gassy conditions (Warren and Kempton, 1997).

Evaporite solution breccias can also focus the deep meteoric flow of radiogenic groundwaters and so control the distribution of economic uranium deposits. For example, in the uranium district of southern Black Hills, South Dakota, Gott et al. (1974) showed how an extensive blanket of collapse breccia and trans-stratal breccia chimney fills were produced by the dissolution of gypsum and anhydrite beds in the upper part of the Late Palaeozoic Minnelusa Formation (Figure 7.52). Up to 83 m of evaporites

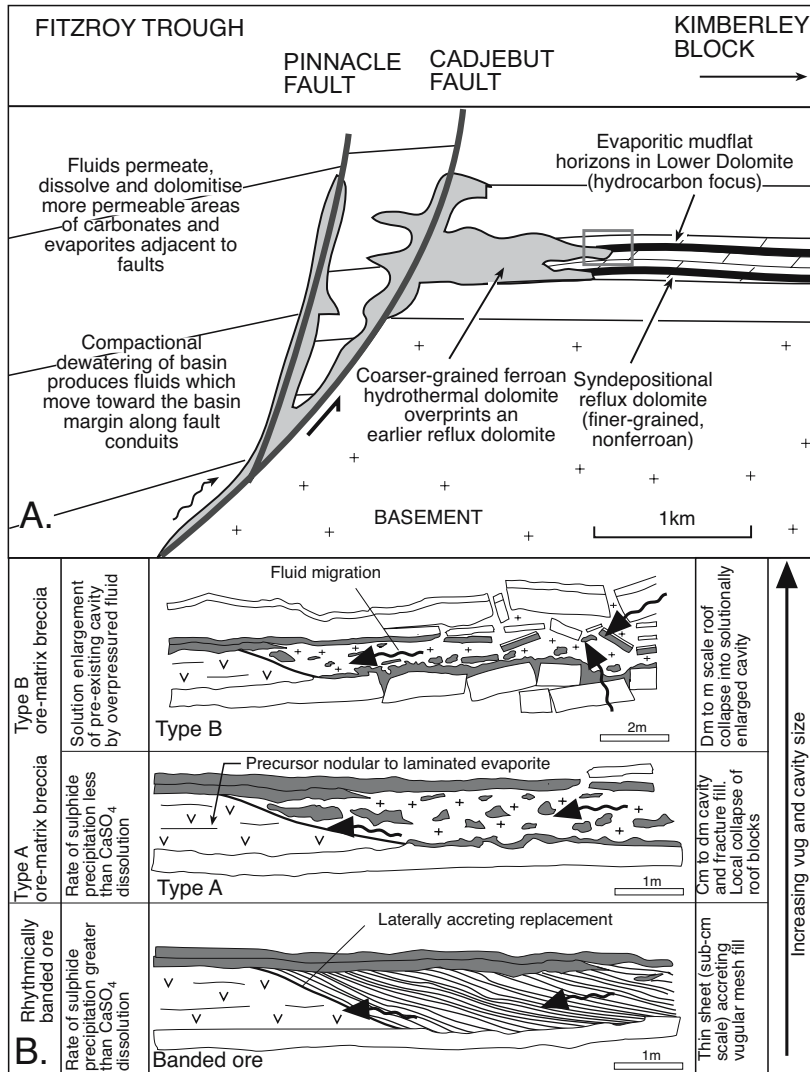


Figure 7.51. Cadjebut MVT ore, NW Australia. A) Schematic cross section showing the relationship between basal fluids moving up along regional extensional faults to act as sources for burial dolomite in the platform carbonates, and the focusing/replacement effect of sulphate beds in the evaporitic mudflat sediments of the Lower Dolomite (rectangle indicates zone of sulphide mineralisation). B) Schematic showing controls on ore texture reflect an interplay between rate of supply of metalliferous fluid and the rate of evaporite dissolution (after Warren and Kempton, 1997).

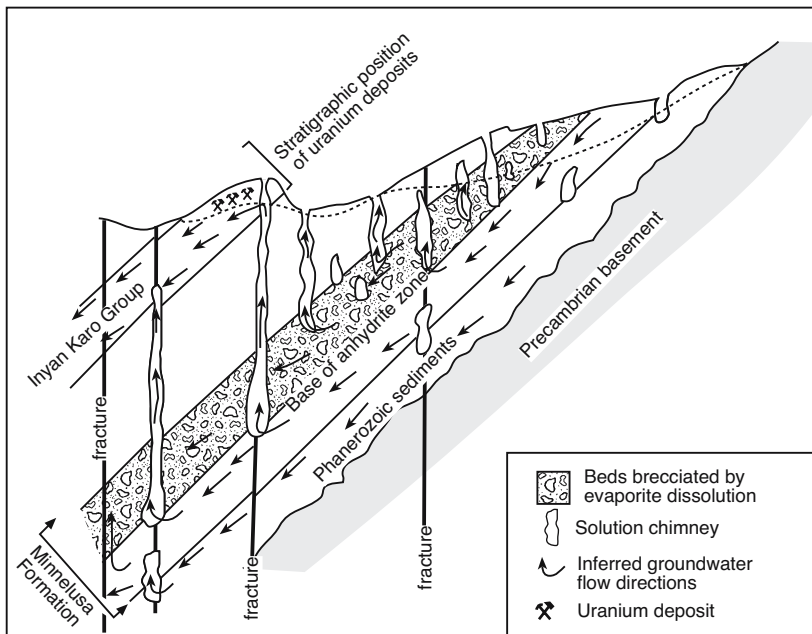


Figure 7.52. Infiltrated uranium mineralisation in the Cretaceous Inyan Kara Group sandstones, southern Black Hills (South Dakota). Solution collapse chimneys and breccias in the Late Palaeozoic Minnelusa Formation transport uraniferous groundwaters to precipitation sites (modified from Gott et al., 1974).

were removed and numerous breccia chimneys were created that extend up to 430 m vertically into Cretaceous continental sandstones of the Inyan Kara Group (Figure 7.52). The chimney fill consists of downward displaced sandstone blocks that were later cemented by calcite. Gott et al. argue that the breccia chimneys created a plumbing system through which artesian oxidised waters leached and transported uranium from deeply buried uraniferous sands and granites up into the Cretaceous section (Figure 7.12). There they encountered organic-entraining Cretaceous sands and so precipitated carnotite-dominated infiltrations along redox interfaces.

Filled vugs and nodules

Replaced nodules and characteristic vug shapes are some of the most used indicators for the former presence of evaporites in both the core and outcrop (Table 7.1). They define former crystal clusters and nodules of gypsum, anhydrite or halite in a matrix composed of mud or silt. Unlike the interiors of halite or anhydrite beds, buried evaporite nodules in a non-evaporite matrix are not isolated from the ongoing effects of crossflowing nearsurface and basinal waters. Whenever an undersaturated pore fluid flushes the matrix, it also dissolves or replaces the salts.

Resultant replaced crystals and vug fills are composed of varying combinations of silica, calcite, dolomite, celestite, baryte and strontianite. Internal textures and nodule fabrics can be spectacular and include; linings and splays of silicified and calcitised evaporite crystallites, evaporite moulds and residues, calcitised evaporitic dolomites (dedolomites), crosscutting drusy dissolution veins and solution enlargement fabrics, with late stage hydrothermal precipitates often infilling the last porosity. Despite the diagenetic complexity, most nodules and vugs mimic the shape of the evaporite parent and this typically leads to recognition of the evaporite connection. When mineralised, vug fill can weather out of the softer matrix to create dispersed surfaces of nodules or clustered piles, leading to descriptions of such outcrops as “Mendip potatoes.”

An open vug in a rock indicates that something has dissolved, while a nodule composed of chert or calcite indicates that something has been replaced or filled. Deciding whether or not that something had an evaporite forebear is frequently dependant on shape and texture. Smooth walled nodules, especially ones now composed of chert or baryte, are a commonplace replacement in normal marine sediment and need not indicate an evaporite precursor. A reliable evaporite indication of a syndepositional CaSO_4 nodule only comes if the rugose irregular surface texture and the shape of the precursor anhydrite nodule or layer remains. In other words, nodules with surfaces of irregular ridges and vugs, textured like the flowerets of a cauliflower, likely indicate an evaporite antecedent. Such nodules are usually described as cauliflower textured (e.g. cauliflower chert or cauliflower vug). If Magadi-style silicate gels were the nodule's parents, then nodule surface should show remnant crocodile-skin texture. Without this, or if only smooth walled nodules shaped like cucumbers and melons are present then a thin section of the nodule, especially of its outer portion is needed as this is where small relict crystallites or replaced lath outlines may still be visible.

Similarly, if single coarse-grained crystals or crystal clusters (desert roses) were either dissolved or replaced and now constitute open or filled moulds, then the original crystal shape

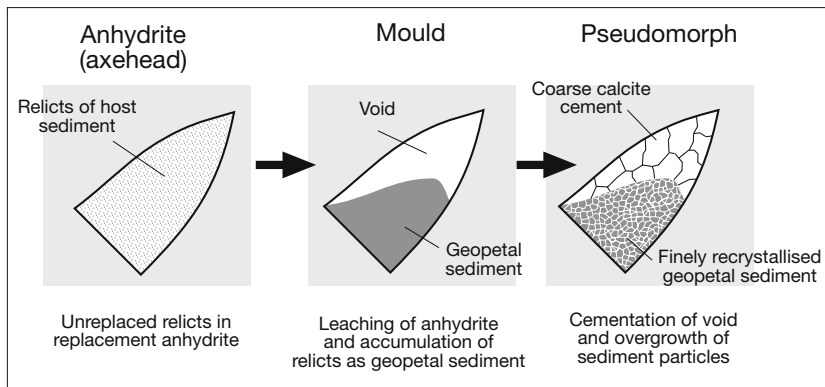


Figure 7.53. Replacement of axe-head anhydrite by carbonate spar showing how void shape needs to be preserved for reliable genetic interpretation. The fill is also a geopetal.

should be clearly discernable in order to reliably proclaim its parenthood (Figure 7.53). If lenticular gypsum was replaced, it should have the bird-beak shape of its precursor, while lenticular anhydrite replacements should be axe-head or barrel shaped (Figures 1.16, 1.26). If displacive halite clusters were replaced there should be evidence of cubes and hoppers on the outside of the vug or nodule.

Preservation of the shapes of evaporite crystals with similar outlines creates difficulties when trying to separate silicified replacements of beds of growth-aligned gypsum from beds of nahcolite/trona. Yet it is the separation of these pseudomorphs that is the fulcrum to arguments on the nature of early Archean seawater (Figure 2.31). Both gypsum and trona have a monoclinic bladed form and both can form nodules or grass-like beds of growth-aligned prisms. Once the actual salt has gone, defining original salt mineralogy and separating crystals with similar shapes using partly altered pseudomorphs can be very difficult.

Silicified evaporites

Silicified anhydrite nodules and CaSO_4 crystals are widely reported and reliably documented in sediments as old as Early Archean and as young as Holocene (Table 7.11).^{7.6} Quartzine and^{7.7} lutecite (aka length-slow chalcedony) typically infill or replace nodules that preserve characteristic cauliflower shapes of the antecedent anhydrite/gypsum nodule (Figure 7.54a; Arbey, 1980). According to Folk and Pittman (1971), rates of nucleation and crystallization are the main controls on crystal size and variety of silica precipitating in a void in a dissolving nodule. Rates in turn depend on the level of silica saturation or its concentration in the mother brine (Figure 7.54b).

High (alkaline) pH levels in the mother solution tend to ionize dissolved silica. Neutral or low pH levels favour silica crystallites made up of combined $\text{Si}(\text{OH})_4$ groups. These tend to polymerise into spiral chains at lower pH and higher concentrations. At high concentrations and high pH the silica precipitates possess a fibrous chalcedonic form reflecting their rapid rates of precipitation. High pH at the precipitation site means silica crystallites also tends to be present in solution as single ionized tetrahedra that attach themselves one by one to the growing surface, so

creating fibres of quartz with the c axes oriented parallel to the long axis of the growing fibres (length-slow). Under low pH or in non-sulphate settings the silica is polymerized into spiral silica chains that attach tangentially to the growth surface of the silica gel, with their c-axes parallel to the growing crystal surface and perpendicular to the eventual direction of the fibres (Figure 7.54c; length-fast; Folk and Pittman, 1971).

Milliken (1979) summarised the typical petrographic and hand specimen scale features of silica that replaced CaSO_4 nodules in Mississippian sediments of southern Kentucky and northern Tennessee (Figure 7.55). Such nodules typically have knobby irregular cauliflower-like surfaces. Diagnostic internal textures include: 1) length-slow chalcedony after lathlike evaporites, especially anhydrite; 2) quartzine; and 3) small amounts of lutecite associated either with megaquartz that shows strong undulose extinction, or with euhedral megaquartz (Chowns and Elkins, 1974). The megaquartz often encloses small blebs of residual anhydrite.

Many buried calcium sulphate nodules are silicified in a multistage process that involves both replacement and void filling (West, 1964; Chowns and Elkins, 1974). The process commences about the margins of a nodule (stage 1) with a volume for volume replacement of anhydrite by microcrystalline quartz. It normally ends with the growth of euhedral drusy

^{7.6} Quartzine is a form of chalcedony composed of fibres having a positive crystallographic elongation parallel to the c axis.

^{7.7} Lutecite is a form of chalcedony characterised by fibres that are seemingly elongated about 30°C to the c axis.

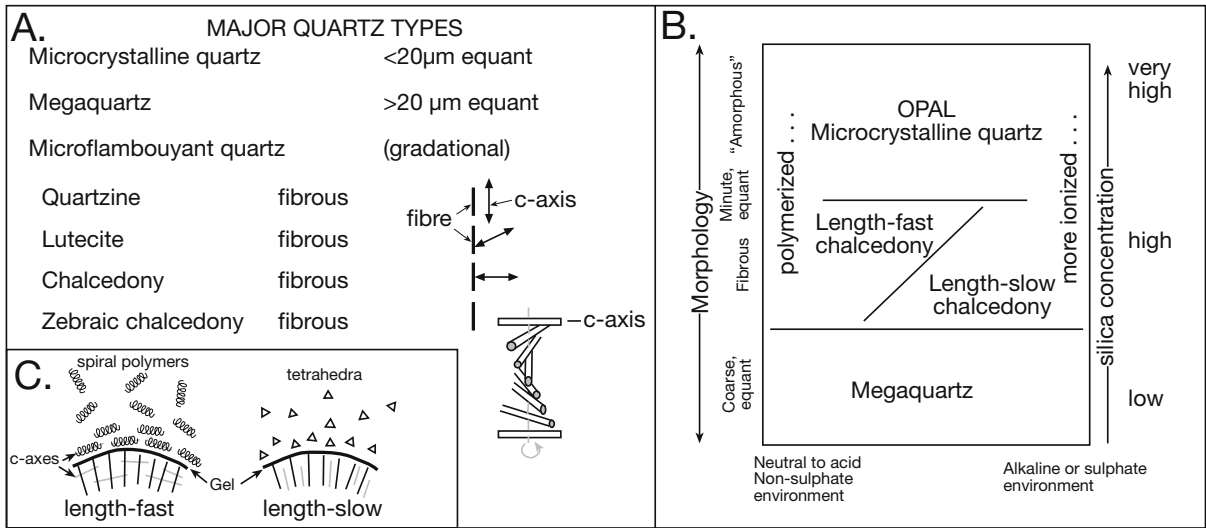


Figure 7.54. Chalcedony as an indicator of vanished evaporites. A) Major quartz types based on crystal size and orientation of chalcedony fibres with respect to c-axis (after Milliken, 1979). B) Style of chalcedony precipitate is controlled by the degree of polymerization, which in term reflects environment of precipitation. C) Crystallite orientation (single tetrahedra versus spiral polymers) with respect to growth surface controls formation of length slow versus length fast crystals - see text (B and C after Folk and Pittman, 1971).

quartz crystals into a central vug (stage 2 and 3). This mode of replacement exemplifies textures seen in texture style A in Figure 7.55.

Stage 1 chalcedony mimics or pseudomorphs the felted lath textures of the precursor anhydrite in the outer portion of the nodules. The pseudomorphs occur as radiating or decussate aggregates with a distinctive flow pattern. Identical decussate and flow textures occur in laths that make up sabkha anhydrite nodules and define their explosive mode of growth (Figure 1.26). As well as the silicified lath microtexture, outlines of larger crystals that predated anhydritisation and silicification may also be preserved by the nodule margin, these crystal outlines vary from prismatic to bladed. Many silicified nodules still retain the knobby cauliflower outline of its precursor anhydrite, other nodule edges preserve the interfacial outlines of gypsum or trona or borate precursors.

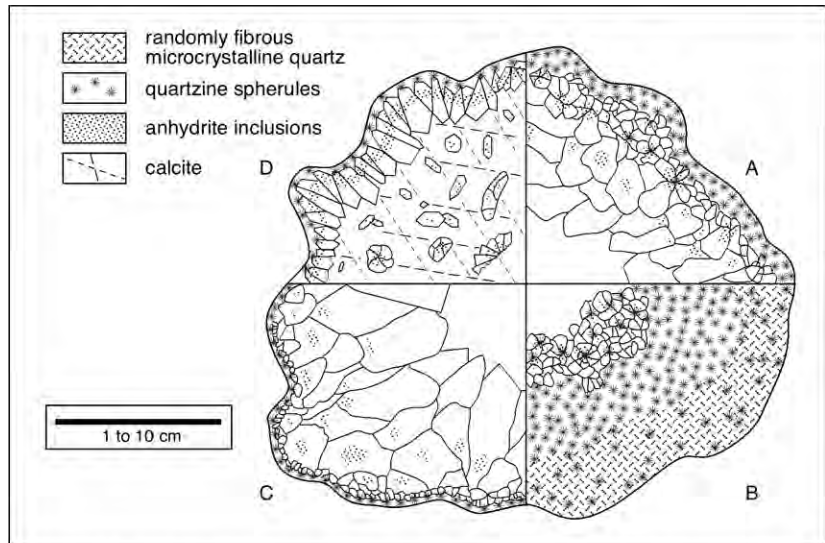


Figure 7.55. Texture in silicified-calcitized anhydrite nodules. A) Most common style of nodule with thin rim of spherulitic quartzine followed inward by megaquartz characterised by increasing crystal size and with frequent anhydrite inclusions. B) Nodule with a large proportion of fibrous quartz. Thick rim of spherulitic quartz passes inward to strongly undulose megaquartz. Some of the megaquartz has anhydritic nuclei. C) Nodule with a thin rim of spherulitic quartzine passing inward to a large proportion of megaquartz. D) Nodule with megaquartz rim and an interior filled with calcite. Calcite may have filled a cavity or replaced earlier silica. Late stage cavity-fill calcite is often defined by a thin rim of authigenic baryte or sulphide, prior to precipitation (modified from Milliken, 1979).

Occurrence and age of host	Comments	Reference
Silica precipitates in Holocene alkaline lakes along the Coorong coastal plain, South Australia. Type area for "Coorong style" chert.	Direct precipitation (?bacterially mediated) of opal-cristobalite in small mm-scale vugs in and on the surface of tepee-overprinted strandzone magnesite/dolomite crusts around the edge of Milne Lake and probably in crusts in other lakes accumulating evaporitic lacustrine dolomite, magnesite, hydromagnesite, aragonite and gypsum.	Peterson and von der Borch (1965)
Nodules and polygons of chert in diatomaceous beds of the late Pleistocene High Magadi beds, Lake Magadi, Africa. Type area for "Magadi-style" chert.	Chert in nodules and polygons is a weathering product of sodium silicate gels. Conversion involves shrinkage and induration. It creates a characteristic "crocodile-skin" texture on the surface of newly formed chert. This texture is associated with soft sediment deformation in the surrounds and sodium carbonate salts in adjacent sediments.	Eugster, 1967; Jones et al., 1967; Hay, 1968
Pleistocene nodules in saline mudflats, Lake Olduvai, Africa.	Magadi-style chert nodules (crocodile-skin) formed by replacement of a sodium silicate (magadiite) precursor.	Hay and Kaiser, 2001
Double-terminated euhedral quartz in Pleistocene sabkha dolomite, offshore Al Jabyl, Saudi Arabia (Pleistocene "Herikimer diamonds").	Megaquartz as individual crystals and clusters of crystals and overgrowths on detrital quartz. Individual crystals up to 1 mm long, many with shallow dolomite mould impressions on their crystal facies, some partly, or completely, engulf dolomite rhombohedra.	Chafetz and Zhang, 1998
Quartz geodes and nodular chert in Campanian (Cret.) marly clays and calcarenites, Basque-Cantabrian Basin, Northern Spain.	Silica replacement of cauliflower geodes and chert as spherulitic fibrous quartz (quartzine-lutecite). There are small anhydrite laths included in some of the mega-quartz crystal fills.	Gomez-Allday et al., 2002
Quartz geodes and chert hosted in Triassic red mudstones, Bristol district of the UK.	Silica replacement in open voids after cauliflower textured anhydrite. Loose euhedral double-terminated quartz crystals aggregating on bottom of some geodes after the CaSO ₄ is dissolved and are called "Bristol Diamonds."	Tucker, 1976a
Nodules developed in a single layer in Bundsandstein (Triassic) redbeds, Iberian Range, Central Spain.	Cauliflower shaped chert nodules and geodes, some are filled with concentric layers of quartz and carbonate, others are still open and partially filled and fractured. Relict anhydrite textures and rare laths, bacteria played a role in dolomitisation of some nodules.	Alonsa-Zarza et al., 2002
Chert nodules in Triassic of North Carolina, USA.	Cauliflower chert with relict anhydrite.	Wheeler and Textoris, 1978
Nodules and crystals in Lower Purbeck Beds, (Jurassic) Dorset, UK.	Silica replacement of individual and clustered gypsum bird-beaks and enterolithic anhydrite nodules (with small relics of anhydrite preserved).	West, 1964; 1973
Discrete horizons, scattered nodules in layers and individual replaced crystals in Seven Rivers, Yates and Tansill formations, Guadalupe Mountains, (Permian) Delaware Basin, USA.	Cauliflower nodule and geodes. Nodules, bird-beak gypsum, axehead anhydrite were all replaced by silica and calcite spar. Initial replacement by black megaquartz (with anhydrite, dolomite, water and hydrocarbon inclusions). This was followed by blocky calcite spar fill of voids created by late-stage dissolution of remaining anhydrite (telogenetic).	Ulmer-Scholle et al., 1993
Thin layers of chert nodules in fluvio-lacustrine muds sandwiched in acidic volcanics of the Lower Permian Bolzano Volcanic Complex, Northern Italy.	Magadi-style chert showing soft-sediment deformation and shrinkage cracks (crocodile-skin), imply a sodium silicate parentage. Transformation to quartz and concomitant (re)crystallization created a variety of silica textures, dominated by microflamboyant quartz.	Krainer and Spötl, 1998
Fist-sized nodules and geodes in layers and dispersed zones in Fort Payne Fm., Warsaw Limestone, St Louis Limestone (Mississippian) of south-central Kentucky and Tennessee, USA.	Concludes that megaquartz characterized by strong undulose, radial extinction, the existence of anhydrite laths included in megaquartz crystals with 'cubic' appearance terminations, the growth of spherulitic, fibrous-radial quartz aggregates (quartzine-lutecite), and crusts of zebraic chalcedony are all evidence of silica replacing anhydrite nodules.	Milliken, 1979
Fist-sized nodules and layers in Fort Payne Fm. and Warsaw Limestone, (Mississippian) near Woodbury, Tennessee, USA.	Silica replacement of anhydrite to form cauliflower cherts with outlines reminiscent of the nodules in the Abu Dhabi sabkha. Soft sediment deformation in the surrounding matrix argues silicification took place prior to complete induration of matrix. Silica was derived from sponge spicules.	Chowns and Elkins, 1974

Table 7.11. Selected examples of silicified evaporites.

Stage 2 microquartz and quartz fill can assume euhedral faces as they grow into voids created by the dissolution of the nodule. At the same time the quartz may continue to engulf and pseudomorph small areas of residual anhydrite or other less

common evaporite salts. Quartz crystals precipitated at this stage are commonly zoned, with more anhydrite inclusions found within the inner zone of the pseudomorph. Some quartz crystals are doubly terminated and probably grew via the support

of a dissolving meshwork of anhydrite. With the final dissolution of the supporting mesh these quartz crystals sometimes dropped to the floor of the void to create a geopetal indicator. Such highly birefringent anhydrite spots define cauliflower nodules in 2.2 Ga sediments in the Yerrida Basin, Australia (El Tabakh et al., 1999).

Stage 3, the final stage of the void fill is typified by the precipitation of coarse drusy euhedral quartz with no included anhydrite. This coarse quartz resembles coarse vein quartz.

Sometimes the processes of void fill may be arrested to leave a hollow core in the silica-lined geode. The void may be filled by a different burial stage cement such as baryte, sparry carbonate (e.g. ferroan dolomite or calcite), or even metal sulphides. This is the case with the large (up to 1 m diameter) silicified cauliflower-shaped anhydrite nodules of Proterozoic Malapunyah Formation of the McArthur Basin in Northern Australia where baryte, then metal sulphides and then sparry calcite typify the latter stages of void fill (pers. obs.). Similar fracture-filling baryte characterises the later diagenetic stages of silicified and calcitised anhydrite nodules in the Triassic Bundsandstein redbeds of the Iberian Range of central Spain (Figure 7.63; Alonso-Zarza et al., 2002). Such geodes are typically excellent indicators of burial cement stratigraphy in a mudstone matrix that otherwise preserves few indicators of the evolving pore fluid chemistry.

Cauliflower chert may retain no evidence of former anhydrite lathes mimicked in chalcedony, but can be completely filled by various styles of coarser-grained megaquartz. The resulting nodules still retain the outline of the precursor evaporite nodule (Figure 7.56). Work on diagenetic timing of numerous silicified CaSO_4 nodules (e.g. Milliken, 1979; Geeslin and Chafetz, 1982; Gao and Land, 1991; Ulmer-Scholle and Scholle, 1994) shows that most silica replacement begins with shallow burial, either in the zone of active phreatic flow or in the upper portion of the zone of compactional flow (probably at depths of less than 500-1000 m). Early silica replacement in the zone of active phreatic flow is indicated by a lack of compressional flattening of the nodule, by the preservation of delicate surface ornamentation and the preservation of

compactional drapes around replaced nodules. If replacement of an anhydrite nodule occurs later in the burial cycle, many anhydrite nodules have by then become flattened or sluggy and no longer retain a rugose surface. The result can be a series of “cucumbers” rather than “cauliflowers.”

Milliken’s (1979) isotopic evidence implies much silica replacement in the nodules she studied was relatively early in the burial cycle at temperatures that were $< 40^\circ\text{C}$. Silica was supplied by throughflushing pore fluids with compositions ranging from seawater to mixed meteoric-seawater. Of course, nodule replacement by silica or calcite does not have to happen on the way down in the burial cycle, it may also happen during uplift back into the telogenetic realm, where the strata have once again entered the zone of active phreatic flow.

Until recently, there were no documented examples of the process of evaporite replacement by quartz in Quaternary sediments. Now, autochthonous, doubly-terminated, euhedral megaquartz crystals have been observed infilling voids in a gypsum- and anhydrite-bearing Pleistocene sabkha dolomite sequence in the Arabian Gulf, as well as forming overgrowths on detrital quartz grains (Chafetz and Zhang, 1998). These siliceous sabkha precipitates are forming within metres of the present sediment surface with a silica source that is probably recycled biogenic material. Individual quartz crystals attain lengths of 1 mm. Many quartz crystals faces preserve impressions of dolomite rhombs or they partly, or completely, engulf dolomite rhombohedra. This process of replacement is early burial, to see the full suite of silica replacement textures and

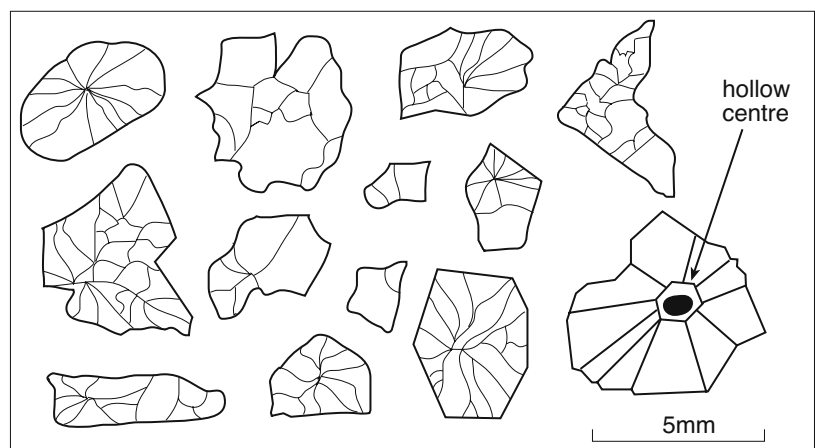


Figure 7.56. Sketches showing various shapes of the quartz nodules and internal arrangements of megaquartz crystals from replaced anhydrite nodules in the Mesoproterozoic Wollgorang Formation of northern Australia and the Neoproterozoic Gaissa Sandstone/Porsanger Dolomite of Finnmark, Arctic Norway (in part modified from Tucker, 1976b).

the variations in timing of the replacement means one must study ancient evaporite sequences.

Overall, the texture of silica infill or replacement in a nodule is dependent on the rate of sulphate dissolution, timing of silica precipitation and rate of silica supply. Some nodules are dominated by the early *lit par lit* replacement textures (styles A and C in Figure 7.55), others have textures indicating silica cements growing into an open phreatic void left after the complete dissolution of the CaSO_4 . Such nodules may still retain a hollow centre where the anhydrite once resided (Figure 7.56). When a silica-filled geode did not start to accumulate silica until after all the CaSO_4 dissolved, the main evidence for an evaporite precursor comes from the shape of the replaced nodule and its stratigraphic position within the evaporitic depositional

sequence, e.g. beneath an erosional surface that defines the top of the capillary zone.

Not all the anhydrite nodules, now replaced by silica, were syndepositional. Maliva (1987) showed that nodular anhydrite, now indicated by quartz geodes in the Sanders Group of Indiana, actually precipitated in the subsurface, while its surrounding matrix of normal marine Sanders Group sediment was still un lithified (Figure 7.57). Anhydrite nodules formed in the subsurface during early burial as hypersaline reflux brines sank into the normal marine limestones of the Ramp Creek and Harrodsburg Formations. Silica subsequently replaced the anhydrite. These geodes are almost invariably associated with the development of reflux dolomite.

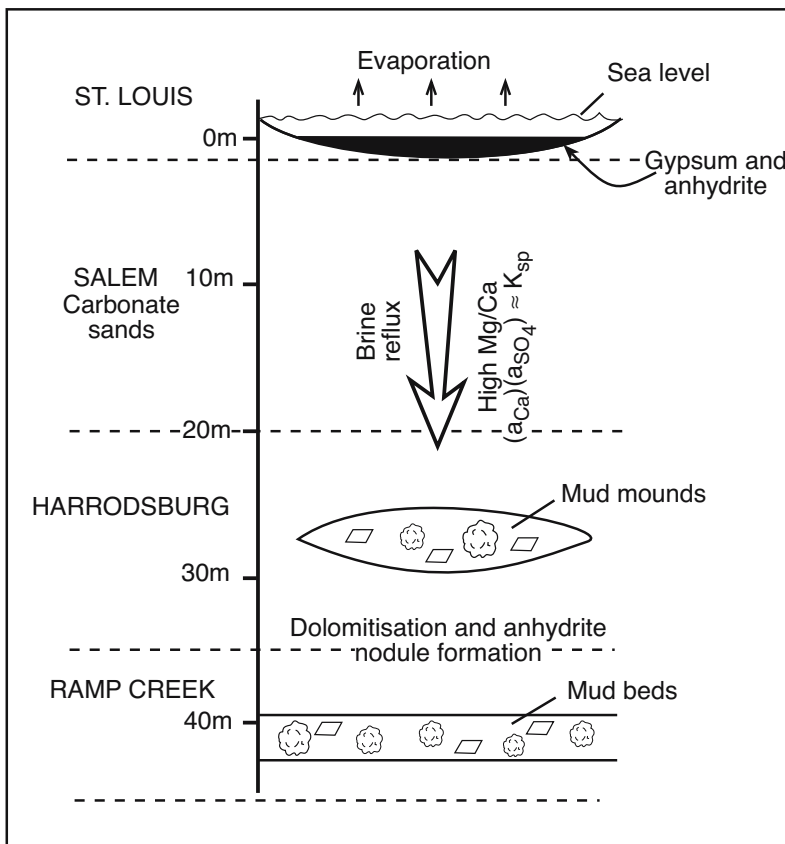


Figure 7.57. Precipitation of anhydrite and gypsum during St. Louis Limestone deposition formed a dense magnesium- and sulphate-rich brine that percolated downward and seaward through the then un lithified sands of the Salem Limestone. Dolomitisation of carbonate mud mounds and beds in the Harrodsburg and Ramp Creek Formations released calcium causing pore waters to become supersaturated with respect to anhydrite, resulting in the precipitation of anhydrite nodules that were later silicified (after Maliva, 1987).

Similarly, not all silica replacing anhydrite in a particular region need come from the same source or be emplaced by the same set of processes. Silicified nodules within middle-upper Campanian (Cretaceous) carbonate sediments from the Lafio and Tubilla del Agua sections of the Basque-Cantabrian Basin, northern Spain preserve cauliflower morphologies, together with anhydrite laths enclosed in megaquartz crystals and spherulitic fibrous quartz (quartzine-lutecite). All this shows that they formed by ongoing silica replacement of nodular anhydrite (Gómez-Alday et al., 2002). Anhydrite nodules at Lafio were produced by the percolation of saline marine brines, during a period corresponding to a depositional hiatus. They have $\delta^{34}\text{S}$ and $\delta^{18}\text{O}$ mean values of +18.8‰ and +13.6‰ respectively, consistent with Upper Cretaceous seawater sulphate values. Higher $\delta^{34}\text{S}$ and $\delta^{18}\text{O}$ (mean values of +21.2‰ and 21.8‰) characterise nodules in the Tubilla del Agua section and are interpreted as indicating a partial bacterial sulphate reduction process in a more restricted marine environment. Later calcite replacement and precipitation of geode-filling calcite in the siliceous nodules occurred in both sections, with $\delta^{13}\text{C}$ and $\delta^{18}\text{O}$ values indicating the participation of meteoric waters in both regions. Synsedimentary

activity of the Penacerrada diapir (Kueper salt - Triassic)), which lies close to the Lafio section, played a significant role in driving the local shallowing of the basin and in the formation of the silica in the nodules. In contrast, eustatic shallowing of the inner marine series in the Tubilla del Agua section led to the generation of morphologically similar quartz geodes, but from waters not influenced by brines derived from the groundwater halo of a diapir.

The chemistry that controls the precipitation of silica as it replaces calcium sulphate in early diagenesis is not well understood. Is it a response to biogenic or abiogenic changes in pH and alkalinity? When opal cristobalite was observed filling mm-scale fenestral vugs in strandzone crusts in a Holocene dolomite/magnesite lake in the Coorong it was considered an inorganic precipitate (Peterson and Von der Borch, 1965). It formed where the pH of surface waters fluctuated between 10.2 and 8.5, and the season fall in pH was considered to drive inorganic precipitation of silica dissolved in the schizohaline lake waters. It came to be considered the type area for inorganic evaporitic precipitation of chert and a style of chert formation known as "Coorong-style." In the last decade sulphate-reducing bacteria have been shown to form dolomite in hypersaline coastal salinas in Brazil (Chapter 4) and some have applied similar notions to interpret the Coorong lake carbonates, that is, they are bacterially mediated precipitates (Rosen et al., 1988; Wright, 1999). The notion that silica precipitation in "Coorong-style" cherts is also microbially mediated is a distinct possibility.

Birnbaum and Wireman (1985) argued that bacterial degradation of organic matter must be important in forming silica precipitates in most evaporites. They demonstrated, through experiment, the strong influence of bacterial sulphate reduction on silica solubility. The ability of sulphate-reducing bacteria to remove silica from solution is related to local changes in pH and to hydrogen bonding within amorphous silica, followed by polymerization to higher weight molecules. During silica replacement of sulphate evaporites, the pore fluid becomes depleted in dissolved sulphate as it is reduced to H_2S by the action of anaerobic sulphate-reducing bacteria, which metabolise sulphate from an anhydrite or gypsum substrate. Where this selective dissolution of the sulphate occurs in the presence of amorphous silica the reaction is accompanied by the precipitation of silica. Hence the microscale mimicry of the lath outlines in the outer parts of many replaced nodules. According to Birnbaum and Wireman it reflects bacterially-mediated silica replacement of the nodule in relatively shallow burial settings where bacteria flourish.

Abiological processes, including thermochemical sulphate reduction are more important at greater burial depths where bacteria no longer survive. Providing matrix permeability is retained, silica replacement can continue into the thermobaric stage and can even persist into exhumation. Replacement under a thermobaric regime is frequently indicated by the preservation of hydrocarbon inclusions in the infilling silica cement.

Not all silicified nodules in evaporitic lacustrine sequences are replacements of $CaSO_4$ nodules, some form by transformation of sodium silicate gels. In the saline alkali lakes of the African rift valley, magadiite ($NaSi_7O_{13}(OH)_3 \cdot 3H_2O$) is a common sodium silicate associated with volcanogenic sediments (Eugster, 1969). It forms beds and nodules in sediments outcropping about the margins of many of the trona-containing lakes in the East African Rift, including Lake Magadi and Lake Natron. Other sodium silicates such as kenyaite and Na-Al silicate gels and zeolites are also present locally in the African rift lakes.

Magadiite nodules in Lake Magadi weather into cherts called Magadi-style cherts with a characteristic reticulate or "crocodile-skin" surface created by shrinkage during the transformation from sodium silicate gel to chert nodule. When buried, Magadiite rich layers in the diatomaceous host sediment pass along strike into outcrop and into beds of crocodile skin chert (Figure 4.39). Conversion of magadiite to bedded and nodular chert is thought to take place close to the sediment surface and be related either to the mobilisation and flushing of sodium by dilute waters in these shallow environments or to spontaneous conversion to chert in deeper brine-saturated zones. Eugster et al., (1967) proposed that magadiite is precipitated by diluting silica-rich, sodium carbonate brines with fresher waters. Mixing lowers the pH, and although the pH change may have been as little as 0.5, a decrease in pH from 10.3 to 9.8 lowers amorphous silica saturation by more than 500 ppm (Figures 4.38b, 7.58). Silica solubility changes very little when pH varies below a maximum of 8. Highly alkaline sodium carbonate waters containing abundant SiO_2 readily form in the Magadi rift valley via weathering and rapid subsurface hydrolysis of labile volcanic materials. Given the hydrogeochemistry needed for highly alkaline brines, evaporite minerals likely to be found in association with Magadi-style cherts are the sodium carbonates (trona, gaylussite or pirssonite; searlesite); gypsum is not present (Figure 2.12; Hardie and Eugster, 1970).

Surdam et al. (1972) listed the following textures as indicators of Magadi-style cherts that have evolved from a sodium silicate gel: 1) Preservation of the soft-sediment deformation features of the putty-like magadiite, such as enterolithic fold-

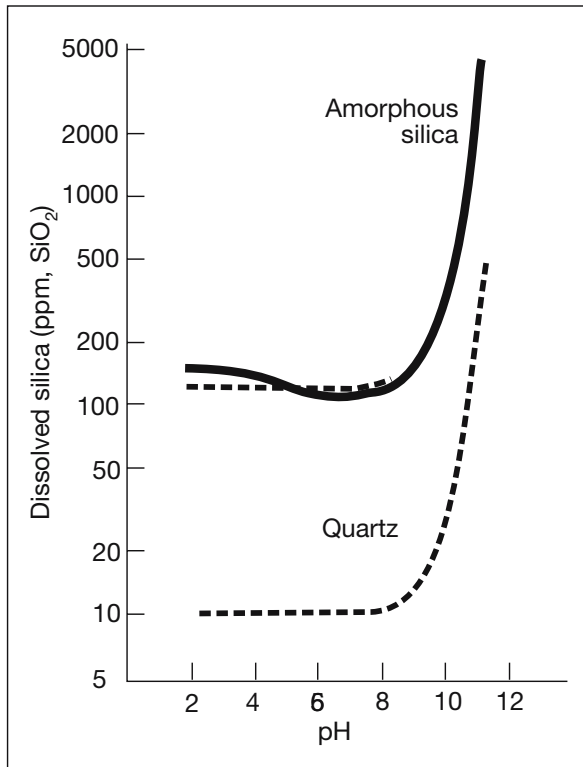


Figure 7.58. Silica solubility curves at 25°C. Solid line shows experimentally determined variation in solubility of amorphous silica with respect to pH. Dashed lines bracket the quartz solubility field (after Krauskopf, 1967 - see also Figure 4.38b).

ing, lobate nodular protrusions, casts of mudcracks and trona crystals, and extrusion forms; 2) Contraction features, such as reticulate cracks and polygonal ridges on the surface of the chert, reflect the loss of volume in the transition (crocodile skin chert). In Phanerozoic strata an ability to separate cauliflower cherts (after gypsum/anhydrite nodules) from crocodile-skin cherts (associated with silicate gels in trona/natron soda lakes) is considered important in defining marine-fed versus continental hydrologies. However, it has yet to be shown that any of these textures are unique to magadiite-chert transitions.

Ancient Magadi-style chert nodules crop out in lacustrine rocks of the Middle Devonian (Middle Old Red Sandstone) Orcadian Basin, Scotland (Parnell, 1986) and the fluviolacustrine sediments of the Permian Balzano volcanic complex in Italy (Krainer and Spötl, 1998). The Scottish cherts are replacive nodules within organic-rich laminates and are the deposits of a stratified alkaline lake. Nodules exhibit soft sediment deformation features including sediment injection along shrinkage fractures within the nodules and preserved stellate quartz pseudomorphs after an evaporite mineral, possibly trona. Nodules were nucleated about vertical cracks in the host sedi-

ment and show polygonal or parallel aligned patterns. Thus the precipitation of the magadiite precursor must have occurred from nearsurface alkaline groundwaters flushing through partially consolidated sediments.

The Italian cherts form thin layers within a fluviolacustrine succession sandwiched between acidic volcanic rocks of the Lower Permian Balzano Volcanic Complex in northern Italy. These cherts are interpreted as analogues to Magadi-style abiogenic chert (Krainer and Spötl, 1998). They show soft-sediment deformation features, shrinkage cracks, and well-preserved palynomorphs that document early diagenetic silica precipitation, volume loss by dehydration, and consolidation prior to mechanical compaction of the enclosing sediment. Similar chert layers were also noted in Triassic playa deposits of North Carolina replacing evaporite siliceous gels in 60 cm-thick siliceous beds intercalated with 20 cm-thick limestone tufa beds (Wheeler and Textoris, 1978).

But evaporite-associated chert can probably accumulate in any number of highly alkaline settings, with or without trona. White magadiite veins constitute rectilinear polygons (1-3 metres across) in playa sediments in Alkali Lake, Oregon, and in adjacent muds associated with alkali salts and brines (Rooney et al., 1969). The same beds do not host substantial volumes of sodium bicarbonate salts. Jones et al. (1967) noted up to 2,700 ppm of dissolved silica in the present-day brines from Alkali Lake playa. Such values represent a substantial supersaturation with respect to amorphous silica, even at the playa's current pH levels, which are near 10.5 (Figure 7.58). This level of supersaturation, in the absence of extensive trona suggests that these lacustrine sodium silicates precipitated directly from a hypersaline silica-saturated solution without the need for a sodium silicate precursor. The debate as to how, where and when crocodile-skin chert can precipitate continues, as yet unresolved.

In thin section, Schubel and Simonson (1990) showed that chert with a magadiite precursor has a characteristic rectilinear or gridwork orientation of quartz crystals, visible in thin section. The texture seems to be inherited, a pseudomorph after the original spherulitic magadiite structure, which shows similar extinction patterns due to presence of 10-20 μm spherical aggregates of plate-like crystals. This microscale pseudomorphing implies a direct volume-for-volume replacement of magadiite by chert. Unfortunately the level of detailed preservation needed to make such distinctions is not usually preserved in older cherts where megaquartz dominates the fill. It is useful in separating cherts from magadiite precursors versus chert from other hypersaline associations in Neogene strata, and

perhaps in a few examples it can be utilised in rocks from as far back as the Mesozoic.

As mentioned earlier, Folk and Pittman (1971) and Folk and Siedlecka (1974) concluded that length-slow chalcedony (lutecite) in chert nodules is a useful indicator of the former presence of evaporites (both anhydrite or magadiite precursors). But the occasional presence of length-slow chalcedony in nonevaporitic regimes, such as in turbidites and basalts, has shed suspicion on its absolute reliability. Heaney (1995) further refined the significance of lutecite by showing that in the early stages of its diagenetic evolution it is largely composed of a form of silica called moganite. Moganite is a polymorph of SiO_2 that is microcrystalline, fibrous and optically length-slow. Water content is $\approx 2\%$, slightly higher than chalcedony and lower than opal (6–10%). It is abundant in, but not restricted to, cherts formed in evaporitic environments. Nonevaporitic silica precipitates typically contain between 5 and 15 wt% moganite, whereas undeniably evaporitic specimens contain between 20 and 75 wt% moganite. No chert from nonevaporitic settings has been found to contain more than 25 wt% moganite. Consequently, enhanced moganite concentration (> 20 wt%) in microcrystalline silica is a valuable indicator for vanished evaporites. Heaney noted a frequent association of moganite with “Magadi-style” chert and suggested that moganite is a diagenetic alteration product of the hydrous Na-silicate magadiite. Unfortunately moganite is a metastable phase and all samples analysed by Heaney that are older than Cretaceous contain little or no moganite.

The transformation of magadiite to moganite must occur over hundreds to thousands of years in alkaline lake systems, whereas the inversion of metastable moganite to quartz requires tens of millions of years. But the moganite-evaporite association is broader than magadiite in soda lake cherts as moganite is forming as an authigenic phase in inland playas of central Australia and these Na-Cl brine systems never contained trona, magadiite or volcanoclastics (English, 2001). The source of silica is a deeply weathered granitic terrain soaked in stagnant brines.

When dealing with chert nodules, lutecite is only a reliable evaporite indicator when it occurs in suitable host lithologies, is stacked into appropriate vertical sequences and occurs in association with other indicators of “the evaporite that was.” The only undeniable single indicator that a chert has an evaporitic parentage is when relicts of the precursor salt still remain within the nodule.

Calcitisation and dedolomitisation

Calcitisation and dedolomitisation are two often-associated diagenetic processes affecting both evaporite salts (anhydrite/gypsum) and evaporitic dolomites. Calcitisation of evaporites refers to the replacement of an evaporite bed by calcite or limestone. Dedolomitisation refers to the conversion of a dolomite to a limestone. Calcium sulphate evaporites are calcitised in two settings; the meteoric, via groundwater flushing and spar fill of the resulting voids, and in the deeper subsurface, via sulphate reduction (both bacterial and thermochemical). Waters in deeper burial settings situated below the active phreatic tend toward anoxia and can carry organics as suspended or dissolved hydrocarbons.

As well as replacement, the flushing of bedded evaporites by surface-derived, low-sulphate meteoric waters also brings on evaporite rehydration, dissolution. Calcite cements typify the nearsurface, while anhydrite conversion, via slow hydration, characterises the deeper near stagnant portions of the same meteoric flow system (e.g. Figure 7.37b). Replacement is often bioepigenetic in shallower settings and thermochemical in even deeper and hotter settings. Thus the products of calcitisation tend to have diagnostic isotopic signatures.

Calcitisation of evaporites

Like silicification, the calcitisation of evaporite crystals and nodules can occur at any time in the burial cycle; whenever the throughflushing waters are undersaturated with respect to the evaporite salts and supersaturated with respect to CaCO_3 (Table 7.12). In South Australia, hollow aragonite (micrite rind) pseudomorphs after Holocene gypsum grow in the shallow subsurface about edges of coastal salinas in areas of active marine phreatic flushing (von der Borch et al., 1977; Warren, 1982a). Similar early pseudomorphs after bottom-nucleated gypsum have been recognised in the Lower Carboniferous of the Vesder region, Belgium (Figure 7.18; Swennen et al., 1981). There the process was under the influence of sulphate-reducing bacteria and the precipitates in zones of dissolved crystals are now composed of sparry calcite. Later in the burial history, compaction- or thermobaric-derived waters can leach CaSO_4 or other salts from the system to create characteristic voids that are then filled by burial-stage calcite. Examples of this other end of the burial spectrum include spectacular Au-enriched silica-rimmed dolomitic nodules after anhydrite in the Triassic redbeds of Spain (Bustillo et al., 1999; Alonso-Zarza et al., 2002).

Occurrence and age	Comments	Reference
Gypsum replacement in sub-tepee limestones in Holocene carbonate, Marion Lake, Australia.	Aragonite skins formed on dissolving gypsum prisms in the boxwork limestone forming where a prism of less saline marine seepage water interacts with the outer edge of the Holocene gypsum fill. This an excellent example of a gypsum-shaped crystal void in the midst of its creation.	Warren, 1982a
Calcitised gypsum beds in Miocene-Pliocene sediments, Calatayud Basin, northern Spain.	Early calcitization of lacustrine evaporite (gypsum, anhydrite) and/or magnesium carbonate (dolomite, magnesite) deposits driven by the encroachment of meteoric waters either at the contact of these deposits with overlying freshwater or where percolating freshwater enters at very shallow burial depth. Calcitization occurs during the interaction between magnesite and Ca-enriched waters derived from the dissolution of gypsum or glauberite.	Sanz-Rubio et al., 2001; Canaveras et al., 1998
Calcitised beds in Tertiary lacustrine dolomites, Madrid basin, central Spain.	Mineralogy of bedded carbonates is now dominated by calcite and the limestones contain moulds of gypsum. Occurrences of calcitised dolomite textures in these facies suggests the influence of fresher water during expanding lacustrine cycles or further subsurface interactions with less saline groundwater.	Calvo et al., 1995
"Gypsum-ghost" limestones adjacent to selenite lithofacies in the Miocene of northern Carpathian Foredeep, Poland.	Mass-balance chemistry shows a deficit of calcium and sulphur contents in the limestones compared to the composition of the selenitic gypsum and implies that the gypsum-ghost limestones system was open to mass transfer and cannot be related to simple and regionally extended replacement of solid sulphate rocks by limestones plus native sulphur; it is a transitional facies.	Gasiewicz, 2000
Calcitised Danian dolocretes in lacustrine beds, Provence Basin, France.	Dolocretes deposited around the palaeolake or playa margin subsequently leached and calcitised. Dolomite rhombs can be hollow. Fabric-destructive calcitization attributed to drop in the lake level, when the upper part of the dolocrete was subjected to vadose flushing, whereas the fabric-preserving calcitization (poikiliotopic) resulted from rise in lake level.	Colson and Cojar, 1996
Marbles in the Muttelbury Nappe, Jurassic Lovelock Formation, West Humboldt Range, Nevada.	Outcropping rauhwacke sheets are interlayered and interlensed with non-breccia marble slabs. The marble slabs are calcitised anhydrites from the original décollement of the thrust. They were produced biopigenetically by the action of sulphate-reducing bacteria on the CaSO ₄ antecedent.	Speed, 1974, 1975
Calcitization of the Permian Raisby/Cadeby Formation, UK.	Groundwater flushing converts nodular calcium sulphate into spar-filled cauliflower-shaped geodes. Fill is multistage telogenetic and with a consistent unroofing history outlined in zoned calcite linings of the geode fills.	Lee and Harwood 1989; Lee, 1990
Calcitization of Permian Karstryggen Formation, Central East Greenland.	Groundwater driven karstification on "the way down" created spar filled vugs after nodular anhydrite and was often associated with the precipitation of celestite.	Scholle et al., 1990, 1993
Calcitised anhydrite in Poplar and Ratcliffe beds in association with Watrous Formation, Mississippian, Williston Basin, USA.	Anhydrite calcitization occurred only after the Watrous unconformity was shallowly buried by redbeds, and replacement probably involved sulphate-reducing bacteria. Replacement calcite contains pseudomorphs and relicts of anhydrite, and pseudomorphs of secondary gypsum, indicating calcitization occurred only after original Mississippian gypsum was altered to anhydrite.	Kendall 2001
Dedolomites in the Mississippian Madison Group of Wyoming and Utah.	Two types of fracture-related dedolomites, one precedes and one postdates regional dolomitisation. The early dedolomite occurred as active groundwaters flushed anhydritic sequences during shallow burial. The later post-stylolitisation fracture-associated dedolomite records chemistries and isotopic signatures of deep tectonic-vein mineralisation.	Budai et al., 1984
Calcitised anhydrite, Winnipegosis Formation, Middle Devonian, Saskatchewan.	Calcitization of organic layers and anhydrite section occurred before compaction and was driven by the activities of sulphate reducing bacteria. It preserves characteristic structures of antecedent (lamination, nodular outlines).	Shearman and Fuller, 1969; Wardlaw and Reinson, 1971
Calcite-filled pseudomorphs in the Cambrian Parakeelya Alkali member of the Observatory Hill Formation, Australia.	Calcite pseudomorphs after trona and shortite occur in the perennial lake and saline mudflat facies of this alkaline playa. Cauliflower-shaped vugs are more commonplace in overlying marine section. Fills are composed of poikilotic calcite with dull luminescent cores and alternating dull and semiluminescent rims. Replacement occurred deep and in association with sulphate reduction.	Southgate et al., 1989; White and Youngs, 1980

Table 7.12. Selected examples of calcitization and dedolomitization in evaporitic settings.

Thus carbonate replacement of calcium sulphate is not depth specific and is driven by various hydrological processes (Pierre and Rouchy, 1988):

- 1) Sulphate dissolution during flushing by bicarbonate-rich waters derived from:
 - dissolved atmospheric CO₂,
 - oxidation of organic compounds (marine or terrestrial),
 - thermal decarboxylation of organic matter.
- 2) Bacterial sulphate reduction in organic-rich or hydrocarbon-flushed sediments. Sulphate reduction may also be later and deeper where it is abiotic and thermochemically induced (Chapter 9).

Late-stage calcite replacement of evaporite nodules postdates silicification in the Tosi Chert, Wyoming (Ulmer-Scholle and Scholle, 1994). It was thermochemically driven and was associated with hydrocarbon migration. Similar pseudomorphic replacement by calcite or dolomite of euhedral trona and shortite crystals occurs in the saline facies of the Cambrian Lake Parakeelya Member, South Australia. It was mesogenetic and took place during burial diagenesis as basinal brines flushed the system at temperatures of up to 110°C. The catabaric dissolution and removal of the sodium carbonate salts took place either coincident with or following the generation of hydrocarbons (Southgate et al., 1989).

Calcitisation of evaporite nodules is most widely documented where meteoric waters react with an evaporite bed in the active phreatic zone and not in the deep subsurface (Table 7.12). Meteoric flushing can occur soon after an evaporite unit is

deposited (early mesogenetic replacement “on the way down”) or it can occur after deeply buried evaporite units are uplifted back into the zone of active meteoric throughflow (telogenetic or “on the way back up”). And, as we have already seen, the replacement process can continue “while at the bottom” or wherever epithermal fluids flush calcium sulphate nodules. This can be as part of an active volcanogenic system (Bustillo et al., 1999) or even in association with the cycling of seawater through hydrothermal anhydrite in mid ocean ridges (Warren, 1999; Chapter 9). In hydrologically mature sedimentary basins, uplift-related meteoric flow is typically forced by head-driven circulation from high-elevation recharge areas (Figure 8.10), which can drive calcitisation and replacement to depths of more than a thousand metres.

One of the best documented examples of calcitised evaporites forming long after deposition and burial of the primary salt beds (“on the way back up”) comes from the onshore Permian Raisby Formation of the UK. There, alteration processes related to relatively recent re-entry into the zone of active meteoric flushing, can be studied both in outcrop and in core. The Raisby Formation (formerly the Lower Magnesian Limestone) is the first major carbonate unit deposited in the English Zechstein series and outcrops as escarpments and coastal cliffs along the NW coast of the UK (Figure 7.59). It is overlain by the Ford Formation (formerly Middle Magnesian Limestone), a classic wedge-shaped carbonate shelf succession, which today crops out in a north-south belt up to 5 km wide. It is interpreted as a barrier reef/shoal sequence with backreef and lagoonal facies composed of white to buff, soft, bedded oolitic and fine grained dolomite. The reef faces is buff to brown hard massive

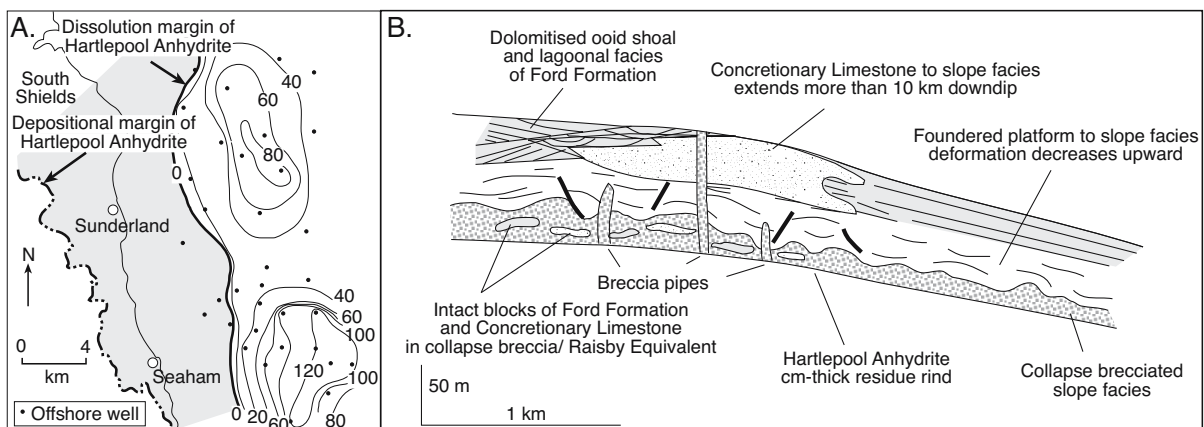


Figure 7.59. Evaporite dissolution in the Permian Zechstein on the NW coast of England. A) Extent of the dissolution zone of the Hartlepool Anhydrite from offshore anhydrite to onshore dissolution residue. Hartlepool isopachs in metres. B) Facies patterns in the Raisby and related formations that make up the Zechstein unit formerly known as Magnesian Limestone. The cross section shows the relationship to dissolution residues of the Hartlepool Anhydrite seen in coastal outcrops where the anhydrite has dissolved.

to rubbly reef dolomite and associated talus, passing up into algal-laminated dolomite with oncoliths. Bryozoa, crinoids, brachiopods, bivalves and gastropods are abundant, except near the top of the buildups where stromatolitic and encrusting algae dominate and define the transition into more hypersaline conditions. Its slope and basin facies today consist of seaward dipping buff fine-grained dolomite. Offshore to the Raisby Formation lies the Hartlepool Anhydrite (Figure 7.59a). Onshore the former position of the Hartlepool Anhydrite is defined by a regionally extensive dissolution residue at the base of the Raisby (Figure 7.59b).

Outcropping Raisby dolomites contain nodular cavities, pores and pseudomorphic voids, which are lined or filled by calcite spar. Deep borehole cores sampling the Raisby Formation may still retain nodules and euhedral crystals of gypsum and anhydrite that are near-identical in size and shape to the cavities and pseudomorphs now seen in outcrop. This indicates that

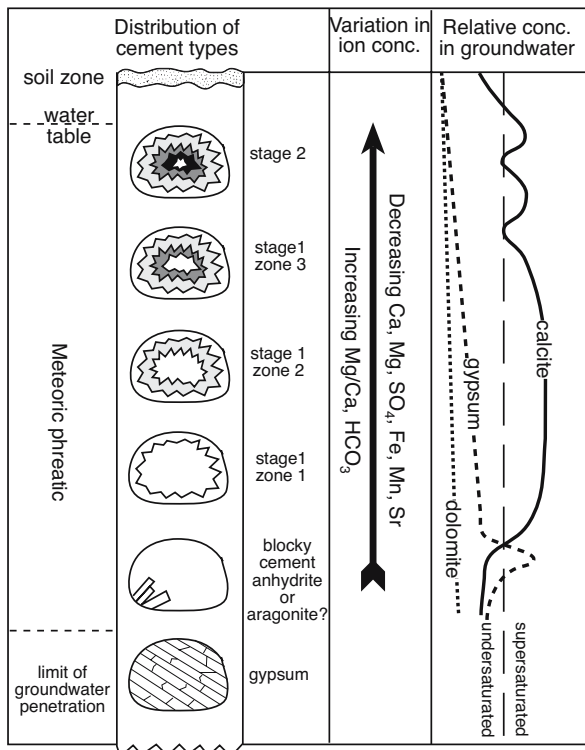


Figure 7.60. Nodule evolution in the Raisby Formation, UK. Vertical axis indicates distance from the land surface, but may also indicate evolution through time of any one cavity. The lowermost cavity is filled with gypsum derived by rehydration of buried anhydrite. Contact with meteoric water causes dissolution of gypsum followed by local anhydrite pore cement that is then replaced by calcite. Succeeding calcite fill of cavities indicates increasing oxygenation and activity of groundwater system (after Lee and Harwood, 1989).

calcium sulphate nodules were once abundant in the subcropping Raisby Formation, but almost all the original salts have since been removed by crossflows of meteoric groundwaters.

Thus calcitisation of evaporite nodules is still active in appropriate zones of groundwater flushing along much of the coastal zone of NW England (Figure 7.59, 7.60; Lee and Harwood, 1989; Lee, 1994, 1995). Much earlier in the burial history of the Raisby Formation, primary Permian gypsum was replaced by anhydrite nodules. Later, coarser replacive burial anhydrite formed, postdating both pressure-solution and any further dehydration of any residual primary gypsum. During further mesogenetic burial, some of the anhydrite in the nodules was replaced by catabaric baryte, dolomite and sphalerite. Upon uplift of the Raisby Formation during the Tertiary, any remaining nodular anhydrite was telogenetically rehydrated to porphyroblastic gypsum. With further exhumation the gypsum was then dissolved by meteoric groundwaters and multiple stages of meteoric calcite cement precipitated within the voids (Figure 7.60). All meteoric phreatic waters in this part of the UK are currently undersaturated with respect to dolomite and saturated with respect to calcite. Thus the calcite void fills in the Raisby Formation are made up of clear, inclusion-free, non-ferroan, low-magnesian telogenetic calcite.

There is an enigmatic episode of what was interpreted by Lee and Harwood (1989) as a widespread, but minor nearsurface anhydrite cement. It precipitated after regional exhumation had rehydrated all the buried anhydrite to gypsum and the gypsum had dissolved to form voids (Figure 7.60). This early blocky crystal phase predated calcite void fills. It is encased in zone 1 calcite and is now replaced by calcite. Its blocky rectilinear prism termination precludes either a gypsum or a baryte precursor. The process and the mechanism which could have created an anhydrite-saturated pore water in the voids after gypsum leaching, in what must have been a shallow unroofing setting, is not well understood. Lee and Harwood (op. cit.) argue that if it is a calcite pseudomorph of anhydrite it perhaps indicates a short-term increase in salinity of nearsurface pore waters brought on by widespread meteoric dissolution of large volumes of subjacent halite.

The succeeding calcite infill of the leached gypsum nodules occurred in two phreatic (isopachous) stages; Stage 1 crystals are circumvoid equant, while stage 2 crystals are coarser, circumvoid and columnar (Figure 7.60). Under cathodoluminescence the stage 2 columnar crystals are nonluminescent and alternate with internal sediment layers. Stage 1 crystals show three geochemically distinct cathodoluminescence zones probably

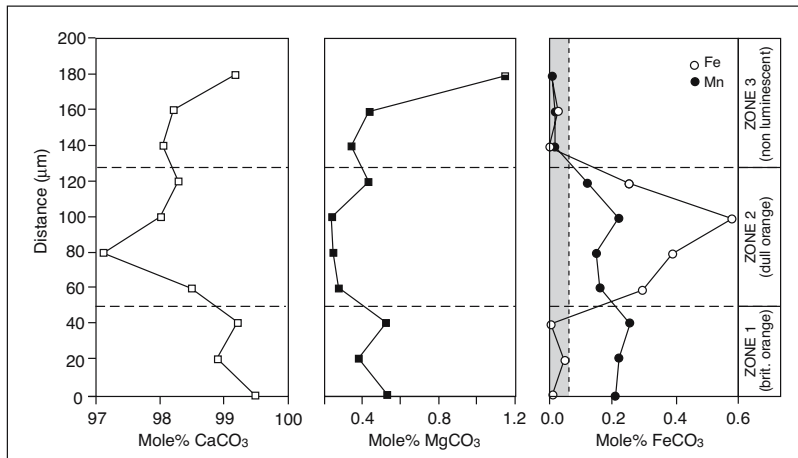


Figure 7.61. Microprobe traverse through a Stage 1 cement crystal growing inward from the nodule wall showing distinct geochemical differences between Zone 1 (bright orange), Zone 2 (dull orange) and zone 3 (nonluminescent). Shaded areas indicate values are below reliable detection limits (after Lee and Harwood, 1989).

related to increasing oxygenation of the crossflowing pore waters (Figure 7.61). The successive zonation reflects increasing groundwater flow in the phreatic zone as the exhumed rocks approach the landsurface. Stage 1 – zone 1 (bright orange) cement has high Mn and low Fe and Mg values. Stage 1 – zone 2 (dull orange-luminescent) has relatively high Fe and Mn and low Mg values. Stage 1 – zone 3 (nonluminescent) has negligible Mn and little Fe in the calcite. Stage 2 cements have much higher Mg levels than stage 1, while the orange luminescing cements (zones 1 and 2) contain much higher levels of Sr than zone 3 or stage 2 cements (Figure 7.61). This geochemical and cathodoluminescent zonation in calcitised nodule in the Raisby Formation is typical of increasing oxygenation in the pore fluids. It tracks the telogenetic passage of the uplifted strata into an increasingly oxygenated and active groundwater system. But what of the early blocky calcite that Lee and Harwood (op. cit.) interpreted as post-gypsification anhydrite?

The process of meteoric calcitisation of CaSO_4 nodules is complicated in some parts of the Zechstein subcrop in central Germany by the presence of neofomed aragonite growing in anhydrite/gypsum vugs (Peckmann et al., 1999). It may be this calcite replacement of aragonite prisms that gives the unusual blocky crystal outlines that were interpreted as an unusual post-gypsification anhydrite in the preceding discussion of the Raisby Formation. Similar misinterpretations of blocky elongate calcite prisms as pseudomorphs after gypsum not as aragonite cementstone replacements have complicated the evaporite history of the Proterozoic MacArthur Basin in northern Australia (Warren, 1999; Chapter 8). Low $\delta^{13}\text{C}$ values (-10‰ PDB) of

the aragonite inclusions growing in the Zechstein gypsum nodules indicate that some of its carbon is derived from organic matter that has been oxidized by bacterial sulphate reduction (see Figure 9.43a). The residual aragonite inclusions bear rhomb-shaped crystals of calcite that replace former dolomite. Elevated Mg/Ca ratios due to this dedolomitization may have promoted the precipitation of aragonite instead of calcite during gypsification. This aragonite has precipitated in the near-surface meteoric–vadose zone in recent times, it is a telogenetic precipitate. Aragonite crystals display a platy habit, while SEM analyses show that two types of micro-rods are associated with these plates (Peckmann et al., 1999). The mineralized micro-rods are

interpreted to be fossilized bacteria. Aragonite inclusions, most of which contain organic-rich aggregations, yield a distinctive biomarker pattern. High concentrations of specific unsaturated fatty acids are clearly indicative of newly produced organic matter and reflect the presence of a discrete microbial community being associated with the formation of the aragonite. At one locality the aragonite is accompanied by native sulphur and the formation of sulphur was mediated by H_2S -oxidizing bacteria. This is corroborated by the presence of densely packed curved aragonite rods representing permineralized bacterial cells on and within the sulphur.

So far, most of our discussion has emphasised the importance of bicarbonate-rich meteoric circulation in calcitising exhumed calcium sulphate beds. But is this always so? The work of Peckmann et al., (1999) shows that aragonite can be a local product of bacterial sulphate reduction acting on gypsum nodules during exhumation of diapir crests. Kendall (2001) argues that biogenic sulphate reduction can be a more widespread process in shallow burial and that bacterial metabolism can calcitise widespread evaporite beds beneath unconformities, independent of active meteoric circulation. He cites beds of anhydrite nodules that are locally replaced by calcite, pyrite and celestite beneath an unconformity atop Mississippian anhydrites of Saskatchewan (Figure 7.62a). Triassic clastics (Watrous Formation) immediately above the unconformity are green (reducing), rather than red (oxidising), and there is a regionally developed subunconformity alteration zone, where carbonates are dolomitized, and porosity is filled with anhydrite.

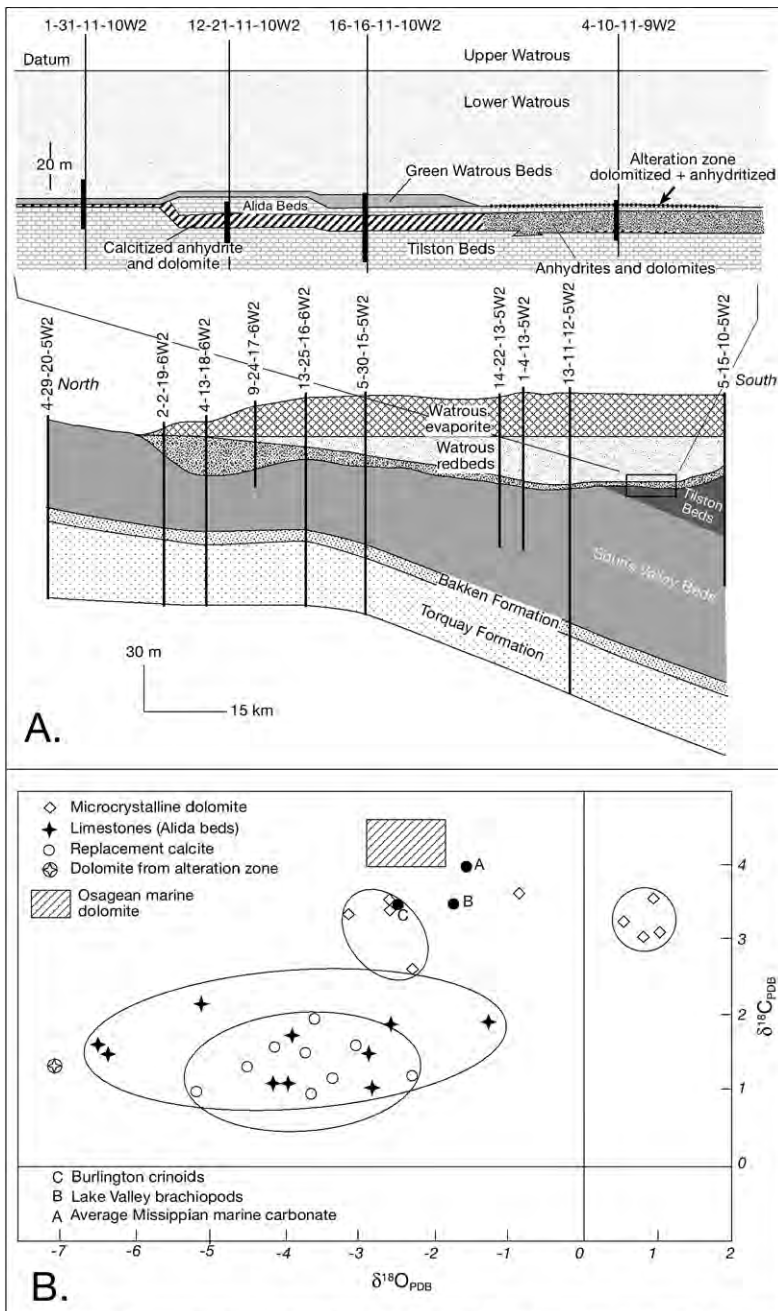


Figure 7.62. Bacterial calcitization, Saskatchewan (after Kendall, 2001). **A)** Diagrammatic section showing the regional unconformity, the northwards disappearance of older Triassic, Permian, Pennsylvanian and late Mississippian strata, and the northwards overstep of the Watrous by Jurassic deposits. Inset shows anhydrite (or calcitised anhydrite) and dolomite constitute the Tilston Evaporite. Most of Tilston Beds and overlying Alida Beds are limestones. Note the very thin calcitised anhydrite zone at the base of the Tilston Anhydrite (arrowed), and a dolomitised zone beneath the unconformity in the 4-10-11-9W2 well. **B)** Carbon-oxygen isotopic ratio cross-plot of calcites that have replaced anhydrite, host rock dolomites, and limestones of overlying Alida Beds. Note overlap of limestone and replacement calcites, and the distinct of dolomite values.

The unconformity lacks karstic features (unlike equivalent age surfaces in the USA), and probably formed in a hyperarid climate. Mississippian anhydrites near the unconformity are not preferentially dissolved, nor were they extensively hydrated. Anhydrite calcitisation probably involved sulphate-reducing bacteria and occurred only after the unconformity was shallowly buried by red beds. Hydrogen sulphide, generated by bacteria in saline brines reduced red bed pigments to form the green halo. Replacement calcite contains pseudomorphs and relicts of anhydrite, and pseudomorphs of secondary gypsum. These indicate calcitisation occurred only after original Mississippian gypsum was altered to anhydrite and this, in turn, was partially converted back to secondary gypsum beneath the unconformity.

Replacement occurred concurrently with the formation elsewhere of a dolomitised zone beneath the unconformity. Sulphur isotopic ratios of replacement pyrite are depleted relative to Mississippian sulphate values, consistent with the activities of sulphate-reducing bacteria. $\delta^{34}\text{S}$ values for Mississippian Tilston and overlying Frobisher Evaporite anhydrites cluster around +18 to +19 ‰, comparable with Mississippian sulphate evaporite values worldwide (Figure 2.23). Values from the much younger replacement anhydrite porphyroblasts, and one value from anhydrite in the dolomitised zone are similar. Sulphides, associated with replacement calcite from the Filmore area, have $\delta^{34}\text{S}$ values that are depleted (by up to 19 ‰) relative to the Mississippian sulphates. Whole-rock analyses of Mississippian (Alida and Tilston Beds) limestones exhibit a narrow range of $\delta^{13}\text{C}$ ratios of +1.5 to +2.2 ‰, averaging +1.8 ‰ but have a wider range in $\delta^{18}\text{O}$ -1.2 to -6.4 ‰, averaging -3.86 ‰ (Figure 7.62b). Carbon and oxygen are both depleted compared with estimated Mississippian marine carbonate values; almost certainly due to the addition of later diagenetic cements (Kendall, 2001).

Mississippian dolomites have heavier $\delta^{13}\text{C}$ values (+2.6 to +3.6 ‰) and appear to be less altered. Their $\delta^{18}\text{O}$ ratios, however, are more varied. Two populations are present: one has preserved Mississippian compositions or is slightly depleted (-2 to -3‰ $\delta^{18}\text{O}$), but most are heavier - clustering around values of +0.9‰ $\delta^{18}\text{O}$, possibly reflecting precipitation from evaporated Mississippian sea water (Figure 7.62b). A single analysis of dolomite from the dolomitized zone has a markedly different composition from the early diagenetic Mississippian dolomites. Replacement calcites have a narrower range of isotopic compositions, averaging -3.9 $\delta^{18}\text{O}$ and +1.5 $\delta^{13}\text{C}$. These averages are almost the same as those calculated for whole-rock analyses of the Mississippian limestones (-3.9 $\delta^{18}\text{O}$ and +1.8 $\delta^{13}\text{C}$). But the carbon isotopic ratios of replacive calcites, do not support this interpretation, rather they are identical to those of Mississippian limestones (Figure 7.62b).

Kendall (2001) argues simple replacement of sulphate by porewater bicarbonate (in equilibrium with host limestones) is unlikely because protons generated during the reaction should have created acidic conditions in which calcite would have dissolved. He notes a full explanation of the calcitisation remains elusive, but may involve replacement occurring in an active arid-zone groundwater system and/or bacterial sulphate reduction occurring upstream of the site of calcitisation.

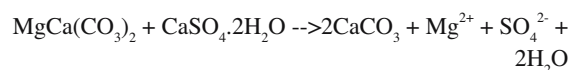
Bustillo et al., (1999) describes some unusual mineralized and silicified carbonate-rich nodules hosted in Lower Triassic red mudstones in Central Spain (Figure 7.63). From their borders to their centres, the nodules (geodes) display a characteristic zonation of; a) a millimetric carbonate crust, b) a quartz rim, c) massive dolomite centres, d) gold-bearing iron-rich infills (haematite laths and goethite with up to 7000 ppm of gold) and e) uplift related calcite cements that sometimes seal the central hollow. Textural evidence indicates that the geodes were originally nodular anhydrite, subsequently replaced by quartz and dolomite. The resultant porosity from this replacement (“on the way down”), or porosity created by later dissolution, has been filled by epithermal gold-bearing iron-oxide hydroxides, romanechite and calcite.

$\delta^{13}\text{C}$ values indicate the participation of meteoric waters in an early burial environment, which was characterized by both a sub-desert climate and a temperate-tropical climate. Oxygen signatures reflect very variable temperatures for all minerals, with the exception of late stage calcite, which was precipitated at <38°C (“on the way up”). Iron-oxide temperature values in the gold rich cores can reach up to 85°C (epithermal stage). The mineralogical assemblages denote a multistage history to the nodules characterised by early silica, then dolomite infill of

a dissolving nodule (early diagenetic replacement “on the way down”) followed by the epithermal activity (“at the bottom”). This mineralization is linked to the Late Hercynian, calc-alkaline volcanism of Central Spain (the Hiendelaencina mining district). Once again, the evaporite replacement process is ongoing, not early versus late, but throughout the burial cycle.

Dedolomitisation of matrix

Dedolomitisation of the host matrix is frequently associated with calcitisation of entrained evaporite nodules. Dedolomitisation describes the conversion of a dolomite back to a limestone by the growth of calcite rhombs within the dolomite matrix.



This process can continue until the dolomite is converted to a limestone, or it may be arrested when the calcitisation of the matrix is no more than partial. Dedolomitisation has long been interpreted as a product of evaporite diagenesis and is typically ascribed to telogenetic calcium-rich groundwaters derived from a nearby dissolving gypsum/anhydrite or glauberite unit (Lucia, 1961; Warrak, 1974; Lee, 1994). An evaporite association is the emphasis of the dedolomitisation discussion in this section; but dedolomitisation can also occur under the influence of calcium-rich basinal waters (mesogenetic), where the elevated levels of calcium are independent of evaporite dissolution. For example, Land and Prezbindowski (1981) documented dedolomitisation from hot, calcium-rich brines moving up into a dolomite reservoir in the Cretaceous Edwards Group of the Gulf Coast. They attributed the high calcium content of these brines to the authigenic albitisation of plagioclase in downdip sandstones.

Evaporite-derived dedolomites are often associated with evaporite dissolution breccias, which indicate the now dissolved bed that supplied the excess calcium needed to dedolomitise (Lee, 1994). Dedolomite under this scenario forms via the reaction of calcium sulphate-rich solutions with a preexisting dolomite to produce calcite with magnesium sulphate as a possible byproduct. The latter is rarely preserved, as it is highly soluble, and either remains as dissolved ions in the escaping waters or is quickly redissolved and flushed by through-flowing groundwaters (Shearman et al., 1961). The CaSO_4 dissolution process is often driven by meteoric flushing of nearsurface oxidising waters and former ferroan dolomites are preferentially replaced. The resulting calcitised dolomites are outlined by intervals stained red with iron oxides and hydroxides.

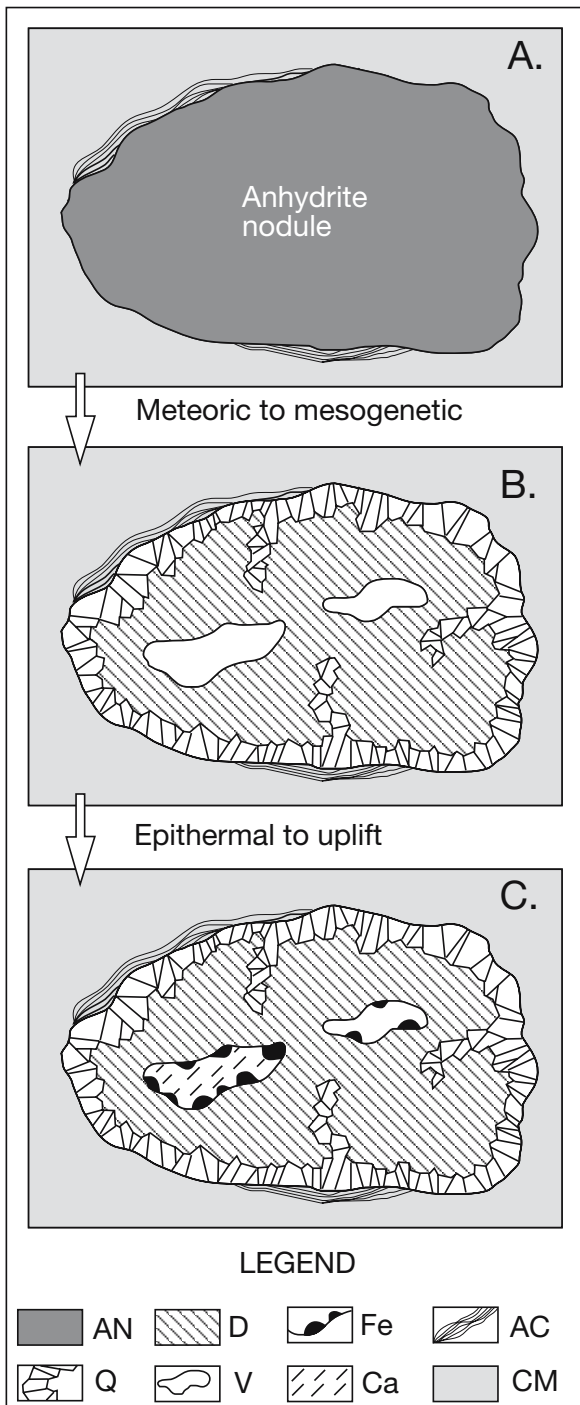


Figure 7.63. Model of the Tordelrabano geodes, Spain (after Bustillo et al., 1999). Abbreviations: AN, anhydrite; D, dolomite; Fe, oxides and hydroxides of iron; AC, carbonate crust; Q, quartz; V, voids; CA, calcite; CM, mudstones. A) Anhydrite nodules form in mudstones from early hypersaline fluids. Later, a crust (probably edaphic) forms around the anhydrite nodule. B) Replacement of the anhydrite by dolomite and quartz from continental groundwaters. Voids form by dissolution of anhydrite or dolomite. C) Filling of the voids by hydrothermal minerals (gold-bearing hematite-goethite). Subsequent precipitation of tectogenic calcite.

Dedolomites created by meteoric flushing of calcium-sulphate evaporite salts typically occur beneath exposure surfaces, dissolution breccias or unconformities. Well-exposed and studied examples of dedolomites, associated with karstification of a shallowly buried sulphate system, typify Miocene lacustrine sequences of the Madrid Basin in central Spain and the Calatayud Basin of NE Spain (Cañaveras et al., 1996; Arenas et al., 1999; Sanz-Rubio et al., 2001). A variety of calcite fabrics, initiated by dedolomitisation and calcitisation of magnesites, formed in association with well-defined solution collapse breccias (Figure 7.64). Dominant dedolomite textures are made up of sutured calcites and radial-fibrous calcites, the latter consisting of pseudospherulite mosaics and fibrous crusts. Other subordinate dedolomite fabrics consist of micro- to mesocrystalline mosaics of rhombic, occasionally zoned calcites, as well as reworked pseudospherulite crystals.

The diagenetic carbonate zone (DCZ) that hosts these textures in the Madrid basin overlies and grades laterally into lacustrine dolomite (lower dolomite unit - LDU) and evaporites (evaporitic unit - EU), and in turn is capped by a palaeokarst or exposure surface (Figures 7.36, 7.64a; Cañaveras et al., 1996). The boundary between the DCZ and the LDU is transitional and is defined by grading in the %MgCO₃ profile (Figure 7.64b). Mg values range from 0.1 to 1.2% in the dedolomites of the DCZ and micrites of upper limestone unit (ULU) and from 8 to 14% in the underlying dolomites of the LDU.

Geochemical evidence indicates dedolomitisation occurred in the shallow subsurface in early burial (< 40 m depth) via the throughflushing of oxidizing meteoric-derived ground waters (Cañaveras et al., 1996). $\delta^{18}\text{O}$ values of the dedolomites in the DCZ average -6.7‰ and range from -6.1 to -7‰ , while $\delta^{13}\text{C}$ averages -8.2‰ and ranges from -7.4 to -9.2‰ . The $\delta^{18}\text{O}$ values in the LDU average -0.3‰ while $\delta^{13}\text{C}$ averages -6.1‰ . Isotope values in the ULU range from -6.4 to -6.8‰ in $\delta^{18}\text{O}$ and from -8.2 to -8.9‰ in $\delta^{13}\text{C}$ (Figure 7.64c). The values of the dedolomites are consistent with precipitation from meteoric waters and give precipitation temperatures of 8 to 12°C. Vertical trends in $\delta^{18}\text{O}$ and $\delta^{13}\text{C}$ can be used to define the average position of the water table in the DCZ at the time the dedolomites were forming (Figure 7.64d). This too supports a palaeokarst model characterized by an irregular shallow water table and a narrow vadose zone (Cañaveras et al., 1996). The

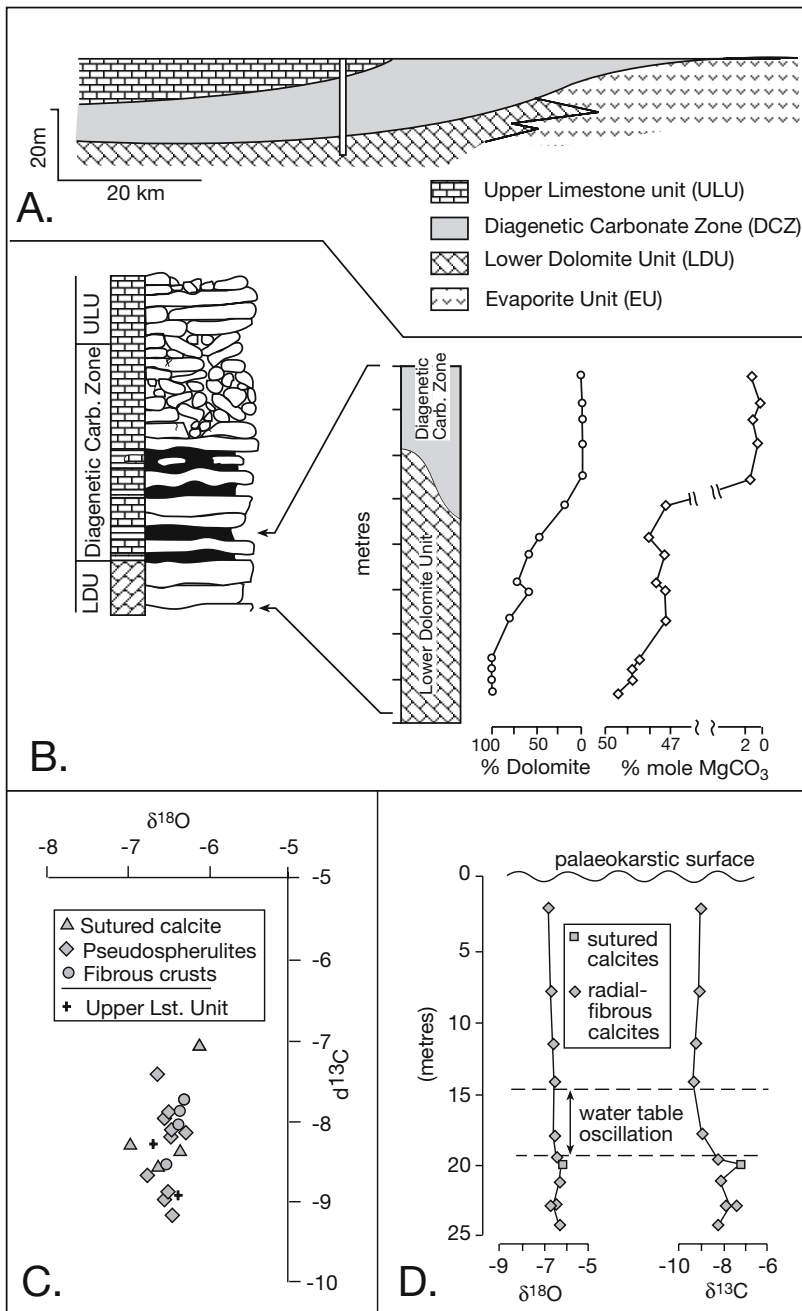


Figure 7.64 Dedolomite in the Madrid Basin, Spain. A) Distribution of the main subunits in Middle to Upper Miocene lacustrine units of the Madrid Basin, central Spain. B) Shows the position of the solution collapse breccia in controlling the dedolomites and the nature of the contact between the lower dolomite unit (LDU) and the dedolomites of the diagenetic carbonate zone. C) Oxygen-carbon crossplot of different types of calcite that make up the dedolomite. D) Vertical trends in $\delta^{18}\text{O}$ and $\delta^{13}\text{C}$ in section of the Diagenetic Carbonate Zone (DCZ). The zone of carbon depletion between 15 and 20 metres below the palaeokarst surface corresponds to a trend of more constant $\delta^{18}\text{O}$ values above this interval and more variable values below. These observations are consistent with the preservation of a palaeo-water table within the DCZ (after Cañaveras et al., 1996).

diagenetic system behaved as an open system for nearly all trace elements analysed; but in the shallower zone (vadose zone) the system was partially closed with respect to strontium. The dedolomitisation was driven by two combined hydrographical patterns: authigenic recharge through limestone aquifers and allogenic recharge from adjacent mountains (Figure 8.10).

Dedolomites can also be formed via evaporite dissolution in the deeper subsurface mesogenetic realm where dissolution-derived basal brines are escaping into the basin margin. Budai et al. (1984) suggested a sub-surface setting for burial dedolomites of the Mississippian Madison Group of Wyoming and Utah. Two stages of fracture-related dedolomite are present, one that precedes and one that postdates regional dolomitisation. The early dedolomite occurred as active groundwaters flushed evaporitic sequences during shallow burial (on the way down in the burial cycle). The later post-styolitisation fracture-associated dedolomite records chemistries and isotopic signatures of deep burial and tectonic-vein mineralisation. Associated with this late dedolomite are calcitised anhydrite nodules and stylolite-bitumen-related dedolomites that also indicate burial-related episodes of dedolomitisation. This episode of dedolomitisation took place during hydrocarbon maturation as basal brines were moving through the Madison reservoir. Then hot Ca-enriched brines were able to dissolve anhydrite and dolomite, while at the same time precipitating calcite along stylolitisised seams and within anhydrite nodules.

Country	Host rock age	Reference	Strand/evaporite	Subaerial exposure	Hydro-thermal	Assoc. clastics	Assoc. baryte	Celestite $^{87}\text{Sr}/^{86}\text{Sr}$	Oceanic $^{87}\text{Sr}/^{86}\text{Sr}$	Interpreted Sr Source
Algeria-Tunisia	Eocene	Chabou-Mostefai et al., 1978	Yes	Yes	-	Yes (updip)	No	-	-	Groundwater influx from granitic source
Argentina	Cretaceous (Neocomian)	Brodtkorb et al., 1982	Yes	Minor	Yes	Yes (above)	Some	0.7072	0.7072	Seawater
Canada	Carboniferous Mississippian	Kendall, 2001	Yes	Yes	No	Yes (above)	No	-	-	Shallow brine drives bact. sulphate reduct.
Germany (FRG)	Jurassic (Malm)	Müller, 1962	Yes	Some local	Some local	Some (above)	No	-	-	Seawater
Great Britain	Triassic (Rhaet)	Wood and Shaw, 1976		Minor	No	Some	Minor	0.7105	0.7076	Groundwater alteration of older limestones
Greenland	Permian (Kazanian)	Scholle et al., 1990	Yes	Yes (extensive)	Minor locally	Yes (below)	No	0.71344	0.7068	Groundwater from redbeds
Italy	Pliocene	Babieri and Masi, 1984	-	-	-	-	Yes	-	-	Evaporites
Mexico	Cretaceous (Albian)	Kesler and Jones, 1981	Yes	Minor to none	Minor	Yes (below)	Yes	0.70765	0.7072	Limestone diagenesis; groundwater
Norway	Silurian (Wenlock)	Olaussen, 1981	Yes	Yes (extensive)	No	Yes (above)	No	-	-	Groundwater alteration of aragonitic limestone
Poland	Permian (Zechstein)	Hryniv and Peryt, 2003	Yes	Yes	No	Yes (below)		-	-	Groundwater alteration of Ca sulphate beds
Spain	Eocene	Taberner et al., 2002	Yes	Yes	no	Yes (above)	Some	0.70776 - 0.70784	0.7071	Groundwater leaching Sr in overlying redbeds
Spain	Miocene	Martin et al., 1984	Yes	Yes (extensive)	No		No	-	-	Marine Sr: mixing zone precipitation
Turkey	Miocene	Tekin et al., 2001	Yes	yes	-		No	0.70782 - 0.7087	0.7083	Volcanics
United States	Silurian	Carlson, 1987	Yes	Yes	Some	No	No	-	-	Dolomite or evaporite dissolution
United States	Carboniferous Mississippian	Frazier, 1975	Yes	Some	Yes	Yes	No	-	-	Seawater brines
USSR (former)	Permian (Lower)	Zaritsky, 1961	Yes	Possible	-	Yes	Yes	-	-	Seawater; groundwater redistribution

Table 7.13. Worldwide occurrences of celestite and associated properties (in part after Scholle et al., 1990; Hanor, 2004).

Celestite as an indicator?

Celestite (SrSO_4) occurs as crystals, nodules and cements in many bedded carbonates, particularly karstified limestones, but also in dolomitic and marly hosts. Evaporite-associated celestite

may replace or pseudomorph individual evaporite crystals, or it may be isopachous and passively fill fissures, vugs and nodular cavities created by the dissolution of an evaporite precursor, or it may form interclast cements within dissolution breccias. Internal textures preserved within a celestite nodule replacing

an evaporite or an intergranular aggregate depend on the ratio of rock to fluid interaction and the timing of flushing.

Celestite, in association with baryte and strontianite can form massive intervals in diapir caprocks and haloes about the dissolving edges of salt allochthons. Caprock occurrences were discussed in the previous chapter and will not be discussed here. SrSO_4 in a bedded evaporitic carbonate host forms either as a primary precipitate from brines (Wood and Shaw, 1976) or, more usually, by the diagenetic interaction of gypsum or anhydrite with groundwater-borne Sr-rich waters (Table 7.13). In this case the dissolution of a calcium-sulphate-containing bed supplies the SO_4 , which then combines with Sr to precipitate as celestite, typically in zones of mixing between hypersaline and meteoric waters. West (1964, 1965, 1973, 1979) discusses the evaporite-celestite association in detail and the interested reader is referred to these benchmarks. Scholle et al. (1990) is recommended for a more general summary of celestite occurrence in sediments worldwide.

Strontium occupies calcium sites in the gypsum or anhydrite lattice, where it can be enriched ten times over the Sr content in enclosing dolostones (Carlson, 1983). Strontium levels are around 2,000 ppm in marine gypsum and 5,000 ppm in anhydrite of marine origin (Stewart, 1968). Leaching of such gypsum/anhydrite can create Sr-rich waters, as can the dissolution of aragonite. Documented sources of strontium-rich waters capable of precipitating celestite include:

- Marine-derived brines (Frazier, 1975; Baker and Bloomer, 1988)
- Waters formed during the conversion of aragonite to calcite (Nickless et al., 1975)
- Waters formed during the dolomitisation of limestones (Wood and Shaw, 1976)
- Waters formed during the conversion of gypsum to anhydrite (Kushnir, 1982; Orti et al., 1998)
- Waters formed during the dissolution of subaerially exposed gypsum (Taberner et al., 2002)
- Resurgent basinal waters that have leached Sr from feldspars and clays in arkosic redbeds (Scholle et al., 1990)
- Red bed successions prograding atop a carbonate evaporite system and carrying a progradational meteoric hydrology that leaches Sr from the redbeds (Taberner et al., 2002)
- Shallow subunconformity waters with elevated Sr from bacterially-mediated calcitisation of anhydrites (Kendall, 2001)

West (op. cit.) notes that sedimentary celestite has, in most cases, formed by direct replacement of gypsum or anhydrite; it tends to remain, even when exposed at the surface as it is much less soluble than either of those minerals. West's papers

on celestite occurrences and controls in the Jurassic Purbeck evaporites of the UK remain as highlights in competent scientific documentation of field relationships and observation-based interpretation of process. He concludes that celestite formed by the selective removal of strontium from groundwater by reacting with dissolving beds and nodules of calcium sulphate. Groundwaters containing a large proportion of calcium ions and a small proportion of strontium ions most commonly exist where limestones occur in proximity to the site of precipitation. Celestite is less common where sandstones are the aquifers adjacent to a gypsum bed. The groundwater may be ascending or descending as it reaches the CaSO_4 . Celestite beds of appreciable thickness are thus formed in Purbeck strata at the upper and lower boundaries of gypsum or anhydrite beds in contact with these groundwaters. Purbeck celestite replaced both nodular anhydrite and bird-beak gypsum roses (West, 1964). Ongoing flushing by bicarbonate-rich groundwaters locally converted celestite to calciostrontianite (Salter and West, 1966).

Carlson (1987) documented groundwater-driven replacement of calcium sulphate salts by celestite in Silurian carbonates of northwestern Ohio. Associated textures indicate evaporite dissolution and karstification. Celestites occur along the western margin of the Ohio (Cayugan) basin within the Greenfield Dolomite and undifferentiated Salina dolostones. The celestite replacements are more durable than the original evaporite salts, which have long since vanished from the outcropping carbonate. Replacement styles include: lenticular and prismatic crystals, replaced cauliflower nodules of anhydrite and laminar celestite beds replacing laminated evaporites. Remnants of the replaced material can be preserved as euhedral, deeply embayed outlines or within internally zoned growth bands that entrain inclusions of dolostone and anhydrite. Poikilotopically enclosed remnants of anhydrite in celestite prisms with lenticular outlines show simultaneous extinction in thin section, possibly indicating that at the time of celestite replacement the gypsum was a single crystal and not a felted anhydrite mat. Alternatively, these lenticular crystals may be after axe-head anhydrite, implying a possibly later origin for at least some of the CaSO_4 than argued by Carlson. Other nodular and laminar celestite pseudomorphs display relict chickenwire and enterolithic structures indicating a primary anhydrite parentage.

Early, almost syndepositional, replacement of CaSO_4 nodules by celestite occurred in both the vadose and the active phreatic zone of the evaporitic Silurian Steinsfjord Formation of the Oslo Region, Norway (Figure 7.65; Olausson, 1981). Marl and carbonate host sediments were deposited in supratidal, intertidal, and restricted subtidal environments. Celestite oc-

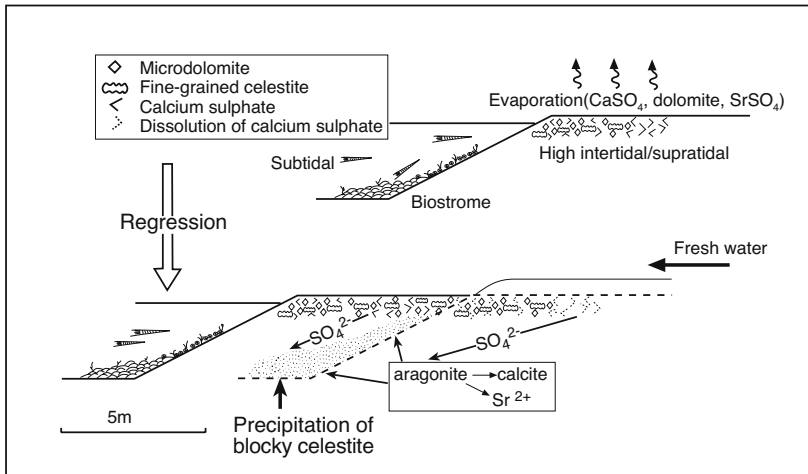


Figure 7.65. Formation of early celestite replacement in the Brattstad Member of the Steinsfjord Formation, Norway. Strontium is derived from freshwater leaching of anhydrite and aragonite (after Olausen, 1981).

curs in two distinct textural associations within these peritidal sediments: 1) as aggregates of tiny celestite crystals in nodular dolomicrites of the high intertidal facies, or 2) as anhedral or euhedral prismatic crystals infilling intrapores and interpores in the low intertidal to subtidal facies. Celestite is thought to have precipitated from SO_4 -enriched porewaters via the solution of calcium sulphate. Solution occurred early during evaporitic mudflat progradation as it was flushed by land derived meteoric waters (Figure 7.65). Released sulphate then reacted with strontium generated by an aragonite to dolomicrite transformation within the high intertidal and an aragonite to calcite transformation in the low intertidal-subtidal.

A similar progradational hydrology is documented in fracture-filling cements at La Tossa reef near Igualada, NE Spain, but in this case it was driven by a meteoric hydrology that continued to focus Sr flow well after the time of gypsum accumulation (Taberner et al., 2002). Fissure cements in other Eocene reefs along the same basin margin, such as Calders reef, tend to be dominated by baryte with only minor celestite. All reefs in the basin grew atop delta-lobe sandstones and prodelta marls, which at La Tossa, but not Calders reef, are overlain by Upper Eocene evaporites and hypersaline carbonates (Figure 7.66a). Stable isotopic analyses of all reef carbonates indicate meteoric recharge was responsible for aragonite stabilization and calcite cementation.

Celestite precipitation at La Tossa began as reef stabilization occurred in early burial. Strontium needed for celestite precipitation was partly derived in situ from dissolution of aragonite corals in the reef and more basinal counterparts. However,

$^{87}\text{Sr}/^{86}\text{Sr}$ data also suggest that Sr at La Tossa was also derived from dissolution of the overlying nearby evaporites (Figure 7.66b; Taberner et al., 2002). As the reef became lithified and stabilized, early burial fluid flow was increasingly focused in fractures and the cavities that linked them. The amount of residual strontium released from aragonite dissolution and recrystallization would have built up to supersaturated levels in the remaining interstitial fluids in the fractures.

^{18}O isotopic data suggest that local meteoric waters at La Tossa (a celestite-rich area) were enriched in Sr compared with those responsible for stabilization in other reefs in the area

where fracture-filling cements are richer in baryte, with lesser celestite (Figure 7.66b). At Calders, as in the La Tossa reef, meteoric cementation was completed before sulphate (baryte and minor celestite) cements precipitated in fractures and dissolution cavities. Calders reef is directly overlain by fluviodeltaic facies, related to the progradation of the St Llorenç del Munt fan-delta and so were susceptible to groundwater invasion immediately after deposition (Figure 7.66a). Baryte may have formed in preference to celestite as a result of more efficient flushing of Sr from Calders reef before sulphate authigenesis.

Relatively low $\delta^{34}\text{S}$ and $\delta^{34}\text{S}$ enrichment ratios show that celestite at La Tossa reef formed from residual sulphate in pore waters after bacterial sulphate reduction. Taken together they also imply that there was a prior episode of sulphate recycling at La Tossa. Meteoric water reaching the La Tossa reef and nearby basinal areas was most probably charged with SO_4 from the dissolution of nearby younger Upper Eocene marine evaporites. This sulphate-rich groundwater, combined with organic matter present in the sediments, fuelled bacterial sulphate reduction in the meteoric palaeoaquifer (Figure 7.66a). A progressive build-up of SO_4 and Sr concentrations occurred, it became relatively more important in time and drove ongoing celestite precipitation as more and more evaporites were dissolved.

In the other reefs (Calders Reef) a similar ongoing post stabilization source for Sr from dissolving gypsum was not present and so the volumes of celestite cement in their fractures are less. Furthermore, meteoric recharge at La Tossa post-dated the 34 Ma (Upper Eocene) time of evaporite deposition. Reef complexes in other parts of the same basin (e.g. Calders Reef)

were stabilized by direct contact with waters from the deltaic wedge well before the time of any evaporite formation.

One of the most impressive examples of celestite precipitated in an active phreatic hydrology at a gypsum-limestone boundary is the karst-associated celestite mineralization of Upper Permian successions in the Karstryggen Formation, central East Greenland (Scholle et al., 1990). With an area of 80 km² and a potential resource of 25-50 tonnes at a grade of 50-60% and local high grade zones of more than 90% celestite it constitutes one of the world's largest strontium deposits. It formed as a replacement of the margins of a pre-existing gypsum body that had precipitated in one of several small structurally-controlled evaporite basins along the edge of a larger marine embayment. Celestite replaces both carbonate and evaporite minerals, as well as forming a passive void infill in pre-existing karst. The

timing of celestite emplacement at the boundary of the gypsum is not well constrained. The sulphate came from the dissolution of calcium sulphate, while the isotopic values indicate the strontium-rich waters came from the deep meteoric or compactional flushing of underlying red beds.

Not all evaporite-hosted celestite requires flushing of the edge of a sulphate bed by meteoric hydrologies. Celestite precipitating waters can also come from mixing of waters sourced in the burial dewatering of hydrated salts. Paleokarst cavities in the Lower Werra Anhydrite (Zechstein) of northern Poland are usually filled by bluish semitransparent anhydrite and more rarely by celestite, polyhalite, halite, and carbonate (Hryniv and Peryt, 2003). In small karst cavities (a few centimetres across), rims of rod-like anhydrite crystals arranged in narrow bundles line the fissures, with the inner part of the cavity filled

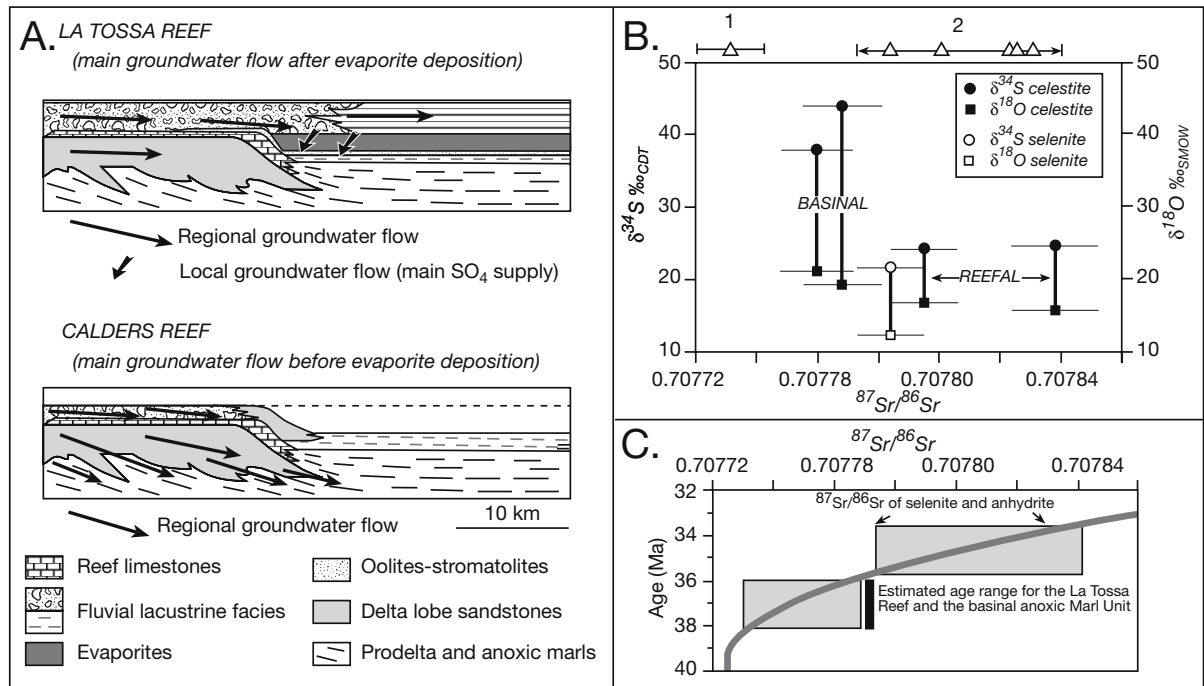


Figure 7.66. Celestite in the Eocene La Tossa and Calders reefs, Spain (after Taberner et al., 2002). A) Early diagenetic paleohydrology determined for the basin margin La Tossa reef at Igualada, compared with the interpreted flow system at Calders reef. Arrows indicate the direction of fluid flow. The reef at Calders was flushed by lateral groundwater flow before evaporite deposition, whereas the major meteoric influence at La Tossa, Igualada, occurred after evaporite deposition and featured a local ongoing meteoric flow system that leached SO₄ and Sr from basinal evaporites. B) Combined δ³⁴S and δ¹⁸O – ⁸⁷Sr/⁸⁶Sr cross-plot for celestite samples filling cavities in La Tossa reef and basinal sections. Isotopic ratios for the marginal selenitic gypsum are also plotted. The strontium isotopic composition are plotted as open triangles for stage 2 (meteoric-stabilisation) calcite cement from the reef (1) and the range of ⁸⁷Sr/⁸⁶Sr values for the Upper Eocene Lower Anhydrite Unit and selenitic gypsum (2). Celestite cements in reef fractures show δ³⁴S, δ¹⁸O and ⁸⁷Sr/⁸⁶Sr ranges that are closer to those of the Upper Eocene evaporites, whereas those celestites that depart from these values are from the basinal samples and later stage calcite cements in the reef. C) Temporal variation in marine ⁸⁷Sr/⁸⁶Sr values. Except for near the inflection point, the errors in age estimates are incorporated in the thickness of the line. The measured ⁸⁷Sr/⁸⁶Sr values from the evaporites give an age of 34 ± 0.9 Ma for their formation. The age of the reef is constrained by the stratigraphic relationships with the evaporites and by comparison with outcropping reefs from the eastern margin of the basin.

by a mosaic aggregate of short prismatic crystals of anhydrite and celestite, as well as coarse irregular anhydrite. Celestite crystals and fan-shaped aggregates, as well as spherulites of anhydrite, are rare in the smaller cavities and fissures. In bigger cavities (some ten centimetres across), multiple zones of fibrous anhydrite are arranged in different directions in the middle part of the cavity fill. The innermost parts of the larger karst cavities still remain as hollow in some cases, with the cavity walls encrusted by coarse, well-developed crystals of anhydrite and celestite.

Karst cavities in the Lower Werra Anhydrite developed in the subsurface by dissolution of CaSO_4 strata in halite-rich intervals flushed by gypsum dehydration waters. During gypsum dehydration, dissolution of halite increased the sodium chloride content of the solution and thus the solubility of calcium sulphate (Figure 2.11b). Dissolved calcium sulphate was leached by diffusion and/or downward flow in the interstitial spaces, and the minerals in karst cavities precipitated from the same solutions as solutions became oversaturated. The work of Hryniv and Peryt (2003) shows that karst in sulphate deposits can develop non-telogenetically during ongoing burial and dewatering in a system without uplift and/or near-surface meteoric flushing.

So far, we have considered celestite as tied to direct dissolution of former bedded and nodular calcium sulphates, typically with nodular and enterolithic textures that indicate the evaporite association. But there are also laterally extensive stratiform and layered celestine deposits that are sufficiently rich in strontium to be mineable and hosted in epeiric carbonates. De Brodtkorb et al. (1982) described such an economic celestite-baryte deposit in Early Cretaceous strata from the extra-Andean region of Neuquen, west central Argentina. The ores are located in the sub-Andean Mesozoic belt and show a conspicuous stratabound character with an aerial extent that closely relates to the presence of regionally extensive platform sulphates. Isotopic $^{87}\text{Sr}/^{86}\text{Sr}$ data confirm an evaporitic origin for this celestite (Table 7.13). Host sediments were deposited during the transition to an epicontinental marine shelf environment from an earlier saltern. The celestite is always hosted in saline and hypersaline facies as these beds were the source of the sulphate. Celestite forms as either syngenetic nodular beds with texture similar to those described earlier, or as more epigenetic stratabound ores composed of “in situ” celestite with texture showing stalactite growth and cavity infilling in its carbonate host, possibly as replacements of bedded saltern sulphates. There are also epigenetic vein-type ores. Open fill textures are interpreted as burial phreatic, precipitated by mesogenetic Ba-enriched solutions dripping into gas filled

dissolution cavities in a previously karstified (?bathypheatic) sulphate evaporite and carbonate host. Some have argued these enigmatic stratiform ores are primary seawater-derived precipitates, others see their origin as mesogenetic replacements of bedded calcium sulphate salterns.

Many stratiform celestites, including the Argentinian ores, have crystals encasing inclusions of solid hydrocarbons and textures showing they precipitated in association with saddle dolomite, burial anhydrite and metal sulphides. Hanor (2004) documents the worldwide association of such stratiform sediment-hosted celestite with epeiric carbonate platforms (Table 7.13). He notes their association with bedded platform sulphates and also points out that the largest known sedimentary celestine occurrences, each with several million metric tons of SrSO_4 , cannot be readily explained as primary precipitates or near-surface meteoric replacements of nodular sulphate evaporites. The largest deposits, as in South America and Greenland, tend to occur as epigenetic replacements in carbonate and evaporite hosts within epeiric platforms that range in age from Silurian to early Pliocene. There is variable evidence of associated hydrothermal activity in these deposits, and Sr isotopes typically have a more radiogenic signature than the prevailing seawater of the time (Table 7.13). Hanor argues the key to explaining the origin of these massive sediment-hosted celestites lies in determining why celestite is the replacement phase in these deposits and not baryte (BaSO_4), which is orders of magnitude less soluble.

Hanor (op. cit.) concludes that stratiform celestite hosted in epicontinental platforms did not form syndepositionally from Sr-enriched brines created by the evaporation of seawater. Sr is removed from concentrating marine brine during the halite stage of evaporation as a dispersed sulphate phase and not as precipitate bedded celestite. The association of large stratiform celestine deposits with marine platform carbonate–evaporite sequences most likely reflects, at least in part, the significant difference in the geochemical behaviour of Sr and Ba during mesogenetic diagenesis.

Concentrations of Sr in subsurface sedimentary fluids are buffered by silicate–carbonate mineral assemblages. Concentration of Sr in solution in modern subsurface waters increases significantly with increasing salinity (Figure 8.27). The concentration of Ba, in contrast, is controlled by equilibrium with the baryte solid phase and is inversely related to the concentration of dissolved sulphate in subsurface fluids (Figure 7.67a; Hanor, 2004). Basinal fluids having the highest Sr/Ba ratios are also the most saline and have moderately high levels of sulphate

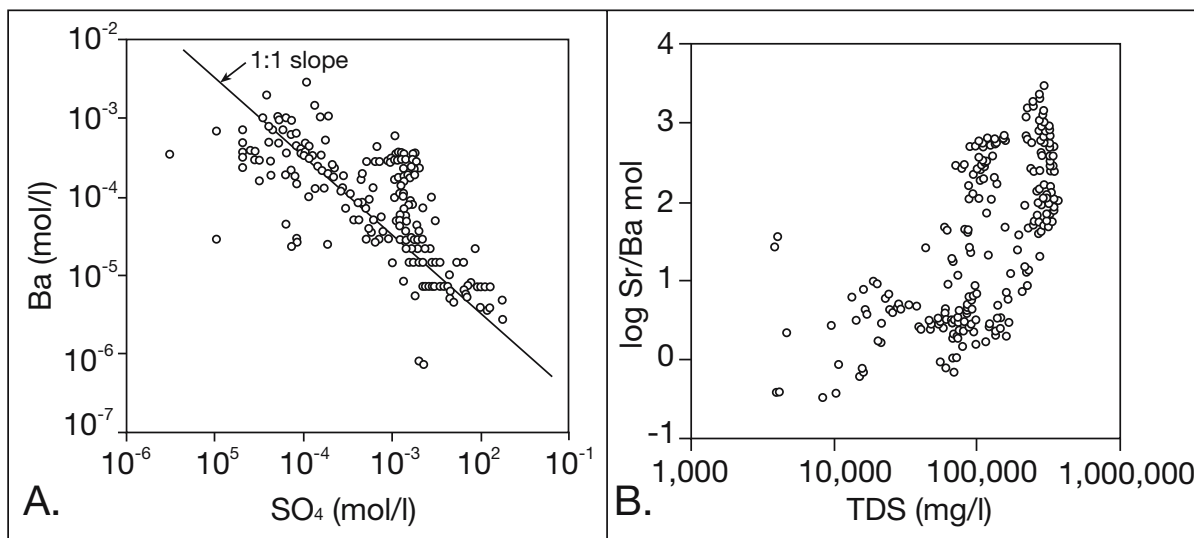


Figure 7.67. Ba in subsurface basinal brines (after Hanor, 2004). A) Variation in dissolved Ba versus dissolved sulphate in basinal brines. B) Variation in Sr/Ba ratio versus the salinity of basinal brines. See Figure 8.27 for Sr trend.

(Figure 7.67b). Thus hypersaline mesogenetic brines flushing through a carbonate platform will be more likely to be saturated with celestine rather than baryte. The precursors to such waters were produced in hypersaline pans and salterns by the evaporation of seawater. As these brines reflux into underlying or laterally adjacent sediments, they leach substantial amounts of Sr as they attempt to achieve chemical equilibrium with their host sediments. In contrast barium concentrations in subsurface reflux brines are kept relatively low by the presence of dissolved sulphate. Precipitation of widespread mesogenetic celestine occurs where these diagenetically altered reflux fluids come into contact with beds containing calcium sulphate minerals and/or sulphate-rich waters. Thus Hanor argues, the stratiform celestite ores of the world are not recrystallised primary precipitates or derived in meteoric mixing zones. They are the result of deeply circulating hypersaline brines moving through an anhydritic epeiric platform under a hydrological drive that is tied to platform restriction and creation of dense reflux brine. The elevated Sr does not come from the parent connate water, but from rock-fluid (brine) interactions with buried platform carbonates. Hydrocarbons are often mobile in the same sediments at the same time.

Not all celestite - calcium sulphate associations are hosted in sediments. An unusual late-stage celestite is intimately associated with hydrothermal $CaSO_4$ (now gypsum) in the Asaka gypsum mine (Koriyama City, Japan). Celestite occurs on the sides of fibrous (satinspar) gypsum in the mine area. The satinspar indicates telogenetic alteration. The celestite is interpreted by Matsubara et al. (1992) as a hydration product

of strontian anhydrite (SrO up to 0.94 wt %), which occurs in the same area. The hydration is very late, associated with uplift and meteorically-driven conversion of strontian anhydrite to gypsum, where the $SrSO_4$ molecule remains intact during the conversion and eventually crystallises as celestite. Warren (1999; Chapter 9) discusses the worldwide occurrence of hydrothermal anhydrites and their association with high-temperature sulphide mineralisation.

Fluorite as an indicator?

Fluorite (CaF_2) and baryte ($BaSO_4$) are not uncommon as hydrothermal phases in mineralised sedimentary carbonates. Compared to sediment-hosted celestite, the range of mesogenetic associations is more cosmopolitan and their appearance in a carbonate platform host typically reflects the carbonate's high susceptibility to replacement, especially when flushed by somewhat acidic, cooling hydrothermal and basinal fluids.

According to Richardson and Holland (1979), the solubility of fluorite in NaCl solutions increases with increasing temperature at all ionic strengths up to about $100^\circ C$ (Figure 7.68). At NaCl concentrations above 1.0 M, the solubility of fluorite increases continuously above $100^\circ C$, and it increases also with increasing $CaCl_2$ and $MgCl_2$ concentrations in the NaCl dominant solutions. According to Munoz et al., 1999, this means that most nonmagmatic fluorite-carrying basinal waters in a sedimentary basin are derived in part from interactions with dissolving evaporites. Evaporite-derived fluorine can even be involved in the formation of rubies (gem corundum) in meta-

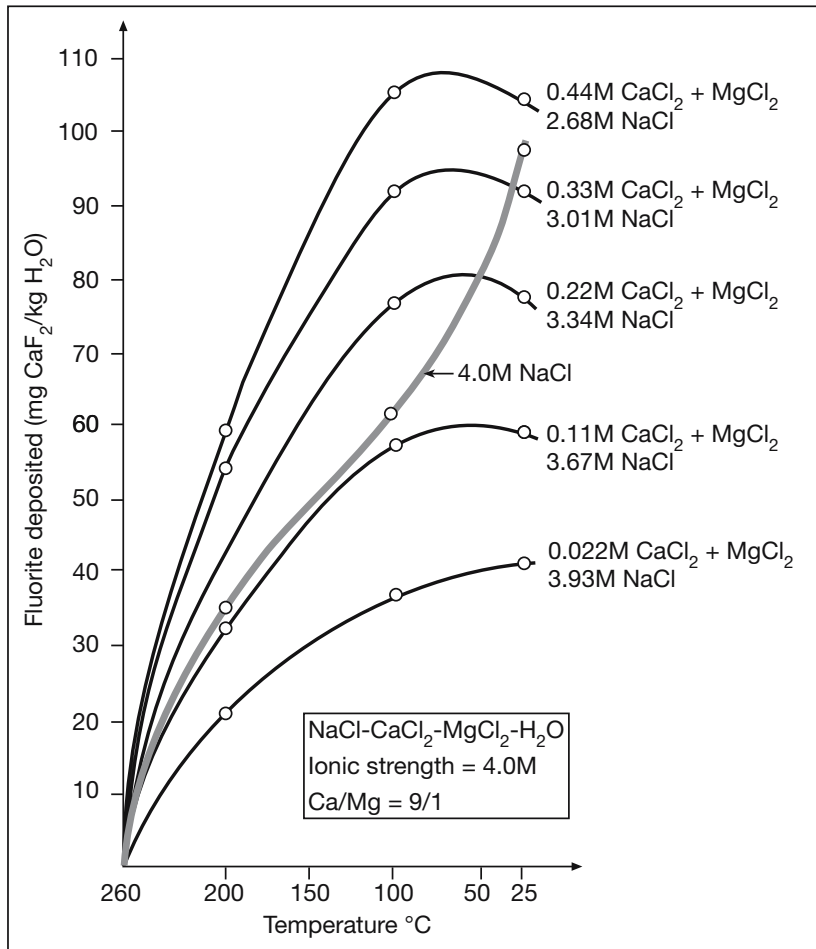


Figure 7.68. Quantity of fluorite precipitated by cooling of $\text{NaCl} \pm \text{CaCl}_2 \pm \text{MgCl}_2 \pm \text{H}_2\text{O}$ solutions with Ca/Mg ratio of 9:1 and an ionic strength of 4 M from 260° to 25°C (after Richardson and Holland, 1979).

evaporites (Garnier et al., 2005). The interaction allows such hydrothermally circulated waters (high salinity and CaCl_2 -bearing) to attain the elevated levels of dissolved fluorine required to precipitate significant volumes of fluorite during subsequent brine cooling. Elevated salinities in the subsurface can come from evaporite dissolution or from brine reflux. Much of the nonmagmatic fluorite dissolved in these saline brines is sourced by subsurface flushing of organic-rich black shales.

For example, fluorite is a minor late stage mesogenetic cement in Devonian carbonates in the Keg River Formation, Canada (Aulstead and Spencer, 1985). The fluorite was carried to the site of precipitation by rising and cooling basinal brines that had flushed deeply buried bedded evaporites and organic laminites. Similar late-stage fluorite cements in voids and fractures have precipitated from structurally-focused basinal brine flows in the

Jurassic reefal carbonates in Zaghuan Province in north-eastern Tunisia, in the Smackover Formation of the Gulf of Mexico, in the Upper Permian Karstryggen Formation of Greenland and in many other buried and faulted carbonate platforms subject to metal sulphide and saddle dolomite emplacement (Souissi et al., 1997). All these fluorites precipitated from highly saline brines in deep halokinetic settings where mesogenetic salt dissolution dominates. Likewise, the isotopic signatures of authigenic fluorites in a number of European fluorspar deposits show the supplying hydrothermal waters were sourced in, or carried by, brines from dissolving or tectonically juxtaposed evaporites. Examples include vein fluorites (Pb-Zn-F) associated with the Permian Haselgebirge evaporites in the Austrian Alps (Göttinger and Grum, 1992) and massive fluorites in veins that crosscut Cambro-Ordovician clastics in the southwestern Massif of Albigeois, France (Munoz et al., 1999). There is also a halokinetic/hydrocarbon/thrust link to crosscutting fluorite veins in Jurassic carbonates of the Koh-i-Maran, Baluchistan in the North Kirthar Range, Pakistan (Guilhaumou et al., 2000). Clearly, the dissolution of deeply buried halite

(both bedded and diapiric) can supply the saline chloride brine needed to act as a fluoride and metal carrier in nonmagmatic sedimentary systems (Warren, 2000b).

Fluorite also forms a widespread, but volumetrically minor, early diagenetic and even syndepositional authigenic mineral phase in some evaporitic matrices where its precipitation may even be related to solar concentration of a surface brine. For example, fluorite has precipitated as ooids and pellets in a 40 cm thick tuff bed in the Gila Conglomerate of New Mexico (Sheppard and Mumpton, 1984). Fluorite also occurs as sparse isotropic euhedral cubes (50–200 μm diameter) within primary gypsum nodules at depths of 235–240 m below the present land surface in Eocene carbonate mudstones of Florida. Celestite also occurs in the same sediment. Cook et al. (1985) argued that the

Florida fluorite was syndeositional with the precipitation of gypsum in the capillary zone of an Eocene sabkha mudflat. If so, it was ultimately derived by the evaporative concentration of normal seawater. Additional fluoride in the parent pore waters may have been derived by fluvial transport of salts weathered from Appalachian volcanics.

Cook et al.'s conclusion is perhaps supported by the work of Kazakov and Sokolova (1950) who documented sedimentary fluorite in various marine carbonates/evaporites in Russia in hosts that range in age from Cambrian to Cretaceous. In related laboratory experiments they observed that fluorite can precipitate from seawater brines concentrated three to four times by volume, especially if an additional (fluvial or volcanic) source of dissolved fluoride was available in the depositional setting.

In a similar fashion, Sheppard and Mumpton (1984) explain the primary precipitation of early diagenetic fluorite using the analogy of high fluoride alkaline lakes in the East African Rift, such as Lake Magadi, Lake Natron and Lake Manyara (Table 4.3). Subsequent to Surdam and Eugster's (1976) documentation of fluorite as a common authigenic phase in Pleistocene sediments of the Magadi Basin, Icole et al. (1990) documented stromatolitic layers in lower Pleistocene lacustrine beds along the western edge of Lake Natron, Tanzania that are mainly composed of fluorite rather than calcium carbonate. Without doubt these are early rather than burial diagenetic precipitates. Moreover, Pleistocene fluorite is replaced by dolomite in the uppermost parts of some of these layers, but this replacement still preserves the original sedimentary texture. Fluorite is also reported in sediments of Lake Bogoria, Kenya, in an interval that also contains sodium silicate gels (magadiite; Renaut and Tiercelin, 1994). There is even a palaeobiological response to the high levels of fluorine in saline lake waters in the rift valley. Many fossil fish, preserved in the Plio-Pleistocene phosphoric lacustrine sediments of Lake Manyara, are hyperostitic (enlarged and fused bone structures), a biological response to elevated fluorine levels in the lake waters (Schlüter and Kohring, 2002).

Crocker (1979) proposed that granular blockspars (fluorite) ore in the Proterozoic Transvaal Supergroup of South Africa indicates primary syndeositional endogenic fluorite mineralisation and is a special precipitative stage tied to Precambrian dolomite evaporite facies. Rouchy et al. (1987) documented an association between fluorite, native sulphur and Visean (Carboniferous) evaporites. In an earlier paper, Amieux (1980) showed fluorite was a characteristic diagenetic stage in the black shale to evaporite transitional facies within the Ludian (Lower

Oligocene) sediments of the Mormoiron Basin, Vaucluse, southeastern France. There the major fluorite precipitation phase postdates major dolomitisation and gypsification but precedes celestite and silicification.

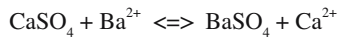
But, fluorite is not solely sourced or carried in evaporite brines, nor deposited only in a sedimentary host. That is just the focus of fluorite discussion in this chapter. Fluorite can be found in fissure veins and stockworks in granitic rocks, greisens, pegmatitic carbonatites, metamorphics, and igneous rocks that include volcanic sublimates (Hodge, 1986). These are not tied to an evaporite source. Nor are the vein and stratified (manto) fluorite deposits that are associated worldwide with areas of rifting and faulting where fluoride-rich hydrothermal fluids migrate up from the lower crust or mantle to replace carbonate hosts (Van Alstine, 1976).

Baryte as an indicator?

Baryte, like fluorite, is a widespread hydrothermal precipitate or replacement. In the sedimentary realm it occurs in a wide variety of settings ranging from lakes and soils to cold seeps and vents on the deep open ocean floor. Its occurrence is not specific to evaporitic sequences, but it is a commonplace replacement/cement in evaporitic hosts. This is especially true in those parts of a basin where evaporite-focused fluid flow brings together hot Ba-rich basinal brines (Cl-rich waters flushing and leaching arkoses (alkali feldspars and micas), redbeds, volcanics and volcanoclastics) and sulphate-rich waters from dissolving sulphate evaporites (anhydrite beds, halokinetic basal anhydrites, allochthon décollements, dissolution residues and diapir caprocks).

Economically, baryte's occurrence is mostly as gangue in various hydrothermal beds and veins entraining metalliferous ores (Warren, 2000b). Baryte also forms stratiform layers, veins, nodules and cavity fills in sulphate-rich sediments, especially in the early Archean, and is also a commonplace precipitate in black smokers and volcanic hosted massive sulphide (VHMS) deposits. In such cases much of the sulphate is nonevaporitic, it comes to the precipitation site either as sulphide in solution which is oxidised to sulphate at the site of deposition or as sulphate ions carried by hydrothermally circulated seawater. Baryte is also a widespread precipitate in deepwater cold seeps, mud volcanoes, springs and brine lakes on the supra-allochthon floor of the Gulf of Mexico (Fu et al., 1994) and their Neogene caprock counterparts (Saunders and Thomas, 1996). In the following section we will focus only on barytes with an obvious evaporite association.

Baryte can directly replace sedimentary gypsum or anhydrite throughout a rock layers diagenetic history. At 25°C and 1 bar, the value of the equilibrium constant, K , for the replacement reaction:



as calculated from Gibb's Free Energy values, and assuming pure solids is:

$$K = 10^{5.5} = a_{\text{Ca}^{2+}} / a_{\text{Ba}^{2+}}$$

Thus, it is thermodynamically feasible for baryte to replace calcium sulphate at earth surface temperatures whenever the activity ratio of ($a_{\text{Ca}^{2+}}/a_{\text{Ba}^{2+}}$) is less than $10^{5.5}$, a condition met in many subsurface waters (Mossman and Brown, 1986). At more elevated temperatures the limiting activity ratio is even less due to the retrograde solubility of anhydrite.

Loosely arranged platy crystals of baryte form pseudomorphs after lenticular gypsum in Quaternary soils from central Australia (Sullivan and Koppi, 1993). In older sedimentary deposits, evaporitic baryte typically replaces nodular forms with irregular and coalesced outlines reminiscent of anhydrite or gypsum, or forms stratiform layers. In several such cases, isotopic analysis indicates the sulphate in the nodules and layers was remobilised from a calcium sulphate precursor such as; caprock sulphate (von Gehlen et al., 1962), sedimentary gypsum (Kesler et al., 1988; Parafinuk, 1989), or anhydrite-rich evaporites (Mossman and Brown, 1986; Frimmel and Papesch, 1990).

Stratiform baryte is often found as a late stage precipitate in association with pervasive ferroan carbonate haloes in the alteration zones around growth faults and salt welds in halokinetic provinces. These haloes tend to define zones where escaping Ba-rich hypersaline basinal waters are flowing out of the basin via halokinetically-focused fault conduits, often feeding stromatolitic baryte seeps on the seafloor (Warren, 1999, 2000b). Sometimes these iron- and barium-rich ascending fluids interact with sulphate present in anhydrite or gypsum nodules, other times with sulphate beds or dissolution residues or with seawater sulphate. Modern examples of salt focused brine outflow in halokinetic provinces tend to occur in relatively deepwater muddy hosts. This is where the most active salt allochthon flow occurs, as on the continental slope and rise of the Gulf of Mexico or the tectonic high of the Mediterranean ridges. Because brine lakes are commonplace in such settings, it precipitates baryte in association with organic- and pyrite-rich laminites under the influence of sulphate reducing bacteria (Chapter 9).

Baryte in cores from the Magnet Cove baryte mine region, Nova Scotia, show a wide variety of massive stratiform to nodular textures. Isolated light coloured baryte nodules, typically hosted in a matrix of ferroan dolomite, show complete gradations from chickenwire to enterolithic and are interpreted as a direct replacement of precursor nodular anhydrite hosted in intertidal and supratidal platform carbonates (Mossman and Brown, 1986)). The mine itself exploited a lenticular to stratiform mass of baryte, not nodules (Figure 7.69a; Boyle, 1962). Unfortunately the Magnet Cove Baryte Mine ceased operations 20 years ago and the mine pit and shaft workings are now flooded. Boyle described the structure of the deposit as “exceedingly complex.” The region is marked by two major sets of faults oriented east-west and northwest-southeast. At the now abandoned Walton deposit the dominant feature is an east-west fault zone in the footwall of the baryte mass that joins a northwest fault that lies close to the hanging wall of the baryte mass.

Much of the baryte ore in the Magnet Cove deposit is associated with the Pembroke Formation (Figure 7.69a). Regionally the Pembroke Formation is a complex multi-origin breccia intimately associated with halokinesis and base metal mineralisation and regionally it is tied to former salt and thrust welds (Lavoie et al., 1998; Warren, 2000b). Faults in the Magnet Cove Mine are pre-ore and constitute brecciated intervals over several metres wide. Post-ore movement also brecciated the baryte and sulphides. The age of the faulting is probably post-Triassic. The ore-hosting sequence is the outcropping remnant of a halokinetic and allochthonous evaporite zone at the top of the Horton Group and it lies along the regional salt weld of the Ainslie Detachment. The likelihood of halokinetically focused extensional faults carrying Ba-rich basinal fluids into sulphate-rich horizons was not considered in the published literature on the Magnet Cove mine. But all the work on the mine geology, and its mineralogy, was published before notions of salt allochthons, rauhacke and burial anhydrite existed.

Similar halokinetic fault-focused salt welds define the position of the massive baryte deposit in the Neoproterozoic Oraparinna diapir and other baryte occurrences associated with halokinetic structures in the Flinders Ranges of South Australia (pers. obs.). The similarities between Magnet Cove and Oraparinna in both structural style and position atop a halokinetic breccia are obvious (Figure 7.69b). Unlike Magnet Cove, the baryte occurrence in the Oraparinna diapir was recognised as a halokinetic association (Dalgarno and Johnson, 1968). The ore at Oraparinna occurs in 1-2 metre wide extensional fracture fills. Like Magnet Cove, the detailed evolution of the Oraparinna diapir is yet to be fully documented in the light of modern ideas of salt

allochthons and salt-cored thrusts. Suprasalt minibasins can be seen to separate the various diapir outcrops throughout the Flinders Ranges and clearly illustrate the evolution of an active extensional diapiric province into a subsequent compressional regime. As in Magnet Cove, a geological map of the structure shows a distribution of facies that reflect the strong influence of diapiric and subsequent thrust breccia (rauhwacke) on the adjacent facies and faults (Figure 7.69b). Salt flow and passive diapirism controlled both the position of a collapse graben atop the Oraparinna diapir during its “falling diapir” stage and focused the subsequent compression of the same succession. What is yet to be studied in the Oraparinna Baryte Mine is the timing of baryte emplacement relative to salt dissolution and faulting in this succession.

A likely younger analog for baryte emplacement about salt structures is the fracture fills atop the Machar diapir in the North Sea (Figure 10.47). Many individual fractures host multiple generations of carbonate, baryte and fluorite growth (Doran et al., 2004). Fluid-inclusions in the fracture-fills show maximum salinities (22 wt% NaCl eq.), suggesting that fluids had dissolved salt from the diapir during their ascent. Maximum fluid-inclusion temperatures (150°C) from wells spanning the crest and flank of the Machar structure, are much hotter than expected for present depths of 1900 to 2800 metres. Carbon isotope signatures of the fracture-filling calcites range from +2 to +7 $^{13}\text{C}_{\text{PDB}} \text{‰}$ and exceed those of tightly constrained chalk matrix 0 to +3 $^{13}\text{C}_{\text{PDB}} \text{‰}$. Thus at least some of the carbon was derived externally to the chalk. Oxygen isotopes from fracture filling calcites (16 to 25 $^{18}\text{O}_{\text{SMOW}} \text{‰}$) are depleted relative to chalk matrix values (24 to 29 $^{18}\text{O}_{\text{SMOW}} \text{‰}$). The combined data sets indicate that fracture-filling material could not have formed from lo-

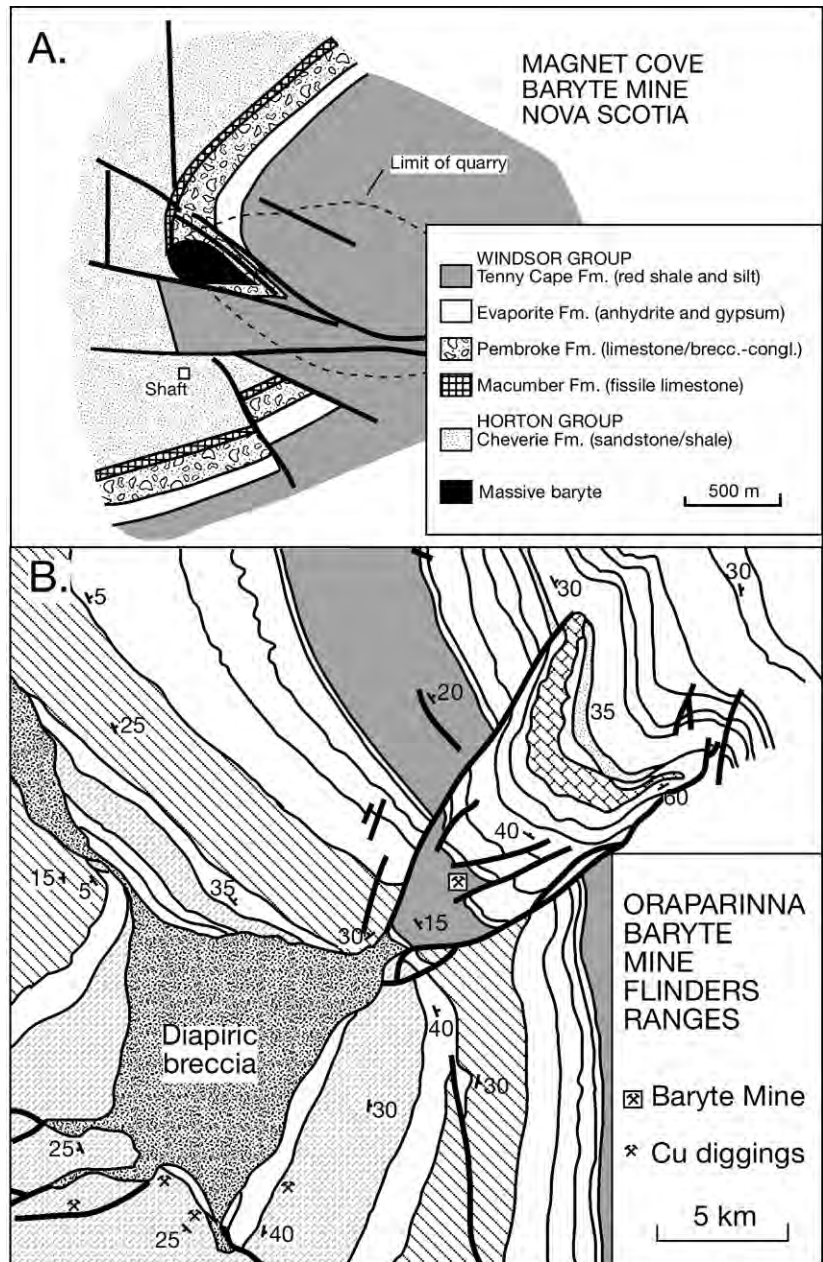


Figure 7.69. Massive and vein-fill baryte deposited via halokinetic focusing. A) Geology of the Carboniferous halokinetic section in the vicinity of the Magnet Cove Baryte Mine, Nova Scotia (after Boyle, 1962). B) Oraparinna Baryte Mine located in the compressed zone of an original falling diapir (Neoproterozoic Oraparinna Diapir) Flinders Ranges, South Australia (Redrafted from regional geological map of Dalgarno and Johnson, 1966; see Figure 7.23 for regional setting of the Oraparinna Diapir).

cal chalk matrix pore-fluids. The likely explanation is pulsed expulsion of hot saline and hydrocarbon-bearing fluids from geopressed sandstones in the adjacent rim syncline that are then cemented on cooling into fractures at shallow depths.

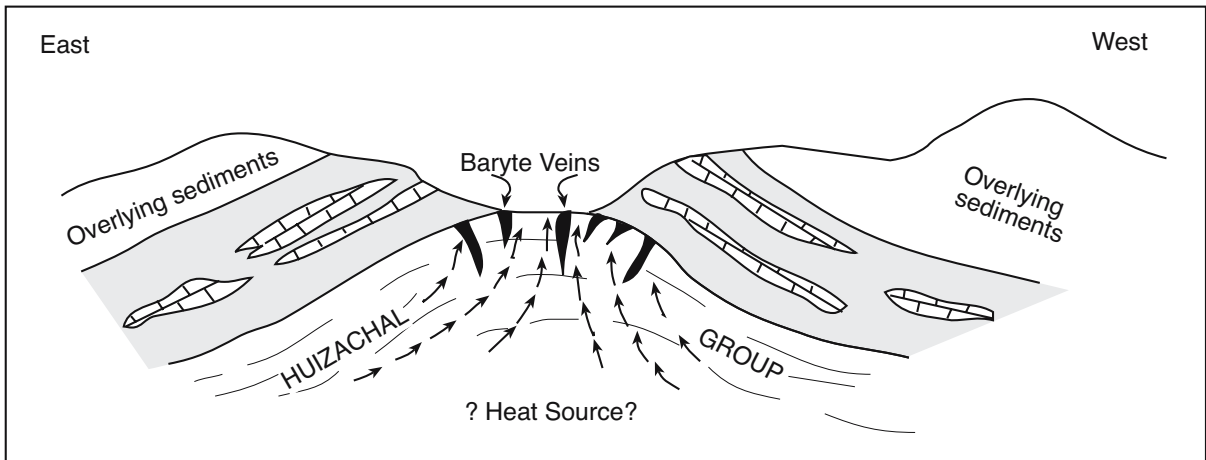


Figure 7.70. Highly schematic E-W cross section through the Galeana district showing localisation of baryte veins at the contact with the Huizachal red beds, directly beneath the Olvido gypsum (grey). Baryte formed as ascending Ba-rich waters ponded beneath the gypsiferous residues (caprocks to allochthonous salt) of the Olvido Fm. (modified from Kesler et al., 1988).

A similar set of hypogene chloride-rich waters flowing along faults probably controlled the formation of mined willemite (Zn-oxide ore) in Cambrian ooid grainstones and archeocyathid mounds in the vicinity of the Beltana diapir in the Flinders Ranges, situated some 80 km northwest of the Oraparinna diapir (Groves et al., 2003). There the ore was first emplaced during a series of Cambro-Ordovician compressional events that reactivated salt numerous diapirs and salt flows, which were first emplaced during Neoproterozoic extension and loading.

Yet another halokinetically focused baryte association is documented in the Galeana Baryte District of Mexico. Gypsum residues of the evaporitic Olvido Formation (Upper Jurassic) form an anticlinal trap, seal and sulphate source to barium carried by basinal waters which had flushed the underlying redbeds of the Huizachal Group. Baryte occurs mostly as monomineralic veins and lenses in a limestone matrix along this contact (Figure 7.70; Kesler et al., 1988; Conklin, 1974). Halites and anhydrites of the halokinetic Olvido Formation created the seal and the faulted structures that focused ore precipitates.

The Galeana district now lies at the western margin of the Sierra Madre Oriental in southern Nuevo Leon, Mexico, and it has been one of the leading BaSO_4 producers for the country. Ore-grade baryte fills reactivated steeply dipping ($50\text{--}88^\circ$ NW) fractures striking $\text{N}40\text{--}50^\circ\text{E}$ and, to a lesser extent, steeply dipping ($60\text{--}85^\circ$ SW) fractures striking $\text{N}60\text{--}80^\circ\text{W}$, all formed at the crest of the San Marcos anticline (Figure 7.70). Massive baryte veins also carry up to 10 wt% SrSO_4 . Baryte formed when ascending barium-rich basinal brines ponded beneath, and partially dissolved, the relatively impervious halites of the Olvido Formation to create the anhydrite precursors to the

gypsiferous residues that now define the outcrop of the Olvido Formation in the Galeana district. After baryte precipitated subsalt, the anticlinal crest was erosionally breached and so exposed mineable baryte at the surface.

Regionally, the Olvido Formation defines the salt-cored Sabinas fold belt, which is made up of a number of salt allochthon tiers and salt-cored detachments. This fold belt is now in compression and thrust welds are common, in part in response to the Laramide orogeny. But when Ba-rich fluids were migrating it may well have been in its earlier stage of halokinetic extension (as was likely the case in the Oraparinna diapir). The spectacular salt allochthons of the La Popa basin, detailed in Chapter 6, are part of the same Sabinas fold belt and were also created by the flowing salt of the Olvido Formation.

Baryte is also a widespread authigenic phase in bedded sandstones of the Salt Wash Member in the Late Jurassic Morrison Formation on the Colorado Plateau (Breit et al., 1990). There it forms as intergranular cements, poikilotopic cements, euhedral crystals and replacements of detrital grains. Areas that contain abundant baryte in the sandstone host coincide with the extent of evaporites in the underlying halokinetic Pennsylvanian Hermosa Formation. A genetic link between the baryte and the dissolving evaporite is reinforced by similar ranges in sulphur isotope data in both lithologies ($\delta^{34}\text{S}$ range from $+8\text{‰}$ to $+14\text{‰}$). Sulphate, derived from the dissolving evaporites, is thought to have risen along faults into the Morrison Formation; a process perhaps aided by halokinetic focusing. Evidence of a fault conduit for the Ba-rich waters is further supported by $^{87}\text{Sr}/^{86}\text{Sr}$ ratios in the baryte cements, which tend to decrease with increasing distance from the supplying fault (from 0.7103

to 0.7084; Breit et al., 1990). This trend reflects the mixing of radiogenic strontium from waters ascending the faults ($^{87}\text{Sr}/^{86}\text{Sr} = 0.7100$), with strontium in waters derived by dissolution of early diagenetic carbonate cements in the sands ($^{87}\text{Sr}/^{86}\text{Sr} = 0.7080$). As the $^{87}\text{Sr}/^{86}\text{Sr}$ values along the faults exceed those in the underlying Hermosa anhydrite it is thought that radiogenic strontium was also added to the ascending waters by reactions between the rising brine and the arkosic horizons that intersect the fault conduit (Figure 10.60). These same arkosic sands are also a source of the copper in ores in similar structural settings in the nearby Lisbon Valley. A similar isotopic argument is used to show an evaporitic sulphate association for mesogenetic baryte mineralisation in the orefields of the northern Pennines (Crowley et al., 1997).

Local concretions of baryte precipitates in sandstones can create rosettes known as “sand rosettes” or “desert roses,” where the baryte acts as a poikilitic cement that encases sand grains. Such baryte is thought to have been precipitated by reactions between soluble sulphate (usually from nearby dissolved gypsum or anhydrite) and basinal waters carrying BaCl_2 . Baryte spar is a commonplace burial cement in reservoir sandstones where two basinal brines mix. The hydrodynamics of such deep mixing is often driven by tectonics, for example, the inversion tectonics

of the North Sea (later in this chapter). Oxidised pyrite can also act as a source of sulphate in subsurface waters, especially in the vicinity of dewatering organic-rich shales.

A more enigmatic but significant baryte-evaporite associations is found in early Archaean metasediments (Figure 2.31). Some of these beds constitute the oldest sediments in the world, namely the ≈ 3.46 Ga Warrawoona Formation at North Pole, Western Australia, with equivalents in South Africa. Both areas are characterised by baryte beds with obvious growth-aligned textures (Figure 7.71). Interpretations are that the baryte either pseudomorphs bottom nucleated subaqueous gypsum or that it represents a primary seafloor precipitate. The proponents of both interpretation are still involved in heated discussion (e.g. Shen and Buick, 2004 versus Runnegar et al., 2001).

Baryte can also be associated with meta-evaporite sequences. Stratabound baryte-hyalophane sulphidic orebodies, which were recently discovered at Rozna (in the Moldanubian zone of the Bohemian Massif, Czech Republic), are hosted within the high-grade metamorphosed complex (Kribek et al., 1996). The host entrains a meta-evaporitic succession and is composed of migmatitic biotite or sillimanite-biotite gneiss and amphibolite, with rare intercalations of marble, calcsilicate gneiss and lenses of coarsely crystalline anhydrite. Similar sequences were discussed in Warren (1999) in Chapter 6, which dealt with meta-evaporites.

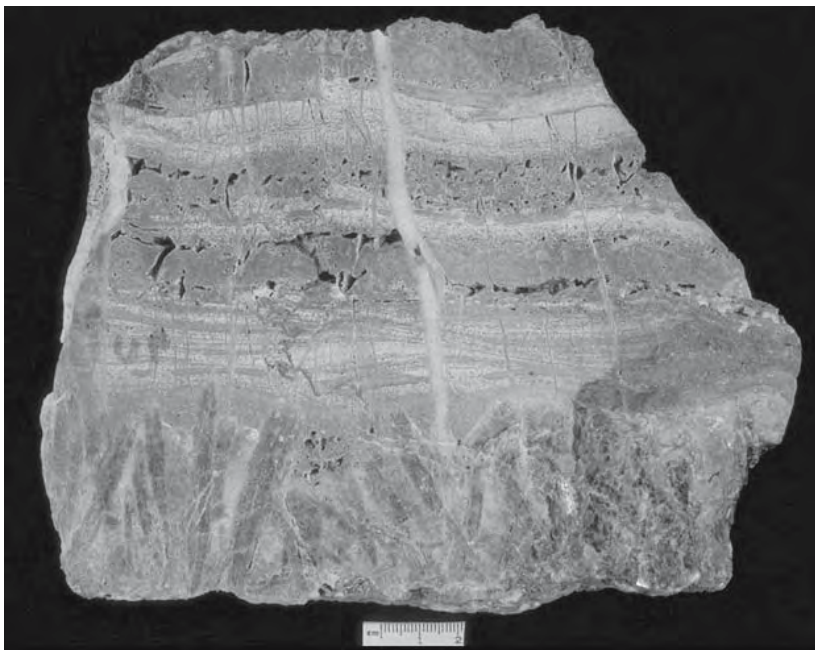


Figure 7.71. Lower third of specimen is composed of growth aligned baryte (is it a possible replacement of bottom-nucleated gypsum or, is it a primary baryte precipitate, associated in some areas with silicified marine-derived nahcolite evaporites?). The sulphate layer is overlain by current-rippled and silicified volcanoclastic sands. Sample collected from the early Archaean 3.45 Ga Warrawoona Fm. near North Pole, Western Australia.

Authigenic anhydrite as a burial salt

As we have seen, some forms of silica, calcite, dolomite, celestite, fluorite and baryte are hydrothermal precipitates that mimic the outline of their evaporite precursor. They form syndepositionally, mesogenetically and telogenetic ally, wherever waters of appropriate chemistry can cool, heat, mix or change redox state. We shall now see that evaporite salts, especially anhydrite spar, can also precipitate mesogenetically. Precipitation occurs in relatively stable subsurface waters, so crystals tend to be coarse and poikilotopic, often co-associates to late-diagenetic calcite, saddle

Occurrence and age of host	Burial anhydrite fabric and subsurface temperature at time of precipitation	Reference
Yacoraitite Fm. (Upper Cretaceous), Argentina.	Sparry anhydrite cement, containing hydrocarbon inclusions and brine, fills intergranular, mouldic and vuggy porosity in a carbonate host. Indicates anhydrite precipitated at 121-137°C from 17% equiv. wt. NaCl brine (NaCl-MgCl ₂ -Na ₂ SO ₄ -NaHCO ₃ -NaCO ₃ basinal brine).	Cesaretti, 2000
Maha Sarakham Fm. (Upper Cretaceous), NE Thailand.	Coarsely crystalline saddle dolomite rhombs float within a matrix of coarse, recrystallized anhydrite spar in the Basal Anhydrite. Isotopes indicate dolomite precipitated at temperatures ≈ 72-123°C.	El Tabakh et al., 2003
Smackover Fm. sandstones, (Upper Jurassic), Gulf of Mexico.	Anhydrite both as poikilotopic spar masses in which detrital grains are replaced and as smaller patches that have replaced single detrital grains. Precipitation temperatures >100°C. Anhydrite is a relatively late cement and postdates all other volumetrically significant authigenic phases in the sandstones, including K-feldspar, dolomite, quartz, and most calcite cements.	Dworkin and Land, 1994
Smackover Fm. dolomites, (Upper Jurassic), Gulf of Mexico.	Anhydrite spar partially replaced allochems and prebitumen calcite cements in mesogenetic pores. Solid bitumen precipitated where hydrocarbons were present. Emplaced in temperature range 100-150°C.	Heydari, 1997, 2000
Khuff Fm. (Upper Permian-Lower Triassic), Abu Dhabi, UAE.	Burial stage poikilotopic crystals fill pore spaces between the detrital carbonate components. Crystals are typically 500 μm in length but locally may reach up to 3 mm.	Worden et al., 1995, 2000
Prider Fm. (Lower Permian) Kansas, USA.	Burial stage poikilotopic anhydrite cement replaces echinoderm fragments, parts of oncoides, some dolomite spar, and some stylolite seams. Precipitation occurred in the range 65-90°C, with a few samples possibly up to 150°C.	Luczaj and Goldstein, 2000
Rotliegende Fm. (Lower Permian), onshore and offshore NW Europe.	Poikilotopic sparry anhydrite enclosing sand grains. Distribution shows a strong fault/fracture control. Precipitation temperatures in the range 120-140°C.	Gauthier et al., 2000; Sullivan et al., 1994
Swan Hills Fm. (Middle to Upper Devonian), Canada.	Coarse bladed crystals of sparry anhydrite enclosing dolomite clasts and possibly related to faults. Fluid inclusions in the anhydrite show crystals formed from basinal fluids at temperatures in excess of 90°C.	Duggan et al., 2001
(Silurian) Gascoyne Basin, Australia.	Sparry anhydrite includes blocky poikilotopic cement filling interparticle and mouldic pore spaces in oolitic horizons, and as a bladed cement in larger, often vuggy pore spaces. Formed at elevated subsurface temperatures.	El Tabakh, et al., 2004
St Peter Sandstone (Ordovician) Michigan Basin, USA.	Late stage sparry anhydrite cements that precipitated in crosscutting fractures and postdates with late stage dolomite that had precipitated at higher temperatures.	Winter et al., 2000

Table 7.14. Selected examples of sparry burial anhydrite.

dolomite, hydrocarbons and metal sulphides. Conditions are typically anoxic and thermochemical sulphate reduction is likely (Table 7.14). Calcium and sulphate are carried by chlorine-rich saline basinal brines, generated by the dissolution of evaporites, and capable of precipitating their dissolved load at chemical interfaces. This may be in strata adjacent to the dissolving evaporite bed or some distance away and along fluid escape conduits such as faults and fractures (Table 7.14).

Morphologically near-identical coarse poikilotopic anhydrite cements can also form during early syndepositional brine reflux within brine-saturated pores beneath an accumulating evaporite (Purvis, 1989; Luczaj and Goldstein, 2000). These syndepositional reflux salts are true evaporites in that they formed in a hydrology driven by solar evaporation. In contrast, burial salts that form in brines generated by the subsurface

dissolution of salt beds are not true evaporites as they are not directly precipitated by processes driven by solar evaporation, nor do they replace the volume occupied by primary and secondary evaporite salts (Table 1.1). They are, in reality, evaporite transformation salts or burial salts. Distinguishing early reflux evaporite cements from later burial salts can require detailed petrographic and isotopic study, especially in the absence of saddle dolomite or metal sulphides.

Not all burial or sparry anhydrite is associated with evaporites. Anhydrite is a retrograde salt, so intergranular and replacive anhydrite cement precipitates when unmodified connate seawater is heated above 150°C (Blount and Johnson, 1969). This is a widespread process in hydrothermal circulation cells in midoceanic ridges and is probably also active in the deeper portions of many sedimentary basins (Figure 2.11a; War-

ren, 1999). Aqueous sulphides can be oxidised to sulphates, which then precipitate as an authigenic CaSO_4 phase, which often happens in surface regions of pyrite oxidation such as in mine wastes, especially when microbially facilitated. But this oxidative sulphate source is relatively uncommon in the deep subsurface where pore waters are typically anoxic and reducing.

Anhydrite is a late stage burial salt in quartzose Rotliegende reservoir sands in Leman Field, North Sea and throughout regions of deeply buried Rotliegende Formation (Figure 7.72a; Sullivan et al., 1994; Gauthier et al., 2000). Poikilotopic anhydrite spar in Leman field is best developed along coarser-grained sand laminae, suggesting their inherent higher permeabilities influenced sites of precipitation. The same sparry anhydrite cement also encloses late authigenic ankerite, ferroan dolomite and pressure-solved cemented grains, showing its deep burial origin. Anhydrite tends to be best developed in and near fractures forming cements zones up to 0.5cm wide and 0.5m

long in Leman core. Crystals in fractures are bladed, coarsely crystalline and tend to grow subparallel to the fracture walls. Cemented coarse-grained laminae and anhydrite-filled fractures frequently intersect suggesting both styles represent the same generation of anhydrite cement.

Timing is best resolved using Sr and O isotopic analysis of the anhydrite cements. Oxygen isotope compositions indicate precipitation temperatures between 120°C and 140°C in waters with a $\delta^{18}\text{O}$ composition similar to the present day formation waters ($\approx 0\text{‰}$ SMOW; standard mean ocean water). These are the maximum inferred burial temperatures for the Rotliegende sandstone in Leman Field. Such temperatures occurred during the Late Jurassic-Early Cretaceous, at the start of basin inversion with maximum burial depths of 3.5-4 km (Figure 7.72b). When corrected for their 150 Ma precipitation age, the Sr isotope ratios in the various anhydrite burial cements, and their Sr contents, are highly variable. ($^{87}\text{Sr}/^{86}\text{Sr}$) ratios range from 0.70797 to 0.71129 and Sr contents from 351 to 2952 ppm

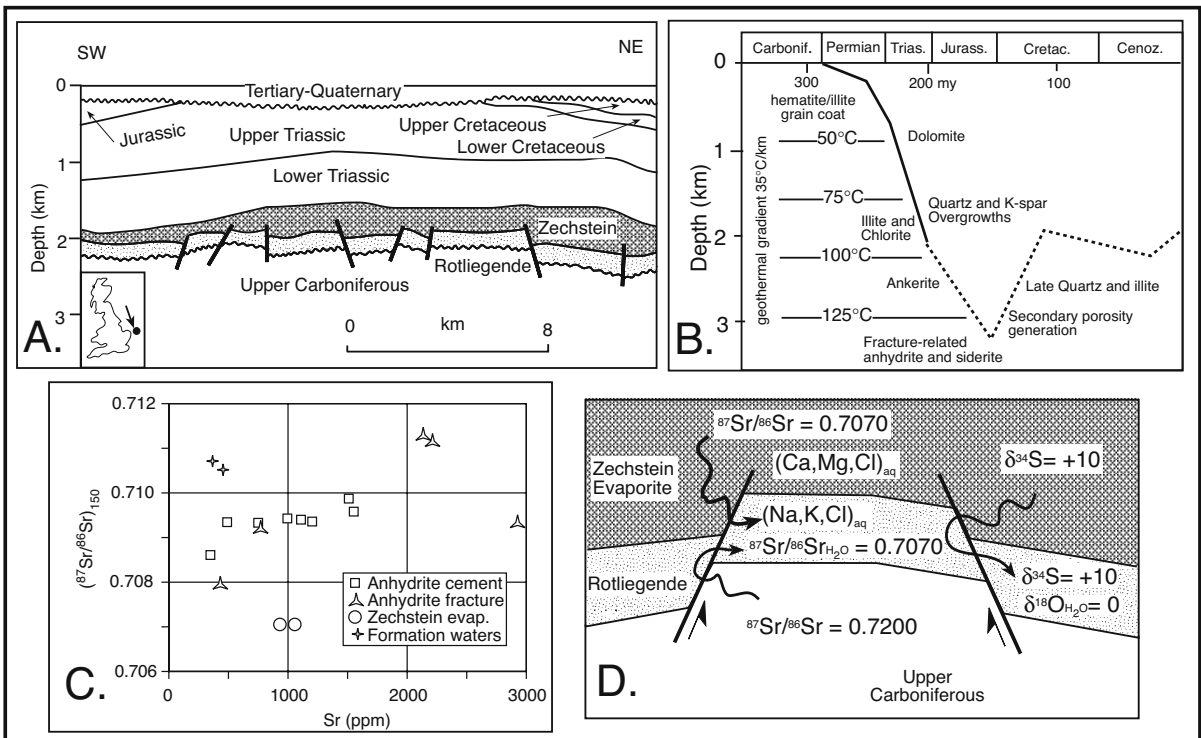


Figure 7.72. Late stage anhydrite in Leman Field, North Sea. A) Location of the Leman gas field and regional geological cross section. B) Subsidence history of Rotliegende reservoir sandstone showing time and temperature of anhydrite precipitation postdates other diagenetic events and precedes secondary porosity formation. C) Strontium isotopic ratios and composition of various anhydrite burial salts compared with formation waters and Zechstein salts. There is a general trend of increasing isotopic ratio with increasing Sr content. D) Schematic section showing major sources of sulphur, strontium and carbon along with their migration from above and below the Rotliegende and subsequent mixing that precipitated anhydrite cements and fracture fill (modified form Sullivan et al., 1994).

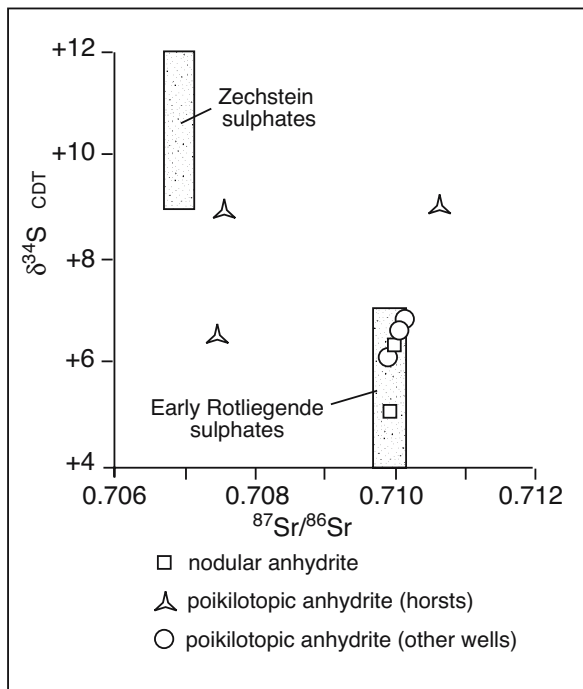


Figure 7.73. Plot of sulphur versus strontium isotopic ratios for coarse anhydrite cements from the German Rotliegende. It clearly shows the affinity of anhydrite cements in horst blocks for Zechstein sources rather than an early Rotliegende signature (after Gaupp et al., 1993).

(Figure 7.72c). Fracture-filling anhydrite spar also traverses this entire strontium range, implying an origin from the same fluid. There is also a general trend of increasing Sr ratio with increasing Sr content of the anhydrite burial salts.

According to Sullivan et al. (1994) the late stage anhydrite indicates an unusual, short-lived, catastrophic event that juxtaposed the Zechstein evaporites and sandstones. The resulting geometry facilitated cross-formational fluid flow via fractures that were tectonically induced by inversion. At that time pore fluids were squeezed from the overlying Zechstein evaporites and underlying Carboniferous mudstones into the lower pressures of the Rotliegende regional aquifer (Figure 7.72d). Mixing of the two waters precipitated dolomite and anhydrite cement, which in turn produced a Na-K-Cl formation water. This pore water was lower in Ca+Mg than the overlying Zechstein, which in turn supplied most of the sulphate and some of the Sr to the anhydrite cements. Like the isotopic evidence, the chemical evidence shows the burial anhydrite precipitated from extremely saline formation waters derived by deep subsurface mixing of Zechstein evaporite brines and deeply circulating meteoric waters. Even today, the Zechstein brines in the Leman Field are extremely saline (165,530–238,531 mg/l), with cation/chloride

ratios indicating ongoing mixing of Zechstein marine evaporite brines with fossil meteoric water.

Onshore in northern Germany the Rotliegende gas reservoirs also contain coarse authigenic poikilotopic anhydrite cements, particularly in the vicinity of faults. Cross-formational flow of Zechstein fluids and fault-related fluid flow was responsible for this anhydrite, especially during times of mixing tied to fault activity (Gaupp et al., 1993; Gauthier et al., 2000). This is clearly seen in the isotopically distinct values of burial anhydrite within horst blocks compared to samples with similar authigenic and nodular anhydrite styles, but from wells outside of the horsts (Figure 7.73). Anhydrite cements in sands atop horst blocks show affinities to Zechstein sulphates. In contrast, anhydrites in the other wells, where uplift has not juxtaposed Rotliegende sands to Zechstein fluids, retain an isotopic signature typical of early Rotliegende time. Once again, this observation underlines the importance of active faulting in facilitating brine mixing, which then precipitates authigenic minerals in the deep burial setting.

Late stage anhydrite and halite cements also characterise deeper burial cements in the aeolian and fluvial feldspathic sandstones of the Upper Jurassic Norphlet Formation and other Smackover sandstones of the Gulf Coast (McBride et al., 1987; Dworkin and Land, 1994). Coarsely crystalline anhydrite, along with quartz and ferroan dolomite, precipitated as intergranular cements. Anhydrite averages 3% by volume (maximum 21%) in Norphlet wells in Mississippi and 1.3% in Alabama. It occurs as scattered sparry crystals, in spherical and poikilotopic patches up to several centimetres across and can completely cement some sand laminae. All the anhydrite cements are patchily distributed in the Norphlet reservoirs and, as in the Rotliegende, tend to be better developed in the coarser sand laminae.

Oxygen isotopic values from the anhydrite averages 15.6 ‰ (SMOW). According to Dworkin and Land (1994) this burial anhydrite precipitated in near oxygen (and strontium) isotopic equilibrium with ambient burial fluids at temperatures of between 90°C and 100°C at depths ≈2.3 km (Figure 7.74a). Authigenic halite cements, along with late stage carbonates, followed at temperatures up to 120°C (<3km burial). Subsequent dissolution of the cements, along with some labile detrital grains, created secondary porosity that makes up at least half of the economic porosity in the Norphlet tight gas sand reservoirs in this region. Potassium-rich brines, generated by dissolution of nearby bitterns, tended to stabilise K feldspar in the Norphlet so that authigenic K-spar can even coat quartz grains, as well as its more commonplace occurrence as overgrowths on detrital K-spar grain substrata.

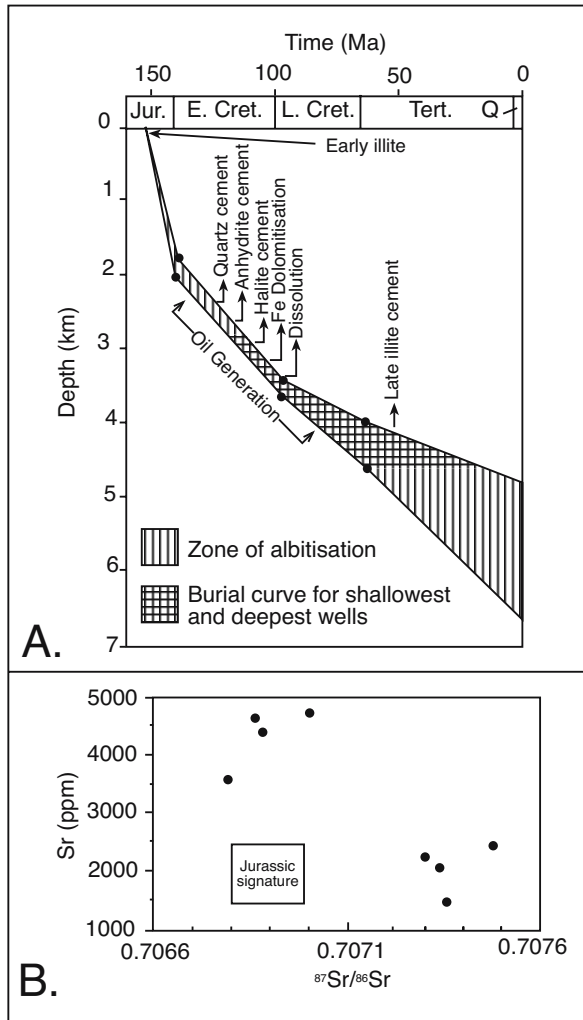


Figure 7.74 Norphlet Formation. (after Dworkin and Land, 1994) A) Burial evolution and diagenetic history. B) Sr isotope signatures.

Dworkin and Land (1994) argue that the expected isotopic composition and trace-element concentration of a marine brine-reflux-derived anhydrite cement in Smackover Formation quartzose sands should be: $\delta^{34}\text{S}_{\text{CDT}} = +16\text{‰}$, $\delta^{18}\text{O}_{\text{SMOW}} = +14\text{‰}$, $^{87}\text{Sr}/^{86}\text{Sr} = 0.7069$, $\text{Sr} = 1500\text{--}2500$ ppm, $\text{Ba} < 20$ ppm, and $\text{Mg} > 200$ ppm (the box in Figure 7.74b). When geochemical analyses of Smackover anhydrite cements are compared with the predicted composition, it is apparent that most of the coarsely crystalline anhydrite is not a marine reflux cement. Rather, two groupings or generations of anhydrite cement can be distinguished using a strontium isotope to strontium content crossplot (Figure 7.74b). An early cement, that may have been derived from slightly modified Late Jurassic sea water (possibly via reflux), is characterised by its Jurassic isotopic

signature and high strontium content ($>3,200$ ppm). A second group of cements, that represent the bulk of coarsely crystalline cements in the Smackover sandstones, has a depleted strontium content ($<3,000$ ppm) and an elevated isotopic ratio. It may have precipitated later in the burial history or may represent burial recrystallisation of the first cement. It probably formed at slightly higher temperatures, which would have maintained relatively low strontium concentrations, and in the presence of pore fluids that had radiogenic Sr isotopic compositions. Such radiogenic pore fluids were probably derived from waters that were involved in the burial dissolution of feldspars.

As well as in Smackover sandstones, dissolution-derived sulphate-rich basal brines also precipitate anhydrite burial salts in Smackover carbonates of the Gulf of Mexico (Figure 7.75; Heydari and Moore, 1989; Heydari, 1997). Precipitates are made up of orthorhombic laths and blades that form spars replacing both allochem grains and calcite cements. The anhydrite spar and the calcite spar formed prior to reaching the oil window and are post stylolitisation. The arrival of liquid hydrocarbons and the precipitation of solid bitumens temporarily retarded further precipitation of calcite, anhydrite and dolomite burial cements. Later, the anhydrite was dissolved and replaced by a more finely crystalline calcite spar and elemental sulphur via thermochemical sulphate reduction processes. This occurred

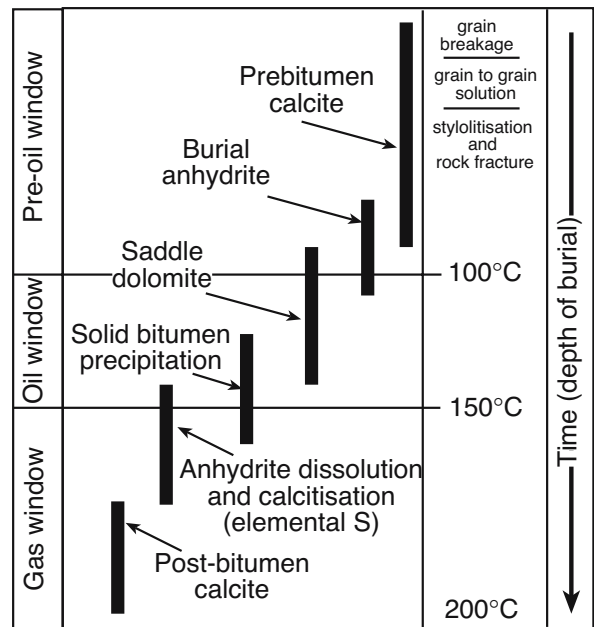


Figure 7.75. General paragenetic sequence for the Smackover Formation in the northern Gulf of Mexico showing approximate temperature range of various events (after Heydari and Moore, 1989; Heydari, 1997).

at the higher temperatures that typify the gas window (Figure 9.42c).

Dissolution-derived late burial anhydrite is also widespread in the Lower Cretaceous carbonates of the Pearsall and Lower Glen Rose Formations, South Texas (Woronick and Land, 1985). As in the Smackover, the anhydrite spar formed late, after the development of saddle dolomite cements. It crystallised mostly as bladed to fibrous anhydrite laths some 0.1 - 6.0 mm in length. Much of this anhydrite fills preexisting intergranular pore space in the carbonates, but it can also replace fossils, matrix material and earlier calcite cements. Once formed, it was subject to corrosion and replacement by calcite. $\delta^{18}\text{O}_{\text{SMOW}}$ values for the anhydrite range from 19.5-22.9‰, values that are much more enriched than the Cretaceous seawater sulphate (+15‰). Woronick and Land (1985) interpret these enriched values as proof that none of the subsurface anhydrite in the Pearsall and the Glen Rose (including some associated nodular anhydrite) was precipitated directly from Cretaceous seawater. They argue that even the nodular anhydrite (previously used as a sabkha indicator) was not primary but had recrystallised in the subsurface. This is supported by $\delta^{34}\text{S}_{\text{CDT}}$ values of the anhydrite and the modern Edwards Formation brines, which lie between 20 and 26‰. Directly precipitated Cretaceous marine evaporites should have $\delta^{34}\text{S}_{\text{CDT}}$ values of less than +16‰ (Figure 2.23).

They envision a basinward flowing deep meteoric aquifer, driven by hydrostatic flow, that was essentially saturated with respect to calcite, dolomite and CaSO_4 . Periodically the meteoric waters mixed with upwelling hotter basinal fluids that were derived from more deeply buried and dissolving Jurassic salts. These basinal fluids contained abundant carbon dioxide, calcium, strontium (radiogenic) and barium, together with small amounts of lead, zinc and hydrocarbons. Mixing of the two waters caused the precipitation of burial anhydrite, as well as other burial cements, including saddle dolomite and metal sulphides.

Other carbonate platform sequences that entrain burial anhydrite cements derived from evaporite dissolution and upflow of sulphate-enriched basinal waters include the Devonian Keg River and Swan Hill formations of Alberta (Aulstead and Spencer, 1985; Duggan et al., 2001) and carbonate reservoirs in the Middle Ordovician Trenton Group, SW Ontario (Middleton et al., 1993).

All these example of sparry burial anhydrite demonstrate the obvious association between advanced dolomitisation of

platform carbonates and the precipitation of later diagenetic poikiloprotic and replacive anhydrite spar. This process, also called anhydritization by Kendall and Walters (1978), is widely observed and significantly reduced porosity in potential reservoir dolomites in the Devonian of Canada, the Permian Khuff of the Saudi Arabia and the Emirates, the Zechstein of NW Europe, the Jurassic of the Gulf of Mexico and the Arab cycles of the Middle East (see Chapter 10). As yet, it has attracted the interest of relatively few researchers and documentation is sparse. As a process it should characterise burial diagenesis in most deeply buried sulphate evaporite systems.

Enigmatic outlines in pseudomorphs

This chapter discusses how evaporites can be replaced by various minerals at any time in their burial and uplift history. So far, I have focused on the more commonplace evaporites — namely, gypsum, anhydrite and halite morphologies — that are pseudomorphed by silica, calcite, dolomite, baryte and celestite. These three evaporite salts constitute more than 90-95% of modern and ancient precipitates, but there are also carbonate or silica pseudomorphs preserving the outlines of other evaporite salts, such as trona, gaylussite, pirssonite, glauberite, thenardite and other less common precipitates. Figure 7.76 illustrates some of the idealised and a few of the more typical shapes of these somewhat less common salts. If their euhedral forms are well preserved by their carbonate or siliceous replacements, they can be recognised still.

But all evaporites are soluble, so the preservation of a crystal form is often accompanied by enlargement or partial collapse of the void during the replacement process. This complicates the process of recognition and is, for example, the main reason why Archean baryte at North Pole is still variably interpreted.

Sodium carbonate salts are more likely to alter to calcite with burial as they already contain elevated levels of bicarbonate ions when they are deposited (Table 7.15; Southgate et al., 1989; Finkelstein et al., 1999). When preserved as isolated replacement crystals in a mudstone matrix, their calcitic pseudomorphs have easily confused or misinterpreted with gypsum, baryte of other lenticular forms.

Misidentifying a pseudomorphs can lead to significant differences in the interpretation of depositional setting. In the case of the Upper Oligocene Creede Formation, southwestern Colorado, the interpretation of lenticular calcite in lacustrine laminites, as either ikaite or gypsum, is one of the pivotal pieces of evidence in defining the lacustrine depositional setting as

Mineral	Formula	Crystal Habit	Brine Type
Gaylussite [#]	Na ₂ Ca(CO ₃) ₂ ·5H ₂ O	Often elongated; also flattened wedged-shaped.	Na—CO ₃ —Cl
Glauberite ^{#,**}	Na ₂ Ca(SO ₄) ₂	Tabular, prismatic, dipyramidal, and may be rounded or step-like.	(Mg) Na—SO ₄ —Cl
Gypsum ^{**}	CaSO ₄ ·2H ₂ O	Thin to thick tabular; elongate; step-wise depressions or rough; acicular; prismatic with nearly equant cross section. Lenticular crystals with rounded or irregular terminations. Warped or curved irregular surfaces, long prismatic crystals occur bent into irregular or hoop-shaped forms.	(Mg) Na—SO ₄ —Cl
Ikaite	CaCO ₃ ·6H ₂ O	Distinct asymmetry with a tendency toward a sigmoidal shape when viewed from the side and square-prismatic in overall shape that taper to the ends; strongly ribbed normal to the length.	Na—CO ₃ —SO ₄ —Cl
Mirabilite ^{**}	Na ₂ SO ₄ ·6H ₂ O	Short prismatic to acicular crystals.	Na—CO ₃ —SO ₄ —Cl and (Mg) Na—SO ₄ —Cl
Pirssonite [#]	Na ₂ Ca(CO ₃) ₂ ·2H ₂ O	Short prismatic; also tabular or pyramidal.	(Mg) Na—CO ₃ —Cl
Thenardite ^{**}	Na ₂ SO ₄	Dipyramid; tabular; rarely prismatic.	Na—CO ₃ —SO ₄ —Cl and (Mg) Na—SO ₄ —Cl

Table 7.15. Evaporite minerals susceptible to replacement by calcite and likely to show lozenge or discoidal outlines. (#) indicates likely diagenetic mineral; (***) indicates a depositional association (after Finkelstein et al., 1999).

deep, cold, fresh, and profundal versus shallower, periodically meromictic and hypersaline (Larsen and Crossey, 1996 vs Finkelstein et al., 1999).

Because ikaite is only stable at near freezing temperatures, it is typically converted to thinolitic calcite (syn. jarrowites, devil's horn calcites, glendonites). Internally, ikaite pseudomorphs may preserve a characteristic granular structure made up of sand-sized, rounded to rhombic, calcite grains set in a matrix of sparry and spherulitic cements (Shearman et al., 1989; Shearman and Smith, 1985). But the shape of a thinolitic calcite is easily confused with the outlines of other evaporite salts that have no implication of degassing in CO₂-saturated coldwater spring seeps (e.g. Figure 4.23).

Likewise, the recognition of ikaite in Neoproterozoic glacial sediments interlayered with pisolites and ooids can be used to imply that the high supersaturation of Precambrian seawater meant that coated grains were possible cold water precipitates. They were not exclusively tropical precipitates, unlike pisolites and ooids in today's oceans and inferred for similar coated grain textures throughout the Phanerozoic (James et al., 2005). Alternatively the interlayering of glendonites and coated grains can be used to support a "freeze or fry" climate model tied to "Snowball Earth."

For years, before ikaite was shown to be a cold water deposit, not an evaporite, many crystals described as ikaite were considered named in a way that could be used interchangeably with the mineral gaylussite, or ikaite was described as pseudo-gaylussite. In terms of depositional setting, ikaite and gaylussite are not

coprecipitates, but from older literature associations one could easily think they were.

Separating ikaite/gypsum/gaylussite is not the only difficult choice when attempting to identify the precursor to a fuzzy edged angular outline now filled by a later mineral phase. Other problem pseudomorph associations include baryte/siderite/gypsum; acicular aragonite/gypsum; pyrite/halite and even anhydrite/gypsum. The difficulty in deciding on the likely precursor of a possible pseudomorph, when the replacement process can destroy to varying degrees the original outline, emphasises the need to look at all sources of evidence when interpreting any ancient succession now leached of the original salts or the daughter products.

Summary

Evaporites are soluble in most subsurface situations. Even preserved evaporite beds show varying degrees of dissolution about their edges. The longer an evaporite bed remains in the subsurface the more likely it is to dissolve. Preservation or loss it is not a question of whether an evaporite will dissolve in the subsurface, but when. This is why there are few preserved beds of evaporite salts older than Neoproterozoic. As thick evaporite units dissolve they leave behind characteristic breccias and other textures and replacements that allow the recognition of former extensive salt beds. The breccias can be interstratal beds or trans-stratal chimneys, distinguishing the two forms differentiates between blanket or more focused inflows. Dissolution can be driven by basal fluids escaping from below or by fluids

infiltrating from above. Salt units may not dissolve until they have flowed into diapirs and welds (halokinetic breccias) or have acted as décollement surfaces in fold and thrust belts (rauhwacke). All evaporite salt units will ultimately dissolve, many disappear in the diagenetic realm while others may be preserved until they attain metamorphic grades or interact with a magmatic body.


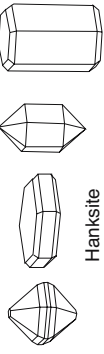
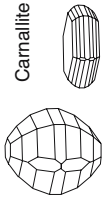
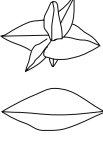

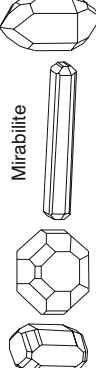
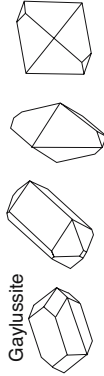

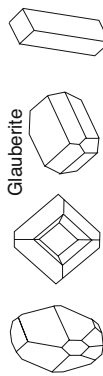
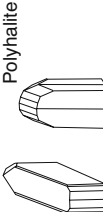
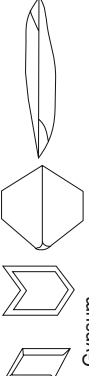

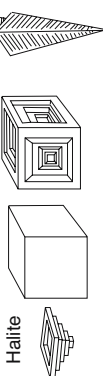
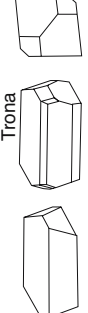
<p>Orthorhombic; Massive, granular, stumpy prisms, flat plates; Perfect (001) and good (010) cleavage; H=3.0-3.6; SG = 2.9-3.0; Tasteless.</p>  <p>Anhydrite</p>	<p>Hexagonal; Tabular or prismatic; good (0001) cleavage, uneven fracture; Weakly effervescent in dilute acid; H = 3.0 - 3.5; SG = 2.56; Deliquescent; Salty taste.</p>  <p>Hanksite</p>
<p>Orthorhombic; Massive, coarsely crystalline, bipyramids; Rare as euhedral crystals that tend to be barrel shaped; No cleavage, conchoidal fracture; H= 1.0-2.5; SG = 1.6; Very bitter taste, very hygroscopic or deliquescent.</p>  <p>Carnallite</p>	<p>Stable at temperatures $\approx 0^{\circ}\text{C}$ then converts to calcite (glendonite). Extensive deposits about coldwater springs in saline lakes (Mono lake) and relict in Lake Lahontan. Previously known as pseudogavlussite, thinnolite, devil's horns and White Sea horns.</p>  <p>Thinnolite (Ikaite)</p>
<p>Orthorhombic; Botryoidal, granular, fibrous; Perfect (010), distinct (011); H= 1.63-1.67; SG = 1.75; Sharp taste, deliquescent, only stable below 27°C; In dry air quickly loses water and turns to powder.</p>  <p>Epsomite</p>	<p>Monoclinic; Prismatic, tabular, acicular, granular fibrous, massive; perfect (001) also (001) (010) (011), conchoidal, H = 1.5 - 2.0; SG = 1.49; Taste cool then weakly saline and bitter; disintegrates to powdery thenardite on exposure.</p>  <p>Mirabilite</p>
<p>Monoclinic; Individual crystals dispersed in clay host in playas; In Venezuelan lakes called clavos or nasis; (110) perfect; conchoidal; H = 2.5-3; SG = 1.99. Reacts with acid; Calcite replacement common.</p>  <p>Gaylussite</p>	<p>Monoclinic; friable aggregates; prismatic; perfect (101), good 100; H= 2.5; SG = 2.21; Fibrous pseudomorphs.</p>  <p>Natron</p>
<p>Monoclinic; Tabular parallel to c, tabular by extension of (111), prismatic, good (001) poor (110) conchoidal; H = 2.5 - 3.0; SG = 2.7 - 2.85; Slightly saline taste; On hydration converts to gypsum and mirabilite; typically slushy, crumbly.</p>  <p>Glauberite</p>	<p>Triclinic; Prismatic, massive, massive fibrous, lamellar; Good (100) cleavage; H = 2.5 - 3.5; SG 2.78; Tasteless; Alters to gypsum when in contact with humid air.</p>  <p>Polyhalite</p>
<p>Monoclinic; Plates, needles, fibres, massive (alabaster), swallowtail and palmate twins; Perfect (010) cleavage, good (111) (100); H = 2.0; SG = 2.3-2.4; Tasteless.</p>  <p>Gypsum</p>	<p>Orthorhombic; wedge shaped crystals; distinct (010), conchoidal; H= 3.0; SG = 2.60; Secondary alteration salt in trona depositing regions.</p>  <p>Shortite</p>
<p>Cubic; Perfect cleavage, conchoidal; Cubes, hoppers, rats, fibrous; H = 2.5; SG = 2.1 - 2.2; Salty taste.</p>  <p>Halite</p>	<p>Monoclinic; typically fibrous nodular or columnar massive, (100) perfect, uneven to subconchoidal fracture; H = 2.5 - 3.0; SG = 2.14; taste alkaline; Effervesces in acids.</p>  <p>Trona</p>

Figure 7.76. Characteristic shapes of some of the various depositional evaporite salts and their physical properties.

Chapter 8: Burial hydrology and chemistry

Burial hydrology

In Chapter 2 we discussed the hydrology of evaporite deposition and early diagenesis, in this chapter we consider subsequent hydrological stages in a sedimentary system, that is burial, followed by uplift. Thick, buried and dissolving evaporites influence subsurface hydrology and formation water chemistries in a sedimentary basin, as do thermal and pressure regimes.

Flushing by basinal pore waters drives alteration, recrystallisation and dissolution of evaporites within four hydro-tectonic realms, namely (Figure 8.1; Table 8.1):

- 1) Passive-margin burial,
- 2) Pull-apart burial,
- 3) Collision margin burial, and
- 4) Post-orogenic burial.

The first three are often sequential, while the fourth can be part of, or adjacent to, the other three. Salt beds and allochthons act as foci for escaping basinal fluids within all these realms. Subsurface breaching of a stratiform salt aquitard, either by dissolution or halokinesis, typically focuses the outflow of basinal fluids. Fluids may rise or sink through a breach, depending on the local temperature and pressure regimes. Fluids flowing through the breach will mix with other basinal or meteoric fluids with differing chemistries and physical properties so that authigenic phases, including burial salts and metal sulphides, are common precipitates at or near the breach.

The passive margin burial realm is characterized by updip extensional tectonics, differential loading, growth faulting, relatively slow and steady subsidence and, in most salt-floored passive margins, by salt flow (Figure 8.1a). Compressional tectonics are commonplace in downdip positions. The Mesozoic and Tertiary evolution of the Gulf of Mexico and Atlantic-margin basins are typical examples of this salt-lubricated hydrologic

style. The shallower parts of this realm, down to $\approx 1-2$ km depth, are typified by active phreatic circulation. Below is the zone of compactional flow, which entrains both horizontal (average rates of 6 cm/year) and vertical flow regimes (average rates of

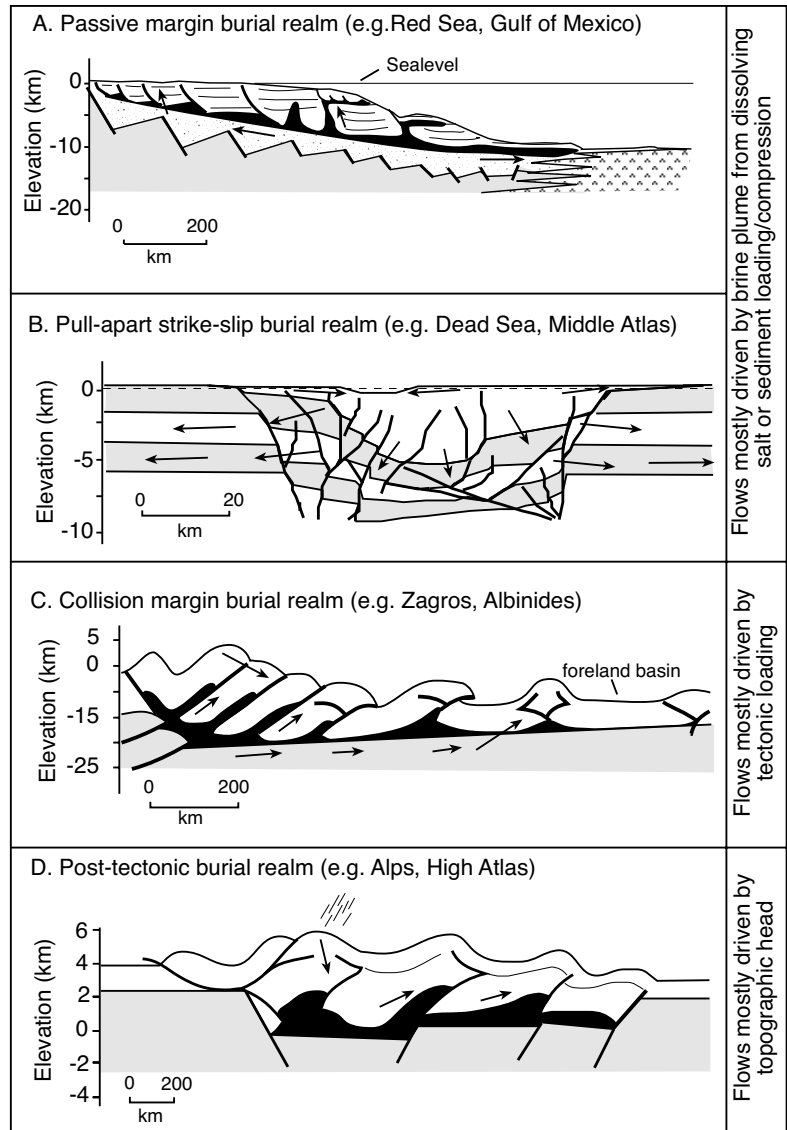


Figure 8.1. Hydrotectonic flow patterns. A) Passive margin circulation with water flow driven by sediment compaction and catabaric/thermohaline flow. Gravity drives nearsurface flow. B) Pull-apart circulation where dissolution-derived brine plumes from rapidly-buried thick evaporites drive deep lateral circulation into basement aquifers. C) Collision margin circulation where thrust sheet emplacement and loading drives burial water from sediments caught up in the orogenic belt into the craton interior. D) Post-tectonic circulation where deep burial flow in the basin sediments is driven by gravity head supplied by the adjacent weathering mountain belt. Note the varying vertical and horizontal scales.

	Location and age of brine source	Role of salt	Reference
Passive Margin burial	Gulf of Mexico, Jurassic	Fluid flow in Mio-Pliocene sediment near salt diapir crest is driven by brines derived from dissolution of salt mass. Suballochthon brine flow is focused by sheet geometry and evolutionary stage.	Cassidy and Ranganathan, 1992; Dworkin and Land, 1996
	Gulf of Lions, France, Miocene	Stratiform Late Miocene evaporite layer forms a widespread blanket that focuses fluid circulation and heat flow in units below salt.	Burrus and Audebert, 1990
	Canning Basin margin carbonates, Australia, Devonian	Chloride-rich metal carrying brines, created by dissolution of Silurian salt dissolving in basin centre, escaped along extensional faults into basin margin to form saddle dolomites and MVT deposits.	Warren and Kempton, 1997; Middleton and Wallace, 2003.
Pull-apart	Dead Sea, Middle East Miocene	Dissolution of Dead Sea halite acts as brine source in many deep water wells as far as 100 km away from the rift. Brine supplied for last 3-6 Ma with its layering and flow direction structurally controlled.	Gvirtzman and Stanislavsky, 2000 Stanislavsky and Gvirtzman, 1999
Collision margin burial	Timor Gap, Northwest Australia, Silurian	Mio-Pliocene inversion event reactivated fault-focused brine flow to surface breaches supplied from Mesozoic reservoirs with the brine originally derived from Silurian salt.	O'Brien et al., 1999; Lisk et al., 2000
	Pyrenees, Southern France and Northern Spain, Triassic	Evaporitic basinal fluids became syntectonic fluids in igneous basement. Brine direction was an evolving system with flow intensity and style of injection controlled by the structural stage of overthrust.	Bitzer et al., 1998; Travé et al., 2000; McCaig et al., 2000
	Slave Point Formation, Canada Devonian	Post Cambrian to pre-Cretaceous compression, associated with orogeny, squeezes basinal brine through carbonates of southern Rockies and drives formation of saddle dolomites of Presqu'île and MVT deposits.	Nesbitt and Muehlenbachs, 1994; Morrow et al., 2002
Post Orogenic burial	Ebro Basin, Spain, Triassic	Dissolution of buried evaporites caught up in the hydrology of compressional belt supplied much of the ionic content to active evaporite systems in the Miocene outflow zones in adjacent foreland depressions.	Sánchez et al., 1999; Salvany et al., 1994
	San Andres Formation, west Texas, Permian	Modern, deeply circulating Na-Cl brines in arkosic sandstone aquifers acquired their high salinity through the dissolution of halite and so displaced Permian age reflux brines.	Bein and Dutton, 1993; Stueber et al., 1998
	Alberta Basin Canada, Devonian	Two brine system; a 'heavy brine' that is a residual Middle Devonian evaporitic brine and a 'light brine' that probably originated from dilution of 'heavy brine' by deeply-circulating meteoric fluids in post-Laramide time.	Michael et al., 2003

Table 8.1. Selected example⁴ basinal fluid circulation.

0.15 cm/year). Deeper still, or in zones of thermal anomalies around growing salt structures and shale diapirs, is the zone of thermohaline flow.

Away from local thermal anomalies, temperatures increase steadily with depth according to regional geothermal gradients, which range from 15–30°C/km in most passive margins. Nonevaporitic sediments shallower than 2–3 km depth are typically hydrostatically pressured, while deeper strata, especially thick impervious shales in rapidly accumulating depocentres such as suprasalt minibasins, tend to be geopressed. A transition to overpressuring can occur at much shallower depths (\approx 1 km or less) where evaporites, not shales, are the predominant basin aquitard (e.g. Jowett et al., 1993). This reflects very rapid rates of basinwide evaporite sedimentation and a complete loss of intrasalt porosity at shallow depths within these basinwide units.

Pull-apart or transform burial is characterised by extensional tectonics and rapid subsidence, along with high sedimentation rates in the basin depocentre (Figure 8.1b). Pull-apart basins are an integral part of intraplate and interplate strike-slip fault zones in both rift and collision settings and tend to form at bends or sidesteps in the main strike-slip fault system (Figure 5.27). When located in arid zones, the fill in a rapidly subsiding basin can entrain thick salt beds, which subsequently become halokinetic. Such salt masses typify modern pull-aparts, such as the Dead Sea basin in the Middle East and Salar de Antofalla in NW Argentina (Stanislavsky and Gvirtzman, 1999; Kraemer et al., 1999). Rapid burial, so typical of this setting, quickly moves thick salt sequences into the subsurface, while contemporaneous salt solution can move large volumes of dense hypersaline brines into adjacent aquifers. High rates of subsidence and sediment fill, along with consequent overpressuring, means

porosity in associated nonevaporitic sediments can be maintained to much greater depths compared to similar lithologies in a typical passive margin deposit.

The collision margin burial realm is characterized by compressional tectonics, thrust faulting, extensive fracturing of strata and episodic movements of basal fluids often in response to tectonic loading (Figure 8.1c). Hot (100° to $>250^{\circ}\text{C}$), saline and highly pressured fluids are driven laterally out of the collision zone via porous and permeable horizons, typically toward the craton or continental interior and vertically along faults and fractures (Oliver, 1986). Such systems tend to characterise foreland basins, which in arid regions can become areas of interior drainage that quickly fill with various salts (Figure 5.27), as in seen in the widespread Miocene marine evaporites of the Zagros/Arabian Gulf region and the lacustrine trona deposits of the Eocene Green River Formation in the USA.

Buried evaporite beds caught up in a compressional suture are likely to be pressurized and remobilised, while crossflows of less saline basal fluids, as they are squeezed out of the collision zone, can drive evaporite dissolution further toward the basin edge. The resulting chloride-rich brines may in turn become metal carriers. Compression-driven hydrologies can precipitate widespread burial dolomites and Pb-Zn deposits, both within the orogenic belts and in the adjacent continental interior (see Warren, 1999, 2000b; for a discussion of various examples). The similarity between geochemistry of fluid inclusions in sphalerite in strata-bound sulphide deposits and that of oil field brines in the U. S. Gulf Coast sedimentary basin led Sverjensky (1986) to conclude that oil field brines can readily evolve into ore-forming solutions.

The post-orogenic burial setting is characterized by a lack of intense tectonic activity, the dominance of topographically driven flow, and by relatively high fluid flow rates, which in zones of deep artesian circulation range from 1 m/year to 30m/year (Figure 8.1d) Flow is driven by elevation gradients created during uplift in the preceding orogenic phase. Post-orogenic fluid flow takes over once the main phase of tectonic collision ends. This hydrologic style drives the dissolution of many buried salt units in continental interiors and encompasses the generation of Na-Cl brines, as is occurring today in the Permian and Michigan basins of the USA, the European Alps and the High Atlas.

Steep topographic gradients about basin edges of all three basin stages can create topographically-driven nearsurface fluid flow

rates as high as 20 m/year in aquifers in the high relief portions of the basin (rift rim, transform edge, and orogenic uplift zones). These are much higher rates compared to flow in low relief topographic settings such as passive margins and intracratonic sags, where nearsurface regional flow rates are typically ≈ 1 m/yr, with local thermal- and density-driven flow rates up to 10 m/year. Fracturing and karstification in any aquifer system creates higher local flow rates that can be orders of magnitude greater than that measured in the matrix.

Gradients within shallow aquifers beneath the more central parts of a basin's depocentre are less than in the steep-sided tectonically active margins, but can still be of the order of metres per year. Deeper aquifers in all basins have much slower flow rates (compared to near surface rates) and are typically measured in metres per year or less. Free convection cells driven by the buoyancy forces associated with temperature and salinity fields about salt allochthons have flow rates in typical temperature and density drive convection cells ≈ 1 m/yr, depending on thickness of the aquifer, fluid-density gradient, and regional permeability (Hanor 1987). Flow rates in deep aquifers within the cores of orogenic belts are typically \approx cm/year and dissipate quickly when stress is alleviated (Garven, 1995). Regional flow rates generated by compaction in a mud-rich sedimentary basin are typically much less than a cm/year, with locally or temporally higher rates during fault or microfracture venting of overpressured zones.

The presence of a subsurface evaporite unit as it flows and dissolves creates brine and density inhomogeneities that facilitate active and long term brine mixing interfaces and much higher local rates of subsurface fluid flow. For example, flow rates within descending brine plumes beneath thick buried and dissolving Miocene salt masses in the Dead Sea region are as high as 10 m/year (Stanislavsky and Gvirtzman, 1999). These rates approach those in aquifers in the margins of a high relief basin. Throughout all sedimentary basins containing flowing and dissolving salt the flow gradients tend to be highly variable.

Fluids in subsiding sedimentary basins

The zones of compactional and thermobaric flow lie beneath the zone of active phreatic circulation. They, rather than the active phreatic, dominate the greater part of the sediment pile accumulating in the extensional zone in a passive margin, in the subsiding foreland depression fill of a compressional regime and in the rapidly subsiding parts of pull-apart basins.

Compactional fluids

The compactional regime is characterised by the upward and outward expulsion of pore waters formerly trapped within the compacting sediment pile. If fluid cannot freely escape the compacting sediment may become overpressured. Compactional waters include connate waters, waters modified by brine-rock interactions, and meteoric waters originally buried within shale, sand or carbonate aquifers. Compactional or consolidation-related flow is a typical response to basin subsidence and ongoing sedimentary loading, which drives out interstitial fluids from compressible and hydraulically conductive buried strata. As it needs overburden loading to drive it, compactional fluid flow is characteristic of the mechanical dewatering stages of the basin's burial history and it dominates the early subsiding and filling stages of a sedimentary basin. Compactional loading of more mature sediment piles can be reactivated in regions of thrust sheet stacking, which can renew brine expulsion from the buried matrix (Garven, 1995). In this case it is the loading of the thrust sheets and the lateral compression of the basin that drives further fluid expulsion. It is a process that is quickly alleviated once thrust stacking ceases (Bitzer et al., 1998).

Compactional flow as an early-burial fluid migration mechanism is typical of young rapidly subsiding nonevaporitic basins, where it dominates mud-rich sections deeper than 1,000-2,000m (e.g. many Tertiary basins in SE Asia). Sediment ages in these basins typically range up to a few tens of millions of years. Differences in pressure heads between adjacent areas are the main driving force to fluid flow and the systems are often

compartmentalised by growth faults and mud diapirs. Most expelled fluid tends to move upward through still porous overlying strata during the earliest stages of compaction (Magara, 1986). Then, in the later stages of compaction, as interbedded clays become relatively impermeable, the principal direction of fluid migration becomes stratigraphic and is controlled by interbedded permeable beds of less compacted and variably cemented sandstones and carbonates.

In contrast, a subsiding basin succession entraining a widespread evaporite bed always contains a highly effective aquitard/aquiclude, almost as soon the salt is deposited. If water-saturated sediments are compacting beneath a thick rapidly accumulating unit of basinwide evaporites, its underside deflects the otherwise upward flow of escaping compactional waters (Figure 8.2a). Rising compactional water is initially undersaturated with respect to the evaporite salt but its underside quickly becomes a zone of salt dissolution and accreting insoluble residues (Chapter 7). Water flows obliquely along the underbelly of the dissolving evaporite bed until it reaches a breach in the salt or the edge of the bed. There fluid flow may once again become strongly vertical. As a general rule of thumb, thick evaporite units in a subsiding basin will focus and pond upward-escaping compactional waters and restrict regions of brine escape to areas atop fractures, growth faults, dissolution-induced breaches, or dissolution edges of the evaporite unit. Halokinesis, through its inherent thickening and thinning of bedded salt, may help focus fluid escape via welds into breached salt withdrawal basins, typically situated between growing salt anticlines, allochthon sheets and diapirs (Figure 8.2c).

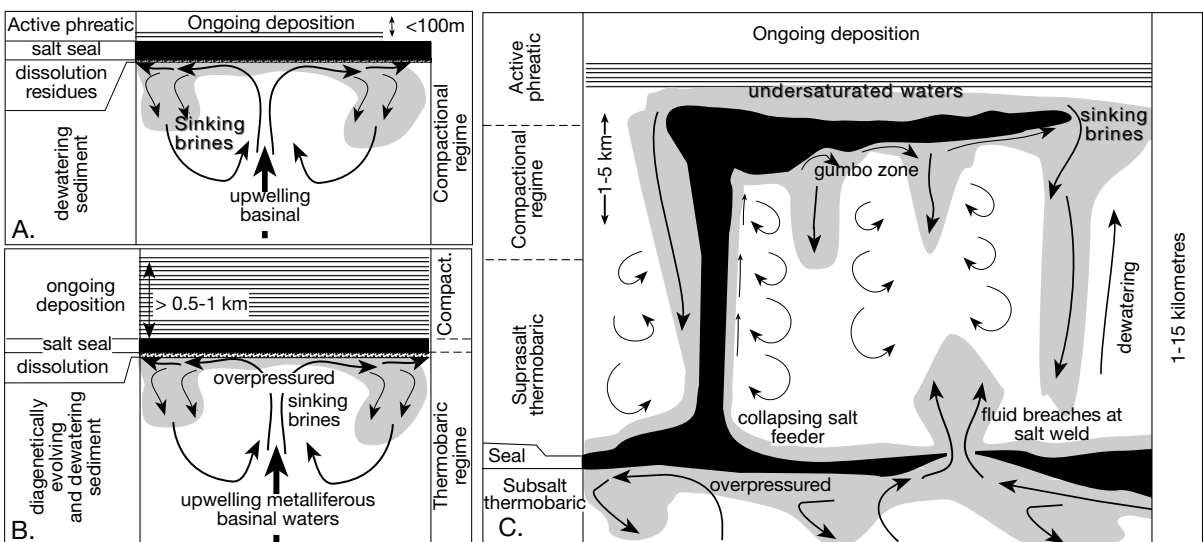


Figure 8.2. Brine flow regimes. A) Compactional regime. B) Thermobaric regime. C) Flow regimes in diapiric province, also shows potential region for escape of hydrocarbon bearing or possibly metalliferous fluids at breach zones in flowing salt bed (salt welds, growth faults, fault welds, etc.).

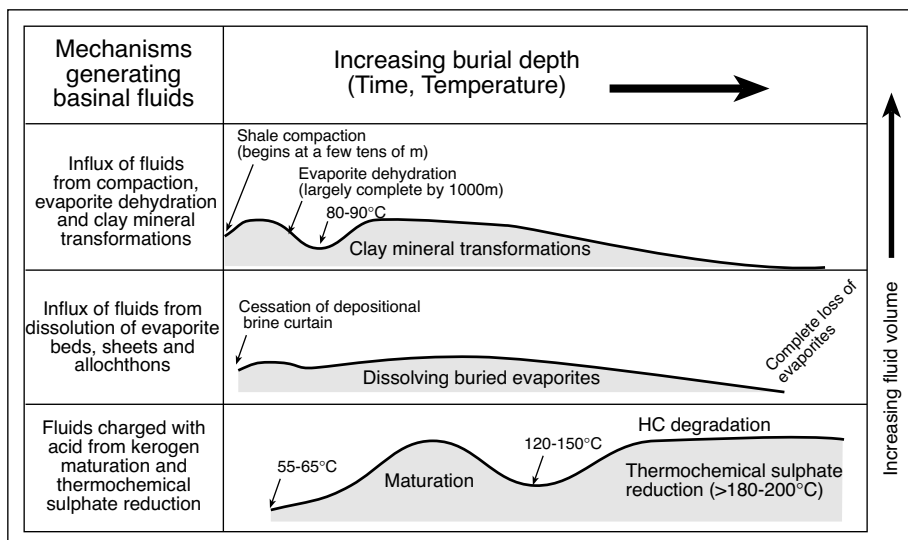


Figure 8.3. Mechanisms that release thermobaric waters into a basin with thick buried evaporites. Increasing burial releases fluids (brines, acids or gases) as indicated by the shaded portions of each row. The fluids would interact and when undersaturated with respect to the salt mass may have increased the rate of salt dissolution. (No vertical scale is implied).

Thermobaric fluids

Thermobaric fluid flow occurs in the deeper parts of a sedimentary basin where the temperatures and pressures are greater and is intimately related to compactional flow in its uppermost parts (Figure 8.2b, c). By definition, it is a zone of widespread diagenetic alteration where significant volumes of “new” thermobaric water are released by dehydration of clay minerals, catagenesis or the dehydration of hydrated evaporite minerals, such as gypsum or carnallite. Fluids in the thermobaric regime move in response to pressure gradients generated by the related phase changes, such as the generation of hydrocarbons, or the release of mineral-bound water, or ongoing lithostatic loading (Figure 8.3). Density contrasts created by salinity or temperature gradients beneath or adjacent to a dissolving salt bed can drive convective flow of thermobaric pore water. Chemical changes in the sediment matrix mean thermobaric waters frequently contain methane, carbon dioxide and hydrogen sulphide derived from the thermal alteration of organic matter, as well as metals leached from basinal shales and volcanoclastics.

Low permeabilities of deeply buried sediment between or below impervious evaporite beds mean typical rates of fluid flow in intra or subsalt beds are typically slow (mm-dm/year) except in zones of seismic pumping. As in compactional zone hydrologies, it is in the interval adjacent to a salt bed where overpressure tends to develop. Rates of fluid flow and the rate of creation of mixing zone interfaces can be enhanced by the formation of temperature anomalies in the buried sediment,

which are tied to the higher conductivity of salt.

Fluid density tends to increase in thermobaric waters in contact with the dissolving edges of salt units and the direction of brine flow is typically focused by the salt edge. These brines have locally anomalous chemistries and can drive diagenetic alteration when mixed with less dense brines derived from adjacent sediments. For example, the Slave Point, Sulphur Point and Keg River formations of Northeast British Columbia contain numerous gas fields, particularly along the

preferentially dolomitized reefal shelf edge margin (Morrow et al., 2002). The typical reservoir facies is a coarse-crystalline white dolomite known as the Presqu’ile Dolomite. It follows the shelf edge within the Slave Point Group, but coarse-crystalline dolomite is also regionally extensive within underlying strata. The dolomite is made up of two geochemically distinct but related phases, both precipitated from thermobaric waters (Figure 8.4a).

The organic-rich Klua Shale, the Otter Park Shale, and marlstones equivalent to the Sulphur Point and Slave Point formations are aquicludes that blocked the upward and lateral flow of warm dolomitising brines derived from dissolution of buried evaporites (Figure 8.4b). Presqu’ile dolomitization along the Slave Point shelf edge is interrupted in places where the Klua Shale extends shelfward underneath the Slave Point Formation. The Watt Mountain shale was also a regional aquiclude that prevented upward circulation of dolomitising fluids in areas behind the Slave Point shelf edge. The flow of dolomitising NaCl-CaCl₂-MgCl₂-H₂O brine solutions began early in the shallow subsurface perhaps even as their brine source (Slave Point evaporite) was still being deposited. This precipitated dolomite cements (type 1) at temperatures > 50°C, during northwestward-directed shallow subsurface brine reflux from the Elk Point evaporite basin. This was followed by later upward-directed subsurface convective flow of NaCl-CaCl₂-MgCl₂-H₂O and NaCl-MgCl₂-H₂O brines, generated by the

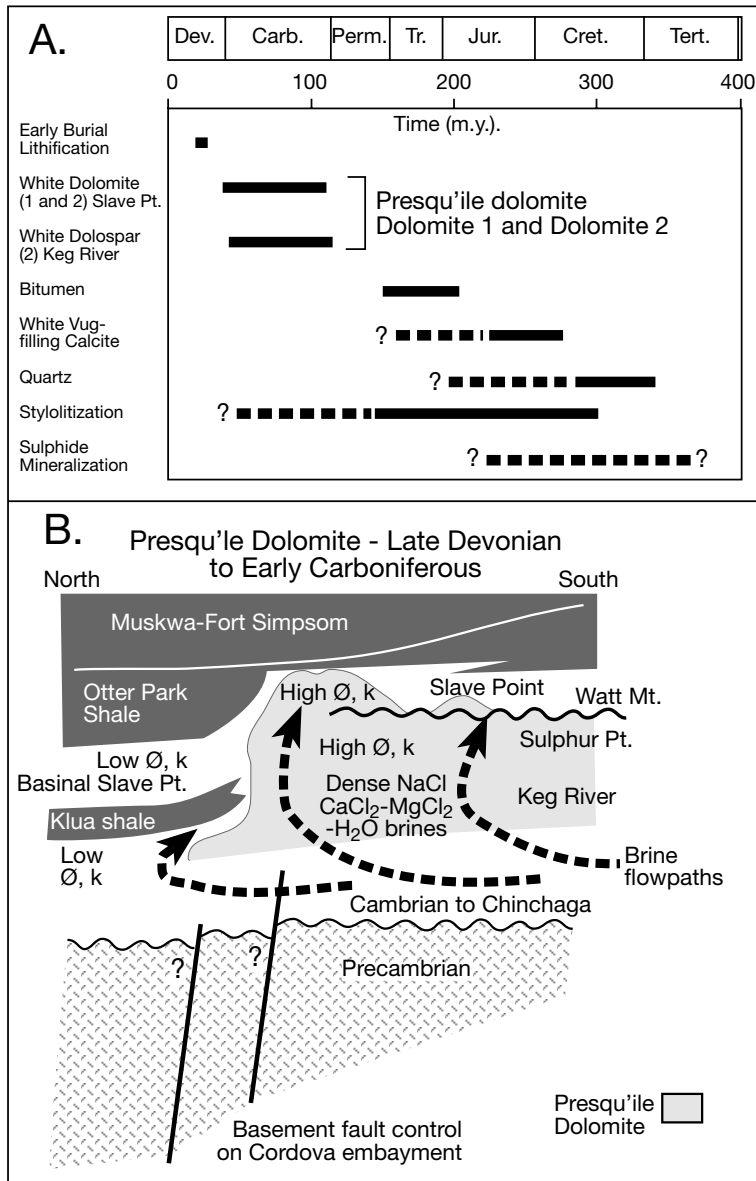


Figure 8.4. A) Chart of diagenetic events for the Keg River to Slave Point strata. Presqu'ile dolomitization (dolomite 1 and dolomite 2) precedes the thermal maturation of organic material and the emplacement of reservoir bitumen. Calcite cementation coincides approximately with the onset of gas generation followed by minor quartz and sulphide (sphalerite and galena) cementation. B) Schematic reconstruction of time of dominant Presqu'ile dolomitization around the Cordova embayment. Dense residual Elk Point brines flowed downdip and northwestward by gravity displacement of less dense subsurface fluids. This flow was confined beneath the Watt Mountain Formation shale. The absence of this confining layer allowed upward flow of brines into the overlying porous Slave Point Formation, where downdip brine flow may have been deflected upward against the low permeability basin fill of shaly units of the Cordova embayment. Initially, dolomitization occurred at temperatures below 50°C , but an increase in basal heat flow and ongoing burial caused dolomite precipitation to continue at 130°C (after Morrow et al., 2002).

ongoing burial dissolution of evaporites, mixing with less saline thermobaric waters escaping from nearby shale and so precipitating later dolomite cements (type 2). These type 2 dolomites are much less voluminous than type 1 and precipitated at temperatures $\approx 130^\circ\text{C}$ during the Late Devonian-Carboniferous. Later lower salinity brines that precipitated late calcite cements and some latest type 2 dolomite may have interacted with connate fluids of marine origin or, less likely, with meteoric fluids (Morrow et al., 2002).

The importance of a buried, slowly dissolving, salt mass in focusing thermobaric fluid flow throughout much of a basin's burial history was also illustrated by Wolfgramm and Mumm (2000). They used fluid inclusion analyses to reconstruct the spatial and temporal variation of fluid composition and thermal properties within sediments beneath the Zechstein salt in northeast Germany. Precipitates from early thermobaric fluids, migrating in the deeper parts of the basin, were characterised by complex salinities, with sulphur contents that increased toward the contact with the Zechstein. This suggests a partial exchange with the overlying evaporites. Inclusions of coexisting fluids dominated by NaCl, CaCl_2 and KCl are largely restricted to authigenic minerals in the Upper Carboniferous sediments and Rotliegende volcanics located in juxtaposition to the overlying evaporites. Younger, secondary fluid inclusions, sometimes containing gas phases, show increasing temperatures related to further burial. Thermal properties of all fluid inclusions indicate steep thermal gradients below the base of the Zechstein and Rotliegende sediments. This documents convective or advective heat and associated focused subsalt fluid flow in the deeper thermobaric parts of the basin. Throughout its burial history the Zechstein salt mass acts as the seal to a widespread convective system until its continuity is broken by salt withdrawal and thinning.

Deep flow in pull-apart basins

Another variation on this compaction/thermobaric theme is the evolving hydrology created by rapid subsidence and fluctuating tectonics that typify transtensional basins or pull-apart basins. The best-documented example of hydrological evolution associated with a salt mass in such a setting is the Dead Sea (Stanislavsky and Gvirtzman, 1999). Deep saline pores brine in the Dead Sea region are in part a residual product of intensively evaporated seawater that seeped into the depression back in the Miocene to accumulate as a widespread marine-fed basinwide halite. In places in the Dead Sea depression (e.g. Mt Sedom and surrounds), this halite is still near the surface, kept there by ongoing salt flow (Figure 8.5a). Dissolution of buried Miocene salt and the associated migration of a residual brine today drives zones of dolomitization within the adjacent

Cretaceous carbonate aquifers. This dissolutional brine occurs in deep wells located more than a 100 km from the Dead Sea depression. The feasibility of such longterm lateral migration of brine from Dead Sea evaporites over the past 3-6 m.y., was verified by palaeohydrologic modelling (Stanislavsky and Gvirtzman (1999).

Their results show that two basin-scale ground-water systems coexist in the present Dead Sea rift valley, one atop the other but with opposite flow directions (Figure 8.5b, c). The upper system is a topography-driven flow of meteoric water fed from the surrounding highlands, which flows eastward into the rift via shallow aquifers (<1 km deep). The second system is a density-driven migration of the Dead Sea brine moving in the opposite direction (westward) through deep Jurassic and Triassic aquifers (upto 4-5 km deep). This deep flow is

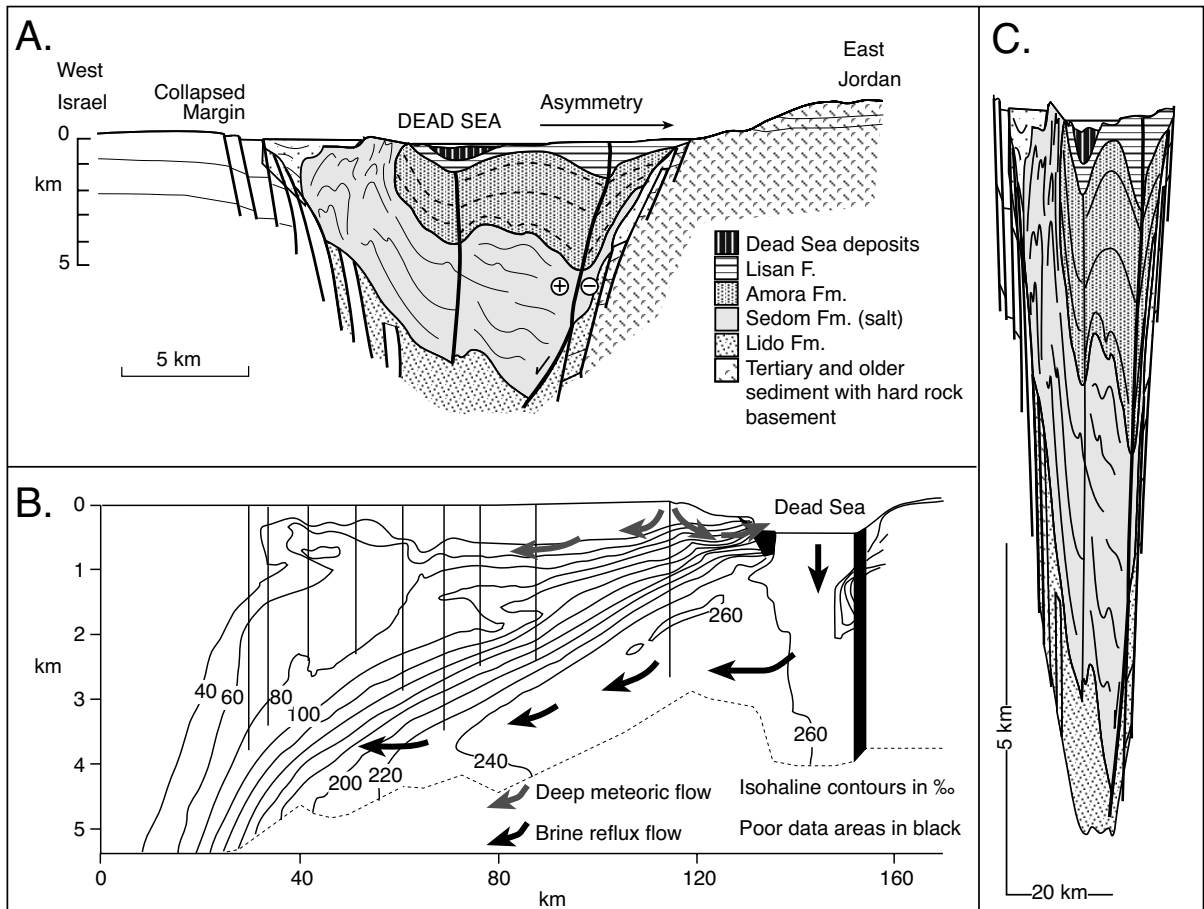


Figure 8.5. A) Dead Sea cross section showing asymmetric nature of fill. Shallow hard rock basement (aquiclude) occurs to the west of the basin fill (after Zak, 1980). B) Present deep westerly brine flow driven by dissolution of deeply buried Miocene salt (after Stanislavsky and Gvirtzman, 1999). C) Schematic geology based on 8.5a (which is a same scale section) stretched to match the same proportions as the vertically exaggerated scale of 8.5b so as to better demonstrate the importance of dissolving Miocene salt in driving deep brine flow.

maintained by ongoing dissolution of the thick halokinetic Miocene evaporites.

The longterm configuration of these flow systems has been modified by the hydrological evolution of the Dead Sea depression. There was an earlier (1.5 to 2.0 Ma) pervasive westward intrusion of brine into adjacent somewhat shallower (1-2 km) aquifers. The total mass of salt that entered the Cretaceous Judea and Kurnub aquifers at that time was 1.9×10^{11} and 3.9×10^{10} kg of salt per 1 metre width slice of cross section (Stanislavsky and Gvirtzman, 1999). Subsequent subsidence meant more than 80% of that earlier shallow outward-directed brine pulse seeped back into the Dead Sea depression. In contrast, for more than 2 million years, deep highly-saline dissolution-derived density-driven brines have been flowing westward toward the Mediterranean from the Dead Sea Basin. They have displaced older pore waters in deeply buried (2-4km) Jurassic and Triassic aquifers across a lateral distance of more than 150 km. Clearly, this is a region where ongoing brine flushing of adjacent deep aquifers is driven by salt dissolution.

Flow in and adjacent to Collision Belts

Compactional and thermobaric flow regimes are active as long as sediments are accumulating within areas of subsidence. With the cessation of sedimentation/subsidence, or with tectonic uplift, compaction driven flow decreases and ultimately ceases and most overpressure dissipates. When a mature basin, which is characterised by hydrological equilibrium in its sediment pile, then undergoes collision, overthrusting and basin inversion, a whole new set of disequilibrium processes are set up and can drive renewed deep-fluid migration (Figure 8.1c). Reverse faults and thrust welds in stacked thrust sheets in growing overthrust belts can focus fluid escape, while the thrust sheet loading acts as a huge press. Compression drives thermobaric waters out of the deeper parts of the compressing basin into the shallower basin margins, with periodic fault release sucking fluid into the fault ("squeegee" mode).

Some authors have explained MVT sulphides as forming in the basin margin zones of compressional terranes where these escaping chloride-rich metalliferous "squeegee" waters mix with topographically driven meteoric waters (Oliver, 1986). This process was thought capable of precipitating sulphides in passive margin carbonate platforms located hundreds of kilometres in front of the active thrust belt. Subsequent modelling of fluid flow and heat transport in compacting and dewatering thrust belt by Deming et al. (1990) showed flow velocities created by the "squeegee" effect are in the order of centimetres

per year and thermal anomalies of the order of 5°C, neither are sufficient to make significant contributions to mass and energy transfer. Likewise, Bethke and Marshak (1990) argued that rates of fluid expulsion in convergent margins are far too low to produce efficient advective heat transport. Most models assume systems that are tectonically and laterally homogenous with isotopic aquifers.

The inherent assumption in this modelling of chemical equilibrium between porewater and the enclosing rock in a sedimentary basin is probably justified by the inherently low flow rates associated with long term widely dispersed leakage (homogenous drainage) of compactional fluids in nonevaporitic mineralogically stable sediments. But assumptions of homogeneity of fluid flow are weaker in areas when episodic and focused dewatering (seismic pumping) is occurring in association with a mass of compressed impermeable salt. Flow velocities about the edges of any compressed but impervious salt mass can be locally high in relation to reaction rates. Drilling in compressional terranes in the Middle East and the Gulf of Mexico shows overpressure beneath sealing salt sheets periodically approach lithostatic. Vein textures and inclusion studies show hydrofracturing tends to occur preferentially and numerous times in zones of sediment adjacent to salt lubricated décollement. As fluid is sucked into these near-salt zones during fault release (typically along the base of the décollement) it doesn't come from the salt (it is impervious) but from the adjacent sediment. Then as compression takes over once more we have a system where the pore fluids drawn into the region of contact with the salt are renewed in an undersaturated state with respect to the salt mass and so are capable of dissolving salt as they are squeezed out ("squeegee" mode) along the underside of the salt mass. This gives a mechanism that drives the ongoing creation of chloride-rich waters capable of constant renewal and of carrying hydrocarbons and metals. The redox front across this interface and breach points in the salt are both capable of focusing base and precious metal precipitation (Warren 2000b).

Hence, inversion-related thrust faulting, which juxtaposes potential aquifers against pressured and dissolving evaporite beds, can mobilise focused thermobaric brine escape from deep aquifer systems. It can move hydrocarbons and metals, while at the same time precipitate late-stage authigenic evaporite cements. This is clearly seen in the authigenic sulphate cements in the Rotliegende Formation in Leman Field in the Southern Permian Basin of the North Sea (Figure 7.72; Gaupp et al., 1993; Sullivan et al., 1994).

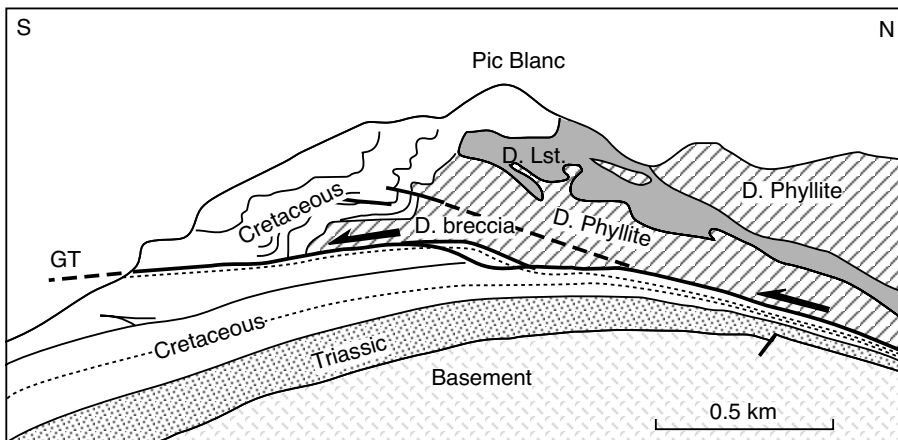


Figure 8.6. Detailed cross-section through the Plan de Larri in the central-western Pyrenees centred on the Gavarnie Thrust (GT; after McCaig et al., 2000). D. phyll. is mostly low grade Devonian phyllite; D. Lst. is mostly low grade Devonian carbonate; the Triassic section is Upper Triassic shales, carbonates and evaporites; D. breccia is a Late Cretaceous breccia weld that in outcrop composed mostly of Devonian clasts; Cretaceous is mostly Upper Cretaceous carbonates.

Coarse-grained burial-stage poikilotopic anhydrite cements increase in abundance in the vicinity of faults cutting the Rotliegende sands. Isotopic data show this late stage anhydrite precipitated at maximum burial of 3.5–4 km during the Late Jurassic–Early Cretaceous, that is, at the start of basin inversion. The data indicate an unusual, short-lived catastrophic event of cross-formational fluid flow along fractures and reactivated faults induced by basin inversion. Late stage magnesite and dolomite cements may also be related to influx of the same subsurface brines.

Remobilisation of basinal brine during inversion typically occurs during a compressional event many millions of years after first burial (Wilson cycle) and may revitalise the formation and migration of hydrocarbons. For example, saline chloride-rich formation waters in Mesozoic hydrocarbon traps in the Timor Sea, Northern Australia are sourced in more deeply buried Palaeozoic evaporites (O'Brien et al., 1999; Lisk et al., 2000). Some 5.5 Ma there was a transient fluid flow event, driven by Mio-Pliocene inversion, and associated far-field fault reactivation, driven by the collision of the Australian plate with SE Asia. It had a major impact on the seal integrity of numerous fault dependant hydrocarbon traps in the Timor Sea and allowed hot (90–130°C), highly saline (>200,000 ppm) brines from deep Palaeozoic evaporite-derived brines to migrate up the reactivated faults to chemically and thermally overprint the reservoir and other shallower intervals. Apatite fission track data suggest that this regional episode of fluid migration was short and lasted for between 10,000 and 100,000 years. It resulted in the development of a prominent, localised Late Tertiary heating

'spike', that if ignored can significantly affect the accuracy of modelled thermal histories in the region.

High pressures associated with collision and thrusting can drive salt-derived fluids into lithologies where they would not otherwise be present, such as when evaporitic basinal fluids become syntectonic fluids in igneous basement. For example, deep basinal brines, derived from dissolving Triassic evaporites, were driven via fractures and shears into hard rock basement (phyllites and gneisses)

of the Pyrenees during the Hercynian orogeny (Figure 8.6; McCaig et al., 2000, discussed in detail later in this chapter). Worldwide, it is likely that dense salt-dissolution-derived brines, sourced deep in the basin by ongoing salt solution, are involved in a number of alteration and mineralisation events in the same general area of the basin. But they occur as short-lived diagenetic pulses or events ($\approx 10^5$ – 10^6 years) spread over hundreds of millions of years, even as the basin passes through all stages of the Wilson tectonic cycle (i.e. rift, collision and post-collision; Figure 5.27). Even after a salt bed has passed into the metamorphic realm it, and its dense brine halo, will continue to act as a source of Na and Cl. In this case the ions come not from halite (gone by 450°–500°C) but from compressed scapolite cages and other meta-evaporitic daughter phases, e.g., the Mt Isa–Cloncurry region of Australia (Warren, 1999; Chapter 6).

Flow in post-orogenic hydrologically-mature basins

After inversion or uplift, evaporite beds re-enter the zone of deep meteoric (artesian) circulation and active phreatic flow (telogenesis). Meteoric fluids enter via infiltrating rainfall and groundwater as strata are increasingly flushed by meteoric waters (Figure 8.1d). Gravitational sinking, driven by topographic gradients and recharge along the uplifted margin of the basin, is the most important mechanism driving fluid migration. This gravity-driven circulation is sometimes termed centripetal flow, as it encompasses flow into the basin centre

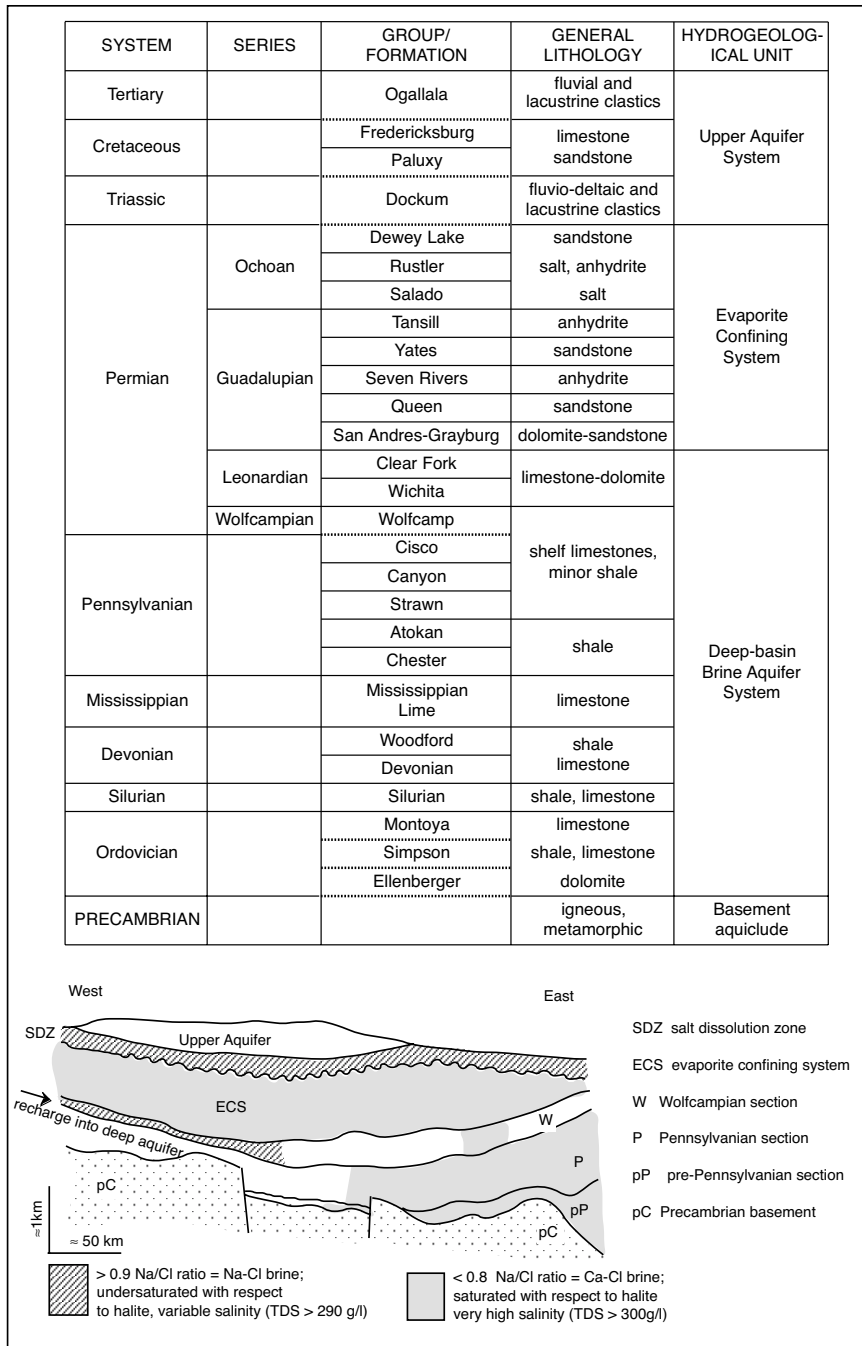


Figure 8.7. Na/Cl molal ratios define subsurface hydrology in Permian Basin, west Texas and Oklahoma. The relict Ca-Cl brines are held in place by the low permeabilities of the evaporite confining zone, while Na-Cl brines derived by halite dissolution are to be found in the salt dissolution zone (SDZ) and the Wolfcampian section (W) of the deep basin aquifer (after Bein and Dutton, 1993). The upper part of the figure shows the relevant stratigraphy of the region, centred on the Central Basin Platform and the occurrence of the major hydrogeologic units within this stratigraphic framework (after Stueber et al., 1998).

from the surrounding highland areas. It is opposite to centrifugal flow, which characterises the compactional, thermobaric and compressional regimes.

Three conditions must be met to allow topography driven flow: 1) the basin needs to be partially elevated above sealevel/brine level, 2) the flow system requires ongoing water replenishment via infiltrating rainfall and groundwater, and 3) aquifers must have sufficient permeability at depth to allow the entry of waters. An exception to the general requirement of a meteoric feed and suprasedalevel hydrologies is a subsealevel foreland basin or saline giant undergoing evaporative drawdown, such as the Mediterranean in the Late Miocene (Messinian), where seawater was the major groundwater feed (Figure 5.27).

Another exception to the general assumption that centripetal flow is driven by a potentiometric head that is always supplied by the uplift, may occur in glacial times. Today the Williston Basin in Manitoba has a hydrology controlled by recharge in the Rocky Mountains, but in the Pleistocene glacial periods this may have not been true. The thickness of the continental ice sheet over subglacial lakes may have provided sufficient hydrologic head to reverse the regional-scale flow system of evaporite-dissolution derived basinal brines in the Williston Basin (Grasby and Betcher, 2000).

Salt dissolution in the post-orogenic continental realm feeds brine into adjacent deeply-circulating confined aquifers beneath thick well preserved evaporite intervals. Over the last 5-10 million years, subsurface Na-Cl brines in various subsalt sandstone aquifers along the edges of the Anadarko, Midland and Palo Duro Basins have acquired their high salinity through the dissolution of halite by deep meteoric circulation of groundwaters. These basins make up the northern portion of the Permian Basin of west Texas and Oklahoma (Figure 8.7; Bein and Dutton, 1993).

Topographically driven, initially fresh, meteoric water moved into the western half of the deep-basin brine aquifer through nearsurface salt dissolution zones and then downward as Na-Cl brines seeped along the various deep aquifers to depths of thousands of metres (SDZ = salt dissolution zone in Figure 8.7). Above the deep aquifer are Ca-Cl basinal brines that are relict Permian mixtures of descending evaporitic brines and connate Permian and Pennsylvanian seawaters. Little or no Neogene meteoric Na-Cl brine has penetrated this Ca-Cl brine zone, which is hosted by the evaporite confining system (ECS). The lack of ingress reflects the extremely low permeability of deeply buried halite and intrasalt shale, anhydrite- or halite-cemented strata that dominate the ECS ("block of ice" analogue). Ages of the Ca-Cl brine in the ECS, based on ^4He and ^{40}Ar analyses of carbonates in the central part of the deep aquifer, range from 100 to 300 Ma (Zaikowski et al., 1987), making it a true "fossil" groundwater. This is the same salt where viable halobacteria have been cultured from brine inclusions preserved in its chevron halite (Vreeland et al., 2000).

To the south of the Palo Duro Basin, in the carbonate platform of the eastern Central Basin platform in west Texas, halite beds occur only in Upper Permian (upper Guadalupian and Ochoan) strata in the Permian Basin. As in the Palo Duro Basin, late stage uplift has influenced pore water composition of some of the original reflux brines in the more permeable subsalt beds. Extremely saline evaporated seawater apparently descended into adjacent Palaeozoic carbonates during halite deposition in the Late Permian, mixing with and displacing marine formation waters by buoyancy-driven convective flow (brine reflux; Stueber et al., 1998). These modified evaporitic brines were the dominant fluids in the Palaeozoic carbonates until the late Tertiary, when topographically-driven meteoric water began to flow into deeper Palaeozoic strata from outcrops and nearsurface aquifers in southeastern New Mexico in association with tectonic uplift that began at 5-10 Ma.

Meteoric water dissolved halite and anhydrite from Permian evaporites near the basin margin and seeped eastward along the regional hydraulic gradient, while mixing with and displacing modified evaporitic brine in the deeper parts. These meteoric waters, driven topographically, have now migrated large distances to displace saline waters deep and drive biodegradation in a basin characterised by numerous oil reservoirs with solution-gas drives.

The original dense brine that sank from Salado and Rustler evaporites into the underlying carbonates of the Central Basin Platform during the Late Permian may not have been of uniform composition, making it more difficult to separate it chemically from brines influenced by connate water or any subsequent deeply circulating meteoric waters. That is, initial brine composition was not solely of a composition that resulted from 23-fold concentration of seawater (Figure 8.8: Stueber et al., 1998). Multiple depositional cycles in Salado evaporites, as described by Lowenstein (1987a), represent periodic invasions of seawater into the Salado basin, followed by progressive drawdown and concentration of brine. Therefore, the degree of seawater concentration reached during each cycle probably varied, and the projection of the data trend plotted to a 23-fold concentration in the upper panel of Figure 8.8 is an oversimplification (Stueber et al., 1998).

The dense brines that began to sink into underlying carbonates during the Late Permian probably had a range of initial compositions along the seawater evaporation trajectory and lay somewhere to the right of the halite precipitation point (Figure 8.8a). The range of Br concentrations above 450 mg/l observed in formation waters from the 365 m (1200 ft) thick Pennsylvanian-Wolfcampian carbonate section in the Central Basin Platform below the Salado and Rustler evaporites is largely a relic of this inhomogeneity.

The present locations of the most saline formation-water compositions below the seawater evaporation trajectory in the Permian of west Texas probably indicate relict evaporitic brines mixed with seawater when they entered the carbonate strata, much like the mixing that has been documented for the Messinian drawdown (Figure 5.33) and is occurring today in the Dead Sea depression. As the brine mixed with phreatic seawater, each evaporitic brine composition along the seawater evaporation trajectory to the right of halite saturation would have been displaced along a line essentially parallel to the portion of the seawater evaporation trajectory prior to halite precipitation (Figure 8.8a, b). When the range of data points

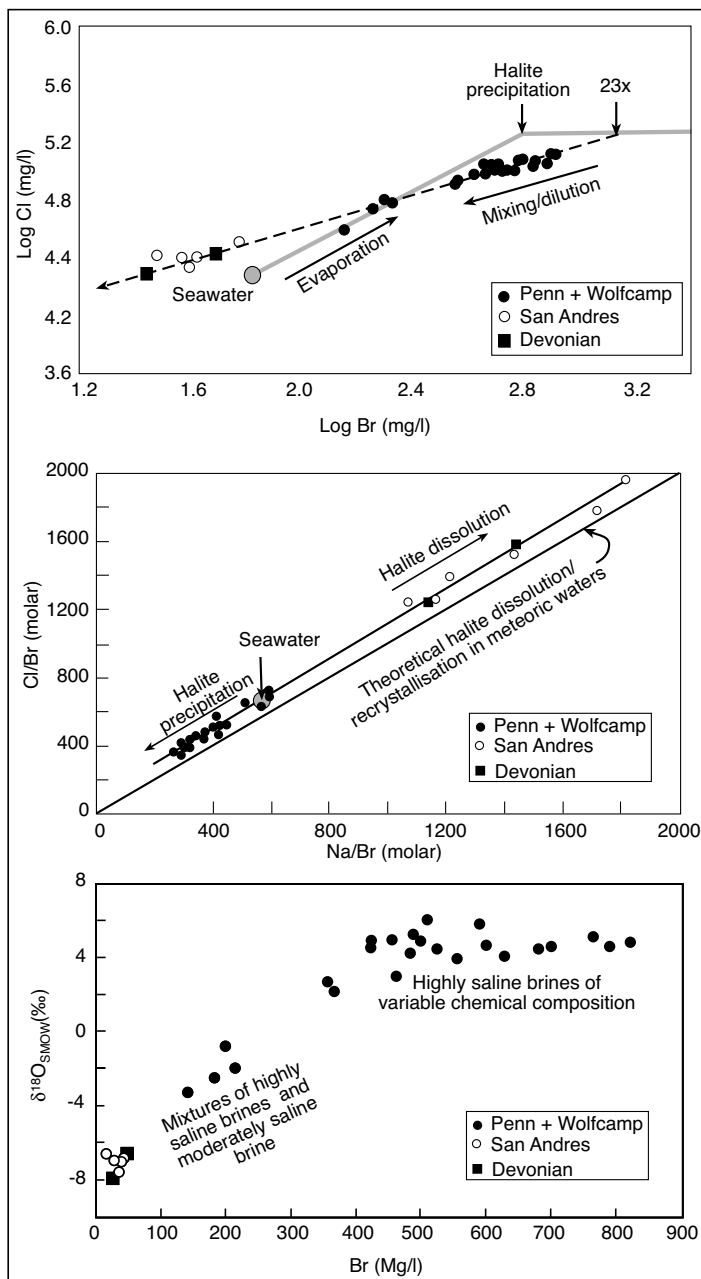


Figure 8.8. Chemical character of 32 formation-water samples from carbonate reservoirs in the Southwest Andrews area (after Stueber et al., 1998). A) Log Cl versus log Br. Seawater evaporation trajectory is from Carpenter (1978). SW = seawater composition; Halite precipitation = 450 mg/l = 2.65 Log Br (mg/l). Dashed line marks the likely mixing trend among the brines. B) Cl/Br vs. Na/Br molar ratios in formation waters relative to the compositional trend formed by seawater evaporated past halite precipitation and seawater that has dissolved halite. Regression line drawn through data points has $r^2 = 0.99$. The range of theoretical compositions that result from dissolution and recrystallisation of halite in fresh water is also shown. C) Oxygen isotope composition plotted against Br concentration.

representing formation waters with present Br levels greater than 450 mg/l is projected along such lines back to the seawater evaporation trajectory to the right of halite saturation, a range of seawater evaporitic concentration between 11-fold and 16.5-fold is indicated for the more saline waters. The concentration dissolution trends are also clearly seen in the Cl/Br and Na/Br crossplot, while the $\delta^{18}\text{O}$ - Br crossplot clearly shows the effect of meteoric mixing (dilution) on both these values (Figure 8.8b and c, respectively).

Thus, modified evaporitic connate brines were the dominant precipitative fluids for cements and replacement in the Palaeozoic carbonates of the Central Basin Platform and the Palo Duro Basin until the late Tertiary, when meteoric water began to flow into deeper Palaeozoic strata from outcrops and nearsurface aquifers in southeastern New Mexico, in association with tectonic uplift that began at 5-10 Ma. Neogene meteoric water dissolved halite and anhydrite from Permian evaporites near the basin margin and sank eastward along the regional hydraulic gradient, mixing with and displacing the modified evaporitic brine in deeper hydrogeologic systems of the Devonian and San Andres aquifers. The mixing curve is indicated by the dashed line, lowered Br values and the negative $\delta^{18}\text{O}$ signatures (Figure 8.8 a and c). These late Cenozoic meteoric fluids probably are responsible for widespread biodegradation of oil in the San Andres/Grayburg interval in the Andrews oilfield area. More regionally such deep meteorically driven dissolution of gypsum/anhydrite beds supplied sulphate-ions for the bacterial production of reduced sulphur with the organics supplied by trapped and upwelling hydrocarbons. This reduced sulphur was then oxidised to form economic accumulations of natural sulphur in west Texas (Chapter 11; Hentz and Henry, 1989; Lee and Williams, 2000).

The Alberta Basin, Canada, is another area of post orogenic fluid circulation where evaporite-derived subsurface waters currently interact with less saline deeply circulated meteoric waters within artesian aquifers (Figure 8.9a; Michael et al., 2003). Regionally, the Devonian succession contains two brines types (a 'light brine' with TDS

< 200 g/l and a 'heavy brine' with TDS >200 g/l), and both brines are pressurized by the potentiometric head supplied by the Rocky Mountains to the west.

The interface between the two brine types is typically lobate and controlled by permeability variations in the host aquifer, as evidenced by concurrent, steep changes in hydraulic head, and salinities (Figure 8.9a). Hydraulic heads in the lower two aquifers (Elk Point and Woodbend-Beaverhill Lake), range from 625 to 750 m, whereas heads in the upper two aquifers (Winterburn and Wabamun) range from 500 to 800 m. This implies that the Ireton is an effective aquitard between the lower two and the upper two aquifers. According to Michael et al. (2003) the geological and hydrogeochemical data suggest the following processes determined the present composition of the 'light' and 'heavy' brines: original seawater, evaporation of brines beyond gypsum onset but below halite saturation, dolomitization, clay dehydration, gypsum dewatering, thermochemical sulphate reduction, and halite dissolution. As in the San Andres Fm., the two brines can be separated by Na/Cl proportions; lighter brines show values >0.9 indicative of derivation from halite dissolution, while heavy brines tend to show values <0.7 reflecting a more relict marine-derived signature (Figure 8.9b).

An influx of meteoric (from the south) and metamorphic (from the west) waters is recognized only in the 'light brine.' Albitisation (sodic replacement) is unequivocally identified only

in aquifers hosting the "heavy brine." The "heavy brine" is likely a residual Middle Devonian evaporitic brine from the Williston Basin of the Elk Point Basin, or it may have originated by partial dissolution of thick, laterally extensive Middle Devonian evaporite deposits to the east. The "light brine"

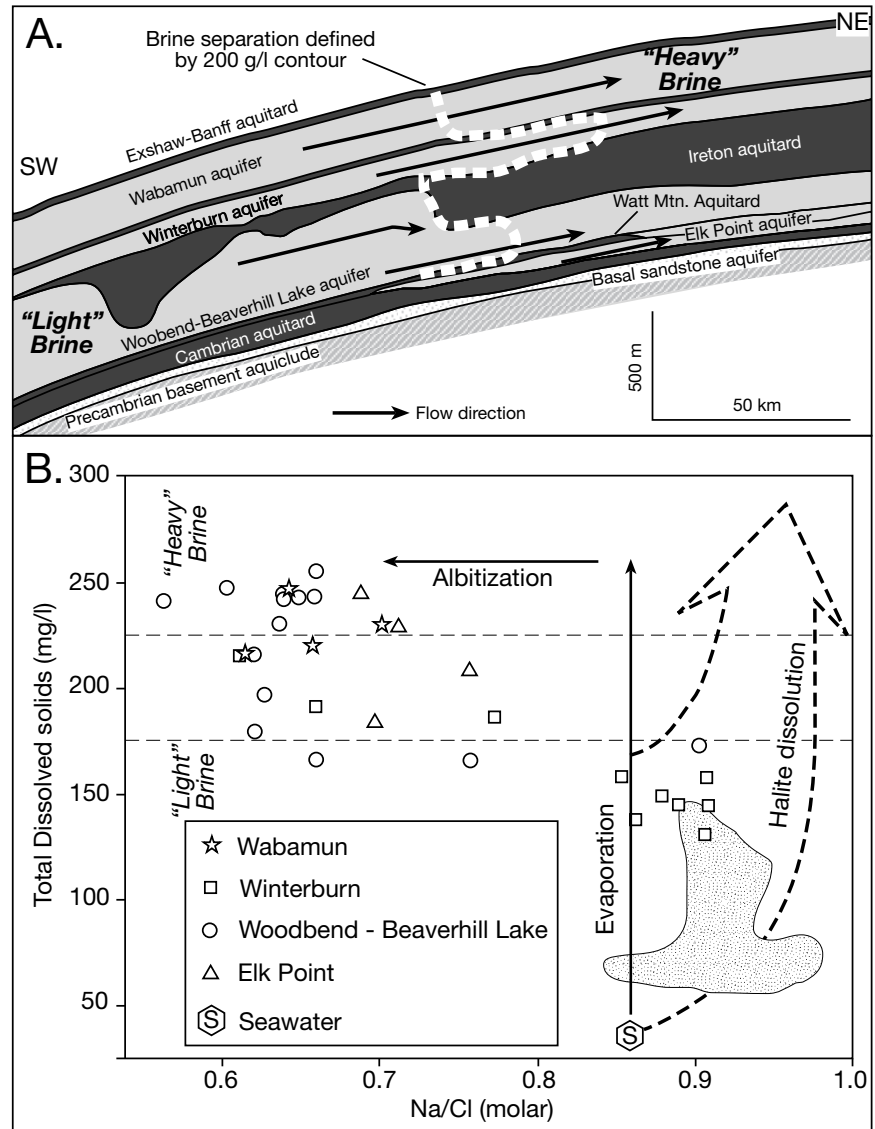


Figure 8.9. Basin fluids in Devonian of Alberta Basin (after Michael et al., 2003). A) Hydrogeological cross-section perpendicular to the deformation front to the west showing conceptually the differential advancement of the less saline formation water displacement front against a high-saline connate brine reservoir in the Cambrian-Devonian hydrostratigraphic group. B) Distribution of Na/Cl ratios versus salinity in Devonian formation waters showing some processes that may have influenced the brines. The stippled area shows the distribution of hydrochemical measurements for Mississippian strata where halite dissolution driven by deep meteoric circulation controls much of the hydrochemistry of the deep aquifer.

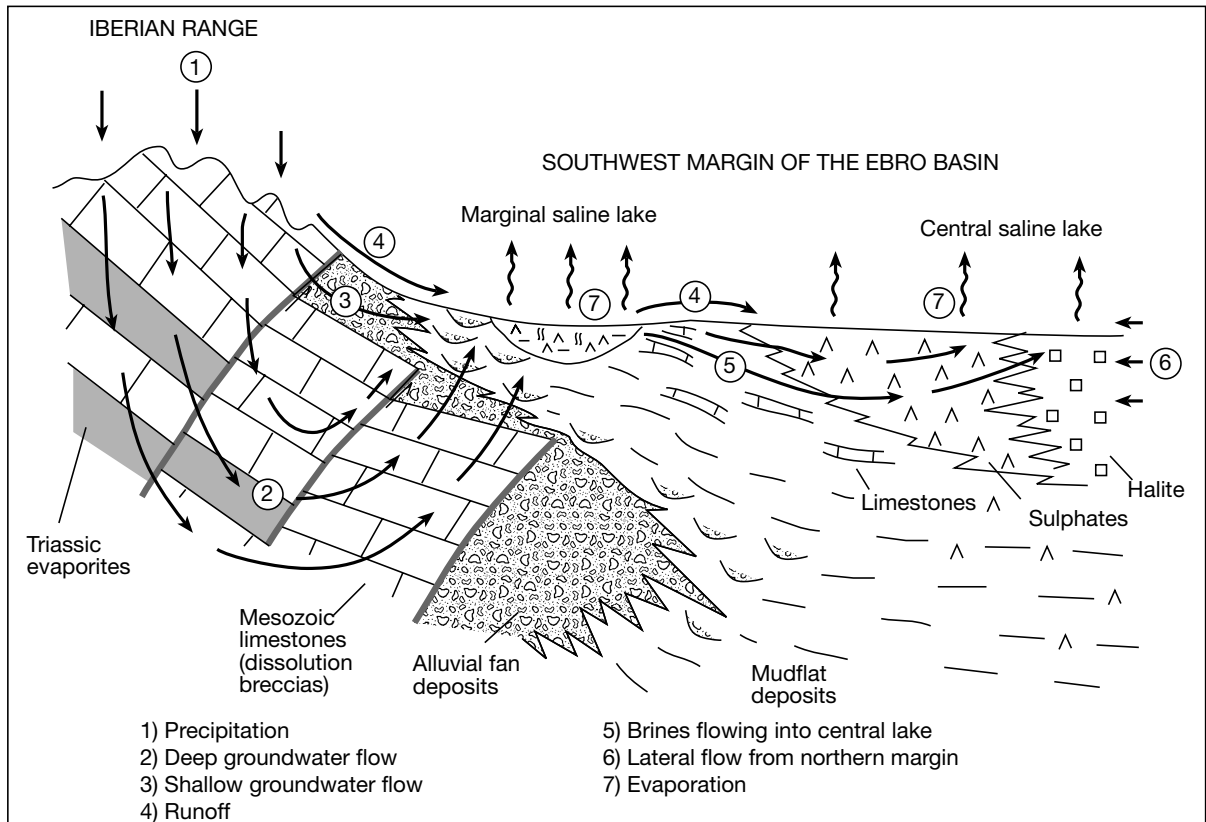


Figure 8.10. Palaeohydrologic pattern of the compressional (thrust) margin of the Miocene Ebro Basin, Spain (after Salvany et al., 1994). The Miocene lacustrine evaporites in the Ebro Basin are ultimately derived from the deep meteoric leaching of Triassic evaporites in the Iberian Range along the southern margin of the basin. Ongoing surface and nearsurface evaporative fractionation of shallow brines divided the Miocene chemical sediments into a series of bioturbated carbonate-rich gypsum lakes and a more central gypsum-halite-rich lake system.

probably originated from dilution of 'heavy brine' by deeply circulating meteoric fluids in post-Laramide times, similar to the dilution seen in the San Andres aquifer.

So far, we have discussed brine styles in the deeply buried portions of post-orogenic aquifers. But, when buried evaporites are caught up in the hydrology of compressional belts and subject to syn- and post-orogenic deep meteoric flow, their dissolution can supply much of the ionic content to actively accumulating evaporite systems in the outflow zones in an adjacent foreland depression. This was the case in the Miocene saline lakes of the Ebro Basin of NE Spain (Sánchez et al., 1999; Salvany et al., 1994). The current saline lakes in the same area (such as Lake Banyoles and Salada Mediana) are considered to be karstic relics of a more active saline hydrology that was set up during the Early and Middle Miocene, via intense compressional deformation and associated high relief in the basin margin.

Evaporite sedimentation at that time took place under a gravity-fed continental brine hydrology not connected to the sea (Sánchez et al., 1999). The sedimentation around the margins of the Ebro Basin was detrital, originating from alluvial systems that surrounded large saline and carbonate lakes in lacustrine systems that in their central depressions were dominated by playa depressions up to 100 km long and 30–50 km wide.

Three concentric hydrologically controlled and segregated subenvironments characterised the lacustrine depression: (1) central lake areas dominated by gypsum and halite pans; (2) intermediate lake areas with pervasive laminated gypsum and anhydrite as well as diagenetic glauberite, and (3) marginal lake areas with nodular diagenetic anhydrite, which gradually passed into distal alluvial plains (Figure 11.54). In some marginal lake areas that were isolated from the central lacustrine

systems there were small evaporitic lakes up to a few kilometres across. There local deposits of carbonate, gypsum and anhydrite precipitated from moderately concentrated brines, along with abundant diagenetic chert (Salvany et al., 1994).

Evaporitic successions in the central gypsum-halite lake area attain thicknesses of more than 200 m (Figure 7.44a) and almost all of it was derived from evaporation of deeply circulated meteoric waters that had dissolved Mesozoic evaporites and carbonates in folded basement in the adjacent Iberian Highlands (Figure 8.10). Most of the carbonate-rich marginal lakes corresponded to zones of the first diffuse emergence of this deep groundwater. Waters then fractionated as they moved toward the lowest parts of the lake depression. Since the Miocene the groundwater hydrology has evolved and matured to that of today where focused springs, rather than diffuse resurgence zones, define zones of initial groundwater outflow (Sánchez et al., 1999).

In summary, dissolving subsurface evaporites contribute to basinal pore salinities, chemistries and can drive fluid flow and mineral alteration at all stages of burial and uplift, and continue to do so as long salt and permeability live on in the sediment pile.

Alteration, pressure cells and salinity-driven convection

All water-bearing sediments compact and alter within the zones of compaction and thermobaric waters, as various connate or subsurface waters escape from the sediment pile. Pore waters issuing from compacting sands, shales and limestones are typically not halite-saturated, so salt masses tend to dissolve wherever fluids from dewatering sediment piles come into contact with salt beds or allochthons.

Evans and Nunn (1989) and Ranganathan and Hanor (1988) analysed salinity-driven convection in permeable sands near salt structures in the Gulf Coast. Sarkar et al. (1995) modelled salinity-driven free convection in less permeable shale-dominated media beneath a dissolving salt sheet or allochthon. Morton and Land (1987), Land (1991), and McKenna and Sharp (1997) noted salinity inversions in the south Texas portion of the Gulf of Mexico basin, where more saline pore waters (including brines > 100,000 ppm total dissolved solids) overlie less saline waters (\approx 20,000 ppm). Strong buoyancy gradients exist where such inversions occur, as the shallower pore waters are both cooler and more saline than deeper pore

waters. Most of these hydrologies are maintained by the rise of brine along fractures and faults from basal depths where deeply buried salt is actively flowing and dissolving. Convective return of brine occurs in areas away from the supplying structure (Sharp et al., 2001).

Haloed, convection and saltout

Over time, the ongoing dissolution of the edges of a salt bed, allochthon or salt wall sets up a dense subsurface brine halo. As it builds, the halo becomes so saline and dense that it starts to drive free convection. Saline pore waters slowly sink beneath the underbelly of the dissolving salt bed or allochthon, or spread laterally atop the upper side of a salt bed or edge of a diapir. Pore water from the salt underbelly sink to depths where it reheats, flows laterally and then rises to return once more to the underside of the evaporite bed to complete the convection cell (Figures 8.2a,b, 8.11). Such density-driven convective circulation is an important mechanism of depositing and remobilising pervasive secondary salts (burial salts) in subsalt beds that were originally nonevaporitic. It also creates basal “caprock” residues along the underside of the bed or allochthon.

Buried evaporite beds in contact with adjacent aquifers become sites of phreatic salt flushing as soon as the solar-driven active phreatic brine reflux hydrology starts to dissipate. Hence, burial dissolution of salt from its edges inward begins as soon as the bed enters the zone of compactional water flow (Chapter 7). This explains why the upper and lower contacts of many thick ancient evaporite beds are not depositional contacts. Rather they are zones characterised by dissolution residues, recrystallisation and pressure solution textures. For the same reason, well preserved primary and syndepositional textures in bedded evaporites are rarely found at the contacts with adjacent nonevaporite lithologies. Depositional fabrics are best preserved internally within an evaporite bed, away from the edges where basal fluids are eating into and altering the original evaporite textures. Diagenetic waters continue to dissolve or “melt” evaporite contacts until the evaporite dissolves or all effective permeability is lost in the adjacent beds.

The modelling of plumes beneath salt beds and subhorizontal allochthonous salt sheets, such as occur in the Gulf of Mexico, shows free convection has the potential to be a significant mechanism in both salt dissolution and mass transport, even if the sediments beneath the salt have permeabilities as low as 0.01 md (Figure 8.11; Sarkar et al., 1995). In such low permeability sediment it will take some 10 My for the sub-salt convection to develop to full strength. Once active, an average

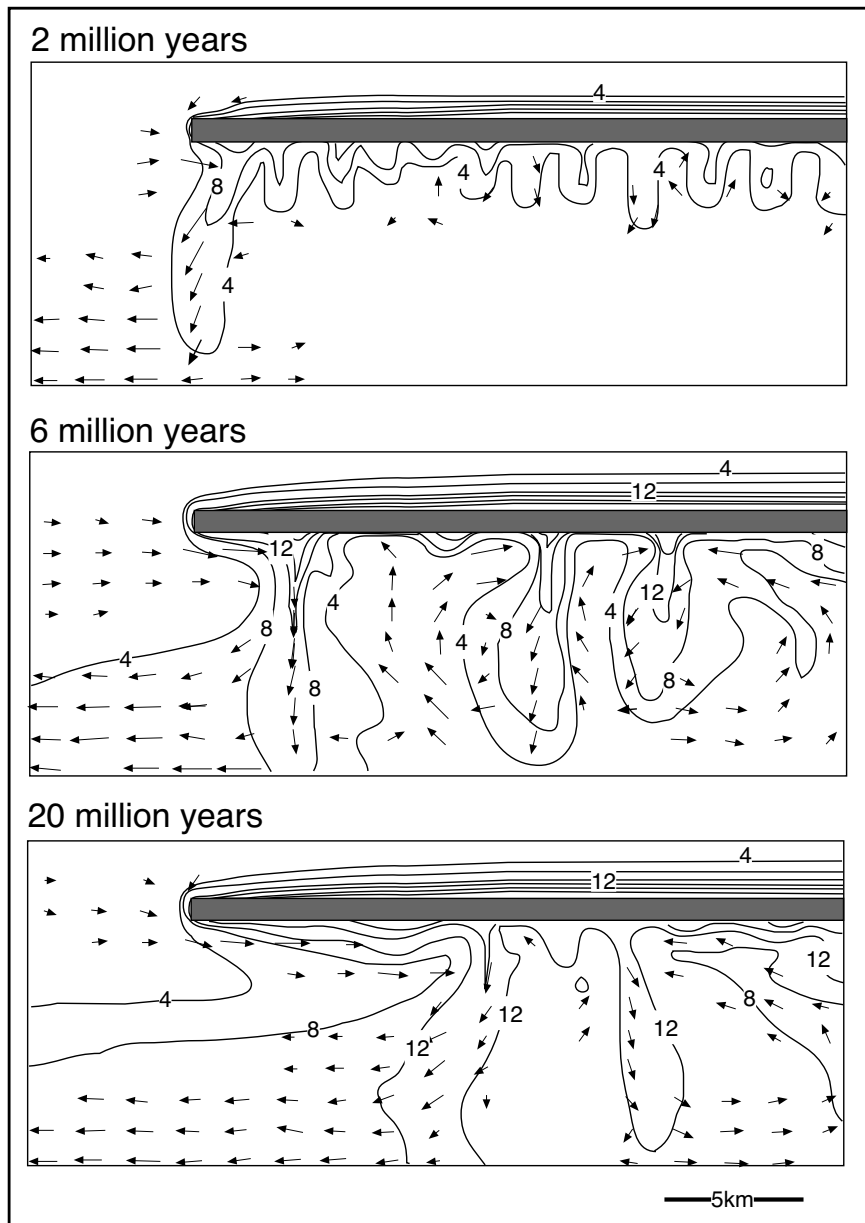


Figure 8.11. Modelled temporal evolution of brine plumes associated with ongoing dissolution of a salt sheet in a shale matrix at times of 2, 6 and 20 My. Salt sheet is grey (after Sarkar et al., 1995). Contours of plumes are given in terms of salinity difference: calculated as pore water salinity minus seawater salinity (3.5%). Numbers are in wt %. The leftmost plume is mostly fed by ongoing dissolution of the salt edge. Vertical exaggeration is 2x.

of 3-5-m of salt is dissolved off the underbelly every million years, with a maximum darcy flux of 3 mm yr^{-1} . Measured matrix permeabilities of overpressured shales immediately beneath allochthonous salt (the gumbo zone) are much higher than 0.01 md and so the actual flow and dissolution rates are much higher.

dissolution of the salt stem is quickly filled, either by salt from the stem, or, if dissolution is rapid enough, by the collapse of sedimentary beds against the stem to form “downthrown” slivers and blocks (Chapter 6). As dissolution of the salt

Chloride-rich density-derived convective flow cells are an inherent part of the hydrology beneath all dissolving evaporite seals. They continue to cycle subsalt pore water over and over through the underlying sediment column until subsalt permeability is shut down by compaction and thermobaric cementation. It can move volatile-entraining chloride-rich brines through base-metal and organic-containing shales and cupiferous redbed beneath buried salt beds and sheets. Wherever such waters break out from beneath the salt seal into suitably prepared ground, the associated cooling and brine mixing can precipitate metal sulphides or facilitate the focused escape of liquid and gaseous hydrocarbons (Warren, 2000b). Breaches typically occur via growth faults, salt welds or via seismic pumping along thrusts and thrust welds; all these features centrifugally drain basinal pore waters from beneath a salt bed or allochthon sheet. Simultaneously, the escape can drive other diagenetic reactions such as secondary porosity formation (via brine mixing and changes in $p\text{CO}_2$) or the precipitation of authigenic burial cements.

Where halite dissolution is occurring along the flank of a salt stock or diapir (shale sheath), the resulting dense pore fluids move into adjacent upturned permeable beds (Figure 8.2c). Any cavity created by local

stem proceeds, the resulting high salinity (high density) pore brines can spall off a sinking brine halo that is maintained by ongoing dissolution. Such high salinity pore waters tend to sink away from the stem down the more porous extensional portions of adjacent steeply dipping beds. Unlike the self-limiting rate of salt loss associated with the undersides of subhorizontal salt geometries, steeply dipping beds about a salt stem create a plumbing system with a tendency to self drain and so facilitate further dissolution of the stem and the set up of conditions suitable for the “salt-out” of rising hydrocarbons.

Hydrocarbons are less soluble in brines than in fresher waters. Price (1976, 1981) noted that at standard temperature and pressure (STP) the solubilities of n-pentane and methyl-cyclohexane decreased from 40 ppm in fresh water to 3 ppm in water with a salinity of 300,000 ppm. This means hydrocarbons dissolved in less saline basinal waters tend to “salt out,” or exsolve, in the vicinity of brine plumes adjacent to a salt stock or along the underside of a salt bed or allochthon. “Salting out” is a direct result of the increase in the salinity of the carrier fluid as the salt body is approached and the associated decrease in hydrocarbon solubility (Figure 8.12). The accumulation of oil and gas along the underside of a salt seal, or adjacent to a salt stock, drastically slows the rate of salt dissolution. Halite is near insoluble when in direct contact with exsolved hydrocarbons rather than pore waters. Such conditions help explain why hydrocarbon legs adjacent to a salt stem have a propensity to stack one atop the other with the hypersaline halo hydrology of the stem acting as a highly efficient seal. Of all the various evaporite traps, stacked salt-stem focused and sealed, steeply-inclined reservoir beds are among the most highly productive regions in the world in terms of barrels of oil equivalent (BOE) per unit area (Figure 10.45a; Halbouty, 1979).

Large-scale vertical migration of subsurface waters and crude oils via shears and fractures against salt structures was noted in the Louisiana Gulf Coast by Hanor and Sassen (1990). They concluded that the vertical upward flux of brine and hydrocarbons in this system followed fault and fracture permeability in sediments adjacent to the salt and did not otherwise move vertically through shales sandwiched between the various sand reservoirs. In the immediate region about the salt stem they found that higher salinities were localised in the same areas where hydrocarbon production occurred over and around the

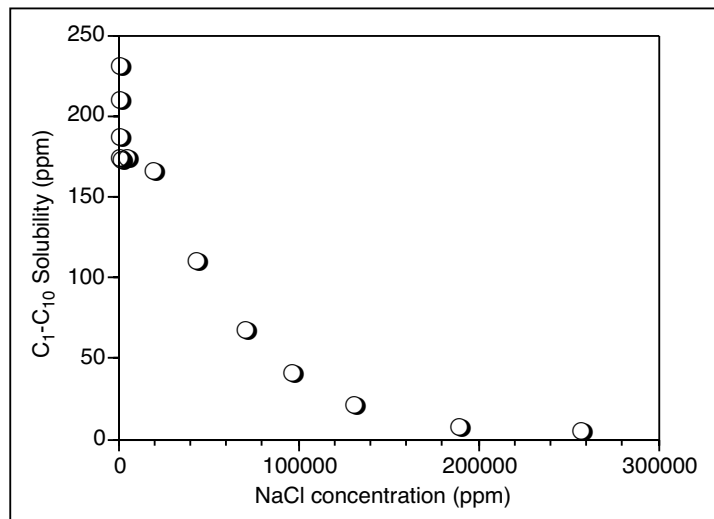


Figure 8.12. Aqueous solubility of a C₄ - C₁₀ petroleum distillation fraction as a function of NaCl concentration at a near constant temperature ($\approx 195^\circ\text{C}$) and pressure (765 bars). Replotted from data in Table 4 of Price (1981).

salt domes. This implies dissolution of salt is driven by the same warm fluids rising from geopressured intervals and carrying with them the hydrocarbons to shallower depths. Thus, most of the vertical fluid transport out of the deeper levels in a halokinetic basin is focused into the zone of structural disturbance adjacent to diapir stems.

Put simply, salt stems, beds and allochthons create temperature, salinity and fracture discontinuities that induce fluid flow. As long as sediments adjacent to a subsiding/flowing stratiform salt bed or allochthon can maintain some degree of permeability, much of the more interesting subsurface hydrology occurs in and around brine haloes centred about intervals or masses of slowly dissolving salt. Ongoing dissolution, alteration and flow near the edge of the bed or stem and extending into adjacent beds creates chemical and pressure gradients that exert significant influence of the style and patterns of subsurface fluid flow. This in turn exerts a strong influence on the location and style of various hydrocarbon and metal accumulations (see Chapters 9 and 10).

Evaporites as pressure seals

Abnormal formation pressure is any pressure that exceeds or falls below the normal pressure to be expected at a given depth. A formation can only be abnormally pressured if the following conditions are met; 1) there must be porosity as the formation must have the means of storing a pressurized fluid, 2) there must be a horizontal and vertical seal. An

Fluid type	Density (gm/cc)	API (degrees)	Salinity (g/l)	Gradient (kPa/m)
Brine	1.250	-18	374	12.25
	1.20	-14	398	11.76
	1.115	-8	222	11.27
	1.125	-6	182	11.02
	1.100	-3	147	10.78
	1.075	0	108	10.54
	1.050	3	71	10.29
Seawater	1.025	7	35	9.99
Freshwater	1.000	10	0	9.80
Heavy oil	0.950	18		9.31
Light oil	0.850	35		8.33
Distillates	0.650	88		6.37
Deep gas	0.500			4.90
Shallow gas	0.300			2.94

Table 8.2. Pressure gradients of various fluid columns, including brines of different salinities.

abnormally pressured zone will be unable to retain its pressure differential if it is adjacent to a permeable boundary.

Normal or hydrostatic pressure is the pressure exerted by a column of fluid extending down to the depth of interest, for a typical porewater column it increases at a rate around 0.465 psi per foot of depth (≈ 10.5 kPa/m). Hence, the normal pressure expected at 10,000 feet is 4,650 psi; abnormal pressure at this depth would be higher or lower than 4,650 psi (32 MPa). In reality a hydrostatic pressure gradient will vary slightly depending on the salinity of the pore fluid (Table 8.2). For fresh water the gradient is 0.43 psi/ft (9.8 kPa/m) and for a salt-saturated solution it is 0.53 psi/ft (11.9 kPa/m).

Pressure gradients are classified as:

- Underpressured (subnormal): <0.465 psi/ft
- Normally pressured: 0.465-0.65 psi/ft
- Moderately overpressured: 0.65-0.8 psi/ft
- Highly overpressured: 0.8-0.9 psi/ft
- Extremely highly overpressured: >0.9 psi/ft

About 80% of the abnormally pressured basins of the world appear to be controlled by low permeability seals (Hunt, 1990). Most intervals of abnormal pressure can be related to: faults, thick shales, extensive salt seals, or various combinations. Overpressured cells are the most common type of abnormal pressure and are characterised by fluid-supported pressures (typically geopressed rather than hydropressed^{8.1}).

Underpressured cells are matrix-supported pressure seals and are not as common as overpressured cells. They may be the result of the depletion of a reservoir of all its fluids, or they can form by surface exposure of the permeable bed at a topographic depth greater than interval where the pressure is being measured or where it is penetrated by the drill bit, or they form by the uplift of a fully enclosed and compacted formation. Both underpressured and overpressured cells are sealed or isolated from their surrounds, otherwise pressures would quickly return to normal. Evaporites play important roles in this isolation due to their inherent low permeabilities. A salt unit does not generate overpressure as it lacks porosity, but due to its exceptional seal capacity can hold back substantially pressurized fluid columns.

Possible causes of abnormal pressuring in sediment pore waters held back by the evaporite seal are numerous and can overlap in the same sequence. They are:

1. *Epeirogenic Movements:*

- a) Compactional disequilibrium during subsidence associated with rapid deposition (geopressed). Porosity reduction beneath a rapidly accumulating mass of sediment is inhibited by the difficulty in expelling pore fluids from relatively impervious sediment. As water is not very compressible, most of the overlying sediment's weight is then borne by the pore water rather than the matrix so creating high fluid pressures in the undercompacted unit. Thus the creation of overpressures by compaction disequilibrium typically requires high sedimentation rates (or erosion rates for underpressure) and a permeability seal or aquitard.
- b) Uplift and topographic recharge (artesian) means that in areas of recharge (high elevation and descending flow) the fluid pressures are below hydrostatic. In areas of discharge (low elevation and ascending flow) the fluid pressures are above hydrostatic (hydropressed). If a seal is present adjacent to the artesian aquifer, then overpressure or underpressure can develop.

2. *Hydrocarbon Generation:*

Maturation of trapped organic matter generating fluids that

^{8.1} Geopressures are found in units of rock in which the free flow of fluids has been effectively prevented by either the in-situ formation of an impermeable barrier bed, or the appropriate placement of such a barrier through tectonic activities such as: folding, faulting, or diapiric action of shale or salt.

A hydro-pressured zone is a sequence where hydraulic communication to the surface is maintained and the excessive pressure is due to the weight of the overlying fluids (typically a topographic head - artesian waters).

1psi/ft=22.5 kPa/m=0.0225MPa/m=22.5 MPa/km

1MPa = 145.038 psi

cannot easily escape to the surface. Higher density kerogen is replaced by lower-density oil and gas, which requires more volume for the same mass.

3. *Clay conversion:*

Volume changes in reactions involving clay mineral transformation with the associated release of fluid. For example, under high pressure and temperature, structural water is expelled from smectite as it converts to illite.

4. *Aquathermal Pressuring:*

Water expands with temperature more than mineral grains do. Thus, as sediments are heated with burial, the expansion of water generates fluid pressure. This effect is much smaller than compaction disequilibrium and requires a near perfect pressure seal to be effective.

5. *Buoyancy Forces:*

Created by density differences between reservoir fluids.

6. *Tectonic Stresses:*

Compressive and dilational regional stresses create pressure cells.

7. *Osmotic Pressures:*

Created by membrane filtration by shales and clays with associated water flow to equalize brine concentrations.

Other than this list of possible causes our discussion will now consider only intervals of abnormal pressure where evaporites have played a role in the creation or retention of anomalous pressure, typically by acting as a highly effective permeability barrier. For a more general discussion on overpressuring, its causes and effects, the reader is referred to Hunt's excellent paper or more recent papers by Yu and Lerche, 1996 and Osborne and Swarbrick, 1997.

Unlike thick shales, evaporites better fit Hunt's (1990) definition of a true pressure seal, which he defined as an impermeable rock with zero transmissivity maintained over long periods of geologic time. Little subsalt fluid escapes through a salt mass, which until breached tends to hold back all the compactional and thermobaric waters, gases or liquid hydrocarbons coming from beds below. In contrast, shales leak all these fluids to varying degrees. Pore fluid pressures tend to rise rapidly in porous sediments beneath the rapidly aggrading salts of a basinwide evaporite seal or in fined-grained sediments accumulating atop active salt withdrawal basin (minibasin) and so both subsalt and suprasalt associations can quickly become overpressured (Figure 8.13; Burrus and Audebert, 1990; Yassir and Bell, 1994; Lerche and Petersen, 1995).

The early onset of subsalt overpressure, and consequent slowing of subsalt fluid escape means that brine-saturated shales and silts below the contact with the salt can remain unconsolidated or semiconsolidated (hence porous and overpressured) to much greater depths and ages than would compacting shales without an evaporite cover. This is the case in many Permian shale beds beneath Zechstein evaporite pressure seals in northern Germany. Drilling through sharp pressure boundaries into shales in order to reach underlying potential reservoir sands can be a problem, as can drilling through porous rafts of Permian anhydrite or overpressured dolomite suspended in halokinetic salt (Finnie et al., 2001). Despite their Permian age, subsalt Zechstein shales tend to retain fresh, highly porous and plastic physical proper-

Salt-maintained overpressure

Salts (especially halite) are second only to clathrates in ability to form effective seals to rising brines and hydrocarbons, including methane (Figure 10.4a). Sharp pressure boundaries tend to characterise the contacts with many salt seals and evaporites create the highest and sharpest depth-related pressure differentials known in sedimentary basins in both overpressured and underpressured settings (Fertl, 1976). Salt-sealed overpressured intervals can be as shallow as a few hundred metres below the surface or deeper than 6000 m.

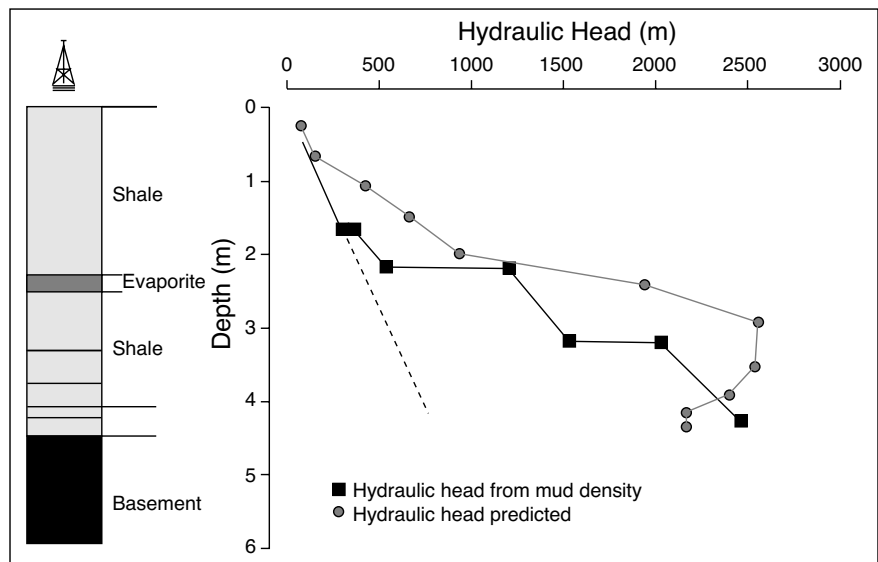


Figure 8.13. Overpressure beneath Messinian evaporites in the Gulf of Lions in the Mediterranean, as indicated by mud densities in the offshore well drilled at kilometre 155 and by predictive modelling (after Burrus and Audebert, 1990).

ties, so that when intersected by the drill bit they are prone to severe heaving, especially below depths of 1-2 km (Thomeer and Bottema, 1961; Williamson et al., 1997).

Similar heaving shales beneath thick salt beds and allochthons are commonly encountered in the Gulf of Mexico, Russia, the Middle East, Asia and North Africa (Fertl, 1976). Overpressured rafts of porous Neoproterozoic platform carbonate and basinal silicilyte suspended in halokinetic halite are widespread in the South Oman Salt basin (Figure 10.54). In all cases the salt seal itself appears normally pressured, but its lack of permeability means it can hold back a substantial fluid column until the drill bit breaches its porous and overpressured underside. Wells through halokinetic salt are also subject to longterm creep and this too can create long term well stability problems (Chapter 12).

Some of the highest measured bottom-hole pressures (formation pressures) in the world, and some of the highest wellhead flow pressures (measured while wells are in production), are found in subsalt reservoirs. These high pore pressures can occur not just in compressed muds but in evaporite-sealed fractured and vuggy carbonates that are not particularly young. For example, highly overpressured intervals occur in deeply buried Jurassic Smackover Formation dolomite reservoirs in the gas and condensate fields of the Central Mississippi salt basin in the Gulf of Mexico region. Salt rollers in the Jurassic Louann Salt are associated with deeply buried growth faults that cut the overlying Smackover carbonate reservoirs. The faults sole above the Smackover and are cut off within the anhydrite seal (Haynesville and equivalents), and so fail to leak fluid from intervals below the anhydrite seal (North, 1985). Down to depths of 3,600 m the fluid pressure gradients approximate hydrostatic (0.465 psi/ft or 10.5 kPa m⁻¹). By 6,000 m a powerfully overpressured zone is entered and the gradient increases to 1.0 psi/ft or 20.35 kPa m⁻¹. This approximates the lithostatic (overburden) stress for that depth.

Another example of an overpressured basin in older strata lies beneath the Permian salt seal of the Tengiz oilfield in the Precaspian basin of western Kazakhstan. The structure traps some 25 x 10⁹ BBL of oil in an upper Palaeozoic carbonate platform (Figure 8.14a; Anissimov et al., 2000). It is part of the giant Palaeozoic carbonate platform of the Primorsky Bend on the northeast Caspian Coast. The reservoir is made up of Upper Devonian to middle Carboniferous carbonates that are variably overlain by a 150-200m thick shale and then sealed by thick Permian halite. This halite enables overpressuring

with pressure gradients beneath the seal of $\approx 20 \text{ kPa m}^{-1}$, values similar to those in the Smackover and once again approaching lithostatic. Gradients in the nearby water-filled Karaton structure are slightly less due to pressure loss through a breach in the evaporite seal (Figure 8.14b).

Likewise, the Permian salts of the Zechstein Group form seals to overpressured gas reservoirs in aeolian Rotliegende sands of the southern North Sea (Fertl, 1976). In the Groningen gas field in the Netherlands, one of the world's largest gas fields ($\approx 100 \text{ tcf}$), the gas reservoir is only slightly overpressured (0.5 psi/ft or 11.3 kPa m⁻¹). But formation pressures in Rotliegende sands below Zechstein salt in northern Germany are much higher ($\approx 0.9 \text{ psi/ft}$ or 20.5 kPa m⁻¹), and in some areas in the Main Zechstein dolomite (Hauptdolomit) once again approach lithostatic (1.0 psi/ft or 22.6 kPa m⁻¹).

One of the most impressive examples of the ability of an evaporite seal to generate and maintain an overpressured subsalt cell comes from the Alborz discovery in Central Iran (Gretener, 1982). The discovery well had drilled through some 400 metres of normally to slightly overpressured Tertiary salt (halokinetic) to penetrate some 5 cm into the fractured Qum Limestone (Oligo-Miocene). Then the entire drill string and mud column were blown back out the hole. At that time the mud pressure was 55 MPa (8,000 psi) at a reservoir depth of 2700 m (8,800 ft) a pressure depth ratio of 20.5 kPa/m or 0.91 psi/ft. In 82 days the well released 5 million barrels of oil and a large but unknown quantity of gas before it self-bridged and the flow died.

Some of the oldest documented occurrences of preserved overpressure, associated with producible hydrocarbons, come from blocks of Neoproterozoic silicilyte, encased within the halokinetic Ara Salt of Oman. Initial fluid pressures within fractured slivers of the Athel Silicilyte in the South Oman Salt Basin can be as high as 19.8 kPa m⁻¹ (Figure 10.54; Amthor et al., 1998).

All these older examples of salt-sealed overpressure clearly illustrate the ability of evaporites to maintain seal integrity over time frames of 250-500 Ma and atop pressure fields approaching those that induce hydrofracturing. In contrast, most compacting and subsiding shaly sediments, with permeabilities ranging from 10⁻⁴ to 10⁻⁸ darcies, are thought to be too permeable, by several orders of magnitude, to preserve overpressures for time frames longer than 200-250 million years (Lee and Williams, 2000).

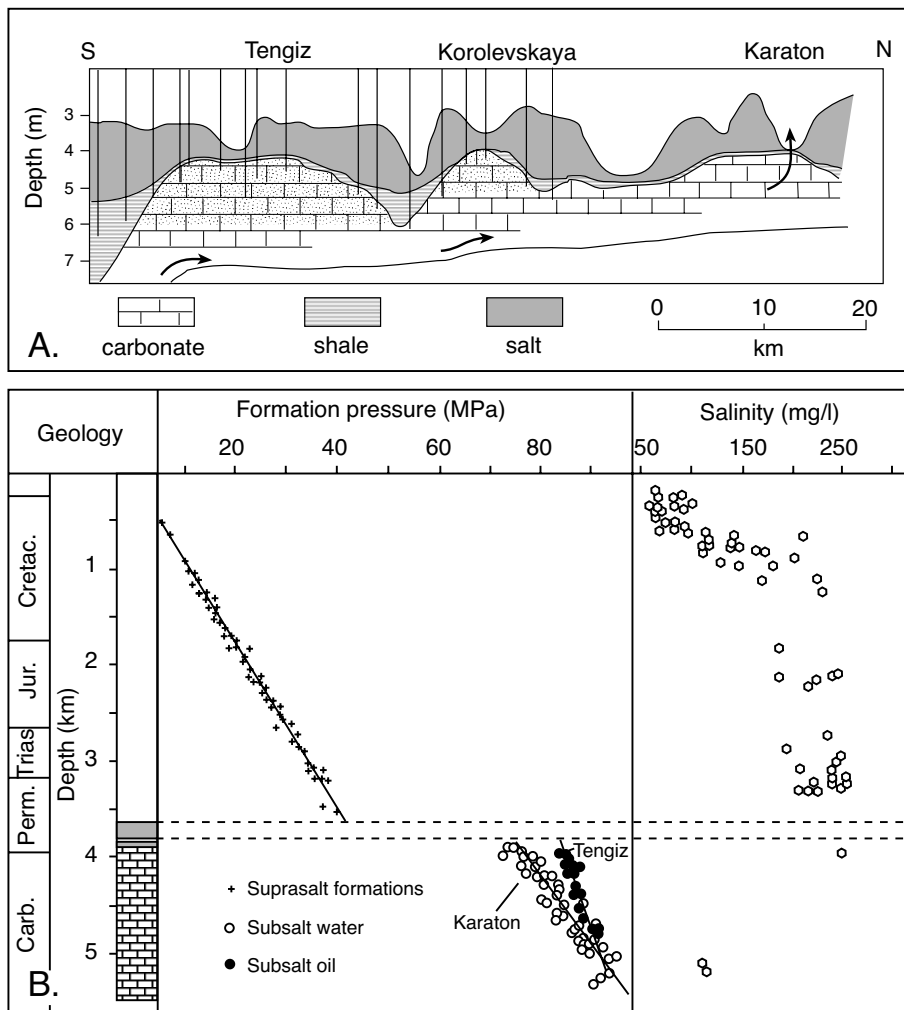


Figure 8.14. Tengiz oil field, Karzakistan. A) East west cross section showing how the evaporite seals the oil in a number of carbonate buildup traps. When the salt is breached at the Karaton structure the oil has escaped and the structure is water filled. B) Measured pressure plotted against depth, clearly shows the base of the evaporite (shaded grey) is the top of the overpressure (after Anissimov et al., 2000).

If hydrofracturing occurs with associated pressure release, growth-pulsed fibrous cements of halite, gypsum and carbonate may precipitate in new fracture nets immediately beneath the evaporite seal. But in systems where the evaporites are subsequently dissolved only carbonate vein fills and their fracture nets will remain as brittle sediment indicators beneath a layer of dissolution breccia or insoluble residues.

Salt's impervious nature and its ability to flow, while intrasalt beds fracture, leads to interesting pressure scenarios wherever rafts are caught up in masses of halokinetic salt. Fracturing of intrasalt beds and encasement in flowing salt is an

inherent mechanism in almost all autochthonous and allochthonous salt masses (Chapter 6). It explains unexpected pressure rises when drilling through thick sequences of salt on the way to testing subsalt hydrocarbon traps or creating purpose built salt storage cavities (Chapters 10 and 12 respectively). Porous blocks intersected in drilling halokinetic salt can be isolated or clustered (Figure 8.15). Common practice is to bleed them down, since they usually have limited extent within the salt mass. At the well site the observed rate of depletion should give some idea of how long the process may take. In the worst case scenario one raft will “blow-out” into another leaving the rig operator to wait until equilibrium is established. Generally, no pressure transitions are observed prior to drilling into a raft, reflecting their isolated nature within the salt.

In the Zechstein, for example, the Z3 bioclastic layer of dolomite, Plattendolomit, is deposited on top of the Z2 Stassfurt halite (Figure 5.48). A CaSO_4 layer was precipitated as gypsum, followed by the Z3 evaporites and the Leine halite (Finnie et al., 2001). Water from the gypsum was expelled as the sulphate dewatered and transformed into anhydrite. The overlying halite did not permit the upward movement of this water and so it forced into the adjacent porous platy dolomites. The Plattendolomite, already contained fluid and so excess fluid was accommodated in part by pressure-driven leaching.

When the Zechstein's most mobile salt layer, the Z2 Stassfurt halite, begins to move, it carries with it the overlying Platten/

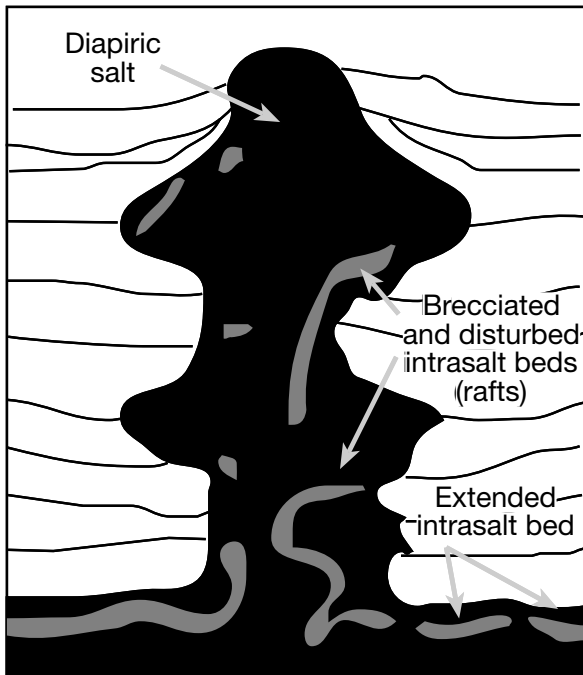


Figure 8.15. Likely distribution style of isolated overpressured blocks of deformed and fractured intrasalt beds (shaded grey) in a diapir or salt wall (based in part on modeling of Koyi, 2001).

Hauptanhydrite, which begins to buckle and deform much more brittlely than the surrounding halite. Eventually these intrasalt beds fractured into discrete rafts and were carried along by the flowing Stassfurt salt as it pierced the base of the Z3 (Figure 8.15). Rafts floating in the salt becomes overpressured by either; i) being uplifted to shallower depths where they continue to hold their deeper pressures because of the surrounding impermeable salt, or ii) overpressures are generated in the raft by the folding and squeezing nature of almost all subsurface salt creep in the inverted structures of the North Sea (Chapter 6).

As well as these examples of overpressure associated with older evaporites, overpressure readily develops in salt-sculpted Tertiary basins, as occurs beneath some, but not all, shallow salt allochthons in Green and Mahogany canyon regions in the Gulf of Mexico (Figure 6.22a; Beckman, 1999). Where salt allochthons are climbing the stratigraphy, subsalt sealing and associated overpressure can occur beneath the salt mass at higher levels than is achieved in overpressured shale basins. Extreme overpressuring is commonplace in subsalt settings in the Gulf of Mexico at depths of 3000-4000 m. Gas being generated at greater depths in these regions can be trapped under the salt seal at pressures approaching lithostatic. It means drilling under the allochthonous salt on the Gulf Coast slope can intersect undercompacted sediments that are moderately to extremely overpressured (Hunt et al., 1998). This influence of Jurassic salt on pressure gradients in the Neogene stratigraphy of the Gulf of Mexico is seen in the increased mud weights typically required for safe drilling once an evaporite allochthon is breached by the drill (Table 8.3). Most wells intersecting salt allochthons in the deepwater realm of the Gulf of Mexico are overpressured at some depth below the base of salt with mud weights controlling pressures ranging from 14 to 17.5 ppg.

In the offshore Mahogany area, salts sheets are encountered below 2,300m (7,500 ft) seafloor with an average thickness of 1,150 m (3,800 ft; Walton and Urband, 1997). The interval of disturbed sediments (gumbo), first sealed below the salt as the allochthon sheet rolled into place across the seafloor, now extends 300-500 m (1,000-1,500 ft) below the salt base. Formation temperature at the salt base is around 75°C (170°F). Rotary sidewall cores in the salt show the salt is very dense and competent. Fracture gradient checks performed in and below the salt mass by pump-in leak-off tests, approach 0.988 psi/ft (19 ppg). The fracture pressure is only 0.5 ppg higher than the pore pressure in those wells. Yet in other subsalt wells the

Well	Top salt (m)	Base salt (m)	Total salt thickness (m)	Total well depth (m)	Mud weight above salt (ppg)	Mud weight below salt (ppg)	Density profile (gm/cc) (above/in salt/below)	Sonic log below salt (μsec/ft)
West Cameron, Block 505, No.2	4,300	4,780	480	5,640	12	18	2.45/2.05/2.25	140
Garden Banks, Block 171, No. 1	2,590	2,925	335	3,230	12	14	2.15/2.05/2.25	140
Vermillon, Block 356, No. 1 South	2,592	3,231	639	5,180	13	18	no data	140
South Marsh Island, Block 200, No.1	2,685	2,987	302	n/a	15.6	17.2	2.15-2.25/2.05/2.15-2.25	130

Table 8.3. Typical mud weights used to drill overpressured suballochthon intervals in the Gulf of Mexico (after O'Brien and Lerche, 1994).

underlying disturbed sediments cannot support a mud column of 16.9 ppg (0.879 psi/ft gradient). Pore pressure gradient decreases as drilling progresses below the salt, until the sediments became more competent and less affected by the influence of early sealing beneath the salt allochthon trap.

But subsalt pressures in allochthon basins are very unpredictable, as it is not the salt itself that generates abnormal pressure (it lacks porosity). The overpressure comes from the inability of basinal fluid to move through the salt mass or to drain freely from thick underlying shales. For adjacent sediment to be abnormally pressured, fluid must be generated by compactional or thermobaric processes in the sediments beneath the salt. The salt mass itself is only the barrier to this escaping fluid. So, where sediments immediately below a salt mass are not carrying overpressured fluids, the contact with the salt is not overpressured. In fact, lower than regional pressure gradients can be found below some salt allochthons, as well as the more typical higher pressures. For example, a few subsalt wells in the Mississippi Canyon have mud weights indicating much lower subsalt pressures (11 to 12.5 ppg mud weights). Such lowered pressures may indicate zones of rapid salt solution and creation pore space via dissolutional collapse. Nor can overpressure be correlated to the thickness of the overburden atop a salt allochthon. The only generalisation that can be made is that, if abnormal pressures are present immediately beneath or adjacent to a salt mass, the pressure boundary will typically be sharp and correspond to the contact with the salt mass.

Thick shale-rich suprasalt successions in the withdrawal sinks (minibasins) of some more deeply buried salt units are also overpressured (Figures 6.30, 6.31). Shale-sealed sands sometimes show evidence of permeability connections through shale gouge zones about salt masses. Shaker (2004) argues that at the scale of salt-rooted minibasins, higher pressure gradients tend to occur in areas where the salt was present, while lower gradients tend to occur in areas where the salt has been withdrawn into adjacent allochthons. But this is a dynamic situation in which seal rupture (often along growth faults in the edges of minibasins and atop a zone of thinned salt) is followed by a cycle of fluid movement, a pressure drop, resealing, and renewed pressure buildup from the continuous generation of thermogenic gas. It creates dynamic pressure regimes where overpressuring beneath salt allochthons can occur a number of times in the minibasin history (McBride et al., 1998a, b).

Such an active growth fault at the edge of a salt-cored minibasin creates a fluid conduit to the numerous shallower reservoirs in Eugene Island South Addition Block 330, offshore Louisiana.

The fault was intersected and sampled at a depth of 2460 m in the extended "Pathfinder" well (Figure 8.16; Anderson et al., 1994). Oil and gas in this region is being produced from Neogene reservoirs as young as 400,000 years old and the field is located beneath numerous active seafloor seeps. Eugene Island is the largest Pleistocene oil field in the world and is surrounded mostly by gas-dominated fields in the south additions of offshore Louisiana. More than 600 million BBL of oil equivalent has been produced from this field since its discovery in 1971 (Figure 8.16a, b). Sediments filling the minibasin consist of alternating sequences of sands and shales that are likely floored by deepwater turbidites from the ancestral Mississippi River delta. The studied fault sits atop a breached salt allochthon and defines the edge of a classic Gulf Coast minibasin (Figure 6.58).

In spite of the removal of what was once an underlying salt allochthon via earlier salt evacuation, deeper sediments are still geopressured. The pressure buildup reflects ongoing rapid deposition of thick deepwater shale above the evacuating salt allochthon. Rapid mud deposition produced permeabilities in the lower part of the minibasin fill that were too low for the compacting pore fluids to escape. Oil and gas today still seeps from silty shales adjacent to the fault zone, which are naturally fractured. Coring revealed that fracturing extends at least 100 m from the growth fault into the shales of the upthrown block. Hydrocarbons in the fault zone are geochemically identical to those sampled from producing reservoirs located within sands that abut shallower splays of the same fault zone system (Figure 8.16b, c). Hydrocarbons did not flow from the growth fault at economically viable rates during drillstem tests. Analysis of fluid pressures shows that the main 'A' fault is currently a profound lateral permeability barrier, with an 1800 psi water pressure differential across it. Even so, Anderson et al. (op cit.) noted that the larger the drawdown pressures applied across perforated intervals, the lower the permeabilities of the fault zone. Flowable hydrocarbons are present and must be partially supporting the matrix. The balance between tectonic stresses and pore pressures, within the relatively tight zone defined by the growth fault, was found to be such that with an increase in pressure of 500 psi or so, large volumes of fluid could be transmitted from depth, suggesting a method that may allow production from such deep zones in the future.

Pressure data in Block 330 supports the notion of periodic fluid flow in the fault being driven by "seismic pumping" within salt-floored extensional basins. The term seismic pumping comes from an analogy to a hand-driven water pump used to raise water from a water well. As the handle of the pump lifts the piston

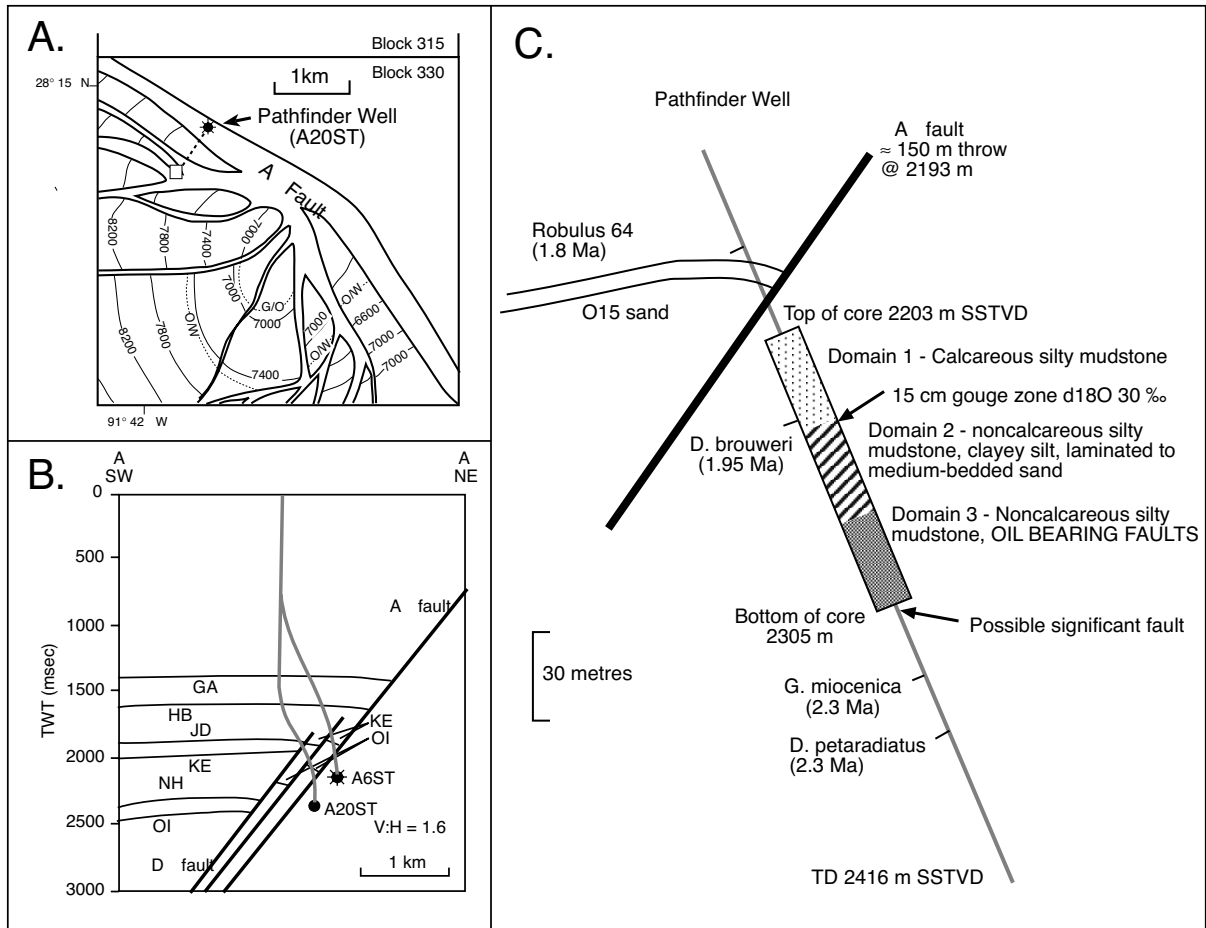


Figure 8.16. Growth fault characteristics, Block 330 Eugene Island, Louisiana. A) Structure contour map of O1 sand, showing position of the Pathfinder well. B) Southwest-northeast cross section AA' showing Pathfinder (A20ST) and A6ST well trajectories, the 'A' fault, subsidiary structures and selected sand tops. Depth in milliseconds two-way travel time (TWT); 1 ms approximately corresponds to 1 m depth in this section. C) Summary cross section of core from Pathfinder well showing core location relative to 'A' Fault zone and biostratigraphic markers. SSTVD = subsea true vertical depth (after Anderson et al., 1994).

it creates a low pressure region that draws in water across a one-way valve into the pump cavity. Then as the action of the handle is reversed it compresses the water beneath the piston forcing water out of the pump faucet. Likewise seismic pumping is related to cycles of dilatancy and fault release in the region of the fault. Extensional dilatancy in the fault and its vicinity draws in pore waters (and hydrocarbons) from its surrounds. This is followed by an episode of fault release, whereby overburden loading now compresses and drives water up along the fault into higher levels. Hence, with seismic pumping active in a normal fault or growth fault, the episode of fault release (earthquake) drives fluid up along the steeply dipping fault.

Seismic pumping of fluid is also possible in a reverse fault or thrust scenario. Once again the time of fault release is the time when fluid is sucked into the fault plane ("squeegee mode" mentioned earlier). But the low angle of the thrust means it does not easily drain up the fault to the surface but remains under subsequent compression to act as a fracture propagator, as evidenced in multistage fracture filling mineralisation associated with the thrust. This is especially so in sediment beneath salt-lubricated (and sealed) thrusts.

Based on their studies of the Eugene Island growth fault, Anderson et al. (1994) and Losh et al. (1999, 2002) concluded that hydrocarbon migration associated with the fault was episodic. It was driven by pressure increases deep within the

geopressed turbidites of the subsalt play, which rose until stresses reopened fractures in the various fault zones that connected with the upper reservoir chambers. At that time, large volumes of hydrocarbons were released rapidly as transient bursts towards the surface. With each pressure release, the faults closed back up. Losh et al. (1999) modelled coupled heat and mass flux in the A6ST well and concluded that the palaeothermal anomaly in the fault zone was short-lived, having a duration of less than 150 years. The anomaly could have been produced by a $2 \times 10^6 \text{ m}^3$ pulse of fluid ascending the fault at an actual velocity of over 1 km/yr (darcy flux of 330 m/yr) from 3 km deeper in the basin. Simple Darcy law computation indicates transient fault permeability on the order of 110 md during this flow. Pulsing of fluid up weld-floored growth faults is probably the norm. Put another way, with added pressure, fluid (including oil and gas) is expelled up the fault zone, but then the very act of releasing the fluids drops the pressure and the fault becomes tight once more. Over and over, the cycle repeats. A pulse of high-pressure fluid ascending the fault lowers effective stress in the fault zone sufficiently to produce a significant transient increase in fault permeability. If the fluid is in an area of the fault adjacent to downthrown, relatively low pressure reservoir sands, the fluid will discharge into them. Permeability in and adjacent to the fault then decreases, such that fluid cannot re-enter the fault zone and escape from the reservoir.

On the broader scale, salt's ability to deform with its accumulating overburden into growth fault-defined minibasins means pressure cells in suprasalt sediments not only show episodic changes in a high-gradient vertical pressure transition, they can also be subject to rapid lateral changes in pressure. Many lateral seals in this situation are subvertical and tend to follow fault trends with their geopressed tops sometimes defined by high temperature carbonate cements. Using a 3D model of fluid flow history in the Eugene Island area, Anderson et al. (1991) concluded that many convective heat flow anomalies at the surface indicated the upward movement of hot subsurface fluids along various salt-floored growth faults. Many of the larger fluid compartments in this laterally restricted system consist of a series of smaller compartments, each with a single top seal and several side seals, which are active growth faults (Gordon and Flemings, 1998). Similar episodic salt movement of various fault-defined pressure cells within the Jurassic Smackover Formation, atop the Louann Salt of the Mississippi Salt Basin, US Gulf Coast, has created a boxwork of large fluid compartments. Adjacent internal pressures ranging from normal (hydrostatic) in one compartment to 70 MPa (10,000 psi) above normal on the other side of the fault.

Pressure changes and drilling

When attempting to control bottom hole pressures during drilling, overpressures beneath evaporites are more of a problem to predict than when drilling thick variably pressured shales (e.g. Zilberman et al., 2001). Most current overpressure control methods, which use slightly overbalance methods of mudweight to minimise formation damage, were developed in shale sequences where there is typically a well-defined transition over tens to hundreds of metres into the zone of overpressure. Transitions are often identifiable by changes in resistivity, density and sonic signatures in MWD (measurement while drilling) logs. Close monitoring of bottom hole pressure and the recognition of this transition zone allows the drilling engineer to set casing, if needed, and to increase mud weight before entering the zone of overpressure. Evaporite seals can be much thinner (down to 3 m), with sharp pressure transitions at their lower boundaries. A sharp dissolutional contact along the underside of almost all thick evaporites and the inherent ability of a salt mass to support high fluid overpressure beneath intervals as little as 3-4 m thick means there can be little, if any, development of a pressure transition zone. Highly pressured sediments can be entered immediately below the base of the evaporite (e.g. Alborz discovery, Iran), whereas pressures appear normal as the evaporite is drilled.

If a basal anhydrite (upside-down caprock; see Chapter 7) has developed on the underside of a halite mass, there may be a slowing of the drill penetration rate immediately prior to entry into the overpressured interval. However floating anhydrite or dolomite rafts in diapiric halite also slow drill penetration rates. In one situation pressure tends to bleed off with time; in the other the well is susceptible to a major blowout.

Low strength casing set in a thick halokinetic salt mass, which tends to heave over time, will deform and can even shear during the active life of the well. Likewise, "drilling on" through heaving and often geopressed shales beneath a salt allochthon (gumbo) is a challenge for the drilling engineer, further compounded by the possibility of encountering heaving intrasalt "shales" or overpressured intrasalt anhydrite and dolomite rafts on the way to the lower contact (e.g. Seymour et al., 1993; Zilberman et al., 2001). Salt is also a good conductor of heat and impacts the local geothermal gradient (see later). It may be that heat is conducted to trapped formation fluids below the salt, so that overpressure of porous intrasalt rafts is further enhanced through restrained thermal expansion of these "shale" beds.

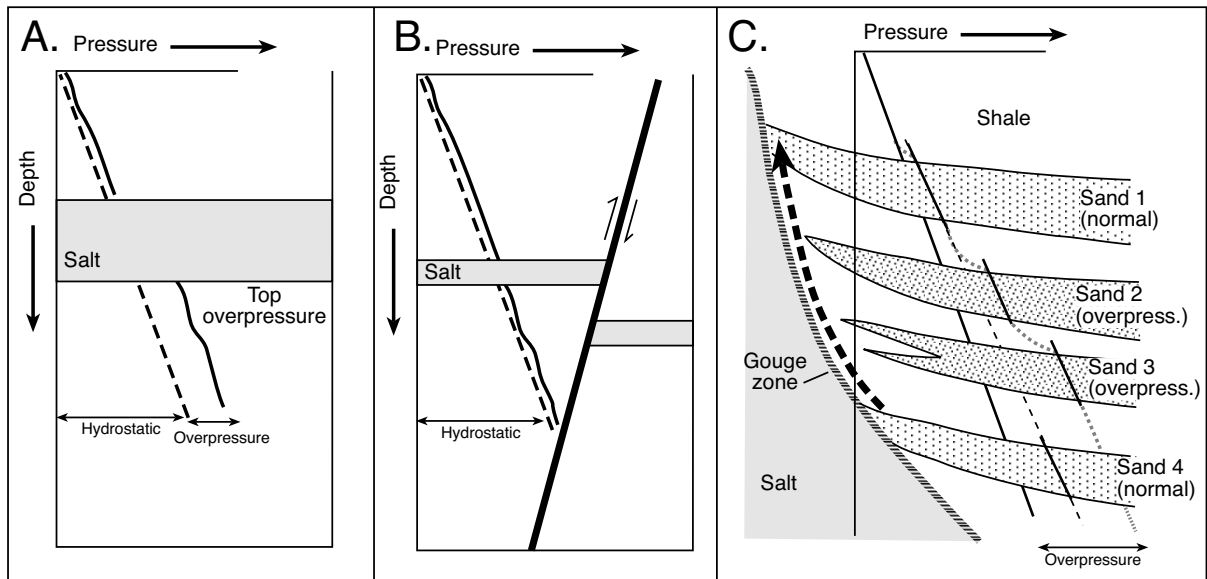


Figure 8.17. Pressure profiles of various evaporite profiles. A) Overpressure beneath a thick laterally extensive salt bed or allochthon. B) Normally pressured beneath a thin discontinuous (faulted) salt layer. C) Overpressure in suprasalt sands encased in shale. Sands which are in contact with the shale gouge tend to be in pressure connection, while those which are not are independently pressured (in part after Shaker, 2004).

Important factors controlling subsalt pressure distribution below both primary beds and allochthons are:

- Lateral extent and thickness of the salt body (Figure 8.17a; diameter of drainage collection)
- Presence of areas of halokinetically thinned, or faulted or discontinuous salt (Figure 8.17b; leakage)
- Depth of salt burial, salt buried at shallower depths (>1-2 km) may not have developed widespread overpressured intervals in the underlying sediments (with allochthons this is often due to a lack of lateral or updip seal)
- Rate of burial, slow burial may have allowed overpressure to dissipate in the subsalt beds
- Presence of a widespread sand-rich section underlying the salt may facilitate drainage and loss of pressure. More laterally restricted sand-rich sections under the salt can form both an excellent trap and reservoir for hydrocarbons (Figure 8.17c)
- Presence of a shale sheath or gouge about a salt structure. Suprasalt sands that connect to this gouge may be overpressured but tend to be in pressure connection. Intervening sands that are unconnected to the gouge can be independently overpressured (Figure 8.17c).

In summary, any actively subsiding and rapidly filling sedimentary basin containing widespread thick evaporite beds or allochthons is prone to subsalt overpressuring. The evaporite bed typically becomes the top of a shallow zone of geopressure and an evaporite in this situation can be thought of as a pres-

sure seal. An evaporite's ability to act as a pressure seal and so create overpressure in the underlying sediments can begin once the underlying sediment enters the zone of compactional dewatering and can continue well into the thermobaric regime. Salt's ability to act as a pressure seal is destroyed once it dissolves or its lateral continuity is breached, as occurs during salt allochthon evacuation. However the process of salt evacuation is often rapid and facilitates deposition of rapidly-emplaced thick deepwater muds within the lower parts of the minibasin fill. Growth faults, first instigated by the salt evacuation and soling into the salt weld, continue to act as escape foci for episodic pulses of upward-flowing hydrocarbon and metal-rich waters, even after the salt has moved on. Zones of salt breaching begin as foci for escaping pressured and metal-rich basinal fluids, they continue to act as episodic suppliers of volatiles, which typically move upward with the escaping basinal waters via the salt welds and growth faults that cut through the evaporite bed.

Salt-generated Underpressure

Most naturally underpressured cells are created by a combination of uplift and erosion or glacial rebound. Pressures in an underpressured interval are less than would be expected if a normal hydrostatic gradient was present. Reduction of lithostatic load in natural situations is most often related to erosion of a low permeability sediment pile, this typically creates an elastic

dilation of rock-pore volumes and so induces underpressuring. In regions of former ice sheets, fluid underpressuring is often tied to a rapid load reduction via melting of the glacier and associated isostatic rebound. Anthropogenically induced underpressure is often associated with hydrocarbon extraction.

One of the most striking examples of salt-associated underpressuring comes from the Keyes Field in the Oklahoma Panhandle. It has produced gas from a depth of 1460 metres (4790 ft) for more than 50 years and its pressure-depth gradient is shown in Figure 8.18 (Hunt, 1990; Powley, 1980). Keyes Field is located in an area of the Amarillo Uplift that rose by around 1500 m (4,920 ft) during the Laramide orogeny and later cooled. Fluid pressures above the Keyes gas sand and down to the Blaine Anhydrite show a normal gradient of 44.5 psi/100ft. Below the Blaine there are two anomalous pressure cells. The upper anomalous cell extends from the base of the Blaine Anhydrite to the top of the Wellington Salt seal (at a depth of 853 m or 2,800 ft). Fluid pressure at its top (≈ 1000 ft - 305m depth) starts at zero and increases down to the top of the Wellington Salt. The gradient in this upper cell is 44

psi/100ft. The lower cell extends from the base of the Wellington Salt to the top of the Precambrian basement. Beneath the Wellington Salt pressures once again start around zero, then increase along a gradient of 0.465 psi/ft (10.5 kPa/m). Overall the Keyes Field is underpressured for its current depth by some 9 Mpa (1,300 psi). Lithologies at the base of each of the pressure cells support the full weight of the overburden.

That both evaporite beds are acting as highly effective seals to their respective pressure regimes is indicated by the fact that fluid pressures start again at zero in the zone immediately beneath each evaporite. In terms of hydrocarbon components, underpressured compartments are important in that they indicate isolation of rocks in the underpressured cell, prior to extraction this isolation has prevented water washing and biodegradation of accumulated oils at depths where these processes would otherwise be important influences on oil quality.

Temperature anomalies and brine flow

Thermal anomalies associated with buried salt have been known since the 1930s (Hawtof, 1930) and can have significant influence on the maturation state of source rocks for hydrocarbons. Such anomalies are related to halite's higher thermal conductivity compared to most rock types (Figure 8.19a). Thermal differentials drive basin fluid circulation, especially in sediments adjacent to interval of halokinetic salt. At room temperature the thermal conductivity of salt is typically three times that of adjacent shales. At 150°C its thermal conductivity is about two thirds of its 25°C value and still more than twice that of an adjacent now compacted shale. Thus a salt bed or salt structure, with its much higher conductivity, exerts a strong influence on the thermal depth profile in an evaporite-en-training basin (Figure 8.19b).

When conductive salt remains as a bed, it raises the temperature gradient in sediments atop the salt bed, lowers the temperature gradient in the salt layer and makes beds below the salt layer cooler than they would be if the salt was not present (Mello et al., 1995). For example, with a 1 km-thick salt bed encased in shale, sediments below the salt are 20°C cooler than they would be if salt were not present (Figure 8.20a). According to Mello et al. (1995) the cooling effect is proportional to the thickness of the salt layer. All subsalt sediments are subject to non-transient cooling effects that last as long as the salt remains. Such temperature differences obviously affect organic maturation in sediments above and below the salt layer.

If the salt bed has flowed and a salt diapir is present, but with its crest buried well below the sediment surface, the conductive spine

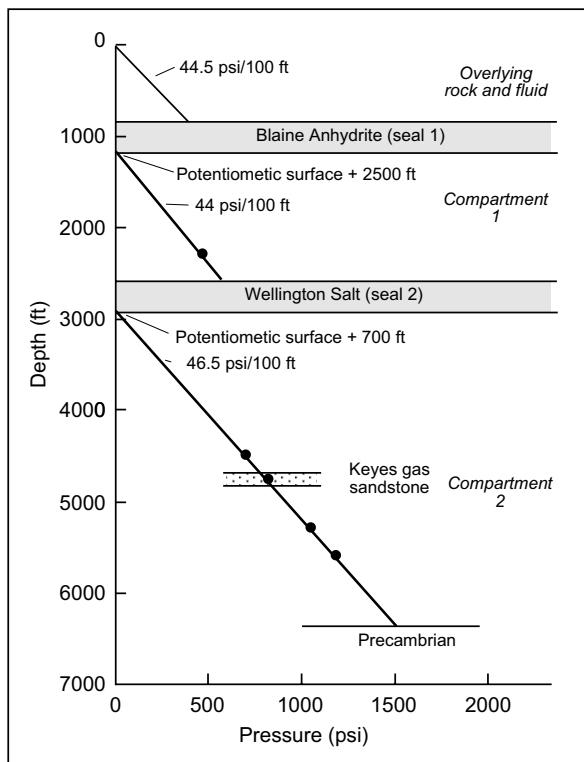


Figure 8.18. Pressure-depth gradient for the Keyes gas field, Cimarron and Texas counties, Oklahoma. Underpressured intervals are due to uplift and the maintenance of isolated pressure cells across evaporite aquicludes (after Hunt, 1990, Powley, 1980).

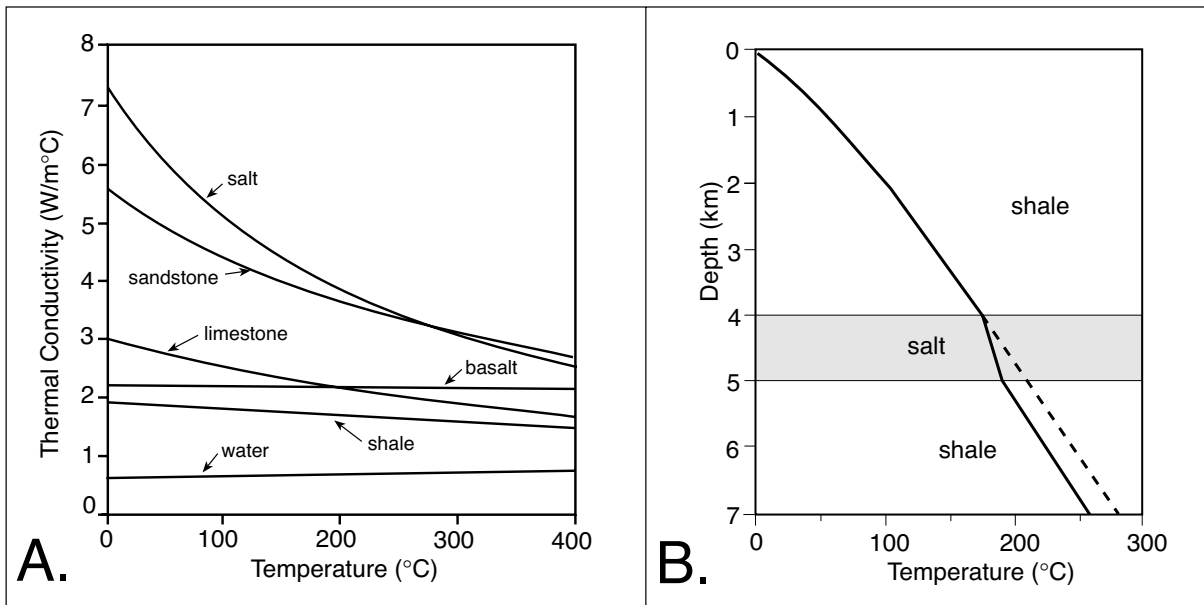


Figure 8.19. Thermal properties of salt. A) Thermal conductivity of various rock grain types (zero-porosity lithologies) and water as a function of temperature. B) Vertical steady-state temperature gradient for a shale section with salt (solid line) and without salt (dashed line). The temperature plot (A) was used to construct the steady state profiles of Figures 8.20 and 8.21 (after Mello et al., 1995).

of salt sets up a thermal dipole with a positive anomaly atop the spine and a negative anomaly at its base (Figure 8.20b). Sediments atop the spine are hotter than they would be without the salt, while sediments below the structure are cooler. Elevated vitrinite reflectance values above buried salt structures have been recognised in the oil industry for many years. However, the cooling effects on beds below a salt bed, diapir or sheet were largely ignored until the work of Mello et al. (1995).

If the diapir crest is at the sedimentation surface, as it is during the passive salt diapir stage, the structure acts as a thermal monopole. The salt spine acts as a sink that channels or drains heat to the surface (Figure 8.20c). In this situation temperatures around and beneath the salt spine and its source layer are less than would exist in a basin without salt. The amplitude of the negative anomaly locally reaches -85°C and its cooling effect extends out for more than three times the diameter of the salt spine (Mello et al., 1995).

The contrast in thermal regimes where a thermal dipole is created when the salt crest is deeply buried versus a monopole where the crest is at the surface raises the question, how close to the surface need a diapir crest be before it starts to act as a heat sink rather than a heat source? Modelling by Mello et al. (1995) suggests the following rule of thumb; the maximum negative anomaly amplitude is reduced $10\text{--}15^{\circ}\text{C}$ for every

250 m of increase in the depth to the top of the salt spine (assuming a shale-rich host). The amount of heat drained from a basin is thus sensitive to the depth to the top of a salt structure and the length of time for which the salt remains at or near the surface before the structure is buried. Basins characterised by syndepositional salt flow and the maintenance of salt spines near the surface will produce the coldest situation with respect to subsalt sediments. This mechanism may help explain why many oil-prolific salt basins still produce large amounts of hydrocarbons today, when some thermal calculations, which do not account for salt effects, suggest that most of the known source rocks in the basin should be overmature (Mello et al., 1995).

Of course, simple salt spines, as modelled in Figure 8.20b and c, are usually part of a much more voluminous allochthonous salt complex, where salt sheets form layers or tiered canopies at a number of different stratigraphic levels. Figure 8.21 presents a thermal model for such a system based on structures in the Gulf of Mexico. The salt sheet is modelled as a steady-state regime in a shale host; it lies within 500 m of the sediment-water interface and still connected with the mother salt bed. It should generate three negative thermal anomalies (Mello et al., 1995):

- a negative thermal anomaly beneath the salt source layer (mother bed);

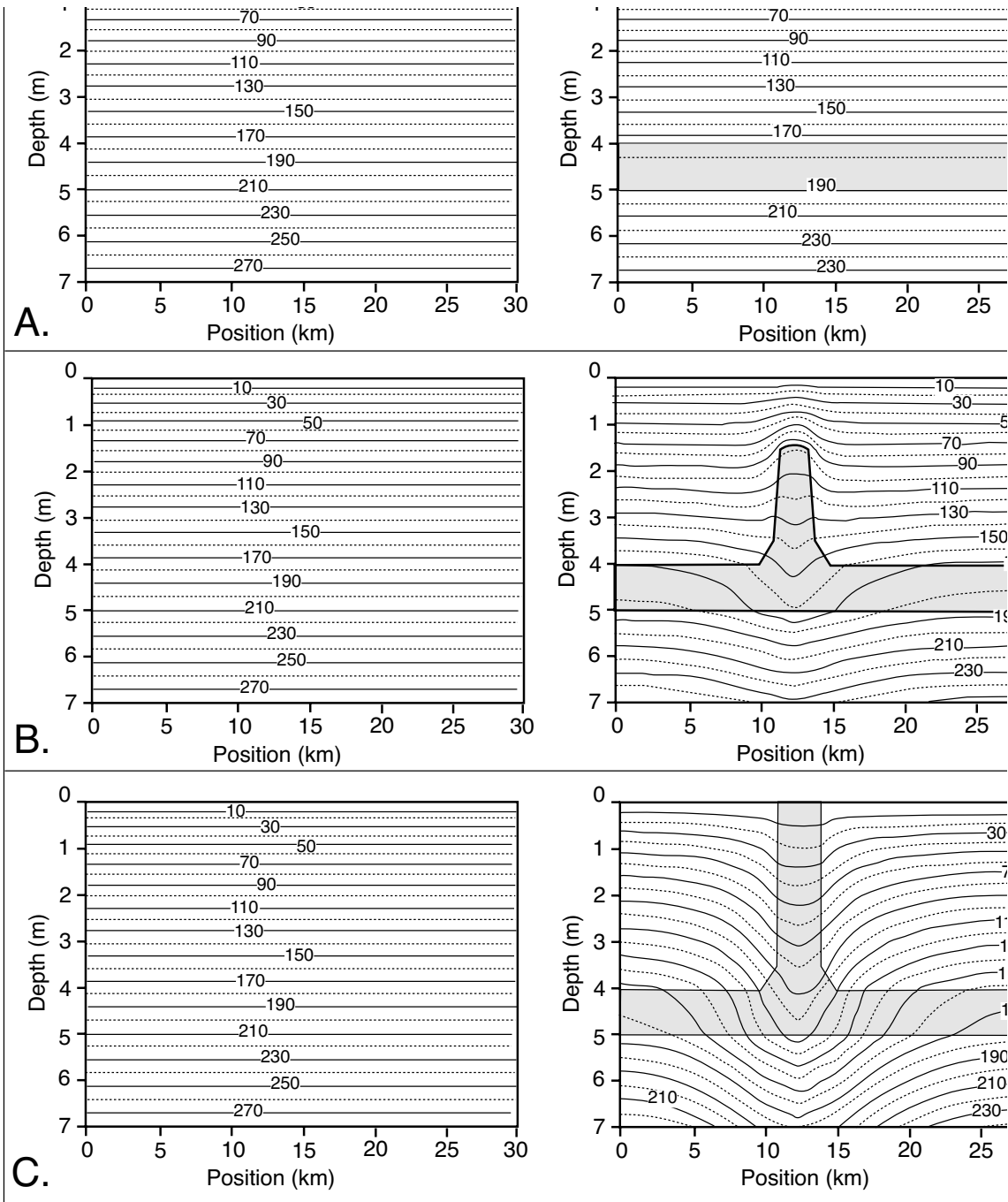


Figure 8.20. Model of steady-state temperature distribution for a shale section containing salt with varying geometries (shown on right hand side) versus the same shale section with no salt (left hand side). All calculations use shale and salt thermal properties and gradients given in Figure 8. A) Salt layer, note that sediments below the salt layer are 20°C cooler than in a shale section with no salt. B) Salt diapir that is connected to its source layer and is not in contact with the surface. Notice the elevated temperatures atop the salt spine and the reduced temperatures beneath the spine - a thermal dipole. C) Salt diapir that is connected to its source layer and is also at the sediment surface. The salt spine acts as a highly efficient heat drain that collects and channels heat from around and beneath the spine and delivers it to the surface. In this situation there is no heating associated with the spine, only cooling - a thermal monopole (after Mello et al., 1995).

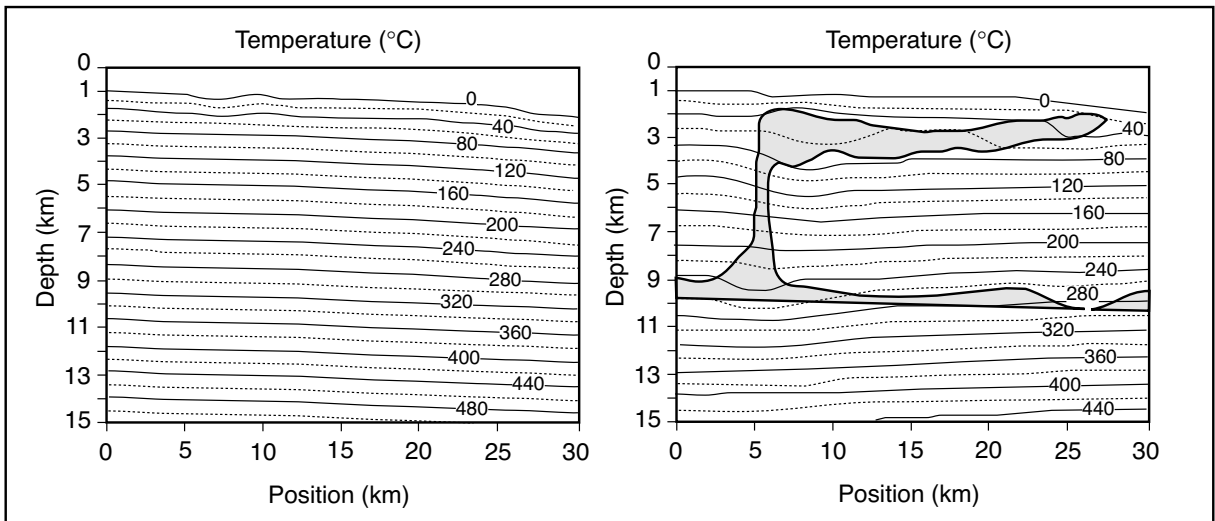


Figure 8.21. Model of steady state temperature distribution created by the emplacement of an allochthonous salt sheet (right hand side) versus profile in a shale section with no salt (left side) Three major negative anomalies are associated with this geometry: a zone of cooling beneath the sheet; a negative or cooling anomaly associated with the dome, which feeds the sheet; and a zone of cooling beneath the lower sheet (after Mello et al., 1995).

- a thermal anomaly associated with the salt stem that feeds the allochthonous salt sheet;
- a thermal anomaly below the salt tongue itself.

There are also some positive anomalies above the salt dome and its tongues, but these are small ($<15^{\circ}\text{C}$) compared with the magnitude of the negative thermal anomalies. The minimum anomaly with the greatest magnitude is $\approx 82^{\circ}\text{C}$ located directly beneath the salt dome (Figure 8.21; position 5 km, depth 10 km). The salt source layer or mother bed contributes only -10°C of the thermal anomaly in the deepest parts of the section. Constructive interference between the salt sheet and the feeding salt spine creates a local thermal anomaly of -55°C at the inside inflection point of the two structures (Figure 8.21; position 7.5 km and depth 4.5 km).

Fluid flow in halokinetic basins

Temperature models do not just indicate the maturation state of source rocks, but as most subsurface heat in a sedimentary basin is transported by fluid flow, also define fluid flow patterns in the subsurface. The thermal anomalies around salt structures by definition also drive brine flow and may be enhanced by density plumes created during salt dissolution (Figure 8.11).

Suprasalt fluid flow and alteration

Like dissolution from the underbelly of a salt layer, dissolution atop and adjacent to a salt spine can create free convecting density plumes in adjacent minibasin sediments (Figure 8.2c). In this case the thermal drive created by the thermal anomalies interacts with the density drive to speed up flow rates in fluids convecting adjacent to the salt spine. If the crest of a diapir has risen to where it lies once again in the active phreatic flow regime, intense dissolution-generated plumes can set up at even shallower depths. Both scenarios generate dense plumes of chloride-rich brine.

Using a dense network of well log data collected in the vicinity of the Bay St. Elaine salt dome in SE Louisiana, Cassidy and Ranganathan (1992) calculated salinity profiles in various strata surrounding the now buried dome crest (Figure 8.22). Salinities range from approximately 4 to 12 wt.%, with most isosalinity lines sloping away from the salt dome. On the southwestern side of the dome (cross sections OA and OC), salinities are 2-4 wt.% higher at a given depth than on opposite sides of the dome, possibly reflecting a greater rate of salt dissolution and enhanced fluid transfer of heat. Lowest salinities occur on the northeastern side (cross sections OA' and OC', Figure 8.22). On all sides of the dome, salinities increase with depth from the shallowest sands to a surface that roughly coincides with the top of overpressured sediments. Within the overpressured section, salinities decrease as depth increases, to levels on some flanks that are one-half the maximum value found in the

hydrostatically pressured zones. For example, the saltiest waters in cross section OC have a salinity of 12 wt.% and occur just above the shale sheath. Within the shale sheath, salinities of interstitial waters are as low as 6 wt.%. Similarly, in section OC', the saltiest waters have a salinity of more than 10 wt.% at a depth of 3 km. In hydrostatically pressured sections on the southwestern flank (cross sections OA and OC) and the northwestern flank (cross section OB), salinities are greatest near the dome and decrease away from the dome. In the overpressured section as well as in the shallower parts of sections OA' and OC', salinities are lowest adjacent to the dome, and increase away from the dome, perhaps reflecting a salt-stem-focused resupply of freshened waters from below. Salinity contours are deflected downward near the fault on the southeastern side of the dome (cross section OB'), but seem unaffected by the faults on the northeastern side (cross section OA').

In a hydrostatically pressured section, one would expect elevated salinities near the salt dome, assuming that the dome is the major source of dissolved salt (Hanor et al., 1986). However, the observed salinity distribution (Figure 8.22) in the vicinity of the Bay St. Elaine dome cannot be explained merely by radial diffusion^{8.2} of salt as it is dissolved from the dome into a static downwelling fluid column. With radial diffusion, the salt concentration should be highest near the dome and decrease away from the dome. A common observation in the subsurface waters of the Gulf Coast is that salinities of interstitial waters in the overpressured suprasalt section are actually lower than salinities of waters at the base of the hydrostatically pressured section (Figure 8.23; Hanor et al., 1986). However, the lobe of relatively fresh water (salinity of less than 6 wt.%) next to the dome in cross sections OA' and OC' (Figure 8.21) dips too steeply to be explained merely by the slope of the overpressured section near the dome.

Cassidy and Ranganathan, (1992) argue that the observed salinity pattern and Bay St. Elaine indicates fresher overpressured pore waters are now escaping upward in a halo around the diapir, especially on the northeastern flank of the dome (cross sections OA' and OC'), where the areas of highest salinity are separated from the dome by relatively fresh (salinity of less than 6 wt.%) pore waters. The low salinity of waters immediately adjacent to the northeastern flank of the dome also may

reflect a greater degree of insulation of the salt dome from dissolution on this flank. They note an alternate explanation is that the pore waters may be upwelling at a slight distance away from the salt-sediment contact, thereby retaining their low salinities as they ascend. The presence of faults on the northeastern side (cross section OA') does not appear to affect the salinity contours. There are not enough control points under the fault in section OB' to evaluate the sealing versus nonsealing nature of the fault.

The salinity field documented about the Bay St. Elaine dome is in striking contrast to the salinity fields mapped around the Bay Marchand and Welsh domes (Figure 8.23 a, b). There, much saltier waters occur next to the domes in sands feeding an adjacent brine plume. The plume extends as a brine layer sourced in regions near the dome tops down to the zone of freshened and geopressured waters at some depth below (Bennett and Hanor, 1987, Hanor 1994a, b). Bay Marchand dome is part of a deep-seated allochthonous salt ridge that also includes the Caillou Island and Timbalier salt domes (Figures 8.23a, 10.44). Something like 7.2×10^{11} kg of solid NaCl must have been dissolved to account for the elevated salinities around the Bay Marchand dome (Bruno and Hanor, 2003). This mass is equivalent to something 0.3 km^3 or a 300m reduction in the height of the current dome. This is a lower limit to the total volume of salt dissolved from the dome as it is based on dissolved ions creating the pore content only of the current system. Most likely, there were earlier pore volumes from dissolved salt that are now flushed from the system. In Welsh dome, the zone of highest salinities occurs atop the crest of the dome and not in a sinking plume off to the side of the dome (Figure 8.23b). Bennett and Hanor (1987) calculated that in this system the volume of brine in the current porosity corresponds to dissolution of at least 2 km of salt from the structure. A lack of a crestal collapse graben over this structure implies salt is still being replenished in the diapir stem. The salinity pattern above Welsh Dome cannot be explained by downwelling of salt dissolution-derived brines. Rather, the upward transport of dense high-salinity brines to levels well above the salt crest is perhaps indicative of episodic expulsion of saline fluids rising along the dome edge.

The salinity halo about St Gabriel dome is characterised by a crestal zone that is fresher than the more saline brine layers/plumes on either side of the dome crest (Figure 8.23c). It is yet another brine distribution pattern in this region of the Gulf Coast and may reflect a situation of fresher upwelling geopressured waters, which are locally displacing a more saline brine layer created by dome crest dissolution.

^{8.2}Diffusion is the movement of ions from areas of high concentration to low concentration and follows Fick's first and second laws. Diffusion is a slow process even in liquids and even slower in a porous medium because ions can migrate only through the pores and the rate depends on pore throat size.

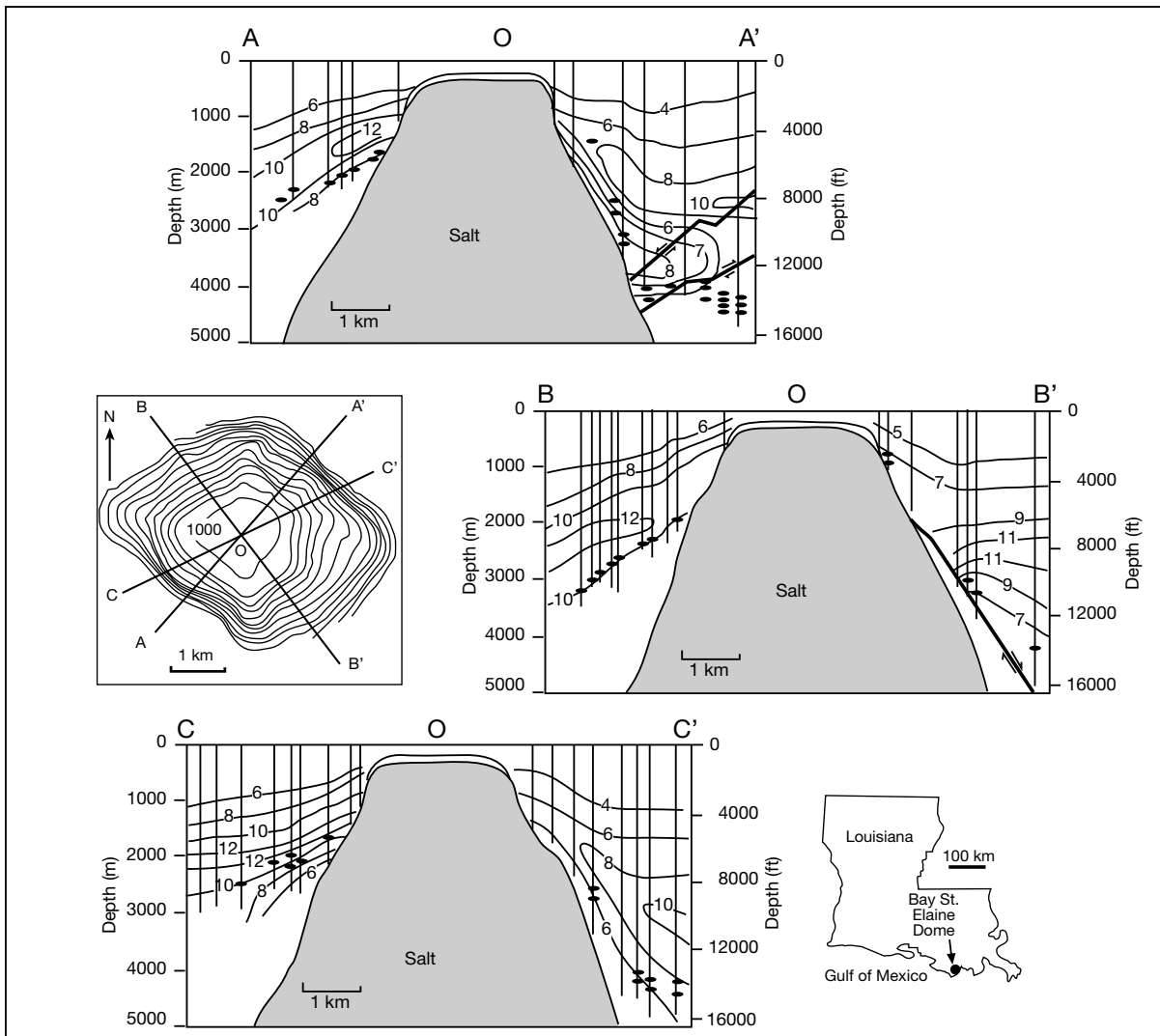


Figure 8.22. Cross sections of pore water salinity (wt%) about the Bay St. Elaine salt dome, Louisiana (depth contours on plan view are 1000 ft). Sections OA' and OC' show lobes or plumes of relatively fresh subsurface waters (<6 wt%) adjacent to the NE flank of the dome. Black ellipses on wells show intersected hydrocarbon zones (after Cassidy and Ranganathan, 1992).

Clearly, salt is still dissolving from the crests of shallowly buried salt structures in the Gulf Coast, this is especially so where there is a well-developed brine plume indicating solute transport directed away from the salt (Bay Marchand and Darrow domes). Clearly also, there are nearby domes in the same region where this brine is locally displaced by salt stem-focused upwellings of subsurface waters. These waters may be more saline (Welsh Dome) or less saline (Bay Marchand and St Gabriel). The interactions are complex and there is no simple single model to explain the variety of pore salinity fields. They vary according to differences in the rates of crestal salt dissolution versus rates of stem-focused upwelling and are

tied to the laterally varying mechanics of compaction flow and salt withdrawal, fluid buoyancy effects, and different suprasalt permeability fields (Cassidy and Ranganathan, 1992).

Density inversion created by the nearsurface dissolution of a diapir crest, in conjunction with a thermal drive and overpressured shales, is sufficient to drive large-scale suprasalt convective cells in the Gulf of Mexico with flow rates of metres per year (Hanor, 1994a). This is two to three orders of magnitude faster than the mm/yr rates that are typical of the thermobaric zone in nonevaporitic basins. Similar elevated flow rates typify the dissolving crests of many structures in the North Sea diapir fields (Williams and Ranganathan, 1994).

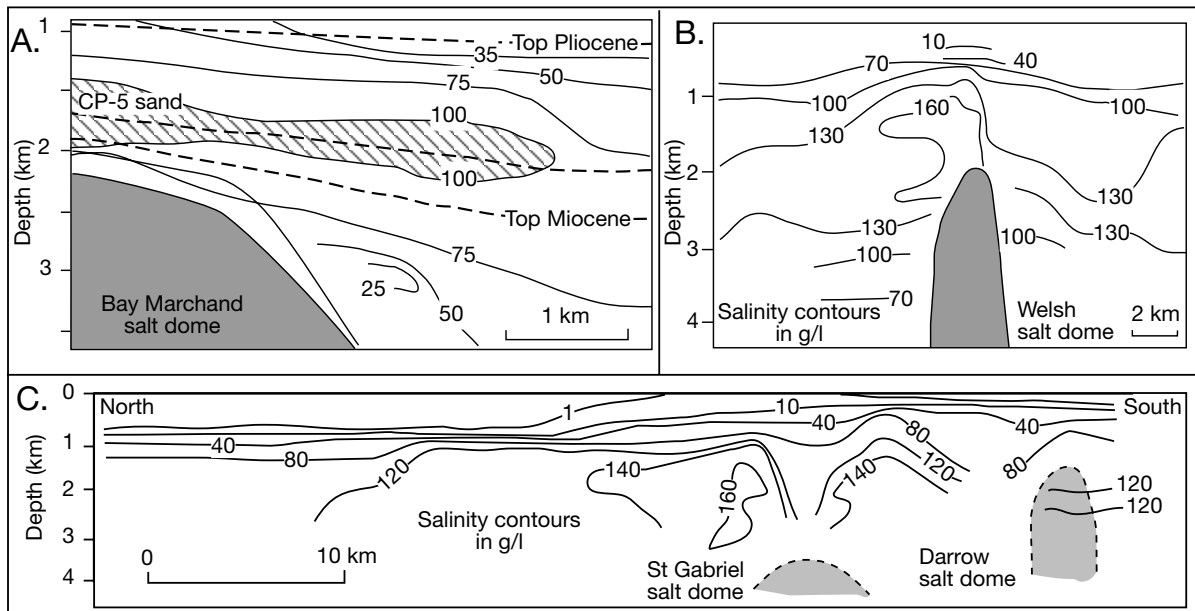


Figure 8.23. Cross section of salinities in the vicinity of several diapirs in the of the Louisiana Gulf Coast showing the various shallow salinity plumes (g/l) generated by subsurface brine dispersion away from the dissolving crests of the salt domes. A) East west section on the southwest flank of the Bay Marchand Dome. The cross hatched axis of the high salinity plume corresponds to the CP-5 Sand (after Bruno and Hanor, 2003). B) Welsh dome section where a regional high salinity layer (<130 g/l) sits atop a zone of overpressure, with higher salinity in the vicinity of the dissolving salt crest (after Bruno and Hanor, 2003). C) Salinity fields mapped around the St. Gabriel dome where saline waters occur near to, but not atop, the dome crest. Darrow dome data are limited but appear to follow the regional pattern of high salinity water near dome crest (after Bennett and Hanor, 1987).

Circumsalt fluid flow drives diagenetic alteration in sediments adjacent to a salt stem. This is demonstrated by zones of calcitic alteration on the west flank of the West Hackberry Dome, Louisiana Gulf Coast (Figure 8.24a; McManus and Hanor, 1993). Drilling has defined some 5×10^{10} kg of authigenic calcite-pyrite cement in Miocene sands adjacent to the salt spine at depths of 1.4 to 2.1 km, across a 1.5×1.5 km area. The Sr, C and S isotopic compositions of the cements show Ca and S were derived from dissolution of the salt-dome anhydrite cap and that carbonate was derived both by thermochemical oxidation of methane and by sulphate reduction, possibly at temperatures as low as 70°C. Constraints on the maximum aqueous concentrations of Ca, which can be released by dissolving diapiric salt, require that more than 5×10^9 m³ of aqueous fluid, equivalent to a fluid volume/pore volume ratio of >250:1, were involved in destroying salt, transporting Ca and SO₄, and precipitating these cements. Thus, the presence of such cements about a salt structure requires a dynamic subsurface mass-transport regime involving either large volumes of throughflushing fluid or fluids that are extensively recirculated.

An equivalent to this subsurface calcite/pyrite cement halo outcrops in a quarry in the Eocene Carrizo Sandstone adjacent to the Butler salt dome, east Texas (Figure 8.24b; Enos and Kyle, 2002). The Carrizo is a fine- to medium-grained quartzarenite to sublitharenite with up to 42-50% cement, principally poikilotopic calcite with local pyrite. Shallow drill holes in the surrounds of the quarry shows cemented zone is delimited by a steeply dipping normal fault, which is radial to the northeast part of dome crest. Cements extend southeast of the fault as a lenticular body some 750 m across and thickest near the fault where it is more than 25 m thick. Pyrite concretions are found on both northwest and southeast sides of the fault, as well as along the fault plane, whereas the calcite cement is present only to the southeast of the fault. $\delta^{13}\text{C}$ values for the calcite (-19 to -37‰) suggest bicarbonate was supplied mainly by bacterial oxidation of methane, whereas $\delta^{18}\text{O}$ data for calcite (-6 to -9‰) indicate meteoric water was involved in supplying diagenetic fluid. $^{87}\text{Sr}/^{86}\text{Sr}$ values for calcite (~0.7073) are within the range for Middle Jurassic seawater, suggesting that dissolution of anhydrite from the Louann Salt provided the Ca. Pyrite is more ³⁴S-rich ($\delta^{34}\text{S}$ range of 10 to 16‰) than typical sulphides in Gulf Coast salt dome cap rocks and is interpreted to represent H₂S supplied from deep sour gas reservoirs.

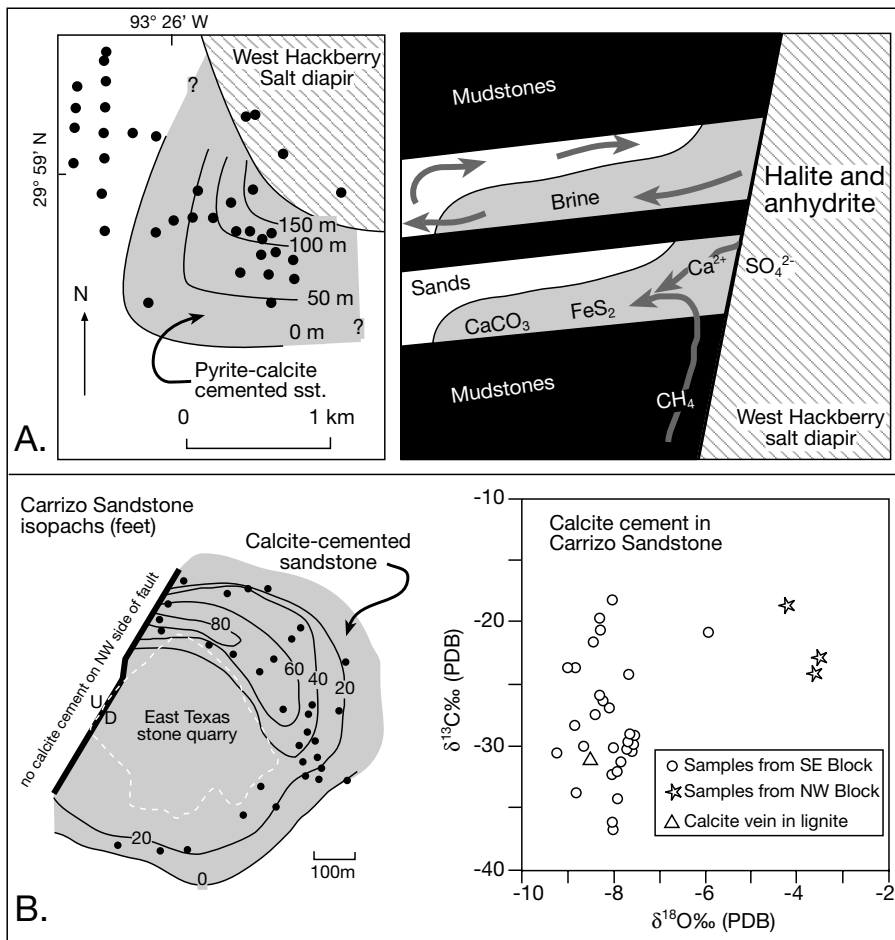


Figure 8.24. Pyrite and calcite cements in diapir edge sands. **A)** West Hackberry Dome, Louisiana showing cumulative thickness in metres of cemented sands, black dots show borehole control. Model schematic shows hydrological circulation at the time of cementation. Dense brines with Ca and SO_4 derived from dissolution of salt stock flow down basal parts of sand beds. Upward flow of less dense fluid above brine plume. Thermogenic methane migrates up side of dome. Thermal reduction of S and oxidation of C results in precipitation of calcite and iron sulphides (after McManus and Hanor, 1993). **B)** Isopach map of the cemented zone in the subcropping Carrizo Sandstone based on drill information (black dots). The NE-trending fault forms the northwestern boundary of the cemented zone. The detailed thickness of the cemented zone within the quarry is unknown but probably was 40 ± 20 ft. Also shown are the carbon and oxygen isotope compositions of calcite cements in the Carrizo Sandstone

Early H_2S supply from deep sour gas reservoirs was channelled upward along the flank of the nearby Butler Dome and outward along the radial fault, resulting in early pyrite precipitation along the fault zone and in adjacent sediments. Early pyrite cements along the fault may have formed a barrier to subsequent fluid circulation, blocking the northwestward movement of both Ca-rich waters from the dome and deep natural gas moving along the fault, thus confining calcite precipitation to the southeast of the fault. Bacterial oxidation of this thermogenic gas resulted

in calcite precipitation, although mixing with shallow ground water bicarbonate may account for the broader range in $\delta^{13}\text{C}$ values in the calcite cement. Enos and Kyle (2002) propose that this type of cementation occurs in similar settings associated with circumsalt hydrocarbon leakage to shallow levels and may represent a previously unrecognized self-sealing type of hydrocarbon trap.

Rapid upward advection^{8.3} of hot brines along the flanks salt domes in the Northern Gulf of Mexico Basin and in the Danish Central Trough seems to require an adjacent and deeper overpressured shale or mudstone succession to focus flow up the sides of the salt structure (Williams and Ranganathan, 1994). Their upward passage influences pore fluid chemistry interfaces, especially redox fronts, near the stem. This creates higher temperature gassy fluid haloes with interfaces that can precipitate metal sulphides and other diagenetic minerals. Inclusions in some of these diagenetic precipitates indicate temperatures were

^{8.3} Advection is a general term used to describe transport of fluids, solids and heat through porous media. It requires permeability to move pore fluids so that ion transport is related to the average linear velocity of water in the pores, which is equal to Darcy velocity divided by effective porosity. In the vicinity of a dissolving salt bed it is associated with dispersion, which describes movement within groundwater as ions or contaminants spread out by mechanical mixing and diffusion. For example, a slug of brine into fresh porewaters mixes with the fresh as it moves away from the dissolution front. The brine covers a larger area as its concentration declines.

some 40° to 80°C above the ambient temperature of the laterally adjacent sediment. Williams and Ranganathan (1994) conclude that thermal perturbations in excess of 60°C can be repeatedly produced near the margins and crests of salt domes via focused dewatering of thick strongly overpressured minibasin intervals around the dome.

Dewatering can be triggered and stopped by cyclically pulsing the permeability at the salt stem-sediment interface (analogous to seismic pumping - Figure 8.16). Modelling shows the upwelling thermal plumes about the dome crest will dissipate within 100,000 years from the cessation of dewatering (Williams and Ranganathan, 1994). Stratigraphically shallow and gravitationally unstable brine plumes from salt dissolution, once formed, will also dissipate once the salt has dissolved, but fade more slowly by sinking and mixing on a 1 m.y. time frame.

Burial dewatering of hydrated salts

So far we have focused on hydrologies in halite-rich shale-dominated basins undergoing various styles of salt flow and dissolution. Halite is the dominant mineral in most thick basinwide evaporite successions, but in some basins anhydrite, not halite, is the dominant salt. In such settings there can be interesting subsurface hydrological effects tied to dewatering of the gypsum precursor to the anhydrite. Conversion occurs whenever a thick gypsum bed is buried and passes into the thermobaric zone. As the burial temperature rises above 60°C, bedded gypsum alters and dewateres to nodular or laminar anhydrite, with an accompanying 39% decrease in rock volume. Potentially, at around a kilometre of burial, this can generate a pressure kick that is significantly in excess of hydrostatic. The conversion of gypsum to anhydrite also defines the depth below which calcium sulphate stylolites cannot form (Figure 1.37).

Conversion depth influences early organic maturation and rock strength (Jowett et al., 1993). Because gypsum dehydration occurs during shallow burial, it is unlikely to be responsible for overpressures that occur at greater depths, where the primary role of the evaporite in the pressure system is as a pressure seal to underlying compacting fine-grained sediments or as a facilitator, via its evacuation, to the rapid accumulation of thick piles of geopressed sediment.

Conversion to anhydrite is accompanied by a four- to six-fold increase in thermal conductivity (gypsum ≈ 0.8 W/m·K; anhydrite ≈ 5.6 W/m·K) and the consumption of heat. At 25°C the transformation of gypsum to anhydrite releases 4 kcal/mole.

In a hydrologically-open compacting sediment pile, gypsum conversion is typically complete by 800-1000 metres of burial, corresponding to a total pressure of ≈ 250 -300 atm (25-30 MPa). Transformation may occur at much shallower depths if the pore fluids are saline, or may not be complete until greater depths if the overlying unit is overpressured (Figure 8.25; Jowett et al., 1993; Testa and Lugli, 2000). When modelling organic maturation in an ancient calcium sulphate basin, via thermal modelling and backstripping techniques, it is important to know the depth at which the gypsum to anhydrite conversion occurred.

In a simple sensitivity test, using a basal heat flow of 2×10^{-6} cal/cm²/s or 2 HFU's, Jowett et al. (1993) calculated the thermal gradient through bedded anhydrite is 18°C/km, while through gypsum it is 63°C/km. With such large differences in thermal gradient, using the wrong lithology over a particular burial depth range can create large errors in organic maturation modelling. For example, assuming 500 m of anhydrite instead of 800 m of decomposing gypsum will produce a 42°C discrepancy at the base of the evaporite unit (Figure 8.25a versus 8.25b). Such an error significantly effects thermal maturation, so that a source beneath the anhydrite would not reach the oil window, while that beneath the gypsum would.

The temperature, and hence the depth at which the transformation occurs depends on the activity (salinity) of the pore waters where the transformation is taking place. Transformation to anhydrite occurs at progressively higher temperatures as the activity of water ($\alpha_{\text{H}_2\text{O}}$) increases. When pore fluids have an $\alpha_{\text{H}_2\text{O}}$ of 0.93 (equivalent to precipitation of gypsum from seawater) the transformation takes place at 52°C (Figure 8.25c; Hardie, 1967). When the water is at halite saturation with an $\alpha_{\text{H}_2\text{O}}$ of 0.75 the transformation occurs at 18°C. The $\alpha_{\text{H}_2\text{O}}$ in pore waters in ancient evaporites is indicated by the associated lithologies. If a thick anhydrite bed (deposited as gypsum) is associated with normal siliciclastics (shales and sandstones), the $\alpha_{\text{H}_2\text{O}}$ of the burial fluids at the time of transformation was ≈ 0.93 and occurred at a temperature $\approx 50^\circ\text{C}$. If the anhydrite retains evidence of coeval halite, or early diagenetic halite cement, then the temperature was around 20°C at the time of transformation and so occurred at much shallow depths, perhaps within metres of the surface (Hovorka, 1992).

When gypsum converts to anhydrite, the molar volume of the solid phase decreases by $\Delta V_s = -28.37$ cm³/mol of anhydrite formed, corresponding to a volume decrease of some 39% (Zen, 1965; Hanshaw and Bredehoeft, 1968). But the released fluid means there is a corresponding increase in molar volume of pore fluid of $\Delta V_f = 36$ cm³ for the 2 mol of water created by the

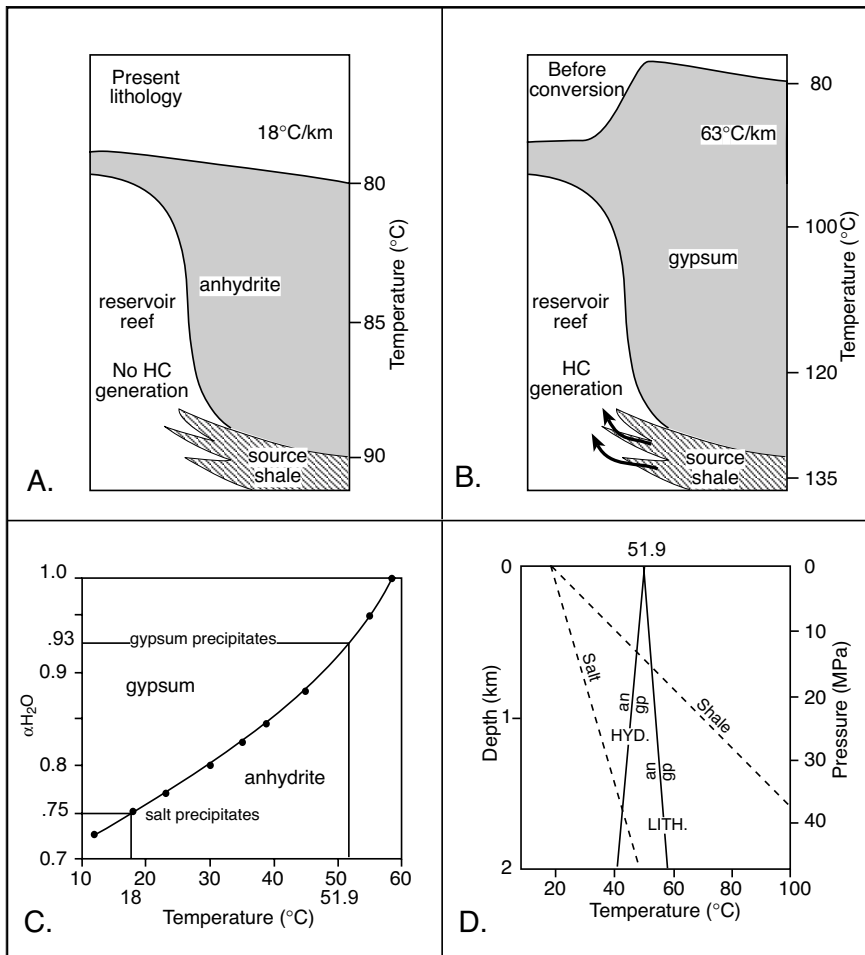


Figure 8.25. Gypsum to anhydrite conversion (after Jowett et al., 1993). A) In an evaporite basin containing 500 m of anhydrite, the calculated palaeothermal temperature implies the underlying source would not reach the “oil window.” B) If the conversion to anhydrite is later, so that the basin can be decompacted prior to gypsum converting to anhydrite, then the low thermal conductivity of the gypsum increases the geothermal gradient and the source rocks do reach the “oil window.” C) The laboratory relationship between the activity of water and the temperature of the gypsum to anhydrite conversion (after Hardie, 1967). D) Depth relationship for the temperature of the gypsum-anhydrite conversion below a shale insulator and a shale conductor. Conversion of gypsum to anhydrite occurs where the temperature line intersects the geothermal gradient in the overlying rock. Hence the conversion depth is much greater beneath halite (conductor) than beneath shale (insulator) (after MacDonald, 1953; Hardie, 1967, Hanshaw and Bredehoeft, 1968).

conversion. Because pressures on the fluid (P_f) and pressures on the solid (P_s) are different, the molar entropy change (S) and the molar volume change (ΔV) are related by the equation (Hanshaw and Bredehoeft, 1968):

$$dP_s/dT = S/(\Delta V_s + V_f dP_f/dP_s)$$

The measured entropy change is $\Delta S = -135.84 + 65.17 \log_{10} T - 0.043T$ (Hardie, 1967), where T is the temperature in degrees Kelvin.

In a hydrostatically pressure system with free drainage allowing escape of the conversion water (e.g. gypsum with intercalated sand beds or porous carbonates) the overburden pressure is taken up only in the solid phases, so favouring the denser solid phase (anhydrite). In this situation, $dP_f/dP_s = \rho_f/\rho_s \approx 0.4$, and the slope on a dP_s/dT on a P-T plot is negative. That is, the conversion temperature decreases with depth and gypsum converts at shallower depths (Figure 8.25d). If, on the other hand, the water from the conversion cannot freely escape from the decomposing gypsum, pore fluids may become geopressed (e.g. escaping pore fluids from a buried gypsum bed sealed beneath a thick widespread salt unit and intercalated with tight shales or lime mudstones). Overburden pressure is then taken up in both the solid and fluid phases. In this case P_f can approach P_s , dP_f/dP_s approaches unity, and the slope of dP/dT becomes positive (Hanshaw and Bredehoeft, 1968). Then the conversion temperature increases with depth and for a given geothermal gradient the conversion of gypsum to anhydrite occurs at progressively greater depths. Hanshaw and Bredehoeft (1968) calculated the lithostatic conditions created by the conversion can only be maintained for a “geologic instant,”

even when the confining beds have hydraulic conductivities as low as 10^{-10} cm/s ($\approx 10^{-3}$ md as in a tight shale).

Most natural systems lay somewhere between the hydrostatic and the lithostatic curves, the dominance of one over the other is difficult to quantify, it can only be estimated by looking at the nature and thickness of the overburden and the intercalated lithologies within the converting calcium sulphate bed. If the

water of hydration cannot drain freely from the dewatering gypsum, the bed converts to a quicksand-like consistency, typically indicated by thick nodular sequences of enterolithic folds with crestal fold vergences that may be oriented in the direction of minimum stress (Warren, 1991). Escaping conversion water ultimately seeps into adjacent strata and escapes the unit. This escaping water of crystallisation can help lubricate nearby growth faults and other relatively shallow slippage features, including nappes.

Based on the ubiquitous presence of flow-aligned anhydrite textures in décollement sutures in the European Alps and elsewhere (e.g. Jordan and Nuesch, 1989; Jordan et al., 1990) it seems that a common effect of sulphate dehydration is an initial decrease in the intrinsic strength of the CaSO_4 unit and an enhanced ability to act as a lubricant. Laboratory testing of mechanical strength during the dehydration of gypsum to bassanite ($\text{CaSO}_4 \cdot 1/2\text{H}_2\text{O}$) under closed drainage supports these observations (Figure 8.26). There is a large decrease in differential stress under undrained conditions at temperatures $\approx 110^\circ\text{C}$, indicating high pore pressures induced by gypsum dehydration (Heard and Rubey, 1966; Murrell and Ismail, 1976). Thus a non-draining dehydrating gypsum bed can act as a zone of weakness or décollement at the base of a thick salt or shale succession. However, in the low temperatures of the laboratory the reaction product is bassanite not anhydrite; a mineral that, like dolomite, is very difficult to manufacture under the kinetic restraints of the laboratory, but is abundant in the real world.

Building on earlier work, but now using varying degrees of pore fluid drainage, the experiments of Olgaard et al. (1995) and Ko et al. (1995) clearly show that under well drained conditions the weakening of the gypsum tends to occur only in the early stages of the dehydration reaction. Their experiments were run at varying temperatures ($23^\circ - 150^\circ\text{C}$), at confining pressures that mimic free to limited drainage (0.1-200 MPa), and at strain rates 0.7×10^{-7} to $6 \times 10^{-5} \text{ s}^{-1}$. As more porosity was created by ongoing dehydration there followed a rapid decrease in pore pressure. The experimental peak in pore pressure corresponded to an observed weakening and embrittlement in the gypsum. Under drained conditions this weakening occurred in the first 1% of the reaction. Ultimate strength was recovered within 3% of the reaction and ultimately exceed that of pure gypsum. They concluded that, unless the surrounding rocks had very low permeabilities, the pore pressures during real world dehydration could only equal or exceed lithostatic pressures during the earliest stage of the gypsum dehydration reaction.

Microstructural observations of Ko et al. (1995, 1997) showed that the initial stage of loss of water of crystallisation creates isolated areas of dehydrated gypsum surrounded by new fluid-filled porosity. Excess pore pressures develop as long as this porosity is not interconnected or fluid is produced faster than it can escape through any newly forming interconnected porosity. Under slow fluid leakage conditions an excess pore pressure first develops, which leads to weakening; but this is followed by strengthening (shown by time arrow in Figure 8.26). The timing of the development of minimum strength and maximum pore pressure is controlled by the drainage evolution of the various mosaics or networks of dehydrated gypsum within the converting gypsum unit. While the dewatered regions are isolated, a pore pressure can build up, which, as it becomes more pervasive, weakens the gypsum. But, as the locally dehydrated intervals start to fuse with each other, pore fluids can now flow from one area to another and ultimately escape into the adjacent non-calcium sulphate surrounds. This strengthening of the dewatering gypsum over time marks an internal transition from undrained to drained behaviour.

As well as acting as a lubricant, escaping water of crystallisation can act as a catalyst in dissolution-precipitation reactions within units subjacent to the dewatering evaporites. As buried

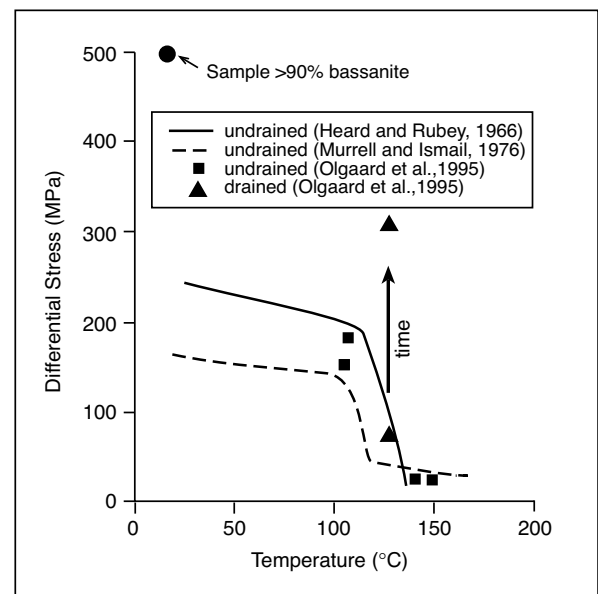
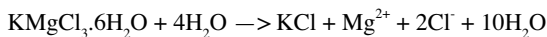


Figure 8.26. Plot showing differential strength of dehydrating gypsum decreases above 110°C in undrained conditions where the water of crystallisation cannot freely escape. Under drained conditions there is an initial decrease in differential strength followed by an increase. This is shown by samples at either end of time arrow (after Ko et al., 1995).

gypsum dewatering to anhydrite the escaping water is saturated with respect to CaSO_4 but undersaturated with respect to other evaporite minerals, including any nearby carbonates (Sass and Ben-Yaakov, 1977) as well as any halite and the bittern salts. As such water seeps through the surrounding rocks it can leach minerals to create secondary porosity or bring about mineralogical transformations. Throughflow of such waters has dissolved marine carbonate grains to form anhydrite-filled moulds during Permian brine reflux in the shallow subsurface of the Palo Duro Basin, Texas (Bein and Land, 1982). With complete dewatering, a gypsum bed that is 100 m thick will convert to a 62 m anhydrite bed (Borchert and Muir, 1964; p. 133). This releases a total of 48.6 m^3 of water per square metre of cross-sectional area. At 30°C this volume of CaSO_4 -saturated water can dissolve 8.1 m^3 of halite or 54 m^3 of carnallite or convert 81 m^3 of carnallite to sylvite:



Similar fluid rock interactions in the subsurface obviously influence many of the minerals and burial cements we now see in evaporites and adjacent beds. As well as basinal fluids derived from dissolving evaporites, fluids from dewatering evaporites (especially gypsum and the hydrated bittern salts, such as carnallite) may also exert a substantial influence on the diagenetic and metallogenic evolution of the sediment pile.

Brine-rock burial evolution

Approximately 20% by volume of most sedimentary basins is made up of pore water of varying salinity, temperature, pressure and ionic proportions. Pore waters in sedimentary basins are mostly calcium chloride waters with major cations present in the proportion $\text{Na} > \text{Ca} > \text{Mg}$ (Figure 5.27; Collins, 1975). More than 70% of oil field waters are either saline (10,000–50,000 mg/l) or brines (>50,000 mg/l). More than 50% of the world's basinal waters are more saline than seawater (>35,000 mg/l). All formation waters (aka subsurface or basinal waters) originate from meteoric, marine, or hydrothermal sources (Moldovanyi and Walter, 1992). Mechanisms proposed to account for elevated salinities of subsurface waters compared to most nonevaporitic surface waters include; membrane filtration or reverse chemical osmosis (reviewed by Graf, 1982), expulsion of evaporatively concentrated (connate) seawater (Rittenhouse, 1967; Carpenter, 1978; Stoessell and Moore, 1983), halite and potash salt dissolution (e.g., Land and Prezbindowski, 1981; Hanor, 1988), and meteoric water-rock interactions in sediments over thermal anomalies or in tectonically active areas (Hardie,

1990). Most of these alternatives can be rejected as significant factors in brine formation (Land 1987; Hanor, 1994a, b). It is now generally accepted that subsurface brines more saline than 100,000 to 120,000 mg/l are mostly related to evaporites via their depositional brine aprons or their subsequent dissolution haloes. Significant modifications to the connate fluid chemistry must occur during burial diagenesis in response to changing solution-mineral equilibria with increasing temperatures.

Several workers have suggested all basin water ionic compositions indicate mixtures in varying proportions of a) brines associated with evaporite residues, b) head-driven deeply circulating meteoric inflows and c) compaction waters (Kharaka et al., 1985; Egeberg and Aagaard, 1989; Moldovanyi and Walter, 1994; Land, 1995a, b). For much of the ensuing discussion we concentrate on subsurface brine chemistries associated with connate brines or evaporite dissolution.

Brine chemistry at depth

Hanor (1994a, b) studied the chemistry of basinal waters worldwide and divided them into three groups; a) Na-HCO_3 and Na-acetate waters, typically with $\text{TDS} < 10,000 \text{ mg/l}$, b) Cl -dominated halite undersaturated waters with salinities between 10,000 and 250,000–300,000 mg/l, these waters include Na-Cl waters and Na-Ca-Cl at higher salinities and, c) Cl -dominated halite-saturated waters, with salinities typically in excess of 300,000 mg/l. Major cation concentrations show a systematic trend with increasing concentration. Ca and K become increasingly dominant, while Na and pH decrease with increasing brine concentration, especially above 300,000 mg/l (Figure 8.27). In moderately saline waters, the monovalent cations Na and K have 1:1 slopes when plotted against TDS , while the divalent cations Mg , Ca and Sr show 2:1 slopes. The pH of moderately saline waters lie in the range 7–9, while high salinity brines are in the range 3–4. Most highly concentrated basinal brines are acidic; this has important implications for the leaching and transport of metals in the relatively low temperature range (<200°C) that typifies sedimentary basins (Warren, 2000b).

Well-defined ionic trends with increasing salinity seen in Figure 8.27 led Hanor (1988, 1994a, b) to suggest that the chemistry of most deep subsurface brine in salt-entraining basins is controlled by the subsurface dissolution of halite and the subsequent buffering of pore water compositions via interactions with multiphase silicate-carbonate mineral assemblages. Dissolution of halite produces a progressively more NaCl -dominated fluid without any systematic increase in K , Ca , Mg and Sr ions, which are supplied by fluid interactions

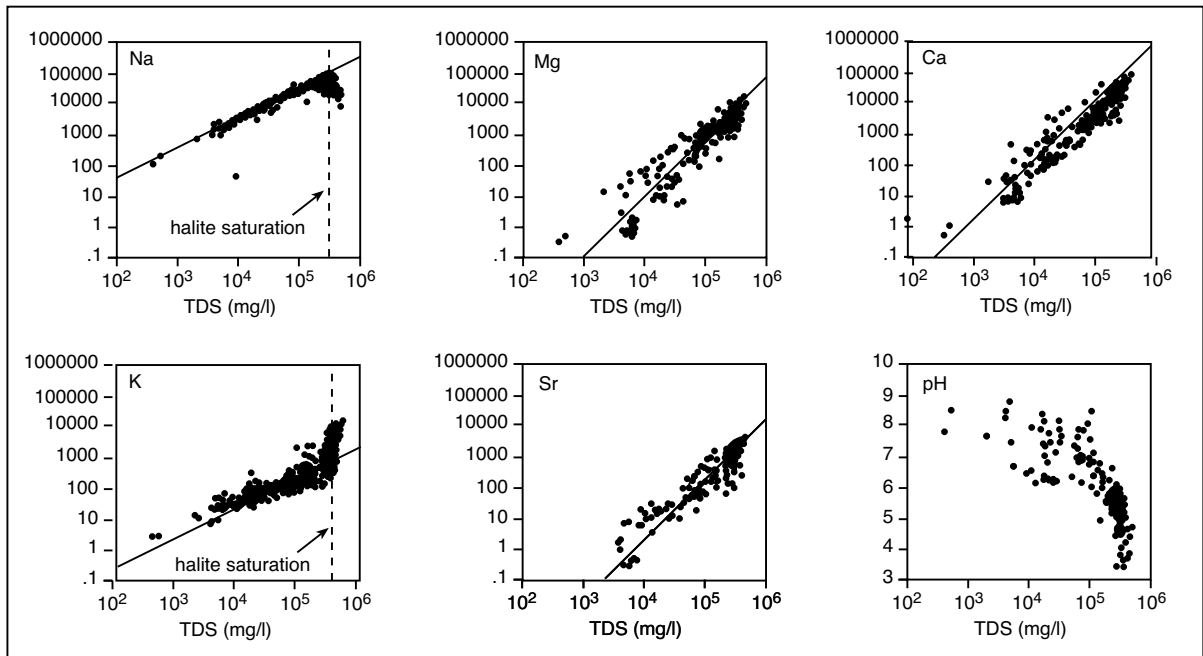


Figure 8.27. Scatter plots of the covariance of log Na, Mg, Ca, K, Sr and pH with log TDS (total dissolved solids) for typical saline basinal waters worldwide (after Hanor 1994a). Note the 1:1 slopes for Na and K and the 2:1 slopes for the divalent cations. All values, except for pH, are in mg/l.

with the adjacent silicate-carbonate assemblages. Such water-rock interactions explain the Na–Ca–Cl brines so common in subsurface brines. These proportions cannot be explained by a simple evaporitic concentration of seawater beyond gypsum saturation and the retention of connate reflux waters. Marine brines precipitating halite contain little or no Ca^{2+} as it has been depleted by CaCO_3 and gypsum/anhydrite precipitation (Figure 2.5). Volumetrically important subsurface reactions capable of modifying connate brines towards higher $\text{Ca}/(\text{Na}+\text{Ca})$ values include dissolution of anhydrite, albitisation of plagioclase feldspars, and dolomitization of limestones (Land 1987). Potassium (as well as Ba and perhaps Sr) can come from albitisation or illitisation of K-feldspar, especially in redbed and volcanoclastic sequences.

In terms of anions, the inherently high solubility of dissolving evaporites means they typically supply unbuffered components into pore waters, the most obvious being chlorine and bromine (Ranganathan, 1991). Other than halite cement, there is no source of chlorine in nonevaporitic lithologies (except minor hydroxyl-bearing minerals such as mica or apatite). Hence, average chlorine content in nonevaporitic basins worldwide is only 48,640 mg/l ($\text{Br} = 155 \text{ mg/l}$), while the average for basins entraining buried salt or their dissolution breccias is 118,392 mg/l ($\text{Br} = 1583 \text{ mg/l}$; Worden, 1996). Palaeozoic

basin brines also show higher average chlorine contents than Mesozoic basins, which are in turn higher than Tertiary basins (Worden, 1996). The difference probably reflects the longer time for more pervasive evaporite solution and circulation in the older basins. Worden (1996), like Hanor, concluded that in an evaporite-entraining basin the dissolution of halite is the major control on the chlorine content of subsurface waters.

If dissolution of thick buried salt explains the elevated salinity of deeply buried highly saline basinal brines, then any sediment undergoing burial will ultimately come into contact with these brines. It will experience water-rock diagenetic interactions tied to basinal fluids derived from this dissolving evaporite and these interactions will occur in the later deeper stages of the rock's burial history. The tie of basinal brine chemistry to buried dissolving salt is clearly seen in the pore water chemistry of the deeply buried Permian Gharif Formation in the Ghaba Salt Basin of Oman (see Figure 10.54a for basin location; Hartmann et al, 2000). The degree of diagenetic overprint varies, depending on burial history. Sandstone at shallow depth ($>2600 \text{ m}$) shows intense dissolution of aluminosilicate and carbonate minerals, combined with minor kaolinite precipitation and compaction, whereas deeply buried sandstone ($>2600 \text{ m}$) is highly compacted and tightly cemented by quartz, carbonate, and sulphate minerals.

The Lower Gharif in the Ghaba Basin consists of coastal-plain siliciclastic rocks passing upward into the marine bioclastic–oolitic Haushi limestone. The Middle Gharif is characterized by fluvial cross-bedded sandstone interbedded with red–brown, mottled siltstones and mudstones containing calcrite and root traces. The top part consists of alluvial-plain mudstone with less calcrite. None of the three formations entrain evaporites. The cementation history in these Gharif sands illustrates what is a typical depth-related set of burial cement stratigraphies for many sedimentary basins.

Eight carbonate cement phases were differentiated in the sands of the Gharif Fm. by Hartmann et al. (2000). In general, the sequence is: calcrite/dolocrete, calcite I/dolomite I and calcite II as consecutive eogenetic phases all predating early quartz I, this is followed by burial diagenetic dolomite II and calcite III/Fe-dolomite/ankerite. Calcrite and dolocrete are present in fluvial sandstone of the Middle and Upper Gharif. Trace amounts of calcite I and dolomite I overgrow reworked caliche nodules. Pore-occluding, poikilitic, brightly luminescent calcite II is present in shallow wells and in the Huqf–Haushi outcrops. Later-formed, patchy poikilitic, brightly luminescent calcite III is restricted to samples from depths of <2600 m. Dolomite II is present in some wells as small, red-luminescent rhombohedra.

Fe-dolomite/ankerite occurs in various amounts (0–27%) as intergranular rhombohedra that fill pores and corrode earlier quartz I and feldspar overgrowths.

Caliche carbonates have $\delta^{18}\text{O}$ and $\delta^{13}\text{C}$ values from -0.3 to -0.7‰ and -1.8 to -2.2‰, respectively (Figure 8.28a). Pristine shell material and “whole-rock” shallow-marine Haushi limestone (Lower Gharif) show $\delta^{13}\text{C}$ values between 0.5 and 5‰ and $\delta^{18}\text{O}$ values ranging from -1.6 to -2.6‰. The stable-isotope composition of early calcite II ranges from -7 to -10‰ and from -19 to -23‰ for $\delta^{18}\text{O}$ and $\delta^{13}\text{C}$, respectively. Calcite III, which formed after calcite II, has $\delta^{18}\text{O}$ values of -4 to -9‰ and $\delta^{13}\text{C}$ values of -2 to -14‰ (Figure 8.28b). Fe-dolomite/ankerite has $\delta^{18}\text{O}$ values ranging from -4 to -9.5‰ and $\delta^{13}\text{C}$ values of -3 to -11‰ (Figure 8.28a). All these isotopic values of the various cements in these sandstones are consistent with ongoing burial diagenesis in an environment characterised by increasing temperature in the presence of hydrocarbons. The calcite II cements formed from meteoric waters that infiltrated the Gharif sands during the late Triassic Early Jurassic. This was followed by burial and the entry of high salinity pore water from dissolution of the Ara salt. During this time of deeper burial and more saline pore waters the Fe-dolomite and ankerite cements precipitated.

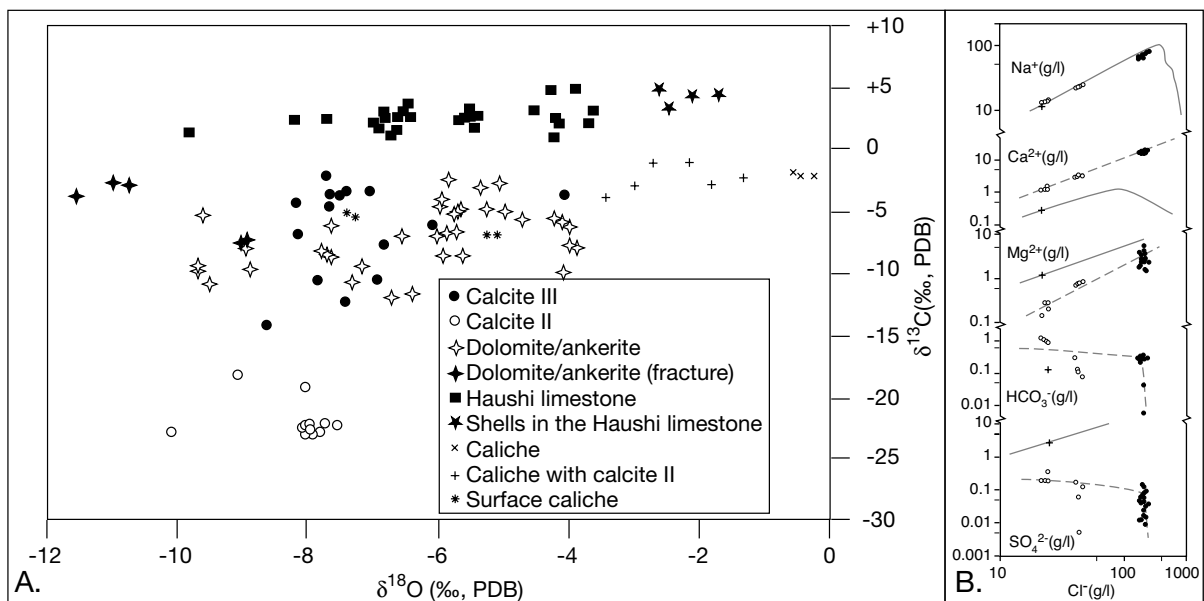


Figure 8.28. Hydrological signature of the Permian Gharif Formation, Oman. A) Stable isotope signatures of Gharif Formation minerals - see text for explanation of trends. B) Variation in dissolved cations and anions as a function of dissolved chloride in Gharif Formation pore waters. Open symbols represent low-salinity brines influenced by meteoric waters. Closed symbols are highly saline brines derived from subsurface dissolution of the Ara Fm. salt. Dashed lines represent the present trends between dissolved ions and chloride. Solid lines are the seawater evaporation dilution lines from Carpenter (1978). Crosses represent the seawater concentration for each dissolved ion (after Hartmann et al., 2000).

The current pore waters in the Gharif are Na–Cl brines with various amounts of Ca, Mg, SO_4 , and HCO_3 (Figure 8.28b; Hartmann et al., 2000). Dissolved Na increases with increasing Cl along the seawater evaporation–dilution curve (Carpenter 1978) confirming dissolving halite as the main ion source to the present saline brines. Values for Mg and Ca also increase, but values for Mg are depleted and those of Ca are enriched relative to the seawater evaporation–dilution curves, imply ongoing rock–fluid interactions. In addition, all brines are depleted in sulphate, but mostly enriched in bicarbonate compared to seawater, perhaps reflecting sulphate reduction processes (Figure 8.28b).

With time and burial the carbonate minerals precipitating from the evolving pore waters of the Gharif Fm. in the Ghaba Salt Basin evolved from depositional pore waters of low salinity (<50 g/l) with $\delta^{18}\text{O}_{\text{SMOW}}$ values of -0.5 to -1.5 ‰ in the more marine Lower Gharif to 2 ‰ in the arid fluvial Middle and Upper Gharif (Figure 8.28b). During subsequent shallow burial (Late Triassic to Early Jurassic), the pore water in the Gharif members changed to high-salinity brines (≈ 180 g/l) with $\delta^{18}\text{O}_{\text{SMOW}}$ values of -4 to -7 ‰. The current highly saline, deep-burial pore water with a heavy $\delta^{18}\text{O}$ signature (0.5–5 ‰) is the result of rock–water interactions in what is a rock-dominated system. Thus present porewater compositions in the deeper parts of the basin, as indicated by both isotopic and ionic compositions, mainly reflect interaction with pore fluids derived by deeper subsurface dissolution of underlying Neoproterozoic Ara Group evaporites. This process is coupled to the precipitation of late diagenetic carbonates and sulphates. Subsequent recharge of isotopically light surface water was driven by inversion along the uplifted southeastern basin margin and was driven by obduction of the Oman Mountains in the Late Cretaceous and the creation of the Huqf–Haushi Arch (Figures 10.5b, 10.54a).

Ceriani et al. (2002) documented a similar post-rift burial infiltration of saline brines in non-evaporitic sediments deposited in an evaporite-floored aborted rift. They studied the evolution of quartz overgrowths and burial dolomite cements in the Upper Sarir Sandstone (Lower Cretaceous) in Abu Atifel oilfield in the Sirt Basin, Libya. Fluid inclusions along the grain-overgrowth boundary of early quartz overgrowths yield homogenization temperatures from 130 to 141 °C and salinities between seawater and freshwater. Aqueous fluid inclusions in later quartz overgrowths have homogenization temperatures from 114° to 129°C and salinities between 18 and 21 wt. % NaCl equivalent. Fluid inclusions in adjacent dolomite burial cements have variable homogenization temperatures (120–141°C) and high salinities (20–22 wt. % NaCl equivalent).

This cooling trend in homogenization temperatures of fluid inclusions, tied to increasingly saline pore waters, is the result of quartz cements first forming in a bath of hot, low-salinity, connate fluids at a burial depth around 2.5 km. These hot fluids were flowing through the Sarir sands, driven by the increased heat flow related to regional rifting of the Sirt Basin. Later quartz overgrowths and burial dolomite cements precipitated during a time of regional cooling tied to the end of the rifting. Authigenesis occurred at a depth of around 3.8 km and was driven by the cooling of pore fluids concurrent with the invasion of dense saline fluids from subadjacent areas of salt deposition and brine reflux. The most likely brine source was a reflux plume from a thick section of Eocene evaporites, although dissolution of subadjacent Cretaceous salts cannot be entirely ruled out (Ceriani et al., 2002). A similar evaporite-associated reflux model was used to explain cool pore brines associated with U-rich dolomitization and subsequent anhydrite precipitation and replacement in the lower Krider Member of the Nolans Limestone in the Hugoton Embayment in Kansas (Luczag and Goldstein 2000).

Worldwide, the ionic proportions in a subsurface saline brine can reflect either the original make-up of the waters in the pores at the time of deposition (such as connate waters in inclusions in Guadalupian chevron halite in west Texas; Figure 8.7) or the effects on ongoing subsurface fluid flow and rock reactions changing the original depositional proportions (as in the salt-dissolution-derived Na–Cl waters of the Gharif Formation). Connate waters are subsurface waters with chemistries near-identical to those of waters which were present in the pores at the time of deposition (Hanor, 1994a). The term connate comes from the Latin (*connatus = born with*). Connate properties of subsurface brines include connate isotopic properties, connate Br/Cl ratios and other ionic proportions. Very few subsurface waters are truly connate because chemical alteration and diagenesis (water-rock interaction) influences the chemical make-up of most. Some authors use the term connate interchangeably with the more general term subsurface water, but to avoid confusion its use should be preserved for those waters and brines that are truly connate (Hanor 1994a). Most basinal brines are not connate, this is especially obvious in subsurface regions where thick evaporites are dissolving creating high salinity Na–Cl dominated brines.

With evaporite-associated subsurface waters there is still considerable debate about the role of residual evaporated seawater (=connate brine) in the chemistry of basinal brine versus dissolving buried evaporites (Moldovanyi and Walter, 1994). In part, the debate centres on the ability of thick evaporite sections

to store connate brine from the time of deposition due to the early creation of evaporite seals by early porosity loss. Most halite-dominated sequences are tight by 100-500 m burial. A “connate” versus “water-rock interaction” argument is made more difficult by requisite hydrology needed to precipitate and preserve a thick, near monomineralic, evaporite sequence. Significant volumes of salts can only accumulate where ongoing brine reflux drives the associated flux of considerable volumes of brine into the adjacent underlying sediments where it disperses into the regional flow system (as in the Sarir Sandstone).

This is the concept of brine disposal, brine leakage, brine reflux or the brine curtain as enumerated by Holser (1979), Sandford and Wood (1991), Rosen (1994) and Warren (1999), respectively. It is summarised in Chapters 2 and 5. The drawdown hydrology that typified the depositional hydrology of most ancient evaporite settings means that substantial volumes of relatively unmodified but dense pulses of concentrated seawater (=connate) or continental brines can be drawn into and stored in sediments about and beneath the evaporite bed and its brine curtain (Figure 2.52). This refluxed connate brine could be stored in subadjacent continental strata (e.g. fluvial or aeolian sediments) as well as in a marine host and can be released later during burial diagenesis and compactional flushing. The question becomes not whether connate pore waters were present beneath and within a thick evaporite bed, but when were these waters flushed from the system and how much water rock interaction took place during and after that flushing.

One reason for confusion between connate and dissolution derived subsurface waters is that some older studies did not distinguish between brine samples collected from porous beds encased within an evaporite sequence and those pore waters collected in adjacent more permeable sediments located above and below an evaporite bed. When this distinction is made, those brines collected within sediments with relict pore fluids encased by a bedded salt unit (with chevrons) are typically found to be connate brines, while those outside the evaporite succession are more likely to reflect chemistries related to salt dissolution and ongoing water rock interaction. For example brines within an evaporite aquitard and a nearby deep brine aquifer in the Palo Duro Basin of west Texas have $\delta^{37}\text{Cl}$ values of -0.4 to 0.0‰ (Figure 2.27b; Eastoe et al., 1999). They were not generated by dissolution of halite.

Another possible confusion in terms of a meteoric versus dissolution origin of diagenetic cements in carbonates in evaporite entraining basins lies in the possible misinterpretation of oxygen isotope signatures of some burial cements precipitated from

hypersaline pore waters. The work of Dickson et al (2001) on carbonates of the Central Basin Platform west Texas underlines this dilemma. Pennsylvanian to Lower Permian cyclic platform carbonates from the Southwest Andrews area of west Texas are now 3 km below the landsurface. Isolated samples of brachiopod shell, zones of calcite cement, and saddle dolomite from limestone cores of the Southwest Andrews oilfields were analysed isotopically in order to determine if: (1) diagenesis was dominated by early, meteoric processes, as suggested by earlier bulk rock isotope studies, (2) whether significant burial diagenesis occurred in hypersaline waters, and (3) whether most burial cements are allochthonous or internally derived.

Bulk isotopic analyses of the limestones show systematic variation in $\delta^{13}\text{C}$ and $\delta^{18}\text{O}$ that historically have been interpreted according to a geochemical model tied to length of subaerial exposure and stratigraphic position (Figure 8.29; Dickson et al., 2001). Chemically zoned calcite cements show four growth stages. Stage 1 and 2 cements have average $\delta^{13}\text{C}$ values of -4.6‰ and average $\delta^{18}\text{O}$ of -5.0‰, and most are thought to have precipitated early during subaerial exposure while bathed in meteoric waters. A few stage 1 cements with average $\delta^{13}\text{C}$ values of -4.7‰ and $\delta^{18}\text{O}$ of -1.4‰ apparently precipitated below the sediment surface from modified seawater in a sulphate reduction zone.

But stage 3 and 4 calcite cements precipitated later, thin sections show they are postcompaction and now compose up to 25% of the total rock volume. They have $\delta^{13}\text{C}$ values (-0.2 to -4.4‰) that vary according to stratigraphic position, and are similar to bulk rock samples of the host limestone. Their $\delta^{13}\text{C}$ values indicate these later cements are locally derived via dissolution of adjacent strata. $\delta^{18}\text{O}$ values of stage 3 and 4 cements (-5.5 to -3.5‰) are isotopically indistinguishable from the stage 1 and 2 cements precipitated from meteoric water (Figure 8.29a). The expected decrease in $\delta^{18}\text{O}$ expected from elevated temperatures during burial (the present formation temperature is $\approx 55^\circ\text{C}$) has been negated by their precipitation from late Permian hypersaline brine with $\delta^{18}\text{O}$ values of +5‰. These stage 3 and 4 cements are composed of sparry calcites and saddle dolomites with $^{87}\text{Sr}/^{86}\text{Sr}$ values that are lower than $^{87}\text{Sr}/^{86}\text{Sr}$ values for contemporaneous Permian marine carbonate (≈ 0.70830 ; (Figure 8.29b). This indicates incorporation of Sr with low $^{87}\text{Sr}/^{86}\text{Sr}$ values (0.70672 to 0.70682), which were derived from the same late Permian hypersaline brines. Entry into normal marine carbonates was driven by ongoing brine reflux during the deposition of the overlying Permian evaporites.

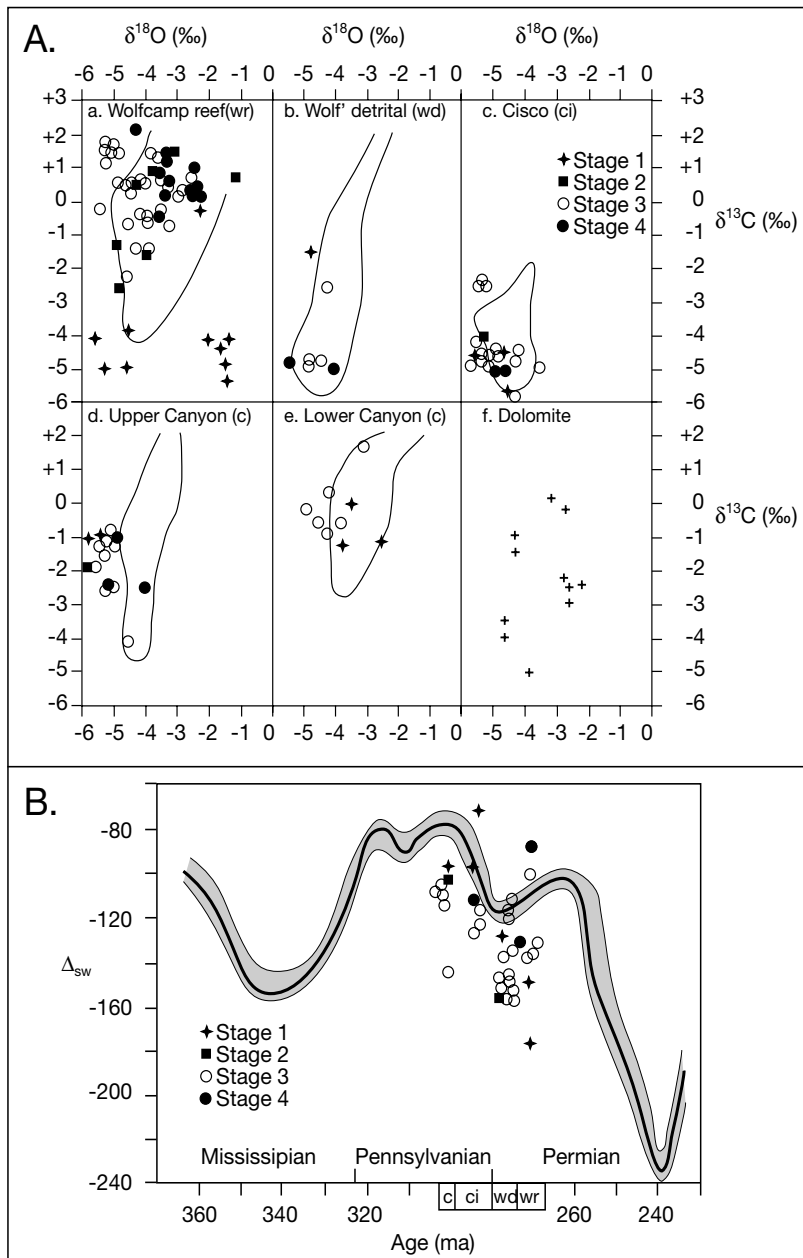


Figure 8.29. Isotopes from the Palaeozoic carbonate platform of the southwest Andrews area, west Texas (after Dickson et al., 2001). A) Carbon-oxygen isotope scatter-plots (A-E) of calcite cement crystals from Wells V7, X1, and Parker "B" 12. The cements are zoned and are grouped into four stages, stage 1 being the oldest and stage 4 being the youngest. Plots are listed by stratigraphic occurrence a) Wolfcampian reef, b) Wolfcampian detrital, c) Cisco, d) Upper Canyon, and e) Lower Canyon intervals, while f) is a carbon-oxygen isotope scatter plot of data from individual crystals of saddle dolomite in all stratigraphic intervals, except the Wolfcampian detrital. B) $^{87}\text{Sr}/^{86}\text{Sr}$ data from selected separated cement stages (1-4) of the same calcite crystals as in A) plotted on the late Palaeozoic seawater strontium isotope curve and its 76% confidence band (grey; curve from Denison et al., 1998). Δ_{sw} is defined as: $\Delta_{\text{sw}} = \left(\frac{^{87}\text{Sr}/^{86}\text{Sr}_{\text{unknown}}}{^{87}\text{Sr}/^{86}\text{Sr}_{\text{modern seawater}}} \right) \times 10^5$.

Dickson et al. (2001) went on to conclude that the buried platform carbonates of Southwest Andrews area have several diagenetic features, all driven by the creation of a reflux curtain, that are probably more common in ancient evaporite-associated limestones than previously recognized. They note: (1) Burial cements have $\delta^{18}\text{O}$ values similar to meteoric cements yet they were precipitated from later hypersaline pore waters with $\delta^{18}\text{O}$ values some 5 ‰ greater than contemporary seawater. (2) Deep-burial cements have $\delta^{13}\text{C}$ values similar to the bulk rock because carbon was derived from pressure dissolution of nearby carbonate. (3) Bulk-rock isotope values are characteristic of marine limestones subjected to meteoric diagenesis, yet they have suffered substantial deep burial diagenesis under the influence of hypersaline waters.

The chemical and isotopic compositions of highly saline water in evaporite-entraining basins complicate simple notions of meteoric versus normal-marine burial diagenesis, especially in intervals close to the dissolving evaporites. Most pore waters are not simply derived during the congruent dissolution of halite beds, nor are they only connate brines (Land, 1995a; Levet et al., 2002). Na and Cl dominate the ionic composition of most sedimentary brines, even in basins that lack preserved evaporites, with the next most abundant cation being Ca and the next most abundant anion Br. This is not the ionic hierarchy of seawater, where the next most abundant cation is Mg and the next most abundant anion is SO_4 , hence most subsurface waters in a sedimentary basin are no longer connate outside of sediments encased in salt.

Today, the three mostly commonly offered explanations for the formation of Na-Ca-Cl basinal brines are (Land,

1995b): 1) preservation of seawater-derived brines that have precipitated halite (raises the Br/Cl ratio) as well as participated in dolomitization and CaSO_4 precipitation (exchanges Mg for Ca and removes calcium sulphate from the brine), 2) subsurface halite dissolution accompanied by salt recrystallisation (partitions bromide into the brine) in association with the dissolution of detrital anorthite (component of detrital plagioclase) - this mechanism may include the deep circulation of meteoric water or escaping compactional waters from thick shale sequences, and 3) reverse osmosis (shale membrane filtration) driven by pressure resulting from compaction, whereby water molecules, uncharged species and small and univalent cations preferentially pass through the shale, so creating calcium, chloride and bromine rich residual brines. Some or all of the mechanisms may be acting concurrently in most sedimentary basins (Demir and Seyler, 1999).

Effects and indications of water-salt interactions

This chapter has shown that dense subsurface waters derived from dissolving evaporites, tend to move through permeable sediments or along permeable conduits such as faults and fractures. They drive various diagenetic processes and flow is typically maintained by density gradients (indicated by thermal or salinity changes). Ongoing diagenesis (or rock-fluid interaction) in nonevaporitic strata also means ionic concentrations of most basin waters are buffered and controlled by the solubility of minerals in the sediment. The low solubility of the common cement minerals such as calcite and quartz means large fluxes of pore waters through nonevaporite lithologies are required to move and precipitate significant volumes of such cements (Bjørlykke and Gran, 1994). In contrast, in the temperature range of sedimentary basins, little water flows through the interior of a salt bed or allochthon. But inherently high solubility means that when the edges of a dissolving evaporite unit are flushed by basinal water crossflows, the dissolving salt contributes large volumes of ions to adjacent more permeable sediments. Even so, most basin brines, even in intervals adjacent to the dissolving evaporite, have salinities well below halite saturation (350–400 g/l). A possible exception is the Michigan Basin where some of the higher salinity basinal brines are clearly halite-buffered (Wilson and Long, 1993).

Solution of buried evaporites explains why: a) salinities increase in a systematic almost linear fashion with depth in sedimentary basins with bedded evaporites near the base of the sequence (Dickey, 1979); b) salinity around active salt stems/domes indicates the advective flow of waters up along the

stem and then horizontally into overlying beds (Hanor, 1988; Bray and Hanor, 1990); c) pore waters in sediments adjacent to a dissolving halite-dominated section lack sulphate, while evaporite sections with a greater proportion of gypsum/anhydrite can generate sulphate waters (Pluta and Zuber, 1995); d) in halokinetic provinces such as the central graben of the North Sea the salinity of the pore waters correlates better with the inverse distance to the nearest evaporite mass than it does to burial depth (Gran et al., 1992); and e) why there is no significant increases in salinity with depth in the northern North Sea (59–62°N), which is an area with no known evaporites (Bjørlykke and Gran, 1994).

The total volume of salts in the world's oceans is about $2.2 \times 10^7 \text{ km}^3$ and there is about the same amount of Cl in the world's sedimentary basins (salts and porewaters) as there is Cl in the modern ocean (Borchert and Muir, 1964). This means that of all the major sediment types, evaporites have the shortest mass half ages estimated to be $\approx 2 \times 10^8$ years (Garrels and Mackenzie, 1981). Hence, there are no significant potash or thick halite deposits older than Neoproterozoic (Warren, 2000c). Evaporite dissolution throughout burial and metamorphism and the associated discharge of Na-Cl rich brines into the basin's subsurface waters, and ultimately to the ocean, explains much of the short mass residence time for chloride. For the same reasons, the residence time for Cl in the world's oceans is the longest of any element and is of the same order ($\approx 2.2 \times 10^8$ years) as halite's mass half-life (Land, 1995a).

Hence, the chlorinity of the Precambrian oceans could not be more than around 50% different from today's. It also means that when large ancient basinwide salt basins rapidly accumulated their salts via drawdown, they could have substantially altered oceanic salinity. For example, the Permian Zechstein evaporites of northwest Europe, with a volume of $2.4 \times 10^6 \text{ km}^3$, is equivalent to some 10% of the volume of the current oceanic reservoir.

High concentrations of the ions from dissolution of buried salts typically indicate effective diffusive or advective transport of the ions from the salt-sediment contact and concentrations usually decrease further away from salt beds or domes (Figure 8.23). Steep gradients or abrupt changes in subsurface salinity, rather than gradual changes, typically indicate limited advective mixing of pore water across a permeability barrier (Bjørlykke and Gran, 1994). Near a subsurface evaporite unit the chemical composition of the pore water concentrations are high and can approach equilibrium with the major evaporite minerals (typically halite or anhydrite). Burial cements can precipitate

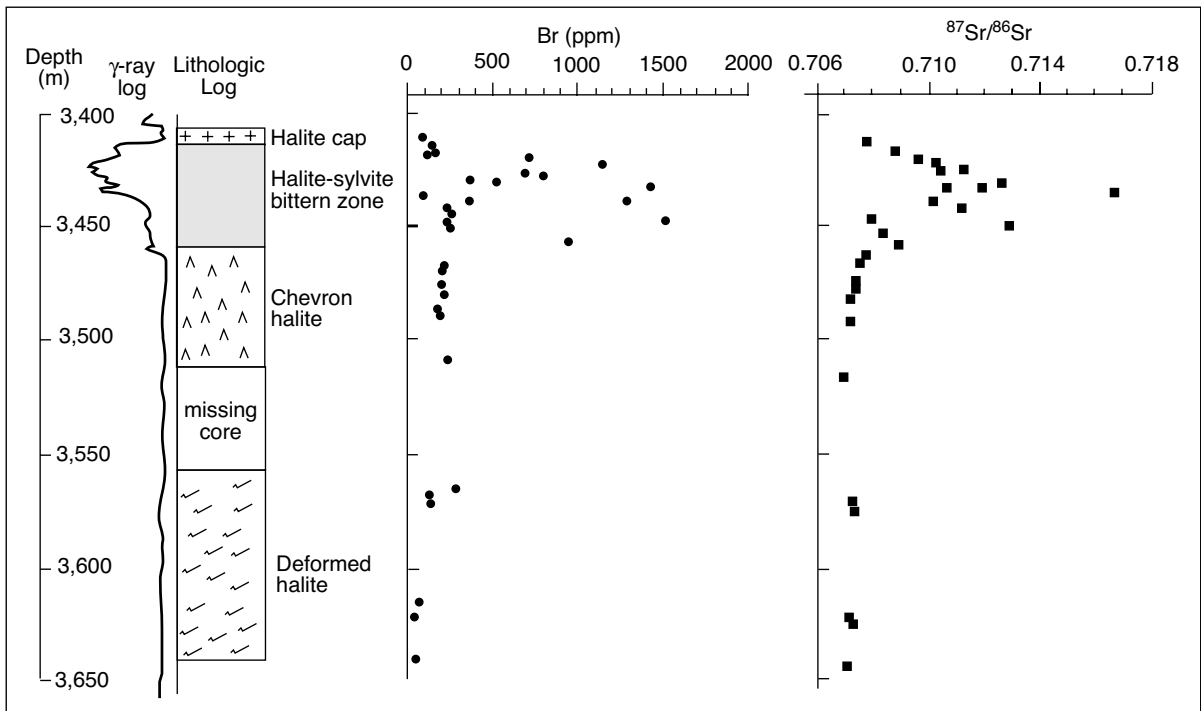


Figure 8.30. Gamma-ray log, lithologic log, Br concentration and $^{87}\text{Sr}/^{86}\text{Sr}$ ratio in whole rock samples from the cored interval through the Louann Salt in the Champion-Klepac #1 well (after Land et al., 1995). The well was drilled to a total depth of 4,800 m. Based on the monotonous gamma log, pure halite, at least 1,050 m thick, underlies the cored interval.

in pores in this zone when saturation is reached. The precipitation of evaporitic burial cements is even more likely when subsurface waters of differing salinities and compositions are mixed (Chapter 2; Sullivan et al., 1994).

Subsurface halite-dominated sequences dissolve in two ways; by incongruent or congruent dissolution. Incongruent dissolution occurs typically at low water rock ratios, whereby the halite recrystallises as more soluble components are lost to adjacent pore fluids. For example, when halite recrystallises in the presence of waters with a bromine content less than that of the original salt-precipitating (connate) water, it will become bromine depleted. At the same time the pore waters become relatively enriched in bromine, supplied by the rupture and dispersion of bromine-enriched connate fluid inclusions during the recrystallisation process. Congruent dissolution is the total or bulk dissolution of salt via throughflushing basinal brines. It forms subsurface Na-Cl brines with high chlorine contents and higher Br/Cl ratios compared to nonevaporitic subsurface waters (Worden, 1996).

Congruent dissolution of potassium-rich bittern salts is an even more effective means of creating-Br enriched hypersaline wa-

ters as minerals like sylvite entrain order-of-magnitude higher levels of bromine compared to sedimentary halite. Congruent or incongruent dissolution of K-salts leads to waters that are bromine-enriched relative to evaporated seawater. Hanor (1994a) proposed that K-salt dissolution explained the bromine enrichment seen in many basinal brines in sedimentary basins with buried evaporites.

Incongruent dissolution is used to explain the bromine depletion of recrystallised Jurassic halite remaining in diapir crests in the Gulf of Mexico (Stoessel and Carpenter, 1986) and is thought to be an important process in regions of salt flow and deformation worldwide (Land et al., 1988; Land et al 1995). In the Champion-Klepac #1 well in the Gulf of Mexico, sylvite occurs atop a thick halokinetic halite succession at the top of the diapiric Jurassic Louann Salt (Figure 8.30; Land et al., 1995; Land, 1995a, b). The well recovered some 150 metres of salt, which is underlain by more than another kilometre of salt. The bittern sequence lacks MgSO_4 salts, giving a mineralogy that, according to Hardie (1990), is a prime candidate for a nonmarine, possibly hydrothermal, brine source, or perhaps indicates evaporation of a Jurassic seawater with ionic proportions different from today (Figure 2.30).

Alternatively, Land et al. (op. cit.) argue the sylvite is the result of incongruent halite solution. The present bittern zone, encased in recrystallised halite, is interpreted to be a diagenetically modified “fractionated residue” created during the dissolution of more soluble marine bittern phases that were once present along with the sylvite. Sylvite is less soluble in halite-saturated subsurface waters than other bittern salts, which were primary coprecipitates (kieserite, epsomite, carnallite, etc; see Figures 2.7, 2.8). Incongruent formation of recrystallised halite and the associated accumulation of the sylvite residue supplied Mg, Br and SO_4 to the escaping pore brines.

Bromine values from deformed halite lower in the Klepac core can be used to argue that incongruent halite dissolution and recrystallisation can supply bromine to escaping pore fluids. Br values in the primary halite chevron-dominated succession beneath the bittern succession is uniform and centred around 200 ppm (range 170–234 ppm). This fits into the range of typical marine values (Holser, 1979). Values in the deformed salt are much lower, averaging 110 ppm and decreasing to values of 29–60 ppm in the lower portions of the core. Did the bromine escape during incongruent recrystallisation of the flowing salt, or was the halite reworked and recrystallised at the time of deposition? Resolution hinges on an improved understanding of how flowing salt recrystallises (Figure 6.3). Over a time frame of millions of years can the outer portions of a thick flowing salt periodically pressurise and leak fluid, or is the flow mechanism purely one of localised halite recrystallisation, pressure solution and edge dissolution within a relatively closed hydrology? At the present time we simply do not have the answer.

Crustal cycling of brines?

Shield brines, which are ubiquitous hypersaline waters in open faults and fractures at depths > 1 km in Precambrian rocks around the world, are among the most enigmatic of all crustal fluids with respect to their age and origin (Bottomley et al., 2002). Not only do shield brines have very high salinities (upto 300 g/l), which are comparable to sedimentary formation brines in evaporite-floored basins, their chemical compositions are of the Ca-Cl type and their O and H isotopic compositions plot well above the global meteoric water line in $\delta^{18}\text{O}$ versus $\delta^2\text{H}$ space (i.e., they are depleted in ^{18}O or enriched in ^2H relative to meteoric water). Arguments for both in situ water-rock interactions (Frape et al., 1984), and ancient, concentrated marine sources have been presented to explain their compositions and widespread occurrences (Bottomley et al., 1994, 1999) and to model per descendum flow paths for some types of shield-hosted ore deposits (e.g. Mernagh et al., 1994).

Bromine elevation in a pore water in a sedimentary host is readily explained by the subsurface dissolution of the more saline evaporite salts, but saline Na-Ca-Cl type groundwaters and brines also occur in deep mines over extensive areas of the Canadian Precambrian Shield. These waters have elevated Br/Cl ratios which imply the chlorinity of these waters was derived from the deep infiltration of residual evaporitic brines, perhaps as remnants of the great marine/hypersaline apron that typify strata of the Palaeozoic era in this region (Bottomley et al., 1994, 1999). Boron concentrations in these waters are generally low (< ≈ 2 mg/l) relative to seawater or to Alberta Basin Devonian formation waters. However, the $^{11}\text{B}/^{10}\text{B}$ ratios of these waters are significantly greater than the average value for continental crustal rocks. Moreover, Bottomley et al. argue that the boron isotopic ratios generally trend to higher values with increasing chlorinity, which supports the conclusion from the Br-Cl relationship that most of the chloride in these shield brines is of marine origin, rather than a product of water/basement rock interactions. In a subsequent paper Bottomley (2002) used ^{129}I measurement to determine the minimum age of brines in basement fractures in the Con gold mine in Yellowknife (Northwest Territories), and found the brines are at least Cretaceous and probably Devonian. He concludes a Pleistocene age and cryogenic origin is impossible.

Yet seawater freezing has been proposed by Herut et al. (1990) and Starinsky and Katz (2003) as an alternative explanation for the saline chemistry of Canadian Shield brines (Figure 8.31). Based on minerals present in salt lakes in Antarctica such as Lake Bonney and Vanda Lake, we know that seawater freezing can form various sodium and magnesium salts and high salinity brines. Thick beds of mirabilite occur on the McMurdo Ice Shelf. From experiment, we know that when seawater freezes at -1.9°C , a small amount of calcium carbonate is the first salt to drop out, usually as aragonite. Next, sodium sulphate precipitates as mirabilite at -8.2°C , sodium chloride as hydrohalite ($\text{NaCl}\cdot 2\text{H}_2\text{O}$) at -22.9°C , and then sylvite + $\text{MgCl}_2\cdot 12\text{H}_2\text{O}$ at -36° (Nelson and Thompson, 1954). At -54°C this cryogenic sequence of salts ultimately produces a calcium chloride brine slurry that precipitates antarctite ($\text{CaCl}_2\cdot 6\text{H}_2\text{O}$). One of the few places in the world where this mineral occurs naturally is in a brine lake known as the Don Juan Pond in the Dry Valleys (Wright Valley) of Antarctica, where the TDS of the bottom brine can exceed 500 kg/m^3 (Torii and Ossaka, 1965).

Up to the point of halite precipitation, seawater freezing has the same effect on chlorine-bromine relationships in residual brines as solar-driven evaporation. So, seawater freezing beneath thick ice sheets may be an important process controlling

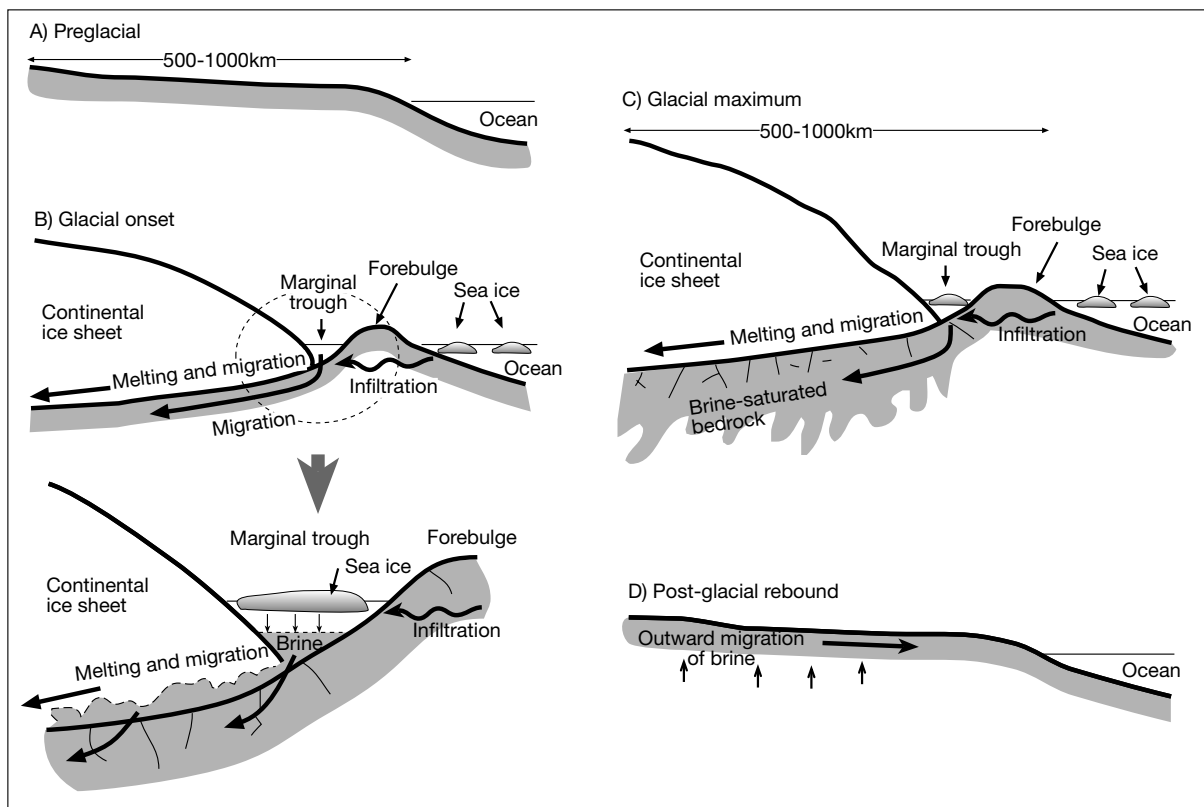


Figure 8.31. Isostatic and hydrological evolution of a marine-cryogenic basin: A) Continent-ocean boundary before the onset of a glacial cycle. B) An ice sheet develops on the continent, depressing the crust underneath and forming a forebulge along the coast. Seawater infiltrates into the marginal trough between the ice edge and the forebulge and sea ice crystallizes on its surface. The resultant brine sinks to the bottom and infiltrates the underlying sediments and rocks via cracks and shear zones and by non-equilibrium melting of the ice sheet base. Then, it migrates inland, along the inclined ice-rock contact, towards the center of the depression. Loss of brine from the trench is compensated by fresh seawater flow through the forebulge. C) During the glacial maximum the basement rocks below the ice sheet become saturated with brine. D) Increased melt water head developing during glacial decline, accompanied by postglacial lithospheric rebound, drive the brines outwards from the center of the glaciostatic depression to their present sites (after Starinsky and Katz, 2003).

the composition of formation waters seeping into fractures and cracks in sub-glacial hard rock sequences. However, recent work on the origin of the various salts in Antarctic salt lakes has shown that, while the mirabilite in Lake Bonney and Vanda Lake are derived by seawater freezing, the antarctite in Don Juan Pond may not be. Rather, it formed by freezing of a resurgent brine that was created by water-rock interactions in a deeply circulated groundwater moving through fractures within a granite host (Takamatsu et al., 1998).

At the other end of the temperature spectrum, the possible creation of hypersaline brines beneath the evaporite basin in a hard-rock basement host, via infiltration of connate waters, leads to an interesting quandary. Have hypersaline basinal brines entered and influenced the chemistry of the hard rock basement that lies

beneath most evaporite-floored sedimentary basins (such as the Gulf of Mexico), or are these waters juvenile residuals from magmatic or metamorphic fractionations (Markel and Bucher, 1998)? Land (1995b) argues for the former. Using quantified mass volume and element residence times he concludes that as the porosity of rocks is reduced during burial, discharge of saline formation waters contributes to crustal chloride cycling. During deep burial, corrosive saline formation waters dissolve metastable detrital minerals derived from crustal/basement rocks and transfer incompatible elements such as Li and B from the igneous crust to the sedimentary crust. Likewise, albitisation transfers Ca from the crustal silicate (igneous) mineral reservoir to the crustal carbonate and aqueous (sedimentary) reservoirs. Metamorphism, and then melting of albite-enriched rocks, accounts for the elevated sodium contents of igneous rocks relative to sedimentary rocks. In this way average sediments

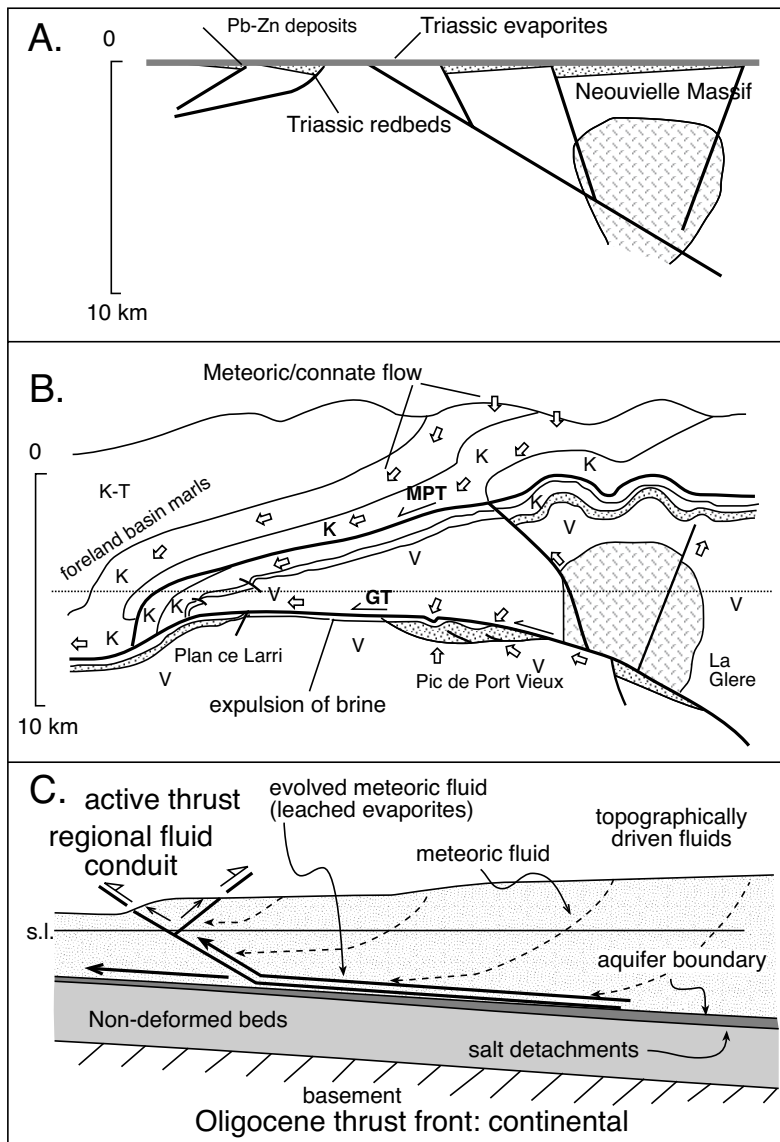


Figure 8.32. Model for fluid evolution and mixing in the Pyrenees. A) Situation at the end of the Triassic: Brines from marine-fed Triassic evaporites sink and displace older formation waters in the underlying redbeds and fractured basement rocks. Pb-Zn deposits formed along normal faults sometime between the Triassic and the middle Cretaceous, due to circulation of metalliferous basinal brines, probably due to density convection. B) Situation during Eocene thrusting. Section above the present exposure level is conjectural (above dashed line). Detail of part of section below thrust line is given in Figure 8.6. Arrows show inferred directions of fluid flow. Note local movement of fluid into the Pic de Port Vieux culmination driven by dilatancy. V = Variscan basement (Silurian and Devonian phyllites, Cambro-Ordovician schists and late granitoids). K = Cretaceous to Palaeocene carbonates. K-T = Tertiary marls and flysch of the foreland basin, locally interthrusted with Cretaceous carbonates. GT = Gavarnie Thrust. MPT = Mont Perdu Thrust. (A & B after McHaig et al., 2000; Horizontal and vertical scales are equal, but there is no precise correspondence between the two diagrams). C) Fluid flow in the El Guix anticline during the Oligocene when deeply circulating and evolved meteoric waters mixed with evaporitic waters from Triassic evaporites that also created the décollement for the thrust plane (after Trave et al., 2000).

have become enriched through time in Ca, Cl, Br, S, Li, and B, and depleted in Na relative to average igneous crust.

In support of the ability of evaporite brines to enter and so influence basement chemistry during metamorphism and overpressuring, McCaig et al. (2000) documented evaporite-derived Na-Cl brines in inclusions in the northern end of the Alpine shear zone, Europe (Figure 8.6; 8.32a,b). They occur where the shear cuts the Neouvielle granodiorite in the Hercynian Axial Zone and also to the south in several localities in the footwall and hangingwall of the Gavarnie Thrust on the southern margin of the Axial Zone. Inclusion fluids generally decrease in salinity from 27-35% at the northern end of the transect to 7-22% on the southern margin of the Axial Zone. The evaporitic origin is seen in the Cl-Br-Na systematics of the fluid inclusions, which show chemistries consistent with a change from halite to halite + sylvite precipitation with progressive evaporation. The fluids in the basement shear zones are interpreted to have essentially the same evaporitic origin as those still contained in nearby Triassic sediments. Brine inclusions in the sediments have Cl/Br ratios lower than seawater indicating relict signatures derived by marine evaporation and halite precipitation in the upper Triassic. It is possible that final concentration of brines in the Neouvielle Massif also involved retrograde hydration reactions via removal of water by precipitation of hydrous minerals.

The somewhat lower salinities seen at the southern margin of the Axial Zone are interpreted by McCaig et al. to reflect mixing of evaporite-derived brines with a higher level fluid (connate or meteoric water) circulating within the Mesozoic carbonates of the higher thrust sheets. At one locality where Triassic evaporites are still present, high Cl/Br ratios at relatively

low salinities are present in inclusions within the underlying Triassic redbeds, but low Cl/Br ratios at higher salinities are seen lower in the sequence. This is consistent with dissolution of halite by a dilute fluid, but with limited penetration downwards.

In a related paper, Trave et al. (2000) demonstrate the involvement of evaporite-related fluids in sediments atop the evaporite-lubricated thrust of the Al Guix anticline in the Pyrenees of NE Spain (Figure 8.32). The El Guix anticline is the southernmost structure of the south-Pyrenean fold-and-thrust belt. Compressional activity in the area represents the latest stages of Alpine compressional tectonics and overprints the Upper Eocene-Oligocene fluvio-lacustrine deposits that overlie halokinetic Triassic evaporites. Based on a detailed structure of the timing and chemistry of various microfracture cements, Trave et al. (2000) conclude that the Pyrenean fold-and-thrust belt and its deformed southern foreland basin were hydrologically compartmentalised, both in time and space. During the early Eocene, when the thrust front affected soft-sediment in the Ainsa basin, the thrust faults were dominated by medium-scale fluid flow cells. Fluids in the basin were largely formation fluids derived from Eocene marine waters with a minor meteoric influence. During the middle Eocene; coeval with the Gavarnie thrust emplacement, the thrust fault was dominated by medium scale fluid flow system and a fluid that was basically a hypersaline Sr-rich brine stored within Triassic redbeds. No evidence was found of any significant input of either surface or metamorphic fluids during this time. During the same period, the thrust faults in the crystalline basement of the central Pyrenees were dominated by a large scale fluid flow mainly derived from the underlying silicate rocks as a result of metamorphic devolatilisation reactions. During the Oligocene, the most external part of the fold-and-thrust belt developed on top of a salt detachment horizon (Figure 8.32c). Then the thrust front affected mostly cemented continental materials of late Eocene-Oligocene age and the thrusts were conduits for meteoric fluids and also for evolved meteoric fluids migrating a short distance upwards after being in contact with the underlying evaporitic beds focused by the décollement.

Thus, the fluid history in the Pyrenean collision zone evolved through a series of stages in time and space, linked also to economic accumulations of base metals: (1) Upper Triassic evaporite formation with sinking of brines into underlying redbeds and fractured basement rocks; (2) Circulation of brines with formation of Pb-Zn deposits along faults at some time between the Triassic and the Upper Cretaceous; (3) Renewed extension with erosion of Triassic rocks in many areas and further

draw down of Triassic brines into the basement; (4) Deposition of Upper Cretaceous and Palaeocene-Eocene carbonates containing connate waters of marine origin; (5) Formation of the Pyrenean thrust belt with overpressuring and expulsion of the brines along shear zones and faults; (6) Creation of topography with a high-level circulation system in the Mesozoic thrust sheets driven largely by topography (McCaig et al., 2000). At the southern margin of the Axial Zone there was limited mixing of the deeper, overpressured brines from evaporitic sediments with more dilute, hydrostatically pressured fluids (Trave et al., 2000). A similar interaction between hydrothermal ($\approx 200^\circ\text{C}$) fluid circulation, associated with the cooling of a granite mass, and hypersaline fluid circulation driven by sinking of dense hypersaline brines, derived in Triassic evaporitic rifts of the Western Approaches, is important in controlling the fracture-related low temperature base metal and uranium accumulations of South Cornwall (Gleeson et al., 2001).

Chapter 9: Halotolerant life in feast or famine (a source of hydrocarbons and a fixer of metals)

Introduction

A source rock for hydrocarbons is generally considered to be a fine-grained rock that, during its burial and heating, generates and releases enough fluids to form commercial accumulations of oil or gas (Figure 9.1a). Back in 1981, Kirkland and Evans made the observation that some 50% of the world's oil sequestered in carbonate reservoirs may be associated with mesohaline micritic source rocks. Heresy or not, the notion that much of the oil in carbonate reservoirs, sealed by evaporite

salts, may also have also been sourced in earlier less saline, but still related evaporitic (mesohaline) conditions, is worthy of consideration. The association between mesohaline waters, the accumulation of organic-rich sediments and the evolution of the resulting evaporitic carbonates into source rocks has been noted by many, including: Woolnough, 1937; Sloss, 1953; Moody, 1959; Dembicki et al., 1976; Oehler et al., 1979; Malek-Aslani, 1980; Kirkland and Evans, 1981; Jones, 1984; Hite et al., 1984; Eugster, 1985; Sonnenfeld, 1985; Ten Haven et al., 1985; Warren, 1986; Evans and Kirkland, 1988; Busson, 1991; Edgell, 1991; Beydoun, 1993; Benali et al., 1995; Billo, 1996; Aizenshtat et al., 1998; Carroll, 1998; Schreiber et al., 2001. As long ago as the middle of last century, Weeks (1958, 1961) emphasised the importance of evaporites as caprocks to major hydrocarbon accumulations. He also pointed out that many of the cycles of deposition that involve organic-rich carbonate marls or muds also end with evaporites. Many of these authors have noted the association of Type I-II hydrogen-prone kerogens in evaporitic source rocks and related their occurrence to the ability of halotolerant photosynthetic algae and cyanobacteria to flourish in saline settings. Such kerogens tend to be oil-prone rather than gas prone (Figure 9.1a).

Much of the organic matter preserved in evaporitic carbonates, and the resulting source rocks, originated as mesohaline planktonic blooms (a pelagic "rain from heaven") or from the benthic biomass (an "in situ" accumulation). It was typically laid down via a succession of pulses of organic matter (often pelleted) sinking to the bottom of a layered brine column. Each pulse indicates a short period when surface brines were diluted and halotolerant producers (mostly cyanobacteria and algae) flourished in the surface waters. That is to say, the laminated mesohaline mudstones that constitute evaporitic source rocks reflect biological responses to conditions of "feast or famine" in variably layered bodies of brine. Warren (1986) referred to the schizohaline salinity cycles of saline settings as repetitive episodes of "life or death."

Before it becomes a source rock the organic matter buried in organic-rich sediment undergoes numerous compositional changes, first dictated by microbial agencies and then by thermal stress (Horsfield and Rullkotter, 1994). This continuum of processes is called thermal maturation. Based on vitrinite reflectance (R_o) measurements of macerals in a maturing source rock, can be divided into three consecutive stages: ⁹¹diagenesis (eogenesis) ($R_o < 0.5\%$), catagenesis ($0.5\% < R_o < 2.0\%$), and

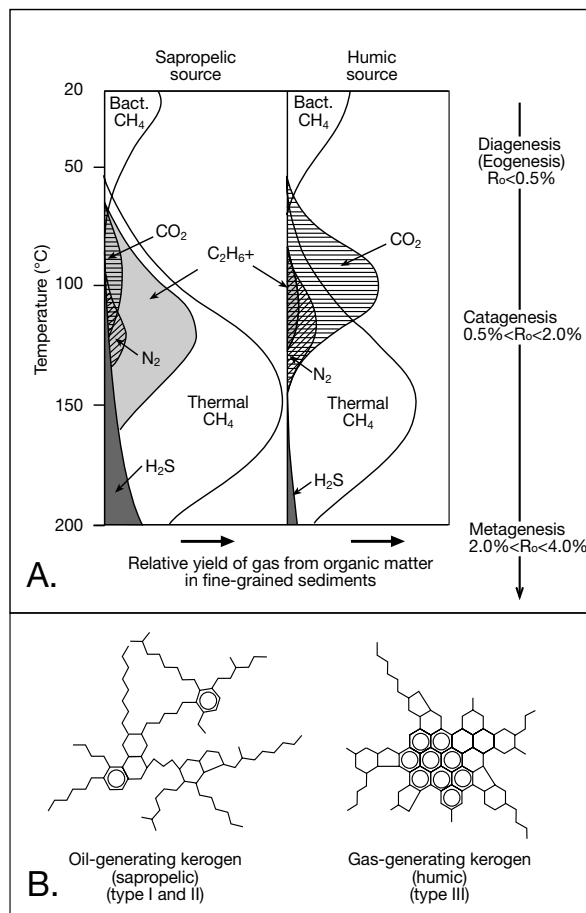


Figure 9.1. Organics and source rocks. A) Relative volumes of gases and liquids derived from a sapropelic and a humic source rock (after Hunt, 1996). Evaporitic source rocks tend to be sapropelic and contain less iron as a reductant so they are also likely to generate more H₂S. B) Molecular structure of typical oil-generating (sapropelic) and gas-generating (humic) organic matter showing the greater preponderance of long-chain hydrocarbons in the sapropelic material (after Hunt, 1996).

metagenesis ($2.0\% < R_o < 4.0\%$), with the oil generation window in the R_o range of 0.5-1.3% (≈ 65 -150°C). Reflectivity is measured by shining a beam of monochromatic light (with a wavelength of 546 nanometres) on to a polished surface of the vitrinite macerals and measuring the percentage of the light reflected with a photometer. Put simply, it measures the degree of darkening (roasting?) of the organics associated with heating of the rock during burial.

As originally defined, macerals are the microscopic organic components of coal and consist of an irregular mixture of different chemical compounds, which are analogous to minerals in inorganic rocks, but differ from minerals in that they have no fixed chemical composition and lack a definite crystalline structure. Macerals change progressively both chemically and physically during ongoing burial and heating, as the rank of macerals (coaly material) advances or the maturity of the organics increases. Macerals in any sediment can be classified into three major groups: vitrinite, inertinite, and exinite. Vitrinite is derived mostly from woody plant tissue and includes the macerals collinite and telinite, most coals have a high percentages of vitrinite macerals. The inertinite group comprises fusinite, micrinite, sclerotinite, and semi-fusinite, which are all rich in carbon but poor sources of volatiles. The exinite macerals, characterized by high hydrogen content (and hence excellent liquid hydrocarbon generating potential), include alginite, cutinite, resinite, and sporinite. Alginites are commonplace macerals in evaporitic settings, while vitrinites are rare, reflecting a lack of higher plants in most hypersaline settings. A lack of vitrinite and poor calibrations to alginite maturation indices can lead to poor correlations between actual source rock maturity and that indicated by vitrinite based estimates in evaporitic source rocks.

Transformation of organic matter to liquid and gaseous hydrocarbons is the result of thermal cracking of kerogen (the solid organic assemblage in a rock that is insoluble in organic solvents and encompasses numerous macerals). Kerogen is the major global precursor of petroleum and its formation, mostly via biologically-induced alteration of plant and animal detritus, is complete by the end of eogenesis. Around 90 percent of the

organic material in a source rock at the onset of catagenesis is dispersed kerogen, consisting of a range of residual materials with basic molecular structures that take the form of stacked sheets of aromatic hydrocarbon rings in which atoms of sulphur, oxygen, and nitrogen also occur. Attached to the ends of the rings are various hydrocarbon compounds, including normal paraffin chains (Figure 9.1b). Mild heating of kerogen over long periods of time results in the cracking of the kerogen molecules and the release of the attached paraffin chains.

Further heating, perhaps assisted by the catalytic effect of clay mineral transformation and evaporite dewatering in the source rock matrix, may then produce soluble bitumen compounds, followed by the various saturated and unsaturated hydrocarbons, asphaltenes, and others of the thousands of hydrocarbon compounds that make up crude oil mixtures. Thus kerogen cracking is induced by burial and heating and it releases micropetroleum (a mixture of liquid and gaseous hydrocarbon products that are soluble in organic solvents) into the pore system of the source rock. The maturity and evolution of the kerogen is paralleled and indicated by increasing maceral (vitrinite) maturity. Once released into the pores of the source rock, micropetroleum migrates toward the surface via secondary migration pathways and along the way a portion of this material can be trapped in a variety of reservoirs of varying quality.

The nature of the organic precursors to kerogen exerts a strong influence on kerogen structure and bulk composition, and hence on subsequent oil- and gas-generating characteristics. Source rock kerogens enriched in long chain hydrogens (aliphatics or paraffins) tend to be oil-prone type I sapropelic source rocks and associated with algal, bacterial and archaeal precursors (indicated by C_2H_6+ in Figure 9.1a), while kerogens that are strongly depleted in long-chain hydrogens are typically type III humic (vitrinitic) source rocks associated with organics from higher plants. They tend to generate gases consisting mostly of methane (dry gas), sometimes with associated hydrogen sulphide or nitrogen. Like hydrocarbons, hydrogen sulphide is generated both biochemically and thermochemically.

Obviously, not all source rocks are evaporitic. Organic matter accumulating in mesohaline sediment is derived from the activities of the ^{9.2}halotolerant and halophilic biomass, mostly algae, bacteria and archaea. Kerogen derived from burial of this organic

^{9.1}The term diagenesis, as used by petroleum geochemists, describes processes of organic modification or alteration in the presence of pore waters where circulation is driven by surface processes. This usage is much more restrictive than the sedimentological use of the term which encompasses all alteration or modification from the time of sediment deposition until the onset of metamorphism. In order to minimise any possible confusion, the term eogenesis is preferred by many workers.

^{9.2} *Halotolerant* organisms can tolerate high salt concentrations but grow better at somewhat lower salinities.

Halophilic organisms grow best at very high salt concentrations and can be killed by lower salinities.

Haloxene organisms cannot tolerate high concentrations of salts.

matter will be composed of their somewhat altered remains, as will the expelled hydrocarbons. Sapropelic organic matter is created by decomposition and polymerization of high-lipid organic materials (with aliphatic long-chain hydrocarbons), which are commonplace in algal and bacterial sediments deposited under anaerobic conditions. Hence, sapropelic organic matter tends to be associated with oil-prone Type I or Type II proto-kerogens (Figure 9.1b). Humic organic matter tends to contain less long chain hydrocarbons and so constitutes a large proportion of the more gas-prone source rocks found in coaly sediments and in dispersed terrestrial organics deposited in prodelta settings. It is mostly associated with Type III protokerogens.

Unoxidised evaporitic organic matter tend to be hydrogen-rich and oil-prone; its sapropelic kerogens (Type I or Type I-II) contain higher proportions of long chain hydrocarbons from cyanobacterial, archaeal and bacterial precursors. Higher plant material, which is the source of much of the humic component in nonevaporitic kerogen simply does not accumulate in large volumes in an evaporitic source rock; higher plants need fresh water and do not flourish in hypersaline waters.

This chapter summarises and classifies evaporitic source rocks, looks at controls on organic enrichment in saline environments, and at the styles of hydrocarbon generation and metal fixing associated with organic-prone mesohaline evaporites. The following chapter looks at how evaporites form the seals and traps to reservoirs that store the generated hydrocarbons.

Evaporitic Source rocks

Amass balance of oil in the global petroleum system indicates that 40% of the world's generated oil is lost to the surface, 58% is dispersed in the subsurface as oil, gas and pyrobitumens somewhere between source and reservoir, and 2% is to be found in pooled accumulations suitable for exploitation (Hunt,

1996). It also shows that the estimated reserves, plus ultimate undiscovered resources, for conventional oil and gas are about the same, each is about 2×10^{12} BOE (barrels of oil equivalent) or $3.2 \times 10^{11} \text{ m}^3$.

A plot of Phanerozoic source rocks shows that more than 90% of the world's discovered original reserves of oil and gas comes from six intervals of geological history, covering only 35% of Phanerozoic time (Figure 9.2; Klemme and Ulmishek, 1991). The six intervals are: 1) Silurian, which generated 9% of the world's recoverable reserves, 2) the Upper Devonian (Tournisian), 8%; 3) Pennsylvanian-Lower Permian 8%; 4) the Upper Jurassic, 25%; 5) the Middle Cretaceous, 29% ; and 6) the Oligo-Miocene, 12.5%. More than 78% of the world's oil and gas is sourced in sediments deposited in restricted or silled anoxic systems located in intrashelf basins on platforms, or in restricted areas formed by circular and linear sags. Four of the six stratigraphic intervals occurred in worldwide first-order sealevel highs (transgressions) associated with greenhouse climatic conditions and the deposition of mostly sapropelic

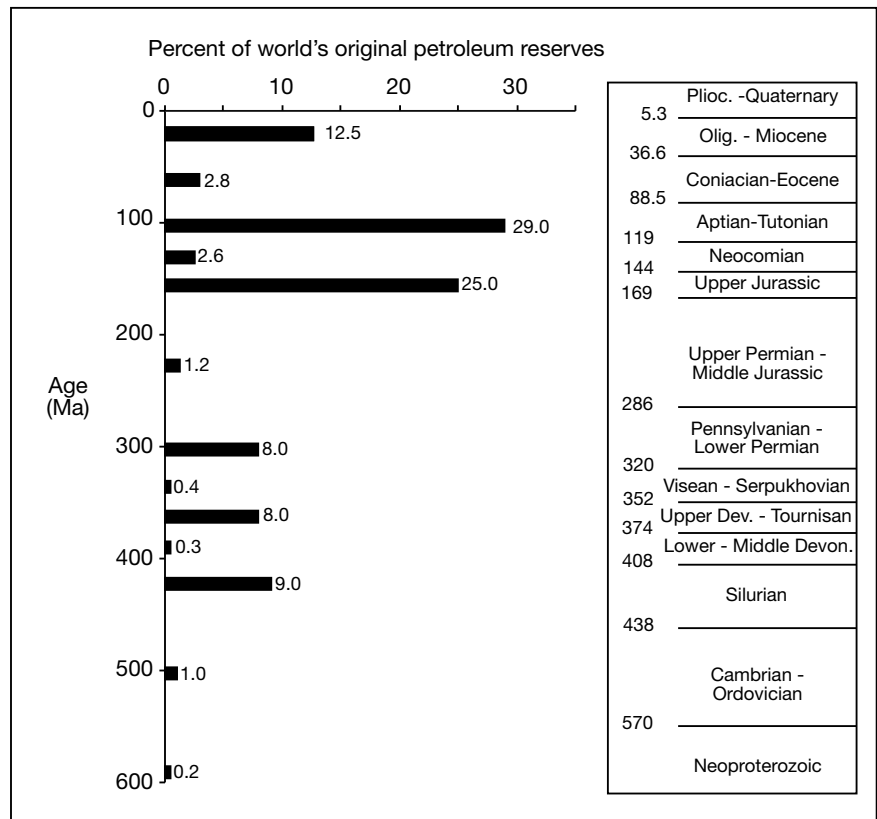


Figure 9.2. Time distribution of effective source rocks as a percentage of the world's original petroleum reserve generated by these rocks (after Klemme and Ulmishek, 1991).

organic matter. The other two, Pennsylvanian-Lower Permian and the Oligo-Miocene, which source 20.5% of the world's oil and gas, occurred during times of lowered sea level (regressions) and deposited mostly type III kerogens (Hunt, 1996). These were times of polar glaciation (icehouse climate mode). Something like two-thirds of the world's oil was generated in Tethyan basins in a system that covers less than a fifth of the world's land area and continental shelves. The efficiency of the Tethyan petroleum system, centred on the countries of the Middle East was facilitated by the deposition of widespread platform evaporite seals, such as the platform anhydrites of the Hith and Khuff formations and the basinwide halites of the Fars/Gachsaran (Chapter 10), as well as gentle structuration of the reservoirs beneath these platform seals via draping, often in association with the flow and dissolution of Infracambrian Hormuz salt, or in foreland fold belts driven by the Zagros collision.

A common theme to most source rocks, both evaporitic and non-evaporitic, is that they require anoxic conditions to accumulate and preserve their organics. This in turn requires some way of restricting the influx of oxygenated waters to the depositional site and is usually accomplished by thermal or density stratification of a water body, typically in a setting where plankton flourish periodically in the upper water mass. This is why so many subaqueous evaporitic settings are also settings where organics tend to accumulate. By definition, evaporites require restricted inflow conditions to accumulate, they are also typically areas of density-stratified waters with high salinities in the lower denser more saline water mass. Levels of dissolved gases are negligible to nonexistent in the lower brine body as it does not easily exchange with the atmosphere, so encouraging long-term bottom anoxia (Figure 2.37b).

This does not mean all of the world's source rocks were deposited in evaporitic settings, only that the restricted conditions that favour the accumulation of evaporites are similar to conditions that favour the accumulation of some types of organic-rich bottom sediments. In arid climates any minor changes in inflow conditions, such as hydrographic isolation from the ocean, can easily force a transition from one into the other. Hence the common association of source rocks with layered basin waters typical of the early mesohaline phase and the onset of evaporitic sedimentation in many lacustrine/epiiric settings (Table 9.1). In the marine realm, the same need for tectonic or eustatic restriction to create a basin suitable for source rock accumulation (intraself, circular or linear sag) also explains why, if further restriction and hydrographic isolation from the ocean ensues, the same region is easily covered by a sequence of salts (Figure 5.27).

Worldwide, studies of ancient evaporitic basins have shown that organic-rich mesohaline sediments can accumulate beneath ephemeral surface brines, in salterns, or in basin and slope settings in both marine and continental settings (Kirkland and Evans, 1981; Oehler, 1984; Warren, 1986; Evans and Kirkland, 1988; Rouchy 1988; Busson, 1992). The most prolific accumulations of organics in ancient evaporitic sediments tend to have been deposited as laminated micritic carbonates beneath density-stratified moderately-saline (mesohaline) anoxic water columns of varying brine depth.

There are three, possibly four, major mesohaline density-stratified settings where organic-rich laminites (source rocks) accumulate in saline settings that are also associated with, or evolve into, evaporite deposits (Figure 9.3; Table 9.1):

- 1) Basin-centre lows in marine-fed evaporitic drawdown basins (basinwides).
- 2) Mesohaline intraself lows atop epiiric evaporitic platforms.
- 3) Saline-bottomed lows in perennial underfilled saline lacustrine basins.
- 4) Closed seafloor depressions in halokinetic deepwater marine slope and rise terrains.

Basin Setting 1: There are two depositional styles for basin-centre or basinwide mesohaline source rocks; a) Basin-centre drawdown laminites intercalated and often sealed by basinwide salts, b) Basin centre laminites where the basin margin is a shallow, restricted, at times evaporitic, platform surrounding a slightly mesohaline deepwater starved-basin centre with bottom waters that were never drawdown or concentrated to where basinwide salts precipitated. Matrices in setting 1b basin-centre laminites range from fine-grained limestones through marls to siliciclastic muds.

In source setting 1a) the basin is largely isolated from a surface marine connection and high levels of organics accumulate as radiogenic "black shales" (typically carbonate laminites), which are intercalated with, and overlain by, thick basinwide evaporite salts (typically halite-dominated). These laminites accumulate on the bottom of mesohaline density-stratified stagnant brine pools in topographically closed parts of the basin floor during the early stages of hydrographic isolation and drawdown. Inactive, typically subaerial, shelf margin reefs and pinnacles typically lie updip or encircle the basin-centre lows (Chapter 5). Subsequent encasement of these platform buildups and other potential reservoirs by "fill and spill" evaporites means these basins easily become highly focused hydrocarbon flow systems. Hydrocarbons accumulate in the reefs or shelf margin

shoals beneath basinwide evaporite seals. Such systems typify the marine-fed Silurian reef/Salina Salt association in the Michigan Basin, USA (Gardner and Bray, 1984), the Devonian Rainbow Reef reservoirs of the Black Creek/Muskeg Basin of Alberta (Clark and Philp, 1989) and Messinian marls of the Lorca Basin, Spain (Russell et al., 1997).

Expulsion efficiencies suffer from encasement and widespread salt plugging of the potential source rocks in many evaporite-rich setting 1a basins. This tends to retain volatiles in the source beds

until the whole system becomes overmature. For example, in the Gibson Dome No. 1 well, in the Paradox Basin almost all of the black shales intercalated in the halite cycles in the Paradox Member are mature enough to have generated oil (Hite et al., 1984). But the hydrocarbons have been largely retained in this mature source rock, reflecting the highly efficient sealing effects of the intercalated evaporite beds and salt cements (mostly halite). Only where the black shales are intercalated or in contact with porous carbonates have the hydrocarbons escaped. The source potential of these shales is very high, the "Gothic shale" is capable of generating almost 5,000 barrels per acre. But that potential is never more than partially realised. Paradox "shales" are responsible for an accumulative production of a little more than 400 million barrels of oil and about 1 TCF of gas in the Paradox Basin in fields such as Ismay and Aneth (Peterson and Hite, 1969).

This problem of evaporite plugging plagues many basinal source rocks where the basin centre evolved to accumulate basinwide evaporites and is one of the main reasons for the dearth of large onshore oilfields beneath bedded salt or within intrasalt carbonates in the Zechstein basin of NW Europe. Organic-

rich source intervals such as the Stinkdolomit, Stink-kalk, and Stinkscheifer are widespread, but the associated oil accumulations are never more than localised and small scale. Setting 1a sediments can be characterised by very rich organic source beds but the intercalated seals prevent most of the volatiles from ever escaping into a reservoir. In later burial diagenesis, as dissolution of salt interbeds facilitates contact with basinal waters carrying Cu, Pb and Zn, they can play an important role as a reductant and metal fixer (Warren, 2000b).

Basin Setting 1b: Basin-centre mesohaline accumulations in this setting are much more efficient petroleum producers than style 1a as they lack intercalated beds of basinwide halite or

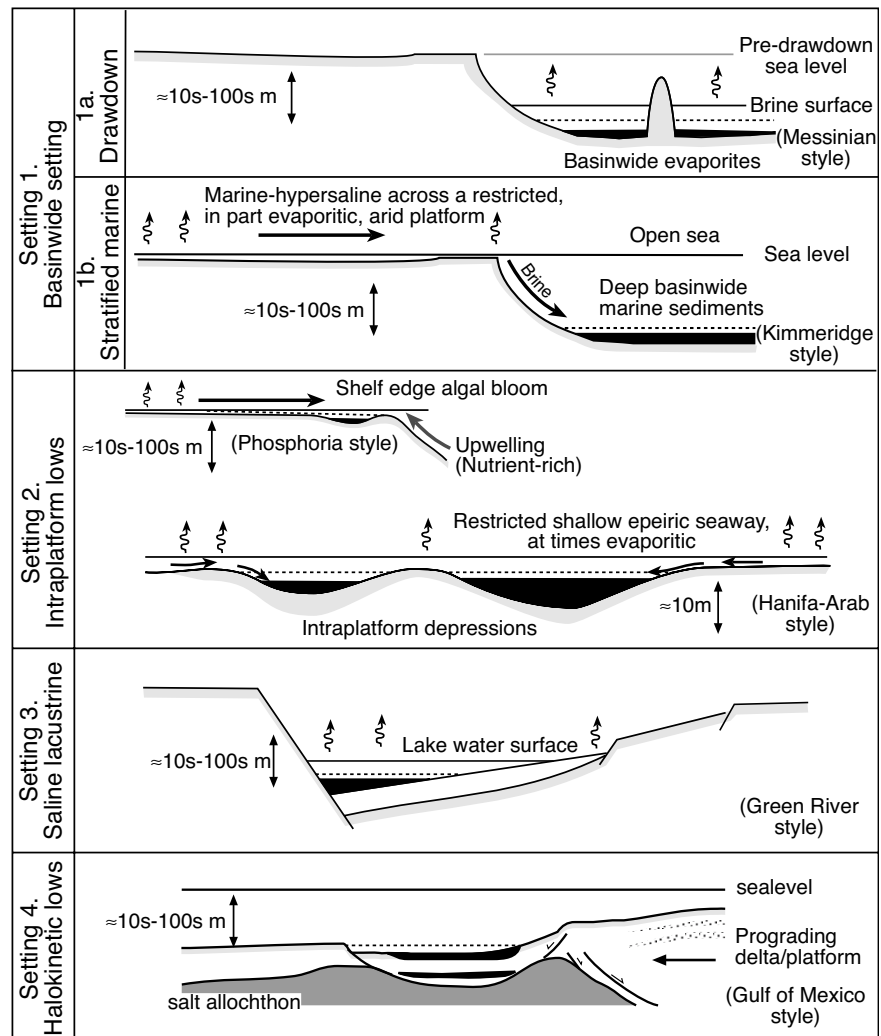


Figure 9.3. Dominant depositional styles for evaporitic source rocks (mesohaline laminites shaded black). All the water bodies show evidence of salinity-related density stratification (indicated by dashed line), also reflected in an associated heliothermic stratification.

Formation/Group locality and age	Basin Style	Characteristics and depositional setting	Reference
Messinian carbonates Lorca Basin, Spain Late Miocene	1a Basinwide evaporite marginal basin	Organic-rich laminated mudstones deposited in pre-evaporitic mesohaline marginal basins with density- and salinity-stratified brine columns. The basin underwent sporadic phases of circulatory restriction with marked production and preservation of organic matter, culminating in evaporitic sedimentation (latest Miocene). As the water in this basin evolved toward evaporitic conditions, a number of organic-rich depositional phases (>25 wt.% TOC) occurred. During the early parts of these phases, the upper water was nutrient rich and comparatively normal marine, and the bottom water was anoxic and more saline. This was followed by rising salinities in the surface waters, holomixis and short phases of evaporite formation.	Benali et al., 1995 Russell et al., 1997 Rouchy et al., 1998
Gessoso-Solffera Formation, Sicily Late Miocene (Messinian)	1a Basinwide evaporite marginal basin	Biomarker compositions from immature organic sulphur-rich marl samples from 10 of the 14 evaporite cycles in an Italian Messinian evaporitic basin (Vena del Gesso) indicate large variations in the composition of species in the water column (e.g. dinoflagellates, diatoms and other algae, cyanobacteria, methanogens, green sulphur bacteria and bacterivorous ciliates) and in contributions from the continent (i.e. land plants) within each marl bed and between marl beds. The marl beds were deposited within a stratified lagoon where anoxic conditions extended into the photic zone for much of the time.	Damste et al., 1995 Keely et al., 1995
Organic-rich marls, Gulf of Suez Middle to Late Miocene	3 Rift basin continental to transitional marine	Inclusion studies show evaporitic environment of deposition (reducing conditions and high salinities), favoured oil generating kerogen. Carbonate minerals and inclusions trapped in gypsum indicate possible mixing of marine water with a brine of restricted occurrence at the time source rocks were deposited.	Kholief and Barakat, 1986 Rouchy et al., 1995
Bresse and Valence salt basins, France Palaeogene	3 Rift basin continental to transitional marine	Organic matter is mostly immature and occurs in intercalated non-halite beds. Type III kerogen is tied to terrigenous deposition. Type I kerogen is abundant in mesohaline evaporitic laminites of Valence basin. Type II is more abundant in Bresse basin. Organics accumulated beneath a perennially stratified brine column of up to tens of metres. Syndepositional dissolution of halite may have aided the accumulation of significant amounts of oil-prone organic matter in non-soluble brecciated residues.	Curial et al., 1990
Salt IV Formation, Mulhouse Salt Basin, Europe Lower Oligocene	3 Rift basin continental to transitional marine	Biomarker assemblages are dominated by acyclic isoprenoids, especially phytane ($0.13 < Pr/Ph < 0.52$), n-alkanes with specific distribution patterns, and steranes. Large differences in distributions indicate changes in palaeoenvironment. The largest changes are in desmethyl- and methylsterane distributions and are probably linked to occasional reconnection of the stratified evaporite basin to the sea, leading to a dinoflagellate bloom in the upper waters of a density-stratified brine column.	Damste et al., 1993 Hofmann et al., 1993a, b Hollander et al., 1993 Keely et al., 1993
Eocene Qianjiang and Lower Eocene-Paleocene Xingouzhu Formation of Jiangling-Dangyang area, Jiangnan Basin of northwest China Eocene-Paleocene	3 Foreland flexure basins, mountain-front fault depressions	Anoxic evaporitic lacustrine source rocks generated most of the crude oils. High salinity and low Eh enhanced preservation of oil-prone organic matter and facilitated incorporation of sulphur. Anoxia and the unusual presence of abundant sulphate as gypsum resulted in microbial reduction of sulphate to sulphide and incorporation of this sulphur into the kerogen. Biomarkers show that source rock in the Sha 13 well (1322 m) was deposited under more saline, lower Eh conditions than the Ling 80 well (1808 m), although both are from the Qianjiang Formation. Sha 13 sample is more organic-rich (6.62 vs. 1.27 wt.% TOC), has a higher hydrogen index (794 vs. 501 mg HC/g TOC) and faster reaction kinetics. Kerogen from the Sha 13 sample is Type I because it has a high hydrogen index and an atomic S/C ratio (0.074).	Huang and Shao, 1993 Jiang and Fowler, 1986 Peters et al., 1996 Ritts et al., 1999 Hanson et al., 2001
Green River Formation, Wyoming and Utah Eocene	3 Foreland flexure basin from Laramide orogeny	Laminated organic mudstones and oil shales deposited in deeper anoxic bottom waters of a perennial saline and density-stratified alkaline lake. Gilsonite and tabbyite bitumens are associated with Parachute Creek Member, deposited during a major expansion and freshening of ancient Lake Uinta. Compound specific isotopic analyses of β -carotene and phytane ($\delta^{13}C = -32.6$ to -32.1 ‰) from these bitumens reflect input from primary photosynthetic producers such as cyanobacteria. Sterane $\delta^{13}C$ values (-34.5 to -29.2 ‰) reflect contributions from lacustrine algae, while extremely depleted $\delta^{13}C$ values for methylhopanes (-58.1 to -61.5 ‰) suggest input from methanotrophic bacteria. Variations in the $\delta^{13}C$ values of the α - β -hopanes (-51.4 to 37.7 ‰) imply additional input from other bacterial sources. The wurtzilite bitumen generated from the saline facies of the Green River Formation was deposited during a later regression of Lake Uinta. Compound specific isotopic analyses of phytane ($\delta^{13}C = -30.1$ ‰) and steranes ($\delta^{13}C = -29.6$ to -26.7 ‰) from this bitumen indicate continued input from primary producers and eukaryotes. The higher relative concentrations of gammacerane ($\delta^{13}C = -26.9$ ‰) indicate increasing input from aerobic species. Slight enrichment in $\delta^{13}C$ in the wurtzilite extract (and several biomarkers) suggests sulphate-reducing bacteria outcompeted methanogens, thereby, eliminating the influence of methanotrophs in this later saline stage of deposition.	Ruble et al., 1994 Katz, 1995
Shahejie Formation, Shengli Oil Province, East China Eocene	3 Continental half-graben Palaeogene rift with Neogene subsidence	Source rock is mainly the lower part of the Third Member (Es 3) of Eocene Shahejie Formation and is a lacustrine organic-rich dark mudstone/oil shale with good quality Type I-II kerogen at the oil-generative stage at $Ro = 0.4$ - 0.8 %. First Member (Es 1) of Oligocene portion of Shahejie Formation has excellent oil potential in the nearby Gunan Basin but is immature in the Fulin Basin. Oil and rock samples from both basins can be grouped into three major biomarker families. First family shows low Pr/Ph (<1), a high gammacerane index (>0.3) and notable beta-carotene, typical of carbonate-evaporite environments. It exists in Es 1 rocks and the related oils and is early mature [β $\beta/(\beta + \alpha)$] = 0.2 - 0.3, and S/(R + S) = 0.10 - 0.20]. Second family shows high Pr/Ph (>1), a low gammacerane index (<0.2) and abundant 4-methyl steranes, indicative of freshwater lacustrine conditions like those in Es 3. It shows higher maturation [β $\beta/(\beta + \alpha)$] = 0.30 - 0.50 and S/(R + S) = 0.35 - 0.55] and notable diasteranes. Third family is transitional, has source and maturity ratios between the above families, and occurs in the Es3 unit samples from the basin interior.	Chen et al., 1996

Table 9.1. Characteristics and settings of evaporitic source rocks; for basin setting, 1 = basin centre; 2 = intrashelf; 3 = lacustrine. See text and Figure 9.3 for further detail on the significance of basin setting.

Formation/Group locality and age	Basin Style	Characteristics and depositional setting	Reference
Bucomazi Formation, Cabinda, offshore Angola Cretaceous	3 Rift basin continental to transitional marine	The Lower Congo hydrocarbon habitat is dominated by the Pre-Salt Bucomazi petroleum system. These lacustrine, often super-rich, laminated evaporitic sediments reveal considerable organofacies variations between their early lacustrine basin fill and later sheet drape development with three major depositional regimes reflecting salinity and water depth control. ¹³ C depleted basal sediments, showing strong gammacerane/4-methyl sterane signatures, were segregated by a major isotopic excursion. This event represents the transition from an early saline playa lake to a deeper water salinity-stratified mesohaline lake supporting a high level of bottom anoxia. For the intermediate sediments, sterane and tricyclic diterpane abundances, plus sterane/hopane ratios, had marine connotations and can be interpreted as the result of intermittent marine incursions. Foreshadowing irreversible oceanic incursion, a resurgence of gammacerane abundance in the uppermost sediments typified littoral-shallow marine depositional conditions.	Burwood et al., 1992 Burwood et al., 1995 Burwood and Mycke, 1996
Lagoa Feia Formation, Campos Basin, Brazil Early Cretaceous	3 Rift basin continental to transitional marine	Rift-stage lacustrine sediments are the source rock of all petroleum so far discovered in the Campos Basin, the most prolific oil province in Brazil. These organic-rich shales were deposited in anoxic brackish to saline lakes. Petroleum migration pathways involve direct contact between source and reservoir rocks within the rift sequence. Later migration to the marine sequence reservoirs is related to windows in the halokinetic salt layer connected to growth faults and unconformities.	Trindade et al., 1995 Mello and Maxwell, 1991
Kimmeridgian Shale, North Sea Jurassic	1b Evap-carb platform surrounding sediment-starved deep marine basin centre generated by ongoing Permian-Mesozoic rifting	Seawater flowed southwards from Boreal Ocean into Tethyan Ocean but evaporation in the shallow waters of the archipelago of islands and shoals created waters of increased salinity and in some cases local strong brines and evaporites, which sank and flowed as saline bottom currents (from 34-42‰) into deeper water. Areas of ponded deeper mesohaline water were commonplace in the more rapidly subsiding grabens, separated by sills, denser waters accumulated until they were able to spill over the sills. In this way more saline waters migrated along the seafloor depressions, their paths being determined by local tectonic features, but mostly in a north to south direction. A stable water stratification ensued, the halocline being at about 50 m water depth and periods of widespread increased salinity are marked by "hot" shales.	Cooper et al., 1995 Miller, 1990
Shelf margin laminites, Arabian Gulf from NW Iraq through the Arabian Gulf to central Oman (e.g. Diyab, Tuwaiq and Hanifa Formations) Upper Jurassic	2 Density- stratified intrashef basins surrounded by evaporitic platform. Some lows are possibly tied to salt withdrawal	Organic-rich laminated mudstones and wackestones deposited in pre-salt intrashef, mesohaline basins on a gently downwarped epeiric platform. Intrashef basins that retain organics all have a density and salinity stratified water column with mesohaline bottom carbonates. These basins source more than 90% of the hydrocarbons in the Middle East. They are argillaceous dolomitic limestones that feed the most prolific petroleum system in the world and underlie the world's richest reservoir: the Arab D in the Arab Formation. One of the most prolific source units is the Hanifa Fm. in the Arabian Basin of Saudi Arabia. In the deeper parts of the intrashef Arabian Basin (waters ≈30m deep) the Hanifa is composed of laminite muds and marls, while in the surrounding shelf it is dominated by grainstones and packstones. Within the Hanifa laminites there are discrete but minor primary laminae of anhydrite (originally gypsum), as well as early diagenetic anhydrite nodules, both indicators of occasional hypersalinity. There are also laminae of fibrous calcite, which some authors have interpreted as another indicator of hypersalinity. The Hanifa is a widespread and prolific source, it can entrain more than 30 metres of laminites; total organic carbon exceeds 1%, with some sections having more than 5%. The kerogen is predominantly hydrogen rich, the generated oils have a high sulphur content, a Pr/Py <1, and a predominance of even-numbered normal alkanes.	Ayres et al., 1982 Palacas, 1984 Evans and Kirkland, 1988 Droste, 1990 Beydoun, 1993 Carrigan et al., 1995 Whittle and Alsharan, 1996
Smackover trend of Mississippi, Alabama and Florida, northeastern Gulf of Mexico Upper Jurassic	2 Shallow restricted-circulation salinity stratified intrashef basin on a broad carbonate platform	Oil and gas in this trend are generated from algal-rich light-brown to black laminated lime mudstones (argillaceous content <6%) of the Lower Smackover Formation. Deposition occurred in intraplatform depressions surrounded by a broad carbonate platform. Bottom waters were stratified with slightly saline waters supplied from the broad platform surrounds and the shoaling carbonate system was sealed by the sulphate evaporites of the Buckner Anhydrite.	Oehler, 1984
Todilto Formation Todilto Basin, USA Middle Jurassic	3 Foreland flexural basin (lacustrine?)	The Limestone Member of the Todilto Fm. is a widespread carbonate laminite up to 3m thick, overlain in the subsurface by up to 30 m of CaSO ₄ known as the Gypsum Member, although it is mostly anhydrite. The Limestone Member is the source rock for 6 known hydrocarbon accumulations in the sands of the underlying Entrada Fm, while it and the overlying CaSO ₄ are the seal. The quantity of TOC is low (≈1%) for such a thin source rock and it has some unusual characteristics compared to most evaporitic source rocks. Laminite couplets are 0.15 mm thick yet are laterally continuous for up to 3.7 km and form widespread cohesive "sheets", which invariably contain remnants of vascular plants. The Todilto is probably lacustrine with a marine seep hydrology, similar in hydrology to the coastal salinas of southern Australia. The organics reflect the growth of a healthy conifer cover in its surrounds and its waters were density-stratified lacustrine, probably fed via a marine seepage inflow and periodic seasonal runoff. This maintained a density-stratified brine column, first at carbonate saturation during deposition of the Limestone Member, then at gypsum saturation during the deposition of the Gypsum Member.	Vincelette and Chittum, 1981 Evans and Kirkland, 1988
Organic mudstones intercalated with evaporites, Mandawa Basin, Tanzania Triassic	3 Rift basin continental to transitional marine	Total organic carbon (TOC) values range from 1.23 to 7.41% (wt) of kerogen Type II/III. The evaporite (hypersaline) influence is indicated by the presence of C-24-tetracyclic terpanes, gammacerane and C-35-homohopanes. The relative abundance of tricyclic terpanes (C-19-C-28+) with respect to pentacyclic terpanes (C-27-C-35) seem to change with depth, whereby the tricyclic/hopanes ratio apparently increases with depth. The mixed organic input from marine and terrestrial precursors are indicated by mixed abundances of C-27-, C-28-, C-29- steranes.	Kagya, 1996

Table 9.1 cont'd. Characteristics and settings of evaporitic source rocks.

Formation/Group locality and age	Basin Style	Characteristics and depositional setting	Reference
Sub salt-allochthon oil seeps, Windsor Group, Nova Scotia, Canada Carboniferous	3 Rift basin continental to transitional marine	The oil seeps are either associated with upper Horton Group (Ainslie Formation) or basal Windsor Group (Macumber Formation) sediments. The biomarker distributions of the samples are similar to Stoney Creek oils and their lacustrine carbonate source rock (Albert Shale) of the Moncton Sub-basin, New Brunswick, as are oils from seeps in the Pugwash Salt mine.	Fowler et al., 1993
Black shales in the Paradox Member of the Hermosa Formation, Paradox Basin, USA Carboniferous (Pennsylvanian)	1a Foreland flexural basin	Organic-rich black shales (informally known as the Cane Creek, Chimney Rock, Gothic shales) form a carbonate laminite basal sequence to a number of salting-upward evaporite cycles in the Paradox Member. Mineralogically the shales are between 30-50% calcite or dolomite with clays and quartz sand forming the remainder of the matrix. TOC values of 5% of hydrogen-prone organics in the black shales are usual, with values of 10% not uncommon and the highest values more than 20%. The organics are mixtures of halotolerant debris and marine-style organics formed when surface waters were at marine salinities, as well as occasional terrestrial organics washed into the basin from the surrounding hinterland.	Evans and Kirkland, 1988 Hite et al., 1984
Oil Shales, Junggar Basin, NW China Upper Permian	3 Controversial, with tectonic interpretations ranging from foreland flexure to regional transtensional basin	Junggar Basin is one of the largest oil-producing basins in China, its Upper Permian oil shales are among the thickest and richest lacustrine source rocks in the world. Together the Jingjingzigu, Lucaogou, and Hongyanchi Formations of the southern Junggar Basin comprise over 1000 m of organic-rich lacustrine facies. They record an evolution from relatively shallow, evaporative lakes to freshwater lakes with fluvial systems. Jingjingzigu Formation was deposited in a perennial saline lake characterized by low TOC and HI, and biomarker features (such as abundant β -carotane) consistent with a specialized saline or hypersaline biota. Biomarker distributions in Jingjingzigu Formation extracts most closely resemble oils from the giant Karamay oilfield. Overlying Lucaogou Formation represents one of the richest and thickest lacustrine source rock intervals in the world, yet it contradicts conventional lacustrine source rock models in at least two important aspects. First, deposition occurred at middle palaeolatitudes (39-43° N) rather than in the tropics. Second, limited nutrient supply in a drainage basin dominated by intermediate volcanic rocks appears to have caused low to moderate primary productivities. Stable salinity stratification and low inorganic sedimentation rates in a deep lake nonetheless resulted in deposits with up to 20% TOC and HI near 800. Overlying Hongyanchi Formation has 1-5% TOC but low HI, and was deposited in freshwater oxic to sub-oxic lakes.	Carroll, 1998 Carroll et al., 1992 Tang et al., 1997
Ravnefeld Formation, East Greenland Upper Permian	3 Rift basin continental to transitional marine	The Ravnefeld Formation is subdivided into five units that can be traced throughout the Upper Permian depositional basin. Two of the units are laminated and organic rich, and were deposited under anoxic conditions. They are considered good to excellent source rocks for liquid hydrocarbons with initial average TOC (total organic carbon) values between 4 and 5% and HI (hydrogen index) between 300 and 400. The cumulative source rock thickness is between 15 and 20 m. The source rocks are separated and enclosed by three units of bioturbated siltstone with a TOC of less than 0.5% and an HI of less than 100. These siltstones were deposited under relatively oxic conditions. The organic geochemistry of the source rocks is typical for marine source rocks with some features normally associated with carbonate/evaporite rift environments [low Pr/Ph (pristane/phytane), low CPI (carbon preference index), distribution of tricyclic and pentacyclic terpanes]. The establishment of anoxic conditions and subsequent source rock deposition was controlled by eustatic sea level changes.	Christiansen et al., 1993
Phosphoria Formation, Little Sheep Creek, Montana Permian	1b Foreland flexure basin	Correlations between biomarker indicators of anoxia and salinity suggest that anoxia was in part the result of a chemocline separating normal marine waters above from more saline bottom waters. Anoxia and salinity in the bottom waters increased with time making conditions in the basin progressively more hostile to benthic organisms.	Dahl et al., 1993
Kupferschiefer Formation, NW Europe Permian	1a Rift basin, restricted marine	Thin, widespread organic-rich laminated mudstone deposited in shallow mesohaline marginal sea-lakes with waters which were <100m deep and mostly 10-30 m deep. Surface exchange with Zechstein ocean was restricted by palaeohighs.	Bechtel and Puttmann, 1997
Anhydritic lacustrine beds, East Shetland Platform, North Sea Middle Devonian	3 Rift basin, restricted marine	The UKCS well 9/16-3 drilled on the western flank of the Beryl Embayment indicates local development of hypersaline environments equivalent to the Achanarras/Sandwick fish bed. Shows close affinity with contemporaneous Middle Devonian source rocks of the Inner Moray Firth and crude oil in Beatrice oil field.	Duncan and Buxton, 1995
Muskeg Formation and Lower Keg River Member, Alberta, Devonian Canada	1a Rift basin, restricted marine	Laminated organic-rich bituminous mudstones deposited in pre-evaporitic density stratified water columns. Vertical migration from the Muskeg formation to the Muskeg Reservoirs may have occurred through local fracturing of anhydrites driven by the dissolution of Black Creek halite.	Clark and Philp, 1989 Stasiuk, 1994
Laminated evaporitic A-1 mudstones, Michigan Basin Silurian	1a Rift basin, restricted marine	Biomarker characteristics indicate a carbonate/evaporite source rock deposited under hypersaline conditions in a strongly reducing environment. The source rocks occur in the basin centre in organic-rich laminites of the inter-reef A-1 Salina Formation, a mesohaline carbonate deposited beneath a density stratified brine column.	Gardner and Bray, 1984 Obermajer et al., 1998 Obermajer et al., 2000
Chandler Formation, Amadeus Basin, Australia Lower Cambrian	1a Foreland flexure	Thin bituminous pre-evaporitic carbonate mudstone deposited subaqueously in a restricted basin immediately prior to the deposition of the thick halites of the Chandler Formation.	Bradshaw, 1988
Hormuz Series, Arabian Gulf and counterparts in Oman, India and Pakistan Neoproterozoic to Early Cambrian	1 Rift basins, restricted marine	Almost all the Persian Gulf and large areas of southern Iran and northeastern Arabia are underlain by a thick sequence of sediments, known as the Hormuz Series, or the Huqf Group in Oman. It is made up of interbedded salt, anhydrite, dolomite, shale and sandstone. It is not only the cause of many salt-dome-related oil and gas fields but is also considered to have been a major source rock for hydrocarbons in Ordovician, Devonian, Carboniferous, Permian and perhaps younger reservoirs.	Amthor, 2000 Edgell, 1991 Grantham et al., 1988 Peters et al., 1995 Terken and Frewin, 2000

Table 9.1 cont'd. Characteristics and settings of evaporitic source rocks.

anhydrite, which otherwise plug and cement source intervals. Style 1b source rocks develop where dense mesohaline bottom waters pond in the deeper parts of deep density-stratified restricted-marine basins. Slightly elevated bottom brine salinities are maintained by a series of dense brine underflows, fed from nearby shoalwater evaporitic platforms (Figure 9.3). A deepwater “marine” centre typifies such basins, along with widespread evaporitic and shoal water carbonate sediments in the surrounding platforms and shelves. Setting 1b basins are best thought of as stunted or underdeveloped basinwide evaporite systems. Development of the basinwide evaporite hydrology was suspended prior to the basin centre drawdown reaching the state of complete hydrographic isolation, which is needed for widespread salt precipitation. Evaporitic conditions (mostly bedded anhydrites) dominated on isolated platform depressions about the basin margin. Typical examples of this style of association are Kimmeridge shales of the North Sea (Miller, 1990; Cooper et al., 1995), organic-rich laminites of the Cherry Canyon Formation in the Permian Delaware Basin of west Texas (Jones, 1984) and possibly some of the Devonian laminites of the Alberta Basin (Clark and Philp, 1989).

In this setting, waters in the deepwater basin centre remain starved of sediment and density-stratified, with the upper less saline part of the water column typified by normal marine water maintained through surface connections to the open ocean. The little sediment matrix that does accumulate in the basin centre settles into an anoxic thermally/density stratified bottom so that the sediment matrix of the source laminites is dominated by a planktonic or nektonic biota and a more or less constant elevated organic content. Carbonate banks or reefs in the surrounding platform grade landward through lagoonal and evaporitic platform facies in to terrestrial clastics. At times of slightly lowered sea level these epeiric platforms can go evaporitic and so deposit widespread platform salts (Chapter 5). Such basins show a centrifugal salinity gradient where the highest salinity areas are in the surrounding shallow evaporite platforms, which supply dense saline waters that trickle and seep basinward to pond in seafloor lows at the anoxic base of a density stratified water column.

With setting 1b, the formation of evaporites and saline waters about the basin edge is not typically followed by the deposition of basin-centre evaporites. At the time the deepwater organic laminites are accumulating, the deep basin centre waters lie at the bottom of the thick density-stratified water column in a semi-enclosed seaway. Bottom brines may be no more than 3-5‰ more saline than the normal marine waters. For example, at the time the Purbeck evaporites were accumulating on

the adjacent platform, the anoxic bottom waters in the marine basin centre, atop the accumulating Kimmeridge shales, had salinities around 42‰, temperatures $\approx 30^{\circ}\text{C}$ and densities ≈ 1.0270 . The overlying near normal marine waters had salinities of 34-39‰, surface temperatures of 26°C in the south and as low as 6°C further north in the region of the Boreal Ocean inflow and densities around 1.0267 (Miller, 1990).

Basin Setting 2: Upper Jurassic source rocks of the Middle East are well studied examples of the epeiric shelf or marine evaporitic platform settings and typify style 2 source rocks, which are deposited within local somewhat deeper, density-stratified mesohaline intrashelf lows (Figure 9.4; Table 9.1; Ayres et al., 1980; Evans and Kirkland, 1988; Droste, 1990; *pers obs.*). In the Tethyan of the Middle East this style of source rock feeds a petroleum system that is probably the most efficient in the world. It evolved from Upper Jurassic source rock accumulators (typically with TOC's $\approx 1\%$ and occasionally up to 6-10%) into evaporitic mudflats sealing the mostly bioclastic reservoirs of the carbonate platform of the Arab cycles, beneath the regional Hith Anhydrite seal, which was deposited on a saltern-covered platform (Figure 10.9). The laminite source rocks in the various intrashelf depressions were deposited at times of widespread epeiric carbonate deposition and stagnant oceanic circulation.

It was a time when much of the Arabian platform was covered by a warm shallow greenhouse sea precipitating varying combinations of carbonates and evaporites. Denser warmer waters, generated by evaporation of epeiric waters and water of the surrounding evaporitic mudflats, were concentrated to where they were somewhat more saline than normal seawater. Dense brines then trickled and seeped over the shallow seafloor into the lower parts of restricted intrashelf basins, to create density-stratified water bottoms that were not more than tens of metres deep and no more than 10-30‰ more saline than seawater (Ayres et al., 1982). Ongoing mixing and dilution of the bottom-hugging brines during their passage to the lows meant the basal water mass in the intrashelf lows, although saline, rarely attained gypsum saturation (mostly mesohaline anoxic brines). The overlying column was usually near normal marine salinity. Salt withdrawal and dissolution of salt diapirs and allochthons, sourced in the Precambrian Hormuz salt, perhaps helped create the intrashelf depressions and may also have played a role in generating a portion of the bottom brines. As the source rocks of the style 1b Kimmeridge Clays accumulated, halokinesis and salt solution of Zechstein mother salt probably also played a role in generating local briny anoxic bottoms (Clark et al., 1999).

One of the most prolific intrashelf source rocks in the Middle East is the Hanifa Formation deposited in the intrashelf Arabian Basin of Saudi Arabia (Figures 9.4, 10.10; Droste, 1990). It sources most of the hydrocarbons reservoirs in the Arab cycles of Saudi Arabia and is regionally sealed by the Hith Anhydrite. The organic-rich portion of the Hanifa, deposited in the “deeper” parts of the intrashelf basin (waters $\approx 30\text{m}$ deep), is composed of laminite muds and marls, while in the surrounding Arabian shelf it is dominated by grainstones and packstones. All Hanifa facies can be locally overprinted with later anhydritic burial and

reflux cements and later diagenetic dolomites. As the various depressions filled with laminites they shallowed to where the stratification was lost and the sediment became an open marine packstone-wackestone, equivalent to sediments deposited over the rest of the Arabian Platform.

Later episodes of hydrographic isolation of the platform, via buildup of a transgressive platform rim and a slight fall in sea level, then drove deposition of anhydritic saltern or mudflat caps of the various Arab cycles A-D and ultimately the deposition of

the regional Hith Anhydrite seal (Figure 10.10). Within parts of the Hanifa laminites there are discrete laminae and thin beds of primary anhydrite, as well as early diagenetic anhydrite nodules, both indicators of periodic hypersalinity. Likewise, the restricted evaporitic caps to some of the source cycles in basin margins to the Hanifa Formation in the Arabian Basin can locally preserve aligned gypsum ghosts, indicating a subaqueous gypsum precursor in the shallower parts of the epeiric seaway (Figure 9.9). Similar, but volumetrically less prolific, intrashelf source rocks characterise parts of the Lower Smackover Formation (Upper Jurassic) of the north-eastern Gulf of Mexico, as in the Mississippi Interior Salt Basin (Oehler, 1984), and parts of the Cretaceous Sunland Formation of Florida (Palacas et al., 1984).

A variation on this density-stratified mesohaline epeiric platform-depression style of source rock accumulation is the phosphate and organic-rich sediment of the Phosphoria Formation in the USA (Stephens and Carroll, 1998). This laminated unit

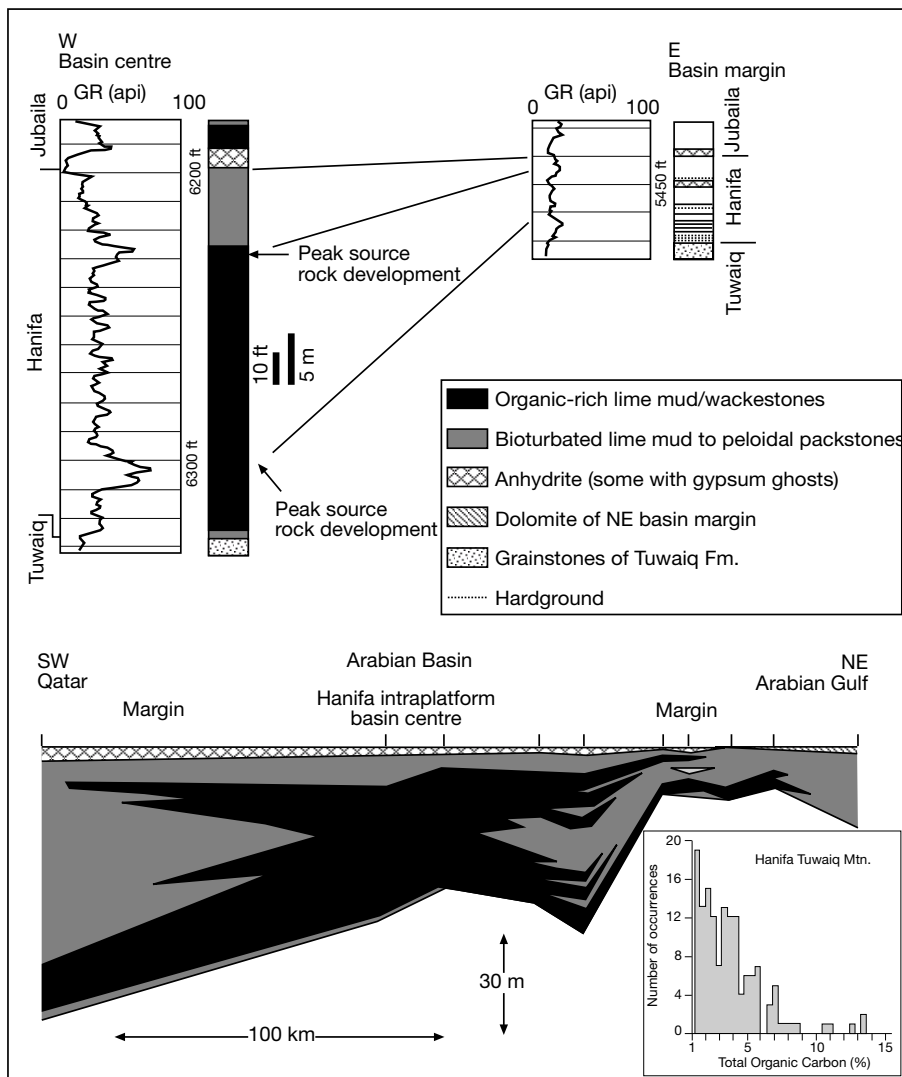


Figure 9.4. Characteristics of the Hanifa Formation, Saudi Arabia, a setting 2 intraplatform basin source rock that was deposited beneath relatively shallow and anoxic mesohaline bottom waters in a slight depression on the shelf and was surrounded by epeiric evaporitic sedimentation, as indicated by the presence of anhydrite in the Hanifa Fm. (after Droste, 1990). Peaks in the organic content of these carbonate mudstones are indicated by peaks in the gamma curve. TOC inset in lower right is redrafted from Carrigan et al., 1995.

sources much of the oil in Wyoming and was deposited in shelf edge depressions of the Phosphoria Sea adjacent to an area of marine upwelling. The nutrient-rich waters facilitated algal blooms near and atop the shelf edge, while bottom-hugging brines, seeping seaward from the evaporitic hinterland, ponded in stagnant shelf edge depressions. Overlap of the two systems created local anoxic shelf-edge mesohaline depressions with anoxic bottom waters that preserved a rain of organics detritus from the overlying algal blooms (Figure 9.3). This system requires an epeiric evaporitic hinterland to supply bottom-hugging brines and, like the saltern-sealed Jurassic intrashelf depressions of the Middle East, has no modern counterpart.

Basin setting 3: These source rocks accumulated in sediment-starved or underfilled saline lakes in arid climates. The laminites typically accumulated in the early continental stage of infill in an opening rift, prior to its opening into a marine-fed marginal evaporite basin, or in the restricted lacustrine stage of a foreland flexure in a collision belt (Figures 5.27, 9.3). Modern underfilled saline rift lakes have some of the highest rates of organic productivity known and can accumulate high levels of organics within carbonate laminites. Some of these lacustrine laminites accumulate beneath deep density-stratified water columns, while others accumulate as “moat facies” or microbial mudflats about lake margins (Figure 9.3; Table 9.1). The likelihood of numerous water level changes during the life of a saline lake especially effect laminites deposited in shoal water moats and margin mudflats and so can lower their preservation potential (Bohacs et al., 2000). Most oil-prone style 3 lacustrine source rocks were deposited at the bottom of perennial salinity-stratified hydrologies, with water column depths measured in metres to tens of metres, not as subaerially exposed algal mudflats. Examples include the Wilkins Peak Member of the Eocene Green River Formation, USA, the Lagoa Feia Formation of the Alagoas portion of the Campos Basin in Brazil, the Bucomazi Formation in offshore West Africa and the Jingjingzigou Formation in the Junggar Basin, China (Table 9.1).

The desiccation needed to form underfilled lacustrine succession typically means that saline lacustrine phases have lesser aerial extents compared to times of freshwater deposition.

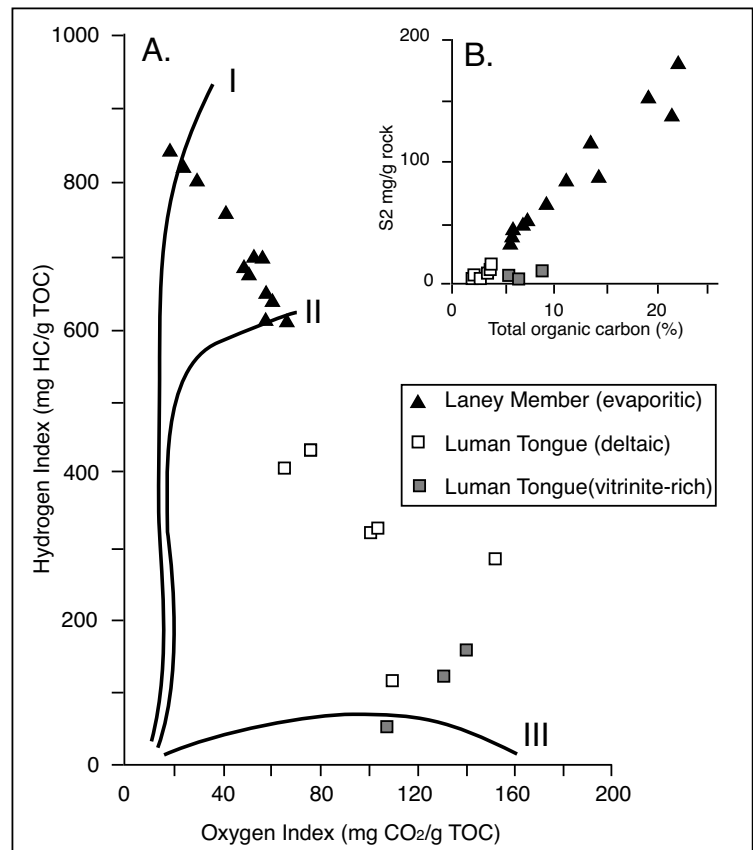


Figure 9.5. Kerogen character of Laney Member and Luman Tongue of the Eocene Green River Formation, USA. A) Hydrogen and oxygen indices. B) Pyrolysis yields of hydrocarbon-equivalents (mg/g rock) plotted against organic carbon percentages. (after Horsfield et al., 1994).

But this does not necessarily mean the evaporitic lacustrine source rocks are less prolific than their freshwater counterparts. Within the Green River Formation there are two associations (fresh and saline) of lacustrine organic laminites exemplified by the Luman Tongue and the Laney Member (Figures 5.10, 9.5; Horsfield et al., 1994). The Luman Tongue consists of organic-rich mudstones deposited as profundal sediments at a time when lake waters were relatively fresh. Proximal organic-poor sediments, as well as coals and thin sandstones, were deposited in the lake plain. The highest levels of TOC in the Luman Tongue are found in lake margin deposits, which contain a mixture of alginite and vitrinite, but they have a low hydrogen index and a low petroleum generation potential. In fact, the petroleum generation potential of these freshwater deposits is no more than moderate.

In contrast, the organic percentages of the carbonate laminites of the Laney Shale are much higher (6-22%) and they are hydrogen prone. The most organic-rich samples were deposited in the

lowest parts of the lake and are composed mostly of alginite with relatively minor contributions from higher plants. The much higher petroleum potential of the Laney shale reflects the marked density stratification of Lake Gosiute waters at the time the Laney was accumulating. At that time bottom anoxia was stabilised by the perennial highly saline bottom waters (Fischer and Roberts, 1991). The vertical transition from saline lacustrine Jingjingzigou Formation to the highly prolific brackish oil shales of the lacustrine Lucaogou Formation in the Permian Junggar Basin of NW China may represent a similar dissolution induced transition in the lake water column and help explain the lakes unusual latitude (Table 9.1; Carroll, 1998).

Basin Setting 4: is an increasingly documented open-ocean evaporite-associated source rock setting where density-stratified saline bottom brines and organic-enriched laminites accumulate in brine-bottomed depressions atop and adjacent to shallow and dissolving salt allochthons (Figures 9.3, 9.33). With burial these laminites may act as source rocks, but unlike the restricted settings of the preceding three styles, deposition typically occurs beneath open marine water atop continental slope and rise sediments. The laminites accumulate on the floor of deep brine pools that form on or near the margins of actively flowing and dissolving shallow salt allochthons. This association is discussed in detail later in this chapter and it is also a significant setting for the formation of base metal-hosting laminites as in Tunisia and the Red Sea (Warren, 2000b). As yet it is not a widely documented environment for hydrocarbon source rocks, but it may in part explain the higher than expected source potential of many prodelta and slope muds in the passive margin fill of evaporite-floored halokinetic rifts.

Source rocks of settings 1a, 2 and 3 are typified by the accumulation of mm-scale layers of oil-prone organics typically in a matrix of fine carbonates. Setting 1b typically contains higher levels of siliciclastic fines and in many cases is a basinal marl or occasionally a laminated siliciclastic carbonate shale. The matrix of setting 4 laminites tends to be composed of whatever detrital sediment is accumulating atop the salt allochthon. In many situations, such as the Gulf of Mexico and the Mediterranean allochthon terranes, this matrix is a siliciclastic mud/clay laid down at the distal ends of prodelta wedges. In others, such as the Jurassic and Cretaceous of the Arabian Gulf and the Triassic of Tunisia, the matrix was carbonate mud.

The presence of mesohaline and marine carbonate muds, rather than aluminosilicate clays, in the matrix of many organic-rich evaporitic source rocks can change maturity and migration parameters. Mesohaline carbonate source rocks are susceptible to early generation of bitumens and volatiles compared with

terrigenous shales. The proportion of bitumens (extractables) in the organics of carbonate source rock is high compared to that of shales as most mesohaline carbonates are largely isolated from high levels of terrigenous influx and the associated load of “spent” or oxidised organic matter (Warren, 1986). For the same reason much of the early asphaltic product in a mesohaline carbonate laminite begins to migrate early in the burial history, whereas similar materials are held longer in the lattice of aluminosilicate clays (Warren, 1986; Cordell, 1992). Espitalie et al. (1980) showed that carbonate source rocks are likely to provide larger volumes of hydrocarbons for pooling than analogous terrigenous shales for the same levels of TOC. Geochemical analyses show that heavy oils from carbonate source rocks can form at marginally mature stages and at lower temperatures than required for oil generation from terrigenous shales, although much of the key data is ambiguous (Jones, 1984).

Evaporitic source rocks deposited from mesohaline waters are a reality (Table 9.1), let us now look to the modern and at relevant processes to see why this is so.

Halobiota: adaptations and biomarkers

As long ago as 1826 during his voyage on the *Beagle*, Charles Darwin described biological aspects of the production of solar salt from an inland lake some 23 km from El Carmen, Patagonia. Although unfamiliar with bacteria (after all, Louis Pasteur was only a 4 year-old child at the time), he recognised that there was a “putrefying life-form” in the mud; that algae caused a green colour on the lake; that flamingoes fed on the brine shrimp and worms; and that other “infusorial animalcula” were part of the salt producing system. Yet in 1957, in his classic book on evaporites, Lotze made the statement: “Nicht das Leben, sondern der Tod beherrscht die Salzbildungsstätten” (Not life, but death rules the locales of salt deposition). Likewise, the name of the Dead Sea in the Middle East comes from the time of the Roman occupation when it was given the Latin name *Mortuum Mare* for its perceived lifelessness.

For millennia, saline environments have been visualised as biotal deserts, largely devoid of biological activity and hence were sedimentary systems with little source rock potential. Like Sir Charles Darwin, we now know that this is not the case. Rather, almost all modern saline environments and water bodies are sites of periodic but intense organic activity, where numerous highly specialized algal, bacterial and archaeal species grow and die

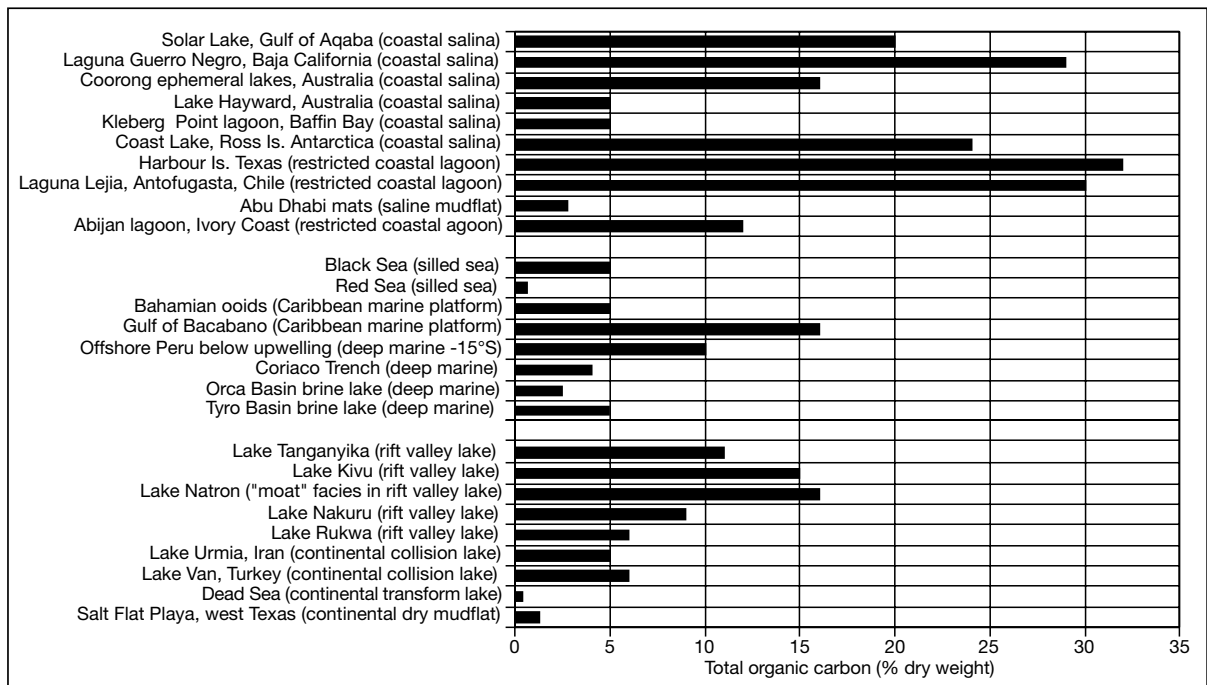


Figure 9.6. Total organic carbon (TOC as dry wt. percent) in various modern saline settings (compiled from various sources listed in this chapter and Warren, 1986).

(cycles of feast or famine). Occasionally, they can leave behind substantial volumes of oil-prone organic residues in laminated bottom sediments, especially in mesohaline carbonates, which on burial can evolve into prolific source rocks. Even in modern saline settings, where evaporite depositional settings are not as diverse or widespread as those of much of the past, conditions are such that mesohaline carbonates can preserve high levels of total organic carbon (TOC; Figure 9.6).

Metabolic pathways in producers and consumers

Before we discuss how halotolerant and halophilic biomass accumulates in saline environments, we need to review some basic biology and biochemistry. Our understanding of the taxonomy and biogeochemistry of two groups, the cyanobacteria (bacteria) and the archaea that can dominate the biota of many hypersaline waters, has undergone quantum change in the last two decades. In the late 1970s, Professor Carl Woese proposed, on the basis of ribosomal RNA affiliations (gene mapping), that life be divided into three domains instead of two, namely: Eukaryota, Eubacteria, and Archaeobacteria (Woese and Fox, 1977; Woese 1993). He later decided that the term Archaeobacteria was a misnomer, and shortened it to Archaea and the term Eubacteria to Bacteria (Figure 9.7; Woese et al., 1990).

DNA base-pair studies show that Archaea are as different from Bacteria as from *Homo sapiens*, but Woese's notion of three domains of life did not take the biological world by storm. Before the advent of hybridization and genome mapping, the inferred evolutionary relationships among microbes were contradictory and very messy. Species or interspecies relationships were not easily established on the basis of intricacies of differences in cellular structure, which are minimal, or by staining, or by the fossil record, which is not species specific. For example, based on their morphology, the archaeal *Halobacteriaceae* can be grouped with the bacterial gram-negative rods (a gram positive or gram negative description indicates whether or not the microbial cell wall reacts with Gram's stain). The advent of gene-based classification threw classic morphological and stain-based groupings into disarray. All the dust from this confrontation between morphology and gene-mapped subdivisions of the biological realm has yet to settle.

The initial chagrin of those botanists and zoologists versed in classic ecological and cladistic techniques to Woese's laboratory-based tripartite classification is understandable; after all, in his nonanthropocentric regime the realms of botany and zoology are relegated to a few twigs on the outermost branches of the Eukaryan limb (Figure 9.7). Even today some books and articles today still refer to archaea as types of bacteria.

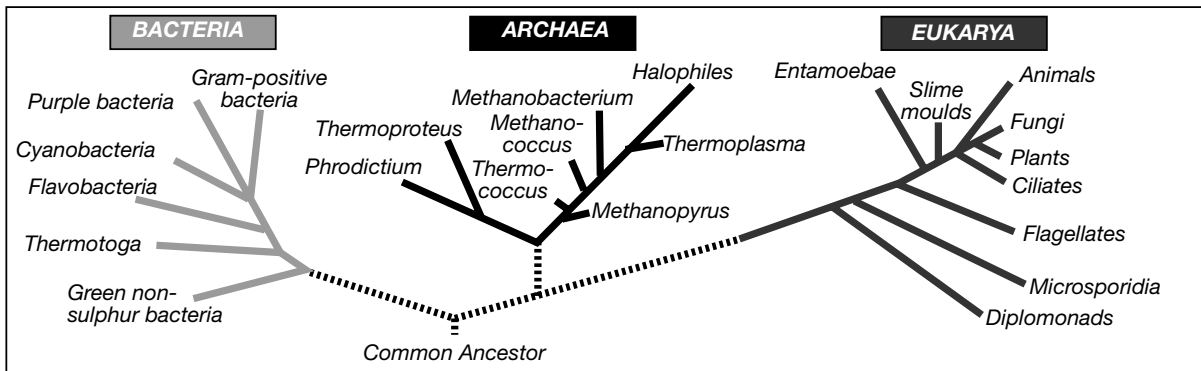


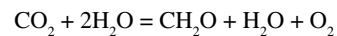
Figure 9.7. Tripartite classification of the domain of life based on genetic differences (as proposed by Woese et al., 1990).

Many microbiologists still feel Woese's system gives too much prominence to the microbial. In this Woese's detractors may be wrong. Estimates of the subsurface microbial biomass, known as the subsurface lithoautotrophic microbial ecosystem or SLiME, place it as high as 100 trillion tonnes (1×10^{14} to 1×10^{18} grams of carbon; Pedersen, 1993; Fredrickson and Onstott, 1996). As such, if it could be stacked above ground, this amount of "gray goo" would cover the earth with a biological layer some 15 metres thick. Since the surface biosphere mass is approximately 4.6×10^{17} grams of carbon, the biomass of the rock-bound subsurface microbial biosphere may well exceed that of the surface biosphere. Woese's tripartite conclusions are slowly moving into the general biological literature.

Cyanobacteria, formerly known a blue-green algae, are now placed in the bacterial kingdom as cells lack a membrane-bound nucleus, like all prokaryotes, but they are not totally at home there. Unlike any other bacteria, they photosynthesise aerobically. Instead of the bacteriochlorophyll pigments found in purple and green bacteria, blue-greens contain chlorophyll-a, as do all eukaryotic^{9,3} phototrophs, and produce free oxygen as a photosynthetic byproduct. Yet they lack the organized chloroplasts of eukaryotes and have their photosynthetic apparatus distributed peripherally in thylakoids within the cellular cytoplasm. Cyanobacteria are often a significant component of modern laminated microbial mats in saline settings that are often called "algal mats" or "cryptogalaminites" in ancient strata. A more correct description for these ancient counterparts is microbial mat or microbialite (Chapter 1).

All three domains of life are represented in saline environments, although most higher plants and animals only survive at the lower end of the mesohaline range. Photosynthesising^{9,3} autotrophic cyanobacteria (prokaryote) and algae (eukaryotes) are the dominant primary producers in modern mesohaline waters, along with lower and varying inputs from the higher

plants and photosynthesising bacteria. When nutrients are available, halotolerant alga and cyanobacteria constitute the bulk of the planktonic biomass in the upper layer of a stratified brine column and construct the upper parts of microbial mats in oxygenated settings wherever light penetrates to the sediment surface. Although the cyanobacteria are prokaryotic, like eukaryotic algae and higher plants, they are photoautotrophic and require oxygen to photosynthesise. The typical aerobic photosynthetic reaction is:



That is, carbon dioxide and water react in the presence of chlorophyll and sunlight to form carbohydrate plus water plus oxygen.

All aerobic photosynthesising organisms that split water molecules and generate oxygen, contain varying proportions of the pigments chlorophyll-a, phycobilin and β -carotenes. Chlorophyll-a is a green pigment that absorbs red and blue-violet light, hence the green colour of photosynthesising cyanobacteria and plants. It is made up of molecules that contain a porphyrin 'head' and a phytol 'tail' (Figure 9.19a). The polar (water-soluble) head is made up of a tetrapyrrole ring and a magnesium ion complexed to the nitrogen atoms of the ring, its phytol tail typically extends into the lipid layer of the thylakoid membrane.

^{9,3}*Autotrophs* (literally "self feeders") are organisms capable of producing organic compounds from simple inorganic compounds.

Heterotrophs (literally "feeders on others") use organic molecules synthesized outside their body as a source of energy and carbon.

Chemoautotrophs use endogenous light-independent reactions to obtain energy, these reactions involve inorganic molecules and an electron donor other than water and do not release oxygen.

Lithoautotrophs depend upon inorganic compounds as electron donors for energy production.

Photoautotrophs use light as a source of energy and CO_2 as a source of carbon (oxygenic photosynthesis).

Chlorophyll-b is a closely related molecule and occurs only in green algae and plants, while chlorophyll-c is found only in the photosynthetic members of the Chromista kingdom (includes diatoms, kelp and coccoliths), as well as in dinoflagellates (which are alveolates along with the foraminifera).

Phycobilisome pigments are water-soluble proteins that occur only in the cyanobacteria and red alga (rhodophytes). They absorb light in the blue-green, yellow, and orange regions of the spectrum compared to chlorophylls, which absorb light in the blue and red regions. Its presence allows communities to photosynthesize into deeper waters and sediment depths where only the longer wavelengths penetrate (blue-green spectrum). Phycobilin molecules are linear tetrapyrroles and are structurally related to chlorophyll-a, but lack the phytol side chain and the magnesium ion (see biomarker discussion later in this chapter). They must pass their absorbed photic energy to chlorophyll and so occur in chlorophyll-rich oxygen-evolving photic reaction centres called chloroplasts. Cyanobacterial chloroplasts make up an extensive, intracellular system of flattened, membranous sacs, called thylakoids, the outer surfaces of which are studded with regular arrays of phycobilisome granules.

Carotenes are accessory water-insoluble pigments in most oxygenic photosynthesizers and are directly attached to cellular membranes. They are orange-red or yellow in colour and absorb the blue-violet and blue-green wavelengths missed by chlorophyll. Structurally they are isoprenoids (terpenes) and are what give autumn leaves their colour when deciduous plants re-absorb chlorophyll in preparation for winter. In the hypersaline realm, carotene pigments from algae like *Dunaliella* sp. and some Archaea are what give the characteristic red or pink^{9,4} colours to brines where they are blooming.

In contrast to the cyanobacteria, all other photosynthetic bacteria in saline waters are^{9,3} chemoautotrophs. The green and purple sulphur bacteria take their hydrogen atoms from biologically or volcanogenically produced H₂S and generate sulphur as a waste product (hence their names; Table 9.2). They utilize a single type of photosynthetic reaction centre with a different photosynthetic pigment (bacteriochlorophyll) to the cyanobacteria and higher plants. It absorbs light of longer, less energy-rich wavelengths compared to chlorophyll and phycobilin. Green sulphur bacteria (Chlorobiaceae) and purple sulphur bacteria (Chromatiaceae) typically oxidise this H₂S via anoxygenic photosynthesis and produce native sulphur or sulphate, but some species can use inorganic elemental sulphur, sulphide, or thiosulphate as the electron donor. In contrast the purple and green nonsulphur bacteria use electrons from organic substrates or hydrogen gas (Table 9.2).

The following simplified equation typifies photosynthesis in purple or green sulphur bacteria:



That is; carbon dioxide and hydrogen sulphide react in the presence of bacteriochlorophyll and sunlight to form a carbohydrate (such as glucose) as well as water and sulphur. Light-absorbing pigments of the purple and green sulphur bacteria consist of various bacterial chlorophylls (a-d) and carotenoids. Phycobilins and chlorophylls, characteristic of the cyanobacteria, are not found in these chemoautotrophs.

^{9,4}The pink to purple colours that typify many hypersaline water bodies comes from concentrations of mostly carotenoid pigments present in the cytoplasm of various halophilic microorganisms. Most haloarchaea are red due to a high content of C-50 carotenoids of the bacterioruberin series in the cell membrane. Photosynthetic cyanobacteria and eukaryotes (e.g., unicellular green algae of the genus *Dunaliella*) contribute to the pigmentation of the hypersaline waters thanks to the presence of chlorophylls and C-40 carotenoids (mostly all-*trans*- and 9-*cis*-β-carotene). Chloroplasts in *D. salina* and *D. parva* accumulate large quantities of this β-carotene at their peripheries in the form of droplets (plastoglobuli) and so blooms appear brown-red, not green like most other algae and cyanobacteria. The carotene seems to act as photo-protective ‘sun-screen’ to protect chlorophyll integrity and shield cellular DNA from the high levels of irradiance that characterizes the normal habitat of halophilic *Dunaliella*. It may also act as a ‘carbon sink’ to store excess carbon produced during photosynthesis under conditions where growth is nutrient-limited but photosynthetic carbon fixation must continue.

Chlorophylls absorb red and blue wavelengths much more strongly than they absorb green wavelengths, so chlorophyll-bearing cyanobacteria and most photosynthesizing plants appear green. In contrast, the carotenoids and phycobiliproteins strongly absorb green wavelength, so microbes and algae with large amounts of carotenoid pigments appear yellow to brown, those with large amounts of phycocyanin appear blue, and those with large amounts of phycoerythrin appear red.

Pigment levels can indicate the stratification of the microbial community in any photoresponsive biomass in a brine column. Red wavelengths (long wavelengths) in white light are absorbed in the first few metres of a brine column or the uppermost millimetre or two of a microbial mat (chlorophyll utilizers flourish). The blue and green wavelengths (shorter) reach deeper into the brine column.

Halophilic archaea were first investigated microbiologically as a common cause for spoilage of salted fish, with their carotene imparting a characteristic red colour. None of the halophilic Archaea have proved to cause disease, so their effects on salted foodstuffs are largely aesthetic. Haloarchaeal spoilage explains the red colour and the foul smell in “red herring.” The phrase “throw in a red herring” means to mislead. Spoiled salted fish were once used by poachers to distract hunting hounds. Poachers would interpose themselves between the prey and the hunting party and drag a sack of red herring across the trail to mislead the dogs, who would follow the scent trail left by the red herring and not the prey. This would give the poachers the opportunity to bag the prey.

Many purple and green sulphur bacteria store elemental sulphur as a reserve material that can be further oxidized to SO_4 by using it as a photosynthetic electron donor. Some of the green sulphur bacteria are probably the most energetically efficient of all phototrophic organisms, they are capable of living photosynthetically in environments where light intensities that are less than 0.01% of typical daylight.

All the groups we have discussed to date are primary producers that are light-dependant and along with halotolerant photosynthetic eukaryotes made up the base of the food chain in most modern hypersaline ecosystems. But there and another class of microbes, the 9,3 lithotrophs and chemotrophs than can metabolise independent of a light source. Modern purple and green chemoautotroph sulphur oxidising communities inhabit the narrow oxygenated interface at the edge of anoxic H_2S -rich chemistries where hydrogen sulphide is bubbling up from below. In saline microbial communities they generally inhabit an unlit layer beneath the lit-community of aerobic cyanobacteria and purple bacteria above (photosynthesizers) and the community of sulphate reducers and fermenters below. This is true in both mats and stratified brine columns (Figure 9.8). Lithotrophic microbes are also a common halocline component in deep seafloor seep communities and in caverns formed by the action of sulphuric acid (Figure 7.45).

Lithotrophic sulphur-oxidisers do not require light to metabolise (chemoautotrophs not photoautotrophs) include both bacteria (e.g. *Thiobacillus sp.*) and archaea (e.g. *Sulpholobus sp.*). Other lithotrophic bacteria use substances such as nitrate and reduce it to nitrite (e.g. strains of *Nitrobacter sp.*). *Sulpholobus* is an archaeal hot spring dweller and transforms H_2S to elemental sulphur, it flourishes at temperatures in excess of 90°C and can live in environments where pH hovers around 1, such as the gypsum wall coats and snottites in sulphuric acid caves (Figure 7.49). *Thiobacillus sp.* are widespread in marine and hypersaline settings, where they oxidize thiosulphate and elemental sulphur to sulphate. For example a unicellular halophilic, chemoautotrophic sulphur-oxidizing bacterium, *Thiobacillus halophilus*, was described in a hypersaline salt lake in western Australia where it grows in waters with salinities of up to 240‰ (Wood and Kelly, 1991). In the last few years, many of the sulphur-oxidizing bacteria originally classified under the genera *Thiobacillus* have been reclassified into the α , β , and γ subclasses of the Proteobacteria. It probably means there is a broader range of sulphur-oxidising forms in hypersaline environments than current species listings suggest and that the informal separation of sulphur oxidisers into the purple and green bacterial groups is still confused.

Archaea, life's third domain, are mostly extremophiles that thrive in highly stressed conditions, including the extremely saline (Kates et al., 1993). Archaea are further subdivided into two kingdoms: 1) the Crenarchaeota; of which all members presently isolated are either thermophiles that metabolise sulphur (via sulphur oxidation, respiration and reduction) or are psychrophiles (cold-dwelling), and 2) the Euryarchaeota; a diverse group, which includes the halophilic *Halobacteriaceae*, some thermophiles and all methanogens (Table 9.2). Some sulphur-oxidizing Archaea are also acidophiles that can grow at a pH approaching zero, others are hyperthermophiles growing at temperatures of up to 115°C on the deep seafloor.

Archaea and Bacteria that require extreme salinities to metabolise are called halophiles, those that can tolerate salinities in excess of 25‰ are termed hyperhalophiles, most modern hyperhalophiles are Archaea. Many aerobic halophilic Archaea (order Halobacteriales) are moderate thermophiles with growth optima at temperatures between 35° and 50°C and sometimes even higher. This may be an adaptation to high temperatures that typify stratified waters in heliothermic salt lakes worldwide. One of the most impressive extremophiles is *Halobacterium lacusprofundi*, it is both a halophile and a psychrophile and thrives in microbial mats in the supersaline (≈ 350 ‰) cold bottom waters ($< 0^\circ$ to 11.7°C) of meromictic Deep Lake in Antarctica (Franzmann et al., 1988). The lake lies in an isolated depression in the Vestfold Hills with a brine surface that is some 50 metres below sea level. Its waters are thermally and chemically stratified and the bottom water mass is too saline to freeze.

Halophilic Archaea in hypersaline depositional settings typically function as 9,3 heterotrophs (decomposers) with the ability to facultatively photosynthesize whenever conditions are suitable. Other Archaea are anaerobic chemo-autotrophs that are sulphur dependant and can flourish in the dark (Table 9.2). They thrive in the vicinity of hydrothermal/volcanogenic vents in saline lacustrine rifts or in marine hydrothermal brine springs atop salt allochthons or in the basal waters of density-stratified brine lakes and seaways. They also inhabit subsurface hypersaline brines that characterize bathypneatic hydrologies atop dissolving sulphate caps of salt allochthons. Sulphur-dependant Archaea resemble ancestral prokaryotes, as do modern methanogenic Archaea, and in the early Archean were the dominant life forms (Figure 9.7). All methanogens are obligate anaerobes and today thrive in three habitats; a) bodies of anaerobic mesohaline to fresh water (e.g. the warm anoxic bottom brines of Solar Lake, b) haloes about anoxic brine springs and, c) the anaerobic digestive tracts of ruminants and some molluscs. Today all

Phylum or family		Informal Group	Dominant metabolic pathways and lifestyles	
Prokaryotes	Halo-adapted Bacteria	Cyanobacteria	Cyanobacteria (T, L) Aerobic oxygenic photolithotrophs with chlorophyll-a plus phycobiliproteins for light gathering; they use hydrogen by splitting water as electron source and generate oxygen; use the Calvin cycle to generate carbohydrates; some heterocystous cyanobacteria (<i>Anabena</i> , <i>Nostoc</i>) form heterocysts, which facilitate nitrogen-fixation.	
		Proteobacteria	Purple sulphur bacteria (T, L)	Anaerobic obligate photoautotroph (use H ₂ S or S ₂ , not water) and may form sulphur granules. Contain bacteriochlorophyll a or b. Group includes many sulphur and sulphate-reducers (e.g. <i>Desulfovibrio</i>).
			Purple non-sulphur bacteria (T, L)	Oxygen-tolerant anaerobic facultative photoautotroph (use hydrogen from simple organic compounds, but not from water, as the electron donor). Contain bacteriochlorophyll a or b.
		Chlorobiaceae	Green sulphur bacteria (T, L)	Anaerobic obligate photoautotroph (use H ₂ S or sulphur as electron donor, not water). Sulphur deposited extracellularly. Contain chlorophyll a and bacteriochlorophyll c or d.
		Flexibacteria	Green non-sulphur bacteria (L)	Anaerobic thermophilic photoheterotroph in sulphide-rich zones, but are capable of autotrophy. Remove hydrogen in simple organic molecules (such as ethanol, lactic acid or pyruvic acid) or hydrogen gas substrate. Can grow lithotrophically or organotrophically under appropriate conditions, or as thermophilic aerobic organotrophs.
		Spirochaetes	Spirochaetes (L)	Free-living obligate anaerobe in waters like Mono Lake, also symbiotic, parasitic. Aerobic, microaerophilic, facultatively aerobic, or anaerobic organotrophs; catabolize carbohydrates, amino acids or lipids.
		Bacteriacea	Flavobacteria (L)	Anaerobic organotrophs, e.g. halocline dwellers in Urania Basin; <i>Bacteroides</i> ferments sugars to acetate and succinate, whereas <i>Flavobacteria</i> ferments glucose (almost exclusively). Chemoautotroph, parasite.
	Archaea	Euryarchaeota	Halophile (L)	Aerobic photoautotroph, chemoautotroph that require very high salinities (1.5-5.5 M, prefer 3-4 M) and complex nutrients for growth. CO ₂ fixed via Calvin cycle. Anaerobic respiration used by some <i>Halobacterium</i> species with nitrate, sulphur, thiosulphate as terminal electron acceptors.
			Methanogen (T)	Strictly anaerobic chemoautotrophs; <i>Methanopyrus</i> is an extreme thermophile; some can fix nitrogen. Lithotrophs generate methane using hydrogen and carbon dioxide (<i>Methanobacterium</i> , <i>Methanothermus</i> , <i>Methanococcus</i> , <i>Methanogenium</i> , <i>Methanoplanus</i>). Organotrophs - generate methane from methyl groups of formate, methanol (<i>Methanosphaera</i> , <i>Methanosarcina</i> , <i>Methanococcoides</i>) or acetate.
		Crenarchaeota (sulphoarchaea)	Thermophile (T)	Obligate anaerobic chemotrophs that require temperatures above 50°C for growth (sometimes higher than 70°C) and use sulphur as electron acceptor (except <i>Sulpholobus</i> , which uses oxygen or ferric iron). Organotrophs oxidize organic compounds for energy (oxygen or sulphur serves as final electron acceptor). Lithotrophs - can also grow organotrophically using sulphur as an electron acceptor.
			Acidophile (T)	Acidophilic thermophilic aerobic chemoautotroph, organotroph.
		Nanoarchaeota	Symbiont on <i>Ignococcus</i> (T)	Hosted on hot vent Archaea in Iceland. Its cell is only 400 nm long.
		Korarchaeota	New group of extreme thermophile (T)	Only described from RNA samples (if it is a real phylum then it is the closest to life's universal ancestor of the earliest Archaeon ~3.7 Ga).

Table 9.2. Summary of metabolic styles of prokaryotes focusing on Archaea and halophilic Bacteria (T = thermophilic; L = can construct laminated microbial communities).

biogenic methane passed into the atmosphere from the guts of animals as well as from decomposing organics in salterns, swamps, marshes, paddy fields, dumps and sewage works is the work of a few dozen species of methanogenic Archaea. It is a little modified group with a clear ancestral line extending back to the early Archean (Margulis and Dolan, 2002).

Halophilic Bacteria as a group is more biochemically divergent than the halophilic Archaea and capable of using a range of aerobic and anaerobic metabolic styles (Table 9.2). Some halophilic purple and green sulphur bacteria are chemo-autotrophic halophiles that can function independent of a light source, while other halotolerant and halophilic bacteria (including cyanobacteria) are oxygenic photoautotrophs (oxidisers). Within the anaerobic halophilic bacteria of the order Haloanaerobiales there are several moderately thermophilic representatives. *Haloferoxanthus orenii*, the first truly thermophilic halophile discovered, was isolated from Chott El Guettar, a warm saline lake in Tunisia. It grows optimally at 60°C and up to 68°C at salt concentrations as high as 200‰ (Cayol et al., 1994). The halophilic *Acetohalobium arabaticum* strain Z-7492 has a temperature optimum of 55 °C (Kevbrin et al., 1997). Under suitably stressed conditions many halophilic bacteria become heterotrophic, utilising either anaerobic or aerobic respiration pathways.

By evolving the ability to symbiogenetically split water as a hydrogen source some 2.5 billion years ago, and so excrete oxygen, the prokaryotic cyanobacteria ultimately enabled the eukaryotic lineages to flourish and displace anaerobic Bacteria and Archaea as the world's primary producers (Margulis and Dolan, 2002). By the Mesoproterozoic this had allowed eukaryotic photosynthesis to develop and ultimately led to the evolution of the higher plants. As oxygen became more plentiful in the ocean and the atmosphere, it was increasingly difficult for anaerobes to flourish in most surface waters. Some retreated to the inhospitable and typically anaerobic environments where they still flourish today, others acquired aerobic bacteria as endosymbionts and today thrive in the aerobic/dysaerobic conditions that typify the hypersaline bottom waters of many density-stratified brine bodies.

Many halotolerant and halophilic Bacteria and Archaea living in hypersaline surface waters are heterotrophs and usually feed on the remains of other organisms. Heterotrophic metabolism shows variation in the terminal electron acceptor. In aerobic respiration it is oxygen and the breakdown product is CO₂, in anaerobic respiration it may be sulphate or nitrate and the breakdown product is H₂S or nitrite (Table 9.2). In all life

forms, including ^{9,3}heterotrophs, energy is obtained from high energy electrons using cyclic or non-cyclic electron transport schemes during which the energy is transferred into and stored as adenosine triphosphate (ATP), while low energy electrons are released by the end reaction. Adenosine triphosphate (ATP) is the basis of all life as it is the energy-carrying molecule found in the cells of all living things. ATP captures chemical energy obtained from the breakdown of food molecules and releases it to fuel other cellular processes.

Exceptions to this general metabolic scheme are the fermenters, like the methanogens, where energy is stored in the form of proton-motive force (PMF), as well as in ATP. Fermentation may be the only metabolic mechanism in halotolerant and halophilic species that inhabit the lowermost living parts of a microbial mat or flourish in the vicinity of the halocline in layered brine column communities, while it may be an emergency system in others (Table 9.2; Figure 9.8). Fermentation always occurs under anaerobic conditions when there is no electron acceptor. It breaks down an organic compound, such as a sugar or amino acid, into smaller organic molecules that then accept the electrons released during the breakdown of the energy source. As glucose is broken down to lactic acid, each molecule of glucose yields only two molecules of ATP, and considerable quantities of glucose must be degraded to provide sufficient energy for microbial growth. Only a relatively small output of energy is obtained per glucose molecule consumed, as the organic molecule is only partially oxidized. Hence, the presence of fermentative halotolerant Bacteria and Archaea and their less efficient metabolisms, rather than oxic decomposers, facilitates preservation of larger quantities of organic end products (proto-kerogens).

Methanogenesis and sulphate reduction are two terminal anaerobic biomineralization pathways in hypersaline systems that convert low molecular-weight products of other bacterial processes (degradation of polymers, fermentation) into CO₂ and methane (Teske et al., 2003). Sulphate-reducing bacteria are physiologically and phylogenetically highly diverse compared to the methanogens and range across a number of bacterial groups. They are capable of oxidizing a wide variety of low-molecular weight compounds (short-chain fatty acids, alcohols, alkanes, aromatic compounds, acetate) to CO₂. When biochemical conditions are suitable for growth the range of sulphate-reducing bacteria is limited only by sulphate availability. When sulphate is depleted, methanogenic archaea become the dominant anaerobic microbial population. Autotrophic methanogens (all Archaea) utilize hydrogen as an energy source for the reduction of CO₂ to methane; specialized genera of metha-

nogens are also capable of inter- and intramolecular disproportionation of C_1 and C_2 carbon compounds (methanol, methylamines, acetate) to methane and CO_2 .

Where methane and sulphate coexist in any anoxic environment (for example, at the interface of sulphate-reducing and methanogenic sediment layers, or at methane seeps and vents beneath marine or hypersaline waters), sulphate-dependent anaerobic methane oxidation takes place whereby methane of biogenic origin is oxidized to CO_2 with sulphate as the terminal electron acceptor (Teske et al., 2003).

The varying metabolic pathways of the microbial communities inhabiting a layered brine column create an interdependent layered microbial ecosystem that reflects the varying degrees of light penetration, oxygenation and anoxia within a variably layered brine body (Figure 9.8). A similar layered pore fluid community (greater anoxia with depth) also characterises microbial mats (Figure 9.17). Oxygenic photosynthesizers (mostly alga and cyanobacteria) characterize the upper well-lit oxic portions of the brine column. Below this community of producers, the remainder of the euphotic zone is characterised by downward decreasing light levels and the increasing dominance of oxygenic decomposers (bacteria, zooplankton and metazoans) over producers, with secondary production occurring in the microbial community (green and purple sulphur bacteria) that floats atop the halocline. If light penetrates to anoxic waters below the halocline, anoxic photosynthesizers flourish there (sulphur-oxidising phototrophic bacteria and archaea). As light levels fall away in the anoxic waters below, the biota is increasingly dominated by the anaerobic decomposers (sulphate-reducers, methanogens and fermenters). If light does not reach the halocline, specialised forms of chemosynthetic green and purple sulphur oxidisers (not photoautotrophs - e.g. some flavobacteria) occupy the narrow interface at the halocline created by the contact between oxic and anoxic waters. In schizohaline settings subject to periodic freshening of the surface waters, the associated bloom of halotolerant produc-

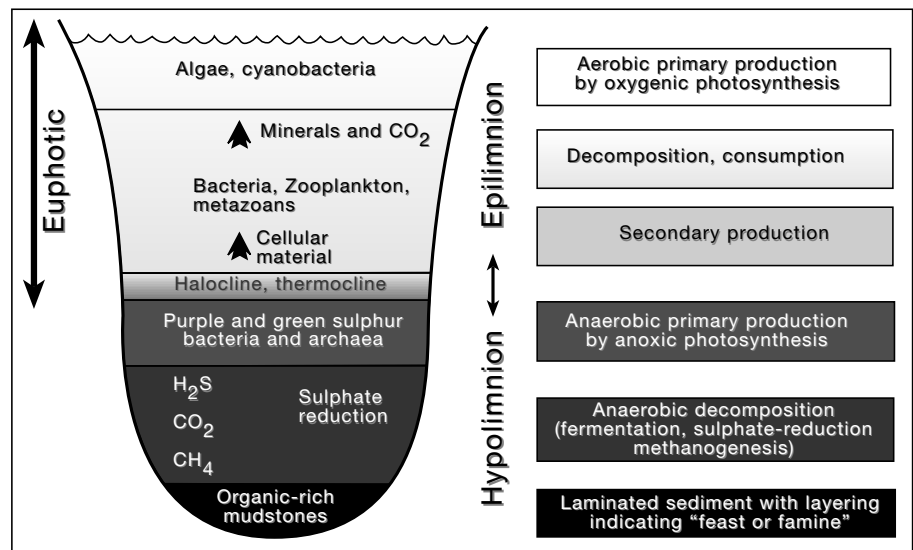


Figure 9.8. A layered brine lake (not to scale) with anoxic waters below the halocline and oxic waters above controls the distribution of the microbial communities via their metabolic requirements and pathways.

ers (alga and cyanobacteria) in the upper water column can swamp the ability of the various decomposers to degrade all the organic matter before it reaches the bottom and so laminated organic-rich and hydrogen-prone mesohaline carbonates can then accumulate on the bottom.

Salinity tolerance in the halobiota

Progressive brine concentration leads to sequential blooms of diverse macro and microbial species adapted to different ranges of salinity (Figures 9.9, 9.10). As modern surface brine is concentrated from 60‰ to around 200‰, dense eukaryotic algal and cyanobacterial populations appear, grazed by ostracods, brine shrimp and brine fly larvae (Figure 9.9a, b). Halotolerant protists are also found feeding in this salinity range, along with yeasts and other fungi. Halotolerant microbial mats cover the bottom of many hypersaline ponds and shallow lakes at this stage. In anoxic waters in this salinity range there are a variety of sulphur-oxidizing, sulphate-reducing, homoacetogenic, methanogenic and heterotrophic bacteria and archaea flourishing at the base of stratified brine columns or in the lower parts of mesohaline microbial mats. Increasing osmotic stress and loss of appropriate habitat as a water body shrinks with ongoing desiccation means much of the macroscopic stenohaline benthic fauna dies off or dies back to refugia about springs and seeps (Figure 9.9c). From about 240‰ to more than 320‰, halophilic archaea and bacteria come to dominate. As ever more elevated salinities are attained,

most other biological activity first slows and then ceases. At the elevated salinities where halophiles and hyperhalophiles flourish, a few eukaryotes, such as brine shrimp, and a handful of algae, including various *Dunaliella sp.* (a naked unicellular biflagellate green alga), are the only other living forms that the halophilic microbes encounter (Figure 9.9a, b).

Primary producers

A variety of obligate and facultative halophytic higher plants (angiosperms) can survive in moderate-to-high salinity conditions that surround saline pans and lakes. Many such terrestrial halophytes must survive long periods of drought and live where vadose soils completely desiccate, such plants are called xero-halophytes. Xero-halophyte adaptations include, deep and extensive roots, high levels of water storage (cacti), highly reduced leaf areas sometimes reduced to spines and scales, fine hairs on the leaf surface, sunken stoma and stoma that only open at night and permanently rolled leaves or leaves with a propensity to roll in drought and so reduce their surface area. They have leaves with salt bladders that can excrete salt with the evaporation water (e.g. saltbush genera such as *Atriplex*, *Halimione*, *Rhagodia* and *Chenopodium*), so that over time the leaf can be covered by extruded salt crystals. Most xero-halophytes cannot survive in water-logged saline conditions where roots are subject to long term low oxygen conditions. There the halophytic succulents tend to dominate and constitute a group generally known as the samphires, they include genera such as *Salicornia*, *Arthrocnemum*, *Halocnemum* and *Halosarcia*). These succulents are capable of surviving on the landward edges of saline mudflats and pans where they can be continually immersed in saline waters for weeks to months.

Then there are the hydro-halophytes that grow in settings subject year round to partial or completely submersed by brine. Modern hydro-halophytes are most common along the lower salinity edges of mesohaline waters (e.g. mangroves on the landward side of Khor al Bazam in Abu Dhabi) but cannot flourish in environments where longterm salinity is more than 5-10‰ above seawater. For example, mangrove seedlings cannot survive immersion for more than 48 hours in concentrated seawater with a salinity of 60‰. Salt in adult mangroves is preferentially stored in the bark and in old leaves so that it is dispersed back into the environment when the leaves or bark are shed.

Continually submersed halophytic angiosperms are largely restricted saline-tolerant varieties of seagrass. All marine seagrasses die back once bottom salinities exceed 60-70‰. For example, four species of *Halophila sp.* collected in Redfish

Bay, Texas, were able to grow in tanks with salinities of up to 74‰, without chlorophyll levels being affected, but only for a relatively short period of time (McMillan and Moseley, 1967). In more continental settings the subaqueous angiosperm with the highest salinity tolerance is *Ruppia sp.* (aka duckweed or widgeon-grass), with an occurrence range of 0.6-390 g/l TDS (seawater salinity \approx 31-34 g/l TDS = total dissolved solids). It thrives in normal marine waters, but also in the schizohaline coastal lakes of the Coorong region of southern Australia. There perennial *Ruppia sp.* communities occupy deeper (up to metres deep), well lit permanent water bottoms with salinities of 12-50 g/l. Annual or seasonal communities inhabit shallow lake bottoms, characterised by less permanent waters with seasonal surface water salinities up to 230 g/l prior to complete lake desiccation (Brock, 1982a, b). In ephemeral lakes in Western Australia, Geddes et al. (1981) found healthy *Ruppia sp.* growing in waters of 4-78 g/l TDS, but at 82-142 g/l, only drupelets (fruits) were present. *Ruppia* taxa are opportunist plants that die back to root mats when salinities rise or the saline lake dries out. They quickly return once surface waters return to salinities suitable for growth.

Preservation potential of organics from xero-halophytes is low as the organic matter is typically oxidised and degraded in the desert soils. Halophytes growing in submersed or brine saturated soils are more likely to be preserved. Kenig et al. (1990) found that, along with intertidal microbial mats, the other major contributors to organic matter preserved in the modern supratidal sediments of the Abu Dhabi sabkha were derived from mangroves (especially cuticle from *Avicennia sp.*) and lagoonal seagrasses (especially *Halodule sp.*).

Charophytes are another group of opportunistic submersed halotolerant plants that flourish in lower salinity regions of a saline lake or lakewide at times of brine freshening (Figure 9.9a). They are thought to show strong affinities to green alga, although some taxonomists link them more closely to bryophytes (Burne et al. 1980). Parts of their structure may become calcified, typically the oogonia or female reproductive organs. These are readily preserved as fossils and can be a major contributor to the numerous calcispheres found in ancient saline mudstones and lunettes. *Lamprothamnium papulosum* is the most common charophyte in the saline lakes of Australia. Studies of this species in saline lakes in the Coorong region Australia, show it can be part of a healthy bottom community at 70‰, although it does not generally successfully germinate or grow above 53‰ (Burne et al. 1980). This is two to three times the typical salinity association documented for charophyte occurrences in brackish lakes in the northern Hemisphere.

Charophytes can regenerate in ephemeral saline lakes after considerable periods of desiccation, although for germination and growth to take place this does require a transient period of suitably freshened water cover. It means charophytes in saline lakes are opportunist species that dieback or retreat to “seep” refugia in harsh times. Widespread oogonia horizons in evaporitic sediments indicate episodes of freshening as in the carbonate lakes of the Coorong and the coastal gypsum salinas in the “Chain of Lakes” at the southern end of Yorke Peninsula, South Australia (Figure 4.7a). Likewise, sediment layers with the remains of *Lamprothamnium papulosum* in Fuente de Piedra, southern Spain, indicate times of freshening in a saline lake with a flora typically dominated by *Dunaliella sp.* (Garcia and Niell, 1997).

Rather than higher plants, halotolerant green algae and cyanobacteria, are the dominant primary organic producers in moderately hypersaline (mesohaline to penesaline; 60-200‰) settings. With elevated salinities restricting the grazers, green algal densities in a surface brine layer can be more than 10^5 ml^{-1} . Mesohaline algae are mostly obligately aerobic, photosynthetic, unicellular microorganisms. Green algae of the genus *Dunaliella*, e.g. *Dunaliella salina*, *D. parva*, and *D. viridis*, are ubiquitous in modern brine lakes, such as Great Salt Lake, Hutt Lagoon and the Dead Sea, where they constitute the base of the food

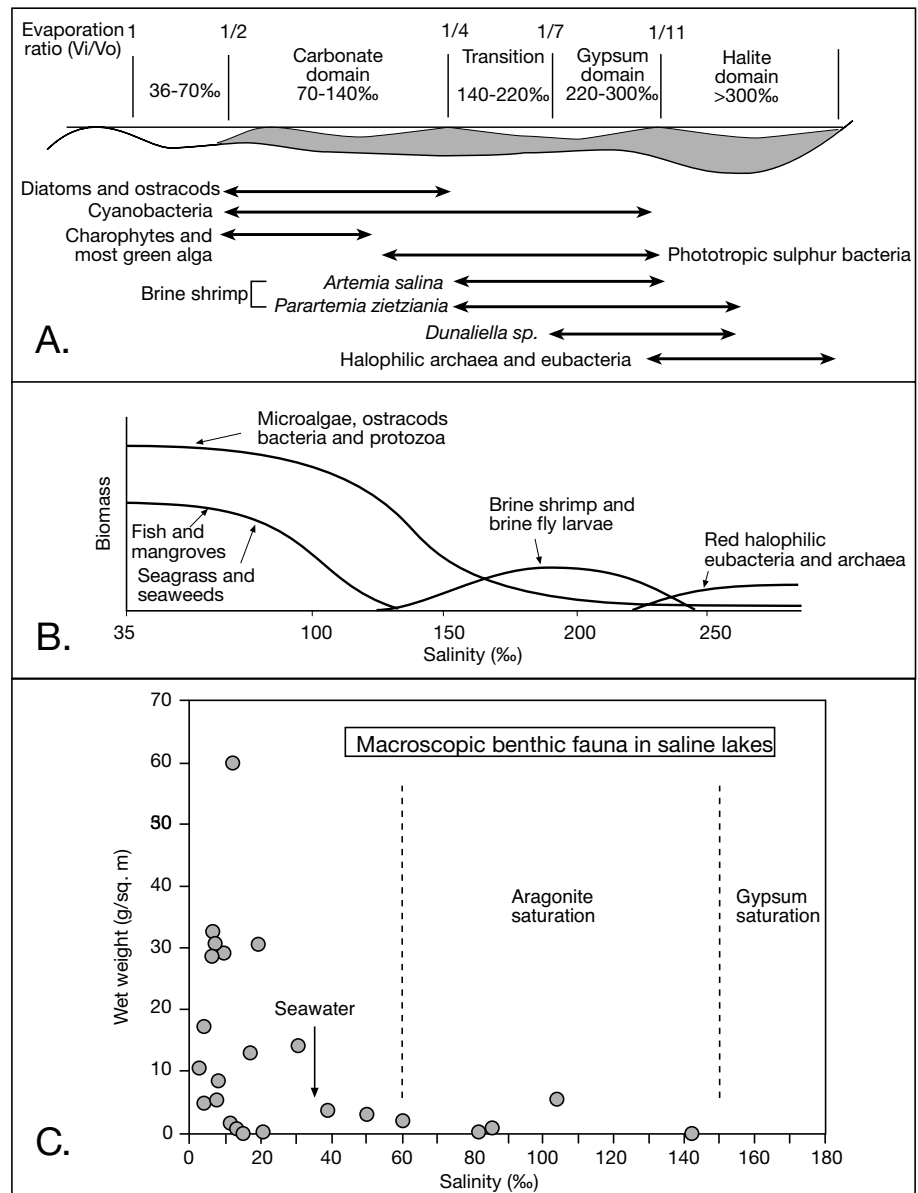


Figure 9.9. Salinity tolerances. A) Typical salinity ranges of the halotolerant biota where V_i is the volume of inflow to the basin and V_o is the volume of outflow (includes evaporation and reflux; after Barbé et al., 1990). B) Typical salinity ranges and biomass proportions of the biota in modern marine saltwork ponds. C) Standing crop (g/m^2) of the macroscopic benthic fauna in selected athalassic (nonmarine) saline lakes of the world (after Hammer, 1986).

chain for the halotolerant fauna (Figure 9.10a; DasSarma and Arora, 2001). Planktonic blooms of photosynthetic microbes can colour saline waters pink or red, especially at the higher end of this salinity range. Most species of green algae are moderate halophiles, with only a few extreme halophiles, e.g. *Dunaliella salina*, *Dunaliella viridis* and *Asteromonas gracilis*.

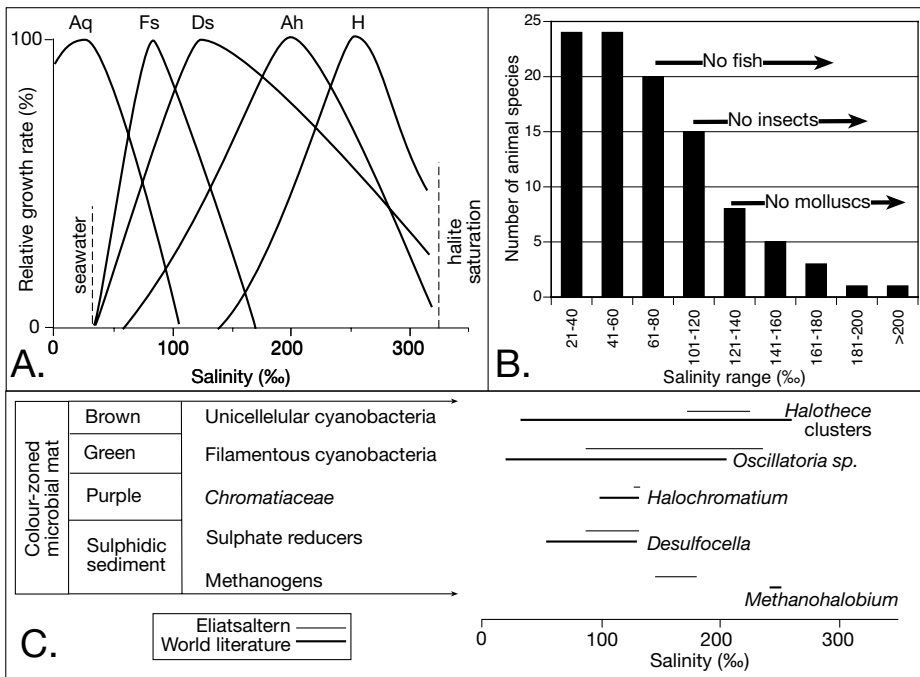


Figure 9.10. Salinity tolerances. **A)** Optimal ranges of selected halotolerant and halophilic micro-organisms. *Agmenellum quadraplicatum* (Aq) is a slightly halotolerant cyanobacterium, *Fabrea salina* (Fs) is a moderately halophilic protist, *Dunaliella salina* (Ds) is a halophilic green alga, *Aphanothece halophytica* (Ah) is an extremely halophilic filamentous cyanobacterium, and *Halobacterium sp.* (H) is an extremely halophilic archaea (after Das Sarma and Arora, 2001). **B)** Decrease in variety of animal species in saline lakes of southeastern Australia (after Bayly and Williams, 1973). **C)** Range of observed optimum salinities for phototrophs in various microbial layers and for the sulphate-reducing bacteria and methanogenic bacteria in microbial crusts. It plots the ranges for a mat from a gypsum saltern in Eliat, Israel and compares values to those in the worldwide literature (plotted from data listed in Table 2 in Sørensen et al., 2004).

The halophilic *Dunaliella parva* is the sole primary producer in Dead Sea brines, with several species of haloarchaea dependent on its periodic blooms (Figure 9.26). *Dunaliella sp.* can survive in marginward refugia, even when the upper and low water layers in the Dead Sea are NaCl-saturated. *Dunaliella salina* is one of the most environmentally tolerant eukaryotic organisms known and can cope with a salinity range from seawater to NaCl saturation, and a temperature range from $<0^{\circ}\text{C}$ to $>38^{\circ}\text{C}$.

Halophilic *Dunaliella sp.* can contain high levels of β -carotene and pigment levels tend to increase with increasing salinity. It means that blooms in hypersaline pans can be harvested and processed to manufacture β -carotene. *Dunaliella salina* contains more than 10 times the levels of β -carotene compared to other halophilic *Dunaliella* species and at higher salinities cells can contain as much as 10-14% β -carotene dry weight, so it is the preferred commercial species (Moulton and Burford, 1990). Two of the largest β -carotene producers in the world are Western Bio-

technology Ltd. (Perth, Western Australia) and Betatene Ltd. (now Cognis Nutrition and Health, Melbourne, Victoria), both began operations in 1986 in Australia. Both operators grow the algae in large and shallow (approx. 20 cm deep) wind-stirred ponds constructed either on the bed of the hypersaline coastal salina known as Hutt Lagoon, or formed by artificially expanding and isolating a lagoon flat. Each of the artificial production ponds atop the surface of Hutt Lagoon is 5 ha in area and was constructed using earthen berms. The Hutt Lagoon production plant has a total current pond area of 50 ha and there are also smaller ponds for research purposes. Ponds used by Betatene Ltd. at Whyalla in coastal South Australia are even larger. High salinity is maintained in the shallow pond waters using a combination of wind-driven mixing, solar evaporation and seawater pumped into the ponds. Uncontrolled episodes of freshening (rainfall) can lower pond salinities. This can favour the growth of the less carotenogenic species (*D. viridis*, *D. minuta* and *D. parva*) as well as allowing grazing protozoa such as the ciliate *Fabrea salina* and the amoeba *Heteroamoeba sp.* to invade the pond. Such invasions can rapidly decimate algal production.

Along with *Dunaliella sp.*, numerous species of cyanobacteria flourish at the elevated salinities where the activities of metazoan grazers are severely limited. Typically they construct laminated microbial mats and stromatolites in water-covered mesohaline areas and peripheral strandzone mudflats (Figure 1.3). Various cyanobacterial species constitute the upper parts of these microbial "high rises" with species dominance in the layer changing according to their tolerances to salinity and light (Figures 9.10c, 9.17). *Microcoleus chthonoplastes* is a

cosmopolitan mat former and is the dominant filamentous blue-green in flat laminated mats in Guerrero Negro in Baja California Sur, Mexico, in Solar Lake in the Sinai and in Deep Lake in South Australia. In Guerrero Negro it grows best in brine-covered pans with a salinity range of 60-95‰. *M. chthonoplastes* tends not to do as well beneath pan waters with longterm salinities above 100‰. In Solar Lake it flourishes beneath waters with an annual salinity range of 45-180‰ and it still manages to photosynthesise, although not all that well, at salinities approaching 300‰. *Spirulina subsalsa*, another filamentous form, flourishes in mats worldwide at salinities of up to 150-180‰. At higher salinities and higher light intensities the nonfilamentous unicellular and coccoid cyanobacterial species come to dominate. The unicellular *Aphanothece halophyta* dominates mat surfaces in Guerrero Negro in pans with surface salinities up to 200‰. In Sabkha Gavish in the Sinai it occurs across an even broader salinity range of 250-330‰. Why the same cyanobacterial species seems to have different salinity ranges in different parts of the world is not clear. It may reflect a response to differing temperature regimes or to different rates of change in salinity of the waters atop the growing mats.

Diatoms (halotolerant bacillariophytal algae with siliceous tests) are another commonplace primary producer in mesohaline and lower penesaline environments (Figure 9.9a). They flourish at times of freshened lake waters or in perennial seepage and dissolution ponds (posas) about the edges of some salars, where they become a major detrital component in some lacustrine stromatolites (Figure 1.3c). Some varieties of diatoms can live in lake brines with longterm salinities around 120‰, while the upper limit for diatom growth is around 180‰ (Clavero et al., 2000). The most halotolerant diatom taxa in the saltern ponds of Guerrero Negro are *Amphora subacutiuscula*, *Nitzschia fusiformis* (both *Amphora* taxa), and *Entomoneis* sp.; all grow well in salinities ranging from 5 to 150‰. Three strains of the diatom *Pleurosigma strigosum* were unable to grow in salinities of less than 50‰ and so are true halophilic alga.

Anoxygenic halotolerant to halophilic sulphur-oxidising photobacteria are another group of primary producers and can create dense biolaminae in a variety of a sulphide-rich environments. Sulphur-oxidising bacteria are further divisible into purple and green sulphur bacteria according to their respective bacteriochlorophylls and carotenoids (Table 9.2). Modern halophilic phototrophic sulphur-oxidising bacteria are filamentous CO₂-fixers (both green and purple sulphur bacteria) utilising sulphide as an electron donor for their photosynthesis (Figure 9.11a). In modern saline environments they grow in niches where light reaches into anoxic, sulphide-containing

bottom water layers or pore waters a few millimetres below the surface of a microbial mat. Different species thrive in different salinities ranging from seawater to halite precipitating (Figure 9.11b). Most of the H₂S they metabolise is biogenic from nearby sulphate reducers, except perhaps around well-lit brine springs and hydrothermal vents where it can be thermogenic.

In contrast to the cyanobacteria and alga that use oxygen, these bacterial phototrophs are anaerobes that use H₂S as an electron donor to produce various oxidised sulphur metabolites, the final product being sulphate or sulphur (Figure 9.11a). Commonplace sulphur-oxidising primary producers in mesohaline waters and microbial mats include; *Chromatium salexigens*, *Thiocapsa halophila*, and *Rhodospirillum salinarum*, with optimal growth in these species between 60 and 110‰ (Figure 9.11b; Caumette, 1993; Ollivier et al., 1994). Phylogenetic studies in the last two decades have removed fully halophilic species, once classified as *Ectothiorhodospira* sp., into a new genera the *Halorhodospira*; that is *Ectothiorhodospira* is the basonym for the halophilic grouping *Halorhodospira*. Shallow brines of the small soda lakes in the Wadi Natrun may be coloured an intense purple-red, due to the development of *Halorhodospira halophila*. *Halorhodospira abdelmalekii*, and *Halorhodospira halochloris* show green pigmentation in pure cultures while *Halorhodospira halophila* is red. Small puddles in hypersaline locations may show separate development of green- and red-coloured species of *Halorhodospira*, while top layers of the sediments of Wadi Natrun lakes (Egypt) show separate layers of the green-coloured and the red-coloured *Halorhodospira* sp. (Imhoff et al., 1979).

Halorhodospira abdelmalekii, *Halorhodospira halochloris*, and in particular *Halorhodospira halophila* are among the most halophilic phototrophic bacteria known (Imhoff, 1988). Isolates of *Halorhodospira halophila* from soda lakes in the Wadi Natrun have salt optima of 250‰ total salts and can survive in halite-saturated solutions (Figure 9.11b). The moderate halophile *Ectothiorhodospira marismortui* is a strict anaerobe found in the hypersaline growths about sulphur springs in the Dead Sea, where spring waters at the time of collection had a pH around 5.2, a salinity ≈ 170‰ and a temperature of 40°C. Isolates of this species grew poorly at a pH of 5.5 but thrived in the neutral pH range between 7 and 8 (Oren et al., 1989).

The ingesters, grazers and pelletizers

Large numbers of a relatively few species of halotolerant invertebrates can survive, graze and produce pellets in low to moderately mesohaline environments (Figure 9.10b). As in the

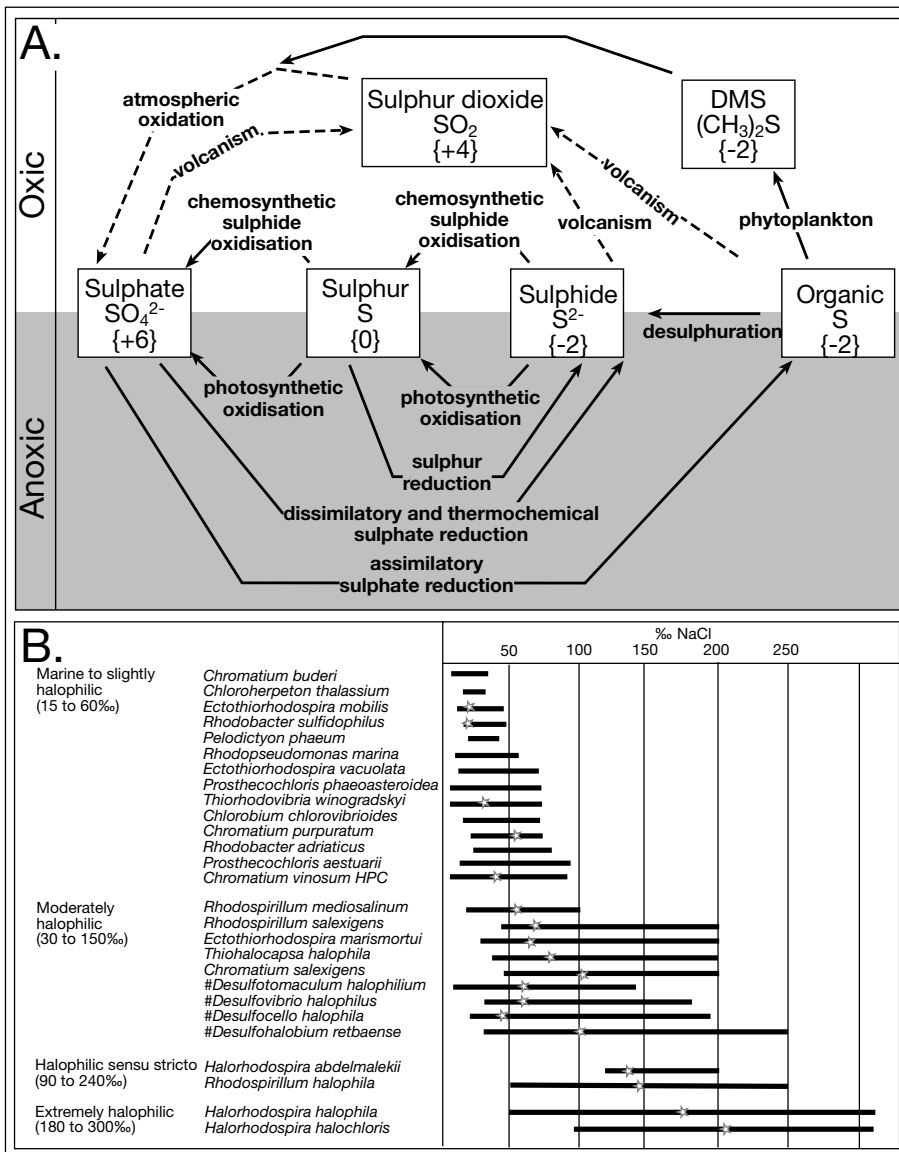


Figure 9.11. Sulphur cycle and salinity tolerance. A) Summary of the sulphur cycle showing the two types of microbially-mediated sulphur oxidation photosynthetic versus chemosynthetic (oxidation states of sulphur are shown in parentheses). Microbial pathways shown by solid lines; broken lines show geological processes involving sedimentary organic-sulphur, calcium sulphate (gypsum/anhydrite) and Fe-sulphide (pyrite). B) Salinity tolerances in phototrophic halophilic bacteria including sulphate-reducers(#). Star on bar indicates the salinity for optimal growth (in part after Caumette, 1993; Ollivier et al., 1994).

oceans, faecal pellets of the zooplankton are very important in rapidly moving organic matter to the water bottom in brine lakes and salterns. It is a mechanism that quickly moves suspended planktonic algal and bacterial debris from an oxygenated freshened water layer into a sediment layer beneath hypersaline anoxic bottom brine. There the anaerobic decomposers are

far less efficient destroyers of long chain hydrocarbons than their aerobic counterparts. Examples of pellet producers that feed on alga and bacteria during times of freshening and feast include; copepods, brine shrimp, ostracods and molluscs such as *Fragum erugatum*.

Fragum erugatum thrives beneath the mesohaline bottom waters of Shark Bay, Australia where it can survive salinities in Hamelin Pool of up to 70‰, but flourishes at salinities around 50-55‰. In the well-lit low nutrient mesohaline bottoms where it filter feeds, its metabolic efficiency is greatly enhanced by the rich xooanthellate flora that symbiotically populate its mantle (Berry and Playford, 2002). During intense storms (hurricanes or cyclones) the remains of this almost monospecific community have been washed into beach ridges that now define the edge of Hamelin Pool.

A more unusual marine association of symbiosis in molluscs living in hypersaline waters occurs on the deepsea bottom of the Gulf of Mexico. There, even though they cannot tolerate elevated salinities, biostromes of chemosynthetic molluscs rim the halocline-defined edge of methane-saturated brine lakes, situated atop salt allochthons. Biostromes are dominated by *Calyptogena* clams, along with serpulid worms, sea anemones, galatheid crabs (stone crabs like *Paralomis* sp.), swimming holothurians and amphipods (Macdonald et al., 1990). The worms and molluscs are chemotrophs with symbiotic

chemosynthetic microbes inhabiting their flesh and thriving on the H₂S and methane escaping across the halocline.

On land, insects flourishing about the edges of hypersaline lakes include halotolerant brine flies, such as *Ephydra hians* and *E. gracillis*. They hatch their eggs in microbial mats and organic scum about the strandlines of modern saline lakes, where their larvae feed and pupate before emerging as adults (Figure 9.9b). Both the larvae and the adult flies are scraper-gatherers feeding on the cyanobacteria and diatoms in benthic mats. The term *mono*, used in the name Mono Lake, California, is a Yokut Indian word for naturally salted brine-fly pupae, a local delicacy before European settlement. Brine-fly larva are well adapted to saline conditions and adults often form thick flying and feeding carpets around the edges of salt lakes. *Ephydrella marshalli* larvae collected from subaqueous benthic mats about the edges of commercial salt works/lagoons on Port Phillip Bay, Victoria, have survived several days immersed in hypersaline sodium chloride media at ≈200‰ (upto 5850 mOsm/l; Marshall et al., 1995). Likewise larvae of dolichopodid brine fly *Hydrophorus plumbeus* collected in Mono Lake survived immersion for a week in NaCl brine with a salinity as high as ≈190‰ (5600 mOsm/l; Herbst and Bradley, 1988). Adult flies have extra long body hairs that enable them to encase themselves in an air bubble and so walk about on the underside of the water surface of a brine lake. They do this to gain access to richer food sources and to lay eggs.

But, in terms of preservation potential in evaporitic settings the remains of most flies and insects, and their carapaces, rank low unless encased in saline concretions (Park and Downing, 2001). Then the three-dimensional preservation of soft tissues is possible via replacement by silica-based minerals as well as calcite, celestite, apatite, and gypsum. But the more usual evidence of arthropods and other invertebrates living in saline settings is via mineralisation of the organics and matrix in faecal pellets.

Halotolerant pellet-producing planktonic crustaceans include; ostracods such as *Cypridis torosa*, *Paracyprideinae sp.*, *Diacypris compacta*, and *Reticypris herbsti*, copepods such as *Nitocra lacustris* and *Rob-*

ertsonia salsa, and brine shrimp such as *Artemia salina*, *Parartemia zietzianis* and other related species. Halotolerant ostracod remains are a common component of mesohaline sediments and flourish at times of freshened surface water layers (Figure 9.12). For example, *Platycypris baueri* has the broadest salinity range of any ostracod found in Australia, it is able to survive at salinities ranging from 5‰ to 195‰, but is much more abundant in the middle of this salinity range and does best in waters with salinities above 70‰ (De Deckker 1981). Yet, it was not present in this upper range during the 1989 flood of Lake Torrens, Australia, when it occurred only at much lower salinities (Figure 9.12; Williams et al., 1998). The species diversity plot in Lake Torrens shows a typical saline pan biotal response to strandline retreat. This allows the halotolerant terrestrial insect population to follow the retreating strandline to scavenge and feed on the decomposing victims of the increasing salinity in the retreating brine sheet. Thus they are found scurrying about the edges of highly saline water sheets but do not actually inhabit the water.

Brine shrimp (*Artemia sp.*), another pellet producer, survive across a wide range of salinities from 25 to 340 ‰, with their optimal range around 60–100‰ (Post and Youssef, 1977). They are well adapted to the fluctuating oxygen and salinity levels that characterize mesohaline ecosystems. Encysted *Artemia* eggs, with their natural cyst coat of glycerol and trehalose hatched after 4 years of anoxic storage in a laboratory, something that the eggs of most arthropod species cannot achieve (Wharton, 2002). Geddes (1975a-c) argued increased osmotic stress is the dominant limit on the upper salinity tolerance of adult Australian brine shrimp (*Parartemia zietzianis*) and this is probably also true for most, if not all, *Artemia sp.* in hypersaline waters

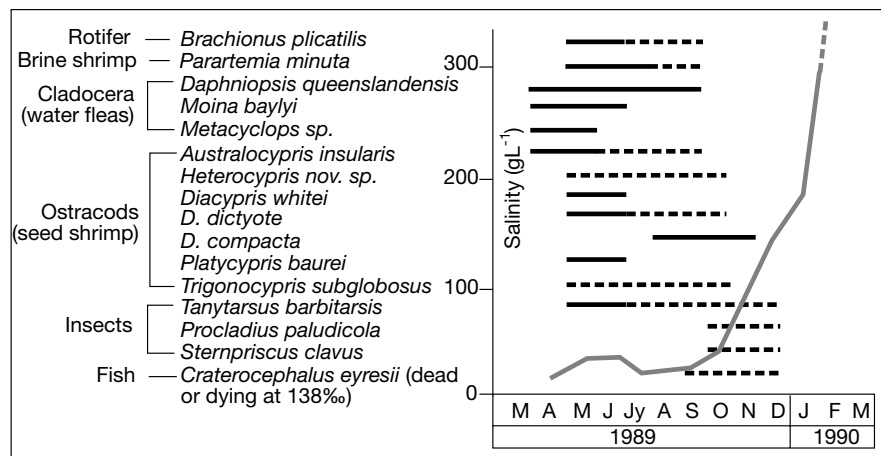


Figure 9.12. Salinity related occurrences of major macrofauna during the 1989 flooding of Lake Torrens, Australia (after Williams et al., 1998).

(Geddes, 1981). Halotolerant ostracods and brine shrimp feed on plankton living in the upper water mass of density-stratified brine columns but can also ingest benthic mats wherever a less saline water mass intersects the lake margin or when bottom waters salinities are suitably lowered (De Deckker, 1981; De Deckker and Geddes, 1980).

Historically, based on studies in the Northern Hemisphere such as in Great Salt Lake, brine shrimp have long been considered to be obligate planktonic filter feeders. Any grazing of benthic mats was assumed to take place by accident when the organisms' constant random swimming knocked pieces from the mats into the brine column where it was ingested. But observation of the feeding habits of brine shrimp feeding on microbial scum in the subaqueous gypsum domes of Lake Inneston, South Australia (pers obs.) and on the benthic mats of Lake Haywood in Western Australia (Savage and Knott, 1998) show that brine shrimp are capable bottom feeders that choose to feed on benthic mats in shallow hypersaline lakes. They will alter their normal planktonic feeding pattern to do so. The animals roll over so their ventral surface faces the benthic mat and their phyllopods continue to beat although all forward motion has ceased. The phyllopods brush the mat, releasing diatoms and cyanobacterial cells, along with crystallites, which are then ingested by the shrimp (Savage and Knott, 1998). Both ostracods and brine shrimp produce large amounts of pelleted carbonate detritus, which is a common component of many ancient evaporitic laminites and source rocks.

Halotolerant gastropods, another pellet producer, follow a lifestyle that allows them to graze on halotolerant algae and plants. Modern examples, such as *Coxiellada* sp., flourish during short periods of freshening in saline environments and are quite common in saline lakes in central Australia and the schizohaline lakes of the Coorong region and the maar lakes in Victoria, Australia. These coxiellids withstand lake desiccation and high salinities (up to 124‰) by sealing its aperture with mucous along the edge of its operculum (De Deckker 1982). Nevertheless, it cannot survive in lakes that remain dry for several years and requires a relatively high frequency of flooding to survive. Low beach ridges, composed almost exclusively of dead coxiellid tests, define the strandzones of many Australian salt lakes. Isolated tests of immature coxiellid gastropods can be found in penesaline sediments well away from the freshened lake margin (e.g. in the somewhat deeper water lacustrine clays of Lake Eyre and some Coorong Lakes). They may have been deposited there as a result of juveniles of the species traveling and grazing upside down along the underside of water-air interface, held there by surface tension forces. As the feeding

gastropods grow they become too heavy and lose contact with the air-brine interface. They sink through the salinity-layered water column, only to osmotically desiccate and die in the anoxic hypersaline bottom waters. Complete shells are incorporated in the bottom laminites to give some characteristic biometrics in a biocoenosis of these lacustrine sediments (mostly diminutive adults and very few juveniles).

Some marine foraminifera are commonplace epibionts on marine seagrasses and where seagrasses can live and survive, so can some species of foram. This is evidenced by the rich foraminiferal biota living on seagrass banks in Shark Bay, Western Australia where seawater salinities ranging from 40-56‰ (Davies 1970), and occasionally up to 70‰, yet even at this level of salinity stress a few porcellanous taxa still grow and survive. One of the most impressive halotolerant forams is *Peneroplis planatus*. In Khor al Bazam, Abu Dhabi, it is epiphytic on seagrass in lagoon waters with a salinity of 42‰ and on seaweed growing in the same lagoon in salinities ranging up to 70‰ (Murray, 1970).

The ability of some marine foram species to survive in a range of salinities has led to some interesting death assemblages in continental lacustrine sediments. Viable marine foraminifera living in continental saline lakes was documented in Australian salt lakes by Cann and De Deckker (1981). Some species can encyst and survive fluctuating salinities and periods of desiccation in both coastal and inland salt lakes, whereas others can only be found in permanent waters. Forams in continental settings generally prefer salinities and/or chemistries of lakes that approach that of sea water, optimum growth and the appearance of new generations typically occur at these values.

Two species that flourish during short periods of flooding in the inland salt lakes in Australia (such as Lake Eyre) are *Ammonia beccarii* and *Elphidium crispum*. *A. beccarii* requires water chemistries and salinities similar to sea water, i.e. with sodium and chloride as dominant ions. Although this species can survive a broad range of salinities (from 7‰ to 67‰), it grows and reproduces most successfully at salinities between 20‰ and 40‰ (Cann and De Deckker 1981; De Deckker 1982). Encysted forms of *A. beccarii* cannot survive summer droughts in modern coastal salinas and it requires permanent surface water to survive in these lakes. *E. crispum* is a marine foram species that thrives in ephemeral saline lakes of the Coorong without needing avian replenishment after a drought. It can survive summer evaporative episodes by encysting in numbers necessary for widespread re-establishment in the following winter freshening. The salinity range of this species is

as yet unknown, although it is thought to survive at relatively high salinities (De Deckker 1982). Encysted forms of both species are carried hundreds of kilometres inland on the feet and bodies of coastal sea birds, which flock every few years to newly flooded inland salt lakes, such as Lake Eyre, to nest and feed (a time of “feast”). If surface water salinities are suitable the forams bloom. Later as salinities in these inland lakes increase once more, the foram population dies back and tests are deposited in a lacustrine sediment matrix (Ludbrook, 1965). Ancient counterparts preserving evidence of this opportunistic lifestyle could create a palaeontological dilemma.

Halotolerant protists, like the forams just discussed, lack a cell wall, can be planktonic or benthic and typically ingest algae and bacteria. Protists are unicellular eukaryotes that were once classified as single-celled animals under the general term protozoa, but as some are not animals this term is now obsolete. Protists are phylogenetically grouped in the Eukaryota at the same level as animals, plants and fungi. Protists encompass groups such as the rotifers, forams, radiolaria. Identified protist species living in hypersaline waters include the moderate halophile *Fabrea salina* from Hutt Lagoon in Australia, where it feeds on populations of *Dunaliella salina*, and the extreme halophile *Porodon utahensis* from the Great Salt Lake, Utah (DasSarma and Arora, 2001). Salt-tolerant rotifers (aka wheel animalcules) include species such as *Brachionus angularis* and *Keratella quadrata*.

Fungi, mostly yeasts (unicellular fungi), are another significant component of a saline salt lake biomass, some are black halophiles that occur in their highest numbers in waters at the onset of halite saturation (Gunde-Cimerman et al., 2000). They are ^{9,3}chemoheterotrophic eukaryotes that grow best in aerobic conditions on carbohydrate substrates at moderate temperatures and in acidic to neutral pH brines. *Debaromyces hansenii* is a halotolerant yeast that when isolated from seawater can grow aerobically in salinities up to 250‰ and is capable of assimilating hydrocarbons. A saprophytic hyphomycete (a minute fungi), *Cladosporium glycolicum*, was found in the Great Salt Lake Utah, growing on submerged wood panels at a salinity exceeding 260‰.

The vertebrates

The highest brine salinity at which viable vertebrates have been observed living in a permanent brine is around 60‰. For example, the white-lipped or alkaline tilapid fish (*Oreochromis alcalica*) lives in such mesohaline waters in African rift lakes and even flourishes at 36–40°C and pH ≈ 10.5 in thermal spring

and moat brines about the edges of Lake Natron and Lake Magadi. Desert pupfish in the Sonoran Desert can survive for short periods in waters of drying pans that are as saline as 100–140‰ (Helfman et al., 1997, p.313). But tilapids are one of the few higher organisms that can tolerate perennial hypersalinity (DasSarma and Arora, 2001). Some birds feed on the periodic planktonic blooms that occur at times of freshening in nutrient-rich hypersaline environments. One of the most spectacular examples of avian exploitation of the halotolerant plankton is the pink flamingo population of African rift lakes. Stilts, gulls and pelicans are other opportunist avians that feed on halobiotal blooms that occur in periodically freshened saline lakes.

Throughout the Neogene, hippopotami (*Hippopotamus amphibius*) are probably the largest vertebrates capable of leaving traces of its presence in semi-arid to arid lake-margin sediments. This is especially so in regions of muddy organic-rich sediments near brackish lake margin springs, as in the saline-alkaline mudflats rimming the crater lake of the Ngorongoro Crater, Tanzania (Deocampo, 2002). In such an environment the organic content of muds that infill hippopotami trackways or furrows leading to the spring is as high as 17% TOC versus organic contents around 6–7% in mudflat sediments adjacent to the trackways.

Bacterial decomposers and chemosynthesisers

The habitat range of the halobiota described so far largely exists in, or near, an environment where light penetrates to the sediment surface. But there is also a range of halotolerant and halophilic organisms that can flourish in environments where light may no longer penetrate. These are the decomposers, fermenters and chemosynthesisers and it is their biochemical signature that is frequently found as biomarkers in many ancient source rocks.

Bacterial sulphate reducers

Dissimilatory sulphate reduction can occur up to quite high salt concentrations and black, foetid sulphide-containing sediments form the bottom to modern coastal salinas and salt works, well into the penesaline salinity range (Oren, 2001). Amongst the bacteria, the most salt-tolerant sulphate reducer is the halophilic *Desulphohalobium retbaense*. Isolated from Lake Retba in Senegal, it is capable of growing at NaCl concentrations of up to 250‰ (Ollivier et al., 1994). Two other sulphate-reducing halophilic isolates are *Desulfovibrio halophilus* and *Desulfovibrio oxyclinae*, which can tolerate NaCl concentrations of up to 180–225‰ (Figure 9.11b; Caumette, 1993; Krekeler et al., 1998). Another isolate, similar to *Des-*

ulfovibrio halophilus has been collected in brine pool samples from the allochthon-associated deep-water brine lakes on the floor of the Red Sea. There it grows at salinities up to 240‰, but only slowly. No viable bacterial sulphate-reducing communities have been collected at the more extreme salinities where halite precipitates. Some sulphate reducers may also be alkalophiles; for example, *Desulfonatronovibrio hydrogenovorans* is a H₂-utilising sulphate-reducing bacterium isolated from the trona beds of Lake Magadi that functions optimally at pH 9.5 and 3% w/v NaCl.

Most halophilic and halotolerant sulphate reducing bacteria are incomplete oxidisers that grow on lactate and produce acetate. Dissimilatory sulphate reduction provides relatively little energy, and therefore the need for sulphate reducers to spend a substantial part of their available energy budget for the production of organic osmotic solutes may set the upper limit to the salt concentration at which these bacteria can grow (Oren, 2001 and later discussion). The oxidation of lactate to acetate and CO₂ yields much more energy. Recently, the first halophilic acetate-oxidizing sulphate-reducing bacterium was isolated: *Desulphobacter halotolerans*. It was collected from the hypersaline bottom sediments of Great Salt Lake, Utah, and found to have a rather restricted salinity range, being unable to grow above 13% NaCl (Brandt and Ingvorsen, 1997). Even so, it possesses the highest NaCl-tolerance reported for any member of the genus *Desulphobacter*.

Bacterial chemosynthesisers (sulphur oxidizers)

Because oxygen and sulphide flux in hypersaline environments occur in opposing gradients, the growth of halotolerant and halophilic sulphur-oxidising bacterial chemosynthesisers is confined to narrow oxic zones of chemical overlap (Figures 9.8, 9.11a). This narrow niche occurs at the interface between the oxygenated layer created by the primary producers and the underlying anoxic layer created by the sulphate reducers. In stratified brine columns, it defines a narrow aerobic zone immediately atop the halocline where chemical gradients are stabilized by density and temperature differences between the cooler less saline surface waters and the warmer more saline bottom layers (Figure 9.8). Ongoing bacterial growth via sulphur chemosynthesis (not the photosynthetic purple and green sulphur bacteria discussed earlier) occurs at many subphotic haloclines where the chemical gradient of rising sulphide is stabilized by the salinity contrast that prevents pervasive vertical mixing (e.g. Figure 2.48). In layered microbial mats it is defined by a layer of purple and green sulphur-oxidising bacteria which flourish below the depth of light penetration. This interesting

group of secondary producers, which often inhabit haloclines, is discussed later in this chapter in the context of secondary organic production in saline brine columns.

Extremophiles (mostly Archaea)

As surface water salinities rise above 200-240‰, rates of oxygenic photosynthesis in algae and cyanobacteria slow and ultimately cease. Halophilic bacteria and archaea come to dominate, mostly as decomposers and fermenters (Figure 9.9). Of the halophilic bacteria, two groups are well represented in elevated salinity ranges; the fermentative bacteria belonging to the family Haloanaerobiaceae and the halophilic members of the autotrophic sulphur-oxidizing bacteria of the family Ectothiorodospiraceae (Figures 9.11b, 9.13). Both families were discussed earlier in this chapter. As the name suggests, the group loosely called halobacteria^{9.5} flourish in supersaline waters, most halobacteria are not bacteria but archaea, belonging to the family Halobacteriaceae.

One species of halophilic bacteria is worthy of special mention is *Salinibacter ruber* as, unlike most other Bacteria, it can flourish in the range of extreme salinities that until recently were considered to be the exclusive province of Archaea. It is a new genus and species (Oren, 2002). *Salinibacter* is a motile rod, pigmented red (probably by a carotenoid) with an absorption maximum at 482 nm and a shoulder at 506-510 nm. Because of the red pigmentation, colonies of this bacteria in superhaline waters have probably been overlooked in the past. Historically, red colonies growing at salinities in excess of 250 g/l have been widely considered to be archaeal. But this bacteria organism is no less halophilic than the archaeal halophiles: no growth was obtained below 100 g/l NaCl, and for optimal growth concentrations between 150 and 230 g/l are required. The physiological properties of *Salinibacter* are unusual for most bacteria: the organism apparently uses KCl to provide osmotic balance, while lacking high concentrations of organic osmotic solutes. Thus, its physiology resembles that of the halophilic Archaea more than that of other aerobes within the domain Bacteria.

We shall now concentrate on salinity ranges of halophilic archaea (haloarchaea). All known extremely halophilic archaea stain gram negative, do not form resting stages or spores and reproduce

^{9.5}The term halobacteria (as opposed to the family Halobacteriaceae that encompasses the halophilic Archaea) is a terminological carry over from the old two-part morphology-based classification of life (see earlier discussion of Woese and his influence on microbial nomenclature).

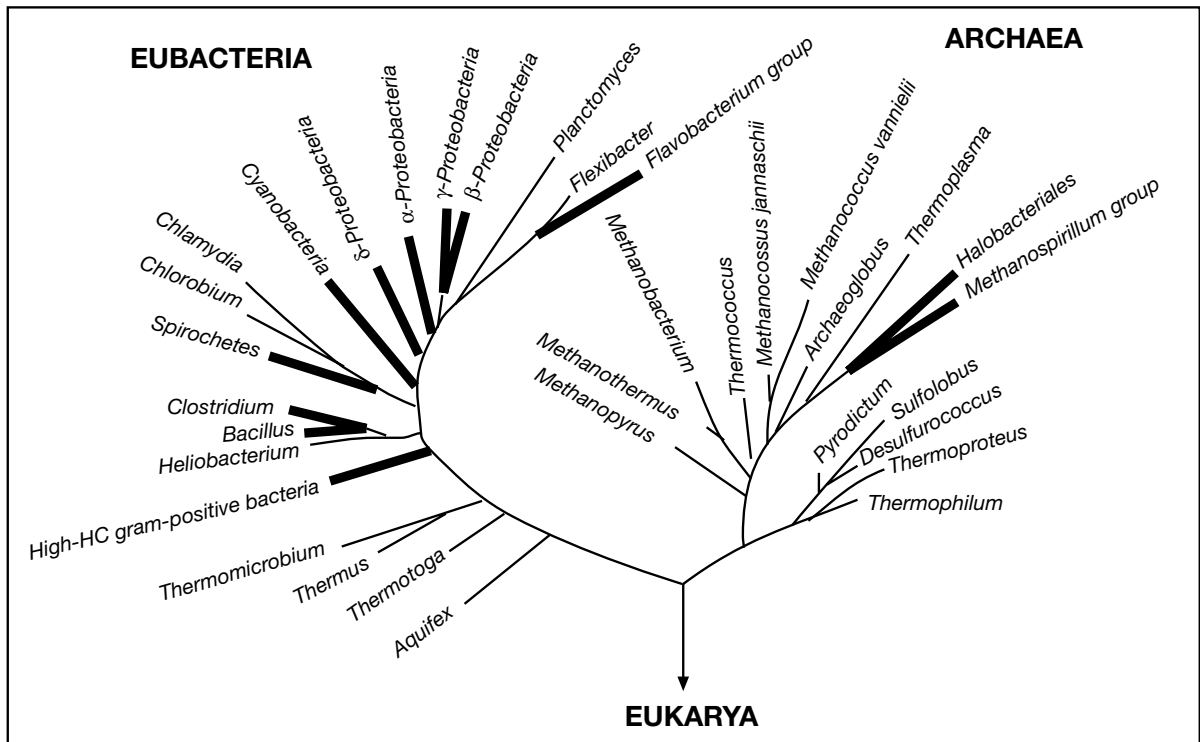


Figure 9.13. Phylogenetic tree of the Bacteria and the Archaea, based on 16S rRNA sequencing comparisons, Bold lines indicate branches containing representatives able to grow at or near optimal rates at NaCl concentrations exceeding 15% (after Ventosa et al., 1998).

by binary fission or budding (Table 9.3). They are morphologically diverse and cell shapes include spheres, spiral, rods, lobed, plate-shaped, irregular-shaped or pleomorphic. They may exist as single cells, as aggregates or form filaments. Cell diameter range from 0.1 to 15 μm and the length of a filament can be up to 200 μm . Currently, in the family Halobacteriaceae there are around 15 genera with 40 species of extreme halophiles (Oren, 2002), Some genera are monotypic: *Halobacterium*; *Halobaculum*; *Natrosobacterium*; *Natrialba*; *Natrosomonas*. The other genera are: *Natrarococcus* (2 species); *Haloarcula* (2 species); *Halococcus* (2 species); *Haloferax* (4 species); *Halorubrum* (5 species), and an eleventh genus, *Haloterrigena*, has recently been proposed (DasSarma and Arora, 2001).

Cosmopolitan haloarchaea genera are *Halobacterium*, *Haloferax*, *Haloarcula* and *Halococcus* (Table 9.3). Haloarchaeans prefer near somewhat acidic to near neutral pH brines and so are commonplace in marine-fed brines, seeps, sea-bottom brine lakes and continental salt lakes. Some Archaea flourish in caprock brines, along with the sulphate-reducing bacteria and are also resident in sulphuric acid caves. *Halococcus sp.* are strict aerobes, their name reflects their coccoid cell shapes; they form pairs, tetrads, sarcinae or irregular clusters. Cells

produce several orange or red carotenoid and retinal pigments needed to better cope with high levels of ultraviolet light that characterise supersaline brine sheets. *Haloferax* prefers high Mg waters and is a major constituent in the halophilic biota of the Dead Sea. The pleomorphic *Haloarcula* typically grows with square and triangular shapes, with straight edges, sharp corners, and is very flat. It is very similar in appearance to the interstices in a mass of halite crystallites. These highly angular shapes are unusual for a lifeform and only possible because internal salt concentrations are as high as they are outside the cell (see cellular adaptations). It means there is little or no net osmotic pressure on the cell wall, allowing it to adapt such high surface-area shapes. Similar shapes are not possible for organisms with 'normal' ionic strengths in the cell interior. Their cell shapes show surfaces and outlines that are indicative of "minimization of surface energy," whereby curved edges and spheroid outlines dominate.

Of the recognized genera of haloarchaea, two have representatives that live only in high pH soda lakes such as Wadi Natrun and Lake Magadi, they are *Natronobacterium* and *Natronococcus*. They grow in highly alkaline brines (pH 9-11) with very low levels of Mg (<0.024 g/l). This group or Archaea is not found in marine-fed salterns or less alkaline continental systems,

Feature	Halobacterium	Halococcus	Haloarcula	Haloferax
NaCl (g/l) required	>120	>120	>90	>90
optimal	204-263	204-263	117-175	117-175
Oxygen requirements	aerobe/facultative anaerobe	strict aerobe	aerobe/facultative anaerobe	strict aerobe
pH optimum	5.5-8.5	5.5-8.5	5.5-8.5	5.5-8.5
Temperature optimum (°C)	20-40	30-37	30-55	35
Pigment	Bacteriorhodopsin Halorhodopsin	Carotenoids Retinian type pigments	Bacterioruberin Retinian type pigments	Bacterioruberin Retinian type pigments
Mg (g/l) required	>0.12	>0.1	>0.12	>0.49
optimal	0.12-1.22		0.12-1.22	0.49-1.215
Size (µm)	0.5-1: 2 x 1.6	0.8-1.5	n/a	1.3 x 2.3
Shapes	irregular rods	cocci	pleomorphic	irregular rods, disks
Gram (+ or -)	+	- (+)	-	-

Table 9.3. Characteristics of the main halophilic archaea (after Perthuisot and Castanier, 2000).

(Grant et al., 1999). How *Natronobacterium* and *Natronococcus* survives in soda lakes is a problem for them (or at least for us, trying to understand how they get can away with it). At such elevated pH levels any protons (H^+) pumped to the outside of a cell by electron transport or rhodopsin membranes, are sucked up by the hydroxyl ions and gone forever. Even though the resulting electric potential is still there, it can't be harvested by an ATPase-based metabolism unless it can recycle protons from outside the cell (see next section). How they get around this problem is not known, and it is probably the issue that limits the upper pH range of life.

Methanogenic archaea, as the name implies, produce methane as a byproduct of their autotrophic metabolism. Methanogens are all Archaea and constitute the strictest anaerobic grouping known. In saline settings, most methanogens do best in anoxic waters with salinities less than 150‰. No other group of living things breathe methane and so their metabolic enzymes are unique (as are the related biomarkers). Several, mostly moderate halophilic, methanogens have been identified in saline ecosystems and include *Methanohalophilus halophilus* from a microbial mat in Shark Bay, *M. mahii* from the Great Salt Lake, and *M. portucalensis* from a coastal saltworks in Portugal (DasSarma and Arora, 2001). The slight halophile *Methanosalsus zhilinae* is also an alkaliphile and a slight thermophile. The extremely halophilic methanogen, *Methanohalobium evestigatum* comes from a salt lake in the Crimea; it has a NaCl optimum of 260‰ and is also a thermophile with a temperature optimum of 50°C. Worldwide these and other methanogens form the base level in chemosynthetic foodchains in salt lakes and are common contributors to the chemosynthetic biota of deep-sea brine pools atop salt allochthons in the Gulf of Mexico (Figure 9.40).

Methanogenesis oxidizes hydrogen using metabolic mechanisms that are not sufficiently efficient to rip out all the hydrogen from the carbon chains. As a biochemical process it occupies a terminal position in the degradation of carbohydrates in the reaction cycle of hypersaline ecosystems. Methanogenic Archaea in hypersaline environments utilise noncompetitive organic substrates such as methanol, methylated amines, and dimethyl sulphide, which originated largely from the breakdown of osmoregulator amines (osmolytes). Methanogens do not utilise carbon dioxide, acetate and hydrogen, which are the substrate for the sulphate-reducing bacteria living nearby. The reason for this metabolic restraint is the greater effectiveness of sulphate-reducing bacteria, which are out-competing methanogens for hydrogen and acetate (i.e. methanogens eat the leftovers).

Cellular adaptations to hypersalinity.

Halotolerant and halophilic species have developed special biochemical mechanisms to cope with the tendency to desiccate in the high osmotic pressures of mesohaline and hypersaline waters namely; slime, osmolytes, halo-adapted membranes and specialized proteins. Halotolerant cyanobacteria constitute a significant component of the upper layers in microbial (algal) mats in modern sabkhas and shallow brine lakes where they are subject to both periodic desiccation and hypersalinity. Such microbial mats show a worldwide recurrence of a few well-adapted cosmopolitan cyanobacterial species in the upper stories of a microbial mat; *Microcoleus chthonoplastes*, *Lyngbya sp.*, *Entophysalis sp.*, and *Synecococcus sp.* All are slimy; they are embedded in matrices of extracellular polymeric mucous that

stores large amounts of water. It protects the cell from osmotic stress and acts as a buffer against extreme temperatures and ultraviolet rays (Gerdes et al., 2000a).

Other halotolerants and all halophiles adapt to osmotic stress at the intracellular level. *Dunaliella parva*, a halotolerant unicellular green alga that flourishes in mesohaline waters (optimum = 120‰, survival 20–340‰), distributes glycerol throughout its cytoplasm to increase the total solute concentration in the cell and so better cope with the high osmotic pressure induced by its high salinity surrounds. Glycerol is an osmotically active substance (osmolyte) that takes up space in the cellular fluids. It lowers the relative water content of the cell and so raises the internal osmotic pressure. Cytoplasmic concentration of glycerol in *Dunaliella parva* can reach 7 mol/l and can constitute over 50% of the dry weight of cells growing in salinities ≈280‰. Glycerol is used as an osmolyte in other halotolerant and halophilic algae, as well as by yeasts, fungi and brine shrimp. Halotolerant and halophilic prokaryotes also use a variety of other sugars, sugar alcohols, amino acids and compounds derived from them (such as glycine betaine and ectoine) as osmolytes, leading to characteristic biomarker assemblages in ancient saline sediments.

Halophilic archaea have two main intracellular defence mechanisms to cope with the extreme osmotic gradients induced by hypersaline to supersaline conditions. One is a modification of the plasma (cell) membrane; the other is an adaptation of the protein structure itself. Unlike most life, the plasma membrane of halophilic archaea is dominated by rhodopsins and the cell membrane does not actively exclude salts, so the overall internal salt concentration in haloarchaeal cytoplasm is high. But the cell membrane is selective, it tends to exclude sodium, while actively pumping potassium into the cell against a thousand-fold concentration gradient. The total ionic strength remains the same on both sides of the plasma membrane, but the ratios of specific ions differ inside and outside the cell wall. Potassium is the dominant cation within the cell. Many cell functions require potassium, but would be disrupted by high levels of sodium. Cells of halophilic archaea can contain up to 4 moles/litre of potassium chloride, which is eight times its concentration in seawater. Anaerobic fermentative halophilic bacteria of the order Haloanaerobiales use a similar “high potassium in the cell” strategy.

Rhodopsins (bacteriorhodopsins) constitute much of the protein in the purple patches in the cell membranes of photo-active haloarchaea. Patches contain 25% lipids and 75% protein, all of which is bacteriorhodopsin (Figure 9.14a). Bacteriorho-

dopsin structure is arranged in groups of 3 protein molecules surrounded by a lipid with a few more lipids in the centre of the molecular cluster. These light-sensitive purple pigments convert light energy into chemical energy (proton pump) and so power the cell's ion pump (Figure 9.14b). Thus, the purple membrane is a site of photosynthesis, but not the chlorophyll-based photosynthesis of cyanobacteria and eukaryotes. Purple membranes obtain energy from light but, unlike chlorophyll, do not use light to generate reducing power and cannot fix CO₂. Haloarchaea with purple membranes are still mostly heterotrophic but can function as facultative autotrophs in low oxygen conditions where they supplement their metabolic power with photosynthesis via the purple membrane patches. Almost all of this extra energy is used to pump potassium across the cell membrane and so maintain the cellular ionic balance (Figure 9.14b).

As an example of the adaptive chemistry of this halophilic lifestyle, consider the archaea *Halobacterium halobium*. Its cell carries a combination of orange-red carotenoids: mostly β-carotene (C-40) and bacterioruberins (C-50). It is an aerobic-facultative anaerobe. When oxygen levels fall, as often happens in hypersaline water bodies, but light still penetrates the brine, anaerobic photophosphorylation takes place in the cell membrane in the absence of chlorophylls and redox carriers. Waters and sediments where *H. halobium* flourishes then take on a blue or purple tint, as in the Dead Sea. In the past, prior to gene sequencing studies, bacteriorhodopsin's characteristic purple colour led to many haloarchaea in their photoactive stage being described as a separate species of purple bacteria. In the same brines but with higher oxygen levels the main cellular metabolism of *H. halobium* is heterotrophic, not photoautotrophic. Cells in the heterotrophic mode are mostly coloured by carotenoids and now waters where it is thriving appear red, not blue-purple. This is its more normal respiratory metabolic mode in hypersaline waters, where it depends on b and c cytochromes as well as cytochrome oxidase to create ATP via the breakdown of glycerol and the other cellular contents from the now dead algae and cyanobacteria. This cytochrome mediated pathway is not a particularly effective metabolic pathway for decomposers living at lower salinities. But in hypersaline waters these more efficient metabolisers cannot function. So, these highly salt-adapted halophilic cells can respire and produce ATP using their red membranes (carotenoids), under little or no stress from any other competing life forms, even if brines maintain relatively high levels of oxygen. The adaptive chemistry of *H. halobium* means it acts as a decomposer in oxygenated water, and as an anaerobic phototroph in dysaerobic to anoxic, but lit, hypersaline waters.

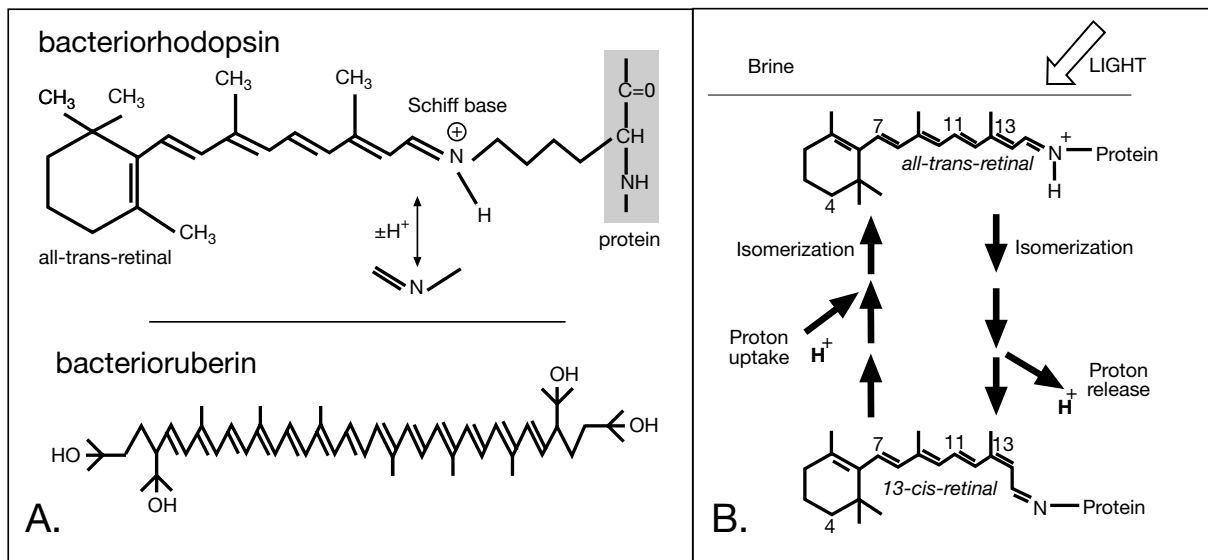


Figure 9.14. Bacteriorhodopsin proton pump (MW = approximately 25,000), A) Molecular structure emphasising retinal. Overall, bacteriorhodopsin is a protein that has 7 alpha-helical segments each spanning the halobacterial cell membrane. It contains one molecule of retinal per protein molecule which is bound via a Schiff base to the side chain $-NH_2$ group of a lysine residue. The Schiff base lysine is located 40 amino acids from the N-terminus and is near the outside of the membrane in the second helical segment. Interaction of retinal with the protein causes a large red shift, and hence light absorption is at 560-570 nm. The pigment looks purple when bound to the protein. Also shown is the structure of bacterioruberin. B) Photon pumping; light rapidly changes the "straight" all-trans form of retinal in bacteriorhodopsin into the "bent" 13-cis form of retinal, with a concomitant release of a proton outside the cell membrane. The 13-cis form spontaneously returns to the all-trans form in a light-independent reaction, with the concomitant uptake of a proton from within the cell.

There it can survive, although at lower metabolic rates, by using its purple membrane patches (bacteriorhodopsin) to pump protons across the cell membrane (Oesterhelt and Marwan, 1993; Kates et al., 1993). Interestingly, the same species can colour the waters it inhabits either red or purple in response to changing oxygen levels.

Bacteriorhodopsin in the purple membrane of haloarchaea is best described as a two-dimensional oriented crystal containing the pigment molecule retinal. When bacteriorhodopsin captures a photon with its retinal "antenna" this induces isomerization of the retinal, which then becomes detached from the protein, triggering conformational changes in the protein itself (Figure 9.14b). This eventually leads to a bleaching and the pumping of a photon across the cell membrane. Bacteriorhodopsin has an orderly orientation or "sidedness" in the plasma membrane, such that when it releases hydrogen/ Na^+ ions in an illumination and bleaching cycle, the hydrogen ions are expelled only at the outer side of the membrane (ion pump). Conversely when bacteriorhodopsin regains its colour the necessary hydrogen can only approach from the inside of the membrane. Thus a cycle of bleaching and recovery sets up a hydrogen ion pump, which in turns sets up an energy gradient that drives ATP synthesis.

What is so impressive about bacteriorhodopsin is its extreme durability and stability. It survives intact at temperatures up to $140^\circ C$ and can reliably run through a photocycle more than 10 million times. There are a large number of intermediates in the bacteriorhodopsin reaction cycle, each of which can be addressed by light of a specific wavelength. This has led many to proclaim its potential in the development of biomolecular computers and biological solar cells. Synthetic bacteriorhodopsin is a working bistable optical switch, it can be fabricated in a monolayer by self-assembly and reliably store data with 10,000 molecules per bit. In the early 1970s it was extensively studied in the former Soviet Union as a way to counteract the West's dominance in semiconductors, some of this research is still classified as a state secret in Russia today.

Some halophilic archaeal strains, including *Halobacterium salinarum*, contain another rhodopsin pigment in their purple membrane called halorhodopsin. It acts as a Cl^- pump, once again generating energy in highly saline conditions. It is usually present in the cell membrane in much smaller amounts than bacteriorhodopsin, but contains the same retinal pigment. It too absorbs light, which it converts to an ion gradient. However instead of pumping protons out, like bacteriorhodopsin, it pumps chloride ions inwards, which helps maintain osmotic

balance in highly saline conditions. Since chloride ions have a negative charge, moving chloride inwards is equivalent in terms of energy to moving a proton outwards. Thus halorhodopsin generates a chloride ion gradient, which also supplies energy to the cell.

All this membrane adaptation merely shifts the osmotic balance problem from the cellular to the molecular level. Ions within the cell's cytoplasm still compete with proteins and other biomolecules for that universal solvent, water. In order to cope with high osmotic stress at the molecular level, halophilic archaeal proteins have evolved to maintain a high negative charge on the protein surface. This attracts water molecules and envelops the protein in a protective shroud of bound water.

For example, in the Dead Sea halophilic archaea (*Haloarcu-
marismortui*) the proteins of its metabolic enzyme (malate de-
hydrogenase) and its electron transfer protein (ferredoxin) are
both wrapped in coats of acidic amino acid sidechains, both of
which carry a negative charge in neutral media. This predomi-
nance of charged amino acids on the surface of enzymes and
ribosomes stabilizes the hydration shell of various cytoplasm
molecules in high salinity intracellular surroundings, even when
the extracellular brines are well into the halite saturation field.
High-density surface charge binds water molecules to the pro-
tein surface much more ef-
fectively than any mesophile
protein. Hence, *Haloarcu-
la* proteins do not dehydrate or
unfold (denature) even when
exposed to extremely high
salinities. But, high levels
of shielding cations (mostly
potassium) are lost via
osmosis in low salinity en-
vironments and an excess of
negatively charged ions then
destabilizes the molecular
structure by ionic repulsion
and the proteins lyse or dis-
integrate. Any species using
a “salt in cytoplasm” strategy
has an innate restriction to
highly saline environments
(obligate halophiles). Ironi-
cally, the intracellular acids
that unfold normal proteins
counteract this tendency in
the halophiles.

In summary, bioadaptations at the cellular level to highly saline conditions can be divided into two groups of responses (Oren, 2001):

a) **The “high-salt-in” option.** Accumulation of salts in the cytoplasm at concentrations equal to or higher than those of the outside medium. Generally KCl is used as the main intracellular salt. Aerobic halophilic archaea (family *Halobacteriaceae*) utilise this strategy, as do fermenting bacteria, bacterial acetogenic anaerobes (*Haloanaerobium*, *Halobacteroides*, *Sporohalobacter*, *Acetohalobium*), and some sulphate reducers. This strategy is energetically relatively inexpensive, but requires far-reaching adaptations by the intracellular enzymatic machinery to the presence of high salt concentrations. Cells utilising this strategy show limited adaptability to changing salt concentrations (obligate halophiles) and have achieved success only after a long and complex evolutionary history.

b) **The “low-salt-in” option.** Exclusion of salts from the cytoplasm and the accumulation of organic osmotic ‘compatible’ solutes (osmolytes) to provide osmotic balance. This strategy is used by halophilic and halotolerant eukaryal microorganisms, by most salt-requiring and salt tolerant bacteria, and also by halophilic methanogenic archaea. This strategy is energetically expensive; the energetic cost depends on the type of organic

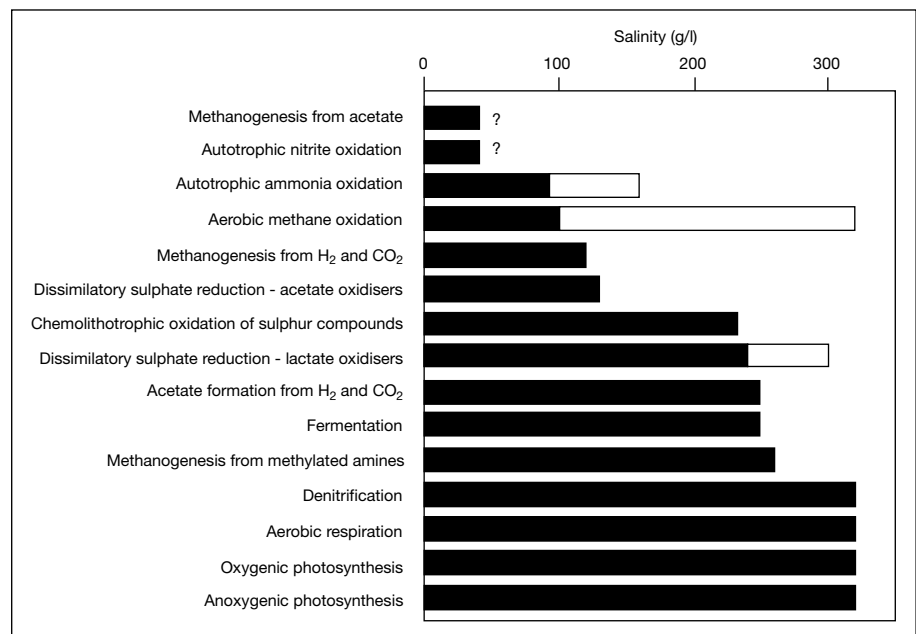


Figure 9.15. Approximate upper salinity limits of selected microbial metabolic pathways (after Oren, 2001 and references therein). Values presented are based on laboratory studies of pure cultures (black bars) and on activity measurements of natural communities in hypersaline environments (white bars).

solute synthesized. No major modification of the intracellular machinery is needed in comparison to non-halophiles, and in most cases cells can rapidly adapt to changes in salinity, as exemplified by *Dunaliella salina*.

As Oren (2001) clearly illustrates, organisms living in increasingly high salinity environments have to devote increasing large proportions of their bioenergetic budgets to osmoregulation, either to synthesize organic solutes or to activate and maintain ionic pumps. This creates a natural salinity-related control over various metabolic pathways, their energy efficiencies and hence their biomarker distributions in the resulting sediments. The following metabolic styles function best at high salinities (Figure 9.15):

1. Those processes that use light as an energy source (and are generally not energy-limited).
2. Heterotrophs (bacteria as well as archaea) that perform aerobic respiration, denitrification, and other dissimilatory processes that yield large amounts of ATP.
3. All types of metabolism performed by organisms that use the 'high-salt-in' strategy, even if the efficiency and amount of ATP obtained in their dissimilatory metabolism is low.

Growth of phototrophic microorganisms in hypersaline surface waters is generally limited by the availability of inorganic nutrients and not by lack of light energy (Oren, 2001). Accordingly, both oxygenic (*Dunaliella sp.*, cyanobacteria) and anoxygenic phototrophs (*Halorhodospira*, *Thiohalocapsa*, *Halochromatium*), all produce organic solutes for osmotic stabilization. They may be found up to very high salt concentrations and in several cases can survive well into the halite saturation field. However, in the case of chemolithotrophs and anaerobic heterotrophs the amount of energy generated in the course of their dissimilatory metabolism is often insufficient to supply the demands of cell growth, osmotic adaptation, and life maintenance. Longterm growth and survival in hypersaline environments is not possible in such species. The 'high-salt-in' strategy is preferable for strongly energy-limited organisms (haloarchaea and fermentative halophilic bacteria) as it is energetically much less costly than the production of organic osmotic solutes. Clearly, salinity controls the various metabolic styles at the cellular level (Figure 9.15; Oren, 2001). Biomarker distributions indicative of the various metabolic pathways will likewise become salinity-related indicators in the rock record.

Life in a layered microbial mat?

The laminated sediments (biolaminites) that typify many evaporitic carbonates and described by sedimentologists using the general, and perhaps somewhat dated, terms algal mats and cryptogalaminites are in effect microbial "high rises," as are many living stromatolites (Chapter 1). They, and their entrained biomarkers, indicate the activities of an ecologically layered microbial community. As a mat surface accretes, its organic constituents are buried. The biochemical make-up of the initial halobiota, which flourished in the hypersaline conditions at or above the mat surface, is altered by the metabolic activities of various decomposers flourishing below.

In order to investigate early or syndepositional changes in the dominant organic constituents and the main diagenetic processes, Grimalt et al. (1992) studied organic profiles in cross sections through two different cyanobacterial mats in a modern marine-fed salina in southern Europe. Changes in lipid composition were compared to the vertical distributions of the various microbial populations. Vertical distributions in the lipid patterns were defined using enrichment cultures from typical species of cyanobacteria, diatoms, purple bacteria, sulphate-reducers and methanogens obtained from the layered mats.

Cyanobacteria *Phormidium valderianum* and *Microcoleus chthonoplastes* were the dominant primary producers in the sampled mats, they occurred almost as monocultures in the upper 6 mm of the mats (Figure 9.16). Worldwide, these and other cosmopolitan filamentous cyanobacterial photosynthesizers are the most obvious organisms in most mesohaline algal mats. Their chlorophyll creates a green layer a few mm thick beneath a sticky or slimy mucosic surface. As layers of these mucilaginous-sheathed cyanobacteria aggrade via periodic growth spurts, it creates biolamination (Chapter 1).

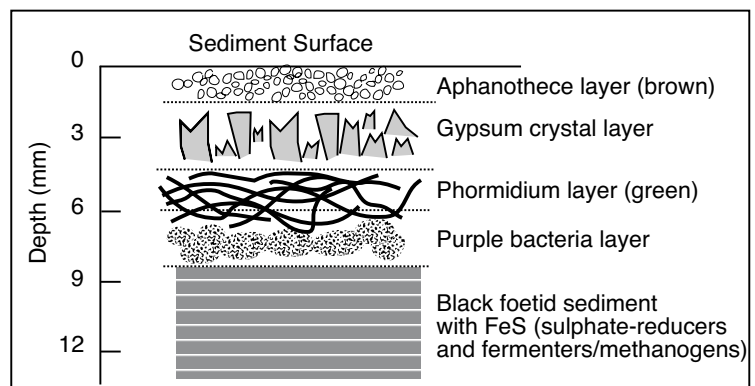


Figure 9.16. Typical microbial community in an evaporitic laminite in a modern coastal salina with salinity in the range 130 to 200 ‰ (after Caumette, 1993).

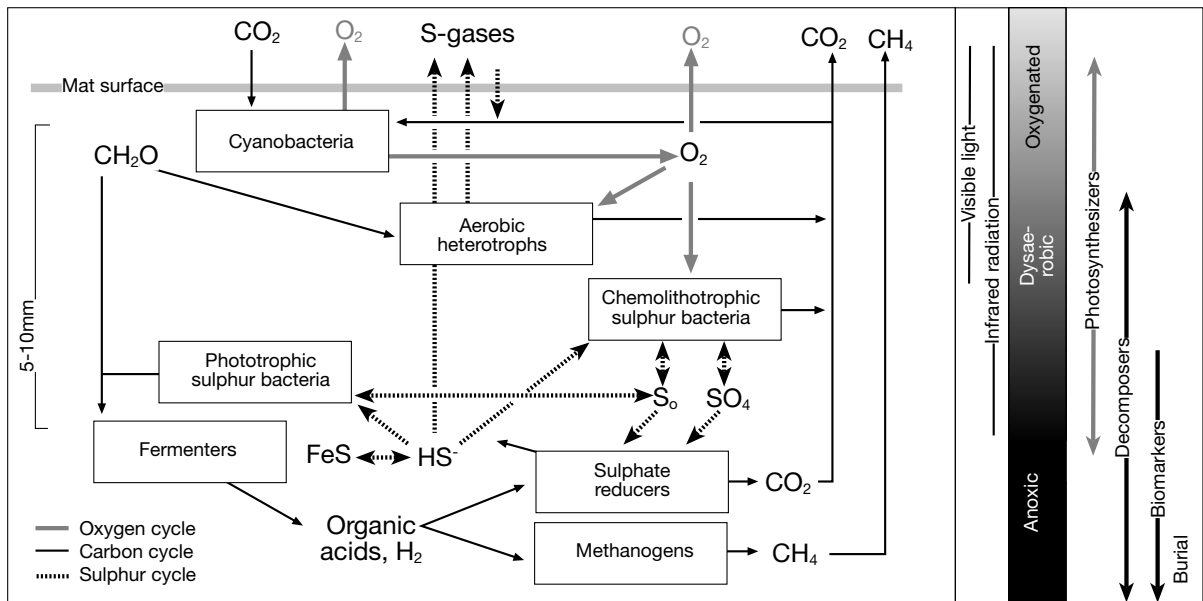


Figure 9.17. Inter-relationships between microbes and the oxygen, carbon and sulphur cycles in the uppermost 5-10 mm of a microbial mat. The oxic-anoxic transition shifts lower in the mat in the daytime and higher in the mat at night (photosynthesis has stopped).

Below the cyanobacteria is a layer of aerobic to dysaerobic heterotrophs (bacteria and archaea), which in the presence of oxygen break down the organic materials produced by the living cyanobacteria (mostly abandoned algal sheaths and slime; Figure 9.17). But because oxygen is only produced by photosynthesis, these organisms can only perform this process during daylight. The next layer below is dominated by chemolithotrophic sulphur bacteria, these are lifeforms that use the redox energy contained in the biochemical gradient between reduced sulphur compounds produced by sulphate reducers (below) and oxygen produced by the cyanobacteria (above). Utilising this redox gradient these purple sulphur bacteria synthesize organic matter and create the characteristic purple-orange layer seen below the green layer in an aggrading microbial mat. Because they can only metabolise in a suitable redox gradient, they need to locate themselves exactly within this gradient, so they are typically the most motile forms in a microbial mat. The redox gradient lies deeper in the mat community during the day due to oxygen production by the cyanobacteria, but it rises and can even reach the mat surface in the dark of night (Figure 9.18). Below the chemolithotrophs are the phototrophic sulphur bacteria. They are anaerobic photosynthesizers that fix sugars by utilising the infrared portion of the light spectrum as they convert sulphide to sulphate. Infrared radiation penetrates deeper into microbial sediment than the visible light used by the cyanobacteria.

Below them are the sulphate reducers, fermenters, and methanogens (Figure 9.17). Fermenters are relatively inefficient decomposers and do not completely break down the organics but break them into alcohols, lactates and other compounds exploited by other decomposers. During the day the sulphate reducers metabolise organics deep in the microbial mat via anaerobic respiration utilising a variety of chemicals including manganese, nitrate, sulphate and even CO_2 . At night they rise somewhat with redox gradient and at times of prolonged bottom brine anoxia and brine column turbidity can even reach the mat surface or enter the lower parts of a density-stratified brine column (Figure 9.18; Des Marais, 2003). They are very important decomposers in most mesohaline microbial mats and give the lower parts of a mat its characteristic "rotten egg" smell. They generally consume up to a third of the organic carbon present in a typical mesohaline microbial mat.

Deeper in the mat are the methanogens. All are anaerobes and utilise simple compounds created by the fermenters (CO_2 and hydrogen, along with organic components such as methanol, acetic acid, formic acid and methylamines) to produce methane. This metabolic pathway produces little biochemical energy and is usually the "last resort" community and makes up the lowermost living layer in the microbial high-rise.

Grimalt et al. (1992) found that the uppermost layers, dominated by cyanobacteria, typically leave no more than minor traces in

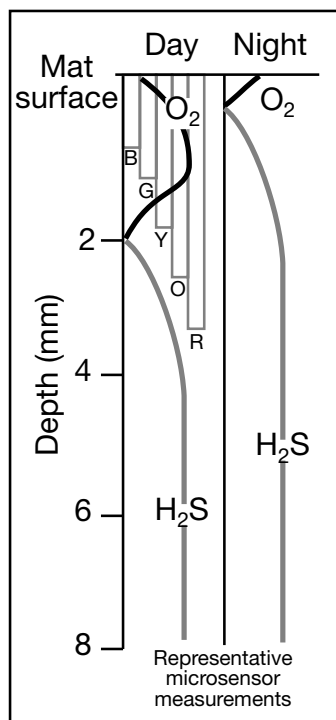


Figure 9.18. Schematic of vertical gradients of O_2 and H_2S during the day and at night. The vertical bars at upper left represent the relative depths of penetration of blue (B), green (G), yellow (Y), orange (O), and red (R) light. Profile is for a filamentous micritic mat. Profiles in filamentous and unicellular mats are qualitatively similar, although the depth scale (mm) of such profiles tends to be greater for unicellular mats. It will also be deeper in mats growing in an around clear crystals such as gypsum or halite, which act as light tubes (after Des Marais, 2003).

sediment at the base of benthic mat communities or within the brine column at the halocline of a density stratified brine body. Defining where halotolerant and halophilic decomposers lived in ancient microbialites is not possible from their organic signatures alone; it requires a sedimentological interpretation of the sediment matrix, which is usually a laminite. But, as discussed in Chapter 1, evaporitic laminites and biolaminites are subaqueous sediments with near identical textures beneath stratified and unstratified brines across water depths ranging from less than a metre deep to hundreds of metres.

the solvent-extractable lipids (biomarkers) in buried mat sediments. Rather, the predominant fatty acid distributions in the lower parts of a mesohaline mat sediment parallel the compositions observed in the enrichment cultures of purple bacteria and appear to be mixed with acids characteristic of heterotrophic bacteria, including purple bacteria and sulphate-reducers. In other words, the organic signatures, even as the mats were accumulating a few millimetres above, were those of the decomposers not the primary producers. This implies that many biomarkers used to typify organic production in hypersaline settings typically do not come from organics of the primary producers but from the products of the decomposer community.

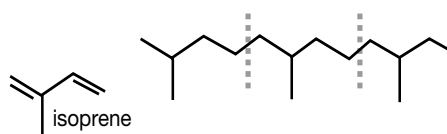
Anaerobic decomposers flourish within the

Biomarkers and microbial responses to changing salinities

Salinity-controlled transitions between a halotolerant and halophilic biota can be seen, indirectly in their organic residues and subsequent biomarkers. Biomarkers can be thought of as molecular or chemical fossils with a basic carbon skeleton derived from once-living organisms. Biomarkers are found in all modern sediments, as well as in petroleum and rock extracts and can provide information about species diversity, depositional environment, thermal maturity, migration pathways and hydrocarbon alteration (Table 9.4; Brocks and Summons, 2003; Peters et al., 2005).

Commonly accepted environmental generalisations based on biomarker distributions include the notion that variation in the ratio between the 96 isoprenoids pristane and phytane indicates oxidising versus reducing conditions (this assumes pristane and phytane are both breakdown products of chlorophyll). In an oxidising environment the cleavage of the phytol side chain of chlorophyll is followed by decarboxylation to produce phytane (Figure 9.19a). In a reducing environment the sidechain cleavage of chlorophyll is followed by its reduction to ultimately produce pristane. Low pristane/phytane ratios are thought to indicate reducing conditions, while higher values (>1) indicate oxidising conditions (Table 9.4). But Philp and Lewis (1987) have shown that the chemistry of chlorophyll breakdown is much more complicated in many natural systems and that variations in the ratio may also indicate varying inputs from the archaea, which contain much higher levels of phytane chains than bacteria. Values of pristane/phytane less than 0.5

⁹⁶Isoprenoids are a major class of nonsaponifiable lipids that occur in plants, animals, and bacteria and are characterized by chains of modular groups of five carbon atoms in which the typical pattern has four of the carbon atoms in a linear chain and a single carbon attached at the carbon one position removed from the end of the chain. The term isoprenoid is derived from the name of the five-carbon, doubly unsaturated branched hydrocarbon isoprene, which could in principle be the simplest monomeric chemical precursor for this class of compounds.



Isoprenoids are also known as terpenes. Terpenes are usually grouped according to the number of isoprene (C_5H_8) units in the molecule: monoterpenes ($C_{10}H_{16}$) contain two such units; sesquiterpenes ($C_{15}H_{24}$), three; diterpenes ($C_{20}H_{32}$), four; triterpenes ($C_{30}H_{48}$), six; and tetraterpenes ($C_{40}H_{64}$), eight. The carotenoid pigments are the best known tetraterpenes in the geological realm.

Indication	Biomarker	Detail
Hypersaline	Gammacerane	High relative to C ₃₁ hopanes in oils derived from sources deposited under hypersaline depositional conditions. High values indicate stratified water column during source deposition (Sinninghe Damste et al., 1995).
	Pristane/phytane	Very low values (< 0.5) in oils derived from source rocks deposited under hypersaline conditions, indicates substantial contribution of phytane from halophilic archaea (ten Haven et al., 1987; 1988).
	C ₂₁ to C ₂₅ isoprenoids enriched in δ ¹³ C	C ₂₁ to C ₂₅ isoprenoids enriched in δ ¹³ C relative to biomarkers of phytoplanktonic origin consistent with halophilic archaea (<i>Halobacteria</i>) as the dominant source (Grice et al., 1998).
	2-methylhopanoids and the MTTC ratio	Specific polar side-chain groups and sometimes an additional methyl substituent at position 2 of the hopane skeleton as being largely of cyanobacterial origin (Summons et al., 1999). Cyanobacteria are commonplace in mesohaline waters and the MTTC ratio can be used to characterise cyanobacterial versus archaeal inputs. MTTC ratio is defined as 5,7,8-trimethylchroman/total MTTCs. (Peters et al., 2005).
Anoxic	C ₃₅ homohopanes	High relative to total hopanes in oils derived from source rocks deposited under anoxic conditions (Peters and Moldowan, 1993). Abundance of C ₃₅ homohopanes in oils (relative to C ₃₁ -C ₃₄ homohopanes) is correlated with source rock hydrogen index (Dahl et al., 1994).
	Pristane/phytane	>1.0 can indicate anoxic conditions, but the ratio is affected by many other factors (see text).
	Isorenieratane and derivatives	Presence in oil indicates anoxic photic zone during source rock deposition, these compounds are biomarkers for green sulphur bacteria (Summons and Powell, 1987).
	V/(V+Ni) Porphyrins	High = reducing conditions (Lewan, 1984).
	28,30-bisnorhopane	High in certain reducing environments (Schoell et al., 1992; Moldowan et al., 1994).
Lacustrine	Botryococcane	Presence = lacustrine source. Absence = meaningless (e.g., Moldowan et al., 1985).
	β-Carotane	Presence = lacustrine source. Absence = meaningless (Jiang and Fowler, 1986).
	Sterane/Hopanes	Low in oils derived from lacustrine source rocks. (Moldowan et al., 1985).
	C ₂₆ /C ₂₅ tricyclic terpanes	> 1 in many lacustrine-shale-sourced oils (Zumberge, 1987).
	Tetracyclic polyprenoids	High in oils from freshwater lacustrine sources (Holba et al., 2000).

Table 9.4. Depositional significance of selected biomarkers.

may indicate hypersaline conditions where archaea dominated (Grice et al., 1998).

Differences in the distribution of n-alkanes are also thought to indicate depositional differences in the organic contributors. Waxes in higher plants have significant concentrations of the long chain C₂₂₋₃₆ alkanes^{9.7} with a pronounced odd/even distribution, such organics tend to be relatively rare in evaporitic source rocks, unless surface waters were freshened by periodic runoff from the land. Much of this terrestrial organic material is oxidized and biodegraded before it makes it to the

^{9.7} Aliphatic hydrocarbons are any chemical compound belonging to the organic class in which the atoms are not linked together to form a ring. They are divided into three main groups according to the types of bonds they contain: alkanes, alkenes, and alkynes. Alkanes (n-alkanes) have only single bonds and a continuous chain structure, alkenes contain a carbon-carbon double bond, and alkynes contain a carbon-carbon triple bond. Aromatic hydrocarbons are classified as either arenes, which contain a benzene ring as a structural unit, or non-benzenoid aromatic hydrocarbons, which are characterized by special stability but which lack a benzene ring as a structural unit.

final site of deposition on the brine pool floor. In contrast a high algal input is thought to be characterised by n-alkanes in the C₁₆₋₁₈ region.

At its simplest, much of the utility of biomarkers in saline environments comes from salinity-related differences in contribution to organic matter of the general categories of primary producers (autotrophs), namely prokaryotes (cyanobacteria and bacteria) and eukaryotes (higher plants, algae) and archaea. Most triterpanes are associated with prokaryotic sources, whereas steranes tend to be produced by eukaryotes. Thus, the triterpane/sterane ratio can be a rough measure of the prokaryote/eukaryote contribution to the organic material. As salinity increases, the less salinity-tolerant eukaryotic organisms (mostly green algae) give way to more halotolerant bacteria and cyanobacteria (tricyclic and ^{9.8}hopane producers) with a corresponding increase in the triterpane/sterane ratio (e.g. Summons et al., 1999). Thus high alkalinity/salinity settings are characterised by tricyclics (C₂₀-C₂₄; m/z 191), β-carotene (C₄₀H₅₆ compound; m/z 125) and gammacerane (C₃₀ triterpane;

m/z 191), all with prokaryote sources. Hence, high levels of gammacerane and β -carotene in ancient organic signatures are typically associated with nonmarine highly saline environments (Peters and Moldowan, 1993; Peters et al., 2005).

Lipids, entrained as organic residues in modern evaporitic carbonates and gypsums from modern saline pans (mesohaline and lower penesaline waters), are mostly derived from heterotrophic bacteria acting on cyanobacteria and green algae (Figures 9.16, 9.17). The resulting n-alkane distributions show a high predominance of n-docosane. In the modern evaporitic carbonate domain (mesohaline), the C_{20} highly-branched isoprenoid olephines, tetrahymanol (from bacterivorous ciliates) and large amounts of phytol are precursors to most lipids found in buried evaporitic sediments. In contrast, the main lipid contributors to organics preserved in modern halites and bittern beds are the extremely halophilic archaea and their organic signatures are enriched in the isoprenoids, especially phytane (Table 9.4; Barbé et al., 1990; Wang, 1998).

Likewise, Waples et al. (1974) and ten Haven et al. (1986), noted that Tertiary sediments deposited in many saline evaporitic lagoons retain high concentrations of regular C_{25} isoprenoids. They related it to the activities of the photolithotrophic *Chlorobiaceae* sp., an anaerobic green sulphur bacteria, known to flourish at the halocline of modern saline lakes. It is thought to have flourished in similar stratified settings in ancient mesohaline to hypersaline seaways. Its biochemistry leads to the preservation of a series of 1-alkyl-2,3,6-trimethyl benzenes, thought to be derived from the breakdown of its aromatic carotenoids in sulphate- and sulphide-rich brines (Summons and Powell, 1987). Ten Haven et al. (1988) went on to propose that there are a number of biomarkers indicating likely hypersalinity at the time of deposition including; short sidechain steranes, $5\alpha(H)$, $14\beta(H)$, $17\beta(H)$ pregnanes and homopregnanes, as well as high gammacerane indices (gammacerane/ C_{30} hopane). Gammacerane is a pentacyclic C_{30} triterpane thought to be a diagenetic alteration product of tetrahymanol (Table 9.4). The principal source of tetrahymanol are bacterivorous ciliates, such as

protists like *Tetrahymena*. Thus the presence of tetrahymanol is not restricted to any particular environment but the presence of tetrahymanol (and its daughter gammacerane) in large amounts suggests the presence of a stratified water column and possibly hypersalinity in the depositional setting (Table 9.4; Sinninghe Damste et al., 1995; Peters et al., 2005 p.576).

For Archaea, the cell membrane itself, due to its high thermal stability, is a good candidate for a biomarker. Archaeal cytoplasmic membranes do not contain the same lipids that prokaryotes and eukaryotes do. Instead, their membranes are formed from isoprene chains (ether lipids) made up from C_5 isoprenoid units (as for the side chains of ubiquinone) rather than C_2 units (ester lipids) in the normal fatty acids of the non-archaea (Figure 9.19b). Halophilic Archaea do not have fatty acids, rather the cell wall is constructed of lipids, mainly of glycerol, connected to phytanyl chains some twenty carbons in length by ether bonds to form phytanylic diether. Typically these are organized in bilayers that make up the cell wall. In the case of archaea living in extreme conditions, two glycerol molecules can be connected to a double chain of phytanol to create a tetraether structure of forty carbons (Figure 9.19c). Phytane-rich isoprene derivatives indicative of ancient archaea have been found in Mesozoic and Palaeozoic evaporitic sediments, and more generally in older Precambrian sediments (Hahn and Haug, 1986). Interestingly, their chemical traces have even been tentatively identified in sediments from the Isua district of west Greenland, the oldest known sediments on Earth, some 3.8 billion years old. Biomarker evidence for green and purple sulphur bacteria is found in Palaeoproterozoic marine sediments from northern Australia in the form of a new carotenoid biomarker - okenane (Brocks et al., 2005).

Bacterioruberin constitutes the purple patches in the archaeal cell wall and we have already discussed its stability with respect to high temperatures in the living environment. It may well constitute an excellent as yet unrecognised biomarker for haloarchaea in ancient evaporitic sediments that were precipitated in moderate to extreme salinities (Brocks and Summons, 2003). The likely fossil equivalent of bacterioruberin is perhydro-bacterioruberin, but it has yet to be discovered in geological samples. However, it is worth bearing in mind that some high-molecular weight biomarkers may have escaped detection because they are difficult to analyse using conventional GC-MS methods.

^{9.8}Hopanooids are a group of compounds (triterpenoids) produced by prokaryotic organisms, and the diagenetic alteration products of these compounds (found in oils, rock extracts and sediment extracts). Just as steroids (steranes) are a useful group of biomarkers for identifying input from various eukaryotic organisms (e.g., plants and animals), an analogous group of compounds, hopanooids, are a useful group of biomarkers for identifying input from various bacteria. Hopanooids serve the same function in bacteria as sterols do in eukaryotes: they act as cell wall rigidifiers. In petroleum and its source rocks, hopanooid biomarkers exist as a subset of a group of compounds called triterpanes (isoprenoids).

Do biomarkers indicate hypersalinity?

Work in modern hypersaline systems clearly shows that archaea and bacteria can both flourish as heterotrophs in upper penesaline and supersaline waters at salinities higher than 200-250‰ and that cyanobacteria and some green algae can still survive and grow at these salinities (Caumette, 1993; Olivier et al., 1994). Hence, respective biomarker signatures in ancient counterparts will not be mutually exclusive and none of the biomarker indicators listed in Table 9.4 are exclusive indications of hypersalinity.

Also, some of the widely used biomarker-derived maturity indicators for low maturity oils, such as low levels of diasteranes, T_s/T_m ratios < 1, somewhat low homohopane and sterane isomerization values, all historically derived from studies in ancient marine settings, are not as reliable when applied to relatively young saline-lacustrine oils, such as those sourced from hypersaline Oligocene laminites in the northern Qaidam Basin, China (Hanson et al., 2001). These sediments and their outcrop equivalents have vitrinite reflectance values in the range 0.68 - 1.0, all within the oil window (Figure 9.1). The discrepancy between mature indications coming from vitrinite studies and the immature indications derived from various sterane isomerization ratios in these young hypersaline-sourced oils are perhaps explained by a lack of time for various sterane equilibria to develop. Some of these hypersaline oils come from hydrogen-rich type I lacustrine source sediments in the Qaidam Basin fill that may be as little as 3 million years old. But some other so-called maturity indicators, such as the low levels of diasterane probably are better tied to deposition of the source

organics in noncarbonate shales accumulating in hypersaline waters (Philp et al., 1991).

The fluctuating salinities that controls life in the depositional setting of all modern and ancient evaporites means that there is no simple single biomarker indicator for hypersalinity in any ancient sediment. For example, the 2-methyl hopanoids are thought to indicate a cyanobacterial association (Table 9.4) and cyanobacteria are commonplace in mesohaline waters. But the presence of cyanobacteria and hence 2-methyl hopanoids

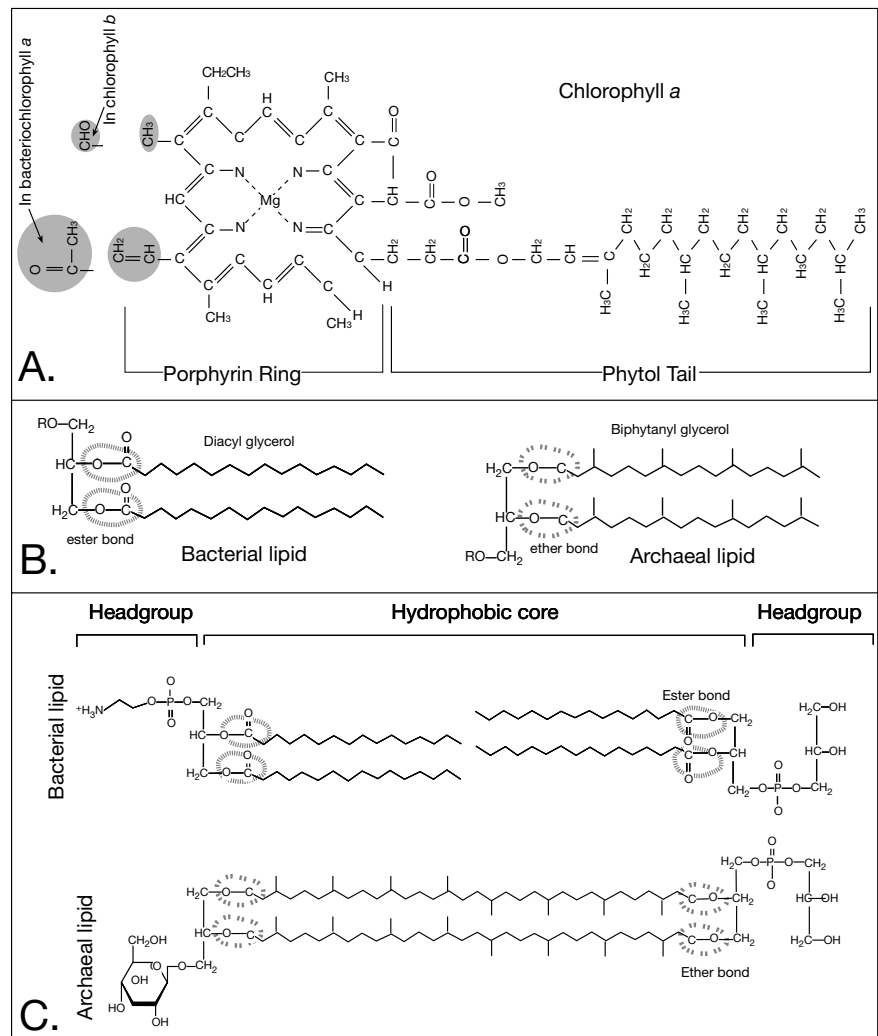


Figure 9.19. Various molecular structures. A) Chlorophyll a structure showing porphyrin ring and phytol tail. Alternate structures from bacteriochlorophyll a and chlorophyll b. B) Phosphatidylanolamine forms a bi-layer lipid in bacterial cells. The acyl chain is usually, but not always straight. Some bacterial lipids have a methyl branch of a cyclohexyl group at the end of the acyl chain, other lipids have one or more unsaturated bonds and the connection of glycerol to the acyl chain is via an ester linkage. C) Lipids are monolayers in Archaea and the phytanyl chain contains isoprenoid-like branches. An ether linkage connects the phytanyl chain. Archaeal membranes also contain bilayer-forming diether lipids.

are not limited to this setting. Likewise, the pentacyclic triterpenoid gammacerane is present in trace amounts in almost all bitumens and oils, but tend to be more abundant in sediments that were deposited under a stratified water column. This is a hydrological condition that is typical of, but not exclusive to, hypersaline lacustrine settings (Sinninghe Damste et al., 1995). A similar argument can be made for low pristane/phytane ratios that are used as indicators of both reducing conditions (assumes a chlorophyll precursor) and halophilia (assumes an archaeal precursor).

All biomarker signatures are indirect and somewhat ambiguous indicators of hypersalinity via assumptions of the relative make-up the original primary producers. In addition all traces of biomarkers from the primary producers preserved in ancient strata have been overprinted by the effects of syndepositional decomposers and likely subsequent mixing from various sources during catagenesis. The overprinting effects of the decomposers in microbial laminites are clearly seen when molecular characteristics of modern hypersaline sediment from the Ejnür salt lake (northern China) are compared to Tertiary (Eocene) core samples from Qianjiang Formation (hypersaline lacustrine) of Jiangnan Basin, central eastern China (Figure 9.20a; Wang et al., 1998). N-alkanoic acids in saline sediments from both areas (Ejnür and Jiangnan) show a pronounced even-over-odd predominance (EOP) and a bimodal distribution. In the lower molecular weight range, the C_{16} and C_{18} components are prominent, with the former dominant. For higher homologues (greater than or equal to C_{20}), docosanoic (C_{22}) and tetracosanoic (C_{24}) acids dominate the n-alkanoic acid homologues in the Jiangnan and Ejnür samples, respectively. Alkanoic acids with an isoprenoid skeleton are more abundant in Jiangnan samples, including C_{20} , C_{21} , C_{24} , C_{25} and C_{30} homologues, with a C_{25} component (3,7,11,15,19-pentamethyleicosanoic acid) most pronounced in the lower part of the Qianjiang Fm. The carbon skeletons of these isoprenoid acids in both units are attributed to archaeal decomposers.

Iso and *anteiso* branched carboxylic acids are prevalent in both the Ejnür samples and in the upper portion of the Qianjiang Formation. They derive from bacteria, probably sulphate-reducing bacteria, and their abundance clearly shows once again the importance of bacterial decomposers, along with haloarchaea, to the biochemical signature of organic matter in modern and ancient saline lake sediments. The presence of hopanoid acids and a 3-carboxy steroidal acid further attest to contributions from bacterial and eukaryotic sources, respectively. The occurrence of particular carboxylic acids in the Jiangnan samples illustrate these compounds, indicators

of halotolerant and halophilic decomposers, can survive as biomarkers in hypersaline source rocks.

Across a broader time and geographic scale, acyclic isoprenoid hydrocarbons are the dominant components in organic matter extracted from sedimentary cores and oils sampling various hypersaline settings in China; the results encompass the Tertiary Jiangnan salt lake basin, the Cretaceous Taian salt lake basin, and the Triassic, Permian and Cambrian Yangtze evaporitic marine platforms (Wang, 1998). Inland saline lake basins in China such as Jiangnan and Songpu are characterized by a tremendous predominance of phytane (C_{20}), which ranges up to 15% of the total extract. The evaporitic marine sediments are also unique in retaining a complete series of super-long-chain acyclic isoprenoids, up to C_{40} (Figure 9.20a). These isoprenoids in the marine evaporites possess head-to-head, tail-to-tail or regular linkages that indicate significant contribution from various archaea to the biomarker signature, i.e. a mixed archaeal contribution from halophiles, methanogens and acidothermophiles. Based on the split in distribution and composition of isoprenoids between the inland salt lakes and the evaporitic marine platform settings, Wang (1998) concluded that the archaeal biota in modern and Cenozoic inland salt lake sediments of China are likely dominated by halophilic archaea, while the halobiotal signatures of Mesozoic and Palaeozoic evaporitic marine sediments were predominantly those of methanogens and acidothermophiles. He also found that the concentration of the various chlorine salts in the sediments is more directly proportional to the abundance of phytane than to sulphate, once again indicating the dominance of halophilic archaea in waters at the halite precipitation stage. He also noted that reduced species of sulphur, sulphide and organic sulphur compounds in the anoxic brines played a key role in the preservation and formation of the abundant phytane in these inland salt lake basins.

A predominance of degraded green algal and cyanobacterial biomarkers in mesohaline settings can be recognised in biomarkers preserved in even older, but organically immature, evaporitic source rocks. The degree of methylation of 2-methyl-2-trimethyl-tridecylchromans (MTTCs) and the abundance of maleimides and bacteriochlorophylls implies a euhaline to mesohaline (≥ 30 -40‰) marine-fed setting for the accumulation and preservation of organics during Kupferschiefer sedimentation in the Permian of NW Europe (Figure 9.20b; Bechtel and Puttmann, 1997; Pancost et al., 2002). These biomarkers are thought to be derived from green/purple sulphur bacteria (decomposers) within organic-rich laminites and suggest that the bottom waters were saturated with H_2S at the time of deposition. Maximum water depths were probably less than 100 metres

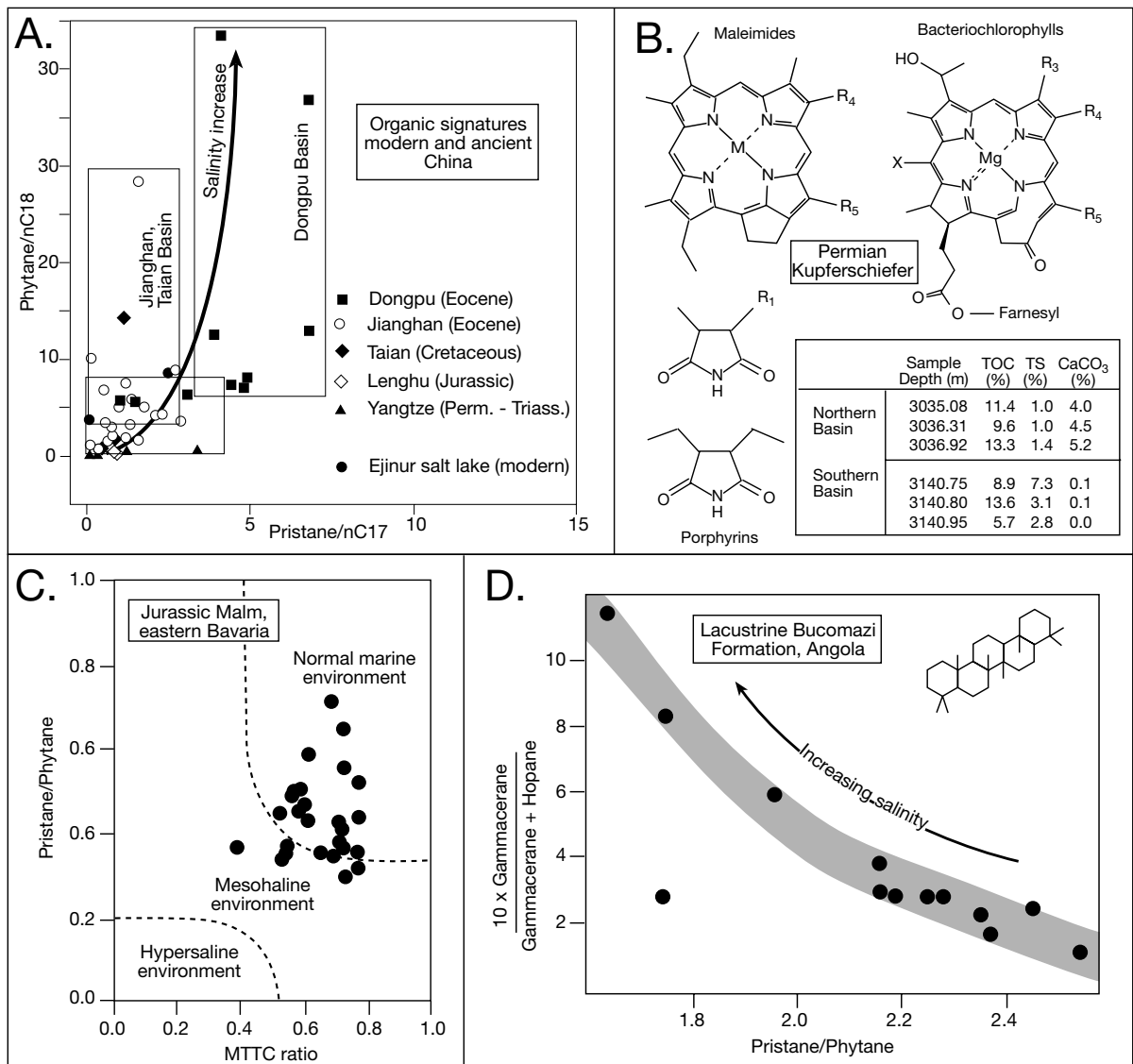


Figure 9.20. Biomarkers. A) Cross plot of Pristane/nC₁₇ versus Phytane/nC₁₈ ratios for various saline/hypersaline settings in China (after Wang, 1998). B) Structure and properties of representative bacteriochlorophylls, maleimides and porphyrins from source rocks in the northern and southern Zechstein basins, offshore NW Europe (after Pancost et al., 2002). Compare with primary structures shown in Figure 9.19a. C) Relationship between pristane/phytane and the methyltrimethyltridecylchroman (MTTC) ratio in Jurassic Malm carbonates of eastern Bavaria (after Schwark et al., 1998). The MTTC ratio is defined as 5,7,8-trimethylchroman/total MTTCs. D) Variations in pristane/phytane ratio and the gammacerane index for oils from lacustrine source rocks in Angola (Inset shows gammacerane structure). Independent biomarker evidence suggests a marine source for the point that lies off the shaded trend (after Peters et al., 2005).

(it was a stratified mesohaline drawdown basin at the onset of Zechstein salinity; see Chapter 5). Decomposers probably lived near the brine boundary between the photic zone and the anoxic (euxinic) bottom water at typical water depths of 10-30 metres below the water surface, as in modern marine-fed density-stratified systems, much like in Lake Mahoney today

(Figure 9.28). Primary production in the upper water column was dominated by photosynthetic cyanobacteria or green algae, while sulphate reduction in the sediment was tied to the availability of abundant sulphate and organic detritus from the overlying water column.

Methanogenesis was also active during Kupferschiefer deposition. This is reflected in the light carbon isotopic composition of organic matter that had originated via recycling of CO₂ generated by methane-oxidizing bacteria in the water column (Bechtel and Puttmann, 1997). Saccate pollen is the only morphologically preserved body fossil in organic matter within this laminated Kupferschiefer sediment, all other traces of cellular morphologies are gone. Euxinic conditions were confirmed by Pancost et al. (2002) over a much larger area of Kupferschiefer deposition than studied by Bechtel and Puttmann. They concluded that almost all of the Kupferschiefer seaway was subject to periods of photic zone euxinia and stratification during the early mesohaline history of the Zechstein Sea.

By themselves, high pristane/phytane ratios, high amounts of gammacerane, and MTTC ratios are not totally reliable indicators of hypersalinity. More reliable determinations can be made when two or more of these biomarkers are crossplotted and the resulting output shows a consistent trend. Figure 9.20c plots pristane/phytane ratio against the MTTC ratio in the Jurassic Malm Zeta laminites of eastern Bavaria in SW Germany (Schwark et al., 1998). The output shows a covariant decrease in the two measures which is interpreted as indicating a trend from normal marine to mesohaline deposition.

A similar covariant trend can be seen in saline lacustrine source rocks when the pristane/phytane ratio is crossplotted against the gammacerane index in mesozoic source rocks from the offshore of west Africa (Peters et al., 2005). Figure 9.20d plots variations in pristane/phytane (a redox and archaeal indicator) and gammacerane index (an indicator of salinity stratification in saline waters) for oils from a set of lacustrine source rocks. Increasing salinity in the depositional setting explains the covariant trend in the plot, whereby higher salinity was accompanied by density stratification and associated reduced oxygen levels in bottom waters. Independent biomarker evidence suggests a marine source for the point that plots off the shaded salinity trend in this figure (after Peters et al., 2005).

Although the levels of entrained organics are very low, similar covariant trends in pristane/phytane and gammacerane occur in C₂₁₋₂₅ isoprenoids, along with relatively heavy δ¹³C signatures, in biomarkers extracted from the Miocene halites of the halokinetic Sedom Formation in Israel. They indicate a predominance of halophilic archaea when the salt was deposited in a CO₂ limited system (Grice et al., 1998; Schouten et al., 2001).

In addition to the signature from their particulate organics, modern brines can also contain large amounts of dissolved organic matter (DOM), with levels that increase with increasing salinity (Hite and Anders, 1991). This liquified organic is

often entrained within brine inclusions in halite and other salt crystals and is not picked up in standard TOC determinations. Levels of volatile fatty acid (VFA), especially acetic acid, are also high in these saline brines. The relative contribution of DOM to the source potential is poorly understood in subsurface evaporitic systems where crossflowing basal brines are dissolving buried halite.

Organic enrichment

The amount of organic matter preserved in an evaporitic sediment, with the potential to become a source rock, is a function of three factors as expressed in the equation (Bohacs et al., 2000):

$$\text{Organic Enrichment} = (P - De)/(Di)$$

where P is production, De is destruction and Di is dilution.

Maximum enrichment occurs when production is maximised and destruction and dilution are minimised. Production at mesohaline salinities is mostly via photosynthetic fixation of CO₂. It includes autochthonous organic matter, formed at or near the site of accumulation and derived from algae, bacteria and aquatic plants, as well as allochthonous organic matter carried in during floods (Bohacs et al., 2000). Katz (1990) showed that varying levels of solar input and water chemistry/stratification exert the largest effects on overall primary production in mesohaline settings. Initial destruction of organic matter is mostly a function of the efficiency of the various scavengers and grazers, which is typically a function of the availability of oxygen (Demaison and Moore, 1980). In increasingly saline settings, bacteria then archaea dominate the scavenger/decomposer population, while the health of the metazoan grazers is largely inhibited by higher salinities (with the possible exception of brine shrimp). Dilution by an influx of minerals to a possible area of organic enrichment can limit levels of organic enrichment by decreasing the proportion of organic matter relative to inorganic matrix. The source of dilution can be detrital clastics or evaporite precipitates.

Dissolved gas levels and temperature changes associated with heliothermal bottoms can create extreme levels of environmental stress in communities attempting to cope with hypersalinity. For example, oxygen is supplied to any water body via exchange with the atmosphere and as a byproduct of photosynthesis of the biota living in the waters. In well-oxygenated water columns most of the organics produced by primary production are de-

stroyed by microbial respiration and the conversion of organic matter back to CO_2 . Much of the improved preservation potential associated with “higher than marine” bottom salinities in mesohaline to hypersaline settings on biotal diversity reflects the effect of increasingly low levels of dissolved oxygen in the bottom and pore waters. Oxygen levels in natural brines tend to decrease with increasing salinity (Figure 9.21a). If not enhanced by the activities of bottom-living aerobic photosynthesizers, natural bottom brines will be dysaerobic to anaerobic by the time salinities reach halite saturation (Kinsman, 1973; Warren 1986). Likewise, all artificial NaCl solutions hold less O_2 at higher salinities and temperatures (Figure 9.21b).

Dissolved CO_2 shows a similar depletion in nutrient-poor waters characterised by little biological activity. Dissolved CO_2 levels in marine-fed modern salt pans decrease to around 50% of the original value as the brine concentration increases from 1.5 to 4 times that of seawater (Lazar and Erez, 1992). CO_2 concentration in brine is also pH dependent; CO_2 content approaches zero in a marine brine at a pH of 8.5-9.0, which is the alkalinity of a brine with a salinity around 70‰ (Moberg et al., 1932). Likewise, measurements of CO_2 in the Dead Sea in 1992 showed its solubility was about 20% of seawater (Barkan et al., 2001). Algae and cyanobacteria, which are dependant on CO_2 for photosynthesis, will suffer shortages at higher salinities.

There can also be increased thermal stress in increasingly hypersaline water bodies. The specific heat of a brine decreases as the salinity increases (Kaufmann, 1960). For example, when the salinity of the surface waters of the Dead Sea increased from 210‰ in the 1940s to 275‰ in the early 1980s, the specific

heat decreased from 3,085 J/kgK to 2,985 J/kgK (Niemi et al., 1997; p. 127). Specific heat is the amount of heat needed to raise one gram of a substance by 1°C. For a given amount of heat input, a unit volume of hypersaline water will show a greater increase in temperature than a less saline water. The resulting greater increase in temperature in a hypersaline water compared to a less saline water can detrimentally effect many thermally-intolerant species. Given the same degree of insolation, it also means density-stratified water columns are heliothermic, with bottom brine tending to be hotter than fresher surface waters. The differences can be substantial, with bottom waters approaching temperatures of 60°C in some

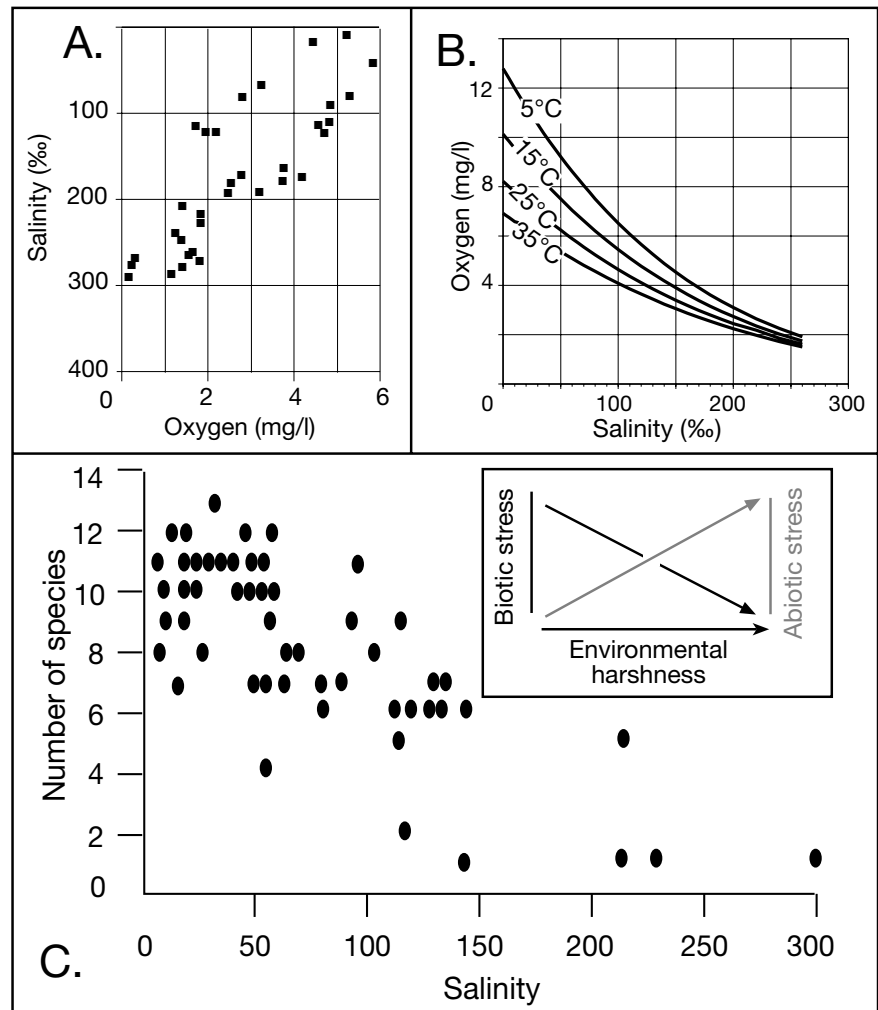


Figure 9.21. Biodiversity and oxygen levels in modern hypersaline settings. A) Measured oxygen levels in present-day surface brines under increasing salinity. Oxygen content of modern seawater ≈ 5.4 mg/l (after Warren, 1986). B) Predicted oxygen values for pure NaCl solutions (replotted from Table 2 in Sherwood et al. (1992)). C) The effect of increasing salinity on metazoan species diversity in the saline lakes of the Coorong region, South Australia (after De Decker and Geddes, 1980).

density-stratified perennial desert lakes such as Solar Lake in the Sinai (Figure 2.48).

An even more interesting association of halophilic microbes comes from the heliothermal lakes of the Vestfold Hills in Antarctica where three hypersaline lakes, Organic Lake, Ekho Lake and Deep Lake, have been studied in some detail (Bowman et al., 2000). The lakes are subsealevel relics of an earlier marine embayment, isolated from the ocean by uplift some 6 ka, but still receiving salt input via marine aerosols. Organic Lake is a shallow meromictic brine lake with waters as much as 7.5 metres deep and an oxycline at 4-5 m. Its surface waters are moderately saline (8 g/l) and their temperature fluctuates between -14 to +15°C. Bottom waters are perennially saline with a TDS of 210 g/l and a near constant temperature of -7°C. Ekho Lake is 42 m deep, meromictic and heliothermally heated with bottom waters maintaining a year-round temperature of 15-16°C. Salinities range from 14 g/l at the surface down to 160-180 g/l on the lake bottom, which is permanently anoxic below an oxycline at 12-20m. The most hypersaline lake is Deep Lake. Its waters are upto 36 m deep, but unlike the other two lakes it is holomictic and aerobic all the way down to the sediment-water interface. Although salinities are around 320 g/l its water temperatures can be as low as -18°C. The biota in holomictic Deep Lake is almost 100% haloarchaeal and it is home to that very robust microbe *Halobacterium lacusprofundi*, (Franzmann et al., 1988; see earlier). The biotal make up of the two meromictic lakes is more complex with varying combinations of the Proteobacteria and Cytophagales. Ekho Lake also contains a number of the Haloanaerobiales, perhaps reflecting its warmer year-round bottom temperature.

But the dominant biomass control in hypersaline and supersaline environments, at least for most multicellular life, is not dissolved gas or even temperature, but the increase in osmotic pressure that comes with increasing salinity. At a concentration of 300‰, sodium chloride brine exerts an osmotic pressure on a cell of more than 100 atmospheres (Bass-Becking, 1928; Reed et al., 1984). Cells of species that typically inhabit marine or brackish waters quickly desiccate in such brines, leading to rapid death (e.g. Geddes, 1975b), hence the adaptations at the cellular level that typify halotolerant and halophilic organisms.

The tendency of bottom waters in many deeper hypersaline water masses to become anoxic, hotter, and osmotically pressured, has helped create many ancient lagerstätte associations (fossil “death communities”), with inherent excellent preservation of fine details in the entrained fossil forms. For example, the widely known Cretaceous Solnhofen micritic plattenkalk

of Bavaria preserves the feathers of the bird-like dinosaur *Archaeopteryx* and many “death-dance” trackways of finely preserved marine crustaceans that once wandered into the hypersaline and anoxic bottom water layers of the Solnhofen lagoon. Similarly, the communities of chemosynthetic mussels, which inhabit nutrient-rich deep dark bottoms about the edges of modern anoxic brine lakes atop dissolving salt allochthons, can suffer mass extermination when sediment slumps occur and mollusc biostromes, carried along by the slump, end up in the anoxic H₂S-rich, death-dealing hypersaline waters of the brine lake (MacDonald, 1992).

High pore water salinities, extreme osmotic stress, a propensity for anoxia in the stratified bottom waters, anoxic pore brines and high bottom temperatures all tend to exclude aerobic burrowing and grazing animals from evaporitic bottom sediments. This minimises a biota that would otherwise oxidise and destroy microbial debris in similar sediments deposited beneath less saline waters.

Biological responses to variably layered brines: Cycles of “feast or famine”

Brines in modern evaporitic depressions are typically layered, with denser more saline waters supporting an ephemeral mass of less dense inflow water (Figure 2.37b). The bottom layer in a perennial brine system tends to be more stable compared to the upper and its physical condition changes little until stratification is lost via mixing of the two water masses (Figure 2.37b). Once mixing occurs the waters in the lake can completely evaporate. Conditions in the floating less dense upper layer are both ephemeral and variable, with wide fluctuations in salinity before desiccation or mixing. When salinities are lowered, this upper layer periodically supports a widespread planktonic bloom (feast). Then, as ongoing evaporation concentrates the upper layer, conditions become increasingly less suitable for life (famine) and a mass die-off occurs, first of the haloxene species, then the halotolerants, then the halophiles. The bloom and the following dieback creates a pulse of organic matter that can swamp the abilities of the anaerobic decomposers in the lower water column to strip it of its hydrogen. Organics can then reach the sediment interface with their long-chain alkanes still largely intact. In conditions where light penetrates to the bottom of the brine column, even when the waters atop the sediment surface are oxygenated, the halotolerant primary producers can be sufficiently productive and the underlying anoxic decomposers sufficiently inefficient that substantial volumes of hydrogen-rich microbial matter can be retained into burial.

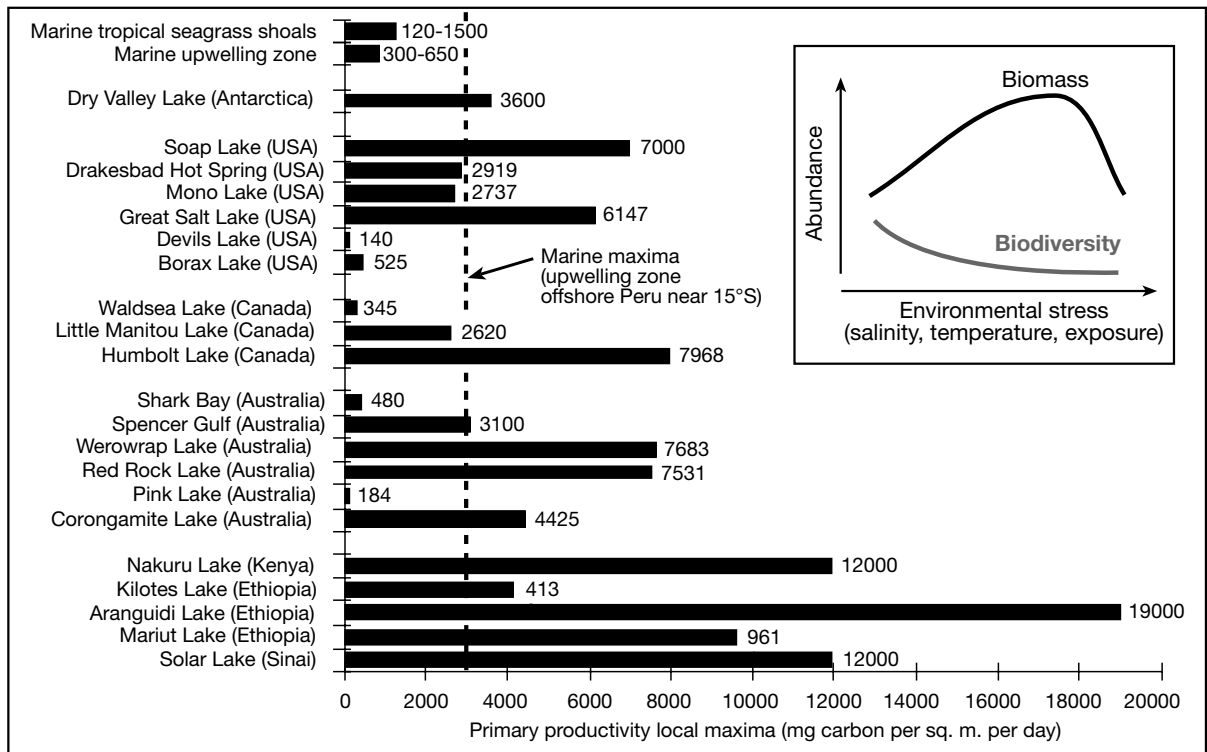


Figure 9.22. Organic productivity (maxima) in various saline ecosystems. Typical marine upwelling zone $\approx 250\text{-}500\text{ mg C/m}^2\text{day}$ (the dashed line is world marine maxima based on offshore Peru); tropical shoal water seagrass banks $\approx 500\text{-}1200\text{ mg C/m}^2\text{day}$; open marine waters are less than $100\text{ mg C/m}^2\text{day}$ and average $20\text{ mg C/m}^2\text{day}$ and coastal waters $40\text{-}50\text{ mg C/m}^2\text{day}$. But, preservation is more important than production rate in terms of source potential. Compiled from sources listed in Warren (1986) and this chapter.

When surface water salinities are suitable, evaporite basins have some of the highest measured rates of organic productivity in the world (Figure 9.22; Warren, 1986). When biodiversity is low and salinity is high, a proliferation of well-adapted species can generate productivity levels that are much higher than those observed in most nonevaporitic settings. These saline systems are indicative of general principles seen in all stressed ecosystems, namely, as the harshness or abiotic stress in a system increases the biotic stress decreases on a few well-adapted species (less predators and grazers). The total biodiversity (number of species) decreases, while at the same time the biomass (total mass of organisms in the system) initially increases (Garcia and Niell, 1993). Ultimately, it too declines as conditions become unsuitable for any life (see insets in Figures 9.21c and 9.22)

Salinity change influences organic productivity:
The flamingo connection in East Africa lakes

One of the most visually impressive indications of periodic but very high levels of organic productivity in a well adapted biota in a salinity-stressed layered water body resides in the

“flamingo connection.” This is a connection between flamingoes, mesohaline planktonic blooms and saline lakes, first noted in the geological literature for the east African rift lakes by Kirkland and Evans (1981) and well documented in Lake Nakuru by Vareschi (1982).

Flamingoes are filter feeders thriving on the dense halotolerant cyanobacterial blooms in the shallows of saline lakes around the world. Two species of flamingo flock in huge numbers in the East African rift lakes, namely, the greater and the lesser flamingo (*Phoenicoptus ruber roseus* and *P. minor* respectively), the lesser flamingo has spectacular pink-red coloration. These bright pink waders feed and breed in rift lakes where cyanobacterial blooms can be so dense that a secchi disc disappears within a few centimetres of the lake's water surface (Warren, 1986). Lake Natron is a major breeding ground for flamingoes in East Africa and is the only regular breeding site for the lesser flamingo in Africa (Simmons 1995). It has the highest concentration of breeding flamingoes in any lake in East Africa. Both the greater and the lesser flamingo are found there, with the lesser flamingo outnumbering the greater by a hundred to one. Lesser

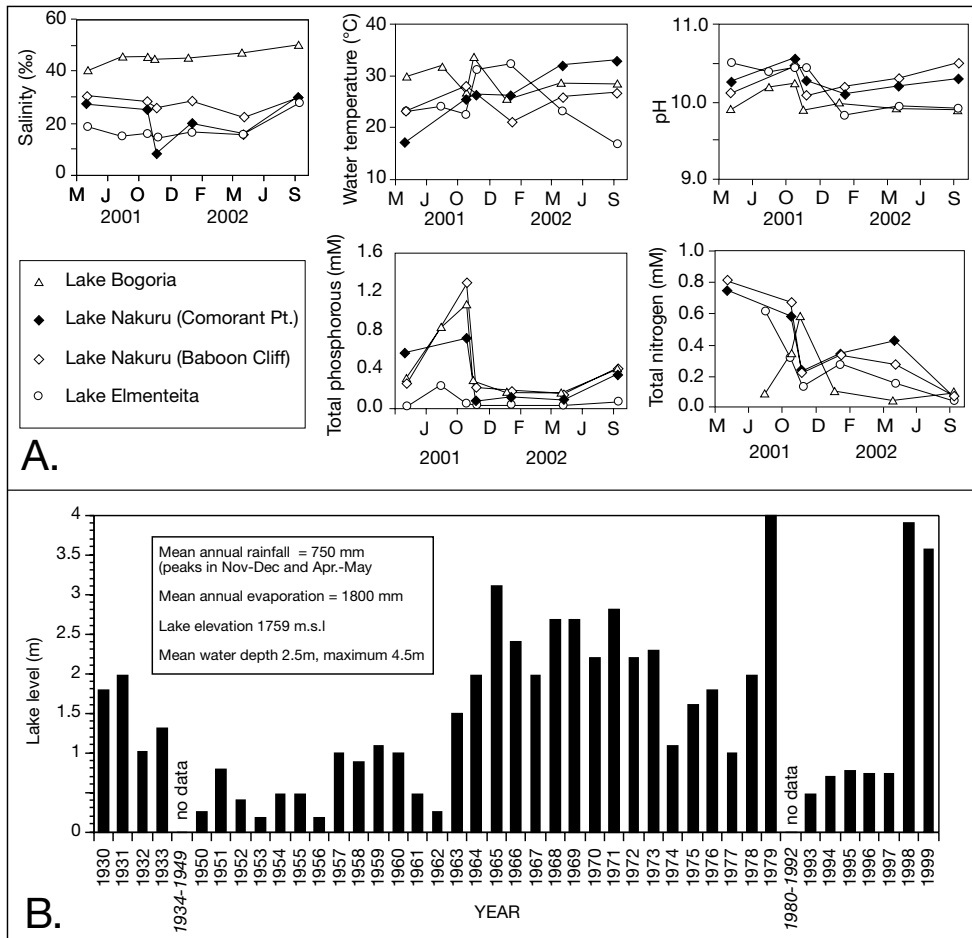


Figure 9.23. Physico-chemical features of saline African Rift valley lakes. A) Physico-chemical changes in soda lake water of the African rift valley lakes from June 2001 to September 2002 (after Ballot, 2004). B) Lake levels in Lake Nakuru from 1930 to 1999. Data are not sufficiently detailed to record times of complete lake drying or drought and there are also substantial times when no data were collected/published (1934-1949 and 1978-1992 (replotted from Vareschi, 1978).

flamingoes bred at Lake Natron in 9 out of 14 years from 1954 to 1967. But while Lake Natron is an essential breeding site, it is not a focal feeding site for flamingoes. Major feeding sites in the rift valley are Lakes Nakuru and Bogoria (formerly Lake Hannington) in Kenya, which are somewhat less saline and so have a greater abundance of mesohaline plankton, especially *Spirulina sp.* (Figure 9.23a). Lakes Nakuru and Bogoria have less than half the areas of Lakes Natron and Magadi, which in turn have small areas compared to most ancient lacustrine evaporites (Figure 5.3)

Millions of flamingoes typically consume more than 200 tons of plankton a day from Lake Nakuru, a shallow saline soda lake with a pH ≈ 10.5 and a typical annual salinity range of 5-30‰ (Figure 9.23a). The lake measures some 6.5 km by 10 km, with eutrophic waters in the lake centre up to 4.5 metres deep

(Figure 9.24a; Vareschi, 1978, 1979, 1982). The feeding style of the birds is to wade through the shallows, with head upside down and beaks waving side to side across the water surface. They are mostly nocturnal feeders and will feed for up to 12-13 hours in a 24 hour period.

The main phytoplankton component in Lake Nakuru waters is the cyanobacterium, *Spirulina platensis* (aka *Arthrospira platensis*). It is the main food component for the lesser flamingoes feeding in both Lake Nakuru and Lake Bogoria (Figure 9.25). In Lake Nakuru it is also consumed by one species of introduced tilapid

fish and one species of copepod and a crustacean. Rotifers, waterboatmen, and midge larvae also flourish in the waters of Lake Nakuru. The mouth-breeding tilapid *Sarotherodon alcalicum grahami* was introduced to the lake in the 1950s to control the mosquito problem and they have flourished ever since, at times displacing the flamingoes as the primary consumers of planktonic algae. Their introduction increased the number of fish-eating birds such as pelicans in the lake (Vareschi, 1978).

Flamingo beaks have evolved to filter plankton from saline to brackish surface waters and are equipped with a feeding system unlike any other bird on earth. By swinging their upside-down heads from side to side and using their tongues to swish water through their beaks, flamingoes siphon the

lake water through the beak filters to trap the cyanobacterium *Spirulina* and other plankton. Flamingoes can filter as many as 20 beakfuls of plankton-rich water a second. Spacings of the filters in the beak of the greater flamingo are wider than those in the beaks of the lesser flamingo. Greater flamingoes feed mostly on zooplankton, while lesser flamingoes feed almost solely on *Spirulina*, thus in any saline lake where the two birds co-exist they do not compete for the same food source.

Spirulina provides high levels of the red pigment phycoerythrin (a protein from the light-harvesting phycobilin family) to the food chain. It accumulates in flamingo feathers to give the birds their world famous coloration (hence the “flamingo connection”). This is not the same pigment that turns waters red in Lake Natron and Lake Magadi. Lesser flamingoes, with their narrower spacings of beak filters survive largely on *Spirulina*, and so have a more intense pink colour than greater flamingoes, a species that sits higher in the lake food chain and so get its feather colour second-hand from the lake zooplankton. As well as possessing very high levels of phycoerythrin in its cytoplasm, *Spirulina* is also unusual among the cyanobacteria in its unusually high protein content (some ten times that of soya). In Lake Chad, and in some saline lakes in Mexico, *Spirulina* accumulates as a lake edge scum that has been harvested for millennia by the local people (including the ancient Aztecs) and used to make nutritious biscuits. A lack of cellulose in the *Spirulina* cell wall means it is a source of plant protein readily absorbed by the human gut, making it a potentially harvestable food source in saline water bodies in regions of desertification.

In 1972 Lake Nakuru waters held a surface biomass of 270 g/m^3 and an average biomass of 194 g/m^3 but, as in most hypersaline ecosystems, Nakuru's organic production rate varies drastically from year to year as water conditions fluctuate (Figure 9.24b; Vareschi, 1978). *Spirulina platensis* was in a long-lasting bloom in 1971-1973, and accounted for 80-100% of the copious phytoplankton biomass in those years. In 1974, however, it almost disappeared from the lake and was replaced by much smaller coccoid cyanobacteria that dealt better with elevated salinities. When the relatively large filaments of *Spirulina sp.* dominate the lake plankton, a flamingo's beak filters between 64 and 86% of the plankton held in each mouthful of lake water (Vareschi, 1978). When the much smaller coccoids come to dominate the filters are much less efficient feeding mechanism. The change in plankton species is also tied to a serious reduction in algal biomass (and protein availability), which in 1974 was down to 71 g/m^3 in surface waters and averaged 137 g/m^3 in the total water mass. As a result the flamingo population feeding

in the lake declined from 1 million to several thousands and the flamingoes moved to other lakes where *Spirulina* were flourishing (Vareschi, 1978).

The lower salinity limit for a *Spirulina* bloom is $\approx 5\text{‰}$ and it does better when salinity is more than 20‰ . The species dominance of *Spirulina* and its higher biomass in somewhat more saline lake waters is clearly in the near unispecific year-round biomass of nearby Lake Bogoria (salinity 40-50‰). Its surface salinity is higher year round than Lake Nakuru (salinity $\approx 30\text{‰}$) and the somewhat fresher Lake Elmenteita (salinity $\approx 20\text{‰}$; Figure 9.23a). Because of this, Lake Bogoria is a more reliable food source for feeding flamingoes compared to either Nakuru or Elmenteita (Figure 9.25). Birds tend to migrate there to feed when conditions for *Spirulina* growth are not ideal in other nearby alkaline lakes (too fresh or too saline). This was the case in 1999 when high rainfall and dilution of lake waters caused the *Spirulina* levels to fall in both Nakuru and Elmenteita.

A driving mechanism for the abrupt change in biomass in Lake Nakuru in the period 1972 -1974 was not clearly defined. It was thought to be related to increased salinity and lowering of lake levels, driving the growth of coccoid species other than *Spirulina sp.* that were better adapted to higher salinity, but offering less protein to the feeding birds (Figure 9.24b; Vareschi, 1978). There is also the simple fact that ever more saline waters cover ever smaller areas on the lake floor. There have been times in the last 70 years when most of the lake has dried up and pools of saline water only a few tens of centimetres deep remained (Figure 9.23b).

During the mid to late 1970s and in the 1980s the lake returned to more typical inherent oscillations in water level and salinity (schizohalinity). The *Spirulina* and flamingo populations in Nakuru returned to impressive numbers. From the 1990s more reliable long-term data sets on physical lake condition and flamingo numbers have been compiled (Figure 9.24d). In 1993, 1995 and 1998 feeding flamingo populations in Lake Nakuru were once again at very low levels and the remaining bird population was stressed. In 1998, unlike 1974, the stress was related to freshening driving the decrease in *Spirulina* biomass, not increased salinity and desiccation. This freshening favoured a cyanobacterial assemblage with strains that possibly also produced toxins. In the preceding bountiful year (1996), the *Spirulina*-dominated biomass had bloomed at times when salinities were favourable and died back at times of elevated salinities and lake desiccation, as in 1974. By 2000 formerly low salinities had once again increased making surface waters

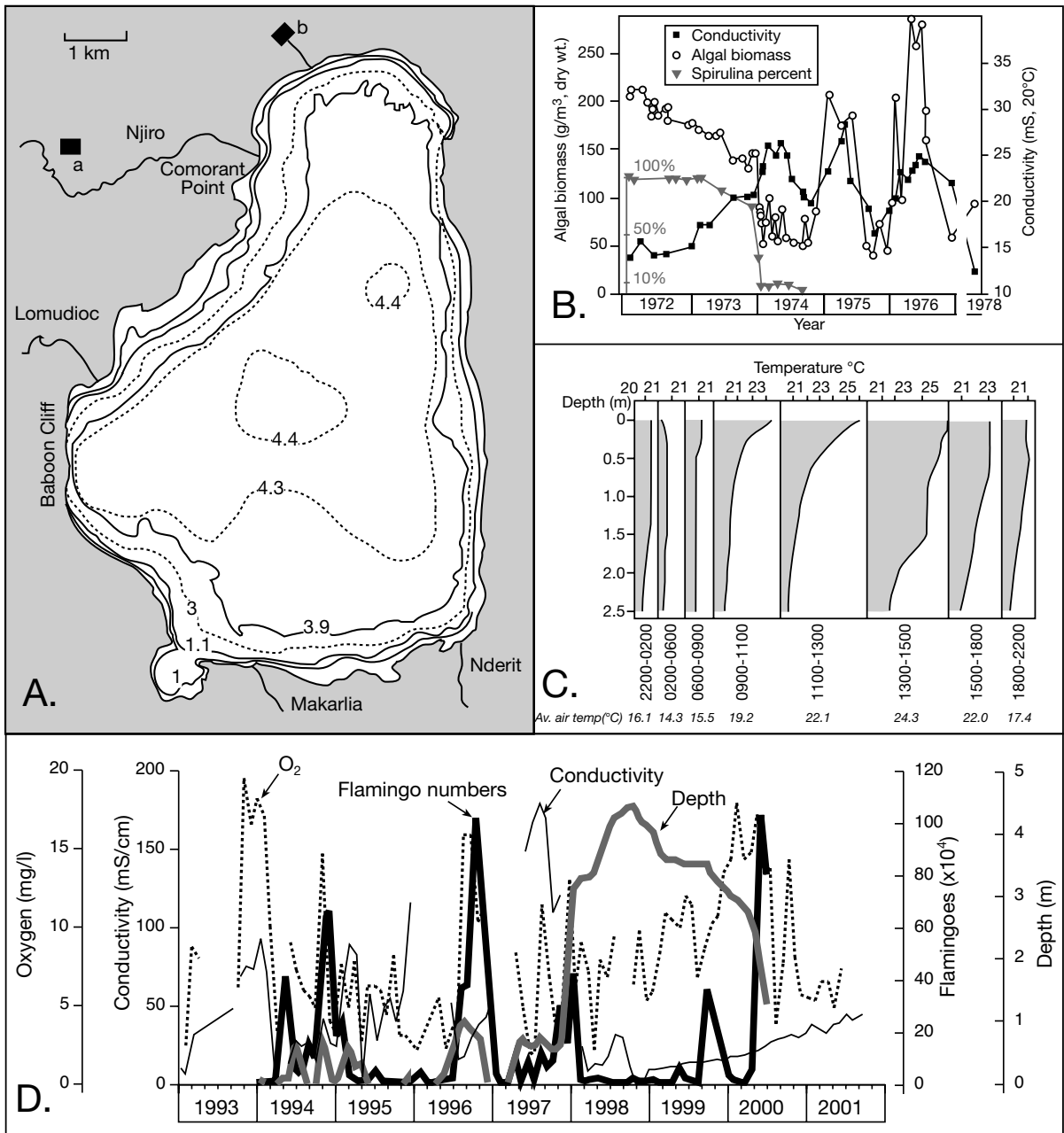


Figure 9.24. Lake Nakuru (A-C after Vareschi, 1982). A) Lake bathymetry (Dec 1979) and strandzone changes. Solid isopleths are actual shorelines at different lake levels over a 20 year period; from outer to inner are December 1979, January 1969, January 1967 and January 1961. Dashed isopleths are based on soundings taken in December, 1971. Two sewage plants are located at a and b. B) Trends of algal biomass and conductivity of lake water during 1972-1978. The percent contribution of *Spirulina platensis* to the total algal biomass is also shown. C) Mean water temperature profiles at different times of day from 1972-1973. D) Monitored water depths, conductivities, oxygen levels and flamingo numbers at Lake Nakuru for the period 1993 to mid 2001. Water depth and flamingo data only available from 1994 to mid 2000. Data is digitised and replotted to a common time scale from data in a progress report by Odadda et al. discussing current conditions in the Lake Nakuru area (downloaded from <http://www.worldlakes.org> on Feb 2, 2004)

suitable for another widespread *Spirulina* bloom and the associated return of high numbers of feeding flamingoes.

And so it seems that breeding flamingoes come to Lake Nakuru to feed in large numbers when there is water in the lake with appropriate salinity and nutrient levels to facilitate a *Spirulina* bloom. In some years when heavy rains occur, lake levels rise significantly and the lake waters, although perennial, stay in the lower salinity tolerance range for *Spirulina platensis*, keeping cyanobacterial numbers and protein levels at the lower end of the spectrum, as in the El Niño period between October 1997 to April 1998. Once lake levels start to fall, salinities and rates of salinity change return to higher levels, then water conditions once again become appropriate for a *Spirulina* bloom. But environmental stress on the flamingoes also comes with elevated salinities and desiccation moving lake waters into salinities at the upper end of *Spirulina* tolerance.

One of the reasons Lake Nakuru is suitable for cyanobacterial and algal growth at times of *Spirulina* bloom is the maintenance of suitable temperatures and oxygenation in the upper water mass. The lake develops a daily thermocline in the upper 1.5 metres of the column that dissipates each day in the late afternoon via wind mixing. Overturn recycles nutrients (derived from decomposition of bird and other droppings) back to the oxygenated surface waters to facilitate an ongoing bloom the next day (Figure 9.24c).

Numbers of flamingoes feeding in Lake Nakuru and Lake Bogoria are used in popular press as indicators of the environmental health of the lakes. Thousands of birds died in Lake Nakuru in 1995 and more than 30,000 birds may have died in Lake Bogoria in the first half of 1999. Some environmentalists argued in the popular press that mass die-offs and their perception of lowered numbers of flamingoes in Lake Nakuru and Lake Bogoria in the 1990s were indicators of uncontrolled forest clearance, an uncontrolled increase in sewerage encouraging eutrophication, and increase in heavy metals from increasing industrial pollutants in the lake and general stress on the bird population from tourists and the drastic increase in local human population centred on the town of Nakuru (third largest in Kenya). Numbers of people in the town, which is the main city in the rift valley, have grown by an average of 10% every decade for the past 30 years.

But like much environmental doomsday argument it is more based on opinionated prediction than on scientific fact (aka the Chicken Little fixation: it sells more newspapers than “good news” stories). When numbers of feeding flamingoes in

Lake Nakuru are compiled across the 1990s it is obvious that flamingo numbers oscillate widely, but it is also obvious that the peak numbers in 2000 are equivalent to the peak in 1996. A longterm fall in numbers of feeding flamingoes in the lake is not based on scientific reality.

Likewise, when studies were done on the cause of the mass die-off in Lake Bogoria in 1999, it was found to have a natural not an anthropogenic cause (Krienitz et al., 2003). The flamingoes had ingested the remains of toxic cyanobacteria that constitute part of the population of the microbial mats that had bloomed to form a floor to the fresh water thermal spring areas about the lake edge. There the mats are dominated by thermally tolerant species; *Phormidium terebriformis*, *Oscillatoria willei*, *Spirulina subsalsa* and *Synechococcus bigranulatus*. The influence of cyanotoxins in the deaths of the birds is reflected in autopsies which revealed: (a), the presence of hot spring cyanobacterial cells and cell fragments (especially *Oscillatoria willei*), and high concentrations of the cyanobacterial hepato- and neurotoxins in flamingo stomach contents and faecal pellets; (b), observations of neurological signs of bird poisoning - birds died with classic indications of neurotoxin poisoning - the ophistotonus behaviour (neck snapped back like a snake) of

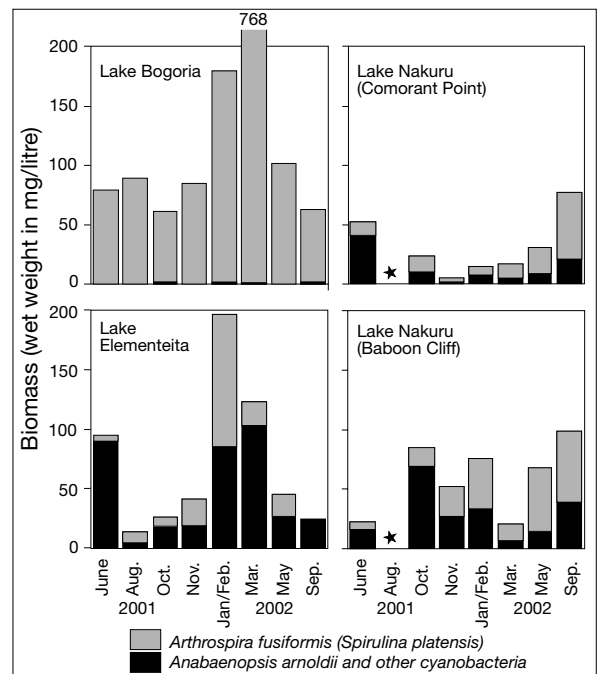


Figure 9.25. Changes in the biomass and the proportion of *Spirulina platensis* in various African rift valley soda lakes from June 2001 to September, 2002. Lake Bogoria is more saline than Nakuru than Elementeita (see Figure 9.23; after Ballot, 2004).

the flamingoes in the dying phase, and the convulsed position of the extremities and neck at the time of death. Cyanobacterial toxins in stomach contents, intestine and faecal pellets were 0.196 g g^{-1} fresh weight (FW) for the microcystins and 4.34 g g^{-1} FW for anatoxin-a. Intoxication with cyanobacterial toxins probably occurred via uptake of detached cyanobacterial cells when birds come daily to the springs to drink and wash their feathers after an overnight feeding session in the saline waters of the lake proper.

When heavy metal studies were undertaken in Nakuru lake sediments, the amount of heavy metals (Cd, Cr, Cu, Hg, Ni, Pb, Zn) were found to be in the typical range of metals in sediments in lakes worldwide. The exception is Cd, which is elevated and can perhaps be ascribed to anthropogenic activity (Svengren, 2002). All other metals are present at low levels, especially if one considers that Lake Nakuru lies within a labile catchment where the bedrock is an active volcanogenic-magmatic terrane.

Rise and fall of lake levels, drastic changes in salinity, a periodically stressed biota, and a lack of predictability in water character are endemic to life in saline ecosystems (cycles of “feast or famine”) and are what controls the number of feeding flamingoes in Nakuru and Bogoria. Oscillations in one or more of these factors are not necessarily anthropogenically induced. In general, sufficient base-line scientific data in this schizohaline ecosystem is not yet available and so accurate determinations of the relative import of increased human activity versus natural environmental stresses on longterm bird numbers are not possible.

Nearby Lake Magadi is also characterised by seasonal freshening, high productivity levels and bright red waters. In this case the colour comes from haloalkaliphilic archaea, not cyanobacteria. Archaeal species belonging to the genera *Natronococcus*, *Natronobacterium*, *Natrialba*, *Halorubrum*, *Natronorubrum* and *Natronomonas*, all occur in soda brines of Lake Magadi. Lake centre brines where this biota flourishes is at trona/halite saturation with a pH up to 12. Stratified moat waters around the trona platform edge are less chemically extreme and moat bottom sediments preserve elevated levels of organics ($\approx 6\text{--}8\%$). Lake Magadi also harbours a varied anaerobic bacterial community in the moat waters, including cellulolytic, proteolytic, saccharolytic, and homoacetogenic bacteria (Shiba and Horikoshi, 1988; Zhilina and Zavarzin, 1994; Zhilina et al., 1996). When the homoacetogen *Natroniella acetigena* was isolated from this environment its pH growth optimum was found to be 9.8–10.0, and it continued to grow in waters with pH up to 10.7 (Zhilina et al., 1996).

Regionally, salinities in the east African rift valley lakes range from around 30–50‰ total salts (w/v) in the more northerly lakes in the rift (Figure 9.23a; Bogoria, Nakuru, Elmenteita, and Sonachi) to trona and halite saturation ($>200\%$) in lakes to the south (Lakes Magadi and Natron). Yet across this salinity range a combination of high ambient temperature, high light intensity and a continuous resupply of CO_2 , makes these soda lakes amongst the highest in the world in terms of their seasonal planktonic biomass (Grant et al., 1999) and also places them among the world’s most productive ecosystems (Figure 9.22; Melack and Kilham, 1974). Organic production is periodic, and pulses of organic product periodically swamp the ability of the decomposers and so accumulate as laminites in the lake centres.

As we have seen, the less alkaline lakes are dominated by periodic blooms of cyanobacteria, while the hypersaline lakes, such as Magadi, can on occasion support blooms of cyanobacteria, archaea and alkaphilic phototrophic bacteria (Jones et al., 1998). Halotolerant and halophilic biota living in the variably saline and layered water columns constitute small-scale “feast or famine” ecosystems, which at times of “feast” are far more productive than either tropical seagrass meadows or zones of marine upwelling (Figure 9.22).

The “flamingo connection” supports a general observation that short periods of enhanced organic productivity are followed by episodes of lessened productivity in various schizohaline lake waters worldwide. It reflects the general principle that increased environmental stress favours the survival of a few well-adapted halotolerant species, to the detriment of others better suited to life in a less saline or less stressed environment. This same general principal of schizohaline ecosystems can be clearly seen in the decrease in invertebrate species (grazers and predators) with increasing salinity in the carbonate lakes of the Coorong of Southern Australia, where only brine shrimp remain alive in waters with salinities in excess of 200‰ (Figure 9.21c).

“Feast or Famine” in the Dead Sea

Effects of occasional freshening on biomass in stratified brine columns that are supersaline, not mesohaline, is clearly seen in the present “feast or famine” productivity cycle of the Dead Sea (Figure 9.26; Oren and Gurevich, 1995; Oren et al., 1995). *Dunaliella sp.*, a unicellular green alga variously described in the past as *Dunaliella parva* or *Dunaliella viridis*, is the sole primary producer in the Dead Sea waters. Then there are several types of halophilic archaea of the family Halobacteriaceae, which utilise organic compounds produced by the algae.

Two distinct periods of organic productivity (feast) have been documented since the lake became holomictic in 1979 (Oren, 1993, 1999). The first mass developments of *Dunaliella* sp. (up to 8,800 cells/ml) began in the summer of 1980 following a dilution of the saline upper water layers by the heavy winter rains of 1979-1980. The rains drove a rapid rise of 1.5 metres in lake level and an increase in the level of phosphates in the lake's surface waters (Figure 4.42b). This bloom was quickly followed by a blossoming in the numbers of red halophilic archaea (2×10^7 cells/ml), *Dunaliella* numbers then declined rapidly following the complete remixing of the water column and the associated increase in salinity of the upper water mass. By the end of 1982 *Dunaliella* had disappeared from the main surface water mass. Archaeal numbers underwent a slower decline.

During the period 1983-1991 the lake was holomictic, halite-saturated and no *Dunaliella* blooms were observed. Viable halophilic and halotolerant archaea were probably present in refugia about the lake edge during this period, but in very low numbers. Then heavy rains and floods of the winter of 1991-1992 raised the lake level by 2 metres and drove a new episode of meromictic stratification as the upper five metres of the water column was diluted to 70% of its normal surface salinity. High densities of *Dunaliella* reappeared in this upper less saline water layer (up to 3×10^4 cells/ml) at the beginning of May 1992, rapidly declining to less than 40 cells/ml at the end of July 1992 (Figure 9.26). An associated bloom of haloarchaea (3×10^7 cells/ml) continued past July and continued to impart a reddish colour to the surface and nearsurface waters.

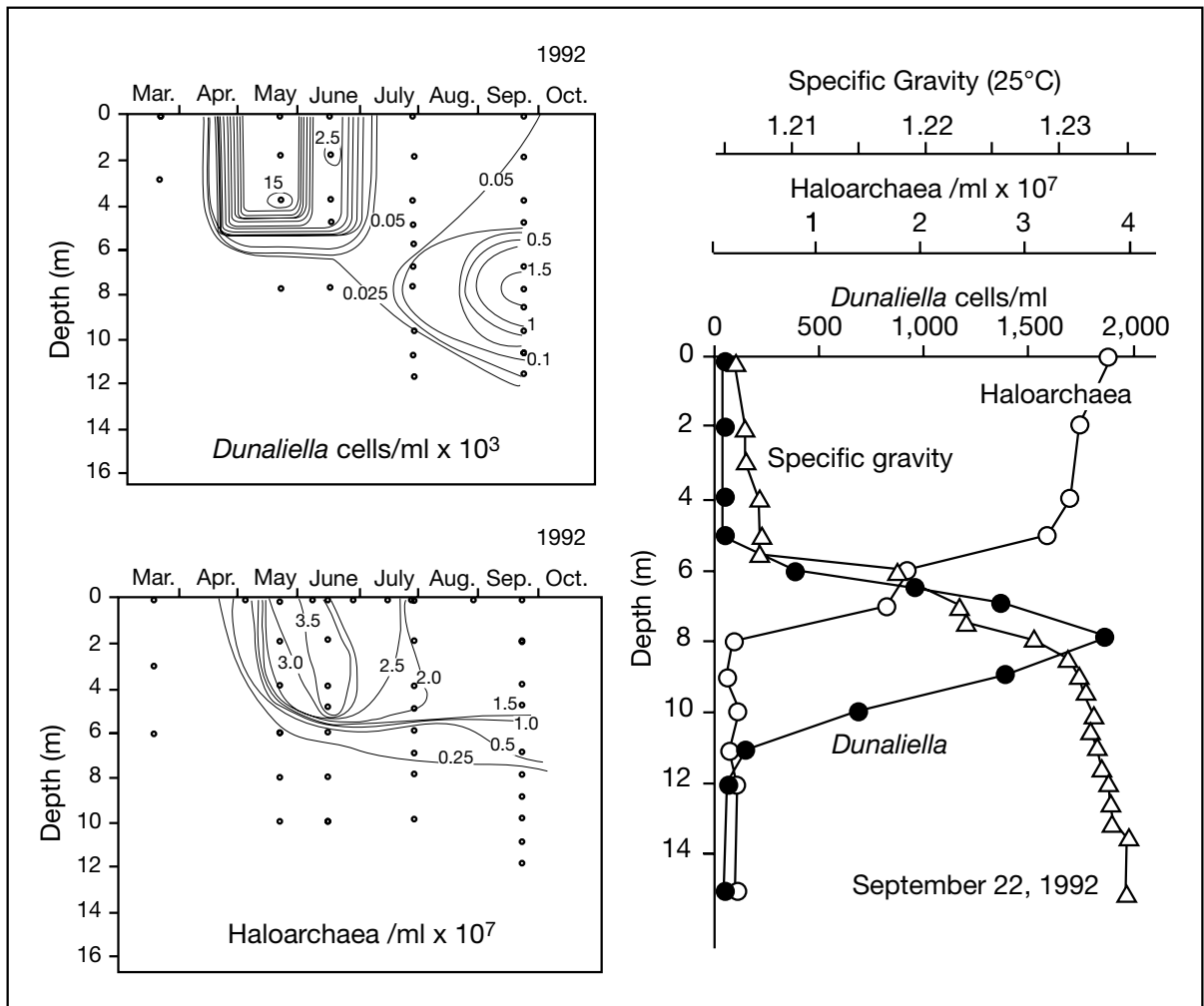


Figure 9.26. Changes in the vertical distribution of *Dunaliella* and halobacteria during the flood-induced density stratification of the Dead Sea in 1992 (after Oren, 1993). Note the vertical distribution of *Dunaliella* and haloarchaea relative to the halocline on September 22, 1992.

Much of the archaeal community was still present at the end of 1993 but the amount of carotenoid pigment per cell had decreased two- to three-fold between June 1992 and August 1993 (Oren and Gurevich, 1995). No new algal and archaeal blooms have developed since the winter floods of 1992-1993. A remnant of the 1992 *Dunaliella* bloom maintained itself at the lower end of the pycnocline at depths between 7 and 13 m (September 1992- August 1993), perhaps chasing nutrients rather than light. Its photosynthetic activity was low, and very little stimulation of archaeal growth and activity was associated with this algal community. It seems that once stratification ends and the new holomictic period begins, the remaining Archaeal community, which was largely restricted to the upper water layers above the halocline, spreads out more evenly over the entire upper water column until it too dies out.

Coloration of the Dead Sea waters from the initial algal bloom allowed Oren and Ben Yosef (1997) to use Landsat images, collected in May 1991 and in April and June 1992, to plot the development of the *Dunaliella sp.* bloom. In contrast, the carotenoids of the subsequent archaeal bloom did not produce a recognizable signal in the images. The April 1992 image obtained at the time of the onset of the algal bloom, prior to its lakewide spread, suggested it originated in the shallow areas near the shore of the lake where light penetrated to the bottom of the brine column. It was probably instigated by resting cells that had survived in near surface sediment of the shallow lake margin.

The ultimate decline of the lakewide bloom of halophilic archaea in the Dead Sea appears to be related to viral infection (Oren et al., 1997). For example, in October 1994, during the decline of the halophilic archaeal population in the upper 20 m of the Dead Sea water column, there were between 0.9 and 7.3×10^7 virus-like particles per ml of brine. Virus-like particles outnumbered archaea by a factor of 0.9-9.5 (averaging 4.4). Water samples collected during 1995 contained low numbers of both archaea and virus-like particles ($1.9-2.6 \times 10^6$ and $0.8-4.6 \times 10^7 \text{ ml}^{-1}$ respectively in April 1995), with viral numbers sharply declining afterwards (less than 10^4 ml^{-1} in November 1995-January 1996). Oren et al. (*op cit.*) suggest that viruses play a major role in the decline of halophilic archaeal communities in many other hypersaline environments where protists and metazoa are absent.

The Dead Sea and the African Rift Valley are examples of “feast or famine” in planktonic submersed settings. Enhancement of productivity (feast) during periodic freshening is also seen in halotolerant microbial mats in marine-margin mudflats. A study

of benthic mats in Storr’s Lake in the Bahamas showed that a reduction in brine salinity from 90‰ to 45‰ significantly enhanced CO_2 and N_2 fixation rates, but additions of inorganic nutrients and dissolved organic carbons (DOC) did not show any significantly enhanced rates compared with the salinity controls (Pinckney et al., 1995). That is, dissolved organic carbon/dissolved organic nitrogen uptake in the mats was not influenced over the entire range of salinities (45-90‰) seen in this study of mesohaline growth. Rather, abiotic stress, induced by hypersaline conditions in these Bahamian lagoons, created lower productivity in the saline-tolerant (haloxene) microbial mats, even when nutrient levels were high. When the osmotic stress on the biota was relieved by a lowering of salinity, mats underwent enhanced primary production and nitrogen fixation. Changing nutrient levels were far less significant than changing salinity levels as controls on mat productivity. Salinity-induced stress in these halotolerant microbial mats outweigh nutrient level, which is the typical limiting factor regulating phototrophic growth in normal marine and brackish waters.

Feast or Famine in the Messinian

“Feast or famine” cycles as just noted in the African rift lakes and the Dead Sea suggest that periodic freshening of surface waters in stratified brine bodies (usually by meteoric water or seawater influx) should facilitate the accumulation of organic-rich pulses to the bottom sediments in similar stratified brine bodies in the past. The notion that subsequent accumulation of a thick salt seal atop mesohaline source rocks, once the basin was cut off from a surface marine connection, helps explain the intimate association between evaporites and hydrocarbon seen in the many occurrences listed in Table 9.1. Now we shall test this notion by considering a likely ancient counterpart.

Organic-rich evaporitic marls were deposited beneath stratified brines in the Lorca Basin, located within the tectonically evolving Betic Cordillera of southeastern Spain. It was a rapidly subsiding basin in an open-marine setting during much of the Miocene (Benali et al., 1995). By the Upper Miocene (Messinian) the basin was accumulating thick diatomite-bearing sediments (Tripoli Unit), which are overlain by the Main Messinian Evaporite series. This evolution from marls to gypsum/halite beds records the onset of the “salinity crisis” throughout the Mediterranean region (Figure 5.40). Restriction by the time of the deposition of the Tripoli Unit in the Lorca Basin led to intercalations of thin precursor evaporitic layers, mostly subaqueous and sabkha Ca-sulphates, with diatomites (Figure 9.27; Rouchy et al., 1998). Prior to the main salinity crisis, the alternation of evaporites and diatomite cycles indicates periodic

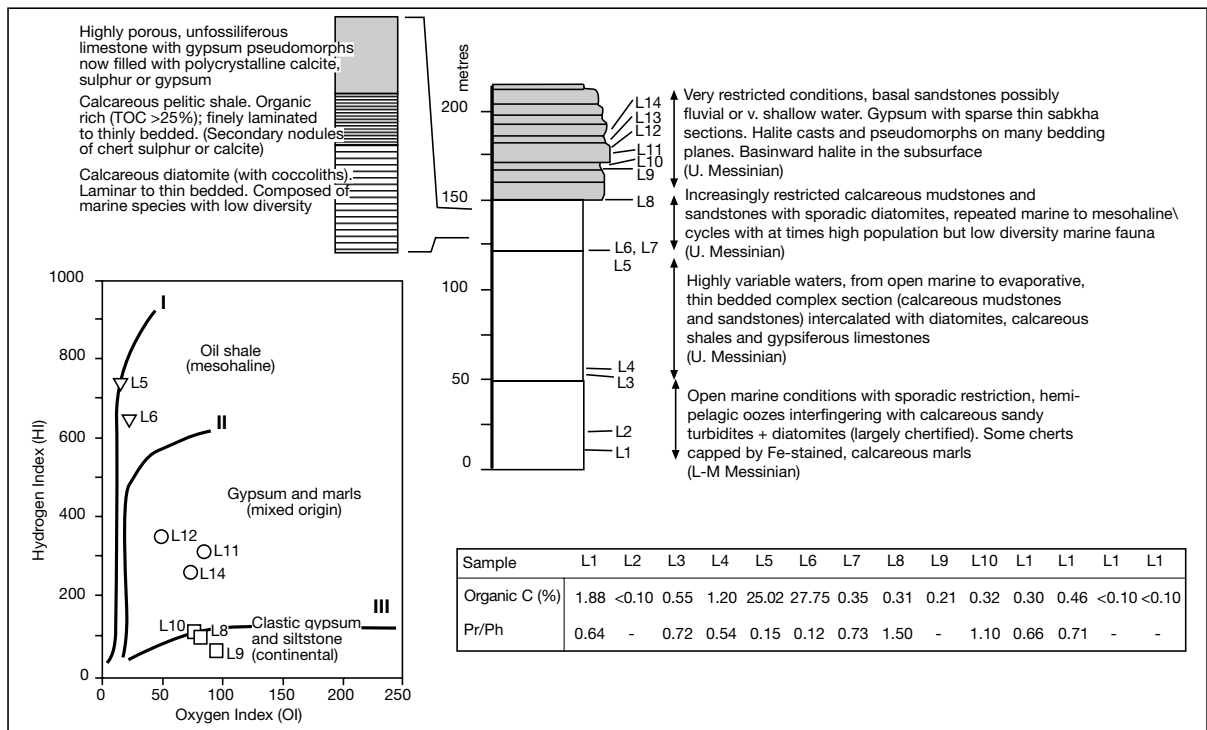


Figure 9.27. Lorca Basin, Spain, showing organic character of normal marine, mesohaline and evaporitic sediments (after Benali et al., 1995).

restriction and the development of mesohaline conditions, followed each time by an episode of marine reflooding.

Schizohalinity drove both the varying levels of primary production in surface waters and the preservation of organic matter in the hypersaline bottom sediments, finally culminating in widespread evaporative sedimentation in the latest Miocene. As basin waters evolved toward perennial hydrographic isolation and holomixis there were unusual evaporative conditions that heralded the main salinity crisis. These were a number of salinity-stratified mesohaline surface floods when the resulting anoxic bottoms accumulated oil shales with up to 25% TOC (Figure 9.27; expanded section). When oil shales were accumulating, the system was meromictic; upper water mass was nutrient-rich and mesohaline with near normal marine salinities, while the bottom waters were anoxic and somewhat more saline than surface waters (Benali et al., 1995). Later in the basin history, when mixed gypsum marls and clastic gypsum sequences were accumulating, the oil-prone quality of any potential kerogen in the basin was diluted by rapid deposition of gypsum precipitates and an influx of oxidised organic detritus.

The formation of organo-sulphur compounds, replacement of sulphates by carbonates and the high levels of elemental

sulphur are other byproducts of early diagenetic/microbial processes occurring in the Lorca oil shale. The high abundance of phytane, 2,3-dimethyl-5-(2,6,10-trimethylundecyl)-thiophene, mid-chain C_{20} isoprenoid thiophenes and bithiophenes and bis-O-phytanyl and O-phytanyl-O-sesterterpanyl glycerol ethers indicates that the organic matter in these sediments was deposited under anoxic hypersaline conditions (Table 9.4; Russell et al., 1997). Isopranyl glycerol ethers occur in sulphur-bound macromolecular matter, which contrasts with the low concentrations of these compounds as free lipids. However, the distribution of these isopranyl glycerols is paralleled by the occurrence of free phytanic acid in both the oil shales and intercalated laminated carbonates and by 3,7,11,15,19-pentamethyleicosanoic acid in the laminated carbonates. A high level of input from bacterial decomposers is indicated by 2-hydroxytetracosanoic acid, n-octadec-11-enoic acid, hopanoic acids and the distributions of iso- and anteiso- C_{15} and C_{17} homologues and minor amounts of iso- C_{16} and anteiso- C_{14} . These branched fatty acids are characteristic of sulphate-reducing bacteria, which would have inhabited the anoxic bottom brine. The relative proportions of the iso- and anteiso-compounds in the total fatty acid distributions are tied to the proportion of reduced sulphur in the sediments.

As in Lake Nakuru and the Dead Sea, cyanobacterial and halotolerant algal blooms in freshened surface waters created these organic-rich Messinian carbonates. Blooms of halotolerant species, followed by die back, drove cycles of “feast or famine” in the Lorca oil shales.

The where and when of productivity

Most biological studies in freshwater lakes and in the oceans have found that the highest levels of organic productivity (primary productivity) occur annually within the zone of maximum light penetration in the upper few metres of the water column. Long term salinity stratification or meromixis in the perennial waters of an evaporite basin, can change the locus of maximum organic productivity, especially in situations where the required nutrients lie at or below the halocline. Haloarchaea in the Dead Sea can survive by facultative photosynthesis long after their primary food source has died back (Figure 9.26). But is there a more general layering of the halobiota in stratified brines where the chemical interface created by the coming and going of the halocline allows life to flourish via chemosynthesis, not photosynthesis? If so, then bacterial productivity in upper fresher waters of a layered brine column may come to rely on nutrients supplied from permanently saline and anoxic bottom waters.

Mahoney Lake is a small 30m deep meromictic salt lake in British Columbia, Canada, with a halocline that separates a variably oxygenated mixolimnion⁹⁹ from a permanently anoxic monimolimnion at a depth of around 6 m in the lake brine column (Figure 9.28a). It has been a saline meromictic/holomictic system for the last 9,000 years, with some meromictic episodes lasting as long as 1,100 years (Overmann et al., 1996). Heterotrophic bacterial production in the lower mixolimnion at times exceeds concomitant primary production in the upper waters of the same mixolimnion by a factor of 7 (Figure 9.28b). In this highly productive interval lives an extremely dense population of the phototrophic purple sulphur-oxidising bacterium *Amoebobacter purpureus*, which is present year round along the lake halocline. The Mahoney Lake halocline harbours the densest population of phototrophic sulphur bacteria ever reported in a natural body of water. It is sufficiently abundant to form the base of a food chain where it constitutes 70% of the diet of planktonic copepods living in the upper water mass.

Each year, following ice melt, a layer of freshened water enters the lake, creating a well defined uppermost oxygenated layer in the mixolimnion, which disappears within a few months. For example, the stability of the mixolimnion declined sharply

between May and July 1993, in parallel with the disappearance of the low-salinity uppermost surface water layer, the warming of the lower waters of the mixolimnion, and the resulting loss in density stratification (Overmann et al. 1996). This allowed mixing across the perennial halocline and the release of nutrients into the lower parts of the mixolimnion. For most of an annual cycle any bacterial growth in the lower mixolimnion is limited by the supply of inorganic phosphorus or nitrogen, which can come from above or below. In Mahoney Lake, liberation of phosphorus from upwelling of the remains of purple sulphur bacteria in the lower waters, and degradation of allochthonous dissolved organic carbon floating at the halocline, act as a carbon source for the bacteria and so render heterotrophic bacterial production largely independent of photosynthetic phytoplankton cycle in the overlying waters of the uppermost mixolimnion.

Similar purple bacterial layers cap the haloclines of brine lakes on the deep seafloor of the Urania Basin in the Mediterranean Sea. This bacterial community utilises sulphur compounds crossing the brine interface from anoxic waters below and thrives many thousands of metres below the euphotic zone (Sass et al., 2001). Sulphur-oxidising bacterial communities, independent of light penetration, probably occur atop marine suprasalt brine-lake haloclines worldwide.

The effect of salinity stratification on productivity in many saline lakes does not follow the predictable annual cycle seen in Lake Mahoney and in most freshwater temperate dimictic lakes (dimictic = seasonally mixed). This lack of annual cyclicality in

⁹⁹ Jargon of lacustrine stratification

Mixolimnion: the upper, low density, freely circulating water layer of a meromictic lake.

Monimolimnion: the deep, usually salty, layer of a meromictic lake, typically it is a perennially stagnant or noncirculating water mass.

Meromixis: a condition in a lake (meromictic lake) where the bottom noncirculating water mass is adiabatically isolated from the upper water mass.

Holomixis: a condition in a lake describing complete overturn and mixing of the lake water mass.

Hypolimnion: is the lowermost water mass in a lake, characterised by a generally uniform temperature (or density) profile.

Eutrophic lake: a lake characterised by an abundance of nutrients and a seasonal deficiency of oxygen in the hypolimnion. Waters are usually shallow and sediments are organic-rich laminites.

Oligotrophic lake: a lake characterised by a deficiency in nutrients and an abundance of oxygen in the hypolimnion. The bottom sediments typically contain low levels of organics and the water column is deep.

Monomictic Lake: –A lake which undergoes one period of complete mixing during the year separated by one period of thermal stratification.

the organic production is clearly seen in the timing of meromictic stages of the Dead Sea (Figure 9.26). Multiple years of stratification without breakdown is also characteristic of Mono Lake, California where photosynthetic activity was measured in its hypersaline and stratified waters during an 8-yr period from 1982 to 1990 (Jellison and Melack, 1993). Exceptionally large volumes of freshwater runoff in 1982 and 1983 led to a 2.6-m rise in surface elevation of Mono Lake and the onset of a new period of meromixis in the lake (Figure 4.21). In 1984 chemical stratification accounted for a density difference of $1.2\text{--}1.5 \times 10^{-2}$ gm/cc between the 2 and 28 m water depths. At the same time the midsummer density difference between 2 and 28 m depths that was due to temperature was approximately 0.5×10^{-2} gm/cc. Salinities ranged from 77 to 98 gm/l across the interface and sodium, chloride, sulphate, and carbonate were the major ions in both the upper and lower water mass.

This eight-year time frame in Mono Lake spans the onset (1983), persistence (1984–1987), and breakdown of meromixis (1988). Following the onset of meromixis, the algal biomass in the lake each spring and autumn decreased from 1984 to 1986: annual primary photosynthetic production was reduced from $269\text{--}462 \text{ gC m}^{-2}\text{yr}^{-1}$ (1984–1986) compared to nonmeromictic conditions of $499\text{--}641 \text{ gC m}^{-2}\text{yr}^{-1}$ (1989 and 1990). A gradual increase in photosynthetic production then occurred, even before meromixis ended, because of increased vertical flux of ammonium from the anoxic saline bottom, due to deeper mixing and the buildup of ammonium in the monimolimnion. Annual primary production in the lake was greatest in 1988 ($1,064 \text{ gC m}^{-2}\text{yr}^{-1}$) when the weakening of chemical stratification and eventual breakdown of meromixis in November of that year allowed a large upward influx of ammonium (source of nitrogen) into the euphotic zone.

Another transition from monomixis to meromixis occurred in Mono Lake from 1994 to 1995 (Figure 9.29; Melack and Jellison, 1998). During the preceding monomictic conditions in 1993 and 1994, the lake had thermally stratified in March and

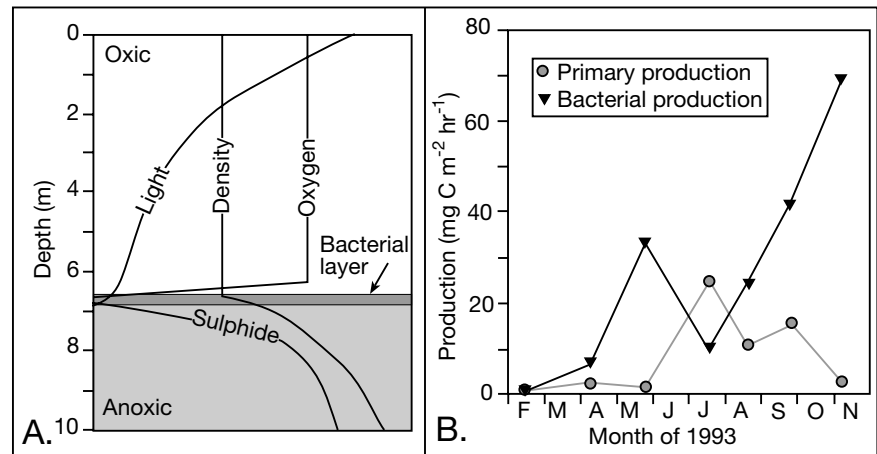


Figure 9.28. Lake Mahoney, Canada. A) Stratification in the brine column showing the position of the purple sulphur-oxidising bacterial community at the halocline. B) Integrated primary production and bacterial production in the mixolimnion during 1993. Both were measured simultaneously during incubation around solar noon (after Overmann et al. 1996).

had mixed to the bottom by each December. During meromictic conditions in 1995, 1996 and 1997, the absence of holomixis during winter once again resulted in persistent anoxic conditions beneath the chemocline, the accumulation of ammonium in the monimolimnion, its depletion in the mixolimnion, and low mixolimnetic chlorophyll concentrations in the spring and autumn. The meromictic state continued until mixing in 2003 and was preceded by a trend of year-to-year deepening of the chemocline, which indicates increasing lability to mixing in a meromictic lake (Figure 9.29). The same deepening of the halocline marks the transition to holomixis in the Dead Sea (Figure 4.43).

The TOC content of a core through the laminites of Mono Lake, sampling the last 300 years, shows an overall tendency toward increasing TOC content in the period 1700–1800, then a consistent trend hovering around 6% but with wider variations in TOC in the last 60 years, since the diversion of the inflow to the Los Angeles water supply in 1941 (Figure 9.30; Benson et al., 2003). The highest values of TOC in the core occur in this time frame, 14% around 1970, as do some of the lowest, e.g. around 4% in 1943 and 1980. Clearly, the perennially anoxic saline bottom waters of the lake, with a pulse of productivity (a time of feast) in those years when the lake transitions from meromictic to holomictic, have facilitated the preservation of organics at levels that in ancient counterparts would characterize a source rock. Whether the fluctuations in TOC levels in the bottom sediments reflect varying intensities in algal blooms or some other factor related to the volume of organics reaching the bottom is not yet defined.

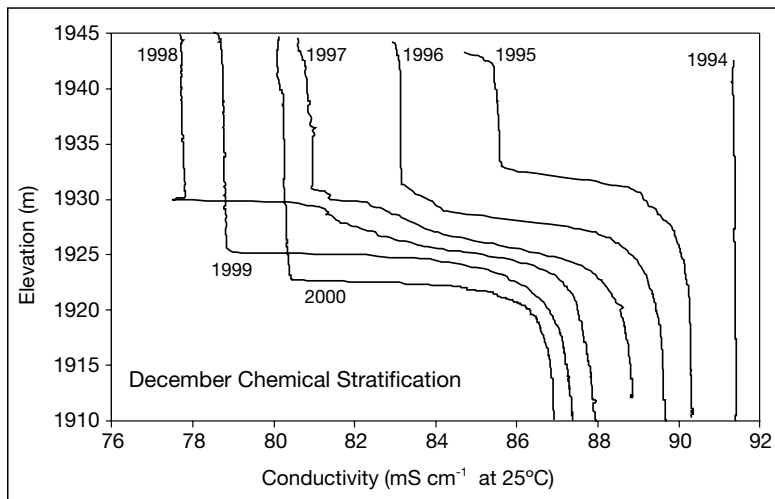


Figure 9.29. Mono Lake, California, conductivity profiles in December for the years 1994-2000 (figure was redrafted from a database downloaded from file://www.monobasinresearch.org/toc.htm, last accessed Dec. 28, 2004).

Predicting preservation of benthic organics

Predicting how organic productivity in surface waters relates to organic preservation under a variable layered brine column is difficult. It is commonly assumed in source rock modelling that saline waters at the base of a stratified saline water column are anoxic and will always favour the preservation of organic matter produced by plankton (Demaison and Moore, 1980). The effectiveness of stratified brines in the preservation of pelagic organic matter originally produced in photic and oxygenated water is especially obvious when comparing open marine and density-stratified hypersaline environments. Estimates for the preservation efficiency of primary organic matter in the modern shallow open-marine oxygenated bottoms centre around 0.1% (Menzel and Ryther, 1970), while on the floor of the anoxic Black Sea it is about 4% (Deuser, 1971). In contrast, preservation efficiency beneath density-stratified hypersaline lakes and epeiric seaways subject to times of feast or famine can be as high as 85% (Hite and Anders, 1991). This vast improvement in preservation in part reflects the “salting effect” of a perennial dysaerobic to anoxic saline bottom brine

layer and the periodic proliferation of a photosynthetic biomass in a freshened upper brine body. Plankton that is blooming in a stratified brine column is liable to mass mortality as ongoing evaporation increases nearsurface salinities to intolerable levels (“feast or famine”). Schizohaline surface waters means most organic-rich evaporitic mesohaline sediments are deposited as laminites, facilitated by repetitive “life and death cycles” in the halobiota (Warren, 1986).

Yet mesohaline to moderately penesaline bottom waters of some density-stratified shallow modern brine lakes are oxygenated, not anoxic. Bottom microbial mat communities below such waters are dominated by halotolerant oxygen-producing photosynthesising benthic cyanobacteria.

These benthic primary producers create and maintain elevated oxygen levels in the well-lit bottom waters immediately above the mat and are the hypersaline equivalents of marine seagrasses. But, benthic microbial mats tend to be anoxic no more than a few millimetres below such photosynthesising surface layers of microbes (Figure 9.18). Burial via mat aggradation tends to quickly move newly created cyanobacterial organics into an anoxic regime, where organic preservation is much more likely

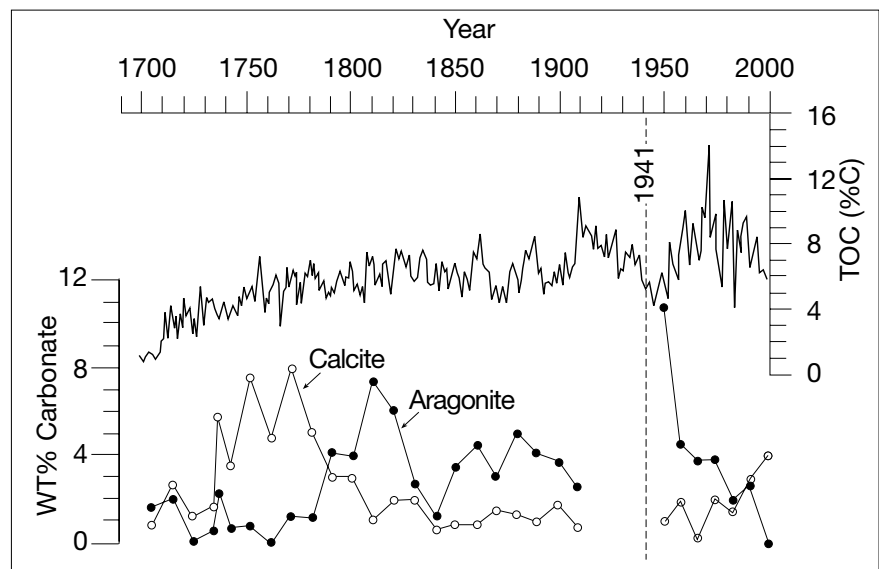


Figure 9.30. TOC and carbonate proportions in a core through Mono Lake laminites deposited in the last 300 years (after Benson et al., 2003).

(Figure 9.6). Unlike marine seagrass banks, the association of permanent bottom hypersalinity and anoxia a few mm below the sediment brine interface, tends to prevent most burrowers from entering the bottom sediment. Burrowing is a major mechanism for maintaining oxygenation in normal marine sediment, where it tends to prevent substantial accumulations of organic matter in bottom sediments.

Lake Hayward, Australia is meromictic and a good case in point; it is a shallow perennial hypersaline coastal salina filled by brines less than 2 metres deep. Photosynthesis via its benthic microbial mat community, is normally sufficient to supersaturate the bottom with dissolved oxygen, even during periods of brine column stratification, yet bottom sediments contain 5-7% TOC (Burke and Knott, 1997). Laminated microbial mats in the permanently submersed mesohaline centre of the lake are dominated by photosynthesising cyanobacteria *Cyanothece sp.*, while *Microcoleus sp.* are dominant in the biolaminites of the lake's seasonally desiccated strandzone. In daylight the oxygen saturation can be as high as 270% in the uppermost photosynthesising mat and the immediately overlying bottom waters (Burke, 1995). However, after an unusually dry year in 1987, the lake salinity in the upper waters increased to 260 g/l and gypsum precipitated across the lake (Figure 9.31; Burke and Knott, 1997). Turbidity generated by gypsum crystallisation in the brine mass was sufficient to obscure the benthos completely, despite the shallowness of the lake (secchi curve in Figure 9.31). As a result, the amount of benthic oxygenic photosynthesis was greatly reduced and benthic mats degraded. During brine stratification in the following winter (1988), bottom waters became anoxic and supported a healthy population of purple sulphur-oxidising bacteria.

However, during the next few years, after each subsequent brine column overturn, healthy cyanobacterial mats

were re-established and they were able to again supersaturate the bottom waters with oxygen year round. The development of a healthy microbial mat community in Lake Hayward prevents periodic bottom anoxia, whereas nearby meromictic lakes, that do not contain a healthy halotolerant microbial benthos, tend to annual anoxia during stratification. The lake illustrates a general principle that healthy halotolerant microbial mat functions as a strong homeostatic mechanism in allowing longterm stability of elevated oxygen levels in bottom waters of the shallow brine lake, but an increase in salinity can make the bottom anoxic.

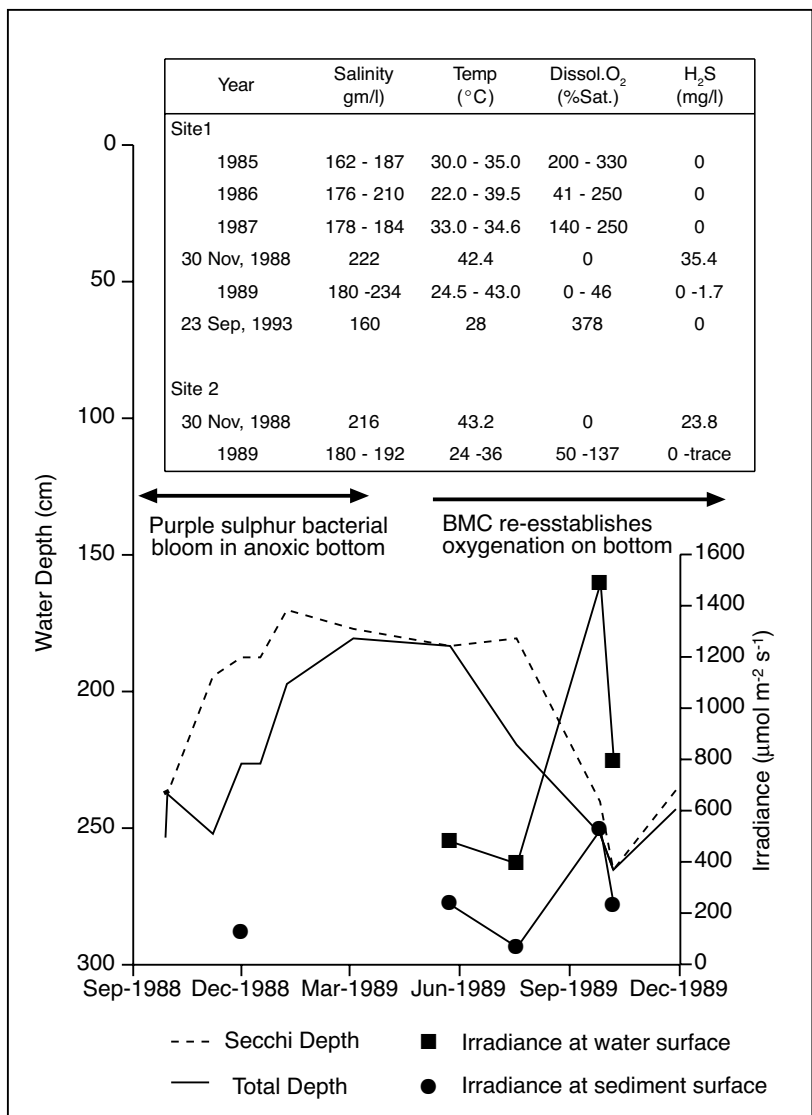


Figure 9.31. Effect of gypsum precipitation on benthic microbial communities and oxygenation in Lake Hayward, West Australia (compiled from data in Burke and Knott, 1997).

benthic mats in low nutrient systems formed from salinities

Gypsum precipitation in the brine column is not the only cause of brine column turbidity and bottom anoxia in shallow waters. Planktonic blooms (a time of feast) can also substantially reduce light penetration to the bottom of a shallow brine lake (Horsfield et al., 1994). If the bloom is intense it can prevent benthic cyanobacteria from photosynthesising. The shaded part of system eutrophies as decomposing planktonic remains rain down through the now dark brine column. Decomposition in the upper portions of the column uses up all the oxygen in the water column. The oxic-anoxic interface rises from the sediment into the brine column, killing off any oxygen-requiring benthic species. Such hypertrophication overwhelms the delivery of oxygen to the bottom by the photosynthetic benthos and facilitates higher levels of organic delivery to bottom sediments than occurs with the benthic mats. This eutrophic and slimy bottom style of deposition naturally characterises the central portions of Solar Lake, Egypt (Figure 4.11). It may explain why the TOC of its bottom sediments, accumulating beneath pore waters that are perennially anoxic, are elevated compared with microbially-bound bottom sediments of Lake Hayward (Figure 9.6; 15-20% versus 5-6%).

In a study of eutrophication in modern saltfields Javor (2000) found that in shallow gypsum and the pre-gypsum ponds there was an interesting inverse relationship between the level of nutrients (nitrates and phosphates) in the brine column and the development of microbial mats on the water covered pan floor. In a high nutrient brine system (eutrophic or well-nourished) the algae and bacteria flourished as planktonic forms and the biomass buildup in the upper parts of the brine column tended to shade the sediment surface so that there was little or no development of a microbial mat and bottom waters were dys-aerobic to anoxic. In a low nutrient system there was little or no planktonic development of algae or bacteria and microbial mats tended to flourish on the perennial pond floor. She found

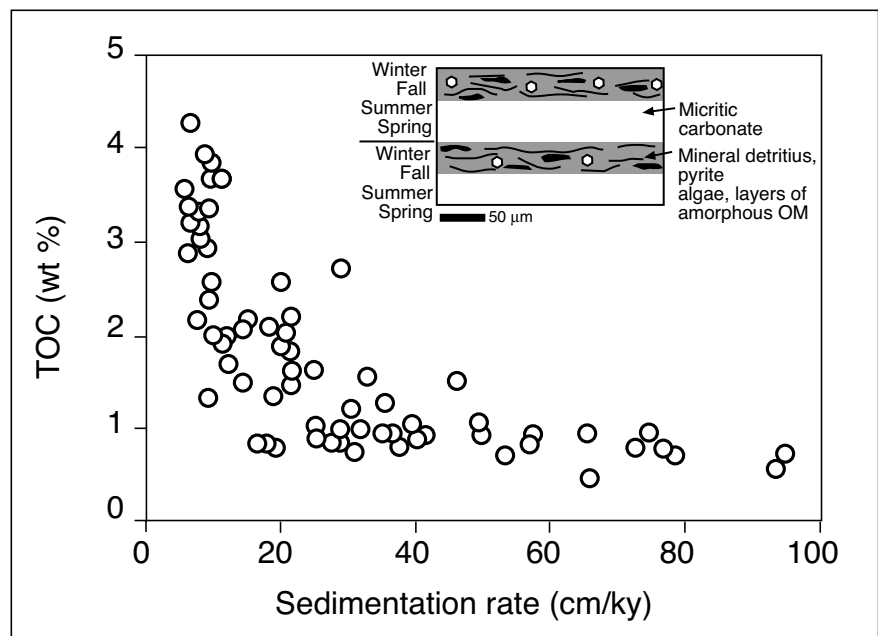


Figure 9.32. Sedimentation rate versus percent of total organic carbon content (TOC) in laminite marls from the Oligocene evaporites of the Mulhouse Basin, Europe. Inset shows the scale and mineral /organic distribution in the laminae (varve couplets) of the sampled intervals (after Hofmann et al., 1993b).

of 50,000 ppm to gypsum saturation. At lower salinities mats were destroyed by the feeding activities of invertebrates and fish (Figure 9.9).

Most benthic microbial mats beneath hypersaline waters depend, in large part, on nutrients recycled by the bacterial decomposers that make up the underside of the living part of the mat. Even if nitrogen and phosphorus levels in the overlying brines are low, there may be sufficient nutrient recycling within the mats to allow the bottom mats to continue to grow. Javor (*op. cit.*) found that once a gypsum crust becomes well established over the floor of a crystalliser pond there was little recycling of nutrients from beneath the crust. From this point downstream in the crystalliser pans, nitrate and phosphate nutrients concentrated by evaporation were recycled into the biomass living in the brine column and not within the benthic mat. In oligotrophic gypsum ponds the gypsum crust is stable and the bottom waters are oxygenated. In eutrophic gypsum ponds at the same salinities the bottom waters become anoxic and sulphate-reducing bacteria flourish. In these systems the gypsum dissolves and the bottom is typically covered by a black slimy organic-rich mud containing no more than a few

embayed and dissolved gypsum remnants, much like the central facies in Solar Lake (Figure 4.11). If portions of this slimy bottom become suspended and are flushed into the next stage of the crystalliser brine stream they create a problem in the final product known as “black spot.” Brine shrimp are often added to the mesohaline ponds of a saltworks to control planktic blooms and so minimise “black spot.”

That organic enrichment occurs naturally in the mesohaline carbonate stage and not in subsequent gypsum or halite layers is clearly seen in the evaporitic marls and salts of the Oligocene Mulhouse Basin (Figure 9.32; Hofmann et al., 1993b). This deposit is one of a few ancient evaporitic settings where organic chemistry has been studied in a logical and detailed fashion, rather than as spot samples. Organic matter occurs mostly in finely laminated carbonate marls (varves), which can contain up to 7% TOC, anhydrite beds contain 0.08-0.78% TOC, halite beds 0.01-0.25% TOC and the potash beds <0.1% TOC. The marls are characterized by thin, continuous bedding parallel laminae that are not disturbed by any bioturbation.

They are interpreted as seasonal varves with the clay and carbonate forming alternate layers in the couplet (see inset in Figure 9.32). In spring and summer the increased temperature in surface waters favoured precipitation of micritic carbonate, in autumn and winter the phytoplankton died back and rain-fall/runoff transported clastic debris into the basin. On the basis that the laminar couplets are varves, Hofmann et al., (1993b) were able to plot the relationship between sedimentation rate and TOC content in the marls (Figure 9.32). Marls deposited during times of low sedimentation rate tend to be organic-rich, while marls deposited at times of higher sedimentation tend to contain lower amounts of organics. They concluded that the even lower levels of organics in the more saline salt beds (anhydrite and halite) indicate even more dilution because of inherently higher sedimentation rates.

Proximity of organic-rich mesohaline laminites to ancient bedded evaporites has lead some geologists to postulate that bedded salts are potentially also organic-rich sediments with the same level of source potential as mesohaline carbonates. This is not borne out by TOC analysis of evaporitic salts in the Mulhouse Basin. Likewise, worldwide measurements of total organic matter levels in ancient CaSO_4 and NaCl lithologies tend to be normal or depleted (Katz et al., 1987). Mesohaline carbonates, not higher salinity salts, are the source rocks to ancient reservoirs (Figure 9.3). But, levels of dissolved organic matter and volatile fatty acids rise in increasingly saline brines

and may be considered potential mobile or liquid sources if caught up in intercrystalline interstices and inclusions (Anders and Hite, 1991). Levels of DOM and VFA may be high in such penesaline salts and could be released in the subsurface when halite beds are dissolved by crossflows of surface brines. But in general the typically low levels of solid organic matter in bedded halite reflects the higher depositional rates of evaporitic salts when compared with evaporitic carbonates (dilution effect). Under the same rate of supply of detrital organics, the higher rate of halite accumulation dilutes the associated organic content compared to carbonate sequences.

Whatever the finer controls on accumulation levels, observations of organic accumulations in modern and ancient mesohaline saline systems show that peaks or pulses in primary production (“feasts”) in density-stratified brine lakes are controlled by two factors; 1) the occasional presence of an ephemeral less saline surface water mass, and 2) a periodic supply of nutrients (nitrate/ammonia and phosphate), possibly from a combination of inflow/runoff and leakage from the lower hypersaline water mass. The biota contributing the organic pulse, which ultimately reach the bottom sediments to form organic-rich laminae, are largely dependant on the timing of photosynthetic activity. Modern saline lakes with a well defined annual freshening of surface waters will deposit varved evaporitic carbonates (e.g. Lake Tanganyika with up to 7-11% TOC in deep bottom laminites; Cohen, 1989), while other brine lakes and seaways, with less predictable stratification, may form similar carbonate laminites, but the organic layering may not be annual (Dead Sea, Mono Lake).

Populations of purple-sulphur oxidising bacteria define the position of the oxic-anoxic interface in hypersaline settings. They reside a few millimetres below the mat surface beneath shallow brines with healthy cyanobacterial mats on the bottom. In deeper brines they reside at the halocline. Shading of a healthy cyanobacterial mat, either by planktonic blooms or mineral saturation in the brine column, allows the oxic-anoxic interface to rise from within the mat into the brine column and bring with it its healthy population of purple bacteria. If organic debris from a planktonic bloom settles to the sediment surface at this time there is less likelihood it will be broken down by fermenters and decomposers before it is buried. Hence, elevated TOC levels from times of planktonic feasting are more likely to be preserved.

Life, brine seeps and dissolving salt allochthons

There is an association between chemosynthetic communities, saline anoxic bottom brines, organic-enriched laminites, metal sulphides and salt allochthons in some modern marine slope and rise settings (Warren, 2000b). Historically, a relatively deep

open marine setting was not considered an area where hypersaline bottom brines facilitated the accumulation of organic and metal sulphide-rich mesohaline sediments. Yet it is in seafloor settings where shallow salt allochthons are actively flowing and dissolving and, as such, is a zone of potential mesohaline source rocks (Figure 9.3).

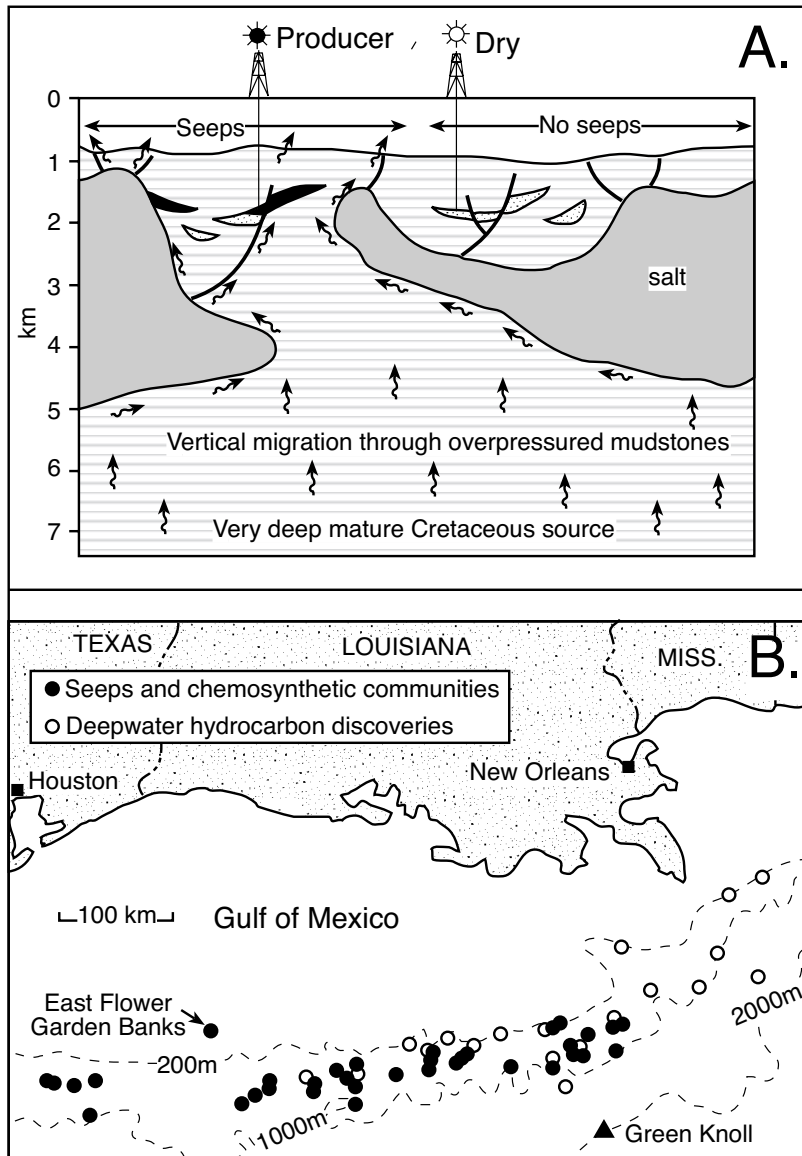


Figure 9.33. Brine seeps. A) Model of hydrocarbon migration and seepage in the deepwater Gulf of Mexico. Seepage indicates a change in the salt continuity in an intrasalt basin, but it does not indicate the presence of an effective migration pathway to a specific hydrocarbon trap. B) General association of seeps, chemosynthetic communities and hydrocarbon discoveries in the deepwater Gulf of Mexico (after Thrasher et al., 1996).

When an allochthonous salt sheet lies just beneath the seafloor it dissolves from the edges inward as it releases and focuses chloride-rich brines into its surrounds. Any subsalt brine forms a dense chloride-rich plume that sinks into the underlying sediments to become caught up in subsalt convection cells (Figures 8.2, 8.23). As it convects it mixes with escaping basal brines, whereby upward brine passage is focused along the dissolving undersides and edges of the salt mass, before it finally seeps and vents to the seafloor (Figure 9.33a). Such brine-issuing vents occur at 1920m-deep seafloor on top of Green Knoll, an isolated salt diapir rising seaward of the Sigsbee Escarpment in the northern Gulf of Mexico. Methane- and chloride-rich vent brines are supplied in part by congruent seawater dissolution of the underlying Louann salt, and in part by hydrocarbon-rich basal waters escaping from deeper within the salt sealed sediment column (Table 9.5; Aharon *et al.* 1992). In the Gulf of Mexico the venting Na-Cl brines are up to seven times saltier than ambient seawater and the geometry of their subsurface passage to the seafloor largely reflects breaks in the continuity of allochthonous salt sheets that underlie much of the continental slope (Figure 9.33b; Thrasher et al., 1996).

Venting of hydrocarbon-rich (methane) hypersaline anoxic brines onto the seafloor, both by lateral flow and by diffusion upward through the underlying clastic sediments, gives rise to seafloor seeps, methane hydrates and methane-

saturated anoxic brine lakes ranging in diameter from 1m to 20km. Only microbes (extremophiles) can inhabit the bottom waters and sediments of the brine lakes, while spectacular chemosynthetic mollusc-tube worm biotopes form in normal marine waters about the brine lake edges. Venting brines can either seep and dissipate via mixing with oxygenated marine bottom waters on the open ocean floor to form spectacularly red braided channelways or can seep into closed depressions on the seafloor to form lakes of density-stratified anoxic bottom brine. It is here on the floor of these brine pools that organic- and sulphide-enriched laminites accumulate.

Seepage and drainage onto an open ocean bottom creates loosely consolidated red-orange iron-oxide deposits, with surfaces characterised by anastomose and braided patterns (Aharon et al. 1992). Similar iron-oxide deposits are found about the edges of the Red Sea brine pools. The ferric iron now in the seafloor oxides was originally extracted during the flushing of buried sediment by salt-dissolution-driven convection of anoxic pore waters in the peridiapiric and salt sheet surrounds (Hanor, 1994a). Once vented onto the oxygenated seafloor, the dissolved iron precipitates as haematite and other ferrous hydroxides. In this scenario the seafloor surface itself constitutes a redox front between the reduced basin brines and oxygenated marine waters. Figure 9.34a and b, shows clearly that red iron oxides are stable in the oxygenated conditions that typify the open seafloor (see also Sheu and Presley, 1986a, b).

In contrast, in the more reduced conditions in highly saline subsurface waters and bottom waters of brine pools, precipitated iron phases are dominated by pyrite, siderite and other ferroan carbonates. The pH does not vary widely in such reduced saline settings (Figure 9.34b), and the relationship between pyrite and siderite becomes clearer when activities of dissolved sulphur or dissolved bicarbonate are plotted against Eh. Pyrite is the

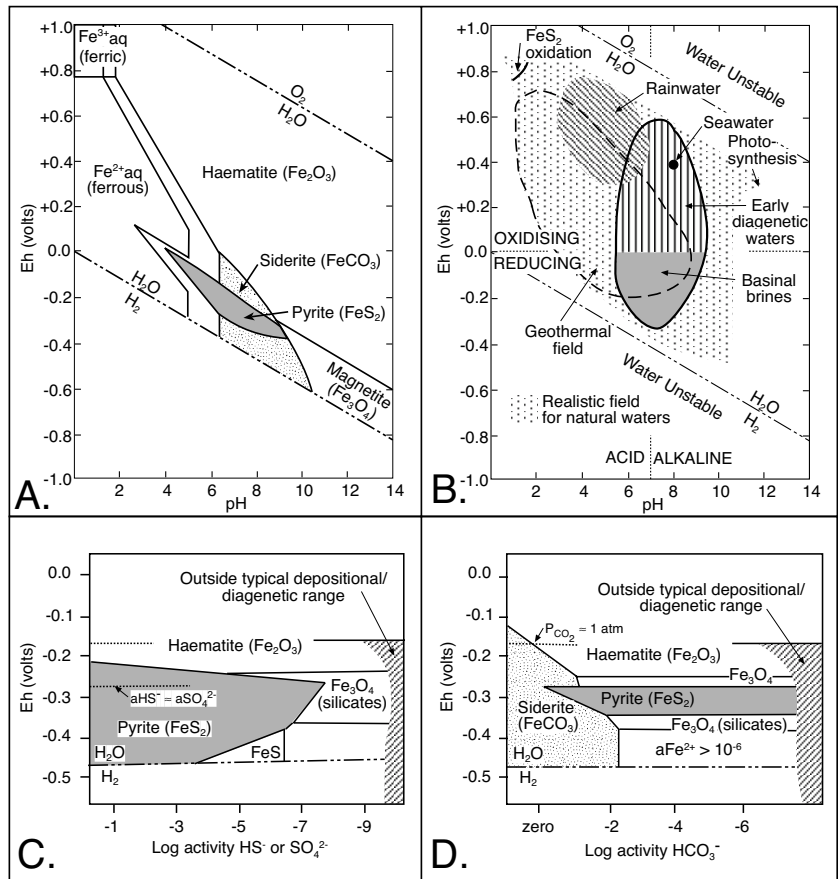


Figure 9.34. Iron stability: phase diagrams showing the stability of iron mineral phases with respect to A) and B) Eh and pH, C) Eh and sulphide/sulphate activity and D) Eh and bicarbonate activity (after Garrels and Christ, 1965; Hesse, 1986; Taylor and Curtis, 1995).

stable phase in anoxic conditions where levels of dissolved sulphide are high (Figure 9.34c), while siderite and other ferroan carbonates are the stable phases under anoxic conditions where the activities of dissolved sulphide are very low and bicarbonate activities are high (Figure 9.34d).

On its way to the surface the same brine chemistry precipitates the pyrite and ferroan carbonate cements in peridiapiric sands as around the Hackberry dome and in the Carrizo sand outcrop (Figure 8.24). It also explains the formation of iron silicates, such as chamosite and berthierine (the Fe_3O_4 silicates in Figure 9.34c, d), in anoxic environments where the activities of both sulphide and bicarbonate are very low. This siliceous Fe-phase chemistry has important implications in terms of the reduction state of Archean and Proterozoic seawater chemistry and the precipitation of banded iron ores (Chapter 2).

	World Mean	Vent GK2	Vent GK11	GOM Surface	GOM Deep
Na	469	3810	1625	500	486
K	10.2	30.1	171.7	10.3	11.1
Ca	10.3	29.3	17.7	8.8	9.7
Mg	52.8	33.1	46.9	53	50.6
Cl	545	3903	1898	589	553
Br	0.84	1.3	2.1	0.86	0.85
SO ₄	28.2	43.6	40.5	30.5	29.7
HCO ₃	1.8	1.8	3.6	2.0	2.0
Sr	0.09	.0617	90.2	.0684	.0845
Li	0.024	.0357	46.3	.0297	.0293
Mn	0.007	.0985	.0723	-	.0017
Fe (x10 ³)	0.06	>1.7	<0.6	-	<0.2
δ ¹⁸ O _{SMOW}	0	0.1	-0.1	1.7	-0.15
δ ¹³ C _{PDB}	0	-2.4	-3.7	0.6	0.6
Cl (‰)	19.37	138.4	67.3	20.9	19.6
T (°C)	25	4.2	4.2	29.3	4.2
pH	8.1	7.35	7.25	8.0	7.6
Depth m	0	1922	1918	0	1958

Table 9.5. Chemistry (mmol/kg) of two venting Green Knoll brines versus surface and deep seawater from the Gulf of Mexico - GOM (after Aharon et al., 1992).

Dense anoxic brines pond in lakes on the modern deep seafloor wherever vented brines can seep into closed depressions. The lows tend to form via local subsidence atop dissolving shallow allochthonous salt sheets or atop areas of salt withdrawal where the underlying salt is flowing into adjacent growing salt structures (growth-fault and rim syncline depressions). The redox interface in such seafloor pools is located at the halocline and so is some metres or tens of metres above the seafloor.

For example, the Orca Basin in the Gulf of Mexico is a closed intraslope depression at a depth of 2,400 metres, some 600m below the surrounding seafloor (Figure 9.35a). Its bottom is filled by a 200m column of highly saline (259‰) anoxic brine that is more than a degree warmer than the overlying seawater column (Figure 9.35b). The pool is stable and has undergone no discernable change since it was first discovered in the 1970s. It is a closed dissolution depression fed by brines seeping from a nearby subsurface salt allochthon (Addy and Behrens, 1980). A large portion of the particulate matter settling into the basin is trapped at the salinity interface between the two water bodies. Trefry et al. (1984) noted that the particulate content was 20-60 μg/l above 2,100m and 200-400 μg/l in the brine column below 2,250m. In the transition zone, the particulate content was up to 880 μg/l and contained up to 60% organic matter.

A core from the bottom of the Orca brine pool captured laminated black organic-enriched pyritic mud from the seafloor to 485 cm depth and entrains 3 intralaminite turbidite beds of grey mud with a total thickness of 70cm (Addy and Behrens, 1980). This is underlain by grey mud from 485 cm to the bottom of the core at 1079 cm. The laminated black mud was deposited in a highly anoxic saline environment, while grey mud deposition took place in a more oxic setting. The major black-grey boundary at 485 cm depth has been radiocarbon dated at 7900 ± 170 years and represents the time when escaping brine began to pond in the Orca Basin depression. Within the dark anoxic laminates of the Orca Basin there are occasional mm- to cm-thick red layers where the iron minerals are dominated by haematite and other iron hydroxides and not by pyrite. These layers represent episodes of enhanced mixing across the normally stable oxic-

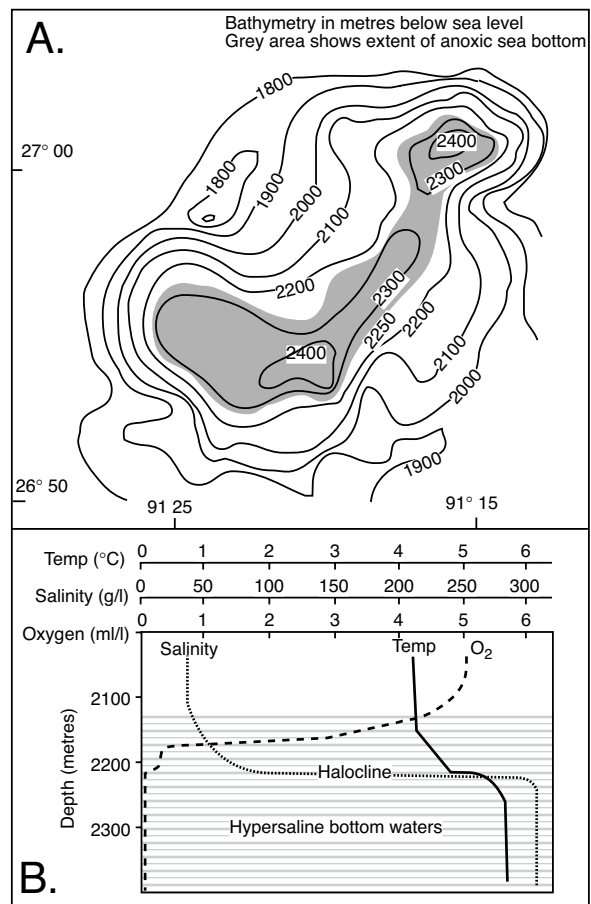


Figure 9.35. Orca Basin, northern Gulf of Mexico. A) Location and bathymetric profile (in metres below sealevel). Grey area outlines the extent of deep highly saline anoxic bottom waters created by the dissolution of nearby allochthonous salt. B) Temperature, salinity and dissolved oxygen profile in the basin (after Williams and Lerche, 1987).

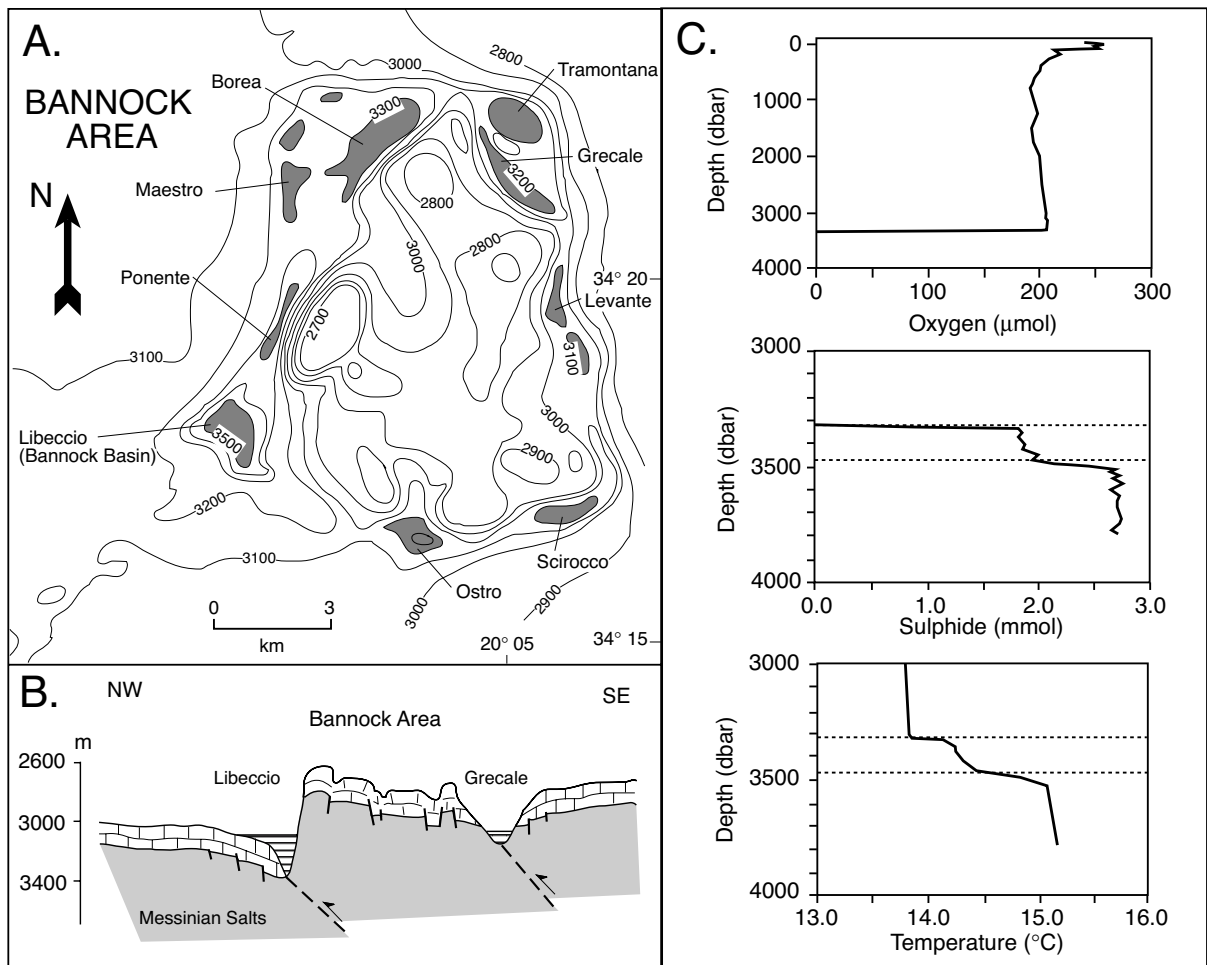


Figure 9.36. Brine pools in the Bannock Basin, Mediterranean Ridge. A) Bathymetry of Bannock area, seafloor contours in metres (after Camerlenghi, 1990). B) Interpreted cross section based on seismic profiles (after Camerlenghi, 1990). C) Water column and brine column characteristics (oxygen, sulphide and temperature profiles; replotted from data tables in Bregant et al., 1990).

anoxic halocline and indicate the short-term destruction of bottom brine stratification.

Brine pools also form in the salt-floored compressive terrain of the accretionary complex of the Mediterranean Ridge where sheets of Miocene evaporites have been folded and thrust to shallow depths below the deep seafloor. The consequent dissolution of Messinian evaporites creates saline brine pools such as the Bannock, Tyro, Discovery, L'Atalante, and Urania brine lakes and basins (Westbrook and Reston, 2002). The Discovery, L'Atalante, and Urania brine lakes constitute what is sometimes referred to as the "anoxic lake region" of the Mediterranean Ridge. The "anoxic lake region" and the brine lakes of the Tyro Basin lie on the growing front of the Hellenic side of the accretionary wedge, while Bannock Basin is located

atop the toe of the accretionary complex (Figure 9.36). Brine lakes on the Hellenic side of the ridge are a response to sediment deformation with a strong diapiric component. Fluids are driven out of the compacting pre-Messinian sediments as it is overridden by the growing Messinian wedges (Figure 5.51). Rising fluids dissolve and breach the evaporite cover wherever it is thin, leading to the escape of hypersaline fluids both ahead of the deformation front and through the pre-Messinian wedge. In contrast, the brine lakes of the Bannock Basin are a result of a seamount as it was dragged into the accretionary complex by the subducting African plate. The disturbance created as it ploughed through evaporites of the accretionary complex allowed hypersaline fluids to escape to the seafloor.

All these lakes occur on the deep-sea floor of the Mediterranean, thousands of metres below the euphotic zone, within depressions that entrain bottom waters more than ten times as saline as Mediterranean seawater. In the Bannock Basin the various brine-filled depressions or sub-basins create a closed outer moat around a central seafloor mound that is 10 km across (Figure 9.36a). The chemical composition of the Tyro Basin bottom brine is related to the dissolution of the underlying halite-dominated evaporites, while the chemical composition of the Bannock Basin (Libeccio Basin in the Bannock area) implies derivation from dissolving bittern salts (de Lange et al., 1990). In the “anoxic lakes region”, sodium chloride is predominant source in the L’Atalante and Urania lakes, but L’Atalante is much richer in potassium chloride than the other lakes. The Discovery basin brine is almost exclusively the product of dissolution of magnesium chloride (bischofite)

salts. It has a density of 1330 kg/m³ which makes it the densest naturally occurring brine yet discovered in the marine environment (Wallmann et al., 2002). Its concentration profile in sediment beneath the brine lake shows the age of this lake is between 700 and 2000 yr. The high concentration of magnesium chloride drives dissolution of biogenic calcium carbonate, but facilitates excellent preservation of siliceous microfossils and organic matter.

Biomarker associations of the organics accumulating in these brine lakes define two depositional styles: typical marine and hypersaline (Burkova et al., 2000). Algal and bacterial biomarkers typical of saline environments were found in layers 0.60 to 0.75 m below the sediment surface in the Tyro Lake Basin, as well as normal marine indicators derived from pelagic fallout (“rain from heaven”). Saline indicators include; regular C-25

isoprenoids, squalane, lycopane, isolycopane, tetraterpenoid and tetrapyrrolic pigments, monoalkyl-cyclohexanes, tricyclic diterpanes, steranes, hopanes, bio- and geohopanes. According to Burkova et al. (2000), the saline organic signatures come from microbial mat layers, redeposited from a Messinian source into the sapropels of the modern depression. Alternatively, they may indicate the activities of a chemoautotrophic community, which flourishes at the halocline or around active brine vents. As in the Orca Basin, the organic content of the bottom sediments of the Mediterranean brine pools is much higher than is found in typical deep seafloor sediment (Figure 9.37a).

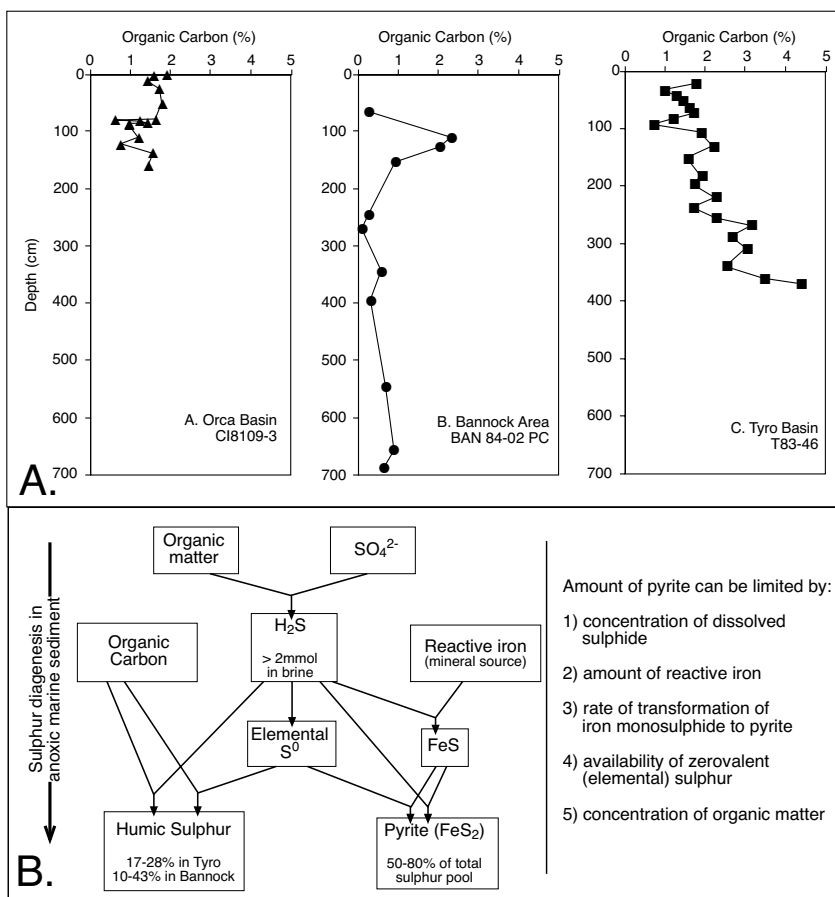


Figure 9.37. Organic characteristics of brine pool bottom sediment. A) Total organic carbon as % dry weight versus depth (plotted from Tyro and Orca data in Table 1 of Sheu, 1987, and Bannock data from Hennecke et al., 1997). B) Modes of occurrence of sulphur in brine pool bottom sediments (after Hennecke et al., 1997).

Anoxic hypersaline brines in Mediterranean brine lakes are highly sulphidic and among the most sulphidic bodies of water in the marine realm, with H₂S concentrations consistently greater than 2-3 mmol (Figure 9.37c; Henneke et al., 1997). The brine body below the Urania chemocline contains up to 11 mM hydrogen sulphide, making it the most sulphidic water body in the known marine realm.

Region of brine occurrence	Salinity (‰)	pH	O ₂ (μM)	H ₂ S (mM)	SO ₄ (mM)	Ca (mM)	Cl (mM)	PO ₄ (μM)	NH ₄ (μM)
Urania Basin (Mediterranean)	200	6.8	0	8.6-11	85	34	2,830	41.2	ND
Libeccio Basin (Bannock area - Medit.)	321	6.5	0	1.67	99	21	5,333	12	3,080
Tyro Basin (Mediterranean)	ND	6.75	0	2.15	49	34	5,350	10	1,260
Orca Basin (Gulf of Mexico)	258	5.5	0	0.60	47	32	5,000	82	500
Seawater (Mediterranean)	39	8.2	200	0	31	11	660	0.2	0.2

Table 9.6. Chemical make-up of various salt allochthon-associated brine pools compared to oxygenated seawater from the Mediterranean (after Sass et al., 2001).

In contrast, there is little to no H₂S in the anoxic bottom brine of the Orca Basin (Table 9.6). There the iron concentration is 2 ppm, a value more than 1000 times higher than in the overlying Gulf of Mexico seawater. Such high levels of reducible iron in the Orca Basin are thought to explain the lack of H₂S in the bottom brine and a preponderance of framboidal pyrite in the bottom sediments (Sheu, 1987). Both the Orca Basin and the brine pools on the floor of the Mediterranean show sulphate levels that can be more than twice that of the overlying seawater.

Pyritic sulphur is the main phase of inorganic reduced sulphur in the Tyro and Bannock basins, where it makes up 50-80% of the total sulphur pool. It is also present at the same levels in cores from the two basins, that is, around 250 μmol per gram dry weight (Figure 9.37b; Henneke et al., 1997). Humic sulphur accounts for 17-28% of the total sulphur pool in the Tyro Basin and for 10-43% in the Bannock Basin. Sulphur isotope data show negative δ³⁴S values for both pyritic sulphur, with δ³⁴S = -19‰ to -39‰; and for humic sulphur, with δ³⁴S = -15‰ to -30‰; indicating that both pyritic and humic sulphur originated from microbially produced H₂S within the brine column.

Marine sediment fills in all the active brine lakes of the Mediterranean Ridge range in age from Holocene to Late Pleistocene and are typically made up of turbidites interlayered with laminated intervals composed of alternating green gelatinous muds and grey reduced oozes. Usually, the density of the bottom brine layer in the Bannock region is high enough to support a layer of finely dispersed organic debris, allowing substantial bacterial mats to float at the seawater-brine interface (halocline) and so form suspended deep mid-water bacterial mats (Erba, 1991). While the organics float on the oxic side of the halocline they are subject to oxidation and biodegradation (Figure 9.8). Owing to the high density of the bottom brines, moving this floating organic material to the floor of density-stratified brine pools appears at first to be a difficult proposition. Bottom sediments in the Urania Basin for example contains very little particulate organic matter (>1% TOC). Yet, organic contents in the anoxic

bottom muds beneath Tyro and Orca basins can be as high as 4-5% organic carbon (Figure 9.37a). The propensity for organics to remain suspended at the halocline can be overcome when mineral crystals, including pyrite, precipitate at the interface via diffusive brine mixing in combination with bacterial sulphate reduction. Newly formed crystals attach to organic matter floating at the halocline to create a combined density that carries the suspended pellicular organics to the pool floor. In such a brine pool scenario, the redox front that fixes pyritic sulphur occurs at the halocline, and not at its more typical marine position located at or below the sediment-seawater interface.

Organic debris, first formed at the halocline, then accumulated as pellicle layers within the pyritic bottom muds (laminites). Pellicular debris is also carried to the bottom during the emplacement of turbidites when the halocline is disturbed by turbid overflow (Figure 9.38; Erba, 1991). Hence, pellicular layers are typically aligned parallel to lamination, or are folded parallel to the sandy bases of the turbidite flows, or line up parallel to deformed layers within slumped sediment layers. Individual pellicle layers are 0.5 to 3 mm thick and dark greenish-grey in colour. Similar pellicular layers cover the surface of, or are locked within, recent gypsum crystals recovered from bottom sediments of the Bannock area. This gypsum is growing today on the bottom of the Bannock Basin, atop areas about the brine pool margin that are directly underlain by dissolving Miocene evaporites (Corselli and Aghib, 1987). Other than the Dead Sea, it is one of the few modern examples of a deepwater evaporite, but its seepage-fed genesis means it is a poor analogue for deepwater basinwide salt units.

The community of bacteria and archaea flourishing at the halocline in sulphidic marine brine pools is quite diverse and largely independent of primary production in the euphotic zone. Bottom brine in the Urania brine lake has a salinity of 162‰ and the chemocline of the brine lake is some 3490m below the ocean surface, so only a very small amount of phytoplanktonic organic carbon ever reaches the 20m thick chemocline. Yet the oxic waters of the upper part of the chemocline support a rich

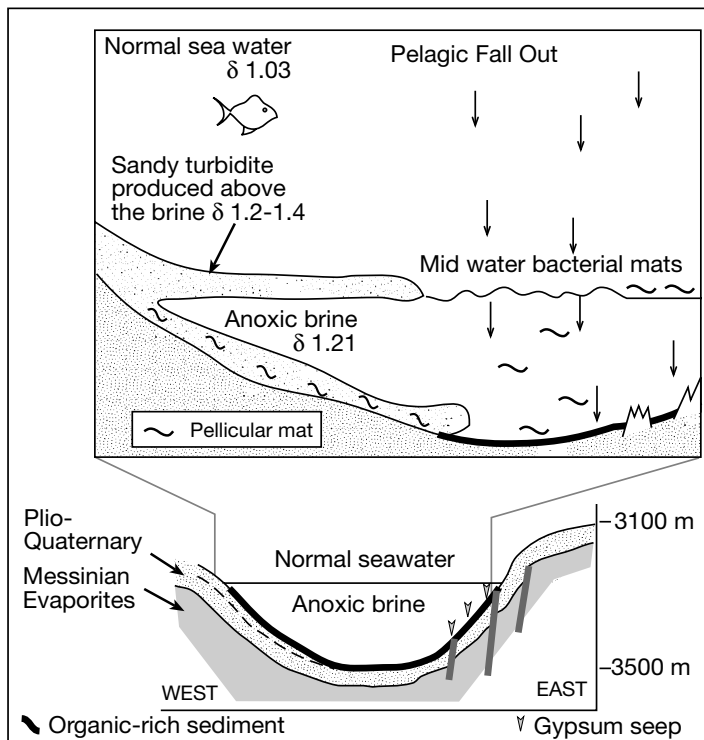


Figure 9.38. Formation and sedimentation model for pellicles in Mediterranean seafloor brine lakes. Bacterial (pellicular) mats grow mid-water at the interface between normal seawater and anoxic brine and trap biogenic and inorganic particles. When pelagic sedimentation prevails, pellicles sink to the basin floor after load increases to breach levels at the halocline interface (right side). Occasional turbidity currents and sediment slumping disrupts the interface, destroys the floating mat layer and transports fragments of pellicles to the basin bottom as part of coarser sandier layers (after Erba, 1991).

bacterial assemblage in the interface between the hypersaline brine and the overlying seawater, much like the bacterial community atop the halocline in Lake Mahoney (Figure 9.39; Sass et al., 2001). Sulphide concentration increases from 0 to 10 mM within a vertical interval of 5 m across the interface. Within this chemocline, the total bacterial cell counts and the exoenzyme activities are elevated. Bacterial sulphate reduction rates measured in this layer are $\approx 14 \text{ nmol SO}_4 \text{ cm}^{-3} \text{ d}^{-1}$ and are among the highest in the marine realm. They correspond to the zone of maximum bacterial activity in the chemocline. Particulate organic content is 15 times greater than that in the overlying normal marine waters. Employing 11 cultivation methods, Sass et al. isolated a total of 70 bacterial strains from the chemocline. These strains were identified as the flavobacteria, *Alteromonas macleodii*, and *Halomonas aquamarina*. All 70 strains could grow chemo-organoheterotrophically under oxic

conditions. Twenty-one of the isolates could grow both chemo-organotrophically and chemo-lithotrophically (decomposers and fermenters). While the most probable numbers in most cases ranged between 0.006 and 4.3% of the total cell counts, an unusually high value of 54% was determined above the chemocline with media containing amino acids as the carbon and energy source.

In another brine lake, the Kebrut Deep on the deep floor of the Red Sea, halophilic archaea flourish in hypersaline waters below the chemocline. Under strictly anaerobic culture conditions, novel halophiles were isolated from samples of these waters and belong to the halophilic genus *Halanaerobium*. They are the first representatives of the genus obtained from deep-sea, anaerobic brine pools (Eder et al., 2001). Within the genus *Halanaerobium*, they represent new species which grows chemoorganotrophically at NaCl concentrations ranging from 5 to 34%. They contribute significantly to the anaerobic degradation of organic matter, which formed at the brine-seawater interface and is slowly settling into the bottom brine.

Neither Tyro or Bannock Basin bottom sediments show a significant correlation between pyritic sulphur and the organic carbon in the bottom sediments, suggesting predominantly syngenetic pyrite formation in bottom sediments of these brine lakes (Henneke et al., 1997). That is, both pyritic and humic sulphur preserved in the bottom sediments formed either in the lower water column or at the sediment-brine interface, not in the sediment itself. Ongoing diagenetic processes within the bottom sediments only form an additional 5% of the total pyrite. Van der Sloot et al. (1990) clearly showed that metal sulphides, as well as organics and other minerals, precipitate at the brine-seawater interface in the Tyro Basin. They found extremely high concentrations of Co (0.015%), Cu (1.35%) and Zn (0.28%) in suspended matter at the halocline. These high particulate Co, Cu and Zn concentrations correspond to sharp increases in dissolved sulphide across the interface (a redox front), and indicate precipitation of metal sulphides at the interface (Figure 9.36c). Humic sulphur in the bottom sediments correlates with the pyritic sulphur distribution and is related to the amount of gelatinous pellicle derived from bacterial mats growing at the halocline between oxic seawater and bottom brine (Erba, 1991, Henneke et al., 1997).

Additionally, the degree of pyritisation in the sediments (DOP ≈ 0.62) indicates that present-day pyrite formation is limited by the reactivity of Fe in the Bannock and Tyro basins and not by the availability of organic matter, the latter being the process that limits pyrite formation in most normal marine settings. The degree of pyritisation (DOP) is defined as [(pyritic iron)/(pyritic iron + reactive iron)]. Raiswell et al. (1988) showed that DOP in ancient sediments can distinguish anoxic from normal marine sediments. Anoxic sediments show DOP values between 0.55 and 0.93, while normal marine sediments have DOP values less than 0.42. The DOP levels in the Bannock and Tyro basins confirm observations made in ancient anoxic sediments. Thus, although the Tyro and Bannock basin brines differ in their major element chemistry, reflecting a different salt source, their reduced sulphur species chemistry appears to be similar, but significantly different from normal marine systems and capable of precipitating metal sulphides above the sediment surface.

Pools of hypersaline, anoxic brines, underlain by laminated pyritic organic-rich sediments, are far more widespread in halokinetic terrains than just in the Orca, and Mediterranean Ridge basins. For example, similar brine seeps and pools have now been documented atop and adjacent to numerous salt allochthons along much of the continental slope of the Gulf of Mexico. In the Green Canyon area, wherever shallow allochthonous salt sheets are dissolving just beneath the seafloor, organic-enriched pyritic sediments are also commonplace (Figure 9.40a, b; Reilly et al., 1996). Similar cool-seep systems are active today along the foot of the Florida Escarpment and the Blake Ridge, where they are focused and in part fed by subadjacent dissolving salt allochthons (Paull et al., 1992).

Edges of salt allochthons do not just focus the upward flow of escaping subsurface waters into brine lakes along minibasin margins, they also focus the upward escape of gaseous and liquid hydrocarbons. Where sea bottom temperatures are suitable, gas hydrates can form atop focused outflow zones.

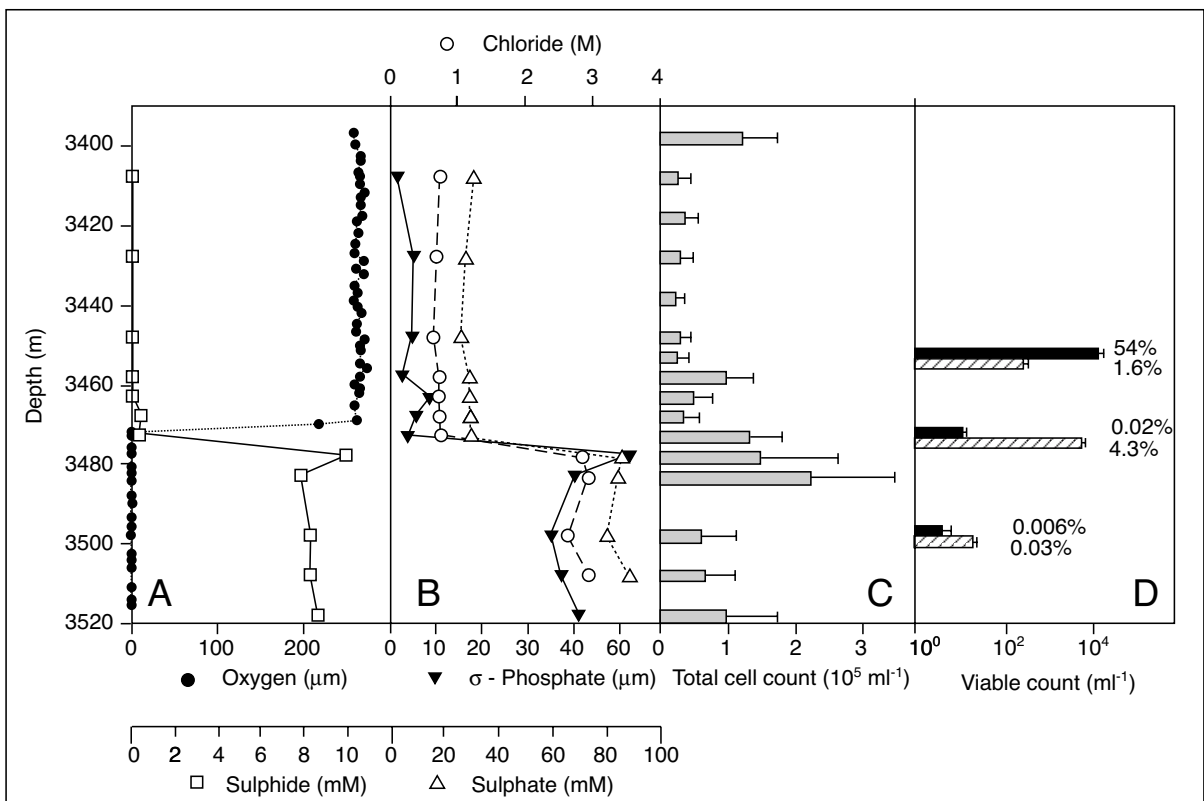


Figure 9.39. Physicochemical parameters, total cell counts, and MPN across the oxic-anoxic boundary of the Urania Basin, Mediterranean Ridge (after Sass et al., 2001). A) Oxygen and sulphide concentrations; B) Sulphate, orthophosphate and chloride concentrations; C) Total cell counts; D) Viable cell counts in anoxic media containing the amino acid mixture (solid bars) and in oxic media containing thiosulphate (cross-hatched bars). The percentages are relative to the total cell count and the error bars indicate standard deviation.

A light-independent chemosynthetic seep biota can grow and flourish in regions of hydrocarbon (methane) and H_2S focused outflow (Figure 9.40b).

Gas hydrate or clathrate is an ice-like crystalline mineral in which hydrocarbon and nonhydrocarbon gases are frozen within rigid molecular cages of water. They can be thought of gaseous permafrost. Their occurrence is not just tied to the cold temperature portion of the deep seafloor; clathrates are the dominant seals to large gas reservoirs in the permafrost regions of Siberia. Methane hydrates are commonplace associations where methane (often biogenic) occurs just below the deep cold seafloor and can accumulate in many seafloor regions independent of any evaporite occurrence. Clathrate formation on the seafloor requires bottom temperatures not encountered until the seafloor bottom lies beneath a water column 450-500 m deep.

Beneath the clathrate covered seafloor, temperature increases with depth and this limits the depth at which gas hydrates will occur; below it an accumulation of free gas is likely.

Thus, clathrates are not unique to, but are often very obvious about, salt allochthon edges where salt flow induces extensional faulting (Chapter 6). This in turn acts as focusing mechanism for escaping thermogenic and biogenic methane and other gases (Figure 9.40; MacDonald et al., 2000, 2003). Rapid burial of organic-entraining sediments in supra-allochthon minibasins encourages the creation of biogenic methane that sources much of the gas escaping to the seafloor. Hence, in the salt allochthon province of the northern Gulf of Mexico there is a definite association between brine pool chemosynthetic communities, thicker gas hydrates and the edges of minibasins (Figure 9.40; Reilly et al., 1996; Milkov and Sassen, 2001).

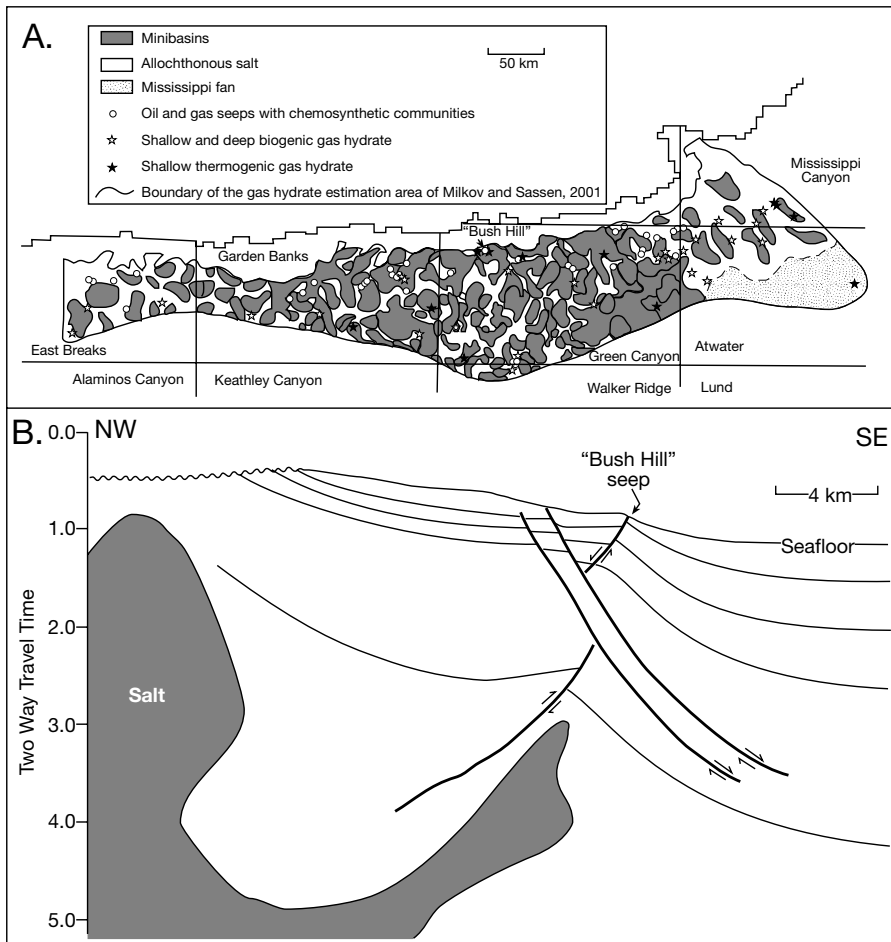


Figure 9.40. Seeps in the northern Gulf of Mexico. A) Documented occurrences of seeps and methane hydrates (after Milkov and Sassen, 2001). B) Interpretation of seismic line showing strong structural control on location of the chemosynthetic seep at "Bush Hill" (after Reilly et al., 1996).

The escape of nutritive methane and H_2S from these brine-filled pockmark pools and lakes supports symbiont-containing mussel and tubeworm communities, which can construct dense biostromes around the brine pool rims. This mussel-tubeworm dominated biota is the cold water equivalent of the chemosynthetic hydrothermal communities flourishing in the vicinity of black smoker vents (MacDonald, 1992; MacDonald et al., 2003). In both settings it is methane and sulphide, not light, that provides the energy source for the bacteria and archaea that make up the base of the food chain. Methanogenic archaea live symbiotically on the mussels' gills, take in methane and convert it to nutrients that nourish the mussels. Seep mussels (*Bathymodiolus childressi*) continually waft methane-rich water through their gills to help the archaea grow and periodically harvest some

of the excess growth. Their lifestyle means that seep mussels need to live near a supply of dissolved gas, they may inhabit isolated zones on the floor where gas is bubbling out but do best about the edges of methane-saturated brine pools and will grow in any fringe area to the pool, wherever they can keep their siphons above the halocline.

Likewise, the polychaete tubeworms (*Hesiocaeca methanicola*) are chemotrophs with a microbe-dependant metabolism. Microbial sulphate reducers live in the anoxic sea-floor sediments near seeps as they convert escaping hydrocarbons and seawater sulphate into H_2S . Tubeworms take up this hydrogen sulphide, along with oxygen, and provide them as nutrients to sulphur-oxidising bacteria living symbiotically in trophosome structures that extend for up to 75% of the length of the tube worm.

Interestingly, when they were first collected, figuring out what these giant tubeworms (*Riftia pachytila*) lived on in deep dark waters was especially mystifying because they had no mouths, guts, or anuses! They were first thought to be absorbing tiny food particles through their skin. The function of the trophosome was unknown but thought to be related to dealing with toxicity not feeding, after all these structures were lined with what was thought to be extruded sulphur crystals. It is now known that the sulphur-oxidising bacteria, which inhabit the trophosome cells, use H_2S to produce nutrients in the form of organic carbon for the tubeworms to metabolise. Elemental sulphur is the common metabolic intermediate in sulphur-oxidising bacteria (Figure 9.11a). Tubeworm colonies or “bushes” in cold seep regions of the Gulf of Mexico are typically rooted in the H_2S -rich muds giving the colony a morphology similar to a tree or shrub, with “roots” extending into the earth and branches extending above. Growing individuals actively extend down into the H_2S -rich mud as well as up into the O_2 -rich water column. It seems that these tubeworm shrubs can absorb H_2S through their “roots” and O_2 through their “branches” (Freytag et al., 2001).

Although individuals may live for more than 300 years, vagaries in the rate of brine and nutrient supply to the seafloor mean many mussels and tubeworms colonies can be overwhelmed by a rising halocline and so die in a short space of time. Their partially decomposed remains can spread out as part of the organic-rich debris atop the halocline, along with bacterial, algal and faecal residues, where it is acted upon by a rich community of aerobic and anaerobic decomposers. If it is mineralised it sinks to the anoxic bottom, where it is largely preserved and protected from further biodegradation. The inherently unstable nature of the seafloor in the vicinity of active salt allochthons and brine lakes means parts of the biostrome are periodically

killed “en masse” as sediment about a brine pool edge collapses, slumps and slides into anoxic pool waters, carrying with it the chemosynthetic community. As well as further elevating levels of preserved organics in the brine pool bottom sediments, this process also creates potential fossil lagerstätte (“death communities”). Cretaceous counterparts to these methanogenic brine systems have been documented in the Canadian Archipelago where methane-rich mound seeps, dominated by fossiliferous fibrous calcite and aragonite hardgrounds, grew atop growth faults activated by salt diapirism in the Sverdrup Basin (Savard et al., 1996).

If the evaporite indicators in ancient counterparts of all these brine pool/seep systems are not recognised, then, once the associated allochthonous salt sheets have dissolved or moved on, the evaporites that focused the accumulation of organic-rich pyritic brine pool sediments will become an enigma (Warren, 2000b). In the Phanerozoic, any remaining organic constituents will be made up primarily of marine plankton, a benthic marine biota and bacteria from a normal marine setting. Sediments above and below the pyritic pellicular laminites are also made up of normal marine deepwater deposits. There will be little geochemical evidence to show that these organic-rich pyritic sediments were preserved in a hypersaline deep marine environment. Evidence of the significance of evaporites in creating such a sequence will only come from sedimentological and structural analysis of core or outcrop from below and adjacent to the laminites, and the recognition of halokinetic breccias, salt welds, chemosynthetic biostromes and marine-cemented hardgrounds within a deeper water marine sediment matrix.

Subsurface organic-sulphate reactions

As organic matter in evaporitic sediments is buried it becomes hotter, it can also be anomalously heated locally by intrusions and crossflows of fault-focused hydrothermal fluid. It is altered in a number of ways, all tied to rates of temperature increase in the presence or absence of oxygen in the pore fluids (Figure 9.41). The subsurface interface between hypersaline waters (typically with reducing dysaerobic to anaerobic chemistries) and less saline waters (typically with more oxidised and oxygenated chemistries) creates redox fronts in aquifers adjacent to subsurface evaporites and is often defined by a colour transition from green (reduced) to red (oxidising) in the sediment matrix. Less saline waters tend to dissolve evaporites and create secondary porosity (mostly vuggy and collapse fracture), while

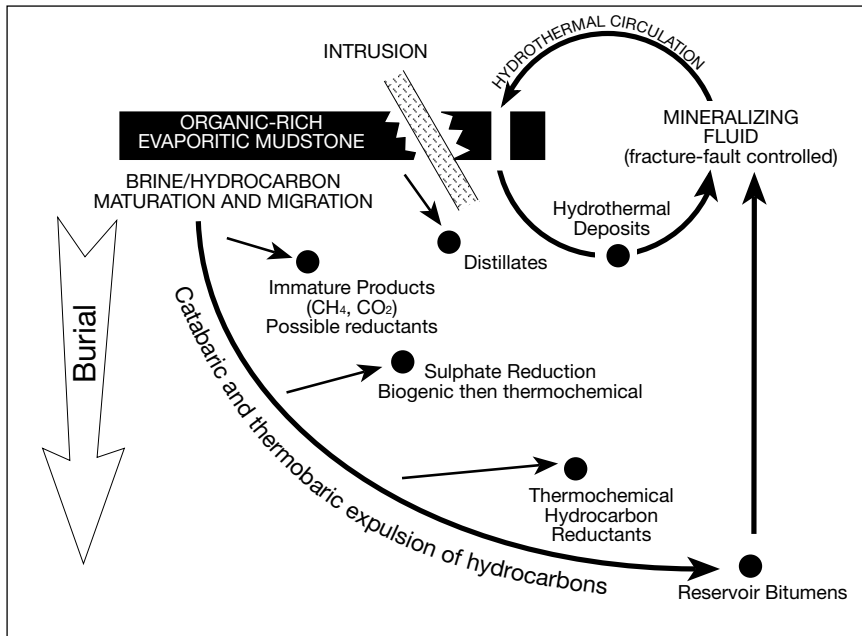


Figure 9.41. The role of organic-rich evaporitic mudstones in burial diagenesis. The mudstones can act as a source of hydrocarbons and as a reductant for metals.

at the same time chloride or sulphate passes into solution. Where the sulphate in solution interacts with the organics in the vicinity of the redox interface, H_2S is generated via sulphate reduction. It can dissolve any adjacent carbonate, which is reprecipitated as calcite cement, along with pyrite and other metals on the reducing side of the interface (Figure 9.41). Much of the H_2S that is found in elevated amounts in an evaporitic basin is bacterially or thermochemically generated by sulphate reduction from sulphate carried by brine and derived from dissolving sulphate beds. Additional H_2S in an evaporite basin can be generated from local magmatic and biogenic sources.

Any association of dissolved sulphate and hydrocarbons (organic matter) is thermodynamically unstable in all diagenetic settings and the chemical response is sulphate reduction (Machel, 2001). Sulphate reduction reactions can be bacterially mediated through the activities of sulphate-reducing bacteria (bacterial sulphate reduction-BSR) or inorganically mediated under conditions of increased temperature and pressure (thermochemical sulphate reduction - TSR). Both scenarios require the presence of preserved organic matter, or its more evolved subsurface equivalent in the form of hydrocarbons (oil or gas), and result in similar but not identical carbonate cements, mostly calcite. The bacterially mediated system operates at lower burial temperatures

<110°C, mostly <60–80°C, in a temperature range equivalent to vitrinite reflectances R_o of 0.2–0.3. Thermochemical sulphate reduction processes require temperatures of more 120°C and R_o values ranging from 1.0 to 4.0 (Figure 9.42).

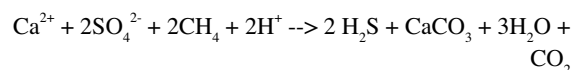
Bacterial sulphate reduction (BSR)

BSR takes place in surface and nearsurface environments where sulphate-reducing bacteria utilise dissolved sulphate and organics/hydrocarbons to produce H_2S (Figure 9.42a, c; Trudinger et al., 1985; Machel, 1987, 2001; Hill, 1995; Riciputi et al., 1996; Aref, 1998b). So far we have discussed bacterial sulphate reducers in the context

of stratified brine columns, where they flourish in anoxic waters beneath the halocline, or in benthic cyanobacterial mats where they occupy the low anoxic portions of the mat. In this section we will look at the nature of BSR in the subsurface.

Bacterial sulphate reduction occurs at temperatures typically <80°C, although hyperthermophilic archaeal sulphate-reducers (*Archaeoglobus* sp.) can grow around hydrothermal vents on the deep ocean floor at temperatures up to 110°C. In regions with normal geothermal gradients the temperature range <60–80°C corresponds to burial depths from the surface down to 2000–2500m. BSR processes and bacterial sulphate reducers are widespread in many other anoxic subsurface sediments unrelated to evaporites. But the discussion in this section concentrates on those types of sulphate reduction that are commonplace in regions of dissolving evaporites and saline pore waters. Such systems tend to form bioepigenetic limestones and cements with textures and isotopic signatures indicating its evaporite precursor or association.

Bacterial sulphate reduction is usually expressed by the equation;



At pH<6-7 the produced H₂S is undissociated; at pH>6-7, H₂S dissociates so that H₂S → H⁺ + HS⁻ (Hill, 1995). In this equation, SO₄ indicates dissolved sulphate, which is derived either from shallow phreatic refluxing brine/seawater or from dissolving sulphate evaporites such as gypsum, glauberite, or anhydrite. CaCO₃ represents bioepigenetic limestone products, which typically precipitate as cements or replacements of precursor evaporite sulphates. CH₄ represents a host of possible organic compounds or hydrocarbons, mostly organic acids and other products of aerobic or fermentative biodegradation.

There are two well established genera of sulphate-reducing bacteria, *Desulphovibrio* and *Desulphotomaculum*, they seem to be quite unrelated to each other and their relation to other bacterial groups is also obscure.

Members of better known genus, *Desulphovibrio*, are mesophilic (prefer a moderate temperature range) and can be moderately halophilic (Figure 9.11b); the genus is thought to contain seven species at the present time. *Desulphotomaculum* species are somewhat more difficult to isolate and purify. They are characterised by spore formation and are sometimes thermophilic; only one moderately halophilic strain has been reported in the five recognised *Desulphotomaculum* species (Postgate, 1984).

Mesophilic isolates of the genus *Desulphovibrio* will typically not grow above 45°C. Thermophilic isolates of the *Desulphotomaculum* genus have been grown at temperatures as high as 70°C - the most common species of thermophile being *Desulphotomaculum nigrificans*. However, Rozanova and Khudyakova (1974) isolated an apparent *Desulphovibrio* sp. having a

maximum growth temperature of 85°C, while Zobell (1957) claimed that he had isolated viable sulphate-reducing bacteria from an oil-bearing reservoir where growth was occurring at 104°C under a pressure of 1000 atm. Both these higher temperature reports were not biologically documented under noncontaminated conditions. The upper temperature limit for subsurface biogenic sulphate reduction is usually considered to be 80-85°C (Trudinger et al., 1985), a reasonable estimate for documented sulphate reducers in most evaporitic and shallow subsurface settings. It means the most vigorous bacteriogenic reduction (>50°C) typically extends from any nutrient-rich brine column oxic-anoxic interface down to redox fronts at burial depths of a kilometre or so.

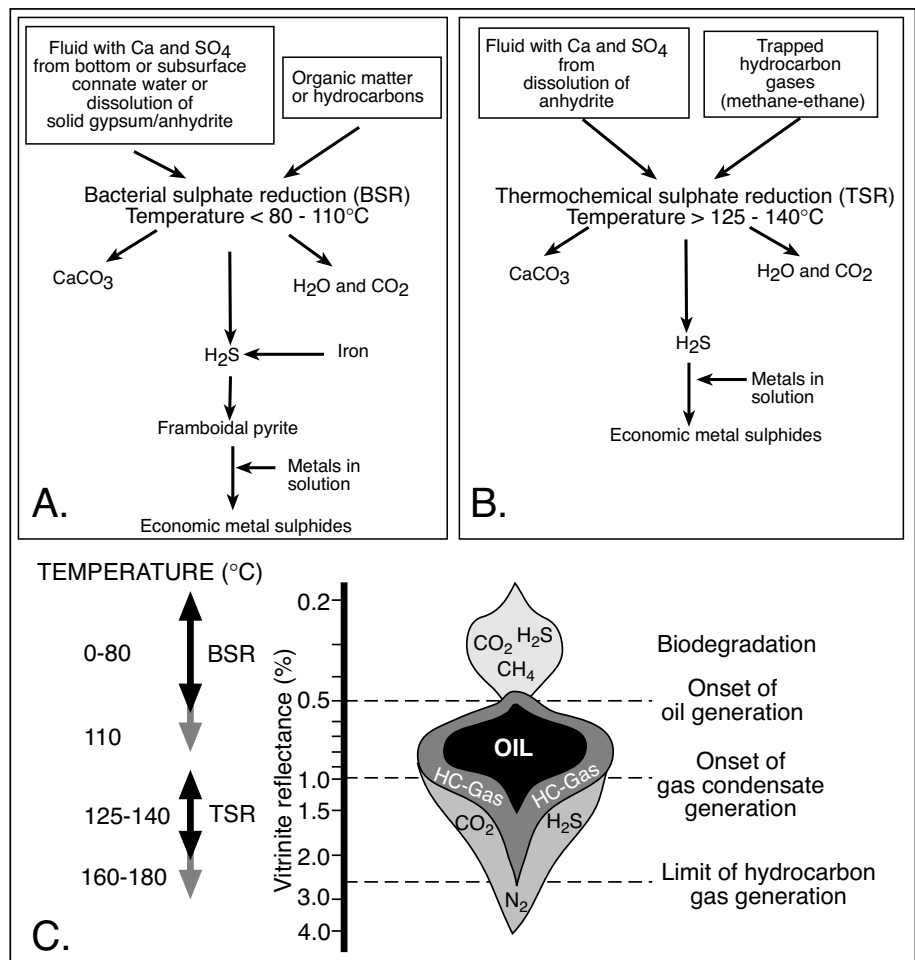


Figure 9.42. Chemical pathways and thermal regimes associated with sulphate reduction. A) Bacterial sulphate reduction - BSR. B) Thermochemical sulphate reduction - TSR. C) Thermal regime and hydrocarbon generation stages tied to characteristic values of vitrinite reflectance (in part after Machel, 2001; Warren, 2000b) Note that there is a lack of biogenically produced pyrite framboids during thermochemical sulphate reduction.

Under suitably pressurized deep-sea bottom conditions, and perhaps some subsurface conditions, biogenic sulphate reduction may extend into higher temperature regions. Work in the anhydritic deep-sea hydrothermal vent sediments of the Guaymas Basin in the Gulf of California has revealed biologically-mediated sulphate reduction by hyperthermophilic Archaea at temperatures up to 110°C, with an optimal rate at 103-106°C (Huber et al. 1989; Jørgensen et al., 1992). But such hyperthermophilic sulphate reducers are not recovered from formation brines of most subsurface hydrocarbon-rich settings, otherwise sweet oils would be a rare style of oil occurrence at temperatures less than 110°C (Machel, 2001).

Bacterial sulphate reduction in evaporitic settings typically occurs near an aerobic/anaerobic interface. It may be a density interface in a layered brine column, it may be at the aerobic-anaerobic interface just below the sediment surface, it may be at an oil/water contact at greater depths, or it may be a subsurface diffusion or mixing zone, focused by faults, fractures and bedding boundaries. Wherever hydrocarbons are involved, most sulphate-reducers cannot directly digest long chain n-alkanes (paraffins) as nutrients. Instead, they depend on metabolic residues of hydrocarbon biodegradation, such as the various organic acids produced by aerobic biodegradation of oil (Davis and Kirkland, 1970; Machel, 1987). Thus, sulphate reducers are anaerobes but typically depend on aerobic bacteria to create suitably biodegraded hydrocarbon substrates.

Sulphate-reducing bacteria then oxidize the biodegraded hydrocarbons to HCO_3 and bitumen residues, while simultaneously reducing the dissolved sulphate to H_2S . Where methane is the main carbon source, all the methane is oxidized into HCO_3 , and no bitumen residue forms (Machel, 1989). Production of H_2S favours the precipitation of carbonate cement or the replacement of dissolving sulphates by calcite. H_2S may escape into the atmosphere or come into contact with dissolved oxygen in an aquifer or a diffusion zone, where it is oxidized into elemental sulphur, as in most shallow sulphur deposits (Chapter 11; Berner, 1980).

Growth of sulphate-reducing bacteria is typically restricted to anoxic pore waters with a pH of 5 - 9. The creation of anoxic microniches means there are many saline depositional situations where the bacterial sulphate-reducers flourish locally, usually within millimetres of oxygenated seawater or brine. For example, at the local scale much of the micrite precipitated as marine stromatolite laminae in metre-high structures in tidal channels of the Bahamas (Chapter 1) are a byproduct of bacterial sulphate reduction. This BSR-induced precipitation

occurs within millimetres of normally oxygenated seawater (Visscher et al., 2000). Likewise BSR controls the precipitation of microbial carbonate in mm-layered mats in a modern hypersaline lake on Eleuthera Island in the Bahamas (Dupraz et al., 2004) and primary dolomites in Brazilian coastal salines (Figure 4.16). At broader subsurface scales, anoxic interfaces suitable for BSR tend to form near the dissolving margins (top or bottom) of shallow salt beds and allochthons, or within diapir caps, or near fractures and other breaches in dissolving calcium sulphate beds. These are all sulphate-rich environments where focused crossflow and mixing occurs between reduced basinal waters and more oxic waters.

Sulphate-reducing bacteria are responsible for the laminar vuggy bioepigenetic limestones that make up the caprocks of the Gulf Coast and Zechstein diapirs (Kyle and Posey, 1991; Peckmann et al., 1999), the Castile Formation mounds (castiles) of the Gypsum Plain, Culberson County, west Texas, the Messinian Gessoso Solifera of Sicily, as well as numerous other calcitic limestones that replace sulphate evaporites worldwide (Figures 6.63, 7.9, 7.45a, 11.58, 11.59). Subsequent weathering of the encasing gypsum means calcitic buttes can form irregular steep-sided hills in areas, as in the Castiles rising 3 to 30 m above the Gypsum Plain of west Texas (Kirkland and Evans 1980). Castile calcite masses did not precipitate at the surface, they originally formed hundreds of metres below the surface (Figure 7.45a). The bacterial/hydrocarbon association of these bioepigenetic limestones is clearly seen in their negative $\delta^{13}\text{C}$ signatures (Figure 9.43a). Carbon in calcite making up a Castile is sourced by the breakdown of organic matter or hydrocarbons and does not come from dissolution of marine limestone. Sulphate-replacing calcites formed by BSR are typically ^{13}C depleted, and this isotopic signature, along with their more negative sulphur isotope signature (compared to marine sulphates), is used to characterise BSR-induced calcites worldwide (Figures 9.43 and 7.48).

Widespread bioepigenetic limestone buttes or castiles today outcrop in areas of exhumed Miocene evaporites along the margin of the Red Sea (Aref, 1998b; Pierre and Rouchy, 1988). There the carbonate masses are vuggy and form irregularly stratiform limestones within or capping beds of sulphate evaporites. As in the Castiles of west Texas and the diapir caprocks of the Gulf Coast, the Red Sea buttes are stained by hydrocarbon residues and smell of hydrocarbons when broken with a hammer. Associated natural sulphur (S_2) is usually yellow, but may be brown to black due to bitumen staining. The carbonate masses replacing the gypsum or anhydrite are made up of varying amounts of aragonite, calcite, or dolomite. $\delta^{13}\text{C}_{\text{PDB}}$ mean values

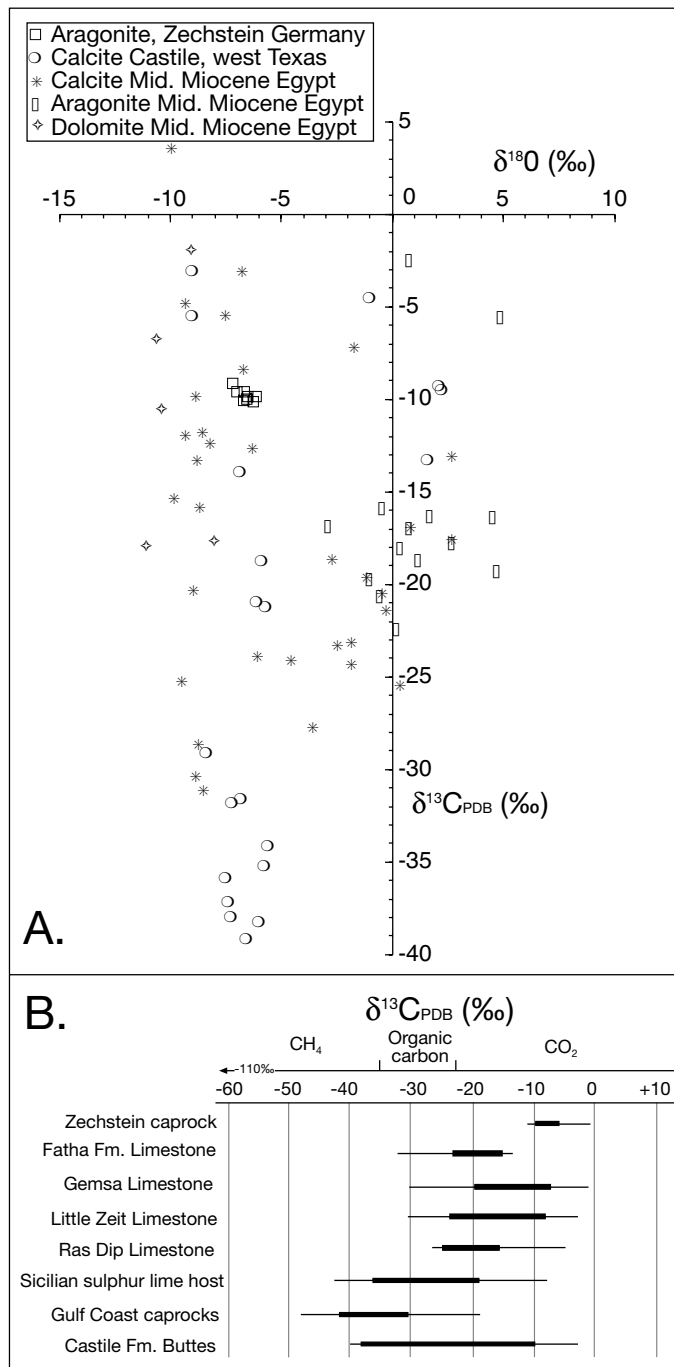


Figure 9.43. Stable isotope signatures of bacterial calcite. A) Outcropping samples from calcite buttes of the Castile Formation, Delaware Basin, west Texas, various Middle Miocene outcrops along the Red Sea coast and aragonite inclusions in gypsum of Zechstein, Germany. B) Bioepigenetic carbonates from Miocene of Gulf of Suez, caprocks in the Gulf of Mexico, sulphur deposits of Sicily and Castile Fm. buttes in west Texas. Thin line indicates range, thick line plots standard deviation about mean (Both figures replotted from data in Aref 1998b; Jassim et al., 1999; Kirkland and Evans, 1976; Peckmann et al., 1999; Pierre and Rouchy, 1988 and references therein).

for carbonate minerals typical of organic-derived signatures and ranging from -3.3 to -31.3 ‰ (Figure 9.43a). There is some overlap, but most are heavier than the $\delta^{13}\text{C}$ values of nearby crude oils (-28.1 to -29.3 ‰). Oxygen values from the Red Sea castiles define two groups. One is clustered around 0 ‰ and is dominated by aragonitic mineralogies with lesser calcite and is thought to indicate BSR replacement of gypsum that occurred soon after deposition. The other group is mostly calcite and dolomite, its $\delta^{18}\text{O}$ values range from -6 to -11 ‰ and is interpreted as a later meteoric-influenced BSR, occurring during halokinetic uplift and flushing of rising diapir caps by fresher groundwaters, this stage is akin to that forming the patchy BSR limestones in caprocks atop coastal plain diapirs in the Gulf of Mexico.

Microbial creation of stratiform bioepigenetic limestone is a widespread but under-recognised process at the dissolving edges of many gypsum/anhydrite masses. It typifies near surface seeps in the Fergana and Amudarya depressions of central Asia and the Mesopotamian depression in Iraq (Jassim et al., 1999). Bedded examples of coarsely crystalline gypsum replaced by texturally similar bioepigenetic calcite characterise contacts of some Upper Miocene gypsum outcrops in the Lorca Basin (Rouchy et al., 1998). Likewise the Ratynsky Limestone, with its characteristic light carbon signature and sulphur association, is a bioepigenetic limestone bed that defines the top of outcropping and subcropping artesian gypsum karst in the western Ukraine (Andrejchuk and Klimchouk, 2001).

Thermochemical sulphate reduction (TSR)

During thermochemical sulphate reduction, H_2S is produced as sulphate is inorganically reduced, via inorganic reactions with hydrocarbons, at temperatures typically in excess of 140°C, which is much too hot for any life (Figure 9.42b, c; Worden et al., 1995; Heydari 1997; Machel, 2001). Reactive hydrocarbons caught up in the TSR reaction are mostly branched and n-alkanes, followed by cyclic and mono-aromatic species in the gasoline range. Historically, the efficiency of thermochemical sulphate reduction in producing H_2S was inferred from experimental evidence or from levels of sour gas (H_2S) in deep oil and gas wells, rather than direct observation of subsurface processes (Trudinger et al., 1985; Noth, 1997). This has now

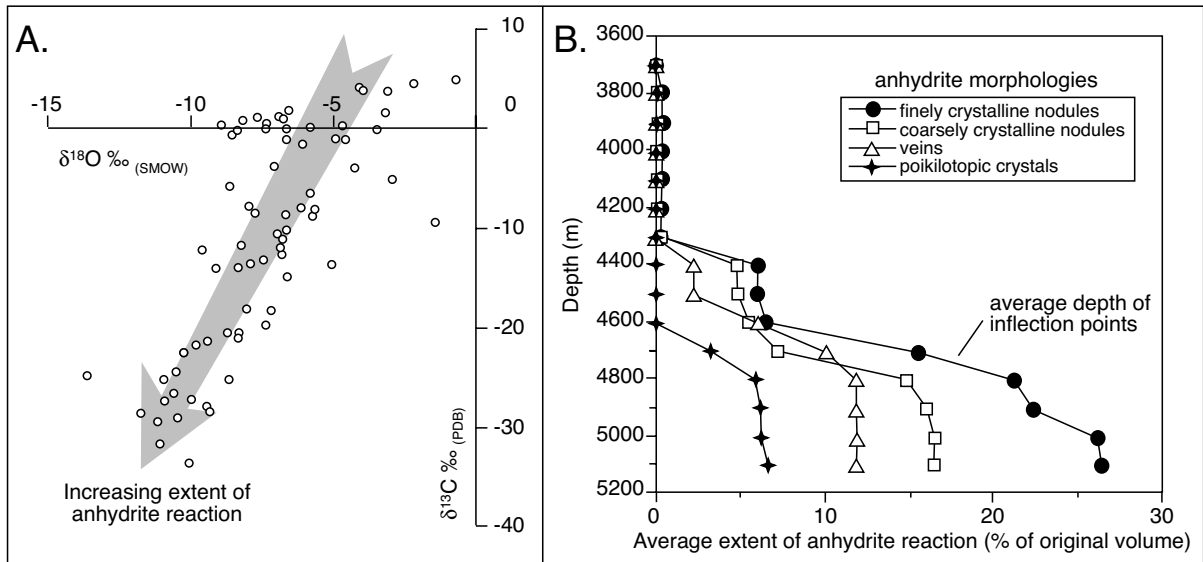
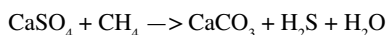


Figure 9.44. Thermochemical sulphate reduction in the Permian Khuff Fm., UAE. **A)** Stable isotopes of thermochemical calcite. Arrow shows trend of increasing calcite reaction. **B)** Depth versus the average extent of anhydrite replacement by calcite for the different types of anhydrite. Anhydrites with smaller crystal sizes are more reactive at any given burial depth. (after Worden et al., 2000).

changed with the direct documentation of TSR-produced H_2S (sour gas) in gas reservoirs in the Permian Khuff Formation of Abu Dhabi (Worden et al., 1995, 1996; Worden and Smalley, 1996). In Khuff reservoirs hotter than 140°C , anhydrite has been partially replaced by calcite, and hydrocarbon gases have been partially or fully replaced by H_2S . That is, anhydrite and hydrocarbons have reacted to produce calcite and H_2S .

Worldwide, the lowest temperature at which TSR occurs may be lower than the 140°C seen in the Khuff Fm. Machel (1998) suggests that the onset of TSR occurs in a range from $100\text{--}145^\circ\text{C}$ depending on variations in chemical kinetics, which will differ from basin to basin. If so, then one can expect TSR-derived H_2S to form at shallower depths than the 4000 m suggested by the work of Worden et al. (1995) or Heydari (1997).

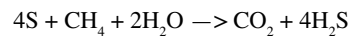
Carbon and elemental sulphur isotope data from the gases and minerals in the Khuff Fm. show that the dominant general reaction is (Worden et al., 1995, 1996; Worden and Smalley, 1996; Heydari, 1997):



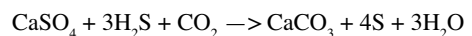
Gas chemistry and isotope data also show that C_2+ gases react preferentially with anhydrite via reactions like:



Sulphur is generated by this reaction and is locally present, but is also consumed by the reaction:



The frequently quoted and experimentally observed reaction between anhydrite and H_2S with CO_2 to produce calcite and sulphur:



has been shown, by gas chemistry, calcite $\delta^{13}\text{C}$ and sulphur $\delta^{34}\text{S}$ data, to be insignificant in the Khuff Formation.

Rather, a direct reaction between hydrocarbons and anhydrite occurs in solution. It takes place within residual pore waters that are initially dominated by carbonate dissolved out of the marine carbonate matrix. The first-formed replacive calcite thus contains carbon that was derived principally from a marine dolomite matrix with a $\delta^{13}\text{C}$ signature of 0 to $+4\text{‰}$. Continuing reaction leads to the progressive domination of pores water derived by TSR carbonate, with a minimum $\delta^{13}\text{C}$ of about 30‰ (Figure 9.44a). The spread of carbon isotope values in the replacive calcite shows that in the earliest stages of TSR the ambient formation water was dominated by bicarbonate derived from dissolution of the matrix dolomite. As TSR commenced, the first-formed aqueous carbonate species plus the newly dissolved calcium from the dissolving anhydrite led to

supersaturation with respect to calcite. However, this calcite was initially dominated by the dolomite-derived carbonate and thus inherited the dolomite's heavier carbon isotope signature. As TSR proceeded, the methane-derived carbonate came to dominate, leading to ever more negative $\delta^{13}\text{C}$ and $\delta^{18}\text{O}$ values in the resulting calcite (Fig. 9.44a).

When petrographically determined amounts of replacive calcite in the Khuff Formation are plotted as a function of depth (Figure 9.44b) it shows that TSR starts around 4300 m depth (corresponding to a present-day temperature of 140°C) for all of the anhydrite types apart from the coarsest (poikilotopic variety), which shows signs of reaction only below 4500m. This implies that availability of sulphate from anhydrite is the rate-limiting step during the earlier stages of reaction when

anhydrite is replaced *in situ* by calcite on the very edges of anhydrite nodules and crystals (Worden et al., 2000). Later, as TSR proceeds, and the thickening calcite rind begins to isolate the anhydrite from the dissolved methane, the reaction becomes transport controlled. TSR ceases once calcite has effectively armour-plated (totally isolated) the remaining anhydrite. Finely crystalline anhydrite underwent more extensive and more rapid TSR than coarser anhydrite crystals because these had a greater ratio of surface area to volume, allowing more and faster dissolution and requiring more calcite to isolate them from methane. Localized loss of H_2S occurs in the Khuff reservoir by reaction with indigenous Fe-bearing clays. Consequently, Khuff reservoirs with a relatively high siliciclastic content have less H_2S than would be expected from the advanced state of anhydrite replacement with calcite in these units.

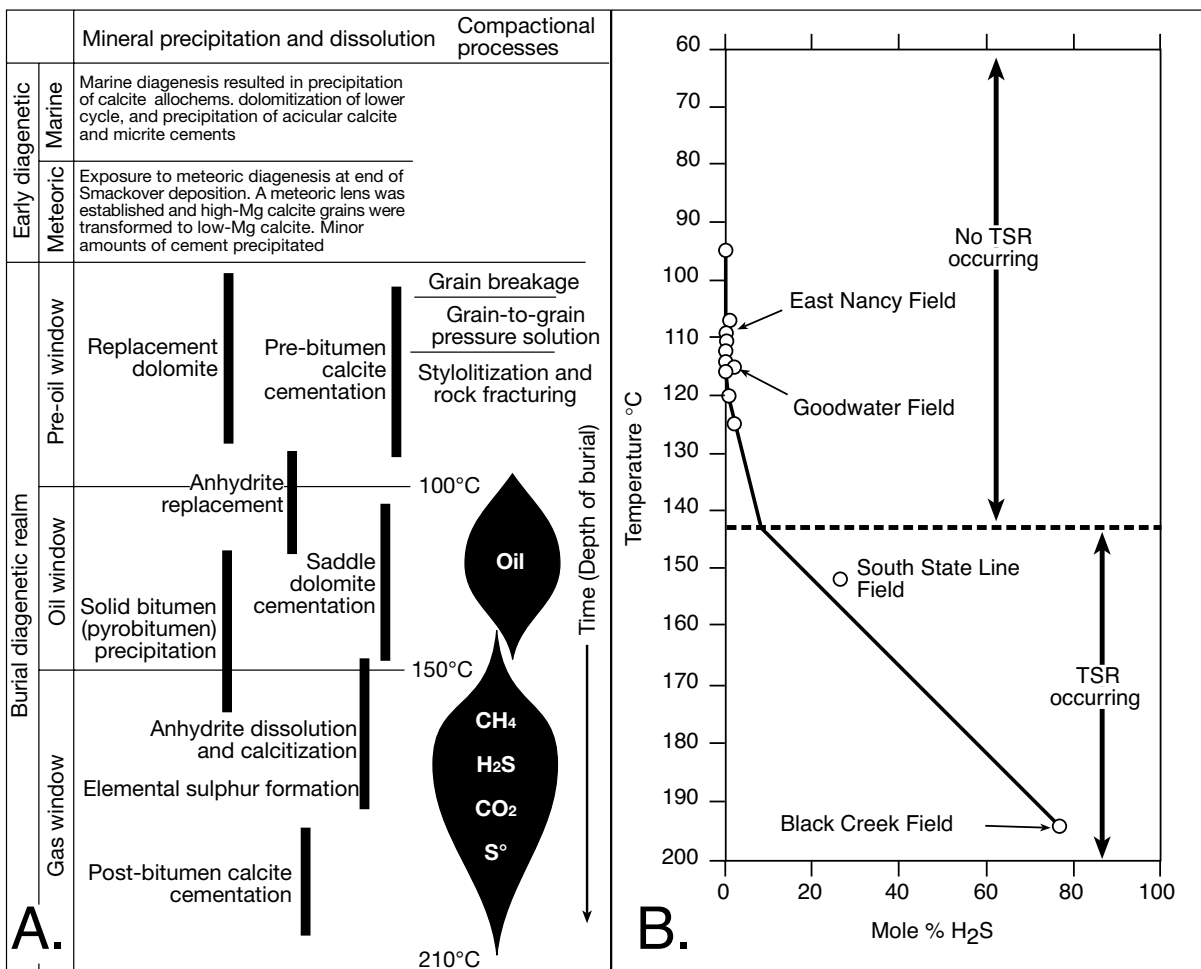


Figure 9.45. Thermochemical sulphate reduction in the Smackover Formation, Gulf of Mexico. A) Paragenetic sequence of the Smackover Formation at Black Creek Field summarizing major products of marine, meteoric, pre-oil window, oil window, and gas window diagenetic stages. B) Concentrations of H_2S in Mississippi Smackover reservoirs vary consistently with temperature (after Heydari, 1997).

Thermochemical sulphate reduction produces substantial volumes of very low salinity subsurface water in the vicinity of the reaction zone. Locally, the salinity of formation water in evaporite lithologies undergoing TSR is, therefore, not necessarily high. In the Khuff reservoir the water salinity and isotope data show that the original formation water was locally diluted between four and five times by water from TSR (Worden et al., 1996). A typical Khuff gas reservoir rock volume calculation suggests that initial formation water volumes can only be increased by about three times as a result of TSR. The extreme local dilution shown by the water salinity and $\delta^{18}\text{O}$ data in the Khuff must, therefore, reflect transiently imperfect mixing between TSR water and original formation water. Dissipation of this water into surrounding lithologies may aid further dissolution of adjacent evaporites. TSR is believed to cause the dilution of formation waters by up to 50% locally and up to 30% on a reservoir scale (Worden et al., 1996; Yang et al., 2001). On the other hand, there might be other reactions involved in TSR, some of them consuming water, so that the amount of water produced is probably highly variable and, according to Machel (2001), negligible at a regional scale.

Anhydrite dissolution and calcitisation in the Jurassic Smackover Formation in Mississippi, USA, does not occur below temperatures of 140–150°C, suggesting that, as in the Khuff, it is a thermochemical process (Figure 9.45a). Gas window diagenesis in deeply buried dolomitized Smackover reservoirs is largely driven by thermochemical sulphate reduction. Reaction of sulphate with H_2S generated S^0 that, in turn, reacts with CH_4 to form more H_2S in a self-reinforcing cycle (Heydari, 1997, 2001). Closed-system diagenesis prevents the escape of H_2S and, with sulphate abundantly available (Buckner Anhydrite). Without Fe^{2+} to remove H_2S by pyrite precipitation, the reaction continues until all hydrocarbons are consumed. TSR-generated CO_2 results in precipitation of postbitumen calcite with low $\delta^{13}\text{C}$ compositions.

Concentration of H_2S in Mississippi Smackover reservoirs varies consistently with temperature (Figure 9.45b; Heydari, 1997). Reservoirs studied are of the same age (150 Ma), similar lithology (clean oolitic limestone), and bounded by impermeable layers (Buckner anhydrite above and lime mudstones below). Heydari (1997) found that concentration of H_2S is very low in reservoirs that have experienced temperatures of 120°C for more than 50 m.y. It suggests that TSR has not occurred, and therefore it is not a time-dependent process (not kinetically driven). High H_2S concentrations occur in reservoirs with temperatures in excess of 140°C and increase with temperature, suggesting TSR is occurring and so it is a temperature-dependent process (thermodynamically driven).

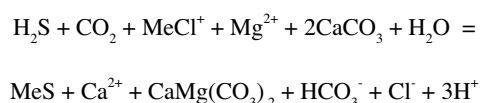
Where anhydrite and methane remain in reservoirs warmer than 140°C, thermochemical sulphate reduction continues into the low temperature end of the metamorphic realm (>200°C). Alonso-Azcarate et al. (2001) documented vein deposits containing native sulphur, gypsum, quartz and rare sphalerite in the very low-grade metasediments of Cervera del Rio Alhama in the Mesozoic Cameros Basin of NE Spain. In outcrop the veins are hosted by lacustrine evaporites, which now comprise alternations of dolomite and recrystallised gypsum (which was anhydrite during metamorphism) layers. Fluid inclusion homogenization temperatures and quartz-sulphate oxygen isotope geothermometry indicate formation of the veins around 225°C. Fluid inclusions contain sulphur along with a gas phase comprising H_2S , N_2 , CO_2 and minor CH_4 . These are all reactants and products of sulphur generation via thermochemical sulphate reduction (TSR) in the anchizone, which utilised organic matter, followed by a partial re-oxidation of some H_2S by SO_4 to produce sulphur. These TSR reactions differ from those observed in most petroleum-related sour gas settings in that there is no evidence for secondary carbonate precipitation and in that significant S isotopic fractionation exists between sulphate (around + 20‰) and reduced products (sulphur is around - 11‰).

H_2S , natural gas and metallogeny

H_2S (sour gas) is bacterially produced from organic matter by BSR at lower temperatures and nonbiogenically by TSR at higher temperatures (Figures 9.42). In deep evaporite-sealed oil and gas provinces, the proportion of bacteriogenic H_2S that becomes one of the many constituent of the trapped natural gas is negligible compared to that produced by TSR (Hunt, 1996). However, further updip, the proportion of bacteriogenically-produced H_2S can be much higher. H_2S is one of the ^{9,10}deadliest gases produced naturally in large amounts. At nearsurface conditions it is almost three times as soluble as CO_2 and more than 70 times as soluble as methane (Figure 7.47). Its critical temperature of 100.4°C is also much higher than that of CO_2 . Above this temperature all undissolved H_2S is in the gas phase. Large quantities of both CO_2 and H_2S gas are thermochemically generated at temperatures greater than 120°–140°C in mature to overmature source rocks. Peak generation for methane is around 140°C, while H_2S has not yet reached its peak generation at temperatures of 170°C (Figures 9.42c, a). H_2S forms best at temperatures beyond where petroleum geochemists have already lost interest, but its genesis is of great importance in the formation of base and precious metal deposits (Warren, 2000b).

Because of its high reactivity, it is difficult for H₂S to migrate from its source to a distant reservoir (Hunt, 1996). Away from direct contact with deeply buried and reactive anhydrite, H₂S in most oil and gas reservoirs is largely the product of sulphate reduction from sulphate ions in solution or the thermal decomposition of sulphur-containing oil. Interestingly, all the natural gas reservoirs with high thermochemical H₂S contents, listed in Table 9.7, are interbedded with anhydrites, or have anhydrite above or below the reservoir horizon. At its critical temperature of 104°C and a pressure of 14 MPa (2,000 psi), H₂S is forty times more soluble in water than at surface conditions.

Wherever H₂S in solution comes into contact with metalliferous chloride brine it is likely to be involved in a number of metal sulphide forming reactions. Sulphide products range from the cool shallow biogenic precipitation of syngenetic framboidal pyrite to the formation of hot, hydrothermal sulphides, which often also involve dissolution and alteration of the adjacent rock matrix. For example, in a Mississippi Valley type (MVT) scenario, a metal sulphide phase typically coprecipitates with hydrothermal or saddle dolomite in bathyphreatic or vuggy porosity at temperatures in the range of 60 - 180°C (Hill, 1995):



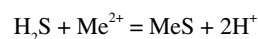
^{9.10} At very low concentrations of less than 10-100 ppm it smells like rotten eggs and there is a common misapprehension that its foul odour is a warning. At 100 ppm the gas kills the sense of smell in 3-15 minutes and will cause you to cough or your eyes to water. Over 100 ppm your eyes and throat may begin to sting. At 200 ppm, your eyes and throat will begin to burn and you will get headaches. Only 600 ppm, or 0.06 of 1% will cause death, if you are not treated very quickly. Over 1,000 ppm causes respiratory paralysis and a sudden agonizing death from asphyxiation.

H₂S is also heavier than air, invisible, highly explosive and can destroy steel and rubber seals very quickly. Modern drill rig floors are all fitted with sniffers.

Region	Reservoir Age	Lithology	Depth (m)	% H ₂ S in total gas
South Texas, USA	Upper Jurassic (Smackover)	Limestone	5,793-6,098	98
Alberta, Canada	Devonian	Limestone	3,800	87
Mississippi, USA	Upper Jurassic (Smackover)	Limestone	5,793-6,098	78
Irkutsk, Russia	Late Cambrian	Dolomite	2,540	42
Wyoming, USA	Permian (Embar)	Limestone	3,049	42
Asmari-Bandar Shapur, Iran	Jurassic	Limestone	3,600-4,800	26
Lacq, France	U. Jurassic and L. Cretaceous	Dolomite and limestone	3,100-4,500	15
East Texas, USA	Upper Jurassic (Smackover)	Limestone	3,683-3,757	14
Alberta, Canada	Mississippian	Limestone	3,506	13
Weser-Ems, Germany	Permian (Zechstein)	Dolomite	3,800	10
South Texas, USA	Late Cretaceous (Edwards)	Limestone	3,354	8
Pont d'As-Meillon, France	Upper Jurassic	Dolomite	4,300-5,000	6
Urals-Volga, Russia	Late Carboniferous	Limestone	1,500-2,000	6

Table 9.7. Regions of natural gas deposits with high H₂S contents. In all these the deposit is stored in a carbonate reservoir that is interbedded with anhydrite, or there is an anhydrite unit above or below the deposit (after Hunt, 1996).

The formation of metal sulphide from hydrogen sulphide generated by TSR can be expressed in the general reaction;



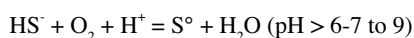
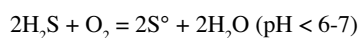
Such reactions create acid, which in turn is capable of forming secondary porosity in a deeply buried limestone host. It is why bathyphreatic vuggy porosity with sphalerite stalactites are found in many MVT ore deposits, such as Cadjebut in Western Australia where these metalliferous dripstones formed in methane-rich bathyphreatic vugs and pores (Figure 7.51; Warren and Kempton, 1997).

When considering the association of sulphate evaporites with mineralisation it is important to realise that it is not the sulphate evaporites that are directly responsible for the precipitation of metal sulphides during sulphate reduction (Warren 2000b). Rather, evaporite dissolution or reaction places sulphate/sulphide in a fluid medium so that it can react with liquid or gaseous hydrocarbons. It is this sulphate-entraining solution that is reduced in the presence of organic matter or hydrocarbons

to form H_2S . And it is the H_2S in solution that then precipitates the metal sulphides at or near a redox interface, which is a zone where slightly more oxidised metalliferous chloride brines can interact with a H_2S buildup on the reduced side of the interface.

Thus, ore textures in areas where sulphate evaporites are dissolving and metal sulphides are precipitating are most likely to be open space or porosity-fill textures. Ore textures and the degree of layering will depend on a number of factors including: the size of the dissolution front (interpore versus laminar versus vug versus solution-collapse cavern), the rate of fluid crossflow at the interface, the degree of stability of the redox interface, and the distance the sulphate ion travels before it is reduced (Warren and Kempton, 1997). Precipitation of the metal sulphides may occur directly across from a dissolving sulphate evaporite where it is producing H_2S on the other side of a fluid-filled interface. Or it may occur after H_2S derived from TSR has seeped and migrated into a closed structure (aka prepared ground) higher in the sedimentary succession.

When H_2S accumulates at an interface where oxygen is present and large volumes of metalliferous brines are absent, it can form accumulations of native sulphur, rather than metal sulphides, via the reactions:



Elemental sulphur can form and persist near a redox interface where $\text{Eh} \approx -0.2$ to $+0.2$. This is thought to be the mechanism that generated the economic evaporite-associated sulphur deposits in hydrocarbon leakage haloes within the Gulf of Mexico diapir caprocks and the stratiform sulphur of Culberson Co. west Texas (Figure 11.59). The presence of abundant free sulphur (S°) in peridiapiric Pb-Zn deposits such as Bou Grine is used by some workers to argue that in such situations the supply of metals to a sulphate/sulphide reduced environment was the reaction-limiting step (Bechtel et al., 1996).

Sulphur sourced from TSR in the deep subsurface may not all be consumed by the reaction of methane and water, especially where metalliferous fluids are not present in sufficient quantities to form metal sulphides. However, as sulphur melts at temperatures between 113° and 120°C , any such sulphur formed during TSR (requires temperature $> 140^\circ\text{C}$) will be molten. Such sulphur occurrences typically occur in deep stratigraphic zones dominated by carbonate and calcium sulphate lithologies

(Hunt, 1996). For example, molten sulphur was recovered from a depth of 6,098 m (20,000 ft) in the Jurassic Smackover carbonate-evaporite sequence in southern Mississippi on the US Gulf Coast. It was also recovered from the Cambro-Ordovician Arbuckle limestone-dolomite at a depth of 9,586 m (31,441 ft) in the Bertha-Rogers well in the Anadarko Basin, Oklahoma. Wells in the Permian Zechstein dolomites in western Germany have recovered molten sulphur from depths between 3,000 and 4,300 m (10,000 - 14,000 ft).

Elemental sulphur reacts with H_2S to form polysulphides, which are powerful oxidants that quickly convert any saturated hydrocarbons to thiopenes, thiols and sulphides (Hunt, 1996). This reactivity means that all the hydrocarbons from pentane, through butane, propane, ethane and finally methane are oxidised to CO_2 at elevated temperatures in the presence of H_2S . Hence, it is no surprise that whenever molten sulphur is recovered on a drillstem test, no appreciable amounts of methane or the higher hydrocarbons are present.

Importance of mesohaline organics and sulphate reduction in stratiform base metal ores

In order to illustrate the commonplace association between mesohaline organics, bedded evaporites and stratiform base metal mineralisation we shall consider only one such style - the giant Lubin copper deposit of Poland. It is an example of a basinal subsalt bedded setting in what is a widespread diagenetic association of base metals and evaporites. But it is only part of the much broader evaporite-base metal-salt allochthon association, which controls the occurrence of many significant base metal deposits through time. The interested reader is referred to Warren (2000b) for a more detailed discussion of this topic.

Sulphate reduction in the Permian basal Zechstein sediments has focused the deposition of large quantities of Cu, Pb and Zn ores in Kupferschiefer-style deposits in Poland and smaller scale deposits in Germany. The Kupferschiefer mining districts of southwestern Poland (Cu deposits of the Fore-Sudetic Monocline and the North Sudetic Trough) are ranked among the largest productive Cu deposits of the world (Bechtel et al., 2002). For example, the Lubin deposit in Poland has estimated ore reserves of 2600 Mt at grades $>2\%$ Cu, 30–80 g Ag/t, and 0.1 g Au/t (Kirkham 1989). Annual production of the district in 1999 was 520,000 t Cu, 1351 t Ag, and 13,800 t crude lead. Additional metals recovered include 66 t technical selenium, 1722 t Ni sulphate, approx. 490 kg Au, 30 kg Pt, 15 kg Pd and, depending on the price, As, Re, and Zn. Economic reserves con-

Deposit, Location (Age of Host)	Reserve (10 ⁶ tonnes)	Cu (%)	Pb (%)	Zn (%)	Evaporite Role	Evaporite Association
BEDDED OR STRATABOUND DEPOSITS						
Kupferschiefer-style, Lubin, Poland (Permian)	≈2,000	>2	-	-	Subsalt, stratiform with brine focus creating the Rote Faule contact and adjacent redox precipitates	Anhydrite and halite in Zechstein hangingwall and anhydrite in Rotliegende footwall
Kupferschiefer-style, Mansfeld, Germany (Permian)	≈7.5	≈2.9	-	±1.8	Subsalt, stratiform with brine focus	Anhydrite and halite in Zechstein hangingwall and anhydrite in Rotliegende footwall
Redstone River, Canada (Neoproterozoic)	small	2.7	-	-	Intrasalt stratabound with subsalt focus to upwelling brine	Algal limestone host with abundant nodular CaSO ₄
Creta, Oklahoma, USA (Permian)	1.9	2	-	-	Intrasalt bedded (breccia), adjacent redox precipitates	Redbed - evaporitic mudflat host with abundant nodular CaSO ₄
Corocoro, Bolivia (Tertiary)	≥7	≈5	-	-	Intrasalt bedded (breccia), brine reductant	Redbed - greenbed host with gypsum and baryte in veinlets and disseminated nodules
Gays River, Nova Scotia (Carboniferous)	2.4	-	8.6	6.3	Subsalt with subsalt focus to upwelling brine. Local supplier of sulphur via TSR	Anhydrite both within main ore zone and as cement in disseminated ore
Nanisivik, Baffin Island (Proterozoic)	6.5	-	1.5	12	Intrasalt?, bedded	Host is a stratiform karst cavern: evaporites and pseudomorphs in lateral equivalent beds
San Vicente, Peru (Triassic - Jurassic)	12	-	1	12	Intrasalt, bedded. Local supplier of sulphur via TSR	Ore hosted in cryptalgal laminites with pseudomorphs after CaSO ₄ in barrier-lagoon host
Cadjebut, NW Australia (Devonian)	3.8	-	17% (Pb+Zn)		Intrasalt, bedded (breccia). Local supplier of sulphur via TSR	Bedded anhydrite as lateral equivalent to each ore lense and linked by evaporite dissolution breccias
Largentière, France (Triassic)	9.6	-	0.7	3.7	Intrasalt	Disseminated CaSO ₄ cements and nodules within evaporitic lagoonal beds
ALLOCHTHON-ASSOCIATED DEPOSITS						
Atlantis II Deep, Red Sea (Holocene)	150-200	0.8	yes	5-6	Suprasalt allochthon acts as focus to resurging Cu-Zn-Cl brine (salt partially covers ridge basalts)	Dissolving allochthon underbelly supplies Cl-rich metalliferous brine to deep seafloor brine lake. Hydrothermal anhydrite is interbedded with laminites
Dzhezkazgan, Kazakhstan (Carboniferous)	≈400	1.5	0.1-1.0	-	Suprasalt diapiric, anticlinal focus to brine flow	Interbedded redbed and greybed host with CaSO ₄ and halite in underlying salt anticline and lateral equivalents
Dongchuan deposits, China (Mesoproterozoic)	10-100	1.0-1.5	-	-	Suprasalt allochthon or intrasalt breccia. Allochthon acts as focus to resurging metalliferous brine	Stratabound ore in cryptalgal laminites adjacent to diapiric breccia
Lisbon Valley, Utah, USA (Cretaceous)	small >0.15	1.4	-	-	Suprasalt allochthon, salt movement creates ore-hosting faults in overburden	Ore in vein and pore fills adjacent to faults created by halokinesis
Jubilee, Nova Scotia (Carboniferous)	Not economic	n/a	n/a	n/a	Subsalt allochthon (tectonic breccia) stratiform, subsalt focus to brine flow	Interstratified fractured carbonate and anhydrite ore host created by regional salt-induced gravity slide
Bou Grine, Tunisia	7.3	-	2.4	9.7	Suprasalt, peridiapiric, brine focus via halokinesis	Ore in peridiapiric organic-rich pyritic laminates adjacent to halite allochthons
Gulf Coast USA (Tertiary)	Not economic	n/a	n/a	n/a	Suprasalt allochthon capstone, brine focus via halokinesis	Anhydritic caprock undergoing bacteriogenic alteration in association with reservoired hydrocarbons

Table 9.8. Some of the many base-metal deposits formed in the diagenetic realm in association with bedded, dissolving and flowing evaporites (after Warren, 2000b).

sist of 31 million t Cu and 81,000 t Ag. The average content of the reduced Cu–Ag ore is 2.1% Cu, 59 ppm Ag, 550–2000 ppm Pb, 33–71 ppm Ni, 20–140 ppm Co, 25–84 ppm Mo, 56–242 ppm V, 20–60 ppb Au, 11–15 ppb Pt, and 10 ppb Pd.

Some mineralisation in the Kupferschiefer was early and associated with bacterial sulphate reduction (especially in the

Kupferschiefer itself, as indicated by syndeositional framboidal pyrite) but much of the economic Cu mineralisation is later. It is a burial diagenetic product, typically precipitated at a redox front created at an interface between dissolving Zechstein evaporites and upwelling basinal waters (metalliferous chloride brines). Mineralisation occurred in an association of evaporite-capped beds at the top of a thick continental volcanic

and redbed sequence, which were deposited atop a Permian continental rift basin passing up into sag filled with basinwide evaporites (Figure 9.46a).

Stratabound Cu–Ag Kupferschiefer deposits were long considered classic examples of syngenetic mineralisation driven by bacterial sulphate reduction (e. g. Wedepohl, 1964). However, detailed work in Poland in the last two decades has shown that the Cu mineralisation cuts depositional boundaries. Richest intervals of mineralisation define low-angle transgressive metal zones associated with the redox edge of diagenetic Rote Faule units (Figure 9.46b; Jowett et al. 1987; Jowett 1992; Oszczepalski, 1994; Large and Gize 1996).

Rote Faule (literally ‘red rot’) actually describes a nonmineralised burial diagenetic zone and loosely encompasses any barren red-coloured rocks typically found near high-grade ore. It is defined by various types of red colour created by the diagenetic formation of disseminated authigenic haematite and goethite in an oxidised haematitic interval adjacent to reduced highly-mineralised intervals. Pyrite and the original organics of the Zechstein carbonate and the Kupferschiefer mudstones, are oxidised and largely removed in Rote Faule intervals (Oszczepalski 1989; Bechtel et al., 2002). The isotopic and organic signatures in its diagenetic precipitates indicate mother fluids fed by deep basin circulation (Bechtel et al., 2002). Rote Faule is not formation specific and occurs in the Weissliegende, Kupferschiefer and Zechsteinkalk strata (Figure 9.46b, c).

Ore sulphides in the Kupferschiefer were largely precipitated in zones where H_2S , carried by brines flushing the TSR zone along the dissolving underside of the Zechstein evaporites, mixed with the rising metalliferous waters. That is, the Rote Faule indicates redox interfaces where ascending slightly-oxidising chloride-rich basinal brines, which carried Cu, Pb and Zn, mixed with dissolution-fed brines carrying TSR-derived H_2S . Base metal precipitation occurred on the far side of subhorizontal oxidation–reduction front indicated by the edge of the Rote Faule.

Sulphides are arranged in three distinct haloes around ‘Rote Faule’, in the order Cu, Pb and Zn (Figure 9.46b, c). Thus, around and above the Rote Faule, the base metals are zoned laterally and vertically in successive mineralisation belts of chalcocite, bornite, chalcopyrite, galena and sphalerite. The overlying evaporitic Zechstein sediments enhanced and focused the precipitation of Cu, both by forming prepared ground at the time of deposition (pyritic and organic-rich

evaporitic laminite host) and during diagenesis by creating a stable dissolution hydrology, which held back hydrocarbons and through dissolution of the Werra Anhydrite Fm. created H_2S by thermochemical sulphate reduction. The thickness of the basinwide evaporites of the Zechstein meant the dissolution front was a stable subsurface interface that focused the large volumes of economic mineralisation into a redox zone immediately adjacent to the Rote Faule boundary.

Levels of mineralisation in the Kupferschiefer adjacent to a Rote Faule interval are typically far higher than background levels in the Kupferschiefer shale (Figure 9.46c). Mineralisation transgresses depositional boundaries as it is tied to the Rote Faule/saline brine interface and not to the depositional pattern and distribution of the Kupferschiefer shale. Thus copper ore is not just hosted in the organic laminites of the Kupferschiefer and the Zechsteinkalk, it also occurs in parts of the Weissliegende aeolian sandstone, a unit that at the time of deposition was exceptionally free of organics, laminites and pre-ore sulphides (Figure 9.46c). To the dismay of many syngeneticists, this positionally clean aeolian sandstone hosts half the economic Cu-sulphides in the Lubin district.

Methane was likely an ephemeral component in the Weissliegende sands, as was authigenic anhydrite cement. Jowett (1992) demonstrated that the widespread sparry anhydrite cements in the Weissliegende at Lubin, along with the trapped methane beneath the evaporite seal, set up burial chemistries suitable for thermochemical sulphate reduction and the precipitation of Cu-sulphides in the Weissliegende host. As well as acting as a seal to the methane, the overlying Zechstein evaporites were also a likely source for the anhydrite burial cements. Clearly, Cu, Pb and Zn mineralization at Lubin is a basinal pore water process, not directly tied to the occurrence of organics or pyrite in the Kupferschiefer. Rather, mineralisation occurred wherever hydrocarbons or organics came into contact with calcium sulphate and thermochemical H_2S was formed. Either the hydrocarbons or the sulphate-forming H_2S could arrive at the mineralisation site in solution. Metals other than the original framboidal pyrite present at the mineralization site were carried in by the basinal waters ascending through the thick underlying redbeds.

Geometries of mineralisation suggest that the dissolving underside of the Zechstein sediment pile acted as a long-term fluid focus and seal; it maintained an ongoing interface with upwelling metal-rich slightly oxidising chloride-rich basinal waters and could be located either in the mesohaline Kupferschiefer or its lateral equivalents in the Weissliegende. Tight Zechstein salts also created a pressure seal that aided hydrofracturing in the

maturing organic laminates of the Kupferschiefer, as evidenced by numerous sulphide–calcite veinlets in the Kupferschiefer. An inherent lack of permeability in widespread thick evaporites also meant the upper side of the Zechstein salt beds prevented downward percolation of fresh oxygenated waters, which would otherwise have destroyed the stability of the redox front at the edge of the Rote Faule.

Mineralisation at Lubin underlines the longterm impervious nature of any thick evaporite unit and its underlying salt-plugged halo, even as it dissolves in the subsurface. It means that until

it is breached its underside is an excellent seal to migrating hydrocarbons (both liquid and gaseous). Thus the organics required for the sulphate reduction process may not only be locally derived from organic-rich sediments, they may have seeped and flowed into the subsalt interval as a hydrocarbon charge trapped directly beneath the evaporite seal. The requirement for organics in the sulphate reduction process and the ability of evaporite beds to act as a seal explains, at least in part, the ubiquitous worldwide association of evaporites, hydrocarbons/ organic matter, and diagenetically created (TSR) base metal deposits. Put simply, bedded sulphate salt beds, chloride-rich

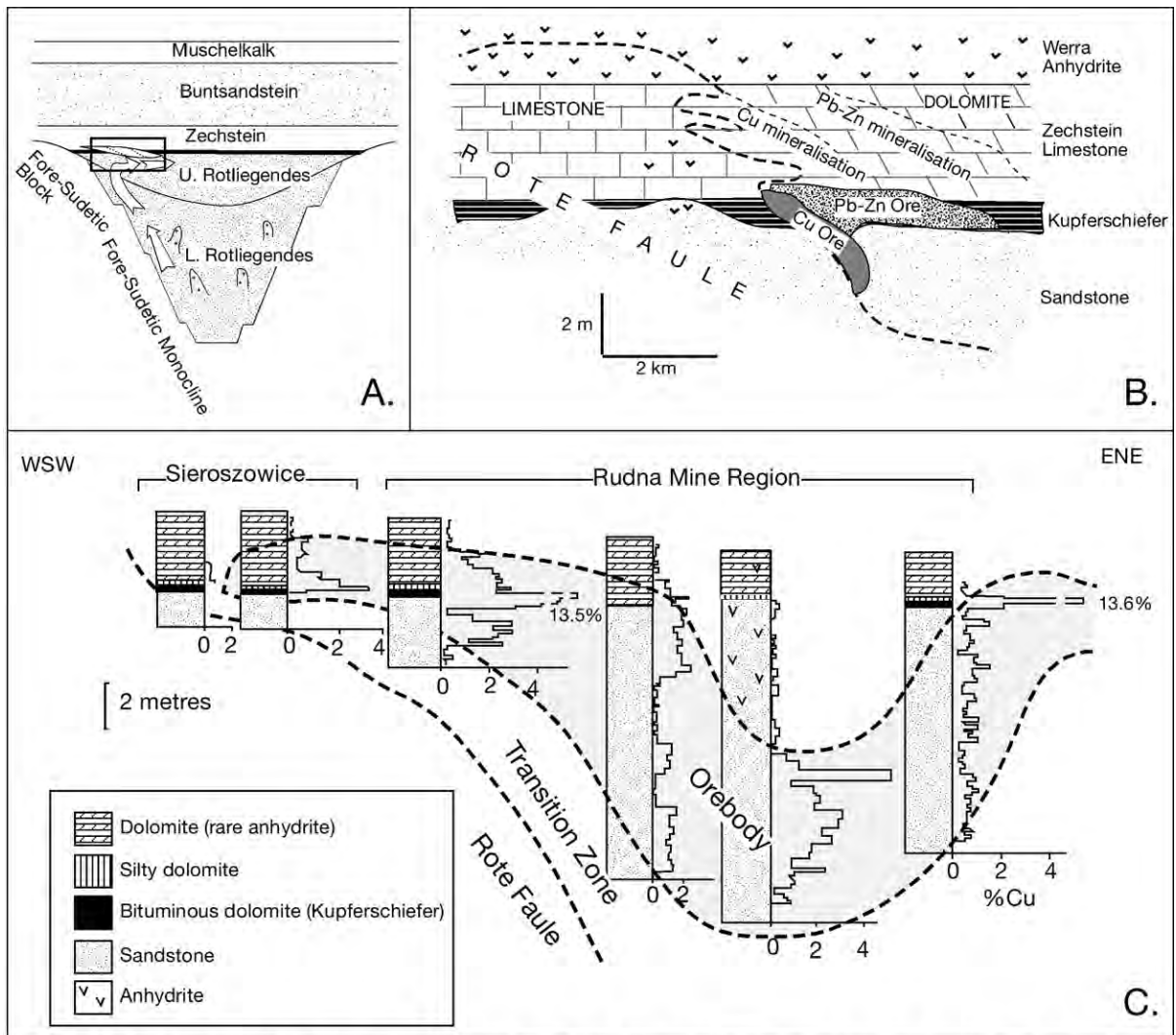


Figure 9.46. Rote Faule and its relation to the Kupferschiefer (after Warren, 2000b and references therein). A) Regional cross-section showing the focusing of the upwelling basinal water beneath the Zechstein evaporites. B) Enlargement of region of Rote Faule [see box in (A)] showing how the mineralisation and its zonation is tied to the Rote Faule not the Kupferschiefer. C) Distribution of Cu in the ore zone showing higher Cu enrichment (≈13%) in the Kupferschiefer, but by far the greater volume of ore resides in the sandstones beneath the Zechstein evaporite seal.

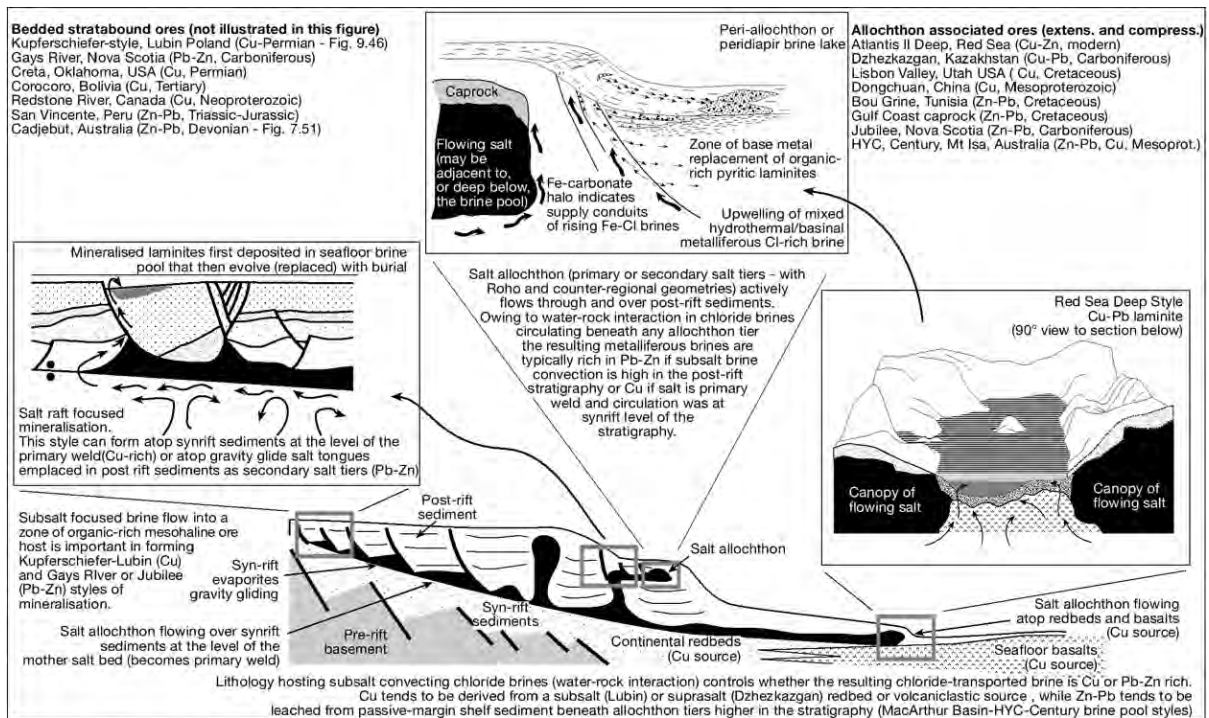


Figure 9.47. Model of salt-allochthon-controlled base-metal (sedex) accumulations. Note the importance of the subsalt lithologies in controlling the mineralogy of the precipitates. Cu is not easily transported too far from its source beds whereas Pb-Zn can be carried much further. The volume of sediment being leached of its metals beneath the focusing salt unit is controlled by the continuity of the salt bed. Also listed are various Cu and Pb-Zn deposits associated with bedded evaporites (after Warren, 2000b).

salt beds, autochthons and allochthons are transient features in most sedimentary basins that through dissolution and flow can dissolve, focus and fix base metals.

This is so not just for base metals associated with bedded platform sulphates, but also for deposits in halokinetic basins (Table 9.8). In Chapter 8 we saw that upward escape of chloride-rich metalliferous basinal brines is typically focused along the underside of thick basinwide evaporite units. Deeply circulating metalliferous subsalt brines typically escape into overlying strata at breach points in the salt body. Such breach points may be the feather-edge of the evaporite bed or extensional faults that cross-cut the flowing and deforming salt body or zones of halokinetic touchdown. Some of these faults may be induced by the basinward flow of salt; others may be large regional basin-defining structures. Any calcium sulphate bed, or an evaporitic carbonate bed rich in mesohaline organics, can act as a supplier of reductants to fix base metals carried by the escaping metal-rich chloride brines (created deep in the basin by halite dissolution). Mineralised redox fronts can occur in subsalt, intrasalt and suprasalt positions and in both bedded and allochthonous salt associations (Figure 9.47).

In all these evaporite-associated low-temperature diagenetic ore deposits there are four common factors that can be used to recognise suitably prepared ground and so improve the ability of an exploration model to predict likely sites of ore occurrence within a basin (Warren, 2000b): (i) a dissolving evaporite bed acts either as a supplier of chloride-rich basinal brines capable of leaching metals, or as a supplier of sulphur and organics that can fix metals; (ii) where the dissolving bed is acting as a supplier of chloride-rich brines, there is a suitable nearby source of metals that can be leached by these basinal brines (redbeds, thick shales, volcanoclastics, basalts); (iii) there is a stable redox interface where these metalliferous chloride-rich waters mix with anoxic waters within a pore-fluid environment that is rich in organics and sulphate/sulphide/H₂S; and (iv) there is a salt-induced focusing mechanism that allows for a stable, long-term maintenance of the redox front, e.g. the underbelly of the salt bed (subsalt deposits), a dissolution or halokinetically maintained fault activity, the overburden (suprasalt deposits), a stratabound intrabed evaporite dissolution front (intrasalt deposits).

Metal sulphide ores formed by TSR and BSR fixation can have near identical textures, both are typically pore or vug-filling cements or evaporite replacements (Machel et al., 1995). One way to help differentiate the origin of the precursor H_2S is via sulphur isotope analysis of ore sulphides that, if possible, is tied to $\delta^{13}C$ and $\delta^{18}O$ analysis of the various gangue carbonate cements and matrix signatures that bracket the ore minerals. H_2S derived via bacterially mediated sulphate reduction tends to be isotopically light and so tends to exhibit more negative δ values (Figure 9.48). This is true of both the sulphur in the sulphides and of the carbon in any late stage dolomite or calcite cements. Unlike carbon and sulphur isotopes, oxygen is more thermally sensitive below $200^\circ C$ and is better used as a geothermometer (Emery and Robinson, 1993).

For example, isotopic values of bacterially reduced sulphide in subsurface waters of the Permian Basin west Texas, is typically in the range -32 to 0 ‰ on the CDT scale. These values are significantly lower than the isotopic composition of sulphate from Permian marine sulphate evaporite, which lie in the range $+9.6$ to $+13$ ‰ (Figure 2.23a). Reoxidation of sulphide to sulphate or sulphur by oxygen in the fluid mixing zones does not cause significant fractionation. Lighter isotopic values in modern cave sulphur in Guadalupe Mountain caves ($\delta^{34}S_{CDT} = -25.8$ to -20 ‰) and in the Culberson mine (-4.7 ‰) indicate bacterial sulphate reduction reactions, rather than abiogenic precipitates (Figure 7.48; Hill, 1995). A hydrocarbon source is indicated by the light carbon isotope character of associated biogenic calcite in the Culberson mine ($\delta^{13}C_{PDB} = -44.2$ to -18.6 ‰; Hill, 1995). The depleted $\delta^{13}C$ values are significantly lower than would be expected in marine carbonates, which normally fall in the range of -4 to $+4$ ‰. The scatter in the data could arise from mixing in varying proportion of fluids. More depleted values (less than -30 ‰) probably reflect oxidation of source hydrocarbons, whereas the heavier ^{13}C was perhaps derived from isotopically heavier fluids of the deep basin.

H_2S from thermochemical reduction is not biologically fractionated, and so $\delta^{34}S$ values of the ore sulphide tend to reflect the isotopic signature of its evaporite precursor (Worden et al., 1997). Limited experimental work on deeply buried anhydrite undergoing thermochemical reduction suggests

that the sulphur isotopic composition of the derived H_2S is isotopically similar to, or a few per mille lighter than, the precursor anhydrite (Krouse et al., 1988). Thus $\delta^{34}S$ and $\delta^{13}C$ values under TSR are much higher (more positive) than its BSR equivalent, while the $\delta^{18}O$ reflects elevated temperatures of late stage diagenetic spar formation (more negative).

But this isotopic distinction between bacterial and thermochemical sources is not as clear cut as it first appears; sulphur need not have come from the reduction of evaporitic sulphate, it may also come from organically derived sulphur in oil trapped in the host rock. Under this scenario the sulphur has low $\delta^{34}S$ values, similar to any associated hydrocarbons (Kesler et al., 1994). The range of values for these hydrocarbon systems is similar to that from bacterially mediated sulphate reduction. This overlap underlines the need for matrix characterisation, which ties stable isotope determinations to detailed petrographic and sedimentological understanding of the ore host. For example, if the ore sulphur was locally sourced, then calcite may have replaced the precursor anhydrite. This calcite should be sampled for carbon and oxygen isotope analyses to see if its genesis parallels that of any ore sulphides. In addition, even though sulphate salts no longer remain, the “salt that was” textures should still be present.

Hydrothermal cracking in saline rift lakes

Not all the hydrocarbons found in evaporitic sediments have necessarily evolved from millions of years of kerogen burial into depths where temperatures exceed $60^\circ C$. In some evaporitic situations the heating and evolution is much more rapid, driven

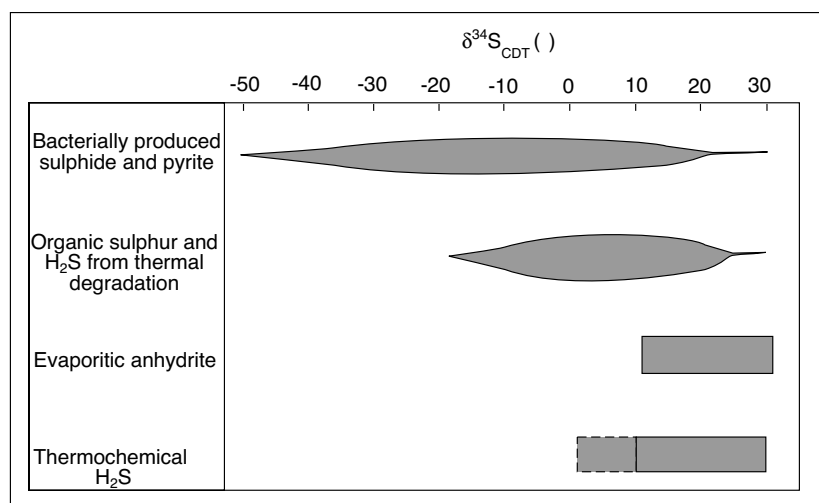


Figure 9.48. Typical ranges of naturally occurring sulphur isotopes under thermochemical and bacterial sulphate reduction (after Emery and Robinson, 1993).

by the near surface circulation of hydrothermal waters. Such heating may be commonplace in evaporite accumulating areas where the evaporite depression was tectonically induced. Hence, hydrothermal hydrocarbons may be an integral part of source rock evolution of the early brackish to mesohaline lacustrine fill of evaporite-sealed rift successions, with organics typically accumulating on the bottom of density/salinity stratified lakes (Tiercelin et al., 1993).

One such example is the oil seeping onto the lake floor off Cape Kalamba in Lake Tanganyika at the south end of the Ubwari Peninsula (Simoneit et al., 2000). The area lies at the intersection of faults controlling the morphology of the northern basin of the Tanganyika Rift. Oil samples collected at the surface of the lake 3-4 km offshore from Cape Kalamba lack typical suites of polynuclear aromatic hydrocarbons. This indicates an origin via hydrothermal alteration of immature biomass in the organic-rich mesohaline sediments of the lake bottom. Based on the constituents of the modern bottom sediments, the prime producers were diatoms and cyanobacteria, which constitute most of the 6% TOC that is found in sediments on the modern deep lake floor. Compositions of the oils and nearby tar balls demonstrate a $<200^{\circ}\text{C}$ temperature during formation/generation, similar to the fluid temperatures identified at the Pemba

hydrothermal site some 150 km north of Cape Kalamba. Hydrothermal petroleum generation seems to have occurred in the lake depression slightly before 25 Ka, during a drier climatic environment when the lake level was lower than today. Hydrothermal smokers or chimneys also occur on the subaqueous floor of the Lake Tanganyika (Barrat et al., 2000). It may well be that the deposition of any future overlying evaporite seal in this underfilled lacustrine situation may focus the flow of micropetroleum into more appropriate landward sands, but ancient economic lacustrine counterparts of this style of hydrothermal oil have yet to be documented.

Not all hydrothermally-cracked oil is found in rift-valley fills or is associated with sedimentary CaSO_4 . More impressive in terms of hydrocarbon volumes and origins are the oils forming in the hydrothermally-flushed deepwater sediments on floor of the Guaymas Basin in the Gulf of California (Figure 9.49a). Radiocarbon dates show this oil forms in association with thermochemical sulphate reduction in less than 5,000 years (Didyk and Simoneit, 1989; Peter and Scott, 1991). But unlike the rift association of east Africa, the anhydrite in this hydrocarbon system is hydrothermal and is created by the convective heating of seawater (retrograde solubility). The isotope signatures of the anhydrite, as well as the hydrothermal baryte

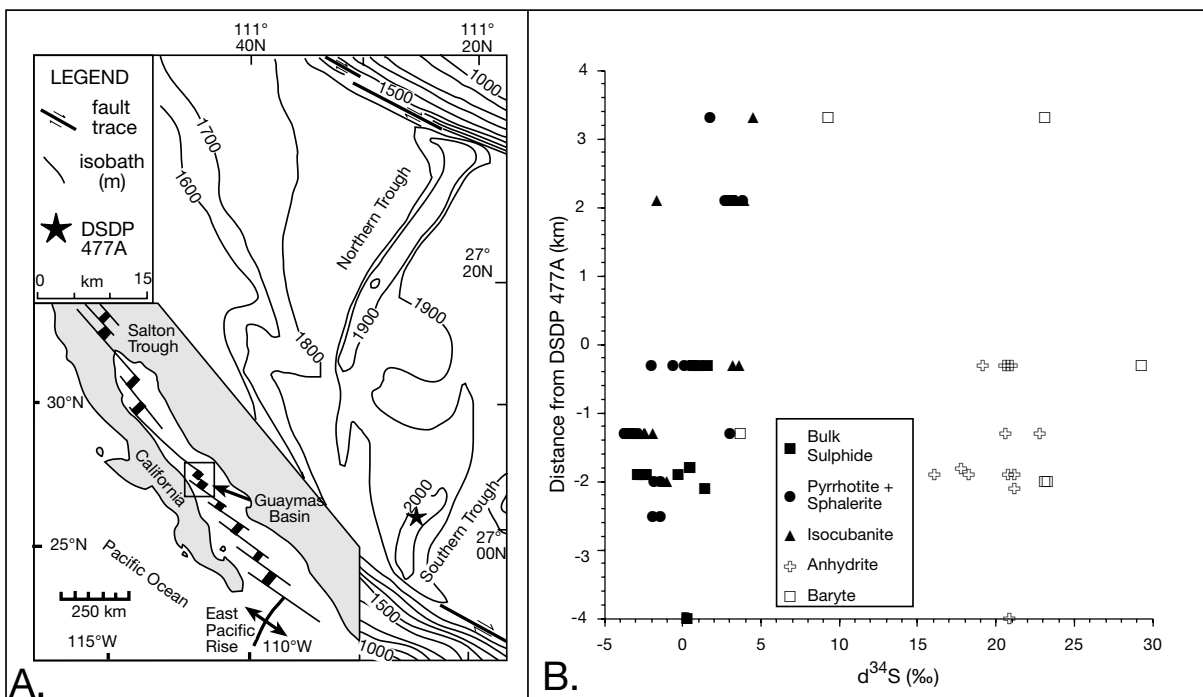


Figure 9.49. Guaymas Basin. A) Location of DSDP drill hole 477A. B) Sulphur isotopes from hydrothermal anhydrite and baryte and various sulphide phases in seafloor samples from the Southern Trough in the vicinity of DSDP 477A (replotted from isotope data in Peter and Shanks, 1992).

and metal sulphide phases show sulphur signatures reflecting their genesis from hydrothermally heated seawater. Notably, the sulphur isotope field of this hydrothermal anhydrite is the same as that of modern evaporitic anhydrite and gypsum (Figure 9.48 c.f. 9.49b).

Although the evidence is clear for hydrothermally-cracked hydrocarbons migrating through sediments at active spreading centres, the inherent association with active faulting and tectonism in modern ocean spreading centres means most hydrocarbon product is lost to the overlying seawater column through a lack of appropriate long-term traps and seals (Kvenvolden and Simoneit, 1990). Perhaps such systems are more likely to trap oils in areas where there is a fortuitous association between hydrothermal circulation and downdip end of salt allochthons flowing basinward across the deep seafloor, as in some parts of the Red Sea troughs.

At the older end of this hydrothermally-cracked oil spectrum are oil remnants in the 3.2 Ga Early Archaean deep-sea volcanogenic massive sulphide deposits of northwest Australia (Rasmussen and Buick, 2000). Archean seawater lacked sufficient sulphate or Ca to form anhydrite. There the oil was preserved in fluid inclusions within hydrothermal baryte, and as pyrobitumens intergrown with polymetallic sulphides. Petrographic textures show that the oil was emplaced and thermally altered (cooked) before late-stage sulphide mineralization. Its presence implies subseafloor hydrothermal petroleum generation was active during the Early Archaean, possibly providing an energy and carbon source for a subsurface microbiota that was metabolizing hydrothermal sulphur species.

Summary

Source rocks accumulate beneath density-stratified saline water and sediment columns in evaporitic settings with layered hydrologies subject to oscillations in salinity and brine level (Figure 9.3). Saline-associated organic matter is not produced at a constant rate. Rather, it is produced as pulses by a halotolerant community responding to relatively short times when less stressful near- or at-surface conditions prevailed in the layered hydrology (Figure 9.50). This happens in any layered brine lake or epeiric seaway when an upper less saline water mass forms atop nutrient-rich brines or in wet mudflats when pore waters freshen in and atop the uppermost few millimetres of a microbial mat.

The resulting bloom (a time of “feasting”) by halotolerant algal, bacterial and archaeal photosynthesizers is a time of exponential growth characterized by very high levels of organic productivity (Figure 9.50). In mesohaline waters where light penetrates to the bottom, the organic-producing layer is typically the upper algal and bacterial portion of a benthic laminated microbialite (typically characterized by elevated numbers of cyanobacteria). In stratified brine columns (oligotrophic and meromictic) the typical producers are planktonic algal or cyanobacterial communities inhabiting the upper water mass. Halotolerant autotrophic microbial communities, living off the remains of this plankton, float mid-water at the halocline of the density-stratified brine columns. Similar communities of aerobic and anaerobic biodegraders also constitute the living layers below the mm-thick primary producing layers of benthic microbialites beneath oxygenated bottom waters.

Short pulses of extremely high productivity in turn create a high volume of organic detritus settling through the water column and/or building up in benthic microbial mats. Then, with the end of the freshening event, the ongoing intense aridity that characterizes all evaporitic depressions means salinities, temperatures and osmotic stresses increase rapidly in the previously freshened water mass, first leading to a slowing of growth, followed by a time of mass die-off in the once flourishing community (“famine;” Figure 9.50). These increasingly salty surface waters can at first no longer support haloxene forms. Then halotolerant life dies back and finally, by the halite pre-

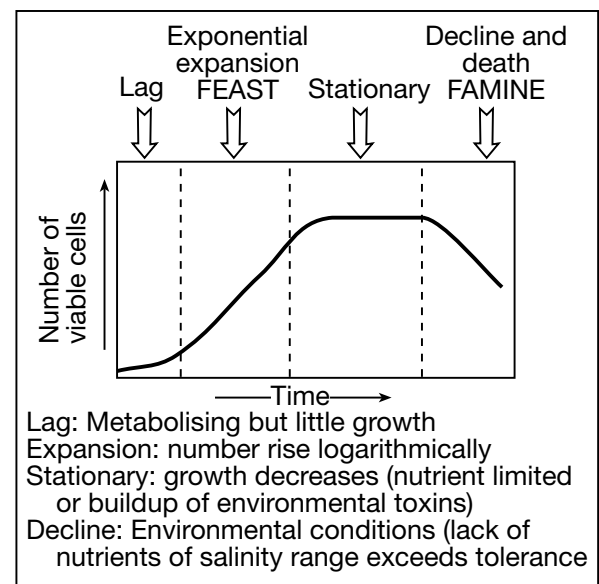


Figure 9.50. Typical growth curve as a population expands into a vacant ecological niche. In a layered brine system it is created by the freshened surface water and ends with holomixis.

cipitation stage, only a few halophilic Archaea remain (typically acting as heterotrophs and fermenters).

The pulses of organic matter created during a freshening event create a laminated bottom sediment. Hydrogen-rich algal and bacterial debris is best preserved within sediments where pore waters are anoxic and remain so until this kerogen is sufficiently buried to generate liquid and gaseous hydrocarbons. Increasing rates of mineral precipitation at higher salinities means levels of hydrogen-prone organics are highest in sediments deposited in schizohaline waters that remain in the mesohaline field. Once ambient salinities pass into the penesaline and supersaline, the proportion of organics accumulating in the bottom sediment becomes insignificant as it is overwhelmed by the large volumes of gypsum and halite reaching or accumulating on the bottom (or trona and glauberite in some continental penesaline/supersaline waters).

Feast and famine is a response of the biota to environmental conditions that are first eminently suitable and then increasingly adverse (Figure 9.51). It is a biological response to rapid niche creation and expansion as the freshened water layer sets up in the evaporitic depression. This creates a vacant ecological niche in to which microbial life rapidly expands, flourishes and then once more dies back as drying or brine concentration shrinks suitable niche space. Longterm stability in any ecosystem leads to domination by “specialist” species that are well adapted, diverse and efficient in terms of energy flow-nutrient utilisation. This biodiverse community takes up and recycles carbon very efficiently through the system and the potential for large volumes of carbon passing into the burial realm is low and hence source potential is also low (a good

example is a tropical coralgal reef). In contrast a schizohaline system is one defined by high habitat instability, a lack of habitat permanence that encourages opportunistic lifestyles (cycles of “feast or famine”). Opportunists expand rapidly into any suitable niche space, but then just as quickly die back as conditions become adverse. Such systems are characterised by high biomass pulses and low species diversity leading to pulses of organics accumulating in the evaporitic depression, with the remains likely to be buried and “pickled” beneath anoxic bottom brines and pore waters, giving such systems a higher source rock potential (Figure 9.51).

Some hypersaline settings are intermediates in that their waters are constantly hypersaline, stressful to most life but suitable to a few well adapted species. These are usually populated by a few very specialized species (e.g. “high-salt-in” halophiles) that can survive and flourish in conditions where most life dies. They photosynthesise and metabolise successfully in these hypersaline conditions (often for example living near haloclines), but do so at rates that are much slower than the growth rates attained by “opportunists” at times of “feast.” Even though heterotrophic, these well-adapted halophiles cannot ingest all the debris raining down on them at times of feasting in the waters above.

Once we attempt to take our understanding of microbial community dynamics from modern into ancient saline systems we must also account for changes in both scale and depositional diversity. Put simply, there are no modern same scale analogs for large ancient marine fed evaporite depressions (Figure 5.27). We can show that organic-rich carbonate laminites forming in the African rift valley lakes today have similar counterparts in

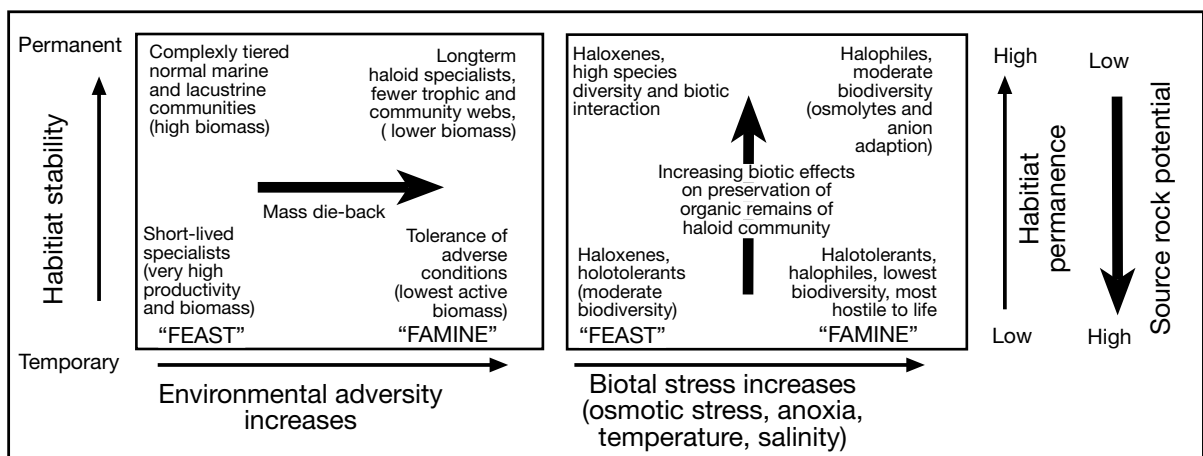


Figure 9.51. Schematic summary (‘halomancy’) of the interrelationships between habitat stability, environmental stress or adversity, biodegradation, anoxia and source rock potential in an evaporite basin.

the ancient rift valley source rocks, for example in the Cabinda Basin of Angola and the Mesozoic lacustrine basins of South America (Table 9.1). Likewise, we are in the early stages of documenting ancient counterparts of supra-allochthon brine lakes with anoxic bottoms rich in organics.

But these are small-scale features. There are no modern counterparts for most ancient large-scale evaporite depressions. They required varying combinations of greenhouse eustasy (epeiric seaways) and tectonics-climate in order to create huge subsealevel depressions filling with evaporitic carbonates and salts (marine-seepage rifts, soft collision belts and far-field intracratonic sags). Yet it was in the resulting salinity-layered intraplatform epeiric depressions and restricted basin centres that schizohaline waters and stable longterm brine plumes formed across time scales that allowed evaporite source rocks to accumulate (Figure 9.3 and Table 9.1). As for most ancient evaporite styles, the present is not a suitable time for studying scales of evaporite development, but process and texture can be seen in small-scale Holocene deposits.

Chapter 10: Oil and gas associations

Introduction

Worldwide, bedded and allochthonous evaporites are highly effective seals. Even though evaporites constitute less than 2% of the world's sedimentary rocks, one-half of the world's largest oilfields are sealed by evaporites, the other half are sealed by shales (Figure 10.1; Grunau, 1987). Kirkland and Evans (1981) argued that evaporites overlies or seal carbonates containing an estimated 50% of the world's known total petroleum reserve. Of the world's 25 largest oil fields, Grunau (*op. cit.*) found that 17 fields are capped by Mesozoic seals, six by Tertiary seals and only two by Palaeozoic seals. Eleven are situated in the seal depth-interval of 1,000-2,000 m; ten are in the 2,000-3,000 m interval; three in the 0-1,000 m interval; and one at a depth greater than 3,000 m.

Of the world's 25 largest gas fields, nine are sealed by evaporites and sixteen by shales and hydrates. Sixteen are capped by Mesozoic seals, 7 by Palaeozoic seals, and only two by Tertiary seals. Fourteen are in the 1,000-2,000 seal-depth interval, nine in the 2,000-3,000 m interval; and two in the 0-1,000 m interval. As one would expect, more gas fields than oilfields

are sealed by Palaeozoic caprocks, and more oilfields than gas fields by Tertiary caprocks. Surprisingly, the seal depth intervals for the 25 largest oil and gas fields do not differ significantly. However, Grunau argues many "supergiant" gas accumulations below depths of 3,000 metres have either not yet been discovered, or have not yet been put in production (e.g. much of the Khuff gas in North Dome in the Middle East).

The exemplary ability of evaporites to act as seals holding back large hydrocarbon columns is clearly seen in the Middle East, where Ghawar, the world's largest oil field, is sealed by bedded evaporites of the Arab Formation and the overlying Hith Anhydrite seal. This seal holds back an estimated remaining reserve of more than 100-200 billion barrels. Evaporites also seal Safaniya the world's largest offshore field, also in Saudi Arabia, with estimated reserves of more than 25-30 billion barrels of oil and 5 billion cubic feet of natural gas. Likewise evaporites are the seal to North Field in offshore Qatar, the world's largest single gas field (non-associated gas) with more than 500 tcf of reserves (Alsharhan and Nairn, 1997). This gas is reservoir and sealed in the evaporitic dolomites of the

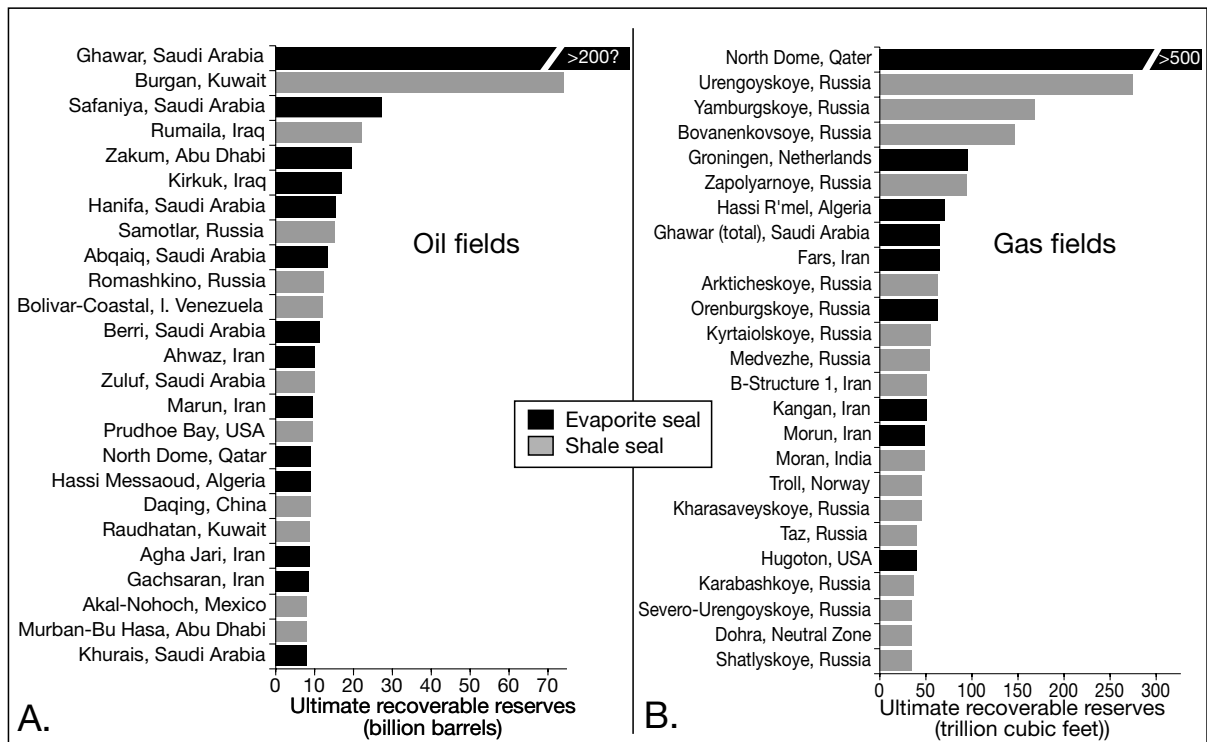


Figure 10.1. Seal type and ultimate recoverable reserves in 25 of the world's largest oil and gas fields (in part after Grunau, 1987).

		Effect of evaporite on nearby reservoir		Effect of seal itself	
		Depositional	Subsurface/diagenetic	Depositional	Subsurface/diagenetic
Bedded salt	Suprasalt	Presence of brine, either from salt dissolution or deposition of nearby salt can prevent accumulation of carbonates or siliciclastics containing a normal marine biota.	Solution of bedded salt creates collapse sinks and fronts that can enhance deposition of porous sediments or encourage collapse fracturing in overlying beds	Not applicable	Dissolution of salt creates a dense brine plume that aids in the formation of hydrodynamic traps
	Intrasalt		Solution of surrounding salt creates fractured and brecciated intrasalt beds that can stack into porous solution breccias	Not applicable	Permeable intervals are encased in bedded salt
	Subsalt	Evaporite bed acts as a source of Mg-rich brine that improves permeability of underlying or adjacent bed (creation of mouldic porosity and brine reflux dolomite)		Evaporite bed acts as top seal and/or lateral seal to reservoir (well documented)	Evaporite bed acts as a source of saturated brine for cement plugging of underlying or adjacent unit
Halokinetic	Suprasalt	Shallow halokinetic salt focuses the deposition of porous sediment around areas of uplifted seafloor or land surface. Can also influence the formation of slumps and CCD-related sedimentation	Dissolution of the upper salt surface creates a caprock reservoir	Salt flows carries blocks of anhydrite/dolomite and allochthon dissolution creates salt ablation (retreat) breccias	Passage of salt allochthon creates adjacent zones of alteration/cementation that may continue to act as a barrier to fluid flow even when the salt is no longer present (weld)
	Intrasalt	Not applicable	Salt flow can break up, fracture and rotate organic-rich intrasalt beds, allowing them to become self-sourcing reservoirs encased in a halokinetic salt seal	Brecciation of intrasalt bed leads to overpressured blocks within the salt mass	Salt flow allows salt unit to maintain seal integrity
	Subsalt	Not applicable	Brine plume created on the underside of a dissolving salt allochthon can alter underlying beds, which in some situations (eg fluid breakthrough) can enhance permeability of underlying beds via dolomitisation/fracturing	Salt allochthon acts as top seal or lateral seal to reservoir sands (well documented). The ability of salt to maintain seal integrity under both extension and compression is significant	Passage of salt allochthon creates adjacent zones of alteration/cementation that may continue to act as a barrier to fluid flow even when the salt is no longer present (weld)

Table 10.1. Role of evaporites in creating hydrocarbon reservoirs and traps.

Permian Khuff Formation and recent announcements (2003) by the Qatari Government have documented more than 900 tcf of certified non-associated gas in the structure.

According to Klemme (1983) all the supergiant^{10.1} gas fields in the world are overlain directly, or somewhat directly, by laterally extensive evaporite beds or by permafrost carapaces with their attendant gas hydrates. Most of the giant Russian gas fields (mostly in Siberia) have hydrate seals, while those of the Middle East are mostly sealed by evaporites. In 53% of the gas fields that have a net recovery of 3.5 tcf or more, evaporites are either associated with the reservoirs or form the trap (Billo, 1996). All of the giant gas fields in thrust belts have an evaporite seal (Downey, 1984) reflecting salt's ability to maintain seal integrity as it deforms, while underlying sediments fracture into salt-sealed reservoirs. Deforming shallow salt allochthons in

the Gulf of Mexico and elsewhere, not only control the seafloor topography focusing deposition of nearby sand and carbonate buildups, but later can flow over these deposits to create the seal (Figure 6.63). Halokinesis creates both suprasalt and subsalt traps. The presence of an impervious salt bed or allochthon also helps maintain higher than expected porosities and pressures in underlying reservoirs (Figure 8.14).

^{10.1}A giant oil field contains more than 0.5×10^9 barrels of expected ultimate recoverable oil, while a supergiant contains more than 5×10^9 barrels (Fitzgerald, 1980). The equivalent separation between giant and supergiant gas fields is 0.5×10^9 and 5×10^9 BOE, respectively.

BOE is barrels of oil equivalent on a BTU basis; 1 barrel of oil = 5.61 ft^3 , so the respective cutoffs for giant and super giant gas fields are 3 and 30 tcf (trillion cubic feet).

In the gently folded belt in front of the main Zagros deformed zone in Iran and Iraq an intimate association exists between sediment deposition, salt flow and the creation of salt-sealed reservoirs. This foreland basin is an area undergoing compression and syndepositional folding where crests are still growing at the surface (growth folds) and so controlling the distribution and structuration of both reservoir and seal. The same collision system also created the restriction that allowed the Fars-Gasharan seal to precipitate. It is an area with a great deal of potential for future evaporite-associated discoveries, as evidenced by the 1999 discovery of the Azadegan oil field, near Ahwaz in the Zagros Fold Belt of southern Iran. As announced by the NIOC (National Iranian Oil Company) in September 1999 the structure holds a possible 24-26 billion barrels of oil in place over an area of more than 520 km², with something like 5-6 billion barrels of recoverable oil. If the size of the projected field is confirmed by ongoing drilling, it will become one of the world's supergiant fields. To put this level of reserves into some perspective, 26 billion barrels of oil in place is more than the total known reserves in China.

Predicting the position and quality of potential reservoirs in evaporite terranes is difficult without integrating notions of feedback between deposition, diagenesis and structural evolution. Therein lies the difficulty in placing evaporite-associated reservoirs and traps in classic terms of structural, stratigraphic and diagenetic traps. When classifying a field with an evaporite trap, the fact that salt is so mobile, so soluble, and so diagenetically active, separates it from other trap styles in a petroleum system. It means that a salt unit, by its comings and goings, plays ongoing and multiple roles in generating reservoirs and traps from the time of deposition through diagenesis to structuring. Tying the resulting oil and gas field to a static and categoric breakdown is near impossible as salt-induced structuring, diagenesis and deposition are often penecontemporaneous and in a state of intimate feedback.

Over the years, I have come to regard such pigeonholes for salt-associated traps as next to useless in predicting likely positions of hydrocarbons in evaporitic provinces. Rather, as a salt unit is typically the most obvious feature on a seismic section, especially in carbonate terrains, I use a much simpler classification of; "Where's the salt?" At their simplest, evaporite-associated reservoirs all occur adjacent to either bedded or halokinetic salt (or their solution residues; Table 10.1). With bedded or halokinetic salt or solution breccias, there are three possible positions of potential reservoir, namely; subsalt, intrasalt and suprasalt (Figure 10.2). Within a single hydrocarbon fairway there may be reservoirs sitting in more than one position. Where I can, I further classify each reservoir in terms of the relative roles of deposition, diagenesis and structure as controls on the position of the targeted hydrocarbon accumulations.

Consider this, when a seal bed with a vertical permeability of 10⁻⁸ darcies is a mile long on each side and is cut by a single fracture 6 μm wide, then the drainage through that single fracture is equivalent to the total fluid flux through the square mile of

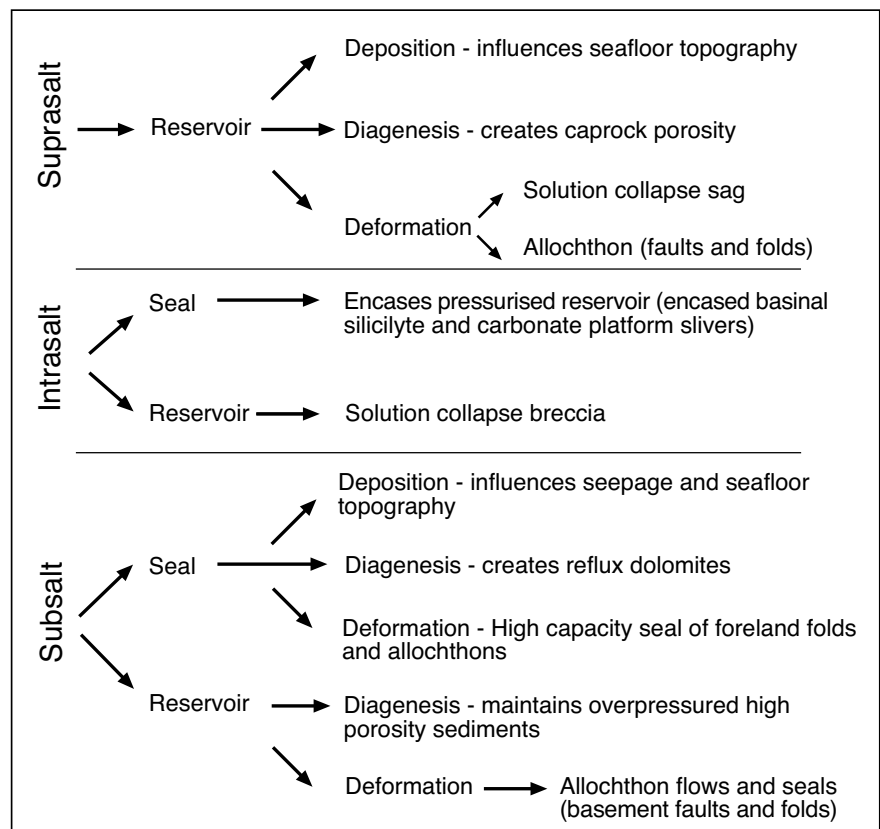


Figure 10.2. Classification of evaporite seals and associated reservoirs relative to the salt body position and the dominant mechanisms.

seal. Downey (1984) calculated that a single fracture 25 μm wide atop a 150 m oil column would leak oil at rate of more than 150 million barrels per million years. Understanding and predicting lateral continuity of both bedded and halokinetic salt seals is an important exploration and development tool.

Continuity of ancient saltern and mudflat seals and their ability to resist fracturing via reannealing means salt beds can gather and constrain subsalt hydrocarbons over large drainage areas. In suprasalt traps, the role of salt in creating reservoirs and traps ranges from stratigraphic seal through diagenetic trap to a creator of structural traps (anticlinal [halokinetic], fault and drape traps). The key factor in assessing the capacity of any seal, including salt, is timing of any microfracturing or fracturing relative to hydrocarbon emplacement in an underlying or adjacent potential reservoir. In other words, does any loss of seal capacity precede or postdate possible storage of hydrocarbons in the reservoir? We shall soon examine a number of examples from various bedded and halokinetic reservoir associations. First, we need to consider why salt units are excellent seals; it's a discussion where salt's inability to maintain ongoing penetrative fractures cannot be overestimated.

Seal capacity of evaporites

In Chapter 9 we saw there is a depositional association between evaporites and some types of organic-rich oil-prone source rocks. In Chapter 6 we saw how salt flows created structures capable of trapping substantial volumes of hydrocarbons. But, of the various reasons for the evaporite-hydrocarbon association (source, trap and seal), the most commonly cited is the efficiency of evaporite layers in holding back substantial hydrocarbon columns for lengthy periods of time, even as adjacent nonevaporite strata fracture and leak. Using a worldwide database of 350 giant oilfields, Macgregor (1996) showed oil pools are dynamic short-lived phenomena, with a median age of 35 Ma. A third of them show evidence for post-entrapment destructive processes, particularly erosion, fault leakage, gas flushing and biodegradation. Biodegradation began in many cases prior to complete filling of the trap. Re-entrapment of oil released from spilling or breached traps was common to all regions. He found the main controls on oilfield preservation to be post-entrapment tectonism and seal type, with temperature and hydrodynamic regimes being secondary factors. He concluded the potential for giant oilfields is greatest in tectonically quiescent basins with evaporite seals. As areas for the best development of this association he cites as the Middle East centred on Saudi Arabia/UAE and the Permian Basin of the

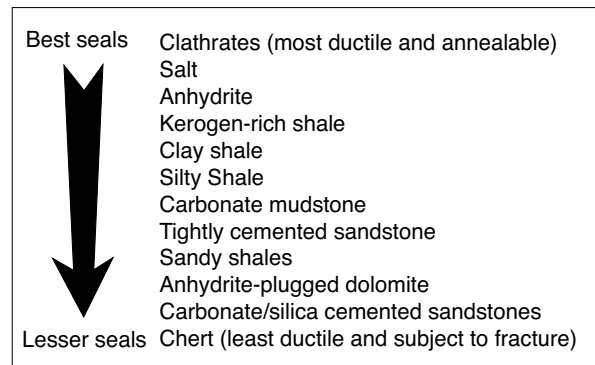


Figure 10.3. Differing ability to form a seal is related to a rock's inherent ductility in the subsurface (in part after Downey, 1984).

southwest USA. Billo (1996) noted a similar association when discussing the same areas.

So why do evaporites seal?

In terms of seal capacity and resistance to fracturing, the most effective sedimentary seals are gas hydrates, followed by evaporites, then shales (Figure 10.3; Downey, 1984). To seal an economic accumulation of hydrocarbons, any sealing surface or lithology needs to be laterally continuous, maintain a constancy of properties over large areas, be relatively ductile, and be widespread over a sedimentary basin. A fundamental requirement for any effective seal is that the minimum^{10.2} displacement pressure of the lithologic unit comprising the sealing

^{10.2}The minimum capillary pressure required to force oil or gas from one water-filled pore to the next.

^{10.3}Gas or methane hydrates (more precisely called clathrates) are the solid form of mostly methane trapped in a crystalline framework of ice and are only found in low temperature seafloor or permafrost conditions. They seal the onshore supergiant fields of west Siberia and the Timan-Pechora basins of Russia and occur also as solid bacterial-associated products in the seafloor in many of the world's oceans where water depths exceed 500 m. Seafloor clathrates are thought to contain more than 20 quadrillion cubic metres of methane. In oil equivalents this is around 15 trillion m^3 (116 trillion barrels), more than 30 times the volume of oil and gas reserves thought to exist in the world (Hunt, 1996).

^{10.4}Synonymous with minimum displacement pressure.

^{10.5}In most oilfield applications the millidarcy (md), which is 0.001 darcies, is used as a measure of permeability. Permeability is fundamentally a L^2 unit. In SI it is expressed in μm^2 , which is 10^{-12}m^2 . In conventional metric use it is expressed in m^2 (metres squared) or cm^2 . The conversion between oilfield and SI units is 1 darcy = $9.869 \times 10^{13} \text{m}^2$. In practical terms, 1 md and $1 \mu\text{m}^2$ are essentially equivalent, while in terms of hydraulic conductivity, 1 darcy = 10^{-5}m/s .

surface be greater than the buoyancy pressure of the hydrocarbon column in the subjacent accumulation. Hence, the size of the pore throats and the density of entrained hydrocarbons and water are of great importance in determining whether or not a particular lithology can act as a seal. Density/buoyancy differences between oil and gas means there are fields, such as some evaporite-cemented San Andres Formation mudstones in the Permian Basin of Texas, where dolomitic mudstones act as a seal to liquid hydrocarbons, yet flow gas.

Any lithology can be a seal, but other than ^{10.3}clathrates, evaporites are the most effective, regardless of hydrocarbon type and structural setting (Figure 10.3). Unlike the low temperatures requirements for a clathrate seal, evaporite seals, with their extremely high ^{10.4}entry pressures, very low permeabilities and large lateral extents, can maintain seal integrity over wide areas, even when exposed to a wide range of subsurface temperature and pressure conditions. A typical shale seal has a permeability $\approx 10^{-1}$ to 10^{-5} md, with rare values as low as 10^{-8} md (Figure 10.4a). Quantitative measurement of evaporite permeability is beyond the capacity of standard instruments used in the oil industry and is mostly a topic of study for engineers working with waste storage caverns (see Chapter 12). Their work shows halite has permeabilities^{10.5} that are less than 10^{-21} m² (10^{-6} md) with some of the tighter halites $\approx 10^{-7}$ to 10^{-9} md and massive anhydrite $\approx 10^{-5}$ md (Beauheim and Roberts, 2002). Cement bonds behind well casings are much more permeable than any evaporite bed that an oil well

intersects. If an oil well is abandoned without appropriate well completion, water seeping into the cement bond behind degraded casing can access the salt and the associated salt leaching can lead to problems in long term ground stability (Table 12.4). Concerns in terms of long term stability of a sealed access well,

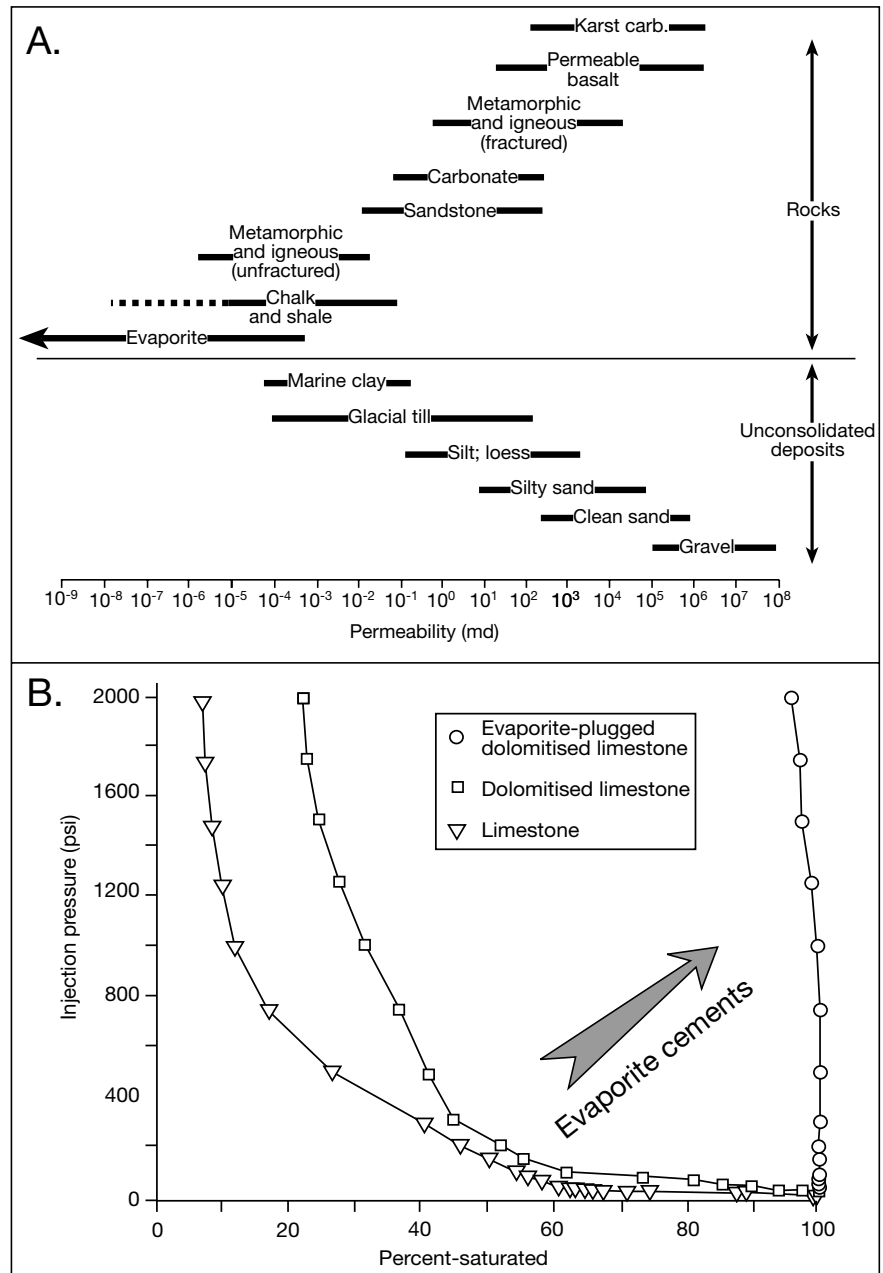


Figure 10.4. Seals. A) Relative ranking of permeability of various lithologies (in part after Beauheim and Roberts, 2002) B) Hg-injection curves from representative lithologies in a sequence undergoing reflux dolomitisation and overdolomitisation (from Warren, 1992).

rather than leakage through the salt itself, is the most important issue to be addressed in the longterm storage of radioactive materials and other high level hazardous waste within purpose-designed isolation cavities in salt (Table 12.5).

Little or no leakage will take place through a laterally continuous evaporite seal when the reservoired hydrocarbon is oil. Even when the reservoired hydrocarbon is methane, little or no loss occurs, even by diffusion. The much greater efficiency of evaporite seals is clearly seen in the total hydrocarbon volumes held back by the two lithologies. Total worldwide shale sediment volume in the crust is more than an order of magnitude greater than that of evaporites, yet the split between reservoired hydrocarbons below a shale or an evaporite seal is roughly 50:50 (Grunau, 1987).

Typical bedded evaporites, especially beds composed of monomineralic assemblages such as massive nodular anhydrite or massive halite, have entry pressures in excess of 3000 psi. Most impure evaporite beds have entry pressures greater than 1000 psi, as do many evaporite-plugged reflux dolomites (Figure 10.4b). Contrast this with most shales, which tend to be water-bearing (mostly bound and structural water) and have typical entry pressures between 900 and 1500 psi. Even though such shales are respectable seals, over time shale allows substantial diffusive leakage of methane and even liquid hydrocarbons via inherent microporosity, less so if the shales are organic-rich. Even ignoring salts ability to reanneal under stress, an evaporite seal has much lower intrinsic permeability that helps maintains its integrity. With permeabilities of 10^{-7} md, a hydraulic gradient of 0.01, and a porosity of 0.01, a brine would take somewhere between 3 and 30 million years to flow 1 metre into an unfractured halite seal, while anhydrite, which has permeability some 100 times higher, a brine would take between 30,000 and 300,000 years to flow 1 metre into the seal (Beauheim and Roberts, 2002). Evaporites are excellent longterm seals to substantial hydrocarbon columns.

With the likely exceptions of clathrates, thick halites and perhaps anhydrites, almost all fine-grained subsurface rocks will at some time in their burial history be subject to microfracturing and leakage. Otherwise, organic-rich mudstones and shales could not act as source rocks and there would be no primary migration of hydrocarbons. In contrast, rather than fracturing, most salt seals tend to lose their seal integrity either through dissolution windows or through salt-flow-induced breaches, which are defined by areas of overburden touchdown and focused subsalt leakage. Thick salt beds experience brittle fracture only at very shallow nearsurface and typically vadose conditions, such as Salar Grande in South America (Figure 3.47).

Halite's very high ductility and its ability to flow, reanneal and re-establish lattice bonding by solution creep (Figure 6.3b) when subject to stress give it a low susceptibility to fracturing. The ability of a halite unit to maintain seal integrity, and so prevent the escape of hydrocarbons, reflects a combination of an ability to flow and reanneal under stress, and the small size of molecular interspace in its ionically-bonded NaCl lattice. Massive bedded halite units contain few, if any, interconnected pore throats. The distance between NaCl lattice units is 2.8×10^{-10} m, while the smallest molecular diameter of a hydrocarbon molecule (methane) is 3.8×10^{-10} m. In reality, the only way that hydrocarbons can migrate through an unfractured halite bed, even by diffusion, is if the halite contains impurities that render it locally porous and make it brittle during deformation.

Whether buried halite beds that enclose organic intrabeds can release volatiles during catagenesis is still a matter of some discussion among organic geochemists. The longterm lack of fracture or pore throats in buried salt beds is why organic-rich intrasalt carbonate or shale laminites tend to be inefficient source rocks in style 1a source rocks (Figure 9.3). Likewise, possible flushing and maturation effects are poorly understood in subsurface situations where encased organic-rich beds are in contact with hydrated salts converting to their anhydrous equivalents (such as gypsum to anhydrite or carnallite to sylvite, mirabilite to thenardite). Loss of water of crystallisation has the potential to allow organic-rich fluids to escape as the hydrated salts transform to their anhydrous forms. But such burial transformations typically occur in the first few hundred metres of burial and may only allow immature hydrocarbons to escape into adjacent more porous sediments (Hite and Anders, 1991). There they must be stored, mature and remigrate in later burial if they are to act as source rocks on encased organic-rich beds (Warren, 1986). Many intrasalt organic-rich beds survive well into the metamorphic realm and evolve into graphitic quartzites and marbles encased in meta-evaporitic albitites and scapolites. However, some thin impurity-rich salt beds may fracture when overpressured (e.g. Figure 6.4).

As a general rule, even as a halite bed fractures, its inherent lack of strength and the consequent ability to flow means any microscale intercrystalline fractures quickly reanneal by a combination of flow and pressure solution induced recrystallisation. Current consensus is that some thin impurity-rich salt beds interlayered with carrier beds do leak small amounts of volatiles, but much less efficiently than thicker organic-rich mudstones and shales; whereas organics encased in thicker salt beds probably cannot leak until the enclosing salt dissolves. Evaporite beds and allochthons constitute some of the strongest longterm

subsurface barriers to the vertical migration of hydrocarbons in a sedimentary basin.

Environments favouring seal continuity

When assessing any hydrocarbon accumulation the top, lateral and bottom seals must be identified and evaluated. Theoretically, the thickness of a seal does not contribute to seal capacity: a clay shale (4-10 μm particle size) with an entry pressure of 600 psi is theoretically capable of sealing a 900 m oil column. In reality, it is unlikely a shale bed only a few cm thick is a laterally continuous, unbroken, unbreached unit capable of maintaining stable lithic character over a sizeable area. A thin evaporite perhaps could be, but a thicker seal provides many layers of contingent sealing beds and so gives a larger probability of a sealing surface being continuous over an entire prospect. Evaporite seals more than 30 m thick are considered excellent, while shale seals more than 50 m thick and evaporite seals more than 10 m thick are considered adequate.

Seal continuity rather than measured seal capacity is the most important factor in assessing seal quality. In the laboratory, one can measure the displacement or entry pressure necessary to force a given hydrocarbon mixture through a rock sample under given conditions of temperature and pressure. However, there are many difficulties in extrapolating quantitative data from a capillary pressure test on a 4-8 inch (10-20 cm) diameter core into a reliable prediction of the seal character across the entire sealing surface. A simple domal closure of 2,950 ha (6,400 acres) provides a ratio between a typical seal sample (4-inch diameter whole core) and the area of top seal of 1 to 3.5 billion. Average values of seal properties measured from core without a reliable geological model for the reservoir are next to useless in quantifying seal integrity. What is needed is knowledge of the likeliest weakest points in the seal across the structure of interest. It's the difference between a guarantee that you will on average survive if you swim in these shark- and stinger-infested waters, versus you are advised not to swim in this lagoon. Most of us prefer the second option, it's the same when investing tens of millions of dollars in exploration and development wells.

Saltern and deepwater evaporite beds make excellent seals because the density-stratified hydrology of their depositional setting guarantees there was little lateral variation in depositional rock properties over large areas of the salt-covered basin floor (Chapters 2 and 5). Evaporite-plugged mudflat units also make effective seals, as do platform carbonates plugged by evaporite cements precipitated from dense reflux brines. But high levels of entrained impurities, less predictable depositional topography

and lateral variations in early diagenetic fluid flux rates means both these seal types are more subject to problems with lateral continuity as well as stress fracture and failure.

Deposition of saltern evaporites atop the various Arab cycle carbonate reservoir sands of Saudi Arabia and the Emirates not only formed the highly effective Hith seal (Figure 10.5a), but aided in the preservation of underlying reservoir porosity and permeability by preventing later entry of meteoric waters (from above) capable of precipitating eogenetic carbonate cements.

Once dissolution starts to thin a previously effective seal, it begins to leak. Even the Hith Anhydrite can leak once it is less than 10 m thick, as can be seen by the migration of Jurassic-sourced oil in Cretaceous reservoirs along the edge of the Hith Anhydrite (Figure 10.5a; Hawas and Takezaki, 1995). In my opinion, this leakage in the thinned Hith can be tied to increasing proportions of dolomite residues near the dissolutional feather edge of the Hith and a consequent propensity for brittle responses near this edge, with local faulting tied to collapse fracturing. There would be little loss of seal capacity in an anhydrite bed as thin as 10 metres if it remained as relatively pure nodular anhydrite.

Leakage is obvious in Al Rayyan Field, Qatar, where the upper Arab anhydrite, the intra "C" anhydrite, and the intra "D" anhydrite of the Arab Formation do not form effective seals and only the Hith acts as a regional seal for the field (Brown and Loucks, 2001). The intra "C" and intra "D" beds are interpreted as depositionally discontinuous with relatively high dolomite contents. This reflects original shoalwater carbonate deposition in the cycle capstones, which were deposited as thinned, and perhaps pinched-out, evaporitic mudflats onlapping the carbonate shoal. Likewise, the intra "C" sabkha unit, with its higher fraction of intercalated porous dolomite intrabeds, promotes seal failure via fracturing and faulting. The discontinuous salina deposits in the intra "D" anhydrite also lack sufficient lateral continuity to form an effective seal over the structure. Brown and Loucks (op. cit.) found that the major cause of seal failure in the thin, upper anhydrite is fault offset, whereby fault throw exceeds seal thickness. The high fraction of brittle dolomite in these anhydrite intrabeds results in wider seal damage zones, allowing greater potential for along-fault leakage. In contrast, where fault throw in the field does not exceed the thickness of the Hith, nor the thickness of the middle, and lower anhydrites in the Arab cycles in the field, the evaporites capping the various intra-Arab cycles remain as intact seals. Faults intersecting these beds also cause less structural (brittle fracture) damage due to the higher anhydrite fractions of the beds, so that along-fault leakage from connected intrasalt beds is minimal.

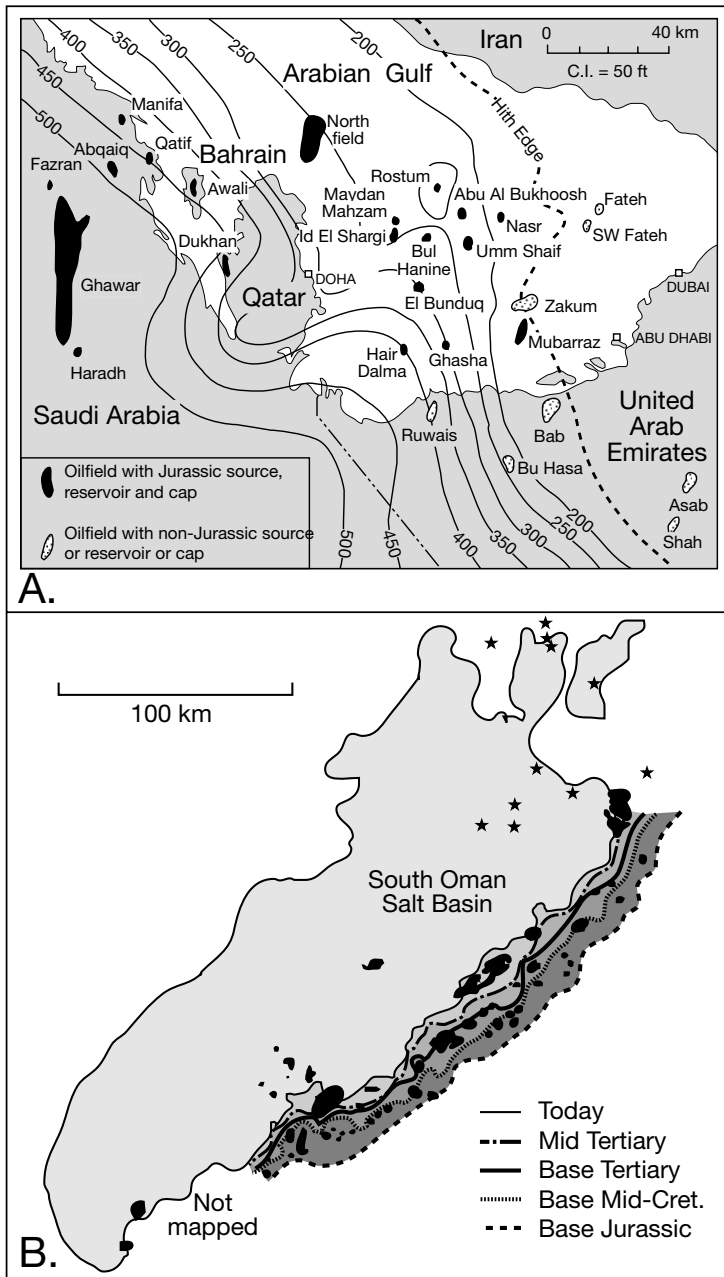


Figure 10.5. Evaporites as seal and a control of charge distribution. A) Hith Anhydrite isopach showing thickening from the UAE west into Saudi Arabia and some of the main fields producing from Jurassic reservoirs in this region (in part after Alsharhan and Kendall, 1994). Note the lack of Jurassic reservoirs to the east of the Hith erosional edge showing the effectiveness of the saltern evaporite in holding back substantial oil and gas columns sourced in Hanifa mudstones (see Figure 9.4). B) Distribution of charge in the oil and gas fields along the highly productive eastern margin of the South Oman Salt Basin is controlled by the retreating dissolution edge of the Neoproterozoic Ara Salt and the underlying Huqf Fm. source rock, which became mature in the Cretaceous. Oil fields shaded black, stars indicate gas fields (after Terken et al., 2001).

Hydrocarbon migration and trapping in the south Oman salt basin, with its subsalt Neoproterozoic Huqf source rock, is strongly controlled by the continuity of the Neoproterozoic Ara Salt. In the centre of the basin, where the salt is still present, there is an additional substantial volume of oil still trapped in intrasalt organic-rich siliceous stringers of the Athel silicilyte (Amthor et al., 1998; Terken et al., 2001). In the peripheral syncline along the east flank, salt dissolution is the controlling parameter of structural style and trap formation (Heward, 1990), and retreat of the salt edge is the main factor for charge timing (Figure 10.5b). Traps in Palaeozoic clastics in the eastern basin margin were initially formed by halokinetic structuring, and subsequently filled by salt dissolution breaches driving dissolution drape and oil emplacement. The subsalt Neoproterozoic Hufq source rock began to generate oil in the middle of the Cretaceous and the retreat of the salts dissolution edge can be mapped in the successive fillings of the various fields that define the productive eastern margin of the basin.

Salt dissolution has today removed most of the salt along the east flank of the south Oman salt basin, and its timely removal is largely responsible for the present-day hydrocarbon-filled structures (Figure 10.5b). Oil accumulations mimic a negative image of the salt structures first formed during the earlier halokinetic stage as early salt withdrawal basins then became inverted into oil bearing turtle structures. Anticlines resulted from drape of strata over Haima and Al Khalata turtle structures and drape over deeper laterally discontinuous siliceous and carbonate stringers floating in the Ara Salt. Where salt dissolution occurred, formerly salt-encased stringers leaked and became the grounded remnants that now form chaotic solution residue horizons both in outcrop and in the subsurface (Terken et al., 2001; Peters et al., 2003).

Wherever marine carbonate reservoir sands are sealed by salterns or basinwide salt beds, the width of the subeconomic transition zone from economic reservoir into an overlying depositional seal is typically narrow and sharp.

Such seals are created as basin isolation drives rapid platform or basinwide drawdown (e.g. anhydrites capping the Arab cycles in Ghawar or Salina Fm. salt seals of the Michigan Basin). The narrow transition reflects hydrographic isolation that typifies the onset of marine fed saltern and basinwide evaporite precipitation (Chapter 5: a corollary of Walther's Law).

In contrast, a continuous depositional transition from reservoir to seal generates an uneconomic hydrocarbon-filled gradational passage into a seal. Such gradational transitions from reservoir to seal characterise many nonevaporite sealed stratigraphic traps, such as reef-grainstone shoals drowned beneath onlapping lagoonal shales, or point bar sands buried beneath floodplain muds. Likewise, some brine reflux traps beneath evaporitic mudflats are created by salt plugging of platform carbonates. They tend to show subeconomic transitions from reservoir to seal both vertically and laterally. Much of the hydrocarbon can lie in partially plugged porous dolomites that are "not quite reservoir, hardly seal" (Figure 10.4b). Compared to pure-evaporite seals, both salt-plugged and shale seals are much more prone to longterm leakage and the creation of thicker transition zones from reservoir to seal. Understanding and predicting the distribution of salt plugging is a significant problem in reliably modelling reserves and production estimates in evaporite-sealed reservoirs worldwide.

The transition from a potential dipping reservoir sand into a near vertical diapir stem or a subhorizontal salt allochthon also forms sharp effective lateral and top seals. The passive mode of salt emplacement creates a sharp rather than a transitional boundary. Syndepositional stacking of reservoir sands against a passive diapir stem seal in the Gulf of Mexico has created some of the most productive acreage anywhere in the world (in terms of recovered bbl/acre; Halbouty, 1979). Sharp contacts also create potentially hazardous sharp transitions into zones of high overpressure (see Chapter 8).

Reservoirs and traps

At its simplest, evaporite-associated reservoirs occur adjacent to either bedded or halokinetic seals (or their solution residues) in subsalt, intrasalt or suprasalt positions (Table 10.1). Bedded salt seals are further subdivided into lacustrine, platform or basinwide settings, while halokinetic salt seals are either autochthonous or allochthonous.

Bedded salt seals

The main function of bedded evaporites in the evaporite hydrocarbon association is as a seal to subsalt accumulations of oil and gas (Table 10.2). In many cases, high levels of primary intergranular porosity in grain-dominated limestones are preserved beneath a salt seal (e.g. Jurassic Arab cycles on the Arabian Peninsula) or intercrystalline porosity forms in variably dolomitized subsalt limestones (e.g. San Andres reservoirs on the Central Basin Platform fields of west Texas). Impermeable evaporite beds and salt-plugged dolomites capping various upward-shoaling platform cycles, effectively seal off underlying porous carbonates from later surface-driven influxes of freshwater or sulphate-bearing fluids. The evaporite horizon is never a potential reservoir, unless it dissolves into a solution breccia or if intergranular salt cements are leached from previously salt-plugged sands or dolomites.

In the early stages of salt deposition, especially of gypsum salterns atop a marine platform, there is usually an associated hydrological system of basinward flushing dense brines (reflux). Circulation is driven by gravitational instability, set up by an updip dense brine plume or brine curtain that typically forms below accumulating evaporites (Figure 2.50). At its periphery this refluxing plume mixes with and displaces less dense subsurface and connate waters to create or enhance the reservoir properties of adjacent subsalt limestones via reflux dolomitization.

As dense Mg-rich brines seep downdip from the platform saltern or mudflat they create intervals of porous dolomites in more distal zones, located seaward of overdolomitised evaporite-plugged areas. In some cases the most extensively dolomitised carbonates in these more distal zones are high-energy, shallow water grainstones and packstones. These were the sediments with the higher permeabilities at the time of dolomitisation. However, in areas of pervasive syndepositional marine cementation, some originally porous carbonates may have already lost much of their intergranular permeability via overgrowths of isopachous rim cements. In this situation the less cemented platform mudstones act as aquifers to the refluxing brines and so are preferentially dolomitised. Likewise, in more restricted portions of an epeiric carbonate platform where the only sediment beneath a salt seal is lagoonal mud, it is dolomitised and sometimes converted into a reservoir with intercrystalline permeability (e.g. the Levelland-Slaughter trend in the San Andres Fm, west Texas and New Mexico). In some muddy platform carbonates, only the pelletal and sandy burrow fills retain sufficient permeability to be dolomitised, while their muddier surrounds are not (e.g. Red River Dolomite of North

Dakota). Whatever the setting, the rule of thumb is that refluxing brines will preferentially dolomitise whatever carbonate facies is capable of acting as an aquifer at the time of reflux.

The economic significance of reflux dolomite was first noted in the 1960s in the various evaporite-associated Permian dolomite reservoirs of west Texas (Adams and Rhodes, 1960). Reflux dolomitisation also controls porosity/permeability distribution in the finer-grained parts of some Jurassic Arab Formation reservoirs in Saudi Arabia, as well as the Permian Khuff Formation in the Arabian Gulf, the Smackover Formation carbonates of the Gulf of Mexico, and many other oil and gas fields across the globe where dolomites occur beneath an evaporite seal (Sun, 1995; Warren, 2000a). Yet, in other depositionally similar evaporitic settings, some of the mesohaline laminites that underlie bedded salts are not dolomitised, typically because they were evaporite-cemented in the strandzone prior to the onset of reflux flushing. They were too tight to transmit the volumes

of Mg-rich brine needed for dolomitisation. Syndepositional permeability in units deposited immediately after a transition into widespread evaporite deposition, controls the type and extent of brine reflux.

Worldwide, Phanerozoic dolomite reservoirs are defined by four syndepositional associations (Sun, 1995; Warren, 2000a): (1) evaporitic mudflats in a carbonate platform, most often a ramp profile (roughly equivalent to peritidal-dominated carbonate of Sun, 1995), (2) saltern-sealed platform carbonates with mudflat development over palaeotopographic highs - this system typically develops across an epeiric platform behind a rimmed shoal profile (roughly equivalent to subtidal carbonate associated with evaporitic tidal flat/lagoon of Sun, 1995), (3) basinwide evaporite seal (subtidal carbonate associated with basinal evaporites of Sun, 1995), and (4) nonevaporitic carbonate sequences associated with topographic highs/unconformities: platform-margin buildups or burial related fault/fracture

Field or area	Reservoir and age	Reservoir	Trap Type	Seal	Reference
Gulf of Suez	Rudeis and Belayim Middle Miocene	Cyclic shallow ramp lagoonal carbonates deposited within a restricted embayment	Dolomites created by brine reflux	Massive basinwide evaporites	Orszag-Sperber et al., 1998 Sun and Estaban, 1994
Mesopotamian Platform	Euphrates-Jeribe Early Miocene	Locally dolomitised and packstones, with red algae, mollusks and benthic foraminifers	Reflux dolomites, skeletal buildups and biostromes	Saltern and mudflat evaporite cap	Buchbinder, 1996 Sun and Estaban, 1994
Oolitic to siliciclastic ramp reservoirs, offshore Angola	Pinda Group (Albian)	Littoral sandstones with interparticle porosity to various types of dolomitised marine shelf to shoreline carbonates with mouldic, vuggy, and intercrystalline porosity	Late Cretaceous segmentation of the reservoir series by salt tectonic gravitational gliding into halokinetic "turtle-back" and raft	Evaporitic mudflats/shales	Eichenseer et al., 1999
Sunniland Field, Southern Florida	Sunniland limestone, Early Cretaceous	Dolomitised bank margin grainstones and mudstones	Low relief anticlinal trap, possibly halokinetic	Massive saltern anhydrite	Halley, 1985 Loucks and Crump, 1985
Walker Creek Field, Chatom Field, and Mt Vernon Field, Gulf of Mexico Basin, Arkansas, USA	Smackover Formation, Jurassic (Oxfordian)	Oolitic-pisolitic dolomitised limestone retaining varying levels of primary intergranular porosity and calcite cement	Up-dip and down-dip depositional pinchout of oolitic grainstone bars, modified by halokinetic faulting (underlying Louann Salt)	Saltern and mudflat (Buckner Anhydrite)	Chimene, 1991; Feazel, 1985; Druckman and Moore, 1985
Appleton Field, Gulf of Mexico Basin, Alabama, USA	Smackover Formation, Jurassic (Oxfordian)	Dolomitised algal peloid ooid grainstone with intercrystalline and vuggy porosity	Combination structural-stratigraphic trap Up-dip and down-dip depositional pinchout of oolitic grainstone bars on high of crystalline basement	Saltern and mudflat (Buckner Anhydrite)	Haywick et al., 2000 Petta and Rapp, 1990
Ghawar, Qatif, Uthmaniya and other Arab Fm. fields in Saudi Arabia	Arab Formation, Late Jurassic (Tithonian and Kimmeridgian)	Partially dolomitised skeletal, peloidal and oolitic grainstone (Arab D), peloidal/oolitic/ skeletal grainstone (Arab C)	Low amplitude anticlines related to basement faulting and possible halokinesis of Hormuz Salt	Nodular anhydrites and tight mudstones of Arab cycles and the overlying Hith Anhydrite	Cantrell et al., 2001 Saner and Sahin, 1999, 2000 Meyer et al., 1996 Wilson, 1985
McElroy Field, Central Basin Platform, Texas, USA	Grayburg Formation, Permian (Lower Guadalupian)	Dolomitised shelf carbonates ranging from mudstones to fusilind wackestones	N-S trending asymmetrical anticline with steeper eastern limb. Permeability pinches out to west due to increasing evaporite plugging (anhydrite and gypsum)	Evaporites and siltstones of the Queen Formation; Anhydrite plugged porosity is heterogeneous.	Harris and Walker, 1990

Table 10.2. Some of the many Tertiary to Permian platform reservoirs and fields sealed by bedded evaporites.

Field or area	Reservoir and age	Reservoir	Trap Type	Seal	Reference
Ghawar, Qatif, Uthmaniya and other Khuff Fm. fields in Saudi Arabia	Khuff Formation (Members A-C), Permian	Dolomitised and leached peloidal grainstones, wackestones and mudstones, variable anhydrite cements	Low amplitude anticlines related to basement faulting and possible halokinesis of Hormuz Salt	Saltern cap and varying development of evaporitic mudflats	Al Jallal, 1995; Dasgupta et al., 2002
Reeves Field, Midland Basin and Levelland-Slaughter trend, Northern Platform, Permian Basin, Texas USA	San Andres Formation, Permian	Dolomitised skeletal wackestones and mudstones	Stratigraphic with structural assist via draping over former shelf edge	Strandline anhydrites of the San Andres Formation	Chuber and Pusey, 1985
Pecos Slope Field, Permian Basin, New Mexico, USA	Abo Formation, Permian (Leonardian)	Fluvial sandstone	Tectonically fractured stratigraphic wedge-out of fluvial clastics	Anhydrite of the Yeso Formation	Bentz, 1992
Tarchaly, Rybaki, Sulecin, Barnowko--Buszewo fields, west Poland and Thuringian basin fields, East Germany	Zechstein main dolomite; Early Permian	Dolomitised oolitic/pisolitic grainstones and mudstones	Shelf margin buildup beneath evaporite seal, structurally assisted	Zechstein anhydrite cap (basinwide)	Depowski and Peryt, 1985; Peryt and Dyjaczynski, 1991; Gorski et al., 1999; Karnin et al., 1996
Aneth Field, Paradox Basin, Utah	Hermosa Formation (one main reservoir, several semi-isolated intervals), Pennsylvanian	Leached and recrystallized oolitic limestone and dolomitised mudstone	Dolomitised carbonate mound	Evaporitic organic-rich dolomitic shale	Peterson, 1992
Lisbon Field, Utah, USA	Leadville Formation; Mississippian	Dolomitised (sucrosic) and karstified platform carbonates (wackstone-packstone)	Faulted anticline beneath supra-unconformity halokinetic evaporites of the Paradox Basin	Paradox Salt (basinwide)	Miller, 1985
Stanley Field, Williston Basin, North Dakota, USA	Mission Canyon Formation; Mississippian	Pisolitic-oolitic limestone with local skeletal marine grainstone. Fenestral porosity with primary interparticle and intraparticle	Updip facies change to fractured evaporitic mudflats and porous grainstones from downdip wackestone and mudstone	Massive platform anhydrite of the Rival Member top seal	Beach and Giffin, 1992
Elkhorn Ranch Field, Williston Basin, North Dakota, USA	Mission Canyon Formation; Mississippian	Dolomitised skeletal mudstones and wackestones	Hydrodynamic trap where structure assists in localising accumulation, but trap stratigraphic passage is into an anhydrite seal	Massive platform anhydrite top seal of the Mission Canyon Formation	DeMis, 1992
Glenburn Field, Williston Basin, North Dakota, USA	Mission Canyon Formation; Mississippian	Pisolitic limestone exhibiting subaerial exposure and vadose diagenesis with porosity pinchouts via evaporite plugs	Solution collapse anticline in underlying Devonian Salt	Massive saltern anhydrite and ferruginous shale caps, structurally assisted (anticlinal)	Borchert et al., 1990 Gerhard, 1985
Little Knife Field, Williston Basin, North Dakota, USA	Red River, Duperow, Mission Canyon; Ordovician, Devonian, Mississippian	Dolomitised shallow shelf to evaporitic mudflat carbonates	Combination anticlinal nose and porosity pinchout	Massive Mission Canyon platform anhydrite top seal, lateral change to nonporous carbonates	Wittstrom, 1990 Lindsay and Kendall, 1985
A and E pools, Rainbow Field, Canada	Keg River Formation, Rainbow Member, Middle Devonian (Givetian)	Dolomitised limestone and limestone	Pinnacle reef enclosed in evaporites and bituminous carbonates	Muskeg Member evaporites	Schmidt et al., 1985
Pinnacle reef fields, Michigan Basin, SE Michigan USA	Guelph Formation and equivalents; Middle Silurian	Dolomitised and karstified pinnacle reefs	Pinnacle reef enclosed in evaporites and bituminous carbonates	Salina Group evaporites	Gill, 1985; Obermajer et al., 2000
Medicine Pole Hills Field, Killdeer Field, Pennel Field, Williston Basin, North Dakota, USA	Guelph Formation and equivalents; Middle Silurian	Sucrosic dolomites of evaporitic mudflats (intercrystalline and vugular porosity)	Combinations of anticlinal noses and porosity pinchout, preferential dolomitisation at top of anticline and evaporite karst	Red River Anhydrite	Fischer et al., 1990; Clement, 1985; Montgomery, 1997

Table 10.2 cont'd. Some of the many Palaeozoic platform reservoirs and fields sealed by bedded evaporites.

controls. Three of the four worldwide dolomite-hydrocarbon associations show an intimate association with evaporites. Brine reflux is the dominant process in dolomite creation in all three, although it can be overprinted by later burial dolomites.

Dolomite reservoirs created by brine reflux can be subdivided using the dominant depositional style of the evaporite capstone, namely, platform and basinwide (Figure 5.7). In platform-evaporite-sealed dolomite associations, the evaporite seal is typically ≈ 5 –10 metres thick (although it can be 20–30m thick) and is usually anhydrite interlayered with shoaling platform carbonates. This evaporite cap can be further subdivided into evaporitic mudflat or saltern-dominated. Basinwide seals to carbonate reservoirs tend to be thick (>100 m) and halite prone in the basin centre and to cap carbonate buildups about the basin edge. Such buildups grew prior to the saline giant stage. Ongoing or longterm reflux beneath accumulating evaporites in both platform and basin settings can “overdolomitise” the reservoir and encourage evaporite plugging leading to occlusion of effective porosity (Warren, 2000a for summary). In platform settings such porosity-depleted overdolomitised zones tend to be most common in regions of restricted carbonate deposition beneath leaky evaporitic mudflats (these are the typical caps to Sun’s peritidal association). These sediments tend to accumulate in the more updip evaporite-dominated portions of a carbonate platform, where underlying carbonates have been flushed for extended periods by hypersaline brines. With basinwide-sealed associations, a later burial overprint and pervasive intra-reservoir karst/fracturing event seem to be needed to create and maintain economic porosity levels.

“Peritidal” muddy carbonate with evaporitic mudflat seals

Evaporitic mudflats dominate the ephemeral water portions of an evaporite basin. As discussed in Chapter 5, the use of a tidal nomenclature is not appropriate in highly restricted to hydrographically isolated epeiric setting where evaporites are accumulating. Strandzone rather than the intertidal and supratidal of the peritidal is more appropriate, but peritidal terms are used in the following discussion to conform to historic subdivisions. Strandzones can create dolomite-forming hydrologies within stacking muddy epeiric platform carbonates whereby highly saline Mg-rich brines, sourced in the mudflats, seep into adjacent restricted lagoonal marine carbonates (Figure 10.6). Without subsequent fracturing, leaching and other diagenetic enhancements to their permeability, such fine-grained mimetic sydepositional dolomites constitute few economic reservoirs. Those intervals that do constitute reservoir tend to

be low permeability systems, which are patchily distributed in a host formation that is extensively plugged with variable levels of evaporite cement. Enhancements to this generally low and patchy permeability can occur if karst, fracturing or burial leaching subsequently modify the host lithology. Early diagenetic permeability tends to increase where the dolomitised marine mudflat was located further out on the platform and away from areas of most intense dolomitisation and evaporite plugging.

Ordovician Red River Fm., Williston Basin, USA and Canada

The Red River Formation was deposited in an epeiric sea-way that occupied the Williston Basin in the Middle to late Ordovician. The Williston Basin is located on the southern edge of the Canadian Shield, straddling the US-Canadian border and centred on Saskatchewan and North Dakota. The basin itself is circular, about 800 km across, and is filled with up to 4600 m of Phanerozoic sediments. The Palaeozoic succession is predominantly carbonate and up to 2 km thick. It is overlain by a Mesozoic succession of mainly fine terrigenous clastic rocks up to 1.5 km thick and a Tertiary succession of mostly coarse terrigenous clastics that is less than a kilometre thick. The maximum thickness of the Red River Fm. occurs in the basin centre close to Bismarck, North Dakota, and where it is slightly more than 200m thick (Pu and Qing, 2003; Longman and Haidl, 1996).

Within the basin are several major epeirogenic structures, of which the Cedar Creek anticline and Nesson anticline are the most prominent. Both anticlines have long episodic histories of farfield tectonic movement. Elsewhere in the basin, the subsurface dissolution of Palaeozoic evaporites resulted in collapse and inversion structures in post-Middle Devonian strata, such as the Birdbear structure (McTavish and Vigrass, 1987).

Red River strata consist of three carbonate-evaporite depositional sequences known as the A, B and C cycles (Figure 10.6a, b; Pu and Qing, 2003). Each sequence starts with a burrowed, normal-marine mudstone to wackestone and packstone at the base, followed by a laminated mudstone representing more restricted mesohaline deposition, which in turn is overlain by a bedded to enterolithic evaporative mudflat anhydrite which can be traced over much of the basin. Industry terminology informally defines these evaporites as capstones to the “A,” “B,” and “C” cycles. Some workers also distinguish a lower “D” zone that lacks an anhydrite cap (Figure 10.6b). In ascending order, a typical Red River cycle consists of: 1) locally dolomitized burrowed carbonate mudstones and skeletal wackestones that define a

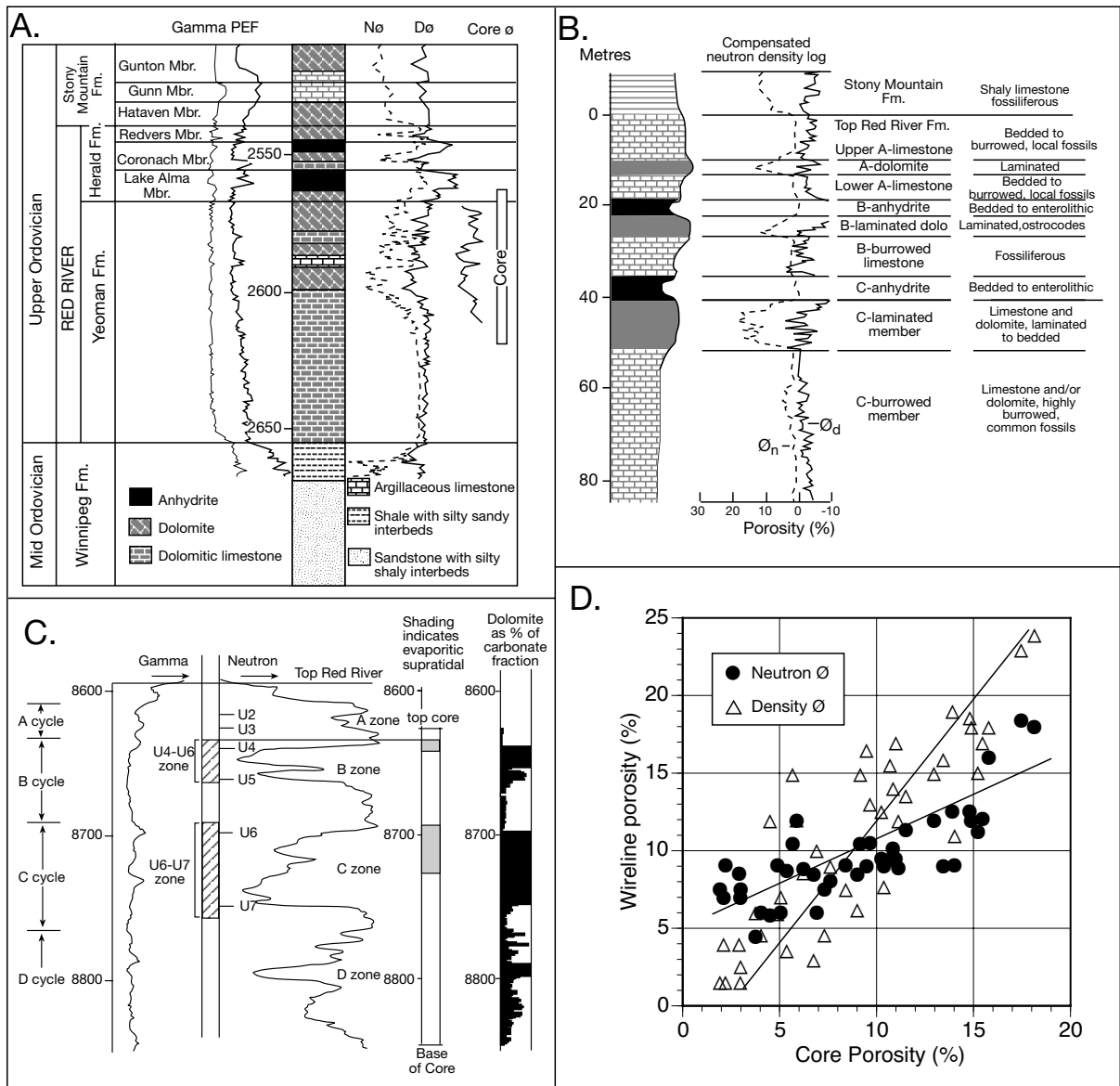


Figure 10.6. Evaporitic mudflat (peritidal) style of deposition in the Ordovician Red River Dolomite, North America. A) Red River stratigraphy with wireline data from well 7-3-7-11W2 in Midale area, Saskatchewan (after Pu and Qing, 2003). B) Typical section showing detailed sedimentary character of the main cycles (after Longman et al., 1983). C) Core section in the Cabin Creek Field, shows the close relationship between dolomite occurrence and evaporite beds (after Clement 1985) D) Relationship between core porosity, neutron log and density log porosity in well 14-16-7-11W2 in Midale area Saskatchewan (after Pu and Qing, 2003).

“Burrowed Member,” which is around 9 m thick in the B zone and up to 90 m thick in the C zone; 2) irregularly laminated carbonate mudstones that constitute a 3-12 m-thick “Laminated Member;” and 3) an impure 3-6 m capping anhydrite showing nodular-mosaic, nodular, or enterolithic textures (Figure 10.6c). All members thin toward the edge of the basin where the anhydrites disappear completely.

Subtidal lithologies in each cycle are classic Zone X sediments composed of partially dolomitized burrowed biomicrite wackestones with fragments of echinoids, brachiopods, bryozoans, trilobites, molluscs, ostracodes, and gastropods, and lesser amounts of solitary corals and stromatoporoids (Figure 5.16). These subtidal dolomitic units are poorly bedded and heavily bioturbated and were laid down in a quiet-water epeiric platform setting.

The Red River Formation is 90 to 180 m thick in Cabin Creek Field on the Cedar Creek anticline in Montana, on the southwest side of the Williston Basin. Its lower part is a tight bioturbated marine limestone (Ruzyla and Friedman, 1985). The average depth to pay across Cabin Creek Field is 2750 m, with a 15.2 m net pay thickness, a productive area of 30.5 km² (7620 acres), and an estimated 224 million barrels of oil in place. Here, and throughout much of the Williston Basin, economic porosity is largely restricted to bioturbated and partially dolomitized platform limestones.

The overlying strandline (intertidal?) portions of a cycle are dolomitic biomicrite wackestones, deposited under somewhat more energetic bottom conditions (Zone Y). These deposits are still muddy but contain graded beds, crossbeds, ripple marks, imbricate shell lags and conglomerates. They also contain allochems characteristic of strandlines, such as oncolites, ooids, intraclasts, and peloids. The overlying anhydritic sediments in each cycle (Zone Z) include wavy-laminated micritic dolomites and organic-rich mudstones, along with evidence of completely restricted and at times subaerial conditions in the form of desiccation cracks, erosion surfaces, intraclast breccias, solution collapse breccias, and nodular anhydrites. This capstone in the vicinity of the Cabin Creek anticline was deposited on the platform in a mosaic of sabkhas and salinas within an evaporitic mudflat.

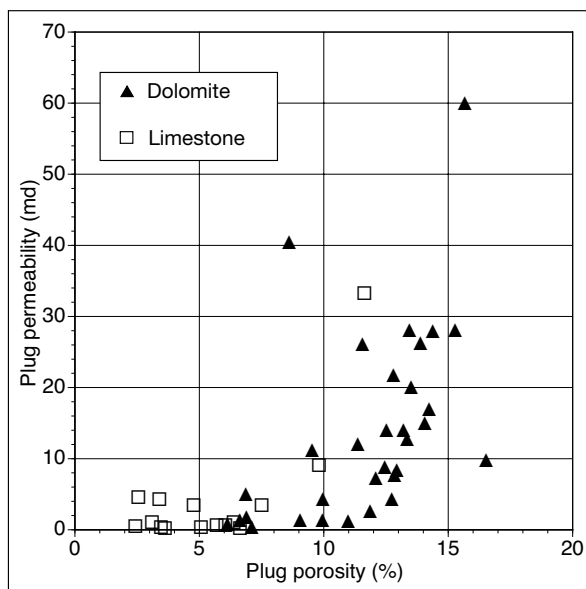


Figure 10.7. Cross plot of core porosity and permeability in the Red River Formation in well 3-8-1-11W2, Midale Field, Saskatchewan. Clearly shows the improvement in porosity and permeability associated with dolomitisation (replotted from Pu and Qing, 2003).

Evaporitic strandzone sediments in the reservoir interval in Cabin Creek Field show evidence of subsequent leaching; they contain empty gypsum and anhydrite moulds, corroded anhydrite crystals and solution collapse breccias. Early micritic dolomites of the supratidal are mimetic but units tend to be overdolomitised and salt plugged and so are relatively poor quality reservoirs. Upper contacts of the evaporite-cemented dolomite intervals are typically sharp, often erosional and pass abruptly up into the limestones of the next cycle suggesting exposure prior to the passage into the next cycle. This style of transition also characterises sediments in modern evaporite mudflats and sabkhas. In contrast, the bases of the various dolomite intervals are transitional and conformable with the underlying marine limestone interval, typical of brine transition driven by an early reflux hydrology.

As in Cabin Creek Field, Red River dolomite throughout the rest of the Williston Basin is mostly of two types; a) a mimetic evaporitic-mudflat reflux mesohaline dolomite, which is primary and precipitated penecontemporaneously as wavy-laminated or peloidal mudstones intercalated with the strandline (supratidal) carbonates; and b) an associated, perhaps slightly later, somewhat coarser-grained brine-reflux dolomite, which dolomitized underlying portions of the intertidal and subtidal sediments immediately below and downdip of the micritic mudflat dolomite (Pu and Qing, 2003; Clement, 1985; Longman et al., 1983). The proportion of dolomite decreases downward from the base of each evaporitic mudflat (supratidal) unit due to the sinking and mixing of dense hypersaline waters, which originated in the strandzone (supratidal?). Brine reflux dolomites selectively replace skeletal fragments and burrows of the marine carbonate platform. Within productive areas, dolomitised limestones consistently show improved porosity and permeability compared to nearby undolomitised limestones (Figure 10.7).

Red River reservoirs throughout much of the Williston Basin are not hosted in mesohaline mudflats, but in porous dolomitised marine lenses some 27 to 43 metres below the "C" Anhydrite Member. Permeable lenses vary in thickness from less than 3 metres up to 60 metres thick and are up to 1.5 km across (Figure 10.8). The lateral extent of these porous lenses and the possible interconnections between them is poorly understood because most producing fields are small and consist of only a few wells. Most cored reservoir intervals are dominated by *Thalassinoides-like* burrow networks, with individual dolomitised burrows 1-2 mm to >1 cm across within a less dolomitised matrix. Reservoir porosities are typically less than 15% and permeabilities less than 30 md, with most wells showing a poor relationship between porosity and permeability (Figure 10.7). Porosity development seems to be related to the degree of dolomitization,

with some porosity enhancement of partially dolomitised intervals occurring during later burial by partial dissolution of residual calcite matrix. The initial formation of dolomite may well have been bacterially mediated and focused along organic-rich linings of the burrows (Gingras et al., 2004). The mechanism was perhaps similar to that of the sulphate-reducing bacteria forming modern dolomites in the mesohaline salinas of Brazil (Figure 4.16). Dolomite-lined burrow meshworks acted as a focus for subsequent dolomitisation.

There is general agreement that dolomites of the mottled Red River C member are genetically related to Mg-rich brines seeping through restricted marine muddy carbonates. These dense hypersaline basin waters were depleted of their calcium and sulphate, either through attendant deposition of aragonite and gypsum, or perhaps by ongoing bacterial sulphate reduction. What is not agreed is whether the dolomitising brines were descending or ascending at the time of widespread dolomitisation. Longman et al. (1983) argued that brine migration was localised by “holes” in the anhydrite mudflat seal (Figure 10.8a). Fracturing, minor faulting, or early expulsion of subsurface waters from the carbonate host probably formed the “holes.” When the descending Mg-rich hypersaline brines first entered the underlying carbonate sediments beneath the “holes” they were oversaturated and precipitated cryptocrystalline dolomite (overdolomitisation), but as they migrated away from the holes they lost their potency and produced rhombs floating in a dissolving calcitic matrix. This calcite may have been precipitated as an early diagenetic phase or left as unreplaced vestiges of original calcite (or aragonite subsequently altered to calcite) during dolomitization.

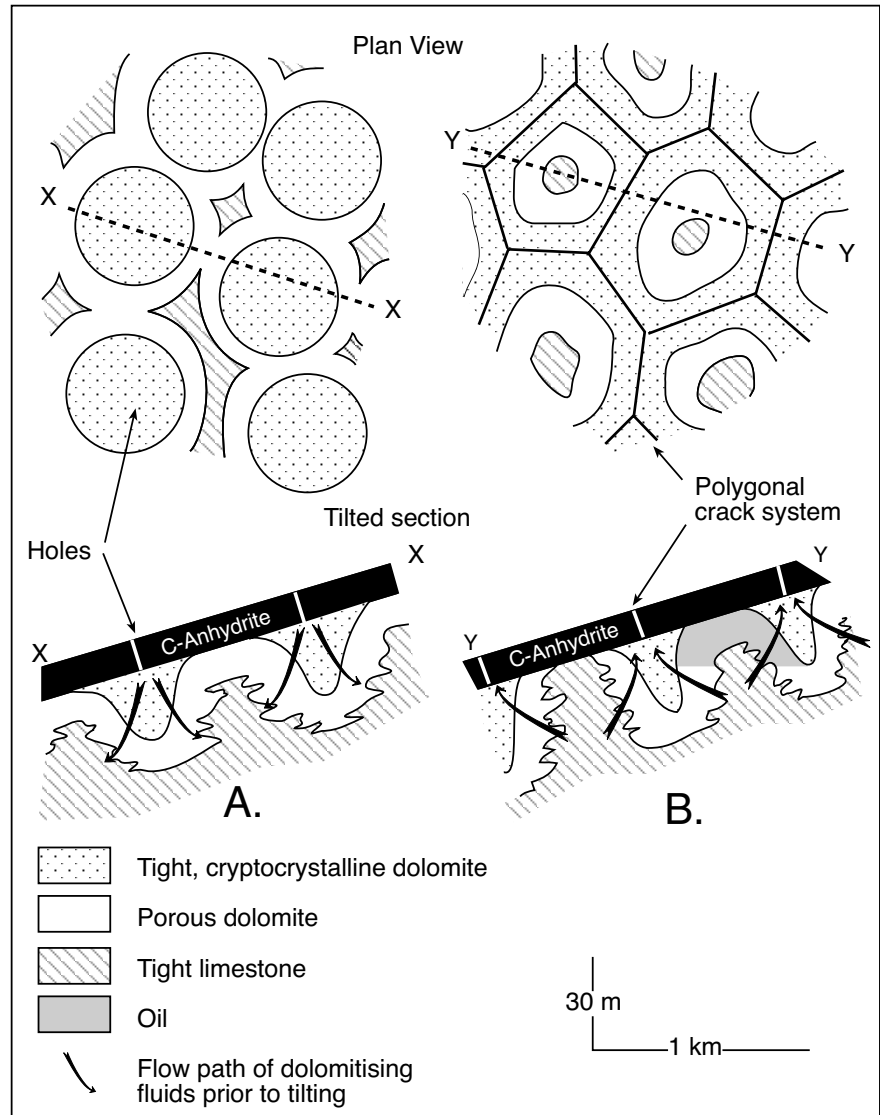


Figure 10.8. Models explaining the occurrence of patchy diagenetic dolomite that characterises much of the reservoir in the various fields in the Red River Formation. A) The descending hole model of Longman et al., 1983. B) the ascending megapolygon model of Kendall (1983). See text for discussion.

Perkins (1991) agreed with the brine reflux model for the widespread mimetic dolomite fabric but went on to argue that following further burial, limestones tended to chemically compact through pressure solution, whereas late stage fractures were localized in the more brittle dolomitised portions of the Red River Formation. These fractures served as conduits for late stage leaching fluids, possibly associated with hydrocarbon generation, which locally enhanced porosity in dolomite intervals adjacent to active fractures through the removal of associated calcite. On the scale of individual burrows, late-stage leaching is reflected in “overly porous” dolomite haloes

around cemented burrow centres and highly porous dolomite seams along stylolitic contacts.

Kendall (1983) also agrees with a brine reflux model but argues that once the gypsum cap was deposited (prior to its burial conversion to anhydrite) it was an aquifer not an aquitard and that the brine flux could just as easily been upward and focused via brine resurgence through more permeable intervals in the gypsum bed. He goes on to suggest that the control on the dolomite intensity was a series of megapolygonal sutures, much like the resurgence of saline groundwaters seen atop giant polygonal cracks in Pleistocene playas (Figure 2.41).

The complexity of dolomite-reservoir to seal interrelationships in the Red River Dolomite is symptomatic of similar relationships in many other mudflat-associated dolomite reservoirs (Warren, 2000a). The dolomitization process is ongoing from deposition through burial and uplift. Likewise, the burial

evolution of the adjacent evaporite seal is also ongoing from first deposition until complete subsurface dissolution. The evaporitic interval can act as both as a source of fluids, as in reflux dolomites and dissolving salt beds, or as a focus to fluid access as when rising basinal fluids pool and spread beneath a laterally extensive evaporite seal, or where a breached salt bed or allochthon facilitates the ingress of fluids either from below or above the breach. Generally, dolomite reservoirs contain multiple styles of dolomite created at different times in the hydrological evolution of the adjacent evaporite seal (Warren, 2000a).

Platform carbonates with saltern seals

Porosity in saltern-sealed carbonates typically occurs as multiple zones within stacked shallowing-upward evaporitic cycles that pass into mudflats near the basin edge or intrabasin highs (Warren 2000a). The saltern evaporite platform reservoir

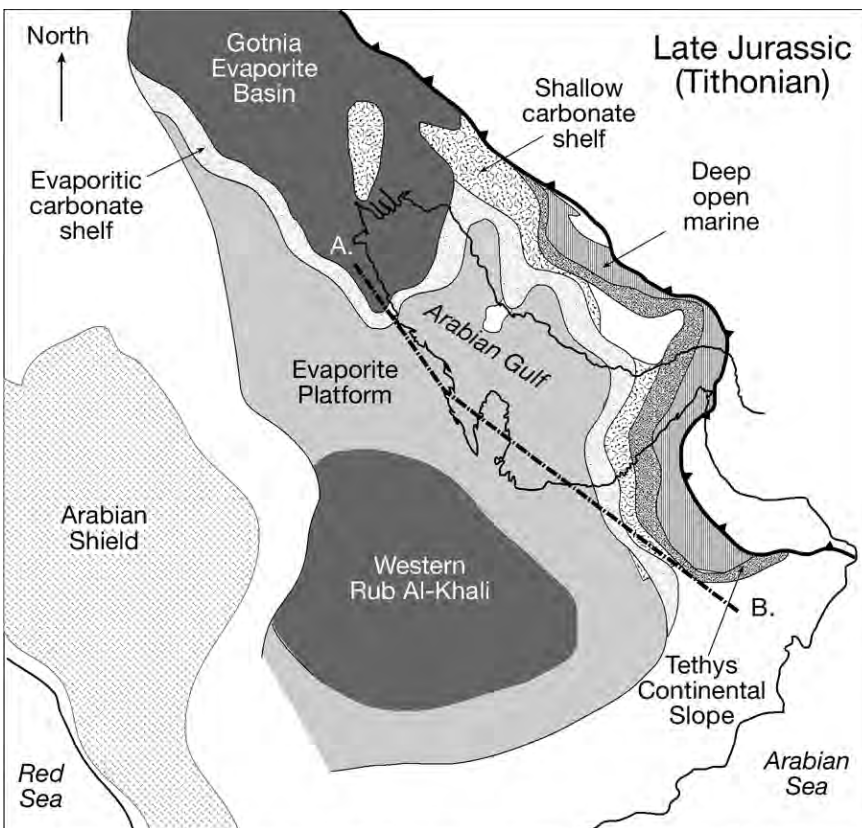


Figure 10.9. Late Jurassic Tithonian palaeogeography of the Arabian Gulf (after Al-Husseini, 1997). Deposition of the four carbonate-anhydrite cycles of the Arab Formation and the overlying Hith Anhydrite constitute the dominant regional reservoirs and caprocks. The western Rub' Al-Khali and Gotnia basins were inland salterns characterised by halite rather than platform-wide anhydrite, which is the dominant evaporite salt in the Arab and Hith formations.

grouping in part corresponds to the “subtidal carbonate associated with evaporitic tidal flat/lagoon” grouping of Sun (1995). Each economic zone is formed by porous, partially to completely dolomitized subtidal limestones. Reservoirs are typically capped by tight, dominantly saltern evaporites, with local highs indicated by seal transitions from saltern into evaporitic mudflat. Reservoir quality in the subtidal carbonate is related to depositional facies and varying intensities of diagenetic overprint.

Reflux dolomitisation is a common permeability enhancing mechanism beneath many leaky pans and saltern seas (as in the reef-rimmed Permian Basin of west Texas). But retention of relict primary porosity in epeiric limestones beneath tight sub-salturn units, rather than intensity of reflux dolomitization near the platform edge, is a significant control on reservoir quality in the Middle East (as evidenced by the

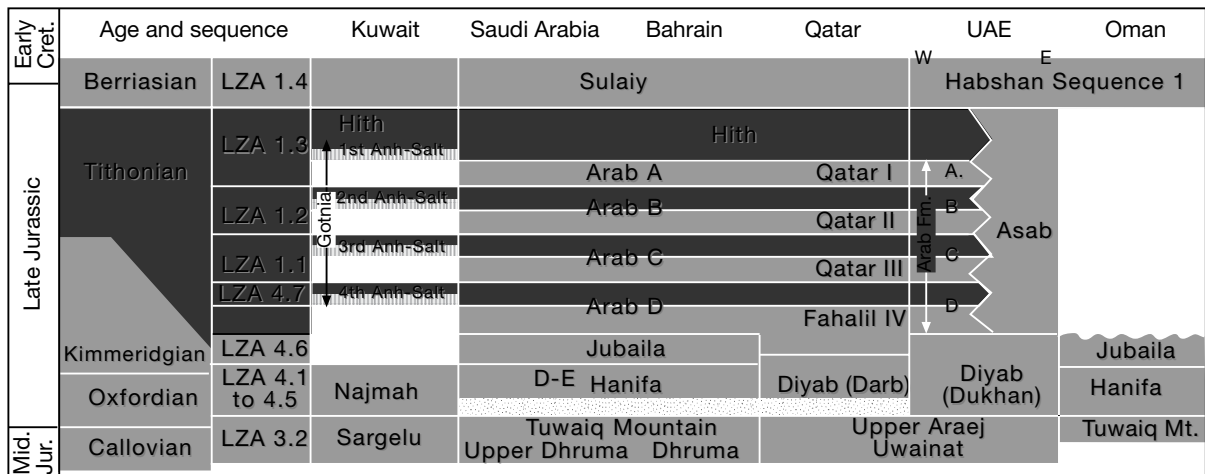


Figure 10.10. Stratigraphy of the Late Jurassic sediments of the southern Arabian Gulf (after Al-Husseini, 1997).

many saltern-sealed interior mounds and shoals making up the main Arab D reservoirs across the Arabian Peninsula; Figure 10.9). In both settings, better quality reservoirs tend to occur in higher energy, grain-dominated limestones (oolitic/peloidal/pisolithic packstones) or dolostones, but quality reservoirs can also form in lower-energy lagoonal dolomudstone/wackestone with an overprint of coarsely crystalline dolomite.

Finely crystalline, mud-dominated mimetic dolomites typically form a thin cap beneath a saltern seal or stacks in updip evaporitic mudflat positions, where they lie nearer the brine source. Such mudflat dolomites are typically low permeability sediments that require further diagenetic enhancement to attain reservoir quality (see previous section).

Jurassic Arab Formation, Arabian Gulf

The Late Jurassic (late Kimmeridgian) Arab Formation within and around the Arabian Gulf hosts some of the most prolific oil fields in the world, including Ghawar and Safaniya fields (Lucia et al., 2001; Sahin and Saner, 2001; Meyer et al., 2000; Cantrell et al., 2001; Alsharhan and Kendall, 1994; Wilson, 1985). This prolific petroleum system includes several regional organic-rich source rocks, stacked reservoirs and multiple seals (Al-Husseini, 1997). Jurassic strata were deposited across a broad platform (Murriss, 1980) that is sometimes characterized as “layer cake.” Chronostratigraphic correlation from outcrops to wells, well to well, and from country to country, defines a late Jurassic regional anhydritic sealed carbonate platform encompassing large intrashelf basins with grainier rims. At times of hydrographic isolation, the platform evolved into a widespread saltern that with further isolation was characterised

by halite-filled depressions known as the Gotnia and Rub Al-Khali salt basins (Figure 10.9; Al-Husseini, 1997).

The proposed regional stratigraphic framework for the Jurassic, as defined by Al-Husseini (1997), is as follows; 1) Upper Triassic-?Lower Jurassic continental clastics (Minjur Formation and equivalents) and the subsequent pre-Toarcian unconformity indicating regional erosion and non-deposition over the Arabian platform. 2) A Toarcian sequence (Marrat Formation and equivalents) providing a basal Jurassic regional datum, except in Oman. 3) Late Toarcian and Aalenian corresponding to a substantial sea-level lowstand and a regional depositional hiatus. 4) The Middle Jurassic Dhruma Formation corresponding to four different sequences with a major intervening hiatus. The Upper Dhruma Member, together with the Tuwaiq Mountain Member, forms the topmost sequence (Figure 10.10). The correlation between the Dhruma, Tuwaiq Mountain, Hanifa and Jubaila formations, to their equivalents in other Arabian Gulf countries, still requires clearer definition. 5) The Arab and Hith Anhydrite formations are Tithonian, based on their sequence assignment, while the Sulaiy Formation is Berriasian and straddles the Jurassic- Cretaceous boundary. The four Tithonian Arab Formation carbonates (A-D members) were deposited as transgressive to early highstand deposits, while the Tithonian Arab, Gotnia and Hith anhydrites are perhaps late highstand deposits which overstep inland salterns (Gotnia and western Rub’ Al-Khali basins). Each carbonate and overlying anhydrite cap in the four Arab cycles (Arab A-D) are interpreted as complete third-order cycles (Al-Husseini, 1997). The equivalents to the Kimmeridgian Jubaila Formation and Tithonian Arab carbonates are absent because of non-deposition in Kuwait. The Tithonian Hith Anhydrite provides a regional stratigraphic datum in the Arabian Peninsula, except in Oman

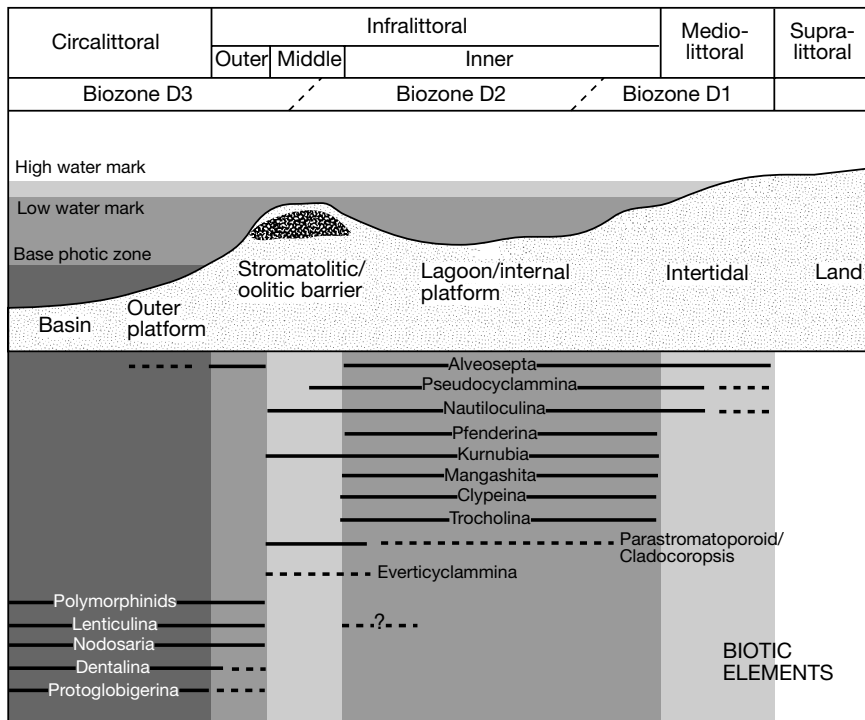


Figure 10.11. Palaeoenvironmental distribution of various biotic elements within the Arab-D reservoir (Wyn Hughes, 1996).

and the eastern United Arab Emirates (UAE). There the Arab and Hith Anhydrite formations are absent as they have been eroded or were never deposited, so the former eastern and southeastern extent of the Hith is not well understood.

The main reservoirs within this prolific petroleum system are oolitic-peloidal grainstones and dolomitized limestones, within a regionally extensive, mostly muddy, carbonate platform that is now called the Arab Formation. The Arab Formation is typically divided into four cycles (A through D from base to top); all cycles can produce, but the Arab D is the most productive over much of the Gulf. Each cycle shoals up from a more marine base to restricted-marine, variably dolomitised, limestone to mudflat dolomites and evaporites. The lower portion of the Arab D is typically a bioclastic lime mudstone or wackestone with normal marine fossils. Away from topographic highs, local organic-rich mudstones were deposited in intrashelf basins and are lithologically identical to similar intrabasinal successions in the underlying Diyab Formation. The lower Arab D is overlain by a middle unit of clean washed calcarenite, largely composed of sorted and rounded skeletal particles and ooids (grainstone-packstone), and an upper variably developed thin dolomitic mudflat sequence, which grades across a metre or two of anhydrite-plugged carbonate into massive to nodular anhydrites

of the Arab D capstone. This anhydrite was deposited within a regional sulphate saltern/pan with local, but still widespread, evaporite mudflats atop local highs. Evaporitic mudflats also encircled the depositional edges of the basin. Microfossil and macrofossil content in the marine portion of the Arab D is a useful discriminant of water depth and restriction (Figure 10.11; Wyn-Hughes, 1996)

Atop the anhydrite-capped marine-dominated limestone and dolomite of the Arab D are the more restricted cyclic carbonates-anhydrites of the Arab A-C. These sediments in the United Arab Emirates show depositional relationships that correspond to the outline of the current and possibly the late Jurassic edge of the evaporite basin, although exact detail has

been obscured by edge dissolution and erosion (Figure 10.12). Wireline signatures in the anhydrite caps to the various A-C cycles in oil fields in both Saudi Arabia and eastern Abu Dhabi indicate evaporite mudflats made up of mosaics of sabkhas, ephemeral brine pans and salinas (personal observation) and are very similar to signatures in shoal water portions of the Arab D capstone. As in the Arab D cap, the proportion of subaqueous anhydrite increases in the capstone away from the crests of many fields, showing that many current highs were also highs in the Jurassic. Unbreached anhydrite caps in all Arab D cycles are highly effective seals, for example the anhydritic cap to the Arab D holds back a 400m-oil column in Ghawar Field, Saudi Arabia. Wireline signatures in the crest of the field indicate a mosaic of salinas and sabkhas.

The Asab Formation in the eastern United Arab Emirates is laterally equivalent (although not necessarily time equivalent) to the Arab Formation (Figure 10.12). Definitions of Arab-A, -B, and -C vary from field to field across the Gulf and do not necessarily represent the same chronostratigraphic unit. The combined Arab-ABC is defined by Grötsch et al. (2003) as a lithostratigraphic unit composed of high-frequency dolomite-anhydrite shallowing-upward cycles capped by the massive

Lower and Upper Hith Anhydrite. The top of the underlying Arab-D reservoir in the eastern UAE is typically picked at the top of a clean gamma-ray trend, which is usually an oolitic and bioclastic grainstone section. Its top typically coincides with the first occurrence of a gamma kick, indicative of a black marker limestone that commonly contains pyrite. However, in my opinion, this marker is not always a depositional unit and may be a dissolution residue created by fluid crossflow along the underside of the anhydrite sealing the Arab D. Although a useful correlative marker of the reservoir top, it probably does not represent a time-line.

If we assume the Arab D is the base of the section throughout the Arabian Peninsula, then the difficulty in breaking out three separate cycles (Arab A-C cycles) atop the Arab D reflects the high degree of textural similarity of all restricted and dolomitised evaporite-capped shoaling cycles. The inherent lack of an entrained time-significant fossil assemblage and the vagaries of syndepositional evaporite dissolution in all evaporitic mudflats makes detailed well-to-well correlation at the level of the

Arab A-C very difficult. There are more than three anhydrite beds in the A-C interval (Figure 10.12). Short but significant episodes of subaerial exposure and freshening characterised the brine sheets depositing these marine-fed mudflat cycles. Intraformational evaporite dissolution residues, sometimes show high gamma kicks and without reference to core can be easily misinterpreted as maximum flooding surfaces.

Capping the cycles of the Arab Formation is a thick regional unit of subaqueous saltern anhydrite, the Hith Anhydrite, which extends over much of the Arabian Gulf region. In Saudi Arabia and the eastern UAE, it holds back almost all of the oil and gas sourced in Jurassic mudstones. It is only at the edge of the Hith in the central and western UAE that Jurassic sourced oil is found as widespread accumulations in the overlying Cretaceous succession (Figure 10.5a, 10.12).

Deposition of the various widespread anhydrite caps in the Arab Formation across the Arabian Plate indicate higher order sealevel falls, within what was a second order sequence ac-

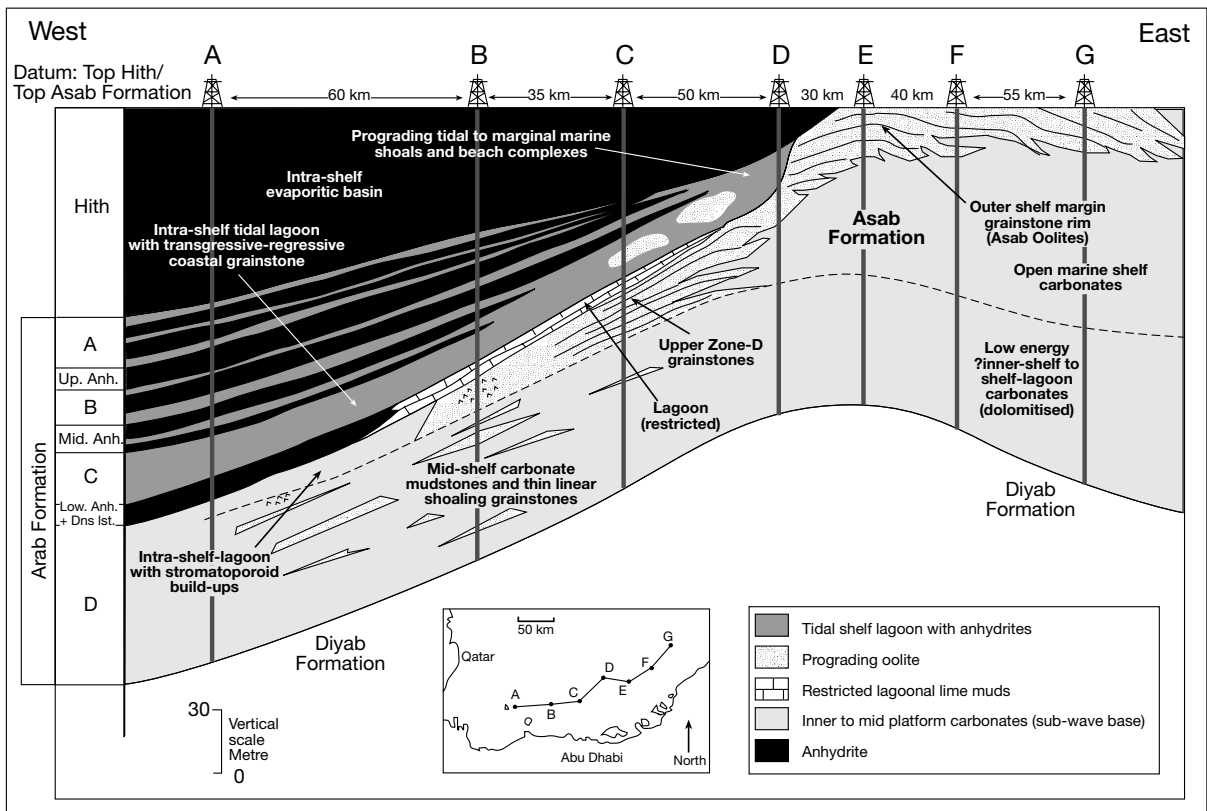


Figure 10.12. Schematic east-west cross-section of the Arab and Hith formations, offshore Abu Dhabi. Note: Datum is possibly affected by erosion and evaporite dissolution with the amount of truncation increasing to the east. Facies relationships between wells are schematic (after Al Silwadi et al., 1996).

cumulating during the late Kimmeridgian. For much of this time, when evaporites were not accumulating, open-marine to restricted-marine epeiric carbonates were the dominant sediments (Figure 10.12; Sharland et al., 2001; Al-Saad and Sadooni, 2001). During the preceding Hanifa and Jubaila time (middle Oxfordian and early Kimmeridgian, respectively), local organic-rich intrashelf basins deposited starved-basin sequences of laminated organic-rich dark-coloured marls and mudstones (Figure 9.4; Ayres et al., 1982).

Prior to hydrographic isolation that marked the end of the Arab D, oolite/peloidal shoals and patchy coral-algal stromatoporoid banks were deposited as local higher energy shoals across the muddy epeiric platform that typified marine stages of Arab Formation deposition across the Arabian Peninsula (Figure 10.11). Regionally, similar but more laterally continuous Kimmeridgian equivalents to these higher energy marine carbonates lined the epeiric platform margin. This band of shelf-edge shoals was a hydrodynamic barrier that periodically restricted free surface exchange between Arabian Platform waters and deeper open-marine (Tethyan) waters to the east and facilitated deposition of the various anhydrite capstones (Figure 10.9). This shoal-rimmed margin thus separated a muddy interior epeiric platform, with its intrashelf depressions, from the deeper openwater marine slope carbonates. Edges of the various intrashelf basins of the epeiric shelf behind the main shelf margin shoal were ramp-style progressions around somewhat deep ($\approx 30\text{m}$) intrashelf basins (Sharland et al., 2001). Much of the regional platform-margin shoal rim was destroyed during later continental collision.

Regionally, much of the reservoir quality in the undolomitised or poorly dolomitised limestone reservoirs in the Arab D can be directly tied to partially-preserved primary porosity in grainstone (oolid, skeletal and peloid) shoals and local reefal (stromatoporoid) debris aprons in the epeiric interior seaway. In many parts of the platform interior (e.g. the offshore UAE) the shoaling of the Jurassic seafloor and the formation of seafloor shoals in the Arab Formation was facilitated by salt structures sourced in the Precambrian Hormuz salt.

After deposition of the Arab D, ongoing higher order eustatic changes formed the numerous parasequences that make up the widespread A-C cycles of the Arab Formation in the epeiric shelf interior. Eustatic fluctuations drove periodic marine flooding episodes on the platform, followed by filling of accommodation space, hydrographic isolation and capping by evaporites and exposure surfaces. With each transgression another more open marine platform unit defined the base of a cycle and

was deposited as marine to mesohaline, skeletal-poor peloid wackestones/mudstones. Local shoaling on the epeiric platform led to progressively higher bottom energies culminating in thin local buildups of ooid and peloid grainstones that are now producing intervals in the Arab ABC.

Progressive platform restriction followed, via a combination of active carbonate aggradation and high order falls in relative sealevel (3rd to 5th order), which periodically exposed the shelf margin within an environment of net evaporation across the arid platform. This drove numerous brining-upward depositional cycles in the Arab ABC, with most, but not all culminating in the deposition of mudflat gypsum. Gypsum beds were porous at the time the various Arab ABC sulphates were deposited and brine reflux drove the formation of mimetic dolomites in the immediately underlying limestones. Dolomitisation is less pervasive, but still significant, in terms of reservoir quality in the underlying Arab D (Figure 10.13b). Thus syndepositional reflux dolomitisation occurred many times during the accumulation of evaporite caps to the various muddier units of the Arab Fm. and each probably indicates platform restriction related to higher order sealevel falls or local halokinetically- or basement fault-induced seafloor uplift. Some evaporite beds associated with these higher-order relative sealevel falls were leached by a subsequent rise in sealevel, so that all that remains of some of these higher order evaporite deposits are nodules cementing carbonate remnants in thin dolomites, along with widespread cm-scale dissolution surfaces and residues, often associated with gamma peaks in the wireline log (pers. obs.).

Any model explaining reflux dolomitisation on the Arabian Shelf as only occurring during the deposition of the four major cycle caps in the Arab Formation is too simplistic, as is the notion that the reservoir sediments of the Arab D cycle are the same as those of the subsequent A-C cycles. Given that the Arab D is the dominant producer throughout the Arabian Peninsula, we shall now focus on the detail of its reservoir characteristics and any relationship to diagenesis, perhaps tied to reflux and vertical crossflows that were focused by its evaporite seal.

The best-documented and regionally largest accumulation of hydrocarbons in the Arabian Peninsula occurs in Ghawar Field in Saudi Arabia (Figure 10.1). It not only stores hydrocarbons in the Jurassic section, but also entrains rich gas reserves in the underlying Permian Khuff Formation and with more than 150-200 billion barrels of recoverable oil is the world's largest single oil-filled structure. The following discussion will only deal with the Jurassic section in Ghawar. Detailed studies of various aspects of Ghawar and its outcrop equivalents in Saudi

Arabia have been published by Cantrell et al., 2001; Cantrell and Hagerty, 1999, 2003; Douglas et al., 1996; Lucia et al., 2001; Meyer et al., 1996, 2000; Powers, 1962; Saner and Sahin, 1999; Stenger et al., 2003; Wyn Hughes, 1996. The following section is a summary of aspects of this work, along with some comments of my own.

Ghawar Field, Saudi Arabia

The Arab-D carbonate reservoir of the Upper Jurassic Arab Formation in the onshore Ghawar Field was discovered in 1948. Following further separate discoveries in culminations along the structure's main axis, five production areas were quickly identified as parts of a single giant Ghawar oil field (Stenger et al., 2003). From north to south Ghawar is made up of Ain Dar, Shedgum, Uthmaniyah, Hawiyah and Haradh (Figure 10.13a). At the Arab-D level, the field is a NNE-trending composite anticline, 230 km long and about 30 km wide, with a productive area of more than 693,000 acres in a single, pressure-continuous reservoir. Ghawar accounts for more than half of Saudi Arabia's cumulative oil production.

Within the Jurassic section the Ghawar produces from the evaporite-sealed Arab D, with the reservoir section extending down into mudstones of the uppermost Jubaila Formation. Production layering is typically broken out into 4 zones

with the main production intervals broken into further finer subdivisions (Figures 10.14). Limestones of Zone 1 and 2 typically constitute the best quality Arab D reservoirs (Figure 10.13b). Arab-C, Hanifa and Fadhili oil reservoirs are also present in parts of the field, but the Arab-D reservoir accounts for nearly all of the oil reserves and production. Production began in 1951 and reached a peak of 5.7 million barrels per day in 1981. This is the highest sustained oil production rate achieved by any single oil field in world history. At the time that this record was achieved, the southern areas of Hawiyah and Haradh had not yet been fully developed. Production was restrained after 1981 for market reasons, but Ghawar remains the world's most important oil field. Cumulative production by year end 2000 was about 51 billion barrels of oil.

Across the field the Arab-D reservoir is comprised of a series of stacked shallow water, platformal carbonate sediments deposited as a cleaning-up and a shallowing-up carbonate succession stacked into metre-scale cycles or parasequences. The bulk of the reservoir is comprised of limestone, though some dolomite is present. Anhydrite is present in the reservoir as cement, but typically in minor amounts (Table 10.3). The cleanest and most porous rocks - hence the most favourable in terms of production - are situated in the grainier upper portion of the reservoir (Zone 2) Interparticle porosity predominates in the various reservoirs, though locally, other porosity types are important; for example, mouldic and intercrystalline porosity

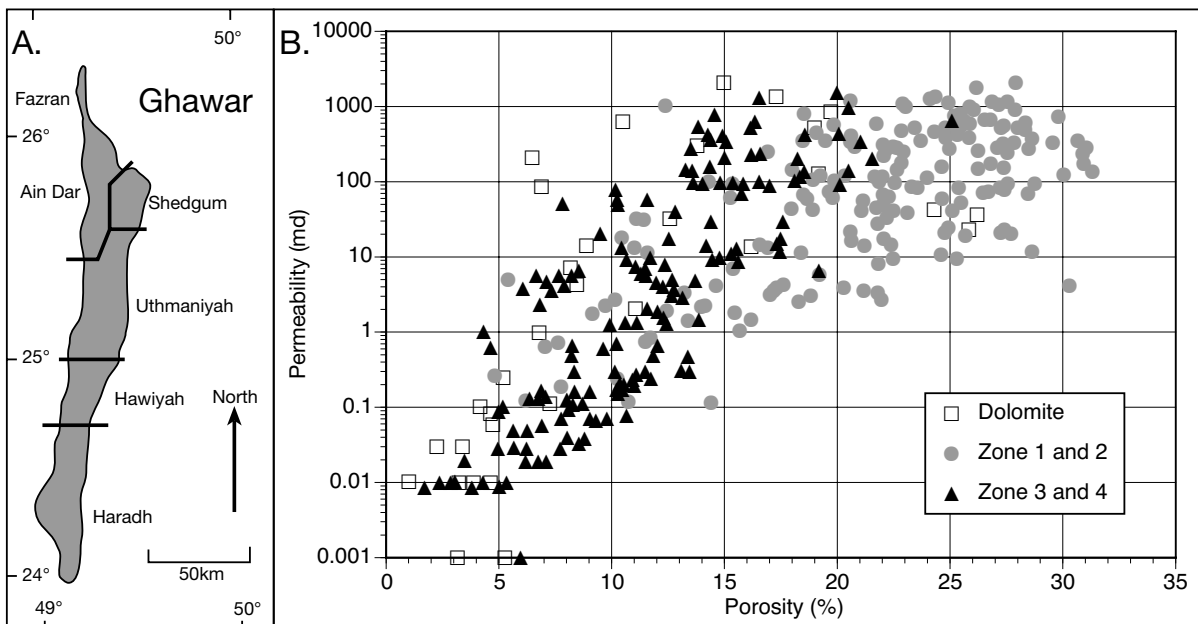


Figure 10.13. Poroperm crossplot of typical Zone 1 and 2, Zone 3 and 4 and dolomites from cores in the Arab D reservoir of Ghawar Field, Saudi Arabia (after Cantrell and Hagerty, 2003).

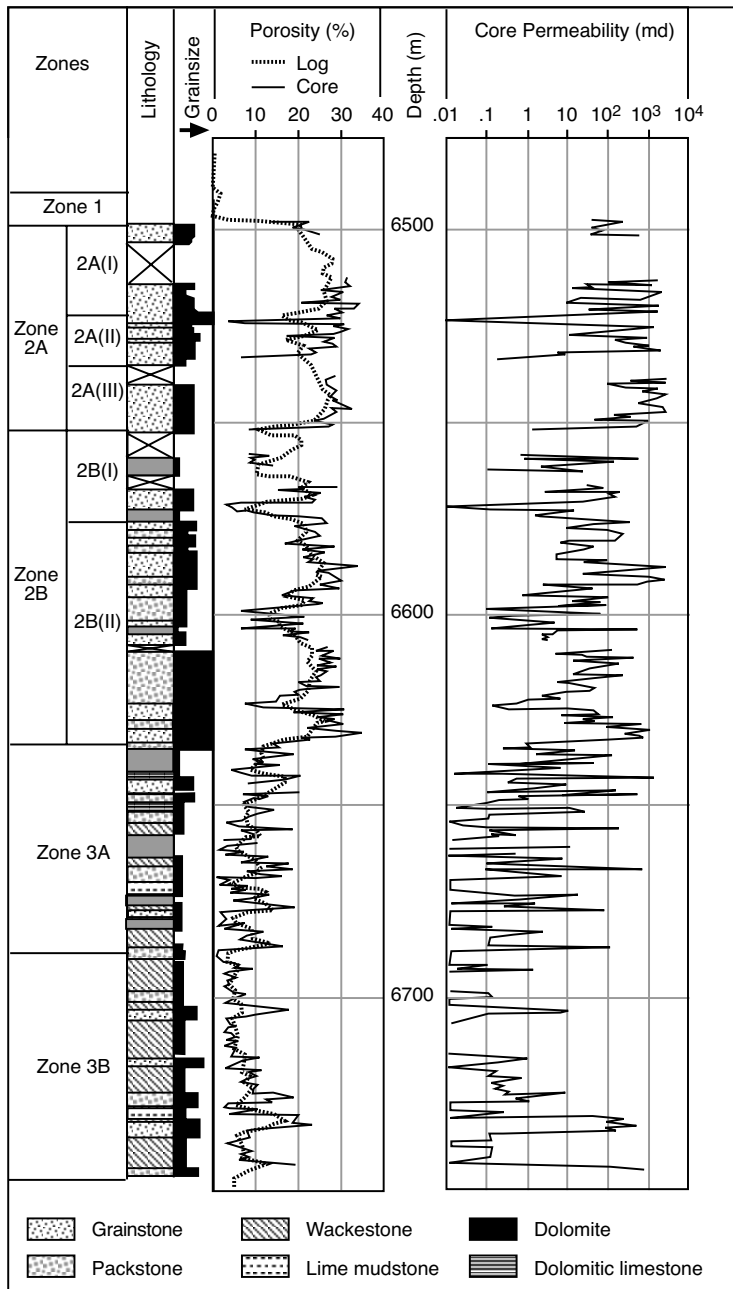


Figure 10.14. Reservoir zonation, porosity and permeability in the Arab D Formation in Uthmaniyah Field, which is an operational area within the much larger Ghawar Field, Saudi Arabia. (after Saner and Sahin, 1999).

in dolomitized portions of the reservoir. Each of the major upward-shoaling cycles that make up the Arab D was initiated in deeper subtidal water that shoaled to near sea-level. The proportion of skeletal grainstones and packstones, along with ooid grainstones, increase within each cycle and within the Arab

D overall. The top of the Arab-D carbonate is characterized by a thinner unit of dolomitized carbonate mudstone (Zone 1), capped by an evaporite seal.

By far the most abundant reservoir rock texture in the Arab-D is packstone; likewise, the most abundant reservoir lithofacies is skeletal-oolitic (SO; Tables 10.3, 10.4; Cantrell and Hagerty, 2003). The other significant lithofacies in the Ghawar reservoir are: *Cladocoropsis* (a characteristic finger-shaped and sized stromatopoid) lithofacies (CLADO), stromatopoid-red algae-coral lithofacies (SRAC), bivalve-coated grain-intraclast lithofacies (BCGI), micritic lithofacies (MIC) and dolomite lithofacies (DOLO), all of which are described in detail by Mitchell et al. (1988). Similar, if not identical, lithofacies make up Arab D reservoirs in other fields in Saudi Arabia and the western United Arab Emirates. In a detailed petrographic and petrophysical characterisation of the Ghawar Arab D reservoir Cantrell and Hagerty (2003) defined seven related limestone reservoir rock types based on the values of: (1) the amount of cement, (2) the amount of matrix (lime mud), (3) the grain sorting/grain packing, (4) the dominant pore type, and (5) the size of the largest moulds (Tables 10.4, 10.5; Figure 10.15).

At the broadest scale of reservoir classification the Arab D reservoirs are either limestone or dolomite (Table 10.5). In terms of porosity and permeability in the limestones, the amount of matrix is the most important of these five parameters and breaks down into three reservoir types (I-III). Cantrell and Hagerty (op cit.) break our two broad families, A and B in each of the three reservoir types (Table 10.5), Family, A, is relatively coarse-grained and poorly sorted rock with relatively large moulds. Family, B, is a generally fine to medium-grained, well-sorted rock with few or small moulds. Together this constitute 6 families of reservoir rock in the Arab D. Reservoir rock type IV is a seventh limestone family in Ghawar. Type IV limestones contains more than 10 percent cement, this modifies pore size distribution enough to warrant a separate limestone reservoir family (Figure 10.15). Each of the seven limestone types are characterized

limestone family in Ghawar. Type IV limestones contains more than 10 percent cement, this modifies pore size distribution enough to warrant a separate limestone reservoir family (Figure 10.15). Each of the seven limestone types are characterized

Lithofacies	Skeletal-Oolitic (SO)	<i>Cladocoropsis</i> (CLADO)	Stromatoporoid Red Algae-Coral (SRAC)	Bivalve-Coated Grain-Intraclast (BCGI)	Micritic (MIC)	Dolomite (DOLO)
Depositional types	Grainstone, mud-lean packstone, packstone	Mud-lean packstone, grainstone, packstone	Mud-lean packstone, grainstone, packstone, boundstone	Packstone, mud-lean packstone, grainstone, wackestone	Wackestone, mudstone, packstone	Indeterminate
Major grain types	Micritized grains, Foraminifers (including Miliolids), Dasycladacean algae, ooids, bivalves	Micritized grains, <i>Cladocoropsis</i> , Dasycladacean algae, foraminifers (including Miliolids)	Micritized grains, stromatoporoids, corals, foraminifers (including Miliolids)	Micritized grains, bivalves, coated grains, intraclasts, foraminifers	Micritized grains, bivalves, foraminifers (including <i>Kurnubia</i>), intraclasts	Anhedral to euhedral dolomite rhombs
Minor grain types	Echinoderms, stromatoporoids, corals, <i>Cladocoropsis</i> , gas-tropods, composite grains, intraclasts, ostracodes, red algae, brachiopods	Stromatoporoids, echinoderms, bivalves, corals, ooids, gastropods, brachiopods, composite grains, red algae	<i>Cladocoropsis</i> , bivalves, echinoderms, Dasycladacean algae, intraclasts, coated grains, composite grains, gastropods	Miliolid foraminifers, corals, stromatoporoids, Dasycladacean algae, echinoderms, gastropods, <i>Cladocoropsis</i>	Coated grains, Miliolid foraminifers, Dasycladacean algae, intraclasts, ostracodes, echinoderms, gastropods, stromatoporoids, corals	Relict and leached bivalves, <i>Cladocoropsis</i> , stromatoporoids, Intraclasts, echinoderms, ind. grains
Sedimentary structures	Cross bedding, burrows, hardgrounds, fining upward graded beds, borings, horizontal laminae	Burrows, hardgrounds, cross bedding, horizontal laminae	Burrows, borings, hardgrounds, fining upward graded beds, cross-bedding	Burrows, hardgrounds, borings, fining upward graded beds, cross bedding	Burrows, hardgrounds, wavy laminae, horizontal laminae, borings, fining upward graded beds	Relict burrows?, hardgrounds?, carbonaceous? laminae
Pore types	Interparticle, mouldic, intraparticle, intercrystalline, fracture	Interparticle, intraparticle, mouldic, intercrystalline	Interparticle, mouldic, intraparticle, intercrystalline, fracture	Interparticle, mouldic, intraparticle, intercrystalline, fracture	Interparticle (within burrow fills), intraparticle, mouldic, intercrystalline, fracture, vug?	Intercrystalline, mouldic, fracture
Diagenetic modification	Leaching and recrystallization, isopachous bladed calcite cement, dolomitization, physical compaction, stylolitization, equant calcite cement, kaolinite emplacement, anhydrite emplacement / replacement, silicification	Leaching and recrystallization, dolomitization, equant calcite cement, stylolitization, anhydrite emplacement, silicification	Leaching and recrystallization, dolomitization, anhydrite emplacement, stylolitization, isopachous bladed calcite cement, equant calcite cement, pyrite, dedolomitization	Leaching and recrystallization, dolomitization, stylolitization, equant calcite cement, anhydrite emplacement, isopachous bladed calcite cement, pyrite	Leaching and recrystallization, dolomitization, stylolitization, anhydrite emplacement, pyrite, silicification, equant calcite cement, kaolinite	Dolomitization, leaching, anhydrite emplacement, equant calcite cement, stylolitization, kaolinite, dedolomitization
Distribution (Ghawar Zone/ Formation)	1, 2A, 2B, 3A, 3B	2A, 2B	2A, 2B, 3A, 3B, Jubaila	2B, 3A, 3B, Jubaila	1, 2A, 2B, 3A, 3B, Jubaila	1, 2A, 2B, 3A

Table 10.3. Characteristics and distribution of carbonates lithofacies, Arab-D reservoir, Ghawar Field (after Cantrell and Hagerty, 2003).

by distinctive porosity-permeability relationships (Figure 10.15). Similar matrix-lean limestone reservoir characterise better quality reservoirs in Abqiq Field in Saudi Arabia and the Jurassic Arab Formation reservoirs of Qatar (Figure 10.16 and 10.17, respectively).

Dolomites in Ghawar constitute reservoir rock type V and are further subdivided according to their dolomite crystal texture, although stratigraphic position and porosity can also be effective pointers in their classification (Table 10.5; Figure 10.18a; Cantrell and Hagerty, 2003). The four dolomite textures are: fabric preserving (Vfp), sucrosic (Vs), intermediate (Vi) and

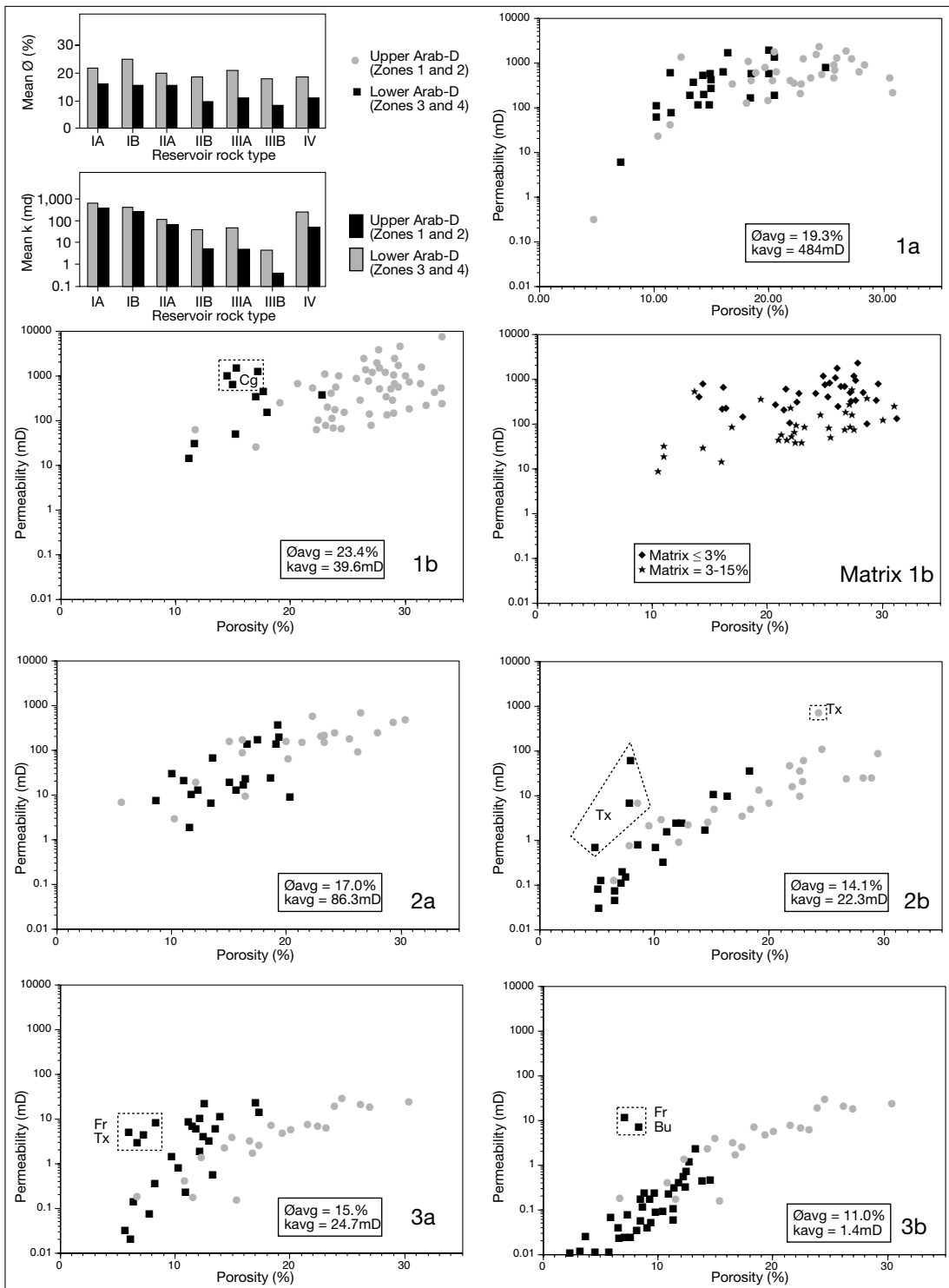


Figure 10.15 Porosity-permeability cross plots of individual limestone reservoir rock types as defined in Table 10.5 (after Cantrell and Hagerty, 2003). Outliers from the main poroperm trends are labeled according to their non-uniformity or textural characteristics (Bu=burrows; Cg=coarse grained; Fr=microfractures; Tx=textural variations; kavg=average permeability, in millidarcies; Øavg=porosity, in percent bulk volume).

Texture	Lithofacies						Total
	SO	CLADO	SRAC	BCGI	MIC	DOLO	
Grainstone	24	-	8	6	6	5	44
M. I. Packstone	30	4	15	19	-	-	68
Packstone	61	9	34	65	14	-	183
Wackestone	2	-	2	2	26	-	32
Mudstone	-	-	-	-	22	1	23
Boundstone	-	-	2	-	-	-	2
Indeterminate	-	-	-	-	-	26	26
Total (samples)	117	14	61	92	62	32	378

Table 10.4. Interrelationships between texture, lithofacies and modes of occurrence in Arab D reservoir in Ghawar Field, Saudi Arabia (after Cantrell and Hagerty, 2003). See Table 10.3 for a description of the various lithofacies units.

mosaic (Vm). The mimetic Vfp dolomite is only found in Zone 1 of the Arab-D (immediately below the anhydrite cap) where it is the major dolomite type. Sucrosic (Vs) dolomite occurs in dolomites with more than 12% porosity, Vm less than 5% and Vi between 5 and 12%. Vfp dolomites have pore systems similar to their precursor limestone, but the pore systems of the other dolomite types are unique.

Powers (1962) and Lucia et al. (2001) concluded that once an interval in the Ghawar Field of Saudi Arabia is dolomitised, its reservoir quality is tied to the proportion of dolomite and dolomite crystal size (Figure 10.18b, c). In general, when dolomites are compared to limestones in the Arab D they show lower porosities (Figure 10.13). This is clearly seen in wireline-based porosity histograms of Zone 1 in the Arab D from Abqaiq Field, a supergiant field with 17 billion barrels of proven reserves, in eastern Saudi Arabia (Figure

10.16; Sahin and Saner, 2001). In part, this decrease in porosity with dolomitisation is a reflection of the originally lower precursor porosity in muddier transitional sediments that typically underlie a mudflat or saltern seal (mimetically dolomitised Zone 1 carbonates - Vfp).

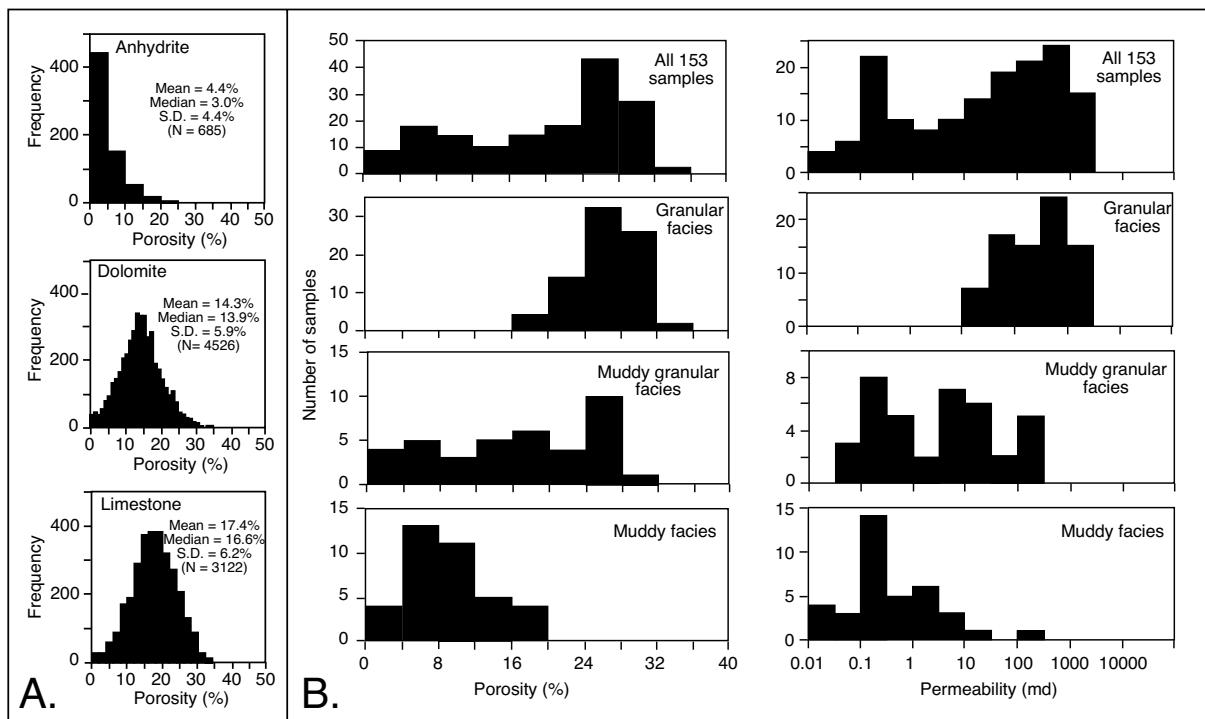


Figure 10.16. Petrophysical character of the Arab D, Abqaiq Field, eastern Saudi Arabia (after Sahin and Saner, 2001). A) Well log porosity for each of the three wireline defined lithologies in Zone 1 of the Arab D. B) Core plug-defined distribution of porosity and permeability in the various limestone dominated lithofacies of the Arab D.

Limestone							Dolomite				
Cement	<10						>10				
Matrix	0-15		16-40		>40		Texture				
Sorting	>0.5 (Poor)	>0.5 (good)					Fabric preserved (Reservoir zone 1)	Sucrosic (Ø >12%)	Intermediate (Ø 5-12%)	Mosaic (Ø >5%)	
Pore Type			BP < MO + WP	BP > MO + BP							
Largest Mould (mm)			>0.3		>0.3	>0.3					
Reservoir Rock type	IA	IB	IIA	IIB	IIIA	IIIB	IV	Vfp	Vs	Vi	Vm

Table 10.5. Classification of reservoir rocks, Arab-D reservoir, Ghawar Field (after Cantrell and Hagerty, 2003).

Anhydrite-derived, corrected porosity in wireline-defined anhydrites in Zone 1 is greater than zero in Abqaiq Field, eastern Saudi Arabia (Figure 10.16a; Sahin and Saner, 2001). This value comes not from the actual anhydrite beds, which are tight, but from the thin dolomite stringers that are intercalated within the anhydrite; they sit at the limits of vertical resolution of the wireline tool in such finely layered sequences. Controls on the Arab D reservoir are similar to those in Ghawar, with limestone matrix type rather than dolomitisation as the prime control (Figure 10.16b). Once the proportion of dolomite in a muddy succession attains 80-90%, the reservoir character substantially improves compared to its muddy limestone precursor (Figure 10.18b).

In many fields the dolomitisation process is most pervasive in lime mudstones below an evaporite unit or its former solution residues (e.g. Zone 1 in Ghawar). The reason why dolomites can form excellent reservoirs in tight mud-rich lime precursors

in many mudstone of the Arab cycles (and the Permian Khuff of Saudi Arabia and San Andres of west Texas) is the development of intercrystalline porosity. Hence, within the muddier facies of Ghawar there is a significant tie of reservoir quality to dolomite percent and crystal size, as in the coarsely crystalline sucrosic intervals in the dolomitised interval of Ghawar. Crystal size in the dolomites is related to reservoir quality with coarser crystals defining the higher porosity/permeability intervals, probably reflecting a propensity for larger pore throats and remnant dissolution voids in the more coarsely crystalline dolomites (Figure 10.18c). Locally such coarsely crystalline dolomite can create high permeability “super-k” layers (Meyer et al., 2000).

But dolomites in the Arab Formation in Saudi Arabia are not from a single generation of reflux dolomite, nor are the dolomitized units laterally homogenous. When dolomite is subdivided by texture and stratigraphy (not porosity as was done in Table

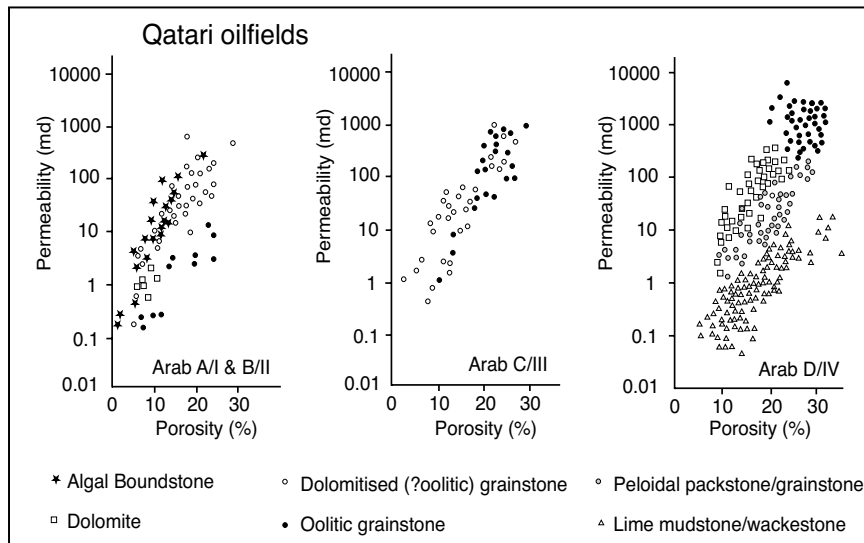


Figure 10.17. Porosity and permeability in the Arab A through D in Qatari oilfields showing the importance to reservoir quality of graininess in the limestones and dolomitization in the Arab D (Alsharhan and Nairn, 1993).

10.5) then five types of dolomite occur in the Arab D reservoir in Ghawar Field, namely (Figure 10.19; Cantrell et al., 2001):

- 1) Finely crystalline, non fabric preserving (NFP) dolomite in Zone 3 (lower Arab D) with considerable preserved calcite, low oxygen isotope values and generally poor reservoir quality. Dolomite is typically associated with hiatal surfaces.
- 2) Medium crystalline NFP dolomite with elevated oxygen isotope values and very poor reservoir quality in Zone 2 (upper Arab D). Occurs essentially as dolomite beds with little or no reservoir quality.
- 3) Medium to coarsely crystalline (NFP) dolomite with low

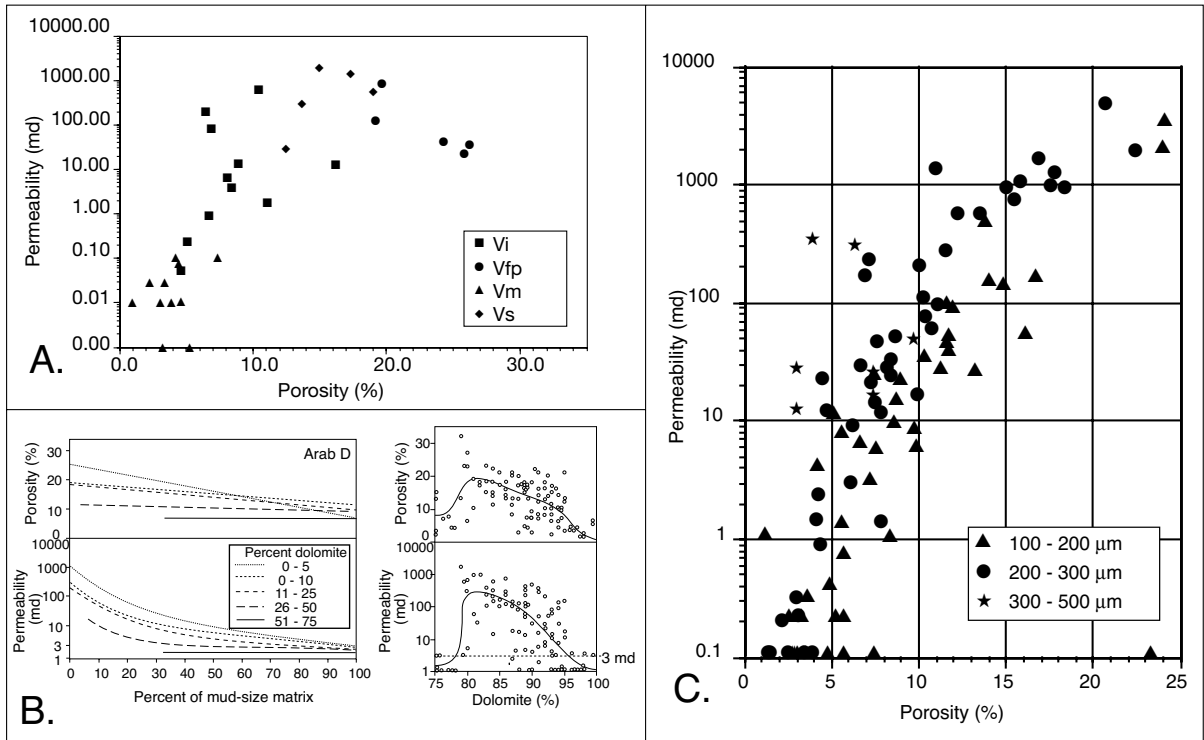


Figure 10.18. Reservoir properties of dolomites in the Arab D, Ghawar Field, Saudi Arabia. A) Textural-petrophysical classification of dolomite reservoirs (after Cantrell and Hagerty, 2003). B) Effect of mud size and dolomite percentage on porosity and permeability in the Arab D in Ghawar Field. There is a drastic increase in permeability when the dolomite proportion is between 80 and 90% (after Powers, 1962). C) Interparticle porosity permeability crossplot for dolomites of various crystal sizes (after Lucia et al., 2001).

oxygen isotope values and very good reservoir quality in Zone 2. Petrographically it is similar to medium-crystalline NFP dolomite but shows a lighter isotopic signature. It is an important reservoir component as it occurs in ‘super k’ intervals (Meyer et al., 2000). It is characterised by a high degree of intercrystalline porosity and locally retains leached mouldic porosity (typically after *Cladocoropsis*).

4) Finely crystalline fabric preserving (FP) dolomite in Zone 1 (uppermost Arab D) with elevated oxygen isotope values and generally fair to poor reservoir properties. It is minor in terms of overall reservoir volume in the Arab D and also occurs in association within and below the overlying C-D anhydrite transition. Typically it forms layers or thin sheetlike beds in Zone 1. Reservoir quality typically reflects the characteristics of the overprinted limestone facies, most of which were relatively mud free and partially cemented mud-lean packstones.

5) Rare locally occurring saddle dolomite (not sampled in the Cantrell et al., 2001 study).

Overall, dolomite comprises around 14% of the Arab D in Ghawar, with the highest proportion in Zone 1 below the anhydrite cap (Figure 10.20, 10.21; Cantrell et al., 2001). Zones

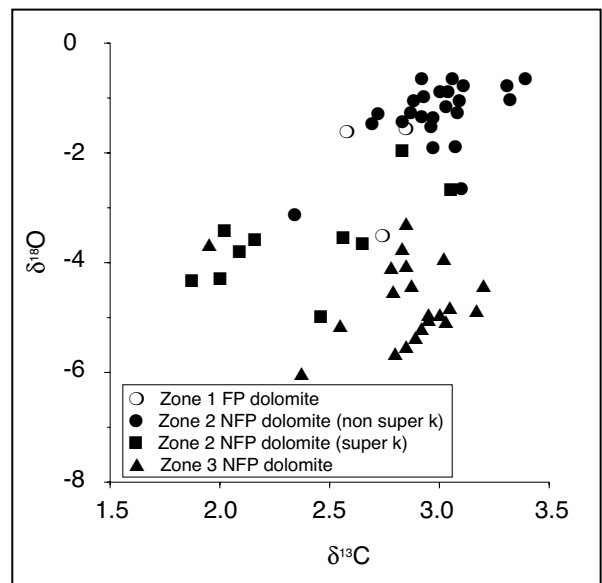


Figure 10.19. Isotopic compositions of dolomites in Arab D, Ghawar Field, Saudi Arabia, based on textures (after Cantrell et al., 2001).

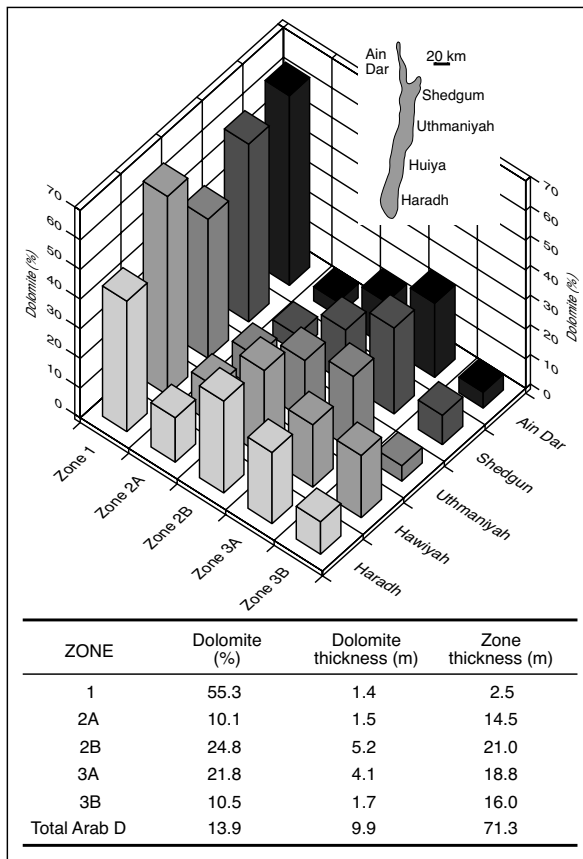


Figure 10.20. Block diagram shows average percent dolomite in different Arab D reservoir zones for each field area of Ghawar Field, Saudi Arabia. The table summarises dolomite percent for all Arab D in Ghawar Field (data re-charted from Cantrell et al., 2001).

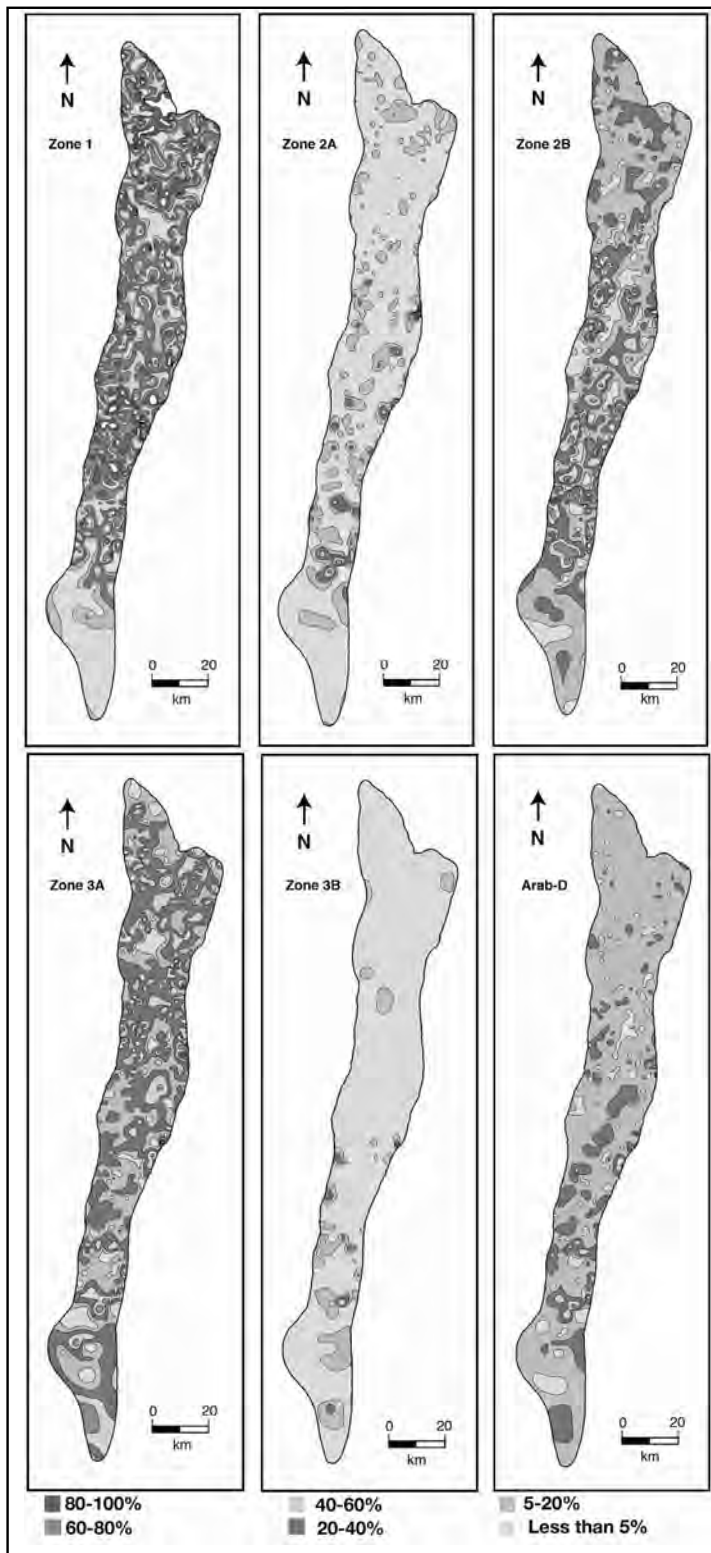
2B and 3A have less dolomite, but it is still a significant fraction of the reservoir matrix. Dolomite is a relatively insignificant contributor to reservoir matrix in Zones 3B and 2A. Within each reservoir zone much of the total dolomite percentage in a well comes from individual layers, which are intercalated with limestones. Laterally many of these dolomite layers can vary greatly in the proportion of dolomite (e.g. Zone 2B). On a Ghawar-wide basis dolomite increases systematically from north to south in Zones 2A and 2B, but zone 3A displays an inverse trend by generally decreasing from north to south (Cantrell et al., 2001).

When Cantrell et al. (2001) mapped dolomite distribution over Ghawar Field they identified a series of parallel linear trends of high dolomite content that extended for tens of kilometres along northeasterly trends (Figure 10.21). These trends are especially obvious in Zone 2B but are also discernable in Zones 2A and

3A. Locally the trends connect areas of pervasive dolomitisation, where much of the section (virtually 100% of Zones 1, 2A, 2B and 3A) is replaced by dolomite. There may also be some saddle dolomite in these same areas, but it is rare. Northeast trends are present, but less obvious, in southern Ghawar. The trends suggest some structural control to the dolomite distribution and, according to Cantrell et al. (2001), indicate diagenetic patterns that are responses to a series of underlying fractures or faults. These structural features facilitated movement of dolomitising fluids into the reservoir.

As for the dolomites in the Red River Formation discussed previously, what is not clear in Ghawar is whether the dolomitising fluids (other than zone 1 dolomites) were ascending or descending when they drove the dolomitising process. Similar fault- and fracture-controlled distributions of dolomite have been documented by Warren and Kempton (1997) in metalliferous evaporite-sealed Devonian carbonates of the platform margin of Canning Basin, Australia and by Hurley and Budros (1990) in the Silurian Scipio Albion Trend in Michigan. Dolomite's propensity for ongoing alteration and replacement in Ghawar, and its proximity to a fluid-focusing evaporite layer (first as a fluid source and then as a seal) throughout its burial history, means the origin of the Ghawar dolomites is probably not a simple unidirectional fluid flow story (Warren, 2000a). Fractures in the host carbonates may have been conduits for descending reflux fluids early in the burial history, but may have then acted as conduits for upwelling fluids later in the field's burial history. During this upwelling stage, various unbreached evaporite seals acted to pond and store escaping basinal fluids. Such flow reversals would overprint early formed dolomites with later burial signatures.

Partially preserved primary pore spaces in the Arab D limestones throughout the region typically remain as well-defined relicts in evaporite-sealed banks of weakly dolomitised coral-stromatoporoid reefs and skel-oid grainstones and grain dominant packstones. These build-ups and shoals are also characterised by leached moulds of stromatoporoid and coral branches and other aragonite allochems. Yet there is little evidence of meteoric diagenesis or karst and little or no evidence of later pervasive diagenesis and calcite cementation once the overlying evaporite cap was deposited. Much of the leaching in the reservoir seems to have been early and perhaps was an integral part of the same reflux hydrology that was dolomitising portions of the Arab Formation adjacent to evaporite beds. Considering their age (≈ 150 Ma) and relatively deep current burial (1200 - 3000 m), this preservation of widespread primary void skeletal moulds in any limestone is unusual.



Wilson (1985) argued the early emplacement of the evaporite capstones atop limestone buildups and the subsequent deposition of the Hith Anhydrite was what preserved economic porosity levels into the burial realm. Burial beneath saltern and mudflat sediment in an environment that was consistently arid and hot meant that once all the gypsum had converted to tight nodular anhydrite beds within the first few hundreds of metres of burial, the resulting seals slowed fluid flow and largely prevented further influx of suprasalt subsurface waters, which would otherwise drive pervasive shallow subsurface cementation in most of the carbonate.

The relatively pristine relict porosity in the reservoir limestones, with solution-mouldic and variably-dolomitised overprints that characterises the Arab D in Ghawar, is a reservoir style that is part of a wider association seen in many evaporite-sealed limestone and dolomite reservoirs worldwide. Such reservoirs tend to show widespread leaching of aragonite allochems without associated karst surfaces or meteoric calcite cements. High Mg-calcite allochems (red algae, echinoids, crinoids) in the same sequence are relatively unaltered or mimetically replaced by dolomite. The process driving this precompaction leaching was not entry of meteoric waters, but flushing and brine mixing driven by early burial throughflushing of hypersaline marine brines (Sun, 1992). As well as the enhancing porosity in the Arab cycles, such evaporite-associated reflux waters have enhanced porosity levels in formerly aragonitic sediments of the Permian San Andres Fm. of west Texas, and the Miocene carbonates of the Middle East and SE Spain.

Slaughter-Levelland Trend, west Texas and New Mexico

Another region of variably dolomitised limestone forming high-volume evaporite-sealed reservoirs within an epeiric carbonate platform is the Slaughter-Levelland trend of New Mexico and Texas

Figure 10.21. Map of the percent dolomite in the various reservoir zones of the Arab D in Ghawar Field, Saudi Arabia (after Cantrell et al., 2001). Clearly shows a linear fracture-related distribution Zone 2 and in the total plot for the Arab D (right hand side of figure).

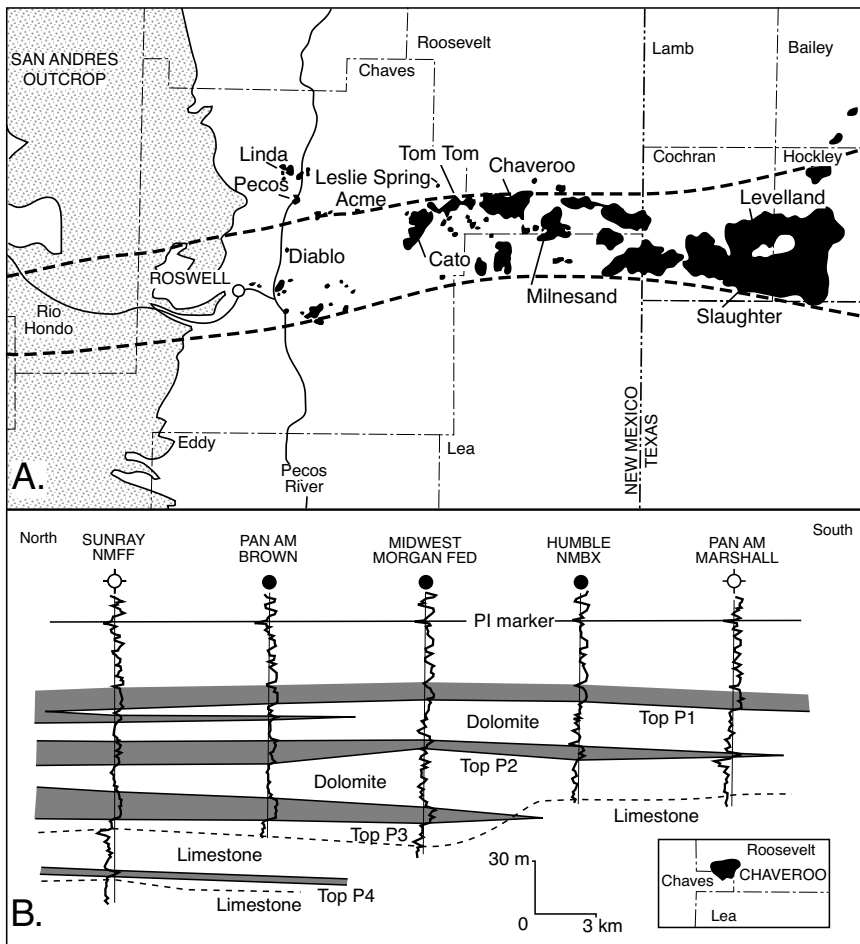


Figure 10.22. San Andres Formation in the Levelland-Slaughter trend near Roswell, New Mexico (after Elliott and Warren, 1989; Warren, 1991). A) North-south section through Chaves and Roosevelt counties in the vicinity of Chaveroo Field. B) Map of the Levelland-Slaughter trend and its equivalents in the San Andres outcrop belt west of Roswell.

(Figure 10.22a). There the main play is in the Permian San Andres Formation with the occurrence of better quality reservoir defined by the transition from platform carbonates in the south into updip massive anhydrites and halites in the north. The lower member of the San Andres contains two evaporite-sealed intervals (P_1 and P_2) that form the main reservoirs (Figure 10.22b). The producing style is a stratigraphic-diagenetic trap defined by updip pinchout (to the north) from a porous dolomite into nonporous evaporite-plugged dolomite beneath regionally extensive evaporite seals. Production from most dolomite reservoirs in the trend is slow but constant.

Cleaning-upward cycles in the lower member can be divided into 5 lithofacies groupings (P_1 to P_5) stacked into shoaling upward successions, with each cycle being 15 -50 m thick

(Elliott and Warren, 1989). Shaly carbonate mudstones define the base of each cycle; they are the initial low-energy deeper water deposits formed atop a flooding surface. These laminar mudstones are overlain by more massive biomicritic packstones and wackestones (≈ 10 m thick) containing brachiopods, bryozoa, crinoids, molluscs, and cephalopods, sometimes forming what may be local low relief bioherms with phylloid algal debris. These various mudstones were deposited on an open marine shelf, initially below wave base and under low-energy conditions.

Next comes the dolomitized intervals (typical matrix porosities 10-12%; permeabilities 20-30md), which constitute the main reservoir in the trend (Figure 10.23a). It is by far the most variable carbonate unit and in places retains remnants of primary texture, giving three variably dolomitised subtypes:

1. Wispy laminated to microstylolitized biomicrites, intramicrites, and peloidal micrites and packstones that entrain poorly preserved open marine faunas. Skeletal material is typically preserved as moulds, which near to the anhydrite cap are filled or partially filled with anhydrite cement. This is the most common reservoir unit in the Slaughter-Levelland trend.
2. Oolitic peloid-foram grainstones, which were deposited as localized shoals (uncommon unit in the Slaughter-Levelland trend).
3. Inter- to supratidal mudstones with fenestra, pisolites, biolaminites, and possible desiccation cracks (uncommon unit in the Slaughter-Levelland trend).

Next comes a massive to laminar anhydrite unit that historically was interpreted as a sabkha deposit (Ward et al., 1986). It is metres-thick in the Slaughter-Levelland trend and is made up of a dm-scale interbedded nodular anhydrite and laminated

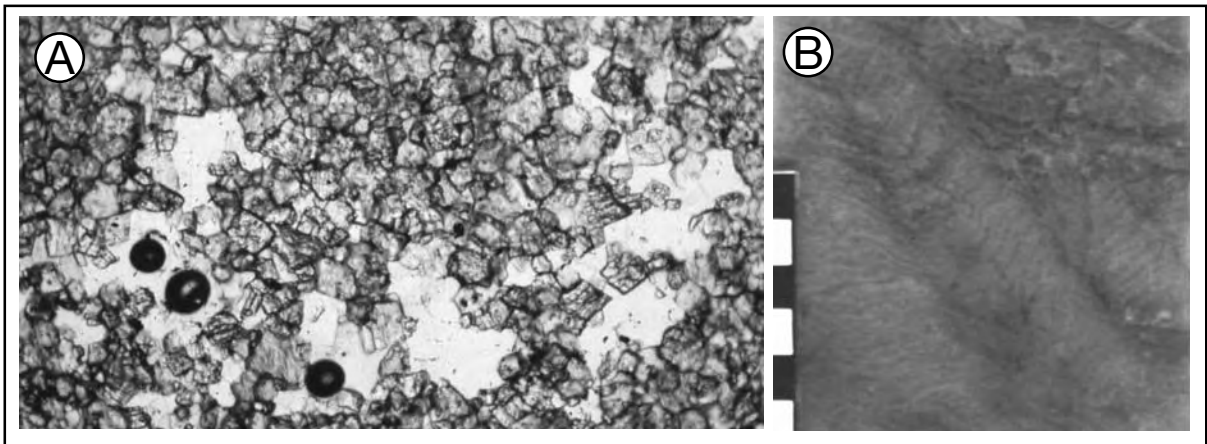


Figure 10.23. Lithofacies of the San Andres Formation. A) Dolomitised pel-mouldic wackestone/packstone showing angular highly altered peloidal outlines, moulds can be plugged by anhydrite (image is about 2 mm wide). b) Elongate nodules of anhydrite typical of the seal facies showing remnant subaqueous gypsum ghosts with internal swallowtail-V's still visible (scale bar in cm).

anhydrite. Some cores immediately to the north of the field preserve vertically aligned anhydrite nodules (gypsum “ghosts”), which pass downward into laminated and bedded nodular mosaic anhydrite (Figure 10.23b). The alignment, the lamination, the purity, the thickness of the units, and the fact that it is laterally equivalent to subaqueous platform gypsum to the north implies that in the Levelland–Slaughter area this unit was laid down near the depositional edge of a saltern (Elliott and Warren, 1989). In the Palo Duro Basin, situated further to the north of the Slaughter-Levelland trend, the equivalent to the various saltern anhydrite caps are overlain by saline-pan halites.

To the west of Roswell the outcrop equivalents to the anhydrite seals are dissolution breccias, which can be used as a regional mapping datum in the vicinity of the Rio Hondo outcrops (Elliott and Warren, 1989). Lateral facies changes can be seen in each outcropping cycle, showing the carbonate intervals were deposited as facies mosaics on an extensive relatively low energy muddy carbonate marine platform, with each cycle separated by evaporites.

The mosaic distribution of the reservoir carbonates and a lack of grainstone and shoreline/strandline shoals either in outcrop or the subsurface, led Elliott and Warren (1989) and Warren (1991) to revise the reservoir model for San Andres deposition the Levelland-Slaughter

Trend. In contrast to previous models that saw the reservoirs in the Slaughter Levelland trend as sabkha-sealed depositional pinchouts, they argued sabkhas are a relatively minor component in the widespread subaqueous saltern seal. Rather than a stratigraphic control the reservoir dolomites were created by brine reflux through relatively muddy epeiric platform carbonates via brines fed from up dip salterns (Figure 10.24; Warren, 1991).

This saltern edge model of San Andres deposition offered a different exploration strategy for the San Andres reservoirs on the Northwestern Shelf of the Permian Basin and elsewhere (Warren, 1991). Generally, saltern-associated reservoirs do not form by updip pinchout of marine grainstones and mudstones

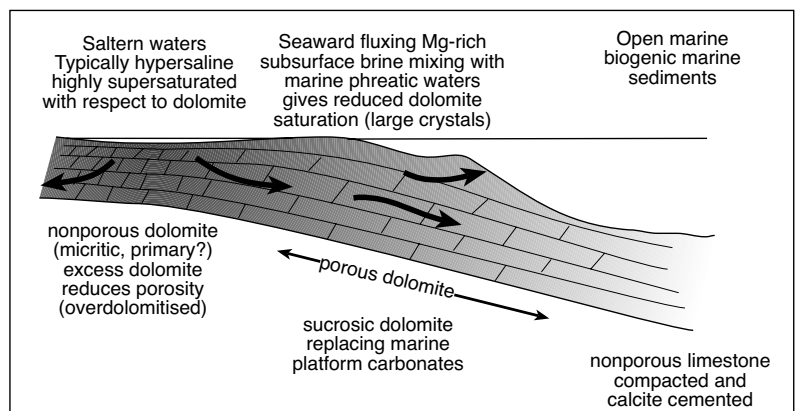


Figure 10.24. Reflux brines drive dolomitisation in marine carbonates some distance downdip from intervals of more restricted shoreward carbonate that tend to be overdolomitised and evaporite plugged (after Saller and Henderson, 1998 and Elliott and Warren, 1989).

into stacked sabkhas. Rather, the reservoir trend marks the transition from an updip, evaporite-plugged, partially-dolomitized subtidal–intertidal section into a dolomitized, subtidal–intertidal sequence characterized by intercrystalline and relict interparticle porosity. Unlike areas closer to the source of the reflux brines and beneath the saltern proper, these regions are not pervasively plugged with evaporite cements. This dolomitised zone passes down-dip into more tightly-cemented open marine subtidal

limestones. Updip plugging was driven by episodes of widespread evaporite deposition and the associated sluggish reflux of supersaturated brine into the underlying newly forming dolomites. The down-dip subtidal–intertidal section saw some evaporitic plugging, but it did not suffer the longterm massive influx of evaporite cements experienced further updip. Its more marine-marginal position allowed the porosity to remain open and magnesium-rich solutions associated with brine reflux to

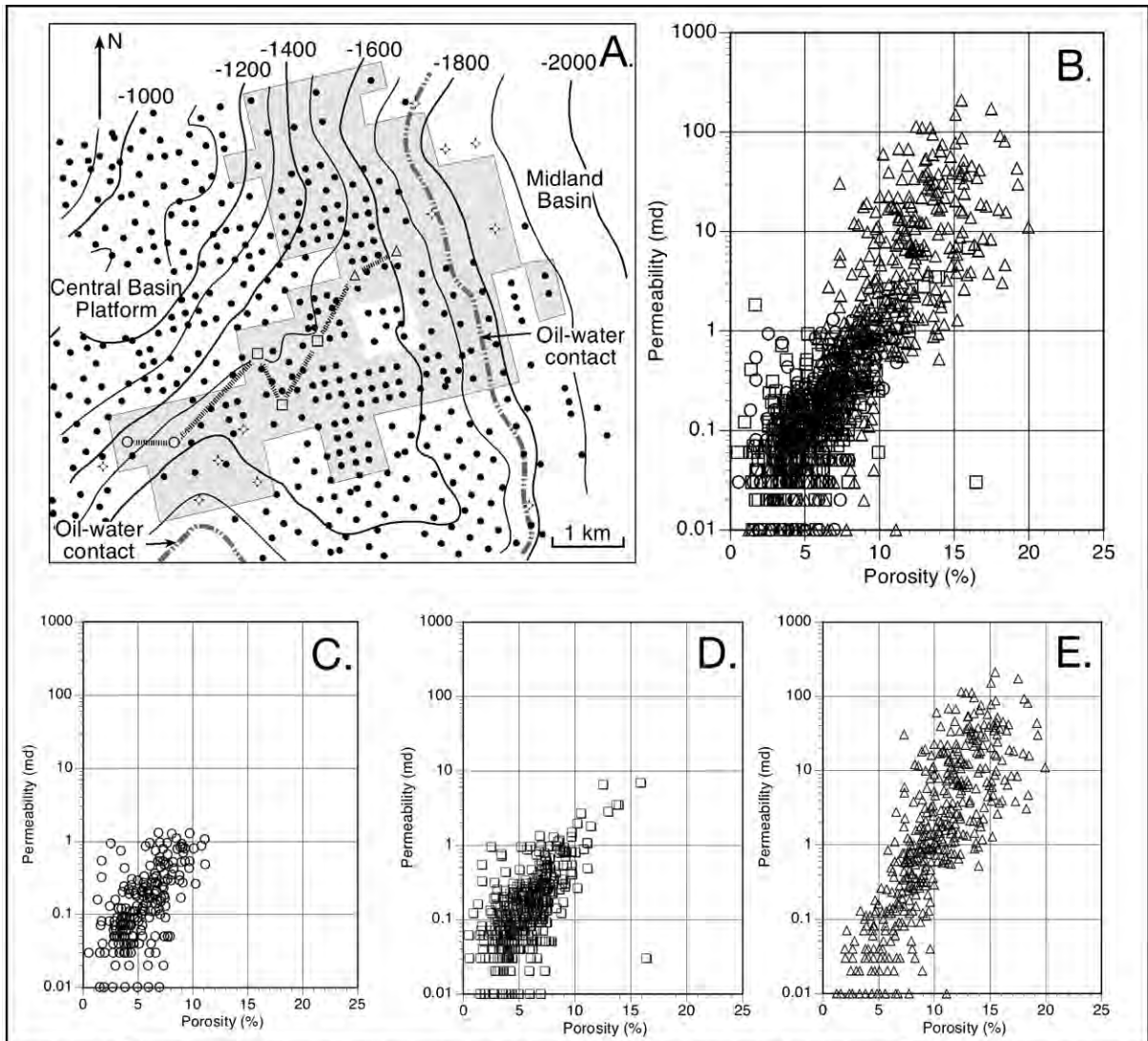


Figure 10.25. Porosity and permeability increase in the Moss unit of the Grayburg Formation in South Cowden Field, west Texas (redrafted and replotted from Saller and Henderson, 1998). A) Map of distribution of wells used in data compilation. The dolomitised transect used to compile data in B-E runs from the overdolomitised evaporite-plugged platform (O) to a dolomitised transitional zone (□) to the more basinward partially dolomitised platform wells with minor evaporite plugging (Δ) B) porosity permeability from all measured plugs in wells along the transect. C) Porosity-permeability from evaporite plugged platform interior wells, D) Transition zone wells. E) Porosity permeability from reservoirs in wells more distal to the evaporite-plugged platform interior. The plots B to E show an obvious increase in reservoir quality in the crossplots that corresponds to a decrease in evaporite plugging and an increase in dolomite crystal size along the downdip reflux pathway (as shown in Figure 10.24).

enter the carbonates to evolve into more coarsely crystalline dolomites. The Levelland-Slaughter reservoir trend is not a palaeoshoreline, nor is it a stratigraphic pinchout trap. It is a diagenetic front and trap with the best reservoir quality defined by the zone immediately down-dip of the thinning edge of the San Andres saltern (Warren, 1991).

Dolomitised limestones Central Basin Platform, west Texas

The same diagenetic control to reflux dolomite intensity seen at the regional scale in the Levelland Slaughter trend is also true at the oil field scale on the Central Basin Platform to the south. Saller and Henderson (1998) noted similar variations in reflux-related "dolomite intensity" controlling reservoir properties in the evaporite-sealed North Riley Field at the northern margin of the Central Basin platform and in South Cowden Field on the east-central margin of the Central Basin platform, Texas (Figure 10.25a, b). The main reservoir units in North Riley Field are permeable dolomites of the Leonardian (Permian) Clear Fork Formation, while dolomites of the Grayburg Formation (Guadalupian, Permian) are the main reservoir in South Cowden Field. Replacive dolomitization and the creation of intercrystalline porosity in both fields was driven largely by the reflux of evaporatively concentrated seawater circulating shortly after deposition of the original limestone matrix.

Ongoing reflux-driven evaporite plugging means porosities and permeabilities are lower in platform-interior dolomites and higher in dolomites near the platform margins in both fields (Figure 10.25c through e). Reservoir porosity and permeability are not strictly facies dependent in either field. As in the Slaughter-Levelland trend, Saller and Henderson (*op cit.*) found the distribution of porosity and permeability is largely the result of location within the diagenetic dolomitising system and to a lesser extent reflects the original depositional permeability of the limestones.

Due to inherently higher brine densities beneath an evaporite-depositing lagoon or saltern, the dense saline dolomitising brines, generated by evaporative concentration of seawater in restricted evaporitic mudflats and salterns, percolated downward and seeped basinward (refluxed) through the sediments. Refluxing brines, supersaturated with respect to dolomite and calcium sulphate, precipitated large quantities of dolomite and anhydrite cement in the proximal parts of the reflux system. This lowered dolomite saturation in waters flowing into distal portions of the reflux system. Lower dolomite saturations resulted in less dolomite, fewer nuclei and larger crystals (not

overdolomitised) along with more intercrystalline porosity and permeability retention in distal parts of the system (Figure 10.24). Many platform-interior wells in both fields are structurally higher than wells near the platform margin, yet structurally lower wells near the platform margin are more porous and permeable, and have produced three to ten times more oil than the platform-interior wells (Saller and Henderson, 1998).

Reservoirs in the Jurassic Smackover Fm., Gulf of Mexico

More than 1 billion barrels-equivalent of oil and gas has been discovered in the Smackover of the northeastern Gulf Coast Basin (Prather 1992a, b). The majority of these hydrocarbons are found in a few large fields such as Jay, Big Escambia Creek, Blackjack Creek, Chunchula, and Hatter's Pond, and the fields in the Mobile Bay complex. Except for the fields in the Mobile Bay complex, which have Norphlet Sand reservoirs, the Smackover Formation is the primary hydrocarbon reservoir in the large fields and many smaller fields, such as Vocation, Barnett, Uriah, and Appleton. Like the Arab D in the Middle East, the richness of Smackover hydrocarbon system in the region is a result of the co-occurrence of microlaminated lime mudstone source rocks, dolostone reservoir rocks, and an evaporite cap, all within an overall shoaling depositional package (Moore, 1984; Heydari, 1997).

The Smackover Formation forms a subsurface arc about the Gulf of Mexico and was deposited in a transgressive-regressive event during Upper Jurassic (Oxfordian) time (Figure 10.26a). It is underlain by the siliciclastic eolian-wadi Norphlet Formation in more marginward areas and by the Louann Salt Formation further out in the Basin. The Smackover, and the overlying Buckner Anhydrite Member of the Haynesville Formation, were deposited in three depositional stages that correspond to periods dominated by marine transgression, aggradation, and ultimately progradation. The Buckner Evaporite and its equivalents, which form the seal to the various upper Smackover fields was interpreted as sabkha until the mid 80s (Lowenstein, 1987). But in the 90s its interpretation changed to an evaporitic mudflat, a mosaic of sabkhas and salinas passing up and laterally into a saltern (Mann, 1990, 1992; Prather 1992a, b; Benson et al., 1996).

The Smackover is a combination of platform dolomites, shelf-margin oolitic and peloidal grainstones, and slope and basin limestones. It can be subdivided into three informal units, the lower, middle, and upper Smackover (also known as Smackover C, B and A, respectively). Each unit was deposited

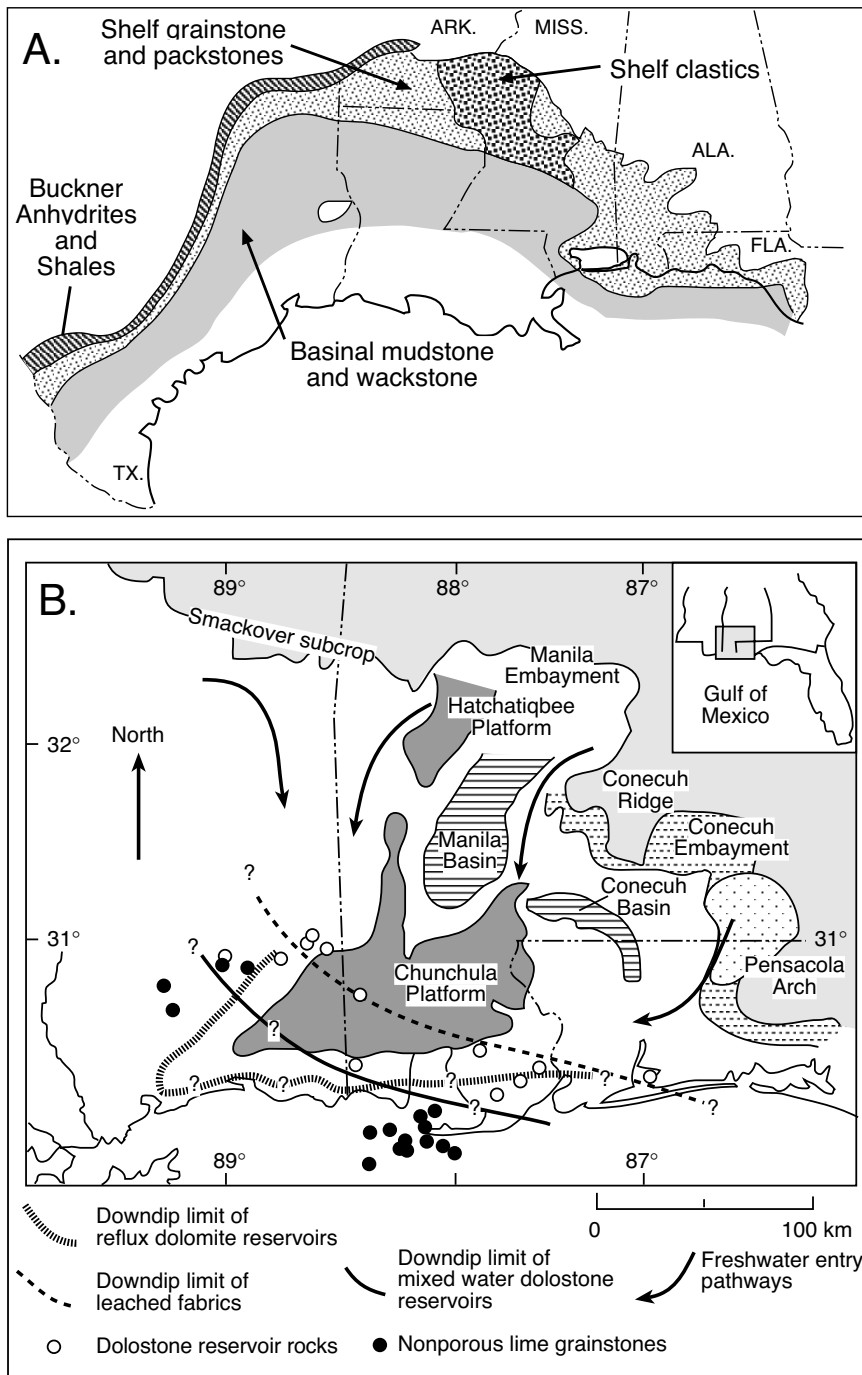


Figure 10.26. Smackover Formation, Northern Gulf of Mexico. A) Generalised map of Smackover distribution along the coast of the United States (after Melas and Friedman, 1992). B) The downdip limit of reflux and shallow burial mixed water zones occurs between dolostone reservoir rocks and nonporous lime grainstones (after Prather, 1992a).

in a different depositional setting on a gently shoaling carbonate ramp. Lower Smackover deposition accompanied a rapid sea level rise that inundated most palaeohighs in the basin to produce a depositional system that was first transgressive and then aggradational in nature (Benson et al., 1996; Prather, 1992a, b). Most sediments in the lower Smackover are basinal and consist of laminae of dark brown to black mudstones, alternating with laminae of pyrite and siliciclastic silt or sand. Locally they are organic rich and have acted as widespread source rocks for the hydrocarbons in the overlying Smackover sands (Heydari, 2000). The style of the laminae in the lower Smackover changes upward from very thin parallel laminae near the base to slightly thicker irregular laminae higher in the section. Algal patch reefs grew in lower Smackover time around the periphery of some palaeohighs, driven by the rising sea.

The middle Smackover is composed of sediments deposited on a low-energy, open-marine platform, laid down as sedimentation caught up with relative subsidence. Short-term sea level fluctuations produced numerous shallowing-upward packages (parasequences) in the middle Smackover. Two lithofacies are typical of the middle Smackover: a wispy-laminated, crustacean-pellet carbonate mudstone containing a sparse pelagic fauna and a densely burrowed skeletal-pellet wackestone containing a benthic fauna. Tidal flat, lagoon, and shoal complexes formed in

topographically higher parts of the northern Gulf, while sub-wavebase sediments were deposited in deeper waters and away from salt structure-induced seafloor shoals.

The upper Smackover consists of several grain-supported lithofacies deposited in shoal settings ranging from strandzone (tidal) bars and channels to beaches, islands, and algal-stromatoporoid reefs. Burrowed pellet and oncolite packstones and algal-stromatoporoid boundstones formed as moderate-energy outer shoals, and sequences of crossbedded mixed allochem, oolite, and oolitic grainstones comprised the current-reworked inner shoals. During upper Smackover deposition, sea level was relatively stable allowing the Smackover to aggrade and prograde. Upper Smackover deposits are peritidal or strandzone dominated. Short-term sea level fluctuations produced shallowing upward packages capped by exposure surfaces in crestal locations and deposited widespread syndepositional isopachous marine cements of aragonite (now calcite).

During lower Buckner deposition, evaporitic mudflats formed over the crests of the palaeohighs and passed off-structure and landward into salterns. Short-term sea level fluctuations produced a series of higher-order shallowing-upward evaporitic mudflat cycles behind the main oolite shoal. Development of subaqueous gypsum increased during ongoing restriction of the northern Conech Embayment and ultimately led to widespread deposition of the subaqueous saltern evaporite seal that defines the upper Buckner Anhydrite. This unit seals most Smackover reservoirs.

Dolomitised upper Smackover facies constitute the most productive reservoirs. In fact, dolomitisation and leaching are critical to the preservation of economic levels of porosity throughout the Smackover in the northern Gulf of Mexico (Figure 10.27). Historically, a minimum of 4% porosity and 0.1 md permeability in Smackover carbonates is considered to be reservoir grade (Becher and Moore, 1976). Economic Smackover porosity is of three main types:

1. Partially preserved primary interparticle porosity
2. Leached mouldic porosity
3. Intercrystalline porosity within coarsely crystalline dolomites

Most reservoirs are found in: a) grainstone shoals, b) fractured and dolomitised sediments of the inner-shelf and, c) algal stromatoporoid buildups (Mancini et al., 2000). The best reservoirs in Arkansas, Louisiana and eastern Mississippi are in dolomitized intervals that preserve incompletely cemented interparticle and mouldic porosity (Figure 10.26a). The updip

Smackover close to the palaeoshoreline in this region often contains leached mouldic porosity due to mixed-water flushing. In east Texas, Alabama, and Florida, the precipitation of dolomite with intercrystalline porosity has enhanced the reservoir potential of the Smackover grainstones.

Dolomitization is almost always required to form a reservoir in inner-shelf Smackover sediments and enhances the reservoir character in the grainier shoal sediments. A rule of thumb in the region is that a minimum of 80% dolomite is necessary for consistently good reservoir quality (Figure 10.27), but rocks that are 100% dolomite, or dolomites with pervasive evaporite cements, are not good reservoirs. Individual reservoirs can be as thick as 10 metres, with porosities as high as 26%, and matrix permeabilities as great as 6.5 md. Although enhanced reservoir quality is often related to reflux dolomitization, the distribution of dolomite, like that of the interparticle porosity and the mouldic porosity, is in large part inherited from porosity trends in the original depositional setting.

Geochemical and petrographic data suggest that calcite/aragonite alteration and dolomitization took place in: (1) phreatic seawater-seepage, (2) brine reflux, (3) nearsurface mixed-water, (4) shallow-burial mixed-water, and (5) deeper burial environments. These settings overlapped in time and space to form a

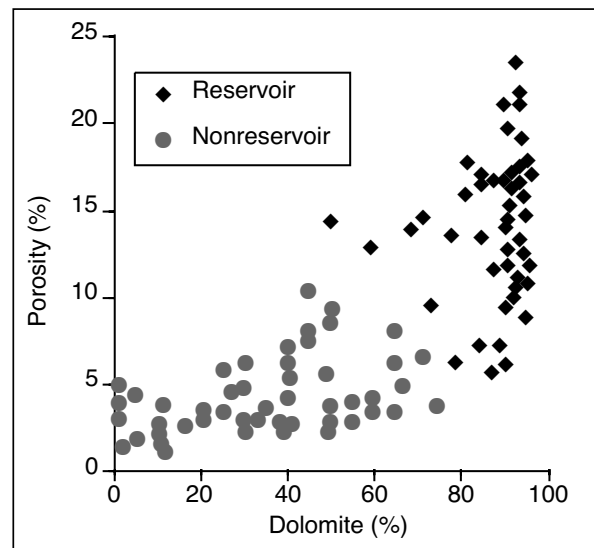


Figure 10.27. Relationship between porosity and the degree of dolomitisation in Jay Field, Conech Embayment. The lower Smackover facies in the field shows low porosity and are relatively less dolomitised compared to the upper Smackover grainstones, which have high porosity and are extensively dolomitised (data from point count data and are replotted from Melas and Friedman, 1992).

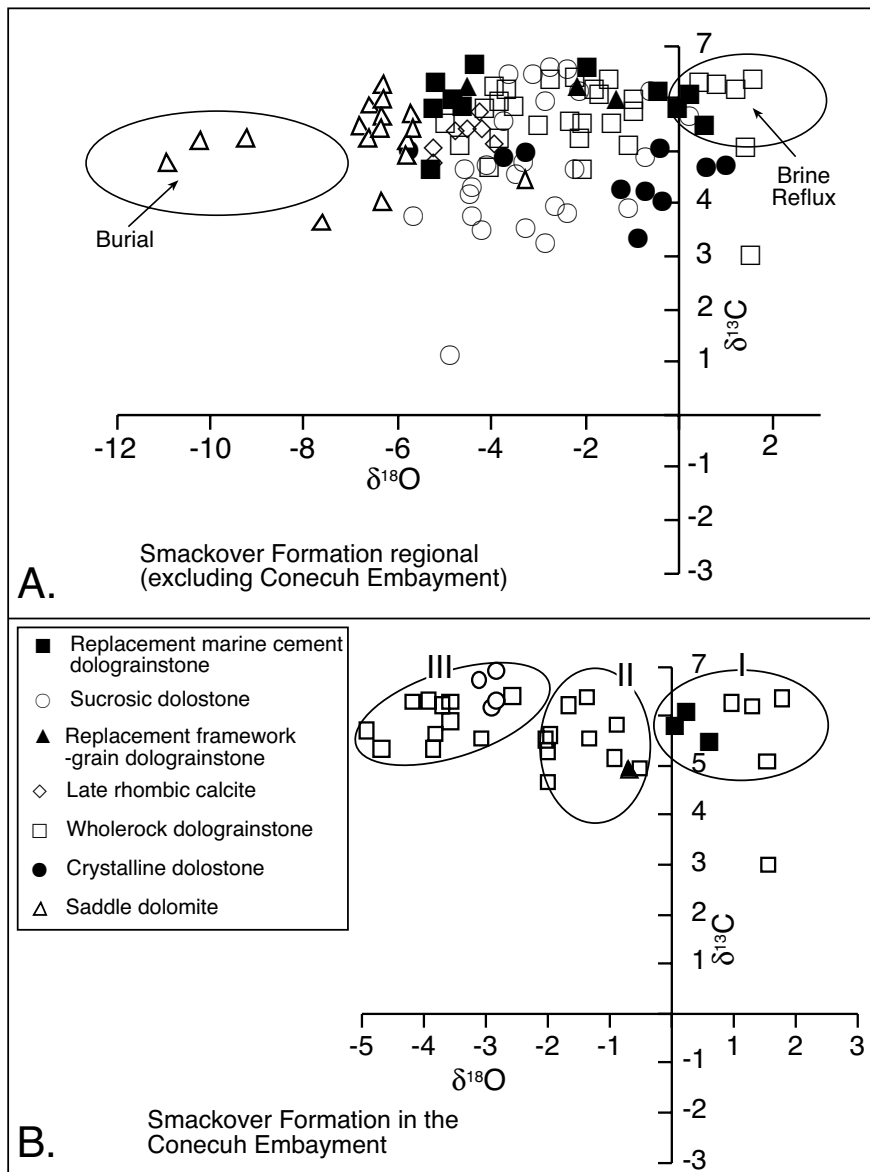


Figure 10.28. Stable isotopic signatures of the Smackover Formation, Northern Gulf of Mexico (after Prather, 1992a). A) Plot of $\delta^{18}\text{O}$ and $\delta^{13}\text{C}$ of dolomites from the Northern Gulf of Mexico, excluding the Conecuh Embayment and deeper burial dolomites. B) Plot of $\delta^{18}\text{O}$ and $\delta^{13}\text{C}$ of dolomites from Conecuh Embayment.

“platform-scale” dolostone composed of a complex mixture of dolomites and authigenic cements (Prather, 1992a). Of the five, the brine reflux and the deeper burial settings can be thought of as end members of a diagenetic spectrum creating dolomites. They are also the most easily separable of the five using isotopic signatures (Figure 10.28a). The other three form a related but overlapping group of subsurface alteration features.

Texturally, without isotopic data and with the exception of early isopachous rim cements, it is very difficult to assign origins to the various replacements and cements that typify the Smackover reservoirs.

Brine reflux dolomitization of the upper Smackover was largely driven by movement of hypersaline brines during deposition of the overlying Buckner Anhydrite member of the Haynesville Formation. Flushing by dense brine explains the distribution of early dolomite in southeastern Alabama and western Florida (Barrett, 1986; Saller and Moore, 1986; Worrall and Warren, 1986). Such beds show an enrichment in $\delta^{18}\text{O}$ indicative of precipitation from evaporated brines and constitute thin zones within the upper 5-7 m of the Smackover throughout the Conecuh Embayment. Replacement of precursor marine cements by dolomites rich in ^{18}O places this phase of dolomitization early in the paragenetic sequence, consistent with a reflux origin. Thicker zones (5-15 m) of isotopically-enriched reflux dolomite occur locally around the Conecuh Ridge, Pensacola Arch, and over the Chunchula Platform (Figure 10.26b). Time-slice lithofacies maps show that these thicker dolomite zones correspond to the locations of coastal evaporitic mudflats, which were first established on palaeotopographic highs within a pericontinental setting (Prather 1992a). These zones show aggradational geometries produced during an early regressive phase of Smackover/Haynesville deposition. Thicker zones of enriched dolostone probably formed in these areas because of the ongoing aggradation of the reflux dolostone host through time.

Texturally, without isotopic data and with the exception of early isopachous rim cements, it is very difficult to assign origins to the various replacements and cements that typify the Smackover reservoirs.

Brine reflux dolomitization of the upper Smackover was largely driven by movement of hypersaline brines during deposition of the overlying Buckner Anhydrite member of the Haynesville Formation. Flushing by dense brine explains the distribution of early dolomite in southeastern Alabama and western Florida (Barrett, 1986; Saller and Moore, 1986; Worrall and Warren, 1986). Such beds show an enrichment in $\delta^{18}\text{O}$ indicative of precipitation from evaporated brines and constitute thin zones within the upper 5-7 m of the Smackover throughout the Conecuh Embayment. Replacement of precursor marine cements by dolomites rich in ^{18}O places this phase of dolomitization early in the paragenetic sequence, consistent with a reflux origin. Thicker zones (5-15 m) of isotopically-enriched reflux dolomite occur locally around the Conecuh Ridge, Pensacola Arch, and over the Chunchula Platform (Figure 10.26b). Time-slice lithofacies maps show that these thicker dolomite zones correspond to the locations of coastal evaporitic mudflats, which were first established on palaeotopographic highs within a pericontinental setting (Prather 1992a). These zones show aggradational geometries produced during an early regressive phase of Smackover/Haynesville deposition. Thicker zones of enriched dolostone probably formed in these areas because of the ongoing aggradation of the reflux dolostone host through time.

Thin zones of enriched dolostones similar to those over most of the Conecuh embayment also occur sporadically around the flanks of the Chunchula Platform, Manila Basin rim, and the flanks of the Hatchatigbee Platform (Figure 10.26b). The downdip limit of thin reflux dolostones tentatively, inferred from very limited well control, appears to parallel depositional strike. Thinness or absence of enriched dolomite zones updip of this line may be associated with rapid progradation of the shoreface/coastal-sabkha couplet resulting in rapid lateral shifting of reflux zones, which prevented aggradation of reflux zones and allowed little time for refluxing brines to circulate deeper into the upper Smackover grainstones.

Brine reflux was driven by Buckner deposition and was tied to regional drawdown hydrology in the region behind the oolite shoals. Drawdown driving the reflux also influenced porosity evolution in the adjacent Smackover shoals that formed the isolating sill. For example, the drop in relative sea level in the Conecuh Embayment during the Oxfordian (Prather, 1992b) exposed thick submarine oolite sand bars of the upper Smackover on the southern flank of the Conecuh Basin. It created a subaerial sill, which separated the Conecuh Basin from the Gulf, as more than 100 m of Buckner salts were laid down as a saltern within the isolated intraplatform sag. The sill today consists of a thick (18–55 m) lower unit of medium to finely crystalline sucrosic dolostone and oolite dolograinstone overlain by a thinner upper unit of finely crystalline oolite dolograinstone. $\delta^{18}\text{O}$ analysis indicated that the dolostone in the sill is composed of three populations of dolomite. Two populations of dolomite depleted in ^{18}O occur in the lower sill (Figure 10.28b, groups II and III). A third population found in the upper part of the sill is relatively enriched in ^{18}O (Figure 10.28b, group I). The contact between the upper and lower units is gradational over about 1 m and has no apparent relationship to stratal boundaries. This contact was first noted by Vinet (1982) in wells from Jay, Blackjack Creek, and Big Escambia Creek fields, and was subsequently located in more wells by Prather (1986).

The association of a relatively abrupt localized geochemical and lithologic discontinuity within rocks beneath a sill that was subaerial during a sea level lowstand suggests the discontinuity may represent a fossil water table (Prather 1992a). If this is the case, the following events must have taken place: (1) partial dolomitization of the lower unit as seawater seeped through the sill to recharge the saltern brines in the Conecuh Basin, (2) complete dolomitization of the upper unit by reflux processes as the upper sill was buried during aggradation and progradation of Buckner evaporites (fill and spill sedimentation of the basin),

and (3) continued burial dolomitization of the lower unit by ^{18}O -depleted dolomitizing fluids. Each of these events gave rise to each of the three isotopic groups of dolomite from the sill: (1) seawater seepage dolomite with $\delta^{18}\text{O}$ values of -0.6 to -1.9 ‰, (2) reflux dolomite with $\delta^{18}\text{O}$ values of 2.0 to 1.0 ‰, and (3) later burial dolomites with $\delta^{18}\text{O}$ values of -2.6 to -4.6 ‰ (Figure 10.28b).

An earlier nearsurface mixed-water environment, locally affected sediments from the surface to several tens of metres thick in the vicinity of local freshwater entry points. Freshwater entered the Smackover either through groundwater sinks (exposed palaeohighs or islands) or via the updip part of the regional groundwater flow system. Under these conditions, freshwater supply to coastal areas of the Northern Gulf, such as the Conecuh embayment, probably was limited to what was supplied by the updip drainage system between the Conecuh ridge and Pensacola arch. These waters leached aragonite allochems, leaving behind hollow grains preserved only by their micrite envelopes. The $\delta^{18}\text{O}$ contents of these replacement dolomites are slightly depleted relative to seawater-seepage dolomites, slightly enriched relative to later rhombic dolomite cements, and closely associated with freshwater-phreatic calcite cements, suggesting a nearsurface mixed-water origin. Dolomite-replaced precursor marine cements, with only slightly depleted $\delta^{18}\text{O}$ compositions relative to seawater-seepage dolomites, have been encountered only in the Conecuh embayment. This is consistent with the notion that they are connected to isolated mixing zones. Their localized distribution probably reflects the limited extent of freshwater environments in such an arid climate.

Rhombic dolomite crystals of the shallow-burial mixed-water environment typically have cloudy cores and clear rims. These rhombic dolomite cements overgrow neomorphic fabrics, which formed after a period of leaching and sparry calcite precipitation. Paragenetic relationships show that vuggy and oomouldic pores within the Conecuh embayment and throughout the Northern Gulf region are virtually contemporaneous (Prather 1992a). Extensive leaching of this kind suggests considerable local artesian influxes of fresh to brackish water after evaporite deposition had ceased. The wide band of leached fabrics that parallels the updip limit of the Smackover suggests freshwater entry probably occurred along the Smackover outcrop in western Alabama and where Haynesville alluvial-fan sandstones interfinger with upper Smackover grainstones around the Conecuh Ridge and Conecuh embayment (Figure 10.26a). Leaching trends similar to this are described by Moore and Druckman (1981) from the updip Smackover of Arkansas and Louisiana.

Their marginward position suggests that the downdip limit of leached fabrics is controlled by a change from less stable aragonite oolites updip to more stable calcite oolites downdip. In eastern Mississippi, Alabama, and Florida, however, the trend of leached fabrics is perpendicular to depositional strike. Therefore, the distribution of leached fabrics in the east is more likely related to the downdip position of a zone of undersaturated groundwater (Figure 10.26b). Sparry calcites that line the large vugs in the Smackover of the Conecuh embayment have somewhat depleted $\delta^{18}\text{O}$ signatures and low $\text{Fe}^{++}/\text{Mn}^{++}$ ratios, which suggest precipitation in warm, slightly reduced, fresher subsurface waters. Abrupt changes of formation-water redox conditions or trace-element concentrations outlined by cathodoluminescent zonation patterns indicate these spars probably precipitated at sufficiently shallow burial depths to receive some recharge of oxidized fresher water from the surface after evaporite deposition had ceased.

These isotopically depleted dolostones of the deeply circulating regional fluid mixing stage constitute the signature of the most widespread reservoir rocks in the Smackover. They define areas where deeply circulating meteoric fluids (artesian waters) mixed with marine-phreatic or basinal brines and overprinted sediments from a few metres to hundreds of metres below the Buckner seal. They are confined to grain-supported and boundstone rock types below the Haynesville Formation, suggesting that the fresher water inflows, which mixed with formation brines, were confined to an aquifer lying below the evaporites and fine-grained siliciclastic rocks of the Haynesville Formation. By the time they were circulating they were excluded from the now-tight carbonate mudstones and wackestones of the lower Smackover Formation. Recharge of the regional aquifer probably occurred as phreatic head rose along the Smackover/Haynesville subcrop during basinward tilting. Associated progradation of the overlying Cotton Valley strandline drove basinward migration of a thick continental freshwater lens atop the saltern evaporites.

In a tectonically stable area such as the Gulf Coast, large variations in recharge of regional confined aquifers, like the Smackover, are likely to occur only in response to substantial fluctuations of sea level (Harrison and Summa, 1991). Maximum downdip limit of the regional mixed-water zone and associated dolomite reservoirs is likely, therefore, to have occurred during prominent sea level lowstands, such as those proposed for the Valanginian (Haq et al., 1987). The distribution of dolomite depleted in ^{18}O suggests that the interpreted regional mixed-water zone must have migrated downdip a minimum of 193 km from points of recharge along the Smackover subcrop and the Conecuh embayment (Prather 1992a).

Later precipitation of saddle dolomite in the deeper burial environment has been linked to chemical compaction of dolostones, thermochemical sulphate reduction, hydrocarbon migration, and epigenetic sulphide emplacement (Heydari, 1997). Their depleted $\delta^{18}\text{O}$ values suggest formation temperatures higher than the other Smackover dolomites (Figures 9.45a, 10.28a). Hydrocarbon inclusions suggest that the saddle dolomites are late burial cements that were at least contemporaneous with hydrocarbon migration, which began in the middle Early Cretaceous. In the Smackover, as in the Arab D, evaporites played an early role in the formation of reflux dolomite and then a subsequent role as a focus (aquiclude) for regional flows of deeply circulating groundwaters and basinal waters.

Middle East reservoirs sealed by bedded basinwide evaporites

As well as saltern evaporites sealing and driving alteration processes in intercalated platform carbonates, there a number of reservoirs sealed by thick caps of basinwide salts. Where the traps are stratigraphic, permeability tends to be developed in dolomitised carbonates beneath bedded seals. Such reservoirs tend to be patchy and of lesser quality compared to reservoirs hosted in the downdip areas of the saltern-sealed traps discussed in the previous section. But where the subsalt traps are structural, broadly-drained anticlinal culminations, as in the Miocene successions of the foreland fold belt of the Zagros in Iraq and Iran, the fields are large and many are supergiants. This structural association reflects ability of evaporites to maintain seal integrity under deformation, while the underlying and intercalated dolomites and limestone fracture. This structural association is discussed in more detail later in the chapter, for now our discussion will focus on the effects of syndepositional reflux dolomitisation on reservoir quality below basinwide evaporites.

Eocene and Miocene associations, Middle East

Carbonate platform and sandstone reservoirs beneath Tertiary-age basinwide seals in the Arabian Gulf and the Gulf of Suez have been overprinted to varying degrees by reflux dolomite. The evaporites define two main age-related saline associations: Lower Eocene and Middle Miocene (Figure 10.29). The Eocene evaporites are saltern evaporites precipitated in an intracratonic sag on the continental side of a foreland bulge in front of the rising Zagros chain (Alavi, 2004). Across the Gulf they constitute widespread 10-20m thick anhydrite/gypsum units within the Rus Formation and its equivalents. Salts in the Rus can perhaps also be considered the youngest example of wide-

spread platform evaporites and accumulated immediately prior to the onset of icehouse eustasy (Chapter 5). Miocene basinwide seals in the region are better known and more significant economically as they form caps to the Asmari limestone. They accumulated in the isolated foreland deep in front of the Zagros suture (Alavi, 2004) and make up the Fars/Gachsaran formations in the Northern Arabian Gulf. Their dissolution residues typify outcrops in the Dam Formation of Qatar and Saudi Arabia (Dill et al., 2005). Similar Middle Miocene basinwide evaporites are also highly effective seals to producing intervals in the rift-infilling Ras Maalab Group in the Gulf of Suez (Alsharhan, 2003).

Eocene evaporites (bedded anhydrites) of the Rus Formation seal platform carbonate reservoirs in the northern Arabian Gulf (Iraq and Iran). Reservoir quality tends to be patchy and constitute the upper portions of thicker stacked Mesozoic pay horizons in giant and supergiant fields of the Northern Gulf. In the 45 by 25 km anticline that is the Nahr Uhm supergiant field in Iraq the structural closure for the various pay zones varies with depth and ranges from 200 metres for the Dammam (Eocene) down through the Rus Formation to about 800 metres for the Lower Cretaceous Yamama reservoir. The Cretaceous is the main production focus for many of the huge fields of Iraq and Kuwait. In the western and southern Gulf (Kuwait, Saudi Arabia, Qatar and the Emirates), the Rus Formation outcrops or subcrops and is typically leached of its bedded evaporites (Dill et al., 2003). Once leached of its salts it constitutes an important aquifer capable of producing potable groundwater. Only dissolution residues and collapse horizons remain in outcrop as indicators of the former presence of widespread bedded evaporites in the Rus Formation, along with associated slumps, digitate stromatolites, hollow cauliflower cherts and calcite nodules (pers. obs).

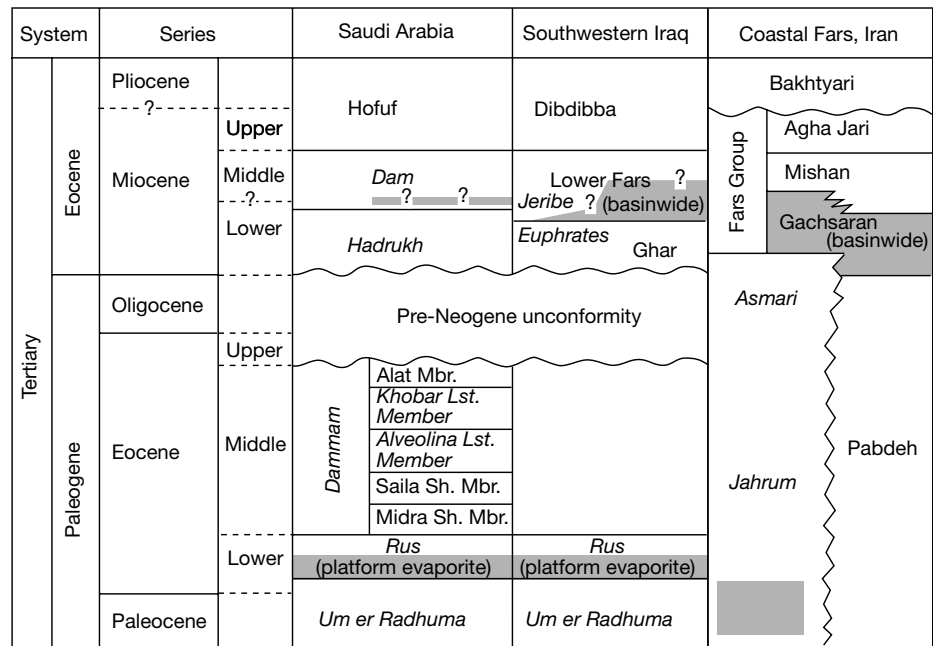


Figure 10.29. Schematic Tertiary Stratigraphy of the Arabian Gulf, with evaporite-entraining successions shaded grey (in part after Tleel, 1973; Sharland et al. 2001, Alavi, 2004).

But the most productive reservoirs in the northern Arabian Gulf are Miocene and are platform or deeper water carbonates (Asmari, Euphrates, Jeribe formations) that are sealed by Middle Miocene bedded salts of the Lower Fars/Gachsaran and equivalents (Figure 10.29). Core analysis of lower Miocene platform carbonates below these seals in Iraq show that open-marine subtidal carbonates have moderate to good porosity (10-35%), but have highly variable permeabilities ranging from less than 1 md to several hundred millidarcies. Restricted tidal flat (evaporitic mudflat) carbonates intercalated in the same sections are tight (Figure 10.30a, 10.31; Sun and Esteban, 1994). In general, the best reservoir quality in the lower Miocene carbonates of the Middle East occurs in: (1) mud-lean skeletal packstones in which leached mouldic and vuggy porosity is well connected (e.g., Euphrates and Jeribe formations of Iraq and Syria), (2) oolitic packstones-grainstones with well-preserved primary intergranular porosity (e.g., local occurrence in the Jeribe Formation of Iraq), (3) coarsely crystalline dolomite (e.g., Euphrates and Jeribe formations of Iraq and Asmari Formation of southwestern Iran); and (4) highly fractured carbonates (e.g., Asmari Formation of southwestern Iran). Dolomitisation in many reservoirs substantially improves reservoir quality, especially in intervals hosting coarsely crystalline dolomites (Figure 10.30b).

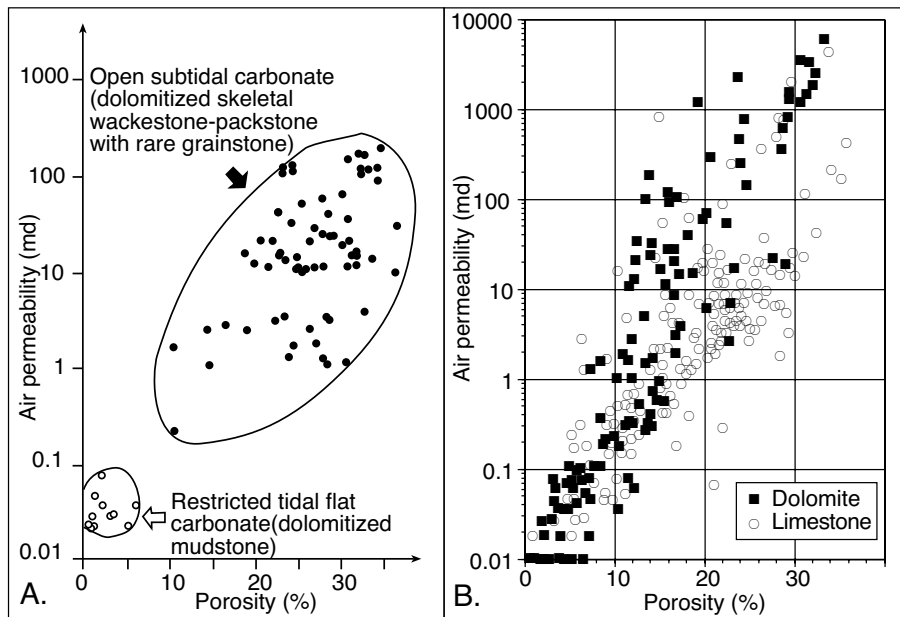


Figure 10.30. Poroperm in the Tertiary of the Middle East. A) Permeability versus porosity in Lower Miocene carbonates (replotted from Sun and Esteban, 1994). B) Permeability versus porosity in Kirkuk Field, Iraq, showing the improvement in reservoir quality typical of dolomitised limestone successions (Cretaceous-Miocene).

In the Middle Miocene carbonates of the Gulf of Suez and the Red Sea, the spatial tie of the dolomites to basinwide rift evaporites, and their preferential distribution along the former platform margins, together with their relatively heavy oxygen isotopic values (averaging +4.65‰; Sun and Esteban, 1994), all suggest that the bulk of the dolomite was formed by the lateral migration of evaporitic basinal brines into the shallow platform. The formative hydrology was driven by the rise of brine levels associated with the evaporite filling the basin centre (Sun, 1992; see also “spill and fill” discussion in Chapter 5 and later in this chapter). In contrast, downdip reflux of descending hypersaline brines, generated within platform salterns, were the main cause of extensive dolomitization in the lower Miocene carbonate reservoirs of the Middle East. Differences in the two styles of hydrology can be recognised by mapping isotopic signatures of cements in cores from well to well and documenting the close stratigraphic relationship of reservoir quality to the transition zones between open marine platform carbonates (now dolomitized) and mapping (in seismic) the positions of restricted saltern evaporites or their residues.

Reservoir porosities in many of the evaporite-sealed Tertiary carbonate successions bear little relationship to depositional facies, rather they are strongly influenced by the distribution of anhydrite cements, burial corrosion, dolomite crystal size and fracture intensity. Undolomitised carbonates in the reservoir-

hosting formations typically occur only in local areas: (1) encased units in marls, (2) platform interiors, and (3) areas with active freshwater drainage. This association of undolomitised intervals with basin margins or marine-cemented and exposed shoals is similar to that in the Smackover and San Andres formations.

Dolomite preferentially replaces magnesium-calcite skeletal grains (red algae, benthic foraminifera, and echinoderms) and micritised nonskeletal grains (oids and peloids) throughout most of the dolomitised Miocene carbonate section of the Arabian Gulf and the Gulf of Suez (Sun and Esteban 1994). Micrite matrix, internal muddy sediments, and micritised outer margins of aragonitic skeletons are also extensively replaced by dolomite. The replacement dolomites are subhedral to anhedral, finely crystalline (<10 μm) and show excellent preservation of original depositional fabric (mimetic dolomitization), indicating that the dolomitisation was either syndepositional or relatively early in burial (Warren, 2000a). Less common are coarsely crystalline dolomite cements lining secondary mouldic pores, often after dissolved evaporites. Sucrosic dolomites (40-80 μm, euhedral-subhedral) occur locally in some mixed carbonate-siliciclastic facies.

A particular diagenetic feature of evaporite-associated Miocene dolomite reservoirs of the Middle East is extensive leaching of skeletal aragonite without prominent karst surfaces or predolomite calcite cements (Figure 10.31; Oswald, 1992; Sun, 1992). Mouldic and even vuggy porosity is well developed in carbonate hosts that contained abundant skeletal aragonite, whereas precursors dominated by high-Mg calcite bioclasts, such as red algae, echinoderms, and benthic foraminifera, are commonly mimetically replaced by reflux dolomite, with only minor moulds and other dissolution voids. As such, these nonvuggy units tend to show better-behaved poroperm relationships and more predictable wireline to core responses. Sun (1992) proposes that invading hypersaline brines rather

than fresh waters were the cause of large-scale leaching of skeletal aragonite.

With progressive burial and compressional folding, these Miocene dolomites have experienced repeated episodes of anhydrite cementation, fracturing, and late stage corrosion of pore walls (Sun and Esteban, 1994). Anhydrite cementation is the most widespread porosity-occluding process. In many cases, both primary and mouldic porosities are almost entirely filled by anhydrite cements. Laterally, the distribution of anhydrite cements is highly variable in these Miocene reservoirs, but as a general rule, they are more abundant in relatively coarse, grain-supported carbonates, or those carbonates containing abundant skeletal aragonite, suggesting that original porosity and permeability played a major role in controlling access by later sulphate-bearing fluids. Brine-driven dolomitization and skeletal aragonite dissolution during the early diagenetic stage produces excellent permeability networks. It enabled ongoing active circulation of anhydrite precipitating fluids and, if some permeability remains, even controlled the subsequent ingress of later burial fluids (including oil and gas).

Tectonically-induced fractures are common in the Lower Miocene carbonates of the Middle East, particularly along the Taurus-Zagros belt where these carbonates are intensively folded and fractured. There appear to have been several stages of fracturing. Most of the early formed fractures were occluded

by anhydrite cements, whereas relatively late-formed fractures, which postdate anhydrite cementation, remain open and effective. In places where the carbonate hosts have a relatively low matrix porosity and permeability, such as the Asmari Limestone in southwestern Iran, fracturing plays a vital role in enhancing the reservoir quality (McQuillan, 1985). The mechanism of production in most Asmari reservoirs of southwestern Iranian oil fields is related mainly to open fractures beneath the Fars/Gachsaran seal (Figure 10.57), although variations in matrix porosity (e.g., mouldic or intercrystalline) locally influence production.

According to Sun and Esteban (1994) the last diagenetic event before hydrocarbon emplacement in Miocene carbonates of the Middle East was burial corrosion through which reservoir quality was improved, particularly in the hydrocarbon-producing reservoirs of the Gulf of Suez and Iraq. These late stage corrosive events bear little or no relationship to depositional facies or stratigraphic position. Corrosion preferentially affects anhydrite cements, relatively fine-grained sediments, and matrix materials. Typically, the current reservoir quality of many Miocene carbonates in the Middle East reflects the intensity of such corrosive events. The combination of vugs and chalky microporosity, which dominates effective porosity in the matrix of most producing Miocene reservoirs, was largely produced by late stage corrosion. Other important porosity types, including moulds, intergranular pores, and fractures, were enlarged by

corrosive processes. The distribution of such burial pore types is characterized by a lack of linear or branching passages related genetically to identifiable recharge and discharge points, making these reservoirs difficult but locally prolific producers.

Intensity of late stage corrosion is perhaps tied to levels of sulphuric acid created by the mixing of waters with different H₂S contents, or by oxidation of H₂S in an evaporite-rich hydrocarbon environment (Sun and Esteban, *op. cit.*). In places, organic acids released through source rock maturation may have

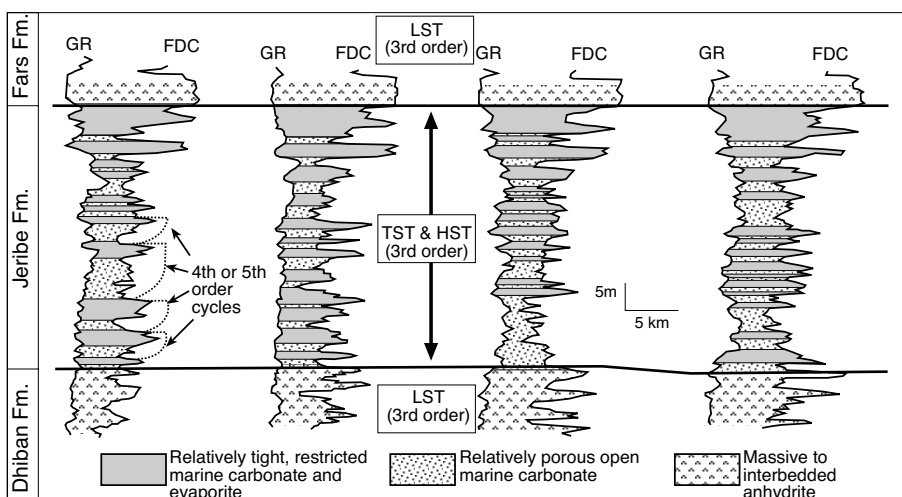


Figure 10.31. Stratigraphic cross section of the Lower Miocene succession in the Middle East, centred on Iraq, showing higher order (4th or 5th) platform evaporite cyclicity within a 3rd order depositional sequence, which is made up of a lowstand evaporite of the Dhiban Formation, followed by transgressive and highstand platform carbonates of the Jeribe Formation, followed by lowstand evaporites of the Lower Fars (after Al-Murani, 1986; Sun and Esteban, 1994). Note the high porosity in the open marine carbonate intervals in the Jeribe Formation, while the intercalated restricted marine carbonates and evaporites are tight (see Figure 10.30a).

also contributed to the late stage corrosion. The development of the permeability network and the availability of migration pathways (faults and fractures) regionally connecting acidic subsurface fluids were two key factors controlling the degree to which fine-grained dolomites or anhydrite cements were corroded.

Silurian pinnacle reef fields, Michigan Basin

Since the late 1960s, production from the numerous evaporite-encased Niagaran reefs of the Michigan Basin has been the main local source of oil and gas production for the state of Michigan (Figures 10.32, 10.33; Gill, 1977, 1985, 1994; see Figure 5.52 for detail on seal geology). Productive reef-substrate areas range from around 40 acres (0.16 km²) to 840 acres (3.4 km²). Recoverable reserves in individual pinnacles range from 30,000 to 22 MM BBL of oil equivalent (BOE). The ten largest fields in the Niagaran pinnacle play were found by drilling of the first 25% of the exploration wells. The discovery per wildcat peaked at 1.55 MM BOE after 500 wildcats, and declined stead-

ily thereafter to a level of 0.02 MM BOE per well after 1,900 wildcats, indicating that the play has reached a state of maturity, as does the move to horizontal drilling to improve recovery efficiency. About 25% of the discovered reserves were found in 5% of the fields, indicating a more even reserve distribution pattern than in many other reefal plays, perhaps a reflection of the high efficiency of basinwide evaporites as seals to pinnacle reefs. Consequently, the relative rate of growth of discovered reserves was slower than in other reef plays.

Downdip pinnacle reefs in the Michigan Basin illustrate a major negative to any relatively un-fractured reef play that is sealed by thick basinwide evaporites. That is, the deposition of a thick sequence of salt atop and adjacent to the reef buildup typically leads to high volume flow of dense saturated brines through the underlying porous strata at the culmination of the reef (potential reservoirs). This tends to overdolomitise and extensively plug most of the uppermost porosity with salts. This is clearly seen in the Niagaran trend shown in Figure 10.33a, which shows a band of evaporite-plugged pinnacle reefs down-dip of the main pinnacle reef play. Within the pinnacle reef play the occurrence of oil updip of the gas accumulations is an indication of classic Gussow style migration and segregation (Figure 10.33b).

Why updip reefs remain as reservoirs and the downdip reefs are salt plugged is an interesting quandary. In my opinion it reflects the likely recharge hydrology that effected the basin when it was hydrographically isolated and the A1 and A2 halites were being deposited. As we saw in Chapter 5, the potentiometric surface created by hydrographic isolation creates a marine-fed seepage margin to a drawdown saline giant (Figure 5.32). Toward the basin edge, this head was sufficient to displace any dense reflux brines from the surrounding basinwide brine plume and so allow deeply circulated seawater to rise through the pinnacle reefs and from part of the marine-feed outflow zone. Crest of pinnacle reefs allowing groundwater egress have characteristic seepage carbonate caps (pisolite, tufa, stromatolite and anhydrite haloes) that differentiate them from the surrounding halite plain. Pinnacles further out in the basin did not have sufficient head to prevent the ingress of sulphate-saturated waters and so their porosity was plugged. Reef caps to these salt-plugged reefs lack or have attenuated indicators of seepage outflows. This palaeohydrology also explains why oilfields in pinnacle reefs that acted as marine seeps, such as the Bell River Mills gasfields, not only produce from the reef facies but also produce from the A1 carbonate fringe. Back in the Silurian these units were part of a single flow unit supplying pressurized phreatic seawater to the basin (Figure 10.32). The hydrology that established the active seep reefs can be used as

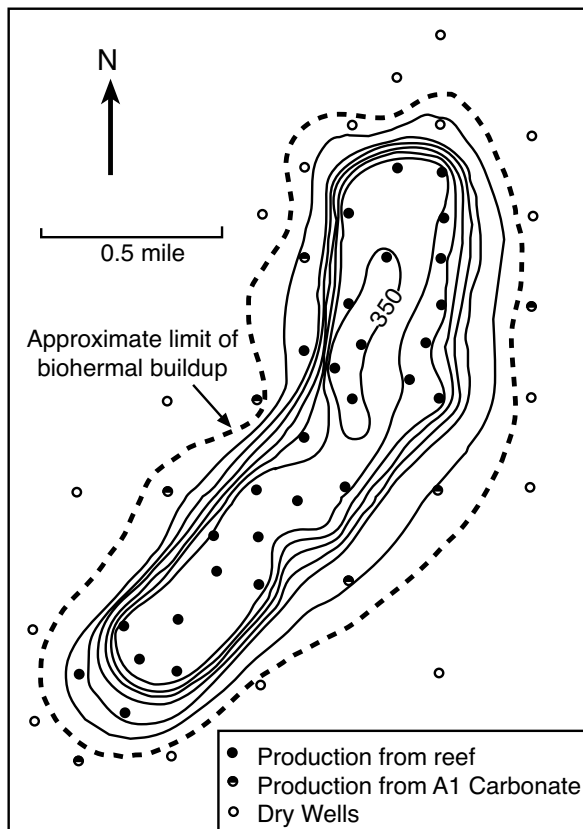


Figure 10.32. Belle River Mills gasfield. Cumulative thickness or isopach of biohermal and organic reef stages, configuration at termination of organic reef stage (after Gill, 1985).

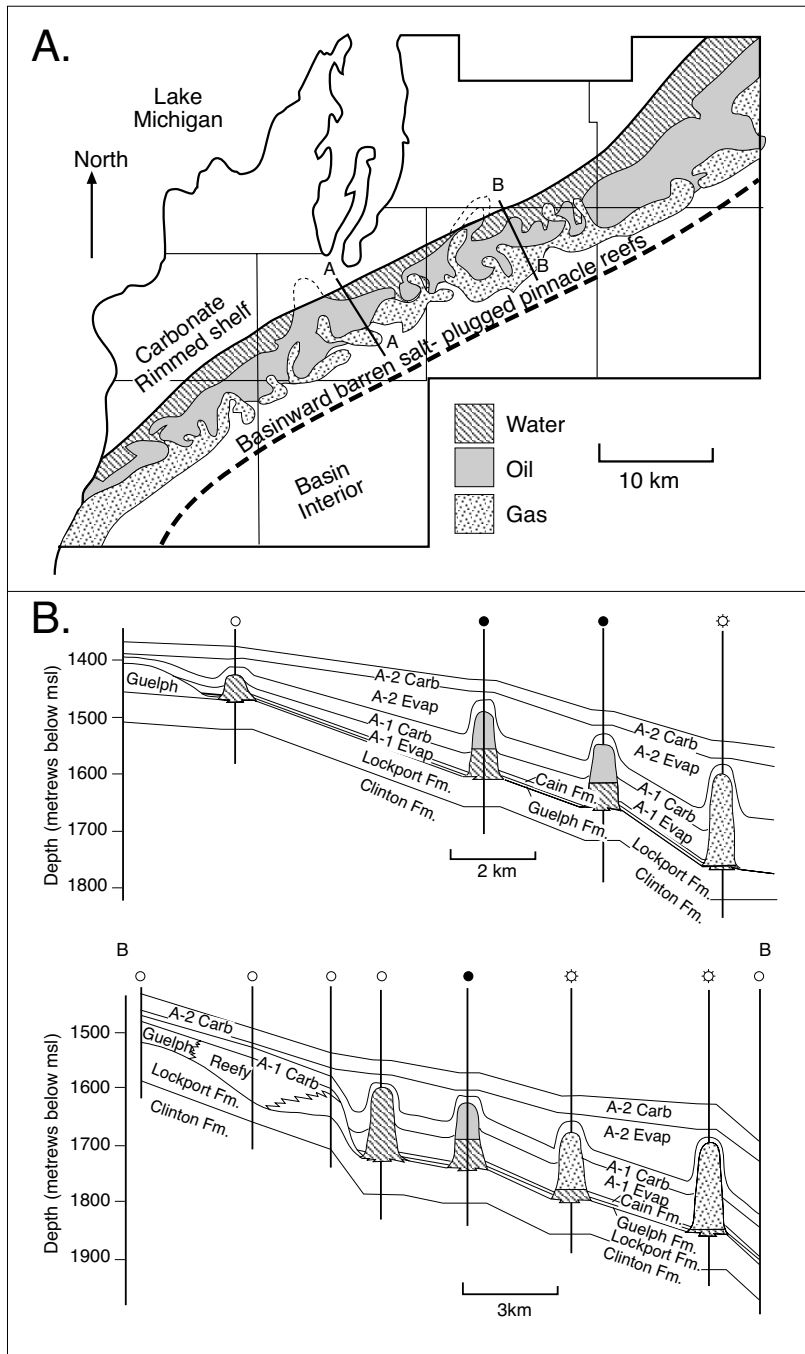


Figure 10.33. Evaporite-sealed Silurian pinnacle reefs in the Northern Michigan Basin. A) Distribution of salt plugged, gas-, oil- and water-bearing reefs. AA' and BB' show the positions of cross sections in Figure 10.25b. B) Cross sections through the pinnacle reef belt showing classical Gussow-migration controlled separation of oil and gas in the reefs. Pinnacles in positions more basinward than shown are not economic due to widespread salt plugging (after Gill, 1985).

an exploration and development tool in such drawdown basins.

Another interesting feature of the Niagaran pinnacle reef play is that many fractures and adjacent pinnacle matrices are overprinted by late stage saddle dolomite and calcite, with ponding of the precipitating fluids driven by circulation of late stage basinal fluids beneath the highly effective evaporite seal (Cercone and Lohmann, 1986). The source of these basinal fluids is not well understood, but is thought to be from the leaching of underlying Ordovician shales.

This argument is supported by the occurrence of fault and fracture-controlled hydrothermal (thermobaric) dolomite reservoirs in Ordovician (sub-Niagaran) marine carbonates in a syncline that defines the oilfields of the nearby Scipio Albion trend (Figure 10.34). Metal sulphides, baryte and coarse sparry anhydrite are coprecipitates from the basinal fluids that formed this set of late-stage coarsely crystalline saddle dolomite. Yoo et al. (2000) argued for an evaporite source to these fluids. Later in this chapter we shall return to this association in a discussion of structurally-focused hydrothermal dolomite overprints and density-driven deep convective circulation cells below the dissolving undersides of highly effective evaporite seals.

Yet again, the presence of a thick sequence of bedded evaporites has exerted a strong influence on reservoir distribution and quality on reservoir distribution and quality well into burial. The Salina salts today acts as highly effective seals to oil and gas accumulations in the

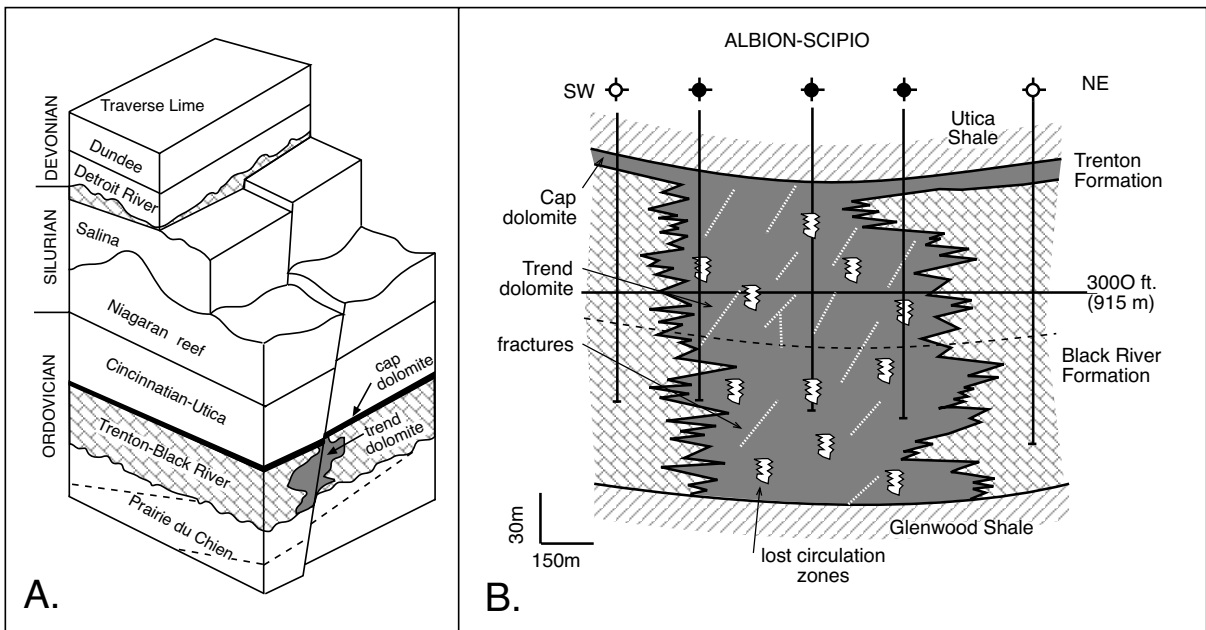


Figure 10.34. Fault-focused late dolomitisation in the Scipio-Albion trend, Michigan (after Hurley and Budros, 1990). A) Structural stratigraphic interpretation of the Albion-Scipio trend. The fault/fracture set that controls dolomitization is pre Devonian. B) Structural cross section of the Scipio-Albion Field. Note that the field is located in a synclinal trend (not usual for a hydrocarbon trap) and there is a rapid lateral transition from a regional nonreservoir limestone into a permeable reservoir dolomite that also hosts late stage anhydrite and other authigenic burial salts. Lost circulation and fracture zones in such fields are common indicators of secondary dolomite-hosted porosity. Note that the seal is a shale not evaporite in this system but the chloride-rich basinal brine responsible for the hydrothermal dolomite has a chemistry strongly influenced by evaporite dissolution deeper in the basin.

pinnacle reefs. During the early drawdown stage the formative hydrology perhaps allowed some pinnacle reefs to remain open, while others further out in the basin were plugged by evaporite cements from brine reflux. Then during later burial the salt bed focused the flow of upwelling basinal waters and the precipitation of later authigenic cements both along its underside and within the salt-sealed pinnacle reefs.

Evaporite-sealed platform and reefs, Devonian, Canada
Early Devonian (pre-Keg River time) in the Alberta Basin of Canada was dominated by multiple-cycle platform evaporite deposits ending with deposition of planar anhydrite sheets of the Chinchaga Formation and shales of the Ashern Formation (Tinker and Kirby, 1991). The lower Keg River/Winnipegosis was deposited as a marine carbonate ramp in shallow waters <75 m deep. Contemporaneous faulting and uplift during Middle Devonian time initiated development of a platform margin composed of stacked, porous (15-25%) packstone and grainstone shoals (Figure 10.35a). Pinnacle and bank growth in on or near the platform edge was contemporaneous with epeiric shelf deposition. Keg River/Winnipegosis deposition ended

with restriction of the basin and subsequent deposition of the basinwide evaporites of the Middle Devonian Muskeg/Prairie Formation (Figure 11.19).

Since the initial discoveries in the mid-1960's, the Keg River/Winnipegosis has produced hydrocarbons from a variety of dolomitic trap types with the largest volumes coming from evaporite-sealed pinnacle reefs. In 1991, Tinker and Kirby listed the following produced volumes; Rainbow/Zama sub-basin (>650 MMBO cum.) and in equivalents in southern Saskatchewan (>2 MMBO cum.); shelf-margin carbonates at Temple Field (>3 MMBO cum.); middle shelf carbonates at Senex (>2 MMBO cum.); inner shelf carbonates in northeastern Montana, southern Saskatchewan, and southern Alberta (>10 MMBO cum.); and inner shelf siliciclastics at Utikima Lake (>75 MMBO cum.). Historically, regions of high production in Middle Devonian carbonates lay to the west and northwest of Calgary, where evaporites acted as the seal for most of the higher volume fields with Keg River/Winnipegosis production (Figure 10.35a). Production in the Rainbow-Zama sub-basin has been declining since the late 1980s. More recent discoveries are smaller and lie along the basin edge, mostly in a region

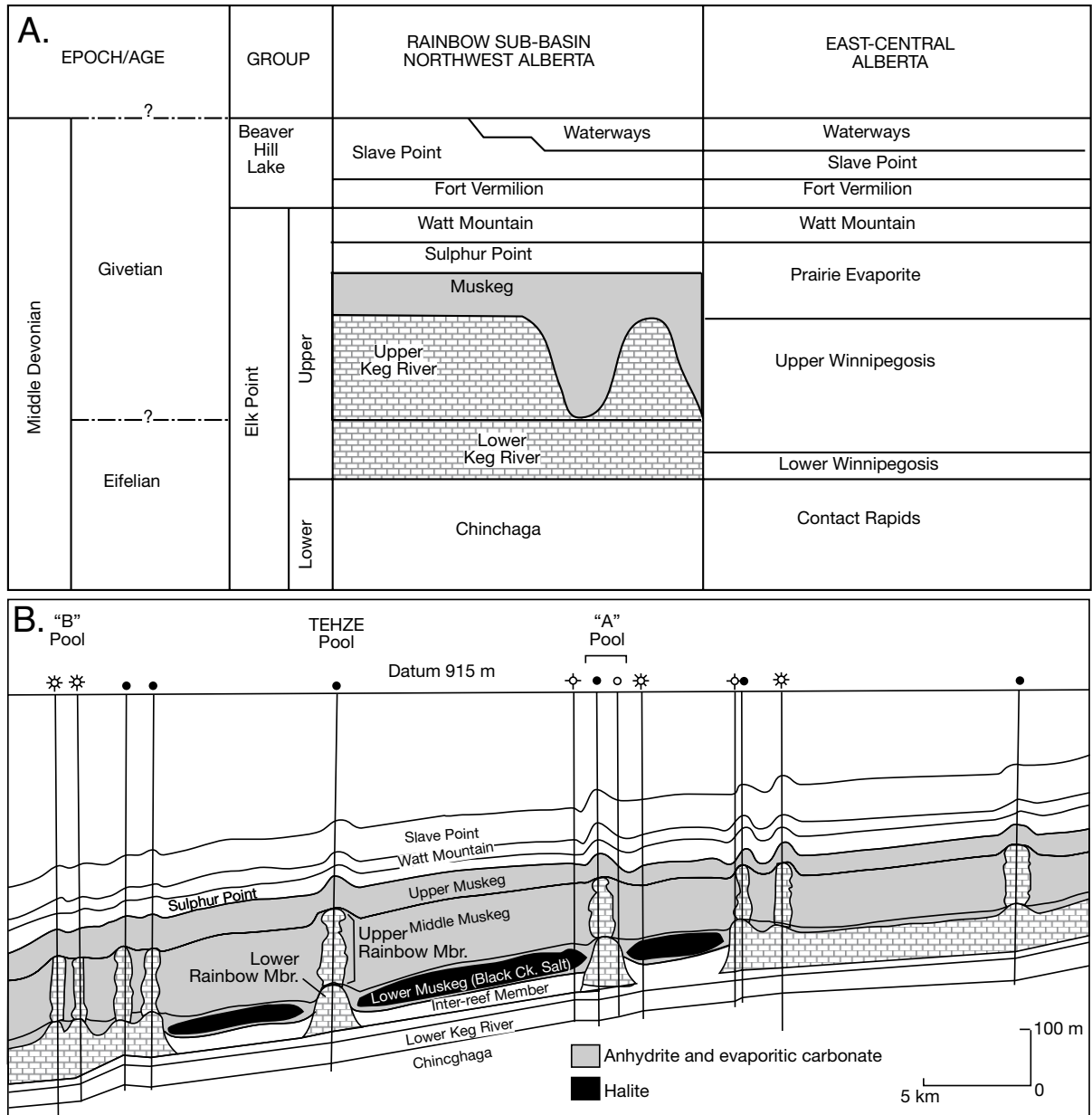


Figure 10.35. Rainbow Basin, Alberta. A) Middle Devonian stratigraphy of the Rainbow Sub-basin and East-Central Alberta (after Chow et al., 1995). B) NE-SW cross section through the mature Rainbow area showing development of carbonate platform in the Upper Keg River and the platform evaporite seal created by the basinwide anhydrite salts of the Muskeg Formation (after Schmidt et al., 1985).

some hundreds of kilometres to the north of the areas of classic production and extending into British Columbia. There the evaporite seal is missing (whether from dissolution or lack of deposition is still contested) and much of the economic porosity is in patchy zones of late stage hydrothermal dolomites, now beneath shale seals.

Today, through enhanced recovery and directional drilling, the Middle Devonian Keg River/Rainbow pools in the mature production area of the Rainbow/Zama sub-basin have produced more than 1.1 billion-barrels of oil, mostly from evaporite-sealed pinnacle reefs and platform dolomites. Historically, the most productive reservoirs have been pinnacle buildups encased by basinwide evaporites of the Muskeg/Prairie formations

(Figure 10.35b; Schmidt et al., 1985; Majid, 1987). Reservoirs in buildups in the upper member of the Keg River Formation consist of floatstone, rudstone and boundstone, with wackestone, packstone, and grainstone matrix. The principal faunal constituents are crinoids, brachiopods, stromatoporoids, corals, and *Stachyodes sp.*, all indicators of open marine sedimentation prior to the onset of evaporite precipitation. Reservoir porosity is a combination of primary intergranular and intragranular and secondary vuggy textures in partially dolomitised intervals. The primary role of the evaporite is as a seal to accumulations in the more permeable carbonates, but evaporite precipitation also drove reflux dolomitization and anhydrite plugging of the reef and platform strata during its precipitation as a saltern seal facies in the basinwide succession.

Prior to the basin's hydrographic isolation the buildups in the upper Keg River member in Alberta were patch reefs or banks, which grew in an open marine epeiric interior seaway fronted by Presqu'île barrier to the west-northwest. Water depth was the main factor controlling the distribution of the more porous intervals of the bank and patch reef facies. The back reef of the main platform became more restricted and anhydrite was precipitated at times of hydrographic isolation prior to the main basinwide event. At times of open marine connection patch reefs were developed in areas of deeper water, whereas banks were formed in shallower areas of an open lagoon. A direct relationship between the thickness of overlying platform anhydrite seal and hydrocarbon occurrences in the platform carbonates of the Keg River Formation was defined by Majid (1987). He concluded that trends beneath the platform evaporite seal can be reliably modelled using depositional fabric and seal thickness. Where the thickness of the anhydrite is more than 10 metres atop areas of patch reefs, it constitutes an adequate seal. In contrast, buildups covered by less than 10 metres of anhydrite constitute regions of higher risk.

Areas of more recent exploration focus in the Keg River and its equivalents are located mostly in British Columbia to the north of the classic areas of Rainbow reef and platform production just described. There, late stage dolomitisation exerts a more significant control over reservoir quality and porosity development does not always follow the depositional plumbing predicted by depositional facies. But effective porosity development still requires what Morrow et al. (2001) termed a "hydrostratigraphic template," first created by a combination of depositional fabric and early reflux dolomitisation. The high-salinity chloride-rich late stage brines driving this burial dolomitisation were largely sourced in regions of dissolving salts (Figure 8.4).

Such a hydrostratigraphic template defines hydrocarbon occurrences in the July Lake gas pool of the Keg River Platform and the Helmet and Peggo gas fields in the Slave Point Formation, all located along the shelf-to-basin transition of the Cordova Embayment in northeast British Columbia. There, burial-stage, coarsely crystalline replacement dolomites and associated saddle dolomite cements and zebra dolomites form a widespread diagenetic facies in the Middle Devonian Presqu'île barrier that extends southwestward from outcrop near Pine Point to the subsurface of the Foothills in northeastern British Columbia. Dissolution and subsequent precipitation of coarsely crystalline burial and saddle dolomites creates hydrocarbon reservoirs with intercrystalline porosity in otherwise tight limestone hosts. The same system hosts sub-salt breccia Mississippi Valley-type Pb-Zn deposits at nearby Pine Point. Porous burial dolomites replacing blocky sparry calcite cements, occur continuously across the sub-Watt Mountain unconformity. They postdate stylolites and earlier replacement dolomites, overlap sulphide mineralization and show regional oxygen isotope signatures that are indicative of deep hot saline basinal fluids escaping via fault and fracture feeds into the adjacent carbonate platform sediments (Figure 8.4; Qing and Mountjoy, 1994).

Recognition of late stage dolomite as a reservoir-former led to a re-examination of core from some of the producing intervals in platform-interior dolomites in the more mature Rainbow sub-basin to the south. Previously, platform carbonate production away from the main pinnacle reef plays had been related to what were considered in the 1970s to be thin pinnacle reefs, biostromes and low relief shoals, all with a depositional control to the reservoir plumbing. But the mechanism and chemistry of porosity retention was never well documented by the explorationists. Subsequent core and thin section studies in the same dolomitized platform intervals established that production was actually tied to later secondary porosity, not relict primary porosity. It was mostly associated with dolomitized subtidal facies at the bases of stacked metre-scale evaporitic depositional cycles (Muir and Dravis, 1995). For example, the Keg River and Muskeg pools on Comet Platform are combination structural-stratigraphic-diagenetic traps with reservoir quality strongly influenced by fracture intensity. Reservoir facies are confined principally to fractured platform-interior beds of restricted subtidal *Amphipora*-peloidal dolopackstones and dolowackestones. They constitute the base of anhydritic 7-12 m thick depositional cycles, which are correlatable across the Comet Platform.

Better quality reservoirs in the platform interior occur at or near the base of each major cycle and result from dissolution

of the platform carbonate, tied to the precipitation of burial dolomite cements. For example, the Keg River pool on the western edge of the Rainbow-Zama sub-basin is locally dominated by spectacular zebra dolomites with vuggy porosity tied to anhydrite dissolution, while Muskeg pool dolomites all exhibit mouldic and vuggy porosities (Muir and Dravis, 1992). Termination of stylolites and fractures into these secondary pore types confirm their burial origin.

Regional tectonic influences on oil pool development in the Comet Platform are indicated by horizontal fractures, vertically-oriented stylolites, and spectacular burial-stage evaporite solution-collapse breccias. Pools are localized over regional fault and fracture trends that affected the carbonates, but did not fracture the evaporite seal, and are related to reactivation of the Great Slave Lake shear zone. Faults and fractures aided burial diagenesis and the creation of late secondary porosity development by focusing the ascent of hot, dolomite-dissolving basement-derived and calcium-rich basal fluids. Seismic data indicate these faults were largely collapse structures generated by salt loss and subsalt breaching in the underlying Cold Lake Salt Formation. Further, some of these faults localized precipitation of massive diagenetic anhydrites (retrograde precipitates) that now provide updip side closure to some pools. This current understanding of reservoir control is a long way from the simple early notions in the 1970s of relict primary porosity in a carbonate biostrome.

Dissolution by hot, basement-derived fluids throughout most of the region is supported by the presence of diagenetic fluorites, megaquartz and polysulphide minerals, helium gas, fluid inclusions, and high carbon dioxide and hydrogen sulphide gases in these hydrocarbon pools. Thus, these platform-interior pools are combination structural-stratigraphic-diagenetic traps with reservoir quality tied to reactivated basement faults and are not directly to depositional porosity in pinnacle reef occurrences. Once reservoir quality in platform cycles was tied to salt solution

Field	Discovery (year)	Depth (m)	Temp (°C)	Oil gravity (API)	Cumulative Oil (MMBO)	Original oil column (m)
Wasson	1936	1520	41	31	1712	137
Slaughter-Levelland	1936-1945	1490	-	30	1514	-
Yate	1926	460	28	31	1172	137
Goldsmith	1936	1310	35	36	756	91
Seminole	1935	1580	42	37	525	80
S. Cowden-Foster	1932	1650	48	35	501	244
N. Cowden	1930	1340	46	35	488	244
McElroy	1926	880	30	32	466	122
Vacuum	1929	1400	38	38	432	-
Hobbs	1928	1230	-	34	297	76
Sand Hills	1944	980	30	33	248	152
Midland Farms	1944	1460	39	46	242	-
Means	1934	1340	38	29	229	70
Dune	1938	1010	31	34	183	244
Eunice-Monument	1929	1100	-	32	175	-
Maljamar	1926	1100	-	37	145	-
Jordan	1937	1130	31	35	129	91
Waddell	1927	1070	31	34	101	91

Table 10.6. Characteristics of fields in the San Andres Formation of west Texas, which are sealed by bedded salts composed of anhydrite and halite.

induced fractures, rather than to inferred low relief pinnacles, it permitted correlation of larger 7-12 metre-thick composite cycles over distances of several kilometres. This meant reservoirs could be more effectively zoned (Muir and Dravis, 1995). By 1989, daily cumulative oil production rates in platform dolomites were increased from 500 m³/day (1988) to 1400 m³/day as a direct result of this revised understanding of reservoir layering. It also led to improved conformance, sweep, and minimization of oil sandwich loss in these miscible- and gas-flooded pools and to more effective horizontal well design.

Once again, reservoir quality in the Rainbow-Zama sub-basin, and equivalents to the north, is in large part tied to the ongoing diagenetic evolution of the dolomitised host and its strong interaction with evaporite aquicludes, dissolution brines, salt solution induced fracturing and basal fluids. As Warren (2000a) observed, ancient dolomite is never a single-phase mineral. In all areas of Keg River associated production there are at least two styles of dolomite present, an earlier brine reflux dolomite, created when the overlying evaporite was porous and a supplier of dense Mg-rich brines and a later dolomite formed when the evaporite bed was a seal that focused and facilitated convective circulation in sediments beneath.

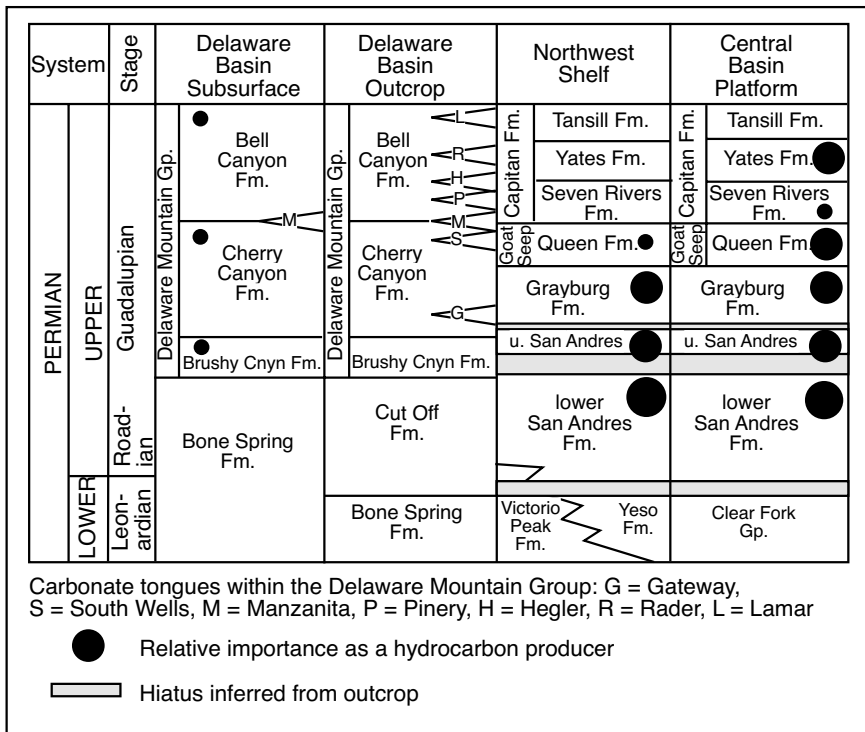


Figure 10.36. Stratigraphy of the latest Leonardian-Guadalupian units of the Permian Basin, west Texas (after Kerans et al., 1994). Almost all of the fields on the Northwest Shelf and the Central Basin Platform are sealed by bedded mudflats or saltern evaporites.

Reservoir quality tied to bedded seals

Depositional facies preserved in a sealing salt bed atop an oil or gas field can be useful indicators of palaeotopography, energy levels and volumes of syndepositional authigenic cements in the reservoir. Lowermost facies in a bedded evaporite seal can typically be related to the topography of the reservoir’s upper contact at the time the seal was precipitated. This means wireline signatures of the seal can be used to differentiate stratigraphic traps from simple drape traps. Drape traps are created by compactional or structural draping some time after the reservoir and seal were deposited. Wireline signatures through seal facies in this scenario typically show no depositionally-controlled thickness changes or internal depositional differentiation between top seal and lateral seal.

In contrast, repeated evaporitic transgressions over an underfilled carbonate or siliciclastic platform can deposit alternating cyclic carbonates/siliciclastics and evaporites in broad, shallow to ephemeral brine environments. Depositional textures in the sealing evaporites are then controlled by the permanence and depth of the saltern and evaporitic mudflat brines. Top seals to preexisting highs such as shelf margin reefs or shoals,

dune crests or slope carbonate buildups show internal fabrics related to palaeorelief. Such topography-related facies mosaics typify the wireline and core textures in the lower levels of the basinwide evaporites sealing the Silurian pinnacles of the Michigan Basin,. Nodular mosaic anhydrites of supratidal sabkhas dominate evaporitic mudflat seal facies atop the crests of underlying pinnacle reefs, while subaqueous saltern facies, made up of bedded massive/mosaic anhydrite and allochthonous dolomite-anhydrite breccias, typify the lateral seals (Figures 5.51,5.52). Similar textural transitions occur between sabkha and salina seals that make up the top seal to karstified shelf margin reservoirs of the Permian San Andres reservoir of Yates Field, west Texas, as well as other Guadalupian sequences in the Permian Basin of west Texas. Around two thirds of the

reservoirs in Permian rocks of west Texas and New Mexico are sealed by bedded platform evaporites (Figure 10. 36; Table 10.6), most show an intimate relationship between evaporite facies in the seal and reservoir quality beneath (Ward et al., 1986; Warren , 1991; Sarg, 2001).

Yates Field, west Texas

Yates Field, located in the southernmost Central Basin Platform of west Texas, is one of the most prolific reservoirs ever discovered in the United States (4 billion barrels original oil in place). It is shallow (305-460m; 1000-1500ft) and produces mostly from the Upper Permian San Andres Formation, with additional secondary production from stringers in the overlying Grayburg, Queen and Seven Rivers Formations. The field covers approximately 100 km² with more than 1600 wells in the field. The field is now largely depleted of recoverable hydrocarbons.

At the level of the Permian section it sits on the structurally highest point of the Central Basin platform. Structural closure

is dominated by a broad asymmetric domal or anticlinal feature, which appears to be formed by the intersection of two separate tectonic structures that combine to create the horseshoe-shaped high that defines the outline of the field. Yates Field was discovered in 1926, high pressures, supplied by the combined gravity segregation, bottom water and gas cap drives, resulted in unusually high initial production rates and it produced by depletion drive until 1976. As pressure depleted throughout that half century, free gas evolved and migrated rapidly through the natural fracture system to the structural top of the field to form a slowly expanding gas cap drive beneath its evaporite seal. The efficiency of the evaporite seal atop the fractured reservoir system can be seen in an official proration test on the Mid-Kansas Oil and Gas Co. and Transcontinental Oil Co. #30 I. G. Yates "A" well, which in 1929 lists a daily potential production of 204,681 barrels (Hennen and Metcalf, 1929) in a system that is less than 500 m below the land surface.

Yates Field is one of a number of fractured dolomitic reservoirs in San Andres Formation of west Texas with an evaporite top-seal centred on the Seven Rivers Formation (Guadalupian). Systems tracts in the seal facies are characterized by stacked successions of metre-scale, brining upward parasequences deposited across an epeiric platform interior. Depositional facies in the seal in all these fields can be used to infer palaeotopography in the underlying San Andres reservoir and to separate the relative importance of deposition, drape and tilt in controlling the hydrocarbon distribution in carbonates below the seal.

Evaporite deposition during Seven Rivers time in Yates Field occurred in two major settings, sabkha (subaerial mudflat) and salina (subaqueous) in an evaporitic mudflat seal, with their areal separation controlled by the positions of underlying carbonate shoals. Wireline character through areas of subaqueous anhydrite is blocky, indicating 10-30m thick sequences of relatively pure subaqueous evaporite. Wireline signatures in areas of sabkha in the seal facies are richer in dolomite matrix and individual cycles are thinner (≈ 1 m) giving a stacked spikier wireline signature to both the gamma and the neutron-density logs (Figure 10.37; Warren, 1991). Subaqueous signatures dominate in what were the topographic lows, while subaerial evaporites are more common above what were the topographically higher parts of the seaway floor. When seal facies are defined in this way, mapped and related to production statistics across the field, it shows that for cumulative production in the Yates Field unit, as of October 1986, only 85 million barrels of oil had been produced from under the thick salina accumulations, whereas almost 985 million barrels had been produced from the area under the sabkhas. Yet the two styles of anhydrite deposition cover roughly equivalent areas of seal over the field (Figure 10.38; Warren, 1991).

Assuming that the M datum in the Seven Rivers approximates a level depositional surface, then the thick anhydrite in the lower Seven Rivers indicate palaeo-lows, while thin areas define ancient highs (Figure 10.37). Massive anhydrite is found only over the central and western parts of the field. The

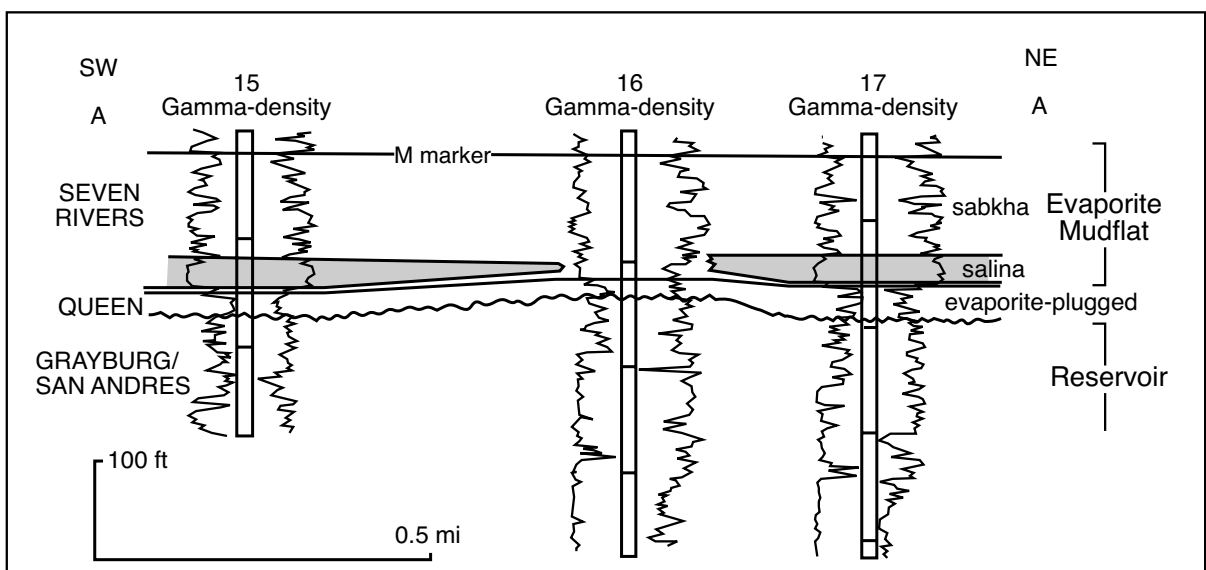


Figure 10.37. Yates Field, west Texas. Use of wireline logs to define depositional setting of the seal facies in the Seven River Fm. atop the San Andres Reservoir. Shows how the position of the salinas in the evaporitic mudflat defines the off structure positions (after Warren, 1991) Figure 10.38a shows location of this section.

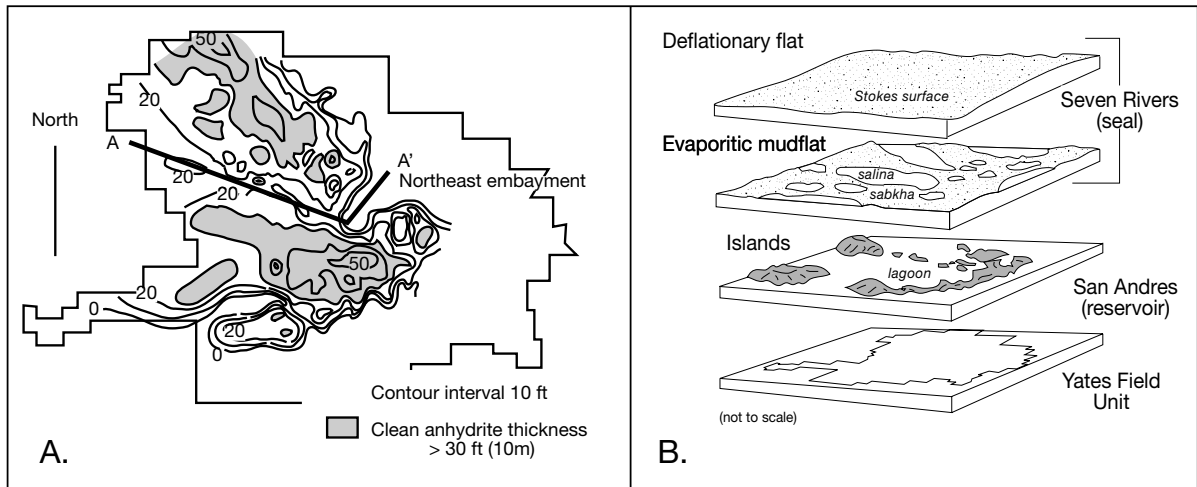


Figure 10.38. Yates Field, west Texas (after Warren 1991). A) Isopach of the massive anhydrite that typifies much of the base of the Seven Rivers seal to the field, thicknesses were mapped based on core and log signature. Clearly shows the subaqueous evaporites formed in lows that define the palaeotopography and hence quality of the underlying reservoir (see text). B) Geological evolution of Yates Field region. During San Andres time the reservoir (fusulinid grainstone) was a set of karstified carbonate islands. By Seven Rivers time the reservoir was buried but the underlying palaeotopography (and the associated differential compaction) was still sufficiently developed to control the position of the depositional lows (salinas) and highs (sabkhas).

anhydrite thins to zero roughly parallel to the platform margin, and shelfward of the San Andres shelf edge. The isopach map of the massive clean anhydrite (Figure 10.38a) shows closed contours surrounding pod-shaped areas of salina anhydrite (originally gypsum) up to 15 m (50 ft) thick. Two salina areas were generally present in Yates Field during early Seven Rivers time, one on the northern and the other on the southern side of the field. The north and south salina ponds are flanked by smaller pod-shaped thicks and are separated by a line of zero evaporite trending north-northwest through the central part of the field. This linear feature is referred to as the northwest trend. Massive anhydrite is also absent in cores and logs in the northeast corner of the field and forms what appears to be an embayment largely devoid of evaporite at the basal level of the Seven River and so defines the area of production called the “northeast embayment.”

Evaporite facies distribution in the basal part of the Seven Rivers Formation was controlled by palaeotopography, which was in turn controlled by the depositional facies relationships in the underlying San Andres Formation (Figure 10.38b). The San Andres lagoon was an area that was positionally low and one that remained low throughout Queen and Seven Rivers deposition, because of dewatering and mudstone compaction. When sufficiently karstified and fractured to hold producible fluids, the lagoon muds are still poorer quality reservoirs compared to adjacent fusulinid shoals. The lagoonal low was covered by a thick section of massive salina anhydrite that

today provides a lateral seal to the adjacent sabkha-capped reservoirs. Sabkha-crested topographic highs sit atop the more permeable reservoir intervals, which are made up of karstified and fractured San Andres mounds and shoals (Craig, 1988). The platform-edge fusulinid grainstones to packstones that are the main reservoir in Yates Field were cemented, fractured and karstified early. The lack of early burial compaction, compared to adjacent lagoonal mudstones, meant areas atop mounds and shoals remained as highs during early burial.

During lower Seven Rivers time, the then-buried San Andres depositional segregation still controlled the facies mosaic in the evaporite seal. Once this marine-fed evaporite system filled the available accommodation space, subsequent depositional style was controlled by a series of aggrading Stokes surfaces within an aggrading eolian sandflat/mudflat. At times of higher eolian sand flux the mudflat became a deflationary sand flat (Figure 10.38b). Such deflationary sandflats can constitute reservoirs in other parts of the Central Basin Platform, as in North Ward-Estes Field.

North Ward-Estes Field, Texas

North Ward-Estes Field, Ward County Texas, is the largest and most prolific of a chain of producing fields in the Guadalupian Yates Formation, which extends along the western margin of the Central Basin platform for approximately 150 km, with a width of 1.5-6.5 km (Figure 10.39a; Andreason, 1992). Cumulative

oil production within the North Ward-Estes Field from 1929 through 1989 was more than 365 million BBL, with oil-in-place estimated at more than 1 billion BBL. Siliciclastic reservoirs in the middle shelf provide most of the hydrocarbon production within the trend, whereas associated interbedded dolomites contributed patchy minor amounts of economic porosity to this play. Porosity distribution in the various Ward-Estes reservoir layers is best modelled using a depositional model based on a continent-coupled eolian to evaporitic mudflat to shelf setting, with superimposed early evaporite dissolution at the strandzone. Hydrocarbon traps form on gentle structural culminations sealed by updip evaporites. Hydrocarbon maturation and migration from the Delaware basin to the shelf reservoirs occurred during the Cretaceous and early Tertiary (Hills, 1984).

In his comprehensive analysis of the late Guadalupian (Permian) Yates Formation reservoir sands, Andreason (1992) showed that the siliciclastic facies were part of a broad, evaporative mudflat that extended across a wide area of platform behind the Capitan reef. Cyclic sea level fluctuations produced a succession of dolomites, evaporites, and siliciclastics as the evaporative coastal plain oscillated across the Yates shelf. Moving landward,

the environments were; (1) lagoon, (2) intertidal algal flat, (3) beach ridge, (4) siliciclastic sabkha, and (5) sand sheet/playa mud flat/salina/salter (Figure 10.39a). Evaporitic cycles, which formed on the inner shelf and landward, grade upward from massive subaqueous-dominant anhydrites into nodular mudflat anhydrites with increasing volumes of siliciclastic mudstone interbeds (playa mudflats). Carbonate-based depositional cycles consist of basal lagoonal peloid and skeletal dolostones, which grade upward into tidal-flat dolostones, beach-ridge sandstones, and finally into siliciclastic sabkhat.

The characteristic disrupted (haloturbated) textures of the Yates siliciclastics were created by surficial and interstratal halite growth during seasonal flooding and subsequent desiccation in a sabkha environment (Andreason, 1992). A siliciclastic accretionary complex, composed of stacked beach ridges and detrital sabkhas, formed behind a pisolitic strandzone. Local siliciclastic accumulations also occurred over sinks or depressions produced by the dissolution of underlying bedded sulphates. Such dissolution breccias are defined by stacked horizons, made up of sharp clast-to-clast angular rudstones to floatstones with sharp basal contacts with the underlying

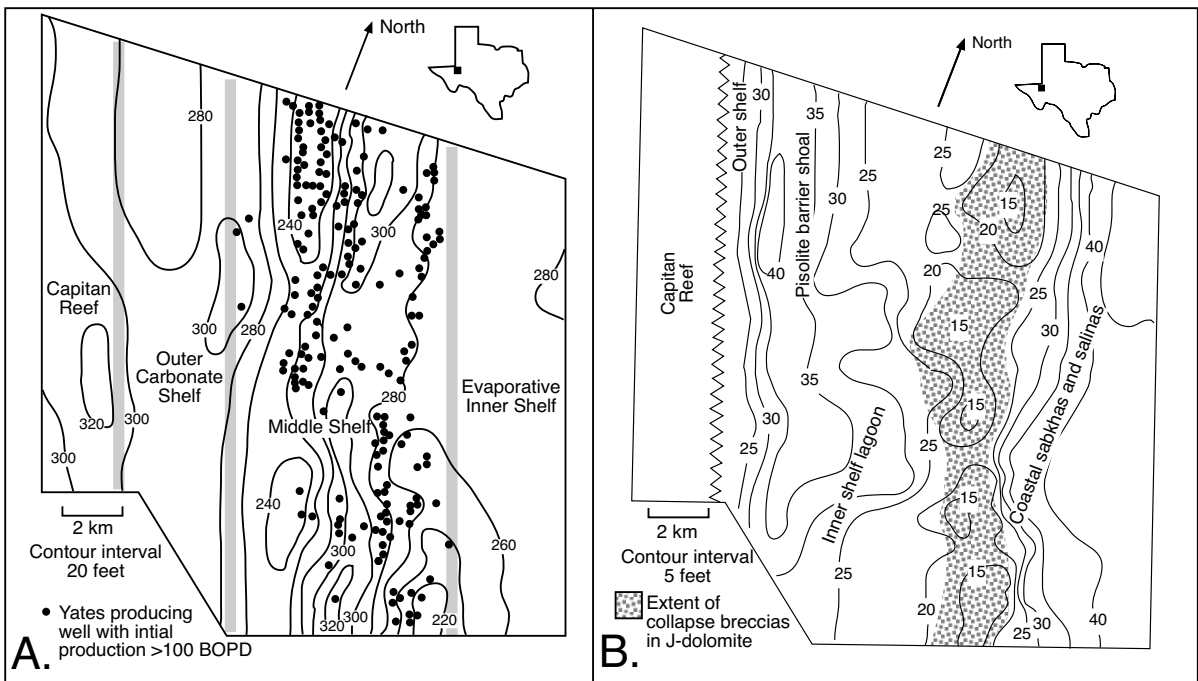


Figure 10.39. Characterisation of Yates Fm., Ward-Estes Field (after Andreason, 1992). A) Total Yates interval isopach showing Yates shelf is divisible into; 1) an outer shelf that includes the Capitan Reef, the backreef flats and the pisolite shelf crest, 2) a middle shelf composed of stacked beach ridges and siliciclastic sabkhas, and 3) evaporitic mudflats made up of extensive flats, salinas and stabilised sand sheets. Hydrocarbons are concentrated in the middle shelf. B) Isopach of the intra-Yates J-Dolomite unit. Shade unit defines the extent of the evaporite collapse breccias that separates inner shelf lagoon from evaporitic mudflat. Depression defined by collapse was filled with greater thicknesses of overlying siliciclastic sand.

crystalgalaminated dolostones and sharp to gradational crackle upper contacts with the overlying subtidal carbonates (peloidal and fossiliferous dolostones). Because of pervasive soft-sediment deformation atop the dissolving mudflat evaporites, these intervals are easily misidentified in core as storm beds or erosive marine transgressive surfaces. Breccia beds correlate

with anhydrite beds (mostly subaqueous) in the inner shelf and with dolomitic mudstones to the west (middle to outer shelf). That dissolution was early is indicated by the excellent correlations between the zone of collapse and a region of differential thickening within the overlying siliciclastics (Figure 10.39b). What is unclear is whether dissolution was driven by a relative sea level rise or fall.

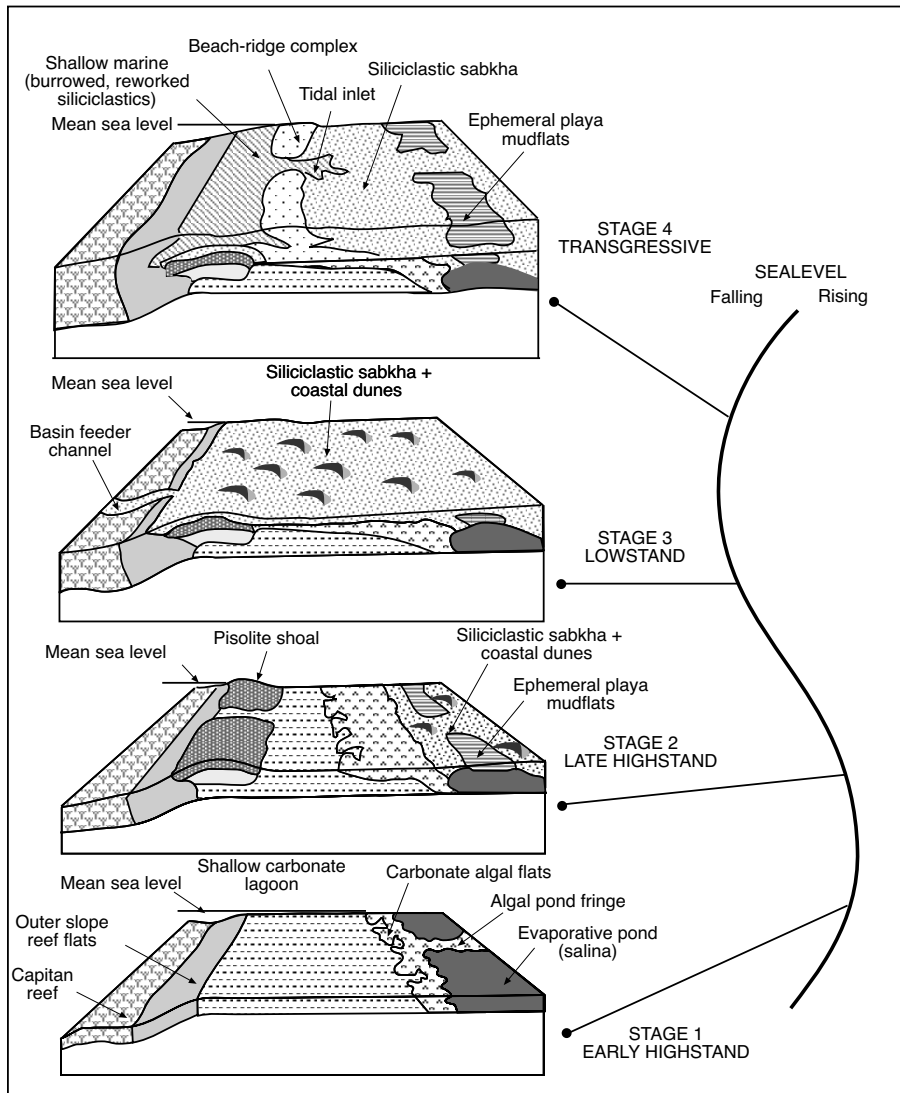


Figure 10.40. Evolution of Yates Shelf (after Andreason, 1992). Early highstand (Stage 1) is characterised by shelf submergence, lagoonal carbonate deposition across the middle shelf and massive evaporites precipitating in embayments and isolated ponds on the inner shelf. As the shelf becomes more emergent during late highstand (stage 2), broad tidal flats extend across the middle shelf and the pisolitic shelf crest becomes re-established. Eolian driven siliciclastics bypass the shelf during lowstand (Stage 3) and deposit within the Delaware Basin. As sealevel rises during the transgressive phase (Stage 4), beach-ridge complexes and siliciclastic sabkhas accrete and prograde in response to a rising water table. This is the phase when most of the siliciclastic Yates reservoirs were deposited.

As we saw in Chapter 2, preservation of evaporites into the early burial realm depends on the maintenance of a narrow range of saline conditions. Dissolution occurs if undersaturated fluids contact the bed at any time during the evaporite's deposition or shallow burial, either from an influx of fresh, meteoric water or from "freshened" seawater. Solution breccias of the lower Yates occur only in the middle shelf and develop preferentially along the seaward extent of the region of massive epeiric saltern sulphates, suggesting dissolution was driven by influxes of normal marine water during relative sealevel rises (Andreason, 1992).

The boundary between the collapse breccias and the massive sulphates marks the position of a concentration boundary on the submerged shelf where evaporative outflow exceeds marine free inflow and gypsum saturation was reached. Andreason argues this concentration boundary was shifted laterally relative to the magnitude of the sea level rise. When located seaward of this concentration boundary and given

sufficient time, evaporites originally present within the now-disturbed siliciclastic facies and the massive sulphate deposits underwent dissolution. Although the shelf position of the collapse breccias strongly suggests dissolution during a relative sea level rise, the possibly of dissolution by meteoric waters during periods of subaerial exposure and sealevel falls cannot be totally excluded.

The Yates Formation is part of the Seven Rivers, Yates, and Tansill trilogy, which in ascending order comprise the shelf-equivalent formations of the upper Guadalupian Capitan reef and represent a complex of lagoonal, coastal and evaporitic platform environments (Figures 5.21a and 10.36). The Yates Formation is unique among upper Guadalupian shelf formations in the Permian Basin in that it marks a period of major siliciclastic shelf deposition, as compared with predominantly carbonate and evaporite deposition of the Seven Rivers and Tansill formations (Figure 10.40; Andreason, 1992). The increased siliciclastic influx onto the shelf, particularly along the western margin of the Central Basin Platform and the northern margin of the Delaware Basin, probably indicates filling of the Midland Basin, which was located to the east. Eolian and wadi-driven siliciclastics, derived from the distant hinterlands to the east and northeast and previously trapped by the shallow Midland pontic sea, The erg migrated across the vast deflationary region of the filled Midland Basin and Central Basin Platform to prograde into the Delaware Basin. Siliciclastics and evaporites had reached the southern portions of the Central Basin platform from the northeast (Midland Basin) by the beginning of the late Guadalupian, as evidenced by the prevalence of these deposits within the upper Queen Formation (Tucker and Chalcraft, 1991).

It was a depositional setting much like the modern coastal zone of eastern Saudi Arabia and southeast Qatar (Figures 2.40, 3.15), but in a coastal strandzone under greenhouse, not icehouse, eustatic control. Throughout the late Guadalupian, the Midland Basin was a site of siliciclastic, anhydrite, and halite deposition within eolian, evaporative mudflat, and playa environments (Ward et al., 1986). In addition, the advancement of a siliciclastic wedge within the upper Seven Rivers Formation from the northeast onto the Central Basin Platform supports the possibility of siliciclastics migrating across the Midland Basin by the close of Seven Rivers deposition. Palaeogeographic reconstructions by Handford (1981) place prevailing winds from the northeast, off the Central Basin Platform. These eolian systems prograded across the Yates Shelf during periods of relative sea level fall and subaerial exposure of the shelf (Figure 10.40).

What is most important in terms of exploration and development models based on this setting is that the thickening and stacking of the better quality reservoir sandstones was controlled by an aggrading marine fed saline water table at the edge of an aggrading pisolitic shoal. Accommodation space for the sands was created by the syndepositional dissolution of a saltern edge along the seaward side of what is now a zone of thick stacked anhydrite beds. The generation of accommodation space for thicker better quality quartzose sands was diagenetically not depositionally controlled. The resulting thickened intervals of higher quality quartzose reservoir sands were then sealed by bedded saltern anhydrites of the Tansill Formation.

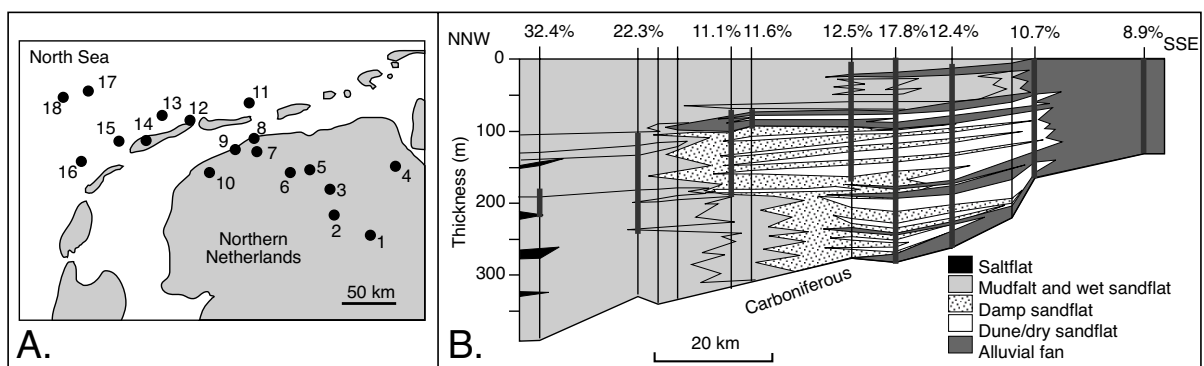


Figure 10.41. Characterisation of Rotliegende Sand reservoirs (after Amthor and Okkerman, 1998). A) Well locations in Northern Netherlands and North Sea. B) Cross section (perpendicular to depositional strike) of the Rotliegende Sand (Slochteren Sandstone) showing the major depositional environments. The average abundance of dolomite and anhydrite (total indicated in percent) increases in a NNE direction from the proximal alluvial fan and dunes/dry sand flat to the distal desert lake (saline pan and mudflat) environments.

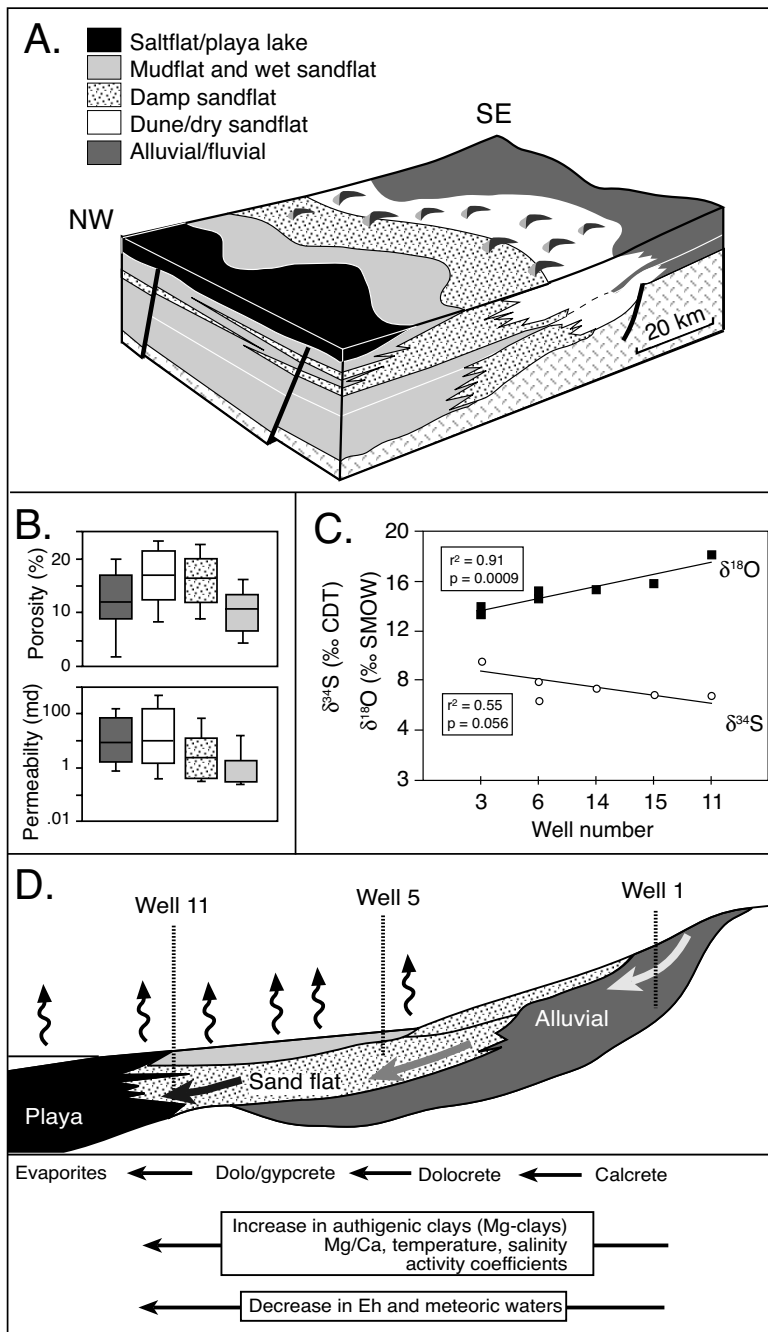


Figure 10.42. Rotliegende of Northern Netherlands (after Amthor and Okkerman, 1998). A) Depositional setting. B) Distribution of porosity and permeability, indicating a relationship between depositional environment, early diagenesis, and reservoir quality. C) $\delta^{34}\text{S}$ and $\delta^{18}\text{O}$ of anhydrite cements relative to geographic well position; oxygen isotopic compositions increase progressively from proximal to distal wells, whereas the sulphur isotopic compositions decrease. Such depletion in $\delta^{34}\text{S}$ and concomitant enrichment in $\delta^{18}\text{O}$ is the result of progressive evaporation in an arid alluvial to marginal desert-sabkha Rotliegende depositional setting. D) Conceptual model of groundwater evolution and its precipitates across an alluvial to sand flat/playa profile with the likely positions of three Rotliegende wells from Figure 10.41a indicated.

Rotliegende sands of Northern Netherlands and North Sea

Rotliegende Formation sandstones in the southern North Sea are important Lower Permian gas reservoirs, with recoverable reserves of $4.25 \times 10^{12} \text{ m}^3$ (150 tcf; Figure 10.41a; Glennie, 1990; Sweet, 1999), they also host much of the onshore gas of the Netherlands and NE Germany including the giant Groningen gas field in the Netherlands. Rotliegende reservoirs in the Netherlands are mostly sandstones and conglomerates deposited in an arid alluvial to marginal desert sand/mudflat and fluvial environments. They are intercalated with shales and evaporites deposited in saline lake/playa settings (Figure 10.41, 10.42a). The northward transport of metamorphic, volcanic, and sedimentary rocks shed from Variscan highlands supplied most of the siliciclastics. In the Netherlands, reservoir quality was significantly affected by early diagenetic processes in a marginal desert/playa lake environment (Figure 10.41b, 10.42a,b; Amthor and Okkerman, 1998).

Further offshore in the southern Zechstein Basin, burial-related products and processes are perhaps more significant and have received more attention than early diagenetic processes as controls on reservoir quality (Figures 7.72, 7.73). According to Amthor and Okkerman (op. cit.) these earlier studies of burial anhydrite cements have largely neglected the effects that early diagenesis can have on reservoir quality and well productivity of Rotliegende sandstones. They argue that much of the precipitation of the main porosity-occluding cements (dolomite, anhydrite, and quartz) occurred early, not late, in the diagenetic history of the Rotliegende reservoirs of the Northern Netherlands and was tied to variations in the syndepositional hydrology. Oxygen isotope values of dolomite cements ($\delta^{18}\text{O}_{\text{SMOW}} = 18.4$ to 23.4 ‰) suggest that meteoric water played a major role throughout the diagenetic history (Figure

10.42c), and that precipitation of the cements occurred at low temperatures (<80° C) characteristic of a desert and shallow burial. The strontium isotopes of dolomite cements ($^{87}\text{Sr}/^{86}\text{Sr} = 0.70935$ to 0.71387) and the sulphur isotopes of anhydrite cements ($\delta^{34}\text{S}_{\text{CDT}} = 6.7$ to 9.7%) are consistent with formation from continental water within a restricted basin and rule out Permian or younger seawater seeps as a source for these cements (Figure 2.23a).

The early diagenetic origin of the cements is also suggested by the fact that the majority of sandstone samples have lost more porosity via cementation than through compaction. Most samples with high amounts of porosity loss via cementation (20%) were affected by early dolomite and anhydrite cements (Figure 10.41b). The relative abundance of dolomite and anhydrite cements can be correlated with depositional environment. Wet depositional environments with water tables close to the surface (interdune and fluvial sandstones) show the highest amount of dolomite and anhydrite cements, whereas dry environments with relatively deep water tables (e.g., dune sandstones) are characterized by low amounts of cements (Figure 10.42d). The precipitation of early diagenetic cements has strongly influenced the present-day porosity patterns in the reservoir, with depositional environments interpreted as depositionally “drier” showing less cements. Early capillary and vadose precipitation of cements significantly altered the porosity patterns in the sandstones and playa mudstones. In effect, the intensity of subsequent cementation in this system largely tracks the palaeohydrology of the depositional setting. A similar set of syndepositional palaeohydrological factors controls subsequent reservoir quality in the Carboniferous eolian sabkha reservoir sands in the anhydritic Juruá Formation in the Solimões Basin (Elias et al., 2004). This is the largest gas sand reservoir in Brazil.

Personalised ramblings on the bedded-evaporite hydrocarbon association

According to Sun and Esteban (1994) the preservation of both primary and secondary porosity in evaporite-associated carbonates is due to varying combinations of the following factors. (1) A relatively arid climate, which means a relatively limited recharge of fresh groundwater, thus minimizing meteoric leaching and calcite cementation. (2) The presence of an extensive cap of impermeable mudflat dolomite and anhydrite. It effectively seals off the underlying permeable carbonate from ongoing early phreatic cementation as it slows or stops surface-groundwater driven flushing by large volumes of meteoric or sulphate-bearing fluids. (3) Early marine cementation and

hypersaline reflux dolomitization, which strengthens the rock framework, thus retarding physical compaction and making it more likely to fracture. (4) The presence of thick evaporites atop carbonates, which tend to form pressurised buffer zones below the salt seal. A thick evaporite retards mechanical compaction in sediments beneath it via the early onset of overpressure, it also prevents an influx of surface-derived cementing waters into the carbonate reservoir.

This listing, and others in the literature like it, do outline some of the reasons for the evaporite-hydrocarbon association, but do not offer predictive tools for explorationists or development geologists. As such they are largely ignored in designing exploration or development programs in evaporite-sealed systems. To create a predictive understanding of reservoir quality beneath evaporite seals is a more difficult task as it requires knowledge of evaporite texture and the ability to construct models of seal-related diagenesis in the carbonates below the seal.

The importance of recognising depositional differences

Our discussion so far has demonstrated that bedded evaporites constitute seals to all of the world’s largest oil and gas accumulations. Without exception, the largest of the various oil and gas fields sealed by bedded evaporites are hosted in partially dolomitized marine platform carbonates. In most giant and supergiant fields the evaporites not only hold back the hydrocarbon column, but also helped create and maintain reservoir quality. The most impressive examples are the various Arab D reservoirs in the Middle East, with slightly smaller but still very significant accumulations in oil pools in San Andres Formation of west Texas. In all these examples the depositional porosity of the reservoir has been altered and sometimes enhanced by brine-related allochem leaching and early reflux-driven dolomitisation. The degree of meteoric overprint at this early burial stage of diagenesis is minor to nonexistent. Syndepositional edge-of-evaporite dissolution from seawater freshening can occur and it led to substantial thickening of high quality groundwater-controlled eolian depopods in the billion barrel North Ward-Estes Field. Deeply circulating regional meteoric influx, mixing with brines of the reflux plume, can also occur in reservoirs below evaporite seals and influence reservoir quality, as in the Smackover Formation reservoirs of the Gulf of Mexico.

In my experience, most variation in subevaporite reservoir quality is the end product of a combination of depositional facies and varying intensities of evaporite plugging, dissolution,

reflux dolomitisation and burial stage cementation. Lateral and vertical variations in all but the latter are indicated by facies variations in the seal itself. Yet, for much of the oil industry, evaporite plugging and reflux dolomitization are associations that geological and geophysical staff do not quantitatively integrate into a reservoir model (other than via loosely controlled geostatistical formulations). The relevance of evaporite at any scale beyond the consideration of its seal integrity is not part of most reservoir studies (The typical question to be asked and answered of the evaporite in a petroleum system is; Is it thick enough? The magic numbers worldwide for answering yes are; greater than 10 metres thick for a clean anhydrite seal, and greater than 5-10 metres thick for halite!). Once the integrity of an evaporite seal or cap to a potential reservoir is established, further study of the seal properties or textures is not considered relevant, other than hoping for, or establishing, its lateral persistence. Rather, subsequent study and measurement focuses on the properties of the reservoir itself.

Attempting to better understand diagenetic intensity in the reservoir using signatures from wireline tools is typically considered too difficult, or the possibility is not even understood. Yet, as any carbonate geologist will testify, diagenesis is what distinguishes properties in a carbonate reservoir from those in a sandstone. Pervasive, but variable, diagenetic intensity is what controls carbonate reservoir quality in every evaporite-sealed petroleum system worldwide. Almost all of the matrix quality in the world's giant and supergiant evaporite-sealed carbonate fields was established during deposition and early burial. This is when surface topography controls intensity of circulation in the diagenetic hydrology (Chapter 2). It can be locally enhanced by later fracture development and perhaps the formation of coarsely crystalline saddle dolomites (typically fed by fractures and faults).

In petroleum systems exemplified by the examples of Yates and North Ward-Estes fields, reservoir quality is predictably tied to the style and position of the early evaporite hydrology and is indicated by evaporite textures in the seal. The same approach is also useful in other reflux-dominated carbonate reservoirs, as in the Arab and Khuff formations in the Middle East.

Much more reliable prediction and modelling (both seismic and reservoir scale) is done by the oil industry in sandstone-shale associations than in carbonate-evaporite systems. Our understanding of reservoir problems in a carbonate reservoir is more often post-mortem than predictive. More reliable maps of anhydrite plugging at the reservoir level and flow unit correlations for waterfloods in carbonates are sorely needed. In

evaporite-sealed systems it requires the integration of field-scale maps of seal facies with maps of reservoir properties in intervals below the seal. This is not currently done by most oil companies. Worldwide the focus of the map is in the reservoir itself and it is almost never related to seal facies.

The first step is the construction of a map of the facies mosaic preserved in the seal, using wireline-based core-calibrated image and conventional logs. At the local scale such a map uses separation of sabkha from salina signatures, at the broader scale it uses wireline based separations of evaporitic mudflat from saltern. Next a field-wide map of reservoir quality is constructed or existing maps of quality can be checked by recalibration to existing core and wireline/image data (in a producing field this data is available at varying degrees of reliability). The field-wide facies mosaic map derived from the seal is then overlain on the fieldwide map of reservoir quality and production data. A match or mismatch of the two outputs tests whether the early burial hydrology and associated palaeotopography has controlled much of the reservoir leaching/dolomitisation and anhydrite plugging.

These maps can then be used to better define untested reservoir zones. In a depositional seal, rather than a drape seal, the better quality reservoir sweetspots are typically beneath mudflat seals. If the evaporite seals across platform cycles are sufficiently thick and possess sufficient impedance contrast, then seismic facies can be constructed over the area of interest and be used to better identify potential sweetspots and other directional drilling targets in the field. This approach of integrating evaporite signatures into maps of reservoir properties is especially useful in carbonates beneath epeiric platform anhydrite beds in systems that have not been substantially overprinted by later stage burial alteration.

But porosity/permeability in an evaporite-sealed system continues to evolve to varying degrees, long after the reservoir has subsided into the mesogenetic realm and early evaporite plugging (via brine reflux) of the subsalt interval has ceased. In some fields the burial overprints are significant and can control reservoir quality, in others they do not. Porosity evolution in the mesogenetic realm is typically driven by focused vertical and lateral flow of ascending basinal brines. Close to their feeders, these waters pervade permeable intervals below the evaporite seal and so overprint the platform carbonate/dolomite to varying degrees, especially atop zones where active faults and fractures cut the reservoir but do not penetrate the evaporite seal. In more diagenetically mature fields, such as the Keg River pools in the western Rainbow-Zama sub-basin, much of the lateral variation

in reservoir quality is tied to burial stage leaching of anhydrite cements, the precipitation of saddle and zebra dolomite, and the formation of coarse, patchy but connected, intercrystalline burial-stage porosity. Now the reservoir altering fluids are fed by ascending brines rising along faults and fractures, these structures are sometimes visible in seismic and this association can be used as an exploration tool. Zones of most intense alteration tend to occur in haloes around the fault or in zones immediately below the evaporite seal and sometimes the drilling target is a narrow zone at the base of a synclinal trough (as in Scipio Albion trend, Michigan Basin). Convincing management to drill a syncline is not an easy task!

In more diagenetically mature portions of a basin, these fault-focused ascending basinal waters can carry high levels of metals and can form MVT deposits via thermochemical sulphate reduction (as in the growth fault-fed accumulations of lead and zinc in the Devonian Platform of the northern edge of the Canning Basin, Australia). In such stratiform MVT deposits the evaporites are typically long gone and all that indicates their former presence are laminar beds of metal sulphides with their coarsely crystalline dolomite gangue.

Even in less diagenetically mature supergiant oil and gas fields, where relict depositional porosity is the dominant control over reservoir quality and reservoir topography can be defined in the wireline signature of the seal, the early stages of overprint from ascending basin fluids will have locally altered reservoir quality, especially in the vicinity of active faults and fractures (as in the Arab D reservoir in the 150 billion barrel-plus Ghawar Field of Saudi Arabia).

The importance of recognising dissolution

Listings of controls of permeability in evaporite-sealed systems, such as that by Sun and Esteban (op. cit.), also underline another problem with many current field-scale geological studies of reservoir quality controls in evaporitic successions. Such studies, even where core is available, have typically not considered the likely presence in many evaporitic platform reservoirs of thin horizons that once were much thicker sequences of bedded evaporite. Yet bedded evaporites are highly soluble both at the surface and in the subsurface (Chapters 1 and 7), their residues are widespread and they can create regional markers easily misidentified in wireline as a correlatable well-to-well flooding surface.

Carbonate reservoirs worldwide are made up of stacks of platform cycles or parasequences, some with and some without

evaporitic capstones. When they were deposited, evaporite capstones in both ramp and platform settings typically mark the tops of zones of shoaling and perhaps cleaning-upward carbonate parasequences. Associated reflux brines were often responsible for formation of stratiform reflux dolomites in the carbonates below, along with variable levels of intergranular anhydrite cement that plug the upper portions of the carbonate cycle. Sometimes the evaporite capstones are absent because they were never deposited, other times the evaporitic capstones to these parasequences have been leached, along with the evaporite plugging cements in the underlying reservoir intervals.

Post-dissolution, all that may be left of a former bedded saltern evaporite is 5-50cm thick stratiform layer of fines, made up of insoluble residues that once were dispersed in the evaporite bed (eolian silts, clays and dolomite rhombs). The overlying succession often shows a characteristic vertical transition of mosaic to crackle breccia or into a zone of syndepositional solution collapse. Leaching of former anhydrite cements from intergranular positions in the carbonates below the residuum layer can create a high permeability interval below the residuum layer. Sometimes beds on either side of the dissolution residue layer may retain nodules of chert, baryte with minor relict anhydrite. The nodules, when present tend to be dispersed as a band on either side of the residuum layer. Using cores and FMI imagery, the associated breccias, sharp bases, crackled and fractured tops, along with slumps into karstic accommodation space created by salt dissolution can be used to define the former positions of these now dissolved parasequence tops.

Unfortunately, many practising geologists in the oil industry are well versed in sequence stratigraphic principles, but not accustomed to thinking and interpreting stratiform surfaces from well to well other than as a depositional interface or perhaps as a marine or subaerial exposure surface. When they see residual horizons in core and an associated clast-to clast breccia they tend to interpret it as either a storm bed or as zones of seafloor disturbance and starved sedimentation "formed at a time immediately prior to the creation of a maximum flooding surface." These layers of dissolution residuals are often clay rich and radiogenic and so show up as spikes on the gamma log through the carbonate platform. If the now dissolved bed was previously associated with an underlying zone of anhydrite cement, then dissolution of this anhydrite can create a zone of high permeability in the interval below the gamma kick.

Without core or image log control, intervals with such high gamma signatures can be easily misidentified as thin shales or mudstones that define flooding surfaces along the muddy base

of the next parasequence cycle. Widespread gamma kicks in a carbonate reservoir can then be miscorrelated well-to-well as depositional surfaces beneath low permeability muddy carbonates at the base of the next shoaling cycle. They are then tied from well to well and used to define regional flooding surfaces. These are in turn used as intrareservoir well-to-well markers to zone up the reservoir into flow units across a field. This misidentification is especially common in correlation studies done in thick carbonate sequences, largely lacking any other markers, and where the team conducting a reservoir zoning study uses a sequence stratigraphic framework for correlation and quality prediction between wells. As discussed in Chapter 5 most sequence stratigraphic and seismic studies currently conducted in carbonate terrains do not deal well with the “comings and goings” of evaporite beds.

Such inappropriate interpretations are not too much of a problem when the reservoir is in the early stages of primary production, or if the field is a single-phase gas field. But they become problematic when the same layer-cake reservoir model is utilised in developing notions of linked flow units via what are considered viable well to well correlations. In the more mature stages of planning of field development it is very important to reconsider any laterally continuous zone in the field, especially if defined by a gamma kick atop or within what is often a dolomitized or high porosity level. It should be redefined for what it is based on its signature in core or a core calibrated image log and not assumed that it is always indicative of some sort of well-to-well marine flooding surface.

Gamma kicks in wirelines taken through anhydritic evaporite platform carbonates do not necessarily indicate depositional shale/micrite. Rather, if it is indicating a solution residuum layer, then depending on how and when it formed and how the overlying section was let down, some of these stratiform residuum horizons may indicate a set of formative processes that have created widespread crosscutting extensional fractures and microfractures in the overburden. In other words, did undersaturated water access the dissolving evaporite from the side, top or base of the former evaporite bed? - as discussed in Chapter 7. Thus gamma kicks associated with an evaporite residuum can be associated with laterally extensive zones of higher fracture permeability above or below the marker. If the creation of the residuum layer was tied to the dissolution of former anhydrite cements in the underlying carbonates then high permeability occurs below the marker. If the formation of the residuum was created by lateral solution loss, then solution induced fracturing can occur across a retreating front in the layer above. In either case there is the distinct possibility

that adjacent high flow units are joined by dissolution induced vertical fractures.

Such a misidentified system becomes more problematic once production induces an oil-water interface rise. Water then penetrates unexpectedly into what were projected to be longterm productive intervals based on depositional assumptions of well-to-well marker or flooding surface correlations. Unrecognised high-permeability vertically-linked zones will drastically reduce sweep efficiencies when production planning of a waterflood continues to evolve based on inappropriate correlations of intra-reservoir permeability. There will be early and unexpected water breakthroughs during the waterflood. Depositional marker-based models do not account for likely vertical fluid transfer via cross fractures that developed at the time of evaporite dissolution. Nor does a sequence-stratigraphic-focused team tend to consider the possibility that likely zones of highly interconnected permeability can be formed by the leaching of former anhydrite or even halite cements in the grainy interval below the now dissolved evaporite unit (e.g. some very high permeability intervals that cut across depositional facies in the carbonate host).

But the reality is that most reservoir models for waterfloods and longterm production must be constructed over large areas of a producing field where closely spaced core to wireline calibrations are not available. The two endmember modes of marker occurrence (dissolution residue versus marine shale) can sometimes be separated using a high resolution conventional wireline tool, such as the MFSL, or better yet an image log. Many residue horizons are systematically associated with a halo of anhydrite or chert nodules on either side of the gamma kick, flooding surfaces typically are not and marine chert nodules, if present, tend to occur within the marker and not above. Clearly, any wireline-based definition of a dissolution surface can be complicated by the development of patchy high density, high resistivity carbonate cements. In this situation wireline separation of the two styles of picks is best done by an interpreter with an understanding of the significance of evaporite cements in the reservoir and who is using a core-calibrated set of wireline and image log signatures, rather than just conventional log shape.

Changing directions of brine flux in an evaporite-sealed system

At the regional scale, brine reflux flushing is most active in the early stages of evaporite deposition, when the evaporite beds retain porosity and permeability and concentrated Mg-rich

brines sink from the overlying free brine pool, through the still permeable bedded evaporite (usually gypsum), and into the underlying sedimentary succession. Elliott and Warren (1989), Saller and Henderson (1998) and Lucia (1999) all point out that the downward cyclic transition from a relatively impervious overdolomitised and salt-plugged platform dolomite (typically with thick intercalated saltern and mudflat seals) into partially dolomitized subtidal platform carbonate reservoirs (with thinner seals) corresponds to a downward decrease in the flux of saturated reflux brines and an increase in dolomite crystal size. This corresponds to a downward decrease in dolomite saturation as the refluxing brines sink deeper and further from the brine source. Thus, the better reflux-enhanced platform reservoirs occur in structures not directly beneath the thicker accumulations of saltern salts, where salt plugging, overdolomitisation and mimetic dolomite dominate. Better potential reservoirs tend to occur more toward the seaward margin of the thickest saltern accumulation where coarser dolomite, partial dolomitization and thinner evaporites are found.

Long term salt plugging, tied to large volumes of saturated brine reflux, means that most hydrocarbon accumulations sealed by basinwide evaporites are typically smaller and less productive fields compared to their platform counterparts (e.g. the relatively small volumes of hydrocarbons in salt-encased Silurian pinnacles of the Michigan Basin and the pinnacles of platform edge of the Rainbow-Zama sub-basin). A lack of widespread potential reservoir in the muddy deepwater setting that immediately predates most basinwide evaporite beds adds to the likelihood of smaller accumulations beneath basinwide salt seals, compared to platform settings. Even so, thick massive basinwide evaporites trap and preserve some of the oldest oil and gas fields in the world (e.g. fields producing from platform carbonate slivers suspended in the Neoproterozoic Ara Salt of Oman).

Most reservoirs associated with bedded basinwide evaporites are in pinnacle reefs where karstification or later subsalt burial corrosion has reinvigorated the reservoir quality. Sun (1995) found porosity distribution in dolomite reservoirs associated with basinwide evaporites typically show no direct relationship to stratigraphic position or depositional trend. His conclusions emphasise the problems of reliable porosity prediction in a syndepositional hydrological system characterized by large autocyclic fluctuations in hydrologic base level (≈ 1 km) over time frames of thousands of years (Chapter 5). It also indicates a lack of differentiation of strandzone versus basin-centre reflux dolomites by most workers, yet both dolomite styles typify basinwide evaporite settings (Warren, 2000b). Unlike

the dolomites associated with platform evaporites, this group of reservoirs cuts across both icehouse and greenhouse periods as basinwide evaporites require tectonics that are independent of sealevel character (Chapter 5).

An evaporite bed can only act as a seal once it has lost its intrinsic permeability. For a gypsum bed converting to anhydrite this happens somewhere in the first 500-1000 m of burial, while for halite it can happen as shallow as a hundred metres below the landsurface. Until then, the permeable evaporite bed facilitates brine reflux, but once tight it only supplies brines to its surrounds via dissolution of its edges and focuses fluid flow along its underside. This transition in rock properties has an interesting effect on diagenesis and explains much of the later stage dolomitisation overprint on early reflux dolomites that are seen in many evaporite-sealed reservoirs (e.g. Canadian pinnacle reef traps and the dolomites of the Arab cycles in Saudi Arabia). As the evaporites were accumulating they flushed the underlying carbonates with dense sinking Mg-rich brines. Once buried and tight, the evaporite seal then prevents the free vertical escape of hot rising brines, which pond in carbonates immediately below the slowly dissolving underside of the evaporite seal. The resulting chemical interface drives salting out of hydrocarbons, creates of burial porosity, and drives the precipitation of authigenic or burial cements, including coarse sparry dolomite. It means most dolomitic reservoirs below an evaporite seal retain evidence of diagenesis first driven by descending reflux brines, which were created as the evaporite seal precipitated. Then later the same subsalt carbonate gathers a new diagenetic signature (of varying intensity) via the seal-focused flushing of hot ascending basinal brines moving along active subseal fractures.

Halokinetic salt traps

In many parts of the world, such as offshore Brazil, offshore west Africa, the North Sea and the Gulf of Mexico, a significant part of the association of evaporites with hydrocarbons can be tied to salt's ability to flow, and by its flow generate large and numerous structural and stratigraphic traps. The emplacement of broad sheets of salt against more porous sediment greatly improves the efficiency of hydrocarbon drainage, both in terms of area drained and in tightness of the reservoir seal (Demaison and Huizinga, 1991; Hindle, 1997).

We saw in Chapter 6 how advances in 3D depth migration and computing power, still occurring today, have revolutionized subsalt and suprasalt hydrocarbon exploration. Only a decade

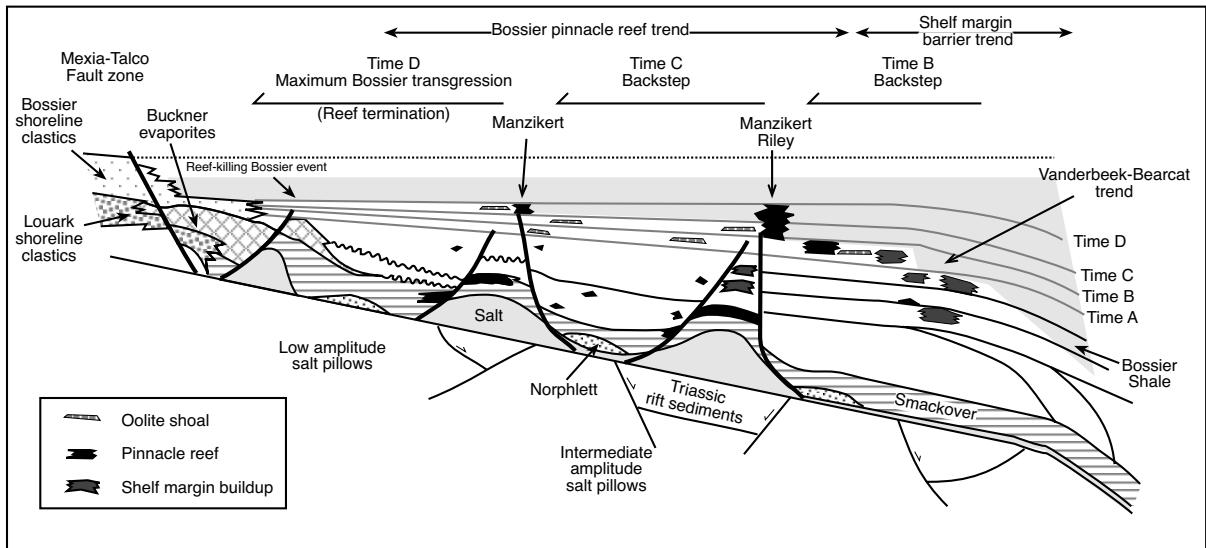


Figure 10.43. Regional model of the development of outboard shelf/ramp margin buildups (structural control to shelf margin) and the “inboard” pinnacle reefs growing in seafloor shoals created by salt pillows in the Marquez Platform, East Texas Basin in Upper Cotton Valley to Lower Bossier time (after Montgomery et al., 1999a).

or so ago, most seismic reflection information in halokinetic provinces was acquired as 2D data; today, most seismic data is acquired as 3D data volumes. The 3D cube provides a dense grid of subsurface information, which can be used to more accurately map salt body contacts and shapes. Older vintage seismic used mathematical models for conventional migration and processing that assumed that the acoustic properties of subsurface sediments did not make abrupt lateral variations. This assumption obviously breaks down near salt structures; a solution required cheap computing power, more sophisticated depth migration techniques and denser data grids. Positioning of contacts in older vintage data can sometimes be improved using more recent processing algorithms and greater computing power, offering a cheaper but less accurate alternative to reshooting a grid.

The notion that salt flow was a horizontal as well as a vertical process was increasingly accepted by the late 1980s. It opened up a whole new set of subsalt or more correctly suballochthon plays in the deep waters of the slope and rise in the circum Atlantic salt basins and similar terranes elsewhere in the world. At the same time drilling technology was improving rapidly, along with geosteering capabilities and broader MWD logging tool suites. Each year wells were being spudded in progressively deeper water. For example, ultradeepwater exploration in Gulf of Mexico, in the decade through to the early millennium, has found more than 3-4 billion BOE in nine major discoveries, in a hydrocarbon exploration province previously considered mature (Enger and Logan., 2001).

But before we discuss the sub-allochthon traps we will look at the suprasalt trap, which was the classic exploration association in halokinetic regions prior to the 1980s. Historic limitations in seismic resolution meant that examples of suprasalt-related oil and gas traps were done in the context of subvertical thumb-like appendages of salt fed by a direct connection to a mother salt bed below. Interpretations of the many producing structures in the onshore and shelf waters were biased toward this older notion of strongly vertical salt flows with salt pillows as the precursor to subvertical diapir stems. We now know that many nonpiercing pillow structures can be compressional features created during inversion or foot of slope gravity gliding (Figure 6.34). Other pillows do form in response to depositional loading as a flow stage preceding the diapiric stage (Figure 6.15). This is the classic model of Trusheim (1960) and based on his extensive work in the Zechstein salt structures of northern Germany. More recent work, even in this classic area, shows thumb-like geometries and associated assumptions of a connection to a more deeply buried mother salt bed are not necessarily correct (Mohr et al., 2004). Isolated rising blebs cut off from the source layer are more likely in the mature portions of many salt basins undergoing compression and inversion. This notion perhaps offers some possibilities for future sub-salt flange sealing plays even in very mature regions of onshore and shelf exploration in the Gulf of Mexico and onshore Europe. But, such traps are likely to be small and discontinuous. Currently the possibility of drilling giant structures in the deep waters of the Gulf of Mexico and other circum Atlantic salt basins are more appealing to the exploration economics of large and mid-sized oil companies.

Supradiapiric traps

Oil and gas reservoirs atop salt structures are as varied as the shapes and timings of the salt structures that caused them. Salt buoyancy means areas above shallow actively flowing salt structures are topographic highs, while the areas between are topographic lows (Table 6.3; Figure 6.51). Fluvio-deltaic, coastal, and submarine slope deposits are usually sand poor over the salt crest (Figure 6.50). Most of the coarser-grained sediments in either setting is deposited in troughs as various types of channel fill and beach deposit, especially in landscape depressions atop zones of active salt withdrawal. In continental settings the pinchout of the high-porosity sand occurs along the flanks of a salt structure, usually well down-dip from the crest. Occasionally, reservoirs can form in the muddy crestal sediments in a continental setting due to diagenesis associated with subaerial exposure and/or unconformities. In arid coastal areas the crest could have been covered by evaporitic mudflats as environments tied to the development of early dolomite in pelleted mudstones with the associated formation of good intercrystalline porosity (Figure 6.56).

In nonpiercement structures in shelf settings the high-porosity sediments tend to form atop or immediately adjacent to a suprasalt crestal shoal (Figures 6.57). Boundstones, skeletal and oolitic grainstones, and well-winnowed siliciclastics are found on such highs. For example, studies by Mancini and Benson (1980) and Ahr and Palko (1981) of the Jurassic Smackover Formation reservoirs in southwest Alabama and Louisiana show that reservoirs often occur in oolitic-pisolitic grainstones located over salt pillow crests, while Montgomery et al. (1999a, b) describe hydrocarbon accumulations in numerous inboard Jurassic (Cotton Valley - Bossier) reefs atop salt pillows and diapirs in the East Texas Basin (Figure 10.43). Similar Jurassic stromatolite and coral stromatoporoid reefs are found in the Smackover atop other salt pillows, such as the Walker Creek Field, Arkansas, in the Hico Knowles Field, Louisiana (Baria et al., 1982), and Hatters Pond in southwest Alabama. There the Smackover buildups are typically 3 - 40 m (10 - 130 ft) thick, commonly elongate, and several square kilometres in plan.

Reef rubble zones throughout the Smackover trend tend to have reservoir-quality porosity, but reef boundstones are economic only when extensively leached, dolomitized, and fractured. Such alteration can create commercial production from reef crests with mean porosities of 15% and permeabilities of 20 md. Hatters Pond Field is typical of a field where the reef crest is tight and depositional facies crosscut the reservoir trend. The distribution of the reef was controlled by the position of the Jurassic high above a growing autochthonous salt pillow, while the trap was created during Cretaceous faulting associated with the structure's diapiric stage (Worrall and Warren, 1986). The level of the reservoir dolomite lies well below the reef crest and above a dolomite unit characterised by post-hydrocarbon saddle dolomite. As in bedded evaporites, the initial porosity controls in carbonate reservoirs atop salt pillows and diapirs are often depositional, but are usually complicated by closures and alteration haloes related to fault welds and subsequent fluid flow.

Siliciclastic examples of closure forming high capacity suprasalt reservoirs by sand-shale juxtaposition across clay-smeared extensional faults can be seen atop salt structure crests in the West Bay Field in Louisiana and the Heidelberg Field in Mississippi (Halbouty, 1979). Bay Marchand - Caillou Island Field is a classic example of this style of fault-controlled suprasalt sand reservoir above the crest of salt structure (Figures 8.23a, 10.44). The three diapirs that constitute the field are passive diapirs atop a salt wall feed. Under the new paradigms of flow that have been developed since this structure was documented by Frey and Grimes (1970), it can now be seen to be the remnant of what was an active salt feeder systems with the current fault weld once acting as a salt wall

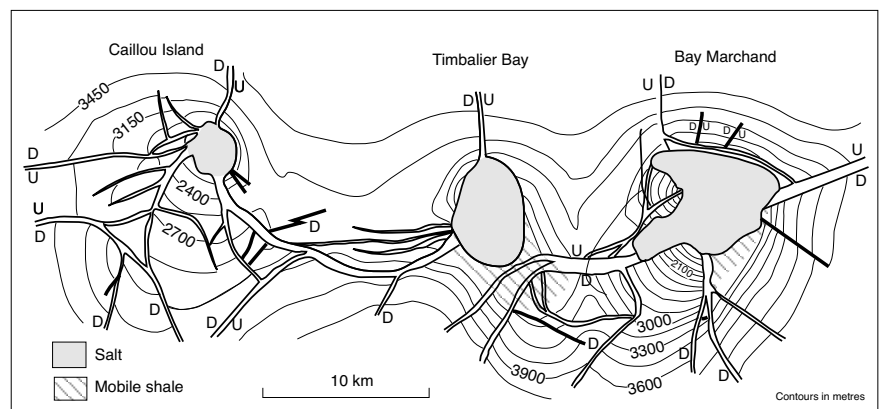


Figure 10.44. Structure contours (in metres) on the productive Upper Miocene sand in the vicinity of the Bay Marchand - Timbalier Bay - Caillou Island diapirs, coastal Louisiana. Diapirs merge at depth into a salt wall and occur along a main extensional fault linking all three domes, each with its own association of radial faults (after Frey and Grimes, 1970).

feeding diapiric allochthons higher in the section. Most of the extension driving the faulting was a response to gravity gliding and salt deflation and not the active intrusion visualised in the original interpretation. The faults show radial, peripheral, or tangential patterns relative to the salt stock. Elsewhere in the Gulf of Mexico similar faults have downfaulted, uplifted, or overthrust sands against impervious shales and multiple stacked reservoirs are stacked up against the fault (e.g. Bryan Salt Mound, Brazoria County, Texas).

Many of the numerous radial faults drawn in older interpretations of suprasalt traps (pre-1990), were published prior to the industry's recognition of salt's intrinsic lack of strength under tension. These interpretations tended to visualise faulting (mostly inferred rather than intersected) as a response to buoyancy and active salt intrusion. This is understandable as in most cases much of the salt that fed into an allochthon has long since dissolved or moved on to higher levels in the stratigraphy, via what are now deflated salt welds. In more recent interpretations of the same structures the faults are seen to be a response to salt withdrawal and to downbuilding in the adjacent sediments. High resolution seismic has shown that many of the inferred radial faults of older interpretations do not exist. Such faults were inferred in order to explain discontinuities between sands in adjacent areas. In reality, many of these discontinuities, are more often a response to unconformities and depositional pinchouts rather than fault-outs, especially in flank traps.

For example, a reinterpretation of the Cote Blanche Field in Louisiana in the mid 1990s, based on newly acquired 3D seismic reduced the number of radial faults in the crest of the field to nine, compared to more than thirty in mid 1970s vintage 2D interpretations. But radial faults do exist about salt structures and are largely a response to salt deflation during the passive stage of diapirism or are a response to later basin inversion and diapir squeezing. In halokinetic extensional terranes that have been subject to later compression, such as parts of the North Sea, offshore UK and Norway, many of the earlier radial faults are reactivated and have evolved into inversion structures (Figure 6.42).

Syndepositional suprasalt traps occur in the sand-rich edges to withdrawal synclines, along with associated pinchouts onto the diapir crest (Figure 10.45a). An example of this type of reservoir is the West Saratoga Field, Hardin County, Texas. There, multiple Yegua sand reservoirs shale out as they pass into the Saratoga Salt Dome (Galloway et al., 1983). The secondary peripheral sink continued to subside as the diapir grew (downbuilding), resulting in steep dips in the sand units as they shale out into the diapir stem (Figure 10.45a) Subsequent loss of salt supply and cap rock formation may cause loss of salt volume and local collapse around the salt stem (Figure 10.45b). Steeply dipping suprasalt reservoirs are characterized by stacked thick oil columns, which may approach 300 m (1,000 ft) where they pile one atop the other alongside the salt or a clay-smear

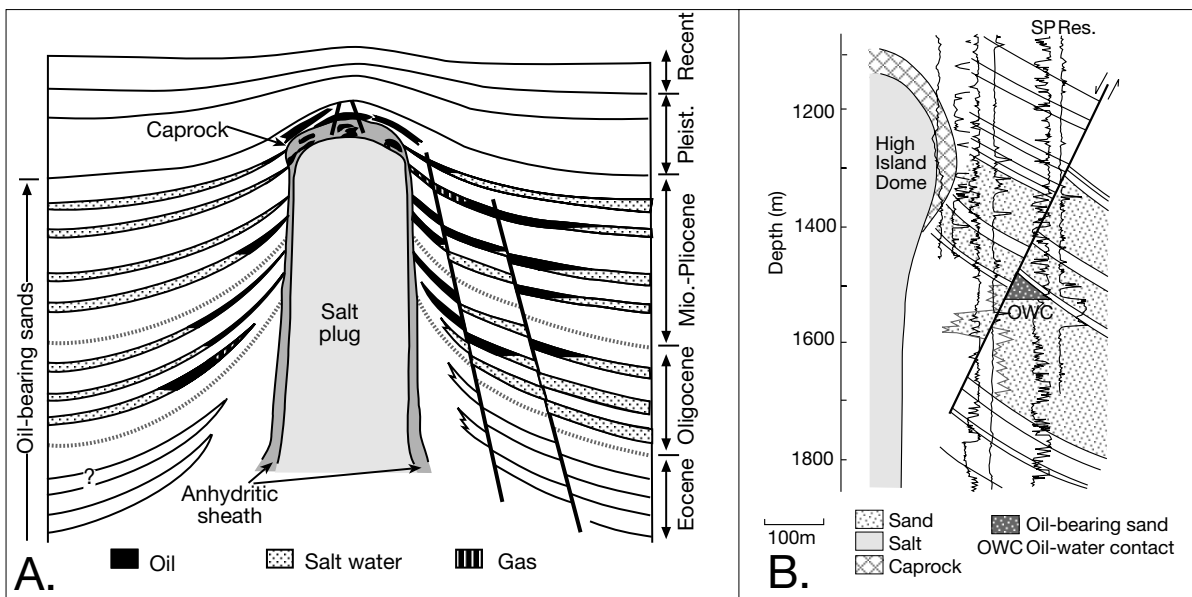


Figure 10.45. Reservoir sands in the Gulf of Mexico A) Stacking of Tertiary-age peripheral reservoir sands creates some of the most productive acreage in the world (after Halbouty, 1979). B) Cross section of the south flank of the High Island Dome, Chambers County, Texas, where the trap is interpreted as due to peripheral faulting juxtaposing a reservoir sand to a shale seal across the fault (after Galloway et al., 1983).

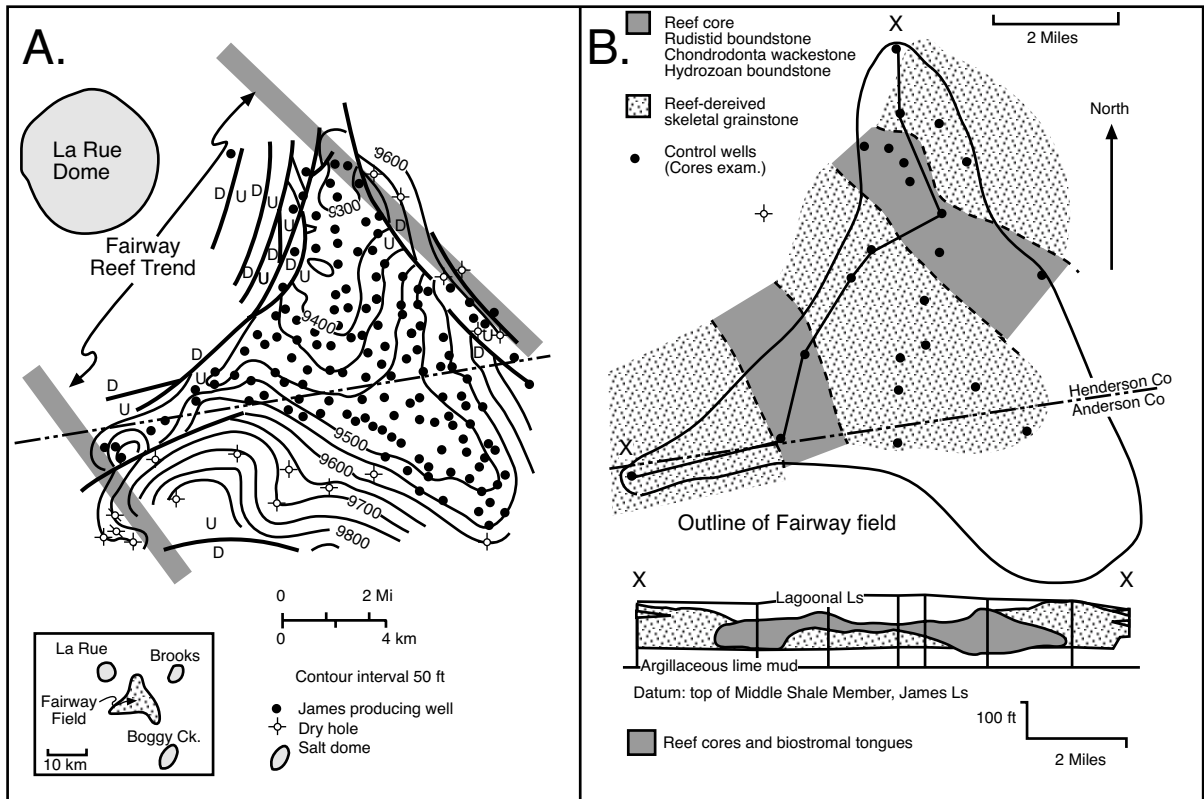


Figure 10.46. Fairway Field, East Texas Basin (after Achauer, 1985). A) Structure map on top of Cretaceous James Limestone Fairway Field, Henderson and Anderson Counties, Texas. The trap is a fault bounded southeast-plunging nose crossed by the northwest trending James Reef Complex. Inset shows Fairway Field formed atop a turtle structure between three salt domes. B) Facies map and interpreted depositional setting of the James Limestone. The main reef core lies in the northwestern part of the field, while satellite reefs to the southeast and southwest are composed of corals, stromatoporoids, algae, and rudists. Carbonates sands and gravels were deposited in the southern part of the field; while elsewhere, muddy lagoonal sands are the dominant lithology.

fault weld. Efficient gravity segregation aided by water influx results in high recovery efficiencies.

Grainstone shoals and reefs may rim the diapir or allochthon crest in carbonate shelf settings. With ongoing subsidence, these units tend to aggrade into a porous rim around the salt stem. A good example of this style of grainstone trap is the West Purt Field in the East Texas Basin, where the reservoir (Rodessa Limestone, Lower Cretaceous), is a fractured mollusc peloid grainstone and rudstone unit abutting the northwest side of the Brushy Creek Diapir (Lomando et al., 1984). The same style of carbonate facies, growing around diapirs and salt welds, now outcrops as the various carbonate lentils associated with the La Popa weld in Mexico (Figure 6.59).

Pulsing salt emplacement, with numerous switches from active to passive, means that any sediment deposited above a passive allochthon or diapir crest is temporary. Whatever the

depositional setting atop the crest, it is shed periodically into the structure's flanks. The resulting salt ablation unconformities can cut into flanking coarser grained deposits, which may then be sealed by subsequent finer-grained deposition or by the encroachment of allochthonous salt (Figure 6.62). The resulting unconformities and truncational traps can be located some distance from the diapir stem. The dip of such unconformity traps is as steep as the dip of the adjacent shaled-out sands. Unconformity traps have thick oil columns and can stack, but show a limited lateral extent away from the salt stem. A good example occurs along the north side of Nash Dome in Texas, where steeply dipping Frio sands (Oligocene) are truncated by multiple dome-flank unconformities.

Stacked flank traps dominate below the crestal level of many producing salt structures in the onshore Gulf of Mexico, reflecting sedimentation about a salt system during the passive stage of its growth. The crest of the structure maintained

its position in earth space while the flanks subsided so that most flank traps are of two interrelated types (Figure 10.45a; Halbouty, 1979): a) Traps created by sedimentation and erosion contemporaneous with salt movement; b) Traps created by the relative upward movement of the salt (downbuilding). Stacked flank and unconformity traps have yielded greater volumes of hydrocarbons per acre than any other type of trap in the Gulf of Mexico (Halbouty, 1979).

The diapir stage is also the time when turtle structure anticlines form in the salt-withdrawal basins between diapirs (Figure 6.17). The region above a turtle is often a topographic high where high-energy shelf sands and reefs accumulate atop an anticlinal drape, creating an excellent trap for the subsequent accumulation of hydrocarbons. A good example is the giant Fairway Field in Lower Cretaceous James Reef Limestones in Henderson and Anderson counties, east Texas (Terriere, 1976, Achauer, 1985). The reservoir is a rudist-reef complex above a shoaling turtle structure and is situated on a saddle between the salt-withdrawal areas of Boggy Creek, Brushy Creek, and La Rue Domes (Figure 10.46).

The growth of a turtle structure between the La Rue, Brooks and Boggy Creek diapirs converted what was a muddy area of open shelf limestones into a shoal area of rudist reefs and grainstone shoals. Postdepositional faulting truncated the northwestern and northeastern margins of the trap, which is now a southeast-plunging nose (Figure 10.46a). Reservoir porosity is largely secondary and is better quality in the meteorically leached portions of mechanically deposited rudist grainstone belts rather than in the reef proper (Figure 10.46b). Secondary porosity tied to halokinetic activity after the reef growth stopped is also the case in many other rudist grainstone buildups atop or adjacent to salt structures in the Gulf of Mexico and the Middle East (e.g. Mishrif Formation

in Umm al Dalk Field, UAE). The main control on reservoir quality in these Cretaceous oil and gas fields is karstification and exposure, driven by periodic seafloor shoaling near or atop the underlying salt structure. Pervasively dolomitised Albian oolite pisolite sands also form extensive reservoirs atop turtle structures in the offshore of Angola (Eichenseer et al., 1999).

Chalk reservoirs above salt structures, such as Danian chalks in Ekofisk, Machar and Medan fields in the North Sea, often had the crestal reservoir properties enhanced by the movement of subadjacent salt during basin inversion (Figure 10.47). Tension was created in the chalk above the growing salt structure and this led to gravitationally-induced microfracturing (D'Heur, 1990a). Oil migrated up these fractures in the chalk and, when the oil column in the fracture system was 50 to 100 m tall, the buoyancy force was sufficient to overcome the high entry pressures inherent in narrow pore throats. Oil was then stored in the matrix as well as in the various fractures. Hardman and

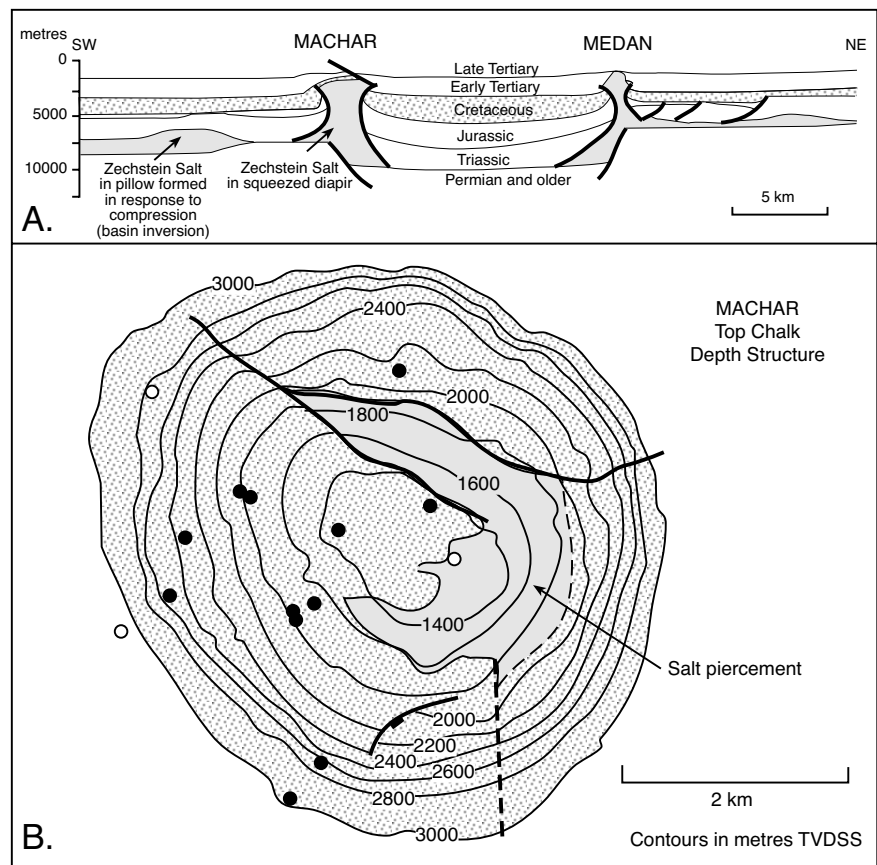


Figure 10.47. Machar Field, UK sector North Sea. A) Interpretive cross section showing position of field and a geometry that is a response to compression of a formerly extensional salt structure. B) Contoured top of chalk in metres TVDSS showing zone of piercement of Zechstein salt (after Foster and Rattey, 1993).

Kennedy (1980) postulated that this process explains why high-relief features in the North Sea chalk/salt structures have better oil saturations and why low-relief traps can have water-wet matrix porosity. Early entry of oil into matrix pores and the associated overpressures then retarded the normal sequence of chalk lithification with burial by inhibiting chemical diagenesis and reducing overburden pressure on the matrix grains (D'Heur, 1990a, b). These processes were most effective in reservoirs above the centre of the salt structure and with time migrated out into the flank reservoir; hence the reduction of porosity and increase in water saturation radially and the concave-upward oil water contact at West Ekofisk.

In a recent study of fracture distribution in chalks reservoirs from a number of rejuvenated diapir fields in the North Sea, including Machar, Davison et al., 2000b found that almost all (>99%) faults and fractures observed are extensional, and form at high angles (>70°) to bedding. Fracturing in the chalks is a response to the rejuvenation of salt flow as the North Basin underwent mild inversion in response to the Alpine Orogeny. The greatest amount of interconnected fracturing and brecciation (natural rubble zones) in the chalk is in wells at or near the crests of the diapirs (Figure 6.47a). The fractures are commonly open, indicating that deformation has continued until the present day, and/or cementation has been inhibited owing to the presence of hydrocarbons, which began to accumulate in the fractures after chalk deposition. Close to the diapir contact (<50 m), the fractures in the chalk are cemented with calcite or anhydrite, which is interpreted to be due to increased fluid flow concentrated along the diapir contact.

This plume of rising saline fluids rising along the dissolving diapir has created a celestite halo in the cap of Machar Field. The fracture intensity within the chalk does not vary consistently from base to top at any one position on the diapir. Reservoir productivity in the chalk is significantly enhanced by fracture permeability over the crest of the diapir structure, where intrinsic permeability in the chalk is insufficient to sustain economic flow rates. However, the chalk is absent on parts of the crest due to non-deposition or downslope sliding (Figure 6.47b; Davison et al., 2000a). These are areas where salt sometimes made it to the Cretaceous seafloor as small allochthon wings off the main salt trend stem. Stylolite and dissolution residue seams, which are parallel to bedding, can slow vertical flow rates in the chalk (Davison et al. 2000b). They are made of clays and other insolubles and show very low permeabilities on the order of nannodarcies.

Understanding the fault and fracture network in Machar chalk as a response to diapir squeezing and the rise of the diapir crest created a new fracture and fault model. Using this knowledge in the field development plan, along with greatly improved seismic imaging, controlled acidising of the chalk, and steered MWD drilling technology, converted Machar from a field that appeared subeconomic in the early appraisals of the late 1980s with test wells returning at best 8,000 bopd to the current producing field with acidised intervals in fractured zones capable of reliably producing at rates of up to 30,000 bopd.

Even as a diapir crest becomes buried and caprock formation comes to dominate, potential reservoirs can still be created. Caprocks host hydrocarbons in many Gulf of Mexico domes show porosities as high as 40%, with porosity types ranging from pinpoint to vuggy to cavernous. Caprock reservoirs in the Gulf of Mexico onshore are shallow and so were attractive targets in the early heyday of drilling in Texas. Many of the famous early Texas reservoirs were in caprocks; examples include Spindletop (the most famous), Sour Lake, and Humble. Caprock reservoirs tend to be made up of relatively small, but numerous, pools. Today, most onshore diapir crests have been drilled and offshore the small size of possible caprock pools means they are not primary targets in most exploration programmes.

Traps can occur below a salt wing (remnant allochthon) or an overhang in a squeezed salt structure with a shape like an inverted teardrop. Prolific production comes from beneath the overhang of Barber Hill Dome in Chambers County, Texas; High Island Dome in Galveston County, Texas; Batson Dome in Hardin County, Texas; and the Weinhausen-Eicklingen salt dome in the Zechstein Basin of northwest Germany (Figure 10.48). Sands below the Barber Hill overhang in east Texas have produced more than 100 million barrels of oil (Halbouty, 1979). All these traps are onshore and were interpreted under the classic styles of Trusheim's pillow to diapir model using the notion that salt was capable of sill-like intrusion at depth. Today they would be interpreted as remnant allochthons created by passive diapirism or allochthons created by reactivated flow due to salt squeezing.

Allochthon plays in the deepwater realm

Throughout the last three decades the deeper offshore province of Gulf of Mexico has been a focus for the development of improved deepwater drilling and seismic technology as deepwater exploration expands into a deepwater realm where much trap structuration is a response to salt flow. Accordingly, as much

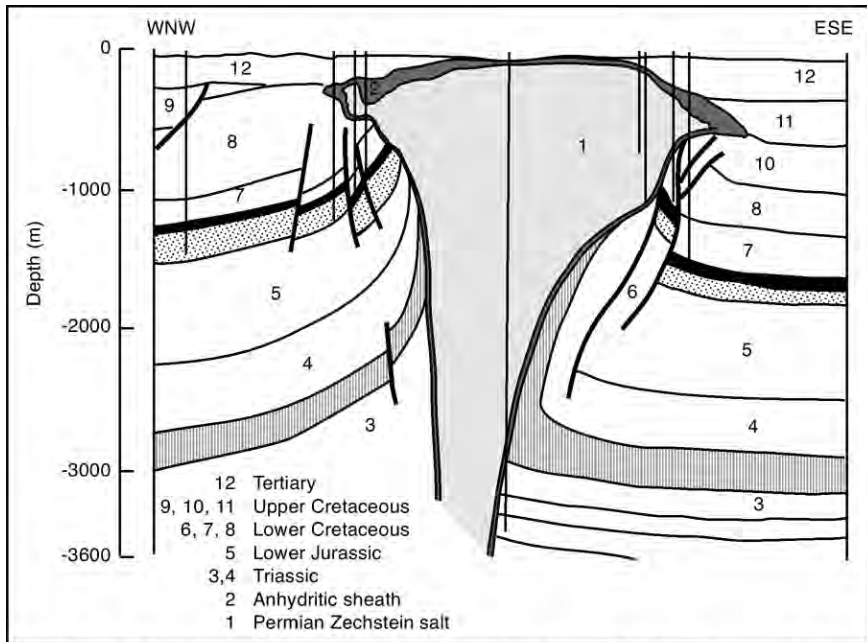


Figure 10.48. Cross section through traps below flank overhangs of the Weinhausen-Eicklingen salt dome, Hanover Basin, northern Germany (after Lotze, 1957). The current geometry also suggests that the structure also underwent compression in the Alpine orogeny.

of the published exploration paradigm for salt allochthon plays comes from the Gulf of Mexico and the examples and models cited in this section largely come from there. However, similar paradigms of allochthon development are being used to drive

two largest deepwater fields found to date are Mars (750 mmbbl oil equivalent) and Thunder Horse (1,000 mmbbl oil equivalent and possibly as high as 3,000 mmbbl). Thunder Horse was not discovered until 1999, a quarter century after the 1975 discovery

exploration in other circum Atlantic basins. As yet this work is not as extensively documented as the Gulf of Mexico, but is a rapidly expanding dataset (see Figures 6.18, 6.37, 6.38).

Since 1975 over 21.2 billion barrels of oil equivalent have been discovered in the deepwater Gulf of Mexico, while some 9.2 tcf of gas and 2,200 mmbbl were produced between 1979 and the end of 2002. Deepening water depths of the various discoveries reflect this time-related technological development (Figure 10.49a; Table 10.7). There were 232 commercial fields discovered in the Gulf during the period from 1975 to the end of 2003 (Cossey, 2004). The current mean size of these discoveries is 94.3 mmbbl oil equivalent. The

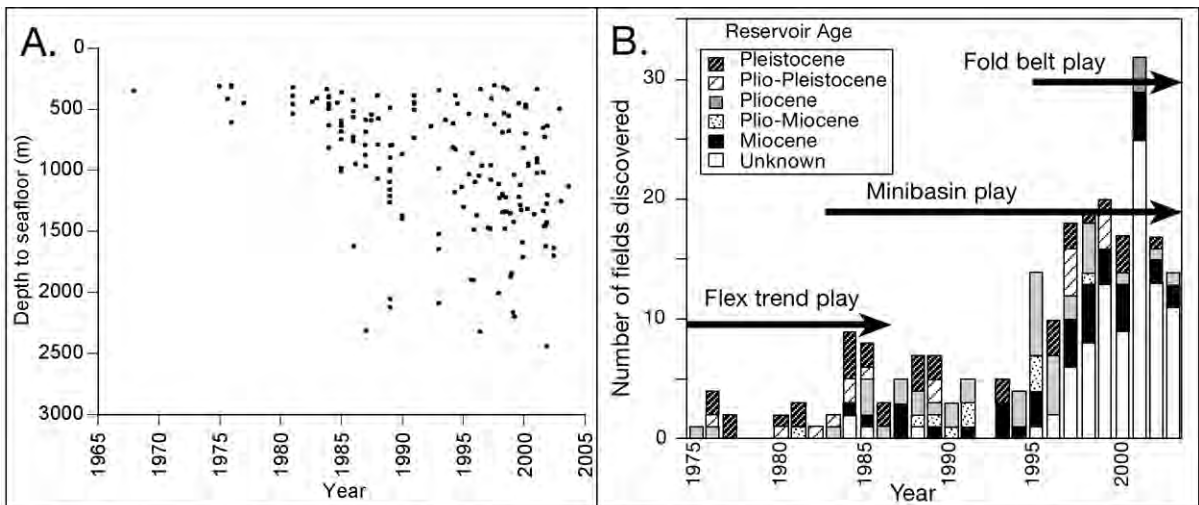


Figure 10.49. Deep water exploration in the Gulf of Mexico. A) Water depth to seafloor for deepwater discoveries in the period 1965-2003 (replotted from Appendix 1, a data table in Richardson et al., 2004). Plot clearly shows the technology-driven expansion of the oil industry into greater drilling depths in this salt allochthon province - see also Table 10.7. B) The number of discoveries for the years 1975-2003, showing reservoir age and dominant play type. It also shows the large increase in discoveries from 1995 onward after the passing of the Royalty Relief Act removed some government tax restrictions to deepwater exploration. There were no discoveries in 1978, 1979 or 1992 (after Richardson et al., 2004; Cossey, 2004).

of Cognac, the first deepwater field (Table 10.7). Initial well flow rates in the deepwater province did not exceed 10,000 bbl/day until 1995, some 20 years after the discovery of Cognac. Three years later, individual well rates at Ram-Powell and Troika had exceeded 20,000 bbl/day.

Several early subsalt wells were accidental subsalt penetrations where operators were drilling to test anomalous seismic reflectors and found salt where they expected hydrocarbons. The first subsalt well drilled in the Gulf of Mexico Outer Continental Shelf was Placid Oil Company's Ship Shoal 366 well in 1983. This well encountered three separate salt intervals, but only 90 metres of subsalt sediment were penetrated. Over the next several years, sporadic subsalt drilling continued. One of the more interesting early subsalt wells was Diamond Shamrock's 1986 well, South Marsh Island 200, which encountered a reservoir-quality sand with a massive 245m net thickness. The potential for worldclass reservoir sands beneath salt allochthons became apparent with this well, but the absence of reliable subsalt targeting from existing seismic technology limited drilling activity.

Porosity and permeability in what are producing deepwater sands in these subsalt fields can be impressive, even though deposition has occurred on deepwater bottoms, situated well out on the continental slope and rise, sometimes in regions that were more than 100 km from their contemporary shorelines. Sands in the Auger Field (Garden Banks 426) retain porosities of 26% and permeabilities up to 350 md. Pliocene and Pleistocene turbidite sands in Green Canyon 205 Field have reported porosities ranging from 28 to 32% with permeabilities between 400 md and 3 darcies. Connectivity in these deepwater sheet sands and amalgamated sheet and channel sands is high for deepwater turbidite reservoirs worldwide and recovery efficiencies are in the 40-60% range (Cossey, 2004). The high production potential of ultra-deepwater reservoirs in the Gulf of Mexico deepwater was documented by production results in Troika and Mars fields where flow rates from turbidite sands are as high as 31,000 and 50,000 barrels of oil per day per well, respectively, far surpassing the previous Gulf of Mexico single well record of 12,000 barrels of oil per day at Auger. This compares to 500-1,000 b/d from a good well on the shelf in the Gulf of Mexico. Although these fields do not compare in size (storage) to the Middle East, they generate Middle

Project Name	Area/ Block	Metres to seafloor	Discov- ered	First Product	Est. equiv. reserves MMbbl
Atlantis	GC 699	1869.3	1998	-	575
Auger	GB 426	871.7	1987	1994	220
Baha	AC 600	2322.6	1996	-	
Bullwinkle	GC 65	412.4	1983	1989	
Champlain	AT 63	1358.5	2000	-	
Cognac	MC 195	311.8	1975	1979	
Diana	EB 945	1371.6	1990	2000	
Europa	MC 935	1179.6	1994	2000	160
Gemini	MC 292	1034.2	1995	1999	
Genesis	GC 205	789.4	1988	1999	
K2	GC 562	1221.0	1999	-	
Lena	MC 280	304.8	1976	1984	
Mars	MC 807	894.0	1989	1996	750
Mensa	MC 731	1620.9	1986	1997	
Neptune	VK 826	588.3	1987	1997	800
Penn State	GB 216	442.0	1991	1999	
Pompano	VK 990	393.2	1981	1994	
Popeye	GC 116	609.6	1985	1996	
Ram-Powell	VK 956	980.2	1985	1997	
Thunder Horse	MC 778	1844.0	1999	-	>1,000
Troika	GC 244	829.4	1994	1997	200
Ursa	MC 809	1158.2	1989	1999	400
Zinc	MC 354	450.5	1977"	1993	

Table 10.7. Some of the salt allochthon related discoveries in the deepwater Gulf of Mexico (compiled in part from Richardson et al., 2004).

Eastern rates of production. The surprising discovery in 1994 of how productive these reservoirs were in tests at Shell Oil's Auger platform entirely changed the company's cost structure for this deepwater play.

Regional plays in the Gulf of Mexico

Regionally, there are three subsalt-associated allochthon trends in the deepwater Gulf of Mexico (Figure 10.49b, 10.50a): i) Flex trend, ii) Minibasin, and iii) Fold belt (Cossey, 2004). The term subsalt is used by explorers to describe plays obscured by a salt canopy. The flex trend describes the shallowest region of the three (in terms of water depth) and it covers a geographic area encompassing the outermost shelf and uppermost slope. Geologically it constitutes the halokinetic zone in front of the Plio-Pleistocene Roho, and is an area where there is no wide-spread salt canopy. It can be further divided into a "toe thrust"

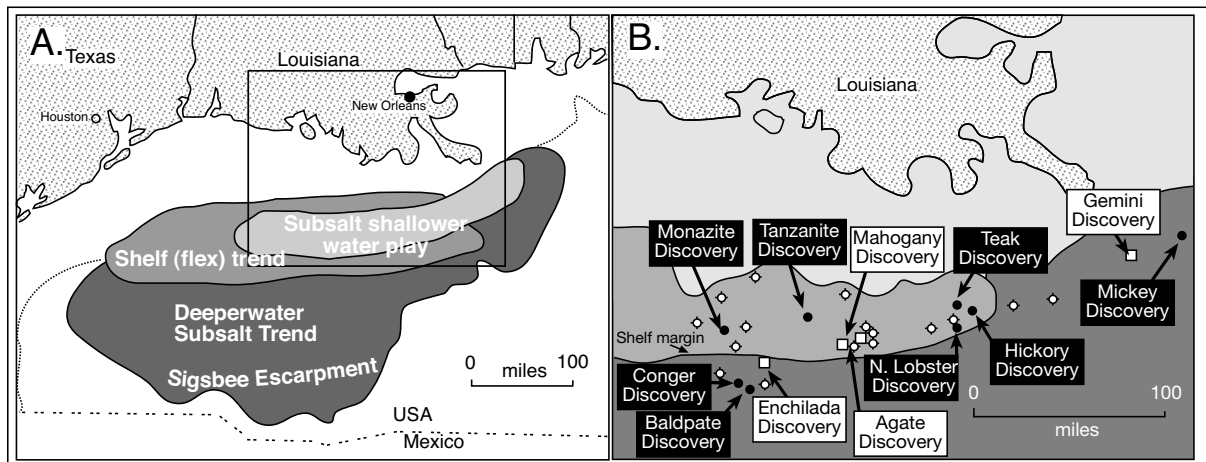


Figure 10.50. Allochthon-related discoveries in the Gulf of Mexico. A) Distribution of shelf and deep water salt plays in the Northern Gulf of Mexico. (in part after Cossey, 2004). B) Selected early discoveries, until the mid 1990s, in the updip slope and rise minibasin province in the eastern Gulf of Mexico (not in as deep water as most of today's targets).

belt and a “primary basin” belt (Figures 6.30; 10.51a; Shinol, 2000 as reported in Shirley, 2000). Large volumes of salt have been lost in this region via allochthon evacuation, dissolution and weld creation. In terms of salt allochthon evolution much of the Flex trend and the Primary Basin region has evolved well past the canopy stage and the area is now a relict thrust fold belt (Figure 10.51b). The minibasin play, as the name implies, encompasses sand deposition associated with the development salt depopods and minibasins (Figure 6.25). It is typically located in somewhat deeper water than the exploitation began in 1983 with the discovery of Bullwinkle. The fold belt trend is located beneath and downdip of the canopy belt and encompasses reservoirs developed by compressional folding at the downslope end of a developing allochthon belt. It constitutes the deepest water region of current areas of exploration activity in the Gulf of Mexico (Figures 6.34; 10.51).

Flex trend exploration began in the early 1970s with the discovery of Cognac Field located just beyond the present-day shelf edge where there is a “flex” in the sea floor profile (Cossey, 2004). Some of the larger flex discoveries were Lena, Zinc, Pompano and Green Canyon 18. Most discoveries in the Flex Trend are fields with small reserves, characterised by discontinuous sands with producing wells showing fairly low flow rates. Exploration wells in this trend generally targeted “bright spots” on 2-D seismic. Gemini, for example, showed up as a very strong event on the seismic. Texaco was so confident of its Gemini prospect that based on a very strong event on the seismic they stopped drilling and set casing just before entering the pay zones. In fact, this hydrocarbon-indicating anomaly could be seen on non-processed, mid-1980s vintage 2D seismic.

Exploration for minibasin plays typically targets the flanks of intraslope basins where reservoir sands pinch out and form combination structural/stratigraphic traps, or it targets zones of drape over turtle structures. Many minibasins plays are sealed and obscured by allochthonous salt, which can fuse into a salt canopy. Some of the larger mini-basin fields discovered to date are Auger, Mars, Diana, Genesis, Troika and Europa. Ram-Powell was discovered in 1985 and is a very large, stratigraphic trap developed in a more unrestricted mini-basin. Larger minibasins typically have turtle structures developed in their centres. The first mini-basin fields brought on-line (Bullwinkle in 1989, Auger in 1994) produced at much higher than expected rates, had better than expected aquifer support and needed fewer wells to develop them. Much of the early production from these minibasin fields ended up being facilities constrained.

Suballochthon exploration for minibasin traps in the deepwater offshore Gulf of Mexico was first successful south of New Orleans in the region known as the “Isolated Salt Tablets” province or Florida slope. It is located in the easternmost Mississippi Canyon area in waters 1,000 to 2,000 metres deep (Figure 10.51a; Shirley, 2000; Hall, 2002). Productive reservoirs are Pliocene to Miocene unconfined turbidites occurring some 3,000-4,500 metre seafloor. These are usually sealed beneath allochthonous salt and are considered combination structural/stratigraphic traps. Exxon made the first deepwater subsalt discovery of oil and gas in this region with its Mississippi Canyon 211 well. This prospect, nicknamed “Mickey” because of the resemblance of three allochthon sheets in plan view to the head and ears of “Mickey Mouse” has hydrocarbons

below salt canopy and lies beneath 1310 m (4,300 ft) of water (Figure 10.50b). Reserve estimates for “Mickey” range between 50 to 150 million barrels of oil equivalent, but the discovery was deemed subeconomic and has yet to be put on production. The “Mickey” discovery indicated the prospectivity of subsalt plays in this region and focused exploration efforts into sub-allochthons, both on the shelf and in deeper water.

As drilling technology and subsalt imaging improved throughout the later 80s and into the 90s, subsalt exploration moved into progressively deeper water. Drilling now could reliably reach larger potential suballochthon minibasin structures, including turtles located further out in the Gulf (Richardson et al., 2004). Minibasin fields currently contain the largest economic resource base in the deepwater Gulf. The subsalt “Mahogany” Field, operated by Phillips Petroleum, is a minibasin play that was discovered in 1993 by the Ship Shoal 349 well in the Mission Canyon region. This field, which began production in December 1996, was the first commercial subsalt oil development in the Gulf of Mexico. In 1994, Shell Offshore, Pennzoil, and Amerada Hess announced another significant minibasin discovery in Garden Banks 128 well, nicknamed “Enchilada” (as in the idiomatic “it’s the big enchilada”). Enchilada has combined reserves estimated at 400 bcf of gas and 25 million bbl of oil/condensate (DeLuca, 1999), and was brought online in July of 1998. In 1996 nine subsalt wells were drilled and three were discoveries. The largest discovery (Anadarko and Chevron) was “Gemini” in Mississippi Canyon Block 292 with estimated reserves of 250-300 Bcf of gas and 3-4 million bbl of condensate (DeLuca, 1999). It currently produces from a single reservoir using a subsea system.

Gemini was the first deepwater subsalt production in the Gulf of Mexico - and showed explorers the potential for prolific production from the deeper water portion of the subsalt play.

In June 1999 one of the Gemini wells tested around 76 million cubic feet of gas and 1,370 barrels of condensate a day. Agate Field in Ship Shoal 361 was discovered in 1996 by Anadarko and Phillips and is now producing through a tieback into the neighbouring Mahogany platform. Anadarko, along with partner BHP, also announced a second subsalt discovery in 1996 in Vermilion 375, called Monazite. The discovery well revealed multiple pay zones, but because of problems during testing, the hole was plugged and abandoned. Amerada Hess and Oryx made a major discovery in late 1997 in their Penn State prospect in Garden Banks 216, the field came on stream in 1999 through a tieback to the Baldpate production facilities.

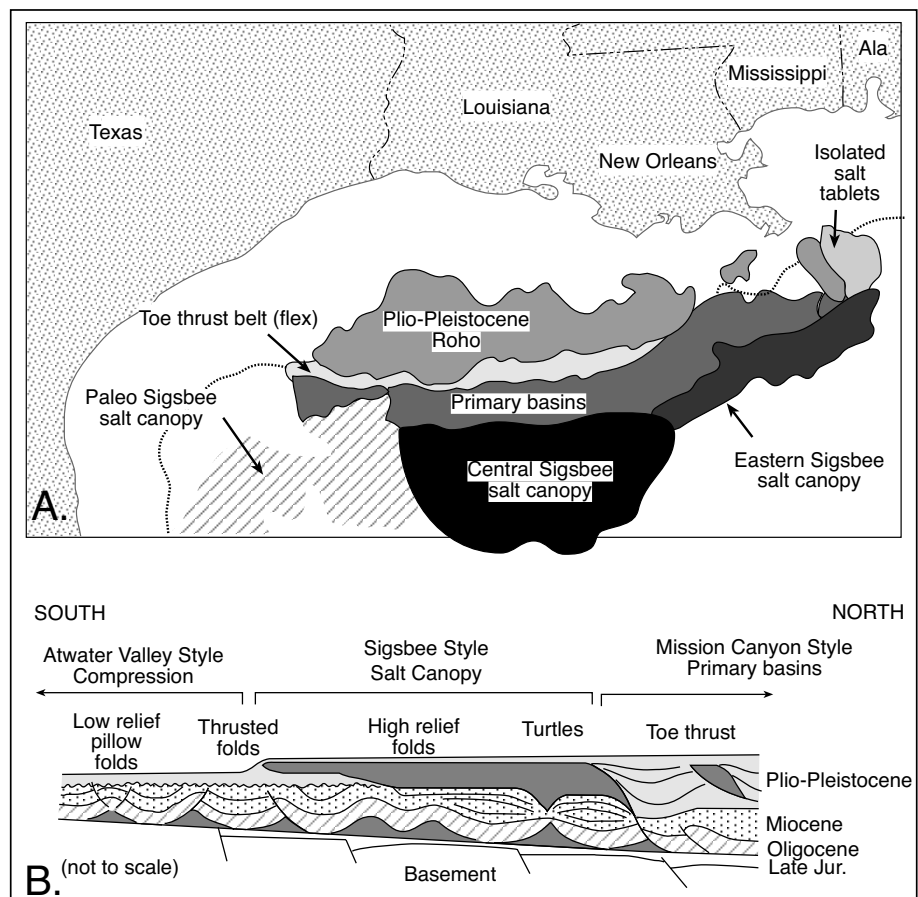


Figure 10.51. Distribution of the various salt fairways in the Northern Gulf of Mexico. Also shows an idealised south to north cross section illustrating typical subsalt and suprasalt structures where the position of the salt defines major play types. Note that the low relief pillow folds in the south are autochthonous and probably define the original southern extent of thick Jurassic salt in the basin.

In July of 1998, Anadarko announced a subsalt discovery at the Tanzanite prospect in 95 m (314 ft) of water in Eugene Island 346 with reserves estimated at 140 million BOE. Later in 1998, Anadarko also announced the discovery of their Hickory prospect in Grand Isle 116 in 97 m (320 ft) of water. The discovery well, drilled to a total depth of 6580 m (21,600 ft), penetrated approximately 2400 m (8,000 feet) of salt before passing into the reservoir, via one of the thickest sections of salt ever drilled in the Gulf of Mexico. Reserves are estimated at 40 million BOE (DeLuca, 1999).

Thunder Horse Field (formerly known as Crazy Horse Field) in Mississippi Canyon Blocks 776, 777 and 778 is a substantial minibasin discovery with a turtle style of reservoir development. It is located in the Boarshead Basin, 200 km south-east of New Orleans and is the largest deep water discovery made to date in the Gulf of Mexico (Enger and Logan, 2001). It has estimated reserves of greater than a billion barrels of oil equivalent in early and middle Miocene sands at about 7,000 - 8500 m (23,000-28,000 feet) depth. BP-Amoco has said reservoir characteristics are excellent and compared Thunder Horse favourably to Magnus Field in the UK North Sea, where wells flowed at rates exceeding 20,000 bbl/day at peak. Thunder Horse shows that deepwater subsalt sands can be highly productive, even at depths well below 7500 m. It is one-and-one-half to twice the size of the next biggest structures in the region (Enger and Logan, 2001) and is one of three large discoveries on turtle structures. The other two are Pluto (aka BS and T; Mississippi Canyon 718) and Mensa (Mississippi Canyon 731). Both the Thunder Horse and Pluto discoveries are partially covered by shallow salt canopies.

Methods of most effectively exploring for minibasin plays are still emerging, especially if a turtle is obscured by a salt canopy (Shirley, 2000). Deeper turtle structures are difficult to image on 3D seismic data, especially beneath thick salt canopies and there are no diagnostic hydrocarbon-indicating amplitudes (bright spots) related to this play, so structures rather than accumulations are targeted. Geologically, turtle structures can be complicated as these structures were synclines at the time they were receiving sediments (Figure 6.17). Then the structure inverted due to ongoing salt withdrawal. That in itself implies there is a complex relationship between timing of trap formation, hydrocarbon charge and migration. The key uncertainty with turtle structures in this style of play is whether a trap was in place during the hydrocarbon migration phase. Also, there can be crestal faulting on these structures that can degrade the top seal of the traps, but the size of the potential discoveries makes the risk worthwhile.

Petroleum systems in the fold belt feature underlying high relief salt cored folds (mostly to the west) and thrust folds to the east in what Hall (2002) calls the Atwater Valley style structural province. Lower and middle Miocene turbidite reservoirs extend across the crests of folds, which typically formed during foot of slope compression in the mid-Miocene to Early Pliocene (Figure 6.34). Three major fold belt trends are currently considered prospective: the Mississippi Fan, the Perdido and the Port Isabel fold belt, all are located in deeper water downdip of the salt canopy/minibasin trend. The Fold Belt play began to be exploited in 1995 with BP-Amoco's discovery of Neptune in Atwater Valley 575 in the Mississippi Fan fold belt. Soon thereafter BP discovered Atlantis and Mad Dog (Hall, 2002). K2/Timon was found just north of the earlier discoveries, and more recently Texaco discovered the Champlain Field in the middle of Atwater Valley, extending the play further east.

To date, there have been five separate discoveries in this Mississippi Fan belt, although four have been centred in the fold belt of the western part in a small area of the southeast Green Canyon area. All are near the edge of the Sigsbee Escarpment and within 50 km of each other in water depths ranging from 1,200 to 3000 metres (4,000 to 6,500 ft). Target reservoirs are found in the 5,000 to 8,000 m (17,000 to 26,000 ft) depth range, and the structures can be prolific with greater than 300 million barrels of oil equivalent. Mad Dog is currently the most prolific of the fold belt discoveries, with reserve estimates ranging from 400 to 800 million barrels of oil equivalent from about 100 m of net hydrocarbon pay in a large, high relief fold under the edge of the Sigsbee Escarpment. Atlantis, however, is now vying with Mad Dog in terms of size. The first appraisal well at Atlantis added significant additional sand section, bringing the total net pay to 150 m (500 ft).

Current seismic quality in this part of the fold-belt province is good to fair, but companies are exploring very high relief features, which are difficult to miss. For example, Mad Dog is a 3,000 m relief feature. Even though imaging is not the best quality, it's hard to overlook a 3,000-metre-tall structure in the subsurface. Plays in the area known as the Eastern Sigsbee Escarpment do not involve the search for the subtle trap! The province's western portion is relatively well drilled now, so the play's future lies in taking the charge risk and moving east to determine how far the play will extend (Shirley, 2000). In contrast, the Perdido Fold Belt Play is under explored. The play is similar to the Mississippi Fan Fold Belt Play in that it consists of very large compressional fold belt structures. Like the Mississippi Fan Fold Belt Play, the compressional folds

extend a considerable distance landward beneath the Sigsbee Salt Canopy. However, the plays differ in the age of the structures and the targeted reservoir.

So, exploration drilling in the deepwater Gulf of Mexico in 2002 and 2003 has found over 2 billion BOE (Richardson et al., 2004). Today (late 2004) the traditional deepwater mini-basin plays are still providing many successful exploration opportunities (e.g. the Thunder Horse and North Thunder Horse discoveries in southern Mississippi Canyon), but recent discoveries in new fold belt deepwater plays continue to expand the exploration potential of the deepwater Gulf of Mexico. Some 99% of total production in the deepwater Gulf of Mexico is from Neogene reservoirs (Pleistocene, Pliocene, and Miocene; Figure 10.49a); however, several recently announced deepwater discoveries encountered large potential reservoirs in sands of Paleogene age (Oligocene, Eocene, and Paleocene). This older portion of the geologic section has been very lightly tested and the discovery of reservoirs of this geologic age may open wide areas of the fold belt in the Gulf of Mexico to further drilling.

How suprasalt becomes subsalt

Salt-withdrawal minibasins are characterized by Karlo and Shoup (2000) as either; (1) shelf-loaded, or (2) slope-loaded (Figure 10.52). Salt withdrawal minibasins on the shelf, which mostly host fluvio-deltaic reservoirs of the northern Gulf of Mexico, are rooted in autochthonous salt at depths of 12,000-14,000 m (40-45,000 ft). They typically show continuous subsidence in a seaward-migrating belt of sediment loading from the Cretaceous onward, with some basins beginning to fill with sediment even earlier in the Jurassic. The basins are aligned in sub parallel linear trends with salt domes intermittently dispersed along the bounding faults. Updip they tend to be simple minibasins while their downdip extent is defined by stepped counter-regional fault basins, often with a secondary turtle structure on the 'step,' along with some local Roho development (Figure 6.30; Karlo

and Shoup, 2000). Associated salt masses grade from simple diapirs updip into larger volume, overhung salt domes and successively into salt wings and allochthons downdip. Block 330 is one such system (Figure 6.58).

Plio-Pleistocene Roho systems are shelf-loaded features (Figures 10.53) with updip zones of extension marked by a series of nested highly listric faults, which display a characteristic horseshoe geometry in map view (Figures 6.30, 10.53b; Karlo and Shoup, 2000). Deltaic sands and shales tend to be stacked in lower parts of the seafloor in a feedback between depositional loading of the rotated wedges associated with these growth faults. The central portion of the same depositional system is typically manifest as a complicated zone of remnant salt, perched diapirs, salt-floored faults, and strike-slip faults. Basinward of this region is the compressional toe, which consists of a melange of salt and deformed sediment. All faults sole into the evacuated remnant of the original salt tablet, which typically overlies a salt-withdrawal minibasin. In map view, the overall geometry of the salt-based detachment system is constrained by the geometry of the salt tablet upon which it is forming.

Slope-loaded minibasins (turbidite reservoirs) are similar to shelf minibasins in terms of sand distributions, but involve much more salt than the shelf systems (Figure 10.52). The slope withdrawal basins are flanked by salt walls with little fault rim development. Formation began with ponding of turbidites trig-

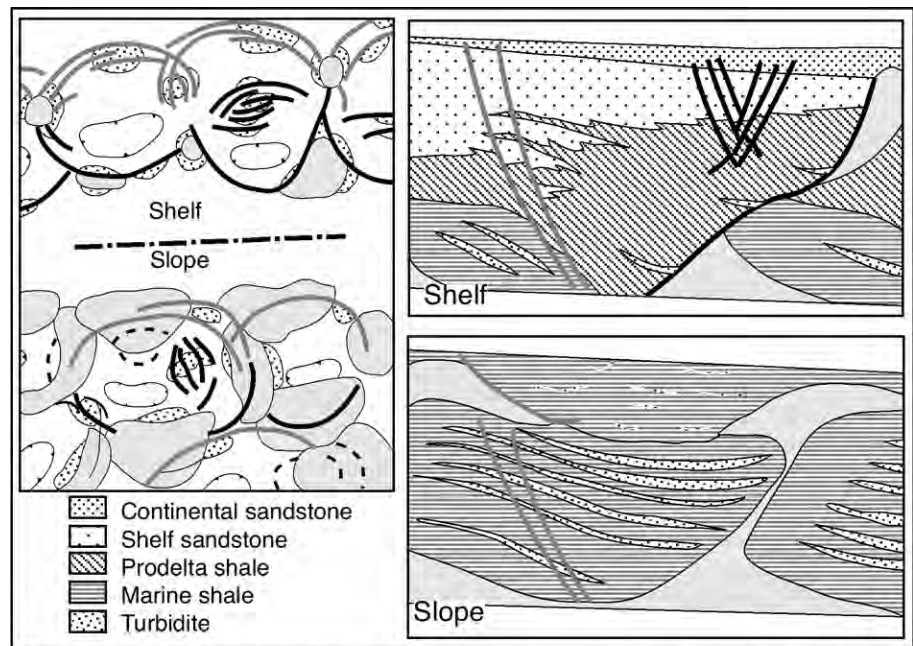


Figure 10.52. Model of reservoir styles showing distribution of subsalt traps in both shelf and deepwater minibasin (primary basin) settings (after Karlo and Shoup, 2000).

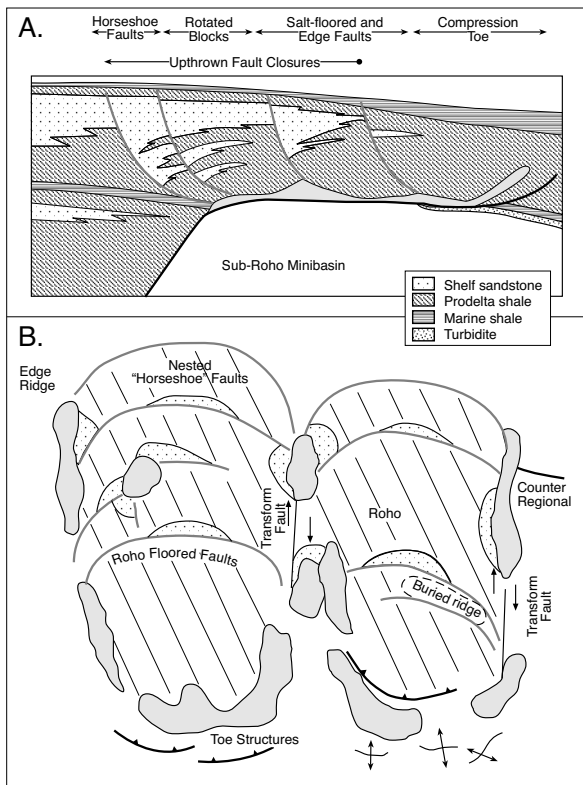


Figure 10.53. Model of reservoir styles showing distribution of Roho (suprasalt) traps in both shelf and deepwater minibasin (primary basin) settings (after Karlo and Shoup, 2000).

gering loading and the creation of diapirs. Because of the great thicknesses of autochthonous salt involved, turbidite ponding is more or less continuous, so long as there is salt withdrawing from the basin. Should the depocentre shift during the diapiric phase, a salt wing forms during the hiatus and overflows the basin resulting in the formation of a salt canopy. Once the allochthonous salt has been evacuated, subsequent turbidite deposition bypasses the basin.

Intrasalt halokinetic plays

Not as yet in full production, but still worthy of consideration, is the intrasalt halokinetic play exemplified by cherty overpressured stringer reservoirs encased in the Precambrian Ara Salt Formation of the Ara Group in Oman. These intrasalt targets of Athel Formation silicilyte represent one of the more complex deep oil exploration plays in onshore Oman and constitute a significant part of Petroleum Development Oman's undrilled prospect portfolio (Reinhardt, 1999; Peters et al., 2003). During the late 1970s to early 80s Petroleum Development Oman (PDO) drilled several significant oil and

gas shows in intrasalt objectives within the Neoproterozoic Ara Salt of the South Oman Salt Basin (Figure 10.54). These potential reservoirs were in porous (15-25%), overpressured siliceous microlaminated sediments that were stratigraphically trapped and encased in halokinetic salt at depths of 3 to 4 km. Based on these intersections, the size of potential intrasalt pools was thought to be large, with individual slabs or slivers of possibly oil-saturated silicilyte seen in seismic to be up to 2x6 km across and more than 300 metres thick.

In 1989 and 1995, respectively, Al Noor and Al Shomou were drilled as two sliver prospects in the Athel Formation (silicilyte). The first two wells in the Al Noor Field encountered over 300 m of pay within low permeability fractured intervals that well tests showed had levels of 8 to 9 md per metre. Reserves of $15.0 \times 10^6 \text{ m}^3$ oil were calculated from these early intersections with an expectation of oil-in-place in the fields of up to 2 billion barrels (Wong et al., 2000). Oil recovered from the wells was attractive, although it was largely hosted in an unusual reservoir of microlaminated organic-rich chert (silicilyte is a general term for a fine-grained silica rock). The oil is light (48° API) with a viscosity of 0.3 to 0.36 mPas^{-1} and a bubble point of 277 bar. The initial solution gas-oil-ratio was 400 to $550 \text{ m}^3/\text{m}^3$, with H_2S levels of 1.5 mol% and CO_2 levels of 3 mol%. It was recovered from wells with early flow rates of up to 8,800 bbls/day. Average well flow rates varied between 40 to $110 \text{ m}^3/\text{day}$ prior to reservoir stimulation, post-stimulation figures have not been released. The silicilyte slivers define a play type worth pursuing, but a number of dry holes drilled after the initial successful wells defined inherent complexities with respect to reservoir quality prediction, hydrocarbon charge, production behaviour, and seismic imaging. Inherently high variability in the silicilyte permeability both vertically and laterally means successful future exploitation must involve targeted directional drilling and reservoir stimulation.

Varying thicknesses created by deep salt pillows atop potential reservoir slivers, and the occurrence of reservoir slivers near the base of the thick halokinetic salt unit, has hampered reliable seismic positioning of these deep (>3000 m) intrasalt reservoir objectives. Likewise, pressure transient tests in the intersected reservoir indicate an effective reservoir permeability that is one-tenth of that measured using cleaned core plugs (O'Dell, 1998). The difference in well and plug determinations is likely caused by a combination of pressure-sealed fractures and the pervasive plugging effect of bitumen in the reservoir (bitumens are removed in standard plug preparation) Uncertainty in these and many other aspects of silicilyte understanding meant that until very recently the Athel Silicilyte was not pursued as a high

value target within the PDO exploration portfolio. Improvements in seismic processing, targeted hydrofracturing, and geosteering technology, means it is possible to now pursue salt-encased permeable slivers as difficult but viable exploration targets.

Recently, wells in the two known silicilyte fields were the successful subject of what was perhaps one of the largest fracture jobs in the region to date. PDO also instigated a number of detailed sedimentological and engineering studies to better understand what characterises reservoir versus non-reservoir associations in the silicilyte slivers. This work is also of broader geological interest as the Ara Group is one of the few sequences in the world where ongoing deposition straddles the Precambrian-Cambrian boundary (Al-Husseini et al., 2003). This broader more academic work established a regional geological framework for silicilytes, carbonates and platform sulphate evaporites of the Ara Group and better defined the stratigraphy of the South Oman Salt Basin. Silicilyte slivers of the Athel Formation currently occupy a more central subsalt basinal position encased in basin-centre halokinetic halite and so are not easily correlated to the carbonates of the platform margin.

The Neoproterozoic/Early Palaeozoic Ara-Group is the terminal subdivision of the Huqf-Supergroup of Oman. Deposition of the Huqf spanned several tens of millions of years during the Vendian Neoproterozoic and early Cambrian. The Ara Group in the South Oman Salt Basin is made up of five to six 3rd-order carbonate-evaporite cycles (Figure 10.55; Schröder et al., 2000a, b, 2003, 2005; Gorin et al., 1982). Wherever the salt seal is breached, the Neoproterozoic organic-rich evaporitic sediments of the Huqf Supergroup have sourced most of the oil and gas stored in halokinetically structured suprasalt Phanerozoic reservoir sands and there is a concentration of large fields along the dissolution edge of the salt (Figure 10.5b; Terken et al., 2001). Oil generation from this ancient source rock began in the middle of the Cretaceous.

Depositional cycles in the Ara Group tend to be lithologically symmetric, with thick dolomitised carbonate platforms sandwiched between anhydrite, halite, and some thin intervals of potash salts (Figure 10.55). The sedimentology constitutes what is a typical marine-fed continental sag succession fill. In each cycle the carbonate is interpreted as representing the initial flooding of the basin platform, with the subsequent progradation of a carbonate ramp system prior to a basinwide episode of evaporite fill. Today all the sulphate is platform anhydrite, but it retains pseudomorphs after selenitic gypsum, showing it was originally deposited as a gypsum saltern (Schröder et al.,

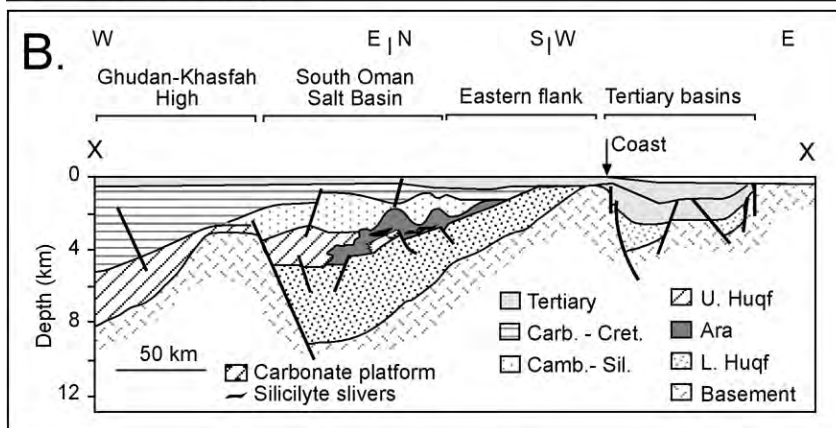
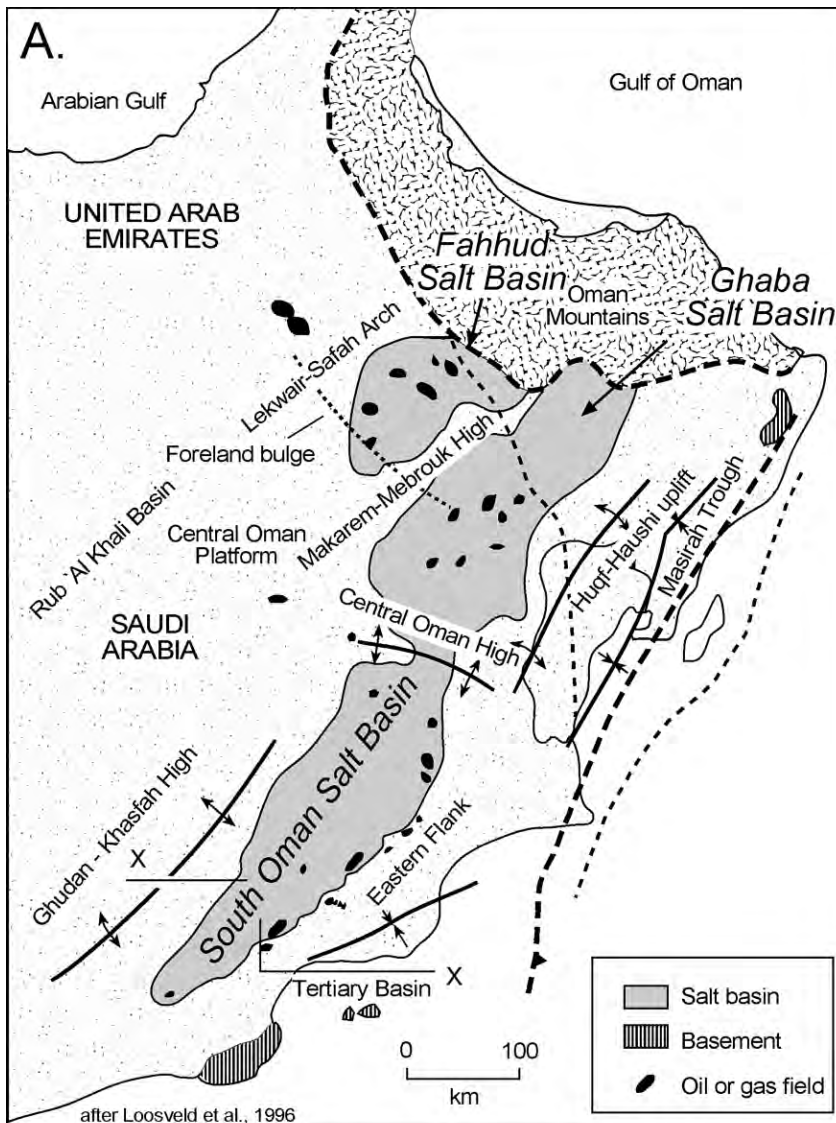
2003). Well-preserved sedimentary structures (e.g. palmate gypsum morphologies and desiccation cracks) suggest a shallow (<5 m deep) subaqueous environment for the various carbonate-sulphate platform cycles. Sabkha deposits represent only a minor fraction of the total platform evaporite volume. Following times of basinwide saltern sulphate accumulation, brine depths shallowed further and thick beds of basin centre halite precipitated, along with thin beds containing potash salts. Evaporite geochemistry indicates a marine source with some minor contributions from continental and/or hydrothermal waters (Schröder et al., 2003).

Much of the halite in the Ara Group was subsequently recrystallised during halokinesis. Most of the deformation evident in the Ara Group is taken up in intervals of flowing salt rather than by internal deformation and folding of the platform carbonates and sulphates. Halokinetic salt also encases the silicilyte slivers or blocks in the more central portions of the South Oman Salt Basin and is why it is difficult to place the various slivers into a depositional reconstruction of the basin. Are these laminated organic-rich cherty slivers still near their original somewhat deeper water depositional position in the basin palaeogeography, or have they slide tens of kilometres or more into the basin via salt-lubricated gravity gliding and raft tectonics? The latter scenario would create a more complex jumble of slithers with porosity distributions largely unrelated to current block orientations.

Internally, the various carbonate and sulphate facies of the undeformed platform blocks are simple to interpret. Energy related facies developed in different water depths in an into-the-basin deepening ramp system, within what was an intracratonic rift or sag. Salt layers in the Ara Group are roughly equivalent to the Hormuz Formation to the north (Schröder 2003; Sharland et al., 2001). Finely laminated organic-rich dolomites and some thrombolite buildups of the carbonate platform facies occupied an outer to middle ramp setting, typified by lower energies and outcrop out the margins of the basin. Further out in the current basin they are overlain by shallow water platform mudstones, packstones, and evaporites (Figure 10.55).

Several factors are listed by Schröder et al. (2000b, 2003) as explaining the porosity dichotomy between Neoproterozoic platform carbonates and basin centre silicilytes:

- Downward circulation of saline brines caused mimetic dolomitisation and deterioration of reservoir characteristics in underlying platform carbonates. Any lithofacies close to overlying evaporites also suffered from evaporite cementa-



tion - i.e. shallow water carbonates at the top of stringers, as well as thin stringers.

- Early maturation of organic matter flushed the pore networks in the deeper water siliceous organic-rich laminites (silicilytes) with hydrocarbons that then prevented subsequent cementation by later carbonate and evaporite cements.
- Early reflux brines tended to flush the larger connected pores of the shallower and higher energy grainier carbonate units (e.g. thrombolite shoals) and so they were more easily filled with evaporite cements than the smaller hydrocarbon-rich pore networks of the basin centre silicilyte laminites.

Porosity evolution in the laminites contrasts with that of thrombolite buildups and shallow water packstones where high porosities have been almost completely plugged by dolomite and evaporite cements, so typical of a depositional association with a basinwide evaporite unit. Thus production in Al Noor and Al Shomou fields comes from salt-encased organic rich blocks of chert of the Athel Silicilyte, not from platform dolomite sulphate successions, which are typically too tight and too evaporite-cemented to produce.

The Athel Silicilyte is part of the Athel Formation in the Vendian to

Figure 10.54. Salt Basins of Oman. A) Map view of three main salt basins. Palaeozoic strata are the main oil and gas producers, not Neoproterozoic platform carbonates or Athel Fm. silicilyte slivers, which occur more toward the centre of the South Oman Salt Basin. B) Cross section through the South Oman Salt Basin, schematically showing position of laminites and slivers in the Ara Salt (after Loosveld et al., 1996 and Schröder et al., 2000a, b).

Early Cambrian Huqf Supergroup. It is a unique source and reservoir rock in the South Oman Salt Basin and is not equivalent in depositional style to the platform setting of the various carbonate-sulphate stringers and blocks (Peters et al., 2003). According to Sharland et al., (2001) silicilyte forms km-scale stratiform blocks encased in a thick halokinetic halite, which also separates the A2 and A3 carbonate stringers. Within slivers the Athel Fm. silicilyte is typically made up of metre-scale interlayers of finely microlaminated, porous silicilyte alternating with non-porous silica-cemented silicilyte. The latter act as vertical baffles to flow within the reservoir. In the absence of outcrop analogues, borehole-imaging logs are extensively used to delineate and to correlate reservoir units. FMI shows that more than 70% of the lithofacies in the Athel Fm. are constituted of beds thinner than 1 metre. Cemented fractures (some with fibrous halite fills) are locally common, typically reducing the horizontal connectivity. The rock matrix consists up to 80% of microcrystalline quartz with high amounts of intercrystalline microporosity (up to 30%). The very small modal crystal size of 2-3 micron and widespread bitumens in the silicilyte pore throats result in microdarcy levels of reservoir permeability (Amthor et al., 1998; Peters et al., 2003). The present-day thicker (distal) silicilyte sections in the basin tend to have a higher average porosity than thinner (proximal) sections toward the platform.

The silicilyte play is an unusual basinal evaporite association, characterized by light and sour oil, hard overpressures and a high-porosity, low-permeability silica matrix (0.2-0.3 md) constituting a fine-grained microlaminated chert that is consistently rich in organic matter (Wong et al., 2000; Amthor et al., 1998; Amthor and Frewin, 1999). Encasing halite has prevented hydrocarbon expulsion from the

silicilyte, explaining inherently high formation pressures ≈ 19.8 kPa/m and high present-day oil saturations $\approx 65-90\%$. The absence of oil expulsion is evident from Rock Eval data, which are characterized by high production indices. A good correlation between S_1 and the generative potential S_1+S_2 suggests that hydrocarbons were indeed generated in situ and did not result from migration of hydrocarbons generated at deeper horizons. This also fits with the typical tight character of source rocks in style 1a basinwide evaporite settings (Chapter 9). As a source rock the Athel Formation silicilyte is also unique (Terken et al., 2001). Finely disseminated kerogen occupies up to 10% of the rock volume, with a third of the organic matter concentrated in stylolites. Source rock extracts reflect the Infracambrian age of the formation, namely; light $\delta^{13}C_{PDB}$ of -37 to -35‰, a strong predominance of C29 over C28 steranes, and high 24-isopropyl/n-propyl cholestane ratios. The kinetic behavior of the Athel is similar to that of the Miocene Monterey Forma-

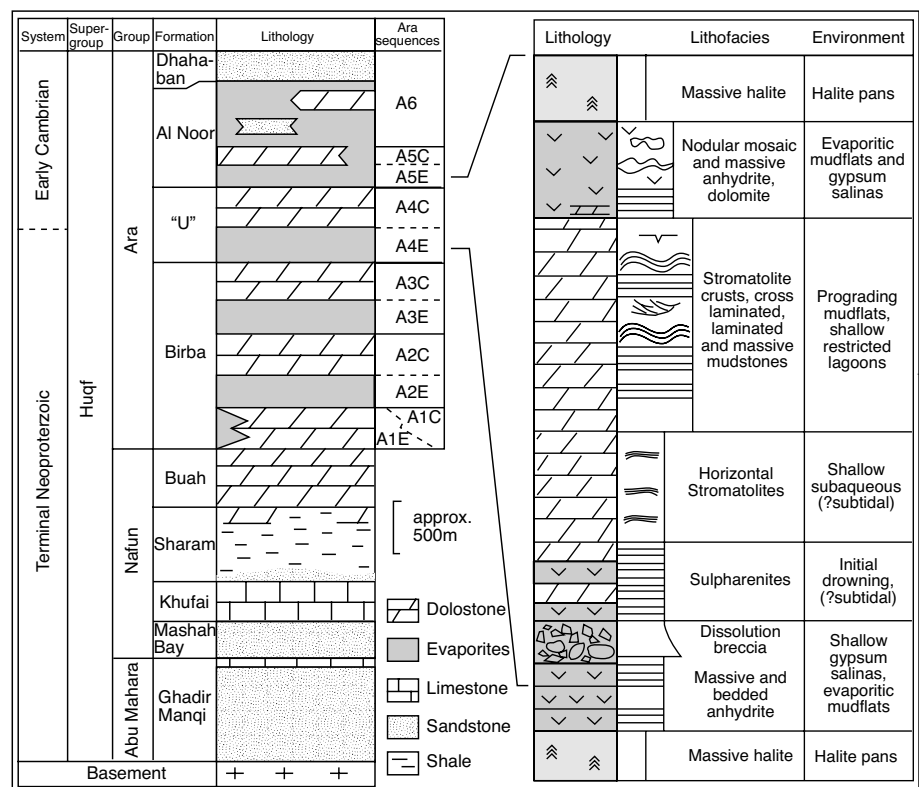


Figure 10.55. Stratigraphy of the Neoproterozoic-Early Cambrian Huqf Super group and a typical platform cycle (A4) in the Neoproterozoic Ara Formation of the South Oman Salt Basin (after Schröder et al., 2000a, b; 2003, 2005). Further out in the now chaotic central parts of the basin, some consider the Athel Silicilyte was originally deposited as a time-equivalent to the A4 carbonate, others argue it once lay immediately atop the unconformity capping the A3 carbonate (more likely). It can even be argued that in the original basin centre stratigraphy, prior to halokinesis, there was more than one level of mesohaline silicilyte deposition. This quandary could perhaps be resolved by more detailed determinations of basinwide versus platform evaporite signatures using wirelines and cores from across the basin).

tion, which, like the Athel, generates oil at low temperatures. Thin microfractures control production and much of the oil in fractures in this silicilyte reservoir is probably self-sourced from the adjacent matrix.

Based on the hydrology of Phanerozoic evaporite basin drawdown, I would argue that the time of Athel Silicilyte deposition probably corresponded to a hiatus in the accumulation of the platform carbonates. The palaeogeographic setting at the time of silicilyte deposition was that of a relatively-shallow restricted marine-fed sag basin. Silicilyte probably accumulated in the somewhat deeper density stratified (meromictic) portions of this rift or intracratonic sag basin immediately prior to the onset of a basinwide episode halite deposition in the central parts of the basin. At that time the basin was bound by exposed and hydrographically isolated carbonate-sulphate platforms along the basin edge. Waters in the basin centre at that time were probably mesohaline and density stratified, with the lower deeper parts of the brine column periodically if not perennially anaerobic (see Chapter 9 - basinwide mesohaline source rocks - style 1a). The silica matrix is considered to have been biochemically (bacterially) precipitated as primary microcrystalline quartz precipitates at ambient surface temperatures (Amthor and Frewin, 1999).

Inflow was via a hydrographically restricted entrance that with cutoff evolved into a marine seepage feed to a halite drawdown basin. Silica levels in Neoproterozoic seawater that were much higher than the biologically-limited silica chemistries of Phanerozoic seawater. Bottom stratification resulted in the preservation of substantial amounts of organic matter in the silicilyte and the formation of hydrocarbon source rocks of exceptional quality and thickness (SPI = 28-65 ton HC/m²; Amthor et al., *op. cit.*). The highest rates of silica accumulation are likely to have been in the distal parts of what were silicilyte half-graben depressions located well away from the source of clastic and carbonate input, much like the diatomites that typify Quaternary chert phases in the African and Turkish subaqueous lacustrine settings (Chapter 4).

Thick organic-rich basinal laminites are not uncommon in many marine-fed Proterozoic basins without an evaporite fill (e.g. oil and gas shales of the Velkerri Fm. of Central Australia; Warren et al., 1998). What makes the slivers in the Ara salt so economically interesting is that their organic maturation took place encased in halite. The liquid fraction could not leak away, so the matrix permeability did not degrade to levels where it was subeconomic, unlike the Mesoproterozoic oil shales of northern Australia and many other Proterozoic oil shales.

Subsalt reservoirs in compressional provinces

There are more than a dozen world-scale fold and thrust belts that have at some time slipped atop a layer of evaporites (Figure 6.33; Davis and Engelder, 1987). Such movement in a zone of horizontal compression often results in “thin-skinned” or gravity-driven tectonics and the deposition of sediments atop salt-cored growth folds. Deformation in the overlying rocks produces seafloor or landscape topography and syndepositional inhomogeneity in overburden porosity and thickness, as well as stress instability in the salt bed. Both processes can initiate diapirism and allochthon breakout in a compressional terrain. Even when there is no development of piercement from salt-cored anticlines, folds show considerable anticlinal thickening in the salt layer, and associated synclinal thinning, as in the Jura and the SE Zagros. Any diapirism typically follows fault planes or tensional shears in the overburden (Figure 6.46b, c).

Overburden deformation styles tend to have geometries that are controlled by the regional state of stress, and that geometry is frequently inherited by the salt structures. The close correspondence between the elongate salt structures of the North Sea and northern Germany to regional tectonic fabric clearly demonstrate this relationship (Figure 6.42). Perhaps the best-studied hydrocarbon province controlled by salt-influenced folding and thrusting is in the Zagros Mountain region of the Arabian Gulf. In terms of hydrocarbon volumes it is certainly the most prolific fold belt in the world and holds as much as a third of the total reserves of the Middle East. Beydoun et al. (1992) estimated that there is more than 200 billion barrels of recoverable hydrocarbon in the Zagros foreland basin.

Zagros Fold belt, Iran

Oil accumulations in anticlines of the Zagros Basin are the result of a Late Tertiary foreland basin foldbelt growing at the outer edge of the vast hydrocarbon-rich Palaeozoic-Mesozoic passive margin shelf of the Arabian plate (Beydoun et al., 1992; Versfeld, 2001). This foreland succession shares many of the same source rocks and salt seals as the relatively undeformed petroleum system of the Arabian Plate to the south. The compressionally driven folding and thrusting began in the Eocene and continues today, still driven by the collision of the Arabian and Iranian plates. Miocene uplift of the growing alpine belt and subsidence of the adjacent foreland created a hydrographically isolated subsealevel depression in an arid climate (Figure 5.27). The Fars/Gachsaran basinwide evaporite precipitated and today seals many of the giant and supergiant fields in the region.

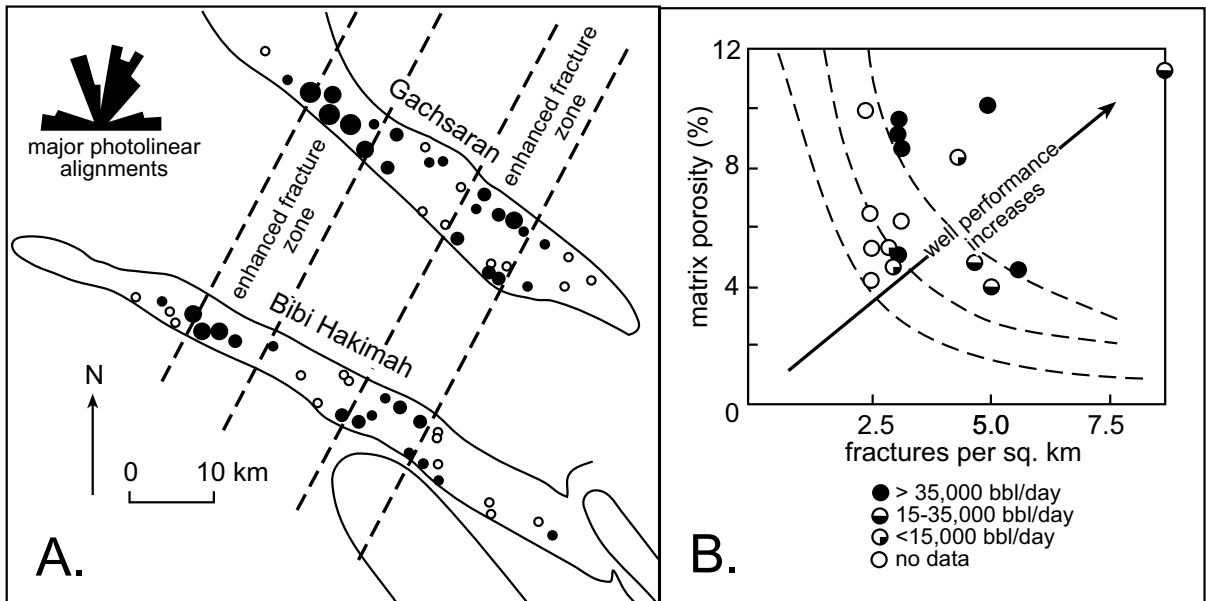


Figure 10.57. Gachsaran and Bibi Hakimeh fields, Iran (after McQuillan, 1985). A) Formline map; areas of solid circles are proportional to maximum allowed production rates. Open circles are non-commercial or nonproducing wells. High production wells lie in zones of enhanced fracturing induced by deformation controlled by basement features. B) Well production rates in Bibi Hakimeh Field as a function of matrix porosity and fracture density.

situated below Asmari production levels in the same wells in the same fold structures (multiple or stacked columns).

In its main producing area the Asmari Fm. is predominantly a shallow-water non-reefal micritic platform limestone containing minor dolomite. Matrix porosity and permeability are low (typical porosities of up to 15% and matrix permeabilities of up to a few millidarcies). The unit owes its excellent reservoir qualities to extensive brittle fracturing induced by Neogene compression (Figure 10.57). Wells intersecting fractured intervals of Asmari Limestone have tested at rates of up to 19,080 m³/day (120,000 bbl/day) and have sustained production rates of 12,700 m³/day (80,000 bbl/day), with estimated averages for wells producing from the fractured Asmari in various fields ranging from 3,180 to 3,975 m³/day (20,000 to 25,000 bbl/day). Where wells fail to penetrate fracture intervals in the Asmari in the same fields they are essentially nonproductive (Figure 10.57; Beydoun et al., 1992).

Second, the continent-to-continent approach prior to final collision and suturing created a subsealevel soft suture belt that in the Miocene hydrographically isolated the basin from the ocean and so deposited the Lower Fars or Gachsaran Formation as a marine-fed basinwide evaporite seal to the growing folds (Figure 5.27; Kashfi, 1983, 1985). The presence of this impermeable unit, with its anhydrite base and halite top, is

critical in sealing reservoirs in the Asmari Limestone and its equivalents and in maintaining seal integrity atop growing whaleback anticlines as underlying carbonates fractured and faulted. Erosion or nondeposition of the Lower Fars seal on growing folds to the northwest and southeast of the main producing Asmari folds in Iran and in parts of Iraq has destroyed the trapping potential of many otherwise suitable whaleback growth folds. And third, in the SE portion of the Zagros Belt, continent-to-continent collision acted as a huge bellows to the underlying Hormuz salt which by flowing up toward the surface further exaggerated the structural closure of many existing nearsurface folds and also reactivated older Jurassic structures further out in the Gulf.

Although the presence of an evaporitic seal overlying a reservoir is always good news for sealing hydrocarbons, a thick underlying salt unit deformed into salt structures that breakout onto the surface is not always so useful in terms of accumulating large quantities of hydrocarbons in large broadly draining structures. Along-strike changes in the tectonic style of the Zagros Mountains demonstrate this point. The NW part of the Zagros fold belt is the most prolific hydrocarbon area and is characterized by a thick and relatively deep section of fractured Asmari. It has been gently folded into whaleback anticlines and sealed beneath laterally continuous Gachsaran/Fars evaporites (Ala, 1982; McQuillan, 1985). There is no halokinetic surfacing of

Hormuz Salt in the Dezful area to break up the continuity of these broad anticlines. Oil fields in this part of the outer Zagros fold belt were relatively easy to define back in the 1920s by a combination of seeps and surface mapping and with development wells stepping out along anticlinal axes.

But salt cored folds in the region of the Zagros fold belt in southeast Iran are characterized by namakiers sourced in the underlying Hormuz Salt (Figure 6.45). Most of the fields in this region are relatively small and gas prone (Ala, 1982; Versfeld 2001). There the Asmari is thinner and often outcrops as erosionally-breached salt-cored anticlines. In addition the Fars Gachsaran is less evaporitic and more carbonate rich (Gill and Ala, 1972). The style of deformation in this area is uplift with salt-cored transtensional shear faults and greater vertical components to the fault breaches compared to areas to the west. This greater intensity and verticality perhaps relates to withdrawal of thick successions of Hormuz salt into adjacent salt diapirs and glaciers. During ongoing periods of vertical

uplift and diapir induced breaching many hydrocarbons either escaped through fractures in the exposed Asmari and its less evaporite-rich cap or underwent secondary migration, possibly becoming trapped on the western side of the Oman Mountains (Kashfi, 1983). Gravity-driven shear faults developed in association with salt intrusions and a poor development of an evaporite seal, probably facilitated the migration and escape of hydrocarbons.

The presence of a thicker Hormuz section in this part of the Arabian Gulf may well have prevented the transferral of the fracture system from the basement into the Asmari, the same fracture system that McQuillan (1985) uses in explaining the prolific production of the giant fields in the thrust belts further to the Northwest. Offshore from the Southern Zagros some large structural accumulations in the Tertiary strata may still remain to be discovered, but future onshore exploration will probably be for smaller stratigraphic or combination traps situated about and sealed by halokinetic structures.

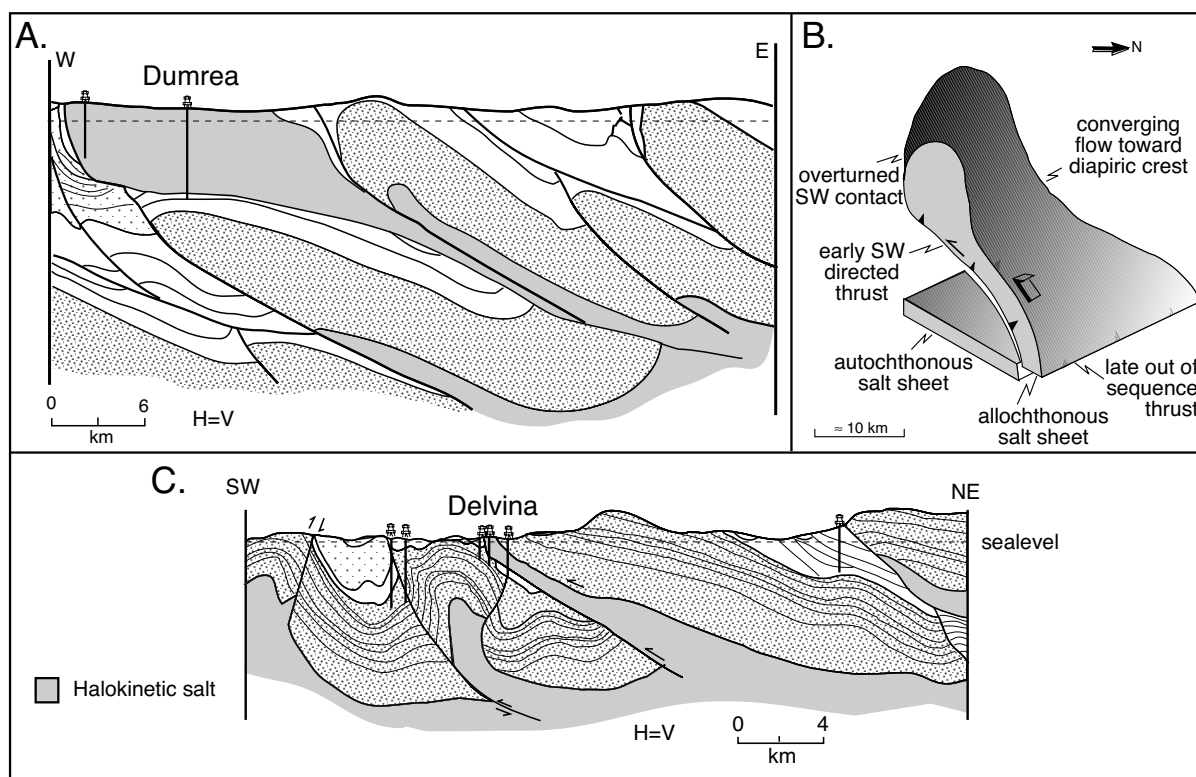


Figure 10.58. Giant fields in the Albanides, Ionian Basin. A) West-east-trending cross section through the Dumrea evaporite body showing the structure of Dumrea Field. B) Three-dimensional block diagram of the Dumrea diapir. C) Cross section of the Delvina gas condensate field trapped below a thrustured Triassic evaporite sheet (after Velaj et al., 1999; Velaj, 2001).

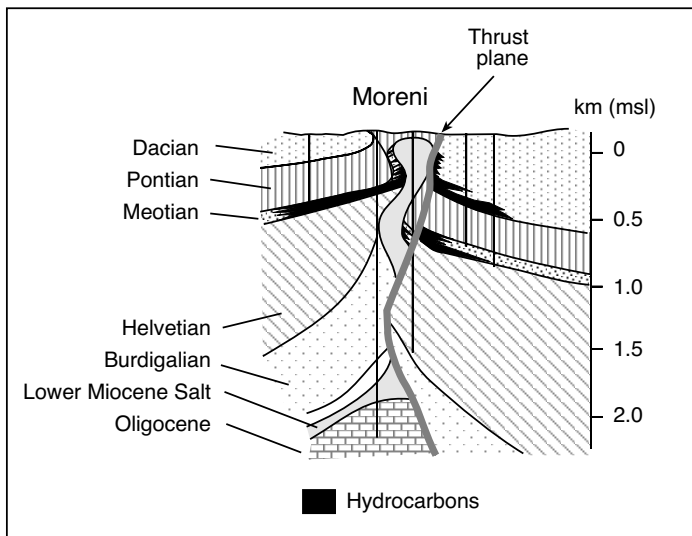


Figure 10.59. Cross section through the Moreni-Gura Ocniței oilfield, the largest field in the Carpathian foredeep. Productive sandstones are Pliocene in age. Structure is a sheared anticline where lower Miocene salt (grey) has lubricated the thrust and now forms a lateral seal to multiple reservoir sands. Also note the greater concentration of oil on the right side of the thrust, which is the downthrown side of the principal fault (after Paraschiv and Olteanu, 1970).

Alpine fold belt in Albania and Romania

Giant salt-sealed highly deformed salt structures characterise onshore oil fields in the compressional Alpine fold and thrust belt of the Ionian basin in Albania. The Triassic evaporites form a regional detachment layer (e.g. Figure 7.24c), but are also cut by thrust ramps that carry evaporites to the surface in their hanging walls (Figure 10.58; Velaj et al., 1999). Contraction of the Ionian zone reached a peak in the late Oligocene–Miocene Alpine Orogeny during an intense episode of overthrusting and major folding. The oil and gas fields in the region produce mainly from fractured Cretaceous–Eocene carbonates (e.g., Balshi-Hekal, Visoka, Gorisht-Koculi, Cakrani, Amonica, Finiq-Krane, and Delvina fields). Where a detachment is located at the top of the evaporite section, salts are dragged up in the footwall along thrusts. Faults develop both at the base and the top of the evaporite. Simple shear deformation along the thrusts causes greater than 80% thinning of the evaporite, so that thinned salt sheets of only 40–200 m thickness are now preserved in regions where the original evaporite thickness was in excess of 2000 m. Where thrust ramps cut through the evaporite and cause repetition of the complete evaporite layer, salt is remobilised into salt-filled compressional anticlines or it escapes at the surface to produce smeared-out allochthonous extrusions capable of sealing large volumes of hydrocarbons.

The most spectacular example of this is the Dumrea structure, where the mobilised evaporites have a complex shape that evolved from an overthrust allochthonous sheet, which today subcrops at the modern landsurface (Figure 10.58a). The Dumrea salt allochthon is up to 5.6 km thick, as proved by drilling, and has been displaced laterally by up to 25 km. It has the effective geometry of a giant sheath fold (Figure 10.58b). Untested traps still exist below the allochthonous evaporites and good quality non-biodegraded hydrocarbons are possible at depth, as was the case in the Delvina Field in southern Albania (Figure 10.58c). Shallower oil fields in the Albanides, not sealed by evaporites, typically contain very heavy oil due to ongoing bacterial degradation (e.g., Balshi-Hekali and Patos-Marinza fields).

The nearby Romanian section of the Carpathians Mountains of eastern Europe is another collisional thrust-fold Alpine belt where hydrocarbon accumulation is intimately related to the presence of smeared basinwide evaporites, in this case of Lower Miocene age (Figure 10.59; Paraschiv and Olteanu, 1970). Most of the reservoirs are Pliocene lacustrine sands, interbedded with fine-grained marls. The latter may well have been both source and seal. Suitable Pliocene sands with sufficient thicknesses and favourable reservoir facies only occur in the Ploiesti area at the convexity of the Carpathian Bend. Like the Zagros Mountains and the Albanides this hydrocarbon province is another halokinetic province where the original basinwide evaporites have been squeezed into a compressive layer during large scale thrust movement. Where thrust ramps toward the present surface the Miocene salt defines stocks, sills, dyke-like masses and other irregular shapes, whose original injection pathways were perhaps controlled by pre-existing diapirs, faults, folds and fault/fold intersections.

Rocky Mountain fold belt, USA

Deformed basinwide salt also plays a role in sealing the Nugget Sandstone reservoir in the Painter and East Painter fields of the Rocky Mountain thrust belt in the USA and the much more gently deformed sequence of Leadville Formation carbonates in the Lisbon Field, Utah. The Mississippian Leadville Limestone reservoir in Lisbon Field in the northern Paradox Basin, Utah, lies below a thick section of halokinetic Paradox salt and has produced some 50 mmbbl and 760 bcfg since its discovery in 1959 (Figure 10.60a). The trap is an elongate, asymmetrical,

northwest-trending salt-cored anticline with nearly 600 m of structural closure (Figure 10.60b; Miller 1985). The field is bound on its northeast flank by a major, basement-involved normal fault with nearly 760 m of displacement. A number of smaller northeast-trending normal faults dissect the reservoir into segments with fractured sweetspots located close to these secondary faults (Miller 1985). The Leadville Limestone was deposited as an open-marine, carbonate-shelf system with local crinoid banks, mud mounds and peloid/oolitic shoals. Two dolomite types characterise the Leadville reservoir, a tight stratiform micritic mimetic dolomite and a later coarser saddle dolomite. Solution-enlarged fractures and breccias are also common in the reservoir interval. The dichotomy in dolomite type and the association of the saddle dolomite with faults and fractures is similar to the evaporite-focused occurrences seen in Ghawar Field. But in the case of Lisbon Field the evaporite seal has gone one stage further. It has maintained its seal integrity even when the salt first underwent extension in the Palaeozoic and then compression during the Laramide orogeny. The oil in the structure is thought to be sourced from the overlying and now fractured Gothic Shale member in the Paradox Salt.

More highly deformed salt in the Painter and East Painter fields maintains its seal integrity atop the deformed and fractured reservoir intervals in the giant Painter and East Painter fields. The same salt also acts as the isolating décollement surface to the overlying overthrust plane (Figure 10.61a). The Painter reservoir structure consists of a rounded asymmetric fold in the Jurassic Nugget Sandstone reservoir (eolian) sealed by the Gyp-

sum Spring Member of the Twin Creek Limestone and the overlying salt. Significant thickening was accommodated in the underlying ductile Ankareh shales and the Thaynes limestones, which comprise the core of the structure (Figure 10.61b; Mitra, 2002). The forelimb of the structure is steep to overturned. A series of small-scale imbricates cut through this limb, but the displacement on these faults is relatively small and does not control the geometry and structural relief of the structure. The tightness of the structure also results in the formation of one or more out-of-syncline thrusts on the forelimb, which terminate upward within the salt unit and downward within the Twin Creek limestones. These out-of-syncline thrusts were folded during the later stages of deformation.

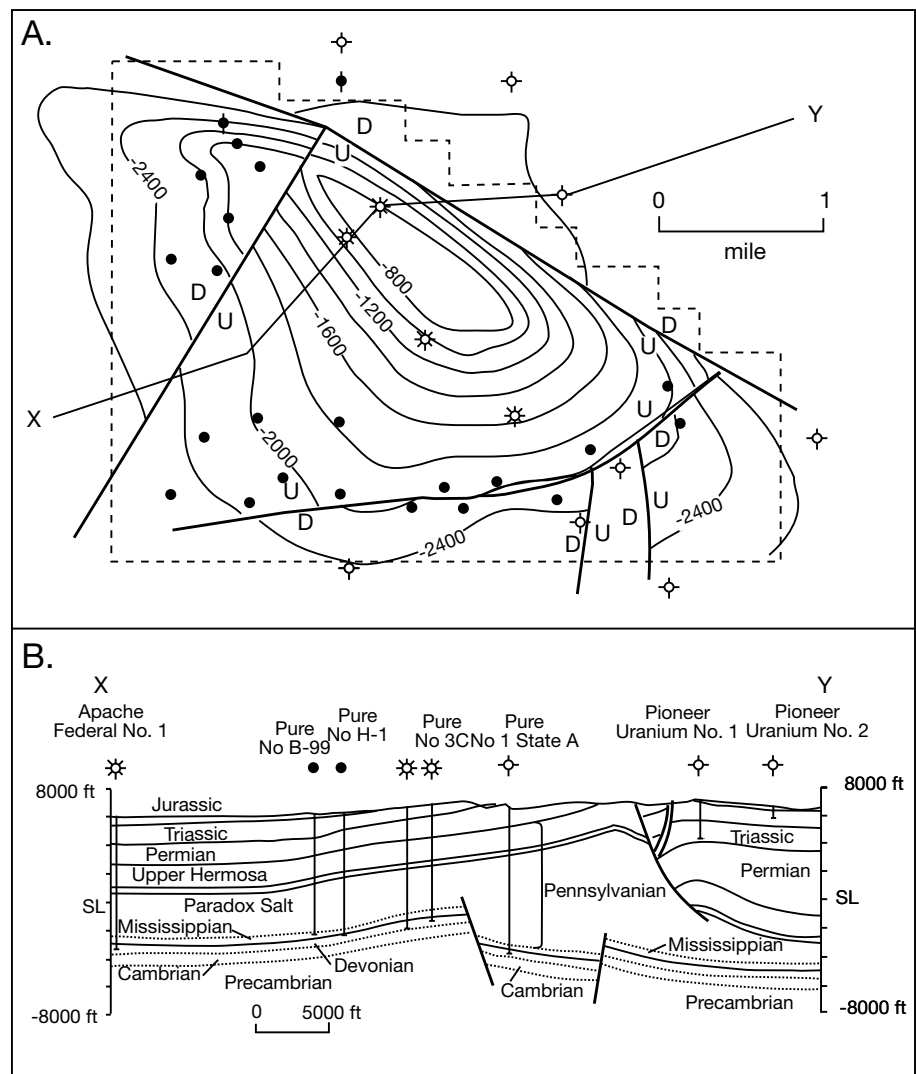


Figure 10.60. Lisbon Field, Utah. A) Depth to top of the Leadville Formation (Contours in feet subsealevel). B) Regional cross section X-Y across the field showing its position beneath the seal of halokinetic Paradox Salt (after Miller 1985).

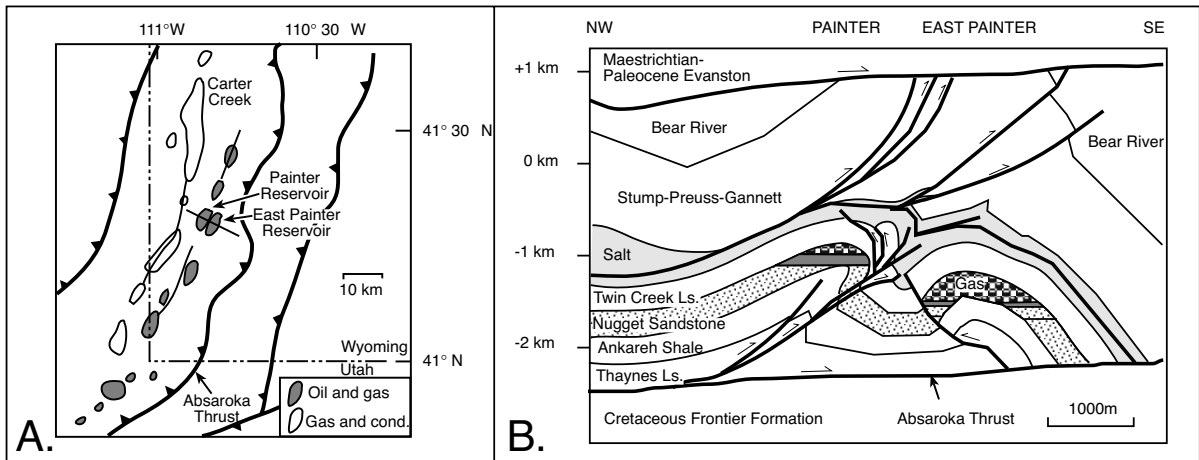


Figure 10.61. A) Geologic map of the Idaho-Wyoming-Utah fold and thrust belt showing some of the major oil- and gas-producing structures in the Absaroka thrust sheet. B) Interpretive cross section through the Painter reservoir and East Painter reservoir structures. (after Mitra, 2002).

The East Painter reservoir structure is a west-vergent detachment fold, formed above the hanging-wall cutoff of the Mesozoic units atop the Cretaceous detachment (Figure 10.61b). The steep frontlimb of this structure is also cut through by a west-vergent thrust. The convergence of the two opposite-vergent structures results in significant disharmonic folding within the Twin Creek limestones and the overlying salt. Interestingly, the hydrocarbons stored in the Nugget Formation sands were sourced in stratigraphically younger but now underlying Cretaceous mudstones (Lamb, 1980).

Evaporite Solution

Collapse-related traps can form early within the depositional setting, or much later during catbaric salt removal. A dissolving subsurface salt unit creates zones of differential collapse, which can induce economic levels of fracturing in the overburden. Where the effects of a shallow dissolution edge reach the landsurface it creates a depression, which focuses deposition of sand, mud or even reefal buildups around its rim (Figure 7.7a; subsidence trough). If it does not reach the surface it still affects brittle overburden as it creates fractures that increase permeability. Either style of dissolution creates anomalous fluid movements, diagenetic haloes, and reservoir modification that can form a structural anomaly at the seismic scale. Salt dissolution breccias that define the position of former salt units or intervals of former salt cements can contribute to the permeability of the fractured overburden interval.

An association between salt collapse, fracturing and oil production is proven in the oil and gas fields of southeast Saskatchewan, southeastern Montana and southwestern North Dakota (Smith and Pullen, 1967; Swenson 1967). Examples include reservoirs in Upper Devonian carbonates of the Hummingbird Field (Birdbear Formation), and the Dolphin, Fryburg, Kisbey, Flat Lake, Medoria-Scoria, Outlook, Star Valley, Tatagwa, Tule Creek, Walpole and West Hope fields. In their study of reservoir porosity in Devonian reef and bank carbonates of western Canada Beales and Oldershaw (1969) make the observation that, “much of the so-called primary porosity in reef reservoirs may be evaporite solution porosity.” Salt collapse depressions in the landscape also focused deposition of Cretaceous reservoir sands in the Mannville Formation in Westhazel Field. Subsurface salt bed leaching and collapse has also contributed to porosity distribution in various North Sea fields (Jenyon and Taylor, 1983; Lohmann, 1979) and to the fracture-focused creation of porosity in hydrothermal dolomites in the platform carbonates of the Rainbow/Zama Basin.

The various salt collapse reservoirs in Devonian carbonates of Canada are typified by fractures and solution-enlarged vuggy to karstic pore systems in what are otherwise dense carbonates. These reservoirs have porosities exceeding 20-30% and permeabilities in the range of darcies. The fields are small but their location makes them economic. Hummingbird Pool has produced more than 3 million barrels and Kisbey more than 1.6 million barrels. The Hummingbird oil pool was discovered in September 1966 on the northwest flank of the Williston Basin by drilling a semi-circular collapse-fill structure covering 2.6 km², thought to be a pinnacle reef prior to drilling (see

Figure 7.5 for location of Hummingbird Trough). Oil in the Hummingbird structure is produced from fractured 15 m-thick algal and bioclastic limestones of the Mississippian Charles Formation and 17m-thick vuggy dolomites of the Devonian Birdbear Limestone. The structure was created by local solution collapse followed by complete regional dissolution during multiple episodes of Prairie Evaporite solution loss during the Late Devonian and Early Mississippian.

Synthesis of the various styles of dissolution induced traps in the Alberta Basin of Canada and the Williston Basin in the USA shows the dissolution process is broad ranging, variable in terms of timing and tied to the dissolving edge of the Prairie Evaporite (Figure 7.5) Compactional drapes can create a rollover anticline that is closed over the dissolved edge of a residual salt body (Figure 10.62a; Anderson et al., 1988; Anderson and Knapp, 1993, Parker 1967). Local solution or collapse can form a sediment-filled sink that transforms to an inverted thick with the ongoing solution of the surrounding salt (Figure 10.62b; a “pseudo-reef” - Anderson and Hunt, 1964). Or subsidence can form a focused sand infill within a solution-induced depression on the land surface (Figures 7.7, 10.62c); or it can form as a remnant of a formerly widespread sand unit that was ultimately preserved only in sediment-filled depressions within the salt bed (Figure 10.62d). Seismic is very useful in defining the

lateral and vertical extent of many collapse anomalies and, if properly acquired and processed, can be used to define internal stratigraphy and reservoir development. Salt collapse structures can lead to focused oil entrapment in fractures in what otherwise may be a “tight” overburden lithology (Figure 7.8). A breach in a dissolving salt bed can also create structural and stratigraphic closure in the overburden. This is especially so if the collapse anomaly occurs “on-salt”, i.e. within a breach surrounded by, or adjacent to, the dissolving salt edge.

Ongoing fluid throughflow prior to oil emplacement in intervals above a dissolved salt bed or collapse chimney may have become pervasively cemented and thus rendered impermeable. Even so, the interval may then provide a seal for fractured and leached reservoirs still being created along the downdip side of the adjacent collapse basin. Collapse structures in the carbonate overburden may be multistage structures located “off-salt”, i.e. in areas where all salt has been removed, as in the classic “Hummingbird” oil trap. Hummingbird drape was created by sequential collapse and its pinnacle-like appearance in seismic gave it the name “pseudo-reef” in early exploration programmes in the Alberta Basin (Figure 10.62b). When dissolution is early, sediments often thicken above the areas of dissolution and thin in the areas over the remaining salt outlier. These overlying sediments can develop the same types of porosity patterns that

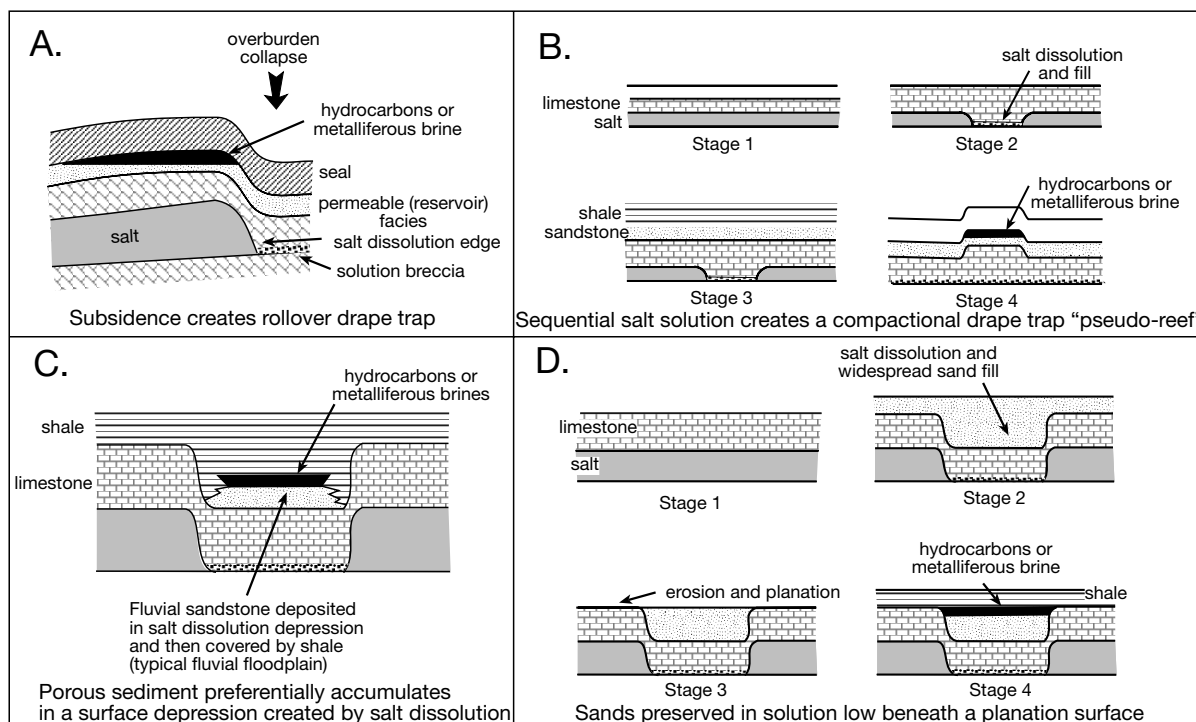


Figure 10.62. Styles of structural and diagenetic trap created by localised salt solution (in part after Anderson et al., 1988).

form above salt ridges. Sometimes the salt dissolves in stages and so creates sequential thickened beds up section as the locus of salt dissolution shifts. In Figure 10.62b, two areas of sediment thickening are created by salt dissolution; the first forms in stage 2, the second in stage 4. This and later differential compaction and drape can create reservoirs above salt remnants (high in stage 2) or by later differential compaction (stages 3 and 4). Other solution traps may be “on-salt,” the result of compactional drape over a single stage fill of a salt solution trough such as at Kisbey Field (Figure 10.62c, d).

Collapse has also created reservoirs in quartz sands such as Berry Field and the Westhazel pool in Lower Cretaceous fluvial sandstones of Alberta. These reservoirs were created by depositional focusing of fluvial sands at the migrating edge of the dissolving subsurface salt of the Prairie Evaporite (Hopkins, 1987). Compared with most stratigraphic traps in Cretaceous sands in the region, the Berry Field is unusual in its occurrence on the flank of a local structural high within a larger regional structural depression. This unusual synclinal setting for the reservoir is a direct indication of its origin as a fluvial system within a landscape position controlled by salt solution.

The Westhazel General Petroleum Pool of west-central Saskatchewan, Canada, produces from the GP member of the Lower Cretaceous Mannville Group and is an excellent example of reservoir stacking in a salt dissolution trough (Figure 10.63; Anderson and Cederwall, 1993). The reservoir facies consists of fine- to medium-grained quartzose sandstones. The lateral

uniformity and coarsening upward appearance of this unit and the uniform thickness of the underlying and overlying shales indicates that the General Petroleum Member was deposited in a relatively shallow, marine environment. The pool was discovered in 1971 and produced in excess of 60,000 m³ (380,000 barrels) of heavy oil from the marine sandstones of the General Petroleum (GP) Member.

This reservoir is structurally closed across the updip, eastern dissolutional edge of the underlying Middle Devonian rock salt of the Leofnard Member of the Prairie Evaporite. The leaching of these salts occurred in post-Mannville time in the Westhazel area and caused the regional southwest dip of the General Petroleum member to be locally reversed (Figure 7.5). The thin, 10 m-thick reservoir facies at Westhazel does not exhibit a diagnostic signature on either seismic or gravity data. Rather, it is the updip edge of the salt, across which the reservoir is closed, that can be mapped using geophysical techniques.

On seismic data, the dissolutional edge of the Prairie salt is characterized by: (1) a subtle decrease in the amplitude and lateral coherency of the underlying Winnipegosis event; (2) a gradual thinning of key encompassing Palaeozoic intervals; (3) dip reversal along the Beaverhill Lake (Late Devonian) event; (4) dip reversal along the Mannville (Lower Cretaceous) event; and (5) time-structural “push down” of Lower Cretaceous and underlying reflections in areas of recent salt dissolution (salt is characterised by fast seismic velocities). On the gravity profile, the edge of the salt is manifested as a 1.5 mGal anomaly. The

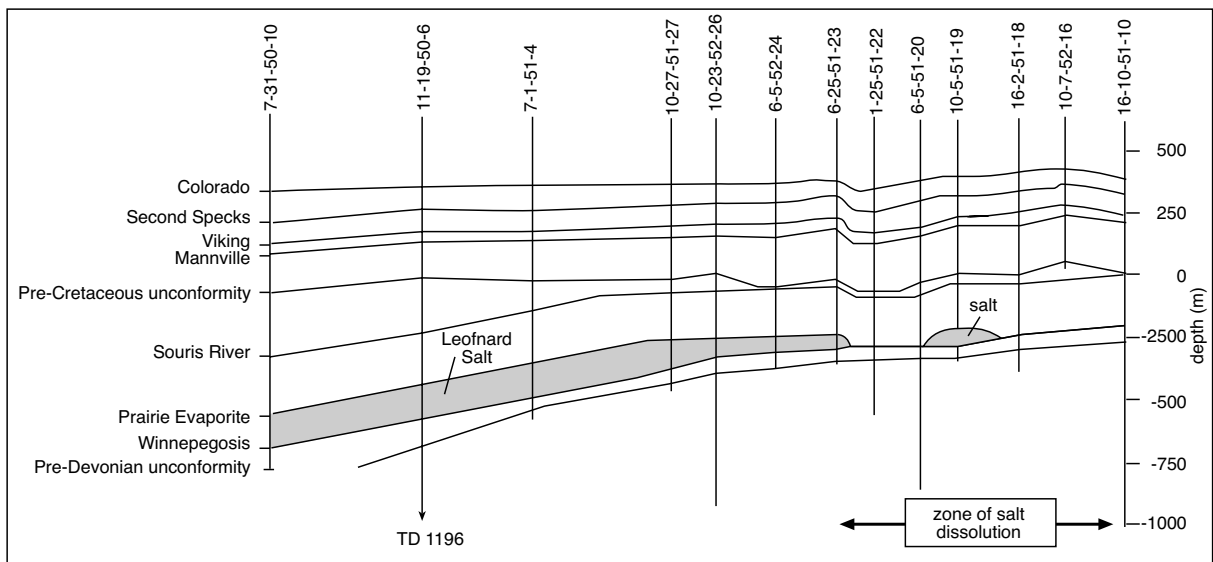


Figure 10.63. Schematic section illustrating the eastern dissolutional edge of the Prairie Formation. The Westhazel study area straddles T50 and T51 in R23W3M - see Figure 7.5 for location (after Anderson and Cederwall, 1993).

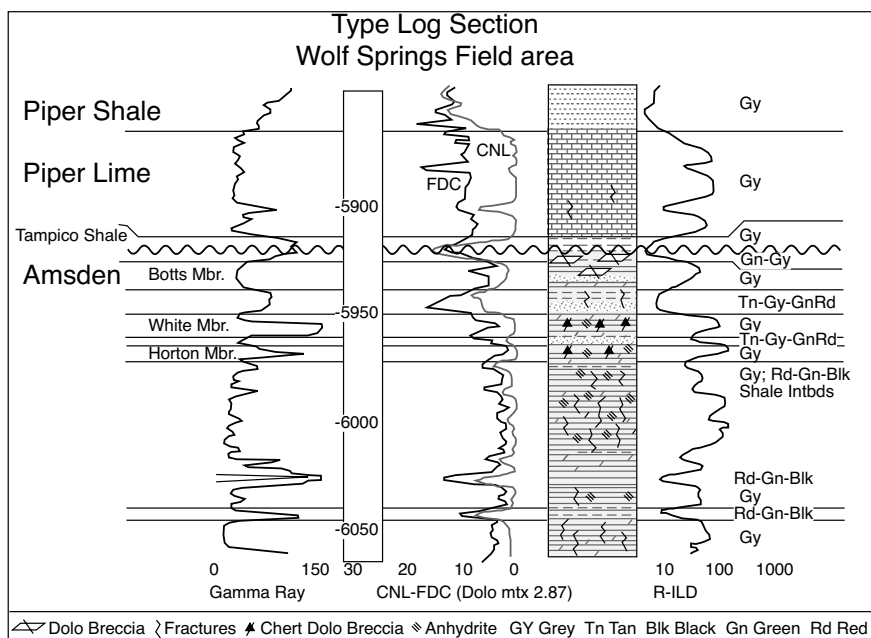


Figure 10.64. Type log for the Wolf Springs Field area. The Botts, White, and Horton members of the upper Amsden are readily discernible as resistive kicks. The White and Horton members correspond to the zones of solution-collapse breccias. The Botts member is a shaly dolomite breccia. The lithologies shown in the Amsden and Piper formations represent compilations assembled from cores in the area (after Luebking et al., 2001).

interpretation of both geophysical data sets is consistent with available geologic control. For more detailed information on salt solution traps the interested reader is referred to an excellent summary paper by Anderson and Knapp (1993).

Occasionally, the solution breccia created by the dissolution of salt can itself act as the reservoir rather than just fracturing and structuring the overburden. This is the case with Wolf Springs Field (north and south pools) and South Wolf Springs Field, located in Yellowstone County, Montana (Luebking et al., 2001). The Wolf Springs fields are unconformity-related combination structural and stratigraphic traps (Luebking et al., 2001). The fields are located on a structural closure on the Custer anticline, where porosity and permeability development exhibits a northeast-southwest orientation perpendicular to structural strike of the anticline. The solution-collapse breccias pinch out laterally into either dense dolomites or anhydrite-plugged collapse breccias. The overlying shaly dolomite breccia of the Botts Member, located just below the Piper unconformity, and the Jurassic Piper Limestone together provide the top seal.

The Wolf Springs and South Wolf Springs fields were discovered in 1955 and 1957, respectively, and have produced more than 5.7 million barrels of oil from the Pennsylvanian Amsden Formation. Amsden reservoir rocks in the area are fractured and

brecciated cherts and dolomites that occur in several laterally persistent and mappable zones (Figure 10.64). The Amsden was deposited in a peritidal to sabkha setting, where evaporite minerals, mainly anhydrite, were once common. These evaporites were partly replaced by silica (chalcedony and chert) soon after deposition. Later dissolution of the remaining evaporites not long after the silicification event, or during the preMiddle Jurassic unconformity, produced the solution-collapse chert breccias that now serve as the best reservoir facies in the field. Subtle variations in the diagenetic history of these breccias are a major factor in shaping reservoir quality.

Interestingly, not all hydrocarbon-reservoirs in salt entraining basins typified by stratiform breccias in carbonate platforms are related to earth-bound dissolution processes. The Cantarell oil field in the Campeche Platform of Mexico, with a current daily production of 1.3 million barrels of oil, is probably the most voluminous oil-producing unit with fracturing related to a bolide impact event. The K-T breccia reservoir itself, its ejecta horizon and its sealing muds are related to the same bolide event that wiped out the dinosaurs (Grajales-Nishimura et al., 2001).

Chapter 11: Evaporites as exploited mineral resources

A history of salt usage

Sodium chloride (halite), the most common industrial evaporite salt, is used in some form by virtually every person in the world. There are more than 14,000 reported usages of halite and more than 30 references to salt in the Bible. Halite, along with other salts, has long played a very important role in human affairs. Some 3,200 years ago Bronze-Age Celtic miners were extracting salt near Hallstatt in Austria, from a network of several kilometres of galleries up to 300 metres below the surface. Seventeen hundred years later some ten pages deal with salt in the "De Re Metallica" by Georgius Agricola (Georg Bauer), both mining it and producing it from seawater. Published in 1556, his was the first book on mining to be based on field research and observation. Until the 19th Century and the advent of refrigeration, salt's main uses were as a preservative and as a much sought after additive to flavour foodstuffs (Kurlansky, 2002). Without salt, the human metabolism cannot function. Even today, most people think of salt in terms of sprinkling it on their food, or in colder climates they may also think in terms of road de-icing. These are in fact lesser modern usages of halite; its main use is as a feedstock in the chemical industry.

The human body's need for salt gave it military significance; the earliest recorded war over access to a supply of salt was over a salt lake in China in 3000 BC. The words, 'war' and 'peace' originate from the words for salt and bread in ancient Hebrew and Arabic. In the American Civil War the salt production facilities in Saltville, Va., Virginia's Kanawha Valley and Avery Island, Louisiana, were early targets of the Union Army. The North fought for 36 hours to capture Saltville, Va., where the salt works were considered crucial to the Rebel army - so crucial that Confederate President Jefferson Davis offered to waive military service to anyone willing to tend coastal salt kettles to supply the South's war effort. In addition to dietary salt, the Confederacy needed this precious mineral to treat wounds, tan leather, dye cloth for uniforms and to preserve meat and other foodstuffs. Thousands of Napoleon's troops died during his retreat from Moscow, because for lack of salt their wounds would not heal.

Early hominids lived on the edge of the saline Lake Olduvai (Hay and Kyser, 2001) and salt was part of their diet. In ancient Greece it was so valuable that the slave trade involved an exchange of salt for a slave and gave rise to the expression, "not worth his salt." Some 4,700 years ago the Peng-Tzao-Kan-Mu was published in China. It is probably the earliest known treatise on pharmacology, with detailed discussions

of the palliative and curative powers of more than 40 kinds of salts, including descriptions of two methods of recovering usable salts from brine. In 2200 BC the Chinese emperor Hsia Yua declared that Shandong Province must supply the Imperial Court with salt. An ancient Chinese philosopher once called salt "the sweetest thing on earth."

In Europe, the first recorded industrial production of pan salt took place in Italy some 2500 years ago when Ancus Martius, one of the early Roman kings, began letting sea water into an enclosed basin, then allowing the sun to evaporate the water to create a salt residue. The importance that Rome attached to the salt works and port at Ostia was such that the main highway along which the salt was carried to Rome was called the Via Salaria. Like Venice after it, the city of Rome based much of its early commerce on trading salt. Special salt rations paid to early Roman soldiers were known as "salarium argentum", the forerunner of the English word "salary." With a near monopoly on supply to Rome, the traders in the port of Ostia raised the salt price so high that the state was forced to take over the industry in 506 BC.

When Julius Caesar landed in Britain in 55 BC, he brought his salinators with him, but found that even the backward Britons were extracting salt by pouring brine on to hot stones. The Romans, however, used iron pans in which they boiled the brine, and Caesar established a brine-based salt works in Cheshire and subsequently in other localities. The towns in Britain where salt was made can be distinguished to this day by the termination "wich", an Anglo-Saxon descriptor for a place where salt was made and includes towns like Greenwich, Ipswich, Droitwich, Northwich and Middlewich. Merchants in 12th-Century Timbuktu in Africa, the gateway to the Sahara Desert and the seat of renowned scholars, valued salt as highly as books or gold. In Tibet, Marco Polo noted that tiny cakes of salt, manufactured from salt lakes in the high plains of Tibet were pressed with images of the Grand Khan and used as coins. Salt is still carried by camel trains and still used as money among the some of the nomadic tribes of the Sahara and Ethiopia's Danakil Plains. The ancient Maya made salt at Salinas de los Nueve Cerros, Guatemala, an area where natural salt springs flowed into a river gully, giving easy trading access to downstream customers. This site was the only large-scale source of salt for the interior Lowland Maya. Maya technology included solar evaporation and firing of brine from salt springs in special large ceramic bowls that are the largest receptacles ever found in any Maya sites.

Type	Mineralogy	Source	Uses
Ammonium Chloride	NH ₄ Cl	Brine Processing	Fertiliser, industrial additive
Ammonium sulphate	(NH ₄) ₂ SO ₄	Brine Processing	Fertiliser
Borate	B ₂ O ₃	Borax (tincal), Boracite, Colemanite, Hydroboracite, Kernite, Ulexite	Glass, ceramics, fibreglass, textile manufacture, agricultural chemicals, pharmaceuticals, flux cleansing agent, water softener, preservative and fire retardant
Bromine (sodium bromide)	Br ₂ , NaBr	Brine Processing	Additive
Calcium sulphate	CaSO ₄	Gypsum, secondary after anhydrite	Construction industry, plaster, cement retardant, soil enhancer
Iodine	I ₂	Brine Processing	Animal feed supplements, catalysts, inks and colorants, pharmaceutical, photographic equipment, sanitary and industrial disinfectant, and stabilisers
Lithium	Li	Brine Processing, hectorite in some saline clays	Production of ceramics, glass, and primary aluminium, battery technology, pharmaceutical
Magnesium carbonate, Magnesium oxide, Magnesium sulphate	MgCO ₃ , MgO, MgSO ₄	Brine Processing, magnesite, electrolytic processing	Majority used for refractories. A constituent in aluminium-base alloys, used for packaging, transportation, and other applications. Remainder is consumed in agricultural, chemical, construction, environmental, and industrial applications
Potash	KCl, KNO ₃ , K ₂ SO ₄	Sylvite, sylvinitite, brine processing	Fertiliser, chemical industry
Sodium carbonate	Na ₂ CO ₃	Trona, solvay process, brine processing	Glass manufacture, chemicals, soap and detergents, pulp and paper manufacture, water treatment, and flue gas desulphurisation
Sodium chloride	NaCl	Halite, brine processing	Food processing, chemical and industrial products, chloralkali industry, swimming pool additive, stockfeed additives
Sodium sulphate	Na ₂ SO ₄	Mirabilite, thenardite, glauberite, brine processing	Detergent powder, glass, pulp and paper
Strontium	Sr	Celestite, strontianite	Television faceglass (decreasing use), ceramic magnets, colouring agent in pyrotechnics and signals
Sulphur	S ₂	Biogenic sulphur, Frasch process	Agricultural chemicals, chemicals manufacture, metal mining, and petroleum refining

Table 11.1. Evaporite salts as a mineral resource.

Salt's economic value meant it was taxed by governments from the ancient Chinese and Romans to late medieval Europe. In 2200 BC the Chinese Emperor Hsia Yu levied a salt tax as one of the world's first documented taxes. Mary Queen of Scots was perhaps the first European head of state to have the idea of making salt a source of governmental revenue. She granted a patent to an Italian to make salt in Scotland and then placed a heavy tax on it, which she appropriated to herself. Elizabeth, Queen of England, and Mary's lifelong "dear sister" and eventual executioner, thought this an excellent idea and likewise taxed English salt making. Salt tax was a source of great resentment to everyone, English and Scots alike, and smuggling grew to alarming proportions. In 1785, the Earl of Dundonald wrote that every year in England, 10,000 people were arrested for salt smuggling. During Queen Anne's reign, the salt tax rose to £30 a ton, an enormous amount of money in those days. The whole of England arose in rioting protest, with the result that the salt tax was finally abolished.

In Burgundy, salt was taxed at more than 100% as it came from the salt-works. This tax was extended to the whole of France when Burgundy was absorbed and the notorious salt tax "la gabelle" became a necessary input to the government's finances. Cardinal Richelieu said that salt was as vital to France as American silver was to Spain. The repeal of the salt tax was a major goal of the revolutionaries of 1789, but Napoléon restored the salt tax to pay for his foreign wars as soon as he became Emperor and it continued until 1945 to feed French government coffers. It is said that income from a salt pan in southern Spain largely financed Columbus' voyages. The Erie Canal, an engineering marvel that connected the Great Lakes to New York's Hudson River in 1825, was called "the ditch that salt built" as salt taxes paid for half of the cost of construction. The "Great Hedge of India," the mid-18th century colonial equivalent of the Great Wall of China, stretched 3,700 km from the western border of Punjab down to the Bay of Bengal. It was manned by 12,000 men and planted by the British to minimise

salt smuggling into Bengal and enforce the collection of the Indian salt tax. As late as the 1940s the people of India under the leadership of Mahatma Gandhi protested British taxes on salt supply. In 1930 he led a 200-mile march to the Arabian Ocean to symbolically collect untaxed salt for India's poor.

Salt, because of its value in the ancient world, still has religious significance. Ancient Greek worshippers consecrated salt in their rituals. Jewish temple offerings included salt; on the Sabbath, Jews still dip their bread in salt as a remembrance of those sacrifices. Covenants in both the Old and New Testaments were often sealed with salt, explaining the origin of the word "salvation." In the Catholic Church, salt was or is used in a variety of purifying rituals. Jesus called his disciples "the Salt of the Earth", a statement that was commemorated by the Catholic church until Vatican II, by placing a small taste of salt on a baby's lip at his or her baptism. In Leonardo Da Vinci's famous painting, "The Last Supper," Judas Escariot has just spilled a bowl of salt - a portent of evil and bad luck. In Buddhist tradition, salt repels evil spirits. That's why in many Asian cultures it's customary to throw salt over your shoulder before entering your house after a funeral: it scares off any evil spirits that may be clinging to your back. In 1933, the Dalai Lama was buried sitting up in a bed of salt. Shinto religion also uses salt to purify an area. Before sumo wrestlers enter the ring for a match - which is actually an elaborate Shinto rite - a handful of salt is thrown into the centre to drive off malevolent spirits. In the American Southwest, the Pueblo worship the Salt Mother. Other native American tribes had significant restrictions on who was permitted to eat salt. Hopi legend holds that the angry Warrior Twins punished mankind by placing valuable salt deposits far from civilization, requiring hard work and bravery to harvest the precious mineral.

Today, halite is a cheaply produced commodity extracted either from mines or salt pans. In the production of table salt, processing, packaging and marketing are the major costs. An exception to the low sale price of modern salt is "Fleur de Sel de Geurande" a delicate gourmet form of white seasalt that is still hand-produced on the fens along the coast of Brittany. It costs \approx US\$40/kg and is produced by "paludiers" only on suitable summer days when halite rafts can be raked from the brine surface of specially maintained coastal salt pans, which are floored with grey clay. According to the local legend it only forms when the wind blows from the east (from the sea). It and the cheaper grey salt (sel gris), which is scraped from the pan floors and also prized by gourmands, has been produced this way since Pre-Roman times. Impurities like this clay are called grey spot or black spot in highly efficient mechanised

production plants elsewhere in the world and are considered undesirable in the end product. It says something about French marketing skills, and perhaps the gullibility of middle-class gourmands with too much money and time on their hands, that each year the gourmet industry successfully markets dirt-polluted salt for top prices.

Salts other than halite have a diversity of usage (Table 11.1). Potash salts are used mostly as agricultural fertiliser, while the sodium salts, halite-trona-glauberite, are major feedstocks in the formation of a wide range of industrial chemicals. Gypsum is used in plaster and cement manufacture throughout the world. This chapter first focuses on the potash salts and then on the other industrial salts and the products of alteration associated with evaporite salts, such as sulphur and zeolites; emphasis is on depositional and diagenetic modes of formation. Halite and gypsum (anhydrite), the two most commonplace salts, are not considered in the same detail as the other salts in this chapter as their deposition and diagenesis was discussed in earlier chapters.

Annual production figures and tables for the various salts in this chapter were compiled from the raw data sheets in various pdf-format documents held on the US Geological Survey web site <<http://minerals.er.usgs.gov/minerals/pubs/commodity/>>. In addition to the cited references, other very useful sources used extensively in the compilation of this chapter were the excellent books on industrial minerals by LeFond (1983), Harben and Bates (1990), Garrett (1995, 1998, 2004) and Harben and Kuzvart (1996).

Potash salts

Natural potash evaporites are part of the bittern series precipitated at the surface or in the shallow subsurface at the higher concentration end of the evaporation series. Today the deposition of thick beds of potash minerals at the earth's surface is a relatively rare occurrence. The extremely high solubility of potash means it can only accumulate in highly restricted, some would say highly continental, settings (Cendon et al., 2003). Where it does occur as beds in the modern playas of Qaidam in China and in the Danakil Depression of Africa, carnallite, not sylvite, is the precipitated salt. This has led some to postulate that carnallite is the primary marine potash phase, while sylvite is a secondary diagenetic mineral formed by incongruent dissolution of carnallite. Others have argued that ancient sylvite was sometimes a primary precipitate deposited by the cooling of highly saline surface or nearsurface brines

Mineral	Composition	K ₂ O %	Comments
<i>Chlorides</i>			
Sylvite	KCl	63.2	Principal ore mineral
Carnallite	MgCl ₂ ·KCl·6H ₂ O	16.9	Ore mineral and contaminant
Kainite	4MgSO ₄ ·4KCl·11H ₂ O	19.3	Important ore mineral
<i>Sulphates</i>			
Polyhalite	2CaSO ₄ ·MgSO ₄ ·K ₂ SO ₄ ·2H ₂ O	15.6	Ore contaminant
Langbeinite	2MgSO ₄ ·K ₂ SO ₄	22.7	Important ore mineral
Leonite	MgSO ₄ ·K ₂ SO ₄ ·4H ₂ O	25.7	Ore contaminant
Schoenite (picromerite)	MgSO ₄ ·K ₂ SO ₄ ·6H ₂ O	23.4	Accessory
Glaserite (aphthitalite)	K ₂ SO ₄ ·(Na,K)SO ₄	42.5	Accessory
Syngenite	CaSO ₄ ·K ₂ SO ₄ ·H ₂ O	28.7	Accessory
<i>Associated minerals</i>			
Halite	NaCl	0	Principal ore contaminant
Anhydrite	CaSO ₄	0	Common ore contaminant
Bischofite	2MgCl ₂ ·12H ₂ O	0	Accessory contaminant
Bloedite (astrakanite)	Na ₂ SO ₄ ·MgSO ₄ ·2H ₂ O	0	Accessory
Loewite	2MgSO ₄ ·2Na ₂ SO ₄ ·5H ₂ O	0	Accessory
Vanthoffite	MgSO ₄ ·3Na ₂ SO ₄	0	Accessory
Kieserite	MgSO ₄ ·H ₂ O	0	Common ore contaminant
Hexahydrite	MgSO ₄ ·6H ₂ O	0	Accessory
Epsomite	MgSO ₄ ·7H ₂ O	0	Accessory
<i>Ores</i>			
Sylvinitite	KCl+NaCl	10-35	Canada, USA, Russia, Brazil, Congo, Thailand
Hartsalz	KCl + NaCl + CaSO ₄ + (MgSO ₄ ·H ₂ O)	10-20	Germany
Carnallitite	MgCl ₂ ·KCl·6H ₂ O + NaCl	10-16	Germany, Spain, Thailand
Langbeinitite	2MgSO ₄ ·K ₂ SO ₄ + NaCl	7-12	USA, Russia
Mischsalz	Hartsalz + Carnallite	8-20	Germany
Kainitite	4MgSO ₄ ·4KCl·11H ₂ O+NaCl	13-18	Italy

Table 11.2. Potassium salts.

or from seawater with ionic proportions different to those of today (Figure 2.30).

Phanerozoic potash salts comprise two distinct groups: MgSO₄-rich and MgSO₄-poor. Potash salts have not been recovered from Precambrian sediments other than in minor amounts in the Neoproterozoic Ara Salt of Oman. Potash deposits rich in MgSO₄ are composed of some combination of gypsum, anhydrite, polyhalite, kieserite, kainite carnallite and bischofite. Potash deposits free of, or poor in, MgSO₄ are dominated by some combination of halite, carnallite, and sylvite. This latter group constitutes a majority of exploited Phanerozoic potash. The hydrogeochemical significance of the two groups was

discussed in Chapter 2; this chapter emphasises the geology of potash salts.

Potash is the generic term for a variety of ore-bearing minerals, ores and refined products, all containing the element potassium in water-soluble form (Table 11.2). It was originally used to describe the mixture of potassium carbonate and potassium hydroxide crystals, which were recovered in heated iron “pots” from boiling the washings of wood (or other plant) “ashes,” both the recovered potash salts were caustic. Lye meant sodium hydroxide and potash lye was potassium hydroxide, a higher grade product that was used in the manufacture of higher-grade softer or facial grade soaps.

Since the 1950s the terms potash or potash salts have been used commercially as general descriptions of potassium chloride (KCl or muriate of potash), potassium sulphate (K₂SO₄ or sulphate of potash), potassium-magnesium sulphate (K₂SO₄ MgSO₄ or sulphate of potash magnesia), potassium nitrate (KNO₃ or saltpetre), or mixed sodium-potassium nitrate (NaNO₃ +KNO₃ or Chilean saltpetre). The most common naturally occurring potash minerals are carnallite and sylvite, with sylvite the most economically important. Other common potassium-entraining evaporite ores include: kainite, kieserite, langbeinite, leonite and polyhalite (Table 11.2).

In 2004 there were 14 potash producing countries, including small volumes from the Ukraine and Chile. The North Americas produce 36% of the world’s total potash production, eastern Europe and Russia some 30%, western Europe 19%, and the

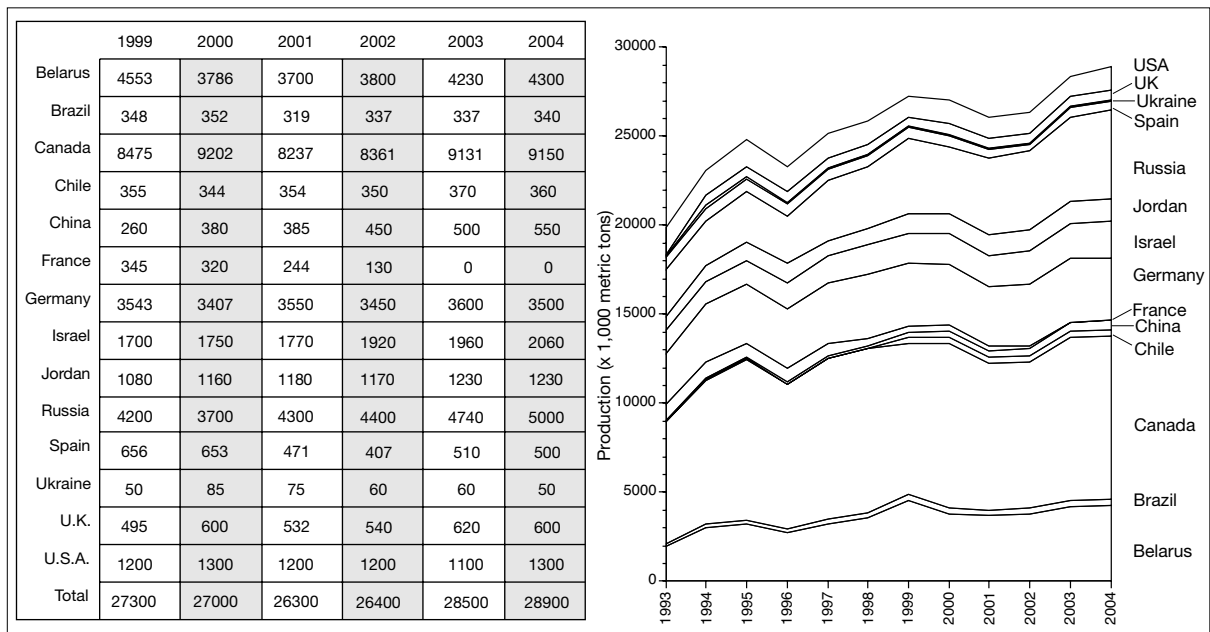


Figure 11.1. World potash production in thousand metric tons^{11.1} of K₂O equivalent - (compiled from USGS on-line data tables downloaded from <http://minerals.usgs.gov/minerals/pubs/commodity/> last accessed 30 September, 2005).

Dead Sea 11% (Figure 11.1). Of total world production, just ten companies control 90%, and the five largest companies control more than 75%. Canada, the world's largest producer holds more than 35% of the world's potash reserves, and recovers potash by conventional underground mining of bedded sylvinite deposits. Production is centred on the Devonian Elk Point Basin in Saskatchewan, with lesser production in the Maritime Provinces and Quebec. Devonian potash is also mined in the Pripyat depression of Belarus. Permian potash is mined from the northern margin of the Delaware Basin in New Mexico, USA; from the Zechstein of Europe (Germany, UK and the Netherlands); and from the Upper Kama Basin in the Russian Federation in the Solikamsk region west of the Urals. Oligocene potash is extracted from the Rhine graben in France, while Miocene potash is mined in the Stebnik area in the western Ukraine. In Spain, in the northern part of the Ebro Basin near the border with France, potash is produced from Eocene-Oligocene lake sediments. In Utah, potash is solution mined from Tertiary playa deposits and recovered from the brine by solar evaporation and flotation. Israel uses similar solar technology to produce large volumes of potash from lake brines created naturally from recycled marine Miocene evaporites and connate waters buried beneath the

floor of the Dead Sea. In California, potash and coproducts, borax pentahydrate, soda ash and saltcake, are recovered from various subsurface playa brines using mechanical evaporation. Sylvite is also a byproduct of nitrate processing in the Atacama Desert of Chile, South America.

The fertiliser industry uses more than 90-95% of produced potash, and the chemical industry uses the remainder in the manufacture of soaps and detergents, glass, ceramics, synthetic rubber and numerous industrial chemicals. About 70% of the potash is produced as potassium chloride and sylvite is the preferred ore mineral in most mines. Potassium sulphate and potassium magnesium sulphate, required by certain crops and soils, comprise about 25% of potash production. Retailers typically sell potash, or potash blended with other fertilisers, in dry or liquid form. Potash is a source of soluble potassium, which is one of the three primary plant nutrients; the others are fixed and soluble phosphorus and nitrogen. Mankind's use of these three nutrients, in commercial forms, started the "Green Revolution" in agriculture.

Other uses of the various potash salts include KCl as a mud additive to stabilise reactive clays in oil well drilling. It is also used in aluminium recycling, in various steel heat-treating processes, metal electroplating, snow and ice melting, and water softening. Potassium chloride is used by the chlor-alkali industry to produce potassium hydroxide. The alkali potassium hydroxide

^{11.1} 1 metric ton (tonne) = 1,000 kilograms = 2,204.6 pounds
1 metric ton (tonne) = 0.9842 ton (imperial)

is used for industrial water treatment and is the precursor of; potassium carbonate, several forms of potassium phosphate, many other potassic chemicals, and is the main ingredient in soap manufacture. The alkaline salt potassium carbonate is used with strontium and barium carbonate in the faceglass for televisions and computer monitors (used as radiation screen, but is a decreasing use with advent of digital flatscreens), alkaline batteries, food products, pharmaceutical preparations, photography, some fire extinguishers, animal feed supplements, and as a catalyst for synthetic rubber manufacture. Generally, the nonagricultural uses account for no more than 5-10% of annual world consumption.

Although it is today a low cost commodity, the importance of potash to world agricultural economy means it is worthwhile gaining a detailed understanding of how potash salts accumulate in a variety of depositional and diagenetic settings. First, we shall look at some Quaternary deposits and then at some ancient counterparts.

Quaternary potash

Natural modern potash accumulations are rare: there are only two well documented examples of substantial Quaternary potash accumulations, namely, the Qaidam Basin in China and the Danakil Depression in Ethiopia. Other examples where carnallite or sylvite are forming today are either minor efflorescences and thin crusts in continental lakes, playas and soils, or are artificial products, either precipitated by enhanced solar pond evaporation of seawater, as in Lake McLeod in Australia, or by evaporation of lake and pore waters pumped into surface pans as in the Dead Sea in the Middle East. Sylvite occurs naturally as a widespread pedogenic salt along with nitrates in the hyperarid regions of the Atacama Desert in Chile.

Playas of the Qaidam Basin

The high plateau region of northern Qinghai-Xizang in west central China north of Tibet contains large endorheic lake basins with thick fills of Mesozoic and Cenozoic nonmarine sediments (Figure 11.2). The modern at-surface playas and salt lakes are subject to intense evaporation and are characterised by hypersaline brines and in some by accumulations of potash and borate evaporites. Lake Dabuxum is of special geological interest as it is one of the few localities in the world where significant quantities of potash salts are precipitating today (Yang et al., 1995; Vengosh et al., 1995; Casas et al., 1992).

The Qaidam Basin is a large intermontane sedimentary and structural basin at the northern margin of the Qinghai-Tibet

Plateau. With an area of 120,000 km², it has an extent that approaches that of some of the moderate to small ancient continental "saline giants," but the active-salt accumulating salt lakes are a much smaller proportion of the basin and only occupy its lower parts (Figures 5.5, 11.2). The Plateau encompasses a large, tectonically active plain, bound by mountains, filled with clastic and evaporite sediments and is totally isolated from the ocean (Figure 11.2). The Kunlun Mountains bound the basin to the south, the Altun mountains to the west and the Qilian Mountains (that reach 5,000 m above sea level) bind the northern portion of the basin. The basin centre has an average elevation of 2,800m and contains numerous shallow to ephemeral saline lakes and dry saline pans.

The Qarhan playa or salt plain, with an area of some 6,000 km², is the largest saltflat in the Qaidam Basin and is underlain by bedded halite (Figure 11.3). It is a broad flat plain floored by a layered halite pan crust with a permanent groundwater brine lens located 0 to 1.3m below the surface. The surface crust consists of a chaotic mixture of fine-grained halite crystals and mud, with a rugged, pitted upper surface (Schubel and Lowenstein, 1997). Vadose diagenetic features, such as dissolution pits, cavities and pendant cements, form where the salt crust lies above the water table. Interbedded salts and siliciclastic sediments underlie the crust to reach thicknesses of up to 75m, and over the last 50,000 years have formed the potash-hosting Qarhan Salt plain or playa (Kezao and Bowler, 1985). Patchy carnallite, hosted in bedded halite, occurs in karst cavities in the upper 13m of the Qarhan playa sequence (Figure 11.3).

The compositions of fluid inclusions in primary (chevron) halite in the various Qahan salt crusts represent preserved lake brines and indicate relatively wet conditions throughout most of the Late Pleistocene (Yang et al., 1995). Oxygen isotope signatures of the inclusions record episodic freshening and concentration during the formation of the various salt units interlayered with lacustrine muds. Desiccation, sufficient to allow halite beds to accumulate, occurred a number of times in the Late Quaternary: 1) in a short-lived event \approx 50,000 ka, 2) from about 17 - 8,000 ka, and 3) from about 2,000 ka till now (Figure 11.3). Modern halite crusts in Qahan playa contain the most concentrated brine inclusions, suggesting that today may be the most desiccated period recorded over the last 50,000 years. Measurements of inclusions in early diagenetic halite that formed from shallow groundwater brines (clear halite spar between chevrons), confirm the climatic record derived from primary (chevron) halite. The occurrence of carnallite-saturated brines in fluid inclusions in the diagenetic halite in the top 13 m of Qahan playa sediments also imply a diagenetic, not depositional origin

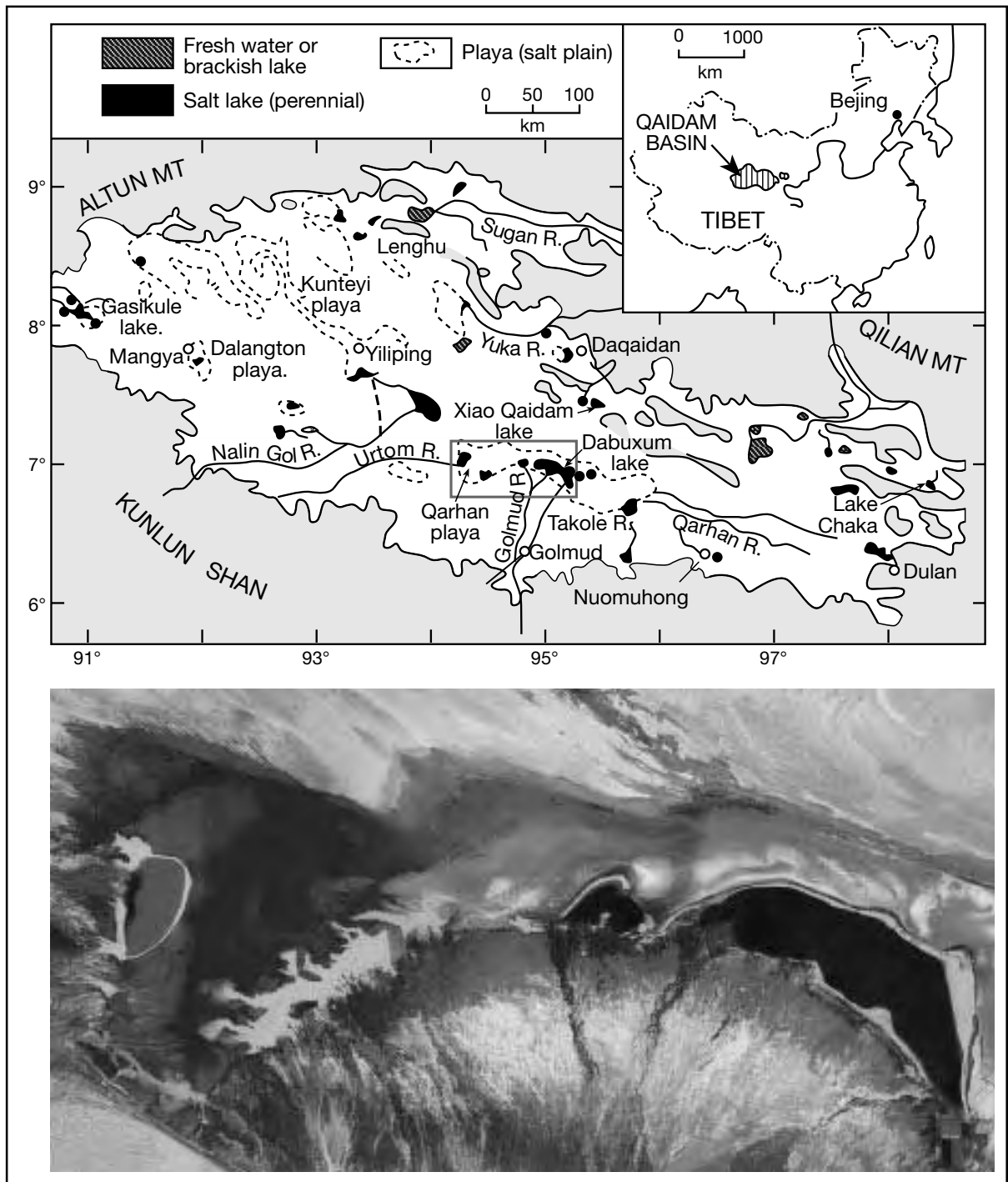


Figure 11.2. Location of salt lakes, freshwater lakes and playas in the Qaidam Basin, China. The Landsat image shows the Golmud fan delta feeding into Lake Dabuxum and the adjacent Qahan playa salt flat, the lake on the eastern side edge of the Qahan playa salt flat is Xiao Lake. Grey box on locality map shows position of the satellite image (Landsat image courtesy of NASA).

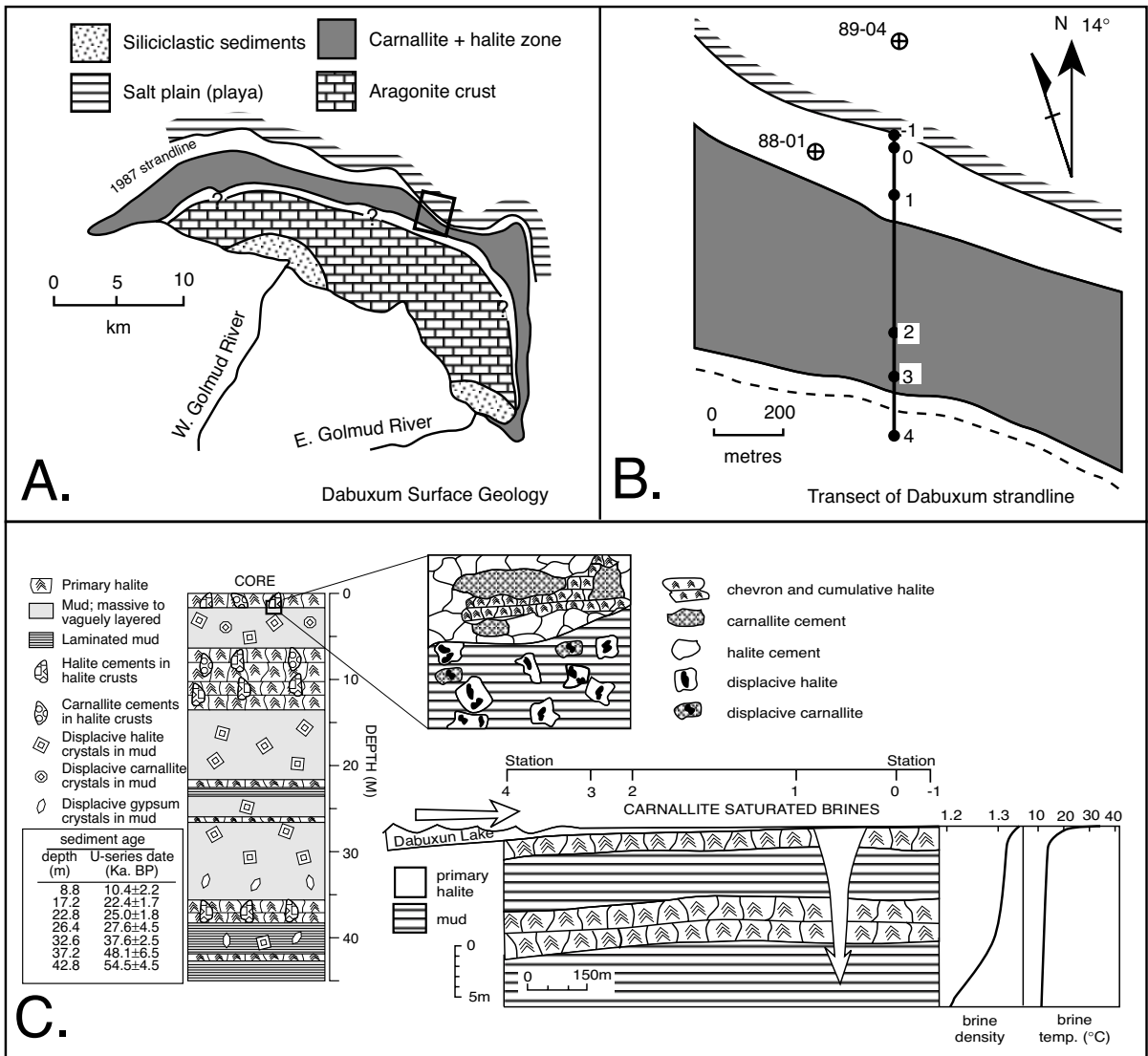


Figure 11.3. Geology of carnallite in Lake Dabuxum area of the Qahan playa, Qaidam Basin. A) Distribution of surficial sediment types also showing the position of enlarged region seen in B - see Figure 11.2 for location. B) Strandline geology of the northern shore of Lake Dabuxum showing position of coring traverse as shown as inset in C. C) Cross section showing how the process of brine cooling forms carnallite cement in the karstic voids in shallow subsurface halite crusts and creates karst-filling cement textures (after Casas et al., 1992).

of carnallites that locally accumulated in the same voids as the more widespread microkarst halite cements.

Today the salt plain of the Qahan playa encloses 10 shallow perennial saline lakes and is fed mostly from the Kunlun Mountains (Kunlun Shan). The largest lake on the Qarhan Salt Plain is Dabuxum Lake; an area where carnallite has recently accumulated along the strandline (Figure 11.2; Casas et al., 1992; Casas, 1992). The greatest volume of water entering the lake comes from the Golmud River (Figures 11.2, 11.3a).

Cold springs, emerging from a linear karst zone some 10 km to the north of the strandline, also supply solutes to the lake. Thus, evaporation of a mixture of river water and spring water creates the carnallite-saturated brines of the Dabuxum Lake system (Lowenstein et al. 1989).

Surface sediments of Dabuxum Lake are zoned (Figure 11.3a, b). The southern part of the lake, closest to the Golmud River delta, is underlain by fine-grained siliciclastic sediments that pass lakeward into a centimetre-thick aragonite crusts, which

floor much of the water-covered area of the lake. A small island in the centre of Dabuxum Lake is made up of mud and silt laminae coated by microcrystalline aragonite and mud chip breccias cemented with aragonite. Stacked halite pan crusts define most of the subaerial Qahan playa saltflats to the north of the perennial lake.

Surface efflorescent crusts of halite and carnallite accumulated along the edges of Dabuxum Lake from 1987-1989 with carnallite reaching thicknesses of up to 0.3 m along a strandline zone approximately 1 km wide. The water-covered lake area at that time was approximately 250 km² and waters were less than 1m deep (Casas et al., 1992). The carnallite crust was brine-saturated, poorly cemented and had a mushy consistency. It was dominated by equigranular, anhedral carnallite crystals up to 5 mm in diameter. Thin sub-centimetre layers of very fine grained (submillimetre) carnallite and siliciclastic mud occurred within the carnallite mush. Individual carnallite crystals in the mush were often linked with textures identical to rafts or films of fine-grained carnallite, which could be seen floating on the surface of the very shallow brines near the lakeshore. Rafts were being blown onto the strandline or left behind on the lake floor as the drying brine sheets retreated from the northern strandzone of the lake. Strandline carnallites underwent extensive syndeositional diagenetic modification depending on daily temperature and weather conditions. In a single two-week period, dominated by fine sunny weather with daily temperatures up to 35°C, carnallite precipitated in the afternoon as rafts, or as centimetre-size, needle shaped skeletal crystals, or as efflorescent puffs of submillimetre crystals on evaporitic mudflats wherever the brine level was below the surface.

Light rains and strong southwest winds are common in the summer in Qaidam Basin. During such storms Dabuxum lake waters are blown over the halite-encrusted north shore and pond as thin brine sheets (Figure 11.3b). For example, vigorous winds on 6 and 10 August 1988 shifted the northern lakeshore several hundred metres north (Casas et al., 1992). These overlapping open lake waters were at or slightly below halite saturation and considerably below carnallite saturation. The carnallite strand zone was modified and partly dissolved after being covered by these waters but was re-established during subsequent warm days. In a subsequent large flood, during July to September 1990, the Dabuxum Lake area expanded from 250 km² to 800 km², while the associated freshening of the expanded lake completely dissolved the carnallite crust. Clearly, surface carnallite along the north

shore of Lake Dabuxum is an ephemeral strandzone sediment with little or no preservation potential.

However, carnallite has been widely precipitated and preserved in the upper 13 m of the 45m thick interbedded clay-halite succession that underlies the modern Lake Dabuxum strandline (Figure 11.3c). These subsurface carnallites are diagenetic void-filling cements and displacive crystals, which indicate a carnallite distribution with a strong temperature control. As dense carnallite-saturated lake brines sank into the underlying sediment they cooled and so precipitated carnallite in preexisting karst holes and pits in the halite bed (Figure 11.3c; Casas et al., 1992). The voids in the halite were created by earlier lowerings of the water table, alternating with times of freshening of the lake waters, with both events occurring numerous times prior to the accumulation of the present salt crust. This style of secondary nearsurface carnallite as early cements in the active phreatic zone is texturally analogous to much of the secondary carnallite and sylvite karst-fill fabric seen in ancient potash deposits in Thailand, Canada and the USA.

Danakil Depression, Ethiopia

The Danakil Depression (aka Dallol Depression) of Eritrea is an area of intense hydrothermal activity related to rift magmatism and deep brine cycling, located in the axial zone of the Afar rift near the confluence of the East African, Red Sea and Carlsberg rifts (Holwerda and Hutchison, 1968; Hutchinson and Engels, 1970; Hardie, 1990). The depression is the northern part of the Afar depression and runs parallel to the Red Sea coast but is some 50 to 80 km inland and separated from the sea by the Danakil Mountains. It is 185 km long, 65 km wide, with a floor 116 metres below sea level in the deepest part of the depression. A shallow volcano-tectonic barrier behind Mersa Fatma prevents hydrographic recharge or even seawater seepage into the current depression from waters of Howakil Bay, which is some 50-60 km WNW of Ito Aichil on the Red Sea coast. In terms of daily temperature the floor of the Danakil is one of the hottest places on earth; year round the daily temperature is above 34°C and in summer every day tops 40°C, with some days topping 50°C.

A halite-floored elongate saltpan covers the deepest part of the Danakil Depression over an area some 40 km long and 10 km wide, (Figure 11.4). The pan's position is asymmetric; it lies near the depression's western edge, some 5km from the foot of the escarpment to the Balakia Mountains, but some 50 km from the eastern margin of the depression. Pleistocene halite beds, exposed by uplift, deflation and water table lowering,

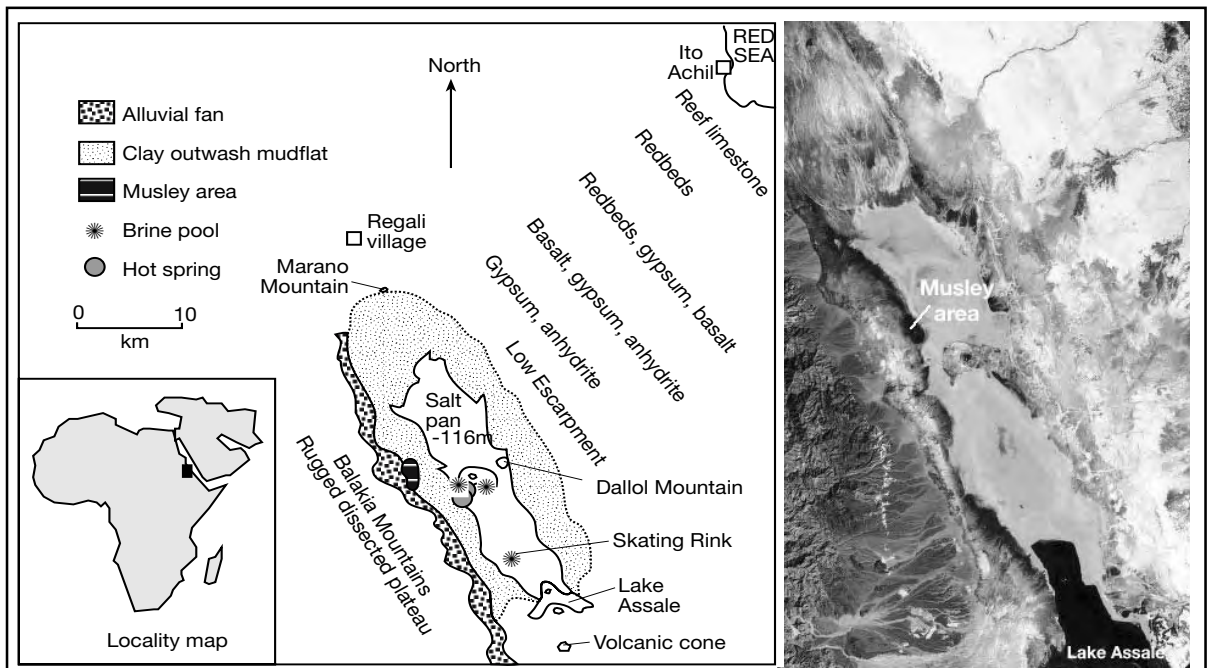


Figure 11.4. Location and geological features of the saline pan located in the northern half of the Danakil Depression, Eritrea (geological map after Holwerda and Hutchison, 1968; Landsat image courtesy of NASA).

outcrop about the salt crusted parts of the northern Danakil, and form low flat-topped plateaus or mesas on the plain, which are heavily dissected and eroded by occasional storm runoff and rainfall. More than 970 metres of halite-dominated Quaternary evaporites have accumulated beneath the present salt pan of the Northern Danakil, along with interbeds of gypsum, anhydrite and shale (Holwerda and Hutchison, 1968; Augustithis, 1980). Similar bedded evaporites probably underlie the entire Danakil depression, but lava flows and alluvium obscure much of the southern part of the depression beyond Lake Assale (Figure 11.4).

In the Musley area the km-thick subcropping Quaternary halite fill contains one and perhaps two dipping potash beds (Figure 11.4). The upper potash bed lies at a depth of 38-190 metres and has been cored in a number of wells, while the lower bed is at a depth of 596m near the western end and it has been interpreted only from gamma logs. Both units dip to the east and the deepest they were encountered by the drill was at 683 and 930 m, respectively.

The upper potash interval in the Musley area is between 15 and 40 metres thick; it consists of a basal member rich in fine-grained laminated kainite (4-14m thick), an intermediate carnallite member (3-25 m thick), and an uppermost stratiform sylvinite member (0-10 m thick) with lenses of carnallite, kieserite,

kainite or polyhalite. It is overlain by and eroded and etched with a 4-15 m-thick halite unit. Finely laminated and layered textures show that kainite and carnallite members are primary or syndepositional precipitates.

Core through the sylvinite member has three types of barren zone within it: a) the entire sylvinite bed is replaced by a relatively pure stratiform halite with dispersed nodules of anhydrite, b) zones up to 23 m across of pure crystalline halite within the sylvinite bed and c) linear potash depleted zones defined by coarsely crystalline halite. Bedding plane spacing and layering in the halite in styles a and b are similar to that in the adjacent sylvite bed. Contact with throughflushing freshened waters probably created most of the barren zones in the sylvinite. Fluid crossflow may also have formed the sylvite of the upper member via selective surface or nearsurface leaching of $MgCl_2$ from its carnallite precursor (Holwerda and Hutchison, 1968). Due to its secondary origin, the proportion of sylvite in the sylvinite member decreases as the proportion of carnallite increases, along with kieserite, polyhalite and kainite.

Beneath the sylvinite member, the carnallite member contains a varied suite of non-commercial potash minerals that in addition to carnallite include, kieserite, kainite (up to 10% by volume) and polyhalite, along with minor amounts of sylvite. Minor anhydrite is common, while bischofite and rinneite may

occur locally, along with rust-red iron staining. Sylvite is more abundant near the top of the carnallite member and its proportion decreases downward, perhaps reflecting its groundwater origin. Kainite is the reverse. The sylvinite member and the carnallite member also show an inverse thickness relationship. Bedding in the carnallite member is commonly contorted with folded and brecciated horizons interpreted as slumps. The base of the carnallite member is defined as the level where carnallite forms isolated patches in the kainite before disappearing entirely.

The kainite member is composed of nearly pure, fine-grained, dense, relatively hard, amber-coloured kainite with $\approx 25\%$ admixed halite. Texture and colour are characteristic of the unit, but even more so are the distinct “ruler-straight” bedding planes in the kainite, a striking contrast to the wavy, contorted and irregular bedding planes of the carnallite and sylvinite members. The preponderance of MgSO_4 salts in these Pleistocene evaporites means they most likely formed by the evaporation of seep-supplied seawater.

This is in marked contrast to the present hydrology of the Danakil Depression (Hardie, 1990). Today hot springs, rich in basinal CaCl_2 , supply and maintain the active brine pools and lakes of the Depression. Lake Giulietti (Lake Afrerá), with an area of 70 km^2 and a floor some 120m below sea level, is located within the active volcanic field of the southern Danakil. Both the inflowing hot springs ($40 - 50^\circ\text{C}$) and the brines of the lake itself are rich in CaCl_2 and poor in MgSO_4 . Extensive concentration of these lake waters will eventually lead to deposition of an MgSO_4 -poor series of salts dominated by sylvite, carnallite, halite and CaCl_2 salts. This will be in marked contrast to the thick underlying MgSO_4 -rich Pleistocene evaporites of the Musley area. It seems that seawater was much more important as a brine source in the Pleistocene than today.

Interaction between hot basinal groundwaters and volcanic bedrock is the likely explanation of the present inflow chemistry. Dissolution of the earlier highly soluble potash evaporites in preference to the less

soluble Mg-salts also plays a part. Many hot brine springs in the geothermally active area in around the Danakil salt pan are rich in FeCl_2 , sulphur and manganese, clearly indicating a hydrothermal interaction of saline groundwaters with volcanics and giving a bright red-orange colour to many of the mineral assemblages precipitating in and about active springs.

Inland chotts and coastal sabkhas in North Africa

Chott el Djerid in southern Tunisia is an endorheic playa where ephemeral carnallite crusts accumulate as efflorescences and intercrystalline cements in the uppermost parts of the central portions of the saline pan facies (Figure 11.5; Bryant et al., 1994a, b). The chott has an area of approximately $5,360 \text{ km}^2$ in a drainage basin with an area of $10,500 \text{ km}^2$. Mean annual rainfall for the area is 80–140 mm, the mean annual temperature is 21°C and evaporation, which is highest between May and September, has a mean annual value of 1500 mm.

Chott el Djerid is the largest in a zone of chotts formed where a series of regional aquifers emerge to create a region of discharge playas along the northeast extremity of the Bas Saharan Artesian Basin (Figure 11.6a). The basin covers most of the Algerian and Tunisian Sahara, extends into Morocco and Libya

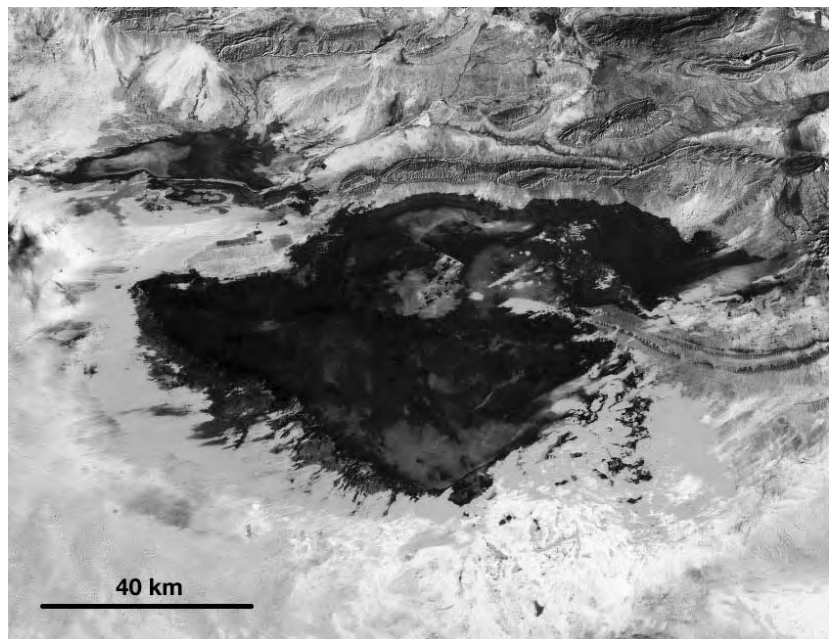


Figure 11.5. Chott el Djerid, Tunisia, showing the extensive saline mudflat that characterises the lowermost part of this inland depression. A surface geology map of the saline mudflat in northeastern portion of this region is given in Figure 11.6c. (Landsat image courtesy of NASA).

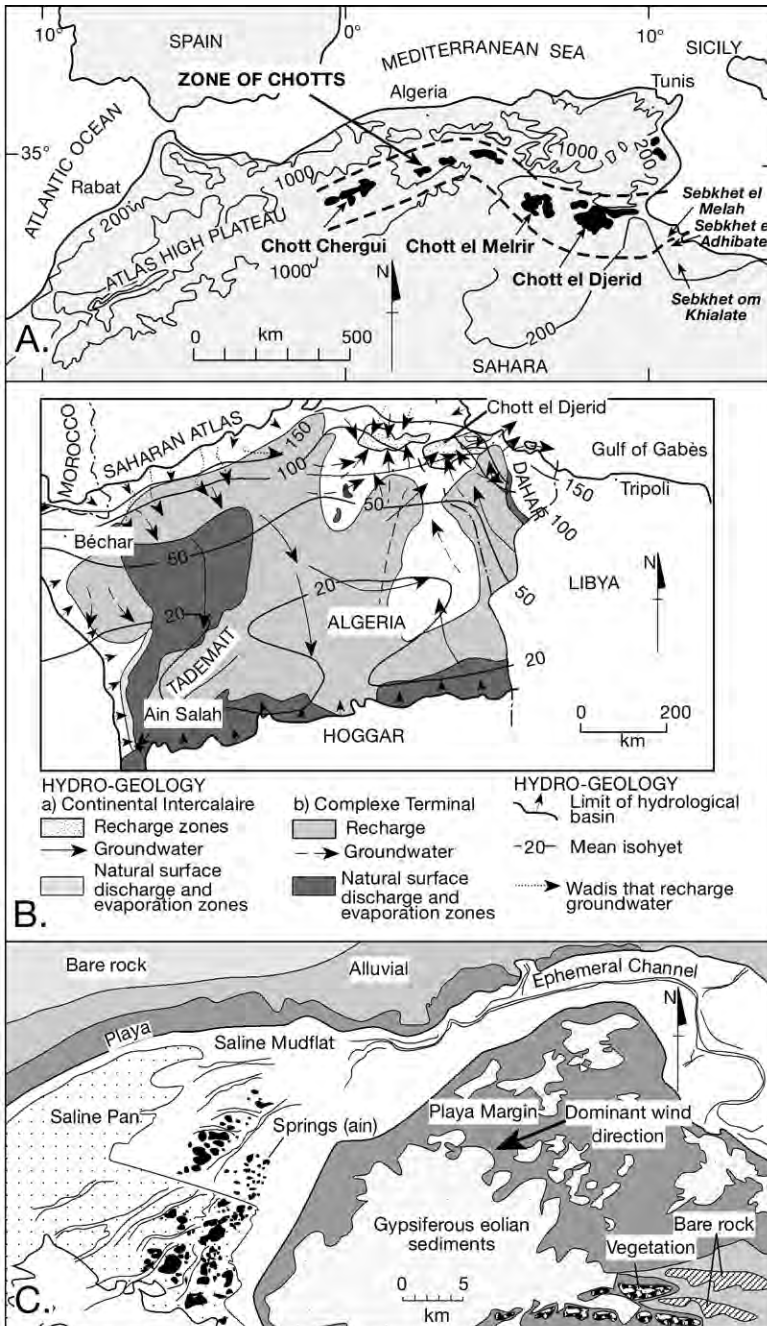


Figure 11.6. Chott el Djerid. A) Locality showing Zone of Chotts as regional groundwater outflow zone. B) Regional hydrology. C) Facies in northeastern corner of Chott el Djerid (after Bryant et al., 1994a).

and encloses the whole of the Grand Erg Oriental. The zone of chotts defines the major discharge area of the “Complexe Terminal” aquifer system, which is made up of permeable Turonian dolomites and Upper Cenomanian limestones and intercalated evaporites, along with some Mio-Pliocene sands

and conglomerates (Figure 11.6b). Discharging continental groundwaters seep into the chotts beneath the edges of thin Quaternary clay aquitards that also form the bottoms to the playas. The same clay bed facilitates temporary ponding of waters supplied by winter floods onto the central playa facies. All the chotts in the “Complexe Terminal” occupy the lowest areas on the north African interior; Chott el Melhir in Algeria is 40 m below sea level, Jar-d and Gharsah lakes in Chott el Djerid are 16 m and 21 m below sea level, respectively. Like the interior basins along the southern edge of the Great Artesian Basin of Australia, the chotts are deflationary rather than accretionary depressions and have lost something like 15-20m of late Quaternary fill via eolian deflation (Blum et al., 1998).

The lowest and more central part of Chott el Djerid is a halite pan covered with an ephemeral halite crust. It is surrounded by gypsum mudflats that in turn passes marginward into a broad evaporitic mudflat and dry sandflat. Much of the mudflat surface is covered by gypsum petees and adhesion ripples (Figure 11.6c). Parts of the sandflat are transitional into aeolian-overprinted sediments with characteristic wind-blown sand streaks, wind-rippled sand sheets mounds and shadow dunes, all of which are cross cut by wadi channels that feed surface water into the central depression during times of flood (see Chapter 3 for more detail on this ephemeral-stream-dune-saline lake association). To the north, beyond the sands flats are the low-relief alluvial fans of the Atlas foothills (Figure 11.5). To the south of Chott el Djerid is the transition into the Saharan erg, the outer edges of which are characterized by low-relief, isolated sand mounds that mostly lack well-defined slip faces and are separated by interdunal sabkhas.

A flood occurred in the northeast portion of Chott el Djerid in January 1990 after an intense storm period when more than

120 mm of rain fell (Figure 11.7) Its aftermath showed that Chott el Djerid undergoes four evolutionary stages as it desiccates to salinities where small volumes of potash salts precipitated as thin efflorescent crusts and pore cements in uppermost parts of the saline mudflat (Bryant et al., 1994a): (1) initial flooding, (2) evaporative concentration of lake waters, (3) the movement of concentrated thin brine sheets over the playa surface as a result of wind action, and (4) total desiccation of the lake by September 1990, some nine months after the initial flood.

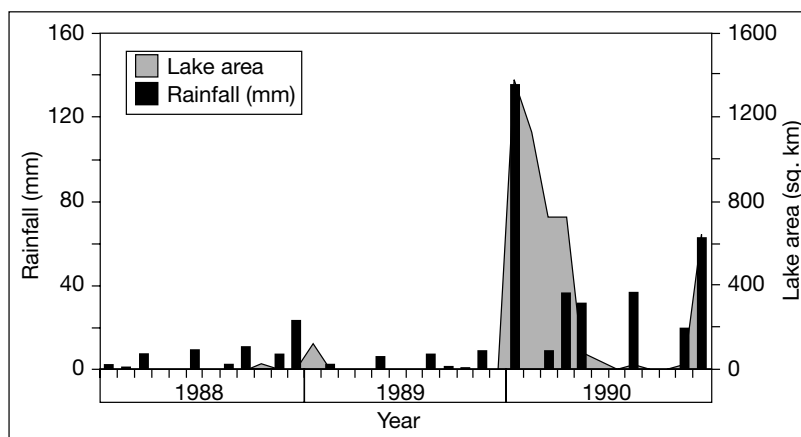


Figure 11.7. Rainfall and lake areas recorded on the Chott el Djerid from 1987 to 1990. (after Bryant, 1999).

Surface waters and seeps in the chott have a consistent $\text{Ca-SO}_4\text{-Cl}$ rich and $\text{HCO}_3\text{-CO}_3$ poor chemistry, reflecting the recycling of older (Pleistocene - Cretaceous) evaporites within the catchment area. As the lake desiccates and shrinks, these waters concentrate to produce an Na-Mg-K-Cl-SO_4 continental brine with ionic proportions similar to those of modern seawater (Table 11.3), but the brine source is continental not marine, although the contribution from marine aerosols has not been quantified. During desiccation, saturation of surface water was reached first with respect to gypsum and then with halite and ultimately with potash minerals. The total brine volume in the chott is $\approx 5 \times 10^9 \text{ m}^3$ and average subsurface salinity $\approx 330 \text{ ‰}$. Brines tend to be more potash rich on the western side of the playa and more sulphate rich on the eastern side (Kbir-Arigoib et al., 2001). After complete desiccation, the main mineral phases in the crystal mush on the floor of the many saline pans across the surface of the chott are gypsum and halite. The ephemeral carnallite is present mostly as thin cm-scale layers within small haematite-stained areas near the centre of the various pan depressions on the chott floor (Figure 11.6c). The carnallite is ephemeral and it redissolves with each new flood of the chott. Its mode of occurrence is typical of the hydrologically decoupled mode of salt crusts in many modern artesian fed playas and its preservation potential is very low (Chapter 2).

Sabkhat om Khialate with an area of 75 km^2 is another area of minor potash precipitation. It a small sabkha depression in the interior desert, well inland of the coastal plain and south of Sabkhat el Melah (Figure 11.6a). Fed by continental waters, it is covered by a thin ephemeral salt crust a few decimetres thick, which contains a mixture of halite, gypsum, and thenardite (Na_2SO_4). Further toward the pan margin are thin efflorescent

crusts made up almost solely of the thenardite with minute amounts of carnallite.

Yet another modern area of ephemeral carnallite formation in North Africa is the near coastal mudflats of Sabkha el Melah and the smaller Sabkha el Mehabeul. Both mudflats are situated on the northern edge of the Djefara coastal plain near the town of Zarzis, Tunisia. Sabkha el Mehabeul is the more isolated of the sabkhas; today it is a continental endorheic depression and has not been hydrographically connected to the nearby Mediterranean since the Late Pleistocene. It retains preserved carnallite and kieserite interstitial cements in thin layers deposited in the last 2000 years, along with minor occurrences of magnesite and huntite (Stengele and Smykatz-Kloss, 1995; Schulz et al., 2002). The larger Sabkha el Melah is still hydrographically connected to the open sea by a channel that opens in times of flooding and turbulent seas. Where brine escapes onto the salt flat there are 6-8m dissolution holes in the surface of the sabkha edge. Brines in these sabkhat are homogeneous and contain more magnesium, potassium, and chloride than brines from other less saline coastal sabkhas (Table 11.3).

Evaporites are concentrically zoned in the sabkha salt crusts and in the upper 0.5 metres of underlying sediment. Zonation is

Locality	Na	K	Ca	Mg	Cl	SO_4
Chott el Jerid	100	9.0	0.7	12	197	12
Sabkhat el Melah	45	7.7	0.2	50	200	28
Sabkhat el Adhibate	88	3.6	1.0	12.6	150	37
Sabkhat om Khialate	43	0.8	0.4	3.3	24	74

Table 11.3. Average composition (g/l) of Tunisian chott and sabkha brines (after Kbir-Arigoib et al., 2001).

more evident in Sabkha el Melah where gypsum and anhydrite occur at the rim of the sabkha depression, while increasing amounts of halite occur towards the centres of local depressions that are ephemeral saline pans. Traces of mirabilite and carnallite can occur in the shallow subsurface sediments in the centres of some lows on the sabkha (< 1 m depth), but only in the innermost and lowermost zones of these ephemeral saline pan facies. Polyhalite also occurs in the Sabkha el Melah sediments and, like similar occurrences in Ojo de Liebre Lagoon, Mexico, it forms as a replacement of gypsum under the influence of increasingly saline pore water (Perthuisot, 1975; Pierre, 1985). The separation of the Sabkha el Mehabeul from the ocean since the Upper Pleistocene has enabled a more advanced stage of diagenetic maturity and brine evolution in its sabkha fill. Anhydrite dominates over gypsum across the sabkha and the concentric zonation of the pan minerals in local depressions is much less obvious. Notably, in both these coastal sabkhas, carnallite, is no more than a minor mineral phase and is found mostly as efflorescent crusts, with little preservation potential.

This lack of preserved bedded potash in modern marine-fed depressions characterises Holocene coastal sabkhas and salinas worldwide. Clearly, in terms of marine-fed potash deposits, the present day coastal setting is a poor key to understanding widespread bedded potash accumulations of the past (Chapter 5).

Sylvite in the Amadeus Basin, Australia

To the south of Alice Springs in the Amadeus Basin of Central Australia there are a number of small saline playas (areas < 50 km²) with thin ephemeral sylvite/glauberite crusts (Arakel and Hong Jun, 1994). Yet there are no documented sylvite crusts in any of the larger playas of the region, such as Lake Amadeus (area ≈ 750 km²). The absence of potash precipitates in the larger playas reflects the nature of the inflow hydrologies to groundwater seeps in the region (Jankowski and Jacobson, 1990). Both types of playa experience the same arid climate; median and mean annual rainfall in the region are 190 mm and 220 mm, respectively, mostly falling in summer (Dec.-Feb.); while annual evaporation is ≈ 3300 mm. All the playas are ultimately supplied by a combination of surface runoff and seepage from a large regional groundwater outflow system that discharges into this chain of playa lakes along an outflow zone some 500 km long (Figure 11.8).

The difference in the mineralogy of the surface salt crusts between the smaller and larger playas lies in the depth to

which the various playa groundwater systems tap into the regional hydrology. Throughout the artesian discharge zone, the various playa salt crusts form by capillary evaporation of resurging groundwaters. All the playa sediments entrain highly concentrated brines; typically, these are sodium-chloride rich waters with appreciable magnesium and sulphate and very low concentrations of calcium and bicarbonate (Table 2.6). The larger playas in the chain, exemplified by Lake Amadeus, have dual shallow and deep groundwater inflow paths. The smaller playas, exemplified by Spring Lake and the Na₂SO₄ lakes of the Karinga Creek drainage system, have only shallow inflow paths. Brines in the larger playas such as Lake Amadeus are continually diluted by mixing with upwelling deep groundwaters tapping into the regional hydrology (Figure 11.8). This gives larger playas a stable recharge hydrology so that halite saturation rarely occurs in the playa sediments and thick halite crusts cannot form (Chapter 2). In contrast, smaller playas tend to be uncoupled from the deep recharge system so pore saturation with respect to gypsum/halite is reached rapidly in the capillary zone of their mudflats (e.g. Spring Lake). Subcropping groundwaters in both lake Amadeus and Spring Lake are undersaturated with respect to glauberite and sylvite. Yet both minerals accumulate as ephemeral efflorescent crusts about the edges of Spring Lake not Lake Amadeus due to its inherently higher local salinities and its rapidly transitioning lake surface, which because it is located well above the regional groundwater discharge level can attain short-term bittern saturation (Figure 2.14). The continual recharge of artesian waters beneath both small and larger playa depressions of this region means there is little longterm preservation of any salts, and zero potential for potash preservation.

The hydrology of the large central Australian playas, and, for the same reasons, the artesian outflow hydrologies of the salt lakes/playas to the south such as Lake Eyre and Lake Frome are just not suitable settings for the longterm accumulation of thick beds of potash salts. Their position in zones of regional meteoric outflow means they are too fresh and too deflationary and the underlying groundwater prism is too fresh to allow thick sequences of bedded salts to accumulate. Similarly unsuitable seepage hydrologies are also why there are no substantial bedded accumulations of Quaternary potash in the Chotts of Tunisia. As we discussed in Chapter 5, you need a deep depression with a saline feed and a stable hypersaline brine curtain to accumulate thick sequences of bedded salts, and in the case of potash salts that brine curtain must be maintained at the upper bittern end of the concentration range. Zones of shallow rising meteoric groundwaters never underlie such systems.

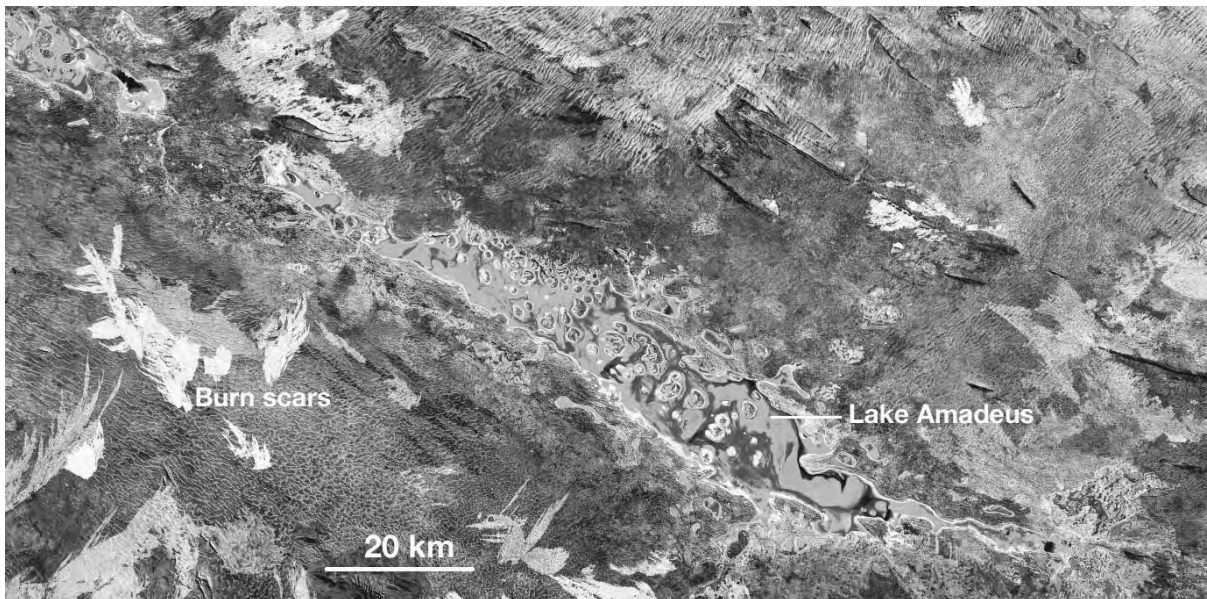


Figure 11.8. Lake Amadeus, Northern Territory, central Australia. This salt lake lies in a drainage chain that forms the central part of the 500-km long groundwater outflow belt (and palaeochannel network) along the northern edge of the Victoria desert. (Landsat image courtesy of NASA).

Potash from brine pumping

Potash is not only mined, it is also produced by brine processing in solar evaporation pans. A mother brine liquor can be pumped into solar evaporation pans from nearby salt lakes or salt flats, as for example, potash produced by the solar concentration of Dead Sea waters (Figure 11.9). Or mother brine can be extracted by solution mining of potash horizons some hundreds of metres below the surface, as it is in operations near Moab, USA, and in the Belle-Plaine operation near Regina, Canada where a brine is recovered from the Prairie potash at a depth of 1800m. Often, the solution recovery exploits potash source beds not suitable for extractive mining due to great depth, structural complexity or propensity for water flood in a precursor conventional mine. The latter was the case at Patience Lake Mine in Saskatchewan, Canada, where two floods in the mid 1980s closed down the conventional mine operation. The former underground mine workings were abandoned and allowed to fill with water so that in 1988 the operation converted to a solution mining/brine recovery setup.

Whatever the brine source, in order to recover potash once the brine is at the surface, it must be subjected to varying combinations of mechanical crystallisation, natural crystallisation (solar evaporation) and flotation. A series of linked fractionation ponds have been built to concentrate Dead Sea brine to the carnallite stage in the Southern Basin of the Dead Sea (Figure 11.9). This is done by the Dead Sea Works Ltd. (DSW), at Sedom on the

Israeli side, and by the Arab Potash Company (APC) at Ghor al Safi on the Jordanian side. Potash is extracted from carnallite slurries created by sequential evaporation in a series of linked, gravity-fed fractionation ponds. The area of the concentration pans is some 130 km², within the total area of 1,000 km² of the Dead Sea floor. The first stage in the evaporation process is pumping of Dead Sea water into header ponds to the gravity-fed series of artificial fractionation pans that now cover the Southern Basin floor. Saturation stages of the evolving brines are monitored and waters are moved from pan to pan as they are subject to the ongoing and intense levels of natural solar evaporation (Figure 11.10b, c; Karcz, 1987). As it concentrates, minor gypsum, then voluminous halite precipitates on the pan floor. Unlike seawater feeds to conventional coastal saltworks with salinities $\approx 35\%$, the inflow brine pumped to the header ponds from the Dead Sea already has a salinity that is $>300\%$. Massive halite precipitation occurs once the brine attains a density of 1.235 ($\approx 340\%$) and reaches a maximum at a density of 1.24 (Figure 11.10b). Evaporation is allowed to continue in the halite header ponds until the original water volume pumped into the pond has been halved, then the concentrated brine is pumped through a conveyance canal into a series of smaller evaporation ponds where carnallite, along with minor halite and gypsum precipitates (Figure 11.10c).

The resulting carnallite ($\text{KCl}\cdot\text{MgCl}_2\cdot 6\text{H}_2\text{O} + \text{NaCl}$) is crushed, slurried with the residual brine and then filtered using floating

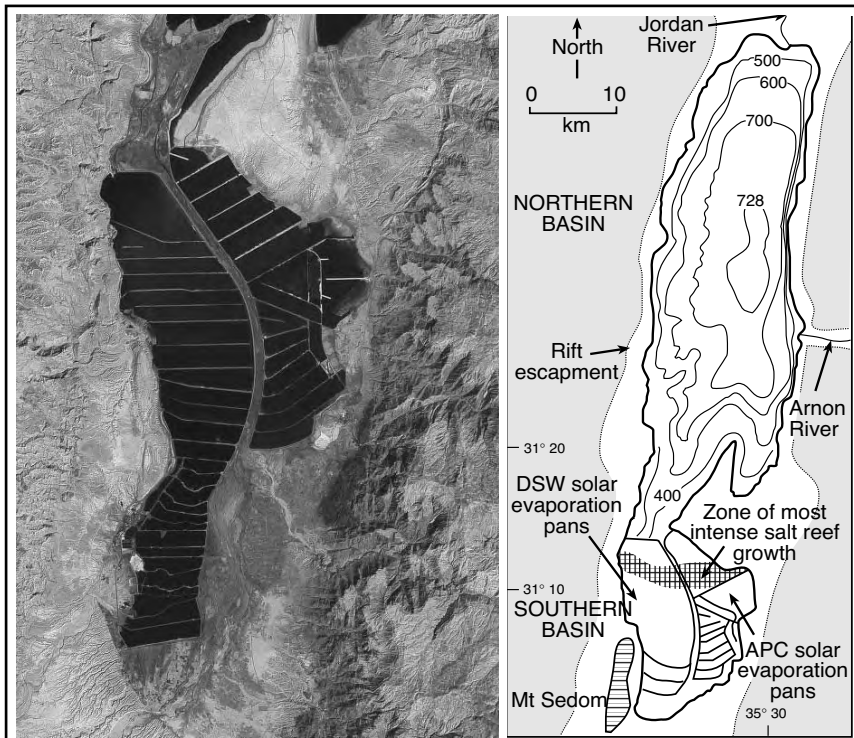


Figure 11.9. Evaporation pans at the southern end of the Dead Sea. The water surface in the Dead Sea is around 415 m below sea level; the Southern Basin is covered only by a thin ephemeral brine sheet maintained by pumping of brines from the Northern Basin where waters attain depths of more than 300m, seafloor isobaths are in metres below sea level (Landsat image courtesy of NASA).

dredges, which then pump the slurry from the pans to the refining plant. This raw product is used to manufacture potash, salt, magnesium chloride, magnesium oxide, hydrochloric acid, bath salts, chlorine, caustic soda and magnesium metal. Residual brines after carnallite precipitation contain about 11-12 g/l bromide and are used for the production of bromine, before the waste brine is returned to the Dead Sea. Israeli potash production currently exceeds 1.3 million tonnes per year while Jordanian production is around a million tonnes per year.

Potassium chloride (mostly sylvite) was originally refined from the carnallite slurry by hot leaching or flotation at the Dead Sea Works, but with a purer carnallite feed, sylvite is now produced more economically in a cold crystallisation plant. Sylvite is produced in the early stages of slurry processing by addition of water to dissolve the magnesium chloride. If the carnallite slurry contains only a small amount of halite, the solid residue that remains after water flushing is mostly sylvite. Successful cold crystallization depends on a high quality feed. If a large amount of halite is present in the feed slurry, the resulting solid residue is sylvinite, not sylvite. This needs to be further

refined by hot crystallization, a more expensive extraction method based on the fact that the solubility of sylvite varies greatly with increasing temperature, while that of salt remains relatively constant (Figure 11.10a). Potash brine is hot leached from the sylvinite, the remaining halite filtered off, and the brine is cooled under controlled conditions to yield sylvite.

Residual brine then undergoes electrolysis to yield chlorine, caustic soda and hydrogen. Chlorine is then reacted with brine filtered from the pans to produce bromine. The caustic soda is sold, and the hydrogen is used to make bromine compounds, with the excess being burnt as fuel. Bromine distilled from the brine is sold partly as elemental bromine, and partly in the form of bromine compounds produced in the bromine plant at Ramat Hovav (near Beer Sheva). This is the largest bromine plant in the world, and Israel is the main exporter of bromine to

Europe. About 200,000 tons of bromine are produced each year. Residual magnesium chloride-rich solutions created by cold crystallisation are concentrated and sold as flakes for use in the chemical industry and for de-icing (about 100,000 tons per year) and dirt road dedusting. Part of the $MgCl_2$ solution is sold to the nearby Dead Sea Periclase plant (a subsidiary of Israel Chemicals Ltd.). At this plant the brine is decomposed thermally to give an extremely pure magnesium oxide (periclase) and hydrochloric acid.

The artificial salt ponds of the Dead Sea are unusual in that they are designed to trap and discard most of the halite precipitate rather than harvest it. Most other artificial salt ponds around the world are shallow pans purpose-designed as ephemeral water-holding depressions that dry out so that halite can be scrapped and harvested. In contrast, the Dead Sea halite ponds are purpose-designed to be permanently subaqueous and relatively deep ($\approx 4m$). Brine levels in the ponds vary by a few decimetres during the year and lowstand levels generally increase each winter when waste brine is pumped back into the northern basin.

When the plant was first designed the expectation was that halite would accumulate on the floor of the early fractionation ponds as horizontal beds and crusts, beneath permanent holomictic brine layers. The expected volume of salt was deposited in the pans each year (Talbot et al., 1996), but instead of accumulating on a flat floor aggrading 15-20 cm each year, halite in some areas built large numbers of macroscopic mounded reefs (salt mushrooms; Figure 1.25). Then, instead of each brine lake being homogenized by wind shear across these large subaqueous ponds, the salt reefs separated the larger early ponds into thousands of smaller polygonal compartments in which the brines developed different compositions. Carnallite slurries crystallized in reef compartments from where it could not be easily harvested, so large volumes of potential product were locked up in the early fractionation ponds. Attempts to drown the reefs by maintaining freshened waters in the ponds during the winters of 1984 and 1985 were only partly successful. The current approach to the salt reef problem in the early fractionation ponds is to periodically breakup and remove them by a combination of blasting and dredging.

In Israel, Dead Sea Salt Work's (DSW) production rose to 2.9 Mt KCl in 2000, continuing a series of increments from the previous four years and reflecting an investment in expanded capacity, the streamlining of product throughput in the mill facilities, the effects of dredging of salt mushrooms, and increased salinity of the Dead Sea due to extended drought conditions. On the other side of the truce line in Jordan, the Arab Potash Co. Ltd. (APC) output rose to 1.9 Mt KCl in 2000. APC is also in the process of removing salt mushrooms from its ponds which, when completed will increase carnallite capacity by over 50 000 t/y. The company is continuing with an expansion program aimed at increasing potash capacity to 2.5 Mt/y by late 2005.

Brine extraction for potash with subsequent solar pan concentration also takes place on the edges of Great Salt Lake and the Bonneville Salt Flats in Utah (Figure 4.17). On the east and west shores of Great Salt Lake near Ogden, Utah, brines are concentrated in the more than 160 km² of solar ponds within a total area of 4,100 km² of the Great Salt Lake. During normal summer conditions, 90% of the halite present in the

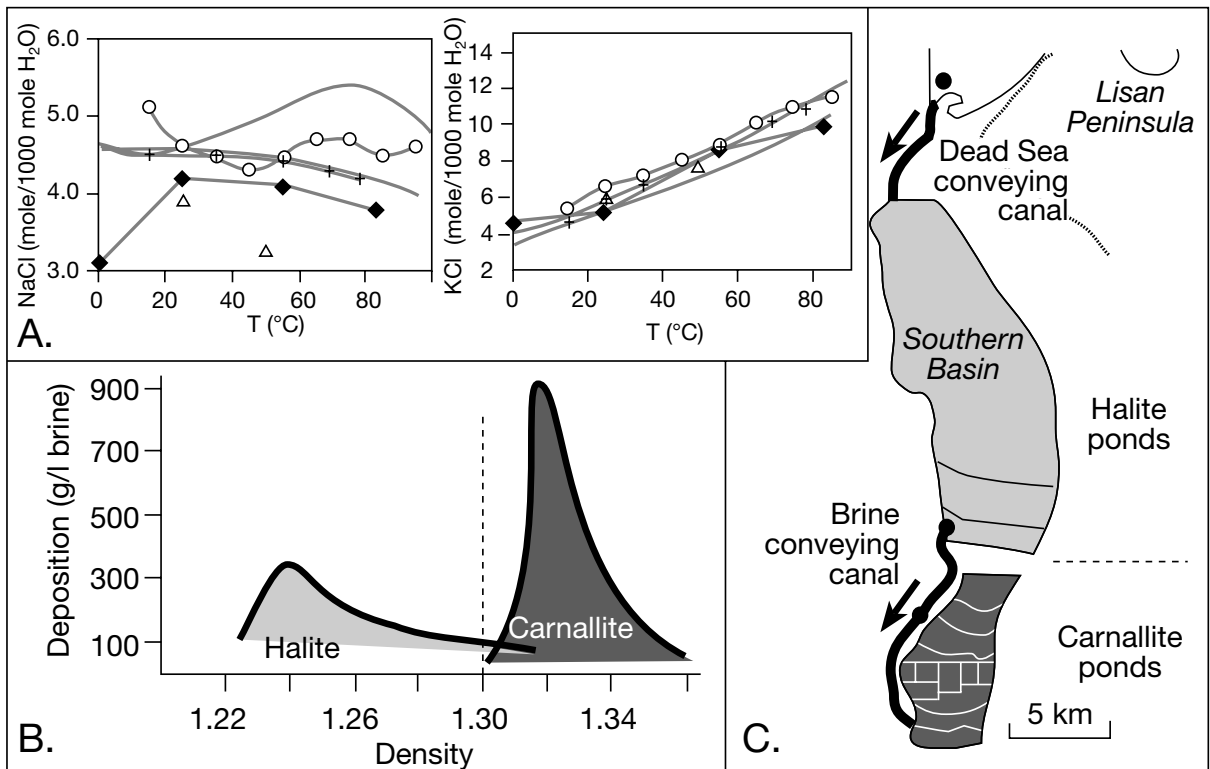


Figure 11.10. Dead Sea potash chemistries and fractionation. A) Halite solubility does not change greatly with temperature while KCl solubility trebles over the same range. B) Showing the relationship between increasing concentration (density) and the transition from halite to carnallite precipitation. C) Design of sequential evaporation pans at the Israeli Sedom plant, southern Basin of the Dead Sea (after Karcz, 1987).

brine is precipitated with little contamination by other salts. Mirabilite is a winter precipitate in the ponds. Once potassium salts begin to precipitate from the saturated brine they form a complex mixture of double salts, such as kainite, schoenite and carnallite, while magnesium precipitates as bischofite, a highly hydrated magnesium chloride. This salt sequence is one of the more complicated solar pond systems in the world. Various salts are sequentially extracted from the fractionation stream and purified to produce the following end products; sodium chloride, potassium sulphate, sodium sulphate and magnesium chloride hexahydrate.

Formerly the solids were harvested from the Great Salt Lake pans using front-end loaders and trucks, and transported to the processing plants. Recently, the Behrens Trench was completed, this is a 35 km underwater canal on the floor of the Great Salt Lake that transports saturated brine product from the western shore solar ponds across the lake to its processing facilities on the eastern shore. Since 2000 the Great Salt Lake plant has produced more than 550,000 tonnes of sulphate of potash. But the earlier history of salt workings about the strandline of Great Salt Lake illustrate one of the major problems in solar pond extraction atop saline mudflats in continental lakes. Record floods in 1984 filled the ponds with fresh water and destroyed much of the infrastructure. Harvesting did not recommence until the early 1990s. Rapid and at times substantial changes in lake level are endemic to saline lacustrine systems and must be planned for in the development of a saltworks.

Potash is also produced by evaporative concentration of solution-mined brine extracted from Pennsylvanian potash evaporites in Paradox member of the Hermosa Formation in the Cane Creek anticline in the northern part of the Paradox Basin in Utah near the town of Moab. There are at least 29 evaporite cycles in the Hermosa Formation, which are dominated by varying combinations of limestone, dolomite anhydrite and halite. Potash occurs near the top of 18 of these cycles, all located immediately above a thick halite bed (Raup, 1966). Eleven of the 18 are of sufficient thickness and quality to be considered economic. The target potash bed is a 3.4m-thick sylvinite bed some 1200 m below the surface and averaging 25-30% K_2O . Salt beds in the halokinetic Cane Creek anticlinal core are characterised by numerous discontinuities and faults and can dip quite steeply.

The Utah brine operation began in 1972, when an unsuccessful conventional mine was abandoned, flooded and converted to the current solution mined- evaporation processed operation. The former mine was not successful due to the high degree

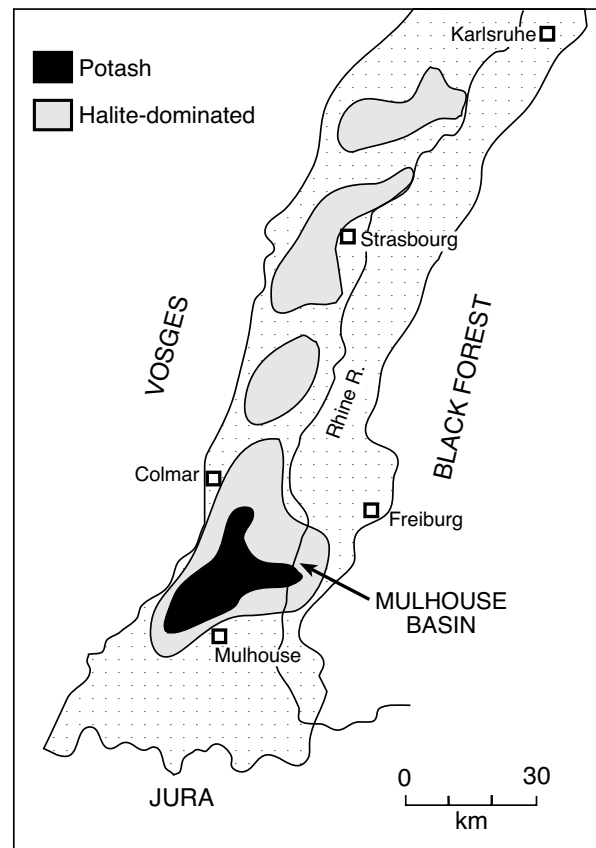


Figure 11.11. Mulhouse Basin, Rhine Graben, showing how the potash dominant section is the southernmost of a number of bedded halite deposits in the graben (see also Figure 5.3).

of deformation of the target ore horizon, which consists of sylvinite layers 2.5-15 cm thick alternating with anhydrite layers less than 3 mm thick. The ore is overlain by 12 m of shaly dolomite and underlain by 43 m of halite. Fold wavelengths are ≈ 30 -120 m and amplitudes range from 6-30 metres (Evans and Linn, 1970). The decision to convert the conventional mine, which had begun operations in 1965, to a solution mine was made after 550 km of 2.7 x 4.9 m rooms and entries had been completed and a number of potentially dangerous "gassy" (methane) intersections had occurred. Brines are today pumped to the surface where they are evaporated in solar pans with the resulting slurry flotated and purified. Solution mining for potash is also profitable in Saskatchewan, where solution mining operations have been active at Belle-Plaine since 1964 and in the abandoned Patience Lake Mine since 1988.

Ancient (Pre-Quaternary) potash

The salt works in the southern end of the Dead Sea are highly efficient producers of potash and account for more than 10% of

the world's annual production. But the other 90% comes from the extraction and mining of potash from ancient evaporite successions. Many of which are saline giants, such as the Canadian deposits and have no modern counterpart (Chapter 5). We shall now look at some of the more important of these ancient potash occurrences.

Rhine Graben

Oligocene evaporites in the Mulhouse Basin in the Rhine Graben contain sylvite with subordinate carnallite, but lack the $MgSO_4$ salts characteristic of the evaporation of modern seawater (Figure 11.11). The Rhine Graben is a Tertiary rift, some 150 km long and 10-25 km wide that straddles the Franco-German border as it runs from Basle in Switzerland to Frankfurt in Germany. With an area of 400 km², the Mulhouse Basin is the southernmost of a number of Oligocene evaporite basins that occupied the graben depression. Total fill of Oligocene lacustrine evaporites is some 1,700m and is dominated by anhydrites, halites and mudstones. The sequence is underlain by Eocene continental mudstones with lacustrine fossils and local anhydrite (Lowenstein and Spencer, 1990; Hardie, 1990; Gely, et al., 1993).

The Oligocene halite section includes two thin, but important, potash zones: the Couche inferieure (Ci; 3.9m thick), and Couche superieure (Cs; 1.6m thick; Figure 11.12). Both potash beds are made up of stacked, thin, parallel-sided cm-dm-thick beds (averaging 8 cm thickness), which are in turn constructed of couplets composed of grey-coloured halite overlain by red-coloured sylvite. Each couplet has a sharp base that separates the basal halite from the sylvite cap of the underlying bed. In some cases the separation is also marked by a bituminous parting. The bottom-most halite in each dm-thick bed consists of halite aggregates with cumulate textures that pass upward into large, but delicate, primary chevrons and cornets. Clusters of this chevron halite swell upward to create a hummocky boundary with the overlying sylvite. The sylvite member of the couplet consists of granular aggregates of small clear halite cubes and rounded grains of red sylvite (with some euhedral sylvite hoppers) infilling the swales in the underlying hummocky halite. The sylvite layer is usually thick enough to bury the highest protuberances of the halite, so that the top of each sylvite layer, and the top of the couplet, is flat. Dissolution pipes and intercrystalline cavities are noticeably absent, although some chevrons show rounded coigns. Intercalated marker beds formed during times of brine pool freshening are composed of a finely laminated bituminous shale with dolomite and anhydrite.

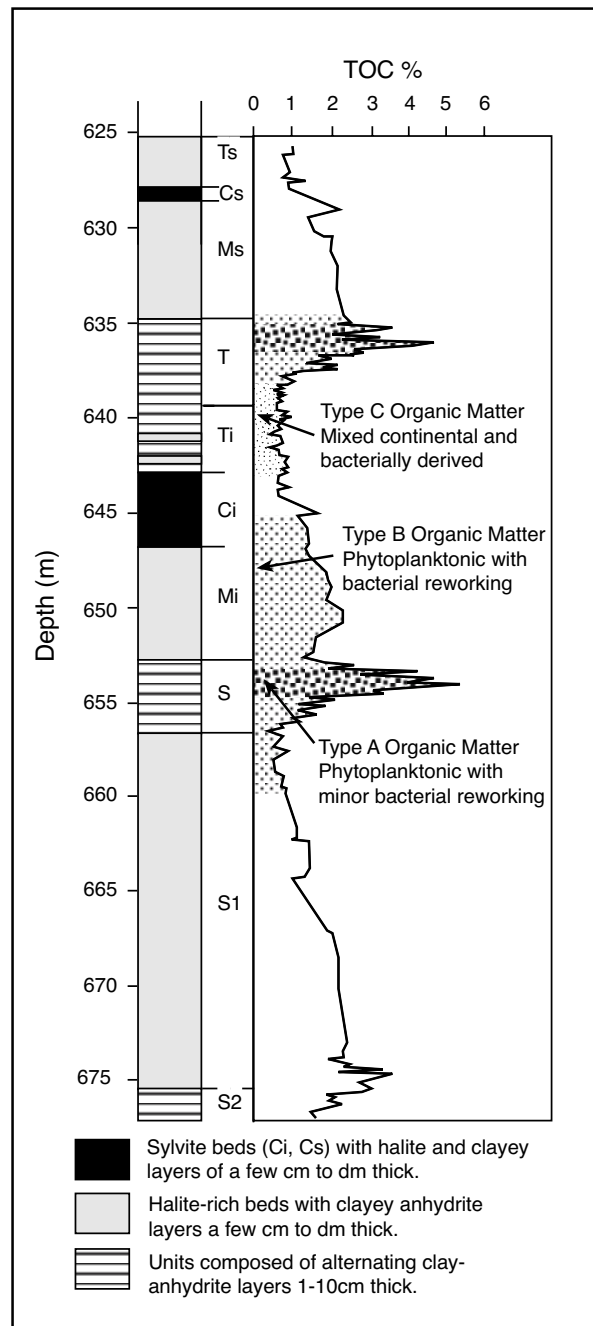


Figure 11.12. Typical section through the potash intervals of the Upper Salt. The log also illustrates the amount and style of total organic carbon (TOC%) extracted from marly layers in the various units. Curve is smoothed using a moving three point average (after Gely et al., 1993).

The sylvite-halite couplets appear to record unaltered settle-out and bottom-growth features of a primary chemical sediment that accumulated in a shallow perennial surface brine pool.

The sylvite layers, like the halite layers, are interpreted as primary subaqueous deposits (Lowenstein and Spencer, 1990). Based on their crystal size, the close association with cumulate halites in the sylvite layers, and the manner in which they mantle underlying chevron halites, sylvites are interpreted as precipitates first formed at the air-brine surface (or within the upper brine) that then sank to the bottom to form well sorted accumulations. Similar cumulate sylvite deposits are found on the floor of modern Lake Dabuxum in China during its more saline phases (Figure 11.2). The current mosaic textural overprint in the Mulhouse sylvite layers was probably produced by postdepositional modification of the crystal boundaries, much in the same way as mosaic halite is formed by recrystallisation of raft and cumulate halite during shallow burial (Figure 1.18). Inclusion studies in both the sylvite and the halites average 63°C, suggesting solar heating of surface brines as precipitation took place. Similar high at-surface brine temperatures are not unusual in many modern brine pools, especially those subject to periodic density stratification and heliothermometry (Figure 2.48).

TOC values in the sylvite interval also imply preservation of a primary sylvite deposit. TOC levels fluctuate in a rhythmic

manner related to the salinity of the depositional brines (Figure 11.12; Gely et al., 1993). The highest TOC values are found in marls near the top of the clay-anhydrite layers and the lowest values are recorded near the top of the halite-rich beds where the sylvite (and the highest brine concentrations) would have occurred. The organic matter is mainly algal (A and B groups), while a third category of organic material (C group) is derived from a mixture of continental inflow and in situ bacterial productivity. The sylvite bed (Ci) occurs at the transition from Type B to Type C, indicating a change of brine chemistry from the hypersaline brines of the halite/sylvite pans to the freshened waters that precipitated the more organic-rich marls (See “feast and famine” discussion in Chapter 9).

Khorat Plateau, Thailand

Potash in the halite-dominated Cretaceous Maha Sarakham Formation is preserved within two basins: the northern Sakon Nakhon Basin (which also extends into Laos) and the southern Khorat Basin. These basins underlie much of the Khorat Plateau in NE Thailand and are separated by the highlands of the Phu Phan Range (Figure 11.13a). It is likely that a single larger evaporite basin encompassing at least the area of the

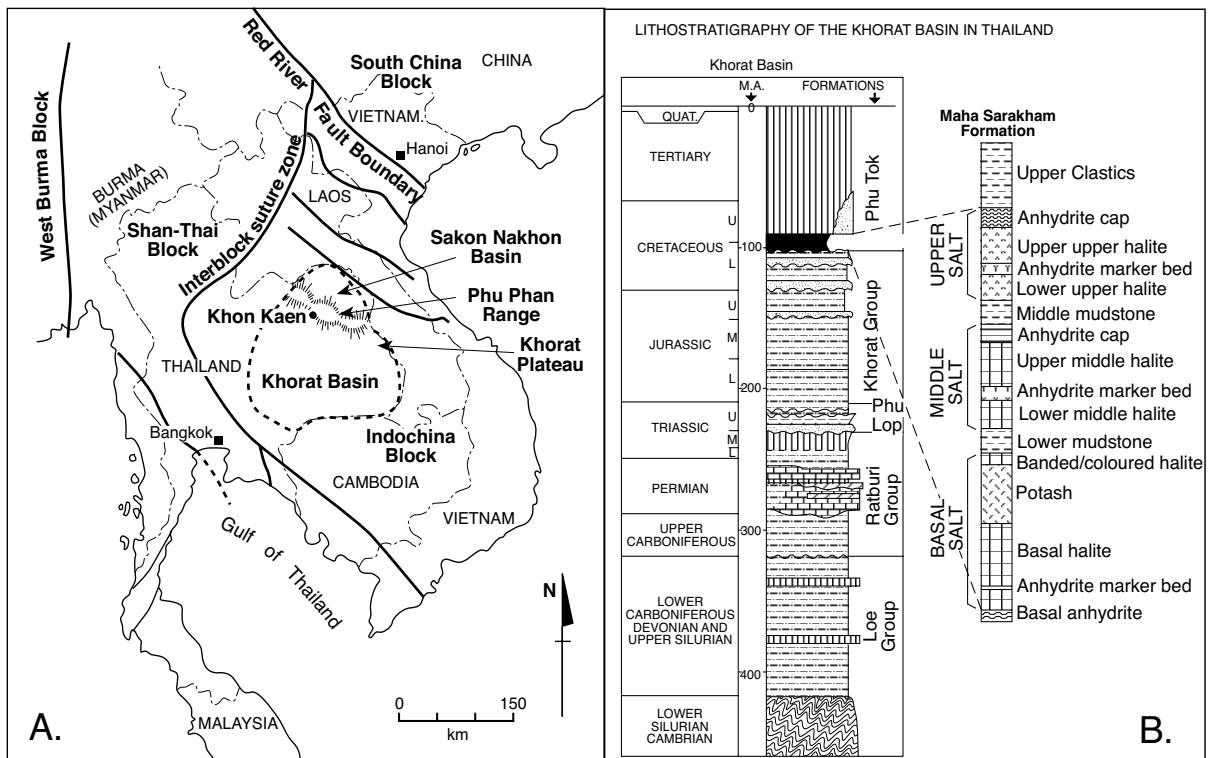


Figure 11.13. Potash in Thailand. A) Locality map showing location and tectonic setting of the Khorat Plateau, the Khorat Basin and the Sakon Nakhon Basin. B) Stratigraphy of the Khorat Basin and the Maha Sarakham Formation, NE Thailand (after Mouret, 1994; Suwanich, 1986).

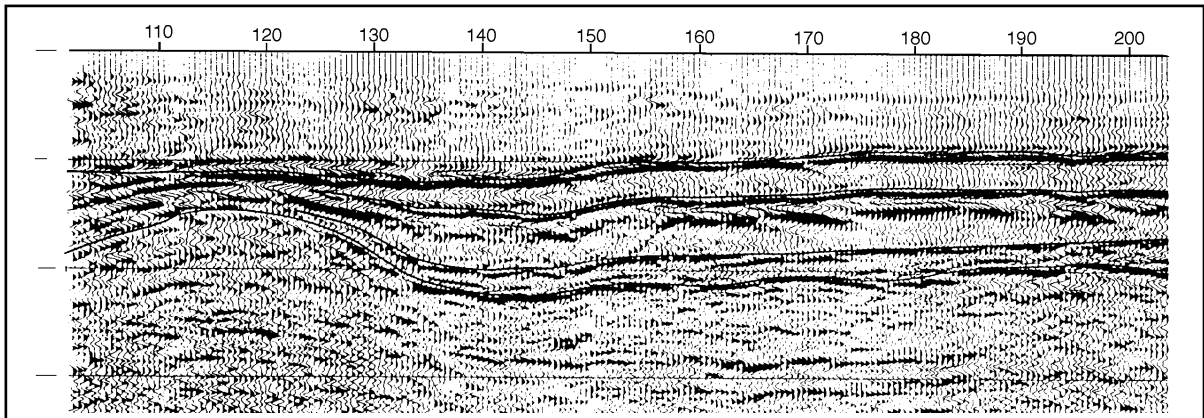


Figure 11.14. Seismic image of Maha Sarakham Formation, from the Khon Kaen area showing a salt pillow in the Lower Salt Member and the syndepositional reduction in sedimentary thickness in units above this structure (seismic line supplied by CRA-RTZ).

present day Sakon Nakhon and Khorat Basins existed at the time of deposition. These deposits represent one of the last saline giants preserved in SE Asia and suggest an extreme arid period during Cretaceous time within a subsealevel marine-fed depression, possibly created by transpressional collision events that preceded the Himalayan Orogeny (see Morley, 2004 for possible timing of collision). The evaporite sequence lacks $MgSO_4$ salts consistent with our current understanding of the evolution of Cretaceous seawater chemistry (Figure 2.30). The current margins of both basins are dissolutional, as are the upper and lower contacts of the salt units.

In those parts of the stratigraphy largely unaffected by evaporite dissolution the Maha Sarakham is composed of three salt beds—Lower, Middle and Upper Salt members—each overlain by a clastic mudstone—Lower, Middle and Upper Clastic members—(Figure 11.13b). Where the Maha Sarakham has not been thinned, either by dissolution or salt flow, it is 250–300 m thick. In areas of salt dissolution it thins to <100 m, while in halokinetic regions it can be more than a kilometre thick (Figures 7.29, 11.14). Evaporite minerals include halite; the sulphates gypsum and anhydrite, along with a variety of halite-hosted potash phases dominated by carnallite and sylvite with accessory tachyhydrite. Portions of the bedded halite display intricate depositional, dissolutional and diagenetic features that rank amongst the most pristine I have seen preserved in an ancient evaporite (Figure 11.15).

Middle and Upper Salt members are generally flat lying and correlatable from well to well. In contrast, seismic and geomorphologic analysis shows that the Lower Salt of the Maha Sarakham has flowed in some parts of the basin so that thicknesses are much more variable from well to well (Figure

11.14). Textures in the Lower Salt Member range from well preserved depositional textures in its upper part immediately below the potash entraining intervals to pervasive flowage features lower in the section. Petrographic evidence for salt flowage includes overburden-controlled elongate flattening of crystals and pervasive halite recrystallisation that has destroyed original bedding features. In wells that pass deeper into the Lower Salt Member there is often a transition down core from pristine depositional textures into flowage textures, implying that flow into the pillows was fed mostly from the deeper parts of the Lower Salt Member. This is also consistent with the upper portions of the salt unit still being deposited while the lower parts of the same unit were flowing.

At the regional scale, the halokinetic features follow curvilinear trends that are typically subparallel to the present basin margin. Some pillows in the Lower Salt Member, especially those associated with sylvinite along the western margin of the basin, were probably syndepositionally initiated, as they are truncated by sediments of the Lower Clastic Member (Figures 11.13b, 11.14). Locally, other salt flow features are probably still active today, driven by laterally shifting surface river systems, including the Mekong and its tributaries. For example, $CaSO_4$ caprocks outcrop today in Laos in the erosional riverbanks of the Nam Theun river one of the major tributaries to the Mekong (pers. obs; Figure 7.7c).

Initiation of the salt flow in the Maha Sarakham halite is probably diachronous and driven by sediment loading from various depocentres moving across the salt bed. In the Cretaceous the depocentres were tied to the deposition of the Lower Clastic Member; today they are tied to the fluvial deposits of the Mekong and its tributaries. Such feedback systems

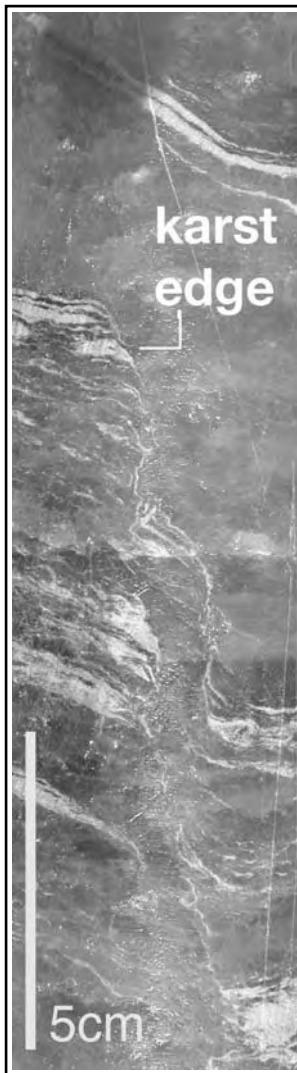


Figure 11.15. Typical multistage dissolution collapse and fill in Maha Sarakham Fm. by chevron halite. Cavities are sometimes filled by clear sylvite, not halite.

between depositional loading (sediment thicks) and salt buildups (pillows and anticlines) and salt dissolution characterise the western margin of the Maha Sarakham in the vicinity of Khon Kaen (Figures 11.14). As well as being seen seismically, the relationship between surface landform and the underlying structuring of the salt can be imaged using currently available topographic maps, aerial photography and satellite imagery.

Like much of the halite in the Maha Sarakham, the petrography, depositional style and preservation quality of potash in the Lower Salt Member has been complicated by dissolution and halokinesis (Hite and Japakasetr, 1979; Sessler, 1990; El Tabakh et al., 1995; Utha-aroon et al., 1995). In terms of the potash minerals, carnallite dominates over sylvite throughout the basin, while traces of tachyhydrite are also found preserved as enclosed euhedral to subhedral crystals in halite.

Potash is widely dispersed as minor shows across the

basin. The only well studied and significant potash-rich zones are in the upper section of the Lower Salt Member along the western margin of the Khorat Plateau. The potash interval is dominated by carnallite (up to 20-30m thick), which forms a widespread stratiform unit along the western margins of both the Khorat and Sakon Nakhon basins. It is locally capped by lesser sylvinite (< 6 m) and covered by a bed of colour-banded red and grey halite (up to 6 m thick). This colour-banded halite preserves pristine depositional textures and is in turn overlain by the Lower Clastic Member.

A complete interval in the potash-entraining region at the top of the Lower Salt Member is divisible into (Figure 11.13b):

- (4) Uppermost colour banded halite (0-6m),
- (3) Sylvinite zone (0-6m),
- (2) Carnallitite zone (0 up to 15-30m),
- (1) Lower zone of massive to bedded halite with traces of carnallite (50-300m).

The lower zone (1), is dominated by massive, colourless, inclusion-free halite, which is made up of stacks of beds 0.2-0.5 m thick. The upper portion of this halite interval retains pristine depositional textures, including aligned bottom-nucleated growth forms, clay dissolution stringers and microkarst pits. This halite zone is underlain by clean recrystallised mosaic halite, which may stack into intervals that are hundreds of metres thick in halokinetic zones. Often this clean halite is dominated by biaxially flattened or necked and recrystallised lensoidal textures, a texture indicative of salt flow. Minor anhydrite stringers and nodules (≈ 1 cm thick) crosscut the axes of cores often with steep inclinations that also suggest flowage. This form of anhydrite is microcrystalline and lacks any of the original gypsum ghost structures so well preserved in thicker regional marker beds, especially those in the middle and upper halite members (Figure 11.13b).

The carnallitite zone (2) is typically 15-25 m thick near the western edge of the current structural basin but can also disappear near the outermost parts of the basin where it has been dissolved by surface driven crossflows of meteoric water. Three types of halite are found in the carnallitite zone: (a) inclusion-rich, cloudy, chevron halite; (b) clear, recrystallised, coarsely crystalline halite; and (c) granular, fine-grained halite. The first typifies preserved bottom-nucleated beds, the second typifies massive halite beds with poorly defined upper and lower contacts and suggests textures associated with macro and micro karstification, while the third type is found as disseminated halite in carnallite-filled voids. Anhydrite and other insoluble residues are scarce in the carnallitite zone. Halite that hosts carnallite is often crosscut by dissolution surfaces, clay stringers, collapsed halite beds and karst cavities can be coated with microcrystalline to coarsely crystalline carnallite (Figure 11.15).

Many of the carnallite-filled voids are subvertical and narrow downward. This implies a syndepositional vadose karst prior to the precipitation of the carnallite cement. Textures in this zone are identical to those found in the bedded potash deposits of the modern Qahan Playa and indicate the water table was subject to large oscillations. The carnallitite interval in the Maha

Sarakham was subject to syndepositional brine freshening, subaerial exposure and water table lowering related to climatic changes and tectonic tilting in the depositional basin.

The sylvinite zone (a mixture of halite and sylvite) directly overlies the carnallite zone and is up to 6 m thick. It is not always present. Its contact zone is transitional with the underlying carnallite zone, although sylvite crystal-clusters in the transition zone typically show sharp non-horizontal edges. Sylvite is present in its halite host as: a) individual and small crystal clusters of up to 1 cm size, making up amoeboid-shaped forms; b) coarsely crystalline massive beds up to 5 cm thick; c) even layered, thick beds of up to 4 cm thick; d) irregular medium to coarsely crystalline patches within massive halite beds and as patches sometimes rimming preexisting carnallite crystals; and e) massive sylvite units up to 25 cm across. In almost all cases, dark grey clayey matrix surrounds the larger sylvite crystals and/or alternates with the subhorizontal sylvite beds. Petrographically, sylvite crystals exhibit euhedral crystalline forms, either as individual crystals or as clusters of crystals.

At the transition between the carnallite and sylvinite zones some dissolution cavities can be 25 cm across (in core) and filled with single clear sylvite crystals. Higher in the sylvinite interval the sylvite tends to occur as stratiform primary layers showing subhorizontal bedding, and ranges from 10 cm to 1 m thick. Individual primary sylvite crystals can reach up to 2 cm in size in the primary layers. Macroscopically, sylvite layers are not homogeneous and several types of sylvite may coexist within single layers along with fine clastic components and halite.

Halite beds alternating with sylvite layers range in thickness from 1 cm to 15 cm. Where not destroyed by the processes of dissolution and recrystallisation, these halite beds can still exhibit relict bedding and occasionally are milky from inclusions in the preserved chevrons. But most of the halite in the sylvinite zone is clear and coarsely recrystallised, with geometries suggesting repeated episodes of dissolution followed by precipitation as passive void-fill cements. Traces of anhydrite are present throughout the sylvinite zone, along with traces of tachyhydrite. Anhydritic cm-diameter nodules are locally present, as are white nodules dominated by microcrystalline borate minerals (boracite and tyreskite).

More than one sylvite-rich interval may occur in the sylvinite zone. Workers in the region who have used a strict stratigraphic approach have often reported intervals with more than one sylvite layer as representing fault-repeat sections. Such an

approach underscores the limitations of using a non-process based layer-cake stratigraphy in an evaporite succession. What is occurring is not associated with a fault-repeat of a single sylvite bed, but the vagaries of a sylvite-filled anastomose karst system being intersected a number of times in a single core. Contacts of many of the so-called repeat beds show classic insoluble-rich geopetal linings.

Colour banded halite (4) constitutes the uppermost part of the Lower Salt Member. It is coarsely laminated and retains pristine depositional textures (mostly chevrons) with little or no evidence of recrystallisation. There is often a sharp upper dissolution contact with the overlying Lower Clastic Member, defined by a diagenetic horizon made up of anhydritic dissolution residues (see Chapter 7).

The origin of the richest sylvite zone (3) is related in part to the action of actively refluxing, possibly freshened brines working on an actively rising (pillowing) carnallite/halite precursor. For example, in the Khon Kaen region (Figures 11.14, 11.16a), the Lower Salt Member has flowed into a pillow structure and the overlying strata are truncated beneath an alluvial cover. The synclinal structure associated with the rim of this pillow is also a zone where sylvinite thickens at the expense of the underlying carnallite (Figure 11.16a). This sylvinite is capped by the Lower Clastic Member, which is in turn capped by the Middle Halite Member. Core from the Middle Halite Member in this region shows predominantly undisturbed subhorizontal bedding and still retains perfectly preserved primary textures, such as chevrons and halite intercrystal karst, along with a regional dm-thick marker bed made up of subaqueous swallowtail gypsum pseudomorphed by halite/anhydrite (pers. obs. of core).

Facies geometries suggest that sylvite deposited along the western margin of the Khorat Plateau was: a) precipitated after the deposition of the carnallite; b) prior to deposition of the Lower Clastic Member; c) fed from lateral inflow, probably driven by a potentiometric head generated by relative uplift of an adjacent growing salt pillow; d) related to the cannibalisation of the uplifted carnallite bed atop a growing salt pillow; e) precipitated early, either as pond-bottom nucleates and floundered raft cumulates or as downward-fluxing karst-filling cements in the rising margins of the brine pool; and f) then covered by subaqueous colour-banded halite, fed via the dissolution of halite from a now carnallite-depleted pillow crest (Figure 11.16b). Sylvite precipitation was driven both by solar evaporation on the pond floor (as in the Mulhouse Basin) and by subsurface cooling of downward flushing potassium-saturated brines (as in the Qaidam Basin). Similar potash recycling into

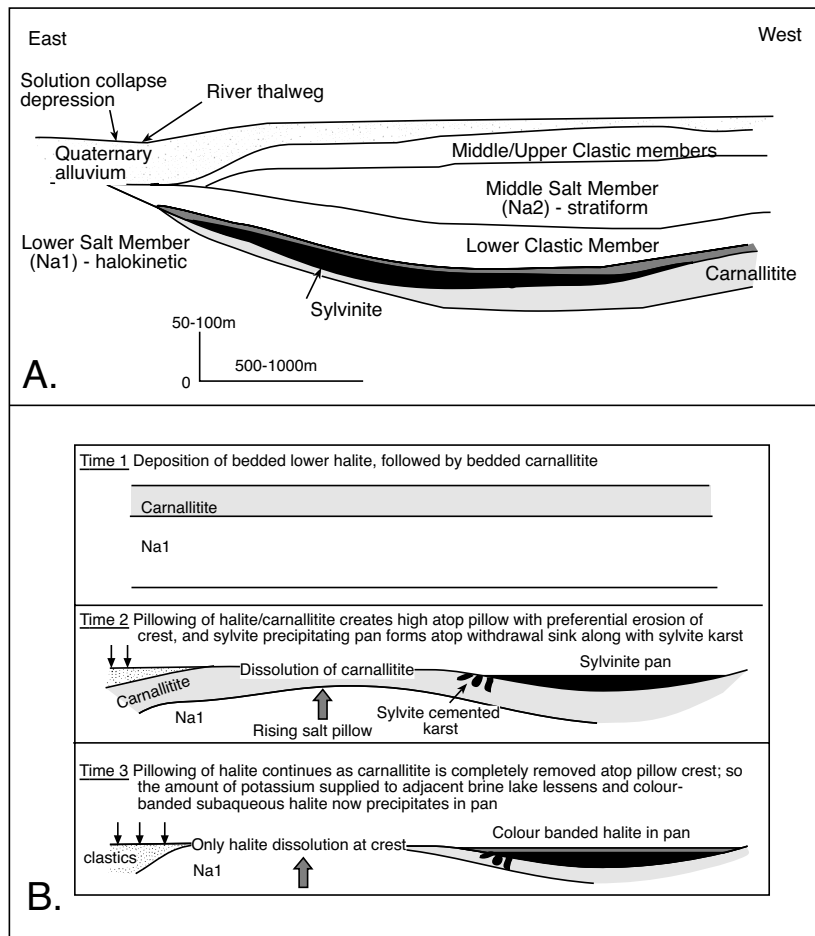


Figure 11.16. Sylvite controls in the Maha Sarakham Formation along the western margin of the Khorat Plateau near Khon Kaen, Thailand. A) Generalised schematic of current sylvite distribution based on well data in the region. B) Sequential development of pillow and the erosion of crest facies controlling first the formation of sylvite and then the colour banded halite within brine-entraining rim syncline depressions (see text for full explanation). Schematic based on author's research and field work in the region.

modern playa depressions in rim synclines is occurring around outcropping crests of diapirs fed by Miocene salt in the Qum Kuh region of central Iran (Figure 3.62). The Iranian potash is probably reworked from a Miocene source layer in the diapiric salt (Rahimpour-Bonab and Kalantarzadeh, 2005).

In terms of potash exploration in Khon Kaen region and elsewhere in Thailand, it is important to note that the thickest potentially exploitable sylvinite fairways lie in rim synclines adjacent to syndepositionally breached salt pillows. They do not form laterally extensive horizons and are not akin to the Devonian sequences of Canada discussed in the next section. These pillows were deforming the carnallite zone and uplifting previously formed carnallite beds into a periodically refreshed

hydrological setting. Simultaneously, sylvite was precipitating on the pan floor and in karstic voids in the halite about the pan rim. It was the super-imposed pillow hydrology that was karstifying the halite at the same time that the upper portion of the carnallite member was dissolving and supplying K-rich brines to the pool floor. The raising of the sedimentation surface, via pillowing, explains why some of the sylvite forms clear coarse-crystal fills in large karst holes in the halite, while other sylvite is a primary precipitate.

The potash geology of the Maha Sarakham has a number of technological challenges for a conventional sylvite mining operation. Its geology should be carefully and publicly documented before the onset of any major mining operation. Maha Sarakham potash tends to occur in the upper part of the lower halite unit, and about the current dissolutional edge of the basin it is sometimes without a substantial thickness of halite atop the potential ore interval. Such a halite bed is a required back when mining as it can support the mine roof as ore is extracted. Mine backs are typically more than 5-10m of halite above the potash level in mines in Canada and New Mexico and 1-2 metres in the robotically extracted potash ores of the Boulby Mine, UK. The overlying

lower clastic unit in the Thai succession is typically not well-indurated sediment, so maintaining mine headwall stability should be a major consideration in mine planning. Likewise, tilting, dissolution and flowage of the Lower Salt means some sylvite layers show bed inclinations of up to 70° to 80° to the drill core axis, implying sylvinite beds have dissolved or flowed. This means the bed thicknesses must be ascertained as a true thickness and not be indicated solely by assay thickness in core or wireline intersections in wells. Such high dips are also problematic in designing a mine plan utilising conventional mine equipment where access and assumptions of stratiform stratigraphy dominate. Within areas where depths to be mined are as shallow as 350-400 metres there may be long term

problems of ground subsidence (see problematic mines and brinefields in Chapter 12). Further out in the basin there may be some intervals of potash in the Maha Sarakham Formation that are more deeply buried and more amenable to solution mining, rather than conventional room and pillar extraction. To date, this has not been the focus of any potash exploration programme in Thailand. All studies of the feasibility of extracting potash in the last three decades have focused on shallower areas of potash about the dissolution overprinted basin edges, where potash tends to occur at depths more amenable to conventional mining (e.g. planned operations at Bamnet Narong and Udon Thani).

Permian potash, Europe and North America

The Zechstein Basin stretches from northern Britain, south-east across the North Sea through the Netherlands, Denmark, Germany and Poland to the edge of the Hercynian massifs (Harz, Rhine and Bohemian mountains). Potash extracted from the Permian Zechstein evaporites provides 20% of the world's potash. The Zechstein succession was deposited in a huge drawdown seaway and is today made up of four evaporite cycles: the Z1-Werra Series, Z2-Stassfurt Series; Z3-Leine Series and Z4-Aller Series (Figures 5.48, 5.49). Each has a general sequence of clastics, carbonates, one or two phases of sodium and potassium salts, regressive halite or anhydrite, and carbonate. Potash beds of Z1 and Z2 are primarily composed of sylvite (KCl), carnallite ($KCl \cdot MgCl_2 \cdot 6H_2O$) and kieserite ($MgSO_4 \cdot H_2O$) and rapid lateral changes are common. The Zechstein 2 potash bed interval locally attains a true thickness of about 15 metres.

German potash

Some active German potash mines in the Stassfurt member (Z3) are more than 100 years old. The Z3 seams are mostly sylvinitic and ore zones are mostly free from higher levels of Mg-salts. In general the average grade of halokinetic potash (sylvinitic type) is 17 to 18 % K_2O , which is low by Canadian standards. However, the extracted products can be utilised economically due to proximity of the market, mining efficiencies and high levels of government farming subsidies throughout the European community.

Two potash cycles are exploited in the Z1 in the Werra -Fulda Basin southeast of Kassel, while two potash beds in the Z2 and Z3 are mined near Hanover. Formations near Hanover in northwestern Germany occur in diapiric salt domes. There the salt and potash mines are located along salt walls that trend

along strike for over 20 km and are 800 to 1000 metres wide (Figure 6.9a). In the Hanover area, potash is mined between depths of 300 and 900 m, along a steeply-dipping seam some 2 to 30 metres in width (the increased width is due to multiple, tight folds). In the southern potash-mining district of Werra-Fulda, two seams are mined at depths of 300 to 900 metres with thicknesses of between 2 and 4 metres. These seams are even lower in grade than in the Hanover area, but unit extraction costs are lower as seams gently dip and are not folded.

Boulby potash, UK

Elsewhere in Europe, potash is extracted from the Aller Series in the Netherlands and the potash member of the Boulby Halite in the Z3 (Teese Group) at the southeast boundary of Cleveland County NE England. The Boulby Potash bed is underlain by a thick sequence of salt that makes up the majority of the Boulby Halite Formation (Figure 11.17). This is in turn underlain by the Billingham Main Anhydrite and Upper Magnesian Limestone Formations of the Teese Group. The Boulby Mine is the only current exploitation of Zechstein potash in England (Holmes, 1991). The first of two shafts at Boulby was completed in 1973 (Figure 11.17). It quickly became apparent that ore grade in this potash deposit, which sits atop the thick halites of the Boulby Halite Formation, was characterized by both brine-controlled mineral migration (karst) and gravity-induced plastic flow of the potash bed. Deformation of the potash bed is ongoing today and has led to a number of mining problems over the years, exacerbated by high temperatures of 40°C or more at the deepest workings (≈ 1300 m below land surface), and occurrence of local highly pressurised nitrogen gas pockets in the salt. Problems include one gas blowout (in 1976) with sufficient pressure to turn a continuous miner onto its side. However, the high-grade of the ore and its relative simple mineralogy (in comparison with many other European Zechstein potash ores) make processing straightforward and so the deposit is economic. The virtual absence of magnesium minerals is particularly relevant to economic processing of the ore stream.

The Boulby Potash interval consists of a sylvinitic bed with gneissic and augen-like flow textures, along with tectonically-rounded rock fragments from adjacent intrasalt beds. The sylvinitic has a bed thickness of < 1 metre to 20 metres over lateral distances of 20 to 30 metres and mined units generally range between 0 and 8.5 metres in thickness. There are five distinct ore types, all of which exhibit rapid lateral changes, although each type may predominate over mine areas more than a kilometre across. The average KCl content in the ex-

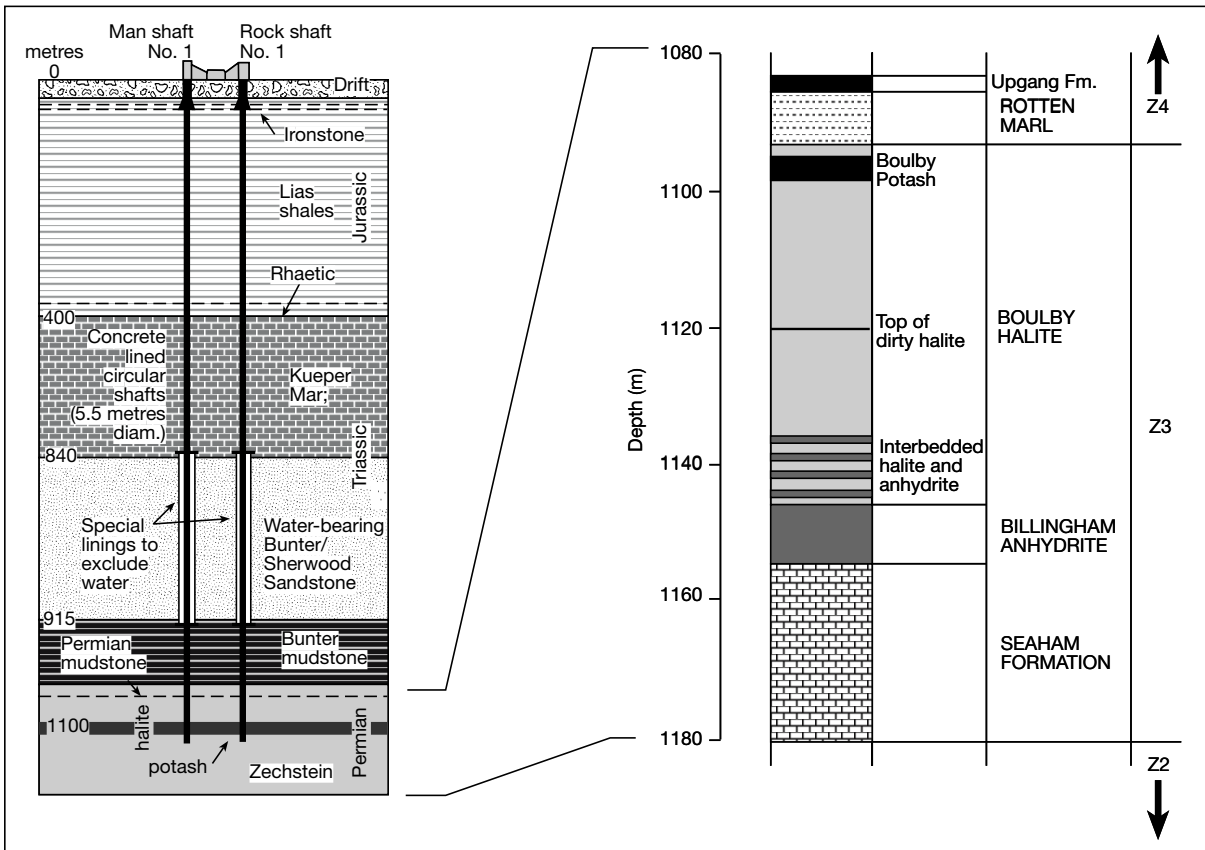


Figure 11.17. Stratigraphy of the Boulby Mine, Sussex, UK (after Holmes, 1991).

exploited parts of the Boulby Halite is 26 % KCl. As in the New Brunswick ores (Figure 11.21b), the Boulby potash sylvinitic ore is characterized by marked thickness changes reflecting flowage thickening and is related to the high differential stresses created by halokinesis of potash encased in halite. Thickening of highly mobile potash intervals can locally enrich several of the ore beds to grades in excess of 50 % KCl.

Locally, clay content in a projected ore zone can be anomalously high and exert a major detrimental effect on ore grade as do unexpected elevated levels of anhydrite, magnesite, pyrite, quartz and boron minerals, which together can exceed 15%.

The Carnallitic (Rotten) Marl Formation of the Staintondale Group, composed primarily of dehydrated clay minerals and halite, overlies the Boulby Halite Formation. As the name implies the Rotten Marl is a "salt-clay." It tends to be structurally incompetent as it lacks any significant cementing mineral binding the soft clay. The bed is further weakened by steeply dipping discontinuities in some parts of the mine area from a combination of flow and dissolution features and it must be

well characterised before mining can proceed. A minimum of 1.5-2 metres of salt in the mine back (roof) is maintained to ensure no significant roof collapse. The Carnallitic (Rotten) Marl Formation sits in sharp contact with the overlying Uppgang Formation, which in turn is overlain by the Upper Anhydrite Formation and Upper Halite Formation of the Zechstein Cycle 4 of the Staintondale Group. The Staintondale Group is in turn overlain by more than a kilometre thick Upper Permian and Triassic marine and continental clastic sediments, which include highly pressurised brines in sands of the Triassic Sherwood Formation (Figure 11.17).

The potash zone is worked using a variation of the room and pillar method. Ore is extracted from the rooms (potash panels) using "continuous miner" equipment, similar to that used in coal mines. Mine development work is carried out in relatively thick stable halite located some 30 metres below the potash zone. Ramps are then driven upward from the development roadway level into the potash zone, which is less structurally stable. Even the access roads are liable to instability due to high lithostatic pressures at these depths; so long horizontal slots

are cut into roadway walls for stress relief. Although the basic concept of roadway development in salt to access room-and-pillar potash panels was sound, determining the most efficient mining system proved difficult and it was not until 1984 that mining costs were sufficiently reduced to achieve profitability. By the mid-1990s, output had stabilised at 16,000t/d – 2.8Mt/y from six production sections. To cope with greater stresses in the ore below 1,200m and to raise output above 3Mt/y, in 2001 the miner operator (ICL Fertilizers) converted its continuous miners to remote-controlled operation (so they can be used safely without prior blasting and gas relief in shaly, gassy sections of the potash ore).

New Mexico potash, USA

Potash is mined from the Salado Formation in the Carlsbad Potash District of the Permian Basin of New Mexico. The area produces more than 70% of all the potash mined in the United States. Potash was first discovered in this region in the mid 1920s during drilling for oil and the first potash mine was opened in 1931. Various potash minerals occur in eleven ore zones numbered 1 through 11 (in ascending order) in a 215 m thick cyclic interval known as the McNutt interval located in the middle of the Salado Formation (Figure 11.18a, Table 11.4; Lowenstein, 1987b). Zone 1 is the richest, but is now exhausted. Production is now mostly from zones 3, 5, 7 and 10. The major ore minerals are sylvite and langbeinite, with accessory leonite, kainite, carnallite, polyhalite, kieserite, bloedite, halite and anhydrite. A typical ore is 60% halite, 30% sylvite, 5% langbeinite, and 2% of polyhalite and insolubles. Langbeinite is produced from zone 4, and mixed sylvite-langbeinite from zone 5. For example, in the IMC Global Inc operation, the ore on the 900 foot (275 m) level is primarily sylvinites with some langbeinite. The 260 m (850 foot) level ore is langbeinite. The 244 and 213 m (800 and 700 foot) level ores are a mixture of the two. IMC Global Inc. produces muriate from sylvinites ore, Sul-Po-Mag from langbeinite, and sulphate by combining the two minerals. Several mines in this potash district have been closed in the last decade, and it is unlikely that they will be reopened.

The potash ore zone in New Mexico lies above and immediately basinward of the older Permian basin margin, as defined by the position of the underlying Capitan Reef (Figure 11.18a). This location corresponds to a likely

surface depression and water sink at the time of deposition. It was probably a zone of differential subsidence in the underlying sediments located at the hinge between indurated platform edge carbonates and muddier basin centre sediments. It was also the spill point of the aggrading basin-filling evaporite cycles that make up the basinwide evaporites of the Castile and Salado formations. The significance of fill and spill hydrology as loci of changes in mineralogy was discussed in Chapter 5. The nearby underlying Capitan Fm. reef crest also acts as a focus to any subsequent rise of artesian or escaping basinal waters (Figures 7.9, 7.45a).

Two types of lithologic cycles dominate the ore zones in the Carlsbad Potash District (Figure 11.18b; Lowenstein, 1987b). Type I cycles begin with mixed siliciclastic carbonate (magnesite) mudstone, followed by anhydrite polyhalite with gypsum crystal pseudomorphs, overlain by halite and capped by muddy halite. Type II cycles begin with halite that grades transitionally upsection into muddy halite and pseudomorphs after gypsum, which retain subaqueous bottom-aligned growth habits or mechanically deposited sedimentary structures (ripples, cross beds, etc.). In the anhydrite-polyhalite parts of the cycles there are many pseudomorphs of primary gypsum textures that are now replaced by anhydrite, polyhalite, halite or sylvite. Sylvite and carnallite are most common in the muddy halite parts of the cycles where they occur as millimetre- to centimetre-sized anhedral crystals. Both the blood-red sylvite and the purple carnallite colours in the ore zone come from micrometre-sized plates of haematite. Potash crystals may be internally zoned; with dark haematite-rich bands developed at the crystal rims, and progressively lighter bands, depleted in

Zone	Mineralogy	Potential
11	Mostly carnallite, minor sylvite and leonite	Noncommercial to date
10	Sylvite, sylvinites	2nd best in district (high clay (6-7%))
9	Carnallite, kieserite, minor sylvite	Noncommercial to date
8	Sylvite	Moderate reserves, future potential, high clay
7	Sylvite	Moderate reserves, moderate clay (3-4%)
6	Carnallite, kieserite, minor sylvite	Noncommercial to date
5	Sylvite and langbeinite	Moderate reserves trace clay (1%)
4	Langbeinite and sylvite	Main source of langbeinite; mixed ore
3	Sylvite	Historically, 3rd in sylvite production
2	Carnallite, kieserite, minor sylvite	Noncommercial to date
1	Sylvite	Formerly major sylvite producing zone (now exhausted)

Table 11.4. Zone and properties of the McNutt ore Zone, New Mexico, listing mineralogy and potential (after Griswold, 1982).

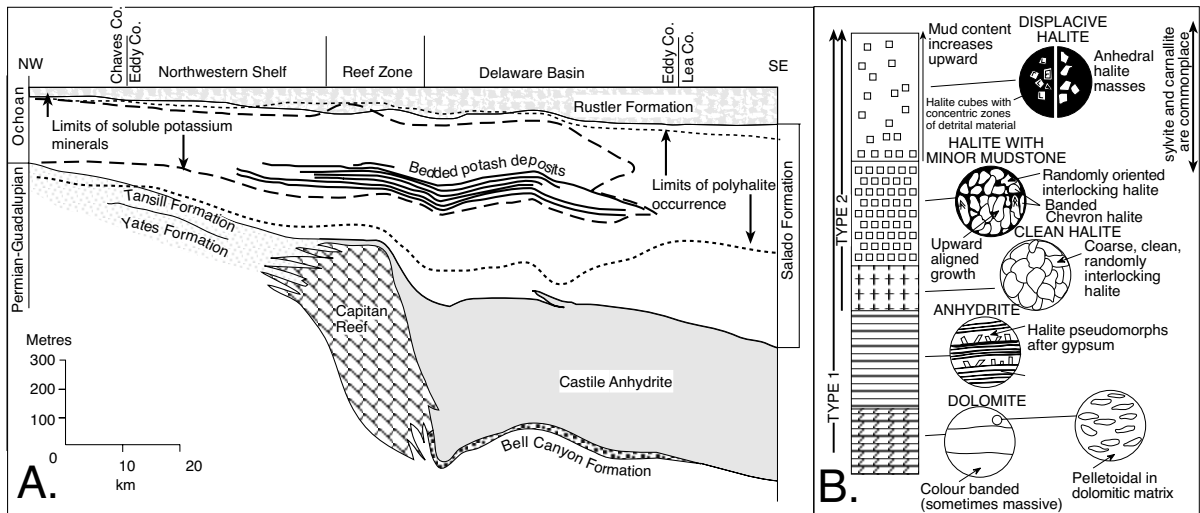


Figure 11.18. Potash in the Carlsbad Potash District, New Mexico. A) Stratigraphic section in southeastern New Mexico showing distribution of bedded potash (McNutt ore zone) about basin margin (after Bates, 1969). B) Idealised halite-dominated depositional cycles that host the ore beds (after Lowenstein, 1987b).

haematite, in the cores of the crystals. Ore zones are hosted in stacked halite beds, up to 1 metre thick with up to 50% sylvite and carnallite. Thin sections of the ore show poikilitic textures, with several halite crystals encased in single carnallite or sylvite crystals. The sylvite and carnallite occupy areas equivalent in size and shape to the void spaces in modern saline pan halites and are interpreted as pore-filling cements (Lowenstein and Spencer, 1990).

Given that Quaternary halite beds lose porosity by 100 metres depth, it is likely that the bulk of the stratiform potash ores within the McNutt potash zone were emplaced syndepositionally or very early during shallow burial. That the ore is early is reinforced by an argon date of 250 ± 0.6 Ma for deposition obtained from langbeinites in the McNutt ore zone, with subsequent local recrystallisation events at 245 and 94 Ma (Renne et al., 2001). Like their more recent analogues, this Permian potash precipitated as stratiform units in depressions in a saltern to mudflat terrain subject to exposure and shallow karsting in bedded halite beds. Much of the ore precipitation was driven by cooling of warm refluxing shallow brine. Later in its burial history the ore zones were subject to recrystallisation from fluid crossflows (descending or ascending), most likely driven by local or region tectonic events. This explains the irregular distribution of the stratiform Carlsbad potash salts and their general lack of fine texture in a halite host that away from the ore zones still retains the original chevron halite texture and why the stratiform potash zone ores frequently cross depositional boundaries in primary halite beds.

West Canadian potash (Devonian)

The Middle Devonian Prairie Evaporite Formation is a potash-entraining halite sequence deposited in the Elk Point Basin, an early intracratonic phase of the Western Canada Sedimentary Basin (Chiple and Kyser, 1989). Devonian halite constitutes a large portion of the four formations that make up the Elk Point Group: 1) the Lotsberg (Lower and Upper Lotsberg Salt), 2) the Cold Lake (Cold Lake Salt), 3) the Prairie Evaporite (Whitkow and Leofnard Salt), and 4) the Dawson Bay (Hubbard Evaporite). At that time the Elk Point Basin covered most of Alberta, the southern half of Saskatchewan, southwest Manitoba and extended south into the USA (Figures 7.5, 11.19a). Its Pacific coast was near the present Alberta-British Columbia border, and the Elk Point Basin was centred at approximately 10° S latitude. The basin was bound to the north and west by a series of tectonic ridges and arches; but due to subsequent erosion, the true eastern extent is unknown (Mossop and Shetton, 1994). Hydrographic isolation of the basin resulted in the deposition of a drawdown sequence of basinwide evaporites in an intracratonic sag and include the various potash entraining intervals in the Prairie Evaporite Formation.

Today the remnants of the Middle Devonian Prairie Evaporite Formation constitute a bedded unit some 500 metres thick, which lies atop the irregular topography of the platform carbonates of the Winnipegosis Formation (Figure 11.19b). Above the Prairie Evaporite Formation is a series of cyclic Devonian limestones, dolomites and evaporites that make up the Dawson Bay, Souris River, Duperow and Nisku Formations. Lying

unconformably on these deposits are the Lower Cretaceous sands of the Mannville Group, which are in turn overlain by younger Cretaceous shales and capped by Quaternary glacial sediments. The Prairie Evaporite Formation is continuous over a large portion of southern Saskatchewan, except where locally removed by dissolution. The dissolution process is ongoing and at various times has created stratigraphic traps for hydrocarbons (e.g. Figure 10.63).

Potash geology

Potash deposits mined in Saskatchewan are all found within the upper 60-70 m of the Prairie Evaporite Formation at depths of more than 400 to 2750 metres beneath the surface of the Saskatchewan Plains. Within the Prairie Evaporite there are four main potash-bearing members, in ascending stratigraphic order they are: Esterhazy, White Bear, Belle Plaine and Patience Lake members (Figure 11.19b). Each member is composed of various combinations of halite, sylvite, sylvinitic, and

carnallite (Fuzesy, 1982). The Belle Plaine member is separated from the Esterhazy by about 15 m of halite, its thickness ranges from 0-18 m and averages around 9 m. The Patience Lake member is separated from the Belle Plaine by 3-12 m of halite its thickness ranges from 0-21 m and averages 12 m (Holter, 1972). In total the Prairie Evaporite Formation does not contain any $MgSO_4$ minerals (kieserite, polyhalite) and indicates a Devonian seawater chemistry somewhat different from today's (Figure 2.30).

As early as 1860, salt springs and seepages near the edge of the Elk Point Basin indicated the presence of widespread salt in Western Canada (Figure 7.5). Rock salt was first sampled in 1907, while potash beds were intersected in Saskatchewan in 1942 during the sinking of oil and gas wells. The potential of commercial grades of potash mineralisation was not recognized until 1946. Canadian potash deposits are among the richest and largest on earth, containing around 5 billion tons of ore in a mineable band up to 50 miles wide, which stretches

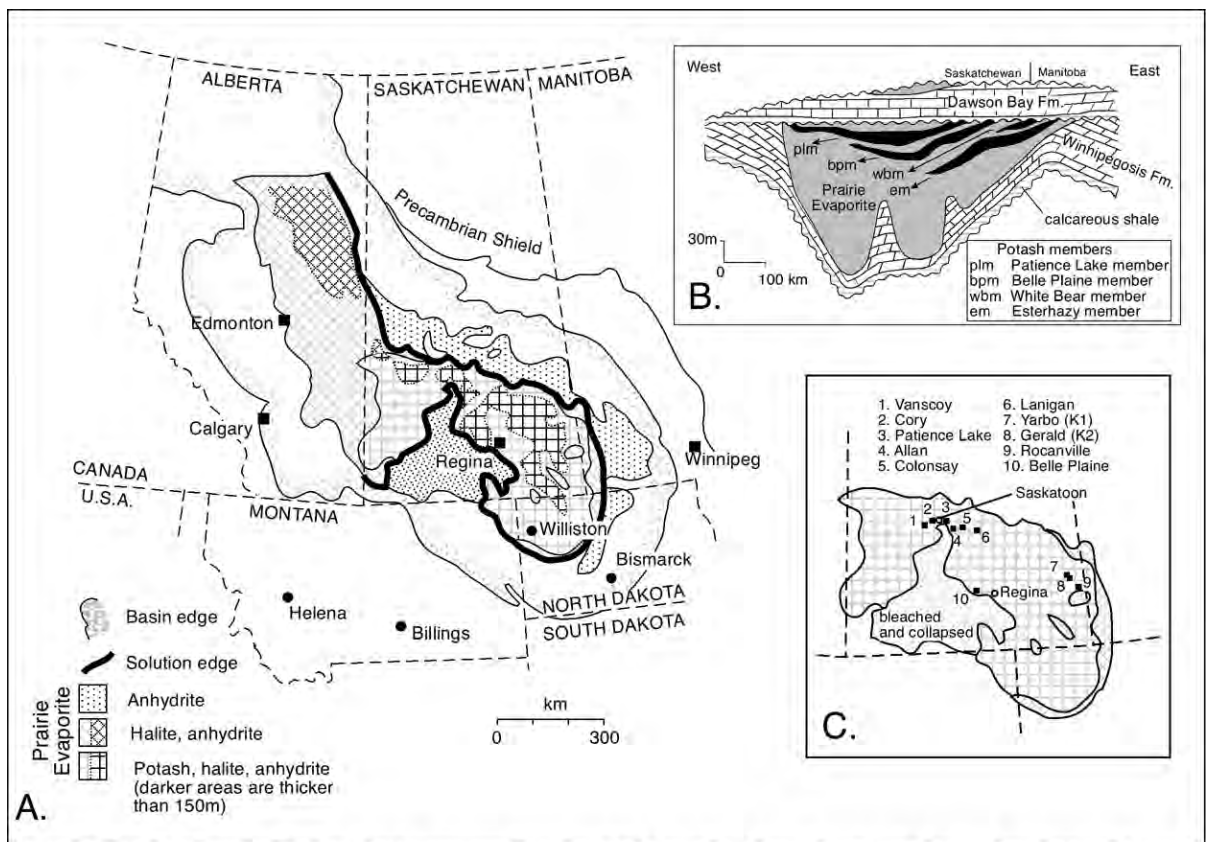


Figure 11.19. Potash in the Elk Point Basin, western Canada. A) Regional geology showing thickest salt and potash intervals in the Prairie Evaporite and its dissolution edge (see also Figure 7.5). B) Cross section of basin showing distribution of potash members. C) Map of potash mines in the basin (compiled and modified from Worsley and Fuzesy, 1979; Fuzesy, 1982; Boys, 1993).

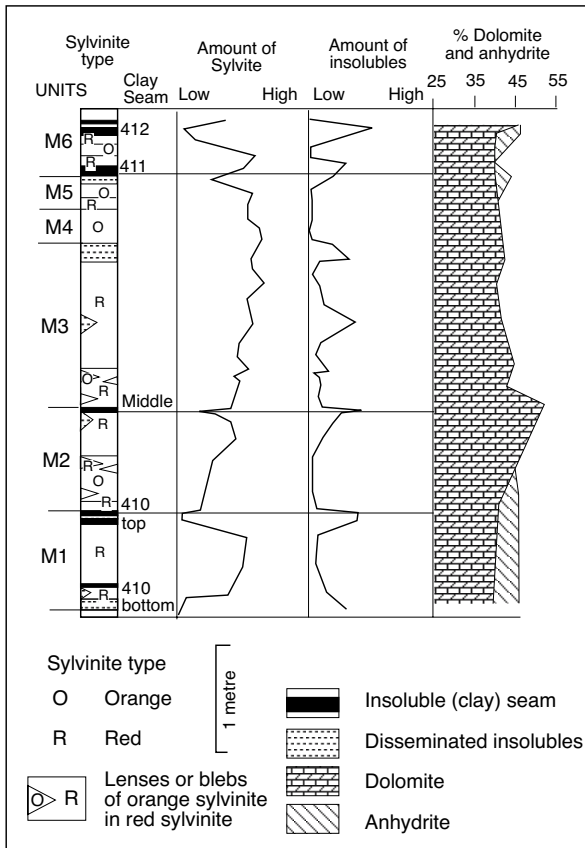


Figure 11.20. Ore section in the Patience Lake member of the Prairie Evaporite Formation in the PCS Cory potash mine (after Boys, 1993).

some 725 km (450 miles) across the province (Figure 11.19). Canada today supplies more than 30% of the world’s annual potash production.

The Prairie Evaporite is more than 200 m thick in the potash mining district in Saskatoon and 140 m thick in the Rocanville area to the southeast. The Patience Lake member is the main target for conventional mining near Saskatoon. The Esterhazy potash member rises close to the surface in the southeastern part of Saskatchewan near Rocanville and on into Manitoba. This is a region where the Patience Lake member is thinner or completely dissolved (Figure 11.19b). Over the area of mineable interest in the Patience Lake member centred on Saskatoon the ore bed currently slopes downward only slightly in a westerly direction, but deepens more strongly to the south at a rate of 3-9 m/km. Mines near Saskatoon are at depths approaching a kilometre and so are nearing the limits of currently economic shaft mining. The main shaft for the Colonsay Mine, which took IMC Global Inc. more than 5 years to complete through

a water-saturated sediment column, finally reach the target ore body at a depth of 960 metres. Such depths and a southerly dip to the ore means that the conventional shaft mines near Saskatoon define a narrow WNW-ESE band of activity (Figure 11.19c). To the south potash is recovered from greater depths by solution mining; the Belle Plaine operation leaches potash from the Belle Plaine member at a depth of 1800m.

The Prairie Evaporite typically thins southwards in the basin; although local thickening occurs where carnallite, not sylvite, is the dominant potash mineral (Worsley and Fuzesy, 1979). The Patience Lake member is mined at the Cory, Allan and Lanigan mines, and the Esterhazy Member is mined in the Rocanville area (Figure 11.19c). Ore mined from the 2.4 m thick Esterhazy Member in eastern Saskatchewan contain minimal amounts of insolubles ($\approx 1\%$), but considerable quantities of carnallite (typically 1%, but up to 10%) and this reduces the average KCl grade value to an average of 25% K_2O . The converse is true for ore mined from the Patience Lake potash member in western Saskatchewan near Saskatoon where carnallite is uncommon in the Cory and Allan mines. The mined ore thickness is a 2.74-3.35 metre cut off the top of the 3.66-4.57metre Prairie Lake potash member. Ore grade is 20-26% K_2O and inversely related to thickness. The insoluble content is 4-7%, mostly clay and markedly higher than in the Rocanville mines.

A typical sylvinitic ore zone in the Patience Lake member can be divided into six units, based on potash rock-types and clay seams (Figure 11.20, M1-M6; Boys, 1993). The units are mappable and can be correlated throughout the PCS Cory Mine with varying degrees of success, dependent on partial or complete loss of section from dissolution. Potash deposition appears to have been cyclic, expressed in the repetitive distribution of haematite and other insoluble minerals. Desiccation polygons, desiccation cracks, microkarst pits and chevron halite crystals indicate that the Patience Lake member that entrains the potash ore was deposited in a shallow-brine, salt-pan environment.

Clay seams form thin stratigraphic layers throughout the potash ore zone(s) of the Prairie Evaporite, as well as disseminated intervals, and constitute about 6% of the ore as mined. Insoluble minerals found in the PCS Cory samples are, in approximate order of decreasing abundance: dolomite, clay [illite, chlorite (including swelling-chlorite/chlorite), and septechlorite], quartz, anhydrite, haematite, and goethite. Clay minerals make up about one-third of the total insolubles: other minor components include: potassium feldspar, hydrocarbons, and sporadic non-diagnostic palynomorphs (Boys, 1993).

Potash salts probably first formed as secondary precipitates just beneath the sediment surface and were modified to varying degrees by ongoing fluid flushing in the burial environment. The cyclic depositional distribution of disseminated insolubles was possibly due to a combination of source proximity and the strength of the winds blowing detritals out over the brine seaway. Possible intrapotash unconformities, created by dissolution of overlying potash-bearing beds, are indicated by an abundance of residual haematite in clay seams. Except in, and near, dissolution and collapse features, the secondary redistribution of insolubles, other than iron oxides, is insignificant.

Bedded halite away from the ore zones generally retains primary depositional textures typical of halite precipitation in shallow ephemeral saline pans (Brodylo and Spencer, 1987). Crystalline growth fabrics, mainly remnants of vertically elongate chevrons, are found in 50-90% of the halite from many intervals in the Prairie Evaporite. Many of the chevrons are truncated by irregular patches of clear halite that formed as early diagenetic cements in syndepositional karst.

Halite associated with the potash ore lacks well-defined primary textures and is atypical when compared with the well-preserved depositional textures in the non-ore sequences. From the regional petrology and the lower than expected Br levels in halite in the Prairie Evaporite Formation, Schwerdtner (1964), Wardlaw and Watson (1966) and Wardlaw (1968) postulated a series of recrystallisation events forming sylvite as a result of periodic flushing by hypersaline solutions. This origin as a secondary precipitate is supported by observations of intergrowth and overgrowth textures (McIntosh and Wardlaw, 1968), large-scale collapse and dissolution features (Gendzwill, 1978), radiometric ages (Baadsgaard, 1987) and palaeomagnetic orientations of the diagenetic haematite linings associated with the emplacement of the potash (Koehler et al., 1997).

Dating of clear halite crystals associated with the ore zone shows that the exceptionally coarse and pure secondary halites forming pods in the mined potash horizons may have precipitated as soon as early burial or have formed as late as Pliocene-Pleistocene. Even today, alteration and remobilisation of the sylvite appears to be an ongoing process, perhaps related to the encroachment of the current dissolution edge or the ongoing stoping of chimneys fed by deep artesian circulation (Figure 7.4).

Halite-sylvite (sylvinite) rocks in the ore zone show two end member textures, the most common is a recrystallised polygonal mosaic texture with individual crystals ranging from millimetres to centimetres and sylvite grain boundaries outlined

by concentrations of blood-red halite. The other end member texture is a framework of euhedral and subhedral halite cubes enclosed by anhedral crystals of sylvite. This is very similar to ore textures in the Salado Formation of New Mexico; which formed by early passive precipitation in karstic voids.

Petrographically, the halite-carnallite (carnallitite) rocks display three distinct textures. Most halite-carnallite rocks contain isolated centimetre-sized cubes of halite enclosed by poikilitic carnallite crystals. The halite cubes are typically clear, with occasional cloudy crystal cores that retain patches of syndepositional growth textures (Lowenstein and Spencer, 1990). The second texture is coarsely crystalline halite-carnallite with equigranular, polygonal mosaic textures. The third type, which is rare, contains interlayered halite and carnallite with a primary bedding style similar to that in the Oligocene potash of the Rhine Graben. In zones where halite overlies anhydrite, most of the halite is clear with only the occasional crystal showing fluid inclusion banding.

Clay minerals, which tend to occur as long continuous seams or markers in the potash zones, are mainly composed of detrital chlorite and illite and authigenic septechlorite, montmorillonite and sepiolite (Mossman et al., 1982; Boys, 1990). Of the two chlorites, septechlorite is the more thermally stable. The septechlorite, sepiolite and vermiculite very likely originated as direct products of settle-out or early diagenesis under hypersaline conditions of what was originally eolian dust settling onto a huge brine seaway. Absence of the otherwise ubiquitous septechlorite from Second Red Beds west of the zero-edge of the evaporite basin supports this concept.

The fluids

Analysis of waters, which are currently found in the various Canadian potash mines and the collapse anomalies in the Prairie Evaporite, further supports the notion that recrystallising fluids had access to the evaporite minerals throughout the burial history of the Prairie Formation (Chiple, 1995; Koehler et al., 1997). Likewise, the Rb-Sr isotope systematics of crystal layers in both halite and sylvite indicate that the Prairie Evaporite was variably recrystallised during fluid events at 371, 284, 241, 185, 147, 85, 35 and 0.5 Ma. These ages are all more recent than original deposition and correspond to ages of various tectonic events that affected the western margin of North America.

Chemical compositions of inclusion fluids in the Prairie Evaporite, as determined by their thermometric properties, reveal at least two distinct waters: a Na-K-Mg-Ca-Cl brine,

variably saturated with respect to sylvite and carnallite; and a Na-K-Cl brine that is the result of fluid-rock interaction and did not result from simple evaporation of seawater to the sylvite facies (Chipley, 1995). This is supported by δD and $\delta^{18}O$ values of inclusion fluids in halite and sylvite, which range from -146 to 0‰ and from -17.6 to -3.0‰, respectively. Most of the preserved isotope values are different from those of evaporated seawater, which should have δD and $\delta^{18}O$ values near 0‰. Furthermore, the δD and $\delta^{18}O$ values of inclusion fluids are probably not the result of precipitation of the evaporite minerals from a brine that was a mixture of seawater and meteoric water. The low latitude position of the basin during the Middle Devonian (10-15° from the equator), the required lack of meteoric water to precipitate basinwide evaporites, and the expected δD and $\delta^{18}O$ values of any meteoric water in such a setting, make this an unlikely explanation. Rather, the δD and $\delta^{18}O$ values of inclusion fluids in the halites reflect ambient and evolving brine chemistries as the fluids in inclusions in the various growth layers were intermittently trapped during the subsurface evolution of the Prairie Formation in the Western Canada Sedimentary Basin. They also suggest that nonmarine pore water has been a major component of the crossflowing basinal brines throughout much of the recrystallisation history (Chipley, 1995).

Other significant potash deposits

Canadian Maritimes (Mississippian of Nova Scotia and New Brunswick)

The Carboniferous geology of the Maritime Provinces and Quebec is characterised by a series of northeast trending fault-bound grabens or half grabens containing clastics and evaporites (mostly halite) up to 10 km thick

(Roberts and Williams, 1993). The Windsor Group (Visean) in Nova Scotia and New Brunswick hosts $MgSO_4$ -poor potash evaporites in several continental intermontane basins that were created by extension-driven post-Acadian strike-slip faulting with the salt then subject to halokinesis first by extension and then subsequent compression. The same evaporite unit that hosts the potash ore also acts as a seal to MVT deposits at Gays River and Jubilee (Figure 11.21a). Exploitable potash at New Brunswick was discovered in the 1970s by the New Brunswick Mineral Resources Branch of the Geological Survey, with the first intersection occurring in 1969-1970 during

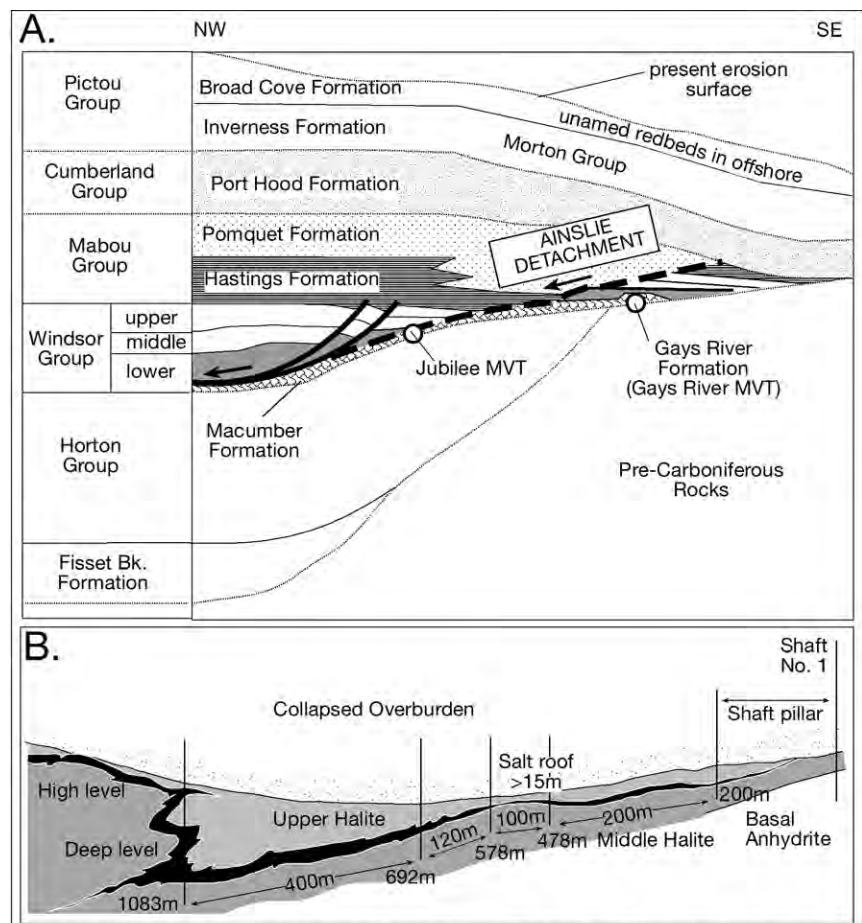


Figure 11.21. Potash in New Brunswick and Nova Scotia. A) Schematic cross-section of the stratigraphy and position of the regional Ainslie Detachment, in Nova Scotia, a major allochthon feature associated with salt flow and gravity gliding into the basin. Lubricating evaporites of the lower Windsor Group (Carrols Corner Formation) are shaded grey. Note the salt raft tectonics geometry with thickening of the Mabou Group in the salt-withdrawal sink. Jubilee-style base metal deposits are hosted in the salt tectonites created by the detachment. In contrast, the Gays River-style of deposit is formed at the evaporite-encased underbelly contact adjacent to the salt-encased reefal buildup. In the case of the Jubilee deposit it was focused by the feather edge of the salt unit (after Lynch et al., 1998; Warren, 2000b). B) Distribution of sylvinite ore zone (black), enclosed in halite an anticlinal structure in a New Brunswick potash mine.

a drilling program designed to define a halite resource suitable for hydrocarbon storage.

Of particular interest for potash extraction is the Cassidy Lake Formation in the Moncton Sub-basin. It entrains structurally complex potash ore and is much more deformed than most of the world's conventionally mined potash occurrences, with ore thicknesses ranging from 0-45 metres (Figure 11.21b). Seismic and borehole evidence from the Windsor Group shows that the Cassidy Lake Formation (rock salt and potash) is separated from the underlying Upperton Formation (anhydrite) by a low-angle décollement surface marked by the presence of mylonitic salt and cataclastic limestone and anhydrite. Much of the halokinetic deformation occurred above the regional décollement separating the Cassidy Lake Formation from the underlying Upperton Formation. Flow has been complex within the salt body itself, resulting in structural repeats of the salt stratigraphy through recumbent to inclined isoclinal folds and sheath folds. Deformation was syntectonically mobilised by gravity sliding, thrusting and folding atop the regional décollement surface, with the most intense deformation being taken up in the highly deformable sylvinites.

The Potash Member in the Cassidy Lake Formation consists of cm-scale beds of halite and halite+sylvite and minor rinneite and polyhalite. The exploited ore is sylvinite running 20-30% K_2O . The Upper Salt Member atop the potash ore is 2.5 - 20 m thick and composed of interlayered thin beds and laminae of argillaceous halite, sylvinite and claystone-anhydrite (Anderle et al., 1979). Because of structural thickening in this halokinetic salt, it entrains what is perhaps the thickest exploited bed of KCl salts in the world in a domelike anticline fold with a highly complicated internal structure dominated by isoclinal and sheath folds. The depth to ore in this structure ranges from 580 to 850 m below the surface and in thickness the ore zone ranges from a few metres to 30 metres (Figure 11.21a). The variable inclination and thickness of the ore zone means mining procedures are more variable than those used in extracting potash from the Prairie Evaporite. In intervals where the ore zone is relatively flat, continuous front procedures are used, similar to Saskatchewan. Where the ore zone is more steeply inclined, classic drill and blast procedures are followed.

In Nova Scotia salt, not potash, is the main product from Pugwash Mine within equivalent age evaporites, but the operations in the halite show a similar structural complexity in the salt to the New Brunswick operation. Figure 11.22 shows a refolded fold in the Pugwash Mine: the axial plane

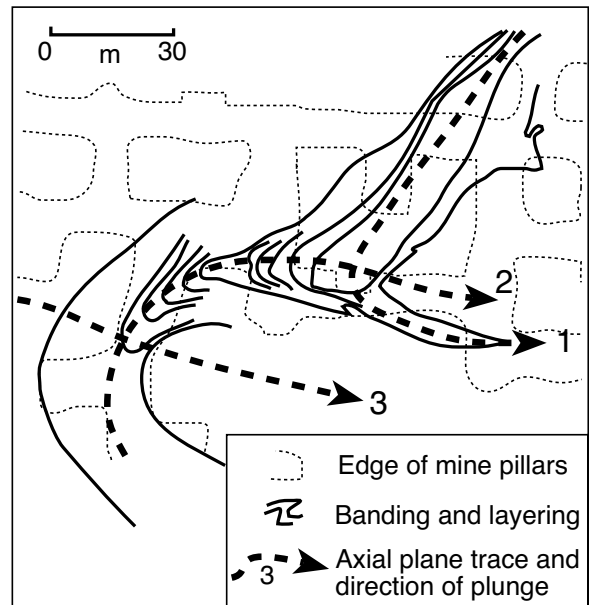


Figure 11.22. Refolded fold in sylvite-halite, Pugwash Mine, Nova Scotia (after Evans, 1967).

of the initial antiform (axial trace 1) was folded and the nose (axial trace 2) of the resultant synform was folded (axial trace 3). The axial planes of each of the folds have the same axial orientations as the axial plane traces of the other two clearly demonstrating an inherently high degree of plasticity during deformation (Evans, 1967).

Borates are commonplace coprecipitates in particular horizons in the Cassidy Lake Formation: for example, danburite occurs in the Basal Halite; while boracite, hydroboracite, szaebelyite, hilgardite and ulexite are found in the Upper Salt Member of the Windsor Group. Where the Clover Hill Formation overlies the Cassidy Lake Formation the contact is typically a thin "residual" bed made up of laminated clayey anhydrite, borates and quartz grains. It is not a depositional contact but the result of ongoing post deformational "sub-rosion" at the evaporite-nonevaporite interface, similar to that documented at the upper and lower contacts of the Maha Sarakham Fm. in Thailand. In 1997, Potash Company of Canada (Potacan) closed its 890,000-ton mine at Cassidy Lake, near Sussex, N.B., because of flooding related to intersection of an unexpected salt "horse." The mine was converted to a solution mine, leaving one conventional mine (Sussex Mine) currently exploiting the New Brunswick potash ore in this structurally complex region.

Cretaceous trans-Atlantic potash: west Africa and Sergipe Basin, Brazil

Cretaceous (Aptian) evaporites were deposited in a series of growing rifts created as Africa separated from South America. Today the remnants of these beds are to be found on opposite sides of the Atlantic in the Sergipe-Alagoas and Gabon-Congo basins. In the Sergipe Basin the evaporite sequence (Ibura member of the Muribeca Formation) is a $MgSO_4$ -free potash deposit composed of stacked cycles of halite, carnallite and sylvite up to 800m thick. More than 750,000 t/yr of potash ore is extracted from the Ibura Member by the Companhia Vale do Rio Doce's at its conventional potash mine in Sergipe State. Several of the cycles in the Ibura Member are composed of thick halite (more than tens of metres thick) containing the highly soluble $CaCl_2$ mineral tachyhydrite (Figure 11.23; Meister and Aurich, 1972; Wardlaw, 1972; Wardlaw and Nicholls, 1972; Borchert, 1977). The Sergipe deposits are characterised by thick cycles with a characteristic upward trend: halite (100%) → halite (35-90%) + carnallite (10-65%) → tachyhydrite (5-100%). Wardlaw (1972) showed that these deposits are primary as they contain bottom-growth features and primary bedding in the halite-carnallite units. Documented textures also suggest that there were episodes of syndepositional karstification and flowage within the carnallite, creating near identical textures to those seen in Thailand and the Qaidam Basin, but not yet documented as analogs when Wardlaw studied the sequence back in 1972. In the upper part of the evaporite sequence a sylvinitic bed sits atop a carnallite + halite bed and is overlain by a halite bed; a mineralogical evolution that is similar to that of the Thai and many other potash successions.

The various potash minerals in the Sergipe Basin show a systematic lateral zonation away from the anticlinal domes that also define the three main oil-producing structures in the Sergipe Basin. This suggests that more soluble potash salts have been leached from the crests of the structures (Borchert, 1977). Near the top of the anticlinal slope there is only rock salt, further out on the anticlinal arms there are intercalated sylvinitic layers, which in turn pass outward into carnallitic and tachyhydritic beds. There are no documented halokinetic structures beneath the anticlines and syndepositional uplift driving the leaching was related to drape over underlying horsts. In my opinion, given the similarity of the sequencing and layering to the Maha Sarakham the possibility of synprecipitational focusing of the ore via halokinesis is a viable alternative.

Similar cyclic potash sequences constitute similar age beds on the African side of the Atlantic, there the beds are also free of $MgSO_4$ salts and may carry thick tachyhydrite units. Beds show a similar layering and sequencing in and around salt domes as in Brazil (Borchert, 1977; de Ruiter, 1979). Within the Congo Basin the most extensive and thickest potash deposits occur in the coastal Kouilou region where ten evaporite intervals are recognised, with a cumulative thickness of potash beds of more than 100m. Carnallite is the predominant potash mineral, while some cycles also contain bischofite and tachyhydrite. Carnallite grades to sylvite in the upper parts of some beds. The region is halokinetic and may be suitable for future solution mining of potash and magnesium. Further inland, for nine years in the 1970s, the equivalents of these evaporite cycles were conventionally mined for sylvite in the Holle mine area. Production was from the uppermost sylvinitic layers atop

carnallite with extraction at rates of 360,000 to 450,000 tonne/year. Geological and water problems prevented the mine from ever reaching its target production level of 720,000 tonne/yr. Operations ceased in 1978 when an aquifer was penetrated and the mine was flooded.

Neither the Sergipe nor the Congo evaporite mineralogies can be derived from the evaporation of modern day seawater. Yet both deposits retain bottom-nucleated crystal fabrics that show that the carnallite is primary implying different seawater chemistry in the Cretaceous (Figures 2.30, 11.23).

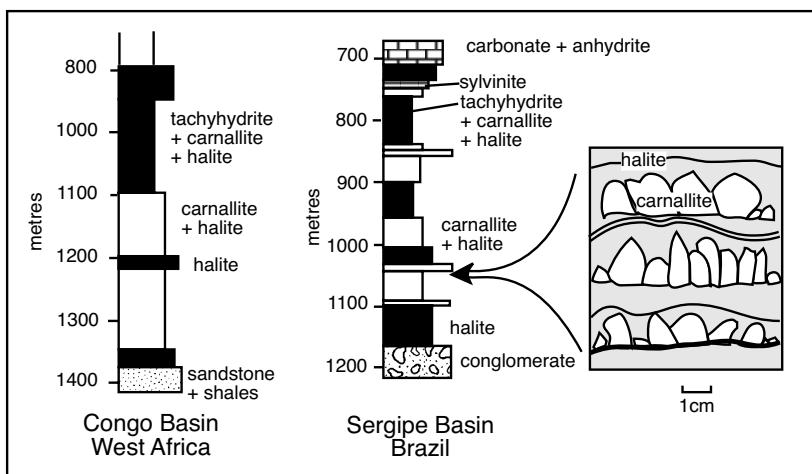


Figure 11.23. Similarities in potash sequences from the Sergipe and Congo Basins (after Hardie, 1990). Inset on the right shows primary layering and bottom-growth features of the Sergipe halite-carnallite subfacies (after Figure 2 in Wardlaw, 1972).

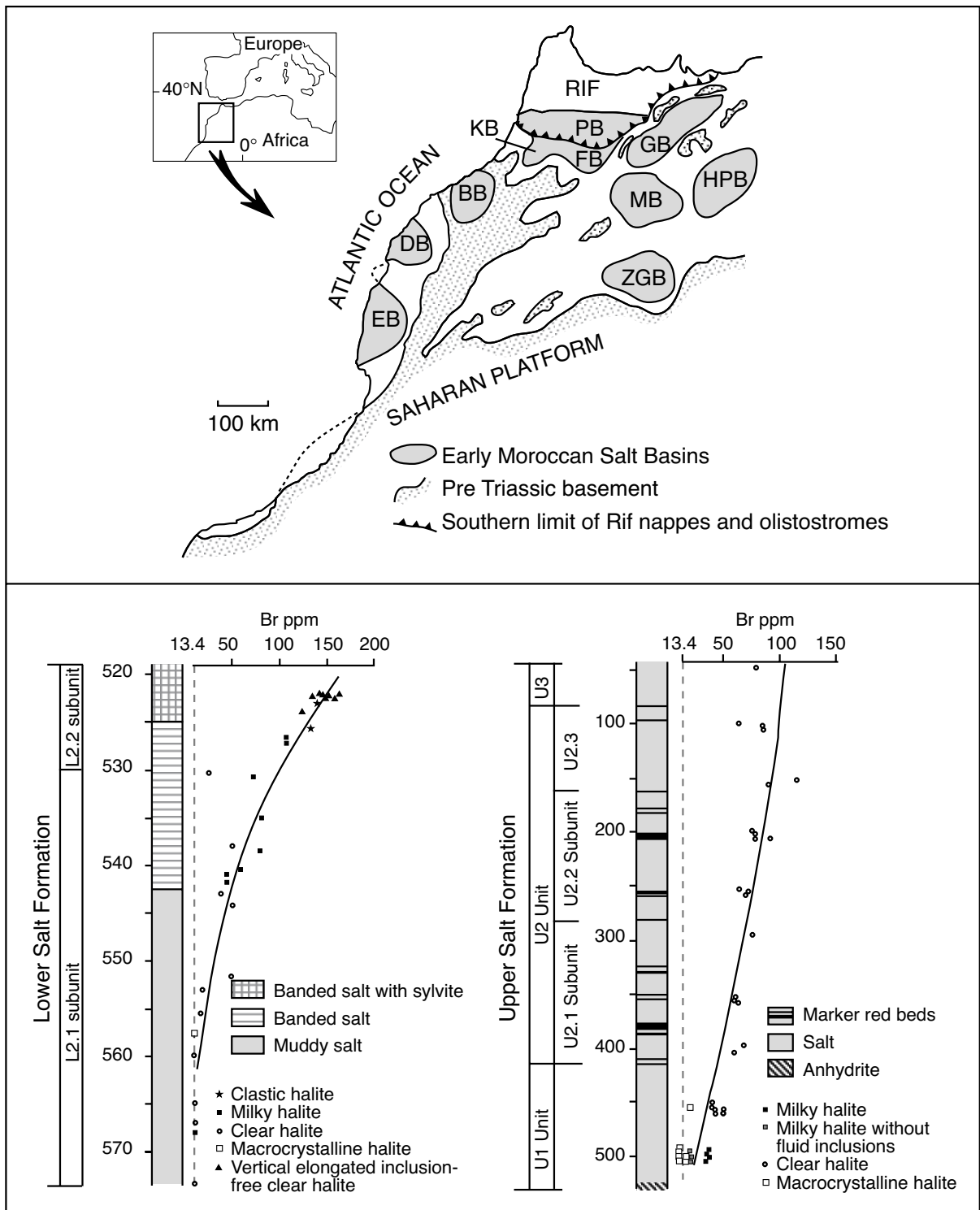


Figure 11.24. Salt in Morocco. A) Location of major Lower Mesozoic Moroccan Salt Basins. Key: BB: Berrechid Basin; DB: Doukkala Basin; EB: Essaouira Basin; FB: Boufekrane Basin; GB: Guerif Basin; HPB: Haut-Plateaux Basin; KB: Khemisset Basin; MB: Moulouya Basin; MM: Moroccan Meseta; PB: Prerif Basin; ZGB: Ziz-Guir Basin. B) Stratigraphy and bromine profiles from the Lower and Upper Salt Formations in the Khemisset Basin, northwestern Morocco (after Et-Touhami, 1996).

Moroccan Meseta (Late Triassic)

Salt basins formed in Morocco as rifts evolved into subsealevel intracratonic sags during the Triassic breakup of the supercontinent Pangaea. As a result, nonmarine redbeds and evaporites fill the many Late Triassic (Keuper) to early Liassic half grabens that make up the Moroccan Meseta (Figure 11.24a). Thick basalt flows (up to 500m) underlie and overlie these saline deposits (van Houten, 1977; Clement and Holser, 1988; Lorenz, 1988). In four of the sub-basins, including the Khemisset Basin, evaporites interbedded with basalts carry varying concentrations of potash. The potash intervals consist essentially of halite, carnallite, sylvite and rinneite, with less than 1% of other minerals (anhydrite, kieserite, bischofite, douglasite; Salvan, 1972). Once again this is a $MgSO_4$ -depleted potash sequence and indicate a largely marine-derived Ca-Cl source with ionic proportions different from today (Figure 2.30b).

The most detailed work on the stratigraphy of the potash intervals to date is by Et-Touhami (1996), who studied the succession in the Khemisset Basin. Strata in the centre of the Khemisset Basin are Late Triassic to Early Liassic and made up of five formations (from base to top); Lower Clay Formation, Lower Salt Formation, the Basaltic Formation, Upper Salt Formation and the Upper Clay Formation (Figure 11.24b). Potash occurs toward the top of the Lower Salt Formation (LSF). The LSF is subdivided into two informal units known as L1 and L2. The lower unit (L1) is composed mostly of red-brown chaotic mudstone interbedded with red beds, especially toward its base. The upper unit (L2) is further divided into the L2.1 and L2.2 subunits (Figure 11.24b). Subunit L2.1 is made up of black chaotic to massive banded salt with some local inclusions of potash. Subunit L2.2 is made up of massive banded halite with potash layers (sylvite and carnallite), along with thin stringers of anhydrite and polyhalite. As in Thailand and Brazil, the sylvite unit tends to occur near the top of a colour banded halite unit and sits directly atop a carnallite succession. Locally the halite crystals in the carnallite unit retain relict chevron fabrics and vertically-elongate inclusion-free halites identical to those interpreted as syndepositional relicts in the Mallowa Salt of the Canning Basin, Australia (Cathro et al., 1992). Slumps and synprecipitatorial karstic textures also characterise the carnallite. A bromine profile through the LSF shows the potash was precipitated in the most saline stage of the accumulation ($Br > 100\text{ppm}$; Figure 11.24b).

The LSF in the Khemisset Basin is covered by vesicular to highly altered lavas and flows of the Basaltic Formation, which also retains local lenticular intercalations of claystones, limestones and evaporites. Atop this is the Upper Salt Formation, a unit

composed of generally flat lying salt beds intercalated with siliciclastic mudstones and siltstones. It is divided into Units 1 - 3, with local potash inclusions sometimes found in Unit 3. The bromine profile of the Upper Salt Formation shows lower concentrations than the LSF and does not appear to have attained the bitter stage for long enough periods to accumulate thick beds of potash ($Br < 100\text{ppm}$; Figure 11.24b).

How does potash form?

Our discussions so far suggest there are two groups of processes controlling ore grade in ancient potash salts. One sees the potash salts, carnallite and sylvite, as primary precipitates or as syndepositional to early diagenetic replacements forming within metres of the depositional surface via brine reflux and brine cooling. The other visualises sylvite as forming later in burial via ongoing incongruent dissolution of precursor carnallite. Both views are valid but, if used exclusively, are perhaps a little too dogmatic. My own view is that, owing to its high solubility, the various textures found in ancient potash salts reflect variegated and evolving origins that are dependent on how many times and how pervasively in its burial history an evolving brine chemistry came into contact with the potash beds (Warren, 2000c). In other words, various forms and textures of potash may dissolve, recrystallise and backreact with each other from the time a potash salt is first precipitated until it is exploited. Textural and mineralogical evolution depends on how open is the hydrology of the system at various stages during its burial evolution. Alteration can occur syndepositionally, in brine reflux or during flushing by compactional or thermobaric subsurface waters. Tectonism (extensional and compactional) during the various stages of a basin's burial evolution acts as a bellows driving fluid flow within a basin, so forcing and speeding up the focused circulation of potash-altering waters.

A similar, but less intense, textural evolution can also be seen in the burial history of the less soluble salts. For example, $CaSO_4$ can flip-flop from gypsum to anhydrite depending on temperature, pore fluid salinity and the state of uplift/burial. This means that, as in gypsum/anhydrite sequences, there will be primary and secondary forms of both carnallite and sylvite that can alternate during deposition, during burial and during any deep meteoric flushing.

In Thailand, both primary potash precipitation and shallow diagenetic backreactions seem to have worked simultaneously with hydrologies that were first driven by early salt diapirism. Then alteration continued into deeper burial and finally by uplift, driven by the regional gravity drive of throughflushing

fluids whose flow was focused along nearby clastic aquifers. The Canadian examples show how carnallite/sylvite has continued to evolve with the evolution of basinal and deeply flushing suprasalt and subsalt meteoric waters as they came into contact with variably dissolving salt units.

Whatever model, or combination of models, is used to explain the origin of the major potash salts, the most important economic corollary is that, wherever a potash bed is in contact with mobile pore fluids, these highly soluble salts are continually subject to dissolution, mobilisation and reprecipitation. When trying to understand the distribution of potash ore in a halite-dominated sequence the ability of the potash salts to flow, dissolve, alter and reprecipitate must be accounted for in any predictive exploration model or development programme. Its ability to dissolve at various times in its diagenetic history also explains variations in that most important feature of any mine — ore grade.

Controls on potash quality: Anomalies, leaching and problematic mine waters

Just as the first rule for safe halite mining is “stay in the salt”, worldwide, the problem areas in most potash mines can be related to thinning or disappearing ore seams in zones that show evidence of dissolution and solution collapse (Boys, 1990, 1993; Woods, 1979). Increased water inflows in Saskatchewan potash mines can be consistently linked to salt anomalies, that is, to natural areas of little or no potash within the potash ore bed (Gendzwill and Martin, 1996). Other than intersecting old open well bores in the potash ore zone, most episodes of flooding, including the complete loss of working mines, stem from uncontrolled water inflows that followed from an intersection with an anomalous non-ore zone.

Geology of the potash ore quality in three salt anomalies were studied by Boys (1993) in the PCS Cory mine, Canada, which extracts potash from the Patience Lake member of the Prairie Evaporite Formation. He defined five postburial facies in the vicinity of the salt anomalies, all related to a current or previous crossflow of water undersaturated with respect to potash (Figure 11.25a). Where undersaturated groundwater continually interacts with a sylvinitic bed it ultimately dissolves all the salts to leave behind only insoluble residues in a solution collapse breccia (facies 1). This potash-free interval is at the other end of the facies continuum defining salt anomalies in the PCS mine (Figure 11.25a; facies 1 through 5). At the other end of the groundwater-potash interaction spectrum are beds composed of completely recrystallised and often potash-enriched sylvinitic

(facies 5). These sweetspots lie adjacent to leached beds where recrystallised halite (facies 4) passes laterally into collapse breccias with blocks of anhydrite and halite (facies 3 and 2; solution residues made up of the less soluble salts), which in turn pass laterally into the most mature dissolution breccias of facies 1, where no evaporite salts remain. When a drive or a test hole passes out of the ore into facies 1 the potential for water problems is high.

In his model, salt anomalies indicate proximity to collapse structures that act as conduits for overlying (or possibly pressurised underlying?) formation waters. The crossflow drives a halo of pervasive leaching and recrystallisation in the Prairie Evaporite Formation. The same fluids that cause widespread recrystallisation, and possibly enrichment of the potash salts at the outer edge of the salt anomaly, also dissolve water-filled cavities in the more central parts of the anomalies. The intensity of the leaching and the geometry of the leached halo is variable, while the timing of major leaching events in the Prairie Evaporite is still poorly constrained. Boys (1993) postulates at least two major water crossflow events in the PCS mine, possibly driven by uplift and tectonism: one occurred in the Late Devonian, the other in the Cretaceous.

Similar leached solution cavity-fill features that create salt anomalies occur in the Boulby Potash Mine in the UK, although most of the features are now halite-cemented and consist of lenses of coarse pure translucent secondary halite (Figure 11.25b). Intersected zones are up to 2 metres across and typically overlie a band of halite encrusted with red haematite (Woods, 1979). The amount of anhydrite at the base of many cavities is greater than would accumulate as a simple insoluble residue implying they formed from waters close to CaSO_4 saturation. According to Woods (1979), the cavities formed in the subsurface from CaSO_4 -saturated brines that were involved in dissolving the carnallite and sylvite. The resulting brines became supersaturated with respect to CaSO_4 causing halite to precipitate and accumulate on the cavity floor.

At a smaller scale, I have observed similar CaSO_4 -floored dm-scale cavities in core from the Maha Sarakham potash intervals in Thailand and in this case they formed early, syn-precipitationally to bedded sylvinitic in adjacent salt withdrawal depressions (Figure 11.16). It seems that phreatic dissolution is commonplace in many potash intervals worldwide. The infill, however, is not always halite; and in Thailand, in the heavily recrystallised sylvinitic zones, some of these anhydrite-floored cavities have been filled by coarse-grained clear sylvite made up of single crystals more than 30 cm across.

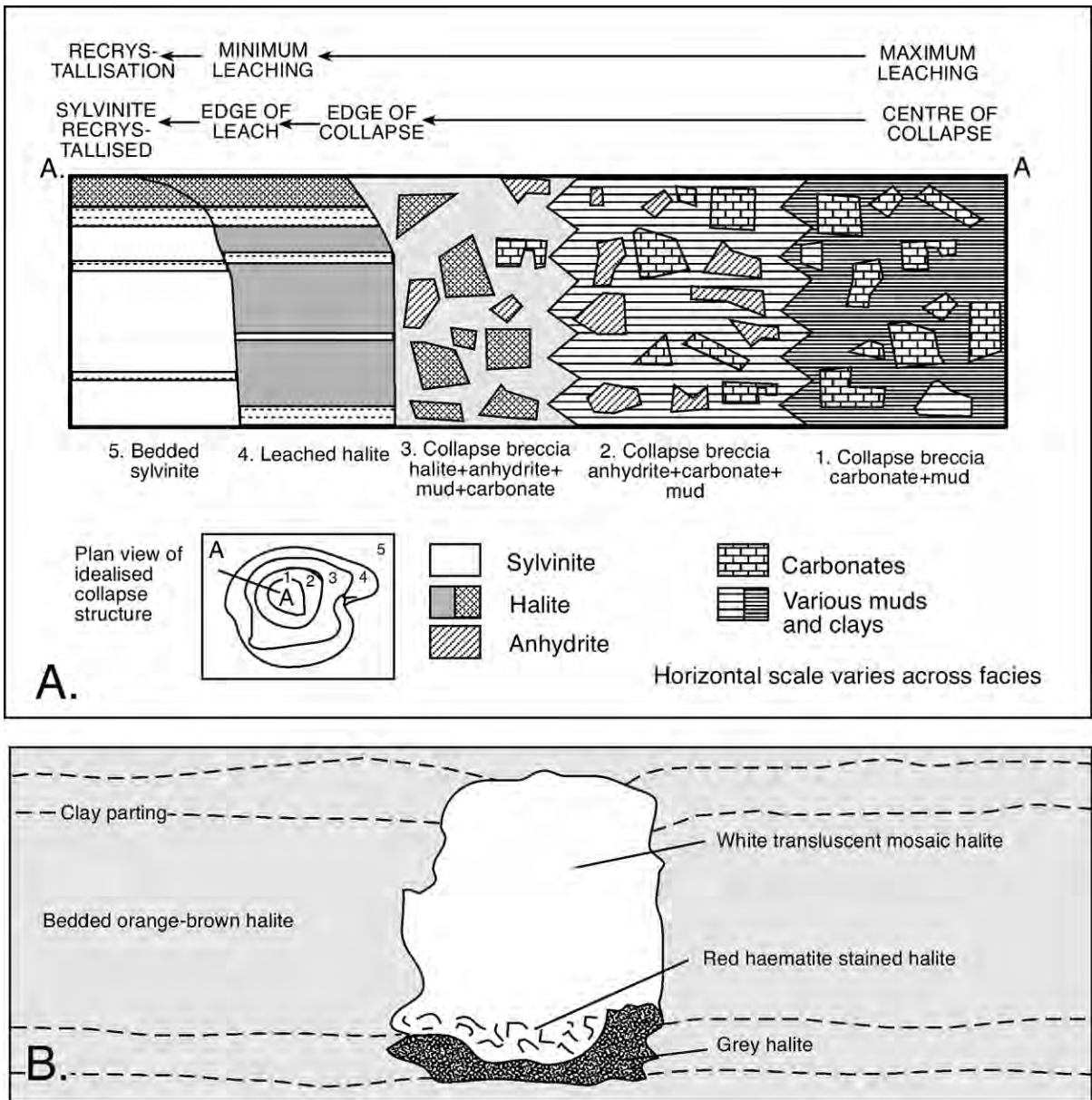


Figure 11.25. Potash solution features. A) Cross section A-A' through half of an idealised collapse structure in the Prairie Evaporite Formation (after Boys, 1993). B) Recemented solution cavity in the Boulby Halite, Boulby Mine, UK. This is probably equivalent to facies 3 in Figure 11.25a but is located below the main potash zone (after Woods, 1979).

Salt anomalies (barren zones in potash ore) also form crosscutting intervals in the Permian potash ores in New Mexico (Linn and Adams, 1966). Locally called “salt horses” (a miner’s corruption of salt horst), these crosscutting irregular zones range from 0.3 to 100 metres in width and 3 to 200 metres in length. Beds in salt horses are thinner than the equivalent beds in ore. Contacts between salt horses and ore are sharp and colour

of the clay changes from grey in ore to brown in salt horses, perhaps indicating more oxygenated crossflushing waters. Pods and lenses of langbeinite, leonite, kainite, recrystallised halite, and recrystallised sylvite occur in McNutt ore near the salt horses, while disseminated polyhalite of the typical marker bed is locally concentrated into intergranular seams and pods in or near horses. According to Linn and Adams (op. cit.)

the NaCl-saturated brines creating the horses entered the ore zone from below and formed horses by the selective leaching of sylvite. This is a mechanism similar to that of Boys (op. cit.) except that he concluded unsaturated fluids entered from above. Fluid entry from below is not unreasonable in the New Mexico situation, as the evaporites along the western margin of the Delaware Basin sit atop an aquifer that entrains deeply circulating meteoric waters (Figures 7.9, 8.7, 11.59b).

Effects of the leaching events that produce the salt anomalies and loss of potash in Canada or elsewhere, range from weak to strong, from selectively preserving delicate laminae and chevron textures, to deforming and destroying salt beds (Boys, 1990). Good preservation of iron oxides in halite may indicate that the leaching was weak or of short duration. In many leach anomalies fed from above, salinity indicator minerals increase downward in a structure, possibly because fluids exit downward and NaCl-saturated fluids tend to follow the chemical gradient provided by potash beds. Or, in my opinion, it zones downward because all brines tend to density stratify and the denser more saturated waters in a downward growing dissolution feature would tend to have ponded at its bottom. Early stages of stratification are seen in the perched waters on blind-bottomed sub-vertical karst holes in Mt Sedom, Israel (Figure 7.39a).

Identifying proximity to a salt anomaly is obviously important in terms of ore quality and mine safety (Boys, 1990). Geological

indicators of proximity to a halite anomaly include: a change in insoluble seam colour from greenish-grey to mottled brown and greenish-grey (probably corresponds to increasingly oxidised fluids in the crossflow structure), unusual local increases in ore grade, large patches of sylvite-poor potash crosscutting units near the top of the ore zone, and drops in topography >10m of the marker seams across an anomaly. For example, within 5 m of a large salt anomaly, Boys (1990) found large blebs (>200 cm² on the mine wall) of sylvite-poor potash that crosscut the units of an incomplete potash cycle near the top of the main ore zone. Anhydrite, a less soluble salt, is also more common in a salt anomaly than in the adjacent ore. Once into the anomaly facies, possible indicators of a nearby major collapse feature include: stretched clay seams; folded beds; small collapse features (1-20 m scale); and split clay seams with salt appearing to be injected into the seam.

In a study of “barren bodies” in the Subiza Mine, Navarra, Spain, Cendon et al. (1998) recognised a syndepositional mechanism of “salt horse” formation (Figure 11.26). It was controlled by brine pool stratification, not various diagenetic processes tied to subsurface crossflow. The Subiza potash deposit contains a 100 m thick Upper Eocene succession of alternating claystone and evaporites (sulphate, halite, and sylvite). The evaporites accumulated in an elongated basin that is one of the depocentres within the 250 km long South Pyrenean foreland basin (Figure 8.10). Slope instability along the margin of the basin, perhaps

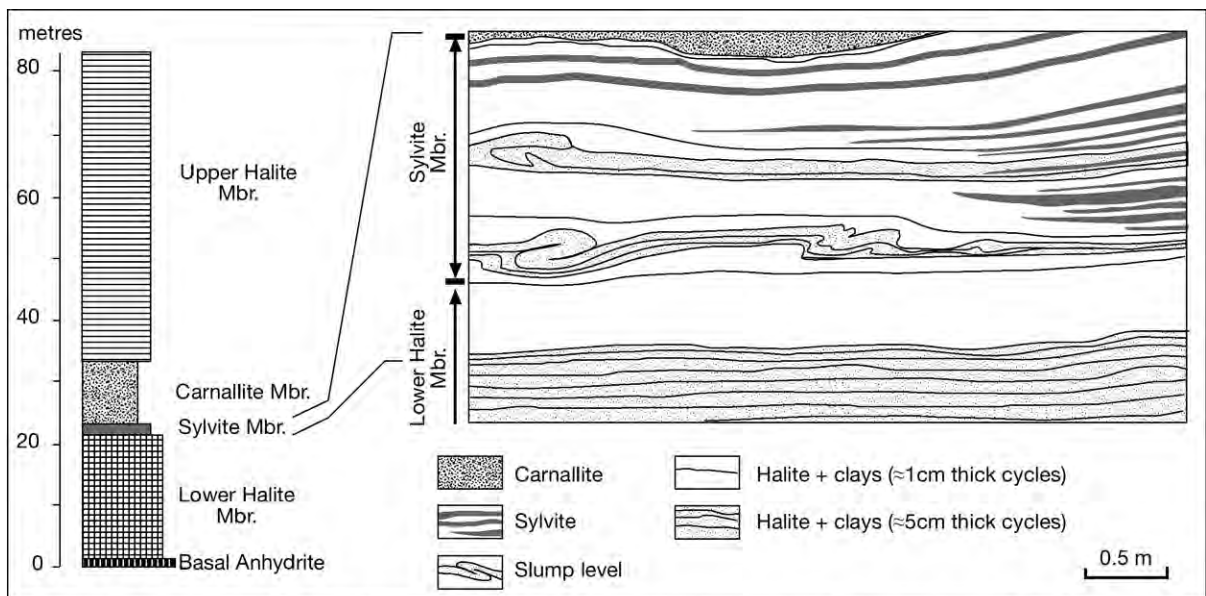


Figure 11.26. Stratigraphy of Upper Eocene potash section based on sequence cored in Biurrun borehole and tied to a mine wall sketch from Subiza Mine, showing barren body made up of two superimposed slump structures with corresponding upper sections, where the overlapping sylvite beds evolve from absent to continuous (after Cendon et al., 1998).

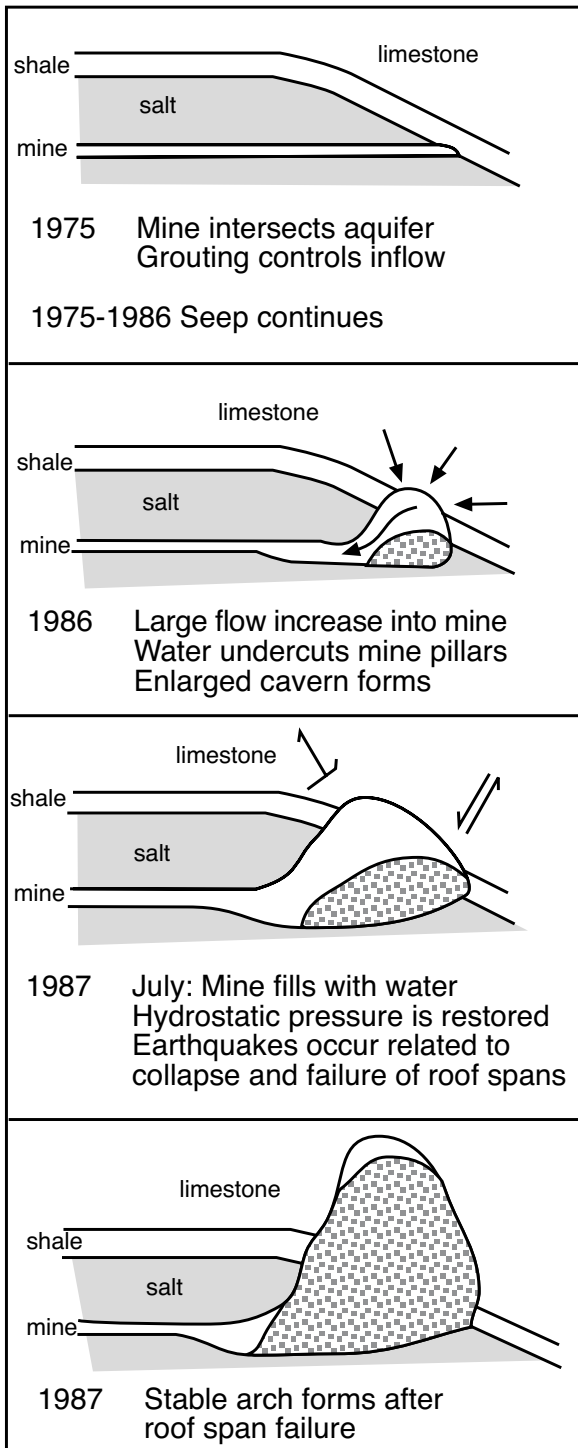


Figure 11.27. Sequence of events controlling the flooding of the Patience Lake Mine (after Gendzwill and Martin, 1996).

promoted by tectonism, created mass wasting of the evaporite beds. This formed subaqueous mounds 0.5-2 m high and tens of metres across. As evaporation progressed, a stratified brine system formed and encroached over the mounds. Halite precipitated at the air-brine interface and sank to the bottom of the basin, along with terrigenous clays. Sylvite, however, precipitated only from the cooling of a lower denser bottom hugging brine. This brine was warm where it formed about the basin edge and cooled as it seeped into the deeper parts of the basin floor. As many mound crests extended into the upper less saline brine, the sylvite could not precipitate over these subaqueous highs. With progressive accumulation, the lower brine ultimately covered the mounds as sylvite beds overlapped the mound tops.

This model, however, is in my opinion problematic in terms of its hydrological restraints: it requires a hydrological system that encapsulates sylvite saturation and precipitation in the cooling lower brine with simultaneous halite precipitation in the upper brine. As discussed in Chapter 3, such a system is extremely difficult to maintain over time frames that allow metre-thick beds of evaporites to accumulate. A more likely hydrology is perhaps a desiccating and concentrating single brine body, which reached halite saturation at the “lake full” stages while the mounds were still covered with brine. It did not reach sylvite saturation until ongoing drying of the brine lake had lowered the level to where the crests of the mounds were exposed. Whichever model is accepted, what is most important in terms of potash geology is that breached syndepositional salt horses or barren zones are less likely to possess subsequent subsurface hydrologies that will flood mines, as compared with horsts induced by subsurface leaching. This type of salt anomaly would not be tied to a zone of potential inflow in an active mine. Using and applying it as an interpretation of salt anomalies in an ore zone outside of the region where it was documented has significant implications in terms of mine safety.

Intersecting unexpected salt anomalies, especially those associated with flowing undersaturated brines should always be noted and dealt with as early as possible in a mine plan. Otherwise these zones can impair or destroy a potash mine. In the 1970s the Patience Lake potash mine operation, located on the eastern outskirts of Saskatoon, encountered a natural collapse structure. Grouting managed to control the inflow and mining continued. Then, in January of 1986 the rate of water inflow began to increase dramatically from the same fractured interval (Figure 11.27; Gendzwill and Martin, 1996). At its worst, the fractures associated with the structure were leaking $75 \text{ m}^3/\text{minute}$ (680,000 bbl/day) of water into the mine. The

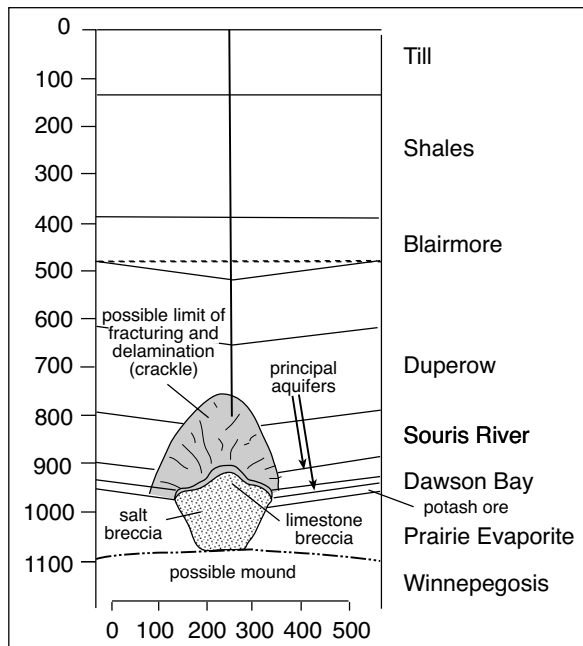


Figure 11.28. Dimensions of the salt collapse chimney that was breached in the Rocanville Mine in 1984 (after Prugger and Prugger, 1991).

water was traced back to the overlying Cretaceous Mannville and possibly the Duperow formations. Finally, in January 1987 the mine was abandoned. It took another 6 months for the mine to fill with water. Subsequent seismic shot over the offending structure suggested that the actual collapse wasn't even penetrated, the mine had merely intersected a fracture within a marginal zone of partial collapse (Gendzwil and Martin, 1996). Part of the problem was that the water was undersaturated and quickly weakened pillars and supports, so compromising the structural integrity of the workings. The unexpected intersection of one simple fracture system resulted in the loss of a billion dollar mine.

Patience Lake mine now operates as a solution mine by pumping KCl-rich brine from the flooded mine workings to the surface. The operation has a capacity to produce more than a million tonnes of potash annually. It works by circulating heated brine through the flooded mineshaft into the former workings, which extend up to 18 km from the main shaft. Heated recovered potassium-rich brines are pumped into surface crystallization ponds where the liquor evaporates and cools. Sylvite, potash, and other salt crystals form and settle to the bottom of the pond. This potash sludge is pumped from a floating dredge to the processing plant, while the cooled NaCl-saturated pond brine is reheated and re-injected into the mine to repeat the process.

Prugger and Prugger (1991) documented the successful treatment of an underground inflow into the Rocanville mine that occurred in 1984. In this case the mine was saved. It began when a mine entry accidentally penetrated a salt collapse structure that then began to leak brine into the mine at rates exceeding $10 \text{ m}^3/\text{min}$ (90,576 bbl/day). Seismic showed that the structure was roughly circular and relatively small in size (300m in diameter), and was isolated from other collapse structures (Figure 11.28). A grout well was drilled from the surface and encountered the collapse upon penetrating the carbonates of the overlying Duperow Formation, suggesting that fracturing associated with the collapse structure had extended as a blind chimney a considerable distance up from the Prairie level. Unlike the Patience Lake Mine flood, a combination of grouting and bulkhead emplacement in Rocanville succeeded in sealing off the inflow, thus saving the mine. Also unlike Patience Lake, the brine from the breached structure was halite-saturated so limiting the amount of dissolution damage. Different outcomes between the loss of the Patience Lake Mine and recovery from flooding in the Rocanville Mine may reflect the difference between intersecting a chimney that made its way to the Cretaceous landsurface and is now overlain by a wide-draining set of sediments versus intersecting a blind chimney that never broke out at the landsurface.

Other economic salts

So far we have discussed potash and concluded that the larger accumulations are marine-derived and accumulated in tectonic (mega-halite) basins with no Quaternary counterpart. We shall now discuss various accumulations of other evaporite salts that are exploited as economic resources. Almost without exception, they are lacustrine precipitates, formed by the evaporation of waters with nonmarine ionic proportions and in depositional settings that have same-scale Quaternary counterparts.

Borate salts (tincals)

Boron (from the Arabic *Buraq* or the Persian *Burah* meaning to glitter or shine) is a highly dispersed element in nature - averaging 3-20 ppm in the earth's upper crust, as estimated by various authors, and 4.6 ppm in seawater. It is both a volatile and mobile element and so tends to be enriched in the later stages of both magmatic crystallisation and volcanic eruptions and a few small economic deposits are found in skarns where late stage magmas have intruded carbonates. But most recoverable deposits of borate salts involve lacustrine deposits

Borate Mineral	Composition	B ₂ O ₃ %	Remarks
<i>Na Borates</i>			
Borax (tincal)	Na ₂ B ₄ O ₇ ·10H ₂ O	36.5	Major ore mineral in USA and Turkey
Kernite	Na ₂ B ₄ O ₇ ·4H ₂ O	51.0	Major mineral often converts to borax
Tincalconite	Na ₂ B ₄ O ₇ ·5H ₂ O	47.8	Intermediate or accessory mineral + manufactured endproduct
<i>Na-Ca Borates</i>			
Ulexite	NaCaB ₅ O ₉ ·8H ₂ O	43.0	Major ore mineral particularly in South America
Probertite	NaCaB ₅ O ₉ ·8H ₂ O	49.6	Secondary/accessory mineral
<i>Ca Borates</i>			
Colemanite	Ca ₂ B ₅ O ₁₁ ·5H ₂ O	50.8	Major ore mineral, particularly in Turkey. Secondary after inyoite
Meyerhoffite	Ca ₂ B ₅ O ₁₁ ·7H ₂ O	46.7	Intermediate ore mineral, rarely survives at surface
Priceite (pandermite)	Ca ₂ B ₄ O ₁₀ ·7H ₂ O	49.8	Ore mineral in Bigadic, elsewhere minor
Inyoite	Ca ₂ B ₆ O ₁₁ ·13H ₂ O	37.6	Minor ore mineral
<i>Other Borates</i>			
Sassolite	B(OH) ₃	56.4	Natural boric acid (fumarole, hot springs), once extracted in Italy
Hydroboracite	CaMgB ₆ O ₁₁ ·6H ₂ O	50.5	Secondary ore mineral
Szaibelyite (Ascharite)	MgBO ₂ (OH)	41.4	Ore in Russia and China (meta-evaporite ores)
Boracite	Mg ₃ B ₇ O ₁₃ ·Cl	62.2	Associated with potash especially in Europe
Howlite	Ca ₂ SiB ₃ O ₈ (OH) ₅	44.5	Accessory mineral
Bakerite	Ca ₄ B ₄ (BO ₄)(SiO ₄) ₃ (OH) ₃ ·H ₂ O	42.1	Accessory mineral
Tunellite	SrB ₆ O ₉ (OH) ₂ ·3H ₂ O	55.1	Accessory mineral
Tertschite	Ca ₄ B ₁₀ O ₁₉ ·2H ₂ O	65.1	Accessory mineral
Kurnakovite	Mg ₂ B ₉ O ₁₁ ·15H ₂ O	37.3	Accessory mineral

Table 11.5. Boron minerals in various exploited deposits.

in arid settings that were strongly influenced by volcanic activity at the time lake deposition occurred. They tend to involve abundant tuffs and basalts in the drainage basin, a semi-arid climate and a standing body of brine that at times becomes sufficiently concentrated to accumulate boron salts. A protective layer of other impervious less-soluble evaporite salts, such as gypsum or anhydrite, typically forms a carapace that prevents subsequent redissolution.

Four minerals comprise more than 90% of the borate salts used by the borate industry; the sodium borates - borax (tincal), kernite, the calcium borate - colemanite, and the sodium-calcium borate - ulexite (Table 11.5). Water content of the various borates tends to decrease with burial and to increase with exposure and weathering. Borax is the primary mineral in many US deposits, but with burial and dewatering it converts to tincalconite and kernite. If kernite is exposed to weathering or throughflowing groundwater it reconverts to borax.

US Borax, a member of the Rio Tinto Borax Group, is the largest global miner of B₂O₃, mostly of tincal ore. The company is also

the world's largest manufacturer of refined borate products. US Borax supplies almost half of the world's demand for industrial and speciality borates from its Kramer borate deposit at Boron in southern California's Mojave Desert. Turkey is the world's largest producer of borate ore, mining more than 1 Mt (1.1 million st) of salable product each year (Figure 11.29) including refined materials from Kirka and Bandirma. This makes Turkey the second largest producer of refined boron compounds after the USA. The government organization, ETI Holding A. S., is the sole producer of Turkish borate compounds through its subsidiary ETIBORA. S. Combined production of Turkey and the United States accounts for more than 50% of the global borate output on a product-ton basis. Additional volumes of mineral concentrates and refined products are also produced in South America, Russia and China. South American production is concentrated in Bolivia, Peru, Chile and Argentina.

In terms of dollar value the most commercially dominant boron salt is the pentahydrate salt (Na₂B₄O₇·5H₂O; tincal). It is used in very large quantities in the manufacture of insulation fibreglass and sodium perborate bleach. Boric acid is also an

important boron compound with major markets in textile fibreglass and in cellulose insulation as a flame retardant. Next in order of importance is borax ($\text{Na}_2\text{B}_4\text{O}_7 \cdot 10\text{H}_2\text{O}$; sodium tetraborate decahydrate), which is used principally in laundry products. Use of borax as a mild antiseptic is minor in terms of both dollars and tons. Amorphous boron is used in pyrotechnic flares to provide a distinctive green colour, and in rockets as an igniter. Boron compounds are also extensively used in the manufacture of borosilicate glasses. Other boron compounds show promise in treating arthritis. The isotope boron-10 is used as a control for nuclear reactors, as a shield for nuclear radiation, and in instruments used for detecting neutrons. Boron nitride has remarkable properties and can be used to make a material almost as hard as diamond. The nitride also behaves like an electrical insulator but conducts heat like a metal. It also has lubricating properties similar to graphite. The hydrides are easily oxidized with considerable energy liberation, and have been studied for use as rocket fuels. Demand is increasing for boron filaments, a high-strength, lightweight material chiefly employed for advanced aerospace structures. Boron is similar to carbon in that it has a capacity to form stable covalently bonded molecular networks.

Historically, borates (as a component of natron salts) were used 4000 years ago in mummification. At the same time borax (in a purer form than natron) was imported from the Far East for use as a gold flux by the ancient Babylonians. The word tincal comes from the Babylonian *tincar* meaning "Far East." By the 8th century AD, the Arabs around Mecca, Medina and Baghdad were using imported borax (*tincar*) as a kiln additive or flux to

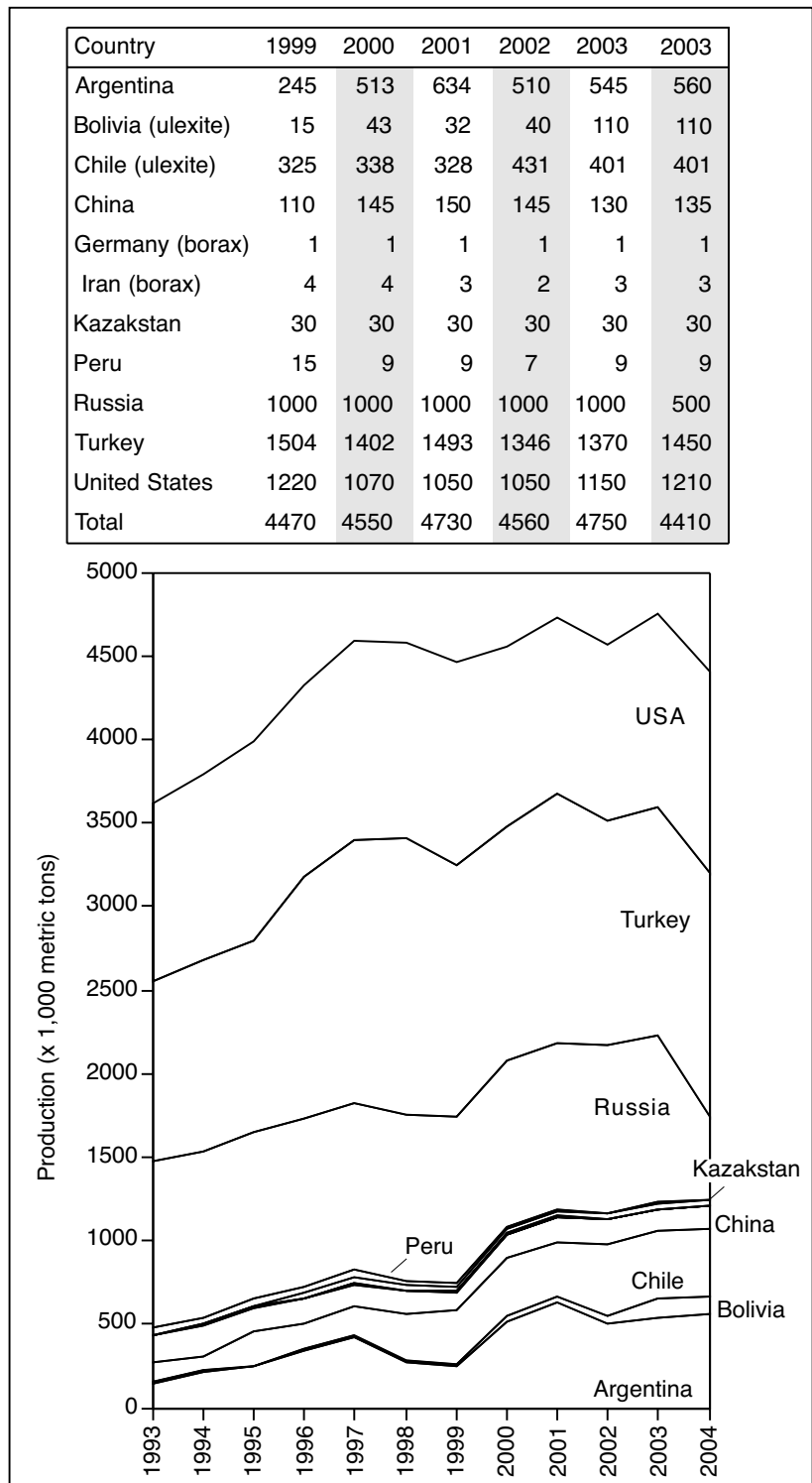


Figure 11.29. Borate production (thousand metric tons of boric oxide B_2O_3 equivalent), compiled from USGS on-line data tables downloaded from <http://minerals.usgs.gov/minerals/pubs/commodity/> last accessed 30 September, 2005.

braze or harden precious metals, especially gold. Borax glazes were used in China from AD 300, and boron compounds were used in glassmaking in ancient Rome. By the Middle Ages, borax from Tibet was regularly imported into Europe. At the time borax was very expensive, and this limited its use principally to the precious metal trade where goldsmiths used it as a soldering agent and in the refining of metals and assaying of ores. Quantities traded were small, its method of production was a tightly held secret of the alchemist's guild, and its source in the borate pavements precipitated in the salt lakes of Tibet remained a mystery until the second half of 18th century. As such it was a valuable traded commodity along the Tibet to Europe trade route travelled by Marco Polo. Tibetan borax was transported over the Himalayas into India in bags tied to the necks of sheep.

Today, borate's supply routes are much more mundane, but the volumes consumed in the chemical industries are huge (Figure 11.29). Currently, borax (tincal) is the preferred sodium borate ore as it needs little processing, crushes freely and dissolves readily in water with a rate of solubility that increases steeply with increasing temperature. "Tincal" is the old general name for borax in the chemical industry and is sometimes used to distinguish the naturally occurring borax ore mineral (tincalonite) from the chemically identical manufactured salt called tincal. Kernite (a source for boric acid manufacture) is present in large tonnages in the USA and Argentina. It is less suitable as an ore salt than borax or tincalonite despite its high B_2O_3 content. Kernite has excellent cleavage, but crushes into fibres that tend to mat and clog handling equipment. It also is much less soluble in water than borax and so is less suitable as a feedstock for the manufacture of pentahydrate. Colemanite is the preferred calcium-bearing borate; it is the least soluble of the commercial borates and only slowly dissolves in water, but is highly soluble in acid solutions. Szaebelyite, a magnesium borate, was the principal source of borate in the former Soviet Union and is the main ore mineral in the Proterozoic meta-evaporite ores of the Liaoning Province, China.

Turkish borates

The borate district of western Anatolia has 5 districts, from west to east they are: Bigadic, Sultancayir, Kestelek, Emet, and Kirka (Figure 11.30). Turkish borates have been mined for the last fifteen centuries. Proven borate reserves are 532 million tonnes with total estimated reserves of 987 million tonnes. Colemanite is mined at Bigadic, Emet, and Kestelek, ulexite is mined at Bigadic, and tincal at Kirka. Borax and colemanite ores are refined and concentrated at the Kirka and Bandirma plants. Bigadic borates are extracted from what is

the largest colemanite/ulexite deposit in the world, with high-grade colemanite and ulexite ores running 30% and 29% B_2O_3 , respectively.

The Kestelek deposit is 27 km southeast of the town of Mustafa Kemalpaşa in the province of Bursa. The borate ore zone there makes up part of an interbedded succession of marl, limestone, tuffaceous limestone, tuff and borate layers (Figure 11.30; Helvacı and Alonso, 2000). Borate layers are typically hosted in clays. Colemanite is present as nodule to boulder size masses (up to 1 m in diameter), and as thin layers of fibrous and euhedral crystals. Colemanite, ulexite and probertite predominate and sparse hydroboracite is also present locally. The Kirka stratigraphic succession comprises borates that are intimately interbedded with and penetrating into marls, claystones, zeolitized tuffs and tuffaceous epiclastic materials in bedded lacustrine sediments. The main boron mineral is borax with lesser amounts of colemanite, ulexite and other borate minerals. Volcano-sedimentary rock units in the Sultancayir deposit include borate-bearing gypsum intercalated in a sandy claystone unit. Calcium borates, mainly pandermite (priceite) and howlite, but also colemanite and bakerite, are interspersed within the Sultancayir gypsum.

All the exploited Turkish borate ores were originally precipitated as early Miocene (16–20Ma) perennial saline lake sediment within a series of northeast-southwest-trending elongate basins, which are underlain by a Palaeozoic and Mesozoic basement composed of ophiolites, marbles and schists (Figure 11.30; Helvacı, 1995). The Bigadic, Emet and Kirka lacustrine basins of western Turkey are hosted by Tibet-type extensional graben structures. The grabens developed during Miocene continent-to-continent collision along the Izmir-Ankara suture zone complex, where calc-alkaline volcanism was simultaneous with borate sedimentation. This volcano-sedimentary sequence consists of (from bottom to top) basement volcanics and volcanoclastics, lower limestone, lower tuff, lower borate zone, upper tuff, upper borate zone and olivine basalt (Figure 11.30). Borates in the upper zone occur in units up to 30 metres thick beneath a sediment cover that is 25 to 410 metres thick, while the lower borate zone is up to 65 metres thick and is found at depths between 150 and 950 metres.

All these Neogene borate deposits have thin sedimentary covers and have never been deeply buried (Helvacı and Orti, 1998). Borate precipitation occurred mostly in subaqueous settings, but in lake systems encompassing a range of evaporitic settings, from stable playa mudflats to deeper perennial lakes, the latter typically shoaling to shallow lakes and playa lakes.

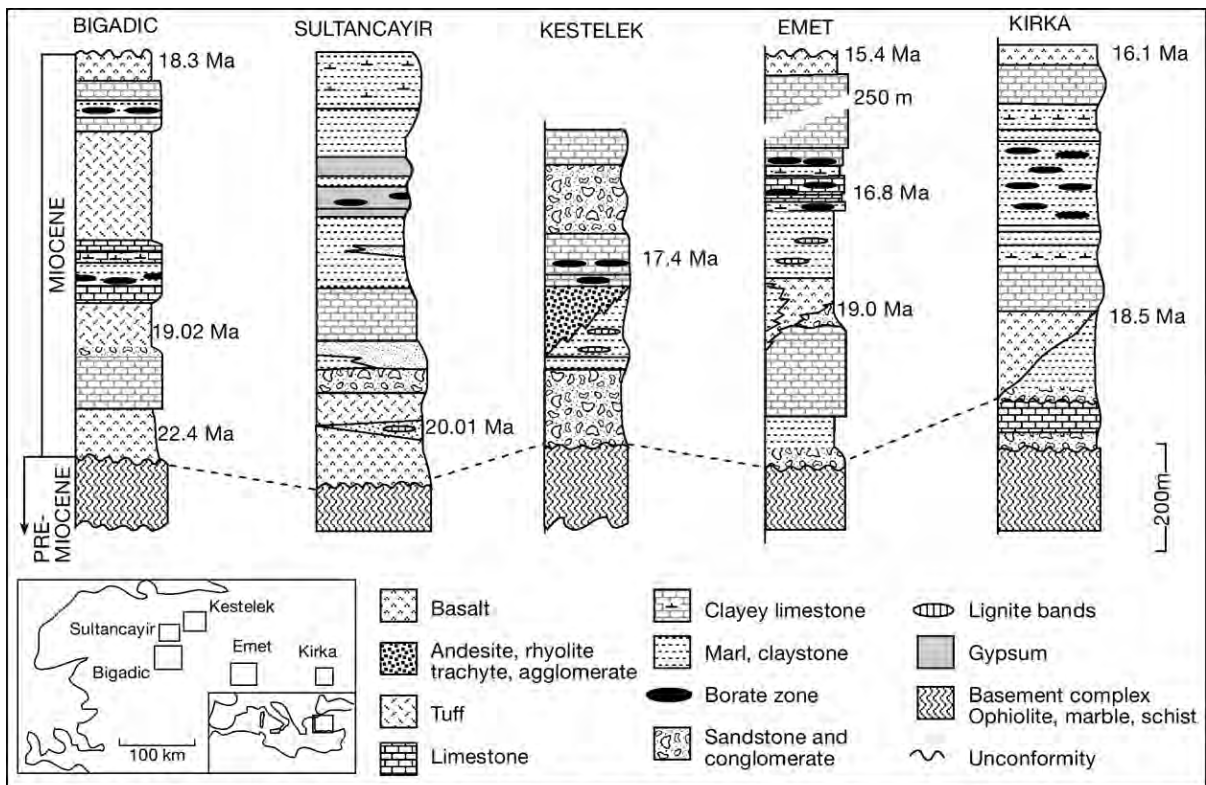


Figure 11.30. Representative sections of the various Miocene borate deposits in western Turkey. All occur in local extensional rifts in a volcanogenic continent-to-continent collision setting (after Helvacı and Alonso, 2000).

Shallowing-upward cyclicality is commonplace in all ore beds and all ores precipitated in lakes in a hydrothermally active volcanogenic terrain (Figure 11.30). Colemanite tends to occupy the deposit's depositional margins, while laminated borax is more common in the centres of the lacustrine basins, with a zone of ulexite separating the two (Inan et al., 1973). This mineral zonation is syndepositional and cannot be ascribed to later burial diagenetic processes.

When details on these obviously primary deposits began to come to the world scientific literature in the mid 1970s the prevailing notion of borate or zones as thermal replacements during deep burial (based on the US deposits and the work of Foshag, 1921 and Garrels and Christ, 1959) were challenged. When details of the primary borate textures in South American deposits became known in the mid 1980s even some of the strongest proponents of the thermal replacement model for borate ores began to admit the possibility of a primary or syndepositional origin for the zonation of the world's borate deposits.

Borate minerals at Bigadic form two ore zones, now separated by thick tuff beds that have been transformed to montmorillonite,

chlorite, and zeolites (mainly heulandite) during diagenesis (Figure 11.31; Gundogdu et al., 1996; Helvacı and Orti, 1998). Colemanite with lesser ulexite predominates in both zones; but other borates, including howlite, proberite, and hydroboracite are present in the lower borate zone; whereas inyoite, meyerhofferite, pandermite, tertschite(?), hydroboracite, howlite, tunellite, and rivadavite are found in the upper borate zone (Helvacı, 1995). Calcite, anhydrite, gypsum, celestite, K feldspar, analcime, heulandite, clinoptilolite, quartz, opal-CT, montmorillonite, chlorite, and illite are also found in the Bigadic deposit.

Nodules of colemanite and ulexite predominate in both borate zones at Bigadic (Figure 11.31). Agglomerated colemanite and ulexite nodules construct alternating bedded horizons with relatively sharp boundaries. Because these minerals are readily dissolved and reprecipitated, early secondary masses of pure and transparent colemanite and ulexite are often encountered in cavities, nodules and cracks. Some nearsurface colemanite and ulexite beds are now so weathered they are completely replaced by calcite.

processes also produced small howlite nodules embedded in unconsolidated colemanite nodules.

In contrast to the colemanite-ulexite dominance at Bigadic, laminated lacustrine borax is volumetrically and economically the most important zone in the Kirka borate deposit (Helvacı and Orti, 2004). The deposit is symmetrically zoned in a lateral sense with a central body of Na borate (borax), an intermediate zone of Na–Ca borate (ulexite), and a marginal zone of Ca borate (colemanite; Figure 11.32a). The same mineral zonation is also developed in a vertical sense, although it is somewhat asymmetrical because of the presence of a discontinuous Mg borate horizon overlying the central body of borax. Older studies, based on analogies with US borate deposits, attributed the zonation to a diagenetic overprint on the margins of the original syndepositional borax-clay laminates of the lake (Inan et al., 1973). More recent work has shown that the Kirka sequence is depositionally fractionated and that the zonation represents a hydrologically controlled separation of evaporite minerals in a lake basin actively accumulating sediment (Helvacı and Orti, 2004). Lateral gradients in salinity in the mudflats passing into the perennially subaqueous centre conditioned the concentric pattern of the facies at Kirka. Thus, the various borax lithofacies zones (chemical, clastic, mixed) seen in the central ore body reflect precipitation in a lake that evolved with subsidence and climate. Conditions oscillated from predominantly subaqueous with variable brine depths (perennial lake stage), to an interstitial sabkha or mudflat setting (playa-lake stage). The evaporative concentration of

the boratiferous waters in the lake, together with the periodic changes in temperature of the water mass are the main controls on the crystallization of borax.

Helvacı and Orti (2004) found no petrographic evidence for a thermally induced inyoite-to-colemanite transformation, as previously proposed by the diageneticists and went on to argue

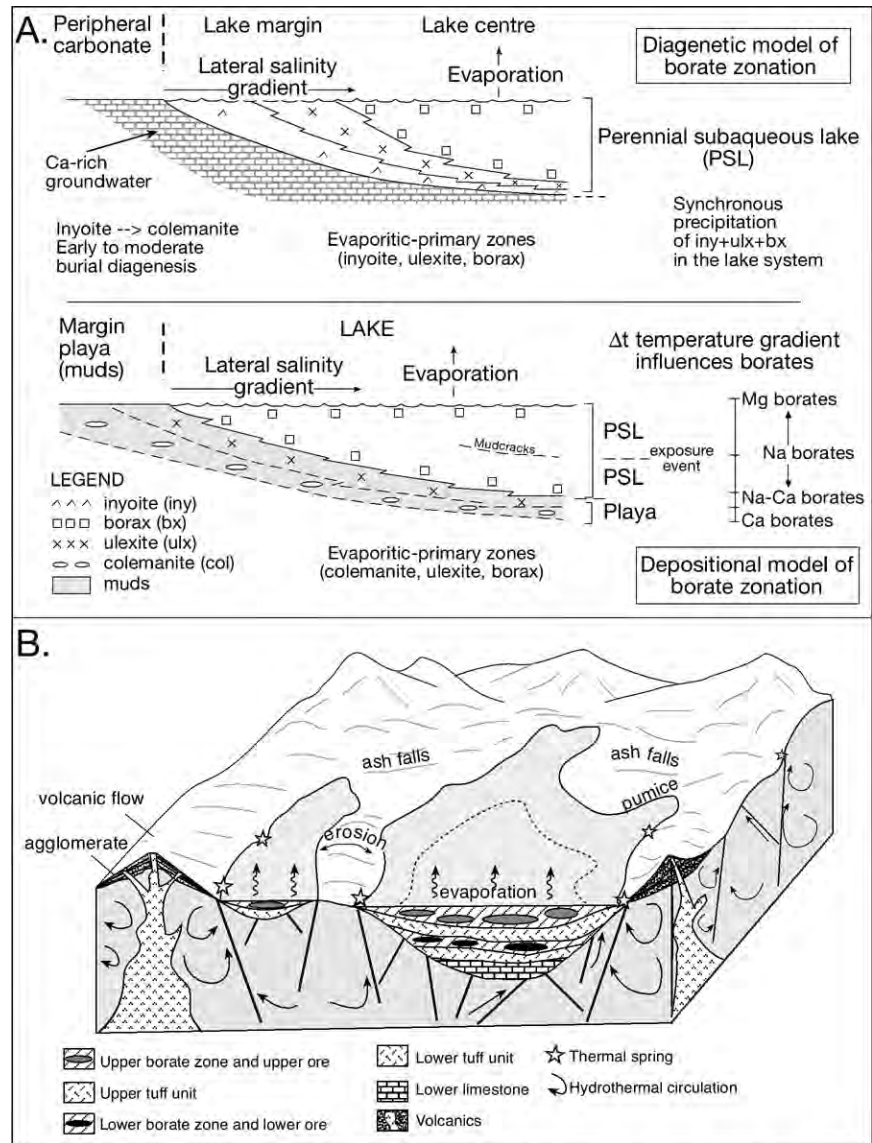


Figure 11.32. Depositional setting and zonation of Turkish borate deposits. A) Two models used to explain the zonation of Turkish borates; one uses diagenetic flushing by Ca-rich subsurface waters (after Inan et al., 1973), the other explains the zonation as a depositional separation (after Helvacı and Orti, 2004). B) playa stage of the Bigadic Deposit (after Helvacı, 1995). Deposition occurred under arid to semi-arid conditions within separate or interconnected perennial saline lakes located in an active volcanic area within lakes fed by borate-rich thermal springs.

that the moderate burial depths in all the various Turkish borate deposits are insufficient for the generalized transformations required by the diageneticists (Figure 11.32a). Rather the Mg borates represent evaporitic precipitates from the fractionation of the initial boratiferous inflow, they are not burial driven reaction products between pre-existing borates and groundwaters. Thus the mineral zonation in Kirka is primary, not only for borax and ulexite in the subaqueous dominated parts of the lake, but also for both the colemanite forming the marginal playa dominated zones and for the Mg borates overlying the central body of borax in Kirka. This same argument of syndepositional not burial flushing can be applied to Bigadic, which is then seen to be a deposit accumulating under predominantly playa conditions (Figure 11.32b).

Almost all workers now accept that the borax-clay laminite texture that dominates the core of the Bigadic deposit is subaqueous. Crystal outlines have a characteristic growth-aligned borax (palisade) texture in mm-cm thick layers separated by clay segregations. This is a texture similar in many ways to the hydroboracites of South American salars (Figure 11.34) and the Kramer deposit in the USA. Borax crystals in the lower portions of the lower borate unit in Kirka show zigzag tops mantled by clay, while borax layers in the upper parts of the same unit show erosional tops. The same textural transition from zig-zag to truncation is seen in meromictic gypsum lakes as the depositional surface aggrades across the zone of saturation in a permanently subaqueous brine lake (Figure 2.49). The nodular Turkish borate ore of the playa margin is more enigmatic; it may be an early diagenetic playa mudflat precipitate or it may be an early alteration halo created by centripetal flushing of the borax core by subsurface waters (Figure 11.32a).

Initial volcanogenic waters that fed the alkaline perennial saline lake(s) were low in Cl and SO₄, and high in boron and Ca, with subordinate Na. Boron isotope data from the Turkish deposits are consistent with colemanite being precipitated from a more acidic brine than ulexite, with borax being precipitated from a brine that was more basic (Helvacı, 1995; Palmer and Helvacı, 1995, 1997). Borax precipitation and replacement to create ore grade beds typically occurred in a laminated gypsiferous host, either syndepositionally or in very early burial, perhaps in stratified brines where solar-derived brines mixed with upwelling boron-rich hydrothermal solutions (Figure 11.32). With further burial the anhydritisation of gypsum began at depths that were less than 250m. At the same time, anhydrite also replaced some of the earlier formed borates (priceite, bakerite and howlite), along with associated celestite. Subsequent uplift and exposure of some parts of the sequence rehydrated nearsurface anhydrite

to secondary gypsum and partially transformed priceite and howlite into secondary calcite.

South American Borates

In the Andes of South America there are more than forty borate deposits hosted in Cenozoic volcanogenic-sedimentary rocks in a 880-km-long stretch along the common borders of Argentina, Bolivia, Chile and Peru (Figure 3.38). This area is a high plateau that was created in the late Cenozoic during a non-collisional compressional orogens. Most deposits are small aprons or cones of borax and ulexite near volcanic vents, with reserves measured in thousands of tonnes. But in the larger endorheic basins, where volcanogenic brines can pond and concentrate, there are beds of ulexite, borax and inyoite in salars ranging up to hundreds of square kilometres in area, with reserves of ulexite ore measured in millions of tonnes (Figure 3.37). Two main styles of occurrence characterise the borate salts in this region; 1) nodular borate locally known as “papas” (potato or cottonball borate), and 2) bedded borates usually interbedded with lacustrine muds and locally known as “barras, bars or bancos”. Nodules are often the preferred texture to mine as they tend to create a purer product when cleaned and air dried (can be > 28% B₂O₃; Garrett, 1998).

The main borate reserves are in the Argentinian Andes in the Pastos Grandes Basin within a 1500-m-thick volcanoclastic and lacustrine stratigraphic unit known as the Sijes Formation. During deposition of the Sijes Formation there were 3 major pulses of borate generation. These pulses are easily identifiable in the central part of the basin but become indistinct and tend to thin out toward the edges (Helvacı and Alonso, 2000). Along its approximately 30 km outcrop, the Miocene Sijes Formation is characterized by a string of borate deposits and occurrences. The borate-bearing members of the Sijes formation are from the base to top as follows: Monte Amarillo (hydroboracite), Monte Verde (colemanite-inyoite) and Esperanza (colemanite). The Tincalayu and Loma Blanca areas are important principally for borax occurrences whereas in modern active salars, borax and ulexite are the dominant borate salts (Helvacı and Alonso, 2000). Ulexite was also the first evaporite to precipitate in the Pleistocene Blanca Lila Formation near Salar Pastos Grandes, followed by gypsum then halite (Vandervoort, 1997).

Typically, South American salars with substantial borates have a central zone, consisting of a relatively thick halite, surrounded by a thinner marginal sulphate zone consisting of a variety of sulphate minerals, as well as variable amounts of halite, ulexite and other borates (Figure 11.33a; Ericksen, 1993; Helvacı and

Alonso, 2000). Salars that are filled mostly with gypsum lack this zonation. The borate zonation may be symmetrical (bull's-eye pattern) with sulphate surrounding a central halite core, or asymmetrical with the halite zone crowded against one side of the salar. This is the situation in Salar de Atacama where tectonic tilting has displaced the lowest part of the brine sink to the southern end of the playa (see Figure 11.41). Both the halite and sulphate zones are typically underlain by gypsum and this in turn by siliciclastics. Alternating arid and pluvial climatic episodes in the Andes since the mid-Miocene, means the playas are filled by alternating salt beds and siliciclastics (Figures 3.40, 3.45).

Most borate-rich salar deposits in South America have undergone relatively little deformation since they were first emplaced. As a result, borates are extracted from a number of open pit operations in the Andean Altiplano (Alonso, 1991). Borax Argentina, a member of the Rio Tinto Borax Group, extracts sodium borate ores at its Tincalayu Mine, high in the Argentinian Andes Mountains (altitude of 4100 metres). Nearby, hydroboracite is extracted at Sijes, and ulexite from two dry lakebeds, Salar Cauchari and Salar Diablillos, all in the Salta province. Originally developed in 1976, Tincalayu is now Argentina's largest open pit operation measuring more than 1.5 km (1 mile) across and 100 m (330 ft) deep and extracts ore at a rate of 100,000 tons per year. In Bolivia, ulexite is extracted from mines in the Salar de Uyuni (Figure 3.42). In Chile, borates are extracted from Salar de Surire; the largest single ulexite deposit in the world with reserves reported to be ≈ 1.5 million tonnes of 35% boron oxide. The salar is located some 4,250 metres above sealevel and within the borders of the Monumento Natural de Surire national park of Chile.

Almost all the borate salts described so far are enigmatic, perhaps syndepositional replacements of gypsum, but in the Sijes Formation (Miocene, central Andes, NW Argentina)

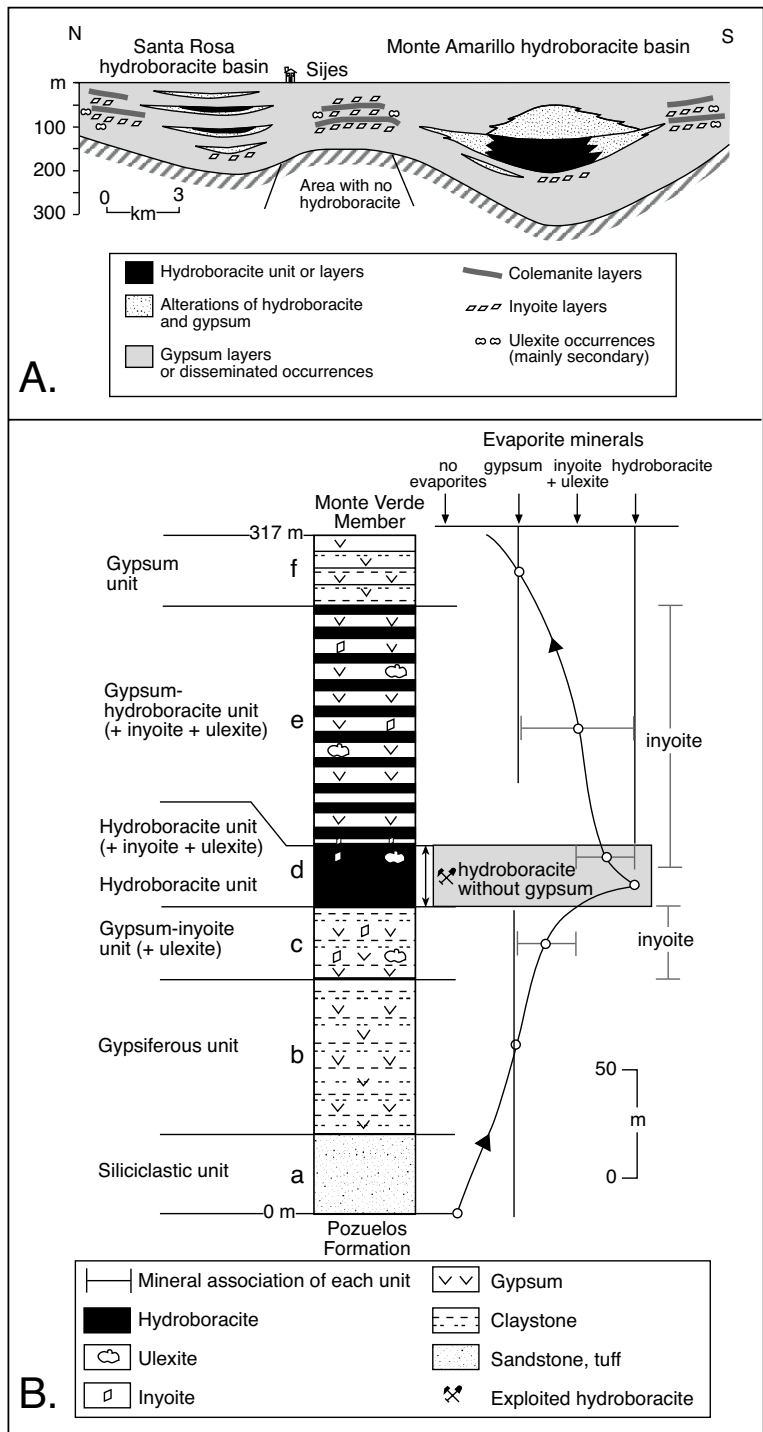


Figure 11.33. Hydroboracite in the Monte Amarillo Member, Sijes Sierra, northern Argentina. A) Borate facies distribution in the Santa Rosa and Monte Amarillo basins. B) Type section of the Monte Amarillo Member showing distribution of the various borate minerals and the relative position of the exploited horizon (after Orti and Alonso, 2000).

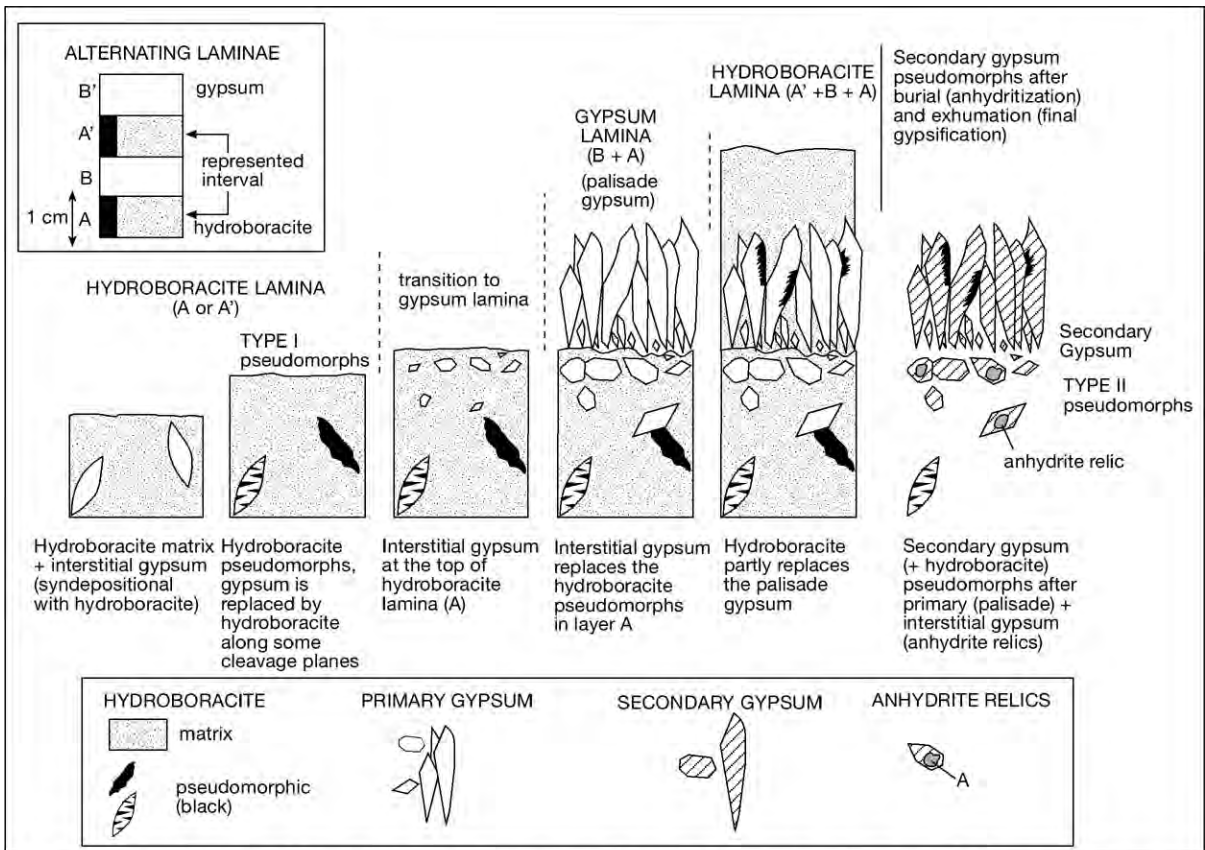


Figure 11.34. Syndepositional formation of hydroboracite pseudomorphs after gypsum in primary hydroboracite successions composed of alternating cm-scale beds of hydroboracite and gypsum precipitates. Most of the hydroboracite is primary, not secondary (after Orti and Alonso, 2000).

some of the hydroboracite is thought to be a primary precipitate (Orti and Alonso, 2000). This area encompasses the largest known hydroboracite accumulation in the world. In outcrop, the sulfate minerals in the Sijes Fm, are mostly secondary gypsum and minor anhydrite, while the borate minerals are hydroboracite with subordinate inyoite and colemanite, and some ulexite. The Sijes Formation (Miocene) has four members; three of them are fine-grained siliciclastic, tuffaceous, and chemical-evaporitic in nature (the Monte Amarillo Member, the Monte Verde Member, and the Esperanza Member), while the other member is dominantly a coarse-grained siliciclastic (the Conglomerate Member). The overlying Blanca Lila Formation (Pleistocene) is made up of claystone and evaporites (including borates). Much of the hydroboracite resides in the Monte Amarillo member.

The Monte Amarillo Member accumulated in two coeval, shallow lacustrine Miocene subbasins (Figure 11.33a): 1) The Monte Amarillo hydroboracite subbasin, and 2) The Santa Rosa

hydroboracite subbasin. The Monte Amarillo hydroboracite subbasin encompasses the borate districts to the south of the Sijes village and is an area where hydroboracite has been mined since 1985. This district is located at an altitude of 3900 m and lies near the palaeogeographic center of the Monte Amarillo subbasin. The Santa Rosa hydroboracite subbasin, includes the borate districts to the north of the Sijes village and is located at an altitude of 3900 m. This subbasin occupies a marginal position with respect to the Monte Amarillo subbasin. In these subbasins, the hydroboracite layers are fine-grained, light brown, and difficult to break with a hammer. Because of these characteristics, they had for long time been confused with limestones. In both subbasins, gypsum accumulated in the margins and the hydroboracite in the centers, the intermediate zones being characterized by mixed gypsum hydroboracite layers.

The type section of the Monte Amarillo Member is 317 m thick, contains an inyoite unit 36 m thick at the base, which is overlain by a hydroboracite unit 137 m thick (Figure 11.33b;

Alonso, 1986). This hydroboracite unit has variable amounts of inyoite and ulexite. Gypsum layers are ubiquitous in the Monte Amarillo Member. Samples of two tuff levels located close to the base and at the top of this section were dated as 6.81 ± 0.18 and 6.25 ± 0.15 Ma, respectively, which indicates a depositional period of about 630,000 years for the Monte Amarillo Member during the Upper Miocene (Alonso 1986).

Alternations between gypsum and hydroboracite laminae are present in the transition from gypsum units to hydroboracite units in the Monte Amrillo member and contain fabrics that indicate both the borates and the gypsum-anhydrite were primary or syndepositional precipitates (Orti and Alonso, 2000). Fine-grained hydro-boracite matrix commonly cements and partly replaces the precursor gypsarenite crystals in the gypsum laminae (Figure 11.34). In addition, micronodules of hydroboracite can displace or replace gypsum laminae. Two styles of pseudomorphs after interstitially grown (precursor) gypsum are preserved in hydroboracite laminae. Type I corresponds to hydroboracite pseudomorphs after euhedral, lenticular or tabular gypsum crystals. Many of these pseudomorphs are thin, curved, lenticular or slightly deformed, and now composed of fine-grained hydroboracite crystals. Others are made up of parallel prisms of hydroboracite that project inward from the boundaries of the pseudomorph with the centre commonly occupied by secondary gypsum bearing anhydrite relics. Parallel arrangement of the prisms suggests replacement of the precursor gypsum along the main cleavage plane (010). Type II corresponds to secondary gypsum pseudomorphs after equant to prismatic, commonly zoned (precursor) gypsum crystals. These pseudomorphs are located in the uppermost parts of hydroboracite laminae and grade into secondary gypsum pseudomorphs that constitute the overlying gypsum lamina. Type II pseudomorphs crosscut and replace type I pseudomorphs suggesting that type II pseudomorphs postdate type I.

Alternations between gypsum laminae (with aligned crystal outlines) and hydroboracite laminae imply bottom precipitation in a shallow subaqueous environment, where fine-grained, soft hydroboracite mud encased the gypsum in the laminated gypsarenites. The prevalent microcrystalline or fibrous textures of hydroboracite suggest a primary origin for these alternations in which precipitating conditions oscillated from gypsum to hydroboracite. Hydroboracite matrix appears to have precipitated interstitially within the open fabric of the (precursor) gypsarenite under syndepositional conditions (Orti and Alonso, 2000). This precipitation, together with associated partial replacement of (precursor) gypsum crystals, occurred during the sedimentation of the overlying hydroboracite lamina (Figure

11.34). In the hydroboracite laminae, type I pseudomorphs seem to correspond to (precursor) gypsum crystals that grew interstitially in the hydroboracite matrix when the borate concentration of the brine was relatively low. It appears that these crystals were very soon replaced by the hydroboracite matrix. The deformation of the pseudomorphs that are formed by fine-grained hydroboracite suggests that the replacement process took place in a soft matrix under syndepositional conditions. However, when this replacement occurred as a growth of prisms along the gypsum cleavage planes, the pseudomorphs remained undeformed and consistent. In general, this mechanism was less penetrative, and many pseudomorphs had a mixed hydroboracite–gypsum composition. Presumably, in these mixed pseudomorphs, the anhydrite replacement of the gypsum postdates the partial hydroboracite replacement. These pseudomorphs changed to hydroboracite–anhydrite during burial, and to hydroboracite–secondary gypsum in final exhumation. Type II pseudomorphs seem to correspond to (precursor) gypsum crystals that grew interstitially toward the tops of the hydroboracite laminae during precipitation of the overlying gypsarenite layer.

Beds dominated by primary gypsum (gypsarenite) and syndepositional anhydrite were first precipitated during deposition of the Monte Amarillo Member, in association with limited amounts of calcium borates (colemanite, inyoite). This was followed by beds containing hydroboracite (calcium/magnesium borate) and alternating gypsum and hydroboracite layers also formed. The hydroboracite at this level in the stratigraphy is mainly a primary mineral, although it also replaced some gypsum under syndepositional conditions (Figure 11.34). The formation of colemanite, which occurred during early diagenesis, is linked to brines precipitating calcium sulphates (gypsum and anhydrite), whereas inyoite coexists with brines precipitating both calcium sulphate and magnesium-bearing borates. Transformations among the various borate minerals during burial diagenesis were not detected by Orti and Alonso (2000). Primary gypsum was transformed into anhydrite from the onset of early diagenesis through to moderate burial diagenesis. The boron source of these deposits is volcanic/hydrothermal activity in the central Andes during the Miocene.

North American borates

The United States is the world's largest producer of boron compounds and the second largest producer of borate ore. Domestic producers exploit saline brines and bedded playa deposits such as Searles Lake in California (Smith, 1979) or their Tertiary counterparts at Boron and the nearby Death Valley area (Kisler

and Smith, 1983). In the Death Valley area the borates were deposited 6 Ma and there are more than 23 deposits. In all the borate ore is contained in the lower 150m of the 2,100m thick Pliocene Furnace Creek Formation. The interiors of most of the ore deposits preserve unaltered bedding planes and uniform depositional patterns. There are few to no indicators of syndepositional alteration (slumps, pseudomorphs) in the centres of the deposits but considerable evidence for alteration and replacement about the deposit's edges. The agglomerated nodular structure of much of the originally exploited ore meant that earlier miners in Death Valley described the various exposures of borate ore as ^{11,2}cottonball or cotton-tail (like a fluffy rabbit tail). Regionally a series of projected shoreline features can be traced from the Billie to the Boraxo to the Sigma-White Monster mines and residues of ancient geothermal spring mantle deposits are locally present (Garrett, 1998).

The exploited massive borate facies in the various Death Valley deposits are made up of thick, massive borate layers, locally containing host rock clasts with sharp to diffuse boundaries. Borate formation first took place at or below the sediment/water interface. The composition of the borate deposits in Death valley varies from mainly colemanite to zoned accumulations, with colemanite surrounding a core of probertite and ulexite. High Ca/Na ratios favored primary deposition of hydrated Ca-borates, which early workers argued were subsequently transformed by diagenetic dehydration to colemanite (Foshag, 1921; Christ and Garrels, 1959). Gradual depletion of Ca and decreasing Ca/Na ratios in the mother brine resulted in Na-Ca-borate precipitation, while any renewed onset of elevated Ca/Na ratios again caused Ca-borate deposition.

These older models for the formation of colemanite as a burial replacement of ulexite and inyoite via flushing by "intruding warm borax solutions" never clearly addressed a number of textural and conceptual problems, namely (Garrett, 2001); 1) Where did these conversion liquours come from? 2) How did they maintain their chemical uniformity? 3) How did they totally and completely pervade and replace what where impermeable units, 4) What was the required voluminous Ca source needed to accomplish the transformation and 5) Where did the residual brine go? In addition, why are there no widespread disruption texture and slump structures both within and above the bedded salts and why are commonplace colemanite alteration minerals like priceite, ginorite, nobleite and gowerite absent. A similar

^{11,2}Interestingly, the mineral name colemanite is named after one of the early miners in the Death Valley region, Mr. William T. Coleman, he could really say that he made a name for himself mining cottonball.

set of problems beset the older notions that the dehydration of borax to kernite indicates a deep burial conversion process. The problems are yet to be solved.

One of the largest deposits in the Death Valley area is the Billie orebody, a 1,100m long lens of ulexite, proberite and colemanite, interbedded and surrounded by limey laminated lacustrine mudstone and shale. Fault activity controlled the position of the lake bed borates and some beds now have local dips of upwards of 45°. The Billie orebody is currently mined by the American Borate Company; the deposit has an average thickness of 45 - 55m and a width of 220m, and a regional dip of 20-30° toward the southeast. Reserves are 2,700,000 metric tons of ulexite-proberite at 27% B₂O₃ and 11,000,000 metric tons of colemanite and 21% B₂O₃ (Garrett, 1998).

The borate ore zone at Billie Creek is hosted by shales of the Furnace Creek Formation and is made up of metre-scale units of nodular borate, mainly colemanite, interbedded with laminated mudstones deposited in a saline lacustrine environment during extension of the basin. The hosting laminites lack features of syndepositional exposure or wave-reworked deposition, indicating that the borate-hosting sediment first accumulated on the floor of a density-stratified perennial lake (Tanner, 2002). The presence of interbedded sulphate minerals in this facies suggests that salinity in this lake was elevated. Metre-scale mounds of porous limestone with a clotted-micritic fabric define spring-apron tufas that formed where groundwater discharged along fault-fed outflows about the edge of a more saline water mass.

The Kramer deposit near Boron, California, in the Mojave Desert is 140 km north northeast of Los Angeles. The total borate area (including the ulexite and colemanite rims) is 8 km (east-west) by 1.6 km (north-south). The Kramer deposit within this area is about 1600m long, 800m wide by 100m thick, and consists of a lenticular central mass of borax/kernite with interbedded montmorillonite-smectite clay. Borate ore reserves currently exceed 100 Mt (110 million st). The original borax target was 45-305 metres deep and dipped 10-15° to the south. The deposit was discovered in 1913 and was developed as an underground operation during the 1920s. It was converted to an open-pit operation in 1957. Since that time, the operation has grown to become the largest mining operation in California. The pit is now more than 2.4 km (1.5 miles) wide and 245 m (800 ft) deep. Ores are part of the shale member of the Kramer beds, which include an arkose member above and the Saddleback Basalt below.

The age of the deposit is 19 ± 0.7 Ma and it defines a small sub-basin in a much larger Tertiary lacustrine basin. It is encased in arkosic sands, silts and minor volcanics and limestones. Sedimentation in the basin was interrupted by flows of acidic lava (olivine basalt to latite) known as the Saddleback Basalt, it constitutes the base to the borate ore zone and also interfingers with other sediments of the basin fill. The upper part of the basalt in the mine area has fractures filled with ulexite and searlesite and its contact with the overlying sediments is defined by an "apple green" siliceous shale that contains ostracod carapaces. The color of the shale reflects its creation by the basalt reacting with lake waters. Bernard and Kistler (1966) defined the sedimentology of borate beds above the Saddleback Basalt. First is a 7.6-15 m thick footwall shale, further divisible into an initial barren (≈ 3.7 m) shale and then a ulexite zone. This is a layer of greenish-gray at times black fissile shale that is thinly laminated, micaceous and at times contorted. Locally it encloses lenses of arkosic sandstone and coarse conglomerate. Above this are the borax beds interbedded with clay and shale along with some beds and lenses of tuff, arkosic sand and conglomerate. The low permeability of these lacustrine shales is thought to have helped preserve the borax by preventing entry of groundwaters. Laterally and vertically away from the deposit's borax/kernite core, the borate facies changes to ulexite and colemanite, and the levels of shale interbeds and clay impurities in the borates become more significant (Bowser

and Dickson, 1966). The deposit is believed to have formed in a shallow Mid-Miocene saline lake, fed by Na- and B-rich thermal springs, a response to the later stages of volcanism. Saline sodium-borate-bearing thermal spring waters, being denser, sank to the lake bottom, cooled, and precipitated borax as they cooled. The original lake position was controlled by faulting contemporaneous with the accumulation of the borax. Continued fault movement, associated with the middle Pliocene uplift of the Mojave Block, tilted and dropped the lake sediments, which are now buried by more than 760 m of late Miocene and Pliocene arkosic sediment. Older models argue that deeply buried portions of the borax deposit were altered, via water loss, to kernite at this time. Renewed movement in late Pliocene–Pleistocene uplifted the deposit and drove some erosion of the original borate so that the outer portions of the kernite facies were rehydrated at that time. The deposit was then covered by 9 to 21 m of Pleistocene and Recent sands and gravels (Barnard and Kistler, 1966, Siefke, 1991).

Searles Lake in southeastern California is located in the lower central portion of a small block-faulted desert valley with a drainage area of 1600 km² and located midway between Boron and Death Valley (Figure 11.35). In the Pleistocene counterpart to the lacustrine evaporites that entrain the exploited Neogene deposits of Boron and Death Valley. The central pan, some 103 km² in extent, overlies a crystalline mush of mixed salts

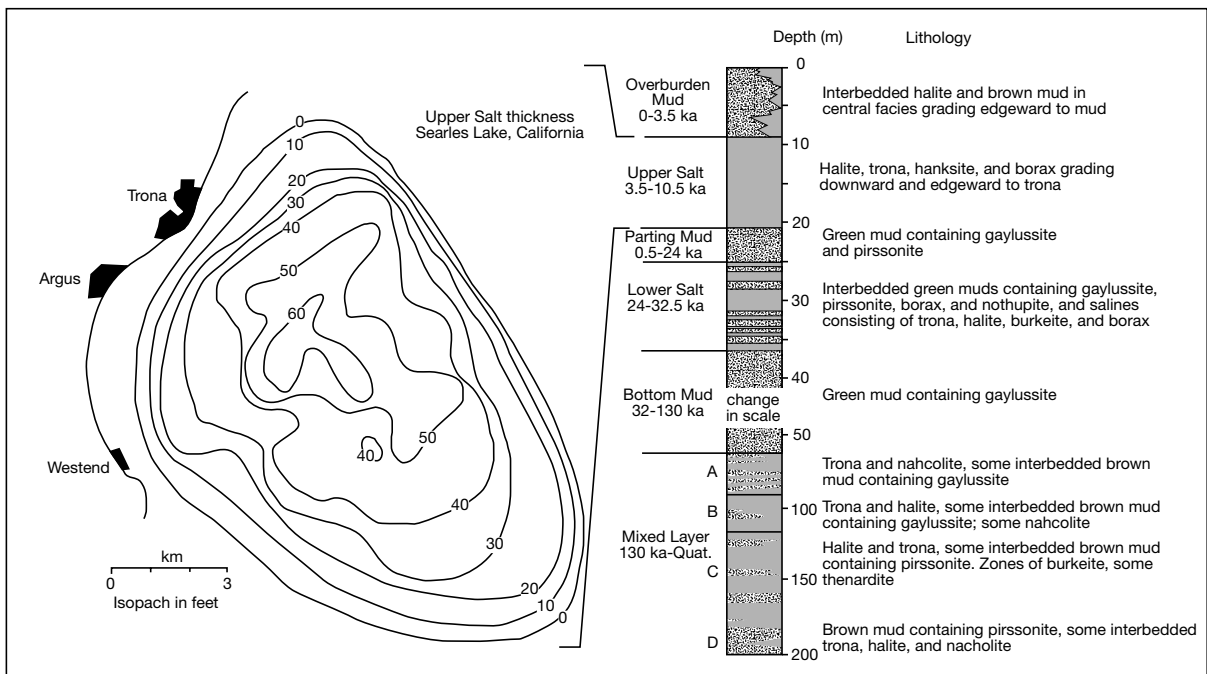


Figure 11.35. Searles Lake, California showing isopach of the "Upper Salt" in feet and the stratigraphy of the three salt layers and the intervening clays (after Smith, 1979).

dominated by sodium carbonates, but also with borax, clays, and hypersaline interstitial brines. The brine recovery operation is a multicomponent chemical system and borax is only one of the products recovered; others include sodium sulphate, lithium compounds, potash, bromine and other salts. Boron was supplied to the lake via thermal springs along the Sierra Nevada frontal faults in Long and Owens Valleys (Smith, 1979).

There are two main solution-mined salt horizons beneath the central pan: the “upper salt,” some 9 to 27 m thick (averaging 15 m), with a brine content averaging 1.0% B_2O_3 ; and the “lower salt,” some 8 to 14 m thick, (averaging 12 m), with a brine content averaging 1.2% B_2O_3 . The upper salt is overlain by a recent surficial mud and salt crust some 7 to 9 m thick and is separated from the lower salt by 3 to 6 m (average 4 m), of relatively impervious clays called the “parting muds” (Figure 11.35) The upper two salt beds accumulated in the period 3.5-40 Ka. There is also a much deeper salt bed with a mineralogy dominated by trona-nahcolite-halite with lesser amounts of burkeite-thenardite.

The salt mush in both the upper and lower salt beds is quite porous (0.35-0.40) and the stored brine is pumped via a series of wells into adjacent saltworks where borate, sodium bicarbonate and sodium sulphate salts are recovered. A constant resupply of brine to the mush beds is maintained by natural recharge and percolation of dilute refinery effluent, which is pumped back into the mush beds. The two salt horizons are pumped separately as they differ somewhat in chemical makeup and therefore require different plant treatments. Historically, until 1979, the upper salt was the solution mining target, since then the lower salt has been mined as a trona target and processed using carbonation.

Other Borate deposits

Borates in China are found in salt lakes on the Qinghai-Xizang (Tibet) Plateau, where typical lake waters contain 85 mg/l of boron oxide (Figure 11.2; Sun and Li, 1993). The maximum value of boron oxide in the brine is around 1,500 mg/l. However, the largest economic borate reserves in China occur not in Quaternary/Tertiary lakes but in the Precambrian meta-evaporites of Liaoning Province. Reported reserves are 44 million tonnes of boromagnesite with 8.4% boron oxide content. The deposits in the Liaoning Province represent 64% of the country's total boron resources and 90% of these deposits are associated with banded iron formations.

The world's only exploited marine borate deposit is in the Inder district of Kazakstan (former USSR), north of the Caspian Sea. The borates form bedded lenses that are up to 3 metres thick and hosted in the gypsiferous caprock in the 100+ km² crest of a large Permian salt dome. Ores are magnesian borates, rather than the more commonplace sodian-calcian borates. Mineralisation is centred on fractures near the top of the dome, where borates have precipitated in a matrix of gypsum, clay and anhydrite. The fluids precipitating borate are thought to be derived from intrusive geothermal springs (Garrett, 1995) Boron is also extracted from the brines of nearby Lake Inder. This salt lake has a surface salt crust along with about 30m of brine-saturated salt, which contains potassium chlorides and bromides as well as borax (Kisler and Smith, 1983). Unlike the other economic borate deposits of the world, this deposit is sourced by dissolving Permian marine salts, it is not tied to volcanism, hence the association with the magnesian salts.

Its marine origin is obvious in its boron isotope signature, which is clearly much more enriched in ¹¹B than nonmarine sediments (Figures 2.25; Swihart et al., 1986). The clear separation of nonmarine and marine borate salts using boron isotopes is also used to define parentage of various meta-evaporitic tourmalines in the meta-evaporites of Liaoning, China. Isotope analysis is a useful technique for determining boron source long after the original salts have evolved into lattice components of high temperature and high pressure minerals (see Warren, 1999; Chapter 6).

There are more than 112 separate borate deposits (12 contained 98% of the reserves) in the Liaoning area on the Liaoning Peninsular in northeast China the main ore mineral is szaibelyite (aka ascharite) and szaibelyite-ludwigite, with some suanite. All are Mg-borates and are hosted along with magnesite and magnetite in fractured marbles. Deposits are thought to be meta-evaporitic skarns originally deposited as lacustrine borates interbedded with volcanic tuffs (Peng and Palmer, 2002).

Borate minerals do occur in marine evaporites other than the Inder deposit, but not in sufficient amounts to be economic targets. For example, potash ore processing of the Zechstein potash ores in Germany leaves behind borates in the mud residues. At times this borate has been recovered as a small-tonnage byproduct (Garrett, 1998). Borates such as priceite and howlite are present in minor amounts in the Cretaceous marine evaporites of the Maha Sarakham Fm. in Thailand, in the Mesozoic evaporites of the Atlantic margin in Nova Scotia, Brazil and west Africa, and in the Permian evaporites of the Delaware Basin, USA (Chapter 7). In all cases it seems that the

levels of boron in the marine bitters were never sufficient to create economic levels of borate salts, that requires hydrothermal circulation, usually in a volcanic basin.

Rock gypsum and rock salt

The depositional, diagenetic and geological settings of halite and gypsum/anhydrite (the most commonplace evaporite salts) were discussed in detail in earlier chapters, and will not be repeated here, only aspects relevant to economic exploitation and production are presented.

Gypsum

Annual world production of gypsum exceeds 100 million metric tonnes (Figure 11.36). Seven countries account for some two-thirds (66%) of world production. In descending order of production they are; the United States (23%), Iran (9%), Canada (8.5%), China (8%), Spain (7.5%), Mexico (6.5%) and Thailand (4.5%). Canada, Spain, Mexico and Thailand export much of their crude gypsum, while Iran and China internally consume most of the gypsum they produce. About 75% of US gypsum production comes from Oklahoma, California, Iowa, Texas, Nevada, Michigan and New Mexico.

Gypsum's main usage is in the construction industry, mostly as calcined (burnt) gypsum in the manufacture of wallboard. In

fact, the word gypsum is derived from the Greek word *gypsos* meaning "to cook" in reference to calcined gypsum. Because gypsum quarries in the Montmartre district of Paris furnished calcined gypsum to much of Europe since the Middle Ages the calcined product is sometimes called "Plaster of Paris." Gypsum's utility to the construction industry stems from its hydrated character. When gypsum is calcined at 160°C it loses 1.5 moles of its combined water to form calcium sulphate hemihydrate (CaSO₄·1/2H₂O) or "Plaster of Paris." When mixed with water the hemihydrate can be spread, cast or moulded into the desired form, which then sets to a rocklike hardness. When spread between sheets of heavy paper and allowed to set it makes the plasterboard or wallboard used worldwide in the "dry wall" industry. Uncalcined finely crushed gypsum and anhydrite are used as retarding agents in Portland cement; the set of the cement is slowed, but the tensile strength is not lessened.

When applied as soil conditioners, gypsum and anhydrite can have beneficial effects. They decrease the salinity of salty soil, improve the permeability of clayey soil and provide sulphur, calcium and catalytic support, so decreasing fertilizer use and maximising the economics of crop production. Uncalcined gypsum is also used as a filler in a diverse range of products including paint, paper and toothpaste, as a flux in the smelting of certain nickel ores, in the manufacture of crayons, in asbestos packing gaskets and when in the form of alabaster as a medium for sculpting. Natural anhydrite is also crushed to

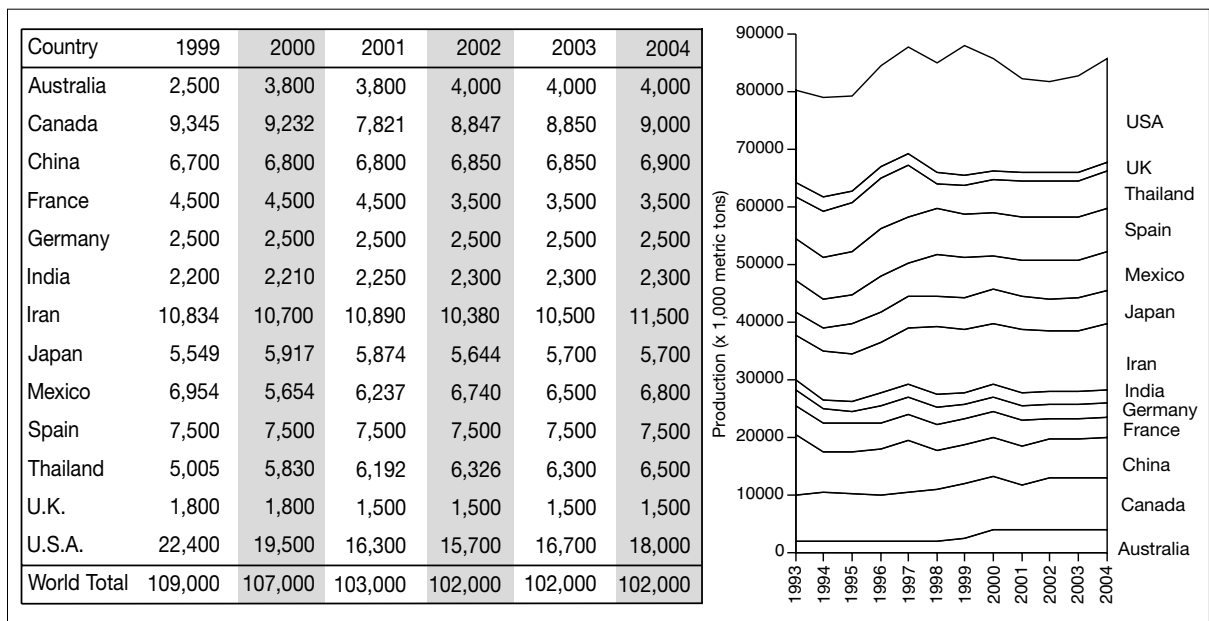


Figure 11.36. World gypsum production (in 1,000s metric tons) of nations producing more than 1,500,000 metric tons per year (compiled from <http://minerals.usgs.gov/minerals/pubs/commodity/> last accessed 30 September, 2005).

less than 7mm (30% of which is dust), then mixed with water and an accelerator (Fe_2SO_4 and K_2SO_4), to form quick-setting, high strength roadside packs. Aerated anhydrite products are sometimes used to fill cavities in mines or in spaces above road arches. Anhydrite has been used as a filling and packing material in the coal mining industry of West Germany since the mid 1960s. Other minor uses for calcined gypsum include dental plaster, modelling casts, moulds, surgical casts and drilling muds.

Most CaSO_4 production is either from quarrying or mining. In North America and Europe, gypsum is mined at relatively shallow depths in areas where ancient buried anhydrite beds or diapir caprocks have reconverted to gypsum during uplift and erosion. The Maritimes region of eastern Canada and the USA produces the most gypsum from a single area in the world, with more than 6 million metric tonnes extracted each year from Mississippian strata of the Windsor Group. There is also substantial US production from Tertiary playa deposits in the Salton Trough, California. Spain is Europe's leading gypsum producer, with the main production from bedded Tertiary lacustrine deposits. In Germany, the greater volume of its gypsum is mined from the rehydrated crests of near surface salt structures of Permian Zechstein salt. Secondary targets are the Middle Muschelkalk and minor production comes from the Keuper. In the UK, the most important beds are Permo-Triassic in age, except for those in Sussex, which are Jurassic. In the southern Hemisphere, substantial volumes of high-grade gypsum are quarried, processed and shipped from

Holocene coastal lakes in southern (>1,000,000 tonnes/year) and western Australia (300,000-500,000 tonnes/year). This production supplies the construction industry of Australia and many other parts of Southeast Asia. Small amounts of coarsely crushed gypsum are used as aggregate to pave unsealed minor roads in many places in southern Australia. Under the region's semi-arid to arid climate gypsum aggregate tends to compact and set into a hard flexible crust.

Rock salt (halite)

Annual world production of rock salt has today reached more than 210 million tons. Approximately one third of the total is produced by solar evaporation of seawater or inland brines; another third is obtained by mining of rock salt deposits. The balance is obtained from processing of recovered brines, mainly via solution mining. The largest volumes of salt production are concentrated in 15 nations, which together produce more than 80% of the world's total production (Figure 11.37). Important commercial rock salt deposits are found in the Silurian of northeastern North America; the Devonian of western Canada (also a major producer of potash); the Permian of Russia, western Europe, the midwest of North America, the Jurassic of the US Gulf Coast and the Miocene of the Middle East. In Europe and North America the salt is recovered either by hard rock mining (mostly room and pillar methods) or by solution mining where water is pumped down a well to dissolve the salt and then recovered as brine. In warmer climates, such as Australia, Spain and Mexico, large volumes of salt are

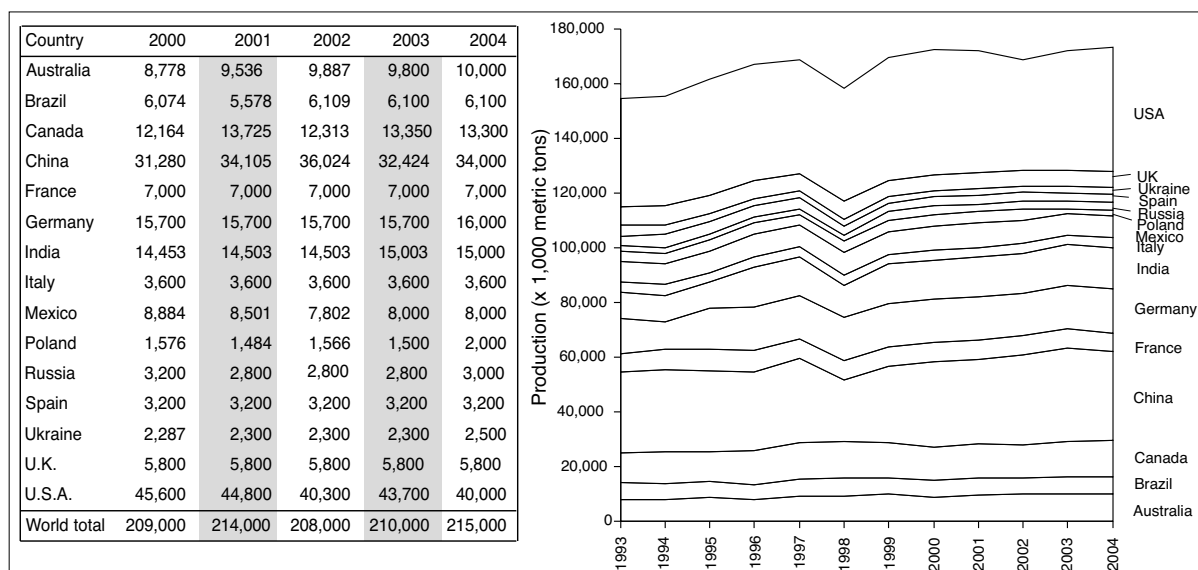


Figure 11.37. Salt (NaCl) production from countries producing >2,000,000 metric tons (values in thousand metric tons - (compiled from <http://minerals.usgs.gov/minerals/pubs/commodity/> last accessed 30 September, 2005).

recovered by solar evaporation of seawater or less commonly of inland playa waters.

World resources of rock salt are practically unlimited and total production levels have remained near static since the early 1990s. The majority of usage worldwide is in the chemical industry, some 60% of total rock salt production is processed to supply sodium and chlorine chemicals that are then used to manufacture a multiplicity of products (Table 11.1). The principal basic chemicals, chlorine and sodium hydroxide (caustic soda) are manufactured from brine via electrolysis. Sodium chloride is reacted with limestone in the Solvay process to produce sodium carbonate (soda ash), and with sulphuric acid to produce hydrochloric acid and sodium sulphate (salt cake). The chloralkali industry also uses substantial quantities of salt. Most of its output is polyvinyl chloride and vinyl chloride monomers; chlorine is another product. The second largest user of salt is mankind itself. Humans metabolise around 30% of the total salt produced to support their physiological functions and eating habits. Salt for food is probably the most "taken for granted" commodity in the world today, available from thousands of sources in hundreds of qualities as table, cooking and industrial salt for food production (see history of salt usage, earlier in this chapter). Salt usage in the northern hemisphere increases in the winter months when salt is used to de-ice frozen roadways ($\approx 10\text{-}15\%$ of world annual production).

Iodine, bromine and lithium salts

Iodine is either recovered from saline brine associated with natural gas production (e.g. southern Kanto gasfield, Japan), oilfield brines (e.g. Woodward, Oklahoma) or mined from lakes and saline soils (Atacama Desert - Chile). Subsurface brine now provides more than 80-85% of iodine produced each year. Japan today controls over 30% of the world capacity, Chile 54% and the USA about 10% (Figure 11.38). Reserves of iodine brines are vast in Japan, nearly inexhaustible, but production rate is limited by problems of land subsidence. Chilean reserves are also vast, but producers can experience climate-related variations in ore quality that affect production costs. Compared with Japanese and Chilean reserves, the US reserves are smaller, but are still estimated to be sufficient for domestic use for another century at current production rates.

Chile is now the largest producer of iodine in the world and the sole producer of commercial quantities of iodine from a non deep-brine source. For example, substantial iodine is recovered as a byproduct in the processing of Chilean nitrate

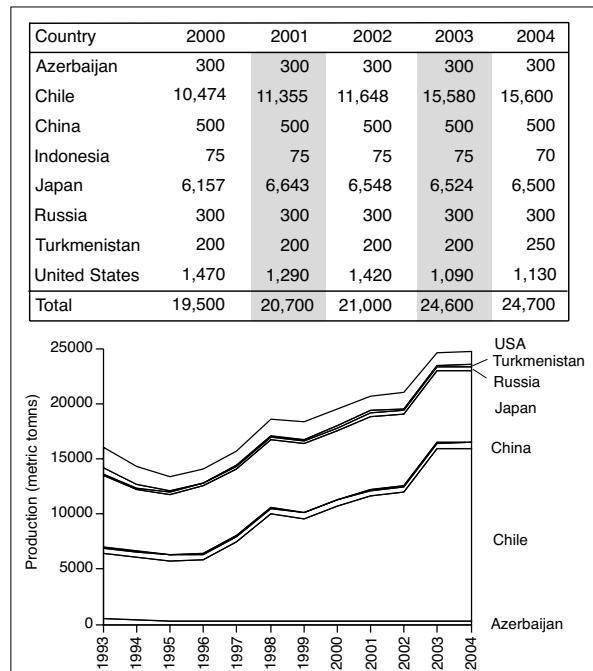


Figure 11.38. World iodine production (in thousand kilograms of elemental iodine - compiled from <http://minerals.usgs.gov/minerals/pubs/commodity/> last accessed 30 September, 2005).

deposits in the Atacama Desert (e.g. at Coya Sur, in northern Chile - see nitrates in following section). The ultimate source of Chilean iodine is thought to be leaching of Tertiary volcanics (Ericksen, 1993). Iodine salts occur in caliche ores, largely as the minerals lautarite (CaI_2O_6) and dietzite ($7\text{CaI}_2\text{O}_6 \cdot 8\text{CaCrO}_4$), and is leached from the nitrate ore using an alkaline solution during the extraction of potassium nitrate and sodium sulphate. Ore layers are 1-3 metres thick and overburden is less than 1 metre. The nitrate deposit with which it is associated is huge, it is some 15 to 75 km wide and parallels the coast for more than 720 km (Figure 11.42). Processing of the quarried ore involves crushing, leaching with fresher water, thickening, filtration, and calcium iodate (with sodium nitrate) precipitation. Many of the iodine plants use solar evaporation ponds to thicken the leachate.

In contrast to the volcanic association of iodine in the Chilean deposits, most of the iodine in the subsurface brines of marine sedimentary basins comes from an organic source (Worden, 1996). In fact, many such subsurface waters are enriched in iodine by up to three orders of magnitude relative to seawater evaporation. Organic material is the main reservoir of iodine in recent marine environments. Organic-rich sediments or their volatiles (hydrocarbons) are the main sources of iodine in

Country and Company	Location	Capacity	Brine source
<i>Azerbaijan</i>			
Neftechala Bromine Plant	Baku	4,000	Underground brines
<i>China</i>			
Laizhou Bromine Works	Shandong	30,000	Underground brines
<i>France</i>			
Atochem	Port-de-Bouc	12,000	Seawater
Mines de Potasse d'Alsace S.A.	Mulhouse	2,300	Bitterns of mined potash
<i>India</i>			
a) Hindustan Salts Ltd.	Jaipur	1,500	Seawater bitterns
b) Mettur Chemicals	Mettur Dam		
c) Tata Chemicals	Mithapur		
<i>Israel</i>			
Dead Sea Bromine Co. Ltd.	Sedom	190,000	Bitterns of potash production
<i>Italy</i>			
Societa Azionaria Industrial Bromo Italiana	Margherita di Savoia	900	Seawater bitterns
<i>Japan</i>			
Toyo Soda Manufacturing Co. Ltd.	Tokuyama	20,000	Seawater
<i>Spain</i>			
Spain: Derivados del Etilo S.A.	Villaricos	900	Seawater
<i>Turkmenistan</i>			
Nebitag Iodine Plant	Vyska	3,200	Underground mines
Cheicken Chemical Plant	Balkan	6,400	Underground mines
<i>Ukraine</i>			
Perekopsky Bromine Plant	Krasnoperckopsk	3,000	Underground mines
<i>United Kingdom</i>			
Associated Octel Co. Ltd.	Amlwich	30,000	Seawater
<i>USA</i>			
Albemarle Corp.	Union Co., Ark.	25,000	Well brines
Albemarle Corp.	Columbia Co., Ark.	310,000	Well brines
Great Lakes Chemical Corp.	Union Co., Ark.	335,000	Well brines
Dow Chemical Co.	Mason Co., Mich.	25,000	Well brines

Table 11.6. Bromine production methods in 1997 (in metric tons of bromine content - compiled from <http://minerals.usgs.gov/minerals/pubs/commodity/> last accessed 28 December, 2004).

most sedimentary basins. Iodine enrichment in brines is often tied to proximity to hydrocarbon pools and iodine increases in concentration in pore waters with increasing depth of burial at a faster rate than bromine (Martin et al., 1993).

Downstream uses of iodine include animal feed supplements, catalysts, inks and colorants, pharmaceuticals, photographic equipment, sanitary and industrial disinfectant and stabilisers.

An effort is now underway to eliminate iodine-deficiency disorders by fortifying world salt supply with iodine. Iodine deficiency is the Third World's leading cause of mental health problems in the form of severe retardation, deaf-mutism and partial paralysis, along with more subtle problems such as clumsiness, lethargy, and reduced learning capacity. Globally, 2.2 billion people live in iodine-deficient areas, especially in mountainous areas located well away from the sea coast. Iodine is an essential part of the thyroid hormone, a substance that contributes to brain development during foetal life and later metabolism.

In Tibet for example, some remote mountain villages have birthing data that show 13% of newborns suffer from cretinism. This is because of low iodine levels in the soils and the fact that local salt is harvested from salt lakes where glaciation and deep weathering have long ago removed iodine from soils. The present soil waters and runoff, that ends up collecting and evaporating in the salt lakes, contains little or no iodine (Lee, 2001). Salt harvested from the lakes, when carried to the villages and sold, is 50% cheaper than local salt that has

been fortified (sprayed) with iodine. A lower cost makes natural salt a more attractive product to peasants in the villages, most of whom are subsistence-level farmers. Harvested salt is usually bartered or exchanged for an equivalent weight in rice. In an attempt to improve the health of the people, selling non-iodised salt has been made illegal by the Chinese government. But a lower price and the fact that the salt harvesters usually barter their salt for an equivalent weight in rice, and have done so

for hundreds of years, make the harvested natural salt more attractive than the more expensive iodised product. To maintain their own subsistence level livelihoods, the salt harvesters are spreading rumours that animals and people fed iodized salt will be infertile.

In rural China and Mongolia, the government's policy of introducing iodized salt to the agrarian population has been much more successful. In the 1980s the rates of goitre (indicated by an enlarged thyroid and an indicator of iodine deficiency) in the general population of China were as high as 40%. By making noniodized salt illegal and keeping the price of the iodised salt low, the current rate of goiter in the general population is now somewhere near 5%. Iodization programs in salt and milk products in the western world since the 1920s had largely eliminated the problem of iodine-deficiency by the 1960s. Ironically, in some in parts of the western world now lacking a government-enforced iodine program, the popular anti-science "new-age" push for healthier back-to-nature and organic food products is an evergrowing market trend. Accordingly, there has been a move away from iodised salt and iodised milk to make it more "natural." Now the rate of incidence of iodine-deficiency in the general population, and in children especially, is growing once more. In Australia, for example, the iodine intake in the population is currently half what it was five years ago, but most Australians are unaware that a problem exists (Li et al, 2001; MacDonnell et al., 2003).

The word bromine comes from the Greek *bromos* meaning stench and was discovered in 1825 when Antoine Balard extracted it from seawater bitterns. The United States and Israel dominate the world's elemental bromine output of about 5.2 Mt (5.7 million st). Azerbaijan, Ukraine, France, United Kingdom, China, Japan and India contribute most of the rest. Bromine is recovered from modern brines in Searles Lake and the Dead Sea, as well as from formation waters in the Gulf of Mexico and the Michigan Basin, and seawater in Japan and Spain (Table 11.6, Figure 11.39). For example, a brine averaging 5000 ppm Br is recovered for processing from depths around 2500m in the upper Reynolds Oolite Member of the Upper Jurassic Smackover Formation in Union Co, southern Arkansas (Kyle, 1991). The elevated Br content in this brine indicates natural leaching of the underlying Louann Salt. Since 1957 bromine has been produced at Beersheva, Israel, as a byproduct from bitterns associated with potash, chlorine and caustic soda production. There solar evaporation concentrates lake brines pumped from the Dead Sea and derived from Miocene evaporites buried beneath the lake floor (Figure 11.9). After the potash slurry is processed, residual bitterns are treated with chlorine

to recover bromine. The bromine-free bitterns are then further processed to recover magnesium. The Dead Sea effluent feed-brine for bromine recovery contains 11,000-12,000 ppm of bromine and is one of the richest bromine brine feeds currently in commercial operation. Brine reserves are also huge, with the Dead Sea waters containing more than 1 billion tonnes of bromine. In Germany, bromine is produced as a byproduct of potash mined from the Zechstein salt.

Since 1973, when the United States produced 71% of the world supply, its market share has decreased; a result of environmental constraints and the emergence of Israel as the world's second largest producer. Today, the United States produces 40% of the world's bromine, Israel 38%, China 8%, the United Kingdom 9% and other countries combined 5% (Figure 11.39).

Traditionally, the major market for bromine was in the production of ethylene dibromide; a lead scavenger in gasoline antiknock compounds. However, this market has been in

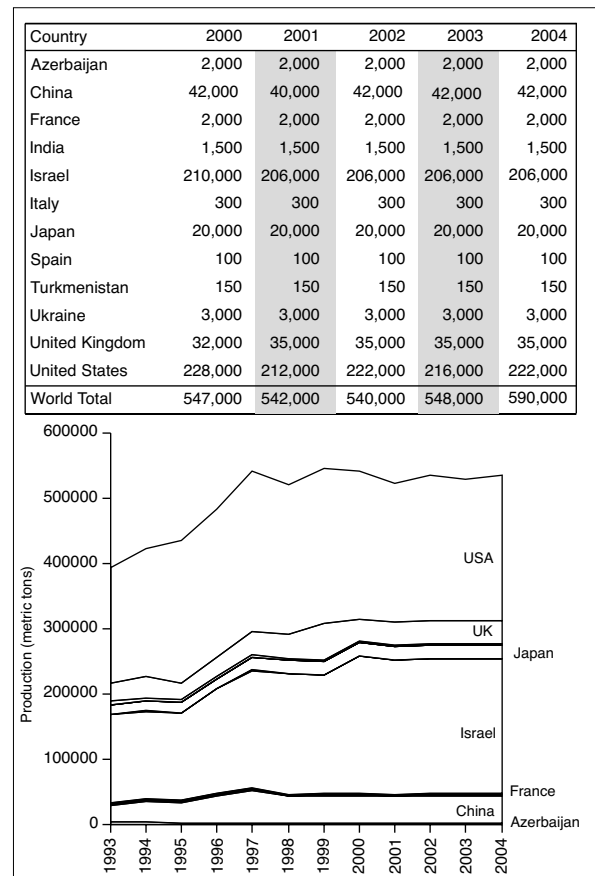


Figure 11.39. World bromine production (in metric tons of bromine content - compiled from <http://minerals.usgs.gov/minerals/pubs/commodity/> last accessed 30 September, 2005).

Country	Source	1999	2000	2001	2002	2003	2004
Argentina	Lithium carbonate from brine	1,592	2,161	0	906	2,850	4,970
"	Lithium chloride from brine	2,794	5,182	4,512	4,729	4,700	6,303
Australia	Spodumene in pegmatite	75,824	81,891	63,433	79,085	124,410	125,000
Brazil	Spodumene in pegmatite	11,122	10,875	9,084	12,046	12,100	12,100
Canada	Spodumene in pegmatite	22,500	22,500	22,500	22,500	22,500	22,500
Chile	Lithium carbonate from brine	30,231	35,869	31,320	35,242	41,667	42,500
China	Spodumene pegmatite and carbonate from brine	12,500	13,000	13,000	13,000	13,500	14,000
Portugal	Lepidolite in aplite-pegmatite	14,862	9,352	11,571	16,325	16,000	16,000
Russia	Minerals not specified in Siberia	2,000	2,000	2,000	2,000	2,000	2,200
United States	Spodumene (closing) + brine	W	W	W	W	W	W
Zimbabwe	Amblyonite, eucrytite, lepidolite, petalite, spodumene in pegmatite	36,671	37,914	36,103	33,172	12,131	12,000

Table 11.7. World lithium production (metric tons) and sources (compiled from USGS on-line data tables, downloaded from <http://minerals.usgs.gov/minerals/pubs/commodity/myb/> last accessed 30 September, 2005). w = withheld to avoid disclosing company proprietary data.

decline in past three decades as more and more countries legislate to adopt the catalytic converter and lead-free gasoline. Flame retardants are now the largest end use and account for more than 30% of the US bromine market. Other uses include intermediates in chemical manufacture of dyes, fragrances and pharmaceuticals; it is also used in photographic compounds, as bleach, as an additive in drilling fluids, and in the production of methyl bromide, a pre-plant soil fumigant.

Lithium occurs in more than 140 minerals, with mined production of lithium ore concentrates mostly from nonevaporitic spodumene pegmatites. Three major lithium miners supply the majority of worldwide demand for solid lithium ore concentrates. They are; Sons of Gwalia in Australia (largest), Tanco in Canada, and Bikita Minerals in Zimbabwe (Table 11.7).

Cheaper prices and abundant supply means there has been a move away from ore to brine as the major source of lithium in the past two decades and brine is today the major supplier of the world's lithium market, with Chilean salars as the dominant source. Production of lithium carbonate from a brine rather than an ore concentrate is much less energy intensive and much more environmentally friendly. Today there are substantial lithium carbonate brine operations in Salar de Atacama, Chile and Salar del Hombre Muerto, Argentina, along with smaller volumes recovered from multicomponent brine operations in Searles Lake, California, and Clayton Valley, Nevada. Salar operations can now produce lithium throughout the year whereas histori-

cally the brine extraction operations were seasonal and subject to downtime related to solar floods.

The highly competitive nature of the current supply market makes some published lithium figures suspect. It is a market where availability of known reserves exceeds projected needs by a ratio of more than 2:1 and lithium carbonate from brine is perhaps now supplying as much as 60-80%

of the world's needs. A ready cheap supply of lithium from brine operations has led to a fall in the real price of lithium by up to 50% since the mid 1990s. The market today is highly competitive with more spodumene operations and low capacity brine operations closing each year. United States production from brine was surpassed in 1998 by Chile and today only one lithium carbonate focused brine operation is still active in the USA (Table 11.7). The United States remains the world's largest consumer of lithium.

Lithium compounds are consumed in the production of ceramics, lubricants, glass, and primary aluminium. Lithium is electrochemically reactive and has unique properties, so there are many ongoing commercial lithium usages in the new high tech fields of industrial production, including the rapidly expanding lithium battery technologies. Lithium needs may expand much faster than currently projected and so ameliorate

Location	Country	Lithium (ppm)	Reference
Salar de Atacama	Chile	1,000-7,000	Risacher and Alonso, 1996
Salar del Hombre Muerto	Argentina	100-700	Saller and O'Driscoll, 2000
Salar de Uyuni	Bolivia	100-500	Risacher and Fritz, 2000
Lake Zabuye	Tibet	700-1,000	Chen, 1986
Clayton Playa, Nevada	USA	100-300	Davis et al, 1986
Searles Lake, Ca	USA	70	Kunasz, 1983
Great Salt Lake, Utah	USA	30-60	Kunasz, 1983
Qinghai Lake	China	100	Kunasz, 1983

Table 11.8. Lithium contents of some salar and playa brines.

the current oversupply and consequent low price.

Only the geology of the saline brine sources is discussed in detail in this section, the interested reader is referred to Garrett (2004) for a full discussion of all lithium raw materials. Subsurface lithium in playa sediments typically occurs either as a brine component (Table 11.8) or as lithium bearing minerals such as hectorite — $[\text{Na}_{0.33}(\text{Mg},\text{Li})_3\text{Si}_4\text{O}_{10}(\text{F},\text{OH})_2]$ — a clay mineral of the smectite group where the replacement of aluminium by lithium and magnesium is essentially complete. Hectorite is still mined in its type area, near Hector, California. It has a soft, greasy texture, a candlewax-like appearance and feels like modelling clay when squeezed between the fingers. As a colloid, hectorite's unique thixotropic properties for emulsion stabilizing, gelling, suspending, binding, bodying and disintegrating, means it sells for more than US\$2,000 a ton. Associated authigenic clays include stevensite and saponite and it lies adjacent to a colemanite deposit. It, along with associated authigenic clays and zeolites, is the diagenetic result of alkaline brines flushing volcanoclastic playa sediments.

Lithium carbonate is still produced from playa brines in Searles Lake, California and Clayton Valley, Nevada. Historically, the Clayton Valley playa has produced about one-third of the US lithium requirements, but its economic viability is now suffering from fierce market competition. The playa has an area of 50 km² and an elevation of 1400 m. It lies in the rain-shadow of the Sierra Nevada, with an annual rainfall \approx 130 mm and an evaporation rate of \approx 1380 mm. Near surface sediments consist of a mixture of clays (smectite, illite, chlorite, kaolin) and salts (halite and gypsum) and widespread pedogenic calcite. Lithium in the brines is derived by the weathering and leaching of the volcanoclastics of the Tertiary Esmeralda Formation and Quaternary ash-fall tuffs (Figure 11.40; Davis et al., 1986). Lithium content is highest on the eastern side of the playa adjacent to the outcropping marls of the Esmeralda Fm. Before it is leached, lithium is held in the clay fraction of the playa sediments and is probably part of the clay structure (hectorite is a widespread minor component in the Clayton Valley clays).

Lithium-rich brine, averaging 0.023% (230 ppm) lithium in a background NaCl concentration of 200,000 ppm, is pumped

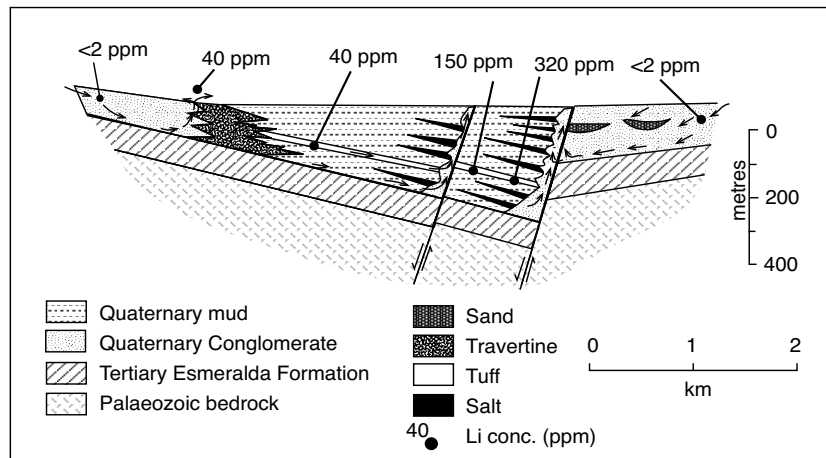


Figure 11.40. Generalised cross section of Clayton Valley Playa, Nevada. Shows the relative position of the major tuff-bed aquifer, inferred directions of groundwater flow and representative lithium concentrations (ppm) in the various aquifers and springs (after Davis et al., 1986).

from depths of 100–300m in the Clayton Valley playa via a number of gravel-packed wells. It then progresses through a series of fractionating evaporation ponds. Some of the brine feed also shows elevated levels of radon gas. Lithium concentration in the liquor increases to 6,000 ppm over the course of 12 to 18 months in the solar evaporation pans. When the lithium chloride level reaches optimum concentration, the liquor is pumped to a recovery plant and treated with soda ash to precipitate lithium carbonate, which is then removed through filtration, dried, and shipped.

Chile has emerged in the last decade as the most important lithium carbonate producer from a lake brine, largely through the exploitation of Salar de Atacama, Chile (Figure 11.41). The salar lies on the Tropic of Capricorn at an altitude of 2,300 m in the Desierto de Atacama, some 200 km inland from Antofagasto. In its more central portions this salt-encrusted playa contains a massive halite unit (nucleus) that is more than 900 m thick, with an area \approx 1,100 km². Fringing saline muds, with an area \approx 2,000 km², surround this nucleus (Figure 3.45).

The current salt crust atop this halite nucleus contains a sodium chloride interstitial brine that is rich in Mg, K, Li, and B (Alonso and Risacher, 1996). Lithium contents of the pore brines range from 200–300 ppm in the marginal zone, some 500–1,600 ppm in the intermediate zone and 1,510–6,400 ppm in the salt nucleus. This central zone averages 4,000 ppm lithium. Main inflows to the salar drain volcanic formations of the Andean Highlands located to the east of the basin (Figure 11.41). Salts dissolved in inflow waters have a double origin. Weathering of volcanic rocks supplies K, Li, Mg, B and, to a lesser extent, Na and

Ca. Leaching of ancient halokinetic evaporites with a mother salt layer beneath the volcanic formations provides additional amounts of Na, Ca, Cl, SO_4 to the most saline inflow waters. The mass-balance of the upper nucleus of the salar centre shows a strong excess of NaCl with respect to the bittern solutes Mg, K, Li, B. According to Alonso and Risacher (1996) this suggests that the nucleus did not originate from evaporation of inflow waters similar to the present. Rather the excess of NaCl is due to NaCl-rich inflow waters that formerly drained the Cordillera de la Sal, a Tertiary-age evaporitic ridge along the western rim of the present-day salar.

The average sedimentation rate of halite in the lake centre is ≈ 0.1 mm/year, based on the age of an ignimbrite interbedded with the salt. This slow aggradation rate implies a climatic setting of long dry periods and inactivity alternating with short wet periods during which large amounts of water, and so large amounts of salt, accumulated in the basin centre. The lack of peripheral lacustrine deposits and the high purity of the salt also suggest that the main salt unit is not the remnant of an ancient deep saline lake, but originated mostly from evaporation of waters supplied by subsurface and subterranean saline seeps.

Brines are pumped from 30 metre deep holes in the salt into solar evaporation ponds. In the ponds they are concentrated by a factor of 25, generating a final brine strength of 4.3% Li. During evaporation processing and the production of potassium chloride and potassium sulphate the ion ratios are constantly monitored and adjusted to avoid the precipitation of lithium potassium sulphate. The high initial lithium content of the brines and the extremely arid setting (3200 mm pan evaporation and <15 mm precipitation) means that only 90 hectares of evaporation ponds are required for the current operation, this is only 5% of the area required at Clayton Valley, Nevada. Borate (as perborate) is recovered at levels of 0.84 g/l during lithium extraction. Increasing volumes of lithium are also produced by new salar brine processing facilities in Salar de Hombre Muerto, Argentina and Salar de Uyuni, Bolivia.

Nitrate salts (nitratite and salt petre)

Nitrogen is abundant on and near the earth's surface where it makes up 78% of the world's atmosphere. It, along with potassium and phosphorus, make up the three essential plant nutrients. Natural deposits of nitrate are rare because of the extreme solubility of nitrate salts in water; synthetic sources

of nitrate today far outweigh the natural sources, with natural sources supplying less than 0.3% of the world's nitrogen needs.

Nitrate salts precipitate as efflorescent crusts in several of the world's deserts including; the Namibian Desert, the Abu Dhabi sabkhas and Death Valley. They are only present in mineable quantities in the Atacama Desert of Chile, where deposits occur in a narrow zone between the low-lying Pampa del Tamarugal to the east and the hills of the Coastal Range to the west (Figure 11.42a; Ericksen, 1981, 1983; Searl and Rankin, 1993). This area contains nitrate-rich soils, as well as surfaces encrusted with nitrate-bearing salts, saline-cemented regolith, and nitrates accumulating in closed basin playas or salars. Commercial concentrations develop in and atop weathered rock

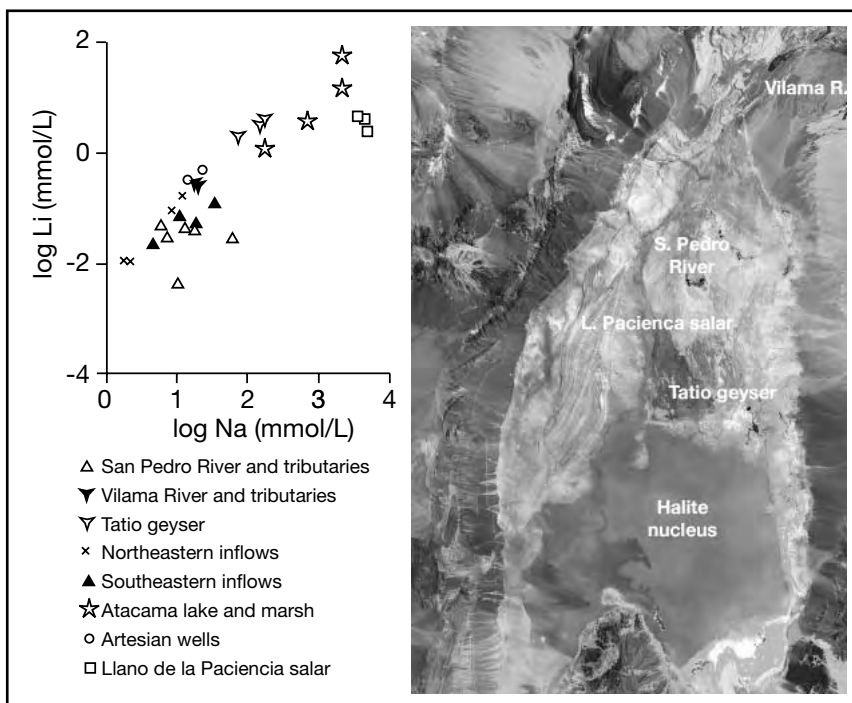


Figure 11.41. Lithium content of waters in the Salar de Atacama basin, Chile (after Carmona et al., 2000). Tectonic tilting of the basin floor has crowded the halite nucleus up against the southwestern margin of the playa and controlled halite thickness within the salar (see Figure 3.45; Landsat image courtesy of NASA).

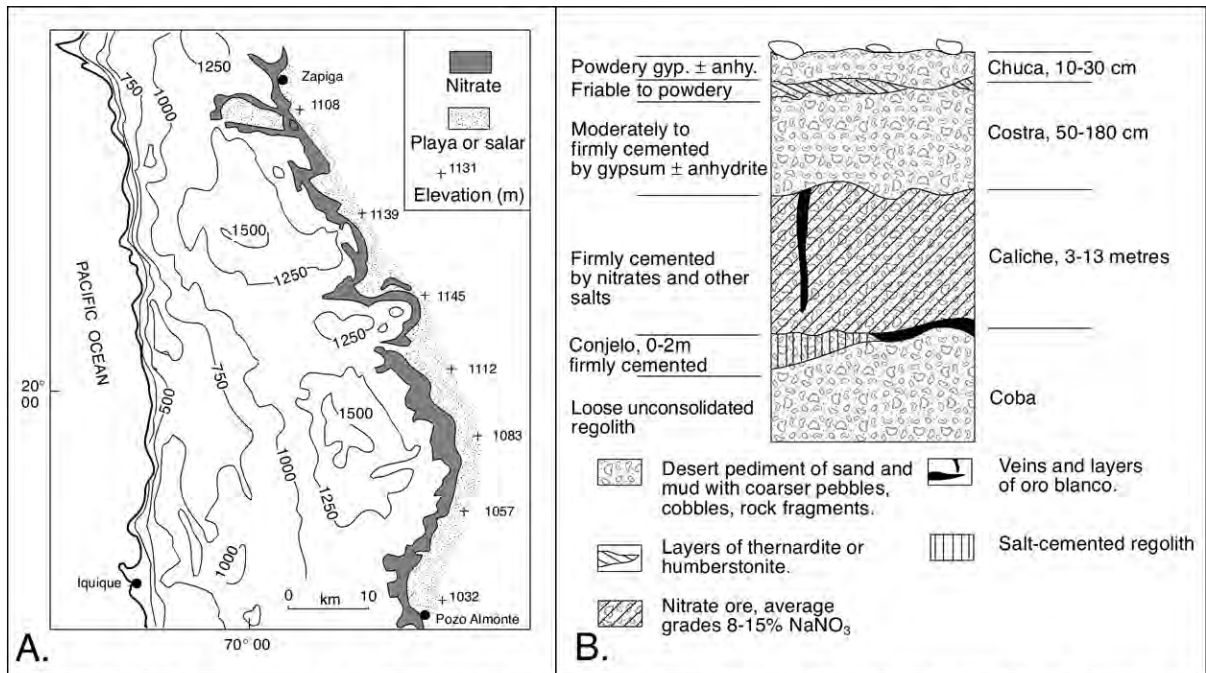


Figure 11.42. South American nitrates. A) Sketch of northernmost Chilean nitrate field, which is located along the eastern side of the Coastal Range, and marginal to salars and clay playas on the western side of Pampa del Tamarugal (see also Figure 3.37). B) Typical regolith profile through alluvial-type nitrate deposits in a Chilean nitrate field (after Ericksen, 1981, 1993).

types ranging from granite to limestone and shales. Nitrates can be found in all topographic positions from hilltops to hillsides to playa and valley floor. The richest accumulations tend to be on the lower slope of hills situated marginal to salars and playas (Ericksen, 1993).

Prior to the invention of synthetic sources by Germany in the First World War, the Chilean nitrates were the main source of salt petre in gunpowder, nitroglycerin and other explosives. At its peak in the first twenty years of last century there were more than 250 actively mined concessions in the Atacama Desert, with production of 4 million tonnes/year and a local population of more than 300,000 people. At the time the local name for the nitrate ore was “oro blanco” or white gold.

Chilean ores have an average composition of: 7-10% NaNO₃; 4-10% NaCl; 10-30% Na₂SO₄; and 2-7% Mg, Ca, K, Br, and I (Table 11.9; Ericksen, 1983; Searl and Rankin, 1993). Highest purity nitrate ore occurs as stratiform pedogenic seams about 20 cm thick, located some 3-7 m below the desert surface. The ore, a form of

hypersaline desert caliche, is part of a sequence of pedogenic layers; with coba at the base, through caliche and costra, to chuca as the overburden. The nitrate-entraining caliche zone is typically 1-3 m thick (Figure 11.42b). It can be alluvial caliche, where the saline minerals, including the nitrates, cement the regolith; or it can be bedrock caliche, where the economic salts form impregnations, irregular masses, veins and fracture-fills in porous or fractured bedrock.

The dominant nitrate in the Atacama is mostly nitratite (=soda nitre or Chilean salt petre). A number of other unusual highly soluble salts have also accumulated, along with the nitrates, and include iodates, perchlorates, chromates and dichromates, as well as the more familiar borates, sulphates and chlorides. It is the only known region in the world that contains natural perchlorate. The salts formed at the more saline end of a phreatic precipitation sequence made up of progressively more soluble

Mineral	Composition	Characteristics	Occurrence
Nitratite (soda nitre)	NaNO ₃	Rhombohedral cleavage	Main ore mineral in Atacama Desert
Nitre (salt petre)	KNO ₃	Acicular	Secondary salt
Darapskite	NaSO ₄ · NaNO ₃ · H ₂ O	Monoclinic	Minor salt
Humberstonite	K ₃ Na ₇ Mg ₂ (SO ₄) ₆ (NO ₃) ₂ · 6H ₂ O	Prismatic	Minor salt

Table 11.9. Typical nitrate minerals in the Atacama Desert, Chile.

evaporitic minerals: silicates (zeolites); calcite; Ca-, Na-, (K-) and Mg-sulphates; Na- and K-Mg-nitrate-sulphates; nitratine; and small amounts of iodates, Na- and K-Mg-iodate-sulphates, chromates, borates and perchlorates (Pueyo et al., 1998). Two specific precipitation trends were distinguished within this more general regional sequence; a Na-trend characterised by an association of glauberite-darapskite-(hectorfloresite), and a K-Mg-Na-trend related to bloedite-polyhalite-humberstonite-niter-(fuenzalidaite).

The only remaining active nitrate mine in the Atacama Desert is an open pit, the Maria Elena deposit, which exploits nitrate ore from stratiform seams just below the desert surface (Callao et al., 2002). Ores are hosted mostly by breccias or sandstones (volcaniclastics and tuffs) with the ore minerals occurring as mm-metre scale rinds about breccia or sandstone clasts. Nitrate contents in the ore seams vary between 7.5 to more than 20 wt % and NaCl between 8.6 to 40 wt %. Locally abundant are the sulphates thenardite, anhydrite, bloedite, polyhalite, hexahydrate and glauberite, which reflect part of 7.5 to 19.7 wt % content of Na_2SO_4 . Other salts present in minor contents include a variety of sulphates (kieserite, woodwardite, loeweite); nitrates (humberstonite, darapskite and nitre); borates (calciborite, strontiborite); chlorides (sylvite, nantokite) and iodates (bruggenite). The IO_3 contents vary between 0.026 to 0.074 wt %.

What is most amazing about the Atacama deposit is the age of the desert host and stability of its geomorphic features; nitrate soils are thought have been at the surface since the mid-Miocene, so allowing the gradual buildup of large volumes of pedogenic salines in the soils including the exploited nitrates (Table 11.9; Alonso et al., 1991). The Atacama Desert is one of the driest places on earth, its hyperaridity is the result of the rainshadow effect of the High Andes and the strong atmospheric temperature inversion along the coast (Figures 2.2a). Average annual rainfall in the Atacama Desert is less than a centimetre, and as much as twenty years can pass between rainstorms and similar conditions have prevailed since the middle Miocene.

Parental brines for the deposits are the hypersaline discharge portions of a regional phreatic system, which Pueyo et al. (1998) consider to be older than 6 Ma. At that time the main physiographic features were similar to today, but the climate was more humid. The precipitating parental fluids were derived from a variety of meteoric sources: westward flowing Andean groundwater, coastal fogs, occasional rainfall and Andean-derived surface floodwaters. Evaporation was involved in the nitrate paragenesis; it is the only mechanism effective

enough to saturate a brine with these very soluble supersaline minerals. Nevertheless, the nitrate ores do not show typical displacive nodular and enterolithic evaporitic textures, rather, the salts tend to passively infill veins, fractures or pre-existing matrix porosity and the various salts have largely accumulated through passive growth. Locally, some of the host silicate and carbonate lithologies have also undergone a small degree of active salt replacement.

The unusual mineralogy of the nitrate ore reflects the extreme chemical evolution of the precipitating brines through multiple episodes of salt precipitation and remobilisation during transport to the nitrate horizons. The ultimate source of the nitrate is tropospheric nitrogen first carried inland as nitrate in sea fogs (Rech et al., 2003; Ericksen, 1993). The upwelling coastal waters of Chile and associated coastal fogs contain high concentrations of nutrients and dissolved solutes. The average concentration of dissolved solutes in Chilean coastal fog are: 9.1 ppm SO_4 ; 0.8 ppm NO_3 ; 1.8 ppm Cl; 4.81 ppm Na; 0.4 ppm K; 1.0 ppm Ca; 0.6 ppm Mg. Sea spray moves these solutes as aerosols into a coastal fog; sulphate in sea spray comes mostly from outgassing of biogenic marine sulphur (e.g. Figure 2.19). As sea fog moves inland over the Atacama, it evaporates and so deposits dissolved solutes, which are then fractionated by pedogenic and downslope meteoric processes. To form an ore grade buildup in the soil requires multiple pedogenic fractionation episodes driven by dissolution, reprecipitation and recrystallisation within hyperarid desert soils. Millennia of these processes vertically separates the highly soluble nitrate salts from less soluble sulphate salts in the overlying profile (Figure 11.42b).

Magnesite and magnesia salts

Magnesium is the eighth most abundant element in the earth's crust and is widely distributed in numerous minerals. Magnesium is named after ancient *Magnesia*, a district in Thessaly, Greece. Among the more commercially important magnesium minerals are magnesite, brucite, dolomite, olivine, talc and serpentine (Table 11.10), as well as the magnesium sulphate and chloride salts recovered from natural brines and concentrated

Mineral	Formula	Deposit Exploited
Magnesite	MgCO_3	Sparry or cryptocrystalline
Dolomite	$\text{Ca}_{(1-x)}\text{Mg}_x(\text{CO}_3)_2$	Not utilised
Brucite	$\text{Mg}(\text{OH})_2$	Weathering byproduct
Brunnerite	$\text{Mg}_{(1-x)}\text{Fe}_x(\text{CO}_3)_2$	Sparry (magnesite associated)

Table 11.10. Sedimentary minerals and deposit types used as a source for magnesium oxide or magnesium metal.

seawater (e.g. epsomite, bischofite, carnallite). World resources of magnesite, dolomite and magnesium-bearing evaporite minerals are enormous. Magnesium-bearing extractable brines are estimated to constitute a potential resource measured in billions of tonnes, and magnesium can be economically recovered from seawater off arid coasts.

As well as being extracted by concentrating seawater, magnesium is also produced by processing of continental evaporitic and subsurface basinal brines in the USA, the Netherlands, Israel and Mexico. In the Netherlands the brine is formed by solution mining of magnesium/potassium-bearing horizons (carnallite, bischofite and kieserite) in the Permian Zechstein section (Figure 12.5b). Mg-rich continental brines of the Dead Sea are also processed for magnesium after bromine is extracted. When pumped into the saltworks, Dead Sea brine already contains 42,430 ppm of magnesium (30 times seawater levels), which when evaporated and processed produce caustic-calcined and ^{11,3} dead-burned magnesia, along with small amounts of magnesian chloride.

Electrolytic processes recover much of the world's currently produced magnesium. The majority of magnesium compounds are used for refractories in the die casting industry and due to a high strength to weight ratio usage in the automobile industry is expected to double in the next decade. Currently, the aluminium industry is the largest consumer of magnesium, where it is a constituent in aluminium-base alloys used for packaging, transportation, and other applications. The remainder is consumed in agricultural, chemical, construction, environmental, and industrial applications. Annual world magnesia production (from magnesite) is more than 3.1 Mt (3.4 million st), mostly from China, USA, North Korea, Russia and Turkey. Although no specific production figures are available, China and the United States probably account for more than one-half of the world's capacity for the production of magnesium compounds from seawater and brines.

^{11,3} *Dead-burned magnesite* (or refractory magnesia) refers to the granular product produced by firing magnesite, magnesium hydroxide, or other materials reducible to magnesia at temperatures in excess of 1,450°C

Calcined magnesia is the result of 800 to 1,000°C heat being applied, frequently in a rotary kiln, to magnesite or other materials reducible by heat to magnesia. It is heated to such a degree that less than 10% ignition loss remains and the product displays absorptive capacity or activity.

Fused magnesia is produced by heating high grade magnesite to a molten state for up to six hours in electric arc furnaces to temperatures approximately 3,000°C. The resultant product, at 96 to 98% MgO, has a favorable high density of 3.50 g/cc and relatively high chemical stability, strength, and resistance to abrasion.

Geological occurrences of magnesite are either microcrystalline (micritic) or macrocrystalline (sparry). There are three geologic modes of magnesite occurrence: 1) Small scale micritic deposits accumulating in Quaternary alkaline lake and mudflats (Table 11.11); 2) Laterally continuous, stratiform sediment-hosted deposits, which can be cryptocrystalline (micritic) or coarsely crystalline (sparry). Sparry deposits tend to occur more frequently in Precambrian strata; 3) Clustered hydrothermal deposits that form sparry magnesites at or near ultramafic complexes of all ages. Styles 2 and 3 form almost all of the currently exploited geological sources of magnesite. Discussion of style 3 lies outside the sedimentological focus of this book and the interest reader is referred to Pohl and Siegl (1986). Sparry style 2 occurrences constitute a large portion of current refractory magnesia ores. Style 1 deposits offer small-scale analogues for the sort of low temperature brine chemistry that has produced many sedimentary magnesite deposits. It suggests a requirement of waters enriched in magnesium, commonly hypersaline, and an association with microbes.

But, as with ancient evaporitic dolomite (Warren, 2000a) and ancient marine-fed evaporites (Chapter 5), there are fundamental problems when comparing brine chemistries of recent and ancient sedimentary magnesites. Today magnesite is a nonmarine evaporite precipitate (Table 11.1). Magnesite is easily manufactured in the lab using inorganic chemical techniques, but as for inorganically produced dolomite, it requires temperatures much too high to be realistic in a modern marine sedimentary system. Likewise there are intrinsic problems with comparisons of scale and diversity, leading many to express their studies of ancient magnesite in terms of "solving the magnesite problem." Modern sedimentary magnesite occurrences are nonmarine bedded, micritic, laterally limited and lacustrine; most ancient sedimentary magnesites are marine-associated, stratiform, microsparry to sparry, laterally and vertically extensive, and diagenetically altered.

Within Style 2, magnesite occurs in two commercially exploited forms, coarse crystalline (sparry) magnesite and cryptocrystalline magnesite (Pohl, 1990). Sparry magnesite deposits tend to be larger and purer (70-90% MgCO₃) than most cryptocrystalline magnesite deposits (purity <12% MgCO₃) and are the preferred ore deposit style. Much of the world's sediment-hosted coarsely crystalline magnesite is Precambrian and typically occurs as variations on a theme of fault-controlled, high temperature, hydrothermal alteration of dolomitic shelf sediment. Magnesites (sparry and micritic) are much more widespread in the Precambrian than the Phanerozoic leading to suggestions that magnesite was a primary evaporitic carbonate or even a normal marine mineral in Precambrian seas.

Location	Style	Reference
Coorong lagoon, southern Australia	Primary magnesite precipitates (with magnesian dolomite) in a number of hypersaline-schizohaline coastal lakes fed by continental brines. Nearby lakes contain hydromagnesite-aragonite associations.	Alderman and von der Borch, 1963; Warren, 1990
Clipperton Atoll, Pacific Ocean	Magnesite occurs at the bottom of the atoll lagoon. Some 2,850 years ago the lagoon became sufficiently isolated to be density stratified. At present the upper 14 to 15 m of the water column has a salinity of 14‰, while the underlying water mass up to a maximum depth of 34 m is marine (salinity of 33 to 34‰).	Bourrouilh-Le Jan et al, 1985
Lake Bonneville, Great Salt Lake depression, Utah	Magnesite was found in association with aragonite and dolomite in five cores taken through saline laminites near the shore of former Lake Bonneville. The dark layers contain about twice as much magnesium as the light layers. The light-colored laminations contain more clay minerals than carbonate.	Graf et al., 1961; Bissell and Chilingar, 1962
Lake Yao, Chad	Magnesite occurs in beaches of Lake Yao, a saline lake in northern Chad. Occurs in a sequential paragenesis going from the lake up to the beach: changes from calcite, aragonite, magnesium calcite, dolomite, huntite, magnesite, sodium carbonates (nahcolite, thermonatrite, trona), sodium sulphates (burkeite, thenardite), halite and sylvite. Accompanying brine has pH≈10.	Gac et al., 1977
Lake Walyungup, (coastal lake) Western Australia	Hydromagnesite in the littoral zone replacing aragonite, particularly within the mesoclot fabric of stromatolites, but also in sediments (strandline and dune sand, crusts) derived by erosion of stromatolites.	Coshell et al., 1998
Playa Pito and Playa Gualla, salt lakes southeast of Zaragoza, Spain	Diagenetic association with dolomite, calcite, gypsum, halite, thenardite, and bloedite, increases with depth (from 5 to 30%). Tends to form in mixing zone about playa edge where hypersaline lake brines mix with brackish groundwaters.	Pueyo-Mur and Inglés-Urpinell, 1987
Tuz Gölu, Turkey	Magnesite and huntite are early diagenetic minerals in saline mudflat formed by transformation of dolomite in the presence of pore fluids with a high Mg/Ca ratio.	Irion and Mueller, 1968; Camur and Mutlu, 1996
Sabkha El Melah, Tunisia	Minor phase in coastal sabkha, probably replacing aragonite.	Perthuisot et al., 1972
Sabkhat of Abu Dhabi	Magnesite is a minor phase (possibly after huntite) found only in the upper 10 - 20 cm of the Abu Dhabi supratidal.	Kinsman, 1967; Bush 1973
Salda Gölu, Turkey	Extensive areas of hydromagnesite shorelines and basin center turbidites formed by mechanical breakdown of hydromagnesite microbialites.	Braithwaite and Zedef, 1993, 1996
Saline lakes, British Columbia, Canada	Simple monomineralic biolaminated carbonate or sulphate layers as well as beds composed of complex mixtures of aragonite, magnesite, hydromagnesite, mirabilite, gypsum, epsomite, and/or bloedite.	Last, 1997

Table 11.11. Selected examples of Holocene occurrences of sedimentary magnesite.

Major Phanerozoic cryptocrystalline magnesite deposits occur in Australia, Greece, Turkey and India, most are considered potential, rather than actual, ore deposits. Worldwide, almost all Phanerozoic cryptocrystalline magnesite sediments are evaporitic lacustrine sediments, but like their Holocene counterparts, most deposits are too small or too impure to be commercially viable. The huge Tertiary lacustrine/pedogenic deposits in the vicinity of Rockhampton, Australia, are a possible exception, as are the Neogene huntite-magnesite-hydromagnesite lacustrine deposits in the Kozani Basin, Northern Greece and the Bela Stena region of southeastern Serbia (Stamatakis, 1995).

Extensive drilling in eastern Australia in the 1980s, centred on Rockhampton, outlined several large lacustrine magnesite deposits, namely; Marlborough, Kunwarara, Merimal and Yaamba.

Of these, the most viable, but as yet not yet fully realised, economic accumulation is the Kunwarara deposit. It contains some 550 million tonnes of potential magnesite ore, including 260 million tonnes in a soil-covered nearsurface "blanket" ore composed of 40-45% cryptocrystalline magnesite.

The Kunwarara deposit, situated some 60 km northwest of Rockhampton, has a proven area of 31 km². All this magnesite is stratiform, micritic, and constitutes a blanket deposit that varies in thickness from 1m to 26m, with an average thickness of 7.75 m. It lies below a humus-rich black clay ranging in thickness from 0.4 to 12m, with an average thickness of 7.75m (Figure 11.43; Burban, 1990; Hill, 1993). Experimental extraction at Kunwarara commenced in the mid 1990s; in 2001, Australian Magnesium Corporation Limited mined 2.7 Mt of crude magnesite ore at Kunwarara, which was beneficiated to produce

594,674 tonnes of magnesite. This produced 117,872 tonnes of dead-burned magnesia, 54,346 tonnes of calcined magnesia and 21,781 tonnes of electro-fused magnesia.

Most of the Kunwarara magnesite occurs as mm-metre diameter nodules and lumps in a matrix of soft magnesitic mudstone that is underlain by dolomitic mudstone, sandstone or gravel. The deposit is thought to have formed via secondary alteration of magnesian-rich lacustrine sediments. In the Marlborough area, magnesite occurrences are more lenticular and occur in palaeochannels in the regolith, as well as in nodules, veins and stockworks in the weathered zone of ultramafic basement rocks. The formation of all the Queensland magnesite deposits involved erosion of deeply weathered lateritic soils on magnesium-rich serpentinites with subsequent deposition as fluvial/lacustrine sediments, which were then subject to further evaporatively-driven pedogenic enrichment.

A partial modern analogue for Kunwarara is the magnesite-rich sequences of Salda Golu in southern Turkey (Figures 1.6, 4.29; Schmid, 1987). Based on this comparison, the following conditions are thought to have formed the Kunwarara deposits:

- Deep weathering of primary stockwork-bearing serpentine rocks and subsequent erosion by heavy rains.
- Water and groundwater transport of eroded and dissolved magnesian materials into a lake depression.
- Deposition and crystallisation of magnesite muds in an ephemeral mudflat (capillary evaporation). Agglomeration of material into cryptocrystalline nodules.
- Periodic waves and sheet flooding carries away non-crystallised impurities such as SiO_2 , Al_2O_3 and CaO .

- Flushed impurities deposited in adjacent shallow lakes, which, with a lowering of lake levels, then acted as matrix for later magnesite nodules.
- Magnesite layers were compacted and covered by soil. Pedogenesis also formed a silica-rich skin on the nodules, while pedogenic magnesite continued to crystallise in the nodule horizon.

In contrast to the pedogenic precipitation of pedogenic magnesite in Tertiary lake depressions, much of the cryptocrystalline magnesite in Precambrian sediment is thought to be a primary precipitate from marine-fed brines. The “Magnesite Problem” is most obvious when comparing the disparity between the abundance of primary or syndepositional cryptocrystalline magnesite in Precambrian restricted marine settings and the paucity of cryptocrystalline magnesite in similar modern marine-fed evaporitic settings. Magnesite in the coastal lakes of the Coorong forms from evaporation of continental not marine waters (Figure 4.4). The disparity probably reflects differences in the ionic proportions in Precambrian and modern oceans, especially the relative lack of sulphate and calcium, as well as extreme carbonate saturation in Precambrian oceans (Chapter 2).

Two well-documented examples of widespread Precambrian magnesite are the Palaeoproterozoic Tulomozerskaya Formation of the Fennoscandinavian Shield (Melezhik et al., 2001) and Neoproterozoic Skillogalee Formation of the Flinders Ranges in southern Australia (Frank and Fielding, 2003). The latter is currently exploited in a small way (10,000 t/year), but its primary sedimentary structures are very well preserved and in the vicinity of Leigh Creek its inherently high purity

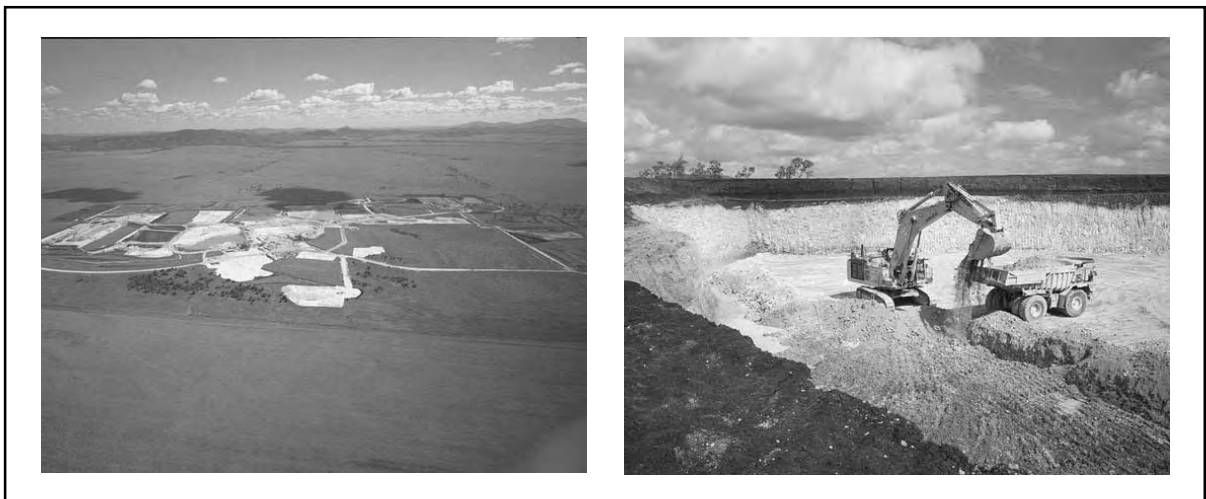


Figure 11.43. Kunwarara mine operations near Rockhampton, Queensland.

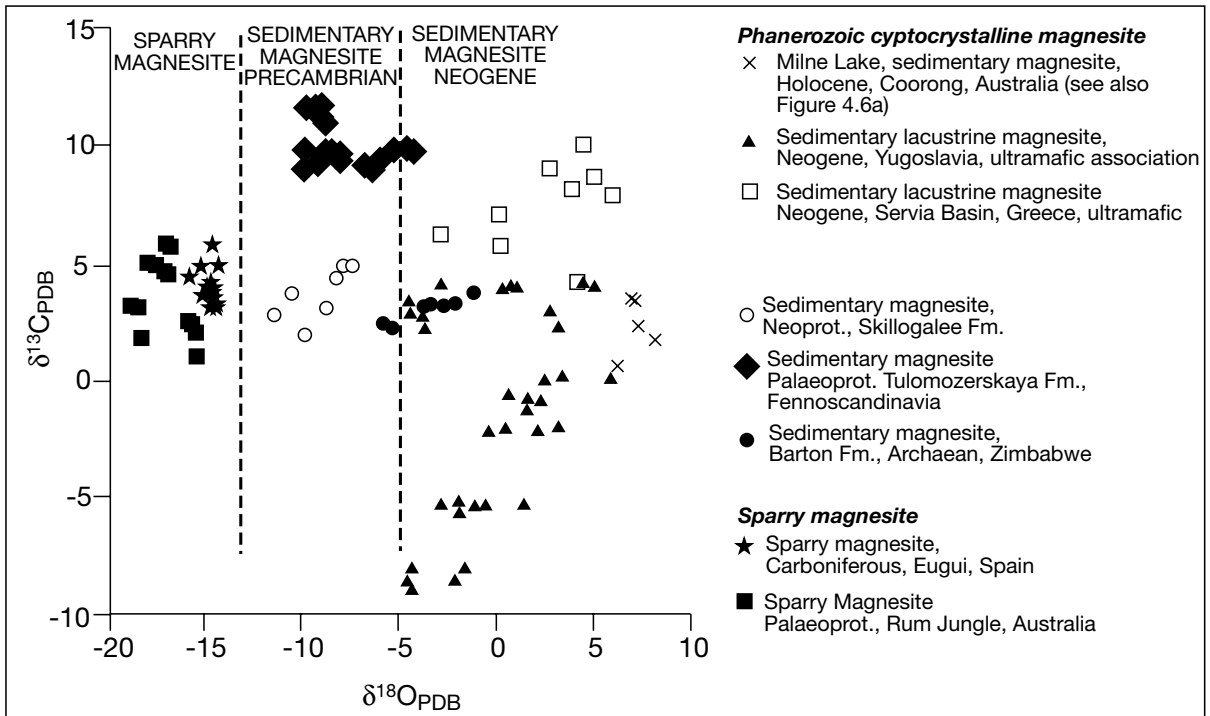


Figure 11.44. Stable isotope signatures of sparry, lacustrine and cryptocrystalline Precambrian magnesites (in part after Melezhik et al., 2001).

gives it the potential for much higher levels of exploitation (Keeling and Mauger, 1998). Metamorphism and coarser recrystallisation has destroyed more of the fine primary detail in the Fennoscandinavian strata. Both areas still retain abundant textures from their primary marine-fed evaporite association (stromatolites, mudcracks, tepees, evaporite pseudomorphs, intraclastic horizons, dissolution breccias). Some more highly metamorphosed Precambrian sparry ore deposits can be huge; a single Proterozoic sparry magnesite deposit in Liaoning Province of China extends for some 60 km and reportedly contains some 130 Gt of ore.

Warren (1999, Chapter 8; 2000b) notes that extensive stratiform Proterozoic sparry brunnerites and siderites in northern Australia sit atop halokinetic autochthonous and allochthonous dissolution breccias. The spars formed as subsurface replacements of precursor platform carbonates in suprasalt overburden. Extensional tectonics focused the escape of subsalt ferroan basinal brines via withdrawal breaches in the salt and then up along active suprasalt growth faults. The same faults also supplied dense metalliferous brines to brine lakes on the seafloor to create the laminites of base metal (sedex) deposits (Figure 9.46). Some of the sparry textures in these replaced platform carbonate were misidentified in earlier work as sparry replacements of

lenticular gypsum (Muir, 1979). They are not. The magnesite, brunnerite and siderite crystal clusters grew poikilotopically in buried but relatively permeable horizons within open marine platform carbonates and in thin section many lenticular crystals still retain poikilotopically enclosed marine allochems. The lenticular crystal shapes, especially of siderite and brunnerite are that of nascent precipitates fed by ascending Precambrian brines. Brunnerite formed when Fe-rich brines permeated dolomite beds, while siderite was the favoured precipitate in pores of a limestone precursor.

A somewhat analogous halokinetic Phanerozoic system is seen in the Upper Burano (Triassic) evaporites of the Apennines. It is a highly deformed halokinetic evaporite-sparry magnesite hydrothermal replacement system, with fluid crossflow focused along extensional fault conduits that feed replacement haloes in platform dolomites (Figure 7.26; Lugli et al., 2002).

A comparison of stable isotope signatures from various types of magnesite deposits shows a clear separation in oxygen isotope signatures between Neogene lacustrine magnesites, Precambrian cryptocrystalline magnesites, and Precambrian sparry magnesites, with each group showing successively more negative values (Figure 11.44). This difference, at least

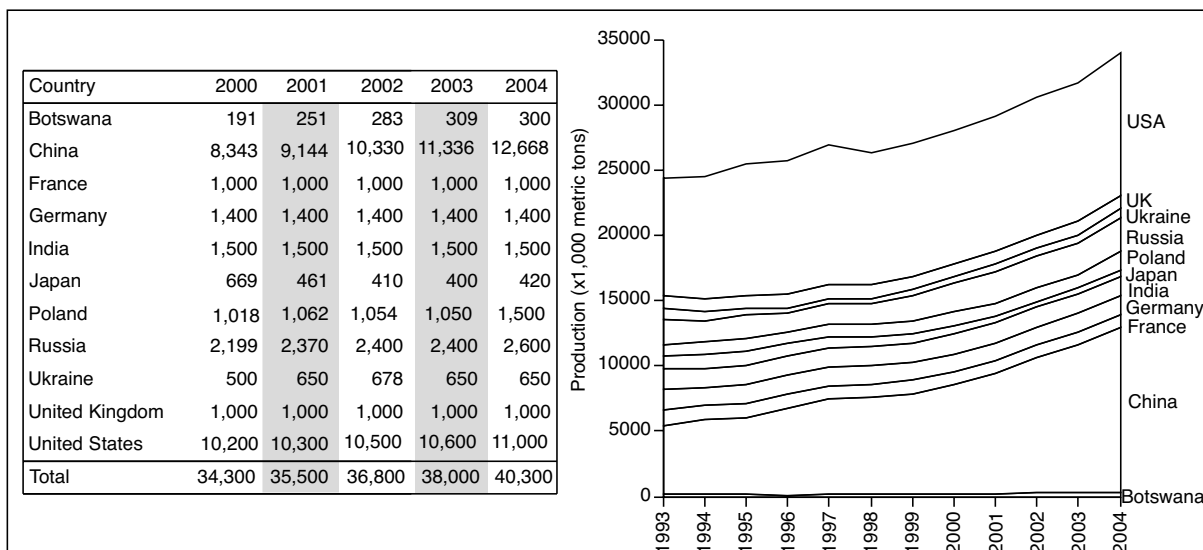


Figure 11.45. World soda ash production (in thousand metric tons) (compiled from USGS on-line data tables, compiled from <http://minerals.usgs.gov/minerals/pubs/commodity/> last accessed 30 September, 2005).

in part, reflects the higher hydrothermal temperatures that characterise the sparry magnesite association. Within the cyptocrystalline magnesites it also reflects the likelihood that Precambrian carbonates have in general experienced higher burial temperatures for longer periods than Neogene lacustrine precipitates (Melezhik et al., 2001). Carbon isotope signatures are much more variable and relate in part to the variable supply of carbon from pre-existing carbonate minerals, levels of organic contribution and amounts of meteoric input.

Sodium carbonate salts (trona)

The word trona is a derivative of the Arabic word *natrun*, from which we also derive the English word natron. Mineralogically natron (not *natrun* as originally used by the ancient Egyptians and then the Arab alchemists) describes the decahydrate form of sodium carbonate and is one of a number of sodium carbonate minerals (Table 11.12). Sodium carbonate (aka *soda ash*) end usage is mostly in glass manufacture followed by chemicals, soap and detergents, pulp and paper manufacture, water treatment, and flue gas desulphurisation. Sodium carbonate's prime use in ancient Egypt, in the form of *natrun* quarried from salt lakes (a trona-halite mix), was an integral part of the mummification^{11.4} process.

In many countries local supply of sodium carbonate (aka soda ash) is synthetic, created using the Solvay process, which utilises halite and limestone as raw materials with an ammonia catalyst within the carbonating towers. Annually, roughly twice as much

^{11.4} Ancient Egyptians are famous for their perfection of the art of mummification. A key ingredient in the process was *natrun*, which is composed of halite+trona. The ancients knew its preservative properties rivalled those of halite and it also absorbs water readily, making it an excellent desiccant/preservative. *Natrun* is found in large quantities in the beds of several Egyptian playa lakes (Wadi Natrun and El Kab, as well as Behiera in the nearby Libyan desert) and it has been mined and traded from these localities for thousands of years. Writings as old as the reign of Ramese III (1198-1166 B.C.) refer to these deposits. The preservative qualities must have been immediately apparent to the ancient Egyptians from its effects on any wild life, which had died in these lakes. There is some evidence that the Egyptians artificially precipitated *natrun* by isolating shallow basins of lake waters for faster evaporation, as is still done in parts of the depression today. For purification and preservation, *natrun* was preferred over halite because it chemically attacks and destroys grease and fat and so is a superior drying agent (as is sodium borate). It is found not only in tombs and in pits, along with other discarded embalming materials, but also forms nodules and residues in the mummies themselves.

There is some debate over the method in which the *natrun* was used for mummification by the ancient Egyptians. Some argue it was used in a way similar to the contemporary method for "salting" fish. Dry *natrun* would be sprinkled over the body, perhaps with sawdust, or spread with linen cloths. Others with a more prosaic bent, believe the body was immersed in vats containing a *natrun* solution. Such a wet method would have been odiferous and accelerated putrefaction, thus counterproductive to the preservation of the body, although it makes for good Hollywood images. A dry body is also more readily bandaged as well as being more amenable to the attachment of amulets and other jewellery. Although mummification has supernatural trappings in popular culture, its basis is rooted in simple chemistry and processes as mundane as salting fish.

Mineral	Formula	Na ₂ CO ₃ (equiv.%)
Trona	NaHCO ₃ ·Na ₂ CO ₃ ·2H ₂ O	70.4
Thermonatrite	Na ₂ CO ₃ ·H ₂ O	85.5
Nahcolite	NaHCO ₃	63.1
Bradleyite	Na ₂ PO ₄ ·MgCO ₃	47.1
Pirssonite	CaCO ₃ ·Na ₂ CO ₃ ·2H ₂ O	43.8
Northupite	Na ₂ CO ₃ ·NaCl·MgCO ₃	40.6
Tychite	2MgCO ₃ ·2Na ₂ CO ₃ ·Na ₂ SO ₄	42.6
Natron	Na ₂ CO ₃ ·10H ₂ O	37.1
Dawsonite	NaAl(CO ₃)(OH) ₂	35.8
Gaylussite	CaCO ₃ ·Na ₂ CO ₃ ·5H ₂ O	35.8
Shortite	Na ₂ CO ₃ ·2CaCO ₃	34.6
Burkeite	Na ₂ CO ₃ ·2Na ₂ SO ₄	27.2
Hanksite	2Na ₂ CO ₃ ·9Na ₂ SO ₄ ·KCl	13.6

Table 11.12. Minerals containing sodium carbonate.

soda ash is produced worldwide by the Solvay process than by trona extraction. Major producers using the Solvay method include; China, Germany, India and Russia (Figure 11.45). Until the 1960s, soda ash in the USA was almost totally derived from Solvay plants situated near industrial markets in the country's northeast. Today the position in the USA is reversed: trona is mined from the Eocene Green River Basin, Wyoming, or processed from lacustrine brines in Searles Lake and Owens Lake, California. Large-scale subsurface operations in Wyoming mine trona using various combinations of room-and-pillar, longwall and shortwall extraction methods.

Solution mining and multicomponent recovery methods process brines extracted from trona beds in Searles Lake (Figure 11.35). Dilute sodium hydroxide (NaOH - commonly called caustic soda) is injected into the lake beds to dissolve trona. The recovered solution is treated with carbon dioxide gas in carbonation towers to convert the sodium carbonate (Na₂CO₃) in solution to sodium bicarbonate (NaHCO₃), which precipitates as nahcolite and is filtered out (Figures 2.13, 12.9). The crystals are again dissolved in water, precipitated with carbon dioxide, and filtered. The product is then calcined to produce dense soda ash. Sodium bicarbonate, sodium sulphate, potassium chloride, potassium sulphate, borax, and other minor minerals are produced as coproducts from sodium carbonate production from brines in Searles Lake, California. Likewise, sodium bicarbonate, sodium sulphite, sodium tripolyphosphate, and chemical caustic soda are manufactured as coproducts during processing of mined trona at several of the Wyoming soda ash plants. A number of naturally occurring evaporite minerals

contain Na₂CO₃, but only trona is economically extracted or solution mined at this time (Table 11.13).

There is a common misconception among some geologists that the presence of thick-bedded trona indicates a carbonatite-rift source area. Certainly there are some geologically scenic trona deposits in the African rift that are surrounded by volcanoes spewing natrocarbonatites, but these are volumetrically minor deposits, even in terms of the volume of rift sediment fill and especially compared to the volumes of ancient trona precipitating in evaporitic seaways of the Archaean (Figures 2.31, 2.32). Even today, all that is needed to form sodium carbonate brine is a suitably alkaline inflow water, depleted in sulphate and chloride. Most continental ground waters in metamorphic, volcanic, or igneous terrains will produce alkaline solutions upon evaporation (Hardie and Eugster, 1970). The relative absence of chloride and sulphate in these types of rocks permits solutions to become relatively enriched in Na and CO₂ and so follow the appropriate "closed basin" concentration pathway leading to trona/nahcolite (Figure 2.12). Mechanisms driving the appropriate chemical evolution leading to trona are varying combinations of mineral precipitation, selective dissolution of efflorescent crusts, degassing of brines, and/or redox reactions (Jones et al., 1977).

Ground water percolating through siliceous soils, such as those developed on granite or windblown sand, can become highly alkaline and enriched in sodium carbonate (Garrels and Mackenzie, 1981). Very high carbon dioxide concentrations (up to 10% of soil gas) can be the result of intense biological activity in the depositional brine. The Pretoria pan and the Sua Pan in Botswana are examples showing elevated sodium carbonate in soil waters. The construction of solar evaporators using this water can produce substantial volumes of trona each dry season. In soda lakes such as Lake Magadi and Lake Natron, the deposition of monomineralic beds of trona may be aided by the continual generation of biogenic CO₂ from the halobiota flourishing in alkaline lake waters (Chapter 9; The Flamingo connection).

In regions characterised by an abundance of limestone or dolomite, or even a drainage basin leaching older marine evaporites, the inflow waters to the saline depression contain too much chloride, sulphate, and calcium to produce a trona brine. Even in some areas draining igneous and volcanic terrains, the inflow waters mix with other basinal waters or with other rock and soil types and so trona cannot precipitate.

Trona in North America

The lacustrine Green River Formation (Eocene) in the Green River Basin in Sweetwater County, southwest Wyoming contains the world's largest known resource of natural sodium carbonate in the form of bedded trona (Figure 11.46). The scale of current extraction, and the possibility for future expansion for the various Wyoming operations is huge. For example, General Chemical's Green River Basin plant has identified trona ore reserves of more than 500 million tonnes and currently maintains more than 200 km of underground workings. Total identified trona resource in the basin is more than 47 billion tonnes, dwarfing any other known natural trona resource. For comparison, the combined identified total resource for Searles and Owens lakes is slightly in excess of 815 million tonnes. America today produces over 10 million tonnes of trona per year and is a net exporter of product. Lesser production is periodically extracted from Quaternary Lake Magadi in the East

African rift ($\approx 250,000$ metric tonnes/year) and from alkaline lakes in Mexico.

The Eocene Green River Formation is divided in ascending order into the Tipton Shale, Wilkins Peak Member, and the Laney Shale. The trona resource lies wholly within the lacustrine Wilkins Peak Member. The Wilkins Peak ranges from about 183 to 410 m (600 to 1,350 feet) in thickness and consists of marlstone, oil shale, trona, siltstone, mudstone, and numerous laterally persistent thin layers of tuff. These sodium carbonate-rich sediments were deposited in two large lakes that occupied several lacustrine sedimentary-structural basins in Colorado, Wyoming, and Utah (Figure 11.46; Dyni 1996). These basins include the Green River, Washakie, and Sand Wash Basins in southwest Wyoming and northwest Colorado, the Piceance Creek Basin in northwest Colorado, and the Uinta Basin in northeast Utah. Eocene Lake Gosiute is the northern

	Location	Comments	Reference
QUATERNARY	Lakes Magadi, Kenya Lake Natron, Tanzania (Magadi is dredged)	Bedded and stacked trona crusts, beds up to 40 m thick precipitated in the saline pan of Lake Magadi and a bed some metres thick precipitated in the pan of Lake Natron.	See this chapter and Chapter 4 for detail
	Interdunal pans, NE Lake Chad, (collected)	Evaporation of groundwaters to form trona-halite-gaylussite crystals crusts and efflorescences in the capillary zone of interdunal depressions.	Eugster and Maglione, 1979
	Sua Pan, Makgadikgadi Basin, Botswana (panned and harvested)	Deepest part of a three pan complex separated by dune covered ridges. Pan surface comprises brine-saturated sand and clay layers with surface efflorescence of trona and halite. Seasonally flooded by Nata River.	Massey, 1973
	Otiwalunda salt pans, Namibia	Trona, thenardite, halite and burkeite efflorescences characterise seasonal crusts in the lower parts of the pans.	Schneider and Genis, 1991
	Pretoria salt pan, South Africa (exploited from 1915-1922)	Meteorite impact crater (200 ka) with trona efflorescences forming on pan when it dries after a flood.	Wagner, 1922
	Wadi Natron, Egypt 100 km west of Cairo (panned and harvested)	Low depression 23 m below sea level, with trona halite crusts accumulating as lake waters desiccate.	Atia et al., 1970
	Lake Texcoco, 20 km NE of Mexico City	Artificial salt lake created after storm channels were diverted to a formerly brackish lake in the early 1900s. Percolation of the resulting dense brine has precipitated trona in underlying sediments.	Alcocer and Williams, 1996
NEOGENE	Nors (salt lakes), Inner Mongolia; e.g. Chagan	Chagan Nor contains three 1-2 m thick trona beds deposited in the last 20,000 years in layers that alternate with fresher water mudstones.	Zheng et al., 1992; Xu, 1992
	Eocene Green River Fm. Wyoming (conventional and solution mining)	Area of more than 3,100 km ² . Contains 42 trona beds, 25 of which have a thickness of 0.91 m or more (which is considered the lower limit of economic significance) and each covering an area of about 175 km ² . Eleven of these beds exceed 1.83 m in thickness.	See this chapter and Chapter 4 for detail
	Wucheng deposit, Eocene, Henan Province China (conventional and solution mining)	Ore body contains about 77% trona and 23% nahcolite, and lies 650 to 970 m deep in beds 0.3-3.0 m thick. 36 ore beds each associated with oil shale (similar to Eocene Green River).	Zhang, 1985
	Beypazari trona deposit, Miocene of NE Turkey, 30 km west of Ankara	Areal extent of the trona deposit is estimated to be 8 km ² . Deposited as two lensoidal trona bodies within a 70- to 100-metre-thick zone in the lower part of a lacustrine shale. Total of 33 trona beds: 16 in the lower trona lens and 17 in the upper. Total thickness of the lower sequence is 40-60 m; upper trona ≈ 40 metres. The interval between the lower and the upper trona sequence is 30-35 metres.	Helvacı, 1998

Table 11.13. Selected trona occurrences, their properties and method of exploitation.

lake that once occupied the Green River, Washakie, and Sand Wash Basins. The southern lake, Eocene Lake Uinta, occupied the Uinta and Piceance Creek Basins in Utah and Colorado. The Uinta Mountain Uplift, an east-west positive structural element, separated the two lakes, although they may have been connected during part of their existence on the east side of the uplift. At its maximum extent, Lake Uinta covered about 57,000 km² (22,000 square miles), and Lake Gosiute, about 38,850 km² (15,000 square miles).

During much of Green River time, the lakes were closed with no outlets (Figure 5.10). The Green River Formation consists of a variety of lacustrine sedimentary rocks, including sandstone, claystone, shale, dolomitic marlstone, oil shale, and numerous, generally thin beds of volcanic tuff deposited in the two lakes (Dyini 1996). Typically, the Green River sediments grade from fine-grained sandstone, mudstone, claystone, and shale in shoreward areas of the lakes into carbonate-bearing sediments enriched in organic matter toward basin centre (Dyini, *op. cit.*).

The lateral transition from siliciclastic to carbonate-enriched rocks is also reflected in vertical sequences of the Green River Formation in the Green River, Piceance Creek, and Uinta Basins. This indicates increasing salinity of the alkaline lake waters as divalent cations of calcium and magnesium were precipitated as calcite, Mg-calcite, and dolomite in lake fringe mudflats, while dissolved sodium, bicarbonate, and chloride continued to accumulate in waters in saline pans in the lower parts of the basin. A lack of sulphate in the trona pans perhaps reflects bacteriogenic sulphate reduction in the lake brines, as is occurring in modern lakes in the African rift valley. Associated hydrolysis of detrital silicate minerals and glassy volcanic ash (zeolites) also contributes additional dissolved bicarbonate, sodium, and other ions to the lake brines. Tuffaceous debris amounts to roughly 5% of the total sediments in the Green River Formation.

During drier periods the Eocene lakes shrank and large volumes of saline sodium bicarbonate minerals were deposited,

either as bottom nucleates in shallow brine sheets or as displacive intrasediment nodules in mudflats. The more abundant sodium salts include trona, nahcolite, shortite, dawsonite, halite, and less commonly eitelite and wegscheiderite. The most important lake desiccation event occurred during Wilkins Peak and Parachute Creek time when vast deposits of trona and nahcolite were precipitated in the Green River and Piceance Creek Basins, respectively (Figure 11.47). During two later desiccation events, nahcolite was deposited as nodules and possibly some thin beds in the Birds-nest zone in the eastern Uinta Basin, Utah. Finally, during a later desiccation event, bedded sodium salts were deposited in the Uinta Basin near Duchesne, Utah (Dyini, 1996). Interbedded dolomitic oil shales separate these desiccation events and represent biochemical deposition from relatively dilute lake waters during expanded lake phases. Trona beds were deposited in the lowest sectors of the various basins during times when surface waters were extremely shallow to ephemeral with brine chemistries akin to those in

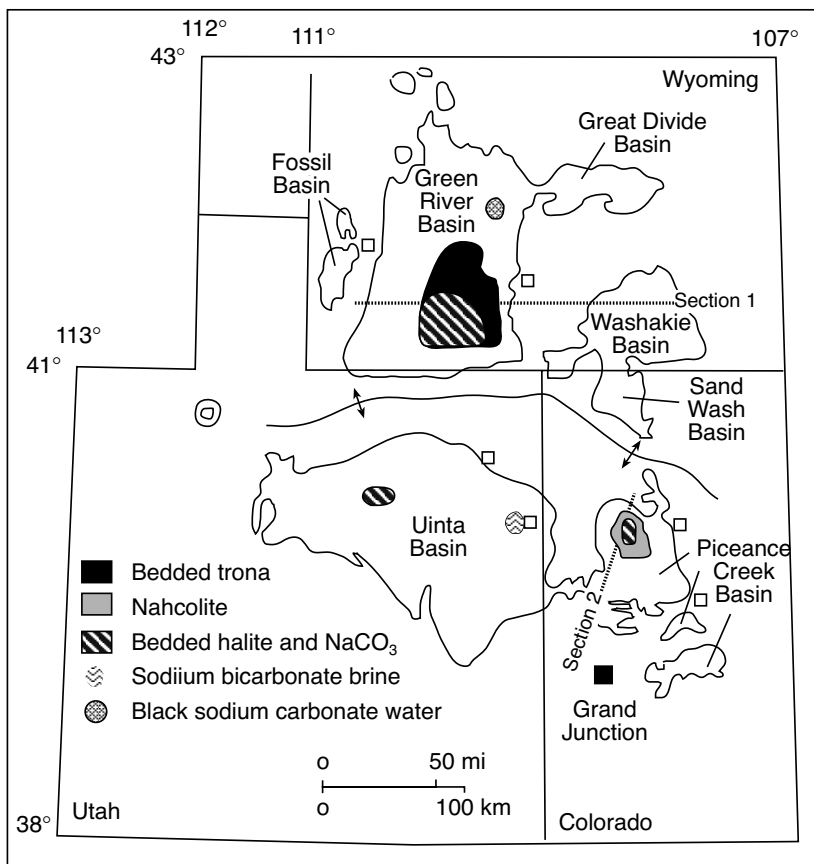


Figure 11.46. Areal distribution of the Green River Formation and the locations of sodium carbonate deposits in Utah, Colorado, and Wyoming (after Dyini, 1996).

modern Lake Magadi (Surdam and Wolfbauer, 1975; Fischer and Roberts, 1991). Centripetal groundwater inflows subsequently dissolved some of the sodium salts, as evidenced by the presence of solution breccias and solution cavities in cores collected in marginward parts of the Green River Formation. At least two areas today contain sodium carbonate brine pools of unknown size, but that are possibly exploitable brine resources (Figure 11.46).

Currently mined trona ore in the Green River Basin is restricted to the Eocene Wilkins Peak Member of Wyoming. Culbertson (1966) defined 42 beds of trona, up to 14 metres thick in the member, at depths ranging from 120m to over 1,000m. He numbered the thickest and economically most important of these beds from 1 to 25 in ascending order (Figure 11.48). These trona beds are remarkable for their purity and continuity compared to other large lacustrine trona deposits elsewhere in the world. Sulphate minerals are essentially absent, and other than halite, the chief impurities are thin dolomitic marlstone stringers and vertical seams of mudstone created by extension and injection of water saturated mud. Faults cutting the trona are rare and bed dips are typically less than a degree, making them eminently suitable for mining. Toward the depocentre in the southern part of the basin some of the trona beds grade laterally into mixed halite and trona (south of dashed line in Figure 11.48). Nahcolite is abundant in some beds in the lower part of the evaporite stratigraphy making them less suitable mining targets. Dyni (1996) also notes that nahcolite, wegscheiderite, northupite, and possibly shortite become locally abundant, as well as quartz, toward the depositional centre of the mixed halite and trona interval of bed 17 (one of the most important ore targets) when it is traced into the southern part of the basin.

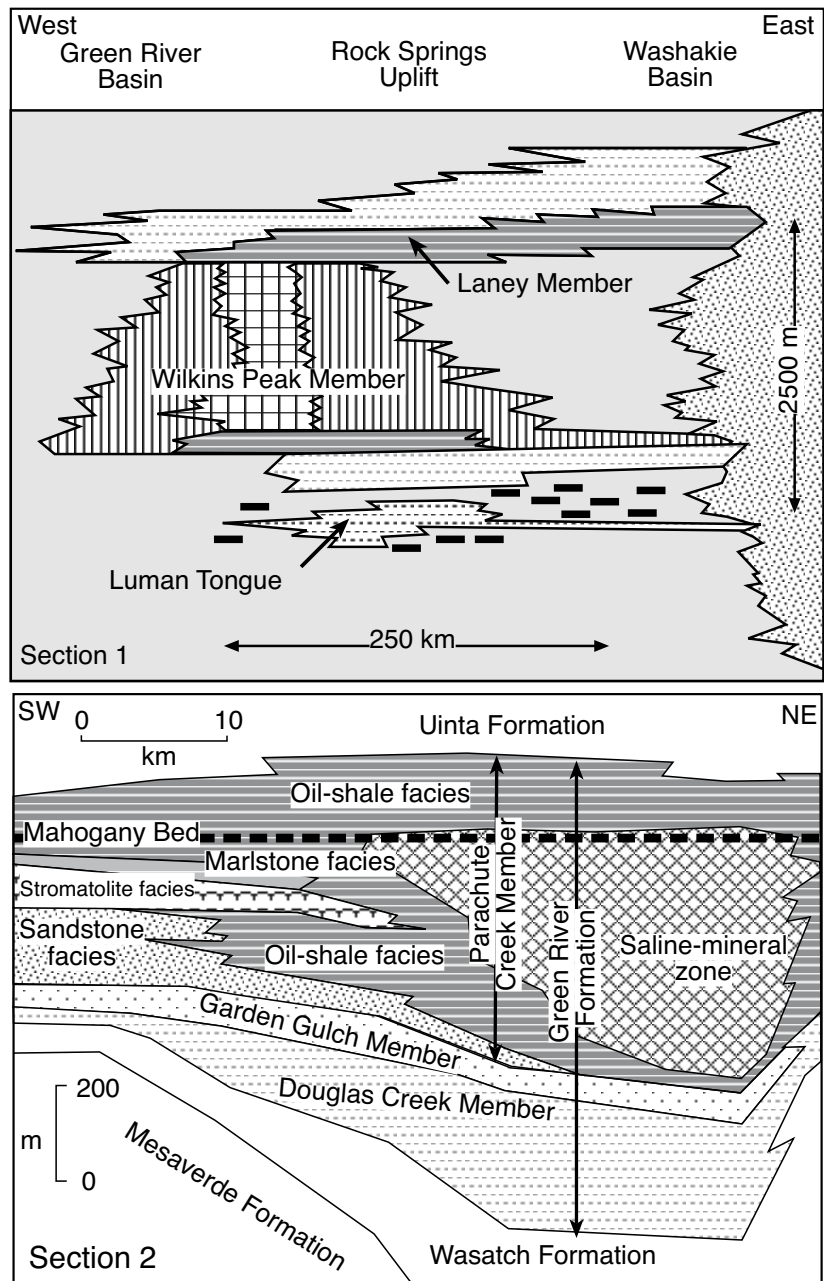


Figure 11.47. Stratigraphy of the Eocene Green River Formation showing interrelationships between various members and facies in the Green River Basin (section 1) and the Piceance River Basin (section 2). Locality of sections indicated on Figure 11.46.

The Wyoming trona district currently produces about 8.2 million mt (9 million tons) of refined soda ash annually from five underground mines that extract a total of about 16.3 million mt (18 million tons) of trona ore (Dyni, 1996). Trona bed 17 where it is more than 1.2 m (4 feet) thick, underlies about 2,000 km² (775 square miles) of the basin and ranges from 1.2 to

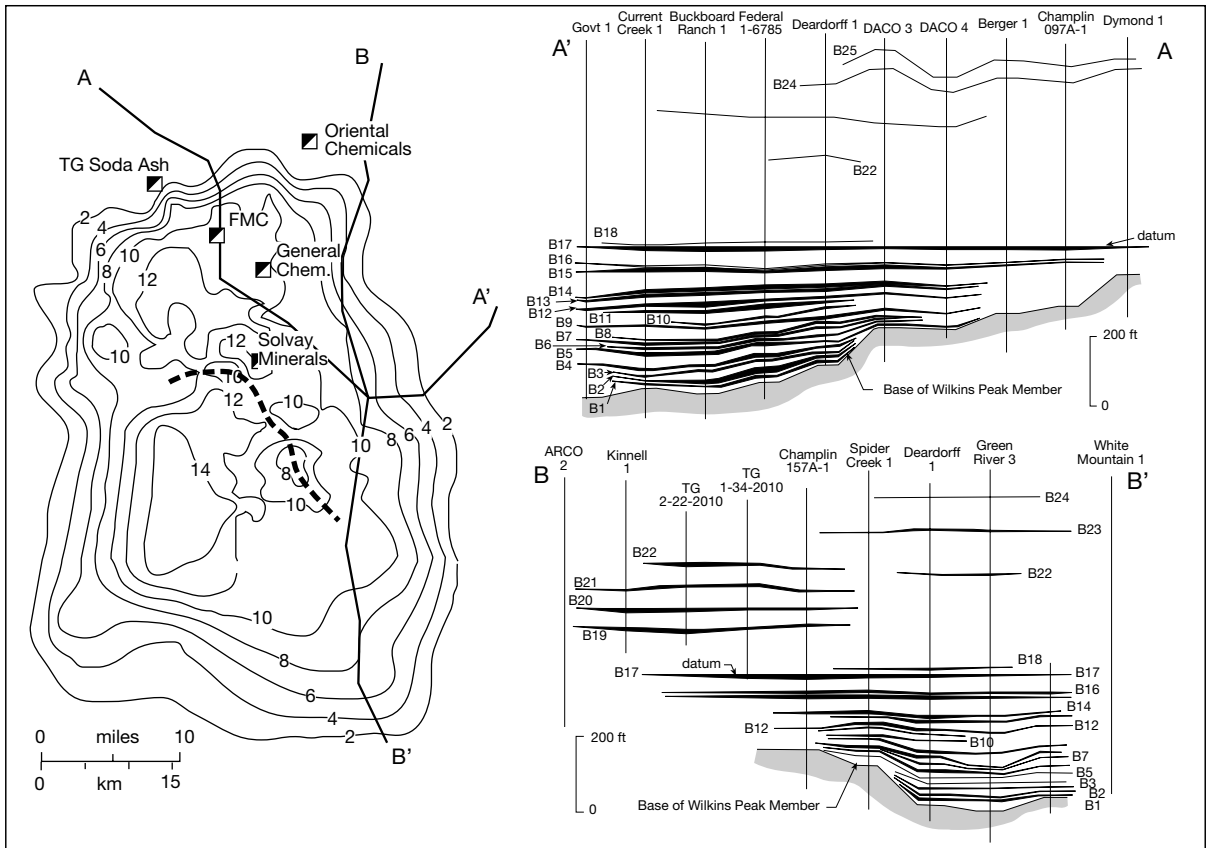


Figure 11.48. Trona distribution in the Wilkins Peak Member of the Eocene Green River Formation in Wyoming. Isopach is of Bed 17 and is in feet. Heavy dashed line indicates approximate northern extent of halitic facies. Cross sections use Bed 17 as a datum; halitic facies are not shown and the wells are equally spaced in the cross sections (after Dnyi, 1996 and Wiig, Dnyi and Grundy, 1995).

5.2 m (4 to 17 feet) in thickness (Figure 11.48; Dnyi, 1996). Twenty-two of the 25 numbered beds listed by Dnyi (1996) are estimated to contain 115 billion mt (127 billion tons) of trona ore, or 69 billion mt (76 billion tons) of trona in beds containing less than 2% halite. These 22 beds, where they are 1.2 or more metres (4 or more feet) thick, underlie areas ranging from 130 to more than 2,000 km² (50 to more than 775 square miles) at depths of 200 to 915 m (650 to 3,000 feet) below the surface. The trona contains 70.3 wt.% sodium carbonate and it takes about 2 tons of trona ore to produce 1 ton of soda ash. Currently, FMC, General Chemical, and Solvay Minerals mine trona bed 17, TG Soda Ash mines bed 20, and Oriental Chemicals mines beds 24 and 25.

Mining is by vertical shaft using room-and-pillar, short- and long-wall techniques (Dnyi, 1996). At three mines, additional sodium carbonate is recovered from wastewaters from the processing plant, which are used to slurry tailings to abandoned parts of the mines. These waters dissolve additional trona

from the pillars and are then pumped back to the surface to recover the sodium carbonate. The post-mining brine recovery technique has proven to be economical and will probably soon be employed by other mines in the district. Earlier attempts to solution mine trona from vertically drilled holes have been unsuccessful due to nahcolite ‘blinding’ (Figure 12.9).

In the last decade small scale solution mining began in the Parachute Creek member in the Piceance Creek Basin using horizontally drilled holes with nahcolite, not trona, as the planned feed source. If the blinding problem is solved a similar horizontal drilling method may be especially useful in the southern part of the basin where the trona beds are thicker and lie at greater depths. In mid 2004 operations at this facility were scaled back and today it is no longer actively extracting or processing brine (see Chapter 12).

The Parachute Creek Member in the deeper northern part of the Piceance Creek Basin contains a saline facies, which includes

beds of nahcolite and halite, along with scattered crystals, nodules, and coarse-crystalline aggregates of nahcolite commingled with high-grade oil shale (Dyner 1981, 1996). Also included in the saline facies is dawsonite as microscopic crystals in the microcrystalline matrix of the oil shale. The top of the nahcolite-bearing oil shale is a dissolution surface above which meteoric waters have dissolved nahcolite and halite forming a "leached zone" of vuggy brecciated oil shale (collapse breccia), which is up to several hundred feet thick. The leached zone extends upward into the lower part of the Mahogany oil-shale zone, a unit of high-grade oil shale traceable throughout the basin (Figure 11.47). The top of the leached zone is defined by the stratigraphically highest occurrence of the solution breccia (Dyner, 1981). This top can be considered to be the top of the original bedded saline facies in the Parachute Creek Member, although crystal cavities and vugs are found scattered through the upper part of the Parachute Creek Member well above the Mahogany oil shale in a zone 168 to 335 m (550 to 1,100 feet) thick.

The potential nahcolite resource in the Piceance Creek basin is estimated at between 29 and 32 billion short tons (26 to 29 billion mt; Dyner, 1996). It is unlikely that this resource will be exploited as oil shale cannot be removed or damaged under current sodium leasing regulations. The major part of the potential nahcolite resource, which occurs as crystalline aggregates scattered through oil shale, will be difficult to economically mine for soda ash alone. Any solution mining of nahcolite beds in this part of the basin may render portions of the overlying oil shale unsuitable for future in situ or underground mining.

Trona in the African rift

Outside of the USA the largest documented production of natural soda ash is from Lake Magadi, located some 120 km southwest of Nairobi, Kenya. The lake is situated in the lowest part of the East African Rift Valley and has a total area of 100 km² (Figures 4.34, 4.36). It contains more than 30 billion metric tons of trona in a bed between 7 and 40 metres thick and believed to have formed in the last 9,000 years. Thermal springs, driven by the area's volcanic activity, are the major source of sodium in the lake and are sourced from a deep actively circulating groundwater reservoir. Trona precipitates in the more central areas of Lake Magadi as a bottom-nucleated crystal pavement. The annual crop is estimated at 1.5 million tonnes/year, although the bulk of this crop (~75%) redissolves each wet season. When trona-saturated surface brines in Magadi dry up, the brine level stays close to the trona pavement surface. Even during exceptionally dry years the brine surface drops only 1 or 2 cm into the trona bed.

Trona in Lake Magadi has been mined since 1914 and is currently quarried from the pavement using dredging barges. As the solid material is removed by the digger belt, liquor from the surrounding trona drains into the resulting cavity, forming a pool or 'paddock' in which dredges float and move forward. Crystals of trona produced by the dredges are coarse crushed, mixed with lake liquor and pumped as a slurry back to the factory where the liquor is discarded and the crystals washed and centrifuged. The damp crystals are then fed into calciners where the residual moisture, water of crystallisation and carbon dioxide gases are driven off leaving normal soda ash. If for any reason a dredging barge breaks down for more than a day or two, trona precipitating in the paddock about the base of the barge can lock the barge in place. This trona has to be physically chipped away before dredging operations can continue. Replenishment of trona in the lake is so rapid that at present extraction rates the Magadi trona is a renewable resource.

Sodium sulphate salts (Glauber's salts)

Sodium sulphate (salt cake or Glauber's salt) is a common salt in many salt lakes and playas (Tables 11.14, 11.15). Thenardite and mirabilite, respectively, the anhydrous and decahydrate single-sodium sulphate salts, are the commercially important ore salts, with lesser production from glauberite and bloedite (astrakanite) ores. Thenardite, named for the French chemist Louis J. Thenard, is a colourless to white mineral with a specific gravity of 2.67 and a hardness of 2.5 - 3.0. It is stable below 33°C and is extremely hygroscopic below 25°C, converting to the decahydrate mirabilite (Figure 11.49). This mineral contains 55.9% water of crystallisation and forms opaque to colourless needle-like crystals sometimes referred to as Glauber's salt.

Mineral	Formula	Na ₂ SO ₄ (%)
Thenardite	Na ₂ SO ₄	100.0
Hanksite	2Na ₂ CO ₃ ·9Na ₂ SO ₄ ·KCl	81.7
Sulphohalite	2Na ₂ SO ₄ ·NaCl	73.9
Glauberite	Na ₂ SO ₄ ·CaSO ₄	51.1
Loewite	2Na ₂ SO ₄ ·2MgSO ₄ ·5H ₂ O	46.3
Ferronatrite	3Na ₂ SO ₄ ·Fe ₂ (SO ₄) ₃ ·6H ₂ O	45.6
Mirabilite	Na ₂ SO ₄ ·10H ₂ O	44.1
Bloedite	Na ₂ SO ₄ ·MgSO ₄ ·4H ₂ O	27.2
Tychite	2NaCO ₃ ·2MgCO ₃ ·Na ₂ SO ₄	42.5
Aphthalite	(Na,K) ₂ SO ₄	21-38
Tamarugite	Na ₂ SO ₄ ·Al ₂ (SO ₄) ₃ ·12H ₂ O	20.3
Mendozite	Na ₂ SO ₄ ·Al(SO ₄) ₃ ·12H ₂ O	15.5

Table 11.14. Minerals containing sodium sulphate.

	Location	Na-sulphate minerals and modes of occurrence	Reference
QUATERNARY	Cold climate saline lakes, Great Plains, western Canada	Mirabilite and thenardite precipitate at onset of winter cooling. Numerous lakes with a combined recoverable reserve \approx 80 Mt.	Last, 1993b, 1994 (see text for details)
	Laguna del Rey playa, Mexico (brine recovery and concentration)	Bedded crystalline mush that is a mixture of glauberite and astrakanite with sodium sulphate reserve of 350 Mt.	Garrett, 2002
	Gulf of Kara Borgaz, Turkmenistan (brine recovery and concentration)	Bedded crystalline mush that is a mixture of glauberite and astrakanite with sodium sulphate reserve of 2 Gt.	Garrett, 2002
	Lake Acigol, Turkey	Brine-soaked Holocene mudflats locally contain efflorescences of halite, bloedite; thenardite and/or mirabilite, all precipitating from the evaporation of artesian groundwaters.	Mutlu et al., 1999
	Intermontane playa, Tibet plateau, Mongolia	Holocene lacustrine setting depositing upto five mirabilite beds, some with borax minerals, retention of mirabilite in bed indicates episode of colder dry climate in basin.	Wei et al., 2002
	Barkol Salt Lake, China	Bedded mirabilite in saline lacustrine sequence.	Wei et al., 1998
	Playas of Karinga Creek area, central Australia	Mirabilite in thin ephemeral efflorescent salt crusts, indicate seasonal desiccation, flushed with next rain (no bedded successions).	Arakel and Hong Jun, 1994
	Vestfold Hills, Antarctica	Modern salt crusts with thenardite in dry valley (no liquid water).	Gore et al., 1996
	Holocene salt lakes, Taoudenni-Agorgott Basin, northern Mali	Nearsurface sediments locally show high glauberite contents, with lesser bloedite, thenardite or halite. Surficial crust in a nearby ephemeral saline lake in northern Namibia includes a basal thenardite layer, overlain by intervals consisting of burkeite with a palisade-type primary fabric that is separated by layers of fine-grained burkeite.	Mees, 1999, 2001
	Owens Lake, California	Thenardite in modern efflorescent crusts.	Levy et al., 1999
	Badwater Basin, Death Valley, California	Abundant glauberite and gypsum, and relatively small amounts of calcite accumulated in mudflat deposits from dry periods from 0 to 10 ka and 60 to 100 ka.	Li et al., 1997
	Northern part of the Great Salt Lake, Utah	Mirabilite bed accumulated in the cooler interval of the Late Pleistocene, when the lake was a perennial water body.	Colman et al., 2001
	Quaternary Sambhar Salt Lake, Rajasthan, India	Thenardite layer in lacustrine muds.	Sinha and Raymahashay, 2000

Table 11.15. Selected Quaternary occurrences of evaporitic Na-sulphate miner-

Common nongeological usage of the term Glauber's salts can be confusing, it usually refers to mirabilite rather than glauberite (named after the 17th century German iatrochemist, Johann Glauber). The mineral name mirabilite comes from the Latin *sal mirabilis* or "miracle salt" possibly referring to its pharmacological use as a cathartic or laxative in the Middle Ages and its utility in treating a wide variety of gastric complaints.

Solubility related to temperature has an important effect on the crystallization of the various sodium sulphate salts in natural brines, as well as in its commercial production. Sodium sulphate solubility in water generally increases as a nonlinear function of temperature. Below 1.2°C, ice and mirabilite form (Figure 11.49). As the temperature increases above 0°C, increasing amounts of sodium sulphate become soluble. At 32.4°C, a transition point on the solubility curve is reached, whereby the decahydrate melts in its own water of crystallization and

thenardite (the anhydrous form of sodium sulphate) crystallizes. With increasing temperatures, its solubility decreases somewhat. The presence of other dissolved salts changes the transition temperature and solubility characteristics of sodium sulphate (see discussion of double salt effect in Chapter 2).

Natural temperature drops in sodium sulphate-saturated brines are sufficient to allow mirabilite to crystallise in Canadian salt lakes during the autumn transition to winter, and even during cooling on summer nights in higher altitudes. In many places, mirabilite crystals redissolve into the lake brine with the next passage to warmer temperatures, this can be on the next day or with the passage of winter into spring.

Natural sources of sodium sulphate make up over 60% of world production, the balance is a byproduct of various chemical and waste recovery processes. Spain and Mexico are the world's

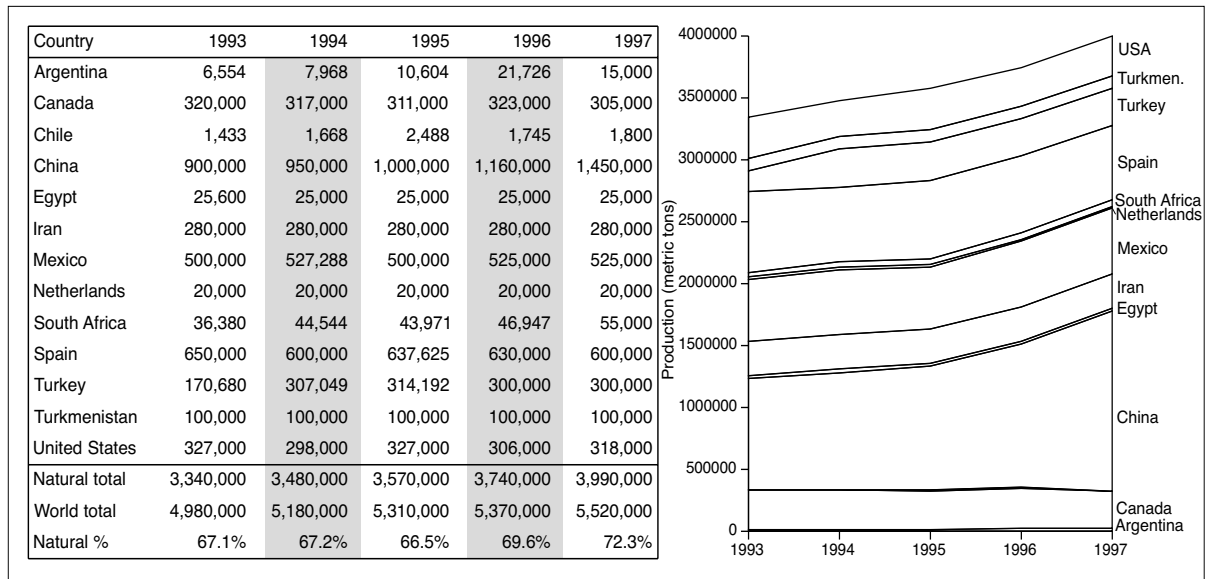


Figure 11.50. World production of sodium sulphate (in metric tons) (compiled from USGS on-line data tables, downloaded from <http://minerals.usgs.gov/minerals/pubs/commodity/myb/> last accessed 30 September, 2005).

highest tonnage miners of sodium sulphate, followed by a group comprising the USA, Canada, Turkey and Iran (Figure 11.50). Of the exploited natural sodium sulphate sources, three are from bedded Quaternary playa deposits namely: Laguna del Rey, Mexico; Searles Lake, California; and the Gulf of Karabogaz, Turkmenistan. There are also natural mirabilite deposits that form annually by winter brine cooling in modern saline lakes such as the Great Salt Lake, Utah, Lake Kuchuk in Russia, some restricted parts of the Aral Sea and numerous small saline lakes on the Great Plains of Canada. Then there are the ancient (Tertiary-age) lacustrine deposits of Spain and Turkey where glauberite and thenardite are the main ore minerals and the modern pedogenic deposits in the Atacama Desert of Chile.

The bulk of sodium sulphate usage is in the manufacture of glass and powdered detergents. It is also used in the pulp and paper industries. Commercial sources of sodium sulphate are mostly crystalline mirabilite, with lesser volumes of thenardite or glauberite and it is typically extracted as brine or mined from salt beds in playas and saline

lakes within cold or arid settings. Sodium sulphate can also be obtained as a byproduct from the production of ascorbic acid, boric acid, cellulose, chromium chemicals, lithium carbonate, rayon, resorcinol, and silica pigments.

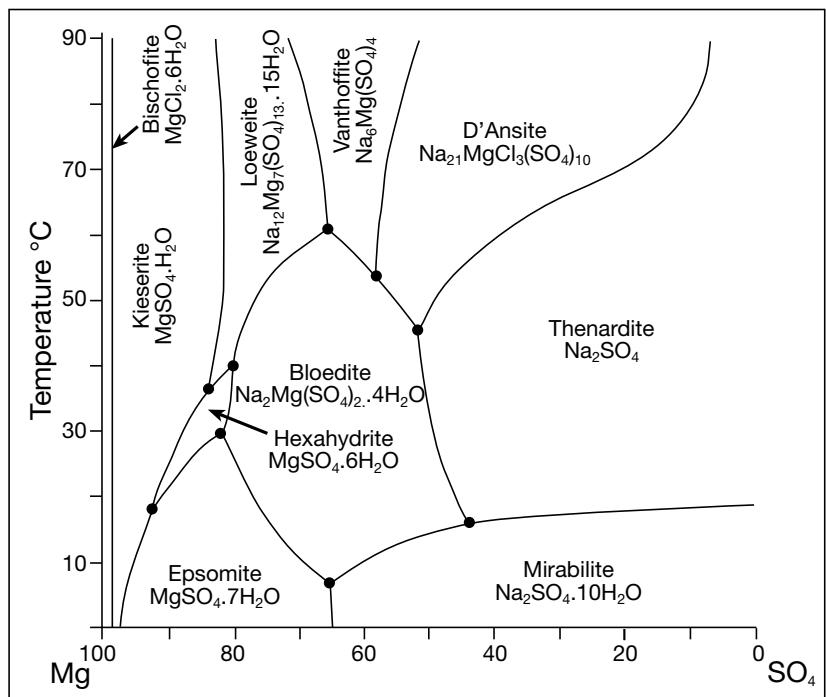


Figure 11.49. Stability diagram of minerals in an NaCl-saturated NaCl-Na₂SO₄-MgCl₂-H₂O system (after Braitsch, 1964).

Canadian deposits

There are an estimated 5.5 million saline lakes in the moraine plain of Canada, creating a concentration and diversity of salt lake environments unequalled in the world (Last, 1989a, b, 1992). Virtually all water chemistry types are represented in these lakes, with Na-Mg-SO₄ brines dominant. Over 80 species of endogenic precipitates and authigenic minerals have been identified as lake precipitates, the most common being calcium/calcium- magnesium carbonates (calcite/dolomite) and sodium/sodium- magnesium sulphates (mirabilite/gypsum). All the Canadian production of sodium sulphate in southern Saskatchewan and southeastern Alberta comes from present day or earlier Holocene late autumn-early winter cooling/freezing of playa brines. Precipitation of the ore salts is mostly as mirabilite, which may convert to thenardite with warming. Ore formation is a cryogenic, not solar evaporative, process. Most mirabilite-accumulating lakes are small (< 100km²), shallow (brines < 3-20m deep), with permanent salt beds found only in the lowest portions of some of these hydrologically closed meromictic depressions (Last, 1989a, 1994). Only around

a hundred lakes have salt reserves of more than 100 kt of Na₂SO₄ and their combined recoverable reserves are around 80 Mt (Garrett, 2002).

Large tracts of hummocky and icethrust moraine dominate the region and, in combination with the limited efficacy of fluvial processes under a subhumid to semiarid temperate climate, results in more than 45% of the region being endorheically drained into perennial saline lakes in depressions in the glacial drift. Some of these depressions are elongate and probably occupy pre-ice age river valleys (Little Manitou Lake), others were created by the melting of huge relict blocks of ice left in the moraine after the main front of the ice sheet had retreated (Ingebright Lake), Groundwater seeping from the surrounding moraine, through the underlying valley sands and across underlying bedrock supplies much of the dissolved content, but there is still no consensus as to the ultimate origin of the sodium and sulphate (Last 1989a). The geographic coincidence of many of the more productive lakes to the subsurface solution edge of the Devonian Prairie Evaporite lead Grossman (1968)

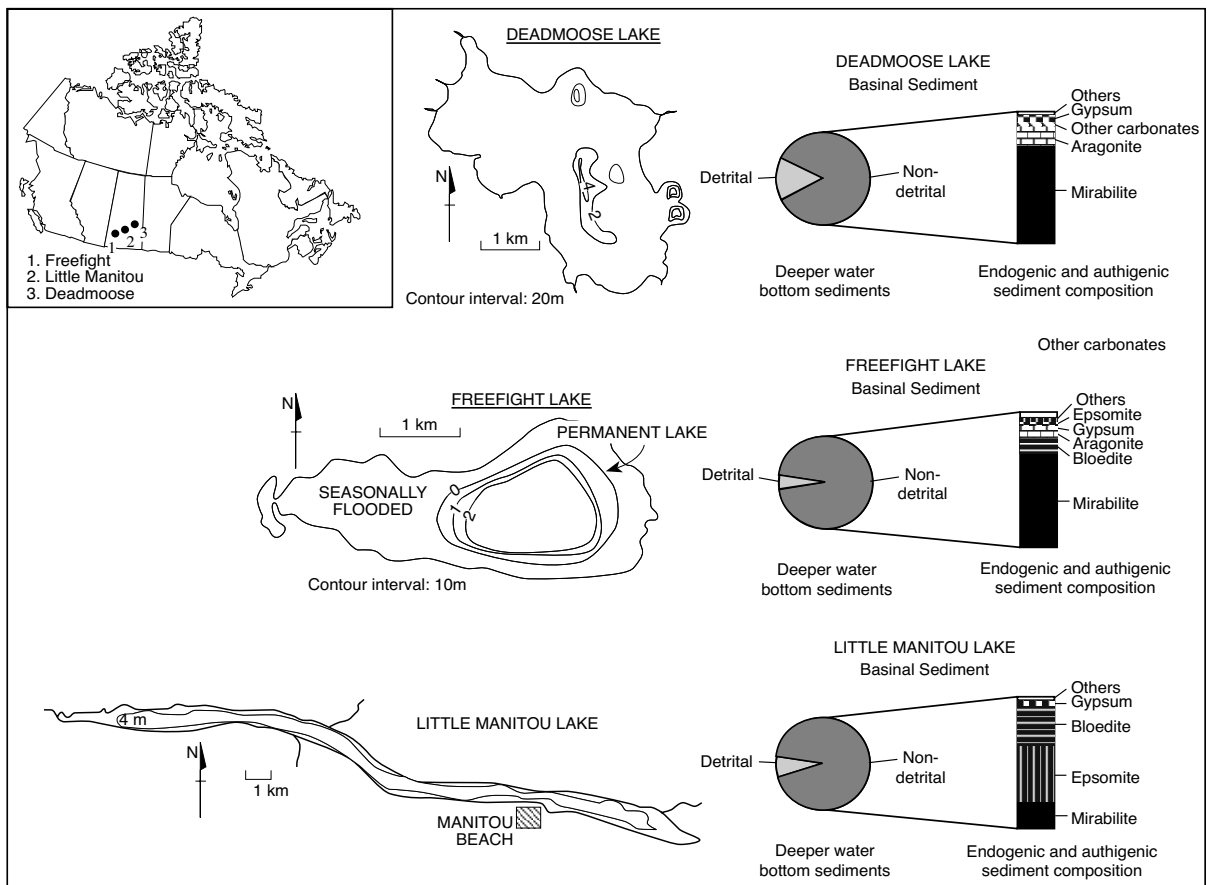


Figure 11.51. Sodium sulphate lakes, Canada, showing bathymetry and bottom sediment composition (after Last, 1994).

to suggest dissolution-derived salt-rich resurging groundwaters were the ultimate source. Others have argued that weathering and leaching of pyritiferous glacial flour is the likely source for the ions, independent of the underlying Devonian salts (Wallick, 1981).

Coldwater precipitates are dredged each year from suitably saline lakes before the mirabilite crusts redissolve with the passage in to the warmer lake waters of spring. Thicker-bedded crystalline thenardite deposits (transformed from primary mirabilite) have accumulated on the bottom of some lake depressions. Each year they retain a saturated brine layer from few centimetres to metres deep but their bottom waters are subject to seasonal warming. Waters in the upper water mass of all the deeper perennial lakes are replenished annually by spring melt. Cryogenic cycling whereby some of the mirabilite redissolves due to heating, can produce lake-bottom brines with salinities that may exceed 400‰. This maintains a perennial curtain or plume of saturated pore brines that preserve thick salt beds in the lower parts of the lake depression.

The saline lakes region of Saskatchewan encompasses some of the largest (Quill, Old Wives) and deepest (Freefight), perennial hypersaline lakes in North America, capable of accumulating bedded salts more saline than evaporitic carbonate. Ingebright Lake in southern Saskatchewan, although it is small in area (< 2km²) has, at 25-40 m-thick, the thickest Holocene evaporite bed in North America and it is dominated by primary precipitates of thenardite, Mg-carbonates and gypsum.

Two recognizable brine styles drive NaSO₄ precipitation and accumulation in the various lakes; intermittent saturation and permanent saturation (Last, 1994). Intermittent brines form seasonally on the bottom and along the shores of the lakes. There mirabilite crystallizes and largely redissolves with each seasonal cycle of cooling and warming. Mirabilite precipitation-dissolution cycles in such lakes can occur in a matter of hours, but as winter sets in, redissolution wanes, causing the crusts to become thicker and more compact. Spring meltwaters in a few lakes with such intermittent brine hydrologies carry in sufficient volumes of fine detritus to mantle salts in the shallower parts of the lakes and so preserve some of the lake precipitates year round. Such beds range in thickness from less than one to several metres, they are relatively impure, and made up of thenardite interstratified with thin layers of mud, clay, and organics.

Thicker purer beds of NaSO₄ tend to accumulate and be preserved beneath the permanent meromictic waters of the deeper

lakes. Hence, Deadmoose, Little Manitou, and Freefight Lakes are lacustrine depressions in the moraine plain where soluble and sparingly soluble NaSO₄ salts accumulate beneath relatively deep permanent brine bodies (up to 20 m deep; Figure 11.51). Both Deadmoose and Freefight Lakes are hypersaline and meromictic systems, with strongly anoxic hypersaline bottom waters. Little Manitou is also hypersaline, but the seasonal density and chemical stratification in the water column usually breaks down in early to midsummer, so allowing mixing of the upper and lower water masses down to the sediment surface.

There are four distinct styles of salt occurrence in these perennial lakes: a) crusts and hardgrounds of the lake edge, b) massive and bedded salts of the lake centre, c) spring or seep deposits, 4) subsurface and groundwater related interstitial and replacive cements (Last, 1989a, b). Relatively thick sections of subaqueous evaporites (mostly thenardite) have accumulated on the bottoms of some of these deep perennial lakes making them one of our better examples of textures in modern "deepwater" evaporites (Last, 1994). These deepwater salts are generally coarsely crystalline, massive to thickly bedded, and interfinger laterally with laminated organic-rich clays and poorly sorted carbonate-clastic debris washed in from nearshore areas. As in the Dead Sea, it seems that the deep water signature to a salt body accumulating in deeper hypersaline waters is not a laminate, but an aggregated bed of coarse crystals growing at the base of a holomictic brine column as crystal meshworks showing little or no preferred growth direction.

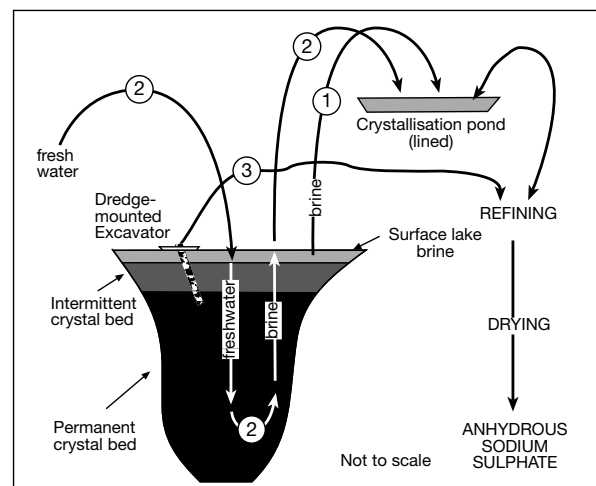


Figure 11.52. Extraction methods in various Saskatchewan sodium sulphate deposits (after Garrett, 2002); 1) Evaporative concentration of lake brine in crystallization pond, followed by precipitation of crystals of Glauber's salt (mirabilite) as the brine cools in autumn; 2) Solution mining of thick crystal beds. The brine return is treated as in 1; and 3) Dredging of lake bottom crystal beds.

Ingebright Lake is the largest salt lake still in production, bed thickness once averaged 6.7 metres of permanent salt. In 1954 the reserves exceeded 11 million tons beneath a lake area of 280 ha (Garrett, 2001). The lake and its drainage area is not large and no streams flow into it. It is fed by numerous springs and seeps about the lake edge, including five large springs that flow year round, supplying a dilute high-sulphate medium carbonate/bicarbonate water to the upper water mass (TDS of 2800 ppm; Cole, 1926). Subaqueous springs also cut up through the mirabilite bed that covers the lake floor. Springs tend to be cold (7°C) in the northern part of the lake, and warmer (15–18°C) and more saline in the south. Each winter these more saline southern springs precipitate large ephemeral mirabilite mounds that are up to 3 metres tall and 6 metres across. The fresher nature of the water supply to the northern springs means they are capable of dissolving all the mirabilite on their rise to the lake floor and so are defined by mud pipes or chimneys cutting up through the mirabilite ore bed (Last, 1993a). This metres-thick mirabilite bed, which covers the perennially subaqueous lake floor, is compact and friable. In the northern part of the lake it contains numerous clay layers that are mostly cm-scale, but as thick as 1 metre at the 7.6 to 9.1 metre level in the lake (Cole, 1926). In the south there is much less mud in the salt and it is more indurated. In the thicker ore bed of the southern part of the lake there are two zones where the mirabilite bed is thicker than 30 metres and one borehole intersected more than 42 metres of relatively pure sodium sulphate.

The mirabilite extraction industry in Canada is in decline, most of the remaining commercial lakes are in southern Saskatchewan. In the early days operators merely mined mirabilite by scraping or blasting, later some of the mirabilite was solution mined (Garrett, 2002). Traditional brine extraction involves pumping of surface brines into storage reservoirs during the summer and then allowing the lower autumn and winter temperatures to precipitate mirabilite (Figure 11.52). The mirabilite is then trucked to the processing plant, where water of crystallisation is removed and product then dried to salt cake in a rotary kiln.

Spanish deposits

Tertiary lacustrine sediments are the major source of sodium sulphate within three large Tertiary basins in Spain that together contain as much as 3 Gt in the form of glauberite or thenardite (Garrett, 2002). Spanish operations recover solid ores for processing, not brine. Ore is mined via room and pillar methods or in-situ leaching extracted via planned face retreat. The “El

Castillar” mine in Toledo Province yields mostly thenardite from an ore averaging 67% Na₂SO₄, 19% CaSO₄ and 12% clay and marl. The ore bed thickness averages 9 metres and it lies atop a 13 metre-thick halite bed. Glauberite is extracted at Cerezo de Riotiròn, Burgos Province, where the deposit is practically horizontal, undisturbed and made up of glauberite in four beds hosted in Miocene lacustrine marls.

The salts have a primary paragenesis of glauberite + anhydrite + dolomite ± chalcedony; the secondary minerals related to hydration and incongruent dissolution of glauberite are mainly gypsum and calcite (Menduina et al., 1984; Salvany and Orti, 1994). Glauberite types are varying combinations of: 1) massive glauberite within fining-upward sequences containing nodular anhydrite; 2) millimetre-scale glauberite layers alternating with dolomicrites; 3) single glauberite crystals dispersed in dolomicritic matrix (Figure 11.53a). There is no mirabilite phase preserved in these deposits.

A ‘perennial saline lake’ model with warm extensive saline mudflats explains the deposit (Figure 11.53b; Salvany and Orti, 1994). Solutes were derived from the phreatic dissolution of Mesozoic evaporites, mainly Ca-sulphates and halite, in the nearby mountains (Figure 8.10; Pyrenees and Iberian Ridge). The precipitation sequence was: carbonate, gypsum-anhydrite, glauberite, halite-polyhalite. Indicators of backreactions of glauberite with gypsum/anhydrite are commonplace because of dissolution resulting from interactions of primary precipitates with less concentrated (meteoric) brines and seeps feeding into the basin margin and supplemented by occasional storm runoff.

That is, glauberite, anhydrite and polyhalite were early diagenetic minerals, which formed via backreactions with a solid precursor (typically gypsum) during early diagenesis. The brines that drove this early alteration reacted with the solid precursor in two ways: 1) reaction of the concentrated brine with the solid phase precipitated during episodes of lowered salinity (e.g. anhydrite alters to glauberite; glauberite alters to polyhalite), and 2) reaction of dilute brines with solid phases precipitated in episodes of higher salinity (e.g. glauberite alters to anhydrite, polyhalite alters to glauberite or anhydrite). Burial led to further transformations of gypsum to anhydrite, and during exhumation and exposure all preexisting sulphates (anhydrite, glauberite, polyhalite) were transformed near the surface into gypsum and now form the weathered cover or carapace seen atop many ore profiles (Figure 11.53a).

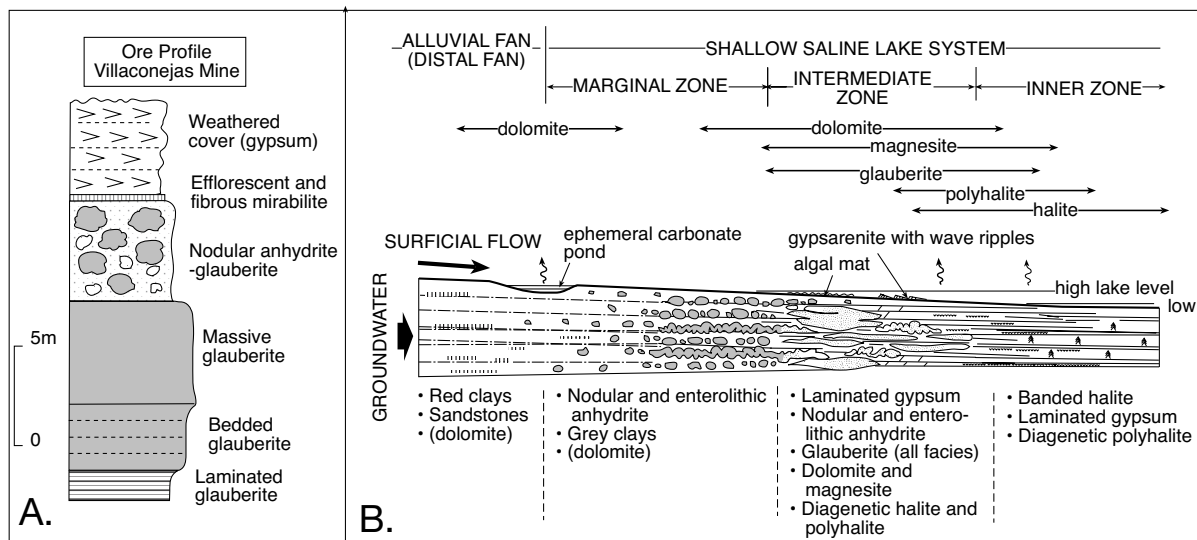


Figure 11.53. Miocene glauberite in Spain. A) Profile of the ore zone in the Villaconejas Mine, Spain. B) Sedimentological model for deposition of Spanish glauberite deposits (after Salvany and Orti, 1994).

Turkish Deposits

Sodium sulphate salts are extracted from the Upper Miocene Kirmir Formation at Cayirhan Mine, Turkey (Figure 11.54; Orti et al., 2002). Unlike the Spanish ores, thenardite (after mirabilite) is a significant depositional component the bedded evaporite portion of this lacustrine ore association. However, none of the mirabilite remains as it converted to thenardite with moderate burial. The Evaporite Member of the Kirmir Formation, which is composed of secondary gypsum at outcrop, can be subdivided into a bedded lower unit and a massive upper unit (Figure 11.54a). Most of the current outcropping and subcropping gypsum of the bedded lower unit has been transformed during exhumation from a glauberite parent. Glauberite layers ("clear glauberite") still remain at depth, as in the Cayirhan mine, where textures suggest it was deposited as a primary, subaqueous, cumulate precipitate on the saline lake floor (Figure 11.54b). But more typically, the glauberite textures are nodular, suggesting it was an early (syndepositional to precompaction) interstitial precipitate, indicating crystal growth occurred just below the sediment surface as passive and displacive crystals within a poorly lithified clayey magnesitic matrix. Thenardite layers in the glauberite beds in the Cayirhan mine, show disruption structures created by syndepositional dissolution and infill (Figure 11.54c). These structures, together with their pseudomorphic textures, suggest mirabilite was the original sodium sulphate lakefloor precipitate. If so, the current thenardite ore is a secondary phase, formed by mirabilite dehydration during early to moderate burial.

The massive upper unit, in which evidence of any sodium-bearing minerals is absent, is characterized by laminated to banded gypsum, with nodular gypsum dominant in the marginal areas of the evaporitic basin. Thick, clast-supported gypsum breccias prevail in the northern, deeper part of the basin. The brecciation of these calcium sulphate layers occurred as a result of syndepositional, gravitational slumping into the deeper parts of the perennial lake during times of lake flow instability driven by active tectonism (Orti et al., 2002).

As well as this ancient resource there are three playa lakes where sodium sulphate is produced from winter brine; they are Acigol, Tersakan and Bolluk and all three use the same basic production method. Surface brine is pumped into a series of solar ponds or small depressions on the lake floor in the summer and autumn. The inflow in some is supplemented by spring or aquifer waters as well as interstitial brine from lake bores or seepage trenches in areas on the lake floor outside of the pans. Salinity of brine in the pans is monitored so that it does not become saline enough to precipitate halite nor fresh enough to dissolve the pan floor where a seed bed some 20-30cm thick of thenardite (with minor mirabilite) was left from the previous year's salt harvest. As the concentrated brine cools from October to December a 50-60 cm thick layer of mirabilite crystallises in the centre of the ponds. From January and on into early spring the residual brine and any spring rainfall is drained from the pan. The flush of this fresher water through the lower part of the now metre-thick salt bed helps re-establish the integrity of the seed layer that will be left behind after harvesting. The

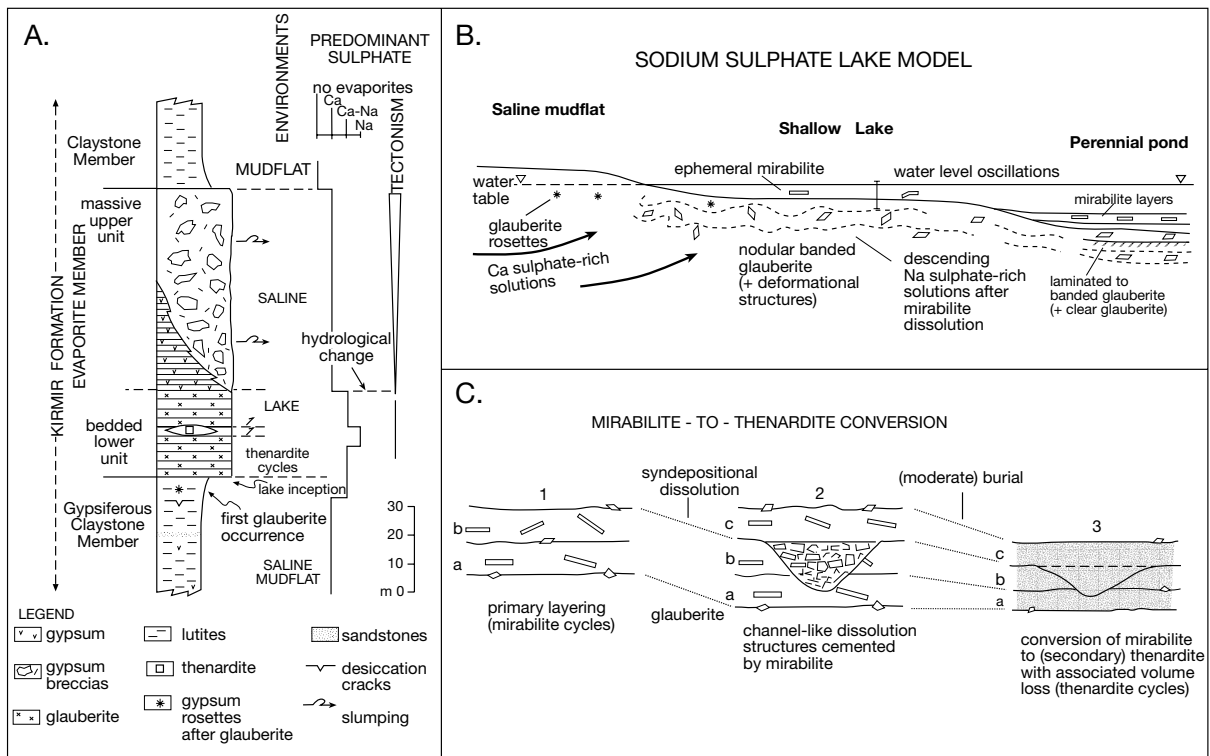


Figure 11.54. Na-Sulphate in the Upper Miocene Kirmir Formation, Turkey (after Orti et al., 2002). A) Stratigraphic occurrence and depositional setting. B) Depositional settings of the lacustrine evaporative system at the time it was precipitating sodium sulphates of the bedded lower unit (Evaporite Member of the Kirmir Formation). C) Interpretation of the genesis of mirabilite and its syndepositional dissolution and final conversion to thenardite during (moderate) burial.

mirabilite slowly dehydrates and by the end of June the bed is largely composed of thenardite, which is scraped from the lake surface and loaded into bags.

The textural transitions associated with this process are interesting and as it ultimately forms a vadose product with textures that are somewhat different to the perennial lakes of Canada but more analogous to the Tertiary deposits just discussed. The mirabilite has two forms, either large thin interlocking elongate hoppers or fine radiating spherules made up of acicular crystals (Garrett, 2001). The 0.6 m-thick mirabilite crust precipitated each winter is characterised by a thin uppermost layer or lamina of thenardite-mirabilite crystals, with some astrakanite. This is underlain by downward-pointing dog-tooth spar crystals of mirabilite, which constitute the bulk of the winter precipitates. They are downward-pointing as mirabilite tends to form rafts or hoppers at the contact between cool air and brine and not to grow upward from the lake floor. Below the coarse crystalline mirabilite is a thin layer of smaller equant mirabilite crystals defining the base of the winter precipitate layer. As the mirabilite bed dehydrates in the following summer it forms small powdery crystals that are easily blown about in the wind and escape the

pan. As summer temperatures reach 30-35°C the mirabilite bed “melts leaving behind some 15% of its former mass as thenardite and a saturated sodium sulphate solution that then continues to precipitate more thenardite. The resulting thenardite layer is composed of hard compact transparent crystals, which can contain numerous solid phase inclusions.

Other sodium sulphate deposits

Most US production of sodium sulphate comes from multicomponent brine processing in Searles Lake, California. As discussed earlier in the sections dealing with borates and trona, this brine resides in the interstices of the lake's salt beds, which contain some 369 million metric tons of Na_2SO_4 and 65 million metric tons of K_2SO_4 , representing $\approx 35\%$ of the total lake brine. These volumes rank it as one of the world's largest exploitable sodium sulphate accumulations. Brine processing in Searles Lake began in 1873 and the first sodium sulphate from brine was produced in 1914. North American Chemicals, Inc. today operates two facilities near Searles Lake, the West End plant and the Argus plant (Figure 11.35). The West End plant

is North America's only source of sodium sulphate where it is recovered as the primary product along with secondary soda ash and borax. Mixed brines are processed (carbonated) with carbon dioxide to precipitate sodium bicarbonate, which is then removed by filtration. The decarbonated brine is cooled three times to produce two successive batches of borax and one of Glauber's Salt (mirabilite). By heating, the sodium bicarbonate is converted to soda ash and the borax is either crystallized as a hydrate or dehydrated to its anhydrous form. The Glauber's salt is washed, melted, and recrystallized as anhydrous sodium sulphate; 99.3% purity can be obtained in this process.

In the brines of the Great Salt Lake, Utah, about 12% of the dissolved salt is sodium sulphate, representing about 400 million tonnes of potential resource. Mirabilite crystallizes naturally during the winter and sinks to the bottom of the lake so that in a cold winter a layer of mirabilite 0.15 to 0.30 m thick occurs seasonally over large portions of the lake floor. It redissolves with the passage into spring. Under favourable conditions, mirabilite rafts are carried by wind and currents to the shore where it can accumulate to a depth of 0.3 m or more. Strand deposits as thick as 3 m have been observed in some very cold windy years.

In the recent past the Great Salt Lake Minerals and Chemicals Corp. has made use of the annual cooling process in its brine pans to manufacture sodium sulphate salts as a secondary product. It operates a facility on the edge of Great Salt Lake for the production of a halite feed to its chemical plant and the coproduction of potassium sulphate and magnesium chloride. Brine is pumped from the Great Salt Lake into solar evaporation ponds where sodium chloride precipitates. Sodium sulphate crystals precipitate in a fairly pure state when winter weather cools the residual brine in the pans to -1 to -4°C. Crystals can be picked up by large earthmoving machinery and stored outdoors each winter until further processing takes place. The harvested salt is melted and anhydrous sodium sulphate precipitated by the addition of sodium chloride to reduce its solubility through the common ion effect. The final product is 99.5% pure NaSO₄. Thus, sodium sulphate is a byproduct of the halite process, but low prices meant it has not been harvested for the last few years.

Beneath the south and southeast parts of the lake there is a metre-thick mirabilite bed below 0.5 m of oolitic sand. To the north, immediately west of Promontory Point, there are much thicker accumulations of bedded mirabilite making up an irregular, 21-metre-thick mirabilite deposit, which is interlayered with clay beds between 4.5 and 9.1 metres thick (Figure 4.19c).

The mirabilite probably accumulated as bedded salt in the colder conditions of the last glacial (probably under a meromictic hydrology similar to that in Ingebright Lake today). Historically, the bed has been blasted and dredged in different parts of the lake and a processing plant was set up on the shores of the lake in the 1930s and 40s.

Ancient lacustrine deposits in the USA containing bedded sodium sulphate are considered non-commercial today, but have been mined in the past at Mesa Verde, Arizona and Rhodes Marsh near Mina, Nevada. The thenardite deposit at Mesa Verde is the only large well-defined ancient sodium sulphate deposit in the USA with projected reserves ≈ 100 Mt (Garrett, 2002). It also has the distinction of probably being the oldest mining operation in the United States. A tunnel in one of the halite beds at the base of the deposit yielded Indian artifacts around 2,000 years old. During the 14th and 15th centuries it was mined more intensively by the Mesa Verde and Rio Verde cliff dwellers, who removed a few thousand cubic metres.

One of the world's larger sodium sulphate deposits and Mexico's major sodium sulphate resource is the brine resource in the Laguna del Rey playa, Coahuila. Today it is a dry playa some 10 km long and 4 km wide. Operating on the lake shore is the world's largest sodium sulphate brine plant (Figure 11.55a). It uses a captive brinefield to solution mine brine from a bed containing 50% glauberite, 20% bloedite (astrakanite), 28% clay and various other sodium and magnesium salts including 1% halite. Minor mirabilite and epsomite are locally present as a cement between the glauberite crystals (Garrett, 2002). The salt body lies some 1-2 metres beneath the present playa floor, is lenticular in cross section, dips slightly to the east and thickens to the south. It has a maximum thickness of 35 metres and an area of 40 km² and contains a resource of some 350 million metric tons of sodium sulphate and 77 million metric tons of magnesium sulphate.

The lower parts of the flat playa surface are marked by an ephemeral halite crust, broken in places by relicts of a now largely inactive dune field. Above the halite crust is a green clay containing abundant gypsum and lesser glauberite and halite. Below the green clay is a red clay bed that immediately overlies the target salt bed. A similar, but much thicker red clay also underlies the main salt mass. Porosity in the salt mass is around 26% and is filled with a brine that when pumped from this salt bed contains more than 26% sodium sulphate (Figure 11.55b). A brinefield of more than 70 wells pumps brine to the surface from a depth of some 24-25 metres below the playa surface. Wells are gravel packed for the lower 12 m and the

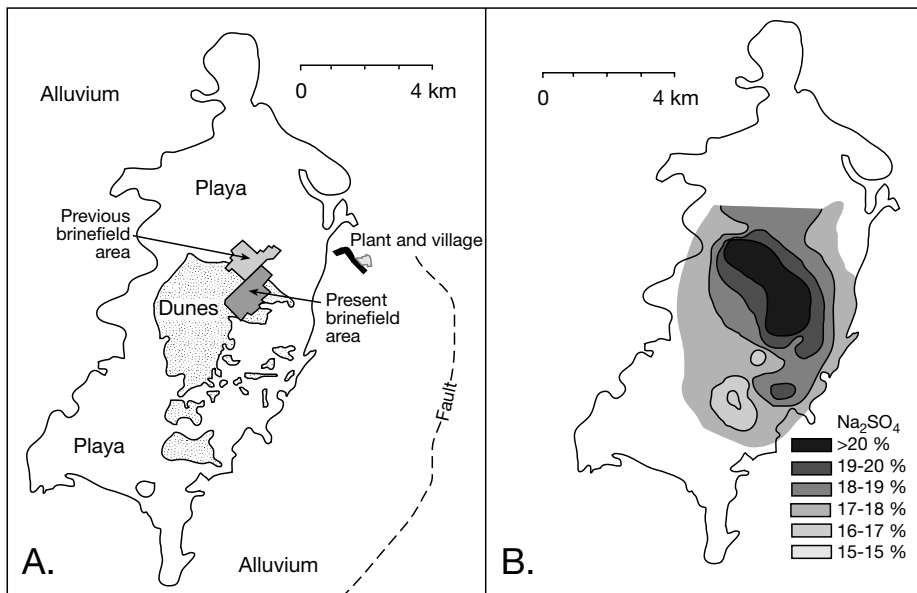


Figure 11.55. Laguna del Rey, Coahuila, Mexico. A) Distribution of surface features, brinefields and production plant. B) Distribution of Na_2SO_4 in brines in the shallow subsurface bed in the salt bed (after Garrett, 2001).

brinefield pumps around 113 litres/sec of 25°C 200 g/l sulphate to the recovery plant (Garrett, 2002). The ultimate source of the ions now accumulating in the playa depression is thought to be halokinetic gypsum capped marine evaporites that subcrop in the surrounding highlands.

Modern saline lakes, similar to the cold playas of Canada, are the major source of sodium sulphate in the former USSR and extend from the Black Sea to western China. Examples include Selenga Lake in the eastern Transbaikal, Lakes Azhbulat, Ebeity and Tengis in Kazakhstan, and the Batalpashinsk and Tambukan Lakes between the Black and Caspian Seas. The enormous potential of these deposits can be illustrated in Lake Azhbulat where some 40 Mt of mirabilite is deposited each winter. On the Kulunda Steppe, western Siberia, lacustrine deposits consist of sodium chloride in the upper layers and mirabilite below. The largest sodium sulphate lake in the region, Lake Kuchuk, southwest of Novosibirsk, covers an area of some 150 km^2 . It contains an estimated 600 Mt of sodium sulphate in brines and underlying strata and each winter between 380,000 and 640,000 tonnes of mirabilite drop out of solution.

Sodium sulphate also occurs as mirabilite-glauberite beds in the shallow subsurface of the Kara-Bogaz-Gol (Gulf of Kara Bogaz) on the eastern side of the Caspian Sea (Figure 11.56a). For much of the Holocene Kara-Bogaz-Gol has been connected via a narrow 500m-wide inlet to the Caspian Sea, which flows

water from the Caspian to Kara-Bogaz-Gol at a rate of 25-44 metres/minute. The inflow is replacing water lost by evaporation from Kara-Bogaz-Gol and the water level in the gulf is consistently 0.5-3 metres below that of the Caspian Sea. This makes it one of the few modern examples of a drawdown basin with a highly restricted hydrographic connection between one isolated seaway and another ($A_0:A_1 = 2 \times 10^7$; Figure 5.28). It is sufficiently restricted to allow gyparenite to accumulate on the brine-covered lake bottom. Water level in the Caspian Sea has varied considerably

over the Quaternary and so Kara-Bogaz-Gol may have periodically lost its supply from the Caspian. In earlier times of cooler temperatures that allowed winter freezing of a perennial water body, some 3 to 8 metre-thick beds of cryogenic sodium sulphate formed and are today composed of varying amounts of calcite-hydromagnesite-gypsum-halite-epsomite-mirabilite-glauberite.

In Turkish, Kara-Bogaz-Gol means "lake of the black throat," so named because the gulf is continually gulping down the waters of the Caspian. There is an interesting anthropogenic aspect to the natural loss of water from the Caspian to the Gulf and the periodic salting of Kara-Bogaz-Gol. Early last century (prior to 1929) the Caspian sealevel was around -26 masl and Kara-Bogaz-Gol was almost entirely water-filled (as it is today; Figure 11.56b). The water-covered surface area was around $18,000 \text{ km}^2$ and its maximum water depth was around 9 metres. The annual volume of water flowing through the inlet was high, somewhere between 18 to 26 km^3 and the difference in level between waters of the Caspian and Kara-Bogaz-Gol was around 0.45 metres. From 1929 until 1940 there was a 1.8 fall in the level of the Caspian Sea and by 1948 the Caspian level was -27.87 m. The volume of inflow to the Gulf fell to 12 - $14 \text{ km}^3/\text{yr}$ by the late 1940s and to $8 \text{ km}^3/\text{yr}$ in 1956. Differences in water level between Caspian and the Gulf increased to 3.17 m in 1947 and 3.80 m in 1955. By 1957-1959 the water-covered

area in Kara-Bogaz-Gol had fallen to around 13,000 km². By 1977 water levels in the Caspian was -29.02 masl, it had fallen fell by more than 3 metres since 1929 (Figure 11.56b) and the 1977 water surface in Kara-Bogaz-Gol was 4.5 metres lower than the Caspian. The strandline of southern Kara-Bogaz-Gol had retreated by 50-60 km in 50 years. This ongoing drop in water level in Kara-Bogaz-Gol since 1929 meant numerous salt works flourished in the increasingly exposed and accessible brine flats.

The ongoing fall of the Caspian Sea level from 1929 and well into the 1970s, was thought by the Russian Government to be related to the continuous loss of water from the Caspian to Kara-Bogaz-Gol. After all, the climate in the Kara-Bogaz-Gol was arid, the annual evaporation rate was 1000-1500 mm and annual rainfall around 70 mm. Russian government scientists argued that damming the entryway would stop the Caspian spilling into the Gulf and so arrest the fall in the Caspian water level. This notion of interfering in a natural saline system was opposed by a number of Turkmeni scientists who argued that the rise and fall of the Caspian and the variable filling in Kara-Bogaz-Gol were natural processes and had been noted in the texts of ancient Islamic scholars living in the region. Ignoring the argument that rise and fall of brine level in isolated saline waters bodies, such as the Caspian, was the normal situation, a decision was made in 1977 by the central administration in Moscow that the entryway would be dammed. Central administration scientists had concluded that sufficient water would still remain in Kara-Bogaz-Gol after damming to allow the salt industry to continue its operations. The dam was not actually constructed for another 3 years. Ironically, the

natural fall in the level of the Caspian had reversed in 1977 and had began to rise once more, with a corresponding rise in waters levels in the Gulf. From 1977 until 1995 the Caspian level rose by the same 3 metres it had dropped since the 30s. However a decision had been made back in 1977 to dam the

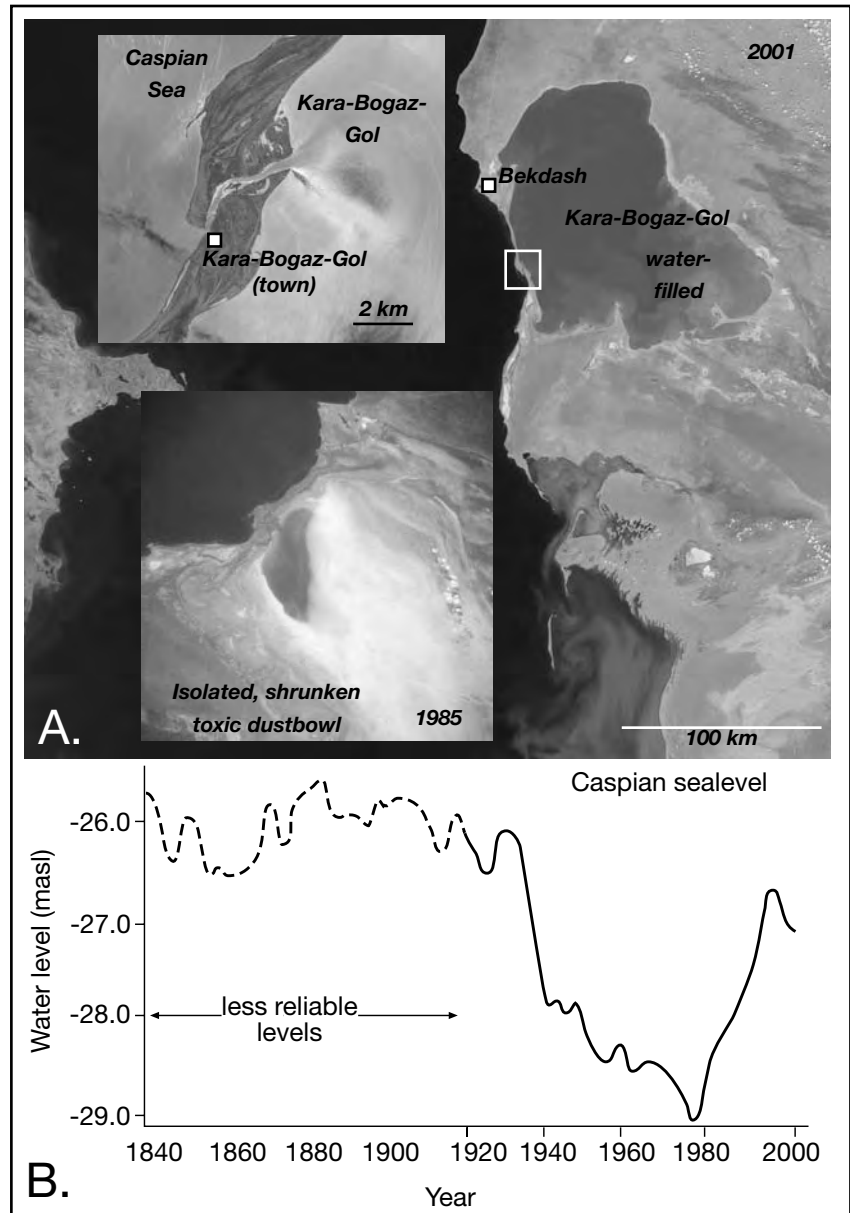


Figure 11.56. A) Kara-Bogaz-Gol (Gulf of Kara Bogaz), Turkmenistan, located on the edge of the Caspian Sea. The compilation of images shows the current water-filled situation (in 2001) after the artificial dam across the entryway was breached. Upper inset shows the nature of the very narrow entryway between the Caspian on the left and the outflow plume in Kara-Bogaz-Gol on the right (position of image indicated by rectangle). Lower inset shows the desiccated and dusty situation in Kara-Bogaz in 1985 when the entryway was dammed. (Images courtesy of NASA). B) Historical levels of the Caspian Sea.

entryway, so in 1980, even though the Caspian water level was rising once more, Russian engineers dammed the entry strait between the Caspian and Kara-Bogaz-Gol.

This complete loss of hydrographic connection to the Caspian did not have the desired effect, which was by then an irrelevancy, but egos and the authority of the Russian Empire was involved. Rather, the damming of the inflow resulted in rapid desiccation of Kara-Bogaz-Gol, so that by 1983 only a small brine covered area remained in the lowest part of the gulf depression (Figure 11.56). Much of the former brine lake floor had turned into a saline dust bowl, blowing high levels of sodium salts onto downwind irrigated pasture lands. By 1984 the villages surrounding Kara-Bogaz-Gol had turned into ghost towns. In 1984, in an attempt to restore the ecosystem, eleven large diameter pipes were laid across the dam so that Caspian water could be pumped back into Kara-Bogaz at a controlled rate. In 1992, after the fall of the Soviet Empire, this approach was abandoned and the dam was completely demolished by order of the president of the newly independent Turkmenistan. As it refilled from 1992 to 1995, the gulf water level rose by some 6 metres and since then its water level has once again matched that of the Caspian Sea and it is once again fulfilling its role as a natural desalinator of the waters of the Caspian.

Today, the water chemistry of the main open water body in the centre of the gulf is an Na-Mg-Cl brine, with a density of 1.2 g/cm^3 , and pH values that range between 7.2 and 9 (Giralt et al., 2003). Surface water temperatures range from 4°C in December to 25°C in July. These temperature fluctuations are seen in the precipitation of different mineral phases during the year. Calcite, aragonite and perhaps hydromagnesite usually precipitate from lake waters in spring, gypsum in summer (via solar evaporation), and crusts of cryogenic mirabilite and halite precipitate on the shores and mudflats of the embayment edge throughout the winter. Gypsum (as lenticular sand-sized grains) is the only sulphate phase seen in cores sampling surface sediments from beneath today's central water body (Giralt et al., 2003).

In the last 0.5 million years three separate Mg-Na-SO₄-rich salt layers (glauberite/bloedite/halite) have formed across the gulf, perhaps forming best in glacial episodes when the connection to the Caspian was reduced compared to today, and year round temperatures were much lower. Such glacial conditions favoured a perennial lake to pan mode of cryogenic mirabilite precipitation, much like winter salting in saline lakes in Canada today. Today a gypsum/glauberite layer is forming from the summer transformation of the mirabilite, epsomite and bloedite that accumulates each winter about the edges

Kara-Bogaz-Gol. A somewhat similar glauberite/bloedite/mirabilite/gypsum mineralogy started to form in the 1980s as capillary efflorescences across the whole floor of the gulf. At the time the Kara-Bogaz-Gol depression was converting to a saline dust bowl. But since 1992, with a return to the high water levels of today, glauberite no longer accumulates on the floor of the lake, only gypsum. The only glauberite forming today is that accumulating about the exposed margins of the gulf where high-calcium groundwaters dissolve and transform earlier winter precipitates of astrakanite, epsomite and mirabilite into capillary precipitates of glauberite.

Natural winter precipitates of sodium sulphate salts in this natural evaporation basin have been used commercially since at least the 1920s. Back then, the produced commodity was just whatever accumulated on the shore from wave action, especially on the southern shores of the Gulf during winter. The salt was scraped and harvested by hand and shipped to the Caspian using animals and barges. In the early 1930s, the port town of Kara-Bogaz-Gol was established on the Caspian side of the entryway, in order to trans-ship salt from the barges to the Caspian. Its population grew to a peak of 7,000 in 1936, (Figure 11.56). By the late 1930s, the gulf had become too shallow for barge traffic and the port town of Kara-Bogaz-Gol was abandoned in 1941. The falling water levels in the gulf also meant that by the end of the 1930s manual collection of naturally formed salt in the southern part of the gulf had stopped as well. The industry had to shift north to its present centre located inland of the town of Bekdash, which is a town of about 10,000 people on the shores of the Caspian Sea. Canals were built inland of Bekdash on the increasingly exposed mudflats that defined the strandzone of the Gulf. The canals were designed to feed gulf waters into large settling basins, which were filled with lake brines in the summer and left to cool in winter when mirabilite precipitated. Bekdash eventually became the centre of the salt industry of Kara-Bogaz-Gol and in the 1960s and 70s supplied chemical feedstock to much of the Russian chemicals industry in the satellite states surrounding the Caspian Sea. By the end of the 1930s, the falling water level drove increased salinities and a shift toward higher volumes of sodium chloride precipitates from ponded gulf waters, an unwanted by-product in the sodium sulphate industry. Profitability fell, and the salt pan-based industry waned through the 1940s. In the 1950s production technology shifted to extraction and processing of subsurface brines. Bekdash was reinvigorated as it was connected to a major brine extraction site via a 24-km pipeline. In 1963 construction began at Bekdash on a modern plant for increased year-round production of salines, independent of natural evaporation. This plant was completed in 1973.

The brines for the processing plant are extracted from the buried glauberite/bloedite/epsomite beds beneath the margin of the gulf. These beds still constitute a huge potential resource containing more than 3 Gt of sodium sulphate. Currently, sodium sulphate brines are solution mined using a single high capacity captive well and a mine planning approach that is a leftover from the former Soviet Union (see Chapter 12). Unlike the monitored gentle extraction of 113 litres/sec of intercrystalline sodium sulphate brine spread over more than 70 wells in Laguna del Rey brinefield, this single well into the Kara-Bogaz salt layers blasts out 126 litres/sec to the pipeline feeding the processing plant. Within the first 10 years of operation it had largely drained all the high salinity brines from its immediate vicinity and created a short circuit for less saline brine entry into the well bore. Ongoing drawdown and associated coning meant brine strength supplied to the plant has dropped to almost unusable levels. Once set up, coning from overpumping is difficult to reverse. The highly competitive state of today's sodium sulphate industry probably means that, without new capital injection for a better planned and monitored set of brinefields, the Kara-Bogaz salt industry will have to close.

A new anhydrous natural sodium sulphate operation in China, with an annual capacity of 200,000 tons, came onstream in mid 2003. The plant, operated by Dayang Chemical Limited Company, is located in Xishunhe Town, Hongze County, Jiangsu Province. The company, which is a joint venture between a Chinese company and an Indonesian firm, extracts mirabilite

from a large sodium sulphate deposit in east China. Little has yet been published on the geology of this lacustrine deposit. It has a proven area of more than 8.4 square kilometres, and a likely reserve of up to 150 million tons. In combination with a second facility with an annual capacity of up to 600,000 tons, and in production since the year 2000 (operated by Jiangsu Nanfeng Chemical Co. Ltd., which is a joint venture between Shanxi Nanfeng Group and Hongze Chemical Group, which is the Chinese operating arm of the Spanish Crimidesa Group), this now makes China the world's largest natural sodium sulphate producer with a combined capacity of 800,000 tons per year.

Sulphur salts (brimstone)

Sulphur may be found alone as native or elemental sulphur, or as a gregarious element in combination with many other elements, including metal sulphides and evaporitic sulphates. It is a common byproduct of bacterial and thermochemical sulphate reduction with the sulphate supplied by dissolving anhydrite or gypsum. Worldwide, documented resource of elemental sulphur amounts to about 5 billion tonnes. It occurs in evaporite and volcanic deposits or as sulphur associated with natural gas, petroleum, tar sands, and metal sulphides. Current uses for sulphur are: phosphate fertilizer production - 70%; petroleum alkylation catalysis (the conversion of one kind of hydrocarbon into another) - 15%; metals industry processes (leaching and pickling) - 7%; chemicals - 4%; and other uses - 4% (Ober, 2000).

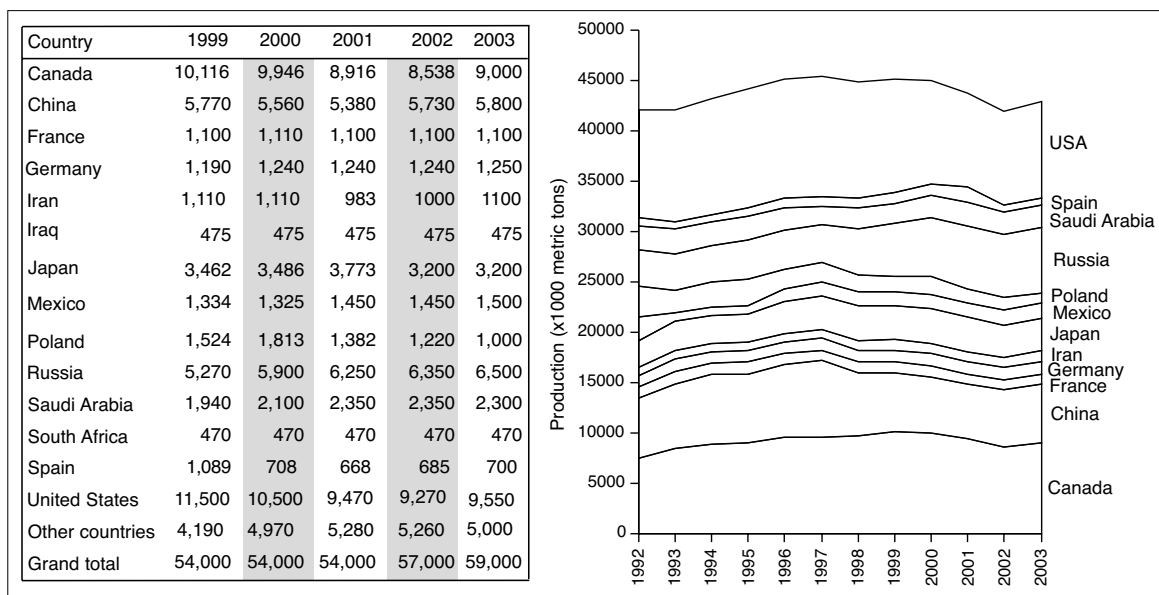


Figure 11.57. World production of sulphur (thousand metric tons - compiled from USGS on-line data tables, compiled from <http://minerals.usgs.gov/minerals/pubs/commodity/> last accessed 30 September, 2005). Grand total is an estimate of total world sulphur, not just tabulated major producers.

Usage history and industry trends

Native sulphur was known to the ancients as brimstone or “the stone that burns” (following details on historical usage are taken in large part from US Geological survey, <<http://pubs.usgs.gov/openfile/of01-197>> accessed December 28, 2004). Early man used sulphur as a colorant for cave drawings, as a fumigant, in medicine, and as incense. By 2000 BC, the Egyptians began using sulphur in the bleaching of linen textiles. Homer refers to its use as a fumigant in the Odyssey. During the Peloponnesian War, in the fifth century BC, the Greeks used burning sulphur and pitch to produce suffocating gases. The Romans combined brimstone with tar, pitch, and other combustible materials to produce the first incendiary weapons. This technology was lost in the “Dark Ages.” Muslims, through the use of alchemy during the “Golden Age of Arabic Science” around AD 700, probably were the first to produce sulphuric acid and this is

today the major use of sulphur. Sulphuric acid is a chemical workhorse throughout the world's chemical industries. Early uses of sulphur were relatively limited in terms of quantities and the small quantities needed were mined, typically from volcanic vent deposits.

Sulphur is a necessary ingredient in gunpowder, which was developed by the Chinese during the time of Confucius (557?-479 BC). Crusaders returning from the Holy Land in the early 1300s brought with them the knowledge of gunpowder. Gunpowder was first used effectively in Europe at the Battle of Crécy (1346). Its introduction led to profound social and political changes and for the first time made sulphur an important tradeable mineral commodity. Sicilian sulphur deposits, hosted in Messinian evaporites, satisfied European demand throughout the Renaissance and continued to supply much of the world's

sulphur into the last century. But attempts to stabilize the price of Sicilian sulphur at high levels by French controlling interests in 1838 led to the development and use of alternative sources. In 1833, a French chemist, Michel Perrett, developed a reasonably economical method of obtaining sulphur dioxide by roasting pyrite. His invention led to the development of a rotary furnace in 1870 that made pyrite a profitable raw material for sulphuric acid production. By 1880, sulphuric acid throughout the world was being produced from pyrite, except in the United States where import tariffs on iron and copper sulphides prevented a shift away from native sulphur. These import tariffs were removed in 1890 and 1894 respectively, and by 1900 burnt pyrite had become the principal acid-making material in the United States.

Native sulphur deposits occur in a number of evaporite basins in America and Europe, and several attempts were made to mine sulphur from salt dome cap rock in Louisiana between 1870 and 1890 using conventional underground mining techniques. These efforts were all frustrated by the patchy nature of caprock sulphur ore and

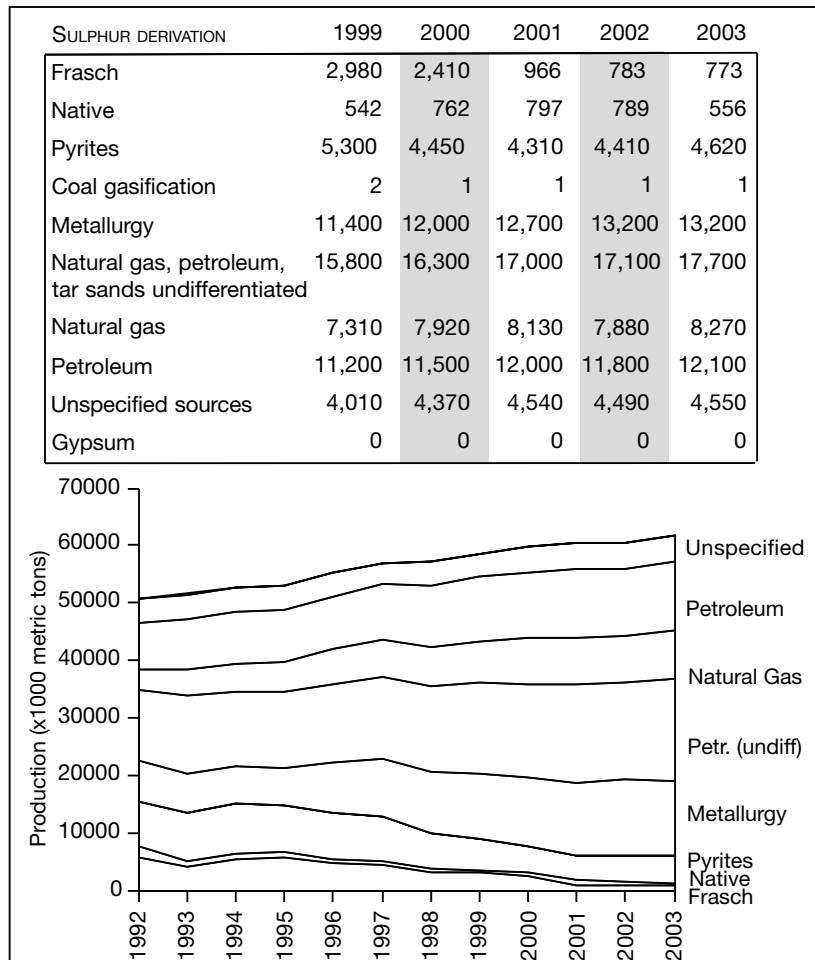


Figure 11.58. Processes of sulphur manufacture - worldwide (in thousand metric tons) compiled from USGS on-line data tables - compiled from <http://minerals.usgs.gov/minerals/pubs/commodity/> last accessed 30 September, 2005).

collapse-prone overburden. In 1894, Herman Frasch developed a method of recovering native sulphur using hot water and compressed air. It is a form of chemically-targeted solution mining and comprises a well made up of three concentric pipes (casing) ending in the ore zone. Pressurized superheated water is pumped down the outermost pipe in the string. The resulting steam melts the sulphur, while air pressure applied via the innermost pipe forces the molten sulphur to the surface via the intermediate space in the pipe string. Sulphur was first commercially obtained using the Frasch method in 1895 by the Union Sulphur Company at Sulphur Mines dome, Calcasieu Parish, LA. The Frasch method was also employed in 1912 at Bryan Mound, Brazoria County, Texas, and later at many other domes scattered about the US Gulf Coast.

Worldwide, the production of mined or extractive sulphur has been falling since the mid 1990s. Poland is the only country still producing more than a million tonnes of native sulphur from evaporite-related deposits, using either the Frasch method or conventional mining (Figures 11.57, 11.58). In August 2000, Freeport Sulphur closed its Main Pass Mine, offshore Louisiana, which was extracting sulphur from a diapiric caprock, it was the country's last remaining Frasch mine. Freeport has sold the mine's assets and it is unlikely that it will ever reopen. In the previous year, Freeport had closed the Culberson Mine in west Texas, which was using the Frasch method to recover sulphur from bacteriogenic deposits hosted in bedded Permian evaporites. Polish Frasch sulphur production still remains above 1 Mt/yr and is likely to stabilize at this level, although production is now threatened by low international prices due to flooding of the market with byproduct sulphur.

Mined sulphur production in Iraq in 2000 was estimated to be about 200 kt (220,000 st). Iraq, though, has the potential to produce between 1 and 2 Mt/a (1.1 million and 2.2 million st/yr). Production is currently at a low level because United Nations sanctions emplaced in the 1990s forbade exports. So Iraqi production is being run at a level sufficient only to meet domestic demand. Today, small quantities of native sulphur are still mined in Asia, Europe, and North and South America. The use of pyrite as a sulphur source has significantly decreased in the last two decades because of pollution concerns. China, South Africa, and Spain are now the only countries in the top 15 sulphur producers whose prime sulphur source is pyrite; together these three nations account for more than 80% of all pyrite-based production.

Although mined sulphur production is decreasing worldwide, world production of recovered sulphur is increasing (Figure 11.58). The growth comes from sulphur recovery from sour gas processing plants and from the refining of sour crude oils. Chemically recovered elemental sulphur is now the predominant sulphur source in Canada, France, Germany, Iran, Russia, Saudi Arabia, and the United States, and an important sulphur source in Japan and Mexico (Figure 11.57). In many countries this form of sulphur is recovered in compliance with environmental regulations that restrict the sulphur content of the fuels sold or used by a processing facility. Growth in sulphur recovery continues to out pace sulphur demand, resulting in increased stocks worldwide, as increasingly stringent environmental regulations force producers to limit atmospheric emissions of sulphur dioxide.

In addition to the currently known native sulphur resource, the amount of natural sulphur held as sulphate in gypsum and anhydrite is almost limitless. Some 600 billion tonnes are contained in coal, oil shale, and shale rich in organic matter, but low-cost recovery methods are lacking.

Types of sulphur deposits

Most large nearsurface accumulations of natural sulphur are the results of chemoautotrophic bacteria living on hydrocarbons or organic matter and dissolving anhydrite/gypsum, either in diapiric caprocks or in stratiform layers near the dissolving edges of anhydrite/gypsum beds. (Ruckmick et al., 1979). Such deposits are classified as biopigenetic and are intimately linked to the formation of microbial calcite. Bacteriogenic production can take place up to a kilometre or more below the landsurface (Figure 9.42). The same bacterial sulphate reduction process also forms much small volumes of native sulphur in modern anoxic marine or lacustrine muds, termed biosynthetic deposits by Ruckmick et al. (1979). These are not economic. Thermogenic deposits of molten sulphur form as the result of thermochemical sulphate reduction acting at much higher burial temperatures in association with natural sour gas (Figure 9.45). There are also deposits of native sulphur in volcanic terrains, usually as vein and fracture fills; a few still are mined in a small way and may be locally important (see history). Lastly there is oxidative native sulphur, which according to Ruckmick et al. (1979) are widespread but typically small sulphur occurrences formed at surface or at depth wherever hydrogen sulphide (regardless of origin) is oxidised. An example would be the dispersed native sulphur that occurs in the Carlsbad and Lechuguilla caves in New Mexico (Figure 7.45). We shall only discuss biopigenetic occurrences in this section.

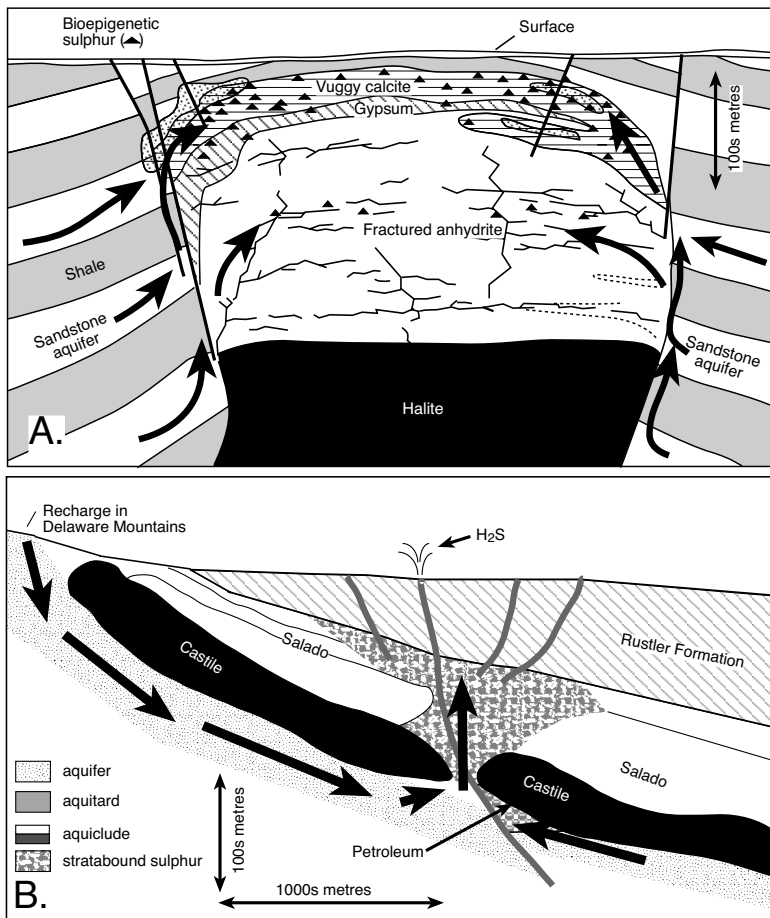
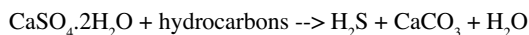


Figure 11.59. Conceptual models for the origin of evaporite-related elemental sulphur. A) Genetic model for diapir caprocks. B) Genetic model for stratabound or stratiform sulphur and the formation of subsurface castiles in the Permian Castile Formation of west Texas and New Mexico (after Ruckmick et al., 1979 - see also Figure 7.45a).

Biology of native sulphur

Native sulphur is microbially produced from calcium sulphate by the bacterial degradation (sulphate reduction) of anhydrite and gypsum in the presence of organic matter or hydrocarbons at temperatures of up to 110°C (Figure 9.42);



Sulphate-reducing bacteria chemoautotrophically metabolise migrating hydrocarbons and sulphate minerals within the evaporites to produce hydrogen sulphide and vuggy bacteriogenic calcite. The H_2S is then oxidized by infiltrating meteoric water to form elemental sulphur. This reaction takes place in the mixing zone between shallow meteoric waters and deep basin fluids in both bedded and diapiric precursors

(Aref, 1998b). Fine specks of sulphur and calcite replace gypsum in the early stages. With increasing replacement, sulphur and calcite form networks and patches within the gypsum (rehydrated anhydrite), which expand until gypsum remains only as relict splotches in massive vuggy calcite with pores lined with sulphur.

Dominant species of bacteria acting on the CaSO_4 change with salinity and temperature (Figure 9.11b); *Desulphovibrio desulphuricans* is active at normal shallow subsurface temperatures, *Desulphovibrio orientis* is active at moderate temperatures and *Clostridium nigrificans* dominates in hotter conditions. These bacterial reducers consume organics or hydrocarbons as a source of energy, but use sulphur instead of oxygen as a hydrogen acceptor and so produce hydrogen sulphide, calcite and water as byproducts. In addition to west Texas and the Gulf of Mexico, large deposits of bioepigenetic sulphur replacing gypsum/anhydrite occur in the Mishraq sulphur deposits (Barker et al., 1979), in the Polish sulphur deposits (Pawłowski et al., 1979), and in the Gulf of Suez (Youssef, 1989; Aref, 1998b).

Occurrences and textures

In sulphur-entraining caprocks atop diapirs in the Gulf Coast and Mexico, the CaSO_4 ore host is first created by dissolution of halite in the rising salt stem (Figure 6.64). This leaves behind a residual carapace or caprock of anhydrite that phreatic groundwater flushing then converts to gypsum at shallower depths (Figure 11.59a; Ruckmick et al., 1979). In the stratiform sulphur ore district of Culberson County, west Texas, requisite ore-forming fluids including basinal hydrocarbons and deeply circulating meteoric groundwaters migrated upward from underlying carrier beds, along steeply dipping normal faults, into the Salado Formation host (Figure 11.59b). Likewise, native sulphur occurs in the Red Sea Coast at Ras Gemsa, where an uplifted horst block, containing middle Miocene oil and gas bearing strata, is overlain and sealed by evaporite-carbonate layers (Youssef, 1989). In all cases the native sulphur resides in pores and vugs of these bio-epigenetic limestone beds.

In its unaltered subsurface state the Castile Formation of the Delaware Basin is made up of laminar anhydrite. Its underside acts as a seal and a focus for hydrocarbons seeping up from the oil kitchen in the deeper parts of the Delaware Basin and for deeply circulating meteoric waters (Figures 7.45a, 11.59b). Previously mineralised castiles now outcrop and subcrop about the edge of the Delaware Basin. The trap was naturally prepared for sulphur accumulation by a series of faults and collapse anticlines, activated or reactivated by evaporite dissolution about the basin edge. These extensional fractures acted as hydrological foci during the creation of porous dissolution collapse breccias or chimneys that crosscut the anhydrite beds of the Castile and the overlying Salado and Rustler formations (Figure 11.59b). Once the dissolution breccia/karst system was created it focused the ascent of petroleum-bearing waters from the underlying carrier beds (Bell Canyon Sandstone aquifer). As hydrocarbon-bearing waters flushed through the breccia, sulphate-reducing bacteria converted anhydrite to limestone and deposited sulphur in newly created fractures and vugs.

Locations of stratiform sulphur in this style of deposit are always structurally controlled. Individual sulphur deposits in west Texas are generally small, although the now closed Duval Mine in Culberson County, Texas, had original sulphur ore reserves of more than 55 Mt, between depths of 70 and 380 metres (Davis and Kirkland, 1979). The Fort Stockton Mine in Pecos County was located on the culmination of a leaky northwest-southeast trending anticline in the Salado Formation with a structural closure of 20 m (65 ft) in mine area (Figure 11.60; McNeal and Hemenway, 1972). Sulphur ore was largely confined to diagenetic limestone hosts that made up the A, B, and C units. Tops of the B and C units were defined by radiogenic clay marker beds and the top of the A was defined as the top of the Salado Formation. Sulphur in the ore zones sat mostly within dispersed vugs, fractures and fenestra in solution collapse breccia units, so it was more amenable to Frasch processing rather than conventional mining. As the ore was mined by steam injection, the more permeable megavug,

mesovug and megafenestral ore zones were prime targets in the steam-mined interval. Intervals with mesointercrystalline and mesofenestral porosity greatly increasing the efficiencies of recovery by facilitating improved steam circulation through sulphur impregnated intervals.

Similar stratiform sulphur occurs along the Red Sea coast of Egypt where accumulations range from small and noncommercial (Gebel Abu Gerfan and Ras Dip) to economic deposits (Gemsa; Aref 1998b). Sulphur crystals vary in morphology, colour, and size, it forms fine disseminations at Abu Gerfan, Gemsa and Gebel El Zeit; fracture and cavity fillings at Gemsa and Little Zeit; and sulphur nests at Gemsa and Shagar. The size of the sulphur aggregates ranges from a few millimetres to 5 cm diameter and crystal morphologies range from anhedral to subhedral to euhedral orthorhombic. Occurrences vary in colour from clear or turbid yellow crystals that may be encrusted with bitumen, to brown or black bitumen-stained sulphur varieties. Within outcropping calcite castiles along the Red Sea coast these epigenetic sulphur crystals can fill vugs or fractures in the host rocks, or they can replace gypsum or anhydrite along cleavage planes or intercrystalline crystal boundaries. They also may pervasively replace gypsum and calcite units to form network or meshwork patterns.

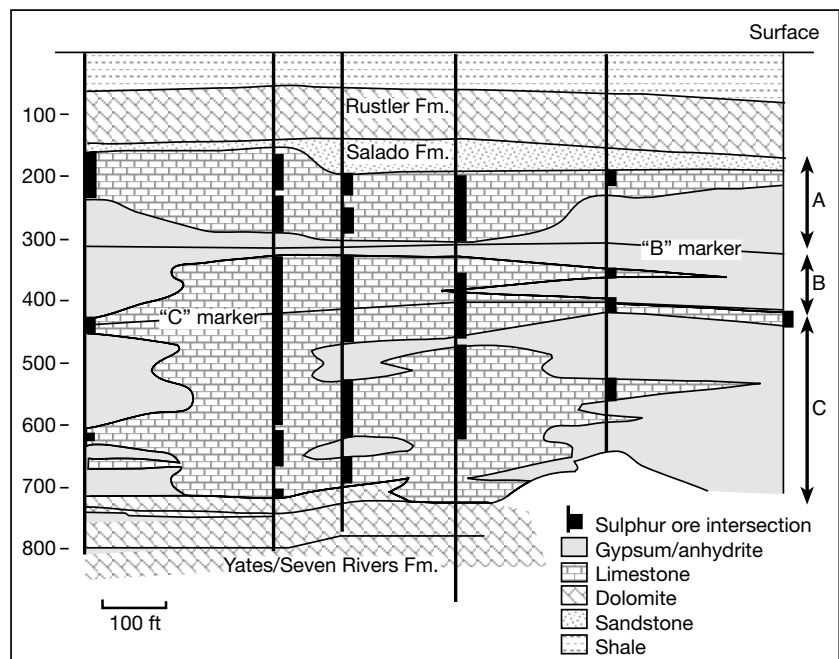


Figure 11.60. West-East cross section through the Fort Stockton anticline showing sulphur occurrence is largely confined to the dissolved remnants of the Castile and Salado Formations (after McNeal and Hemenway, 1972).

Bio-epigenetic sulphur was mined in Poland as early as the fifteenth century, and although declining, annual sulphur production in Poland still exceeds 1-2 million tonnes. Native sulphur deposits today occur beneath fluvioglacial outwash in the Vistula Valley, some 190 km south of Warsaw, and in the area around Lublin. All deposits lie within a Middle Tortonian gypsum host and are part of the 3,000 m thick fill of Miocene sediments that accumulated during the Alpine Orogeny in the foredeep north of the Carpathian Front (e.g. Figure 12.17a).

Polish sulphur is either extracted by conventional open-pit mining or by the Frasch hot-water/steam method (Pawlowski et al., 1979). The sulphur occurs in several styles; the most commercially important is as disseminated microcrystalline sulphur in a fine-grained poorly lithified calcitic marl host. This form of sulphur makes up 15% to 80% of the exploited rock mass and averages 30%. It is pale coloured and may occur in rounded concretionary masses, in thin irregular stringers, or in thick masses of high purity. A secondary ore mode is as coarser recrystallised forms that are bright yellow and typically occurs as crystals lining vugs and along fractures and seams. Masses of this coarsely crystalline form commonly grade into the microcrystalline form. Non-commercial occurrences constitute finely divided sulphur in interstices in growth-aligned bottom-nucleated gypsum crystals and as dispersed sulphur cements in sandstone beds. Both styles contain less than 15% sulphur in forms that are difficult to concentrate.

The main difference between North American, Polish and Red Sea sulphur occurrences is that the ore host is rehydrated and exhumed anhydrite in North America, while the Polish and Red Sea ore hosts have never been sufficiently buried to convert primary gypsum to anhydrite. This is also the case in the sulphur deposits of Sicily, which are hosted in Messinian gyp-

sum with immature hydrocarbons bleeding from the mine walls (pers. obs.).

Bacterial reduction of sulphate in all native sulphur ore hosts causes significant depletion of $\delta^{34}\text{S}$ in H_2S relative to the parent sulphate and a similar depletion in the sulphur derived from it (Thode and Monster, 1973). Reoxidation of sulphide to sulphate or sulphur by O_2 in the fluid mixing zone does not cause significant isotopic fractionation. Hence the lighter sulphur isotopic composition of oxidative sulphur in Guadalupe Mountain caves ($\delta^{34}\text{S}_{\text{CDT}} = -25.8$) and in the stratiform sulphur of the Culberson mine (-4.7‰) (Figure 7.48; Hill, 1996). A hydrocarbon source of the biochemical reaction is also indicated by the light carbon isotope character of epigenetic calcite in the Culberson mine ($\delta^{13}\text{C}_{\text{PDB}} = -44.2$ to -18.6‰ ; Figure 9.43; Hill, 1995). These depleted $\delta^{13}\text{C}_{\text{PDB}}$ values are significantly lower than would be expected in marine carbonates, which normally fall in the range -4 to $+4\text{‰}$.

Zeolites - molecular sieves

Like clays, zeolites are hydrated aluminosilicates made up of alkaline and alkaline earth metals. Their varying tetrahedral structures break them out into seven related aluminosilicate groups with some non-claylike properties (Table 11.16). Most clays have a layered crystalline structure and are subject to shrinking and swelling as water is absorbed and removed

Mineral structure (channel size in angstroms)	Typical unit cell content	Void volume	Specific Gravity	CEC (meq/gm)
Group 1: Single 4-ring				
Analcime (1.6 x 4.2; irregular)	$\text{Na}[\text{AlSi}_2\text{O}_6] \cdot \text{H}_2\text{O}$	0.18	2.24-2.39	4.54
Phillipsite (4.2 x 4.4)	$(\text{K}, \text{Na}, \text{Ca}_{0.5}, \text{Ba}_{0.5})_x [\text{Al}_x \text{Si}_{16-3x} \text{O}_{32}] \cdot 12\text{H}_2\text{O}$	0.31	2.15-2.20	3.87
Laumontite (5.0 x 5.3)	$\text{Ca}_4[\text{Al}_8\text{Si}_{16}\text{O}_{48}] \cdot 18\text{H}_2\text{O}$	0.34	2.20-2.23	4.25
Group 2: Single 6-ring				
Erionite (3.6 x 5.2)	$\text{K}_2(\text{Na}, \text{Ca}_{0.5})_8 [\text{Al}_{10}\text{Si}_{26}\text{O}_{72}] \cdot 30\text{H}_2\text{O}$	0.35	2.02-2.08	3.12
Group 3: Double 4-ring				
A (Linde: 4.2)	$\text{Na}_{12}[(\text{AlO}_2)_{12}] \cdot 27\text{H}_2\text{O}$	0.47	1.99	3.12
Group 4: Double 4-ring				
Chabazite (3.7 x 4.2)	$(\text{Ca}_{0.5}, \text{Na}, \text{K})_4 [\text{Al}_4\text{Si}_8\text{O}_{24}] \cdot 12\text{H}_2\text{O}$	0.47	2.05-2.10	3.81
Group 5: Complex 4-1, T_5O_{10}				
Natrolite (2.6 x 3.9)	$\text{Na}_2[\text{Al}_2\text{Si}_3\text{O}_{10}] \cdot 2\text{H}_2\text{O}$	0.23	2.20-2.26	5.26
Group 6: Complex 5-1, T_8O_{16}				
Mordenite (2.9 x 5.7)	$(\text{Na}_2, \text{Ca}, \text{K}_2)_4 [\text{Al}_6\text{Si}_{40}\text{O}_{96}] \cdot 28\text{H}_2\text{O}$	0.28	2.12-2.15	2.29
Group 7: Complex 4-4-1, $\text{T}_{10}\text{O}_{20}$				
Clinoptilolite (3.9 x 5.4)	$(\text{Na}, \text{K}, \text{Ca}_{0.5}, \text{Sr}_{0.5}, \text{Ba}_{0.5}, \text{Mg}_{0.5})_6 [\text{Al}_6\text{Si}_{30}\text{O}_{72}] \cdot 20\text{H}_2\text{O}$	0.34	2.16	2.54

Table 11.16. Properties of some important zeolites (in part after Breck, 1974).

between the expanding and contracting lattice layers. In contrast, zeolites lack this expandable layered lattice. Rather, they have a rigid, 3-dimensional crystalline structure consisting of a network of interconnected tunnels and cages, separated by tetrahedral latticework. Water moves freely in and out of these pores, while the zeolite framework remains rigid. A dehydrated zeolite framework, with its honeycomb of passageways, is capable of absorbing large quantities of fluids and gases in place of the removed water, without ever changing volume. In fact, the word zeolite comes from the Greek *zein* meaning “to boil” (lit. *boiling rock*) as described by early chemists who had seen water boiling out of the rock pores when it was heated, but without obvious changes in rock volume.

Their rather unusual cage- or sieve-like lattice structure gives zeolites some useful characteristics (Table 11.16: Breck 1974):

- a high degree of hydration;
- a rigid structure with a low density and large void volume when dehydrated;
- a stable crystal structure when dehydrated;
- a set of mineral specific cation exchange properties;
- a set of uniform molecular-sized channels in many dehydrated crystals;
- a controlled variable set of physical properties such as electrical conductivity;
- an ability to adsorb selected gases and vapours;
- catalytic properties.

Because each member of the zeolite family has a unique aperture size, the molecules admitted to the framework are restricted to those of appropriate dimensions. This selective nature of the various zeolite structures makes them extremely useful as molecular sieves with numerous industrial applications.

Zeolites also have the ability to exchange cations, whereby one charged ion is exchanged for another in the crystal structure. The ability of a zeolite to do this is measured by its cation exchange capacity (CEC; Table 11.16). Compared to clays, zeolites have high CEC's, which are lattice specific and reflect varying degrees of alumina substitution for silica in the lattice tetrahedra to create lattice specific zones of surface charge. Exchange sites on natural zeolites are primarily occupied by 3 major cations: potassium (K), calcium (Ca), and sodium (Na), although other elements such as magnesium (Mg) may also be present. Exchange sites on a particular zeolite may contain nearly all K, nearly all Na, some Ca or Mg, or a combination of these and this controls which zeolites are suitable for a particular application.

In agriculture, zeolites are used as preservative agents (desiccants), soil conditioners, fertilizer extenders, herbicides, pesticide and fungicide carriers, animal food additives and odour controllers. Zeolites with K exchange sites are useful as longterm K release fertilisers. Other uses include dimension stone, lightweight aggregate, pozzolan and numerous filtration/treatment uses, such as natural gas purification, nuclear waste treatment and disposal, and oil spill, sewage and effluent cleanup. Chabazite is used to remove CO₂ and H₂S from sour natural gas, while clinoptilolite can remove ammonia in tertiary sewage treatment and for odour control in pet-litter. It also relieves ammonia stress in cud-chewing animals and it can strip base metals from effluents. Clinoptilolite is also highly effective in the cleanup of radioactive waste as it strongly adsorbs strontium and cesium, two of the longest-lived radioactive ions. It was used in the cleanup of Three Mile Island spill and was fed to children affected by the Chernobyl disaster.

Geological controls on saline zeolitization

There are six major geological settings where zeolites are found, of which saline lacustrine settings are one (Table 11.17). Most zeolites are altered volcanoclastics, with the larger number of exploited zeolite deposits formed by groundwater flushing of volcanoclastics within saline lacustrine settings. Zeolites are not preserved in rocks where metamorphic grade exceeds zeolite facies and so their occurrence decreases with age. More than 30 different zeolite minerals have been identified in Cenozoic rocks, only 7 in Mesozoic strata, 2 in the Early Palaeozoic, 4 in the Late Palaeozoic, one in the Neoproterozoic and none in the Archaean (Iijama, 1980). The interested reader is referred to Mumpton (1981) or Iijama (1980) for a full discussion of all the geological settings forming zeolites, we shall only consider zeolites formed in saline lacustrine settings.

Natural zeolites typically form by the reaction of pore waters with labile material, typically with volcanic glass, but also with poorly crystalline clay, plagioclase or silica. Formation of zeolites is favoured by elevated ratios of Mg and pH to Na, K and Ca in waters interacting with volcanics, conditions that characterise saline groundwaters in many closed hypersaline basins, especially in tectonically active depressions (continental rifts and collision belts). Chemical composition of the protolith glass, grain size and permeability of the host vitric tuff, are the important factors in controlling the mineralogy of a zeolite. A preponderance of sodic-rich zeolites such as analcime, mordenite, phillipsite, natrolite and clinoptilolite is probably a more common outcome in evaporitic compared to nonevaporitic zeolite associations, reflecting high levels of

Mode of occurrence	Temp °C	Zeolite species	Examples
Alkaline saline lake and percolating groundwater, semi arid (in basic tephra)	20-50	Ph, Cp, Ch, Er, Mo, Gi, Fa, Go, Na, An, (He)	Zeolitic tuffs of ancient Lake Tecopa, Shoshone, California
Percolating groundwater in a semi-arid setting (in acid tephra - vitric tuff)	20-50	Ph, Cp, Er, Mo, Fe, Th, Me	Altered tuffs of the John Day Formation, central Oregon
Nearshore or deep sea volcanoclastic sediment halmyolysis	4-50	Ph, Cp, (An)	Massive, clinoptilolite-rich tuff near Kurdzali, Bulgaria
Shallow burial diagenesis (low-temp. hydrothermal)	25-100	Sc, He, St	Massive, clinoptilolite-rich tuff near Kurdzali, Bulgaria
Deep burial diagenesis (mod. temp. hydrothermal)	100	La, An	Massive, clinoptilolite-rich tuff near Kurdzali, Bulgaria
Low grade metamorphic (high temp. hydrothermal)	>200	Wa, Yu, An	Altered tuffs and sandstones Wairakei, New Zealand
Magmatic primary	high	An	Nishi-Iburi District, Hokkaido, Japan
			An: analcime; Na: natrolite;
He: heulandite; Th: thomsonite; Me: mesolite; Sc: scolecite; St: stilbite; La: laumontite; Wa: wairakite; Yu: yugawaralite.			

Table 11.17. Geological occurrence of some natural zeolites (in part after Iijama, 1980; Mumpton, 1983).

Na in most saline brines. Other factors influencing chemical composition of sedimentary zeolites are salinity, pH, ratios of alkali and alkaline-earth ions in the pore waters, along with temperature, pressure and partial pressure of water in the fluid-filled pore spaces.

Of the various factors controlling which portions of a volcanoclastic sequence will be zeolitised in a saline lacustrine basin, pH of the flushing solution is the most important (Hay, 1981; Hall, 1998). Any alteration of natural volcanic glass is pH dependant, silicate glasses are most rapidly decomposed in strongly alkaline solutions. For example, Mariner and Surdam (1970) showed experimentally that the rate of dissolution of rhyolitic glass increases 20-fold as the pH is raised from 8.5 to 11.5 (see also Figure 7.58).

The pH of interstitial water is typically the most important control on zeolitization. Surface water and groundwater in many volcanic areas is acidic, but zeolitization requires neutral to alkaline conditions (Hall, 1998). Therefore, any acidic interstitial water must be removed or neutralized before zeolitization can take place. Conditions favouring zeolitization occur if there is likely to be an influx of slightly alkaline (bicarbonate-bearing) groundwaters. This change in pore water can occur via deposition or redeposition of ash in a standing body of alkaline water (not uncommon in saline depressions), or if there is reheating of ash via hydrothermal circulation pushing alkaline saline groundwater through the ash bed. Alkaline water can come from leaching of overlying or neighbouring limestone. Arid hypersaline depressions are associated with density-induced

circulation cells that favour the replacement of original acidic pore water with more alkaline brackish to hypersaline brines. Zeolites can also form rapidly in alkaline soils where vadose flushing tends to reduce the amount of acidic pore water (Hay 1963; Renaut 1993b). The reaction of volcanic glass with water is itself conducive to a rise in pH, because the dissolution mechanism involves a cation exchange reaction at the glass surface, whereby H_3O^+ enters the glass from the solution, while Na and K enter the solution from the glass (Casey and Bunker 1990).

Saline lacustrine zeolites are commonplace in endorheic alkaline basins in block-faulted terrains (such as the Basin and Range province of the USA; Shepard and Gude, 1968), in trough valley depressions associated with rifting (such as Lake Magadi or Lake Bogoria in the Eastern Rift Valley of Kenya; Surdam and Eugster, 1976) and in Tibet-type grabens formed in depressions in compressional terrains (such as Emet and Kirka basins, Turkey; Gundogdu et al., 1996). Most saline Neogene basins that retain exploitable volumes of zeolites still retain large volumes of highly reactive, silica-rich, vitric, volcanic material and evaporite beds. Bedded evaporites or their dissolution residues in a volcanic terrain are the product of a density-driven throughflushing brine system that must have displaced the original acidic waters. And so evaporite horizons are excellent pointers in a basin to a level in the stratigraphy where ash alteration and zeolites are likely (Figure 11.61).

Zeolites precipitate in volcanic hosts in timeframes measured in thousands to hundreds of thousands of years, depending on

brine alkalinity, the precursor mineralogy and the climate (typically semi-arid rather than hyperarid). Groundwaters driving zeolite formation in saline settings are typically sodium-rich, often with elevated carbonate-bicarbonate contents and a pH level maintained above 9 (soda lakes). Favourable hostrocks are freshly deposited rhyolitic to dacitic, vitric tuffs, especially those levels of the volcanoclastic succession time equivalent to alkali-rich saline mudflats and saline pans. Saline aluminosilicate gels (kenyaiite, magadiite) can form pointer minerals at these levels and can act as zeolite precursors (Chapter 4). Associated saline rocks can be bedded evaporites (trona, halite, borate), with interlayered mudstones, oil shales, diatomites (which can be an additional silica source in many alkaline lakes), bedded or nodular Magadi-style cherts and volcanoclastic conglomerate/sandstone.

Zeolitic alteration haloes in exposed marginward saline sediments of Lake Bogoria in the Kenya Rift Valley provide a useful Quaternary analog for many older saline lacustrine zeolites (Renaut, 1993b). Late Quaternary fluviolacustrine siltstones, mudstones and claystones (Loboi Silts) make up the northern margins of this saline, alkaline lake and contain up to 40% authigenic analcime and minor natrolite. The zeolitic sedimentary layers are reddish brown and up to 1 m thick. The amount of analcime increases upward in the profile, but decreases with distance from the saline lake. Altered sediments hosting the zeolites show many pedogenic features including; zeolitic root mats, rootmarks, concretions and carbonate rhizoliths. Residual patches of calcrete locally cap the zeolitic rocks. The zeolitic profile about the edge of Lake Bogoria is interpreted as an exhumed palaeosol, which defines a former landsurface on the saline mudflat of the paleolake.

Analcime in the Bogoria mudflat is made up of submicroscopic (0.5-2.5 μm) subhedral and euhedral crystals, which have an average Si/Al ratio of 2.33 (as determined by X-ray microanalysis) or 2.18 (as determined from the d-value of analcime peak). Analcime formed diagenetically in these lake-marginal sediments via reaction of silicate detritus with alkaline Na_2CO_3 rich pore waters, which had concentrated during sabkha-like capillary evaporation and evapotranspiration.

Poorly ordered clay minerals were probably the main matrix reactants. Authigenic illite may have been a byproduct of the reactions forming the analcime. The saline pore waters of the mudflat probably supplied additional Na, and possibly K and SiO_2 to the process of zeolitisation. Calcrete and rhizoliths formed during or shortly after the main period of zeolitisation with the Ca sourced by dilute runoff and seepage waters. Authigenic smectite was precipitated in open pores following analcime formation. Zeolites have formed in similar saline mudflat settings in other nearby alkaline lakes such as Lake Magadi, where zeolites are associated with magadiite nodules (Figure 4.39).

Microcrystalline zeolite-bearing vitric tuffs, chiefly composed of analcime, chabazite, clinoptilolite, mordenite, phillipsite and sometimes erionite, are typical of mined saline lacustrine zeolites worldwide. Ore deposits are typically layered and may consist of one to several stacked zeolite layers separated by sub-economic or barren beds. Cutoff grade for zeolite ore varies greatly depending on mineralogy and cementation intensity. For example, a 10 to 20 centimetre thick ore bed at Bowie in North America contains 60 to 80% chabazite. This zone would not be economic if the main ore mineral was clinoptilolite. Most commercial clinoptilolite deposits contain between 50% and 90% zeolite.

Current large-scale commercial exploitation of saline lacustrine zeolites takes place in the Basin and Range province of the United State (Surdam and Sheppard, 1978) and the Andes

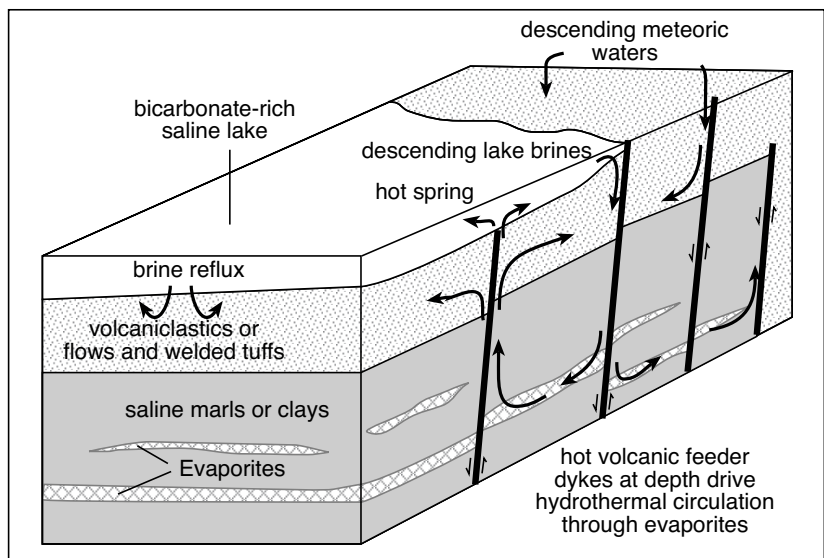


Figure 11.61. Schematic showing possible circulation mechanism in a saline lacustrine system where volcanics are altering and weathering to various zeolites.

(Hartley et al., 1991). For example, zeolites are extracted from saline lacustrine strata in the San Simon Valley, Arizona. The valley is underlain by 700 m of Pliocene to Holocene flat-lying fluvial and lacustrine rocks. Ore horizons occur within what is known as the “older alluvial fill,” which is a zeolitised Pliocene tuff and part of a more regional tuff marker bed within the Green Lake Beds (Sheppard et al., 1978). Thickness of individual zeolitic tuff layers ranges from 10 cm to 10 m with areal extents from tens to hundreds of square kilometres. The most common zeolites in this succession are chabazite, erionite and clinoptilolite, with small quantities of analcime in the southern part of the deposit. Parent materials include volcanic glass, biogenic silica, clays, plagioclase and quartz. Non-zeolite authigenic minerals in the tuff include smectite clays, calcite, halite, gypsum and/or thenardite. Chabazite, the main commercial mineral, constitutes up to 80% of the bed in the ore zone.

These zeolites crystallised after the accumulation of volcanic ash as throughflushing saline alkaline groundwaters reacted with the ash in the lake mudflat. Factors controlling intensity of alteration in the Green Lake Beds included the original lake bottom topography, depth and cation content of the saline-alkaline lake waters and proximity to postdepositional erosion surfaces (Eyde and Eyde, 1987). Zeolitic alteration ceased when an extensive system of younger palaeochannels deeply eroded the Green Lake Beds. Erosion indicates a change in the base level and a fall in groundwater level that removed the beds from the zone of active saline flushing. Erosion left only a few dissected remnants of the original tuff marker so that the “high grade zeolite bed” now outcrops in the various channel walls, where it is now mined. Former channels and the Green Lake Beds are now overlain by a section of halite-cemented brown mudstone known as the Brown Lake Beds, which largely prevented any later surface-driven meteoric alteration of the zeolites.

Throughflushing saline waters will first generate analcime and then K-feldspar with more complete alteration. In ancient zeolitised lacustrine deposits this is reflected in a commonplace transition from unaltered finely crystalline volcanoclastic glass and tuff near a palaeostrandline, through a series of immature alkaline silicic zeolites to analcime to potassic and sodic authigenic feldspars in the lake centre (Eugster, 1986; Hay et al., 1991). Volcanic glass is initially converted to zeolites such as clinoptilolite and mordenite before being altered to analcime. Under ultrasaline conditions when the K/Na activity ratio is sufficiently high (from earlier halite precipitation), analcime is then converted to K-feldspar. Tuff beds deposited

during the most saline and alkaline phase of Lake Gosiute in the Eocene Green River Formation typically exhibit such K feldspar alteration. Beds that remain soaked in somewhat less saline brines still remain at the analcime alteration stage (Smith et al., 2003).

Likewise, basin-centre Quaternary deposits in the various saline east African rift valley lakes typically exhibit more alteration in the lake centres, suggesting that as Pleistocene saline lakes shrank and concentrated, sediments in the lowest (central) positions were more exposed to increasingly saline and alkaline fluids.

Such pointers to the intensity of alteration outline Cretaceous Lake T'oo'dichi' in the Four Corners region of the USA (Figure 11.62; Turner and Fishman, 1991). This large alkaline saline lake occupied the entire eastern part of the Colorado Plateau region during deposition of the Brushy Basin Member of the Upper Jurassic Morrison Formation. At its maximum it extended from Albuquerque, New Mexico, to Grand Junction, Colorado, and occupied a region that encompassed the San Juan and ancestral Paradox basins, making it one of the largest ancient alkaline, saline lakes known; it was more than twice the size of Eocene Lake Uinta. As yet, zeolites have not been found in sufficient quantity to be exploited in this ancient lake system.

The lake was typically shallow and frequently evaporated to dryness, although the water table was probably never far beneath the surface and widespread bedded salt did not form (Figure 11.62; Turner and Fishman, 1991). Intermittent streams carried detritus from source areas to the west and southwest far out into the lake basin, a reflection of a low depositional gradient and the ephemeral brackish nature of the lake. Prevailing westerly winds carried silicic volcanic ash to the lake basin from an arc region to the west and southwest. A lateral hydrogeochemical gradient, characterized by increasing salinity and alkalinity from the margin of the lake to the centre, developed in pore waters of the lacustrine sediments and resulted in alteration of the ash to a variety of authigenic minerals that define concentric zones within the lake basin. The basinward progression of diagenetic mineral zones is smectite to clinoptilolite to analcime ± potassium feldspar to albite in the lake centre. A concomitant lateral zonation of mixed-layer illite/smectite developed, from highly smectitic in the outermost zones to highly illitic in the central zone.

Authigenic albite and illitic mixed-layer clay, minerals typically thought to require elevated temperatures for formation in non-saline burial settings, crystallized during early diagenesis

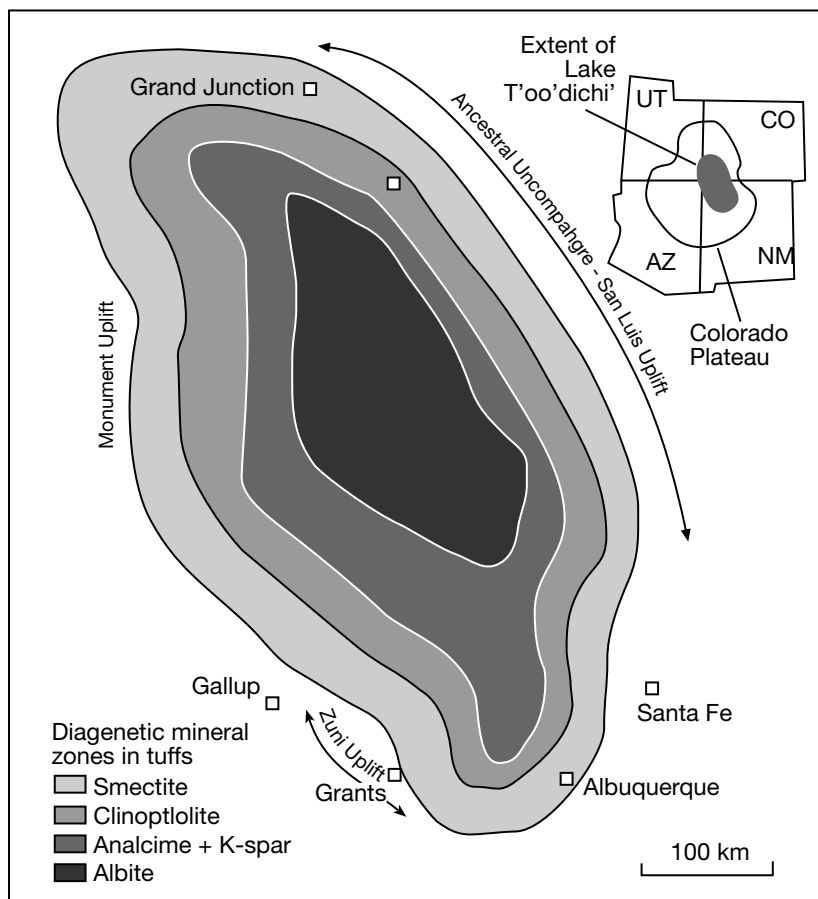


Figure 11.62. Basinward progression of concentric alteration haloes in the tuff lithofacies in the lacustrine Brushy Basin Member of Jurassic Lake T'oo'dichi' (after Turner and Fishman, 1991). This ancient alkaline lake occupied the combined San Juan-Paradox Basin area and was bound by structurally active uplift areas (related to an active volcanic arc that lay to the west).

at syndepositional temperatures in the lacustrine sediments of Lake T'oo'dichi'. Other examples of syndepositional authigenic albite are documented in saline lacustrine sediments of the Eocene Green River Fm. (Cole, 1985), Miocene tuffs near Boron, California (Williamson, 1987) and albite rims to evaporite pseudomorphs in the Triassic lacustrine mudstones of the Passaic Formation of the Newark Basin (El Tabakh et al., 1997).

Throughout burial, and on into the zone of metamorphism, zeolites can continue to react with evolving pore fluids as new minerals are formed by the replacement of earlier zeolites. Ongoing alteration in deep burial also explains the abundance of albitised metasediments and metavolcanics in meta-evaporitic settings and the loss of natural zeolites with increasing geological age.

But not all sodic zeolites in saline lakes need a volcanoclastic precursor. Analcime occurs in the basal anhydrite of the Navarra potash in a late Eocene basin that contained no volcanoclastics. Rosell and Orti (1980) interpreted it as a result of the interaction of highly concentrated brines with detrital clays. Likewise, authigenic analcime is forming today in playa muds in central Australia in endorheic systems that have never entrained volcanoclastics (English 2001). For example, Lake Lewis playa in the Northern Territory lies in a hydrologically closed intermontane basin in a low relief terrain in which clay-rich palaeolacustrine sediments are infused with highly evolved sodic brines. Near-stagnant lake waters, fed by groundwaters flowing through the Proterozoic Arunta granite-gneiss terrain and through arkosic alluvium and its weathering products, source the silica and sodium needed to precipitate analcime. Supersaturation of groundwaters with respect to SiO_2 and the availability of catalytic ions, coupled with high rates of evaporation, favours precipitation of opal and chalcedonic silica from solution near the groundwater discharge zone about the lake strandline. Moganite, a distinctive silica polymorph that is commonly associated with evaporites, is amongst the various silica species precipitated in association with the analcime (Chapter 7).

Downgradient from the zone of silica precipitation, beneath the playa proper, the brines become SiO_2 -deficient. Long periods of weathering and diagenesis of the lacustrine clays, immersed in semi-stagnant brines, has transformed detrital minerals into amorphous or gelatinous aluminosilicates. Hence, various aluminosilicate phases have become metastable in the long-term presence of evolved SiO_2 -deficient interstitial brine. Analcime is stable in this relatively stagnant Na-rich brine and is crystallizing authigenically below the watertable from these amorphous and gelatinous aluminosilicates in the more central parts of the lake depression. No volcanic rocks

or pyroclastic sediments are involved in this diagenetic occurrence of analcime. The appearance of analcime in Lake Lewis probably commenced within the last 100,000 years and is ongoing (English, 2001).

Summary

Evaporite salts and their diagenetic coproducts form mineable resources in a wide range of depositional and environmental settings. Potash deposits range in age from Quaternary to Devonian; no economic potash deposits are known to occur in Precambrian strata. The wide age range of preservation for highly soluble potash beds reflects the impervious nature of a thick salt mass once it is buried. Even though the various potash salts are highly soluble, undersaturated solutions often cannot reach them until a thick protective wrap of tight halite has been etched away. Both enrichment and depletion in the ore itself also reflects the long burial diagenetic history of this relatively impervious salt mass and the focusing of diagenesis about its dissolving edges.

Large potash accumulations, such as in the Zechstein and Prairie evaporite basins form in subsealevel marine seepage-fed depressions (Table 11.18; Figure 5.27). Their size and extent reflects an ongoing supply of brine across depositional areas that were one to two orders of magnitude larger than seen in any Neogene continental salt lake. They formed at times when the basin floor was subsealevel but tectonically isolated from any surface connection with the ocean (soft collision belts, farfield flexures, zipping and splitting stages of supercontinent). Large-laterally extensive ancient potash deposits are not the result of evaporation of nonmarine waters. To form, they needed high levels of salinity on the basin floor to occur for long enough and to be maintained deep enough into the subsurface for thick potash sections to be precipitated and preserved. It requires a brine hydrology that is not present on the earth's surface today. Modern approximations to a potash accumulating system are all lacustrine and are all smaller scale. Our best modern examples come from the highly arid continental salt lakes of the Qaidam depression of inland China.

Aside from ancient marine-fed saline giants and the Chinese foreland collision basins, the other major depositional setting for economic accumulations of potash is active continental rift grabens. Some, such as the Pleistocene Danakil Depression, had a Pleistocene seawater spring feed. Other small potash accumulations, such as the Mulhouse Basin in the Rhine Graben, perhaps had nonmarine feeds. In all cases, the greater volume

of inflowing ions within the depression was via brine springs, rather than surface runoff.

Without exception, nonpotash bedded salt resources (sodium carbonates or sulphates) formed in continental lacustrine or playa settings. They owe their existence to the unusual ionic compositions that come from groundwater leaching, under highly arid conditions, in appropriate bedrock terrains. Quaternary continental examples have same scale and same ionic proportions in the brines as their ancient lacustrine counterparts (Figure 5.3).

It is simply a matter of chemistry that these types of lacustrine deposits do not form from Phanerozoic seawater. Phanerozoic seawater simply never had the make-up necessary to precipitate borates, nitrates, sodium carbonates or sodium sulphates. This chemical evolution can only happen with nonmarine brines, typically where nonmarine waters drain into an arid, highly isolated depression in the continental landsurface. The effect of isolation and concentration in producing appropriate brine chemistries is often enhanced by the presence of nearby mountains. Mountains act both to form a rain shadow zone and to create topographic head, which drives deep circulation of meteoric groundwaters. In continental lakes in both rift valleys and collision belts, the creation of the mountains is tied to an active tectonic regime and volcanism, which in turn tends to create enhanced hydrothermal circulation and labile volcanoclastic aquifers in hydrographically closed depressions where saline waters are ponding. Borates, for example, form via the lacustrine concentration of spring inflows that have passed through active volcanogenic terrain. Likewise, the trona beds of Lake Magadi reflect nonacidic groundwater and hydrothermal/basin brine leaching (low sulphate, high bicarbonate waters).

All bedded non-potash deposits discussed in this chapter accumulated in endorheic depressions, often in the rain shadow of a nearby mountain range. This situation is most obvious in the various South American salars, they lie in intermontane depressions with floors that are thousands of metres above sea level, yet they drain and pond hypersaline waters for long periods of time, sufficient to allow salt beds hundred of metres thick to accumulate. Likewise mountains and volcanoes influenced local climate and helped create the Neogene successions of NE Turkey and the Basin and Range playas in the USA. Long-term aridity for more than 6 Ma tied to rain shadow effects, in combination with offshore upwelling, explains the hyperarid nitrate regolith of Atacama Desert.

Location	Age	Mine-able	Tectonic setting and brine feed	Depositional setting	MgSO ₄	Main potash minerals	Style and origin of potash
Qaidam Depression, China	Quaternary	Yes	Foreland basin	Continental playa	Yes	Carnallite, lesser sylvite	Void filling cements and displacive crystals via cooling of syndepositional sinking brines.
Danakil Depression, Ethiopia	Quaternary	Possibly	Rift aulocogen	Continental playa	Yes	Primary carnallite, kainite, secondary sylvite	Seaward seepage into Pleistocene subsealevel rift depression.
Chott el Djerid, North Africa	Quaternary	No	Endorheic depression	Continental discharge playa depression	No	Ephemeral halite-carnallite crusts	Brine evaporation in an area of regional artesian aquifer discharge.
Small plays in Amadeus Basin, Australia	Quaternary	No	Endorheic depression	Continental discharge playa depression	No	Ephemeral halite-sylvite crusts	Brine evaporation in small playas atop, but not connected to, zones of artesian aquifer discharge (only rare and minor occurrences of potash salts).
Dead Sea Depression, Middle East	Quaternary	No	Continental trans-form or "pull-apart" basin	Artificial brine recovery and pan evaporation	No	Carnallite slurry with sodium and magnesium chloride	Sequential evaporation of brine pumped from pores and dissolution cavities in subsurface Miocene evaporites.
Solfiera Fm., Caltanissetta Basin, Sicily (Messinian)	Late Miocene	Yes	Foreland basin (marine-fed)	Continental depression fed by seawater seepage	Yes	Syndepositional carnallite and early secondary sylvite	Syndepositional carnallite and secondary sylvite via brine cooling within karsted halite host. Deposited in early stage of a basinwide seaway drawdown.
Mulhouse Basin, France	Oligocene	Yes	Continental rift graben	Continental salttern, bedded	No	Primary carnallite and sylvite	Interlayered primary potash and halite cm-scale couplets with settle-out/bottom growth textures.
Maha Sarakham Fm., NE Thailand	Cretaceous	Yes	Continental foreland basin	Continental salttern, now halokinetic in part	No	Syndepositional carnallite and early secondary sylvite, also tachyhydrite	Syndepositional carnallite and secondary sylvite via brine cooling within karsted halite host.
Transatlantic potash basins, West Africa and Brazil	Cretaceous	Possibly	Continental rift graben (marine-fed)	Continental saltterns, now halokinetic in part	No	Primary carnallite and sylvite, also tachyhydrite	Bottom growth textures in both halite and halite layers in cm-scale stacked couplets.
Moroccan Meseta, Northern Africa	Late Triassic (Keuper)	Possibly	Continental rift graben (marine-fed)	Continental saltterns, now halokinetic in part	Rare	Not known - no detailed petrography available	Potash/halite evaporites interbedded with redbeds and basaltic lava flows.
Windsor Group, Canadian Maritime Provinces	Carboniferous (Viséan)	Yes	Continental rift graben (marine-fed?)	Continental saltterns, now halokinetic in part	No	Syndepositional carnallite and sylvite within primary halite. Associated borates	No detailed petrography yet published. Some thickening of potash units on salt pillow margins.
Z1, Z2 and Z3 evaporite intervals in Zechstein Basin, Europe	Permian	Yes	Basinwide marine evaporite (suture) (marine-fed)	Mostly saltterns, occasional deeper water, now halokinetic in part	Yes	Syndepositional carnallite and sylvite within primary halite	Carnallite as void fill during early brine reflux. Incongruent dissolution of carnallite to form sylvite. Potash units thickened by salt flow.
Salado Fm., Delaware Basin, New Mexico, USA	Permian	Yes	Basinwide marine evaporite (suture) (marine-fed)	Mostly saltterns, occasional deeper water, now halokinetic in part	Yes	Syndepositional carnallite and sylvite within primary halite	Carnallite and sylvite precipitated as void fills during early brine reflux.
Prairie Evaporite Fm., Elk Point Basin, Canada	Devonian	Yes	Basinwide evaporite (intracratonic) (marine-fed)	Mostly saltterns, occasional deeper water	No	Syndepositional carnallite and sylvite within primary halite	Syndepositional potash textures, often overprinted by later alteration events related to tectonically driven episodes of fluid flushing by basinal brines or deeply circulating meteoric waters.

Table 11.18. Summary of major potash evaporite occurrences as discussed in this text (see Chapter 5 for geological detail).

Location	Age	Tectonic setting	Depositional setting	Main minerals	Style and origin of mineralisation
BORATES					
Bigadic, Turkey	Miocene	Tibet-style grabens in collision arc	Volcanogenic playa/mudflats	Colemanite, ulexite	Precipitated as secondary nodules and fissure-fills within unconsolidated sediments, just below the sediment-water interface.
Boron, California	Miocene	Basin and Range	Volcanogenic saline lake/mudflats	Borax/kernite core facies with more distal ulexite, proberite and colemanite	Borax/kernite core facies with more distal ulexite, proberite and colemanite.
Salars, South America	Miocene	Intermontane grabens	Saline lakes and mudflats	Borax, ulexite, hydroboracite and inyoites	Borax, ulexite, hydroboracite and inyoites.
Meta-evaporites, Liaoning Province	Proterozoic	Amphibolite-grade metamorphics	Saline playa and mudflats	Boromagnesite	Metamorphosed lacustrine beds associated with banded iron formations and volcanics.
NITRATES					
Atacama Desert, South America	Neogene	Intermontane depressions	Intermontane depressions	Pedogenic nitratite with associated iodates, perchlorates, bromates and chlorides	Hyperarid conditions have prevailed since the mid-Miocene allowing buildup of highly soluble salts in the desert regolith.
SODIUM CARBONATES					
Lake Magadi, East African Rift, Tanzania	Holocene	Continental rift graben	Volcanogenic perennial saline lake	Cumulates and bottom-nucleated trona blades	Trona accretes each year as bottom growths atop 15m thick trona beds, which are sometimes deformed into pressure ridges (petees).
Wilkins Peak Member, Green River Basin, USA	Eocene	Foreland basin	Arid lacustrine interval in Tertiary basin fill	Trona beds and nodules with associated oil shales and dolomites	Subaqueous bottom growth on the floor of saline lakes and intrasediment nodules beneath the surface of desiccated mudflats.
SODIUM SULPHATES					
Continental playas in lowlands of Alberta and Saskatchewan	Holocene	Spring-fed hypersaline depressions on Northern Great Plains of Canada	Hypersaline, meromictic, perennial continental salt lakes	Coarsely crystalline, massive to thickly bedded mirabilite with lesser epsomite, bloedite, gypsum, magnesite and aragonite	Cooling of freestanding lake brine causes subaqueous bottom and nodular mirabilite to form.
Tertiary lacustrine deposits, Toledo Province, Spain	Miocene	Continental foreland basin to nearby Pyrenees and Iberian Ridge	Hypersaline, mudflats of continental salt lakes	Glauberite with lesser anhydrite, gypsum chalcedony, dolomite and magnesite	Glauberite with lesser anhydrite, gypsum chalcedony, dolomite and magnesite.

Table 11.19. Summary of nonpotash salt resources discussed in this chapter (all are continental saline lacustrine deposits).

The high solubility of the nonpotash salt resources, and their formation as lacustrine, not marine, precipitates explains their limited thicknesses, their mostly Neogene ages and their relatively small size compared to marine evaporites (Table 11.19; Figure 5.3). A lacustrine depositional setting, with its inherent lack of a huge isochemical brine reserve (seawater), means bed thicknesses and salt volumes will always be less than that of bedded salts accumulating in marine-fed saline giants. Inherent high solubility of lacustrine salt beds (trona, mirabilite, glauberite) in a hydrology susceptible to drastic changes in water supply and water table, means lacustrine salts are rarely found in rocks with pre-Cenozoic ages.

The Proterozoic borates of Liaoning Province are an obvious exception. The impervious nature of this succession, its metavolcaniclastic host, and the formation of a silicified envelope around the borates, relatively soon after their precipitation, allowed these salts to be preserved, although as a meta-evaporite. As a rule of thumb for salt exploration in a frontier area, those arid basins with post Mid-Tertiary ages should be considered much more prospective than any older basins. You should not expect to find trona or thenardite or other soluble lacustrine phases in large amounts in Palaeozoic successions and will probably not find them at all in Precambrian strata, at least not without a meta-evaporite silica genesis and a transformation into mineral phases such as tourmaline and scapolite.

Chapter 12: Solution mining and cavern use

Introduction

Salt solution mining is just what it says, the mining of various salts by dissolving them and pumping the resulting brine to the surface. It is predicated on the solubility of the targeted salt; the “rule of thumb” in the solution mining industry is that every 7 - 8 m³ of freshwater pumped into a cavity will dissolve 1 m³ of halite. Water or undersaturated brine is injected through a purpose-designed well drilled into a salt bed to etch out a void or cavern. The resulting “almost saturated” brine is then extracted for processing. It usually targets salts at depths greater than 400 to 500 metres and down to 2,000 m (Figure 12.1). The current deepest salt solution operation is in the northern Netherlands in Zechstein salts at a depth of 2,900 metres. At depths greater than 2,000m ongoing salt creep tends to reduce cavern size. Some operating brinefield caverns are as shallow

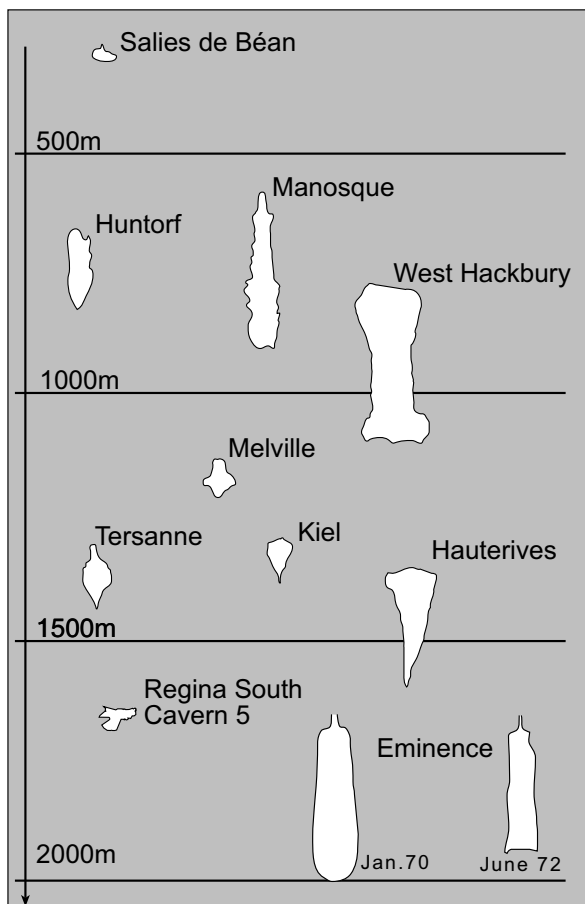


Figure 12.1. Depth profiles of various salt caverns, all are in salt domes except Regina South and Salies de Béan, which are in bedded salt. Eminence shows the volume changes after 18 months due to salt creep (see Figure 12.30).

as 150 metres, but this can lead to catastrophic chimneying and stoping in sediments above cavity. With deeper operations the landsurface tends to subside into a bowl of subsidence, as it does above many conventional mines. Cavern shape and the upward rise of the cavern roof is today controlled by an inert fluid blanket pumped in and maintained at the top of the zone of active brine creation. Early solution wells did not use this blanket technology as brinefield operators expected surface sinks, collapses and regular abandonment of caved wells.

In a solution mining saltworks, where production of various chemical salts is the main aim, saline brine is withdrawn from the expanding cavern and often pumped into solar evaporation pans to manufacture salts of designated grade, mineralogy and quality. Brine product from the pans, either solids or slurries, or a brine feed direct from the solution cavern, is piped to a nearby chemical processing plant designed for particular chloralkali, magnesia or other chemical products. Wells located near the site of a chemical plant and designed to capture brine of a particular chemistry are called captive brine wells.

The advantage of solution mining over conventional mining or surface evaporation pans is that product quality and the extraction operation is not as subject to the vagaries of climate or rock strength. Specific subsurface mineralogies can be targeted by the well bore to obtain a specific feedstock or chemical product without the need to get men and equipment from the surface to the mine face. Solution mining can exploit folded and disturbed beds or deep-lying strata, situations not easily mined using conventional techniques.

As well as halite, which historically has been the most common commercial target, other solution-mined salts include; potash (sylvite, sylvinite, carnallite), trona/nahcolite (sodium carbonate/sodium bicarbonate), borates (borax, ulexite, colemanite), sodium sulphates (mirabilite, thenardite) and magnesium chlorides. Today the cavern produced by solution mining may have a greater value than the extracted brine, particularly for a ubiquitous salt like halite. If appropriately designed, a cavity can be used for hydrocarbon or waste storage and even for energy generation.

Diapiric salt masses tend to be the preferred medium for solution mining as the salt mass undergoing designed dissolution is typically large, thick and tends to be homogenous. This makes it easier to purpose design in terms of both cavern shape and volume. Bedded salts tend to be less vertically homogenous

and more subject to caving and roof collapse, although ongoing improvements in directional and horizontal drilling mean these deposits can be exploited. Rather than the brine product, more and more the cavern itself and its use as a storage vessel, is the rationale for solution mining.

The solution mining process

Solution mining is an alternative to mechanical excavation of salt ores (Richner et al., 1992). Since most waste components in solution mining are not soluble they are left behind to settle to the bottom of the expanding cavern as the brine product is removed to a surface processing facility. Unlike conventional mining, there are no large above-ground waste piles and tailings impoundments. However, the possibility of collapse and karstification atop brinefields means contamination and leakage into nearsurface and surface waters are potential problems. Monitoring of landsurface stability reduces the possibility of such uncontrolled collapse and environmental degradation.

History of salt solution wells

The Chinese have been using brine wells, a form of solution mining, for more than 2,000 years (Yuanxiong and Chengxun, 1983). Designed-use shaft wells were sunk as early as 300 BC in the Szechuan and Yunnan provinces. By 1035 AD the Chinese in the Szechuan area were using percussion drilling to recover deep brines, a technique that would not come to the West for another 600-800 years. European travellers to China in 1400-1700 AD reported salt and natural gas production from brine wells, some of which had been sunk deeper than 450 metres and at least one well was more than 1,200 metres deep. Salt production in China at that time was prodigious, with more than 10,000 wells in operation. Marco Polo reported annual production in a single province of more than 30,000 tons.

Practically all the materials used in Chinese brine recovery wells, including ropes, casing and derricks, were made from wood or wood fibre, mostly bamboo. Bamboo is salt resistant and salt kills microbes and algae that would cause it to rot. Pipeline joints were sealed by mud or a mixture of lime and tung oil. Manpower was used both to power the drilling process and to raise the brine. A sharp iron wedge bit (resembling a spade or shovel) was suspended on a levered rope at the end of a bamboo tube so that it kept pounding and pulverising the rock at the bottom of the drill hole (Figure 12.2a inset). At the surface the drilling tool and drill string (bamboo) were suspended

from the end of a “spring pole.” The raising and lowering of the percussion head at the base of the hole was supplied either by workmen running up a short incline and jumping down, one after the other, onto a small platform attached to the spring pole or by a single workman alternately standing on a wooden lever pole and stepping off (Figure 12.2a; Deutsch, 1978). As the drill assembly was raised after each descent another worker rotated the drill string assembly so it would strike the base of the hole in a different position. After three to five years, a successful well could have penetrated up to several hundred metres to intersect a brine or natural gas target. In 1835 the Xinhai well reached a depth of more than 1 km using this bamboo percussion technology. Interestingly, the deepest percussion well in Europe around the same time was in Germany where a percussion well reached 535m in 1835. A likely reason for this shallower depth was that the Europeans used rope to suspend the drill tool, while the Chinese used bamboo.

Periodically, pulverised rock was bailed from the base of the deepening hole. This was done by pouring water down the hole to create a slurry. The slurry was extracted by lowering a weighted hollowed-out bamboo pipe with an interior leather flap on its lower end. When lowered into the slurry the flap would open and jiggling the pipe up and down when on the base of the hole forced rock slurry into the pipe. Then the pipe was raised with the weight of the slurry forcing the leather flap closed.

Later, once the hole had achieved its target depth, brine in the Szechuan area was often recovered from the well by the same means, namely, using a long bamboo bailer with a leather valve at its bottom. When a brine-filled tube was suspended over a nearby storage tank, a poke from a stick would open the valve releasing the brine (Figure 12.2b). Alternatively, a section of bamboo with pith left in place was cut by a series of holes located just below each pith level creating a series of small buckets. The weighted bailer was lowered into the brine pooled at the base of the brine well and brine flowed into the holed pith sections. Then the bailer was raised and inverted over the storage tank.

Often the storage tank was connected by bamboo piping to the salt boiling house (Figure 12.2c). Other bamboo pipes, located just below a natural gas wellhead were used to capture escaping methane and pipe it to the boiling house to fire the salt crystallisers (iron pans).

From the pipe technology developed at the Szechuan brine works, Chinese throughout the country learned to build irrigation and plumbing systems (Kurlansky, 2002). Farms, villages, and

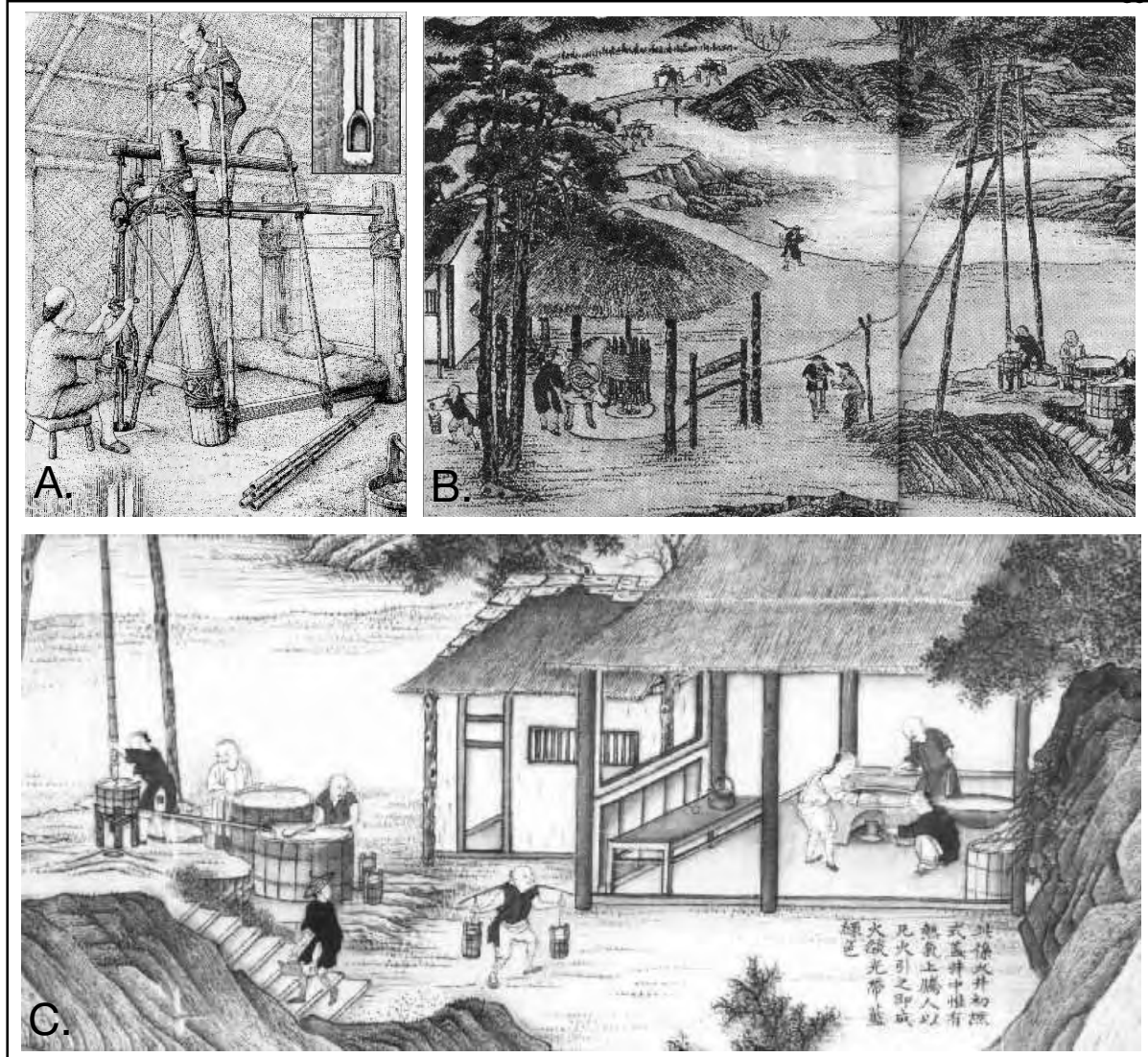


Figure 12.2. Solution mining and brine recovery technology in saltworks of the Szechuan region of China in the mid-eighteenth century. A) Man-powered percussion drilling using a human weighted lever system to raise the drill bit. Inset shows typical spade like iron drill bit that was suspended on bottom of bamboo drill string. B) Animal-powered brine hoisting from a deep solution well. C) Transfer of brine to iron pans for boiling of the brine product and recovery of salt. Boiling plants often using piped natural gas (No bamboo piping from well head to boiling house is shown in this image).

even houses were fitted with bamboo plumbing. By the time of the Norman conquest of England, Su Dongpo, a bureaucrat born in Sichuan, was building sophisticated bamboo urban plumbing networks. Large bamboo water mains were installed in Hangzhou in 1089 AD and in Canton in 1096 AD. Holes and ventilators were installed for dealing with both blockages and air pockets.

In Europe, near Lorraine, France, much simpler designed-use brine shaft wells were sunk by hand as early as 858 AD (something the Chinese had been doing since at least 250 BC). In 1381 AD the Duke of Lorraine, the Bishop of Metz and the

Duke of Bar, formed a salt cartel that operated brine wells at Chateau-Salins and Salonne (Deutsch, 1978). By 1740 brine was raised in the region using horse-driven pumps and in 1758 steam-driven pumps were drawing brine from wells that were more than 100 metres deep. By 1839 salt was being directly mined in an underground operation at Dienze that employed over 400 miners. By 1830 in the USA there were more than 60 brine wells in operation in Kanawha region near the confluence of the Kanawha and Ohio rivers. Numerous brine wells were in operation in New York State by 1880, while large-scale brine recovery operations in the various playas of the Basin and Range were underway by the early 1900s. Today, steel-cased

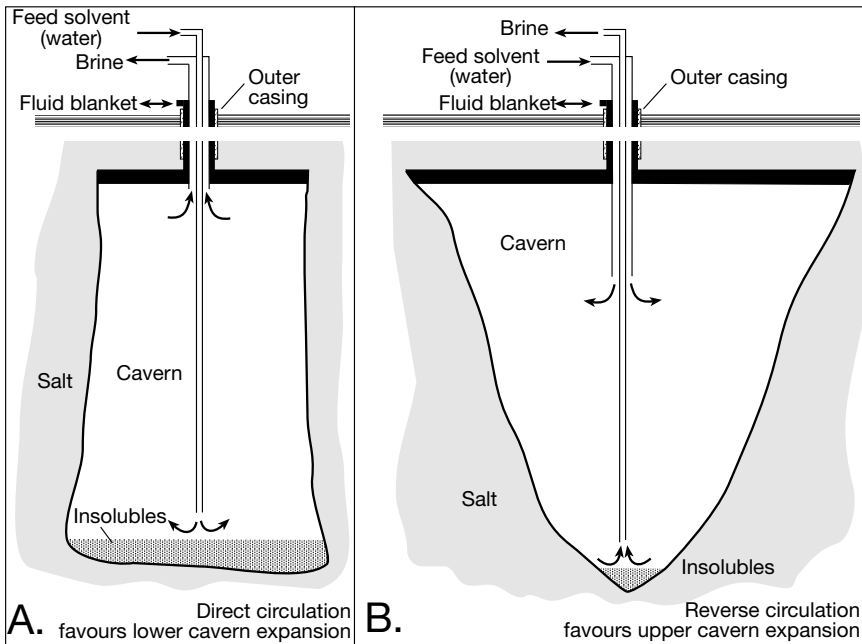


Figure 12.3. The solution mining process. A) Direct brine circulation where feed solvent is injected through the tubing string and brine is withdrawn through the annular space between the tubing string and the final casing. Cavern shape tends toward cylindrical with slightly expanded lower section. B) Reverse-circulation where the feed solvent enters the cavity through the annulus and brine is withdrawn through the tubing string. Cavern tends to be wider at top than base ("morning glory"). In both cases the outermost casing allows feed of the blanket solution into the uppermost part of the cavern, so protecting the cavern roof. Varying the volume of blanket in the cavern can be used to help shape the cavity.

brine wells are consistently drilled to depths of more than 1-2 km to extract brine product or to excavate custom-built salt caverns for hydrocarbon or waste storage.

Well and cavern design

The design of a salt solution well consists of two or more columns of steel pipes (casing strings) with the smaller inside the larger. Fresh water or undersaturated brine (feed solvent), needed to drive the solution process in an expanding cavern, is pumped into the well to create a cavity in the targeted salt. The resulting brine is then returned to the surface for processing and recovery.

The first step in solution mining salt is to drill an appropriate-diameter borehole, large enough to accommodate all the required pipes (casing). This means solution wells are wider than most oil and gas or water wells. Near the surface, the borehole is widest to allow for installation of several concentric layers of pipe casing (Figure 12.3). The outermost layer of casing, known as the surface casing, is cemented in place to prevent

any leakage and contamination of nearby groundwaters. Surface casing does not typically extend all the way down to the cavern roof. The final casing string (or long string casing), which is also cemented in place, is set at some depth below the top of the target salt so that during dissolution a reasonable thickness of salt remains in place as a salt roof to the expanding solution cavity. In modern wells there is another string next to the outer casing string that controls the thickness of the fluid blanket.

Generally, one or more non-cemented casing strings, the tubing strings, are placed inside the final casing string. In modern designed-use caverns, non-cemented casing or tubing strings first extend to a depth near the planned base of the cavern. Under this design scenario, strings can be rotated and raised (snubbed or pulled) as the cavern grows and the bottom fills with debris. Depending on the size of the cavern and the amount of impurities present, more than 20 metres of impurities (dolomite-anhydrite residues and fragmented roof blocks) can sit on the bottom of an active solution cavern (Crossley, 1998; Tomasko 1985). Some older interconnected multi-well brinefields did not have non-cemented strings in each well.

Salt subjected to undersaturated crossflow in an expanding solution cavity tends to leach 1.5 to 2 times faster vertically than horizontally (fresher water is less dense than brine and tends to accumulate in the upper part of a cavity). Vertical leaching tends to be even faster if there are gas inclusions in the brine giving it even greater buoyancy. An inert low density fluid blanket is usually pumped into a solution cavern to prevent rapid upward stoping and ultimate collapse of the cavern roof, along with its cemented casing string, into the growing cavity. Roof blanketing, sonar imaging and designed cavern shaping typifies almost all current commercial solution mining operations.

Blanketing fluid is inert so it does not dissolve the target salt, and is always less dense than the feed solvent or the produced brine. It always floats to the top of the cavern where it insulates the roof from the effects of dissolution. Older blankets were one of a number of different types of oil, typically diesel or crude, but today are increasingly composed of other fluids including LPG, nitrogen and compressed air. Nitrogen and less often compressed air tend to be the fluids of choice as they do not have the environmental and safety issues associated with a hydrocarbon blanket. Generating a blanket requires the addition of a devoted column of pipes in the well string and the blanket is usually pumped in/out via the annular space between the outer and middle casing pipes (Figure 12.3).

There are several methods for developing and shaping caverns. In the direct circulation method, feed solvent is injected through the tubing string and brine is withdrawn through the annular space between the tubing string and the final casing (Figure 12.3a). In the reverse-circulation method, feed solvent enters through the annulus and the brine is withdrawn through the tubing string (Figure 12.3b). As less dense water in a salt cavern tends to float on a more concentrated brine, a “morning glory” type cavity with a much wider top than base is likely to be formed by what is called reverse circulation, especially in cavities grown without the aid of a fluid blanket. A more cylindrical cavity is formed by direct circulation. During cavern excavation, the volume of the blanket fluid is increased or decreased to help shape the cavity.

Detailed discussion of the engineering aspects involved in well design and cavern shaping is largely outside the geological focus of this book. Various authors, such as Remson et al. (1966), have outlined the general procedures for controlling the shape of the solution mine cavities, and many articles, such as that of Shock (1985) and Jacoby (1974), have been written on basic solution mining techniques for various salts. Extensive bibliographies also have been prepared on solution mining, such as those by Dahl (1985) and Nigbor (1982). Combinations of these various methods and other more complicated solution mining approaches are now well understood and can be used to obtain any desired cavern geometry or well-to-well interconnections (API, 1994).

If a particular brine product is the goal of a solution mining operation, rather than the cavern itself, then the extracted brine typically is evaporated or treated at the surface to produce a crystallized product. In this case an “almost saturated” brine product is mandatory in the rising casing string. Dilute brine is too expensive to process, while supersaturated brine can

block the raising string with unwanted precipitates. When a single-hole solution mining well is first drilled, the flow rate through the cavity and up the pipe is usually kept very low to maintain higher levels of brine concentration. As the surface area of the cavity and the cavity volume increase with time, the extracted brine flow rate can be progressively raised. In a year or so comparatively high flow rates can be maintained. The life of a successful brine well can be quite long, up to 30-40 years. If the solution process is maintained from a single well the area around the well will eventually subside, or the borehole roof carrying the casing strings will weaken and cave, disrupting the brine flow. Even if the roof doesn't cave, salt will dissolve from around the casing string and it will eventually corrode and fall into the cavity.

Historically, captive wells designed for brine recovery and not for storage were expected to be abandoned or to fail. Most such wells started out as reasonably good producers, but ultimately failed by breakage or damage to the casing string by corrosion, by roof caving or by subsidence-related shearing/collapse of the casing string (Deutsch, 1978). Failure could occur soon after a well evolved into a high-capacity performer or decades later. Most brinefield operators learnt that many of their oldest wells were their most reliable producers. Many captive brinewells “die” during their “infancy,” but if they live through the usual “childhood diseases” of roof collapse and casing shear, the chance of failure lessen as they get older. Some older brinefield wells in bedded salts, that is, wells that had produced for 20 to 30 years, seemed to be immune to caving and were abandoned only when the target salt layer was exhausted.

Predicting which wells survive in a brinefield is difficult. An analysis of some 60 wells drilled between 1887 and 1925 clearly shows this trend of long-lived survivors (Figure 12.4).

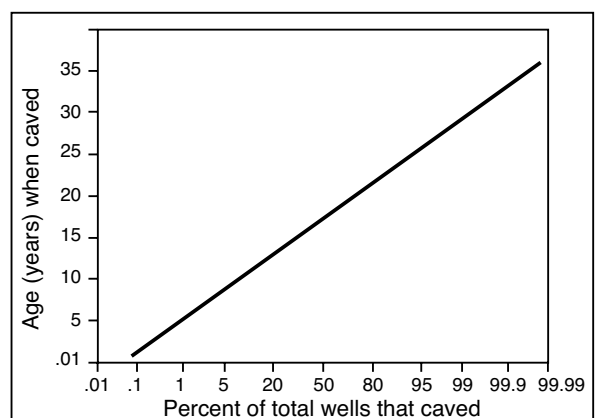


Figure 12.4. Schematic of the “life expectancy” of a set of brine wells (Deutsch, 1978).

One possible explanation for “long-life” wells is that early cave-ins distributed fallen rock in such a way that the lowest part of the tubing string was protected from damage by later cave-ins. Alternatively, as the roof of a growing salt cavity reached a greater and greater span, it could either cave with serious results for the well, or it could very gradually subside until it was supported by silt or projections and debris at the bottom of the cavity. A brine well in the latter situation would continue to be a good producer, even with a very shallow cavity. Well failure or poor performance is somewhat random in nature, and can occur unexpectedly. Consequently, and because of slow initial production rates, most captive brinefield operators employ many wells, abandoning nonproducers and bringing new ones on-line.

In all cases, mud and other insolubles, as well as some salt falls accumulate as muddy breccias at the base of the expanding cavity. In wells where salt layers other than halite are the target and are encased in thick halite, the initial borehole is typically drilled through the target bed(s) to some distance into the underlying halite mass. As the cavity then expands, it creates a sump below the target bed where insolubles can accumulate. In any solution cavity it will be necessary to raise the bottom casing string (snubbing) above the level of the insolubles, otherwise the well will need to be plugged and abandoned. This is also true if the casing has been severely bent or damaged by the rock-falls from the roof. Normally these problems occur very slowly, and the cost of the initial capital and well operation is such that the total mining expense is very low compared to conventional room and pillar extraction.

Many land areas above brinefields, which were active in the 18th or 19th centuries and were over-exploited, are today subject to collapse. But few records of well placement or even the position of the brinefield were kept in older areas of extraction (as in Hutchison, Kansas - see case histories later in this chapter). This leads to all manner of environmental and civil engineering problems in the vicinity of many former brinefields. But not all engineering and subsidence problems in areas of nearsurface salt are anthropogenic (Figure 7.41). Salt dissolves and the large collapse cavities form naturally at the landsurface in time scales measured in days or weeks. Outside of areas atop poorly managed or historical brinefields, separating anthropogenic sinkholes from natural dissolution cratering is very difficult. A cynic might conclude that many causative interpretations depend in large part on which interest group is paying the consultancy bill.

Solution well styles

Various techniques have been employed in brinefields over the last 150 years to improve brine production costs and to increase the amount of brine produced per well. Today the dissolution process for single wells can involve multiple concentric or independent tubing strings, various fluid injection/production depth combinations, as well as several different roof-protection combinations involving blankets of different types of hydrocarbons including crude oil, LPG, and gases such as nitrogen and CO₂. Blanket design now also includes solids such as floatable cements and hollow spheres (Richner et al., 1992). Multiple-well interconnections can be achieved in a planned manner using appropriate geological understanding along with combinations of roof padding, well deviation/horizontal drilling and hydraulic fracturing.

Expert design of solution wells is for the most part dependant on geological understanding of the salt to be exploited. Required knowledge includes: dip and thickness variations of the target bed; mineralogical composition, homogeneity, insoluble levels and dissolution behaviour of the target salt bed and adjacent salt layers; distribution and mineralogy of intrasalt beds; structural integrity of confining beds. Caverns engineered in salt domes tend to be more reliable and predictable structures than caverns engineered in bedded salts and are more suited to product storage especially if the product is stored under pressure. Compared to dome salt, bedded salt in the vicinity of a solution well tends to be thinner and bound above and below by more permeable formations. Bedded salt is also more likely to enclose layered intrasalt beds with varying levels of solubility and fracture intensity (anhydrite, shale and dolomite intrabeds) and so tends to supply significantly higher quantities of impurities to the cavity floor. The most stable cavern shape for purpose-designed storage resembles a giant carrot or cucumber embedded deep in a mass of salt. This ideal shape is next to impossible in bedded salt, and to continue the vegetable garden analogy, jack-o-lantern pumpkins are a more likely outcome.

Historically, the earliest single wells had top injection (reverse circulation) and no roof pad or blanket. These Tully-method wells had the advantage of low investment costs along with rapid development of saturated brine flow (Richner et al., 1992). Unfortunately, this technique tended to create unstable morning-glory caverns subject to roof failure and their design inherently limits brine recovery to the upper portions of any targeted salt mass. Casing damage was likely even in the very early stages of cavern growth. “Tully” wells are not used

today and belong to a time in human history when landscape damage was seen as a positive indicator of “progress.” In the 1920s and 30s Detroit-method wells, with direct circulation via a bottom tubing injection, became the preferred method for excavating single well brine producers as they tended to create more stable cylindrical caverns, less subject to early collapse and loss of the well.

In the 1930s the “Trump” method, a multiple well technique, was introduced to exploit bedded salts. It involved direct circulation and the use of a roof pad or blanket (Figure 12.5a). Multiple wells were completed near the base of the targeted salt formation. The aim was to create large diameter undercuts near the base of the target salt bed and then allow the undercut caverns to expand beneath their blankets until adjacent cavities met. Historically, wells utilising the Trump method were between 61 and 183 metres apart. Once an interwell connection occurred, the wells were changed from two independent circulation wells, into two-well or multiple-well operations. One (or more) well(s) became the injector(s) for feed solvent and the other(s) became the brine producer(s) (Figure 12.5a). In this way the salt formation between the two wells was more efficiently recovered by the rising cavity roof and the per well brine production rates and tonnages were markedly improved compared to the older single “Tully” method wells. Using the Trump method entails a 12-24 month period of cavern development during which arrangements must be made for the usage or disposal of unsaturated brine.

recommended a 91m well spacing in bedded salt and about 18 months from the onset of feeder brine pumping to a time when an appropriate and consistent quality brine product could be recovered. He noted that cavity development and brine field subsidence in general can be controlled to a greater degree using the “Trump” procedure rather than a single Tully well. It entails relatively low production costs and high flow rates per mature well. However, the padded rising roof of the cavity is not a structurally competent shape, and roof falls ultimately occur. Constant raising of the casing is often required, especially in the downdip feed wells. The production or uphole wells are

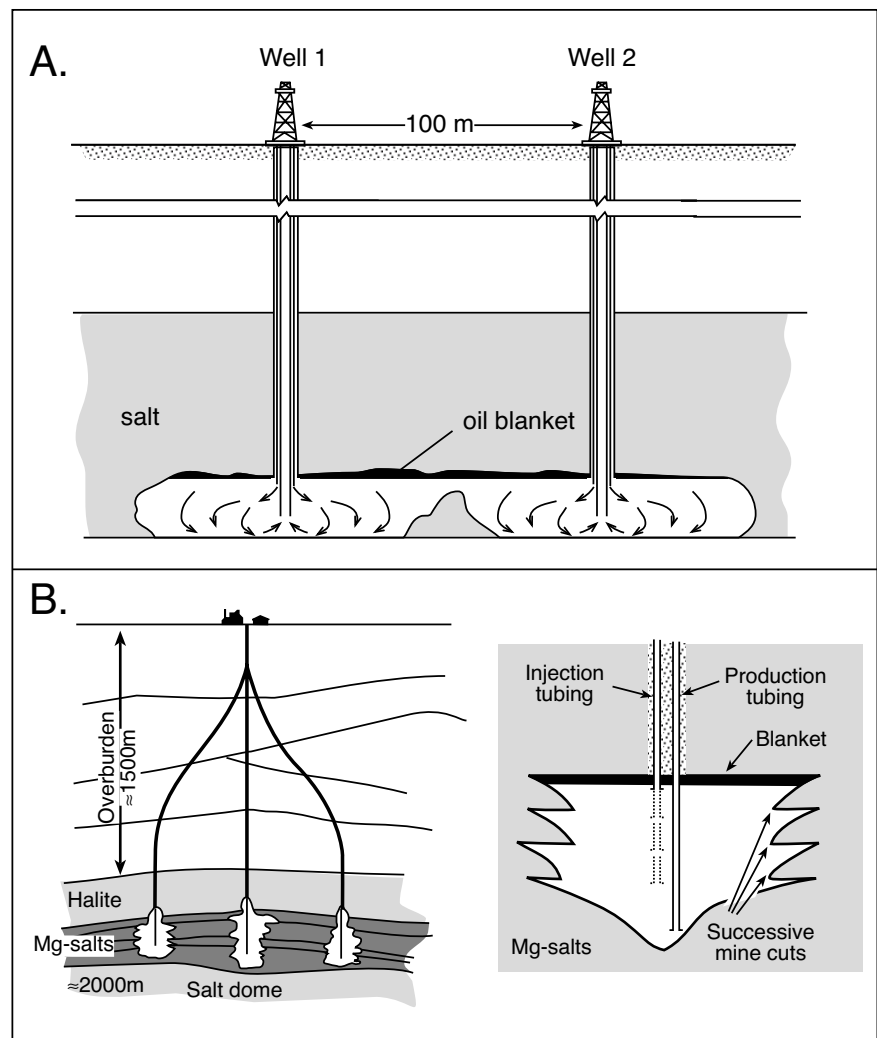


Figure 12.5. Methods of solution mining. A) Joining wells by using an oil pad or blanket in combination with reverse circulation (after Henderson, 1974). B) Schematic of deviated wells in magnesium salts at the NedMag plant in Veendam, Netherlands, showing solution mining method of upward retreating successive cuts with positions controlled by the blanket (after Currie and Walters, 1985).

Henderson (1974) reviewed this multiwell method of solution mining for halite targets. For maximum efficiency, he

particularly vulnerable, and generally weaken and fail first (see the Romanian SALROM disaster in case studies).

Specific examples of the mining of very thin beds of salt using one- or two-hole methods were reported from a brinefield in China by Yuanxiong and Chengxun (1983). Single-well, nonblanketed, production of a salt bed 1 to 6 m thick at a depth of over 1,000 m in 12 wells over a five-year period averaged 20,000 to 30,000 t/yr of salt per well (maximum 70,000 t/yr), with a well life of four to eight months. Both the casing and tubing tended to deform, bend, and break from roof falls. Well life was longer in zones with a more stable roof. However, when oil pads were employed on a single two-pipe well 935 m deep within a 17-m-thick salt, the well was fairly quickly producing 50 t/day of salt as a saturated brine. Well life and productivity were much improved. Two other wells were then connected by using oil pad control to test against the single well extraction method. The wells were 1,042 m deep, 71.7 m apart, and operating in a salt bed some 17 to 20 m thick. Cavity height during excavation was maintained about 2 m above the base of the salt. By 100 days the flow rate in each well was 10 m³/hr with an “almost saturated” exit brine, and in 500 days the wells were interconnected. In a third set of wells at 1,004 m depth, 16-m-thick salt, and 68-m spacing, it only took 180 days to make the connection. About 26,000 tons of salt were “wet mined” in making each cavity, and the daily salt output was 300 to 400 t/day per well at the end of this period. Blanketed reverse circulation (top injection, bottom production) was employed to better control roof height and allow faster horizontal cavity growth. Over 50% recoveries of the entire thin salt beds were obtained with excellent economics and minimal surface subsidence using this procedure.

Today, most single well solution mining operations utilise a modified annular injection method, known as variable point injection, where both the tubing string and the casing string are positioned near the lowermost level of salt to be dissolved. Undercuts of more than 100 m diameter are achieved using a gaseous or liquid roof pad. In captive wells, brine production rates of more than 13 litres/sec have been obtained once the blanket is withdrawn. As solution proceeds both the tubing string and the casing strings are raised clear of the accumulating insolubles (snubbed). This type of well is also capable of achieving planned-cavity shapes suitable for waste storage.

An interesting test of the efficiency of both single-well and two-connected-wells solution mining systems targeting a thin bed of sodium borate was described by Taylor (1970). An 8.8-metre thick layer of borate ore, which was 107 metres below

the land surface with a 72% ore grade, was solution-mined in a series of tests. At the completion of the tests the cavities were physically mined (entered) and inspected. No roof padding was employed during the tests. Hot water at 102° to 110°C was injected as a feed into the 21°C formation and a 15 litre/min flow produced an “almost saturated” borax solution with an exit temperature around 77°C. As the test progressed, feed temperature was steadily decreased and the allowable flow rate of the saturated solution steadily increased. On later cavern entry it was found that broad morning glory holes had formed and large amounts of insolubles had accumulated on the cavern floor. Clay and shales from the roof had fallen as intraclasts with a “sand and gravel” structure. Cavity bottoms were dominated by this material, rather than by fine bottom slimes usually postulated to dominate cavity bottoms. Some slabs of borate remained encased in the pile of insolubles, where they remained buried as unleached blocks.

Techniques in potash operations

Texas Gulf solution mines potash-rich brine from deformed salt beds in the Paradox Formation at Moab, Utah and then uses solar concentrators to achieve a product appropriate for processing. The IMC Kalium operation near Moose Jaw, Saskatoon, recovers potash brine by solution mining a sylvinite bed (Belle Plain Member) 9 to 15 metres thick at a depth of 1,650 m using a patented solution and recovery method (Figure 11.19). To capture the ore, hot undersaturated brine feed is pumped into the dissolution cavity. Concentrated potash brine is then returned to the surface processing plant, which uses a sequential evaporation-crystallization process to recover potash and recycle hot NaCl-rich brine to the subsurface for another leach cycle. In the dry steam driven evaporation stage in the processing plant, moisture is removed and the recovered brine is brought to saturation point. But halite and sylvite have different temperature responses (Figure 11.10a). Halite is crystallized first by evaporating the recovered brine, then potash is recovered by cooling the remaining hot, saturated solution.

The NedMag solution mining facility near Veendam in the Netherlands produces magnesium from magnesium chloride brine by solution mining a Zechstein salt dome, targeting beds that are a mixture of carnallite (KCl.MgCl₂.6H₂O), bischofite (MgCl₂.6H₂O) and halite (NaCl), with some sylvite (KCl) and kieserite (MgSO₄.H₂O). Target beds at Veenham average 100 metres (combined) thickness at depths between 1,400 and 1,800 m. About a 100 metres of halite lies above the target magnesium salts and more than 1,400 m occur below. Beds were accessed by a total of 12 solution wells drilled between

1972 and 1991. Nine of these wells were still operational in 2000 with average brine production per well around 25 m³/h. NedMag has recently excavated one of the deepest solution mining cavities in the world at 2,890 metres. Each year the NedMag plant produces in excess of 150,000 tonnes of high purity synthetic dead-burned magnesia and more than 70,000 tonnes of magnesium chloride in liquid or solid form. A similar solution-mined operation producing MgCl₂ brine by targeting bischofite beds is planned for a large deposit near Volgograd in Russia.

The mining procedure at Veendam utilizes a backstepping solution cavity method (Figure 12.5b). Cavity extent is limited to ≈100 m diameter (perhaps now extended to 150 m), and the brine is maintained at the original downhole (lithostatic) pressure. Wells are designed to be plugged and abandoned at full pressure. Considerable insoluble rockfall and mud deposition is encountered from the laminated intrasalt formations and the various impurities in the NedMag target beds. This requires frequent raising of both the injection (to control the cavity diameter) and the withdrawal of pipes (to prevent blockages; Figure 12.5b).

Cavern pressures are kept relatively low in the producing caverns (average of 10 MPa or 100 bars) and well below the far field rock stresses. This facilitates salt creep into the cavern, but the lower viscosity of the magnesium salts compared to halite means they are preferentially squeezed like toothpaste into an active solution cavern at a rate far greater than the creep of the adjacent halite. Hence, the bischofite beds supply far greater volumes to the dissolution cavern than the adjacent halite beds with convergence rates contributing 30–40% of the produced MgCl₂-brine volume. This method has been called “squeeze mining” and the brine product from squeeze caverns can be very pure. For example, four wells producing brine from “squeeze caverns” at Veendam are almost saturated with respect to bischofite, rendering a high quality brine product with less than 1% by weight of non-magnesium chloride salts.

All of the halite in the dissolution cavern must be leached along with the potash in order to keep the face of the solution cavity open and dissolving rapidly. Otherwise, a buildup of salt and insolubles on the active dissolution face cause blinding. Bottom casings are raised (snubbed) periodically to keep above the buildup of insolubles. As with all solution brine operations, flow rates are kept low enough to produce a transparent “almost saturated” brine. Because the targeted potash bed is thin, well capital and operating costs are comparatively high, but are reported to be still less than conventional potash min-

ing. Relevant published potash solution mining articles and processing patents include; Bach et al. (1985), Day (1967), Dillard et al. (1975) and Schlitt (1982).

Carnallite, like trona, shows incongruent solubility so that in beds composed of mixtures of carnallite, sylvite and halite, the sylvite tends to be left behind as a less soluble component that can slow the rate of dissolution (surface blinding). Furthermore, the solubility of halite, sylvite, and kieserite is very low in strong MgCl₂ solutions. However, by carefully maintaining the proper MgCl₂ concentration in the Veendam cavern brines and monitoring solution flow rates using variably pressurised waters, NedMag has minimised blinding in bischofite beds (Steenge 1979). For successful magnesium chloride recovery, the solution rate, the dissolving surface and the produced brine at Veendam must be maintained at all times at an ‘almost saturated’ condition. The operations at Veendam are a worldclass example of targeted and monitored solution mining with a set of process technologies specifically designed for the brine product. Historically, high levels of carnallite in some potash beds in the Zechstein have made them a poor choice for a KCl targeted beds in both solution and conventional mining operations. But NedMag has recently begun to use a patented process to produce brines that are also saturated with respect to carnallite from carnallitic beds previously considered subeconomic.

Lithology effects shape

So far, much of our discussion of shapes of solution cavities has assumed that the thick salt targeted for dissolution is relatively homogenous. But halite masses typically contain thinner intercalated layers, composed either of less soluble salts, such as anhydrite or dolomite, or of more soluble salts, such as carnallite or bischofite (as at Veendam). An assumption of target bed homogeneity in solution planning can lead to problems during the leaching process.

With less soluble salt layers intersecting a cavern edge there is a tendency to form unsupported ledges and bevels, which eventually collapse to the floor of the expanding cavity. This can damage the roof in the vicinity of the feeder pipe, break the drill string, or force the operator of a suitably designed well to raise the well pipe off the former cavity floor (snubbing). In the case of more soluble beds, their rapid solution can leave behind blocks of unstable halite, which have a propensity for collapse, or it can lead to cavity shapes that become enlarged in one direction and encroach on the structural integrity of the well design, especially when there are adjacent solution cavities.

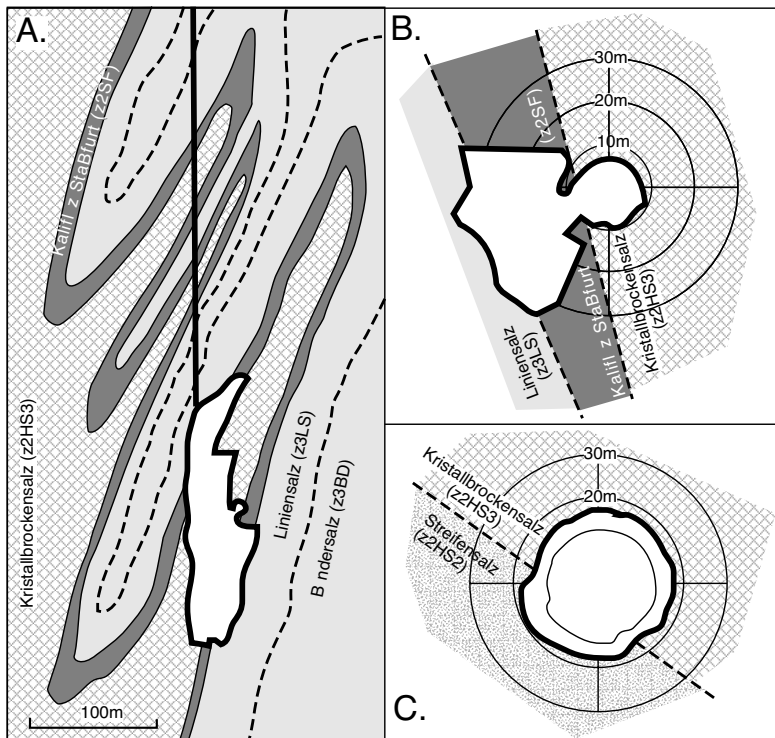


Figure 12.6. Effect of salt geology on cavern shape in diapiric Zechstein Salt. A) Vertical section through a cavity in Zechstein Salt in Germany showing preferential enlargement into potash-rich Kaliflöz Stassfurt horizon (shaded grey). B) Horizontal slice showing strongly asymmetrical shape formed as cavity develops preferentially into the potash facies of the Kaliflöz Stassfurt. C) Horizontal slice in a cavity in two halite lithologies where differences in crystal size and proportion of insolubles create a slight asymmetry that is maintained during growth (after Wilke et al., 2001).

The best studied and modelled examples of lithology variation effecting cavity shape come from the monitored cavities in the Zechstein salts of onshore Germany (Wilke et al., 2001). Of the four major Zechstein formations in the northwest European Zechstein basin, the Staßfurt formation (Zechstein 2) occurs in sufficient thickness (more than 800 m), to flow in to salt pillows and diapirs and so is the most important target unit for solution-leached caverns in this part of Europe (Figures 5.48). The underlying units of Werra formation, along with older salt units of the Rotliegende, are typically inactive and many beds are still attached to the basement. Salt of the overlying Leine formation (Zechstein 3) contains relatively thick beds of anhydrite and dolomite. It has an original thickness of 200 m, lies above the Staßfurt formation and is typically caught up in the Zechstein flows, but it needs the underlying thick halite of the Zechstein 2 to flow and carry it along.

High quality documentation of the internal structures of the German diapirs during potash mining has produced an excel-

lent data set on which to model the likely geological complexity of these Zechstein structures (Figure 6.9a). This work caused the German salt experts, Richter-Bernberg and Horfrichter to conclude that of the Z2 and the Z3 series, the Hauptsalz member of the Staßfurt formation is most suitable for designed-use cavern construction and that the upper part of Staßfurt be avoided where possible due to inherently higher proportions of highly soluble potash and magnesium layers. Likewise the overlying Hauptanhydrit of the Z3 has a propensity to create unstable anhydrite blocks during halite leaching and is not considered suitable for controlled cavity creation. Since their pioneer work, the goal has been to avoid solution mining in this transition zone between Zechstein 2 (Staßfurt Formation) and Zechstein 3 (Leine Formation). Nevertheless several caverns have been leached in these strata, some without any problems, others with intensive preferred leaching directions (Figure 12.6a, b; Wilke et al., 2001).

Structural elements in salt diapirs, largely crystal size and anhydrite distribution patterns in non-potash containing intervals lead to slight changes in cavern development. For this reason a sonar-measured cavern shape can be used to re-interpret a pre-existing geological map. For example, the horizontal section in Figure 12.6c outlines the contact between the Kristallbrockensalz (Z2A-HS3) and the Streifensalz (Z2-HS2), which leaches slightly faster due to its finer halite crystal size and more widely dispersed insolubles. Figure 12.6a, b are examples of preferred leaching along a relatively undisturbed potash seam. It lies several metres above a previously interpreted contact between the Kristallbrockensalz (Z2-HS3) and the Streifensalz (Z2-HS2). This later geological interpretation along the borehole provoked concerns that the potash layer would be intersected as cavern proceeded and led to a modified plan for cavern creation.

Experience in this terrain has shown that where potash layers of the Kaliflöz Staßfurt cross the drill axis a number of times it is not possible to perform a controlled leaching in one step. Rather, the leach design has to be planned as a number of mining steps to avoid a premature achievement of the maximum

allowed cavern diameter in the vicinity of the potash layers (Wilke et al., 2001).

Such a controlled leaching program, tied to lithological variation, is called blanket management and proceeds in a series of back steps as described by Wilke et al. (2001; Figure 12.7):

- Blanket depth is kept below the 50° dipping potassium seam at a distance such that the expanding cavern wall will not touch the seam while it is expanding towards the maximum allowed diameter.
- After reaching 80% of the planned cavern volume below the seam, the blanket is raised to a position slightly above the dipping seam to allow some upwards leaching along its occurrence.
- After some weeks of development of the original borehole, the blanket is pumped down to once again cover the more soluble part of the leached section.
- Continue leaching and continuously add “oversize” amounts to the blanket to be sure the more soluble section is covered.
- Raise the blanket to prepare a new leaching step, before snubbing the pipes. Maintain the blanket in the section of the potassium seam to continue protecting that area.
- Change the injection point depths shortly before the maximum diameter is reached below the seam and while the production point is still sufficiently deep to approach to

the maximum allowable shape in this part of the cavern. All the upper section of the cavern is then allowed to expand toward planned diameter.

In the case of caverns intersecting highly soluble intrasalt beds it is especially important to create “as much as possible” cylindrical caverns below the level of any seam. This approach means that the largest allowable storage volume is created inside the project’s rock mechanical parameters. At the same time the hole shape must be monitored often enough to avoid uncontrolled expansion in the highly soluble (potash) layers.

Well pad design

Some modern brinefields and storage sites are made up of single wells with concentric casings extending into individual caverns. Others consist of several adjacent brine wells extending into a single large cavern. Yet others create multiple caverns off a cluster pad. Brine is withdrawn either through the outer concentric casing in a single well cavern, or through a separate casing in a multiple well cavern. Once active, the size and shape of solution-mined caverns can be measured and controlled with cavern sonar and operating techniques (Crossley, 1997, 1998).

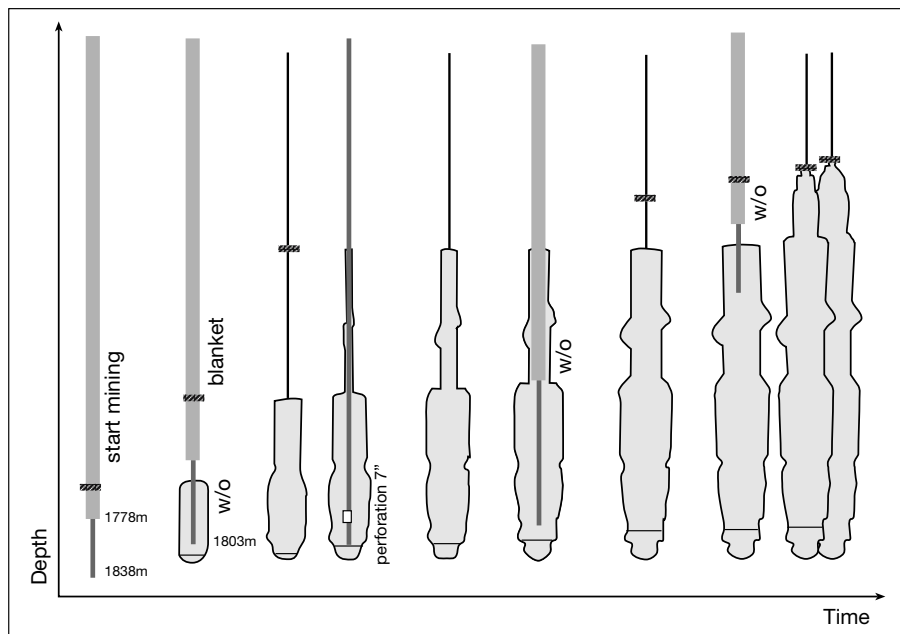


Figure 12.7. Solution mining for a gas storage cavern using a blanket management plan designed to control breakout across an inclined potash bed that cuts the storage cavern twice along its planned length (as shown in 12.6a). The scheme uses a combination of blanket management and sequential snubbing. See text for details (after Wilke et al., 2001).

Single drill pads typically sit atop vertical wells, they offer maximum flexibility in cavern depth range and minimisation of hole damage (Figure 12.8a). Snubbing or pulling pipe is relatively straightforward in a vertical well due to low frictional losses. There is minimal borehole contact and good control on any twisting of the drill string needed to free it if it has become stuck. In all solution wells the initial borehole shape is important as it can strongly influence the shape of the subsequent cavern. Vertical holes suffer minimal borehole asymmetry, which is often created by excessive one-sided hole wear during the drilling phase of an inclined well.

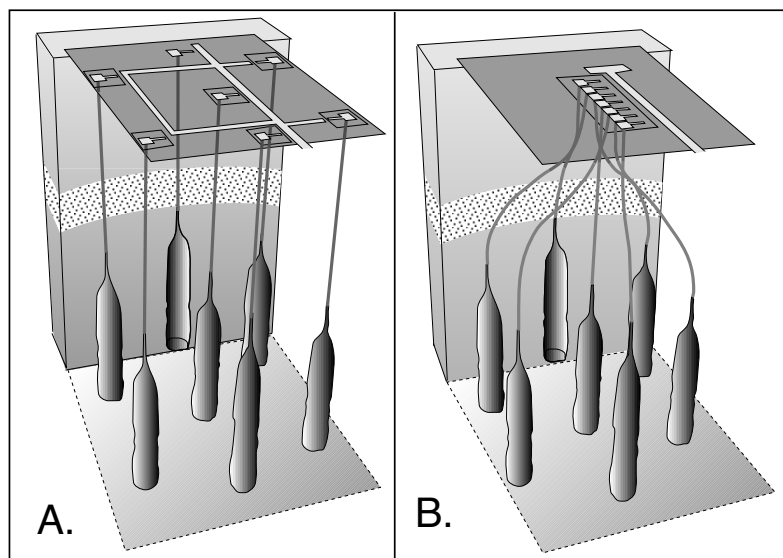


Figure 12.8. Well pad design. A) Single well pads. B) Cluster pad.

Cluster well pads allow multiple caverns to be created beneath a large pad and are a cheaper alternative to single well pads (Figure 12.8b). They have lower infrastructure costs and land area requirements, they need only a single access road, one field pipeline for the brine product, one set of power supply cables to the pad, and the surveillance of only one site. However, compared to single well pads, they suffer from less flexibility in ongoing planning and maintenance. The need for directional drilling and the degree of deviation means it may be difficult or even impossible to turn the leaching strings or the cables after a cluster pad well is activated. Rotating a tubing string is a technique frequently used to free the coupling on the last cemented casing shoe if it has become stuck during production. Once a cluster well group is completed is difficult to later modify production casings, but this can be an ongoing need in some hydrocarbon storage caverns. Cluster wells, which require an S-shaped drilling path, may not be feasible in regions where the targeted salt is shallow. Cluster pads only work if target salt bodies are more than 600-700m below the surface. A rough rule of thumb is that directed drilling can give deviations of some 1.5° every 10 metres of vertical depth.

Casing couplings should be engineered in the early stages of well completion design and are a critical feature in most cluster pad wells, especially those used for hydrocarbon storage. Once operational, it is virtually impossible to turn the leaching string in a deviated well. To compensate, the outermost leaching casing should be fitted with an integral coupling below the casing shoe of the last cemented casing string. That way, couplings do not stick in the vicinity of the casing shoe. When a cavern is to be

used for gas storage the more expensive option of integral couplings should be included in design of the brine withdrawal string. This prevents the sticking of casing in the vicinity of the production-string casing shoe. If a cavity is to be used for gas storage, the brine withdrawal string must be raised under gas pressure as the cavern is first filled with gas.

Deciding on single well pads versus cluster pads influences the design of the casing string and the completion specifications. With a cluster pad the likely depth and homogeneity of the target salt must be known prior to the commencement of drilling. Successful directional drilling of S-shaped wells is best achieved using measurement while drilling (MWD) techniques. MWD techniques are now standard methods in

the oil and gas industry and should perhaps be more widely considered for single well pads. MWD allows the operator to better deal with any unexpected deviations encountered during the drilling of vertical or inclined wells.

Blinding and phase chemistry

Halite is the targeted salt for most solution-mined brinefields and is one of the simplest chemical systems to cope with in the subsurface. Thick halite deposits, if associated with only carbonate and calcium sulphate impurities, are chemically well-behaved during dissolution and their basic brine chemistry was discussed in Chapter 2. But today, there are a growing number of solution mining operations that target salts with more complex dissolution chemistries, such as the borate or sodium carbonate salts, where covering or blinding the cavern surface with a layer of less soluble salts is a strong possibility.

All non-halite targets require a predictive understanding of brine phase chemistry. The intricacies of phase chemistry of brines and salts is largely outside the evaporite focus of this book and a detailed consideration of the various precipitation outcomes requires a book in its own right (see Usdowski and Dietzel, 1998). To illustrate what is possible we will look at some of the complexities and possible problems using current understanding of simple phase equilibria and dissolution kinetics for trona (after Haynes, 1997). Kerr-McGee currently solution mines soda ash at Trona, California and until recently

American Soda operated a directionally drilled solution mine facility for a nahcolite target bed in Colorado.

Phase chemistry - trona solution mining

The ternary phase equilibria of the sodium carbonate system $\text{Na}_2\text{CO}_3\text{-NaHCO}_3\text{-H}_2\text{O}$ is temperature dependant (Haynes, 1997 see also Figure 2.13). When trona is dissolved in pure water it follows the dissolution path A-A' (Figure 12.9a). If the system is at 40°C, an undersaturated brine following the trona dissolution path will encounter the 40°C isotherm at X. Further trona dissolution means the brine is now supersaturated with respect to nahcolite. At some point this mineral begins to drop out of solution, while the brine follows the path X-Y. At Y, solid nahcolite, solid trona and a brine liquor corresponding to point Y (17% Na_2CO_3 and 5.6% NaHCO_3) are all in equilibrium. A similar precipitation sequence will occur at other temperatures from 25° to 87°C, showing that sodium carbonate solubility doesn't change much over this range, while the wt% of bicarbonate doubles in the residual brine (Y to Z). Wagscheiderite forms above 87°C (Figure 12.9b). The formation of the less soluble nahcolite is the reason many early field tests attempting to solution mine trona mention "blinding" of the dissolution surface whereby a coat of nahcolite forms atop the dissolving trona, slowing or preventing further dissolution.

"Blinding" problems can be avoided if temperatures for brine extraction are kept high or if the feed solvent is not pure water but a solution of Na_2CO_3 . The effect of high temperature can be seen as a byproduct of shale-oil recovery experiments conducted by Shell Oil in the Piceance Creek Basin. In 1970-

72, the Company experimented with warm water and steam injection in an attempt to recover oil from nahcolite-bearing oil shales of the Parachute Creek Member on a 10-acre site in Rio Blanco County, Piceance Basin Colorado. In addition to the expected oil, Ireson (1990) reported that large amounts of sodium carbonate brine were co-produced at higher recovered brine temperatures (Figure 12.10).

In 1990, solution mining of Boies nahcolite bed began near Rifle, Colorado. Where mined, the Boies bed is about 7.6 m (25 feet) thick and at a depth of 610 m (2,000 feet; Day, 1974). Such a thin target bed means solution mining is most efficient if it involves directional drilling. A vertical hole is sunk to a hundred metres or so above the target bed, the hole is then turned so it enters the target bed at a slight angle and then is drilled horizontally along the base of the bed. Hot water is then injected into the bed to dissolve the nahcolite and form an expanding cavity. Sodium carbonate brine is recovered from another vertical hole drilled into the cavity some hundreds of feet from the injection hole.

Until 2004, American Soda PPL solution mined nahcolite using this hot extraction methods on a lease near Parachute, Colorado and adjacent to White River Nahcolite's property. First, pressurized hot water was injected into bedded nahcolite at depths of some 450 to 600 metres subsurface. Nahcolite was returned to the surface as a highly saturated NaHCO_3 solution. In the first quarter of 2002, the company drilled 26 wells but anticipated that as the solution cavities expanded, production would be maintained using half that number. Idle wells were to be held in reserve to ensure an uninterrupted source of feed

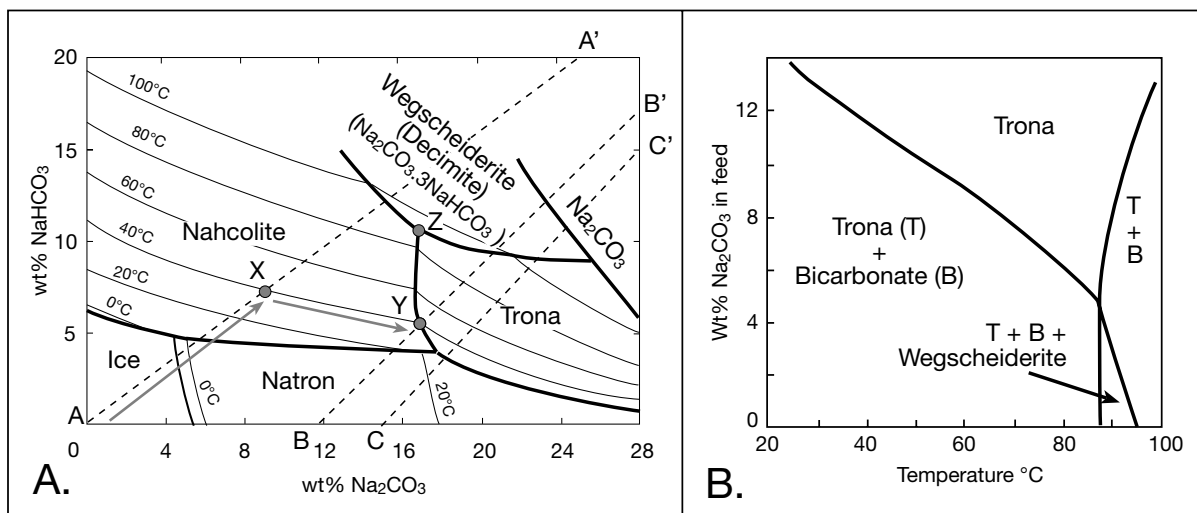


Figure 12.9. Trona stability (after Haynes, 1997). A) Stability of major sodium carbonate minerals in the temperature range 0-100°C. B) Stability fields of various precipitates, trona is in excess in all phases.

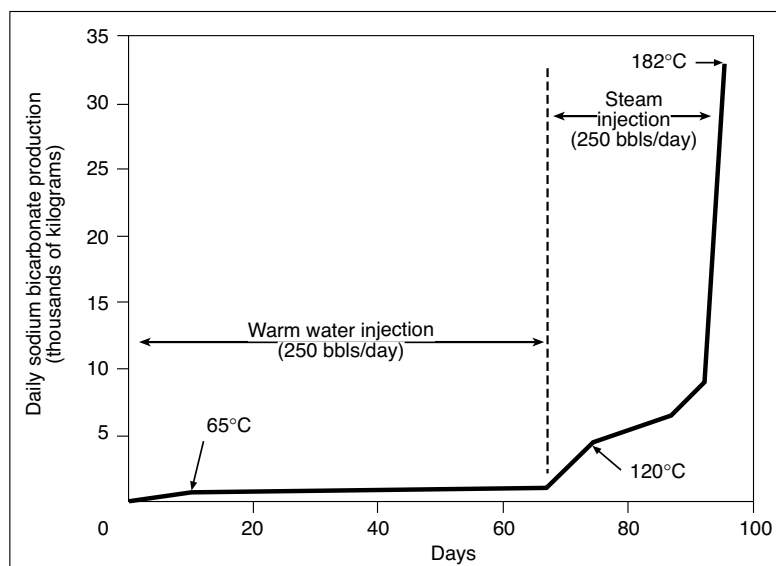


Figure 12.10. Daily production of sodium bicarbonate from Shell's shale-oil recovery experiment in the Piceance Creek Basin, Colorado (from Ireson, 1990).

brine. At the brinefield plant, CO_2 was stripped from the well liquor ahead of pipeline transport. This created a brine solution more suitable for pipeline transport and also gave a relatively low-cost source of CO_2 . Brine was pumped 70 km (44 miles) from the brinefield to the Parachute Creek processing plant using an insulated, pressurized, closed-loop pipeline. At the plant, the incoming brine passed through crystallisers, was dried and packaged for shipping. Recycled hot water from the processing plant was then piped back to the minesite to leach more nahcolite. The 1,000-acre upper site was the prior location of Unocal's shale oil upgrading plant and much of the former infrastructure was used by American Soda. Unfortunately, the operation was deemed uneconomic and was shut down in late 2004.

Solution mining nahcolite in the Piceance Creek Basin suffers some unusual problems that can be expensive to control (Dyini, 1996). Problems include: 1) Cavern shapes in the Boise must be tightly controlled and regularly monitored as the Boise bed is very close to a natural dissolution surface in the immediate overburden, a breakthrough into this overlying water-bearing leached zone would be detrimental to controlled solution mining in the target bed; 2) The Boise bed actually consists of two nahcolite beds, the lower one is thinner and also contains halite, so exact bed targeting is very important both during directional drilling and in cavity expansion during production; 3) The Boise bed grades laterally into mixed halite and nahcolite toward the basin's chemical depocentre,

accidentally dissolving halite in this region would contaminate brine product with high levels of sodium chloride; 4) Oil shale which overlies the Boise Bed cannot be mined or damaged under current sodium leasing regulations. Given the major part of the known nahcolite resource today occurs as crystalline aggregates scattered through oil shale, it difficult to target mine for soda ash alone. Current legislation makes the solution mining of soda ash difficult, if not impossible, over much of the extent of the Boise Bed as it could render parts of the overlying oil shale unsuitable for future in situ leaching or underground mining. Under current legislation, any oil shale that is damaged by solution mining must be stockpiled for future oil recovery.

A possible future method to solution mine trona, not nahcolite, could use an initial feed solvent that contains Na_2CO_3 in solution (Haynes, 1997). For example, a 15 wt% Na_2CO_3 solution proceeds along the line C-C' in Figure 12.9a. This intersects the 40°C isotherm well into the trona stability field and no sodium bicarbonate (nahcolite) will form. The line B-B' separates fields at 40°C where nahcolite and trona are likely precipitates and corresponds to a value of 11.9 wt% Na_2CO_3 on the abscissa. This is the minimum feed solvent composition that will insure that no nahcolite is precipitated during the dissolution process. Critical "excess carbonate lines" were similarly determined by Haynes (1997) at other temperatures and are plotted as the solid phase existence fields of Figure 12.9b. Trona is present in all stability fields as it is the excess phase.

Another way to avoid nahcolite blinding in a trona target bed is to maintain a caustic solution for the feed (Haynes, 1997). The phase relationships in Figure 12.9 are well known to the trona industry but their utility is greatly lessened in situations where impurities are present in the dissolving trona or in situations where other reagents need to be introduced to the solvent feed (see Haynes, 1997 for details). Clearly an understanding of the phase equilibria and temperature susceptibility of any targeted salt system is fundamental to any successful solution mining operation.

Cavern Usage	Product stored	Distribution and specifications	Operational mechanism
Hydrocarbons	Liquid hydrocarbons- Crude oil, distillate, naphtha, etc	More than 16 storage sites encompassing more than 190 caverns. Largest volume stored in USA (SPR), storage also in France, Mexico and Germany.	Due to reduced compressibility but relatively low density of product and immiscibility with water, caverns are operated by a brine compensation mechanism. This requires above ground facility (ponds) for storing excess brine when the caverns are filled with hydrocarbons. Brine compensation enlarges the cavern during each recovery cycle, hence cavern shape must be continually monitored throughout life of facility. Less pressure variation occurs in caverns used for liquid storage compared to gas, so caverns can be much larger for liquid storage (more than 1 million m ³) in a single cavern. Salt creep is less critical for liquid storage compared to gas.
	Liquefied hydrocarbons- LPG, ethylene, ethane	Around 110 storage sites with over 190 caverns. Major sites in Sarnia (Canada) and Mount Belvieu (USA). Sites also in Morocco, France and Germany.	
Compressed air storage	Energy generation via electrical demand-peak shaving	Two plants currently in operation worldwide- Huntorf Germany and Alabama Electric Cooperative, USA.	Air is compressed and stored in a salt cavern using cheap electricity. Then stored air is expanded through a gas turbine to produce high value, peak electricity. Caverns cycle daily.
Waste storage	Industrial waste	Limited number of facilities in operation in USA and Europe, most caverns used to store oil-field wastes or industrial chemicals.	Waste is stored as a "final repository" hence cavern must be emptied prior to filling with pelleted waste (avoids groundwater contamination), or an inert blanket of suitable density must be used to separate waste (pasty consistency) from the brine. Waste is also stored as both "inerted" bulk material and in containers in old salt mines in Germany.
	Nuclear waste	Operational site at WIPP, New Mexico, USA. Waste is isolated by plugs made from a crushed mix of salt and compacted clay.	

Table 12.1. Use of salt caverns as storage facilities (after Grappe, 2000).

Use of Salt Caverns

Less and less the rationale to create a solution mined salt cavern is the production of brine or a particular chemical feedstock. In the past few decades, the number of purpose-built storage caverns, shaped using solution mining techniques, has expanded rapidly and an industry centred on the construction of salt caverns for hydrocarbon and waster storage has evolved and continues to expand (Thoms and Gehle, 2000a, b). Today’s commercial brine producers are also aware of potential storage opportunities, they still use controlled solution mining techniques to produce their required brine feed, but at the same time their ultimate goal is to produce a tight cavern suitable for future hydrocarbon or longterm waste storage (Table 12.1).

Hydrocarbon Storage

Crude oil or unrefined petroleum and light hydrocarbons can be safely stored below ground in liquid form in brine-compensated salt caverns (Table 12.2; Veil et al., 1996; Grappe, 2000; Thoms and Gehle, 2000a). Light hydrocarbons currently stored in salt caverns include propane, butane, ethane, ethylene, and other products extracted by refineries that can be transported and stored as liquids. In recent years natural gas^{12.1} has been stored in salt caverns in increasing volumes, this entails much higher storage pressures and a greater need for pressure integrity in

the access well(s) and couplings compared to liquids storage. Natural gas is a clean burning energy source and has become a prime source of energy worldwide, especially in gas-fired power plants, which now constitute some 25% of gas usage in the United States (Thoms and Gehle, 2000a). Earlier last century natural gas was flared as a oilfield byproduct. By the 1970s it was thought to be in short supply, but it is now known to exist in adequate volumes for the foreseeable future.

As early as 1916 there was a German patent taken out to cover the solution mining of salt caverns for the storage of crude oil and distillates. The earliest oil storage in caverns was in bedded salt in Canada early in World War II. A few years later in 1949 liquefied petroleum gas (LPG) was stored in caverns in bedded Permian salts near Kermit, Texas. Crude oil was stored in salt caverns in England during the “Suez Crisis” in the 1950s. In 1975, the US Congress created the Strategic Petroleum Reserve (SPR) program to provide sufficient petroleum reserves to reduce the impact of interruptions to future oil supplies. The SPR today consists of more than 60 caverns in domal salt bodies across the United States, with a total capacity of 680 million barrels (108 x 10⁶ m³).

^{12.1}Natural gas is a naturally occurring mixture of hydrocarbon gases, principally methane with lesser quantities of ethane, propane, butane, and other gases.

Country	Light Hydrocarbons	Crude Oil	Natural Gas
Canada	6,620	-	552,720
Denmark	-	-	xxxx
France	xxxx	-	xxxx
Germany	xxxx	xxxx	5,040
Iraq	xxxx	-	-
Mexico	-	1,500	-
Morocco	xxxx	-	-
Poland	-	-	143,000
Russia	465-750	-	60-180
USA	85,220	102,100	3,423,250

Table 12.2. Hydrocarbon storage (1000 m³) in salt caverns, xxxx indicates storage but volumetric data is not available (after Thoms and Gehle, 2000a).

The first storage of natural gas in a salt cavern was at Unity Saskatchewan in 1959, followed soon after in 1961 in Marysville, Michigan USA. Gas storage caverns were first purpose engineered in 1963 in Saskatchewan, Canada, in bedded Devonian salt at depths of 1,100 metres. This was followed in 1964 by the first purpose-engineered gas cavern in a salt dome at Eminence, Mississippi, at a depth of 1,740-2,040 metres (Figure 12.1). European gas storage in salt domes began in Tersanne, France in 1970 at depths of 1,400-1,500 metres and near Kiel, Germany in 1971 at depths of more than 1,300 metres. Compressed air energy storage (CAES) for peak electricity generation began in 1978 in the Huntorf dome near Hamburg, while in 1991 a second CAES plant was commissioned in the McIntosh salt dome, near Mobile, Alabama.

Hydrocarbons in a salt cavern are stored in what is in effect a pressure vessel, where high pressure fluids are contained within a stiff impervious envelope using a system of pipes and valves that allow fluids to be placed, sealed and periodically withdrawn from the cavity. Salt caverns differ from standard surface storage tanks in the following way (Bérest & Brouard, 2003):

1. The “container” consists of the access well and the cavern proper. Typically, the height (depth) of such a system is ≈1 km. The access well(s) is equipped with several casing strings or tubes, one inside the other, containing fluids (brine and hydrocarbons) at different densities. Even small differences in fluid densities result in very different column weights within the concentric annuli that make up the well. At the same depth, the gap between fluid pressures in adjacent annuli can be several MPa (Figure 12.11). If the concentric fluids accidentally come into direct contact it creates unstable situations where accidents and spills are more likely.

2. The volume of a storage cavern is very large (up to 1,000,000 m³). Even a small pressure drop in the cavern results in a significant change in the volume of the stored product. Liquid compressibility, an often negligible consideration in most above-ground storage tanks, plays a significant role in the safe operation of large underground caverns.

Interactions between these two factors explain most industrial accidents involving hydrocarbons in salt caverns (see case histories).

Storage facilities for liquids (oil, naphtha, kerosene, gasoline) and liquefied hydrocarbons (LPG, ethylene, propylene) are operated by the “brine compensation” method. As brine is injected through a central tube at the bottom of the cavern, an equivalent volume of product is withdrawn through the annular space between the steel cemented casing and the central brine tube. When the cavern is idle, the brine is at atmospheric pressure at ground level. In the brine tube, however, the pressure is in proportion to the depth and specific density of brine, which is around 1200 kg·m⁻³ (Figure 12.11). If the interface between the oil and brine is 1000 m below ground level, the pressure in the brine column at this point is approximately 12 MPa. Brine pressure and product pressure are equal at the interface in the cavern between brine and product. Above this point,

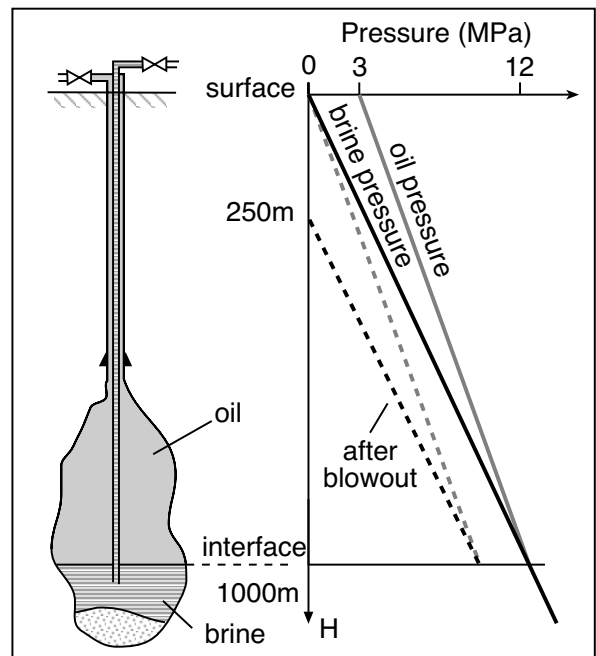


Figure 12.11. Typical pressure regime in a salt cavern used for oil storage. Situation after a blowout is graphed as dashed lines (after Bérest & Brouard, 2002).

the pressure in the product-filled annular space reduces gradually, and more slowly than in brine because the density of the stored product is lower (of the order of 900 kg.m⁻³ for oil, and 500 kg.m⁻³ for LPG).

Thus at any given depth, the pressure in the annular space containing the product is higher than the pressure in the central brine-filled tube. The difference is greatest at ground level, where in a 1 km deep example it is 3 MPa (for oil storage) or 7 MPa (for LPG storage). At the wellhead, the stored product applies pressure to the valve controlling the annular space. If this valve fails, the product is ejected suddenly, and the brine level in the central string drops until a new pressure balance is reached (see West Hackberry blowout in case histories).

For a valve failure in an oil-storage cavern, with an oil density of 900 kg.m⁻³ and with the initial brine oil storage interface at a depth of 1000 m, the top level of the brine in the central tubing will come to rest at a depth of 250 m below the surface (Figure 12.11; Bérest and Brouard, 2003; Bérest et al., 1999). The weights of the brine column and the oil column will then be equal at the interface depth in the cavern. If both fluids were incompressible, the volume of expelled oil following valve failure would be small because the central tube capacity in the access well is only a few tens of litres per metre length of casing. In reality, due to differences in liquid compressibility in oil and brine in the cavern itself, much more oil is expelled. The compressibility factor of brine is $B_b = 2.7 \times 10^{-4} \text{ MPa}^{-1}$; the compressibility factor of the cavern is $B_c = 1.3 \times 10^{-4} \text{ MPa}^{-1}$ (this figure can vary, depending on the elastic properties of rock salt and the cavern shape; see Bérest et al., 1999.); and the compressibility factor of the oil is $\approx B_o = 6 \times 10^{-4} \text{ MPa}^{-1}$. If y is the ratio between the stored-oil volume and the cavern volume, the global compressibility

$$\text{is } B = B_c + y B_o + (1 - y) B_b$$

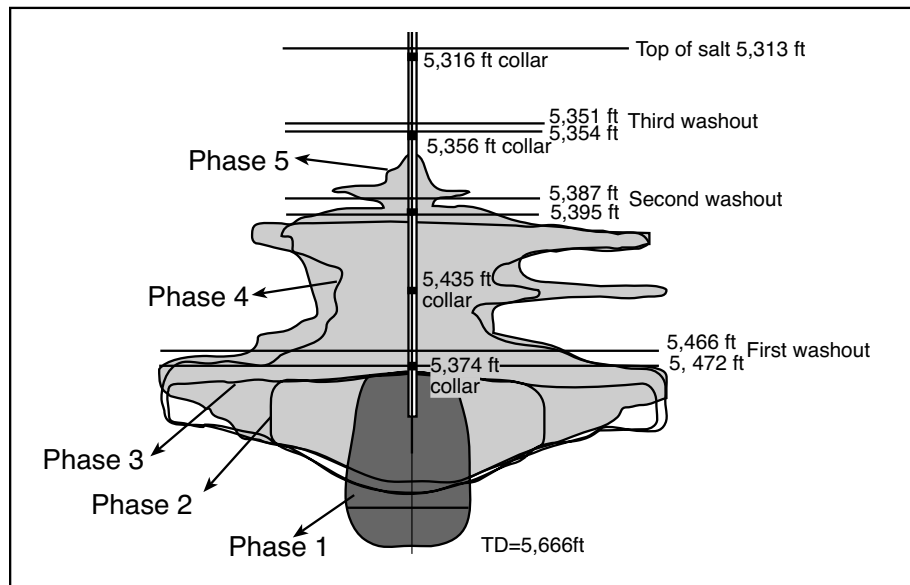


Figure 12.12. Outline (cross section) of Cavern 5, Regina South cavern field, leached into the bedded salt of the Devonian Winnipegosis Salt, Canada. Shows changes in cavern shape over time (Phase 1 to 5) due to ongoing brine compensation (after Crossley, 1998).

Following the wellhead valve failure, the pressure of the entire body of stored fluids (oil and brine) will be reduced by $\Delta P = 3 \text{ MPa}$ (in a 1 km deep example). If the cavity contains $V = 500,000 \text{ m}^3$ of oil and very little brine ($y \approx 1$), then, because of the compressibility, the amount ejected will be

$$B.V.\Delta P = (6 \times 10^{-4} \text{ MPa}^{-1} \times 500,000 \text{ m}^3) \times 3 \text{ MPa} = 900 \text{ m}^3.$$

For liquefied product, a limited amount of LPG would first be expelled in liquid form. (However, this amount will be larger than in the case of oil, as the compressibility factor of LPG is larger, $B_p = 3 \times 10^{-3} \text{ MPa}^{-1}$). This liquid would evaporate gradually after running over the ground, and a heavier-than-air gas cloud would form. Accidental ignition of such a gas cloud is likely (see Brenham explosion in case histories).

Brine pumped into a cavern to compensate for displaced product must be less than totally saturated with respect to the encasing salt. This prevents any salt crystallising in the access casing, but it also leaches salt from the cavern wall. Regular product cycling using brine compensation increases the size of a salt cavern. Caverns used by oil storage companies in North America typically increase in size by about 1 to 2 percent a year. Some of the older caverns in the USA and Canada are now twice as large as when they were first filled (Figures 12.12, 12.13).

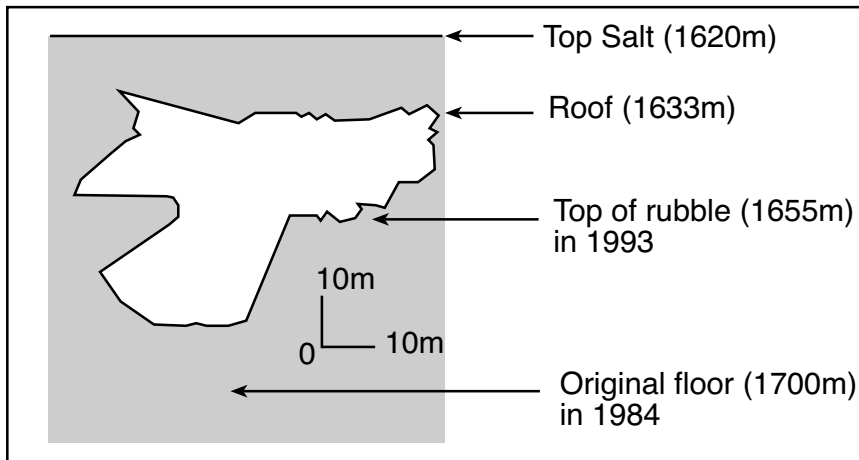


Figure 12.13. Outline (cross section) as of 1993 of Cavern 5, Regina South, leached into the bedded salt of the Devonian Winnipegosis Salt, Canada. It is one of a number used for brine-compensated gas storage. Changes in floor level show how its shape has changed since 1984 (after Crossley, 1998).

Unfettered enlargement of a storage cavern can evolve into a stability problem as the retreating salt roof and walls are increasingly susceptible to sloughing, caving, fusion and associated damage to the long casing string. Cavern expansion has led to industrial accidents at some storage facilities and during the 1980s emphasized the need for better legislative definitions of safe storage and cavern life in the USA (see Mineola fire in case histories). The worst case expansion scenario is total roof failure and the formation of a sinkhole connecting the surface to the underlying storage cavern. This is highly unlikely in modern, well maintained and monitored storage facilities around the developed world. The recognition of such a possibility required the complete drainage of the former SPR facility on Weeks Island, Louisiana (see case histories).

Natural gas storage caverns operate under much higher pressures than those storing liquid hydrocarbons. Internal pressure not brine compensation cycles the stored product. Purpose-designed salt caverns are ideal for the storage of natural gas, especially when excavated in salt domes. They are stable and will not disintergrate in an explosion. They are safe and out of sight and so can be located near demand centres. They act as huge pressurised cavities with low gas cushion^{12.2} requirements of around 33% of the total storage volume. Unlike other gas storage facilities above and below ground, a salt cavern also offers very high deliverability and rapid product cycling.

^{12.2}Cushion gas is the volume of gas needed to fill a cavern to where the gas pressure is sufficient to supply a significant flow of gas to the surface.

Caverns deal readily with peak demand, gas shaving and any rapid demand fluctuations. Operators can change from injection to withdrawal in 15 minutes and back to injection in 30 minutes.

The main disadvantage to natural gas storage in a solution cavern is the relatively high cost of construction compared to other forms of underground storage (e.g. using depleted oil and gas fields or suitable aquifers). But purpose-built salt cavity facilities are consistently safer and cleaner than all other types of storage. As an example of cost, consider the purpose built “Big Hill” facility in Texas; completed in 1992, it

is a 14.3 million cubic metre, solution-mined cavity operated under the U.S. Petroleum Reserve. The leaching cost (in 1992 dollars) was \approx \$1.80 per cubic metre of salt excavated, and the total cost of the project (including land acquisition, design, site development, pipeline development, drilling, hydrocarbon interfaces, etc.) was \$21.80 per cubic metre. Part of the higher cost for salt caverns reflects the need for controlled circulation and safe disposal of large volumes of cycled water required during the construction stage. But construction and maintenance costs are low compared with above ground storage facilities, which also suffer from much lower cycling rates, storage volumes, a higher likelihood of catastrophic damage during an accident and a need for higher gas cushions.

Life expectancy of a storage cavern may be as little as forty years for existing caverns made with older solution leach technologies, or a century or more in purpose-engineered facilities constructed with current technologies. Deep caverns in thicker relatively homogenous salt bodies (as typifies many salt domes) are the safest hydrocarbon storage facilities currently known for natural gas and liquids.

Waste Disposal

Salt caverns can be used for the safe disposal of various types of hazardous waste (Table 12.1; Grappe, 2000; Dusseault and Davidson, 1999). Until recently, the major users of solution caverns as waste repositories were within the same salt-based and hydrocarbon-based industries that generated the cavities.

Nonradioactive waste disposal

Since 1959, alkali wastes from local “soda ash” production has been pumped back into “worked out” solution caverns of the Holford brinefield, located some 30 km south of Manchester, England. The Holford brinefield operator is authorised to dispose of 200 tons per day of brine mud solids from the purification of crude brine, and 250 tons per day of alkali wastes from local soda ash production. In addition, the operator is authorised to dispose of organic residues from the production of perchloroethylene, trichloroethylene, and other related chlorohydrocarbons into specially designated caverns that contain alkaline material designed to neutralise any free acid in the wastes. Brine displaced from the caverns by the emplacement of solids is used to slurry additional solids back to the caverns. The US salt mining industry also disposes of impurities generated during above-ground brine purification processes into salt caverns. Wassman (1983) reported that the Dutch pumped wastes from a brine purification plant in to a nearby salt cavern. Concentrated magnesium chloride brine has also been stored in caverns in the Netherlands. In Mexico, sulphate purged from salt evaporators is being disposed of in salt caverns.

In addition to brine wastes, salt caverns are now also used to dispose of oilfield wastes. The state of Texas recently legislated that six salt caverns can be used for the disposal of nonhazardous oilfield waste and one cavern for the disposal of naturally occurring radioactive waste. The states of Louisiana and New Mexico are developing similar legislation. Canada has recently authorised disposal of oil field wastes into several caverns near Edmonton and Unity, Saskatchewan. Oil field products slated for disposal in salt caverns include; used drilling fluids, drill cuttings, completion and stimulation waste, produced sand, tank bottoms, and soil contaminated by crude oil or produced water.

Disposal caverns used in hydrocarbon waste disposal act like large oil/water/solids separators. The solids in the incoming waste settle to the bottom of the cavern while the lighter oils and hydrocarbons rise to the top of the cavern, where they can be removed. Incoming waste displaces clean brine, which is either sold as a product or disposed of. Cavern pressure integrity in a cavern to be put to such a use should be defined, tested and access controlled before the cavern is filled with oil field waste. It should be regularly monitored throughout the waste emplacement cycle, and optimally, for some period of time after waste emplacement has ended and before the cavern is finally sealed.

The main concern in any waste liquid storage is what will be the longterm response of the cavern once it is filled. Will it maintain its integrity for hundreds or even thousands of years? In a detailed study of rock property responses based on more than a decade of detailed rock mechanics studies in the laboratory, in the field and in abandoned salt cavities, Bérest and Brouard (2001) concluded that storing hazardous waste in salt caverns is an appealing solution when the toxicity of the waste vanishes after a few decades or centuries.

A suitable selection of cavern fluid pressure in the storage cavity will prevent too fast a convergence rate and allow a small amount of rock-mass fluid flow to be directed toward the cavern, preventing any fluid seepage from the cavern. Bérest and Brouard (2001) recommend that such storage facilities be shallower than 1000m to minimise the effects of creep and published cavern convergence curves for both a brine and a fuel-oil support medium (Figure 12.14). As is to be expected, cavern convergence or creep rates are much higher when less dense fuel oil rather than brine is the support medium in the cavern.

Radioactive waste

Radioactive waste disposal in salt caverns is much more problematic as toxicity can remain for millennia and stability must be maintained across such timeframes. Such timelengths include the possible to and fro of icesheets over much of North America and Europe. A key question to be resolved is whether medium and high level waste should be stored above or below the watertable.

Mainland Europe has adopted rigorous technical regulations for hazardous waste management. Germany, for example, requires that all waste, which cannot be stored for extended periods above ground without posing a serious threat to the biosphere, even after undergoing treatment, should be stored underground in suitable geologic formations. In the early 1960s the German Federal Government (former West Germany) decided that radioactive waste is to be stored exclusively in deep geological formations of the continental crust. Whereas the German nuclear industry was to be responsible for waste processing, intermediate disposal and conditioning, the German Government was to be responsible for final disposal. To this end the German Government contracted DBE, a company especially founded for this purpose in 1979, to plan, construct and operate the final radioactive waste repositories of the German Government. Until unification, DBE activities centred on the Gorleben

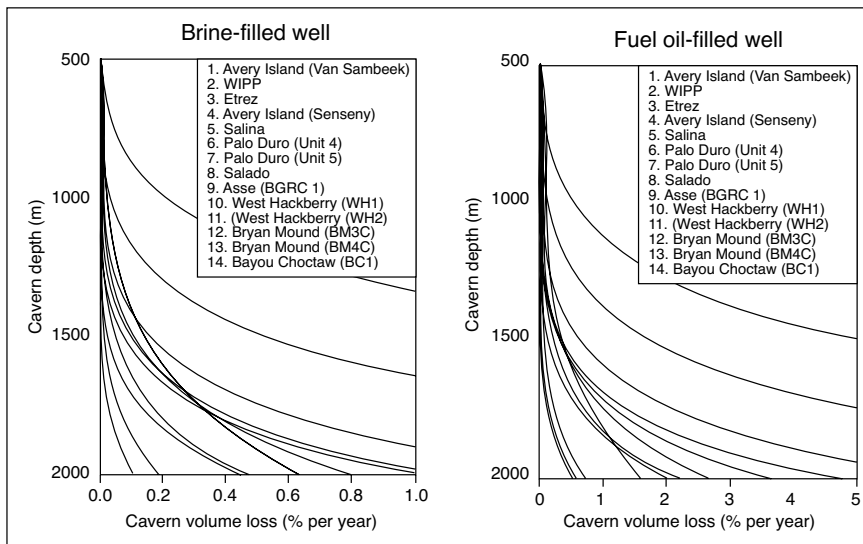


Figure 12.14 Calculated annual convergence of a sealed salt cavern filled with brine or fuel oil and expressed as percent volume loss (Bérest and Brouard, 2001).

and Asse salt domes and on the Konrad iron ore mine. Up to 1979, the Asse facility was also used as an experimental final repository for low-level wastes. In the following two decades the focus of experimental studies shifted to the purpose-designed Gorleben facility in the Gorleben salt dome.

Since March 1999, the WIPP site in New Mexico, USA, has been receiving radioactive waste for storage. This is a purpose-built salt cavern constructed by conventional mining techniques in bedded salt, not by solution mining. Like an unpressurized solution cavern, it is subject to the same creep, closure, temperature and pressure considerations and its depth of some 500 m below the surface places it in a depth range where karst penetration and lateral discontinuities including upward stoping chimneys are possible, if highly unlikely, in the next few hundred millennia. At this stage no salt solution cavern is used for nuclear waste storage in the USA, because of a legislated requirement for reversibility (Grappe, 2000). Unfortunately in some ways, much of the research effort by the DOE in the USA has focused on the relatively shallow WIPP site in a region of chimneying and deep subsalt artesian circulation and not on the development of deep purpose-built storage caverns in diapiric salt. Then again, no-one wants a radiogenic waste storage facility in the much more highly populated Gulf of Mexico rim.

In the context of the ability of diapiric salt caverns to safely store nuclear waste in a cavern space with adequate confinement and salt cover it's worthwhile looking at the response of salt caverns to nuclear detonations (Thoms and Gehle, 2000a).

Two 5-kiloton devices were detonated in salt as events within the “Ploughshare” and “Project Dribble” test programs. The event “Gnome” of Ploughshare took place in 1961 in bedded salt near Carlsbad, New Mexico, and the event “Salmon” of Project Dribble occurred in 1964 in the Tatum Dome near Hattiesburg, Mississippi. Three additional events involving explosions of natural gas were performed in the cavity in the Tatum salt stock first created by the Salmon event. The salt stock completely contained all the blasts and the original cavern was only enlarged by 17 metres (55 feet) by the original nuclear explosion. To date no leakage of radioactivity has been reported atop the Tatum dome. Salt domes maintain seal integrity even when subject to the rigours of nuclear explosions within the cavern!

The suitability of purpose-built caverns deep in salt domes for the disposal of hazardous chemical and even low level nuclear wastes has been recognised by governments and companies worldwide, but applications to construct such waste disposal facilities have also raised such strong public objections that few permissions have been given anywhere in the developed world. As that famous German, Chancellor Bismarck, once said, “When a man says he approves of something in principle, it means he hasn't the slightest intention of putting it into practice.”

Problems in salt mines, well-bores and storage facilities

Dissolution and collapse of near-surface and at-surface salt is a natural and ongoing process. When such salt bodies are penetrated by drilling or parts of the salt mass are extracted in a poorly supervised fashion, the resulting disturbance can speed up natural solution and collapse, sometimes with unexpected environmental consequences (Table 12.3). In this context it is of interest to quote part of the introduction in a paper by Zuber et al. (2000) dealing with flooding and collapse events in Polish salt mines.

Location	Timing and size	Explanations & implications	Reference
Ocele Mari Brinefield, Romania	Partial collapse of the roof of a much larger solution cavern occurred on 12 September 2001, it formed a large collapse crater and forced a brine flood down a nearby valley. Subsequent collapse and flooding occurred on July 15, 2004.	Poorly monitored salt leaching under the former Soviet regime between 1970 and 1993 created a gigantic cavern as salt pillars separating adjoining caverns were inadvertently dissolved and the cavern roof migrated toward the surface. The resulting cavern was filled with 4 million cubic metres of brine and was more than 350 metres across. It broke through to the surface at its northern end in 2001, with further collapse in 2004.	von Tryller, 2002
Ground subsidence in brinefields near Krakow, Poland (Lezkowice/Barycz brinefields)	At the Barycz brinefield, 33 sinkholes up to 27 metres wide and 27 metres deep appeared between 1923 and 1993, the region is subject to numerous landslides.	A large deep sinkhole which was formed between 1984 and 1986 above the Lezkowice brinefield. Pollution of the ground-water system via poorly managed wells and broken pipes allowed high salinity waters to reach the nearby Raba River. In 1983 the river salinity reached 206 mg/l.	Garlicki, 1993 Zuber et al., 2000
Collapse at Compagnie des Salins Gellenoncourt saltworks near Lorraine, France	On March 4, 1998, a sinkhole more than 50 m across and 40 m deep formed atop the SG4 and SG5 brinefield caverns, France. It was an induced collapse.	The SG4 and SG5 caverns, drilled in 1967, unexpectedly joined in 1971. By 1982 the salt cushion in the roof had dissolved out putting the cavity roof in direct contact with a 25m thick marl. In October 1992 the marls broke free, exposing a large section of the cavity roof to direct contact with the brittle Dolomite de Beaumont. Collapse was induced by enlarging the cavity by injecting 300,000 m ³ of fresh water.	Buffet, 1998
Cargill saltworks collapse, near Hutchinson, Kansas	Collapse started on October 21, 1974. Within 4 hours the crater was 60 metres across and after 3 days had created a circular depression some 90 metres in diameter and nearly 15 metres deep.	Uncontrolled brine extraction since 1888 certainly contributed to the Cargill collapse. Post-mortem analyses showed that several warning signs, especially an enlarging bowl of subsidence, had been noted, but ignored. After the collapse the brine field and the loss of part of the saltworks infrastructure the brinefield was abandoned.	Walters, 1978 Hendron and Lenzini, 1983 Dyini, 1986
Brinefield sinkholes at Windsor, Ontario and Point Hennepin, Michigan	On February 19, 1954, near Windsor, a water filled depression some 120 - 150 metres across and up to 7.5 metres deep formed within a few hours, destroying much of the surface plant. On January 9, 1971 at Point Hennepin the first collapse crater formed, after a few months it stabilized with a diameter of 65 metres. A second crater developed in April and May 1971 measuring some 120 metres across, with a depth of 35 metres.	The similarity in the geology of the Windsor and the Detroit sites as well as the rapidity of the collapse, along with the size and steepness of the collapse craters, led Nieto and Russell, (1985) to question the collapse mechanism of Terzaghi (1971). They argued his notion of steep upward caving from more than 300 to 400 metres below the surface and centred on solution caverns in the Salina Salt could not explain the craters or their subsidence history. Instead, they proposed a collapse scenario based on a loss of cohesion in pressurised Sylvania sandstone and in the presence of water.	Terzaghi, 1971; Nieto and Russell, 1984
Retsof Mine collapse, New York State	Loss of the Retsof Salt Mine began with a magnitude 3.6 earthquake in the early morning hours of March 12, 1994. Two large, circular collapse features some 100 metres apart developed a month apart at the land surface above two collapsed mine rooms.	Catastrophic breakdown driven by collapse of a small pillar and panel section in the mine some 340 metres below the surface. Collapse of the "back" was accompanied by an initial inrush of brine and gas (methane) into the mine and by a sustained inflow of water via the overlying fractured limestone. A month later on April 18 an adjacent mine room collapsed. \	Gowan and Trader, 1999; Payment, 2000

Table 12.3. Events associated with brinefields (see text for full description).

“Catastrophic inflows to salt mines, though quite frequent, are seldom described in literature and consequently students of mining and mine managers remain, to a high degree, ignorant in this respect. Contrary to common opinion, inflows are seldom caused by unavoidable forces of nature. Though some errors were unavoidable in the past, modern geophysical methods are, most probably, quite sufficient to solve the majority of problems (e.g., to determine a close presence of the salt bound-

ary). Detailed study of the recent catastrophic floods, which happened in Polish salt mines, shows that they usually occur, or have strong negative impacts, due to human errors. Most probably similar human errors caused catastrophic inflows to salt mines in other countries. It seems that a knowledge of the real history of catastrophes, better education of mine engineers and the application of modern geophysical methods could lead to the reduction of floods in salt mines.”

Case histories: caving brinefields

Abandoned brine fields can be areas with major environmental problems as many old wells are undocumented and unmonitored. Like areas of natural solution collapse (e.g. Figure 7.42), they can become zones of catastrophic ground failure, this is especially problematic if located near cities or towns (Table 12.3). Some of the most outstanding examples of how not to solution mine a resource and how not to control ground subsidence effects are to be found in east European countries that are still trying to deal with the environmental outcomes of being former satellite states of the Soviet Union.

Ocnele Mari Brinefield, Romania

SALROM, a government-owned company, solution mines Badenian (Miocene) halite in the Valcea Prefecture of Romania (Figure 12.15a). Production from Field 2 was shut down on March 5 1991 when earth vibrations were noted by SALROM workers. A subsequent sonar survey showed that poorly monitored brinefield leaching between 1971 and 1991 had created a gigantic merged cavern as salt pillars separating adjoining caverns were inadvertently dissolved (Figure 12.15b); the upper parts of the captive boreholes 363, 364, 365, 366, 367 and 369 had merged into a common cavern. The cavern was filled with some 4.5 million cubic metres of brine, was less than a hundred metres below the landsurface, was more than 350 metres across and was overlain by loosely consolidated sandy marls (von Tryller, 2002; Zamfirescu et al., 2003). The cavern was overlain by a bowl of subsidence and, even though mining operations in the region of the cavern completely

stopped in 1993, the ground above continued to subside to a maximum of 2.2 metres prior to the September 2001 collapse. In the period 1993 - 2001 the cavern continued to enlarge and the northern part of the cavity expanded by some 25-35 m (see inset in Figure 12.15b showing sonar surveys 1995 -2001).

The 1993 sonic survey of the cavern showed it was so large and shallow that its roof must ultimately collapse, predicting when was the unknown. The fear was that if it collapsed cata-

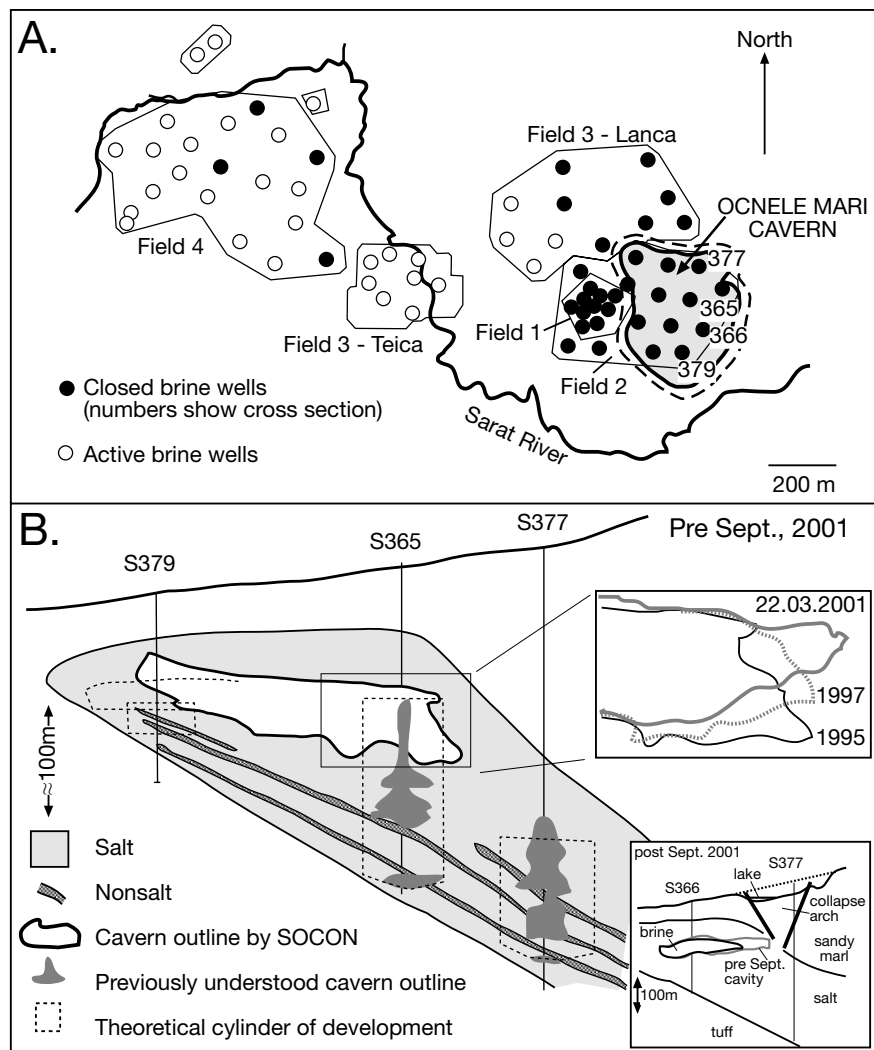


Figure 12.15. Ocnele Mari brinefield, Romania. A) Locality map showing various active and inactive brinefields as well as the likely extent of the large solution cavern defined by SOGON. B) Interpretive cross section showing locality of cavern and proximity to land surface, the inset shows sonar defined outlines and the upward migration of the cavern from 1995 to 2001. This ultimately led to a partial collapse of the cavern roof in this zone on September 12, 2001, as seen in lower inset (redrafted from SMRI data files at <http://www.solutionmining.org>; von Tryller, 2002; Zamfirescu et al., 2003).

strophically, it could release a flood of at least a million cubic metres of brine. Brine could be released either over several hours (least damaging scenario) or instantly forming a wave of escaping water several metres high that would flood the nearby Sarat River valley for many kilometres downstream. There were 22 homes on top of the cavern that would be immediately affected; also at risk were the hundreds and perhaps thousands of residents in the area of the saltworks and river valley below, as well as the local ecology and the civil/industrial infrastructure. Ongoing brine delivery from other nearby operational SALROM caverns to the large Olchem and Govora chemical plants would also be disrupted. When collapse did ultimately occur (twice in the period 2001 - 2004), each episode took place over a number of hours and so a catastrophic wave of water did not eventuate.

According to SMRI (Solution Mining Research Institute) there was no good engineering solution to prevent the Ocele cavern roof from collapsing. Prior to collapse, brine in the cavern exerted pressure against the roof helping to hold it up; removing even a small amount of brine would remove hydraulic pressure that could possibly trigger a catastrophic collapse. Nor was it practical to fill the cavern with sand and industrial wastes as suggested by the Romanian government. It would take too long and it was unsafe to place men and equipment on top of the still expanding cavern. Even if it could be done, only the areas directly below the injection wells would be filled. The best solution was to construct a dam as close to the cavern as possible, and then perhaps trigger a controlled collapse by pumping out the cavern brine.

A partial collapse of the cavern roof atop well 377 occurred on 12 September of 2001, the ensuing brine flood killed a child and injured an older man. The collapse began at 7 pm with brine spilling out of wells 365 and 367. Southward of well 377 a collapse cone some 10 metres across started to form and fill with brine. The cone continued to expand and fill with water until its southern lip was breached. Water spilled out of the cone and down the hill slope. The flow rate of the expelled flow reached a maximum of 17 m³/sec at 3 am on September 13th, with flow continuously exceeding 10 m³/sec for a period of more than 6 hours around that time. By 7 am flow was down to 4-5 m³/sec and by 7 pm, 24 hours after the flow began the flow rate was 0.4-0.5 m³/sec. Some 24 hours after the onset, roof collapse had formed a water-filled lake with an area of 2.4 ha (see inset in Figure 12.15b; Zamfirescu et al., 2003).

A second roof collapse occurred on July 13, 2004. Realitatea Romaneasca, Romania, reported that ground collapse occurred

on 9:30 pm July 13, 2004, possibly triggered by heavy, recent rains. The wellhead of bore 365 was destroyed in this collapse and many other well heads in Field 2 had been destroyed by ongoing subsidence in the period 2001-2004. This collapse was the culmination of a series of collapse-related events that began on Monday July 11. It was planned that a purpose-built earthen dam would contain the brine flood. But when the roof fall occurred at 9:30 pm, the dam was breached 30 minutes later by some 250,000 m³ of salt water. Flow rate through the breach reached a maximum of 6 m³/sec. Collapse did not occur until just after local authorities had evacuated people from 50 homes in the area around the cavern. Most of the brine forced out by the roof collapse escaped into the Sarat (Olt) River. The government attempted to dilute the effects of this flush of salt water by releasing fresh water into the river from nearby dams. Environmental effects of this brine flush on the river ecology are still being evaluated, but fortunately, unlike the 2001 event, there was no loss of life.

Subsidence in Old Belvedere Spinello, Italy

The Old Belvedere Spinello brinefield is located near Crotona, in southern Italy. It was originally operated via brine wells interconnected by hydraulic fractures. This area, now referred to as the "Old Mine," exhibits subsidence effects ranging from sinkholes to bowl subsidence and landslides. The brinefield lies in a valley atop layered salt. The character of the salt varies down the valley from a modestly deformed bi-crested salt anticline in the "Old Mine" area to a laterally compressed and thickened domelike anticline lower down the valley. Brinefield mining began over the less deformed salt in the upper valley and gradually moved down the valley toward thicker more deformed salt. Relatively strong formations overlie the less deformed salt of the "Old Mine" brinefield area. Over the more recently mined domelike salt target, located further down the valley, these brittle formations are replaced by relatively weak overburden strata. For a short distance on one side of the valley near the "Old Mine" the crest of the salt anticline lies against a fault running beneath the toe of a steep hill. From this point the top of the salt dips steeply in the direction of brine wells located some distance away in the valley axis.

A sinkhole first appeared in the vicinity of brining operations in the less deformed salt at the "Old Mine" end of the brinefield. Another sinkhole soon appeared updip beneath the toe of the previously mentioned steep hill and more than 360 m from the nearest active brine well of the "Old Mine" area. Salt solutioning had apparently migrated updip within the salt formation for a considerable distance from the brine wells to

where it had dissolved a large cavity at the toe of the hill. The sinkhole that formed over the uphill cavity destroyed the strength of the soils at the toe of the nearby hill. A landslide plunged into the sinkhole, driving brine from the sinkhole cavity as a destructive downstream flood.

Since then no sinkholes have appeared in the more recently mined end of the brinefield, with its weak overburden materials. Instead, gradual bowl subsidence dominates this part of the field. Solution mining is now carried out in what is called the new Belvedere Spinello Brinefield using a number of single well, sonar monitored salt caverns (Guarascio, et al., 1995).

Brinefield and mine collapse near Krakow, Poland

This former salt mining region, centred on the Wieliczka Mine, lies close to Krakow in south of Poland, and has been mined since the 13th century. There are two main problem sites, Barycz and Lezkowice. The Lezkowice site is near Krakow and lies about 10 km east of Wieliczka (Figure 12.16). The Barycz site, located to the immediate west of Wieliczka Mine, covers an area of one square kilometre, and is two kilometres wide at its maximum extent. It was first solution mined in 1923. Miocene salt at Barycz is relatively flat lying, around 30 metres thick, and some 230 to 280 metres below the land surface. Salt at Lezkowice is steeply dipping and can be found as patchy subcrops as shallow as 40 metres below the surface. Salt was solution mined at Lezkowice from the nearsurface to depths of more than 450 metres. Both sites are covered by

15-20 metres of unconsolidated Quaternary sediments (sands, gravels and peats).

At its most active the Barycz brinefield consisted of more than 900 solution wells about 50 metres apart. In 1993 after 70 years of exploitation the field had produced some 10 million tons of salt, equivalent to a unit 3 metres thick across the whole of the exploited area. There was significant surface subsidence in the brinefield from the onset of solution mining, with ground displacements of 10 to 30 cm noted between 1926 and 1934. Thirty three sinkholes up to 27 metres wide and 27 metres deep appeared in the brinefield between 1923 and 1993, and the region was subject to numerous landslides. By 1993 the field was exhausted and the landsurface was pockmarked by stagnant brine-filled subsidence cones and sinkholes, often centred on abandoned wells. As the land is considered unusable for agriculture it is currently used as a waste dump by the nearby town of Krakow ($\approx 800,000$ inhabitants).

Obvious depletion of the Barycz brinefield meant that in order to maintain a feedstock for nearby chemical industries the saltworks needed to shift to the Lezkowice site in 1968. There the brinefield wells were sited 35 metres apart with a 300 m wide "exclusion" zone between the brinefield and the nearby Raba River. Brine well production was supposed to be limited to 8-10 years and the cavities monitored by sonar to prevent the problems experienced at Barycz. Exploitation actually continued unabated for 20 years until January 1988 when the brinefield was finally shutdown. Overexploitation led to the fusion of

numerous cavities, the unfettered escape of brine into the environment and the nearby Raba River. Some 5.1 million tons of salt were extracted over the 20 year life of the brinefield (corresponds to 17 million cubic meters of brine product). In an attempt to prevent further ground collapse, loam and ash waste from a nearby power station were injected into some of the cavities. Even taking into account the re-injection of some 1.10 million cubic meters of waste, the cumulative volume of the cavities remaining beneath the Lezkowice site in 1990 was of the order of 1.45 million cubic metres.

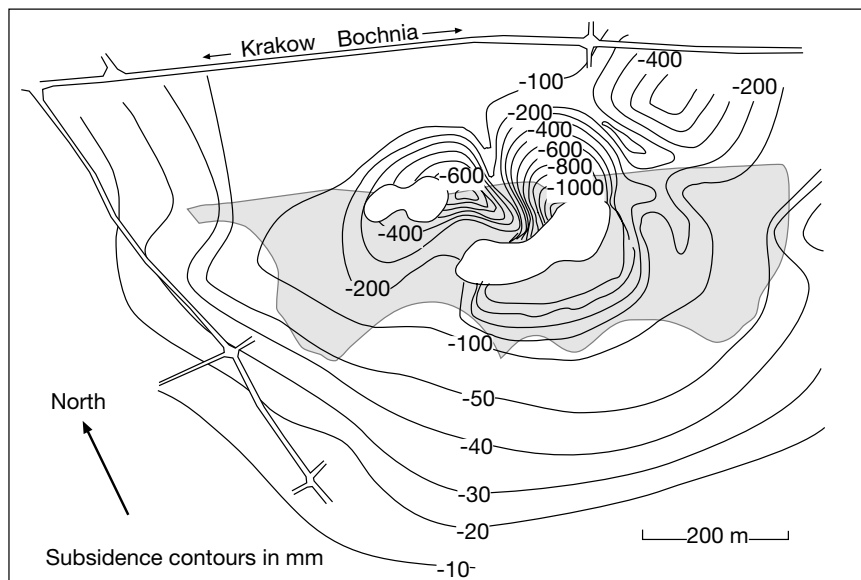


Figure 12.16. Subsidence at the Lezkowice brinefield site between 1974 and 1988, contours in mm. Area of the former brinefield is shaded grey (after Garlicki 1993).

Subsidence measurements were made at Lezkowice from the beginning of the exploitation in 1968. Measurements carried out between 1974 and 1988 show two principal zones where subsidence exceeds 80 cm (Figure 12.16) Garlicki, 1993). The most significant area of subsidence lies at the centre of the brinefield, but extends beyond the exploited zone, in particular in the northeast. Subsidence reaches 1.20 meters in the brinefield centre. The second major subsidence zone, where subsidence was higher than 80 cm, is located in the northern part of the brinefield. There is a third zone of subsidence with depressions of more than 50 cm to the east of the former brinefield.

Between August 1988 and June 1991, subsidence increased by 40 cm in the western part, and 80 cm in the central part; sagging in the central part had lengthened along an east-west axis and the depression bowl had migrated 150 metres east. The first large deep (22 m) sinkhole at Lezkowice started to form in 1984, and continued to grow until 1986. After the first few months the sinkhole was filled by the brinefield operator with more than 250,000 m³ of sandy and argillaceous waste materials. Another large sinkhole formed nearby between 1988 and 1989, but it was no more than 3 metres deep. Still more sinkholes appeared between 1988 and 1990 with a total a volume of more than 300,000 m³, all were filled using waste residues.

Garlicki (1993) estimates that the large deep sinkhole, which formed between 1984 and 1986, was a response to the uncontrolled dissolution of a steeply dipping layer of salt that lay no more than a few metres beneath the Quaternary cover. There was significant salinization of the Quaternary aquifer in the region due a combination of brine leakage from poorly maintained pipelines and casings, and the uncontrolled solution flushing of shallow salt. The resulting brine percolated through sands and gravel aquifers and easily breached the “exclusion” zone to reach the River Raba. River salinity reached 206 mg/litre in 1983 but returned to lower levels after the operator drilled drainage sumps.

Unfortunately, although the two areas are separated by a shallow salt ridge, the world heritage Wieliczka Mine with its unique salt sculptures and carvings in the upper levels of the mine, lies less than a few kilometres from the Barycz brinefield. Throughout its history the mine has been subject to flooding and freshwater influx. Even though a dehumidification program for the mine air has now removed the sculptures and carvings in the mine from the endangered sites list, it is in a constant state of possible destruction by flooding (Zuber et al., 2000). Exploited Miocene salt in Wieliczka mine is made up of two intervals: the lower one consists of layered salt which was

strongly tectonically deformed, while the upper interval consists of salty clays with large salt blocks (Figure 12.17). The salt deposit, and the adjacent flysch sediments were overthrust from the south and are relatively well documented by the mining operations. Tertiary-age water-bearing Chodenice beds make up the northern boundary of the deposit and are much less well studied. They consist mainly of clays, slightly cemented sandstones and sandstone conglomerates that were probably strongly fractured during Miocene folding (Figure 12.17). The main water inflow into the mine network occurs along the southern boundary with the Chodenice beds.

Seven centuries of exploitation, beginning in the 13th century, has created more than 2000 chambers with the total volume of about 7.5×10^6 m³ and over 190 km of galleries in nine main levels and several local midlevels. Throughout the 700 years of mine history there were many catastrophic intrusions of water and loose sand, largely caused by a lack of knowledge of the boundary of the salt and the high permeability of adjacent rocks. Zuber et al. (2000) gives a simplified historical record of inflow rates to the mine in m³ day⁻¹ as: 6 in 1381–1819, 31 in 1820–1919, 50 in 1925–1960, 135 in 1960–1971, 500 to 418 in 1972–1991, and about 900 in 1992. In 1991, there were about 260 inflows with very low flow rates and several larger inflows at the fourth, fifth, sixth and seventh mine levels. These large inflows considerably increased the total water inflow to the mine in the last several decades. One of the most catastrophic inflows started in 1992 in the Mina gallery at the fourth level and was so intense that the lower flooded sections of the mine had to be abandoned (Figure 12.17b). Shortly before the First World War that gallery had crossed the salt boundary and stopped 20 m beyond the salt deposit in gypsum and clay cover (Figure 12.17a). After the Second World War, the gallery was not accessible due to rock falls, and slag used to fill in the Dunajewski chamber cut across the Mina gallery. Water was seeping downward through the slag deposit and exiting at the fifth level (Badeni gallery) at a rate of 4–5 litres per minute and TDS of 300 g/l (Zuber et al., 2000). Serious trouble with inflows started during a reconstruction of the Mina gallery aimed at ponding the inflow behind a dam where it could be pumped from the mine. A catastrophic influx began on the night of 13 April 1992 when the flow rate increased to 200–300 litres per minute (290–430 m³ day⁻¹), i.e., nearly equal to the sum of all other inflows to the mine at that time. Pumps then in use were not able to pump it out. In consequence, the gallery was filled nearly to the ceiling with water and mud, but the water drained or was pumped out after a few days. An even more catastrophic flood began on September 13, 1991 and overwhelmed the pumps and the newly constructed

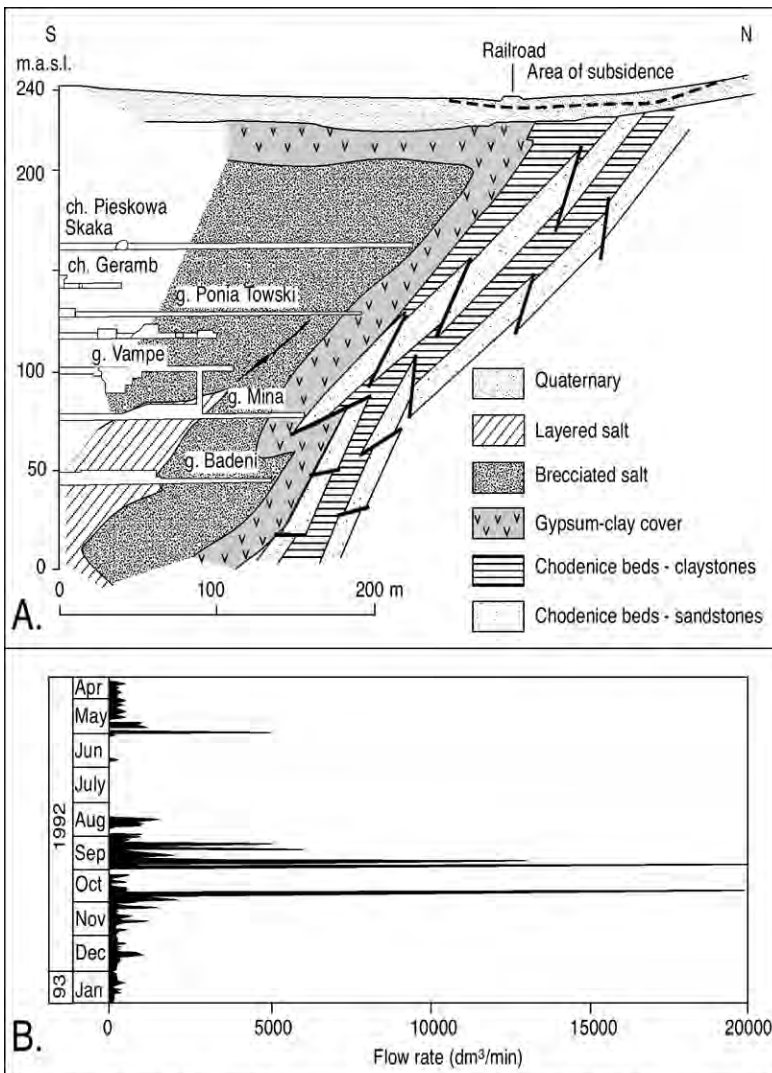


Figure 12.17. A) Wieliczka Mine cross section through the northern boundary in the region of the Mina Gallery. B) Inflow rates into the Mina Gallery during 1992-93 (after Garlicki and Wilk, 1993; Zuber et al., 2000).

dams. Influxes exceeded 10,000 litres per minute. Inflows to the Mina Gallery continued to show a similar pulsing well into 1993 (Figure 12.17b). Operations in the lower levels ceased soon after and the mine today is no longer exploiting solid salt although brine processing still takes place. This processing is expanding the proportion of cavities in the lower levels of the mine and will ultimately destabilise the tourist areas. But if brine is not removed and processed, the resulting rising waters will also enter the tourist levels of the mine.

The pore pressure release created by the flooding drove considerable subsidence at the surface. Walls surrounding a historic

Franciscan monastery partially caved and huge cracks appeared in the walls of the buildings both inside the monastery itself and around it, making some sites structurally unsafe. In October 1992 the surface subsidence in the wake of the successive floods was as deep as 0.5 m.

The pulsed nature of the inflow prior to the final flood argues for more than one water source to the Mina level (Zuber et al., 2000). Initially, the Chodenice beds in the vicinity of the Mina gallery were drained of water, then either waters stored in the Chodenice beds west and east of the Mina gallery were drained, or there was a hydraulic contact established with the sands of the Tertiary Grabowiec beds (Figure 12.17a). The Grabowiec beds are mostly confined aquifers filled with Holocene waters. In any case, the increased influx at the Minas level did not influence the flow rate of other inflows, and the local recharge, especially within the subsidence cone atop the mine, was negligible.

The pulsed character of the measured inflow was probably driven by natural instability of adjacent rocks, and by unsuccessful attempts to stop the inflow. Wash out (suffosion) periods occurred during times with high inflow rates. These were followed by land subsidence, which led to clogging (colmatation) when the flow rates and hydraulic pressures dropped (Zuber et al., 2000). A temporary colmatation lead to an increase of the water table level in the Chodenice beds, this drove an increase in hydraulic head until pressure breakout occurred and the whole cycle repeated.

That the pulsing process is quite complicated is shown by differences in water levels observed in a number of boreholes in the northern region of the mine adjacent to the Mina gallery (Garlicki et al., 1996). In general, when the water pressure builds-up sufficiently, dams, or any other anthropogenic sealing forms in this area of the mine are easily destroyed or moved from their positions because they cannot be anchored in stable rocks. The Chodenice beds are naturally unstable and

additionally deformed and weakened by ongoing exposure to water crossflows. If the exiting water is recharged indirectly through the Grabowiec sands, the inflow rate to the mine can perhaps be reduced, but only if their basal sections are sealed in the region of the contact with the Chodenice beds. If the water comes from the distant parts of the Chodenice beds, the inflow rate can be reduced by pumping in wells installed at distances sufficient to avoid further rock destabilization in the vicinity of the gallery. Undoubtedly, any such operation would be a very expensive undertaking.

When the inflow to the Mina gallery developed to catastrophic dimensions in the early 1990s, the mine management showed a remarkable lack of scientific or engineering sophistication and no understanding of simple hydrological principles. They called on and paid generously for dowsing and witching methods to solve the flooding problem. The dowzers claimed that an underground “river” flows through the mine at the rate of 1.5 m³/s. Following the advice of witches and dowzers, a 100-m-long trail was buried about 1 metre below the ground

surface, it was supposed to stop the inflow of the underground “river” at a depth of 170 m, and to change the “rivers” flow direction upwards (Zuber et al., 2000). Today, the flooding of the lower mine continues, the tourist region of the mine area is still under constant threat of renewed flooding, but the witches and dowzers are happy and counting their spare zlotys.

Induced collapse in the Gellenoncourt saltworks, France

On March 4, 1998, a sinkhole more than 50 m across and 40 m deep formed atop the SG4 and SG5 brinefield caverns in the Gellenoncourt saltworks near Lorraine, France (Figure 12.18; Buffet, 1998). It was an induced collapse designed to prevent a possible uncontrolled future ground collapse. The problem started in 1967 with the beginning of the exploitation of salt layers in the Keuper Fm. In total the Keuper is more than 150 m thick with five salt layers at its base, passing up into variegated and poorly consolidated marls and sandstones and capped by the Dolomite du Beaumont. The top of the

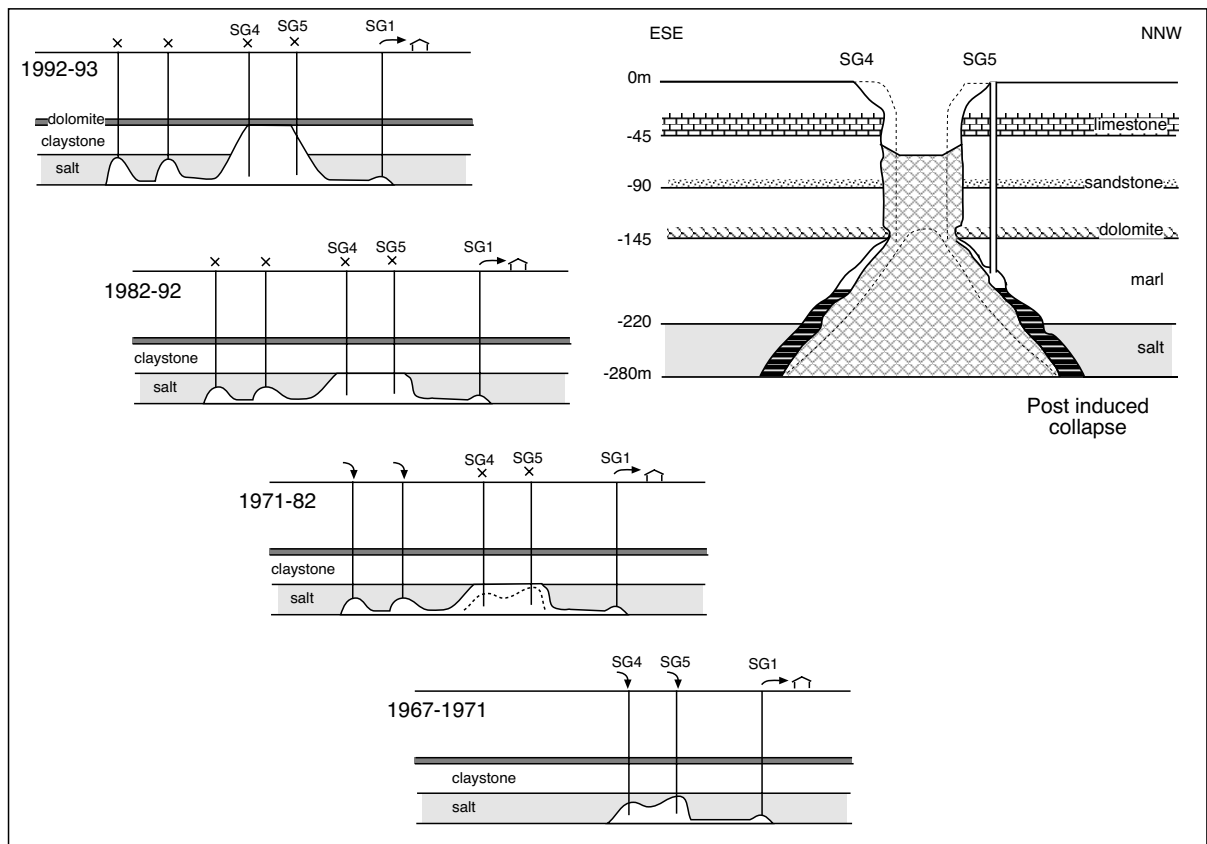


Figure 12.18. Series of chronological panels showing the evolution of the SG4-SG5 cavity in the Gellenoncourt saltworks, France. The larger panel shows the shape and size of the final induced collapse crater (after Buffet, 1998).

salt is some 220 m below the surface and divided into 5 beds numbered 1 to 5 from top to bottom, with the solution mining program designed to leach beds 1 through 3 in the region of SG4 and SG5 caverns (Figure 12.18). Five wells, SG1 to SG5, were joined using hydrofracturing in February 1967. Theoretically the process was designed to leave a substantial salt pillow atop all the cavities and so separate the solution cavities from the overlying marls (Figure 12.18; 1967-1971). The SG4 and SG5 caverns unexpectedly joined in 1971. Brine injection to these two wells was stopped, but crossflowing brines flowing to the producing SG1 well continued to excavate these two caverns. By 1982 the salt cushion in the roof of the SG4-SG5 cavern had completely dissolved away, placing the cavity roof in direct contact with the base of the marls.

From 1982 until October 1992 there was no further upward growth of the cavern roof. Then a 25 m-thick section of the variegated marls in the roof broke free and fell to the cavern floor, leaving a large section of the cavity roof in direct contact

with the brittle Dolomite de Beaumont. This stiff dolomite layer prevented any further immediate collapse of the roof and consequent propagation of the cavity to the surface. But continued growth of the roof span beneath the dolomite would mean a later, larger, perhaps catastrophic collapse. In 1995 the operator tried to induce a controlled collapse by placing a submerged pump in the cavity and pumping out brine to create an exposed upper face. But this didn't work. The next approach was to further enlarge the roof span by injecting 300,000 m³ of freshwater into the cavity. Collapse occurred on March 4, 1998, forming a 50 m wide crater. To protect the surrounding countryside from any brineflood damage a dam was constructed to capture any brine overflow, but in the actual event it was not needed.

Retsof Mine, New York State, USA

The 1994 flooding of the Retsof Mine, New York State USA, took place over a period of weeks. Prior to abandonment, the 24 km² area of workings made it the largest underground salt mine in the USA and the second largest in the world (Figure 12.19). It had been in operation since 1885 and each year it produced a little over 3 million tons of halite. It supplied more than 50% of the total volume of salt used to de-ice roads across the United States.

The eventual loss of the Retsof Salt Mine began in the early morning hours of March 12, 1994 with a magnitude 3.6 earthquake. The quake was caused by the catastrophic breakdown of a small mine pillar and panel section some 340 metres below the surface and was accompanied by surface collapse of an area atop the mine that was some 180 by 180 metres across and 10 metres deep. This all occurred at the southern end of the mine near the town of Cuylerville. A month later on April 18 an adjacent mine room collapsed to form a second collapse crater. The initial March 12 collapse in the mine was accompanied by an inrush of brine and gas (methane) and by a sustained intense inflow of water at rates in excess of 70 m³/min, via the overlying now fractured limestone back (Gowan and Trader, 1999).

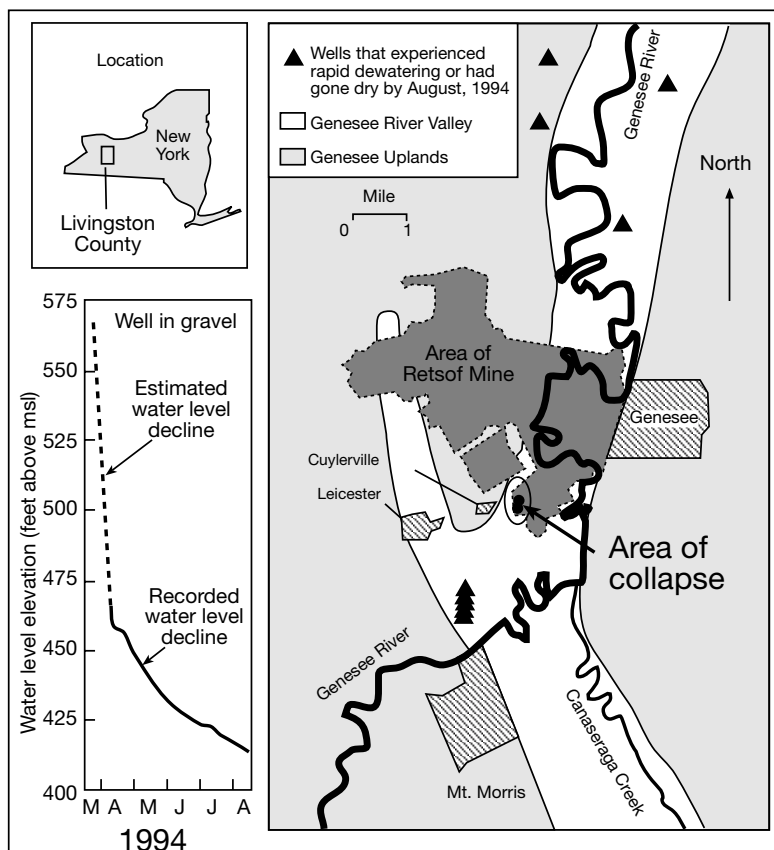


Figure 12.19. Locality plan of the Retsof mine and the area of collapse along with a selected hydrograph from a well in the Genesee River valley (March 12 to August 12 1994; after Tepper et al., 1997).

In a little more than a month, two steep-sided circular collapse features, some 100 metres apart, indented the landscape above the two collapsed mine rooms. The northernmost feature, which was more than 200 metres across, included a central area that was about 60 metres wide and had subsided about 6 to 10 metres. The southernmost feature, which was about 270 metres in diameter, included a central area that was about 200 metres wide and had subsided about 20 metres (Figure 12.19). Fractures extending up from the broken mine back created hydraulic connections between aquifers that previously had been isolated from each and provided new high volume routes for rapid migration of perched groundwaters to the mine level.

Water flooded into the mine at rates that eventually exceeded 60,000 litres per minute and could not be controlled by pumping or in-mine grouting. Within weeks the entire mine was flooded. Associated aquifer drawdown caused inadequate water supply to a number of local wells in the months following the collapse; some dried up (Figure 12.19; Tepper et al., 1997). Aside from the loss of the mine and its effect on the local economy, other adverse effects included abandonment of four homes, damage to other homes (some as much as 1.5 kilometres from the sinkholes), the loss of a major highway and bridge, loss of water wells and prohibition of public access to the collapse area. Land subsidence, possibly related to compaction induced by aquifer drainage to the mine, even occurred near the town of Mt. Morris some 3 miles southwest of the collapse area.

Post-mortem examination of closure data from the two failed mine panels showed an anomalous buildup of fluid pressure above the panels in the period leading up to their collapse. The initial influx of brine and gas following the first collapse coincided with the relief of this excess pressure. Gowan and Trader (1999) demonstrated the existence of pre-collapse pressurized brine cavities and gas pools above the panels and related them to nineteenth-century solution mining operations. They also documented widespread natural gas and brine pools within Unit D of the Syracuse Formation approximately 160 ft above the mined horizon in the Retsof Mine. Such brine accumulations apparently formed long before solution mining began in the valley, driven by the natural circulation and accumulation of meteoric waters along vertical discontinuities, which connected zones of dissolving salt to overlying fresh water aquifers.

Sinkhole problems Cargill saltworks, Kansas

A number of sinkholes appeared in the 1950s and 1970s around brine wells near Hutchinson, Kansas, an area where numerous wells were extracting brine from bedded Permian salts. For

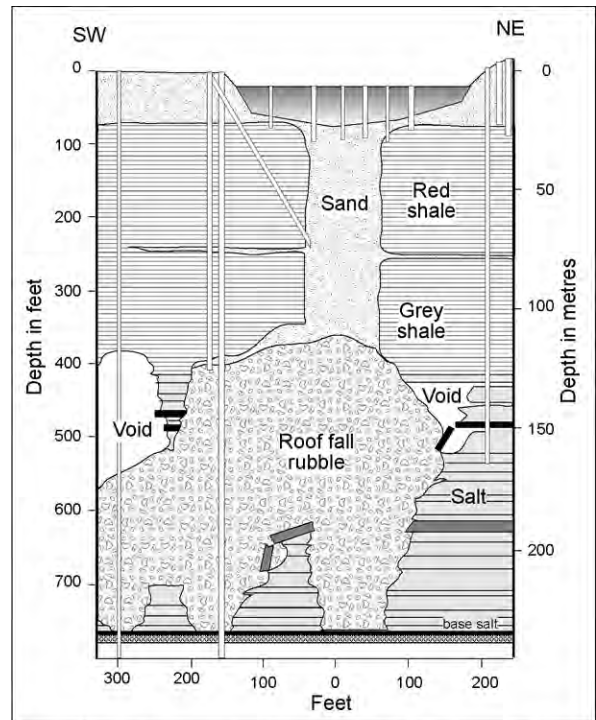


Figure 12.20. Cross section through south sinkhole at the Cargill collapse site showing the fused solution voids in the Permian Hutchinson Salt, which led to catastrophic cavern roof collapse (after Walters, 1978).

example, the Cargill collapse sink near Hutchinson, Kansas, started to form on October 21, 1974. Within 4 hours it was 60 metres across, after 3 days it had created a circular depression some 90 metres across and nearly 15 metres deep. The initial collapse left the tracks of the Missouri-Pacific Railroad spectacularly suspended 6 metres above the water that accumulated in the sinkhole. There was no loss of life at the site.

The Permian Hutchinson salt at this site is about 105 metres thick and occurs at a depth of some 130 metres (Martinez et al., 1998). The salt is overlain by 110 metres of Permian shales, and these, in turn, are covered by about 20 metres of water-saturated, loose Quaternary sands (Figure 12.20). Locations of some of the earliest brine wells in this property are unknown, and the early dissolution methods were not documented (see Hutchinson gas explosion). The sink developed in an area that was part of an active brine field at the time of collapse and would have included both operating and abandoned wells. Embraced within the sinkhole itself was a captive brine well that was drilled in 1908 and plugged and abandoned in 1929.

Earlier uncontrolled brine extraction in the region since 1888 certainly contributed to the Cargill collapse. Post-mortem

analysis showed that several warning signs, especially an enlarging bowl of subsidence, had been noted, but ignored. Post-event drilling revealed a large elongate solution gallery underlay the crater (Dyini, 1986; Hendron and Lenzini, 1983; Walters, 1978). The cavern paralleled a line of brine-producing wells that were hydraulically connected. Prior to collapse the span of the cavern roof was more than 400 metres long and a little less than 90 metres wide. This growing roof span had ultimately exceeded the bridging capacity of overlying Permian shales. Successive overlying rock layers collapsed into the stoping cavity atop the salt, forming an expanding bowl of subsidence at the surface until the uppermost shale layer finally dropped into the water-filled void. At this point, loose water-saturated Quaternary sands quickly sank into the cavity, creating the surface sink. The sand continued to flow until it filled a subsurface chimney some 30 metres in diameter (Figure 12.20).

This, and other nearby sinkholes in the Hutchison region, formed atop breached salt caverns where bedded salt lay at shallow depths in areas with easily broken shaly overburden. As a result of numerous collapses the State of Kansas now requires caverns created by solution wells to be acoustically monitored and a salt roof of at least 12 metres be maintained over captive brine caverns.

Brinefield subsidence, Windsor, Ontario

Subsidence, followed by collapse, destroyed a portion of the suprastructure of an active salt works near Windsor, Ontario. It was the end result of solution mining of the Silurian Salina salt for a period of 50 years. The first well in the brinefield was drilled in 1902, but intensive exploitation began in 1922, from 1922 to 1953 some 25 wells were drilled. Most were completed in

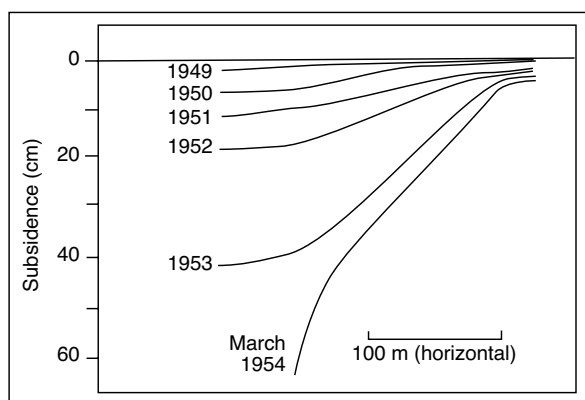


Figure 12.21. Subsidence profile over the margin of the collapse zone in Windsor, Ontario (after Terzaghi, 1971).

the “Lower Salt” at depths around 480 metres (Terzaghi, 1971). Most wells were cased and cemented to depths below the base of the “Middle Salt” between 370 and 390 m. All of the early captive wells circulated water without a blanket, so dissolution was rapid and upward stoping poorly constrained.

Prior to the 1954 collapse an area that was some 300 metres across had subsided some 40 cm over a period of 5 years. Cracks in several buildings on the site were first noted in 1948 and measurements were then made of the subsidence cone up until the collapse. During the first two years of monitoring (1948-1950) maximum subsidence was 6.3 cm (Figure 12.21). The general trend over the 5 years of monitoring was that the cone of subsidence was becoming increasingly deep at increasing speed. By the fifth year of monitoring the depth of the basin had increased another 23 cm making for a total drop of 40 cm in the landsurface since the beginning of monitoring. The rate of subsidence climaxed on February 19, 1954 with a catastrophic failure when a water-filled depression, some 120-150 metres across and up to 7.5 metres deep, swallowed much of the surface plant. Prior to the 1954 collapse an estimated $4.25 \times 10^6 \text{ m}^3$ of salt had been dissolved. Contrary to the initial expectations voiced in 1948, collapse was not centred on wells of the brinefield, but beneath the saltworks itself.

The February 19th collapse event was spectacular, the 9 hours it took to pass to completion shows how quickly such events can proceed. The first signs of a pending collapse were noted between 8 and 9 am with small ground tremors and vibrations. By 10:30 am it was obvious a crater was forming in the centre of the bowl of subsidence, which was visibly sagging. Around midday the crater started to fill with water, first by draining a nearby marsh and later with water from broken pipes. Around 1:15 pm there was a rapid 1 metre drop in the ground defining the edge of the crater accompanied by a 1.2 m high water spout issuing from a crack along part of the crater edge. Throughout the early afternoon other cracks and water jets appeared. The escaping waters were black and smelt of H_2S . By the mid afternoon the collapse had ceased and had constructed a 150 metre wide water-filled sinkhole in the middle of a 600 metre wide cone of subsidence.

Sinkholes in the Detroit River

In 1971 several sinkholes developed in and around Hennepin Point and on nearby Grosse Isle. Both sites are located next to the Detroit River, SE Michigan, near Detroit and 10 km downriver from the Windsor collapse site. The sinkholes were the result of 30 years of solution mining of the “Lower Salt” of

Silurian Salina Group salts at depths of more than 320 metres. Production of brinefield salt at Point Hennepin began in 1943 using unblanketed brine wells. Salt cavities quickly met to form larger cavities. The largest was made up of two galleries called the Northern gallery and Central gallery. Ground subsidence atop this large cavity was first noticed in 1960. The rate of subsidence was constant until the end of 1967. From then it accelerated until the first collapse crater formed above the Northern Gallery on January 9, 1971. Its subsidence history is near identical to the 1954 Windsor site. After a few months of expansion this first crater stabilized with a diameter of 65 metres. In April and May 1971 a second crater then developed above the Central gallery. This crater, some 120 metres across and up to 35 metres deep, was larger than that above Northern gallery. By May, another companion crater, some 60 metres in diameter, had formed next to the larger sinkhole.

The similarity in the geology of the Windsor and the Detroit sites, as well as the rapidity of the collapse, along with the size and steepness of the collapse craters, led Nieto and Russell (1984) to question the upward caving or stoping collapse mechanism of Terzaghi (1971). They argued his notion of steep upward propagation and caving from more than 300 to 400 metres below the surface could not explain the steepness of the three surface craters or their rapid, near catastrophic subsidence. Instead, they proposed a collapse scenario based on loss of cohesion in the Sylvania sandstone layer some distance atop the Silurian salt bed. Their collapse scenario is now accepted for both the Windsor and Point Hennepin events (Figure 12.22).

Intensive solution leaching of the lower layer of Salina salt, and to a lesser degree the two other salt beds in the Salina Group, formed a basin of subsidence in the overlying strata. At the landsurface this cone of subsidence was initially small and slowly evolved outward. It became unstable when it had attained surface slopes of more than 2 mm/m and a diameter of more than 500 metres. As the cone expanded out and up, strata atop the growing cavity salt cavity responded by downwarping

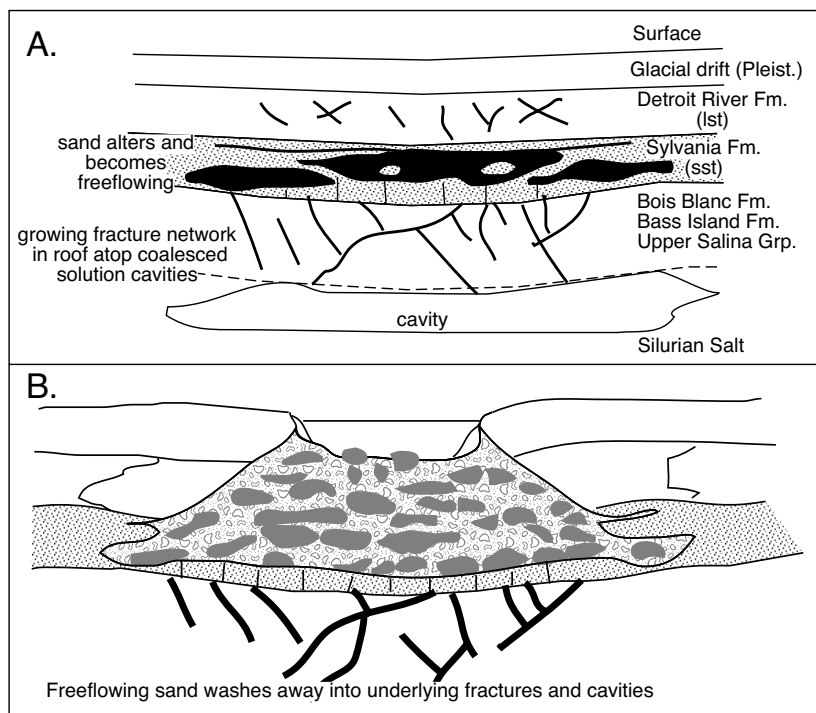


Figure 12.22. Collapse mechanism for the Windsor and Detroit events. **A)** A growing cone of subsidence causes fractures in the carbonate overburden and pervasive disaggregation and cavity growth in the Sylvania sandstone. **B)** Catastrophic collapse of the overburden into cavities in the Sylvania sandstone not into cavities in the Salina salt drives sinkhole formation at the landsurface (in part after Nieto and Russell, 1984).

elastically into the underlying cavity and then fracturing, but not necessarily collapsing. Downwarping created compressive stresses in the higher part of each cohesively downwarping overburden unit. Expanding joints in the lower part of each unit took up the corresponding tensile stress. Compression increased in the higher part of each layer until it reached its compressional limit, the layer then fractured. Like the adjacent carbonate beams, the Sylvania sandstone bed initially deformed elastically until a rupture, driven by internal compression, formed in the higher part of the bed.

What was different in the Sylvania layer compared to the limestone beams atop the cavity was its fracture response to compressional stress. When plugs of the Sylvania sandstone were subjected to triaxial compression testing it was found the plugs failed by pervasive grain rotation, not by fracture (in contrast, plugs of the underlying dolomites all failed by fracture). Instead of a cracked plug at the end of a test, what was left in the stress jacket after a test of Sylvania Sandstone was freeflowing sand grains. In the real world, a network of growing fractures and solution channels in the underlying Bois Blanc and Bass Island formations allowed the disaggregated

Location	Timing and Size	Explanations and implications	Reference
Haoud Berkaoui oilfield, near Ouarlaga, Algeria	In October 1986 a crater 200 metres in diameter, 75 metres deep formed. It has expanded until now when the cavity is more than 230 by 600 metres across. Its outward progression is still continuing at a rate of 1 metre per year (Thought by environmentalists to be the "largest anthropogenic sinkhole in the world").	In 1978, an oil exploration well with a 2500 m Ordovician target was abandoned because of stability problems in Triassic salt at a depth around 650 metres. The well was abandoned without casing near the bottom of the well. A second well was drilled in 1979 located 80 metres from the previous well. In March 1981, the lining of this well broke because of cavity formation at around 550 metres, which is the level of salt. In October a surface crater formed, centred on these two wells. Dissolving salt may be salinising the crossflowing artesian waters, leading to undocumented, but possible, degradation of freshwater oases in the region.	Morisseau, 2000
Wink Sink, Texas, and Whitten Ranch Sink, New Mexico	On June 3, 1980 the Wink Sink formed a 110 m wide and 34 m deep collapse crater. It was centered on the Hendrick 10 A well in the Hendrick oil field. Whitten Ranch Sinkhole or collapse crater formed sometime between August 31 and September 5, 1998 and was up to 23 m wide and 33m deep.	It appears likely that the natural processes of salt dissolution, cavity growth and resultant chimney collapse atop the Permian Capitan reef were accelerated by oil drilling and extraction activity in the immediate area of the sinkholes in the early part of last century. Large water filled sinkholes (as in the "Bottomless Lakes" of New Mexico) are a natural part of the landscape in the region and were collapsing long before the arrival of man.	Baumgardner et al., 1982 Powers, 2000 Johnson, 2001
Panning Sink, Kansas	It formed in April 1959 with a diameter of 90 metres and had a water surface more than 18 metres below the sinkhole lip.	Formed by subsidence and collapse around an already tilted and abandoned salt-water-disposal (SWD) well - Panning 11A.	Walters, 1978, 1991
Lake Peigneur, Jefferson Island Louisiana	On November 20, 1980, Lake Peigneur disappeared in hours as it drained into an underlying salt mine cavern. Within hours, a collapse sinkhole 0.91 km ² in area developed in the SE portion of the lake and in 12 hours the underlying mine had flooded and 2 days later the lake had refilled with water.	An oil well being drilled from barges and platforms in lake intersected an abandoned part of an active salt mine in the salt dome that underlies the lake. Water from the lake and the intervening natural collapse features entered the mine workings. The Lake itself is a natural dissolution depression.	Autin, 2002 Thoms, 2000b Thoms and Gehle, 1994
Sinkhole atop Weeks Island, storage facility, Louisiana	An active sinkhole some 10 metres across and 10 metres deep, first noted near the edge of the SPR facility in May 1992. A second, much smaller sinkhole was noticed early February 1995, but it lay outside the area of cavern storage.	The sinkhole led to the decision to drain the facility of its hydrocarbons. Drainage and remediation was completed in 1999 at a cost of US \$100 million. This facility was not purpose built but was an old salt dome mine facility. In hindsight, based on an earlier event, one might fault the initial DOE decision to select this mine for oil storage. A groundwater leak in the mine in 1978 may have been a forewarning of events to come. Injection of cement grout into the flow path controlled the leak at that time, but it could just as easily have become uncontrollable and formed a sinkhole.	Neal and Meyers, 1995 Bauer et al., 2000
Mont Belvieu sinkhole, Texas	July 30, 1993 a sinkhole crater formed between two brine storage wells. The crater stabilized in a few hours with a diameter of 12 metres and a depth of 6 metres. It was filled with sand a few days later.	Large volumes of brine are periodically cycled in and out of the brine cavern in the caprock. It is used to drive the withdrawal of the stored hydrocarbons in other deeper storage caverns. Using a system that stores saline brine in a caprock, even without the possibility of the collapse of a brine well, means there is a possibility of groundwater contamination from leaked storage brines.	Cartwright et al., 2000

Table 12.4. Events associated with oil wells or storage (see text for full description).

Sylvania sands to infiltrate into the saltwork galleries. Collapse of overburden into resulting cavities in the Sylvania then followed. The catastrophic collapse of the landsurface was facilitated by expanding shallow cavities in the sandstone, not the deeper cavities in the Salina Salt.

Case histories: caving and leaking wells

Petroleum-industry activities have unintentionally aided and produced dissolution cavities via exploration, production or brine disposal wells drilled in, or through, subsurface salt units (Table 12.4; Martinez et al., 1998). Ongoing corrosion of access wells to storage caverns, or the continued expansion of

caverns as stored product is cycled, can also have unexpected and sometimes disastrous results. If a storage cavity becomes too large for the roof to be self-supporting, successive roof failures may cause cavities to migrate upward and reach the land surface. Documented surface collapses and sinks, which can be directly related to oil drilling and poor brine disposal practices, all involve boreholes drilled long ago, typically in the 1920s to 1950s. This was at a time of different public perceptions of development and long before the application of modern engineering safeguards pertaining to drilling-mud design, casing placement and the use of salt-tolerant cements. It can be more than 30 or 40 years after a well was plugged and abandoned before the problem becomes obvious at the surface. There will be more problems related to old wells in the future.

Wink Sink, west Texas

Wink Sink, located 3 km north of the town of Wink in Winkler County, Texas, is centred on an abandoned oil well within the giant Hendrick oilfield. Hendrick 10A had produced oil from 1928 to 1951 and was the foci of the sink crater, while a second nearby operational oil well was plugged and abandoned soon after the collapse began (Figure 12.23). Wink sink first formed on June 3, 1980 and within 24 hours had expanded to a maximum width of 110 metres. Two days later, the maximum depth of the sinkhole was 34 metres with a volume estimated at 159,000 m³ (Johnson 1987, 1989). The collapse was the surface expression of an underlying dissolution cavity that had migrated upward by successive roof failures until it breached the land surface. The instigating cavity had first developed in halite beds of the Permian Salado Formation, some 400 metres below (Figure 12.23).

The location of Wink Sink atop the Guadalupian Capitan Reef trend places it in a region of natural ongoing dissolution of salt and associated chimneying, which first occurred atop

the reef aquifer as early as Salado time (Figure 7.9). Wink Sink lies in an evaporite karst region where water filled sinkholes as large as, and larger than, Wink Sink are a natural part of the subsurface landscape of the Permian Basin (e.g. water-filled sinkholes that make up the various lakes in Bottomless Lakes State Park, New Mexico). Such structures were collapsing long before the arrival of man. Sediments in collapse chimneys in the vicinity of Wink Sink indicate caving events had occurred at various times from the late Permian, to Triassic, to the Cenozoic (Johnson 1987; Baumgardner et al., 1982).

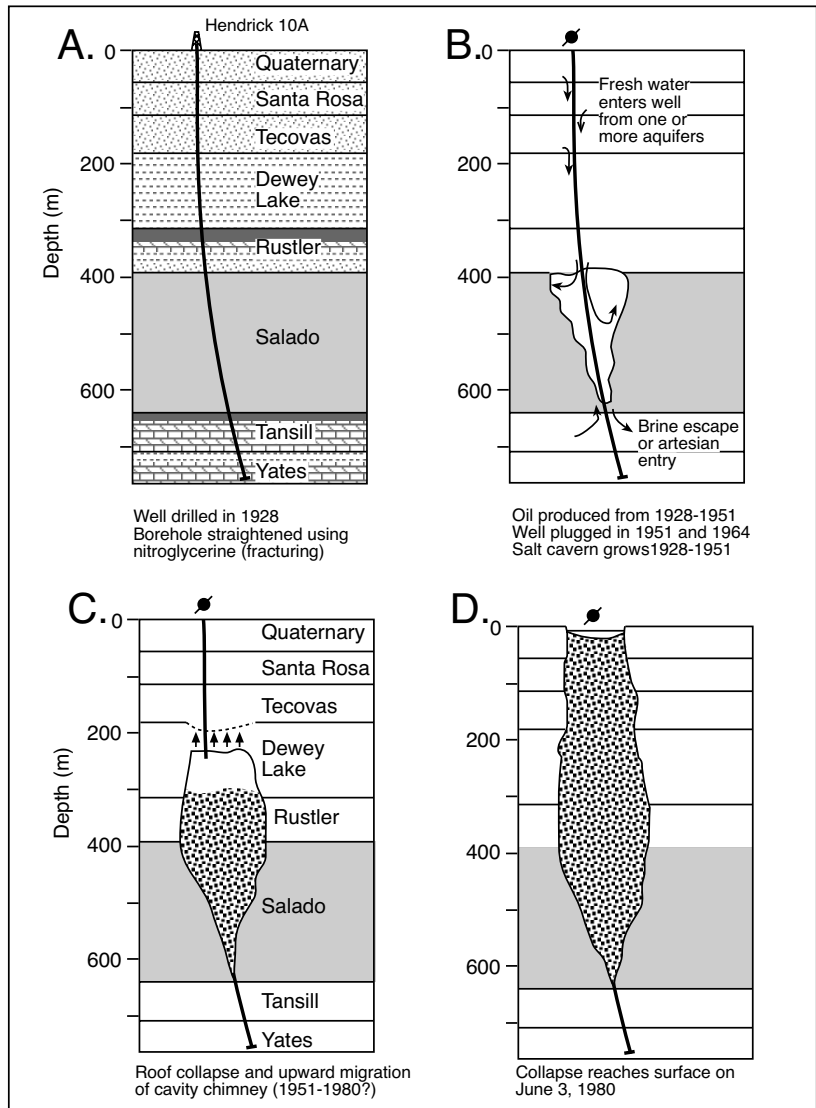


Figure 12.23. East-West section through Hendrick well 10-A in Wink Sink, west Texas (after Johnson, 1987). Undersaturated meteoric and artesian water circulated along borehole margins to dissolve the salt and create a salt cavern, which migrated to the land surface by successive roof failures ("chimneying"). See Figure 7.9 for location of the Wink Sink.

But the natural processes of salt dissolution, cavity growth and resultant chimney collapse were perhaps accelerated by drilling and inappropriate well management practices in the immediate area of the sinkhole in the early part of last century. Drilling and completion of the Hendrick well 10A during the late 1920s was consistent with standard industry practices of the time (Figure 12.23a). But in retrospect, several factors and events related to the drilling and ongoing exploitation of the borehole probably contributed to development of a surface sink centred on the well. These include the probable use of a fresh-water drilling fluid, use of nitroglycerine to straighten the hole, the strong possibility of poor cement jobs that inadequately sealed off the salt beds behind the casing, possible corrosion of casing and cement fretting by salt water, and the removal of some critical casing during the final plugging of the well in 1964.

Poor cement jobs and fractures in cement linings behind the well casings opened a vertical pathway for movement of undersaturated fluid up or down the borehole surrounds (Baumgardner et al., 1982). Surface casing in the well was originally set at a depth of 122 m, approximately at the base of the Santa Rosa fresh-water aquifer. If the casing were set too shallow to seal off the aquifer, or if undersaturated waters were present in some of the siltstone or sandstone beds of the underlying Tecovas Formation, undersaturated waters would have leaked into the borehole surrounds (Figure 12.23b). Also, the cement job at the base of this surface casing in 1928 was probably not suitable for the subsurface conditions. It was done at a time when salt tolerant cements were not yet in use. Fracturing of the original cement possibly occurred during later workover, re-entry, and plugging operations. Fractures could have focused water flow from the Santa Rosa into the borehole surrounds at the level of the Salado Salt (Figure 12.23c).

Baumgardner et al. (1982) pointed out that the absence of cement plugs or cement linings in the Hendrick 10A borehole below a depth of 669 metres during the period from 1928 to 1951 would have allowed water to move upward under artesian pressure from the Guadalupian aquifer at the base of the Salado Formation. In my opinion this is the more likely mechanism driving dissolution as it creates a density inversion in the hydrology that moves fresher waters upward into the salt. Contamination from above requires the less saline (lighter) waters of the Santa Rosa aquifer to displace brine (denser). Casing in the well may have also been perforated by corrosion. In addition the pumping of large amounts of saline water between 1928 to 1951, when it was used as a brine well, would have caused a substantial crossflow of undersaturated water and aided further corrosion of the casing (Hendrick Field brines ranged from 5,000 to 48,000 ppm dissolved solids; Johnson 1987).

Drilling, completion, and plugging procedures combined to create a conduit that enabled fresh water to better circulate in the vicinity of the borehole and so dissolve salt. When the dissolution cavity was large enough, the roof failed and overlying strata collapsed into the cavity (Figure 12.23d). The Wink collapse underlines the importance of appropriate well design specifications, reliable maintenance during well life, and the need for adequate plugging and abandonment procedures specifically designed for wells passing through salt intervals.

Panning Sink, Barton County, Kansas

Panning Sink on the Panning Lease formed in April 1959 by subsidence and collapse around an already tilted and abandoned salt-water-disposal well (Figure 12.24). The Panning 11A well had been abandoned in the previous January because of uncontrolled wellhead tilting. Walters (1978) reported that a 90-metre-wide water-filled sinkhole formed in about 12 hours, with a water surface more than 18 metres below the lip of the sinkhole. Four days later the crater had widened and the water surface was only 4 metres below the crater edge.

The suspect well, originally drilled as an oil producer in 1938, penetrated 91 metres of Permian Hutchinson salt at a depth of 298 metres on its way to the Arbuckle Group reservoir. Freshwater drilling fluids used in drilling the well dissolved the salt in the borehole to an excessive diameter (≈ 1.4 metres) and this washed-out zone was not cemented behind the 15.2-centimeter-diameter casing. Conversion of the borehole to an salt-water-disposal well from 1946 to 1958 injected a large quantity ($\approx 1.6 \times 10^6 \text{ m}^3$) of unsaturated oilfield brines (with a total concentration about the same as seawater) into the well and so further dissolved the salt behind the well casing. Ongoing exposure to undersaturated brine formed a large cavern, and with successive roof falls, this water-filled void migrated upward to ultimately cause the surface crater.

Gorham oil field, Russell County, Kansas,

Some 1,397 oil wells in the Gorham oil field have produced some 100 million barrels of oil, making it a giant oil field. The largely depleted Gorham oil field is now the site of slow subsidence of a major highway (Interstate 70) above salt-dissolution zones in the equivalents of the Permian Hutchinson salt. A number of wells in the field, drilled on 4-hectare spacings in 1936 and 1937, had penetrated 75 metres of the Wellington Salt at depths around 390 metres (Walters, 1991). The wells are now plugged and abandoned, but some of them contain corroded casing that had been left in the boreholes above, within, and below

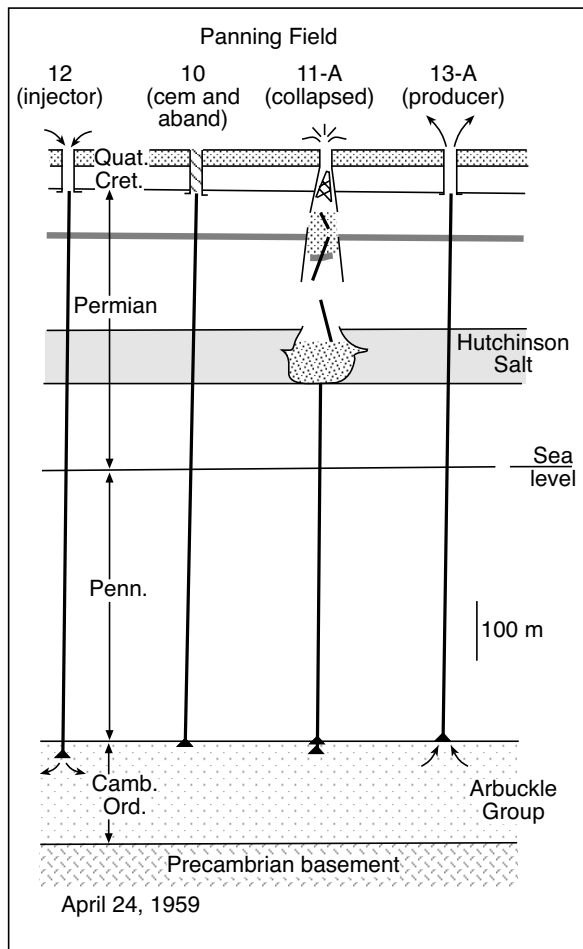


Figure 12.24. Schematic cross section through Panning Field, Kansas, showing the situation on April 24, 1959 (after Johnson, 2001; Walters, 1978).

the salt unit. As a result unsaturated water has flowed up and down some of the boreholes, dissolving large volumes of the salt. Subsidence was further aided by disposal of waste oilfield brines that were re-injected when unsaturated with respect to halite. Subsidence of I-70 pavement is occurring at rates that are less than 0.3 metre per year, but cumulative subsidence from the highway's construction through to 1987 was 4 metres in two of the sinks atop the field, and 0.3 metre in a third sink. It meant rebuilding parts of I-70 in 1971 and again in 1986. Even so, incidents of rapid dissolution induced subsidence atop wells drilled through the Wellington Salt and its equivalents are rare events, in Kansas the ratio of wells intersecting salt and being associated with at-surface subsidence is something like 1:10,000 (Walters, 1978).

Sinkhole at Bayou Choctaw Dome, Louisiana

In 1954 the "No.7 brine well" in the Bayou Choctaw salt dome, Louisiana, collapsed during brine production, probably because of loss of its salt roof atop a growing solution cavern. A sinkhole formed at the site over a period of several days, and was quickly filled with nearby surface water. A rig that was producing brine at the time fell into the collapsing depression and was never seen again. The collapse created a large near-circular lake, about 210 metres in diameter, which today is still a water-filled structure and known locally as "cavern lake" (Stanczuk, et al., 1976).

Grand Saline sinkhole, Texas

In 1976 the Grand Saline sink emerged at the surface within the city of Grand Saline, Texas. The sink occurred at the site of a former brine well that penetrated the top of the Grand Saline salt dome at a depth of 60 metres and had produced brine from 1924 through 1949. The sink eventually grew to a diameter in excess of 15 metres, and a total of 8,500 cubic metres of silt and clay was displaced into the underground cavity. A house was endangered by this collapse, and, during the collapse a pipeline broke and sewage flowed into the sinkhole.

Haoud Berkaoui oilfield, Algeria

In October 1986 a crater, some 200 metres across and 75 metres deep, formed in the Haoud Berkaoui oilfield, near Ouarlaga, Algeria (Morisseau, 2000). Today it continues to expand and is now some 230 by 600 metres across. Its outward progression is continuing at a rate of 1 metre per year. The collapse is centred on two oil wells drilled in the late 1970s. In 1978 an oil exploration well with a 3200m target was abandoned at a depth of around 600 metres because of well stability problems - 600m is the level of Senonian salt in the region. By this level the well had already passed through 50 metres of anhydrite (220-270m depth), interbedded anhydrite clay and dolomite 270m -450 m depth). These are sediments that, in their undisturbed state, are likely aquicludes to any access by unconfined phreatic groundwaters. Prior to drilling it was thought that the Senonian halite extended continuously to a depth of 600 m in the well and in turn was underlain by 50 m of anhydrite (600-650m depth). Below the halite-anhydrite is a artesian aquifer (Albian) with a hydraulic potential in this area of 2.5 MPa (\approx 250 m head)

The first well was abandoned without any casing near the bottom of the well, probably facilitating the escape of artesian waters. A second well, drilled in 1979, was located some 80 metres

from the previous well. It successfully obtained its Ordovician target. But in March 1981, the lining of this second well broke, probably because of cavity formation at a level around 550 metres (once again the regional level of salt) and the well was lost. On October 1, 1986 a large crater formed, centred on these two wells. The diameter of the initial subsurface cavity that stopped to the surface is estimated to have been around 300 m. Once the cavity breached the surface the initial ascending artesian supply to the cavity was $\approx 2,000 \text{ m}^3/\text{hr}$.

As in Wink Sink, Texas, the loss of these wells, in this case during their active life, emphasises the need for caution when planning abandonment in a salt bed, especially when it is highly likely that the salt is a seal to a regional artesian system. The fact that the first well was lost during drilling argues that a breach was already present in the salt bed and a cavity was already stopping its way to the surface. But it is also possible that the inappropriate completion and cementation of casing levels, prior to the well's abandonment, may have accelerated cavity expansion. In hindsight, the loss of the second well some 3 years later, situated so close to the first and dealing with the same cavern-ridden geology, was highly likely as was cavity collapse 5 years after that.

Lake Peigneur, Louisiana

On November 20, 1980, one of the most spectacular sinkhole events associated with oilwell drilling occurred atop the Jefferson Island dome just west of New Iberia. Lake Peigneur disappeared as it drained into an underlying salt mine cavern and a collapse sinkhole, some 0.91 km^2 in area, developed in the SE portion of the lake (Autin, 2002). In the 12 hours following the first intersection the underlying mine had flooded and the lake was completely drained.

Lake Peigneur is a natural water-filled salt solution depression atop the Jefferson Island salt dome, which is one of the salt cored islands in the Five Islands region of the Gulf Coast (Figure 7.13a). The lake is about 2.4 km in diameter with a bean-shaped configuration with a topographic promontory along the southeast shore of the lake rising to more than 23 m above sea level and the surrounding delta plain. Nearby was the site of the infrastructure of the Jefferson Island salt mine (Figure 12.25a).

Drainage and collapse of the lake began when a Texaco oilrig, drilling from a pontoon in the lake, breached a unused section of the salt mine some 1000 feet (350 metres) below the lake floor. Witnesses working below ground described how a wave of water instantly filled an old sump in the mine measuring

some 200 ft across and 24 feet deep. The volume of floodwater engulfing the mine corridors couldn't be drained by the available pumps. At the time of flooding the mine had 4 working levels and one projected future level. The shallowest was at 800 feet, it was the first mined level and had been exploited since 1922. The deepest part of the mine at the time of flooding was the approach rampways for a planned 1800 foot level. In 58 years of mine life some 23-28 million m^3 of salt had been extracted. Prompt reaction to the initial flood wave by mine staff allowed all 50 personnel, who were underground at the time, to escape without anything more than a few minor injuries.

The rapid flush of lake water into the mine, probably augmented by the drainage of natural solution cavities in the caprock below the lake floor, meant landslides and mudflows developed along the perimeter of the sinkhole, and that the lake was enlarged by 28 ha. The surface entry hole in the floor of Lake Peigneur quickly grew into a half-mile-wide crater. Eyewitnesses all agreed that the lake drained like a giant unplugged bathtub—taking with it trees, two oil rigs (worth more than \$5 million), eleven barges, a tug boat and most of the Live Oak botanical gardens. It almost took local fisherman Leonce Viator Jr. as well. He was out fishing with his nephew Timmy on his fourteen-foot aluminium boat when the disaster struck. The water drained from the lake so quickly that the boat got stuck in the mud and they were able to walk away! The drained lake didn't stay dry for long, within two days it was refilled to its normal level by Gulf of Mexico waters flowing backwards into the lake depression through a connecting bayou. But, since parts of the lake bottom had slumped into the sinkhole during the collapse, the final water level in some sections was higher than before relative to previous land features. It left one former lakefront house aslant under 12 feet of water.

Of course, an anthropogenically induced disaster like this attracted the lawyers like flies to a dead dingo. On 21 November 1980, the day after the disaster, Diamond Crystal Salt filed a suit against Texaco for an unspecified amount of damage. On 25 November, Texaco filed a countersuit against Diamond Crystal. The Live Oak Gardens sued both Diamond Crystal and Texaco. Months later, the State of Louisiana was brought into the suit since the incident occurred on state land. One woman sued Texaco and Wilson Brothers (the drillers) for \$1.45 million for injuries (bruised ribs and an injured back) received while escaping from the salt mine. Less than a week before the scheduled trial, a out-of-court settlement was reached between the major players. Texaco and Wilson Brothers agreed to pay \$32 million to Diamond Crystal and \$12.1 million to the Live Oak Gardens.

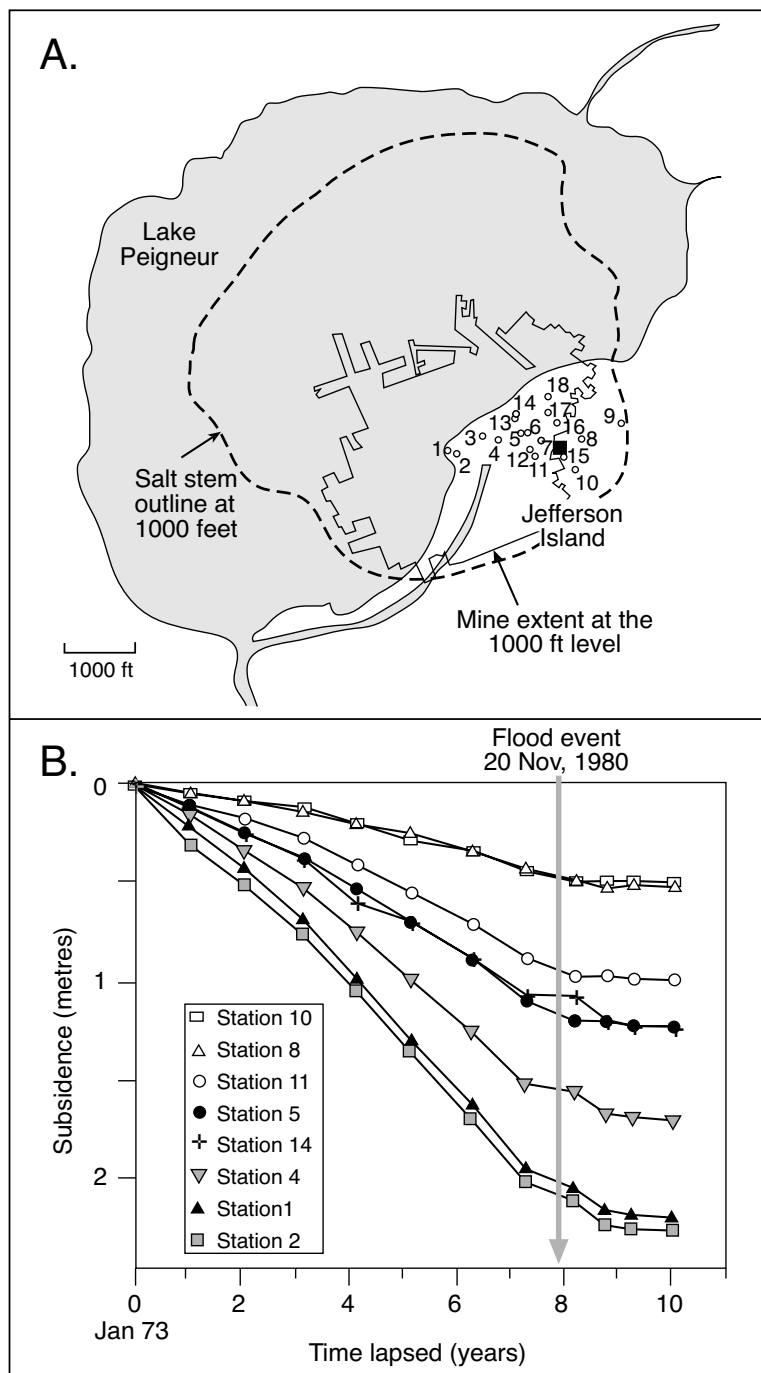


Figure 12.25. Lake Peigneur, Jefferson Island, Louisiana. A) Plan view showing the extent of Lake Peigneur and the position of the surface monitoring stations (1-18) with selected data plotted as 12.25b. Also shown is the extent of the mine workings at 1000 feet subsurface and the outline of the salt stem at the same level. Black square indicates the position of the now flooded No. 1 shaft. B) Ten years of surface subsidence data showing the drastic decrease in subsidence that followed the flooding of the mine workings (see Figure 7.13 for locality; after Thoms and Gerhle, 1994).

An ongoing environmental catastrophe that was anticipated by environmental groups at the time of the accident never materialized. The lake quickly returned to its natural freshwater state and with it the wildlife was largely un-affected. Nine of the barges eventually popped back up like corks (the drilling rigs and tug were never to be seen again). The torrent of water helped dredge Delcambre Canal so that it was two to four feet deeper. And of course, the former 1 metre deep Lake Peigneur was now 400 metres deep in the vicinity of the borehole!

Interestingly, the filling of the mine workings with water drastically slowed the rate of land subsidence atop the mine (Figure 12.25b). Measurements had been carried out between 1973 and 1983, some 7 years before the accident and continued for 2 years afterwards (Thoms and Gerhle, 1994). Slowing reflects the post-accident reduction in the total pressure exerted on the roof of the mine to half its pre-accident levels. Prior to the accident there was no hydrostatic pressure to alleviate some of the lithostatic pressure exerted by the weight of the overburden and so land subsidence above the mine workings was relatively rapid.

Although this incident is not directly related to any solution mining operation and no human lives were lost (although three dogs perished), it clearly illustrates the speed of potential leakage following a breach in a cavern roof in any shallow storage facilities filled with low density fluids. It also illustrates the usual cause of such disasters – human error in the form of a lack of due diligence, a lack of forward planning and a lack of communication between various private and government authorities. It also illustrates that filling a solution cavity with water slows the rate of subsidence atop a large salt cavity and that waters after the disturbance will return quietly to a state of density stratification.

The incident had wider resource implications as it detrimentally affected the profitability of other salt mines in the Five Islands region (Autin, 2002). Even as the legal and political battles at Lake Peigneur subsided, safe mining operations at the nearby Belle Isle salt mine came into contention with public perceptions questioning the structural integrity of the salt dome roof. Horizontal stress on the mineshaft near the level where the Louann Salt contacts the overlying Pleistocene Prairie Complex had caused some mine shaft deterioration. Broad ground subsidence over the mine area was well documented and monitored as was near continuous ground water leakage into the mine workings. The Peigneur disaster meant an increased perception of continued difficulty with mine operations and an increased risk of catastrophic collapse was considered a distinct possibility. In 1985, a controlled flooding of the Belle Isle salt mine was completed as part of a safe closure plan.

Subsidence over the nearby Avery Island salt mine (operated by Cargill Salt) has been documented since 1986. This is oldest operating salt mine in the United States and has been in operation since the American Civil War and the mine has recently undergone a major reconstruction and safety workover. Mine management and landowners did not publicly disclose the technical details of rates of subsidence, but field observations reveal the nature of the subsidence process. Subsidence along the mine edge coincided with a topographic saddle above an anomalous salt zone located inside the mined salt area, ground water flowed into the mine, and there were a number of soil gas anomalies associated with the mine. Small bead-shaped sinkholes were initially noticed in the area in 1986, then over several years, a broad area of bowl-shaped subsidence and areas of gully erosion formed (Autin, 2002). Reconstruction has now stabilised this situation. Much of the subsidence on Avery Island is a natural process that occurs atop any shallow salt structure. Dating of middens and human artifacts around salt solution induced water-filled depressions atop the dome show it is a natural process that extends back beyond the 3,000 years of human occupation documented on the island.

Compared to the other salt domes of the Five Islands, Cote Blanche Island has benefited from a safe, stable salt mine operation throughout the mine life (Figure 7.13; Autin, 2002). Reasons for this success to date are possibly; (i) mining operations have not been conducted as long at Cote Blanche Island as other nearby domes, (ii) the Cote Blanche salt dome may have better structural integrity than other islands, thus allowing for greater mine stability (although it too has anomalous zones, a salt overhang, and other structural complexities), and (iii) the salt is surrounded by more clayey (impervious) sediments

than the other Five Islands, perhaps allowing for lower rates of crossflow and greater hydrologic stability.

Case Histories: storage caverns

The world's demand for fuel means it must be held in sufficient quantities near centres of distribution so as to insure security of supply. Deciding where and how mankind stores substantial volumes of hydrocarbons (or in the future the much more volatile hydrogen) in or near populated areas will always be a problem. There have been a few accidents in below ground storage facilities and some of them are listed in this section. However, when the environmental and safety records of above and below ground fuel storage facilities are compared, the below ground facilities are an order of magnitude safer and less environmentally hazardous. Problems with storage caverns in salt hosts are related either to the utilisation of non-purpose built caverns or to human error and poor management practices.

Weeks Island, Louisiana

The Weeks Island Strategic Petroleum Reserve (SPR) facility on Weeks Island, Louisiana, lay some 30 km SE of Jefferson Island (Figures 7.13a, b, 12.26). It utilized abandoned room and pillar caverns of the Morton Salt Company mine and so was unusual compared to other purpose-built storage caverns of the Strategic Petroleum Reserve (SPR). It was purchased in the 1970s, a time that was early in the annals of the SPR and at the height of the 1970s oil crisis. Occupying a former salt mine it was the shallowest of all the SPR facilities across the USA (150-220 metres below the land surface). It was not a custom built facility nor was it constructed by solution mining technologies.

Following oil fill in 1980-1982, the facility stored some 72.5 million BBL of crude oil in abandoned mine chambers. Then in November 1995, the Department of Energy (DOE) initiated oil drawdown procedures, along with brine refill and oil skimming, plus numerous plugging and sealing activities. In 1999, at the end of this recovery operation, about 98% of the crude oil had been recovered and transferred to other SPR facilities in Louisiana and Texas; approximately 1.47 MMBL still lies in the now plugged and abandoned cavern system.

The cause of this drainage and abandonment was an active sinkhole some 10 metres across and 10 metres deep, first noted near the edge of the SPR facility in May 1992 and apparently formed about a year earlier. The growing depression was located on the south-central portion of the island, directly

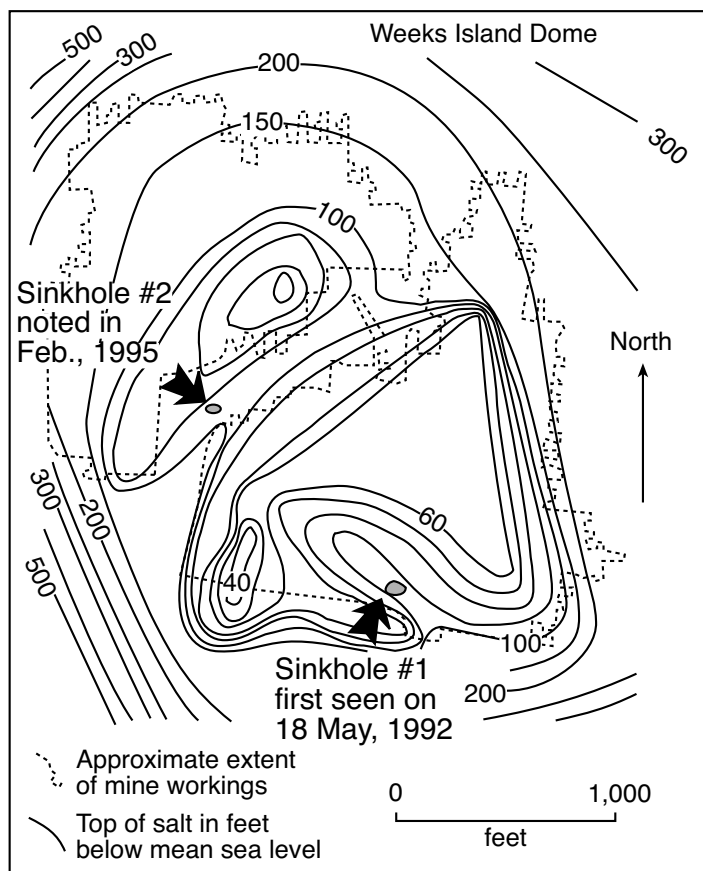


Figure 12.26. Strategic Petroleum Reserve facility, Weeks Island, Louisiana. Top of salt contours showing how sinkholes developed in depressions atop the upper part of the salt. The sinkholes occur in regions near the edge of the cavern with the potential for foundering of the cavern roof into the chambers of the former Morton Salt mine.

over a subsurface trough, which is obvious in the top-of-salt contour (Figure 12.26; Neal and Myers, 1995). Earlier shallow exploratory drilling around the Department of Energy service and production shafts in 1986 had identified the presence of irregularities and brine-filled voids along the top of salt in this region. A second, much smaller sinkhole was noticed in early February 1995, but it did not constitute a serious threat as it lay outside the area of cavern storage.

Neal (1994) pointed out that Kupfer's 1976 map of that part of the mine located beneath the first sinkhole showed black salt. Black salt in Gulf Coast salt mines is often associated with anomalous leached zones where salt was subject to unpredictable movement and sometimes to collapse. The volume of this sinkhole (estimated as 650 m³ when first noted), its occurrence over a trough in the top of salt and its position directly above

the oil-filled mine caverns, meant it was of concern to the SPR authorities, especially in terms of the stability of the roof of the storage cavern.

Investigations undertaken in 1994 and 1995 into the cause of the active surface sinkholes verified that water from the aquifer above the Weeks Island salt dome was seeping into the underground oil storage chambers at the first site (Neal and Myers, 1995; Neal et al., 1995, 1997). The drainage and decommissioning of the Weeks Island facility followed. Beginning in 1994, and continuing until abandonment of the facility a saturated brine was injected directly into the throat of first sinkhole, which lay some 75 metres beneath the surface. This essentially arrested further dissolution and bought time for DOE to prepare for the safe and orderly transfer of crude oil to another storage facility. To provide added insurance during the oil transfer stage, a "freeze curtain" was constructed in 1995. It consisted of a 54 well installation around the principal sinkhole that froze the overburden and uppermost salt to a depth of 67 metres (Martinez et al., 1998). Until the mine was completely filled with brine and its hydrocarbons removed, this freeze wall prevented groundwater flow into the mine via the region of black salt around the sinkhole. Dealing with this sinkhole was costly. Mitigation and the removal and transfer of oil, including dismantling of infrastructure (pipelines, pumps etc.), cost a total of nearly US\$100 million; the freeze curtain itself cost nearly \$10 million.

In hindsight, based on an earlier leak into the mine while it was an operational mine and the noted presence of black salt in a shear zone in the mined salt, one might fault the initial DOE decision to select this mine for oil storage. In 1978 groundwater had already leaked into a part of the mine adjacent to the sinkhole and was forewarning of events to come (Martinez et al., 1998). Injection of cement grout into the flow path controlled the leak at that time, but it could just as easily have become uncontrollable and formed a sinkhole then. But in 1978 the technology needed to understand the salt physics, salt solution and mine conditions and so predict future events had not been developed. The world, and the United States, was in the middle of an oil crisis and as a former US President once observed, "It's hard to drain the swamp when you're up to your arse in alligators!"

Explosions and fires from cavern leakage

Almost all the explosions and fires described in this section are caused either by human error, poor forward planning, a lack of due diligence by the storage company or operator or a combination of these factors. In all cases the salt caverns themselves did not fail. In spite of these accidents, cavern storage is still one of the safest ways to store what are very large volumes of highly explosive materials. Consequences are far graver, and death rates much higher, when explosions and fires have occurred in above ground fuel storage tanks.

The West Hackberry explosion

On September 21, 1978 a blowout and explosion occurred at the West Hackberry salt dome storage facility in southern Louisiana (USA). It killed one worker, released 10,000 m³ of oil to the surface and cost US \$14-20 million (1980 dollars) in cleanup and remediation. The incident occurred during workover operations on one of the access wells to the No. 6 cavity.

Understanding the causes of the explosion requires a few background comments on the casing strings in the well and the workover specifications (Figure 12.11). The well completion was made up of an outer 12.75-in (32.4 cm) casing string cemented to a depth of 2632 ft (816m). Cemented inside was another 9.62-in (24.4 cm) diameter casing string some 2603 ft (807 m) long. This was probably added after the “initial” completion to improve oil tightness when the cavity was converted to oil storage. An innermost 5.5-in (14 cm) diameter pipe string was used to withdraw brine whenever oil was pumped in to the cavity (see Figure 12.27).

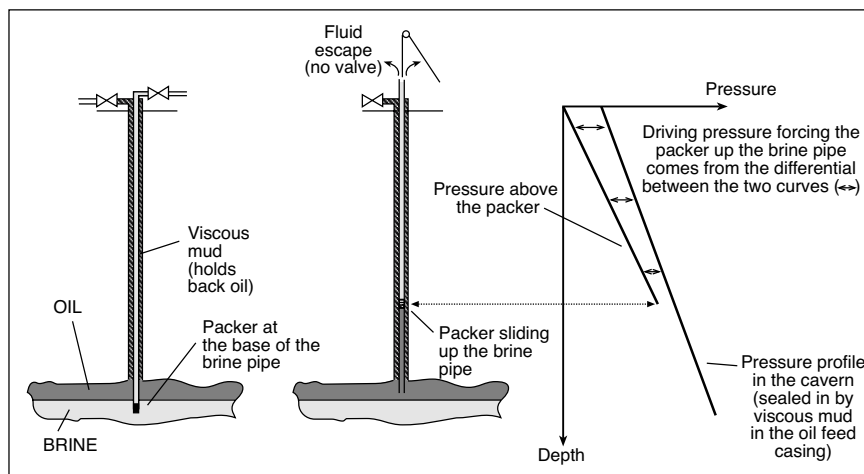


Figure 12.27. Schematic of the pressure differentials that caused the West Hackberry blowout and explosion (see also Figure 12.11).

On the day of the explosion the workover consisted of withdrawing the 5.5-in innermost tubing string, repairing a leak on the 12.75-in casing, and reinforcing the wellhead equipment. To accomplish this, the annular space between the innermost pipe string and the 9.62-in casing had been filled with high-viscosity mud. This was designed to bring wellhead pressure in the oil string to zero. Once the annular space was filled, a packer was set at the bottom of the 5.5-in brine pipe to seal it off from the cavity. Work then commenced on pulling the 5.5-in pipe; however, after 14 pipe lengths had been stacked, the packer slipped as increasing differential pressure started to push it up to the surface. As the packer rose, the pressure (brine to oil differential) on it increased. Soon the packer shot up and out on to the surface, forming an oil geyser (blowout) that continued until the pressure differential had dissipated. By that time an estimated 72,000 barrels (10,000 m³) had shot up into the air, caught fire and killed one of the drilling crew.

A poor understanding of the pressure distribution in the fluid columns when the workover was designed is the main reason for the incident. As planned, the workover was extremely delicate, it was attempted without drawing down the oil pressure in the cavern. As the oil was under high pressure (sealed in by viscous mud in oil feeder casing) as the workover began it was liable to expand violently if any mishap upset the status quo. Injecting the viscous mud at the top of the well was a good precaution against any failure of the topside valve on the oil-filled annular space, but it had absolutely no effect on the dangerous situation at the bottom of the cavity and if the packer failed, which it did, there was no way of preventing a blowout.

A comprehensive but simple precaution would have been to release the pressure on the oil in the cavity by drawing down the top surface of the brine in the access well to about one-quarter of its total original height. The volume of oil needed to be withdrawn was, of course, exactly equal to the volume that was expelled in the blowout. This relatively small volume of oil could easily have been stored temporarily in another cavity on the site. So doing would have rendered the workover situation entirely safe.

The Brenham explosion

A disastrous explosion occurred on April 7, 1992, following the outflow of LPG onto the surface from a well atop a storage cavern in the Brenham Salt Dome. The blast occurred some 110 km northwest of Houston. It killed a 6-year old boy and two adults, injured 21 persons, damaged more than 40 homes and snapped trees like matchsticks, while denuding acres of rolling farmland. In all it caused an estimated US\$ 9 million in damage to property within a 5 km radius. Seismographs at three Texas universities within 120 km of the scene recorded surface tremors ranging from 3.5 to 4.0 on the Richter scale. Windows were rattled in homes more than 200 km away.

The Brenham storage facility consisted of a 380,000-bbl (60,000-m³) cavern filled with LPG (a mixture of propane, ethane, n-butane and other gases). The cavern was linked to ground level by a 13-3/8-in diameter, 2,702-ft long cemented casing (Figure 12.28). A central brine pipe (2,871-ft long) allowed injection and withdrawal of brine. LPG was injected to or withdrawn from three distinct pipelines. Brine was provided by two above-ground brine ponds. The wellhead was equipped with a shutdown valve. The Brenham station was operated remotely by a dispatcher in Tulsa, Oklahoma (Bérest and Brouard, 2003).

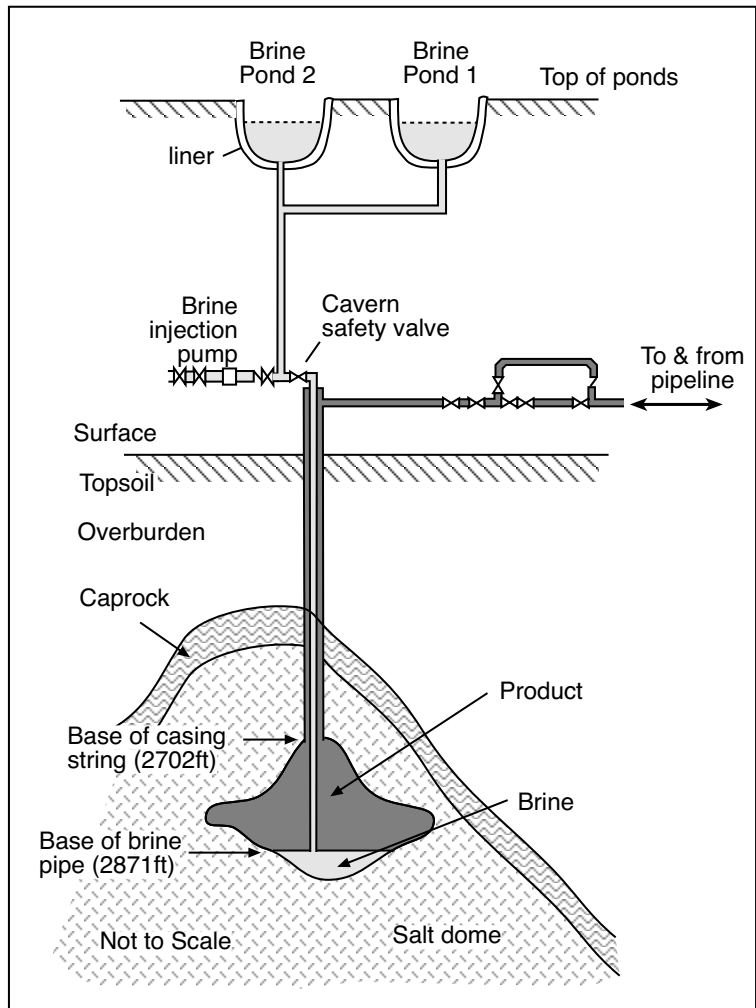


Figure 12.28. Schematic of the situation at the time of the Brenham explosion.

At 5:43 am on April 7, 1992, additional LPG was injected in the cavern. The brine/LPG interface unexpectedly reached the 1-in diameter weep hole located in the lower part of the central tubing, some 1 ft above the tubing base. The weep hole was supposed to provide warning in case of imminent overfilling. LPG flowed into the central brine tubing, leading to lower density in the fluid in the central column, partial vaporization and expansion of the lighter gases, a pressure drop in the cavern and, ultimately, a large flow of gas through the weep hole and the tubing base alike.

Brine, followed by liquefied gas, daylighted at the brine pond surface. Back-calculation proved that 3,000 to 10,000 bbl (500 to 1,600 m³) of liquefied gases were expelled via the ponds. The release of gas into the atmosphere activated gas detectors

at ground level. (Such activation was apparently a relatively frequent event at this station, and alarms were often unrelated to an actual gas leak). The dispatcher in Tulsa was not able to interpret correctly the somewhat confusing information delivered by the telemetric system - a unique signal was sent, whatever had activated a number of detectors. The shutdown valve (or cavern safety valve) was assumed to have immediately reacted to the high pressure level (100 psi) in the brine tubing at the wellhead, but the system failed.

A subsequent National Transport Safety Board (NTSB) investigation confirmed the local operator had overfilled the storage cavern to where LPG had escaped into an adjoining brine storage pit through the brine injection system via an open valve. Product had then evaporated and, being heavier than air,

formed a low-lying cloud 30 feet high and several hundred yards long. At 7:08 am the “mushroom-shaped” vapour cloud was ignited by an automobile driving into the foggy cloud near the storage facility.

According to the NTSB report, Mapco (the operator of the facility) was not aware of the volume of product in storage at the site. Some 338,995 barrels were actually stored instead of the 288,000 bbl estimated by Mapco. NTSB concluded that the management procedures had lacked oversight adequate to confirm employee measurements. Nor did the company have the ability to balance cavern receipts against withdrawals. In addition, employee measurement procedures did not adequately take into account specific gravity variations of the NGLs in storage.

Aside from the computation errors, NTSB said other contributing factors included:

- a) Inadequate positioning of the brine pipe weep hole - in a post accident redesign it was moved to 6 feet above the base of the brine pipe,
- b) A lack of several fail-safe features on the cavern's shutdown system - this system had included a brine pressure-sensing line designed so that when a large pressure build-up was sensed in the brine line it switched a spring that, when triggered, sent an electrical signal in a chain containing a fusible link whose fusion should have closed the brine safety valve and so prevented product leakage back up the brine pipe. It is extremely likely that one or two manual valves were closed on this sensing line at the time of the explosion, isolating it from the main body of the brine pipe, so making the emergency shutdown system ineffective. Ironically, the shutdown valve was activated when heat from the explosion burned the fuse and triggered valve closure (it shut the barn door after the horse had bolted).
- c) Inadequate emergency response training and procedures, along with poor communication among Mapco employees responding to the alarms and to the obvious surface emergency.

Early media coverage sensationally reported that “A Salt Dome Has Blown Up”. However the cavern storing the leaked liquids later passed a mechanical integrity test and is still in use today. It was operational supervision and safety procedures that failed dismally, not the cavern. After this accident, the Railroad Commission of Texas issued new regulations (effective in 1994) mandating that LPG storage caverns be protected by at least two overfill detection and automatic shut-in methods.

Barber's Hill explosion and collapse

On October 3, 1980 a gas-fed explosion occurred in a residence in Mont Belvieu, a Texan town that sits atop the Barbers Hill diapir, some 60 km west of Houston. Barbers Hill dome is the largest subsurface LPG storage facility in the U.S. with over 126 active solution-mined caverns storing between 75 and 300 million barrels of light hydrocarbon products. The explosion was ignited by a woman who sustained burns when turning on her dishwasher. Two weeks earlier, on September 17, 1980, a drop in pressure had been recorded in one of the nearby cavities storing liquefied petroleum gas (70% ethane, 30% propane). The cavern was emptied of product and filled with brine. Subsequent investigation showed a leak had occurred through a corroded casing joint in the access well. The well in question had originally been drilled in 1958. Leaking gas seeped through the surrounding soil to accumulate in the foundations of the residence where the explosion occurred. In the days that followed, gas daylighted haphazardly in residential areas around the site of the original explosion. Holes were drilled into the water table to find and vent pockets of gas. Residual gas saturations in the soils forced the evacuation of 73 families for nearly seven months and a drastic fall in property values.

A few years later, on July 30, 1993, there was another event that further lowered Mont Belvieu property values. In a few hours a sinkhole crater formed between two brine wells in the EGP Fuel Storage facility (Cartwright et al., 2000). The crater stabilized with a diameter of 12 metres and a depth of 6 metres. A well that was near the problem site had to be abandoned after the sinkhole formed. It was not a hydrocarbon storage well so the environmental implications of a collapse-induced abandonment were not as significant it would have been for a failed hydrocarbon cycling well. The cause of the sinkhole is contentious but it is thought that brine cycling in the two wells may have contributed to the collapse. Detailed subsidence work in the cone of subsidence about the sinkhole suggest that it was there prior to the collapse and if it had been monitored the data could have been used as an indicator of the likelihood of collapse (Cartwright et al., 2000).

Brine injection that drives brine compensated withdrawal of the stored hydrocarbons periodically requires large volumes of brine in short time frames. But in Mont Belvieu there was not sufficient above ground infrastructure to store the large volumes of brine needed for product cycling. To give access to large volumes of brines quickly, brines were pumped down brine storage wells with bases in shallow caprock caverns. Wells adjacent to Mont Belvieu sinkhole were two such wells.

Mineola propane fire

In 1995 there was an underground fire that burned for several days at a salt dome storage cavern operated by Suburban Propane near Mineola in East Texas, some 145 km east of Dallas. The cavern in which the blow-out occurred extended from 1200 ft to 2500 ft (350-750 m) subsurface. The blowout occurred when a salt wall separating two storage caverns had become so thin from the enlargement associated with brine compensation (product cycling) that it cracked (Gebhardt et al., 2001). This allowed stored propane product to flow from one cavern to an adjacent cavern that was empty of product and undergoing testing. Pressurised nitrogen was being injected into the adjacent brine filled cavern as part of a standard mechanical integrity test. The testing may have contributed to the penultimate pressure buildup that allowed propane product to leak into shallow depths via a casing leak (Bérest and Brouard, 2003). The leaking well had originally been drilled as an oil producer in the late 1950s, four decades before the accident. Liquefied gas escaped through the soil in a halo that extended as far as 100 feet from the well. The escaping gas ignited and burned releasing heavy black smoke. Extinction of the fire was not a viable option, as dangerous re-ignition and flash back was likely. The innovative kill techniques applied to this well are described in Gebhardt et al. (2001).

There are potential problems with longterm intercavern integrity as all salt caverns will enlarge during product cycling, so the Texas Railroad Commission now legislates what is an acceptable degree of enlargement before a storage cavern must be plugged and abandoned.

Hutchinson explosion

On January 17, 2001, a gas explosion and fire destroyed two businesses in downtown Hutchison in central Kansas (Allison, 2001). The next day in a mobile home park 3 miles away another explosion occurred and 2 residents died of injuries received. The explosions were tied to geysers spewing gas and water, and their appearance caused the excavation of hundreds of Hutchison residents. Pathways to the landsurface at both explosion sites and to the various active geysers across town were directly tied to abandoned wells that were once used to solution mine the Hutchison Salt.

The January 17-18, 2001 eruptions of gas and brine, driving 30-ft (10m) geysers in the town, resulted from the loss of 143 MMcf of gas from the Yaggy natural gas storage facility located 7 miles down the road from the town community of 40,000

people (Figure 7.8). Oneok Inc., owned and operated the Yaggy field through a subsidiary company called KGas. Upon review of pressure records, KGas officials realized that the S-1 cavern had probably been leaking at a low level at least since the pod of caverns had been refilled with natural gas on January 14, and perhaps longer. At the time, technicians did not think much of a minor pressure drop, as it was a routine situation associated with filling the cavern. When the caverns are pressurized, the natural gas is compressed, raising its temperature. Once in the caverns, the pressurized gas begins to cool and condense, resulting in a slight pressure decrease. It was common practice to then “top off” the cooled caverns with additional gas to fill the caverns to the final storage pressure.

The Yaggy field of salt caverns was originally developed in the early 1980s to hold propane. Wells were drilled to depths of about 650-900 feet (200-300 m), into the lower parts of the Hutchinson Salt Member and cased with steel. The roof of each cavern was about 40 feet (12m) below the top of the salt layer. The company had difficulty making a financial success of the operation and eventually ceased operations. All of the storage wells were filled with brine and then plugged by partially filling them with concrete. KGas acquired the facility in the early 1990s and converted it to natural gas storage (by definition this is a pressurized storage system). Plugged wells were drilled out to return the feeder wells and caverns to use. At the surface the wells in the Yaggy facility are 300 feet (90m) apart. At the time of the crisis, Yaggy had about 70 wells, of which 62 were feeders to active natural gas storage caverns. More than 20 new wells had been drilled and were being used to create new caverns for expansion of the field storage capacity.

At full capacity, the field could hold 3.5 billion cubic feet (Bcf) of gas at pressures of about 600 pounds per square inch and at the time of the accident it was supplying up to 150 MMcf (million cubic feet) of gas per day. Yaggy is the only natural gas storage field in salt caverns in the state of Kansas. Other salt caverns in Kansas are used for brine-cycled storage of liquid hydrocarbons, such as propane, at much lower pressures than the natural gas at Yaggy.

Records show that when KGas drilled the concrete out from the well casing in S-1 well to return the well to operation, they encountered a steel casing coupler that had fallen into the concrete in the well during the plugging operations (Allison, 2001). During the workover this object may have deflected the drill bit against the side of the well casing damaging and weakening it. A post accident down-hole video in S-1 shows a large curved slice in the casing at that depth. The city's

geological consultant described it as looking “like a kitchen knife cutting into a can.” Prior to the Yaggy facility approval by state authorities the S-1 had a satisfactory casing pressure test, as required by the Kansas Department of Health and Environment. The test was thought to demonstrate the integrity of the casing at that time. However, the well at the depth of the leak was never tested to the maximum pressure that would be experienced in service.

The route followed to the surface by the escaping gas is still not completely documented. Initial seismic surveys in early February 2001 at first indicated a possible subsurface sand channel through which the escaping gas flowed up from the storage facility. But that was not borne out by a study of regional well logs or the 22% success rate in drilling for suspected gas pockets (Watney et al., 2003) or subsequent seismic interpretation (Nissen et al., 2004). The most likely candidate carrier is thought to be a fractured intrasalt dolomite, which facilitated drainage to the crest of the anticline culmination that underlies the town of Hutchinson.

There are more than 600 NGL-LPG salt storage caverns in bedded Hutchinson salt in the state of Kansas, the most of any state in the USA. Kansas also has plans for more natural gas storage caverns, although Gulf Coast salt dome caverns are 10-20 times larger. The mix of bedded salt and permeable rock formations around Hutchinson, the presence of natural dissolution irregularities and the fact that Hutchinson has been an area of solution mining since the late 1800s is a real problem for storage of high-pressure fluids. Once the S-1 well was breached, numerous unplugged brine wells that were long ago drilled within the Hutchinson Salt and abandoned, without appropriate documentation, routed the escaping gas to the surface. Such wells are directly tied to the downtown fire that first heralded the problem, and to the two deaths that occurred in the explosion in the mobile home park a few days later. Work since the explosion has pointed out numerous problems to be addressed in a region of bedded salt that appears in many ways not to be a suitable site for future natural gas storage projects. Even so, the salt storage cavern itself did not leak, the access piping was the problem due to well workover damage.

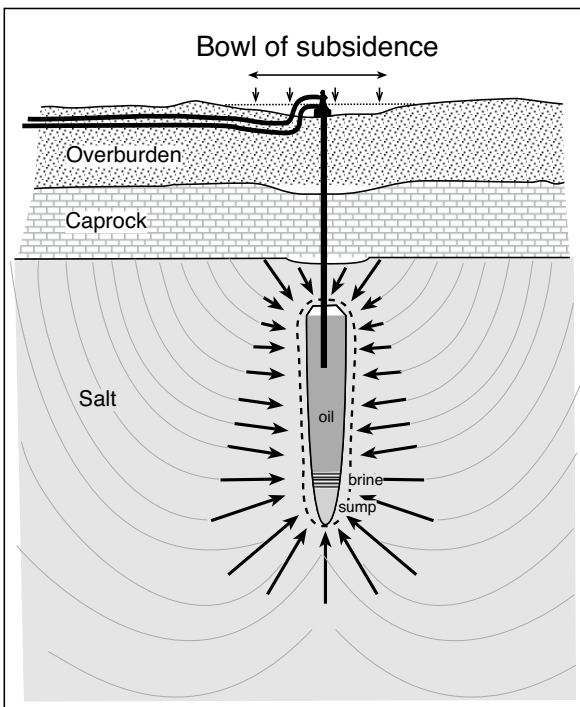


Figure 12.29. After the cavern has formed and is filled, salt creep causes the cavern to shrink from its original size (dashed shape) into a somewhat smaller configuration. This induces subsidence and possible collapse in the zone above the cavern. At the surface this process forms a “bowl of subsidence” (in part after Thoms, 2000).

Recognising and preventing potential cavern problems

Three factors can contribute to the breaching and collapse of solution-mined cavities, namely creep, uncontrolled leaching, and the presence of anomalous zones in what had been assumed to be homogenous salt. Anomalous zones may be unexpected regions of highly soluble salts (potash salts), of fractured intrasalt beds, or zones of much older natural leaching (e.g. black salt), which may contain pressurized brine or gas (methane or nitrogen). In brinefields and some salt mines the anomalous zones tend to occur near intersections with poorly documented older well bores. The same set of factors generates many of the operational problems in conventional salt mines (Chapter 11).

Salt Creep

The principal factors influencing the rate of salt creep are; a) cavern depth and overburden characteristics - pressure and temperature gradients, b) internal cavity pressure, c) cavern shape, salt properties (e.g. variations in halite crystal size, moisture content). Left alone, and not subject to fresh water incursion, salt (especially halite and the potash salt) will creep into an unbreached storage cavern until differential pressures are equalised. Salt cavities are generally stable at depths between a few

hundred metres and about 2000 metres depth (Figure 12.1). Below that depth there is an elastic-plastic transition zone for salt behaviour somewhere below 1000 to 2000 metres. Cavities below this zone can be relatively unstable and show large volume decreases through rock creep with the transition depth depending on the composition of the salt, the geothermal gradient and the overburden pressure. Effects of salt cavity creep, due to inadequate internal pressuring, were first noted in the 1970s by the operators of some large purpose-built storage caverns. The Eminence cavern in Mississippi, built at 1700-2000m, lost 40% of its volume in just two years post construction, while Tersanne in France lost 30% to salt creep (Figure 12.30). Such losses in storage capacity were potentially expensive, but when adjustments were made to cavern depths and minimum gas storage pressures, the volume loss stopped. Today both facilities are still operational and have recovered much of their volume loss (Thoms and Gehle, 2000a). Salt creep occurs at slower rates above the transition zone; measured rates are mm - cm per year in salt mines in Kansas and Texas with depths up to 600 m.

Like mines, salt cavities built above or within the transition zone can be extremely stable and when properly located, designed and operated may lose only a few percent volume a year. Some cavities in salt above the transition zone can remain remarkably stable even if emptied of product. For example, in the 1950s, a lenticular cavern with a roof span 366 metres was excavated by solution mining in the Bryan Mound salt dome in Texas, which is also the site for the later Strategic Petroleum Reserve programme. The cavern has an unusual shape compared to the "carrot" shape of later purpose-designed caverns in the Mound. It was has an average depth of 550 metres, a cavity height of 55 metres and an unsupported span of more than 360 metres. After excavation, it was filled with LPG but subsequently lost wellhead pressure and so was abandoned (emptied). Thirty years later, measurements indicated that this cavern is still

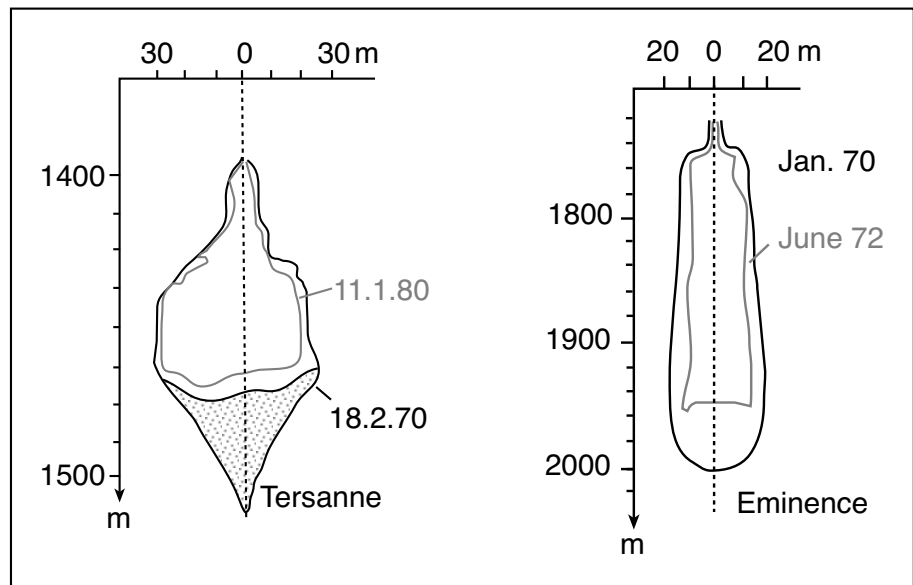


Figure 12.30. Creep effects in Tersanne (France) and Eminence (Mississippi) showing shrinkage with time (Dotted shading indicates the distribution of insolubles in the Tersanne cavern).

remarkably stable, having lost only about 4 percent of its total volume since abandonment.

Salt creep is accelerated by large differences between natural lithostatic pressure (in the salt) and the pressure in the cavern. The rate of creep also depends on variations in the proportions and physical properties of the various salt minerals and the configuration of nearby nonevaporites (e.g. carbonate, anhydrite or potash beds in halite). To minimise creep, operational pressures in a fluid-filled storage cavern should be as high as allowed, this is especially true in facilities used to store natural gas. But this may encourage leakage and gas loss in facilities lacking structural integrity (see Hutchison explosion in case histories).

When a cavern is active, overburden creep will typically drive ongoing subsidence at the landsurface in the form of a subsidence bowl or depression (Figure 12.29). The length of the delay between creep into a cavern and its expression at the surface depends upon cavern depth, mode of cavern operation, thickness of salt cover and character of overburden materials or roof beams (Neal 1991). Ground effects atop shallow caverns usually show up more quickly than those above deeper caverns, subsidence over some storage caverns has been detected only after a decade or more of operation (Thoms, 2000).

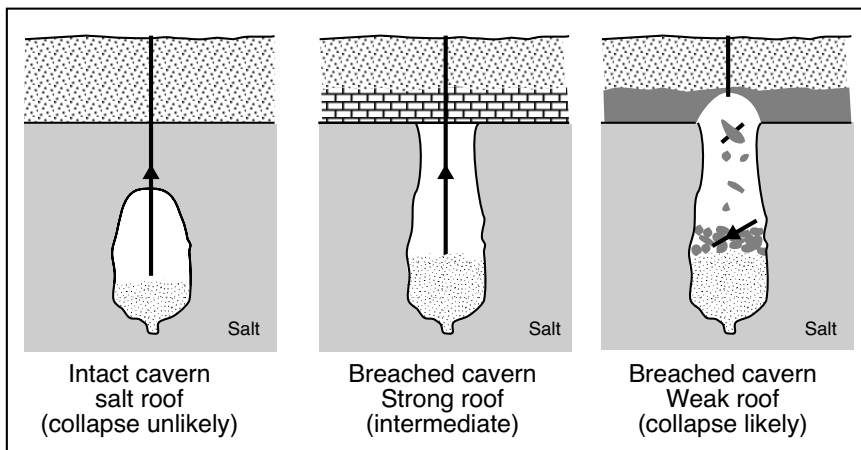


Figure 12.31. Preservation of a salt roof or the presence of strong overburden spanning the cavern roof makes cavern collapse less likely.

Salt falls versus roof collapses

Salt fall from the cavern roof, as distinct from catastrophic roof collapse and chimneying, occurs in most caverns especially in bedded salt. In a storage cavern it is part of the preliminary construction/leaching phase and also occurs during later storage cavern expansion driven by product cycling. Providing an adequate salt pillow is left as part of the cavern's design, roof falls are not considered detrimental by most operators, as they generally do not greatly affect containment volume. They may sometimes damage casing strings "hanging" from the roof of the cavern.

Most damaging to a salt cavern and possibly to the surface environment is total collapse of a cavern's roof span. It may ultimately lead to the formation of a sinkhole at the landsurface. Such surface expressions atop a brinefield may be delayed for some time after operations have ceased. Typical causes of sinkholes in brinefields are uncontrolled solution leaching, the unexpected intersection of soluble (potash-rich) seams in the salt roof, or the presence of natural brine lenses from natural karstification near the outer parts of a salt mass (see case histories).

Figure 12.31 illustrates the range of probabilities for salt fall and collapse in salt cavities: a) is an intact cavern with adequate salt cover - salt falls are a part of the operational running of the cavern, b) is a breached cavern with a strong roof, still capable of spanning the cavern - ultimately ongoing salt solution it will drive it into a breached system, while c) illustrates a breached cavern system that may soon develop into a sinkhole at the surface - it is the result of total salt removal beneath a weak cavern roof.

Ongoing brine compensation (product cycling) means any storage cavern has the potential to expand until it collapses. To prevent potentially dangerous collapses and product leakage, the shape of a storage cavern must be monitored throughout its life. Some materials found above salt formations, such as reactive shales exposed to brine, may take time to weaken. This means a delayed collapse event, it can occur years after the cessation of solution operations. Occasionally the salt roof to a cavern in stage b) may be taken out with the intent of instigating

collapse (see the SG4 case history). Deliberate oversolutioning is being considered to create desirable wetlands via sinkholes in the former ICI brinefield near Teeside, England.

Ground subsidence

Salt creep means the ground surface over an intact cavern will deform into a shape resembling a wide shallow bowl, hence the name bowl subsidence. Bowl subsidence over intact salt caverns is a response to movements at depth which are transferred to the surface with diminishing amplitude over a wide cone of influence. Subsidence of the landsurface above a salt cavern is normal and to be expected, especially above shallower storage caverns (Figure 12.32). This surface response is similar to "trough subsidence" at the surface above "long-wall" or "room and pillar" mining operations. As the boundaries of such mines advance the accompanying ground movements manifest as moving linear depressions in the landscape called areas of trough subsidence by mining engineers. Bowl subsidence above a salt cavern is not a problem unless the roof span breaches and the rate of ground subsidence increases.

Measured land subsidence rates vary above salt caverns constructed for storage of US Strategic Petroleum Reserve (SPR). Rates atop storage domes in the 1980s ranged up to 40 - 50 mm/year in SPR facilities in Texas and Louisiana (e.g. Figure 12.32a). Rates above the much deeper Tersanne cavern in France are much lower \approx 6-8 mm/year than those of the Gulf Coast (Figure 12.32b), even after the cavern had shrunk relatively rapidly in the 1970s (Figure 12.30). Since the late 1980s, almost all purpose-built storage caverns have been filled and

maintained at higher pressures than in the 1970s. Pressurizing has mitigated salt creep and surface subsidence effects in land areas atop many of these domes (Thoms, 2000).

For example, the Bryan Mound Dome, located southeast of Houston on the Texas Gulf Coast, was one of the first domes to host SPR caverns. The SPR site's subsidence rate was 24.4-36.6 mm per year from 1982 to 1988; when subsequently pressurized from 1988 to 1994 the subsidence rate fell to 6.1-24.4 mm per year; and was 3.1-15.2 mm per year from 1994 to 1999. That is, the median subsidence rate atop Bryan Mound decreased by 70% following the increase in cavern pressure. Rates at the more recently constructed Big Hill SPR site ranged from 6.1-15.2 mm per year from 1989 to 1994; and from 6.1-9.1 mm per year from 1994 to 1999. By contrast, the subsidence rate at another SPR site, West Hackberry, was still high, approximately 76.2 mm per year after pressurization. The reason for the much lower rate at Big Hill is thought to reflect the very thick (300m+) brittle caprock covering the Big Hill salt stock (Linn and Culbert, 1999; Bauer, 1999).

Estimates of rates of acceptable bowl subsidence atop product cycling caverns can be calculated using influence functions based on linear elasticity, the same mathematics used by mining engineers. This works well if the displacements are small, continuity prevails, and if appropriate effective reaction moduli can be estimated for the various inhomogeneous overburden materials above the caverns. Assumptions of mathematical linearity are often incorporated into methods for fitting subsidence models to existing databases in order to predict future trends of subsidence over cavern fields. But different leaching rates and inhomogeneous distributions of subsurface features means predictions are often of limited use. More sophisticated three dimensional finite element computer programs have been used recently to analyse subsidence over brinefields incorporating closely spaced caverns with relatively complicated subsurface geometries (see Kunstman and Mazur, 2000).

Surface indicators of breached caverns

Measuring subsidence above an active storage cavity over a number of years is a useful tool to monitor the state of the cavern and the likelihood of any sinkholes appearing at the surface. Subsidence over breaching caverns, where the integrity of the roof span is finally lost, generally involves three stages (Figure 12.33; Thoms, 2000): 1) initial overburden collapse into breached cavern; 2) upward caving via "chimneying" through indurated strata (which engineers sometimes describe as "stiff soils"), and 3) transition to bowl subsidence in more plastic

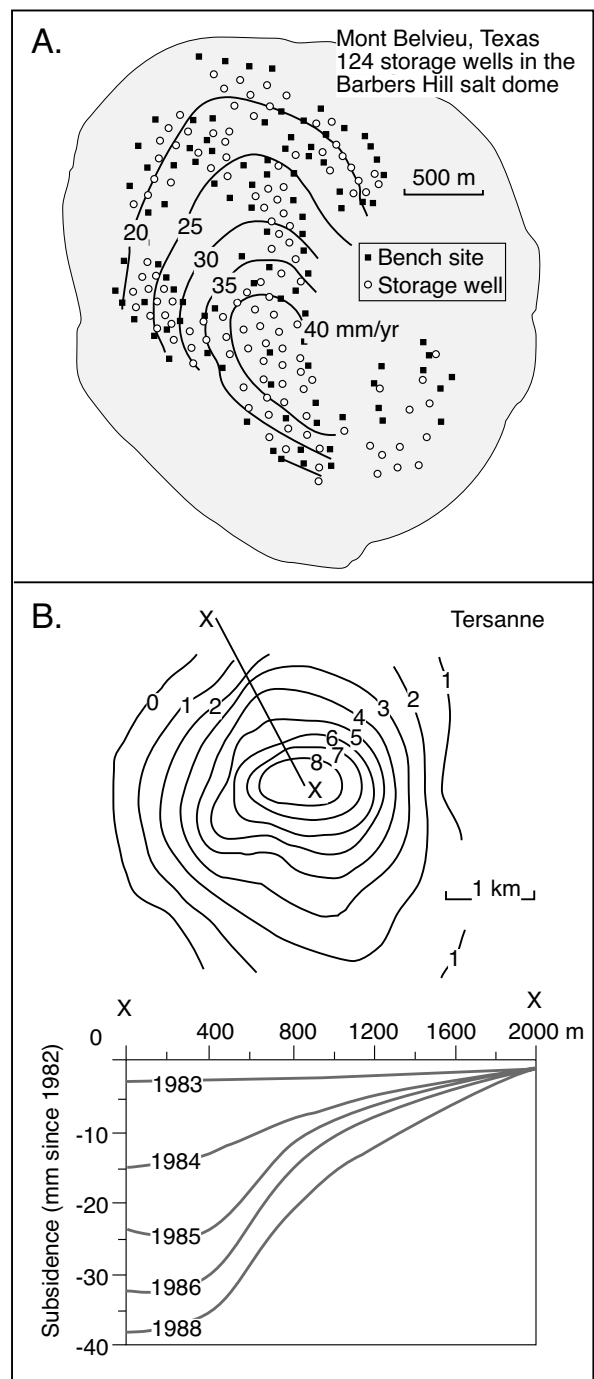


Figure 12.32. Landsurface subsidence above storage caverns. A) Subsidence contours in mm/year atop the Barbers Hill salt dome in the vicinity of Mont Belvieu, Texas (after Ratigan, 1991). B) Subsidence contours in mm/year atop the Tersanne storage cavern, France. Lower panel plots successive subsidence profiles from 1983 to 1988 along the line X-X' (after Bérest and Brouard, 2003; Durup, 1991).

soils near the surface. Following initial roof span collapse, local conditions determine whether caving or bowl subsidence will dominate. After an initial breach and collapse, Stage 2 caving stops vertically through indurated strata as an upward migrating cavity atop a growing chimney. The cavity diminishes in height as it rises because of the bulking of caved materials into the stopping chimney. In Stage 3 the caving mechanism transforms into bowl subsidence as more plastic horizons (weathered strata and soils) are encountered nearer the surface. Breached caverns typically manifest at the surface as relatively deep subsidence bowls, sometimes with sinkholes near their centres.

Stage 2 caving can be bypassed or be arrested if the breached cavern is overlain only by plastic overburden or the cavern is too small to contain all the bulking debris from the overlying strata. In the latter case, the bulking materials fill the cavity to where they can support the roof once more, so arresting further upward migration. Localized bowls of subsidence will usually be seen at the surface over the arrested cavity. With time, the bulked materials may consolidate and allow some additional upward migration of the cavity, and so drive additional subsidence.

Among the various subsidence features, sinkholes are of greatest concern as they are rapidly expressed surface features of typically downdropped plugs of surface material encircled by near vertical sides. They occur when Stage 2 caving dominates all the way to the surface. Concentric fissuring and collapse of the landsurface atop a sinkhole can form within hours of the structure first breaking through to the surface. Overburden

materials rapidly slip and fall into the growing water-saturated core with a huge potential for property damage and even loss of life (see case histories).

Monitoring and minimizing collapse

Subsidence effects, and even active sinkholing were once ignored by brinefield operators but changes in rates of subsidence, along with sonar monitoring of cavern shape, are now used as indicators of the state of the cavern. Responsible operators now conduct periodic or continuous subsidence surveys, and if anomalous effects are recognised, preventative action can be taken.

Routine monitoring of subsidence over storage cavern fields can be performed with conventional land surveying methods. A network of reference points or monuments is set up that effectively spans a brinefield or storage facility (Figures 12.32a). A tie-in is often made to an established reference point located some distance away from the influence of the field. Differences in elevations of points over time intervals between surveys can then be interpreted as velocities of vertical movement (Figures 12.25b, 12.32). It is important to perform surveys at about the same time each year to minimize effects of natural seasonal factors, e.g., soil temperature and rainfall. For some cavern fields it may be more efficient to make use of the Global Positioning System (GPS) for subsidence monitoring. Regulatory agencies often require that subsidence over storage caverns be routinely monitored and reported. Standard techniques for this

purpose are given in Swarts (1993), Watts (1991) and Wong (1982).

More sophisticated automated methods for monitoring subsidence are justified when there is a significant risk of environmental or property damage, as in an area where there is a high probability of sinkhole development in close proximity to residences or storage pipelines and other infrastructure. Such a system might consist of an array of strategically placed tiltmeters, geophones, and inclinometers, with remote read-out and telemetry components. This system should be capable of collecting and

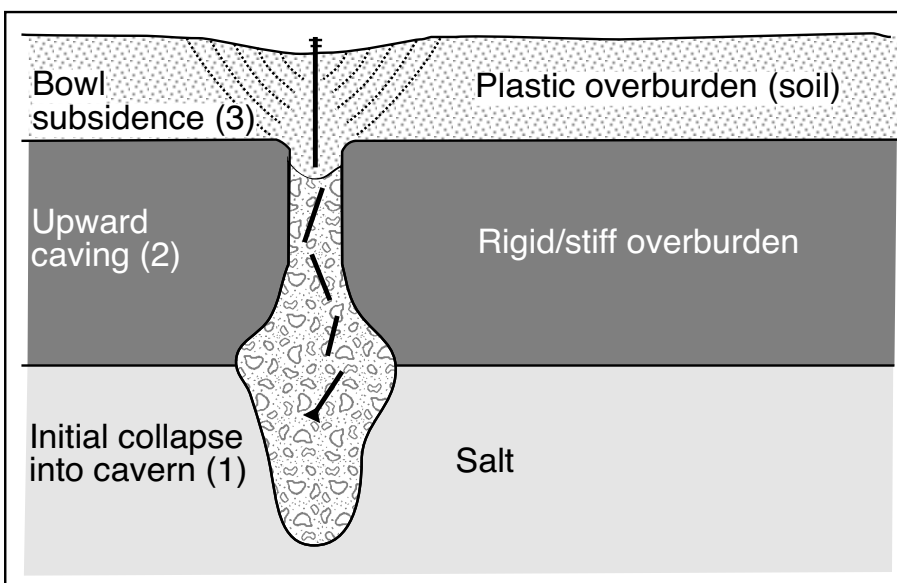


Figure 12.33. Three stages of cavern collapse and sinkhole growth (after Thoms, 2000).

sending data to a comprehensive analysis station at selected time intervals or when activated by a precursor event. Significant events may consist of accelerating localized surface movements, microseisms, and fissures.

Monitoring ground subsidence and cavern shape allows a cavern operator to minimize the effects of subsidence by:

Minimising subsidence from salt creep - As noted earlier, salt creep into caverns causes longterm bowl subsidence at the surface. It follows that bowl subsidence can be mitigated by minimizing salt creep in caverns. The most direct method for minimizing salt creep in existing hydrocarbon storage caverns is to operate them at the highest practical pressures at all times. The determination of the highest practical cavern pressures and operating schedules will involve consideration of site-specific cavern rock mechanics, economic and regulatory factors, as well as the potential impact of subsidence (Rokahr, et al., 1998).

Maintaining adequate salt cover - In order to avoid possible collapse that might ultimately lead to sinkholes, an adequate salt cover must be maintained over salt caverns during solution mining and product cycling. Regulatory agencies generally now require that caverns be monitored to ensure that an adequate salt roof is maintained above caverns. Downhole "wireline" logging technology, e.g. sonar, is available to periodically check shapes and sizes of caverns and the location of the salt roof (Crossley, 1998).

So how stable is a storage cavern?

Sites that are most suitable for a storage cavern lie within relatively homogenous regions of salt located deep in a diapiric salt mass, typically more than a kilometre below the landsurface and hundred of metres below the upper surface of the salt. Even today, many salt caverns used for various types of storage were first used for the commercial production of brine or hydrocarbons, although the number of purpose-built facilities increases year by year. Some older caverns now have shapes and spans or are at shallower depths that make them marginally suitable for future storage or waste disposal. Likewise the access wells to these caverns were drilled some time ago and suffer the effects of corrosion and older cement technologies. These older non-purpose built caverns do however make excellent "in-situ" laboratories to test the strength and integrity of salt formations. For example one brine cavern in the Bryan Mound Dome in Texas now has a roof span of 335 metres, yet it has not collapsed (Thoms and Gehle, 2000a).

Natural gas storage caverns, with their inherent need for the deep cycling of internal pressures, place much greater demands on the integrity of the surrounding salt than caverns used for liquids storage. Salt cavities for natural gas storage were first designed with relatively small storage volumes but designs over the last three decades have increased in size. In Germany the maximum permitted volumes of gas for storage in salt caverns started at 350,000 m³, increased to 500,000 m³ and for the past ten years has been set at 700,000 m³. In the US cavern volumes for gas storage are not specifically regulated, but a design-specified cavern for natural gas storage with a volume of 15 mmbbl (6.5 Bcf) and a roof span of more than 100 metres is now underway in the Napoleonville Dome in south Louisiana (completion 2007).

Cavern Plugging

When a salt cavern used for hydrocarbon storage reaches the end of its life it must be plugged in a way that does not allow for any later environmental degradation. Wells can not be plugged using the same relatively straightforward methods used to seal an oil or gas well that has reached the end of its useful life. Oil and gas wells are usually sealed by simply installing a "plug" of alternating intervals of different grouts. Sealing and abandoning a brinewell or a salt cavern is not the same as plugging an oil and gas well for two main reasons (Ratigan 2000):

- 1) Brine wells are generally completed with much larger casings than oil and gas wells.
- 2) The fluid pressure in the abandoned salt cavern is still joined to the casing string and it rises after plugging.

The first is not a significant deterrent to plugging and abandoning a storage well, appropriate modern grouts and methods are offered by most service companies. Essentially all of the uncertainties associated with cavern sealing and abandonment are a direct result of the second factor, rising fluid pressure and its effects on the access well(s).

Once a cavern is sealed and abandoned, salt begins to flow or creep into the opening and continues to flow until pressure differences between the salt and the cavern interior vanish. Plugs in former access wells to abandoned caverns must be capable of holding back this pressure, otherwise brine or stored waste product may be squeezed back up the well bore. Fluid flow paths out of the cavern are schematically depicted

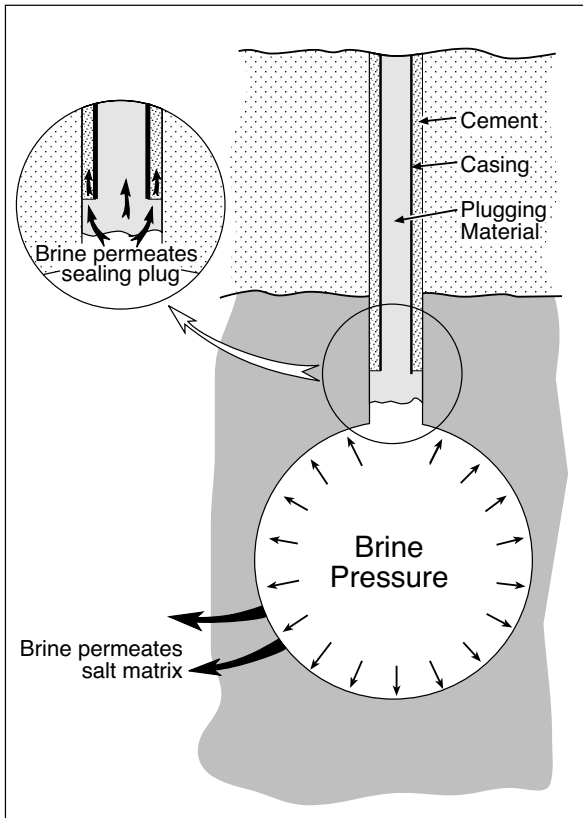


Figure 12.34. Factors influencing cavern integrity once a cavern has been plugged and abandoned (after Ratigan, 2000).

in Figure 12.34, while Table 12.5 summarizes the effects of the various processes contributing to fluid flow and pressure changes in a sealed salt cavern (Ratigan 2000).

It is not just salt creep that increases the fluid pressure in an abandoned cavern. Solution mining and product cycling results in a significant disruption of the thermal environment in the salt. Feed solvent injected into the formation to create the cavern is

almost always cooler than the salt formation, as is most stored product or waste. Continual leaching of a cavern to its final shape can result in a significant cooling of the salt surrounding the cavern, particularly near the cavern boundary. Unless a cavern has been inactive for a long period of time (tens of years), the fluid in the cavern will be at a lower temperature than the “pre-cavern” temperature of the rock salt. Thus, when the cavern is sealed, heat will flow from the salt mass to the cavern fluid and its temperature will rise in response. A rise in fluid temperature expands the fluid volume and, since the cavern is sealed, the cavern fluid pressure will rise.

Unless the cavern was idle for some years prior to its plugging, cavern fluid is not 100 percent saturated with sodium chloride. Salt dissolution may occur after a cavern is sealed and tends to lessen the effects of pressure rise. So, even after sealing, dissolution of the cavern wall continues until the enclosed fluid approaches halite saturation. This increases in the cavern volume and so tends to decrease the cavern fluid pressure. Salt dissolution is an endothermic chemical reaction, which further reduces the temperature of the fluid, and so further reduces fluid pressure in the cavern.

A number of other interactive processes can effect the stability of a storage cavern and its plugged entry hole, depending on the nature of any waste stored in a sealed cavern. Differential settling and compaction cause the various wastes pumped into the cavern to separate into layers. Various chemical reactions can then occur within or between layers of waste, or between the waste and the surrounding salt. All can cause unexpected pressure build-up and so drive fluid penetration of the plug seal. Gas can also be produced in a sealed storage cavern, either by bacterial degradation of waste materials or by natural degassing corrosion of the surrounding salt. This too leads to a buildup in fluid pressures and places increased stress on the cavity plug and the cavern walls.

Process	Influence on Fluid Pressure	Time Scale
Salt creep	Increases cavern fluid pressure at a monotonically decreasing rate	Majority of the pressure rise occurs years to tens of years after sealing
Fluid heat transfer between salt and cavern	Causes cavern fluid expansion and increases cavern fluid pressure at a decreasing rate	Majority of pressure rise within tens of years to many tens of years after sealing
Salt dissolution and cavern fluid saturation	Increases cavern volume and decreases fluid temperature, which in turn, causes a decrease in fluid pressure	Majority of pressure decrease within years after sealing
Cavern fluid escape into salt	Decrease in cavern fluid pressure	Continues indefinitely
Cavern fluid escapes via sealing plug/or casing cement	Decrease in cavern fluid pressure	Continues indefinitely

Table 12.5. Factors influencing fluid pressure in a plugged cavern (after Ratigan, 2000)

Even though salt has extremely low permeabilities, pressurised cavern fluid may slowly seep into the surrounding salt. This will reduce the volume of fluid in the cavern, and thus help ameliorate the pressure exerted on the salt by the cavern fluid. However, the entry of cavern fluids into the salt will also alter the salt matrix stresses, increase the rate of creep and the intrinsic permeability of the salt.

Before a cavern is sealed, the amount of cavern fluid that permeates the salt cavern walls is negligible. After the cavern is sealed and the cavern fluid pressure rises, the amount of cavern fluid that permeates the cavern wall must increase, both because the pressure gradient (driving the fluid transport) increases and because the salt permeability increases. If the cavern fluid pressure cannot be reduced sufficiently through the diffusional flow it is possible that fractures could develop in the salt. This would in turn reduce the cavern fluid pressure, but obviously increases the likelihood of a possible leak of cavern fluid into adjacent formations. Whether or not a fracture or fractures develop depends on the rate of cavern fluid pressurization. Low pressurization rates would not be expected to result in fracturing of the salt, rather the salt would flow and anneal. Very high rates of pressurization might well produce a brittle fracture.

But, as mentioned earlier, the salt itself is probably not the weakest link in terms of seal integrity. Pressurized cavern fluid will tend to first breach or fracture the sealing plug/casing shoe. Diffusional or fracture-induced flow could then occur through the sealing cement plug or the cement between the salt borehole wall and the deepest casing (Figure 12.34 inset).

As well as dissolution creating potential seal problems, there is also the longer term problem of ongoing local rise of smaller salt spines within a diapir (Figure 6.9c), which can shear casing and allow a breach to form in the well string. This was the situation in the at-surface well collar in well S-5 in the Sour Lake oilfield atop the Sour Lake diapir in Hardin County, Texas (Looff, 2001). In 1998 the well casing sheared, driven by a rising spine of salt in what was overall a degrading or dissolving diapir crest. The 13 5/8-inch casing string, set in salt caprock, was being pushed upward inside the 16 inch casing. This fractured the cement between the two strings and the 16-inch casing string, that had been welded to the wellhead, which was sheared off its foundation as it was displaced upward by several inches.

Storage in salt creates a complex situation with various processes and mechanisms driving cavern pressures in opposite

directions. A study of the stability of such systems is a study in multivariate rock mechanics, grout physics and pore fluid chemistry, well beyond the sedimentological emphasis of this book (see Munson, 1997; Lee and De Souza, 1998 for a discussion of some of the basic considerations). As yet, our models of salt and grout response of time frame of hundreds or even thousands of years do not allow us to reliably predict exact conditions under which pervasive fracturing or leakage will occur. Accordingly, most storage facilities are “over-engineered” to reduce the possibility of longterm failure (Ratigan 2000).

Summary

Solution mining with appropriate monitoring and timely plugging offers major advantages in generating chemical feedstock compared to room-and-pillar mining techniques. Drilling injection and production wells cost less than sinking deeper shafts and opening underground workings. It also provides safer operating conditions as underground miners are not needed.

In terms of problems with solution cavities and storage facilities it is important to note that a salt mass used for storage has never failed or leaked. The weak point in these systems is in the well, its casing and its grout. Even so, almost all the problems related to well failure are more a matter of human error, either by negligence, or a lack of understanding by on-the-ground personnel. There is a general rule of thumb when it comes to salt cavities salt mines and that is, “keep it in the salt!” Most failures and breaches occur when a leaching or a mining operation allows the cavity to contact the edge of the salt. There undersaturated water crossflows can exaggerate any uncontrolled dissolution problems.

The rapidly expanding technologies of deep purpose-built and monitored storage caverns located well within geologically suitable salt masses, will lead to future safer storage of hydrocarbons and hazardous wastes. Almost all the problems documented in the USA and elsewhere come from storage operations utilising caverns constructed by earlier less-defined solution methods. Even so, in all the incidents related to various storages in salt caverns the integrity of the cavern has never been threatened by any accident. All incidents to date can be traced back to poor management practises or utilisation of facilities that are not necessarily suitable. Salts caverns are probably one of the safest ways to store hydrocarbons and dispose of hazardous materials.

References

- Aal, A. A., E. El-Barkooky, M. Gerrits, H. J. Meyer, M. Schwander, and H. Zaki, 2001, Tectonic Evolution of the Eastern Mediterranean Basin and its Significance for the Hydrocarbon Prospectivity of the Nile Delta Deepwater Area: *GeoArabia*, v. 6, p. 363-384.
- Abed, A. M., and R. Yaghan, 2000, On the paleoclimate of Jordan during the last glacial maximum: *Palaeogeography Palaeoclimatology Palaeoecology*, v. 160, p. 23-33.
- Abu-Jaber, N. S., 1998, A new look at the chemical and hydrological evolution of the Dead Sea: *Geochimica et Cosmochimica Acta*, v. 62, p. 1471-1479.
- Abu-Zeid, M. M., A. R. Baghdady, and H. A. El-Etr, 2001, Textural attributes, mineralogy and provenance of sand dune fields in the greater Al Ain area, United Arab Emirates: *Journal of Arid Environments*, v. 48, p. 475-499.
- Achauer, C. W., 1982, Sabkha anhydrite; the supratidal facies of cyclic deposition in the Upper Minnelusa Formation (Permian), Rozet Fields area, Powder River basin, Wyoming, in C. R. Handford, Loucks, R. G., Davies, G. R., ed., *Depositional and diagenetic spectra of evaporites; a core workshop*, v. 3: Tulsa, OK, SEPM Core Workshop, p. 193-209.
- Achauer, C. W., 1985, Facies morphology and major reservoir controls, James Atoll Reef, Fairway Field, Texas, in P. Roehl, and P. Choquette, eds., *Carbonate petroleum reservoirs – a casebook*: New York, Springer-Verlag, p. 485-494.
- Ackermann, R. V., P. W. Schlische, and P. E. Olsen, 1995, Synsedimentary collapse of portions of the Lower Blomidon Formation (Late Triassic), Fundy Rift Basin, Nova Scotia: *Canadian Journal of Earth Sciences*, v. 32, p. 1965 - 1976.
- Adams, J. E., and H. N. Frenzel, 1950, Capitan barrier reef, Texas and New Mexico: *Journal of Geology*, v. 58, p. 289-312.
- Adams, J. F., and M. L. Rhodes, 1960, Dolomitisation by seepage refluxion: *American Association of Petroleum Geologists Bulletin*, v. 44, p. 1912-1920.
- Addy, K. S., and E. W. Behrens, 1980, Time of accumulation of hypersaline anoxic brine in Orca basin (Gulf of Mexico): *Marine Geology*, v. 37, p. 241-252.
- Aghashahi, E., and H. Zomorodian, 1981, Gravity study of Qum salt dome in Iran: *Journal of Earth and Space Physics*, v. 10, p. 21-24.
- Aharon, P., Y. Kolodny, and E. Sass, 1977, Recent hot brine dolomitization in the "Solar Lake," Gulf of Elat; isotopic, chemical, and mineralogical study: *Journal of Geology*, v. 85, p. 27-48.
- Aharon, P., H. H. Roberts, and R. Snelling, 1992, Submarine venting of brines in the deep Gulf of Mexico: observations and geochemistry: *Geology*, v. 20, p. 483-486.
- Ahr, W. M., 1973, The carbonate ramp: an alternative to the shelf model: *Transactions of Gulf Coast Association of Geological Societies*, v. 23, p. 221-225.
- Ahr, W. M., and G. J. Palko, 1981, Depositional and diagenetic cycles in Smackover limestone-sandstone sequences, Lincoln Parish, Louisiana: *Transactions of Gulf Coast Association of Geological Societies*, v. 31, p. 7-17.
- Aitken, J. D., 1981, Stratigraphy and sedimentology of the upper Proterozoic Little Dal Group, Mackenzie Mountains, Northwest Territories: *Campbell, F. H. A. Proterozoic basins of Canada. Paper Geological Survey of Canada*, v. 10, p. 47-71.
- Aitken, J. D., and D. G. Cook, 1969, *Geology, Lake Belot, District of Mackenzie: Geological Survey of Canada Map 6*.
- Aizenshtat, Z., I. Miloslavski, D. Aschengrau, and A. Oren, 1998, Chapter 8: Hypersaline depositional environments and their relation to oil generation, in A. Oren, ed., *Microbiology and biogeochemistry of hypersaline environments*, CRC Press, p. 89-108.
- Aktas, G., and J. D. Cocker, 1995, Diagenetic and depositional controls on reservoir quality in Khuff and Unayzah sandstones, Hawtah trend, central Saudi Arabia: *Middle East Petroleum Geosciences Conference: Geo-94*, v. 1: Manama, Bahrain, Gulf PetroLink, 44-52 p.
- Al-Aasm, I. S., and J. J. Packard, 2000, Stabilization of early-formed dolomite: a tale of divergence from two Mississippian dolomites: *Sedimentary Geology*, v. 131, p. 97-108.
- Al-Bakri, D. H., F. I. Khalaf, and Al-Ghadban, 1984, Mineralogy, genesis, and sources of surficial sediments in the Kuwait marine environment, northern Arabian Gulf: *Journal of Sedimentary Petrology*, v. 54, p. 1266-1279.
- Al-Farraj, A., 2005, An evolutionary model for sabkha development on the north coast of the UAE: *Journal of Arid Environments*, v. 63, p. 740-755.
- Al-Hurban, A., and I. Gharib, 2004, Geomorphological and sedimentological characteristics of coastal and inland sabkhas, Southern Kuwait: *Journal of Arid Environments*, v. 58, p. 59-85.
- Al-Husseini, M., J. E. Amthor, J. P. Grotzinger, and J. Mattner, 2003, Arabian Plate Precambrian-Cambrian Boundary interpreted in Oman's Ara Group: *GeoArabia*, v. 8, p. 578-580.
- Al-Husseini, M. I., 1997, Jurassic sequence stratigraphy of the western and southern Arabian Gulf: *GeoArabia*, v. 3, p. 361-382.
- Al-Jallal, I. A., 1991, Depositional Environments, Lithofacies Types, and Reservoir Development of the Permian Khuff Formation in Eastern Saudi Arabia: *Bulletin American Association of Petroleum Geologists*, v. 75, p. 1401.
- Al-Jallal, I. A., 1995, The Khuff Formation: its regional reservoir potential in Saudi Arabia and other Gulf countries: depositional and stratigraphic approach, in M. I. Al-Husseini, ed., *Middle East Petroleum Geosciences Conference, GEO'94*: v. 1: Manama, Bahrain, Gulf PetroLink, Bahrain, p. 103-119.
- Al-Murani, G. S. G., 1986, *Sedimentology and petrophysical aspects of the middle Miocene Jeribe Formation, East Baghdad field, Iraq*: doctoral thesis, University of Oxford, Oxford, 256 p.
- Al-Saad, H., and F. N. Sadooni, 2001, A new depositional model and sequence stratigraphic interpretation for the Upper Jurassic Arab "D" reservoir in Qatar: *Journal of Petroleum Geology*, v. 24, p. 243-264.
- Al-Sarawi, A. M., 1988, Morphology and facies of alluvial fans in Kadmah Bay, Kuwait: *Journal of Sedimentary Petrology*, v. 58, p. 902-907.
- Al-Sarawi, M., A. Al Zamel, and I. A. Alrifaiy, 1993, Late Pleistocene and Holocene sediments of the Khiran area (south Kuwait): *Journal of the University of Kuwait-Science*, p. 145-157.
- Al-Zamel, A., and M. Al-Sarawi, 1998, Late Quaternary Sabkha sedimentation along Kadmah Bay Coast, Kuwait, Arabian Gulf: *Arab Gulf Journal of Scientific Research*, v. 16, p. 471-495.

- Ala, M. A., 1982, Chronology of trap formation and migration of hydrocarbons in Zagros Sector of Southwest Iran: *Bulletin American Association of Petroleum Geologists*, v. 66, p. 1535-1541.
- Alavi, M., 2004, Regional stratigraphy of the Zagros fold-thrust belt of Iran and its proforeland evolution: *American Journal of Science*, v. 304, p. 1-20.
- Alcocer, J., and W. D. Williams, 1996, Historical and recent changes in Lake Texcoco, a saline lake in Mexico: *International Journal of Salt Lake Research*, v. 5, p. 45-51.
- Alderman, A. R., and H. C. W. Skinner, 1957, Dolomite sedimentation in the southeast of South Australia: *American Journal of Science*, v. 255, p. 561-567.
- Alderman, A. R., and C. C. von der Borch, 1963, Dolomite reaction series: *Nature*, v. 198, p. 465-466.
- Alexander, L. L., and P. B. Flemings, 1995, Geologic evolution of a Pliocene-Pleistocene salt-withdrawal minibasin - Eugene Island Block 330, offshore Louisiana: *AAPG Bulletin*, v. 79, p. 1737-1756.
- Ali, Y. A., and I. West, 1983, Relationships of modern gypsum nodules in sabkhas of loess to compositions of brines and sediments in northern Egypt: *Journal of Sedimentary Petrology*, v. 53, p. 1151-1168.
- Allan, R. J., J. A. T. Bye, and P. Hutton, 1986, The 1984 filling of Lake Eyre, South Australia: *Transactions Royal Society South Australia*, v. 110, p. 81-87.
- Allen, P. A., and P. F. Hoffman, 2005, Extreme winds and waves in the aftermath of a Neoproterozoic glaciation: *Nature*, v. 433, p. 123-127.
- Alley, N. F., 1998, Cainozoic stratigraphy, palaeoenvironments and geological evolution of the Lake Eyre Basin: *Palaeogeography Palaeoclimatology Palaeoecology*, v. 144, p. 239-263.
- Allison, G. B., and C. J. Barnes, 1985, Estimation of evaporation from the normally 'dry' Lake Frome in South Australia: *Journal of Hydrology*, v. 78, p. 229-242.
- Allison, M. L., 2001, The Hutchinson Gas Explosions: Unraveling a Geologic Mystery: *Kansas Bar Association, 26th Annual KBA/KIOGA Oil and Gas Law Conference*, v. 1, p. 3.1-3.29.
- Alonso, H., and F. Risacher, 1996, Geochemistry of the Salar de Atacama. 1. Origin of components and salt balance [Spanish]: *Revista Geologica de Chile*, v. 23, p. 113-122.
- Alonso, R., 1991, Evaporitas neógenas de los Andes Centrales, in J. J. Pueyo, ed., *Génesis de Formaciones Evaporíticas. Modelos Andinos e Ibéricos*, Universitat de Barcelona. *Estudi General*, v. 2, p. 267-329.
- Alonso, R. N., 1986, Ocurrencia, posición estratigráfica y génesis de los depósitos de boratos de la Puna Argentina: *Doctoral thesis, Universidad Nacional de Salta, Argentina*, 196 p.
- Alonso, R. N., T. E. Jordan, K. T. Tabbutt, and D. S. Vandervoort, 1990, Giant evaporite belts of the Neogene central Andes: *Geology*, v. 19, p. 401-404.
- Alonso-Azcarate, J., S. H. Bottrell, and J. Tritlla, 2001, Sulfur redox reactions and formation of native sulfur veins during low grade metamorphism of gypsum evaporites, Cameros Basin (NE Spain): *Chemical Geology*, v. 174, p. 389-402.
- Alonso-Zarza, A. M., Y. Sánchez-Moya, M. A. Bustillo, A. Sopena, and A. Delgado, 2002, Silicification and dolomitization of anhydrite nodules in argillaceous terrestrial deposits: an example of meteoric-dominated diagenesis from the Triassic of central Spain: *Sedimentology*, v. 49, p. 303-317.
- Alpers, C. N., R. O. Rye, D. K. Nordstrom, L. D. White, and B.-S. King, 1992, Chemical, crystallographic and stable isotopic properties of alunite and jarosite from acid-hypersaline Australian lakes: *Chemical Geology*, v. 92, p. 203-226.
- Alsharhan, A. S., 1993, Facies and sedimentary environment of the Permian carbonate (Khuff Formation) in the United Arab Emirates: *Sedimentary Geology*, v. 84, p. 89-99.
- Alsharhan, A. S., 2003, Petroleum geology and potential hydrocarbon plays in the Gulf of Suez rift basin, Egypt: *American Association Petroleum Geologists - Bulletin*, v. 87, p. 143-180.
- Alsharhan, A. S., and C. G. S. Kendall, 2003, Holocene coastal carbonates and evaporites of the southern Arabian Gulf and their ancient analogues: *Earth Science Reviews*, v. 61, p. 191-243.
- Alsharhan, A. S., and C. G. S. Kendall, 1994, Depositional setting of the Upper Jurassic Hith Anhydrite of the Arabian Gulf; an analog to Holocene evaporites of the United Arab Emirates and Lake MacLeod of Western Australia: *Bulletin American Association of Petroleum Geologists*, v. 78, p. 1075-1096.
- Alsharhan, A. S., and A. E. M. Nairn, 1993, Geology and hydrocarbon habitat in the Arabian Basin - the Mesozoic of the State of Qatar: *Geologie en Mijnbouw*, v. 71, p. 265-294.
- Alsharhan, A. S., and A. E. M. Nairn, 1997, *Sedimentary Basins and Petroleum Geology of the Middle East*: Amsterdam, The Netherlands, Elsevier Science, 942 p.
- Alsop, G. I., D. J. Blundell, and I. Davison, 1996, *Salt Tectonics: Special Publication*, v. 100: London, Geological Society, 310 p.
- Alsop, G. I., J. P. Brown, I. Davison, and M. R. Gibling, 2000, The geometry of drag zones adjacent to salt diapirs: *Journal of the Geological Society*, v. 157, p. 1019-1029.
- Amery, G. B., 1969, Structure of Sigsbee Scarp, Gulf of Mexico: *American Association of Petroleum Geology Bulletin*, v. 53, p. 2480-2482.
- Amery, G. B., 1978, Structure of continental slope, northern Gulf of Mexico, in A. H. Bouma, C. T. Moore, and J. M. Coleman, eds., *Framework, facies, and oil-trapping characteristics of the upper continental margin*, AAPG Studies in Geology, v. 7, p. 141-153.
- Amiel, A. J., and G. M. Friedman, 1971, Continental sabkha in Arava Valley between Dead Sea and Red Sea: Significance for origin of evaporites: *Bulletin American Association of Petroleum Geologists*, v. 55, p. 581-592.
- Amieux, P., 1980, Exemple d'un passage des 'black shales' aux evaporites dans le Ludien (Oligocene inferieur) du bassin de Mormoiron (Vaucluse, Sud-Est de la France). (Example of a transition of black shales to evaporites in the Ludian (Lower Oligocene) of the Mormoiron Basin, Vaucluse, south-eastern France): *Bulletin, Centres de Recherches Exploration-Production Elf- Aquitaine*, v. 4, p. 281-307.
- Amin, A., and K. Bankher, 1997b, Causes of land subsidence in the Kingdom of Saudi Arabia: *Natural Hazards*, v. 16, p. 57-63.
- Amin, A. A., and K. A. Bankher, 1997a, Karst hazard assessment of eastern Saudi Arabia: *Natural Hazards*, v. 15, p. 21-30.
- Amit, R., E. Zilberman, N. Porat, and Y. Enzel, 1999, Relief inversion in the Avrona Playa as evidence of large-magnitude historical earthquakes, southern Arava Valley, Dead Sea Rift: *Quaternary Research*, v. 52, p. 76-91.
- Amthor, J., and J. Okkerman, 1998, Influence of early diagenesis on reservoir quality of Rotliegende sandstones, northern Netherlands:

- Bulletin American Association of Petroleum Geologists, v. 82, p. 2246-2265.
- Amthor, J. E., 2000, Precambrian carbonates of Oman: A regional perspective (abs): *GeoArabia*, v. 5, p. 47.
- Amthor, J. E., and N. L. Frewin, 1999, Enigmatic Origin of a Late Pre-Cambrian Laminated Chert: Have Bacteria Done It? Bulletin American Association of Petroleum Geologists AAPG Annual Meeting San Antonio, Texas, April 11-14, 1999, v. 83 (13).
- Amthor, J. E., W. Smits, and P. Nederlof, 1998, Prolific Oil Production from a Source Rock- The Athel Silicilyte Source-Rock Play in South Oman (abs.): Bulletin American Association of Petroleum Geologists, AAPG Annual Meeting, Salt Lake City, Utah, May 17-20, 1998, v. 82 (13).
- Anati, D. A., 1998, Dead Sea water trajectories in the T-S space: *Hydrobiologia*, v. 381, p. 43-49.
- Anati, D. A., 1999, The salinity of hypersaline brines: concepts and misconceptions: *International Journal of Salt Research*, v. 8, p. 1-16.
- Anati, D. A., Gavrieli, and A. Oren, 1995, The residual effect of the 1991-93 rainy winter on the Dead sea stratification: *Israel Journal of Science*, v. 44, p. 63-70.
- Andler, J. P., K. S. Crosby, and D. C. E. Waugh, 1979, Potash at Salt Springs, New Brunswick: *Econ. Geol.*, v. 74, p. 389-396.
- Anderson, J. E., J. Cartwright, S. J. Drysdall, and N. Vivian, 2000, Controls on turbidite sand deposition during gravity-driven extension of a passive margin: examples from Miocene sediments in Block 4, Angola: *Marine & Petroleum Geology*, v. 17, p. 1165-1203.
- Anderson, N. L., R. J. Brown, and R. C. Hinds, 1988, Geophysical aspects of Wabamun salt distribution in southern Alberta: *Can. Jour. Expl. Geophys.*, v. 24, p. 166-178.
- Anderson, N. L., and D. A. Cederwall, 1993, Westhazel General Petroleum Pool; case history of a salt-dissolution trap in west-central Saskatchewan, Canada: *Geophysics*, v. 58, p. 889-897.
- Anderson, N. L., J. Hopkins, A. Martinez, R. W. Knapp, P. A. Macfarlane, W. L. Watney, and R. Black, 1994a, Dissolution of bedded rock salt; a seismic profile across the active eastern margin of the Hutchinson Salt Member, central Kansas: *Computers and Geosciences*, v. 20, p. 889-903.
- Anderson, N. L., and R. Knapp, 1993, An overview of some of the larger scale mechanisms of salt dissolution in Western Canada: *Geophysics*, v. 58, p. 1375-1387.
- Anderson, N. L., A. Martinez, J. F. Hopkins, and T. R. Carr, 1998, Salt dissolution and surface subsidence in central Kansas - A seismic investigation of the anthropogenic and natural origin models: *Geophysics*, v. 63, p. 366-378.
- Anderson, R. N., L. M. Cathles III, and H. R. Nelson, 1991, "Data Cube" depicting fluid flow history in Gulf Coast sediments: *Oil and Gas Journal*, v. 89, p. 50-55.
- Anderson, R. N., P. Flemings, S. Losh, and J. A. Austin, 1994b, Gulf of Mexico growth fault drilled, seen as oil, gas migration pathway: *Oil and Gas Journal*, v. June 6, 1994, p. 97 & ff.
- Anderson, R. Y., W. E. J. Dean, D. W. Kirkland, and H. I. Snider, 1972, Permian Castile Varved Evaporite Sequence, West Texas and New Mexico: *Geological Society of America Bulletin*, v. 83, p. 59-85.
- Andreason, M. W., 1992, Coastal siliciclastic sabkhas and related evaporative environments of the Permian Yates Formation, North Ward-Estes field, Ward County, Texas: *American Association of Petroleum Geologists Bulletin*, v. 76, p. 1735-1759.
- Andrejchuk, V. N., and A. B. Klimchouk, 2001, Geomicrobiology and redox geochemistry of the karstified Miocene gypsum aquifer, western Ukraine: The study from Zoloushka Cave: *Geomicrobiology Journal*, v. 18, p. 275-295.
- Andrejchuk, V. N., and A. B. Klimchouk, 2004, Mechanisms of karst breakdown formation in the gypsum karst of the fore-Ural region, Russia (from observations in the Kungurskaja Cave): *Speleogenesis and Evolution of Karst Aquifers 2 (2)*, available at www.speleogenesis.info, (online journal).
- Anissimov, L., E. Postnova, and O. Merkulov, 2000, Tengiz oilfield: geological model based on hydrodynamic data: *Petroleum Geoscience*, v. 6, p. 59-65.
- API, 1994, Design of solution-mined underground storage practices: Washington, DC, American Petroleum Institute, Recommended practice 1114.
- Aqrawi, A. A. M., and G. Evans, 1994, Sedimentation in the lakes and marshes (Ahwar) of the Tigris Euphrates delta, southern Mesopotamia: *Sedimentology*, v. 41, p. 755-776.
- Arakel, A. V., 1980, Genesis and diagenesis of Holocene evaporitic sediments in Hutt and Leeman lagoons, Western Australia: *Journal of Sedimentary Petrology*, v. 50, p. 1305-1326.
- Arakel, A. V., and T. Hong Jun, 1994, Seasonal evaporite sedimentation in desert playa lakes of the Karinga Creek drainage system, central Australia, in R. W. Renaut, and W. M. Last, eds., *Sedimentology and geochemistry of modern and ancient saline lakes*: Tulsa, OK, Society for Sedimentary Geology; Special Publication, v. 50, p. 91-100.
- Arakel, A. V., G. Jacobson, and W. B. Lyons, 1990, Sediment-water interaction as a control on geochemical evolution of playa lake systems in the Australian arid interior: *Hydrobiologia*, v. 197, p. 1-12.
- Arbey, N., 1980, Silicification des évaporites: *Bulletin, Centres de Recherches Exploration-Production Elf- Aquitaine*, v. 4, p. 309-365.
- Aref, M. A. M., 1998a, Holocene stromatolites and microbial laminites associated with lenticular gypsum in a marine-dominated environment, Ras el Shetan area, Gulf of Aqaba, Egypt: *Sedimentology*, v. 45, p. 245-262.
- Aref, M. A. M., 1998b, Biogenic carbonates - are they a criterion for underlying hydrocarbon accumulations - an example from the Gulf of Suez region: *Bulletin American Association of Petroleum Geologists*, v. 82, p. 336-352.
- Aref, M. A. M., 2003, Classification and depositional environments of Quaternary pedogenic gypsum crusts (gypcrete) from east of the Fayum Depression, Egypt: *Sedimentary Geology*, v. 155, p. 87-108.
- Aref, M. A. M., O. E. A. Attia, and A. M. A. Wali, 1997, Facies and depositional environment of the Holocene evaporites in the Ras Shukeir area, Gulf of Suez, Egypt: *Sedimentary Geology*, v. 110, p. 123-145.
- Arenas, C., and G. Pardo, 1999, Latest Oligocene-Late Miocene lacustrine systems of the north-central part of the Ebro Basin (Spain): sedimentary facies model and palaeogeographic synthesis: *Palaeogeography Palaeoclimatology Palaeoecology*, v. 151, p. 127-148.

- Arenas, C., A. M. A. Zarza, and G. Pardo, 1999, Dedolomitization and other early diagenetic processes in Miocene lacustrine deposits, Ebro Basin (Spain): *Sedimentary Geology*, v. 125, p. 23-45.
- Arkin, Y., and A. Gilat, 2000, Dead Sea sinkholes - an ever-developing hazard: *Environmental Geology*, v. 39, p. 711-722.
- Armenteros, I., B. Daley, and E. Garcia, 1997, Lacustrine and palustrine facies in the Bembridge Limestone (Late Eocene, Hampshire Basin) of the Isle of Wight, Southern England: *Palaeogeography Palaeoclimatology Palaeoecology*, v. 128, p. 111-132.
- Armstrong, A. K., 1995, Facies, diagenesis, and mineralogy of the Jurassic Todilto Limestone Member, Grants uranium district, New Mexico, New Mexico Bureau of Mines Bulletin No. 153, 41 p.
- Armstrong, L. A., A. Ten Have, and H. D. Johnson, 1987, The geology of the Gannet fields, central North Sea, in J. Brooks, and K. W. Glennie, eds., *Petroleum Geology of NW Europe*: London, Graham and Trotman, p. 533-548.
- Arp, G., 1995, Lacustrine bioherms, spring mounds, and marginal carbonates of the Ries-impact-crater (Miocene, southern Germany): *Facies*, v. 33, p. 35-89.
- Arp, G., A. Reimer, and J. Reitner, 2001, Photosynthesis-induced biofilm calcification and calcium concentrations in Phanerozoic oceans: *Science*, v. 292, p. 1701-1704.
- Arthurton, R. S., 1973, Experimentally produced halite compared with Triassic layered halite-rock from Cheshire, England: *Sedimentology*, v. 20, p. 145-160.
- Asmar, B. N., and P. Ergenzinger, 1999, Estimation of evaporation from the Dead Sea: *Hydrol. Process*, v. 13, p. 2743-2750.
- Assereto, R. C., and R. L. Folk, 1976, Brick-like texture and radial rays in Triassic pisolites of Lombardy, Italy: A clue to distinguish ancient aragonitic pisolites: *Sedimentary Geology*, v. 16, p. 205-222.
- Asserto, R. I. A. M., and C. G. S. C. Kendall, 1977, Nature, origin, and classification of peritidal tepee structures and related breccias: *Sedimentology*, v. 24, p. 153-210.
- Astin, T. R., and D. A. Rogers, 1991, 'Subaqueous shrinkage cracks' in the Devonian of Scotland reinterpreted: *Journal of Sedimentary Petrology*, v. 61, p. 850-859.
- Atia, A. K. M., E. E. Hilmy, and S. M. Bolous, 1970, Mineralogy of the Salt Deposits of Wadi El Natrun: Arab Republic of Egypt, Desert Institute Bulletin, v. 20, p. 49-74.
- Augustithis, S. S., 1980, On the textures and treatment of the sylvinite ore from the Danakili Depression, Salt Plain (Piano del Sale), Tigre, Ethiopia: *Chem. Erde*, v. 39, p. 91-95.
- Aulstead, K. L., and R. J. Spencer, 1985, Diagenesis of Keg River Formation, northwestern Alberta; fluid inclusion evidence: *Bulletin of Canadian Petroleum Geology*, v. 33, p. 167-183.
- Autin, W. J., 2002, Landscape evolution of the Five Islands of south Louisiana: scientific policy and salt dome utilization and management: *Geomorphology*, v. 47, p. 227-244.
- Autin, W. J., and R. P. McCulloh, 1995, Quaternary geology of the Weeks and Cote Blanche islands salt domes: *Gulf Coast Association of Geological Societies Transactions*, v. XLV, p. 39-46.
- Ayora, C., D. I. Cendon, C. Taberner, and J. J. Pueyo, 2001, Brine-mineral reactions in evaporite basins: Implications for the composition of ancient oceans: *Geology*, v. 29, p. 251-254.
- Ayora, C., J. Garciaiveigas, and J. Pueyo, 1994, The chemical and hydrological evolution of an ancient potash-forming evaporite basin as constrained by mineral sequence, fluid inclusion composition, and numerical simulation: *Geochimica et Cosmochimica Acta*, v. 58, p. 3379-3394.
- Ayres, M. G., M. Bilal, R. W. Jones, L. W. Slenz, M. Tartir, and A. O. Wilson, 1982, Hydrocarbon Habitat in Main Producing Areas, Saudi Arabia: *American Association of Petroleum Geologists Bulletin*, v. 66, p. 1-9.
- Azer, S. R., and R. G. Peebles, 1998, Sequence stratigraphy of the Arab A to C members and Hith Formation, offshore Abu Dhabi: *GeoArabia*, v. 3, p. 251-268.
- Baadsgaard, H., 1987, Rb-Sr and K-Ca isotope systematics in minerals from potassium horizons in the Prairie Evaporite Formation, Saskatchewan, Canada: *Chemical Geology*, v. 66, p. 1-15.
- Babel, M., 1990, Crystallography and genesis of the giant intergrowths of gypsum from the middle Miocene evaporites of southern Poland: *Arch. Min.*, v. 44, p. 103-35.
- Babel, M., 1991, Dissolution of halite within the middle Miocene (Badenian) laminated gypsum of southern Poland: *Acta Geologica Polonica*, v. 41, p. 165-182.
- Babieri, M., and U. Masi, 1984, Sr geochemical evidence on the origin of celestite-barite deposits at Pian dell'Organo in the Tolfa Mountains area (Latium, central Italy): *Mineralogy and Petrology*, v. 28, p. 33-37.
- Bach, J., I. Fitz, N. Gueschow, V. Rentjes, H. J. Kretzchmar, and M. Krafki, 1985, Recovery of carnallite by isothermal solution mining, German (East) patent DD221235A1, VEB Kombinat Kali, p. 8.
- Bachman, G., and R. B. Johnson, 1973, Stability of Salt in the Permian Salt Basin of Kansas, Oklahoma, Texas and New Mexico: *U. S. Geol. Surv. Open-File Rept.*, v. 4339-4.
- Bachman, G. O., 1981, Geology of Nash Draw, Eddy County, New Mexico: *U. S. Geol. Surv. Open-File Rept.* 81-3.
- Bachman, G. O., 1984, Regional geology of Ochoan evaporites, northern part of Delaware Basin: *New Mexico Bureau of Mines and Mineral Resources, Circular*, v. 184, p. 22.
- Badaut, D., and F. Risacher, 1983, Authigenic smectite on diatom frustules in Bolivian saline lakes: *Geochimica et Cosmochimica Acta*, v. 47, p. 363-375.
- Bahroudi, A., and H. A. Koyi, 2003, Effect of spatial distribution of Hormuz salt on deformation style in the Zagros fold and thrust belt: An analogue modelling approach: *Journal of the Geological Society*, v. 160, p. 719-733.
- Baker, B. H., 1958, Geology of the Magadi Area: *Geological Survey of Kenya Report*, v. 42, p. 81 p.
- Baker, D. M., R. J. Lillie, R. S. Yeats, G. D. Johnson, M. Yousuf, and A. S. H. Zamin, 1988, Development of the Himalayan frontal thrust zone: Salt Range, Pakistan: *Geology*, v. 16, p. 3-7.
- Baker, P. A., C. A. Rigsby, G. O. Seltzer, S. C. Fritz, T. K. Lowenstein, N. P. Bacher, and C. Veliz, 2001, Tropical climate changes at millennial and orbital timescales on the Bolivian Altiplano: *Nature*, v. 409, p. 698-701.
- Baker, P. A., and S. H. Bloomer, 1988, The origin of celestite in deep water carbonate sediments: *Geochim. Cosmochim. Acta*, v. 52, p. 335-339.
- Baker, P. A., and M. Kastner, 1981, Constraints on the formation of sedimentary dolomite: *Science*, v. 213, p. 214-216.
- Balch, D. P., A. S. Cohen, D. W. Schnurrenberger, B. J. Haskell, B. Valero-Garces, J. W. Beck, H. Cheng, and R. L. Edwards, 2005,

- Ecosystem and paleohydrological response to Quaternary climate change in the Bonneville Basin, Utah: *Palaeogeography, Palaeoclimatology, Palaeoecology*, v. 221, p. 99-122.
- Balk, R., 1953, Salt Structure of Jefferson Island Salt Dome, Iberia and Vermilion Parishes, Louisiana: *Bulletin American Association Petroleum Geologists*, v. 37, p. 2455-2474.
- Balkwill, H. R., 1978, Evolution of Sverdrup Basin, Arctic Canada: *Bulletin American Association Petroleum Geologists*, v. 62, p. 1004-1028.
- Ballot, A., 2004, Cyanobacteria in Kenyan Rift Valley lakes: A biological and toxicological study: Doctoral thesis, Fachbereich Biologie, Chemie, Pharmazie der Freien Universität Berlin.
- Barbeau, D. L., 1999, A Flexural Model for the Paradox Basin: *Bulletin American Association Petroleum Geologists*, v. 83, p. 1881-1882.
- Barbé, A., J. O. Grimalt, J. J. Pueyo, and J. Albaiges, 1990, Characterization of model evaporitic environments through the study of lipid components: *Organic Geochemistry*, v. 16, p. 815-828.
- Baria, L. R., D. I. Stouder, P. M. Harris, and P. D. Crevello, 1982, Upper Jurassic reefs of Smackover Formation, United States Gulf Coast: *American Association Petroleum Geologists Bulletin*, v. 66, p. 1449-1482.
- Barkan, E., B. Luz, and B. Lazar, 2001, Dynamics of the carbon dioxide system in the Dead Sea: *Geochimica et Cosmochimica Acta*, v. 65, p. 1.
- Barker, J. M., D. E. Cochran, and R. Semrad, 1979, Economic geology of the Mishraq native sulfur deposit, northern Iraq: *Economic Geology*, v. 74, p. 484-495.
- Barley, M. E., J. S. R. Dunlop, J. E. Glover, and D. I. Groves, 1979, Sedimentary evidence for an Archaean shallow-water volcanic-sedimentary facies, eastern Pilbara Block, Western Australia: *Earth and Planetary Science Letters*, v. 43, p. 74-84.
- Barnard, R. M., and R. B. Kistler, 1966, Stratigraphic and Structural Evolution of the Kramer Sodium Borate Body, Boron, California: Second Symposium on Salt, Northern Ohio Geological Society, Cleveland, OH, v. 1, p. 133-150.
- Barrat, J. A., J. Boulegue, J. J. Tiercelin, and M. Lesourd, 2000, Strontium isotopes and rare-earth element geochemistry of hydrothermal carbonate deposits from Lake Tanganyika, East Africa: *Geochimica et Cosmochimica Acta*, v. 64, p. 287-298.
- Barrett, M. L., 1986, Replacement geometry and fabrics of the Smackover (Jurassic) Dolomite, southern Alabama: *Gulf Coast Association of Geological Societies Transactions*, v. 36, p. 9-18.
- Barton, D. C., 1933, Mechanics of formation of salt domes with special reference to Gulf Coast salt domes of Texas and Louisiana: *American Association Petroleum Geologists Bulletin*, v. 17, p. 1025-1083.
- Bartov, Y., M. Stein, Y. Enzel, A. Agnon, and Z. Reches, 2002, Lake Levels and Sequence Stratigraphy of Lake Lisan, the Late Pleistocene Precursor of the Dead Sea: *Quaternary Research*, v. 57, p. 9-21.
- Bass-Becking, L. G. M., 1928, On organisms living in concentrated brines: *Tijdsch. Ned. Dierk. Ver.*, v. Series 3, p. 6-9.
- Bates, R. L., 1969, Potash Minerals: Geology of the industrial rocks and minerals: New York, Dover Publ., 370-385 and 439-440 p.
- Bathurst, R. G. C., 1980, Deep crustal diagenesis in limestones: *Revista Instituto Investigaciones Geológicas, University of Barcelona*, v. 34, p. 89-100.
- Baud, A., and J. L. Haglund, 1996, Enhanced subsalt exploration utilizing the basal salt shear model: *Transactions of Gulf Coast Association of Geological Societies*, v. XLVI, p. 9-14.
- Bauer, S., 1999, Analysis of subsidence data for the Bryan Mound site, Texas: Sandia Report, SAND99-1739, Sandia National Laboratories.
- Bauer, S. J., B. L. Ehgartner, and J. T. Dale, 2000, Geotechnical studies associated with decommissioning the Strategic Petroleum Reserve facility at Weeks Island, Louisiana: a case history: *Proc. S.M.R.I. Fall Meeting Technical Session, San Antonio*, p. 146-156.
- Baumgardner, R. W., A. D. Hoadley, and A. G. Goldstein, 1982, The Wink Sink; a case history of evaporite dissolution and catastrophic subsidence: Formation of the Wink Sink, a salt dissolution and collapse feature, Winkler County, Texas., v. Bureau of Economic Geology, The University of Texas at Austin, Report of Investigations No. 114, 38p.
- Bayly, I. A. E., and W. E. Williams, 1973, Inland waters and their ecology: Hawthorn, Vic., Longman Australia.
- Beach, D. K., and J. W. Giffin, 1992, Stanley Field, USA Williston Basin, North Dakota, in N. H. Foster, and E. A. Beaumont, eds., *Treatise of Petroleum Geology; Atlas of Oil and Gas Fields: Stratigraphic Traps III*: Tulsa, OK, American Association Petroleum Geologists, p. 389-420.
- Beadle, L. C., 1974, Inland waters of tropical Africa: London, Longman, 365 p.
- Beales, F. W., and A. E. Oldershaw, 1969, Evaporite-solution brecciation and Devonian carbonate reservoir porosity in western Canada: *Am. Assoc. Petroleum Geologists Bull*, v. 53, p. 503-512.
- Beauheim, R. L., and R. M. Roberts, 2002, Hydrology and hydraulic properties of a bedded evaporite formation: *Journal of Hydrology*, v. 259, p. 66-88.
- Becher, J. W., and C. H. Moore, 1976, The Walker Creek Field - A Smackover diagenetic trap: *Transactions of Gulf Coast Association of Geological Societies*, v. 26, p. 34-56.
- Bechtel, A., A. Gratzner, W. Püttmann, and S. Oszczepalski, 2002, Geochemical characteristics across the oxic/anoxic interface (Rote Fäule front) within the Kupferschiefer of the Lubin-Sierszowice mining district (SW Poland): *Chemical Geology*, v. 185, p. 9-31.
- Bechtel, A., M. Pervaz, and W. Puttmann, 1998, Role of organic matter and sulphate-reducing bacteria for metal sulphide precipitation in the Bahloul Formation at the Bou Grine Zn/Pb deposit (Tunisia): *Chemical Geology*, v. 144, p. 1-21.
- Bechtel, A., and W. Puttmann, 1997, Palaeoceanography of the early Zechstein Sea during Kupferschiefer deposition in the Lower Rhine Basin (Germany) - A reappraisal from stable isotope and organic geochemical investigations: *Palaeogeography Palaeoclimatology Palaeoecology*, v. 136, p. 331-358.
- Bechtel, A., S. M. Savin, and S. Hoernes, 1999, Oxygen and hydrogen isotopic composition of clay minerals of the Bahloul Formation in the region of the Bou Grine zinc-lead ore deposit (Tunisia): evidence for fluid-rock interaction in the vicinity of salt dome cap rock: *Chemical Geology*, v. 156, p. 191-207.
- Bechtel, A., Y. N. Shieh, M. Pervaz, and W. Puttmann, 1996, Biodegradation of hydrocarbons and biogeochemical sulfur cycling in the

- salt dome environment - inferences from sulfur isotope and organic geochemical investigations of the Bahloul Formation at the Bou Grine Zn/Pb ore deposit, Tunisia: *Geochimica et Cosmochimica Acta*, v. 60, p. 2833-2855.
- Beckman, J., 1999, Study reveals overpressure sources in deep-lying formations: *Oil and Gas Journal*, v. September, p. 137.
- Begin, Z. B., W. Broecker, B. Buchbinder, Y. Druckman, A. Kaufman, M. Magaritz, and D. Neev, 1985, Dead Sea and Lake Lisan levels in the past 30,000 years: Geological Survey of Israel, Preliminary report, v. GSI/29.8, p. 18 p.
- Begin, Z. B., A. Ehrlich, and Y. Nathan, 1974, Lake Lisan, the Pleistocene precursor of the Dead Sea: *Bulletin Geological Survey Israel*, v. 63, p. 30.
- Behr, H.-J., and C. Röhrlich, 2000, Record of seismotectonic events in siliceous cyanobacterial sediments (Magadi cherts), Lake Magadi, Kenya: *International Journal of Earth Sciences*, v. 89, p. 268-283.
- Behr, H. J., H. Ahrendt, H. Martin, H. Porada, J. Rohrs, and K. Weber, 1983, Sedimentology and mineralogy of Upper Proterozoic playa-lake deposits in the Damara orogen, in H. Martin, and F. W. Eder, eds., *Intracontinental Fold Belts*: Berlin, Springer-Verlag, p. 577-610.
- Bein, A., and A. R. Dutton, 1993, Origin, distribution, and movement of brine in the Permian Basin (USA) - A model for displacement of connate brine: *Geological Society of America Bulletin*, v. 105, p. 695-707.
- Bein, A., S. D. Hovorka, R. S. Fisher, and E. Roedder, 1991, Fluid inclusions in bedded Permian halite, Palo Duro Basin, Texas; evidence for modification of seawater in evaporite brine-pools and subsequent early diagenesis: *Journal of Sedimentary Petrology*, v. 61, p. 1-14.
- Bein, A., and L. S. Land, 1982, San Andres carbonates in the Texas Panhandle: sedimentation and diagenesis associated with magnesium-calcium-chloride brines: Bureau of Economic Geology, University of Texas, Report of Investigation, v. 121, p. 48 pp.
- Bein, A., and L. S. Land, 1983, Carbonate sedimentation and diagenesis associated with Mg-Ca-Chloride brines: The Permian San Andres Formation in the Texas Panhandle: *Journal of Sedimentary Petrology*, v. 53, p. 243-260.
- Bell, C. M., 1989, Saline lake carbonates within an Upper Jurassic-Lower Cretaceous continental red bed sequence in the Atacama region of northern Chile: *Sedimentology*, p. 4.
- Bell, C. M., 1997, Saline lake turbidites in the La Coipa area, Northern Chile: *Revista Geologica de Chile*, v. 24, p. 259-267.
- Bell, C. M., and M. Suarez, 1993, The depositional environments and tectonic development of a Mesozoic intra-arc basin, Atacama region, Chile: *Geological Magazine*, p. 417-430.
- Bellah, A. M., and H. Hassouba, 1995, Quaternary sediments from the coastal plain of northwestern Egypt (from Alexandria to el Omayid): *Carbonates & Evaporites*, v. 10, p. 8-44.
- Bellanca, A., J. P. Calvo, P. Censi, R. Neri, and M. Pozo, 1992, Recognition of lake-level changes in Miocene lacustrine units, Madrid Basin, Spain. Evidence from facies analysis, isotope geochemistry and clay mineralogy: *Sedimentary Geology*, v. 76, p. 135-153.
- Bellanca, A., and R. Neri, 1986, Evaporite carbonate cycles of the Messinian, Sicily; stable isotopes, mineralogy, textural features, and environmental implications: *Journal of Sedimentary Petrology*, v. 56, p. 614-621.
- Belloni, S., B. Martins, and G. Orombelli, 1972, Karst of Italy, in M. Herak, and V. T. Springfield, eds., *Karst: Important karst regions of the Northern Hemisphere*: Amsterdam, Elsevier, p. 85-128.
- Belous, I. R., S. I. Kirikilitza, M. L. Levenshteyn, E. K. Rodina, and V. N. Florinskaya, 1984, Occurrences of mercury in northeastern Donbass salt dome: *Internat. Geol. Rev.*, v. 26, p. 573-582.
- Ben-Avraham, Z., T. M. Niemi, D. Neev, J. K. Hall, and Y. Levy, 1993, Distribution of Holocene sediments and neotectonics in the deep north basin of the Dead Sea: *Marine Geology*, v. 113, p. 219-231.
- Ben-Avraham, Z., T. Niemi, C. Heim, J. Negendank, and A. Nur, 1999, Holocene stratigraphy of the Dead Sea: Correlation of high-resolution seismic reflection profiles to sediment cores: *Journal of Geophysical Research-Solid Earth*, v. 104, p. 17617-17625.
- Benali, S., B. C. Schreiber, M. L. Helman, and R. P. Philp, 1995, Characterisation of organic matter from a restricted/evaporative sedimentary environment - Late Miocene of Lorca Basin, south-eastern Spain: *American Association of Petroleum Geologists - Bulletin*, v. 79, p. 816-830.
- Benan, C. A. A., and G. Kocurek, 2000, Catastrophic flooding of an aeolian dune field: Jurassic Entrada and Todilto Formations, Ghost Ranch, New Mexico, USA: *Sedimentology*, v. 47, p. 1069-1080.
- Benison, K. C., and R. H. Goldstein, 1999, Permian paleoclimate data from fluid inclusions in halite: *Chemical Geology*, v. 154, p. 113-132.
- Benison, K. C., and R. H. Goldstein, 2000, Sedimentology of ancient saline pans: An example from the Permian Opeche Shale, Williston Basin, North Dakota, USA: *Journal of Sedimentary Research Section A-Sedimentary Petrology & Processes*, v. 70, p. 159-169.
- Benison, K. C., and R. H. Goldstein, 2001, Evaporites and siliciclastics of the Permian Nippewalla Group of Kansas, USA: a case for non-marine deposition in saline lakes and saline pans: *Sedimentology*, v. 48, p. 165-188.
- Benison, K. C., and R. H. Goldstein, 2002, Recognizing acid lakes and groundwaters in the rock record: *Sedimentary Geology*, v. 151, p. 177-185.
- Benito, G., A. Perezgonzalez, F. Gutierrez, and M. J. Machado, 1998, River response to Quaternary subsidence due to evaporite solution (Gallego River, Ebro Basin, Spain): *Geomorphology*, v. 22, p. 243-263.
- Bennett, S. S., and J. S. Hanor, 1987, Dynamics of subsurface salt dissolution at the Welsh Dome, Louisiana Gulf Coast, in I. Lerch, and J. J. O'Brien, eds., *Dynamical geology of salt and related structures*: New York, Academic Press Inc, p. 653-677.
- Benson, J., L. M. Pultz, and D. D. Bruner, 1996, Paleotopographic Vs Eustatic Controls on Deposition of the Smackover Formation, Appleton Field, Escambia County, Alabama (Abs.): *Bulletin American Association of Petroleum Geologists*, v. 80, p. 1495.
- Benson, L., B. Linsley, J. Smoot, S. Mensing, S. Lund, S. Stine, and A. Sarna-Wojcickig, 2003, Influence of Pacific Decadal Oscillation on the climate of Sierra Nevada, California and Nevada: *Quaternary Research*, v. 59, p. 151-159.
- Benson, R. H., K. Rakic-El Bied, and L. W. McKenna, 1997, Eustatic implications of late Miocene depositional sequences in the Melilla Basin, northeastern Morocco: *Sedimentary Geology*, v. 107, p. 147-165.
- Bentz, L. M., 1992, Pecos Slope Field - USA, Permian Basin, New Mexico, in N. H. Foster, and E. A. Beaumont, eds., *Treatise of*

- Petroleum Geology; Atlas of Oil and Gas Fields: Stratigraphic Traps III: Tulsa, OK, American Association Petroleum Geologists, p. 129-153.
- Berner, R. A., 1980, Early Diagenesis - A theoretical approach: Princeton NJ, Princeton University Press, 241 p.
- Bethke, C., and S. Marshak, 1990, Brine migration across North America: the plate tectonics of groundwater hydrology: *Ann. Rev. Earth Planet. Science*, v. 18, p. 287-315.
- Beydoun, Z. R., 1993, Evolution of the northeastern Arabian plate margin and shelf - Hydrocarbon habitat and conceptual future potential: *Revue de l'Institut Francais du Petrole*, v. 48, p. 311-345.
- Beydoun, Z. R., 1998, Arabian Plate oil and gas: why so rich and prolific? *Episodes*, v. 21, p. 74-81.
- Beydoun, Z. R., M. W. Hughes Clark, and R. Stoneley, 1992, Petroleum in the Zagros Basin: A Late Tertiary foreland basin overprinted onto the outer edge of a vast hydrocarbon-rich Palaeozoic-Mesozoic passive-margin shelf, in R. W. Macqueen, and D. A. Leckie, eds., *Foreland basins and fold belts*: Tulsa, OK, American Association of Petroleum Geologists Memoir 55, p. 309-339.
- Biddle, P. G., 1983, Patterns of drying and moisture deficit in the vicinity of trees on clay soils: *Geotechnique*, v. 33, p. 107-126.
- Bigham, J. M., and D. K. Nordstrom, 2000, Iron and aluminum hydroxy-sulfates from acid surface waters, in C. N. Alpers, J. L. Jambor, and D. K. Nordstrom, eds., *Sulfate Minerals: Crystallography, Geochemistry, and Environmental Significance*, Mineralogical Society of America, *Reviews in Mineralogy and Geochemistry*, No. 40, p. 351-403.
- Billo, S. M., 1986, Petrology and kinetics of gypsum-anhydrite transitions: *Journal of Petroleum Geology*, v. 10, p. 73-86.
- Billo, S. M., 1996, Geology of marine evaporites favorable for oil, gas exploration: *Oil & Gas Journal*, v. 94, p. 69-73.
- Birnbau, S. J., and J. W. Wireman, 1985, Sulfate-reducing bacteria and silica solubility; a possible mechanism for evaporite diagenesis and silica precipitation in banded iron formations: *Canadian Journal of Earth Sciences*, v. 22, p. 1904-1909.
- Bischoff, J. L., J. P. Fitts, and K. M. Menking, 1993a, Sediment pore waters of Owens Lake Drill Hole OL-92, in I. S. Smith, and J. L. Bischoff, eds., *Core OL-92 from Owens Lake, southeast California*, U.S. Geological Survey Open-File Report 93-683 (available online at <http://pubs.usgs.gov/of/of93-683/report.html>).
- Bischoff, J. L., R. Julia, W. E. C. I. Shanks, and R. J. Rosenbauer, 1994, Karstification without carbonic acid; bedrock dissolution by gypsum-driven dedolomitization: *Geology*, v. 22, p. 995-998.
- Bischoff, J. L., S. Stine, R. J. Rosenbauer, J. A. Fitzpatrick, and T. W. Stafford Jr, 1993b, Ikaite precipitation by mixing of shoreline springs and lake water, Mono Lake, California, USA: *Geochimica et Cosmochimica Acta*, v. 57, p. 3855-3865.
- Bissell, H. J., and G. V. Chilingar, 1962, Evaporite type dolomite in salt flats of western Utah: *Sedimentology*, p. 200-210.
- Bitzer, K., A. Travé, J. M. Carmona, and F. Calvert, 1998, Fluid flow in foreland basins during emplacement of thrust sheets: modelling the south-Pyrenean Ainsa basin: *Bull. Soc. Geol. France*, v. 169, p. 627-634.
- Bjørlykke, K., and K. Gran, 1994, Salinity variations in North Sea formation waters; implications for large scale fluid movements: *Marine & Petroleum Geology*, v. 11, p. 5-9.
- Black, T. J., 1997, Evaporite karst of northern lower Michigan: *Carbonates & Evaporites*, p. 81-83.
- Blount, C. W., and F. W. Dickson, 1969, The solubility of anhydrite (CaSO₄) in NaCl-H₂O from 100 to 450° C and 1 to 1000 bars: *Geochimica Cosmochimica Acta*, v. 33, p. 227-245.
- Blum, M., G. Kocurek, M. Deynoux, C. Swezey, N. Lancaster, D. M. Price, and J. C. Pion, 1998, Quaternary wadi lacustrine aeolian depositional cycles and sequences, Chott Rharsa basin, Southern Tunisia, in A. S. Alsharan, K. W. Glennie, G. L. Whittle, and G. C. S. C. Kendall, eds., *Quaternary Deserts and Climate Change*: Rotterdam, A. A. Balkema, p. 539-552.
- Bobst, A. L., T. K. Lowenstein, T. E. Jordan, L. V. Godfrey, T. L. Ku, and S. D. Luo, 2001, A 106 ka paleoclimate record from drill core of the Salar de Atacama, northern Chile: *Palaeogeography Palaeoclimatology Palaeoecology*, v. 173, p. 21-42.
- Bogoch, R., B. Buchbinder, and M. Magaritz, 1994, Sedimentology and geochemistry of lowstand peritidal lithofacies at the Cenomanian-Turonian boundary in the Cretaceous carbonate platform of Israel: *Journal of Sedimentary Research Section A-Sedimentary Petrology & Processes*, v. 64, p. 733-740.
- Bohacs, K. M., A. R. Carroll, J. E. Neal, and P. J. Mankiewicz, 2000, Lake-basin type, source potential, and hydrocarbon character: An integrated sequence-stratigraphic - geochemical framework, in E. H. Gierlowski-Kodesch, and K. Kelts, eds., *Lake basins through space and time*, v. 46: Tulsa, American Association Petroleum Geologists Studies in Geology, p. 3-34.
- Bookman, R., Y. Enzel, A. Agnon, and M. Stein, 2004, Late Holocene lake levels of the Dead Sea: *Geological Society of America Bulletin*, v. 116, p. 555-571.
- Booth, J., and N. Sattayarak, 2000, Multiple inversion of the Khorat Plateau Basin, NE Thailand, with the formation and preservation of a productive gas play: *Bulletin American Association Petroleum Geologists*, v. 84, p. 1395-1518.
- Borchert, H., 1977, On the formation of Lower Cretaceous potassium salts and tachyhydrite in the Sergipe Basin (Brazil) with some remarks on similar occurrences in West Africa (Gabon, Angola etc.), in D. D. Klemm, and H. J. Schneider, eds., *Time and strata-bound ore deposits*: Berlin, Germany, Springer-Verlag, p. 94-111.
- Borchert, H., and R. O. Muir, 1964, Salt deposits--The origin, metamorphism and deformation of evaporites: London, D. Van Nostrand Co., Ltd.
- Borchert, R., D. Fischer, R. Johnson, and L. C. Gerhard, 1990, Glenburn Field - USA, Williston Basin, North Dakota, in E. A. Beaumont, and N. H. Foster, eds., *Treatise of Petroleum Geology; Atlas of Oil and Gas Fields: Stratigraphic Traps I*: Tulsa, OK, American Association Petroleum Geologists, p. 91-106.
- Borer, J. M., and P. M. Harris, 1991, Lithofacies and cyclicity of the Yates Formation, Permian Basin: Implications for reservoir heterogeneity: *AAPG Bulletin*, v. 75, p. 726-779.
- Bosak, P., J. I. Bruthans, M. Fillippi, T. Svoboda, and J. Smid, 1999, Karst and salt caves in salt diapirs, SE Zagros Mountains (Iran): *Acta Carsologica*, v. 28, p. 41-75.
- Bottomley, D. J., D. C. Gregoire, and K. G. Raven, 1994, Saline groundwaters and brines in the Canadian Shield; geochemical and isotopic evidence for a residual evaporite brine component: *Geochimica et Cosmochimica Acta*, v. 58, p. 1483-1498.

- Bottomley, D. J., A. Katz, L. H. Chan, A. Starinsky, M. Douglas, I. D. Clark, and K. G. Raven, 1999, The origin and evolution of Canadian Shield brines: evaporation or freezing of seawater? New lithium isotope and geochemical evidence from the Slave craton: *Chemical Geology*, v. 155, p. 295-320.
- Bottomley, D. J., R. Renaud, Z. Kotzer, and I. D. Clark, 2002, Iodine-129 constraints on residence times of deep marine brines in the Canadian Shield: *Geology*, v. 30, p. 587-590.
- Boucot, A. J., and J. Gray, 2001, A critique of Phanerozoic climatic models involving changes in the CO₂ content of the atmosphere: *Earth-Science Reviews*, v. 56, p. 1-159.
- Boulter, C. A., and J. E. Glover, 1986, Chert with relict hopper moulds from Rocklea Dome, Pilbara Craton, Western Australia; an Archean halite-bearing evaporite: *Geology*, v. 14, p. 128-131.
- Bourrouilh, L.-J. F., J. L. Carsin, P. M. Niasussat, and Y. Thommeret, 1985, Sédimentation phosphatée actuelle dans le lagon confiné de l'Île de Clipperton (Océan Pacifique). Datations, sédimentologie et géochimie: *Sciences géologiques, Mémoire, Strasbourg*, v. 77, p. 109-124.
- Bowler, J. M., 1973, Clay dunes: their occurrence, formation and environmental significance: *Earth-Science Reviews*, v. 9, p. 315-338.
- Bowler, J. M., 1983, Lunettes as indices of hydrologic change; a review of Australian evidence: *Proceedings of the Royal Society of Victoria*, v. 95, p. 147-168.
- Bowler, J. M., 1986, Spatial variability and hydrologic evolution of Australian lake basins; analogue for Pleistocene hydrologic change and evaporite formation: *Palaeogeography, Palaeoclimatology, Palaeoecology*, v. 54, p. 21-41.
- Bowser, C. J., and F. W. Dickson, 1966, Chemical zonation of the borates at Kramer, California: *Second Symposium on Salt, Northern Ohio Geological Society, Cleveland, OH*, v. 1, p. 122-132.
- Boyer, B. W., 1982, Green River laminites: Does the playa-lake model really invalidate the stratified lake model? *Geology*, v. 10, p. 321-324.
- Boyle, R. W., 1962, *Geology and Geochemistry of the Magnet Cove Barium-Lead-Zinc-Silver Deposit, Walton, Nova Scotia*: *Canadian Mining Journal*, v. 83, p. 104-110.
- Boys, C., 1990, *The geology of potash deposits at PCS Cory Mine, Saskatchewan: Master's thesis, University of Saskatchewan; Saskatoon, SK; Canada*.
- Boys, C., 1993, A geological approach to potash mining problems in Saskatchewan, Canada: *Exploration & Mining Geology*, v. 2, p. 129-138.
- Bradley, W. H., and H. P. Eugster, 1969, *Geochemistry and paleolimnology of the trona deposits and associated authigenic minerals of the Green River Formation of Wyoming*: U. S. Geological Survey Professional Paper, v. 469B, p. 71p.
- Bradshaw, J., 1988, *The depositional, diagenetic and structural history of the Chandler Formation and related units, Amadeus Basin, central Australia*: PhD thesis, University New South Wales (Australia).
- Bradshaw, J., 1991, *Description and depositional model of the Chandler Formation; a Lower Cambrian evaporite and carbonate sequence, Amadeus Basin, central Australia*: *Bulletin - Australia, Bureau of Mineral Resources, Geology and Geophysics*, v. 236, p. 227-244.
- Braga, J. C., J. M. Martín, and R. Riding, 1995, Controls on microbial dome fabric development along a carbonate-siliciclastic shelf-basin transect, Miocene, SE Spain: *Palaios*, v. 10, p. 347-361.
- Braithwaite, C. J. R., and V. Zedef, 1994, Living hydromagnesite stromatolites from Turkey: *Sedimentary Geology*, v. 92, p. 1-5.
- Braithwaite, C. J. R., and V. Zedef, 1996, Hydromagnesite stromatolites and sediments in an alkaline lake, Salda Golu, Turkey: *Journal of Sedimentary Research A: Sedimentary Petrology and Processes*, v. 66, p. 991-1002.
- Braitsch, O., 1964, The temperature of evaporite formation, in A. E. M. Nairn, ed., *Problems in palaeoclimatology*: New York, Wiley, p. 479-490.
- Brandt, K. K., and K. Ingvorsen, 1997, *Desulfobacter halotolerans* sp. nov., a halotolerant acetate-oxidizing sulfate-reducing bacterium isolated from sediments of Great Salt Lake, Utah: *Systematic and Applied Microbiology*, v. 20, p. 366-373.
- Bray, R. B., and J. S. Hanor, 1990, Spatial variations in the subsurface pore fluid properties in a portion of southern Louisiana: implications for regional fluid flow and solute transport: *Trans. Gulf Coast Assoc. Geol. Soc.*, v. 40, p. 53-64.
- Breck, D. W., 1974, *Zeolite Molecular Sieves*: New York, Wiley-Interscience, 771 p.
- Bregant, D., G. Catalano, G. Civitarese, and A. Luchetta, 1990, Some chemical characteristics of the brines in Bannock and Tyro Basins: salinity, sulphur compounds, Ca, F, pH, At, PO₄, SiO₂, NH₃: *Marine Chemistry*, v. 31, p. 35-62.
- Breit, G. N., M. B. Goldhaber, D. R. Shawe, and E. C. Simmons, 1990, Authigenic barite as an indicator of fluid movement through sandstones within the Colorado Plateau: *Journal of Sedimentary Petrology*, v. 60, p. 884-896.
- Brenchley, P. J., J. D. Marshall, G. A. F. Carden, D. B. R. Robertson, D. G. F. Long, T. Meidla, L. Hints, and T. F. Anderson, 1994, Bathymetric and isotopic evidence for a short-lived Late Ordovician glaciation in a greenhouse period: *Geology*, v. 22, p. 295-298.
- Brennan, S. T., and T. K. Lowenstein, 2002, The major-ion composition of Silurian seawater: *Geochimica et Cosmochimica Acta*, v. 66, p. 2683-2700.
- Brennan, S. T., T. K. Lowenstein, and J. Horita, 2004, Seawater chemistry and the advent of biocalcification: *Geology*, v. 32, p. 473-476.
- Bretz, J. H., 1952, A solution cave in gypsum: *Journal of Geology*, v. 6-, p. 279-283.
- Briere, P. R., 2000, Playa, playa lake, sabkha: Proposed definitions for old terms: *Journal of Arid Environments*, v. 45, p. 1-7.
- Briggs, L. I., 1958, Evaporite facies: *Journal of Sedimentary Petrology*, v. 28, p. 46-56.
- Briggs, L. I., D. Gill, D. Z. Briggs, and R. D. Elmore, 1980, Transition from open marine to evaporite deposition in the Silurian Michigan Basin, in A. Nissenbaum, ed., *Hypersaline brines and evaporitic environments: Developments in Sedimentology*, v. 28: Amsterdam, Elsevier, p. 253-270.
- Brock, M. A., 1982a, *Biology of the Salinity Tolerant Genus Ruppia L in Saline Lakes in South-Australia. I. Morphological Variation within and between Species and Ecophysiology*: *Aquatic Botany*, v. 13, p. 219-248.
- Brocks, J. J., G. D. Love, R. E. Summons, A. H. Knoll, G. A. Logan, and S. A. Bowden, 2005, Biomarker evidence for green and purple sulphur bacteria in a stratified Palaeoproterozoic sea: *Nature*, v. 437, p. 866-870.
- Brocks, J. J., and R. E. Summons, 2003, Chapter 8.03: Sedimentary hydrocarbons, biomarkers for early life, in W. Schlesinger, ed.,

- Treatise in Geochemistry, v. 8: Amsterdam, Elsevier, p. 53.
- Brock, M. A., 1982b, Biology of the Salinity Tolerant Genus *Ruppia* L in Saline Lakes in South-Australia.2. Population Ecology and Reproductive- Biology: *Aquatic Botany*, v. 13, p. 249-268.
- Brodylo, L. A., and R. J. Spencer, 1987, Depositional environment of the Middle Devonian Telegraph Salts, Alberta, Canada: *Bulletin Canadian Petroleum Geology*, v. 35, p. 186-196.
- Brogly, P. J., I. P. Martini, and G. V. Middleton, 1998, The Queenston Formation - Shale-dominated, mixed terrigenous- carbonate deposits of Upper Ordovician, semiarid, muddy shores in Ontario, Canada: *Canadian Journal of Earth Sciences*, v. 35.
- Brongersma-Sanders, M., 1972, Hydrological conditions leading to the development of bituminous sediments in the pre-evaporite phase [with discussion]: in *Geology of saline deposits; Geologie des depots salins*. Unesco Earth Sci. Ser. No.
- Brookfield, M. E., 2003, The enigma of fine-grained alluvial basin fills: the Permo-Triassic (Cumbrian Coastal and Sherwood Sandstone Groups) of the Solway Basin, NW England and SW Scotland: *International Journal Earth Science (Geol. Rundsch.)*, v. 93, p. 282-296.
- Brown, A. A., and R. G. Loucks, 2001, Evaluation of Anhydrite Seals through Depositional, Structural, and Lithological Analysis; Example from the Jurassic Arab Formation, Al Rayyan Field, Qatar (abs.): *Bulletin American Association of Petroleum Geologists*, v. 85(13).
- Brun, J.-P., and X. Fort, 2004, Compressional salt tectonics (Angolan margin): *Tectonophysics*, v. 382, p. 129-150.
- Bruno, R. S., and J. S. Hanor, 2003, Large-scale fluid migration driven by salt dissolution, Bay Marchand Dome, offshore Louisiana: *CGCAGS Transaction*, v. 53, p. 97-107.
- Bruthans, J., M. Filippi, J. Smíd, and L. Palatinus, 2002, Trí Nahácu (Three Nudes) and Ghar-e Daneshyu caves - The world's second and fifth longest salt caves: *The International Caver 2002*, Swindon, U.K., p. 27-36.
- Bruthans, J., J. Smid, M. Filippi, and O. Zeman, 2000, Thickness of cap rock and other important factors affecting the morphogenesis of salt karst: *Acta Carsologica*, v. 29, p. 51-64.
- Bruthans, J., and O. Zeman, 2003, Factors controlling exokarst morphology and sediment transport through caves: Comparison of carbonate and salt karst: *Acta Carsologica*, v. 32, p. 83-99.
- Bryant, R. G., 1999, Application of AVHRR to monitoring a climatically sensitive playa. Case study: Chott el Djerid, southern Tunisia.: *Earth Surface Processes & Landforms*, v. 24, p. 283-302.
- Bryant, R. G., N. A. Drake, A. C. Millington, and B. W. Sellwood, 1994a, The chemical evolution of the brines on Chott el Djerid, southern Tunisia after an exceptional rainfall event in January 1990, in R. W. Renault, and W. M. Last, eds., *Sedimentology and geochemistry of modern and ancient saline lakes*, v. 50: Tulsa, Okl, SEPM/Society for Sedimentary Geology; Special Publication, p. 3-12.
- Bryant, R. G., B. W. Sellwood, A. C. Millington, and N. A. Drake, 1994b, Marine-like potash evaporite formation on a continental playa; case study from Chott el Djerid, southern Tunisia: *Sedimentary Geology*, v. 90, p. 269-291.
- Buchardt, B., C. Israelson, P. Seaman, and G. Stockmann, 2001, Ikaite tufa towers in Ikka Fjord, southwest Greenland: Their formation by mixing of seawater and alkaline spring water: *Journal of Sedimentary Research Section A-Sedimentary Petrology & Processes*, v. 71A, p. 176-189.
- Buchbinder, B., 1996, Miocene carbonates of the eastern Mediterranean, the Red Sea and the Mesopotamian Basin: geodynamic and eustatic controls, in E. K. e. a. Franseen, ed., *Models for carbonate stratigraphy from Miocene reef complexes of Mediterranean regions*, SEPM/Society for Sedimentary Geology; Concepts in Sedimentology and Paleontology, v. 5, p. 89-96.
- Buck, M. J., D. C. Ford, and H. P. Schwarcz, 1994, Classification of cave gypsum deposits derived from oxidation of H₂S, in I. D. Sasowsky, and M. V. Palmer, eds., *Breakthroughs in Karst Geomicrobiology*: Colorado Springs, Colorado, Karst Waters Institute, p. 5-9.
- Budai, J. M., K. C. Lohmann, and R. M. Owen, 1984, Burial dedolomite in the Mississippian Madison Limestone, Wyoming and Utah thrust belt: *Journal of Sedimentary Petrology*, v. 54, p. 276-288.
- Budd, D. A., A. H. Saller, and P. M. Harris, 1995, Unconformities and porosity in carbonate strata, v. American Association of Petroleum Geologists Memoir 63: Tulsa, Okla, American Association of Petroleum Geologists.
- Buffet, A., 1998, The collapse of Compagnie des Salins SG4 and SG5 drilling: *Proc. S.M.R.I. Fall Meeting, Rome*, p. 79-105.
- Buick, R., 1992, The antiquity of oxygenic photosynthesis; evidence from stromatolites in sulphate-deficient Archaean lakes: *Science*, v. 255, p. 74-77.
- Buick, R., and J. S. R. Dunlop, 1990, Evaporitic sediments of early Archaean age from the Warrawoona Group, North Pole, Western Australia: *Sedimentology*, v. 37, p. 247-277.
- Burban, B., 1990, Kunwarara magnesite deposit, in F. E. Hughes, ed., *Geology of the mineral deposits of Australia and Papua New Guinea*, Australasian Institute of Mining and Metallurgy Monograph Series, Volume 14 (2), p. 1675-1677.
- Burchette, T. P., and V. P. Wright, 1992, Carbonate ramp depositional systems: *Sedimentary Geology*, v. 79, p. 3-57.
- Burk, C. A., M. Ewing, J. L. Worzel, A. O. J. Beall, W. A. Berggren, D. Bukry, A. G. Fischer, and E. A. J. Pessagno, 1969, Deep-sea drilling into the Challenger knoll, central Gulf of Mexico: *Bulletin American Association Petroleum Geologists*, v. 53, p. 1338-1347.
- Burke, C. M., 1995, Benthic microbial production of oxygen supersaturates the bottom water of a stratified hypersaline lake: *Microbial Ecology*, v. 29, p. 163-171.
- Burke, C. M., and B. Knott, 1997, Homeostatic interactions between the benthic microbial communities and the waters of a saline lake: *Marine & Freshwater Research*, v. 48, p. 623-631.
- Burkova, V. N., E. A. Kurakolova, N. S. Vorob'eva, M. L. Kondakova, and O. K. Bazhenova, 2000, Hydrocarbons of the hypersaline environment of the Tyro deep-sea depression (eastern Mediterranean): *Geochemistry International*, v. 38, p. 883-894.
- Burliga, S., 1996, Kinematics within the Klodawa salt diapir, central Poland, in G. I. Alsop, D. J. Blundell, and I. Davison, eds., *Salt tectonics*: London, United Kingdom, Geological Society of London Special Publication, v. 100, p. 11-21.
- Burne, R. V., J. Bauld, and P. De Deckker, 1980, Saline lake charophytes and their geological significance: *Journal of Sedimentary Petrology*, v. 50, p. 281-293.
- Burne, R. V., and L. S. Moore, 1987, Microbialites; organosedimentary deposits of benthic microbial communities: *Palaaios*, v. 2, p. 241-254.
- Burns, K. L., O. Stephansson, and A. J. R. White, 1977, The Flinders Ranges breccias of South Australia — diapirs or décollement? *Quarterly Journal Geological Soc. London*, v. 134, p. 363 - 384.

- Burri, E., 1986, Various aspects of karstic phenomena in the urbanised area of Gissi and neighbouring areas (southern Abruzzo, Italy): *Le Grotte d'Italia*, v. 4, p. 143-161.
- Burri, P., R. du Dresnay, and C. W. Wagner, 1973, Tepee structures and associated diagenetic features in intertidal carbonate sands (lower Jurassic, Morocco): *Sedimentary Geology*, v. 9, p. 221-228.
- Burrus, J., and F. Audebert, 1990, Thermal and compaction processes in a young rifted basin containing evaporites; Gulf of Lions, France: *American Association Petroleum Geologists - Bulletin*, v. 74, p. 1420-1440.
- Burwood, R., 1984, Carbonate source rocks for six million barrels of oil per day – Zagros fold belt, southwestern Iran, in J. G. Palacas, ed., *Petroleum geochemistry and source rock potential of carbonate rocks*, American Association of Petroleum Geologists Studies in Geology 18, p. 206.
- Burwood, R., S. M. De Witte, B. Mycke, and J. Paulet, 1995, Petroleum geochemical characterisation of the lower Congo Coastal basin Bucomazi Formation, in B. Katz, ed., *Petroleum source rocks*: Berlin, Springer Verlag, p. 235-263.
- Burwood, R., P. Leplat, B. Mycke, and J. Paulet, 1992, Rifted Margin Source Rock Deposition - a Carbon Isotope and Biomarker Study of a West African Lower Cretaceous Lacustrine Section: *Organic Geochemistry*, v. 19, p. 41-52.
- Burwood, R., and B. Mycke, 1996, Coastal Angola and Zaire; a geochemical contrast of the lower Congo and Kwanza Basin hydrocarbon habitats (abs): *Bulletin American Association of Petroleum Geologists*, v. 80, p. 1277.
- Bush, P., 1973, Some aspects of the diagenetic history of the sabkha in Abu Dhabi, Persian Gulf, in B. H. Purser, ed., *The Persian Gulf: Holocene carbonate sedimentation and diagenesis in a shallow epicontinental sea*: New York, Springer Verlag, p. 395-407.
- Busson, G., 1980, *Evaporite deposits; illustration and interpretation of some environmental sequences*: Paris, France, Ed. Technip, 266 p.
- Busson, G., 1991, Relationship between different types of evaporitic deposits, and the occurrence of organic-rich layers (potential source-rocks): *Carbonates and Evaporites*, v. 6, p. 177-192.
- Bustillo, M. A., J. Garcia-Guinea, J. Martinez-Frias, and A. Delgado, 1999, Unusual sedimentary geodes filled by gold-bearing hematite laths: *Geological Magazine*, v. 136, p. 671-679.
- Butler, G. P., 1966, Early diagenesis in the recent sediments of the Trucial Coast of the Persian Gulf: Doctoral thesis, University of London, 251 p.
- Butler, G. P., 1969, Modern evaporite deposition and geochemistry of coexisting brines, the sabkha, Trucial coast, Arabian gulf: *Journal of Sedimentary Petrology*, v. 39, p. 70-89.
- Butler, G. P., 1970, Holocene gypsum and anhydrite of the Abu Dhabi sabkha, Trucial Coast; an alternative explanation of origin: 3rd Symposium on Salt, Northern Ohio Geological Society, v. 1, p. 120-152.
- Butler, G. P., P. M. Harris, and C. G. S. C. Kendall, 1982, Recent evaporites from the Abu Dhabi coastal flats, in C. R. Handford, R. G. Loucks, and G. R. Davies, eds., *Depositional and diagenetic spectra of evaporites; a core workshop*, v. 3, SEPM Core Workshop, p. 33-64.
- Butler, R. W. H., W. H. Lickorish, M. Grasso, H. M. Pedley, and L. Ramberti, 1995, Tectonics and sequence stratigraphy in Messinian basins, Sicily; constraints on the initiation and termination of the Mediterranean salinity crisis: *Geological Society of America Bulletin*, v. 107, p. 425-439.
- Bäurle, G., O. Bornemann, F. Mauthe, and D. Michalzik, 2000, Origin of stylolites in Upper Permian Zechstein Anhydrite (Gorleben Salt Dome, Germany): *Journal of Sedimentary Research*, v. 70, p. 726-737.
- Bérest, P., J. Bergues, and B. Brouard, 1999, Static and dynamic compressibility of deep underground caverns: *Int. J. Rock Mech. & Mining Sci.*, v. 36, p. 1031-1049.
- Bérest, P., and B. Brouard, 2001, Storage of tritiated water in salt caverns: In Proc. KIWIR 6th International Workshop on Key Issues in Waste Isolation Research, ENPC, P. Delage ed., Presses de l'Ecole Nationale des Ponts et Chaussées, Paris, p. 497-511, 2001.
- Bérest, P., and B. Brouard, 2002, Safety of salt caverns used for underground storage: Proc. 8th Portuguese Congress for Geotechnique, 15-18 April 2002, Lisbon, Portugal.
- Bérest, P., and B. Brouard, 2003, Safty of salt caverns used for underground storage: *Oil and Gas Science and Technology - Rev. IFP*, v. 58, p. 361-384.
- Caja, M. K., I. S. Al-Aasm, R. Marfil, M. Tsige, T. Martin-Crespo, and R. Salas, 2003, Multiphase carbonate cementation related to fractures in the Upper Jurassic limestones, Maestrat Basin (Iberian Range, Spain): *Journal of Geochemical Exploration*, v. 78-9, p. 33-38.
- Calaforra, J. M., and A. Pulido-Bosch, 1999, Gypsum karst features as evidence of diapiric processes in the Betic Cordillera, Southern Spain: *Geomorphology*, v. 29, p. 251-264.
- Calaforra, J. M., and A. Pulido-Bosch, 2003, Evolution of the gypsum karst of Sorbas (SE Spain): *Geomorphology*, v. 50, p. 173-180.
- Callao, S., E. Arce, and A. Andia, 2002, Mineralogía, química e inclusiones fluidas en lo depositos de nitratos de Maria elena, Lla region, Chile: *Bol. Soc. Chil. Quím.*, v. 47, p. 181-190.
- Calvo, J. P., M. M. Blanc-Valleron, J. P. Rodriguez Arandia, J. M. Rouchy, and M. E. Sanz, 1999, Authigenic clay minerals in continental evaporitic environments: *International Association Sedimentologists Special Publication*, No. 27, p. 129-151.
- Camerlenghi, A., 1990, Anoxic Basins of the eastern Mediterranean: geological framework: *Marine Chemistry*, v. 31, p. 1-19.
- Camoin, G., J. Casanova, J. M. Rouchy, M. M. Blancvalleron, and J. F. Deconinck, 1997, Environmental controls on perennial and ephemeral carbonate lakes - the central Paleo-Andean basin of Bolivia during Late Cretaceous to Early Tertiary times: *Sedimentary Geology*, v. 113, p. 1-26.
- Camur, M. Z., and H. Mutlu, 1996, Major-ion geochemistry and mineralogy of the Salt Lake (Tuz Golu) basin, Turkey: *Chemical Geology*, v. 127, p. 313-329.
- Cann, J. H., and P. De Deckker, 1981, Fossil Quaternary and Living Foraminifera from Athalassic (Non-Marine) Saline Lakes, Southern Australia: *Journal of Palaeontology*, v. 55, p. 660-670.
- Cantrell, D. L., and R. M. Hagerty, 1999, Microporosity in the Arab Formation Carbonates, Saudi Arabia: *GeoArabia*, v. 4, p. 129-154.
- Cantrell, D. L., and R. M. Hagerty, 2003, Reservoir rock classification, Arab-D reservoir, Ghawar field, Saudi Arabia: *GeoArabia*, v. 8, p. 129-154.
- Cantrell, D. L., P. K. Swart, C. R. Handford, C. G. S. C. Kendall, and H. Westphal, 2001, Geology and production significance of dolo-

- mite, Arab D reservoir, Ghawar Field, Saudi Arabia: *GeoArabia*, v. 6, p. 45-60.
- Carlson, C. A., F. M. Phillips, D. Elmore, and H. W. Bentley, 1990, Chlorine-36 tracing of salinity sources in the Dry Valleys of Victoria Land, Antarctica: *Geochimica et Cosmochimica Acta*, v. 54, p. 311-318.
- Carlson, E. H., 1983, The occurrence of Mississippi Valley-type Mineralization in northwestern Ohio, in G. Kisvarsanyi, S. K. Grant, W. P. Pratt, and J. W. Koenig, eds., *International Conference on Mississippi Valley Type lead-zinc deposits; Proceedings*, University of Missouri Rolla, Mo, p. 424-435.
- Carlson, E. H., 1987, Celestite replacements of evaporites in the Salina Group: *Sedimentary Geology*, v. 54, p. 93-112.
- Carlson, E. H., 1992, Reactivated interstratal karst - example from the late Silurian rocks of western Lake Erie (USA): *Sedimentary Geology*, v. 76, p. 273-283.
- Carozzi, A. V., I. A. Orchueta, and M. L. R. Schelotto, 1993, Depositional models of the Lower Cretaceous Quintuco-Loma Montosa Formation, Neuquen Basin, Argentina: *Journal of Petroleum Geology*, p. 421-450.
- Carpenter, A. B., 1978, Origin and chemical evolution of brines in sedimentary basins: Oklahoma Geological Survey Circular, v. 79, p. 60-77.
- Carrigan, W. J., G. A. Cole, E. L. Colling, and P. J. Jones, 1995, Geochemistry of the Upper Jurassic Tuwaiq Mountain and Hanifa Formation petroleum source rocks of eastern Saudi Arabia, in B. Katz, ed., *Petroleum source rocks*: Berlin, Springer Verlag, p. 67-87.
- Carroll, A. R., 1998, Upper Permian lacustrine organic facies evolution, southern Junggar basin, NW China: *Organic Geochemistry*, v. 28, p. 649-667.
- Carroll, A. R., and K. M. Bohacs, 1999, Stratigraphic classification of ancient lakes: Balancing tectonic and climatic controls: *Geology*, v. 27, p. 99-102.
- Carroll, A. R., S. C. Brasell, and S. A. Graham, 1992, Upper Permian lacustrine oil shales, southern Junggar Basin, Northwest China: *American Association Petroleum Geologists - Bulletin*, v. 76, p. 1874-1902.
- Carter, N. L., 1976, Steady-state flow of rocks: Review of Geophysics and Space Physics, v. 14, p. 301-360.
- Carter, N. L., and F. D. Hansen, 1983, Creep of rocksalt: *Tectonophysics*, v. 92, p. 275-333.
- Carter, N. L., S. T. Horseman, J. E. Russell, and J. Handin, 1993, Rheology of rock salt: *Journal of Structural Geology*, v. 15, p. 1257-1271.
- Cartwright, M., M. McLaughlin, J. Ratigan, and D. Blankenship, 2000, A sinkhole at the EGP Fuels Company LPG storage terminal Mount Belvieu Texas: Proc. S.M.R.I. Fall Meeting Technical Session, San Antonio, p. 128-143.
- Casanova, J., 1986, East African Rift stromatolites, in L. E. Frostick, R. W. Renaut, I. Reid, and J. J. Tiercelin, eds., *Sedimentation in the African Rifts*, *Journal of the Geological Society of London*, Special Publication No. 25, p. 201-210.
- Casanova, J., and D. Nury, 1989, Biosédimentologie des stromatolites fluvio-lacustres du fossé oligocene de Marseille: *Bull. Soc. Geol. Fr.*, v. 8, p. 1111-1128.
- Casas, E., 1992, Modern carnallite mineralisation and Late Pleistocene to Holocene brine evolution in the nonmarine Qaidam Basin, China: Doctoral thesis, State University of New York at Binghamton.
- Casas, E., and T. K. Lowenstein, 1989, Diagenesis of saline pan halite; comparison of petrographic features of modern, Quaternary and Permian halites: *Journal of Sedimentary Petrology*, v. 59, p. 724-739.
- Casas, E., T. K. Lowenstein, R. J. Spencer, and P. Zhang, 1992, Carnallite mineralization in the nonmarine, Qaidam Basin, China; evidence for the early diagenetic origin of potash evaporites: *Journal of Sedimentary Petrology*, v. 62, p. 881-898.
- Casey, W. H., and B. Bunker, 1990, Leaching of mineral and glass surfaces during, in M. F. Hochella, and A. F. White, eds., *Mineral-Water Interface Geochemistry*, *Reviews in Mineralogy*, v. 23, p. 397-426.
- Cassidy, D. P., and V. Ranganathan, 1992, Groundwater Upwelling, Near Bay St. Elaine Salt Dome in Southeastern Louisiana, as Inferred from Fluid Property Variations: *Bulletin American Association of Petroleum Geologists*, v. 76, p. 1560-1568.
- Castanier, S., J. P. Perthuisot, M. Matrat, and J. Y. Morvan, 1999, The salt ooids of Berre salt works (Bouches du Rhone, France): the role of bacteria in salt crystallisation: *Sedimentary Geology*, v. 125, p. 9-21.
- Castanier, S., J. P. Perthuisot, J. M. Rouchy, A. Maurin, and O. Gueorget, 1992, Halite ooids in Lake Asal, Djibouti; biocrystalline build-ups: *Geobios*, v. 25, p. 811-821.
- Catho, D. L., J. K. Warren, and G. E. Williams, 1992, Halite saltern in the Canning Basin, Western Australia; a sedimentological analysis of drill core from the Ordovician-Silurian Mallowa Salt: *Sedimentology*, v. 39, p. 983-1002.
- Caumette, P., 1993, Ecology and physiology of phototropic bacteria and sulphate-reducing bacteria in marine salterns: *Experientia*, v. 49, p. 473-481.
- Cayol, J. L., B. Ollivier, B. K. C. Patel, G. Prensier, J. Guezennec, and J.-L. Garcia, 1994, Isolation and characterization of *Halo-thermothrix orenii* gen. nov., sp. nov., a halophilic, thermophilic, fermentative strictly anaerobic bacterium: *Int. J. Syst. Bacteriol.*, v. 44, p. 534-540.
- Cañaveras, J. C., S. Sanchezmoral, J. P. Calvo, M. Hoyos, and O. S., 1996, Dedolomites associated with karstification - an example of early dedolomitisation in lacustrine sequences from the Tertiary Madrid basin, central Spain: *Carbonates & Evaporites*, v. 11, p. 85-103.
- Cañaveras, J. C., S. Sanchezmoral, E. Sanzrubio, and M. Hoyos, 1998, Meteoric calcitization of magnesite in Miocene lacustrine deposits (Calatayud basin, NE Spain): *Sedimentary Geology*, v. 119, p. 183-194.
- Cendon, D. I., C. Ayora, J. J. Pueyo, and C. Taberner, 2003, The geochemical evolution of the Catalan potash subbasin, South Pyrenean foreland basin (Spain): *Chemical Geology*, v. 200, p. 339-357.
- Cendon, D. I., C. Ayora, and J. P. Pueyo, 1998, The origin of barren bodies in the Subiza potash deposit, Navarra, Spain - Implications for sylvite formation: *Journal of Sedimentary Research Section A-Sedimentary Petrology & Processes*, v. 68, p. 43-52.
- Ceriani, A., A. Di Giulio, H. Goldstein, and C. Rossi, 2002, Diagenesis associated with cooling during burial: An example from Lower Cretaceous reservoir sandstones (Sirt basin, Libya): *Bulletin American Association Petroleum Geologists*, v. 86, p. 1573-1591.

- Cercone, K. R., 1988, Evaporative sea level drawdown in the Michigan Basin: *Geology*, v. 16, p. 387-390.
- Cercone, K. R., and K. C. Lohmann, 1986, Diagenetic history of the Union 8 pinnacle reef (Middle Silurian), northern Michigan, USA, in B. Purser, and J. Schroeder, eds., *Reef diagenesis*: Berlin, Germany, Elsevier, p. 381-398.
- Ceriani, a., A. Di Giulio, H. Goldstein, and C. Rossi, 2002, Diagenesis associated with cooling during burial: An example from Lower Cretaceous reservoir sandstones (Sirt basin, Libya): *Bulletin American Association Petroleum Geologists*, v. 86, p. 1573-1591.
- Cesaretti, N. N., J. Parnell, and E. A. Dominguez, 2000, Pore fluid evolution within a hydrocarbon reservoir: Yacoraite Formation, (Upper Cretaceous), Northwest Basin, Argentina: *Journal of Petroleum Geology*, v. 23, p. 375-398.
- Chabert, C., and P. Courbon, 1997, Atlas de cavités non calcaires du monde: Union Int. Spéléol. au prés Madame Carle, Paris, p. 1-120.
- Chabou-Mostafai, S., J. J. DeVolce, Y. Fuchs, G. Memant, and M. Riviere, 1978, Sur les niveaux a celestite de Tunisie centrale et du sud-Constantinois: *Sciences de la Terre*, v. 22, p. 293-300.
- Chafetz, H. S., and R. L. Folk, 1984, Travertines: depositional morphology and the bacterially constructed constituents: *Journal of Sedimentary Petrology*, v. 54, p. 289-316.
- Chafetz, H. S., and J. L. Zhang, 1998, Authigenic euhedral mega-quartz crystals in a Quaternary dolomite: *Journal of Sedimentary Research Section A-Sedimentary Petrology & Processes*, v. 68, p. 994-1000.
- Channer, D. M. D., C. E. J. de Ronde, and E. T. C. Spooner, 1997, The Cl-Br-I composition of ≈ 3.23 Ga seawater: Implications for the geological evolution of ocean halide chemistry: *Earth and Planetary Science Letters*, v. 150, p. 325-335.
- Charrach, J., 1986, Genesis of halite islands in the southern basin of the Dead Sea: Israel Geological Society, Annual Meeting, p. 26-27.
- Chekunov, A. V., V. K. Garvish, R. I. Kutas, and L. I. Ryabchun, 1992, Dnieper-Donets palaeorift: *Tectonophysics*, v. 208, p. 257-272.
- Chen, J. Y., Y. P. Bi, J. G. Zhang, and S. F. Li, 1996, Oil-source correlation in the Fulin basin, Shengli petroleum province, East China: *Organic Geochemistry*, v. 24, p. 931-940.
- Chen, K., and J. M. Bowler, 1986, Late Pleistocene evolution of salt lakes in the Qaidam Basin, Qinghai Province, China: *Palaeogeography, Palaeoclimatology, Palaeoecology*, v. 54, p. 87-104.
- Chen, X. Y., J. R. Prescott, and J. T. Hutton, 1990, Thermoluminescence dating on gypseous dunes of Lake Amadeus, central Australia: *Australian Journal of Earth Sciences*, v. 37, p. 93-101.
- Chen, Y., 1986, Hydrochemistry and evolution of interstitial brine in the Zhabuye saline lake of Tibet. (Chinese): *Bulletin of the Institute of Mineral Deposits, Chinese Academy of Geological Sciences*, v. 18, p. 176-184.
- Chimene, C. A., 1991, Walker Creek Field - USA, Gulf of Mexico Basin, Arkansas, in E. A. Beaumont, and N. H. Foster, eds., *Treatise of Petroleum Geology; Atlas of Oil and Gas Fields: Stratigraphic Traps II*: Tulsa, OK, American Association Petroleum Geologists, p. 55-117.
- Chipley, D. B. L., 1995, Fluid history of the Saskatchewan sub-basin of the western Canada sedimentary basin: Evidence from the geochemistry of evaporites: Doctoral thesis, University of Saskatchewan.
- Chipley, D. B. L., and T. K. Kyser, 1989, Fluid inclusion evidence for the deposition and diagenesis of the Patience Lake Member of the Devonian Prairie Evaporite Formation, Saskatchewan, Canada: *Sedimentary Geology*, v. 64, p. 287-295.
- Chivas, A. R., A. S. Andrew, W. B. Lyons, M. I. Bird, and T. H. Donnelly, 1991, Isotopic constraints on the origin of salts in Australian playas; I, Sulphur: *Palaeogeography, Palaeoclimatology, Palaeoecology*, v. 84, p. 309-322.
- Choquette, P. W., and L. C. Pray, 1970, Geologic nomenclature and classification of porosity in sedimentary carbonates.: *Bulletin American Association of Petroleum Geologists*, v. 54, p. 207-250.
- Chough, S. K., S. B. Kim, and S. S. Chun, 1996, Sandstone/chert and laminated chert/black shale couplets, Cretaceous Uhangri Formation (southwest Korea): depositional evenets in alkaline lake environments: *Sedimentary Geology*, v. 104, p. 227-242.
- Chow, N., and F. Longstaffe, 1995, Dolomite of the Middle Devonian Elm Point Formation, Southern Manitoba - intrinsic controls on early dolomitization: *Bulletin of Canadian Petroleum Geology*, v. 43, p. 214-225.
- Chow, N., and A. D. George, 2004, Tepee-shaped agglutinated microbialites: an example from a Famennian carbonate platform on the Lennard Shelf, northern Canning Basin, Western Australia: *Sedimentology*, v. 51, p. 253-265.
- Chowns, T. M., and J. E. Elkins, 1974, The origin of quartz geodes and cauliflower cherts through the silicification of anhydrite nodules: *J. Sediment. Petrol.*, v. 44, p. 885-903.
- Christ, C. L., and R. M. Garrels, 1959, Relations among sodium borate hydrates at the Kramer deposit, Boron, California: *American Journal of Science*, v. 257, p. 516-528.
- Christiansen, F. G., S. Piasecki, L. Stemmerik, and N. Telnaes, 1993, Depositional environment and organic geochemistry of the Upper Permian Ravnjeld Formation source rock in East Greenland: *Bulletin American Association of Petroleum Geologists*, v. 77, p. 1519-1537.
- Chuber, S., and W. C. Pusey, 1985, Productive Permian carbonate cycles, San Andres Formation, Reeves field, West Texas, in P. O. Roehl, and P. W. Choquette, eds., *Carbonate petroleum reservoirs*: New York, Springer-Verlag, p. 289-307.
- Cita, M. B., 1983, The Messinian salinity crisis in the Mediterranean: A review, in H. Berckhemer, and K. J. Hsu, eds., *Alpine Mediterranean Geodynamics Review*, v. 8, American Geophysical Union; *Geodynamics Series*, p. 113-140.
- Clark, D. N., 1980a, The sedimentology of the Zechstein 2 Carbonate Formation of eastern Drenthe, the Netherlands, in H. Fuchtbauer, and T. Peryt, eds., *The Zechstein basin with emphasis on carbonate sequences*, E. Schweizerbart'sche VbH: *Contributions to Sedimentology* 9, p. 131-165.
- Clark, D. N., 1980b, The diagenesis of Zechstein carbonate sediments, in H. Fuchtbauer, and T. Peryt, eds., *The Zechstein basin with emphasis on carbonate sequences*, E. Schweizerbart'sche VbH: *Contributions to Sedimentology* 9, p. 167-203.
- Clark, J. A., J. A. Cartwright, and S. A. Stewart, 1999, Mesozoic dissolution tectonics on the West Central Shelf, UK Central North Sea: *Marine & Petroleum Geology*, v. 16, p. 283-300.
- Clark, J. A., S. A. Stewart, and J. A. Cartwright, 1998, Evolution of the NW margin of the North Permian Basin, UK North Sea: *Journal of the Geological Society*, v. 155, p. 663-676.

- Clark, J. P., and R. P. Philp, 1989, Geochemical characterization of evaporite and carbonate depositional environments and correlation of associated crude oils in the Black Creek basin, Alberta: *Bulletin of Canadian Petroleum Geology*, v. 37, p. 401-416.
- Clarke, J. D. A., 1994, Evolution of the Lefroy and Cowan palaeodrainage channels, Western Australia: *Australian Journal of Earth Sciences*, v. 41, p. 55-68.
- Clarke, P., and J. Parnell, 1999, Facies analysis of a back-tilted lacustrine basin in a strike-slip zone, Lower Devonian, Scotland: *Palaeogeography Palaeoclimatology Palaeoecology*, 151(1-3):167-190, v. 151, p. 167-190.
- Clauzon, G., J. P. Suc, F. Gautier, A. Berger, and M. F. Loutre, 1996, Alternate interpretation of the Messinian salinity crisis: controversy resolved? *Geology*, v. 24, p. 363-366.
- Clavero, E., M. Hernandez-Marine, J. O. Grimalt, and F. Garcia-Pichel, 2000, Salinity tolerance of diatoms from thalassic hypersaline environments: *Journal of Phycology*, v. 36, p. 1021-1034.
- Clement, G. P., and W. T. Holser, 1988, Geochemistry of Moroccan evaporites in the setting of the North Atlantic Rift.: *Journal of African Earth Sciences*, v. 7, p. 375-382.
- Clement, J. H., 1985, Depositional sequences and characteristics of Ordovician Red River Reservoirs, Pennell Field, Williston Basin, in P. O. Roehl, and P. W. Choquette, eds., *Carbonate petroleum reservoirs: a case book*: New York, Springer Verlag, p. 71-84.
- Clemmensen, L. B., 1978, Alternating aeolian, sabkha and shallow-lake deposits from the Middle Triassic Gipsdalen Formation, Scoresby Land, East Greenland: *Palaeogeography, Palaeoclimatology, Palaeoecology*, v. 24, p. 111-135.
- Clemmensen, L. B., W. T. Holser, and D. Winter, 1984, Stable isotope study through Permian Triassic boundary: *Bull. Geol. Soc. Denmark*, v. 33, p. 253-260.
- Clemmey, H., and N. Badham, 1982, Oxygen in the Precambrian atmosphere; an evaluation of the geological evidence: *Geology*, v. 10, p. 141-146.
- Closson, D., 2005, Structural control of sinkholes and subsidence hazards along the Jordanian Dead Sea coast: *Environmental Geology*, v. 47, p. 290-301.
- Cloud, P. E., 1972, A working model of the primitive earth: *Am. J. Sci.*, v. 272, p. 537-548.
- Cobbold, P. R., K. E. Meisling, and V. S. Mount, 2001, Reactivation of an obliquely rifted margin, Campos and Santos basins, southeastern Brazil: *Bulletin American Association Petroleum Geologists*, v. 85, p. 1925-1944.
- Cobbold, P. R., P. Szatmari, L. S. Demercian, D. Coelho, and E. A. Rossello, 1995, Seismic and experimental evidence for thin-skinned horizontal shortening by convergent radial gliding on evaporites, deepwater Santos Basin, Brazil, in M. P. A. Jackson, D. G. Roberts, and S. Snelson, eds., *Salt tectonics: a global perspective*, AAPG Memoir, v.65, p. 305-322.
- Cody, R. D., 1976, Growth and early diagenetic changes in artificial gypsum crystals grown within bentonite muds and gels: *Geological Society America Bulletin*, v. 87, p. 1163-1168.
- Cody, R. D., and A. M. Cody, 1988, Gypsum nucleation and crystal morphology in analog saline terrestrial environments: *Journal of Sedimentary Petrology*, v. 58, p. 247-255.
- Cohen, A. S., 1989, Facies relationships and sedimentation in large rift lakes and implications for hydrocarbon exploration: Examples from Lake Turkana and Tanganyika: *Palaeogeography Palaeoclimatology Palaeoecology*, v. 70, p. 65-80.
- Cohen, A. S., and C. Thouin, 1987, Nearshore carbonate deposits in Lake Tanganyika: *Geology*, v. 15, p. 414-418.
- Cole, R. D., 1985, Depositional environment of oil shale in the Green River Formation, Douglas Creek Arch, Colorado and Utah, in M. D. Picard, ed., *Geology and Energy Resources, Uinta Basin of Utah*: Salt Lake City, Utah, Utah Geological Association, p. 211-224.
- Collenette, P., and D. J. Grainger, 1994, Mineral Resources of Saudi Arabia (not including oil, natural gas and sulfur): DGMR Special Publication, v. SP-2, p. 322.
- Collins, A. G., 1975, Geochemistry of oil field waters: *Developments in Petroleum Science*, 1: Amsterdam, Elsevier, 496 p.
- Colman, S. M., K. Kelts, and D. A. Dinter, 2002, Depositional history and neotectonics in Great Salt Lake, Utah, from high-resolution seismic stratigraphy: *Sedimentary Geology*, v. 148, p. 61-78.
- Colson, J., and I. Cojan, 1996, Groundwater dolocretes in a lake-marginal environment - An alternative model for dolocrete formation in continental settings (Danian of the Provence Basin, France): *Sedimentology*, v. 43, p. 175 - 188.
- Conklin, J., 1974, Structural geology of the Huizachal-Peregrina Anticlinorium: *Pan American Geological Society, Geology of Huizachal-Peregrina Anticlinorium*, p. 21-31.
- Cook, D. J., A. F. Randazzo, and C. L. Sprinkle, 1985, Authigenic fluorite in dolomitic rocks of the Floridan Aquifer: *Geology*, v. 13, p. 390-391.
- Cooper, A. H., 1986, Subsidence and foundering of strata caused by the dissolution of Permian gypsum in the Ripon and Bedale areas, North Yorkshire: Harwood, Gill M., Smith, Denys B. *The English Zechstein and related topics*. Univ. Newcastle upon Tyne, Newcastle upon Tyne, United Kingdom. Geological Society Special Publications, v. 22, p. 127-139.
- Cooper, A. H., 1995, Subsidence hazards due to the dissolution of Permian gypsum in England: Investigation and remediation, in B. F. Beck, ed., *Karst Geohazards - Engineering and Environmental Problems in Karst Terrane*. Proceedings of the fifth multidisciplinary conference on sinkholes and the environmental impacts of karst, Gatlinburg, Tennessee: Rotterdam, A.A. Balkema, p. 23-29.
- Cooper, A. H., 1998, Subsidence hazards caused by the dissolution of Permian gypsum in England: geology, investigation and remediation, in J. G. Maund, and M. Eddleston, eds., *Geohazards in Engineering Geology*, v. 15: London, Geological Society, London, p. 265-275.
- Cooper, A. H., and A. C. Waltham, 1999, Subsidence caused by gypsum dissolution at Ripon, North Yorkshire: *Quarterly Journal of Engineering Geology*, v. 32, p. 305-310.
- Cooper, A. M., 1991, Late Proterozoic hydrocarbon potential and its association with diapirism in Blinman #2, Central Flinders Ranges.: Honours thesis, University of Adelaide - National Centre Petroleum Geology and Geophysics.
- Cooper, B. S., P. C. Barnard, and N. Telnaes, 1995, The Kimmeridge Clay Formation of the North Sea, in B. Katz, ed., *Petroleum source rocks*: Berlin, Springer Verlag, p. 89-110.
- Cordell, R. J., 1992, Carbonates as hydrocarbon source rocks, in G. V. Chilingarian, S. J. Mazzullo, and H. H. Rieke, eds., *Carbonate reservoir characterisation: a geologic-engineering analysis, part 1: Developments in Petroleum Science*, v. 30: Amsterdam, Elsevier, p. 271-329.

- Coron, C. R., 1982, Facies relations and ore genesis of the Newfoundland Zinc mines deposit, Daniel's Harbour, western Newfoundland: Doctoral thesis, University of Toronto (Canada).
- Corselli, C., and F. S. Aghib, 1987, Brine formation and gypsum precipitation in the Bannock Basin (eastern Mediterranean): *Marine Geology*, v. 75, p. 185-199.
- Cosgrove, J. W., 2001, Hydraulic fracturing during the formation and deformation of a basin: A factor in the dewatering of low-permeability sediments: *Bulletin-American Association of Petroleum Geologists*, v. 85, p. 737-748.
- Coshell, L., and M. R. Rosen, 1994, Stratigraphy and Holocene history of Lake Hayward, Swan Coastal Plain, Western Australia, in R. Renaut, and W. Last, eds., *Sedimentology and Geochemistry of Modern and Ancient Lakes*, v. 50: Tulsa OK, SEPM Special Publ., p. 173-188.
- Coshell, L., M. R. Rosen, and K. J. McNamara, 1998, Hydromagnesite replacement of biomineralized aragonite in a new location of Holocene stromatolites, Lake Walyungup, Western Australia: *Sedimentology*, v. 45, p. 1005-1018.
- Cossey, S. P., 2004, Celebrations began with cognac: AAPG Explorer, v. September 2004.
- Cota, L., and G. Baric, 1998, Petroleum potential of the Adriatic offshore, Croatia: *Organic Geochemistry*, v. 29, p. 559-570.
- Cotton, J. T., and H. A. Koyi, 2000, Modeling of thrust fronts above ductile and frictional detachments: Application to structures in the Salt Range and Potwar Plateau, Pakistan: *Geological Society of America Bulletin*, v. 112, p. 351-363.
- Council, T. C., and P. C. Bennett, 1993, Geochemistry of ikaite formation at Mono Lake, California: implications for the origin of tufa mounds: *Geology*, v. 21, p. 971-974.
- Cowan, G., 1993, Identification and significance of aeolian deposits within the dominantly fluvial Sherwood Sandstone Group of the East Irish Sea Basin, UK., in C. P. North, and D. J. Prosser, eds., *Characterization of Fluvial and Aeolian Reservoirs*: London, Geological Society of London Special Publication 73, p. 231-245.
- Crabaugh, M., and G. Kocurek, 1993, Entrada Sandstone - example of a wet eolian system, in K. Pye, ed., *The Dynamics and Environmental Context of Aeolian Sedimentary Systems*, Geological Society London, Special Publication No. 72, p. 103-126.
- Craig, D. H., 1988, Caves and other features of Permian karst in San Andres dolomite, Yates field reservoirs, west Texas, in N. P. James, and P. W. Choquette, eds., *Paleokarst*: New York, Springer-Verlag, p. 342-363.
- Cramez, C., and M. P. A. Jackson, 2000, Superposed deformation straddling the continental-oceanic transition in deep-water Angola: *Marine and Petroleum Geology*, v. 17, p. 1095-1109.
- Crocker, I. T., 1979, Fluorite mineralisation in the dolomite of the Transvaal Supergroup, South Africa: *Geological Society of South Africa, Special Publication*, v. 6, p. 73-82.
- Crossley, N. G., 1997, Downhole probes evaluate cavern integrity: *Oil and Gas Journal*, v. March 3, 1997, p. 74-79.
- Crossley, N. G., 1998, Sonar surveys used in gas-storage cavern analysis: *Oil & Gas Journal*, v. May 4, 1998, p. 98-108.
- Crowley, S. F., S. H. Bottrell, M. D. B. McCarthy, J. Ward, and B. Young, 1997, $\delta^{34}\text{S}$ of Lower Carboniferous anhydrite, Cumbria and its implications for barite mineralisation in Northern Pennines: *Journal of the Geological Society*, v. 154, p. 597-600.
- Cucchi, F., and L. Zini, 2003, Gypsum karst of Zagros Mountains (I.R. Iran): *Acta Carsologica*, v. XXXII, p. 69-82.
- Culbertson, W. C., 1966, Trona in the Wilkins Peak Member of the Green River Formation, southwestern Wyoming: *Geological Survey research*.
- Cunningham, K. I., and K. I. Takahashi, 1992, Evidence for petroleum-assisted speleogenesis, Lechuguilla Cave, Carlsbad Caverns National Park, New Mexico: Barker, Charles E., Coury, Anny B. Abstracts of the U. S. Geological Survey, central region.
- Cunningham, K. J., R. H. Benson, K. Rakicelbied, and L. W. McKenna, 1997, Eustatic implications of Late Miocene depositional sequences in the Melilla Basin, Northeastern Morocco: *Sedimentary Geology*, v. 107, p. 147-165.
- Curial, A., D. Dumas, and G. Dromart, 1990, Organic matter and evaporites in the Paleogene West European Rift: The Bresse and Valence salt basins (France), in A. Y. Huc, ed., *Deposition of Organic Facies*, v. 30: Tulsa, OK, American Association Petroleum Geologists, *Studies in Geology*.
- Currie, P. K., and J. V. Walters, 1985, Finite element modelling of cavity behaviour in the solution mining of magnesium salts, in W. J. Schlitt, ed., *Salt and Brines '85*: New York, Amer. Inst. Min. Met. Petr. Eng., p. 87-96.
- Curtis, R., G. Evans, D. J. J. Kinsman, and D. J. Shearman, 1963, Association of dolomite and anhydrite in the Recent sediments of the Persian Gulf: *Nature*, p. 679-680.
- Cytryn, E., D. Minz, R. S. Oremland, and Y. Cohen, 2000, Distribution and Diversity of Archaea Corresponding to the Limnological Cycle of a Hypersaline Stratified Lake (Solar Lake, Sinai, Egypt): *Applied & Environmental Microbiology*, v. 66, p. 3269-3276.
- Czapowski, G., 1987, Sedimentary facies in the oldest rock salt (Na 1) of the Leba elevation (northern Poland), in T. M. Peryt, ed., *The Zechstein Facies in Europe*, v. 10: Berlin, Springer-Verlag *Lecture Notes in Earth Sciences*, p. 207-224.
- Czapowski, G., T. M. Peryt, and O. B. Raup, 1992, Carbonate-anhydrite-halite cycles in the Roet (Lower Triassic) of western Poland: *Bulletin - Polish Academy of Sciences: Earth Sciences*, v. 40, p. 161-164.
- D'Heur, M., 1990a, West Ekofisk Field--Norway Central Graben, North Sea, *Structural Traps IV: Tectonic and Nontectonic Fold Traps*, American Association Petroleum Geologists, Special Publication, p. 57-83.
- D'Heur, M., 1990b, Eldfisk Field--Norway Central Graben, North Sea, *Structural Traps IV: Tectonic and Nontectonic Fold Traps*, American Association Petroleum Geologists, Special Publication, p. 27-56.
- D'Onfro, P., 1988, Mechanics of salt tongue formation with examples from Louisiana slope (abs): *American Association of Petroleum Geology, Bulletin*, v. 72, p. 175.
- Dahl, J., J. M. Moldowan, and P. Sundararaman, 1993, Relationship of biomarker distribution to depositional environment - Phosphoria Formation, Montana, USA: *Organic Geochemistry*, p. 1001-1017.
- Dahl, J. E., J. M. Moldowan, S. C. Teerman, M. A. McCaffrey, P. Sundararaman, M. Pena, and C. E. Stelling, 1994, Source rock quality determination from oil biomarkers I. - An example from the Aspen Shale, Scully's Gap, Wyoming: *Bulletin American Association Petroleum Geologists*, v. 78, p. 1507-1026.

- Dahl, L. J., 1985, Solution Mining Bibliography, in W. J. Schlitt, ed., Salt and Brines '85, Amer. Inst. Min. Met. Petr. Eng., p. 169-174.
- Dailly, G. C., 1976, A possible mechanism relating progradation, growth faulting, clay diapirism and overthrusting in a regressive sequence of sediments: Canadian Petroleum Geology Bulletin, v. 24, p. 92-116.
- Dalgarno, C. R., and J. E. Johnson, 1966, Parachilna Sheet, South Australia.
- Dalgarno, C. R., and J. E. Johnson, 1968, Diapiric structures and late Precambrian-early Cambrian sedimentation in Flinders ranges, South Australia: American Association Petroleum Geologists, Memoir, v. 8, p. 301-314.
- Damnati, B., and M. Taieb, 1995, Solar and ENSO signatures in laminated deposits from Lake Magadi (Kenya) during the Pleistocene/Holocene transition: Journal of African Earth Sciences, v. 21, p. 373-382.
- Damste, J. S. S., J. W. De Leeuw, S. Betts, Yue Ling, and P. M. Hofmann, 1993, Hydrocarbon biomarkers of different lithofacies of the Salt IV Formation of the Mulhouse Basin, France: Organic Geochemistry, v. 20, p. 1187-1200.
- Damste, J. S. S., N. L. Frewin, F. Kenig, and J. W. De Leeuw, 1995, Molecular indicators or palaeoenvironmental change in a Messinian evaporitic sequence (Vena del Gesso, Italy). 1. Variations in extractable organic matter of ten cyclically deposited marl beds: Organic Geochemistry, v. 23, p. 471-483.
- Dardeau, G., and P. C. Graciansky, 1990, Halokinesis and alpine rifting in the Alpes-Maritimes (France): Bull. Centres Rech. Explr.-Prod. Elf Aquitaine, v. 14, p. 443-464.
- Darragi, F., M. Gueddari, and B. Fritz, 1983, Mise en évidence d'un fluoro-sulfate de sodium, la kogarkoite, dans les croutes salines du Lac Natron en Tanzanie (Presence of Kogarkoite ($\text{Na}_3\text{SO}_4\text{F}$) in the salt paragenesis of Lake Natron in Tanzania: Comptes-Rendus des Seances de l'Academie des Sciences, Serie 2: Mecanique-Physique, Chimie, Sciences de l'Univers, Sciences de la Terre, v. 297, p. 141-144.
- Darragi, F., and Y. Tardy, 1987, Authigenic trioctohedral smectites controlling pH, alkalinity silica and magnesium concentrations in alkaline lakes: Chemical Geology, v. 63, p. 59-72.
- Das, N., J. Horita, and H. D. Holland, 1990, Chemistry of fluid inclusions in halite from the Salina Group of the Michigan Basin; implications for Late Silurian seawater and the origin of sedimentary brines: Geochimica et Cosmochimica Acta, v. 54, p. 319-327.
- Dasgupta, S., M. R. Hong, and I. A. Al-Jallal, 2002, Accurate reservoir characterization to reduce drilling risk in Khuff-C carbonate, Ghawar field, Saudi Arabia: GeoArabia, v. 7, p. 81-100.
- DasSarma, S., and P. Arora, 2001, Halophiles: Encyclopedia of Life Sciences (Nature Publishing Group www.els.net), p. 1-9.
- Davies, G. R., 1970, Carbonate bank sedimentation, eastern Shark Bay, Western Australia, in B. W. Logan, G. R. Davies, J. F. Read, and D. E. Cebulski, eds., Carbonate Sedimentation and Environments, Shark Bay, Western Australia, American Association of Petroleum Geologists Memoir, v. 13, p. 85-168.
- Davies, P. B., 1984a, Deep Seated Dissolution and Subsidence in Bedded Salt Deposits: Doctoral thesis, Stanford University.
- Davies, P. B., 1984b, Structural analysis of a deep seated salt dissolution collapse chimney; implications for nuclear waste disposal: Neues Jahrbuch fuer Mineralogie, Abhandlungen, v. 149, p. 163-175.
- Davis, D. G., 1980, Cave development in the Guadalupe Mountains. A critical review of recent hypotheses: Natl. Speleol. Soc. Bull., v. 42, p. 42-48.
- Davis, D. M., and T. Engelder, 1985, The role of salt in fold-and-thrust belts (Canada): Tectonophysics, v. 119, p. 67-88.
- Davis, D. M., and T. Engelder, 1987, Thin-skinned deformation over salt, in I. Lerche, and J. J. O'Brien, eds., Dynamical geology of salt and related structures: New York, Academic Press, p. 301-337.
- Davis, J. B., and D. W. Kirkland, 1970, Native sulfur deposition in the Castile formation, Culberson county, Texas: Econ. Geol., v. 65, p. 107-121.
- Davis, J. B., and D. W. Kirkland, 1979, Bioepigenetic sulfur deposits: Economic Geology, v. 74, p. 462-468.
- Davis, J. R., I. Friedman, and J. D. Gleason, 1986, Origin of the lithium-rich brine, Clayton Valley, Nevada: US Geological Survey Bulletin, v. 1622, p. 131-138.
- Davison, I., G. Alsop, N. Evans, and M. Safaricz, 2000a, Overburden deformation patterns and mechanisms of salt diapir penetration in the Central Graben, North Sea: Marine & Petroleum Geology, v. 17, p. 601-618.
- Davison, I., G. I. Alsop, and D. J. Blundell, 1996a, Salt tectonics: some aspects of deformation mechanics, in G. I. Alsop, D. J. Blundell, and I. Davison, eds., Salt tectonics, Geological Society, London; Special Publication, v. 100, p. 1-10.
- Davison, I., I. Alsop, P. Birch, C. Elders, N. Evans, H. Nicholson, P. Rorison, D. Wade, J. Woodward, and M. Young, 2000b, Geometry and late-stage structural evolution of Central Graben salt diapirs, North Sea: Marine & Petroleum Geology, v. 17, p. 499-522.
- Davison, I., D. Bosence, G. I. Alsop, and M. H. Al-Aawah, 1996b, Deformation and sedimentation around active Miocene salt diapirs on the Tihama Plain, northwest Yemen, in G. I. Alsop, D. J. Blundell, and I. Davison, eds., Salt tectonics, v. 100, Geological Society, London; Special Publication, p. 23-39.
- Davison, I., D. Bosence, I. Alsop, and M. A. H. Al Aawah, 1995, Deformation and sedimentation above and below Miocene salt diapirs and their overhangs, NW Yemen: Proceedings of GCCSEPM Foundation 16th Annual Research Conference, Salt Sediment and Hydrocarbons, Dec 3-6, 1995, p. 33-40.
- Davison, I., M. Insley, M. Harper, P. Weston, D. Blundell, K. McClay, and A. Quallington, 1993, Physical modelling of overburden deformation around salt diapirs: Tectonophysics, v. 228, p. 255-274.
- Day, R., 1974, White River Nahcolite Solution Mine: Proceedings of the SME Annual Meeting, Albuquerque, NM, February, 14-17.
- Day, R. W., 1967, Solution mining of carnallite, US Patent 3,555,212, Reynolds Metals, p. 5.
- de Brodtkorb, M. K., V. Ramos, M. Barbieri, and S. Ametrano, 1982, The evaporitic celestite-barite deposits of Neuquen, Argentina: Mineralium Deposita, v. 17, p. 423-436.
- De Celles, P. G., and G. Mitra, 1995, History of the Sevier orogenic wedge in terms of critical taper models, Northeast Utah and Southwest Wyoming: Geological Society of America Bulletin, v. 107, p. 454-462.
- De Deckker, P., 1981, Ostracods of Athalassic Saline Lakes - a Review: Hydrobiologia, v. 81-2, p. 131-144.
- De Deckker, P., and M. C. Geddes, 1980, Seasonal fauna of ephemeral saline lakes near the Coorong Lagoon, South Australia: Australian Journal of Marine and Freshwater Research, v. 31, p. 677-699.

- De Lange, G. J., J. J. Middleburg, C. H. van der Weijden, G. Catalano, G. W. Luther, III, D. J. Hydes, J. R. W. Woittiez, and G. P. Klinkhammer, 1990, Composition of anoxic hypersaline brines in the Tyro and Bannock Basins, eastern Mediterranean: *Marine Chemistry*, v. 31, p. 63-88.
- De Meer, S., and C. J. Spiers, 1999, Influence of pore-fluid salinity on pressure solution creep in gypsum: *Tectonophysics*, v. 308, p. 311-330.
- De Putter, T., J. M. Rouchy, A. Herbosch, E. Keppens, C. Pierre, and E. Groessens, 1994, Sedimentology and palaeo-environment of the upper Viséan anhydrite of the Franco-Belgian Carboniferous basin (Saint-Ghislain borehole, southern Belgium): *Sedimentary Geology*, v. 90, p. 77-93.
- De Ronde, C. E. J., M. J. Dewit, and E. T. C. Spooner, 1994, Early Archean (>3.2 Ga) Fe-oxide rich, hydrothermal discharge vents in the Barberton Greenstone belt, South Africa: *Geological Society of America Bulletin*, v. 106, p. 86-104.
- De Ronde, C. E. J., and T. W. Ebbesen, 1996, 3.3 BY age of organic compound formation near sea-floor hot springs: *Geology*, v. 24, p. 791-794.
- De Ruiter, P. A. C., 1979, The Gabon and Congo basins salt deposits: *Econ. Geol.*, v. 74, p. 419-431.
- De Vogel, S. B., J. W. Magee, W. F. Manley, and G. H. Miller, 2004, A GIS-based reconstruction of late Quaternary paleohydrology: Lake Eyre, arid central Australia: *Palaeogeography, Palaeoclimatology, Palaeoecology*, v. 204, p. 1-13.
- Dean, W. E., 1978, Trace and minor elements in evaporites, in W. Dean, and B. C. Schreiber, eds., *Marine evaporites*, Society of Economic Paleontologists and Mineralogists, Short course notes, v. 4, p. 86-104.
- Dean, W. E., and R. Y. Anderson, 1982, Continuous subaqueous deposition of the Permian Castile evaporites, Delaware Basin, Texas and New Mexico: Handford, C. R., Loucks, R. G., Davies, G. R. Depositional and diagenetic spectra of evaporites; a core workshop. S. E. P. M. Core Workshop, v. 3, p. 324-353.
- Dean, W. E., and T. D. Fouch, 1983, Lacustrine Environment, in P. A. Scholle, D. G. Bebout, and C. H. Moore, eds., *Carbonate Depositional Environments*, American Assoc. Petroleum Geologists Memoir, 33, p. 96-130.
- Decima, A., J. A. McKenzie, and B. C. Schreiber, 1988, The origin of "evaporative" limestones: An Example from the Messinian of Sicily: *Journal of Sedimentary Petrology*, v. 58, p. 256-272.
- Deffeyes, K. S., F. J. Lucia, and P. K. Weyl, 1965, Dolomitization of Recent and Plio-Pleistocene sediments by marine evaporite waters on Bonaire, Netherlands Antilles, in L. C. Pray, and R. C. Murray, eds., *Dolomitization and limestone diagenesis A symposium*. Soc. Econ. Paleontologists and Mineralogists Spec. Pub., v. 13, p. 71-88.
- Degens, E. T., H. K. Wong, S. Kempe, and F. Kurtman, 1984, A Geological Study of Lake Van, Eastern Turkey: *Geologische Rundschau*, v. 73, p. 701-734.
- Dejonghe, L., 1990, The sedimentary structures of barite: examples from the Chaudfontaine ore deposit, Belgium: *Sedimentology*, v. 37, p. 303-323.
- Dellwig, L. F., 1955, Origin of the Salina Salt of Michigan: *Journal Sedimentary Petrology*, v. 25, p. 83-110.
- Dellwig, L. F., and R. Evans, 1969, Depositional processes in Salina salt of Michigan, Ohio, and New York: *Bulletin American Association of Petroleum Geologists*, v. 53, p. 949-956.
- DeLuca, M., 1999, Forty-six wells designated subsalt in the Gulf of Mexico: *Offshore*, v. January Issue, p. 50.
- Demaison, G. J., and B. J. Huizinga, 1991, Genetic classification of petroleum systems: *Bulletin American Association of Petroleum Geologists*, v. 75, p. 1626-1643.
- Demaison, G. J., and G. T. Moore, 1980, Anoxic environments and oil source bed genesis: *American Association of Petroleum Geologists Bulletin*, v. 64, p. 1179-1209.
- Demange, J., G. M. di Paola, J. Lavigne, M. Lopoukhine, and L. Stieljes, 1971, Etudé géothermique de Territore Francais des Afars et des Issas: Nov. 70, Avr. 71, Rapp. 71, SGN 262 GTM Bureau de Recherches Géologiques et Minières, Orléans.
- Dembicki, H. J., W. G. Meinschein, and D. E. Hattin, 1976, Possible ecological and environmental significance of the predominance of even carbon number C20 - C30 n-alkanes: *Geochimica et Cosmochimica Acta*, v. 40, p. 203-208.
- Demercian, S., P. Szatmari, and P. R. Cobbold, 1993, Style and pattern of salt diapirs due to thin-skinned gravitational gliding, Campos and Santos basins, offshore Brazil: *Tectonophysics*, v. 228, p. 393-423.
- DeMille, G., J. R. Shouldice, and H. W. Nelson, 1964, Collapse structures related to evaporites of the Prairie Formation, Saskatchewan: *Geological Society America Bulletin*, v. 75, p. 307-316.
- Deming, D., J. A. Nunn, and D. G. Evans, 1990, Thermal effects of compaction-driven groundwater flow from overthrust belts: *J. Geophys. Research*, v. 96, p. 2485-2499.
- Demir, I., and B. Seyler, 1999, Chemical composition and geologic history of saline waters in Aux Vases and Cypress Formations, Illinois Basin: *Aquatic Geochemistry*, v. 5, p. 281-311.
- DeMise, W. D., 1992, Elkhorn Ranch Field -USA, Williston Basin, North Dakota, in N. H. Foster, and E. A. Beaumont, eds., *Treatise of Petroleum Geology; Atlas of Oil and Gas Fields: Stratigraphic Traps III: Tulsa, OK*, American Association Petroleum Geologists, p. 369-388.
- Denison, R. E., D. W. Kirkland, and R. Evans, 1998, Using strontium isotopes to determine the age and origin of gypsum and anhydrite beds: *Journal of Geology*, v. 106, p. 1-17.
- Deocampo, D. M., 2002, Sedimentary structures generated by *Hippopotamus amphibius* in a lake-margin wetland, Ngorongoro Crater, Tanzania: *Palaios*, v. 17, p. 212-217.
- Depowski, S., and T. Peryt, 1985, Carbonate petroleum reservoirs in the Permian dolomites of the Zechstein, Fore-Sudetic area, western Poland, in P. O. Roehl, and P. W. Choquette, eds., *Carbonate petroleum reservoirs*: New York, Springer-Verlag, p. 251-264.
- Des Marais, D. J., 2003, Biogeochemistry of Hypersaline Microbial Mats Illustrates the Dynamics of Modern Microbial Ecosystems and the Early Evolution of the Biosphere: *Biological Bulletin*, v. 204, p. 160-167.
- Desborough, G. A., 1978, Abiogenic-chemical stratified lake model for the origin of oil shale of the Green River Formation: an alternative to the playa lake model: *Bulletin Geological Society of America*, v. 89, p. 961-971.

- Deuser, W. G., 1971, Organic carbon budget of the Black Sea: Deep Sea Research, v. 18, p. 995-1004.
- Deutsch, Z. G., 1978, Brine wells and pipelines, in D. W. Kuafmann, ed., Sodium Chloride: The production and properties of salt and brine: Washington DC, American Chemical Society, p. 142-185.
- Dewing, K., and P. Copper, 1991, Upper Ordovician stratigraphy of Southampton Island, Northwest Territories: Canadian Journal of Earth Sciences, v. 28, p. 283-291.
- Diaz, G. C., M. Mendoza, J. Garcia-Veigas, J. Pueyo, and P. Turner, 1999, Evolution and geochemical signatures in a Neogene forearc evaporitic basin: the Salar Grande (Central Andes of Chile): Palaeogeography Palaeoclimatology Palaeoecology, v. 151, p. 39-54.
- Dickey, P. A., 1979, Petroleum Development Geology: Tulsa, OK, PPC Books Division of the Petroleum Publishing Company, 398 p.
- Dickson, J. A. D., I. P. Montanez, and A. H. Saller, 2001, Hypersaline burial diagenesis delineated by component isotopic analysis, Late Paleozoic limestones, west Texas: Journal of Sedimentary Research, v. 71, p. 372-379.
- Didyk, B. M., and B. R. T. Simoneit, 1989, Hydrothermal oil of the Guaymas Basin and implications for petroleum formation mechanisms: Nature, v. 342, p. 65-69.
- Dietzel, M., and I. Letofsky-Papst, 2002, Stability of magadiite between 20 and 100°C: Clays and Clay Minerals, v. 50, p. 657-666.
- Dill, H. G., S. Nasir, and H. Al-Saad, 2003, Lithological and structural evolution of the northern sector of Dukhan anticline, Qatar, during the early Tertiary: with special reference to sequence stratigraphic bounding surfaces: GeoArabia, v. 8, p. 201-226.
- Dill, H. G., R. Botz, Z. Berner, D. Stüben, S. Nasir, and H. Al-Saad, 2005, Sedimentary facies, mineralogy, and geochemistry of the sulphate-bearing Miocene Dam Formation in Qatar: Sedimentary Geology, v. 174, p. 63-96.
- Dillard, D. S., J. G. Davis, and R. L. Every, 1975, Solution mining potassium chloride from subterranean deposits, Canada Patent 961,408, p. 18.
- Dimroth, E., and M. M. Kimberley, 1975, Precambrian atmospheric oxygen; evidence in the sedimentary distributions of carbon, sulfur, uranium, and iron: Canadian Journal of Earth Sciences, v. 13, p. 1161-1185.
- Donovan, R. N., 1993, Evaporites in the Middle Devonian of the Orcadian Basin near Berriedale, Caithness: Scottish Journal of Geology, v. 29, p. 45-54.
- Doran, H., R. S. Haszeldine, C. Taberner, and A. E. Fallick, 2004, Fluid Migration around the Machar Salt Diapir UK Central North Sea: Impact on Porosity and Permeability of a Fractured Carbonate Reservoir (abs) presented at AAPG Annual Meeting, Dallas, Texas, April 18-21, 2004: Bulletin American Association Petroleum Geologists, v. 88 (13).
- Douglas, J. L., and S. A. Members of the 'Ain Dar/Shedgum Modeling Team, 1996, Geostatistical Model for the Arab-D Reservoir, North 'Ain Dar Pilot, Ghawar Field, Saudi Arabia: An Improved Reservoir Simulation Model: GeoArabia, v. 1, p. 267-284.
- Downey, M. W., 1984, Evaluating seals for hydrocarbon accumulations: Bulletin American Association of Petroleum Geologists, v. 68, p. 1752-1763.
- Draper, J. J., and A. R. Jensen, 1976, The geochemistry of Lake Frome, a playa lake in South Australia: Bureau of Mineral Resources Journal of Australian Geology Geophysics, v. 1, p. 83-104.
- Driese, S. G., 1985, Interdune pond carbonates, Weber sandstone (Pennsylvanian-Permian) Northern Utah and Colorado: Journal of Sedimentary Petrology, v. 55, p. 187-195.
- Driscoll, R., 1983, The influence of vegetation on the swelling and shrinking of clay soils in Britain: Geotechnique, v. 33, p. 93-105.
- Dronkert, H., 1985, Evaporite models and sedimentology of Messinian and Recent evaporites: GUA Papers of Geology, Series 1, v. 24, p. 283 pp.
- Droste, H., 1990, Depositional cycles and source rock development in an epeiric intra-platform basin; the Hanifa Formation of the Arabian Peninsula: Sedimentary Geology, v. 69, p. 281-296.
- Droste, J. B., and R. H. Shaver, 1985, Comparative stratigraphic framework for Silurian reefs: Michigan Basin to surrounding platforms, in K. R. Cercone, and J. M. Budai, eds., Ordovician and Silurian Rocks of the Michigan Basin and its Margins, Michigan Basin Geological Society Special Paper No. 4, p. 79-94.
- Druckman, Y., 1981, Sub-recent manganese-bearing stromatolites along shorelines of the Dead Sea, in C. Monty, ed., Phanerozoic stromatolites; case histories: Berlin, Federal Republic of Germany, Springer-Verlag, p. 197-208.
- Druckman, Y., and C. H. Moore, 1985, Late subsurface secondary porosity in a Jurassic grainstone reservoir, Smackover formation, Mt Vernon Field, Southern Arkansas, in P. O. Roehl, and P. W. Choquette, eds., Carbonate petroleum reservoirs: New York, Springer-Verlag, p. 369-383.
- Drury, M. R., 1999, Stepping stones; The making of our home world, Oxford University Press, 409 p.
- Drury, M. R., and J. L. Urai, 1990, Deformation-related recrystallization processes: Tectonophysics, v. 172, p. 235-253.
- Du Plessis, P. I., and J. P. Leroux, 1995, Late Cretaceous alkaline saline lake complexes of the Kalahari Group in northern Botswana: Journal of African Earth Sciences, v. 20, p. 7-15.
- Duane, M. J., and A. Z. Al-Zamel, 1999, Syngenetic textural evolution of modern sabkha stromatolites (Kuwait): Sedimentary Geology, v. 127, p. 237-245.
- Duane, M. J., A. Al-Zamel, and C. J. Eastoe, 2004, Stable isotope (chlorine, hydrogen and oxygen), geochemical and field evidence for continental fluid flow vectors in the Al-Khiran sabkha (Kuwait): Journal of African Earth Sciences, v. 40, p. 49-60.
- Duggan, J. P., E. W. Mountjoy, and L. D. Stasiuk, 2001, Fault-controlled dolomitization at Swan Hills Simonette oil field (Devonian), deep basin west-central Alberta, Canada: Sedimentology, v. 48, p. 301-323.
- Dulhunty, J. A., 1977, Salt crust solution during fillings of Lake Eyre: Transactions Royal Society South Australia, v. 101, p. 147-151.
- Duncan, W. I., and N. W. K. Buxton, 1995, New evidence for evaporitic Middle Devonian Lacustrine sediments with hydrocarbon source potential on the East Shetland Platform, North Sea: Journal of the Geological Society, v. 152, p. 251-258.
- Dunham, R. J., 1972, Capitan Reef, New Mexico and Texas: Facts and questions to aid interpretation and group discussion: Midland, Texas, Permian Basin Section SEPM Publication No. 72-14.

- Dupraz, C., and A. Strasser, 1999, Microbialites and micro-encrusts in shallow coral bioherms (Middle to Late Oxfordian, Swiss Jura Mountains): *Facies*, v. 40, p. 101-130.
- Dupraz, C., P. T. Visscher, L. K. Baumgartner, and R. P. Reid, 2004, Microbe-mineral interactions: early carbonate precipitation in a hypersaline lake (Eleuthera Island, Bahamas): *Sedimentology*, v. 51, p. 745-765.
- Durup, J. G., 1991, Relationship between subsidence and cavern convergence at Tersanne (France): Proc. SMRI Spring Meeting, Atlanta.
- Dusseault, M. B., and B. C. Davidson, 1999, Design and management of salt solution caverns for toxic waste disposal: *Journal of Canadian Petroleum Technology*, v. 38, p. 56-61.
- Dutkiewicz, A., A. L. Herczeg, and J. C. Dighton, 2000, Past changes to isotopic and solute balances in a continental playa: clues from stable isotopes of lacustrine carbonates: *Chemical Geology*, v. 165, p. 309-329.
- Dutkiewicz, A., and C. C. von der Borch, 1995, Lake Greenly, Eyre Peninsula, South Australia; sedimentology, palaeoclimatic and palaeohydrologic cycles: *Palaeogeography, Palaeoclimatology, Palaeoecology*, v. 113, p. 43-56.
- Dutkiewicz, A., C. C. Von der Borch, and J. R. Prescott, 2002, Geomorphology of the Lake Malata-Lake Greenly complex, South Australia, and its implications for Late Quaternary Palaeoclimate: *Transactions of the Royal Society of South Australia*, v. 126, p. 103-115.
- Duval, B., C. Cramez, and M. P. A. Jackson, 1992, Raft tectonics in the Kwanza Basin, Angola: *Marine and Petroleum Geology*, v. 9, p. 389-404.
- Dworkin, S. I., and L. S. Land, 1994, Petrographic and geochemical constraints on the formation and diagenesis of anhydrite cements, Smackover sandstones, Gulf of Mexico: *Journal of Sedimentary Research, Section A: Sedimentary Petrology and Processes*, v. 64, p. 339-348.
- Dworkin, S. I., and L. S. Land, 1996, The origin of aqueous sulfate in Frio pore fluids and its implication for the origin of oil field brines: *Source*, 11, no.3 (1996) p. 403-408: *Applied Geochemistry*, v. 11, p. 403-408.
- Dyni, J. R., 1981, Geology of the nahcolite deposits and oil shales of the Green River Formation in the Piceance Creek Basin, Colorado: Doctoral thesis, University of Colorado, Boulder, 182 p.
- Dyni, J. R., 1996, Sodium carbonate resources of the Green River Formation: United States Geological Survey, Open File Report, v. 96-729, p. 39 p.
- Dyni, R. C., 1986, Subsidence investigations over salt-solution mines, Hutchinson, Kansas: United States Bureau of Mines Information Circular 9083.
- Dyson, I. A., 1998, The Christmas tree diapir and salt glacier at Pinda Springs, central Flinders Ranges: *MESA Journal*, v. 10.
- Dyson, I. A., 1999, The Beltana Diapir — a salt withdrawal minibasin in the northern Flinders Ranges: *MESA Journal*, v. 15, p. 40-46.
- Dyson, I. A., 2004, Christmas tree diapirs and the development of hydrocarbon reservoirs; A model from the Adelaide Geosyncline, South Australia: In: Salt-sediment interactions and hydrocarbon prospectivity: concepts, applications and case studies for the 21st Century. Papers presented at the 24th Annual Gulf Coast Section SEPM Foundation Bob F. Perkins Research Conference, Houston Tx, December 5-8, 2004 (CD publication), p. 79-96.
- Eardley, A. J., 1938, Sediments of Great Salt Lake, Utah: *Bulletin American Association of Petroleum Geologists*, v. 22, p. 1305-1411.
- Eastoe, C. J., A. Long, and L. P. Knauth, 1999, Stable chlorine isotopes in the Palo Duro Basin, Texas: Evidence for preservation of Permian evaporite brines: *Geochimica et Cosmochimica Acta*, v. 63, p. 1375-1382.
- Eastoe, C. J., A. Long, L. S. Land, and J. R. Kyle, 2001, Stable chlorine isotopes in halite and brine from the Gulf Coast Basin: brine genesis and evolution: *Chemical Geology*, v. 176, p. 343-360.
- Eastoe, C. J., and T. Peryt, 1999, Stable chlorine isotope evidence for non-marine chloride in Badenian evaporites, Carpathian mountain region: *Terra Nova*, v. 11, p. 118-123.
- Ece, O. I., 1998, Diagenetic transformation of magnesite pebbles and cobbles to sepiolite (Meerschaum) in the Miocene Eskisehir lacustrine basin, Turkey: *Clays & Clay Minerals*, v. 46, p. 436-445.
- Ece, O. I., and F. Coban, 1994, Geology, occurrence and genesis of Eskisehir Sepiolites, Turkey: *Clay and Clay Minerals*, v. 42, p. 81-92.
- Eckardt, F. D., and B. Spiro, 1999, The origin of sulphur in gypsum and dissolved sulphate in the Central Namib Desert, Namibia: *Sedimentary Geology*, v. 123, p. 255-273.
- Eckardt, F. D., H. Viles, N. Drake, G. A. S., and K. White, 2001, The role of playas in pedogenic gypsum crust formation in the Central Namib Desert: A theoretical model: *Earth Surface Processes and Landforms*, v. 26, p. 1177-1193.
- Eder, W., L. L. Jahnke, M. Schmidt, and R. Huber, 2001, Microbial diversity of the brine-seawater interface of the Kebrit Deep, Red Sea, studied via 16S rRNA gene sequences and cultivation methods: *Applied & Environmental Microbiology*, v. 67, p. 3077-3085.
- Edgell, H. S., 1991, Proterozoic salt basins of the Persian Gulf area and their role in hydrocarbon generation: *Precambrian Research*, v. 54, p. 1-14.
- Edgell, H. S., 1996, Salt tectonism in the Persian Gulf Basin, in G. I. Alsop, D. J. Blundell, and I. Davison, eds., *Salt tectonics*, v. 100: London, United Kingdom, Geological Society of London Special Publication, p. London, United Kingdom.
- Egeberg, P. K., and P. Aagaard, 1989, Origin and evolution of formation waters from oil fields on the Norwegian Shelf: *Applied Geochemistry*, v. 4, p. 131-142.
- Egemeier, S. J., 1981, Cavern development by thermal waters: *National Speleological Society Bulletin*, v. 43, p. 31-51.
- Egenhoff, S. O., A. Peterhansel, T. Bechstadt, R. Zuhlke, and J. Grottsch, 1999, Facies architecture of an isolated carbonate platform: tracing the cycles of the Latemar (Middle Triassic, northern Italy): *Sedimentology*, v. 46, p. 893-912.
- Eggenkamp, H. G. M., R. Kreulen, and A. F. K. Van Groos, 1995, Chlorine stable isotope fractionation in evaporites: *Geochimica et Cosmochimica Acta*, v. 59, p. 5169-5175.
- Eggink, J. W., D. E. Riegstra, and P. Suzanne, 1996, Using 3D seismic to understand the structural evolution of the UK Central North Sea: *Petroleum Geoscience*, v. 2, p. 83-96.
- Eichenseer, H. T., F. R. Walgenwitz, and P. J. Biondi, 1999, Stratigraphic Control on Facies and Diagenesis of Dolomitized Oolitic Siliciclastic Ramp Sequences (Pinda Group, Albian, Offshore Angola): *Bulletin American Association Petroleum Geologists*, v. 83, p. 1729-1758.

- Eisenberg, L., 2003, Giant stromatolites and a supersurface in the Navajo Sandstone, Capitol Reef National Park, Utah: *Geology*, v. 31, p. 111-114.
- El Anbaawy, M. I. H., M. A. H. Al Aawah, K. A. Al Thour, and M. E. Tucker, 1992, Miocene evaporites of the Red Sea Rift, Yemen Republic; sedimentology of the Salif halite: *Sedimentary Geology*, v. 81, p. 61-71.
- El Sayed, M. I., 1993, Gypcrete of Kuwait: field investigation, petrography and genesis: *Journal of Arid Environment*, v. 25, p. 199-203
- El Tabakh, M., K. Grey, F. Pirajno, and B. C. Schreiber, 1999, Pseudomorphs after evaporitic minerals interbedded with 2.2 Ga stromatolites of the Yerrida basin, Western Australia: Origin and significance: *Geology*, v. 27, p. 871-874.
- El Tabakh, M., R. Riccioni, and B. C. Schreiber, 1997, Evolution of Late Triassic rift basin evaporites (Passaic Formation) - Newark Basin, eastern North America: *Sedimentology*, v. 44, p. 767-790.
- El Tabakh, M., B. C. Schreiber, C. Utharoon, L. Coshell, and J. K. Warren, 1998a, Diagenetic origin of Basal Anhydrite in the Cretaceous Maha Sarakham Salt - Khorat Plateau, NE Thailand: *Sedimentology*, v. 45, p. 579-594.
- El Tabakh, M., B. C. Schreiber, and J. K. Warren, 1998b, Origin of fibrous gypsum in the Newark rift basin, eastern North America: *Journal of Sedimentary Research Section A-Sedimentary Petrology & Processes*, v. 68, p. 88-99.
- El Tabakh, M., C. Utharoon, L. Coshell, and J. K. Warren, 1995, Cretaceous saline deposits of the Maha Sarakham Formation in the Khorat Basin, Northeastern Thailand: *International Conference on Geology, Geochronology and Mineral Resources of Indochina 22-25 November 1995, Khon Kaen, Thailand*, v. Core Workshop Notes, p. 20 pp.
- El Tabakh, M., C. Utharoon, J. K. Warren, and B. C. Schreiber, 2003, Origin of dolomites in the Cretaceous Maha Sarakham evaporites of the Khorat Plateau, northeast Thailand: *Sedimentary Geology*, v. 157, p. 235-252.
- Elias, A. R. D., L. F. De Ros, A. M. P. Mizusaki, and S. M. C. Anjos, 2004, Diagenetic patterns in eolian/coastal sabkha reservoirs of the Solimões Basin, Northern Brazil: *Sedimentary Geology*, v. 169, p. 191-217.
- Eliassen, A., and M. R. Talbot, 2005, Solution-collapse breccias of the Minkinfjellet and Wordiekammen Formations, Central Spitsbergen, Svalbard: a large gypsum palaeokarst system: *Sedimentology*, v. 52, p. 775-794.
- Elliott, L. A., and J. K. Warren, 1989, Stratigraphy and depositional environment of lower San Andres Formation in subsurface and equivalent outcrops; Chaves, Lincoln, and Roosevelt counties, New Mexico: *Bulletin American Association of Petroleum Geologists*, v. 73, p. 1307-1325.
- Elorza, M. G., and F. G. Santolalla, 1998, Geomorphology of the Tertiary gypsum formations in the Ebro Depression (Spain): *Geoderma*, v. 87, p. 1-29.
- Emery, D., and A. Robinson, 1993, *Inorganic Chemistry: Applications to Petroleum Geology*: Oxford, Blackwell Scientific Publications, 254 p.
- Engel, A. S., M. L. Porter, B. K. Kinkle, and T. C. Kane, 2001, Ecological assessment and geological significance of microbial communities from Cesspool Cave, Virginia: *Geomicrobiology Journal*, v. 18, p. 259-274.
- Enger, S., and A. Logan, 2001, Ultra-deepwater play paces gulf, North America: *Oil & Gas Journal*, v. 99, p. 80-85.
- English, P. M., 2001, Formation of analcime and moganite at Lake Lewis, central Australia: significance of groundwater evolution in diagenesis: *Sedimentary Geology*, v. 143, p. 219-244.
- Enos, J. S., and J. R. Kyle, 2002, Diagenesis of the Carrizo Sandstone at Butler Salt Dome, East Texas Basin, U.S.A.: Evidence for Fluid-Sediment Interaction Near Halokinetic Structures: *Journal of Sedimentary Research*, v. 72, p. 68-81.
- Enzel, Y., R. Bookman, D. Sharon, H. Gvirtzman, U. Dayan, B. Ziv, and M. Stein, 2003, Late Holocene climates of the Near East deduced from Dead Sea level variations and modern regional winter rainfall: *Quaternary Research*, v. 60, p. 263-273.
- Epstein, J. A., B. Zelvianski, and G. Ron, 1975, Manganese in sodium chloride precipitating for mixing Dead Sea brines: *Israel J. Earth Sci.*, v. 24, p. 112-113.
- Epstein, J. B., 2001, Hydrology, Hazards, and Geomorphic Development of Gypsum Karst in the Northern Black Hills, South Dakota and Wyoming, in E. L. Kuniansky, ed., U.S. Geological Survey Karst Interest Group Proceedings, St. Petersburg, Florida February 13-16, 2001: Denver, Co, U.S. Geological Survey, Water-Resources Investigations Report 01-4011, p. 30-37.
- Erba, E., 1991, Deep mid-water bacterial mats from anoxic basins of the eastern Mediterranean: *Marine Geology*, v. 100, p. 83-101.
- Ericksen, G. E., 1981, Geology and origin of the Chilean nitrate deposits: *US Geological Survey Prof. Paper*, v. 1188, p. 37 pp.
- Ericksen, G. E., 1983, The Chilean nitrate deposits: *American Scientist*, v. 71, p. 366-374.
- Ericksen, G. E., 1993, Upper Tertiary and Quaternary continental saline deposits in the central Andean region: *Geological Association of Canada Special Paper*, v. 40, p. 89-102.
- Ericksen, G. E., and R. Salas, 1989, Geology and resources of salars in the central Andes, in G. E. Ericksen, M. T. Cañas Pinochet, and J. A. Reinemund, eds., *Geology of the Andes and its relation to hydrocarbon and mineral resources*. Earth Science Series 11: Houston, TX, Circum Pacific Council for Energy and Mineral Resources, p. 151-164.
- Erol, O., 1978, The Quaternary history of the lake basins of central southern Anatolia, in W. C. Brice, ed., *The Environmental History of the Near and Middle East Since the Last Ice Age*: London, Academic Press, p. 111-139.
- Eschner, T. B., and G. Kocurek, 1988, Origins of relief contacts between eolian sandstones and overlying marine strata: *Bulletin American Association Petroleum Geologists*, v. 72, p. 932-943.
- Espitalie, J., M. Madee, and B. Tissot, 1980, Role of mineral matrix in kerogen pyrolysis: influence on petroleum generation and migration: *Bulletin American Association of Petroleum Geologists*, v. 64, p. 59-66.
- Esteban, M., 1980, Significance of upper Miocene coral reefs of the Western Mediterranean: *Palaeogeography Palaeoclimatology Palaeoecology*, v. 29, p. 169-188.
- Esteban, M., 1996, An overview of Miocene reefs from Mediterranean areas: general trends and facies models, in E. K. e. a. Franseen, ed., *Models for carbonate stratigraphy from Miocene reef complexes of Mediterranean regions*, v. 5, *SEPM/Society for Sedimentary Geology*; Concepts in Sedimentology and Paleontology, p. 3-53.

- Esteban, M., and L. C. Pray, 1983, Pisoids and pisolite facies (Permian), Guadalupe Mountains, New Mexico and West Texas, in T. M. Peryt, ed., *Coated Grains*: Berlin, Springer-Verlag, p. 503-537.
- Et-Touhami, M., 1996, L'origine des accumulations salifères du Trias marocain: apport de la géochimie du brome du sel du bassin de Khemisset (Maroc central) The origin of Moroccan Triassic salt deposits: contribution of Br geochemistry in the halite-rock from the Khemisset Basin (central Morocco) [French]: *Comptes Rendus de l'Académie des Sciences Serie II Fascicule A-Sciences de la Terre et des Planètes*, v. 323, p. 591-598.
- Eugster, H. P., 1967, Hydrous sodium silicate from Lake Magadi, Kenya: precursors of bedded chert: *Science*, v. 157, p. 1177-1180.
- Eugster, H. P., 1969, Inorganic bedded cherts from the Magadi area, Kenya: *Contributions Mineralogy and Petrology*, v. 22, p. 1-31.
- Eugster, H. P., 1970, Chemistry and origin of the brines of Lake Magadi, Kenya: *Special Publ. Geol. Soc.*, v. 3, p. 215-235.
- Eugster, H. P., 1971, Origin and deposition of trona: *Contribution to Geology (Trona issue)*, v. 10, p. 49-55.
- Eugster, H. P., 1980a, Geochemistry of evaporitic lacustrine deposits: *Annual Review of Earth and Planetary Sciences*, v. 8, p. 35-63.
- Eugster, H. P., 1980b, Lake Magadi, Kenya, and its precursors, in N. A., ed., *Hypersaline brines and evaporitic environments*, Elsevier *Developments in Sedimentology* 28, p. 195-232.
- Eugster, H. P., 1985, Oil shales, evaporites and ore deposits: *Geochimica et Cosmochimica Acta*, v. 49, p. 619-635.
- Eugster, H. P., 1986, Lake Magadi, Kenya; a model for rift valley hydrochemistry and sedimentation? in L. E. Frostick, R. W. Renaut, I. Reid, and J. J. Tiercelin, eds., *Sedimentation in the African rifts*, *Geological Society Special Publication* 25, p. 177-189.
- Eugster, H. P., and L. A. Hardie, 1978, Saline Lakes, in A. Lerman, ed., *Lakes; chemistry, geology, physics*: New York, NY, Springer-Verlag, p. 237-293.
- Eugster, H. P., and G. Maglione, 1979, Brines and evaporites of the Lake Chad basin, Africa: *Geochim. Cosmochim. Acta.*, v. 43, p. 973-982.
- Eugster, H. P., and R. Surdam, 1973, Depositional environment of the Green River Formation of Wyoming: A preliminary report: *Bulletin Geological Society of America*, v. 84, p. 1115-1120.
- Evans, D. G., and J. A. Nunn, 1989, Free thermohaline convection in sediments surrounding a salt column: *Journal of Geophysical Research-Atmospheres*, v. 94, p. 12,413-12,422.
- Evans, G., 1995, The Arabian Gulf: A modern carbonate-evaporite factory, a review: *Cuadernos de Geología Ibérica*, v. 19, p. 61-96.
- Evans, G., V. Schmidt, P. Bush, and H. Nelson, 1969, Stratigraphy and geologic history of the sabkha, Abu Dhabi, Persian Gulf: *Sedimentology*, v. 12, p. 145-159.
- Evans, R., 1967, The structure of the Mississippian evaporite deposit at Pugwash, Cumberland County, Nova Scotia: *Economic Geology*, v. 62, p. 262-273.
- Evans, R., 1978, Origin and significance of evaporites in basins around Atlantic margin: *Bulletin American Association Petroleum Geologists*, v. 62, p. 223-234.
- Evans, R., and K. O. Linn, 1970, Fold relationships within evaporites of the Cane Creek Anticline: *Third Symp. on Salt: North Ohio Geol. Soc.*, v. 1, p. 286-297.
- Evans, R., and D. W. Kirkland, 1988, Evaporitic environments as a source of petroleum, in B. C. Schreiber, ed., *Evaporites and hydrocarbons*: New York, NY, United States, Columbia Univ. Press, p. 256-299.
- Ewing, M., and J. Antoine, 1966, New seismic data concerning sediments and diapiric structures in Sigsbee Deep and upper continental slope, Gulf of Mexico: *American Association Petroleum Geologists Bulletin*, v. 50, p. 470-504.
- Eyde, T. H., and D. T. Eyde, 1987, The Bowie chabazite deposit, in H. W. Peirce, ed., *21st Forum on the Geology of Industrial Minerals*, v. 4, Arizona Bur. Geol. and Min. Tech Spec. Paper., p. 133.
- Farmer, P., D. Miller, and A. Pieprzak, 1996, Exploring the subsalt: *Oilfield Review*, Spring 1996, p. 50-64.
- Faulds, J. E., B. C. Schreiber, S. J. Reynolds, L. A. Gonzalez, and D. Okaya, 1997, Origin and paleogeography of an immense, nonmarine Miocene salt deposit in the basin and range (Western USA): *Journal of Geology*, v. 105, p. 19-36.
- Fay, R. O., and D. L. J. Hart, 1978, Geology and mineral resources (exclusive of petroleum) of Custer County, Oklahoma: *Bull. Okla. Geol. Surv*, v. 114.
- Feazel, C. T., 1985, Diagenesis of Jurassic grainstone reservoirs in the Smackover Formation, Chatom Field, Alabama, in P. O. Roehl, and P. W. Choquette, eds., *Carbonate petroleum reservoirs*: New York, Springer-Verlag, p. 357-367.
- Feldmann, M., and J. A. McKenzie, 1997, Messinian stromatolite-thrombolite associations, Santa Pola, SE Spain: an analogue for the Palaeozoic? *Sedimentology*, v. 44, p. 893-914.
- Feldmann, M., and J. A. McKenzie, 1998, Stromatolite-thrombolite associations in a modern environment, Lee Stocking Island, Bahamas: *Palaeos*, v. 13, p. 201-212.
- Feng, Z., Y. S. Zhang, and Z. K. Jin, 1998, Type, origin, and reservoir characteristics of dolostones of the Ordovician Majiagou Group, Ordos, North China platform: *Sedimentary Geology*, v. 118, p. 127-140.
- Ferguson, J., G. Jacobsen, W. R. Evans, R. A. Wooding, C. J. Barnes, and S. W. Tyler, 1992, Advection and diffusion of groundwater brines in modern and ancient salt lakes, Nulla groundwater discharge complex, Murray Basin, southeast Australia, in J. Kharaka, and A. S. Maest, eds., *Rock-Water Interactions Proceedings*: Balkema, Rotterdam.
- Ferrarese, F., T. Macaluso, G. Madonia, P. A., and U. Sauro, 2002, Solution and recrystallisation processes and associated landforms in gypsum outcrops of Sicily: *Geomorphology*, v. 49, p. 25-453.
- Fertl, W. H., 1976, *Abnormal Formation Pressures*: Amsterdam, Elsevier Scientific, 382 p.
- Finkelstein, D. B., R. L. Hay, and S. P. Altaner, 1999, Origin and diagenesis of lacustrine sediments, upper Oligocene Creede Formation, southwestern Colorado: *Geological Society of America Bulletin*, v. 111, p. 1175-1191.
- Finnie, A. B., 2001, A Case Study of High Pressure Brine Flows within the Zechstein Supergroup of the Southern North Sea: SPE Paper 67781 Presented at the SPE/IADC Drilling Conference held in Amsterdam, The Netherlands, 27 February-1 March 2001.
- Fischer, A. G., and L. T. Roberts, 1991, Cyclicity in the Green River Formation (lacustrine Eocene) of Wyoming: *Journal of Sedimentary Petrology*, v. 61, p. 1146-1154.
- Fischer, A. G., and M. Sarnthein, 1988, Airborne silts and dune-derived sands in the Permian of the Delaware Basin: *Journal of Sedimentary Petrology*, v. 58, p. 637-643.

- Fischer, D., T. Heck, and L. C. Gerhard, 1990, Medicine Pole Hills Field, Williston Basin, North Dakota, in E. A. Beaumont, and N. H. Foster, eds., *Treatise of Petroleum Geology; Atlas of Oil and Gas Fields: Stratigraphic Traps I: Tulsa, OK*, American Association Petroleum Geologists, p. 229-255.
- Fisher, R. S., 1988, Clay minerals in evaporite host rocks, Palo Duro Basin, Texas Panhandle: *Journal of Sedimentary Petrology*, v. 58, p. 836-844.
- Fisher, W. L., and P. U. Rodda, 1969, Edwards Formation (Lower Cretaceous), Texas: Dolomitization in a Carbonate Platform System: *Bulletin American Association Petroleum Geologists*, v. 53, p. 55-72.
- Fitzgerald, T. A., 1980, Giant oil field discoveries 1968-1978; An overview, in M. T. Halbouty, ed., *Giant oil and gas fields of the decade 1968-1978: Tulsa, OK*, American Association of Petroleum Geologists Memoir 30.
- Fletcher, R. C., M. R. Hudec, and I. A. Watson, 1995, Salt glacier and composite sediment-salt glacier models for the emplacement and early burial of allochthonous salt sheets, in M. P. A. Jackson, D. G. Roberts, and S. Snellson, eds., *Salt tectonics: a global perspective*, AAPG Memoir, v. 65, p. 77-108.
- Flinch, J. F., A. W. Bally, and S. G. Wu, 1996, Emplacement of a passive-margin evaporitic allochthon in the Betic Cordillera of Spain: *Geology*, v. 24, p. 67-70.
- Folk, R. L., 1993, SEM imaging of bacteria and nannobacteria in carbonate sediments and rocks: *Journal Sedimentary Petrology*, v. 63, p. 990-999.
- Folk, R. L., 1999, Nannobacteria and the precipitation of carbonate in unusual environments: *Sedimentary Geology*, v. 126, p. 47-55.
- Folk, R. L., and J. S. Pittman, 1971, Length-slow chalcidony; a new testament for vanished evaporites: *Journal Sedimentary Petrology*, v. 41, p. 1045-1058.
- Folk, R. L., and A. Siedlecka, 1974, The "schizohaline" environment: its sedimentary and diagenetic fabrics as exemplified by late Paleozoic rocks of Bear Island, Svalbard: *Sedimentary Geology*, v. 11, p. 1-15.
- Fontes, J. C., and R. Letolle, 1976, ^{18}O and ^{34}S in the upper Bartonian gypsum deposits of the Paris Basin: *Chem. Geol.*, v. 18, p. 285-295.
- Fontes, J. C., P. Pouchan, J. F. Saliege, and G. M. Zuppi, 1980, Environmental isotope study of groundwater system in Republic of Djibouti: *Arid Zone Hydrology - Proceedings of Advisory Group Meeting*, p. 237-267.
- Ford, D., and P. Williams, 1989, *Karst geomorphology and geology*: London, Chapman and Hall.
- Ford, D. C., 1997, Principal features of evaporite karst in Canada: *Carbonates & Evaporites*, v. 12, p. 15-23.
- Fort, X., J.-P. Brun, and F. Chauvel, 2004, Salt tectonics on the Angolan margin, synsedimentary deformation processes: *American Association Petroleum Geologists - Bulletin*, v. 88, p. 1523-1544.
- Forti, P., S. Galdenzi, and S. M. Sarbu, 2002, The hypogenic caves: a powerful tool for the study of seeps and their environmental effects: *Continental Shelf Research*, v. 22, p. 2373-2386.
- Foshag, W., 1921, The origin of the colemanite deposits of California: *Economic Geology*, v. 16, p. 194-214.
- Foster, P. T., and P. R. Rattey, 1993, The evolution of fractured chalk reservoir: Machar oilfield, UK, North Sea: *Petroleum Geology of Northwest Europe*, Barbican Conference Proceedings, Geological Society of London, v. 2, p. 1445-1452.
- Fouke, B. W., C. J. Beets, W. J. Meyers, G. N. Hanson, and A. J. Melillo, 1996, Sr-87/Sr-86 chronostratigraphy and dolomitization history of the Seroe Domi Formation, Curacao (Netherlands Antilles): *Facies*, v. 35, p. 293-320.
- Fowler, M. G., A. P. Hamblin, D. J. MacDonald, and P. G. McMahon, 1993, Geological occurrence and geochemistry of some oil shows in Nova Scotia: *Bulletin of Canadian Petroleum Geology*, v. 41, p. 422-436.
- Frakes, L. A., J. E. Francis, and J. I. Syktus, 1992, Climate modes of the Phanerozoic: the history of the earth's climate over the past 600 million years: New York, Cambridge University Press, 274 p.
- Frank, T. D., and C. R. Fielding, 2003, Marine origin for Precambrian, carbonate-hosted magnesite? *Geology*, v. 31, p. 1101-1104.
- Franzmann, P. D., E. Stackebrandt, K. Sanderson, J. K. Volkman, D. E. Cameron, P. L. Stevenson, T. A. McMeekin, and H. R. Burton, 1988, *Halobacterium lacusprofundi* sp. nov., a halophilic bacterium isolated from Deep Lake, Antarctica: *Syst. Appl. Microbiol.*, v. 11, p. 20-27.
- Frape, S. K., P. Fritz, and R. H. McNutt, 1984, The role of water-rock interactions in the chemical evolution of groundwaters from the Canadian Shield: *Geochimica et Cosmochimica Acta*, v. 48, p. 1617-1627.
- Frazier, W. J., 1975, Celestite in the Mississippian Pennington Formation, central Tennessee: *Southeast. Geol.*, v. 16, p. 241-248.
- Fredrickson, J. K., and T. C. Onstott, 1996, Microbes deep inside the Earth: *Scientific American*, v. Oct. 1996, p. 68-73.
- Frey, M. G., and W. H. Grimes, 1970, Bay Marchand--Timbalier Bay--Caillou Island Salt Complex, Louisiana: *American Association Petroleum Geologists - Memoir*, v. 14, p. 277-291.
- Freytag, J. K., P. R. Girguis, D. C. Bergquist, J. P. Andras, J. J. Childress, and C. R. Fisher, 2001, A paradox resolved: Sulfide acquisition by roots of seep tubeworms sustains net chemoautotrophy: *Proceedings of the National Academy of Sciences of the United States of America*, v. 98, p. 13408-13413.
- Friedman, G. M., A. J. Amiel, M. Braun, and D. S. Miller, 1973, Generation of carbonate particles and laminites in algal mats - Examples from sea-marginal hypersaline pool, Gulf of Aqaba, Red Sea: *Bulletin American Association of Petroleum Geologists*, v. 57, p. 541-557.
- Friedman, G. M., and V. Shukla, 1980, Significance of quartz euhedra after sulphates; example from the Lockport Formation (Middle Silurian) of New York: *Journal of Sedimentary Petrology*, v. 50, p. 1299-1304.
- Frimmel, H. E., and W. Papesch, 1990, Sr, O and C isotope study of the Brixlegg barite deposit, Tyrol (Austria): *Economic Geology*, v. 85, p. 1162-1171.
- Frumkin, A., 1994a, Hydrology and denudation rates of halite karst: *Journal of Hydrology*, v. 162.
- Frumkin, A., 1994b, Morphology and development of salt caves: *National Speleological Society, Bulletin*, v. 56, p. 82-95.
- Frumkin, A., 1996, Determining the exposure age of a karst landscape: *Quaternary Research*, v. 46, p. 99-106.

- Frumkin, A., 1998, Salt cave cross-sections and their paleoenvironmental implications: *Geomorphology*, v. 23, p. 183-191.
- Frumkin, A., and Y. Elitzur, 2002, Historic Dead Sea Level Fluctuations Calibrated with Geological and Archaeological Evidence: *Quaternary Research*, v. 57, p. 334-342.
- Frumkin, A., and D. C. Ford, 1995, Rapid entrenchment of stream profiles in the salt caves of Mount Sedom, Israel: *Earth Surface Processes & Landforms*, v. 20, p. 139-152.
- Frumkin, A., and E. Raz, 2001, Collapse and subsidence associated with salt karstification along the Dead Sea: *Carbonates & Evaporites*, v. 16, p. 117-130.
- Fryberger, S. G., 1986, Stratigraphic traps for petroleum in wind-laid rocks: *Bulletin American Association of Petroleum Geologists*, v. 70, p. 1765-1776.
- Fryberger, S. G., T. S. Ahlbrandt, and A. S., 1979, Origin, sedimentary features and significance of low-angle eolian "sand sheet" deposits, Great Sand Dunes National Monument and vicinity, Colorado: *Journal of Sedimentary Petrology*, v. 49, p. 733-746.
- Fryberger, S. G., A. M. Al Sari, and T. J. Clisham, 1983, Eolian dune, interdune, sand sheet, and siliciclastic sabkha sediments of an offshore prograding sand sea, Dhahran area, Saudi Arabia: *Bulletin American Association of Petroleum Geologists*, v. 67, p. 280-312.
- Fryberger, S. G., A. M. Al Sari, T. J. Clisham, A. R. R. Syed, and G. A. H. Khattab, 1984, Wind sedimentation in the Jafurah sand sea, Saudi Arabia: *Sedimentology*, v. 31, p. 413-431.
- Fu, B., P. Aharon, G. R. Byerly, and H. H. Roberts, 1994, Barite chimneys on the Gulf of Mexico slope. Initial reports on their petrography and geochemistry: *Geo-Marine Letters*, v. 14, p. 81-87.
- Fuersich, F. T., S. Freytag, J. Roehl, and A. Schmid, 1995, Palaeoecology of benthic associations in salinity-controlled marginal marine environments; examples from the lower Bathonian (Jurassic) of the Causses (southern France): *Palaeogeography, Palaeoclimatology, Palaeoecology*, v. 113, p. 135-172.
- Fuzesy, A., 1982, Potash in Saskatchewan: Report Saskatchewan, Department of Mineral Resources.
- Fürst, M., 1976, Tektonik und Diapirismus der östlichen Zagrosketten: *Z. dtsh. geol. Ges.*, v. 127, p. 183-225.
- Gac, J. Y., 1980, Géochimie du bassin du Lac Tchad: *Travaux et Documents ORSTOM*, v. 123, p. 54 pp.
- Gac, J. Y., A. Al-Droubi, H. Paquet, B. Fritz, and Y. Tardy, 1977, Chemical model for origin and distribution of elements in salts and brines during evaporation of waters. Application to some saline lakes of Tibesti, Chad: *Physics and Chemistry of the Earth*, New York, v. 11, p. 149-158.
- Galdenzi, S., 1990, Un modello genetico per la Grotta Grande del Vento: *Mem. Ist. It. Speleol.*, v. II.
- Galdenzi, S., and T. Maruoka, 2003, Gypsum deposits in the Frasassi Caves, central Italy: *Journal of Cave and Karst Studies*, v. 65, p. 111-125.
- Galdenzi, S., and M. Menichetti, 1995, Occurrence of hypogenic caves in a karst region: Examples from central Italy: *Environmental Geology*, v. 26, p. 39-47.
- Galloway, W. E., T. E. Ewing, C. M. Garret, N. Tyler, and D. G. Bebout, 1983, Atlas of major Texas oil reservoirs: The University of Texas at Austin, Bureau of Economic Geology special publication, 139 p.
- Gansser, A., 1957, Die geologische Erforschung der Qum Gegend, Iran: *Ver. Schweiz. Petrol. Geol. u. Ing.*, B., p. 1-16.
- Gao, G., S. D. Hovorka, and H. H. Posey, 1990, Limpid dolomite in Permian San Andres halite rocks, Palo Duro Basin, Texas Panhandle; characteristics, possible origin, and implications for brine evolution: *Journal of Sedimentary Petrology*, v. 60, p. 118-124.
- Gao, G., and L. S. Land, 1991, Nodular chert from the Arbuckle Group, Slick Hills, SW Oklahoma: a combined field, petrographic and isotopic study: *Sedimentology*, v. 38, p. 857-870.
- Garber, R. A., 1980, The sedimentology of the Dead Sea: PhD thesis, Rennsaler Polytechnic, 170 p.
- Garber, R. A., and G. M. Friedman, 1983, Coated grains along the Dead Sea shore, in T. Peryt, ed., *Coated Grains*: New York, Springer Verlag, p. 163-168.
- Garber, R. A., G. M. Friedman, and A. Nissenbaum, 1981, Concentric aragonite ooids from the Dead Sea: *Journal of Sedimentary Petrology*, v. 51, p. 455-458.
- Garber, R. A., P. M. Harris, and J. M. Borer, 1990, Occurrence and significance of magnesite in Upper Permian (Guadalupian) Tansill and Yates formations, Delaware Basin, New Mexico: *AAPG Bulletin*, v. 74, p. 119-134.
- Garber, R. A., Y. Levy, and G. M. Friedman, 1987, The sedimentology of the Dead Sea: *Carbonates and Evaporites*, v. 2, p. 43-57.
- Garcia, C. M., and F. X. Niell, 1993, Seasonal Change in a Saline Temporary Lake (Fuente-De-Piedra, Southern Spain): *Hydrobiologia*, v. 267, p. 211-223.
- Garcia-Guinea, J., S. Morales, A. Delgado, C. Recio, and J. M. Calaforra, 2002, Formation of gigantic gypsum crystals: *Journal of the Geological Society*, v. 159, p. 347-350.
- Gardner, W. C., and E. E. Bray, 1984, Oil and source rocks of the Niagaran Reefs (Silurian) in the Michigan Basin, in J. G. Palacas, ed., *Petroleum geochemistry and source rock potential of carbonate rocks*, v. 18: Tulsa, Ok, American Association of Petroleum Geologists, *Studies in Geology*, p. 33-44.
- Garea, B. B., and C. J. R. Braithwaite, 1996, Geochemistry, isotopic composition and origin of the Beda dolomites, block NC74F, SW Sirt Basin, Libya: *Journal of Petroleum Geology*, v. 19, p. 289-304.
- Garfunkel, Z., and Z. Ben-Avraham, 1996, The structure of the Dead Sea: *Tectonophysics*, v. 155-176.
- Garfunkel, Z., I. Zak, and R. Freund, 1981, Active faulting in the Dead Sea Rift: *Tectonophysics*, v. 62, p. 37-52.
- Garleff, K., H. Kugler, A. V. Poschinger, H. Sterr, H. Strunk, and G. Villwock, 1997, Germany, in C. Embleton, and C. Embleton, eds., *Geomorphological hazards of Europe*, Vol. 5. *Developments in Earth Surface Processes*, v. 5, p. 147-177.
- Garlicki, A., 1993, Solution mining of Miocene salts in Poland and its environmental impact, in H. a. T. Hoshi Kakihana, ed., *Proc. 7th Symp. on Salt*, Kyoto, Japan, April 1992: Amsterdam, Elsevier Science, p. 419-424.
- Garlicki, A., M. Pulina, and J. Rozkowski, 1996, Karst phenomena and their influence on the ground-waters threat in the Wieliczka salt mine (in Polish): *Przegląd Geologiczny*, v. 44, p. 1032-1038.
- Garlicki, A., and Z. Wilk, 1993, Geological and hydrogeological background of the recent water damage in Wieliczka Salt Mine (in Polish): *Przegląd Geologiczny*, v. 3, p. 183-192.
- Garnier, V., D. Ohnenstetter, and G. Giuliani, 2005, Fluor-rich aspidolite: a witness of evaporite implication in the genesis of ruby Nangimali (Azad-Kashmir, Pakistan) marbles (in French). *Comptes Rendus Geosciences*, v. 336, p. 1245-1253.

- Garrels, R. M., and C. L. Christ, 1965, *Solutions, minerals, and equilibria*: San Francisco, W. H. Freeman, 450 p.
- Garrels, R. M., and F. T. Mackenzie, 1981, *Evolution of sedimentary rocks*: New York, W. W. Norton and Co.
- Garrett, D. E., 1995, *Potash: Deposits, processing, properties and uses*: Berlin, Springer, 752 p.
- Garrett, D. E., 1998, *Borates: Deposits, processing, properties and use*: Amsterdam, Elsevier.
- Garrett, D. E., 2002, Sodium sulfate - 5,000 years of mining and production of salt cake: *Mining Engineering*, February, 2002, p. 17-22.
- Garrett, D. E., 2004, *Handbook of lithium and natural calcium chloride*, Elsevier Academic Press, 460 p.
- Garrett, P., 1970, Phanerozoic stromatolites: noncompetitive ecologic restriction by grazing and burrowing animals: *Science*, v. 169, p. 171-173.
- Garrison, R. E., and N. J. McMillan, 1999, Evidence for Jurassic continental rift magmatism in northeast Mexico: Alloctenic meta-igneous blocks in El Papalote diapir, La Popa Basin, Nuevo Leon, Mexico, in C. Bartolini, J. L. Wilson, and T. F. Lawton, eds., *Mesozoic sedimentary and tectonic history of north-central Mexico*, Geological Society America Special Paper 340, p. 319-332.
- Garven, G., 1995, Continental-scale groundwater flow and geologic processes: *Annu. Rev. Earth Planet. Sci.*, v. 23, p. 89-117.
- Gasiewicz, A., 2000, Comparative study of major element geochemistry of gypsum-ghost limestones and selenite lithofacies from the Miocene of northern Carpathian Foredeep: implication to the model of massive replacement of solid sulphates by calcium carbonates: *Chemical Geology*, v. 164, p. 183-218.
- Gaullier, V., and B. C. Vendeville, 2005, Salt tectonics driven by sediment progradation: Part II - Radial spreading of sedimentary lobes prograding above salt: *Bulletin American Association Petroleum Geologists*, v. 89, p. 1081-1089.
- Gaupp, R., A. Matter, J. Platt, K. Ramseyer, and J. Walzebeck, 1993, Diagenesis and fluid evolution of deeply buried Permian (Rotliegende) gas reservoirs, northwest Germany: *Bulletin-American Association of Petroleum Geologists*, v. 77, p. 1111-1128.
- Gauthier, B. D. M., R. C. W. M. Franssen, and S. Drei, 2000, Fracture networks in Rotliegend gas reservoirs of the Dutch offshore: implications for reservoir behaviour: *Geologie en Mijnbouw/Netherlands Journal of Geoscience*, v. 79, p. 45-57.
- Gautier, F., G. Clauzon, J. P. Suc, J. Cravette, and D. Violant, 1994, Age et durée de la crise de salinité messinienne: *C. R. Acad. Sci. Paris Ser. 2*, v. 318, p. 1103-1109.
- Gavish, E., 1974, Geochemistry and mineralogy of a Recent sabkha along the coast of Sinai, Gulf of Suez: *Sedimentology*, v. 21, p. 397-414.
- Gavish, E., 1980, Recent sabkhas marginal to the southern coasts of Sinai, Red Sea, in A. Nissenbaum, ed., *Hypersaline brines and evaporitic environments*, Elsevier, Amsterdam, p. 233-251.
- Gavish, E., W. E. Krumbein, and J. Halevy, 1985, Geomorphology, mineralogy and groundwater geochemistry as factors of the hydrodynamic system of the Gavish Sabkha, in G. M. Friedman, and W. E. Krumbein, eds., *Hypersaline ecosystems; the Gavish Sabkha*, v. Ecological Studies Vol. 53: New York, Springer, p. 186-217.
- Gabrieli, 1997, Halite deposition in the Dead Sea: 1960-1993, in T. Neimi, Z. Ben-Avraham, and J. R. Gat, eds., *The Dead Sea*, Oxford University Press, p. 161-171.
- Ge, H. X., M. P. A. Jackson, and B. C. Vendeville, 1997, Kinematics and dynamics of salt tectonics driven by progradation: *AAPG Bulletin-American Association of Petroleum Geologists*, v. 81, p. 398-423.
- Gebhardt, F., D. Eby, and D. Barnette, 2001, Utilizing coiled tubing technology to control a liquid propane storage well fire, A case history: *Proc. SMRI Spring Meeting*, Orlando, p. 301-308.
- Geddes, M. C., 1975a, Studies on an Australian brine shrimp, *Parartemia zeitziانا Sayce* (Crustacea: Anostraca). I. Salinity tolerance: *Comp. Biochem. Physiol.*, v. 51A, p. 553-559.
- Geddes, M. C., 1975b, Studies on an Australian brine shrimp, *Parartemia zeitziانا Sayce* (Crustacea: Anostraca). II. Osmotic and ionic regulation: *Comp. Biochem. Physiol.*, v. 51A, p. 561-571.
- Geddes, M. C., 1975c, Studies on an Australian brine shrimp, *Parartemia zeitziانا Sayce* (Crustacea: Anostraca). III. The mechanisms of osmotic and ionic regulation: *Comp. Biochem. Physiol.*, v. 51A, p. 573-578.
- Geddes, M. C., P. De Deckker, and W. C. Williams, 1981, On the chemistry and biota of some saline lakes in Western Australia: *Hydrobiologia*, v. 81, p. 201-222.
- Geeslin, J. H., and H. S. Chafetz, 1982, Ordovician Aleman ribbon cherts; an example of silicification prior to carbonate lithification: *Journal of Sedimentary Petrology*, v. 52, p. 1283-1293.
- Geluk, M. C., 1998, Internal tectonics of salt structures: *Journal of Seismic Exploration*, v. 7, p. 237-250.
- Geluk, M. C., 2000, Late Permian (Zechstein) carbonate-facies maps, the Netherlands: *Geologie en Mijnbouw*, v. 79, p. 17-27.
- Gely, J. P., V. M. M. Blanc, D. F. Fache, M. Schuler, and M. Ansart, 1993, Characterization of organic-rich material in an evaporitic environment; the lower Oligocene of the Mulhouse Basin (Alsace, France): *Geologische Rundschau*, v. 82, p. 718-725.
- Gendzwil, D., and N. Martin, 1996, Flooding and loss of the Patience Lake potash mine: *CIM Bulletin*, v. 89, p. 62-73.
- Gendzwil, D., and J. Unrau, 1996, Ground control and seismicity at International Minerals and Chemical (Canada) Global Ltd: *CIM Bulletin*, v. 89, p. 52-61.
- Gendzwil, D. J., 1978, Winnipegosis mounds and Prairie Evaporite Formation of Saskatchewan - seismic study: *American Association Petroleum Geologists - Bulletin*, v. 62, p. 73-86.
- Gerdes, G., K. Dunajtschik-Piewak, H. Riege, A. G. Taher, W. E. Krumbein, and H.-E. Reineck, 1994, Structural diversity of biogenic carbonate particles in microbial mats: *Sedimentology*, v. 41, p. 1273-1294.
- Gerdes, G., T. Klenke, and N. Noffke, 2000a, Microbial signatures in peritidal siliciclastic sediments: a catalogue: *Sedimentology*, v. 47, p. 279-308.
- Gerdes, G., W. E. Krumbein, and N. Noffke, 2000b, Evaporite Microbial Sediment, in R. E. Riding, and S. M. Awramik, eds., *Microbial Sediments*: Berlin Heidelberg, Springer-Verlag, p. 196-208.
- Gerhard, L. C., 1985, Porosity development in the Mississippian pisolitic limestones of the Mission Canyon formation, Glenburn field, Williston basin, North Dakota., in P. O. Roehl, and P. W. Choquette, eds., *Carbonate Petroleum Reservoirs*, Springer-Verlag, p. 191-205.
- Gertman, I., and A. Hecht, 2002, The Dead Sea hydrography from 1992 to 2000: *Journal of Marine Systems*, v. 35, p. 169-181.

- Gibling, M. R., G. C. Nanson, and J. C. Maroulis, 1998, Anastomosing river sedimentation in the Channel Country of central Australia: *Sedimentology*, v. 45, p. 595-619.
- Giles, K. A., and R. K. Goldhammer, 2002, Isolated to Coalesced Carbonate Buildups Developed on Passive Salt Diapir Bathymetry, La Popa Basin, NE Mexico (abs): *American Association Petroleum Geologists - Bulletin*, v. 86 (13 supplement).
- Giles, K. A., and T. F. Lawton, 1999, Attributes and evolution of an exhumed salt weld, La Popa basin, northeastern Mexico: *Geology*, v. 27, p. 323-326.
- Gill, D., 1977, Salina A-1 sabkha cycles and the Late Silurian paleogeography of the Michigan Basin: *Journal of Sedimentary Petrology*, v. 47, p. 979-1017.
- Gill, D., 1985, Depositional facies of Middle Silurian (Niagaran) pinnacle reefs, Belle River Mills gas field, Michigan Basin, SE Michigan, in P. O. Roehl, and P. W. Choquette, eds., *Carbonate petroleum reservoirs: a case book*: New York, Springer Verlag, p. 123-139.
- Gill, D., 1994, Niagaran reefs of Northern Michigan. 1. Exploration portrait: *Journal of Petroleum Geology*, v. 17, p. 99-110.
- Gill, W. D., and M. A. Ala, 1972, Sedimentology of the Gachsaran Formation (Lower Fars Series), Southwest Iran: *American Association Petroleum Geologists - Bulletin*, v. 56, p. 1965-1974.
- Gillespie, R., J. W. Magee, J. G. Luly, E. Dlugokencky, R. J. Sparks, and G. Wallace, 1991, AMS radiocarbon dating in the study of arid environments: examples from Lake Eyre, South Australia: *Palaeogeography Palaeoclimatology Palaeoecology*, v. 84, p. 333-338.
- Gingras, M. K., S. G. Pemberton, K. Muelenbachs, and H. G. Machel, 2004, Conceptual models for burrow-related, selective dolomitization with textural and isotopic evidence from the Tyndall Stone, Canada: *Geobiology*, v. 2, p. 21-30.
- Giralt, S., R. Julià, S. Leroy, and F. Gasse, 2003, Cyclic water level oscillations of the KaraBogazGol-Caspian Sea system: *Earth and Planetary Science Letters*, v. 212, p. 225-239.
- Gleeson, S. A., J. J. F. M. Wilkinson, F. M. Stuart, and D. A. Banks, 2001, The origin and evolution of base metal mineralising brines and hydrothermal fluids, South Cornwall, UK: *Geochimica et Cosmochimica Acta*, v. 65, p. 2067-2079.
- Glennie, K. W., 1989a, A summary of tropical desert sedimentary environments, present and past: *Geological Association of Canada Special Paper*, v. 36, p. 67-84.
- Glennie, K. W., 1989b, Some effects of the Late Permian Zechstein transgression in northwestern Europe: *Geological Association of Canada Special Paper*, v. 36, p. 557-565.
- Glennie, K. W., 1990, Outline of North Sea history and structural framework, in K. W. Glennie, ed., *Introduction to the petroleum geology of the North Sea (3rd edition)*: Oxford, Blackwell Scientific Publications, p. 34-77.
- Glennie, K. W., 1998, The desert of southeast Arabia: a product of Quaternary climatic change, in A. S. Alsharhan, K. W. Glennie, G. L. Whittle, and C. G. S. C. Kendall, eds., *Quaternary Deserts and Climatic Change*: Rotterdam, A. A. Balkema, p. 279-291.
- Glennie, K. W., and A. T. Buller, 1983, The Permian Weissliegendes of NW Europe: the partial deformation of eolian sands caused by the Zechstein transgression: *Sedimentary Geology*, v. 35, p. 43-81.
- Goede, A., T. C. Atkinson, and P. J. Rowe, 1992, A giant late Pleistocene halite speleothem from Webbs Cave, Nullarbor Plain, southeastern Western Australia: *Helictite*, v. 30, p. 3-7.
- Goldstein, R. H., 2001, Fluid inclusions in sedimentary and diagenetic systems: *Lithos*, v. 55, p. 159-193.
- Gomis-Yagues, V., N. Boluda-Botella, and F. Ruiz-Bevia, 2000, Gypsum precipitation/dissolution as an explanation of the decrease of sulphate concentration during seawater intrusion: *Journal of Hydrology*, v. 228, p. 48-55.
- Goodall, I. G., G. M. Harwood, A. C. Kendall, T. McKie, and M. E. Tucker, 1992, Discussion on sequence stratigraphy of carbonate-evaporite basins; models and application to the Upper Permian (Zechstein) of Northeast England and adjoining North Sea: *Journal of the Geological Society of London*, v. 149, p. 1050-1054.
- Goodall, T. M., 1995, *The Geology and Geomorphology of the Sabkhat Matti Region (United Arab Emirates): a Modern Analogue for Ancient Desert Sediments from North-west Europe*: Doctoral thesis, University of Aberdeen, Aberdeen, Scotland.
- Goodall, T. M., C. P. North, and K. W. Glennie, 2000, Surface and subsurface sedimentary structures produced by salt crusts: *Sedimentology*, v. 47, p. 99-118.
- Goodfellow, W. D., and I. R. Jonasson, 1984, Ocean stagnation and ventilation defined by $\delta^{34}\text{S}$ secular trends in pyrite and barite, Selwyn Basin, Yukon: *Geology*, v. 12, p. 583-586.
- Gorbunova, K. A., 1979, Morphology and hydrogeology of gypsum karst (in Russian): *Univ. Perm. All Union Karst and Speology Inst.*, p. 222-223.
- Gordon, D. S., and P. B. Flemings, 1998, Generation of overpressure and compaction-driven fluid flow in a Plio-Pleistocene growth-faulted basin, Eugene Island 330, offshore Louisiana: *Basin Research*, v. 10, p. 177-196.
- Gordon, W. A., 1975, Distribution by latitude of Phanerozoic evaporite deposits: *Journal of Geology*, v. 83, p. 671-684.
- Gore, D. B., D. C. Creagh, J. S. Burgess, E. A. Colhoun, A. P. Spate, and A. S. Baird, 1996, Composition, distribution and origin of surficial salts in the Vestfold Hills, East Antarctica: *Antarctic Science*, v. 8, p. 73-84.
- Gorin, G. E., L. G. Racz, and M. R. Walter, 1982, Late Precambrian - Cambrian Sediments of Huqf Group, Sultanate of Oman. AAPG Bulletin 66: 2609-2627: *American Association Petroleum Geologists - Bulletin*, v. 66, p. 2609-2627.
- Gornitz, V. M., and B. C. Schreiber, 1981, Displacive halite hoppers from the Dead Sea; some implications for ancient evaporite deposits: *Journal of Sedimentary Petrology*, v. 51, p. 787-794.
- Gorski, M., Z. Wojtkowiak, and S. Radecki, 1999, Barnowko-Mostno-Buszewo (BMB): the largest crude oil deposit in Poland: *Petroleum Geoscience*, v. 5, p. 5-15.
- Gott, G. B., D. F. Wolcott, and C. G. Bowles, 1974, Stratigraphy of the Inyan Kara Group and localisation of Uranium deposits, Southern Black Hills, South Dakota and Wyoming: *US Geol Surv. Prof. Paper*, v. 763, p. 1-57.
- Gowan, S. W., and S. M. Trader, 1999, Mine failure associated with a pressurized brine horizon: Retsof Salt Mine, western New York: *Applications & Environmental & Engineer*, v. 6, p. 57-70.
- Graf, D. L., 1982, Chemical osmosis, reverse chemical osmosis, and the origin of subsurface brines: *Geochimica et Cosmochimica Acta*, v. 46, p. 1431-1448.

- Graf, D. L., A. J. Eardley, and N. F. Shimp, 1961, A preliminary report on magnesium carbonate formation in Glacial Lake Bonneville: *Journal of Geology*.
- Grajales-Nishimura, J. M., E. Cedillo-Pardo, C. Rosales-Dominguez, D. J. Morán-Zenteno, D. J. Alvarez, P. Claeys, J. Ruíz-Morales, J. García-Hernández, P. Padilla-Avila, and A. Sánchez-Ríos, 2000, Chicxulub impact: The origin of reservoir and seal facies in the southeastern Mexico oil fields: *Geology*, v. 28, p. 307-310.
- Gran, K., K. Bjørlykke, and P. Aagaard, 1992, Fluid salinity and dynamics in the North Sea and Haltenbanken derived from well log data, in A. Hurst, C. M. Griffiths, and P. F. Worthington, eds., *Geological Application of Wireline Logs II*, Geological Society London Special Publication, 65, p. 327-328.
- Grande, L., 1980, Paleontology of the Green River Formation, with a review of the fish fauna: *Bull. Univ. Geol. Surv. Wyoming*, v. 63, p. 333p.
- Grant, S., W. D. Grant, B. E. Jones, C. Kato, and L. Li, 1999, Novel archaeal phylotypes from an East African alkaline saltern: *Extremophiles*, v. 3, p. 139-145.
- Grantham, P. J., G. W. M. Lijmbach, J. Posthuma, M. W. Hughes Clarke, and R. J. Willink, 1988, Origin of crude oils in Oman: *Journal of Petroleum Geology*, v. 11, p. 61-80.
- Grappe, J., 2000, Alternative uses of underground caverns: An introduction to the technology of solution mining; Spring 2000 Technical Class, Solution Mining Research Institute, Hague, Netherlands, p. 154-178.
- Grasby, S. E., and R. Betche, 2000, Pleistocene recharge and flow reversal in the Williston basin, central North America: *Journal of Geochemical Exploration*, v. 69-70, p. 403-407.
- Gregory, G., C. Killey, and S. Stewart, 2002, Dahl Hit, Saudi Arabia, Cave Survey map; last accessed on September 15, 2005, <http://www.saudicaves.com/ainhit/17ain.jpg>.
- Gregory-Wodzicki, K. M., 2000, Uplift history of the central and northern Andes: A review: *Geological Society of America Bulletin*, v. 112, p. 1091-1105.
- Gretener, P. E., 1982, Another look at Alborz nr. 5 in Central Iran: *Bull. Ver. schweiz. Petroleum Geol. u. -Ing.*, v. 48, p. 1-8.
- Grice, K., S. Schouten, A. Nissenbaum, J. Charrach, and J. S. S. Damste, 1998, Isotopically heavy carbon in the C-21 to C-25 regular isoprenoids in halite-rich deposits from the Sedom Formation, Dead Sea basin, Israel: *Organic geochemistry*, v. 28, p. 349-359.
- Griffin, D. L., 1999, The late Miocene climate of northeastern Africa: Unravelling the signals in the sedimentary succession: *Journal of the Geological Society*, v. 156, p. 817-826.
- Griffin, D. L., 2002, Aridity and humidity: two aspects of the late Miocene climate of North Africa and the Mediterranean: *Palaeogeography, Palaeoclimatology, Palaeoecology*, v. 182, p. 65-91.
- Grimalt, J. O., R. De Wit, P. Teixidor, and J. Albaiges, 1992, Lipid biogeochemistry of Phormidium and Microcoleus mats: *Organic Geochemistry*, v. 19, p. 509-530.
- Griswold, G. B., 1982, Geologic overview of the Carlsbad potash-mining district: Circular New Mexico Bureau of Mines and Mineral Resources, v. 182, p. 17-22.
- Grossman, I. G., 1968, Origin of the sodium sulphate deposits of the northern Great Plains of Canada and the United States: *U. S. Geol. Surv. Prof. Pap.*, v. 600-B, p. 104-109.
- Grotzinger, J. P., 1986a, Cyclicity and paleoenvironmental dynamics, Rocknest Platform, northwest Canada: *Geol. Soc. America Bull.*, v. 97, p. 1208-1231.
- Grotzinger, J. P., 1986b, Shallowing upward cycles of the Wallace Formation, Belt Supergroup, northwestern Montana and northern Idaho: *Montana Bureau of Mines Geol. Spec. Pub.*, v. 94, p. 143-160.
- Grotzinger, J. P., and J. F. Kasting, 1993, New constraints on Precambrian ocean composition: *Journal of Geology*, v. 101, p. 235-243.
- Grotzinger, J. P., and A. H. Knoll, 1995, Anomalous carbonate precipitates - Is the Precambrian the key to the Permian: *Palaios*, v. 10, p. 578-596.
- Grotzinger, J. P., and A. H. Knoll, 1999, Stromatolites in Precambrian carbonates: Evolutionary mileposts or environmental dipsticks? *Annual Review of Earth & Planetary Sciences*, v. 27, p. 313-358.
- Grotzinger, J. P., and J. F. Read, 1983, Evidence for primary aragonite precipitation, lower Proterozoic (1.9 Ga) Rocknest dolomite, Wopmay orogen, northwest Canada: *Geology*, v. 11, p. 710-713.
- Grotzinger, J. P., and D. H. Rothman, 1996, An abiotic model for stromatolitic morphogenesis: *Nature*, v. 383, p. 423-425.
- Groves, I. M., C. E. Carman, and W. J. Dunlap, 2003, Geology of the Beltana Willemite Deposit, Flinders Ranges, South Australia: *Economic Geology*, v. 98, p. 797-818.
- Grunau, H. R., 1987, A worldwide look at the cap-rock problem: *Journal of Petroleum Geology*, v. 103, p. 245-266.
- Guarascio, M., G. Fernandez, and R. L. Thoms, 1995, Updated evaluation of sinkhole potential at the Belvedere Spinello Brinefield: SMRI Fall Meeting, Sept 25 - Oct 1, 1995, Hanover, Germany, p. 43 p.
- Gueddari, M., 1984, *Geochemie et thermodynamique des evaporites continentales: etude de lac Natron en Tanzanie et du Chott el Jerid en Tunisie*. (Geochemistry and thermodynamics of continental evaporites: a study of Lake Natron in Tanzania and the Chott el Djerid in Tunisia). *Sciences Geologiques - Memoire*, v. 76, p. 143 pp.
- Guglielmo, G., B. C. Vendville, and M. P. A. Jackson, 2000, 3-D Visualization and Isochore Analysis of Extensional Diapirs Overprinted by Compression: *American Association Petroleum Geologists - Bulletin*, v. 84, p. 1095-1108.
- Guilhaumou, N., N. Ellouzi, T. M. Jaswal, and P. Mougou, 2000, Genesis and evolution of hydrocarbons entrapped in the fluorite deposit of Koh-i-Maran, (North Kirthar Range, Pakistan): *Marine and Petroleum Geology*, v. 17, p. 1151-1164.
- Guiraud, R., 1965, *Geologie et hydrogeologie du bassin versant du Chott el Hodna; resume des connaissances actuelles*: Algeria, *Serv. Geol., Bull. No.*, v. 33, p. 51-66.
- Gunatilaka, A., 1990, Anhydrite diagenesis in a vegetated sabkha, Al-Khiran, Kuwait, Arabian Gulf: *Sedimentary Geology*, v. 69, p. 95-116.
- Gunatilaka, A., and S. Mwangi, 1988, Continental sabkha pans and associated nebkhas in southern Kuwait, Arabian Gulf: *Geophysical and Geochemical Exploration*, v. 12, p. 308-311.
- Gunatilaka, A., A. Saleh, and A. Al-Temeemi, 1980, Plant-controlled supratidal anhydrite from Al-Khiran, Kuwait: *Nature*, v. 288, p. 257-260.
- Gunatilaka, A., A. Saleh, A. Al-Temeemi, and N. Nassar, 1987, Calcium-poor dolomite from the sabkhas of Kuwait: *Sedimentology*, v. 34, p. 999-1006.

- Gunde-Cimerman, N., P. Zalar, S. de Hoog, and A. Plemenita, 2000, Hypersaline waters in salterns – natural ecological niches for halophilic black yeasts: *FEMS Microbiology Ecology*, v. 32, p. 235-240.
- Gundogan, I., and C. Helvaci, 2001, Sedimentological and petrographical aspects of Upper Miocene evaporites in the Beypazari and Cankiri-Corum basins, central Anatolia, Turkey: *International Geology Review*, v. 43, p. 818-829.
- Gundogdu, M. N., H. Yalcin, A. Temel, and N. Clauer, 1996, Geological, mineralogical and geochemical characteristics of zeolite deposits associated with borates in the Bigadic, Emet and Kirka Neogene lacustrine basins, western Turkey: *Mineralium Deposita*, v. 31, p. 492-513.
- Gurer, O. F., and A. Gurer, 1999, Development of evaporites and the counterclockwise rotation of Anatolia, Turkey: *International Geology Review*, v. 41, p. 607-622.
- Gussow, W. C., 1968, Salt diapirism: importance of temperature, and energy source of emplacement, in J. Braunstein, and G. D. O'Brien, eds., *Diapirism and diapirs*: Tulsa OK, American Association of Petroleum Geologists Memoir 8, p. 16-52.
- Gustavson, T. C., S. D. Hovorka, and A. R. Dutton, 1994, Origin of satin spar veins in evaporite basins: *Journal of Sedimentary Research, Section A: Sedimentary Petrology and Processes*, v. 64, p. 88-94.
- Gustavson, T. C., W. W. Simpkins, A. Alhades, and A. D. Hoadley, 1982, Evaporite dissolution and development of karst features on the Rolling Plains of the Texas Panhandle: *Earth Surface Processes and Landforms*, v. 7, p. 545-563.
- Gutiérrez, F., 1996, Gypsum karstification induced subsidence - effects on alluvial systems and derived geohazards (Calatayud Graben, Iberian Range, Spain): *Geomorphology*, v. 16, p. 277-293.
- Gutiérrez, F., and A. H. Cooper, 2002, Evaporite dissolution subsidence in the historical city of Catalayud, Spain: *Damage appraisal and prevention: Natural Hazards*, v. 25, p. 259-288.
- Gvirtzman, H., and E. Stanislavsky, 2000, Palaeohydrology of hydrocarbon maturation, migration and accumulation in the Dead Sea Rift: *Basin Research*, v. 12, p. 79-93.
- Gómez-Alday, J. J., F. Garcia-Garmilla, and J. Elorza, 2002, Origin of quartz geodes from Lano and Tubilla del Agua sections (middle-upper Campanian, Basque-Cantabrian Basin, northern Spain): isotopic differences during diagenetic processes: *Geological Journal*, v. 37, p. 117-134.
- Götzinger, M. A., and W. Grum, 1992, Die Pb-Zn-F Mineralisationen in der Umgebung von Evaporiten der Nördlichen Kalkalpen Österreich - Herkunft und Zusammensetzung der fluiden Phase: *Mitt. Ges. Geol. Bergbaustud Österr* (Vienna), v. 38, p. 47-56.
- Habermehl, M. A., 1980, The Great Artesian Basin: *BMR Journal Australian Geology and Geophysics*, v. 5, p. 9-38.
- Habermehl, M. A., 1982, Springs in the Great Artesian Basin - Their Origin and Nature.: Bureau of Mineral Resources, Australia, Report 235, BMR Microfilm MF 179.
- Habermehl, M. A., 1988, Springs of the Great Artesian Basin: Aspects of Hydrogeologic, Hydrochemical, and Isotopic Characteristics: SLEADS Conference 88, Salt Lakes in Arid Lands, p. 30 pp.
- Habermehl, M. A., 1996, Groundwater Movement and Hydrochemistry of the Great Artesian Basin, Australia: In *Mesozoic Geology of the Eastern Australia Plate Conference*, Geol. Society of Aust. Inc., Extended Abstracts, No. 43, pages 228-236.
- Habicht, K. S., and D. E. Canfield, 1996, Sulphur isotope fractionation in modern microbial mats and the evolution of the sulphur cycle: *Nature*, v. 382, p. 342-343.
- Hafid, M., 2000, Triassic-early Liassic extensional systems and their Tertiary inversion, Essaouira Basin (Morocco): *Marine & Petroleum Geology*, v. 17, p. 409-429.
- Hahn, J., and P. Haug, 1986, Traces of Archaeobacteria in ancient sediments: *System. Appl. Microbiol.*, v. 7, p. 178-183.
- Halbouty, M. T., 1979, Salt domes, Gulf region, United States and Mexico: Houston, Texas, Gulf Publishing, 561 p.
- Hall, A., 1998, Zeolitization of volcanoclastic sediments: The role of temperature and pH: *Journal of Sedimentary Research*, v. 68, p. 739-745.
- Hall, S. H., 2002, The role of autochthonous salt inflation and deflation in the northern Gulf of Mexico: *Marine and Petroleum Geology*, v. 19, p. 649-682.
- Hallager, W. S., M. R. Ulrich, J. R. Kyle, P. E. Price, and W. A. Gose, 1990, Evidence for episodic basin dewatering in salt-dome cap rocks: *Geology*, v. 18, p. 716-719.
- Hallam, A., 1981, Facies interpretation and the stratigraphic record: San Francisco, W. H. Freeman and Co., 291 p.
- Halley, R. B., 1977, Ooid fabric and structure in the Great Salt Lake and the Geologic record: *Journal of Sedimentary Petrology*, v. 47, p. 1099-1120.
- Halley, R. B., 1985, Setting and geologic summary of the Lower Cretaceous, Sunniland field, Southern Florida, in P. O. Roehl, and P. W. Choquette, eds., *Carbonate petroleum reservoirs*: New York, Springer-Verlag, p. 443-454.
- Hammer, U. T., 1986, Saline lake ecosystems of the world (*Monographiae Biologicae*, Vol. 59): Dordrecht, Netherlands, Dr. W. Junk Publishers, 632 p.
- Handford, C. R., 1981a, A process-sedimentary framework for characterizing Recent and ancient sabkhas: *Sedimentary Geology*, v. 30, p. 255-265.
- Handford, C. R., 1982, Sedimentology and evaporite genesis in a Holocene continental sabkha playa basin – Bristol Dry Lake, California: *Sedimentology*, v. 29, p. 239-253.
- Handford, C. R., 1990, Halite depositional facies in a solar salt pond: A key to interpreting physical energy and water depth in ancient deposits? *Geology*, v. 18, p. 691-694.
- Handford, C. R., 1991, Marginal marine halite; sabkhas and salinas, in J. L. Melvin, ed., *Evaporites, petroleum and mineral resources*, v. 50, Elsevier Developments in Sedimentology, p. 1-66.
- Handford, C. R., A. C. Kendall, D. R. Prezbindowski, J. B. Dunham, and B. W. Logan, 1984, Salina-margin tepees, pisoliths and aragonite cements, Lake MacLeod, Western Australia; Their significance in interpreting ancient analogs: *Geology*, v. 12, p. 523-527.
- Handford, C. R., and C. H. J. Moore, 1976, Diagenetic implications of calcite pseudomorphs after halite from the Joachim Dolomite (middle Ordovician), Arkansas: *Journal of Sedimentary Petrology*, v. 46, p. 387-392.
- Handford, H. R., 1981b, Coastal sabkha and salt pan deposition of the lower Clear Fork Formation (Permian), Texas: *Journal of Sedimentary Petrology*, v. 51, p. 761-778.
- Hanna, M. A., 1953, Fracture Porosity in Gulf Coast: *American Association Petroleum Geologists - Bulletin*, v. 37, p. 266-281.

- Hanor, J. S., 1987, Kilometer-scale thermohaline overturn of pore waters in the Louisiana Gulf Coast: *Nature*, v. 327, p. 501-503.
- Hanor, J. S., 1988, Origin and migration of subsurface sedimentary brines: *SEPM Short Course Notes*, v. 21, 248 p.
- Hanor, J. S., 1994a, Origin of saline fluids in sedimentary basins, in J. Parnell, ed., *Geofluids; origin, migration and evolution of fluids in sedimentary basins: Geological Society Special Publications*, v. 78: London, United Kingdom, Geological Society of London, p. 151-174.
- Hanor, J. S., 1994b, Physical and chemical controls on the compositions of waters in sedimentary basins: *Marine & Petroleum Geology*, v. 11, p. 31-45.
- Hanor, J. S., 2000, Barite-celestine geochemistry and environments of formation, in C. N. Alpers, J. L. Jambor, and D. K. Nordstrom, eds., *Reviews in Mineralogy and Geochemistry - Sulfate Minerals: Crystallography, Geochemistry, and Environmental Significance*, v. 40, Mineralogical Society of America, p. 193-263.
- Hanor, J. S., 2004, A model for the origin of large carbonate and evaporite hosted celestine (SrSO₄) deposits: *Journal Sedimentary Research*, v. 74, p. 168-175.
- Hanor, J. S., J. E. Bailey, M. C. Rogers, and L. R. Milner, 1986, Regional variations in physical and chemical properties of south Louisiana oil field brines: *Gulf Coast Association Of Geological Societies, Transactions*, v. 36, p. 143-149.
- Hanor, J. S., and R. Sassen, 1990, Evidence for large scale vertical and lateral migration of basinal waters, dissolved salt, and crude oil in the Louisiana Gulf Coast, in D. Schumacher, and B. F. Perkins, eds., *Gulf Coast oils and gases: The characteristics, origin, distribution and exploration and production characteristics. Ninth Annual Research Conference Proceedings, GCSSEPM Foundation, October 1, Austin TX: Tulsa, SEPM*, p. 283-296.
- Hanshaw, B. B., and J. D. Bredehoeft, 1968, On the maintenance of anomalous fluid pressures; 2, Source layer at depth: *Geol. Soc. Amer., Bull.*, v. 79, p. 1107-1122.
- Hanson, A. D., B. D. Ritts, D. Zinniker, J. M. Moldowan, and U. Biffi, 2001, Upper Oligocene lacustrine source rocks and petroleum systems of the northern Qaidam basin, northwest China: *AAPG Bulletin-American Association of Petroleum Geologists*, v. 85, p. 601-619.
- Hao, C., 1987, Translated title: A discussion on the results of electrical prospecting for Shuangbei gypsum deposit, Hebei: *Kancha Diqiu Wuli Kancha Diqiu Huaxue Wenji=Contribution to the Exploration [of] Geophysics and Geochemistry*, v. 5, p. 234-240.
- Hao, F., S. T. Li, Y. C. Sun, and Q. M. Zhang, 1998a, Geology, compositional heterogeneities, and geochemical origin of the Yacheng gas field, Qiongdonggan Basin, South China Sea: *American Association of Petroleum Geologists Bulletin*, v. 82, p. 1372-1384.
- Hao, F., S. T. Li, Y. C. Sun, and Q. M. Zhang, 1998b, Abnormal organic matter maturation in the Yinggehai Basin, South China Sea: Implications for hydrocarbon expulsion and fluid migration from overpressured systems: *Journal of Petroleum Geology*, v. 21, p. 427-444.
- Haq, B. U., J. Hardenbol, and P. R. Vail, 1987, Chronology of fluctuating sea levels since the Triassic: *Science*, v. 235, p. 1156-1167.
- Harben, P. W., and R. L. Bates, 1990, *Industrial Minerals; Geology and world deposits*: London, UK, Industrial Minerals Division, Metal Bulletin Plc, 312 p.
- Harben, P. W., and M. Kuzvart, 1996, *Industrial Minerals: A world Geology*: London, Industrial Minerals Information Ltd., Metal Bulletin Plc, 462 p.
- Hardie, L. A., 1967, The gypsum-anhydrite equilibrium at one atmosphere pressure: *American Mineralogist*, v. 52, p. 172-200.
- Hardie, L. A., 1968, The origin of the Recent non-marine evaporite deposit of Saline valley, Inyo county, California: *Geochimica et Cosmochimica Acta*, v. 32, p. 1279-1301.
- Hardie, L. A., 1984, Evaporites: Marine or non-marine? *American Journal of Science*, v. 284, p. 193-240.
- Hardie, L. A., 1990, The roles of rifting and hydrothermal CaCl₂ brines in the origin of potash evaporites: an hypothesis: *American Journal of Science*, v. 290, p. 43-106.
- Hardie, L. A., 1991, On the significance of evaporites: *Annual Review Earth and Planetary Science*, v. 19, p. 131-168.
- Hardie, L. A., 1996, Secular variation in seawater chemistry: an explanation for the coupled secular variation in the mineralogies of marine limestones and potash evaporites over the past 600 m.y.: *Geology*, v. 24, p. 279 - 283.
- Hardie, L. A., A. Bosellini, and R. K. Goldhammer, 1986, Repeated subaerial exposure of subtidal carbonate platforms, Triassic, Northern Italy: evidence for high frequency sea level oscillations on a 10,000 year scale.: *Paleoceanography*, v. 1, p. 447-457.
- Hardie, L. A., and H. P. Eugster, 1970, The evolution of closed-basin brines: *Spec Pub. Mineral. Soc. Am.*, v. 3, p. 273-290.
- Hardie, L. A., and H. P. Eugster, 1971, The depositional environment of marine evaporites: A case for shallow, clastic accumulation: *Sedimentology*, v. 16, p. 187-220.
- Hardie, L. A., and T. K. Lowenstein, 2004, Did the Mediterranean Sea dry out during the Miocene? A reassessment of the evaporite evidence from DSDP Legs 13 and 42A cores: *Journal of Sedimentary Research*, v. 74, p. 453-461.
- Hardie, L. A., J. P. Smoot, and H. P. Eugster, 1978, Saline lakes and their deposits: a sedimentological approach, in A. Matter, and M. E. Tucker, eds., *Modern and Ancient Lake Sediments*, v. 2, International Association Sedimentologists Special Publication, p. 7-41.
- Hardman, R. F. P., and W. J. Kennedy, 1980, Chalk reservoirs of the Hod Fields, Norway: The sedimentation of the North Sea reservoir rocks, *Geilo: Norsk Petroleumforening, Section XI*.
- Harmon, R. S., T. C. Atkinson, and J. L. Atkinson, 1983, The mineralogy of Castleguard Cave, Columbia Icefields, Alberta, Canada: *Arctic and Alpine Research*, v. 15, p. 503-516.
- Harris, P. M., and S. D. Walker, 1990, McElroy Field, Central Basin Platform, Permian Basin, Texas, in E. A. Beaumont, and N. H. Foster, eds., *Treatise of Petroleum Geology; Atlas of Oil and Gas Fields: Stratigraphic Traps I: Tulsa, OK, American Association Petroleum Geologists*, p. 195-227.
- Harrison, H., and B. Patton, 1995, Translation of salt sheets by basal shear: *Proceedings of GCCSEPM Foundation 16th Annual Research Conference, Salt Sediment and Hydrocarbons, Dec 3-6, 1995*, p. 99-107.
- Harrison, J. C., 1995, Tectonics and kinematics of a foreland fold belt influenced by salt, Arctic Canada, in M. P. A. Jackson, D. G. Roberts, and S. Snelson, eds., *Salt tectonics: a global perspective, AAPG Memoir, v.65*, p. 379-412.

- Harrison, W. J., and L. L. Summa, 1991, Paleohydrology of the Gulf of Mexico Basin: *American Journal of Science*, v. 291, p. 109-176.
- Hartley, A., S. Flint, and P. Turner, 1991, Analcime: a characteristic authigenic phase of Andean alluvium, northern Chile: *Geological Journal*, v. 26, p. 189-202.
- Hartley, A. J., and G. May, 1998, Miocene gypcrettes from the Calama Basin, northern Chile: *Sedimentology*, v. 45, p. 351-364.
- Hartmann, B. H., K. Ramseyer, and A. Matter, 2000, Diagenesis and pore-water evolution in Permian sandstones, Gharif Formation, Sultanate of Oman: *Journal of Sedimentary Research Section A-Sedimentary Petrology & Processes*, v. 70, p. 533-544.
- Harvie, C. E., J. H. Weare, L. A. Hardie, and H. P. Eugster, 1980, Evaporation of sea water; calculated mineral sequences: *Science*, v. 208, p. 498-500.
- Harwood, G. M., 1980, Calcitized anhydrite and associated sulphides in the English Zechstein First Cycle Carbonate (EZ1 Ca), in H. Fuechtbauer, Peryt, T. M., ed., *The Zechstein Basin, with emphasis on carbonate sequences.*, E. Schweizerbart'sche VbH: Contributions to Sedimentology, v. 9, p. 61-72.
- Havholm, K. G., and G. Kocurek, 1994, Factors controlling eolian sequence stratigraphy: clues from super bounding surface features in the Middle Jurassic Page Sandstone: *Sedimentology*, v. 41, p. 913-934.
- Hawas, and H. Takezaki, 1995, A Model for Migration and Accumulation of Hydrocarbons in the Thamama and Arab Reservoirs in Abu Dhabi, U.A.E. (abs.): *Bulletin American Association of Petroleum Geologists*, v. 79, p. 1221.
- Hawtof, E. M., 1930, Results of deep well temperature measurements in Texas, in *Earth temperature in oil fields*: *API Production Bulletin*, v. 205, p. 62-108.
- Hay, R. L., 1963, Zeolitic weathering in Olduvai Gorge, Tanganyika: *Geological Society America Bulletin*, v. 74, p. 1281-1286.
- Hay, R. L., 1968, Chert and its sodium-silicate precursors in sodium-carbonate lakes of east Africa: *Contributions to Mineralogy and Petrology*, v. 17, p. 255-274.
- Hay, R. L., 1970, Silicate reactions in three lithofacies of a semi arid basin, Olduvai Gorge, Tanzania: *Mineralogical Society of America Special Paper*, v. 3, p. 237-255.
- Hay, R. L., 1981, Geology of zeolites in sedimentary rocks, in F. A. Mumpton, ed., *Mineralogy and geology of natural zeolites*, *Min. Soc. America Reviews in Mineralogy*, v. 4, p. 165-175.
- Hay, R. L., S. G. Guldman, J. C. Matthews, R. H. Lander, M. E. Duffin, and T. K. Kyser, 1991, Clay mineral diagenesis in core KM-3 of Searles Lake, California: *Clays & Clay Minerals*, v. 39, p. 84-96.
- Hay, R. L., R. E. Hughes, K. T. K., H. D. Glass, and J. Liu, 1995, Magnesium-rich clays of the Meerschaum Mines in the Amboseli, Tanzania and Kenya: *Clays & Clay Minerals*, v. 43, p. 455-466.
- Hay, R. L., and T. K. Kyser, 2001, Chemical sedimentology and paleoenvironmental history of Lake Olduvai, a Pliocene lake in northern Tanzania: *Geological Society of America Bulletin*, v. 113, p. 1510-1521.
- Hay, W. W., 1996, Tectonics and climate: *Geologische Rundschau*, v. 85, p. 409-437.
- Haynes, H. W., 1997, Solution mining of trona: *In Situ*, v. 21, p. 357-394.
- Hayward, A. B., and R. H. Graham, 1989, Some geometrical characteristics of inversion: *Geological Society of London Special Publication*, v. 44, p. 17-39.
- Haywick, D. W., M. B. Hall-Brown, and L. Pfeiffer, 2000, Smackover Reservoir Diagenesis in the Appleton Oilfield, Escambia County, Alabama (abs): *Bulletin American Association of Petroleum Geologists*, v. 84, p. 1680.
- Heaney, P. J., 1995, Moganite as an indicator for vanished evaporites: a testament reborn? *Journal of Sedimentary Research A: Sedimentary Petrology & Processes*, v. A65, p. 633-638.
- Heard, H. C., and W. W. Rubey, 1966, Tectonic implications of gypsum dehydration: *Geol. Soc. America Bull*, v. 77, p. 741-760.
- Heaton, R. C., M. P. A. Jackson, M. Bahahmoud, and A. S. O. Nani, 1995, Superposed Neogene extension, contraction, and salt canopy emplacement in the Yemeni Red Sea, in M. P. A. Jackson, D. G. Roberts, and S. Snelson, eds., *Salt Tectonics: a global perspective*: Tulsa, AAPG Memoir 65, p. 333-351.
- Heckel, P. H., 1974, Carbonate buildups in the geologic record: a review: in *Reefs in Time and Space*, in L. F. Laporte, ed., *Reefs in Time and Space, Selected Examples from the Recent and Ancient*, v. 18: Tulsa, OK, Soc. Econ. Paleontologists & Mineralogists Spec. Pub. p. 90-105.
- Helfman, G., D. Facey, and B. Collette, 1997, *The diversity of fishes*: Oxford, UK, Blackwell Publishing, 1006 p.
- Helvacı, C., 1995, Stratigraphy, mineralogy, and genesis of the Bigadic Borate deposits, Western Turkey: *Economic Geology*, v. 90, p. 1237-1260.
- Helvacı, C., 1998, The Beypazari trona deposit, Ankara Province, Turkey., in J. R. Dyni, and R. W. Jones, eds., *Proceedings of the first international soda ash conference; Volume II*: Laramie, WY, Public Information Circular - Geological Survey of Wyoming, v. 40, p. 67-103.
- Helvacı, C., and R. C. Alonso, 2000, Borate Deposits of Turkey and Argentina: A Summary and Geological Comparison: *Turkish Journal of Earth Sciences*, v. 9, p. 1-27.
- Helvacı, C., and F. Orti, 1998, Sedimentology and diagenesis of Miocene colemanite-ulexite deposits (western Anatolia, Turkey): *Journal of Sedimentary Research Section A-Sedimentary Petrology & Processes*, v. 68A, p. 1021-1033.
- Helvacı, C., and F. Orti, 2004, Zoning in the Kirka borate deposit, western Turkey: Primary evaporitic fractionation of diagenetic modifications? *Canadian Mineralogist*, v. 42, p. 1221-1246.
- Hemley, J. J., P. B. Hostetler, A. J. Gude, and W. T. Mountjoy, 1969, Some stability relations of alunite: *Economic Geology*, v. 64, p. 599-612.
- Henderson, K., 1974, Methods of joining two or more wells for brine production, in A. H. Coogan, ed., *Fourth Symposium on Salt*, v. 2: Cleveland, N. Ohio Geol. Soc., p. 211-218.
- Hendron, A. J., and P. A. Lenzini, 1983, Subsidence investigation at Well #56, Carey Salt Brinefield, Hutchison Kansas: *SMRI Research Project Report*, v. 83-0001-SMRI, p. 67.
- Henneke, E., G. W. Luther, G. J. Delange, and J. Hoefs, 1997, Sulphur speciation in anoxic hypersaline sediments from the Eastern Mediterranean Sea: *Geochimica et Cosmochimica Acta*, v. 61, p. 307-321.

- Hennen, R. V., and R. J. Metcalf, 1929, Yates Oil Pool, Pecos County, Texas: American Association Petroleum Geologists - Bulletin, v. 13, p. 1509-1556.
- Henriksen, S., and T. O. Vorren, 1996, Early Tertiary sedimentation and salt tectonics in the Nordkapp Basin, Southern Barents Sea: Norsk Geologisk Tidsskrift, v. 76, p. 33-44.
- Hentz, T. F., and C. D. Henry, 1989, Evaporite-hosted native sulfur in Trans-Pecos Texas; relation to late-phase Basin and Range deformation: *Geology*, v. 17, p. 400-403.
- Herbst, D. B., and T. J. Bradley, 1988, Osmoregulation in Dolichopodid Larvae (*Hydrophorus-Plumbeus*) from a Saline Lake: *Journal of Insect Physiology*, v. 34, p. 369-372.
- Herdendorf, C. E., 1984, Inventory of the morphometric and limnologic characteristics of the large lakes of the world: Ohio State University Sea grant Program Technical Bulletin, v. OHSU-TB-17, p. 78 p.
- Herries, R. D., and G. Cowan, 1997, Challenging the 'sheet-flood' myth: the role of water-table-controlled sabkha deposits in redefining the depositional model for the Ormskirk Sandstone Formation (Lower Triassic), East Irish Sea Basin, in N. S. Meadows, S. Trueblood, M. Hardman, and G. Cowan, eds., *Petroleum Geology of the Irish Sea and Adjacent Areas*: London, Geological Society of London Special Publication 124, p. 253-276.
- Herut, B., I. Gavrieli, and L. Halicz, 1998, Coprecipitation of trace and minor elements in modern authigenic halites from the hypersaline Dead Sea brine: *Geochimica et Cosmochimica Acta*, v. 62, p. 1587-1598.
- Herut, B., A. Starinsky, A. Katz, and A. Bein, 1990, The role of sea-water freezing in the formation of subsurface brines: *Geochimica et Cosmochimica Acta*, v. 54, p. 13-21.
- Hesse, R., 1986, Early diagenetic pore water/sediment interaction: Modern offshore basins: *Geoscience Canada*, v. 13, p. 165-197.
- Heward, A. P., 1990, Salt removal and sedimentation in southern Oman, in A. H. F. Robertson, M. P. Searle, and A. C. Ries, eds., *The geology and tectonics of the Oman region*, Geological Society of London, Special Publication, v.49, p. 637-652.
- Heward, A. P., S. Chuenbunchom, G. Makel, D. Marsland, and L. Spring, 2000, Nang Nuan oil field, B6/27, Gulf of Thailand: karst reservoirs of meteoric or deep-burial origin? *Petroleum Geoscience*, v. 6, p. 15-27.
- Heydari, E., 1997, The role of burial diagenesis in hydrocarbon destruction and H₂S accumulation, Upper Jurassic Smackover Formation, Black Creek Field, Mississippi: *American Association of Petroleum Geologists - Bulletin*, v. 81, p. 26-45.
- Heydari, E., 2000, Porosity Loss, Fluid Flow, and Mass Transfer in Limestone Reservoirs: Application to the Upper Jurassic Smackover Formation, Mississippi: *Bulletin American Association of Petroleum Geologists*, v. 84, p. 100-118.
- Heydari, L. E., and C. H. Moore, 1989, Burial diagenesis and thermochemical sulfate reduction, Smackover Formation, Southeast Mississippi salt basin: *Geology*, v. 17, p. 1080-1084.
- Hilaire-Marcel, C., J. Casanova, and M. Taieb, 1987, Isotopic age and lacustrine environments during late Quaternary in the Tanzanian Rift (Lake Natron), in M. R. Rampino, J. E. Sanders, W. S. Newman, and L. K. Konigsson, eds., *Climate: history, periodicity, and predictability*: New York, NY, United States, Van Nostrand Reinhold Co., p. 117-123.
- Hill, B. F., 1993, Magnesite and magnesia production by Queensland Magnesite (Operations) Pty Ltd at Kunwarara and Rockhampton, Qld, in J. T. Woodcock, and J. K. Hamilton, eds., *Australasian mining and metallurgy; the Sir Maurice Mawby Memorial volume*: Melbourne, Victoria, Australia, Australasian Institute of Mining and Metallurgy, v. 19, p. 1388-1393.
- Hill, C. A., 1990, Sulphuric acid speleogenesis of Carlsbad Caverns and its relationship to hydrocarbons, Delaware Basin, New Mexico and Texas: *American Association of Petroleum Geologists Bulletin*, v. 74, p. 1685-1694.
- Hill, C. A., 1995, H₂S-related porosity and sulfuric acid oil-field karst, in D. A. Budd, A. H. Saller, and P. M. Harris, eds., *Unconformities and porosity in carbonate strata*, American Association Petroleum Geologists Memoir 63, p. 301-306.
- Hill, C. A., 2000, Overview of the geologic history of cave development in the Guadalupe Mountains, New Mexico: *Journal of Cave and Karst Studies*, v. 62, p. 60-71.
- Hill, C. A., and P. Forti, 1986, *Cave Minerals of the World*: National Speleological Society, Huntsville, AL, 238 pp.
- Hills, J. M., 1984, Sedimentation, tectonism, and hydrocarbon generation in Delaware Basin, West Texas and Southeastern New Mexico: *American Association Petroleum Geologists - Bulletin*, v. 68, p. 250-267.
- Hindle, A. D., 1997, Petroleum migration pathways and charge concentration - a three-dimensional model: *Bulletin-American Association of Petroleum Geologists*, v. 81, p. 1451-1481.
- Hinnov, L. A., and R. K. Goldhammer, 1991, Spectral analysis of the Middle Triassic Latemar Limestone: *Journal of Sedimentary Petrology*, v. 61, p. 1173-1193.
- Hite, R. J., and D. E. Anders, 1991, Petroleum and evaporites, in J. L. Melvin, ed., *Evaporites, petroleum and mineral resources*, v. 50: Amsterdam, Elsevier Developments in Sedimentology, p. 477-533.
- Hite, R. J., D. E. Anders, and T. G. Jing, 1984, Organic-rich source rocks of Pennsylvanian age in the Paradox Basin of Utah and Colorado, in J. Woodward, F. F. Meissner, and J. L. Clayton, eds., *Hydrocarbon source rocks of the Greater Rocky Mountain Region*: Denver, Rocky Mountain Assoc. Geologists, p. 255-274.
- Hite, R. J., and T. Japakeset, 1979, Potash deposits of the Khorat Plateau, Thailand and Laos: *Economic Geology*, v. 74, p. 448-458.
- Hodell, D. A., R. H. Benson, J. P. Kennett, and K. Rakic-El Bied, 1989, Stable isotope stratigraphy of latest Miocene sequences in northwest Morocco: the Bou Regreg Section: *Paleoceanography*, v. 4, p. 467-482.
- Hodell, D. A., J. H. Curtis, F. J. Sierro, and M. E. Raymo, 2001, Correlation of late Miocene to early Pliocene sequences between the Mediterranean and North Atlantic: *Paleoceanography*, v. 16, p. 164-178.
- Hodge, B. L., 1986, Occurrence and exploitation of fluorite, in R. W. Nesbitt, and I. Nichol, eds., *Geology in the real world - the Kingsley Dunham volume*: London, Inst. Mining Metallurgy, p. p. 165.
- Hodgkins, M., and M. J. O'Brien, 1994, Salt sill deformation and its implications for subsalt exploration: *Leading Edge*, v. August 1994, p. 849-851.
- Hoffman, P. F., I. R. Bell, R. S. Hildebrand, and L. Thorstad, 1977, *Geology of the Athapuscow Aulocogen, East Arm of the Great Slave*

- Lake, District of Mackenzie: Current Research Part A: Geol. Surv. Canada Paper, v. 84-1A, p. 117-146.
- Hoffman, P. F., A. J. Kaufman, G. P. Halverson, and D. P. Schrag, 1998, A Neoproterozoic Snowball Earth: *Science*, v. 281, p. 1342-1346.
- Hofmann, H. J., K. Grey, A. H. Hickman, and R. I. Thorpe, 1999, Origin of 3.45 Ga coniform stromatolites in Warrawoona Group, Western Australia: *Bulletin Geological Society of America*, v. 111, p. 1256-1262.
- Hofmann, P., A. Y. Huc, B. Carpentier, P. Schaeffer, P. Albrecht, B. Keely, J. R. Maxwell, D. J. S. Sinninghe, L. J. W. de, and D. Leythaeuser, 1993a, Organic matter of the Mulhouse Basin, France; a synthesis: *Organic Geochemistry*, v. 20, p. 1105-1123.
- Hofmann, P., D. Leythaeuser, and B. Carpentier, 1993b, Palaeoclimate controlled accumulation of organic matter in Oligocene evaporite sediments of the Mulhouse Basin: *Organic Geochemistry*, v. 20, p. 1125-1138.
- Holba, A. G., E. Tegelaar, L. Ellis, M. S. Singletary, and P. Albrecht, 2000, Tetracyclic polyrenoids: Indicators of freshwater (lacustrine) algal input: *Geology*, v. 28, p. 251-254.
- Holland, D. S., J. B. Leedy, and D. R. Lammlein, 1990, Eugene Island Block 330 Field - USA, offshore Louisiana, in E. A. Beaumont, and N. H. Foster, eds., *Treatise of Petroleum Geology: Atlas of Oil and Gas Fields: Structural Traps III - Tectonic fold and fault traps*: Tulsa, OK, American Association Petroleum Geologists, p. 103-143.
- Holland, H. D., J. Horita, and W. Seyfried, 1996, On the secular variations in the composition of phanerozoic marine potash evaporites: *Geology*, v. 24, p. 993-996.
- Holland, H. D., and H. Zimmermann, 2000, The Dolomite Problem Revisited: *Int. Geol. Rev.*, v. 42, p. 481-490.
- Hollander, D. J., A. Y. Huc, J. S. S. Damste, J. M. Hayes, and J. W. De Leeuw, 1993, Molecular and bulk isotopic analyses of organic matter in marls of the Mulhouse Basin (Tertiary, Alsace, France): *Organic Geochemistry*, v. 20, p. 1253-1263.
- Holliday, D. W., 1970, The petrology of secondary gypsum rocks; a review: *Journal of Sedimentary Petrology*, v. 40, p. 734-744.
- Holmes, R., 1991, Some aspects of the geology of the potash seam at Boulby mine: *Journal of the Open University Geological Society*, v. 12, p. 77-88.
- Holser, W. T., 1966, Bromide geochemistry of salt rocks: Second Symposium on Salt, Ohio Geological Society, p. 248-275.
- Holser, W. T., 1977, Catastrophic chemical events in the history of the ocean: *Nature*, v. 267.
- Holser, W. T., 1979, Mineralogy of evaporites, in R. G. Burns, ed., *Marine Minerals*, v. 6, Mineralogical Society America, *Reviews in Mineralogy*, p. 211-294.
- Holser, W. T., 1984, Gradual and abrupt shifts in ocean chemistry during Phanerozoic time, in H. D. Holland, and A. F. Trendall, eds., *Patterns of Change in Earth Evolution*: Berlin, Springer-Verlag, p. 123-143.
- Holser, W. T., G. P. Clement, L. F. Jansa, and J. A. Wade, 1988a, Evaporite deposits of the North Atlantic Rift, in W. Manspeizer, ed., *Triassic-Jurassic rifting: Continents breakup and the origin of the Atlantic Ocean and Passive margins*, *Developments in Geotectonics*, v. 22: Amsterdam, Elsevier, p. 525-556.
- Holser, W. T., M. Schidlowski, F. T. Mackenzie, and J. B. Maynard, 1988b, Geochemical cycles of carbon and sulfur, in C. B. Gregor, R. M. Garrels, F. T. Mackenzie, and J. B. Maynard, eds., *Chemical Cycles in the Evolution of the Earth*: New York, Wiley, p. 107-173.
- Holter, M., 1972, Geology of the Prairie Evaporite Formation of Saskatchewan, Canada, *Geology of saline deposits (Geologie des depots salins)*, v. 7, UNESCO Earth Sci. Ser., p. 183-189.
- Holwerda, J. G., and R. W. Hutchinson, 1968, Potash-bearing evaporites in the Danakil area, Ethiopia: *Economic Geology*, v. 63, p. 124-150.
- Honty, M., P. Uhlík, V. Sucha, M. Caplovicová, J. Francu, N. Clauer, and A. Biron, 2004, Smectite-to-illite alteration in salt-bearing bentonites (the East Slovak Basin): *Clays and Clay Minerals*, v. 52, p. 533-551.
- Hooper, R. J., Leng Siang Goh, and F. Dewey, 1995, The inversion history of the northeastern margin of the Broad Fourteens Basin, in J. G. Buchanan, and P. G. Buchanan, eds., *Basin inversion*, Geological Society, London; Special Publication, 88, p. 307-317.
- Hopkins, J. C., 1987, Contemporaneous subsidence and fluvial channel sedimentation: Upper Mannville C Pool, Berry Field, Lower Cretaceous of Alberta: *Bulletin American Association of Petroleum Geologists*, v. 71, p. 334-345.
- Horsfield, B., D. J. Curry, K. M. Bohacs, A. R. Carroll, R. Littke, U. Mann, M. Radke, R. G. Schaefer, G. H. Isaksen, H. G. Schenk, E. G. Witte, and J. Rulkotter, 1994, Organic geochemistry of freshwater and alkaline lacustrine environments, Green River Formation, Wyoming: *Organic geochemistry*, v. 22, p. 415-450.
- Horsfield, B., and J. Rulkotter, 1994, Diagenesis, catagenesis, and metagenesis of organic matter, in L. B. Magoon, and W. G. Dow, eds., *The petroleum system - from source to trap*, v. 60, AAPG; Memoir, p. 189-199.
- Hose, L. D., A. N. Palmer, M. V. Palmer, D. E. Northup, P. J. Boston, and H. R. DuChene, 2000, Microbiology and geochemistry in a hydrogen-sulphide-rich karst environment: *Chemical Geology*, v. 169, p. 399-423.
- House, W. M., and J. A. Pritchett, 1995, Fluid migration and formation pressures associated with allochthonous salt sheets in the northern Gulf of Mexico: Gulf Coast Section SEPM Foundation Sixteenth Annual Research Conference, p. 121-124.
- Hovorka, S., 1987, Depositional environments of marine-dominated bedded halite, Permian San Andres Formation, Texas: *Sedimentology*, v. 34, p. 1029-1054.
- Hovorka, S. D., 1989, Depth evolution of the Delaware Basin-Castile/Salado transition, in P. M. Harris, and G. A. Grover, eds., *Subsurface and Outcrop Examination of the Capitan Shelf Margin, Northern Delaware Basin*, v. 13: Tulsa, Oklahoma, SEPM, Core Workshop, p. 441-450.
- Hovorka, S. D., 1992, Halite pseudomorphs after gypsum in bedded anhydrite; clue to gypsum-anhydrite relationships: *Journal of Sedimentary Petrology*, v. 62, p. 1098-1111.
- Hovorka, S. D., 2000, Understanding the processes of salt dissolution and subsidence: *Solution Mining Research Institute Proceedings*, p. 11-24 (PDF file); see also <http://www.beg.utexas.edu/environment/qly/salt/index.htm>.
- Hovorka, S. D., L. P. Knauth, R. S. Fisher, and G. Q. Gao, 1993, Marine to nonmarine facies transition in Permian evaporites of the Palo Duro Basin, Texas; geochemical response: *Geological Society of America Bulletin*, v. 105, p. 1119-1134.
- Howell, P., and A. W. Liebold III, 1992, Sequence Stratigraphy of the Silurian Carbonates and Evaporites in the Michigan Basin: *Bulletin American Association of Petroleum Geologists*, v. 76, p. 56-57.

- Howell, P. D., and B. A. van der Pluijm, 1999, Structural sequences and styles of subsidence in the Michigan Basin: *Geological Society America Bulletin*, v. 111, p. 974-991.
- Hoy, R. B., R. M. Foose, and B. J. O'Neill Jr., 1962, Structure of Winnfield salt dome, Winn Parish, Louisiana: *American Association Petroleum Geologists - Bulletin*, v. 46, p. 1444-1459.
- Hryniv, S. P., and T. M. Peryt, 2003, Sulfate cavity filling in the Lower Werra Anhydrite (Zechstein, Permian), Zdrada area, northern Poland: Evidence for early diagenetic evaporite paleokarst formed under sedimentary cover: *Journal Of Sedimentary Research*, v. 73, p. 451-461.
- Hsu, K. J., W. B. F. Ryan, and M. B. Cita, 1973, Late Miocene Desiccation of the Mediterranean: *Nature*, v. 242, p. 240-244.
- Hsu, K. J., and J. Schneider, 1973, Progress report on dolomitization of Abu Dhabi Sabkhas, Arabian Gulf, in B. H. Purser, ed., *The Persian Gulf: Holocene carbonate sedimentation and diagenesis in a shallow epicontinental sea*: New York, Springer-Verlag, p. 409-422.
- Hsu, K. J., and C. Siegenthaler, 1969, Preliminary experiments on hydrodynamic movement induced by evaporation and their bearing on the dolomite problem: *Sedimentology*, v. 12, p. 448-453.
- Huang, X. Z., and H. S. Shao, 1993, Sedimentary characteristics and types of hydrocarbon source rocks in the Tertiary semiarid to arid lake basins of Northwest China: *Palaeogeography Palaeoclimatology Palaeoecology*, v. 105, p. 33-43.
- Huber, R., M. Kurr, H. W. Jannasch, and K. O. Stetter, 1989, A novel group of methanogenic archaeobacteria (*Methanopyrus*) growing at 110°C: *Nature*, v. 342, p. 833-834.
- Hubert, J. F., and M. G. Hyde, 1982, Sheetflow deposits of graded beds and mudstones on an alluvial sandflat-playa system; the Upper Triassic Blomidon Redbeds, St Marys Bay, Nova Scotia: *Sedimentology*, v. 29, p. 457-474.
- Humphris Jr., C. C., 1978, Salt movement on continental slope, northern Gulf of Mexico, in A. H. Bouma, C. T. Moore, and J. M. Coleman, eds., *Framework, facies, and oil-trapping characteristics of the upper continental margin*, AAPG Studies in Geology, v. 7, p. 69-85.
- Hunt, D., and M. E. Tucker, 1992, Stranded parasequences and forced regressive wedge systems tract; deposition during base level fall: *Sedimentary Geology*, v. 81, p. 1-9.
- Hunt, D. W., W. M. Fitchen, and E. Kosa, 2002, Syndepositional deformation of the Permian Capitan reef carbonate platform, Guadalupe Mountains, New Mexico, USA: *Sedimentary Geology*, v. 154, p. 89-126.
- Hunt, J. M., 1990, Generation and migration of petroleum from abnormally pressured fluid compartments: *Bulletin American Association of Petroleum Geologists*, v. 74, p. 1-12.
- Hunt, J. M., 1996, *Petroleum geochemistry and geology*: New York, W. H. Freeman & Co., 743 p.
- Hunt, J. M., J. K. Whelan, L. B. Eglinton, and L. M. Cathles III, 1998, Relation of shale porosities, gas generation, and compaction to deep overpressures in the US Gulf Coast, in B. E. Law, G. F. Ulmishkek, and V. I. Slavina, eds., *Abnormal pressures in hydrocarbon environments*, v. 70: Tulsa, OK, American Association Petroleum Geologists Memoir, p. 87-104.
- Hurley, N. F., and R. Budros, 1990, Albion-Scipio and Stoney Point fields, U.S.A., Michigan Basin, in E. A. Beaumont, and N. H. Foster, eds., *Stratigraphic traps: I*: Tulsa, OK, AAPG Treatise of Petroleum Geology, Atlas of Oil and Gas Fields, p. 1-37.
- Hussain, M., and J. K. Warren, 1988, Dolomitization in a sulfate-rich environment; modern example from Salt Flat Sabkha (dried playa lake) in West Texas-New Mexico: *Carbonates & Evaporites*, v. 3, p. 165-173.
- Hussain, M., and J. K. Warren, 1989, Nodular and enterolithic gypsum; the 'sabkha-tization' of Salt Flat Playa, West Texas: *Sedimentary Geology*, v. 64, p. 13-24.
- Husseini, M. I., 1989, Tectonic and deposition model of late Precambrian-Cambrian Arabian and adjoining plates: *Bulletin American Association Petroleum Geologists*, v. 73, p. 1117-1131.
- Huston, D. L., and G. A. Logan, 2004, Barite, BIFs and bugs: evidence for the evolution of the Earth's early hydrosphere: *Earth and Planetary Science Letters*, v. 220, p. 41-45.
- Hutchinson, R. W., and G. G. Engels, 1970, Tectonic significance of regional geology and evaporite lithofacies in northeastern Ethiopia: *Philosophical Transactions of the Royal Society*, v. A 267, p. 313-329.
- Icole, M., J.-P. Masse, G. Perinet, and M. Taieb, 1990, Pleistocene lacustrine stromatolites, composed of calcium carbonate, fluorite, and dolomite, from Lake Natron, Tanzania; depositional and diagenetic processes and their paleoenvironmental significance: *Sedimentary Geology*, v. 69, p. 139-155.
- Icole, M., and G. Perinet, 1984, Les silicates sodiques et les milieux évaporitiques carbonates bicarbonates sodiques: une revue: *Revue de Géologie Dynamique et de Géographie Physique*, v. 25, p. 167-176.
- Iijima, A., 1980, Geology of natural zeolites and zeolitic rocks, in L. V. Rees, ed., *Fifth International Conference on Zeolites*, Heyden Publishers, p. 103-117.
- Illing, L. V., A. J. Wells, and J. C. M. Taylor, 1965, Penecontemporary dolomite in the Persian Gulf, in L. C. Pray, and R. C. Murray, eds., *Dolomitization and limestone diagenesis*, Society of Economic Paleontologists and Mineralogists Special Publication 13, p. 89-113.
- Imhoff, J. F., H. G. Sahl, G. S. H. Soliman, and H. G. Trüper, 1979, The Wadi Natrun: Chemical composition and microbial mass developments in alkaline brines of eutrophic desert lakes: *Geomicrobiology Journal*, v. 1, p. 219-234.
- Inan, K., A. C. Dunham, and J. Esson, 1973, Mineralogy, chemistry and origin of Kirka borate deposit, Eskishehir Province, Turkey: *Trans. Inst. Mining Metall., Appl. Earth Sci.*, v. B-82, p. 114-123.
- Ireson, A. T., 1990, Review of the soluble salt process for in situ recovery of hydrocarbons from oil shale with emphasis on leaching [of nahcolite] and possible beneficiation, in J. H. Gary, ed., *Twenty-third Oil Shale Symposium Proceedings*: Golden, CO, Colorado Sch. Mines Press, p. 152-155.
- Irion, G., and G. Mueller, 1968, Huntite, dolomite, magnesite and polyhalite of Recent age from Tuz Golu, Turkey: *Nature*, v. 220, p. 1309-1310.
- Irwin, M. L., 1965, General theory of epeiric clear water sedimentation: *American Association of Petroleum Geologists Bulletin*, v. 49, p. 445-459.
- Jackson, G. D., and T. R. Iannelli, 1981, Rift-related cyclic sedimentation in the Neohelikian Borden Basin, northern Baffin Island, in F. H. A. Campbell, ed., *Proterozoic Basins of Canada*, v. 81-10, Geological Survey Canada Paper, p. 269-302.
- Jackson, M. J., M. D. Muir, and K. A. Plumb, 1987, Geology of the southern McArthur Basin, Bureau Mineral Resources, Canberra, Australia, *Bulletin* 220, 173 p.

- Jackson, M. P. A., and R. B. Cornelius, 1987, Stepwise centrifuge modelling of the effects of differential sediment loading on the formation of salt structures, in I. Lerche, and J. J. O'Brien, eds., *Dynamical geology of salt and related structures*: Orlando, Florida, Academic Press, p. 163-259.
- Jackson, M. P. A., R. R. Cornelius, C. H. Craig, A. Gansser, J. Stocklin, and C. J. Talbot, 1990, Salt diapirs of the Great Kavir, central Iran: *Memoir - Geological Society of America*, v. 177, p. 139 pp.
- Jackson, M. P. A., and C. Cramez, 1989, Seismic recognition of salt welds in salt tectonic regimes: CGSSEPM Found. 10th A. Res. Conf. Prog. Extended Abs., Houston, Texas, p. 72-78.
- Jackson, M. P. A., and M. R. Hudec, 2004, A new mechanism for advance of allochthonous salt sheets, In: *Salt-sediment interactions and hydrocarbon prospectivity: concepts, applications and case studies for the 21st Century*. Papers presented at the 24th Annual Gulf Coast Section SEPM Foundation Bob F. Perkins Research Conference, Houston Tx, December 5-8, 2004 (CD publication), p. 220-242.
- Jackson, M. P. A., D. G. Roberts, and S. Snelson, 1995, Salt tectonics: AAPG Memoir, v. 65, American Society Petroleum Geologists, 454 p.
- Jackson, M. P. A., and C. J. Talbot, 1986, External shapes, strain rates, and dynamics of salt structures: *Geological Society of America Bulletin*, v. 97, p. 305-323.
- Jackson, M. P. A., and C. J. Talbot, 1991, A glossary of salt tectonics: *Geological Circular 91-4*, Bureau of Economic Geology, University of Texas at Austin, 44 p.
- Jackson, M. P. A., and C. J. Talbot, 1994, Advances in salt tectonics, in P. L. Hancock, ed., *Continental deformation*: Tarrytown, NY, Pergamon Press, p. 159-179.
- Jackson, M. P. A., and B. C. Vendeville, 1994, Regional extension as a geologic trigger for diapirism: *Geological Society of America Bulletin*, v. 106, p. 57-73.
- Jackson, M. P. A., B. C. Vendeville, and D. D. Shultz-Ela, 1994a, Structural dynamics of salt systems: *Annual Review of Earth and Planetary Sciences*, v. 22, p. 93-117.
- Jackson, M. P. A., B. C. Vendeville, and D. D. Shultz-Ela, 1994b, Salt-related structures in the Gulf of Mexico: A field guide for geophysicists: *The Leading Edge*, v. August 1994, p. 837-842.
- Jackson, M. P. A., O. N. Warin, G. M. Woad, and M. R. Hudec, 2003, Neoproterozoic allochthonous salt tectonics during the Lufilian orogeny in the Katangan Copperbelt, central Africa: *Geological Society of America Bulletin*, v. 115, p. 314-330.
- Jacobson, G., 1988, Hydrology of Lake Amadeus, a groundwater-discharge playa in central Australia: *BMR Journal of Australian Geology & Geophysics*, v. 10, p. 301-308.
- Jacobson, G., G. E. Calf, J. Jankowski, and P. S. McDonald, 1989, Groundwater chemistry and palaeorecharge in the Amadeus Basin, central Australia: *Journal of Hydrology*, v. 109, p. 237-266.
- Jacobson, G., and J. Jankowski, 1989, Groundwater-discharge processes at a central Australian playa: *Journal of Hydrology*, v. 105, p. 275-295.
- Jacoby, C. H., 1974, Solution mining of evaporites, in F. F. Aplan, ed., *Solution Mining Symposium*: New York, Am. Inst. Min. Met. Petrol. Eng., p. 165-171.
- Jagnow, D. H., C. A. Hill, D. G. Davis, H. R. DuChene, K. I. Cunningham, D. E. Northup, and J. M. Queen, 2000, History of sulfuric acid theory of speleogenesis in the Guadalupe Mountains, New Mexico. 62(2): 54-59.: *Journal of Cave and Karst Studies*, v. 62, p. 54-59.
- James, N. P., and A. C. Kendall, 1992, Introduction to carbonate and evaporite facies models, in R. G. Walker, and N. P. James, eds., *Facies Models: Responses to sea level change*, Geological Association of Canada, p. 265-275.
- Jankowski, J., and G. Jacobson, 1989, Hydrochemical evolution of regional groundwaters to playa brines in central Australia: *Journal of Hydrology*, v. 108, p. 123-173.
- Jankowski, J., and G. Jacobson, 1990, Hydrochemical processes in groundwater-discharge playas, central Australia: *Hydrological Processes*, v. 4, p. 59-70.
- Jassim, S. Z., A. S. Jibril, and N. M. S. Numan, 1997, Gypsum karstification in the Middle Miocene Fatha Formation, Mosul area, Northern Iraq: *Geomorphology*, v. 18, p. 137-149.
- Jassim, S. Z., R. Raiswell, and S. H. Bottrell, 1999, Genesis of the Middle Miocene stratatound sulphur deposits of northern Iraq: *Journal of the Geological Society*, v. 156, p. 25-39.
- Javor, B. J., 1989, *Hypersaline environments*: Heidelberg New York, Springer Verlag.
- Javor, B. J., 2000, Biogeochemical models of solar salterns, in R. M. Geertmann, ed., *8th World Salt Symposium*, v. 2: Amsterdam, Elsevier, p. 877-882.
- Jeanbourquin, P., 1988, Nouvelles observations sur les cornieules en Suisse occidentale: *Eclogae Geologicae Helvetiae*, v. 81, p. 511-538.
- Jeanbourquin, P., 1994, Early deformation of Ultrahelvetic mélanges in the Helvetic nappes (Western Swiss Alps): *Journal of Structural Geology*, v. 16, p. 1367-1383.
- Jellison, R., and J. M. Melack, 1993, Meromixis in hypersaline Mono Lake, California. 1. Stratification and vertical mixing during the onset, persistence, and breakdown of meromixis: *Limnology & Oceanography*, v. 38, p. 1008-1019.
- Jennings, J. N., 1985, *Karst Geomorphology*: London, Blackwell, 293 p.
- Jenyon, M. K., and J. C. M. Taylor, 1983, Hydrocarbon indications associated with North Sea Zechstein shelf features: *Oil and Gas Journal*, v. 81, p. 155-160.
- Jiang, Z., and M. G. Fowler, 1986, Carentenoid-derived alkanes in oils derived from northwestern China: *Organic geochemistry*, v. 10, p. 831-839.
- Johns, R. K., 1968, Investigation of Lake Torrens and Gairdner: Geological Survey of South Australia, Report of Investigation, v. 31.
- Johnson, K. S., 1987, Development of the Wink Sink in west Texas due to salt dissolution and collapse, *Karst Hydrology: Proceedings of the Second Multidisciplinary Conference on Sinkholes and the Environmental Impacts of Karst*, Orlando Florida, 9-11 October 1987: Rotterdam, A. A. Balkema, p. 127-136.
- Johnson, K. S., 1989, Development of the Wink Sink in West Texas, USA, due to salt dissolution and collapse: *Environmental Geology and Water Science*, v. 14, p. 81-92.
- Johnson, K. S., 2001, Sinkholes associated with petroleum boreholes drilled through salt deposits in the USA: *Proc. S.M.R.I. Fall Meeting*, Albuquerque, p. 8-17.
- Jones, B., and R. W. Renaut, 1994, Crystal fabrics and microbiota in large pisoliths from Laguna Pastos Grandes, Bolivia: *Sedimentology*, v. 41, p. 1171-1202.

- Jones, B. E., W. D. Grant, A. W. Duckworth, and G. G. Owenson, 1998, Microbial diversity of soda lakes: *Extremophiles*, v. 2, p. 191-200.
- Jones, B. F., 1965, The hydrology and mineralogy of Deep Springs Lake, Inyo County, California: U. S. Geological Survey Professional Paper, v. 502, p. A1-A56.
- Jones, B. F., 1983, Occurrence of clay minerals in surficial deposits of southwestern Nevada: *Sci Géol. Mém.*, v. 72, p. 81-92.
- Jones, B. F., 1986, Clay mineral diagenesis in lacustrine sediments, in F. A. Mumpton, ed., *Studies in diagenesis*, US Geological Survey Bulletin No. 1578, p. 291-300.
- Jones, B. F., H. P. Eugster, and S. L. Rettig, 1977, Hydrogeochemistry of the Lake Magadi Basin, Kenya: *Geochimica Cosmochimica Acta*, v. 41, p. 53-72.
- Jones, B. F., and E. Galán, 1988, Sepiolite and palygorskite, in S. W. Bailey, ed., *Hydrous Phyllosilicates (Exclusive of Micas)*, v. 19: Washington, Mineralogical Society of America, *Reviews in Mineralogy*, p. 631-674.
- Jones, B. F., J. S. Hanor, and W. R. Evans, 1994, Sources of dissolved salts in the central Murray Basin, Australia: *Chemical Geology*, v. 111, p. 135-154.
- Jones, B. F., S. L. Rettig, and H. P. Eugster, 1967, Silica in alkaline brines: *Science*, v. 158, p. 1310-1314.
- Jones, B. G., B. E. Chenhall, A. J. Wright, J. W. Pemberton, and C. Campbell, 1987, Silurian evaporitic strata from New South Wales, Australia: *Palaeogeography, Palaeoclimatology, Palaeoecology*, v. 59, p. 215-225.
- Jones, D. J., 1953, Gypsum-Oolite Dunes, Great Salt Lake Desert, Utah: *Bulletin American Association Petroleum Geologists*, v. 37, p. 2530-2538.
- Jones, G. D., F. F. Whitaker, P. F. Smart, and W. E. Sanford, 2002, Fate of reflux brines in carbonate platforms: *Geology*, v. 30, p. 371-374.
- Jones, G. D., and Y. Xiao, 2005, Dolomitization, anhydrite cementation, and porosity evolution in a reflux system: Insights from reactive transport models: *Bulletin American Association Petroleum Geologists*, v. 89, p. 577-601.
- Jones, R. W., 1984, Comparison of carbonate and shale source rocks, in J. G. Palacas, ed., *Petroleum geochemistry and source rock potential of carbonate rocks*, v. 18: Tulsa, OK, American Association of Petroleum Geologists, *Studies in Geology*, p. 163-180.
- Jordan, P., T. Noack, and T. Widmer, 1990, The evaporite shear zone of the Jura Boundary Thrust; new evidence from Wisen Well (Switzerland): *Eclogae Geologicae Helvetiae*, v. 83, p. 525-542.
- Jordan, P., and R. Nuesch, 1989, Deformation structures in the Muschelkalk anhydrites of the Schafisheim Well (Jura Overthrust, northern Switzerland): *Eclogae Geologicae Helvetiae*, v. 82, p. 429-454.
- Jordan, T. E., N. Muñoz, M. Hein, T. K. Lowenstein, L. Godfrey, and J. Yu, 2002, Active faulting and folding without topographic expression in an evaporite basin, Chile: *Geological Society of America Bulletin*, v. 114, p. 1406-1421.
- Jowett, E. C., L. M. Cathles III, and B. W. Davis, 1993, Predicting depths of gypsum dehydration in evaporitic sedimentary basins: *Bulletin American Association Petroleum Geologists*, v. 77, p. 402-413.
- Jowett, E. C., A. Rydzewski, and R. J. Jowett, 1987, The Kupferschiefer Cu-Ag ore deposits in Poland: a re-appraisal of the evidence of their origin and presentation of a new genetic model: *Can Journ. Earth Sci.*, v. 24, p. 2016 - 2037.
- Jørgensen, B. B., M. F. Isaksen, and H. W. Jannasch, 1992, Bacterial sulfate reduction above 100°C in deep-sea hydrothermal vent sediments: *Science*, v. 258, p. 1756-1757.
- Kabyshev, B., B. Krivchenkov, S. Stovba, and P. A. Ziegler, 1998, Hydrocarbon habitat of the Dniepr-Donets depression: *Marine & Petroleum Geology*, p. 177-190.
- Kacaroglu, F., M. Degirmenci, and O. Cerit, 1997, Karstification in Miocene gypsum - An example from Sivas, Turkey: *Environmental Geology*, v. 30, p. 88-97.
- Kadioglu, M., Z. Sen, and E. Batur, 1997, The greatest soda-water lake in the world and how it is influenced by climatic change: *Ann. Geophysicae*, v. 15, p. 1489-1497.
- Kagya, M. L. N., 1996, Geochemical characterization of Triassic petroleum source rock in the Mandawa Basin, Tanzania: *Journal of African Earth Sciences & the Middle East*, v. 23, p. 73-88.
- Kah, L. C., T. W. Lyons, and J. T. Chesley, 2001, Geochemistry of a 1.2 Ga carbonate-evaporite succession, northern Baffin and Bylot Islands: implications for Mesoproterozoic marine evolution: *Precambrian Research*, v. 111, p. 203-234.
- Kah, L. C., T. W. Lyons, and T. D. Frank, 2004, Low marine sulphate and protracted oxygenation of the Proterozoic biosphere: *Nature*, v. 431, p. 834-838.
- Kaldi, J., and J. Gidman, 1982, Early diagenetic dolomite cements; examples from the Permian Lower Magnesian Limestone of England and the Pleistocene carbonates of the Bahamas: *Journal of Sedimentary Petrology*, v. 52, p. 1073-1085.
- Kamali, M. R., N. M. Lemon, and S. N. Apak, 1995, Porosity generation and reservoir potential of Ouldburra Formation carbonates, Officer Basin, South Australia: *APEA Journal*, v. 35, p. 106- 120.
- Karacan, E., and I. Yilmaz, 1997, Collapse dolines in Miocene gypsum - An example from SW Sivas (Turkey): *Environmental Geology*, v. 29, p. 263-266.
- Karakitsios, V., and F. Pomonipapaioannou, 1998, Sedimentological study of the Triassic solution collapse breccias of the Ionian Zone (NW Greece): *Carbonates & Evaporites*, v. 13, p. 207-218.
- Karcz, I., and I. Zak, 1987, Bedforms in salt deposits of the Dead sea brines: *Journal of Sedimentary Petrology*, v. 57, p. 723-735.
- Kargel, J. S., J. F. Schreiber, and C. P. Sonett, 1996, Mudcracks and dedolomitisation in the Wittenoom Dolomite, Hamersley Group, Western Australia: *Global & Planetary Change*, v. 14, p. 73-96.
- Karlo, J. F., and R. C. Shoup, 2000, Classifications of Syndepositional Systems and Tectonic Provinces of the Northern Gulf of Mexico: *Search and Discovery Article #30004 (2000)*, <http://www.searchanddiscovery.net/documents/karlo/index.htm>.
- Karnin, W. D., E. Idiz, D. Merkel, and E. Ruprecht, 1996, The Zechstein Stassfurt carbonate hydrocarbon system of the Thuringian Basin, Germany: *Petroleum Geoscience*, v. 2, p. 53-58.
- Kashfi, M. S., 1983, Variations in tectonic styles in the Zagros geosyncline and their relation to the diapirism of salt in Southern Iran: *Journal of Petroleum Geology*, v. 6, p. 195-206.
- Kashfi, M. S., 1985, The Pre-Zagros integrity of the Iranian Platform: *Journal of Petroleum Geology*, v. 8, p. 353-360.

- Kashima, K., 2002, Environmental and climatic changes during the last 20,000 years at Lake Tuz, central Turkey: *Catena*, v. 48, p. 3-20.
- Kasprzyk, A., 2003, Sedimentological and diagenetic patterns of anhydrite deposits in the Badenian evaporite basin of the Carpathian Foredeep, southern Poland: *Sedimentary Geology*, v. 158, p. 167-194.
- Kastner, M., 1984, Control of dolomite formation: *Nature*, v. 311, p. 410-411.
- Kates, M., D. J. Kushner, and A. T. Matheson, 1993, The biochemistry of the Archaea: *New Comprehensive Biochemistry*, v. 26: Amsterdam, Elsevier, 582 p.
- Katz, B. J., 1990, Lacustrine Basin Exploration - Case studies and modern analogues, v. 50, *American Association Petroleum Geologists Memoir*, 340 p.
- Katz, B. J., 1995, The Green River Oil Shale: An Eocene Carbonate Lacustrine Source Rock, in B. J. Katz, ed., *Petroleum Source Rocks*: Berlin, Springer-Verlag, p. 309-332.
- Katz, B. J., K. K. Bissada, and J. W. Wood, 1987, Factors limiting potential of evaporites as hydrocarbon source rocks (abs): *AAPG Bulletin*, v. 71, p. 575.
- Kaufman, A. J., and S. Xiao, 2003, High CO₂ levels in the Proterozoic atmosphere estimated from analyses of individual microfossils: *Nature*, v. 425, p. 279-282.
- Kaufmann, D. W., 1960, *Sodium Chloride*: New York, Reinhold.
- Kautz, K., and H. Porada, 1976, Sepiolite formation in a pan of the Kalahari: *Nues Jahrb. Mineral Monatsh.*, v. 12, p. 545-559.
- Kazakov, A. V., and E. I. Sokolova, 1950, Conditions of formation of fluorite in sedimentary rocks: *Akad. Nauk SSSR Geologicheskii Institut Trudy*, v. 114, p. 22-64.
- Kbir-Arigoib, N., D. B. H. Chehimi, and L. Zayani, 2001, Treatment of Tunisian salt lakes using solubility phase diagrams: *Pure Appl. Chem.*, v. 73, p. 761-770.
- Keeling, J., and A. Mauger, 1998, New airborne HyMap data aids assessment of magnesite resources: *MESA Journal*, v. 11, p. 7-11.
- Keely, B. J., S. R. Blake, P. Schaeffer, and J. R. Maxwell, 1995, Distribution of pigments in the organic matter of marls from the Vena del Gesso evaporitic sequence: *Organic Geochemistry*, v. 23, p. 527-593.
- Keely, B. J., J. W. De Leeuw, J. R. Maxwell, J. S. S. Damste, S. E. Betts, and Ling Yue, 1993, A molecular stratigraphic approach to palaeoenvironmental assessment and the recognition of changes in source inputs in marls of the Mulhouse Basin (Alsace, France): *Organic Geochemistry*, v. 20, p. 1165-1186.
- Keheila, E., H. Khalifa, and A. El-Haddad, 1989, Holocene carbonate facies model, Ras Shukhier hypersaline pool and its surrounding sabkha, west Gulf of Suez, Egypt: *Sedimentary Geology*, v. 63, p. 155-169.
- Kelts, K., and M. Shahrabi, 1986, Holocene sedimentology of hypersaline Lake Urmia, northwestern Iran: *Palaeogeography, Palaeoclimatology, Palaeoecology*, v. 54, p. 105-130.
- Kempe, S., 1972, Cave genesis in gypsum with particular reference to underwater conditions: *Cave Science*, v. 49, p. 1-6.
- Kempe, S., and E. T. Degens, 1978, Lake Van varve record - the past 10,420 years, in E. T. Degens, and F. Kurtman, eds., *Geology of Lake Van*: Ankara, Turkey, MTA Press, p. 56-63.
- Kempe, S., and E. T. Degens, 1985, An early soda ocean? *Chemical Geology*, v. 53, p. 95-108.
- Kempe, S., and J. Kazmierczak, 1994, The role of alkalinity in the evolution of ocean chemistry, organization of living systems, and biocalcification processes: *Bulletin de la Institut Oceanographique (Monaco)*, v. 13, p. 61-117.
- Kempe, S., J. Kazmierczak, G. Landmann, T. Konuk, A. Riemer, and A. Lipp, 1991, Largest known microbialites discovered in Lake Van, Turkey: *Nature*, v. 349, p. 605-608.
- Kendall, A. C., 1983, Unconformity-associated replacement limestones after anhydrite in Mississippian of Williston Basin: *AAPG Bulletin*, v. 67, p. 494-495.
- Kendall, A. C., 1988, Aspects of evaporite basin stratigraphy, in B. C. Schreiber, ed., *Evaporites and hydrocarbons*: New York, Columbia University Press, p. 11-65.
- Kendall, A. C., 1989, Brine mixing in the Middle Devonian of Western Canada and its possible significance to regional dolomitization: *Sedimentary Geology*, v. 64, p. 271-285.
- Kendall, A. C., 1992, Evaporites, in R. G. Walker, and N. P. James, eds., *Facies Models: Responses to sea level change*, Geological Association of Canada, p. 375-409.
- Kendall, A. C., 2001, Late diagenetic calcitization of anhydrite from the Mississippian of Saskatchewan, western Canada: *Sedimentology*, v. 48, p. 29-55.
- Kendall, A. C., and G. M. Harwood, 1989, Shallow water gypsum in the Castile Formation - significance and implications, in P. M. Harris, and G. A. Grover, eds., *Subsurface and outcrop examination of the Capitan Shelf margin, northern Delaware Basin*, v. 13, *SEPM Core Workshop*, p. 451-457.
- Kendall, A. C., and K. L. Walters, 1978, The age of metasomatic anhydrite in Mississippian reservoir carbonates, southeastern Saskatchewan: *Canadian Journal of Earth Sciences*, v. 15, p. 424-430.
- Kendall, C. G. S. C., and P. Skipwith, 1968a, Recent algal mats of a Persian Gulf lagoon: *Journal of Sedimentary Petrology*, v. 38, p. 1040-1058.
- Kendall, C. G. S. C., and P. Skipwith, 1968b, Geomorphology of a recent shallow water carbonate province, Khor al Bazam, Trucial Coast, southwestern Arabian Gulf: *Geological Society of America Bulletin*, v. 80, p. 865-892.
- Kendall, C. G. S. C., and S. P. A. D. E. Skipwith, 1969, Holocene shallow-water carbonate and evaporite sediments of Khor al Bazam, Abu Dhabi, southwest Persian Gulf: *Bulletin American Association of Petroleum Geologists*, v. 53, p. 841-869.
- Kendall, C. G. S. C., and J. K. Warren, 1987, A review of the origin and setting of tepees and their associated fabrics: *Sedimentology*, v. 34, p. 1007-1027.
- Kendall, C. G. S. C., and J. K. Warren, 1988, Peritidal evaporites and their sedimentary assemblages, in B. C. Schreiber, ed., *Evaporites and hydrocarbons*: New York, Columbia University Press, p. 66-138.
- Kenig, F., A. Y. Huc, B. H. Purser, and J. L. Oudin, 1990, Sedimentation, distribution and diagenesis of organic matter in a recent carbonate environment, Abu Dhabi: *Organic Geochemistry*, v. 16, p. 735-747.
- Kennard, J., 1981, The Arrintheta Formation: Upper Cambrian epeiric carbonates in the Georgina Basin, central Australia.:

- Australia Bureau of Mineral Resources, Geology & Geophysics, Bulletin, v. 211, p. 61 pp.
- Kennedy, M., 1993, The Undoolya sequence - Late Proterozoic salt-influenced deposition, Amadeus Basin, central Australia: Australian Journal of Earth Sciences, v. 40, p. 217-228.
- Kennet, J. P., 1982, The Terminal Miocene Event, Global Cooling and the Mediterranean Salinity Crisis, in J. P. Kennet, ed., Marine Geology: Englewood Cliffs, New Jersey, Prentice Hall, p. 738-742.
- Kent, P. E., 1979, The emergent Hormuz salt plugs of southern Iran: Journal of Petroleum Geology, v. 2, p. 117-144.
- Kent, P. E., 1987, Island salt plugs in the Middle East and their tectonic implications, in I. Lerche, and J. J. O'Brien, eds., Dynamical geology of salt and related structures, Academic Press, New York, p. 3-37.
- Kerans, C., and W. M. Fitchen, 1996, Sequence hierarchy and facies architecture of a carbonate-ramp system: San Andres Formation of Algerita escarpment and western Guadalupe Mountains, west Texas and New Mexico: Report of Investigation - Bureau of Economic Geology, Univ of Texas at Austin, v. 235, p. 86p.
- Kerans, C., W. M. Fitchen, W. C. Gardner, and B. R. Wardlow, 1993, New Mexico Geological Society Guidebook: 44th Field Conference, Carlsbad Region, New Mexico and West Texas, p. 175-184.
- Kerans, C., F. J. Lucia, and R. K. Senger, 1994, Integrated characterization of carbonate ramp reservoirs using Permian San Andres Formation outcrop analogs: Bulletin American Association of Petroleum Geologists, v. 78, p. 181-216.
- Kerr, S. D. J., and A. Thomson, 1963, Origin of nodular and bedded anhydrite in Permian shelf sediments, Texas and New Mexico: Bulletin American Association Petroleum Geologists, v. 47, p. 1726-1732.
- Kesler, S. E., H. D. Jones, F. C. Furman, R. Sassen, W. H. Anderson, and J. R. Kyle, 1994, Role of crude oil in the genesis of Mississippi Valley-Type deposits; evidence from the Cincinnati Arch: Geology, v. 22, p. 609-612.
- Kesler, S. E., and L. M. Jones, 1981, Sulfur- and strontium-isotopic geochemistry of celestite, barite and gypsum from the Mesozoic basins of northeastern Mexico: Chemical Geology, v. 31, p. 211-224.
- Kesler, S. E., J. Ruiz, and L. M. Jones, 1988, Strontium isotope geochemistry of the Galeana Barite District, Nuevo Leon, Mexico: Economic Geology, v. 83, p. 1907-1917.
- Kevbrin, V. V., A. M. Lysenko, and T. N. Zhilina, 1997, Physiology of the alkaliphilic methanogen Z-7936, a new strain of Methanosalsus zhilinaeae isolated from Lake Magadi: Microbiology, v. 66, p. 261-266.
- Kezao, C., and J. M. Bowler, 1985, Preliminary study on sedimentary characteristics and evolution of paleoclimate of Qarhan Salt Lake, Qaidam Basin: Scientia Sinica (series B), v. 28, p. 1218-1232.
- Kharaka, Y. K., R. W. Hull, and W. W. Carothers, 1985, Water-rock interactions in sedimentary basins, in G. C. Gautier, Y. K. Kharaka, and R. Surdam, eds., Relationship of organic matter and mineral diagenesis: Tulsa OK, SEPM Short Course Notes, 17, p. 79-272.
- Kholief, M. M., and M. A. Barakat, 1986, New evidence for a petroleum source rock in a Miocene evaporite sequence, Gulf of Suez, Egypt: Journal of Petroleum Geology, v. 9, p. 217-226.
- Khoriby, E. M., 2005, Origin of the gypsum-rich silica nodules, Moghra Formation, Northwest Qattara depression, Western Desert, Egypt: Sedimentary Geology, v. 177, p. 41-55.
- Kiessling, W., E. Flugel, and J. Golonka, 1999, Paleoreef maps: Evaluation of a comprehensive database on Phanerozoic reefs: AAPG Bulletin-American Association of Petroleum Geologists, v. 83, p. 1552-1587.
- King, R. H., 1946, Carnallite-filled mud cracks in Salt Clay: Journal of Sedimentary Petrology, v. 16, p. 14.
- Kinsman, David, J., and J., 1967, Huntite from a carbonate-evaporite environment: Amer. Mineral., v. 52, p. 9-10.
- Kinsman, D. J. J., 1965, Gypsum and anhydrite of recent age, Trucial Coast, Persian Gulf: 2nd Symposium on Salt, Northern Ohio Geological Society, v. 1, 302-326.
- Kinsman, D. J. J., 1969, Modes of formation, sedimentary associations, and diagnostic features of shallow-water and supratidal evaporites: Bulletin American Association of Petroleum Geologists, v. 53, p. 830-840.
- Kinsman, D. J. J., 1973, Evaporite Basins and the Availability of Oxygen in Natural Brines: Int. Symp. Salt, Tech. Program Abstr. Book No.
- Kinsman, D. J. J., 1976, Evaporites; relative humidity control of primary mineral facies: Journal of Sedimentary Petrology, v. 46, p. 273-279.
- Kipfer, R., W. Aeschbachertig, H. Baur, M. Hofer, D. M. Imboden, and P. Signer, 1994, Injection of mantle type helium in Lake Van (Turkey) - the clue for quantifying deep water renewal: Earth & Planetary Science Letters, v. 125, p. 357-370.
- Kirkham, A., 1997, Shoreline Evolution, Aeolian Deflation and Anhydrite Distribution of the Holocene, Abu Dhabi: GeoArabia, v. 2, p. 403-416.
- Kirkham, A., 1998, Pleistocene Carbonate Seif Dunes and their Role in the Development of Complex Past and Present Coastlines of the U.A.E: GeoArabia, v. 3, p. 19-32.
- Kirkland, D. W., R. E. Denison, and W. E. Dean, 2000, Parent brine of the Castile evaporites (Upper Permian), Texas and New Mexico: Journal of Sedimentary Research Section A-Sedimentary Petrology & Processes, v. 70, p. 749-761.
- Kirkland, D. W., and R. Evans, 1976, Origin of limestone buttes, Gypsum Plain, Culberson County, Texas: American Association of Petroleum Geologists, Bulletin, v. 60, p. 2005-2018.
- Kirkland, D. W., and R. Evans, 1980, Origin of castles on the Gypsum Plain of Texas and New Mexico: Guidebook New Mexico Geological Society, v. 31, p. 173-178.
- Kirkland, D. W., and R. Evans, 1981, Source-rock potential of evaporitic environment: Bulletin American Association of Petroleum Geologists, v. 65, p. 181-190.
- Kisler, R. B., and W. C. Smith, 1983, Boron and borates, in S. J. Lefond, ed., Industrial Minerals and Rocks: New York, AIME, p. 533-560.
- Klemme, H. D., 1983, The geologic setting of giant gas fields: Laxemburg, Internation Institute for Applied Systems Analysis, p. 133-160.
- Klemme, H. D., and G. F. Ulmishek, 1991, Effective petroleum source rocks of the world: Stratigraphic distribution and controlling depositional factors: Bulletin American Association of Petroleum Geologists, v. 75, p. 1809-1851.
- Klimchouk, A. B., 1990, Artesian genesis of the large maze caves in the Miocene gypsum of the Western Ukraine: Doklady Akademii Nauk Ukrainskoj SSR, v. Ser. B7, p. 28-32.

- Klimchouk, A. B., 1992, Large gypsum caves in the western Ukraine and their genesis: *Cave Science*, v. 19, p. 3-11.
- Klimchouk, A. B., 1996, Gypsum karst of the world: *Journal of Speleology*, v. 25.
- Klimchouk, A. B., 2000, Speleogenesis of great gypsum mazes in the Western Ukraine, in A. B. Klimchouk, D. Ford, A. N. Palmer, and W. Dreybrodt, eds., *Speleogenesis: Evolution of karst aquifers*: Huntsville, Natl. Speleol. Soc., p. 261-273.
- Klimchouk, A. B., 2003, Unconfined versus confined speleogenetic settings: variations of solution porosity: *Speleogenesis and Evolution of Karst Aquifers 1 (2)*, www.speleogenesis.info, 7 pages. (online journal).
- Klimchouk, A. B., and V. N. Andrejchuk, 2003, Karst breakdown mechanisms from observations in the gypsum caves of the Western Ukraine: Implications for Subsidence Hazard Assessment, *Speleogenesis and Evolution of Karst Aquifers*, *The Virtual Scientific Journal*: www.speleogenesis.info.
- Knauth, L. P., 1998, Salinity history of the Earth's early ocean: *Nature*, v. 395, p. 554-555.
- Knauth, L. P., 2005, Temperature and salinity history of the Precambrian ocean: implications for the course of microbial evolution: *Palaeogeography Palaeoclimatology Palaeoecology*, v. 219, p. 53-69.
- Ko, S. C., D. L. Olgaard, and B. Ueli, 1995, The transition from weakening to strengthening in dehydrating gypsum: Evolution of excess pore pressures: *Geophys. Res. Lett.*, v. 22, p. 1009-1012.
- Ko, S. C., D. L. Olgaard, and T. F. Wong, 1997, Generation and maintenance of pore pressure excess in a dehydrating system. 1. Experimental and microstructural observations: *Journal of Geophysical Research-Solid Earth*, v. 102, p. 825-839.
- Kobluk, D. R., and D. R. Crawford, 1990, A modern hypersaline organic mud- and gypsum-dominated basin and associated microbialites: *Palaios*, v. 5, p. 134-148.
- Koch, A., V. Mathur, R. Nagy, and F. Synder, 1998, Methodology for minibasin ranking in the deepwater Gulf of Mexico: *Intergration of Geologic Models for understanding risk in the Gulf of Mexico*, AAPG Hedberg Research Conference, Galveston Texas.
- Kocurek, G., and J. Nielson, 1986, Conditions favorable for the formation of warm-climate eolian sand sheets: *Sedimentology*, v. 33, p. 795-816.
- Kocurko, M. J., 1979, Dolomitization by spray-zone brine seepage, San Andres, Colombia: *Journal of Sedimentary Petrology*, v. 49, p. 209-214.
- Koehler, G., T. K. Kyser, R. Enkin, and E. Irving, 1997, Paleomagnetic and isotopic evidence for the diagenesis and alteration of evaporites in the Paleozoic Elk Point Basin, Saskatchewan, Canada: *Canadian Journal of Earth Sciences*, v. 34, p. 1619-1629.
- Konishi, Y., J. Prince, and B. Knott, 2001, The fauna of thrombolitic microbialites, Lake Clifton, Western Australia: *Hydrobiologia*, v. 457, p. 39-47.
- Korotkov, A. N., 1974, Caves of the Pinego-Severodvinskaja karst (in Russian): *Geog. Soc. USSR, Leningrad*.
- Kotwicki, V., 1986, *Floods of Lake Eyre*: Adelaide, Engineering and Water Supply Department, 99 p.
- Kotwicki, V., and R. Allan, 1998, La Nina de Australia - contemporary and palaeo-hydrology of Lake Eyre: *Palaeogeography Paleoclimatology Paleocology*, v. 144, p. 265-280.
- Kovalevich, V. M., 1975, Thermometric studies of inclusions in artificial crystals of halite: *Fluid Inclusion Research*, v. 8, p. 96.
- Kovalevich, V. M., 1976, Halite of the salt deposits of Miocene age from the Forecarpathians: *Fluid Inclusion Research*, v. 9, p. 72.
- Kovalevich, V. M., T. M. Peryt, and O. I. Petrichenko, 1998, Secular variation in seawater chemistry during the Phanerozoic as indicated by brine inclusions in halite.: *Journal of Geology*, v. 106, p. 695-712.
- Koyi, H. A., 1988, Experimental modeling of role of gravity and lateral shortening in Zagros mountain belt: *American Association of Petroleum Geologists Bulletin*, v. 72, p. 1381-1394.
- Koyi, H. A., 1991, Gravity overturns, extension, and basement fault activation: *Journal of Petroleum Geology*, v. 12, p. 117-242.
- Koyi, H. A., 1998, The shaping of salt diapirs: *Journal of Structural Geology*, v. 20, p. 321-338.
- Koyi, H. A., 2001, Modeling the influence of sinking anhydrite blocks on salt diapirs targeted for hazardous waste disposal: *Geology*, v. 29, p. 387-390.
- Kraemer, B., D. Adelman, M. Alten, W. Schnurr, K. Erpenstein, E. Kiefer, P. van den Bogaard, and K. Gorler, 1999, Incorporation of the Paleogene foreland into the Neogene Puna plateau: The Salar de Antofalla area, NW Argentina: *Journal of South American Earth Sciences*, v. 12, p. 157-182.
- Krainer, K., and C. Spotl, 1998, Abiogenic silica layers within a fluviolacustrine succession, Balzano volcanic complex, Northern Italy - A Permian analogue for Magadi-type cherts: *Sedimentology*, v. 45, p. 489-505.
- Krauskopf, K. B., 1967, *Introduction to Geochemistry*, McGraw-Hill, 721 p.
- Krekeler, D., A. Teske, and H. Cypionka, 1998, Strategies of sulfate-reducing bacteria to escape oxygen stress in a cyanobacterial mat: *FEMS Microbiology Ecology*, v. 25, p. 89-96.
- Kribek, B., J. Hladikova, K. Zak, J. Bendl, M. Putilova, and Z. Uhlik, 1996, Barite-hyalophane sulfidic ores at Rozna, Bohemian Massif, Czech Republic metamorphosed black shale-hosted submarine exhalative mineralisation: *Economic Geology*, v. 91, p. 14-35.
- Krienitz, L., A. Ballot, K. Kotut, C. Wiegand, S. Pütz, J. S. Metcalf, G. A. Codd, and S. Pflugmache, 2003, Contribution of hot spring cyanobacteria to the mysterious deaths of Lesser Flamingos at Lake Bogoria, Kenya: *FEMS Microbiology Ecology*, v. 43, p. 141-148.
- Krijgsman, W., M. M. Blanc-Valleron, R. Flecker, F. J. Hilgen, T. J. Kouwenhoven, D. Merle, F. Orszag-Sperber, and J. M. Rouchy, 2002, The onset of the Messinian salinity crisis in the Eastern Mediterranean (Pissouri Basin, Cyprus): *Earth & Planetary Science Letters*, v. 194, p. 299-310.
- Krijgsman, W., A. R. Fortuin, F. J. Hilgen, and F. J. Sierro, 2001, Astrochronology for the Messinian Sorbas basin (SE Spain) and orbital (precessional) forcing for evaporite cyclicity: *Sedimentary Geology*, v. 140, p. 43-60.
- Krijgsman, W., F. J. Hilgen, I. Raffi, F. J. Sierro, and D. S. Wilson, 1999, Chronology, causes and progression of the Messinian salinity crisis: *Nature*, v. 400, p. 652-655.
- Krouse, H. R., C. A. Vian, L. S. Eliuk, A. Ueda, and S. Halas, 1988, Chemical and isotopic evidence for thermochemical sulphate reduction by light hydrocarbon gases in deep carbonate reservoirs: *Nature*, v. 333, p. 415-419.

- Krumbein, W. E., Y. Cohen, and M. Shilo, 1977, Solar Lake (Sinai) 4. Stromatolitic cyanobacterial mats: *Limnology and Oceanography*, v. 22, p. 635-656.
- Krumgalz, B. S., A. Hecht, A. Starinsky, and A. Katz, 2000, Thermodynamic constraints on Dead Sea evaporation: can the Dead Sea dry up? *Chemical Geology*, v. 165, p. 1-11.
- Krupp, R., T. Oberthür, and W. Hirdes, 1994, The early Precambrian atmosphere and hydrosphere: Thermodynamic constraints from mineral deposits: *Economic Geology*, v. 89, p. 1581-1598.
- Ku, T. L., S. D. Luo, T. K. Lowenstein, J. R. Li, and R. J. Spencer, 1998, U-series chronology of lacustrine deposits in Death Valley, California: *Quaternary Research*, v. 50, p. 261-275.
- Kulke, H., 1978, Tektonik und Petrographie einer Salinarformation am Beispiel der Trias des Atlassystems (NW-Afrika), in W. Zeil, ed., *Geotektonische Forschungen*, v. 55, p. 1-158.
- Kunasz, I. A., 1983, Lithium raw materials, in S. J. Lefond, ed., *Industrial minerals and rocks: New York, AIME*, p. 869-880.
- Kunstman, A., and M. M. Mazur, 2000, Cavern development and leaching simulation: An introduction to the technology of solution mining; Spring 2000 Technical Class, p. 60-80.
- Kupfer, D., 1976, Shear zones inside Gulf Coast salt stocks help to delineate spines of movement: *Bulletin American Association of Petroleum Geologists*, v. 60, p. 1434-1447.
- Kurlansky, M., 2002, *Salt: A world history*: New York, Walker & Co., 484 p.
- Kushnir, J., 1981, Formation and early diagenesis of varved evaporite sediments in a coastal hypersaline pool: *Journal of Sedimentary Petrology*, v. 51, p. 1193-1203.
- Kushnir, J., 1982, The partitioning of seawater cations during the transformation of gypsum to anhydrite: *Geochimica et Cosmochimica Acta*, v. 46, p. 433-446.
- Kushnir, S. V., 1986, The epigenetic celestite formation mechanism for rocks containing CaSO_4 : *Geochemistry International*, v. 23, p. 1-9.
- Kvenvolden, K. A., and B. R. T. Simoneit, 1990, Hydrothermally derived petroleum: examples from Guaymas Basin, Gulf of California, and Escanaba Trough, northeast Pacific Ocean: *American Association of Petroleum Geologists Bulletin*, v. 74, p. 223-237.
- Kyle, J. R., 1991, Evaporites, evaporitic processes and mineral resources, in J. L. Melvin, ed., *Evaporites, petroleum and mineral resources: Developments in Sedimentology*, v. 50: Amsterdam, Elsevier, p. 477-533.
- Kyle, J. R., and W. A. Gose, 1991, Paleomagnetic Dating of Sulfide Mineralization and Cap Rock Formation in Gulf Coast Salt Domes (abs): *American Association Petroleum Geologists - Bulletin*, v. 75, p. 615.
- Kyle, J. R., and H. H. Posey, 1991, Halokinesis, Cap rock Development and salt dome mineral resources, in J. L. Melvin, ed., *Evaporites, petroleum and mineral resources: Developments in Sedimentology*, v. 50: Amsterdam, Elsevier, p. 413-474.
- Kyle, J. R., and P. E. Price, 1986, Metallic sulphide mineralization in salt-dome cap rocks, Gulf Coast, U.S.A: *Institution of Mining and Metallurgy. Transactions, Section B: Applied Earth Sciences*, v. 95, p. B6-B16.
- Lamb, C. F., 1980, Painter reservoir field giant in Wyoming thrust belt: *Bulletin American Association of Petroleum Geologists*, v. 64, p. 638-644.
- Lambert, S. J., 1983a, Dissolution of Evaporites in and around the Delaware Basin, Southeastern New Mexico and West Texas: Sandia Nat'l. Labs. Report SAND82-0461, Albuquerque, NM, 96 pp.
- Lambert, S. J., 1983b, Evaporite dissolution relevant to the WIPP site, northern Delaware Basin, southeastern New Mexico: Brookins, D. G. Scientific basis for nuclear waste management Vi. Univ. N.m., Dep. Geol., Albuquerque, Nm, United States. p.
- Lambiase, J. J., 1990, A model for tectonic controls of lacustrine stratigraphic sequences in continental rift basins, in B. J. Katz, ed., *Lacustrine Basin Exploration - Case studies and modern analogues*, v. 50: Tulsa, OK, American Association Petroleum Geologists Memoir, p. 265-276.
- Land, L. S., 1985, The origin of massive dolomite: *Journal of Geological Education*, v. 33, p. 112-125.
- Land, L. S., 1991, Evidence for vertical movements of fluids, Gulf Coast sedimentary basin: *Geophysical Research Letters*, v. 18, p. 919-922.
- Land, L. S., 1995a, The role of saline formation water in crustal cycling: *Aquatic Geochemistry*, v. 1, p. 137-145.
- Land, L. S., 1995b, Na-Ca-Cl saline formation waters, Frio Formation (Oligocene), south Texas, USA: *Products of diagenesis: Geochimica et Cosmochimica Acta*, v. 59, p. 2163-2174.
- Land, L. S., R. A. Eustice, L. E. Mack, and J. Horita, 1995, Reactivity of evaporites during burial - An example from the Jurassic of Alabama: *Geochimica et Cosmochimica Acta*, v. 59, p. 3765-3778.
- Land, L. S., J. A. Kupecz, and L. E. Mack, 1988, Louann Salt geochemistry (Gulf of Mexico sedimentary basin, U.S.A.); a preliminary synthesis: *Chemical Geology*, v. 74, p. 25-35.
- Land, L. S., and D. R. Prezbindowski, 1981, The origin and evolution of saline formation water, Lower Cretaceous carbonates, South-central Texas, U.S.A.: *Journal of Hydrology*, v. 54, p. 51-74.
- Landmann, G., G. M. Abu Qudaira, K. Shawabkeh, V. Wrede, and S. Kempe, 2002, Geochemistry of the Lisan and Damya Formations in Jordan, and implications for palaeoclimate: *Quaternary International*, v. 89, p. 45-57.
- Landmann, G., A. Reimer, G. Lemcke, and S. Kempe, 1996, Dating Late Glacial abrupt climate changes in the 14,570 yr long continuous varve record of Lake Van, Turkey: *Palaeogeography Palaeoclimatology Palaeoecology*, v. 122, p. 107-118.
- Langdon, G. S., and J. K. Hall, 1994, Devonian--Carboniferous Tectonics and Basin Deformation in the Cabot Strait Area, Eastern Canada: *Bulletin American Association Petroleum Geologists*, v. 78, p. 1748-1774.
- Langford, R. P., 2003, The Holocene history of the White Sands dune field and influences on eolian deflation and playa lakes: *Quaternary International*, v. 104, p. 31-39.
- Large, D. J., and A. P. Gize, 1996, Pristane/phytane ratios in the mineralized Kupferschiefer of the Fore-Sudetic Monocline, southwest Poland: *Ore Geology Reviews*, v. 11, p. 89-103.
- Larsen, B. D., Z. Ben-Avraham, and H. Shulman, 2002, Fault and salt tectonics in the southern Dead Sea basin: *Tectonophysics*, v. 346, p. 71-90.
- Larsen, D., 1994, Origin and paleoenvironmental significance of calcite pseudomorphs after ikaite in the Oligocene Creede Formation, Colorado: *Journal of Sedimentary Research A: Sedimentary Petrology & Processes*, v. A64, p. 593-603.

- Larsen, D., and L. J. Crossey, 1996, Depositional environments and paleolimnology of an ancient caldera lake - Oligocene Creede Formation, Colorado: *Geological Society of America Bulletin*, v. 108, p. 526-544.
- Last, W. M., 1989a, Continental brines and evaporites of the northern Great Plains of Canada: *Sedimentary Geology*, v. 64, p. 207-221.
- Last, W. M., 1989b, Sedimentology of a saline playa in the northern Great Plains, Canada: *Sedimentology*, v. 36, p. 109-123.
- Last, W. M., 1992, Petrology of carbonate hardgrounds from East Basin Lake, a saline maar lake, southern Australia: *Sedimentary Geology*, v. 81, p. 215-229.
- Last, W. M., 1993a, Salt dissolution features in saline lakes of the northern Great Plains, western Canada: *Geomorphology*, v. 8, p. 321-334.
- Last, W. M., 1993b, Geolimnology of Freeflight Lake: an unusual hypersaline lake in the northern Great Plains of western Canada: *Sedimentology*, v. 40, p. 431-448.
- Last, W. M., 1994, Deep-water evaporite mineral formation in lakes of Western Canada, in R. W. Renaut, and W. M. Last, eds., *Sedimentology and geochemistry of modern and ancient saline lakes*, v. 50, SEPM Special Publication, p. 51-59.
- Last, W. M., and R. E. Vance, 1997, Bedding characteristics of Holocene sediments from salt lake of the Northern Great Plains, western Canada: *Journal of Paleolimnology*, v. 17, p. 297-318.
- Laval, B., S. L. Cady, J. C. Pollack, C. P. McKay, J. S. Bird, J. P. Grotzinger, D. C. Ford, and H. R. Bohm, 2000, Modern freshwater microbialite analogues for ancient dendritic reef structures: *Nature*, v. 407, p. 626-629.
- Lavoie, D., D. F. Sangster, M. M. Savard, and F. Fallara, 1998, Breccias in the lower part of the Mississippian Windsor Group and their relation to Pb-Zn mineralisation: a summary: *Economic Geology*, v. 93, p. 734-735.
- Lawver, L. A., and L. M. Gahagan, 2003, Evolution of Cenozoic seaways in the circum-Antarctic region: *Palaeogeography, Palaeoclimatology, Palaeoecology*, v. 198, p. 11-37.
- Lazar, B., and J. Erez, 1992, Carbon geochemistry of marine-derived brines. I. C-13 depletions due to intense photosynthesis: *Geochimica Cosmochimica Acta*, v. 56, p. 335-345.
- Laznicka, P., 1988, Breccias and coarse fragmentites: petrology, environments, associations, ores: *Developments in Economic Geology*, v. 25: New York, Elsevier, 832 p.
- Leary, D. A., and J. N. Vogt, 1986, Diagenesis of the San Andres Formation (Guadalupian), Central Basin Platform, Permian Basin, in D. G. Bebout, Harris, P. M., ed., *Hydrocarbon Reservoir Studies San Andres/Grayburg Formations, Permian Basin*, SEPM Special Publ. No. 26, p. 67-68.
- LeBlanc, L., 1994, Drilling, completion, workover challenges in subsalt formations: *Offshore*, v. 54, p. 21-22.
- Lee, M. K., and D. D. Williams, 2000, Paleohydrology of the Delaware basin, western Texas: Overpressure development, hydrocarbon migration, and ore genesis: *Bulletin American Association of Petroleum Geologists*, v. 84, p. 961-974.
- Lee, M. R., 1990, The sedimentology and diagenesis of the Raisby Formation (Z1 carbonate), northern England.: Masters thesis, University of Newcastle upon Tyne; Department of Geology.
- Lee, M. R., 1994, Emplacement and diagenesis of gypsum and anhydrite in the late Permian Raisby Formation, north-east England: *Proceedings - Yorkshire Geological Society*, v. 50, p. 143-155.
- Lee, M. R., 1995, Calcite concretions in carbonate rocks of the late Permian Raisby Formation, north-east England: *Proceedings - Yorkshire Geological Society*, v. 50, p. 245-253.
- Lee, M. R., and G. M. Harwood, 1989, Dolomite calcitization and cement zonation related to uplift of the Raisby Formation (Zechstein carbonate), Northeast England: *Sedimentary Geology*, v. 65, p. 285-305.
- Lee, R., and E. De Souza, 1998, The effect of brine on the creep behaviour and dissolution chemistry of evaporites: *Canadian Geotechnical Journal*, v. 35, p. 720-729.
- Lee, R. V., 2001, *Maladies, malaise, and modernization: health and development in Ladakh*: *Asian Affairs*, v. 32, p. 300-306.
- Lefond, S. J., 1983, *Industrial Minerals and rocks (Nonmetallics other than fuels)*: New York, Soc. Mining Engineers of the American Inst. Mining Metallurgical and Petroleum Engineers..
- Lehmann, C., D. A. Osleger, and I. P. Montanez, 1998, Controls on cyclostratigraphy of Lower Cretaceous carbonates and evaporites, Cupido and Coahuila platforms, northeastern: *Journal of Sedimentary Research*, v. 68, p. 1109-1130.
- Lehmann, C., D. A. Osleger, and I. Montanez, 2000, Sequence stratigraphy of Lower Cretaceous (Barremian-Albian) carbonate platforms of northeastern Mexico: regional and global correlations: *Journal of Sedimentary Research Section A-Sedimentary Petrology & Processes*, v. 70, p. 373-391.
- Lehner, P., 1969, Salt tectonics and Pleistocene stratigraphy on continental slope of northern Gulf of Mexico: *Bulletin American Association Petroleum Geologists*, v. 53, p. 2431-2479.
- Leibold, A. W., 1992, Sedimentological and geochemical constraints on Niagara/Salina deposition, Michigan Basin: Doctoral thesis, University of Michigan, 280 p.
- Leibold, A. W., L. M. Walter, T. J. Huston, and N. J. R. O', 1992, Fluid inclusion geochemistry of halite from the Silurian A-1 Evaporite, Michigan Basin: *Abstracts Geological Society of America*, v. 24, p. 334.
- Lemon, N. M., 1985, Physical Modelling of Sedimentation Adjacent to Diapirs and Comparison with Late Precambrian Oratunga Breccia Body in Central Flinders Ranges, South Australia: *American Association Petroleum Geologists Bulletin*, v. 69, p. 1327 - 1328.
- Lemon, N. M., 1988, Diapir recognition and modelling with examples from the Late Proterozoic Adelaide Geosyncline, Central Flinders Ranges, South Australia: Doctoral thesis, University of Adelaide.
- Lemon, N. M., 2000, A Neoproterozoic fringing stromatolite reef complex, Flinders Ranges, South Australia: *Precambrian Research*, v. 100, p. 109-120.
- Lerche, I., and K. Petersen, 1995, *Salt and Sediment Dynamics*: Boca Raton, CRC Press, 322 p.
- Leslie, A. B., G. M. Harwood, and A. C. Kendall, 1997, Geochemical variations within a laminated evaporite deposit: Evidence for brine composition during formation of the Permian Castile Formation, Texas and New Mexico, USA: *Sedimentary Geology*, v. 110, p. 223-235.

- Leslie, A. B., A. C. Kendall, G. M. Harwood, and D. W. Powers, 1996, Conflicting indicators of palaeoceanographic depth during deposition of the upper Permian Castile Formation, Texas and New Mexico, in A. E. S. Kemp, ed., *Palaeoclimatology and Palaeoceanography from Laminated Sediments*: London, Geological Society London Special Publication, No. 116, p. 111-124.
- Letouzey, J., B. Colletta, R. Vially, and J. C. Chermette, 1995, Evolution of salt-related structures in compressional settings, in M. P. A. Jackson, D. G. Roberts, and S. Snelson, eds., *Salt tectonics: a global perspective*, AAPG Memoir, v. 65, p. 41-60.
- Letouzey, J., P. Werner, and Y. Marty, 1990, Fault reactivation and structural inversion; backarc and intraplate compressive deformations; example of the eastern Sunda Shelf (Indonesia): *Tectonophysics*, v. 183, p. 341-362.
- Lévet, S., J. P. Toutain, M. Munoz, G. Berger, P. Negrel, N. Jendrzewski, P. Agrinier, and F. Sortino, 2002, Geochemistry of the Bagnères-de-Bigorre thermal waters from the North Pyrenean Zone (France): *Geofluids*, v. 2, p. 25-40.
- Levy, D. B., J. A. Schramke, K. J. Esposito, T. A. Erickson, and J. C. Moore, 1999, The shallow ground water chemistry of arsenic, fluorine, and major elements: Eastern Owens Lake, California: *Applied Geochemistry*, v. 14, p. 53-65.
- Levy, Y., 1977a, Description and mode of formation of the supratidal evaporite facies in northern Sinai coastal plain: *Journal of Sedimentary Petrology*, v. 47, p. 463-474.
- Levy, Y., 1977b, The origin and evolution of brine in coastal sabkhas, Northern Sinai: *Journal of Sedimentary Petrology*, v. 47, p. 451-462.
- Levy, Y., 1980, Evaporitic environments in the Northern Sinai, in A. Nissenbaum, ed., *Hypersaline brines and evaporitic environments*, Elsevier, Amsterdam, p. 131-143.
- Levy, Y., 1984, Halite from the bottom of the Dead Sea: *Geolo. Surv. Israel Report GSI/48/84*.
- Lewan, M. D., 1984, Factors controlling the proportionality of vanadium to nickel in crude oils: *Geochimica et Cosmochimica Acta*, v. 48, p. 2231-2238.
- Lewis, S., and M. Holness, 1996, Equilibrium halite-H₂O dihedral angles: High rock salt permeability in the shallow crust: *Geology*, v. 24, p. 431-434.
- Leyrer, K., C. Strohmenger, K. Rockenbauch, and T. Bechstaedt, 2001, High resolution forward stratigraphic modeling of Ca-2 carbonate platforms and off-platform highs (Upper Permian, Northern Germany), Springer Verlag.
- Li, J. R., T. K. Lowenstein, and I. R. Blackburn, 1997, Responses of evaporite mineralogy to inflow water sources and climate during the past 100 Ky in Death Valley California: *Geological Society of America Bulletin*, v. 109, p. 1361-1371.
- Li, J. R., T. K. Lowenstein, C. B. Brown, T. L. Ku, and S. D. Luo, 1996, A 100 ka record of water tables and paleoclimates from salt cores, Death Valley, California: *Palaeogeography Palaeoclimatology Palaeoecology*, v. 123, p. 179-203.
- Li, M., G. Ma, K. Guttikonda, S. Boyages, and C. Eastman, 2001, The re-emergence of iodine deficiency in Sydney, Australia: *Asia Pacific J of Clin. Nutr.*, v. 10, p. 200-203.
- Li, Y. H., and S. Gregory, 1974, Diffusion of ions in sea water and in deep-sea sediments: *Geochimica et Cosmochimica Acta*, v. 38, p. 703-714.
- Li, Z. X., C. M. Powell, and R. Bowman, 1993, Timing and genesis of Hamersley iron-ore deposits: *Exploration Geophysics*, v. 24, p. 631-636.
- Liang-Jie Tang, Cheng-Zao Jia, Zhi-Jun Jin, Shu-Ping Chen, Xue-Jun Pi, and H.-W. Xie, 2004, Salt tectonic evolution and hydrocarbon accumulation of Kuqa foreland fold belt, Tarim Basin, NW China: *Journal of Petroleum Science and Engineering*, v. 41, p. 97-108.
- Liebold III, A. W., and P. Howell, 1991, Death of a Carbonate Basin: The Niagara-Salina Transition in the Michigan Basin (abs.): *Bulletin American Association of Petroleum Geologists*, v. 75, p. 619.
- Light, M. P. R., and H. H. Posey, 1992, Diagenesis and its relation to mineralisation and hydrocarbon reservoir development; Gulf Coast and North Sea Basins, in K. H. Chilingar, and G. V. Wolf, eds., *Diagenesis III*: Oxford-Amsterdam-New York, Elsevier, p. 511-541.
- Lindsay, J. F., 1987, Upper Proterozoic evaporites in the Amadeus Basin, central Australia, and their role in basin tectonics: *Geological Society of America Bulletin*, v. 99, p. 852-865.
- Lindsay, R. F., and C. G. S. C. Kendall, 1985, Depositional facies, diagenesis, and reservoir character of Mississippian cyclic carbonates in the Mission Canyon Formation, Little Knife field, Williston Basin, North Dakota, in P. O. Roehl, and P. W. Choquette, eds., *Carbonate petroleum reservoirs*: New York, Springer-Verlag, p. 175-190.
- Linn, J. K., and J. Culbert, 1999, Experience in underground storage of crude oil in salt: *Special Publication 90, Geo-Inst. ASCE*, p. 810 p.
- Linn, K. O., and S. S. Adams, 1966, Barren halite zones in potash deposits, Carlsbad, New Mexico: *Second Symposium on Salt*, p. 59-68.
- Liro, L. M., 1992, Distribution of shallow salt structures, lower slope of the northern Gulf of Mexico, USA: *Marine and Petroleum Geology*, v. 9, p. 433-451.
- Lisk, M., M. M. Faiz, E. B. Bekele, and T. E. Ruble, 2000, Transient fluid flow in the Timor Sea, Australia: implications for prediction of fault seal integrity: *Journal of Geochemical Exploration*, v. 69, p. 607-613.
- Liu, W. G., Y. K. Xiao, Z. C. Peng, Z. S. An, and X. X. He, 2000, Boron concentration and isotopic composition of halite from experiments and salt lakes in the Qaidam Basin: *Geochimica et Cosmochimica Acta*, v. 64, p. 2177-2183.
- Lock, D. E., 1986, The formation of modern epsomite deposits near Lake Eyre, and their significance for Early-Cainozoic weathering in central Australia: *Sediments down under. 12th International Sedimentological Congress, Canberra, Australia, 24-30 August, 1986. International Sedimentological Congress.*, p. 189.
- Lofi, J., C. Gorini, S. Berne, G. Clauzon, A. T. Dos Reis, W. B. F. Ryan, and M. S. Steckler, 2005, Erosional processes and paleo-environmental changes in the Western Gulf of Lions (SW France) during the Messinian Salinity Crisis: *Marine Geology*, v. 217, p. 1-30.
- Logan, B. W., 1987, The MacLeod evaporite basin, western Australia; Holocene environments, sediments and geological evolution: Tulsa, OK, American Association of Petroleum Geologists, Memoir 44, 140 p.
- Logan, B. W., and R. G. Brown, 1976, Shark Bay, University of Western Australia, Excursion Guide, p. 63.

- Logan, G. A., J. M. Hayes, G. B. Hieshima, and R. E. Summons, 1995, Terminal Proterozoic reorganisation of biogeochemical cycles: *Nature*, v. 376, p. 53-56.
- Lohmann, H. H., 1979, Seismic recognition of salt diapirs: *Bulletin American Association of Petroleum Geologists*, v. 63, p. 2097-2102.
- Lomando, A. J., 1999, Structural influences on facies trends of carbonate inner ramp systems, examples from the Kuwait-Saudi Arabian coast of the Arabian Gulf and Northern Yucatan, Mexico: *GeoArabia*, v. 4, p. 339-360.
- Lomando, A. J., T. P. Birdsall, and C. L. Goll, 1984, Deposition and porosity evolution of Rodessa (Lower Cretaceous) grainstone reservoirs, examples from West Purl and Bois D'Arc fields, Texas, in P. M. Harris, ed., *Carbonate sands – a core workshop*, v. 5, Society of Economic Paleontologists Mineralogists Core Workshop, p. 365-390.
- Long, A., C. J. Eastoe, A. S. Kaufmann, J. G. Martin, L. Wirt, and J. B. Finley, 1993, High precision of chlorine stable isotope ratios: *Geochemica et Cosmochimica Acta*, v. 57, p. 2907-2912.
- Long, D. T., N. E. Fegan, W. B. Lyons, M. E. Hines, P. G. Macumber, and A. M. Giblin, 1992a, Geochemistry of acid brines: Lake Tyrrell, Victoria, Australia.: *Chemical Geology*, v. 1-2.
- Long, D. T., N. E. Fegan, J. D. McKee, W. B. Lyons, M. E. Hines, and P. G. Macumber, 1992b, Formation of alunite, jarosite and hydrous iron oxides in a hypersaline system: Lake Tyrrell, Victoria, Australia.: *Chemical Geology*, v. 96, p. 183-202.
- Long, L. E., M. E. Erwin, and R. S. Fisher, 1997, Rb-Sr ages of diagenesis of Mg-rich clay in Permian sediments, Palo Duro Basin, Texas Panhandle, USA: *Journal of Sedimentary Research Section A-Sedimentary Petrology & Processes*, v. 67, p. 225-234.
- Longman, M. W., T. G. Fertal, and J. S. Glennie, 1983, Origin and geometry of Red River Dolomite reservoirs, western Williston Basin: *Bulletin American Association of Petroleum Geologists*, v. 67, p. 744-771.
- Longman, M. W., and F. M. Haidl, 1996, Cyclic deposition and development of porous dolomites in the Upper Ordovician Red River Formation, Williston basin, in M. W. Longman, and M. D. Sonnenfeld, eds., *Paleozoic systems of the Rocky Mountain region, Rocky Mountain Section, Society for Sedimentary Geology*, p. 29-46.
- Looff, K. M., 2000, Geologic and Microstructural Evidence of Differential Salt Movement at Weeks Island Salt Dome, Iberia Parish, Louisiana: *Gulf Coast Association of Geological Societies Transactions*, v. 50, p. 543-555.
- Looff, K. M., 2001, Recent Salt Related Uplift and Subsidence at Sour Lake Salt Dome, Hardin County, Texas: *Gulf Coast Association of Geological Societies Transactions*, v. 51, p. 187-194.
- Loope, D. B., 1984, Discussion: Origin of extensive bedding planes in aeolian sandstones: a defence of Stoke's hypothesis: *Sedimentology*, v. 31, p. 123-125.
- Loope, D. B., and Z. E. Haverland, 1988, Giant desiccation fissures filled with calcareous eolian sand, Hermosa Formation (Pennsylvanian), southeastern Utah: *Sedimentary Geology*, v. 56, p. 403-413.
- Loosveld, R. J. H., A. Bell, and J. J. M. Terken, 1996, The Tectonic Evolution of Interior Oman: *GeoArabia*, v. 1, p. 28-51.
- Loreau, J. P., and B. H. Purser, 1973, Distribution and ultrastructure of Holocene ooids in the Persian Gulf, in B. H. Purser, ed., *The Persian Gulf: Holocene carbonate sedimentation, and diagenesis in a shallow epicontinental sea*: Berlin, Springer-Verlag, p. 279-328.
- Lorenz, J. C., 1988, Synthesis of late Paleozoic and Triassic redbed sedimentation in Morocco, in V. H. Jacobshagen, ed., *The Atlas system of Morocco; studies on its geodynamic evolution*, v. 15: Berlin, Springer-Verlag, Berlin-Heidelberg-New York, Lecture Notes in Earth Sciences, p. 139-168.
- Losh, S., E. Eglinton, M. Schoell, and J. Wood, 1999, Vertical and lateral fluid flow related to a large growth fault, South Eugene Island Block 330 field, offshore Louisiana: *Bulletin American Association of Petroleum Geologists*, v. 83, p. 244-276.
- Losh, S., L. M. Walter, P. Meulbroek, A. Martini, L. M. Cathles III, and J. K. Whelan, 2002, Reservoir fluids and their migration into the South Eugene Island Block 330 reservoirs, offshore Louisiana: *American Association Petroleum Geologists - Bulletin*, v. 86, p. 1463-1488.
- Lotze, F., 1957, *Steinsalz und Kalisalze*: Berlin, Gebruder Borntraeger.
- Loucks, R. G., and J. H. Anderson, 1985, Depositional facies, diagenetic terranes and porosity development in Lower Ordovician Ellenberger Dolomite, Puckett field, west Texas, in P. O. Roehl, and P. W. Choquette, eds., *Carbonate petroleum reservoirs*: New York, Springer-Verlag, p. 19-37.
- Loucks, R. G., and J. O. Crump, 1985, Vertical facies sequences of the Sunniland and Punta Gorda formations in the Lower Cretaceous South Florida Embayment; Natural Resource Management Corporation No. 31-2 Alico core: Bebout, D. G., Ratcliff, D. Lower Cretaceous depositional environments from shoreline to slope; a core workshop. Univ. Tex. at Austin, Bur. Econ. Geol., Austin, Tx, United States.
- Loucks, R. G., and M. W. Longman, 1982, Lower Cretaceous Ferry Lake Anhydrite, Fairway Field, East Texas; product of shallow-subtidal deposition, in C. R. Handford, R. G. Loucks, and G. R. Davies, eds., *Depositional and diagenetic spectra of evaporites; a core workshop*, v. 3: Tulsa, OK, SEPM, p. 130-173.
- Loucks, R. G., and J. F. Sarg, 1993, Carbonate sequence stratigraphy: recent developments and applications, v. *American Association of Petroleum Geologists Memoir 57*: Tulsa, Oklahoma, U.S.A.
- Loutfi, G., and S. El-Bishlawi, 1986, Habitat of hydrocarbon in Abu Dhabi, UAE: *Symposium on the hydrocarbon potential of intense thrust zones*, p. 65-124.
- Lowe, D. R., 1983, Restricted shallow-water sedimentation of early Archean stromatolitic and evaporitic strata of the Strelley Pool Chert, Pilbara Block, Western Australia: *Precambrian Research*, v. 19, p. 239-283.
- Lowe, D. R., and M. M. Tice, 2004, Geologic evidence for Archean atmospheric and climatic evolution: Fluctuating levels of CO₂, CH₄, and O₂ with an overriding tectonic control: *Geology*, v. 32, p. 493-496.
- Lowe, D. R., and G. F. Worrell, 1999, Sedimentology, mineralogy, and implications of silicified evaporites in the Kromberg Formation, Barberton greenstone belt, South Africa: *Special Paper - Geological Society of America*, v. 329, p. 167-188.
- Lowenstein, T. K., 1987a, Evaporite depositional fabrics in the deeply buried Jurassic Buckner Formation, Alabama: *Journal of Sedimentary Petrology*, v. 57, p. 108-116.
- Lowenstein, T. K., 1987b, Origin of depositional cycles in a Permian "saline giant"; the Salado (McNutt Zone) evaporites of New

- Mexico and Texas: Geological Society of America Bulletin, v. 100, p. 592-608.
- Lowenstein, T. K., and L. A. Hardie, 1985, Criteria for the recognition of salt-pan evaporites: *Sedimentology*, v. 32, p. 627-644.
- Lowenstein, T. K., L. A. Hardie, M. N. Timofeeff, and R. V. Demicco, 2003a, Secular variation in seawater chemistry and the origin of calcium chloride basinal brines: *Geology*, v. 31, p. 857-860.
- Lowenstein, T. K., M. C. Hein, A. L. Bobst, T. E. Jordan, T. L. Ku, and S. Luo, 2003, An assessment of stratigraphic completeness in climate-sensitive closed-basin lake sediments: Salar de Atacama, Chile: *Journal of Sedimentary Research*, v. 73, p. 91-104.
- Lowenstein, T. K., J. R. Li, C. Brown, S. Roberts, M., T. L. Ku, S. D. Luo, and W. B. Yang, 1999, 200 ky paleoclimate record from Death Valley salt core: *Geology*, v. 27, p. 3-6.
- Lowenstein, T. K., and R. J. Spencer, 1990, Syndepositional origin of potash evaporites; petrographic and fluid inclusion evidence: *American Journal of Science*, v. 290, p. 43-106.
- Lowenstein, T. K., R. J. Spencer, and P. Zhang, 1989, Origin of ancient potash evaporites; clues from the modern Qaidam Basin, western China: *Science*, v. 245, p. 1090-1092.
- Lowenstein, T. K., M. N. Timofeeff, S. T. Brennan, H. L. A., and R. V. Demicco, 2001, Oscillations in Phanerozoic seawater chemistry: Evidence from fluid inclusions: *Science*, v. 294.
- Lowry, D. C., 1967, Halite speleothems from the Nullarbor Plain, Western Australia: *Helveticite*, v. 6, p. 14-20.
- Lu, F. H., and W. J. Meyers, 1998, Massive dolomitisation of a Late Miocene carbonate platform - A case of mixed evaporative brines with meteoric water, Nijar, Spain: *Sedimentology*, v. 45, p. 263-277.
- Lu, F. H., W. J. Meyers, and G. N. Hanson, 2002, Trace elements and environmental significance of Messinian gypsum deposits, the Nijar Basin, southeastern Spain: *Chemical Geology*, v. 192, p. 149-161.
- Lucas, S. G., and O. R. Anderson, 1994, Ochoan (Upper Permian) stratigraphy and age determinations, southeastern New Mexico and West Texas: *Bulletin American Association of Petroleum Geologists*, v. 78, p. 496.
- Lucia, F. J., 1961, Dedolomitization in the Tansill (Permian) formation: *Geol. Soc. America Bull.*, v. 72, p. 1107-1109.
- Lucia, F. J., 1968, Recent sediments and diagenesis of south Bonaire, Netherlands Antilles: *Journal of Sedimentary Petrology*, p. 845-858.
- Lucia, F. J., 1972, Recognition of evaporite-carbonate shoreline sedimentation, in J. K. Rigby, and W. K. Hamblin, eds., *Recognition of ancient sedimentary environments*, v. 16, Soc. Econ. Paleontol. Mineral., Spec. Publ., p. 190-191.
- Lucia, F. J., J. W. Jennings, and M. Rahnis, 2001, Permeability and rock fabric from wireline logs, Arab-D reservoir, Ghawar Field, Saudi Arabia: *GeoArabia*, v. 6, p. 619-646.
- Lucia, F. J., and R. P. Major, 1994, Porosity evolution through hypersaline reflux dolomitization, in B. Purser, M. Tucker, and D. Zenger, eds., *Dolomites - A Volume in Honour of Dolomieu*, International Association of Sedimentologists Special Publication No. 21, p. 325-341.
- Lucia, J. F., 1999, *Carbonate reservoir characterisation*: Berlin, Springer, 226 p.
- Luczaj, J. A., and R. H. Goldstein, 2000, Diagenesis of the lower Permian Krider member, southwest Kansas, USA: Fluid-inclusion, U-Pb, and fission-track evidence for reflux dolomitization during latest Permian time: *Journal of Sedimentary Research Section A-Sedimentary Petrology & Processes*, v. 70, p. 762-773.
- Ludbrook, N. H., 1965, Occurrence of foraminifera in salt lakes.: *Quarterly geological notes*, Geological Survey of South Australia, v. 14, p. 6-7.
- Luebking, G. A., M. W. Longman, and W. J. Carlisle, 2001, Unconformity-related chert/dolomite production in the Pennsylvanian Amsden Formation, Wolf Springs fields, Bull Mountains basin of central Montana: *American Association of Petroleum Geologists Bulletin*, v. 85, p. 131-148.
- Lugli, S., 2001, Timing of post-depositional events in the Burano Formation of the Secchia valley (Upper Triassic, Northern Apennines), clues from gypsum-anhydrite transitions and carbonate metasomatism: *Sedimentary Geology*, v. 140, p. 107-122.
- Lugli, S., G. Morteani, and D. Blamart, 2002, Petrographic, REE, fluid inclusion and stable isotope study of magnesite from the Upper Triassic Burano Evaporites (Secchia Valley, northern Apennines): contributions from sedimentary, hydrothermal and metasomatic sources: *Mineralium Deposita*, v. 37, p. 480-494.
- Lugli, S., B. C. Schreiber, and B. Triberti, 1999, Giant polygons in the Realmonte mine (Agrigento, Sicily): Evidence for the desiccation of a Messinian halite basin: *Journal of Sedimentary Research Section A-Sedimentary Petrology & Processes*, v. 69, p. 764-771.
- Luján, M., F. Storti, J. C. Balanya, A. Crespo-Blanc, and F. Rossetti, 2003, Role of decollement material with different rheological properties in the structure of the Aljibe thrust imbricate (Flysch Trough, Gibraltar Arc): an analogue modelling approach: *Journal of Structural Geology*, v. 25, p. 867-881.
- Lynch, G., and P. S. Giles, 1996, The Ainslie Detachment: a regional flat-lying extensional fault in the Carboniferous evaporitic Maritimes Basin of Nova Scotia, Canada: *Canadian Journal of Earth Sciences*, v. 33, p. 169-181.
- Lynch, G., and J. V. A. Keller, 1998, Association between detachment faulting and salt diapirs in the Devonian-Carboniferous Maritimes Basin, Atlantic Canada: *Bulletin of Canadian Petroleum Geology*, v. 46, p. 189-209.
- Lynch, G., J. V. A. Keller, and P. S. Giles, 1998, Influence of the Ainslie Detachment on the stratigraphy of the Maritimes Basin and mineralisation in the Windsor Group of Northern Nova Scotia, Canada: *Economic Geology*, v. 93, p. 703-718.
- Lyons, W. B., H. E. Gaudette, and H. C. Gustafson, 1982, Dissolved organic carbon in pore waters from a hypersaline environment: *Organic geochemistry*, v. 3, p. 133-135.
- Lyons, W. B., M. E. Hines, and H. E. Gaudette, 1984, Major and minor pore water geochemistry of modern marine sabkhas: the influence of cyanobacterial mats, in Y. Cohen, R. W. Castenholz, and H. O. Halvorsor, eds., *Microbial Mats: Stromatolites*: New York, A. R. Liss, p. 411-424.
- Lyons, W. B., S. W. Tyler, H. E. Gaudette, and D. T. Long, 1995, The use of strontium isotopes in determining groundwater mixing and brine fingering in a playa spring zone, Lake Tyrrell, Australia: *Journal of Hydrology*, v. 167, p. 225-239.
- Ma, Z. Q., 1998, The geological characteristics and the formative conditions of the Gantang gypsum deposit in Ningxia, China: *Carbonates & Evaporites*, v. 13, p. 100-107.

- Mabelya, L., W. H. V. Helderman, M. A. Vanthof, and K. G. Konig, 1997, Dental fluorosis and the use of a high fluoride-containing trona tenderizer (Magadi): Community Dentistry & Oral Epidemiology, v. 25, p. 170-176.
- Macaluso, T., and U. Sauro, 1996, Weathering and Karren on exposed gypsum surfaces: International Journal of Speleology, v. 25, p. 115-126.
- MacDonald, G. J. F., 1953, Anhydrite-gypsum equilibrium relations: Am. Jour. Sci., p. 884-898.
- MacDonald, I. R., 1992, Sea-floor brine pools affect behavior, mortality, and preservation of fishes in the Gulf of Mexico: lagerstätten in the making? Palaios, v. 7, p. 383-387.
- MacDonald, I. R., M. B. Peccini, and N. L. Guinasso Jr, 2000, Pulsed oil discharge from a mud volcano: Geology, v. 28, p. 907-910.
- MacDonald, I. R., J. F. Reilly, N. L. Guinasso, J. M. Brooks, R. S. Carney, W. A. Bryant, and T. J. Bright, 1990, Chemosynthetic mussels at a brine-filled pockmark in the northern Gulf of Mexico: Science, v. 248, p. 1096-1099.
- MacDonald, I. R., W. W. Sager, and M. B. Peccini, 2003, Gas hydrate and chemosynthetic biota in mounded bathymetry at mid-slope hydrocarbon seeps: Northern Gulf of Mexico: Marine Geology, v. 198, p. 133-158.
- McDonnell, C., M. Harris, and M. Zacharin, 2003, Iodine Deficiency and goitre in schoolchildren in Melbourne, 2001: Med. J. Aust., v. 178, p. 159-162.
- Macgregor, D. S., 1996, Factors controlling the destruction or preservation of giant light oil fields: Petroleum Geoscience, v. 2, p. 197-217.
- Machel, H. G., 1987, Some aspects of diagenetic sulphate-hydrocarbon redox reactions, in J. D. Marshall, ed., Diagenesis of sedimentary sequences: Geological Society Special Publications, v. 36: London, Geological Society, p. 15-28.
- Machel, H. G., 1989, Relationships between sulphate reduction and oxidation of organic compounds to carbonate diagenesis, hydrocarbon accumulations, salt domes, and metal sulphide deposits: Carbonates & Evaporites, v. 4, p. 137-151.
- Machel, H. G., 1993, Anhydrite nodules formed during deep burial: Journal of Sedimentary Petrology, v. 63, p. 659-662.
- Machel, H. G., 1998, Gas Souring by Thermochemical Sulfate Reduction at 140°C: A discussion: Bulletin American Association of Petroleum Geologists, v. 82, p. 1870-1873.
- Machel, H. G., 2001, Bacterial and thermochemical sulfate reduction in diagenetic settings - old and new insights: Sedimentary Geology, v. 140, p. 143-175.
- Machel, H. G., and E. A. Burton, 1991, Burial-diagenetic sabkha-like gypsum and anhydrite nodules: Chemical Geology, v. 90, p. 211-231.
- Machel, H. G., H. R. Krouse, and R. Sassen, 1995, Products and distinguishing criteria of bacterial and thermochemical sulfate reduction: Applied Geochemistry, v. 10, p. 373-389.
- Macumber, P. G., 1992, Hydrological processes in the Tyrell Basin, southeastern Australia: Chemical Geology, v. 96, p. 1-18.
- Magara, K., 1986, Geological models of petroleum entrapment: London, United Kingdom, Elsevier Appl. Sci. Publ.
- Magara, K., M. S. Khan, F. A. Sharief, and H. N. Alkhatib, 1993, Log-derived reservoir properties and porosity preservation of Upper Jurassic Arab Formation in Saudi-Arabia: Marine & Petroleum Geology, v. 10, p. 352-363.
- Magaritz, M., 1987, A new explanation for cyclic deposition in marine evaporite basins; meteoric water input: Chemical Geology, v. 62, p. 239-250.
- Magee, J., G. H. Miller, N. A. Spooner, and D. Questiaux, 2004, Continuous 150 k.y. monsoon record from Lake Eyre, Australia: Insolation-forcing implications and unexpected Holocene failure: Geology, v. 32, p. 885-888.
- Magee, J. W., 1991, Late Quaternary lacustrine, groundwater, aeolian and pedogenic gypsum in the Prungle Lakes, southeastern Australia: Palaeogeography, Palaeoclimatology, Palaeoecology, v. 84, p. 229-257.
- Magee, J. W., J. M. Bowler, G. H. Miller, and D. L. G. Williams, 1995, Stratigraphy, sedimentology, chronology and palaeohydrology of Quaternary lacustrine deposits at Madigan Gulf, Lake Eyre, South Australia: Palaeogeography Palaeoclimatology Palaeoecology, v. 113, p. 3-42.
- Magee, J. W., and G. H. Miller, 1998, Lake Eyre palaeohydrology from 60 ka to the present: beach ridges and glacial maximum aridity: Palaeogeography Palaeoclimatology Palaeoecology, v. 144, p. 307-329.
- Maglione, G., 1980, An example of Recent continental evaporitic sedimentation; the Chadian Basin (Africa), in G. Busson, ed., Evaporite deposits; illustration and interpretation of some environmental sequences: London, Editions Technip, marketed Graham & Trotman, p. 5-9 & 74-91 (photos).
- Maiklem, W. R., 1971, Evaporative drawdown - a mechanism for water level lowering and diagenesis in the Elk Point Basin: Bulletin Canadian Petroleum Geology, v. 19, p. 487-503.
- Maisonneuve, J., 1982, The composition of the Precambrian ocean waters: Sedimentary Geology, v. 31, p. 1-11.
- Majid, A. H., 1987, Exploration Strategy in Keg River Carbonates of Northwestern Alberta, Canada (abs.): Bulletin American Association of Petroleum Geologists, v. 71, p. 588.
- Malek, E., G. E. Bingham, and G. D. McCurdy, 1990, Evapotranspiration from the margin and moist playa of a closed desert valley: Journal of Hydrology, v. 120, p. 15-34.
- Malek-Aslani, M., 1980, Environmental and diagenetic controls of carbonate and evaporite source rocks: Transactions Gulf Coast Association of Geological Societies, v. 30, p. 445-456.
- Maliva, R. G., 1987, Quartz geodes; early diagenetic silicified anhydrite nodules related to dolomitization: Journal of Sedimentary Petrology, v. 57, p. 1054-1059.
- Maltsev, V. A., and D. C. Ford, 1991, The influence of seasonal changes of cave microclimate upon the genesis of gypsum formations in caves: NSS Bulletin, v. 52, p. 99-103.
- Maltsev, V. A., and D. I. Malishevsky, 1990, On hydrothermal phases during later stages of the evolution of Cup Coutunn Cave system, Turkmenia, USSR: NSS Bulletin, v. 52, p. 95-98.
- Mancini, E. A., and D. J. Benson, 1980, Regional stratigraphy of the Upper Jurassic Smackover carbonates of southwest Alabama: Transactions of Gulf Coast Association of Geological Societies, v. 30, p. 151-165.
- Mancini, E. A., J. Benson, B. S. Hart, R. S. Balch, W. C. Parcell, and B. J. Panetta, 2000, Appleton field case study (eastern Gulf coastal

- plain): Field development model for Upper Jurassic microbial reef reservoirs associated with paleotopographic basement structures (E & PNotes): *American Association Petroleum Geologists - Bulletin*, v. 84, p. 1699-1717.
- Manega, P. C., and S. Bieda, 1987, Modern sediments of Lake Natron, Tanzania: *Sciences Geologiques - Bulletin*, v. 40, p. 83-95.
- Mann, C. J., and W. M. Nelson, 1989, Microbialitic structures in Storr's Lake, San Salvador Island, Bahamas Islands: *Palaios*, v. 4, p. 287-293.
- Mann, S. D., 1990, Depositional facies of saltern evaporites of the Buckner Anhydrite Member of the Haynesville Formation of southwestern Alabama: Geological Society of America, Southeastern Section, 39th annual meeting. Abstracts with Programs Geological Society of America, v. 22, p. 24.
- Mann, S. D., and M. D. C. Kopaska, 1992, Depositional history of the Smackover-Buckner transition, eastern Mississippi interior salt basin: *AAPG Bulletin*, v. 76, p. 1463.
- Manzi, V., S. Lugli, F. R. Lucchi, and M. Roveri, 2005, Deep-water clastic evaporites deposition in the Messinian Adriatic foredeep (northern Apennines, Italy): did the Mediterranean ever dry out? *Sedimentology*, v. 52, p. 875-902.
- Marco, S., R. Weinberger, and A. Agnon, 2002, Radial clastic dykes formed by a salt diapir in the Dead Sea Rift, Israel: *Terra Nova*, v. 14, p. 288-294.
- Mariner, R. H., and R. C. Surdam, 1970, Alkalinity and formation of zeolites in saline alkaline lakes: *Science*, v. 170, p. 977-980.
- Marion, G. M., R. Farren, and A. Komrowski, 1999, Alternative pathways for seawater freezing: *Cold Regions Science and Technology*, v. 29, p. 259-266.
- Margulis, L., and M. F. Dolan, 2002, *Early Life: Evolution on the Precambrian Earth*, Jones and Bartlett, 224 p.
- Markl, G., and K. Bucher, 1998, Composition of fluids in the lower crust inferred from metamorphic salt in lower crustal rocks: *Nature*, v. 391, p. 781-783.
- Marshak, S., and T. Flottmann, 1996, Structure and origin of the Fleurieu and Nackara arcs in the Adelaide fold-thrust belt, South Australia - Salient and recess development in the Delamerian Orogen: *Journal of Structural Geology*, v. 18, p. 891-908.
- Marshall, A. T., P. Kyriakou, P. D. Cooper, P. Coy, and A. Wright, 1995, Osmolality of rectal fluid from two species of osmoregulating brine fly larvae (Diptera: Ephyridae): *J. Insect Physiol.*, v. 41, p. 413-418.
- Marshall, J. E. A., D. A. Rogers, and M. J. Whiteley, 1996, Devonian marine incursions into the Orcadian Basin, Scotland: *Journal of the Geological Society*, p. 451-466.
- Martin, J. B., J. M. Gieskes, M. Torres, and M. Kastner, 1993a, Bromine and iodine in Peru Margin sediments and pore fluids - Implications for fluid origins: *Geochimica et Cosmochimica Acta*, v. 57, p. 4377-4389.
- Martin, J. M., and J. C. Braga, 1994, Messinian events in the Sorbas Basin in southeastern Spain and their implications in the recent history of the Mediterranean: *Sedimentary Geology*, v. 90, p. 257-268.
- Martin, J. M., J. C. Braga, C. Betzler, and T. Brachert, 1996, Sedimentary model and high-frequency cyclicity in a Mediterranean, shallow-shelf, temperate-carbonate environment (uppermost Miocene, Agua Amarga Basin, southern Spain): *Sedimentology*, v. 43, p. 263-277.
- Martin, J. M., J. C. Braga, and R. Riding, 1993b, Siliciclastic stromatolites and thrombolites, late Miocene, S.E. Spain: *Journal of Sedimentary Petrology*, v. 63, p. 131-139.
- Martin, J. M., H. M. Ortega, and R. J. Torres, 1984, Genesis and evolution of strontium deposits of the Granada Basin (southeastern Spain): evidence of diagenetic replacement of a stromatolite belt: *Sedimentary Geology*, v. 39, p. 281-298.
- Martinez, J. D., and R. Boehner, 1997, Sinkholes in glacial drift underlain by gypsum in Nova Scotia, Canada: *Carbonates and Evaporites*, v. 12, p. 84-90.
- Martinez, J. D., K. S. Johnson, and J. T. Neal, 1998, Sinkholes in Evaporite Rocks: *American Scientist*, v. 86, p. 38.
- Martini, J. E. J., P. E. Wipplinger, and F. G. Moen, 1997, Mboobo Mkuilu Cave, South Africa, in C. A. Hill, and P. Forti, eds., *Cave Minerals of the World: Huntsville, Alabama, National Speleological Society*, p. 336-339.
- Massari, F., and C. Neri, 1997, The infill of a supradetachment basin - the continental to shallow-marine Upper Permian succession in the Dolomites and Carnia (Italy): *Sedimentary Geology*, v. 110, p. 181-221.
- Massey, N. W. D., 1973, Resources Inventory of Botswana: *Industrial Minerals and Rocks, Mineral Report No. 3*, Geological Survey Dept., Lobatse, Botswana, 30 p.
- Matsubara, S., A. Kato, and E. Hashimoto, 1992, Celestine from the Asaka gypsum mine, Koriyama City, Fukushima Prefecture, Japan: *Min. J. (Japan)*, v. 16, p. 16-20.
- Mattes, B. W., and S. Conway-Morris, 1990, Carbonate/evaporite deposition in the Late Precambrian-Early Cambrian Ara Formation of southern Oman, in A. H. F. Robertson, M. P. Searle, and A. C. Ries, eds., *The geology and tectonics of the Oman region*, v. 49, Geological Society Special Publications, p. 617-636.
- Mawson, S. D., 1929, Some South Australian limestones in process of formation: *Quarterly Journal of the Geological Society*, v. 85, p. 613-623.
- Mazzoli, S., 1994, Early deformation features in syn-orogenic Messinian sediments of the northern Marche Apennines (Italy): *Annales Tectonicae*, v. 8, p. 134-147.
- Mazzullo, S. J., and B. A. Birdwell, 1989, Syngenetic formation of grainstones and pisolites from fenestral carbonates in peritidal settings: *Journal of Sedimentary Petrology*, v. 59, p. 605-611.
- McArthur, J. M., J. Turner, W. B. Lyons, A. O. Osborn, and M. F. Thirlwall, 1991, Hydrochemistry on the Yilgarn Block, Western Australia: ferrolysis and mineralization in acidic brines: *Geochimica et Cosmochimica Acta*, v. 55, p. 1273-1288.
- McArthur, J. M., J. Turner, W. B. Lyons, and M. F. Thirlwall, 1989, Salt sources and water-rock interaction on the Yilgarn Block, Australia: isotopic and major element tracers: *Applied Geochemistry*, v. 4, p. 79-92.
- McBride, B. C., M. G. Rowan, and P. Weimer, 1998a, The evolution of allochthonous salt systems, northern Green Canyon and Ewing Bank (offshore Louisiana), northern Gulf of Mexico: *Bulletin American Association of Petroleum Geologists*, v. 82, p. 1013-1036.
- McBride, B. C., P. Weimer, and M. G. Rowan, 1998b, The effect of allochthonous salt on the petroleum systems of northern Green Canyon and Ewing Bank (offshore Louisiana), Northern Gulf of Mexico: *American Association of Petroleum Geologists Bulletin*, v. 82, p. 1083-1112.

- McBride, E. F., L. S. Land, and L. E. Mack, 1987, Diagenesis of aeolian and fluvial feldspathic sandstones, Norphlet Formation (Upper Jurassic), Rankin County, Mississippi, and Mobile County, Alabama: *AAPG Bulletin*, v. 71, p. 1019-1034.
- McCaffrey, M. A., B. Lazar, and H. D. Holland, 1987, The evaporation path of seawater and the coprecipitation of Br(-) and K(+) with halite: *Journal of Sedimentary Petrology*, v. 57, p. 928-937.
- McCaig, A. M., J. Tritilla, and D. Banks, 2000, Fluid mixing and recycling during Pyrenean thrusting: Evidence from fluid inclusion halogen ratios: *Geochimica et Cosmochimica Acta*, v. 64, p. 3395-3412.
- McClay, K. R., 1990, Extensional fault systems in sedimentary basins: a review of analogue studies: *Marine and Petroleum Geology*, p. 206-233: *Marine and Petroleum Geology*, v. 7, p. 206-233.
- McGowran, B., G. Moss, and A. Beecroft, 1992, Late Eocene and early Oligocene in southern Australia: local neritic signals of global oceanic changes, in D. R. Prothero, and W. A. Berggren, eds., *Late Eocene-Oligocene Climatic and Biotic Evolution*: Princeton, NJ, Princeton University Press, p. 178-201.
- McGregor, D. R., E. C. Pendery, and D. L. McGregor, 1963, Solution caves in gypsum, north central Texas: *Journal of Geology*, v. 71, p. 108-115.
- McGuinness, D. B., and J. R. Hossack, 1993, The development of allochthonous salt sheets as controlled by the rates of extension, sedimentation, and salt supply, in J. M. Armentrout, R. Bloch, H. C. Olson, and B. F. Perkins, eds., *Rates of Geologic Processes*, Gulf Coast Section SEPM Foundation, 14th Annual Research Conference, Houston, Texas, p. 127-139.
- McIntosh, R. A., and W. N. C., 1968, Barren halite bodies in the sylvinite mining zone at Esterhazy, Saskatchewan: *Canadian Journal Earth Sciences*, v. 5, p. 1221-1238.
- McKenna, T. E., and J. M. Sharp Jr., 1997, Subsurface temperatures, fluid pressures, and salinities in the Rio Grande embayment, Gulf of Mexico basin, USA: *Proceedings of the 30th International Geological Congress*, v. 8, p. 263-274.
- McKenzie, J. A., 1981, Holocene dolomitization of calcium carbonate sediments from the coastal sabkhas of Abu Dhabi, U.A.E.: *Journal of Geology*, v. 89, p. 185-198.
- McKenzie, J. A., K. J. Hsu, and J. F. Schneider, 1980, Movement of subsurface waters under the sabkha, Abu Dhabi, UAE and its relation to evaporative dolomite genesis, in D. H. Zenger, J. B. Dunham, and R. L. Ethington, eds., *Concepts and Models of Dolomitization*, SEPM Spec. Publ. 28, p. 11-30.
- McManus, K. M., and J. S. Hanor, 1993, Diagenetic evidence for massive evaporite dissolution, fluid flow, and mass transfer in the Louisiana Gulf Coast: *Geology*, v. 21, p. 727-730.
- McMillan, C., and F. N. Moseley, 1967, Salinity tolerances of five marine macrophytes of Redfish Bay, Texas: *Ecology*, v. 48, p. 503-506.
- McNeal, R. P., and G. A. Hemenway, 1972, Geology of Fort Stockton Sulfur Mine, Pecos County, Texas: *Bulletin American Association of Petroleum Geologists*, v. 56, p. 26-37.
- McNeil, B., H. F. Shaw, and A. H. Rankin, 1998, The timing of cementation in the Rotliegend sandstones of the southern North Sea - A petrological and fluid inclusion study of cements: *Journal of Petroleum Geology*, v. 21, p. 311-327.
- McQuillan, H., 1985, Fracture-controlled production from the Oligocene-Miocene Asmari Formation in Gachsaran and Bibi Hakimeh fields, Southwest Iran, in P. O. Roehl, and P. W. Choquette, eds., *Carbonate petroleum reservoirs*: New York, Springer-Verlag, p. 511-523.
- McTavish, G. J., and L. W. Vigrass, 1987, Salt dissolution and tectonics, south-central Saskatchewan, in C. G. Carlson, and J. E. Christopher, eds., *Proceedings of the fifth international Williston basin symposium*, v. 9, Saskatchewan Geological Society, Special Publication, p. 157-168.
- McWhae, J. R. H., 1953, The Carboniferous breccia of Bellefjorden: *Geol. Mag.*, v. 90, p. 287-298.
- Mees, F., 1999, Textural features of Holocene perennial saline lake deposits of the Taoudenni-Agorgott basin, northern Mali: *Sedimentary Geology*, v. 127, p. 65-84.
- Mees, F., 2001, The development of a burkeite-dominated salt crust - an example of evaporite sedimentation in a saline pan with non-monominerale deposits: *Sedimentology*, v. 48, p. 1225-1233.
- Meisling, K. E., P. R. Cobbold, and V. S. Mount, 2001, Segmentation of an obliquely rifted margin, Campos and Santos basins, southeastern Brazil: *Bulletin-American Association of Petroleum Geologists*, v. 85, p. 1903-1924.
- Meister, F. M., and N. Aurich, 1972, Geologic outline and oil fields of Sergipe Basin, Brazil: *American Assoc. Petrol. Geol. Bull.*, v. 56, p. 1034-1047.
- Melack, J. M., and R. Jellison, 1998, Limnological conditions in Mono Lake: contrasting monomixis and meromixis in the 1990s: *Hydrobiologia*, v. 384, p. 21-39.
- Melack, J. M., and P. Kilham, 1974, Photosynthetic rates of phytoplankton in East-African alkaline saline lakes: *Limnology and Oceanography*, v. 19, p. 743-755.
- Melas, F. F., and G. M. Friedman, 1992, Petrophysical characteristics of the Jurassic Smackover Formation, Jay Field, Conecuh embayment, Alabama and Florida: *American Association of Petroleum Geologists Bulletin*, v. 76, p. 81-100.
- Melezhik, V. A., A. E. Fallick, P. V. Medvedev, and V. V. Makarikhin, 2001, Palaeoproterozoic magnesite: lithological and isotopic evidence for playa/sabkha environments: *Sedimentology*, v. 48, p. 379-397.
- Melim, L. A., 1991, The origin of dolomite in the Permian (Guadalupian) Capitan Formation, Delaware Basin, west Texas and New Mexico: implications for dolomitization models: Doctoral thesis, Southern Methodist University, Dallas, Texas, 200 p.
- Melim, L. A., and P. A. Scholle, 2002, Dolomitization of the Capitan Formation foreereef facies (Permian, west Texas and New Mexico): seepage reflux revisited: *Sedimentology*, v. 49, p. 1207-1227.
- Mello, M. R., and J. R. Maxwell, 1991, Organic geochemical and biological marker characterization of source rocks and oils derived from lacustrine environments in the Brazilian continental margin, in B. J. Katz, ed., *Lacustrine basin exploration case studies and modern analogs*: Tulsa OK, American Association Petroleum Geologists Memoir, 50, p. 77-97.
- Mello, U. T., G. D. Karner, and R. Anderson, 1995, Role of salt in restraining the maturation of sub-salt source rocks: *Marine & Petroleum Geology*, v. 12, p. 697-716.
- Melvin, J. L. e., 1991, Evaporites, petroleum and mineral resources: *Developments in sedimentology*: Amsterdam, Elsevier, 556 p.

- Menduina, J., S. Ordonez, and M. A. Garcia del Cura, 1984, Geologia del yacimiento de glauberita de Cerezo del Rio Tiron (Provincia de Burgos): *Boletín Geológico y Minero, Instituto Geológico y Minero de España*, v. 95, p. 33-51.
- Menning, M., 1995, A numerical time scale for the Permian and Triassic periods: An integrative time analysis, in P. A. Scholle, T. Peryt, and D. S. Ulmer-Scholle, eds., *The Permian of Northern Pangea, 1. Paleogeography, Paleoclimates, Stratigraphy*: Berlin, Springer Verlag, p. 77-97.
- Menzel, D. W., and J. H. Ryther, 1970, Distribution and recycling of organic matter in the oceans, in D. W. Hood, ed., *Organic matter in natural waters*, v. 1, University of Alaska, Institute of Marine Science, Occasional Publication, p. 31-53.
- Merabet, O., and A. Popov, 1971, Les bassins salifères de l'Algérie, in G. Richter-Bernberg, ed., *Geology of saline deposits*: Paris, UNESCO, p. 167-176.
- Mernagh, T. P., C. A. Heinrich, J. F. Leckie, D. P. Carville, D. J. Gilbert, R. K. Valenta, and L. A. I. Wyborn, 1994, Chemistry of low-temperature hydrothermal gold, platinum, and palladium (+/- uranium) mineralization at Coronation Hill, Northern Territory, Australia: *Economic Geology*, v. 89, p. 1053-1073.
- Meshref, W. M., 1990, Tectonic framework, in R. Said, ed., *The Geology of Egypt*: Rotterdam, A. A. Balkema, p. 113-156.
- Mesoella, K. J., J. D. Robinson, L. M. McCormick, and A. R. Ormiston, 1974, Cyclic deposition of Silurian carbonates and evaporites in Michigan Basin. *Am. Assoc. Petrol. Geol. Bull.* 58, 34-62.: *American Association Petroleum Geologists - Bulletin*, v. 58, p. 34-62.
- Meyer, F. O., R. C. Price, I. A. Al-Ghamdi, I. M. Al-Goba, S. M. Al-Raimi, and J. C. Cole, 1996, Sequential stratigraphy of outcropping strata equivalent to Arab-D Reservoir, Wadi Nisah, Saudi Arabia: *GeoArabia*, v. 1, p. 435-456.
- Meyer, F. O., R. C. Price, and S. M. Al-Raimi, 2000, Stratigraphic and petrophysical characteristics of cored Arab-D super k intervals, Hawiyah area, Ghawar field, Saudi Arabia: *GeoArabia*, v. 5, p. 355-384.
- Meyers, W. J., F. H. Lu, and J. K. Zachariah, 1997, Dolomitization by mixed evaporitic brines and freshwater, Upper Miocene carbonates, Nijar, Spain: *Journal of Sedimentary Research Section A-Sedimentary Petrology & Processes*, v. 67 A, p. 988-912.
- Miall, A. D., 1997, *The geology of stratigraphic sequences*: Berlin, Springer-Verlag, 433 p.
- Michael, K., H. G. Machel, and S. Bachu, 2003, New insights into the origin and migration of brines in deep Devonian aquifers, Alberta, Canada: *Journal of Geochemical Exploration*, v. 80, p. 193-219.
- Michalzik, D., 1996, Lithofacies, diagenetic spectra and sedimentary cycles of Messinian (late Miocene) evaporites in SE Spain: *Sedimentary Geology*, v. 106, p. 203-222.
- Middleton, G. V., 1961, Evaporite solution breccias from the Mississippian of southwest Montana: *Journal of Sedimentary Petrology*, v. 31, p. 189-195.
- Middleton, K., M. Coniglio, R. Sherlock, and S. K. Frape, 1993, Dolomitization of Middle Ordovician carbonate reservoirs, southwestern Ontario: *Bulletin of Canadian Petroleum Geology*, v. 41, p. 150-163.
- Milkov, A. V., and R. Sassen, 2001, Estimate of gas hydrate resource, northwestern Gulf of Mexico, continental slope: *Marine Geology*, v. 179, p. 71-83.
- Miller, J. A., 1985, Depositional and reservoir facies of the Mississippian Leadville Formation, Northwest Lisbon Field, Utah, in P. O. Roehl, and P. W. Choquette, eds., *Carbonate petroleum reservoirs*: New York, Springer-Verlag, p. 161-173.
- Miller, R. G., 1990, A paleogeographic approach to Kimmeridge Shale formation, in A. Y. Huc, ed., *Deposition of organic facies*: Tulsa OK, American Association Petroleum Geologists Studies in Geology, 30, p. 13-26.
- Milliken, K. L., 1979, The silicified evaporite syndrome; two aspects of silicification history of former evaporite nodules from southern Kentucky and northern Tennessee: *Journal Sedimentary Petrology*, v. 49, p. 245-256.
- Milroy, P. G., and V. P. Wright, 2000, A highstand oolitic sequence and associated facies from a Late Triassic lake basin, south-west England: *Sedimentology*, v. 47, p. 187-209.
- Minckley, W. L., 1969, Environments of the Bolsón de Cuatro Ciénegas, Coahuila, México: Texas Western Press, The University of Texas at El Paso, Science Series, No. 2, 65 pages.
- Mirandagasca, M. A., J. A. Gomezcaballero, and C. J. Eastoe, 1998, Borate deposits of Northern Sonora, Mexico - Stratigraphy, tectonics, stable isotopes and fluid inclusions: *Economic Geology*, v. 93, p. 510-523.
- Miser, D. E., J. S. Swinnea, and H. Steinfink, 1987, TEM observations and X-ray structure refinement of a twinned dolomite microstructure: *American Mineralogist*, v. 72, p. 188-193.
- Mitchell, J. C., P. J. Lehmann, D. L. Cantrell, I. A. Al-Jallal, and M. A. R. Al Thagafy, 1988, Lithofacies, diagenesis and depositional sequence; Arab-D Member, Ghawar field, Saudi Arabia, in A. J. Lomando, and P. M. Harris, eds., *Giant oil and gas fields - A core workshop*: Tulsa, OK, SEPM core Workshop No. 12, p. 459-514.
- Mitra, S., 2002, Structural models of faulted detachment folds: *Bulletin American Association of Petroleum Geologists*, v. 86, p. 1673-1694.
- Mlynarski, M., and J. Zlotnicki, 2001, Fluid circulation in the active emerged Asal rift (east Africa, Djibouti) inferred from self potential and Telluric-Telluric prospecting: *Tectonophysics*, v. 339.
- Moberg, E. G., D. M. Greenberg, R. Revelle, and E. C. Allen, 1932, The buffer mechanism of seawater: *Scripps Inst. Oceanography Tech. Serv. Bull.*, v. 3, p. 231-278.
- Mohr, M., P. A. Kukla, J. L. Urai, and G. Bresser, 2004, New Insights to the evolution and mechanisms of salt tectonics in the Central European Basin system: An integrated modeling study from Northwest Germany, In: *Salt-sediment interactions and hydrocarbon prospectivity: concepts, applications and case studies for the 21st Century. Papers presented at the 24th Annual Gulf Coast Section SEPM Foundation Bob F. Perkins Research Conference, Houston Tx, December 5-8, 2004 (CD publication)*, p. 90-118.
- Moiola, R. J., and E. D. Glover, 1965, Recent anhydrite from Clayton Playa, Nevada: *Am. Mineralogist.*, p. 11-12.
- Moldovanyi, E. P., and L. M. Walter, 1992, Regional trends in water chemistry, Smackover Formation, southwest Arkansas: geochemical and physical controls: *American Association of Petroleum Geologists Bulletin*, v. 76, p. 864-894.
- Moldowan, J. M., J. Dahl, B. J. Huizinga, F. J. Fago, L. J. Hickey, T. M. Peakman, and D. W. Taylor, 1994, The molecular fossil record of oleanane and its relation to angiosperms: *Science*, v. 265.

- Moldowan, J. M., W. K. Seifert, and E. J. Gallegos, 1985, Relationship between petroleum composition and depositional environment of petroleum source rocks: American Association of Petroleum Geologists Bulletin, v. 69, p. 1255-1268.
- Montañez, I. P., 1994, Late diagenetic dolomitization of Lower Ordovician, Upper Knox carbonates: A record of the hydrodynamic evolution of the south Appalachian Basin: American Association of Petroleum Geologists Bulletin, v. 78, p. 1210-1239.
- Montañez, I. P., and J. F. Read, 1992, Eustatic control on early dolomitization of cyclic peritidal carbonates: evidence from the Early Ordovician Upper Knox Group, Appalachians: Geological Society of America Bulletin, v. 104, p. 872-886.
- Montgomery, S. L., 1997, Ordovician Red River "B" - Horizontal oil play in the southern Williston Basin: Bulletin American Association of Petroleum Geologists, v. 81, p. 519-532.
- Montgomery, S. L., R. Karlewicz, and D. Ziegler, 1999b, Upper Jurassic "Reef" play, east Texas Basin: An updated overview: Part 2 - Inboard trend: American Association Petroleum Geologists - Bulletin, v. 83, p. 869-888.
- Montgomery, S. L., and D. Moore, 1997, Subsalt play, Gulf of Mexico - A review: AAPG Bulletin-American Association of Petroleum Geologists, v. 81, p. 871-896.
- Montgomery, S. L., T. H. Walker, P. Wahlman, R. C. Tobin, and D. Ziegler, 1999a, Upper Jurassic "Reef" play, east Texas Basin: An updated overview: Part 1 - Background and outboard trend: American Association Petroleum Geologists - Bulletin, v. 83, p. 707-728.
- Moody, J. D., 1959, Relationship of primary evaporites to oil accumulation: 5th World Petroleum Congress, New York, v. 1, p. 134-138.
- Moore, C. H., 1984, The upper Smackover of the Gulf rim: depositional systems, diagenesis, porosity evolution and hydrocarbon production, in W. P. S. Ventress, B. M. Bebout, B. F. Perkins, and C. H. Moore, eds., The Jurassic of the Gulf rim, Gulf Coast Section, SEPM, p. 283-307.
- Moore, C. H., A. Chowdhury, and L. Chan, 1988, Upper Jurassic Smackover dolomitization, Gulf of Mexico; a tale of two waters, in V. Skula, and P. A. Baker, eds., Sedimentology and geochemistry of dolostones, SEPM Special Publication No. 43, p. 175-189.
- Moore, C. H., and Y. Druckman, 1981, Burial diagenesis and porosity evolution, Upper Jurassic Smackover, Arkansas and Louisiana: American Association of Petroleum Geologists Bulletin, v. 65, p. 597-628.
- Moreira, N. F., L. M. Walter, C. Vasconcelos, J. McKenzie, and P. J. McCall, 2004, Role of sulfide oxidation in dolomitization: Sediment and pore-water geochemistry of a modern hypersaline lagoon system: Geology, v. 32, p. 701-704.
- Morisseau, J. M., 2000, Uncontrolled leaching of salt layer in an oil field in Algeria: Proc. S.M.R.I. Fall Meeting Technical Session, San Antonio, p. 330-333.
- Morley, C. K., 2004, Nested strike-slip duplexes and other evidence for Late Cretaceous-Paleogene transpressional tectonics before and during India-Eurasia collision, in Thailand, Myanmar and Malaysia: J. Geol. Soc. London, v. 161, p. 799-812.
- Morley, C. K., and G. Guerin, 1996, Comparison of gravity-driven deformation styles and behaviour associated with mobile shales and salt: Tectonics, v. 15, p. 1154-1170.
- Morris, R. C., 1985, Genesis of iron ore in banded iron-formation by supergene and supergene metamorphic processes - a conceptual model, in W. K.H., ed., Handbook of strata-bound and stratiform ore deposits, v. 13, Elsevier, p. 73-235.
- Morris, R. C., 1993, Genetic modelling for banded iron-formation of the Hamersley Group, Pilbara Craton, Western Australia: Precambrian Research, v. 60, p. 243-286.
- Morrow, D. W., 1982, Descriptive field classification of sedimentary and diagenetic breccia fabrics in carbonate rocks: Bulletin of Canadian Petroleum Geology, v. 30, p. 227-229.
- Morrow, D. W., and B. D. Ricketts, 1988, Experimental investigation of sulfate inhibition of dolomite and its mineral analogues: Shukla, Vijai, Baker, Paul A. Sedimentology and geochemistry of dolostones, based on a symposium. Special Publication Society of Economic Paleontologists and Mineralogists, v. 43, p. 25-38.
- Morrow, D. W., L. D. Stasiuk, and Mengwei Zhao, 2001, Dolomitisation and burial diagenesis of Devonian Slave Point and Keg River formations in the Cordova Embayment region of Northeast British Columbia (ext'd abs.): Canadian Society Petroleum Geologists, Rock the Foundation Convention, June 18-22, 2001, p. 026-1 to 026-5.
- Morrow, D. W., M. Zhao, and L. D. Stasiuk, 2002, The gas-bearing Devonian Presqu'île Dolomite of the Cordova embayment region of British Columbia, Canada: Dolomitization and the stratigraphic template: Bulletin American Association of Petroleum Geologists, v. 86, p. 1609-1638.
- Morse, J. W., and F. Mackenzie, T., 1998, Hadean ocean carbonate geochemistry: Aquatic Geochemistry, v. 4, p. 301-319.
- Morton, R. A., and L. S. Land, 1987, Regional variations in formation water chemistry, Frio Formation (Oligocene), Texas Gulf Coast: Bulletin American Association of Petroleum Geologists, v. 71, p. 191-206.
- Morton, R. A., and J. R. Suter, 1996, Sequence Stratigraphy and Composition of Late Quaternary Shelf-Margin Deltas, Northern Gulf of Mexico: American Association Petroleum Geologists - Bulletin, v. 80, p. 505-530.
- Mossman, D. J., and M. J. Brown, 1986, Stratiform barite in sabkha sediments, Walton-Cheverie, Nova Scotia: Economic Geology, v. 81, p. 2016-2021.
- Mossman, D. J., R. N. Delabio, and A. D. Mackintosh, 1982, Mineralogy of clay marker seams in some Saskatchewan potash mines: Canadian Journal of Earth Sciences, v. 19, p. 2126-2140.
- Mossop, G., and I. Shetsen, 1994, Geological Atlas of the Western Canada Sedimentary Basin: Canadian Society of Petroleum Geologists and Alberta Research Council, 504 p.
- Moulton, T. P., and M. A. Burford, 1990, The mass culture of *Dunaliella viridis* (Volvocales, Chlorophyta) for oxygenated carotenoids: laboratory and pilot plant studies: Hydrobiologia, v. 204-205, p. 401-408.
- Mount, T., 1975, Diapirs and diapirism in the Adelaide 'Geosyncline': Doctoral thesis, University of Adelaide.
- Mountney, N. P., and D. B. Thompson, 2002, Stratigraphic evolution and preservation of aeolian dune and damp/wet interdune strata: an example from the Triassic Helsby Sandstone Formation, Cheshire Basin, UK: Sedimentology, v. 49, p. 805-833.
- Mouret, C., 1994, Geological history of NE Thailand since the Carboniferous: Relations with Indochina and the Carboniferous to early Cenozoic evolution model: Proc. Internat. Sympos. on Stratigraphic Correlation of Southeast Asia, Bangkok, p. 132-158.

- Mriheel, I. Y., and A. S. Alhnaish, 1995, Study of Messinian carbonate-evaporite lithofacies, offshore western Libya: *Terra Nova*, v. 7, p. 213-220.
- Muchez, P., T. De Putter, C. Peeters, A. Herbosch, and W. Viaene, 1994, Comparison of the diagenetic evolution of the lower Viséan Belle Roche breccia and the middle Viséan Grande Breche: *Bulletin - Societe Belge de Geologie*, v. 103, p. 149-159.
- Mudd, G. M., 1998, The sustainability of mound springs in South Australia: Implications for Olympic Dam: Paper Presented at the Int'l Association of Hydrogeologists Meeting, Ballarat, Australia. Commission on Mineral and Thermal Waters Meeting, September 21 to 24, 1998, p. 1-13.
- Mudd, G. M., 2000, Mound springs of the Great Artesian Basin in South Australia: a case study from Olympic Dam: *Environmental Geology*, v. 39, p. 463-476.
- Muir, I. D., and J. J. Dravis, 1995, Incorporation of Core and Petrographic Data - Key to Improved Management and Exploitation of Middle Devonian Keg River Carbonate Pools in Rainbow Sub-Basin, Alberta, Western Canada (abs.): *Bulletin American Association of Petroleum Geologists*, v. 79, p. 69.
- Muir, M. D., 1979, A sabkha model for the deposition of part of the Proterozoic McArthur Group of the Northern Territory, and its implications for mineralisation: *BMR Journal of Australian Geology & Geophysics*, v. 4, p. 149-162.
- Mukhopadhyay, A., J. Alsulaimi, E. Alawadi, and F. Alruwaih, 1996, An overview of the Tertiary geology and hydrogeology of the northern part of the Arabian Gulf region with special reference to Kuwait: *Earth-Science Reviews*, v. 40, p. 259-295.
- Mumpton, F. A., 1983, Commercial utilization of natural zeolites, in S. J. LeFond, ed., *Industrial Minerals and Rocks*: New York, American Institute of Mining, Metallurgical and Petroleum Engineers Inc., p. 1418-1431.
- Munoz, M., A. J. Boyce, P. Courjault-Rade, A. E. Fallick, and F. Tollon, 1999, Continental basinal origin of ore fluids from southwestern Massif central fluorite veins (Albigeois, France): evidence from fluid inclusion and stable isotope analyses: *Applied Geochemistry*, v. 14, p. 447-458.
- Munson, D. E., 1997, Constitutive model of creep in rock salt applied to underground room closure: *International Journal of Rock Mechanics & Mining Sciences & Geomechanics*, v. 34, p. 233-247.
- Murray, J. W., 1970, The foraminifera of the hypersaline Abu Dhabi lagoon, Persian Gulf: *Lethaia*, v. 3, p. 51-68.
- Murray, R. C., 1964, Origin and diagenesis of gypsum and anhydrite: *Journal of Sedimentary Petrology*, v. 34, p. 512-523.
- Murray, R. C., 1969, Hydrology of South Bonaire, Netherlands Antilles; a rock selective dolomitization model: *Journal of Sedimentary Petrology*, v. 39, p. 1007-1013.
- Murrell, S. A. F., and I. A. H. Ismail, 1976, The effect of decomposition of hydrous minerals on the mechanical properties of rocks at high pressures and temperatures: *Tectonophysics*, v. 31, p. 207-258.
- Murris, R. J., 1980, Middle East: Stratigraphic Evolution and Oil Habitat: *American Association of Petroleum Geologists Bulletin*, v. 64, p. 597-618.
- Mutlu, H., S. Kadir, and A. Akbulut, 1999, Mineralogy and water chemistry of the Lake Acigol, Denizli, Turkey: *Carbonates and Evaporites*, v. 14, p. 191-199.
- Mutti, M., 1994, Association of tepees and palaeokarst in the Ladinian Calcare Rosso (Southern Alps, Italy): *Sedimentology*, v. 41, p. 621-641.
- Mutti, M., and J. A. T. Simo, 1993, Stratigraphic patterns and cycle-related diagenesis of upper Yates Formation, Permian, Guadalupe Mountains, in R. G. Loucks, and J. F. Sarg, eds., *Carbonate sequence stratigraphy: recent developments and applications*, v. 57, *Memoir American Association Petroleum Geologists*, p. 515-534.
- Myers, A. J., 1960a, Alabaster Caverns: *Oklahoma Geol. Notes*, v. 20, p. 132-137.
- Myers, A. J., 1960b, An area of gypsum karst topography in Oklahoma: *Oklahoma Geol. Notes*, v. 20, p. 10-14.
- Myers, A. J., 1962, A fossil sinkhole: *Oklahoma Geological Notes*, v. 22, p. 13-15.
- Myers, D. M., and C. W. Bonython, 1958, The theory of recovering salt from sea water by solar evaporation: *Journal of Applied Chemistry (Australia)*, v. 8, p. 207-219.
- Müller, D. W., and K. J. Hsu, 1987, Event stratigraphy and paleoceanography in the Fortuna Basin (Southeast Spain): a scenario for the Messinian Salinity Crisis: *Paleoceanography*, v. 2, p. 679-696.
- Müller, D. W., J. A. McKenzie, and P. A. Mueller, 1990, Abu Dhabi sabkha, Persian Gulf, revisited; Application of strontium isotopes to test an early dolomitization model: *Geology*, v. 18, p. 618-621.
- Müller, G., 1962, *Zür Geochemie des Strontiums in Ozeanen Evaporiten unter besonderer Berücksichtigung der sedimentären Coelestinlagerstätten von Hemmelte-West (Süd-Oldenburg)*: *Geologie, Supplement* 35.
- Müller, S., and G. Teitz, 1971, Dolomite replacing "cement A" in biocalcarenes from Fuerteventura, Canary Islands, Spain, in D. P. Bricker, ed., *Carbonate Cements*: Baltimore, John Hopkins Press, p. 376 p.
- Nagy, Z. R., I. D. Somerville, J. M. Gregg, S. P. Becker, K. L. Shelton, and A. G. Sleeman, 2005, Sedimentation in an actively tilting half-graben: sedimentology and stratigraphy of Late Tournaisian-Viséan (Mississippian, Lower Carboniferous) carbonate rocks in south County Wexford, Ireland: *Sedimentology*, v. 52, p. 489-512.
- Nalpas, T., and J. P. Brun, 1993, Salt flow and diapirism related to extension at crustal scale: *Tectonophysics*, v. 228, p. 349-362.
- Nanson, G. C., R. A. Callen, and D. M. Price, 1998, Hydroclimatic interpretation of Quaternary shorelines on south Australian playas: *Paleogeography Paleoclimatology Paleoecology*, v. 144, p. 281-305.
- Neal, J. T., 1991, Prediction of Subsidence Resulting from Creep Closure of Solution-Mined Caverns in Salt Domes, in A. I. Johnson, ed., *Land Subsidence: Proc. Fourth Inter. Symp. on Land Subsidence*, IAHS Publ. No.200, p. 225.
- Neal, J. T., 1994, Surface features indicative of subsurface evaporite dissolution: Implications for storage and mining: *Solution Mining Research Institute, Meeting paper, 1994 Spring meeting, Houston Texas*.
- Neal, J. T., 1995, Supai salt karst features: Holbrook Basin, Arizona, in B. F. Beck, ed., *Karst geohazards: engineering and environmental problems in karst terrane*. Proc. 5th conference, Gatlinburg 1995, Balkema, p. 53-59.
- Neal, J. T., S. Ballard, S. J. Bauer, B. L. Ehgartner, T. E. Hinkebein, E. L. Hoffman, J. K. Linn, M. A. Molecke, and A. R. Sattler, 1997,

- Mine-Induced Sinkholes Over the U.S. Strategic Petroleum Reserve (SPR) Storage Facility at Weeks Island, Louisiana: Geologic Mitigation Prior to and During Decommissioning, SAND96-2387A.: Presented at 6th Multidisciplinary Conference on Sinkholes and the Engineering & Environmental Impacts of Karst, Springfield, Missouri, April 6-9, 1997. Sandia National Laboratories, Albuquerque, NM.
- Neal, J. T., S. J. Bauer, and B. L. Ehgartne, 1995, Sinkhole Progression at the Weeks Island, Louisiana, Strategic Petroleum Reserve (SPR) Site: Solution Mining Research Institute, Fall Meeting, San Antonio, Texas, October 1995. Sandia National Laboratories, Albuquerque, NM.
- Neal, J. T., R. Colpitts, and K. S. Johnson, 1998, Evaporite Karst in the Holbrook Basin, Arizona, in J. Borchers, ed., Joseph F. Poland Symposium on Land Subsidence: Sudbury, MA, Assoc. Eng. Geologists Spec. Pub. 8, p. 373-384.
- Neal, J. T., R. Colpitts, and K. S. Johnson, 2001, Evaporite Karst in the Holbrook Basin, Arizona: SMRI (Solution Mining Research Institute) Report presented at the Fall 2001 Meeting 7 - 10 October 2001 Albuquerque, New Mexico, USA.
- Neal, J. T., A. M. Langer, and P. F. Kerr, 1968, Giant desiccation polygons of Great Basin playas: Geological Society of America Bulletin, v. 79, p. 69-90.
- Neal, J. T., and R. E. Myers, 1995, Salt dissolution sinkhole at the Weeks Island, Louisiana, strategic petroleum reserve storage site, in B. F. Beck, ed., Karst Geohazards: Engineering and environmental problems in karst terrane. Proc. 5th Conference, Gatlinburg 1995, Balkema, p. 61-65.
- Neev, D., and K. O. Emery, 1967, The Dead Sea: Depositional processes and environments of evaporites: Israel Mineral Development Geological Survey Bulletin, v. 41, p. 147 p.
- Neev, D., and J. K. Hall, 1979, Geophysical investigations in the Dead Sea: Sedimentary Geology, v. 25, p. 209-238.
- Nelson, K. H., and T. G. Thompson, 1954, Deposition of salts from seawater by frigid concentration. J. Mar. Res. 13, 166-182.
- Nelson, T. H., 1991, Salt tectonics and listric normal faulting, in A. Salvador, ed., The Gulf of Mexico Basin: Boulder, Geol. Soc. America, p. 73-89.
- Nelson, T. H., and L. H. Fairchild, 1989, Emplacement and evolution of salt sills in northern Gulf of Mexico (abs): American Association of Petroleum Geologists Bulletin, v. 73, p. 395.
- Nesbitt, B. E., and K. Muehlenbachs, 1994, Paleohydrology of the Canadian Rockies and origins of brines, Pb-Zn deposits and dolomitization in the Western Canada Sedimentary Basin: Geology, v. 22, p. 243-246.
- Nettleton, W. D., 1991, Occurrence, characteristics, and genesis of carbonate, gypsum, and silica accumulations in soils: Nettleton, W. D. Occurrence, characteristics, and genesis of carbonate, gypsum, and silica accumulations in soils. U. S. Dep. Agric., Natl. Soil Surv. Lab., Lincoln, NE, United States. SSSA Special Publication, v. 26, p. 1-16.
- Neumann, C. A., B. M. Bedout, L. R. McNeese, C. K. Paull, and H. A. Paerl, 1988, Modern stromatolites and associated mats: San Salvador, Bahamas, in J. Mylroie, ed., Proceedings of the 4th Symposium on the geology of the Bahamas, Bahamas Field Station, 235-250, San Salvador.
- Newell, A. J., 2001, Bounding surfaces in a mixed eolian-fluvial system (Rotliegend, Wessex Basin, SW UK): Marine and Petroleum Geology, v. 18, p. 339-347.
- Newson, T. A., and M. Fahey, 2003, Measurement of evaporation from saline tailings storages: Engineering Geology, v. 70, p. 217-233.
- Nickless, E. F. P., S. J. Booth, and P. N. Mosley, 1975, Celestite deposits of the Bristol area: Inst. Min. Metall., Trans., Sect. B., v. 84, p. 62-63.
- Nicolaides, S., 1995, Origin and modification of Cambrian dolomites (Red Heart Dolomite and Arthur Creek Formation), Georgina Basin, central Australia: Sedimentology, v. 42, p. 249 - 266.
- Nielsen, P., R. Swennen, J. A. D. Dickson, A. E. Fallick, and E. Kerpens, 1997, Spheroidal dolomites in a Visean karst system - bacterial induced origin? Sedimentology, v. 44, p. 177-195.
- Niemi, T., Z. Ben-Avraham, and J. R. Gat, 1997, The Dead Sea - The Lake and its setting, Oxford University Press, 336 p.
- Nieto, A. S., and D. G. Russell, 1984, Sinkhole Development in Windsor-Detroit Solution Mines and the Role of Downward Mass Transfer in Subsidence: In-Situ, v. 8, p. 293-327.
- Nigbor, M. T., 1982, State of the art of solution mining fo salt, potash, and soda ash: US Bureau of Mines, v. OFR 142-82, p. 90 pp.
- Nijman, W., K. H. de Bruijne, and M. E. Valkering, 1999, Growth fault control of Early Archaean cherts, barite mounds and chert-barite veins, North Pole Dome, Eastern Pilbara, Western Australia: Precambrian Research, v. 95, p. 245-.
- Nissen, S. E., W. L. Watney, and J. Xia, 2004, High-resolution seismic detection of shallow natural gas beneath Hutchinson, Kansas: Environmental Geosciences, v. 11, p. 129-142.
- Noffke, N., G. Gerdes, and T. Klenke, 2003, Benthic cyanobacteria and their influence on the sedimentary dynamics of peritidal depositional systems (siliciclastic, evaporitic salty, and evaporitic carbonatic): Earth-Science Reviews, v. 62, p. 163-176.
- Nordstrom, D. K., 1982a, The effect of sulfate on aluminum concentrations in natural waters: some stability relations in the system Al_2O_3 , SO_3 , H_2O at 298 K: Geochimica et Cosmochimica Acta, v. 46, p. 681-692.
- Nordstrom, D. K., 1982b, Aqueous pyrite oxidation and the consequent formation of secondary iron minerals, in J. A. Kittrick, D. S. Fanning, and L. R. Hossner, eds., Acid Sulfate Weathering, v. 10: Madison, WI, USA, Soil Science Society of America Special Publication, p. 37-56.
- North, F. K., 1985, Petroleum Geology: Winchester, Mass, Unwin Hyman Ltd, 631 p.
- Noth, S., 1997, High H₂S contents and other effects of thermochemical sulphate reduction in deeply buried carbonate reservoirs: Geologische Rundschau, v. 86, p. 275-287.
- Nurmi, R. D., and G. M. Friedman, 1977, Sedimentology and depositional environments of basin-center evaporites, lower Salina Group (Upper Silurian), Michigan Basin, in J. H. Fisher, ed., Reefs and Evaporites—Concepts and Depositional Models AAPG Studies in Geology 5: Tulsa, OK, American Association of Petroleum Geologists, p. 23-52.
- O'Brien, G. W., M. Lisk, I. R. Duddy, J. Hamilton, P. Woods, and R. Cowley, 1999, Plate convergence, foreland development and fault reactivation: primary controls on brine migration, thermal histories and trap breach in the Timor Sea, Australia: Marine & Petroleum Geology, v. 16, p. 533-560.

- O'Brien, J., and I. Lerche, 1994, Understanding subsalt overpressure may reduce drilling risks: *Oil and Gas Journal*, v. 92, p. 28-29,32-34.
- O'Dell, P. M., 1998, The Athel: A Challenging Formation in South Oman: SPE 50981; presented at the 1997 SPE Middle East Oil Show held in Bahrain, 15-18 March.
- Ober, J. A., 2000, Sulfur in Minerals Commodity Summaries 2000: U.S. Geological Survey, p. 164-165.
- Obermajer, M., M. G. Fowler, and L. R. Snowdon, 1998, A geochemical characterization and a biomarker re-appraisal of the oil families from southwestern Ontario: *Bulletin of Canadian Petroleum Geology*, v. 46, p. 350-378.
- Obermajer, M., M. G. Fowler, L. R. Snowdon, and R. W. Macqueen, 2000, Compositional variability of crude oils and source kerogen in the Silurian carbonate-evaporite sequences of the eastern Michigan Basin, Ontario, Canada: *Bulletin of Canadian Petroleum Geology*, v. 48, p. 307-322.
- Oehler, D. Z., J. H. Oehler, and A. J. Stewart, 1979, Algal fossils from a Late Precambrian, hypersaline lagoon: *Science*, v. 205, p. 338-340.
- Oehler, J. H., 1984, Carbonate source rocks in the Jurassic Smackover trend of Mississippi, Alabama, and Florida, in J. G. Palacas, ed., *Petroleum geochemistry and source rock potential of carbonate rocks: Tulsa, Oklahoma*, American Association of Petroleum Geologists, *Studies in Geology* No. 18, p. 63-69.
- Oesterhelt, D., and W. Marwan, 1993, Signal transduction in Halobacteria, in M. Kates, D. J. Kushner, and A. T. Matheson, eds., *The Biochemistry of the Archaea*, v. 26: Amsterdam, Elsevier, p. 173-187.
- Ogniben, L., 1957, Secondary gypsum of the sulphur series, Sicily, and the so-called integration: *J. Sediment. Petrology*, p. 64-79.
- Olaussen, S., 1981, Formation of celestite in the Wenlock, Oslo region Norway - evidence for evaporitic depositional environments: *Journal of Sedimentary Petrology*, v. 51.
- Olgaard, D. L., S. C. Ko, and T. F. Wong, 1995, Deformation and pore pressure in dehydrating gypsum under transiently drained conditions: *Tectonophysics*, v. 245, p. 237-248.
- Olive, W. W., 1957, Solution-subsidence troughs, Castile Formation of Gypsum Plain, Texas and New Mexico: *Geological Society of America*, v. 68, p. 351-358.
- Oliver, J., 1986, Fluids expelled tectonically from orogenic belts; their role in hydrocarbon migration and other geologic phenomena: *Geology*, v. 14, p. 99-102.
- Ollivier, B., P. Caumette, J. L. Garcia, and R. A. Mah, 1994, Anaerobic bacteria from hypersaline environments: *Microbiological Reviews*, v. 58, p. 27-38.
- Olson, R. A., 1984, Genesis of paleokarst and strata-bound zinc-lead sulfide deposits in a Proterozoic dolostone, northern Baffin Island, Canada: *Economic Geology*, v. 79, p. 1056-1103.
- Oren, A., 1993, The Dead Sea - Alive again: *Experientia*, v. 49, p. 518-522.
- Oren, A., 1999, Microbiological studies in the Dead Sea: future challenges toward the understanding of life at the limit of salt concentrations: *Hydrobiologia*, v. 405, p. 1-9.
- Oren, A., 2001, The bioenergetic basis for the decrease in metabolic diversity at increasing salt concentrations: implications for the functioning of salt lake ecosystems: *Hydrobiologia*, v. 466, p. 61-72.
- Oren, A., 2002, Molecular ecology of extremely halophilic Archaea and Bacteria: *FEMS Microbiology Ecology*, v. 39, p. 1-7.
- Oren, A., and N. Ben Yosef, 1997, Development and spatial distribution of an algal bloom in the Dead Sea: A remote sensing study: *Aquatic Microbial Ecology*, v. 13, p. 219-223.
- Oren, A., and P. Gurevich, 1995, Dynamics of a bloom of halophilic Archaea in the Dead Sea: *Hydrobiologia*, v. 315, p. 149-158.
- Oren, A., P. Gurevich, D. A. Anati, E. Barkan, and B. Luz, 1995, A bloom of *Dunaliella parva* in the Dead Sea in 1992: biological and biogeochemical aspects: *Hydrobiologia*, v. 297, p. 173-185.
- Oren, A., and F. Rodriguez-Valera, 2001, The contribution of halophilic Bacteria to the red coloration of saltern crystallizer ponds: *FEMS Microbiology Ecology*, v. 36, p. 123-130.
- Orozco, M., J. M. Molina, A. Crespo-Blanc, and F. M. Alonso-Chaves, 1999, Palaeokarst and rauhwacke development, mountain uplift and subaerial sliding of tectonic sheets (northern Sierra de los Filabres, Betic Cordilleras, Spain): *Geologie en Mijnbouw*, v. 78, p. 103-117.
- Orszag-Sperber, F., G. Harwood, A. Kendall, and B. H. Purser, 1998, A review of evaporites of the Red Sea - Gulf of Suez rift, in B. H. Purser, and D. W. J. Bosence, eds., *Sedimentation and Tectonics of Rift Basins: Red Sea - Gulf of Aden*: London, Chapman and Hall, p. 409-428.
- Orszag-Sperber, F., J. Plaziat, F. Baltzer, and B. H. Purser, 2001, Gypsum salina-coral reef relationships during the Last Interglacial (Marine Isotopic Stage 5e) on the Egyptian Red Sea coast: a Quaternary analogue for Neogene marginal evaporites? *Sedimentary Geology*, v. 140, p. 61-85.
- Orti Cabo, F., M. J. J. Pueyo, and O. L. Rosell, 1985, Cartographie de subsurface du Salifere superieur du bassin potassique de Mulhouse (Oligocene, Alsace): Busson, G. Le sel; donnees geologiques en relation avec son exploitation et son utilisation; seance specialisee de la Societe Geologique de France. Salt; geologic data in relation to its exploitation and utilization; Special session of the Geological Society of France. *Bulletin de la Societe Geologique de France*, Huitieme Serie, v. 1, p. 863-872.
- Orti Cabo, F., and D. J. Shearman, 1977, Estructuras y fabricas deposicionales en las evaporitas del mioceno superior (Messiniense) de San Miguel de Salinas (Alicante, Espana): Instituto Investigaciones Geologicas Diputacion Provincial Universidad de Barcelona, v. 32, p. 5-54.
- Orti, F., and B. Alonso, 2000, Gypsum-hydroboracite association in the Sijes Formation (Miocene, NW Argentina): implications for the genesis of Mg-bearing borates: *Journal of Sedimentary Research*, v. 70.
- Orti, F., I. Gundogan, and C. Helvacı, 2002, Sodium sulphate deposits of Neogene age: the Kirmir Formation, Beypazari Basin, Turkey: *Sedimentary Geology*, v. 146, p. 305-355.
- Orti, F., C. Helvacı, L. Rosell, and I. Gundogan, 1998, Sulphate-borate relations in an evaporitic lacustrine environment - the Sultancayir gypsum (Miocene, western Anatolia): *Sedimentology*, v. 45, p. 697-710.
- Orti, F., and L. Rosell, 2000, Evaporative systems and diagenetic patterns in the Calatayud Basin (Miocene, central Spain): *Sedimentology*, v. 47, p. 665-685.

- Orti, F., L. Rosell, and P. Anadon, 2003, Deep to shallow lacustrine evaporites in the Libros Gypsum (southern Teruel Basin, Miocene, NE Spain): an occurrence of pelletal gypsum rhythmites: *Sedimentology*, v. 50, p. 361-386.
- Osborn, W. L., 1989, Formation, diagenesis, and metamorphism of sulfate minerals in the Salton Sea geothermal system, California, U.S.A: Masters thesis, University of California, Riverside; Riverside, CA.
- Osborne, M. J., and R. E. Swarbrick, 1997, Mechanisms for generating overpressure in sedimentary basins: A reevaluation: *American Association Petroleum Geologists - Bulletin*, v. 81, p. 1023-1041.
- Oswald, E. J., 1992, Dolomitization of a Miocene reef complex; Mallorca, Spain: doctoral thesis, State University of New York at Stony Brook, 437 p.
- Oszczepalski, S., 1989, Kupferschiefer in southwestern Poland: sedimentary environments, metal zoning, and ore controls: *Geological Association of Canada Special Paper*, v. 36, p. 571-600.
- Oszczepalski, S., 1994, Oxidative alteration of the Kupferschiefer in Poland: oxide-sulphide parageneses and implications for ore-forming models: *Kwartalnik Geologiczny*, v. 38, p. 651-671.
- Overmann, J., J. T. Beatty, and K. J. Hall, 1996, Purple sulfur bacteria control the growth of aerobic heterotrophic bacterioplankton in a meromictic salt lake: *Applied and Environmental Microbiology*, v. 62, p. 3251-3258.
- Owen, R. B., R. Crossley, T. C. Johnson, D. Tweddle, L. Kornfield, S. Davison, D. H. Eccles, and D. E. Engstrom, 1990, Major low levels of Lake Malawi and implications for speciation rates in cichlid fishes: *Proc. Royal Soc. London Ser. B.*, p. 240-519.
- Paik, I. S., and H. J. Kim, 1998, Subaerial lenticular cracks in Cretaceous lacustrine deposits, Korea: *Journal of Sedimentary Research Section A-Sedimentary Petrology & Processes*, v. 68, p. 80-87.
- Paine, J. G., 1994, Subsidence beneath a playa basin on the Southern High Plains, U. S. A.; evidence from shallow seismic data: *Geological Society of America Bulletin*, v. 106, p. 233-242.
- Palacas, J. G., 1984, Petroleum geochemistry and source rock potential of carbonate rocks, v. AAPG studies in geology No. 18: Tulsa, Okla., U.S.A, American Association of Petroleum Geologist, 208 p.
- Palacas, J. G., D. E. Anders, and J. D. King, 1984, South Florida Basin - A prime example of carbonate source rocks of petroleum, in J. G. Palacas, ed., *Petroleum geochemistry and source rock potential of carbonate rocks*, v. 18: Tulsa, Oklahoma, American Association of Petroleum Geologists, *Studies in Geology*, p. 71-96.
- Palmer, A. N., and M. V. Palmer, 1998, Geochemistry of Cueva de Villa Luz, Mexico, an active H₂S cave [abs.]. *Journal of Cave and Karst Studies*, v. 60, p. 188.
- Palmer, A. N., and M. V. Palmer, 2000, Hydrochemical interpretation of cave patterns in the Guadalupe Mountains, New Mexico: *Journal of Cave and Karst Studies*, v. 62, p. 91-108.
- Palmer, M. R., and C. Helvacı, 1995, The boron isotope geochemistry of the Kirka borate deposit, western Turkey: *Geochimica et Cosmochimica Acta*, v. 59, p. 3599-3605.
- Palmer, M. R., and C. Helvacı, 1997, The boron isotope geochemistry of the Neogene borate deposits of western Turkey: *Geochimica et Cosmochimica Acta*, v. 61, p. 3161-3169.
- Pancost, R. D., N. Crawford, and J. R. Maxwell, 2002, Molecular evidence for basin-scale photic zone euxinia in the Permian Zechstein Sea: *Chemical Geology*, v. 188, p. 217-227.
- Papioanou, F. P., and Z. Carotsieris, 1993, Dolomitization patterns in Jurassic-Cretaceous dissolution-collapse breccias of Mainalon Mountain (Tripolis Unit, Central Peloponnesus-Greece): *Carbonates & Evaporites*, v. 8, p. 9-22.
- Pappalardo, R. T., and A. C. Barr, 2004, The origin of domes on Europa: The role of thermally induced compositional diapirism: *Geophysical Research Letters*, v. 31, p. L01701, doi:10.1029/2003GL019202, 2004.
- Paquet, H., and G. Millot, 1972, Geochemical evolution of clay minerals in the weathered products of Mediterranean climate: *Proceedings, International Clay Conference, Madrid, 21-24 June, 1972*, p. 199-206.
- Parafiniuk, J., 1989, Strontium and barium minerals in the sulfur deposits from the Tarnobrzeg region (SE Poland): *Arch. Min.*, v. 43, p. 41-60.
- Paraschiv, D., and G. Olteanu, 1970, Oil Fields in the Mid-Pliocene zone of the eastern Carpathians (District of Ploiesti, in M. T. Halbouty, ed., *Geology of giant petroleum fields*, American Association of Petroleum Geologists Memoir 14, p. 399-427.
- Park, L. E., and K. F. Downing, 2001, Paleocology of an exceptionally preserved arthropod fauna from lake deposits of the Miocene Barstow Formation, southern California, USA: *Palaios*, v. 16, p. 175-184.
- Park, R. K., 1977, The preservation potential of some recent stromatolites: *Sedimentology*, v. 24, p. 485-506.
- Parker, J. M., 1967, Salt solution and subsidence structures, Wyoming, North Dakota, and Montana: *Bulletin American Association Petroleum Geologists*, v. 51, p. 1929-1947.
- Parnell, J., 1986, Devonian Magadi-type cherts in the Orcadian Basin, Scotland: *Journal of Sedimentary Petrology*, v. 56, p. 495-500.
- Patterson, R. J., 1972, Hydrology and carbonate diagenesis of a coastal sabkha in the Persian Gulf: Doctoral thesis, Princeton University, 473 p.
- Patterson, R. J., and D. J. J. Kinsman, 1981, Hydrologic framework of a sabkha along the Arabian Gulf: *Bulletin American Association of Petroleum Geologists*, v. 65, p. 1457-1475.
- Patterson, R. J., and D. J. J. Kinsman, 1982, Formation of diagenetic dolomite in coastal sabkhas along the Arabian (Persian) Gulf: *American Association of Petroleum Geologists Bulletin*, v. 66, p. 28-43.
- Paukstys, B., A. H. Cooper, and J. Arustiene, 1999, Planning for gypsum geohazards in Lithuania and England: *Engineering Geology*, v. 52, p. 93-103.
- Paul, J., 1980, Upper Permian algal stromatolite reefs, Harz Mountains (F. R. Germany), in H. Fuchtbauer, and T. Peryt, eds., *The Zechstein Basin with emphasis on carbonate sequences*, E. Schweizerbart'sche Verlagsbuchhandlung, Stuttgart, West Germany, p. 253-268.
- Paul, J., 1999, Evolution of a Permo-Carboniferous Basin: The Ilfeld Basin and its relationship to adjoining Permo-Carboniferous structures in Central Germany: *Neues Jahrbuch für Geologie und Paläontologie-Abhandlungen*, v. 214, p. 211-236.
- Paull, C. K., J. R. Chanton, A. C. Neumann, J. A. Coston, and C. S. Martens, 1992, Indicators of methane-derived carbonates and chemosynthetic organic carbon deposits: examples from the Florida Escarpment: *Palaios*, v. 7, p. 361-375.
- Pawlowski, S., K. Pawlowska, and B. Kubica, 1979, Geology and genesis of the Polish sulfur deposits: *Economic Geology*, v. 74,

- p. 475-483.
- Payment, K. A., 2000, Loss of the Retsof salt mine: legal analysis of liability issues, in R. M. Geertmann, ed., Proc. 8th World Salt Symp., Salt 2000, The Hague, v. 1: Amsterdam, Elsevier, p. 399-404.
- Peckmann, J., J. Paul, and V. Thiel, 1999, Bacterially mediated formation of diagenetic aragonite and native sulfur in Zechstein carbonates (Upper Permian, Central Germany): *Sedimentary Geology*, v. 126, p. 205-222.
- Pedersen, K., 1993, The deep subterranean biosphere: *Earth Science Reviews*, v. 34, p. 243-260.
- Pedley, M., J. A. G. Martín, S. O. Delgado, and D. Del Cura, 2003, Sedimentology of Quaternary perched springline and paludal tufas: criteria for recognition, with examples from Guadalajara Province, Spain: *Sedimentology*, v. 50, p. 23-44.
- Pedone, V. A., and R. L. Folk, 1996, Formation of aragonite cement by nanobacteria in the Great Salt Lake, Utah: *Geology*, v. 24, p. 763-765.
- Peel, F. J., C. J. Travis, and J. R. Hossack, 1995, Genetic structural provinces and salt tectonics of the Cenozoic offshore U.S. Gulf of Mexico: a preliminary analysis, in M. P. A. Jackson, D. G. Roberts, and S. Snellson, eds., *Salt tectonics: a global perspective*: Tulsa OK, AAPG Memoir, v. 65, p. 153-175.
- Pegrum, R. M., and N. Mounteney, 1978, Rift Basins Flanking North Atlantic Ocean and Their Relation to North Sea Area: *Bulletin American Association Petroleum Geologists*, v. 62, p. 419-441.
- Peirce, H. W., 1981, Major Arizona salt deposits: *Field Notes, Arizona Geological Survey*, v. 11, p. 1-5.
- Pell, S. D., A. R. Chivas, and I. S. Williams, 2000, The Simpson, Strzelecki and Tirari Deserts: development and sand provenance: *Sedimentary Geology*, v. 130, p. 107-130.
- Peng, Q. M., M. R. Palmer, and J. W. Lu, 1998, Geology and geochemistry of the Paleoproterozoic borate deposits in Liaoning-Jilin, northeastern China: evidence of metaevaporites: *Hydrobiologia*, v. 381, p. 51-57.
- Peng, Q.-M., and M. R. Palmer, 2002, The Paleoproterozoic Mg and Mg-Fe Borate Deposits of Liaoning and Jilin Provinces, Northeast China: *Economic Geology*, v. 97, p. 93-108.
- Perkins, R. D., 1991, Early and late diagenetic alteration of Ordovician Red River carbonates, Tioga Deep Field, Williston Basin, North Dakota: *Bulletin American Association of Petroleum Geologists*, v. 75, p. 652.
- Perthuisot, J.-P., 1975, La sebkha el Melah de Zarzis. Génese et évolution d'un bassin paraliq: *Travaux Laboratoire de Géologie, École Normale Supérieure, Paris*.
- Perthuisot, J. P., and S. Castanier, 2000, The role of extreme halophilic bacteria in the precipitation of salt, in R. M. Geertmann, ed., 8th World Salt Symposium, v. 1: Amsterdam, Elsevier, p. 173-180.
- Perthuisot, J. P., S. Foridia, and A. Jauzein, 1972, Un modele recent de bassin cotier a sedimentation saline; la sebkha el Melah (Zarzis, Tunisie): *Review Geographie Physical Geologie Dynamique*, v. 14, p. 67-83.
- Peryt, T. M., 2000, Resedimentation of basin centre sulphate deposits: Middle Miocene Badenian of Carpathian Foredeep, southern Poland: *Sedimentary Geology*, v. 134, p. 331-342.
- Peryt, T. M., and K. Dyczyński, 1991, An isolated carbonate bank in the Zechstein Main Dolomite Basin, western Poland: *Journal of Petroleum Geology*, v. 14, p. 445-458.
- Peryt, T. M., and V. M. Kovalevich, 1997, Association of redeposited salt breccias and potash evaporites in the Lower Miocene of Stebnyk (Carpathian foredeep, West Ukraine): *Journal of Sedimentary Research Section A-Sedimentary Petrology & Processes*, v. 67 A, p. 913-922.
- Peryt, T. M., F. Orti, and L. Rosell, 1993, Sulphate platform-basin transition of the lower Werra Anhydrite (Zechstein, Upper Permian), western Poland; facies and petrography: *Journal of Sedimentary Petrology*, v. 63, p. 646-658.
- Peryt, T. M., C. Pierre, and S. P. Gryniv, 1998, Origin of polyhalite deposits in the Zechstein (Upper Permian) Zdrada Platform (northern Poland): *Sedimentology*, v. 45, p. 565-578.
- Peryt, T. M., and P. A. Scholle, 1996, Regional setting and role of meteoric water in dolomite formation and diagenesis in an evaporite basin - Studies in the Zechstein (Permian) of Poland: *Sedimentology*, v. 43, p. 1005-1023.
- Peter, J. M., and S. D. Scott, 1991, Hydrothermal mineralization in the Guaymas Basin, Gulf of California, in J. P. Dauphin, and B. R. T. Simoneit, eds., *The Gulf and Peninsula Province of the Californias*, v. 47, AAPG Memoir, p. 721-741.
- Peter, J. M., and W. C. Shanks III, 1992, Sulfur, carbon, and oxygen isotope variations in submarine hydrothermal deposits of Guaymas Basin, Gulf of California, USA: *Geochimica et Cosmochimica Acta*, v. 56, p. 2025-2040.
- Peters, J. M., M. Shuster, H. A. Al-Siyabi, J. B. Filbrandt, J. P. Grotzinger, and M. J. Newall, 2003, Surface-piercing salt domes of interior North Oman, and their significance for the Ara carbonate 'stringer' hydrocarbon play: *GeoArabia*, v. 8, p. 231-270.
- Peters, K. E., M. E. Clark, U. Dasgupta, M. A. McCaffrey, and C. Y. Lee, 1995, Recognition of an Infracambrian source rock based on biomarkers in the Bahewala-1 oil, India: *Bulletin American Association of Petroleum Geologists*, v. 79, p. 1481-1494.
- Peters, K. E., A. E. Cunningham, C. C. Walters, J. G. Jiang, and Z. A. Fan, 1996, Petroleum systems in the Jiangling-Dangyang area, Jiangnan basin, China: *Organic Geochemistry*, v. 24, p. 1035-1060.
- Peters, K. E., and J. M. Moldowan, 1993, The biomarker guide: Interpreting molecular fossils in petroleum and ancient sediments: Englewood Cliffs, NJ, Prentice Hall, 363 p.
- Peters, K. E., C. C. Walters, and J. M. Moldowan, 2005, *The Biomarker Guide: Volume 2, Biomarkers and isotopes in petroleum systems and earth history*, Cambridge University Press, 700 p.
- Peterson, J. A., 1992, Aneth Field -USA, Paradox Basin, Utah, in N. H. Foster, and E. A. Beaumont, eds., *Treatise of Petroleum Geology; Atlas of Oil and Gas Fields: Stratigraphic Traps III*: Tulsa, OK, American Association Petroleum Geologists, p. 41-82.
- Peterson, J. A., and R. J. Hite, 1969, Pennsylvanian evaporite-carbonate cycles and their relation to petroleum occurrence, southern Rocky Mountains: *American Association Petroleum Geologists - Bulletin*, v. 53, p. 884-908.
- Peterson, M. N. A., G. S. Bien, and R. A. Berner, 1963, Radiocarbon studies of recent dolomite from Deep Spring Lake, California: *Journal of Geophysical Research*, v. 68, p. 6493-6505.
- Peterson, M. N. A., and C. C. Von der Borch, 1965, Chert: modern inorganic deposition in a carbonate precipitating locality: *Science*, v. 149, p. 1501-1503.
- Petrichenko, O. I., 1979, Translated title: Methods of inclusions in minerals of saline deposits: *Fluid Inclusion Research*, v. 12, p. 214-274.

- Petta, T. J., and S. D. Rapp, 1990, Appleton Field - USA, Gulf of Mexico Basin, Alabama, in E. A. Beaumont, and N. H. Foster, eds., *Treatise of Petroleum Geology; Atlas of Oil and Gas Fields: Structural Traps IV - Tectonic and nontectonic fold traps*: Tulsa, OK, American Association Petroleum Geologists, p. 299-318.
- Pfeiffer, D., and J. Hahn, 1976, Karst of Germany, in M. Herak, and V. T. Stringfield, eds., *Karst: Important karst regions of the Northern Hemisphere*: Amsterdam, Elsevier, p. 189-223.
- Philippe, Y., 1994, Transfer zone in the southern Jura thrust belt (eastern France): geometry, development and comparison with analogue modelling experiments, in A. Mascle, ed., *Exploration and petroleum geology of France*: Berlin, Springer Verlag, EAPG Memoir, v. 4, p. 327-346.
- Philp, R. P., and C. A. Lewis, 1987, Organic geochemistry of biomarkers: *Ann. Rev. Earth Planet. Science*, v. 15, p. 363-395.
- Philp, R. P., P. Fan, C. A. Lewis, J. Li, and H. Wang, 1991, Geochemical characteristics of oils from the Chaidamu, Shanganning and Jiangnan basins, China: *Journal of Southeast Asian Earth Sciences*, v. 5, p. 351-358.
- Phleger, F. B., 1969, A modern evaporite deposit in Mexico [with discussion]: *Bulletin American Association of Petroleum Geologists*, v. 53, p. 824-829.
- Picard, L., 1943, Structures and evolution of Palestine with notes on neighbouring countries: Jerusalem Hebrew University Dept. Geol. Bulletin, v. 4, p. 1-134.
- Picha, F., 1978, Depositional and diagenetic history of Pleistocene and Holocene oolitic sediments and sabkhas in Kuwait, Persian Gulf: *Sedimentology*, v. 25, p. 427-449.
- Pierre, C., 1982, Teneurs en isotopes stables (^{18}O , ^2H , ^{13}C , ^{34}S) et conditions de genese des evaporites marines; application a quelques milieux actuels et au Messinien de la Mediterranee: Doctoral thesis, Orsay, Paris-Sud.
- Pierre, C., 1985, Polyhalite replacement after gypsum at Ojo de Liebre Lagoon (Baja California, Mexico); an early diagenesis by mixing of marine brines and continental waters: Schreiber, B. Charlotte, Harner, H. Lincoln. Sixth international symposium on salt, v. 6, p. 257-265.
- Pierre, C., 1988, Application of stable isotope geochemistry to the study of evaporites, in B. C. Schreiber, ed., *Evaporites and hydrocarbons*: New York, Columbia University Press, p. 300-344.
- Pierre, C., and J. M. Rouchy, 1988, Carbonate replacements after sulphate evaporites in the Middle Miocene of Egypt: *Journal of Sedimentary Petrology*, v. 58, p. 446-456.
- Pinckney, J., H. W. Paerl, and B. M. Bebout, 1995, Salinity control of benthic microbial mat community production in a Bahamian hypersaline lagoon: *Journal of Experimental Marine Biology & Ecology*, v. 187, p. 223-237.
- Pirajno, F., and K. Grey, 2002, Chert in the Palaeoproterozoic Bartle Member, Killara Formation, Yerrida Basin, Western Australia: a rift-related playa lake and thermal spring environment? *Precambrian Research*, v. 113, p. 169-192.
- Pittman, J. G., 1985, Correlation of beds within the Ferry Lake Anhydrite of the Gulf Coastal Plain: *Transactions Gulf Coast Association of Geological Societies*, v. 35, p. 251-260.
- Pivnik, D. A., and N. A. Wells, 1996, The transition from Tethys to the Himalayas as recorded in NW Pakistan: *Geological Society of America Bulletin*, p. 1295-1313.
- Playa, E., F. Orti, and L. Rosell, 2000, Marine to non-marine sedimentation in the upper Miocene evaporites of the Eastern Betics, SE Spain: sedimentological and geochemical evidence: *Sedimentary Geology*, v. 133, p. 135-166.
- Plaziat, J. C., F. Baltzer, A. Choukri, O. Conchon, P. Freytet, F. Orszag-Sperber, B. Purser, A. Raguideau, and J. L. Reyss, 1995, Quaternary changes in the Egyptian shoreline of the northwestern Red Sea and Gulf of Suez: *Quaternary International*, v. 30, p. 11-22.
- Pluta, I., and A. Zuber, 1995, Origin of brines in the Upper Silesian Coal basin (Poland) inferred from stable isotope and chemical data: *Applied Geochemistry*, p. 447-460.
- Podladchikov, Y., C. Talbot, and A. N. B. Poliakov, 1993, Numerical models of complex diapirs: *Tectonophysics*, v. 228, p. 189-198.
- Pohl, W., 1990, Genesis of magnesite deposits - models and trends: *Geologische Rundschau*, v. 79, p. 291-299.
- Pohl, W., and W. Siegl, 1986, Sediment-hosted magnesite deposits, in K. H. Wolh, ed., *Handbook of statabound and stratiform ore deposits*, v. 14: Amsterdam, Elsevier Science Publishers, p. 233-310.
- Poliakov, A. N. B., Y. Podladchikov, E. C. Dawson, and C. Talbot, 1996, Salt diapirism with simultaneous brittle faulting and viscous flow, in G. I. Alsop, D. J. Blundell, and I. Davison, eds., *Salt tectonics*, Geological Society, London; Special Publication, v. 100, p. 291-302.
- Polkowski, G. R., 1997, Degradation of reservoir quality by clay content, Unayzah Formation, Central Saudi Arabia: *GeoArabia*, v. 2, p. 49-64.
- Polyak, V. J., and N. Guven, 1996, Alunite, natroalunite and hydrated halloysite in Carlsbad Cavern and Lechuguilla Cave, New Mexico: *Clays & Clay Minerals*, v. 44, p. 843-850.
- Polyak, V. J., W. C. Mcintosh, N. Guven, and P. Provencio, 1998, Age of Carlsbad cavern and related caves from Ar40/Ar39 of alunite: *Science*, v. 279, p. 1919-1922.
- Pomoni-Papaioannou, F., and V. Karakitsios, 2002, Facies analysis of the Trypali carbonate unit (Upper Triassic) in central-western Crete (Greece): an evaporite formation transformed into solution-collapse breccias: *Sedimentology*, v. 49, p. 1113-1132.
- Ponder, W. F., 1986, Mound springs of the Great Artesian Basin, in P. De Decker, and W. D. Williams, eds., *Limnology in Australia*: Melbourne, Dr W. Junk, p. 403-420.
- Pope, M. C., J. P. Grotzinger, and B. C. Schreiber, 2000, Evaporitic subtidal stromatolites produced by in situ precipitation: Textures, facies associations, and temporal significance: *Journal of Sedimentary Research Section A-Sedimentary Petrology & Processes*, v. 70, p. 1138-1151.
- Post, F. J., and N. N. Youssef, 1977, Aprocaryotic intracellular symbiont of the Great Salt Lake brine shrimp *Artemia salina* (L.). *Canadian Journal Microbiology*, v. 23, p. 1232-1236.
- Posamentier, H. W., and D. P. James, 1993, An overview of sequence-stratigraphic concepts; uses and abuses, in H. W. Posamentier, C. P. Summerhayes, B. U. Haq, and G. P. Allen, eds., *Sequence stratigraphy and facies associations*, v. 18: Oxford, UK, Special Publication of the International Association of Sedimentologists, p. 3-18.
- Postgate, J. R., 1984, *The sulphate-reducing bacteria*, 2nd Edition, Cambridge University Press.
- Powell, C. M., N. H. S. Oliver, Z. X. Li, D. M. Martin, and J. Ronaszeki, 1999, Synorogenic hydrothermal origin for giant Hamersley iron oxide orebodies.: *Geology*, v. 27, p. 175-178.

- Powell, C. M., W. V. Preiss, C. G. Gatehouse, B. Krapez, and Z. X. Li, 1994, South Australia record of a Rodinian epicontinental basin and its Mid-Proterozoic breakup (≈ 700 Ma) to form the Palaeopacific ocean: *Tectonophysics*, v. 237, p. 113-140.
- Powers, D. W., 2000, Evaporites, casing requirements, water-floods, and out-of-formation waters: potential for sinkhole developments: Proc. S.M.R.I. Fall Meeting Technical Session, San Antonio, p. 186-195.
- Powers, D. W., and R. M. Holt, 2000, The salt that wasn't there: Mudflat facies equivalents to halite of the Permian Rustler Formation, southeastern New Mexico: *Journal of Sedimentary Research Section A-Sedimentary Petrology & Processes*, v. 70, p. 29-36.
- Powers, R. W., 1962, Arabian Upper Jurassic carbonate reservoir rocks, in W. E. Ham, ed., *Classification of carbonate rocks: a symposium*, American Association of Petroleum Geologists Memoir, v. 1, p. 122-192.
- Powley, D. E., 1980, Pressures, normal and abnormal: AAPG Advanced Exploration School, Unpublished Lecture Notes, 38 pp.
- Prather, B. E., 1986, Diagenesis of Smackover Reservoir Rocks in Southeastern Gulf Coast (abs): American Association Petroleum Geologists - Bulletin, v. 70, p. 634.
- Prather, B. E., 1990, Evolution of an Upper Jurassic Carbonate/Evaporitic Platform in the Conecuh Embayment, Northeastern Gulf Coast, U.S.A. (Abs.): American Association Petroleum Geologists - Bulletin, v. 74, p. 742.
- Prather, B. E., 1992a, Origin of Dolostone Reservoir Rocks, Smackover Formation (Oxfordian), Northeastern Gulf Coast, U.S.A.: Bulletin American Association of Petroleum Geologists, v. 76, p. 133-163.
- Prather, B. E., 1992b, Evolution of a Late Jurassic carbonate/evaporite platform, Conecuh Embayment, northeastern Gulf Coast, U.S.A.: American Association Petroleum Geologists - Bulletin, v. 76, p. 164-190.
- Pratt, B. R., 2002, Tepees in peritidal carbonates: origin via earthquake-induced deformation, with example from the Middle Cambrian of western Canada: *Sedimentary Geology*, v. 153, p. 57-64.
- Presley, M. W., 1987, Evolution of Permian evaporite basin in Texas Panhandle: AAPG Bulletin, v. 71, p. 167-190.
- Price, L. C., 1976, Aqueous solubility of petroleum as applied to its origins and primary migration: *Bulletin American Association of Petroleum Geologists*, v. 60, p. 213-244.
- Price, L. C., 1981, Aqueous solubility of crude oil to 400°C and 2,000 bars pressure in the presence of gas: *Journal of Petroleum Geology*, v. 4, p. 195-223.
- Prikryl, J. D., H. H. Posey, and J. R. Kyle, 1988, A petrographic and geochemical model for the origin of calcite cap rock at Damon Mound salt dome Texas: *Chemical Geology*, v. 74, p. 67-98.
- Prugger, F. F., and A. F. Prugger, 1991, Water problems in Saskatchewan potash mining--what can be learned from them? *CIM Bulletin*, v. 84, p. 58-66.
- Pu, R., and H. Qing, 2003, Pool characterization of Ordovician Midale field: Implication for Red River play in northern Williston basin, southeastern Saskatchewan, Canada: American Association Petroleum Geologists - Bulletin, v. 87, p. 1699-1715.
- Pueyo, J. J., G. Chong, and A. Jensen, 2001, Neogene evaporites in desert volcanic environments: Atacama Desert, northern Chile: *Sedimentology*, v. 48, p. 1411-1431.
- Pueyo, J. J., G. Chong, and M. Vega, 1998, Mineralogy and parental brine evolution in the Pedro de Valdivia nitrate deposit, Antofagasta, Chile (Spanish): *Revista Geologica de Chile*, v. 25, p. 3-15.
- Pueyo-Mur, J. J., and M. Inglés-Urpinell, 1987, Magnesite formation in recent playa lakes, Los Monegros, Spain, in J. D. Marshall, ed., *Diagenesis of Sedimentary Sequences*, Geol. Soc. Lond. Spec. Publ. v. 36, p. 119-122.
- Purser, B. H., 1973a, The Persian Gulf: Holocene carbonate sedimentation and diagenesis in a shallow epicontinental sea: New York, Springer-Verlag, 471 p.
- Purser, B. H., 1973b, Sedimentation around bathymetric highs in the southern Persian Gulf, in B. H. Purser, ed., *The Persian Gulf: Holocene carbonate sedimentation and diagenesis in a shallow epicontinental sea*: New York, Springer Verlag, p. 157-177.
- Purser, B. H., and G. Evans, 1973, Regional sedimentation along the Trucial Coast, southeastern Persian Gulf, in B. H. Purser, ed., *The Persian Gulf: Holocene carbonate sedimentation and diagenesis in a shallow epicontinental sea*: New York, Springer Verlag, p. 199-210.
- Purvis, K., 1989, Zoned authigenic magnesites in the Rotliegend Lower Permian, southern North Sea: *Sedimentary Geology*, v. 65, p. 307-318.
- Pysklywec, R. N., and J. X. Mitrovica, 2000, Mantle flow mechanisms of epeirogeny and their possible role in the evolution of the Western Canada Sedimentary Basin: *Canadian J. Earth Science*, v. 37.
- Qing, H., and E. W. Mountjoy, 1994, Origin of dissolution vugs, caverns, and breccias in the Middle Devonian Presqu'ile barrier, host of Pine Point Mississippi Valley-type deposits: *Economic Geology*, v. 89, p. 858-876.
- Queen, J. M., A. N. Palmer, and M. V. Palmer, 1979, Carbonate replacement of sulfate; new mechanism for porosity generation in carbonate rocks marginal to evaporite basins: *Am. Assoc. Pet. Geol., Bull.*, v. 63, p. 512-513.
- Quinlan, J. F., 1978, Types of karst, with emphasis on cover beds in their classification and development: Doctoral thesis, University of Texas at Austin.
- Quinlan, J. F., R. O. Ewers, J. A. Raty, and K. S. Johnson, 1986, Gypsum karst and salt karst of the United States of America: *Atti simposio internazionale sul carsismo nelle evaporiti; Le Grotte d'Italia*, v. 12, p. 419-420.
- Raab, M., G. M. Friedman, B. Spiro, A. Starinsky, and I. Zak, 2000, The geological history of Pliocene-Pleistocene evaporites in Mount Sedom (Israel) and how strontium and sulfur isotopes relate to their origin: *Carbonates & Evaporites*, v. 15, p. 93-114.
- Rack, F. R., 1993, A geologic perspective on the Miocene evolution of the Antarctic Circumpolar Current system: *Tectonophysics*, v. 222, p. 397-415.
- Radke, B. M., 1980, Epeiric carbonate sedimentation of the Ninmaroo Formation (Upper Cambrian-Lower Ordovician), Georgina Basin (Australia). *BMR Journal of Australian Geology & Geophysics*, v. 5, p. 183-200.
- Ragland, D. A., and R. N. Donovan, 1984, The Cool Creek Formation (Ordovician) at Turner Falls in the Arbuckle Mountains of southern Oklahoma: *Oklahoma Geology Notes*, v. 45, p. 132-148.
- Rahimpour-Bonab, H., and Z. Kalantarzadeh, 2005, Origin of secondary potash deposits; a case from Miocene evaporites of NW Central Iran: *Journal of Asian Earth Sciences*, v. 25, p. 157-166.

- Raines, M. A., and T. A. Dewers, 1997, Dedolomitization as a driving mechanism for karst generation in Permian Blaine Formation, southwest Oklahoma, USA: *Carbonates & Evaporites*, v. 12, p. 24-31.
- Raiswell, R., F. Buckley, R. A. Berner, and T. F. Anderson, 1988, Degree of pyritization of iron as a palaeoenvironmental indicator of bottom water oxygenation: *Journal of Sedimentary Petrology*, v. 58, p. 812-819.
- Ram, E., A. Z. Ben, and Y. Kost, 1988, Halite bodies development in the evaporation pan No. 5 of Dead Sea Works: Israel Geological Society, Annual Meeting, p. 92-93.
- Ramage, J. R., 1987, Lithofacies, regional stratigraphy, and depositional systems of the Clear Fork Group (Permian) Palo Duro Basin, Texas Panhandle: Masters thesis, University of Texas at Austin.
- Ranganathan, V., 1991, Salt diffusion in interstitial waters and halite removal from sediments; examples from the Red Sea and Illinois basins: *Geochimica et Cosmochimica Acta*, v. 55, p. 1615-1625.
- Ranganathan, V., 1992, Basin dewatering near salt domes and formation of brine plumes: *Journal of Geophysical Research, B, Solid Earth and Planets*, v. 97, p. 4667-4683.
- Ranganathan, V., and J. S. Hanor, 1988, Density-driven groundwater flow near salt domes: *Chemical Geology*, v. 74, p. 173-188.
- Rasmussen, B., and R. Buick, 2000, Oily old ores: Evidence for hydrothermal petroleum generation in an Archean volcanogenic massive sulfide deposit: *Geology*, v. 28, p. 731-734.
- Ratcliff, D. W., and D. J. Weber, 1997, Geophysical imaging of subsalt geology: *Leading Edge*, v. Feb. 1997.
- Ratigan, J., 2000, A status report on the Solution Mining Research Institute cavern sealing and abandonment program: SMRI Report, 13 p.
- Raup, O. B., 1966, Bromine distribution in some halite rocks of the Paradox Member, Hermosa Formation, in Utah: Second Symposium on Salt; North Ohio Geol. Soc. p. 236-247.
- Raup, O. B., 1970, Brine mixing - an additional mechanism for formation of basin evaporites: *Bulletin American Association of Petroleum Geologists*, v. 54, p. 2246-2259.
- Raup, O. B., 1982, Gypsum precipitation by mixing seawater brines: *Bulletin American Association of Petroleum Geologists*, v. 66, p. 363-367.
- Raup, O. B., and R. J. Hite, 1993, Preliminary data on the lithology, bromine distribution, and insoluble minerals from the A-1 Evaporite Formation, Salina Group, in the JEM Petroleum Corporation, Bruggers 3-7 Core, Missaukee County, Michigan: Open File Report U. S. Geological Survey, v. 93-236, p. 15 p.
- Raymer, D. G., and J. M. Kendall, 1998, Seismic anisotropy in salt structures due to preferred crystal orientation: *Revue de l'Institut Francais du Petrole*, v. 53, p. 585-594.
- Read, J. F., 1985, Carbonate platform facies models.: *Bulletin American Association of Petroleum Geologists*, v. 69, p. 1-21.
- Read, J. F., and A. D. Horbury, 1993, Eustatic and tectonic controls on porosity evolution beneath sequence-bounding unconformities and parasequence disconformities on carbonate platforms, in A. D. Horbury, and A. G. Robinson, eds., *Diagenesis and basin development*, v. 36, AAPG, Studies in Geology, p. 155-197.
- Read, J. F., C. Kerans, L. J. Weber, J. F. Sarg, and F. M. Wright, 1995, Milankovitch sea-level changes, cycles, and reservoirs on carbonate platforms in greenhouse and ice-house worlds: SEPMSociety for Sedimentary Geology Short Course Notes, v. 35, 81 pp p.
- Rech, J. A., J. Quade, and J. Betancourt, 2002, Late Quaternary paleohydrology of the central Atacama Desert (lat 22°-24°S), Chile: *Geological Society of America Bulletin*, v. 114, p. 334-348.
- Rech, J. A., J. Quade, and W. S. Hart, 2003, Isotopic evidence for the source of Ca and S in soil gypsum, anhydrite and calcite in the Atacama Desert, Chile: *Geochimica et Cosmochimica Acta*, v. 67, p. 575-586.
- Reed, R. H., J. A. Chudek, R. Foster, and W. D. P. Stewart, 1984, Osmotic adjustment in cyanobacteria from hypersaline environments: *Arch. Microbiol*, v. 138, p. 333-33.
- Reid, R. P., P. T. Visscher, A. W. Decho, J. F. Stolz, B. M. Beboutk, C. Dupraz, I. G. Macintyre, H. W. Paerl, J. L. Pinckney, L. Prufert-Beboutk, T. F. Steppe, and D. J. DesMarais, 2001, The role of microbes in accretion, lamination and early lithification of modern marine stromatolites: *Nature*, v. 406, p. 989-992.
- Reilly, J. F., I. R. MacDonald, E. K. Biegert, and J. M. Brooks, 1996, Geologic controls on the distribution of chemosynthetic communities in the Gulf of Mexico, in D. Schumacher, and M. A. Abrams, eds., *Hydrocarbon Migration and its Near-Surface Expression*, American Association of Petroleum Geologists Memoir 66, p. 38-61.
- Reinhardt, J. W., J. E. Amthor, and F. Hoogendijk, 1999, Deep Oil Exploration in an Unconventional Reservoir - The Precambrian Intra-Salt Carbonate Play of Oman (abs): *Bulletin American Association of Petroleum Geologists*, v. 83.
- Reinhardt, L., and W. Ricken, 2000, The stratigraphic and geochemical record of Playa Cycles: monitoring a Pangaean monsoon-like system: *Palaeogeography, Palaeoclimatology, Palaeoecology*, v. 161, p. 205-227.
- Reitner, J., G. Arp, V. Thiel, G. P., G. U., and M. W., 1997, Organic matter in Great Salt Lake ooids (Utah, USA) - First approach to a formation via organic matrices: *Facies*, v. 36, p. 210-219.
- Remmelts, G., 1995, Fault-related salt tectonics in the southern North Sea, The Netherlands, in M. P. A. Jackson, D. G. Roberts, and S. Snelson, eds., *Salt Tectonics: A global perspective*: Tulsa, American Association of Petroleum Geologists Memoir, v. 65, p. 261-272.
- Remson, D. R., O. B. Dommers, and F. W. Jessen, 1966, Techniques for developing predetermined shaped cavities in solution mining, in J. L. Rau, ed., *Second Symposium on Salt*: Cleveland, OH, N. Ohio Geol. Soc., p. 297-310.
- Renaut, R. W., 1993a, Morphology, distribution and preservation potential of microbial mats in the hydromagnesite-magnesite playas of the Cariboo Plateau, British Columbia, Canada: *Hydrobiologia*, v. 267, p. 75 - 98.
- Renaut, R. W., 1993b, Zeolitic Diagenesis of Late Quaternary Fluvio-lacustrine Sediments and Associated Calcrete Formation in the Lake Bogoria Basin, Kenya Rift-Valley: *Sedimentology*, v. 40, p. 271-301.
- Renne, P. R., W. D. Sharp, I. P. Montanez, T. A. Becker, and R. A. Zierenberg, 2001, Ar-40/Ar-39 dating of Late Permian evaporites, southeastern New Mexico, USA: *Earth & Planetary Science Letters*, v. 193, p. 539-547.
- Rettig, S. L., B. F. Jones, and F. Risacher, 1980, Geochemical evolution of brines in the Salar of Uyuni, Bolivia: *Chemical Geology*, v. 30, p. 57-79.
- Reuter, F., and V. V. Tolmacev, 1990, Bauen und Bergbau in Sekens und Erdfallgebieten, Ein Ingenieurgeologies des Karstes: *Schriftenreihe für Geologische Wissenschaften*, 28 Akademie Verlag, Berlin.

- Rezak, R., 1985, Local carbonate production on a terrigenous shelf: Gulf Coast Association of Geological Societies Transactions, v. 35, p. 477-483.
- Rezak, R., and T. J. Bright, 1981, Seafloor instability at the East Flower Garden Bank, northwest Gulf of Mexico: *Geo-marine Letters*, v. 1, p. 97-103.
- Riccioni, R. M., P. W. G. Brock, and B. C. Schreiber, 1996, Evidence for early aragonite in paleo-lacustrine sediments: *Journal of Sedimentary Research Section A-Sedimentary Petrology & Processes*, v. 66, p. 1003-1010.
- Richardson, C. K., and H. D. Holland, 1979, The solubility of fluorite in hydrothermal solutions, an experimental study: *Geochim. Cosmochim. Acta*, v. 43, p. 1313-1325.
- Richardson, G. E., L. S. French, R. D. Baud, R. H. Peterson, C. D. Roark, T. M. Montgomery, E. G. Kazanis, G. M. Conner, and M. P. Gravois, 2004, Deepwater Gulf of Mexico 2004: America's Expanding Frontier, v. OCS Report Number MMS 2004-021: New Orleans, U.S. Department of the Interior, Minerals Management Service New Orleans, Gulf of Mexico OCS Region, 150 p.
- Richner, D. R., D'Arcy Shock, J. K. Ahlness, D. R. Tweeton, W. C. Larson, D. J. Millenacker, and R. D. Schmidt, 1992, Solution Mining: In situ techniques, in H. L. Hartman, ed., *SME Mining Engineering Handbook*, v. 2: Littleton, CO, Society for Mining, Metallurgy and Exploration, p. 1493-1528.
- Richter-Bernburg, G., 1957, Isochrone Warven im Anhydrit des Zechstein 2: Germany, *Geol. Landesanst., Geol. Jb. Bd.*
- Richter-Bernburg, G., 1980, Salt Tectonics, Interior structures of salt bodies: *Bull. Cent. Rech. Explor.-Prod. Elf Aquitaine*, v. 4, p. 373-393.
- Richter-Bernburg, G., 1986, Zechstein 1 and 2 anhydrites; facts and problems of sedimentation, in G. M. Harwood, and D. B. Smith, eds., *The English Zechstein and related topics*, v. 22: London, UK, Geological Society Special Publication, p. 157-163.
- Riciputi, L. R., D. R. Cole, and H. G. Machel, 1996, Sulfide formation in reservoir carbonates of the Devonian Nisku Formation, Alberta, Canada - An ion microprobe study: *Geochimica et Cosmochimica Acta*, v. 60, p. 325-336.
- Riding, R., 1979, Origin and diagenesis of lacustrine algal bioherms at the margin of the Ries Crater, Upper Miocene, southern Germany: *Sedimentology*, v. 26, p. 645-680.
- Riding, R., 1991, Classification of Microbial Carbonates, in R. Riding, ed., *Calcareous Algae and Stromatolites*: Berlin, Springer Verlag, p. 21-51.
- Riding, R., 2000, Microbial carbonates: the geological record of calcified bacterial-algal mats and biofilms: *Sedimentology*, v. 47, p. 179-214.
- Riding, R., 2002, Structure and composition of organic reefs and carbonate mud mounds: concepts and categories: *Earth Science Reviews*, v. 58, p. 163-231.
- Riding, R., J. C. Braga, and J. M. Martin, 1999, Late Miocene Mediterranean desiccation: topography and significance of the 'Salinity Crisis' erosion surface on-land in southeast Spain: *Sedimentary Geology*, v. 123, p. 1-7.
- Riding, R., J. C. Braga, J. M. Martin, and I. M. Sanchezalmazo, 1998, Mediterranean Messinian salinity crisis- Constraints from a coeval marginal basin, Sorbas, southeastern Spain: *Marine Geology*, v. 146, p. 1-20.
- Riding, R., J. M. Martin, and J. C. Braga, 1991, Coral-stromatolite reef framework, Upper Miocene, Almeria, Spain: *Sedimentology*, v. 38, p. 799-819.
- Riegl, B., 2003, Climate change and coral reefs: Different effects in two high latitude areas (Arabian Gulfs, South Africa): *Coral Reefs*, v. 22, p. 433-466.
- Risacher, F., B. Alonso, and C. Salazar, 2003, The origin of brines and salts in Chilean salars: a hydrochemical review: *Earth-Science Reviews*, v. 63, p. 249-293.
- Risacher, F., and H. Alonso, 1996, Geochemistry of Salar de Atacama. 2. Water Evolution [Spanish]: *Revista Geologica de Chile*, v. 23, p. 123-134.
- Risacher, F., and H. Alonso, 2001, Geochemistry of ash leachates from the 1993 Lascar eruption, northern Chile. Implication for recycling of ancient evaporites: *Journal of Volcanology & Geothermal Research*, v. 109, p. 319-337.
- Risacher, F., and H. P. Eugster, 1979, Holocene pisolites and encrustations associated with spring-fed surface pools, Pastos Grandes, Bolivia: *Sedimentology*, v. 26, p. 253-270.
- Risacher, F., and B. Fritz, 1991a, Geochemistry of Bolivian salars, Lipez, southern Altiplano: origin of solutes and brine evolution: *Geochimica et Cosmochimica Acta*, v. 55, p. 687-705.
- Risacher, F., and B. Fritz, 1991b, Quaternary geochemical evolution of the salars of Uyuni and Coipasa, central Altiplano, Bolivia: *Chemical Geology*, v. 90, p. 211-231.
- Risacher, F., and B. Fritz, 2000, Bromine geochemistry of salar de Uyuni and deeper salt crusts, Central Altiplano, Bolivia: *Chemical Geology*, v. 167, p. 373-392.
- Rittenhouse, G., 1967, Bromine in oil-field waters and its use in determining possibilities of origin of these waters: *American Association Petroleum Geologists - Bulletin*, v. 51, p. 2430-2440.
- Ritts, B. D., A. D. Hanson, D. Zinniker, and J. M. Moldovan, 1999, Lower-middle Jurassic nonmarine source rocks and petroleum systems of the northern Qaidam basin, northwest China: *Bulletin American Association of Petroleum Geologists*, v. 83, p. 1980-2005.
- Roberts, S. M., and R. J. Spencer, 1995, Paleotemperatures preserved in fluid inclusions in halite: *Geochimica et Cosmochimica Acta*, v. 59, p. 3929-3942.
- Roberts, W., and P. F. Williams, 1993, Evidence for early Mesozoic extensional faulting in Carboniferous rocks, southern New Brunswick, Canada: *Canadian Journal of Earth Science*, v. 30, p. 1324-1331.
- Robertson, A. H. F., S. Eaton, E. J. Follows, and A. S. Payne, 1995, Depositional processes and basin analysis of Messinian evaporites in Cyprus: *Terra Nova*, v. 7, p. 233-253.
- Robinson, B. W., and A. Gunatilaka, 1991, Stable isotope studies and the hydrological regime of sabkhas in southern Kuwait, Arabian Gulf: *Sedimentary Geology*, v. 73, p. 141-159.
- Roca, E., P. Anadon, R. Utrilla, and A. Vazquez, 1996, Rise, closure and reactivation of the Biorb-Quesa evaporite diapir, eastern Prebetics, Spain: *Journal of the Geological Society*, v. 153, p. 311-321.
- Rodríguez-Aranda, J. P., 1995, *Sedimentología de los Sistemas de Llanura Lútica-lago Salino del Mioceno en la Zona Oriental de la Cuenca de Madrid (Taracón-Auñón)*: Doctoral thesis, Universidad Complutense, Madrid, 474 p.

- Rodríguez-Aranda, J. P., and J. P. Calvo, 1998, Trace fossils and rhizoliths as a tool for sedimentological and palaeoenvironmental analysis of ancient continental evaporite successions: *Palaeogeography Palaeoclimatology Palaeoecology*, v. 140, p. 383-399.
- Rodríguez-Aranda, J. P., J. P. Calvo, and M. E. Sanz-Montero, 2002, Lower Miocene gypsum palaeokarst in the Madrid Basin (central Spain): dissolution diagenesis, morphological relics and karst end-products: *Sedimentology*, v. 49, p. 1385-1400.
- Roedder, E., 1984a, The fluids in salt: *American Mineralogist*, v. 69, p. 413-439.
- Roedder, E., 1984b, Fluid Inclusions: *Mineralogical Society of America, Reviews in Mineralogy*, v. 12.
- Roedder, E., and R. L. Bassett, 1981, Problems in determination of the water content of rock-salt samples and its significance in nuclear-waste storage siting: *Geology*, v. 9, p. 525-530.
- Roedder, E., and B. J. Skinner, 1968, Experimental evidence that fluid inclusions do not leak: *Economic Geology*, v. 63, p. 715-730.
- Roehl, P. O., 1985, Depositional and diagenetic controls on reservoir rock development and petrophysics in Silurian tidalites, Interlake Formation, Cabin Creek field area, Montana, in P. O. Roehl, and P. W. Choquette, eds., *Carbonate petroleum reservoirs*: New York, Springer-Verlag, p. 85-105.
- Roehler, H. W., 1993, Eocene climates, depositional environments, and geography, greater Green River Basin, Wyoming, Utah, and Colorado: *U.S. Geological Survey Professional Paper*, v. 1506-F, p. 74.
- Rogers, D. B., and S. J. Dreiss, 1995a, Saline groundwater in Mono basin, California.1. Distribution: *Waters Resources Research*, v. 31, p. 3131-3150.
- Rogers, D. B., and S. J. Dreiss, 1995b, Saline groundwater in Mono basin, California.2. Long term control of lake salinity by groundwater: *Water Resources Research*, v. 31, p. 3151-3169.
- Rokahr, R., K. Standtmeister, and D. Zander-Schiebenhofer, 1998, Mechanical determination of the maximum internal pressure for gas storage caverns in rock salt: *SMRI Fall Meeting*, Oct. 4-7, Rome Italy, 455 p.
- Rooney, T. P., B. F. Jones, and J. T. Neal, 1969, Magadiite from Alkali Lake, Oregon: *American Mineralogist*, v. 54, p. 1034-1043.
- Rosell, O. L., and C. F. Orti, 1980, Presencia de analcima y observaciones diagenéticas en la anhidrita basal de la cuenca potásica de Navarra (Eocene superior, Cuenca del Ebro, España): *Lectures and communications from the First symposium on diagenesis of sediments and sedimentary rocks*. Univ. Barcelona, Dep. Petrol. y Geoquim., Barcelona, Spain. *Revista del Instituto de Investigaciones Geológicas de la Diputación Provincial de Barcelona*, v. 34, p. 223-235.
- Rosen, M. R., 1991, Sedimentologic and geochemical constraints on the evolution of Bristol Dry Lake Basin, California, U.S.A.: *Palaeogeography, Palaeoclimatology, Palaeoecology*, v. 84, p. 309-332.
- Rosen, M. R., 1994, The importance of groundwater in playas: A review of playa classifications and the sedimentology and hydrology of playas, in M. R. Rosen, ed., *Paleoclimate and the Basin Evolution of Playa Systems*: Boulder, Co, Geological Society of America Special Paper No. 289, p. 1-18.
- Rosen, M. R., G. B. Aehart, and M. S. Lico, 2004, Exceptionally fast growth rate of <100-yr-old tufa, Big Soda Lake, Nevada: Implications for using tufa as a paleoclimate proxy: *Geology*, v. 32, p. 409-412.
- Rosen, M. R., L. Coshell, J. V. Turner, and R. J. Woodbury, 1996, Hydrochemistry and nutrient cycling in Yalgorup National Park, Western Australia: *Journal of Hydrology*, v. 185, p. 241-274.
- Rosen, M. R., D. E. Miser, M. A. Starcher, and J. K. Warren, 1989, Formation of dolomite in the Coorong region, South Australia: *Geochimica et Cosmochimica Acta*, v. 53, p. 661-669.
- Rosen, M. R., D. E. Miser, and J. K. Warren, 1988, Sedimentology, mineralogy and isotopic analysis of Pellet Lake, Coorong region, South Australia.: *Sedimentology*, v. 35, p. 105-122.
- Rosen, M. R., J. V. Turner, L. Coshell, and V. Gailitis, 1995, The effects of water temperature, stratification, and biological activity on the stable isotopic composition and timing of carbonate precipitation in a hypersaline lake: *Geochimica et Cosmochimica Acta*, v. 59, p. 979-990.
- Rosen, M. R., and J. K. Warren, 1990, The origin and significance of groundwater-seepage gypsum from Bristol Dry Lake, California, USA: *Sedimentology*, v. 37, p. 983-996.
- Rouchy, J. M., 1986, Sedimentologie des formations anhydritiques givetiennes et dinantiennes du segment varisque franco-belge: *Bulletin de la Societe Belge de Geologie*, v. 95, p. 111-127.
- Rouchy, J. M., 1988, Relations évaporites-hydrocarbures: l'association laminites-récifs-évaporites dans le Messinien de Méditerranée et ses enseignements, in G. Busson, ed., *Evaporites et hydrocarbures*, v. 55, *Mémoires du Muséum national d'Histoire naturelle*, (C), p. 15-18.
- Rouchy, J. M., M. C. Bernet-Rollande, and A. F. Maurin, 1994, Descriptive petrography of evaporites: Applications in the field, subsurface and the laboratory, in T. c. French oil and gas industry association, ed., *Evaporite sequences in petroleum exploration: 1. Geological Methods*, Editions Technip, p. 70-123.
- Rouchy, J. M., G. Camoin, J. Casanova, and J. F. Deconinck, 1993, The central palaeo-Andean basin of Bolivia (Potosi area) during the Late Cretaceous and early Tertiary: reconstruction of ancient saline lakes using sedimentological, paleoecological and stable isotope records: *Palaeogeography, Palaeoclimatology, Palaeoecology*, v. 105, p. 179-198.
- Rouchy, J. M., A. Laumondais, and E. Groessens, 1987, The Lower Carboniferous (Visean) evaporites in northern France and Belgium; depositional, diagenetic and deformational guides to reconstruct a disrupted evaporitic basin: Peryt, Tadeusz M. (ed) *Evaporite basins*. *Lecture Notes in Earth Sciences*, v. 13, p. 31-67.
- Rouchy, J. M., D. Noel, A. M. A. Wali, and M. A. M. Aref, 1995a, Evaporitic and biosiliceous cyclic sedimentation in the Miocene of the Gulf of Suez; depositional and diagenetic aspects: *Sedimentary Geology*, v. 94, p. 277-297.
- Rouchy, J. M., F. Orszag-Sperbe, M. M. Blanc-Valleron, C. Pierre, M. Rivier, N. Combourieu-Nebout, and I. Panayides, 2001, Paleoenvironmental changes at the Messinian-Pliocene boundary in the eastern Mediterranean (southern Cyprus basins): significance of the Messinian Lago-Mare: *Sedimentary Geology*, v. 145, p. 93-117.
- Rouchy, J. M., and C. Pierre, 1979, Données sédimentologiques et isotopiques sur les gypses des séries évaporitiques messiniennes d'Espagne meridionale et de Chypre: *Rev. Geogr. Phys. Geol. Dyn.*, v. 21, p. 267-280.
- Rouchy, J. M., C. Pierre, and F. Sommer, 1995b, Deep-water re-sedimentation of anhydrite and gypsum deposits in the Middle

- Miocene (Belayim Formation) of the Red Sea: *Sedimentology*, v. 42, p. 267-282.
- Rouchy, J. M., and J. P. Saint-Martin, 1992, Late Miocene events in the Mediterranean as recorded by carbonate-evaporite relations: *Geology*, v. 20, p. 629-632.
- Rouchy, J. M., M. Servant, M. Fournier, and C. Causse, 1996, Extensive carbonate algal bioherms in Pleistocene saline lakes of the central Altiplano of Bolivia: *Sedimentology*, v. 43, p. 973-993.
- Rouchy, J. M., C. Taberner, M. M. Blanc-Valleron, R. Sprovieri, M. Russell, C. Pierre, E. Di Stefano, J. J. Pueyo, A. Caruso, J. Dinares-Turell, E. Gomis-Coll, G. A. Wolff, G. Cespuglio, P. Ditchfield, S. Pestrea, N. Combourieu-Nebout, C. Santisteban, and J. O. Grimalt, 1998, Sedimentary and diagenetic markers of the restriction in a marine basin: the Lorca Basin (SE Spain) during the Messinian: *Sedimentary Geology*, v. 121, p. 25-55.
- Roveri, M., M. A. Bassetti, and F. R. Lucchi, 2001, The Mediterranean Messinian salinity crisis: an Apennine foredeep perspective: *Sedimentary Geology*, v. 140, p. 201-214.
- Roveri, M., V. Manzi, F. R. Lucchi, and S. Rogledi, 2003, Sedimentary and tectonic evolution of the Vena del Gesso basin (Northern Apennines, Italy): Implications for the onset of the Messinian salinity crisis: *Geological Society of America Bulletin*, v. 115, p. 387-405.
- Rowan, M. G., 1995, Structural styles and evolution of allochthonous salt, central Louisiana outer shelf and upper slope, in M. P. A. Jackson, D. G. Roberts, and S. Snelson, eds., *Salt tectonics; a global perspective*: Tulsa, AAPG Memoir, v. 65, p. 199-228.
- Rowan, M. G., 1997, Three dimensional geometry and evolution of a segmented detachment fold, Mississippi fan foldbelt, Gulf of Mexico: *Journal of Structural Geology*, v. 19, p. 463-480.
- Rowan, M. G., K. A. Giles, and T. F. Lawton, 2001, A Tale of Two Diapirs: The Effects of Shortening on Passive Growth: *American Association Petroleum Geologists - Bulletin*, v. 86.
- Rowan, M. G., B. S. Hart, S. Nelson, P. B. Flemings, and B. D. Trudgill, 1998, Three-dimensional geometry and evolution of a salt-related growth-fault array, Eugene Island 330 field, Offshore Louisiana, Gulf of Mexico: *Marine & Petroleum Geology*, v. 15, p. 309-328.
- Rowan, M. G., M. P. A. Jackson, and B. D. Trudgill, 1999, Salt-related fault families and fault welds in the northern Gulf of Mexico: *Bulletin-American Association of Petroleum Geologists*, v. 83, p. 1454-1484.
- Rowan, M. G., T. F. Lawton, K. A. Giles, and R. A. Ratliff, 2003, Near-salt deformation in La Popa basin, Mexico, and the northern Gulf of Mexico: A general model for passive diapirism: *Bulletin American Association Petroleum Geologists*, v. 87, p. 733-756.
- Rowan, M. G., and P. Weimer, 1998, Salt-sediment interaction, Northern Green Canyon and Ewing Bank (offshore Louisiana), northern Gulf of Mexico: *American Association of Petroleum Geologists Bulletin*, v. 82, p. 1055-1082.
- Ruble, T. E., A. J. Bakel, and R. P. Philp, 1994, Compound-Specific Isotopic Variability in Uinta Basin Native Bitumens - Paleoenvironmental Implications: *Organic Geochemistry*, v. 21, p. 661-671.
- Ruckmick, J. C., B. H. Wimberly, and A. F. Edwards, 1979, Classification and genesis of biogenic sulfur deposits: *Economic Geology*, v. 74, p. 469-474.
- Ruegg, J. C., M. Kasser, J. C. Lepine, and A. Tarantola, 1979, Geodesic measurements of rifting associated with a seismo-volcanic crisis in Afar: *Geophys. Res. Lett.*, v. 6, p. 817-820.
- Runnegar, B., W. Dollase, R. Ketcham, M. Colbert, and W. Carlson, 2001, Early Archean sulfates from Western Australia first formed as hydrothermal barites, not gypsum evaporites: *Geological Society of America, Annual Meeting, November 5-8, 2001; Session No. 166*.
- Runnells, D. D., 1969, Diagenesis, chemical sediments, and the mixing of natural waters: *Journal Sedimentary Petrology*, v. 39, p. 1188-1201.
- Ruppel, S. C., and H. S. Cander, 1988, Dolomitization of shallow water carbonates by seawater and seawater-derived brines, San Andres Formation (Guadalupean), West Texas, in V. J. Shukla, and P. A. Baker, eds., *Sedimentology and Geochemistry of Dolostones*, v. 43: Tulsa Okla, SEPM Special Publ., p. 245-262.
- Russell, M., J. A. Grimalt, W. A. Hartgers, C. Taberner, and J. M. Rouchy, 1997, Bacterial and algal markers in sedimentary organic matter deposited under natural sulphurization conditions (Lorca Basin, Murcia, Spain): *Organic Geochemistry*, v. 26, p. 605-625.
- Russell, M. J., J. K. Ingham, V. Zedef, D. Maktav, F. Sunar, A. J. Hall, and A. E. Fallick, 1999, Search for signs of ancient life on Mars: expectations from hydromagnesite microbialites, Salda Lake, Turkey: *Journal of the Geological Society*, v. 156, p. 869-888.
- Ruzyla, K., and G. M. Friedman, 1985, Factors controlling porosity in dolomite reservoirs of the Ordovician Red River Formation, Cabin Creek field, Montana, in P. O. Roehl, and P. W. Choquette, eds., *Carbonate petroleum reservoirs: A case book*: New York, Springer Verlag, p. 39-58.
- Sadooni, F. N., 1995, Petroleum prospects of Upper Triassic carbonates in northern Iraq: *Journal of Petroleum Geology*, v. 18, p. 171-190.
- Sage, L., and J. Letouzey, 1990, Convergence of the African and Eurasian plates in the eastern Mediterranean, in J. Letouzey, ed., *Petroleum and tectonics in mobile belts*: Paris, Technips, p. 49-68.
- Sahin, A., and S. Saner, 2001, Statistical distributions and correlations of petrophysical parameters in the Arab-D reservoir, Abqaiq oilfield, Eastern Saudi Arabia: *Journal of Petroleum Geology*, v. 24, p. 101-114.
- Said, R., 1993, *The River Nile: Geology, hydrology and utilization*: Oxford, Pergamon Press.
- Salameh, E., and H. Bannayan, 1993, Water resources of Jordan: Present status and future potentials, Friedrich Ebert Stiftung.
- Salameh, E., and H. El-Naser, 2000, The Interface Configuration of the Fresh-/Dead Sea Water - Theory and Measurements: *Acta Hydrochim. Hydrobiol.*, v. 28, p. 323-328.
- Saleh, A., F. Al-Ruwaih, A. Al-Reda, and A. Gunatilaka, 1999, A reconnaissance study of a clastic coastal sabkha in Northern Kuwait, Arabian Gulf: *Journal of Arid Environments*, v. 43, p. 1-19.
- Saller, A. H., and N. Henderson, 1998, Distribution of porosity and permeability in platform dolomites - Insight from the Permian of west Texas: *AAPG Bulletin-American Association of Petroleum Geologists*, v. 82, p. 1528-1550.
- Saller, A. H., and B. R. Moore, 1986, Dolomitization in the Smackover Formation, Escambia County, Alabama: *Gulf Coast Association of Geological Societies Transactions*, v. 36, p. 275-282.
- Saller, M., and M. O'Driscoll, 2000, Lithium takes charge: *Industrial Minerals*, v. 390 (March), p. 37-47.
- Salter, D. I., and I. M. West, 1966, Calciostromantite in the basal Purbeck Beds of Durlston Head, Dorset: *Mineralogical Magazine*, v. 35, p. 146-150.

- Salvador, A., 1987, Late Triassic-Jurassic paleogeography and origin of the Gulf of Mexico basin: *Bulletin American Association of Petroleum Geologists*, v. 71, p. 419-451.
- Salvan, H. M., 1972, Les niveaux salifères marocains, leurs caractéristiques problèmes, in G. Richter-berenburg, ed., *Geology of Saline deposits*: Paris, UNESCO, p. 147-168.
- Salvany, J. M., A. Munoz, and A. Perez, 1994, Nonmarine evaporitic sedimentation and associated diagenetic processes of the southwestern margin of the Ebro Basin (lower Miocene), Spain: *Journal of Sedimentary Research, Section A: Sedimentary Petrology and Processes*, v. 64, p. 190-203.
- Salvany, J. M., and F. Orti, 1994, Miocene glauberite deposits of Alcanadre, Ebro Basin, Spain: sedimentary and diagenetic processes, in R. W. Renaut, and W. M. Last, eds., *Sedimentology and geochemistry of modern and ancient saline lakes*, SEPM/Society for Sedimentary Geology Special Publication, v. 50, p. 203-215.
- Sanchez-Moral, S., J. C. Cañaveras, L. Laiz, C. Saiz-Jimenez, J. Bedoya, and L. Luque, 2003, Biomediated Precipitation of Calcium Carbonate Metastable Phases in Hypogean Environments: A Short Review: *Geomicrobiology Journal*, v. 20, p. 491-501.
- Sanchez-Moral, S., S. Ordonez, M. A. G. Delcura, M. Hoyos, and J. C. Canaveras, 1998, Penecontemporaneous diagenesis in continental saline sediments - Bloeditization in Quero playa lake (La Mancha, Central Spain): *Chemical Geology*, v. 149, p. 189-204.
- Sancho, C., J. L. Peña, R. Mikkan, C. Osácar, and Y. Quinif, 2004, Morphological and speleothemic development in Brujas Cave (Southern Andean Range, Argentina): palaeoenvironmental significance: *Geomorphology*, v. 57, p. 367-384.
- Sandberg, P. A., 1975, New interpretations of Great Salt Lake ooids and of ancient non-skeletal carbonate mineralogy.: *Sedimentology*, v. 22, p. 497-537.
- Sandler, A., Y. Harlavan, and G. Steinitz, 2004, Early formation of K-feldspar in shallow-marine sediments at near-surface temperatures (southern Israel): evidence from K-Ar dating: *Sedimentology*, v. 51, p. 323-338.
- Saner, S., and W. M. Abdulghani, 1995, Lithostratigraphy and depositional environments of the Upper Jurassic Arab-C Carbonate and associated evaporites in the Abqaiq field, eastern Saudi Arabia: *Bulletin American Association of Petroleum Geologists*, v. 79, p. 394-409.
- Saner, S., and A. Sahin, 1999, Lithological and zonal porosity-permeability distributions in the Arab-D reservoir, Uthmaniyah field, Saudi Arabia: *Bulletin-American Association of Petroleum Geologists*, v. 83, p. 230-243.
- Sanford, W. E., and W. W. Wood, 1991, Brine evolution and mineral deposition in hydrologically open evaporite basins: *American Journal of Science*, v. 291, p. 687-710.
- Sanford, W. E., and W. W. Wood, 2001, Hydrology of the coastal sabkhas of Abu Dhabi, United Arab Emirates: *Hydrogeology Journal*, v. 9, p. 358-366.
- Sanjuan, B., G. Michard, and A. Michard, 1990, Origine des substances dissoutes dans les eaux des sources thermales et des forages de la région Asal-Ghoubbet (République de Djibouti): *Journal of Volcanology & Geothermal Research*, v. 43, p. 333-353.
- Sans, M., J. A. Munoz, and J. Verges, 1996b, Triangle zone and thrust wedge geometries related to evaporitic horizons (southern Pyrenees): *Bulletin of Geological Petroleum Geology*, v. 44, p. 375-384.
- Sans, M., A. L. Sanchez, and P. Santanach, 1996a, Internal structure of a detachment horizon in the most external part of the Pyrenean fold and thrust belt (northern Spain), in G. I. Alsop, D. Blundell, and I. Davison, eds., *Salt tectonics*: London, Geological Society Special Publication, v. 100, p. 65-76.
- Sanz-Rubio, E., M. Hoyos, J. Calvo, and J. Rouchy, 1999, Nodular anhydrite growth controlled by pedogenic structures in evaporite lake formations: *Sedimentary Geology*, v. 125, p. 195-203.
- Sanz-Rubio, E., S. Sanchez-Moral, J. C. Canaveras, J. P. Calvo, and J. M. Rouchy, 2001, Calcitization of Mg-Ca carbonate and Ca sulphate deposits in a continental Tertiary basin (Calatayud Basin, NE Spain): *Sedimentary Geology*, v. 140, p. 123-142.
- Sarbu, S. M., T. C. Kane, and B. K. Kinkle, 1996, A chemoautotrophically based cave ecosystem: *Science*, v. 272, p. 1953-1955.
- Sarg, J. F., 1981, Petrology of the carbonate-evaporite facies transition of the Seven Rivers Formation (Guadalupean, Permian), Southeast New Mexico: *Journal of Sedimentary Petrology*, v. 51, p. 73-96.
- Sarg, J. F., 2001, The sequence stratigraphy, sedimentology, and economic importance of evaporite-carbonate transitions: a review: *Sedimentary Geology*, v. 140, p. 9-42.
- Sarkar, A., J. A. Nunn, and J. S. Hanor, 1995, Free thermohaline convection beneath allochthonous salt sheets - An agent for salt dissolution and fluid flow in Gulf Coast sediments: *Journal of Geophysical Research-Solid Earth*, v. 100, p. 18085-18092.
- Sass, A. M., H. Sass, M. J. L. Coolen, H. Cypionka, and J. Overmann, 2001, Microbial communities in the chemocline of a hypersaline deep-sea basin (Urania basin, Mediterranean Sea): *Applied and Environmental Microbiology*, v. 67, p. 5392-5402.
- Sass, E., and A. Bein, 1988, Dolomites and salinity; a comparative geochemical study: Shukla, Vijai, Baker, Paul A. *Sedimentology and geochemistry of dolostones*, based on a symposium. Special Publication Society of Economic Paleontologists and Mineralogists, v. 43, p. 223-233.
- Sass, E., and Ben-Yaakov, 1977, The carbonate system in hypersaline solutions: *The Dead Sea Brines: Marine Chemistry*, v. 5, p. 83-109.
- Saunders, J. A., and C. T. Swann, 1994, Mineralogy and geochemistry of a cap-rock Zn-Pb-Sr-Ba occurrence at the Hazlehurst salt dome, Mississippi: *Economic Geology*, v. 89, p. 381-390.
- Saunders, J. A., and R. C. Thomas, 1996, Origin of exotic minerals in Mississippi salt dome cap rocks - Results of reaction path modeling: *Applied Geochemistry*, v. 11, p. 667-676.
- Savage, A., and B. Knott, 1998, *Artemia parthenogenetica* in Lake Hayward, Western Australia. II. Feeding biology in a shallow seasonally stratified, hypersaline lake: *International Journal of Salt Lake Research*, v. 7, p. 13-24.
- Savard, M. M., G. Lynch, and F. Fallara, 1996, Burial diagenesis model for the Macumber Formation on Cape Breton Island - implications for the tectonic evolution of the Windsor Group: *Atlantic Geology*, v. 32, p. 53-64.
- Schaad, W., 1995, The origin of Rauhewackes (Cornieules) by the karstification of gypsum [German]: *Eclogae Geologicae Helvetiae*, v. 88, p. 59-90.
- Schauer, M., and T. Aigner, 1997, Cycle stacking pattern, diagenesis and reservoir geology of peritidal dolostones, Trigonodus Dolomite, Upper Muschelkalk (Middle Triassic, SW Germany): *Facies*, v. 37, p. 99-113.

- Scheck, M., and U. Bayer, 1999, Evolution of the Northeast German Basin — inferences from a 3D structural model and subsidence analysis: *Tectonophysics*, v. 313, p. 145-169.
- Scheck, M., U. Bayer, and B. Leweren, 2003, Salt movements in the Northeast German Basin and its relation to major post-Permian tectonic phases—results from 3D structural modelling, backstripping and reflection seismic data: *Tectonophysics*, v. 361, p. 277-299.
- Schenk, C. J., and S. G. Fryberger, 1988, Early diagenesis of eolian dune and interdune sands at White Sands, New Mexico: *Sedimentary Geology*, v. 55, p. 109-120.
- Schenk, C. J., and R. W. Richardson, 1985, Recognition of interstitial anhydrite dissolution; a cause of secondary porosity, San Andres Limestone, New Mexico, and upper Minnelusa Formation, Wyoming: *Bulletin American Association of Petroleum Geologists*, v. 69, p. 1064-1076.
- Schenk, P., and M. P. A. Jackson, 1993, Diapirism on Triton: A record of crustal layering and instability: *Geology*, v. 21, p. 299-302.
- Schenk, P., P. Vonbitter, and R. Matsumoto, 1994, Deep-basin Deep-water carbonate-evaporite deposition of a saline giant - Loch Macumber (Visean), Atlantic Canada: *Carbonates & Evaporites*, v. 9, p. 187-210.
- Schidlowski, M., U. Matzeigkeit, W. G. Mook, and W. E. Krumbein, 1985, Carbon isotope geochemistry and ^{14}C ages of microbial mats from Gavish sabkha and Solar Lake, in G. M. Friedman, and W. E. Krumbein, eds., *Hypersaline ecosystems - The Gavish sabkha*: New York, Springer-Verlag, p. 381-401.
- Schlager, W., and H. Bolz, 1977, Clastic accumulation of sulfate evaporites in deep water: *Journal of Sedimentary Petrology*, v. 47, p. 600-609.
- Schlitt, W. J., 1982, Interfacing technologies in solution mining: *Proc. of the Second SME-SPE Intl. Solution Mining Symp.*, Denver: New York, AIME, 370 p.
- Schlumberger Pty. Ltd., 1994, Through the reef barrier: *Middle East Well Evaluation Review*, v. 15, p. 8-29.
- Schlüter, T., and R. Kohring, 2002, Palaeopathological fish bones from phosphorites of the Lake Manyara area, Northern Tanzania - Fossil evidence of a physiological response to survival in an extreme biocenosis: *Environmental Geochemistry and Health*, v. 24, p. 131-140.
- Schmid, I. H., 1987, Turkey's Salda Lake: a genetic model for Australia's newly discovered magnesite deposits: *Ind. Min.*, v. 239, p. 19-31.
- Schmid, R. M., 1988a, Lake Torrens Brine: *Hydrobiologia*, v. 158, p. 267-269.
- Schmid, R. M., 1988b, Lake Torrens halite accumulation (South Australia): *Zeitschrift der Deutschen Geologischen Gesellschaft*, v. 139, p. 289-296.
- Schmidt, V., I. A. McIlreath, and A. E. Budwill, 1985, Origin and diagenesis of Middle Devonian pinnacle reefs encased in evaporites, "A" and "E" pools, Rainbow field, Alberta, in P. O. Roehl, and P. W. Choquette, eds., *Carbonate petroleum reservoirs*: New York, Springer-Verlag, p. 141-160.
- Schneider, G. I. C., and G. Genis, 1991, Soda Ash and Thenardite, Open File Report MRS 24, Namibia Ministry of Mines and Energy, 18 p.
- Schoell, M., M. A. McCaffrey, F. J. Fago, and J. M. Moldowan, 1992, Carbon isotopic compositions of 28,30-bisnorhopanes and other biological markers in a Monterey crude oil: *Geochimica et Cosmochimica Acta*, v. 56, p. 1391-1399.
- Scholle, P. A., L. Stemmerik, and O. Harpoth, 1990, Origin of major karst-associated celestite mineralization in Karstryggen, central East Greenland: *Journal of Sedimentary Petrology*, v. 60, p. 397-410.
- Scholle, P. A., L. Stemmerik, D. Ulmer-Scholle, G. Diliagro, and F. H. Henk, 1993, Palaeokarst-influenced depositional and diagenetic patterns in Upper Permian carbonates and evaporites, Karstryggen Area, Central East Greenland: *Sedimentology*, v. 40, p. 895-918.
- Scholle, P. A., D. S. Ulmer, and L. A. Melin, 1992, Late-stage calcites in the Permian Capitan Formation and its equivalents, Delaware Basin margin, West Texas and New Mexico; evidence for replacement of precursor evaporites: *Sedimentology*, v. 39, p. 207-234.
- Schouten, S., W. A. Hartgers, J. F. Lopez, J. O. Grimalt, and J. S. S. Damste, 2001, A molecular isotopic study of C-13 -enriched organic matter in evaporitic deposits: recognition of CO_2 -limited ecosystems: *Organic Geochemistry*, v. 32, p. 277-286.
- Schreiber, B. C., 1988a, Subaqueous evaporite deposition, in B. C. Schreiber, ed., *Evaporites and hydrocarbons*: New York, Columbia University Press.
- Schreiber, B. C., and M. El Tabakh, 2000, Deposition and early alteration of evaporites [Review]: *Sedimentology*, v. 47, p. 215-238.
- Schreiber, B. C., and D. J. J. Kinsman, 1975, New observations on the Pleistocene evaporites of Montallegro, Sicily and a modern analog: *Journal of Sedimentary Petrology*, v. 45, p. 469-479.
- Schreiber, B. C., R. P. Philp, S. Benali, M. L. Helman, J. A. de la Pena, R. Marfil, P. Landais, A. D. Cohen, and C. G. S. C. Kendall, 2001, Characterisation of organic matter formed in hypersaline carbonate/evaporite environments: Hydrocarbon potential and biomarkers obtained through artificial maturation studies: *Journal of Petroleum Geology*, v. 24, p. 309-338.
- Schreiber, B. C., and E. Schreiber, 1977, The salt that was: *Geology*, v. 5, p. 527-528.
- Schreiber, B. C., and D. Walker, 1992, Halite pseudomorphs after gypsum; a suggested mechanism: *Journal of Sedimentary Petrology*, v. 62, p. 61-70.
- Schreiber, B. C. e., 1988b, *Evaporites and hydrocarbons*: New York, Columbia University Press, 475 p.
- Schröder, S., J. E. Amthor, and A. Matter, 2000b, Unusual hydrocarbon reservoirs in intrasalt carbonate stringers (Birba Area, Infracambrian Ara Group, S-Oman): *GeoArabia*, v. 5, p. 177.
- Schröder, S., B. C. Schreiber, J. E. Amthor, and A. Matter, 2000a, Evaporites of the Ara Group (South Oman): an essential element of stratigraphy in an Infracambrian salt basin: *GeoArabia*, v. 5, p. 176-177.
- Schröder, S., B. C. Schreiber, J. E. Amthor, and A. Matter, 2003, A depositional model for the terminal Neoproterozoic-Early Cambrian Ara Group evaporites in south Oman: *Sedimentology*, v. 50, p. 879-898.
- Schröder, S., J. P. Grotzinger, J. E. Amthor, and A. Matter, 2005, Carbonate deposition and hydrocarbon reservoir development at the Precambrian-Cambrian boundary: The Ara Group in South Oman: *Sedimentary Geology*, v. 180, p. 1-28.

- Schubel, K. A., and T. K. Lowenstein, 1997, Criteria for the recognition of shallow-perennial-saline-lake halites based on Recent sediments from the Qaidam Basin, western China: *Journal of Sedimentary Research Section A-Sedimentary Petrology & Processes*, v. 67, p. 74-87.
- Schubel, K. A., and B. M. Simonson, 1990, Petrography and diagenesis of cherts of Lake Magadi, Kenya: *Journal of Sedimentary Petrology*, v. 60, p. 761-776.
- Schubert, J. K., and D. J. Bottjer, 1992, Early Triassic stromatolites as post-mass extinction disaster forms: *Geology*, v. 20, p. 883-886.
- Schultz-Ela, D., and P. Walsh, 2002, Modeling of grabens extending above evaporites in Canyonlands National Park, Utah: *Journal of Structural Geology*, v. 24, p. 247-275.
- Schultz-Ela, D. D., 1992, Restoration of cross-sections to constrain deformation processes of extensional terranes: *Marine and Petroleum Geology*, v. 9, p. 372-388.
- Schultz-Ela, D. D., 2003, Origin of "Drag" Folds Bordering Salt Diapirs: *Bulletin American Association Petroleum Geologists*, v. 87, p. 757-780.
- Schultz-Ela, D. D., and M. P. A. Jackson, 1996, Relation of subsalt structures to suprasalt structures during extension: *American Association of Petroleum Geologists Bulletin*, v. 80, p. 1896-1924.
- Schultz-Ela, D. D., M. P. A. Jackson, and B. C. Vendeville, 1993, Mechanics of active salt diapirism: *Tectonophysics*, v. 228, p. 275-312.
- Schulz, E., A. Abichou, T. Hachicha, S. Pomel, U. Salzmann, and K. Zouari, 2002, Sebkhass as ecological archives and the vegetation and landscape history of southeastern Tunisia during the last two millennia: *Journal of African Earth Sciences*, v. 34, p. 223-229.
- Schuster, D. C., 1995, Deformation of allochthonous salt and evolution of related salt-structural systems, Eastern Louisiana Gulf Coast, in M. P. A. Jackson, D. G. Roberts, and S. Snelson, eds., *Salt tectonics: a global perspective*, AAPG Memoir, v. 65, p. 177-198.
- Schwark, L., M. Vliex, and P. Schaeffer, 1998, Geochemical characterization of Malm Zeta laminated carbonates from the Franconian Alb, SW-Germany (II): *Organic geochemistry*, v. 29, p. 1921-1952.
- Schwerdtner, W. M., 1964, Genesis of potash rocks in Middle Devonian Prairie Evaporite Formation of Saskatchewan: *Am. Assoc. Petroleum Geologists Bull.*, p. 1108-1115.
- Searl, A., and S. Rankin, 1993, A preliminary petrographic study of the Chilean nitrates: *Geological Magazine*, v. 130, p. 319-333.
- Sears, S. O., and F. J. Lucia, 1979, Reef growth model for Silurian pinnacle reefs, northern Michigan reef trend: *Geology*, v. 3, p. 299-302.
- Sears, S. O., and F. J. Lucia, 1980, Dolomitization of Northern Michigan Niagara reefs by brine refluxion and fresh water/sea water mixing, in D. H. Zenger, J. B. Dunham, and R. L. Ethington, eds., *Concepts and models of dolomitization*, Society of Economic Paleontologists and Mineralogists, Special Publication 28, p. 215-235.
- Sebag, D., E. P. Verrecchia, S. J. Lee, and A. Durand, 2001, The natural hydrous sodium silicates from the northern bank of Lake Chad: occurrence, petrology and genesis: *Sedimentary Geology*, v. 139, p. 15-31.
- Sellwood, B. W., and R. E. Netherwood, 1984, Facies evolution in the Gulf of Suez area: Sedimentation history as an indicator of rift initiation and development: *Modern Geology*, v. 9, p. 43-69.
- Senalp, M., and A. Al-Duaiji, 1995, Stratigraphy and sedimentation of the Unayzah reservoirs, Central Saudi Arabia, in M. I. Al-Husseini, ed., *Middle East Petroleum Geosciences Conference, GEO'94*, v. 1: Manama, Bahrain, Gulf Petrolink.
- Seni, S. J., 1992, Evolution of salt structures during burial of salt sheets on the slope, northern Gulf of Mexico: *Marine and Petroleum Geology*, v. 9, p. 452-468.
- Seni, S. J., and M. P. A. Jackson, 1983a, Evolution of salt structures, East Texas diapir province; Part 1, Sedimentary record of halokinesis: *Bulletin American Association of Petroleum Geologists*, v. 67, p. 1219-1244.
- Seni, S. J., and M. P. A. Jackson, 1983b, Evolution of salt structures, East Texas diapir province; Part 2, Patterns and rates of halokinesis: *Bulletin American Association of Petroleum Geologists*, v. 67, p. 1245-1274.
- Sessler, W., 1990, Influence of subsrosion on three different types of salt deposits, in D. Heling, P. Rothe, U. Förstner, and P. Stoffers, eds., *Sediments and Environmental Geochemistry*: Berlin, Springer-Verlag, p. 179-196.
- Seymour, K. P., G. Rae, J. M. Peden, and K. Ormston, 1993, Drilling close to salt diapirs in the North Sea: *SPE 26693*, September 1993, p. 193-204.
- Shaker, S. S., 2004, Geopressure compartmentalization in salt basins: Their assessment for hydrocarbon entrapments in the Gulf of Mexico, In: *Salt-sediment interactions and hydrocarbon prospectivity: concepts, applications and case studies for the 21st Century*. Papers presented at the 24th Annual Gulf Coast Section SEPM Foundation Bob F. Perkins Research Conference, Houston Tx, December 5-8, 2004 (CD publication), p. 421-433.
- Shaker, S. S., and M. A. Smith, 2002, Pore Pressure Profile Predictions in the Challenging Supra/Sub-Salt Exploration Plays in Deep Water, Gulf of Mexico: *AAPG Annual Meeting 2002*.
- Sharland, P. R., R. Archer, D. M. Casey, R. B. Davies, S. H. Hall, A. P. Heward, A. D. Horbury, and M. D. Simmons, 2001, *Arabian Plate Sequence Stratigraphy*: GeoArabia Special Publication 2: Bahrain, Gulf Petrolink, 371 p.
- Sharp, J. M., T. R. Fenstermaker, C. T. Simmons, T. E. McKenna, and J. K. Dickinson, 2001, Potential salinity-driven free convection in a shale-rich sedimentary basin: Example from the Gulf of Mexico basin in south Texas: *Bulletin American Association Petroleum Geologists*, v. 85, p. 2089-2110.
- Shaw, A. B., 1964, *Time in Stratigraphy*: New York, McGraw-Hill, 365 p.
- Shaw, A. B., 1977, A review of some aspects of evaporite deposition: *Mountain Geologist*, v. 14, p. 1-16.
- Shearman, D. J., 1963, Recent anhydrite, gypsum, dolomite, and halite from the coastal flats of the Arabian shore of the Persian Gulf: *Geological Society of London, Proceedings*, v. 1607, p. 63-65.
- Shearman, D. J., 1970, Recent halite rock, Baja California, Mexico: *Inst. Min. Metall., Trans., Sect. B.*, v. 79, p. B155-B162.
- Shearman, D. J., 1978, Evaporites of coastal sabkhas, in W. E. Dean, and B. C. Schreiber, eds., *Marine evaporites*: Tulsa Ok., Soc. Econ. Paleontol. Mineral., Short Course Notes.
- Shearman, D. J., and J. G. Fuller, 1969, Anhydrite diagenesis, calcitization, and organic laminites, Winniepegosis Formation, Middle Devonian, Saskatchewan: *Bull. Can. Pet. Geol.*, v. 17, p. 496-525.

- Shearman, D. J., J. Khouri, and S. Taha, 1961, On the replacement of dolomite by calcite in some Mesozoic limestones from the French Jura: *Proceedings Geologists' Assoc.*, London, v. 72, p. 1-12.
- Shearman, D. J., A. McGugan, C. Stein, and A. J. Smith, 1989, Ikaite, $\text{CaCO}_3 \cdot 6\text{H}_2\text{O}$, precursor of the tholinolites in the Quaternary tufas and tufa mounds of the Lahontan and Mono Lake Basins, western United States: *Geol. Soc. Am. Bull.*, v. 101, p. 913-917.
- Shearman, D. J., G. Mossop, H. Dunsmore, and M. Martin, 1972, Origin of gypsum veins by hydraulic fracture: *Inst. Min. Metall. Trans., Sect. B.*, v. 81, p. B149-B155.
- Shearman, D. J., and A. J. Smith, 1985, Ikaite, the parent mineral of jarrowite-type pseudomorphs: *Proceedings of the Geologists' Association*, v. 96, p. 305-314.
- Shelton, J. S., R. P. Papsen, and M. Womer, 1978, Aerial guide to geological features of southern California: *Aeolian Features of Southern California: A Comparative Planetary Geology Guidebook*, Office of Planetary Geology, National Aeronautics and Space Administration, U.S. Government Printing Office, Washington, D.C., p. 216-249.
- Shen, Y., and R. Buick, 2004, The antiquity of microbial sulfate reduction: *Earth Science Reviews*, v. 64, p. 243-272.
- Sheppard, R. A., and A. J. Gude, 1968, Distribution and genesis of authigenic silicate minerals in tuffs of Pleistocene Lake Tecopa, Inyo County, Calif.: *U.S. Geol. Surv. Prof. Paper*, v. 597, p. 38 p.
- Sheppard, R. A., A. J. Gude, and G. M. Elson, 1978, Bowie zeolite deposit, Cochise and Graham Counties, Arizona, in L. B. Sand, and F. A. Mumpton, eds., *Natural Zeolites — Occurrence, Properties, Use*, Pergamon, p. 319-328.
- Sheppard, R. A., and F. A. Mumpton, 1984, Sedimentary fluorite in a lacustrine zeolitic tuff of the Gila Conglomerate near Buckhorn, Grant County, New Mexico: *Journal of Sedimentary Petrology*, v. 54, p. 853-860.
- Sherwood, J. E., F. Stagnitti, M. J. Kokkinn, and W. D. Williams, 1992, A standard table for predicting equilibrium dissolved oxygen concentrations in salt lakes dominated by sodium chloride: *International Journal of Salt Lake Research*, v. 1, p. 1-61.
- Sheu, D. D., 1987, Sulfur and organic carbon contents in sediment cores from the Tyro and Orca basins: *Marine Geology*, v. 75, p. 157-164.
- Sheu, D. D., and B. J. Presley, 1986a, Formation of hematite in the euxinic Orca basin, northern Gulf of Mexico: *Marine Geology*, v. 69, p. 309-321.
- Sheu, D. D., and B. J. Presley, 1986b, Variations of calcium carbonate, organic carbon and iron sulfides in anoxic sediment from the Orca Basin, Gulf of Mexico: *Marine Geology*, v. 70, p. 103-118.
- Shiba, H., and K. Horikoshi, 1988, Isolation and characterization of novel anaerobic, halophilic eubacteria from hypersaline environments of western America and Kenya: In: *Proceedings of the FEMS symposium—The microbiology of extreme environments and its biotechnological potential*, Portugal, p. 371-373.
- Shields, M. J., and P. V. Brady, 1995, Mass balance and fluid flow constraints on regional scale dolomitization, Late Devonian, Western Canada sedimentary basin: *Bulletin of Canadian Petroleum Geology*, v. 43, p. 371-392.
- Shinn, E. A., 1973, Carbonate coastal accretion in an area of longshore transport, NE Qatar, Persian Gulf, in P. B. H., ed., *The Persian Gulf: Holocene carbonate sedimentation and diagenesis in a shallow epicontinental sea*: New York, Springer-Verlag, p. 179-191.
- Shinn, E. A., 1976, Coral recovery in Florida and the Persian Gulf: *Environmental Geology*, v. 1, p. 241-254.
- Shinn, E. A., 1983, Birdseyes, fenestrae, shrinkage pores, and loferites; a reevaluation: *Journal of Sedimentary Petrology*, v. 53, p. 619-628.
- Shinol, J. H., H. S. Sumner, and J. T. Ford, 2000, Subsalt Exploration in the Gulf of Mexico Deep Water (abs): *American Association Petroleum Geologists - Bulletin*, v. 84.
- Shirley, K., 2000, Gulf of Mexico deepwater and subsalt plays: The promise of the best of both worlds: *AAPG Explorer*, v. Oct. 2000.
- Shock, D. A., 1985, Solution mining of soluble salts - its scope and its future, in W. J. Schlitt, ed., *Salt and Brines '85*: New York, Am. Inst. of Min. Met. and Pet. Eng., p. 1-10.
- Sibley, D. F., 1980, Climatic control of dolomitization, Seroe Doni formation (Pliocene), Bonaire, N. A., v. 28, *SEPM Spec. Pub.*, p. 247-258.
- Siedlecka, A., 1972, Length-slow chalcedony and relicts of sulphates; evidences of evaporitic environments in the upper Carboniferous and Permian beds of Bear Island, Svalbard: *Journal Sedimentary Petrology*, v. 42, p. 812-816.
- Siedlecka, A., 1976, Silicified Precambrian evaporite nodules from northern Norway; a preliminary report: *Sedimentary Geology*, v. 16, p. 161-175.
- Siefke, J. W., 1991, The Boron Open Pit Mine at the Kramer Borate Deposit, in M. A. McKibben, ed., *The Diversity of Mineral and Energy Resources of Southern California*, SEG Guidebook Series, v. 12, p. 4-15.
- Sillitoe, R., and H. McKee, 1996, Age of supergene oxidation and enrichment in the Chilean porphyry copper province: *Economic Geology*, v. 91, p. 164-179.
- Simkiss, K., 1977, Biomineralization and detoxification: *Calcified Tissue Research*, v. 24, p. 199-200.
- Simkiss, K., 1989, Biomineralisation in the context of geological time: *Royal Society of Edinburgh Transactions, Earth Sciences*, v. 80, p. 193-199.
- Simmons, R. E., 1995, Population declines, viable breeding areas and management options for flamingos in southern Africa: *Conservation Biology*, v. 10, p. 504-514.
- Simoneit, B. R. T., T. A. T. Aboul-Kassim, and J. J. Tiercelin, 2000, Hydrothermal petroleum from lacustrine sedimentary organic matter in the East African Rift: *Applied Geochemistry*, v. 15, p. 355-368.
- Simpson, E. L., and K. A. Eriksson, 1993, Thin eolianites interbedded within a fluvial and marine succession: early Proterozoic Whitworth Formation, Mount Isa Inlier, Australia: *Sedimentary Geology*, v. 87, p. 39-62.
- Singer, A., 1979, Palygorskite in sediments: detrital, diagenetic or neofomed - A critical review: *Geologische Rundschau*, v. 68, p. 996-1008.
- Singer, A., K. Stahr, and M. Zarei, 1998, Characteristics and origin of sepiolite (Meerschaum) from central Somalia: *Clay Minerals*, v. 33, p. 349-362.
- Sinha, R., and B. C. Raymahashay, 2000, Salinity model inferred from two shallow cores at Sambhar Salt Lake, Rajasthan: *Journal of the Geological Society of India*, v. 56, p. 213-217.

- Sinninghe Damste, J. S., J. Kenig, M. P. Koopmans, J. Koster, S. Schouten, J. M. Hayes, and J. W. De Leeuw, 1995, Evidence for gammacerane as an indicator of water column stratification: *Geochimica et Cosmochimica*, v. 59, p. 1895-1900.
- Sloss, L. L., 1953, The significance of evaporites: *Journal of Sedimentary Petrology*, p. 143-161.
- Smith, D. B., 1971, Possible displacive halite in the Permian Upper Evaporite Group of northeast Yorkshire: *Sedimentology*, v. 17, p. 221-232.
- Smith, D. B., 1972, Foundered strata, collapse breccias and subsidence features of the English Zechstein, in G. Richter-Bernberg, ed., *Geology of saline deposits*: Paris, UNESCO, p. 255-269.
- Smith, D. B., 1996, Deformation in the Late Permian Boulby Halite (EZ3Na) in Teesside, NE England, in G. I. Alsop, D. J. Blundell, and I. Davison, eds., *Salt tectonics*: London, United Kingdom, Geological Society of London special Publication, v. 100, p. 77-88.
- Smith, D. G., and J. R. Pullen, 1967, Hummingbird structure of southeast Saskatchewan: *Canadian Petroleum Geology Bulletin*, v. 15, p. 468-482.
- Smith, G. I., 1979, Subsurface stratigraphy and geochemistry of Late Quaternary evaporites, Searles Lake, California: US Geological Survey, Professional Paper, v. 1043, p. 130 pp.
- Smith, M. E., B. Singer, and A. Carroll, 2003, Ar-40/Ar-39 geochronology of the Eocene Green River Formation, Wyoming: *Geological Society of America Bulletin*, v. 115, p. 549-565.
- Smith, R. M. H., and T. R. Mason, 1998, Sedimentary environments and trace fossils of Tertiary oasis deposits in the central Namib desert, Namibia: *Palaeos*, v. 13, p. 547-559.
- Smoot, J. P., 1983, Depositional subenvironments in an arid closed basin; the Wilkins Peak Member of the Green River Formation (Eocene), Wyoming, USA: *Sedimentology*, v. 30, p. 801-827.
- Smoot, J. P., 1991, Sedimentary facies and depositional environments of early Mesozoic Newark Group, Eastern North America: *Paleogeography, Paleogeology and Paleoclimatology*, v. 84, p. 369-423.
- Smoot, J. P., and T. K. Lowenstein, 1991, Depositional environments of non-marine evaporites, in J. D. Melvin, ed., *Evaporites, Petroleum and Mineral Resources*, Elsevier Science, *Developments in Sedimentology*, V. 50, p. 189-347.
- Sneh, A., 1979, Fan deltas along the Dead Sea rift: *Journal Sedimentary Petrology*, v. 49, p. 541-552.
- Snyder, F. C., and J. A. Nugent, 1995, Teak - Testing a subsalt hydrocarbon trap geometry, South Timbalier Block 260, Gulf of Mexico: *Proceedings of GCCSEPM Foundation 16th Annual Research Conference, Salt Sediment and Hydrocarbons*, Dec 3-6, 1995, p. 257-267.
- Sonnenfeld, P., 1985, Evaporites as oil and gas source rocks: *Journal of Petroleum Geology*, v. 8, p. 253-271.
- Sonnenfeld, P., 1995, The color of rock salt; a review: *Sedimentary Geology*, v. 94, p. 267-276.
- Sonnenfeld, P., and I. S. Al-Aasm, 1991, The Salina Group evaporites in the Michigan Basin, in P. A. Catocinos, and P. A. Daniels, Jr., eds., *Early sedimentary evolution of the Michigan Basin*: Boulder, CO, Geological Society of America, Special Paper v. 256, p. 139-153.
- Soriano, M. A., and J. L. Simon, 1995, Alluvial dolines in the central Ebro Basin, Spain - A spatial and developmental hazard analysis: *Geomorphology*, v. 11, p. 295-309.
- Souissi, F., J. L. Dandurand, and J. P. Fortune, 1997, Thermal evolution of fluids during fluorite deposition in the Zaghwan Province, northeastern Tunisia: *Mineralium Deposita*, v. 32, p. 257-270.
- Southgate, P. N., 1982, Cambrian skeletal halite crystals and experimental analogues: *Sedimentology*, v. 29, p. 391-407.
- Southgate, P. N., 1991, A sedimentological model for the Loves Creek Member of the Late Proterozoic Bitter Springs Formation, Australia: Bureau Mineral Resources (BMR), *Geology and Geophysics, Bulletin*, v. 236, p. 113 - 126.
- Southgate, P. N., I. B. Lambert, T. H. Donnelly, R. Henry, H. Etminan, and G. Weste, 1989, Depositional environments and diagenesis in Lake Parakeelya: a Cambrian alkaline playa from the Officer Basin, South Australia: *Sedimentology*, v. 36, p. 1091-1112.
- Spangenberg, J., L. Fontbote, Z. D. Sharp, and J. Hunziker, 1996, Carbon and oxygen isotope study of hydrothermal carbonates in the zinc-lead deposits of the San Vicente district, Central Peru - Quantitative modeling of mixing processes and CO₂ degassing: *Chemical Geology*, v. 133, p. 289-315.
- Spangenberg, J. E., L. Fontbote, and S. A. Macko, 1999, An evaluation of the inorganic and organic geochemistry of the San Vicente Mississippi Valley-type zinc-lead district, central Peru: Implications for ore fluid composition, mixing processes, and sulfate reduction: *Economic Geology*, v. 94, p. 1067-1092.
- Spathopoulos, F., 1996, An insight on salt tectonics in the Angola Basin, South Atlantic, in G. I. Alsop, D. J. Blundell, and I. Davison, eds., *Salt tectonics*, Geological Society, London; Special Publication, v. 100, p. 153-174.
- Speed, R. C., 1975, Carbonate breccia (rauhwacke) nappes of the Carson Sink region, Nevada: *Geol. Soc. America Bull.*, v. 86, p. 473-486.
- Speed, R. C., and R. N. Clayton, 1975, Origin of marble by replacement of gypsum in carbonate breccia nappes, Carson Sink region, Nevada: *Journal of Geology*, v. 83, p. 223-237.
- Spencer, R. J., 1983, The geochemical evolution of Great Salt Lake, Utah: Doctoral thesis, Johns Hopkins University.
- Spencer, R. J., H. P. Eugster, and B. F. Jones, 1985, Geochemistry of Great Salt Lake, Utah II: Pleistocene-Holocene evolution: *Geochimica et Cosmochimica Acta*, v. 49, p. 739-747.
- Spencer, R. J., and L. A. Hardie, 1990, Control of seawater composition by mixing of river waters and mid-ocean ridge hydrothermal brines, in R. J. Spencer, and I. M. Chou, eds., *Fluid Mineral Interactions: A Tribute to H. P. Eugster*, v. 2: San Antonio, Geochem. Soc. Spec. Publ., p. 409-419.
- Spencer, R. J., and T. K. Lowenstein, 1990, *Evaporites*: Geoscience Canada. Reprint Series, v. 4, p. 141-164.
- Spiers, C. J., P. M. T. M. Schutjens, R. H. Brzesowsky, C. J. Peach, J. L. Liezenberg, and H. J. Zwart, 1990, Experimental determination of constitutive parameters governing creep of rocksalt by pressure solution, in R. J. Knipe, and E. H. Rutter, eds., *Deformation mechanisms, rheology and tectonics.*, Geological Society Special Publication, v. 54, p. 215-227.
- Spindler, W. M., 1977, Structure and stratigraphy of a small Pliocene-Pleistocene depocenter, Louisiana continental shelf: *Gulf Coast Assoc. Geol. Soc. Trans.*, v. 27, p. 180-196.
- Spötl, C., 1989a, The Alpine Haselgebirge Formation, Northern Calcareous Alps (Austria): Permo-Scythian evaporites in an alpine thrust system: *Sedimentary Geology*, v. 65, p. 113-125.

- Spötl, C., 1989b, Complex zoning and resorption in breunnerite from Hall in Tyrol, Austria: Evidence from back-scattered electron microscopy: *Mineralogy and Petrology*, v. 40, p. 225-233.
- Spötl, C., and S. Burns, 1994, Magnesite diagenesis in redbeds - A case study from the Permian of the Northern Calcareous Alps (Tyrol, Austria): *Sedimentology*, v. 41, p. 543-565.
- Spötl, C., F. J. Longstaffe, K. Ramseyer, M. J. Kunk, and R. Wiesheu, 1998, Fluid-rock reactions in an evaporitic melange, Permian Haselgebirge, Austrian Alps: *Sedimentology*, v. 45, p. 1019-1044.
- Stamatakis, M. G., 1995, Occurrence and genesis of huntite-hydromagnesite assemblages, Kozani, Greece - important new white fillers and extenders: *Transactions - Institution of Mining & Metallurgy, Section B*, v. 104, p. 179-186.
- Stanczuk, D. T., F. Tatom, W. Tolbert, J. Simmons, J. Vancil, R. L. Thoms, and C. G. Smith, 1976, The mechanisms and ecological impacts of the collapse of salt dome oil storage caverns: Project No. 5-210-00-567-04, Science Applications Inc. McLean Virginia.
- Stanislavsky, E., and H. Gvirtzman, 1999, Basin-scale migration of continental-rift brines: Paleohydrologic modeling of the Dead Sea basin: *Geology*, v. 27, p. 791-794.
- Stanton Jr, R. J., 1966, The solution brecciation process: *Geological Society of America Bulletin*, v. 77, p. 843-847.
- Starinsky, A., and A. Katz, 2003, The formation of natural cryogenic brines: *Geochimica et Cosmochimica Acta*, v. 67, p. 1475-1484.
- Stasiuk, L. D., 1994, Oil-prone alginite macerals from organic-rich Mesozoic and Paleozoic strata, Saskatchewan, Canada: *Marine & Petroleum Geology*, v. 11, p. 208-218.
- Steenge, W. D., 1979, Solution mining at controlled production rate, Dutch patent, 7,905,287.
- Steinhoff, I., and C. Strohmenger, 1999, Facies differentiation and sequence stratigraphy in ancient evaporite basins - An example from the basal Zechstein (Upper Permian of Germany): *Carbonates & Evaporites*, v. 14, p. 146-181.
- Steinhorn, I., 1983, In situ salt precipitation at the Dead Sea: *Limnology and Oceanography*, v. 28, p. 580-583.
- Steinhorn, I., and J. R. Gat, 1983, The Dead Sea: *Scientific American*, v. 249, p. 102-109.
- Stemmerik, L., J. E. Rouse, and B. Spiro, 1988, S-isotope studies of shallow water, laminated gypsum and associated evaporites, Upper Permian, East Greenland: *Sedimentary Geology*, v. 58, p. 37-46.
- Stengele, F., and W. Smykatz-Kloss, 1995, Mineralogical and geochemical study of Holocene sebkha sediments in southeastern Tunisia: *Chemie der Erde-Geochemistry*, v. 55, p. 241-256.
- Stenger, B., T. Pham, N. Al-Araleb, and P. Lawrence, 2003, Tilted original oil/water contact in the Arab-D reservoir, Ghawar field, Saudi Arabia: *GeoArabia*, v. 8, p. 9-42.
- Stenson, R. E., and D. C. Ford, 1993, Rillenkarren on gypsum in Nova Scotia: *Geographie Physique et Quaternaire*, v. 47, p. 239-243.
- Stephens, N. P., and A. R. Carroll, 1999, Salinity stratification in the Permian Phosphoria sea; a proposed paleoceanographic model: *Geology*, v. 27, p. 899-902.
- Stephenson, R. A., J. T. van Berkel, and S. A. P. L. Cloetingh, 1992, Relation between salt diapirism and the tectonic history of the Sverdrup Basin, Arctic Canada: *Canadian Journal of Earth Sciences*, v. 29, p. 2695-2705.
- Stewart, A. J., R. Q. Oaks Jr, J. A. Deckelman, and R. D. Shaw, 1991, 'Mesothrust' versus 'megathrust' interpretations of the structure of the northeastern Amadeus Basin, central Australia: *Bulletin - Bureau of Mineral Resources, Geology & Geophysics, Australia*, v. 236, p. 361-383.
- Stewart, F. H., 1968, Geochemistry of marine evaporite deposits: *Geological Society America Special Paper*, v. 88, p. 539-540.
- Stewart, S. A., and M. P. Coward, 1995, Synthesis of salt tectonics in the southern North Sea, UK: *Marine & Petroleum Geology*, v. 12, p. 457-475.
- Stewart, S. A., A. H. Ruffell, and M. J. Harvey, 1997, Relationship between basement-linked and gravity driven fault systems in the UKCS salt basins: *Marine & Petroleum Geology*, v. 14, p. 579-602.
- Stieljes, L., 1973, Evolution tectonique récente du rift d'Asal: *Review Geographie Physical Geologie Dynamique*, v. 15, p. 425-436.
- Stiller, M., and Y. C. Chung, 1984, Radium in the Dead Sea: A possible tracer for the duration of meromixis: *Limnology and Oceanography*, v. 29, p. 574-586.
- Stiller, M., A. Nissenbaum, R. S. Kaufmann, and A. Long, 1998, Cl-37 in the Dead Sea system - preliminary results: *Applied Geochemistry*, v. 13, p. 953-960.
- Stiller, M., and L. Sigg, 1990, Heavy metals in the Dead Sea and their coprecipitation with halite: *Hydrobiologia*, v. 197, p. 23-33.
- Stine, S., 1990, Late Holocene fluctuations of Mono Lake, eastern California: *Palaeogeography Palaeoclimatology Palaeoecology*, v. 78, p. 333-381.
- Stoessel, R. K., and A. B. Carpenter, 1986, Stoichiometric saturation tests of $\text{NaCl}_{1-x}\text{Br}_x$ and $\text{KCl}_{1-x}\text{Br}_x$: *Geochimica et Cosmochimica Acta*, v. 50, p. 1465-1474.
- Stoessel, R. K., and C. H. Moore, 1983, Chemical constraints and origins of four groups of Gulf Coast reservoir fluids: *Bulletin American Association Petroleum Geologists*, v. 67, p. 896-906.
- Stokes, W. L., 1968, Multiple parallel truncation bedding planes - a feature of wind-deposited sandstone formations: *Journal of Sedimentary Petrology*, v. 38, p. 510-515.
- Stollhofen, H., S. Gerschutz, I. G. Stanistreet, and V. Lorenz, 1998, Tectonic and volcanic controls on Early Jurassic rift-valley lake deposition during emplacement of Karoo flood basalts, southern Namibia: *Palaeogeography Palaeoclimatology Palaeoecology*, v. 140, p. 185 ff.
- Stover, S. C., S. M. Ge, P. Weimer, and B. C. McBride, 2001, The effects of salt evolution, structural development, and fault propagation on Late Mesozoic-Cenozoic oil migration: A two-dimensional fluid-flow study along a megaregional profile in the northern Gulf of Mexico Basin: *Bulletin American Association of Petroleum Geologists*, v. 85, p. 1945-1966.
- Strauss, H., 1997, The isotopic composition of sedimentary sulfur through time: *Palaeogeography Palaeoclimatology Palaeoecology*, v. 132, p. 97-118.
- Strauss, H., D. M. Banerjee, and V. Kumar, 2001, The sulfur isotopic composition of Neoproterozoic to early Cambrian seawater - evidence from the cyclic Hanseran evaporites, NW India: *Chemical Geology*, v. 175, p. 17-28.
- Strohmenger, C., M. Antonini, G. Jager, K. Rockenbauch, and C. Strauss, 1996b, Zechstein 2 Carbonate reservoir facies distribution in relation to Zechstein sequence stratigraphy (upper Permian, northwest Ger-

- many) - an integrated approach: *Bulletin des Centres de Recherches Exploration-Production Elf Aquitaine*, v. 20, p. 1-35.
- Strohmenger, C., E. Voigt, and J. Zimdars, 1996a, Sequence stratigraphy and cyclic development of Basal Zechstein carbonate-evaporite deposits with emphasis on Zechstein 2 off-platform carbonates (Upper Permian, Northeast Germany): *Sedimentary Geology*, v. 102, p. 33-54.
- Stueber, A. M., A. H. Saller, and H. Ishida, 1998, Origin, migration, and mixing of brines in the Permian Basin: geochemical evidence from the eastern Central Basin Platform, Texas: *American Association of Petroleum Geologists Bulletin*, v. 82, p. 1652-1672.
- Sugitani, K., K. Mimura, K. Suzuki, K. Nagamine, and R. Sugisaki, 2003, Stratigraphy and sedimentary petrology of an Archean volcanic-sedimentary succession at Mt. Goldsworthy in the Pilbara Block, Western Australia: implications of evaporite (nahcolite) and barite deposition: *Precambrian Research*, v. 120, p. 55-79.
- Sullivan, L. A., 1990, Micromorphology and genesis of some calcite pseudomorphs after lenticular gypsum: *Australian Journal of Soil Research*, v. 28, p. 483-485.
- Sullivan, L. A., and A. J. Koppi, 1993, Barite pseudomorphs after lenticular gypsum in a buried soil from central Australia: *Australian Journal of Soil Research*, v. 31, p. 393-396.
- Sullivan, M. D., R. S. Haszeldine, A. J. Boyce, G. Rogers, and A. E. Fallick, 1994, Late anhydrite cements mark basin inversion; isotopic and formation water evidence, Rotliegend Sandstone, North Sea: *Marine and Petroleum Geology*, v. 11, p. 46-54.
- Summons, R. E., and T. G. Powell, 1987, Identification of arylisoprenoids in a source rock and crude oils: Biological markers for the green sulfur bacteria: *Geochimica et Cosmochimica Acta*, v. 51, p. 557-566.
- Summons, R. E., L. L. Jahnke, J. M. Hope, and G. A. Logan, 1999, 2-methylhopanoids as biomarkers for cyanobacterial oxygenic photosynthesis: *Nature*, v. 400, p. 554-557.
- Sumner, D. Y., and J. P. Grotzinger, 1996, Were kinetics of Archean calcium carbonate precipitation related to oxygen concentration: *Geology*, v. 24, p. 119-122.
- Sumner, D. Y., and J. P. Grotzinger, 2000, Late Archean Aragonite Precipitation: Petrography, Facies Associations, and Environmental Significance, in J. P. Grotzinger, and N. P. James, eds., *Carbonate Sedimentation And Diagenesis In The Evolving Precambrian World*, v. 67: Tulsa, SEPM Special Publication, p. 123-144.
- Sumner, D. Y., and J. P. Grotzinger, 2004, Implications for Neoproterozoic ocean chemistry from primary carbonate mineralogy of the Campbellrand Malmani Platform, South Africa: *Sedimentology*, v. 51, p. 1273-1299.
- Sun, D., and B. Li, 1993, Origin of borates in the saline Lakes of China, Seventh Symposium on Salt, v. 2, Elsevier, Amsterdam, p. 177-193.
- Sun, S. Q., 1992, Skeletal aragonite dissolution from hypersaline seawater: a hypothesis: *Sedimentary Geology*, v. 77, p. 249-257.
- Sun, S. Q., 1995, Dolomite reservoirs; porosity evolution and reservoir characteristics: *American Association of Petroleum Geologists Bulletin*, v. 79, p. 186-204.
- Sun, S. Q., and M. Esteban, 1994, Paleoclimatic controls on sedimentation, diagenesis, and reservoir quality - Lessons from Miocene carbonates: *Bulletin American Association of Petroleum Geologists*, v. 78, p. 519-543.
- Supajanya, T., and M. C. Friederich, 1992, Salt tectonics of the Sakon Nakhon Basin, northeastern Thailand: *Journal of Southeast Asian Earth Sciences*, v. 7, p. 258-259.
- Surdam, R. C., and H. P. Eugster, 1976, Mineral reactions in sedimentary deposits of Lake Magadi region, Kenya: *Geological Society of America Bulletin*, v. 87, p. 1739-1752.
- Surdam, R. C., H. P. Eugster, and R. H. Mariner, 1972, Magadi-type chert in Jurassic and Eocene to Pleistocene rocks Wyoming: *Geol. Soc. Am. Bull.*, v. 83, p. 1739-1752.
- Surdam, R. C., and R. A. Sheppard, 1978, Zeolites in saline alkaline lake deposits, in L. B. Sand, and F. A. Mumpton, eds., *Natural Zeolites: Occurrence, properties, use*: New York, Pergamon, p. 145-174.
- Surdam, R. C., and C. A. Wolfbauer, 1975, Green River Formation, Wyoming: a playa lake complex: *Geological Society of America Bulletin*, v. 86, p. 335-345.
- Suwanich, P., 1986, Potash and Rock Salt in Thailand: *Nonmetallic Minerals Bulletin No.2*, Economic Geology Division, Department of Mineral Resources, Bangkok, Thailand.
- Svensen, J. B., 2003, Parabolic halite dunes on the Salar de Uyuni, Bolivia: *Sedimentary Geology*, v. 155, p. 147-156.
- Svengren, H., 2002, A study of the environmental conditions in Lake Nakuru, Kenya, using isotope dating and heavy metal analysis of sediments: Masters thesis, Dept. Structural Chemistry, University of Stockholm, Sweden.
- Sverjensky, D. A., 1986, Genesis of Mississippi Valley-type lead-zinc deposits: *Annual Review of Earth and Planetary Sciences*, v. 14, p. 177-199.
- Swarts, S. W., 1993, Global positioning system (GPS) and its applications for subsidence monitoring: SMRI Spring Meeting, April 26, Syracuse, New York.
- Sweet, M. L., 1999, Interaction between aeolian, fluvial and playa environments in the Permian Upper Rotliegend Group, UK southern North Sea: *Sedimentology*, v. 46, p. 171-187.
- Swennen, R., W. Viaene, and C. Cornelissen, 1990, Petrography and geochemistry of the Belle Roche breccia (lower Viséan, Belgium): evidence for brecciation by evaporite dissolution: *Sedimentology*, v. 37, p. 859-878.
- Swennen, R., W. Viaene, L. Jacobs, and O. J. Van, 1981, Occurrence of calcite pseudomorphs after gypsum in the Lower Carboniferous of the Vesder region (Belgium): *Bulletin de la Societe Belge de Geologie*, v. 90, p. 231-247.
- Swensen, R. E., 1967, Trap Mechanisms in Nisku Formation of northern Montana: *Bulletin American Association of Petroleum Geologists*, v. 51, p. 1948-1958.
- Swett, K., and A. H. Knoll, 1989, Marine pisolites from Upper Proterozoic carbonates of East Greenland and Spitsbergen: *Sedimentology*, v. 36, p. 75-93.
- Swihart, G. H., P. B. Moore, and E. L. Callis, 1986, Boron isotopic composition of marine and nonmarine evaporite borates: *Geochimica et Cosmochimica Acta*, v. 50, p. 1297-1301.
- Szatmari, P., 2000, Habitat of petroleum along the South Atlantic Margins, in M. R. Mello, and B. J. Katz, eds., *Petroleum Systems of the South Atlantic Margins*, v. 73: Tulsa, American Association of Petroleum Geologists Memoir, p. 69-75.
- Sánchez, C., and E. Galan, 1995, An approach to the genesis of palygorskite in a Neogen-Quaternary continental basin using principal factor analysis: *Clay Minerals*, v. 30, p. 225-238.

- Sánchez, J. A., P. Coloma, and A. Perez, 1999, Sedimentary processes related to the groundwater flows from the Mesozoic Carbonate Aquifer of the Iberian Chain in the Tertiary Ebro Basin, northeast Spain: *Sedimentary Geology*, v. 129, p. 201-213.
- Taberner, C., J. D. Marshall, J. P. Hendry, C. Pierre, and M. F. Thirlwall, 2002, Celestite formation, bacterial sulphate reduction and carbonate cementation of Eocene reefs and basinal sediments (Igalada, NE Spain): *Sedimentology*, v. 49, p. 171-190.
- Taimeh, A. Y., 1992, Formation of gypsic horizons in some arid regions soils of Jordan: *Soil Science*, v. 153, p. 486-498.
- Takamatsu, N., N. Kato, G. I. Matsumoto, and T. Torii, 1998, The origin of salts in water bodies of the McMurdo Dry Valleys: *Antarctic Science*, v. 10, p. 439-448.
- Talbot, C. J., 1978, Halokinesis and thermal convection: *Nature*, v. 273, p. 739-741.
- Talbot, C. J., 1979, Fold trains in a glacier of salt in southern Iran: *Journal of Structural Geology*, v. 1, p. 5-18.
- Talbot, C. J., 1992a, Quo vadis tectonophysics? With a pinch of salt! *Tectonophysics*, v. 16, p. 1-20.
- Talbot, C. J., 1992b, Centrifuged models of Gulf of Mexico profiles: *Marine and Petroleum Geology*, v. 9, p. 412-432.
- Talbot, C. J., 1993, Spreading of salt structures in the Gulf of Mexico: *Tectonophysics*, v. 228, p. 151-166.
- Talbot, C. J., and P. Aftabi, 2004, Geology and models of Qum Kuh central Iran: *Journal of Geological Society of London*, v. 161, p. 1-14.
- Talbot, C. J., and M. Alavi, 1996, The past of a future syntaxis across the Zagros, in G. I. Alsop, D. J. Blundell, and I. Davison, eds., *Salt tectonics*, Geological Society, London; Special Publication, v. 100, p. 89-110.
- Talbot, C. J., and M. P. A. Jackson, 1987a, Internal kinematics of salt diapirs: *American Association of Petroleum Geologists Bulletin*, v. 71, p. 1068-1093.
- Talbot, C. J., and M. P. A. Jackson, 1987b, Salt tectonics: *Scientific American*, v. 257, p. 70-79.
- Talbot, C. J., and R. J. Jarvis, 1984, Age, budget and dynamics of an active salt extrusion in Iran: *Journal of Structural Geology*, v. 6, p. 521-533.
- Talbot, C. J., W. Stanley, R. Soub, and N. Alsadoun, 1996, Epitaxial salt reefs and mushrooms in the southern Dead Sea: *Sedimentology*, v. 43, p. 1025-1047.
- Talbot, M. R., K. Holm, and M. A. J. Williams, 1994, Sedimentation in low-gradient desert margin systems; a comparison of the Late Triassic of Northwest Somerset (England) and the late Quaternary of east-central Australia, in M. R. Rosen, ed., *Paleoclimate and basin evolution of playa systems*, v. 289, Special Paper - Geological Society of America, p. 97-117.
- Tang, Z. H., J. Parnell, and F. J. Longstaffe, 1997, Diagenesis of analcime-bearing reservoir sandstones - the Upper Permian Pingdiqian Formation, Junggar Basin, Northwest China: *Journal of Sedimentary Research Section A-Sedimentary Petrology & Processes*, v. 67, p. 486-498.
- Tanner, L. H., 2002, Borate formation in a perennial lacustrine setting: Miocene/Pliocene Furnace Creek Formation, Death Valley, California, USA: *Sedimentary Geology*, v. 148, p. 259-273.
- Taylor, D. G., 1970, Experiments on solution mining of borax at boron, California, in J. L. Rau, ed., *Third Symposium on Salt*, v. 1: Cleveland, N. Ohio Geol. Soc., p. 412-416.
- Taylor, J. C. M., 1990, Upper Permian-Zechstein, in K. W. Glennie, ed., *Introduction to the Petroleum Geology of the North Sea (3rd Edition)*: Oxford, Blackwell, p. 153-190.
- Taylor, K. G., and C. D. Curtis, 1995, Stability and facies association of early diagenetic mineral assemblages; an example from a Jurassic ironstone-mudstone succession, U.K.: *Journal of Sedimentary Research, Section A: Sedimentary Petrology and Processes*, v. 65, p. 358-368.
- Taylor, P. M., and H. S. Chafetz, 2004, Floating rafts of calcite crystals in cave pools, central Texas, U.S.A.; crystal habit vs. saturation state: *Journal of Sedimentary Research*, v. 74, p. 328-341.
- Tekin, E., B. Varol, and G. M. Friedman, 2001, A preliminary study: Celestite-bearing gypsum in the Tertiary Sivas basin, Central-Eastern Turkey: *Carbonates & Evaporites*, v. 16, p. 93-101.
- Teller, J. T., J. M. Bowler, and P. G. Macumber, 1982, Modern sedimentation and hydrology in Lake Tyrell, Victoria: *Journal of the Geological Society of Australia*, v. 29, p. 159-175.
- Teller, J. T., K. W. Glennie, N. Lancaster, and A. K. Singhvi, 2000, Calcareous dunes of the United Arab Emirates and the Noah's flood: the post glacial reflooding of the Persia (Arabian Gulf): *Quaternary International*, v. 68-71, p. 297-308.
- ten Haven, H. L., J. W. De Leeuw, J. Rullkötter, and J. S. Sinninghe Damste, 1987, Restricted utility of the pristane/phytane ratio as a paleoenvironmental indicator: *Nature*, v. 330, p. 641-643.
- ten Haven, H. L., J. W. de Leeuw, and P. A. Schenk, 1985, Organic geochemical studies of a Messinian evaporite basin, northern Apennines (Italy), part I: Hydrocarbon biological markers for a hypersaline environment: *Geochimica et Cosmochimica Acta*, v. 49, p. 2181-2191.
- ten Haven, H. L., J. W. De Leeuw, J. S. Sinninghe Damsté, P. A. Schenk, S. E. Palmer, and J. E. Zumberge, 1988, Application of biological markers in the recognition of palaeo-hypersaline environments, v. 40: London, Blackwell, Geological Society London Special Publication, 123-130 p.
- Ter Heege, J. H., J. H. P. De Bresser, and C. J. Spiers, 2005, Rheological behaviour of synthetic rocksalt: the interplay between water, dynamic crystallisation and deformation mechanisms: *Journal of Structural Geology*, v. 27, p. 948-964.
- Tepper, D. H., W. H. Kappel, T. S. Miller, and J. H. Williams, 1997, Hydrogeologic effects of flooding in the partially collapsed Retsof salt mine, Livingston County, New York: US Geol. Survey Open File Report, v. 97-47, p. 36-37.
- Terken, J. M. J., and N. L. Frewin, 2000, The Dhahaban petroleum system of Oman: *Bulletin American Association of Petroleum Geologists*, v. 84, p. 523-544.
- Terken, J. M. J., N. L. Frewin, and S. L. Indrelid, 2001, Petroleum systems of Oman: Charge timing and risks: *Bulletin American Association of Petroleum Geologists*, v. 85, p. 1817-1845.
- Terriere, R. T., 1976, Geology of Fairway Field, east Texas, North American oil and gas fields, *American Association of Petroleum Geologists Memoir* 24, p. 157-176.
- Terzaghi, R. D., 1971, Brinefield subsidence at Windsor, Ontario, *Third symposium on Salt*, v. 2: Cleveland, Ohio, Northern Ohio Geological Society, p. 298-307.

- Teske, A., A. Dhillon, and M. L. Sogin, 2003, Genomic Markers of Ancient Anaerobic Microbial Pathways: Sulfate Reduction, Methanogenesis, and Methane Oxidation: *Biological Bulletin*, v. 204, p. 186-191.
- Testa, G., and S. Lugli, 2000, Gypsum-anhydrite transformations in Messinian evaporites of central Tuscany (Italy): *Sedimentary Geology*, v. 130, p. 249-268.
- Thiel, V., A. Jenisch, G. Landmann, A. Reimer, and W. Michaelis, 1997, Unusual distributions of long-chain alkenones and tetrahymanol from the highly alkaline Lake Van, Turkey: *Geochimica et Cosmochimica Acta*, v. 61, p. 2053-2064.
- Thode, H. G., and J. Monster, 1973, Sulfur-isotope geochemistry of petroleum, evaporites, and ancient seas [with comment], in D. W. Kirkland, ed., *Marine Evaporites; Origin, Diagenesis, and Geochemistry*, Dowden, Hutchinson and Ross.
- Thomas, D. W., and M. P. Coward, 1996, Mesozoic regional tectonics and South Viking Graben formation - Evidence for localized thin-skinned detachments during rift development and inversion: *Marine & Petroleum Geology*, v. 13, p. 149-177.
- Thomeer, J. H. M. A., and J. A. Bottema, 1961, Increasing occurrence of abnormally high reservoir pressures in boreholes and drilling problems resulting therefrom: *Bulletin American Association Petroleum Geologists*, v. 45, p. 1721-1730.
- Thoms, R. L., 2000, Subsidence and sinkhole development over salt caverns: An introduction to the technology of solution mining: *Spring 2000 Technical Class*, p. 127-141.
- Thoms, R. L., and R. M. Gehle, 1994, The Jefferson Island mine flooding revisited: *Proc. S.M.R.I. Spring Meeting*, Houston.
- Thoms, R. L., and R. M. Gehle, 2000a, A brief history of salt cavern use, in R. M. Geertmann, ed., *8th World Salt Symposium*, v. 1: Amsterdam, Elsevier, p. 207-214.
- Thoms, R. L., and R. M. Gehle, 2000b, Winnfield mine flooding and collapse event of 1965: *Proc. S.M.R.I. Fall Meeting Technical Session*, San Antonio, p. 262-274.
- Thomson, A., P. D. Hine, J. R. Greig, and D. W. Peach, 1996, Assessment of subsidence arising from gypsum dissolution: *Technical Report for the Department of the Environment*. Symonds Group Ltd, East Grinstead. 288 p.
- Thrasher, J., A. J. Fleet, S. J. Hay, M. Hovland, and S. Düppenbecker, 1996, Understanding geology as the key to using seepage in exploration: the spectrum of seepage styles, in S. D., and M. A. Abrams, eds., *Hydrocarbon migration and its near-surface expression*: Tulsa, AAPG Memoir 66, p. 223-241.
- Tiercelin, J. J., and A. Mondeguer, 1991, *The geology of the Tanganyika trough*, in G. W. Coulter, ed., *Lake Tanganyika and its life*: London, Oxford University Press, p. 7-48.
- Tiercelin, J. J., C. Pflumio, M. Castrec, J. Boulegue, P. Gente, J. Rolet, C. Coussement, K. O. Stetter, R. Huber, S. Buku, and W. Mifundu, 1993, Hydrothermal vents in Lake Tanganyika, East African Rift system: *Geology*, v. 21, p. 499-502.
- Timofeeff, M. N., T. Lowenstein, S. Brennan, R. Demicco, H. Zimmermann, J. Horita, and L. von Borstel, 2001, Evaluating seawater chemistry from fluid inclusions in halite: Examples from modern marine and nonmarine environments: *Geochimica et Cosmochimica Acta*, v. 65, p. 2293-2300.
- Tinker, S. W., and K. C. Kirby, 1991, The Keg River/Winnipegosis Petroleum System--Source to Trap Part I (abs.): *Bulletin American Association of Petroleum Geologists*, v. 75, p. 682.
- Tisljar, J., 1992, Origin and depositional environments of the evaporite and carbonate complex (Upper Permian) from the central part of the Dinarides (southern Croatia and western Bosnia): *Geologia Croatica*, v. 45, p. 115-126.
- Tleel, J. W., 1973, Surface geology of the Dammam Dome, Eastern Province, Saudi Arabia: *American Association Petroleum Geologists - Bulletin*, v. 57, p. 558-576.
- Tomasko, D., 1985, A numerical model for predicting the thermal behaviour of caverns in the Strategic Petroleum Reserve: *Doctoral thesis*, University of New Mexico, Albuquerque.
- Tompkins, L. A., V. A. Pedone, M. T. Roche, and D. I. Groves, 1994, The Cadjebut deposit as an example of Mississippi Valley-Type mineralization on the Lennard Shelf, Western Australia - Single episode or multiple events: *Economic Geology*, v. 89, p. 450-466.
- Torii, T., and J. Ossaka, 1965, A new mineral, calcium chloride hexahydrate, discovered in Antarctica: *Science*, v. 149, p. 975-977.
- Toulemont, M., 1984, Le karst gypseux du Lutetien superieur de la region parisienne; caracteristiques et impact sur le milieu urbain: *Revue de Geologie Dynamique et de Geographie Physique*, v. 25, p. 213-228.
- Trappe, J., 2000, Pangea: extravagant sedimentary resource formation during supercontinent configuration, an overview: *Palaeogeography Palaeoclimatology Palaeoecology*, v. 161, p. 35-48.
- Trave, A., F. Calvet, M. Sans, J. Verges, and M. Thirlwall, 2000, Fluid history related to the Alpine compression at the margin of the south-Pyrenean Foreland basin: the El Guix anticline: *Tectonophysics*, v. 321, p. 73-102.
- Trefry, J. H., B. J. Presley, W. L. Keeney-Kennicutt, and R. P. Trocine, 1984, Distribution and chemistry of manganese, iron, and suspended particulates in Orca Basin: *Geomarine Lett.*, v. 4, p. 125-130.
- Trendall, A. F., 1983, The Hamersley Basin, in A. F. Trendall, and R. C. Morris, eds., *Iron Formations: Facts and Problems*: Amsterdam, Elsevier, p. 69-129.
- Trindade, L. A. F., J. L. Dias, and M. R. Mello, 1995, Sedimentological and geochemical characterisation of the Lagoa Feia Formation, rift phase of the Campos Basin, Brazil, in B. Katz, ed., *Petroleum source rocks*: Berlin, Springer Verlag, p. 149-165.
- Truc, G., 1978, Lacustrine sediments in an evaporitic environment: the Ludian (Palaeogene) of the Mormoiron Basin, SE France, in A. Matter, and M. E. Tucker, eds., *Modern and ancient lake sediments*, *International Association Sedimentologists*, Spec. Publ. 2, p. 187-202.
- Trudinger, P. A., L. A. Chambers, and J. W. Smith, 1985, Low-temperature sulphate reduction; biological versus abiological: *Canadian Journal of Earth Sciences*, v. 22, p. 1910-1918.
- Trusheim, F., 1960, Mechanism of salt migration in Northern Germany: *American Association Petroleum Geologists Bulletin*, v. 44, p. 1519-1540.
- Tsui, P. C., and D. M. Cruden, 1984, Deformation associated with gypsum karst in the Salt River Escarpment, northeastern Alberta: *Canadian Journal of Earth Sciences*, v. 21, p. 949-959.
- Tucker, K. E., and R. G. Chalcraft, 1991, Cyclicity in the Permian Queen Formation - U.S.M. Queen Field, Pecos County, Texas (abs): *SEPM (Society for Sedimentary Geology)*, *Core Workshop*, v. 15, p. 385-428.
- Tucker, M. E., 1976a, Quartz replaced anhydrite nodules ('Bristol Diamonds') from the Triassic of the Bristol District: *Geological Magazine*, v. 113, p. 569-574.

- Tucker, M. E., 1976b, Replaced evaporites from the late Precambrian of Finnmark, Arctic Norway: *Sedimentary Geology*, v. 16, p. 193-204.
- Tucker, M. E., 1991, Sequence stratigraphy of carbonate-evaporite basins; models and application to the Upper Permian (Zechstein) of Northeast England and adjoining North Sea: *Journal of the Geological Society of London*, v. 148, p. 1019-1036.
- Tucker, M. E., 1993, Carbonate diagenesis and sequence stratigraphy: *Sedimentology review*, v. 1, p. 51-72.
- Tucker, M. E., 1999, Sabkha cycles, stacking patterns and controls: Gachsaran (Lower Fars/Fatha) Formation, Miocene, Mesopotamian Basin, Iraq: *Neues Jahrbuch für Geologie und Palaontologie-Abhandlungen*, v. 214, p. 45-69.
- Tucker, R. M., 1981, Giant polygons in the Triassic salt of Cheshire, England: A thermal contraction model for their origin: *Journal of Sedimentary Petrology*, v. 51, p. 779-786.
- Turner, C. E., and N. S. Fishman, 1991, Jurassic Lake T'oo'dichi': A large alkaline, saline lake, Morrison Formation, eastern Colorado Plateau: *Geological Society of America Bulletin*, v. 103, p. 538-558.
- Turner, P., D. Pilling, D. Walker, J. Exton, J. Binnie, and N. Sabaou, 2001, Sequence stratigraphy and sedimentology of the late Triassic TAG-I (Blocks 401/402, Berkine Basin, Algeria): *Marine & Petroleum Geology*, v. 18, p. 959-981.
- Tyler, S. W., and R. A. Wooding, 1991, Experimental verification of convection of groundwater beneath salt lakes: *EOS*, v. 72, p. 216.
- Tyler, S. W., S. Kranz, M. B. Parlange, J. Albertson, G. G. Katul, G. F. Cochran, B. A. Lyles, and G. Holder, 1997, Estimation of groundwater evaporation and salt flux from Owens Lake, California, USA: *Journal of Hydrology*, p. 110-135.
- Ullman, W. J., 1995, The fate and accumulation of bromide during playa salt deposition: an example from Lake Frome, South Australia: *Geochimica et Cosmochimica Acta*, v. 59, p. 2175-2186.
- Ullman, W. J., and K. D. Collerson, 1994, The Sr-isotope record of late Quaternary hydrologic changes around Lake Frome, South Australia: *Australian Journal of Earth Sciences*, v. 41, p. 37-45.
- Ulmer-Scholle, D. S., and P. A. Scholle, 1994, Replacement of evaporites within the Permian Park City Formation, Bighorn Basin, Wyoming, USA: *Sedimentology*, v. 41, p. 1203-1222.
- Ulmer-Scholle, D. S., P. A. Scholle, and P. V. Brady, 1993, Silicification of evaporites in Permian (Guadalupian) back-reef carbonates of the Delaware Basin, west Texas and New Mexico: *Journal of Sedimentary Petrology*, v. 63, p. 955-965.
- Ulmishek, G. F., 2001a, Petroleum Geology and Resources of the Dnieper-Donets Basin, Ukraine and Russia: *U.S. Geological Survey Bulletin*, v. 2201-E.
- Ulmishek, G. F., 2001b, Petroleum Geology and Resources of the North Caspian Basin, Kazakhstan and Russia: *U.S. Geological Survey Bulletin* 2201-B.
- Ulmishek, G. F., V. A. Bogino, M. B. Keller, and Z. L. Poznyakevich, 1994, Structure, stratigraphy and petroleum geology of the Dnieper-Donets Basins, Byelarus and Ukraine, in S. M. Landon, ed., *Interior Rift Basins*, v. 59: Tulsa, OK, American Association Petroleum Geologists Memoir, p. 125-156.
- Ulrich, M. R., J. R. Kyle, and P. E. Price, 1984, Metallic sulfide deposits in the Winnfield salt dome, Louisiana; evidence for episodic introduction of metalliferous brines during cap rock formation: *Transactions Gulf Coast Association of Geological Societies*, v. 34, p. 435-442.
- Ulrich, M. R., J. R. Kyle, and P. E. Price, 1985, Textural evidence for origin of salt dome anhydrite cap rocks, Winnfield Dome, Louisiana (abs): *American Association Petroleum Geologists - Bulletin*, v. 69, p. 313.
- Urai, J. L., C. J. Spiers, H. J. Zwart, and G. S. Lister, 1986, Weakening of rock salt by water during long-term creep: *Nature*, v. 324, p. 554-557.
- Udowski, E., and M. Dietzel, 1998, Atlas and data of solid-solution equilibria of marine evaporites: Berlin, Springer Verlag, 316 p.
- Usgilio, M. J., 1849, Etudes sur la composition de l'eau de la Méditerranée et sur l'exploitation des sel qu'elle contient: *Ann. Chim. Phys.*, v. 27, p. 172-191.
- Utha-aroon, C., 1993, Continental origin of the Maha-Sarakham evaporites, northeastern Thailand: *Journal of Southeast Asian Earth Sciences*, v. 8, p. 193-203.
- Utha-aroon, C., L. Coshell, and J. K. Warren, 1995, Early and late dissolution in the Maha Sarakham Formation: Implications for basin stratigraphy: *International Conference on Geology, Geochronology and Mineral Resources of Indochina 22-25 November 1995*, Khon Kaen, Thailand, p. 275-286.
- Valero-Garces, B., C. Arenas, and A. Delgado-Huertas, 2001, Depositional environments of Quaternary lacustrine travertines and stromatolites from high-altitude Andean lakes, northwestern Argentina: *Canadian Journal of Earth Sciences*, v. 38, p. 1263-1283.
- Valero-Garces, B. L., A. Delgado-Huertas, N. Ratto, and A. Navas, 1999, Large C-13 enrichment in primary carbonates from Andean Altiplano lakes, northwest Argentina: *Earth & Planetary Science Letters*, v. 171, p. 253-266.
- Valyashko, M. G., 1956, Geokhimiya broma v protsessakh galogeneza i ispolzovanie sodержaniya broma v kachestve geneticheskogo i poiskovogo kriteriya (Geochemistry of bromine in the processes of salt deposition and the use of bromine content as a genetic and prospecting criterion): *Geokhimiya*, v. 6, p. 570-589.
- Van Alstine, R. E., 1976, Continental rifts and lineaments associated with major fluorospar districts: *Economic Geology*, v. 71, p. 977-987.
- Van Breemen, N., 1982, Genesis, morphology, and classification of acid sulfate soils in coastal plains, in J. A. Kittrick, D. S. Fanning, and L. R. Hossner, eds., *Acid Sulfate Weathering*, v. 10: Madison, WI, Soil Science of America Special Publication, p. 95-108.
- Van der Sloot, H. A., D. Hoede, G. Hamburg, J. R. W. Woittiez, and C. H. Van der Weijden, 1990, Trace elements in suspended matter from the anoxic hypersaline Tyro and Bannock Basins (eastern Mediterranean): *Marine Chemistry*, v. 31, p. 187-203.
- van Houten, F. R., 1977, Triassic-Liassic deposits of Morocco and eastern North America; Comparison: *American Association Petroleum Geologists Bulletin*, v. 61, p. 79-99.
- van Lith, Y., C. Vasconcelos, R. Warthmann, J. C. F. Martins, and J. A. McKenzie, 2002, Bacterial sulfate reduction and salinity: two controls on dolomite precipitation in Lagoa Vermelha and Brejo do Espinho (Brazil): *Hydrobiologia*, v. 485, p. 35-49.
- Van Lith, Y., R. Warthmann, C. Vasconcelos, and J. A. McKenzie, 2003, Microbial fossilization in carbonate sediments: a result of the bacterial surface involvement in dolomite precipitation: *Sedimentology*, v. 50, p. 237-245.
- Van Rensbergen, P., R. R. Hillis, A. J. Maltman, and C. K. Morley, 2003, Subsurface sediment mobilization: Introduction, in P. Van Rensbergen, R. R. Hillis, A. J. Maltman, and C. K. Morley, eds.,

- Subsurface Sediment Mobilization, v. 216: London, Geological Society of London Special Publication, p. 1-8.
- Van Rensbergen, P., and C. K. Morley, 2000, 3D Seismic study of a shale expulsion syncline at the base of the Champion delta, offshore Brunei and its implications for the early structural evolution of large delta systems: *Marine & Petroleum Geology*, v. 17, p. 861-872.
- Van Wagoner, J. C., R. M. Mitchum, K. M. Campion, and V. D. Rahmanian, 1990, Siliciclastic Sequence Stratigraphy in Well Logs, Cores and Outcrops, Amer. Assoc. Petrol. Geol. Methods in Exploration Series, No. 7: Tulsa.
- Van Wagoner, J. C., H. W. Posamentier, R. M. Mitchum Jr., P. R. Vail, J. F. Sarg, T. S. Loutit, and J. Hardenbol, 1988, An overview of the fundamentals of sequence stratigraphy and key definitions, in C. K. Wilgus, B. S. Hastings, C. G. S. C. Kendall, H. W. Posamentier, C. A. Ross, and J. C. Van Wagoner, eds., *Sea-Level Changes: An Integrated Approach*, v. 42: Tulsa, Soc. Econ. Paleontol. Mineral. Spec. Publ., p. 39-45.
- Vandervoort, D. S., 1997, Stratigraphic response to saline lake-level fluctuations and the origin of cyclic nonmarine evaporite deposits - The Pleistocene Blanca Lila Formation, Northwest Argentina: *Geological Society of America Bulletin*, v. 109, p. 210-224.
- Vandervoort, D. S., T. E. Jordan, P. K. Zeitler, and R. N. Alonso, 1995, Chronology of internal drainage development and uplift, southern Puna Plateau, Argentine Central Andes: *Geology*, v. 23, p. 145-148.
- Vareschi, E., 1978, The ecology of Lake Nakuru (Kenya). I. Abundance and feeding of the lesser flamingo: *Oecologia*, v. 32, p. 11-35.
- Vareschi, E., 1979, The ecology of Lake Nakuru (Kenya). II. Biomass and spatial distribution of fish: *Oecologia*, v. 37, p. 321-325.
- Vareschi, E., 1982, The ecology of Lake Nakuru (Kenya). III. Abiotic factors and primary production: *Oecologia*, v. 55, p. 81-101.
- Varol, B., H. Araz, L. Karadenizli, N. Kazanci, G. Seyitoglu, and S. Sen, 2002, Sedimentology of the Miocene evaporitic succession in the north of Cankiri-Corum basin, central Anatolia, Turkey: *Carbonates and Evaporites*, v. 17, p. 197-209.
- Vasconcelos, C., and J. A. McKenzie, 1997, Microbial mediation of modern dolomite precipitation and diagenesis under anoxic conditions (Lagoa Vermelha, Rio de Janeiro, Brazil): *Journal of Sedimentary Research Section A-Sedimentary Petrology & Processes*, v. 67, p. 378-390.
- Vasconcelos, C. O., J. A. McKenzie, S. Bernasconi, D. Grujic, and A. J. Tien, 1995, Microbial mediation as a possible mechanism for natural dolomite formation at low temperature: *Nature*, v. 337, p. 220-222: *Nature*, v. 337, p. 220-222.
- Vearncombe, S., M. E. Barley, D. I. Groves, N. J. McNaughton, E. J. Mikucki, and J. R. Vearncombe, 1995, 3.26 Ga black smoker-type mineralization in the Strelley Belt, Pilbara Craton, Western Australia: *Journal of the Geological Society of London*, v. 152, p. 587-590.
- Veevers, J. J., 2004, Gondwanaland from 650–500 Ma assembly through 320 Ma merger in Pangea to 185–100 Ma breakup: supercontinental tectonics via stratigraphy and radiometric dating: *Earth Science Reviews*, v. 68, p. 1-132.
- Veil, J., D. Elcock, M. Raivel, D. Caudle, R. C. Ayers Jr., and B. Grunewald, 1996, Preliminary technical and legal evaluation of disposing of nonhazardous oil field waste into salt caverns, Washington, USA, Argonne National Laboratory, Report for US Department of Energy, Office of Fossil Energy under contract W-31-109-ENG-38.
- Veizer, J., Y. Godderis, and L. M. Francois, 2000, Evidence for decoupling of atmospheric CO₂ and global climate during the Phanerozoic eon: *Nature*, v. 408, p. 698-701.
- Velaj, T., 2001, Evaporites in Albania and their impact on the thrusting processes, *Journal of the Balkan Geophysical Society*, p. 9-18.
- Velaj, T., I. Davison, A. Serjani, and I. Alsop, 1999, Thrust tectonics and the role of evaporites in the Ionian zone of the Albanides: *AAPG Bulletin-American Association of Petroleum Geologists*, v. 83, p. 1408-1425.
- Vendeville, B. C., 2005, Salt tectonics driven by sediment progradation: Part I - Mechanics and Kinematics: *Bulletin American Association Petroleum Geologists*, v. 89, p. 1071-1079.
- Vendeville, B. C., and K. T. Nilsen, 1995, Episodic growth of salt diapirs driven by horizontal shortening: *Gulf Coast Section Society of Economic Palaeontologists and Mineralogists Foundation. 16th Annual Research Conference, Salt Sediment and Hydrocarbons*, p. 285-295.
- Vendeville, B. C., and M. P. A. Jackson, 1992a, The rise of diapirs during thin-skinned extension: *Marine and Petroleum Geology*, v. 9, p. 331-353.
- Vendeville, B. C., and M. P. A. Jackson, 1992b, The fall of diapirs during thin-skinned extension: *Marine and Petroleum Geology*, v. 9, p. 354-371.
- Vengosh, A., A. R. Chivas, M. T. McCulloch, A. Starinsky, and Y. Kolodny, 1991, Boron isotope geochemistry of Australian salt lakes.: *Geochimica et Cosmochimica Acta*, v. 55, p. 2591-2606.
- Vengosh, A., A. R. Chivas, A. Starinsky, Y. Kolodny, B. Zhang, and P. Zhang, 1995, Chemical and boron isotope compositions of non-marine brines from the Qaidam Basin, Qinghai, China: *Chemical Geology*, v. 120, p. 135-154.
- Vengosh, A., A. Starinsky, Y. Kolodny, A. R. Chivas, and M. Raab, 1992, Boron isotope variations during fractional evaporation of sea water: new constraints on the marine vs. nonmarine debate: *Geology*, v. 20, p. 799-802.
- Ventosa, A., J. J. Nieto, and A. Oren, 1998, Biology of moderately halophilic aerobic bacteria: *Microbiology and Molecular Biology Reviews*, v. 62, p. 504-544.
- Versfelt Jr., P. L., 2001, Major hydrocarbon potential in Iran, in M. W. Downey, J. C. Threet, and W. A. Morgan, eds., *Petroleum provinces of the twenty-first century*, American Association Petroleum Geologists Memoir 74, p. 417-427.
- Vially, R., J. Letouzey, F. Bénard, N. Haddadi, D. G., H. Askri, and A. Boudjema, 1994, Basin inversion along the North African margin, the Saharan Atlas (Algeria), in F. Roure, ed., *Peritethyan Platforms*: Paris, Technip, p. 79-118.
- Vila, J.-M., F. Benkherouf, and A. Charriere, 1994, Interpretation du matériel triasique de la région de l'Ouenza (confins algero-tunisiens): un vaste "glacier de sel" sous-marin albien, à l'image des structures off-shore d'Aquitaine (Interpretation of the Triassic formations in the Ouenza area (Algerian-Tunisian confines): a large submarine Albian "salt-glacier", like the off-shore structures of Aquitaine): *Comptes Rendus - Academie des Sciences, Serie II: Sciences de la Terre et des Planete*, v. 318, p. 109-116.
- Vila, J. M., M. Ghanmi, M. B. Youssef, and M. Jouirou, 2002, The submarine "salt glaciers" of northeastern Maghreb (Algeria and Tunisia), and the US Gulf Coast passive continental margins: Comparisons, special look on the composite "salt glaciers" illustrated

- by the Fedj el Adoum structure (northwestern Tunisia), and global review: *Eclogae Geologicae Helveticae*, v. 95, p. 347-380.
- Vincelette, R. R., and W. E. Chittum, 1981, Exploration for oil accumulation in Entrada Sandstone, San Juan Basin, New Mexico: *Bulletin American Association of Petroleum Geologists*, v. 65, p. 2546-2570.
- Vinet, M. J., 1982, Stratigraphy and dolomitization of the Smackover and Buckner formation (Upper Jurassic) Jay-Big Escambia Creek field area, southern Alabama-western Florida (abs): *Jurassic of the Gulf Coast rim; Gulf Coast Section SEPM*, p. 110-113.
- Visscher, P. T., P. R. Reid, and B. M. Bebout, 2000, Microscale observations of sulfate reduction: Correlation of microbial activity with lithified micritic laminae in modern marine stromatolites: *Geology*, v. 28, p. 919-922.
- Vlasceanu, L., S. M. Sarbu, A. S. Engel, and B. K. Kinkle, 2000, Acidic, cave-wall biofilms located in the Frasassi Gorge, Italy: *Geomicrobiology Journal*, v. 17, p. 125-139.
- Volozh, Y., C. J. Talbot, and A. Ismail-Zadeh, 2003, Salt structures and hydrocarbons in the Pricaspian basin: *Bulletin American Association Petroleum Geologists*, v. 87, p. 313-334.
- Von der Borch, C. C., 1965, The distribution and preliminary geochemistry of modern carbonate sediments of the Coorong area, South Australia: *Geochimica et Cosmochimica Acta*, v. 29.
- von der Borch, C. C., 1976, Stratigraphy and formation of Holocene dolomitic carbonate deposits of the Coorong area, South Australia: *Journal of Sedimentary Petrology*, v. 46, p. 952-966.
- von der Borch, C. C., B. Bolton, and J. K. Warren, 1977, Environmental setting and microstructure of subfossil lithified stromatolites associated with evaporites, Marion Lake, South Australia: *Sedimentology*, v. 24, p. 693-708.
- Von der Borch, C. C., and D. Lock, 1979, Geological significance of Coorong dolomites: *Sedimentology*, v. 26, p. 813-824.
- Von der Haar, S. P., and D. S. Gorsline, 1977, Hypersaline lagoon deposits and processes in Baja California, Mexico, in H. J. Walker, ed., *Research Techniques in Coastal Environments*, Geoscience and Man, v. 18, p. 165-177.
- von Engelhardt, W. H., H. Fuchtbauer, and G. Muller, 1977, *Sedimentary petrology*, Halsted Press, New York.
- von Gehlen, K., H. Nielsen, and W. Ricke, 1962, S-Isotopen Verhältnisse in Baryt und Sulfiden aus hydrothermalen Gangen im Schwarzwald und jüngeren Barytgängen in Süddeutschland und ihre genetische Bedeutung: *Geochim Cosmochim. Acta*, v. 26, p. 1189-1207.
- Von Tryller, H., 2002, The Cavern Field No. 11 in Ocenele Mari - History, Present and Future: *Solution Mining Research Institute Proceedings*, Spring Meeting, 28 April 1 May, 2002, Banff, Canada, p. 10 pp.
- Vreeland, R. H., W. D. Rosenzweig, and D. W. Powers, 2000, Isolation of a 250 million-year-old halotolerant bacterium from a primary salt crystal: *Nature*, v. 407, p. 897-900.
- Wagner, P. A., 1922, The Pretoria Salt-Pan—A Soda Caldera: *Memoir, Union of South Africa Geological Survey*, v. 20, 136 p.
- Waldron, J. W. F., and M. C. Rygel, 2005, Role of evaporite withdrawal in the preservation of a unique coal-bearing succession: Pennsylvanian Joggins Formation, Nova Scotia: *Geology*, v. 33, p. 337-340.
- Walker, R. N., M. D. Muir, W. L. Diver, N. Williams, and N. Wilkins, 1977, Evidence of major sulphate evaporite deposits in the Proterozoic McArthur Group, Northern Territory, Australia: *Nature*, v. 265, p. 526-529.
- Wallace, M. W., 1990, Origin of dolomitization on the Barbwire Terrace, Canning Basin, Western Australia: *Sedimentology*, v. 37, p. 105-122.
- Wallick, E. I., 1981, Chemical evolution of groundwater in a drainage basin of Holocene age, east central Alberta: *Journal of Hydrology*, v. 54, p. 245-283.
- Wallmann, K., F. S. Aghi, D. Castradori, M. B. Cita, E. Suess, J. Greinert, and D. Rickert, 2002, Sedimentation and formation of secondary minerals in the hypersaline Discovery Basin, eastern Mediterranean: *Marine Geology*, v. 186, p. 9-28.
- Walters, R. F., 1978, Land subsidence in central Kansas related to salt dissolution: *Kansas Geological Survey Bulletin* 214, p. 1-82.
- Walters, R. F., 1991, Gorham Oil Field, Russell County, Kansas: *Kansas Geological Survey Bulletin* 228.
- Waltham, D., 1997, Why does salt start to move? *Tectonophysics*, v. 282, p. 117-128.
- Walton, D., and B. E. Urband, 1997, Well design, casing challenges in Gulf of Mexico subsalt drilling: *Offshore*, v. April, 1997, p. 78-82.
- Wang, R. L., 1998, Acyclic isoprenoids - molecular indicators of archaeal activity in contemporary and ancient Chinese saline/hypersaline environments: *Hydrobiologia*, v. 381, p. 59-76.
- Wang, R. L., S. C. Brassell, J. M. Fu, and G. Y. Sheng, 1998, Molecular indicators of microbial contributions to recent and Tertiary hypersaline lacustrine sediments in China: *Hydrobiologia*, v. 381, p. 77-103.
- Waples, D. W., P. Haug, and D. H. Welte, 1974, Occurrence of a regular C25 isoprenoid hydrocarbon in Tertiary sediments representing a lagoonal saline environment: *Geochimica et Cosmochimica Acta*, v. 38, p. 381-387.
- Ward, R. F., C. G. S. C. Kendall, and P. M. Harris, 1986, Late Permian (Guadalupian) facies and their association with hydrocarbons: *Bulletin American Association of Petroleum Geologists*, v. 70, p. 239-262.
- Wardlaw, N. C., 1968, Carnallite-sylvite relationships in the middle Devonian Prairie evaporite formation, Saskatchewan: *Geol. Soc. Amer. Bull.*, v. 79, p. 1273-1294.
- Wardlaw, N. C., 1972, Unusual marine evaporites with salts of calcium and magnesium chloride in Cretaceous basins of Sergipe, Brazil: *Economic Geology*, v. 67, p. 156-168.
- Wardlaw, N. C., and G. D. Nicholls, 1972, Cretaceous evaporites of Brazil and West Africa and their bearing on the theory of continental separation: *Internat. Geol. Congress*, 24th, Section 6, p. 43-55.
- Wardlaw, N. C., and G. E. Reinson, 1971, Carbonate and evaporite deposition and diagenesis, middle Devonian Winnipegosis and Prairie evaporite formations of south-central Saskatchewan: *Bulletin American Association Petroleum Geologists*, v. 55, p. 1759-1786.
- Wardlaw, N. C., and W. M. Schwerdtner, 1966, Halite-anhydrite seasonal layers in the Middle Devonian Prairie Formation, Saskatchewan, Canada: *Geological Society of America Bulletin*, v. 77, p. 331-342.
- Wardlaw, N. C., and D. W. Watson, 1966, Middle Devonian salt formations and their bromide content, Elk Point area, Alberta: *Canadian Jour. Earth Sci.*, v. 3, p. 263-275.

- Warrak, M., 1974, The petrography and origin of dedolomitized, veined or brecciated carbonate rock, the "cornieules" in the Frejus region, French Alps: *Journ. Geol. Soc. Lond.*, v. 130, p. 229-247.
- Warren, J. K., 1982a, The hydrological significance of Holocene tepees, stromatolites, and boxwork limestones in coastal salinas in South Australia: *Journal of Sedimentary Petrology*, v. 52, p. 1171-1201.
- Warren, J. K., 1982b, Hydrologic setting, occurrence, and significance of gypsum in late Quaternary salt lakes, South Australia: *Sedimentology*, v. 29, p. 609-637.
- Warren, J. K., 1983a, Tepees, modern (southern Australia) and ancient (Permian - Texas and New Mexico) - a comparison: *Sedimentary Geology*, v. 34, p. 1-19.
- Warren, J. K., 1983b, Pedogenic calcrete as it occurs in Quaternary calcareous dunes in coastal South Australia: *Journal of Sedimentary Petrology*, v. 53, p. 787-796.
- Warren, J. K., 1985, On the significance of evaporite lamination, in B. C. Schreiber, and H. L. Harner, eds., *Sixth International Symposium on Salt*, v. 6, p. 161-170.
- Warren, J. K., 1986, Shallow water evaporitic environments and their source rock potential: *Journal Sedimentary Petrology*, v. 56, p. 442-454.
- Warren, J. K., 1988, Sedimentology of Coorong dolomite in the Salt Creek region, South Australia: *Carbonates and Evaporites*, v. 3, p. 175-199.
- Warren, J. K., 1989, Evaporite sedimentology: Importance in hydrocarbon accumulation: Englewood Cliffs, Prentice-Hall, 285 p.
- Warren, J. K., 1990, Sedimentology and mineralogy of dolomitic Coorong lakes, South Australia: *Journal of Sedimentary Petrology*, v. 60, p. 843-858.
- Warren, J. K., 1991, Sulfate dominated sea-marginal and platform evaporative settings, in J. L. Melvin, ed., *Evaporites, petroleum and mineral resources: Developments in Sedimentology*, v. 50: Amsterdam, Elsevier, p. 477-533.
- Warren, J. K., 1992, Evaporites and Their Importance to Petroleum Exploration: Manual GL508 Petroleum Geology in the IHRDC Video Library for Exploration and Production Specialists, p. 230 pp.
- Warren, J. K., 1997, Evaporites, brines and base metals: brines, flow and "the evaporite that was": *Australian Journal of Earth Sciences*, v. 44, p. 149-183.
- Warren, J. K., 1999, *Evaporites: their evolution and economics*: Oxford, UK, Blackwell Scientific, 438 p.
- Warren, J. K., 2000a, Dolomite: Occurrence, evolution and economically important associations: *Earth Science Reviews*, v. 52, p. 1-81.
- Warren, J. K., 2000b, Evaporites, brines and base metals: low-temperature ore emplacement controlled by evaporite diagenesis: *Australian Journal of Earth Sciences*, v. 47, p. 179-208.
- Warren, J. K., 2000c, Geological controls on the quality of potash, in R. M. Geertmann, ed., *8th World Salt Symposium*, v. 1: Amsterdam, Elsevier, p. 173-180.
- Warren, J. K., S. C. George, P. J. Hamilton, and P. Tingate, 1998, Proterozoic source rocks - Sedimentology and organic characteristics of the Velkerri Formation, Northern Territory, Australia: *American Association of Petroleum Geologists Bulletin*, v. 82, p. 442-463.
- Warren, J. K., K. G. Havholm, M. R. Rosen, and M. J. Parsley, 1990, Evolution of gypsum karst in the Kirschberg Evaporite Member near Fredericksburg, Texas: *Journal of Sedimentary Petrology*, v. 60, p. 721-734.
- Warren, J. K., and R. H. Kempton, 1997, Evaporite Sedimentology and the Origin of Evaporite-Associated Mississippi Valley-type Sulfides in the Cadjebut Mine Area, Lennard Shelf, Canning Basin, Western Australia., in I. P. Montanez, J. M. Gregg, and K. L. Shelton, eds., *Basinwide diagenetic patterns: Integrated petrologic, geochemical, and hydrologic considerations*: Tulsa OK, SEPM Special Publication, v. 57, p. 183-205.
- Warren, J. K., and C. G. S. C. Kendall, 1985, Comparison of sequences formed in marine sabkha (subaerial) and salina (subaqueous) settings; modern and ancient: *Bulletin American Association of Petroleum Geologists*, v. 69, p. 1013-1023.
- Warthmann, R., Y. van Lith, C. Vasconcelo, and J. A. McKenzie, 2000, Bacterially induced dolomite precipitation in anoxic culture experiments: *Geology*, v. 28.
- Wassmann, T. H., 1983, Cavity utilization in the Netherlands, *Sixth International symposium on Salt*, v. II, p. 191-201.
- Watkins, J. S., G. MacRae, and G. R. Simmons, 1995, Bipolar simple-shear rifting responsible for distribution of mega-salt basins in Gulf of Mexico, in C. J. Travis, H. Harrison, M. R. Hudec, B. C. Vendeville, F. J. Peel, and B. F. Perkins, eds., *Salt, sediment, and hydrocarbons*, SEPM Foundation, Gulf Coast Section, 16th Annual Research Conference Program with Papers, p. 297-305.
- Watney, W. L., S. E. Nissen, S. Bhattacharya, and D. Young, 2003, Evaluation of the Role of Evaporite Karst in the Hutchinson, Kansas, Gas Explosions, January 17 and 18, 2001, in K. S. Johnson, and J. T. Neal, eds., *Evaporite karst and engineering/environmental problems in the United State*, Oklahoma Geological Survey Circular 109, p. 119-147.
- Watson, A., 1985, Structure, chemistry and origins of gypsum crusts in southern Tunisia and the central Namib Desert: *Sedimentology*, v. 32, p. 855-875.
- Watts, R. A., 1991, Subsidence surveys: SMRI Fall Meeting, Oct 29, Las Vegas Nevada, 23 p.
- Webster, D. M., and B. F. Jones, 1994, Paleoenvironmental implications of lacustrine clay minerals from the Double Lakes Formation, southern Great Plains, Texas., in R. W. Renaut, and W. M. Last, eds., *Sedimentology and geochemistry of modern and ancient saline lakes*, v. 50: Tulsa, Society Economic Paleontologists and Mineralogists Special Publication, p. 661-686.
- Wedepohl, K. H., 1964, Untersuchungen am Kupferschiefer in Nordwestdeutschland: Ein Beitrag zur Deutung der Genese bituminöser Sedimente: *Geochemica et Cosmochimica Acta*, v. 28, p. 305-364.
- Weeks, L. G. e., 1958, *Habitat of oil: A symposium*: Tulso, OK, American Association Petroleum Geologists.
- Weeks, L. G. e., 1961, Chapter 5, Origin, migration and occurrence of petroleum, in G. B. Moody, ed., *Petroleum exploration handbook*: New York, McGraw-Hill.
- Wei, E. Y., Z. M. Liu, X. L. Deng, and S. K. Xu, 1998, Biomineralization of mirabilite deposits of Barkol Lake, China: *Carbonates and Evaporites*, v. 13, p. 86-89.
- Wei, L. J., M. P. Zheng, X. F. Liu, K. Q. Cai, and Z. Nie, 2002, Discovery of borax-bearing mirabilite beds in Dong Co, northern Tibet, and its palaeoclimatic significance: *Acta Geologica Sinica-English Edition*, v. 76, p. 271-282.

- Weidlich, O., and M. Bernecker, 2004, Quantification of depositional changes and paleo-seismic activities from laminated sediments using outcrop data: *Sedimentary Geology*, v. 166, p. 11-20.
- Weijermars, R., 1999, Surface Geology, Lithostratigraphy and Tertiary Growth of the Dammam Dome, Saudi Arabia: A New Field Guide: *GeoArabia*, v. 4, p. 199-226.
- Weijermars, R., M. P. A. Jackson, and B. Vendeville, 1993, Rheological and tectonic modeling of salt provinces: *Tectonophysics*, v. 217, p. 143-174.
- Wells, A. J., 1962, Recent dolomite in the Persian Gulf: *Nature*, p. 274-275.
- Wells, A. T., 1980, Evaporites in Australia: *BMR Bulletin*, v. 198: Canberra, Australia, Bureau of Mineral Resources, 104 p.
- Wells, R. T., and R. H. Tedford, 1995, Sthenurus (Macropodiae, Marsupialia) from the Pleistocene of Lake Callabonna, South Australia: *Bulletin of the American Museum of Natural History*, v. 225, p. 1-111.
- Wender, L. E., J. W. Bryant, M. F. Dickens, A. S. Neville, and A. M. Al-Moqbel, 1998, Paleozoic (Pre-Khuff) hydrocarbon geology of the Ghawar area, eastern Saudi Arabia: *GeoArabia*, v. 3, p. 272-302.
- Wenkert, D., 1979, Flow of salt glaciers: *Geophysical Research Letters*, v. 6, p. 523-526.
- West, I. M., 1964, Evaporite diagenesis in the lower Purbeck beds of Dorset: *Proceedings - Yorkshire Geological Society*, v. 34, p. 315-330.
- West, I. M., 1965, Macrocell structure and enterolithic veins in British Purbeck gypsum and anhydrite: *Proceedings of Yorkshire Geological Society*, v. 35, p. 47-58.
- West, I. M., 1973, Vanished evaporites; significance of strontium minerals: *Journal of Sedimentary Petrology*, v. 43, p. 278-279.
- West, I. M., 1979, Review of evaporite diagenesis in the Purbeck Formation of southern England, Symposium on: West European Jurassic Sedimentation - "Sedimentation Jurassique W. European", Association of French Sedimentologists Special Publication No. 1, p. 407-416.
- West, I. M., Y. A. Ali, and M. E. Hilmy, 1979, Primary gypsum nodules in a modern sabkha on the Mediterranean coast of Egypt: *Geology*, v. 7, p. 354-358.
- Westbrook, G. K., and T. J. Reston, 2002, The accretionary complex of the Mediterranean Ridge: tectonics, fluid flow and the formation of brine lakes - an introduction to the special issue of *Marine Geology: Marine Geology*, v. 186, p. 1-8.
- Wharton, D. A., 2002, Life at the limits; Organisms in extreme environments: Cambridge, UK, Cambridge University Press, 307 p.
- Wheeler, W. H., and D. A. Textoris, 1978, Triassic limestone and chert of playa origin in North Carolina: *Journal of Sedimentary Petrology*, v. 48, p. 765-776.
- White, A. H., and B. C. Youngs, 1980, Cambrian alkali playa-lacustrine sequence in the northeastern Officer Basin, South Australia.: *Journal of Sedimentary Petrology*, v. 50, p. 1279 - 1286.
- White, K., and N. Drake, 1993, Mapping the distribution and abundance of gypsum in south-central Tunisia from Landsat Thematic Mapper data: *Zeitschrift fur Geomorphologie*, v. 37, p. 309-325.
- White, W. B., 1988, *Geomorphology and hydrology of karst terrains*: New York, Oxford University Press, 464 p.
- Whiticar, M. J., and E. Suess, 1998, The cold carbonate connection between Mono Lake, California and the Bransfield Strait, Antarctica: *Aquatic Geochemistry*, v. 4, p. 419-454.
- Whittaker, S. G., and E. W. Mountjoy, 1996, Diagenesis of an Upper Devonian carbonate-evaporite sequence: Birdbear Formation, southern Interior Plains, Canada: *Journal of Sedimentary Research A: Sedimentary Petrology and Processes*, v. 66, p. 965-975.
- Whittig, L. D., A. E. Deyo, and K. K. Tanji, 1982, Evaporite mineral species in Mancos Shale and salt efflorescence, Upper Colorado River basin: *Soil Science Society of America Journal*, v. 46, p. 645-651.
- Whittle, G. L., and A. S. Alsharhan, 1996, Diagenetic history and source rock potential of the Upper Jurassic Diyab Formation, offshore Abu Dhabi, United Arab Emirates: *Carbonates and Evaporites*, v. 11, p. 145-154.
- Whittle, G. L., A. S. Alsharhan, and A. Ain, 1995, Observations on the diagenesis of the Lower Triassic Sudair Formation, Abu Dhabi, United Arab Emirates: *Facies*, v. 33, p. 185-194.
- Whitton, B. A., and M. Potts, 2000, The ecology of cyanobacteria: Their diversity in time and space: Berlin, Springer, 704 p.
- Wiggins, W. D., P. M. Harris, and R. C. Burruss, 1993, Geochemistry of post-uplift calcite in the Permian Basin of Texas and New Mexico: *Geological Society of America Bulletin*, v. 105, p. 779-790.
- Wigley, T. M. L., J. J. Drake, J. F. Quinlan, and D. C. Ford, 1973, Geomorphology and geochemistry of a gypsum karst near Canal Flats, British Columbia: *Canadian J. Earth Science*, v. 10, p. 113-129.
- Wiig, S. V., W. D. Grundy, and J. R. Dyni, 1995, Trona resources in the Green River Basin, southwest Wyoming, U.S. Geological Survey Open-File Report 95-476, 88 p.
- Wilgus, C. K., and W. T. Holser, 1984, Marine and Nonmarine Salts of Western Interior, United States: *American Association Petroleum Geologists - Bulletin*, v. 68, p. 765-767.
- Wilke, A. R., C. Hellberg, and O. Bornemann, 2001, Geological interpretation of domal salt structures in the North European Zechstein Formation: Influence on cavern development: *Solution Mining Research Institute Technical Paper Fall 2001 Meeting*, 7 - 10 October, Albuquerque, New Mexico, p. 9 pp.
- Williams, A. F., and J. W. Holmes, 1978, A novel method of estimating the discharge of water from the mound springs of the Great Artesian Basin, Central Australia: *Journal of Hydrology*, v. 38, p. 263-272.
- Williams, D. F., and I. Lerche, 1987, Salt domes, organic-rich source beds and reservoirs in intraslope basins of the Gulf Coast region, in I. Lerche, and J. J. O'Brien, eds., *Dynamical geology of salt and related structures*: New York, Academic Press, p. 751-830.
- Williams, G. K., 1984, Some musings on the Devonian Elk Point Basin, western Canada: *Bulletin of Canadian Petroleum Geology*, v. 32, p. 216-232.
- Williams, M. A. J., D. I. Dunkerley, P. De Deckker, A. P. Kershaw, and T. Stokes, 1993, *Quaternary Environments*: London, Edward Arnold, 330 p.
- Williams, M. D., and V. Ranganathan, 1994, Ephemeral thermal and solute plumes formed by upwelling groundwaters near salt domes: *Journal of Geophysical Research-Solid Earth*, v. B8, p. 15667-15681.

- Williams, W. D., P. De Deckker, and R. J. Shiel, 1998, The limnology of Lake Torrens, an episodic salt lake of central Australia, with particular reference to unique events in 1989: *Hydrobiologia*, v. 384, p. 101-110.
- Williamson, B. M., 1987, Formation of authigenic silicate minerals in Miocene volcaniclastic rocks, Boron, California: Master of Science thesis, University of California, Santa Barbara.
- Williamson, C. R., 1978, Depositional processes, diagenesis and reservoir properties of Permian Deep sea sandstones, Bell Canyon Formation, Texas - New Mexico: Doctoral thesis, University of Texas at Austin.
- Williamson, C. R., and M. D. Picard, 1974, Petrology of carbonate rocks of the Green River Formation (Eocene): *Journal of Sedimentary Petrology*, v. 44, p. 738-759.
- Williamson, D., M. Taieb, B. Damnati, M. Icole, and N. Thouveny, 1993, Equatorial extension of the younger Dryas event - Rock magnetic evidence from Lake Magadi (Kenya): *Global & Planetary Change*, v. 7, p. 235-242.
- Williamson, M. D., S. J. Murray, W. S. Atkins, T. A. P. Hamilton, and M. A. Copland, 1997, A review of Zechstein Drilling Issues: SPE 38483, September 1997, p. 189-196.
- Wilson, A. H., and J. A. Versfeld, 1994, The early Archaean Nondweni greenstone belt, southern Kaapvaal Craton, South Africa; Part I, Stratigraphy, sedimentology, mineralization and depositional environment: *Precambrian Research*, v. 67, p. 243-276.
- Wilson, A. M., W. Sanford, F. Whitaker, and P. Smart, 2001, Spatial patterns of diagenesis during geothermal circulation in carbonate platforms: *American Journal of Science*, v. 301, p. 727-752.
- Wilson, A. O., 1985, Depositional and diagenetic facies in the Jurassic Arab-C and -D reservoirs, Qatif field, Saudi Arabia, in P. O. Roehl, and P. W. Choquette, eds., *Carbonate petroleum reservoirs*: New York, Springer-Verlag, p. 319-340.
- Wilson, J. T., 1966, Did the Atlantic close and then re-open? *Nature*, v. 211, p. 676-681.
- Wilson, T. P., and D. T. Long, 1993, Geochemistry and isotope chemistry of Ca-Na-Cl brines in Silurian Strata, Michigan Basin, USA: *Applied Geochemistry*, v. 8, p. 507-524.
- Winsborough, B. M., J. S. Seeler, S. Golubic, R. L. Folk, and B. Maguire, Jr., 1994, Recent fresh-water lacustrine stromatolites, stromatolitic mats and oncoids from northeastern Mexico, in J. Bertrand-Sarfati, and C. Monty, eds., *Phanerozoic Stromatolites II*: Amsterdam, Kluwer Academic Publishers, p. 71-100.
- Winter, B., J. Valley, J. Simo, G. Nadon, and C. Johnson, 1995, Hydraulic seals and their origin - Evidence from the stable isotope geochemistry of dolomites in the Middle Ordovician St-Peter Sandstone, Michigan Basin: *Bulletin American Association of Petroleum Geologists*, v. 79, p. 30-48.
- Wittstrom, M. D., 1990, Little Knife Field - USA, Williston Basin, North Dakota, in E. A. Beaumont, and N. H. Foster, eds., *Treatise of Petroleum Geology; Atlas of Oil and Gas Fields: Stratigraphic Traps I*: Tulsa, OK, American Association Petroleum Geologists, p. 159-194.
- Wooding, R. A., 1960, Rayleigh instability of a thermal boundary layer in flow through a porous medium: *Journal of Fluid Mechanics*, v. 9, p. 183-192.
- Woese, C. R., 1993, Introduction. The archaea: their history and significance, in M. Kates, D. J. Kushner, and A. T. Matheson, eds., *The Biochemistry of the Archaea*, v. 26: Amsterdam, Elsevier, p. vii-xxix.
- Woese, C. R., and G. E. Fox, 1977, Phylogenetic structure of the prokaryotic domain: the primary kingdoms: *Proc. Natl. Acad. Sci. USA*, v. 74, p. 5088-5090.
- Woese, C. R., O. Kandler, and M. L. Wheelis, 1990, Towards a natural system of organisms: proposal for the domains Archaea, Bacteria, and Eucarya: *Proc. Natl. Acad. Sci. USA*, v. 87, p. 4576-4579.
- Wolfgramm, M., and A. Mumm, 2000, Spatial correlation of fluid inclusion generations: reconstructing fluid flow during basin evolution: *Journal of Geochemical Exploration*, v. 69, p. 397-402.
- Wong, K. W., 1982, A manual on ground surveys for the detection and measurement of subsidence related to solution mining: SMRI Research Project Report, v. 81-0003A-SMRI.
- Wong, S. W., P. M. O'Dell, C. J. de Pater, and J. Shaoul, 2000, Fresh Water Injection Stimulation in a Deep Tight Oil Reservoir: SPE 62618: presented at the 2000 SPE/AAPG Western Regional Meeting held in Long Beach, California, 19-23 June 2000.
- Wood, A. P., and D. P. Kelly, 1991, Isolation and characterisation of *Thiobacillus halophilus* sp. nov., a sulphur-oxidising autotrophic eubacterium from a Western Australian hypersaline lake: *Arch. Microbiol.*, v. 156, p. 277-280.
- Wood, M. W., and H. F. Shaw, 1976, The geochemistry of celestites from the Yates area near Bristol (U.K.): *Chem. Geol.*, v. 17, p. 179-193.
- Wood, W. W., W. E. Sanford, and A. R. S. Al Habshi, 2002, Source of solutes to the coastal sabkha of Abu Dhabi: *Geological Society of America Bulletin*, v. 114, p. 259-268.
- Wood, W. W., W. E. Sanford, and S. K. Frape, 2005, Chemical openness and potential for misinterpretation of the solute environment of coastal sabkhat: *Chemical Geology*, v. 215, p. 361-372.
- Woods, P. J. E., 1979, The geology of Boulby Mine: *Economic Geology*, v. 74, p. 409-418.
- Woolnough, W. G., 1937, Sedimentation in barred basins and source rocks of oil: *American Association Petroleum Geologists - Bulletin*, v. 29, p. 1101-1157.
- Worden, R. H., 1996, Controls on halogen concentrations in sedimentary formation waters: *Mineralogical Magazine*, v. 60, p. 259-274.
- Worden, R. H., and P. C. Smalley, 1996, H₂S-Producing reactions in deep carbonate gas reservoirs - Khuff Formation, Abu Dhabi: *Chemical Geology*, v. 133, p. 157-171.
- Worden, R. H., P. C. Smalley, and M. M. Cross, 2000, The influence of rock fabric and mineralogy on thermochemical sulfate reduction: Khuff Formation, Abu Dhabi: *Journal of Sedimentary Research Section A-Sedimentary Petrology & Processes*, v. 70, p. 1210-1221.
- Worden, R. H., P. C. Smalley, and A. E. Fallick, 1997, Sulfur cycle in buried evaporites: *Geology*, v. 25, p. 643-646.
- Worden, R. H., P. C. Smalley, and N. H. Oxtoby, 1995, Gas souring by thermochemical sulfate reduction at 140°C: *AAPG Bulletin-American Association of Petroleum Geologists*, v. 79, p. 854-863.
- Woronick, R. E., and L. S. Land, 1985, Late burial diagenesis, Lower Cretaceous Pearsall and Lower Glen Rose Formations, south Texas (USA). in N. Schneidermann, and P. M. Harris, eds., *Carbonate cements, SEPM, Tulsa; Special Publication 36*, p. 265-275.
- Worrall, D. M., and S. Snelson, 1989, Evolution of the northern Gulf of Mexico, with emphasis on Cenozoic growth faulting and the role of salt, in A. W. Bally, and A. R. Palmer, eds., *Geology of*

- North America – An Overview: Boulder, CO, Geological Soc. America, p. 97-138.
- Worrall, J. G., and J. K. Warren, 1986, Three-stage dolomitization of the Smackover Formation, SW Alabama; evidence for near-surface and burial-derived fluids: Society of Economic Paleontologists and Mineralogists Midyear Meeting Abstracts, v. 3, p. 118-119.
- Worsley, N., and A. Fuzesy, 1979, The potash-bearing members of the Devonian Prairie Evaporite of southeastern Saskatchewan, south of the mining area: *Economic Geology*, v. 74, p. 377-388.
- Wright, D. T., 1999, The role of sulphate-reducing bacteria and cyanobacteria in dolomite formation in distal ephemeral lakes of the Coorong region, South Australia: *Sedimentary Geology*, v. 126, p. 147-157.
- Wright, D. T., and D. Wacey, 2005, Precipitation of dolomite using sulphate-reducing bacteria from the Coorong Region, South Australia: significance and implications: *Sedimentology*, v. 52, p. 987-1008.
- Wu, S., 1993, Salt and slope tectonics offshore Louisiana: Doctoral thesis, Rice Univ. Houston.
- Wu, S., A. W. Bally, and C. Cramez, 1990b, Allochthonous salt, structure and stratigraphy of the north-eastern Gulf of Mexico. Part II: structure: *Marine & Petroleum Geology*, v. 7, p. 334-370.
- Wu, S., P. R. Vail, and C. Cramez, 1990a, Allochthonous salt, structure and stratigraphy of the north-eastern Gulf of Mexico. Part I: stratigraphy: *Marine & Petroleum Geology*, v. 7, p. 318-333.
- Wyn Hughes, G., 1996, A New Bioevent Stratigraphy of Late Jurassic Arab-D Carbonates of Saudi Arabia: *GeoArabia*, v. 1, p. 417-434.
- Wyn Hughes, G., 1997, The Great Pearl Bank Barrier of the Arabian Gulf as a Possible Shu'aiba Analogue: *GeoArabia*, v. 2, p. 279-304.
- Xiao, Y. K., D. P. Sun, Y. H. Wang, H. P. Qi, and L. Jin, 1992, Boron isotopic compositions of brine, sediments, and source water in Qaidam Lake, Qinghai, China: *Geochimica et Cosmochimica Acta*, v. 56, p. 1561-1568.
- Xu, C., 1993, Clay Mineral Research in Chinese Saline Lakes (in Chinese): Science Press, Beijing.
- Yagmurlu, F., and C. Helvacı, 1994, Sedimentological characteristics and facies of the evaporite-bearing Kirmir Formation (Neogene), Beypazari Basin, central Anatolia, Turkey: *Sedimentology*, v. 41, p. 847-860.
- Yahi, N., R. G. Schaefer, and R. Littke, 2001, Petroleum generation and accumulation in the Berkine basin, eastern Algeria: *Bulletin American Association Petroleum Geologists*, v. 85, p. 1439-1467.
- Yang, C., I. Hutcheon, and H. R. Krouse, 2001, Fluid inclusion and stable isotope studies of thermochemical sulphate reduction from Burnt Timber and Crossfield East gas fields in Alberta, Canada: *Bulletin of Canadian Petroleum Geology*, v. 49, p. 149-164.
- Yang, W. B., R. J. Spencer, H. R. Krouse, T. K. Lowenstein, and E. Cases, 1995, Stable isotopes of lake and fluid inclusion brines, Dabusun Lake, Qaidam Basin, Western China - Hydrology and paleoclimatology in arid environments: *Palaeogeography Palaeoclimatology Palaeoecology*, v. 117, p. 279-290.
- Yaoru, L., and A. H. Cooper, 1997, Gypsum karst geohazards in China, in B. F. Beck, and J. B. Stephenson, eds., *The Engineering Geology and Hydrogeology of Karst Terranes*. Proceedings of the 6th Multidisciplinary Conference on Sinkholes and the Engineering and Environmental Impacts of Karst, Springfield, MO, 6-9 April, 1997, p. 117-126.
- Yassir, N. A., and J. S. Bell, 1994, Relationships between pore pressure, stresses, and present-day geodynamics in the Scotian Shelf, offshore eastern Canada: *Bulletin American Association of Petroleum Geologists*, v. 78, p. 1863-1880.
- Yeats, R. S., and R. J. Lillie, 1991, Contemporary tectonics of the Himalayan frontal fault system: folds, blind thrusts and the 1905 Kangra earthquake: *Journal of Structural Geology*, v. 13, p. 215-225.
- Yechieli, Y., I. Gavrieli, B. Berkowitz, and D. Ronen, 1998, Will the Dead Sea die? *Geology*, v. 28, p. 755-758.
- Yoo, C. M., J. M. Gregg, and J. S. Shelton, 2000, Dolomitization and Dolomite Neomorphism: Trenton and Black River Limestones (Middle Ordovician) Northern Indiana, U.S.A.: *Journal of Sedimentary Research*, v. 70, p. 265-274.
- Yoo, C. M., and Y. I. Lee, 1998, Origin and modification of early dolomites in cyclic shallow platform carbonates, Yeongheung Formation (Middle Ordovician), Korea: *Sedimentary Geology*, v. 118, p. 141-157.
- Young, G. M., 1981, The Amundsen embayment, Northwest Territories: relevance to the upper Proterozoic evolution of North America, in F. H. A. Campbell, ed., *Proterozoic Basins of Canada*, *Geol. Surv. Canada Paper* 81-10, p. 203-218.
- Youssef, E. A. A., 1989, Geology and genesis of sulfur deposits at Ras Gemsa area, Red Sea coast, Egypt: *Geology*, v. 17, p. 797-801.
- Youssef, E. S. A. A., 1998, Sequence stratigraphy of the Upper Jurassic evaporite-carbonate-sequence at the western area of Wadi Al-Jawf-Marib Basin, Yemen: *Carbonates & Evaporites*, v. 13, p. 168-173.
- Yu, Z. H., and I. Lerche, 1996, Modelling abnormal pressure development in sandstone shale basins: *Marine & Petroleum Geology*, v. 13, p. 179-193.
- Yuanxiong, L., and N. Chengxun, 1983, Technical development of solution mining of thinly bedded rock salt deposits of Ziliujing, Sichuan China, in B. C. Schreiber, ed., *Proceedings 6th International Salt Symposium*, v. 2: Alexandria VA, Salt Institute, p. 87-99.
- Zachos, J. C., M. Pagani, L. Sloan, E. Thomas, and K. Billups, 2001, Trends, rhythms, and aberrations in global climate 65 Ma to present: *Science*, v. 292, p. 686-693.
- Zaikowski, A., B. J. Kosanke, and N. Hubbard, 1987, Noble gas composition of deep brines from the Palo Duro Basin, Texas: *Geochimica et Cosmochimica Acta*, v. 51, p. 73-84.
- Zak, I., and R. Freund, 1980, Strain measurements in eastern marginal shear zone of Mount Sedom salt diapir, Israel: *Bulletin American Association Petroleum Geologists*, v. 64, p. 568-581.
- Zak, I., and R. Freund, 1981, Asymmetry and basin migration in the Dead Sea rift: *Tectonophysics*, v. 80, p. 27-38.
- Zamfirescu, F., M. Mocuta, T. Constantinecu, E. Medves, and A. Danchiv, 2003, The main causes of a geomechanical accident of brine caverns at field II of Ocnele Mari - Romania: *RMZ - Materials and Geoenvironment*, v. 50, p. 431-434.
- Zaritsky, P. V., 1961, Celestite from the Lower Permian deposits of the Donbas: *Akademiya Nauk SSR, Doklady*, v. 133, p. 801-804.
- Zen, E. A., 1965, Solubility measurements in the system $\text{CaSO}_4\text{-NaCl-H}_2\text{O}$ at 35 degrees, 50 degrees, and 70 degrees C and one atmosphere pressure: *J. Petrology*, Oxford, p. 124-164.
- Zhang, Y., 1985, Geology of the Wucheng trona deposit in Henan, China: Schreiber, B. C., Warner, H. L. Sixth international symposium on salt.

- Zharkov, M. A., 1981, History of Paleozoic Salt Accumulation: Berlin, Springer Verlag, 308 pp p.
- Zheng, H. B., C. M. A. Powell, and H. Zhao, 2003, Eolian and lacustrine evidence of late Quaternary palaeoenvironmental changes in south-western Australia: *Global and Planetary Change*, v. 35, p. 75-92.
- Zheng, X. Y., M. G. Zhang, J. H. Dong, Z. H. Gao, C. Xu, Z. M. Han, B. Z. Zhang, D. P. Sun, and W. K. J., 1992, Salt Lakes in Inner Mongolia (in Chinese): Science Press, Beijing, p. 1-296.
- Zhilina, T. N., and G. A. Zavarzin, 1994, Alkaliphilic anaerobic community at pH 10: *Curr. Microbiol.*, v. 29, p. 109-112.
- Zhilina, T. N., G. A. Zavarzin, F. Rainey, V. V. Kevbrin, N. A. Kostrikina, and A. M. Lysenko, 1996, *Spirochaeta alkalica* sp nov, *Spirochaeta africana* sp nov, and *Spirochaeta asiatica* sp nov, alkaliphilic anaerobes from the continental soda lakes in Central Asia and the East African Rift: *International Journal of Systematic Bacteriology*, v. 46, p. 305-312.
- Zhu, C., and S. Zhang, 1999, A study of the characteristics of the organic matter in carbonate rocks and source rocks in the Lower Ordovician Majiagou Formation of Ordos Basin: *Journal of the Chengdu Institute of Technology*, v. 26, p. 217-220.
- Zilberman, V. I., V. A. Serebryakov, M. V. Gorfunkel, and G. V. Chilingar, 2001, Prediction of Abnormally High Formation Pressures (AHFP) in petroliferous salt-bearing sections: *Journal of Petroleum Science & Engineering*, v. 29, p. 17-27.
- Zimmermann, H., 2000a, On the origin of fluid inclusions in ancient halite - basic interpretation strategies, in R. M. Geertmann, ed., *Salt 2000 - 8th World Salt Symposium Volume 1: Amsterdam*, Elsevier, p. 199-203.
- Zimmermann, H., 2000b, Tertiary seawater chemistry - Implications from primary fluid inclusions in marine halite: *American Journal of Science*, v. 300, p. 723-767.
- Zimmermann, H., 2001, On the origin of fluids included in Phanerozoic marine halite - basic interpretation strategies: *Geochimica et Cosmochimica Acta*, v. 65, p. 35-45.
- Zobell, C., 1957, The ecology of sulphate-reducing bacteria.: *Sulphate-Reducing Bacteria - their relation to the secondary recovery of oil*, Symposium, St Bonaventure University, (Oct 23-24, 1957).
- Zuber, A., J. Grabczak, and A. Garlicki, 2000, Catastrophic and dangerous inflows to salt mines in Poland as related to the origin of water determined by isotope methods: *Environmental Geology*, v. 39, p. 299-311.
- Zubtsov, S., F. Renard, J.-P. Gratiera, R. Guiguet, D. K. Dysthe, and V. Traskine, 2004, Experimental pressure solution compaction of synthetic halite/calcite aggregates: *Tectonophysics*, v. 385, p. 45-57.
- Zumberge, J. E., 1987, Prediction of source rock characteristics based on terpane biomarkers in crude oils: A multivariate statistical approach: *Geochimica et Cosmochimica Acta*, v. 51, p. 1625-1637.
- Zverev, V. P., 1967, Otsenka nasyshchennosti podzemnykh vod sul'fatom kal'tsiya v diapazone temperature 0-40 degrees C: in *Regional'naya geotermya i rasprostraneniye termal'nykh vod*, p. 308-313.

Index

A

- Abnormal pressure. *See* Overpressure
- Abu Dhabi Sabkha, UAE. *See* Sabkha
- Acid saline lakes
- alunite and other indicators 56, 89
 - hydrology and hydrogeochemistry 88–91
 - Permian redbeds, Kansas 308–310
- Adamovsk salt stock, Ukraine 485
- Albitites
- origin 107
- Algal (cyanobacterial) mats. *See* Microbialites
- Abu Dhabi sabkha 149
- biology 7
 - Ras Muhammad Pool, Sinai 233
 - Solar Lake, Gulf of Elat 232
- Alkaline earth carbonates 77
- Alkalinity
- explained 78
- Alkanes 653
- Allochthonous salt
- as thrust nappe 400
 - attributes 398
 - brine pools on sea floor 676
 - counter-regional faults 401
 - differential loading
 - creation of faults 392
 - effect on sea floor carbonates 433
 - effect on sea floor topography 400
 - emplacement mechanisms 399
 - formation of growth faults 401
 - protective carapace 400
 - regional faults 401
 - subsalt overpressure 403
 - subsalt sedimentation 446
 - suprasalt carbonate sedimentation 437
 - suprasalt clastic sedimentation 440
- Alluvial fans
- Alluvial fan–ephemeral saline lake
 - attributes 181–220
 - attributes 161, 167, 176, 276
- Al Salif diapir, Yemen 434
- Amadeus Basin, Australia
- salt tectonics 422
 - sylvite 804
- Anhydrite
- calcitised 539–544
 - deepwater 35
 - enteroliths via burial 48
 - formation from gypsum 47–50
 - halophyte association 166
 - hydrothermal 4
 - nodules formed in burial 50–51
 - solubility 75
 - stylolites 51
 - thermal stability 602
 - type
 - axe-head or keg barrel 39
 - chicken-wire 40
 - enterolithic (contorted) 40
 - gypsum “ghosts” 48
- Anhydritization
- definition 564
 - Zechstein 367
- Annual production
- borate 832
 - bromine 849
 - gypsum 845
 - halite 846
 - iodine 847
 - lithium 850
 - potash 795
 - sodium carbonate (trona) 861
 - sodium sulphate (mirabilite) 866
 - sulphur 879
- Anoxia
- in source rock accumulations 619
- Antarctica
- cryogenic salts 59, 612
 - ice sheet expansion, Tertiary 289
 - microbes in modern salt lakes 632, 660
- Apennines 361–362
- Arab (Jurassic) Formation, Middle East 721–725
- Archaea
- biomarkers 654
 - defined 629
 - halophilic (haloarchaea) 632
 - isotopic association 656
 - methanogenic 632
 - occurrence
 - Dead Sea, Middle East 666
 - Guaymas Basin 688
 - Red Sea deeps 682
 - photoautotrophic mechanism 647–648
- Archaeobacteria. *See* Archaea
- Artemia. *See* Brine shrimp
- Atmospheric circulation
- creation of deserts 59
- Authigenic “burial” salts
- attributes 45, 50–51, 560–564
- Autotrophs 630

B

- Backreactions
 attributes 83
- Bacteria
 “low salt” in option 649
 defined 629, 629–630
 in saline waters 634
 lipid composition 655, 669
 sulphate reducers
 metabolic character 687
 salinity range 643
 sulphur oxidisers 632, 639
- Bacterial sulphate reduction. *See* sulphate reduction
- Bacteriochlorophyll
 attributes 631
- Bacteriorhodopsins 647
- Baryte
 as evaporite indicator 556–559
 as hydrothermal indicator 106
 occurrences
 Chaudfontaine, Belgium 106
 Galeana baryte, Mexico 558
 Hermosa Fm., USA 558
 Magnet Cove, Nova Scotia 556
 Nondweni greenstones, Africa 105
 North Pole, Australia 105, 559
 Oraparinna diapir, Australia 556
- Basinwide evaporite
 characteristics 324–345
 deep water-deep basin 327
 shallow water-deep basin 328
 shallow water-shallow basin 328
 sequence stratigraphy 347–351
- Bassanite 47, 54, 151, 603
- Belle Roche breccia, Belgium 476
- Bioadaptation
 “High salt-in” option 649
 “Low salt-in” option 649
 at the cellular level 646–648
 to increasing salinity 635–637
- Biomarkers
 attributes 652–656
- Biomineralization
 laminites 7
- Blomiden Formation, Canada
 syndepositional solution breccia 479
- Borates
 Attributes of deposits 831–839
 occurrences
 playas of North America 841
 Sijes Fm., Andes South America 838
 Western Anotolia, Turkey 834
- Boron
 isotope
 indicator of parenthood 96–98
- Bottom nucleated texture
 gypsum 23–26, 129–130
- Boxwork limestone 228
- Box folds 420
- Breccias. *See also* Evaporite solution breccias
 breccia chimneys 460
 classification
 crackle 473
 floatbreccia 473
 mosaic 473
 packbreccia 473
 rubble 473
 halokinetic 481–485
 interstratal 478, 480
 sedimentary 472
 trans-stratal (trans-formational) 478, 480
- Brine
 chemistry, burial 604–610
 chemistry, marine
 bitterns in relation to seafloor flux 74
 changes across time 74
 concentration series 67
 chemistry, nonmarine
 attributes 76–83
 cooling
 potash precipitation 798, 806
 crustal cycling 612
 cryogenic 612
 curtain. *See also* Brine, reflux
 characteristics 333–334
 flow regimes
 deposition 112–138
 hydrology
 deposition 112–138
 marine
 leakage effects precipitates 74
 mixing and precipitation 45, 75
 nonmarine
 chemical evolution 77–78
 chemical types 76
 parenthood indicators 92–98
 ponding 130–138
 potash production from brine wells 805
 reflux
 backreactions 134
 characteristics 130–135, 607, 735, 763–764
 creation of reservoir permeability 713, 719, 724, 732,
 733, 737, 739, 742, 750
 megapolygons 91, 719
 permanency 132–138
 separating marine and nonmarine 83
 specific heat 659
 type
 marine 67–76

- nonmarine 76–83
 - volcanogenic 85
- Brine chemistry
 - Abu Sir sabkha, Nile Coast 169
 - allochthon vent, Gulf of Mexico 676
 - chotts and sabkhas, Tunisia 803
 - continental lakes, Qaidam Basin, China 97
 - continental perennial lakes 238
 - continental playas, Australia 80
 - Dead Sea and surrounds, Middle East 266
 - East African rift valley lakes 257
 - Lake Eyre, Australia, post 1984 flood 204
 - marine-fed coastal lakes 68
- Brine fingers
 - convective megapolygons 91
- Brine fly
 - lifestyle and salinity tolerance 641
- Brine inclusions. *See* Fluid inclusions
- Brine plume. *See* Brine, reflux
- Brine pool
 - bottom stability effects texture 36, 129
 - in allochthon terrane 676–684
 - stratification 25, 117
 - permanency 126
- Brine processing
 - Dead Sea, Middle East 805
 - Ingebright Lake, Canada 870
- Brine shrimp
 - feeding habits (pellets) 241, 642
 - salinity tolerance 641
- Bristol Dry Lake, USA
 - attributes 183
 - displacement halite 40
 - gypsum to anhydrite 48
- Broad Forties basin, North Sea 424
- Bromine
 - attributes of commercial deposits 849
 - levels as indicator of parenthood 92–94
 - Salar Uyuni, Bolivia 191
- Burial
 - cycle of evaporite alteration 2–4, 489–493
 - dewatering of hydrated salts 47–50, 601–604
- Burial cycle
 - mosaic halite 45–46
- Burial salt
 - anhydrite nodules 47–50, 601
 - authigenic indicators 559–564
- C**
- CaCl₂ brines
 - Danakil Depression, Africa 801
 - driving burial diagenesis 45, 102, 105, 571
 - fluorite solubility 553
 - from seawater freezing 612
 - hydrothermal FeCl₂ enrichment 801
 - tachyhydrite 811, 824
- Cadjebut Pb-Zn deposit, Australia
 - evolution of ore textures 528–529, 528–530
 - sphalerite speleothem 478
- Calatayud Basin, Spain
 - karst hazard 519
 - sediment distribution 307
- Calcitisation 539
 - evaporite nodules 541–545
- Callanna Beds, Australia 483
- Capillary evaporation
 - defined 114
 - effects on sedimentation 117
 - in sabkha sediments 152
- Caprock
 - as allochthon carapace 400
- Cargneules 486
- Carlsbad-Lechuguilla cavern 523
- Carnallite
 - crusts and beds 799
 - in Chott el Djerid, Tunisia 801
 - in Danakil depression, Africa 800
 - in Dead Sea depression, Middle East 806
 - in Delaware Basin, USA 817
 - in Khorat Plateau, Thailand 811
 - in Lake Qaidam, China 796–799
 - in Prairie Evaporite, Canada 820
 - in Rhine Graben, Europe 809
 - in Sabkha el Mehabeul, Algeria 803
 - in Sabkha el Melah, Algeria 803
 - in trans-Atlantic basins 824
 - rafts 799
 - void-filling cement 799
- Carnallitite
 - definition 794
- Carson Sink Breccia, USA
 - origin as thrust sheet 490–493
- Castiles
 - mechanism of formation 688
 - occurrences in Texas 466
- Castile Formation, USA
 - deepwater laminite 33
- Caves. *See* Karst
- Celestite
 - attributes in bedded host 548–553
 - hydrothermal 553
 - in diapir caprock 449
 - sources of Sr-rich waters 549
- Cementstone
 - attributes in Precambrian 21, 106, 292
- Cerithid gastropod 148
- Chemocline
 - annual evolution in brine pool 126

- Chemotrophs
 attributes 631
- Chert nodules
 as evaporite indicators 532–539
 textures after evaporites 533
- Chevron folds
 compressional salt tectonics 420
- Chicken-wire. *See* anhydrite
- Chlorine
 isotope
 indicator of parenthood 98–100
- Chott el Djerid, Tunisia
 Quaternary potash evaporite 803
- Clay
 saline authigenesis 54–56
- Clear Fork Formation (Permian), USA
 Central Basin Platform, USA 737
 mudflat to saltern transition 316
- Climate
 change and effect on evaporite 288–292
 Quaternary
 deserts 59–67
- CO₂
 fluctuations and climate 289–290
 microbial mineralisation 7
- Compaction
 pressure profiles 583
- Concentration
 marine brine 68
 non-marine brine 76
- Continentality
 role in creation of deserts 61
- Continental waters 76–89
- Coorong Lakes, Australia
 attributes 223–226
 dolomite 226
 lake mineralogy 79, 224
 laminites 6
 stromatolite lakes 11
- Cornicles 486
- Creep rates 378–380
- Cryogenic salts. *See* Antarctica
 forming basement brines 612
 precipitation suite from seawater 612
- Cyanobacteria
 adaption to increased salinity 635–641
 coccoid 8
 distribution in microbial mat 650–652
 filamentous 8
 oil prone source rock 619
- D**
- Dabuxum Lake, China
 formation of carnallite 798
- Danakil Depression, Africa
 changes in Quaternary inflow chemistry 801
 potash evaporites 799–801
- Dasht-e-Kavir, Iran
 diapir
 internal structures 385
 diapirs and pans 219
- Das Island, Arabian Gulf
 diapiric breccia 483
- Dead Sea, Middle East
 attributes 264–267
 biology and density stratification 666–668
 brine wells for potash 805
 deepwater halite 270
 displacement halite 40
 halolites 28
 karst and falling lake level 125
 laminites 5, 273
 mushrooms of halite 36
 stromatolites 11
 tectonic setting 265
 water level changes 266
- Death Valley playa, USA
 Quaternary history 60
 sedimentary attribute 185
- Debris flows 298, 318, 322, 350, 359, 361
- Decarboxylation
 importance in calcitisation 541
- Dedolomite
 attributes 539–547
- Deepwater evaporite
 attributes 273–275, 298–299, 681, 869
 Dead Sea, Middle East
 halite via brine mixing or cooling 271
 evaporitic carbonate 6
- Deep Springs Lake, USA
 attributes 182
- Density stratification
 attributes 126–129
 Dead Sea, Middle East 268
 Lake Haywood, Australia 126
 Solar Lake, Middle East 128
- Depopod
 defined 432
- Desert
 continental effects 61
 controls on formation 59
 playa types 59
 rain shadow effects 61
 types of continental 59
- Diapir
 breccia
 Blinman diapir, Australia 486
 Oratunga diapir, Australia 483
 definition 376

- falling diapir 396–398
 - in Arabian Gulf 437
 - in Danakil Depression, Ethiopia 384
 - in Flinders Ranges, Australia 438
 - in Gulf of Mexico 395, 410, 421, 440
 - in Jabal al Milh, Yemen 434, 435
 - in Maritime Alps, France and Spain 429
 - in North Sea 388
 - in Santos Basin, Brazil 417
 - shale 450
 - via hot salt intrusion 384
- Diapiric solution breccias 481–486
 - Arabian Gulf 483
 - Flinders Ranges, Australia
 - matrix minerals 484
 - origin by passive flow 484
- Diatom
 - salinity tolerance 639
- Dissolution. *See* karst
- Diversity
 - biological 659
- Dolines
 - collapse 459
 - solution 459
- Dolomite
 - hydrothermal 748
 - limpid 47
 - mimetic 44
 - modern
 - Coorong, Australia 79, 227–228, 238
 - Lagoa Vermelha 236
 - Lake Greenly-Malata, Australia 81
 - reflux 131
 - varieties in Tripolis breccia, Greece 476
- Dolomitization
 - by brine reflux 44, 133
 - in a drawdown basin 337
 - Nijar Platform, Mediterranean 339
- Downbuilding 390
- Drawdown
 - dolomite 337
 - evaporite 117, 126, 227, 230, 232, 306, 320, 328, 332
 - examples
 - Messinian, Mediterranean 352–361
 - Michigan Basin, USA 368–369
 - Zechstein, Europe 362–367
 - sequence stratigraphy 342–347
- Drilling Salt
 - pressure problems 591
- Dry mudflat 178
- Dunes. *See also* eolian
 - gypsum. *See* Lunettes
 - surfaces and palaeohydrology 121
- E**
 - Ebro Basin, NE Spain
 - hydrologic regime 580
 - karst hazard 519
 - Elk Point Basin, Canada
 - dolomitization via drawdown 338
 - Endoheic basin
 - Chott el Djerid, Tunisia 801
 - defined 59
 - Enorama Diapir, Australia
 - effect on stromatolite reef growth 438
 - ENSO - El Nino Southern Oscillation
 - definition 204
 - Lake Magadi, Africa 256
 - Eogenesis 2
 - Eolian 211
 - dune 143, 215
 - erg 212
 - reservoir 755, 758
 - sabkha 211–220
 - Eubacteria. *See* Bacteria
 - Eugene Island “Block 330” field, Gulf of Mexico
 - halokinetic/geological evolution 440
 - Eustacy
 - influence on evaporite deposition 342
 - Eutrophic lake
 - definition 670
 - effects on evaporite salts 674
 - Evaporation rate
 - effect of humidity 64
 - effect of salt crust 65
 - variation with depositional setting 66
 - Evaporite
 - as lubricants 603–615
 - basic requirements 1
 - basinwide 300
 - broad-scale models 300–332
 - burial salt
 - definition 4
 - Comparison to sandstone and carbonates 4
 - continental/lacustrine 300
 - controls on diversity 295–296
 - definition 2
 - distribution of ancient deposits 293–340
 - major minerals 2
 - platform 300
 - primary evaporite
 - attributes 22–38
 - definition 2
 - problems in correlation 335–337
 - secondary evaporite
 - definition 2
 - tertiary evaporite
 - attributes 51–57

definition 4

Evaporites
 climatic control on Quaternary deposits 59–67

Evaporite indicators
 attributes 531–559
 authigenic burial salts 559–564
 baryte 553–555
 calcitised evaporites 539–547
 celestite 548–553
 fluorite 553–555
 silicified evaporites 532–539
 controls on silica 537
 magadiite 261, 262–264, 537

Evaporite metal associations
 low temperature
 in Black Hills U 530
 in Cadjebut Pb-Zn 528–530

Evaporite solution breccias
 “chalky” dolomite 474, 506
 attributes 472–481
 basal anhydrite 498–500
 boxwork texture 477
 breccia geometries 478
 controls 478
 clasts
 description 473
 nature of movement 473
 origin 475
 diapiric 481–486
 dissolution residues
 attributes 472
 gypsum karst 494–500
 preferential solution 493
 evolution of texture 474–478
 focus for sulphide mineralisation 528–531
 hydrocarbon traps 786
 hydrological controls
 postinduration 480
 preferential solution breccias
 attributes 493
 effect on correlation 497
 speleothem textures 477
 stratiform breccia 472, 478–479
 typical vertical sequence 474
 uranium 530

Evaporitic carbonate
 algal mats 232
 attributes 5
 types
 boxwork limestone 228
 laminite 5, 226, 273
 stromatolites 6–57, 228
 tepee 16–18, 228
 travertine 9
 tufa 9, 223–224, 244–246

Evaporitic mudflat
 attributes 178–179, 296–297
 hydrological attributes 113
 Ewaso Ngiro River, Africa 257

F

“Fill and spill” cycles 351
 “Flamingo connection”. *See* Organic matter

Faults
 en echelon 423
 growth faults
 counterregional 401, 407
 regional 401
 intersection in salar beds
 Great Salt Lake, Utah 242
 Salar de Atacama, Chile 198
 Salar Grande, Chile 199
 listric 394, 407, 416
 pseudo-fault 393, 408
 tear faults and salt extrusion 426
 thrust 425

Ferry Lake anhydrite, USA
 stacked saltern cycles 319

Flower Gardens Bank, Gulf of Mexico
 effect of halokinesis on reef growth 438

Fluid flow
 hydrologic regimes
 basinal 571
 collision belts 574
 compactional 570
 depositional 112–138
 subsalt 581
 suprasalt 596
 thermobaric 571
 uplift 575
 metalliferous 696–699

Fluid inclusions
 Death Valley halite, modern 101
 indicator of parenthood 100–101
 Phanerozoic seawater 102
 Silurian halite, Michigan Basin 103

Fluorite
 as evaporite indicator 555
 brine, East African rift 258
 Pleistocene, East African rift 555

Folding
 salt cored
 angular folds 420
 compressional 417
 thin-skinned
 attributes 419–423

Frasch Process
 sulphur extraction method 879

G

- “Greenhouse” climate mode 343, 346
- Gastropod
 - pellet production 642
 - salinity tolerance 642
- Gaylussite
 - pseudo-gaylussite (ikaite) 565
- Gene mapping
 - defining Kingdoms of Life 629
- Glauberite
 - Gulf of Karabogaz 874
 - Lacustrine, Kimir Fm., Miocene, Turkey 871
 - Lacustrine, Miocene, Spain 870
 - Quaternary, Laguna Del Rey playa, Mexico 873
 - via anhydrite replacement 84
- Glendonite 246
- Glen Rose Formation, USA
 - authigenic salts 564
- Graben
 - crestal 396
 - inverted basin 422–423
 - keystone 396
- Great Artesian Basin, Australia
 - hydrology 205
- Great Kavir, Iran. *See* Dasht-e-Kavir, Iran
- Great Pearl Bank, Arabian Gulf
 - attributes 145
- Great Salt Lake, USA
 - attributes 239–243
 - lunette 31
 - mirabilite 873
 - potash production 807
- Green Canyon area, Gulf of Mexico
 - allochthonous salt 408
- Green River Formation, USA
 - nahcolite 905
 - trona 861–863
- Groundwater
 - acid groundwater lakes 88–91
 - planation surfaces 118–119
- Guadalquivir allochthon, Spain 421
- Gumbo zone
 - overpressure in subsalt 403
- Gypsum
 - “ghosts” in anhydrite 48
 - alabastrine 52
 - capillary crusts 184
 - commercial deposits 845
 - conversion to anhydrite 47–50
 - dewatering and intrinsic strength 603–604
 - indicator of bottom stability 25
 - lunettes 31, 229
 - meteoric karst 494–500
 - planation surfaces 130

- solubility 75
- tumuli 463
- types
 - “daisy head” rehydration 506
 - alabastrine 52, 506
 - bottom nucleated 23, 228
 - desert or sand roses 24, 152, 161
 - gypsite 229, 231
 - gypsolite (oolite) 28
 - intrasediment saline seep 274
 - laminated 229
 - lenticular or “bird beak” 23
 - mush 150
 - palmate or fanned 23–57
 - porphyroblastic 52
 - speleothems 507
 - subaqueous, shallow 23
 - turbidites 298
 - uplift textures 51–52

H

- Hadley Cells
 - atmospheric circulation 59
- Halite
 - commercial deposits 846
 - deformation
 - as a “crack stopper” 381
 - as a lubricant 381
 - flow texture complexity 388–389
 - importance of water 380
 - relative strain rates 378
 - solution transfer creep 380
 - density changes with burial 376
 - fluid inclusions, Lake Qaidam 796
 - haloturbation 43, 118
 - karst 40, 496
 - physical properties (density, pressure, strength, viscosity) 376
 - porosity loss with burial 44–45
 - thermal effects 384
 - types
 - burial mosaic 45–46
 - chaotic halite 43
 - chevrons 26
 - crusts 26
 - crusts, karst 41
 - deepwater, Dead Sea, Middle East 271
 - displacement 40
 - halolite (oolite) 28
 - intrasediment 40
 - mosaic 46–47
 - pagoda 40
 - reefs 36–38
- Halite Lake, Coorong Australia

- attributes 226
 - Haloarchaea. *See* Archaea
 - Halobacteria
 - defined 644
 - Halocline
 - attributes 126
 - Hartsalz
 - definition 794
 - Haselgebirge Formation (Permian), Austria
 - tectonic breccias and thrusting 487
 - Hauptdolomit, Europe
 - breccia geometry 478
 - Heliothermal brines
 - Lake Haywood, Australia 126
 - mechanism of formation 116, 659
 - Solar Lake, Gulf of Elat 128, 232
 - Heterotrophs 631, 634
 - Holomixis
 - definition 670
 - Hopper. *See* halite
 - Hutchison gas explosion
 - detail 935
 - Hutchison Salt, Kansas 464
 - Hydrocarbon
 - association with evaporites 705–708
 - compressibility in cavern storage 909
 - slowing of salt dissolution 45
 - solubility in brine 583
 - traps
 - subsalt 446
 - suprasalt 440
 - turtle structure anticlines 396
 - Hydrocarbon accumulations
 - evaporite (bedded)-associated
 - Arab Formation, Middle East 721
 - Levelland-Slaughter field, USA 733
 - Lower Keg River/Winnipegosis, Canada 748
 - Miocene carbonates, Taurus-Zagros belt, Middle East 745
 - North Riley field, USA 737
 - North Ward-Estes field, Texas 754
 - Pinnacle reefs, Michigan Basin, USA 746
 - Red River Formation, USA 716
 - Rotliegende sands, NW Europe 758
 - Smackover-hosted, Gulf of Mexico 737
 - South Cowden field, USA 737
 - Yates field, west Texas 752
 - evaporite (foldbelt)-associated
 - Carpathian foldbelt, Eastern Europe 784
 - Rocky Mountain foldbelt, USA 784–786
 - Zagros Foldbelt, Arabian Gulf 780–783
 - evaporite (halokinetic)-associated
 - Gulf of Mexico 771–775
 - Machar, North Sea 767
 - evaporite (intrasalt)-associated
 - Ara Salt, Oman 776–777
 - Hydrofracture 574, 587
 - Hydrogeochemistry
 - sabkha
 - chloride plateau 165
 - Hydrologic regime
 - active phreatic 113–126
 - active phreatic regime
 - controls on sedimentation 117
 - closed basin 79
 - compaction 570
 - deep meteoric
 - Alberta Basin 578
 - Palo Duro Basin 577
 - leaky basin 74, 80
 - post-orogenic 575–585
 - pull-apart transforms 573–574
 - thermobaric 603–615
 - vadose characteristics 113
 - Hydrology
 - brine curtain 333–335
 - importance in evaporite deposition 332–335
 - no surface connection for thick salt 332
 - Hydrology, brine curtain
 - Mono Lake, California 246
 - Hydrothermal
 - cracking of organic matter 699
 - definition of salt 4
 - dolomite 748
 - Hypersaline
 - defined 68
 - Hypolimnion
 - definition 670
- ## I
- ”Icehouse” climate mode 343
 - Ikaite 11, 245, 565
 - Incongruent dissolution
 - formation of sylvite 47, 71, 73
 - of halite 99, 611
 - Infiltration
 - in the vadose zone 114
 - Inimical waters 318
 - Insects
 - in hypersaline settings 641
 - Interdune sabkha. *See* Sabkha, eolian
 - Intrasalt minibasin 407, 408
 - Inverted basins 422–423
 - Iodine
 - attributes of commercial deposits 847
 - deficiency, effect on human health 848

Ionic
 species in seawater 67
 species in nonmarine waters 76

Island shoal facies
 Abu Dhabi 145

Isotopes
 boron
 indicator of parenthood 96–98
 chlorine
 indicator of parenthood 98–100
 dolomite
 Andrews platform, Texas 609
 Coorong Australia 227
 Gharif (Permian), Oman 606
 Nijar (Messinian), Spain 339
 gypsum
 Lorca (Messinian) Basin, Spain 358
 oxygen
 indicator of parenthood 94–96
 Saline lakes of Andes 9
 strontium
 Andrews platform, Texas 609
 Louann Salt, Gulf of Mexico 611
 sulphur
 indicator of parenthood 94–96
 Precambrian 110

J

Jabal al Milh diapir, Yemen 435
 Jafurah Sand Sea, Saudi Arabia 160, 212
 Janecke diagram
 phase equilibria 71
 Jura fold belt, Europe
 compressional tectonics 419

K

Kainitite
 definition 794
 Kara-Bogaz-Gol
 attributes 874–876
 Karinga Creek drainage system, Australia
 glauberite/sylvite efflorescences 804
 Karst
 examples
 Cadjebut Pb-Zn Mine, Australia 528
 Delaware Basin, west Texas 466
 Five Islands, Louisiana 470
 Holbrook Anticline, Arizona 468
 Hutchison salt, Kansas 464
 Ripon area, England 517
 Uranium Black Hills, USA 530
 Zagros-Hormuz region, Arabian Gulf 471
 gypsum caves 501–506

halite caves 509–510
 hazards, natural 515
 hypogene 521
 karst hazards 515–520
 landforms 458–462
 sulphuric acid speleogenesis 521–528
 Keg River Formation, Canada
 authigenic salts 564
 Kerogen
 defined 618
 Khors
 Southern Arabian Gulf 147
 Kirschberg Evaporite, Texas
 gypsum karst 477, 506
 Kuwait Bay 161
 Kwanza Basin, Angola
 raft tectonics 397

L

Laguna del Rey playa, Mexico 873
 Lakes, Continental saline
 Attributes 238
 controls on formation 282
 Lake (place name)
 Aci (Acigolu), Turkey
 attributes 253
 Amadeus, Australia
 falling water table 124
 potash evaporites 804
 soil throughput controls lake brine 80
 Asal, Africa
 attributes 280–282
 halolites 28
 Banyoles, Spain
 brine evolution and karst 76
 Bogoria, East Africa
 attributes 261
 Bonneville, USA 240–242
 Callabonna, Australia 210
 Chad, Africa
 interdunal sabkha 216
 water level changes 202
 Clifton, Australia
 attributes 223
 Eskisehir, Turkey
 sepiolite (meerschaum) 85
 Eyre, Australia
 attributes 202
 geological history 208
 hydrology 204–205
 Kallakooah interdunal sabkha 216
 pedogenic magnesite 81
 Quaternary history 60
 Frome, Australia

- attributes 208–210
 - Quaternary history 60
 - Great Salt Lake, Utah 239
 - Hayward, Australia
 - brine stratification 126
 - Lagoa Vermelha, Brazil
 - bacterial dolomite 236
 - Lisan (Pleistocene), Middle East
 - Attributes 277
 - MacLeod, Australia
 - attributes 230
 - Magadi, East Africa
 - attributes 255
 - Late Pleistocene sediments 260
 - trona 259
 - Mono Lake, USA
 - attributes 243
 - ikaite 11
 - Natron, East Africa
 - attributes 255
 - Qaidam, China
 - boron isotope 96
 - carnallite rafts 28
 - potash geology 796–808
 - Quaternary history 796
 - Salda, Turkey
 - attributes 250
 - T'oo'dichi' Cretaceous, USA
 - zeolite 887
 - Tanganyika, Africa
 - hydrothermal petroleum seep 700
 - laminites 6
 - Quaternary history 303
 - Torrens, Australia
 - biology and salinity 641
 - Tuz (Tuzgolu), Turkey
 - attributes 252
 - Tyrell, Australia
 - hydrogeochemistry 89–91
 - Urmia, NW Iran
 - attributes 254
 - Van, Turkey
 - attributes 247
 - Laminites
 - deepwater
 - “rain from heaven” mode 33–35
 - Dead Sea, Middle East 273
 - Lake Urmia, Iran 255
 - defined 5
 - halite 27
 - Langbeinitite
 - definition 794
 - Lee Stocking Island, Bahamas
 - stromatolite 12
 - Leman Field, North Sea 561
 - Length-slow chalcedony
 - as evaporite indicator 533, 539
 - Lithium
 - attributes of commercial deposits 850–852
 - Lorca Basin, Spain
 - organic matter (Messinian) attributes 668–670
 - Lufilian foldbelt, central Africa 491
 - Lunettes
 - gypsum 31–33
 - Lutecite
 - as evaporite indicator 533
- ## M
- Madigan Gulf, Lake Eyre
 - salt crust 202
 - Magadiite
 - attributes 537, 538
 - in Lake Magadi, Africa 262
 - Magnesite
 - attributes of commercial deposits 854–857
 - isotopic signature 858
 - pedogenic 81
 - Maha Sarakham Formation, Thailand
 - basal anhydrite 499
 - dissolution
 - stratigraphic evolution 495
 - preferential solution 495
 - Mahoney Lake, Canada
 - biology and density stratification 670–671
 - Malata-Greenly playa, Australia
 - hydrology 81
 - Mallowa Salt, Australia
 - halite textures 40
 - Marine aerosol
 - input to continental waters 86–88
 - Marion Lake, Australia
 - attributes 228
 - gypsum pseudomorphs 541
 - strandline/seepage facies 16
 - Maritime Alps, Europe
 - halokinesis 429
 - Megapolygons
 - attributes 120
 - Meromixis
 - definition 670
 - ectogenic 306
 - Mono Lake, California 244, 671
 - Solar Lake, Gulf of Elat 232
 - Mesogenesis 2
 - Mesohaline
 - definition 68
 - Messinian evaporites, Mediterranean
 - attributes 293
 - diachronous stratigraphy 352

- Microbialite
 attributes 6
 lacustrine 9
 layering in microbial mats 650–652
 marine 12–13
 marine to evaporite transition 13–16
 mineralisation styles 9
 non-stromatolitic 9
 sedimentology 10–11
 travertine 9
- Mineralisation
 Cu-Ag Rote Faule, Europe 696
 Pb-Zn, Cadjebut Australia 528
 uranium, Black Hills, Dakota 530
- Mirabilite
 in chotts and sabkhas of North Africa 804
 in Great Salt Lake, USA 808, 873
 in Ingebright Lake, Saskatchewan 870
 in Turkish salt lakes and pans 871
 occurrences 866
 replaced by thenardite 871
 temperature stability 865
- Mischsalz
 definition 794
- Mitre folds 420
- Mixing. *See* Brine, mixing
- Mixolimnion
 Dead Sea, Middle East 269
 definition 116, 670
 Lake Hayward, Australia 126
 Mono Lake, USA 244
- Moat Facies
 Lake Magadi 259
- Moganite
 as evaporite indicator 539
- Monimolimnion
 definition 670
- Monohydrocalcite
 Lake Fellmongery, Australia 226
- Monomixis
 definition 670
- Monsoons
 Lake Eyre Hydrology 204
- Mount Sedom, Middle East
 in human history 375
 karst and caves 510
- Mulhouse Basin (Oligocene), Europe
 organic matter 675
 sylvite 809
- N**
- Nahcolite
 production from steam flushing 905–906
- Namakiers
 breccia style 485
 Dashti glacier at Kuh-e-Namak, Iran 378
 emergence at tear faults 426
 speed of salt flow 378
- Namib Desert, Africa
 attributes 64
 pedogenic gypsum 87–88
- Neutral buoyancy
 defined 376
 Gulf of Mexico salt 381
- Nitrates
 attributes of commercial deposits 852–854
- Norphlet Formation, USA
 authigenic salts 562
- North Pole, Pilbara
 vents or pseudomorphs? 105
- Nutrients
 organic productivity 627, 643, 674
 recycling in density stratified brine 667
 recycling in microbial mats 674
- O**
- Oil and gas. *See* Hydrocarbon
- Oligotrophic lake
 definition 670
- Organic matter
 “feast or famine”. *See* Source rock
 African rift valley lakes 664
 Dead Sea, Middle East 666
 Lorca Basin, Spain 668
 destruction 658
 evolution into a source rock 617
 Lake Nakuru, Africa
 the “flamingo” connection 662–666
 Lorca Basin (Miocene), Spain 668–670
 organic productivity in saline waters 661
 Storr’s Lake, Bahamas 668
 production 661
 sedimentation rate 674
- Osmotic
 stress 668
- Ostracod
 salinity tolerance 641
- Overpressure
 beneath salt 585–591
 causes 584
 rafts in flowing salt 587
- Owens Lake, USA
 evaporation rates 66
- Oxygen
 solubility in brine 659

P

- Palaeohydrology
 - Stokes surfaces 121
- Palo Duro Basin, USA
 - palaeogeography 315
- Palygorskite
 - authigenic 56
- Pans, Saline 176–211
 - attributes 179
- Paradox Basin, USA
 - potash production from brine wells 808
- Parry Islands Foldbelt, Canada
 - compressional tectonics 419
- Pedogenic Salts
 - Gypsum 28–33
- Pedogenic salts
 - Nitrates 852–854
- Pellets
 - producers in saline waters 639
- Penesaline
 - definition 68
- Permeability
 - halite and anhydrite 709–711
- Persian Gulf. *See* Arabian Gulf
- Petroleum. *See* hydrocarbon
- Phanerozoic evaporite
 - volume through time 295
- Photosynthesis
 - mechanism 630
- Pinnacle reef
 - evaporite-sealed, Keg River (Devonian), Canada 748
 - evaporite-sealed, Michigan Basin (Silurian), USA 746
- Pisolite
 - as indicator of seepage 16, 339, 350
 - in Andean Altiplano 16
 - in Marion Lake, Australia 16
 - Lake MacLeod, Australia 230
 - marine 18
 - seepage 17
 - vadose 16–18
 - via “in situ” alteration 18
- Platform evaporite
 - attributes 310
 - in “greenhouse” climatic mode 346
 - ramp facies 312
 - rimmed shelf facies 318–323
 - sequence stratigraphy 345–346
- Playa
 - attributes of modern playas 59–67
 - capture 124
 - definition 140
 - depositional spectrum 176
 - discharge
 - defined 80
 - falling watertable 125
 - recharge
 - defined 80
- Polygons. *See* megapolygons
- Polyhalite
 - via glauberite replacement 84
- Porosity
 - burial loss in halite beds 44–45
- Potash evaporites
 - attributes 793–891
 - historical terminology 794
 - in Amadeus Basin playas, Australia 804
 - in Chott el Djerid, Tunisia 801–804
 - in Danakil Depression, Africa 799–891
 - in Lake Qaidam, China 796–799
 - potash production, usage 795
 - potash production, worldwide 794
 - production from brine wells 805–809
 - sylvite
 - via incongruent solution 793
 - via primary precipitation 793
 - the “potash problem” 101–105, 794
- Precambrian
 - atmosphere 106–107
 - carbonate textural evolution 21
 - evaporite salts 105
- Pressure
 - abnormal pressures 583–590
 - overpressure 585
 - control using mud weights 403–404
 - Gulf Coast “gumbo” 403–404
 - underpressure 592
 - hydrostatic 583
- Primary evaporite
 - attributes 5–38
 - defined 2
- Problems in evaporite correlation
 - biostratigraphic 336
 - dissolution effects 336, 497
 - rapidity of deposition 336
 - stratigraphic complexity 336
 - use of vertical exaggeration 336
- Pseudomorph
 - aragonite after gypsum 541
 - calcite after gypsum 541
 - crystal morphologies 564
 - gypsum “ghosts” 48
 - halite after gypsum
 - hydrological mechanism 134–136
 - textures 43
 - interpreting ocean history 105–112
 - reaction rims 84

Q

- Qaidam Basin, China
 - boron isotopes 92
 - brine evolution 91
 - source of salts 67
- Qarhan salt plain, China
 - potash geology 796
- Quartzine
 - as evaporite indicator 532
- Quaternary evaporite
 - extent and thickness 293

R

- “Roho” system
 - defined 407
 - Rafted intrasalt blocks
 - Mode of formation 389
 - overpressure 587
 - Rainfall
 - extreme events in deserts 211
 - Raisby Formation, UK
 - evaporite solution breccia 542
 - Ras Muhammad pool, southern Sinai
 - attributes 232
 - Rauhewacke
 - defined 486
 - Lufilian (Katangan) foldbelt, central Africa 492
 - Swiss Alps, Europe 486
 - Red River (Ordovician) Formation, USA 716–720
 - Reefs
 - Proximity to evaporites through time 318
 - Reef growth
 - influence of salt tectonics 438
 - Retrograde solubility
 - Abu Dhabi sabkha 159
 - defined for anhydrite 75
 - of the common salts 455
 - Rollover anticline
 - mode of formation 394
 - Rote Faule
 - Cu-Ag mineralisation, Poland 696
- S**
- “Stokes” surfaces 119–123
 - Sabkha
 - algal mats 6, 149–150
 - Arabian Gulf 143
 - Basin and Range playas, USA 182
 - classification by setting 141
 - continental 181
 - alluvial fan–ephemeral saline lake 181
 - ephemeral stream floodplain - dune field–ephemeral 201
 - continental mudflat and pan
 - attributes 176
 - definition 139–141
 - eolian 211–218
 - hydrological attributes 113
 - limitations of Holocene models 174–176
 - sedimentary model 173
 - Holocene limitations 175
 - textures 38–40
 - Sabkha (place name)
 - Abu Dhabi 143–152
 - intertidal facies 149
 - island shoal facies 145
 - subtidal facies 145
 - supratidal facies 151
 - Bardawil Lagoon, Middle East 170–171
 - Bristol Dry Lake, California 183
 - Coastal, eastern Saudi Arabia 160–161
 - Death Valley playa, California 185
 - Deep Springs Lake, California 182
 - Gulf of Suez 166
 - Kuwait, Al Khiran 166
 - Kuwait, Kadmah Bay 161–164
 - Lake Eyre, Australia 202
 - Lake Frome, Australia 208
 - Nile delta coast, Egypt 168–169
 - Sabkha el Mehabeul, Algeria 803
 - Sabkha el Melah, Algeria 191, 803
 - Sabkha Matti, UAE 217
 - Sabkha Yotvata, Israel 181
 - Saline Valley playa, California 183
 - Shatt el Arab estuary 172–178
 - Umm Ash Shuraybat, Saudi Arabia 217
 - Umm Said sabkha, Qatar 119
 - Salar
 - attributes 187–201
 - Salar de Atacama, Chile 196–198
 - Salar de Uyuni, Bolivia 191–192
 - Salar Grande, Central Andes of Chile 198–201
 - Salda Lake (Saldagolu), Turkey
 - attributes 250
 - stromatolites 11
 - Salinas
 - carbonate 223
 - coastal Australia 222–228
 - Coorong lakes 223
 - gypsum 227–229
 - halite 230–231
 - Lagoa Vermelha, Brazil 236–238
 - Pleistocene, Ras Shukeir, Red Sea coast 234
 - Ras Muhammad Pool, Sinai 232
 - Sleaford Mere, Australia 223
 - Solar Lake, Gulf of Elat 232
 - stromatolites 228
 - Saline mudflat
 - attributes 178–179

- Saline pan
 - attributes 179–180
- Saline Valley playa, California
 - attributes 183
- Saltern
 - attributes 297
- Salts
 - Industrial usage 793. *See also* Annual production
- Salt cake. *See* Sodium sulphate
- Salt canopy
 - attributes 409
- Salt Flat Playa, west Texas
 - tepee crusts 178
- Salt glacier 400, 410, 434
 - breakout 395
 - emergence at compressional tear faults 426
- Salt ramp 395
- Salt roller 394, 416
- Salt solution mining. *See* Solution mining
- Salt strength
 - changes during deformation 389
- Salt tectonics
 - “Roho” system 407
 - contractional
 - anticlinal salt breakout 420
 - décollement 423
 - gravity gliding 414–423
 - inverted basins 422–423
 - mechanisms 414
 - thin-skinned fold and thrust 419–423
 - density and viscosity changes 376–382
 - diapirs
 - active 390, 433
 - evolution of a salt wall 396
 - falling 396
 - lack of faulting 391
 - mock-turtle anticline 396
 - passive 390
 - reactive 389, 433
 - turtle structures 396
 - effect on sedimentation style
 - influence of diapir stage 432–440
 - postkinematic 431
 - prekinematic 431
 - synkinematic 431
 - fold wavelengths 388
 - modelling
 - fluid-brittle overburden 377
 - fluid-fluid 377
 - significance of weakness 381
 - pressure effects 382–384
 - raft tectonics 396–398
 - Kwanza Basin 397
 - mechanisms 397
 - Zechstein Basin 397
 - salt flat 395
 - salt flow textures and rates 388–389
 - salt geometry and sedimentation rate 394–395
 - thermal effects 384
 - triggers to salt flow
 - differential loading 408–410
 - regional extension 389–391
- Salt weld 401, 416
 - attributes 406–410
 - fault weld 402
 - primary weld 402
 - secondary weld 402
- Santos Basin, Brazil
 - salt tectonics 417
- San Andres Formation, USA
 - Levelland-Slaughter trend, USA 733–734
 - saltern 315
 - Yates field, west Texas 752
- Saudi Arabia
 - coastal sabkha 161
- Seal capacity
 - evaporite properties 708–711
- Searles Lake, USA
 - attributes 843
 - borates from brine 843
 - sodium sulphate from brine 872
 - trona from brine 860
- Seawater
 - concentration series 68
- Seawater chemistry
 - changes across time
 - Archaean 105
 - Phanerozoic 102–105
 - Proterozoic 105
- Secondary evaporite
 - defined 2
- Sedimentation, diapiric
 - postkinematic 431
 - prekinematic 431
 - synkinematic 431
- Seismic pumping
 - in compressional regimes 574
 - in salt-floored extensional basins 589
- Selenite
 - Holocene 229
- Sepiolite
 - authigenic 56
- Sepiolite (meerschaum)
 - Lake Eskisehir, Turkey 85
- Sequence stratigraphy
 - attributes 340–372
 - autocyclic controls 350–351
 - basinwide evaporites 342, 347–351
 - problems in methodology 348

- basinwide stages
 - “fill and spill” 351
 - gypsum wedge 350
 - intra-basinal TST 351
- carbonate systems 345
- classic methodology 340
- effect of sealevel 342
- eustacy
 - “greenhouse” climate mode 343
 - “icehouse” climate mode 343
- evolution during drawdown 348–351
- importance of solution breccias 346
- in Zechstein evaporites, Europe 363–368
- platform evaporites 342
 - eustacy and restriction 345–346
- Shale diapir
 - characteristics 450
- Shatt el Arab delta 172
- Sigsbee Scarp, Gulf of Mexico
 - salt allochthons 376, 399
- Sleaford Mere, Australia
 - attributes 223
- Smackover Formation, USA
 - authigenic salts 563
- Smackover Formation (Jurassic), USA 737–739
- Snowball Earth
 - ikaite 565
 - isotopic character 110
 - tepee-like structures 292
 - timing 293
- Sodium carbonate salts. *See* Trona
- Sodium sulphate
 - attributes 865–872
- Soil moisture zone
 - defined 113
- Solar Lake, Gulf of Elat
 - attributes 232
 - heliothermal character 127
- Solubility
 - of common salts 455
- Solution mining
 - cavities
 - cavern plugging 941
 - indicators of breached caverns 939
 - indicators of collapse 938
 - lithology effects cavern shape 901–903
 - predicting ground collapse 940
 - salt creep 936
 - history 894
 - methods of mining
 - cluster well pad 904
 - single well pad 903
 - Trump method 899
 - Tully method 899
 - problems with cavities
 - Barycz and Wieliczka sites, Poland 916
 - Bayou Choctaw, Louisiana 927
 - Cargill saltworks, Kansas 921
 - Detroit River brinefield, USA 922
 - Gellenoncourt saltworks, France 919
 - Grand Saline sink, Louisiana 898, 927
 - Ocelele Mari brinefield, Romania 912
 - Old Belvedere Spinello brinefield, Italy 915
 - Retsof Mine, USA 920
 - Windsor brinefield, Canada 922
 - problems with hydrocarbon storage
 - Barber’s Hill explosion 934
 - Brenham explosion 933
 - Gorham oil field, USA 926
 - Haoud Berkaoui oil field, Algeria 927
 - Hutchison explosion, USA 935
 - Lake Peigneur, USA 928
 - Mineola propane fire, USA 935
 - Panning Sink, USA 926
 - Weeks Island, Louisiana 930
 - West Hackberry explosion, USA 932
 - Wink Sink, USA 925
 - techniques
 - snubbing 897
 - well and cavern design 896
- Solvay method
 - trona production 859
- Source rock
 - “feast or famine” style 701. *See also* organic matter
 - Biomarkers indicating hypersalinity 653
 - classification 619–628
 - basin style 1a 620
 - basin style 1b 621
 - basin style 2 625
 - basin style 3 627
 - basin style 4 628
 - controls on enrichment 658
 - definition 617
- Speleothem
 - gypsum 507
 - halite 514
 - oulopholite (cave flowers) 514
- Sphalerite
 - colloform 530
- Spring Mound. *See* Tufa
- Strain
 - markers
 - in flowing salt 388
 - memory
 - in flowing salt 387
 - rates
 - speed of salt deformation 378
- Strandline/seepage facies
 - attributes 6
 - Elk Point Basin 339

- Stromatolites
 attributes 6
 Coorong Lakes, Australia 226
 cyanobacteria 7
 Dead Sea, Middle East 277
 definition 6
 hydromagnesite 226, 251
 lacustrine 10
 marine 12
 Marion Lake, Australia 228
 microbialite 6
- Strontianite
 in diapir caprock 449
- Subnormal pressure. *See* Underpressure
- Sulphate reduction
 bacterial 686–689
 Dead Sea brine column 273
 thermochemical 689–692
- Sulphur
 attributes of economic deposits 877–881
 isotope
 indicator of parenthood 94–96
- Sulphuric acid speleogenesis 521–528
- Supersaline
 definition 68
- Sylvinitic
 definition 794
- Sylvite
 in Canadian Maritimes 823
 in Danakil Depression, Africa 800
 in Delaware basin, USA 817
 in Khorat Plateau, Thailand 811
 in Lake Amadeus, Australia 804
 in Prairie Evaporite, Canada 820
 in Rhine Graben, Europe 809
 in trans Atlantic basins 824
 in Zechstein Basin, Europe 815
- Syndepositional karst
 carnallite/halite crusts 799
 gypsum/halite crusts 40–41, 129–130, 229
- T**
- Taper angles
 in salt-cored thrusts 381, 420
- Telogenesis 2
- Temperature
 deposition. *See* Fluid inclusions
 gradient and salt mass 593–594
- Tepee
 Abu Dhabi sabkha, UAE 148
 attributes 18–20
 Coorong Lakes, Australia 226
 island shoal facies 17
 Lake MacLeod, Australia 230
 Marion Lake, Australia 20, 228
 Salt Flat Playa, USA 178
 stacking 20
- Tertiary evaporite
 attributes 51–54
 defined 4
- Textural re-equilibration
 “sabkha-ized” sediment 44
 attributes 43–57
 influence of burial 45–50, 601–604
- Thenardite
 phase-stability temperature 867
- Thermalite
 Abu Dhabi sabkha 159
 defined 158
- Thermochemical sulphate reduction. *See* sulphate reduction
- Thinolites 11, 246
- Thrombolite
 Lee Stocking Island 12
 Sleaford Mere, Australia 223
 Storr’s Lake, San Salvador 12
- Thrust belt
 décollement 423
 in Atlas Mountains, N. Africa 422
 in Carpathians, Romania 427
 in Lufilian foldbelt, central Africa 492
 taper angle 423
- Thrust plane breccias (Rauhewacke)
 attributes 486–493
 in Carson Sink, USA 490
 in Haselgebirge Fm, Austria 487
 in Swiss Alps 486
- Total Organic Carbon (TOC)
 Coorong salinas, Australia 225
 Green River Fm. (Eocene), USA 627
 Hanifa Fm. (Jurassic), Saudi Arabia 625
 Mulhouse Basin (Oligocene), France 675
 Quaternary saline association 629
- Travertine 9
- Trona
 as an Archaean marine mineral 107
 blinding in solution mining 905
 in Lake Magadi, Africa 259, 865
 marine or nonmarine? 77
 phase chemistry 79, 905
 Sodium carbonate deposits 859–891
 textures 260
- Tufa
 attributes 9–10
 Deep Springs Lake, USA 183
 El Peinado and San Francisco lakes, Andean Altiplano 9
 High Magadi beds, Africa 260
 Lake Eyre Basin, Australia 206
 Lake Van, Turkey 250
 Mono Lake, USA 244

Salar Uyuni, Bolivia 195
 Salda Golu, Turkey 10
 salina margins, Australia 223
 Tumuli 463

U

Underpressure
 salt-related 592–615
 Uranium, Black Hills, USA 530–531

V

Vadose pisolite. *See* Pisolite
 Van't Hoff
 phase equilibria 69
 Vitahaline
 definition 68
 Vitrinite reflectance
 attributes 617

W

Waste disposal
 in salt storage caverns 910–912
 Water
 Specific heat 659
 Water depth
 saline lakes 283
 Water level changes
 Dead Sea, Middle East 267
 Great Salt Lake, USA 240
 Lake Lisan, Middle East 278
 Lake Urmia, Iran 255
 Lake Van, Turkey 249
 Mono Lake, USA 244
 Weakness of salt
 in salt flow modelling 381
 Weeks Island, Louisiana
 oil storage problems 930
 Wet interdune
 attributes 119–121
 Wilson cycle
 control on basinwide evaporites 331
 squeezed diapirs 425
 thin-skinned salt tectonics 419
 Woese, Carl
 domains of life 629

Y

Yotvata Sabkha, Israel
 attributes 181

Z

Zagros Foldbelt, Middle East
 compressional tectonics 420
 Zechstein evaporites, Europe
 authigenic magnesite 133
 brine evolution 84
 lack of kainite 84
 raft tectonics 397
 sequence stratigraphy 363–368
 Zeolite
 minerals and properties 882–887
 via brine alteration 85